Jovitas Skucas

Advanced Imaging of the Abdomen

Springer

Advanced Imaging of the Abdomen

Jovitas Skucas

Advanced Imaging of the Abdomen

With 489 Figures in 1025 Parts

Springer

Jovitas Skucas, MD
Professor Emeritus, Department of Imaging Sciences, University of Rochester, Rochester, NY, USA

British Cataloging in Publication Data
A catalogue record for this book is available from the British Library.

Library of Congress Control Number 2005924309

ISBN-10: 1-85233-992-6 e-ISBN 1-84628-169-5
ISBN-13: 978-1-85233-992-0

Printed on acid-free paper.

Printed in the United States of America. (BS/EB)

9 8 7 6 5 4 3 2 1

Springer Science+Business Media
springeronline.com

Preface

This book is an attempt to bridge the interface between referring clinicians and radiologists when faced with a patient suspected of having a complex or unusual abdominal condition. The emphasis is on the choice of imaging procedures, expected diagnostic yield, a discussion of pertinent imaging findings, and the possible differential diagnosis. The rapid proliferation of imaging techniques provides a bewildering array of choices to the referring physician. Thus when faced with a suspected biliary abnormality, should one suggest traditional endoscopic retrograde cholangiography, or is noninvasive and noncontrast magnetic resonance (MR) cholangiography or even contrast-aided computed tomography (CT) cholangiography more appropriate? What is the role of CT virtual colonoscopy? Is it limited to colon cancer screening or does it have a role in cancer staging?

This book discusses imaging topics of those structures that fall in the purview of the gastroenterologist, urologist, general surgeon, and related specialist. The anatomic limits of the abdomen are somewhat stretched to include the esophagus superiorly, and the aorta, inferior vena cava, and adjacent structures posteriorly. The emphasis is on new imaging findings and innovations. This book also discusses the clinical aspects of a disease needed to formulate a rational diagnostic approach, but basic research, results of animal studies, and imaging research are not discussed as they are not pertinent to clinical medicine. Because of space limitations, fetal imaging and choosing a contrast agent are not discussed. Also, laboratory findings and therapeutic options are not discussed, except for those having a bearing on subsequent diagnostic studies.

This book is intended to be used as a reference for the atypical and unique presentation and newer diagnostic imaging modalities. Publications of unusual clinical and imaging finding are accentuated, and common imaging studies of common disorders are only mentioned in passing, if they are applicable.

Traditionally, radiology texts have used a pathologically oriented outline. Subsequently it became the custom to discuss disorders from an imaging point of view. An attempt is made here to integrate clinical presentation with pertinent radiologic findings. The material is organized primarily along anatomic organ systems, with some exceptions. For instance, disorders of the adnexa involve the peritoneal cavity, but they are closely related to the female genital tract and thus are included in Chapter 12, Female Reproductive Organs, rather than the peritoneum chapter. Within each organ system the material is subdivided further along broad disorder categories, such as congenital, inflammation, tumors, etc., but a pragmatic clinical approach is adopted. For example, a

history of trauma is usually known and thus imaging findings associated with acute trauma are discussed in separate sections.

It has been said that "to steal from one author is plagiarism, if you steal from many, it's research" (1). With that definition in mind, this work, I hope, is research. The references are rather wide-ranging, but to make the text more readable the number of references is deliberately kept low and information that has diffused in the medical community is not referenced further. The cited references serve both as an acknowledgment to the original authors and as a guide to a more in-depth source on a particular topic.

An abbreviated format has been adopted in presenting published studies. Emphasis is on sensitivity and specificity (or false-positive rate), realizing that these provide an incomplete picture. Where applicable, the measurements given include a standard deviation. To maintain brevity, little additional statistical analysis is provided.

It is assumed that the reader has basic knowledge of abdominal imaging. The technical details about performing and interpreting various imaging modalities are omitted except when pertinent to new techniques and applications. Thus a statement such as

> Tc99m-DTPA scintigraphy and color duplex US . . . could reliably differentiate minimal and not perfused renal allografts . . .

omits that scintigraphy consisted of analogue scans up to 60 minutes postinjection and that time-activity curves over the first 60 seconds after injection of 370 to 440 MBq of technetium-99m-diethylenetriaminepentaacetic acid are obtained and classified by a perfusion score, the time between renal and iliac artery peaks and washout of the renogram curve; similarly, not mentioned is that color duplex ultrasonography (US) consists of a perfusion study in all sections of the graft and vascular anastomoses by color-coded duplex sonography and that maximal blood flow velocity and resistive index in the renal artery are determined by a pulsed Doppler device. Most of these details are intuitive to the specialist performing such a test.

To avoid repetition, the more common imaging findings are not repeated for each imaging modality. Thus if a lesion contains fat, it is stated as such; it is not stated that this fat is hypodense with CT, hyperechoic with US, or hyperintense with T1-weighted MR sequences. The exception is if a specific imaging appearance is unique.

Indications for magnetic resonance imaging (MRI) are still evolving. In addition, as new imaging technology becomes available the imaging modality recommended for a particular application today may not be optimal tomorrow. Thus multislice helical CT techniques continue to expand application of CT angiography and interventional procedures, possibly at the expense of further rapid growth of MRI.

Numerous individuals contributed images to this book and their effort is gratefully acknowledged. Over the years many ex-residents have provided me with interesting studies from their daily practices and these are acknowledged. A special thanks goes to Jolanta Galdikaite, an illustrator in Kaunas, Lithuania, for the line drawings.

Jovitas Skucas, MD

Reference

1. Attributed to the Hollywood ne'er-do-well Wilson Mizner (1876–1933). Quoted in Green J. Chasing the Sun: Dictionary Makers and the Dictionaries They Make. New York: Henry Holt, 1996:19.

Contents

Terminology

The term *tumor* is used in a broad sense for a focal growth, be it inflammatory, developmental, or neoplastic in nature. In solid organ chapters *tumor* is used synonymously with *nodule*.

A number of terms are in general use to describe computed tomography (CT), ultrasonography (US), and magnetic resonance (MR) imaging findings. Although the synonyms listed are self-evident to radiologists, they tend to be confusing to clinicians. For consistency, the following terminology is adopted:

Adopted Terms[1]	Synonyms
CT[2]:	
Hypodense	Hypoattenuating, low attenuation, low opacity
Isodense	Isoattenuating
Hyperdense	Hyperattenuating, high attenuation, high opacity
US:	
Hypoechoic	Hypogenic, hypoechogenic, echopenic, sonolucent
Isoechoic	Isogenic
Hyperechoic	Hypergenic, echogenic
MR[2,3]:	
Hypointense	Low signal intensity
Isointense	Intermediate signal intensity
Hyperintense	High signal intensity

[1] Density, echogenicity, and intensity are usually expressed in reference to an assumed internal standard, generally normal adjacent tissue parenchyma.

[2] CT and MR precontrast and postcontrast appearances of a lesion varies. Also, the early postcontrast appearance (arterial phase) often differs from that seen on delayed images (venous phase or even later).

[3] MR findings vary depending whether T1- or T2-weighted sequences are imaged and on imaging parameters used. To avoid confusion, these MR terms are applied only to precontrast images. The terms hypo- and hypervascular are used to describe tissue appearance after intravenous contrast injection. The term *contrast agent* has a different meaning in MR than usually applied to barium sulfate or the iodinated agents used in angiography and CT. MR contrast agents are not visualized directly; rather, their usefulness is based on their ability to change water proton relaxation times.

I

Digestive System

1

Esophagus

Technique

Dynamic Recording

Videopharyngography, also called modified barium swallow, is an established technique providing dynamic recording in evaluating deglutition. Continuous image detection rather than pulsed fluoroscopy is preferred because transient laryngeal penetration is more difficult to detect with the latter.

Esophageal videofluoroscopy (videoesophagography) is preferred by some radiologists to evaluate esophageal tonicity and peristalsis, while most simply rely on fluoroscopic observation. Especially in a search for subtle peristaltic abnormalities, a recumbent patient position is preferred to eliminate gravity. Manometry and esophageal videofluoroscopy agreed 100% in a setting of normal esophageal function, in 90% for nonspecific motility disorders, 100% in diffuse esophageal spasm, and 90% in achalasia, but only in 50% for a "nutcracker" esophagus (1).

A computer program can quantify esophageal wall motion using data obtained from an esophagogram, but whether such information is of clinical relevance remains to be established.

Speech therapists and some radiologists prefer a lateral view when evaluating swallowing. Nevertheless, a frontal view has much to offer during the pharyngeal phase. In experienced hands, laryngeal penetration is just as readily detected in a frontal position and, in addition, right- and left-sided pharyngeal muscle function can be compared to each other. Oblique views are of occasional value.

High-speed magnetic resonance imaging (MRI) also evaluates dynamic deglutition (*MR pharyngography*), but clinical application of this technique is still evolving.

Barium Studies

Barium sulfate is the preferred contrast agent for intraluminal esophageal studies. Controversy exists, however, in a setting of a suspected leak, with some radiologists, especially in Europe, preferring water-soluble contrast (discussed below; see Trauma).

A barium-rice mixture, mixed in equal proportions, has been proposed to evaluate esophageal motility disorders; a normal esophageal transit time for such a mixture is between 5 and 15 seconds. In patients with esophageal motility disorders, this simple and low-cost technique yields a transit time outside of these limits in over half (2). Nevertheless, it is not often employed and dynamic recording using various consistency barium products is more in vogue.

Children presenting with dysphagia are readily evaluated with an esophagram.

A 11.5-mm barium tablet is commercially available. It serves no useful purpose in the face of an obvious stricture but is useful in detecting a subtle esophageal narrowing. The tablet is

designed to dissolve and thus is retained only temporarily proximal to a stricture. Normally the barium tablet should pass into the stomach within 20 seconds when using a standardized 45-degree incline position and ingesting 60 cc of water after swallowing the tablet; failure of tablet passage under these conditions suggests a persistent narrowing. These conclusions do not apply to a patient in a horizontal position.

A barium tablet has been used to screen for occult esophageal lesions during routine chest radiography but is rarely practiced today. A chewed barium tablet, barium-impregnated marshmallow bolus, and similar contrast have been largely supplanted by standardized meals in evaluating oral and pharyngeal dysfunction.

Computed Tomography

A low-density, high-viscosity barium paste ingested just before computed tomography (CT) scanning aids in outlining the esophageal lumen. A negative oral contrast agent, consisting of a vanilla-flavored paraffin emulsion, has been used during helical CT to evaluate chemotherapy of esophageal cancer (3) but is not widely employed.

Sufficiently rapid image acquisition of a region in question during a single breath-hold is feasible with multislice helical CT, allowing two-dimensional (2D) and 3D reconstructions.

Ultrasonography

The thyroid gland acts as an acoustic window of the cervical portion of the esophagus. The left liver lobe provides an acoustic window for study of reflux and the gastroesophageal junction.

Gray-scale ultrasonography (US) has been used to investigate oral motor function in children with neurologic impairment (4). Its full role is yet to be established.

Endoscopic US (*endosonography*), using a high-resolution 20 MHz transducer, has the potential of becoming the most important imaging modality in esophageal cancer staging and evaluating other intramural lesions. Tumor extension to regional nodes can be detected. The current trend is that endosonography influences patient management, often toward less costly, less risky, and less invasive procedures. Endoluminal US data can provide 3D images, potentially aiding staging, but this technique is too new to draw conclusions.

Fine-needle aspiration biopsy using endoscopic US guidance is feasible.

Magnetic Resonance Imaging

Of all gastrointestinal structures, the esophagus is most prone to respiratory and cardiac motion artifacts. Cardiac-gated techniques are not often used because of the prolonged sequences.

Most radiologists do not opacify the esophagus during MR imaging.

Scintigraphy

Use of esophageal transit scintigraphy varies considerably among institutions and countries. Whether its diagnostic value approaches that of a barium study or manometry is debatable. The current indications for its use are when esophageal manometry is unavailable, when the patient cannot tolerate manometry, when there is clinical suspicion of a motility disorder but the manometry is equivocal, and when a serial response to therapy is desired.

Manometry

Esophageal manometry often serves as a gold standard when evaluating other imaging modalities for detecting and classifying esophageal motility abnormalities. Correlation with eventual clinical diagnoses, however, shows that it is an imperfect gold standard. Although temporal measures of intraluminal pressure at various sites in the esophagus, including the gastroesophageal junction, translate into esophageal tonicity and peristalsis values, many esophageal motility disorders have overlapping findings, and manometry is often simply reported as "nonspecific" or "compatible with" a certain disorder. These findings are, of course, not unique to manometry, and other dynamic imaging modalities also have similar limitations.

Manometry is not complication free. Thus esophageal perforation occurred in a patient during manometry, mediastinitis and bilateral pleural effusions developed, a distal esophageal perforation was detected, and an esophagectomy and gastric pull-through performed (5), but the patient died.

Congenital Abnormalities

Duplication

An esophageal duplication, which is a foregut cyst, is the least common of all esophageal congenital abnormalities. Complete duplication is rare; some of these abnormalities are also associated with gastric duplication. Some duplications communicate with the esophageal lumen, although most do not. With a high superior communication they mimic a branchial pouch fistula. Some lie between the esophagus and trachea or extend into the mediastinum anteriorly. A rare one is intraabdominal in location.

Duplications are often incidental findings, although being lined by alimentary tract mucosa, they can ulcerate. Hemorrhage or secretions increase their size, with the larger ones then obstructing pulmonary vessels or a bronchus. In the very young they are prone to obstruct the esophageal lumen. Similar to other gut duplications, a rare adenocarcinoma and a leiomyosarcoma have developed in these duplications involved all layers and pleural surface.

Conventional radiography or a contrast study reveals an extrinsic or intramural mass adjacent to the esophageal lumen, most often in the lower third of the esophagus. Computed tomography and MRI confirm their cystic nature. They appear as sharply marginated, fluid-filled oval or spherical tumors (Fig. 1.1). Endoscopic US of one cyst showed contiguity of the esophageal muscularis propria with cyst wall muscle layers (6).

A typical duplication is hypointense on T1- and hyperintense on T2-weighted images, although the T2 signal varies depending on cyst protein content. Postcontrast the cyst wall enhances to varying degree; marked enhancement should suggest either inflammation or presence of gastric mucosa.

A rare cancer develops in a foregut cyst. 2-[18F]-fluoro-deoxy-D-glucose (FDG) positron emission tomography (PET) of a foregut cyst adenocarcinoma revealed numerous hypermetabolic regions consistent with metastases (7).

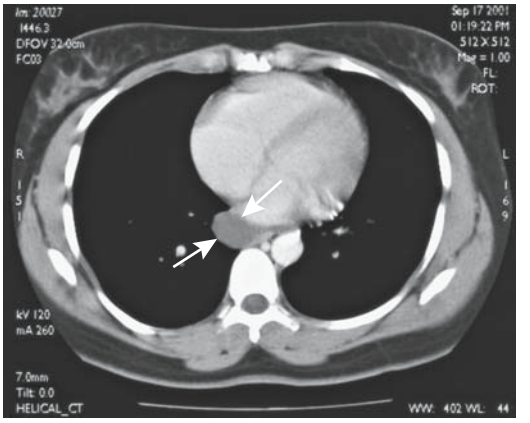

Figure 1.1. Esophageal duplication. Computed tomography (CT) reveals a cyst (arrow) adjacent to the distal esophagus. It did not communicate with the esophageal lumen. (Courtesy of Temil Tirkes, M.D., University of Pennsylvania.)

Bronchogenic Cyst

Bronchogenic cysts are congenital malformations having an epithelial lining. They occur either in the lung or in the mediastinum. When located adjacent to the esophagus they appear to arise from the wall of the esophagus, result in dysphagia, and mimic an esophageal duplication (8). Histologically, both have ciliated epithelium; however, esophageal duplications have two smooth-muscle layers and lack cartilage. Some authors classify both simply as foregut cysts.

Short Esophagus/Congenital Esophageal Stenosis

Most congenital strictures in infants are smooth, elongated, and associated with esophageal foreshortening. In an infant the congenital nature of such a stricture is generally suspected; in older individuals differentiation from complications of reflux esophagitis is problematic.

Multiple ringlike constrictions in the upper or mid-esophagus are occasionally found in young adults with long-standing dysphagia (9); such an appearance is believed to represent residual congenital esophageal stenosis, although a Barrett's esophagus is in the differential.

Atresia/Tracheoesophageal Fistula

Failure of foregut differentiation results in specific tracheoesophageal anomalies. Most

investigators classify these foregut malformations into five types. The nomenclature used varies and it is thus best to describe the actual defect present (Fig. 1.2). Gas in the stomach implies a communication with the tracheobronchial tree. Some H-type fistulas are relatively asymptomatic during infancy and manifest only later in life.

Almost two thirds of neonates with these anomalies also have other defects, with the most common being a cardiac defect, followed by skeletal, neurologic, and renal disorders.

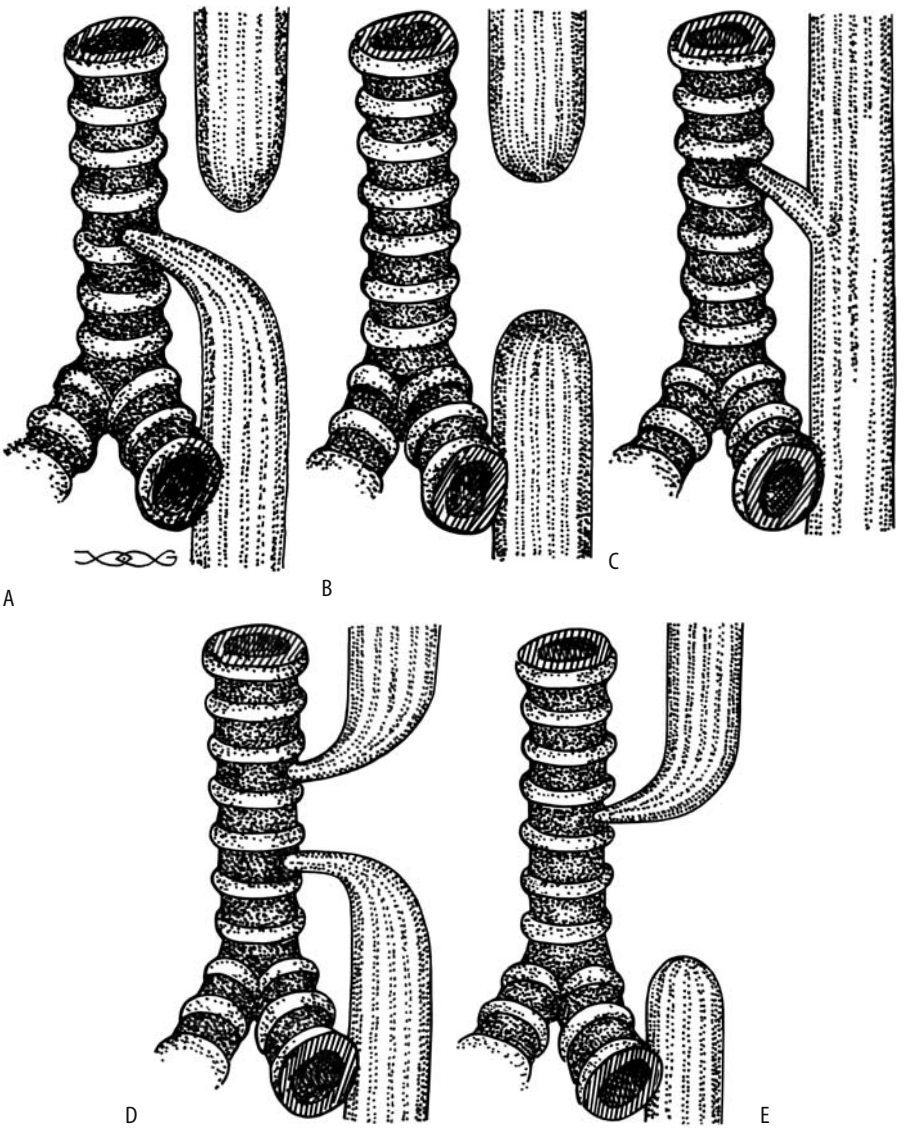

Figure 1.2. Classification of tracheoesophageal fistulas. A: The most common is a proximal esophageal atresia with a distal lateral fistula. B: Isolated esophageal atresia. C: H-type fistula. D: Esophageal atresia with both proximal and distal tracheoesophageal fistulas. E: Distal esophageal atresia and proximal fistula.

Some have a complex bronchopulmonary foregut malformation, including sequestration and duplication. At times the esophageal pouch contains heterotopic pancreatic tissue. One newborn with an esophageal lung (a rare type of communicating bronchopulmonary foregut malformation) also had esophageal atresia, a tracheoesophageal fistula, duodenal stenosis, an annular pancreas, imperforate anus, vertebral anomalies, and ambiguous genitalia (10). In one infant an upper pouch reached 1.5 cm below the tracheal carina while the distal esophagus connected to the trachea 2 cm above the carina, thus also forming a partial esophageal duplication (11); the upper pouch contained heterotopic pancreatic tissue. Rarely, the distal esophagus connects with a lower lobe bronchus, with the involved lung having a systemic arterial blood supply (12).

An increased prevalence of foregut malformations is found in Down syndrome. An association exists between esophageal atresia/tracheoesophageal fistula and congenital distal esophageal stenosis. Complicating the issue are the more common acquired postoperative esophageal strictures. Congenital esophageal stenoses tend to be relatively long, smooth, and circumferential and located at the mid-to-distal esophagus, with a normal caliber superiorly and inferiorly; postoperative strictures, on the other hand, tend to be more focal (Fig. 1.3).

The procedure of choice to evaluate neonates with congenital tracheoesophageal atresia and fistulas is contrast radiography. The role of 3D CT and virtual bronchoscopy is not established, although they appear accurate in defining esophageal atresia and fistulas (13). Small tracheoesophageal fistulas are difficult to detect. Most involve the proximal one third of the esophagus and extend superiorly before communicating with the trachea. A double balloon catheter has been proposed as an aid to evaluate subtle H-type fistulas (14).

Postoperative anastomotic complications include symptomatic stricture, leakage, and recurrent fistula; gastroesophageal reflux is found in over half of these infants, and postoperative esophageal dysmotility is common. Postoperative extrapleural fluid collections in neonates after esophageal atresia repair using an extrapleural surgical approach suggest an anastomotic leak (15); chest radiographs reveal these effusions to be similar in appearance to pleural effusions.

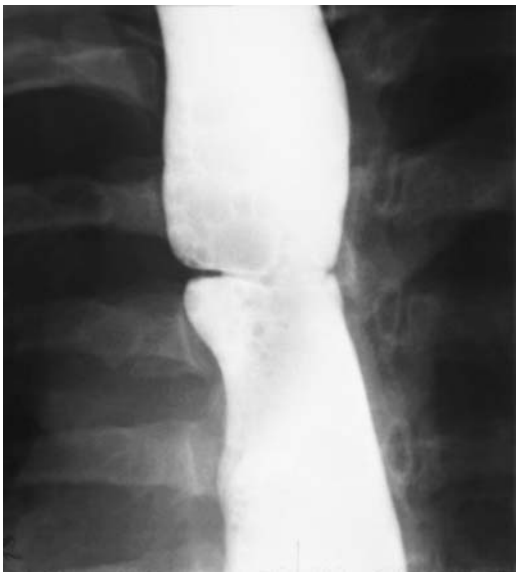

Figure 1.3. Residual deformity in mid-esophagus from a tracheoesophageal fistula repair as a child.

Vascular Anomalies

Embryologically, the great vessels develop from six fetal vascular arches. A normal aorta develops from the fourth arch and pulmonary artery and ductus arteriosus from the sixth. The specific vascular anomaly present depends on the vascular arch remnant; radiologists usually subdivide them based on their radiologic appearance.

Imaging should suggest the type of anomaly present, although at times angiography is necessary to outline the full extent of an anomaly.

Posterior Esophageal Impressions

This is the most common vascular anomaly in this region and is caused by an aberrant right subclavian artery posterior to the esophagus, with an occasional one being between the trachea and esophagus. Similar but reversed finding is found with a right aortic arch and an aberrant left subclavian artery.

Most patients are asymptomatic and it is not uncommon to first detect this anomaly in an adult as an incidental finding. A minority develop dysphagia due to secondary esophageal compression, a condition known as dysphagia lusoria. Occasionally dysphagia lusoria first develops in adulthood and is severe enough to result in poor oral intake and weight loss.

An esophagram is diagnostic; in a frontal position the aberrant artery indents the esophagus from the level of the aortic arch superiorly and to the right, while in a lateral position this indentation is typically posterior to the esophagus. Aortography and CT are superfluous for diagnosis, although useful to define the underlying anatomy if surgical correction is contemplated.

A rare aberrant right subclavian artery aneurysm has eroded into the esophagus.

Posterior Esophageal and Anterior Tracheal Impressions

A vascular ring consists either of a double aortic arch or a right arch together with an aberrant left subclavian artery. A high prevalence of an aberrant left subclavian artery is found in patients with a right aortic arch. The proximal end of the aberrant left subclavian artery, located in the posterior tracheoesophageal space, appears as a diverticular-like aortic outpouching. Magnetic resonance imaging best defines the relationship between involved structures. Esophageal compression and tracheal displacement account for some of the wheezing and dysphagia in these patients.

A barium esophagogram should identify a right aortic arch deformity and suggest an aberrant left subclavian artery but will not detect a vascular outpouching. In symptomatic individuals, the ready availability and low cost of a barium esophagogram make it an ideal screening study.

Anterior Esophageal and Posterior Tracheal Impressions

Abnormal sixth arch development leads to left pulmonary artery originating from the right. Respiratory difficulties predominate in these infants. Either CT or MRI should identify the vascular nature of this anomaly.

Trauma

Blunt trauma is an uncommon cause of esophageal injury. Cardiovascular and lung trauma tend to predominate with a severe injury. Rarely, iatrogenic esophageal injury results from resuscitative measures, at times unsuspected because of minor initial trauma.

An esophageal injury classification scale, devised by the American Association for the Surgery of Trauma, is outlined in Table 1.1.

Hematoma

Although a hematoma is included here under the heading of trauma, it should be kept in mind that some hematomas are spontaneous in origin, especially in patients on anticoagulation therapy. The patient presents with acute chest pain, dysphagia if the hematoma compresses the esophageal lumen, or hematemesis. Pain in some patients is severe enough to suggest spontaneous esophageal rupture (Boerhaave syndrome), an aortic dissection, or acute myocardial infarction.

Some hematomas are huge. A contrast esophagram identifies a smooth or serpiginous intramural tumor (Fig. 1.4). In a still bleeding patient, postcontrast CT reveals extravasation into the hematoma; otherwise, CT simply detects a well-marginated, elongated intramural tumor, initially having an attenuation higher than that of blood.

A contrast study of a hematoma communicating with the esophageal lumen has an appearance similar to an intramural diverticulum; with healing, the hematoma pocket should gradually disappear. A similar imaging appearance is seen with an intramural abscess that drains spontaneously into the lumen.

Table 1.1. Surgical Esophageal Injury Scale

Grade*	Type of injury
I	Contusion or hematoma Partial thickness laceration
II	Laceration ≤50% circumference
III	Laceration >50% circumference
IV	Segmental loss or devascularization ≤2 cm
V	Segmental loss or devascularization >2 cm

* Advanced one grade for multiple injuries, up to grade III.
Modified from Moore et al. (16).

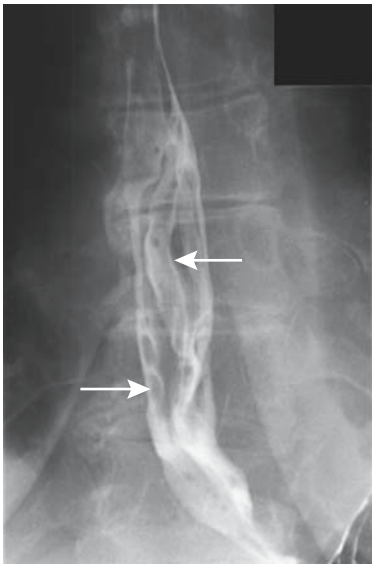

Figure 1.4. Esophageal intramural hematoma. The distal esophagus contains serpiginous folds (arrows) mimicking varices. These findings cleared on a follow-up study.

Most esophageal hematomas resolve with conservative therapy.

Perforation

Clinical

Table 1.2 lists underlying conditions associated with esophageal perforation or fistula. Sudden compression or stretching against an adjacent bony segment account for some perforations during blunt trauma. An occasional cervical spine bony fragment perforates the esophagus.

Table 1.2. Conditions associated with esophageal perforation/fistula

Neoplasm
Primary esophageal
Extrinsic neoplasms
Postsurgical/instrumentation
Erosion by tube or stent
After corrosive ingestion
Penetrating or blunt trauma
Chronic infection
Ingested foreign body
Mallory-Weiss tear
Boerhaave syndrome
Ehlers-Danlos syndrome

The most distal esophageal segment is normally intraabdominal in location, and a perforation here results in a pneumoperitoneum or peritonitis rather than mediastinitis.

Blind attempts to pass a nasogastric tube have led to pharyngeal perforation or a perforation through a Zenker's diverticulum. In newborns, a contrast study through a perforating tube superficially mimics esophageal atresia.

Pain and fever after esophageal instrumentation suggest a perforation, and such a scenario is not an uncommon indication for a prompt esophagram request. The choice of contrast agent to be used is controversial, with junior radiologists leaning toward water-soluble contrast agents while more senior, experienced radiologists tend to prefer barium sulfate. This topic is addressed in more detail below (see Imaging).

Although most localized perforations are managed successfully medically, a more extensive injury requires surgical correction. The success rate of primary repair is highest if performed within 24 hours of injury, thus the reason for performing an esophagram promptly.

Spontaneous esophageal perforation without an underlying abnormality is rare. Patients with Ehlers-Danlos syndrome are somewhat prone to spontaneous esophageal rupture.

Mallory-Weiss Tear

Many Mallory-Weiss tears are not in the esophagus but occur in a sliding hiatal hernia. Prior retching or vomiting is common, although some patients have no antecedent symptomatology. The laceration extends through the mucosa and typically manifests with bleeding, often massive, but most bleeding stops spontaneously. Occasionally, however, even therapeutic endoscopy cannot control bleeding and surgery is necessary.

A Mallory-Weiss tear or even perforation has occurred after ingestion of a colonic lavage solution. Partial obstruction of the esophagogastric junction appears to predispose to these tears.

Boerhaave's Syndrome

Boerhaave's syndrome, or spontaneous transmural esophageal perforation, generally occurs

in the lower third of the esophagus and extends into the left pleural space. Right-sided pleural involvement is less common. This condition has been described in the cervical esophagus (17), but whether such perforation is indeed Boerhaave's syndrome depends on how the syndrome is defined.

Hematemesis is often the initial presentation, with an occasional patient presenting with vomiting and chest pain. Duodenal obstruction, regardless of cause, is associated with Boerhaave's syndrome. A possibility of esophageal perforation is often overlooked and thus a delay in diagnosis and therapy for a condition having an inherent high mortality and morbidity. Nevertheless, an occasional patient is treated medically with satisfactory results.

About 90% of patients with Boerhaave's syndrome have an abnormal chest radiogram (18); hydropneumothorax was found in 50%, pneumomediastinum in 30%, isolated pleural effusion in 25%, and parenchymal infiltrates in 14%. Computed tomography also identifies these findings as well as periesophageal mediastinal fluid. An esophagram using a water-soluble contrast agent should identify the site of perforation and guide surgical therapy (Fig. 1.5). If a diagnosis is delayed, CT is appropriate to detect mediastinitis or a mediastinal abscess.

Figure 1.5. Boerhaave's syndrome. Contrast extravasation (arrow) is just proximal to a hiatal hernia.

Imaging

The most common abnormality after instrumental esophageal perforation is pneumomediastinum, followed by left cardiophrenic angle obliteration. It should be realized that immediately after a perforation a chest radiograph is often normal. In general, a proximal intrathoracic esophageal perforation is more often associated with a right pleural effusion, while a distal perforation leads to a left pleural effusion.

A contrast esophagram is the study of choice to detect an acute perforation. Computed tomography will detect a thickened esophageal wall and adjacent extraluminal fluid, but whether it has a role in early detection of a small leak is questionable.

The choice of contrast agent to be used in a setting of suspected acute esophageal perforation is controversial. A water-soluble agent is used with a suspected acute perforation in the distal esophagus and possible spill into the peritoneal cavity. With a suspected more proximal esophageal perforation a common approach in the United States is to start with a water-soluble agent and switch to barium if a leak is not identified, a practice not without controversy. Some radiologists use barium initially for suspected pharyngeal and proximal esophageal perforations. Granted that barium is retained in soft tissues, but no convincing evidence suggests additional tissue damage by barium beyond what is produced by infected saliva. Similar to the rest of the gastrointestinal tract, damage produced by an esophageal perforation is mostly due to leak of infected esophageal content; additional spill of barium into an already infected cavity adds little, if any, damage. Retained barium in soft tissues is of little consequence aside from possibly hindering future examinations if large amounts are spilled. Thus residual barium was detected in 29% of follow-up radiographic studies performed 4 to 48 days after barium esophagrams identified esophageal leaks in postoperative patients (19); none of the residual barium interfered with new studies. Barium sulfate in soft tissues is not carcinogenic.

Classic teaching held that acute spill of barium sulfate into the peritoneal cavity resulted in acute barium peritonitis having a high morbidity and mortality. While undoubtedly true a generation or more ago, current

commercial barium sulfate products have evolved into considerably safer products inducing less of an inflammatory reaction.

Perforations have been claimed to have been missed when using a 50% to 100% weight/volume barium suspension (20,21), which is counter to other published data (22) and to my experience; higher opacity barium has more x-ray stopping power and better opacifies small tracts than iodinated contrast. Subtle perforations are more readily identified with barium.

Many radiologists in Europe routinely use water-soluble contrast agents for suspected esophageal perforation. Among these agents, in Europe low-osmolality contrast media are usually employed; in the United States a commercial high-osmolality mixture of sodium and meglumine diatrizoate (Gastrografin and related products) is preferred, mostly because of its flavoring agents, which make it somewhat palatable to patients. The high-osmolality agents are contraindicated if spill into lungs is suspected, in which setting United States radiologists prefer the relatively innocuous barium sulfate.

My practice is to use water-soluble contrast agents in a setting of acute trauma if a possibility of intraperitoneal spill exists. With trauma (including abdominal surgery) more than several days old, on the other hand, barium sulfate is preferred. Thus a fluoroscopic study requested for suspected perforation several days after an intraabdominal resection is generally performed with barium sulfate.

Pediatric radiologists in search of a perforation tend to use nonionic, water-soluble contrast agents.

Therapy

Nonoperative therapy in select patients with thoracic esophageal perforations consists of antibiotics, nasoesophageal suction, and total parenteral nutrition. Some of these patients develop esophageal stenoses.

The surgeon usually inquires about a site of perforation; perforations of the lower one third of the intrathoracic esophagus are approached through a left thoracotomy, while more proximal perforations are managed through a right thoracotomy.

A postoperative esophagram establishes esophageal integrity prior to start of oral intake. Most postsurgical disruptions heal spontaneously provided the surgical field is adequately drained and esophagus is patent distally.

Foreign Bodies

Esophageal foreign bodies range from bezoars, impacted food, and a penetrating swallowed bony fragment, to swallowed coins, the latter mostly in young children. Nonfood esophageal bezoars are rare. Often these are associated either with a distal stricture or diffuse spasm. A rare sharp foreign body such as a bone splinter perforates sufficiently deep to result in an esophagoaortic fistula and exsanguination. Food impaction in the esophagus is quite common and is often related to a distal stricture or spasm. At times acute impaction is the first presentation of an esophageal carcinoma (Fig. 1.6).

In an otherwise stable patient, barium is the preferred contrast agent of choice to detect food impaction; with the patient upright, the high specific gravity of barium aids disimpaction. A number of physical maneuvers have been employed as an aid to disimpaction, with most being of dubious value. Spasmolytic drugs have

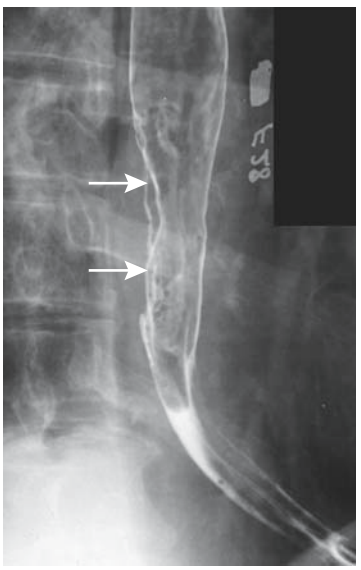

Figure 1.6. Squamous cell carcinoma. An esophagram reveals an eccentric infiltrating cancer (arrows).

been tried in some patients if underlying spasm is suspected. In a multicenter double-blind study using glucagon and diazepam, no significant difference in disimpaction was found among patients given spasmolytic agents versus placebo (23). Effervescent agents have been used to treat esophageal food impaction, with varying success.

Computed tomography has evolved into a reliable technique for detecting small, poorly calcified esophageal foreign bodies to the point that the number of endoscopies for this indication has decreased. A prospective CT study of patients with suspected esophageal fish or chicken bones detected an esophageal foreign body in 30, with a foreign body found during subsequent rigid esophagoscopy in 29 (24). Computed tomography also detects associated inflammatory changes in surrounding tissues.

In pediatric patients some radiologists remove an esophageal foreign body with a balloon catheter. This technique is successful and safe in experienced hands. Of 337 coin extractions attempted using a Foley catheter, pediatric radiologists with training in catheter technique were successful in 96% of patients (25); no complications were encountered.

Wall Thickening

Infection/Inflammation

Reflux and Reflux Esophagitis

Clinical

Gastroesophageal reflux consists either of gastric juice or of duodenal content. Reflux tends to be sporadic and difficult to quantify. One definition of massive reflux is reflux to or above the thoracic inlet either spontaneously or with provocation while in a recumbent position. Reflux is not synonymous with esophagitis; some reflux is associated with little inflamation.

Nonimaging tests for gastroesophageal reflux include direct visualization during endoscopy, the Bernstein acid infusion test and 24-hour esophageal pH monitoring. It should be kept in mind that endoscopy evaluates primarily consequences of gastroesophageal reflux rather than reflux per se. The Bernstein test, currently rarely performed, attempts to duplicate a patient's symptoms during infusion of a weak hydrochloric acid solution into the esophagus. Esophageal pH monitoring is considered the gold standard in detecting reflux. Yet results of 24-hour esophageal pH monitoring show that some patients with endoscopically apparent esophagitis have normal pH monitoring and some without esophagitis have abnormal findings (26).

Gastroesophageal reflux is associated with a hypotensive lower esophageal sphincter that allows reflux. At times, however, reflux occurs even with a hypertensive lower esophageal sphincter. A direct association exists between the presence of a hiatal hernia and gastroesophageal reflux and esophagitis. Patients with a large hiatal hernia are more likely to have abnormal pH monitoring and worse esophagitis than those with a small hiatal hernia.

Heartburn and acid regurgitation are typical clinical symptoms, but presentations vary, at times mimicking cardiac disease. Considerable evidence suggests an association between gastroesophageal reflux and asthma. Reflux in some patients leads to laryngospasm or bronchospasm and triggers an asthmatic attack. Some patients with reflux-associated asthma do not have symptoms referable to the gastroesophageal reflux.

Children with cystic fibrosis have a higher prevalence of gastroesophageal reflux than normals. Metachromatic leukodystrophy also appears to be associated with gastroesophageal reflux.

Even in children, an esophageal stricture secondary to reflux is more common than a congenital stricture. Why some patients form strictures and others do not is not known; presumably those with prolonged reflux and a decreased lower esophageal sphincter pressure are more prone to strictures, but that is conjecture.

Imaging

Reflux is not synonymous with reflux esophagitis. Several hypermotility abnormalities are found in patients with gastroesophageal reflux: more premature cricopharyngeus muscle contractions and increased amplitude and duration of esophageal contractions compared to controls. Patients with reflux have delayed esophageal emptying; emptying is impaired further once esophagitis develops. In adults,

an experienced fluoroscopist readily detects most reflux, if present, together with delayed esophageal emptying during a barium study.

Transabdominal US is used in some centers to detect gastroesophageal reflux in children, although the severity of reflux is difficult to assess and the results are controversial. Some investigators have achieved about 90% agreement with esophagography and 24-hour esophageal pH measurement, especially when color Doppler is added to B-mode US, but others have found US to be an unreliable diagnostic test in screening infants (27).

In most symptomatic patients, however, an upper gastrointestinal examination is performed not to detect reflux but rather to identify complications of reflux. Barium esophagram findings of reflux esophagitis consist of ulcers, nodules, fold thickening, and, eventually, strictures. Ulcers tend to be small, focal, and often barely visible. A number of these ulcers are solitary and are more common on the posterior wall close to the gastroesophageal junction (28). Small isolated ulcers are not unique to reflux esophagitis and are also found with herpes infection, drug-induced esophagitis, Behçet's esophagus, and acute radiation-induced esophagitis.

Small, irregularly shaped nodules, described as *granulations*, are common in the distal esophagus in reflux esophagitis, often intermixed with small ulcers. The overall appearance often is that of granularity, and a double-contrast esophagram is generally necessary for adequate visualization. One should keep in mind, however, that nodularity, especially if varying in size and not discrete, also suggests a superficial spreading carcinoma.

Thickened folds due to inflammation are common and often are associated with ulcers. These folds contain both mucosa and submucosa and, being inflamed, are present with the esophageal lumen either distended or collapsed. Folds varying in size with change in intraluminal pressure should suggest varices. Associated findings are common and include hiatal hernias, intramural pseudodiverticula, scarring, and strictures (Fig. 1.7).

In patients with esophagitis (regardless of cause), CT identified a relatively long segment of circumferential esophageal wall thickening (using a 5-mm threshold) in 55% and a target sign in 17% (29); these CT findings are nonspecific, and other diseases, including an occasional infiltrating cancer, also result in a thickened esophageal wall.

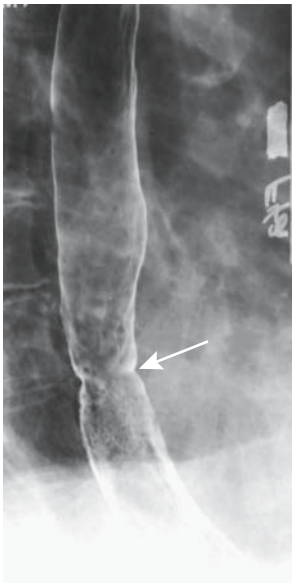

Figure 1.7. Reflux stricture (arrow) in the distal esophagus. A 12-mm barium pill is useful to confirm equivocal strictures.

At times transabdominal US detects a hiatal hernia, but esophagitis is not readily detected. Endoscopic US, on the other hand, readily evaluates the esophageal wall and surrounding structures, detecting esophageal wall thickening due to inflammation and other causes.

A radionuclide gastroesophageal reflux study using technetium-99m (Tc-99m) sulfur colloid is physiologic, readily performed, and provides quantitative data. This test has achieved wider acceptance in pediatric patients than in adults.

Whether one imaging or nonimaging modality is superior to others in guiding clinical therapy is debatable.

Therapy

Almost all patients with massive reflux on barium studies have pathologic acid reflux in the recumbent position (30); therapy for reflux disease can be started in these patients without need for 24-hour pH monitoring. Stricture dilation and temporary stent insertion have a limited role in benign esophageal strictures; strictures recur unless the underlying disorder is treated. Long-term stenting with expandable

metallic stents of benign esophageal strictures results in a high complication rate. Perforation and stent migration are not uncommon complications; stents have been passed per rectum or regurgitated. Nevertheless, in some patients temporary stenting of a benign esophageal stricture is useful. Covered expandable nitinol stents can be removed with a retrieval hook (31).

In many centers laparoscopic antireflux surgery has supplanted open surgery; laparoscopic and open fundoplications achieve similar results. Currently popular operations include the Nissen fundoplication (Fig. 1.8) and the Hill posterior gastropexy repair. Both have a similarly high success rate, although they are not complication free. Acute complications include esophageal or gastric perforation, gastric volvulus and an incarcerated intrathoracic hernia. Esophageal manometry reveals a considerable increase in lower esophageal sphincter resting pressure and sphincter length after fundoplication, and thus provides objective data of fundoplication effectiveness.

Pneumomediastinum detected shortly after laparoscopic fundoplication is probably of little or no significance; pneumothorax, on the other hand, is abnormal and should be investigated, keeping in mind that during a laparoscopic fundoplication the left pleura is entered and results in a pneumothorax (32).

Roughly 10% of patients have fundoplication failure and develop recurrent gastroesophageal reflux. Other complications include refractory dysphagia, intractable gas bloating, chest or abdominal pain, and incapacitating diarrhea, findings due to a tight repair, vagal nerve injury resulting in gastroparesis, and ulcerations. Although dysphagia improves in some patients, others require dilations or even reoperation. Acute dysphagia after a fundoplication usually implies a tight repair; later, esophageal stenosis should be suspected, possibly related to the diathermy dissection performed. Other complications include a slipped or disrupted fundoplication and recurrent hiatal hernia (Fig. 1.9). Unrecognized esophageal dysmotility accounts for occasional dysphagia, but this finding should be detected with preoperative imaging. A gastrobronchial fistula or esophagobronchial fistula is a rare complication. Computed tomography in one patient identified left lower lobe consolidation and left bronchial tree filling with contrast from a left subphrenic abscess, with a fistula confirmed by oral contrast (33).

Dilation for recurrent dysphagia in patients with a slipped fundoplication has a lower success rate than in those with an intact fundoplication.

Many children undergoing a fundoplication are neurologically impaired and thus prone to surgical complications. A fundoplication breakdown, recurrent hiatal hernia, or both are indications for a second antireflux operation (34); complications after a second Nissen fundoplication include bowel obstruction, wound infection, a tight wrap, and pneumonia. Long-term, only 72% of these children remained symptom free.

Figure 1.8. Prominent postoperative Nissen fundoplication. The distal esophagus is narrowed by an edematous fundal wrap.

Barrett's Esophagus

Clinical

A Barrett's esophagus consists of replacement of normal esophageal squamous epithelium by a specialized columnar epithelium, called *heterotopic gastric mucosa*. Such metaplasia is believed to be induced by chronic gastroesophageal reflux, esophagitis, and a unique

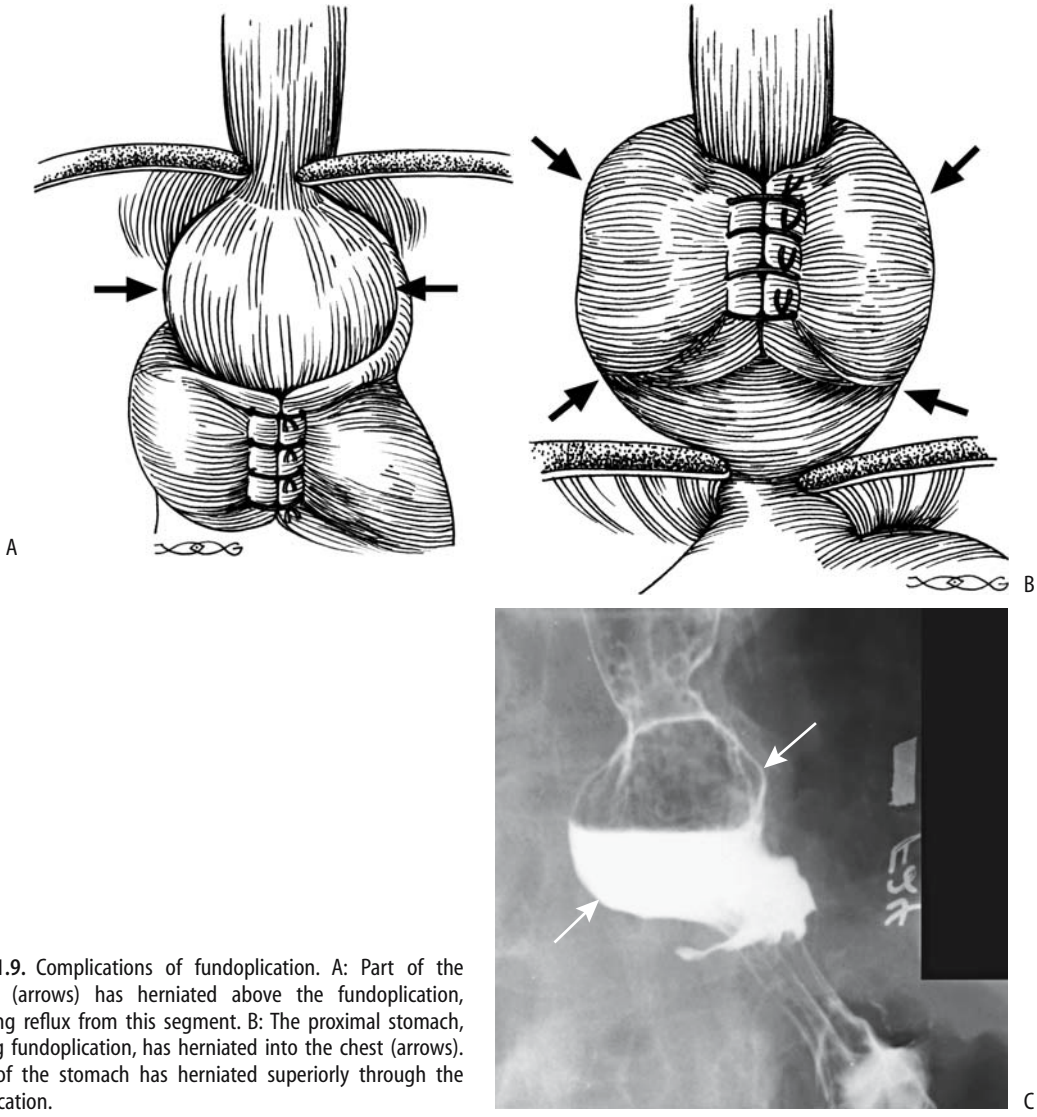

Figure 1.9. Complications of fundoplication. A: Part of the stomach (arrows) has herniated above the fundoplication, permitting reflux from this segment. B: The proximal stomach, including fundoplication, has herniated into the chest (arrows). C: Part of the stomach has herniated superiorly through the fundoplication.

type of healing, although this view is probably an oversimplification; duodenogastric reflux appears to be involved in some patients. A Barrett's esophagus can develop after total gastrectomy and esophagojejunostomy. It is more often encountered in men and in Caucasians. A familial occurrence is evident in some families. For some reason it is uncommon in Japan (35).

Does *Helicobacter pylori* infection play a role in a Barrett's esophagus? In 73 patients with a Barrett's esophagus, *H. pylori* was detected in the esophagus in 15% and in 36% of gastric mucosa (36); all those positive in the esophagus were also positive in the stomach. The presence *of H. pylori* in the esophagus is related to presence of gastric-type mucosa and of concomitant gastric *H. pylori* infection.

Given the increasing survival of cystic fibrosis patients and their propensity for gastroesophageal reflux, they appear to be at increased risk for a Barrett's esophagus.

Occasionally heterotopic gastric mucosa is encountered in the upper one third of the esophagus or even pharynx without other stigmata of Barrett's esophagus, a condition

believed by some to be congenital (37). Complications of such proximal heterotopic gastric mucosa include fistula formation and an adenocarcinoma.

Prevalence of Barrett's esophagus is unknown because both imaging and endoscopy misses some of these lesions. Although at times Barrett's esophagus has a characteristic appearance, mucosal biopsy is necessary for confirmation. Pathologically, the presence of esophageal gland ducts in columnar epithelium-lined mucosa is pathognomonic of Barrett's esophagus but is not often sought.

A Barrett's esophagus is either continuous in extent or patchy and surrounded by normal esophageal mucosa. Most often Barrett's esophagus is located just proximal to the lower esophageal sphincter. Such complications of Barrett's esophagus as ulceration, stricture, dysplasia, and cancer tend to be less prevalent in a short-segment Barrett's.

A Barrett's esophagus is considered premalignant, with an intermediate stage being dysplasia. An ongoing concern is biopsy sampling error and ability to differentiate low-grade dysplasia from high-grade dysplasia, with the latter tissue being at risk for malignant degeneration. Grading of dysplasia is subject to observer variability. The presence of positive tumor markers such as *p53*, c-*erb*-2, proliferating cell nuclear antigen (PCNA), and carcinoembryonic antigen (CEA) or the existence of aneuploidy is used by some to gauge the risk for progression to malignancy, but no firm criteria are available.

Estimates of adenocarcinoma prevalence in patients with Barrett's esophagus vary widely. In a Spanish study, an adenocarcinoma developed at an incidence of 1 per 104 Barrett's esophagus per year (38), while at a Veterans Administration Medical Center in Tucson, Arizona, it was 1 per 208 Barrett's esophagus per year (39). Severe dysplasia commonly surrounds a carcinoma. Some studies suggest that patients with an esophageal adenocarcinoma, presumably arising from Barrett's esophagus, are not at higher risk of developing extraesophageal malignancies, but other reviews have reached the opposite conclusion, finding that patients with Barrett's esophagus are at increased risk of colon cancer.

Occasionally Barrett's esophagus regresses after medical therapy, but such results are inconclusive.

Imaging

A typical barium study of a Barrett's esophagus reveals an irregular or reticular region of barium coating, ulcers, and strictures (Fig. 1.10). Involvement commonly is close to the squamocolumnar junction. The reticular appearance tends to be rather subtle, and a high-quality double-contrast esophagram is necessary to detect these lesions. At times deep ulcers develop, a finding not generally seen in uncomplicated reflux esophagitis.

A double-contrast esophagram in patients with short-segment Barrett's esophagus revealed hiatal hernias in 90%, gastroesophageal reflux in 80%, reflux esophagitis in 35%, and peptic scarring or strictures in 55% (40); a reticular pattern was not seen in these patients.

Endoscopic US shows that the mucosal second hypoechoic layer is significantly thicker in Barrett's patients than in a normal esophagus (41); Barrett's esophagus can be diagnosed with a sensitivity approaching 100% and specificity of 86% if the mucosa hypoechoic layer is thicker than the first hyperechoic layer. More common is detection of focal esophageal wall thickening; such thickening is also found with some carcinomas, and endoscopic US cannot distinguish

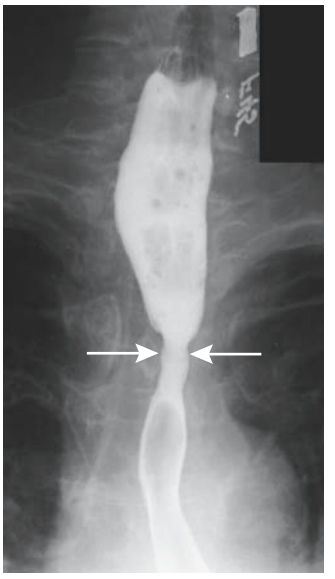

Figure 1.10. Barrett's stricture (arrows). Adenocarcinomatous transformation is in the differential diagnosis.

between benign and malignant causes of wall thickening.

Drug-Induced Inflammation

A specific etiology for drug-induced esophagitis is not known. One postulate suggests that the weak caustic action of many drugs during their stasis in the esophagus results in localized corrosive injury. Numerous drugs are implicated in esophagitis and lead to ulcerations. Common ones include tetracycline derivatives and nonsteroidal antiinflammatory agents. Typically, a pill lodges in the esophagus at sites of normal narrowing such as the aortic arch or proximal to a stricture or due to lack of propulsion. Alendronate, used to treat osteoporosis in postmenopausal women, has led to multiple ulcers and strictures resistant to dilation.

These ulcers tend to be multiple, often shallow, and clustered at one site. Surrounding inflammation, manifesting as thickened folds, is common. An occasional one is large, presumably due to coalescence of smaller ulcers (Fig. 1.11). These ulcers heal readily once the incriminating agent is withdrawn, although an occasional one progresses to esophageal perforation.

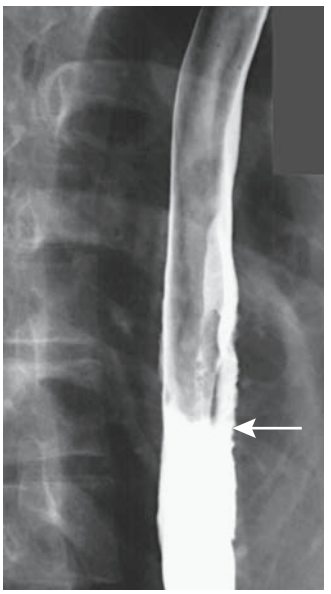

Figure 1.11. Aspirin-induced focal esophagitis. Thickened folds and subtle ulcers are present in the mid-esophagus (arrow).

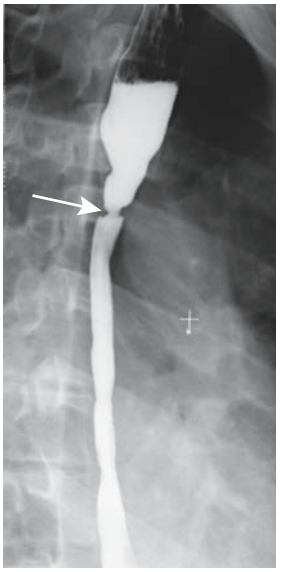

Figure 1.12. Sequela of lye stricture as a child. An esophagram reveals a long stricture involving most of the esophagus. A proximal web-like stricture (arrow) required periodic balloon dilation.

Thermal/Corrosive Injury

Acute thermal injury develops after ingestion of hot substances. Ingestion of solid alkali produces mostly oropharyngeal damage. Liquid alkali, such as drain cleaners, and acid ingestion, such as hydrochloric acid, damage both the esophagus and the stomach and occasionally even extend into the duodenum. Necrosis ensues, and at times it is massive. Unless perforation develops, the acute phase gradually subsides within a week or so, and strictures, at times bizarre in appearance, begin to form. Previous corrosive injury is associated with an increased risk of carcinoma.

On a long-term basis, some type of esophageal dysmotility persists in most patients who ingest corrosives, most often consisting of nonperistaltic low-amplitude contractions. Long strictures are common, at times gradually progressing and manifesting years later (Fig. 1.12).

Most patients with corrosive injury are managed by gastroenterologists who prefer endoscopy rather than radiographic contrast studies to evaluate underlying damage. Lye ingestion is one of the causes of a dark-

pigmented or black esophagus seen during endoscopy.

Crohn's Disease

In the gastrointestinal tract, the esophagus is least likely to be involved by Crohn's disease. When present, dysphagia, odynophagia, and, at times, bleeding develop. Most patients also have gastric and distal ileal involvement.

The most common appearance consists of aphthae. Occasionally these aphthae enlarge and linear ulcers develop. These ulcers have evolved into deep, intramural tracts parallel to the esophageal lumen. A rare Crohn's esophagus presents as a polyposis. Rarely, severe involvement leads to irregular ulcerations and an imaging appearance mimicking other severe inflammation.

Crohn's involvement of the esophagus is one of the more uncommon causes of esophageal stricture or an esophagopulmonary fistula (42).

Phlegmonous Esophagitis

Phlegmonous esophagitis is rare. An infection usually extends from the stomach.

Severe esophageal infection or ischemia could result in esophageal pneumatosis, but in practice it is a rare finding. Occasionally esophageal pneumatosis develops after acute gastric dilatation (43).

Tuberculosis

Primary esophageal tuberculosis is rare. More common is esophageal involvement secondary to extension from an adjacent structure, such as carinal lymph nodes (Fig. 1.13). Clinically, dysphagia and odynophagia predominate. A rare esophageal tuberculosis evolves into an intramural abscess (44). Anecdotal reports describe spontaneous esophageal perforation, and a spontaneous esophageal fistula/sinus tract with no known underlying etiology should suggest tuberculosis.

Radiographic findings vary considerably and include nodularity, stricture, ulcer, and fistula. An intraluminal septum probably represents a fistula with secondary luminal recommunication. Computed tomography reveals mediastinal or other adjacent adenopathy.

A biopsy from a site of ulceration or mass often simply shows epithelioid cell granulomas.

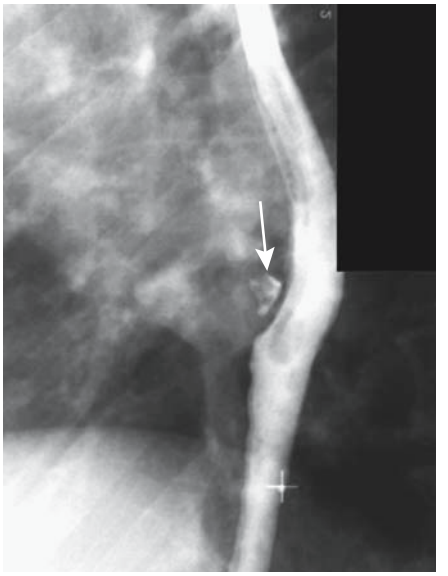

Figure 1.13. Tuberculous sinus tract between esophagus and carinal lymph nodes (arrow) in a patient with dysphagia. Primary disease was in the lymph nodes.

At times culture of the biopsy material reveals *Mycobacterium tuberculosis*, but such cultures are not commonly performed.

Candidiasis

Although occasionally developing without an underlying cause, esophageal candidiasis typically evolves in a setting of immunosuppression, malignancy, diabetes mellitus, debilitation, scleroderma, or drug use. Oral thrush is not always identified. Dysphagia is a common presentation, with or without odynophagia.

A double-contrast barium study differentiates most candida esophagitis from other esophagitides. Varying-size plaques, tending to align to the esophageal longitudinal axis, are a typical appearance of candidiasis (Fig. 1.14). With progression, these plaques coalesce; some become undermined and the appearance is that of a shaggy, irregular outline. A *foamy* esophagus has been described on a double-contrast esophagram (45); it consists of innumerable small, round gas bubbles mixed with barium on top of the barium column. Ulcers are uncommon early but develop with plaque sloughing.

Figure 1.14. *Candida* esophagitis. The esophagus has a shaggy, irregular outline.

Viral Esophagitis

Herpes simplex virus type I esophagitis develops most often in immunocompromised patients. An esophagram typically reveals well-defined ulcers in otherwise normal-appearing mucosa. These ulcers range from punctate to round or, rarely, linear.

Cytomegalovirus and HIV-induced ulcers tend to be large and shallow. The imaging appearance with both is similar, and biopsy is necessary for differentiation.

Histoplasmosis

Primary esophageal histoplasmosis is rare and occurs mostly in immunocompromised patients. More likely esophageal involvement is secondary to one of two circumstances: First, with mediastinal histoplasmosis, resultant adenopathy and inflammation lead to esophageal obstruction and dysphagia. Second, esophageal ulcers and nodules develop in a setting of disseminated histoplasmosis. A histoplasmosis-associated stricture is rare.

Biopsy reveals intracellular histoplasmosis.

Chronic Granulomatous Disease

Chronic granulomatous disease is an inherited disease manifesting in childhood and characterized by recurrent bacterial or fungal infections. The primary defect is a neutrophil granulocyte dysfunction that suppresses the body's ability to kill phagocytosed microorganisms. This condition rarely involves the esophagus, although an occasional child develops esophageal narrowing. Biopsy simply revealed nonspecific inflammation.

This entity differs from the rare chronic granulomatosis found in adults (discussed in Chapter 14).

Eosinophilic Esophagitis

Eosinophilic esophagitis is a rare cause of dysphagia, generally detected in the young. Isolated esophageal involvement does occur, but more common is disseminated disease. Dysphagia and chest pain are typical presentations. An allergic history is common and many of these patients have a peripheral eosinophilia.

Imaging does not play a direct role in the diagnosis but serves primarily to exclude complications, such as strictures and other conditions.

Other

Chronic dysphagia but without symptoms of reflux has been described in patients developing localized esophageal strictures (46); histology reveals esophageal mucosal blistering but no significant inflammation and no concurrent cutaneous or mucous lesions. The authors called this entity *chronic esophagitis dissecans*.

Behçet's Syndrome

Behçet's syndrome involving the esophagus is rare. The few reported patients presented with esophageal ulcers varying in depth (Behçet's syndrome is discussed in Chapter 17).

Radiation

Clinically evident radiation esophagitis is not common. Patients also receiving Adriamycin or actinomycin-D have a considerably lower threshold for radiation esophagitis.

Patients undergoing concurrent chemo- and radiotherapy for lung cancer have a considerably lower threshold for radiation esophagitis which is confined to the radiation field (47); esophagitis was more common in the low-dose chemotherapy group than in those receiving a larger dose.

The imaging appearance ranges from isolated ulcers, usually shallow, to eventual long strictures in the radiation field.

Sarcoidosis

Sarcoidosis typically involves lungs, lymph nodes, and spleen, with gastrointestinal involvement being less common. The hallmark of sarcoidosis is the presence of noncaseating granulomas, although similar histologic findings are found in a number of disorders. In general, single-organ involvement is uncommon and should not be attributed to sarcoidosis. A possibility of sarcoidosis (and its therapy) predisposing to lymphoma has been raised, presumably via an immune system pathway. Sarcoidosis has preceded lymphoma by months or years.

Sufficient mediastinal sarcoid adenopathy can compress and narrow the esophagus lumen. A barium study typically reveals a smooth and narrowed esophageal lumen. Subcarinal adenopathy often splays the right and left main stem bronchi. In most patients esophageal motility is normal. Manometry occasionally reveals nontransmitted contractions and a spastic lower esophageal sphincter. The rare primary esophageal sarcoidosis presents as a focal, circumferential stricture (Fig. 1.15).

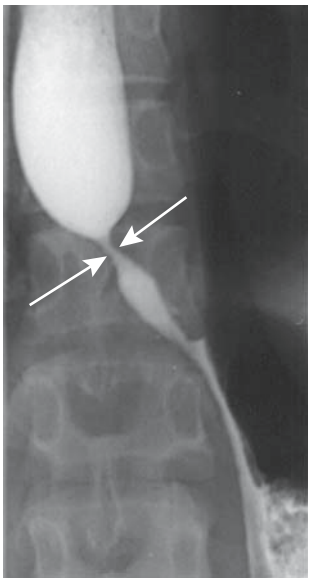

Figure 1.15. Esophageal sarcoidosis manifesting as a circumferential, smooth stricture (arrows).

Fibrosis

Esophageal fibrosis and fibrosis-associated strictures are a common end point for a number of conditions (Table 1.3), and these are discussed in their appropriate sections. In distinction to other parts of the gastrointestinal tract, the relative smoothness of an esophageal stricture is an insensitive guide in distinguishing a benign from a malignant stricture. Also, not all esophageal narrowings represent a stricture; for instance, the distal esophageal narrowing in achalasia is mostly spasm.

Extensive mediastinal fibrosis does lead to esophageal stricture. Generally these strictures have a smooth appearance and tapering margins. Self-expanding stents have been helpful in relieving acute dysphagia in these patients.

Tumors

Nonneoplastic

Sebaceous Glands

Normally sebaceous glands do not exist in the esophagus, although ectopic sebaceous glands have been described. They vary in size; some appear as irregular, lobulated nodules, while a rare patient has multiple rounded polyps arranged in rows.

Histology is diagnostic for these submucosal glands.

Fibrovascular Polyp

Most giant intraluminal esophageal polyps are fibrovascular in origin. An occasional one is a leiomyoma, hamartoma, or some other difficult to classify tumor.

Table 1.3. Etiologies of fibrotic esophageal strictures

Condition	Comments
Reflux esophagitis	Both acid and alkali reflux result in strictures, usually in distal third
Barrett's esophagus	Most strictures are in middle or distal third
Drug induced	Most common in mid-esophagus
Thermal/corrosive	Most strictures are long and in distal segment
Crohn's disease	Strictures tend to be smooth and vary in length
Phlegmonous	Involves distal segment and usually extends into stomach
Infectious	Strictures result from chronic infection
Chronic granulomatous disease	Fibrosis is secondary to recurrent bacterial or fungal infections
Chronic esophagitis dissecans	A rare cause of esophageal strictures
Radiation	Strictures correspond to radiation port and tend to be smooth in outline
Mediastinal fibromatosis	Esophagus tends to be extensively involved
Sarcoidosis	Usually secondary to mediastinal sarcoidosis
Plummer-Vinson syndrome	Appearance more web-like rather than a fibrotic stricture
Epidermolysis bullosa	Ulcerations lead to fibrotic strictures
Pemphigoid	Blistering results in web-like appearance, at times evolving into strictures
Prolonged nasogastric intubation	Long distal esophageal strictures
Intramural (pseudo)diverticulosis	Distal esophageal strictures are probably due to reflux esophagitis

Most fibrovascular polyps originate in the proximal one third of the esophagus, originate in the submucosa, are covered by squamous epithelium, and consist of fibrosis, fat, and stromal tissue. Most present with either lumen obstruction or bleeding. They obstruct when large. Some develop a long pedicle and prolapse, even to the point of laryngeal obstruction. Occasionally CT and MR identify predominantly fat (48).

Being rather mobile, during a barium study these polyps superficially mimic a bolus of food.

Hemangioma

Esophageal hemangiomas are uncommon. Most appear as sessile polyps. Computed tomography reveals marked contrast enhancement. One was hypoechoic on endoscopic US, was confined to the submucosa, and adjacent muscularis propria appeared intact (49).

Heterotopic Pancreas

The term *choristoma* is occasionally used to describe a tumor-like mass of normal tissue in an abnormal location. A heterotopic pancreas is one such tumor.

Obvious heterotopic pancreatic tissue is rare in the esophagus, but intramucosal pancreatic acinar-like cells are not. These pancreatic acinar cells tend to be located on either side of the squamocolumnar junction, but they do not represent ectopic pancreatic tissue.

Benign Neoplasms

Papilloma

The majority of squamous cell papillomas occur in the distal esophagus and most are asymptomatic. Some papillomas are associated with mucosal injury and subsequent regeneration. They are not considered premalignant. They tend to be misdiagnosed as mucosal tags or inflammatory polyps if only small biopsy specimens are available, but the pathologist should suggest a correct diagnosis if papillary projections are identified. Radiologically, most are small, range from smooth to slightly irregular, and vary in size (Fig. 1.16).

Leiomyoma

A leiomyoma is the most common esophageal tumor found at autopsy. Most are intramural in location, single, small, and not detected by imaging. Most are discovered incidentally, and the larger ones result in dysphagia. Most occur in adults.

A rare leiomyoma grows mostly intraluminal, at times even becoming pedunculated, thus suggesting a muscularis mucosa origin. An occa-

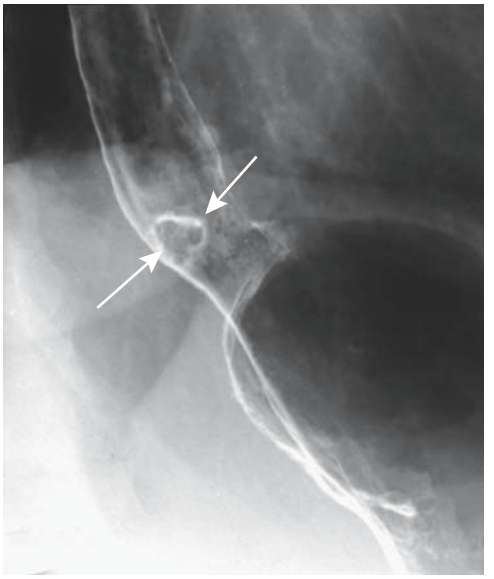

Figure 1.16. Squamous papilloma close to the gastroesophageal junction (arrows).

sional one mimics a fibrovascular polyp, especially if originating in the proximal esophagus. One pedunculated leiomyoma extended 20 cm in a dilated esophagus containing retained foreign material (50); the overall appearance suggested achalasia.

Precontrast, leiomyomas tend to be close to isointense; they enhance homogeneously postcontrast, except for larger ones containing necrosis.

Endoscopic US of a plexiform leiomyoma showed a sharply marginated, hypoechoic intramural tumor containing internal linear echoes (51). Endoscopic US should differentiate whether a leiomyoma originates from muscularis mucosa or muscularis propria; endoscopic lumpectomy is possible for those originating from muscularis mucosa.

Diffuse esophageal leiomyomatosis occurs in X-linked Alport's syndrome, an inherited dominant trait caused by specific gene mutations, and, in fact, diffuse leiomyomatosis and esophageal involvement are often the first manifestations of Alport's syndrome. Progressive dysphagia starting in childhood is typical.

A barium esophagram in leiomyomatosis reveals smooth esophageal narrowing. Computed tomography and endoscopic US identify diffuse esophageal wall thickening.

Malignant Neoplasms

Pharyngeal Tumors

Pharyngeal malignancies originate in any of the three pharyngeal compartments: nasopharynx, oropharynx, or hypopharynx. Most are squamous cell carcinomas, with a minority of lymphomas, adenoid cystic carcinomas, and rare undifferentiated carcinomas. Pharyngeal sarcomas are rare.

Direct visualization continues to be the mainstay of tumor detection, while pharyngography has been supplanted by CT and MRI in evaluating tumor spread. Neck MRI is especially helpful due to its enhanced soft tissue contrast.

Esophageal Carcinoma

Among patients with esophageal carcinoma seen at the Cleveland Clinic Foundation between 1987 and 1994, 74% had an adenocarcinoma and 26% a squamous cell carcinoma (52); no differences existed between the two groups in age, prior gastric surgery, smoking, or alcohol use, but significant risk factors for an adenocarcinoma were male gender, white race, distal cancer location, and the presence of Barrett's esophagus.

Clinical

Squamous Cell Carcinoma: Esophageal squamous cell carcinoma shows considerable regional variation in prevalence. Both tobacco and alcohol use are predisposing risk factors in the Western world, but these do not appear to play a major role in regions of the world where this cancer is especially prevalent. In the United States, tobacco plays a greater role in esophageal squamous cell carcinoma than in adenocarcinoma and is a more prominent factor in women than men (53). Human papillomavirus appears to have a role in carcinogenesis in geographic regions with a high prevalence of this cancer.

A patient with an esophageal squamous cell carcinoma presented with paraneoplastic glomerulonephritis and nephrotic syndrome (54); such an autoimmune phenomenon appears to be induced by tumor antigen

inhibition. The sign of Leser-Trelat (multiple verrucous papules) is also associated with a rare squamous cell esophageal carcinoma (55).

Dysphagia for solid foods is the most common presentation but is a late occurrence.

An association exists between esophageal dysplasia and both esophageal carcinoma and head and neck carcinomas. Patients who have had a prior partial gastrectomy for peptic ulcer disease also appear to be at increased risk. An occasional carcinoma is linked to prior radiation therapy to this region. Increased prevalence is found in patients with achalasia, Plummer-Vincent syndrome, a caustic stricture, or tylosis (keratopalmar keratosis), an autosomal condition.

Simultaneous esophageal squamous cell carcinoma and gastric adenocarcinoma have developed, but whether these have been by chance is conjecture. In a rare patient intramural pseudodiverticulosis is associated with an esophageal carcinoma.

Esophageal squamous cell carcinoma exhibits considerable variability throughout the world. It is one of the leading causes of cancer death in Asia, with an especially high prevalence in northern Iran and northern China. Another focus of high prevalence is found among Zulu and Bantu people in South Africa. In Shanghai, esophageal cancer rates have decreased more than 50% over an 18-year period ending in 1989 (56), in the United States an increase is found among black men, while in Scotland, both adenocarcinoma and squamous carcinoma have been increasing both in men and women.

Adenocarcinoma: Discussed here are adenocarcinomas arising both in the esophagus and in the gastric cardia (at the gastroesophageal junction). Prior literature debated whether the latter tumors should be considered esophageal or gastric in origin, but from a clinical viewpoint little justifies their separate consideration; the resultant surgical approach is similar.

Extensive associated dysplasia is common surrounding an esophageal adenocarcinoma. Many of these patients have a long history of gastroesophageal reflux, and gastric content has thus been implicated in carcinogenesis, but a specific carcinogen has not been identified. Bile and pancreatic juice reflux have also been implicated. No significant association exists between *H. pylori* infection and carcinoma of the gastroesophageal junction; this is in distinction to a significant association between *H. pylori* infection and other gastric adenocarcinomas.

Prevalence of esophageal and gastric cardia adenocarcinoma is increasing in the Western world. Data from the Surveillance, Epidemiology, and End Results (SEER) study in the United States reveal that in white males the incidence of esophageal adenocarcinoma increased >350% since the mid-1970s and currently surpasses squamous cell carcinoma (57); an increase also occurred in black males but was considerably lower.

Not all of these adenocarcinomas develop in a Barrett's esophagus. Barrett's esophagus patients tend to have a better prognosis after surgery, probably because reflux and similar symptoms result in an earlier diagnosis.

These tumors commonly invade the gastric cardia. A rare esophageal adenocarcinoma first manifests as a metastasis.

Small Cell Carcinoma: Primary small cell carcinoma, morphologically indistinguishable from its lung counterpart, is rare in the esophagus. Pathologically these tumors are divided into oat-cell and non–oat-cell varieties. These are aggressive tumors with a poor prognosis, although radiation therapy and chemotherapy does prolong survival.

These tumors vary in size from small mucosal lesions to large fungating masses. Extensive intrathoracic and intraabdominal adenopathy is not uncommon on initial presentation. Imaging studies tend to be similar to those seen in patients with a squamous cell carcinoma. Barium studies reveal a smoothly marginated, sessile, ulcerated tumor located inferior to the carina (58).

A rare association with celiac disease has been raised (59). Also, a rare patient with a small cell esophageal carcinoma has a synchronous squamous cell carcinoma.

Adenoid Carcinoma: An esophageal adenoid cystic carcinoma is rare. They tend to be rather aggressive.

Pathology

Esophageal lymphatics consist of a submucosal network draining into regional lymph nodes. An esophageal malignancy can thus spread readily both longitudinally and circumferentially.

The Lauren classification (discussed in more detail in Chapter 2) appears also useful with esophageal adenocarcinomas. It is an independent prognostic factor. Diffuse-type tumors are associated with a significantly worse prognosis than intestinal-type tumors (60).

Most esophageal varicoid carcinomas are adenocarcinomas, although an occasional squamous cell carcinoma spreads superficially, with invasion limited to submucosa. A varicoid carcinoma involves varying esophageal lengths, occasionally even diffusely involving the entire esophagus. Both endoscopy and endoscopic biopsy have missed these mostly submucosal cancers.

Detection

An esophageal carcinoma is generally first detected either with a barium study or endoscopy, while tumor invasion is evaluated with CT or endoscopic US. Because many of these tumors are hypervascular compared to normal esophageal tissues, postcontrast multidetector CT imaging during the arterial phase also appears useful for initial tumor detection, although currently little data are available in the literature to provide guidance.

Esophagography remains an excellent tool both for diagnosis and follow-up of an esophageal carcinoma. A double-contrast technique and meticulous attention to detail are necessary.

At times an early superficial carcinoma presents as an isolated focus of nodularity identified with a double-contrast esophagram. The differential diagnosis of such a finding includes Barrett's esophagus, focal esophagitis, or even focal glycogenic acanthosis. A more extensive carcinoma is readily detected by a double-contrast barium study, but a biopsy is generally necessary to establish the diagnosis (Fig. 1.17).

Adenocarcinomas tend to have a nodular outline, and a technically high-quality study is necessary to detect smaller tumors (Fig. 1.18). Even when advanced, they tend to infiltrate intramurally, and a bulky intraluminal mass is found only in a minority (Fig. 1.19). Varicoid adenocarcinomas in the distal esophagus mimic varices, but unlike varices, these serpiginous cancers do not change shape and size with degree of esophageal lumen distention, and most experienced radiologists readily differentiate these two conditions (Fig. 1.20). Adenocarcinomas developing in a setting of Barrett's esophagus typically have an initial flat or plaque-like, irregular appearance and tend to be difficult to detect.

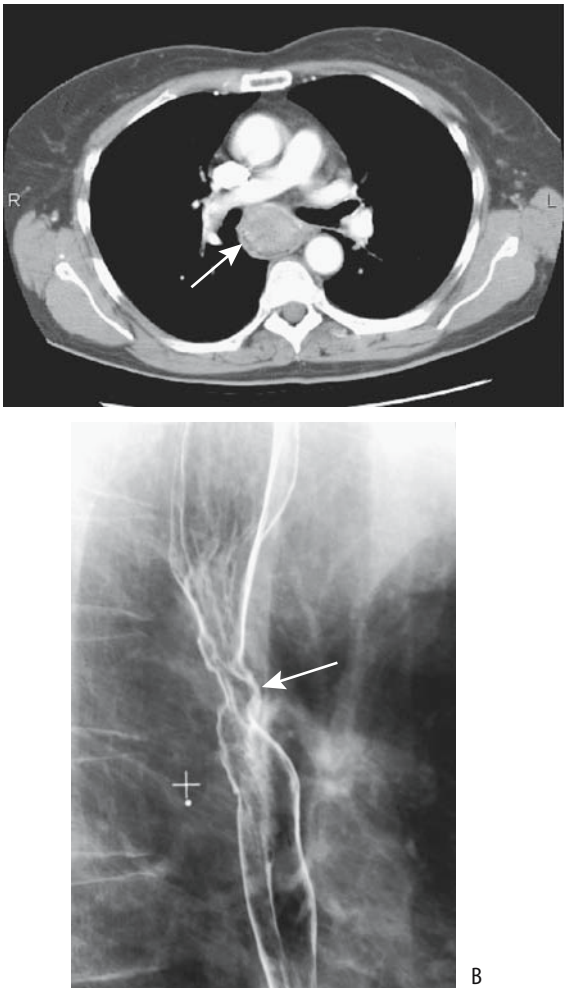

Figure 1.17. Squamous cell carcinoma in mid-esophagus. A: CT identifies a poorly enhancing tumor infiltrating the esophagus (arrow). (Courtesy of Arunas Gasparaitis, M.D., University of Chicago.) B: Ulcerated carcinoma in mid-esophagus (arrow) in another patient.

Staging

Squamous Cell Carcinoma: The tumor, node, metastasis (TNM) system is used for staging

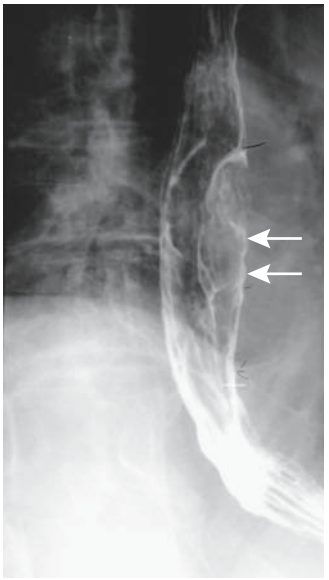

Figure 1.18. Polypoid adenocarcinoma in mid-esophagus (arrows).

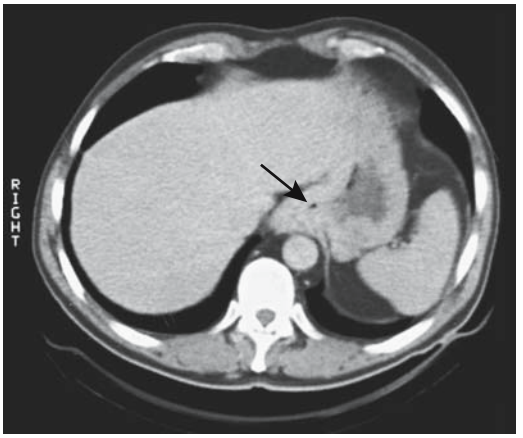

Figure 1.19. Distal esophageal adenocarcinoma. CT reveals diffuse infiltration of surrounding tissues (arrow).

esophageal carcinomas (Table 1.4). Information obtained from imaging is combined with other data to achieve a preoperative stage useful for subsequent prognosis and therapy. From an immediate surgical viewpoint, however, a primary concern is not staging but whether a tumor is resectable or not.

Preoperative imaging is used to detect local and metastatic spread. Computed tomography complements rather than competes with endoscopy and barium studies, which are primarily diagnostic rather than staging modalities. Arterial phase multislice CT shows most tumors to be hypervascular to surrounding normal soft tissues; CT detects tumor intralu-

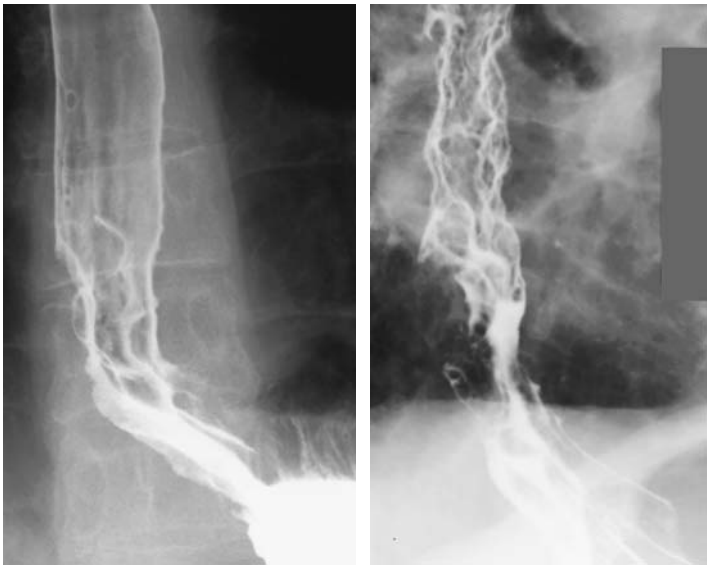

A B

Figure 1.20. Varicoid adenocarcinoma. A: The appearance superficially mimics varices, but the folds are too sharply defined for varices. B: A more advanced varicoid carcinoma.

Table 1.4. Tumor, node, metastasis (TNM) staging of esophageal tumors

Primary tumor:			
Tx	Primary tumor cannot be assessed		
T0	No evidence of primary tumor		
Tis	Carcinoma-in-situ		
T1	Tumor invades lamina propria or submucosa		
T2	Tumor invades muscularis propria		
T3	Tumor invades adventitia		
T4	Tumor invades adjacent structures		
Lymph nodes:			
Nx	Regional lymph nodes cannot be assessed		
N0	No regional lymph node metastasis		
N1	Regional lymph node metastasis		
Distant metastasis:			
Mx	Distant metastasis cannot be assessed		
M0	No distant metastasis		
M1	Distant metastasis		
Stage 0	Tis	N0	M0
Stage I	T1	N0	M0
Stage IIA	T2	N0	M0
	T3	N0	M0
Stage IIB	T1	N1	M0
	T2	N1	M0
Stage III	T3	N1	M0
	T4	any N	M0
Stage IV	any T	any N	M1

Source: From the AJCC Cancer Staging Manual, 6th edition (2002), published by Springer-Verlag, New York, NY, used with permission of the American Joint Committee on Cancer (AJCC), Chicago, IL.

minal extension, invasion, or displacement of tissue planes and blood vessels, obliteration of normal fat planes, and lymph node enlargement. The CT signs pointing toward irresectability are tumor-to-aorta contact angle >45 degrees; obliteration of the fat pad between the tumor, aorta, and spine; and tracheal invasion. Unfortunately, these signs have a high false-positive rate and they should be interpreted judiciously. Some of these patients are cachectic, however, and have little fat that can serve as a landmark.

A CT-specific staging system is used by some to gauge intramural extension and adjacent structure involvement. Intravascular contrast defines major adjacent vessels. A lymph node transverse diameter of 10 mm or more is one criterion used to gauge lymph node metastases, but the results are disappointing. Analysis of 7218 resected lymph nodes in patients with esophageal carcinoma revealed that only 28% of histopathologically proven nodes containing metastases were ≥10 mm in size, whereas 35% of metastatic nodes were 5 to 10 mm, and 36% were <5 mm (61); looking at the reverse, of resected nonmetastatic lymph nodes 7% were >10 mm and the authors concluded that CT cannot assess whether mediastinal lymph nodes are affected. Current data indicate that CT cannot reliably identify nodal involvement. It is useful, however, in detecting extensive spread.

One limitation of endoscopic US in staging esophageal cancers is that often the probe cannot be passed through a carcinoma and the full extent of a tumor cannot be assessed. Also, more distant involvement cannot be evaluated. Endoscopic US often does suggest whether a carcinoma is limited to the mucosa or submucosa, or extends into adjacent tissues. Using endoscopic US criteria, a blinded evaluation of patients with esophageal malignancy attempted to differentiate between tumors limited to the esophageal wall (T1-2) and extraesophageal (T3-4) involvement (62); the accuracy of muscularis disruption and tumor border irregularity was low in differentiating between intra- and extraesophageal disease. On the other hand, tumor maximal thickness was accurate in predicting extraesophageal extension; tumors limited to the esophagus measured 8 ± 1 mm, but extraesophageal tumors had a thickness of 16 ± 2 mm.

In a multicenter retrospective study of 79 patients with invasive (T4) esophageal carcinoma, endoscopic US accuracy was 88% in detecting tumor invasion, whereas CT accuracy was 44% ($p = .0002$) (63); of interest is that in this group of invasive cancers (consisting of both adenocarcinomas and squamous cell carcinomas), overall mortality was not significantly different whether surgery was performed or not.

Gauging lymph node involvement by endoscopic US is problematic. Although some studies have reached a nodal staging sensitivity of 92% (64), others have achieved staging sensitivities of only 60% to 80%. Nevertheless, endoscopic US is more accurate than CT in staging node invasion.

More proximal esophageal squamous cell carcinomas metastasize to cervical lymph nodes. Neck US using a 7.5- or 10-MHz transducer appears useful, keeping in mind that US simply detects lymph nodes, and nodes above a certain

size, such as 5 mm or so in their long dimension, are assumed to be metastatic. Some studies use a short-to-long node dimension ratio >0.5 as an indicator of metastasis.

In patients with an intrathoracic esophageal squamous cell carcinoma, 1.5 T, T1-weighted sagittal MRI could not detect lesions subsequently found to be less than stage T2 (65); detected T3 lesions had a mean diameter of 25 mm, whereas T4 lesions were 34 mm. Nevertheless, future MRI staging of esophageal cancers appears promising. Thus in evaluating depth of mural invasion, T2-weighted MRI (at 1.5 T) agreed in 95% of patients with suspected superficial esophageal carcinoma with final histopathologic evaluation (66); in 5% of specimens MRI staging was higher.

Positron emission tomography has a role in staging both esophageal squamous cell carcinoma and adenocarcinoma. Its spatial resolution is insufficient to evaluate local extension, but it is often more specific than CT or US in detecting nodal involvement, keeping in mind that activity in a primary tumor can mask adjacent lymph node uptake. In 36 patients with a newly diagnosed esophageal cancer, 18F-FDG PET detected abnormal uptake in all (67); in those undergoing a curative esophagectomy, PET and CT correctly identified extent of nodal involvement in 76% and 45% of patients, respectively. The current primary role for PET is in excluding stage IV disease and in following patients postresection. One should keep in mind that esophagitis and adjacent inflammation result in a false-positive PET scan, and this study thus should be obtained only several months or longer after radiation therapy or resection.

Although thoracoscopic staging has been proposed, it is not widely employed.

Adenocarcinoma: Compared to postoperative staging, endoscopic US correctly staged tumor depth invasion in 87% of patients compared to 40% for CT (68) (Fig. 1.21). It was also significantly more accurate (73%) than CT (33%) in staging node invasion. Even if the endoscope probe could not pass through a tumor stricture, US is able to stage. False-positive findings are due to edema or fibrosis, whereas scattered infiltration accounts for false-negative ones.

Lymph node metastasis is uncommon if an adenocarcinoma is limited to the mucosa, is present in <20% of patients when a cancer extends to the submucosa, and increases further with deeper tumor extension (Fig. 1.22).

Complications

Esophageal neoplasms necrose and fistulize to adjacent structures, including trachea and major bronchi (Fig. 1.23). Imaging detection of tumor invasion into the tracheoesophageal fat plane increases the likelihood of future tracheoesophageal fistula formation. Unusual ones include an esophagosubarachnoid fistula (69) and even lower extremity subcutaneous emphysema, with psoas muscles presumably serving as a pathway (70).

Some neoplastic fistulas are iatrogenic. These tissues are friable, and even passage of a feeding tube can result in a perforation and fistula.

Therapy

Therapeutic options available for cure consist of surgical resection, at times in combination with radiotherapy or chemotherapy. Combined chemo- and radiation therapy before esophagectomy for invasive esophageal or gastroesophageal junction cancer did not influence distant metastases but did control local recurrence, achieving a 5-year local tumor control rate of 90%, compared to 64% after esophagectomy only (71); on the other hand, postoperative mortality was 16% in the chemo- and radiation therapy group versus 6% after esophagectomy only.

Some surgeons recommend esophagectomy to all patients able to withstand resection, keeping in mind that such an approach provides no survival benefit; only those patients who are too ill for surgery are referred to palliation, an approach of questionable value.

For cure: Flat esophageal carcinomas and areas of dysplasia are amenable to endoscopic mucosal strip resection. This procedure holds promise as long as a lesion is limited in depth. In general, survival does not depend on tumor location within the esophagus.

Photodynamic therapy cures most early squamous cell carcinomas (Tis and T1a) of the esophagus (72).

Traditional therapy for squamous cell esophageal carcinomas involves resection (where applicable), radiation therapy, and chemotherapy. Patients with stage I and II

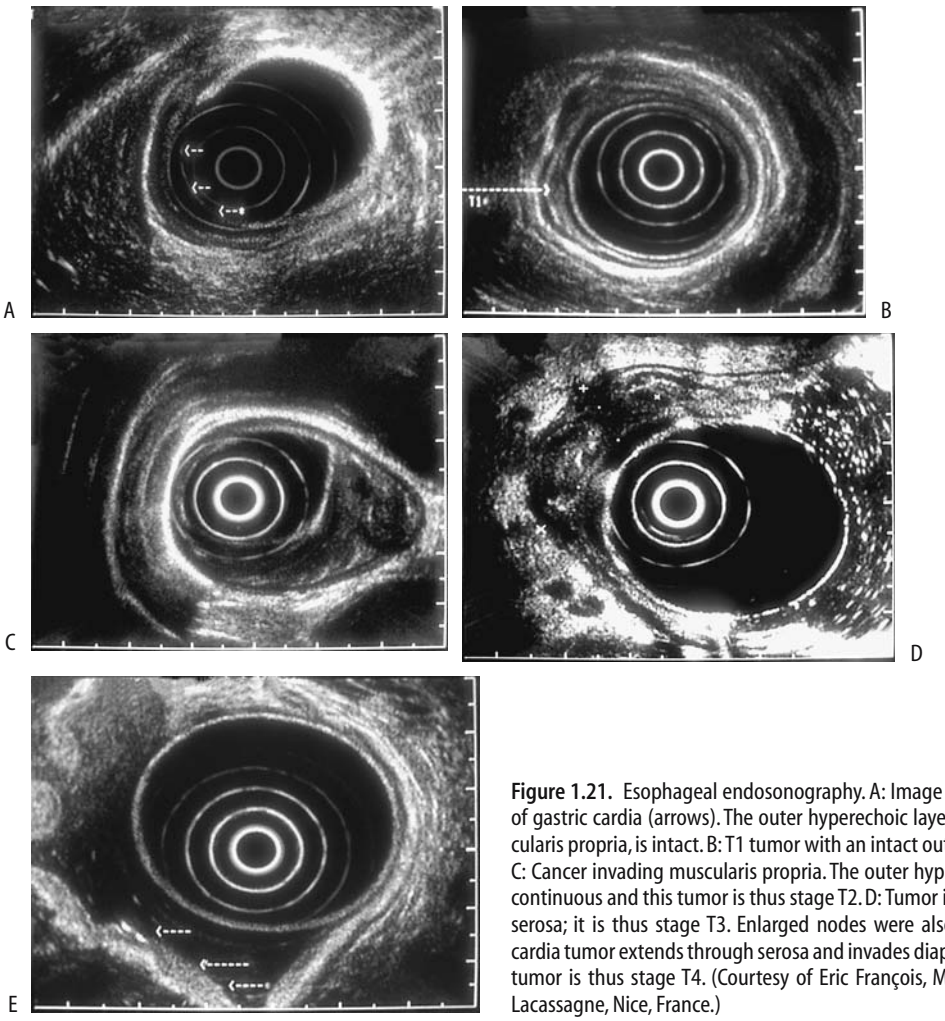

Figure 1.21. Esophageal endosonography. A: Image of superficial cancer of gastric cardia (arrows). The outer hyperechoic layer, representing muscularis propria, is intact. B: T1 tumor with an intact outer hypoechoic layer. C: Cancer invading muscularis propria. The outer hyperechoic layer is discontinuous and this tumor is thus stage T2. D: Tumor invading beyond the serosa; it is thus stage T3. Enlarged nodes were also present. E: Gastric cardia tumor extends through serosa and invades diaphragm (arrows). The tumor is thus stage T4. (Courtesy of Eric François, M.D., Centre Antoine-Lacassagne, Nice, France.)

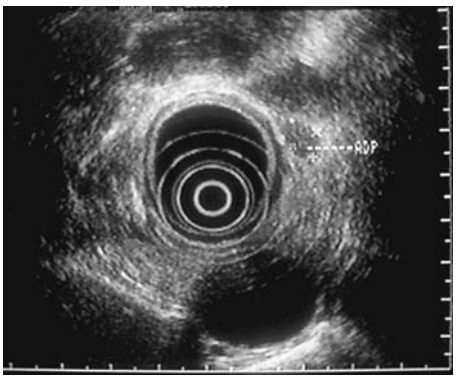

Figure 1.22. Endosonography reveals numerous hypoechoic nodes surrounding the esophagus, (Courtesy of Eric François, M.D., Centre Antoine-Lacassagne, Nice, France.)

cancer achieve greater 5-year survival either with surgery only or surgery plus adjuvant chemoradiotherapy than with primary radiation therapy only.

Either a transhiatal esophagectomy or a transthoracic approach is used to resect a distal esophageal or gastric cardia adenocarcinoma. Both techniques appear to be equally safe and have comparable complications and survival rates.

The 5-year survival for patients undergoing resection of an esophageal adenocarcinoma, without postoperative residual tumor and without lymph node involvement, is about 60–70%.

Computed tomography using a negative oral contrast agent and endoscopy appear comparable in evaluating the response to chemotherapy

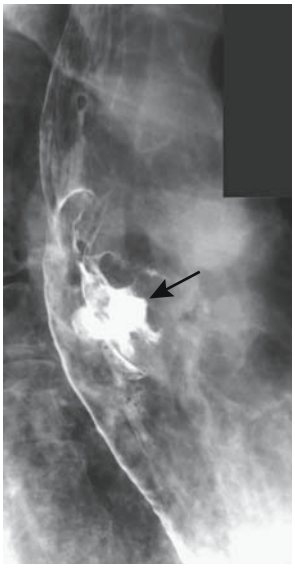

Figure 1.23. Cancer ulcerating into carinal lymph nodes (arrow).

of gastroesophageal junction adenocarcinomas (3).

Although of limited application, transjugular intrahepatic portosystemic shunting (TIPS) can relieve portal hypertension in a cirrhotic patient with esophageal varices and an esophageal adenocarcinoma, allowing subsequent cancer therapy.

Palliation: Therapy of patients with cancer invading adjacent structures is controversial. Palliation of dysphagia in most patients with either squamous cell carcinoma or adenocarcinoma consists of stenting, radiotherapy, laser therapy, or serial dilation of the malignant stricture. Some centers report prolonged survival after chemotherapy, radiotherapy, and esophagectomy combined with regional node dissection.

Indications for stenting an inoperable esophageal carcinoma are obstruction or fistula. The procedure of choice for an inoperable carcinoma, especially in underdeveloped countries, is often a plastic stent inserted under endoscopic guidance without general anesthesia and requiring only a short hospital stay (73).

Numerous commercial stents are available and new ones continue to be introduced. These stents are inserted using either endoscopic or fluoroscopic guidance. Self-expanding metal stents provide dysphagia palliation for a majority of patients. Covered stents provide better long-term palliation than uncovered stents. Comparing Wallstents and knitted nitinol stents, a multicenter study found that procedure-related mortality, early complication rate, and severe persistent pain after stent placement were higher with Wallstents (74); on the other hand, stent dysfunction, reintervention rate, and cost were lower in the Wallstent patients. Mean survival time of patients with malignant dysphagia is longer with covered than with uncovered stents.

In addition to treating strictures, covered metallic stents also are effective in treating inoperable malignant perforations and tracheoesophageal fistulas. Both covered Wallstents and Gianturco stents are popular. A contrast study shortly after the procedure evaluates stent position with respect to the fistula. Therapy with Wallstent endoprostheses or Gianturco stents of esophagorespiratory fistulas or perforations in patients with unresectable esophageal cancer led to closure of 90% of fistulas and all perforations (75).

What is the effect of a magnetic field on various metallic stents? Magnetic resonance imaging quality was not degraded by the titanium alloy Ultraflex stent and nitinol covered Wallstent (76); stainless steel Gianturco stent and modified Gianturco stent have an appreciable attraction force and torque. In particular, the Gianturco stent is pulled toward the head with a force 7× gravity, although whether this is enough of a risk for dislodgment is unknown. In addition, the stainless steel Gianturco stents produce gross artifacts around the stent.

Stent-related delayed complications tend to be more common than immediate complications and consist of recurrent fistula, tumor ingrowth, and tracheal compression by tumor (Fig. 1.24). Complications appear to be similar regardless of whether a stent is used primarily to treat a stricture or to bypass a fistula (Table 1.5). Gastroesophageal reflux is common if the stent straddles the gastroesophageal junction; at times resultant esophagitis is sufficiently severe to mimic an obstruction. Tumor ingrowth and overgrowth after stenting result in recurrent dysphagia and can be treated by balloon dilation or insertion of a second stent. Stents

Figure 1.24. Tygon tube perforation (arrow). Most common site of perforation is at the proximal sleeve.

do migrate proximally and distally, although migration is less of a problem with newer stents. Covered stents tend to migrate more often than uncovered stents; on the other hand, tumor ingrowth occurs with uncovered stents. Stent erosion into adjacent tissues is not uncommon, with most perforations occurring at stent ends.

A nitinol stent broke spontaneously shortly after insertion, and another one broke after laser therapy for tumor ingrowth, possibly due to thermal overload during laser therapy (77); electrocoagulation and laser use should be used with caution around a stent. Another nitinol stent invaginated after initial expansion and shortened to about two thirds of its length, allowing tumor overgrowth (78).

Table 1.5. Complications of esophageal stenting

Reflux
Aspiration
Food impaction
Perforation
Benign strictures at stent edges
Esophagorespiratory fistula
Esophagovenous intravasation
Aortoesophageal fistula
Stent migration
Stent fracture
Stent invagination
Stent twisting/torsion
Tumor ingrowth or overgrowth
Massive hemorrhage
Death

Endoscopic laser therapy is useful in palliating some of these cancers, and reopening rates of >90% can be achieved. Survival did not differ in patients with stages III and IV squamous cell carcinoma whether they underwent esophagectomy or endoscopic laser therapy (79); patients undergoing laser therapy did have a shorter hospital stay, although sequential retreatments are necessary. Complications of laser therapy include esophagotracheal fistulas and hemorrhage. There have been incidents of procedure-related mortality. A prospective randomized trial found that in patients with inoperable esophageal cancer dysphagia palliation was substantially better with stenting than with endoscopic laser therapy (80).

Tumor response to radiotherapy or chemotherapy is estimated by measuring residual tumor size. Tumor volume can be calculated from CT scans by combining adjacent measured tumor areas on each 1-cm slice. The accuracy of this method is similar to results obtained from resected tumor weight and water displacement measurements.

Complications of Therapy: A gastroesophageal anastomotic leak is not uncommon after cancer resection. Most of these leaks are detected by a barium study shortly after surgery, and most smaller ones are managed medically and close spontaneously. Larger ones or those not healing with conservative therapy are amenable to esophageal stenting. In one study, immediate leak occlusion was evident after stenting, and clinical healing occurred in 93% of patients, with a median healing time of 6 days (81).

An esophageal mucocele developed after surgical bypass due to continued secretions in the excluded esophagus (82).

Recurrence/Metastasis

Local recurrence manifest as dysphagia and generally implies extensive disease (Fig. 1.25).

Figure 1.25. Recurrent cancer at gastroesophageal anastomosis. A gastric cardia adenocarcinoma had been resected previously.

Typical metastases are to mediastinal, cervical, and abdominal lymph nodes.

Endoscopic US is an option for early detection of locally recurrent cancer. A study of patients followed by endosonography found that two thirds of patients were still asymptomatic when US detected recurrence (83).

Metastases from an esophageal adenocarcinoma mimicked myositis ossificans (84).

Lymphoma

A primary esophageal lymphoma is rare. Most involvement is secondary, often due to direct spread from mediastinal lymph nodes or stomach. Lymphomas range from polypoid to diffusely infiltrating (Fig. 1.26). An occasional one is primarily intramural and mimics esophageal varices, similar to a varicoid carcinoma.

A lymphoma infiltrating an esophageal squamous cell carcinoma is a rarity; the diagnosis is difficult even for a pathologist because reactive lymphoid infiltration is not uncommon adjacent to a squamous cell carcinoma.

Sarcoma

Some connective tissue tumors are difficult to characterize even with immunohistochemistry, and most authors simply label them as stromal tumors. Whenever possible, however, a specific pathologic diagnosis should be applied to mesenchymal tumors because of differences in therapy and prognosis.

Within the gastrointestinal tract, gastrointestinal stromal tumors (GISTs) are least common in the esophagus and most common in the stomach. These tumors are discussed in more detail in Chapter 2.

Leiomyosarcoma

Although leiomyomas are common in the esophagus, sarcomatous degeneration is not. Most sarcomas present as large bulky tumors varying in size. Their growth rate is variable, although most are slow-growing. The distinction between a leiomyoma and a leiomyosar-

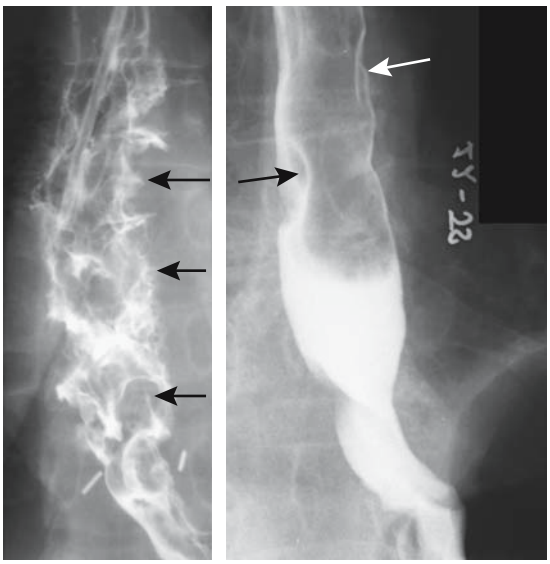

A B

Figure 1.26. Esophageal lymphoma. A: A diffuse infiltrating, ulcerating tumor (arrows) was believed to have been induced by cyclosporin. (Courtesy of Arunas Gasparaitis, M.D., University of Chicago.) B: Recurrent lymphoma presenting as multiple nodules (arrows).

coma is generally made only by the pathologist and even then often with difficulty.

Dysphagia is the usual presentation. An occasional patient manifests with bleeding or pain. Leiomyosarcomas tend to metastasize late in their course.

The vast majority of leiomyosarcomas develop in the esophageal segment containing smooth muscle (i.e., mid-to-distal esophagus). The rare one found more proximally presumably originates either from the vessel wall or muscularis mucosa. Some are sufficiently large that a chest radiograph reveals a mediastinal mass. Squamous cell carcinomas and adenocarcinomas, on the other hand, rarely are sufficiently large at initial presentation to be detected with chest radiography.

Their barium appearance varies from a mostly intramural to a large intraluminal mass. A primarily infiltrating tumor is less common. Larger ones tend to ulcerate. A rare one is pedunculated and occasionally even extends into the stomach. At times a necrotic one communicates with the esophageal lumen, leading to gas and contrast within the tumor.

Computed tomography identifies any exophytic component. These tumors are isointense with skeletal muscle on T1-weighted MRI and hyperintense on T2-weighted MRI.

Other

Although liposarcomas are relatively common throughout the body, they are rare in the esophagus. Some appear polypoid, and imaging suggests a fibrovascular polyp.

A hypopharyngeal liposarcoma grew submucosally into the esophagus (85).

A rare malignant fibrous histiocytoma presents as a soft tissue polyp.

A carcinosarcoma is uncommon in the esophagus. Histologically, these tumors show elements of both squamous cell carcinoma and sarcoma. Histogenesis is believed to involve metaplasia of some carcinomatous cells toward mesenchymal differentiation. Only rarely is a carcinosarcoma a result of simultaneous adjacent tumor development from both epithelial and mesenchymal tissue, identified by distinct immunoreactive and genetic clonalities in the two components.

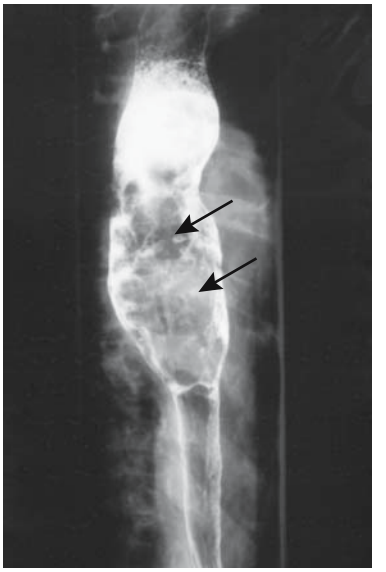

Figure 1.27. A carcinosarcoma presents as an expansile intraluminal polyp (arrows). (Courtesy of Arunas Gasparaitis, M.D., University of Chicago.)

Commonly a carcinosarcoma presents as an intraluminal polyp mimicking a fibrovascular polyp (Fig. 1.27).

Melanoma

Melanocytes are normally present in the esophageal epithelium, and primary melanomas develop in the esophagus, albeit rarely. Many esophageal melanomas, however, are metastatic. These are aggressive tumors associated with a poor prognosis regardless of presentation or appearance.

Common presentations are dysphagia or odynophagia; melena is rare.

Primary melanomas range from an exophytic, pedunculated polyp, often bulky, to an infiltrative lesion, generally not obstructing but distending the esophageal lumen (Fig. 1.28). Endoscopic US shows some of these tumors to be smooth-walled, have discrete margins, and have varying echogenicity (86).

Metastatic melanomas tend to be flat and not visualized with barium studies, although CT and US detect any intramural or extrinsic extension.

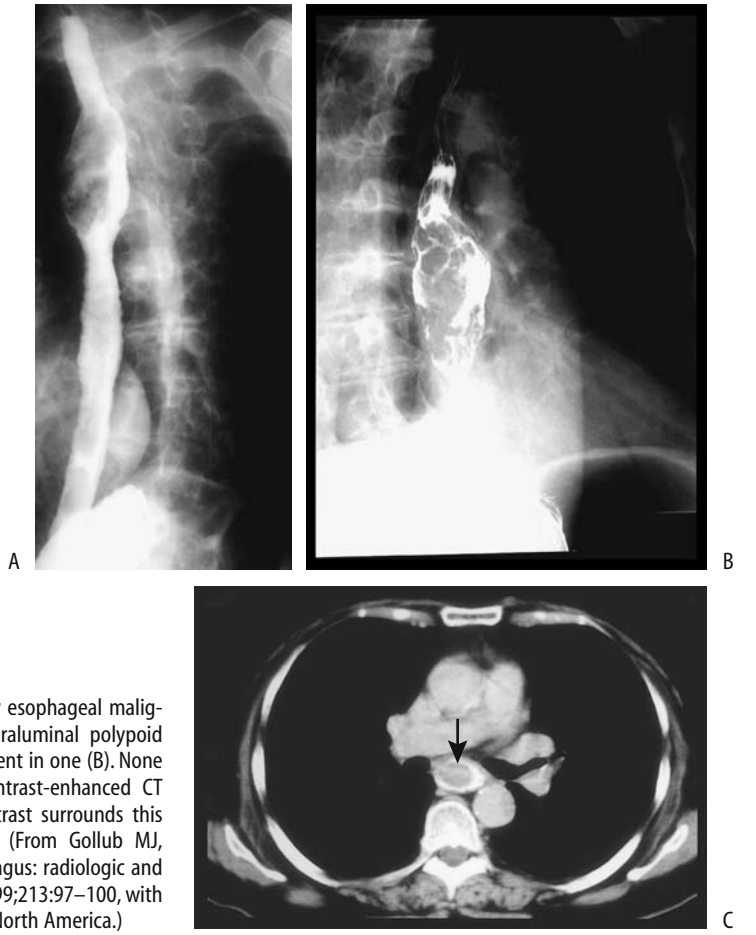

Figure 1.28. A,B: Two patients with primary esophageal malignant melanoma. Both tumors have an intraluminal polypoid appearance. Linear ulcers or fissures are evident in one (B). None resulted in lumen obstruction. C: Oral contrast-enhanced CT reveals an intraluminal tumor (arrow). Contrast surrounds this primary esophageal malignant melanoma. (From Gollub MJ, Prowda JC. Primary melanoma of the esophagus: radiologic and clinical findings in six patients. Radiology 1999;213:97–100, with permission from the Radiological Society of North America.)

Metastases or Direct Invasion

The esophagus is involved either by direct invasion from adjacent structures or metastases. Both result in dysphagia. Lung cancer is the most common secondary malignancy involving the esophagus. Breast cancer metastasis to the esophagus is not uncommon, at times with a latency of many years. A thyroid carcinoma or other malignant tumor in the paraesophageal tissues either invades or metastasizes to the esophagus (Fig. 1.29). Rarely, renal carcinoma, prostate carcinoma, or a bladder transitional cell carcinoma metastasizes to the esophagus. An often overlooked primary is a pancreatic tail carcinoma; these spread to the paraaortic nodes, which then involve the distal esophagus and gastroesophageal junction, with an imaging appearance mimicking a primary gastroesophageal carcinoma (Fig. 1.30).

Management of resultant esophageal narrowing is difficult; these patients readily perforate during bougienage and balloon dilation and form fistulas.

Neuroendocrine Tumors

Neuroendocrine tumors are discussed in more detail in Chapter 14.

Schwannomas

A cervical schwannoma in the retropharyngeal tissues led to dysphagia (87); CT and T2-weighted MRI showed a target lesion, suggestive of a neurofibroma. Some peripheral schwannomas do not enhance on MRI (88).

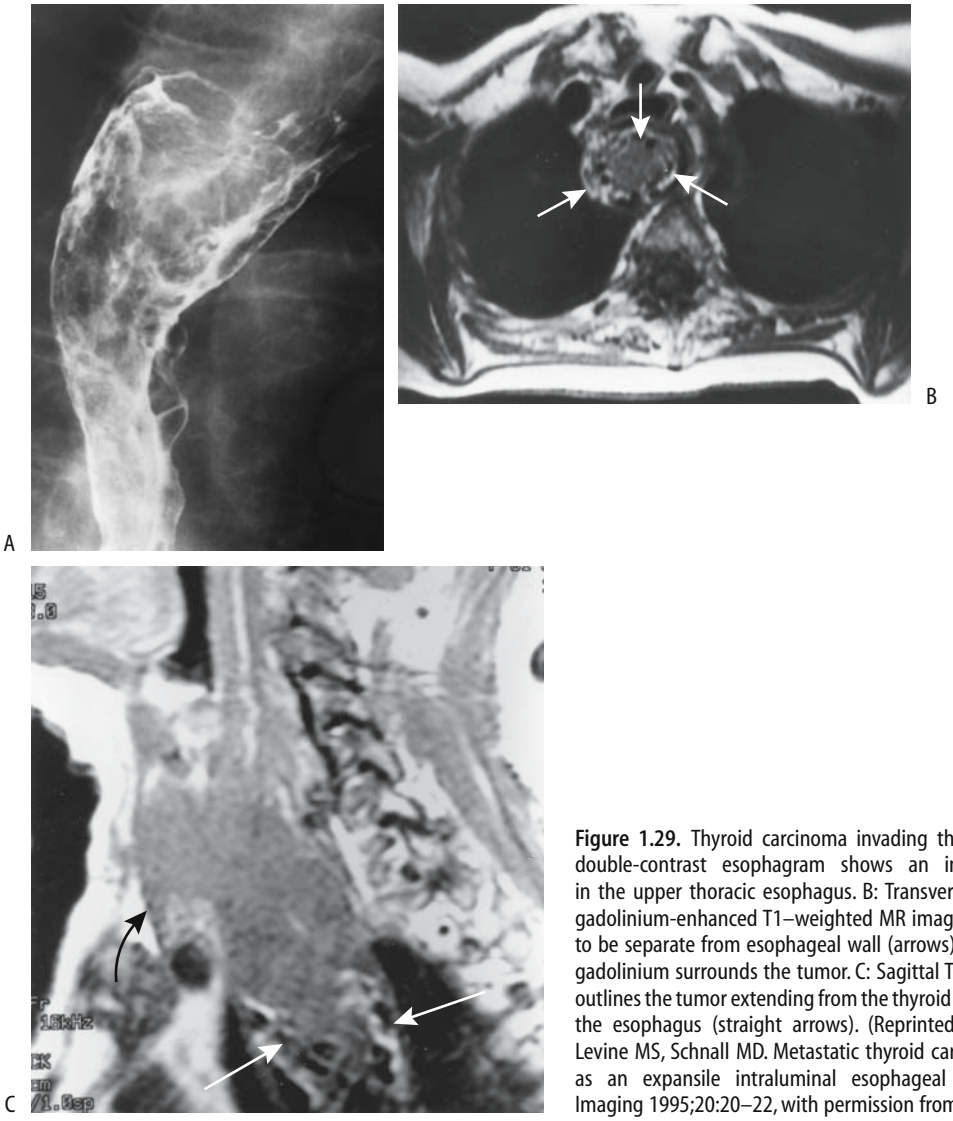

Figure 1.29. Thyroid carcinoma invading the esophagus. A: A double-contrast esophagram shows an intraluminal tumor in the upper thoracic esophagus. B: Transverse postintravenous gadolinium-enhanced T1–weighted MR image shows the tumor to be separate from esophageal wall (arrows). Hyperintense oral gadolinium surrounds the tumor. C: Sagittal T1–weighted image outlines the tumor extending from the thyroid (curved arrow) into the esophagus (straight arrows). (Reprinted from Cooney BS, Levine MS, Schnall MD. Metastatic thyroid carcinoma presenting as an expansile intraluminal esophageal mass. Abdominal Imaging 1995;20:20–22, with permission from Springer.)

Granular Cell Tumors

Most granular cell tumors originate as a solitary painless nodule in the skin, tongue, or larynx. Also known as *Abrikossoff's tumors* and *granular cell myoblastoma*, they are rare in the gastrointestinal tract, with the esophagus being most often involved. Even rarer are multifocal granular cell tumors.

These tumors are not believed to originate from muscle cells and thus are not of myoblastic cell origin and the term *granular cell myoblastoma* appears inappropriate. Investigators favor a neuroectodermal origin and, more specifically, a peripheral nerve Schwann cell origin. Histology and immunohistochemical analysis provide a diagnosis. Their characteristic morphologic feature is eosinophilic cytoplasmic granularity believed to represent an accumulation of lysosome fragments (89), possibly due to a degenerative process. The vast majority are benign, but an occasional malignant one has generated considerable heat about proper management. Some granular cell tumors

Figure 1.30. Pancreatic tail carcinoma spreading to paraaortic nodes and invading distal esophagus. This appearance mimics a primary gastroesophageal carcinoma.

are associated with epithelial hyperplasia and undoubtedly are mistaken for squamous cell carcinomas; endoscopic biopsies identify only about half of these tumors.

A number of these tumors are discovered incidentally. The larger ones result in dysphagia. An occasional one ulcerates. Patients range in age from young adulthood onward.

A barium esophagram reveals an intramural tumor. The appearance is similar to that of a small leiomyoma.

Endoscopic US shows a hypoechoic, solid, intramural tumor (90).

Magnetic resonance imaging in a patient with progressive dysphagia revealed a granular cell tumor to be hypointense on T1-weighted images and mildly hyperintense on T2-weighted images (91); homogeneous contrast enhancement was evident.

Carcinoids

Esophageal carcinoids are rare. The literature is somewhat vague when describing these tumors and such terms as *atypical carcinoids* and esophageal *endocrinomas* are encountered, with the latter term used to describe a number of endocrine-active tumors.

When detected, most esophageal carcinoids are small, solid intramural tumors. Both an esophagram and endoscopy often simply identify a polyp (92); endoscopic US reveals a sharply demarcated, hyperechoic mucosal tumor.

Webs and Rings

Esophageal webs are thin membranes, 1 to 2 mm in diameter, extending completely or partially around the esophageal lumen. Most webs occur singly and are located in the proximal esophagus along the anterior border. Some are part of a benign appearing stricture.

Most smaller webs are incidental findings; more prominent ones are symptomatic (Fig. 1.31). No definite association exists between the remaining esophageal lumen caliber and degree of dysphagia.

Esophageal webs are amenable to balloon dilation; they are readily dilated with 20-mm diameter balloon catheters, a simple and effective therapy.

Figure 1.31. Upper esophageal webs. No underlying disease was found.

Plummer-Vinson Syndrome

A combination of dysphagia, esophageal webs, and iron-deficiency anemia is characterized as the Plummer-Vinson syndrome. Patients are at increased risk of developing a postcricoid carcinoma.

As already mentioned, these webs are readily dilated.

Epidermolysis Bullosa

Epidermolysis bullosa, an inherited autosomal-recessive autoimmune disorder, is characterized by bullous lesions of the skin and bullae, erosions, and ulcerations in the oropharynx and esophagus. Occasionally the esophagus is involved with no cutaneous manifestations. These lesions heal by fibrosis and result in web-like rings.

An association probably exists between epidermolysis bullosa and Crohn's disease.

These webs are readily balloon dilated, although therapy often results in hemorrhage and further fibrosis.

Pemphigoid

Cicatricial pemphigoid, also known as *benign mucous membrane pemphigoid*, results in blistering lesions in the skin and mucous membranes. It rarely involves the esophagus, but when present esophageal blistering results in a web-like appearance, usually in the proximal portion. Some webs evolve into single or multiple strictures, and esophageal dilation is necessary.

One patient with cicatricial pemphigoid was also found to have cervical esophageal intramural pseudodiverticulosis (93).

Dilation, at times multiple, is required for dysphasia induced by these webs. Dilation in one patient led to an intramural dissection extending from the cervical esophagus to the esophagogastric junction (93).

Schatzki's Ring

Occasionally a web-like narrowing is detected at the distant end of the esophagus. Also called *lower esophageal ring* or *mucosal ring*, this narrowing contains not only mucosa but also other esophageal wall layers; it does not represent the squamocolumnar-mucosal junction. These rings, at most several millimeters in thickness, are believed by some to be secondary to reflux esophagitis, although their precise etiology is unknown. They are more common in adults than in children. Their prevalence is difficult to gauge; many subtle ones are not detected on an esophagram without full distention.

Schatzki's rings that are less than 12 or 13 mm in diameter lead to solid food dysphagia. An associated hiatal hernias is common.

Progressive dysphagia to solid food and acute food impaction are typical presentations; associated esophagitis is common.

These rings are best studied with the esophagus maximally distended with barium and gas. An occasional subtle one is identified only with a barium pill impacting at the ring.

Other Webs

Occasionally recurrent upper esophageal webs and cricopharyngeal muscle spasms are associated with esophageal heterotopic gastric mucosa.

Occasionally multiple esophageal webs are detected in a patient with dysphagia, but no predisposing condition is discovered; a congenital etiology is often ascribed. Although these patients respond to web dilation, dysphagia often recurs.

Motility Disorders/Dilation

Dysphagia and Dysmotility

Dysphagia is a common condition and is routinely encountered in most practices. Anatomic and functional abnormalities are common even in young adults. In patients younger than 30 years with dysphagia, a barium esophagram was able to explain symptoms in 70% (94); findings included achalasia, dysphagia lusoria, esophagitis, esophageal dysfunction, stricture, gastroesophageal reflux, and pharyngeal dysfunction.

A number of dysmotility findings are specific for a particular disorder but some cannot be pigeonholed into a specific category; these are often given such terms as *nonspecific esophageal motility disorder* or *lower esophageal sphincter*

dysfunction. In many of these patients a barium tablet is trapped in the proximal or mid-esophagus and in some is associated with symptoms. Autonomic nerve function tests, which assess parasympathetic vagal nerve function, show that patients with a bolus-specific dysmotility disorder have vagal nerve dysfunction (95). Swallowing initiates an esophageal peristaltic contraction after a brief latency and it is this interplay between inhibitory and contractile neurons that establishes subsequent contraction propagation velocity and amplitude.

Esophageal dysmotility has been reported in children who had been breast-fed by mothers who had silicone breast implants (96); the authors believed that dysmotility was chronic.

About a quarter of hospitalized psychiatric patients complaining of anxiety or depression had an abnormal esophageal transit study as measured by krypton-81m scintigraphy (97).

Using a bolus at 22°C and 60°C, esophageal scintigraphy and manometry in patients with intermittent dysphagia found that hot water accelerated esophageal clearance, decreased amplitude and duration of esophageal contractions, and improved symptoms (98); whether this technique should have a role in managing patients with motility disorders is not clear.

Some patients with dysphagia have normal imaging studies and normal endoscopies. Empiric dilation has resolved symptom in some patients with solid food dysphagia but not those with a component of liquid dysphagia.

Penetration and Aspiration

Bolus penetration into the laryngeal vestibule is best approached with a videofluoroscopic swallowing study, and this test is routinely performed in swallowing centers.

Vagus nerve stimulation is used to treat seizures, especially in children with mental and motor disabilities. Some of these children with swallowing difficulties are prone to aspirate when the stimulator is activated continuously (99); the authors recommended that swallowing function be assessed prior to the start of vagus nerve stimulation in these children.

Premature Lower Sphincter Closure

Impaired relaxation of the lower esophageal sphincter is associated with dysphagia. A classic example is achalasia. Some patients with normal sphincter relaxation have premature closure, often associated with more proximal esophageal peristaltic abnormalities, and with reflux suspected as the underlying cause.

Achalasia

Primary

General

Achalasia is a chronic esophageal motor disorder characterized by disordered esophageal peristalsis, often to the point of aperistalsis, and failure of the lower esophageal sphincter to relax. Some achalasia patients have motor disturbances in other parts of the gastrointestinal tract, even biliary tract, and associated abnormal autonomic cardiovascular and other functions. For instance, superior mesenteric artery US in achalasia patients revealed a significantly lower postprandial increase of peak systolic velocity and a significantly higher postprandial decrease of pulsatility index and resistance index (100). An occasional patient also has cricopharyngeal dysfunction. Incomplete upper esophageal sphincter relaxation is associated with achalasia—a finding rare in most other motility disorders.

In general, the primary abnormality in achalasia is incomplete relaxation of the lower esophageal sphincter, although achalasia patients with a normal lower esophageal sphincter relaxation have been described. Dilation and aperistalsis of the more proximal esophagus develop subsequently. For some reason esophageal bezoars are uncommon in achalasia.

Pathologically, patients with achalasia have few or no ganglion cells, but show myenteric inflammation, neural fibrosis, and often a ganglionitis (101); the number of remaining ganglion cells is inversely related to degree of myenteric fibrosis. Advanced achalasia exhibits marked myenteric ganglion cell depletion, extensive neural destruction, and chronic inflammation.

Mean duration of symptoms with newly diagnosed achalasia is generally years. A delay in diagnosis is common.

Vigorous Achalasia

Some patients with achalasia have prominent but uncoordinated contractions in the body of the esophagus, a condition termed *vigorous achalasia*. Pathologically, this entity appears distinct from classic achalasia; the number of ganglion cells in patients with vigorous achalasia is normal. Patients have myenteric inflammation, but no neural fibrosis (101).

Both manometry and barium studies are useful in differentiating between vigorous achalasia and more typical achalasia (Fig. 1.32).

Patients with vigorous achalasia also respond to botulinum toxin injection.

Etiology

The familial form of achalasia rarely manifests prior to puberty. The etiology of primary achalasia is unknown (secondary achalasia is discussed later). A number of viruses have been searched for, with disappointing results. An inconclusive association between varicella infection and achalasia has been raised. An occasional patient develops concomitant achalasia and Guillain-Barré syndrome, for which a viral etiology is postulated.

A 25-year old woman developed both achalasia and megacolon (102); serology for *Trypanosoma cruzi* was negative, and no neuromuscular disorders were evident. Whether this is a rare and unique manifestation of a single disease entity or whether it represents two different diseases is conjecture.

An achalasia-like condition occasionally develops after esophageal and paraesophageal surgery. Truncal vagotomy has been associated with subsequent development of achalasia. This is rare with a highly selective vagotomy.

Achalasia has developed in patients with multiple endocrine neoplasia syndrome type 2 and in secondary amyloidosis. It is rare during pregnancy.

Diagnosis

Using manometry as a gold standard, videoesophagography sensitivity in diagnosing achalasia was 75% and scintigraphy achieved a sensitivity of 68% (103), results lower than those found in a number of clinical practices. In most patients a diagnosis of achalasia with a barium esophagram is straightforward. Vigorous achalasia is more problematic. Of concern in all these patients is not to miss the occasional underlying carcinoma.

Gastroesophageal reflux is rare in untreated achalasia and, if detected, should suggest another diagnosis.

Endoscopic US of the lower esophageal sphincter in patients with achalasia identifies wider than normal longitudinal and circular smooth muscle layers; overlap exists with normality, and a definitive diagnosis of achalasia should be made with caution.

Scintigraphy detects radioisotope retention in a dilated esophagus, a finding also seen with other disorders.

Thyroid scintigraphy detects radioisotope retention in a dilated esophagus, a finding also seen with other disorders. 99mTc-pertechnetate scintigraphy accumulation within a dilated esophagus is presumably due to salivary gland uptake and excretion of tracer with saliva.

Inhalation of amyl nitrate relaxes an otherwise spastic lower esophageal sphincter, but this

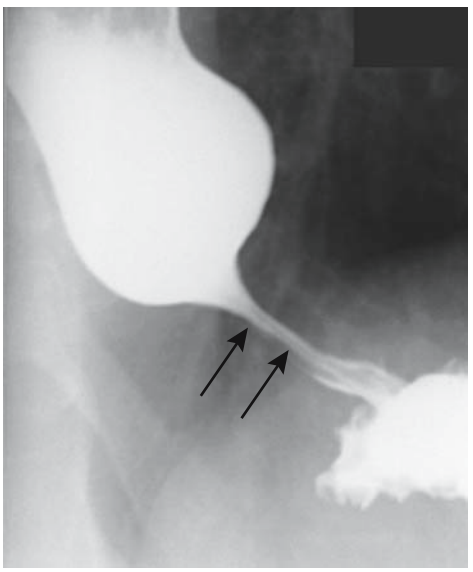

Figure 1.32. Vigorous achalasia. A long, spastic distal esophageal segment (arrows) mimics conventional achalasia. This segment did distend occasionally, distinguishing it from a carcinoma. Uncoordinated contractions were present more proximally (not shown).

maneuver is rarely necessary or performed when evaluating for achalasia.

Complications

A massively distended esophagus can cause tracheal compression and lead to respiratory compromise and stridor; the trachea is usually compressed at the thoracic inlet.

Patients with long-standing achalasia are at increased risk of developing an esophageal carcinoma (Fig. 1.33). These carcinomas are notoriously difficult to detect; they tend to be diffuse, infiltrate submucosally, and develop anywhere in the esophagus rather than being limited to the distal segment.

Retrograde gastroesophageal intussusception is a rare complication (104).

The esophageal wall in achalasia is not unduly thickened. Thus any focal thickening, detected by CT or other imaging, should raise suspicion for a malignancy. Unfortunately, with passage of time many of these patients have already undergone botulism injections, endoscopic dilations, and a possible myotomy, therapies associated with fibrosis and esophageal wall distortion and thickening.

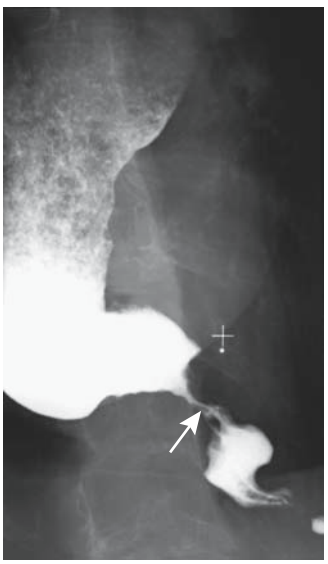

Figure 1.33. Adenocarcinoma in a patient with long-standing achalasia. The narrowed segment (arrow) is longer than usually seen in achalasia and it never changed shape, indicative of stenosis rather than spasm. The distended more proximal esophagus containing secretions can be seen both with primary achalasia and a cancer.

Treatment

Therapy of achalasia consists of a reduction of the lower esophageal sphincter pressure, leading to improved esophageal emptying. Currently botulinum toxin injection is in vogue, with dilation and myotomy reserved for more complex situations. Calcium channel blockers and nitrates, which were used in the past, are currently rarely employed.

Botulinum toxin injection into the gastroesophageal junction improves symptoms in patients with idiopathic achalasia and are occasionally also useful in other, nonachalasia esophageal motility disorders. Treatment with botulinum toxin appears to be as effective as pneumatic dilation in relieving symptoms and improving esophageal function. In most patients, however, symptoms gradually recur, patients become less responsive to subsequent botulinum toxin injection, and the interval between injections shortens to the point that other therapies such as pneumatic dilation or myotomy are contemplated. Response rate to botulinum is greatest in older patients.

Lower esophageal sphincter pneumatic dilation relieves dysphagia for varying lengths of time. This procedure is generally performed under fluoroscopic guidance although some gastroenterologists use endoscopic guidance. At times several balloons in tandem are required to achieve adequate dilation.

Esophageal intramural hematoma and perforation are known risks of pneumatic dilation. Complications of pneumatic dilation appear to be underestimated and underreported. A complaint of prolonged postdilation chest pain suggests a perforation. Some patients develop a diverticular-like outpouchings at the gastric cardia, and dilation should be approached cautiously in the presence of a diverticulum close to the lower esophageal sphincter due to an increased risk of perforation.

Most gastroenterologists believe that a Heller myotomy is the surgical procedure of choice only after failure of medical therapy. Surgeons disagree and believe that a surgical myotomy rather than balloon dilatation should be performed even for early achalasia. A myotomy

relieves dysphagia in over 90% of patients, and they are able to return to a normal diet.

In a prospective, randomized clinical study of the initial stages of megaesophagus managed either by hydrostatic dilation or esophagocardiomyotomy with esophagofundopexy, clinical, radiographic, endoscopic, manometric, and pH follow-up for 3 years showed both treatments to be similar in ameliorating dysphagia, patients had similar esophageal emptying, and both groups developed a reflux esophagitis rate of 5%, although surgery led to a significantly greater reduction of the lower esophageal sphincter pressure (105).

A Heller myotomy is performed either through a thoracotomy or through the abdomen. A transabdominal laparoscopic technique is gaining popularity. The operation consists of dividing the lower esophageal circular muscles. An antireflux procedure such as a fundoplication is often added. Whether adoption of a laparoscopic approach will lead to an earlier surgical referral for these patients, who often undergo multiple endoscopic dilations, remains to be seen.

On a long-term basis, an esophageal stricture, presumably secondary to reflux, is a complication of a myotomy performed for achalasia.

Some patients have a return of peristalsis after a myotomy, especially those with a previous short history of dysphagia and those with limited dilation.

A rare giant epiphrenic diverticulum develops years after a Heller myotomy for achalasia.

Secondary

Neoplastic

Occasionally a patient with a gastroesophageal sphincter region malignancy develops clinical and radiographic findings suggesting achalasia. This condition, which is sometimes called pseudoachalasia, is best termed *secondary achalasia.* Most of these underlying neoplasms are small, intramural in location, range from esophageal and gastric primary tumors to metastases, and many are covered by normal overlying mucosa. Both endoscopic biopsy and barium studies tend to be nondiagnostic; even CT has overlooked these lesions. Manometry likewise is not helpful. Thus even with negative radiographic studies and biopsy results, in the face of clinical suspicion of an underlying malignancy, follow-up studies are warranted.

At times achalasia secondary to a malignancy responds to botulinum toxin injection, thus further confusing the issue. The narrowed segment is eccentric or nodular; it contains abrupt borders in only about half of patients with secondary achalasia, and the tumor can be identified in only a minority (106).

Chagas' Disease

Chagas' disease is a chronic infection caused by the parasite *Trypanosoma cruzi*, which is endemic in Latin America. The parasite is transmitted by hematophagous bugs, which are especially prevalent in rural regions. High tissue and blood parasite levels are found during the acute phase, which evolves into an asymptomatic carrier phase, which in turn evolves into a chronic phase one or several decades later, most often manifesting through cardiac abnormalities.

The presence of Chagas' disease is determined with a serologic test. Dysphagia often precedes any visible esophageal abnormalities. Esophageal findings in infected patients range from normal, a prolongation of contractions in the middle and distal esophageal segments, to the other extreme of a megaesophagus. Once a megaesophagus is established, aperistalsis and a nonrelaxing lower esophageal sphincter are obvious.

Scintigraphy performed with the patient in a recumbent position is a sensitive test for detecting esophageal dysmotility in these patients.

Amyloidosis

Esophageal involvement by amyloidosis is rare, but it is a cause of esophageal motor abnormality. Secondary esophageal amyloidosis is associated with rheumatoid arthritis. Clinically, endoscopically, and radiologically, the appearance mimics that of primary achalasia.

Progressive Systemic Sclerosis (Scleroderma)

Considerable variability in esophageal motility exists in asymptomatic scleroderma patients,

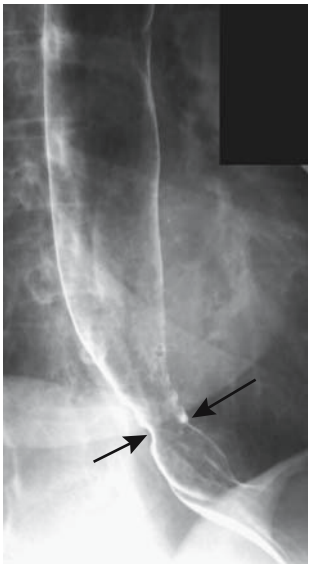

Figure 1.34. Scleroderma. A patulous esophagogastric junction (arrows) and lack of esophageal peristalsis point toward scleroderma. A hiatal hernia is also present.

especially early in their disease; this limits scintigraphy as an initial screening test. Using manometry as a gold standard, videoesophagography achieves a sensitivity of 95% to 100% in diagnosing systemic sclerosis; specificity, however, is considerably lower.

In an occasional patient an apparent causal relationship exists between a cancer and progressive systemic sclerosis.

A barium study in uncomplicated scleroderma is diagnostic (Fig. 1.34). Once a stricture develops due to reflux, the overall appearance mimics achalasia, or, if proximal dilation is only mild, a reflux esophagitis stricture. Rarely, wide-mouthed sacculations develop (107).

Myasthenia

Myasthenia gravis is an autoimmune disorder leading to muscle weakness. Dysphagia is common with oropharyngeal muscle involvement. Imaging findings tend to be nonspecific.

Diffuse Esophageal Spasm

Often called *nutcracker esophagus*, diffuse esophageal spasm is a primary esophageal motor disorder and is a cause of noncardiogenic chest pain. Dysphagia is common. The exaggerated and disordered esophageal contractions are familiar to most radiologists.

Compared to manometry, videoesophagography achieved a sensitivity of 100% in diagnosing diffuse esophageal spasm, whereas the sensitivity for scintigraphy was 67% (103).

Computed tomography reveals smooth, symmetric, circumferential esophageal wall thickening involving the distal two thirds (108); the periesophageal fat is normal in appearance. Endoscopic US also readily measures esophageal muscle width. Distal esophageal wall thickness was readily evaluated by older gastrointestinal radiologists who would coat the esophageal mucosa with barium and identify the outer esophageal wall surface by air in adjacent lung.

Therapy in these patients is symptomatic and usually consists of lower esophageal dilation. Similar to achalasia, lower esophageal sphincter botulinum toxin injection also improves symptoms.

Stroke

Swallowing problems are common during the acute phase after a stroke but most resolve within weeks or several months. Thus aspiration is common immediately after a stroke, detected by videofluoroscopy, but eventually resolves in most patients.

Myotonic Dystrophy

Myotonic dystrophy, a multisystemic disorder, is inherited as an autosomal-dominant trait. In most patients systemic rather than gastrointestinal involvement predominates.

Manometry in patients with myotonic dystrophy reveals a reduction in resting tone of both upper and lower esophageal sphincters and reduced contraction pressure both in the pharynx and esophagus (109); videofluorography shows a hypotonic pharynx and a hypotonic or atonic esophagus is often dilated. These findings are not always associated with dysphagia.

Distal esophageal involvement suggests that in myotonic dystrophy both striated and smooth muscles may be affected.

Globus Pharyngis

A feeling of a lump in the throat, often more prominent during swallowing, was previously called *globus hystericus.* Globus pharyngis has several connotations; some use this term to designate the clinical symptomatology, regardless of whether any underlying disorder is identified, and others limit the term to a diagnosis when other abnormalities are excluded. Etiology of globus pharyngis is not known, although gastroesophageal reflux has been postulated to play a role. These patients usually do not have dysphagia.

Esophageal manometry in consecutive patients with a globus sensation without dysphagia at Helsinki University Hospital detected an abnormality in 67% of these patients, most often consisting of a nonspecific motility disorder, and 62% also had a positive Bernstein test (110).

Published imaging studies do not agree. Some have found normal pharyngeal function and normal pH monitoring, with only an occasional cricopharyngeus muscle dysfunction; others, however, describe pharyngeal stasis, pharyngoesophageal sphincter dysfunction, and nonspecific esophageal peristalsis common; videofluoroscopy combined with static radiography yields more abnormalities than either study alone.

Oculopharyngeal Muscular Dystrophy

Oculopharyngeal muscular dystrophy is a genetic disorder consisting of progressive myopathy involving primarily head and neck muscles. The dysphagia that these patients develop, typically in midlife, is attributed to pharyngeal and upper esophageal striated muscle involvement. Because of a gradual onset of symptoms, some patients develop compensatory mechanisms to cope with their dysphagia even in the face of overt radiologic and manometric findings.

Endoscopy, manometry, and scintigraphic esophageal emptying studies found low pharyngeal pressures, disordered, nonpropulsive peristalsis, and stasis in the middle and lower thirds of the esophagus (111); smooth muscle involvement thus probably also has a role in causing dysphagia in these patients.

Arnold-Chiari Malformation

Dysphagia is occasionally seen in this condition of hindbrain herniation, although in most patients neurologic symptoms predominate. An occasional patient develops disordered esophageal motility and gastroesophageal reflux prior to a diagnosis of Arnold-Chiari malformation; dysphagia and esophageal manometric abnormalities can resolve following posterior craniotomy and decompression.

Parkinson's Disease

Dysphagia is common in Parkinson's disease, with resultant aspiration accounting for a large part in these patients' morbidity and mortality. They have abnormalities in oral, pharyngeal, and esophageal phases of swallowing. Nevertheless, the clinical severity of Parkinson's disease does not predict either the presence or the severity of dysphagia.

Most patients develop an abnormal oral phase consisting of residue and intermittent deglutition (112); pharyngeal phase abnormalities include stasis and delayed laryngeal elevation. Pharyngeal transit and upper esophageal sphincter relaxation are delayed in those with aspiration, with the overall findings suggesting bradykinesia. Occasionally the upper esophageal sphincter does not relax completely. Abnormal esophageal peristalsis, a delay in opening of the lower esophageal sphincter, and increased gastroesophageal reflux are found in these patients (113).

Progressive Supranuclear Palsy

Progressive supranuclear palsy, a degenerative extrapyramidal disease, mimics Parkinson's disease. Dysphagia is common. Uncoordinated lingual movements, excessive oral bolus leakage to the pharynx, vallecular stasis, and abnormal epiglottic motion are common.

Sjögren's Syndrome

Sjögren's syndrome affects the salivary glands. Dysphagia in these patients is primarily due to resultant xerostomia. About one third of patients have abnormal esophageal peristalsis associated with severe dysphagia. Some patients also develop esophageal webs.

MALT lymphomas develop in some patients, usually in organs targeted by Sjögren's syn-

drome, and these lymphomas tend to spread to other mucosal sites (114).

Celiac Disease

Dysphagia tends to develop in patients with well-established celiac disease; various motor abnormalities are detected in some of these patients.

Cervical Osteophyte Dysphagia

Although cervical osteophytes are common, dysphagia associated with these osteophytes is not. In an occasional patient dysphagia develops with moderate-size osteophytes. Complicating the picture is that osteophytes are often present in elderly patients with dysphagia due to neurogenic causes.

Dysphagia Aortica

Dysphagia aortica is secondary to compression of the distal esophagus by the descending aorta and cardiac structures. Such esophageal compression is detected rather frequently, although dysphagia is uncommon. Usually the most severe esophageal compression is close to the gastroesophageal junction.

Other Disorders

Swallowing dysfunction is common in patients with the Guillain-Barré syndrome. Either oral phase, pharyngeal phase, or both are involved. Most severe dysfunction occurs during the acute episode, but some patients have residual swallowing dysfunction after the acute attack clears.

Swallowing abnormalities are common in multiple sclerosis patients, even in asymptomatic ones (115). Dysphagia generally is associated with aspiration.

Diverticula

Conventional

A distinction between a true diverticulum (containing all esophageal wall layers) and a false diverticulum is of academic interest only.

An esophageal intraluminal diverticulum is rare. Its etiology is not known, but pathogenesis centers around specific muscle weakness. Prior trauma appears to play a role in some.

Being lined by esophageal mucosa, it is not surprising that an occasional diverticulum develops a carcinoma.

Zenker's Diverticula

A pharyngoesophageal diverticulum occurs in a weak zone between the inferior pharyngeal constrictor muscles and cricopharyngeus muscle. The pathophysiology of their formation is not settled; proposed mechanisms include swallowing muscle incoordination, cricopharyngeal achalasia, and even gastroesophageal reflux, although most diverticula are not associated with cricopharyngeal muscle discoordination. Nevertheless, a number of surgeons believe that their recurrence rate is increased if a cricomyotomy is not performed.

These diverticula are common. Most smaller ones are asymptomatic, with an occasional small one producing a foreign body sensation. Retention of secretions is common, and reflux of barium from the diverticulum into the hypopharynx and subsequent aspiration are a known complication. At times stasis leads to a bezoar forming within the diverticulum. When the diverticulum is large, it compresses the esophagus and leads to dysphagia. A diverticulum is not an uncommon site for perforation when inserting tubes or endoscopes.

Most of these diverticula expand posterolateral and inferiorly. A rare one extends superiorly into the posterior pharyngeal space. A barium esophagram detects even a small Zenker's diverticulum. Its inner margin should be smooth. Aside from secretions or a bezoar, any irregularity should suggest either inflammation or a neoplasm.

In the United States, diverticulectomy is the traditional therapy, often combined with a cricopharyngeal myotomy. Some surgeons emphasize diverticulopexy, a procedure preferred in high surgical risk patients. In Europe, an endoscopic approach is preferred, with the septum between the diverticulum and esophageal lumen being sectioned.

Complications after an open diverticulectomy include mediastinitis, stenosis at the sphincter level, fistula, and diverticula recurrence. A pneumomediastinum develops in a minority after endoscopic diverticulotomy.

A pouch can no longer be recognized on a postoperative barium study, although after the endoscopic Dohlman procedure a pouch does persist.

Killian-Jamieson Diverticula

Lateral hypopharyngeal pouches, also called *Killian-Jamieson diverticula*, are uncommon. Most are asymptomatic, with an occasional one resulting in dysphagia. They tend not to be associated with aspiration.

These diverticula are detected with a frontal-view pharyngogram. A pseudo–Valsalva maneuver aids in identifying them. Unilateral left-sided diverticula are more common than bilateral or right-sided ones (116).

(Pseudo)diverticulosis

Occasionally encountered are multiple small diverticular-like outpouchings. Etiology of this condition, commonly called *intramural esophageal pseudodiverticulosis*, is unknown. These outpouchings are believed to represent dilated esophageal submucosal glands, probably induced by underlying inflammation. They have developed distal to a benign stricture, in esophageal candidiasis, have been described in vigorous achalasia, are associated with an esophageal carcinoma, and have developed following laser therapy. These outpouchings resolved after radiation therapy for cancer.

Dysphagia is inconstant.

Associated intramural tracking is rather common, especially in patients with diffuse pseudodiverticulosis (117).

Intramural pseudodiverticulosis is readily diagnosed with a barium esophagram. In some patients it is localized, whereas in others it extends diffusely throughout the esophagus. Endoscopy may not detect it because the luminal communications tend to be rather narrow.

Fistula

Some acute perforations (discussed in the previous sections on trauma) evolve into fistulas. Most acquired esophageal fistulas in adults are associated with a malignancy. Nonmalignant fistulas are secondary to erosion by tubes, esophageal or adjacent inflammation/infection, related to surgery, or sequelae of prior perforation (Fig. 1.35).

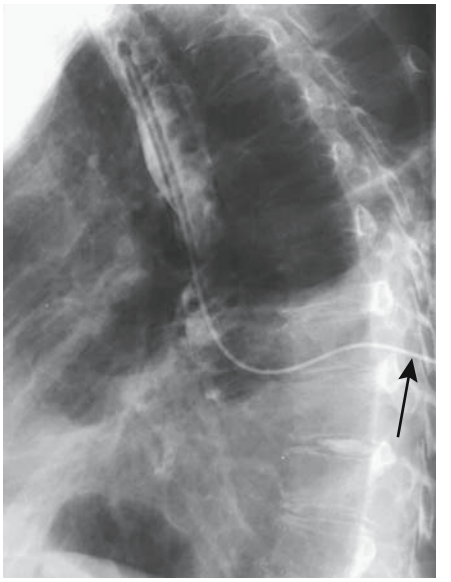

Figure 1.35. Esophagocutaneous fistula. A catheter was threaded into a sinus tract on the patient's back (arrow); injected contrast outlines the esophagus.

A tracheoesophageal fistula developed secondary to ingestion of a disk battery (118).

Vascular Lesions

Dieulafoy Lesions

Dieulafoy esophageal lesions are uncommon. These arteriovenous malformations may bleed, with the patient presenting with massive hematemesis.

Varices

Clinical

Portal hypertension is discussed in more detail in Chapter 17.

In cirrhotic patients with portal hypertension, esophageal varices are the most common site for portosystemic shunting. Most varices eventually drain into the azygos or hemiazygos veins.

Variceal bleeding tends to develop when the portal pressure gradient (portal vein pressure minus inferior vena caval pressure) is above 12 mm Hg. This is not an absolute value, of course, and some patients bleed at lower portal pressure gradients.

Imaging

An initial assessment should include a portal vein study, together with its major branches. Ultrasonography, including color Doppler US, identifies portal vein blood flow, establishes patency, and detects any portal thrombi.

Both barium studies and CT readily detect esophageal varices (Fig. 1.36). Their comparable accuracy is not known. Varices are readily apparent on contrast-enhanced CT; unenhanced, they tend to mimic adenopathy. Computed tomography also detects deeper perforating veins in the distal esophagus that interconnect paraesophageal veins with submucosal veins, a finding also identified by endoscopic US, although bleeding is usually from more superficial ones. Presumably the perforating veins play a role in variceal recurrence after sclerotherapy.

Transabdominal US is not often used to detect esophageal varices, yet in 47 patients with cirrhosis or idiopathic portal hypertension US achieved a respectable 93% sensitivity and 82% specificity when an esophageal wall thickness of at least 5 mm or an irregular wall outline were used as criteria for esophageal varices (119). Another US findings of varices includes hepatofugal venous flow identified by Doppler US.

Senior radiologists undoubtedly remember being taught that subtle esophageal varices are best identified not at the gastroesophageal junction (high pressure zone) but slightly more proximally. Endoscopic US confirms this observation. Endoscopic US also measures size of esophageal varices and wall thickness, but limitations exist; in particular, small varices are difficult to identify with endoscopic US.

In patients with Child-Pugh class A cirrhosis without ascites, an increased renal resistive index (>0.7), measured by duplex Doppler US, significantly correlates with the presence of esophageal varices (120).

T2-weighted MRI using an esophageal receiver probe is an alternate method of evaluating not only esophageal but also periesophageal varices. Magnetic resonance angiography (MRA) also identifies both esophageal

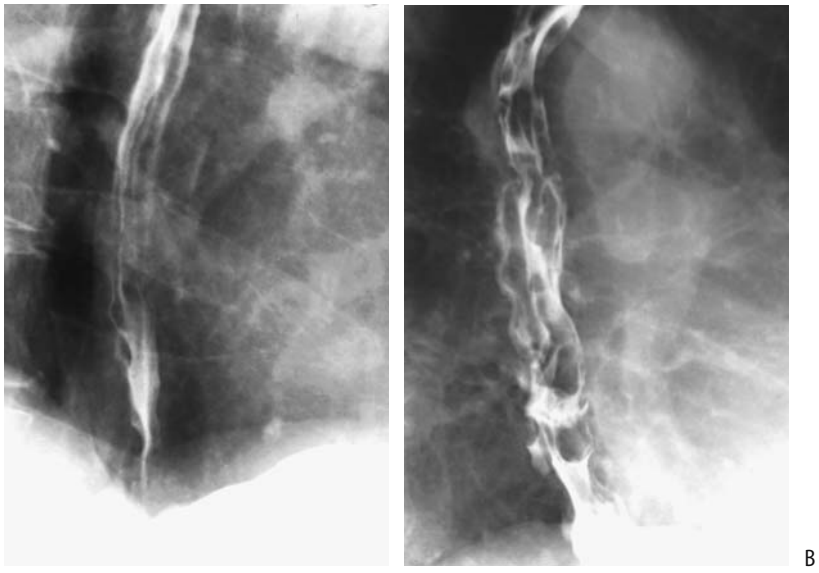

A B

Figure 1.36. Esophageal varices. A: Beaded esophageal folds are evident with the esophageal lumen collapsed. B: Larger varices present even with the lumen distended. Esophagitis does not result in beaded folds.

and gastric varices. It is also useful in detecting variceal recurrence after sclerotherapy.

Therapy

Medical

An initial approach in cirrhotic patients is drug therapy to reduce portal hypertension and thus reduce risk of variceal bleeding, with the most widely used being beta-blockers (medical and surgical therapies of bleeding esophageal varices are discussed in more detail in Chapter 17). Vasopressin infusion is often used as initial therapy for acute variceal bleeding.

On a chronic basis, medical therapy, sclerotherapy, varix ligation, or TIPS significantly reduces the risk of recurrent bleeding. Differences in mortality, however, have been variable. In selected patients liver transplantation is a consideration. Recommendations for use of these various therapies abound in the clinical literature.

Sclerotherapy

In many institutions endoscopic sclerotherapy is the initial therapy for acute esophageal variceal bleeding. A number of studies confirm that the risk of rebleeding and mortality are significantly reduced by sclerotherapy, but success in arresting acute variceal bleeding is not universally achieved. Sclerotherapy and medical therapy probably have similar mortalities. Endoscopic therapy fails in about 15%.

Most often sclerotherapy is performed in a setting of portal hypertension due to cirrhosis, but esophageal varices in patients with noncirrhotic portal fibrosis have also been effectively treated. Sclerotherapy is readily performed in children.

Endoscopic US appears useful in evaluating and following varices after both sclerotherapy and ligation. Presence and size of residual paraesophageal varices can be evaluated.

Is it possible to gauge whether esophageal varices will recur after endoscopic sclerotherapy? The answer depends to some degree on whether other collateral channels are present. Presence or development of other portosystemic collaterals protects to some degree against recurrent esophageal varices after sclerotherapy. Also, a portal pressure increase or splenomegaly developing after sclerotherapy indicates an increased risk for variceal recurrence.

Contrast-enhanced CT postsclerotherapy reveals an enhancing and thickened esophageal wall. The involved esophageal segment is distorted and narrowed. Edema, mediastinal effusion, and pleural effusion develop in some patients.

Intramural thickening and disappearance of submucosal varices and extramural collaterals are endoscopic US findings after sclerotherapy. Ultrasonography determines whether adequate variceal thrombosis was induced by sclerotherapy.

Barium studies and scintigraphy reveal uncoordinated peristaltic contractions and a marked increase in esophageal transit time shortly after sclerotherapy. Many of these patients also develop transient gastroesophageal reflux. These peristaltic abnormalities presumably are due to a sclerotherapy-induced chemical esophagitis, possibly accentuated by peptic esophagitis. In fact, most rebleeding after sclerotherapy is believed to be secondary to esophageal ulcerations related to sclerotherapy. These ulcers are difficult to detect because of underlying distortion. They heal either with no sequelae or progress to strictures, with an occasional one evolving into a sinus tract, an esophagotracheal or esophagopleural fistula, or even an abscess.

The effect of sclerotherapy on esophageal motility appears to be more complex than described above and probably is multifactorial. Thus amplitude of esophageal peristaltic contractions also increase after TIPS, yet resting lower esophageal sphincter pressure is similar before and after TIPS (121); TIPS thus improves esophageal motor function without inducing gastroesophageal reflux.

Sclerotherapy does not increase the risk of developing portal vein thrombosis, but patients with portal hypertension and varices are at increased risk for developing bacterial peritonitis, and sclerotherapy appears to accentuate this risk.

Several patients with esophageal varices, treated by sclerotherapy, later developed a carcinoma near the gastroesophageal junction and at sclerotherapy sites (122,123); whether this is a coincidence or whether sclerotherapy is indeed carcinogenic is speculation.

Ligation

Similar to sclerotherapy, endoscopic band ligation of a varix is effective therapy. Nevertheless, there are differences. Summarizing the published data, endoscopic variceal sclerotherapy and ligation appear equally effective in arresting an acute bleed; ligation requires fewer treatment sessions and is associated with fewer complications, but ligation has a higher variceal recurrence rate than sclerotherapy. A number of investigators believe that ligation should be the first choice therapy for esophageal varices.

After endoscopic variceal ligation an entrapped varix undergoes thrombosis, sloughing, and surrounding fibrosis.

Imaging shortly after ligation reveals ligated varices as smooth nodules that do not change shape, thus distinguishing them from typical varices. Their appearance does mimic other esophageal tumors, but a history of ligation aids in differentiation.

Endoscopic variceal ligation also leads to increased peristaltic activity and prolonged lower esophageal sphincter relaxation.

Other Procedures

Patients with portal hypertension and esophageal varices have also been treated, by TIPS, esophageal transection and devascularization, and by a number of portocaval anastomoses. Embolization of esophageal varices and other endovascular occlusion techniques had a greater role in the past and have been supplanted to a large extent by TIPS. To cite one example of embolization, hematemesis from esophagojejunal varices 5 years after total gastrectomy and Roux-en-Y esophagojejunostomy for carcinoma was treated by embolization after percutaneous transhepatic portography showed that these varices were supplied by an ascending jejunal vein (124) (Fig. 1.37).

Figure 1.37. A: A superior mesenteric venogram, performed via percutaneous transhepatic catheterization in this patient with a total gastric resection, reveals esophagojejunal varices supplied by jejunal veins (arrow). B: Both ethanol and ethanolamine oleate containing iopamidol are injected into the varices through a 3-French catheter. C: Follow-up venogram confirms variceal obliteration. [From Chikamori et al. (138), with permission from Springer.]

Immunosuppression

AIDS

Infection

Dysphagia and odynophagia are common in patients infected with the immunodeficiency virus. The most common infection is candidiasis. If an esophagram reveals ulcerations, infection by cytomegalovirus or herpes simplex should be suspected. The HIV infection per se may result in esophageal ulcers. More than one cause is not uncommon. The specific agent responsible for ulcerations should be sought because therapy is specific. Idiopathic ulcers are treated with steroids.

An occasional AIDS patient with odynophagia develops giant esophageal ulcers. Fragments believed to represent HIV virus are obtained from some of these giant ulcers, which tend to be long and shallow, and some are surrounded by a rim of soft tissue.

Candidiasis

With increasing severity of *Candida* infection, initial discrete scattered plaques coalesce and narrow the esophageal lumen; these plaques consist primarily of desquamated squamous epithelium and inflammatory cells, *Candida* sp., and superimposed bacterial infection. Although ulcers are a common finding in *Candida* esophagitis, most are not due to *Candida* alone. Untreated, *Candida* esophagitis can progress to stenosis.

Viral

Cytomegalovirus esophageal infection is not uncommon in immunocompetent patients. A common finding consists of well-circumscribed multiple, large, but shallow discrete ulcers, although at times inflammation resembles a carcinoma. An occasional ulcer evolves into a bronchoesophageal fistula. Occasionally a cytomegalovirus ulcer heals spontaneously.

In distinction to cytomegalovirus infection, herpes ulcers tend to be small, at times even pinpoint, and multiple in otherwise normal-appearing mucosa (Fig. 1.38). Simultaneous herpes and *Candida* esophagitis is not uncommon and results in a diffuse and irregular appearance.

The HIV esophagitis results in large shallow ulcers and, in absence of other predisposing causes, such a finding should suggest AIDS.

Imaging appearance of cytomegalovirus and HIV esophagitis is similar, and biopsy or mucosal brushing is necessary to differentiate between them (HIV esophagitis is one of exclusion).

Other

Similar to infections at other body sites, these patients are prone to develop unusual esophageal infections. Esophageal involvement with tuberculosis, actinomycosis, mucormycosis, and leishmaniasis has been reported (Fig. 1.39). Actinomyces superinfection of a cytomegalovirus ulcer has led to numerous sinus tracts.

Microorganisms are identified in about half of esophageal biopsies from AIDS patients with clinical esophagitis. Acid-fast bacilli should be searched for; in some of these patients no underlying giant cells are detected.

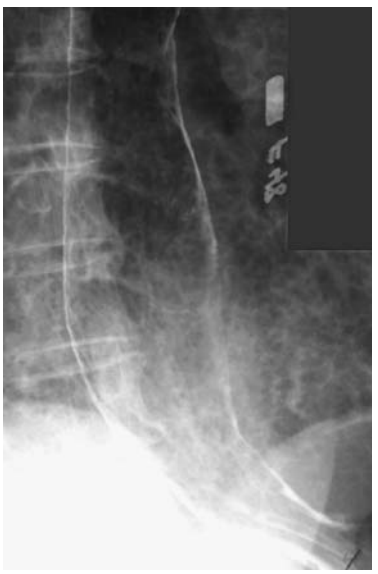

Figure 1.38. Herpes esophagitis in an AIDS patient manifesting with thickened folds and an occasional small ulcer.

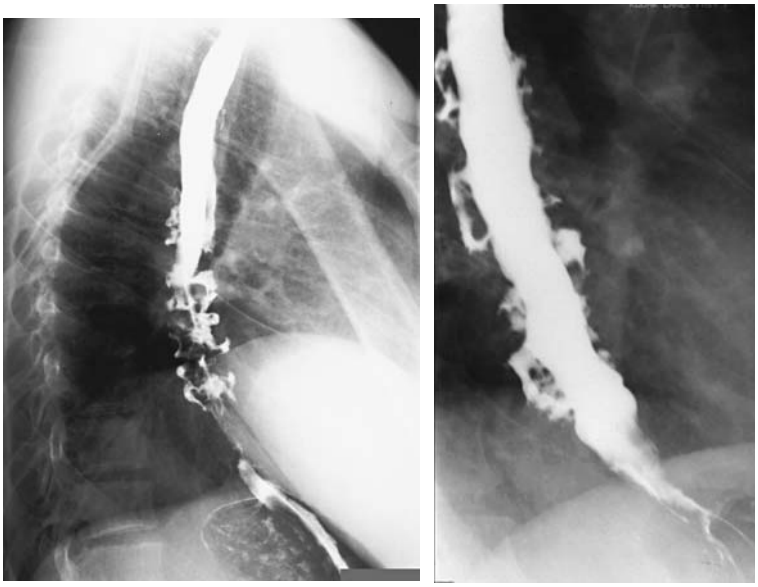

A B

Figure 1.39. Esophageal actinomycosis in an AIDS patient with severe dysphagia. A,B: Two studies show numerous deep ulcers, some extending parallel to the esophageal lumen.

Bacillary angiomatosis, due to *Rochalimaea henselae* infection, causes multiple, diffuse, friable esophageal polyps.

Tumor

The most common esophageal tumors in AIDS patients are Kaposi's sarcoma and non-Hodgkin's lymphoma (Fig. 1.40). Some lymphomas are primary esophageal and consist of large, ulcerating tumors mimicking a sarcoma. Infection, at times with an unusual organism, coexists with some esophageal lymphomas. The occasional Barrett's adenocarcinoma may be fortuitous.

An inflammatory fibroid polyp presented as a long submucosal mass in the distal esophagus.

Radiation therapy has been used to treat esophageal malignancies in AIDS patients. These patients appear to have greater sensitivity to radiation therapy than non-AIDS patients.

Figure 1.40. High-grade, large-cell malignant lymphoma in an HIV patient. A barium esophagram reveals an irregular, almost tube-like esophagus containing extensive ulcers. (From Marnejon T, Scoccia V. The coexistence of primary esophageal lymphoma and Candida glabrata esophagitis. Am J Gastroenterol 1997;92:354–356, with permission from Blackwell.)

Posttransplant

Esophageal webs and strictures develop in graft-versus-host disease. These strictures mimic those seen in reflux esophagitis. Large esophageal bulla have been reported in patients after bone marrow transplantation (125);

whether these are due to a superimposed infectious agent or graft-versus-host disease is conjecture.

Postoperative Changes

Pharyngeal Surgery

Postoperative pharyngography is helpful in following patients after oropharyngeal surgery. Considerable variability exists in the imaging findings and a baseline postoperative imaging study is very helpful in these patients (126). Knowledge of the specific surgical procedure performed aids in differentiating postsurgical fibrosis from tumor recurrence.

Transplanted jejunal patches are used to reconstruct oropharyngeal soft tissue defects. Transplant viability is maintained via vascular anastomoses. Tumors tend to recur at patch margins. Needless to say, such transplanted tissue has a complex CT and MRI appearance during follow-up due to the degree of underlying fibrosis, and differentiation from recurrent tumor is difficult. Nevertheless, these imaging studies are especially useful with tumor recurrence beneath a patch, where clinical access is not feasible.

Postesophagectomy

Gastric pull-through with a cervical esophagogastric anastomosis is a common procedure. Some patients are not given anything per os until an esophagram has excluded a perforation or obstruction. The study also determines how well the intrathoracic stomach empties. Some surgeons advocate peroral water feeding to detect leaks. Many radiologists use a water-soluble contrast agent for this examination. Because of a potential for aspiration, unless an acute intraperitoneal communication is suspected, I prefer barium as a contrast agent. After major barium aspiration delayed CT identifies thickened interlobular septa, subpleural lines, subpleural cysts and centrilobular nodules with barium particles, findings of mild but silent fibrosis (127).

Some patients develop dysphagia years after colonic interposition. Usually by that time marked colonic redundancy has developed and accounts for dysphagia.

Celiac disease became clinically evident in a woman after vagotomy and esophagectomy for hypopharyngeal squamous carcinoma (128); presumably her postoperative hypocalcemia unmasked indolent celiac disease.

An uncommon way of demonstrating an anastomotic leak is with Tc-99m-HIDA scintigraphy.

Examination Complications

The choice of contrast agent to be used in a setting of a suspected esophageal perforation was discussed above (see Perforation).

Endoscopy Related

The most common endoscopy-related complication is perforation. Postprocedure pain is common with a perforation but it sometimes manifests later. Oral contrast for imaging studies should be used with caution until topical anesthesia and sedation wear off. Initially, an esophagram generally has a highest yield, but CT is appropriate once enough time elapses for inflammation or abscess to develop (Fig. 1.41).

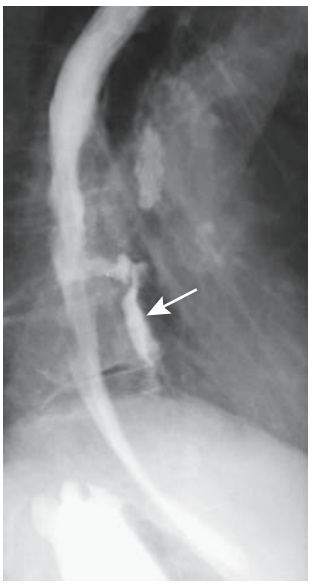

Figure 1.41. Esophageal perforation secondary to endoscopic dilation. Contrast outlines a mid-esophageal cavity (arrow).

Stricture Dilation

Both benign and malignant stricture dilation result in perforation. Risk of perforation varies not only with underlying disease but also with how vigorous an attempt is made. Perforations range from intramural, transmural, to transmural with mediastinal leakage. Most perforations are managed medically, with only an occasional one requiring surgical correction. Some, especially if a fistula is evident, are successfully treated with a stent.

Surgery

Tumor recurrence developed at a thoracoscopic port site after thoracoscopically assisted total esophagectomy for squamous cell carcinoma (129); of interest is that the original tumor was not extracted through this port site.

An occasional neoplasm develops in an interposed colon years after esophageal resection and colonic interposition.

References

1. Brusori S, Braccaioli L, Bna C, et al. [Role of videofluorography in the study of esophageal motility disorders.] [Italian] Radiol Med 2001;101:125–132.
2. Schwickert HC, Schadmandfischer S, Jaeger U, et al. Motility disorders of the esophagus—diagnosis with barium-rice administration. Eur J Radiol 1995;21:131–137.
3. Helmberger H 3rd, Baum U, Dittler HJ, et al. Adenocarcinoma of the gastro-esophageal junction: CT for monitoring during neoadjuvant chemotherapy. Eur J Radiol 1996;23:107–110.
4. Yang WT, Loveday EJ, Metreweli C, Sullivan PB. Ultrasound assessment of swallowing in malnourished disabled children. Br J Radiol 1997;70:992–994.
5. Meister V, Schulz H, Greving I, Imhoff M, Walter LD, May B. [Perforation of the esophagus after esophageal manometry.] [German] Dtsch Med Wochenschr 1997;122:1410–1414.
6. Bhutani MS, Hoffman BJ, Reed C. Endosonographic diagnosis of an esophageal duplication cyst. Endoscopy 1996;28:396–397.
7. Smith SM, Young CS, Bishop AF. Adenocarcinoma of a foregut cyst: detection with positron emission tomography. AJR 1996;167:1153–1154.
8. Zaunbauer W, Amsler UJ, Haertel M. [Bronchogenic cyst. A rare benign esophageal tumor.] [Review; German] Radiologe 1996;36:991–995.
9. Oh CH, Levine MS, Katzka DA, et al. Congenital esophageal stenosis in adults: clinical and radiographic findings in seven patients. AJR 2001; 176:1179–1182.
10. Sumner TE, Auringer ST, Cox TD. A complex communicating bronchopulmonary foregut malformation: diagnostic imaging and pathogenesis. Pediatr Radiol 1997;27:799–801.
11. Yamagiwa I, Obata K, Ouchi T, Sotoda Y, Shimazaki Y. Heterotopic pancreas of the esophagus associated with a rare type of esophageal atresia. Ann Thorac Surg 1998;65:1143–1144.
12. Kemp JL, Sullivan LM. Bronchoesophageal fistula in an 11–month-old boy. Pediatr Radiol 1997;27:811–812.
13. Lam WW, Tam PK, Chan FL, Chan KL, Cheng W. Esophageal atresia and tracheal stenosis: use of three-dimensional CT and virtual bronchoscopy in neonates, infants, and children. AJR 2000;174:1009–1012.
14. Kiyan G, Dagli TE, Tugtepe H, Kodalli N. Double balloon esophageal catheter for diagnosis of tracheoesophageal fistula. Eur Radiol 2003;13:397–399.
15. Donnelly LF, Frush DP, Bisset GS 3rd. The appearance and significance of extrapleural fluid after esophageal atresia repair. AJR 1999;172:231–233.
16. Moore EE, Jurkovich GJ, Knudson MM, et al. Organ injury scaling. VI: Extrahepatic biliary, esophagus, stomach, vulva, vagina, uterus (nonpregnant), uterus (pregnant), fallopian tube, and ovary. J Trauma 1995;39:1069–1070.
17. Grassi R, Romano L, Diettrich A, Rossi G, Pinto A. [Incomplete Boerhaave syndrome of the cervical esophagus.] [German] Aktuelle Radiol 1995;5: 360–362.
18. Hegenbarth R, Birkenfeld P, Beyer R. [Roentgen findings in spontaneous esophageal perforation (Boerhaave syndrome).] [German] Aktuelle Radiol 1994;4:337–338.
19. Gollub MJ, Bains MS. Barium sulfate: a new (old) contrast agent for diagnosis of postoperative esophageal leaks. Radiology 1997;202:360–362.
20. Keberle M, Wittenberg G, Trusen A, Hoppe F, Hahn D. Detection of pharyngeal perforation: comparison of aqueous and barium-containing contrast agents. AJR 2000;175:1435–1438.
21. Keberle M, Wittenberg G, Trusen A, Baumgartner W, Hahn D. [Comparison of iodinated and barium-containing contrast media of different viscosity in the detection of pharyngeal perforation.] [German] Rofo Fortschr Geb Rontgenstr Neuen Bildgeb Verfahr 2001;173:691–695.
22. Buecker A, Wein BB, Neuerburg JM, Guenther RW. Esophageal perforation: comparison of use of aqueous and barium-containing contrast media. Radiology 1997;202:683–686.
23. Tibbling L, Bjorkhoel A, Jansson E, Stenkvist M. Effect of spasmolytic drugs on esophageal foreign bodies. Dysphagia 1995;10:126–127.
24. Eliashar R, Dano I, Dangoor E, Braverman I, Sichel JY. Computed tomography diagnosis of esophageal bone impaction: a prospective study. Ann Otol Rhinol Laryngol 1999;108:708–710.
25. Harned RK 2nd, Strain JD, Hay TC, Douglas MR. Esophageal foreign bodies: safety and efficacy of Foley catheter extraction of coins. AJR 1997;168:443–446.
26. Chan CC, Lee CL, Wu CH. Twenty-four-hour ambulatory esophageal pH monitoring in patients with symptoms of gastroesophageal reflux. J Formos Med Assoc 1997;96:874–878.

27. Milocco C, Salvatore CM, Torre G, Guastalla P, Ventura A. Sonography versus continuous 24 hours oesophageal pH-monitoring in the diagnosis of infant gastroesophageal reflux. Pediatr Med Chir 1997; 19:245–246.
28. Hu C, Levine MS, Laufer I. Solitary ulcers in reflux esophagitis: radiographic findings. Abdom Imaging 1997;22:5–7.
29. Berkovich GY, Levine MS, Miller WT Jr. CT findings in patients with esophagitis. AJR 2000;175:1431–1434.
30. Pan JJ, Levine MS, Redfern RO, Rubesin SE, Laufer I, Katzka DA. Gastroesophageal reflux: comparison of barium studies with 24-h pH monitoring. Eur J Radiol 2003;47:149–153.
31. Song HY, Jung HY, Park SI, et al. Covered retrievable expandable nitinol stents in patients with benign esophageal strictures: initial experience. Radiology 2000;217:551–557.
32. Watson DI, Mitchell P, Game PA, Jamieson GG. Pneumothorax during laparoscopic mobilization of the oesophagus. Aust N Z J Surg 1996;66:711–712.
33. De Backer AI, De Schepper AM, Vaneerdeweg W. Esophagobronchial fistula following redo Nissen fundoplication. Abdom Imaging 2000;25:116–118.
34. Dalla Vecchia LK, Grosfeld JL, West KW, Rescorla FJ, Scherer LR 3rd, Engum SA. Reoperation after Nissen fundoplication in children with gastroesophageal reflux: experience with 130 patients. Ann Surg 1997;226:315–321.
35. Itatsu T, Miwa H, Murai T, et al. Multiple early esophageal cancers arising from Barrett's esophagus, and a review of cases of early adenocarcinoma in Barrett's esophagus in Japan. [Review] J Gastroenterol 1997;32:389–395.
36. Ricaurte O, Flejou JF, Vissuzaine C, et al. Helicobacter pylori infection in patients with Barrett's oesophagus: a prospective immunohistochemical study. J Clin Pathol 1996;49:176–177.
37. Jacobs E, Dehou MF. Heterotopic gastric mucosa in the upper esophagus: a prospective study of 33 cases and review of literature. [Review] Endoscopy 1997;29: 710–715.
38. Sanchez Robles C, Santalla Pecina F, Retamero Orta MD. [Barrett esophagus. An epidemiological study in an area of Spain.] [Spanish] Rev Esp Enferm Dig 1995;87:353–355.
39. Drewitz DJ, Sampliner RE, Garewal HS. The incidence of adenocarcinoma in Barrett's esophagus: a prospective study of 170 patients followed 4.8 years. Am J Gastroenterol 1997;92:212–215.
40. Yamamoto AJ, Levine MS, Katzka DA, Furth EE, Rubesin SE, Laufer I. Short-segment Barrett's esophagus: findings on double-contrast esophagography in 20 patients. AJR 2001;176:1173–1178.
41. Adrain AL, Ter HC, Cassidy MJ, Schiano TD, Liu JB, Miller LS. High-resolution endoluminal sonography is a sensitive modality for the identification of Barrett's metaplasia. Gastrointest Endosc 1997;46:147–151.
42. Stiewe S, Nitzsche H. [Crohn disease of the esophagus with esophageal-pulmonary fistula.] [German] Rofo Fortschr Geb Rontgenstr Neuen Bildgeb Verfahr 1998;169:562–563.
43. Tixedor N, Taourel P, Adell JF, Bruel JM. Extensive esophageal pneumatosis after acute dilatation of the stomach. AJR 1998;171:272–273.
44. Lee KH, Kim HJ, Kim KH, Kim HG. Esophageal tuberculosis manifesting as submucosal abscess. AJR 2003;180:1482–1483.
45. Sam JW, Levine MS, Rubesin SE, Laufer I. The "foamy" esophagus: a radiographic sign of Candida esophagitis. AJR 2000;174:999–1002.
46. Ponsot P, Molas G, Scoazec JY, Ruszniewski P, Henin D, Bernades P. Chronic esophagitis dissecans: an unrecognized clinicopathologic entity? Gastrointest Endosc 1997;45:38–45.
47. Watanabe H, Hirota S, Soejima T, et al. [Endoscopic findings of esophagitis in concurrent chemoradiotherapy for lung cancer.] [Japanese] Nippon Igaku Hoshasen Gakkai Zasshi 1998;58:271–276.
48. Ascenti G, Racchiusa S, Mazziotti S, Bottari M, Scribano E. Giant fibrovascular polyp of the esophagus: CT and MR findings. Abdom Imaging 1999;24:109–110.
49. Yoshikane H, Suzuki T, Yoshioka N, Ogawa Y, Ochi T, Hasegawa N. Hemangioma of the esophagus: endosonographic imaging and endoscopic resection. Endoscopy 1995;27:267–269.
50. Gupta NM, Dhavan S, Bambery P, Goenka MK. Pedunculated large leiomyoma of esophagus. Indian J Gastroenterol 1998;17:33.
51. Higa S, Matsumoto M, Tamai O, et al. Plexiform leiomyoma of the esophagus: a peculiar gross variant simulating plexiform neurofibroma. [Review] J Gastroenterol 1996;31:100–104.
52. Birgisson S, Rice TW, Easley KA, Richter JE. The lack of association between adenocarcinoma of the esophagus and gastric surgery: a retrospective study. Am J Gastroenterol 1997;92:216–221.
53. Ahsan H, Neugut AI, Gammon MD. Association of adenocarcinoma and squamous cell carcinoma of the esophagus with tobacco-related and other malignancies. Cancer Epidemiol Biomarkers Prev 1997;6:779–782.
54. Yedidag A, Zikos D, Spargo B, MacEntee P, Berkelhammer C. Esophageal carcinoma presenting with nephrotic syndrome: association with antineutrophil cytoplasmic antibody. [Review] Am J Gastroenterol 1997;92:326–328.
55. Chiba T, Shitomi T, Nakano O, et al. The sign of Leser-Trelat associated with esophageal carcinoma. Am J Gastroenterol 1996;91:802–804.
56. Zheng W, Jin F, Devesa SS, Blot WJ, Fraumeni JF Jr, Gao YT. Declining incidence is greater for esophageal than gastric cancer in Shanghai, People's Republic of China. Br J Cancer 1993;68:978–982.
57. Devesa SS, Blot WJ, Fraumeni JF Jr. Changing patterns in the incidence of esophageal and gastric carcinoma in the United States. Cancer 1998;83:2049–2053.
58. Levine MS, Pantongrag-Brown L, Buck JL, Buetow PC, Lowry MA, Sobin LH. Small-cell carcinoma of the esophagus: radiographic findings. [Review] Radiology 1996;199:703–705.
59. Saad R, Bellec V, Dugay J, Blanchi A, Foulet A, Renou P. [Association of celiac disease and esophageal small cell carcinoma.] [French] Presse Med 1999;28:277–278.
60. Polkowski W, van Sandick JW, Offerhaus GJ, et al. Prognostic value of Lauren classification and c-erbB-2 oncogene overexpression in adenocarcinoma of the esophagus and gastroesophageal junction. Ann Surg Oncol 1999;6:290–297.

61. Okuda I, Kokubo T, Udagawa H, et al. [Mediastinal lymph node metastasis from esophageal carcinoma: CT assessment with pathologic correlation.] [Japanese] Nippon Igaku Hoshasen Gakkai Zasshi 1997;57:391–394.
62. Brugge WR, Lee MJ, Carey RW, Mathisen DJ. Endoscopic ultrasound staging criteria for esophageal cancer. Gastrointest Endosc 1997;45:147–152.
63. Chak A, Canto M, Gerdes H, et al. Prognosis of esophageal cancers preoperatively staged to be locally invasive (t4) by endoscopic ultrasound (EUS)—a multicenter retrospective cohort study Gastrointest Endosc 1995;42:501–506.
64. Gines A, Bordas JM, Llach J, et al. [Endoscopic ultrasonography in the staging of esophageal cancer. Therapeutic implications.] [Spanish] Gastroenterol Hepatol 1998;21:117–120.
65. Nakashima A, Nakashima K, Seto H, et al. Thoracic esophageal carcinoma: evaluation in the sagittal section with magnetic resonance imaging. Abdom Imaging 1997;22:20–23.
66. Yamada I, Izumi Y, Kawano T, et al. Superficial esophageal carcinoma: an in vitro study of high-resolution MR imaging at 1.5T. J Magn Reson Imaging 2001;13:225–231.
67. Flanagan FL, Dehdashti F, Siegel BA, et al. Staging of esophageal cancer with 18F-fluorodeoxyglucose positron emission tomography. AJR 1997;168:417–424.
68. Holden A, Mendelson R, Edmunds S. Pre-operative staging of gastro-oesophageal junction carcinoma: comparison of endoscopic ultrasound and computed tomography. Australas Radiol 1996;40:206–212.
69. Tibble JA, Ireland AC. Carcinoma of the oesophagus causing paraparesis by direct extension to the spinal cord. Eur J Gastroenterol Hepatol 1995;7:1003–1004.
70. Jager GJ, Joosten F, v.d. Berkmortel FW, Salemans JM. Subcutaneous emphysema of the lower extremity secondary to a perforated esophageal carcinoma. Abdom Imaging 1995;20:23–25.
71. Chidel MA, Rice TW, Adelstein DJ, Kupelian PA, Suh JH, Becker M. Resectable esophageal carcinoma: local control with neoadjuvant chemotherapy and radiation therapy. Radiology 1999;213:67–72.
72. Savary JF, Grosjean P, Monnier P. Photodynamic therapy of early squamous cell carcinomas of the esophagus: a review of 31 cases. Endoscopy 1998;30:258–265.
73. Govil A, Kumar N. Esophageal prosthesis in palliation of malignant esophageal obstruction. [Review] Trop Gastroenterol 1995;16:49–58.
74. Schmassmann A, Meyenberger C, Knuchel J, et al. Self-expanding metal stents in malignant esophageal obstruction: a comparison between two stent types. Am J Gastroenterol 1997;92:400–406.
75. Morgan RA, Ellul JP, Denton ER, Glynos M, Mason RC, Adam A. Malignant esophageal fistulas and perforations: management with plastic-covered metallic endoprostheses. Radiology 1997;204:527–532.
76. Taal BG, Muller SH, Boot H, Koops W. Potential risks and artifacts of magnetic resonance imaging of self-expandable esophageal stents. Gastrointest Endosc 1997;46:424–429.
77. Schoefl R, Winkelbauer F, Haefner M, Poetzi R, Gangl A, Lammer J. Two cases of fractured esophageal nitinol stents. Endoscopy 1996;28:518–520.
78. Loser C, Folsch UR. Self-expanding metallic coil stents for palliation of esophageal carcinoma: two cases of decisive stent dysfunction. Endoscopy 1996;28: 514–517.
79. Pongchairerks P. Endoscopic laser therapy for stage III and IV esophageal cancer. Jpn J Clin Oncol 1996;26:211–214.
80. Adam A, Ellul J, Watkinson AF, et al. Palliation of inoperable esophageal carcinoma: a prospective randomized trial of laser therapy and stent placement. Radiology 1997;202:344–348.
81. Roy-Choudhury SH, Nicholson AA, Wedgwood KR, et al. Symptomatic malignant gastroesophageal anastomotic leak: management with covered metallic esophageal stents. AJR 2001;176:161–165.
82. Erasmus JJ, McAdams HP, Goodman PC. Diagnosis please. Case 5: esophageal mucocele after surgical bypass of the esophagus. Radiology 1998;209:757–760.
83. Fockens P, Manshanden CG, van Lanschot JJ, Obertop H, Tytgat GN. Prospective study on the value of endosonographic follow-up after surgery for esophageal carcinoma. Gastrointest Endosc 1997;46:487–491.
84. Geukens DM, Van de Berg BC, Malghem J, De Nayer P, Galant C, Lecouvet FE. Ossifying muscle metastases from an esophageal adenocarcinoma mimicking myositis ossificans. AJR 2001;176:1165–1166.
85. Wambeek ND. Mendelson RM. Liposarcoma of the hypopharynx. Australas Radiol 1996;40:165–168.
86. Namieno T, Koito K, Ambo T, Muraoka S, Uchino J. Primary malignant melanoma of the esophagus: diagnostic value of endoscopic ultrasonography. Am Surg 1996;62:716–718.
87. Tahri N, Marsot-Dupuch K, Chabolle F, Tubiana JM, Josset P. [An unusual cause of dysphagia: cervical schwannoma of the prevertebral space. Radioclinical correlations.] [French] Ann Radiol 1994;37:547–551.
88. Lee JA, Boles CA. Peripheral schwannoma lacking enhancement on MRI. AJR 2004;182:534–535.
89. Ordonez NG. Granular cell tumor: a review and update. [Review] Adv Anat Pathol 1999;6:186–203.
90. Palazzo L, Landi B, Cellier C, et al. Endosonographic features of esophageal granular cell tumors. Endoscopy 1997;29:850–853.
91. Boncoeur-Martel MP, Loevner LA, Yousem DM, Elder DE, Weinstein GS. Granular cell myoblastoma of the cervical esophagus: MR findings. AJNR 1996;17: 1794–1797.
92. Tanida S, Miyamoto T, Katagiri K, et al. Carcinoid of the esophagus located in lamina propria. J Gastroenterol 1998;33:541–545.
93. Naylor MF, Maccarty RL, Rogers RS. Barium studies in esophageal cicatricial pemphigoid. Abdom Imaging 1995;20:97–100.
94. Lundquist A, Olsson R, Ekberg O. Clinical and radiologic evaluation reveals high prevalence of abnormalities in young adults with dysphagia. Dysphagia 1998;13:202–207.
95. Ekberg O, Olsson R, Nilsson H, Lilja B, Sundkvist G. Autonomic nerve dysfunction in patients with bolus-specific esophageal dysmotility. Dysphagia 1995;10:44–48.
96. Levine JJ, Trachtman H, Gold DM, Pettei MJ. Esophageal dysmotility in children breast-fed by

mothers with silicone breast implants. Long-term follow-up and response to treatment. Dig Dis Sci 1996;41:1600–1603.
97. Roland J, Dhaenen H, Ham HR, Peters O, Piepsz A. Oesophageal motility disorders in patients with psychiatric disease. Eur J Nucl Med 1996;23:1583–1587.
98. Triadafilopoulos G, Tsang HP, Segall GM. Hot water swallows improve symptoms and accelerate esophageal clearance in esophageal motility disorders. J Clin Gastroenterol 1998;26:239–244.
99. Lundgren J, Ekberg O, Olsson R. Aspiration: a potential complication to vagus nerve stimulation. Epilepsia 1998;39:998–1000.
100. von Herbay A, Heyer T, Olk W, et al. Autonomic dysfunction in patients with achalasia of the oesophagus. Neurogastroenterol Motil 1998;10:387–393.
101. Goldblum JR, Rice TW, Richter JE. Histopathologic features in esophagomyotomy specimens from patients with achalasia. Gastroenterology 1996;111:648–654.
102. Martin E, Perez San Jose C, Emparan C, Aguinagalde M, Sabas J. Idiopathic megacolon associated with oesophageal achalasia. Eur J Gastroenterol Hepatol 1998;10:147–150.
103. Parkman HP, Maurer AH, Caroline DF, Miller DL, Krevsky B, Fisher RS. Optimal evaluation of patients with nonobstructive esophageal dysphagia. Manometry, scintigraphy, or videoesophagography? Dig Dis Sci 1996;41:1355–1368.
104. Wong MD, Davidson SB, Ledgerwood AM, Lucas CE. Retrograde gastroesophageal intussusception complicating chronic achalasia. Arch Surg 1995; 130:1009–1010.
105. Felix VN, Cecconello I, Zilberstein B, Moraes-Filho JP, Pinotti HW, Carvalho E. Achalasia: a prospective study comparing the results of dilatation and myotomy. Hepatogastroenterology 1998;45:97–108.
106. Woodfield CA, Levine MS, Rubesin SE, Langlotz CP, Laufer I. Diagnosis of primary versus secondary achalasia: reassessment of clinical and radiographic criteria. AJR 2000;175:727–731.
107. Coggins CA, Levine MS, Kesack CD, Katzka DA. Wide-mouthed sacculations in the esophagus: a radiographic finding in scleroderma. AJR 2001;176:953–954.
108. Nino-Murcia M, Stark P, Triadafilopoulos G. Esophageal wall thickening: a CT finding in diffuse esophageal spasm. J Comput Assist Tomogr 1997;21: 318–321.
109. Costantini M, Zaninotto G, Anselmino M, et al. Esophageal motor function in patients with myotonic dystrophy. Dig Dis Sci 1996;41:2032–2038.
110. Farkkila MA, Ertama L, Katila H, Kuusi K, Paavolainen M, Varis K. Globus pharyngis, commonly associated with esophageal motility disorders. Am J Gastroenterol 1994;89:503–508.
111. Tiomny E, Khilkevic O, Korczyn AD, et al. Esophageal smooth muscle dysfunction in oculopharyngeal muscular dystrophy. Dig Dis Sci 1996;41:1350–1354.
112. Nagaya M, Kachi T, Yamada T, Igata A. Videofluorographic study of swallowing in Parkinson's disease. Dysphagia 1998;13:95–100.
113. Leopold NA, Kagel MC. Pharyngo-esophageal dysphagia in Parkinson's disease. Dysphagia 1997;12: 11–18.
114. Tonami H, Matoba M, Yokota H, Higashi K, Yamamoto I, Sugai S. Mucosa-associated lymphoid tissue lymphoma in Sjögren's syndrome: initial and follow-up imaging features. AJR 2002;179:485–489.
115. Wiesner W, Wetzel SG, Kappos L, et al. Swallowing abnormalities in multiple sclerosis: correlation between videofluoroscopy and subjective symptoms. Eur Radiol 2002;12:789–792.
116. Rubesin SE, Levine MS. Killian-Jamieson diverticula: radiographic findings in 16 patients. AJR 2001; 177:85–89.
117. Canon CL, Levine MS, Cherukuri R, Johnson LF, Smith JK, Koehler RE. Intramural tracking: a feature of esophageal intramural pseudodiverticulosis. AJR 2000;175:371–374.
118. Chiang MC, Chen YS. Tracheoesophageal fistula secondary to disc battery ingestion. Am J Otolaryngol 2000;21:333–336.
119. Kishimoto R, Chen M, Ogawa H, Wakabayashi MN, Kogutt MS. Esophageal varices: evaluation with transabdominal US. Radiology 1998;206:647–650.
120. Colli A, Fraquelli M, Pometta R, Cocciolo M, Visentin S, Conte D. Renovascular impedance and esophageal varices in patients with Child-Pugh class A cirrhosis. Radiology 2001;219:712–715.
121. Iwakiri K, Kanazawa H, Matsuzaka S, et al. Effects of transjugular intrahepatic portosystemic shunt (TIPS) on esophageal motor function and gastroesophageal reflux. J Gastroenterol 1998;33:305–309.
122. Larrubia JR, Mendoza JL, Ciguenza R, Lana R, Gonzalez JF, Espinos D. [Carcinoma of the gastroesophageal junction following variceal sclerosis: more than a coincidence?] [Spanish] Gastroenterol Hepatol 1998;21:6–9.
123. Tanoue K, Hashizume M, Ohta M, Ueno K, Kitano S, Sugimachi K. Development of early squamous cell carcinoma of the esophagus after endoscopic injection sclerotherapy for esophageal varices. Hepatogastroenterology 1995;42:792–796.
124. Chikamori F, Shibuya S, Takase Y. Percutaneous transhepatic obliteration for esophagojejunal varices after total gastrectomy. Abdom Imaging 1998;23:560–562.
125. Minocha A, Mandanas RA, Kida M, Jazzar A. Bullous esophagitis due to chronic graft-versus-host disease. [Review] Am J Gastroenterol 1997;92:529–530.
126. Hahn S, Weber A, Kosling S. [The pharynx following tumor-surgery interventions. The variability of the clinical images in conventional fluoroscopic diagnosis.] [German] Radiologe 2000;40:640–648.
127. Voloudaki A, Ergazakis N, Gourtsoyiannis N. Late changes in barium sulfate aspiration: HRCT features. Eur Radiol 2003;13:2226–2229.
128. ten Bokkel Huinink D, de Meijer PH, Meinders AE. Coeliac disease clinically manifest after vagotomy and oesophagectomy. Neth J Med 1996;49:235–238.
129. Dixit AS, Martin CJ, Flynn P. Port-site recurrence after thoracoscopic resection of oesophageal cancer. Aust N Z J Surg 1997;67:148–149.

2

Stomach

Technique

Contrast Studies

High-density, low-viscosity barium sulfate preparations specially formulated to coat the acidic gastric mucosa are used for double-contrast upper gastrointestinal studies. Some radiologists routinely induce gastric hypotonia, whereas others believe that any improvement in study quality due to hypotonia is limited. If hypotonia is preferred, in the United States the hypotonic agent glucagon is used, but in many other parts of the world scopolamine methylbromide (Buscopan) is employed, except in elderly patients or those where the side effects of scopolamine contraindicate its use and glucagon is then substituted. Pirenzepine, a selective antimuscarinic drug, appears as effective as scopolamine in inducing gastroduodenal hypotonia but without the undesirable side effects (1).

Water soluble agents are discussed in Chapter 4.

In the United States considerable low-resolution digital radiography equipment has been installed, with the primary justification being ease of filming (radiation dose is a separate and complex issue). High-resolution digital radiography equipment is becoming available; thus digital radiography with a four million pixel charge-coupled device achieves a significant improvement over conventional radiography in detecting gastric cancer (2).

Computed Tomography

Computed tomography (CT) contrast agents suitable for upper gastrointestinal tract opacification are similar to those used in the small bowel. Vomiting after ingesting an oral CT contrast agent is not uncommon. Especially in trauma patients, premedication with metoclopramide results in decreased nausea and vomiting.

A positive oral contrast agent is generally used for most of the gastrointestinal tract, but better gastric wall visualization is achieved with oral water. Water does not obscure subtle gastric wall thickening or enhancement. Using a multislice CT technique and a water-filled gastric lumen, normal gastric wall layers are well outlined during arterial or parenchymal phases.

Multislice three-dimensional (3D) CT of the stomach, often called virtual gastroscopy, is gradually achieving clinical acceptance. Virtual gastroscopy using gas for lumen distention and either a water-soluble agent or barium sulfate for mucosal coating has the potential of being competitive both with barium studies and endoscopy.

Three-dimensional CT rendering using shaded-surface display, ray sum display, and virtual gastroscopy with simultaneous visualization of intraluminal and submucosal components of various gastric tumors provides information not available either with barium studies or endoscopy.

Ultrasonography

A 3D ultrasonography (US) system is on the horizon. A position and orientation sensor mechanism is needed for this system to interface with a scanner head.

Similar to the esophagus, endoscopic US evaluates the gastric wall and adjacent structures and can localize a lesion and outline its extent, but the findings are nonspecific. Thus submucosal fibrosis due to a healing ulcer can mimic the appearance of a neoplasm.

Magnetic Resonance

Oral upper gastrointestinal magnetic resonance (MR) contrast agents are discussed in Chapter 4. The stomach is best studied distended. Hypotonic agents are usually not employed.

Endoscopic MR is under development.

Scintigraphy

Gastric emptying scintigraphy has been available for more than 25 years and is discussed later (see Gastric Emptying Studies). Over time, test meals and techniques have been optimized and standardized, and introduction of digital scintigraphy provides dynamic imaging and allows visualization of antral contractions.

Biopsy/Cytology

Percutaneous CT-guided core needle biopsies are readily obtained from gastric wall tumors. Nonendoscopic gastric biopsy can be performed as part of a double-contrast barium upper gastrointestinal study. Such combined barium-and-biopsy studies readily detect *Helicobacter pylori* infection and evaluate suspicious findings, eliminating a need for upper endoscopy in most patients.

Percutaneous gastric biopsies, drainage, and gastrostomies can also be performed using CT guidance. Interestingly, comparing CT-fluoroscopy with conventional CT gastric interventional procedures, the radiation doses were significantly higher with CT-fluoroscopy, but the yields and procedure times were not significantly different (3).

Endoscopic US-guided fine-needle aspiration biopsy also provides cytologic confirmation of suspicious lesions. A multicenter prospective study achieved a fine-needle aspiration cytology sensitivity of 92% and specificity of 93% for lymph node staging, 88% and 95% for identifying extraluminal masses, and 61% and 79% for gastrointestinal wall lesions, respectively (4).

Congenital Abnormalities

Duplication

Gastric duplications are rare. Even rarer is a foregut duplication involving both the esophagus and stomach. Most do not communicate with the true lumen and are located in the antrum, and vary in size considerably. A rare carcinoma has originated in a gastric duplication.

A barium study, US, CT, or magnetic resonance imaging (MRI) should detect most duplications, yet the diagnosis is not always straightforward; a gastric duplication can be misdiagnosed as a pancreatic pseudocyst or a hepatobiliary cystic tumor. Although endoscopic needle aspiration of a gastric duplication cyst is feasible, these mucus-filled duplications tend to recur after simple aspiration. Ultrasonography identifies a multilayered wall, including a hyperechoic mucosa surrounded by hypoechoic muscle layers, findings better seen with endoscopic US.

A congenital double pylorus is rare. A rare double pylorus communicates with a duplication.

Atresia

Agastria and microgastria are very rare anomalies. Microgastria is associated with asplenia. Gastric atresia usually involves the antrum. Antral atresia results in a greatly dilated more proximal stomach and no gas distally, mimicking the appearance of pyloric obstruction (single-bubble sign). Although atresia may be complete, more often it consists of a web-like deformity with a partial opening. In some patients the latter becomes apparent only later in life.

An association has been described between pyloric atresia and epidermolysis bullosa (5).

The differential diagnosis for partial gastric outlet obstruction in the young includes pyloric stenosis, antral web, antral stenosis, antral duplication, and, rarely, aberrant pancreas.

Vascular Anomalies

Vascular anomalies are common in the stomach and are of interest to the surgeon. To illustrate the scope of vascular anomalies, in a gastric cancer study 44% of patients had vascular anatomy differing from normal, and in 13% a double anomaly was detected (6).

Trauma

In a setting of CT performed for abdominal trauma, many centers administer routinely either dilute barium or a water-soluble contrast agent either orally or through a nasogastric tube. Done properly, little risk exists of aspiration or other complications.

Gastric perforation is less common than small bowel or colonic perforations, due, in part, to the relatively thick gastric wall. Most traumatic perforations involve a distended stomach. Inadvertent esophageal intubation and gastric ventilation and cardiopulmonary resuscitation have led to gastric perforation. The Heimlich maneuver can also result in gastric rupture. An intrathoracic stomach after gastric herniation into the thorax is also prone to perforate.

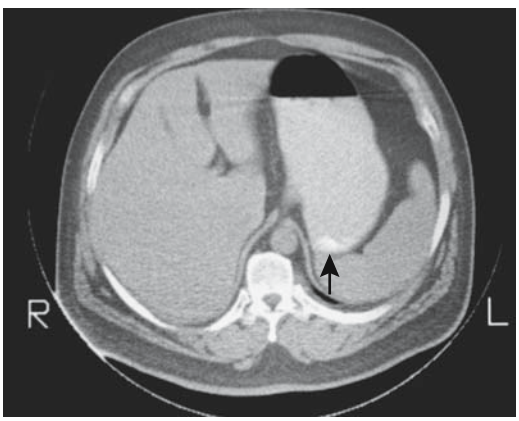

Figure 2.1. Gastric wall calcifications (arrow), years after abdominal trauma.

Spontaneous gastric perforation occurs mostly in neonates. The etiology is unknown; possible overdistention or ischemia appears to play a role. Some of these neonates have been on mechanical ventilation or have had attempted nasogastric intubation. The resultant pneumoperitoneum tends to be large. One useful sign of gastric perforation using a horizontal x-ray beam is absence of an air-fluid level in the stomach; a gastric air-fluid level tends to be present with a more distant perforation.

A rare gastric hematoma eventually calcifies (Fig. 2.1).

Vomiting

A discussion of vomiting has only indirect relevance to imaging studies, nevertheless, an appropriate imaging study must eventually be selected for a patient experiencing serious vomiting. This topic is best approached by considering likely etiologies in various age groups. More detailed discussions of etiologies and relevant imaging studies are included in this and other appropriate chapters.

Gastroesophageal reflux must be differentiated from vomiting. Reflux implies an incompetent gastroesophageal sphincter. Vomiting, on the other hand, is a complex phenomenon consisting of sudden relaxation of the superior esophageal and gastroesophageal sphincters, pylorospasm, forceful antral muscular contractions, sudden diaphragmatic descent, and abdominal muscle contractions forcing gastric content into the esophagus—mechanisms familiar to radiologists who have observed vomiting under fluoroscopy.

In infants, the gastroesophageal sphincter is incompletely developed and reflux is common. What is "normal" reflux and what constitutes "abnormal" has provoked considerable debate in the pediatric literature and is beyond the scope of this chapter. Especially with upper gastroenteric obstruction, a distinction between reflux and vomiting is often blurred. Esophageal obstruction obviously results in neither reflux nor vomiting, and the condition is generally clinically suspected with first feedings. Bilious vomiting in infants suggests sepsis or obstruction distal to the papilla of Vater, with the most common condition being volvulus secondary to midgut malrotation, a surgical emergency.

Pylorospasm, pyloric stenosis, a duodenal or more distal small bowel web, stenosis or atresia, meconium plug syndrome, and various colonic obstructions are other causes of bowel obstruction and vomiting in infants. Rarer causes of obstruction include large diaphragmatic hernias and gastric volvulus.

Conventional radiography is probably still the most optimal initial imaging study in these infants. At times evidence of a gasless abdomen or gut distention to a certain point suggest a diagnosis, and additional imaging simply delays therapy. At other times this study raises suspicion of a specific diagnosis, and a barium study or US is then performed for confirmation or exclusion.

In an older infant or child with clinically evident gastroesophageal reflux or failure to thrive, a barium study is often obtained both for confirmation of reflux and as screening for other abnormalities. Although reflux can also be studied with a pH probe, US, or scintigraphy, these studies do not exclude other disorders. Scintigraphy is of little use in an infant with projectile vomiting, but it is useful in an older cooperative child.

Causes of vomiting in adults are legion. Central neural, toxic, visceral, and metabolic causes are common; the etiologies are difficult to detect, and most do not require imaging studies. Some visceral causes of vomiting, such as acute cholecystitis, are suspected clinically, and appropriate imaging studies obtained. A major direct role of imaging is to detect an underlying bowel obstruction, traditionally performed with a barium study but currently often supplanted by CT.

Wall Thickening

Infection/Inflammation

Helicobacter Infection

Clinical

Helicobacter pylori, a curvilinear motile gram-negative bacillus, is implicated as a cause of inflammation, ulcers, and a number of neoplasms. Prevalence of *H. pylori* varies considerably in different populations. Prevalence is higher in non-Caucasians and increases with age; *H. pylori* colonization occurs at about 3% per year and eradication at 1% per year. Although O blood group patients do have a higher prevalence of peptic ulcer disease, *H. pylori* seroprevalence does not differ between different ABO groups.

H. pylori is easy to diagnose noninvasively and is treatable with antibiotics. A more complex topic is whether all *H. pylori* should be eradicated (a "kill them all" philosophy more in vogue in the 1990s) or whether there are good, neutral, as well as bad *H. pylori*. Presumably *H. pylori* has been a human commensal since time immemorial and produces no known harm in many people. Is it thus worthwhile to suggest blanket antibiotic therapy with its related problems, or should eradication be limited to those at risk for known complications of this infection? Other *Helicobacter* species also appear to play a role. Thus *H. heilmanii* is responsible for acute gastritis in some patients.

One interesting observation is that *H. pylori* infection in Crohn's disease and ulcerative colitis patients is less prevalent than in controls.

A number of studies have found no statistical difference in patients with symptoms and histologic findings compatible with gastritis or peptic ulcer disease between those positive for *H. pylori* and those negative. Likewise, gastric emptying times are not related to *H. pylori* infection. Nevertheless, the relationship between *H. pylori* and peptic ulcer disease is not straightforward, with more aggressive strains being more common in peptic ulcer disease. Antral *H. pylori* infection results in an antral gastritis and a derangement of the usual acid inhibition of gastrin production, which leads to an increase in gastrin release, which in turn promotes excess acid secretion by the noninflamed, more proximal part of the stomach. Chronic gastrin elevation results in hyperplasia of both enterochromaffin-like cells and parietal cells, thus further increasing acid secreting capacity. In some patients chronic infection eventually leads to antral atrophy, gastrin production decreases, and hypochlorhydria ensues.

At times *H. pylori*–induced hypergastrinemia and gastritis suggest Zollinger-Ellison syndrome; eradication of *H. pylori* results in resolution of findings.

The World Health Organization (WHO) classifies *H. pylori* as a carcinogen. Its presence

is associated with a severalfold increased risk of developing a gastric cancer. Carcinogenesis is probably through a sequence of gastritis induction, intestinal metaplasia, dysplasia, and finally development of carcinoma. No difference in prevalence of *H. pylori* infection exists in patients with Lauren intestinal and diffuse types of carcinomas (the Lauren classification is discussed later; see Adenocarcinoma).

Chronic *H. pylori* infection promotes mucosa-associated lymphoid tissue (MALT), and primary gastric non-Hodgkin's MALT lymphoma is strongly associated with *H. pylori* infection, although the *H. pylori* strains involved appear to differ from those associated with peptic ulcer disease. Eradication of *H. pylori* leads to regression of MALT (7) and of low-grade mucosa-associated lymphomas in their early stages, although several years are needed for gastric mucosa to become normal after *H. pylori* eradication.

It should be pointed out that MALT develops not only in a setting of *H. pylori* infection but also in response to other antigen stimulation. Thus reactive lymphoid follicles also develop in the stomach of *H. pylori*–negative celiac patients.

In the presence of the enzyme urease, urea is hydrolyzed to CO_2 and ammonia. *H. pylori* is a common urease-containing bacterium and will produce CO_2 from orally administered urea. The urea breath test consists of having the patient ingest radioactive C-14–labeled urea and then monitoring for the presence of C-14 with a breath analyzer. This test has had limited acceptance. False-positive results are seen in achlorhydria and some other bacterial infection. A serologic test is easier to perform, although the antibody titer remains elevated even after infection has been eliminated.

Imaging

The most common finding of gastric *H. pylori* infection is thickened folds, presumably representing resultant gastritis rather than *H. pylori* infection per se. Other findings include antral nodularity and underlying lymphoid hyperplasia, findings often more evident in children than adults. Antral nodularity usually regresses after *H. pylori* is eradicated.

Gastritis

Clinical

By definition, gastritis signifies inflammation. Some so-called gastritis, such as chemically induced gastritis, often manifests by acute hemorrhage, and histology detects little evidence of inflammation; some authors prefer the term *gastropathy* rather than *gastritis*.

Any discussion beyond the superficial quickly evolves into a number of controversies surrounding the definition of gastritis. A symposium of pathologists in Sydney in 1990 established guidelines for classifying and grading gastritis; these guidelines were modified in Houston in 1994 (8).

For convenience, gastritis is usually subdivided into acute, chronic, and a special or distinctive type. Acute gastritis is generally a clinical diagnosis. Pathologists cannot distinguish between acute and active gastritis. No specific radiologic findings are helpful. Acute gastritis is often categorized under discrete types such as chemical (corrosive) injury, stress-related, phlegmonous, and similar. Chemical gastritis includes not only drug- and alcohol-induced gastritis but also gastric changes induced by bile reflux. Stress gastritis is associated with severe trauma, burns, shock, sepsis, and related conditions, and tends to manifest within days of an insult. Acute hemorrhage is a not uncommon clinical presentation with most acute gastritis, and, in fact, in an occasional patient angiographic therapy using vasopressin infusion is necessary for hemorrhage control.

Numerous subdivisions and synonyms are in vogue for chronic gastritis (Table 2.1). Most pathologists divide chronic gastritis primarily into nonatrophic, atrophic, and special types, yet biopsies in some patients, of necessity, still are classified as indeterminate. No essential difference exists between chronic active and acute erosive gastritis, terms commonly used by pathologists.

Of note is that *H. pylori* is associated with several types of gastritis. *H. pylori*–associated nonatrophic gastritis almost always involves the antrum, with inflammation extending to the gastric body to a varying degree. With autoimmune gastritis, on the other hand, both inflammation and atrophy spare the antrum.

Table 2.1. Classification of chronic gastritis (updated Sydney system)

Type	Etiologies	Synonyms
Nonatrophic	*H. pylori*	Superficial, antral gastritis
Atrophic		
Autoimmune		Antrum often spared
Multifocal	*H. pylori*, diet, other factors	Diffuse gastritis, pernicious anemia–associated gastritis
Special		
Chemical	Chemicals, drugs, bile	Reflux, drug-induced gastritis
Radiation	Radiation therapy	
Lymphocytic	Immune, drugs, gluten, *H. pylori*	Celiac disease–associated gastritis
Noninfectious		
Crohn's		Crohn's gastritis
Sarcoidosis		
Wegener's		
Eosinophilic	Food sensitivity	Allergic gastritis
Infectious	Bacteria, viruses, fungi, parasites	Phlegmonous gastritis

Source: Adapted from Dixon et al. (8).

Also, *H. pylori* gastritis almost always is associated with neutrophil infiltration. *H. pylori* is detected more often in lesions with active rather than chronic inflammation; the presence of *H. pylori* correlates with degree of lymphocyte infiltration, but not with metaplasia or mucosal atrophy.

Pathologists do not agree on a precise definition of *normal*. One controversy is the concept of atrophy, with pathologists using a visual scale of mild, moderate, and marked (8). Atrophy implies loss of glandular tissue and is a common pathway for a number of disorders. Thus *atrophic gastritis* is a descriptive term and not a specific disease. An association between atrophy and metaplasia is not clear, although metaplasia is common in chronic gastritis, regardless of etiology. Some patients with atrophic gastritis develop dysplasia. Follow-up with repeat biopsies reveals that mild dysplasia most often resolves spontaneously, with an occasional one progressing to moderate dysplasia. In summary progression of mild dysplasia is rare, moderate dysplasia changes slowly, and severe dysplasia is an indication for surgery.

Pathologists also gauge activity; thus chronic active gastritis implies the presence of neutrophils, a finding beyond resolution of endoscopy or radiology. Confusing the issue further, some endoscopists do not obtain biopsies but rely on their visual impression to diagnose a specific type of gastritis.

Biopsy tissue, if needed, is usually obtained during endoscopy. An alternate approach is to perform a barium upper gastrointestinal study and at the same time, using a nasogastric tube, obtain fluoroscopically guided gastric biopsies; such fluoroscopic biopsies achieve sensitivities and specificities of over 90% in diagnosing gastritis (9).

Diagnosis

Findings of gastritis on a barium study include aphtha, antral nodularity, thickened folds, coarse areae gastricae, and, at times, lumen narrowing. A number of other disorders, however, have similar findings. Aphtha and coarsened areae gastricae are seen in gastritis, Crohn's disease, MALT lymphoma, some infections such as herpes and cytomegalovirus, and the rare gastric involvement by Behçet's disease (Fig. 2.2) or even mastocytosis (Fig. 2.3).

Occasionally gastric lymphoid hyperplasia is a prominent finding of *H. pylori* gastritis, especially in children. If small, these nodules are difficult to distinguish from aphtha with surrounding inflammation.

Patients ingesting nonsteroidal antiinflammatory drugs on a chronic basis tend to develop gastritis. Some of these patients have a characteristic antral greater curvature flattening.

Aside from biopsy, endoscopists use such macroscopic findings as nodularity, erosions, mucosal hemorrhage, and redness to diagnose

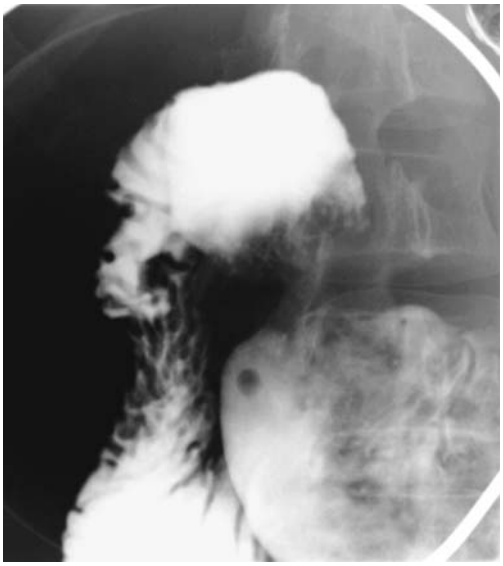

Figure 2.2. Gastric Behçet's disease. Multiple discrete aphtha are scattered in the antrum. Gastritis and Crohn's disease can have similar findings.

gastritis, yet considerable controversy surrounds an endoscopic diagnosis of gastritis. In consecutive patients undergoing endoscopy, macroscopic endoscopy findings achieved a sensitivity of only 40% and a specificity of 84% in detecting *H. pylori* gastritis (10).

Atrophic/Autoimmune

Patients with autoimmune gastritis tend toward achlorhydria and elevated gastrin levels. Histologically, antral G-cell hyperplasia and an increase in endocrine cells are common. Gastric carcinoids tend to develop in these patients. A relationship with gastric carcinoma is not clear.

Radiology has a limited role in autoimmune gastritis.

Chemical

Acid-induced corrosive gastritis tends to be more severe than the more common caustic-induced damage, yet the latter also results in considerable damage, generally in the antrum, at times sufficiently severe to evolve into gastric outlet obstruction. The resultant linitis plastica–like appearance tends to have sharply marginated, irregular borders mimicking a gastric carcinoma; a number of these strictures have been resected in the mistaken notion that they are malignant.

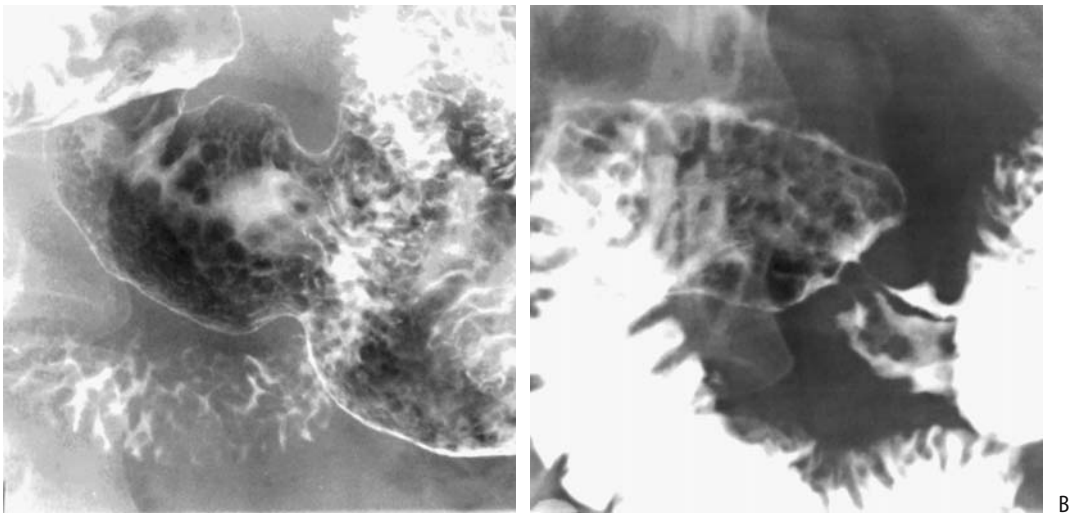

A B

Figure 2.3. Gastroduodenal mastocytosis. Nodules, shown to be infiltrated by mast cells, are scattered throughout the antrum (A) and duodenal bulb (B).

Some of these patients undergo either a simple gastrojejunostomy or a Billroth I or II operation and tend to do well, provided no esophageal stricture develops.

Enterogastric reflux of bile and pancreatic secretions is a well-known cause of gastritis both in patients with an intact stomach and after gastric surgery. Such reflux is detected by technetium 99m (Tc-99m)-HIDA scintigraphy, but has no specific imaging appearance.

Lymphocytic

The role of *H. pylori* in lymphocytic gastritis is not settled; some studies point to no association, whereas others suggest the opposite.

Lymphocytic gastritis is a histologic diagnosis. Histochemical study suggests that lymphocytic gastritis often is part of a generalized lymphocytic gastroenteropathy. In some patients it is associated with celiac disease. It manifests as rugal thickening, nodularity, and erosions. Some authors describe these thickened, serpiginous rugal folds, together with superimposed inflammation, as varioliform gastritis, and at times the imaging appearance suggests Ménétrier's disease. Some patients develop diffuse gastric ulcerations. Duodenitis is often present. These patients also tend to develop a protein-losing gastroenteropathy. An occasional patient presents with a massive hemorrhage.

Collagenous

The recently described entity of collagenous gastritis is rare. Similar to collagenous colitis, its defining characteristic is fibrous thickening of the subepithelial basement membrane. Etiology and pathogenesis are unknown. There are no specific imaging findings.

Granulomatous

In a setting of chronic gastritis some biopsies yield findings compatible with granulomatous gastritis, although a diagnosis of idiopathic granulomatous gastritis is rare; most of these patients have either Crohn's disease or sarcoidosis, with an occasional granulomatous gastritis being secondary to infection, foreign bodies, or other gastropathy.

Peptic Ulcer Disease

Clinical

Peptic ulcers are uncommon in children and rare in infants. Numerous medications induce gastric ulcers. Some nonsteroidal antiinflammatory drugs are associated with giant gastric ulcers. Chemotherapeutic infusion into the hepatic artery for liver neoplasms is occasionally associated with gastric ulcerations. Some of these ulcers tend to be large.

Complications of peptic ulcer disease include stricture and perforation. Anterior wall gastric ulcers tend to perforate into the peritoneal cavity, whereas posterior wall ulcers more often involve the pancreas. A rare gastric ulcer penetrates the spleen or other adjacent structure.

The definition of a giant gastric ulcer varies, but typically an ulcer diameter of 3 cm or more is assumed to represent this entity. These giant ulcers are not a separate pathologic entity, but their significance lies in their worse prognosis due to hemorrhage and need for urgent surgery. A giant gastric ulcer led to a pneumopericardium (11).

A double pylorus in most adults is a complication of peptic ulcer disease; a congenital double pylorus is very rare. These ulcers originate either in the duodenal bulb or distal antrum. An occasional benign gastric ulcer evolves into a gastrojejunal or gastrocolic fistula. Other causes of a double pylorus include a necrotic cancer and prior surgery (Fig. 2.4).

Imaging

The appearance of gastric ulcers on an upper gastrointestinal study is familiar to most radiologists and are not discussed here. In general, a finding of a deep U-shaped deformity at the incisura, irregular soft tissue tumor surrounding the ulcer, and prominent converging folds are associated with a significant delay in ulcer healing, even with adequate therapy.

Ultrasonography is not used for ulcer detection, but if US reveals a "target" sign, consisting of hypoechoic gastric wall thickening surrounding a hyperechoic ulcer lumen, the patient can then be referred for a more appropriate study.

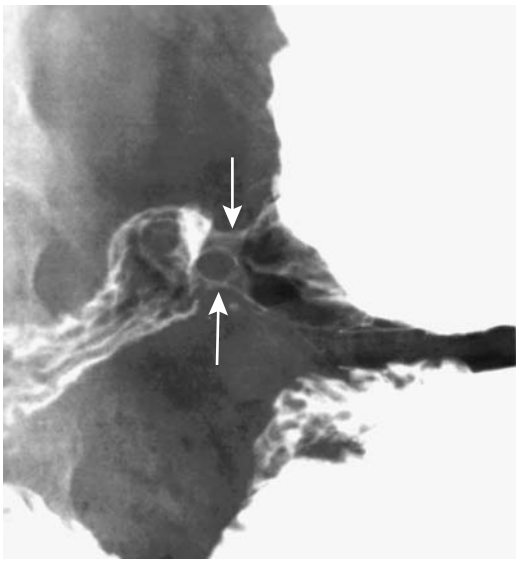

Figure 2.4. Double pyloric channel (arrows). This patient had a prior antrectomy and the two channels were believed to be related to surgery.

Eosinophilic Gastroenteritis

Eosinophilic gastroenteritis is an inflammatory disorder of unknown etiology, considered to be a separate entity from idiopathic hypereosinophilic syndrome, although transitional forms probably exist. Its primary feature is eosinophilic infiltration of discrete or diffuse gastrointestinal tract segments. An occasional patient has eosinophilic infiltration of most if not all of the bowel. About half of these patients have some type of allergy, and a majority have peripheral eosinophilia.

Gastric involvement manifests most often as a narrowed lumen or thickened rugae.

In a rare infant eosinophilic gastroenteritis mimics the clinical findings and US appearance of idiopathic hypertrophic pyloric stenosis.

Eosinophilic gastroenteritis should be differentiated from helminth infestation with its associated eosinophilia.

Crohn's Disease

Prevalence of gastric involvement in Crohn's disease is unknown. When Crohn's disease is evident in the upper gastrointestinal tract, nearly always concomitant small bowel or colonic involvement is also found.

Although chronic gastritis and duodenitis are common in Crohn's disease patients, only an occasional biopsy yields granulomas (12). One should keep in mind that granulomas are not pathognomonic for Crohn's disease; they are also found in sarcoidosis, some infections such as tuberculosis and anisakiasis, as a foreign body reaction, or as an occasional vasculitis. As a practical matter, however, if other causes of granuloma formation are excluded, the presence of noncaseating granulomas is assumed to be due to Crohn's disease.

The imaging appearance of gastric Crohn's disease varies from aphthae to strictures (Fig. 2.5). Scintigraphy in Crohn's patients with nonobstructive disease and no evidence of gastroduodenal disease shows normal gastric emptying, although symptomatic Crohn's patients develop delayed gastric emptying.

Malacoplakia

Malacoplakia is a granulomatous inflammatory disease involving either the gastrointestinal or genitourinary tract. It is discussed in more detail in Chapter 10.

Malacoplakia is rare in the stomach. It originates either in the gastric wall or adjacent structure and infiltrates the stomach. Its primary significance is that it mimics a neoplasm.

Cytomegalovirus

The prevalence of acute viral gastritis is unknown. The most common is cytomegalovirus infection, which is encountered mostly in immunocompromised individuals and occasionally in children, where it tends to present as thickened rugae similar to Ménétrier's disease.

Anisakiasis

Anisakiasis is caused by eating raw fish infected with *Anisakis* larvae. Many reports originate from Japan, but the condition is also encountered in other countries having an acquired culinary taste for raw fish such as sushi and sashimi. Ingestion of undercooked microwaved fish is also implicated. It is uncommon in older individuals and those with prior gastric surgery; rel-

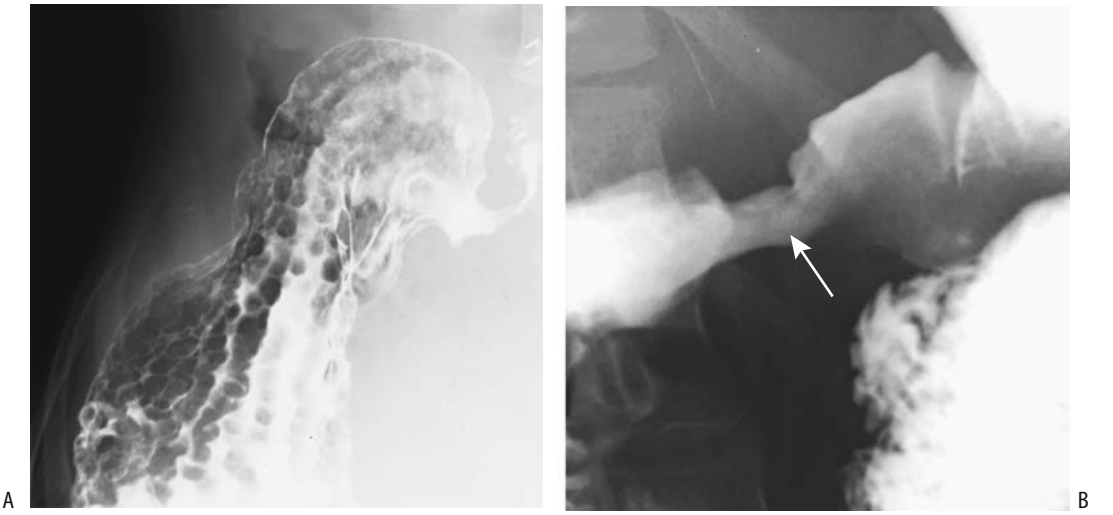

Figure 2.5. Gastric Crohn's disease in two patients. A: Multiple nodules and thick, nodular folds involve the stomach. B: The distal antrum and pyloric region are formless and patulous (arrow).

ative achlorhydria appears to decrease larval toxicity.

Anisakiasis manifests by abdominal pain, at times severe enough to mimic an acute abdomen, shortly after eating infected raw fish. Eosinophilia is not common during the acute episode. Imaging detects gastric wall edema persisting for 1 or 2 days after infection. With a technically excellent double-contrast examination, a small moving curvilinear defect is identified on the mucosa.

Endoscopy identifies larvae adhered to gastric or duodenal mucosa.

Syphilis

Gastric syphilis is mostly of historical interest. It generally follows an indolent course. The gastric wall is infiltrated and thickened, at times suggesting a neoplasm. Histologically, a vasculitis is common.

On a barium study gastric syphilis mimics peptic ulcer disease or even a malignancy. Endoscopy and at times even histology suggest a gastric lymphoma or lymphocytic gastritis.

Tuberculosis

Most patients with gastric tuberculosis also have pulmonary involvement, although primary gastric tuberculosis does exist, especially in Third World countries. Grossly it mimics sarcoidosis and Crohn's disease. Some patients develop gastric ulcers, gastric outlet obstruction, or even massive hemorrhage.

The diagnosis can be established by histology and growth of *Mycobacterium tuberculosis* in an appropriate culture medium.

Histoplasmosis

Most patients with gastrointestinal histoplasmosis are immunocompromised or suffer from disseminated disease.

One patient with African histoplasmosis (*Histoplasma duboisii*) presented with a gastric ulcer that radiologically and endoscopically suggested a malignancy (13).

Emphysematous and Phlegmonous Gastritis

Gastric pneumatosis and *gastric emphysema* are descriptive terms for gas in the stomach wall and *emphysematous gastritis* signifies inflammation, although these terms are used interchangeably to describe gas in the stomach wall. Some use *emphysematous*, *phlegmonous*, and *necrotizing gastritis* interchangeably,

although these terms have different meanings and define different conditions.

Emphysematous gastritis is a rare finding. Involvement ranges from focal to most of the stomach being involved.

Etiologies leading to gas in the stomach wall are listed in Table 2.2. Gastric ischemia as a cause of emphysematous/phlegmonous gastritis is rare except in patients who have had prior extensive surgical gastric devascularization. Rarely, phlegmonous gastritis develops after nongastric surgery (14). Gastric emphysema occasionally develops in a neonate with duodenal obstruction and not due to necrotizing gastritis. Transient gastric emphysema was associated with colonic infarction (15). Some patients with emphysematous gastritis are relatively asymptomatic, and in this subgroup emphysema presumably is neither infectious nor ischemic in origin.

The diagnosis is suggested by imaging and not by endoscopy. Inflammation, edema, and gas develop in the submucosa and deeper layers, with the overlying mucosa being relatively normal. Conventional radiography and CT reveal linear or oval gas collections in the gastric wall. Focal emphysema is better seen with CT than conventional radiography. Ultrasonography reveals focal emphysema as hyperechoic foci with distal reverberations.

Table 2.2. Etiologies of emphysematous gastritis

Associated condition	Comments
Infectious gastritis	Most common cause of emphysematous gastritis
Ischemia	
Trauma	Includes feeding tube and stent perforation, barotrauma
Recent endoscopy	Presumably due to overdistention and mucosal disruption
Gastric ulcer	
Gastric bezoar	
Gastric outlet obstruction	
Massive gastric dilation	Presumably due to necrosis
Gastric perforation	
Ingestion of corrosives	
Gastric amyloidosis	
Immunocompromised status	Due to steroids, chemotherapy, radiation therapy, or AIDS
Increased intrathoracic pressure	
Idiopathic	

Ischemia

Gastric ischemia is discussed in Chapter 17. Overt gastric ischemia is rare. Symptoms tend to be nonspecific, especially with a gradual onset.

Radiation

The stomach is relatively resistant to radiation damage. Deep ulcers have developed months after radiation to adjacent nodes. These ulcers tend not to heal.

Ménétrier's Disease

Ménétrier's disease is one of the protein-losing enteropathies. Clinically, hypoproteinemia is evident and if untreated leads to edema. Fecal α_1-antitrypsin excretion is increased and serves as a marker for protein-losing enteropathy.

Imaging findings consist of marked rugal and gastric wall thickening. Initially the antrum is spared, but eventually the entire stomach becomes involved. Imaging often suggests a malignancy, such as lymphoma. Complicating the issue further is that occasionally Ménétrier's disease undergoes malignant transformation.

A type of Ménétrier's disease occurs in children. Although these children do have a protein-losing enteropathy and gastric rugae are thickened, the condition is transient and probably differs from that seen in adults. Primary cytomegalovirus infection is evident in some children with such a transient form of Ménétrier's disease.

In adults, US reveals mucosal thickening with normal submucosa and muscle layers. In children, US is useful in following disease progression and resolution.

Sarcoidosis

Gastric involvement without systemic sarcoidosis and no lung hilar adenopathy is rare. At times

Figure 2.6. Antral sarcoidosis. The antral lumen is narrowed and folds thickened by a diffuse antral wall infiltrate (arrows).

gastric biopsies yield epithelial cell granulomas, even though imaging identifies no abnormality.

Once established, gastric sarcoidosis manifests as nodules, thickened folds, gastric wall thickening, lumen narrowing, and superficial antral ulcers (Fig. 2.6); the condition thus mimics Crohn's disease and linitis plastica, although a similar appearance is also seen in gastric syphilis, eosinophilic gastritis, polyarteritis nodosa, and phlegmonous gastritis. Rarely, a focus of sarcoid infiltration develops a deep ulcer.

Gastric carcinoma and lymphoma have developed in a setting of gastrointestinal sarcoidosis; whether these associations are fortuitous or not is conjecture.

Amyloidosis

Amyloidosis is probably a blood dyscrasia. It occurs in a primary form and in association with such diseases as chronic infections and multiple myeloma.

Most often gastric amyloidosis leads to diffuse antral wall thickening, at times narrowing the lumen to the point of obstruction. A patient with familial amyloid polyneuropathy had multiple gastric amyloid polyps (16). A patient on hemodialysis and secondary amyloidosis developed phlegmonous gastritis (17).

Endoscopic US reveals gastric wall thickening and loss of normal mucosal and submucosal outline.

Tumors

Bezoars

Gastric bezoars are more common after prior gastric surgery or peptic ulcer disease than in the general population.

Trichobezoars lead to pain, vomiting, and bleeding due to erosions. If sufficiently large, they result in gastric obstruction, or, if they pass into the small bowel, small bowel obstruction. Some trichobezoars extend from the stomach, through the small bowel, to the colon (Rapunzel syndrome). Iron deficiency anemia is not uncommon.

Most small trichobezoars are readily diagnosed by conventional radiographically and CT. Some trichobezoars are associated with gastric pneumatosis. Their MRI appearance varies depending on relative amounts of gas and fluid; the presence of air causes a hypointense appearance both on T1- and T2-weighted images, whereas fluid and other debris result in a hyperintense appearance on T1- and T2-weighted images. It is the larger ones that fill almost the entire gastric lumen that cause a diagnostic dilemma. If in doubt, a barium study is diagnostic.

Because of their consistency, trichobezoars are difficult to remove endoscopically and, especially with larger ones, surgical removal is necessary. Most large gastric phytobezoars are treated surgically, although an occasional one is fragmented endoscopically.

Numerous preparations result in gastric pharmacobezoars, ranging from aluminum hydroxide gel to enteral feeding formulas. Some pharmacobezoars also cause symptoms secondary to continued intragastric release of their active ingredients.

Nonneoplastic Tumors

Cyst

Most small gastric cysts are nonneoplastic and represent intramural collections of gastric secretions. They range from submucosal cystic glands and duplication cysts to cystica polyposa, with an occasional hamartoma and adenomyoma. Their intraluminal projection varies. Some gastric cysts cannot be readily classified.

Cystica polyposa is an uncommon solid and cystic gastric tumor, with most developing proximal to a gastroenterostomy. Their prevalence increases with time after surgery. These tumors consist of epithelial hyperplasia and dysplasia and contain dilated gastric glands that are either limited to the mucosa (gastritis cystica superficialis) or extend into the submucosa (gastritis cystica profunda). Large and mostly intraluminal ones have led to gastric outlet obstruction.

An unclear relationship exists between cystica polyposa and cancer developing in a gastric stump.

Hyperplastic Polyp

A prospective gastroscopy study of resected polyps found 55% to be hyperplastic polyps, 29% inflammatory, and 10% adenomatous (18); other, less common, polyps included fundic gland polyps, carcinoid, early gastric cancer, and a pancreatic rest. All of these polyps were smaller than 2 cm.

Most hyperplastic polyps are discovered incidentally, and are small (less than 20 mm in diameter), smooth, and multiple, and most are found in the antrum. Occasionally hyperplastic polyps enlarge and become lobulated, and their appearance suggests a polypoid carcinoma (19). Whether to simply biopsy these large polyps is debatable; most are resected.

Hyperplastic polyps are usually considered nonneoplastic per se, although some contain dysplasia, carcinoma-in-situ, or even a carcinoma. Pedunculated antral hyperplastic polyps can prolapse into the duodenum. Hyperplastic gastric polyposis is associated with colorectal adenomas. The relationship between hyperplastic polyps and nonfamilial fundic gland polyposis is not clear but these appear to be distinct entities (fundic gland polyps are discussed later; see Nonfamilial Polyposis).

Inflammatory Fibroid Polyp

Inflammatory fibroid polyps are nonencapsulated submucosal lesions composed primarily of loose connective tissue and inflammatory tissue. They also contain varying amounts of myofibroblasts, thus confusing the histologic picture. They occur throughout the gastrointestinal tract; in the stomach they predominate in the antrum.

Most smaller polyps are sessile and are covered by smooth overlying mucosa, whereas larger ones tend to project more intraluminally, ulcerate and bleed (Fig. 2.7). Prolapse into the duodenal bulb leads to gastric outlet obstruction. Endoscopic biopsies tend to be noncontributory, and a polypectomy is necessary for diagnosis.

Endoscopic US of 10 proven gastric inflammatory fibroid polyps showed all to be located in the second and/or third sonographic layer, 90% had an indistinct margin, 80% were hypoechoic, and 90% were homogeneous in appearance (20).

Inflammatory Pseudotumor (Fibrosarcoma)

A so-called inflammatory pseudotumor, also known as *plasma cell granuloma*, *inflammatory fibrosarcoma*, and other terms, is a rare, infiltrating condition of unknown etiology. Although included here under nonneoplastic tumors, whether it is indeed inflammatory or

Figure 2.7. Inflammatory polyp in distal antrum. An adenoma has a similar appearance.

represents a neoplasm is not settled. This condition is discussed in more detail in chapter 14.

A number of these tumors are associated with elevated sedimentation rate. In the stomach they ulcerate and bleed.

Heterotopic Pancreas

Ectopic pancreatic tissue occurs at a number of sites, being most common in the gastric antrum and proximal duodenum, with only an occasional jejunal one found. Histology reveals either complete pancreatic tissue or exocrine pancreas, with only an occasional one consisting mostly of endocrine pancreas. Although often considered innocuous, complications of such ectopic tissue include inflammation, cyst formation, adenocarcinoma transformation, and formation of an endocrine tumor. Pancreatic acinar-appearing cells are occasionally found in gastric mucosa; such metaplasia is often detected around the squamocolumnar junction and differs from ectopic pancreatic tissue.

Ectopic antral pancreatic tissue usually presents as a single submucosal tumor, occasionally up to 3 cm in size. A central umbilication is identified in some.

A common CT appearance is an oval or round tumor containing smooth or serrated margins. About half enhance with contrast similar to normal pancreas (21,22); poorly enhancing ones contain mostly ducts and muscle tissue, with pancreatic acini being sparse. A minority contain a dilated heterotopic pancreatic duct. Of interest is that the CT findings are often interpreted incorrectly as representing other lesions.

Gastric heterotopic pancreatic tissue even led to a pseudocyst.

Teratoma

The stomach is a rare site for a teratoma. These tumors occur primarily in males and often present as bulky, palpable, abdominal masses. They range in location from primarily intraluminal, to intramural, to extrinsic.

Computed tomography and MR are the preferred imaging modalities, identifying both cystic and fatty components and often also suggesting its gastric origin.

Hemangioma

For unknown reasons gastric hemangiomas are rare. Most have manifested by bleeding. They appear similar to other mesenchymal tumors. Several have contained phleboliths, which aid in diagnosis. An occasional one is polypoid.

Extramedullary Hematopoiesis

A barium study in a patient with myelofibrosis revealed multiple gastric polyps (23); biopsy identified extramedullary hematopoiesis in these polyps, a very rare site for hematopoiesis.

Benign Neoplasms

Adenoma

Gastric adenomas are uncommon. Most occur in the antrum. The two most common presentations are bleeding or malabsorption.

Adenomas are at increased risk of malignant transformation and even an occasional small adenoma contains a carcinomatous focus. Also, the presence of an adenoma is associated with an increased risk of developing a gastric carcinoma elsewhere in the stomach. Gastric villous adenomas are associated with synchronous rectal villous adenomas. Probably an association also exists between gastric adenomas and other colonic polyps.

Nonneoplastic polyps and most adenomas have a very similar imaging appearance and most smaller ones are sessile (Fig. 2.8). In a collection of atypical adenomas, four were depressed and three were flat, they were located around the incisura or antrum, they ranged from 10 to 25 mm in diameter, and with a barium study all mimicked an early gastric carcinoma (24); a nodular surface, convergency of folds, and a shallow depression were common.

Solid polyps are homogeneous and hypointense on T1- and hyperintense on T2-weighted MRI (except for lipomas, as discussed below).

Leiomyoma

Gastric leiomyomas are common; a majority are discovered incidentally, often in a stomach resected for other reasons, and are small in size.

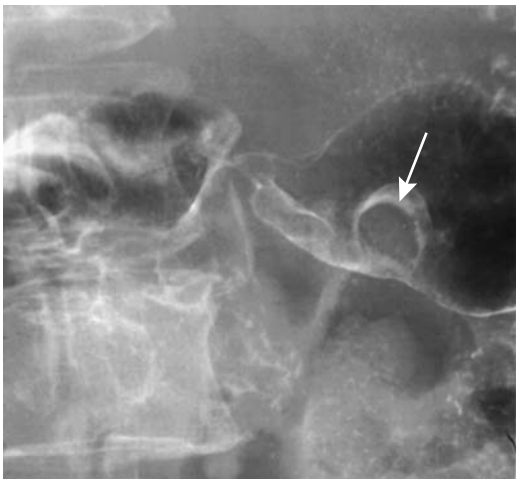

Figure 2.8. Antral adenoma appearing as a sessile polyp (arrow).

They are more common in the fundus than more distally.

For some of these tumors a distinction between leiomyoma and its sarcomatous counterpart is tenuous at best and some are thus labeled as having a variable biologic patterns or simply as gastrointestinal stromal tumors (GISTs) (stromal tumors are discussed in more detail in Chapter 1).

With growth, both benign and malignant ones tend to outgrow their blood supply and become partially necrotic (Fig. 2.9); as a result the larger ones have a heterogeneous, partly necrotic-cystic imaging appearance. A rather prominent contrast enhancement is common in nonnecrotic regions.

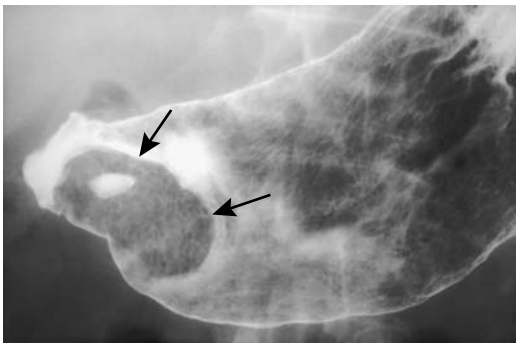

Figure 2.9. Ulcerated antral leiomyoma (arrows). (Courtesy of Arunas Gasparaitis, M.D., University of Chicago.)

Calcifications in a gastric leiomyoma are rare (25) and ossification even rarer.

Lipomatous Tumors

Most gastric lipomatous tumors are lipomas, with an occasional angiolipoma, teratoma, or even a liposarcoma found. Reactive lipomatosis is a nebulous entity encountered occasionally.

Most lipomas are discovered incidentally, most often in the fundus. An occasional one ulcerates, presumably secondary to ischemia, and bleeds. An occasional prepyloric lipoma obstructs or, if polypoid, prolapses into the duodenum and leads to bleeding. Occasionally multiple gastric lipomas are detected.

Barium studies reveal most lipomas as smooth submucosal tumors with or without ulcerations, similar to stromal tumors and lymphomas (26). Computed tomography reveals lipomas to be of homogeneous density of about −30 to −100 Hounsfield units (HU); some have an apparent capsule. Similar to other structures containing fat, lipomas are hyperintense on T1- and hypointense on most T2-weighted images and they lose signal intensity on fat-suppressed T1-weighted spoiled gradient echo (SGE) images. Thus, regardless of location, a lipoma can be distinguished from most other polyps. Distinguishing a lipoma from a liposarcoma, on the other hand, is problematic. Well-differentiated liposarcomas contain thick septa or nodules on T1-weighted MRI, with these septa or nodules becoming hyperintense on fat-suppressed or STIR T2-weighted sequences, findings seen only in a minority of lipomas (27). A heterogeneous appearance or presence of a necrotic or cystic component in a fat-containing tumor should suggest a teratoma or a liposarcoma.

The rare angiolipoma shows marked CT contrast enhancement.

A heterogeneous appearance or presence of a necrotic or cystic component in a fat-containing tumor should suggest a teratoma or a liposarcoma.

Hemangiopericytoma

Hemangiopericytomas can occur in most tissues, but a gastric location is rare.

Polyposis Syndromes

Gastrointestinal polyposis syndromes are discussed in more detail in Chapter 4. Included here are only those aspects pertinent to the stomach.

Nonfamilial Polyposis (Fundic Gland Polyps)

Fundic gland polyps are most prevalent in middle-aged women and are not associated with either gastric adenomas or gastric cancers; they can grow or regress, some even resolving completely. They are not premalignant.

They tend to be small, ranging in size from 1 to 3 mm. A double-contrast upper gastrointestinal study readily detects these polyps.

Familial Polyposis

Upper gastrointestinal polyps are common in a setting of familial adenomatous polyposis. These polyps are either of gastric fundic gland origin (hyperplastic) or adenomas. Most resultant gastric adenocarcinomas arise from adenomas, although a rare adenocarcinoma originates from a hyperplastic fundic polyp.

Occasionally gastric polyps in patients with familial adenomatous polyposis regress on indomethacin therapy.

Peutz-Jeghers Syndrome

Gastric hamartomatous polyps develop in patients with Peutz-Jeghers syndrome. Occasional gastric adenocarcinomas have been reported.

Juvenile Polyposis

Gastric juvenile polyposis, consisting of numerous juvenile polyps scattered throughout the stomach, is rare. Some patients have a family history of intestinal polyposis or have generalized juvenile polyposis, although it is not clear whether gastric juvenile polyposis is a separate entity from generalized juvenile gastrointestinal polyposis.

These polyps predominate in the antrum; with time, some became numerous, larger, and pedunculated. They are associated with adenomas and adenocarcinomas. Eventual gastrectomy is performed either for suspected malignancy or control of protein-losing gastropathy.

Cronkhite-Canada Syndrome

These patients develop characteristic ectodermal abnormalities consisting of dystrophic nail changes and alopecia.

A barium study reveals multiple polyps scattered in the stomach, duodenum, and small bowel. Biopsy of these polyps shows mostly an inflammatory infiltrate and a cystic component. Some of these patients have an elevated carcinoembryonic antigen (CEA) level that decreases after steroid therapy. Anecdotal reports describe bowel adenomas.

Adenocarcinoma

Adenocarcinomas involving the gastroesophageal junction are discussed in Chapter 1. Both clinically and from prognostic and management viewpoints these tumors are closer to esophageal cancers than to more distal gastric cancers. Early gastric cancers are discussed below. Although these tumors are adenocarcinomas and are precursors to more advanced cancers, their clinical presentation and imaging approach are sufficiently different to warrant a separate discussion.

Diffuse scirrhous gastric tumor spread leads to a linitis plastica appearance (Fig. 2.10). Some use the term *linitis plastica* as a synonym for an extensive scirrhous gastric adenocarcinoma, but this term is a descriptive one; several other disorders can have a similar appearance: metastatic carcinoma (breast, etc.), lymphoma, sarcoidosis, prior corrosive ingestion, and even gastric syphilis. Also, at times *H. pylori* gastritis and other benign entities thicken the gastric wall sufficiently to suggest a cancer.

Clinical

The prevalence of gastric cancer, by age, varies considerably throughout the world. In the Far East, gastric cancer is more common in a younger age group than in Europe or North America and their 5-year survival rate is similar to other age groups. On the other hand, gastric cancer in younger American patients is more likely to be associated with distant metastases

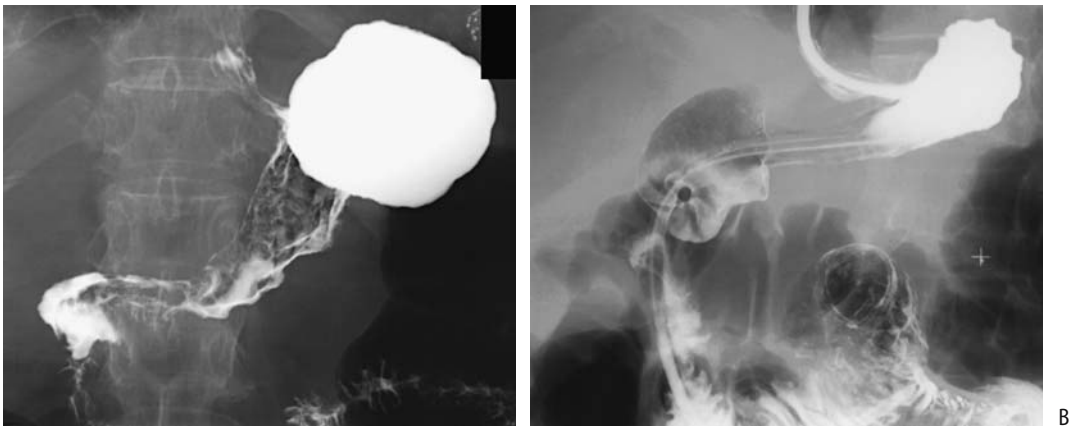

Figure 2.10. Linitis plastica appearance of adenocarcinoma. A: A diffuse infiltrate is present but there is no obstruction. B: Linitis plastica in this patient has progressed to almost complete lumen obstruction. Only the fundus was spared in both patients.

and more adverse features than older patients (28). In Japan, the prevalence of gastric cancer continues to decrease in young patients.

Epstein-Barr virus infection is associated with some gastric cancers, but reported association varies, being greatest in East Asia. These virus-associated cancers tend to be superficial depressed or ulcerated in appearance.

The Netherlands Cohort Study on diet and cancer revealed a strong inverse association between onion consumption and risk of stomach carcinoma (29).

A number of gastric cancer families exist. Transmission tends to be autosomal dominant.

The Leser-Trélat sign consists of eruption of multiple seborrheic keratoses or similar lesions in association with an internal malignancy and is considered to be a paraneoplastic autoimmune phenomenon. Occasionally such seborrheic keratosis regresses after tumor resection but returns with cancer recurrence. Paraneoplastic hypercalcemia occasionally develops. Rare associations exist between gastric cancer and such conditions as acromegaly and polyarteritis nodosa.

An occasional gastric carcinoma perforates; perforation into the peritoneal cavity generally results in an acute abdomen. Among patients with a perforated gastric carcinoma collected from the Japanese literature, perforation occurred with all tumor stages, being 19% with stage I tumors, 12% with stage II, 30% with stage III, and 39% with stage IV tumors (30).

A rare gastric carcinoma is first detected as a metastasis (Fig. 2.11).

Pathology

An adenoma-to-carcinoma transformation sequence, as found with colorectal tumors, is not evident in most gastric tumors. Carcinomas do occur, however, in adenomatous polyposis syndromes. Gastric dysplasia is a precancerous condition. A gastric cancer is often already present when dysplasia is detected.

Epstein-Barr virus–positive early gastric carcinomas have a mostly $CD8^+$ T-lymphocytic surrounding infiltrate, with adjacent gastric mucosa being atrophic and depleted of parietal cells (31). An occasional undifferentiated carcinoma has Epstein-Barr virus limited to tumor epithelial cells, pointing toward a possible pathogenesis for these tumors.

Gastric cancer classifications in use are those of the WHO and the Lauren and Borrmann systems. Lauren subdivides gastric cancer into two types: intestinal and diffuse. The intestinal type tends to be more differentiated than the diffuse type. These classifications are only roughly comparable; the WHO classification of tubular, mucinous, and papillary carcinomas are mostly equivalent to the Lauren classification of intestinal type, and the WHO signet ring and many undifferentiated carcinomas fall into the Lauren diffuse tumor type. The Borrmann classification (Table 2.3) is based on

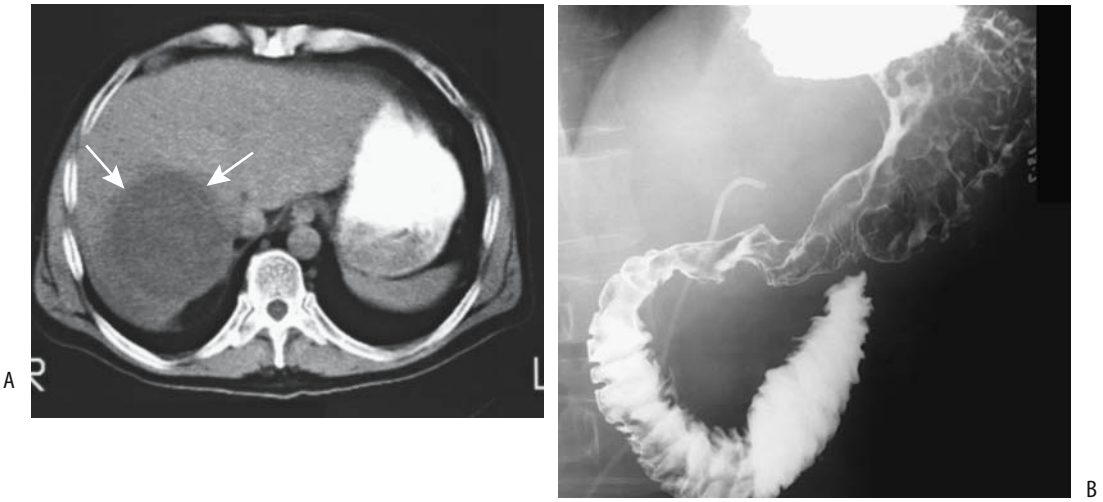

Figure 2.11. Metastatic antral carcinoma. A: A large liver metastasis (arrows) was detected first. B: Only then was a primary antral carcinoma discovered.

gross morphology and is in common use by Japanese and some European investigators.

Lauren intestinal-type carcinomas appear to be related to environmental factors and diet, and in countries with decreasing prevalence of gastric cancer it is the intestinal type that is declining, with little change in diffuse type (32). These two subtypes appear to have different pathogenetic processes. Predisposing atrophic gastritis and intestinal metaplasia and dysplasia more often lead to intestinal type of cancer.

The Goseki classification of gastric cancer is based on intracellular mucus production and degree of tubular differentiation, but this classification does not provide additional prognostic value beyond what was available with the tumor, node, metastasis (TNM) staging and the Lauren classification.

An infiltrating gastric scirrhous carcinoma incites a mostly desmoplastic reaction that leads to a fixed and rigid-appearing gastric wall. Most scirrhous carcinomas result in a linitis plastica appearance, although an occasional one is focal in extent. Lymphoma and some metastases have a similar imaging appearance, but with these tumors the infiltration is primarily by tumor cells.

Table 2.3. Borrmann classification of gastric carcinomas

Type	Description
I	Polypoid tumor with no ulceration
II	Fungating, ulcerating tumor with distinct borders
III	Ulcerating tumor with poorly defined borders
IV	Diffusely infiltrating tumor without ulceration (linitis plastica appearance)

A signet ring cell carcinoma is a poorly differentiated adenocarcinoma, with tumor cells invading surrounding tissues singly or in small groups. Some of these are associated with an intense lymphocytic and plasma cell infiltrate.

Extrahepatic hepatoid adenocarcinomas exhibit true morphologic and immunohistochemical hepatocellular differentiation. The most common site for a primary extrahepatic hepatoid carcinoma is in the stomach. These tumors are aggressive and metastasize readily to the liver. In fact, some of the older studies of a double malignant primary in the stomach and liver probably represent gastric hepatoid carcinomas with liver metastases. Nevertheless, this topic is complex, and not only patients with liver metastasis but also patients with a synchronous primary liver hepatocellular carcinoma have been reported.

Unusual features of gastric hepatoid adenocarcinomas include high levels of serum α-fetoprotein and an ability to secrete bile. An occasional gastric adenocarcinoma has no hepatoid features, but perigastric lymph node

metastases contain hepatoid characteristics, suggesting hepatoid differentiation only in metastatic foci. The histology of these tumors shows an adenocarcinomatous component intermingled with hepatoid regions.

Some degree of neuroendocrine differentiation is common both in conventional and hepatoid gastric cancers. In most tumors endocrine cells are either scattered or grouped in small clusters and are independent of tumor stage or histologic type. One unusual gastric carcinoma variant is the presence of an osteoclast giant cell stromal component. An occasional odd histologic mix is encountered, such as a primary coexistent adenocarcinoma and choriocarcinoma.

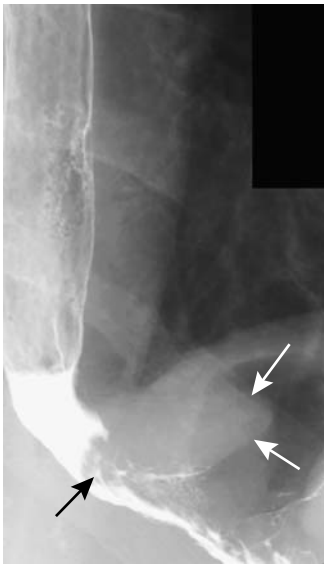

Figure 2.12. Fundal adenocarcinoma (arrows) in a patient evaluated for reflux.

Detection

Imaging

Currently most initial detection of gastric cancer is by endoscopy and biopsy of a suspicious tumor. Barium studies are generally performed for other indications, and gastric cancers are detected incidentally (Fig. 2.12). Nevertheless, an occasional patient still presents with gastric outlet obstruction secondary to an extensive cancer (Fig. 2.13). Currently, many physicians believe that imaging has a role primarily in staging rather than initial cancer detection, yet some studies point to barium having a role in these patients. Thus in patients with pathologically proved scirrhous gastric carcinomas, tumor location and extent were correctly identified by endoscopy in only 33%, while barium studies were accurate in 68% of patients (33); upper gastrointestinal studies reveal thick and irregular folds, ulcerations and nodularity.

Calcifications are rare in primary gastric cancers, with most calcifications developing in well-differentiated mucinous adenocarcinomas, although an occasional scirrhous carcinoma contains calcifications.

Giant gastric ulcers can be either benign or malignant. Statistically, however, a giant ulcer is more likely to be malignant. The presence of fistulas generally signifies an advanced gastric cancer.

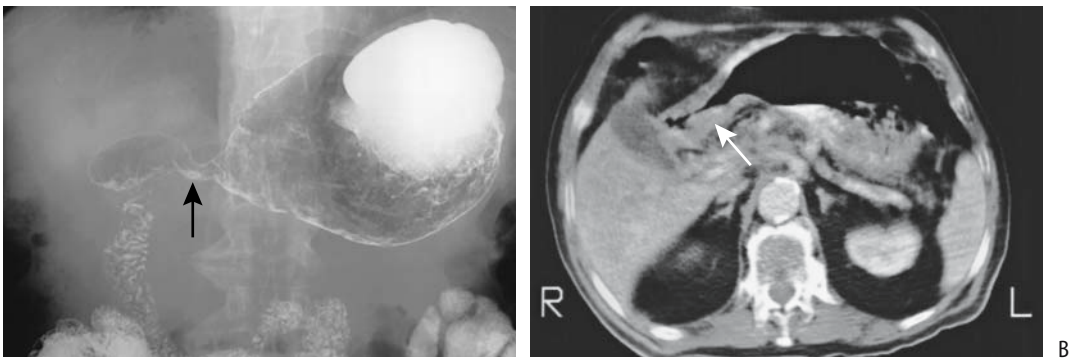

Figure 2.13. Antral adenocarcinoma. A barium study (A) and computed tomography (CT) (B) detect marked antral infiltration (arrow). (Courtesy of David Katz, M.D., University of Massachusetts.)

Many radiologists believe that at initial presentation an antral adenocarcinoma does not spread across the pylorus into the duodenal bulb, the exceptions being if a patient is immunocompromised or during late presentation with extensive tumor spread when bulbar involvement is common. Radiologists use this observation to differentiate among an antral cancer, lymphoma, and peptic ulcer disease, with the latter two readily extending across the pylorus. In a minority of patients, however, transpyloric spread occurs with an antral carcinoma. Duodenal invasion is either direct, through deep muscle layers or lymphatics, or through venules. Barium studies reveal a rigid, open, and eccentric pylorus and a deformed bulb. Computed tomography identifies infiltration extending across the pylorus.

A retrospective review found perceptual error to be the reason for not detecting 41% of 27 carcinomas by upper gastrointestinal radiography performed within 3 years prior to tumor diagnosis (34); the most common overlooked finding was an intramural depression.

Computed tomography tumor detection is aided by gastric distention with water (called hydro-CT). A hypotonic agent helps maintain gastric distention.

In a collection of advanced gastric cancers, a triphasic CT technique achieved a 98% detection accuracy (35); of these, 28% were best seen on parenchymal phase during gradual enhancement from the mucosal side. Computed tomography of a typical gastric carcinoma reveals focal gastric wall thickening and mild-to-moderate arterial phase enhancement. Extensive gastric wall thickening develops with tumor growth, with some tumors exhibiting marked enhancement. Computed tomography can miss early linitis plastica, although when it is well established, CT reveals diffuse gastric wall thickening. When extensive, scirrhous carcinomas result in extensive circumferential infiltration of the stomach, although some of these tumors are plaque-like in appearance. A less common linitis plastica cancer appearance is diffusely thickened gastric rugal folds with no apparent overlying ulcerations; the appearance mimics diffuse lymphoma, less often Ménétrier's disease. Dynamic CT shows most nonscirrhous carcinomas to have either homogeneous contrast enhancement or at least a thin outer layer, whereas scirrhous ones tend toward a gastric wall consisting of two layers: a lower attenuation thick outer layer and a higher attenuation thick inner layer.

Computed tomography arteriography, performed by injecting contrast through a catheter in the celiac trunk, correctly detected seven of eight early gastric cancers and all 13 advanced gastric cancers (36). Computed tomography arteriography is not used as a primary tool for gastric cancer detection, but it is of potential use for cancer staging.

Endoscopic US shows promise in detecting gastric malignancies, achieving sensitivities over 95%. It delineates gastric wall and adjacent structure infiltration. Mucinous carcinomas result in a hyperechoic endoscopic US appearance due to mucinous content and surrounding fibrosis. Endoscopic US of scirrhous carcinomas reveals irregular hypoechoic thickening of submucosa and muscularis propria.

Some scirrhous carcinomas are hypointense on both T1- and T2-weighted images, presumably due to the often associated fibrosis. Such a pattern is seen with linitis plastica. Little enhancement is evident with linitis plastica. Magnetic resonance reveals most gastric cancers as early enhancing thickened gastric wall tumors.

Both intestinal adenocarcinomas and various endocrine neoplasms contain receptors for vasoactive intestinal peptide (VIP) and scintigraphy with I-123 VIP appears advantageous. Binding of labeled VIP by primary tumors and metastases is visible for up to 24 hours in primary and recurrent gastric adenocarcinomas.

Endoscopy

Accuracy of gastric cancer detection with endoscopy varies considerably, especially with diffusely infiltrating cancers that are covered by intact mucosa. Even some biopsies are noncontributory, with cancer cells being dispersed in a fibrous matrix. Tumor location is better appreciated on an imaging study than with endoscopy.

In general, endoscopy of a polyp revealing normal overlying gastric mucosa suggests a mesenchymal tumor. Nevertheless, on rare occasion an adenocarcinoma will be mostly intramural and even invade to the serosa and not be detected by endoscopy or even biopsies.

Early Gastric Cancer

Clinical

Controversy surrounds the definition of an early gastric cancer. In Japan, a diagnosis of an early gastric cancer is made considerably more often than in the West. Some observers believe that an early gastric cancer is simply an early stage of a conventional gastric cancer rather than a different disease entity, an opinion not universally shared. Early gastric cancers tend to be intestinal type rather than diffuse type. In Japan about 10% of early gastric cancers are multiple.

Metastasis to lymph nodes is rare if a gastric cancer is limited to the mucosa; nodal involvement is more common with submucosal tumor spread. In the occasional patient with a recurrence after curative resection for early gastric cancer, recurrence is believed to be secondary to occult metastases in perigastric lymph nodes.

Endoscopic resection of early gastric cancer is performed in some countries for elevated mucosal cancers <2 cm in size and depressed mucosal cancers without ulceration <1 cm in size. Although endoscopic resection is possible for some tumors with submucosal extension, those with deep submucosal invasion are not cured with this approach.

Imaging

Detection and staging cannot be discussed separately for early gastric cancers because the definition already implies that a tumor is limited to the mucosa or at most submucosa. Computed tomography has a limited role in detecting early gastric cancer. Among patients with an early gastric cancer, axial CT identified 64% of tumors, whereas 3D CT images revealed 94% (37). On the other hand, using a triphasic CT technique and a water-filled stomach, another study detected only 23% and achieved a staging accuracy of 15% (35); those early cancers detected were best seen during the arterial or parenchymal phases.

Early gastric cancers detected by CT are polypoid, elevated, or invade submucosa. Wall thickening with early gastric cancers is limited to the inner layer only. These cancers show CT contrast enhancement. Advanced cancers also have contrast enhancement, but gastric wall thickening generally is more diffuse.

Postcontrast CT (mucosal phase, 38 to 45 seconds after the start of contrast injection) in patients with early gastric cancer revealed three patterns (38): (1) localized thickening of an inner hyperenhancing layer; (2) focal interruption of an inner hyperenhancing mucosal layer; and (3) focal protrusion of the inner hyperenhancing layer. The lesions became less distinct on a delayed phase. Overall, CT early gastric cancer detection rate was 57%. Of note is that some advanced gastric cancers had an appearance similar to early gastric cancer. Considerable CT difficulty exists differentiating between T1 cancers with submucosal invasion and more advanced cancers.

Conventional endoscopy and endoscopic US have roughly similar accuracy in determining the depth of invasion with early gastric cancers.

Staging

The TNM staging classification is outlined in Table 2.4. Preoperative staging of gastric cancer is of obvious importance but is fraught with uncertainty. Intraoperative surgical assessment tends to overstage early invasion and understage deep invasion. Microcarcinosis, defined as scattered carcinoma cells within lymph node sinuses or pulp without surrounding stromal reaction, is common in otherwise pN0 tumors; the number of detected tumor cells and involved lymph nodes carries prognostic significance, a significance differing from that found with gross lymph node metastasis.

Primary gastric cancer typically spreads to adjacent lymph nodes and liver. In a prospective study of regional lymph nodes from consecutive patients with primary gastric cancer, the mean diameter of tumor-free lymph nodes was 4.1 mm and those infiltrated by metastases was 6.0 mm (39); a practical problem is that although 80% of tumor-free lymph nodes were <5 mm in diameter, 55% nodes containing metastases were also <5 mm in diameter and the authors concluded that lymph node size is not a reliable indicator for lymph node metastasis. In spite of such findings, many authors assume an arbitrary boundary between normal and metastatic nodes. Currently no imaging modality is sufficiently accurate to reliably predict lymph node involvement. Perigastric lymph

Table 2.4. Tumor, node, metastasis (TNM) staging of gastric carcinoma

Primary tumor:			
Tx	Primary tumor cannot be assessed		
T0	No evidence of primary tumor		
Tis	Carcinoma-in-situ		
TI	Tumor invades lamina propria or submucosa		
T2a	Tumor invades muscularis propria		
T2b	Tumor invades subserosa		
T3	Tumor penetrates serosa		
T4	Tumor invades adjacent structures		
Lymph nodes:			
Nx	Regional nodes cannot be assessed		
N0	No metastases in regional lymph nodes		
N1	Metastases in 1 to 6 regional lymph nodes		
N2	Metastases in 7 to 15 regional lymph nodes		
N3	Metastases in more than 15 regional lymph nodes		
Distant metastasis:			
Mx	Distant metastases cannot be assessed		
M0	No distant metastases		
M1	Distant metastases		
Tumor stages:			
Stage 0	Tis	N0	M0
Stage IA	T1	N0	M0
Stage IB	T1	NI	M0
	T2a,b	N0	M0
Stage II	T1	N2	M0
	T2a, b	N1	M0
	T3	N0	M0
Stage IIIA	T2a, b	N2	M0
	T3	N1	M0
	T4	N0	M0
Stage IIIB	T3	N2	M0
Stage IV	T4	N1–3	M0
	T1–3	N3	M0
	any T	any N	M1

Source: From the AJCC Cancer Staging Manual, 6th edition (2002), published by Springer-Verlag, New York, NY, used with permission of the American Joint Committee on Cancer (AJCC), Chicago, IL.

nodes can be infiltrated by tumor but still be normal in size; conversely, some enlarged nodes do not contain tumor. Compounding the issue is that a nonneoplastic reactive infiltrate develops in some lymph nodes close to a cancer. Such sarcoid-like epithelioid cell lesions are detected in regional lymph nodes in about one third of gastric cancers; they are independent of tumor stage, type, and tumor grade, and do not aid in prognosis.

Fluoroscopic guidance of nasogastric biopsies is feasible to establish boundaries of a known gastric carcinoma, but this technique has achieved only limited acceptance.

Comparing published CT, US, and MR gastric cancer staging results is fraught with difficulty. Sensitivities vary markedly, depending on the basic assumptions used. As a gross approximation, helical CT and endoscopic US appear to provide similar T and N staging accuracies. Most problems arise in differentiating T2 and T3 tumors.

Computed Tomography

Computed tomography staging of gastric cancer has been rather disappointing and continues to be controversial. Some patients have obliteration of adjacent fat planes due to cachexia or inflammation. Some CT studies have achieved a tumor (T) and node (N) staging accuracy of only about 50% (40), although multislice triphasic CT results are more accurate. In general, CT differentiation between T3 and T4 cancers is not sufficiently accurate to predict resectability. It is accurate, however, in detecting distant metastases, and some surgeons rely on CT primarily to detect these metastases. Computed tomography more often suggests correctly unresectability rather than resectability.

Depth of tumor invasion and serosal invasion are believed to be difficult to determine even with helical CT. Yet in establishing serosal invasion, use of hydro-CT, induced hypotonia, and prone patient position has achieved a sensitivity of 100% and specificity of 80% to 87% (41).

The ability of multislice CT to detect lymph nodes depends on node size; roughly half of nodes <10 mm and about 75% of those >10 mm are detected. Detecting tumor in a lymph node is another matter; intrinsically, nothing in the CT appearance suggests that a particular lymph node is involved by tumor.

Staging accuracy of CT arteriography in patients with gastric cancer was 77% for serosal invasion and 76% for regional lymph node metastasis (36); of note is that accuracy for T staging of early gastric cancers was only 50%.

Whether multislice 3D images aid in staging gastric cancers remains to be determined.

Ultrasonography

Ultrasonography detection of motion (the sliding sign) between a gross gastric cancer and pancreas aids in assessing pancreatic invasion. In patients with advanced gastric cancer, the presence of such a US sliding sign yielded 80% sensitivity and 96% specificity in detecting pancreatic invasion (42); the presence of sliding motion by a tumor against the pancreas on respiration or on extrinsic transducer compression and a preserved fat plane between the two structures signified the lack of pancreatic invasion.

Theoretically, endoscopic US with its high resolution should be able to detect submucosal or deeper invasion and thus aid in differentiating early gastric cancer from an advanced one. Published studies suggest that endoscopic US is superior to both CT and intraoperative surgical staging, achieving a T-stage accuracy of about 60% to 90% and an N-stage accuracy of 65% to 70%. Endoscopic US-guided fine needle aspiration cytology is an option for evaluating gastrointestinal wall infiltration and even lymph node staging. Staging is limited for large carcinomas extending beyond the stomach. The most frequent cause of understaging depth of invasion is microscopic tumor spread, whereas surrounding inflammation leads to overstaging. Nodal staging by endoscopic US should be approached cautiously; most published results are on a per patient basis; expressed on a per node basis, accuracy falls considerably, similar to other imaging modalities.

Magnetic Resonance Imaging

Limited data are available about the role of MRI in staging gastric cancer. Gastric distention with an oral contrast agent appears advantageous in these patients, but no major difference between water and gadolinium is apparent (43).

Current evidence suggests no significant accuracy differences in either T or N staging between preoperative MRI and CT. For example, the T stage was overstaged with MRI in 7% and CT in 10% and understaged with MRI in 20% and CT in 23%. The N stage was overstaged with MRI in 10% and CT in 7% and understaged with both MRI and CT in 34% (44). Comparable results have been achieved in other studies. Relative accuracy of lymph node metastases varies considerably between MR studies, ranging from only about 50% to over 90% with some techniques. In general, MRI tends to be superior to CT in T staging, but CT is superior in N staging.

Compared to surgical staging, MRI staging is accurate for 75% to 80% of tumors, being higher for more extensive tumors (45); an interrupted hypointense band or enhancing tumor penetrating through the gastric wall signifies tumor penetrating serosa.

Therapy

For Cure

The highest cure rates are reported from Japan, where early gastric cancer detection is greatest. Outside of Japan, advanced disease is common. In many Western centers most of these cancers are already advanced, and cure rates are dismal. Typical statistics are that only two thirds of gastric cancer patients undergo surgery and of these in only half is tumor resection feasible. Generally age is no barrier, and in patients aged 80 years or older with gastric cancer some investigators achieve crude 5-year survival rates of over 40% in those amenable to curative resection (46). Parameters predicting survival in patients with advanced gastric cancer undergoing potentially curative resection are depth of tumor invasion, lymph node invasion, and tumor histologic classification (Fig. 2.14).

Some patients with an unresectable gastric cancer undergo chemotherapy in an attempt to downstage the cancer. Results of chemotherapy, evaluated by CT, have been mixed. Some gastric hepatoid adenocarcinomas respond to adjuvant chemotherapy.

Palliation

Whether patients with metastatic gastric cancer should undergo palliative resection, even laparoscopic, is questionable. But before we adopt a fatalistic outlook, however, it should be pointed out that although most patients with stage IV gastric cancer have a poor prognosis, some of these patients with a resectable cancer do survive for 5 years or longer.

Palliation with self-expanding flexible metallic stents is an option for inoperable malignant gastric outlet obstruction; both peroral and percutaneous gastrostomy approaches are used. In

Figure 2.14. Recurrent gastric carcinoma after a Billroth II resection 6 months previously for antral cancer. Most of the residual stomach is now infiltrated.

general, results are less favorable than in the esophagus. Successful palliation of patients with malignant gastric or duodenal obstruction using self-expandable covered metallic stents can be achieved in over 75% (47,48). Complications consist of stent migration and fracture. Overall, a stent improves quality of life, restores oral food intake, and relieves vomiting in these patients with a limited life expectancy.

Metastasis/Recurrence

Following gastric cancer resection, the most common recurrence is either in regional lymph nodes or in distal organs. Metastasis to hepatoduodenal nodes leads to obstructive jaundice. Duct obstruction is due to not only compression by surrounding nodes but also direct bile duct invasion from nodes. Patient survival with liver metastasis is short, although an occasional long-term survivor is reported.

Metastasis to cervical lymph nodes currently is seldom encountered. The presence of cervical lymphadenopathy, however, is not pathognomonic of cancer spread, and a biopsy is necessary.

Bone metastases are evaluated by Tc-99m bone scans. Common metastatic sites are spine, then ribs, pelvis, femur, and skull. These sites are also common for other malignancies. A direct correlation exists between bone scan results and serum alkaline phosphatase levels.

Occasionally a gastric carcinoma extends as a tumor thrombus via gastric veins into the portal vein; intraoperative US should be considered when such a tumor thrombus is suspected.

Gastric scirrhous carcinomas readily metastasize to other bowel. Direct spread and invasion to transverse colon via the gastrocolic ligament is a feature of advanced gastric cancers.

More unusual metastases are to pericardium, gallbladder, and skin. Solitary metastases have been to the spleen and bladder. Even leptomeningeal carcinomatosis has developed before a primary gastric cancer became symptomatic.

Adenosquamous/Squamous Cell Carcinoma

Both adenosquamous and squamous cell gastric carcinomas are rare. These tumors have a predilection for the proximal part of the stomach. Squamous metaplasia, presumably from prior mucosal injury, appears to play a role in the origin of squamous cell carcinomas.

Adenosquamous carcinomas tend to invade extensively and even if limited to the submucosa can already have metastasized.

Small Cell Carcinoma

Small cell carcinomas are rare. Their prognosis is very poor compared with that of more common types of gastric cancers.

The imaging appearance of gastric small cell carcinomas is variable and nonspecific; described CT features consist of a bulky exophytic tumor showing little peritumoral infiltration and having little contrast enhancement (49).

A gastric small cell carcinoma developed in a man with a 5-year history of progressive systemic sclerosis (50); serum CEA and neuron-specific enolase levels were elevated, and imaging revealed a sharply marginated and ulcerated tumor. Although esophageal and some

other cancers developing in a setting of progressive systemic sclerosis are not uncommon, gastric cancer is exceedingly rare.

Lymphoma

Clinical

The gastrointestinal tract is the most common extranodal site for non-Hodgkin's lymphoma, with the stomach being most often involved. A study of adults in a Copenhagen county with primary gastrointestinal non-Hodgkin's lymphoma found 50% with gastric lymphomas, 25% with lymphomas of the small intestine, 20% with lymphomas of the colon, and 4% with multifocal involvement (51). A different prognosis and therapy distinguish these lymphomas from nodal lymphomas. B-cell origin lymphomas and MALT lymphomas predominate among patients with primary gastric lymphoma.

A convenient subdivision is into MALT, low-grade lymphomas, high-grade lymphomas, and Burkitt's lymphomas. Various low-grade lymphomas can be identified by their different monoclonal antibodies. Epstein-Barr virus genomes are detected only in an occasional lymphoma. One type of less common T-cell lymphoma is associated with celiac disease.

The relation between tumors of B-cell origin is not clear-cut. Chronic lymphocytic leukemia and lymphocytic lymphoma appear related to different stages of B-cell differentiation; one proposed pathway of B-cell differentiation leads to immunoglobulin M (IgM)-producing plasma cells and manifests as plasmacytoid lymphocytic lymphoma, whereas another produces IgG- or IgA-positive plasma cells and leads to plasmacytoma (and multiple myeloma).

As the term *mucosa-associated lymphoid tissue* (MALT) suggests, it is found in the epithelium. The term *MALT lymphoma* is a descriptive one for lymphoid tissue in this location; nevertheless, it has achieved specific therapeutic and prognostic significance. Current evidence suggests that oncogenesis of MALT lymphomas involves proliferation of autoreactive B cells in response to *H. pylori*–specific T cells, and the genetic instability of these B cells then induces chromosomal abnormalities. Especially in a setting of *H. pylori* gastritis, gastric lamina propria undergoes lymphoid infiltration and lymphoid hyperplasia. Whether this tissue represents a precursor of lymphoma or is indeed lymphoma is a matter of degree and often is controversial. Clinically, most MALT lymphomas are more benign than their nodal counterparts. Low-grade ones tend to be indolent and remain localized for many years. Some spread to other mucosal sites. *H. pylori* is identified in a majority of these patients.

In eradicating *H. pylori*, antibiotic therapy also decreases the amount of lymphoid tissue in most patients, although some continue to be *H. pylori* positive/MALT positive, *H. pylori* negative/MALT positive, or *H. pylori* positive/MALT negative. In an occasional patient, in spite of antibiotic therapy, transition of low-grade to high-grade lymphoma still occurs. Staging with endoscopic US appears useful in predicting response of low-grade MALT lymphomas to *H. pylori* therapy.

Although biopsy is essential for diagnosis, some intramurally located lymphomas have a grossly normal-appearing overlying mucosa, and superficial biopsies are unremarkable.

A number of reports discuss coexisting malignant gastric lymphoma and adenocarcinoma, and this association appears to be more common than expected by chance. Most of the adenocarcinomas are macroscopically early and histologically differentiated, but most lymphomas are advanced and a correct preoperative diagnosis is established in only a minority of these patients. One should also keep in mind that epithelial signet-ring cells are not uncommon adjacent to a MALT lymphoma, and these cells can be confused with a carcinoma; reports of such double carcinoma-lymphoma neoplasms should be viewed with caution.

The TNM staging system also applies to gastric lymphomas.

Pathology

The MALT lymphomas appear to represent a unique and distinct clinicopathologic entity, yet a pathologic diagnosis of MALT lymphoma is not always clear-cut. Pathologists divide these lymphomas into low grade and high grade, with an occasional high-grade and adjacent low-grade lymphoma encountered. With progres-

sion, they infiltrate extensively and develop into advanced gastric lymphomas. Histologically, these tumors are difficult to diagnose, with a correct initial biopsy diagnosis made in only about two-thirds of patients; a biopsy diagnosis can be improved with immunohistochemical and molecular biology techniques.

Low-grade primary gastric lymphomas involve Peyer's patches rather than lymph nodes. Confusing the issue is that reactive lymphoreticular hyperplasia is common in chronic gastritis, especially if associated with *H. pylori* infection, with this lymphoid tissue presumably having a role in a local immune response. Previously called *pseudolymphoma* by pathologists, extensive lymphocytic infiltration or the presence of large lymphoid follicles should raise the suspicion of MALT lymphoma.

Follow-up of patients with gastric lesions difficult to distinguish between reactive lymphoreticular hyperplasia and MALT lymphoma has led to an eventual diagnosis of MALT lymphoma in one half (52); metastases were evident in several patients.

Imaging

The most common imaging appearance of a primary non-MALT gastric lymphoma is that of an ulcerating tumor, an appearance less often seen with small bowel and colon lymphomas. Some of these ulcerating tumors consist of a huge ulcer surrounded by a sparse soft tissue mass. Less common is intramural infiltration. Growing intramurally, these lymphomas tend either to thicken rugae massively or to result in a linitis plastica appearance. Computed tomography in these patients reveals marked circumferential gastric wall thickening (Fig. 2.15).

Lymphoma is more common in the distal half of the stomach. Some extend through the pylorus into the duodenum, but gastric outlet obstruction is not common and helps differentiate lymphoma from an antral adenocarcinoma. Associated adenopathy is common and tends to be more extensive than seen with gastric adenocarcinoma. A rare gastric lymphoma results in a fistula to an adjacent organ.

Endoscopic and imaging findings of low-grade MALT gastric lymphoma ranges from a grossly normal appearance, erosions (flat type), ulcerations (depressed type), and a nodular cobblestone appearance due to lymph follicle prominence, to thickened rugae (elevated type). Only a minority of these lymphomas have focal gastric wall thickening. The appearance thus mimics that of gastritis, ulcer, early gastric carcinoma, or even a metastasis, such as a malignant melanoma or, in an AIDS patient, Kaposi's sarcoma. Multiple nodules mimic a polyposis syndrome. Thickened rugae suggest Ménétrier's disease. The presence of disorganized rugae,

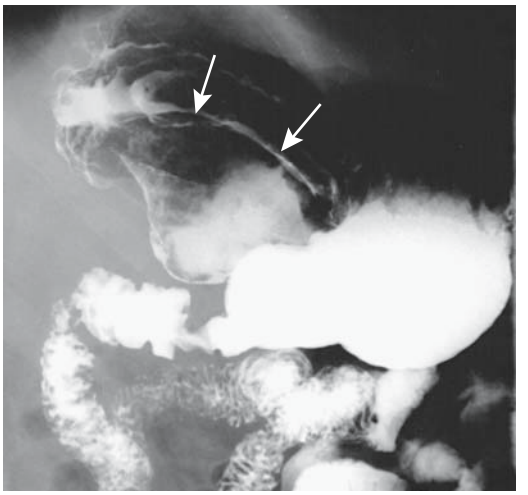

A

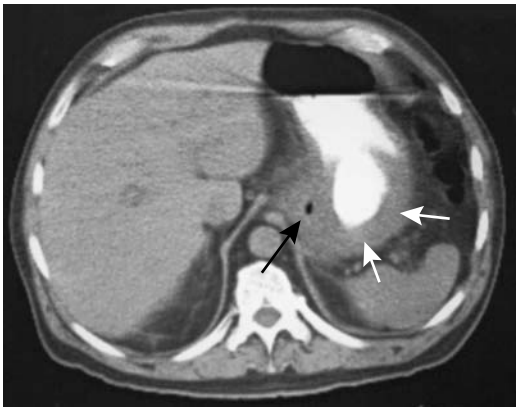

B

Figure 2.15. Gastric lymphoma. A: A barium study reveals a large, ulcerated tumor (arrows) in body of stomach. B: CT shows focal gastric wall infiltration (arrows). An atypical adenocarcinoma is in the differential diagnosis.

poorly defined ulcer margins, and multiple lesions suggests lymphoma. Low-grade MALT lymphomas tend toward a nodular, almost confluent appearance on double-contrast barium studies, and high-grade ones tend toward a more polypoid, ulcerated tumor.

A double-contrast gastrointestinal examination is the preferred imaging test to detect these tumors. Computed tomography is of limited help in detecting low-grade MALT lymphoma. With high-grade lymphoma, CT detects not only a gross tumor but also any associated adenopathy. Computed tomography shows poor enhancement of those tumors with a noticeable intramural component.

Endoscopic US is of limited value in detecting low-grade MALT lymphomas because in some of these tumors the gastric wall is not thickened. Wall thickening, when present, consists predominantly of mucosa alone and/or submucosa. In those with a thickened wall, however, endoscopic US may document regression to a normal-thickness wall, keeping in mind that in some patients the mucosa and submucosa remain thickened even in remission.

After radiation therapy a gastric lymphoma often regresses to a normal appearance. Occasionally seen are radiating folds to a centrally located ulcer or scar.

Computed tomography in a 54-year-old man with primary gastric Burkitt's lymphoma showed marked gastric wall thickening but lymph nodes tend not to be enlarged (53).

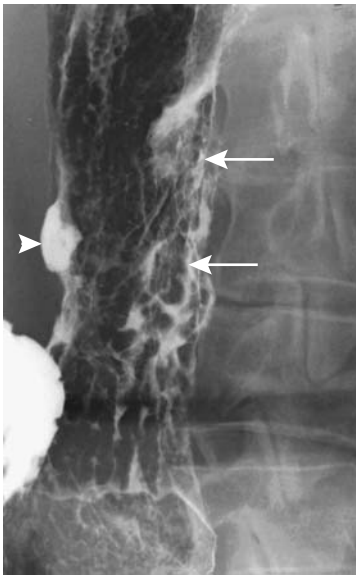

Figure 2.16. Gastric involvement with chronic lymphocytic leukemia results in thick, irregular folds (arrows) and ulcerations.

Leukemia

Leukemic infiltration of the stomach generally does not lead to bleeding.

The imaging appearance of leukemia involving the stomach ranges from normal to the occasional massive rugal thickening (Fig. 2.16). A rare gastric leukemia presents with intraluminal polyps.

Plasmacytoma

Some plasmacytomas grow rapidly. Weight loss and upper gastrointestinal bleeding are typical presentations.

Barium studies of the few reported primary gastric plasmacytomas reveal a varying appearance ranging from a depressed tumor pathologically representing a plasma cell granuloma; a nodular, submucosal tumor containing atypical plasma cells; a sessile polypoid appearance; to extensive gastric wall infiltration. Plasmacytomas appear similar to carcinomas and lymphomas. Aside from confirming intramural infiltration, CT is noncontributory. Plasmacytomas tend to enhance poorly, similarly to lymphomas. Associated adenopathy is not common.

Sarcoma

Some sarcomas manifest by their bulk, whereas others result in chronic blood loss. An occasional one presents with an acute bleed, usually into the stomach but at times intraperitoneally. Hypoglycemia is an occasional presentation.

Presence of a gastric stromal tumor (or an autonomic nerve origin tumor), extraadrenal paraganglioma, and a pulmonary chondroma signifies Carney's triad, with at least two of these findings needed for a presumptive diagnosis. Some evidence suggests that Carney's triad is a disorder of the autonomic nervous system rather than a multiple endocrine neoplasia syndrome or multiple hamartoma syndrome.

Gastrointestinal Stromal Tumors (GISTs)

The terms *stromal tumors, smooth muscle tumors*, and *mesenchymal tumors* are often used interchangeably, although not all mesenchymal tumors are stromal in origin. Also, some authors lump all stromal tumors into one category and simply refer to them as GISTs, others define GISTs as soft tissue sarcomas originating from gastrointestinal tract mesenchymal cells, and still others limit this term primarily to undifferentiated sarcomas. Most sporadic GISTs contain somatic c-*kit* gene mutations, believed to be pathogenetic for stromal tumors originating from interstitial cells of Cajal, and thus GISTs can be defined by the presence of appropriate immunoreactivity, an approach preferred by a number of experts in this field. On the other hand, stromal tumors in neurofibromatosis type 1 patients do not contain detectable c-*kit* gene mutations, and in these patients presumably develop by a different mechanism (54). The term *pure stromal tumor* as a synonym for an undifferentiated tumor appears inappropriate. The major significance of GISTs is their particular sensitivity to imatinib mesylate (Gleevec), a selective tyrosine kinase inhibitor and a cancer therapeutic agent. Most stromal tumors contain mutations in the KIT receptor tyrosine kinase or mutations in the platelet-derived growth factor receptor α (55).

Based on immunohistochemical and other techniques, stromal tumors can be subdivided into (1) those differentiating toward smooth muscle, (2) those differentiating toward neural elements, (3) tumors containing both cell types, and (4) undifferentiated stromal tumors.

Undifferentiated stromal tumors signify those undifferentiated or poorly differentiated tumors of stromal origin, which are difficult to subclassify further.

Gastrointestinal stromal tumors occur most commonly in the stomach, followed by small bowel, then rectum, colon, and least often in the esophagus. The most common stromal tumor in the esophagus is a leiomyoma, and for clinical and prognostic purposes, whenever possible, it should be classified as such. Most stromal tumors originate from muscularis propria, with only a small minority from muscularis mucosa; most of the latter are in the colon and present as intraluminal polyps, although current evidence suggests that these colonic tumors are leiomyomas and not GISTs. Histologically, most GISTs are spindle cell in appearance, with a minority being epithelioid. In the past, many of the latter were classified as leiomyoblastomas or epithelioid leiomyosarcomas (these are discussed in a subsection below). A minority of stromal tumors contain a prominent myxoid component and some of these are at the borderland of being considered GISTs.

Gastrointestinal stromal tumors' malignant potential is estimated based on their mitoses per high power field. Patient survival is significantly related to number of mitoses.

The imaging appearance of GISTs varies markedly; they range from mostly exophytic, intramural, intraluminal, to a dumbbell-shaped appearance (56). They predominate in the gastric fundus and body. Small tumors have a sharp margin, tend to be mostly intraluminal and have a homogeneous density on unenhanced and contrast enhanced images (57); with growth, they become irregular in outline, have a larger extraluminal component and are more inhomogeneous in density. Large ones infiltrate adjacent organs. Presence of metastases establishes malignancy. When detected with barium or CT, many appear large, bulky, and ulcerated (Fig. 2.17). Stromal sarcomas tend to be solitary, multilobulated and mostly exophytic. Necrosis and hemorrhage are common. Interestingly, GISTs rarely obstruct bowel lumen. Ulceration of overlying mucosa is common with the larger ones, accounting for their propensity to bleed. Computed tomography and MRI readily outline the extraserosal extent of both benign and malignant varieties. Coronal and sagittal CT and MRI reconstructions are at times useful in establishing the organ of origin of large GISTs. Postcontrast, these tumors have variable enhancement except in regions of necrosis. Calcifications are rare. These stromal tumors rarely metastasize to lymph nodes, and the presence of enlarged adjacent nodes should suggest another diagnosis. Except when metastases are present, imaging cannot differentiate benign stromal tumors from malignant ones or other solid tumors such as neuroendocrine ones. Endoscopic US findings in 35 benign and malignant stromal cell tumors suggest that a tumor diameter of >4 cm and an irregular extraluminal border, hyperechoic foci, and cystic regions point toward a malignancy (58).

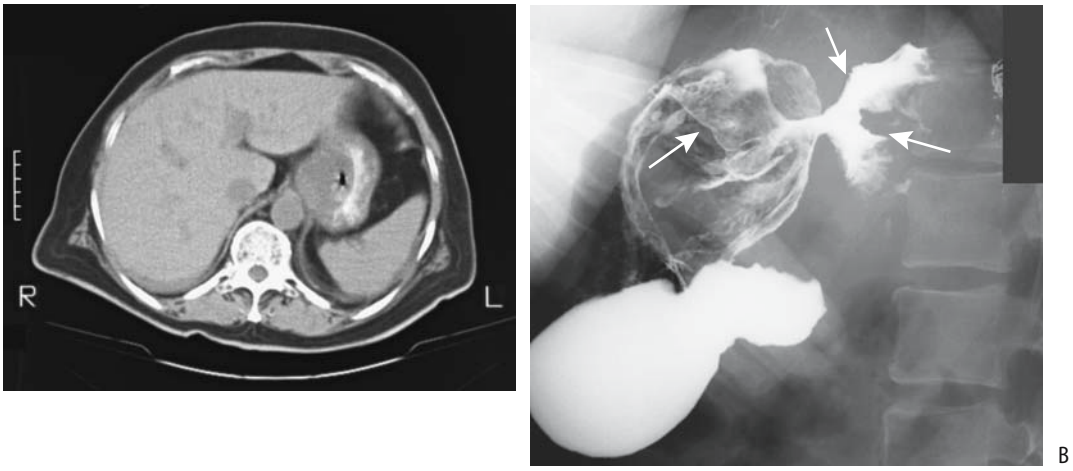

A B

Figure 2.17. Stromal tumors (gastrointestinal stromal tumor, GIST). A: One tumor at the gastric cardia mimics an adenocarcinoma. B: A large ulcerated GIST has replaced most of the gastric fundus (arrows). This appearance would be atypical for an adenocarcinoma.

Preoperatively, a pathologic diagnosis is often not made; endoscopic cytology is generally negative and even endoscopic biopsy is often negative.

Leiomyosarcoma

Most gastric leiomyosarcomas discussed in the older literature would now be classified as GISTs.

Multiple gastric leiomyosarcomas are rare. Imaging readily identifies these tumors (Fig. 2.18). In children, some gastric leiomyosarcomas reveal regions of necrosis and calcification, findings less common in adults.

Prognosis depends on tumor size, degree of mitotic activity, and nuclear grading. A poor prognosis can be predicted if four or more mitoses are identified per 20 high power fields or if severe nuclear atypia is present. Ulceration

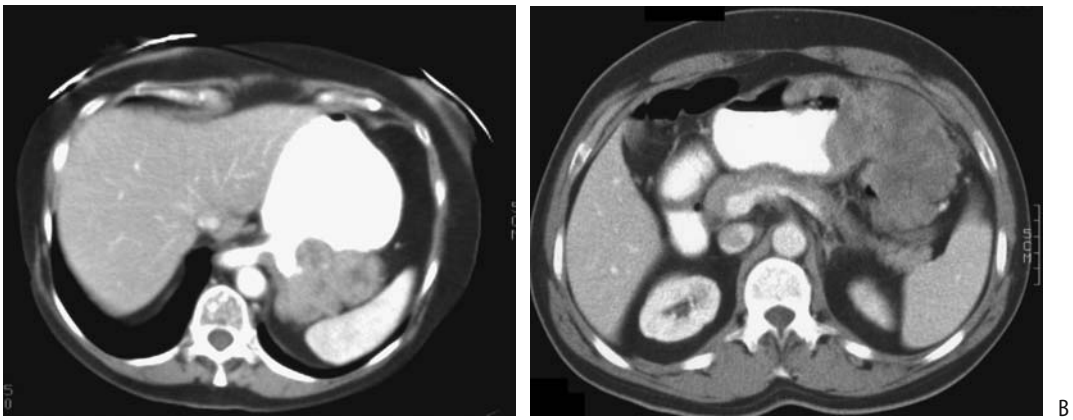

A B

Figure 2.18. A: Gastric leiomyosarcoma with both an intraluminal and an extraserosal component. B: Another patient with a mostly extraserosal gastric leiomyosarcoma. (Courtesy of Harpreet Pannu, M.D., and Elliott Fishman, M.D., Johns Hopkins University.)

and a diameter greater than 6 cm also imply a poor prognosis.

Epithelioid GISTs (Leiomyoblastomas)

Most leiomyoblastomas (also called *epithelioid leiomyosarcomas* or *epithelioid stromal tumors*) tend to be slow growing. About 25% are malignant. Although most are intramural in location, an occasional one grows primarily intraluminal, and even prolapsing into the duodenal bulb. Computed tomography revealed one connected to the serosal surface by a narrow stalk and changing its location in the peritoneal cavity during studies (59).

Their imaging appearance is similar to leiomyosarcomas (Fig. 2.19). Magnetic resonance imaging of a recurrent gastric leiomyoblastoma 14 years after initial presentation revealed a heterogeneous and moderately hypointense signal on T1-weighted images and a heterogeneous and moderately hyperintense signal on T2-weighted images (60); the tumor enhanced somewhat postgadolinium, with enhancement increasing on delayed images. The heterogeneous appearance suggested regions of necrosis.

Liposarcoma

Primary gastric liposarcomas are rare. An occasional one contains sufficient fat to be identified by CT, but in general their imaging appearance is similar to that of other stromal tumors. One presented as a large ulcerated submucosal mass at the incisura (61).

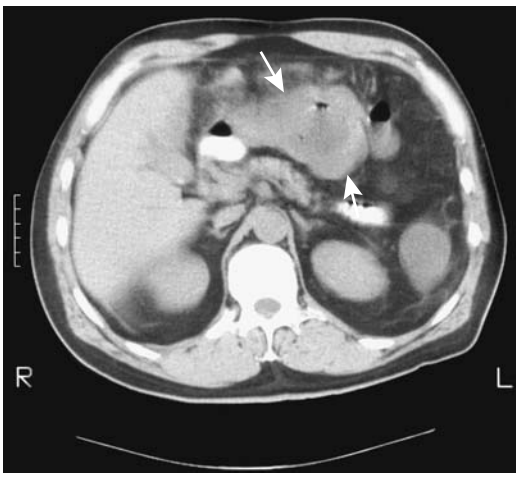

Figure 2.19. Leiomyoblastoma. CT identifies a soft-tissue density tumor (arrows) containing a lucent center and focal gas. It was believed initially to represent an abscess.

Figure 2.20. Kaposi sarcoma seen as a submucosal nodule (arrow) in an AIDS patient.

Histiocytoma

A primary gastric malignant fibrous histiocytoma is very rare. These solid, intramural tumors are similar in appearance to other gastric sarcomas.

Angiosarcoma

A patient on hemodialysis for 21 years was found to have multicentric gastrointestinal angiosarcomas (62); autopsy revealed lung, bone, liver, gallbladder, and lymph node metastases.

Kaposi's Sarcoma

Kaposi's sarcomas are subdivided into the Mediterranean (non-AIDS) type and those associated with AIDS. Patients with Mediterranean Kaposi's sarcoma also develop gastrointestinal tumors. A typical imaging appearance is that of a sessile polyp (Fig. 2.20).

Carcinosarcoma

Occasionally detected is a tumor containing an adenocarcinoma and mesenchymal elements such as a rhabdomyosarcoma or osteosarcoma and that is labeled *carcinosarcoma* by patholo-

Figure 2.21. Pancreatic body adenocarcinoma invading stomach (arrow).

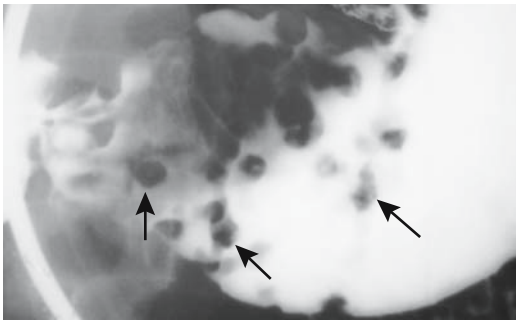

Figure 2.23. Gastric melanoma presenting as multiple polyps (arrows). (Courtesy of Arunas Gasparaitis, M.D., University of Chicago.)

gists (or *sarcomatoid carcinoma*, although these two terms are differentiated by pathology purists). In some cases, an immunocytochemical study suggests that the carcinomatous cells have transformed into sarcomatous cells or even vice versa. A number of these patients have had a previous partial gastrectomy performed years earlier.

Metastasis or Direct Invasion

With the exception of breast cancer and malignant melanoma, metastases to the stomach are not common; more often encountered is direct invasion from adjacent structures. Typical is pancreatic carcinoma, which readily invades the stomach, duodenum, and other adjacent structures (Fig. 2.21). Peritoneal carcinomatosis also involves the stomach. A rare metastasis is from a renal cell carcinoma, at times one resected years previously. Establishing a primary site can be difficult with simultaneous gastric and ovarian carcinomas (Fig. 2.22). These metastatic carcinomas ulcerate, bleed, obstruct, or even perforate.

A vast majority of gastric melanomas are metastatic (Fig. 2.23). Only a rare one is believed to be a primary gastric melanoma, a diagnosis to be made with caution.

Not all tumor diagnosis is straightforward; at times imaging studies and endoscopy with biopsy suggest an inflammatory condition, such

A

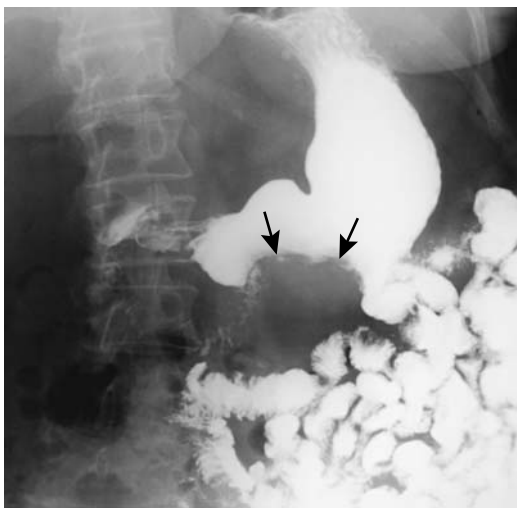

B

Figure 2.22. Patient with ovarian carcinoma (A, arrows) developed gastric metastasis (B), seen as a polypoid tumor involving the greater curvature (arrows). (Courtesy of William Bechtel, M.D., M.D. Anderson Hospital, Houston, Texas.)

as gastric Crohn's disease, when in fact metastatic breast carcinoma or other metastasis to the stomach is responsible for an inflammatory reaction around sparse tumor cells, but this is a limitation of biopsy, and especially cytology, rather than an indictment of imaging or endoscopy.

Neuroendocrine Tumors

Autonomic Nerve Tumor

Gastrointestinal autonomic nerve (GAN) tumors morphologically resemble an enteric plexus and were originally called plexomas or plexosarcomas. They consist of spindle-shaped cells mimicking a smooth muscle tumor, such as a GIST, or schwannoma. They also contain synapse-like structures and contain neurosecretory granules, suggesting a myenteric plexus origin.

Schwannoma

A schwannoma, also known as *neurilemmoma*, *neurinoma*, and *perineural fibroblastoma*, originates from peripheral nerve sheaths (Schwann cells) and is found at peripheral neural tissue sites. Most are benign, with about half of the malignant ones occurring in a setting of neurofibromatosis type 1 (von Recklinghausen's disease). Radiation therapy appears to predispose to schwannoma formation. These are rare tumors in children and are rare in the stomach. Clinically, schwannomas present with bleeding from erosions, obstruction, or, if large enough, a palpable mass.

The imaging appearance is similar to that of other stromal (mesenchymal) tumors. Heterogeneous tumor CT contrast enhancement is evident in some. An occasional schwannoma is partly cystic and shows peripheral contrast enhancement with CT and MRI.

Endoscopic biopsy is not always straightforward with these tumors, at times suggesting a GIST or leiomyoma, with only a resected specimen confirming a schwannoma.

Zollinger-Ellison Syndrome

Zollinger-Ellison syndrome develops as a result of a gastrin-secreting tumor, gastric acid hypersecretion, and resultant severe peptic ulcer disease (gastrinomas are discussed in more detail in Chapter 9). Primary gastric gastrinomas are uncommon; most are in the duodenopancreatic region. Clinically, these patients range from those with atypical peptic ulcer disease to those with malabsorption. Of note is that not all patients with an elevated gastrin level manifest Zollinger-Ellison syndrome.

H. pylori infection is not a risk factor for ulcers in these patients; in fact, prevalence of *H. pylori* infection in patients with Zollinger-Ellison syndrome is lower than in the general population and much lower than in patients with classic peptic ulcer disease.

Carcinoid

Contrary to earlier belief, gastric carcinoids are common and in fact may be the most common gastrointestinal location for these tumors. Gastric carcinoids can be subdivided into several categories:

1. In association with chronic atrophic gastritis, gastric enterochromaffin-like cell hyperplasia and pernicious anemia
2. In association with Zollinger-Ellison syndrome
3. In association with multiple endocrine neoplasia type 1
4. Sporadic carcinoids

Pathogenesis of all except the last type is influenced by promoting agents, such as hypergastrinemia and transforming agents, and carcinoids develop through a hyperplasia–dysplasia–neoplasia sequence. In general, these are associated with a good prognosis. Pathogenesis of the sporadic carcinoids is unknown; these patients have a poor prognosis.

A majority of gastric carcinoids are associated with chronic atrophic gastritis, and about half of these patients have multiple tumors. Gastric enterochromaffin-like cell hyperplasia is common in autoimmune gastritis, and presumably carcinoids found in some of these patients are related to hyperplasia. Evidence suggests that gastric enterochromaffin-like cell carcinoids constitute an independent tumor in multiple endocrine neoplasia type I (MEN-I) syndrome and develop with enteropancreatic and parathyroid MEN-I tumors via inactivation of the MEN-I gene.

The prevalence of gastric carcinoids is increased in a setting of hypergastrinemia. The drug omeprazole leads to an increase in serum gastrin levels and in laboratory animals induces gastric carcinoids. An achlorhydria–hypergastrinemia–carcinoid sequence appears to exist. Hypergastrinemia-associated carcinoids tend to have a benign course and some are managed by endoscopic excision. Sporadic carcinoids occur throughout the stomach and are not related to gastrin levels. They are more likely to be malignant than the other types.

Contrast-enhanced imaging studies are necessary to detect these hypervascular tumors. Carcinoids tend to enhance more than normal gastric wall on contrast-enhanced MR.

Glomus Tumor

Computed tomography of two gastric glomus tumors revealed peripheral nodular or homogeneous arterial phase contrast enhancement, followed by prolonged late phase enhancement (63).

Gastric Dilation

Gastric Emptying Studies

Gastric emptying is influenced by the presence of duodenal acid or fat. Acid in the duodenum induces tonic duodenal constrictions and increases gastric emptying, but bile and fat delay gastric emptying by decreasing duodenal contractility. Animal and vegetable fats have similar effects on gastric emptying (64). Accelerated gastric emptying is found in several conditions, namely non–insulin-dependent diabetes, increased body mass index, hypertension, hyperthyroidism, and after some medications, such as erythromycin. Gastric motility in diabetes mellitus, however, is a complex issue (see Gastroparesis, below). Gastric liquid emptying is accelerated after truncal vagotomy; emptying of solids is also usually increased, but results are inconstant.

Gastric emptying and gastric motility studies are feasible with MRI. Adding gadolinium contrast to a liquid meal results in a bright gastric lumen. Serial 3-D T1-weighted gradient-echo MRI every 5 minutes or so assesses gastric volumes and detects delayed gastric emptying (65). A T1/2 value can be calculated from a plot of gastric emptying. Whether such MR techniques have a role in clinical practice remains to be established.

Similar to MR, gastric emptying scintigraphy using various Tc-99m–labeled solids and liquids generate gastric radioisotope time-activity curves from which a gastric emptying rate and half-times are calculated. A two-point method (at 0 and 120 minutes) correlates well with a multiple point conventional method and saves substantial technologist and camera times (66). An emptying half-time implies exponential emptying, which is not necessarily true and thus introduces a variable; nevertheless, an emptying half-time is often used as a standard. To be reproducible, several corrections are incorporated, including radioisotope decay during test time and variation in tissue attenuation between patients. Men have a faster gastric emptying rate, shorter half-emptying time, and lower residual radioactivity than women. Patient positioning and meal composition and size need be standardized by each laboratory performing these studies and normal ranges established. Also, mechanical gastric outlet obstruction should be excluded prior to the test.

A solid test meal is more reliable and is employed more often than a liquid meal. The radioisotope should not disassociate from the test meal used, otherwise results will approach those of a liquid meal. Initially Tc-99m–sulfur colloid–labeled chicken liver was the test meal used, having been supplanted in most institutions by an egg meal. The half-times obtained with a solid liver meal differ from those of an egg meal; the latter is more of a semisolid consistency.

Other methods of measuring gastric emptying include oral ingestion of acetaminophen in a test meal followed by serial blood sampling for plasma acetaminophen. Breath sampling for $^{13}CO_2$ after a liquid test meal containing ^{13}C-acetate provides a gross estimate of gastric emptying time. Also, in experienced hands a barium upper gastrointestinal study is often adequate to evaluate gastric emptying.

In children, a Tc-99m–sulfur colloid milk scan is useful in evaluating both gastroesophageal reflux and gastric emptying. In-111-DTPA in water is a liquid marker. One

refinement is a dual-phase solid-liquid combination, although the added complexity is not necessary in many patients. Serial imaging allows calculation of activity as a percent of original; the gastric emptying half-time is then calculated.

The sulfamethizole absorption test evaluates gastric motility and gastric emptying. This test relies on a rapid absorption of sulfamethizole from proximal small bowel.

Gastric Outlet Obstruction

Infant Hypertrophic Pyloric Stenosis

Clinical

Etiology of infantile hypertrophic pyloric stenosis (IHPS) is not known. Hypergastrinemia appears to have a pathogenetic role. Genetic factors also are involved; IHPS is encountered more often if a parent or sibling has had the condition. It is more common in boys. A possible connection exists between IHPS and allergic gastroenteropathy; both entities narrow the pyloric region. In some infants IHPS is associated with eosinophilic gastroenteritis; histologically, these infants have pyloric circular muscle hypertrophy and hyperplasia. Jaundice in several infants with IHPS was believed to represent an early manifestation of Gilbert's syndrome (67).

A surprising number of other bowel obstructions have been reported in a setting of IHPS, including a duodenal web, coexisting hypertrophic antral polyp, pyloric mucosal hypertrophy, an adjacent cyst or duplication, and a solid tumor. An occasional infant develops IHPS during the postoperative period after repair of some other congenital condition.

Some infants with cyanotic congenital heart disease undergo prostaglandin infusion therapy and some then develop gastric outlet obstruction. Persistent but asymptomatic gastric distention develops in some infants within 48 hours of initial prostaglandin therapy and in a minority evolves into feeding intolerance with continued prostaglandin therapy; gastric distention resolves in most when prostaglandin therapy is stopped. Although superficially similar to IHPS, these infants have mostly distal antral mucosal involvement. Barium studies reveal antral narrowing; US detects increased gastric mucosal thickening and distal antral and pyloric elongation but no muscular wall thickening. The lobular mucosal thickening consists of alternating hyper- and hypoechoic structures and in these infants lumen narrowing appears to be secondary to mucosal rather than muscle thickening.

Imaging

Whether a surgeon is able to palpate a pyloric "olive" depends on pyloric muscle volume, which can be obtained from US. Whether such pyloric volume calculations are of clinical value is debatable.

If a typical pyloric "olive" is palpable, a strong argument can be made for no preoperative imaging studies. On the other hand, US in experienced hands achieves a high sensitivity and specificity in detecting pyloric stenosis. A major limitation of US is its inability to detect alternative diagnoses in an infant with nonbilious vomiting due to some other cause. Thus in an infant with projectile vomiting, if US excludes pyloric stenosis, a second imaging study, such as a barium examination, is often necessary to identify an esophageal, gastric, or duodenal abnormality to account for the infant's symptomatology. In clinical practice a reasonable compromise seems to be to perform US in those infants with strong suspicion for pyloric stenosis whereas others undergo a barium study.

A number of authors have proposed normal and abnormal ranges of pyloric length, muscle thickness, and muscle volume (Fig. 2.24). Ultrasonography measurement of pyloric muscle thickness and pyloric length is easier if the muscle is enlarged. In healthy infants, pyloric muscle thickness measures about 2 mm and pyloric length about 10 mm; in infants with surgically confirmed IHPS, muscle thickness is about double and pyloric length increased by about 40%. Unfortunately, in actual practice results are not so clear; infants with an initial suspicion of IHPS but a final diagnosis of no IHPS have intermediate measurements. Also, overlap exists between normal and IHPS, and a diagnosis based solely on US measurement of pyloric muscle thickness is not straightforward. In particular, a contracted pylorus imaged tangentially will appear thickened. Some investigators prefer to rely primarily on pyloric length, yet critical analysis reveals diagnostic

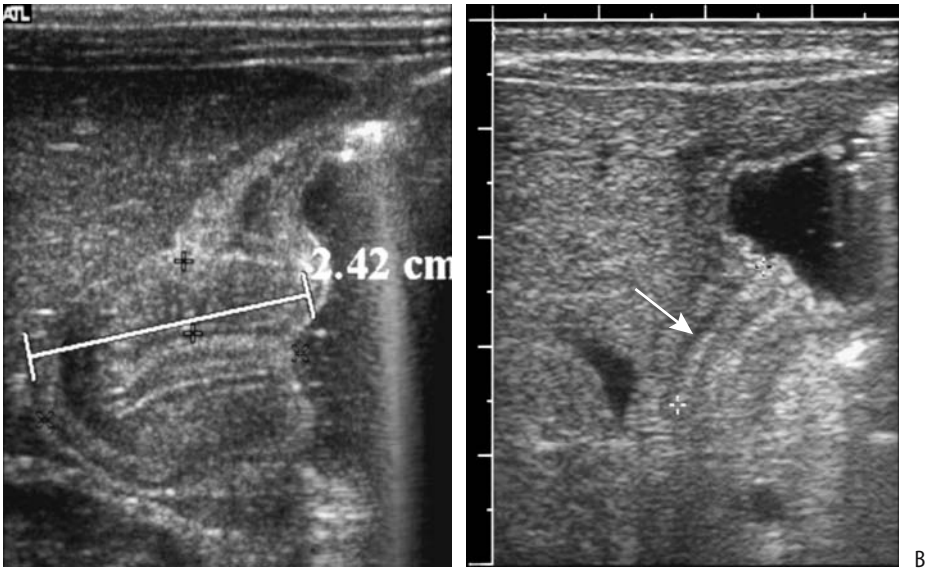

A B

Figure 2.24. Pyloric stenosis. A: Ultrasonography (US) reveals marked pyloric muscle hypertrophy and an elongated pylorus to 24 mm in a 1–year-old boy. B: Ultrasonography in a 2–week-old full-term girl identifies pyloric shouldering and a hypoechoic pyloric muscle layer (arrow). (Courtesy of Luann Teschmacher, M.D., University of Rochester.)

problems similar to those when relying on pyloric width.

The commonly used US term *pyloric muscle thickness* appears to be anatomically incorrect. Closer study of the pyloric wall reveals that hypertrophied mucosa makes up about one third of the pyloric cross-sectional diameter and tends to fill the pyloric lumen (68). To add confusion, the term *pylorospasm* is applied to an apparently thickened pyloric muscle without evidence of IHPS. A time-varying pyloric muscle thickness and an incomplete obstruction to flow should differentiate pylorospasm from IHPS, which is fixed in outline, yet here also a borderline zone exists.

Infants with suspected IHPS and borderline US values for pyloric volume have been treated with an antispasmodic drug (metoclopramide) with inconstant results; obstruction has cleared in some, while others have progressed to IHPS.

IHPS is a rare cause of transient portal venous gas.

Delayed gastric emptying is encountered in some infants with few if any symptoms. Such "pylorospasm" is controversial and of dubious significance.

Therapy

Laparoscopic pyloromyotomy is being performed for IHPS and may result in a shorter hospital stay.

Both US and a barium study remain abnormal for some time after a pyloromyotomy for IHPS. However, no significant delay in gastric emptying should be evident.

In infants with IHPS treated medically, US identifies an initial pyloric channel shortening followed by muscular thinning as symptoms improved (69).

Other Causes in Infants

A congenital antral membrane is a rare cause of gastric outlet obstruction. Partial obstruction is more common than complete and some patients present later in life (Fig. 2.25). A barium study differentiates an antral web from IHPS; with a web a more distally located pylorus can be identified. Difficulty of differentiation exists, however, with complete obstruction.

A rare ectopic pancreas in the distal antrum causes gastric outlet obstruction. Ultrasonogra-

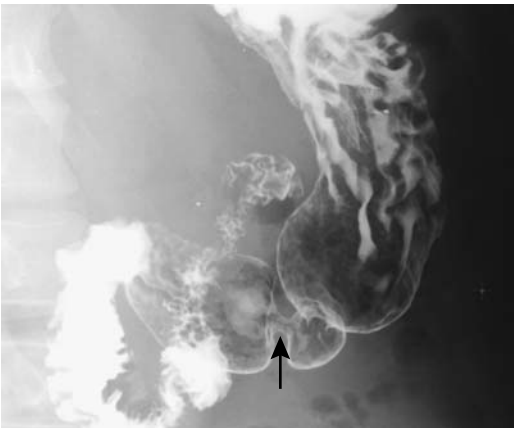

Figure 2.25. Antral web (arrow) in an adult. A peristaltic wave is thicker and changes with time.

phy in a 1-month-old infant with familial hyperlipidemia suspected of IHPS revealed an intense hyperechoic thickened pyloric muscle (70); surgery found a necrotic and inflamed pyloric muscle infiltrated by fat.

Gastric volvulus in infants tends to be part of a complex congenital visceral attachment anomaly, often involving the left hemidiaphragm.

Causes in Adults

In adults, gastric outlet obstruction was more common in the past. Prior to H2 blockers, peptic ulcer disease was the most common cause of gastric outlet obstruction; currently a malignancy is more common. A pedunculated antral polyp prolapsing intermittently through the pylorus into the duodenum is a cause of gastric outlet obstruction. Skill in differentiating between a prolapsing polyp and prolapsed gastric mucosa (which is a normal variant) should be acquired in a radiology residency.

An uncommon cause of gastric outlet obstruction is a cholecystogastric or a cholecystoduodenal fistula and resultant gallstone obstruction (Bouveret's syndrome). This condition is discussed in Chapter 3.

Gastric outlet obstruction secondary to an enlarged gallbladder is rare; based on the few reported patients, a gallbladdder neoplasm or other infiltrative disease should be suspected.

Antral diaphragms occur in both children and adults. Some are congenital, but an antral web in an adult is usually an acquired condition, presumably secondary to prior inflammation. Histologically, these webs consist of normal mucosa without significant inflammation. If sufficiently prominent, these webs and diaphragms result in obstruction.

Hypertrophic pyloric stenosis in adults is rare. In one elderly woman a barium study simply revealed markedly reduced gastric emptying (71). From a clinical and imaging viewpoint, adult hypertrophic pyloric stenosis should be considered only after more common etiologies of gastric outlet obstruction are excluded.

Balloon dilation of peptic ulcer–induced gastric outlet strictures is performed using endoscopic, fluoroscopic, or both modalities for guidance. Older children with delayed gastric emptying refractory to medical therapy have been treated with balloon pyloroplasty using fluoroscopic guidance (72); the full role of such therapy both in children and adults is yet to be established.

Volvulus

In the gastrointestinal tract *torsion* signifies a twist of the organ in question, whereas *volvulus* implies superimposed lumen obstruction. This is not a universally accepted definition; for instance, urologists use the term *torsion* for conditions most gastroenterologists would label as volvulus.

Gastric torsion occurs with hiatal hernias, especially larger ones, even to the point of volvulus. Similarly, volvulus occurs if the stomach herniates through some other point of weakness, such as foramen of Morgagni.

Gastric volvulus is encountered both in the very young and very old. Volvulus occurs either along the gastric longitudinal axis (organoaxial) or transverse axis (mesenteroaxial). The latter is more common; it is occasionally associated with recent trauma. An organoaxial volvulus obstructs either at the proximal point of twist, generally close to the esophagogastric junction, at the distal point, generally in the distal antrum, or at both. The site of greatest obstruction determines which organ is most dilated, and thus the resultant imaging appearance varies (Fig. 2.26).

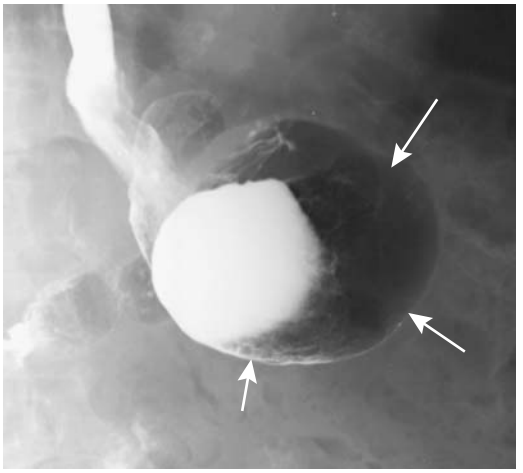

Figure 2.26. Organoaxial gastric volvulus. The stomach is distended (arrows), but some barium does pass into the duodenum and thus neither the proximal nor distal twists are obstructed completely.

In spite of the normally rich gastric blood supply, a sufficiently severe twist results in vascular compromise. If untreated, volvulus progresses to gastric necrosis, with conventional radiography identifying gas in the stomach wall (emphysematous gastritis).

Occasionally passage of a nasogastric tube relieves an acute volvulus. Acute gastric volvulus has been reduced endoscopically, although it tends to recur, and many of these patients require eventual surgical correction. In most patients acute gastric volvulus requires emergent surgical correction. Chronic gastric volvulus, in reality representing either gastric torsion or intermittent acute volvulus (or both), can often be temporized.

Intussusception

Both gastroduodenal and duodenogastric intussusceptions are rare in a nonoperated stomach. Some degree of antral mucosal prolapse into the duodenum, however, is quite common and is a normal variant. At times the lead point of gastroduodenal prolapse is an antral polyp, such as a lipoma, adenoma, or other. Ectopic antral pancreatic tissue also occasionally acts as a lead point for prolapse.

Jejunogastric intussusception is one of the complications of a hemigastrectomy and gastrojejunostomy (Billroth II operation).

Gastroparesis

Gastroparesis is evaluated either with scintigraphy or a barium study. Experienced gastrointestinal radiologists are quite adept at detecting delayed gastric emptying during a barium study. Ultrasonography can evaluate antral motility but is little used for this purpose.

Diabetes Mellitus

Recently diagnosed non–insulin-dependent diabetes mellitus patients have gastric emptying similar to controls. Many long-term diabetics, however, even without obvious gastroparesis, have disordered gastric emptying and delayed gastric emptying, but a minority develop accelerated gastric emptying. Etiology of gastroparesis in diabetic patients is not completely understood, but both an underlying irreversible autonomic neuropathy and a hyperglycemia-associated reversible motility impairment are probably involved. In general, poor correlation exists in diabetics between solid and liquid gastric emptying phases and test results should be interpreted with caution due to individual idiosyncratic variation. Blood glucose concentration at the time of study may account for some of the variations.

Diabetics with severe refractory gastroparesis have a high morbidity. Some of them benefit from jejunostomy tube placement. A rare complication of diabetic coma is gastric necrosis.

Median Arcuate Ligament Syndrome

The median arcuate ligament syndrome is believed to result from celiac axis compression by the fibrous median arcuate ligament, which is part of the diaphragmatic crura. A neural, vascular, or other factor may also be involved. Surgical decompression of the celiac axis leads to resolution of abdominal pain, improved gastric emptying, and restoration of a normal gastric electrical rhythm.

Clinically these patients have symptoms mimicking gastric outlet obstruction, but

imaging detects no obstruction; rather, gastroparesis is suggested.

Other

Patients with chronic liver disease and portal hypertension have delayed gastric emptying of both solid and liquid emptying phases. A number of neoplasms are associated with gastroparesis, presumably representing a paraneoplastic process.

Patients with moderate to severe neurologic trauma tend not to tolerate gastric tube feedings. Using radionuclide imaging to measure gastric solid and liquid emptying, men with either spinal cord or head injury had significantly prolonged gastric emptying compared to controls (73); gastric emptying was more prolonged in those with a high-level injury compared to a low-level lesion. Gastric emptying is impaired in quadriplegics.

In some nondiabetic patients with dyspepsia symptoms and no obvious cause, scintigraphy and barium studies suggest gastroparesis and poor antral motor activity; often a barium study reveals retention of food in the stomach.

Systemic Sclerosis

Most scintigraphy and barium studies show little if any abnormality in gastric peristalsis or emptying in patients with systemic sclerosis. In symptomatic patients with diffuse disease, however, scintigraphic gastric emptying studies using solid food often reveal delayed gastric emptying.

While esophageal and some other cancers are not uncommon in a setting of progressive systemic sclerosis, gastric cancer is exceedingly rare.

Bulimia/Anorexia Nervosa

Acute gastric dilation is a complication of anorexia nervosa during a bulimic attack. A rare sequela is gastric necrosis and perforation. A conventional radiograph should detect gastric dilation and suggest a need for close follow-up. More complex imaging is superfluous but is often obtained when evaluating abdominal symptoms in these patients, often girls or young women.

Figure 2.27. Gastric foreign body. This 3–year-old had swallowed a battery months ago; it was encased by dense fibrosis. (Courtesy of Bevin Bastian, M.D., Memorial Hospital, Rock Springs, Wyoming.)

Swallowed Foreign Bodies

Most swallowed foreign bodies pass through the gastrointestinal tract. Sharp objects and objects retained in the stomach for over a day or so are generally removed endoscopically. Larger objects, including some coins, remaining in the stomach for prolonged time tend to become attached to the gastric wall and are then difficult to remove endoscopically. Some actually appear to embed in the gastric wall (Fig. 2.27).

Metal objects can corrode. In vitro studies show that radiolucent corrosion develops within 24 hours in post-1982 United States zinc alloy pennies when retained in the stomach (74); no such changes were evident in copper-based pre-1982 pennies.

Gastric Hernia

A large hiatal hernia is almost always associated with organoaxial torsion, with the degree of torsion having a direct relationship to the size of the hernia (Fig. 2.28). Up to a 180-degree twist

Figure 2.28. Intrathoracic stomach. With herniation, the stomach tends to rotate and, as in this patient, the greater curvature has rotated 180 degrees and is superior to the lesser curvature. Such a twist predisposes to gastric volvulus.

is present if most of the stomach is in the chest. In spite of the torsion, gastric volvulus develops only in a minority of these patients; a more common problem is obstruction at the hiatus.

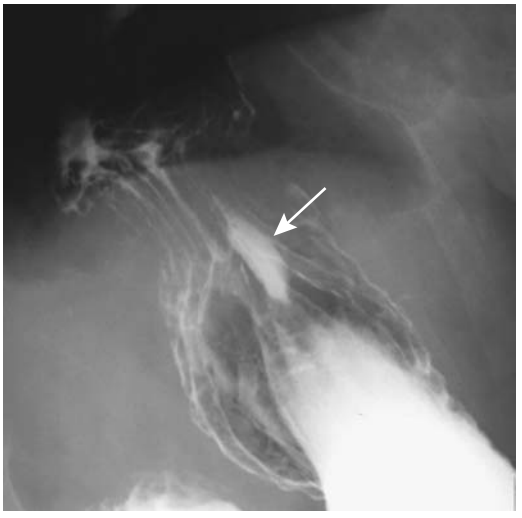

Figure 2.29. A sliding hiatal hernia and ulcer (arrow) at the hiatus.

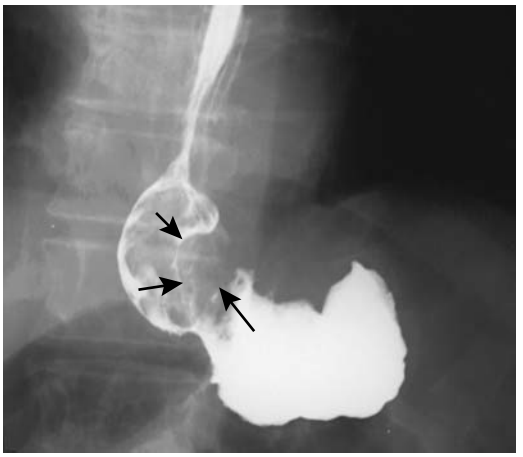

Figure 2.30. Adenocarcinoma (arrows) in a large hiatal hernia.

One of the less common causes of a diaphragmatic hernia is prior surgery. As one example, transdiaphragmatic gastric herniation developed after coronary artery bypass using a right gastroepiploic artery (75).

Occasionally Tc-99m-pertechnetate scintigraphy, performed for other indications, will demonstrate an unsuspected diaphragmatic hernia.

An ulcer is not uncommon in a hiatal hernia; these ulcers are notoriously difficult to detect with a barium study (Fig. 2.29). A perforating ulcer in a hernia involves any adjacent structure, including pericardium and left ventricle. Cancers also develop in hiatal hernias (Fig. 2.30).

Diverticula

Practically the only location where gastric diverticula occur is at the gastric cardia. Some authors label these fundic diverticula. Most so-called antral diverticula represent sequelae of prior peptic ulcer disease, and the use of this term here is inappropriate.

A carcinoma has developed in a fundal diverticulum.

These diverticula are easier to identify with barium than CT or MRI; they have been misidentified as a left adrenal tumor on CT and MRI (76).

Table 2.5. Causes of abnormal gastric communications

To peritoneal cavity:
Acute trauma
Peptic ulcer disease
Neoplasm
Ischemia
To bowel:
Surgical anastomosis
Peptic ulcer disease
Neoplasm
Primary gastric
Primary colonic
Crohn's disease
To biliary tree:
Gallstone disease
Peptic ulcer disease
Neoplasm
To urinary tract:
Staghorn calculus

Perforation/Fistula

A gastric fistula with communication to another organ is less common than in the small bowel or colon. Part of the reason is the relatively thick gastric wall and its relatively rich blood supply, making gastric ischemia uncommon. Nevertheless, numerous abnormal communications involving the stomach have been reported (Table 2.5).

Vascular Lesions (Bleeding)

Clinical

Prophylactic aspirin use is recommended for a number of medical conditions, yet at times even low doses result in gastrointestinal bleeding.

Hematemesis implies bleeding proximal to the ligament of Treitz. Melena, or black tarry stool, usually is from an upper gastrointestinal site but occasionally is secondary to small bowel or even right colonic bleeding (incidentally, black tarry stool is *melenic* stool; *melanotic* stool implies the presence of melanin pigment). Common causes of hematochezia and melena in adults include a duodenal or gastric ulcer. Common etiologies of upper gastrointestinal bleeding in pediatrics range from gastritis and esophagitis to peptic ulcers and varices in older children.

An occasional patient with diabetic ketoacidosis develops upper gastrointestinal hemorrhage; bleeding generally is not severe and is self-limited. The most common cause of such bleeding is erosive esophagitis, less often gastritis and duodenitis.

Although ascariasis is usually associated with small bowel and biliary disorders, upper gastrointestinal ascariasis is a rare cause of gastric bleeding.

Diffuse gastric angiomatosis manifests with bleeding, at times life-threatening. Angiography should be diagnostic. Some of these patients require a total gastrectomy.

Imaging

Several available scintigraphic techniques identify gastrointestinal bleeding. Provided active bleeding occurs at time of scanning, Tc-99m–sulfur colloid detects bleeding rates as low as 0.1 mL/min. Intermittent bleeding tends to be missed because of rapid clearance of the sulfur colloid from circulation.

Tc-99m–red blood cell scintigraphy provides a prolonged blood pool and is more useful with intermittent bleeding. Only several milliliters of extravasated blood is needed for detection. Serial images up to 24 hours are obtained. One cause of false-positive results is secretion of free Tc-99m-pertechnetate into the gastrointestinal tract.

Angiographic detection of bleeding has been largely replaced by contrast-enhanced CT, except when performed as part of therapeutic embolization.

Tumors

Chronic bleeding and resultant iron-deficiency anemia are one of the clinical presentations of gastric carcinomas. Mesenchymal tumors and lymphoma also tend to ulcerate and bleed.

Some hemangiomas also bleed. Multiple gastric hemangiomas are occasionally found in Osler-Weber-Rendu syndrome.

Dieulafoy Lesions

Over a century ago a Parisian surgeon, G. Dieulafoy, described massive gastric bleeding

Table 2.6. Terminology used to describe Dieulafoy-like lesions

Dieulafoy-related terms	Other terminology
Dieulafoy lesion	Gastric submucosal aneurysm
Gastric Dieulafoy's erosion	Solitary large submucosal artery
Dieulafoy-like erosion	Ulceratio simplex
Morbus Dieulafoy—Dieulafoy's disease	Exulceratio simplex
Dieulafoy's syndrome	Solitary exulceratio simplex
Ulcer of Dieulafoy	Submucosal arterial malformation
Dieulafoy vascular malformation	Caliber-persistent artery anomaly
Solitary gastric erosion of Dieulafoy	Cirsoid aneurysm

from an artery close to the mucosa and the term *gastric Dieulafoy's erosion* entered the French medical literature. Over the years this condition has acquired a myriad of names (Table 2.6), with current usage mostly settled on *Dieulafoy lesion*. Although some authors refer to these lesions as gastric *vascular malformation*, this terminology is sufficiently similar to *arteriovenous malformation* to create confusion; Dieulafoy lesions are not related to arteriovenous malformations. Little evidence suggests that these lesions represent a separate disease or syndrome.

Initially these bleeding submucosal arteries were believed to be limited to the stomach, but over the last several decades similar lesions have also been described in the small bowel and colon. It usually consists of a wide-caliber submucosal artery without histologic evidence of a true aneurysm. Etiology and pathogenesis are unknown. A vascular dysplasia, or thrombosis and necrosis of an abnormal submucosal artery are considerations, but the lack of an inflammatory reaction around many of these lesions is puzzling. Bleeding is usually through a small overlying mucosal defect. The surrounding mucosa is normal.

These lesions are found throughout the stomach, although the posterior wall lesser curvature near the cardia is a common site. They are more prevalent in elderly men. Although previously believed to be rare, these lesions come to medical attention mostly when investigating massive, often life-threatening upper gastrointestinal bleeding.

The diagnosis is made from a resected specimen. Lately, however, endoscopists have become enamored with this entity, often making the diagnosis on visual inspection only and then initiating endoscopic therapy. Typical diagnostic criteria used by endoscopists are presence of arterial bleeding or a visible nonbleeding superficial vessel without surrounding ulceration or erosion.

Endoscopic US aids in detecting subtle Dieulafoy lesions; a vessel several millimeters in diameter is detected penetrating through the muscularis propria and extending into submucosa. Partly filling the stomach with water helps identify these vessels.

Arteriography, if performed while the lesion is bleeding, should identify a feeding vessel and site of bleeding. The appearance is different from that seen with angiodysplasia or arteriovenous malformations; neither a tuft of abnormal vessels nor an early draining vein is seen with a Dieulafoy lesion.

Initially these lesions were managed by wedge resection or oversewing, although currently many are managed by endoscopic hemostasis. Focal acute ischemia is a potential complication after sclerotherapy agent injection. Endoscopic lesion localization followed by laparoscopic gastric wedge resection is an option in some patients.

Ectasia

Gastric vascular ectasia is found in two conditions: so-called watermelon stomach and portal hypertensive gastropathy. Both are rare causes of chronic gastric bleeding and iron-deficiency anemia. Whether the underlying pathogenesis differs in a watermelon stomach from portal hypertensive gastropathy is conjecture.

Watermelon Stomach

Gastric vascular ectasia, also called watermelon stomach, is a gastropathy of uncertain pathogenesis, often associated with autoimmune gastritis and connective tissue disorders. An

association appears to exist between watermelon stomach and scleroderma-like diseases (77). Many of these patients also have cirrhosis, portal hypertension, and hypergastrinemia. Antral vascular ectasia is associated with cirrhosis and bone marrow transplantation. Of interest is that histology reveals thicker than normal gastric mucosal capillary walls in these patients (78); gastric mucosal capillary dilation is not a reliable criterion. These capillaries often contain fibrin thrombi. Presence of neuroendocrine cells showing immunoreactivity for serotonin suggest a role for neuroendocrine mediators in this condition.

Clinically these often elderly patients present with anemia and unrelenting chronic blood loss. An occasional one develops a massive bleed.

The diagnosis cannot be made with barium studies. A characteristic endoscopic appearance consists of diffuse erythema and ectatic, tortuous capillaries. Endoscopic US reveals preservation of muscularis propria; these changes regress after laser ablation.

Tc-99m–labeled red cell imaging is useful to localize any bleeding site.

Endoscopic electrocoagulation or laser photocoagulation are often therapeutic; at times antrectomy is necessary. A-interferon therapy may have a role.

Portal Hypertensive Gastropathy

Portal hypertensive gastropathy and gastric vascular ectasia appear similar but probably are separate conditions, although little clear-cut pathologic differentiation exists between these two conditions. Usually ectasia in a watermelon stomach is limited to the antrum, whereas in portal hypertensive gastropathy the proximal stomach is more often involved.

Portal hypertensive gastropathy describes a spectrum of gross findings developing in gastric mucosa in patients with portal hypertension. Cirrhosis is not a prerequisite because noncirrhotic patients with portal hypertension also develop this condition. Gastric intramural vessels dilate, presumably secondary to both portal venous congestion and increased gastric blood flow. Arterial intimal hyperplasia is evident in some patients. Endogenous vasodilator overproduction and decreased vascular sensitivity to vasoconstrictors appear to play a role. The mucosa is atrophied and contains a mosaic pattern and hemorrhagic spots. Varices may or may not be present, although portal hypertensive gastropathy is more severe in those with prominent esophageal varices. Endoscopists classify the condition as mild when either a mosaic pattern or superficial reddening is seen and severe when diffuse cherry red spots are identified. These changes are flat and not detected with imaging, although some patients have thickened and nodular gastric fundal folds (79), a nonspecific finding.

Chronic blood loss is more common than acute massive bleeding. Gastric acid output is decreased and the mucosal barrier becomes impaired.

Endoscopic esophageal variceal sclerotherapy accentuates portal hypertensive gastropathy and gastric varices, and in some patients becomes evident only after sclerotherapy. Some patients bleed from portal hypertensive gastropathy and gastric varices after sclerotherapy.

In patients with portal hypertension and hypersplenism, portal hypertensive gastropathy tends to improve after splenic arterial embolization. Portal hypertensive gastropathy is reversed in most by portosystemic shunting, such as a central splenorenal decompressive shunt and presumably in this subgroup of patients venous congestion is the cause of gastropathy.

Varices

Detection

Isolated splenic vein thrombosis, regardless of etiology, leads to gastric varices without concomitant esophageal varices. Endoscopic US appears superior to endoscopy in detecting gastric varices. Endoscopic Doppler US also quantitates these varices; color Doppler US detects slow, steady flow in gastric varices located in a thickened gastric wall.

A double-contrast upper gastrointestinal tract examination readily detects gastric varices (Fig. 2.31). Most are located close to the gastric cardia and most have a typical verrucoid appearance. A minority of these varices, however, have a conglomerate mass-like appearance (80); in profile, these varices appear as smooth intramural masses having distinct borders, whereas en face they appear as thick, tortuous folds.

Contrast-enhanced CT also detects gastric varices. In particular, 3D CT portography

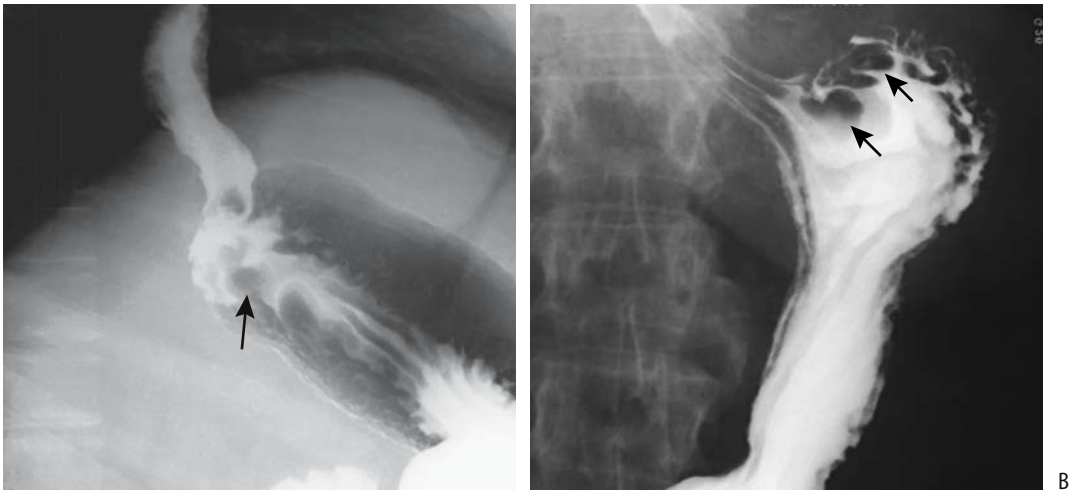

A B

Figure 2.31. A,B: Two examples of fundal varices (arrows).

readily identifies gastric fundic varices. Portography is the gold standard (Fig. 2.32).

Therapy

In distinction to esophageal varices, gastric varices tend to have an extensive network of feeding vessels. Thus control of gastric variceal bleeding by endoscopic sclerotherapy is considerably more difficult. A combination of decreasing the blood flow with band ligation followed by injection of a sclerosing agent is successful in some. At times a combination of sclerotherapy with percutaneous transhepatic variceal obliteration in patients with large gastric varices results in gastric variceal eradication. Transjugular intrahepatic portosystemic shunting (TIPS) does control bleeding from gastric varices but in some patients sclerotherapy achieves better long-term results. In one study the cumulative survival rates at 1 and 5 years were 81% and 40%, respectively, in the TIPS group and 96% and 76% in the sclerotherapy group ($p < 0.01$) (81); subdividing these patients, survival was higher for those in Child-Pugh class A undergoing sclerotherapy rather than TIPS ($p < 0.01$), but no significant differences were found for those in Child-Pugh classes B and C.

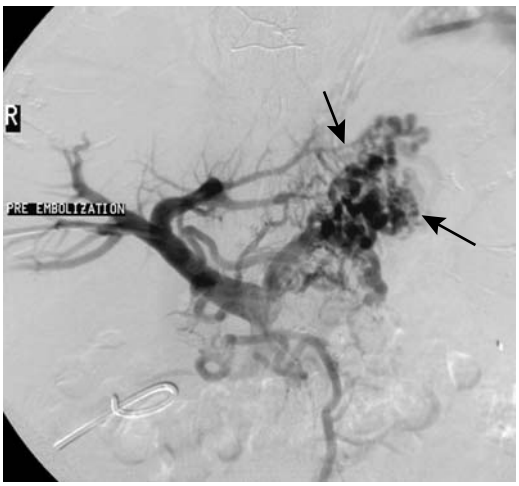

Figure 2.32. Fundal varices (arrows). The study was performed via percutaneous portal vein puncture. (Courtesy of David Waldman, M.D., University of Rochester.)

Emergency TIPS in patients with variceal bleeding is equally effective in controlling gastric fundal variceal bleeding and esophageal variceal bleeding (82). In some patients splenic artery embolization reduces blood flow sufficiently to stop bleeding. An occasional patient requires a splenectomy to control bleeding.

Retrograde transvenous obliteration of gastric varices is feasible in presence of gastrorenal or gastrocaval collaterals. Using a balloon occlusion catheter, sclerosing agents injected into gastric varices led to variceal obliterated (83); gastric varices recur in a minority

of these patients and can be treated with repeat transvenous variceal obliteration. Esophageal varices also developed in some patients treated with endoscopic injection sclerotherapy.

In patients with hepatic schistosomiasis and bleeding gastric varices, emergency endoscopic sclerotherapy achieved hemostasis in 85% (84); patients who did not respond to sclerotherapy underwent emergency surgery.

Immunosuppression/AIDS

Unusual gastric infections develop in AIDS patients, and, in fact, occasionally an initial manifestation of AIDS is a cytomegaloviral or other rare gastric infection. Gastroduodenal involvement with *Mycobacterium avium* is a cause for hemorrhage (85).

Gastric toxoplasmosis is rare even in AIDS, presenting with gastric wall thickening; thickened rugae, and at times even an ulcer.

A barium study in AIDS patients with cryptosporidium gastropathy reveals antral narrowing resembling a carcinoma or Crohn's gastritis; these patients tend to develop varying degrees of gastric obstruction, with the narrowing presumably related to underlying cryptosporidiosis; obstruction clears following therapy.

Emphysematous gastritis, gastric wall necrosis, and gastric perforation are rare conditions reported in HIV-infected patients. Gastric necrosis in one HIV-positive patient was believed to be secondary to a vasculitis (86).

Human herpesvirus type 8 (HHV-8 virus), belonging to the lymphotropic herpes family, is associated with lymphoid neoplasms in immunodeficient patients and with Kaposi's sarcomas (87). This unusual virus contains genes encoding oncoproteins and is believed to also have a role in multiple myeloma, Waldenström's macroglobulinemia and possibly in sarcoidosis.

Non-Hodgkin's lymphoma is considerably more prevalent in AIDS patients than in the general population. Lymphoma tends to be generalized, often involving the gastrointestinal tract. Most are B-cell lymphomas.

AIDS-related Kaposi's sarcomas occur primarily in homosexual patients. Endoscopic US identifies a hypoechoic and nonhomogeneous lesion involving either the submucosa or both the mucosa and submucosa (88).

Postoperative Stomach

Cancer

After a hemigastrectomy, such as for peptic ulcer disease, mucosal dysplasia develops and these patients are at increased risk of developing a carcinoma, often called gastric stump or remnant cancer. These cancers start developing more than 10 years after hemigastrectomy. Biopsy detection of severe dysplasia is a worrisome sign and in this subgroup about half eventually develop an adenocarcinoma, at times at multiple sites. These gastric remnant cancers behave similarly to other gastric cancers.

After Fundoplication

Lumen obstruction after a fundoplication is due to either surrounding edema or too tight of a wrap. The former clears as edema subsides.

Rarely, the stomach herniates proximally through a fundoplication wrap. A gastric perforation can develop within the thoracic cavity, presumably on an ischemic basis.

Afferent Loop Syndrome

Afferent loop obstruction (syndrome) is a complication of a hemigastrectomy and gastrojejunostomy (Billroth II operation) (Fig. 2.33). Most of these obstructions manifest early after surgery, but an occasional stricture develops years later. Obstructive jaundice is a common presentation in these patients, although some have sudden onset of abdominal pain. Afferent loop obstruction is also a cause of recurrent acute pancreatitis.

Adhesions, kinking, internal herniation, or intussusception are causes of early obstruction, whereas stenosis and neoplasm lead to obstruction years later. Some patients do not have actual mechanical obstruction but preferential gastric emptying into the afferent loop leads to chronic distension, a condition more common in a left-to-right rather than a right-to-left gastrojejunostomy. In these latter patients an efferent loop obstruction is also in the differential diagnosis.

Computed tomography reveals a dilated, fluid-filled afferent loop. High-quality conventional radiographs also identify a fluid-filled

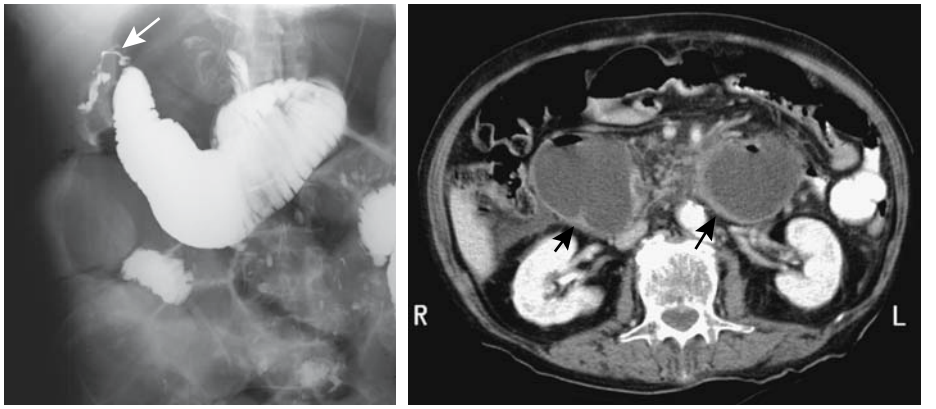

Figure 2.33. A: Blown afferent loop stump (arrow) after a Billroth II resection. The afferent loop is obstructed. B: Another patient with an obstructed afferent loop after a Billroth II resection. Contrast-enhanced CT reveals a dilated, fluid-filled small bowel loop having an enhancing wall (arrows). (Courtesy of Patrick Fultz, M.D., University of Rochester.)

afferent loop, suggesting the diagnosis. An occasional afferent loop syndrome is detected on a postoperative cholangiogram. A barium study should be diagnostic.

A patient developed a large duodenal enterolith in a dilated afferent loop 24 years after a Billroth II anastomosis (89).

Intussusception

An infrequent complication after a Billroth II anastomosis is jejunogastric intussusception (Fig. 2.34). Most often the intussusceptum consists of the efferent loop; less often the afferent loop is involved. Some of these intussusceptions are associated with gastric outlet obstruction, whereas with others the patients are relatively asymptomatic due to partial obstruction. Occasionally this complication develops late after surgery.

Postpancreaticoenteric Anastomosis

A pancreaticoduodenectomy as therapy for carcinoma of the ampulla of Vater, first described by Whipple, currently consists of a hepaticojejunostomy, a gastro- or duodenojejunostomy and a pancreaticoenteric anastomosis (usually a pancreaticojejunostomy). One complication of this operation is breakdown of the pancreaticojejunostomy anastomosis, a region not directly accessible to imaging. Occasionally, a resultant fistula is first detected by contrast injected into

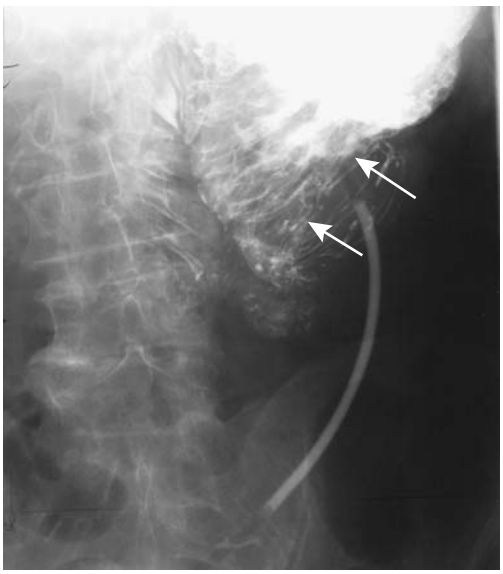

Figure 2.34. Jejunogastric intussusception in a patient with a Billroth II anastomosis. The intragastric valvulae conniventes have a coil spring appearance (arrows). A jejunal feeding tube is in place.

adjacently placed drains. Surgeons attempt to decrease breakdown of the pancreaticoenteric anastomosis by modifying the above technique and performing a pancreaticogastrostomy, where the residual portion of the pancreas drains into the stomach. Radiographically, the anastomosis presents as a broad-based intraluminal mass that should not be confused with a neoplasm.

Morbid Obesity Surgery

Over the years a number of surgical procedures have been designed to control morbid obesity. Because of complications, often metabolic in nature, a jejunoileal bypass is no longer performed. A number of patients with a jejunoileal bypass have had reversal of their bypass, at times with weight gain to previous levels.

A common indication for a barium study is failure to lose weight postoperatively. Not uncommonly these postoperative patients complain of nausea, vomiting, and an inability to eat. A barium study reveals typical postoperative findings with no complications, yet the patients are gradually losing weight and cannot understand why they are unable to eat almost constantly.

Helical CT not only identifies normal postoperative anatomy but is also very useful in detecting complications in these patients (90). Some loculated fluid collections are unrelated to a leak. One should also keep in mind that the residual fundus tends to mimic a loculated fluid collection.

Gastric Bypass

Gastric bypass results in a small proximal gastric pouch that drains via a gastrojejunostomy. The jejunostomy portion consists of a jejunal loop, a more distant jejunojejunostomy, or a Roux-en-Y (Fig. 2.35). The latter two are designed to prevent bile reflux into the gastric pouch. In most patients a gastric bypass leads to significantly more weight loss than with gastroplasty, and currently many surgeons favor gastric bypass. These patients have a high prevalence of gallstones, and some surgeons perform a cholecystectomy at the time of initial surgery.

The major early complication is a leak resulting in an abscess or even peritonitis. A contrast study should be diagnostic. A temptation to simply instill contrast via a nasogastric tube and obtain one or two radiographs without fluoroscopic guidance should be avoided; invariably such an approach leads to a suboptimal and a missed diagnosis in these obese, often critically-ill patients.

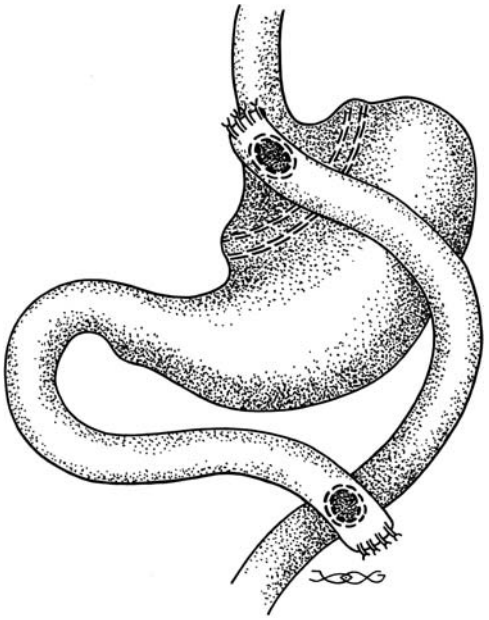

Figure 2.35. Appearance of a side-to-side gastric bypass combined with a Roux-en-Y. A double row of staples divides the stomach into a smaller proximal pouch and a larger excluded segment.

Radiographic study of afferent limb obstruction (the bypassed segment) shows a dilated distal gastric segment and a dilated duodenojejunal loop. The proximal jejunal limb tends to be narrowed as it passes through the transverse mesocolon (91), but actual obstruction at this site is not common.

Late complications encountered with a gastric bypass include anastomotic stenosis and marginal ulcer.

Gastroplasty

Gastroplasty consists of gastric stapling to produce a small pouch at the gastric cardia, with a small opening left into the distal gastric segment. Initially transverse gastric stapling (partitioning) was in vogue, but subsequently

vertical stapling (Mason's vertical banded gastroplasty) became more popular. A silicone ring or polypropylene mesh surrounds the gastric opening.

Laparoscopic gastroplasty leads to about 4% of patients developing early complications (perforation, early slippage, and respiratory problems) and 6% late complications (late slippage, incisional hernia, and port problems) (92). Other complications include gastroesophageal reflux, mesh erosion into the stomach lumen, and staple-line disruption with resultant weight gain.

Reflux esophagitis tends to be more severe with a gastroplasty, although some surgeons believe that gastric restriction operations do not increase the risk of reflux if a functioning antireflux barrier is also performed.

An upper gastrointestinal examination with barium detects both early and late postoperative complications.

Gastric Banding

Gastric banding is an alternative procedure to gastric bypass and gastroplasty (Fig. 2.36). Initially more popular in Europe, it is gaining acceptance in the United States. Adjustable laparoscopic gastric banding around the fundus with an inflatable band connected by a thin tube to an access port permits port puncture and stomal adjustment between the pouch and the stomach for optimal weight loss. Postoperative fluoroscopy confirms the band position and is used for stomal adjustment.

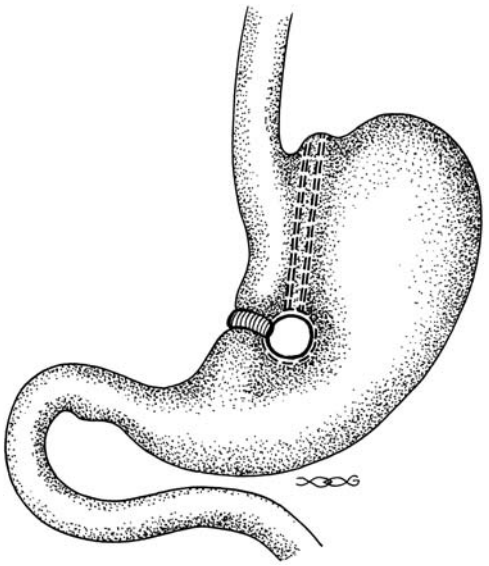

Figure 2.36. Vertical banded gastroplasty. A mesh is wrapped around the stoma located close to the lesser curvature.

Unsatisfactory weight loss occurred in 20% of 98 consecutive postbanding patients (93); late complications, developing in about one third of patients, consist of pouch dilation, herniation, intragastric band penetration (94), disconnection or leaking port (95), and port infection. An unusual complication is a decrease in stoma caliber due to gastritis, found in 3% of patients in one study (96). Marked gastric pouch dilation is a less common complication.

Most complications are readily detected with a contrast study. Computed tomography detects port infection.

Biliopancreatic Diversion

Currently biliopancreatic diversion is gaining in popularity and preliminary results are promising. It consists of a distal gastrectomy and formation of a long Roux-en-Y loop. The biliopancreatic loop from the duodenum inserts at an enteroenterostomy about 200 cm distal to the gastroenterostomy and about 50 cm proximal to the ileocecal valve. Because the biliopancreatic loop is not in direct continuity with the stomach, it does not contain gas. Obstruction of this loop thus leads to CT and US simply showing a markedly dilated, fluid-filled loop of bowel. Obstruction of the gastroenterostomy loop, on the other hand, has the typical radiologic findings of obstruction.

Retained Gastric Antrum

One of the indications for a Billroth II gastrojejunostomy is intractable peptic ulcer disease. If antral mucosa is left behind or if ectopic gastrin-producing cells are present in the retained duodenum, the resultant gastrin output tends to reactivate the patient's peptic ulcer symptoms. The blind afferent loop tip cannot be studied because it is not accessible either to a barium study or endoscopy.

A Tc-99m-pertechnetate scan (Meckel's scan) is worthwhile in this setting. Tracer uptake is

Figure 2.37. A stomal ulcer (arrow) has developed after a previous gastroduodenostomy.

evident both in the residual gastric pouch and in any retained antral remnant. The latter is identified as a focus of radioactivity in the region of the duodenal stump. The reason for such antral uptake, which normally does not contain hydrochloric acid secreting parietal cells, is that pertechnetate uptake is primarily by mucin-secreting cells, which are located throughout the stomach.

After a simple gastrojejunostomy, ulcers tend to occur in the jejunum, opposite the anastomosis (Fig. 2.37).

Gastrostomy

A basic question concerning percutaneous gastrostomies is whether the initial decision to insert a gastrostomy is appropriate. Some of these patients have a poor subsequent clinical course. In a retrospective review, 33% of the surrogates interviewed were uncertain whether a decision to proceed to gastrostomy feedings was correct (97).

Whether a gastrojejunostomy feeding tube with its reduced risk of gastroesophageal reflux is preferred over a gastrostomy should be individualized. Most gastrostomies are permanent, although indications exist for a temporary one: during recovery of swallowing, preparation for surgery with a more proximal obstruction, and for drainage of some fistulas. Gastrostomies are performed surgically, endoscopically assisted, or by using a percutaneous approach with imaging guidance. Among surgeons, a laparoscopic-assisted gastrostomy is becoming popular. A higher tube placement success rate is achieved when using an imaging technique rather than endoscopy (98); at times a hybrid percutaneous-oral approach is easiest. Procedure related mortality rates are highest for surgically placed gastrostomies and lowest with an imaging approach.

Instead of fluoroscopy, at times US is used to guide gastric puncture. Computed tomography–guided gastrostomy or gastroenterostomy is also feasible and often is technically successful when an endoscopic approach is not possible or had failed. Some believe that gastropexy is not necessary, but gastropexy does prevent tube displacement resulting in leakage.

Percutaneous retrograde insertion of gastrostomy or gastrojejunostomy tubes can be performed safely in children. Similar to adults, complications include an extragastric tube location and small bowel or colon transgression. Marked hepatosplenomegaly in children occasionally denies adequate access.

Percutaneous gastrostomy tubes are readily inserted under fluoroscopic guidance using a modified Seldinger technique and without general sedation. Initially this technique was used mostly for patients with an obstructed esophagus where percutaneous endoscopic gastrostomy was not feasible, yet the ease of fluoroscopic gastrostomy tube insertion has led to its wider acceptance. Few contraindications exist for this technique; it has a high success rate and is associated with few serious complications (99).

One option is a pull-type gastrostomy tube, consisting of retrograde esophageal catheterization through the stomach and a gastrostomy tube then pulled through from the mouth into the stomach. This technique, performed either by endoscopists or interventionalists, has a high success rate and few complications.

Ascites is often considered a relative contraindication to a percutaneous gastrostomy, although gastropexy overcomes some of the problems encountered in this subset of patients. Initial paracentesis and prevention of fluid reaccumulation, together with gastropexy, aid in preventing pericatheter leakage. A gastrostomy

or gastrojejunostomy with gastropexy in 45 consecutive patients with ascites was associated with a 7% rate of major complications and one procedure-related death (100); of note is that half of the complications occurred in a setting of peritoneal spread by ovarian carcinoma.

Out of 643 patients referred for fluoroscopically assisted percutaneous gastrostomy or gastrojejunostomy, a catheter could not be placed in 4% of patients due to overlying viscera or prior gastric surgery (101); catheter revision was necessary in 14%, mostly due to tube dislodgment.

Complications associated with percutaneous gastrostomy insertion include bleeding, obstruction, gastric perforation, and peritonitis. Minor leaks and a postinsertion pneumoperitoneum are not uncommon. Catheter dislodgment occurred in 68% of 25 balloon-retained catheters (102), 11% of 75 pigtail-retained catheters (103), and in none of 55 mushroom-retained gastrostomy catheters, and the authors concluded that mushroom catheters are more durable and preferred whenever possible.

Gastrostomy tube insertion through the transverse colon results in a cologastrocutaneous fistula or a colocutaneous fistula. Necrotizing fasciitis is a rare complication. Inserted through the gastrocolic ligament, a gastrostomy tube can end up in the lesser sac, superficially mimicking a correctly inserted tube. Occasional gastric pneumatosis develops after tube gastrostomy. Gastric wall dissection occurred during percutaneous gastrostomy, believed to be due to a tangential puncture of the stomach wall (104).

Several perforations have been associated with a Wills-Oglesby-type gastrostomy tube. Perforations in five patients were related to the distal catheter limb (105); these perforations occurred several months after tube placement, did not lead to peritonitis, and were managed medically.

A gastrostomy catheter can migrate distally, with the catheter tip lodging in the ileum. Occasionally a gastrostomy tube is cut and the inner tube button allowed to pass through the gastrointestinal tract. This procedure has been questioned, as the button has led to bowel obstruction.

In a setting of a malignancy, tumor seeding can occur after insertion of a percutaneous gastrostomy. This complication is more often encountered after endoscopic rather than imaging percutaneous tube insertion (106), probably due to direct tumor implantation during the endoscopic procedure. CT identifies a stomal implant as a lobulated soft tissue tumor in the abdominal wall, less so at the entry or exit sites.

Examination Complications

Rather than use the term *complications* to describe misadventures during endoscopy, the term *negative outcomes* has been proposed (107); this latter system defines, classifies, and grades negative outcomes using a scoring system based on several measures:

Immediate negative outcome (O): effect of complication on completion of endoscopy, change in level of care, change in length of hospitalization, necessity for new invasive procedures

Disability (D): a residual or chronic negative outcome caused by a complication

Death (D): a value varying with circumstances

A quantitative measure is obtained by using an overall ODD score.

Positive blood cultures were detected in 25% of patients undergoing gastroscopy (108); *Staphylococcus* species and *Streptococcus* species were most common.

References

1. Braccini G, Marraccini P, Boraschi P, Marrucci A, Bertellotti L, Testa R. [Usefulness of pirenzepine in the study of the upper digestive tract and the large intestine with double contrast media: comparison with scopolamine methylbromide.] [Italian] Radiol Med 1996;92:733–737.
2. Iinuma G, Ushio K, Ishikawa T, Nawano S, Sekiguchi R, Satake M. Diagnosis of gastric cancers: comparison of conventional radiography and digital radiography with a 4 million-pixel charge-coupled device. Radiology 2000;214:497–502.
3. Spies V, Butz B, Altjohann C, Feuerbach S, Link J. [CT-guided biopsies, drainage and percutaneous gastrostomies: comparison of punctures with and without CT fluoroscopy). [German] Rofo Fortschr Geb Rontgenstr Neuen Bildgeb Verfahr 2000;172:374–380.
4. Wiersema MJ, Vilmann P, Giovannini M, Chang KJ, Wiersema LM. Endosonography-guided fine-needle aspiration biopsy: diagnostic accuracy and com-

plication assessment. Gastroenterology 1997;112: 1087–1095.
5. Ng CC, Hung FC, Hsieh CS, et al. Epidermolysis bullosa letalis with pyloric atresia in an infant. J Formos Med Assoc 1996;95:61–65.
6. Guadagni S, Gola P, Marsili L, et al. Arterial vasculature of the stomach and oncologic gastrectomies. [Review] Surg Radiol Anat 1995;17:269–276.
7. Hsu PI, Lai KH, Tseng HH, et al. Impact of Helicobacter pylori eradication on the development of MALT, gland atrophy and intestinal metaplasia of the antrum. Chin Med J 2000;63:279–287.
8. Dixon MF, Genta RM, Yardley JH, Correa P. Classification and grading of gastritis. The updated Sidney system. Am J Surg Pathol 1996;20:1161–1181.
9. Bender GN, Peller T, Tsuchida A, Kelley JL. Double contrast upper gastrointestinal barium examination with biopsy versus endoscopy with biopsy in dyspeptic patients. Invest Radiol 1995;30:329–333.
10. Loffeld RJ. Diagnostic value of endoscopic signs of gastritis: with special emphasis to nodular antritis. Neth J Med 1999;54:96–100.
11. Chapman PR, Boals JR. Pneumopericardium caused by giant gastric ulcer. AJR 1998;171:1669–1670.
12. D'Inca R, Sturniolo G, Cassaro M, et al. Prevalence of upper gastrointestinal lesions and Helicobacter pylori infection in Crohn's disease. Dig Dis Sci 1998;43: 988–992.
13. Sanguino JC, Rodrigues B, Baptista A, Quina M. Focal lesion of African histoplasmosis presenting as a malignant gastric ulcer. Hepatogastroenterology 1996;43: 771–775.
14. Radhi J, Kamouna M, Nyssen J. Phlegmonous gastritis following coronary bypass surgery. Can J Gastroenterol 1999;13:837–839.
15. Millward SF, Fortier M. Transient gastric emphysema caused by colonic infarction. AJR 2001;176:1331–1332.
16. Greaney TV, Nolan N, Malone DE. Multiple gastric polyps in familial amyloid polyneuropathy. Abdom Imaging 1999;24:220–222.
17. Joko T, Tanaka H, Hirakata H, et al. Phlegmonous gastritis in a haemodialysis patient with secondary amyloidosis. Nephrol Dial Transplant 1999;14:196–198.
18. Papa A, Cammarota G, Tursi A, et al. Histologic types and surveillance of gastric polyps: a seven year clinicopathological study. Hepatogastroenterology 1998;45: 579–582.
19. Cherukuri R, Levine MS, Furth EE, Rubesin SE, Laufer I. Giant hyperplastic polyps in the stomach: radiographic findings in seven patients. AJR 2000;175: 1445–1448.
20. Matsushita M, Hajiro K, Okazaki K, Takakuwa H. Gastric inflammatory fibroid polyps: endoscopic ultrasonographic analysis in comparison with the histology. Gastrointest Endosc 1997;46:53–57.
21. Cho JS, Shin KS, Kwon ST, et al. Heterotopic pancreas in the stomach: CT findings. Radiology 2000;217: 139–144.
22. Park SH, Han JK, Choi BI, et al. Heterotopic pancreas of the stomach: CT findings correlated with pathologic findings in six patients. Abdom Imaging 2000;25: 119–123.
23. Palmer GM, Shortsleeve MJ. Gastric polyps due to extramedullary hematopoiesis. AJR 1998;171:531.
24. Kim SH, Han JK, Yoon CJ, et al. Gastric adenoma with atypical appearance: findings on double-contrast barium study with histopathologic correlation. Abdom Imaging 2000;25:124–128.
25. Ferrozzi F, Tognini G, Zuccoli G, Gabrielli M, Zangrandi A, Campani R. [Gastric stromal tumors. Findings with computerized tomography.] [Italian] Radiol Med 2000; 99:56–61.
26. Thompson WM, Kende AI, Levy AD. Imaging characteristics of gastric lipomas in 16 adult and pediatric patients. AJR 2003;181:981–985.
27. Galant J, Marti-Bonmati L, Saez F, Soler R, Alcala-Santaella R, Navarro M. The value of fat-suppressed T2 or STIR sequences in distinguishing lipoma from well-differentiated liposarcoma. Eur Radiol 2003;13: 337–343.
28. Theuer CP, Kurosaki T, Taylor TH, Anton-Culver H. Unique features of gastric carcinoma in the young: a population-based analysis. Cancer 1998;83:25–33.
29. Dorant E, van den Brandt PA, Goldbohm RA, Sturmans F. Consumption of onions and a reduced risk of stomach carcinoma. Gastroenterology 1996;110:12–20.
30. Adachi Y, Mori M, Maehara Y, Matsumata T, Okudaira Y, Sugimachi K. Surgical results of perforated gastric carcinoma: an analysis of 155 Japanese patients. Am J Gastroenterol 1997;92:516–518.
31. Arikawa J, Tokunaga M, Satoh E, Tanaka S, Land CE. Morphological characteristics of Epstein-Barr virus-related early gastric carcinoma: a case-control study. Pathol Int 1997;47:360–367.
32. Kaneko S, Yoshimura T. Time trend analysis of gastric cancer incidence in Japan by histological types, 1975–1989. Br J Cancer 2001;84:400–405.
33. Park M-S, Ha HK, Choi BS, et al. Scirrhous Gastric Carcinoma: Endoscopy versus Upper Gastrointestinal Radiography. Radiology 2004;231:421–426.
34. Shindoh N, Nakagawa T,Ozaki Y, Kyogoku S, Sumi Y, Katayama H. Overlooked gastric carcinoma: pitfalls in upper gastrointestinal radiology. Radiology 2000;217: 409–414.
35. Takao M, Fukuda T, Iwanaga S, Hayashi K, Kusano H, Okudaira S. Gastric cancer: evaluation of triphasic spiral CT and radiologic-pathologic correlation. J Comput Assist Tomogr 1998;22:288–294.
36. Kim HS, Han HY, Choi JA, et al. Preoperative evaluation of gastric cancer: value of spiral CT during gastric arteriography (CTGA). Abdom Imaging 2001;26:123–130.
37. Lee DH, Ko YT. The role of 3D spiral CT in early gastric carcinoma. J Comput Assist Tomogr 1998;22:709–713.
38. Lee JH, Jeong YK, Kim DH, et al. Two-phase helical CT for detection of early gastric carcinoma: importance of the mucosal phase for analysis of the abnormal mucosal layer. J Comput Assist Tomogr 2000;24:777–782.
39. Monig SP, Zirbes TK, Schroder W, et al. Staging of gastric cancer: correlation of lymph node size and metastatic infiltration. AJR 1999;173:365–367.
40. Dux M, Richter GM, Hansmann J, Kuntz C, Kauffmann GW. Helical hydro-CT for diagnosis and staging of gastric carcinoma. J Comput Assist Tomogr 1999;23: 913–922.
41. Rossi M, Broglia L, Graziano P, et al. Local invasion of gastric cancer: CT findings and pathologic correlation

using 5–mm incremental scanning, hypotonia, and water filling. AJR 1999;172:383–388.
42. Lim HK, Kim S, Lim JH, et al. Assessment of pancreatic invasion in patients with advanced gastric carcinoma: usefulness of the sliding sign on sonograms. AJR 1999;172:615–618.
43. Kim AY, Han JK, Kim TK, Park SJ, Choi BI. MR imaging of advanced gastric cancer: comparison of various MR pulse sequences using water and gadopentetate dimeglumine as oral contrast agents. Abdom Imaging 2000;25:7–13.
44. Sohn KM, Lee JM, Lee SY, Ahn BY, Park SM, Kim KM. Comparing MR imaging and CT in the staging of gastric carcinoma. AJR 2000;174(6):1551–1557.
45. Kang BC, Kim JH, Kim KW, et al. Value of the dynamic and delayed MR sequence with Gd-DTPA in the T-staging of stomach cancer: correlation with the histopathology. Abdom Imaging 2000;25:14–24.
46. Marrelli D, Roviello F, De Stefano A, et al. Surgical treatment of gastrointestinal carcinomas in octogenarians: risk factors for complications and long-term outcome. Eur J Surg Oncol 2000;26:371–376.
47. Park KB, Do YS, Kang WK, et al. Malignant obstruction of gastric outlet and duodenum: palliation with flexible covered metallic stents. Radiology 2001;219: 679–683.
48. Jung GS, Song HY, Kang SG, et al. Malignant gastroduodenal obstructions: treatment by means of a covered expandable metallic stent-initial experience. Radiology 2000;216:758–763.
49. Lee SS, Ha HK, Kim AY, et al. Primary extrapulmonary small cell carcinoma involving the stomach or duodenum or both: findings on CT and barium studies. AJR 2003;180:1325–1329.
50. Shikuwa S, Senju M, Tanaka H, et al. Progressive systemic sclerosis associated with primary small cell carcinoma of the stomach. [Review] J Gastroenterol 1997;32:538–542.
51. Hansen PB, Vogt KC, Skov RL, Pedersen-Bjergaard U, Jacobsen M, Ralfkiaer E. Primary gastrointestinal non-Hodgkin's lymphoma in adults: a population-based clinical and histopathologic study. J Intern Med 1998; 244:71–78.
52. Matsumoto S, Kohda K, Koike K, et al. [Diagnosis and prognosis of reactive lymphoreticular hyperplasia (RLH) or mucosa-associated lymphoid tissue (MALT) lymphoma.] [Japanese] Nippon Shokakibyo Gakkai Zasshi 1998;95:872–879.
53. Andoh A, Takaya H, Bamba M, et al. Primary gastric Burkitt's lymphoma presenting with c-myc gene rearrangement. J Clin Gastroenterol 1998;33:710–715.
54. Kinoshita K, Hirota S, Isozaki K, et al. Absence of c-kit gene mutations in gastrointestinal stromal tumours from neurofibromatosis type 1 patients. J Pathol 2004; 202:80–85.
55. Heinrich MC, Corless CL, Duensing A, et al. PDGFRA activating mutations in gastrointestinal stromal tumors. Science 2003;299:708–710.
56. Levy AD, Remotti HE, Thompson WM, Sobin LH, Miettinen M. Gastrointestinal stromal tumors: radiologic features with pathologic correlation. Radiographics 2003;23:283–304.
57. Ghanem N, Altehoefer C, Furtwangler A, et al. Computed tomography in gastrointestinal stromal tumors. Eur Radiol 2003;13:1669–1678.
58. Chak A, Canto MI, Rosch T, et al. Endosonographic differentiation of benign and malignant stromal cell tumors. Gastrointest Endosc 1997;45:468–473.
59. Rha SE, Sohn KM, Lee SY, Jung HS, Park SM, Kim KM. Pedunculated exogastric leiomyoblastoma presenting as a wandering abdominal mass. Abdom Imaging 2000;25:545–547.
60. Sofka CM, Semelka RC, Marcos HB, Calvo BF, Woosley JT. Metastatic gastric leiomyoblastoma: a case report. Magn Reson Imaging 1998;16:343–346.
61. Seki K, Hasegawa T, Konegawa R, Hizawa K, Sano T. Primary liposarcoma of the stomach: a case report and a review of the literature. [Review] Jpn J Clin Oncol 1998;28:284–288.
62. Usuda H, Naito M. Multicentric angiosarcoma of the gastrointestinal tract. [Review] Pathol Int 1997;47:553–556.
63. Kim JK, Won JH, Cho YK, Kim MW, Joo HJ, Suh JH. Glomus tumor of the stomach: CT findings. Abdom Imaging 2001;26:303–305.
64. Tsai SC, Hsieh JF, Ho YJ, Kao CH. Effects of butter and soybean oils on solid-phase gastric emptying in patients with functional dyspepsia. Abdom Imaging 2000;25:35–37.
65. Lauenstein TC, Vogt FM, Herborn CU, DeGreiff A, Debatin JF, Holtmann G. Time-resolved three-dimensional MR imaging of gastric emptying modified by IV administration of erythromycin. AJR 2003;180:1305–1310.
66. Halkar RK, Paszkowski AL, Jones ME, et al. Two-point, timesaving method for measurement of gastric emptying with diagnostic accuracy comparable to that of the conventional method. Radiology 1999;213:599–602
67. Trioche P, Chalas J, Francoual J, et al. Jaundice with hypertrophic pyloric stenosis as an early manifestation of Gilbert syndrome. Arch Dis Child 1999;81:301–303.
68. Hernanz-Schulman M, Lowe LH, Johnson J, et al. In vivo visualization of pyloric mucosal hypertrophy in infants with hypertrophic pyloric stenosis: is there an etiologic role? AJR 2001;177:843–848.
69. Yamamoto A, Kino M, Sasaki T, Kobayashi Y. Ultrasonographic follow-up of the healing process of medically treated hypertrophic pyloric stenosis. Pediatr Radiol 1998;28:177–178.
70. Veyrac C, Couture A, Bongrand AF, Baud C, Ferran JL. Atypical pyloric stenosis in an infant with familial hyperlipidemia. Pediatr Radiol 1996;26:402–404.
71. Graadt van Roggen JF, van Krieken JH. Adult hypertrophic pyloric stenosis: case report and review. [Review] J Clin Pathol 1998;51:479–480.
72. Skarsgard PL, Blair GK, Culham G. Balloon pyloroplasty in children with delayed gastric emptying. Clin Radiol 1998;41:151–155.
73. Kao CH, ChangLai SP, Chieng PU, Yen TC. Gastric emptying in male neurologic trauma. J Nucl Med 1998; 39:1798–1801.
74. O'Hara SM, Donnelly LF, Chuang E, Briner WH, Bisset GS 3rd. Gastric retention of zinc-based pennies: radiographic appearance and hazards. Radiology 1999;213: 113–117.

75. McCaig J, Varghese JC, Rees MR. Case report: transdiaphragmatic gastric herniation: a rare complication of CABG using the right gastroepiploic artery. Clin Radiol 1996;51:143–145.
76. Privat C, Courthaliac C, Ravel A, Perez N, Boiteux JP, Boyer L. [CT and MRI features of a pseudo adrenal lesion: subcardial diverticulum.] [French] Prog Urol 1999;9:509–512.
77. Fabian G, Tovari E, Baranyay F, Czirjak L. Watermelon-stomach as a cause of chronic iron deficiency anemia in a patient with systemic sclerosis. J Eur Acad Dermatol Venereol 1999;12:161–164.
78. Misra V, Misra SP, Dwivedi M. Thickened gastric mucosal capillary wall: a histological marker for portal hypertension. Pathology 1998;30:10–13.
79. Chang D, Levine MS, Ginsberg GG, Rubesin SE, Laufer I. Portal hypertensive gastropathy: radiographic findings in eight patients. AJR 2000;175:1609–1612.
80. Carucci LR, Levine MS, Rubesin SE, Laufer I. Tumorous gastric varices: radiographic findings in 10 patients. Radiology 1999;212:861–865.
81. Ninoi T, Nakamura K, Kaminou T, et al. TIPS versus transcatheter sclerotherapy for gastric varices. AJR 2004;183:369–376
82. Chau TN, Patch D, Chan YW, Nagral A, Dick R, Burroughs AK. "Salvage" transjugular intrahepatic portosystemic shunts: gastric fundal compared with esophageal variceal bleeding. Gastroenterology 1998; 114:981–987.
83. Hirota S, Matsumoto S, Tomita M, Sako M, Kono M. Retrograde transvenous obliteration of gastric varices. Radiology 1999;211:349–356.
84. Contractor QQ, Contractor TQ, Kher YR. Sclerotherapy in bleeding gastric varices of hepatic schistosomiasis. J Clin Gastroenterol 1996;23:97–100.
85. Collazos J, Blanco MS, Mayo J, Martinez E. Gastrointestinal hemorrhage due to gastroduodenal involvement by Mycobacterium avium complex in a patient with acquired immune deficiency syndrome. J Clin Gastroenterol 1998;26:84–85.
86. Alcantara Gijon F, Bernal Bellido C, Ceballos Garcia R, Gomez Munoz JC. [Gastric necrosis due to vasculitis in an HIV+ patient.] [Review] [Spanish] Rev Esp Enferm Dig 1999;91:152–153.
87. Mikala G, Xie J, Berencsi G, et al. Human herpesvirus 8 in hematologic diseases. [Review] Pathol Oncol Res 1999;5:73–79.
88. Zoller WG, Bogner JR, Powitz F, Liess H, Goebel FD. Endoscopic ultrasound in the diagnosis and staging of gastrointestinal Kaposi's sarcoma. Endoscopy 1995;27: 191–196.
89. Carbognin G, Biasiutti C, El-Khaldi M, Ceratti S, Procacci C. Afferent loop syndrome presenting as enterolith after Billroth II subtotal gastrectomy: a case report. Abdom Imaging 2000;25:129–131.
90. Yu J, Turner MA, Cho S-R, et al. Normal anatomy and complications after gastric bypass surgery: Helical CT findings. Radiology 2004;231:753–760.
91. Smith TR, White AP. Narrowing of the proximal jejunal limbs at their passage through the transverse mesocolon: a potential pitfall of laparoscopic Roux-en-Y gastric bypass. AJR 2004;183:141–143.
92. Chevallier JM, Zinzindohoue F, Cherrak A, et al. [Laparoscopic gastroplasty for severe obesity. 300 cases, evaluation of the first 150.] [French] Presse Med 2000;29:1921–1925.
93. Wiesner W, Schob O, Hauser RS, Hauser M. Adjustable laparoscopic gastric banding in patients with morbid obesity: radiographic management, results, and postoperative complications. Radiology 2000;216:389–394.
94. Rapp-Bernhardt U, Wolf S, Dohring W, Bernhardt TM. [Intragastric penetration as a local complication after performance of gastric banding.] [German] Rofo Fortschr Geb Rontgenstr Neuen Bildgeb Verfahr 2000;172:305–306.
95. Hainaux B, Coppens E, Sattari A, Vertruyen M, Hubloux G, Cadiere GB. Laparoscopic adjustable silicone gastric banding: radiological appearances of a new surgical treatment for morbid obesity. Abdom Imaging 1999;24:533–537.
96. Mortele KJ, Pattijn P, Mollet P, et al. The Swedish laparoscopic adjustable gastric banding for morbid obesity: radiologic findings in 218 patients. AJR 2001;177:77–84.
97. Van Rosendaal GM, Verhoef MJ, Mace SR, Kinsella TD. Decision-making and outcomes for percutaneous endoscopic gastrostomy: a pilot study. J Clin Gastroenterol 1997;24:71–73.
98. Laasch H-U, Wilbraham L, Bullen K, et al. Gastrostomy insertion: Comparing the options—PEG, RIG or PIG? Clin Radiol 2003;58:398–405.
99. Dinkel HP, Triller J. [Percutaneous gastrostomy with balloon PEG balloon replacement tubes by the radiologist. An interventional technique for simple placement of feeding catheters without surgical or endoscopic intervention.] [German] Radiologe 2001; 41:473–477.
100. Ryan JM, Hahn PF, Mueller PR. Performing radiologic gastrostomy or gastrojejunostomy in patients with malignant ascites. AJR 1998;171:1003–1006.
101. Dewald CL, Hiette PO, Sewall LE, Fredenberg PG, Palestrant AM. Percutaneous gastrostomy and gastrojejunostomy with gastropexy: experience in 701 procedures. Radiology 1999;211:651–656.
102. Funaki B, Peirce R, Lorenz J, et al. Comparison of balloon- and mushroom-retained large-bore gastrostomy catheters. AJR 2001;177:359–362.
103. Funaki B, Zaleski GX, Lorenz J, et al. Radiologic gastrostomy placement: pigtail- versus mushroom-retained catheters. AJR 2000;175:375–379.
104. Reimer W, Farres MT, Lammer J. Gastric wall dissection as a complication of percutaneous gastrostomy. Cardiovasc Intervent Radiol 1996;19:288–290.
105. Kanterman RY, Hicks ME, Simpson KR, Malden ES, Picus D, Darcy MD. Nonsurgical management of gastric or duodenal perforation from a Wills-Oglesby-type gastrostomy tube. J Vasc Interv Radiol 1996;7: 737–741.
106. Pickhardt PJ, Rohrmann CA Jr, Cossentino MJ. Stomal metastases complicating percutaneous endoscopic gastrostomy: CT findings and the argument for radiologic tube placement. AJR 2002;179:735–739.
107. Fleischer DE, Van de Mierop F, Eisen GM, et al. A new system for defining endoscopic complications emphasizing the measure of importance. Gastrointest Endosc 1997;45:128–133.
108. Barragan Casas JM, Hernandez Hernandez JM, Garcinuno Jimenez MA, et al. Bacteremia caused by digestive system endoscopy. Rev Esp Enferm Dig 1999; 91:105–116.

3

Duodenum

Congenital Abnormalities

Duplication

As in the rest of the gastrointestinal tract, a duodenal duplication may or may not communicate with the true lumen. Most duplications are located along the first and second parts of the duodenum. An occasional one is discovered incidentally, but most descending duodenal duplications coming to medical attention are associated with pancreaticobiliary abnormalities. An occasional one obstructs the common bile duct; at times a bizarre biliary communication is identified. A duplication can appear as a cystic tumor in the periampullary region. Some are associated with duodenal compression and obstruction or recurrent acute pancreatitis, a presentation more common in children. Rare complications of noncommunicating duodenal duplications include necrosis and perforation resulting in an acute abdomen, becoming infected or even causing an intussusception.

Ultrasonography (US) reveals a hyperechoic inner layer and a hypoechoic outer muscular layer; these layers are better defined with endoscopic US. At times peristaltic activity is identified.

Cholangiopancreatography is helpful in defining any associated ductal anomalies. Often endoscopic retrograde cholangiopancreatography (ERCP) is not successful due to periampullary distortion and magnetic resonance cholangiopancreatography (MRCP) is necessary. A barium study aids in detecting duodenal communication and in narrowing the differential diagnosis considerably. With duodenal communication, the differential includes a duodenal diverticulum and a necrotic tumor. Without duodenal communication, other intramural or extrinsic tumors are in the differential. The presence of stones suggests communication with pancreaticobiliary ducts. With some of these duplications, computed tomography (CT), US, and magnetic resonance (MR) do not establish a site of origin, although imaging should differentiate a duodenal duplication from a choledochal cyst and pancreatic pseudocyst. Also, the clinical presentation is different with the latter two entities. In either case, the underlying pancreaticobiliary ductal anatomy is often atypical and should be defined prior to resection or anastomosis.

Atresia/Stenosis/Web

Duodenal atresia, believed to be due to failure of duodenal recanalization early in gestation, is the most common cause of a high bowel obstruction in a neonate. The most common site for atresia is just distal to the papilla of Vater, and these neonates present with bilious vomiting, whereas the less common atresia proximal to the papilla mimics gastric outlet obstruction. Atresias range from partial to complete; the atretic segment is either string-like or appears as a web.

Table 3.1. Duodenal obstruction in the neonate

Midgut malrotation with volvulus
Duodenal atresia
Duodenal stenosis
Duodenal web
Ladd's bands
Duodenal duplication
Annular pancreas
Anomalous portal vein anterior to duodenum
Tumor or distention in an adjacent structure

Not all neonatal duodenal obstruction is due to duodenal atresia or stenosis (Table 3.1). Midgut malrotation with volvulus in the newborn presents with complete duodenal obstruction and has a similar presentation.

Patients with duodenal atresia are prone to having other anomalies, including an annular pancreas and other pancreaticobiliary anomalies. A rare patient has an anomalous portal vein anterior to the duodenum. The prevalence of duodenal atresia is increased in Down syndrome, in a setting of congenital heart disease, and in those with a tracheoesophageal fistula. Esophageal atresia and duodenal atresia may coexist; in such a setting, unless a tracheoesophageal fistula is present, the stomach fills with fluid and distends. The large bowel is normal in these patients. A microcolon implies an additional, more distal obstruction.

A rare congenital duodenal obstruction in an infant leads to gastric emphysema (1).

An occasional adult develops a partial duodenal obstruction secondary to a web. Duodenal webs are associated with aspirin ingestion (2) and long-term use of nonsteroidal anti-inflammatory drugs (3).

Radiographs reveal no gas distal to the atresia. An exception is with a rare bifid common bile duct anomaly where the bile duct communicates both with proximal and distal duodenal segments.

After repair of duodenal atresia, the duodenal bulb continues to be larger in volume than usual.

Trauma

Blunt trauma is a common cause for a duodenal hematoma (Fig. 3.1). Imaging reveals duodenal wall thickening, at times to the point of obstruction. In its retroperitoneal position close to other major structures, duodenal trauma is commonly associated with injury to the adjacent pancreas and liver. An endoscopic biopsy is a cause of an intramural duodenal hematoma (4). An intramural duodenal hematoma can develop secondary to pancreatitis. An abused child had both a duodenal hematoma and contained duodenal and proximal jejunal perforations (5); duodenal obstruction ensued and exploratory laparotomy found a calcified, fibrotic mesentery and both duodenal and jejunal strictures.

Full-thickness duodenal rupture does occur in patients sustaining blunt duodenal injury; the second duodenal segment is most often involved. Most of these ruptures are associated with other intraabdominal injuries, but one should keep in mind that traumatic retroperitoneal duodenal perforation initially reveals few clinical sign and symptoms. Blunt abdominal trauma can also result in diverticular perforation.

Imaging detection of an early duodenal perforation is difficult. For instance, among traumatic duodenal perforations studied with CT, extravasation of contrast is identified only in a small minority.

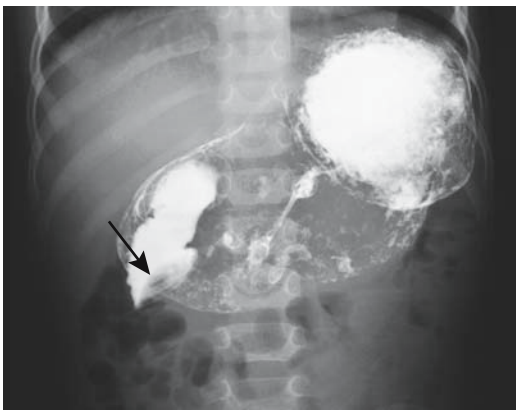

Figure 3.1. Duodenal hematoma (arrow) resulting in a high-grade obstruction. The obstruction resolved spontaneously.

A *veiled right kidney* is a US finding of a retroperitoneal duodenal perforation (6).

A bullet causes not only duodenal but also adjacent organ damage. Fistulas are one sequela, at times to unusual sites such as a pyeloduodenal fistula, if damage is not recognized initially.

Wall Thickening

Infection/Inflammation

Some infections manifest primarily in the proximal small bowel, whereas others are detected distally. For convenience, most small bowel infections are discussed in Chapter 4.

Duodenitis

The term *duodenitis* implies duodenal inflammation and is a histologic diagnosis, although endoscopists often apply this term to a gross reddened mucosa believed to represent inflammation.

Myriad conditions thicken duodenal valvulae conniventes: infections, eosinophilic gastroenteritis, amyloidosis, mastocytosis, lymphangiectasia, infiltrating neoplasms, Crohn's disease, and other entities. Ischemic duodenitis in the absence of prior surgery should suggest a small vessel vasculitis. Using thickened folds as a criterion for duodenitis, an upper gastrointestinal examination in children achieved a 46% sensitivity and 98% specificity for detecting duodenitis, compared to 54% sensitivity and 92% specificity for endoscopy (7); the low sensitivities were due mostly to normal findings for both radiology and endoscopy in children with mild duodenitis.

Peptic Ulcer Disease

The discovery of *Helicobacter pylori* has modified our understanding of peptic ulcer disease pathogenesis. Thus antral infection with *H. pylori* promotes antral gastritis, increased gastrin release, and increased acid production. Duodenal bulb *H. pylori* colonization promotes bulbar gastric metaplasia, leading to further *H. pylori* infection, more inflammation, and further inability to neutralize gastric acid load. In some patients this cycle persists until an ulcer develops. Probably both bulbar gastric metaplasia and bulbar *H. pylori* colonization are necessary to develop a duodenal ulcer. Both the prevalence and the extent of gastric metaplasia and the amount of *H. pylori* in the duodenal bulb in patients with a duodenal ulcer are much higher than in those with a gastric ulcer or chronic gastritis. Eradication of *H. pylori* decreases the amount of acid entering the duodenum, and duodenal inflammation subsides.

Peptic ulcer disease is more prevalent in cirrhotic patients and those in chronic renal failure than in the general population. In cirrhotics, antral *H. pylori* colonization does not appear to play a major role in duodenal peptic ulcer disease.

Postbulbar duodenal peptic duodenitis is uncommon. At times a barium study reveals postbulbar ulcerations, thickened folds, or even a stenosis, and an endoscopic biopsy identifies inflammation; because peptic duodenitis here is uncommon, focal pancreatitis in an annular pancreas or celiac disease should be suspected and an endomysial antibody test obtained. In some patients an endoscopic biopsy revealed villous atrophy.

A barium study of peptic ulcer disease is usually straightforward. Ulcers in unusual locations and recurrent ulcers are more problematic. Peptic ulcer disease in younger children, although uncommon, does result in an unusual presentation and radiologic appearance. Ultrasonography reveals focal duodenal wall thickening, at times even an echogenic line adjacent to the ulcer, but US is rarely employed to detect duodenal ulcers.

Occasionally encountered is a giant duodenal ulcer; cocaine and methamphetamine use is associated with some of these giant ulcers, although many are idiopathic.

Some perforated duodenal ulcers result in a pneumoperitoneum and peritonitis. Other ulcers perforate into an adjacent structure, including pancreas, liver, bile ducts, and adjacent colon. Duodenocolic and duodenocholedochal fistulas secondary to peptic ulcer disease are rare. At times such a perforation clinically mimics myocardial ischemia; conventional radiographs should suggest a correct diagnosis.

Contrast-enhanced CT of a perforating ulcer reveals focal bowel wall thickening, enhancement, and inflammatory changes in surround-

ing tissues. A wall defect at the site of perforation is rarely detected. On the other hand, extraluminal gas bubbles, at times in Morison's pouch, should be sought. A water-soluble upper gastrointestinal contrast study, although out of vogue in a number of institutions, remains a viable alternative.

Crohn's Disease

Duodenal Crohn's disease is notoriously difficult to diagnose. A biopsy is often of little help, most often revealing nonspecific inflammation and only occasionally containing granulomas. Imaging findings include aphtha, a peptic ulcer-like appearance, fistula, a stenotic segment varying in length, or complete obstruction (Fig. 3.2). Presence of thickened folds may be the only clue to Crohn's disease. Fistulas are less common than with ileal involvement. Most duodenocolic fistulas are secondary to colonic Crohn's disease rather than duodenal Crohn's. Occasionally duodenal deformity is secondary to Crohn's disease in an adjacent loop of bowel. A double-contrast barium study should differentiate between primary and secondary duodenal involvement.

A number of patients with duodenal Crohn's have undergone a Billroth I operation in the mistaken belief that their underlying deformity was secondary to peptic ulcer disease. Invariably inflammation and strictures progress.

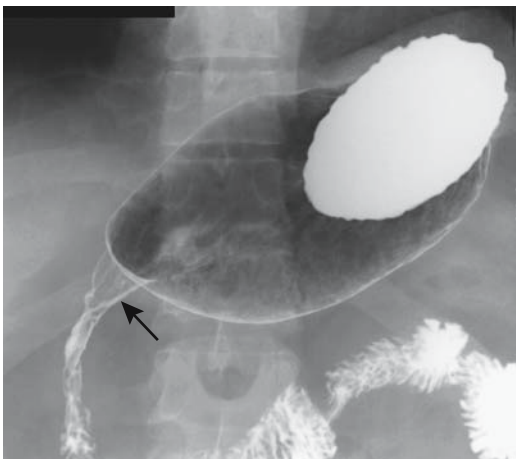

Figure 3.2. Duodenal Crohn's disease in a patient with known ileal disease. A duodenal stricture and effaced valvulae conniventes are evident (arrow). (Courtesy of Daniel Wopperer, M.D., Rochester, New York.)

Diverticulitis

Diverticula are more common in the duodenum than in the rest of the small bowel, yet duodenal diverticulitis is sufficiently rare to be a curiosity. Clinically, duodenal diverticulitis mimics peptic ulcer disease, cholecystitis, or pancreatitis. A number of patients have unsuspected duodenal diverticulitis first detected at exploratory laparotomy for an acute abdomen, an understandable event given the rarity of this condition.

A barium study should detect thickened duodenal folds secondary to duodenal inflammation. Computed tomography identifies any associated inflammation and abscess. Inflammation medial to the duodenal sweep suggests focal pancreatitis (and indeed adjacent portions of the pancreas tend to be inflamed). Perforations lead either to a focal walled-off cavity or peritoneal spill. Extraluminal gas can range from focal bubbles to pneumoperitoneum.

Most duodenal diverticula are peri-Vaterian in location and, when infected, surrounding inflammation thus is centered around the duodenopancreatic interface. Imaging differential diagnosis includes focal pancreatitis (at times suggesting an inflamed annular pancreas) or postbulbar ulcer disease.

Associated with Dialysis and Pancreatitis

Thickened duodenal folds are common in patients on dialysis. Although patients in renal failure have an increased prevalence of peptic ulcer disease, not all dialysis patients with thickened folds have clinical peptic ulcer disease.

Duodenal involvement is common in acute pancreatitis, even to the point of obstruction. Thickened folds are seen in a setting of chronic pancreatitis.

Tuberculosis

Even in endemic regions duodenal tuberculosis is rare, and this diagnosis is thus often not suspected.

Duodenal stenosis was discovered in a 69-year-old man who also had common bile duct

obstruction due to stones (8); Crohn's disease was initially suspected, and therapy with corticosteroids was instituted until tuberculosis was identified.

Sarcoidosis

The liver followed by the stomach are the most common abdominal organs involved. Small bowel sarcoidosis, including duodenal, is uncommon. Gastrointestinal tract sarcoidosis is one cause for a protein-losing enteropathy. Sarcoidosis involving the papilla can obstruct the common bile duct.

Radiographically, sarcoidosis mimics Crohn's disease.

Amyloidosis

Duodenal amyloidosis is uncommon. Clinically, diffuse amyloid infiltration leads to lumen narrowing and, with extensive involvement, obstruction. Occasionally infiltration is polypoid in appearance.

Cystic Dystrophy

An unusual condition, duodenal cystic dystrophy is associated with chronic pancreatitis and presents as focal duodenal wall thickening. At times associated with heterotopic pancreatic tissue, and with about half the affected patients having chronic pancreatitis, the relationship of duodenal cystic dystrophy to duplication cysts is speculation. Most cystic dystrophy foci contain cysts, but an occasional one is solid. Some of these cystic structures suggest dilated ducts lined with exocrine pancreatic epithelium. A rare one evolves into an abscess. Occasionally a thickened duodenal wall progresses to a stricture. Whether this entity is simply inflammation of heterotopic tissue is conjecture. In either case, the spectrum consists of cysts, fibrosis, and possible stricture.

Imaging in patients with duodenal cystic dystrophy reveals a thickened duodenal wall and intramural cysts varying in size. Some of these cysts are >1 cm in diameter, the thickened duodenal wall is isodense on precontrast CT and varies from hypovascular to exhibiting strong contrast enhancement (9). Duodenal cystic dystrophy appears mostly hypoechoic with US.

Necrosis

Caustic ingestion generally results in esophageal and, less often, gastric injury. Occasionally, however, it is associated duodenal injury, even necrosis. In general, contrast imaging is safe in these individuals.

Tumors

Nonneoplastic

Hyperplastic/Metaplastic

Hyperplastic or metaplastic duodenal polyps are uncommon. A rare metaplastic polyp occurs in the duodenal bulb and is associated with *H. pylori*, regressing after anti–*H. pylori* therapy.

Heterotopic Tissue

Heterotopic pancreatic tissue is common in the duodenal wall. This tissue contains acini and ducts, but not islet cells. Occasionally localized inflammation within such heterotopic tissue results in valvulae conniventes thickening and eventually evolves into a duodenal stricture.

Less often encountered in the duodenum is heterotopic gastric tissue. Both chief cells and parietal cells are present.

Hamartoma

Brunner gland hamartomas are most common in the first portion of the duodenum and most occur in middle-aged individuals. Although submucosal in origin, an occasional one becomes pedunculated. Some are several centimeters in size. They consist of proliferating Brunner gland tissue surrounded by fibrosis, fat, and lymphoid tissue. These hamartomas bleed, obstruct if they are large enough, or are simply an incidental finding.

Patients with untreated sprue develop multiple small polyps scattered throughout the duodenal bulb. These polyps probably represent Brunner's gland hyperplasia, although they may represent an intrinsic abnormality of sprue.

An isolated myoepithelial hamartoma is rare in the duodenum; most of these occur in a setting of one of the polyposis syndromes. An isolated duodenal hamartomatous polyp occasionally also contains an adenocarcinoma.

Polyposis Syndromes

Polyposis syndromes are discussed in more detail in Chapter 5. Covered here are only those aspects pertinent to the duodenum.

Patients with familial adenomatous polyposis develop polyps in the stomach, duodenum, small bowel, and colon. True prevalence of duodenal polyposis in these patients is not known, because small adenomas are often not visualized either by imaging or endoscopy. Also, part of the confusion involves a definition of the term *polyp;* not all adenomas in familial polyposis protrude into the lumen. An endoscopic duodenal search of patients with familial adenomatous polyposis detects adenomas in 30% to 60% of patients; these tumors tend to be either flat or flat-topped elevations with a central depression. The most common duodenal location is periampullary. An occasional duodenal polyp is a villous adenoma.

These patients are at increased risk of developing a papilla of Vater carcinoma, and a duodenal adenocarcinoma is a not uncommon cause of death in familial polyposis patients who have had a previous colectomy. They are also prone to developing mesenteric fibromatosis.

Periampullary adenomas have been removed endoscopically, although the long-term results of such therapy are not known. Prophylactic pancreaticoduodenal resection has been performed for severe duodenal polyposis (10).

Bulbar Tumors

Primary duodenal bulb neoplasms are so rare that an average physician will not encounter one in a lifetime of practice. They are probably reportable. Only occasional descriptions exist of bulbar villous adenomas and adenocarcinomas.

An early bulbar cancer (well-differentiated papillary adenocarcinoma) was detected on a barium study as a smooth, sessile polyp (11). A very rare one develops in a setting of a chronic or refractory bulbar ulcer, but bulbar ulcers are not considered to be premalignant.

More common duodenal bulb neoplasms are benign mesenchymal tumors such as leiomyoma or lipoma. A rare metastatic melanoma mimics a benign ulcer; in some parts of the world resected skin tumors are not examined by a pathologist and thus a patient may not be aware of a prior melanoma resection.

Periampullary Tumors

Clinical

Discussed here are tumors originating from the papilla of Vater and adjacent duodenum. Bile duct tumors are covered in Chapter 8, and pancreatic origin tumors are discussed in Chapter 9.

Linguistic purists argue about correct usage, but the terms *periampullary*, *papillary*, and *peri-Vaterian tumor* are synonymously used in the literature and are descriptive terms for tumors of the mid-descending duodenum, papilla of Vater, pancreas adjacent to the papilla, sphincter of Oddi, and even distal common bile duct. Some malignant tumors infiltrate surrounding structures to the point that a specific site of origin cannot be identified. Nevertheless, the site of origin should be sought because of prognostic differences. Thus a carcinoma of the papilla of Vater is associated with a better prognosis than a carcinoma originating from adjacent pancreas.

The two most common periampullary tumors are adenoma and adenocarcinoma. An adenoma, quite often villous, can be quite large and not cause biliary obstruction (Fig. 3.3). These adenomas are premalignant. Once jaundice ensues in a patient with a known peri-Vaterian adenoma, however, malignant degeneration and invasion is likely. An occasional peri-Vaterian carcinoma first manifests as pancreatitis. In general, a cancer originating at the papilla that has not spread through the sphincter of Oddi invades locally; on the other hand, a tumor penetrating through the sphincter tends to metastasize to regional lymph nodes. Also, a malignancy penetrating the duodenal muscularis propria generally has a poor prognosis.

Other papillary tumors are uncommon and an occasional one is difficult to classify. A papilla of Vater adenomyoma produced obstructive jaundice (12). A rare carcinosarcoma and a primary carcinoma containing both glandular and neuroendocrine differentiation have been reported at the papilla.

Patients with von Recklinghausen's disease are prone to developing peri-Vaterian tumors,

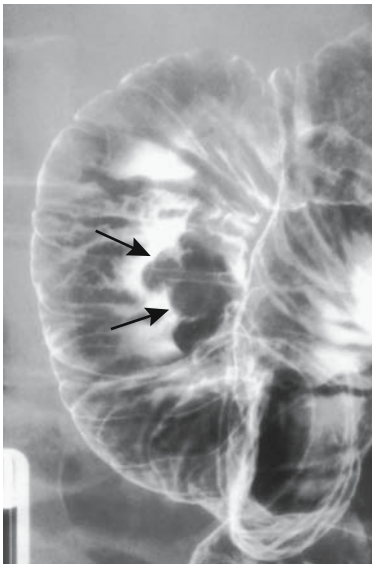

Figure 3.3. Peri-Vaterian villous adenoma (arrows). A focus of carcinoma can readily be present and thus a biopsy showing no cancer is of limited help with these tumors. (Courtesy of Arunas Gasparaitis, M.D., University of Chicago.)

some being rather uncommon, such as a somatostatinoma (13). A very rare peri-Vaterian tumor acts as a lead point for common bile duct prolapse (14).

Imaging

Even when small, some papilla cancers obstruct the bile ducts, yet neither endoscopy nor imaging is able to detect them. With further growth these tumors are readily identified with an imaging study or endoscopic cholangiopancreatography. An occasional periampullary carcinoma is not detected initially at ERCP but becomes evident as a protruding mass only after a papillotomy.

Peri-Vaterian carcinomas range in appearance from primarily polypoid and intraluminal, primarily intramural and infiltrating the duodenal wall, growing mostly into the pancreatic head, to those with a mixed growth pattern. Those growing into the pancreas are often indistinguishable from a cholangiocarcinoma or primary pancreatic carcinoma both by imaging and histology (Fig. 3.4).

Transabdominal US has a limited role in detecting these tumors.

A mostly intramural neoplasm has to be >1 cm or so to be identified by endoscopic US. Nevertheless, of periampullary tumors requir-

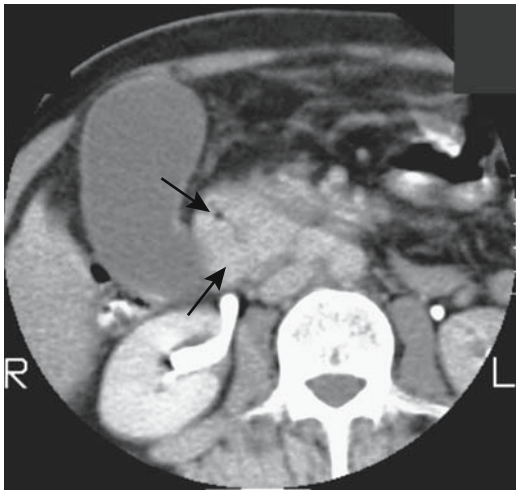

A

B

Figure 3.4. A: Carcinoma of papilla. Contrast-enhanced CT reveals a nonenhancing tumor involving descending duodenum and pancreatic head (arrows). A distended gallbladder is evident. (Courtesy of Patrick Fultz, M.D., University of Rochester.) B: Carcinoma originating close to the papilla of Vater. Extensive bile duct and pancreatic invasion is present. Exact site of tumor origin could not be determined.

ing surgery, endoscopic US can correctly stage 75% to 85% of these tumors; although regional adenopathy is detected, more distant metastases cannot be evaluated. Similar to other imaging, endoscopic US cannot differentiate between benign and malignant adenopathy.

Intraductal US using high-frequency sonographic catheters appears useful in staging papillary cancers. This technique can confirm whether a tumor extends into duodenal submucosa, is limited to Oddi's muscle, or whether it invades pancreas; intraductal US is less sensitive in detecting lymph node metastases.

High-spatial-resolution MRI should identify most periVaterian tumors, in one study achieving a sensitivity of 88% and specificity of 100% in assessing of tumor invasion (15). PeriVaterian carcinomas are hypointense on precontrast T1-weighted images and enhance less than normal pancreas on immediate postgadolinium SGE images. Tumor conspicuity is greatest on immediate postcontrast images. Magnetic resonance cholangiopancreatography in some of these patients shows varying degrees of common bile duct and pancreatic duct dilation.

At most sites biopsy is necessary to establish a histologic diagnosis. In spite of this advice, some surgeons do not obtain a percutaneous biopsy or even retrograde cholangiopancreatography if an imaging study defines the tumor and its proximal extent, arguing that such preoperative studies do not alter a decision for surgical exploration and, in fact, may cause complications. They believe that visualization by noninvasive imaging should suffice.

Tumor, node, metastasis (TNM) staging for papilla of Vater tumors is outlined in Table 3.2.

Table 3.2. Tumor, node, metastasis (TNM) staging of papilla of Vater tumors

Primary tumor:			
Tx	Primary tumor cannot be assessed		
T0	No evidence of primary tumor		
Tis	Carcinoma-in-situ		
T1	Tumor limited to ampulla of Vater or sphincter of Oddi		
T2	Tumor invades duodenal wall		
T3	Tumor invades pancreas		
T4	Tumor invades peripancreatic soft tissues or adjacent organs		
Lymph nodes:			
Nx	Regional nodes cannot be assessed		
N0	No regional lymph node metastasis		
N1	Metastasis to regional nodes		
Distant metastasis:			
Mx	Distant metastases cannot be assessed		
M0	No distant metastasis		
M1	Distant metastasis		
Tumor stages:			
Stage 0	Tis	N0	M0
Stage IA	T1	N0	M0
Stage IB	T2	N0	M0
Stage IIA	T3	N0	M0
Stage IIB	T1	N1	M0
	T2	N1	M0
	T3	N1	M0
Stage III	T4	any N	M0
Stage IV	any T	any N	M1

Source: From the AJCC Cancer Staging Manual, 6th edition (2002), published by Springer-Verlag, New York, NY, used with permission of the American Joint Committee on Cancer (AJCC), Chicago, IL.

Therapy

An ampullectomy has been performed for small benign tumors and T1 carcinomas originating in the papilla of Vater.

Initially performed early in the 20th century, pancreaticoduodenectomy for a periampullary carcinoma was advocated by Whipple in the 1930s, and since then this operation continues to bear his name. Over the years a number of modifications have been introduced, and currently many surgeons opt for a pylorus-preserving variant. The indications for a Whipple procedure have also expanded and now include a potentially curable carcinoma in the pancreatic head (complications and imaging of the postoperative Whipple procedure are discussed in Chapter 9). If a Whipple procedure is contraindicated because of metastatic disease or poor patient condition, insertion of a palliative biliary drainage prosthesis is an option.

Potentially, resection of a peri-Vaterian carcinoma should have a high cure rate. Nevertheless, a number of these patients do not undergo curative resection due to age, poor health, or advanced disease. Catheter stenting in poor surgical risk patients is a viable option. Evidence suggests that preoperative biliary drainage in these patients results in decreased morbidity and shorter postoperative hospitalization (16).

After a Whipple procedure for a peri-Vaterian carcinoma, resection margin tumor involvement is the major prognostic factor for survival. Among consecutive patients who underwent pancreaticoduodenectomy with radical lymphadenectomy for papillary carcinoma, 54% had positive lymph nodes (17); the most common tumor spread was to the posterior pancreaticoduodenal nodes, followed by the inferior pancreaticoduodenal artery nodes and then the paraaortic nodes. Distal metastasis is uncommon for these tumors, at least initially.

Adenoma/Adenocarcinoma

Excepting the periampullary region (discussed above), duodenal adenomas are uncommon. They are considered premalignant. Some contain predominantly a villous component (Fig. 3.5).

About half of small bowel adenocarcinomas occur in the duodenum; their appearance is similar to that of the rest of the small bowel (Fig. 3.6). Patients with celiac disease have a slightly increased prevalence of duodenal carcinoma than the general population. A duodenal carcinoma developing years after a Billroth gastroduodenostomy is probably unrelated to the original surgery. Patients with hereditary nonpolyposis colorectal cancer are probably not at increased risk for developing a duodenal adenoma or carcinoma.

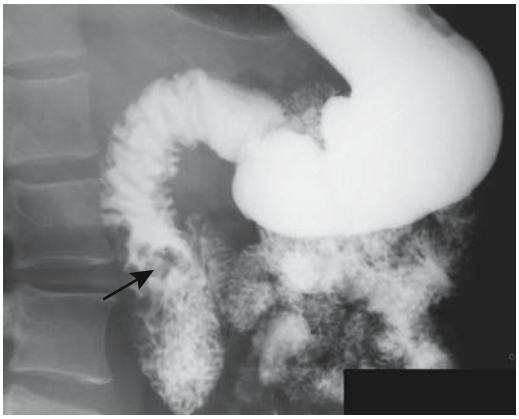

Figure 3.5. Duodenal villous adenoma (arrow).

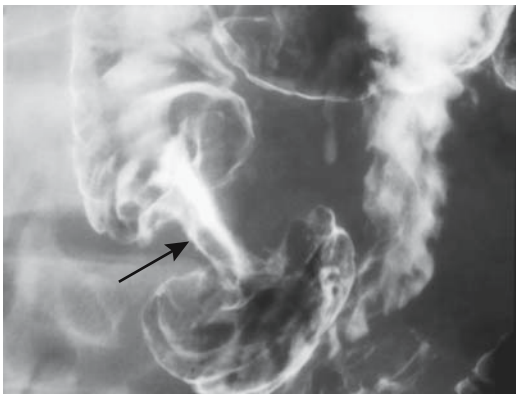

Figure 3.6. Descending duodenal adenocarcinoma (arrow). (Courtesy of Arunas Gasparaitis, M.D., University of Chicago.)

A retrospective multiinstitution review of patients with duodenal adenocarcinomas found a detection accuracy of 82% for duodenography and 88% for endoscopy (18); almost two thirds of these tumors were in the periampullary region. Detecting an adenocarcinoma in the distal duodenum is beyond endoscopic reach, but it can also be difficult with both barium studies and CT (Fig. 3.7).

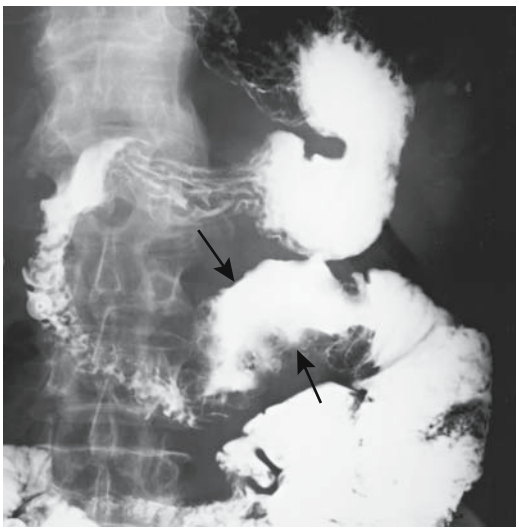

Figure 3.7. Primary necrotic duodenal adenocarcinoma in distal duodenum (arrows). A sarcoma or lymphoma can have a similar ulcerated appearance.

The duodenum shares its blood supply with the pancreas. As a result, depending on tumor location and the extent of infiltration, adequate resection often requires a pancreaticoduodenectomy, although occasionally a pancreas-sparing duodenectomy is feasible.

Endoscopic resection of some duodenal adenomas and carcinomas is practiced in Japan. Saline is injected into the submucosa near the tumor, which is resected using electrocoagulation. Elevated tumors less than 50 mm in diameter have been removed using this technique (19). Larger tumors and depressed ones with or without marginal elevation are resected surgically.

Lymphoma/Leukemia

Mucosa-associated lymphoid tissue (MALT) lymphoma rarely affects the duodenum. At times multiple small erosions are detected. One MALT low-grade B-cell lymphoma in the duodenal bulb was detected by a barium study and endoscopy as multiple elevated, irregularly contoured nodules (20). Adult T-cell leukemia led to varioliform polypoid infiltration in the duodenum (21). Sufficient involvement of adjacent lymph nodes will result in duodenal obstruction (Fig. 3.8).

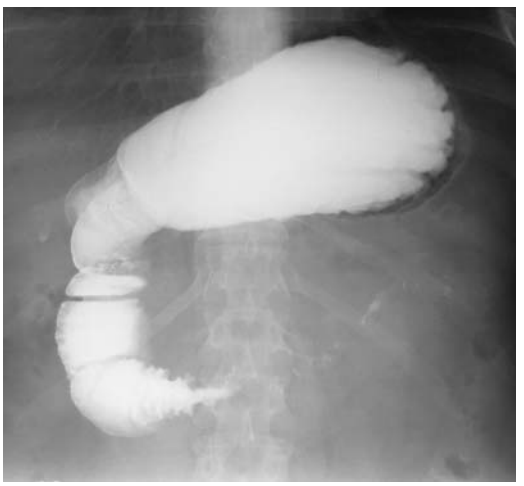

Figure 3.8. Lymphoma obstructing duodenum. Duodenal invasion by an adjacent pancreatic carcinoma or a metastasis to paraaortic nodes has a similar appearance.

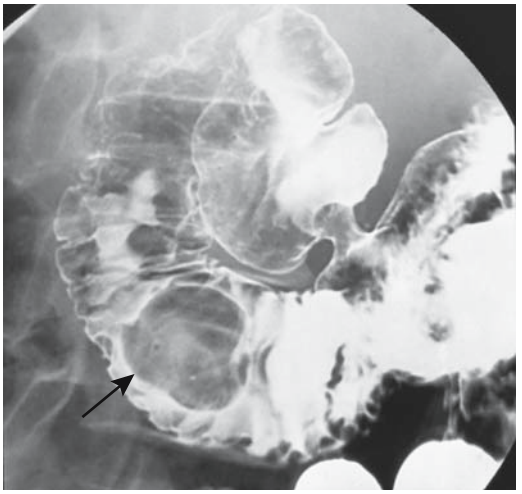

Figure 3.9. Duodenal lipoma (arrow). (Courtesy of Arunas Gasparaitis, M.D., University of Chicago.)

Mesenchymal Tumors

Some duodenal stromal tumors are sufficiently undifferentiated to be difficult to characterize. At times even mitotic activity does not distinguish between benign and malignant tumors. Similar to other mesenchymal tumors, a duodenal leiomyoma may bleed or, if large enough, result in obstruction. Presumably some benign tumors eventually undergo sarcomatous degeneration.

A thallium-201 single photon emission computed tomography (SPECT) myocardial perfusion study revealed prominent uptake in a duodenal leiomyosarcoma (22).

The occasional duodenal lipoma is often an incidental finding (Fig. 3.9). Some are huge. Some become pedunculated and even act as a lead point for an intussusception. A rare one erodes and bleeds.

A barium study reveals a lipoma either as an intramural or intraluminal polyp. The primarily fat composition of a lipoma is identified by CT (assuming that the tumor is detected by CT).

Metastasis or Direct Invasion

A malignancy in any adjacent structure readily invades the duodenum and, similar to a metastasis, readily bleeds or obstructs the duodenal lumen (Fig. 3.10). Thus an advanced right renal cell carcinoma and some pancreatic malignan-

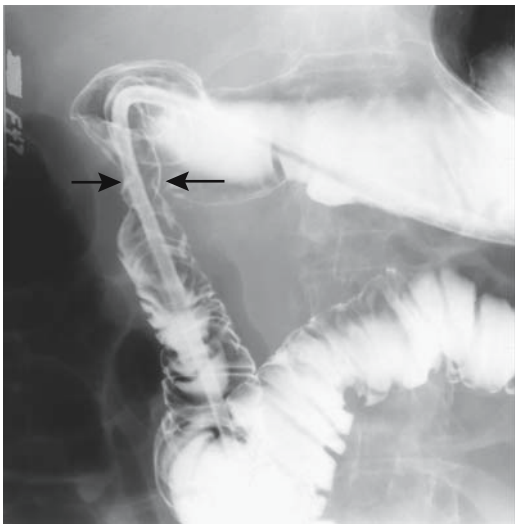

Figure 3.10. Pancreatic carcinoma invading duodenum (arrows). The symmetrical circumferential invasion is somewhat atypical.

cies readily invade the duodenum. A hepatocellular carcinoma spreading to portal lymph nodes will also invade the first or second duodenal segment. Most common metastases involve the pancreaticoduodenal nodes or adjacent paraaortic nodes (Fig. 3.11).

A "bull's-eye" lesion distal to the bulb rarely represents a benign ulcer; more likely it is a metastatic melanoma (Fig. 3.12) or breast carcinoma. Larger melanomas tend to mimic necrotic mesenchymal tumors.

An inoperable cancer patient presenting with gastric outlet or duodenal obstruction should be considered for palliation with a perorally implanted self-expanding endoprosthesis. Occasionally combined biliary and duodenal obstructions can be bypassed with double stents introduced percutaneously.

Neuroendocrine

Carcinoid

Carcinoid tumors are not uncommon in the duodenum. Most are <1 cm in size and benign, and are detected incidentally. Some carcinoids adjacent to the ampulla of Vater are associated with pancreatitis.

Endoscopic US appears to aid in duodenal carcinoid detection and in evaluating the depth of tumor invasion.

High-resolution breath-hold contrast-enhanced magnetic resonance imaging (MRI) detected a 10-mm primary duodenal carcinoid (23).

Endoscopic resection is feasible with some superficial carcinoids.

Gastrinoma

Gastrinomas are discussed in more detail in Chapter 9. Duodenal gastrinomas range from single to multiple and some are associated with synchronous pancreatic tumors. They are somewhat prevalent in patients with multiple endocrine neoplasia (MEN) type I syndrome, and among these patients a majority of carcinoids consist of gastrointestinal submucosal nodules; only a minority of patients with sporadic Zollinger-Ellison syndrome have similar submucosal nodules. Clinically, these patients develop hypergastrinemia and gastric acid hypersecretion.

Duodenal gastrinomas are considerably more malignant than those originating in the pancreas; it is not uncommon to find lymph node metastasis at initial presentation even with a

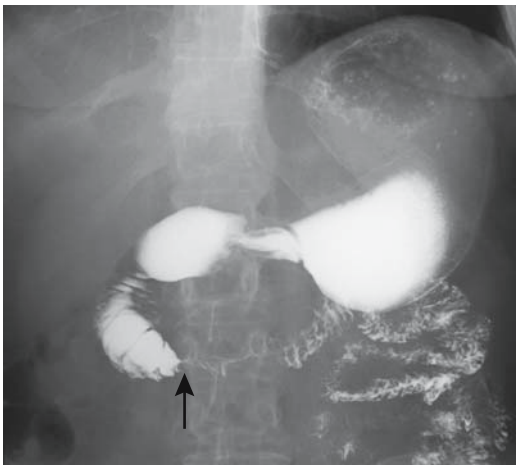

Figure 3.11. Metastatic Merkel cell tumor to third duodenal segment produces partial obstruction (arrow). More common metastases to this location are colon and breast carcinomas.

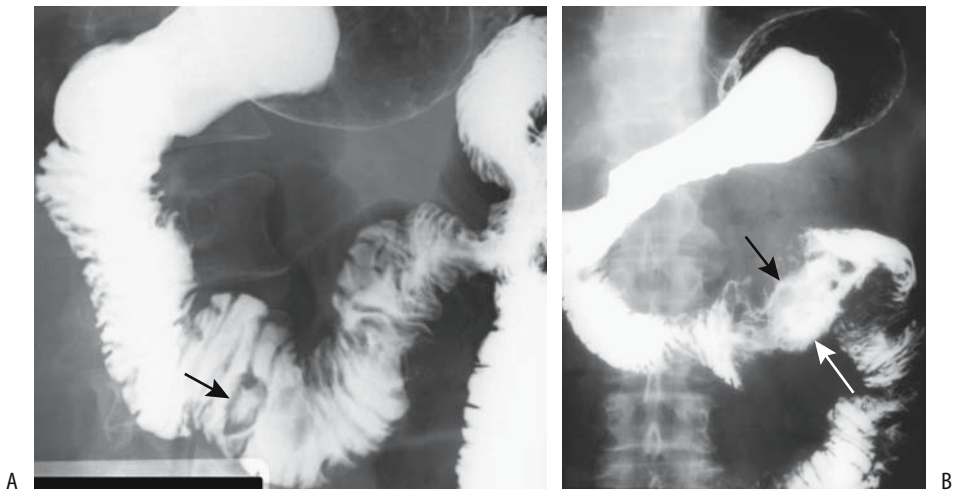

Figure 3.12. Metastatic melanoma. A: A "bull's-eye" appearance (arrow) is typical in the small bowel. (Courtesy of William Bechtel, M.D., M. D. Anderson Hospital, Houston, Texas.) B: A necrotic tumor (arrows) has replaced the fourth duodenal segment. (Courtesy of Arunas Gasparaitis, M.D., University of Chicago.)

small primary tumor. Especially among the small ones located submucosally in the first or second part of the duodenum only a minority are identified by preoperative imaging. A 15-mm submucosal gastrinoma palpated at surgery in the posterior duodenal wall had an enlarged peripancreatic lymph node close to the pancreas head as the only positive preoperative imaging finding, although surgery revealed regional lymph node metastases (24).

Clinically these patients develop hypergastrinemia and gastric acid hypersecretion.

At times selective arterial secretin injection aids in localizing these tumors. Fine-needle aspiration cytology has been performed with some of these tumors.

Paraganglioma

Duodenal paragangliomas are rare, usually benign tumors having a predilection for the periampullary region. An occasional one presents with gastrointestinal bleeding. An occasional periampullary paraganglioma is pedunculated, results in obstructive jaundice, or is simply detected as an incidental duodenal polyp on a barium study.

Paragangliomas appear solid and homogeneous on CT, US, and MRI, and enhance homogeneously postcontrast; they contain a prominent vascular network.

Other

Only a rare schwannoma is reported in the duodenum. Use of water as oral contrast during contrast-enhanced CT aids in identifying these hypervascular bleeding schwannoma.

An occasional small superficial insulinoma can be resected endoscopically.

Dilation/Obstruction

Obstruction by an annular pancreas is discussed in Chapter 9. Paraduodenal hernias are covered in Chapter 14.

Gallstone Ileus

A biliary-enteric fistula caused by an eroding gallstone develops to the stomach, duodenum, or even transverse colon. A majority are to the

duodenum. Rarely, multiple fistulas ensue. Most originate from the gallbladder, with an occasional one evolving from the common bile duct. Once the presence of a fistula is established, the surgeon is interested in whether it communicates with the gallbladder or bile duct, but a surrounding inflammation can make this differentiation difficult at surgery, and often an imaging study will suggest the path of a fistulous communication. An upper gastrointestinal study is generally most helpful with this differentiation, although indirect CT signs, such as whether the gallbladder is contracted and the location of bile duct versus gallbladder gas, can occasionally point toward a correct diagnosis.

Although a gallstone can obstruct anywhere in the gastrointestinal tract, most impact in the distal ileum (but not the terminal ileum); the second most common location is in the duodenum (Bouveret's syndrome), and the patient then presents with gastric outlet obstruction. In addition to duodenal lumen obstruction, at times a stone also leads to bile duct obstruction, and the patient presents with jaundice. Bouveret's syndrome is sufficiently rare that no large series have been published, but common enough that numerous single reports exist. It is unfortunate that some of these patients have died without a simple radiologic study being obtained; a barium study or CT should be diagnostic.

A gallstone does not necessarily need to pass into the duodenal lumen to obstruct. Thus a stone eroding into the duodenal wall but not yet forming a fistulous tract to the lumen will obstruct. An analogy can be made to Mirizzi's syndrome, where an eroding stone leads to bile duct obstruction. A gallstone impacting in an intraluminal duodenal diverticulum is a rare cause of duodenal lumen obstruction. In addition to lumen obstruction, hemorrhage is a common consequence of a stone eroding into the stomach or duodenum.

Most of these stones are approached surgically. Duodenal obstruction by a gallstone has been treated by endoscopic lithotripsy (25).

Superior Mesenteric Artery Syndrome

Duodenal obstruction secondary to compression by the adjacent anteriorly located superior mesenteric artery (SMA) is currently rarely encountered. This condition, called *SMA syndrome*, *cast syndrome*, and *Wilkie's syndrome*, generally develops in thin patients or those suddenly bedridden. A number of patients developed acute SMA syndrome after surgery for severe spinal deformity. It has developed after rapid weight loss due to bowel resection. When fully developed, this syndrome presents a serious management problem; as an extreme, gastric necrosis has ensued.

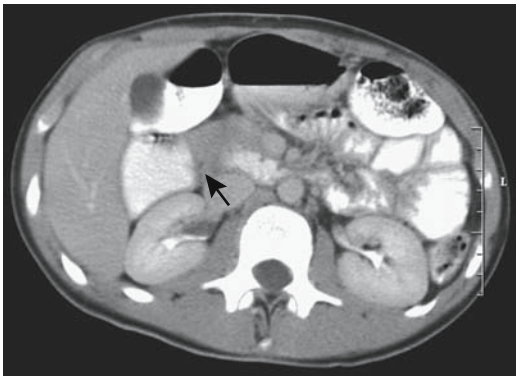

Figure 3.13. Severe superior mesenteric artery syndrome. Oral and intravenous contrast-enhanced CT reveals marked dilation of the descending duodenum and an abrupt cut-off in the third portion (arrow). The superior mesenteric artery and vein had a normal relationship. The patient underwent a duodenojejunostomy. (Courtesy of Patrick Fultz, M.D., University of Rochester.)

Although CT and magnetic resonance angiography (MRA) will detect this condition, the diagnosis is generally straightforward with a barium study (Fig. 3.13).

In most patients, subsequent mobility or weight gain is generally curative. An occasional patient requires a duodenojejunostomy, although SMA syndrome has recurred in a rare patient.

Occasionally, a suddenly bedridden patient develops a similar obstruction more distally in the small bowel.

Intussusception

Normally the extraperitoneal duodenal location should prevent intussusception, although large

polyps do predispose to an intussusception. Thus patients with Peutz-Jeghers syndrome, who tend to have large duodenal polyps, are prone to this complication, and it is often recurrent. Intermittent abdominal pain is common.

A barium study or CT in Peutz-Jeghers patients often detects recurrent duodenojejunal intussusception. Eventual almost complete duodenal obstruction requires surgical polypectomy. At times associated bile duct and pancreatic duct obstruction are sequelae of a duodenojejunal intussusception and on a chronic basis have led to pancreatic atrophy.

Extrinsic Causes

Ileocolic intussusception in the very young is a common occurrence. Occasionally such an intussusception and resultant bowel dilation obstruct the adjacently located duodenum.

Other Obstructions

Duodenal obstruction has been caused by a shiitake mushroom (26).

Chronic adynamic ileus (intestinal pseudo-obstruction) also affects the duodenum. A hereditary autosomal-dominant form is characterized by visceral myopathy manifesting as a megaduodenum (27); histology identified longitudinal muscle vacuolar degeneration and fibrosis.

Diverticula

Peri-Vaterian

Duodenal diverticula are most common in the papilla of Vater region and most are detected incidentally during barium imaging or ERCP. Their CT and MR appearance can be somewhat confusing (Fig. 3.14). For instance, in one study of patients with periVaterian diverticula, MR cholangiography missed 18% and clearly detected only 35% (28). Their content varies considerably. In an occasional patient such a peri-Vaterian diverticulum becomes infected, bleeds, obstructs adjacent duodenal lumen, or even harbors a malignancy. At times bleeding is massive. Adjacent infection or tumor predispose

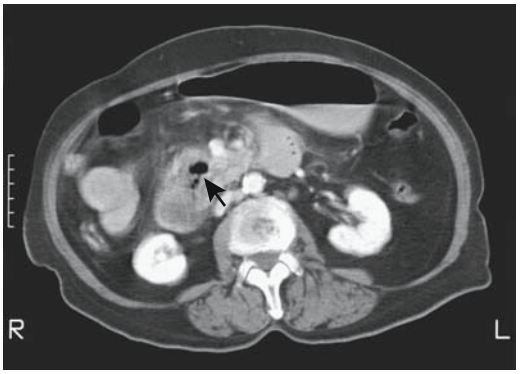

Figure 3.14. Duodenal diverticulum. CT identifies gas in the pancreatic head (arrow). Initially this gas was believed to be in an abscess in this patient with pancreatitis. (Courtesy of Patrick Fultz, M.D., University of Rochester.)

to perforation and fistula formation from a diverticulum to adjacent structures. Ulcers and even an eroding enterolith within a diverticulum have led to duodenal diverticular perforation (29). These perforations are either into the peritoneal cavity or into an adjacent organ.

Patients with a peri-Vaterian diverticulum probably have impaired sphincter of Oddi function, presumably secondary to compression of the adjacent distal bile duct, and many case reports have suggested an increased risk for choledocholithiasis, cholangitis, and pancreatitis in the presence of a peri-Vaterian diverticulum. Yet a retrospective study of 1115 patients undergoing ERCP detected only a moderate, but not statistically significant, relationship between presence of a peri-Vaterian diverticulum and common bile duct stones (30). Several other studies have reached similar conclusions, and if there is an increased risk of choledocholithiasis in patients with a peri-Vaterian diverticulum, it is small.

Some patients with Ehlers-Danlos syndrome develop a large duodenal diverticulum. A peri-Vaterian diverticulum filled with a food bezoar occasionally results in common bile duct obstruction.

Ultrasonography reveals a peri-Vaterian diverticulum as a collection of persistent bright linear or concave echoes close to the pancreatic head.

Intraluminal

Most intraluminal diverticula (also described as a *wind-sock sign*) develop in the second part of the duodenum and most manifest in young adults. Whether all of these diverticula are congenital in origin is conjecture, although some are associated with other duodenal congenital anomalies, including ampulla of Vater malposition. In an occasional patient the ampulla is located in the diverticulum or on its rim. Small ones tend to be incidental findings, but duodenal obstruction, stasis, bleeding, and pancreatitis are occasional sequelae of larger ones.

Whether all of these diverticula are congenital in origin is conjecture, although some are associated with other duodenal congenital anomalies, including ampulla of Vater malposition. At times the ampulla is located on the diverticular rim.

The diagnosis is straightforward with a barium study. Other imaging modalities detect these diverticula if an intraluminal collection of contrast can be identified surrounded by a thin radiolucent line. Their connection to the main lumen ranges from a focal neck to an almost circumferential opening. Their classic wind-sock appearance is pathognomonic, although diagnostic problems occur if the diverticulum is already filled with secretions and little contrast enters its lumen.

Locating the ampulla is obviously important if diverticular excision is contemplated.

Other Diverticula

Most diverticula in the third and fourth portions of the duodenum are incidental findings (Fig. 3.15). Although stasis within such a diverticulum is common, the volume involved is sufficiently small that clinical malabsorption rarely develops.

Bleeding, at times massive, is occasionally encountered from distal duodenal diverticula. Most endoscopy does not reach much beyond the second duodenal segment and simply detects intraluminal blood without identifying a site of bleeding. With active bleeding either a technetium-99m (Tc-99m) red blood cell study or arteriography is the study of choice.

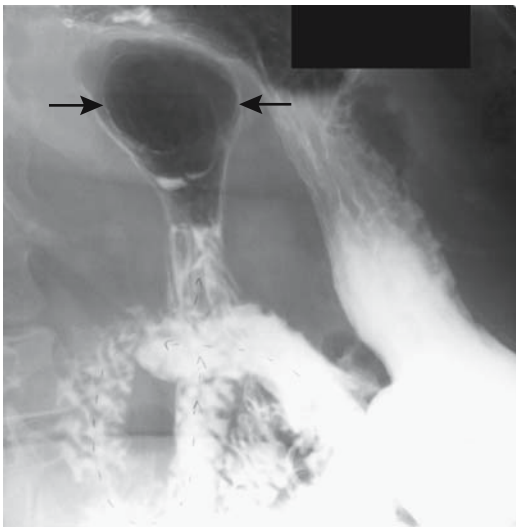

Figure 3.15. Giant diverticulum (arrows) at ligament of Treitz region. (Courtesy of Thomas Miller, M.D., San Louis Obispo, California.)

Melanosis

Occasionally endoscopy reveals melanin-like black or brown spots within the duodenum, usually within the first and second parts. Although such a finding can be secondary to a melanoma, more often no tumor is found. These melanin-like spots represent iron deposition within macrophages. This condition, also known as *pseudomelanosis duodeni*, is more common in the elderly and those with chronic illnesses, and in some appears related to hypertension or antihypertensive medications.

Perforation/Fistula

Although considerably less common than in years past, the most common cause of duodenal perforation in adults continues to be peptic ulcer disease. An acute perforated ulcer is one of the causes of an acute abdomen and usually requires surgical correction. An occasional impacted fish bone results in duodenal perforation, a rare event.

A laparoscopic approach is feasible to treat duodenal perforations. A retrospective study of laparoscopic repair of perforated duodenal ulcers in 35 patients found that conversion to

laparotomy was necessary in 23%, with the causes being a fragile perforation edge, a perforation that could not be identified, and extensive intraabdominal adhesions (31).

Vascular Lesions (Bleeding)

Vascular fistulas are discussed in Chapter 17.

Dieulafoy Lesion

Dieulafoy lesions are rarely described in the duodenum. Their endoscopic appearance is similar to those seen in the stomach.

Varices

Duodenal varices are less common than in the esophagus or stomach. Most of these varices are part of an esophagogastric variceal complex, but an occasional patient develops only isolated duodenal varices. Isolated portal vein thrombosis appears to predispose to duodenal varices that are part of a retroperitoneal portosystemic shunt system. They have been reported throughout the duodenum. The feeding vessel is either the superior or inferior pancreaticoduodenal vein or superior mesenteric vein. Efferent veins drain into the inferior vena cava.

Although most duodenal varices are secondary to portal hypertension, occasionally a mesenteric arteriovenous fistula results in isolated duodenal varices and portal hypertension. A bleeding duodenal varix developed in a setting of splenic vein thrombosis and chronic pancreatitis (32).

Fluoroscopy shows that duodenal varices tend to decrease in size with inspiration.

Devascularization or percutaneous transhepatic obliteration of the varix in question is often the treatment of choice for these varices. Other options for controlling bleeding from these bleeding varices include endoscopic ligation, endoscopic injection sclerotherapy, and transjugular intrahepatic portosystemic shunt (TIPS).

Angiodysplasia/Telangiectasia

A duodenal angiodysplasia bleeding site is least common in the gastrointestinal tract. An occasional duodenal site is found in patients with hereditary hemorrhagic telangiectasia. Some of these angiodysplasias are related either to the major or minor papilla.

Therapy

Endoscopy is often the initial examination performed in patients with upper gastrointestinal bleeding. In some patients, however, endoscopic therapy is not successful in stopping bleeding from a duodenal site, and in these patients arte-

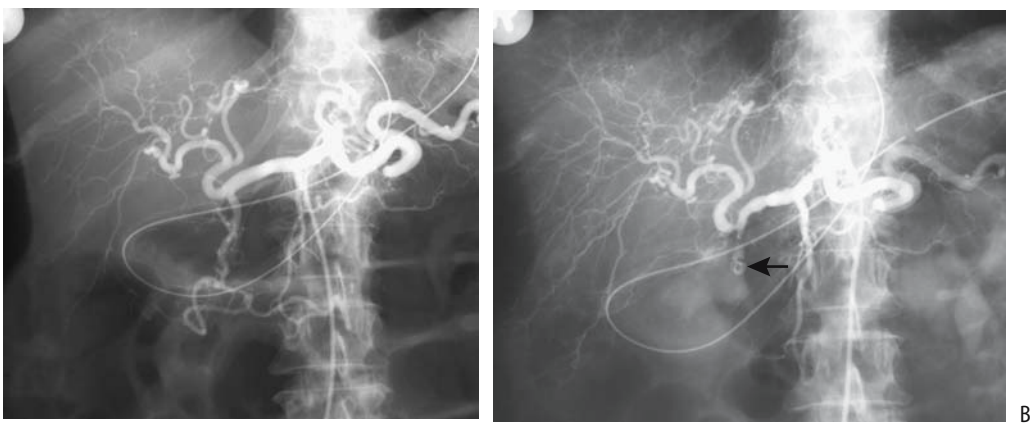

Figure 3.16. Gastroduodenal artery embolization for bleeding duodenal ulcer. Pretherapy arteriogram (A) and coil obstructing gastroduodenal artery (B, arrow). (Courtesy of Oscar Gutierrez, M.D., University of Chile, Santiago, Chile.)

riography and subsequent transcatheter arterial embolization should be considered. Embolization successfully achieves hemostasis in most patients, although the success rate is less than with lower gastrointestinal bleeding (Fig. 3.16). Occasionally single-vessel embolization will not arrest bleeding, and embolization of both gastroduodenal and inferior pancreaticoduodenal arteries is necessary. In spite of the rich duodenal blood supply, such synchronous embolization should be undertaken with caution because of the possible induction of duodenal or pancreatic ischemia.

References

1. Alvarez C, Rueda O, Vicente JM, Fraile E. Gastric emphysema in a child with congenital duodenal diaphragm. Pediatr Radiol 1997;27:915–917.
2. Thiefin G, Barraya R, Ramaholimihaso F, Diebold MD. [Duodenal diaphragm induced by aspirin.] [French] Presse Med 2000;29:1351–1352.
3. Rha SE, Lee JH, Lee SY, Park SM. Duodenal diaphragm associated with long-term use of nonsteroidal anti-inflammatory drugs: a rare cause of duodenal obstruction in an adult. AJR 2000;175:920–921.
4. Sollfrank M, Koch W, Waldner H, Rudisser K. [Intramural duodenal hematoma after endoscopic biopsy.] [German] Rofo Fortschr Geb Rontgenstr Neuen Bildgeb Verfahr 2001;173:157–159.
5. Shah P, Applegate KE, Buonomo C. Stricture of the duodenum and jejunum in an abused child. Pediatr Radiol 1997;27:281–283.
6. McWilliams RG, Blakeborough A, Johnson MI, Weston M. Case report: the "veiled right kidney sign"—an ultrasound finding in retroperitoneal perforation of the duodenum. Br J Radiol 1996;69:1061–1063.
7. Long FR, Kramer SS, Markowitz RI, Liacouras CA. Duodenitis in children: correlation of radiologic findings with endoscopic and pathologic findings. Radiology 1998;206:103–108.
8. Naouri C, Menecier P, Naouri A, Levenq P. [Duodenal tuberculosis: a difficult diagnosis.] [French] Presse Med 1997;26:805–806.
9. Vullierme MP, Vilgrain V, Flejou JF, et al. Cystic dystrophy of the duodenal wall in the heterotopic pancreas: radiopathological correlations. J Comput Assist Tomogr 2000;24:635–643.
10. Causeret S, Francois Y, Griot JB, Flourie B, Gilly FN, Vignal J. Prophylactic pancreaticoduodenectomy for premalignant duodenal polyposis in familial adenomatous polyposis. Int J Colorectal Dis 1998;13:39–42.
11. Bradford D, Levine MS, Hoang D, Sachdeva RM, Einhorn E. Early duodenal cancer: detection on double-contrast upper gastrointestinal radiography. AJR 2000;174:1564–1566.
12. Ligorred L, Morollon MJ, Aragon J, et al. [Obstructive jaundice from an adenomyoma of the ampulla of Vater.] [Spanish] Rev Esp Enferm Dig 1997;89:411–412.
13. Hamissa S, Rahmouni A, Coffin C, Wolkenstein P. CT detection of an ampullary somatostatinoma in a patient with von Recklinghausen's disease. AJR 1999;173:503–504.
14. Smith TR, Berkowitz D, Frost A. Prolapse of the common bile duct with small ampullary villous adenocarcinoma into third part of the duodenum. AJR 2003;181:599–600.
15. Sugita R, Furuta A, Ito K, Fujita N, Ichinohasama R, Takahashi S. Periampullary tumors: High-spatial-resolution MR imaging and histopathologic findings in ampullary region specimens. Radiology 2004;231:767–774.
16. Marcus SG, Dobryansky M, Shamamian P, et al. Endoscopic biliary drainage before pancreaticoduodenectomy for periampullary malignancies. J Clin Gastroenterol 1998;26:125–129.
17. Shirai Y, Ohtani T, Tsukada K, Hatakeyama K. Patterns of lymphatic spread of carcinoma of the ampulla of Vater. Br J Surg 1997;84:1012–1016.
18. Santoro E, Sacchi M, Scutari F, Carboni F, Graziano F. Primary adenocarcinoma of the duodenum: treatment and survival in 89 patients. Hepatogastroenterology 1997;44:1157–1163.
19. Hirasawa R, Iishi H, Tatsuta M, Ishiguro S. Clinicopathologic features and endoscopic resection of duodenal adenocarcinomas and adenomas with the submucosal saline injection technique. Gastrointest Endosc 1997;46:507–513.
20. Kawai T, Tada T, Yokoyama, Joh T, Itoh M. Lymphoma arising in mucosa-associated lymphoid tissue of the duodenal bulb. J Gastroenterol 1998;33:97–101.
21. Gakiya I, Kugai Y, Hayashi S, et al. Varioliform mucosal polypoid lesions in intestinal tract in a patient with adult T-cell leukemia. J Gastroenterol 1997;32:553–557.
22. Shuke N, Tonami N, Takahashi I, et al. Prominent uptake of Ti-201 by duodenal leiomyosarcoma after exercise myocardial perfusion study. Clin Nucl Med 1995;20:299–301.
23. Whitfill CH, Siegelman ES, Rosato EF, Furth EE. Primary carcinoid of the duodenum: detection and characterization by magnetic resonance imaging. J Magn Reson Imaging 1998;8:1175–1176.
24. Takasu A, Shimosegawa T, Fukudo S, et al. Duodenal gastrinoma—clinical features and usefulness of selective arterial secretin injection test. J Gastroenterol 1998;33:728–733.
25. Dumonceau JM, Delhaye M, Deviere J, Baize M, Cremer M. Endoscopic treatment of gastric outlet obstruction caused by a gallstone (Bouveret's syndrome) after extracorporeal shock-wave lithotripsy. [Review] Endoscopy 1997;29:319–321.
26. Hitosugi M, Kitamura O, Takatsu A, Yoshino Y. Autopsy case of duodenal obstruction from impacted mushroom. [Review] J Gastroenterol 1998;33:562–565.
27. Basilisco G. Hereditary megaduodenum. [Review] Am J Gastroenterol 1997;92:150–153.
28. Tsitouridis I, Emmanouilidou M, Goutsaridou F, et al. MR cholangiography in the evaluation of patients with duodenal periampullary diverticulum. Eur J Radiol 2003; 47:154–160.
29. Tsukamoto T, Hasegawa I, Ohta Y, et al. [Perforated duodenal diverticulum caused by enterolith.] [Review]

[Japanese] Nippon Shokakibyo Gakkai Zasshi 1998;95: 895–899.
30. Novacek G, Walgram M, Bauer P, Schofl R, Gangl A, Potzi R. The relationship between juxtapapillary duodenal diverticula and biliary stone disease. Eur J Gastroenterol Hepatol 1997;9:375–379.
31. L'Helgouarc'h JL, Peschaud F, Benoit L, Goudet P, Cougard P. [Treatment of perforated duodenal ulcer by laparoscopy. 35 cases.] [French] Presse Med 2000;29: 1504–1506.
32. Dhadphale S, Sawant P, Rathi P, et al. Bleeding duodenal varix in splenic vein thrombosis and chronic pancreatitis. Indian J Gastroenterol 1998;17:29–30.

4

Jejunum and Ileum

Technique

Contrast Studies

Barium Sulfate

Accepted clinical indications for a barium small bowel study include (1) unexplained gastrointestinal bleeding, (2) suspected small bowel tumor, (3) suspected small bowel obstruction, (4) Crohn's disease, and (5) malabsorption. Computed tomography (CT) has made inroads in some of these indications, especially with suspected obstruction, and whether a barium study or CT is performed varies considerably between institutions. The role of a swallowed capsule is still being established. Nevertheless, a majority of American radiologists both in academia and private practice continue to perform small bowel follow through examinations (1).

This is not the place to discuss relative merits of a conventional small bowel study versus enteroclysis and other more specialized examinations.

The limitations of a conventional small bowel study are well known. Enteroclysis has achieved a sensitivity and specificity of over 90% in detecting abnormalities responsible for a patient's symptoms, and some experts are adamant that the conventional small bowel follow-through examination should be abandoned; still, this examination continues to be performed throughout most of the world.

The small bowel is studied using a barium sulfate suspension in water (including various additives). One novel approach is to substitute a methylcellulose solution instead of water as the suspending agent. Use of a 40% barium suspension in methylcellulose improved small bowel image quality (compared to a water suspension) (2). Whether such a modification is overall advantageous remains to be established.

The peroral pneumocolon and gas-enhanced double-contrast study have carved a very limited niche in the study of suspected small bowel disease. Retrograde ileography using an endoscopically introduced occluding balloon is an option (3); its complexity argues against wide use.

Enteroscopy visualizes the proximal small bowel. Some authors believe that a combination of enteroscopy and enteroclysis via a catheter inserted on enteroscope withdrawal offers the advantages of both studies.

Water-Soluble Agents

Ionic water soluble contrast agents beloved by some surgeons have a very limited role in small bowel studies. They are hyperosmolar and draw fluid into the small bowel lumen, resulting in distention and dilution. Especially in neonates they tend to damage mucosa and induce hypovolemia. Considerably more harm is produced if these agents are aspirated into the lungs than with barium.

Most nonionic agents are still hyperosmolar, but are associated with fewer side effects and complications than ionic agents. They lead to

less dilution and are better visualized in the small bowel than are ionic agents. Nevertheless, for optimal visualization with conventional radiography barium sulfate is preferred in most patients.

Normally ionic water-soluble contrast agents are minimally absorbed after oral use, although idiosyncratic absorption exists. An occasional patient without underlying small bowel disease has sufficient absorption to opacify renal collecting systems, but, in general, such absorption should be viewed with suspicion. Common causes of visualizing the renal collecting systems after oral administration are bowel perforation and impaired bowel mucosal integrity.

Prevalence of contrast sensitivity secondary to oral contrast ingestion is much less than with intravenous (IV) injection, although contrast reactions occur even with dilute solutions, such as used to opacify the gut for CT studies.

Computed Tomography

Conventional

Oral contrast is necessary for adequate evaluation of most small bowel abnormalities. Intraluminal contrast not only identifies small bowel loops, but also reveals any bowel wall thickening, an exception being in patients with suspected high-grade obstruction who are studied without oral contrast. For most examinations, whether a dilute iodine solution or a barium sulfate suspension is used is generally a personal preference. With slower CT units an iodine solution tends to produce fewer streak artifacts than a barium suspension, a problem of little consequence with multislice CT. Commercial barium suspensions tend to taste better than iodine solutions, a factor in examining nausea-prone cancer patients. Iodine taste is often masked by adding sugar and various fruit extracts; although essentially sugar-free iodine contrast agents are available, in general the barium products contain less sugar than corresponding iodine suspensions.

One cannot take commercial barium sulfate preparations designed for fluoroscopic study and dilute them for CT use; such an attempt leads to a very low barium sulfate suspension in water, and within minutes this barium simply settles out of suspension on dependent bowel mucosa, resulting in incomplete lumen visualization and gross artifacts. Commercial CT barium manufacturers overcome this settling tendency, in part, by using rather small barium sulfate crystal particles and various high viscosity antisettling additives.

A concentration of 1.5% to 2.0% small particle barium sulfate preparations is suitable for oral small bowel opacification during abdominal CT; as a further refinement, a 2.0% concentration provided better jejunal contrast, whereas a slightly lower concentration is better suitable for pelvic structures.

Other CT oral contrast agents are feasible and at times preferred. Among whole milk, 2% milk, water, barium suspension, and no oral contrast, whole milk was superior to the others (4).

The term *double-contrast abdominal CT* is used in the trauma literature to specify use of both intravenous and per oral contrast; this is a misuse of the traditional connotation of "double contrast" in radiology and is best avoided to prevent confusion.

Computed Tomography Enteroclysis

Computed tomography enteroclysis consists of bowel intubation with an enteroclysis catheter and instilling a water-soluble contrast agent, a dilute barium suspension, or a methylcellulose suspension followed immediately by CT scanning. Whether a positive contrast agent or a water-density agent together with an intravenous contrast agent to opacify bowel mucosa is superior is not clear. Negative oral contrast agents designed specifically for CT-enteroclysis are also becoming available. Multislice CT performed during a single breath-hold allows three-dimensional (3D) reconstruction.

Computed tomography enteroclysis is a viable alternate in a setting of small bowel obstruction or inflammatory bowel disease and in a search for polyps. It is superior to conventional CT, especially with low-grade bowel obstruction. Whether CT enteroclysis is preferred over conventional enteroclysis is debatable.

Ultrasonography

Conventional ultrasonography (US) does detect small bowel wall thickening. The major limitation of US is in a setting of increased bowel gas, a finding usually present in many small bowel abnormalities.

Magnetic Resonance

Technique

Currently magnetic resonance (MR) has a limited role in small bowel disease, although potential applications exist. After CT enteroclysis, it was only a question of time before MR enteroclysis was also performed. Single breath-hold magnetic resonance imaging (MRI) after enteroclysis with oral iron particles in Crohn's patients detected most stenoses, fistulas, and marked bowel wall thickening with prominent contrast enhancement (5). Magnetic resonance enteroclysis using methylcellulose in patients with suspected inflammatory bowel disease or small bowel obstruction achieves similar results to those obtained with conventional enteroclysis or surgery (6). Another MR enteroclysis study using oral and IV gadolinium–diethylene triamine pentaacetic acid (DTPA) reached similar conclusions, noting that a prerequisite for an excellent study is good bowel distention and a homogeneous appearance (7). Although one study of CT enteroclysis immediately followed by MR found CT sensitivity higher than MR in detecting small bowel wall thickening, wall enhancement and detection of adenopathy (8), the relative merits of CT enteroclysis versus MR enteroclysis remain to be explored.

Although techniques vary, precontrast T1-weighted spoiled gradient echo (SGE) images, T2-weighted images, and early and late post-contrast SGE images are commonly obtained. Single breath-hold MR sequences minimize peristaltic artifacts and aid in evaluating dilated bowel.

Contrast Agents

The primary objective of oral MR bowel contrast agents is to identify bowel lumen and differentiate normal bowel wall from an abnormal process. For most MR enteroclysis, contrast is injected via a nasojejunal catheter.

Oral MR contrast agents are subdivided into positive contrast agents, which predominantly shorten T1 and increase MR signal intensity on T1-weighted images, and negative contrast agents, which either shorten T2 and decrease signal intensity or simply lack hydrogen protons. Positive contrast agents include various iron, manganese, and gadolinium paramagnetic compounds. Their hyperintense signal is useful in detecting a sinus tract; on the other hand, they mask intraluminal contents and make bowel wall visualization difficult.

A distinction between positive and negative contrast agents is not absolute, and MR properties of some contrast agents change both with dilution and MR sequence used. For example, in vivo ferric ammonium citrate is hyperintense on both T1- and T2-weighted turbo spin echo (TSE) and fat-suppression images 20 minutes after contrast administration at concentrations <45 mg/mL (9); on the other hand, at higher concentrations and at 10 to 20 mg/mL, bowel loops are hypointense on T2-weighted TSE and short-time inversion recovery (STIR) images both at 20 minutes and 2 hours. A more relevant issue is whether this contrast improves sensitivity and specificity for detecting abnormalities; the current results are not clear (10). Gadolinium is a positive contrast agent and shortens T1 in the small bowel, but when concentrated in the colon acts as a negative contrast agent.

A dilute barium sulfate suspension is a useful negative agent. Air and water are also MR contrast agents. The perfluorocarbons lack hydrogen protons and do not produce a MR signal on either T1- or T2-weighted images. Their role in the gastrointestinal tract is not established.

Positive contrast agents accentuate motion artifacts, which are reduced by choosing short scanning times. On the other hand, contrast artifacts are more common with negative agents, yet bowel wall detail is accentuated with negative agents. Use of antiperistaltic pharmacologic agents is not common.

Scintigraphy

Technetium-99 m (Tc-99 m)–hexamethylpropyleneamine oxime (HMPAO)–labeled leukocyte scintigraphy is useful in detecting inflammation. Its major application is with a suspected abscess, in Crohn's disease, and other inflammatory processes.

Capsule Endoscopy/Biopsy

Capsule endoscopy is an endoscopic procedure and is not covered in this work, but mentioned must be its relevance to small bowel imaging

studies. The most common abnormal capsule finding is angioectasia and similar submucosal malformations, lesions not detected by imaging studies (11); also, more ulcers are detected with a capsule than with barium or CT.

Percutaneous 18-gauge core biopsies or 21-gauge aspiration of bowel wall tumors using CT and US guidance are performed similarly to other abdominal site biopsies.

Percutaneous Jejunostomy

A percutaneous jejunostomy is believed to be difficult to perform due to inconstant small bowel position and mobility. Yet one study achieved a 95% success rate for new feeding jejunostomies and an 81% success rate for replacement jejunostomies (12); these jejunostomies aid drainage, dilation, stone extraction, and bile duct or intestinal recanalization. Leakage is a possible complication.

During esophagectomy, a loop of jejunum can be surgically fixed to the anterior abdominal wall and marked with metal clips; later these clips can be used as guides for percutaneous access for a feeding jejunostomy in those requiring additional nutritional support.

Congenital Abnormalities

Rotation Anomalies

Midgut malrotation implies an arrest in the usual rotation at any one position, with portions of bowel being not in their usual place, that is, they are malpositioned. Such malposition is usually accompanied by lack of fixation and it is usually this fixation anomaly that allows the bowel to twist and form a volvulus.

Patients with congenital diaphragmatic hernias have a high prevalence of midgut rotational abnormalities, and those with right-sided hernias have a more obvious anomaly than those with left-sided ones. Yet mid-gut volvulus is uncommon among patients operated upon for a congenital diaphragmatic hernia, probably related to postoperative adhesions limiting development of a volvulus in these patients with rotational abnormalities.

Malrotation does occur in each of a pair of identical twins. Midgut malrotation is common in patients with asplenia and polysplenia, and a barium study to detect malrotation is suggested in these patients (situs inversus and heterotaxy syndrome are discussed in Chapter 14).

Presenting symptoms in a setting of malrotation reflect the degree of obstruction and are age dependent. In neonates, bilious vomiting predominates. In older children, pain, bilious vomiting, and failure to thrive are common. Teenagers and young adults tend to have chronic nonspecific pain. Obstruction due to malrotation is accentuated in pregnancy.

With incomplete rotation the cecum is located more medial than usual. Fibrous bands extending diagonally from a malpositioned cecum to the right upper quadrant (Ladd bands) tend to compress adjacent small bowel and result in duodenal or jejunal obstruction of varying severity.

In many of these individuals a diagnosis of malrotation is made either by an upper gastrointestinal examination or a barium enema; the former is more sensitive and is preferred (Fig. 4.1). Subtle rotational anomalies are not uncommon, and the diagnosis is not as straightforward as generally taught. Some children have an unusual duodenal redundancy or a duodenojejunal junction located somewhat more medial than usual. In fact, in some of these children an upper gastrointestinal examination is believed to be grossly "normal." The status of duodenal redundancy with a normal duodenojejunal junction as a marker for subtle intestinal malrotation is not known. The reverse is also true—false-positive diagnoses result from failure to recognize normal variants in jejunum position. Manual epigastric compression during an upper gastrointestinal examination is useful to detect some neonate intestinal malrotations. For instance, manual compression of a near-normal duodenojejunal junction can detect abnormal mobility, suggesting malrotation; in some infants with malrotation and volvulus, manual compression induces contrast to pass beyond the point of obstruction and identifies a twist.

A reversed relationship between the superior mesenteric artery and vein, a sign of midgut volvulus, is not always present with malrotation, and this sign cannot be relied on to detect malrotation. A deep ileocolic intussusception also distorts normal superior mesenteric vessel anatomy.

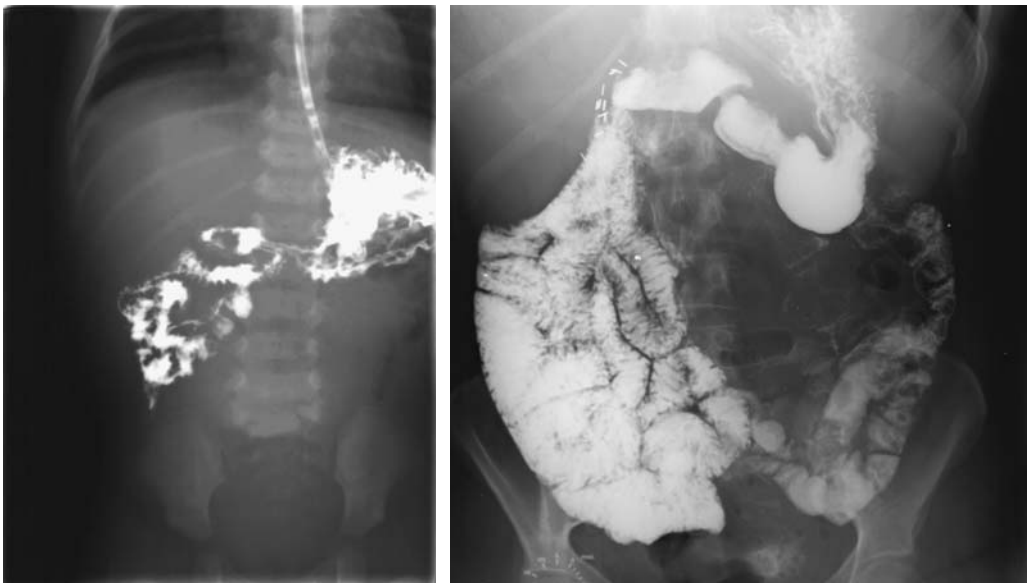

A B

Figure 4.1. A: Midgut malrotation in a newborn. B: Midgut malrotation in a 27–year-old with chronic abdominal pain. Although uncommon, patients this age can develop midgut volvulus as an acute presentation.

Occasionally a malrotation is suspected with radionuclide gastric emptying studies performed for other reasons.

Duplication

A small bowel duplication is lined with intestinal mucosa and is usually intramural in location. It may or may not communicate with the true lumen. Ileal duplications are more common than jejunal. Multiple duplications are rare.

Some patients with a duplication are asymptomatic, whereas others present with a palpable mass or even obstruction. In general, most larger duplications manifest early in life. A communicating ileal duplication is an occasional cause of massive hemorrhage.

Imaging typically shows a duplication as an oval or elongated cystic structure adjacent to bowel lumen. It generally has a thick wall, thus distinguishing it from a mesenteric cyst, which is thin-walled. Ultrasonography reveals the cystic nature of a duplication; in addition, US shows a characteristic inner hyperechoic mucosa and an outer hypoechoic muscle layer.

Many duplications contain ectopic gastric mucosa, and thus scintigraphy (Meckel's scan) detects some. An occasional one contains ectopic pancreatic tissue.

Obstruction

Atresia

Small bowel atresia, believed to be secondary to intrauterine ischemia, ranges from complete to partial and involves the jejunum, the ileum, or both. It is associated with midgut malrotation and is more prevalent in a setting of cystic fibrosis. Autosomal dominance is evident in some families with bowel atresia. Not all atresias are detected in early life; a rare infant develops an ileocolonic fistula to bypass an atretic segment.

Some authors subdivide jejunoileal atresia into four types:

Type I: a short, web-like narrowing

Type II: blind-ending proximal and distal tracts with a fibrous connection

Type III: a short, atretic segment in the proximal jejunum

Type IV: multiple atretic segments

In the rare *apple-peel* type of atresia the distal duodenum or proximal jejunum ends blindly, the distal superior mesenteric artery is absent, and the distal small bowel is foreshortened and spirals around its rudimentary blood supply, appearing similar to an apple peel. This condition presumably is due to a distal superior mesenteric artery occlusion or failure to develop.

Meconium Ileus

Meconium ileus is in the differential diagnosis with a suspected low intestinal obstruction. Almost all neonates developing meconium ileus have cystic fibrosis. Some have an underlying atresia, stenosis, or volvulus. Untreated, meconium ileus may progress to bowel necrosis and perforation (meconium peritonitis is discussed in Chapter 14).

Conventional radiographs reveal a low obstruction. Other findings, such as a bubbly appearance in the right lower quadrant, lack sufficient sensitivity and specificity to be diagnostic.

A water-soluble contrast enema is not only diagnostic but also often therapeutic. It identifies a small-caliber colon (microcolon), but keep in mind that both a meconium ileus and distal small bowel atresia result in a small caliber colon. With a distal ileal obstruction, however, the entire colon has a small caliber; otherwise a colonic abnormality should be sought Meconium ileus results in intraluminal content at the site of obstruction.

Ultrasonography in six neonates with a meconium ileus revealed multiple loops of bowel filled with hyperechoic material (13); this is in distinction to neonates with ileal atresia who have dilated loops of bowel filled with fluid and gas but not hyperechoic content.

A distinction between a meconium ileus and ileal atresia is more than academic, because the former is usually relieved by a contrast enema but the latter requires surgical intervention.

Cystic Fibrosis

Cystic fibrosis, with a recessive-autosomal inheritance pattern, involves multiple organs, with the lungs and pancreas most often affected. A number of affected patients eventually develop chronic liver disease. The sweat test should initially be performed when cystic diagnosis is suspected.

In patients eventually shown to have cystic fibrosis, newborn meconium ileus occurs as an initial presentation only in a minority. On the other hand, those with a meconium ileus almost all have cystic fibrosis.

The bowel wall becomes thickened in these children; histology reveals extensive intramural fibrosis and fatty infiltration, but unlike Crohn's disease, acute inflammation is not a prominent feature.

Distal ileal obstruction due to inspissated intestinal content developing after the neonatal period is called *meconium ileus equivalent*. The prevalence of such obstruction increases with age. Especially during the first such obstructive episode, acute appendicitis is often in the differential diagnosis. A contrast enema is generally diagnostic. Often contrast does not reflux into the terminal ileum. Computed tomography is occasionally used to monitor these patients. The diagnosis can be suspected with US.

Other causes of bowel obstruction in these patients include intussusception and colonic strictures. One child with cystic fibrosis developed partial ascending colon obstruction secondary to diverticulitis (14), a very rare complication indeed.

A number of cystic fibrosis patients now reach adulthood and they are developing new complications, such as cancer, which is not common in the pediatric age group.

A barium enema reveals an irregular and spiculated colon outline, nodules, and loss of haustra. Irreversible and progressive colonic strictures tend to develop, at times to the point of almost complete obstruction.

Thickened small bowel folds and nodularity are familiar to most radiologists. Conventional abdominal radiographs reveal calcifications only in a minority ranging from small specks of calcium to extensive curvilinear calcifications; most calcifications are intramural in location, with a minority being intraluminal or serosal. An occasional newborn with cystic fibrosis has multiple atresias and calcified intraluminal meconium.

Celiac Disease (Sprue)

Clinical

Celiac disease, or gluten-sensitive enteropathy, is a familial genetically determined disease associated with human leukocyte antigen (HLA)-B8-DR3 and manifesting by a digestive tract cytotoxic T-lymphocyte reaction. Affected individuals have a lifelong intolerance to dietary gluten. Certain foods, such as wheat, barley, rye, and others, exacerbate the symptoms of this protein-losing enteropathy. A strict gluten-free diet protects against known complications.

Considerable variability exists in presentation. A latent form of celiac disease appears to exist; affected individuals have subtle small intestine abnormalities consisting of increased intraepithelial lymphocyte levels, abnormal mucosal permeability, and elevated levels of secretory immunoglobulin A (IgA) and IgM antibody to gliadin. Occasionally celiac disease is first diagnosed even in elderly patients, presumably as an expression of silent disease that has been present since childhood. At times unrelated abdominal surgery unmasks latent celiac disease. It does present in the puerperium. It is a complex disease; variants such as celiac disease with immunologic activation of normal small bowel mucosa have been suggested. Some patients have liver disease, detected as a hypertransaminasemia and often labeled a nonspecific reactive hepatitis, which reverts to normal on a gluten-free diet. In an occasional patient an immunologic basis is suggested by finding associated primary biliary cirrhosis, primary sclerosing cholangitis, or autoimmune hepatitis.

Worldwide prevalence of celiac disease varies considerably. An interesting postulate is that the introduction of a high gluten content diet at an early age increases the risk and affects the symptomatology of celiac disease in a specific population. A study involving roughly half of the French pediatric population found an annual incidence of one per 2419 (15); the diagnosis was made before age 2 years in 77% of affected individuals, with the symptoms being failure to thrive, diarrhea, anorexia, abdominal distention, weight under two standard deviations, and short stature.

Orocecal transit time is delayed, and small bowel villous atrophy develops in untreated patients.

Highly sensitive and specific noninvasive blood tests for celiac disease are available, and imaging is relegated to a study of complications. A small bowel biopsy appears superfluous to confirming the diagnosis in symptomatic adults with antibodies to IgA antiendomysial.

Imaging

Patients with celiac disease have fasting or postprandial bowel motor abnormalities, which in most affected individuals are similar to those found in neuropathic disorders (Fig. 4.2). Dilated distal small bowel containing excessive fluid is a late but characteristic finding, at times mimicking partial distal small bowel obstruction. These abnormalities decrease on a gluten-free diet.

Enteroclysis achieves an almost 100% specificity but only about 80% sensitivity in detecting celiac disease in adults (16).

Ultrasonography of infants with known celiac disease detects abdominal fluid and hyperperistalsis in most. The US findings in adults include fluid-filled, dilated small bowel. Disordered motility is common. Bowel wall thickening is mild; marked thickening suggests hypoproteinemia, and asymmetric thickening raises suspicion for a neoplasm. Abdominal fluid is found in a minority. None of these findings are pathognomonic, but detection of several findings should raise suspicion for this disease.

Mild-to-moderate mesenteric adenopathy is common. If an untreated patient is placed on a gluten-free diet, serial CT should show a reduction in node size. Mesenteric lymph node necrosis develops in a rare patient.

Superior mesenteric artery Doppler US in untreated patients reveals significantly higher fasting peak systolic velocity, end diastolic velocity, mean velocity, and flow volume than in controls, and a resistive index that is significantly lower (17). Of interest is that the superior mesenteric artery and portal vein tend to dilate. The effect of therapy on the superior mesenteric artery resistive index is illustrated in Table 4.1.

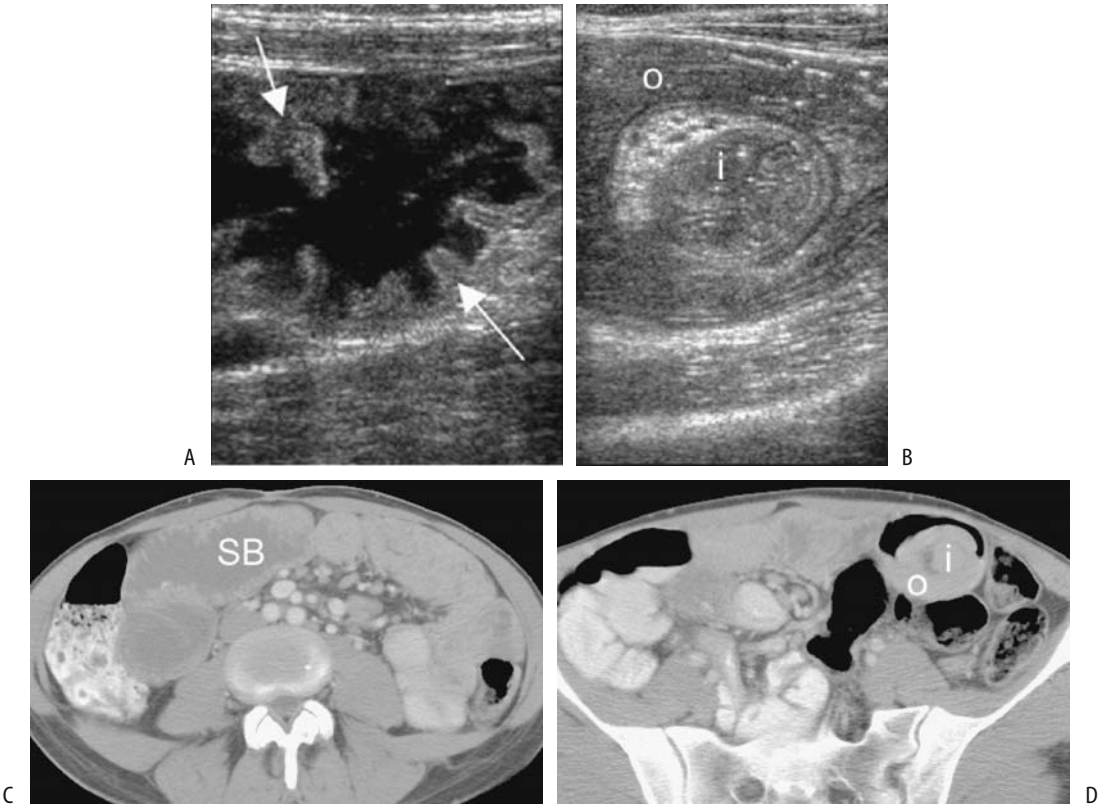

Figure 4.2. Celiac disease. A: Transverse sonogram in a 35–year-old woman reveals dilated, fluid-filled small bowel loops containing prominent folds (arrows). (b) An intussusception is evident in another US image. C,D: Transverse CT after oral and IV contrast also identified dilated fluid-filled small bowel loops (SB). D: An intussusception is evident in the left lower quadrant (i) (Courtesy of Martin E. O'Malley, M.D. *Source:* Wilson SR. Evaluation of the small intestine by ultrasonography. In: Gourtsoyiannis NC, ed. Radiological Imaging of the Small Intestine. Heidelberg, Germany: Springer-Verlag, 2002 with permission.)

Protein-losing enteropathy can be studied with several scintigraphic agents, including Tc-99 m human serum albumin (HSA), Tc-99 m human immunoglobulin, indium 111 transferrin, and Tc-99 m-dextran.

Comparing pretreatment and follow-up enteroclysis in adults with celiac disease, clinical response to a gluten-free diet correlated better with enteroclysis findings than with repeat biopsy (19).

Table 4.1. Superior mesenteric artery resistive indices (RI) in celiac disease

	Number of patients	Overnight fasting	After meal	RI change
Controls	10	0.81 ± 0.02	0.67 ± 0.03	0.14 ± 0.2
Celiac disease				
Untreated	10	0.78 ± 0.05	0.74 ± 0.01	0.04 ± 0.01
Treated	10	0.79 ± 0.03	0.70 ± 0.02	0.09 ± 0.02
Crohn's disease				
Inactive	10	0.82 ± 0.03	0.69 ± 0.04	0.13 ± 0.3
Active	10	0.78 ± 0.03	0.70 ± 0.02	0.08 ± 0.03

Source: Adapted from Giovagnorio (18).

Associated Conditions/Complications

Lymphocytic gastritis develops in a minority of patients with celiac disease. Of interest is that gastric mucosa-associated lymphoid tissue (MALT) regresses in *Helicobacter pylori*–negative celiac patients when treated with a gluten-free diet.

Patients with long-standing celiac disease are at increased risk for malignancies, with small bowel high-grade T-cell lymphoma being most common and tending to involve the proximal small bowel. This is in distinction to lymphoma in normal small bowel, which is usually B cell in origin. Celiac disease and lymphoma have been diagnosed during the same presentation. A common appearance is that of small, discrete nodules varying in size or localized fold thickening. Nodules are not found in uncomplicated celiac disease, and such a finding should suggest superimposed lymphoma. A CT finding of marked adenopathy also suggests lymphoma. At times a barium study outlines a shaggy, ulcerated bowel segment, mimicking inflammatory bowel disease. Complicating the issue is that these lymphomas are often associated with considerable inflammation, and a biopsy may suggest inflammatory bowel disease. Enteropathy-associated lymphoma has a poor prognosis, with malignant ulcers not uncommonly resulting in bowel perforation.

Small bowel adenocarcinomas also occur in these patients. In fact, an occasional patient presents with small bowel adenocarcinoma, and celiac disease is diagnosed only after cancer resection. The prevalence of pharyngeal and esophageal carcinomas is also increased in these patients.

An occasional patient develops intestinal ulcerations, loss of valvulae conniventes, and a thickened, tube-like bowel wall; the overall imaging appearance mimics chronic ischemia.

Type 1 diabetes mellitus is found in an occasional patient with celiac disease diagnosed in adulthood. An anecdotal association exists with primary sclerosing cholangitis, lupus, and antiphospholipid syndrome. Some evidence suggests an increased prevalence of celiac disease in patients with primary biliary cirrhosis. An autoimmune linkage is suggested with idiopathic thrombocytopenic purpura and hepatic granulomatous disease.

Splenic atrophy is common in these individuals. Whether splenic infarction and splenic venous thrombosis in one patient was fortuitous is conjecture (20).

Bone scintigraphy is positive for sacroiliitis in some adults with celiac disease.

Some patients with unresponsive celiac disease are treated with immunosuppressive therapy. A lack of response to therapy should raise the possibility of lymphoma, a setting contraindicating immunosuppressive therapy.

Agammaglobulinemia

An arrest in B-lymphocyte development leads to agammaglobulinemia. The primary defect involves mutations consisting of missense, nonsense, and splice mutations as well as deletion and insertion mutations in the gene encoding Btk (Bruton tyrosine kinase) (21).

Because maternal IgG passes through the placenta, affected newborns initially have normal serum IgG levels, but then these levels decrease and hypogammaglobulinemia ensues. Affected patients are prone to mostly bacterial infections. They have normal resistance to viral infections, except for enteroviral infections, leading to vaccine-related paralytic poliomyelitis and a dermatomyositis-meningoencephalitis syndrome (21). Intestinal giardiasis is common in these patients.

A barium small bowel study often is diagnostic in affected patients; marked lymphonodular hyperplasia is evident throughout the small bowel, especially the jejunum, a site where even in pediatric patients lymphonodular hyperplasia is uncommon (Fig. 4.3).

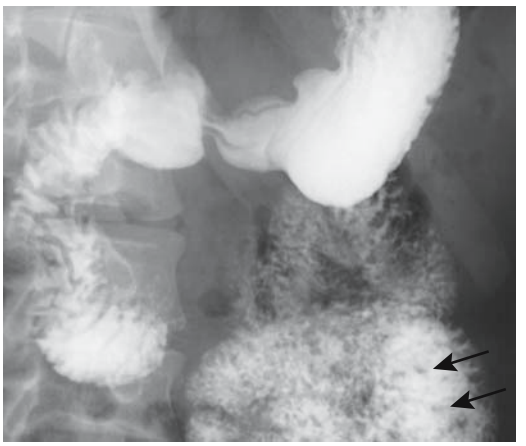

Figure 4.3. Agammaglobulinemia. Small nodules are scattered in the jejunum (arrows).

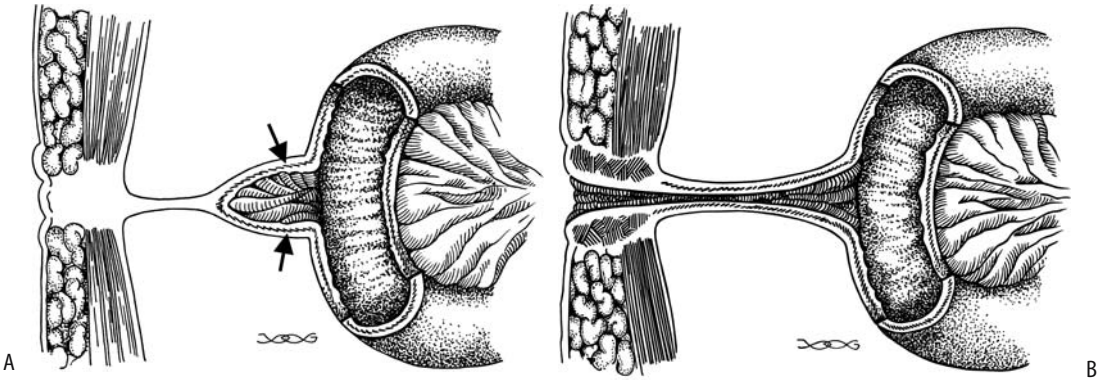

Figure 4.4. A: Diagram of a Meckel's diverticulum arising from the antimesenteric small bowel border (arrows) and connected to the abdominal wall by a fibrous tract. B: Instead of a fibrous tract, an omphalomesenteric duct connects bowel to skin.

Omphalomesenteric Anomalies

Failure of the omphalomesenteric duct to regress results in a residual umbilical sinus, omphalomesenteric cyst, enterocutaneous fistula, or a Meckel's diverticulum.

Cysts and Fistulas

An omphalocele is the presence of midgut structures in the umbilical cord remnant (Fig. 4.4). A variety of intestinal content may be present within the defect. The midgut is malrotated. Some patients have other anomalies.

An omphalomesenteric cyst is formed when both omphalomesenteric duct ends involute, leaving a persistent central cavity. Most are incidental findings, with an occasional one becoming infected or compressing and obstructing an adjacent structure. A persistent fibrous omphalomesenteric remnant between the umbilicus and midgut is a potential source for small bowel volvulus around the fibrous band.

Meckel's Diverticulum

Clinical

A Meckel's diverticulum is the most common congenital gastrointestinal tract abnormality (Fig. 4.5). It results from persistence of the embryonic yolk sac. Most Meckel's diverticula are asymptomatic but they can be involved in two clinical scenarios: More common is the patient presenting with bleeding suspected from gastric mucosa in a Meckel's diverticulum, with bleeding usually being gradual rather than massive. Less often encountered is the patient with sequelae to inflammation or intussusception. Obstruction is more common in patients under the age of 10 years, and perforation is more common in young adults. A rare Meckel's diverticulum first manifests in the elderly.

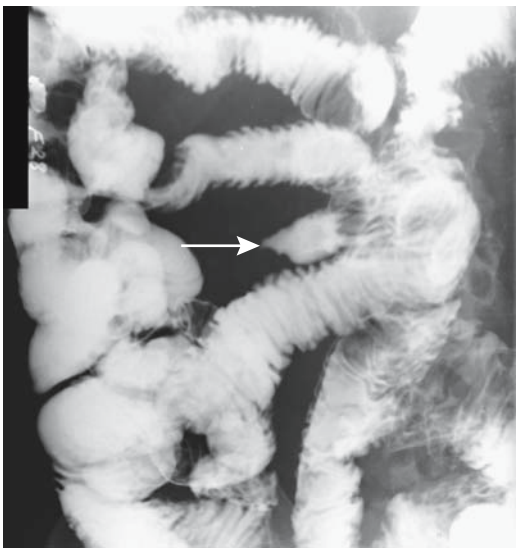

Figure 4.5. Meckel's diverticulum (arrow), detected on a retrograde small bowel examination.

Meckel's diverticula vary in size and shape, with an occasional one being very large. A rare one even has a second outpouching, or daughter diverticulum, connected to the main diverticulum. Ultrasonography reveals an uncomplicated, fluid-filled Meckel's diverticulum as a cyst-like structure. Some of these diverticula mimic an appendiceal mucocele, mesenteric cyst, enteric duplication, or even a cystic ovarian tumor if a separate ovary cannot be identified by imaging.

Complications

Ectopic gastric mucosa is found in 20% to 50% of patients with Meckel's diverticula and "gastritis" is common in those with gastric mucosa; only an occasional one contains *H. pylori*. Similar to the stomach, gastric secretions by this ectopic mucosa are stimulated by hormonal factors. As expected, hemorrhage and perforation develop in a setting of ectopic gastric mucosal tissue.

Incidentally, ectopic gastric mucosa is also found at other sites. As already mentioned, ectopic gastric mucosa is not uncommon in gastrointestinal duplications. In some patients, islands of heterotopic gastric mucosa in the jejunum and ileum account for recurrent small bowel bleeding and accumulation of Tc-99 m-pertechnetate at these sites. The Tc-99 m-pertechnetate concentrates in gastric mucosal mucin secreting cells, and scintigraphy reveals persistent focal activity only if such gastric mucosa is present within the diverticulum. Cimetidine or ranitidine premedication inhibits gastric secretion and helps diminish background activity. Still, both false-positive and false-negative results occur. At times abnormal Tc-99 m-pertechnetate uptake is shown with single photon emission computed tomography (SPECT) but not with planar imaging (22). It should be emphasized that a Meckel's scan detects only the presence of gastric mucosa, rather than hemorrhage or other complications.

Gastric mucosa enhances more than any other bowel mucosa on postcontrast MRI, and any gastric mucosa in a Meckel's diverticulum reveals marked enhancement.

Calculi are not common in a Meckel's diverticulum. An enterolith consists mostly of calcified food residue (phytobezoar). Some stones are multiple, calcified in their periphery, or even faceted. Rarely, a milk of calcium suspension forms in a Meckel's diverticulum (23). Most stones contain enough calcium to be visible with conventional radiography. Computed tomography and US also detect most of these stones.

A stone (or bezoar) passing into the ileal lumen can cause bowel obstruction and mimic gallstone ileus. A rare enterolith within a Meckel's diverticulum obstructs the diverticular communication with bowel lumen and leads to diverticulitis. Imaging should identify such a calcified enterolith; superficially an appendicolith is in the differential.

Perforation of a Meckel's diverticulum is commonly ascribed to ulcerated heterotopic gastric mucosa. An 8-day-old boy perforated a Meckel's diverticulum (24), a highly unusual age for this to occur; no ectopic gastric tissue was found in the resected specimen, and a narrow diverticular neck was believed to have led to poor emptying, subsequent inflammation, and perforation.

Inflammation does result in Meckel's diverticulitis. A CT scan showing a fluid-filled cavity surrounded by a thickened, contrast-enhancing wall suggests diverticulitis.

There is no reason why a Meckel's diverticulum should not be involved by Crohn's disease. Differentiating terminal ileal Crohn's disease (and possibly involving a Meckel's diverticulum) from an inflamed and ulcerated Meckel's diverticulum is another matter; resultant distortion is similar with both.

A Meckel's diverticulum is a potential point for small bowel fixation. Torsion initially involves only the diverticulum, but a sufficient twist leads to ileal volvulus. Adhesions secondary to an inflamed diverticulum form a site for an internal hernia.

An inverted Meckel's diverticulum is a potential lead point for a small bowel intussusception, and in the distal ileum most intussusceptions are due to either a polyp or a Meckel's diverticulum. An inverted Meckel's diverticulum appears as an intraluminal polyp. A barium study reveals an inverted diverticulum as a solitary, elongated, smoothly marginated, often club-shaped intraluminal tumor. This inverted diverticulum often contains fat along its serosal surface, detected by CT as an intraluminal elongated mass containing central fat surrounded by

soft tissue. Ultrasonography shows a target-like structure with a hyperechoic center and identifies a blind-ending, thick-walled bowel loop. An intussuscepting inverted Meckel's diverticulum is difficult to reduce with a barium or air enema.

Conventional radiography detects a perforation or suggests an obstruction; CT and US identify the site of obstruction and any abscesses and often suggest the underlying etiology.

Tumors similar to those found throughout the gastrointestinal tract also develop in Meckel's diverticula. A number of these are detected incidentally when a diverticulum is resected for unrelated reasons. These tumors range from adenomas and carcinomas to sarcomas, and originate from either ileal or gastric epithelium. A leiomyosarcoma originating in a Meckel's diverticulum contained a 4-L cystic component, presumably secondary to necrosis (25). A rare neuroendocrine tumor has developed in a Meckel's diverticulum.

Therapy

If an incidental Meckel's diverticulum is discovered, some surgeons recommend that a diverticulectomy be performed; others argue that the risk of complications, although low, does not justify a prophylactic resection. A morbidity of 2% and zero mortality was found in a retrospective study of 90 patients who had an incidental diverticulectomy (26); using decision analysis the authors concluded that an incidental diverticulectomy in adults should be abandoned.

Bleeding and obstruction are the primary presentations in patients requiring surgery for symptomatic Meckel's diverticula. Less frequent indications for surgery are an acute abdomen due to perforation, diverticulitis, or intussusception.

Trauma

Most radiologists administer both oral and IV contrast prior to a CT trauma study. Oral contrast is generally started early on, often in the emergency department. Its use has been questioned by emergency physicians, who point out the additional time incurred, the extra need to insert a nasogastric tube in some patients, and the alleged lack of efficacy, yet most radiologists involved in trauma care find oral contrast very beneficial and administer it almost routinely.

Bowel distention is common with significant bowel trauma, yet this finding is nonspecific; it occurs with bowel obstruction and peritoneal irritation due to a number of etiologies.

A review of almost 20,000 blunt trauma patients found that hollow-viscus injury occurred with a similar frequency in both children and adults (27); duodenal injuries, however, were more common in pediatric patients.

Shock Bowel

Shock bowel represents a diffuse bowel abnormality developing in hypotensive patients, often in a setting of blunt abdominal trauma. The CT findings of shock bowel consist of diffuse small bowel wall thickening, with increased and prolonged contrast enhancement. Often fluid-filled, dilated small bowel is also identified. The colon generally is less affected than small bowel. These bowel CT findings are secondary to hypoperfusion and, at least initially, are reversible.

Bleeding/Hematoma

Intramural hemorrhage manifests as a region of bowel wall thickening. It ranges from focal to diffuse. Hematomas also develop adjacent to injured bowel, either intra- or retroperitoneal in location. Because of its intraperitoneal location, small bowel trauma often also results in hemoperitoneum rather than a discrete hematoma. Combined bowel wall and mesenteric injury is often present and fluid (blood) between loops of small bowel is a result of trauma to either one.

Intramural hemorrhage is identified as a homogeneous, focal hyperdense bowel wall thickening that does not enhance postcontrast. Unenhanced CT is often helpful in this setting. Generally a bowel wall thicker than 3 or 4 mm (as detected with CT) is assumed to be abnormal, although little evidence in the literature provides quantitative guidance. Some authors

believe that circumferential wall involvement is necessary for bowel to be considered abnormal (28).

A hyperechoic submucosal layer thicker than 2.5 mm, detected by US, implies either submucosal edema or hemorrhage (29).

Most bowel wall hematomas resolve without sequelae; some produce transient small bowel obstruction, but in a few bleeding leads to a stricture requiring surgery.

Perforation

Isolated small bowel perforation due to acute blunt abdominal trauma is uncommon; a number of these are due to seat belt trauma. More serious injury to adjacent solid organs is often more evident. Small bowel perforation tends to be more common on the antimesenteric border.

A pneumoperitoneum and extraperitoneal gas are specific but insensitive findings of a small bowel perforation. The small bowel normally contains little gas, and a number of these perforations manifest later as an intraabdominal abscess rather than as an immediate pneumoperitoneum.

Direct CT evidence of bowel rupture is uncommon. An indirect postcontrast CT sign of small bowel rupture consists of a streaky density within the related mesentery due to blood and other infiltration along the mesenteric vasculature.

Small bowel perforation after blast injury is not common. Anecdotal evidence in three men injured by the explosion of a terrorist bomb suggests that an eventually proven perforation does occur after a finite time delay rather than being a manifestation of delayed diagnosis (30); the authors suggest that patients exposed to a blast injury be observed for at least 48 hours.

Stricture

In an occasional patient ischemia of a crushed bowel segment leads to an infarct. A less severe insult evolves into an eventual fibrosis and stricture with the patient presenting with small bowel obstruction weeks or even months after trauma.

Wall Thickening

Infection/Inflammation

Clinical presentation in a setting of small bowel infection or inflammation varies considerably. Likewise, imaging findings range from minor thickening of valvulae conniventes to marked intramural infiltration. Submucosal edema and hemorrhage, if severe enough, may lead to small bowel obstruction.

Crohn's Disease

Clinical

Epidemiologic data for Crohn's disease patients suggest the presence of a recessive gene having high penetrance, in distinction to ulcerative colitis where a dominant or additive gene having low penetrance is more likely. Numerous investigators have searched for an infective etiology. Although a superimposed infection is not uncommon, identification of an infective etiology for Crohn's disease has not been fruitful and currently no convincing infective etiologic agent is established.

Crohn's disease in two or more members of a family is found in about 10% of patients; similarly, the prevalence among first-degree relatives is about 10 times that of the general population. Conflicting data exist on whether patients with a familial pattern have an earlier age at onset and more extensive disease than those with sporadic disease.

Prevalence of Crohn's disease has increased during the last several decades in several populations. Considerable variation in relative prevalence of Crohn's disease still exists. Crohn's disease is rare in Central and South America. Although rare among the Chinese, prevalence is increasing, at least in Singapore; in 1993, at Singapore General Hospital the prevalence was 27 per 100,000 patients compared with 3.5 per 100,000 patients in 1986 (31). In the United States, distal ileal involvement is most common. In parts of Europe colorectal involvement predominates at the time of diagnosis. In general, colonic involvement is more prevalent in patients with disease manifesting at a later age. The disease is not limited to the bowel, and even extraintestinal sites can be involved.

Crohn's disease has two age peaks of onset. At the more common younger age, Crohn's disease tends to develop after puberty, with only an occasional younger child being affected. Almost all present with abdominal pain, with most children also having weight loss and diarrhea. The second age peak is in the elderly. Here one has to exclude bowel ischemia, which in some patients has a similar clinical presentation and imaging appearance. Nevertheless, enough evidence has accrued to establish that a second peak of onset does indeed occur in the elderly. In general, those having an initial diagnosis made before the age of 20 years have a greater prevalence of family history of Crohn's disease, more small bowel involvement, and they require more frequent surgery than those diagnosed after age 40 years; the older group had more colonic involvement.

Standardized clinical estimates of severity and activity of Crohn's disease have been developed and these allow comparison of published studies.

Chronic abdominal pain is common, often being insidious in onset and progression. Some children present with growth retardation or simply delayed puberty. In a small minority of patients hepatobiliary or joint abnormalities manifest first. Especially in children, a blood count and erythrocyte sedimentation rate are almost always abnormal, and these tests appear reasonable with suspected Crohn's disease.

The literature tends to emphasize gradual disease progression, but in reality two patterns predominate: In a minority, Crohn's disease is unrelenting, progresses rapidly, perforates readily, and relapses after surgery; in a majority a chronic, indolent course marked by periods of exacerbation and quiescence is more common. Clinical evidence suggests that Crohn's disease patients tend to fall into specific categories such as those primarily with inflammation and fibrosis-stenosis and those forming fistulas. Within families, patients tend to have concordance of sites and types of involvement.

Pregnancy appears to have a mild favorable influence; prevalence of disease relapse after pregnancy is somewhat less than before pregnancy.

Five patients with Crohn's disease and leukemia received allogeneic bone marrow transplantation (32); four showed no signs or symptoms of Crohn's disease after transplantation; Crohn's disease relapsed after transplantation in one patient with mixed donor–host hematopoietic chimerism.

Four patients with long-standing Crohn's disease had a spontaneous clinical improvement after becoming HIV infected, suggesting that immune response integrity has a role in Crohn's disease (33). These findings are countered, however, by an HIV-infected patient who developed a new onset of Crohn's disease (34).

Anti–goblet cell autoantibodies are detected in some patients with Crohn's disease and in their first-degree relatives, suggesting that this marker is of possible use in detecting patients susceptible to inflammatory bowel disease.

Intussusception is rare with Crohn's disease; presumably the commonly associated fibrosis prevents it. Nevertheless, occasional enteroenteric intussusception has been reported.

Associated Conditions

A family with both familial polyposis and Crohn's disease, probably a fortuitous association, has been described (35). Several patients have developed synchronous Crohn's disease and myelodysplastic syndrome, and this association appears to be more than chance. Myelodysplastic syndrome probably should be considered in older patients with Crohn's disease and peripheral blood cytopenia, and Crohn's disease should be considered in myelodysplastic syndrome patients developing gastrointestinal symptoms. Isolated associations have been reported with multiple sclerosis, glycogen storage disease, sarcoidosis, rheumatoid purpura, ankylosing spondylitis, Charcot-Marie-Tooth disease, deuteranopia, pachydermoperiostosis, multiple exostosis, and familial ichthyosis.

Remission was induced by chemotherapy in a patient with non-Hodgkin's lymphoma (36); abdominal pain, diarrhea, and bloody stools 1 year later were found to be secondary to Crohn's disease.

An occasional pancreatitis is difficult to place in proper perspective; in some patients it appears related to sclerosing cholangitis, in others to azathioprine therapy, and in still others it appears to be fortuitous. Nevertheless,

pancreatic autoantibodies are detected in some Crohn's patients, and some have impaired pancreatic function.

Differential Diagnosis

On an acute basis, some infections are indistinguishable both clinically and radiographically from Crohn's disease (these are discussed below; see Acute Enteritis). On a more chronic basis, other infections, radiation enteritis, ischemia, Behçet's syndrome, and some neoplasms have a similar appearance. Major venous thrombosis in a young patient or an ischemic stenosis suggests Crohn's disease.

Close clinical and imaging similarity between Crohn's disease and Behçet's syndrome warrants mention (Behçet's syndrome is further discussed in Chapter 17). Behçet's syndrome is often not considered in the differential diagnosis in regions of low prevalence, and undoubtedly some patients have been misclassified. Bowel involvement in Behçet's syndrome manifests as bowel wall thickening enhancing postcontrast, inflammatory polyps, aphthae, or deep ulcers. Deep distal ileal or right colonic ulcers or a frank perforation should suggest Behçet's syndrome.

A primary ileocecal region lymphoma can mimic Crohn's disease. A problem exists for the radiologist who detects typical imaging findings of ileal Crohn's disease in a patient without an established diagnosis. Should lymphoma be mentioned in the differential diagnosis? Although rare in this imaging setting, some radiologists encounter lymphoma mimicking Crohn's disease in their practice.

Another entity bedeviling radiologists who detect ileal wall thickening on CT and suggest Crohn's disease is that a minority of right colon cancers result in similar findings (37); in some patients this thickening is due to direct tumor extension, but in others lymphatic obstruction, congestion, and edema are responsible.

The poorly understood chronic granulomatosis syndrome probably is distinct from Crohn's disease. Whether orofacial granulomatosis is a manifestation of underlying gastrointestinal Crohn's disease is speculative.

The clinical findings and imaging appearance of diffuse intestinal ganglioneuromatosis, especially if involving the distal small bowel, mimic Crohn's disease (38).

Pathologic Findings

Measured intraoperatively, the small bowel in Crohn's patients is significantly shorter than in controls.

Increased intestinal permeability and presence of antineutrophil leukocyte antibodies are two of several theories proposed to explain the findings in Crohn's disease; no definitive proof exists for either one.

One of the hallmarks of Crohn's disease is the presence of noncaseating granulomas. Why these granulomas develop is not clear. Almost half of these granulomas are adjacent to lymphatic vessel. Mucus-secreting cells are found at sites of ulceration and presumably are sequelae of ileal crypt stem cell differentiation.

Ileal ulcers in Crohn's disease tend to have a longitudinal orientation and predominate along the mesenteric side. The short vessels supplying this region are end arteries, and small vessel ischemia is a possible cause of these ulcers.

Imaging

Barium Studies

Whether a conventional small bowel barium study or enteroclysis is performed in an initial search for Crohn's disease is controversial. Some enthusiasts consider enteroclysis the primary imaging method in diagnosing small bowel Crohn's disease, and mild changes, including subtle aphthae and fistulas, are best seen with enteroclysis. With well-established disease a conventional study is generally sufficient and as an initial study is preferred by many investigators due to its simplicity, better patient acceptance, and relatively high yield. A conventional small bowel barium study is often used to follow exacerbation in patients with established disease. A well-performed study detects strictures, obstruction, fistulas, and a phlegmon. It does not differentiate a phlegmon from an abscess. Also, morphologic findings on a small bowel study correlate poorly with clinical activity; scintigraphy achieves better correlation.

A conventional small bowel study reported better mucosal detail, more fistulas, and more

duodenal involvement than enteroclysis performed within 2 weeks (39). Although the authors concluded that if a small bowel study is normal, no need for enteroclysis exists, a number of gastrointestinal radiologists would disagree and recommend enteroclysis, especially when seeking subtle findings.

A peroral pneumocolon or retrograde study evaluates the cecum and distal ileum using a double-contrast technique (Fig. 4.6). It is an underutilized study in select patients with subtle Crohn's disease suspected at these sites.

The most common site of small bowel involvement is the terminal ileum, yet any site can be involved. The imaging appearance varies considerably with more proximal involvement (Fig. 4.7).

At times normal small bowel proximal to a diseased segment is somewhat dilated, even without evidence of distal obstruction, a finding ascribed to peritoneal irritation and resultant mild adynamic ileus. One interesting observation made by monitoring intraluminal pressure with a double-lumen tube during enteroclysis is that Crohn's patients have an elevated intraluminal pressure compared to patients with noninflammatory disease and irritable bowel syndrome (40).

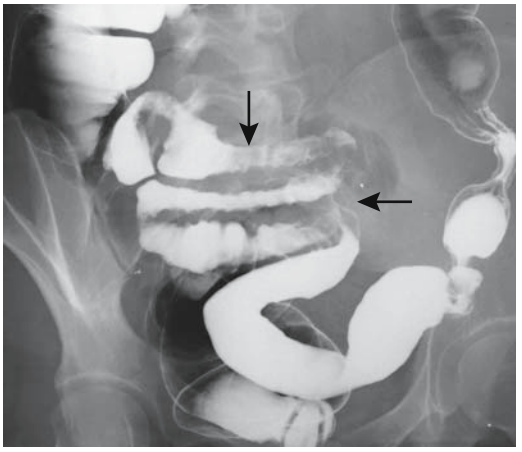

Figure 4.6. Ileal Crohn's disease (arrows) identified on retrograde small bowel study. Similar diffuse bowel wall thickening is also seen with lymphoma.

Computed Tomography

Computed tomography detects bowel wall thickening, increased enhancement of diseased bowel, mesenteric infiltration, fistulas, phlegmon, and abscesses in Crohn's patients. Although some studies have concluded that CT can be an alternative to small bowel barium studies in detecting inflammatory bowel disease (41), but similar to US, it is not sensitive in detecting subtle involvement. Also, one should avoid the trap of simply calling bowel wall thickening in a clinical setting of suspected Crohn's disease "compatible with Crohn's disease"; it is not pathognomonic, and a long differential exists. In spite of some enthusiast's

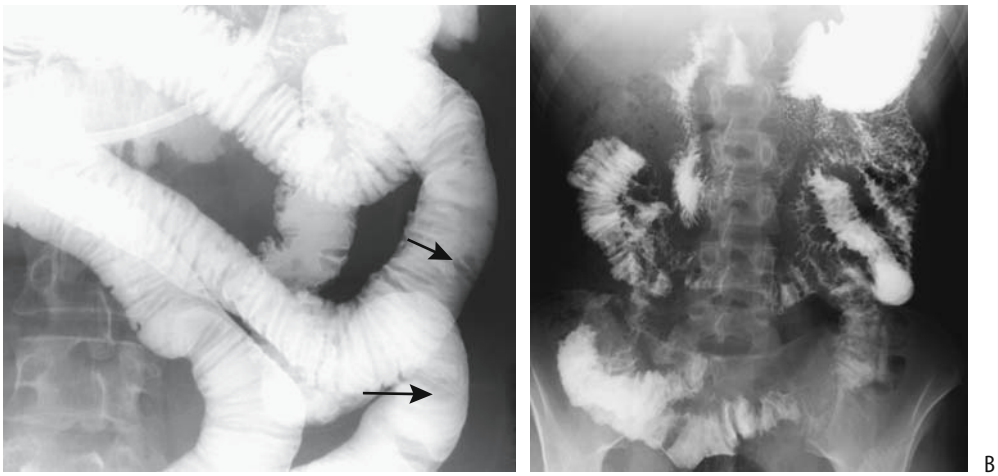

A B

Figure 4.7. A: Jejunal Crohn's disease. Enteroclysis reveals multiple jejunal nodules (arrows). (Courtesy of Steven Martin, M.D., Corning Hospital, Corning, New York.) B: Severe jejunal Crohn's disease mimicking carcinomatosis.

advocacy for CT in suspected early Crohn's disease, the primary role of CT is in more advanced disease, especially in a search for complications. Thus in a setting of exacerbation, CT is the primary imaging test when suspecting an abscess.

Computed tomography achieves a sensitivity of about 70% in identifying abnormal bowel loops, 80% in detecting fistulas, and almost 100% for abscesses; specificities for these findings approach 100%. Computed tomography identifies bowel wall thickening and a homogeneous bowel wall density. A *target sign* (hypodense submucosal layer), although more common in ulcerative colitis, is also found in Crohn's disease.

Computed tomography demonstrates submucosal and mesenteric fat deposition. A diffuse fibrofatty mesenteric infiltrate develops, with adjacent small bowel loops separated by this infiltrate. The normal sharp interface seen with CT between the bowel wall and its mesentery is lost, resulting in an irregular bowel contour and periintestinal blurring. Enlarged mesenteric lymph nodes are common. In general, the involved lymph nodes are smaller than 10 mm in diameter; larger ones should suggest a malignancy or other complication.

Postcontrast, vasa recta dilation and diseased bowel wall contrast enhancement are evident. The involved mesentery is hypervascular, a finding identified with CT and Doppler US. In some patients with active disease the mesenteric vessels feeding diseased bowel segments are dilated, tortuous, with prominence and wide spacing of vasa recta, a CT finding called the *comb sign* (42).

Computed tomography enteroclysis is more accurate than conventional CT not only in detecting Crohn's disease but also in outlining sinus tracts and fistulas. Multiplanar reformatted images aid in image interpretation. A negative contrast agent apears to improve detection of abnormal bowel (43). Whether CT enteroclysis is superior to conventional enteroclysis is not known.

Ultrasonography

Abdominal US achieves sensitivities and specificities of 90% to 95% in detecting Crohn's disease location.

With established disease, small bowel wall thickness is generally >5 mm. Some authors consider an US bowel wall thickness >7 mm to be "diagnostic" for inflammatory bowel diseases (44), a generous thickness indeed, which achieves high specificity, but, similar to CT, a thick bowel wall is not synonymous with Crohn's disease. A stenosis, regardless of etiology, is usually associated with a thickened bowel wall. Effacement of the five bowel wall layers in a thickened bowel wall, as visualized by US, signifies more severe disease activity than if all five wall layers are identified (45). Little data exists on the accuracy of US in detecting mild small bowel abnormalities, such as the presence mostly of aphthae. Likewise, a correlation of bowel wall thickness with disease activity appears rather simplistic.

Doppler US detects significantly greater superior mesenteric artery blood flow in patients with Crohn's disease than in controls (46). Vessel density in affected bowel loops, measured by Doppler US, reflects disease activity (47). Superior mesenteric artery resistive indices (RI) also reflect disease activity (Table 4.1). Whether such Doppler US blood flow measurements are of clinical relevance in detecting or following disease activity remains to be established. These findings of increased blood flow in diseased bowel should be balanced by laser Doppler flowmetry data from surgery revealing that blood flow in a bowel containing aphthae is slightly less than in normal tissue and with inflammation progression bowel blood flow actually decreases (48).

Ultrasonography probably detects most Crohn's-associated abscesses, but the yield for stenoses and fistulas is inconstant and sufficiently low to limit the application of US to specific situations.

Magnetic Resonance Imaging

Magnetic resonance imaging is grossly underused in patients with Crohn's disease. A retrospective comparison concluded that MRI is superior to US in locating affected segments (sensitivity: MRI 98%; US 76%) and in detecting fistulae (sensitivity: MRI 87%; US 31%), stenoses (sensitivity: MRI 100%; US 58%) and abscesses (sensitivity: MRI 100%; US 89%) (49). Its role in pregnant patients is obvious. The use of oral and rectal contrast and bowel distention

aid in visualizing bowel wall thickening. One technique consists of oral contrast using 1000 mL of a 2.5% mannitol solution and imaging in axial and coronal planes using breath-hold T2-weighted half-Fourier acquisition single-shot turbo spin echo (HASTE) and contrast-enhanced T1-weighted fast low-angle shot (FLASH) sequences (50); diseased bowel wall enhances considerably more than normal bowel. Contrary to some earlier studies, poor correlation exists between bowel wall enhancement and the Crohn's Disease Activity Index (50). Inflammation, mesenteric involvement, sinus tracts, and abscesses are depicted by MR. It also has a role in the subset of patients with perianal fistulas being evaluated for surgical correction.

Magnetic resonance imaging identified 80% to 85% of abnormal bowel segments, compared with 60% to 65% by single phase helical CT (51); although moderate or marked mural thickening was identified equally by both modalities, MR was superior in mildly thickened bowel.

Scintigraphy

Scintigraphy does not have a role in initial disease detection; its primary application is in following established disease activity. Although scintigraphic findings correlate with clinical activity and this test is thus useful in disease exacerbation, it appears inferior to other imaging modalities in detecting an abscess, fistula, or bowel obstruction.

Technically, labeling of Tc-99 m–hexamethylpropyleneamine oxime (HMPAO) with leukocytes is easier and study acquisition times faster than a corresponding indium-111 examination. A positive scan represents strong presumptive evidence of inflammable bowel disease and scintigraphy appears to be a simple screening test in differentiating these disorders from such entities as irritable bowel syndrome. This test even detects subclinical bowel inflammation. Thus in one study over half of patients with seronegative spondyloarthropathy and no clinical evidence of inflammatory bowel disease had a positive Tc-99 m-HMPAO leucocyte scan (52). It is, however, nonspecific and does not differentiate among Crohn's disease, ulcerative colitis, infectious enteritis, and inflammation due to such entities as appendicitis. Also, its sensitivity decreases in patients receiving steroid therapy. Thus in a Crohn's patient being treated with steroids, Tc-99 m–leukocyte scintigraphy failed to detect inflammation but an In-111 leukocyte scan did reveal abscesses (53); the effect of steroid-induced chemotaxis on leukocyte-based scintigraphy is not clear.

Technetium-99 m-HMPAO leukocyte scintigraphy appears to have moderate correlation to the Crohn's Disease Activity Index (54) but currently the impact of scintigraphy on other imaging and endoscopic modalities and its clinical implications are difficult to place in perspective. Potentially combined use of CT and Tc-99 m-HMPAO leukocytes scintigraphy appears useful, yet whether the additional information obtained from these two imaging modalities beyond what is available from barium studies does indeed influence clinical management of most patient remains to be established.

Technetium-99 m human polyclonal immunoglobulin scintigraphy appears limited in detecting location or extent of disease. Likewise, In-111 polyclonal immunoglobulin scintigraphy appears less sensitive than Tc-99 m-HMPAO both for diagnosis and in evaluating disease extent and has been replaced by the latter. Radioimmunoscintigraphy with Tc-99 m antigranulocyte monoclonal antibody is also less sensitive than Tc-99 m-HMPAO leukocyte scintigraphy

Scintigraphy with gallium-67 citrate and In-111 leukocytes are of limited use in Crohn's disease.

Complications

Hepatobiliary abnormalities of inflammatory bowel disease are discussed in Chapters 7 and 8. Some of these abnormalities, such as subtly abnormal liver function tests or sclerosing cholangitis, are considered to be not complications but rather a direct manifestation of the disease.

Extraintestinal manifestations are part of the spectrum of findings in Crohn's disease (Table 4.2). Their prevalence varies considerably in different studies.

Musculoskeletal

Arthritis in patients with inflammatory bowel disease ranges from peripheral to axial. Axial

Table 4.2. Extraintestinal manifestations of Crohn's disease

Skin
Pyoderma granulosum
Erythema nodosum
Eyes
Conjunctivitis
Iritis
Uveitis
Joints
Ankylosing spondylitis
Hypertrophic osteoarthropathy
Liver
Sclerosing cholangitis
Cholangiocarcinoma
Other
Abscesses
Thrombophlebitis

involvement tends to be similar to that seen with ankylosing spondylitis. Asymptomatic sacroiliitis is not uncommon; conventional radiography identifies asymptomatic sacroiliitis in considerably fewer patients than CT. An interesting study from Korea found that in Crohn's patients arthritis occurred only in those with colonic involvement (55). Arthritis and erythema nodosum are more frequent in Crohn's disease than in ulcerative colitis.

Osteoporosis is a known complication of Crohn's disease. Some adult and pediatric patients have a marked reduction in bone density and develop vertebral compression fractures. Etiologic factors include the use of steroid therapy, superimposed malnutrition and abnormal calcium, vitamin D, and hormone metabolisms. Bone mineral density evaluation of pediatric Crohn's patients seems reasonable.

Abscess

Abscesses are more common with small bowel or ileocolic Crohn's than with colonic involvement. An occasional sterile abscess develops. Some abscesses involve not only adjacent structures, including spleen, lymph nodes, psoas muscle, liver, pancreas, and abdominal wall, but also the brain. A Crohn's fistula led to a presacral abscess and spondylodiscitis (56). A peroneal abscess in a Crohn's patient resulted in priapism. In some patients Crohn's disease is discovered only after the source for an abscess is sought.

From a clinical viewpoint, differentiation of an abscess from a phlegmon is necessary. Computed tomography is usually employed for this purpose.

Successful percutaneous drainage of Crohn's abscesses has been performed, although the procedure remains controversial. Among percutaneously drained abscessed, 56% were successful (57); successful drainage was associated with fewer fistulas, and the abscesses tended to be first rather than recurrent, spontaneous rather than postsurgical, located in the right lower quadrant, and small. In an acute clinical setting, percutaneous drainage of even a complex abscess is feasible and, if necessary, can be followed by elective surgical drainage. Drainage of an abscess associated with an internal fistula usually does not heal the fistula. A persistent enterocutaneous fistula at the site of catheter insertion is a recognized complication. Perhaps a major consideration for percutaneous drainage of a Crohn's abscess is that it gains time to stabilize a patient for further, more definitive, therapy.

Some surgeons believe that surgical resection of inflamed tissues, including diseased loops of bowel, leads to faster healing and fewer complications.

Fistula/Perforation

Fistulas are common and extend to another loop of bowel, bladder, or other structure not involved by Crohn's disease (Fig. 4.8). In the absence of prior surgery or percutaneous drainage, cutaneous abdominal fistulas are uncommon. A fistula almost always is associated with a phlegmon or abscess. Some fistulas bypass an obstructed bowel segment. Unusual sites include rectourethral and even a rare one into a hip joint. Some of these fistulas are associated with prior resection or abscess drainage.

Suspected cutaneous fistulas are typically studied with fistulography using fluoroscopic guidance. A comparison of US-guided and fluoroscopically guided fistulography in eight patients with Crohn's ileitis and suspected enterocutaneous fistulas found agreement between

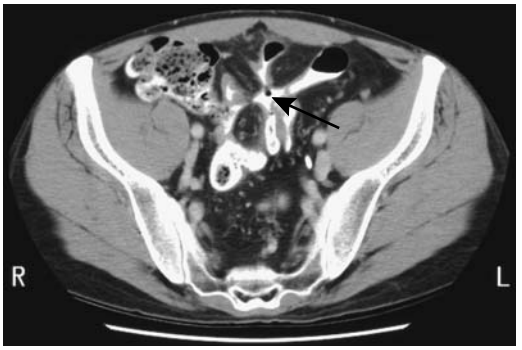

Figure 4.8. Multiple fistulas secondary to Crohn's disease. CT after oral contrast identifies matted loops of small bowel just superior to the bladder (arrow). Fistulas extend between small bowel, colon, and bladder. Other images identified gas within the bladder. (Courtesy of Patrick Fultz, M.D., University of Rochester.)

the two studies in all patients (58); US fistulography was performed using physiologic saline injected through an inserted catheter, with the fistulous tracts appearing as hypoechoic lines extending from the cutaneous opening. One advantage of fluoroscopic guidance is that the amount of contrast injected is easier to estimate by visualizing the extent of the internal communications.

Bowel perforation and peritonitis is infrequent in Crohn's disease, yet most physicians dealing with this disease sooner or later encounter this complication, at times as an initial presentation. A concurrent small bowel obstruction is often also present.

Bleeding/Thrombosis

Chronic blood loss and iron-deficiency anemia are not uncommon with small bowel Crohn's disease. A rare patient presents with major hemorrhage even to the point of exsanguination.

Patients with Crohn's disease are at increased risk of vascular thrombosis. Etiology for thrombosis in these patients is not known; coagulation defects and fibrinolysis have been suggested, although not all patients with thromboembolic complications manifest a coagulation disorder. Inferior vena caval thrombosis and portal vein thrombosis develop, with the latter being more common with ulcerative colitis than with Crohn's disease (Fig. 4.9). Inferior mesenteric vein thrombosis is not uncommon.

Arterial occlusive disease is occasionally found in relatively young Crohn's patients. In some, this appears to be a premature atherosclerosis rather than a vasculitis; these patients often are steroid dependent and have long-standing Crohn's colitis. Some arterial thrombi are at a remote site, including internal carotid arteries.

These thrombi are readily detected with CT.

Malignancy

The prevalence of small bowel adenocarcinoma, lymphoma, and hematologic malignancies in patients with long-standing Crohn's disease is greater than in the general population, although the small numbers involved make prediction uncertain. Current evidence suggests that duration of disease and presence of surgically bypassed loops of bowel are factors in carcinoma development. Other potential pathogenetic factors include chromosomal abnormalities, immunologic dysfunction, and medical therapy for Crohn's disease. These adenocarcinomas develop throughout diseased bowel, including strictureplasty sites and in fistulous tracts.

The imaging appearance of a malignancy in a setting of Crohn's disease is nonspecific and mimics a benign stricture (Fig. 4.10).

Genitourinary

An extensive phlegmon surrounding the terminal ileum occasionally obstructs the right ureter and results in an eventual loss of the right kidney, at times silently. A rare patient develops left-sided hydronephrosis. Renal US to check for hydronephrosis seems worthwhile in a patient with extensive ileal Crohn's disease.

Renal tubular damage appears to be an extraintestinal manifestation of disease and not due to therapy (59).

So-called metastatic Crohn's disease occasionally involves the penis; ulcerations develop and biopsy reveals granulomas.

Other

Thyroid disease is more common with ulcerative colitis than with Crohn's disease. Thyroid volume and free thyroxine increase and some patients develop antithyroid antibodies, even in the absence of clinical thyroid disease. Thyroid volume can be calculated by US.

A weak association between Sweet's syndrome (acute febrile neutrophilic dermatosis), believed to represent a hypersensitivity reaction occurring with parainflammatory and paraneoplastic conditions, and Crohn's disease appears to exist. Erythematous, ulcerated skin nodules develop in these patients; biopsy revealed noncaseating granulomas.

Mesenteric fibromatosis is a rare complication of Crohn's disease, almost always associated with previous intestinal resection. Fibromatosis occurs more often after bowel resection in familial polyposis syndrome.

One example of the protean manifestations of Crohn's disease is a young adult with lung infiltrates, believed to represent sarcoidosis, who also developed peptic ulcer symptoms with gastric outlet obstruction and duodenal stenosis after a Billroth I anastomosis, later thought to be due to Crohn's disease (60); bronchial biopsy revealed noncaseating granulomas.

Ascites occasionally develops during an acute episode. Ascites is not a feature of chronic Crohn's disease; if present, another etiology should be sought.

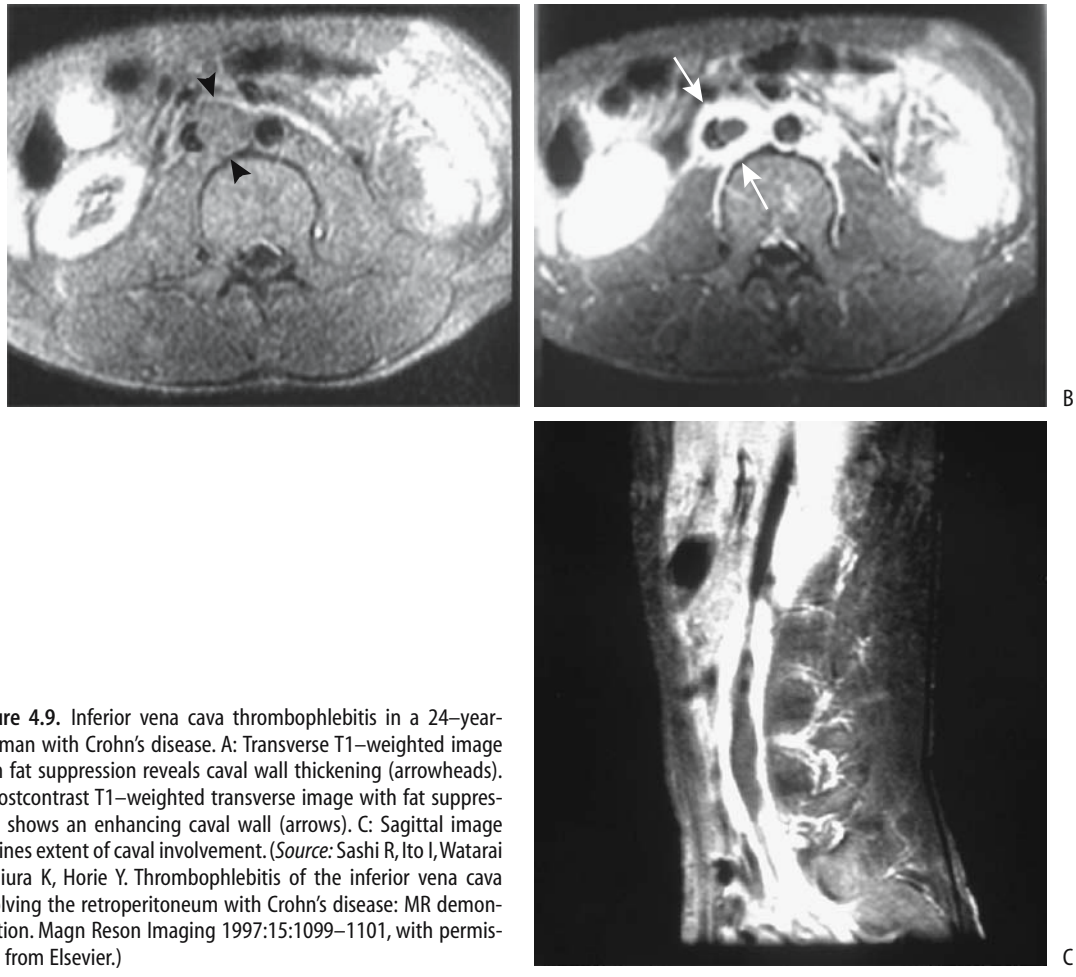

Figure 4.9. Inferior vena cava thrombophlebitis in a 24–year-old man with Crohn's disease. A: Transverse T1–weighted image with fat suppression reveals caval wall thickening (arrowheads). B: Postcontrast T1–weighted transverse image with fat suppression shows an enhancing caval wall (arrows). C: Sagittal image outlines extent of caval involvement. (*Source:* Sashi R, Ito I, Watarai J, Miura K, Horie Y. Thrombophlebitis of the inferior vena cava involving the retroperitoneum with Crohn's disease: MR demonstration. Magn Reson Imaging 1997:15:1099–1101, with permission from Elsevier.)

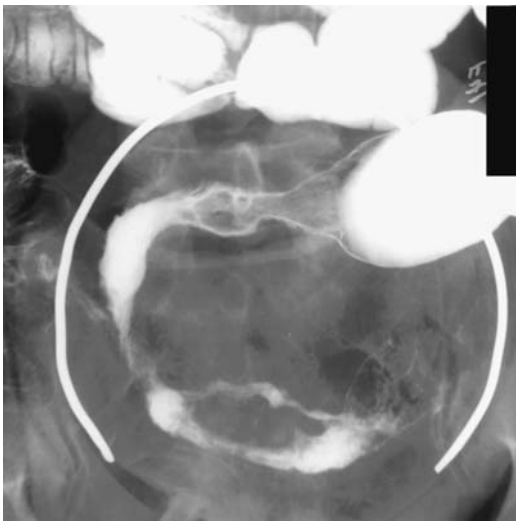

Figure 4.10. Small bowel adenocarcinoma in a setting of long-standing Crohn's disease.

Systemic amyloidosis is a rare but serious complication of Crohn's disease, with the kidneys being the critical target organ. Scintigraphy using a I-123 serum amyloid component targets body amyloid deposits; preliminary evidence suggests a possible role for this test in patients with suspected Crohn's amyloidosis (61).

Outcome

Most patients who have Crohn's disease do not die from it. The Rochester, New York, registry of inflammatory bowel disease patients shows that patient deaths due to Crohn's disease decreased from 44% in the period 1973–1980 period to 6% in the period 1981–1989 (62).

Serial gray-scale US measurement of bowel wall thickness and Doppler US grading are used by some to follow changes in disease activity during medical management.

Typical indications for surgery are failed medical therapy, small bowel obstruction, enteric fistula, and abscess. The most common site for recurrence after surgery is in the preanastomotic neoterminal ileum.

Surgery does not cure Crohn's disease. Surgery can, however, control complications. Published recurrence rates after surgical resection of diseased bowel vary considerably; the observed symptomatic recurrence rate is lower than endoscopy- or biopsy-detected recurrence rate. Also, patients presenting with an acute complication tend to have higher recurrence rates.

The type of surgery performed has little influence on recurrence. Quite often resection margins contain microscopic disease, yet retained disease or length of macroscopic disease-free resection margins probably has little influence on subsequent recurrence.

Strictureplasty avoids a short bowel syndrome developing after an extensive resection and appears useful in managing extensive obstructive Crohn's disease. It does not alter the natural disease course.

A laparoscopic approach continues to gain ground whenever an ileocecal resection or stoma formation are necessary for Crohn's disease.

Chronic Idiopathic Enterocolitis

Also found as an isolated entity, chronic nongranulomatous ulcerative enterocolitis occasionally develops in patients with celiac sprue, lymphoma, hypogammaglobulinemia, and related conditions. Biopsy reveals a chronic inflammatory infiltrate involving small bowel and often also colon. No infection or inflammatory bowel disease is detected during prolonged follow-up. Some patients respond to steroid therapy.

The relationship of chronic granulomatosis syndrome to this condition is conjecture.

Imaging findings in this entity are not established.

Acute Enteritis

In some adults and children acute enteritis causes lymph nodes enlargement. Such enlarged nodes are nonspecific and are found in a number of diseases.

Aside from the two entities discussed, similar clinical presentations are found with *Campylobacter jejuni* enteritis, *Escherichia coli* infection, and *Clostridium difficile* infection. Imaging is often nonspecific and CT simply reveals ileal or cecal wall thickening and enlarged mesenteric lymph nodes. Occasionally marked bowel

dilation is a prominent feature. Clinically, either acute gastroenteritis or Crohn's disease are suspected.

Yersinia *Enterocolitis*

Yersinia enterocolitica, a gram-negative, low temperature growing bacillus, is a common enteric pathogen; in temperate countries gastroenteritis due to yersinia infection usually ranks third after *Campylobacter* and *Salmonella.* It often presents as an acute, self-limiting enteritis with symptoms referable to the right lower quadrant mimicking appendicitis or acute Crohn's disease. Also called *mesenteric adenitis*, this infection most often is due to either *Y. enterocolitica* or *C. jejuni*. Mesenteric lymph node biopsy simply identifies nonspecific follicular hyperplasia.

A number of these patients have been explored for suspected appendicitis; the appendix is found to be unremarkable but terminal ileum is thickened and mesenteric adenopathy identified. Preoperative imaging for suspected appendicitis should differentiate these two conditions. At times Crohn's disease has a similar clinical presentation and even intraoperative appearance; in patients with *Y. enterocolitica* infection the clinical and imaging findings revert to normal within several weeks.

At times *Y. enterocolitica* infection is chronic. Thus CT and US in a woman with weight loss and leukocytosis detected enlarged abdominal lymph nodes. A malignant lymphoma was suspected but bone marrow and lymph node biopsies did not detect a neoplasm (63); serology confirmed a previous *Y. enterocolitica* infection and in 6 months her enlarged lymph nodes regressed.

Occasionally *Y. enterocolitica* results in a small bowel intussusception, presumably secondary to enlarged mesenteric nodes.

Salmonella/Shigella (Enteric Fever)

Enteric fever is caused by *Salmonella* infection, with common serotypes being *S. typhi*, *S. paratyphi*, and *S. enteritidis*. The only reservoir for *S. typhi* is in humans. Histologically, bowel and mesenteric lymph node involvement mimics Kikuchi-Fujimoto lymphadenitis (see Chapter 14) and infection by some other bacteria. The diagnosis is confirmed by culture.

Salmonella and *Shigella* infection results in an acute terminal ileitis. A colitis is also often evident and many of these patients cannot tolerate a barium study, especially a barium enema.

A small bowel barium study in a patient with *Salmonella* ileitis showed terminal ileal spasticity and thickened folds (64); CT revealed a circumferential, homogeneously thickened terminal ileum and mild colonic wall thickening.

A small bowel barium study in a patient with *Shigella* ileitis identified an irregular narrowed lumen, large nodules, and terminal ileal ulcers, and CT showed thickening of the terminal ileal wall and a target configuration (64). In spite of these anecdotal reports, imaging cannot differentiate between most infective agents. The role of CT in differentiating these infections from Crohn's disease is not clear.

Giardiasis

Giardiasis is a protozoan infestation endemic throughout large parts of the world. Clinically it presents with gastroenteritis of varying severity. It is commonly diagnosed from duodenal aspirates or biopsies, although a barium study often suggests the diagnosis.

The radiologic changes are best seen in the duodenum and proximal small bowel; small bowel folds are thickened and distorted. Increased intraluminal secretions are common. Some patients develop disordered peristalsis.

Occasionally giardiasis involves most of the gastrointestinal tract and even biopsies of the terminal ileum and colon yield positive results.

Strongyloidiasis

Infestation with the nematode *Strongyloides stercoralis* leads to vomiting, diarrhea, and rectal bleeding. Disseminated infection is often fatal, especially in the very young and those with diabetes mellitus, malnutrition, and immunosuppression. In others strongyloidiasis smolders for decades, presenting only with occasional relapses.

Imaging reveals thickened valvulae conniventes. With more extensive infestation CT identifies a thickened, poorly marginated bowel wall that enhances postcontrast to varying

degrees; a similar appearance is seen with other acute bowel infections and with obstruction to venous drainage.

The diagnosis is established by identifying duodenal or colonic *S. stercoralis* larvae.

Ascariasis

Ascaris lumbricoides infests a large proportion of the world's population, mostly in developing countries where the condition is encountered mainly in children. During its life cycle the worm travels through the respiratory tract and portal and hepatic veins, and eventually pulmonary alveoli. After further growth, larvae migrate to the larynx, are swallowed, and mature in the small bowel.

Infected patients range from relatively asymptomatic, having nonspecific abdominal symptoms, to bowel obstruction, and the occasional patient develops a perforation and peritonitis. Pancreaticobiliary manifestations develop with worm migration into the biliary or pancreatic ducts. This is not an innocuous condition and patients developing an acute abdomen have a high mortality.

Classically, ascariasis is diagnosed with barium studies, where barium in the worm intestinal tract is identified on delayed views. Computed tomography reveals not only contrast within the worm gut but also the worm coursing through opacified bowel. The worm produces a long, thin, tubular soft tissue structure coiled in small bowel. Computed tomography often reveals the worm only in cross section. In endemic regions, bowel obstruction by worms is recognized on conventional radiographs (Fig. 4.11).

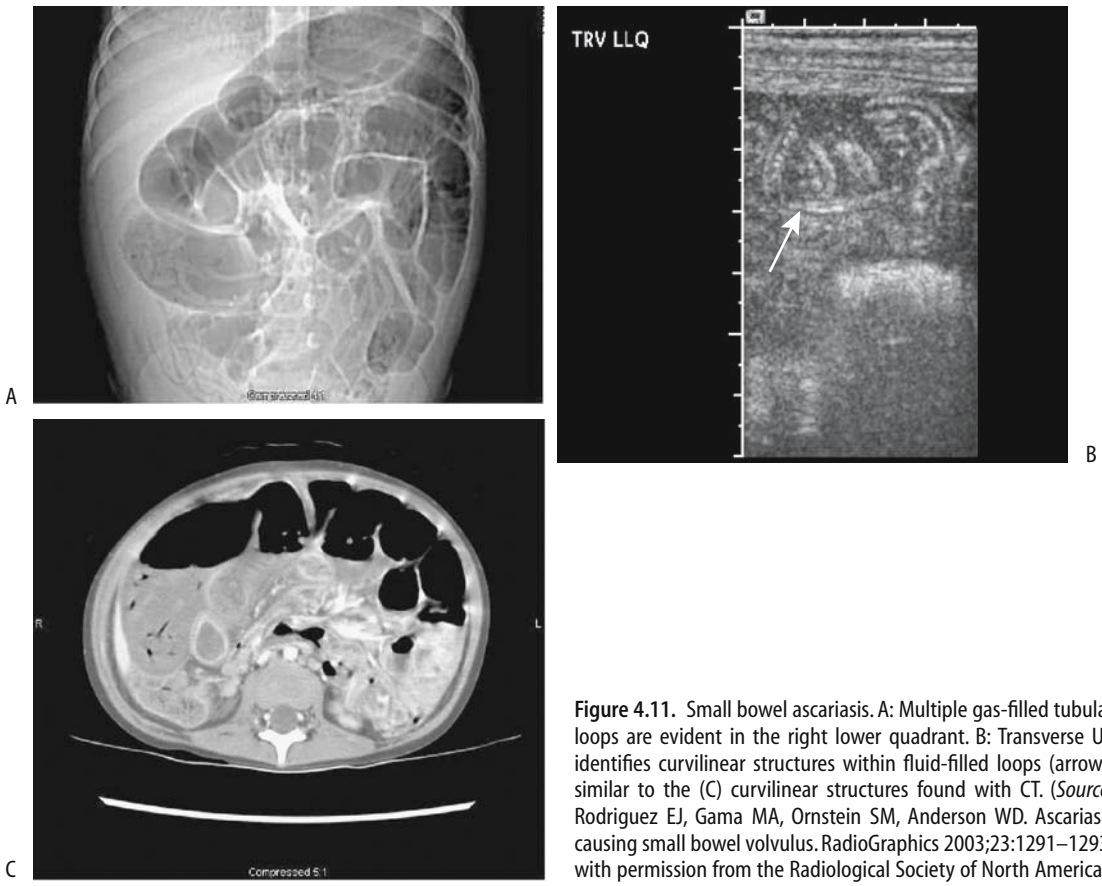

Figure 4.11. Small bowel ascariasis. A: Multiple gas-filled tubular loops are evident in the right lower quadrant. B: Transverse US identifies curvilinear structures within fluid-filled loops (arrow), similar to the (C) curvilinear structures found with CT. (*Source:* Rodriguez EJ, Gama MA, Ornstein SM, Anderson WD. Ascariasis causing small bowel volvulus. RadioGraphics 2003;23:1291–1293, with permission from the Radiological Society of North America.)

Ultrasonography is the most common imaging modality available in some parts of the tropics and is suited to detect ascariasis. Intestinal ascariasis is suspected with US by finding tubular structures within the small bowel lumen. Among 22 individuals with *A. lumbricoides* eggs in their stools, US visualized a worm in six (65); the parasite appears as a large, curved hyperechoic strip, 4 to 6 mm in diameter, and contains an inner, anechoic, longitudinal canal. The US appearance has been described as a winding highway (65).

Whipple's Disease

Whipple's disease is a rare, systemic disorder, often limited to the gastrointestinal tract and lymph nodes, although more generalized manifestations are evident in some. Intestinal symptoms are thought to be secondary to invasion by a rod-shaped gram positive aerobic bacillus, called *Tropheryma whippelii*, found both intra- and extracellularly.

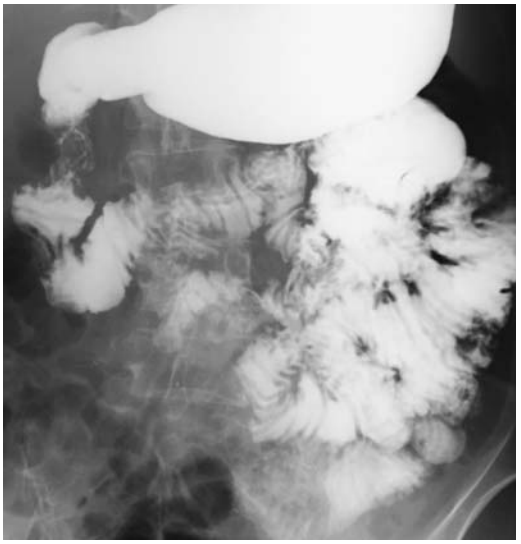

Figure 4.12. Whipple's disease. Jejunal wall and valvulae conniventes are slightly thickened. Giardiasis has a similar appearance.

Table 4.3. Clinical data on 52 French Whipple's disease patients

Sex:	73% male
Clinical manifestations prior to diagnosis:	
Musculoskeletal	67%
Digestive	15%
Generalized	14%
Neurologic	4%
Later manifestations:	
Diarrhea, weight loss, malabsorption	85%
Arthralgia or arthritis	83%
Prominent neurologic symptoms	21%
Cardiovascular symptoms	17%
Mucocutaneous symptoms	17%
Pleuropulmonary symptoms	13%
Ophthalmologic symptoms	10%
Biopsy site for histopathologic diagnosis*:	
Jejunum	90%
Lymph node	6%
Brain	2%
Postmortem jejunum or brain	2%
Response to therapy:	
Favorable	90%
Death	4%
Chronic dementia	2%
Continued digestive symptoms	4%
Relapse**	17%

*Based on 51 patients.
**Seven of 41 patients initially treated successfully.
Source: Adapted from Durand et al. (66).

Table 4.3 summarizes a retrospective clinical Whipple's disease study by the Société Nationale Française de Médecine Interne (SNFMI). An antecedent migratory polyarthritis often precedes gastrointestinal symptoms; the arthralgia is seronegative, symmetric, and migratory, and no joint destruction is evident. Some patients develop sacroiliitis. It is associated with renal amyloidosis and extraintestinal adenopathy.

Small bowel valvulae conniventes and bowel wall are thickened (Fig. 4.12). Intra- and extraperitoneal lymphadenopathy is common. A characteristic feature of Whipple's disease is that involved lymph nodes have a lower CT density than normal. Biopsy reveals foamy macrophages and surrounding lipid, accounting for the CT appearance. Presence of hypodense nodes is not pathognomonic for Whipple's disease, however, and occasionally other infections (especially tuberculosis) or a diffuse neoplasm also exhibit hypodense nodes.

The diagnosis is established by finding periodic acid-Schiff (PAS)-positive material in involved histiocytes. Ultrastructural study identifies bacterial fragments within histiocytes.

Antibacterial therapy is often prolonged but is curative in most.

Cytomegalovirus Infection

Most clinically evident cytomegalovirus infection occurs in immunocompromised patients, and it is a common cause of massive lower gastrointestinal bleeding. Most lesions consist of ulcers and granulation tissue. These findings appear to be due to endothelial infiltration by macrophages and intranuclear inclusion bodies and a resultant cytomegalic vasculitis leading to ischemia and secondary ulceration. The endoscopic appearance of some lesions suggests a malignancy.

Ulcerations presumably account for the massive intestinal hemorrhage developing in some patients. Either jejunum or ileum can be involved. Deep ulcers occasionally result in perforation and peritonitis.

Although angiography does detect a bleeding site, the tangle of vessels induced by this infection can suggest angiodysplasia.

Anisakiasis

Human anisakiasis most often involves the stomach and duodenum. A minority of patients present with findings suggesting an acute abdomen, at times mimicking appendicitis. Laparotomy in two patients revealed an ileitis, with an edematous ileal wall infiltrated by eosinophils and containing *Anisakis* larvae (67).

Ultrasonography detects ascites, small bowel dilation and thickened valvulae conniventes. These are nonspecific abnormalities found in a number of other inflammatory conditions.

Protein-Losing Gastroenteropathy

Protein-losing gastroenteropathy is not a single entity but a description of a type of bowel reaction to a variety of insults. Some of the conditions leading to clinical, imaging, and pathologic findings of protein-losing gastroenteropathy are listed in Table 4.4. These conditions are discussed in their respective sections.

Some imaging tests are useful to detect protein-losing gastroenteropathy in its broad sense rather than being specific to a particular disease. A Tc-99 m-HSA scan is considered positive for protein-losing gastroenteropathy if tracer exudate is identified in the gut. Serial scanning up to 24 hours is necessary to detect bowel activity in some patients. Among patients with suspected protein-losing gastroenteropathy, 96% revealed Tc-99 m-human serum albumin (HAS) in bowel, but among these 28% were positive only on 24 hours images (68); no bowel activity or only slight activity is identified in controls.

Table 4.4. Conditions associated with protein-losing gastroenteropathy

- Eosinophilic gastroenteritis
- Ménétrier's disease
- Radiation enteritis
- Celiac disease
- Intestinal lymphangiectasia
- Extensive amyloidosis
- Certain infections
  - Whipple's disease
  - Tropical sprue
  - Bacterial overgrowth
- Intestinal lymphoma

Drug Related

Some drugs are known to induce small bowel ulcerations and stenoses. Among others, potassium salts and nonsteroidal antiinflammatory drugs are implicated (Fig. 4.13). Some patients develop multiple ulcerations.

Enteroclysis aids in detecting superficial ulcers and subtle stenoses. Thus among patients with drug-induced stenoses, enteroclysis reveals one of three findings: a web-like stricture; a short, smooth stricture; or an ulcerated, circumferential stenosis (69). At times CT detects a thickened, irregular bowel wall.

Ischemia

Ischemia due to major vessel abnormalities and vasculitides are covered in Chapter 17. Isolated colon ischemia is more common than small bowel.

Bowel ischemia ranges from acute to chronic. Early or mild ischemia results in intramural edema or hemorrhage (hematoma), findings similar to those seen as sequelae from a bleeding diathesis, such as anticoagulation therapy

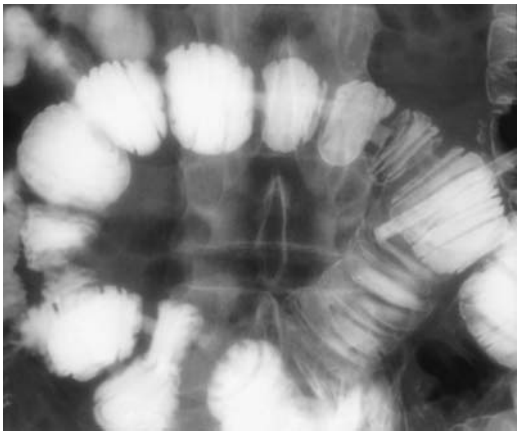

Figure 4.13. Jejunal webs secondary to nonsteroidal anti-inflammatory drug use. (Courtesy of Arunas Gasparaitis, M.D., University of Chicago).

(small bowel bleeding is discussed later, see Vascular Lesions). A partial or gradual decrease in intestinal blood flow opens collateral vessels and bowel stenoses develop.

Computed tomography findings of ischemia vary depending on the severity of the ischemia and whether an infarct has developed (Table 4.5). Aside from reduced wall enhancement, the other signs are relatively nonspecific.

Ultrasonography findings suggesting small bowel ischemia consist of thickened bowel wall and absent blood flow, identified by color Doppler US; bowel wall thickening with readily apparent color Doppler flow suggests inflammation.

Ultrasonography reveals a hematoma as focal bowel wall thickening, at times consisting of a thick, hyperechoic inner layer and a thin, hypoechoic outer layer; the bowel lumen tends to be narrowed, decreased peristalsis is evident, and often fluid is identified between involved bowel loops.

Table 4.5. Computed tomography findings of ischemia in a setting of small bowel obstruction*

Finding	Sensitivity (%)	Specificity (%)
Reduced bowel wall contrast enhancement	48	100
Bowel wall thickening	38	78
Mesenteric fluid	88	90
Mesenteric vein congestion	58	79
Ascites	75	76

*Based on CT findings in 142 patients with acute bowel obstruction and suspected intestinal ischemia.
Source: Adapted from Zalcman et al. (70).

Radiation

The amount of small bowel included in a radiation treatment field is a factor in subsequent radiation enteropathy. Two pretherapy methods are used to calculate bowel volume: a grid method using orthogonal radiographs, and algorithms based on CT data using either polyhedral or cylindric approximations.

Irradiation results in bowel wall thickening and lumen narrowing. During the acute phase edema and hemorrhage predominate, with eventual bowel wall fibrosis developing. Lumen narrowing can be either on an acute basis due to edema or chronic due to stenosis. Some obstructions develop only months or years later.

Radiation therapy induces mesenteric lymph node fibrosis and lymphatic occlusion resulting in lymphatic congestion and is one of the causes of protein-losing enteropathy.

Early vascular-phase CT in patients with irradiated intestine revealed bowel wall thickening in a three-layered pattern, believed to represent early contrast enhancement of the mucosal and muscular-serosal layers and decreased enhancement of submucosa (71); this three-layered appearance gradually faded into homogeneous enhancement during delayed equilibrium.

Angioneurotic Edema

Hereditary angioneurotic edema, a rare condition, is most often encountered in a setting of hereditary deficiency of the complement system. Acquired angioneurotic edema is even less common, although the clinical presentation is similar to the hereditary form. An acute attack, often initiated by mild trauma, involves skin, larynx, or abdominal structures and can be fatal. Abdominal involvement often mimics an acute abdomen.

Computed tomography findings in three patients with visceral angioneurotic edema revealed thickened small-bowel wall, including mucosa, increased wall contrast enhancement,

prominent mesenteric vessels, ascites, and fluid within bowel lumen (72).

Small bowel barium studies show diffuse thickening of valvulae conniventes in addition to bowel wall infiltration. One patient with hereditary angioedema developed focal small bowel involvement, mimicking a tumor on CT (73); if in doubt, a follow-up study should clarify whether these changes are permanent.

Mastocytosis

An uncommon disease, mastocytosis consists of a proliferation of mast cells that originate from $CD34^+$ hemopoietic stem cells in bone marrow. In the past it was believed to represent a reactive or hyperplastic process, but more recent evidence suggests that mastocytosis is a neoplastic condition. Although urinary histamine metabolite levels are suggestive of the diagnosis, bone marrow biopsy is often required.

Clinical manifestations of mastocytosis result from mast cell degranulation and release of mediators inducing local paroxysmal congestion. Bone involvement is most common, followed by digestive tract and hematologic structures.

Thickening of valvulae conniventes and bowel wall develop during the acute attack, reverting to normal between attacks.

Lymphangiectasia

Intestinal lymphangiectasia is one of the protein-losing enteropathies, and it leads to malabsorption, hypoproteinemia, ascites, and edema. It is either congenital or acquired and presumably is secondary to obstruction of lymphatic flow and resultant lymphatic engorgement. Most imaging modalities simply show bowel wall and valvulae conniventes thickening, representing nonspecific findings (Fig. 4.14). A CT *target sign* (*halo sign*), consisting of an inner hypodense ring surrounded by a higher density outer ring, has been described in a patient with intestinal lymphangiectasia (74).

Technetium-99 m-dextran lymphoscintigraphy detects chylous ascites, but this test has a limited role in evaluating intestinal lymphangiectasia. An occasional patient with primary intestinal lymphangiectasia has abnormal intestinal accumulation of tracer during Tc-99 m–methylene diphosphonate (MDP) skeletal scintigraphy.

Figure 4.14. Intestinal lymphangiectasia. Both bowel wall and valvulae conniventes are diffusely thickened.

Amyloidosis

Primary gastrointestinal tract amyloidosis is rare. More often it is associated with multiple myeloma or chronic infection or inflammation such as Crohn's disease. Gastrointestinal amyloidosis occasionally develops in patients on chronic hemodialysis.

If extensive enough, amyloidosis presents with ulcerations, bleeding, ischemia, or even a protein-losing enteropathy. A rare patient develops pneumatosis cystoides intestinalis.

Clinically and with imaging, amyloidosis mimics a number of other conditions. Hypoperistalsis and superimposed bacterial overgrowth are common. Some patients develop a pseudo-obstruction, thickened valvulae conniventes and small nodules scattered throughout the small bowel—findings secondary to mostly submucosal amyloid deposition.

In a patient with secondary amyloidosis and a protein-losing enteropathy, Tc-99m–diethylenetriamine pentaacetic acid (DTPA) HSA scintigraphy identified the protein-losing site (75).

Tumors

Enteroclysis and capsule endoscopy are the current imaging gold standards in detecting primary small bowel tumors, yet for a number of reasons enteroclysis is performed mostly in select centers. In spite of several enthusiastic reports, CT and MR have had a limited role, except for tumors with diffuse involvement such as lymphomas. Undoubtedly the role of MRI will expand in the future.

Nonneoplastic

Splenic Rests

Small bowel splenic rests are not common. Typically they tend to present as submucosal tumors. A number of these patients have had a prior splenectomy, thus these foci presumably represent splenosis. At times in postsplenectomy patients Tc-99m–red blood cell scintigraphy suggests the correct diagnosis and thus needless surgery can be avoided.

Lymphoid Nodular Hyperplasia

Common variable hypogammaglobulinemia syndrome with intestinal lymphoid nodular hyperplasia is one of the hypogammaglobulinemic enteropathies, manifesting by decreased serum immunoglobulins, recurrent respiratory tract infections, and chronic diarrhea. From an imaging viewpoint the primary interest in hypogammaglobulinemia is the commonly associated intestinal lymphoid nodular hyperplasia.

Prominent lymphoid follicles are often detected in children and young adults and are believed to be a normal finding. A similar nodular pattern throughout the small bowel in more elderly patients should suggest hypo- or agammaglobulinemia. Many of these patients also have superimposed giardiasis, leading to thickened valvulae conniventes throughout the proximal small bowel.

Occasionally a lymphoid hyperplasia pattern is detected in an elderly immunocompetent patient with no known hematologic abnormality, leading to a diagnostic dilemma. Ileoscopy in one woman showed multiple soft, pliable, ileal polyps, and biopsies revealed mucosal inflammation consisting of numerous enlarged follicles containing reactive germinal centers and a mixed infiltrate of lymphocytes, plasma cells, and eosinophils (76); enlarged adjacent lymph nodes were detected by CT, and the patient underwent a right ileocolectomy. The final diagnosis was simply lymphoid hyperplasia.

Heterotopic Pancreas

Pancreatic rest tissue (heterotopic pancreas) is occasionally found in the small bowel. Some of these pancreatic rests measure up to several centimeters in size, are vascular, and bleed, generally on a chronic basis. Less common is pancreatitis developing in this heterotopic pancreatic tissue. Presumably some idiopathic small bowel strictures represent fibrosis from prior pancreatitis within a pancreatic rest.

Arteriography of larger small bowel pancreatic rests simply reveals a vascular tumor.

Inflammatory Polyp

Small bowel inflammatory polyps consist of connective tissue infiltrated by inflammatory cells, usually eosinophils. They are not neoplastic in origin. Most inflammatory polyps are located in the ileum and most are solitary. Occasionally one acts as a lead point for an intussusception.

Hemangioma

Jejunal and ileal hemangiomas are not common. They occur in Maffucci's syndrome. Most are discovered incidentally. Gastrointestinal hemorrhage is the most common presentation, with some patients simply becoming anemic. In a rare patient bleeding is intraperitoneal.

A 3-week-old boy with a cutaneous hemangioma and gastrointestinal bleeding also had gastrointestinal hemangiomatosis (77); contrast-enhanced CT revealed diffuse small bowel wall enhancement.

Small bowel hemangiomas vary in size from very small to a large tumor filling the bowel lumen. These are soft tumors and thus some are missed by barium studies. Unless they are actively bleeding, angiography also misses some of these lesions.

Lymphangioma

Lymphangiomas, or malformations of lymphatic tissue, are more common in the mesentery than in small bowel wall (they are discussed in more detail in Chapter 14).

A not uncommon presentation of diffuse lymphangiomatosis is intestinal bleeding.

Occasionally small bowel lymphangiomatosis appears as multiple polyps, and at times both large and small ones are present. If large enough, a small bowel or adjacent mesenteric lymphangioma obstructs the bowel lumen.

Endometriosis

Colonic endometriosis is more common than small bowel involvement. Distal ileal involvement predominates in small bowel endometriosis and results in fibrosis and strictures mimicking ileal Crohn's disease (Fig. 4.15). Complicating the issue is the occasional woman with antecedent Crohn's colitis who develops ileal endometriosis.

Clinical presentation of small bowel endometriosis varies. Symptoms do not necessarily occur cyclically, and these women develop pain, hematochezia, or small bowel obstruction.

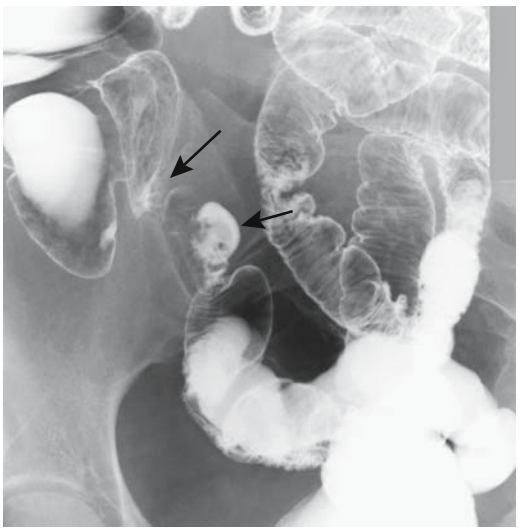

Figure 4.15. Terminal ileal endometriosis (arrows). Superficially it mimics Crohn's disease.

Barium studies in five women revealed endometrial implants within 10 cm of the ileocecal valve in four and more proximal in one (78); findings ranged from an annular infiltration, extrinsic tumor, and spiculations, to a plaque-like tumor. Of interest is that rectosigmoid endometriosis was also found in four who underwent a barium enema.

Benign Neoplasms

Adenoma

Adenomas are most common in the duodenum. Similar to other intraluminal polyps, an adenoma can bleed, intussuscept, or obstruct. When resected, some adenomas already contain a focus of adenocarcinoma.

Adenomas appear as intraluminal soft tissue tumors. Differentiation from carcinoma is based mostly on size and whether bowel wall invasion is present, keeping in mind that for most smaller ones imaging differentiation is not possible.

Leiomyoma

The most common small bowel neoplasm is a leiomyoma. It is rare in neonates but large, congenital ones are in the differential diagnosis of a palpable abdominal mass. An increased leiomyoma prevalence is reported in patients with neurofibromatosis.

Most are small and intramural and are discovered either at surgery or autopsy. Leiomyomas tend to be hypervascular to the point that some mimic an arteriovenous malformation. A mostly intraluminal leiomyoma suggests a muscularis mucosa origin. Yet even one originating from muscularis propria can ulcerate and bleed, at times massively, necessitating arterial embolization even to the point of inducing ischemia in order to stop bleeding.

Occasionally a leiomyoma presents as a giant abdominal or pelvic tumor, often partly necrotic.

Lipomatous Tumors

Small bowel lipomas are common, at times being multiple. In spite of their intramural origin they have a tendency to become pedunculated and then are indistinguishable from

other pedunculated polyps. In fact, a lipoma should be high in the differential diagnosis for a small, smooth pedunculated small bowel polyp. In adults, lipomas are a relatively common lead point for an intussusception. Occasionally multiple lipomas result in multiple intussusceptions and small bowel obstruction.

Computed tomography shows a lipoma as a well-marginated, homogeneous tumor having fat attenuation.

Polyposis Syndromes

The polyposis syndromes are discussed in more detail in Chapter 5. Covered here are only those aspects pertinent to the small bowel.

Although not common, small bowel adenocarcinomas do develop in familial polyposis, even after a colectomy. Whether these carcinomas are more common after a colectomy due to ileal mucosa becoming dysplastic, as some investigators have suggested, is unknown.

Enteroenteric intussusceptions are common in Peutz-Jeghers syndrome (Fig. 4.16). Most are transient, but an occasional one evolves into an obstruction or ischemia. Magnetic resonance in a patient with Peutz-Jeghers syndrome detected a solitary 1.5-cm polyp associated with an enteroenteric intussusception (79); the polyp was isointense to bowel on precontrast images and enhanced similar to bowel both on early and late postcontrast images. A rare finding in Peutz-Jeghers syndrome is small bowel cystica profunda.

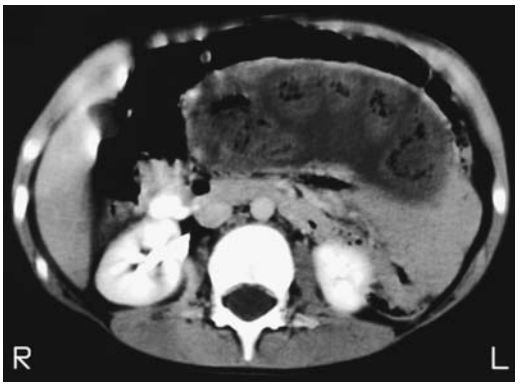

Figure 4.16. Small bowel intussusception in an 8–year-old boy with Peutz-Jeghers syndrome. The greatly dilated small bowel loop contains several nondilated loops in this CT image, reflecting the chronicity of this condition. (Courtesy of Patrick Fultz, M.D., University of Rochester.)

An occasional polyp in a patient with Peutz-Jeghers syndrome undergoes osseous metaplasia.

Malignant Neoplasms

Primary small bowel cancers are not common. The Utah Cancer Registry from 1966 through 1990 found the most common cancer to be a carcinoid (41%), followed by adenocarcinoma (24%), lymphoma (22%), and sarcoma (11%), with a small percentage unclassified (80); an age-adjusted incidence of small bowel cancers was 1.4 per 100,000; for comparison the colon cancer rate was 36 per 100,000 and breast cancer 93 per 100,000.

Carcinoids, lymphomas, and sarcomas decrease in frequency from the ileum to the duodenum (80); the reverse is true for adenocarcinomas. Of interest is that in industrialized countries adenocarcinomas tend to predominate but lymphomas are more common in developing countries (81).

Adenocarcinoma

Patients who have one small bowel adenocarcinoma are at increased risk of developing both other duodenal and jejunal tumors and other carcinomas. The risk of small bowel adenocarcinomas increases with age and is higher among men. Risk factors appear similar to those seen for colon cancer. An increased prevalence is found in patients with Crohn's disease, celiac disease, cystic fibrosis, familial adenomatous polyposis, and Peutz-Jeghers syndrome.

The two current imaging modalities used for diagnosing small bowel cancers are barium studies and CT. The role of CT enteroclysis is promising but not yet established. The diagnosis is not always straightforward. An occasional small bowel adenocarcinoma metastatic to the ovary mimics a primary ovarian carcinoma.

A typical small bowel adenocarcinoma appears as a poorly marginated soft tissue tumor or localized infiltration often obstructing the bowel lumen (Fig. 4.17). A minority necrose extensively, do not obstruct, and mimic a mes-

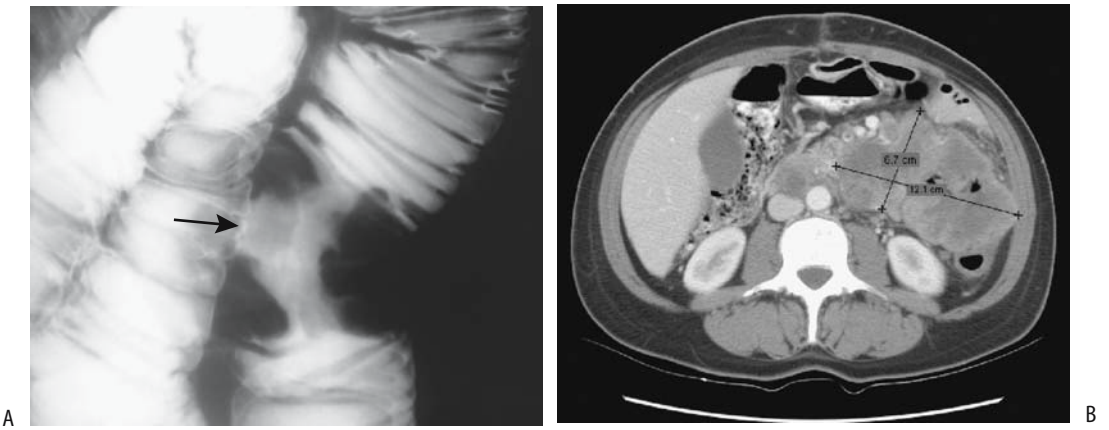

Figure 4.17. Jejunal adenocarcinoma. A: A typical "napkin-ring" stricture is evident (arrow). B: CT in another patient reveals a heterogeneously enhancing tumor (cursors). Several adjacent jejunal loops are encased by this tumor. (Courtesy of Arunas Gasparaitis, M.D., University of Chicago.)

enchymal tumor. A multicentric adenocarcinoma is rare.

The role of MRI is not established. Both precontrast T1-weighted SGE images and postgadolinium fat-suppressed images appear useful in visualizing these tumors. Malignant tumors tend toward heterogeneous enhancement on postgadolinium images.

Few studies have evaluated preoperative staging of small bowel adenocarcinomas (Table 4.6). A retrospective preoperative nonhelical CT study achieved an overall CT staging accuracy of only 47% (82); sensitivity and specificity for detecting adenopathy were 75% and 20% and for detecting distant metastases 58% and 63%, respectively. Staging errors were compounded by the presence of Crohn's disease, other polyps, and small bowel obstruction.

The 5-year survival rate for patients with small bowel adenocarcinoma is about 20%; less than half of patients undergo a "curative" resection.

Lymphoma

Clinical

Patients with Crohn's disease or celiac disease, immunocompromised patients, and those with dermatitis herpetiformis are at increased risk for intestinal lymphomas. Most primary intestinal lymphomas are non-Hodgkin's lymphomas. Lymphomas develop throughout the small bowel, the exception being in the setting of celiac disease, when proximal lymphomas are more common.

Mediterranean lymphoma probably is a variant of primary lymphoma. Weight loss, diarrhea, and general debility predominate in these patients. Affected are mostly young adults. In distinction to the stomach, only a minority of small bowel lymphomas are of the MALT type. Immunoproliferative disease is a rare lymphoproliferative disorder involving the small intestine. It appears to be a manifestation of MALT lymphoma.

Clinical findings range from abdominal pain, malabsorption, and hypoalbuminemia, to perforation, the latter finding seen more often with primary intestinal T lymphomas rather than B type. These T lymphomas tend to be rather aggressive.

Imaging

Primary intestinal lymphoma develops mostly as either a polypoid or an exophytic ulcerated lesion, with only an occasional one infiltrating diffusely (Fig. 4.18). Focal circumferential involvement is common. In some patients the

Table 4.6. Tumor, node, metastasis (TNM) staging of small intestinal adenocarcinoma

Primary tumor:			
Tx	Primary tumor cannot be assessed		
T0	No evidence of primary tumor		
Tis	Carcinoma-in-situ		
TI	Tumor invades lamina propria or submucosa		
T2	Tumor invades muscularis propria		
T3	Tumor invades into subserosa; tumor invades through muscularis propria into surrounding tissue for less than 2 cm (between leaves of mesentery or into retroperitoneum if duodenal)		
T4	Tumor invades adjacent organs; tumor perforates serosa; tumor extends more than 2 cm into retroperitoneum or between leaves of mesentery		
Lymph nodes:			
Nx	Regional lymph nodes cannot be assessed		
N0	No regional lymph node metastases		
NI	Regional lymph node metastasis		
Distant metastases:			
Mx	Distant metastases cannot be assessed		
M0	No distant metastases		
MI	Distant metastasis		
Tumor stages:			
0	Tis	N0	M0
I	T1	N0	M0
	T2	N0	M0
II	T3	N0	M0
	T4	N0	M0
III	any T	N1	M0
IV	any T	any N	MI

Source: From the AJCC Cancer Staging Manual, 6th edition (2002), published by Springer-Verlag, New York, NY, used with permission of the American Joint Committee on Cancer (AJCC), Chicago, IL.

bowel lumen is aneurysmally dilated, in others it is narrowed. Bowel obstruction is not a common feature even with extensive lymphomatous involvement and, if present, should suggest another diagnosis. At times ulcers are quite large and out of proportion to the tumor mass, an appearance mimicking a necrotic mesenchymal tumor (Fig. 4.19).

In the terminal ileum primary lymphomas tend to have a tumor-like appearance; more proximal ones more often are ulcerated. Extensive fistulas are rare with both primary and secondary small bowel lymphoma. Non-Hodgkin's lymphomas also present as multiple polyps scattered throughout the gastrointestinal tract. These polyps range from relatively flat ones, with an overall appearance similar to that of lymphonodular hyperplasia, to mostly intraluminal ones mimicking familial polyposis. A polypoid appearance is more common with Mediterranean lymphomas and in immunocompromised patients.

Therapy

Surgery is performed to obtain a biopsy, establish the extent of involvement, correct any obstruction or perforation, and, at times, debulk.

After cytoreductive chemotherapy some of these patients develop intramural fat deposition, detected by serial CT as fat-attenuating bowel wall thickening. It should be kept in mind that submucosal fat deposition also occurs in inflammatory bowel disease.

Small bowel fibrosis and resultant obstruction are a complication of chemotherapy for intestinal lymphoma.

Sarcoma

Leiomyosarcoma

The pathologic borderland between leiomyoma and leiomyosarcoma is rather murky, and the same applies to a larger extent in radiology. Presence of metastases obviously signifies malignancy. A small bowel leiomyosarcoma often presents as a large tumor with a prominent, irregular central cavity that fills with barium. The cavity tends to overwhelm any surrounding soft tissue component. In spite of the large size, lumen obstruction is not common.

Computed tomography reveals a small bowel mesenchymal neoplasm, regardless of whether it is benign or malignant, as a large, bulky, eccentric mass, often with a low attenuation center or cavity (Fig. 4.20). Some investigators have used specific CT criteria to suggest malignancy but with limited success. The CT findings of 21 leiomyomas and 24 leiomyosarcomas were subdivided into three groups—I, probably benign; II, probably malignant; and III, malignant—and the results compared with histopathologic diagnosis (83). In addition to direct invasion and metastasis, CT findings favoring malignancy included tumor size >5 cm,

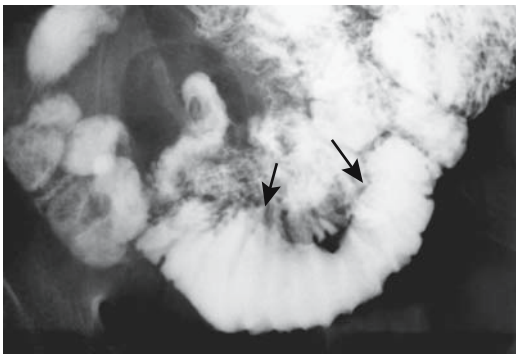

A

B

Figure 4.18. A: Ileal lymphoma (mucosa-associated lymphoid tissue, MALT) presenting as a dilated loop containing thickened valvulae conniventes (arrow). (Courtesy of Arunas Gasparaitis, M.D., University of Chicago.) B: Small bowel lymphoma diffusely thickening bowel wall and obliterating valvulae conniventes.

a lobulated contour, heterogeneous contrast enhancement, mesenteric fat infiltration, ulceration, adenopathy, and an exophytic growth. The presence of calcifications does not aid in differentiating benign from malignant. Similarly to adenocarcinomas, small bowel leiomyosarcomas have been misdiagnosed as ovarian tumors.

The 5-year survival rate for patients with a small bowel sarcoma is about 50%.

Liposarcoma

Many liposarcomas contain little or no fat. Thus a CT finding of attenuation greater than fat in a tumor does not exclude a liposarcoma.

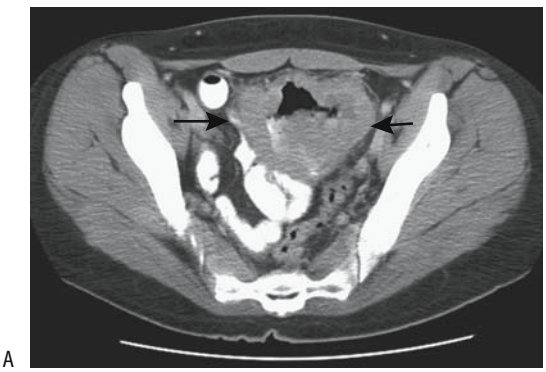

A

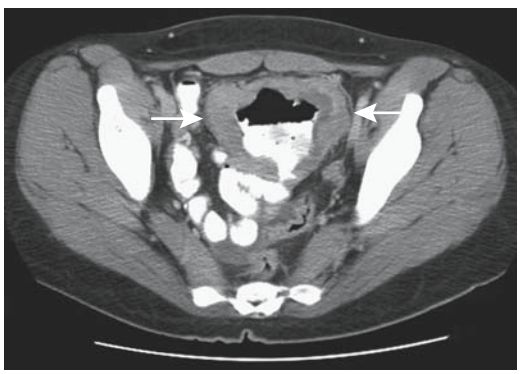

B

Figure 4.19. Non-Hodgkin's lymphoma. A,B: Two CT images reveal a tumor (arrows) with a necrotic center (arrowheads). No bowel obstruction was present.

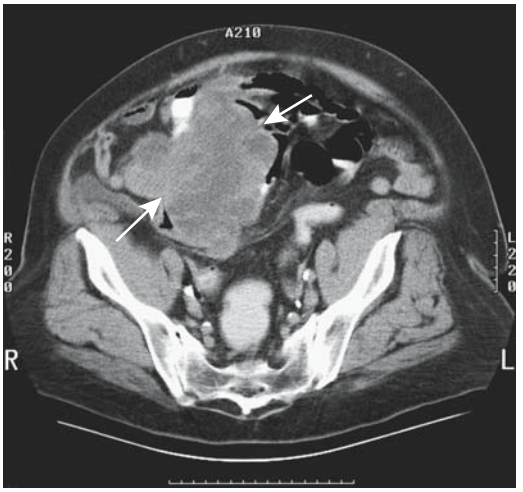

Figure 4.20. Small bowel leiomyosarcoma, probably a gastrointestinal stromal tumor (GIST), in a 47–year-old woman with fever, pain, and a palpable right lower quadrant tumor. Oral and IV contrast-enhanced CT reveals a complex, heterogeneously enhancing tumor (arrows). Other images identified surrounding mesenteric infiltration. (Courtesy of Patrick Fultz, M.D., University of Rochester.)

Other Primary Malignancies

A primary jejunal choriocarcinoma in a man led to melena and a markedly elevated serum β-human chorionic gonadotrophin level (84); the authors suggest metaplasia to primitive trophoblasts as an etiology for this tumor.

Small bowel sarcomatoid carcinomas are rare. They tend to be necrotic, ulcerated, and hemorrhagic. The prognosis was poor in the few reported patients.

Metastasis or Direct Invasion

Tissue from intestinal metastases can be successfully obtained using US-guided 22-gauge fine-needle aspiration or 18-gauge core biopsy (85).

Melanoma

A small bowel melanoma, even if a primary is not known, is most likely metastatic. The time interval between initial skin lesion and detection of intestinal metastases is typically several years. Bleeding and obstruction are common presentations. An Armed Forces Institute of Pathology review of 103 patients with small bowel malignant melanoma suggests two subsets: one occurs in younger patients and is more aggressive with rapid metastasis and early death, and the other is a more indolent form occurring in older patients that tends to metastasize less often (86). A rare melanoma intussuscepts (87).

Most metastatic melanomas to the small bowel present as multiple small, solid nodules scattered haphazardly. An occasional metastasis is solitary, at times quite large, and even cystic in appearance.

Other

Breast, ovarian, lung, and other similar metastases to bowel tend to obstruct, often at multiple sites, or ulcerate and bleed. Their imaging appearance ranges from minor infiltration to large, necrotic tumors (Fig. 4.21). Enteroclysis is necessary to detect subtle ones, keeping in mind that most metastases are closer to the serosa than mucosa (mucosal metastases are rare). The larger ulcerated tumors are detected by most imaging modalities.

Neuroendocrine Tumors

A number of neuroendocrine tumors are of mesenteric origin and rightfully should be discussed in Chapter 14. In clinical and radiologic practice, however, these tumors often are in the differential diagnosis of small bowel and colonic tumors.

Schwannoma/Neurilemmoma

Small bowel schwannomas are uncommon. An occasional one bleeds. These are mostly solid soft tissue tumors.

Neurofibroma

Neurofibromatosis is discussed in more detail in Chapter 14.

Many patients are asymptomatic but an occasional tumor erodes through the mucosa and bleeds or acts as a lead point for an intussusception. When large, tumor bulk may obstruct either the small bowel or adjacent urinary tract.

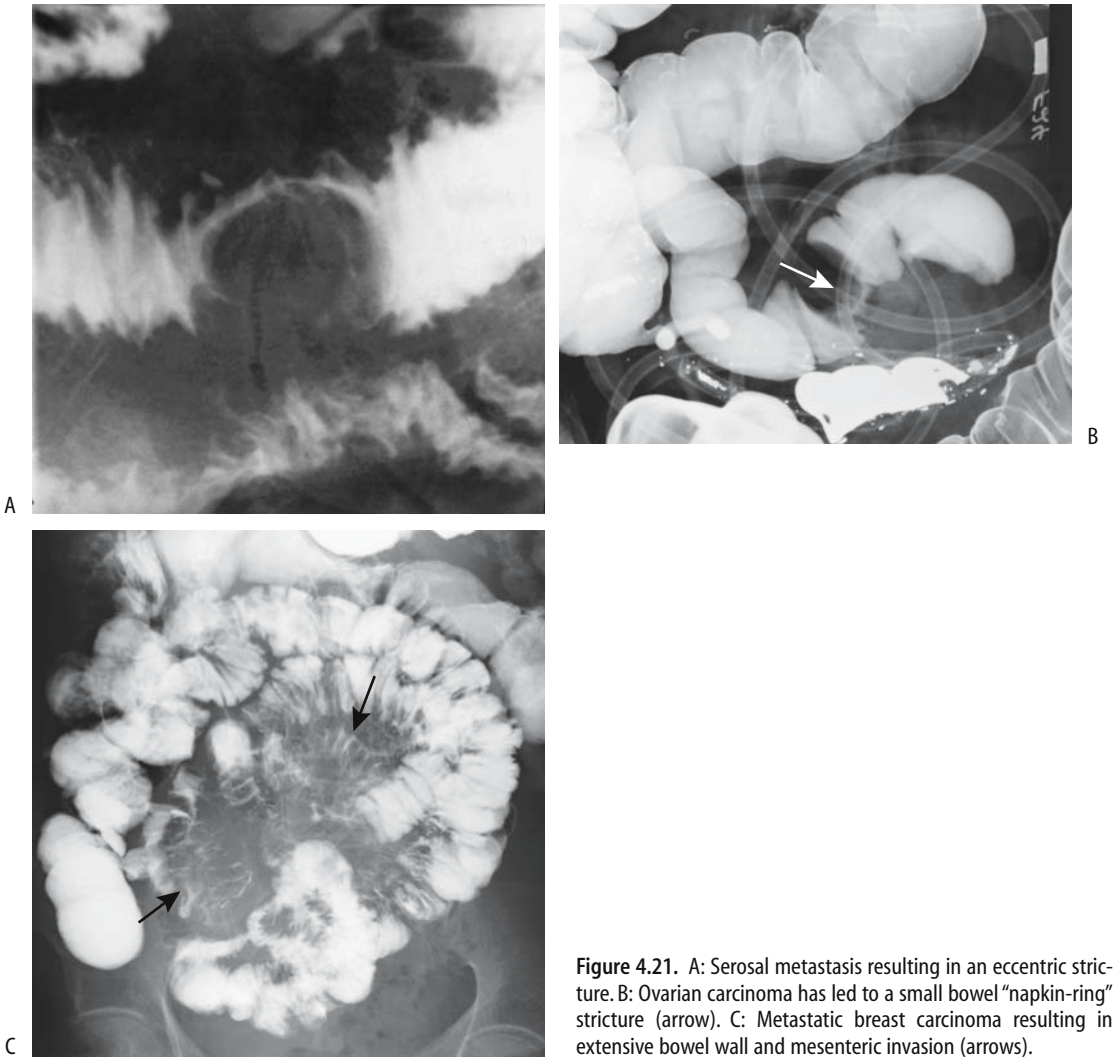

Figure 4.21. A: Serosal metastasis resulting in an eccentric stricture. B: Ovarian carcinoma has led to a small bowel "napkin-ring" stricture (arrow). C: Metastatic breast carcinoma resulting in extensive bowel wall and mesenteric invasion (arrows).

Most nonplexiform neurofibromas occur on the antimesenteric border. Imaging of the few published plexiform neurofibromas shows a mesenteric polypoid or bead-like mass infiltrating a loop of bowel and its associated mesentery (88). The degree of small bowel and mesenteric involvement varies and is reflected on relative barium studies and CT of the involved bowel. Mesenteric angiography and CT angiography are helpful in localizing a bleeding tumor.

Magnetic resonance in a patient with neurofibromatosis revealed duodenal and jejunal polyps 1 to 2 cm in diameter (79); the polyps were isointense to bowel wall and enhanced similarly.

Carcinoid

Clinical

Jejunoileal and colonic carcinoids tend to be rather aggressive tumors, with even small ones

showing local invasion and metastasis. Multiple carcinoids are not uncommon, and a case can be made for searching for additional tumors. Abdominal carcinoids are not limited to bowel wall, and a mesenteric location is often favored.

Elevated serum serotonin and urine 5-hydroxyindoleacetic acid levels suggest liver metastases, although high serotonin activity of some primary carcinoids results in a carcinoid syndrome even without metastasis.

Imaging

Small bowel carcinoids range from intramural polyps to an exuberant desmoplastic reaction to the point of obstruction (Fig. 4.22). Intestinal necrosis is a rare complication.

Computed tomography was normal in 21% of patients with a known midgut carcinoid in spite of biochemical evidence for tumor (89); liver metastases were found in 68%, 20% had mesenteric root involvement, and 24% had extraperitoneal adenopathy, and the authors conclude that CT can miss a primary carcinoid but that it is useful in gauging the extent of tumor spread and as an aid during follow-up. A common CT appearance is a distinct mesenteric tumor, often containing characteristic linear radiating soft tissue spokes, which should be distinguished from mesenteric soft tissue stranding, which is found in a number of infiltrative conditions and is a nonspecific finding. A minority of carcinoids contain calcifications.

Ultrasonography findings tend to be nonspecific.

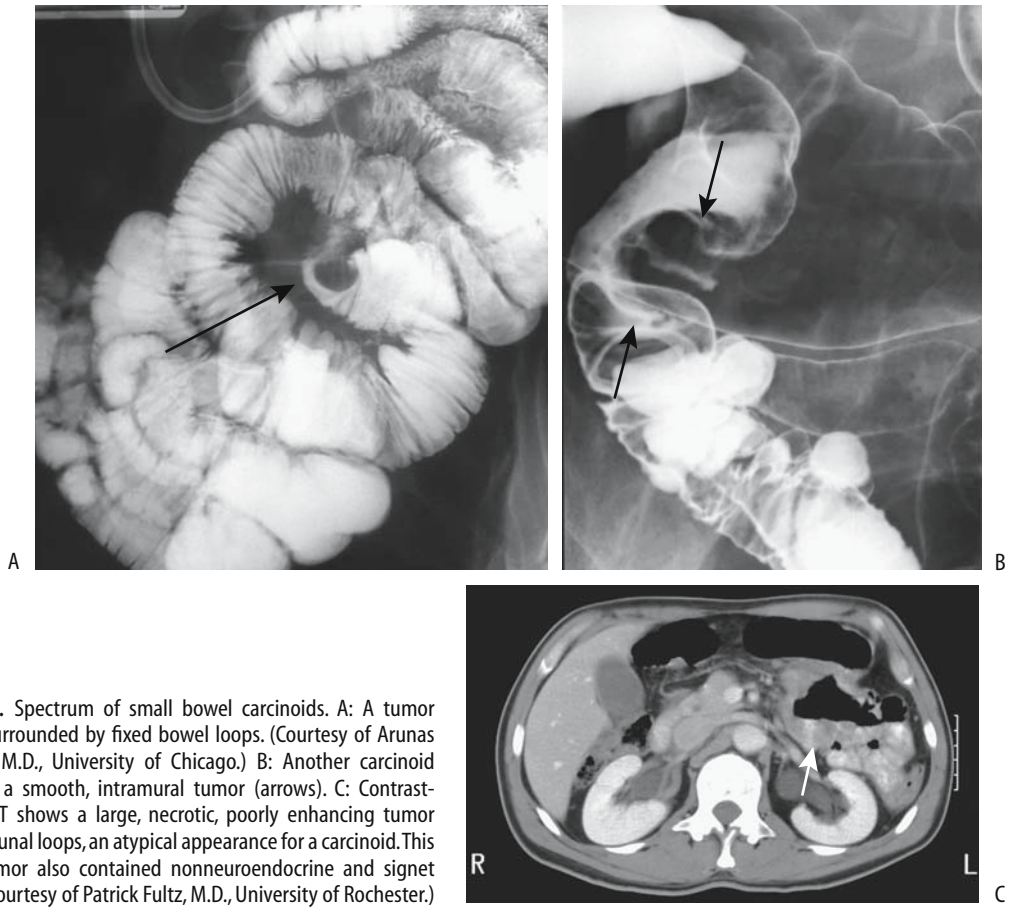

Figure 4.22. Spectrum of small bowel carcinoids. A: A tumor (arrow) is surrounded by fixed bowel loops. (Courtesy of Arunas Gasparaitis, M.D., University of Chicago.) B: Another carcinoid presents as a smooth, intramural tumor (arrows). C: Contrast-enhanced CT shows a large, necrotic, poorly enhancing tumor involving jejunal loops, an atypical appearance for a carcinoid. This complex tumor also contained nonneuroendocrine and signet ring cells. (Courtesy of Patrick Fultz, M.D., University of Rochester.)

Magnetic resonance imaging in patients with carcinoids identified a primary tumor in 67% (90); these tumors were best seen on postcontrast T1-weighted fat-suppressed images, and their appearance ranged from a nodular tumor originating from bowel wall to focal bowel wall thickening having homogeneously moderate contrast enhancement. Mesenteric nodular metastases were associated with mesenteric stranding in most. Most liver metastases were hypervascular with moderate contrast enhancement, although 6% were hypovascular; of note is that some metastases were visible only on immediate postcontrast images. Carcinoids are hypointense both on T1- and T2-weighted MR images. Infiltration from a central tumor into surrounding hyperintense mesenteric fat results in a spoke-wheel appearance.

Carcinoids contain increased somatostatin receptors, and thus scintigraphy with radiolabeled somatostatin analogues is potentially useful. Initial studies with octreotide labeled with radioactive iodine were discouraging but In-111–pentetreotide appears promising; SPECT is more sensitive than planar scintigraphy in detecting both primary carcinoids and metastases. Indium 111–pentetreotide is more sensitive than CT.

Whole-body 18F-dihydroxyphenylalanine (DOPA) positron emission tomography (PET) of a mix of primary tumors, lymph node metastases, and organ metastases achieved an overall sensitivity of 65%; sensitivity of 18-fluorodeoxyglucose (FDG)-PET was 29%, somatostatin receptor scintigraphy 57%, and morphologic procedures 73% (91). The FDG-PET imaging was falsely negative in a patient with a known metastatic carcinoid and a positive octreotide scan (92).

Therapy

Therapy for carcinoids varies depending on tumor size and presence of metastases. Curative radical resection should be considered for small intestine carcinoids. With some metastatic carcinoids a palliative resection decreases symptoms. Medical therapy with somatostatin analogues and α-interferon can prolong survival. The 5-year survival rate for patients with small bowel carcinoids is <50%.

In appropriate patients metaiodobenzylguanidine (MIBG) scintigraphy appears to have a role in planning iodine 131 MIBG therapy.

Dilation

In ancient Greece the term *ileus* described intestinal obstruction. The Romans narrowed this definition to include primarily intestinal volvulus and intussusception, and in this sense *ileus* was used up to the 18th century. The *Oxford English Dictionary* defines *ileus* as a painful affection due to intestinal obstruction. *Ileus* as a synonym for intestinal obstruction, regardless of cause (mechanical ileus, adynamic or paralytic ileus, ischemic ileus, and so on), is used in Europe and Japan, but in the United States *ileus* has been subverted to be synonymous with adynamic ileus only, leading to confusing terminology. Even some of the more respected American medical and surgical textbooks have adopted this narrower definition of ileus.

Mechanical Obstruction

Table 4.7 lists some of the conditions associated with mechanical small bowel obstruction. Both internal and external hernias are common causes of small bowel obstruction; these are discussed in Chapter 14. Ileocolic intussusception is covered in Chapter 5.

Radiologists typically subdivide small bowel obstruction into complete and incomplete. Incomplete obstruction is then subdivided further into low grade, high grade, and similar variants. Restraint should be used in drawing clinical prognostic conclusions from such radiographic classification. Some have equated *incomplete* obstruction to mean *insignificant* obstruction, although these two terms have different meanings. Whether to suggest surgical correction of an incomplete obstruction should be based more on clinical findings (presence of nausea, vomiting, pain, inability to maintain weight, etc.) rather than on a specific radiographic appearance, with some exceptions; thus the presence of bowel wall edema or pneumatosis suggest underlying ischemia.

Detection

Many patients with suspected small bowel obstruction undergo passage of a decompres-

Table 4.7. Conditions associated with mechanical small bowel obstruction

- Intraluminal
  - Bezoar (foreign body)
  - Gallstone
  - Intussusception
  - Parasites
  - Polyp (neoplastic or nonneoplastic)
  - Meconium
- Intramural
  - Infiltrating neoplasm
  - Hematoma and hemorrhage
  - Inflammation
    - Crohn's disease
    - Infection
  - Ischemia
  - Radiation enteritis
  - Congenital stricture
- Extrinsic
  - Adhesions
  - Adjacent inflammation/abscess involving bowel
  - Hernia (internal or external)
  - Volvulus
  - Extrinsic neoplasm, cyst, etc. compressing bowel
  - Congenital bands
  - Endometriosis

sion tube early in their course, even before a definitive diagnosis is established, followed by *watchful observation*, a poorly defined term having a different meanings for different physicians. Gastrointestinal radiologists prefer that these patients undergo imaging studies without undue delay. What should be the sequence of imaging studies?

Because of ready availability, conventional radiographs should be obtained before bowel decompression. Likewise, CT is best performed before bowel decompression. If conventional radiographs do not reveal small bowel dilation, the decompression catheter, preferably a sump-type catheter rather than a simple nasogastric tube, is advanced distal to the pylorus. Barium instilled through the tube provides a fluoroscopic small bowel study, and is used for enteroclysis or as an aid to identify the small bowel during a subsequent CT study.

Occasional but recurrent publications advocate the use of a water-soluble contrast agent to study small bowel obstruction. Although in infants use of a nonionic agent is advantageous, in the study of adult small bowel obstruction the water-soluble contrast agents have little to recommend. Erratic amounts of additional fluid are drawn intraluminally, the already distended bowel becomes even more distended, the patient becomes more uncomfortable, and often the only conclusion possible from such a study is identifying whether the bowel is grossly dilated or not. In fact, some of the studies claiming a superiority for CT over a small bowel contrast study used water-soluble contrast agents rather than barium for the comparison study, leading to preordained results. In most patients, if bowel wall integrity is not compromised, a small bowel contrast study should be performed with barium.

Some investigators use solid, 4-mm radiopaque markers to identify a partial small bowel obstruction (93); the markers coalesced close to the obstruction. This technique is currently little used and appears inferior to more conventional imaging tests.

Small bowel dilation per se, without colonic dilation, is not pathognomonic of obstruction; for example, patients with celiac sprue tend to have dilated, fluid-filled loops of small bowel, with an overall appearance similar to distal small bowel obstruction. On the other hand, regardless of the imaging study performed, small bowel obstruction is implied if proximal small bowel is dilated while more distal loops are collapsed. These dilated proximal loops tend to be filled mostly with liquid intestinal content. Numerous bowel caliber dimensions have been published in an attempt to differentiate between normal and dilated caliber bowel, but these measurements have little use in clinical practice; the borderland between normal caliber and dilated bowel is sufficiently vague and varies considerably depending on site, degree, and age of an obstruction, resultant peristaltic activity, and presence of underlying disease.

The presence of massively dilated small bowel loops suggests a chronic, long-standing obstruction.

Conventional Radiography

A number of investigators advocate CT rather than conventional radiographs when bowel obstruction is suspected clinically. Generally

three questions are raised in this setting: Is obstruction indeed present? Where is the obstruction? What is the etiology of an obstruction? From a surgical perspective the first question is most important and generally both the first and often also the second question can be answered by conventional radiography. The underlying etiology is of less interest to the surgeon, except to exclude ischemia and incarceration, etiologies notoriously difficult to detect early by any imaging modality. Bowel obstruction (or the lack of it) can be approached with either an oral barium study or CT, although many radiology departments have evolved to the point where CT is more readily available and is encouraged.

Conventional radiographs aid in differentiating complete or high-grade partial small bowel obstruction from low grade or no obstruction; findings suggesting a high-grade small bowel obstruction include the presence of gas-fluid levels at a differential height in the same loop and presence of a mean gas-fluid level width ≥25 mm on upright abdominal radiographs (94).

Barium Study

A small bowel barium study is a viable option in the patient with a suspected small bowel obstruction. Contraindications to barium are few: an acute abdomen, suspected bowel perforation, or distal colonic obstruction. Some surgeons still argue for a water-soluble agent to avoid possible barium spillage into the peritoneal cavity during subsequent surgery, an argument of dubious validity; the surgeon should spill neither barium nor the usually infected intestinal contents proximal to a small bowel obstruction.

A number of studies have documented the advantages of enteroclysis over a conventional small bowel study, yet in most institutions enteroclysis is rarely performed in this clinical setting.

Prior to performing a barium study, be it a conventional small bowel study, enteroclysis, or a CT-enteroclysis study, thought must be given to whether another diagnostic study will be needed that is obviated by the intraluminal retention of barium. Even endoscopists complain if their field of view is obscured by barium.

Small bowel obstruction is not a contraindication to an antegrade barium study. Barium proximal to a small bowel obstruction remains in suspension. It does not become more viscous, as happens in the colon, and in the small bowel barium does not influence the degree of obstruction. Contrary to an occasional surgical report (95), barium does not make a small bowel obstruction worse. Likewise, the occasional surgeon's request to use "thin" barium in a setting of small bowel obstruction is meaningless; marked fluid retention proximal to an obstruction invariably leads to barium dilution.

A barium enema with reflux into the small bowel is a viable study in a patient with suspected distal small bowel or colon obstruction. This study differentiates between obstructive ileus and adynamic ileus in most patients and often provides an etiology for an obstruction.

Computed Tomography

Reported CT sensitivities in detecting small bowel obstruction have ranged up to 100%, with examiner enthusiasm and interest in the technique probably influencing results. Nevertheless, a number of studies over the past decade have shown that CT not only detects a small bowel obstruction but also often identifies a cause. CT can correctly distinguished between small bowel obstruction and adynamic ileus in almost all and established a cause of obstruction in most. In general, CT is more accurate in a setting of a high-grade rather than low-grade obstruction.

Comparing conventional radiography and CT in patients with suspected small bowel obstruction, the positive predictive value of conventional radiography was 80% and of CT 95% (96); of interest is that the false-negative rate was 8% with conventional radiography but only 1.6% with CT. Nevertheless, the authors recommended that conventional radiography still be the initial study of choice. The authors did not evaluate and compare their CT results to barium studies.

A blinded retrospective analysis comparing conventional radiography and CT in patients suspected of having a small-bowel obstruction achieved a similar overall accuracy with both examinations (Table 4.8); CT, however, revealed

Table 4.8. Imaging of mechanical small bowel obstruction*

	Sensitivity (%)	Specificity (%)	Accuracy (%)
Overall:			
Conventional radiography	69	57	67
CT	64	79	67
High-grade obstruction:			
Conventional radiography	86		
CT	82		
Low-grade obstruction:			
Conventional radiography	56		
CT	50		

* Data based on 78 patients with suspected small-bowel obstruction.
Source: Adapted from Maglinte et al. (97).

a cause of obstruction in 95%, a finding not usually possible with conventional radiography. The authors concluded that conventional radiography should remain the initial imaging study in patients with suspected small bowel obstruction. Comparing enteroclysis and CT in clinically equivocal small bowel obstruction, CT correctly identified 79% of 43 proven intestinal obstructions (98); CT was most accurate with a complex or long narrowed segment and least accurate with short stenotic segments. It was falsely positive in two patients with mesenteric infarction; enteroclysis had no false positives or false negatives. The author concluded that enteroclysis is more accurate in detecting and localizing an obstruction, but CT is superior in determining the cause of the obstruction and in detecting any underlying strangulation.

A retrospective CT study in children achieved a sensitivity of 87% and specificity of 86% for detecting small bowel obstruction (99); the etiology of the obstruction was correctly identified in 47% of scans.

The conclusions of these studies apply to the patient with a suspected small bowel obstruction where an examination is performed to confirm that an obstruction is indeed present and to suggest an etiology. Another large group of patients consists of those hospitalized with an obstruction but due to delays, often erroneous but well-intentioned, the obstruction has now resolved clinically and the radiologist is asked to suggest an etiology for the previous obstruction. The analogy is similar to a chest radiograph being obtained after pneumonia has cleared. In such a situation enteroclysis appears to be the examination of choice in detecting a subtle underlying tumor, residual adhesion, or similar abnormality; CT is of limited value in such a setting. Also, CT appears to have a limited role in evaluating a partial small bowel obstruction. In such a setting enteroclysis appears superior.

Typical CT criteria for small bowel obstruction consist of a discrepancy between more proximal dilated and more distal nondilated small bowel loops (Fig. 4.23). Distal small bowel obstruction consists of generalized small bowel dilation and a narrowed colon lumen. A CT finding of gas and particulate material in dilated segments of small bowel is considered abnormal, and most of these patients have a more distal small bowel obstruction, although an occasional patient with slow small bowel transit, regardless of etiology, has similar findings. It is, however, an uncommon finding in obstruction.

Thickened bowel wall containing a thin hyperdense component, called a *target sign* or *halo sign*, represents fluid within the bowel wall and is seen with bowel ischemia. A somewhat similar appearance is found with small bowel intussusception and with an inflamed loop, such as in Crohn's disease. This sign is also seen in some normal bowel where it represents fat infiltration and appears related to obesity (100).

Rather than relying on axial images, coronal and sagittal images are often more helpful in

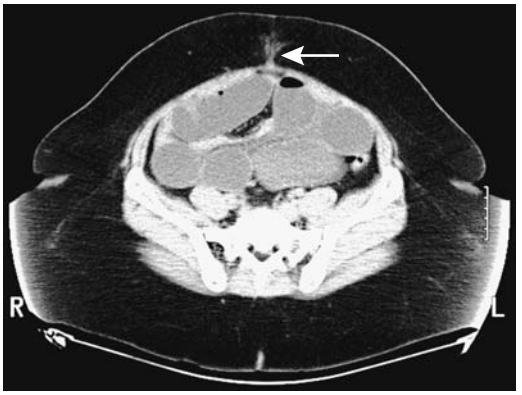

Figure 4.23. An incisional hernia causing small bowel obstruction after laparoscopic surgery. CT identifies both the hernia (arrow) and marked proximal small bowel dilation. (Courtesy of Patrick Fultz, M.D., University of Rochester.)

identifying a point of obstruction and suggesting a possible etiology.

Computed tomography enteroclysis achieves a sensitivity similar to that of conventional enteroclysis in detecting a site of partial small bowel obstruction, assesses the degree of obstruction, and often also identifies a cause of the obstruction. This study is superior to conventional CT, especially in a setting of partial small bowel obstruction. Still, CT enteroclysis should be approached with caution; instillation of large amounts of contrast into a small bowel already distended by an obstruction simply distends it further and risks inducing vomiting and aspiration.

Ultrasonography

Ultrasonography studies of patients with acute abdominal pain have achieved sensitivities of 75% to 95% in detecting an obstruction, yet closer perusal makes it difficult to place these studies in a proper perspective. Ultrasonography is more often employed to study the bowel in Europe rather than the United States or Canada, where it has been supplanted by CT and, to a lesser extent, by MRI.

Conventional US readily identifies extraluminal fluid; such fluid is present in about two thirds of patients with small bowel obstruction.

Duplex Doppler US has been used to differentiate between obstruction and paralytic ileus, with results similar to those obtained during a physical examination, namely, in the early stages of mechanical obstruction. Doppler US reveals hyperperistalsis proximal to the obstruction; in long-standing obstructions, as expected, a decrease in intensity and duration of peristalsis predominates. Dilated and atonic segments are identified in adynamic ileus, although some bowel motility usually is still present. Fluoroscopic observation of contrast-filled loops of bowel identifies similar peristaltic activity, although most fluoroscopists tend to rely little on these observations.

Magnetic Resonance Imaging

Magnetic resonance imaging is not often employed in suspected small bowel obstruction; rather, obstruction is occasionally detected when a study is performed for other reasons. Preliminary evidence suggests, however, that a MR study dedicated to the small bowel is rather accurate. A prospective study of patients with suspected inflammatory bowel disease or small bowel obstruction found that MR enteroclysis findings were similar to those obtained with conventional enteroclysis or surgery (6).

Adhesions

The most common cause of small bowel obstruction is adhesions, usually secondary to prior surgery. The surgery does not necessarily have to involve small bowel. In one hospital, small bowel obstruction due to adhesions was highest after appendicectomy and colonic resections and lowest after gallbladder and pancreatic surgery (101). Even some urologic procedures lead to small bowel obstruction. Adhesions range from single to multiple. Some adhesions fixate or kink a loop of bowel; others, extrinsic to the bowel, act as a nidus for an internal hernia.

Computed tomography reveals an adhesive obstruction as a sharp bowel angulation at the site of obstruction. A barium study identifies an adhesion as a smooth, extrinsic, linear impression at the point of change in bowel caliber.

Cancer

Not all obstructions in patients with a known cancer are secondary to tumor; about one third

have a benign etiology. At times CT can suggest an etiology for intestinal obstruction. Patients with known intraabdominal malignancy and small bowel obstruction often have other sites of obstruction not detectable by CT (102); additional information altering subsequent treatment is often provided by a contrast enema. In fact, the entire gastrointestinal tract should be studied in cancer patients because multiple sites of obstruction are relatively common.

Surgery relieves most small bowel obstructions. In patients with a malignant obstruction, however, surgical relief of an obstruction usually does not influence survival.

Closed Loop Obstruction/Volvulus

A closed loop obstruction consists of a loop of bowel obstructed at two points. The *closed loop* refers to bowel lumen and not blood vessels. In time, increasing intraluminal pressure leads to venous stasis, ischemia, and strangulation. Although many closed loop obstructions eventually evolve into strangulation, from an imaging viewpoint the two entities can be distinguished: a closed loop obstruction implies lumen obstruction; strangulation signifies bowel ischemia. Obstruction in a hernia is a type of closed loop obstruction.

A volvulus is due to intestinal twisting and resultant lumen obstruction. A volvulus is a type of closed loop obstruction if the obstruction involves both inflow and outflow to the twisted loop.

Because etiologies of volvulus differ between infants and adults, these populations are best approached separately.

Infants

Small bowel volvulus in infants is almost always associated with midgut malrotation or nonrotation. Malrotation predisposes to a small bowel twist around its mesentery, which contains the superior mesenteric artery and vein; resultant vascular compromise leads to small bowel necrosis unless emergent surgical intervention ensues. The proximal end of malrotation is in the descending duodenum, distal to the papilla of Vater, and resultant luminal obstruction at this level accounts for the common clinical presentation of bilious vomiting, often within first days of life.

Conventional radiographs often reveal partial rather than complete duodenal obstruction. Complete duodenal obstruction and a gasless distal bowel is more common with duodenal atresia. Ischemia developing in a setting of neglected partial volvulus also results in a gasless abdomen. A conventional radiographic finding compatible with duodenal obstruction is seen only in about half of the infants requiring surgical correction. When present, however, a need for further imaging prior to surgery is debatable.

The duodenal corkscrew appearance on a contrast study is familiar to most radiologists. Barium is used by most, with a minority preferring water-soluble low osmolarity contrast agents. Some advocate US using water as a contrast agent, but such an approach is very operator dependent and not widely practiced.

The usual anatomic relationship of superior mesenteric artery and vein is reversed in malrotation. Ultrasonography reveals a whirlpool, with the superior mesenteric vein and mesentery twisted around the superior mesenteric artery. Although this finding is useful in detecting malrotation both with CT and US, false-positive and false-negative findings do occur. In one study, however, color Doppler US identified a whirlpool sign that rotated clockwise (with caudal movement of the transducer) in 12 of 13 pediatric patients with surgically confirmed midgut volvulus and counterclockwise in three patients without midgut volvulus (103); the sensitivity of this clockwise US whirlpool sign in detecting midgut volvulus was 92% and the specificity 100%, and the authors suggest that color Doppler US should be an initial imaging study in children with suspected midgut volvulus.

Adults

In adults a closed loop small bowel obstruction is most often secondary to adhesions. Small bowel volvulus without a predisposing cause is not common in Western Europe or North America, but in parts of Turkey it represents 13% of small bowel obstruction (104). In some parts of the world volvulus is associated with ingestion of large quantities of milky foods. Ascariasis infestation predisposes to small

bowel volvulus. On a rare occasion a small bowel mesenteric tumor, even a lipoma or lymphangioma, acts as a nidus for a twist, leading to volvulus. A rare cause was a vena cava perforation by a Greenfield filter resulting in small-bowel volvulus (105).

Some adults with chronic small bowel volvulus have few clinical signs and symptoms and some even do not require surgical correction.

The classic conventional radiography description of a closed loop small bowel obstruction is a *coffee bean sign*, often a late finding caused by the mostly fluid-filled dilated loops. The diagnosis is established with barium studies, CT, MRI, or even angiography. Computed tomography shows radial convergence of stretched mesenteric vessels toward a point of obstruction. The involved small bowel loops taper toward the point of obstruction, and two converging bowel loops, representing the afferent and efferent loops, are identified at the point of obstruction. At times such converging loops are identified even before clinical obstruction is evident. Small bowel loops involved in the closed loop are dilated and have a C or U shape. Veins draining the closed loop are engorged. Eventually bowel and mesenteric folds become edematous and radiate toward the site of torsion.

Computed tomography and US of a volvulus reveal a similar appearance to a closed loop obstruction, but a volvulus also contains a twist or whirl due to rotation of the involved loop of bowel and its mesentery; the radiating folds mimic a spoke wheel. Mesenteric edema and ascites are relatively common findings. In a volvulus involving most of the small bowel, the superior mesenteric artery and vein are reversed in their relative positions. A mesenteric twist is not pathognomonic of volvulus but is also seen with adhesions and prior bowel resection.

Ileosigmoid Knot

A rare cause of both small bowel and sigmoid colon obstruction, the ileosigmoid knot consists of ileal loops wrapping around the base of a redundant sigmoid. Both an elongated small bowel mesentery and a redundant sigmoid colon predispose to this entity. The twisted ileal loops readily become ischemic and gangrenous; thus there is a high prevalence of strangulation.

Occasionally conventional radiographs suggest the diagnosis by identifying a small bowel obstruction, a dilated sigmoid colon, and medial displacement of the cecum and distal descending colon. A barium small bowel study simply shows small bowel obstruction, although this study tends to be unsatisfactory due to the often associated peritonitis and superimposed slow bowel transit time. Computed tomography is suggestive by showing a twist, or whirl, of the involved bowel.

Strangulation

In a strangulated obstruction, blood flow to the obstructed loop is compromised, leading initially to ischemia and eventually to bowel necrosis. The diagnostic studies must thus be performed with dispatch.

The most common cause of bowel strangulation is a loop trapped in a hernia, either internal or external. An acute volvulus often also compromises blood supply to the twisted loop and leads to strangulation. Strangulating obstructions are difficult to diagnose both clinically and with conventional radiologic techniques. Enteroclysis should detect a closed loop obstruction, but cannot detect strangulation unless bowel edema or other signs of ischemia are evident. A *target sign*, mesenteric edema or infiltration by blood, and pneumatosis intestinalis are evidence of ischemia. Strangulation progressing to pneumatosis intestinalis, regardless of how diagnosed, signifies bowel wall necrosis.

Computed tomography of a strangulating loop shows a serrated beak at the site of the bowel obstruction. Intramural edema and hemorrhage develop due to ischemia. Contrast-enhanced CT reveals delayed enhancement of diseased bowel loops. Intramesenteric hemorrhage is identified in some patients. Computed tomography findings pointing to a strangulated obstructions rather than a simple small bowel obstruction are poor or no bowel wall enhancement, findings of low sensitivity but high specificity. Less often found are an unusual course for mesenteric vessels and mesenteric vessel engorgement. Ascites develops eventually. Overall, CT identifies about 85% of patients with a strangulated obstruction, keeping in mind that higher sensitivities can be achieved at the expense of lower specificity.

Abnormal US findings are detected in about 90% of patients with bowel strangulation; these consist of small bowel distention, aperistalsis, bowel wall thickening, and intraperitoneal fluid, findings also seen with prolonged simple small bowel obstruction, but with strangulation these findings develop earlier in the course. An US finding of fluid–fluid levels due to intestinal content sedimentation throughout the small bowel is found with small bowel obstruction, regardless of cause, once adynamic ileus ensues. On the other hand, US detection of intraluminal fluid–fluid levels in a segment of adynamic bowel together with peristalsis in other loops suggests a strangulating obstruction (106).

Figure 4.24. Transient jejunojejunal intussusception in a patient with terminal ileal Crohn's disease, a rare association.

Intussusception

Ileocolic intussusception is discussed in the Chapter 5.

Clinical

The final end point of an intussusception is invagination of one loop of bowel (intussusceptum) into another (intussuscipiens). Almost any segment of the small bowel and colon can be involved. Most intussusceptions are antegrade, with only an occasional one being retrograde. Detected on barium studies or CT, most are transient and cannot be duplicated. Experienced radiologists detect random, transient nonobstructing intussusceptions sufficiently often that these are often considered to be a normal variant (Fig. 4.24). Indeed, whether such transient intussusceptions are of clinical significance in the absence of other findings is debatable. Nevertheless, transient intussusceptions are more common than normal in certain disorders, such as celiac sprue.

It is the longer, more persistent intussusceptions, with the intussusceptum consisting not only of bowel but also its associated mesentery, that cause trouble both in adults and children. Among adults with one or more intussusceptions detected with CT or MR, 30% had a neoplastic lead point (107). Both jejunal and ileal polyps, benign and malignant, act as lead points. A Meckel's diverticulum or enlarged lymph nodes occasionally serve as a lead point both in adults and children. Hypertrophied Peyer's patches, a duplication, or even ectopic pancreas are encountered as a lead point mostly in children. Enteric intussusceptions due to metastases are rare. Rare also is an intussusception due to Crohn's disease. Small bowel intussusception is a complication encountered after prior abdominal surgery. At times intussusception is obscured by postoperative or chemotherapeutic findings.

Jejunal intussusceptions in children are not common, and although some are idiopathic, more often a polyp, such as a hamartoma, is a lead point. More distal intussusceptions in young children tend to be idiopathic.

In distinction to infants, the signs and symptoms in most adults with intussusception are nonspecific. An obstruction is not even initially suspected in many patients.

Imaging

Jejunogastric intussusception is one of the complications encountered after a hemigastrectomy and gastrojejunostomy (Billroth II operation). A barium study reveals coiled-spring–appearing jejunal loops within the gastric remnant, thus confirming the diagnosis. Computed tomography or US should also establish the diagnosis; a coiled-spring appearance to the jejunal loops (intussusceptum) within the stomach should be evident.

In children with an ileoileocolic intussusception, an air enema tends to identify the intussusceptum as two or more intraluminal polyps

once it has been reduced to the ileocecal valve; this appearance differs from the smooth or somewhat lobulated appearance found with most simple ileocolic intussusceptions to allow differentiation of ileoileocolic from ileocolic intussusceptions.

Computed tomography of an enteroenteric intussusception reveals a characteristic target lesion containing an intraluminal soft tissue tumor (intussusceptum), asymmetric mesentery, and, at times, a dilated intussuscipiens (Fig. 4.25). When imaged along its long axis, an intussusception has more of a sausage-shaped appearance. Occasionally CT also defines an underlying lead point.

The US appearance of an uncomplicated enteric intussusception is that of a target lesion.

Fluid within bowel provides intrinsic contrast for T2-weighted MRI. A bowel-within-bowel or coiled spring appearance is seen on both axial and coronal images.

Gallstone Ileus

Most gallstones impact in the distal ileum (not in the terminal ileum). The next most common site is in the duodenum (discussed in Chapter 3), and the least common is colonic obstruction, where it occurs proximal to a stricture.

A typical clinical scenario is the elderly woman with no previous abdominal surgery presenting with small bowel obstruction. At the other extreme, gallstone ileus has been detected even in a teenager.

Gallstone ileus is often suspected from a conventional radiographic examination. The classic Rigler triad consists of small bowel obstruction, biliary tract gas, and a distal small bowel calcification, although all three findings are uncommon in any one patient. Similar findings are also evident with CT, and preliminary data suggest that CT allows a more confident diagnosis.

Abdominal US detects small bowel obstruction and does locate an ectopic gallstone in some patients.

Mortality with gallstone ileus remains high, partly due to an often late diagnosis, aged patient population, and frequently coexisting other medical problems.

Foreign Body

Gastrointestinal foreign bodies are encountered in both children and adults (Fig. 4.26). A majority pass spontaneously without complications.

Small bowel bezoars are less common than gastric ones. Risk for bezoars increases after vagotomy and partial gastric resection. An unusual small bowel obstruction developed during enzymatic treatment for a gastric persimmon bezoar (108). Conventional radiographs simply suggest bowel obstruction without identifying a bezoar. Some bezoars contain sufficient gas to suggest pneumatosis intestinalis. A barium study identifies the intraluminal bezoar. Computed tomography findings consist of an intraluminal heterogeneous soft tissue tumor, often containing focal gas.

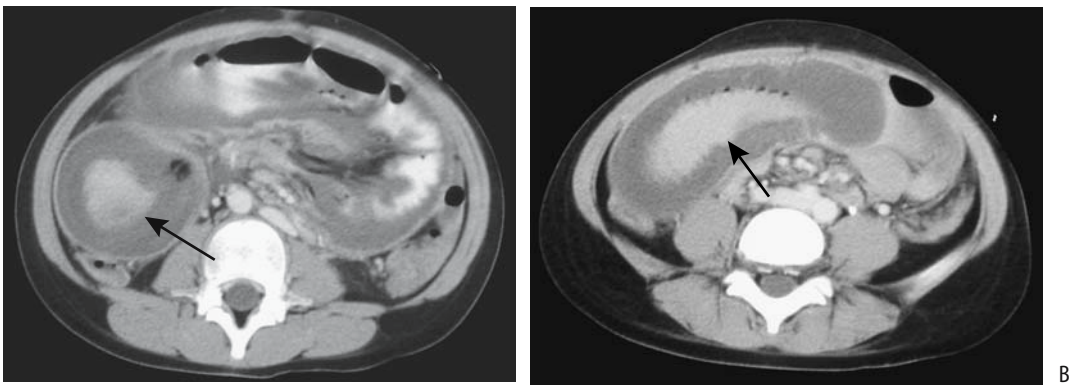

A B

Figure 4.25. Jejunojejunal intussusception in a child. Transverse (A) and longitudinal (B) images identify the intussusception (arrows). Barium outlines the intussusceptum. (Courtesy of Luann Teschmacher, M.D., University of Rochester.)

Figure 4.26. A swallowed tube-like foreign body contains contrast (arrow). (Courtesy of Algidas Basevicius, M.D., Kaunas Medical University, Kaunas, Lithuania.)

A trichobezoar is an uncommon cause of small bowel obstruction. Most are suggested by conventional radiography or a barium study and further imaging is not warranted.

Retained surgical gauze eventually becomes encased in a fibrotic mass that can lead to small bowel obstruction or a fistula and mimic a neoplasm. In a region of the world endemic for tuberculosis, a retained surgical sponge simulated intestinal tuberculosis (109). Retained surgical staples are generally of little significance, although when incorporated in an adhesion they appear next to an obstruction. Occasionally a severed gastrostomy tube obstructs the small bowel.

The current popularity of a high-fiber diet is also not without risk. Thus in one patient recurrent small bowel ileus was caused by ingestion of high-fiber canned asparagus (110).

Other Obstructions

Acute sigmoid diverticulitis is a not uncommon cause of small bowel obstructions; a loop of small bowel becomes trapped by focal inflammation or simply becomes adynamic.

Any intramural infiltration sufficient to narrow the lumen eventually leads to lumen obstruction. Similar to the duodenum, intramural hemorrhage or a hematoma can obstruct the jejunal or ileal lumen; these obstructions tend to be transient, and they clear as a hematoma resolves.

Small bowel obstruction is a rare but major complication during pregnancy. As in the general population, those women who have had previous abdominal surgery are at increased risk of developing a small bowel obstruction.

Eosinophilic gastroenteritis–associated bowel stenosis is a rare cause of small bowel obstruction.

Therapy

Once appropriate imaging studies are obtained and an obstruction diagnosed, an indwelling catheter is useful in decompressing the small bowel; this should make the patient more comfortable and aid the return of bowel function.

Some surgeons claim a purported therapeutic effect by hyperosmotic water-soluble contrast in relieving small bowel obstructions, but radiologists generally scoff at such claims. A prospective, randomized study of patients with suspected postoperative small bowel obstruction comparing the effect of instilling 100 mL of a hyperosmotic water-soluble contrast agent via a nasogastric tube found no difference in length of hospital stay or in the rate of complications, whether a contrast agent was used or not (111).

Traditionally, patients with an unresolving small bowel obstruction underwent a laparotomy. Laparoscopic therapy of small bowel obstruction is also performed, especially in a setting of postoperative adhesions.

Adynamic Ileus

Acute

Peritoneal inflammation, either primary or secondary, leads to bowel paralysis. The resultant adynamic ileus ranges from focal (sentinel loop) to generalized and involves both the small and large bowel. Some surgeons attempt to distinguish between a normal postoperative ileus and adynamic ileus. Most radiologists consider these to be the same entity.

Ingestion of certain raw foods induces adynamic ileus. In Japan, adynamic ileus developed in some patients after eating raw squid (112); the squid contained a specific type of

larva. Acute small bowel angioneurotic edema is also a cause of adynamic ileus.

Acute adynamic ileus can generally be suspected from conventional radiographs; both the small bowel and colon are dilated. Superficially, distal colonic obstruction and an incompetent ileocecal valve mimic these findings.

Chronic (Pseudo-Obstruction)

Chronic adynamic ileus, also called *intestinal pseudo-obstruction*, is not a single entity but an intestinal condition associated with a number of neuropathies and myopathies. Familial visceral neuropathy results in chronic myenteric plexus destruction leading to poor motility and bowel distention on a chronic basis. Myotonic muscular dystrophy and familial visceral myopathy involve intestinal smooth muscle and lead to small bowel dysmotility and distention (Fig. 4.27). Endoscopic biopsy is generally not helpful in these patients because abnormalities are in the external muscle layers. Barium contrast studies are often necessary to exclude mechanical obstruction.

Figure 4.27. Familial oculo-intestinal myopathy in a 21–year-old patient. Enteroclysis reveals marked bowel hypotonia. The bowel wall is of normal thickness. (Courtesy of Arunas Gasparaitis, M.D., University of Chicago.)

At times intestinal pseudo-obstruction is associated with an underlying neoplasms, such as lung carcinoma or carcinoid, with the intestinal dilation presumably secondary to a paraneoplastic process. In some patients intestinal dysmotility resolves after tumor resection. Intestinal pseudo-obstruction and a secretory diarrhea were the initial presentation in a man found to have Crohn's disease (113).

Infants with fetal alcohol syndrome develop intestinal pseudo-obstruction, probably due to an enteric neuropathy.

Various radiopaque markers have been used to measure small bowel transit time, but they have achieved limited clinical application. Gastric emptying, small bowel transit and colonic transit can be combined into a single scintigraphic whole-gut transit time study. The clinical relevance of such a test, however, is not clear.

Therapy with erythromycin and cisapride are often effective therapies in this condition.

Systemic Sclerosis (Scleroderma)

Systemic sclerosis is readily differentiated from celiac disease. In the latter entity the duodenum tends not to be dilated, close to normal small bowel motility is evident, dilation involves primarily the distal small bowel, and more intraluminal bowel content is present—findings differing from those seen in systemic sclerosis.

Some patients with systemic sclerosis develop pneumatosis cystoides intestinalis and even idiopathic pneumoperitoneum. Although a de novo pneumoperitoneum usually suggests a surgical abdomen, some of these patients are managed medically. Nevertheless, an autopsy study of patients with systemic sclerosis found bowel perforation to be more common than expected (114); these perforations ranged from the esophagus to colon, with some being initially silent. The authors suggest that the bowel wall in these patients is inherently weak, and cautioned physicians performing invasive procedures to keep this in mind.

Other Disorders

Collagenous sprue mimics celiac disease both clinically and radiologically. Duodenal and

jejunal biopsies reveal villous atrophy in both entities, but in collagenous sprue collagen is deposited in small bowel lamina propria.

The small bowel is not a major target organ in Chagas disease. An occasional patient develops marked jejunal dilation due to stasis, bacterial overgrowth, and resultant malabsorption.

The small bowel appearance in dermatomyositis is similar to that seen in sprue, although findings in sprue tend to be more striking.

Ehlers-Danlos syndrome is an inherited connective tissue disorder resulting in skin hyperextensibility, articular hypermobility, and tissue fragility. The bowel is dilated. These patients are prone to developing intestinal hemorrhage and bowel perforation.

Generally a carbon-14 D-xylose breath test is used in patients with suspected small bowel bacterial overgrowth. One limitation of this test is that in individuals with gastrointestinal motor dysfunction, delayed gastric emptying tends to prevent carbon-14 D-xylose from reaching the small bowel loops involved by bacterial overgrowth and thus results in a negative test. A liquid phase gastric emptying test performed at the same time as D-xylose test corrects for gastric stasis.

Perforation/Fistula

Bowel perforation and resultant peritonitis is discussed in Chapter 14.

Migration of a biliary stent into the small bowel is generally of little consequence; rarely, it has led to small bowel perforation. An uncommon cause of bowel perforation is a suction biopsy. A swallowed toothpick or sharp bone can lead to small bowel perforation. Some perforations seal over spontaneously and have few, if any, sequelae; others develop into peritonitis or an abscess.

Pneumoperitoneum is the classic sign of bowel perforation. As is well known, not all perforations result in a pneumoperitoneum; intraperitoneal fluid is more common. Computed tomography visualization of bowel wall discontinuity at a perforation site is rare. Oral contrast extravasation likewise is rarely identified, although renal excretion after oral administration of a water-soluble contrast agent should raise suspicion of bowel perforation. A caveat: in some patients orally ingested water-soluble contrast is absorbed from normal bowel. Nonabsorbable barium contrast agents are not used in a clinical setting of suspected acute bowel perforation.

A fistula involving the small bowel can develop to any adjacent structure. In adults most fistulas are secondary to either prior surgery or Crohn's disease. Less often a small bowel malignancy or disorders in adjacent structures lead to a fistula. A small bowel fistula to bone results in osteomyelitis.

Subtle small bowel fistulas and sinus tracts are best studied with enteroclysis.

Most enterocutaneous fistulas are initially managed medically. Fluoroscopically guided fistulous tract and associated bowel catheterization should be considered for those not healing; eventual fistula closure can be achieved in most. Several chronic enterocutaneous fistulas were successfully treated by injecting biologic glue (N-butyl-2-cyanoacrylate-histoacryl) into the fistulous tract (115).

Diverticula

Meckel's diverticula were discussed earlier (see Congenital Abnormalities).

Jejunal and ileal diverticula are not rare. Most are innocuous and considered to be incidental findings (Fig. 4.28). An occasional diverticulum will bleed (at times massively), perforate, or even obstruct the small bowel. A rare diverticulum evolves into diverticulitis or an intra-abdominal abscess, involves extraperitoneum structures, or develops into an abdominal wall abscess. Clinically, ileal diverticulitis mimics appendicitis.

Tumors, including adenocarcinomas and sarcomas, do develop in diverticula; both barium studies and CT detect them, if they are large enough.

Both small bowel and colonic diverticula are more prevalent in patients with connective tissue disorders such as Marfan's syndrome and Ehlers-Danlos syndrome. These patients also develop diverticula-related complications.

Occasionally detected is extensive diverticulosis of the entire small bowel. Stasis, bacterial

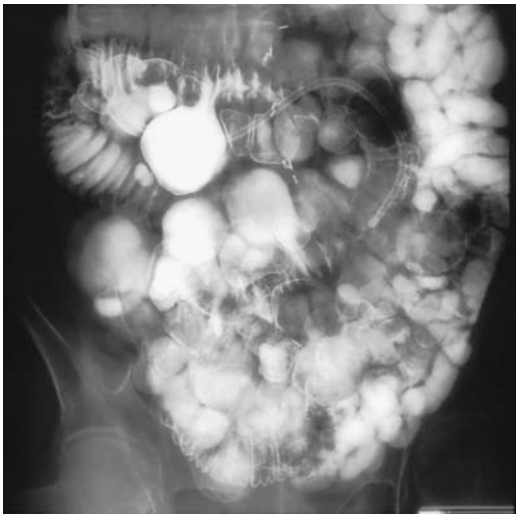

Figure 4.28. Jejunal diverticulosis. Numerous diverticula fill with barium. (Courtesy of Arunas Gasparaitis, M.D., University of Chicago).

overgrowth, and resultant malabsorption develop in these patients.

Pneumatosis Intestinalis

Intramural bowel gas (and it is a gas, not air) is called pneumatosis intestinalis, an uncommon condition. These gas collections range from a linear, oval, to a round appearance, either submucosal or subserosal in location. It should be emphasized that pneumatosis intestinalis is a sign rather than a specific disease and is found in a number of benign and serious conditions (Table 4.9). Some authors, however, limit use of the term *pneumatosis cystoides intestinalis* to a benign condition.

Table 4.9. Conditions associated with pneumatosis intestinalis

Bowel ischemia
Adults with chronic obstructive pulmonary disease
After endoscopic biopsies
Progressive systemic sclerosis and chronic granulomatous disease
Systemic amyloidosis
Myotonic dystrophy
Drug therapy with steroids, chemotherapy
Immunosuppression and immunodeficiency states
Cryptosporidiosis infection in AIDS patients
Following surgical handling of bowel
After jejunoileal bypass surgery and organ transplantation
With malignancies such as leukemia and lymphoma
Associated with gastric ulcer, bowel carcinoma and metastatic disease
In infants with necrotizing enterocolitis
In infants with pyloric stenosis

The most ominous cause of pneumatosis intestinalis is bowel ischemia; in adults a poor prognosis is suggested if both pneumatosis intestinalis and portal venous gas are detected. In the pediatric age group, however, a benign course occasionally ensues for pneumatosis intestinalis associated with gas in both the portal vein and systemic veins.

Little in the imaging appearance of pneumatosis intestinalis allows one to suggest an underlying cause. Thus benign pneumatosis and pneumatosis due to bowel ischemia have a similar appearance. In a minority of patients with benign pneumatosis, imaging also reveals a pneumoperitoneum, presumably secondary to rupture of some of the gaseous blebs.

Pneumatosis intestinalis is readily diagnosed with conventional radiography. With CT, differentiation of colonic pneumatosis involving the left colon from diverticula can be difficult. In general, CT lung windows should be used to detect pneumatosis. Magnetic resonance findings consist of circumferential collections of gas next to or intramural in location; such collections are easier to see with gradient echo images.

Vascular Lesions (Bleeding)

If the underlying condition cannot be otherwise corrected, the therapeutic procedure of choice in controlling an acute hemorrhage often is percutaneous transcatheter vascular embolization. A variety of embolization materials are in use.

Etiology

The list of conditions responsible for life-threatening gastrointestinal hemorrhage is legion (Table 4.10). Discussed here are only those conditions not covered in other sections.

Table 4.10. Causes of jejunal and ileal bleeding

Trauma
Infection
Crohn's disease
Vascular causes
Ischemia
Angiodysplasia
Telangiectasia
Arteriovenous malformation
Dieulafoy lesion
Varices
Ruptured aneurysm
Hemangioma
Meckel's diverticulum
Neoplasm
Other
Ectopic decidua
Bleeding disorder/overcoagulation

Aneurysm

Arterial aneurysms do rupture into the small bowel. Angiography or CT should detect them and, during active bleeding, occasionally even identify contrast extravasation into the small bowel lumen.

Neoplasms

Almost any small bowel neoplasm will bleed either acutely or on a chronic basis. Some of the rarer neoplasms associated with bleeding include:

Small bowel hemangioendotheliomas: They typically manifest through bleeding or, less often, abdominal pain.

Small bowel angiosarcomas: These bleed, ulcerate, or even obstruct. Barium studies and CT should detect these tumors once they reach a certain size. Because of the intermittent nature of bleeding with these highly vascular tumors, scintigraphy may be negative.

Angiodysplasia

The prevalence of angiodysplasia increases with age; most are acquired. An increased prevalence is found in patients with renal failure, von Willebrand's disease, aortic stenosis, pulmonary disease, and cirrhosis, although in some patients such an association is fortuitous. The prevalence is difficult to estimate; often bleeding from an unknown site is ascribed to small bowel angiodysplasia. Angiography detects some angiodysplasia and some are identified by the pathologist, but some are undoubtedly missed because the involved vessels collapse in resected bowel.

If detected by imaging, most angiodysplasias are resected. As an aid to the pathologist, intraarterial injection of a low-viscosity barium sulfate suspension or a dye and water-soluble contrast agent mixture into a resected specimen should reveal any dilated vessels.

Telangiectasia

Telangiectasias of the small bowel are uncommon. Multiple telangiectasias should suggest Osler-Weber-Rendu disease even in the absence of characteristic skin and mucous findings. These lesions are responsible for chronic bleeding.

Varices

Small bowel varices are rare. Some are due to portal hypertension and unusual drainage pathways; thus an occasional varix is encountered in the ileum. Varices also develop secondary to an extensive arteriovenous shunt, such as a large hemangioma. Stomal varices have developed at an ileostomy.

Similar to other sites, small bowel varices are identified by superior mesenteric angiography or percutaneous transhepatic mesenteric venography if access to the site of varices can be achieved.

Small bowel varices have been treated by percutaneous transhepatic embolization, using a transjugular approach, or portosystemic shunting if they are due to portal hypertension.

Dieulafoy Lesion

Dieulafoy lesions were essentially unheard of in the small bowel until the mid-1990s, when a number of case reports were published. These patients present with massive hemorrhage, and most reports describe jejunal rather than ileal Dieulafoy lesions.

Superior mesenteric angiography simply detects a bleeding site and provides rough local-

ization. Intraoperative small bowel endoscopy is helpful to locate the actual bleeding site.

Other

Extrauterine decidua rarely involves the bowel wall. Occasionally such decidua bleed, with bleeding usually intraperitoneal in location. Intraluminal bleeding is unusual.

Bleeding Detection

Barium studies should detect a small bowel tumor if the tumor is sufficiently large. Angiography identifies extravasation if the bleeding is brisk enough and, at times, reveals prominent vasculature, both arterial and venous.

Most physicians encounter occasional patients with intermittent bleeding who have a negative upper gastrointestinal, small bowel, and colon workup for a bleeding site. One approach in these patients is to provoke bleeding with heparin and urokinase, followed by scintigraphy and then mesenteric angiography in those with positive scintigraphy. In 10 such provocative bleeding studies, scintigraphy detected hemorrhage in four and in two of these a source was identified and treated with embolization or surgery (116).

Computed tomography is not the primary modality used to detect gastrointestinal hemorrhage. Anecdotal reports describe detection of intraluminal contrast within the small bowel during CT performed immediately after negative angiography. Such a study must be performed without the use of oral contrast.

Some spontaneous intraluminal bleeding is associated with an intramural hematoma. Computed tomography initially reveals a hematoma to be isodense to blood, but as a clot forms it gradually becomes hyperdense; in time, with clot lysis, its attenuation (density) decreases. A noncontrast (neither oral nor IV) CT is preferred if intramural hemorrhage is suspected; contrast tends to obscure a hyperdense hematoma. The involved small bowel wall is thickened and at times a halo containing a hyperdense ring is detected. Lumen obstruction ensues with sufficient intramural bleeding and the more proximal small bowel dilates.

Intramural hemorrhage results in hyperintense signals on precontrast T1- and T2-weighted MR sequences.

Both colloid and red blood cell scintigraphy detect bleeding sites, although sensitivity of Tc-99m–red blood cell scintigraphy is higher. Especially if upper gastrointestinal sources of bleeding have been excluded by other tests, a Tc-99m–red blood cell scan is very reliable in identifying small bowel bleeding. Occasionally a bleeding site is detected only on dynamic blood flow studies and a first set of static images; peristalsis prevents identification of a bleeding site on subsequent images.

Criticism of the use of scintigraphy exists. In a surgical study from a community hospital, scintigraphy localized an exact bleeding site in only 19% of patients (117); confirmation of an actual site of bleeding was either at surgery or endoscopy. These results do not reflect conclusions reached in most published studies.

In some patients with known bleeding and a negative scintigraphic study within the first several hours, a conservative medical management approach appears appropriate.

Even if angiography does locate a site of hemorrhage, a surgeon still has to find the site in the small bowel. In such a setting a highly selective angiographic catheter left in place after angiography, with subsequent intraoperative methylene blue dye injected through the catheter, is useful to the surgeon in locating the site of bleeding.

Immunosuppression

AIDS

A majority of AIDS patients developing diarrhea are infected with enteric pathogens. Some specific infections tend to be more common in certain geographic regions. For instance, the intracellular protozoan *Leishmania donovani* is common in the Mediterranean basin and is one of the infections often detected in HIV-positive patients in that region. Cryptosporidial oocyst infection involves primarily the proximal small bowel. Several AIDS patients developed pneumatosis intestinalis and cryptosporidiosis infection and the association appears to be more

than coincidental. *Mycobacterium avium intracellulare* infection results in extensive adenopathy. Small bowel perforation has developed due to *M. tuberculosis* in HIV-infected patients. *Pneumocystis carinii* bowel infection leads to lumen obstruction and bleeding. Ileal actinomycosis has been described in an AIDS patient (118). Two or more coexisting organisms are common in these patients.

Gastrointestinal lymphoma in AIDS patients is an aggressive tumor associated with a poor prognosis. These lymphomas develop anywhere from the esophagus to the colon; a polyposis-like appearance is not uncommon. A more unusual lymphoma presentation was as an ulcerated tumor in a Meckel's diverticulum (119).

Patients with AIDS develop nonspecific small bowel ulcers. These ulcers, also occurring in the oropharynx and esophagus, appear to be caused directly by the HIV itself. The ulcers tend not to become stenotic, which is in contradistinction to idiopathic ulcers in non-AIDS patients. Some small bowel ulcers are also secondary to superimposed infection and necrotic tumors.

Graft-Versus-Host Disease

Two types of bowel complications predominate after bone marrow transplantation, namely either a superinfection or acute graft-versus-host disease. The presence of both complications signifies an especially ominous prognosis.

Graft-versus-host disease generally manifests within several months after allogeneic bone marrow transplantation, with the gastrointestinal tract being a primary target organ. Initially it manifests as thickening of valvulae conniventes, followed by diffuse bowel wall thickening and resultant featureless tube-like lumen narrowing, a "pipestem" appearance, and separation of bowel loops (Fig. 4.29). At times CT reveals marked contrast enhancement, a pattern also seen with some superimposed infections and other infiltrating or ischemic conditions. Acute gastrointestinal graft-versus-host disease in adult allogeneic bone marrow transplant recipients occurs with about the same frequency as gastrointestinal infections.

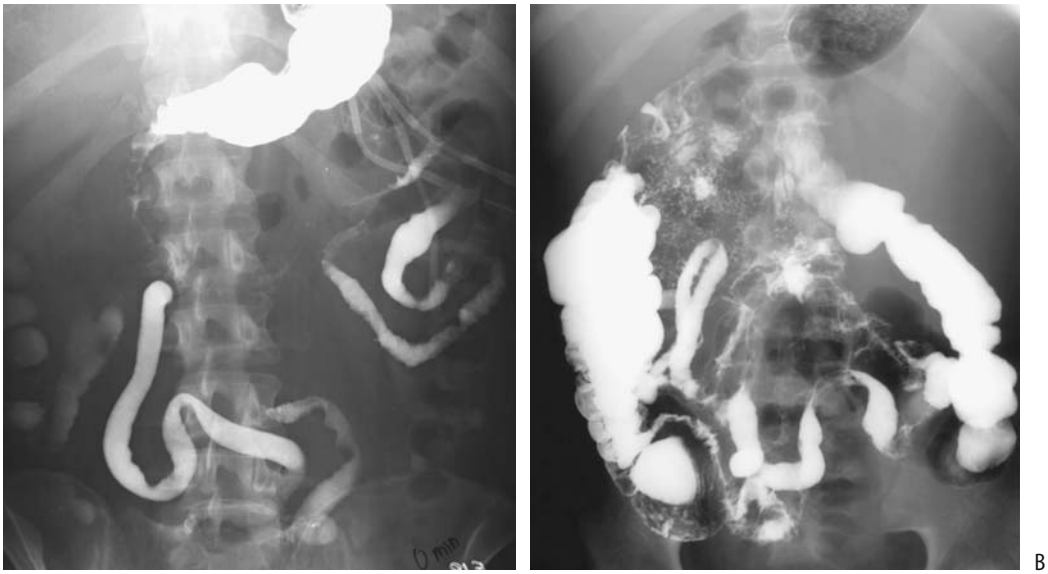

A B

Figure 4.29. A: Graft-versus-host disease after bone marrow transplant. B: Viral gastroenteritis in a bone marrow transplant patient. The two conditions have a similar imaging appearance.

Occasionally massive hematochezia develops secondary to either graft-versus-host disease or viral gastroenteritis.

CT detects small bowel wall thickening, engorgement of vasa recta and mesenteric fat stranding (120); ascites, periportal edema and mucosal contrast enhancement are evident in some patients. Fluid-filled, dilated bowel is common proximal to segments of bowel wall thickening. Bowel wall thickening is related to more severe graft-versus-host disease. Some patients exhibit a thin, enhancing mucosal layer which histologically consists of vascular granulation tissue.

A rare bone marrow transplant patient exhibits prolonged oral barium sulfate adherence to small bowel mucosal, at times for several weeks a finding probably related to severe mucosal disease resulting in a denuded mucosa and barium crystals being trapped within lamina propria.

Magnetic resonance reveals diffuse bowel wall thickening and increased postcontrast bowel wall enhancement (121).

Diffuse invasive gastrointestinal candidiasis presented as adynamic ileus after bone marrow transplantation (122).

Other

A subset of liver and kidney transplant patients develops inflammatory bowel disease while undergoing immunosuppression; histology is consistent with either ulcerative colitis or Crohn's disease. Usually the colon is involved, but some patients have small bowel disease. Some respond to maintenance therapy, but others require a colectomy. Although inflammatory bowel disease in these patients may be fortuitous, the onset and progression of disease while already immunosuppressed is surprising.

Postoperative Changes

Small Bowel Transplantation

Small bowel transplantation is lifesaving in those unable to tolerate chronic total parenteral nutrition. Transplantation is performed either only with small bowel or together with colon, liver, or even several organs. The current indications for small bowel transplantation include short-bowel syndrome, severe intractable diarrhea, cancer, and severe intestinal pseudo-obstruction. Many of these patients have been on prior chronic parenteral nutrition.

Graft rejection rates appear lower if combined liver and small bowel grafts are performed rather than an isolated bowel transplant.

For Obesity

Instead of a gastric bypass, pancreaticobiliary diversion is an alternative procedure for obesity. It consists of a distal gastrectomy, gastroenterostomy, and a Roux-en-Y enteroenterostomy. The enteroenterostomy is created closer to the ileocecal valve than to the stomach.

One complication is obstruction of the pancreaticobiliary loop. It results in a dilated, fluid-filled segment that is difficult to identify with conventional radiography. Computed tomography or MR should be diagnostic.

Currently a jejunoileal bypass is rarely performed. In the occasional such patient where bowel visualization is desired, either a conventional antegrade barium study or enteroclysis defines the in-continuity small bowel but not the excluded loops. With an end-to-end jejunoileostomy and an end-to-side ileosigmoid colostomy of the excluded segment, a barium enema at times defines varying lengths of excluded ileal segment. Such an approach is not feasible with an isoperistaltic end-to-side jejunoileostomy. Computed tomography with axial reconstructions appears reasonable to help define bypassed segments, but little in the literature provides guidance for such an approach.

Examination and Surgical Complications

Ileostomy

The most common site of obstruction after ileostomy construction is at the ileostomy site. A digital examination identifies most of these

obstructions. If needed, a retrograde barium study evaluates the extent of the obstruction.

Short Bowel Syndrome

How short must the small bowel be before a patient develops a short bowel syndrome is difficult to predict. A minimum remaining small bowel length of about 150 cm appears to prevent malabsorption. The remaining length needed to prevent small bowel syndrome also depends on the duration of prior parenteral nutrition.

Isoperistaltic colon interposition is occasionally used to treat short bowel syndrome. The interposed colonic segment functions primarily by slowing intestinal transit. Of interest is that although the interposed colon shows no gross small bowel intestinalization, it adapts by taking on some small bowel features such as an increase in crypt depth and mucosal thickness.

Ileal Pouch

An ileal pouch to anal anastomosis is the operation of choice in patients undergoing a proctocolectomy either for ulcerative colitis or familial polyposis. On a long-term basis the ileal pouch mucosa undergoes metaplasia and tends to mimic colonic mucosa. A late complication is inflammation of this pouch, or pouchitis. Of interest is that pouchitis almost always occurs in patients who had prior ulcerative colitis; presumably such pouchitis represents recurrent ulcerative colitis.

Both a temporary ileostomy and an ileoanal anastomosis are created after a total proctocolectomy. Prior to subsequent ileostomy takedown, pouchography is generally performed to evaluate the ileoanal anastomotic integrity. Disruption of the ileoanal anastomosis as detected by pouchography, is a sensitive but not specific predictor of subsequent sepsis.

A rare complication of total proctocolectomy and ileal pouch formation is duodenal compression due to superior mesenteric artery syndrome.

Catheter Related

A spontaneous knot in a transgastric jejunostomy tube has been reported (123).

References

1. Ha A, Levine M, Rubesin S, Laufer I, Herlinger H. Radiographic Examination of the Small Bowel: Survey of Practice Patterns in the United States. Radiology 2004; 231:407–412.
2. Ha HK, Shin JH, Rha SE, et al. Modified small-bowel follow-through: use of methylcellulose to improve bowel transradiance and prepare barium suspension. Radiology 1999;211:197–201.
3. Taruishi M, Saitoh Y, Watari J, et al. Balloon-occluded endoscopic retrograde ileography. Radiology 2000;214: 908–911.
4. Thompson SE, Raptopoulos V, Sheiman RL, McNicholas MM, Prassopoulos P. Abdominal helical CT: milk as a low-attenuation oral contrast agent. Radiology 1999;211:870–875.
5. Holzknecht N, Helmberger T, von Ritter C, Gauger J, Faber S, Reiser M. [MRI of the small intestine with rapid MRI sequences in Crohn disease after enteroclysis with oral iron particles.] [German] Radiologe 1998;38:29–36.
6. Umschaden HW, Szolar D, Gasser J, Umschaden M, Haselbach H. Small-bowel disease: comparison of MR enteroclysis images with conventional enteroclysis and surgical findings. Radiology 2000;215:717–725.
7. Rieber A, Wruk D, Nussle K, et al. [MRI of the abdomen combined with enteroclysis in Crohn disease using oral and intravenous Gd-DTPA.] [German] Radiologe 1998;38:23–28.
8. Schmidt S, Lepori D, Meuwly JY, et al. Prospective comparison of MR enteroclysis with multidetector spiral-CT enteroclysis: interobserver agreement and sensitivity by means of "sign-by-sign" correlation. Eur Radiol 2003;13:1303–1311.
9. Broglia L, Tortora A, Maccioni F, et al. [Optimization of dosage and exam technique in the use of oral contrast media in magnetic resonance.] [Italian] Radiol Med 1999;97:365–370.
10. Malcolm PN, Brown JJ, Hahn PF, et al. The clinical value of ferric ammonium citrate: a positive oral contrast agent for T1–weighted MR imaging of the upper abdomen. J Magn Reson Imaging 2000;12:702–707.
11. Hara AK, Leighton JA, Sharma VK, Fleischer DE. Small bowel: preliminary comparison of capsule endoscopy with barium study and CT. Radiology 2004;230: 260–265.
12. Cope C, Davis AG, Baum RA, Haskal ZJ, Soulen MC, Shlansky-Goldberg RD. Direct percutaneous jejunostomy: techniques and applications—ten years' experience. Radiology 1998;209:747–754.
13. Neal MR, Seibert JJ, Vanderzalm T, Wagner CW. Neonatal ultrasonography to distinguish between meconium ileus and ileal atresia. J Ultrasound Med 1997;16:263–266.
14. Benya EC, Nussbaum-Blask AR, Selby DM. Colonic diverticulitis causing partial bowel obstruction in a child with cystic fibrosis. Pediatr Radiol 1997;27: 918–919.
15. Baudon JJ, Dabadie A, Cardona J, et al. [Incidence of symptomatic celiac disease in French children.] [French] Presse Med 2001;30:107–110.
16. Lomoschitz F, Schima W, Schober E, Turetschek K, Kaider A, Vogelsang H. Enteroclysis in adult celiac

disease: diagnostic value of specific radiographic features. Eur Radiol 2003;13:890–896.
17. Aliotta A, Pompili M, Rapaccini GL, et al. Doppler ultrasonographic evaluation of blood flow in the superior mesenteric artery in celiac patients and in healthy controls in fasting conditions and after saccharose ingestion. J Ultrasound Med 1997;16:85–91.
18. Giovagnorio F. [Doppler ultrasonography of the upper mesenteric artery in chronic intestinal inflammation.] [Italian] Radiol Med 1999;98:43–47.
19. van den Bosch HC, Tjon a Tham RT, Gooszen AW, Fauquenot-Nollen JM, Lamers CB. Celiac disease: small-bowel enteroclysis findings in adult patients treated with a gluten-free diet. Radiology 1996;201: 803–808.
20. Andres E, Pflumio F, Knab MC, et al. [Splenic thrombosis and celiac disease: a fortuitous association?] [French] Presse Med 2000;29:1933–1934.
21. Ochs HD, Smith CI. X-linked agammaglobulinemia. A clinical and molecular analysis. [Review] Medicine 1996;75:287–299.
22. Connolly LP, Treves ST, Bozorgi F, O'Connor SC. Meckel's diverticulum: demonstration of heterotopic gastric mucosa with technetium-99m-pertechnetate SPECT. J Nucl Med 1998;39:1458–1460.
23. Sanchez Alegre ML, de la Torre J, Guembe P, Alarcon J. Milk of calcium in Meckel's diverticulum. AJR 2000; 174:1466–1467.
24. Yeh JT, Lai HS, Duh YC. Perforated Meckel's diverticulum in a neonate. J Formos Med Assoc 1996;95: 644–645.
25. Cazaban-Mazerolles D, Baylet-Vincent F. [Leiomyosarcoma of Meckel's diverticulum in cystic form.] [French] Presse Med 2000;29:651–653.
26. Peoples JB, Lichtenberger EJ, Dunn MM. Incidental Meckel's diverticulectomy in adults. [Review] Surgery 1995;118:649–652.
27. Allen GS, Moore FA, Cox CS J, Wilson JT, Cohn JM, Duke JH. Hollow visceral injury and blunt trauma. J Trauma 1998;45:69–75.
28. Brody JM, Leighton DB, Murphy BL, et al. CT of blunt trauma bowel and mesenteric injury: typical findings and pitfalls in diagnosis. Radiographics 2000;20:1525–1536.
29. Frisoli JK, Desser TS, Jeffrey RB. Thickened submucosal layer: a sonographic sign of acute gastrointestinal abnormality representing submucosal edema or hemorrhage. AJR 2000;175:1595–1599.
30. Paran H, Neufeld D, Shwartz Kidron D, et al. Perforation of the terminal ileum induced by blast injury: delayed diagnosis or delayed perforation? J Trauma 1996;40:472–475.
31. Law NM, Lim CC, Chong R, Ng HS. Crohn's disease in the Singapore Chinese population. J Clin Gastroenterol 1998;26:27–29.
32. Lopez-Cubero SO, Sullivan KM, McDonald GB. Course of Crohn's disease after allogeneic marrow transplantation. Gastroenterology 1998;114:433–440.
33. Pospai D, Rene E, Fiasse R, et al. Crohn's disease stable remission after human immunodeficiency virus infection. Dig Dis Sci 1998;43:412–419.
34. Lautenbach E, Lichtenstein GR. Human immunodeficiency virus infection and Crohn's disease: the role of the CD4 cell in inflammatory bowel disease. J Clin Gastroenterol 1997;25:456–459.
35. Brignola C, Belloli C, De Simone G, et al. Familial adenomatous polyposis and inflammatory bowel disease associated in two kindreds. [Review] Dig Dis Sci 1995;40:402–405.
36. Veldman W, van Beek M, Keuning JJ, Driessen WM. Regional enteritis complicating malignant lymphoma. Neth J Med 1996;49:82–85.
37. Kim AY, Ha HK, Seo BK, et al. CT of patients with right-sided colon cancer and distal ileal thickening. AJR 2000;175:1439–1444.
38. Charagundla SR, Levine MS, Torigian DA, Campbell MS, Furth EE, Rombeau J. Diffuse intestinal ganglioneuromatosis mimicking Crohn's disease. AJR 2004;182:1166–1168.
39. Bernstein CN, Boult IF, Greenberg HM, van der Putten W, Duffy G, Grahame GR. A prospective randomized comparison between small bowel enteroclysis and small bowel follow-through in Crohn's disease. Gastroenterology 1997;113:390–398.
40. Leppek R, Sauerwald M, Berthold LD, Franzen U, Klose KJ. [Standardized enteroclysis. Monitoring of intralumen pressure in 3 different patient groups.] [German] Radiologe 1998;38:624–631.
41. Jamieson DH, Shipman PJ, Israel DM, Jacobson K. Comparison of multidetector CT and barium studies of the small bowel: inflammatory bowel disease in children. AJR 2003;180:1211–1216.
42. Meyers MA, Mcguire PV. Spiral CT demonstration of hypervascularity in Crohn's disease—vascular jejunization of the ileum or the Comb sign. Abdom Imaging 1995;20:327–332.
43. Reittner P, Goritschnig T, Petritsch W, et al. Multiplanar spiral CT enterography in patients with Crohn's disease using a negative oral contrast material: initial results of a noninvasive imaging approach. Eur Radiol 2002;12:2253–2257.
44. Cammarota T, Bresso F, Sarno A, Astegiano M, Macchiarella V, Robotti D. [Abdominal pain and bowel dysfunction: the diagnostic role of ultrasonography.] [Italian] Radiol Med 2000;100:337–342.
45. Borghi P, Armocida C, Rigo GP, et al. [Advantages of the echographic staging of intestinal Crohn's disease. Correlations of echographic patterns and histological findings.] [Italian] Radiol Med 1998;95:338–343.
46. van Oostayen JA, Wasser MN, Griffioen G, van Hogezand RA, Lamers CB, de Roos A. Activity of Crohn's disease assessed by measurement of superior mesenteric artery flow with Doppler ultrasound. Neth J Med 1998;53:S3–8.
47. Spalinger J, Patriquin H, Miron MC, et al. Doppler US in patients with Crohn disease: vessel density in the diseased bowel reflects disease activity. Radiology 2000;217:787–791.
48. Tateishi S, Arima S, Futami K. Assessment of blood flow in the small intestine by laser Doppler flowmetry: comparison of healthy small intestine and small intestine in Crohn's disease. J Gastroenterol 1997;32: 457–463.
49. Potthast S, Rieber A, Von Tirpitz C, Wruk D, Adler G, Brambs HJ. Ultrasound and magnetic resonance imaging in Crohn's disease: a comparison. Eur Radiol 2002;12:1416–1422.

50. Schunk K, Kern A, Heussel CP, et al. [Assessment of inflammatory activity in Crohn disease with hydro-MRI.] [German] Rofo Fortschr Geb Rontgenstr Neuen Bildgeb Verfahr 2000;172:153–160.
51. Low RN, Francis IR, Politoske D, Bennett M. Crohn's disease evaluation: comparison of contrast-enhanced MR imaging and single-phase helical CT scanning. J Magn Reson Imaging 2000;11:127–135.
52. Alonso JC, Lopez-Longo FJ, Lampreave JL, et al. Abdominal scintigraphy using 99mTc-HMPAO-labelled leucocytes in patients with seronegative spondylarthropathies without clinical evidence of inflammatory bowel disease. Eur J Nucl Med 1996;23: 243–246.
53. Challa S, Lyons KP, Broekelschen P, Milne N. Relative sensitivity of Tc-99m WBC versus In-111 WBC in a patient with Crohn disease and steroid use. Clin Nucl Med 1997;22:700–703.
54. Serrano J, Gomez A, Verdu J, et al. [Abdominal scintigraphy with 99MTc-HMPAO-labelled leukocytes. Utility of the quantification in the evaluation of the inflammatory activity of Crohn's disease and ulcerative colitis.] [Spanish] Rev Esp Med Nucl 1999;18:356–362.
55. Suh CH, Lee CH, Lee J, et al. Arthritic manifestations of inflammatory bowel disease. J Korean Med Sci 1998;13:39–43.
56. Zajac M, Engelhard K, Schuhmann R. [Spondylodiscitis with presacral abscesses caused by fistulization in Crohn's disease of the small intestine.] [German] Rontgenpraxis 2000;52:340–342.
57. Sahai A, Belair M, Gianfelice D, Cote S, Gratton J, Lahaie R. Percutaneous drainage of intra-abdominal abscesses in Crohn's disease: short and long-term outcome. Am J Gastroenterol 1997;92:275–278.
58. Cerro P, Scribano ML, Falasco G, Zannoni F, Spina C. [Ultrasonography in the diagnosis of enterocutaneous fistula in Crohn's disease.] [Italian] Radiol Med 1998;96:214–217.
59. Kreisel W, Wolf LM, Grotz W, Grieshaber M. Renal tubular damage: an extraintestinal manifestation of chronic inflammatory bowel disease. Eur J Gastroenterol Hepatol 1996;8:461–468.
60. Fellermann K, Stahl M, Dahlhoff K, Amthor M, Ludwig D, Stange EF. Crohn's disease and sarcoidosis: systemic granulomatosis? Eur J Gastroenterol Hepatol 1997;9: 1121–1124.
61. Lovat LB, Madhoo S, Pepys MB, Hawkins PN. Long-term survival in systemic amyloid A amyloidosis complicating Crohn's. Gastroenterology 1997;112: 1362–1365.
62. Nordenholtz KE, Stowe SP, Stormont JM, et al. The cause of death in inflammatory bowel disease: a comparison of death certificates and hospital charts in Rochester, New York. Am J Gastroenterol 1995;90:927–932.
63. Trommer G, Bewer A, Kosling S. [Mesenteric lymphadenopathy in Yersinia enterocolitica infection.] [German] Radiologe 1998;38:37–40.
64. Balthazar EJ, Charles HW, Megibow AJ. Salmonella- and Shigella-induced ileitis: CT findings in four patients. J Comput Assist Tomogr 1996;20:375–378.
65. Hoffmann H, Kawooya M, Esterre P, et al. In vivo and in vitro studies on the sonographical detection of Ascaris lumbricoides. Pediatr Radiol 1997;27:226–229.
66. Durand DV, Lecomte C, Cathebras P, Rousset H, Godeau P. Whipple disease. Clinical review of 52 cases. The SNFMI Research Group on Whipple Disease. Societe Nationale Francaise de Medecine Interne. [Review] Medicine 1997;76:170–184.
67. Olveira A, Sanchez Rancano S, Conde Gacho P, Moreno A, Martinez A, Comas C. [Gastrointestinal anisakiasis. Seven cases in three months.] [Spanish] Rev Esp Enferm Dig 1999;91:70–72.
68. Chiu NT, Lee BF, Hwang SJ, Chang JM, Liu GC, Yu HS. Protein-losing enteropathy: diagnosis with (99m)Tc-labeled human serum albumin scintigraphy. Radiology 2001;219:86–90.
69. Schmutz GR, Chapuis F, Morel E, N'Guyen D, Dion C, Regent D. [Drug-induced stenosis of the small bowel. Value of enteroclysis.] [French] J Radiol 1997;78:33–39.
70. Zalcman M, Sy M, Donckier V, Closset J, Gansbeke DV. Helical CT signs in the diagnosis of intestinal ischemia in small-bowel obstruction. AJR 2000;175:1601–1607.
71. Kikuno M, Takahashi K, Shinozaki T, Nakazawa M, Sugawara T, Furuse M. [CT findings of the irradiated intestinal wall: comparison of early vascular phase and delayed equilibrium phase.] [Japanese] Nippon Igaku Hoshasen Gakkai Zasshi 1999;56:703–707.
72. De Backer AI, De Schepper AM, Vandevenne JE, Schoeters P, Michielsen P, Stevens WJ. CT of angioedema of the small bowel. AJR 2001;176:649–652.
73. Nasnas R, Awky J, Aoun N, Haddad S, Slaba S, Atallah N. [Digestive manifestations of hereditary angioneurotic edema. Apropos of a case.] [French] J Radiol 1997;78:1167–1169.
74. Stevens RL, Jones B, Fishman EK. The CT halo sign: a new finding in intestinal lymphangiectasia. J Comput Assist Tomogr 1997;21:1005–1007.
75. Suzuki C, Higaki S, Nishiaki M, et al. 99mTc-HSA-D scintigraphy in the diagnosis of protein-losing gastroenteropathy due to secondary amyloidosis. J Gastroenterol 1997;32:78–82.
76. Vayre-Oundjian L, Boruchowicz A, Bloget F, Triboulet JP, Gosselin B, Colombel JF. [Pseudotumor nodular lymphoid hyperplasia of the ileum.] [Review] [French] Gastroenterol Clin Biol 1997;21:990–993.
77. Scafidi DE, McLeary MS, Young LW. Diffuse neonatal gastrointestinal hemangiomatosis: CT findings. Pediatr Radiol 1998;28:512–514.
78. Scarmato VJ, Levine MS, Herlinger H, Wickstrom M, Furth EE, Tureck RW. Ileal endometriosis: radiographic findings in five cases. Radiology 2000;214: 509–512.
79. Semelka RC, Marcos HB. Polyposis syndromes of the gastrointestinal tract: MR findings. J Magn Reson Imaging 2000;11:51–55.
80. DiSario JA, Burt RW, Vargas H, McWhorter WP. Small bowel cancer: epidemiological and clinical characteristics from a population-based registry. Am J Gastroenterol 1994;89:699–701.
81. Neugut AI, Jacobson JS, Suh S, Mukherjee R, Arber N. The epidemiology of cancer of the small bowel. [Review] Cancer Epidemiol Biomarkers Prev 1998;7: 243–251.

82. Buckley JA, Siegelman SS, Jones B, Fishman EK. The accuracy of CT staging of small bowel adenocarcinoma: CT/pathologic correlation. J Comput Assist Tomogr 1997;21:986–991.
83. Chun HJ, Byun JY, Chun KA, et al. Gastrointestinal leiomyoma and leiomyosarcoma: CT differentiation. J Comput Assist Tomogr 1998;22:69–74.
84. Chan GS, Ng WK, Chua DT, Wu PC. Raised serum hCG in a male patient caused by primary jejunal choriocarcinoma. J Clin Pathol 1998;51:413–415.
85. Ledermann HP, Binkert C, Frohlich E, Borner N, Zollikofer C, Stuckmann G. Diagnosis of symptomatic intestinal metastases using transabdominal sonography and sonographically guided puncture. AJR 2001;176:155–158.
86. Elsayed AM, Albahra M, Nzeako UC, Sobin LH. Malignant melanomas in the small intestine: a study of 103 patients. Am J Gastroenterol 1996;91:1001–1006.
87. Strobel K. [Small intestine invagination in metastatic intestinal malignant melanoma.] [German] Rofo Fortschr Geb Rontgenstr Neuen Bildgeb Verfahr 2001;173:768–769.
88. Seppala R, Prefontaine M, Mikhael NZ. Mesenteric small-bowel polyposis: a diagnostic radiographic sign of neurofibromatosis. AJR 1997;168:434–436.
89. Sugimoto E, Lorelius LE, Eriksson B, Oberg K. Midgut carcinoid tumours. CT appearance. Acta Radiol 1995; 36:367–371.
90. Bader TR, Semelka RC, Chiu VC, Armao DM, Woosley JT. MRI of carcinoid tumors: spectrum of appearances in the gastrointestinal tract and liver. J Magn Reson Imaging 2001;14:261–269.
91. Hoegerle S, Altehoefer C, Ghanem N, et al. Whole-body 18F dopa PET for detection of gastrointestinal carcinoid tumors. Radiology 2001;220:373–380.
92. Jadvar H, Segall GM. False-negative fluorine-18–FDG PET in metastatic carcinoid. J Nucl Med 1997;38:1382–1383.
93. Hennigs S, Jager H, Gissler M, et al. [Small intestinal transit with radio-opaque markers to localize intermittent small bowel obstruction.] [German] Rofo Fortschr Geb Rontgenstr Neuen Bildgeb Verfahr 2000;172:1000–1005.
94. Lappas JC, Reyes BL, Maglinte DD. Abdominal radiography findings in small-bowel obstruction: relevance to triage for additional diagnostic imaging. AJR 2001;176:167–174.
95. Assalia A, Schein M, Hashmonai M. Barium contrast study converts partial small-bowel obstruction into a complete one. Report of 2 cases. S Afr J Surg 1993;31: 102–103.
96. Miyazaki O. [Efficacy of abdominal plain film and CT in bowel obstruction.] [Japanese] Nippon Igaku Hoshasen Gakkai Zasshi 1995;55:233–239.
97. Maglinte DD, Reyes BL, Harmon BH, et al. Reliability and role of plain film radiography and CT in the diagnosis of small-bowel obstruction. AJR 1996;167: 1451–1455.
98. Makanjuola D. Computed tomography compared with small bowel enema in clinically equivocal intestinal obstruction. Clin Radiol 1998;53:203–208.
99. Jabra AA, Eng J, Zaleski CG, et al. CT of small-bowel obstruction in children: sensitivity and specificity. AJR 2001;177:431–436.
100. Harisinghani MG, Wittenberg J, Lee W, Chen S, Gutierrez AL, Mueller PR. Bowel wall fat halo sign in patients without intestinal disease. AJR 2003;181: 781–784.
101. Matter I, Khalemsky L, Abrahamson J, Nash E, Sabo E, Eldar S. Does the index operation influence the course and outcome of adhesive intestinal obstruction? Eur J Surg 1997;163:767–772.
102. Hentel KD, Gollub MJ. Contrast enema before bypass surgery for small-bowel obstruction in the oncologic patient: is it necessary? AJR 2003;181:1361–1364.
103. Shimanuki Y, Aihara T, Takano H, et al. Clockwise whirlpool sign at color Doppler US: an objective and definite sign of midgut volvulus. Radiology 1996;199: 261–264.
104. Gurleyik E, Gurleyik G. Small bowel volvulus: a common cause of mechanical intestinal obstruction in our region. Eur J Surg 1998;164:51–55.
105. Lok SY, Adkins J, Asch M. Caval perforation by a Greenfield filter resulting in small-bowel volvulus. J Vasc Interv Radiol 1996;7:95–97.
106. Clautice-Engle T, Jeffrey RB Jr, Li KC, Barth RA. Power Doppler imaging of focal lesions of the gastrointestinal tract: comparison with conventional color Doppler imaging. J Ultrasound Med 1996;15:63–66.
107. Warshauer DM, Lee JK. Adult intussusception detected at CT or MR imaging: clinical-imaging correlation. Radiology 1999;212:853–860.
108. Nomura H, Kitamura T, Takahashi Y, Mai M. Small-bowel obstruction during enzymatic treatment of gastric bezoar. Endoscopy 1997;29:424–426.
109. Gupta MM, Bandlish MK, Kumar A, Gupta R, Aahi KS. Retained surgical sponge simulating intestinal tuberculosis. Indian J Gastroenterol 1997;16:68–69.
110. Wortler K, Beerwerth W, Peters PE. [Chronic recurrent ileus. Recurrent mechanical ileus of the small intestine caused by a high fiber diet (canned asparagus).] [German] Radiologe 1997;37:95–97.
111. Feigin E, Seror D, Szold A, et al. Water-soluble contrast material has no therapeutic effect on postoperative small-bowel obstruction: results of a prospective, randomized clinical trial. Am J Surg 1996;171:227–229.
112. Morita M, Nakamura H, Urade M, Hirosawa H. [Clinical study of ileus like symptom due to eating of raw firefly squid, Watasenia scintillans.] [Japanese] Nippon Shokakibyo Gakkai Zasshi 1995;92:26–31.
113. Carethers JM, McDonnell WM, Owyang C, Scheiman JM. Massive secretory diarrhea and pseudo-obstruction as the initial presentation of Crohn's disease. [Review] J Clin Gastroenterol 1996;23: 55–59.
114. Ebert EC, Ruggiero FM, Seibold JR. Intestinal perforation. A common complication of scleroderma. Dig Dis Sci 1997;42:549–553.
115. Santos F, Campos J, Freire J, Andrade A, Tavora I, Castelo HB. Enterocutaneous fistulas: an unusual solution. Hepatogastroenterology 1997;44:1085–1089.
116. Malden ES, Hicks ME, Royal HD, Aliperti G, Allen BT, Picus D. Recurrent gastrointestinal bleeding: use of thrombolysis with anticoagulation in diagnosis. Radiology 1998;207:147–151.
117. Garofalo TE, Abdu RA. Accuracy and efficacy of nuclear scintigraphy for the detection of gastrointestinal bleeding. Arch Surg 1997;132:196–199.

118. Litt HI, Levine MS, Maki DD, Sachdeva RM, Einhorn E. Ileal actinomycosis in a patient with AIDS. AJR 1999;172:1297–1299.
119. Patel NR, Oliva PJ, McCoy S, Soike DR, Leeper SC, Thomas E. Massive lower gastrointestinal hemorrhage in an AIDS patient: first case report of ulcerated lymphoma in a Meckel's diverticulum. Am J Gastroenterol 1994;89:133–134.
120. Kalantari BN, Mortele KJ, Cantisani V, et al. CT features with pathologic correlation of acute gastrointestinal graft-versus-host disease after bone marrow transplantation in adults. AJR 2003;181:1621–1625.
121. Worawattanakul S, Semelka RC, Kelekis NL, Sallah AS. MR findings of intestinal graft-versus-host disease. Magn Reson Imaging 1996;14:1221–1223.
122. DiBaise JK, Quigley EM. Fatal diffuse invasive gastrointestinal candidiasis masking as ileus after bone marrow transplantation. J Clin Gastroenterol 1997;24: 165–168.
123. Myers A, Thurston W, Ho CS. Spontaneous knotting of a transgastric jejunostomy tube: case report. Can Assoc Radiol J 1997;48:22–24.

5

Colon and Rectum

Technique

Barium Enema

Contrary to the opinion of some computed tomography (CT) and magnetic resonance imaging (MRI) enthusiasts, a double-contrast barium enema continues to be a viable option in a setting of suspected colitis, colorectal cancer screening and detection, and follow-up after therapy. Similarly, it is a sad reflection on medical practice that occasionally a statement still appears in print that barium sulfate is toxic to the colon (1).

One of the present indications for a barium enema is failed colonoscopy, although in some centers CT colonography is gaining ground and magnetic resonance (MR) virtual colonoscopy is on the horizon. An obvious concern in performing any enema shortly after failed colonoscopy is risk of perforation. Contrary to the experience of some investigators, the author has found barium enemas performed on the same day as colonoscopy to be mostly unsatisfactory; invariably the patient is "tired out" from the colonoscopy, has difficulty cooperating, excessive colonic spasm is often encountered, and residual fluid interferes with mucosal coating. A formal air contrast barium enema, performed a week or so later, tends to be of superior quality.

Proctography

Evacuation proctography, a dynamic imaging modality, evaluates functional and morphologic abnormalities of the anorectal region. This examination, also called *dynamic proctography* or *defecography*, requires specially adopted fluoroscopic equipment, including rapid filming, that is not available in many radiology departments. It has a role in evaluating unexplained constipation, incontinence, rectal prolapse, and rectal pain. It evaluates the presence or absence of a sigmoidocele, rectocele, rectal prolapse, puborectalis muscle contraction, anal canal opening, changes in anorectal angle, and rectal emptying. Resultant findings appear to be independent of contrast agent viscosity used.

Pre- and postproctography questionnaires by referring clinicians revealed that clinicians found this study of major benefit in 40% and of moderate benefit in 40% (2); the primary diagnosis was changed in 18% of patients, intended surgical management became nonsurgical in 14%, intended nonsurgical therapy became surgical in 4%, and type of surgery contemplated changed in 10%.

Although detailed and precise anatomic measurements are possible with this study, their clinical relevance is still not clear. In particular, the borderland between normal and abnormal is poorly defined. Lack of confidence in some

of the findings becomes evident after patient symptoms persist following surgical correction of an alleged abnormality.

Computed tomographic proctography is feasible, but rarely performed. The study is performed with the patient seated; coronal images aid in outlining perineal floor muscles. Sagittal reconstruction allows comparison with conventional proctography.

An open configuration MR system allows image acquisition with the patient in a vertical position. Anorectal angle changes, anal canal function, puborectalis muscle configuration, and pelvic floor dynamics are evaluated at rest and during straining (3). Even if an open MR unit is not available, conventional proctography is gradually being replaced by pelvic floor MRI using an endoanal coil. Suspected fistulas, sphincter lacerations, rectoceles, tumor invasion by low rectal carcinomas, and other pelvic floor disorders are imaged in detail with this technique. Currently this is considered to be the most accurate imaging test of distal perirectal structures, especially the external sphincter.

Two approaches are possible for MR rectal studies: either rectal distention with fluid and use of a surface coil or no distention and use of a rectal MR coil. More studies have addressed the latter technique, but advances in hardware and software design make it difficult to predict which path will be superior. One technique consists of opacifying the rectum with 200 mL of an ultrasonography (US) gel and obtaining a single sagittal T2-weighted gradient echo sequence through the rectum (4); with a 1.5-T MR unit, a temporal resolution of 1.1 second is obtained, allowing imaging at rest and during straining and evacuation.

Using a surface coil in the anal canal, endorectal MRI appears superior to endorectal US in visualizing the external sphincter, although internal sphincter lesions are better evaluated with endorectal US (5).

Colonoscopy

Conventional

The prevalence of incomplete colonoscopy varies considerably among endoscopists and institutions, ranging from several percent up to one third of studies. A majority of incomplete colonoscopies are in women. A prior abdominal hysterectomy is associated with a higher rate of incomplete colonoscopy.

Complete colonoscopy consists in visualizing cecal landmarks, an elusive task in some patients. Attempts to provide photographs of cecal landmarks have met with limited success. Experienced endoscopists display considerable disparity in deciding whether complete colonoscopy had been performed when reviewing photographs of cecal landmarks (6).

The polyp miss rate of colonoscopy was estimated by performing two consecutive back-to-back colonoscopies on the same day (7); overall polyp miss rate was 24%, being 27% for polyps ≤5 mm, 13% for lesions 6 to 9 mm, and 6% for those ≥1 cm. The miss rates for small polyps occurred among essentially all endoscopists.

Polyp size is routinely estimated by endoscopists. Because of endoscopic lens system limitations, apparent measurements tend to be smaller than actual. Lesions in the periphery of the field of view are smaller than in the center. Likewise, size varies with depth of view. Comparing magnified radiographic polyp measurements (which are magnified due to inherent focus-object-film geometry) with the minified endoscopic appearance results in considerable discrepancy.

Laser fluorescence spectroscopy performed during colonoscopy has detected colonic dysplasia with a claimed sensitivity and specificity of over 90% (8).

Computed Tomographic Colonography

The introduction of multidetector CT opened possibilities for complex three-dimensional (3D) colon studies, allowing the entire abdomen and pelvis to be covered with a slice thickness of <3 mm in under 30 seconds, allowing single breath-hold scanning. An effective slice thickness approaching 1 mm should, in theory, detect all relevant polyps. Once lumen distention is introduced, one is well on the road toward CT detection of colon neoplasms. Yet although multiple publications have established the feasibility of screening CT colonography, its role remains undefined.

The terms *CT colonography*, *CT colonoscopy*, and *virtual colonoscopy* have often been used interchangeably to describe a global examination designed to detect colonic tumors regardless of specific images obtained. *Computed*

tomographic colonography appears to better describe this procedure, but *virtual colonoscopy* is ingrained in the literature, although a trend has developed to use *CT colonography* for a global examination consisting of narrow collimation data reconstructed to various combinations of 2D multiplanar reformatting and 3D images and to limit the term *virtual colonoscopy* to specific colonoscopy-like images. *Hydro-CT* is a less often used term to describe colonic distention with fluid during a CT study.

Currently CT colonography is a viable alternate after failed or incomplete conventional colonoscopy. Residual colonic distention is adequate in many patients when CT is performed shortly after incomplete colonoscopy, but additional air insufflation is often helpful. Indications for CT colonography have expanded considerably and in some centers it has mostly replaced conventional colonoscopy for polyp detection, leaving the latter modality for therapy of detected polyps.

Technique

Although CT colonography is generally regarded as a technically easy study, interpretation requires a steep learning curve. Data evaluation time and number of false positive findings decrease with experience. Similar to a barium enema, a colon-cleansing regimen is required with most current CT colonography techniques. Numerous false positives ensue if residual stool is present, thus emphasizing the importance of a colon-cleansing regimen, a difficult task in most practices. One study achieved ideal bowel preparation in only 19% of 200 patients (9). The two bowel preparations commonly employed are a polyethylene glycol electrolyte ("wet") solution or a phospho-soda ("dry") preparation, both given the day prior to CT colonography. Polyethylene glycol electrolyte solution results in considerably more bowel residual fluid.

Current limitations of CT colonography include fluid retention and inadequate luminal distention due to spasm. Similar to a barium enema, polyps tend to be missed if the lumen is not distended. Spasm is minimized by judicious use of an antispasmodic agent. Problems inherent with fluid retention are partly overcome by performing the study with the patient both prone and supine, at the expense of doubling the radiation dose. Nevertheless, acquisition and review of supine and prone images significantly increase polyp detection sensitivity (10), and the trend is to use both positions.

Ingestion of oral contrast agents is generally considered inadequate preparation for CT cancer detection. In practice, colonic lavage combined with oral barium contrast for stool tagging and oral iodinated contrast for electronic fluid marking are useful techniques. A viable option consists of oral contrast combined with laxatives in frail, elderly patients who do not tolerate more vigorous CT colonography or a barium enema, realizing that this technique detects only more bulky tumors.

Air is commonly used to distend the lumen. Carbon dioxide is an alternative agent but the relative merits of one over the other are arguable. Adequacy of distention is evaluated with a CT scout image. With newer CT scanners, if a study is being performed for suspected colitis, especially ischemic colitis, some authors find little advantage for intraluminal contrast.

As an aside, a tap-water enema is often administered if colon visualization is desired during abdominal CT examination. Comparing water, methylcellulose, and ultrasound gel as multislice CT rectal contrast agents, methylcellulose was significantly superior to ultrasound gel in differentiating normal from diseased bowel (11); although better rectal distention was achieved with methylcellulose and ultrasound gel, superior more proximal colon distention was obtained with water. Of these three agents, the authors recommend rectal methylcellulose.

Computed tomographic colonography with multidetector CT results in significantly better colonic distention and yields fewer respiratory artifacts compared to single-detector CT.

Computed tomographic colonography is a viable alternate after failed or incomplete conventional colonoscopy. A prospective study of patients performed within 2 hours of incomplete colonoscopy found that although residual colonic distention was adequate in most patients, additional air insufflation significantly increased colon distention (12).

Once patient scanning is completed, the data are transferred to a workstation for analysis. These are complex examinations, and hundreds of images are generated in transverse, multiplanar reformatted, and 3D endoluminal modes. The relative advantages of axial, coronal, 2D, and 3D display techniques are still evolving;

A B

Figure 5.1. A,B: Two views of three-dimensional (3D) computed tomography (CT) double-contrast virtual colonoscopy. Images can be analyzed from any perspective in space. (Courtesy of Wolfgang Luboldt, M.D., Johann Wolfgang Goethe University, Frankfurt-am-Main.)

in some patients several techniques are necessary to adequately visualize the entire colonic wall. A typical practice is to use primarily 2D multiplanar reformatted imaging for analysis and reserve 3D imaging for specific problems; endoluminal views appear necessary to differentiate polyps from folds. Several commercial 3D endoluminal volume rendering and navigational systems are available and further improvements are to be expected. Adding color (translucency rendering) to 3D aids in ruling out false polyps (13). Interpretation of 2D images is faster; on the other hand, navigation with 3D endoluminal imaging mimics the conventional colonoscopic appearance (Fig. 5.1). A panoramic view perpendicular to the centerline is also feasible, with sequential panoramic video views scanning the colon surface.

Results

Polyp detection sensitivity varies depending on scanning and image reconstruction parameters employed and on polyp size. No consensus exists on preferred viewing modes. For larger polyps a panoramic display results in greater sensitivity than a virtual endoluminal display and 3D displays are more sensitive than 2D displays. Experienced abdominal radiologists achieve similar polyp detection rates using 2D multiplanar reformation and 3D display techniques (14). Computed tomography colonography using axial 2D data and a cine mode and 3D "fly-through" with surface-rendered and multiplanar reformatted images identified the same number of polyps with both techniques (15). A metaanalysis of reported accuracy of CT colonography found a pooled per-patient sensitivity for polyps >10 mm to be 88%, for polyps 6–9 mm 84% and for polyps 5 mm or smaller 65% (16); per-polyp sensitivity for polyps >10 mm was 81%.

CT colonoscopy perforation rates are low and should be similar to those with a barium enema. Rectal perforation is a potential complication with blind air insufflation in a setting of more proximal rectosigmoid obstruction.

Future Studies

Attempts to circumvent a colon cleansing regimen are theoretically feasible by tagging colonic content with ingested barium sulfate, with subsequent digital subtraction of this material. In patients with suspected or known colonic polyps, sensitivity for identifying

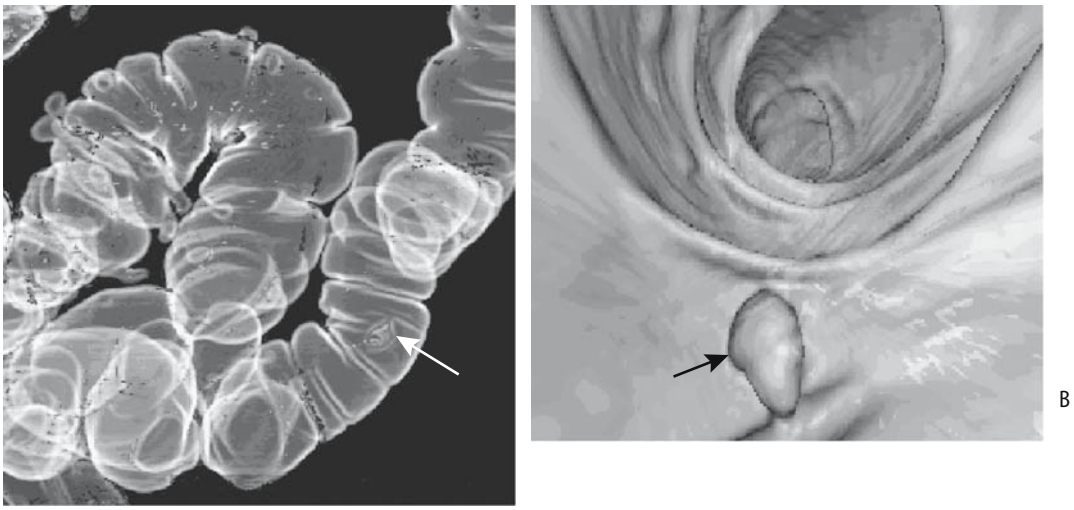

Figure 5.2. Computer-aided polyp detection. A,B: Focal increased tumor perfusion after IV contrast can be automated to "detect" potential neoplasms (arrow). (Courtesy of Wolfgang Luboldt, M.D., Johann Wolfgang Goethe University, Frankfurt-am-Main.)

patients with polyps 1 cm or larger was 80% to 100% if these patients ingested multiple dilute contrast doses over a prior 48 hours (17).

Using signal processing of CT colonography data to identify tumors protruding into bowel lumen, an automated polyp detection algorithm achieved a 64% sensitivity for detecting polyps 10 mm or greater (18). Another approach is to use tumor contrast enhancement superimposed on a virtual double contrast and endoscopic display (19) (Fig. 5.2). Shape-based polyp detection and polyp edge enhancement are helpful in identifying polyps.

Teleradiology of CT colonography using wavelet compression to 1:1, 10:1, and 20:1 ratios detected all lesions >10 mm for all compression ratios, but sensitivities for smaller lesions fell off with increasing compression ratios (20).

A claimed advantage of CT colonography is that extracolonic abnormalities are also detected. Among consecutive patients undergoing CT colonography, important extracolonic findings in 11% led to further imaging studies, and as a result several patients underwent surgery (21). Nevertheless, being designed for optimal colonic imaging, CT colonography is limited in evaluating solid organs (compared to a fine-tuned CT study of a specific organ or abnormality in question).

Magnetic Resonance Colonography

Similar to CT colonography, MR colonography is feasible, with relative advantages of CT versus MR colonography still evolving. Two broad approaches are possible:

1. Bright lumen MR colonography relies on colon filling with a paramagnetic contrast-water enema and T1-weighted gradient-recalled echo (GRE) single breath-hold acquisition, which results in a hyperintense luminal image, with other tissues being hypointense. Multiplanar reformatted 3D images and virtual colonoscopic images are then obtained.
2. Dark lumen MR colonography obtained by colon filling with a tap-water enema, which is hypointense on T1-weighted GRE imaging and an intravenous paramagnetic contrast agent to produce a hyperintense colonic wall. A variant technique is to use gas or air to distend the lumen; gas has no signal.

Another technique consists of colonic distention with fluid and use of T2-weighted spin echo (SE) imaging. The colon is studied both in cross section and using a virtual intraluminal outline. Often a coronal plane is useful.

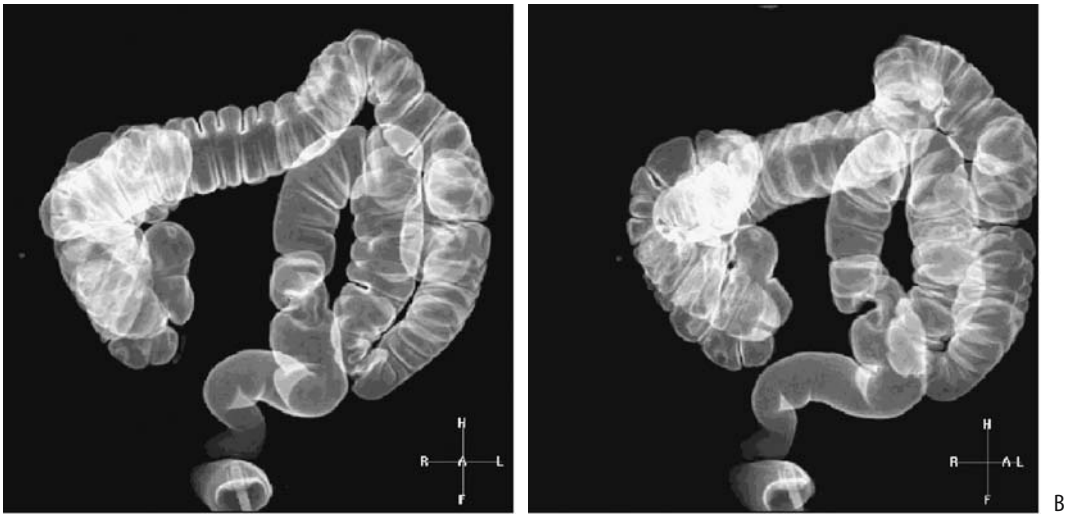

A B

Figure 5.3. A,B: Two 3D double-contrast MR virtual colonoscopy images. Visualization is similar to that obtained with CT (see Fig. 5.1). (Courtesy of Wolfgang Luboldt, M.D., Johann Wolfgang Goethe University, Frankfurt-am-Main.)

The disadvantages of the bright lumen technique include retained air bubbles, which mimic polyps. Therefore, both prone and supine views are necessary. Surface-rendered MR virtual colonoscopic views, orthogonal sections and water-sensitive single-shot fast spin echo (FSE) MR images in patients (post–gadolinium-water enema) achieved a 93% sensitivity and 99% specificity in detecting tumors >10 mm (22). To illustrate the complexity of these studies, they often require instillation of a gadolinium-water enema, prone and supine positioning, breath-hold 3D spoiled gradient recalled echo (SGRE) sequences and also 2D images pre– and post–intravenous contrast, and, wherever necessary, virtual intraluminal images.

Comparing manganese chloride, iron glycerophosphate, and gadolinium-based enemas for use in T1 shortening 3D GRE MR colonography, the contrast-to-noise ratios for the iron enema were highest (23); the authors suggest replacing gadolinium with iron due to cost considerations.

Using a gadopentetate-water enema and breath-hold 3D SGE sequences, a virtual double-contrast display is achieved by calculating signal intensity differences between adjacent voxels and making adjacent voxels with similar intensities lucent while adjacent voxels with different intensities are made opaque (24); the resultant colonic display can be magnified and rotated around its axis for detailed study from different planes (Fig. 5.3).

Some authors use the term *hydro-MRI* when a water, saline, or some other contrast enema is administered prior to MRI. Such an approach is helpful when the study is performed primarily for suspected colonic disease, and it is a step toward formal MR colonography. Confusing the issue is that *hydro-MRI* is also used by some authors if oral water or contrast is ingested prior to a MR small bowel study. Thus the type of contrast (including water and air) and route of administration need to be specified. The term *double-contrast MR imaging* is used by some when both an MR contrast enema and an MR intravenous (IV) contrast agent are employed. Due to its ambiguity, it is probably best avoided.

A typical technique for colon neoplasms consists of breath-hold T2-weighted half-Fourier acquisition single-shot turbo spin echo (HASTE) and gadolinium-enhanced breath-hold fat-suppressed T1-weighted SGE images (25); inflammatory changes appear best on the gadolinium-enhanced breath-hold fat-suppressed T1-weighted SGE images.

Air bubbles with the dark lumen technique are hypointense and blend into the surrounding hypointense water; thus only one patient position is necessary, resulting in a shorter scan time. Likewise, polyps enhance with IV contrast and stool does not. Potentially, the dark lumen

technique is also useful to evaluate colitis because of bowel wall enhancement.

Using lumen distention with CO_2, breath-hold single-shot FSE MRI performed during a CO_2 enema in seven patients with known colon carcinoma detected cancers in all and correctly identified tumor extension through muscularis propria in four (26).

Colon cleansing is required with most of the above methods. Similar to CT colonography, use of an oral paramagnetic contrast agents to label stool (called fecal tagging) in an unprepared colon results in stool being hyperintense and thus blending in with a bright lumen. Or, concentrated oral barium sulfate, which is hypointense and thus useful with a dark lumen technique, is combined with IV gadolinium to enhance the colonic wall and any associated tumors (27). These MR stool-tagging techniques are still in their infancy.

Ultrasonography

Compared to other intraabdominal sites, colon US is rather limited. In some centers it has found a niche in following patients with colonic Crohn's disease but appears less useful with ulcerative colitis and diverticulitis. Its role in pediatric intussusception reduction is well established, less so in adult tumor detection and staging. Ultrasonography findings are not disease-specific. Also, in general, a negative US examination does not exclude disease.

Colon US performed after a water enema is called *hydrocolonic sonography* (occasionally a methylcellulose-water mixture is used). Hydrocolonic US does detect larger polyps but it is very operator dependent and has been overshadowed by CT colonography.

Doppler US evaluates colonic blood flow. Thus viability of an obstructed bowel segment is suspected if Doppler US detects no blood flow. Similarly, in inflammatory bowel disease and in acute appendicitis Doppler flow through a thickened bowel segment can suggest an acute or ongoing inflammation.

The published terminology is somewhat inconsistent for US performed with rectal probes: *Endoscopic* and *endoluminal* US include either a rectal or vaginal probe, whereas the terms *transrectal* and *endorectal* US are used interchangeably. *Anorectal echo-endoscopy* and similar terms are also in use.

Endovaginal US evaluates the rectum and adjacent structures, including puborectalis muscle thickness, sphincter thickness, and sphincter defects. Distending the rectum with a water enema better delineates perirectal tissue planes.

Endorectal US defines surrounding structures. Urogenital structures and perirectal spaces are readily imaged. Both proctography and endorectal US evaluate internal and external rectal sphincters. Three-dimensional endorectal US appears to provide more accurate control of a biopsy needle toward a perirectal lesion than is available with other modalities, although the data for this are sparse. The current primary use of endorectal US is in a setting of rectal cancer and in the workup of evacuation disorders.

Available US miniprobes fit through the working channel of an endoscope. Similar to upper gastrointestinal endoscopic US, the role of flexible colonoscopic US in detecting and staging neoplasms is not yet clear.

Scintigraphy

A gamma camera scintigraphic technique estimates colonic transit, an infrequently used study in clinical practice.

The application of scintigraphy in inflammatory bowel disease and in the bleeding patient is covered in each respective section later in this chapter. Abdominal positron emission tomography (PET) scanning is discussed in more detail in Chapter 14.

Congenital Abnormalities

Malposition

Midgut malrotation is discussed in Chapter 4.

The interposition of small or large bowel into the right subphrenic space, first described by Chilaiditi in 1910, is rarely symptomatic and should be considered a normal variant. Bilateral bowel interposition is rare (28). Some authors use the term *Chilaiditi's syndrome* to describe all such bowel interposition; others limit the term only to the symptomatic patient. Prevalence of such bowel hepatodiaphragmatic interposition appears to depend on patient position and is identified more often with the patient supine.

Detection of bowel interposition is generally straightforward with conventional radiography and barium studies. The appearance is confusing with US, where interposed bowel loops mimic an abnormal mass. Computed tomography detects ascending colon interposition between kidney and psoas muscle (pararenal space) in about 1% (29). Retropsoas interposition is slightly more common with the ascending colon (3%) and descending colon (2%) (30); little retroperitoneal fat favors interposition. A colon interposed posterior to the pancreas, between the spleen and left hemidiaphragm, is rare.

Duplication

Gastrointestinal duplications are associated with both vertebral and genitourinary tract abnormalities. They occur roughly in one out of 4000 births. Least common are hindgut duplications. Most are detected in the young.

Colonic duplications have either a spherical or tubular appearance, with some long duplications mimicking a second colon lumen. Most of these duplications do not communicate with the lumen and occur along the mesenteric border. Occasionally a duplication contains noncolonic mucosa, such as heterotopic gastric mucosa, small bowel, pancreatic, and even respiratory epithelium. The mucosa of some duplications continues secreting and a noncommunicating duplication thus increases in size with time. Imaging identifies an abdominal cystic tumor.

A rare duplication intussuscepts; it acts as a source of cecal volvulus, or is an incidental palpable mass at initial presentation. An occasional one develops a fistula to an adjacent structure. Magnetic resonance imaging is useful with the rare rectal duplication in a neonate to show no posterior extension, thus excluding a meningocele.

Obstruction

Common distal ileal obstructions in neonates are due to meconium ileus and ileal atresia; in the colon obstructions include imperforate anus, meconium plug syndrome, and Hirschsprung's disease. From a practical viewpoint, distal ileal and colonic obstructions in the neonate are lumped together as low intestinal obstructions.

A microcolon in a neonate is a descriptive term of a contrast enema finding rather than a specific disorder and usually suggests distal small bowel obstruction. Colonic disorders associated with a small caliber of the entire colon include total colonic aganglionosis of Hirschsprung's disease and a microcolon seen with prematurity. Conventional radiography usually differentiates between a high and a low intestinal obstruction. A contrast enema is necessary to define the obstruction further.

Atresia

In rectal atresia the anus is normal, with the atretic segment located more proximal. No bowel fistula is identified. Atresia proximal to the rectum is uncommon, although it can occur anywhere in the colon. Colonic stenosis is rare. A contrast enema reveals a small caliber colon distal to the obstructed, atretic segment.

Imperforate Anus

The most common neonatal colonic obstruction is an imperforate anus. Although the term *imperforate anus* implies a single and simple defect, in reality this is a complex deformity often also involving genitourinary tract structures and other anomalies. Cryptorchidism is common; in general, a more superior level of anorectal malformation increases the risk of cryptorchidism.

Rectal atresia differs from an imperforate anus. With an imperforate anus the hindgut does not descend and communicate with the anus, but either ends blindly or forms a fistula in an abnormal location (ectopic anus). An imperforate anus is classified as being high or low using the puborectalis sling as a dividing line. The differentiation between a high and low lesion is often made clinically, and imaging plays a limited direct role. The presence of a perineal dimple or passage of meconium from the genitourinary tract is a useful guide. In some boys conventional radiography reveals gas in the bladder.

The puborectalis muscle tends to be hypoplastic with a high obstruction. With a high lesion, the rectum can end blindly, although more often in boys it terminates in the posterior

urethra, and less often in the bladder or anterior urethra. In girls the rectum tends to terminate in the vagina. Prior to definitive surgery, most high lesions are treated with a bypass colostomy. The underlying anatomy is then studied through the distal colostomy limb (mucous fistula) or, if needed, by cystography and urethrography.

A low lesion is usually associated with a perineal dimple, and no communication exists with the genitourinary tract. A variant of a low lesion is a congenital triad consisting of an anorectal malformation, sacral abnormality, and a presacral tumor, first described by Currarino et al. (31) in 1981 (Table 5.1). Magnetic resonance imaging is useful in this triad to detect a tethered cord.

Imaging aids in detecting any associated renal or sacral abnormalities. Magnetic resonance imaging outlines the hindgut, bony and muscular pelvic anomalies, including the puborectalis muscle and external sphincter, and other surrounding anatomy. T1-weighted images establish whether the puborectalis muscle is hypoplastic. Magnetic resonance imaging tends not to identify small fistulous tracts, however, and a contrast study is useful to define them.

Some boys have a mix of meconium and urine and the meconium calcifies; these calcifications are intraluminal in location, thus distinguishing them from meconium peritonitis. Such a mix of meconium and urine does not occur in girls with anal atresia; calcified intraluminal content in a girl should suggest a cloacal malformation consisting of communication between the urethra and rectum, generally through a single perineal channel.

After surgical correction of an anorectal malformation—such as rectal pull-through(perineoplasty) or posterior sagittal reconstruction (anorectoplasty)—MRI is helpful in detecting complications and to evaluate muscle integrity. Residual internal and external sphincter disruptions are identified.

Table 5.1. Currarino triad: anorectal malformation, sacral abnormality and presacral mass findings in 11 patients

Abnormality	Number
Anorectal malformation	
Low imperforate anus	3
Anorectal stenosis	8
Presacral tumor	
Teratoma	7
Meningocele	2
Dermoid cyst	1
Enteric/dermoid cyst	1
Sacral and other	
Deformed sacrum	11
Tethered cord	2

Source: Date from Lee et al. (32).

Megacystis-Microcolon-Intestinal Hypoperistalsis Syndrome

In the megacystis-microcolon-intestinal hypoperistalsis syndrome the bladder is markedly distended and a contrast enema shows what initially looks like a small-caliber colon. Although the initial appearance suggests an obstruction, no mechanical obstruction is found. A shortened small bowel, at times malrotated, reveals poor or absent peristalsis. Hydronephrosis is common. Hydrometrocolpos and segmental colonic dilation also occur. Etiology of this rare autosomal-recessive disorder is unknown. Neuronal dysplasia is identified in some. This syndrome also occurs without megacystis; with such a presentation it blends into the general category of functional intestinal obstruction in neonates.

The diagnosis should be considered in a newborn with a markedly distended bladder and suspected intestinal obstruction.

Meconium Plug Syndrome

Meconium plug syndrome and small left colon syndrome are probably the same entity. Diabetes in the mother is common. These full-term neonates have colonic obstruction due to inspissated intestinal contents. The colonic lumen is narrowed distally and distended proximally. An abrupt transition between dilated and nondilated bowel is evident in some.

Hirschsprung's disease is in the differential diagnosis.

Hirschsprung's Disease

Pediatric

Hirschsprung's disease is caused by incomplete caudal migration of neural cells, with bowel

distal to the point of migration arrest constituting an aganglionotic segment. By definition, the aganglionotic segment is continuous and extends to the anus; still, rare patients have segmental skip regions. Most often aganglionosis involves the rectum, but occasionally this segment extends more proximally, including the right colon, and the neonate presents with a microcolon. Also uncommon is for aganglionosis to be limited to the internal sphincter region only. To give an example of the varied involvement, in one Central European hospital among 142 children treated for Hirschsprung's disease, 52% had typical rectal involvement, 30% a long colonic segment, in 13% only a very short rectal segment was involved, and 4% suffered from total colonic aganglionosis (33).

For unknown reasons Hirschsprung's disease is uncommon in prematures. The prevalence in boys is several times greater than in girls.

An association exists between multiple endocrine neoplasia (MEN) type IIA and Hirschsprung's disease. Mutations in the *RET* proto-oncogene are found in both entities (patients with MEN type IIB also have colonic abnormalities, including chronic constipation, but any relationship with aganglionosis is not clear). Hirschsprung's disease is more common in patients with Down syndrome. Patients with Ondine's curse (congenital hypoventilation syndrome) and congenital neuroblastoma also develop Hirschsprung's disease; they tend toward total colonic aganglionosis. Both Hirschsprung's disease and ganglioneuroblastomas manifest aberrations of neural crest cell growth and development.

Radiologists generally perform a barium enema when suspecting Hirschsprung's disease. A low-osmolality water-soluble contrast enema has also been used. Although a contrast enema tends to be diagnostic in most, in neonates a transition zone is not well defined during the first several weeks of life, and a normal examination does not exclude the diagnosis (Fig. 5.4). At times uncoordinated contractions are detected in the aganglionic segment.

In total colonic aganglionosis a contrast enema reveals a microcolon or a transition zone in the small bowel, or, rarely, it is even normal.

A definitive diagnosis is made by rectal biopsy. In some infants a full-thickness biopsy is necessary. At times biopsy reveals ganglion cells in the face of an abnormal barium enema, and in such a setting an allergic colitis should be considered in the differential diagnosis.

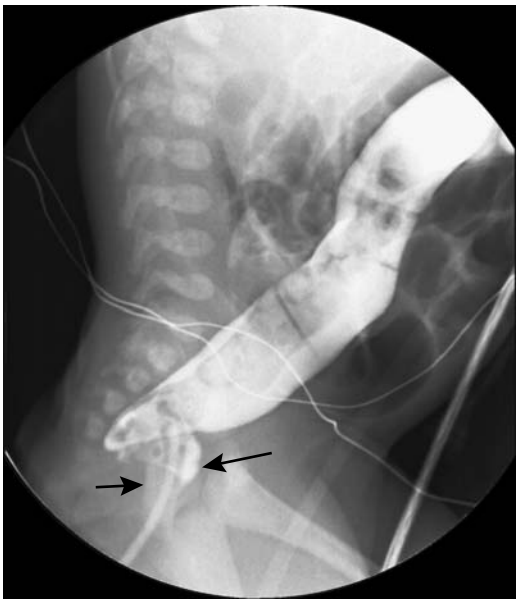

Figure 5.4. Hirschsprung's disease. Barium enema identifies a narrowed rectum (arrows) and a dilated colon more proximally. (Courtesy of Luann Teschmacher, M.D., University of Rochester.)

The usual therapy for established Hirschsprung's disease is an initial colostomy, followed by endorectal pull-through (Soave procedure).

Adult

Occasionally a mild form of what appears to be Hirschsprung's disease is detected in adults. This acquired intestinal aganglionosis is often labeled adult Hirschsprung's disease, but this term is tenuous at best. Biopsy often reveals a ganglionitis and loss of neurons. In some patients, with time, the involved segment becomes more extensive. Whether such acquired intestinal aganglionosis is indeed a variant of Hirschsprung's disease, an allergic manifestation, or some other as yet undefined condition, is speculation.

Presentation in adults is generally similar but milder to that seen in children. It is diagnosed with a barium enema, anorectal manometry, and tissue biopsy. Occasionally adult Hirschsprung's disease mimics rectal Crohn's

disease; manometry helps distinguish between these two.

Allergic Colitis in Infancy

Allergic colitis, such as an allergy to cow milk proteins, tends to mimic the barium enema appearance of Hirschsprung's disease. A barium enema reveals an irregular rectal narrowing and a transition zone (34); rectal biopsies identify ganglion cells and a lamina propria inflammatory infiltrate. Symptoms resolve after diet change.

Cystic Fibrosis

Cystic fibrosis is discussed in more detail in Chapter 4. Mentioned here are findings pertinent to the large bowel. Some authors use the term *fibrosing colonopathy* or *severe indeterminate colitis* to describe colonic changes.

A child with cystic fibrosis developed ascending colon diverticulitis (35).

Patients with cystic fibrosis receiving large doses of pancreatic enzymes develop colonic strictures. Histologically, these strictures consist of chronic inflammation, extensive collagen deposition, submucosa fibrosis, and ulcerations. These strictures are probably different from those seen in Crohn's disease. Confusing the issue is that several of these patients have developed an inflammatory bowel disease. Whether this indeed represents classic inflammatory bowel disease or is a sequela of cystic fibrosis and thus a separate entity is conjecture.

Abnormal barium enema findings are common in children with severe cystic fibrosis and suspected distal bowel obstruction unresponsive to medical management and consist of strictures, loss of haustra, and longitudinal foreshortening. Computed tomography shows bowel wall thickening, mesenteric infiltration, increased pericolonic fat, and mural striation, findings more prominent in the proximal colon.

Patients with cystic fibrosis developing *Clostridium difficile* colitis do not develop watery diarrhea. Therapy for impaction and related conditions is unsatisfactory, and CT detection of a pancolitis in such a clinical setting should suggest antibiotic-associated (*C. difficile*) colitis (36).

Short Colon Syndrome

In the congenital short colon syndrome the colon is either entirely or partially replaced by a dilated pouch. In the partial type some normal-appearing colon is evident between the ileum and a dilated pouch; in the complete variety the ileum inserts directly into a pouch. Some of these infants have associated anorectal malformations and colourinary fistulas. This condition appears to be more common in northern India than in other regions.

Trauma

Perforation

Most colon perforations manifest as a pneumoperitoneum and are readily detected. A retroperitoneal perforation, on the other hand, is more difficult to detect; at times no perforation is evident initially, but an abscess or hematoma develop later.

Penetrating injuries to the colon are usually managed by a diverting colostomy, although the trend is toward primary repair.

Obstetrical Trauma

Endorectal and transvaginal US are useful to evaluate sphincter injury after childbirth trauma, although endorectal MRI appears superior in establishing the site and extent of a tear; MRI also evaluates the integrity of individual anal sphincter muscles.

Wall Thickening

An uncommon cause of colonic wall thickening, generally involving mostly right colon in otherwise asymptomatic cirrhotic patients, is congestion secondary to portal hypertension.

Inflammation/Infection

Detection of Colitis

Focal or diffuse colonic wall thickening is the primary CT finding of colitis. Although such thickening is abnormal, it is nonspecific and occurs not only with various colitides but also

with some tumors and other infiltrative conditions. Similarly, the *target sign* (discussed in Chapter 4) is abnormal but nonspecific; it is, however, a marker for colitis and some infiltrative conditions but is not found with neoplasms. The term *target sign* is also used by ultrasonographers when describing an intussusception. Differentiating patients by clinical presentation, some investigators use the term *colitis* synonymously with *inflammatory bowel disease*, although in a broader sense these are not the same entities.

Using criteria of mucosal thickness >1.5 mm, bowel wall thickness >4 mm, mucosal irregularity, absence of haustra, and terminal ileal thickness >4 mm, hydrocolonic US in ulcerative colitis and Crohn's patients achieved 100% sensitivity in detecting active inflammatory bowel disease and 87% in identifying disease extension (37).

Technetium-99m (Tc-99m)–hexamethylpropyleneamine oxime (HMPAO) leukocyte scintigraphy is a noninvasive test requiring no bowel preparation and is readily performed even in ill patients. It is a sensitive test for inflammation, being positive even in a setting of normal barium studies in patients later shown to have Crohn's disease or ulcerative colitis. In patients with acute inflammatory and infectious colitis, Tc-99m-HMPAO leukocyte scintigraphy achieves sensitivities and specificities >80% in detecting involved segments. Tc-99m–2,3-dimercaptosuccinic acid (DMSA) scintigraphy reaches an overall sensitivity and specificity of >90% in detecting bowel inflammation (38).

18F-fluoro-deoxy-D-glucose (FDG) PET is primarily a neoplasm imaging agent, yet increased uptake is also evident in other hypermetabolic states such as acute enterocolitis.

Inflammatory Bowel Disease

General Findings

The term *inflammatory bowel disease* is reserved by most authors for Crohn's disease and ulcerative colitis. The term is also used by some authors to describe a similar-appearing colitis when a specific underlying disorder is in doubt, at times prefacing the term with *nonspecific* or *indeterminate*.

Some of the infective, drug-related and ischemic colitides mimic inflammatory bowel disease in their appearance; they are classified separately once a specific etiology is established. In particular, an etiology other than Crohn's disease or ulcerative colitis should be sought if a previous colitis resolves. Occasionally described is a nongranulomatous ulcerative enterocolitis manifesting with severe chronic diarrhea; even after an extensive investigation, no specific diagnosis is made.

Most patients with inflammatory bowel disease have a chronic, indolent presentation. An occasional patient, however, is first seen with an acute massive bleed or acute episode of severe colitis. Even toxic megacolon has manifested during an initial presentation.

A number of indices measure disease activity, but most have had limited clinical adoption. An interesting one involves use of the water-soluble radiographic contrast agent iohexol. Urinary excretion of ingested iohexol is significantly higher in patients with active inflammatory bowel disease than in those with quiescent disease or in controls (39).

Several studies have documented a lower seroprevalence of *Helicobacter pylori* infection in patients with Crohn's disease and ulcerative colitis than in controls.

Inflammatory bowel disease is not limited to the bowel, but also involves hepatobiliary, musculoskeletal, ocular, dermatologic, and other organ systems. A possible association with glycogen storage disease type IB exists. An association exists between inflammatory bowel disease and sclerosing cholangitis and cholangiocarcinoma, although a relationship between colonic and bile duct disease activity is not straightforward; after liver transplantation for sclerosing cholangitis, inflammatory bowel disease can be reactivated despite maintenance immunosuppression. Likewise, colon carcinoma has developed after liver transplantation. Thus serial colon cancer screening is necessary after liver transplantation.

Pathologic Findings

The presence of crypt abnormalities, basal plasmacytosis with chronic inflammation, and distal Paneth cell metaplasia point toward inflammatory bowel disease rather than other colitides. Thr histology of a colorectal biopsy

suggests Crohn's disease if epithelial granulomas, microgranulomas, or isolated giant cells are detected; these findings, however, are often lacking from biopsies of patients with obvious Crohn's disease. In some patients a diagnosis of indeterminate colitis is appropriate.

Biopsy in ulcerative colitis reveals an irregular or villous surface, a decrease in mucous content, and crypt atrophy. Initially diffuse small ulcers develop surrounded by inflammation and hyperemia. With disease progression the bowel wall thickens and lumen narrows. The muscularis mucosa thickens markedly and foreshortens, leading to shortening of colonic length. In distinction to Crohn's disease, a vasculitis is uncommon in ulcerative colitis. A transmural lymphocytic phlebitis, however, is detected in some patients.

Postinflammatory polyps, also called pseudopolyps, are a common finding in ulcerative colitis, although they also develop in a number of other colitides, including some infections. With partial healing the overlying mucosa becomes hyperplastic. In some patients these polyps become sufficiently large and extensive to obstruct bowel lumen. These polyps can cause a protein-losing enteropathy.

Differential Diagnosis

Clinical

Although in most patients differentiation between Crohn's disease and ulcerative colitis is straightforward, in a small subset radiologic studies, colonoscopy, and biopsy do not differentiate with any degree of certainty between these two entities. An attempt at differentiation using serologic testing has had rather limited success. Intestinal mucosal lymphocytes isolated mostly from lamina propria contain higher levels of CD19, transferrin receptor, T-cell receptors alpha/beta, and T-cell receptors gamma/delta in ulcerative colitis patients than in Crohn's patients (40); the clinical significance of these findings is not clear.

In a vast majority of patients ulcerative colitis extends from the rectum proximally for varying lengths, with a pancolitis found in a minority. Skip areas are not found, and in a setting of a right-sided colitis with rectal sparing ulcerative colitis should not be in the differential diagnosis. Nevertheless, it is difficult to place some patients in the proper perspective. For instance, a clinical, radiographic, endoscopic, and histologic follow-up in a patient with right-sided colitis consisting of multiple shallow ulcers, erosion, and stenoses and sparing of the rectum and left colon appeared to exclude Crohn's disease, tuberculosis, yersiniosis, Behçet's disease, and ischemic colitis (41); the authors concluded that the patient was indeed suffering from right-sided ulcerative colitis.

Toxic megacolon is generally associated with ulcerative colitis, on rare occasions even being an initial manifestation of this disease. One should keep in mind, however, that toxic megacolon is also encountered in severe acute Crohn's disease and some infectious colitides.

Imaging

The role of double-contrast barium enema and colonoscopy in diagnosing both Crohn's disease and ulcerative colitis is well established. A number of studies have concluded that the double-contrast barium enema and colonoscopy are complementary imaging modalities for optimal detection of all mucosal and structural colonic lesions, with the exception of those that do not distort the mucosa.

The terminal ileum is often involved in Crohn's disease but is spared in ulcerative colitis (with the exception of backwash ileitis). The barium enema appearances of terminal ileal Crohn's disease and backwash ileitis are quite different, and radiologists readily differentiate these entities.

In Crohn's disease CT identifies thickening of diseased bowel in most patients, and in the acute phase such thickening is universal. The bowel wall has a homogeneous appearance in Crohn's disease, but in ulcerative colitis it ranges from homogeneous to a *target sign* (discussed in Chapter 4). The outer colonic contour tends to be smooth in severe ulcerative colitis; in Crohn's disease it can be either smooth or irregular.

Rectal involvement results in presacral space widening and is found both with Crohn's proctitis and ulcerative colitis. Computed tomography shows this widening to be mostly secondary to infiltration by fat-containing linear and nodular soft tissue densities.

In young adults with chronic abdominal pain and bowel dysfunction, some authors establish an arbitrary upper normal US bowel wall thickness, with inflammatory bowel disease suggested if this thickness is exceeded. Thus in consecutive outpatients, use of a 7-mm upper normal bowel wall thickness achieved a sensitivity of 74% and specificity of 98% in suggesting inflammatory bowel disease (42); these findings could be further subdivided into an 84% sensitivity and 98% specificity for Crohn's disease and 38% and 98%, respectively, for ulcerative colitis.

After distending the large bowel with water (hydrocolonic US), US normally differentiates five wall layers having different echogenicities. The colonic wall is hypoechoic and thickened, and these five colonic wall layers cannot be visualized in most Crohn's disease patients, but they tend to be preserved in ulcerative colitis; loss of this layer stratification is due to fibrosis and implies an irreversible change.

Postcontrast MR in colonic Crohn's disease reveals transmural bowel wall enhancement, a finding distinct from typical ulcerative colitis where enhancement is limited to the mucosa and MRI identifies less bowel wall thickening. Thus after lumen distention with oral and rectal fluid, pre– and post–gadolinium (Gd)–diethylenetriamine pentaacetic acid (DTPA) HASTE and dynamic fast low-angle shot (FLASH) axial and coronal images allowed differentiation of Crohn's disease and ulcerative colitis in 81% of 27 patients with inflammatory bowel disease (43). Low-field MRI (0.1 T) tends to overestimate and underestimate disease extension both in Crohn's patients and in ulcerative colitis patients.

Although Tc-99m-HMPAO–white blood cell scintigraphy is very sensitive and specific in detecting colonic inflammation (44), it has a limited role in differentiating active colonic Crohn's disease from ulcerative colitis. Discontinuous uptake suggests Crohn's disease, but some children with ulcerative colitis also have discontinuous uptake.

Crohn's Disease

Clinical

Crohn's disease is discussed in more detail in Chapter 4. Covered here are those aspects related to the colon (Crohn's colitis). Although Crohn's disease is most often found in the distal small bowel, disease confined to the colon and rectum is not uncommon. A later age of disease onset appears related to an increased prevalence of colorectal rather than small bowel involvement.

In a retrospective cohort study of patients with colorectal Crohn's disease, distribution was segmental in 40%, total in 31%, and left-sided in 26% (45); perianal or rectal fistulas developed in 37%. In those patients attaining clinical remission, the 5-year cumulative relapse rate was 67%. Half of these patients underwent a resection within the first 10 years, and half of these ultimately required an ileostomy. Analysis of the cause of death of patients with Crohn's disease during 1973 to 1980 in Rochester, New York, found that Crohn's disease was the causative factor in 44% of deaths, but during 1981 to 1989 deaths due to Crohn's disease decreased to 6% (46).

Imaging

Early colonic manifestations of Crohn's disease consist of lymph follicle prominence and presence of aphthae. These are readily detected with a double-contrast barium enema but are not visualized with CT. The presence of aphthae implies active colitis but is not pathognomonic of Crohn's disease (Fig. 5.5); lymphoid hyper-

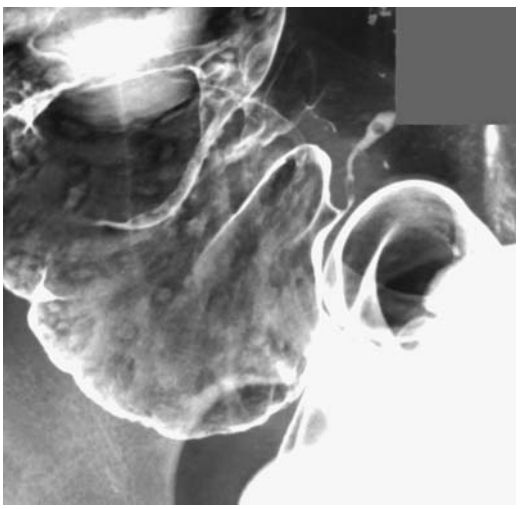

Figure 5.5. Cecal Behçet's disease. Aphthae are scattered throughout. Crohn's disease has a similar appearance.

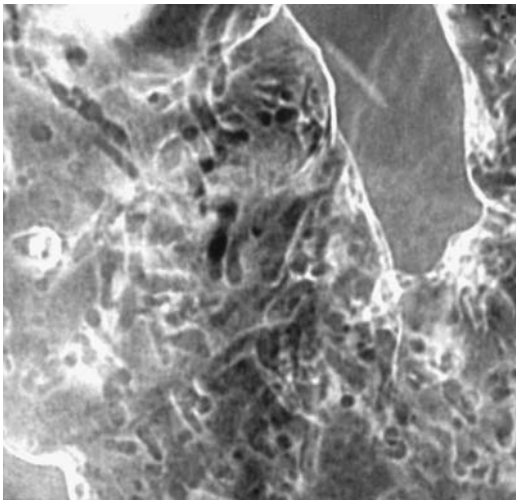

Figure 5.6. Crohn's disease. Extensive filiform polyposis is present. (Courtesy of Arunas Gasparaitis, M.D., University of Chicago.)

plasia, on the other hand, exists without disease activity.

Progression of inflammation leads to filiform polyposis and diffuse intramural thickening (Fig. 5.6). With established disease, the presence of homogeneously thickened bowel wall during an arterial phase CT study generally implies the presence of fibrosis.

Magnetic resonance imaging is very accurate in detecting active Crohn's colitis (Fig. 5.7). After oral bowel opacification with a 2.5% mannitol solution, axial and coronal breath-hold MRI using contrast-enhanced T-1 weighted FLASH and T2-weighted HASTE sequences identified more diseased segments than comparable barium studies (47). Current evidence suggests that a hydro-MRI study is very reliable in both detecting and evaluating the extent of Crohn's disease.

Some authors suggest that specific imaging findings can suggest whether a particular stage of Crohn's disease is reversible or not. Thus presence of a *target sign* suggests that fibrosis has not yet developed and the underlying abnormalities are reversible with appropriate therapy. Whether this is indeed so remains to be proven.

Complications

The earlier literature rarely mentioned cancer developing in a setting of Crohn's disease. Some of these publications should be held suspect because a number of these patients were misdiagnosed. More recent publications document an increased incidence of cancer in bowel involved by Crohn's disease. Typically the interval from initial Crohn's diagnosis until cancer is detected is up to 20 years. Some cancers are multiple. They have developed in a defunctionalized rectal stump. An occasional one involves a Crohn's-induced anorectal sinus tract or fistula.

Patients with inflammatory bowel disease (both Crohn's disease and ulcerative colitis) tend to develop a diffusely infiltrating and metastasizing carcinoma, called linitis plastica of the colon. Most of these are adenocarcinomas. Radiologically, these cancers tend to mimic a benign stricture, and at times even a biopsy is nondiagnostic.

Anal fissures and low anal fistulas are common in Crohn's disease and tend to be associated with an adjacent phlegmon or abscess. Most sinus tracts and fistulas in a setting of Crohn's colitis end blindly or are enteroenteric; an occasional fistula extends to an unusual

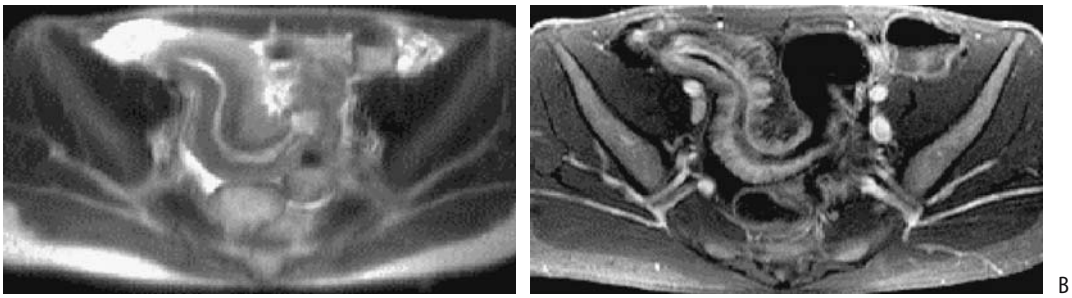

A B

Figure 5.7. Comparison of MR HASTE sequences (A) and contrast-enhanced GRE sequences (B) of bowel segment involved with Crohn's disease. (Courtesy of Wolfgang Luboldt, M.D., Johann Wolfgang Goethe University, Frankfurt-am-Main.)

location. A high or complex anal fistula or a rectovaginal fistula is uncommon, with only a minority of these patients having obvious Crohn's proctitis (the imaging approach to fistulas is discussed later in this chapter; see Fistula).

Most urinary tract fistulas involve the bladder, with only a rare one extending into the ureter, urethra, or Bartholin's gland. A rare colonic fistula crosses the diaphragm; even developing a colobronchial fistula.

Superimposed infections are common and often account for acute flare-ups.

Similar to the small bowel, only a rare colocolic intussusception has been reported in Crohn's colitis.

Ulcerative Colitis

Clinical

In large parts of Europe the incidence of ulcerative colitis in school-age children has been about 1.5 to 2.0 per 100,000 children per year for the last several decades (48). In some parts of the world the reverse is true, namely, the incidence of ulcerative colitis is decreasing while Crohn's disease is increasing. Prevalence is greater in some families and ethnic groups, and an inheritance pattern is evident in some.

The etiology and pathogenesis of ulcerative colitis are unknown. An abnormal immune system response appears to be involved, although whether the immune system itself is abnormal or whether it is responding to some other abnormality is conjecture. Significantly increased secretion of mast cell tryptase, a highly mast cell specific protease, suggests mast cell involvement (49). These patients have a higher prevalence of allergic symptoms, and skin tests show increased rates of immediate and delayed hypersensitivity than controls. The concordance rate of ulcerative colitis is higher in monozygotic twins than in dizygotic twins, although not to the extent seen in Crohn's disease. Thus in a Danish study of nearly 30,000 twins the proband concordance rate among monozygotic twins was 58% for Crohn's disease and 18% for ulcerative colitis and among dizygotic twins the rates were 0% and 4%, respectively (50).

One interesting sidelight is that a previous appendectomy appears to protect somewhat against future ulcerative colitis. Also, in women with known ulcerative colitis, the number of relapses/year after pregnancy is lower compared to a similar period before pregnancy.

Ulcerative colitis usually manifests after puberty, with only a minority detected earlier. Most patients have a chronic, relapsing course. A common clinical finding is bloody diarrhea, and its absence should suggest another diagnosis. Experienced clinicians can probably recall an occasional patient first presenting with fulminant toxic colitis.

Past teaching held that once ulcerative colitis was established, it changed little in extent, a finding no longer believed to be true. Over a several year period idiopathic ulcerative proctocolitis in most patients remains similar in extent, in a minority spreads proximally and, less often, decreases in extent.

Associated Conditions

An association between ulcerative colitis and primary sclerosing cholangitis or pericholangitis is well known. Less well known is an occasional association between pancreatitis and both ulcerative colitis and Crohn's disease. Occasionally pancreatitis manifests before onset of ulcerative colitis. Complicating the picture is an association of acute pancreatitis and azathioprine therapy.

An occasional association exists between ulcerative colitis and pyoderma gangrenosum, glomerulonephritis, systemic lupus erythematosus, sarcoidosis, and Ménétrier's disease. Whether similar genetic or immunologic pathways are involved is speculation.

One patient developed ankylosing spondylitis at age 28 years, ulcerative colitis at age 49 years, and chronic granulocytic leukemia at age 59 years (51). An uncommon association appears to exist between ulcerative colitis and rheumatoid arthritis.

Imaging

The traditional imaging study to diagnose and quantitate the extent of involvement was a double-contrast barium enema. In parts of Europe a single-contrast enema, using air as a contrast agent, is performed. Gastroenterologists prefer colonoscopy and biopsy.

Presacral space widening due to fatty infiltration is common once the disease is established

and is readily apparent with most imaging modalities. Loss of rectal valves of Houston is also common.

Early in the course of disease a CT study is normal and thus for early disease detection CT is not warranted. With more extensive bowel involvement CT identifies a colonic wall *target sign*. The hypertrophied mucosa is seen as a soft tissue density surrounded by a lower density ring representing fatty submucosal infiltration, this in turn is surrounded by a soft tissue density muscularis propria. As already mentioned, such a target sign is not specific for ulcerative colitis, but is also found in a number of other colitides. Bowel wall thickening and lumen narrowing evolve with chronicity.

Ultrasonography assesses both the extent and activity of ulcerative colitis and follows the response to medical treatment. Using a thickened bowel wall and loss of haustra as evidence of disease in patients with active ulcerative colitis, US correctly identified diseased segments in 74% of patients (52); also, US revealed bowel wall thickening decreasing after medical therapy in patients showing clinical improvement.

Doppler US reveals increased portal and mesenteric blood flow and a lower resistance index in the superior mesenteric artery in those with active disease but not in those with quiescent disease. Active Crohn's disease or ulcerative colitis involving the left colon lead to a marked increase in inferior mesenteric artery blood flow (53); compared with controls, Doppler US reveals increased velocity, flow volume, and a decreased pulsatility index. These findings should be balanced against laser Doppler flowmetry of rectal blood flow; flowmetry detected significantly reduced rectal perfusion in those with ulcerative colitis but not Crohn's colitis (54); suggesting that impaired local blood flow plays a pathogenetic role in ulcerative colitis.

Postcontrast MR reveals marked mucosal enhancement of diseased segments and relative submucosal and muscle sparing. Because of this limited transmural involvement, MRI tends to underestimate the extent of disease. A fat-suppression technique is helpful in outlining diseased segments.

Technetium-99m-HMPAO leukocyte scintigraphy is useful in evaluating the extent and sites of disease activity. This noninvasive study predicts and localizes acute inflammation, but a negative study does not exclude acute inflammation. Also, sites of positive leukocyte scintigraphy become negative after leukocyte apheresis or glucocorticoid therapy, and thus leukocyte scintigraphy appears useful in evaluating treatment response. Also, Tc-99m-HMPAO scintigraphy appears to predict proximal disease extension better than CT.

Complications

Perforation in a setting of toxic megacolon is a well-recognized complication of ulcerative colitis. Instead of frank perforation, an occasional patient with severe ulcerative colitis develops retroperitoneal emphysema.

Dysplasia is believed to be a precursor in the pathway to cancer in ulcerative colitis. Detecting dysplasia is generally in the province of a pathologist, although at times the colonoscopic or barium enema appearance suggests this condition by finding nodular protrusions, irregular mucosa, and minute spiculations. If detected incidentally, such a finding warrants a biopsy, yet for cancer surveillance and dysplasia detection most physicians rely on histopathology for these notoriously difficult-to-detect tumors. Cancers developing in a setting of ulcerative colitis typically are flat or plaque-like rather than polypoid or ulcerated as seen in nondiseased bowel. Surrounding diseased mucosa makes early cancer detection even more difficult. An underlying cancer in a colonic stricture is readily missed both radiologically and colonoscopically. In some, previous endoscopy did not reveal either dysplasia or cancer, with an advanced adenocarcinoma being later discovered.

Prevalence of colon cancer increases in a setting of pancolitis. Also, the risk of colorectal dysplasia and carcinoma appears increased by the presence of primary sclerosing cholangitis.

Surveillance colonoscopic biopsies are useful to detect dysplasia, with high-grade dysplasia being considered a precursor to cancer. Nevertheless, in spite of the extensive literature on surveillance colonoscopic biopsies, no consensus exists on its clinical value in patients with ulcerative colitis. In general, surgery should be considered in patients with an underlying stricture even if a biopsy is negative for dysplasia or malignancy.

A number of reports describe primary colonic lymphoma developing in a setting of ulcerative colitis. Complicating the picture are reports of colonic lymphoma misdiagnosed as ulcerative colitis; superficial colonic biopsies in these patients are believed to be compatible with ulcerative colitis, with lymphoma manifesting only several months later. In distinction to ulcerative colitis, colonic mucosal abnormalities resolve after therapy for lymphoma.

Thromboembolic disease is a known complication of ulcerative colitis. Massive pulmonary emboli and even dural sinus thrombosis have occurred.

Pulmonary interstitial fibrosis and fibrosing alveolitis have developed in a setting of ulcerative colitis.

Infections develop readily, and some acute flare-ups are secondary to superimposed infection. Infection should be suspected in a patient being treated with steroids who becomes fulminant. In some countries, ulcerative colitis patients receiving steroids have developed pulmonary or intestinal tuberculosis. Severe infection can result in pseudomembranous colitis developing even without antibiotic use.

Surgery for Colonic Inflammatory Bowel Disease

Surgical approaches to colonic involvement by inflammatory bowel disease consist of (1) total proctocolectomy with an ileostomy, (2) total colectomy with an ileorectal anastomosis, and (3) colectomy with a mucosal proctectomy and ileoanal anastomosis (ileal pouch).

The choice of surgery is influenced by the type of inflammatory bowel disease. A retrospective study of 86 patients with colonic Crohn's disease who underwent a single-stage proctocolectomy and 65 who underwent total colectomy and ileorectal anastomosis found that 29% of proctocolectomy patients and 68% of ileorectal anastomosis patients developed symptomatic recurrence (55); after proctocolectomy the 5-, 10-, and 15-year cumulative reoperation rates for recurrence were 13%, 16%, and 26%, compared to 29%, 46%, and 48%, respectively, after ileorectal anastomosis.

Ileostomy

A total proctocolectomy is curative for bowel manifestations of ulcerative colitis but not Crohn's disease. Some of the extraintestinal complications of ulcerative colitis have a clinical course independent of bowel disease and are not affected by a colectomy. Currently total proctocolectomy is rarely performed on an elective basis for ulcerative colitis because of associated complications, including sexual dysfunction.

Among patients with Crohn's disease who underwent total colectomy, end ileostomy, and an oversewn rectal stump, over half later required a proctectomy (56); of note is that 23% of these patients later developed small bowel recurrence requiring surgery.

Some patients with ileostomies performed for ulcerative colitis develop polyps at their ileostomy stomas; most of these are inflammatory polyps, but an occasional neoplastic polyp also develops.

Ileorectal Anastomosis

A subtotal colectomy leaves behind a diseased rectum with its associated complications, including the risk of cancer.

An interesting retrospective study found that 21% of patients undergoing a subtotal or total colectomy for ulcerative colitis required reoperation for postoperative acute cholecystitis; none of the patients undergoing colectomies for other reasons (mostly cancer) developed acute cholecystitis (57).

Ileal Pouch

An ileoanal anastomosis and creation of an ideal pouch eliminates all diseased rectal mucosa and is the current therapy for both familial polyposis syndrome and ulcerative colitis. An ileoanal anastomosis is performed in two stages: resection, anastomosis, and a diverting loop ileostomy initially, followed by closure of loop ileostomy several months later.

A special ileoanal barium study has been proposed to predict the frequency of bowel movements and measure pouch spasticity (58); with the patient standing, barium sulfate is instilled into the pouch until reflux into more proximal small bowel occurs. The total volume infused and volume voided are measured. The clinical usefulness of such a quantitative test remains to be determined.

A leak, adjacent inflammation, abscesses, and fistula formation are immediate complications related to creation of an ileoanal pouch. A contrast enema is commonly performed to check for stricture, leak, or other complication prior to ileostomy closure. Strictures developing on a more chronic basis are evaluated by endoscopy, pouchography, CT, and endoluminal US. Coronal CT visualizes most anastomoses and adjacent structures. A high accuracy is claimed for endoluminal transpouch US, but this study has not achieved popularity.

Postoperatively, functioning ileal pouch mucosa undergoes colonic metaplasia. Pouch inflammation (pouchitis) is a late complication and develops in about 10% to 30% of patients. Although the underlying cause of pouchitis is not clear, in some patients pouchitis presumably represents recurrent ulcerative colitis. Patients with primary sclerosing cholangitis develop significantly more severe chronic pouch inflammation than those without cholangitis (59). Liver transplantation does not alter the course of pouchitis in most patients. Pouchitis appears to be related to ulcerative colitis because it is uncommon in a pouch created for familial polyposis.

Pouchitis is detected both by a barium study and endoscopy. The final diagnosis is based on histologic findings.

A long-term complication of an ileal pouch is fistula formation. The pouch and any related fistulas are readily evaluated with a barium enema, although MRI is also useful in evaluating pelvic fistulas (60). For poorly understood reasons, cholelithiasis is relatively common in patients after an ileoanal anastomosis; most stones are composed primarily of cholesterol.

One late complication after an ileoanal anastomosis is small bowel volvulus, believed to be related to surgical manipulation and the resultant mesenteric tension.

Diverticulitis

Clinical

Symptomatic diverticular disease tends to manifest in one of two ways: either as an infection evolving into diverticulitis or as a lower gastrointestinal hemorrhage, often massive but typically self-limiting. The latter condition is discussed later in this chapter; see Vascular Lesions (Bleeding).

Acute right colonic diverticulitis is an uncommon diagnosis in the Western world, although the actual prevalence is not known because some of these patients are treated conservatively. A higher prevalence of right colonic diverticulitis is found in the Orient. Among consecutive patients admitted to Singapore General Hospital with diverticular disease, 42% had right-sided diverticula, 34% had left-sided, and 24% had bilateral (61); of these patients, 47% had rectal bleeding, 36% diverticulitis, 12% obstruction, and the rest presented with fistulas. In the West, a correct preoperative diagnosis of right colic diverticulitis is usually not made. A not uncommon scenario is a preoperative diagnosis of acute appendicitis in an adult, found to represent right colonic diverticulitis at surgery. A necrotic cecal carcinoma is also in the clinical differential diagnosis.

Left-sided diverticulitis in younger adults tends to be more virulent than in the elderly. These patients have a higher rate of emergency surgery, and an erroneous preoperative diagnosis, such as appendicitis, is more often entertained.

Imaging

Quite often a patient with typical clinical findings of acute sigmoid diverticulitis does not undergo any imaging but is treated medically. Only in patients with an atypical presentation or those not responding to medical management is CT obtained to evaluate for possible complications. Although CT readily detects diverticulitis, the diagnosis is generally already suspected clinically and a surgeon is more interested in presence of complications. In some European centers, on the other hand, a water-soluble contrast enema and, more recently, CT are obtained during the acute attack.

Ultrasonography has been proposed in a setting of acute diverticulitis; it is of particular value in women for whom a gynecologic abnormality is in the differential diagnosis. A contrast enema should be approached with caution in these generally acutely ill patients; first, a barium enema is contraindicated because of a possible perforation into the peritoneal cavity (keeping in mind that a free perforation is a known complication of acute diverticulitis), and

if a contrast enema is needed a water-soluble contrast agent is employed; second, these sick patients tolerate an enema poorly, spasm is common, and, due to the inherent low radiographic contrast of water-soluble contrast agents, details are difficult to evaluate. Also, although water-soluble contrast agents are innocuous in the peritoneal cavity, with a perforation invariably infected colonic matter is also spilled.

Imaging studies are also requested if a patient does not improve with medical therapy and surgery is contemplated. For this latter indication imaging is performed primarily to exclude complications of diverticulitis, namely abscesses, fistulas, or other abnormalities such as a necrotic tumor.

Further imaging is generally requested once an acute attack has subsided and if an elective resection is contemplated. At this point an abscess is generally not a consideration, as the surgeon is interested in the presence of any other disease, namely, a necrotic, infected cancer. Clinically, such a cancer can mimic diverticulitis. The controversy here revolves around the best modality with which to detect a necrotic colon cancer. In this setting I prefer a double-contrast barium enema over CT, although gastroenterologists argue for colonoscopy. A differentiation between a necrotic cancer and diverticulitis is usually straightforward with a barium enema but can be rather subtle with CT. To illustrate this dilemma, a retrospective study of patients with proved diverticulitis and colon cancer, with readers blinded to diagnosis, found that pericolic inflammation and colonic involvement >10 cm in length were the most significant findings for diverticulitis, whereas enlarged pericolic lymph nodes and intraluminal tumor were the most significant findings for colon cancer (62); using these criteria, a prospective CT study achieved a correct unequivocal diagnosis in only 40% of patients with diverticulitis and 66% of patients with colon cancer (62), not a very satisfactory result. Also, some patients with diverticulitis have enlarged lymph nodes, thus further confusing the differential between diverticulitis and a necrotic cancer.

Table 5.2 outlines typical CT findings in acute sigmoid diverticulitis. Not all findings are, of course identified in any one patient. Most commonly detected is pericolic inflammation.

Table 5.2. Computed tomography findings in acute sigmoid diverticulitis

Focal sigmoid wall thickening
Arrowhead sign (see text)
Inflammation
Pericolic
Sigmoid mesentery
Phlegmon
Abscess
Intramural
Pericolic
Fistula
Obstruction
Sigmoid obstruction
Small bowel obstruction
Portal and mesenteric vein gas
Peritonitis

Although diverticula are often identified, the presence of diverticula is not a sign of diverticulitis. Focal mural thickening is often found in a setting of chronic diverticular disease without evidence of acute inflammation. Some radiologists subdivide CT findings of diverticulitis into mild and severe, with the latter including a mesenteric abscess, fistula, and peritonitis, but such differentiation is generally obvious clinically.

An *arrowhead sign*, consisting of an arrowhead-shaped collection of contrast located within a thickened colon wall, was identified by postcontrast enema CT imaging in 27% of patients with a final clinical diagnosis of colon diverticulitis (63); an inflamed diverticulum, consisting of a rounded, paracolic outpouching with surrounding fat stranding, was found in 33% of these patients. Neither the arrowhead sign nor an inflamed diverticulum was found in any other condition in the authors' study of 150 consecutive patients suspected of diverticulitis, and thus both achieved 100% specificity; of interest is that almost half of the inflamed diverticula identified contained high attenuation material.

The results of US in detecting and evaluating sigmoid diverticulitis are mixed. Comparison studies of CT and US in patients suspected of having acute colonic diverticulitis reveal similar sensitivities and specificities for CT and US; more pericolic diverticular abscesses are identified with CT than US. Either a concomitant adynamic ileus or an obstruction tends to limit adequate US visualization of the region in

question. Some gas-containing abscesses mimic bowel loops. Ultrasonography identifies some noninflamed diverticula, with these diverticula often containing echogenic material. Ultrasonography findings of diverticulitis include bowel wall thickening, seen as a thick hypoechoic layer, and pericolonic fat inflammation, seen as a hyperechoic layer. The suspect diverticulum, if identified, appears as a hyperechoic focus adjacent but outside the colonic lumen. A flask-like or arrowhead-like hypoechoic appearance is occasionally detected in colon segments affected by diverticulitis. Fistulas have a linear, hypoechoic appearance.

Overlying intestinal gas is avoided with endorectal US. Occasionally a perforation, abscess, or fistula not shown on transabdominal US is identified with endorectal US.

Bowel wall thickening, abscesses, fistulas, and sinus tracts are well detected with MRI (Fig. 5.8). Surrounding inflammation appears on T1-weighted images as hypointense stranding within hyperintense fat. The inflammatory component enhances postcontrast. As with CT, a necrotic colon cancer is difficult to distinguish from diverticulitis with MR.

In differentiating right-sided colonic diverticulitis from a carcinoma, detection of an inflamed diverticulum by CT had a mean sensitivity of 87% and specificity of 93%, while preserved wall contrast enhancement had a mean sensitivity and specificity of 90% and 95%, respectively (64). Follow-up US in patients believed to suffer from acute right colonic diverticulitis reveals spontaneous evacuation of the inflamed diverticular content into the colonic lumen.

Complications

Complications of diverticulitis include fistula, abscess, perforation with peritonitis, and obstruction. The latter complication involves either colon or an adjacent loop of small bowel.

Among patients with diverticular fistulas, slightly less than half are colovesical, similar

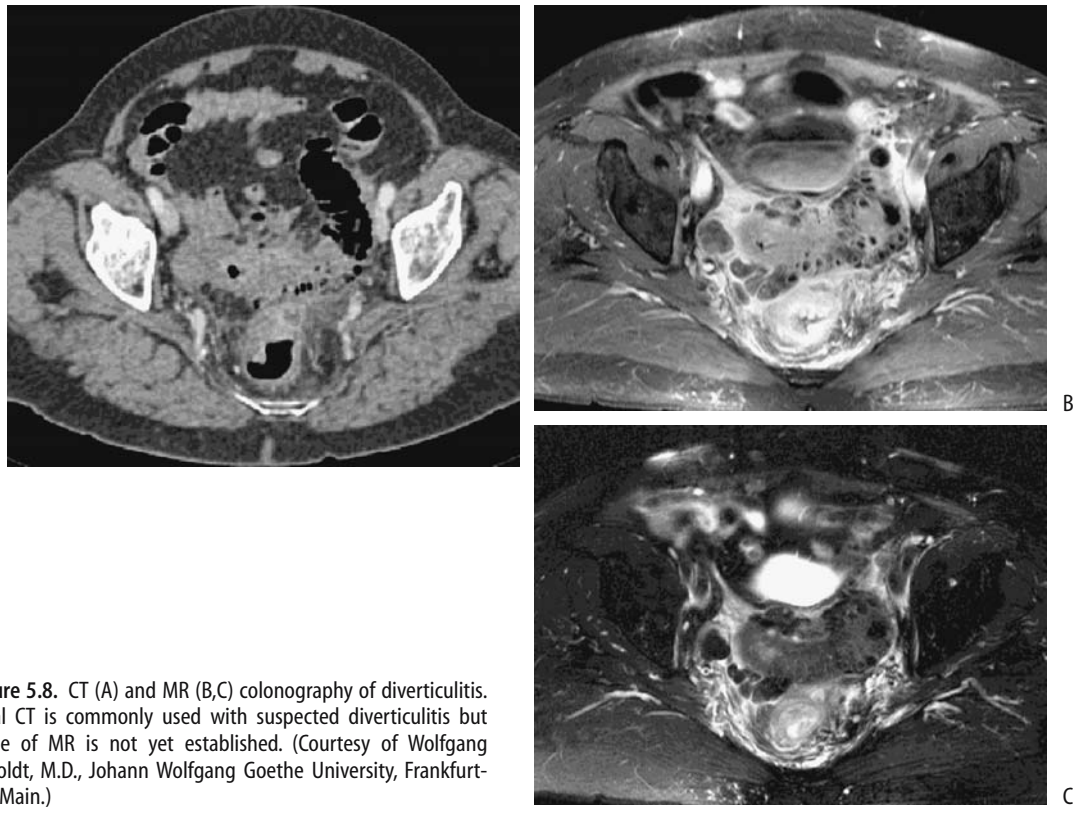

Figure 5.8. CT (A) and MR (B,C) colonography of diverticulitis. Axial CT is commonly used with suspected diverticulitis but value of MR is not yet established. (Courtesy of Wolfgang Luboldt, M.D., Johann Wolfgang Goethe University, Frankfurt-am-Main.)

number are colovaginal and a few percent are colocutaneous and coloenteric. Rare colouterine and colosalpingeal fistulas have been reported. A rare fistula extends into the thigh and presents either as a septic arthritis or as subcutaneous emphysema. A rare complication of sigmoid diverticulitis is vertebral osteomyelitis. Most fistulas are readily detected by CT. In fact, CT is superior to cystoscopy in detecting colovesical fistulas.

Inferior mesenteric vein thrombophlebitis is an underappreciated complication of sigmoid diverticulitis; CT reveals an enlarged and inflamed inferior mesenteric vein. At times gas is identified within the vein lumen. Sigmoid diverticulitis is a common cause of multiple liver abscesses and portal venous gas.

On an acute basis, bowel obstruction is due to inflammation and edema. Small bowel obstruction develops if a loop of small bowel becomes adherent at the site of inflammation or abscess. A persisting obstruction implies a fibrotic stricture and is an indication for resection. A barium enema can generally differentiate between a benign diverticular stricture and one due to cancer. A correct barium enema differentiation between benign and malignant strictures was made in most patients with a documented sigmoid strictures (65); only one benign stricture was called malignant, but caution was advised for benign-appearing strictures; nine malignant strictures were called benign.

Therapy

In general, a first episode of uncomplicated diverticulitis is managed conservatively. Most patients with a typical acute episode treated medically with bowel rest and antibiotics do not undergo surgery. Surgery is considered in those with recurrent attacks or those unresponsive to conservative therapy.

Chronic diverticulitis has been treated laparoscopically. Similar to other laparoscopic procedures, patients have a faster recovery and shorter hospital stay than those undergoing conventional surgery. The procedure costs more than an open resection in the United States because of longer operating room time, but the reverse applies in Germany.

Perforated sigmoid diverticulitis is generally resected, a colostomy performed, and a Hartmann's pouch or mucus fistula created, followed later by a second laparotomy to reestablish colon continuity. One option feasible in some patients is initial percutaneous abscess drainage, followed in a week or so by resection and primary anastomosis, thus sparing the patient a temporary colostomy and a second laparotomy.

Surprisingly, some surgically treated patients continue being symptomatic.

Infective Colitis

Mentioned here are only those infections primarily affecting the large bowel; others are covered in Chapter 4. Patients with salmonella, shigella, or yersinia infection develop bowel wall thickening, a nonspecific finding. Yersinia infection also leads to adenopathy and focal ulcerations of involved bowel (Fig. 5.9).

In patients with acute infectious diarrhea and a single identified enteropathogen, a majority are due to invasive pathogens; the presence of blood in stool is almost pathognomonic for an invasive agent but this finding has a low sensitivity.

Figure 5.9. Yersinia enterocolitis. A barium enema reveals ulcers scattered throughout the rectum.

Escherichia coli

Enterohemorrhagic colitis is caused by a noninvasive *E. coli* serotype, often manifesting in outbreaks due to undercooked food. The contiguous right colon tends to be predominantly involved, with imaging findings mimicking either mild-to-moderate ischemic colitis or Crohn's disease. Computed tomography appears to be more sensitive than conventional radiographs in identifying diseased segments (66).

Hemolytic uremic syndrome associated with *E. coli* infection has an intestinal prodromal phase, with a hemorrhagic acute colitis found in some patients. In fact, in North America, hemolytic-uremic syndrome after *E. coli* hemorrhagic colitis is the main cause of pediatric renal failure requiring kidney transplant. During this prodrome phase color Doppler US reveals a thickened, markedly avascular colonic wall.

Phlegmonous Colitis

Phlegmonous colitis is an often unrecognized and usually fatal condition caused by bacterial infection. In an autopsy study of patients with phlegmonous colitis, all had either underlying hepatic cirrhosis or subacute liver atrophy believed to be due to viral hepatitis (67); phlegmonous colitis was not suspected prior to death. Pathologic findings consisted of cecal involvement (77%), edema and submucosal phlegmonous changes (100%), bacterial infection (100%), no detectable mucosal injury (92%), and acute peritonitis (15%).

At times total colectomy is necessary for adequate disease control.

Amebic Colitis

Amebiasis, or infection by *Entamoeba histolytica*, ranges from asymptomatic carriers to a fulminant and necrotizing colitis. At times during an acute phase the clinical presentation suggests inflammatory bowel disease, with severe intestinal bleeding, progression to fulminant colitis, or even perforation. Colonic mucosal necrosis is common.

Among patients with fulminant amebic colitis seen at a referral center in Mexico, about half also had a coexistent amebic liver abscess (68). The reverse is also true; in 45 patients with amebic liver abscesses, colonoscopy revealed colonic involvement in 58% (69). Most often acute colonic involvement consists of discrete ulcers in the right colon. Coloenteric or rectovaginal fistulas are not common with intestinal amebiasis.

Tuberculous colitis and chronic amebic colitis tend to have a similar imaging appearance, although tuberculosis is more prone to involve mesentery and small bowel (Fig. 5.10).

Schistosomiasis

Schistosoma mansoni, or intestinal bilharziasis, is endemic in West Central Africa, the Arabian peninsula, some Caribbean islands, and the Atlantic Ocean side of South America. Chronic infection tends to localize mostly in mesenteric veins draining the colon; eggs are deposited in submucosal veins and pass into the bowel lumen. Associated portal hypertension, hepatomegaly, and splenomegaly develop eventually. Gastrointestinal bleeding in infected individuals is from two sources: either direct colonic infestation or bleeding esophageal varices secondary to portal hypertension.

Schistosoma japonicum has been eradicated in Japan, and currently is found in China, Thailand, Philippines and Indonesia; *Schisto-*

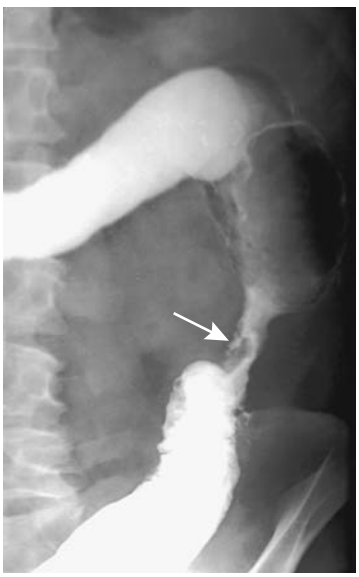

Figure 5.10. Descending colon stricture secondary to amebic colitis (arrow). A tuberculous stricture or one due to inflammatory bowel disease can have a similar appearance.

soma mekongi is mostly in the Mekong valley; these have a similar bowel presentation and are a major cause of liver fibrosis and resultant portal hypertension. *Schistosoma intercalatum*, endemic in central Africa, affects the rectosigmoid and manifests with pain, diarrhea, and rectal bleeding.

Colonic ulcers, neovascularity, fibrosis, and giant cell granulomas surround *S. mansoni* eggs. Hyperemia and telangiectasia are the endoscopic findings of colonic infestation, indicative of increased vascularity, changes also secondary to portal hypertension developing in some patients with schistosomal liver involvement. Such portal colopathy is not pathognomonic for this condition but is also found in patients with portal hypertension due to other causes. A granuloma can mimic an adenomatous polyp during colonoscopy.

Computed tomography reveals a thickened, poorly marginated bowel wall having varying contrast enhancement. These findings presumably reflect underlying inflammation and portal hypertension.

Tuberculosis

Abdominal tuberculosis is discussed in more detail in Chapter 14.

In endemic areas, about 10% of gastrointestinal tuberculosis involves the colorectum and consists of strictures, colitis and, least common, polyps (70). Symptoms tend to be those of chronic infection. A majority of intestinal tuberculosis is secondary to pulmonary involvement.

Biopsies often fail to establish a diagnosis, at times revealing granulomas, although nonspecific inflammation is a more common histologic finding. Resected specimens reveal inflammation, caseating granulomas, and Langhans giant cells, all consistent with tuberculosis, but acid-fast bacilli are rarely isolated.

A not atypical clinical history consists of constipation, weight loss, and abdominal pain, with occasional rectal bleeding. Blood tests and chest radiographs are often noncontributory. Massive rectal bleeding is uncommon.

In its chronic form tuberculosis results in colonic strictures, ileocecal valve deformity, ulcerations, polyps, and fibrous bands, with the right colon and ileum being most often involved. The cecal lumen narrows. A wide, gaping ileocecal valve, often with deformed and thickened valve lips, is a characteristic finding but not always present. The terminal ileum is deformed, narrowed and suggests Crohn's disease. Colonic involvement tends to be segmental, at times involving multiple sites. A tuberculous stricture often mimics a benign-appearing colonic stricture such as is seen in Crohn's disease (Fig. 5.11). Rarely, colonic tuberculosis manifests as a diffuse pancolitis.

Colonic tuberculosis does lead to fistulas, including an occasional duodenocolic fistula, but fistulas and sinus tracts are less common than with Crohn's disease.

Tuberculous rectal involvement is uncommon. A barium enema in these patients reveals a stricture of variable length, deep ulcerations, and a widened presacral space; biopsy simply yields a granulomatous infiltrate. Anal and perianal tuberculosis results in findings similar to Crohn's disease.

Over the years a number of reports described cecal tuberculosis coexisting with a cecal adenocarcinoma. Due to the distortion, even at surgery an underlying carcinoma can be difficult to identify.

These patients respond to antitubercular therapy and often do not require surgery.

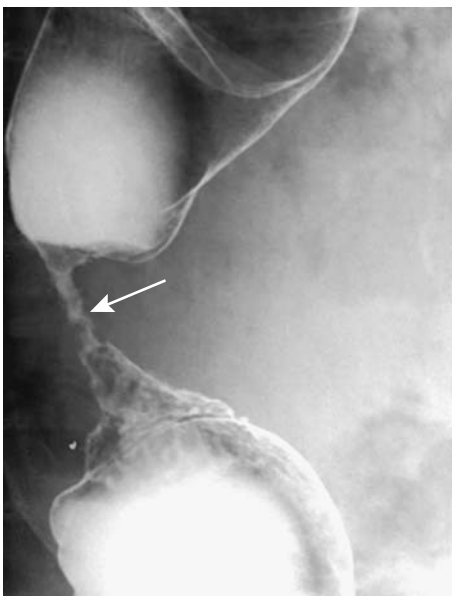

Figure 5.11. Tuberculous colitis presenting as a stricture (arrow). An ameboma, ischemic stricture, or even inflammatory bowel disease can have a similar appearance.

A double-contrast barium enema reveals skip lesions and multiple, transverse, or circumferential ulcers, with the ulcers ranging from shallow to deep and having an uneven, nodular margin. Inflammatory polyps are common, occasionally mimicked a malignancy.

Actinomycosis

Actinomyces israelii, an anaerobic bacterium, is normally found in the upper gastrointestinal tract and here it rarely causes disease. In the pelvis, on the other hand, actinomycosis results in fistulas, inflammatory tumors, strictures, and abscesses. It causes more harm in women and is often associated with intrauterine devices. The diagnosis is often established by culture of a removed contraceptive device.

With colonic involvement, generally rectosigmoid, the induced marked fibrosis tends to mimic a colon cancer by barium enema, CT, and endoscopy, except that a common hallmark of actinomycosis is extensive fistulization, at times even cutaneously, an uncommon finding with a cancer. Thus a barium enema often reveals extensive fistulas, generally more than is seen with diverticulitis or even Crohn's disease. Computed tomography shows a contrast-enhancing tumor, often containing a cystic component. Ileocecal region involvement leads to ileocecal valve enlargement.

Computed tomography of abdominopelvic actinomycosis reveals concentric or eccentric bowel wall thickening of varying contrast enhancement, together with a heterogeneously enhancing tumor adjacent to involved bowel (71). At times an abscess is in the differential diagnosis. Progression over time tends to be gradual, raising further suspicion for cancer. As one example, a barium enema in a patient revealed a tumor at the base of the cecum and a narrowed sigmoid colon, whereas CT identified a mass in the ileocecal region (72); 7 months later adjacent tissues were more infiltrated, the cecum more involved, the sigmoid colon further narrowed, and pelvic extension identified. A pelvic abscess and appendiceal carcinoma were in the differential diagnosis. Laparotomy and histology revealed chronic inflammation involving the ileocecal region, right ureter, fallopian tube, ovary, bladder, psoas muscle, and abdominal wall, and confirmed the underlying actinomycosis. At times aspiration from an infected mass provides the diagnosis.

Even with extensive involvement, once a diagnosis of actinomycosis is established medical therapy rather than resection is generally warranted. In practice, however, the diagnosis is difficult, and some patients are noncompliant with long-term antibiotic therapy.

Anisakiasis

Anisakiasis is considerably more common in the upper gastrointestinal tract than in the colon. Several patients with ascending colon involvement by *Anisakis simplex* larvae presented with an acute abdomen. Imaging identifies focal colonic wall thickening, mimicking diverticulitis or ischemia.

Viral

Herpes simplex colitis leads to aphthae and erosions. Quite often only a short colonic segment is involved.

Cytomegalovirus colitis is rare in immunocompetent patients. Infection has led to fulminant hemorrhagic colitis. Imaging reveals colonic wall thickening and ulceration, in some patients mimicking a neutropenic colitis (Fig. 5.12).

A rare immunocompetent patient develops primary cytomegalovirus colitis, followed by ulcerative colitis, raising the possibility of cytomegalovirus infection triggering the onset of ulcerative colitis.

Typhlitis/Neutropenic Colitis

Typhlitis is not a specific disease but a descriptive term of cecal inflammation. The term was more in vogue at the beginning of the 20th century, prior to appendicitis being identified as a separate entity. Currently the term *typhlitis* is reserved mostly for a primarily neutropenic cecal infiltration developing in a setting of acute leukemia, lymphoma, aplastic anemia, and other immunologic deficiency conditions.

Neutropenic colitis is common in immunocompromised neutropenia patients, most often in patients with hematologic malignancies, transplant patients, and those with AIDS. A viral organism is isolated in some, with cytomegalovirus predominating. Superimposed

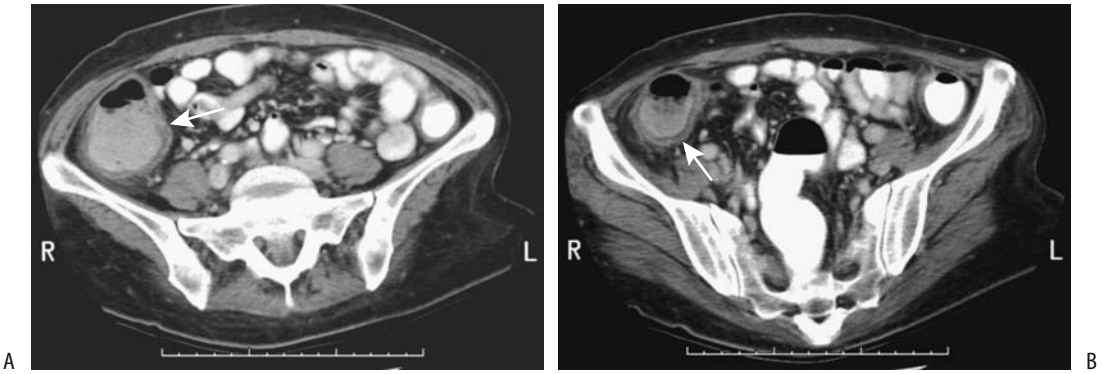

Figure 5.12. Cytomegalovirus colitis. A,B: Two pelvic CT images reveal a dilated, thick-walled colon (arrows). Pseudomembranous colitis is in the differential diagnosis. (Courtesy of Patrick Fultz, M.D., University of Rochester.)

focal ischemia and infection result in bowel wall inflammation and, if severe enough, necrosis. The differential diagnosis often includes primary infection and neoplastic infiltration.

Imaging reveals cecal wall thickening extending for varying lengths into the ascending colon. Lumen distention is an inconsistent finding. Often CT detects a hypodense cecal wall due to edema. Surrounding inflammation, fat stranding, and pericolonic fluid are common.

Drug-Related Colitis

Classification of some of the following conditions is arbitrary. Ischemia is often the final end point.

Antibiotic-Associated (Pseudomembranous) Colitis

Clinical

Whether the term *antibiotic-associated colitis* or *pseudomembranous colitis* is used is a personal choice; some authors simply label this condition *Clostridium difficile* diarrhea. A pseudomembrane is not always identified; then again, an occasional adult develops pseudomembranous colitis, even a fulminant one, without recent antibiotic therapy. A similar condition was already recognized in the preantibiotic era when it was encountered mostly after surgery and manifested as an enteritis. Associated malnutrition, immunodeficiency, and colonic stasis, especially in fragile elderly patients, result in high morbidity and mortality.

Numerous antibiotics and other drugs are responsible for this condition. Antitumoral agents induce a pseudomembranous colitis, presumably due to their combination antimitotic and antibacterial activity. 5-Fluorouracil often results in a mild, nonspecific colitis but rarely leads to florid pseudomembranous colitis. Interferon occasionally results in an acute colitis similar to inflammatory bowel disease. Toxin-producing strains of the anaerobic bacterium *C. difficile* are implicated in almost all instances, although rarely *Staphylococcus aureus*, *Clostridium perfringens*, *Yersinia enterocolitica,* and some strains of salmonella and shigella are involved. Rarely, more than one organism is involved.

Pathogenesis consists of the replacement of normal colonic bacterial flora by *C. difficile* with release of mucosal toxins. Damage is secondary to at least two toxins: an enterotoxin (toxin A), which induces intestinal tissue damage and fluid response, and a cytotoxin (toxin B), which produces an *in vivo* additive effect. A fast and inexpensive enzyme-linked immunosorbent assay (ELISA) test for the enterotoxin is available, although it is not foolproof. Also, an antibody response to these toxins is detected in some asymptomatic carriers.

Complicating the picture is a wide spectrum of clinical presentations ranging from an asymptomatic carrier to a fulminant, life-threatening

toxic megacolon-like condition. Findings are most evident in the colon, although more extensive bowel involvement develops in some patients. Clinically, colitis with fever, elevated erythrocyte sedimentation rate, and elevated white cell count are common.

An experienced observer can suggest the diagnosis during sigmoidoscopy. Biopsy of characteristic plaques confirms the diagnosis. One should avoid making a diagnosis of antibiotic-associated colitis based solely on stool culture for *C. difficile*; asymptomatic carriers exist both in adults and neonates, especially in hospitals.

In spite of adequate medical management, some patients progress to toxic megacolon and perforation. Occasionally a colectomy is necessary. One novel therapy is formation of a colostomy and instillation of vancomycin through the colostomy.

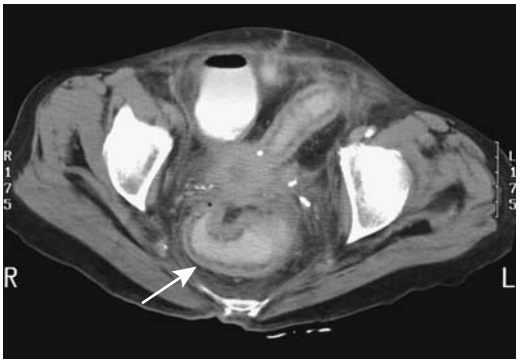

Figure 5.13. *Clostridium difficile* colitis. CT reveals circumferential colonic and rectal wall thicken (arrow). (Courtesy of Patrick Fultz, M.D., University of Rochester.)

Imaging

Conventional radiographs detect only more extreme bowel involvement. A toxic megacolon appearance is indistinguishable from that seen in inflammatory bowel disease.

A barium enema is not necessary and is poorly tolerated by these patients. Performed early in the course of this condition it shows multiple small plaques, a shaggy bowel wall outline, thickened haustra, and bowel wall thickening.

Ascites develops as the condition progresses. Ascites is also found in a number of other colitides (except ulcerative colitis), and its presence does not aid in narrowing a differential diagnosis.

Once pseudomembranous colitis is well established, CT detects nodular haustral thickening, thickened colonic wall ranging from segmental to a pancolitis, ascites, and pericolonic edema (Fig. 5.13); the markedly serrated lumen identified by conventional radiography has been called the CT *accordion sign*. These serrations should not be confused with deep ulcers or sinus tracts. One should keep in mind, however, that the accordion sign is not specific for pseudomembranous colitis and other causes of colonic inflammation or edema also result in this sign.

Arterial phase CT reveals a *target sign*, consisting of a hyperdense inner and outer wall margin with an interposed hypodense submucosa. A number of disorders have a similar abnormal appearance. Although CT can suggest the diagnosis in the appropriate clinical setting, laboratory findings are more sensitive. At one institution, *C. difficile* colitis was explicitly diagnosed at CT with a 52% sensitivity and 93% specificity (73).

Ultrasonography shows a thickened bowel wall and luminal narrowing. Some patients have two concentric bowel wall rings: a thick heterogeneous hyperechoic inner ring composed of plaques and mucosal and submucosal edema, and a thinner hypoechoic outer ring representing muscularis propria.

Indium-111–labeled leukocyte imaging identifies bowel activity. 18F-FDG-PET in a patient with *C. difficile* colitis can result in marked 18F-FDG uptake throughout the colon wall.

Nonsteroidal Antiinflammatory Drug Colopathy

Nonsteroidal antiinflammatory drugs are associated with a nonspecific colitis. Analgesic suppositories cause extensive proctitis, including ulcerations. They have been implicated in collagenous colitis. They also exacerbate a preexisting colitis. Pathogenesis of this condition is unclear, although vascular stenoses and resultant ischemic are likely causes.

These drugs are implicated in erosions and colonic ulcers. An occasional patient develops a

benign-appearing colonic stricture, including short, diaphragm-like colonic strictures (74). Biopsy reveals cryptitis, fibrosis, and granulomas, suggesting Crohn's disease, but the findings clear after drug discontinuation. Colitis recurs with drug rechallenge.

Bloody diarrhea and abdominal pain are typical presentations and, on a more chronic basis, weight loss and iron-deficiency anemia ensue.

Cathartic Colitis

Cathartic colitis is a term applied to the colonic findings developing secondary to chronic stimulant laxative abuse. Often implicated is chronic ingestion of bisacodyl, phenolphthalein, senna, and casanthranol. Anthranoid laxatives such as senna (*Cassia senna*) and cascara (*Rhamnus purshiana*) are commonly used purgatives in treating constipation. After passing unabsorbed to the colon, they are metabolized to active aglycones, which act as laxatives by damaging epithelial cells, thus affecting normal absorption, secretion, and bowel motility. Damaged epithelial cells eventually produce a pigmented mucosal, called *(pseudo)melanosis coli*. This pigmentation gradually disappears after drug cessation. When detected endoscopically, melanosis coli usually implies chronic anthranoid laxative abuse, although melanosis coli has also been described in patients with chronic inflammatory bowel disease (75).

Previous studies suggested that anthranoid laxative use and resultant melanosis coli is tumorigenic, and these patients are at increased risk for colorectal cancer, but a more recent prospective study found no significant risk for either colorectal adenomas or carcinomas (76).

Colonic redundancy and dilation are common in patients with chronic constipation, but loss of haustral folds is found only in those taking laxatives.

Cocaine Colitis

Cocaine colitis is considered a form of ischemic colitis. Left colon lesions predominate and consist of ulcers, hemorrhagic, edematous mucosa, and inflammatory polyps; rectal involvement is common, an unusual finding with classic ischemic colitis. Histologically, lesions range from acute to chronic, probably reflecting repeated cocaine use. When severe, patchy necrosis to the point of perforation and multiple small vessel thrombi develop.

Collagenous/Microscopic/Lymphocytic Colitis

Collagenous colitis and microscopic colitis (also called *lymphocytic colitis*) are recently recognized clinicopathologic conditions, but whether these are separate entities or variations of a single condition is not clear. Little evidence supports two distinct disorders; the immune abnormalities are similar in both and a similar immune mechanism appears involved. The two names reflect their histologic findings. Pathogenesis of both appears to be either inflammatory or autoimmune in nature; a role for infection or drug toxins is speculative.

Collagenous/lymphocytic colitis is most often associated with nonsteroidal antiinflammatory drugs. Underlying rheumatologic and autoimmune diseases are often present; even celiac disease exists in some patients. Some patients have associated gastric and duodenal subepithelial collagenous deposits or Crosby capsule biopsy evident but subclinical small intestinal abnormalities. A possible pathogenetic association between interstitial cystitis and collagenous colitis has been raised. This condition may not be limited to the colon.

Biopsies in both collagenous and lymphocytic colitis reveal intraepithelial lymphocytes, probably a reflection of epithelial injury, and a lamina propria plasma cell and neutrophil infiltrate. In collagenous colitis a thickened collagen band is evident beneath the surface epithelium, a finding missing in microscopic colitis. In an occasional patient microscopic colitis progresses to collagenous colitis.

Symptoms in patients with collagenous colitis tend to be nonspecific, with chronic watery diarrhea and abdominal pain predominating. Most patients are women in their sixth decade or older. Most patients have spontaneous or treatment-related resolution of their symptoms. One unusual association was salmonella osteomyelitis developing in a patient with collagenous colitis (77).

A barium enema or endoscopy reveals no specific abnormality in most patients. In a minority macroscopic erosions and even ulcerations are evident. Endoscopic findings also

include edema, erythema, and an abnormal vascular pattern (78). The diagnosis rests on histopathologic findings.

Diversion Colitis

After surgical bowel diversion and formation of an excluded segment, some patients develop inflammatory changes in the diverted bowel. These consist of aphthae, crypt abscesses, and easy friability. Large ulcerations develop in an occasional patient.

Malacoplakia

Colonic malacoplakia is rare, occurring both in isolation and in association with other diseases. Although not a neoplasm, malacoplakia is locally aggressive and invades surrounding tissues. At times it is multifocal. Kidney transplant patients, in particular, appear prone to develop colorectal malacoplakia; in some, malacoplakia appears related to immunosuppression therapy. It has developed in a colon adenoma, although more often it is associated with a carcinoma, where malacoplakia is located adjacent to the tumor.

Rare clinical manifestations of malacoplakia include massive hemorrhage and cecal perforation.

Imaging usually suggests a malignancy. Some develop multiple polyps. Malacoplakia in one patient was hyperdense on unenhanced CT, hypointense both on T1- and T2-weighted MR images, and enhanced slightly after gadolinium (79); the authors postulated that intracytoplasmic siderocalcific inclusions accounted for the CT and MRI findings.

Other Colitides

A barium enema should be diagnostic of colitis cystica profunda. If large enough, the fluid-filled cysts are also visible with CT or endorectal US (if the rectum is involved).

Occasional reports describe a hot-water enema or some chemical inducing colitis (Fig. 5.14).

Xanthogranulomatous inflammation of the sigmoid colon has led to colonic obstruction.

Kawasaki disease (mucocutaneous lymph node syndrome) in a child can present with fever and focal colitis.

Neonatal Necrotizing Enterocolitis

Clinical

A disease more common in premature neonates, necrotizing enterocolitis (NEC) typically starts with bloody diarrhea or distention several days after birth. Although a number of factors have been postulated, epidemic outbreaks in newborn nurseries implicate an infectious role. The final common pathway is probably ischemia with subsequent mucosal or more severe damage. A condition similar to neonatal NEC occasionally develops in older infants. Many

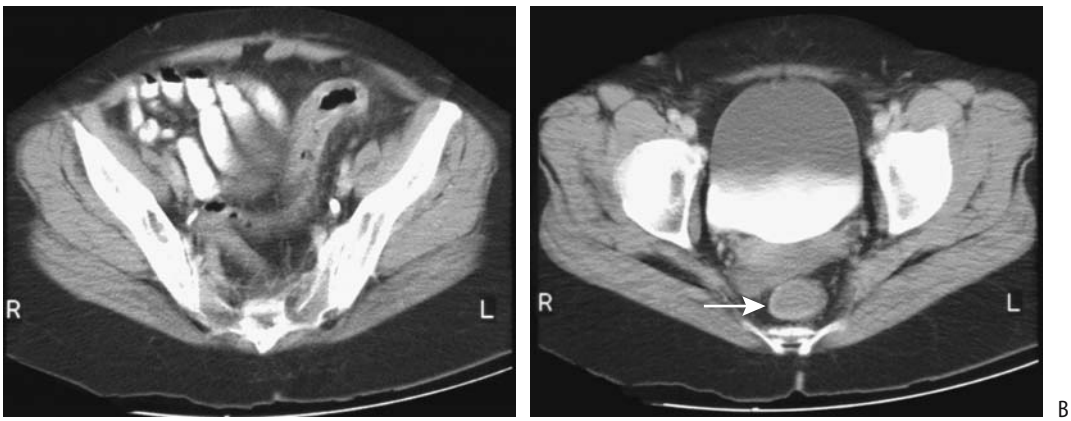

A B

Figure 5.14. Chemical-induced colitis in a patient who was giving herself hydrogen peroxide enemas for constipation. A,B: CT shows marked rectosigmoid wall thickening (arrows). (Courtesy of Thomas Miller, M.D., San Luis Obispo, California.)

have had prior major surgery, and underlying ischemia appears to be a factor.

Necrotizing enterocolitis carries a high mortality, averaging 50% in some centers, with mortality varying inversely with gestational age and birth weight. Extensive bowel resection may result in a short gut syndrome.

Imaging

Any part of the bowel can be involved, although the most common sites are distal small bowel and proximal colon. Involvement ranges from diffuse to segmental. Among neonates undergoing surgery, about a third have NEC totalis (80). Strictures, usually colonic, and more often in the left colon, develop as a late complication.

Conventional radiography early in the course of NEC reveals small bowel dilation, then colonic distention. In some neonates focal regions of bowel lumen narrowing and wall thickening are evident, nonspecific findings. Eventually pneumatosis intestinalis and portal venous gas develop in some, findings almost pathognomonic for NEC in neonates (it is a gas and not air as some of the literature claims). Although in adults portal venous gas carries a grave connotation, in these neonates such gas represents a more benign finding. Complicating the picture, some babies even with severe NEC do not develop pneumatosis or portal venous gas. Ascites is usually a sign of severe NEC, a finding difficult to detect with conventional radiography but readily apparent with US. Although these findings are useful as a guide, they are insensitive in predicting impending perforation.

In neonates with NEC and portal venous gas, venous gas developed within 24 hours of onset of abdominal distention, feeding intolerance, or a finding of rectal blood (80); pneumatosis intestinalis was identified in 80%, and 20% progressed to perforation. Venous gas initially was transient but recurred in some of these neonates.

Urine CT attenuation is increased after enteral iohexol in neonates with NEC; in normal neonates urine CT attenuation is slightly above water. A serial increase in urine CT attenuation coefficients after oral ingestion of iohexol is associated with clinical deterioration (81).

Complications of NEC include perforation, often early in the course. Serial conventional horizontal-beam radiographs are necessary to detect a subtle perforation. Perforation, or impending perforation, is an indication for surgery.

A contrast enema is usually not performed during the acute episode because of a perceived increased risk of perforation. Most strictures are detected with a barium enema later, after the acute insult has resolved. An occasional sequela is an enteroenteric or enterocolic fistula.

If an ileostomy or colostomy is necessary, study of the distal colon is worthwhile prior to ostomy takedown to ensure that no residual strictures exist.

Ischemic Colitis

Clinical

Bowel ischemia and various vasculitides are discussed in more detail in Chapter 17. Isolated colonic ischemia is relatively common, especially in the elderly, and its clinical and imaging manifestations are sufficiently discrete to warrant separate discussion. Colon ischemia is often included under the colitides. Especially when chronic in nature, ischemic colitis and some of the vasculitides tend to mimic inflammatory bowel disease. Some of the conditions associated with colonic ischemia are listed in Table 5.3.

A typical clinical presentation is sudden onset of abdominal pain, distention, and bloody maroon-colored diarrhea. Atypical presentations are relatively common; in a study of patients with eventually proven ischemic colitis, ischemia was initially not suspected clinically in 30% (82). Underlying atherosclerosis, shock, and congestive heart failure are common but not universal findings in these often elderly patients. Sequelae range from a mild, self-limiting condition to major bowel infarction and death.

Most common sites for colonic ischemia are at the splenic flexure and sigmoid. At the splenic flexure a branch of the middle colic artery forms an anastomosis with an ascending branch of the inferior mesenteric artery, feeding the marginal artery of Drummond. This marginal artery is present in less than half the population; the tenuous splenic flexure blood supply only becomes worse with onset of arteriosclerotic disease.

Table 5.3. Conditions associated with ischemic colitis

Arteriosclerotic vascular disease
Venous thrombosis
Low flow states (hypotension, stasis)
Emboli
Atherosclerotic emboli
Cholesterol emboli
Vasculitides
Behçet's syndrome
Cocaine-use colitis
Polycythemia in a smoker
Polycythemia vera and extensive extramedullary hematopoiesis
Takayasu's arteritis
Thromboangiitis obliterans (Bürger's disease)
Systemic lupus erythematosus
Polyarteritis nodosa
Dermatomyositis
Allergic granulomatous vasculitis (Churg-Strauss syndrome)
Other
Associated with oral contraceptives
Massive caustic ingestion
A late complication of hemolytic-uremic syndrome
Familial dysautonomia (Riley-Day syndrome)
During α-interferon therapy

Isolated rectosigmoid ischemia is uncommon, presumably because of collateral blood supply. Occasionally sigmoid colectomy leads to rectal infarction; presumably the superior rectal arteries, which are sacrificed at resection, provide major rectal blood flow.

Colonic infarction in one patient led to transient gastric emphysema (83).

Ischemia after hemorrhagic shock is more common in the small bowel than colon. In the large bowel, the right colon is most often involved, even to the point of ischemic necrosis. Resection in some of these patients reveals no vascular thrombi or emboli, and nonocclusive ischemia is presumably responsible.

A type of ischemic colitis warranting separate mention is that occurring proximal to a colonic obstruction. Also called *obstructive colitis*, it is similar to inflammatory bowel disease. Ischemia in this condition is due to an impaired venous blood flow secondary to a combination of increased endoluminal pressure, underlying atherosclerotic disease that otherwise would be asymptomatic, and other possible factors. The prevalence is about 1% to 5%, mostly in elderly patients. The most common cause of associated obstruction is a carcinoma, less often a benign stricture or diverticulitis; the ischemic segment appears thickened, ulcerated, or even necrotic. At times pneumatosis is evident. Untreated, perforation ensues.

Imaging

The role of imaging during an acute ischemic attack is to confirm that a patient's symptoms are indeed due to colon ischemia rather than to another etiology. Angiography has a lesser role in detecting colon ischemia than in the past. Often identified is atheromatous disease involving major vessels.

Imaging findings during the acute phase consist of bowel wall thickening, seen as thumbprinting, and ulcerations, eventually clearing or evolving into strictures or frank necrosis. An ischemic segment tends to have sharp margins, in distinction to most acute infective colitides, which have poorly defined margins. Computed tomography readily identifies colonic wall thickening; pericolonic stranding is common but is nonspecific. Occasionally seen is a "halo" sign, consisting of an inner hypodense ring surrounded by a hyperdense outer ring, a nonspecific sign also found in some other colitides.

Computed tomography reveals the involved colonic wall to range from a heterogeneous appearance suggesting edema in about two thirds and homogeneous thickening in one third, with occasional intramural gas; wall thickening and segmental involvement are common.

Isolated cecal ischemia or infarction is rare. Clinically, appendicitis is suspected but CT should differentiate these two entities.

Doppler US aids in differentiating between inflammation and ischemia of thickened bowel wall. The absence of color Doppler flow and absence of arterial signal suggests ischemia; in fact, the absence of arterial flow in the wall of an ischemic colon predicts an unfavorable outcome (84).

In-111–labeled leukocyte imaging detects bowel activity in ischemic colitis. Normally In-111 activity is not identified in bowel. A primary purpose of Tc-99m-HMPAO leukocyte scan is to detect inflammation rather ischemia, but in an

occasional patient, this scan reveals marked uptake within an ischemic sigmoid colon.

Conventional radiography in three patients revealed vascular calcifications close to the right hemicolon, a barium enema showed thumbprinting and right colic lumen narrowing, and CT detected colon wall thickening and venous calcifications (85); the authors termed this condition *phlebosclerotic colitis*.

Radiation Proctocolitis

Radiation proctocolitis is a disabling, often delayed manifestation of radiation injury and results in an obliterative endarteritis and ischemia. Because of its proximity to gynecologic structures, the rectum is a common site of involvement. These patients range from asymptomatic to having chronic bleeding, obstruction due to strictures, or fistulas. Bleeding typically develops months after completion of radiation therapy. Before ascribing rectal bleeding to proctitis, however, other causes of gastrointestinal bleeding should be excluded in these patients.

Computed tomography findings following radiation therapy vary. Detected are perirectal fascia thickening, increased perirectal fat density, and, less often, rectal wall swelling. Presacral space widening develops in a minority, increasing with dose. These changes develop soon after start of therapy.

Endorectal US shows thickening of perirectal connective tissue and obliteration of the rectal submucosal echogenic layer along the anterior rectal wall (86).

Magnetic resonance imaging identifies radiation fibrosis as irregular enhancement and high signal intensity, often even years later.

Clinically significant bleeding from radiation-induced proctitis has been managed successfully using a combination of endoscopic yttrium-aluminum-garnet (YAG) laser therapy and application of topical formalin dressings to the rectal mucosa.

The risk for future neoplasms with chronic radiation proctocolitis, even decades after pelvic radiation, is well known to most physicians. Both flat (nonpolypoid) adenomas and rectal carcinomas develop. Imaging is not reliable in detecting small neoplasms in the presence of radiation changes.

Amyloidosis

Amyloidosis ranges from localized to diffuse involvement. When localized, amyloidosis often mimics a benign stricture, rarely, a carcinoma (87). It does not predispose to cancer formation; a finding of localized amyloidosis and a coexistent carcinoma is probably fortuitous. Colonic amyloidosis does ulcerate and bleed; presumably blood vessel wall infiltration by amyloid leads to ischemia and ulceration.

Epiploic Appendagitis

Appendices epiploicae are mostly fat-containing structures arising from colonic serosal surface. They exist throughout the colon. Normally they are not detected with imaging except if surrounded by fluid.

The sudden onset of localized acute abdominal pain is a common presentation for torsion (infarction) of an epiploic appendix. These patients are afebrile, and laboratory findings are normal. Depending on the location, clinically and with imaging the condition mimics acute appendicitis or diverticulitis. Although epiploic appendagitis is a nonsurgical cause of an acute abdomen, it is not uncommon for the diagnosis to be made by either the surgeon or pathologist. Untreated, spontaneous resolution in a week or so is the usual outcome.

Most often epiploic appendagitis occurs in either the ascending or descending portions of the colon and tends to be located anteriorly rather than posterior in the bowel wall circumference (Fig. 5.15). A CT finding of a focal inflammatory tumor or edema adjacent to the colon, especially at sites uncommon for diverticulitis, should suggest this condition. A fat density or almost fat density tumor is a common but not universal finding. Computed tomography in six patients identified a fatty tumor containing a hyperdense rim along the anterolateral colonic wall, together with infiltration of adjacent pericolic fat (88).

Ultrasonography often reveals a small, solid, focal noncompressible hyperechoic tumor at the site of maximum tenderness.

Computed tomography and US findings are strongly suggestive of the diagnosis. Similar findings are seen with segmental omental infarction, although usually these are in a dif-

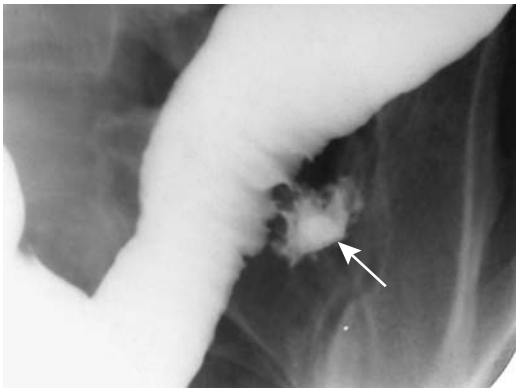

Figure 5.15. Epiploic appendagitis. A barium enema reveals focal extravasation (arrow). The appearance is atypical for diverticulitis.

ferent location. In either case, therapy is similar and surgery is avoided if the condition is suspected.

Follow-up CT shows resolution of inflammation, and although a lesion may still be identified, it should be decreasing in size (88). An occasional infarcted epiploic appendage eventually calcifies; some become detached and float within the peritoneal cavity. One such peritoneal loose body measured 6 cm in diameter (89). The differential diagnosis of calcified peritoneal loose bodies includes gallstones lost during surgery and, unless their mobility is confirmed by imaging with different patient positioning, a calcified leiomyoma or similar tumor.

Tumors

A polyp is an intraluminal growth. It can be benign or malignant, neoplastic, inflammatory, or hyperplastic. It is a descriptive term having a specific morphologic meaning and does not imply a particular histologic connotation. The practice of some authors in using this term synonymously for an adenoma only leads to confusion and should be condemned.

Among colonic polyps <5 mm in diameter, in adults, about 40% to 50% are adenomatous, 40% hyperplastic, and the rest a mix of mucosal tags, lymphoid tissue, and other benign causes. About half are located in the rectosigmoid. In children juvenile polyps predominate. In adults, the percent of adenomatous and carcinomatous polyps increases with an increase in polyp size.

Nonneoplastic Tumors

Hyperplastic Polyps

Small hyperplastic polyps (also called *metaplastic polyps*) are the most common nonneoplastic lesion in the colon and rectum. They tend to be sessile, often are multiple, generally <5 mm in diameter, and most commonly in the rectosigmoid.

A relationship between hyperplastic polyps and the subsequent development of adenomas is controversial. Both share similar lifestyle risk factors. Most colonic hyperplastic polyps are not considered to have a neoplastic potential and are not directly involved in the adenoma-carcinoma cycle, but some larger hyperplastic polyps do develop dysplasia and progress to a cancer. An occasional patient with multiple hyperplastic colonic polyps harbors a colon adenocarcinoma. In addition, follow-up of patients who had hyperplastic polyps suggests that they are more likely to develop adenomas than those without initial polyps (90). An occasional hereditary nonpolyposis colorectal cancer family patient develops colorectal cancers, adenomas, and hyperplastic polyps.

The radiologic and endoscopic appearance of adenomas and hyperplastic polyps <5 mm in diameter is similar. A central umbilication tends to develop with further growth. Some of these small umbilicated tumors, at times called *inverted hyperplastic polyps* by pathologists, are difficult to detect even with a double-contrast barium enema and mimic the appearance of a flat adenoma and adenocarcinoma (91), and thus excision is warranted.

Rare instances of hyperplastic polyposis have been reported. These polyps tend to be larger than isolated ones and the overall appearance mimics multiple adenomatous polyps. Complicating the picture is the occasional patient with hyperplastic polyposis but with some of the polyps containing foci of adenomatous tissue or even an adenocarcinoma.

18F-fluoro-deoxy-D-glucose PET is negative for hyperplastic polyps; FDG does not accumulate in these polyps.

Juvenile Polyp

This polyp is known as a retention polyp, and it consists of inflammatory tissue, fibrosis, and a cystic component. No consensus exists about

whether it is inflammatory or hamartomatous in origin. It is the most common colonic polyp in the pediatric age group, although some are first detected in adults. It is more common in the distal colon and rectum, and most are solitary. A juvenile polyposis syndrome is rare.

Juvenile polyps are not believed to be premalignant; polypectomy of a solitary juvenile polyp does not predispose to future new juvenile polyps and is not associated with a future increased risk of colorectal cancer. Nevertheless, occasional reports describe both an adenoma and an adenocarcinoma associated with juvenile polyps.

Especially in children, a not uncommon presentation is hematochezia. An occasional juvenile polyp intussuscepts.

The polyps' barium enema appearance is similar to that of an adenomatous polyp. Most have a smooth and oval outline. Compression gray-scale US shows them to be hypoechoic, contain small cysts and have an adjacent hyperechoic layer corresponding to the submucosa (92); their color Doppler findings range from hypo- to hypervascular.

Inflammatory Fibroid Polyp

Inflammatory fibroid polyps are uncommon in the colon. Some are found in a setting of inflammatory bowel disease or chronic infections. Most manifest through rectal bleeding. Biopsy simply reveals inflammation.

Similar to an inflammatory pseudotumor, their appearance on a barium enema or colonoscopy suggests a malignancy. They range from a sessile, plaque-like, to a pedunculated polyp in appearance (Fig. 5.16).

Inflammatory Pseudotumor (Fibrosarcoma)

An occasional resected polyp or infiltrating tumor is termed an inflammatory pseudotumor (variously called *inflammatory fibrosarcoma* or *plasma cell granuloma*). These tumors are discussed in more detail in Chapter 14. They originate either in the colon or adjacent soft tissues, including presacral space. Their aggressive nature often suggests a malignancy.

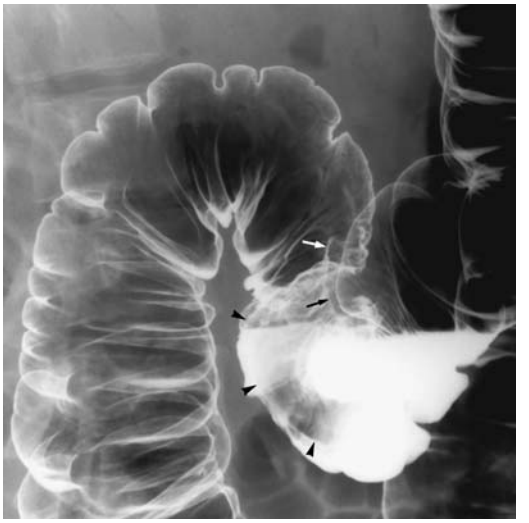

Figure 5.16. Inflammatory fibrous polyp (arrows and arrowheads) in a man with rectal bleeding. Initially a carcinoma was suspected.

These tumors tend to invade and require resection with wide margins.

Hamartoma

Retrorectal hamartomas consist of soft tissue and cysts lined by ciliated epithelium. Also called tail-gut syndrome, they are detected due to their mass-like effect, and occasionally one becomes infected.

Hemangioma

Colon hemangiomas range in size from small, focal submucosal lesions to large, diffuse, infiltrating tumors involving long colonic segments. Most manifest through chronic bleeding and anemia. Even when large, lumen obstruction is rare with a hemangioma (Fig. 5.17).

The full extent of a large hemangioma is evaluated by contrast-enhanced CT or MRI. Rectal cavernous hemangiomas and their surrounding structures are best evaluated by MRI using an endorectal surface coil. These often diffuse rectosigmoid cavernous hemangiomas produce colonic wall thickening and a hyperintense signal on T2-weighted MR images.

Occasionally a hemangioma is detected with a Tc-99m–red blood cell scan.

Figure 5.17. Transverse colon hemangioma (arrows). This pliable tumor mimicked a spastic colonic segment but it would never distend. No obstruction was present, a typical finding even with a large hemangioma.

Lymphoid Nodules

Lymphonodular hyperplasia is quite common in children and is occasionally encountered in adults. The condition occurs both in the small bowel and colon. An association between lymphonodular hyperplasia and several disorders has been described, although currently most investigators believe that in some patients, especially children, the presence of lymphonodular hyperplasia is a normal variant. It is found adjacent to a colonic segment involved by ulcerative colitis, and the presence of these nodules was proposed as a sign of early ulcerative colitis (93). Such lymphoid hyperplasia also develops in posttransplant patients who are under chronic immunosuppression.

These small polyps, up to several millimeters in diameter, are readily detected by both a double-contrast barium enema and colonoscopy. Rarely, enough lymphoid tissue accumulates at one site to result in a larger lymphoid polyp.

Lymphangioma

Cystic lymphangiomas are more common in the mesentery but do occur in the bowel wall. Ultrasonography reveals these lymphangioma to be compressible, anechoic, and possessing posterior acoustic enhancement; as expected, Doppler US identifies no flow. Computed tomography attenuation is near that of water. Endoscopic US reveals septa in the multilocular ones. A double-contrast barium enema identifies a lymphangioma as a submucosal tumor, soft, round, and smooth.

Endometriosis

Colonic endometriosis is discussed here in the tumor section because its appearance often mimics a neoplasm.

Endometriosis signifies the presence of functioning endometrial tissue in ectopic sites. The most common site of intestinal involvement is the anterior rectal region, followed by the appendix and ileocecal region. Endometriosis involving the rectovaginal septum posteriorly and then extending laterally into the uterosacral ligaments and anterior rectal wall results in fibrosis and scarring, eventually leading to a colorectal stricture and obstructive symptoms. Perforation and an acute abdomen are rare complications.

This tissue undergoes change under hormonal stimulation. In symptomatic women pain and altered bowel habits are common presentations. Clinically, endometriosis often mimics inflammatory bowel disease.

Colonoscopy reveals intact mucosa at the site of involvement; mucosal ulcerations occur in a minority and are a cause of rectal bleeding. At times only laparoscopy establishes the diagnosis. With typical anterior rectal wall involvement, barium enema findings are similar to those seen with rectal invasion by a gynecologic tumor (Fig. 5.18) or metastasis to the pouch of Douglas.

Endorectal US achieved a sensitivity and specificity of over 95% in detecting rectovaginal septal infiltration by endometriosis (94). Although these results are impressive, the role of US in providing a differential diagnosis and aiding management is not clear.

Magnetic resonance imaging reveals endometriosis >1 cm in size to be homoge-

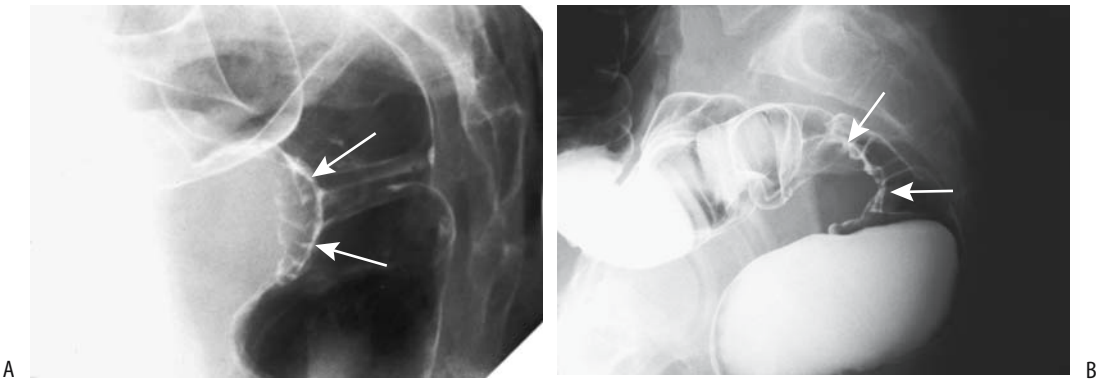

Figure 5.18. A,B: Two women with rectal endometriosis (arrows) identified on lateral barium enema views. The focal, corrugated, anterior rectal wall involvement is typical. A gynecologic cancer growing posteriorly into the rectal serosa has a similar appearance.

neously hyperintense on T1-weighted images and hypointense on T2-weighted images; smaller lesions tend toward a variable T2-weighted signal (95). Some foci contain a cystic component (Fig. 5.19).

Surgery for rectosigmoid endometriosis is technically difficult. At times posterior vaginal wall excision and partial rectal resection are necessary.

Xanthelasma

Xanthelasma is diagnosed histologically as a collection of lipid-laden histiocytes. It develops

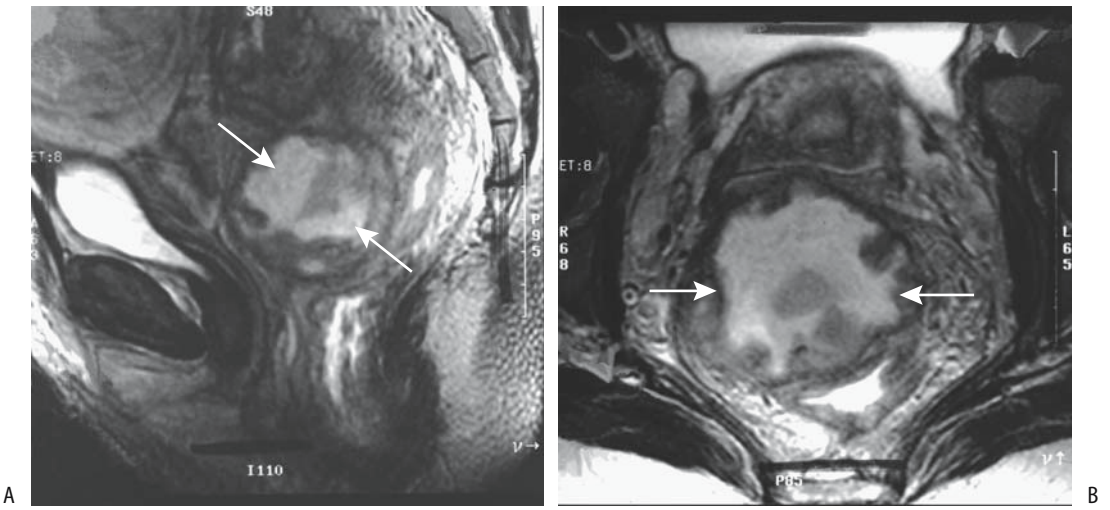

Figure 5.19. Endometriosis involving pouch of Douglas. Sagittal (A) and transverse (B) T2–weighted magnetic resonance (MR) images reveal a heterogeneous tumor between the uterus and rectum (arrows), illustrating how the anterior rectal wall is so often involved. (From Burgener FA, Meyers SP, Tan RK, Zaunbauer W. Differential Diagnosis in Magnetic Resonance Imaging. Stuttgart: Thieme, 2002, with permission.)

in the colonic wall and other structures. Imaging plays no role in this condition.

Benign Neoplasms

Adenoma

The primary importance of colon adenomas is in their potential for carcinomatous transformation. Less often they manifest by bleeding or other complications. More adenomas are detected in the left colon than the right, although over the last several decades a shift toward right-sided polyps is evident, especially in African Americans; in this patient population the malignancy potential for right-sided polyps is similar to that found on the left.

Most small adenomas are tubular or tubulovillous, and a small minority are villous. A larger villous component within an adenoma is associated with a higher risk for high-grade dysplasia and cancer. Villous adenomas are generally excised because even multiple biopsies may miss a focus of carcinoma. Some villous adenomas, however, are treated with endoscopic neodymium (Nd):YAG laser therapy, and one must ensure adequate therapy; incompletely treated ones recur. Complications of laser therapy include stricture, self-limited bleeding, and fistula.

Some villous adenomas regress after nonsteroidal antiinflammatory drug therapy.

The role of *Helicobacter pylori* infection in colon adenoma and carcinoma formation is not clear. Prevalence of *H. pylori* antibodies in patients with colorectal adenomas and carcinomas is greater than in controls.

Adenomas range from pedunculated to sessile. Some have a long stalk, in others a stalk is barely visible. Sessile adenomas range from those with a discrete intraluminal component to relatively rare flat ones, with the latter consisting of an intramural tumor with a nodular or reticular surface and thus being especially difficult to detect either by imaging or endoscopy. Villous adenomas are classically described as frond-like and containing numerous interstices, but such an appearance in found only in a minority. Imaging cannot differentiate most villous adenomas from their tubular counterpart.

Computed tomography suggested several anecdotal villous adenomas by identifying a convoluted surface or residual oral contrast in polyp interstices (96).

Detection of one adenoma implies an increased future risk for another adenoma. Studies provide somewhat conflicting results, but, in general, among patients followed for at least 10 years, those with a large initial adenoma have a significantly higher risk of developing metachronous adenomas.

Leiomyoma

Colorectal leiomyomas are uncommon. Most are asymptomatic, although the larger ones tend to be associated with pain, change in bowel habits, or rectal bleeding. Some are detected incidentally during a rectal examination. Leiomyosarcomas tend to be larger and more inhomogeneous than leiomyomas.

Endorectal US reveals rectal leiomyomas as hypoechoic tumors, similar to other stromal tumors. It is helpful in evaluating tumor extent, but not in differentiating benign from malignant.

Lipoma

Lipomas are intramural in origin and most are single, although diffuse colonic lipomatosis does occur. They vary in size considerably. More often than other stromal tumors, lipomas tend to become pedunculated and act as a lead point for an intussusception. Some lipomas undergo spontaneous autoamputation.

Uncomplicated lipomas have a CT fat density. Intussuscepting ones tend to contain more of a soft tissue density, probably because of associated infarction and necrosis. The lack of fat detected by CT in the lead point of an intussusception thus does not exclude a lipoma.

Endoscopic US identifies colon lipomas as hyperechoic tumors.

Magnetic resonance imaging reveals lipomas as typical fat-density tumors—hyperintense on T1- and hypointense on fat-suppressed T1-weighted images.

Angiomyolipoma

Extrarenal angiomyolipomas are rare. If large enough, an ileocecal valve angiomyolipoma or one in the left colon can obstruct.

Polyposis Syndromes

Not all patients with familial polyposis can be placed in a discrete syndrome. Thus one large family had a tendency to develop mixed colonic adenomatous and hyperplastic polyps, with the characteristic lesion being an atypical juvenile polyp, although some polyps contained mixed histology (97); some of these polyps became malignant. Inheritance in this family appeared to be autosomal dominant.

Familial Adenomatous Polyposis

Familial adenomatous polyposis is a genetic disorder with an autosomal-dominant inheritance and penetrance approaching 100%. Typically these patients develop hundreds to thousands of adenomatous polyps throughout the colon and often also in the rest of the gastrointestinal tract. Gardner's syndrome and familial polyposis coli have the same genetic defect but exhibit different phenotypic expression. Many investigators describe both entities with the term *familial adenomatous polyposis*.

The Swedish Polyposis Registry noted an incidence rate during 1977 to 1996 of 0.86 per million and a prevalence 32 per million at the end of 1996 (98); the median age at polyposis diagnosis of probands was 39 years, while in the call-up group it was 22 years. Importance of earlier detection is evident: 67% of probands and 3% of call-up patients already had colorectal cancer at initial diagnosis, with corresponding mortality rated being 44% and 2%, respectively.

The discovery of a defective gene changed the diagnosis of this condition and now allows direct carrier identification by mutation screening in some but not all patients. The mutation abnormality is complex, and numerous mutations in the adenomatous polyposis coli gene have been identified. The defective gene is a tumor suppressor gene having a role in carcinogenesis. Although gene mutations are often evident in sporadic colorectal adenomas and carcinomas, familial adenomatous polyposis patients already have mutations in this gene.

Polyp count and age are directly related to the risk of cancer. Patients with >1000 polyps had a 2.3 times greater risk of having a cancer than those with <1000 polyps (99); each 10-year age group led to a 2.4-fold difference in cancer risk. Nevertheless, occasional cancers are detected in patients younger than 30 years of age and those having less than 1000 polyps.

A predisposition to adenomatous polyps in familial adenomatous polyposis is best known, but both benign and malignant tumors also develop at other sites. More common extracolonic manifestations include desmoid tumors, often extraperitoneal in location, and gastroduodenal neoplasms. These patients tend to have gastric fundic gland polyposis. Skin, subcutaneous tissue, and bone tumors develop. Some studies suggests an increase in adrenal tumors. Papillary thyroid carcinoma are detected in about 1% to 2% of these patients.

Colon polyps develop and start growing roughly at the time of puberty, and in patients at known risk surveillance is started shortly thereafter. A double-contrast barium enema readily detects familial polyposis, although most gastroenterologists perform endoscopy.

The nonsteroidal antiinflammatory drug sulindac is currently used to treat patients with familial polyposis. Long-term use leads to a marked reduction in the number and size of polyps and, at times, even in their disappearance. Occasionally, however, polyps recur and a malignancy develops.

Because the predominant risk in many of these patients is colon cancer, colon resection is recommended. Procedures performed include the following:

1. Proctocolectomy with ileostomy
2. Total colectomy with ileorectal anastomosis and postoperative rectal surveillance
3. Colectomy, rectal mucosectomy, and ileorectal pull-through (ileal pouch)

Unsatisfactory results with proctocolectomy and ileostomy led surgeons to a total colectomy with an ileorectal anastomosis, but an intact rectal mucosa leaves these patients at risk for developing a future rectal carcinoma. In a Czech study of 55 patients undergoing colectomy and ileorectal anastomosis for familial polyposis, 16% developed a malignant tumor within 16 years (100). Many of these patients have either nodal or distant metastases at the time of rectal cancer detection, and a number of studies

have concluded that a proctocolectomy and ileoanal anastomosis should be the primary operation, instead of colectomy and ileorectal anastomosis.

The Soave procedure—a colectomy, rectal mucosectomy, and ileorectal pull-through—is currently preferred by many surgeons. One unanswered question concerns therapy when small bowel polyps are present. Also, these patients are at increased risk of developing ileal pouch polyps. Among 85 ileal pouches examined, 35% contained adenomas (101); the risk of developing an adenoma at 5, 10, and 15 years was estimated to be 7%, 35%, and 75%, respectively. Those with a pouch adenoma were more likely to also have duodenal adenomas.

Complications of an ileorectal Soave pull-through include anastomotic stricture and leak. Some of these strictures are dilated using either endoscopic or imaging guidance. Most focal perforations heal with time. Although a new ileorectal pull-through is feasible after breakdown of an initial anastomosis, a number of these patients are left with a permanent ileostomy.

As mentioned previously, these patients are at increased risk for mesenteric fibromatosis, or desmoid tumors. Some desmoids form spontaneously, although their prevalence increases after surgery. Desmoids are considered benign, but they are locally aggressive tumors associated with considerably morbidity and mortality. Desmoids are most common in the mesentery, followed by abdominal wall. Abdominal wall desmoids can be excised but recur in about half of patients; mesenteric desmoids are more difficult to excise. A not uncommon history is for a patient to undergo total colectomy, a desmoid tumor develops in the abdominal wall or close to some other surgical incision, a second surgical procedure is performed to resect the desmoid, a more extensive desmoid recurs, etc. An occasional desmoid becomes infected and forms an abscess.

At times skeletal scintigraphy with 99mTc-HDP shows diffuse uptake in regions of fibromatosis.

Medical therapy is feasible for some desmoids. Some regress with tamoxifen therapy.

Data in the Familial Gastrointestinal Cancer Registry in Toronto show that most deaths of patients with familial adenomatous polyposis are still from colorectal cancer (102); the proportion of deaths caused by extracolonic disease is rising, however, probably due to better screening and earlier prophylactic colectomies. Desmoid tumors are especially difficult to manage. Death due to desmoid tumor complications is not uncommon.

Turcot's Syndrome

Turcot's syndrome is a rare hereditary disorder consisting of central nervous system malignant gliomas and colon polyposis. It has manifested in the pediatric age group.

In a 30-year-old Japanese man with histopathologically confirmed glioblastoma multiforme and colonic well-differentiated adenocarcinoma, somatic mutations of *K-ras* and *APC* genes were identified in the colon carcinoma but not in the brain tumor (103); alterations in DNA repair genes presumably play a role in these tumors.

Multiple Hamartoma Syndrome (Cowden's Disease)

Familial multiple hamartoma syndrome, also known as *Cowden's disease*, is an autosomal-dominant condition having high penetrance but variable expressivity. The gene involved, believed to be a tumor suppressor gene, has been mapped to the long arm of chromosome 10 at 10q22–23. Mutations in this gene were identified in 81% of 37 Cowden's disease families (104); these include missense and nonsense point mutations, deletions, and insertions over the entire length of this gene.

Numerous hamartomatous polyps are the usual gastrointestinal tract manifestation of Cowden's disease. One patient presented with numerous round gastric and duodenal polyps and elongated (filiform) small bowel polyps (105). Extraintestinal manifestations vary considerably and range from macrocephaly to various genitourinary defects and other deformities.

Some affected patients develop gastric or colonic carcinomas, although the premalignant status of these polyps is not established. These patients also form various other cancers; in the

abdomen they are at increased risk for renal cell carcinoma, neuroendocrine neoplasms, germ cell tumors, and endometrial neoplasms.

Peutz-Jeghers Syndrome

Peutz-Jeghers syndrome manifests primarily as multiple hamartomatous polyps in the stomach, duodenum, small bowel, and colon. Patients with this syndrome often develop malabsorption and profound anemia or present with recurrent bouts of small bowel obstruction. Intussusceptions and even prolapse of a colonic polyp through the anus have been reported. Skin pigmentation is common.

A hamartoma-to-adenoma transition sequence probably exists, with an increased risk of carcinomatous development, although the cancer risk in these patients is considerably less than with familial polyposis.

A 16-year-old boy with Peutz-Jeghers syndrome diagnosed at age 8 years developed a rectal carcinoid (106).

Cronkhite-Canada Syndrome

Cronkhite-Canada syndrome consists of hamartomatous polyposis in the stomach, small bowel, and colon in association with alopecia and onychodystrophy. It is nonfamilial.

Prior to polyp detection these patients develop changes in taste sensation, dystrophic nails, and alopecia areata, findings suggesting the syndrome during the initial patient contact. Malabsorption is common and leads to hypoproteinemia.

Numerous polyps containing foci of inflammation and cystic regions develop in the stomach and small bowel. Not all of these polyps are hamartomatous; these patients also develop adenomatous polyps and thus are at risk for malignancy.

Juvenile Polyposis Syndromes

The presence of multiple juvenile polyps suggests one of the familial juvenile polyposis syndromes. Three types have been described: polyps limited to the colon, polyps throughout the gastrointestinal tract, and gastric juvenile polyposis. Some patients appear to be at increased risk of developing colon cancer.

The coexistence of familial juvenile polyposis and hereditary hemorrhagic telangiectasia has been described both sporadically and in families. An association of colorectal juvenile polyposis and hereditary spherocytosis has also been raised.

A severe form of juvenile polyposis is seen in the first several years of life. Some of these infants have bloody diarrhea and malabsorption to the point that life cannot be sustained.

Malignant Neoplasms

Adenocarcinoma

Clinical

In North America and Western Europe, colorectal carcinoma ranks second in incidence after lung cancer in men and breast carcinoma in women. It is considerably less common in developing countries. The incidence is increasing in Eastern Europe and Japan. Published cancer data vary not only among countries but also between university and nonuniversity centers. A number of studies show a correlation between meat consumption and colorectal cancer. Still, this topic remains controversial. A French review of available studies concluded, "One cannot state, nor exclude, that meat promotes colorectal cancer" (107).

Regular ingestion of aspirin or other nonsteroidal antiinflammatory drugs decreases the risk of colorectal cancer, although the length of time necessary before a reduction in risk occurs is debated.

Although not common, colorectal cancer does occur in young adults, with case reports describing even patients under 20 years of age. Some studies report clinical presentation and tumor grade to be similar to that in the older population, others report a lower morbidity and mortality; still others suggest dismal results because of advanced stage at diagnosis and an aggressive tumor.

An association between *Streptococcus bovis* bacteremia and the presence of a colon carcinoma is well known. The reason for this bacteremia is puzzling, because bowel *S. bovis* colonization rates in those with colorectal cancer and controls appear similar (108). A similar association exists with *S. sanguis* and colon cancer, and presumably other streptococci species also lead to bacteremia in a setting

of a colon carcinoma. Other rarer associations include pericarditis caused by *Bacteroides fragilis*, an anaerobic colon organism, and *Clostridium septicum* gas gangrene. Liver metastases may become infected. A rare primary colon carcinoma, however, manifests as a primary liver abscess without liver metastases.

A migratory thrombophlebitis precedes some gastrointestinal malignancies, including colon cancer. An occasional necrotizing vasculitis serves the same purpose. The Leser-Trelat sign consists of an association of multiple seborrheic keratoses with an internal malignancy; several colorectal cancers have been reported as a component of the Leser-Trelat sign. A rare association was increasing body hair growth (hypertrichosis lanuginosa) before a rectal cancer was discovered (109).

Genetics

One definition of hereditary nonpolyposis colorectal cancer is that at least three relatives should be affected, one is a first-degree relative of the other two, and that at least two successive generations be involved. An autosomal-dominant inheritance is evident for these hereditary cancers, and they are characterized by early age of onset, the predominance of right-sided lesions, and an increased prevalence of synchronous and metachronous neoplasms. Two subtypes of this syndrome are described:

Lynch syndrome I: cancers limited to the colon and rectum

Lynch syndrome II: similar, but extracolonic cancers also involve the endometrium, ovaries, and stomach

The true prevalence of hereditary nonpolyposis colorectal cancer is debated. About 1% to 2% of patients with colorectal cancer fit a definition of hereditary nonpolyposis colorectal cancer syndrome, although considerable geographic variation in the prevalence of this syndrome exists. Because of the high worldwide prevalence of colorectal cancer, this is one of the more common if not the most common inherited neoplasm currently known. The cumulative risk of colorectal cancer for relatives of patients with a colorectal cancer at or under 45 years begins rising at age 40 years, reaching 5% at age 50 and 10% at age 70 years. The lifetime risk of colorectal cancer among members of families with pathogenic mutations at some of these gene carriers is up to 80%; the risk of nongastrointestinal cancers is also increased for some of these gene carriers. Thus, is an upper urinary tract tumor in a patient with a hereditary nonpolyposis colorectal cancer due to a genetic abnormality or due to chance (110)?

At least five genes have been identified as sites of germline mutations associated with hereditary nonpolyposis colorectal cancer syndrome. Considerable data point to the *p53* gene playing a role in colorectal carcinoma development. Among adenomas, 8% of those containing low-grade dysplasia were *p53* positive compared to 73% of those containing high-grade dysplasia, suggesting a role for the *p53* gene in the transition between adenoma and carcinoma (111), and the observed increase of *p53* expression supports an adenoma–carcinoma sequence. Expression of *p53* in nonpolypoid carcinomas argues for another carcinogenesis pathway.

A large Dutch cancer registry found the relative risk of brain tumors in hereditary colorectal cancer patients and their first-degree relatives to be six times greater than that in the general population (112). The relative lifetime risk for these patients is low, and the authors do not recommend screening for brain tumors.

Associated Conditions

Does a colon polypectomy predict future colorectal cancer occurrence? A Milan colonoscopic polypectomy study of over 1000 patients with adenomatous polyps identified the presence of multiple adenomas and high-grade dysplasia as significant predictors of future cancer (113); presumably this subgroup of patients benefits from increased surveillance.

Prior studies have suggested an association between gallstones (or cholecystectomy) and risk of colon cancer; but more recent prospective studies fail to support this association. The same conclusions have been reached for previous gastric surgery for peptic ulcer disease.

A three- to eightfold increased risk for colon adenomas and carcinomas exists in patients with acromegaly. Patient with acromegaly also develop gastric cancer, pancreatic mucinous cystic tumors and other tumors; the known

tumorigenesis of elevated growth hormone and insulin-like growth factor levels appear to be responsible for these neoplasms.

An increased risk of colon cancer probably exists in patients with a Barrett's esophagus. An association is also suggested with Zollinger-Ellison syndrome with its hypergastrinemia; a significant number of patients with colon carcinoma have increased serum gastrin levels.

Synchronous Cancers

An increased prevalence of synchronous colorectal cancers has long been known. A multiinstitutional database of 4878 colon cancer patients recorded 3.3% having synchronous tumors (114); of these, 8% had more than two tumors at the time of diagnosis. An occasional patient with multiple synchronous colonic adenocarcinomas is reported (115). Considering the highest stage synchronous tumor, survival appears to be the same as for patients with a single colonic tumor (114).

Once one colorectal cancer is diagnosed, the need to study the remaining colon is known to most clinicians (Fig. 5.20). Yet, in spite of this, some patients still undergo cancer resection without preoperative study for synchronous lesions.

A rare patient develops a synchronous colorectal carcinoma and lymphoma, including Hodgkin's disease; this association appears to be fortuitous.

Metachronous Cancers

The definition of metachronous cancer varies. Most authors use this term to describe a second separate cancer, while some also include intraluminal recurrences, arguing that a pathologist cannot readily differentiate recurrences from a new focus of adenocarcinoma.

Metachronous colorectal neoplasms consist of adenomas and carcinomas, related through the adenoma-carcinoma cycle (Fig. 5.21). Patient who have one colorectal cancer resected are at increased risk of developing a second cancer (metachronous cancer). Overall, the prevalence of metachronous cancers ranges from 1% to 5%, but the prevalence of metachronous adenomas is considerably higher. Adenoma surveillance reduces the risk of metachronous colon cancers. Patients with a synchronous adenoma or carcinoma discovered at initial presentation are at significantly higher risk for metachronous adenomas and carcinomas, compared to those without a synchronous tumor.

The interval between first and second cancers ranges from months up to a decade or more. Carcinoembryonic antigen (CEA) levels do not aid in detecting a second cancer.

Screening

Why screen? To a large extent, colorectal cancer screening consists of detecting adenomas, with a reduction of colon cancer mortality achieved by resecting these precancerous adenomas. Among colorectal cancers detected by screening asymptomatic individuals at one Japanese institution, 61% were either stage 0 or stage I; among comparable symptomatic patients only 16% had tumors of these early stages (116).

Controversy exists about the size of adenomas that require resection. Should several-millimeter adenomas found at colonoscopy be resected? Also, what is the chance of a malignancy being present in a small colonic polyp (Fig. 5.22)? Histology of polyps not detected by a CT colonography study revealed that 58% of those 5 mm or smaller were not adenomas and 43% of those 6–9 mm were not adenomas (117). An analysis of over 11,000 adenomas detected during colonoscopy at the Erlangen Registry of Colorectal Polyps detected no invasive carcinoma in adenomas <5 mm (118); the malignancy rate for larger adenomas not only showed a right-sided shift but also the rate was significantly modified by histology, the presence of synchronous lesions, and other factors.

A Japanese study of sessile colonic adenomas <5 mm followed these polyps for an average of 24 months (119); none developed carcinomatous transformation. The authors concluded that polypectomy of these small lesions is not necessary, and they can be followed either radiologically or endoscopically.

Colorectal cancer screening has become prevalent in the Western world. A survey for occult blood, flexible sigmoidoscopy, colonoscopy, and barium enema are the screening modalities used. The role of CT colonography as a routine screening examination is still evolving. Still, only a minority of colorectal

Figure 5.20. Synchronous hepatic flexure adenocarcinoma (A, arrow) and ascending colon adenoma (B, arrowheads). C: Two synchronous adenocarcinomas in another patient, a circumferential cancer in the ascending colon (arrow) and an infiltrating one in the transverse colon (arrowheads).

cancers are detected by screening asymptomatic individuals.

Numerous studies have concluded that fecal occult blood testing is cost effective in detecting colorectal cancer. Although patient recruitment and test sensitivity vary considerably, its low cost makes it attractive. As one example, in a defined region in Spain a participation rate of 56% was achieved and a majority of detected cancers were Dukes' stage A (120); thus an improvement in diagnostic stage is feasible, with, one hopes, an improved survival.

Patients are generally assigned to one of three colon cancer risk categories: average, moderate, and high. Moderate risk includes those with a first-degree relative with a colon carcinoma or large adenoma and those with a prior adenoma or carcinoma. High risk includes those with inflammatory bowel disease, familial polyposis, and nonpolyposis colorectal cancer syndromes. Screening of inflammatory bowel disease patients involves a different concept than for other patients; cancer in these patients does not arise from adenomas, and screening consists of random biopsies and a search for dysplasia.

No consensus has developed in the gastrointestinal literature about surveillance screening time intervals. After an initial colonoscopic polypectomy, whether patients are assigned to follow-up surveillance either every two years or

Figure 5.21. Metachronous colon carcinoma. A barium enema performed through a descending colostomy identifies a right colon cancer (arrow). The patient had had a previous rectal carcinoma resected.

four years does not appear to affect over-all risk of developing a new adenoma. Even if a more protracted study leads to a slight increased risk of new neoplasms, this risk should be counterbalanced by the fewer examinations necessary and thus presumably decreased over-all colonoscopic complication rate. In general, in average-risk individuals the interval between screening examinations can be expanded beyond 5 years, provided the initial examination does not detect a neoplasm.

Assuming a compliance of 60% with initial screening, a hypothetical study of 50-year-old white individuals at average risk for colorectal cancer found the most effective strategy to be annual fecal occult blood testing plus sigmoidoscopy every 5 years starting at age 50 years, followed by colonoscopy if a polyp is detected (121); such a scenario achieved an 80% reduction in colorectal cancer mortality compared with no screening. If, on the other hand, screening compliance is assumed to be 100%, the study concluded that screening more often than every 10 years was prohibitively expensive. Similar to other modeling studies, the optimal recommendations suggested depend on the initial assumptions used.

First degree relatives of colorectal cancer patients are at increased risk for adenomas and cancers. A French case-control colonoscopic screening study of first-degree relatives of colorectal cancer patients (i.e., those of moderate risk) found an odds ratio of 1.5 for adenomas, including an odds ratio of 2.6 for high-risk adenomas (≥1 cm in size or containing a villous component) (122); the prevalence of high-risk adenomas in relatives was higher when the index patient was younger than 65 years, was male, and had a distal rather than proximal cancer.

The above discussion involves mostly conventional colonoscopy; a double-contrast barium enema was not considered as an alternative. Barium enema sensitivity for detecting a carcinoma or larger adenoma is 85% to 95%. Several studies have concluded that a double-contrast barium enema is cost-effective for colorectal cancer screening. Using published estimates of cost and effectiveness of colorectal cancer screening of a double-contrast barium

Figure 5.22. A 15-mm sigmoid adenocarcinoma (arrow) detected on a screening barium enema. Initial colonoscopy could not detect this tumor, probably because of extensive colon redundancy. The patient eventually underwent sigmoid resection.

enema performed every 3 years (or every 5 years with annual fecal occult blood testing), an incremental cost-effectiveness ratio of <$55,600 per life-year saved was achieved, compared to colonoscopic screening with a cost-effectiveness ratio of >$100,000 per life-year saved (123).

Women with previous breast, endometrial, or ovarian cancer are at increased risk of developing a colorectal cancer. Should women with these cancers undergo preoperative barium enema or colonoscopic screening? Reccomendations vary, because risk of colon adenomas and carcinomas is low. A typical one is that in otherwise asymptomatic women under 50 years of age no colon screening is necessary, but in those over age 70 years such screening is recommended.

A double-contrast barium enema is associated with a perforation rate of about 1/25,000, which is less than one tenth that of colonoscopy.

Pathology

Normally proliferating cells are located in colonic crypt bases, on the other hand, transforming growth factor-β (TGF-β) immunoreactive and apoptotic cells are close to the surface, corresponding to normal migration of colonocytes. Distribution of proliferating and TGF-β immunoreactive cells is reversed in adenomatous polyps, suggesting that cell migration in adenomas is not toward the lumen but inward.

Traditionally, development of colorectal carcinomas was ascribed to an adenoma-to-carcinoma transformation sequence. This concept was modified when it was realized that some small adenomas also have a malignant potential, albeit small, and was modified further when flat carcinomas were detected developing de novo from polyp-free mucosa. These flat (also called depressed) carcinomas appear to arise from a different precursor and suggest a different pathway for their carcinogenesis than the adenoma-to-carcinoma cycle. Finally, molecular biology enters the picture by showing a lack of K-*ras* mutations in carcinogenesis of flat colonic carcinomas. A multipotential stem cell is probably located within the mucosa. The presence of neuroendocrine or squamous differentiation in some colorectal carcinomas argues that such differentiation evolves in several directions; such differentiation is more common in the midgut portion of the colon as compared to the hindgut. In general, the presence of neuroendocrine differentiation is associated with a poor prognosis.

Superficial spreading intramucosal tumors (defined as epithelial tumors >30 mm in diameter), consist of both adenomas and carcinomas and tend to be located in the cecum and rectum; most superficial spreading carcinomas have an adenomatous component and consist of a low-grade carcinoma. Thus most superficial spreading tumors develop initially as an adenoma.

One uncommon histologic subtype is a signet ring cell carcinoma. These tumors tend to infiltrate readily, and some even have a scirrhous or linitis plastica appearance. They occur in younger patients; patient survival is shorter than with more typical adenocarcinomas.

A clear cell adenocarcinoma, similar to renal clear cell adenocarcinomas, also develops on rare occasions in the colon.

A rare colon adenocarcinoma <10 mm in size infiltrates the submucosa or invades the submucosal lymphatics or blood vessels. These lesions typically have a polypoid appearance, although an occasional one is flat. An rare early colonic cancer will metastasize to the liver (124).

Proximal and distal colon cancers have different clinical presentations, differ in prognosis, and have different epidemiologic aspects. A study of DNA ploidy and overexpression of nuclear *p53* found proximal tumors to be more often diploid than distal ones and distal tumors to have more *p53* overexpression than proximal ones, suggesting a different carcinogenesis for these tumors (125). Some investigators believe these cancers should be considered different tumors.

Some colorectal adenocarcinomas are associated with considerable mucin production. Different properties between mucinous and nonmucinous colorectal carcinomas suggest different carcinogenic pathways.

A colorectal carcinoma occasionally calcifies. Most of these are mucinous adenocarcinomas. Distinctly unusual, however, is heterotopic bone formation.

Although imaging and colonoscopy can suggest that a particular lesion is a carcinoma, the final diagnosis is established by a pathologist from either a biopsy or a surgically resected bowel. Whether a pre-resection biopsy should

be obtained from a tumor showing obvious malignant imaging characteristics is a matter of opinion and established local practice. Most biopsies of primary colon carcinomas are obtained via colonoscopy (or sigmoidoscopy for rectosigmoid lesions), although percutaneous biopsy using imaging guidance is feasible for larger tumors.

Detection

Barium Enema: The relative roles of barium enema, flexible sigmoidoscopy, and colonoscopy are not established. A number of studies have shown a superiority of colonoscopy over barium enema. The problem with most of these studies is that colonoscopy is used as a gold standard and the studies are performed by gastroenterologists, but barium enemas were performed by general radiologists and the results are often biased against barium enema. A barium enema, however, does detect most pedunculated, sessile and infiltrating colon (Fig. 5.23) and rectal (Fig. 5.24) carcinomas.

In a retrospective multihospital Indiana study, the sensitivity of colonoscopy for detecting colorectal cancer (95%) was greater than with a barium enema (83%) (126); the sensitivity of a double-contrast barium enema (85%) was no different from that of a single-contrast study (82%). Barium enema performed no better in the right than the left colon. Cancers detected by colonoscopy were more likely to be Dukes' class A (25%) than cancers detected by barium enema (10%).

A retrospective colon cancer study from a well-defined geographic region in Norway found that a barium enema correctly detected a cancer in 91% of 386 tumors, a cancer or major precancerous lesion was overlooked in 7%, and the examination was not possible in 2% (127); colonoscopy, on the other hand, correctly detected cancer in 80% of 215 tumors, cancer or a major precancerous lesion was overlooked in 6%, and colonoscopy was technically incomplete in 14%.

Endoscopy (Conventional Colonoscopy): In an Indiana study, colonoscopy performed by gastroenterologists was more sensitive (97%) for cancer detection than those done by nongastroenterologists (87%) (126).

How accurate is colonoscopy in localizing a colorectal cancer? One study of 77 cancers revealed significant errors in tumor localization in 8% (a significant error was defined as a change from the preoperative planned resection to an alternative resection) (128). A retrospective study of colorectal cancers not detected by colonoscopy performed within 3 years of diagnosis suggested that 57% of the cancers were "missed," and 43% were believed not to have been reached, although some right colon cancers recorded as missed may have been not reached (129); the authors suggested that cecal

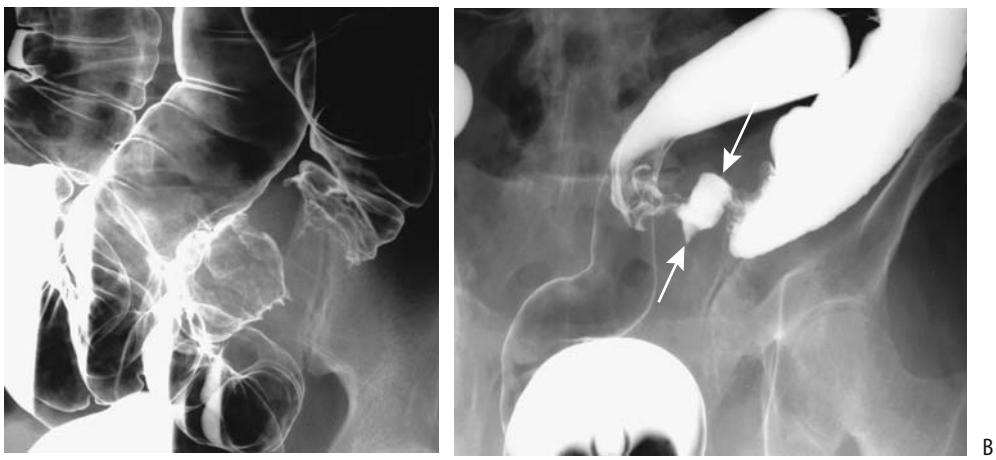

A B

Figure 5.23. Colon adenocarcinoma. A: A double-contrast barium enema identifies a tight circumferential cancer. The entire colon could be studied in spite of the tight obstruction. B: This patient presented both with bleeding and obstruction. Barium enema reveals an ulcerated (arrows), circumferential sigmoid cancer.

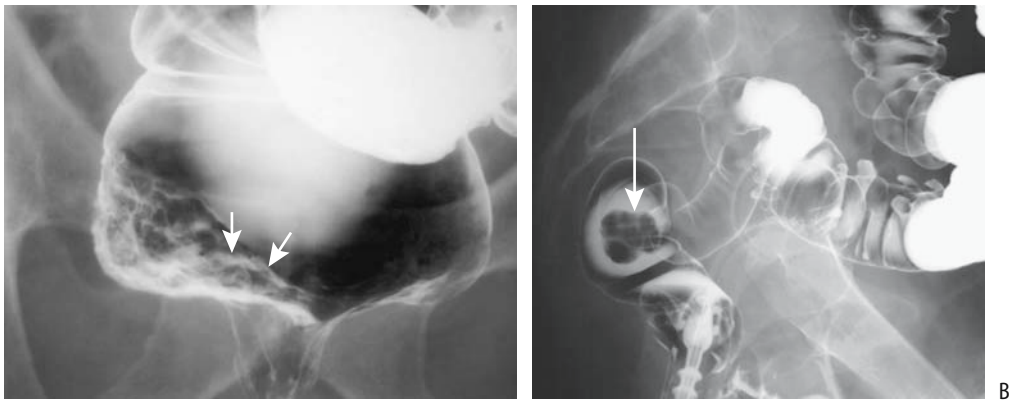

Figure 5.24. A: Distal rectal carcinoma (arrows) presenting as a diffuse carpet-like infiltrate. (Courtesy of Arunas Gasparaitis, M.D., University of Chicago.) B: Polypoid, infiltrating rectal carcinoma (arrow).

intubation should be verified by specific landmarks in all instances, and failure to reach the cecum should be followed by a prompt barium enema or CT colonography.

Computed Tomography: Computed tomography of some large, fungating ascending colon carcinomas infiltrating to pericolic fat identifies segmental distal colonic wall thickening. The histopathology of resected specimens reveals submucosal and subserosal edema, chronic inflammation and fibrosis, or both (130).

Not all focal colorectal tumors detected by CT or MR are neoplastic. An adjacent abscess can readily mimic a necrotic cancer and vice versa (Fig. 5.25). Endometriosis is another example.

Intravenous contrast enhancement aids polyp detection (131); both benign and malignant polyps enhance with contrast, while residual content does not. Enhancement significantly improves visualization of 6–9 mm polyps (75% postcontrast versus 58% precontrast) (132). Contrast also aids detection of local tumor extension and any lymphadenopathy. Most published performance data on CT colonoscopy are summarized in a 2003 book on this topic (133).

Studies suggest that CT colonography is competitive with conventional colonoscopy in detecting both benign and malignant polyps >1 cm. In patients with colonic tumors (confirmed at endoscopy or surgery), axial and multiplanar CT detected all malignancies (134); all missed benign tumors were <8 mm in diameter. Computed tomographic colonoscopy performed the same day as conventional colonoscopy achieved a 58% sensitivity and 52% specificity in identifying polyps, with sensitivity for polyps ≥1 cm being 86% (135).

After bowel preparation and colon air insufflation, 300 patients underwent CT scanning in supine and prone positions using 3-mm collimation and single breath hold (136); transverse CT images, sagittal and coronal reformations, and 3D endoluminal images completed the CT colonography. Using conventional colonoscopy results as a gold standard, this study achieved a sensitivity of 90% for detecting polyps 10 mm or larger, 80% for polyps 5.0 to 9.9 mm, and 59% for polyps <5 mm; of note is that CT colonography detected all carcinomas. Intravenous contrast provides colonic wall and tumor enhancement. Enhancement significantly improved visualization of 6- to 9-mm polyps (75% postcontrast versus 58% precontrast) (9). One potential pitfall for CT colonography is the occasional carpet-like (137) or flat cancer. Most studies suggest that multiplanar 3-D endoluminal images achieve better sensitivity and specificity than 2-D images; nevertheless, in any one patient a combination of images is often necessary for full evaluation.

Computed tomographic colonoscopy is an alternative to barium enema and conventional colonoscopy, especially in frail, elderly patients. Detection of small polyps in these patients is not as relevant as in younger patients.

Ultrasonography: Endorectal US detects rectal tumors. Attempts have been made to

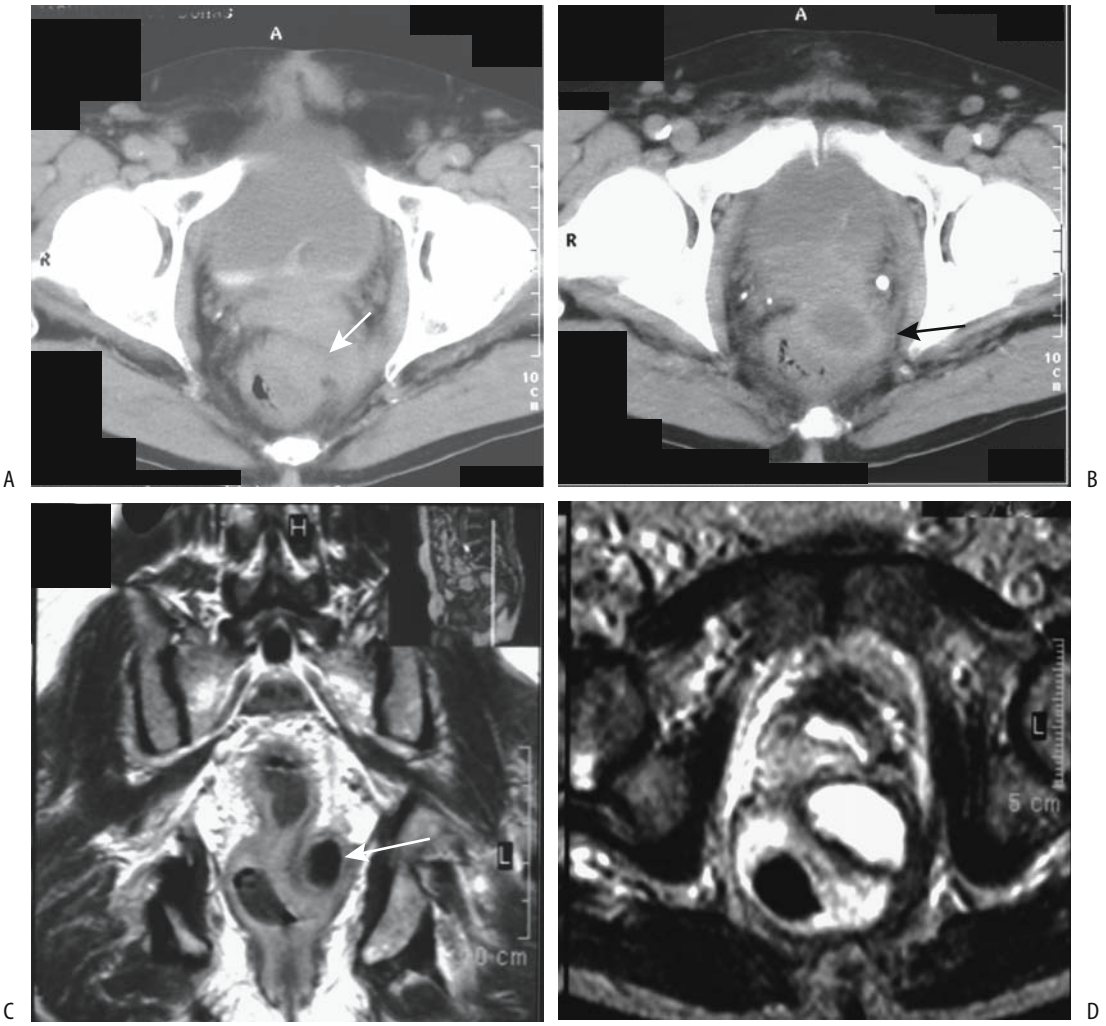

Figure 5.25. Pararectal abscess mimicking a rectal carcinoma. Constipation developed after prostatic resection 4 months previously for benign hyperplasia. A,B: Two pelvic CT images reveal a rectal tumor narrowing the lumen (arrows). C,D: T1– and T2–weighted images show rectal wall thickening and an adjacent fluid-filled structure (arrow), suggesting an abscess or necrotic tumor. (Courtesy of Egle Jonaitiene, M.D., Kaunas Medical University, Kaunas, Lithuania.)

detect a malignancy arising within a rectal villous adenoma, but results have been disappointing. In general, rectal villous adenomas are resected regardless of imaging or biopsy findings.

Uncommon Type/Presentation

Flat (Depressed) Adenomas and Carcinomas: So-called flat (also called *depressed* and *superficial depressed*) colon adenomas and carcinomas do not have a predominant intraluminal growth pattern; rather, they show a tendency toward early submucosal invasion and early metastasis. Nevertheless, they grow slowly. A retrospective collection of nine flat colon carcinomas found an initial mean 12-mm diameter, and it took these cancers an average of 32 months to double in size; a comparable sample of polypoid carcinomas doubled in size, on average, in 9 months

(138); with time, flat cancers continued with a nonpolypoid growth pattern. Cell kinetics and molecular alterations in flat tubulovillous tumors suggest that they represent a distinct entity differing from their polypoid counterpart (139). Some evidence suggests that flat colonic tumors evolve from colonic mucosa overlying lymphoid nodules.

These cancers are less common than those evolving via the adenoma-carcinoma sequence. A higher proportion develop in a setting of inflammatory bowel disease and radiation proctocolitis. Some are rather aggressive and when still small have already metastasized to the liver, but these are rare exceptions.

Comparing flat adenomas and adenocarcinomas evaluated in Stockholm and Tokyo by the same pathologist, the Japanese lesions were more advanced with regard to dysplasia and were more aggressive (140), suggesting the presence of different geographic manifestations. Complicating the picture, in the United States a number of small, flat umbilicated tumors are hyperplastic polyps rather than neoplasms.

Although many radiologists believe that even a technically excellent double-contrast barium enema does not detect most flat colonic neoplasms, a Japanese study suggests otherwise (141); among 97 early flat and depressed colorectal cancers, a double-contrast barium enema detected converging folds and semilunar deformity more often in cancers with moderate-to-massive submucosal extension than in those confined to mucosa or with only focal submucosal extension. Also, deep depressions, an irregular surface in these depressions, and tumors >20 mm were predictive of submucosal extension (141); using these radiographic findings, the authors achieved an overall accuracy of 85% for identifying depth of invasion.

Similar to a barium enema, small flat colon adenomas and adenocarcinomas may not be detected with conventional endoscopy because of their similar translucency to surrounding mucosa. They are identified as a slight mucosal deformity, a slightly more reddish color than surrounding mucosa, and by loss of the vascular network pattern. Undoubtedly these small lesions were often previously overlooked.

Potentially, CT colonography with IV contrast will detect flat neoplasms. These tend to be slightly hypervascular compared to normal colonic mucosa and, especially with the higher resolution available with multidetector CT, should be detectable with a high-quality study.

Linitis Plastica: The rare primary colorectal linitis plastica, or *scirrhous carcinoma*, usually develops in a setting of inflammatory bowel disease and in younger patients than more typical colon cancers. Metastases are not uncommon when such a primary tumor is first identified.

Both colonoscopic and barium enema findings can be subtle, with a typical appearance resembling a benign stricture (Fig. 5.26). Computed tomography reveals these scirrhous carcinomas as circumferential, homogeneously enhancing lesions. The involved colon wall is thickened considerably. The sensitivity in detecting these lesions depends on tumor size and quality of CT study. Endoscopic US of rectal linitis plastica shows a circumferential thickening of the rectal wall, with thickening involving mostly the submucosa and muscularis propria; endoscopic US also detects perirectal fat infiltration.

In general, breast and stomach carcinomas metastatic to the colon have a linitis plastica appearance more often than a primary colon scirrhous carcinoma.

Figure 5.26. Colon linitis plastica. (Courtesy of Arunas Gasparaitis, M.D., University of Chicago.)

Perforation: Previously performed water-soluble contrast enema has been replaced by CT. Computed tomography readily identifies these mostly advanced tumors, with a majority being associated with an abscess near the tumor.

An occasional carcinoma perforates into adjacent soft tissues and leads to extraintestinal gas or subcutaneous emphysema (Fig. 5.27). At times unusual fistulas form. Technetium-99m-DTPA renography in a patient with hematuria revealed sigmoid colon radioactivity extending to the transverse colon (142); a sigmoid adenocarcinoma had invaded the bladder and formed a colovesical fistula.

Do patients with a perforating colon carcinoma have a worse prognosis than those without a perforation? Comparing perforating cancers and obstructing cancers undergoing emergency surgery, no significant difference in survival or disease progression was evident between these two groups (143).

Obstruction: The size of colon cancers when first detected have decreased during the last several decades, yet it is still common in most practices to see a patient first present with colonic obstruction due to a large, bulky tumor. These patients first undergo proximal colon decompression and only later have definitive cancer resection. A sufficiently tight obstruction obviates both a complete barium enema and colonoscopy, studies not only defining an obstructing tumor but also detecting any synchronous neoplasm. In such a setting, preoperative CT colonography is very useful to evaluate the proximal colon. In 19 patients with distal occlusive colorectal carcinomas, preoperative CT colonography identified all occlusive cancers and also detected synchronous lesions—two cancers and 20 other polyps (144), findings confirmed by other studies (145) (Fig. 5.28).

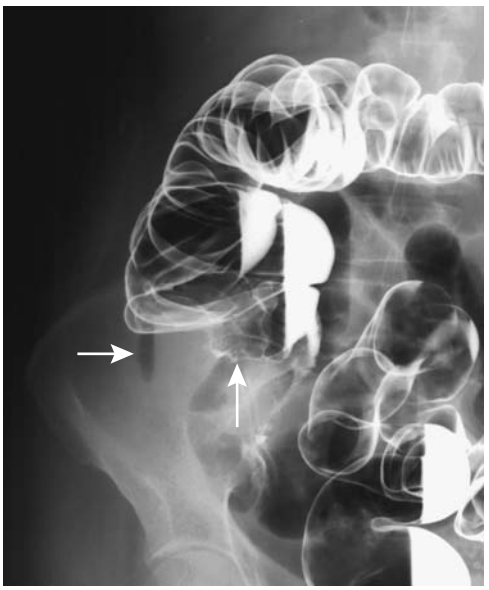

Figure 5.27. Perforated right colon carcinoma (arrows) in a patient suspected to have acute appendicitis. Soft tissue gas in the necrotic tumor mimics an appendiceal abscess.

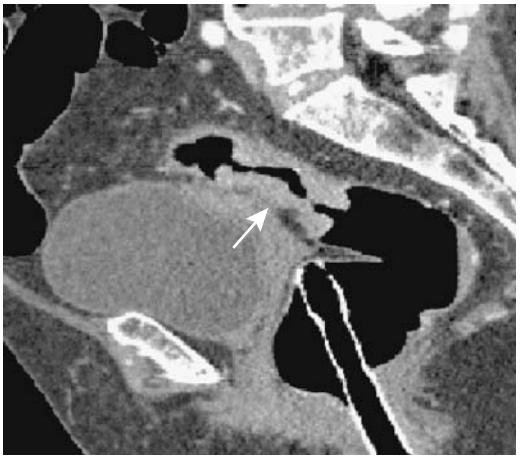

Figure 5.28. Obstructing carcinoma (arrow). CT colonography can also study the proximal colon. Sagittal images are helpful in surgical planning. (Courtesy of W. Luboldt, M.D., Johann Wolfgang Goethe University, Frankfurt-am-Main.)

Expandable intraluminal stents are useful in malignant colonic obstructions. A pretherapy stent placed through an obstruction provides decompression, allows a bowel-cleansing regimen to be employed, and thus obviates a preliminary colostomy (146). After decompression, these patients undergo tumor staging, and a decision is made whether to proceed to cancer resection or whether successful stenting is to be the primary palliative therapy. The success rate in stent placement varies but typically is about 90%; thus stent placement was successful in 88% of 80 patients and bowel obstruction

resolved in 67% (146). A multicenter study of 71 patients with acute malignant obstruction found self-expandable metallic stent placement to be technically successful in 90%, but it was not possible to advance across the obstruction in 3% and the prostheses was poorly positioned in 7% (147).

Stent complications include perforation and stent dislocation. Completely covered stents tended to migrate more than uncovered stents.

Metastasis as the Initial Presentation: Only an occasional colorectal cancer presents first as a metastasis, generally in the liver. A rare rectal cancer spreads via systemic veins, but pulmonary metastases also occur occasionally from a nonrectal site.

Bone and cerebral metastases as an initial presentation are rare. A cecal carcinoma in a cirrhotic patient first presented with umbilical metastasis (Sister Mary Joseph node) (148). A curiosity is a single microscopic metastatic focus in a resected thyroid colloid nodule in a patient with unsuspected sigmoid colon carcinoma and multiple liver metastases (149).

Staging

General: Several staging systems are in use, including the tumor, node, metastasis (TNM) system (Table 5.4). The Dukes staging system was originally designed for rectal carcinomas, but over the years it has been expanded to include colon cancers; a number of modifications and subdivisions have evolved, and if the Dukes system is used, the specific modification employed should be identified.

A small colorectal cancer initially tends to grow more circumferentially rather than longitudinally along the colon wall. Spread occurs via both the lymphatics and hematogenously. A cancer in the intraperitoneal colonic segments is prone to form peritoneal carcinomatosis once the serosal barrier is breached.

Some carcinomas, especially well-differentiated ones, invade extensively into surrounding organs without evident metastasis to lymph nodes or more distant structures. For example, a large transverse colon carcinoma in a 60-year-old woman had invaded the adjacent duodenum and pancreas and was in close contact to the superior mesenteric vein (150); no metastases were evident and en bloc resection revealed no lymph node spread.

Table 5.4. Tumor, node, metastasis (TNM) staging of colorectal tumors

Primary tumor:

Tx	Primary tumor cannot be assessed
T0	No evidence of primary tumor
Tis	Carcinoma in situ: Intraepithelial or invasion of lamina
TI	Tumor invades submucosa
T2	Tumor invades muscularis propria
T3	Tumor invades through muscularis propria into subserosa, or into nonperitonealized pericolic or perirectal tissues
T4	Tumor directly invades other organs or structures, and/or perforates visceral peritoneum

Lymph nodes:

Nx	Regional lymph nodes cannot be assessed
N0	No regional lymph node metastasis
NI	Metastasis in 1 to 3 regional lymph nodes
N2	Metastasis in 4 or more regional lymph nodes

Distant metastasis:

Mx	Distant metastasis cannot be assessed
M0	No distant metastasis
M1	Distant metastasis

Tumor staging:

	AJCC/UICC			DUKES-3*
Stage 0	Tis	N0	M0	—
Stage I	T1	N0	M0	A
	T2	N0	M0	A
Stage IIA	T3	N0	M0	B
Stage IIB	T4	N0	M0	B
Stage IIIA	T1,2	N1	M0	C
Stage IIIB	T3,4	N1	M0	C
Stage IIIC	any T	N2	M0	C
Stage IV	any T	any N	M1	D

AJCC, American Joint Committee on Cancer; UICC, Union Internationale Centre le Cancer.

*Dukes B is a composite of better (T3, N0, M0) and worse (T4, N0, M0) prognostic groups, as is Dukes C (any T, NI, M0 and any T, N2, M0).

Source: From the AJCC Cancer Staging Manual, 6th edition (2002), published by Springer-Verlag, New York, NY, used with permission of the American Joint Committee on Cancer (AJCC), Chicago, IL.

Ability to detect perirectal node involvement varies with node size. In general, malignant nodes are larger than nonmalignant ones, although some normal sized nodes are invaded and some enlarged ones are not. Enlarged lymph nodes can be due to reactive inflammation. In addition, metastatic nodes range from being partially to totally invaded. Similar to metastatic nodes at other body sites, aside from

node size, node metastases do not correlate with a specific imaging appearance. Also, some colorectal cancers metastasize to more distant lymph nodes and bypass closer nodes. Such skipping nodal metastases are detected in about 10% of patients; patients with skipping nodal metastases have a significantly better prognosis than those without bypassed metastases.

Routine preoperative CT and MR colon cancer staging is of limited use because of low accuracy in assessing the depth of tumor invasion and detecting early lymph node invasion, but these examinations are very useful for detecting invasion of adjacent structures and metastasis to distant sites. Almost all colon cancers are resected. Patients with rectal cancer, on the other hand, have additional therapeutic options, and initial staging often determines the type of therapy employed.

The Radiology Diagnostic Oncology Group concluded in 1996 that CT and MRI accuracies were equivalent in depicting transmural tumor spread, assessing lymph node involvement, and detecting liver metastases (151). Due to advances in CT and MR equipment and software design since then, however, these results should be viewed as obsolete.

Staging is best approached by treating rectal and nonrectal cancers separately.

Rectal Carcinoma: Rectal wall penetration and pelvic lymph node involvement are the major prognostic factors in predicting recurrence. Some lymph nodes <5 mm in diameter already contain metastases, a limitation in the imaging prediction of tumor spread. Nevertheless, the sensitivity for detecting positive lymph nodes is greater for rectal tumors than for more proximal colonic tumors because benign perirectal adenopathy is uncommon.

The prevalence of lymph node involvement with rectal cancers is related to tumor depth. Among rectal cancers, lymph node involvement was as follows: T1, 6%; T2, 20%; T3, 66%; and T4, 79% (152). A biopsy finding of lymphatic vessel invasion was highly indicative of lymph node metastasis.

One pathway for the spread of sigmoid and high rectal cancers is via the inferior mesenteric lymph chain, but specific spread is unpredictable and can include the inferior mesenteric lymph nodes, nodes adjacent to rectum, and nodes at the root of the inferior mesenteric artery.

A meta-analysis of articles published up to 2002 found that for muscularis propria invasion by a rectal cancer US and MR had similar sensitivities but US specificity was 86% and MR 69% (153); sensitivity for perirectal tissue invasion was: CT 79%, US 90% and MR 82%, with similar specificities. All three modalities were comparable for detecting lymph node involvement.

Multidetector CT is more accurate in staging more advanced rectal cancers than more superficial ones; CT does not provide rectal wall details. Adding multiplanar reconstruction improves local staging of these cancers.

In 53 consecutive patients with distal rectal carcinoma, CT sensitivity for detecting perirectal and inferior mesenteric lymph node metastases was 53% and specificity 85% (154).

Computed tomography using a water enema (hydro-CT) appears useful in staging rectal cancers. Hydro-CT studies tend to be more accurate than no enema studies; increased accuracy is mostly in detecting invasion within or beyond the muscular layers. A CT study of patients with rectal cancer using a tap water enema, IV contrast, and pharmacologic bowel hypotonia reached a sensitivity of 90% and specificity of 70% in differentiating tumors limited to bowel wall from those invading extrinsically (155).

Conventional US has been largely supplanted by endorectal US in staging rectal carcinomas. Endorectal US is very accurate in T-staging superficial cancers but not more advanced cancers because of limited acoustic range. Some authors express endorectal US staging using TNM nomenclature—called the uTNM classification. Although some results are promising, the overall conclusions are rather pessimistic, especially for detecting lymph node metastasis.

Endoscopic resection should be possible if imaging could differentiate between mucosal and submucosal invasion. A number of stuties of early rectal cancer concluded that endoscopic US is not accurate enough to determine appropriate therapy for these tumors. On the other hand, a more recent study found that endorectal US achieved a sensitivity and specificity of 93% and 71%, respectively, and MRI 100% and 60% for detecting rectal wall penetration (156). Endorectal US does not reliably detect muscularis propria invasion (T2 tumors). Endorectal

US does, detect perirectal fat invasion (T3 tumors). Tumor spread to more distal structures, such as bladder, is more problematic.

Ultrasonography of the distal rectum is more difficult and the tissue planes are less well defined than more proximally, and endoscopic US staging accuracy in the distal rectum is lower than in the middle or proximal segments. On the other hand, endorectal US is accurate in evaluating anal canal infiltration by low rectal cancers. The overall tendency in staging rectal villous tumors with endoscopic US is to overstage rather than understage. Endoscopic US in patients with a rectal adenocarcinoma performed within 2 weeks prior to surgery and radiation therapy overstaged 21% and understaged 9% of patients (157). Overstaging of the depth of invasion is due, in part, to tumors located close to an uninvolved layer, not uncommon adjacent inflammation and hypervascularity, which tend toward a more anechoic appearance than tumor infiltration. Microscopic invasion accounts for some understaging.

After a rectal polypectomy with an adenocarcinoma discovered in the specimen, endorectal US detected residual tumor with a sensitivity of 100% but a specificity of only 44% (158).

How accurate is endorectal US in detecting local lymph node invasion? Considerably more lymph nodes are involved at histologic examination than are detected by US, and a number of studies have concluded that endoscopic US is too unreliable to be used in preoperative patient selection. Some enlarged lymph nodes are due to reactive inflammation and not tumor infiltration. The ability to detect perirectal nodes varies with node size. In general, malignant nodes are larger than nonmalignant ones, although overlap exists. Metastatic nodes range from being partially to totally invaded. Similar to metastatic nodes at other body sites, aside from node size, node metastases do not correlate with a specific imaging appearance. Several studies concluded that endoluminal US does not reliably identify the extent of lymph node involvement. The role of 3D endorectal US in staging rectal carcinoma remains to be established.

Whether patients are treated by radiotherapy or chemotherapy prior to surgery also appears to influence rectal US accuracy. Diagnostic US accuracy for wall infiltration and lymph node detection decreases after preoperative radiotherapy or chemoradiotherapy.

In patients with known rectal tumors, endorectal US and MRI achieve comparable staging results. The advantages of endorectal US are its small-diameter instruments, its ready availability, it is technically less demanding, and it costs less; MRI, on the other hand, is operator independent and also evaluates other sites.

Magnetic resonance imaging using an endorectal coil provides more detail than similar MRI using a surface coil. On the other hand, use of an endorectal coil combined with imaging using external coils appears advantageous in assessing both intramural tumor infiltration and more distal pelvic spread. Little data exists on placing such combined imaging in a proper perspective.

High-spatial resolution MRI using T2-weighted FSE images identifies mesorectal fascia, peritoneal reflection, Denonvilliers fascia and adjacent structures. Magnetic resonance imaging has a tendency to understage rectal carcinomas (Fig. 5.29). Overstaging in some patients is due primarily to the presence of adjacent perirectal inflammation.

Rectal distension by a water enema improves MR detection of rectal wall penetration. Using a rectal ferric ammonium citrate enema, spin echo MRI identifies most rectosigmoid cancers. Preoperative MR staging of rectal cancer achieved a 100% sensitivity and 70% specificity in distinguishing tumor stages worse than Dukes' stage A (159); on T1-weighted images a rectal superparamagnetic contrast enema creates a signal void in a distended lumen while wall contrast enhancement by IV gadolinium differentiates mucosa, muscle layers, and perirectal space, details not obtainable with nonenhanced images.

In a randomized phase II trial, preoperative MR using the superparamagnetic iron oxide rectal contrast agent ferristene and IV contrast achieved a sensitivity of 97% and specificity of 50% in staging carcinomas higher than T2 stage (160); using receiver operator characteristic (ROC) analysis, MR differentiated between T1/T2 and T3/T4 tumor stages with a ROC index of 0.85. Higher viscosity rectal contrast agent formulations were superior to low-viscosity formulations, but no significant differences were found between high and low iron content agents.

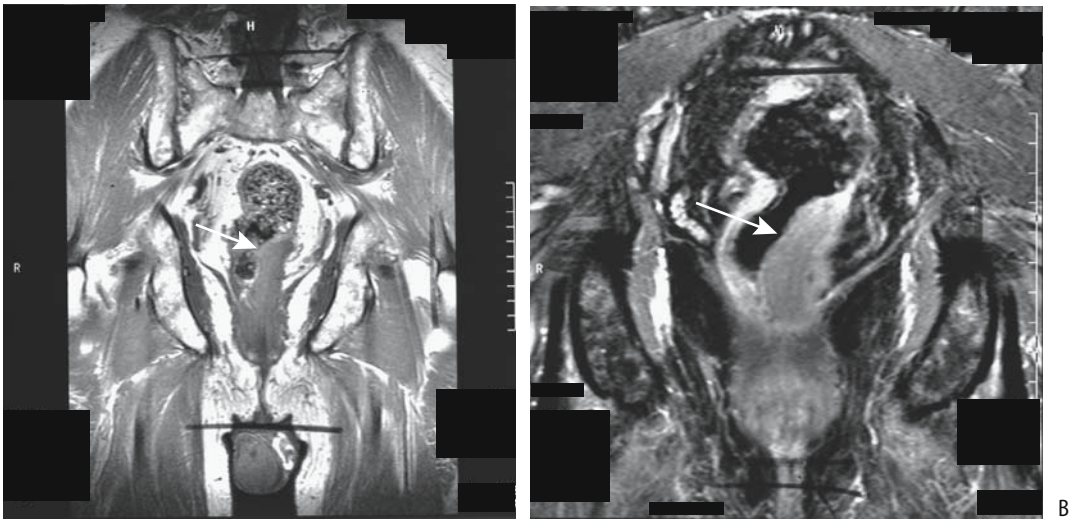

Figure 5.29. Rectal carcinoma. Precontrast (A) and contrast-enhanced (B) coronal T1–weighted MR images identify a left distal rectal tumor (arrows) invading perirectal fat. (From Burgener FA, Meyers SP, Tan RK, Zaunbauer W. Differential Diagnosis in Magnetic Resonance Imaging. Stuttgart: Thieme, 2002, with permission.)

Similar to other imaging modalities, small lymph node metastases are not identified, although iv SPIO agents show promise. Nonmalignant nodes are hypointense or have a hypointense center, while eccentric and hyperintense nodes tend to contain metastases larger than 1 mm in diameter, although overlap does exist (161).

Can MRI predict sphincter salvage in these patients? A prospective MRI study of patients with a low or middle third rectal adenocarcinoma (defined as <12 cm from pectinate line) using rectal and IV contrast and a flexible surface coil achieved 100% sensitivity and 98% specificity in assessing anal sphincter infiltration and 90% sensitivity and 100% specificity in detecting adjacent organ infiltration (i.e., T4 stage) (162); nodal staging, however, was suboptimal—MRI reached a 68% sensitivity and 24% specificity.

Magnetic resonance imaging potentially differentiates between mucinous and nonmucinous rectal tumors. On T2-weighted fast SE images mucinous tumors had significantly higher tumor-to-muscle, tumor-to-fat, and tumor-to-urine signal intensity ratios compared with nonmucinous tumors (163); most mucinous tumors also revealed peripheral post–gadolinium contrast enhancement.

Nonrectal Carcinoma

Although some earlier studies claimed high CT sensitivity and specificity in detecting local tumor extension (T stage), more recent studies are more pessimistic. Local CT staging accuracy increases at higher disease stages. In general, the presence of obvious pericolic spread and nodal involvement is more reliable than negative findings. Nodal involvement is assessed by simply detecting enlarged nodes. Disappointingly, an accuracy of only about 50% has been achieved by a number of studies for nodal metastases.

Most current CT colonography research involves tumor detection, although some evidence suggests that it also should have a role in staging. Thus one study achieved an overall accuracy of 83% in T staging and 80% in N staging when employing contrast enhanced transverse and multiplanar reformated CT colonography, with images obtained in the arterial phase focusing on the suspected neoplasm and portal venous phase images on the entire abdomen and pelvis (164).

The results of hydrocolonic US to detect and stage colorectal carcinomas have been disappointing. Assessment of lymph node involvement is poor.

Comparing different MR studies is difficult because results vary considerably depending on sequences employed. A number of studies have concluded that MR staging accuracy, including nodal involvement, is similar to that obtained with CT. Nevertheless, MRI staging is still in its infancy and future improvements hold promise.

18F-fluoro-deoxy-D-glucose PET appears useful in staging colon cancer. It identifies primary carcinomas (including in-situ carcinomas) but is insensitive in detecting lymph node metastases (165); similar results were obtained with CT. On the other hand, 18F-FDG-PET detects extrahepatic colon metastases missed by other imaging modalities (including CT and MRI); PET detects extraperitoneal nodal metastases, pulmonary metastases, and regional lymph node involvement. Thus PET influences patient selection for hepatic resection.

But 18F-FDG-PET is false-positive in patients with inflammatory bowel or other sites of inflammation.

Radioimmunoscintigraphy holds promise in detecting metastases, but sufficient clinical data are not available on its use in initial staging. Operative gamma probe immunoscintigraphy achieves high sensitivity in detecting liver and extrahepatic abdominal tumor sites but is little practiced.

Therapy

Rather active current research interests involve immunotherapy and genetic therapy. A current trend is toward more aggressive therapy of metastases with such modalities as hyperthermia, cryoablation, and various combination of systemic therapy and surgery. Currently a majority of patients undergo colon cancer resection even in the face of metastases.

For Cure

Endoscopic: A cancer that has not penetrated through the muscularis mucosa is considered a carcinoma-in-situ, and generally endoscopic polypectomy suffices. Terms synonymous with carcinoma-in-situ include *intramucosal carcinoma*, *carcinoma limited to mucosa or lamina propria*, and *superficial carcinoma*. The latter term, however, is sometimes applied to cancers that also involve the submucosa and thus has an imprecise meaning.

Spread beyond muscularis mucosa signifies an invasive cancer and wider excision is indicated, although some pedunculated polyps are resected endoscopically if no vascular or stalk invasion is evident (Fig. 5.30).

One interesting fusion of procedures consists of laparoscopically assisted endoscopic polypectomy for broad-base polyps. Under general anesthesia, endoscopic polypectomy is assisted by laparoscopy and the polyp site is then sutured using a laparoscopic approach.

Surgical: Colorectal cancer surgery is performed in the very old, with cancer-free survival in these elderly patients being quite good. Indications for surgery should be rather liberal; this is in contradistinction to gastric cancer surgery where survival is much more limited.

In addition to preoperative imaging, liver palpation at laparotomy aids in detecting liver metastases at the time of surgery. Intraoperative liver US is also very useful in further staging and patient selection for additional therapy but currently is not widely practiced. The quality of operative US influences considerably the results obtained.

Preliminary results of laparoscopic colon cancer resection are encouraging, with patient survival, tumor recurrence, and mortality being similar to those of open resection. The liver cannot be palpated during laparoscopic colo-

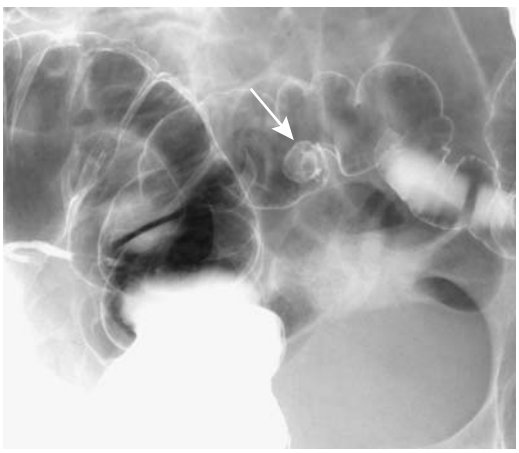

Figure 5.30. Pedunculated sigmoid adenocarcinoma (arrow). The stalk is seen as a circle within this 1-cm round, smooth tumor.

rectal cancer resection, and this useful diagnostic procedure, performed during an open resection, is thus lost. One proposal is that intraoperative laparoscopic US be included as part of laparoscopic colorectal cancer resection; it is possible to scan all liver segments through a single port site for possible metastases. Nevertheless, this is a complex procedure requiring that a radiologist be present in the surgical suite; all parenchymal segments and major intrahepatic vascular and biliary structures need to be identified during the scan. This takes considerable time and effort.

European clinical trials of rectal cancer patients suggest that best results are achieved with radiation therapy followed by surgery. In the United States postoperative radio- and chemotherapy are used for T3 and N1 cancers. One complication after radical surgery for rectal carcinoma is vesicourethral dysfunction.

Radiochemotherapy: Local excision or endorectal radiotherapy are alternate therapies for local control of some select early rectal cancers. A number of studies have established that radiation therapy pre- and postsurgery improves survival. Preoperative radiotherapy appears superior for local tumor control. Radiochemotherapy alone is appropriate in a setting of an unresectable tumor.

Antitumor activity of some chemotherapeutic agents consists of thymidylate synthetase inhibition, an enzyme necessary in DNA synthesis (166); dose-limiting toxicities prevent their more widespread use. Nevertheless, adjuvant therapy with 5-fluorouracil and levamisole does increase the cure rate of stage III (Dukes' C) colon cancer patients. Likewise, radiation therapy combined with chemotherapy appears to have a role in patients with stages II (Dukes' B2) and III rectal cancer.

A combination of adjuvant radiochemotherapy and radical surgery in patients with rectal carcinoma achieves mixed results. Complete response to preoperative chemotherapy and radiation therapy for locally advanced rectal cancer is achieved in a minority. In some patients such therapy also decreases cancer stage, thus permitting a sphincter-saving procedure.

Computed tomography has a major role in planning preoperative radiotherapy.

Serial postcontrast infusion MRI in patients with T3 rectal carcinoma during preoperative radiotherapy provides tumor perfusion data from which a tumor perfusion index (PI) was established (167); the PI increased significantly during the first 2 weeks of therapy, and then decreased. A high initial PI value correlated with subsequent greater lymph node downstaging and thus is potentially of prognostic significance.

Radioimmunotherapy: The use of monoclonal antibody radioimmunotherapy for primary colorectal cancer is still in investigational status. Simultaneous injection of copper 67 and sodium iodide 125–anti-CEA monoclonal antibody in six patients yielded an average Cu-67/I-125 ratio of 1.9 for tumor uptake, 0.7 for blood, and 2.6 for tumor to blood (168); one problem identified by the study was that Cu 67–monoclonal antibody tumor uptake was too low while liver and bowel uptake was considerable.

Other: Ten patients with advanced pelvic cancer (recurrent rectal and ovarian cancer) underwent sequential arterial cisplatinum and mitomycin infusion via an extracorporeal circuit established by isolating pelvic vessels with balloon catheters placed above the aortic and caval bifurcations and pneumatic cuffs at the thighs (169); although the authors established the feasibility for such extracorporeal perfusion, 2-year patient follow-up failed to show a positive response.

Palliation

In the absence of metastases, a preoperative definition of an unresectable cancer is often imprecise. Especially for rectal cancers, unresectability is often established only at surgery.

Patients with unresectable rectal cancer undergo palliation therapy. A combination of local excision, radiation, and chemotherapy is balanced depending on the size of the local tumor spread, the size of the metastases, and life expectancy. Repeat local excision is appropriate for some. Even pelvic reradiation appears to have a role in select patients. Published reports of brachytherapy have been disappointing.

Endoscopic laser therapy using an Nd:YAG noncontact laser performed in patients with obstructing or bleeding inoperable colorectal cancers initially control symptoms in most patients, but symptoms can be expected to recur.

For Obstruction: Most stents are inserted retrograde for palliation of rectosigmoid tumors. An occasional one is inserted antegrade via a percutaneous cecostomy. In addition to relief of obstruction prior to surgery, expandable intraluminal stents decompress the bowel for palliation of a nonresectable tumor, obviating a permanent colostomy (146). A multicenter study of successful palliative stent placement found bowel obstruction resolving within 24 hours of stenting in 96% of patients, with none requiring a colostomy for decompression (170).

Complications, consisting of mild rectal bleeding, abdominal pain, stent malpositioning, obstruction due to fecal impaction, and eventual tumor ingrowth into the stent lumen, are not uncommon. Stents have perforated and migrated.

Among survivors, estimated primary stent patency rate was 91% at 6 months (146).

For Bleeding: An occasional patient with colorectal cancer presents with massive and potentially life-threatening bleeding. Even in a setting of an unresectable tumor, transcatheter embolization should be encouraged. Reembolization is performed if bleeding recurs. Most of these patients eventually die from tumor cachexia rather than exsanguinate.

Recurrence and Follow-Up

General: Although screening for recurrence is commonly practiced, guidelines on specific follow-up have not been established. Screening practices for hepatic and pulmonary metastases vary considerably between hospitals.

Currently a CEA determination is the most common test used to detect cancer recurrence. Carcinoembryonic antigen has a high specificity for tumor recurrence and not uncommonly is positive before imaging. On the other hand, whether frequent CEA determinations prolong survival is not clear.

The role of colonoscopy in screening for local recurrence is rather limited because only about 10% of recurrences are intraluminal. Colonoscopy does have a long-term role, however, in detecting new adenomas and metachronous cancers. Although colonoscopy does have a long-term role in detecting new adenomas and metachronous cancers, preliminary studies suggest, however, that CT colonography is a feasible alternative to both conventional colonoscopy and liver US in following these patients (171).

Both CT and MRI have a major role in detecting recurrence of colorectal cancers, with some studies claiming an accuracy over 90%. A basic question, however, is whether such early recurrence detection influences survival. Current data suggest a rather pessimistic answer. A prospectively, randomized study with patients undergoing either intensive (yearly colonoscopy, liver CT, chest radiography, clinical review, and simple screening) or standard follow-up (structured clinical review and simple screening tests only) found no significant difference in survival between the two groups after a 5-year follow-up (172); yearly colonoscopy failed to detect any asymptomatic local recurrence, and only one asymptomatic curable metachronous colon tumor was found. Liver CT resulted in earlier detection of hepatic metastases but did not increase the number of curative hepatectomies.

Local peritoneal involvement appears to supersede other parameters in estimating patient prognosis. Nevertheless, the clinical significance of malignant cells in the peritoneal cavity is not clear. For instance, in patients with no evidence of peritoneal metastases, peritoneal washing before elective colon resection for adenocarcinoma detected malignant cells in 32% of patients with tumor extending to the serosa (173); the 5-year survival rates were 48% for those with positive washing and 68% for those with negative washing, although multivariate analysis revealed no significant association between positive washing and survival.

Rectal Carcinoma: Recurrence of rectal carcinomas is discussed separately because its recurrence patterns and imaging approach are distinct from those in more proximal colon. Tumor recurrence must be distinguished from postresection fibrosis and surgical deformity (Fig. 5.31). Staging of patients with a proven rectal cancer after radiation and chemotherapy is especially difficult. Both CT and endorectal US overstage these cancers even in patients subsequently found to have no residual cancer. No current imaging modality can reliably distinguish between radiation fibrosis and residual cancer, although MR and scintigraphy show promise (see below). With most imaging a baseline study 2 to 4 months after surgery is

Figure 5.31. A double-contrast barium enema reveals a benign anastomotic stricture (arrow) after sigmoid resection for cancer.

very useful. Postoperative fibrosis retracts over time and gradually develops well-defined margins.

Recurrence after an abdominoperineal resection is most often local. It tends to infiltrate diffusely and is asymmetrical in appearance (Fig. 5.32). No consensus exists on the best imaging modality to evaluate for recurrence. Recurrence detection rates of >90% by endorectal US are being achieved, and this study appears especially useful in this setting.

CT achieves about an 80% sensitivity and specificity in detecting recurrence, while MRI sensitivity is similar but specificity is greater. A typical protocol for these patients consists of CT performed within 2 to 4 months after resection and repeated every 6 to 8 months during the first 2 years (with CEA testing); MRI is reserved for those with a positive or questionable CT finding, those with different clinical symptoms, and those with an increasing CEA. A biopsy is indicated if MRI does not resolve the issue.

Postcontrast CT of active granulation tissue reveals considerable enhancement. Compounding the issue is that local recurrence of rectal cancer results in transient early enhancement at the anastomotic site; whether recurrence can be confidently differentiated from postoperative granulation tissue is not clear.

After rectal cancer resection, the most common CT finding of recurrence is a round or nodular enhancing tumor. A retrospective study of postsurgery or radiotherapy rectal cancer patients who had at least three CT examinations concluded that relapse should be considered if a presacral mass enlarges, appears inhomoge-

A

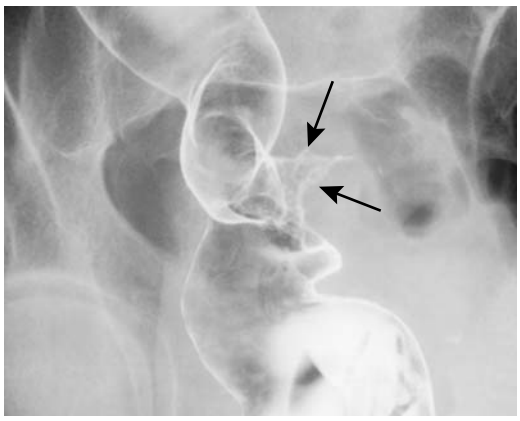

B

Figure 5.32. A: Recurrent rectal carcinoma (arrow) in a patient with a prior rectal cancer resection and a side-to-end low colorectal anastomosis. B: Tumor recurrence at anastomosis in another patient. Barium enema reveals an irregular, ulcerated infiltrating tumor (arrows).

neous, and is asymmetric in outline, or if enlarged lymph nodes develop and infiltrate surrounding structures (174); an unchanged appearance in several follow-up CT examinations is evidence for lack of recurrence. A necrotic recurrence is often difficult to distinguish from an inflammatory mass or abscess.

Some evidence suggests that radiation fibrosis has a somewhat different MR enhancement pattern than postoperative scar tissue. Granulation tissue developing shortly after rectal cancer resection shows marked postcontrast CT enhancement and is hyperintense on T2-weighted MR images. Eventual fibrosis, especially evident after radiation therapy, is hypointense on both T1- and T2-weighted images. Fibrosis shows poor but variable enhancement postcontrast. Retraction of surrounding tissues is common. Fibrosis exhibits an irregular enhancement even years after radiation therapy.

Technetium-99m–labeled anti-CEA antigen-antibody scintigraphy appears to have a role in detecting pelvic recurrence, with sensitivity being similar to that of CT. Sensitivity is greater with an increase in size of a recurrence. In select patients antibody scanning aids in differentiating recurrent tumor from fibrosis.

18F-fluoro-deoxy-D-glucose PET shows increased tumor uptake at recurrence sites; scar tissue has low FDG accumulation. FDG-PET in one study achieved a sensitivity of 82% and a specificity of 65%, but combined PET/CT sensitivity increased to 98% and specificity 96% in differentiating malignant from benign disease (175).

With suspected local recurrence, either transrectal-guided fine-needle aspiration cytology using a 21-gauge needle or a core biopsy with an 18-gauge needle appears appropriate. If a tumor is palpable, digitally guided puncture is feasible; for others, either CT or US guidance is used. Whether 3D endorectal US guidance aids the biopsy of suspected perirectal recurrence remains to be established.

Nonrectal Carcinoma: As a rough estimate, approximately 50% of patients undergoing curative resection for Dukes C colorectal cancer develop a recurrence within 3 to 5 years, and over 90% of them die from their cancer. In those developing a recurrence, almost all colorectal cancers recur within 3 years. Because many recurrent carcinomas consist primarily of an extrinsic component, CT and MRI are well suited for postresection follow-up. A baseline study aids the future differentiation of fibrosis from recurrent tumor.

Superficially, a suture granuloma developing after bowel resection and reanastomosis mimics local recurrence with both colonoscopy and a barium enema.

Considering enhancement within 90 seconds of an abnormal structure on dynamic contrast-enhanced subtraction MRI to signify a malignancy, MR achieved a 97% sensitivity and 81% specificity in differentiating fibrosis from recurrence during follow-up (176); using a finding of high signal intensity on T2-weighted SE images as a criterion for malignancy, sensitivity and specificity were only 77% and 56%, respectively.

Distal Recurrence: For unknown reasons, colorectal cancer metastasis to a fatty liver is uncommon.

Colorectal cancer metastasis to bone is not uncommon. At times bone biopsy is required both for diagnosis and to exclude osteomyelitis. Bone metastasis is more common with rectal and cecal cancers than with other colon cancers. What is uncommon is to find a solitary bone metastasis or a metastasis years later. Signet ring cell cancers appear to have a higher propensity for bone metastasis. Brain metastasis is uncommon but does occur. A rare metastasis occurs within a laparotomy scar.

In women with a prior colorectal adenocarcinoma who then developed a new pelvic tumor, ovarian metastasis was found in 57%, a benign ovarian neoplasm in 26%, and a primary ovarian cancer in 17% (177); among women with a past colorectal cancer, a newly diagnosed uterine cancer was a primary endometrial adenocarcinoma in 73% and metastatic colon cancer in 20%. The rare colorectal carcinoma in adolescent girls frequently metastasizes to the ovaries; these ovarian metastases range from solid, combined solid and cystic, to multilocular cysts, although they tend to be cystic less often than in older patients.

Calcifications in metastatic colon carcinoma are not uncommon; such calcifications are readily identified with CT. Ossification in a metastatic colon carcinoma is rare.

Imaging studies useful in evaluating liver and extrahepatic metastases include conventional chest radiographs, CT, MRI, and scintigraphy.

Resection of liver metastases is precluded in the face of extrahepatic metastases (liver metastases are discussed in more detail in Chapter 7).

Both 18F-FDG-PET and radioimmunoscintigraphy detect earlier local recurrence than is possible with CT or MRI and aid in identifying tumor involving normal size lymph nodes. Their current use, however, is still rather limited and their role in the latter clinical setting is not yet adequately established.

Theoretically, colon cancer detection is improved by combining a monoclonal antibody, which has selective tumor affinity, with PET scanning, which has increased sensitivity and resolution over conventional imaging. To test this hypothesis, an anticolorectal cancer monoclonal antibody (MaB 1A3) was labeled with copper 64, which is a positron emitting radionucleotide (178); such monoclonal antibody-PET scanning achieved a sensitivity of 71% in detecting confirmed tumor sites.

In patients with suspected recurrent colorectal or ovarian carcinoma and normal or equivocal CT or MR studies, indium 111 satumomab pendetide (OncoScint) imaging and FDG-PET imaging are similar in their tumor detection abilities; the radioimmunoconjugate OncoScint is better at detecting carcinomatosis, but PET better detects liver metastases. Indium 111 satumomab liver imaging is suboptimal due to high background levels; nevertheless, it does provide relevant information about extent and location of recurrent colorectal cancer throughout most of the abdomen. It appears especially useful in patients with normal other imaging studies but a rising or high CEA level. An occasional indium 111 satumomab study is false positive, with activity detected in another tumor, such as a nonfunctioning adrenal adenoma.

Single photon emission computed tomography (SPECT) immunoscintigraphy using Tc-99m–anti-CEA monoclonal antibodies shows promise in follow-up after surgery. There are, however, problems in interpreting images because of variations in antibody distribution. It detects local or abdominal recurrence and appears to be more accurate than CT in the abdomen.

Scant literature exists on the usefulness of PET imaging in detecting recurrent colorectal cancer, although PET is more sensitive in detecting early recurrence than CT or MRI. In fact, PET appears to be more sensitive than CEA in detecting tumor recurrence. In previously treated colorectal cancer patients with suspected recurrence, FDG-PET detects >90% of liver and extrahepatic metastases, considerably more than CT. In fact, currently FDG-PET is the most accurate noninvasive modality for staging patients with recurrent metastatic colorectal cancer.

Anaplastic Carcinoma

Colorectal small cell anaplastic carcinomas are rare. Some contain exocrine differentiation. These tumors tend to be aggressive and metastasize early, both to lymph nodes and hematogenously. Staging should include CT of the chest and abdomen and bone scintigraphy.

Adenosquamous/Squamous Cell Carcinoma

These are rare but aggressive colorectal tumors having a predilection for the rectum; some are associated with ulcerative colitis or with other carcinomas.

About 70% of anal carcinomas are squamous and 30% are cloacogenic (179). Imaging has no role in detecting these cancers but aids in staging. They spread mostly locally to the perirectal, inguinal, and iliac nodes; distal spread is to the lungs and liver.

Traditional therapy of anal carcinoma was an abdominoperineal resection, which is rarely performed now, having been supplanted by radiation and chemotherapy.

Lymphoma

Lymphomas range from diffuse gastrointestinal tract involvement to, less often, being limited to the colon. Cecum and rectum are the most common large bowel sites. Primary colon lymphomas tend to present as large intramural infiltrating tumors. Over half of primary colonic non-Hodgkin lymphomas are diffuse large-cell lymphomas.

Clinically, some colonic lymphomas present with signs and symptoms similar to those of an adenocarcinomas; others mimic inflammatory bowel disease. Less common presentations are acute abdomen, intussusception, or simply with an abdominal tumor. A possibility of lymphoma being misdiagnosed as inflammatory

bowel disease from superficial mucosal biopsies has already been mentioned (see Ulcerative Colitis). Some of these patients undergo steroids therapy until a correct diagnosis of lymphoma is made. In fact, lymphoma should be considered in the differential diagnosis of a dense lymphocytic infiltrate obtained from a segment of bowel simulating either ulcerative colitis or Crohn's disease.

Although not common, patients with leukemia have developed colon lymphoma.

Overall, colonic lymphomas appear similar to those seen in the small bowel. A common appearance is that of an intramural infiltrating, sharply marginated tumor. Involved colon tends to be thickened and distorted, an aid in differentiating lymphomas from adenocarcinomas. A lymphomatous large, ulcerated mass is less common. A rare appearance is aneurysmal dilation of the affected colonic segment.

Unlike cecal adenocarcinomas, extension across the ileocecal valve is common with lymphomas, and the site of origin is often difficult to determine; some authors use the term *ileocecal lymphoma* to describe these tumors. Their differential diagnosis includes a mesenchymal tumor and localized Crohn's disease.

Double-contrast barium enema findings in patients with peripheral T-cell lymphoma range from diffuse colonic involvement to focal, and from aphthae, gross ulcers, polyps, and circumferential narrowing to simply ileocecal deformity (180). An occasional lymphoma manifests as multiple polyps in the proximal gastrointestinal tract and numerous aphthae in the colon.

An occasional colonic lymphoma presents as diffuse polyposis. These polyps tend to vary in size, and the barium enema appearance mimics familial polyposis, although the two entities can usually be differentiated on clinical grounds. Most often such lymphomatous polyposis represents B-cell lymphoma.

Sarcoma

Leiomyosarcomas are the most common primary colorectal sarcomas. These sarcomas tend to be larger than carcinomas at first presentation. After resection the 5-year survival depends on the tumor grade.

Endoscopic US identifies rectal leiomyosarcomas as hypoechoic tumors.

Liposarcoma

Magnetic resonance imaging of liposarcomas reveal several patterns. Well-differentiated liposarcomas have MRI characteristics similar to those of a lipoma, consisting of a well-marginated tumor hyperintense on T1-weighted images, hypointense on T2-weighted images, and showing little if any contrast enhancement; less well-differentiated liposarcomas tend toward a heterogeneous appearance, with many containing varying amounts of necrosis. In general, tumor necrosis varies inversely with the degree of tumor differentiation.

Angiosarcoma

Colonic angiosarcomas are rare. A cecal angiosarcoma occasionally intussuscepts.

Histiocytoma

Primary colonic malignant fibrous histiocytomas are rare. Initially these sarcomas are confined to the colon wall, but with growth ulcerate through the mucosa and bleed, or they invade the adjacent soft tissues. Peritoneal implants and lymph node metastases are evident with some. Also, an adjacent extraperitoneal malignant fibrous histiocytoma readily invades the colon and appears as an infiltrating serosal tumor.

Imaging reveals a solid, generally large tumor suggesting a sarcoma or lymphoma.

Pathologic identification of a histiocytoma is not always straightforward. At times an inflammatory fibrosarcoma and a leiomyosarcoma are in the differential.

Carcinosarcoma

Only a few colonic carcinosarcomas have been reported. A question is occasionally raised about whether these represent two separate collision neoplasms, although most carcinosarcomas appear to represent differentiation of a single progeny into two cell types. The presence of retroviral particles in the sarcomatous cells of some of these tumors supports the theory of tumor differentiation from a carcinomatous into a sarcomatous component.

An elevated, fungated, ulcerated tumor is a typical appearance. Most carcinosarcomas carry a poor prognosis.

Melanoma

Most of the rare primary melanomas are found in the rectum, and these patients present with rectal bleeding. They tend not to obstruct.

Primary rectal malignant melanomas tend to be polypoid or fungating, but often already extending to the pelvic side wall at initial presentation (181). A cancer is often suspected. Adenopathy is common. At times a biopsy contains few melanocytes but considerable inflammation, and only after tumor excision is a correct diagnosis made.

A dual rectal melanoma and adenocarcinoma are occasionally reported; presumably such dual collision neoplasms develop by chance.

Both primary and metastatic melanomas have a high tumor-to-background PET activity and FDG-PET scanning is useful to detect unsuspected metastases; PET is also commonly employed for follow-up after therapy.

Metastasis or Direct Invasion to Colon

Metastasis to the colon is not common; more common is direct invasion from an adjacent structure. Thus gynecologic malignancies invade the rectum, or a hepatocellular carcinoma invading the adjacent splenic flexure results in massive bleeding, even to the point of exsanguination.

In a comparison of CT and MRI in predicting bladder or rectal invasion in women with uterine carcinoma, MRI was slightly, but not statistically, superior to CT (182); both provided similar results as rectoscopy.

A long segment of circumferential rectal wall thickening, having a rectal linitis plastica appearance, is most often due to metastatic gastric cancer, but it can be found with other causes of peritoneal carcinomatosis and rectal metastasis (183). Obstructions and fistulas are rare manifestations of lung and breast metastases. A renal cell carcinoma is one cause of a hypervascular metastasis.

A recurrent bladder or prostatic carcinoma invading the rectum can simulate a rectal leiomyoma or result in an annular constricting lesion.

A malignant colon obstruction, either primary colonic or extrinsic, most often due to spread of a gynecologic tumor or peritoneal seeding, is a difficult management problem. Most of these tumors are unresectable, but palliation of bowel obstruction is desirable. Palliation consists, at best, of a proximal colostomy. An occasional option with a single major obstruction is metallic stent placement for decompression if access under fluoroscopic guidance is feasible. Most such treatable obstructions are in the rectum and rectosigmoid, but occasionally a stent can be inserted through a more proximal obstruction (184). Many of these patients, however, have widespread metastases, including to the small bowel, and no viable bypass is feasible.

Rhabdoid Tumor

The rare colonic malignant rhabdoid tumor is diagnosed by a pathologist detecting rhabdoid cells. This tumor is more common in the kidneys. No specific imaging features have been described.

Neuroendocrine Tumors

Colonic neuroendocrine tumors are uncommon, and some are difficult to place in proper perspective. An occasional colorectal poorly differentiated neuroendocrine carcinoma presents with widespread liver metastasis.

These tumors range from benign to malignant. Most are solid, intramural tumors, with an occasional mesenteric one appearing as an extraserosal tumor.

Carcinoid

Rectal carcinoids are more common than colonic ones; a cecal location is most common in the colon. Synchronous carcinoids occur occasionally. Similar-appearing rectal carcinoids have developed in siblings. The malignant potential of rectal carcinoids varies considerably.

Small rectal carcinoids are palpable on digital examination as firm nodules. Endoscopy visualizes small polyps covered by normal-appearing mucosa, with either erythema or a central depression occasionally being found.

Carcinoid syndrome develops mostly in a setting of metastases, with only an occasional rectal carcinoid directly responsible for this syndrome.

Table 5.5. Clinical findings in patients with rectocolic and ileocecal carcinoids

Finding	Reference 185	Reference 186
Number of tumors studied	279*	36**
Tumor size:		
>2 cm	90%	—
Average size	—	6 cm
Prevalence of:		
Metastases	61%	—
Nodal invasion	—	22%
Detection of serotonin		
Immunohistochemical	67%	
Laboratory	69%	
Postoperative 5-year survival rate	65%	26%

* Includes 203 patients with colon carcinoids and 76 with ileocecal carcinoids.
** Includes malignant carcinoids only.

Table 5.5 summarizes the clinical findings from two studies. Between 1964 and 1988, the Alberta Cancer Registry compiled 36 malignant colon carcinoids (excluding ileocecal region and rectum) (186); average age at diagnosis was 68 years, and at presentation 22% of patients were already Dukes C and 86% had invaded pericolic fat. Many malignant carcinoids have already metastasized at initial presentation, with the most common metastatic sites being the liver and lung. In fact, the presence of metastases is often the unequivocal finding establishing malignancy of these tumors. Survival with colonic carcinoids is lower than with rectal or appendiceal carcinoids (or even with colon adenocarcinomas).

Carcinoids range in appearance from a simple polyp to an apple-core infiltrating tumor mimicking an adenocarcinoma. An unusual barium enema finding in the presence of a carcinoid is colon jejunization. Such jejunization presumably is secondary to colonic wall foreshortening induced by the desmoplastic reaction commonly associated with these tumors. A carcinoid located in the posterior rectal wall or adjacent tissues widens the presacral space.

Transrectal US in patients with rectal carcinoids reveals increased echogenicity and a heterogeneous internal echo pattern in some. Small rectal carcinoids tend to be hypoechoic. Pathologically, these findings are associated with increased fibrotic interstitium around nodular tumor nests. Transrectal US can also often reveal depth of invasion and suggest lymph node metastasis.

I-123-metaiodobenzylguanidine (MIBG) scintigraphy evaluates metastatic carcinoids.

Some small carcinoids have been resected endoscopically, although most require surgical excision, similar to adenocarcinomas.

Other Tumors

Schwannomas, or primary nerve sheath tumors, originate more often from peripheral nerves and are rare in the colon. Most are benign. Their imaging appearance is similar to other stromal tumors. A cystic component is occasionally detected.

A rare colonic ganglioneuroma presents as filiform polyposis.

Neurofibromatosis type 1 (von Recklinghausen's disease) is discussed in Chapter 14. Gastrointestinal neurofibromatosis is uncommon and is a late manifestation of von Recklinghausen's disease. Only rarely is colonic neurofibromatosis an initial presentation.

Gastrointestinal neurofibromas range from solitary, to multiple, to plexiform in appearance. An occasional colonic plexiform neurofibroma and neuronal hyperplasia result in disordered mobility, a megacolon, and proximal bowel dilation, similar to other causes of adynamic ileus. Some manifest through gastrointestinal bleeding.

Granular cell myoblastomas are more common in the esophagus. They are rare in the colon. Most are single, but occasional reports describe multiple tumors scattered throughout the large bowel.

Dilatation

Mechanical Obstruction

The two most common causes of colonic obstruction in adults, namely colon cancer and diverticulitis, have already been discussed. Hernias are covered in Chapter 14. Colon obstruction in a setting of cystic fibrosis was covered in a previous section (see Cystic Fibrosis).

Primary causes of intestinal obstruction in elderly patients requiring surgery are an incarcerated hernia and colonic neoplasms.

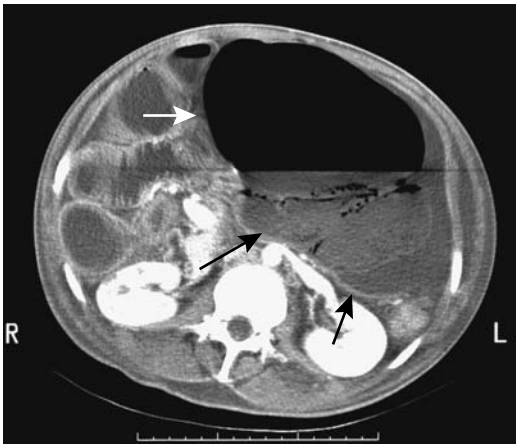

Figure 5.34. Cecal volvulus. CT identifies a massively dilated cecum displaced to the left of midline (arrows). Dilated loops of small bowel on the right are secondary to small bowel obstruction. (Courtesy of Patrick Fultz, M.D., University of Rochester.)

Volvulus

Cecal

Traditionally, cecal volvulus was suggested with conventional radiography and confirmed either with a barium enema or colonoscopy. Most often cecal volvulus is idiopathic (Fig. 5.33), but occasionally it is induced by a more distal partial obstruction. Computed tomography appears to be more accurate than conventional radiography in suggesting the diagnosis (187), and although CT is often performed for suspected cecal volvulus, few studies have evaluated whether it is superior or even equal to a barium enema (Fig. 5.34).

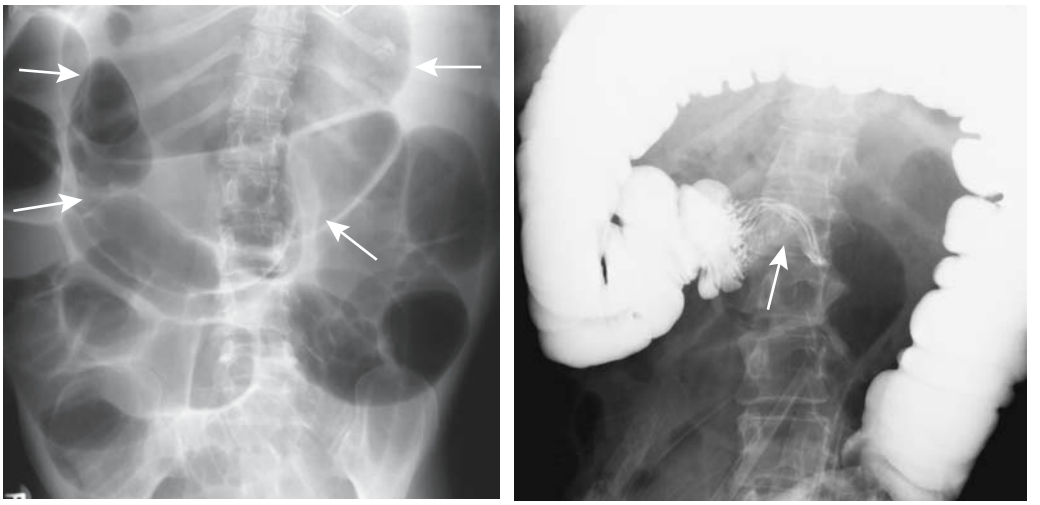

Figure 5.33. Cecal volvulus. A: Conventional radiograph shows a greatly dilated midabdominal loop of bowel (arrows). B: Barium enema reveals a characteristic beak sign (arrow) at the site of twist in the right colon.

In distinction to sigmoid volvulus, a successful therapeutic barium enema or colonoscopy is achieved only in a minority of these patients, and most undergo surgery.

Sigmoid

Sigmoid volvulus ranges from an acute condition, often associated with strangulation, to a chronic setting, with the patient presenting with a gradual onset or intermittent obstruction. An immediate concern is to ascertain that this is indeed idiopathic sigmoid volvulus rather than a sigmoid or rectal cancer-induced colonic obstruction. Sigmoid volvulus occasionally develops during pregnancy and after gynecologic and other abdominal surgery.

Imaging findings of sigmoid volvulus are familiar to most radiologists (Fig. 5.35). A CT whirl pattern consists of a twisted, dilated sigmoid loop and its associated vessels around the mesocolon. If the transverse colon can be identified on radiographs (with the patient supine), a dilated sigmoid colon located cephalad to the transverse colon is an accurate finding of sigmoid volvulus (188).

The preferred therapy for acute sigmoid volvulus is decompression either by endoscopy or barium enema, followed, if indicated, by elective sigmoid resection. Simple sigmoid decompression does relieve obstruction but volvulus tends to recur if no resection or fixation is performed. A surgical nonresective procedure consists of extraperitonealization of the sigmoid colon by placing it in the infraumbilical abdominal wall.

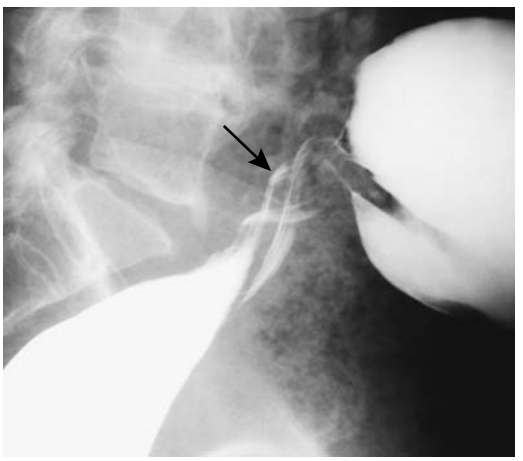

Figure 5.35. Sigmoid volvulus. A lateral view from a barium enema identifies a typical twist (arrow), shows barium in a dilated sigmoid and excludes a carcinoma as etiology for the obstruction.

Transverse Colon

Transverse colon volvulus is rare. It is more common in women. Patients with Chilaiditi's syndrome appear more prone to developing a transverse colon volvulus; lax colonic ligaments predispose to such torsion.

In adults, conventional radiographs are rarely diagnostic of transverse colon volvulus. Barium enema findings vary; even a coil-spring appearance mimicking an intussusception has been reported.

Other

Only rare reports describe splenic flexure volvulus. It occurs in association with systemic sclerosis and has developed in patients with a wandering spleen, generally around the splenic pedicle. It can be associated with small bowel obstruction.

Descending colon volvulus can develop in a setting of an anomalous mesocolon and a redundant bowel.

Intussusception

In an intussusception, a segment of bowel, the intussusceptum, invaginates into the lumen of an adjacent intussuscipiens. Any part of bowel can intussuscept, although a mobile intraperitoneal bowel loop and its associated mesentery are most often involved. The intussusceptum usually invaginates distally, although occasional proximal invagination does occur (for example, a jejunogastric intussusception after a Billroth II operation). Intussusceptions range from transient to fixed. As discussed below, some are reduced with pressure.

By its bulk, an intussusception should obstruct the bowel lumen, although in distinction to pediatric patients, bowel obstruction is not a prominent feature of adult intussusceptions. A more serious consequence, especially in the younger patient, is vascular occlusion of the intussusceptum, generally venous, and resultant ischemia.

Adults

Intussusceptions in most adults have an identifiable lead point and range from enteroenteric, to ileocolic, to colocolic, to rectal prolapse. The most common lead point is a cecal adenocarcinoma (Fig. 5.36); less common is cecal lymphoma or a benign polyp. Rarer lead points in adults consist of pseudomembranous colitis, Meckel's diverticulum, a rare duplication, endometrioma (Fig. 5.37), or even calcified cecal fecaliths. An appendiceal polyp in a patient with Peutz-Jeghers syndrome acted as a lead point for intussusception (189). Although most colonic lipomas are intramural and sessile, they are prone to becoming pedunculated and act as lead points for an intussusception. Not all of these are at the ileocecal region; a number of sigmoid lipoma-associated sigmoidorectal intussusceptions have been reported.

A rectal intussusception is usually a transient phenomenon occurring during straining, is idiopathic, and is associated with constipation. Proctography shows circular infolding of the rectal wall during straining. The criteria defining when such infolding is abnormal are not well established, and minor changes probably are best considered normal variants, but solitary rectal ulcer syndrome (discussed later) is in the differential diagnosis.

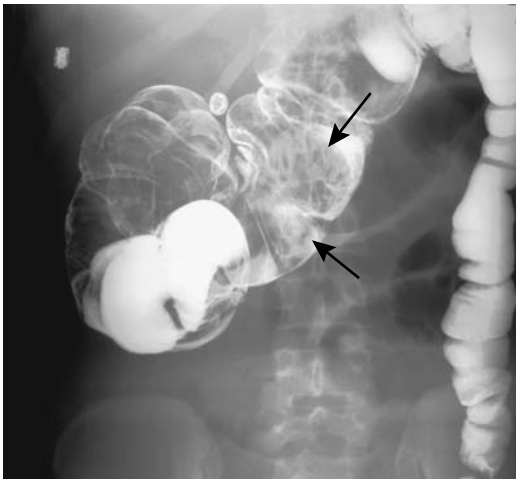

Figure 5.37. Colocolic intussusception (arrows). The lead point was an endometrioma, a highly unusual source for an intussusception.

Computed tomography and MR detect most adult ileocolic intussusceptions but, aside from a lipoma, identification of a lead point is difficult. At times even endoscopic biopsy fails to provide an etiology, and the diagnosis is established only after a right hemicolectomy. Computed tomography findings of an intussus-

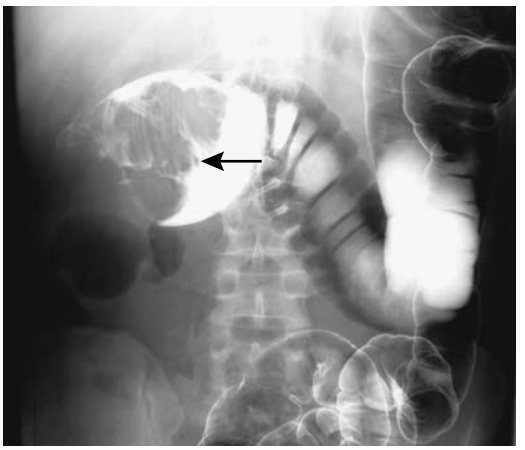

A

B

Figure 5.36. Colocolic intussusception with cecal carcinoma as lead point. A: Barium enema reveals the intussusceptum in the transverse colon (arrow). B: With further pressure the intussusceptum is reduced into the ascending colon.

ception consist of a target or sausage-shaped inhomogeneous soft tissue tumor. The appearance varies depending on the relative orientation of the x-ray beam and intussusception. Colocolic intussusceptions caused by a colonic lipoma can be suggested by US; CT is diagnostic if fat is detected in the lead point, although the lack of fat in the lead point due to infarction and necrosis of an intussuscepted tumor does not exclude a lipoma.

Unenhanced CT has a role if ischemia is suspected in adults with an intussusception; CT findings of a hypodense layer in the intussusceptum or surrounding fluid or gas should suggest vascular compromise (190); lumen obstruction is not always present in an ischemic or necrotic intussusception.

Overlying pneumatosis cystoides intestinalis and enteritis cystica profunda are uncommon associated finding of a colocolic intussusception.

Magnetic resonance imaging also readily identifies intussusceptions, with findings similar to those found with CT. Magnetic resonance imaging reveals concentric bowel rings.

Pediatrics

Clinical

An acute ileocolic intussusception in a young child is a common emergency. Most intussusceptions occur before the age of 2 years and are idiopathic in origin. The rare identifiable lead points, more common in older children, consist of a Meckel's diverticulum, polyp, or even a duplication. Why the reported prevalence of intussusception is greater in some parts of the world is puzzling.

The typical clinical presentation and conventional radiographic findings are well known. Occasionally encountered, however, is an atypical presentation, for instance, bilious vomiting due to an ileocolic mass resulting in extrinsic duodenal obstruction.

One variant is an ileoileocolic intussusception. Prereduction findings are similar to those of an ileocolic intussusception. Once the intussusception was reduced to the cecum, air enemas in nine children with ileoileocolic intussusceptions identified the intussusceptum as two or more separate polypoid components, in contrast to ileocolic intussusceptums, which tend to be either smoothly marginated or somewhat lobular in appearance (191).

Sigmoidorectal intussusceptions also occur in infants and children. In some, the typical clinical presentation of a palpable abdominal mass and colicky pain is absent. These intussusceptions can be misdiagnosed as simple rectal prolapse.

Presumably a surgical consultation has been obtained and a surgeon has examined the child prior to attempted intussusception reduction. The child should be in stable condition, and both the surgeon and the radiologist should be confident that no contraindication exists to a therapeutic enema. Contraindications for reduction include bowel perforation, peritonitis, and hypovolemic shock.

A long-term outcome study in children found an overall recurrence rate of 9%, with about two thirds of children having a single recurrence (192); reducibility was 95% for recurrent intussusceptions, with no perforations. Also, recurrence did not predict an abnormal lead point.

Imaging

Although conventional abdominal radiographs are often obtained first, their value has been questioned. Even experienced observers often differ whether in children with clinically suspected intussusception it is indeed present or absent; the best predictor of intussusception is a soft tissue mass and decreased large bowel gas (Fig. 5.38).

In some centers, US is the initial imaging modality of choice when suspecting an intussusception (Fig. 5.39). In experienced hands US has a high sensitivity and specificity in detecting an intussusception and a contrast enema is then limited to therapy. Viewed in a transverse section, prereduction US shows an intussusception as a doughnut or *target lesion*; it has a reniform shape (*pseudokidney* is the term often used) when viewed in longitudinal section. Scans close to the lead point of an intussusception reveal the intussusceptum as a hypoechoic central structure; scans away from the lead point have a hyperechoic crescent appearance due to mesentery and related vessels being drawn in by the intussusceptum. Although such a US appearance should suggest an intussusception, neither a target nor reni-

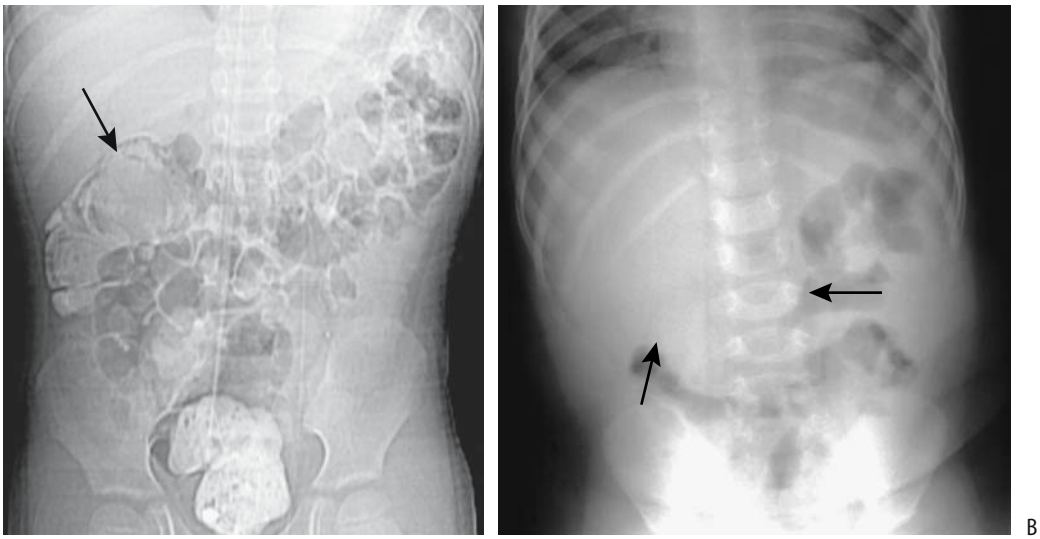

Figure 5.38. Ileocolic intussusception. A: CT scout view identifies an intussusception (arrow) in a 7–year-old. Burkitt's lymphoma was the lead point. (Courtesy of Luann Teschmacher, M.D., University of Rochester.) B: Intussusception in a 10–month-old infant with pain and palpable right upper quadrant mass. A conventional radiograph reveals a soft-tissue tumor in region of transverse colon (arrows). A barium enema confirmed intussusception.

form appearance is pathognomonic. Necrotizing enterocolitis, volvulus, or even stool may mimic this appearance.

At times, because of obscure symptomatology, these patients are studied with CT. Findings of intussusception are straightforward in most. Computed tomography reveals an intraluminal tumor and a *target sign*–like appearance of alternating layers of high and low attenuation. With obstruction, more proximal bowel loops distend with fluid. Necrosis manifests as inflammation, loss of tissue planes, and presence of intraperitoneal fluid.

An extensive ileocolic intussusception distorts normal superior mesenteric vessel anatomy. Thus with the lead point of an intussusceptum at the sigmoid colon or distally, the superior mesenteric vein is located to the left of the superior mesenteric artery.

Published successful intussusception reduction rates range between 70% and 85%, with an occasional report of 90%, regardless of whether a liquid or air is used. A comparison of different contrast agents used is difficult unless the procedure used is standardized. A major factor influencing success rates is the intraluminal pressure achieved rather than any other technical factor. A barium enema bag at 1-m elevation produces greater intraluminal pressure than a typical water-soluble contrast agent or water at the same height. Pressure during pneumatic reduction varies considerably.

At times US identifies fluid within an intussusception, representing trapped peritoneal fluid, seen on axial images as an anechoic crescent between the intussusceptum and intussuscipiens.

Ultrasonography during reduction of an ileoileocolic intussusception reveals a complex frond-like appearance. The intussuscepted small bowel is also surrounded by cecal fluid. These intussusceptions are likewise difficult to reduce.

Contrast Agents

Historically, a barium enema was performed in the pediatric patient suspected of an intussusception. The study not only established a diagnosis but also was therapeutic.

Some radiologists still use barium for reducing intussusceptions, although teaching and pediatric hospitals have changed to a pneumatic technique.

A

B

C

Figure 5.39. Ileocolic intussusception due to large lymph nodes in a 10–year-old. A: CT detects an intraluminal right colic tumor (arrows) suggesting an intussusception. The intussusceptum is seen as a target lesion on a transverse US scan (B) and as an oval tumor on a longitudinal scan (C). Surgery revealed enlarged nodes as a lead point but no neoplasm was identified. (Courtesy of Luann Teschmacher, M.D., University of Rochester.)

A pneumatic reduction of intussusception is safe and successful in most children. Although fluoroscopy is useful for this procedure and is employed by many radiologists, a lead point is difficult to identify. Thus even with successful reduction, the presence of a tumor lead point is not excluded. Still, many radiologists believe that pneumatic reduction is quicker, safer, and more effective than hydrostatic reduction.

Reduction success rate varies with the duration of signs and symptoms. Thus success rate for air reduction was 89% for those symptomatic for <12 hours, 83% for those with symptoms for 12 to 24 hours, and 74% for those symptomatic for >24 hours (193). Several trials of air reduction increase the success rate. A success rate of 70% with one trial of air reduction increased to 91% after a policy of up to three trials was instituted (193).

Some radiologists perform pneumatic reduction under US control. In patients who underwent 52 US-guided pneumatic intussusception reductions, the overall success rate was 92% (194); a pressure of 60 mm Hg was maintained for 30 seconds, and if an intussusception failed to reduce, the procedure was repeated at a pressure of 120 mm Hg. Perforation occurred in two others. The published data of pneumatic reduction under US control are difficult to place in the proper perspective because of the subjective nature of many of these studies.

In some parts of the world pneumatic reduction is performed with no imaging, and the success of reduction is evaluated purely on clinical grounds.

Color Doppler US evaluates whether blood flow is present in an intussusception. The success rate for air reduction is significantly greater in those children with blood flow in the intussusception than in those with absent flow. Lack of Doppler evidence for blood flow, however, should not be a contraindication to attempted reduction, and practical application of such Doppler study remains to be established.

A more recent technique is US-guided intussusception reduction using a saline enema or Hartmann's solution. The sonographic criteria of intussusception reduction include an initial target sign that is later no longer identified, visualization of the ileocecal valve, and fluid refluxing into small bowel; this technique has a success rate of over 90% in reducing an intussusception.

Complications

In some infants only partial intussusception reduction is achieved. In these infants, instead of performing immediate laparotomy, in consultation with the surgeon and if the infant is clinically stable, another attempt at intussusception reduction may be appropriate.

The risk of bacteremia during intussusception reduction is low.

What are the sequelae of a perforation during an intussusception reduction? In 14 perforations (seven using barium and seven air) all children with barium reduction required bowel resection, but only four of the seven with air required resection (195); in addition, the anesthesia time was longer and hospital stay longer in the barium group. Of interest is that perforations are through necrotic bowel only in a minority of these children; presumably increased pressure plays a major role in these perforation. In general, all other factors being equal, the perforation rate is probably similar regardless whether barium or air is used.

Extrinsic Obstruction

Occasionally a distended bladder compresses the rectosigmoid against the sacrum and obstructs on either an acute or chronic basis. Similarly, some gynecologic tumors compress the rectosigmoid without invasion. A barium enema is diagnostic.

A pregnant patient with an ileal pouch–anal anastomosis presented at 36 weeks' gestation with bowel obstruction (196); the obstruction cleared after delivery.

Obstruction by Gallstones

Gallstone ileus most often obstructs in the ileum (discussed in Chapter 4). With a cholecystoduodenal fistula, if a stone manages to pass through the ileocecal valve, colonic gallstone ileus occurs almost always only proximal to a stricture.

Another scenario of colonic gallstone ileus occurs if a cholecystocolic fistula develops; obstruction by the gallstone most often is in the sigmoid colon. If the obstruction is incomplete, a barium enema identifies a cholecystocolic fistula.

Obstruction Due to Motility Abnormalities

Pseudo-Obstruction (Ogilvie's Syndrome)

Etiology

A number of etiologies have been proposed for acute colonic pseudo-obstruction (Ogilvie's syndrome), including an imbalance between sympathetic inhibitory and parasympathetic excitatory colonic innervation. It occurs most often after surgery or trauma (Table 5.6).

Table 5.6. Conditions associated with Ogilvie's syndrome

Common
Recent surgery
Recent trauma
Severe medical condition
Uncommon
Postcesarean section
Leukemia
von Recklinghausen's disease
Multiple endocrine neoplasia (MEN) syndrome type 2
Botulism in infants
Herpes zoster infection
Hypothyroidism
Myotonic dystrophy
Drug therapy
Imipramine
Tocolytic therapy

Some chronically hospitalized or bedridden patients have a chronic megacolon or megarectum, generally of idiopathic etiology. Manometry in these patients reveals abnormal colonic tonicity. Histology of resected specimens from patients with idiopathic megarectum and megacolon reveals hypertrophy of muscularis mucosae and muscularis propria; those with an idiopathic megarectum tend to have decreased innervation density of the longitudinal muscle.

Recurrent acute colonic pseudo-obstruction in a young patient with no evident risk factors was eventually ascribed to toxoplasmosis infection (197); adrenergic bowel denervation was believed to be caused by toxicity or cross-reaction between a toxoplasma antigen and the patient's immune system.

Imaging

The conventional radiographic appearance of Ogilvie's syndrome mimics distal colonic obstruction. Thus if the diagnosis is in doubt, a limited barium enema is indicated and should differentiate between these conditions.

Instead of a barium enema, two additional conventional radiographs often suffice: a right lateral decubitus view of the abdomen followed by a prone lateral view of the pelvis. With these two additional views gaseous distention of the rectum can be achieved in most patients with pseudo-obstruction, while in patients with mechanical obstruction such distention is not found.

Although the cecum is generally most dilated in Ogilvie's syndrome, occasionally some other colonic segment is involved. The rectum tends to be collapsed.

Therapy

Ogilvie's syndrome has been treated successfully with a parasympathomimetic drug such as neostigmine. The success of such therapy suggests that Ogilvie's syndrome is a result of excessive parasympathetic suppression rather than sympathetic overactivity. Colonoscopic decompression has a high success rate, although some patients required multiple decompressions. A decompression tube positioned in either the right colon or transverse colon appears to be equally successful.

Untreated, Ogilvie's syndrome has progressed to perforation and an acute abdomen.

Chagasic

Chagas' disease is a chronic infection caused by the parasite *Trypanosoma cruzi*, which is endemic in rural regions of Latin America. A chronic phase develops several decades after initial infection, most often manifesting through cardiac abnormalities. Colonic abnormalities consist of decreased motility and tonicity, identified as a megacolon. These patients develop small bowel bacterial overgrowth with resultant complications.

Systemic Sclerosis (Scleroderma)

Colorectal dysfunction is common in patients with systemic sclerosis. Hypotonia and stasis develop in some. Constipation is common, but, paradoxically, incontinence is also not uncommon.

T1- and T2-weighted SE MRI magnetization transfer contrast-weighted and dynamic gadolinium-enhanced images in 11 of 14 patients with scleroderma and fecal incontinence revealed forward deviation of an atrophied internal sphincter that had decreased contrast enhancement (198); for comparison, patients with incontinence alone showed no internal sphincter deviation or decreased vascularity but did have significant reduction in external sphincter mass.

Diverticula

Colonic

Colonic diverticula represent outpouchings in the bowel wall. In the past, a distinction was made between true and false diverticula (pseudodiverticula), but common indiscriminate usage has made any such distinction moot.

Prevalence of colonic diverticula varies considerably throughout the world. Their prevalence is increasing in some populations. Right-sided colonic diverticula are more common in Asia than in the West.

Occasionally encountered are calcified stones within a diverticulum. Presumably these stones form as a result of stasis. Superficially such

right-sided diverticular stones mimic gallbladder stones or renal stones.

In rare instances a diverticulum intussuscepts or inverts into colonic lumen and simulates a polyp. Some of these patients have undergone surgery or colonoscopy because the diverticulum could not be distinguished from a polyp. Some of these inverted diverticula have an umbilication that represents the *en face* diverticular opening. Computed tomography of these inverted diverticula reveal a central contrast collection within the lumen, presumably within the diverticulum.

Ultrasonography does not readily identify colonic diverticula. When seen, diverticulitis rather than diverticulosis should be suspected.

Rectal

Rectal diverticula are uncommon and, in general, tend to be larger than the corresponding sigmoid ones. These diverticula tend to be more common in scleroderma patients.

Giant Diverticula

Giant colonic diverticula are sufficiently rare that individual reports are still being published. Most occur in the sigmoid colon. Their etiology is unknown, although several theories are postulated: First, a check-valve mechanism in the diverticular neck allows colonic content to enter but not exit. Or, a localized diverticular infection results in an abscess that eventually communicates with colonic lumen. Although less likely, such a cavity may also represent sequelae of a communicating duplication cyst. In either case, some of these cavities enlarge to giant proportions. Histologically, these giant diverticula do not have a mucosal lining, with the wall consisting mostly of fibrotic tissue, thus suggesting a contained perforation as their etiology.

Patients range from asymptomatic to those presenting with bleeding or an acute abdomen. An occasional giant colonic diverticulum perforates and results in a pneumoperitoneum. Other rare complications include an associated carcinoma, small bowel obstruction, or even volvulus.

These uncommon lesions can be suspected with conventional radiography and are diagnostic with a barium enema when barium flows into the diverticulum, thus establishing its colonic communication (Fig. 5.40). Imaging shows a large gas collection, usually close to the sigmoid colon. The diverticular wall tends to be thin and smooth. Horizontal x-ray beam radiographs often reveal a gas-fluid level. The diverticular wall shows no CT contrast enhancement,

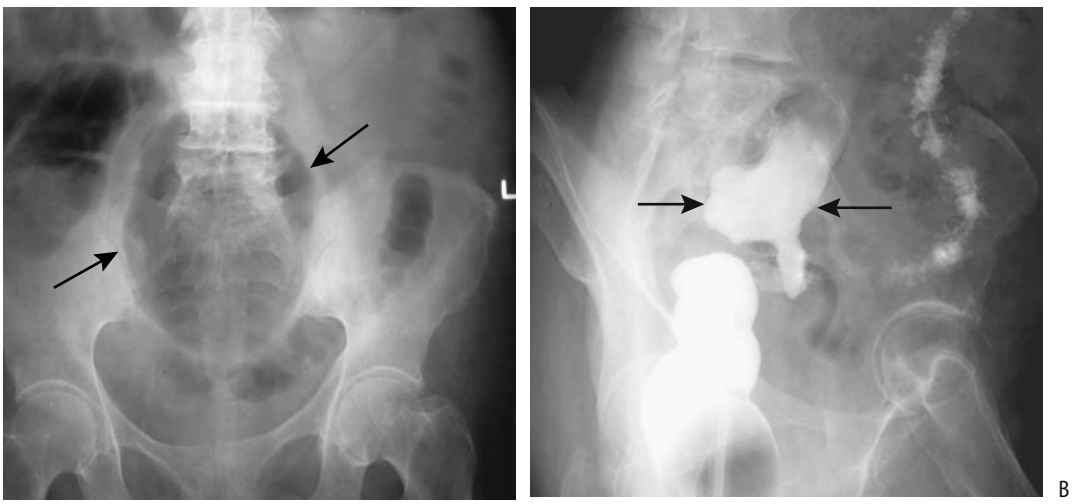

Figure 5.40. Giant sigmoid diverticulum. A: A conventional radiograph identifies a large gas-filled structure (arrows). B: A barium enema confirms a diverticulum (arrows) and establishes its communication with colon.

except if surrounding inflammation is present. Some rare chronic diverticula contain calcifications within their wall.

A thick-walled cavity or any nodularity should suggest a necrotic tumor rather than a giant diverticulum. A communicating duplication is rare in the sigmoid, usually is on the mesenteric side, is seen in a younger patient population, and histology should reveal an epithelial lining containing all layers of the colonic wall.

Most giant colonic diverticula are resected.

Evacuation Disorders

Lax pelvic floor muscles and an abnormal pelvic floor descent are evident in some patients with evacuation disorders, leading to multiorgan interrelated abnormalities; these complex pelvic floor abnormalities, found mostly in women, are discussed in Chapter 12.

Discussed here are primarily evacuation disorders, which in themselves are a diverse and complex group of conditions manifesting mostly by rectal pain and difficulty in evacuation. Rectal incontinence is the other extreme. The nomenclature for various abnormal findings is still evolving, and authors often describe these conditions based on the primary abnormality detected.

Traditionally, proctography evaluated both structural and function, although dynamic MRI is assuming a primary role in evaluating evacuation disorders.

Enterocele

One of the causes of a widened rectovaginal space is a peritoneocele, defined as herniation of the posterior-inferior peritoneal space (cul-de-sac) into a recess between the rectum posteriorly and vagina or bladder anteriorly. Any adjacent intraperitoneal structures can be involved, although most often small bowel is involved and is then called an enterocele. Prolapse of redundant sigmoid (sigmoidocele) is less common. Some of these are capable of partially obstructing the rectum. A distended rectum may conceal a peritoneocele and an enterocele; a radiograph taken with the rectum collapsed should detect this condition.

An anterior enterocele, or anterior vaginal wall hernia containing small bowel, develops in some women who undergo a cystectomy for intractable interstitial cystitis.

Evacuation proctography is the examination of choice to detect the more common posterior enterocele consisting of prolapsed small bowel interposed between vagina and rectum. Small bowel and vaginal opacification are needed during this study. Some enteroceles become evident only at the end of evacuation or on postevacuation radiographs. Of interest is that physical examination detects only half of enteroceles found on proctography (199); the reverse is also true—some enteroceles detected by physical examination are not identified at proctography.

Vaginal US is helpful to detect a posterior enterocele; if one is present, bowel is visualized in the rectovaginal space, especially when bearing down. This examination is highly sensitive and specific in detecting these enteroceles and is an alternative to evacuation proctography.

Rectocele

Although constipation is common in patients with a rectocele, in some patients even a large rectocele is not associated with impaired evacuation. Also, placing rectoceles in clinical perspective can be difficult; constipation is not always relieved after rectocele repair.

Anterior Rectocele

An anterior rectocele consists of a bulge in the anterior wall of the rectum during straining. Although a mild bulge is a normal finding, a typical definition is that the bulge should be >2 cm in extent to be considered a rectocele. Most rectoceles are reduced at rest. They are more common in women, probably due to a weakness of the rectovaginal septum.

Some investigators subdivide anterior rectoceles into two groups: distention and displacement. Manometry in patients with each type revealed a significantly higher anal pressure and a more impaired rectoanal inhibitory reflex in the distention group than in controls or the other group (200); patients in the displacement group have a lower anal pressure, and proctog-

raphy at rest and during evacuation show a significantly higher anorectal angle and a more abnormal pelvic floor descent than in the distention group or in controls. Overall, distention rectoceles have pelvic floor dyssynergia, while displacement rectoceles show a descent in the pelvic floor.

Currently a suspected rectocele or sigmoidocele is most often studied with evacuation proctography. Whether a rectocele is detected or not is mostly independent of contrast agent viscosity. Pelvic MRI, including MR proctography, often provides additional information. Proctography detects most rectoceles, although a majority are also detected on physical examination (201); whether barium is trapped in a rectocele depends mostly on its size.

A rectocele tends to bulge only during straining. Among patients with rectocele shown by proctography, 60% also had paradoxical anal sphincter relaxation (202).

In addition to enteroceles and rectoceles, widening of the rectovaginal space on straining is occasionally due to a peritoneocele. Sigmoidoceles are uncommon.

Posterior Rectocele

Posterior rectal outpouchings include posterior rectoceles and ischiorectal hernias. Posterior or perineal rectoceles are outpouchings of the lower posterior rectal wall through a levator ani muscle defect, usually present only during straining. An ischiorectal hernia is seen as a posterolateral outpouching; these are present at rest.

Posterior rectal herniation also develops after resection of sacral tumors, such as a chordoma.

Rectal Prolapse/Solitary Rectal Ulcer Syndrome

Clinical

Abnormal puborectalis muscle contraction and rectal wall prolapse or intussusception are often implicated in the pathogenesis of solitary rectal ulcer syndrome, a benign condition found mostly in adults. Prolapse ranges from internal to external; the term *intussusception* is appropriate if it is circumferential. Complete rectal prolapse is a clinical diagnosis and generally needs surgical correction. Whether this condition is one syndrome or encompasses a number of disorders is conjecture. Diffuse pelvic floor weakness involving genitourinary structures is found in some women. Chronic constipation, evacuation abnormalities, and rectal prolapse are typical presentations. Confusing the issue, some authors find rectal bleeding to be common, but others believe it is an uncommon finding.

Pressure necrosis and mucosal injury during rectal prolapse and intermittent intussusception appear to play a role, although the pathophysiology is probably multifactorial. Typical histopathologic findings consist of focal mucosal distortion, muscularis mucosa proliferation, and obliteration of lamina propria. An ulcer, accompanied by granulation tissue, is usually located anterior in the rectum but at times extends circumferentially.

Sigmoidoscopy is generally noncontributory in these patients, aside from providing a biopsy and excluding other abnormalities. In some patients manometry reveals decreased external sphincter tone during straining, a nonspecific finding.

Biopsy in patients believed to suffer from solitary rectal ulcer syndrome revealed a solitary ulcer in 78%, multiple ulcers in 11%, granular proctitis in 7%, and rectal inflammation in 4% (203); although voiding proctography missed some ulcers, it identified rectal intussusception in 41%, rectoanal intussusception in 26%, external rectal prolapse in 22%, and mucosal prolapse in 30%. Only one patient had a rectocele. In a majority of patients videoproctography showed that the ulcer wall was first to invaginate.

Solitary rectal ulcer syndrome and an inflammatory cloacogenic polyp have similar histopathologic findings; both are located anterior in the rectum and both tend to be associated with rectal prolapse.

Previous therapy for intractable symptoms included rectocolic resection, a procedure rarely performed today. After elastic binding for rectal mucosal prolapse, follow-up voiding proctography revealed prolapse remission in most patients.

Imaging

A double-contrast barium enema, with emphasis on the anterior rectal wall, is useful to detect

an ulcer and the sequelae of inflammation, but an evacuation study is necessary to evaluate functional abnormalities. Imaging is also often requested prior to surgical repair to evaluate the rest of the large bowel.

In spite of its name, solitary rectal ulcer syndrome does not always present with an ulcer, nor is it always solitary. A common imaging appearance is that of nodularity or an anterior rectal wall irregular polyp. Similar findings are seen with an inflammatory cloacogenic polyp; some mimic a rectal adenocarcinoma.

Voiding videoproctography is the imaging modality of choice for suspected rectal prolapse. Prolapse originates in the midrectum as an intussusception varying in length. Proctography reveals rectal mucosal prolapse as a soft tissue bulge into the rectal lumen, more evident during straining and evacuation than during rest (Fig. 5.41). Mucosal prolapse is more

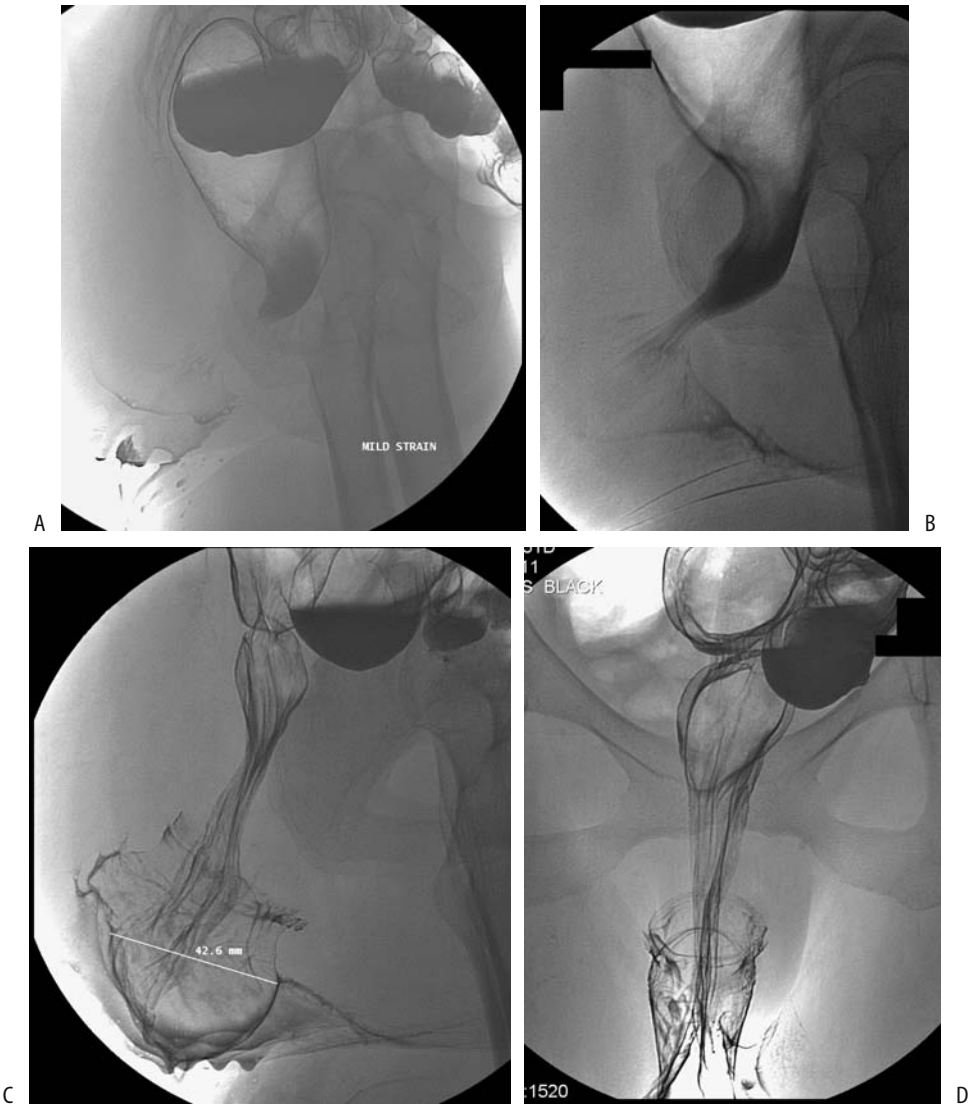

Figure 5.41. Rectal prolapse. A: Initial lateral view is unremarkable. B: Prolapse becomes evident with early straining. Further straining reveals marked prolapse (C, cursor), also identified on a frontal view (D). (Courtesy of Arunas Gasparaitis, M.D., University of Chicago.)

common than intussusception (204). Associated other abnormalities are common and include rectocele, perineal descent syndrome, puborectalis muscle syndrome, and levator ani diastasis, the latter identified with dynamic CT.

At times endorectal US is helpful. Ultrasonography reveals an inhomogeneous and thickened submucosa in the internal and external sphincter regions; the ratio of external to internal anal sphincter thickness is reduced in these patients and muscle hypertrophy identified by US appears useful in some in suggesting the diagnosis.

Puborectalis Syndrome

Puborectalis syndrome is used to describe incomplete relaxation or paradoxical contraction of the puborectalis muscle during evacuation, often with resultant outlet obstruction. At times an isolated finding, it is one of a spectrum of abnormalities detected in constipated patients. The term *pelvic floor dyssynergy* is used by some to encompass a more complex set of findings.

Primary symptom of puborectalis syndrome consists of incomplete or intermittent evacuation. Voiding proctography reveals an abnormal puborectalis muscle impression along the posterior rectal wall, a reduced change in anorectal angle during straining, and prolonged barium pooling in the rectal ampulla; manometry detects an increase in external anal sphincter pressure under straining in about two thirds of these patients (Fig. 5.42). Some patients also have associated rectal mucosal prolapse and a rectocele.

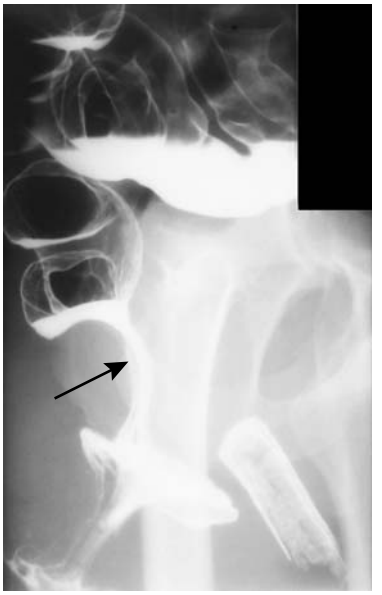

Figure 5.42. Nonrelaxing puborectalis muscle (arrow). This is a contributing factor in solitary rectal ulcer syndrome. (Courtesy of Arunas Gasparaitis, M.D., University of Chicago.)

Anismus/Incontinence

Whether anismus and puborectalis syndrome are the same entity is conjecture. Many authors discuss them together. Some patients with functional outlet obstruction have a megarectum, rectocele, rectal intussusception, mucosal prolapse, or abnormal perineal descent. Reduced change in anorectal angle between rest and evacuation is used by some as a criterion for defining functional outlet obstruction. Although the anorectal angle does change during straining and voiding (and viscosity of the contrast medium used influences the results), the importance of a particular amount of change is questionable. Anorectal angle measurements provide conflicting data, with some studies revealing no significant difference between patients with anismus and controls and others concluding that in most patients with incontinence the anorectal angle is increased at rest.

One study found that 90% of patients with impaired proctographic evacuation had anismus at subsequent anorectal physiologic testing (205).

Endoanal US identifies anal sphincter defects in approximately two thirds of incontinent patients (206); these findings are difficult to place in the proper perspective because in this same study the prevalence of anal sphincter defects in continent patients was 43%. Endovaginal US appears to be as reliable as endoanal US in evaluating the anal sphincter but endovaginal US is more accurate for perianal inflammatory disease (207).

Whether endoanal US or MR is superior is not clear. A retrospective study in women with fecal incontinence concluded that in detecting external and internal sphincter lesions

endoanal MRI agreed better with subsequent surgical findings than did endoanal US (208); endoanal US was not accurate in identifying external sphincter thinning, a finding confirmed in another study (209). Yet another study found not only endoanal US and MRI to be equivalent in detecting external anal sphincter defects, but also US was superior for internal anal sphincter defects (210).

Often a combination of studies is helpful in these patients. As one example, proctography in 38 patients with incontinence identified rectal mucosal prolapse (n = 12), rectocele (n = 10), perineal descent syndrome (n = 8), and external rectal prolapse (n = 3); endoanal US identified 15 sphincter ring interruptions (12 hypoechoic, two mixed, and one hyperechoic) and internal anal sphincter thinning in five; perineography revealed a cystocele in five and a cystourethrocele in one; and manometry showed sphincter hypotonia at rest in 15 (211). Placing these findings in a proper perspective, however, is often challenging.

A separate group of patients with fecal incontinence consists of those with congenital anomalies, such as spina bifida. Some of these often young patients are successfully treated with percutaneous cecostomy tube placement, a procedure having few complications.

Table 5.7. Conditions associated with colonic perforation

Mechanical obstruction (obstructive ileus)
Neoplasm
Benign stricture/obstruction
Volvulus
Herniation
Intussusception
Fecal impaction
Adynamic ileus
Inflammation/infection
Ogilvie's syndrome
Toxic megacolon
Necrotizing enterocolitis
Typhlitis
Ischemic ileus
Severe malacoplakia
Instrumentation
Endoscopy
Barium enema
Biopsy
Foreign body
Toothpick
Other sharp objects
Drug therapy
Ehlers-Danlos syndrome

Perforation

Some of conditions associated with colonic perforation are listed in Table 5.7. Among common etiologies for colonic perforation, patients with a perforating carcinoma have a high mortality. An unusual cause is due to paclitaxel therapy; these perforations appear to be a direct drug effect causing mitotic arrest of the gastrointestinal epithelium. The prevalence of such perforation is not known, although it is associated with a high mortality rate.

Ehlers-Danlos syndrome type IV consists of an inherited collagen disorder. The syndrome can be confirmed by culture of skin fibroblasts. These patients have a defect in either the synthesis or structure of type III procollagen and are prone to spontaneous aortic, small bowel, and colonic rupture. Recurrent colon perforations develop in patients with this syndrome.

A number of reports describe colonic perforation by an ingested sharp bone or toothpick, generally in the sigmoid colon. Among ingested bones, chicken bones seem to predominate.

Spontaneous rectal perforation is rare; one unusual rectal rupture led to small intestine evisceration through the anus (212).

In distinction to upper gastrointestinal perforation from peptic ulcer disease, which tends to result in small amounts of intraperitoneal gas, colonic perforations more often lead to a large pneumoperitoneum. Exceptions, however, are common. Also, some colonic perforations manifest with an abscess rather than pneumoperitoneum.

Nonspecific Ulcer

Grouped under this heading are those colonic ulcerations believed not to be associated with other diseases. Some of these ulcers presumably are ischemic in etiology. Few publications exist on this topic.

Fistula

Diagnostic modalities to evaluate fistulas include fistulography for cutaneous fistulas, CT, MRI using an endorectal coil, and proctosigmoidoscopy, with endorectal US having a major role in perirectal fistulas. Nevertheless, MRI has gradually achieved preeminence.

At times a two-part CT study is found advantageous when searching internal communication for cutaneous fistulas; first, conventional CT is obtained after filling the appropriate bowel with contrast, followed by concentrated contrast injection into any visible fistulas and rescanning using wide window settings.

Colonoscopy is insensitive in identifying colonic fistulas.

Perianal Fistulas

Perianal fistulas are either anovaginal, associated with Crohn's disease, or cryptoglandular in origin. Most perianal infections originate in intersphincteric anal glands located close to the dentate line and spread from there. The Parks classification of perianal fistulas is based on a fistula track relationship to anorectal musculature and consists of four main types: (1) superficial or low, (2) intersphincteric, (3) transsphincteric, and (4) suprasphincteric or high fistula. A horseshoe fistula extends circumferentially.

Almost all external sinus tracts and fistulas located close to the posterior midline are associated with a simple superficial or intersphincteric fistula; on the other hand anterior and posterolateral external sinus tracts and fistulas tend to be complex and often extend transsphincteric or are suprasphincteric in their course. These fistulas must be differentiated from necrotic tumors, infections such as actinomycosis, pilonidal cysts, and similar disorders. Any associated abscesses also need be identified by imaging.

What are the relative roles of US and MRI? No obvious answers have emerged, although current evidence suggests that, overall, MR is superior to US; also, MR is the more active current research front.

Fistulography is traditionally used to study sinuses and external fistulas. Few studies have compared US and MR against fistulography, preferring to use surgical findings as their gold standard. Yet the reliability of surgery as a standard has been questioned; using long-term patient outcome as a gold standard, preoperative contrast-enhanced MR grading achieves higher sensitivity and specificity than surgical exploration in predicting patient outcome (213); in this study surgery was performed without knowledge of MR findings, and outcome was considered unsatisfactory if additional surgery was necessary.

Is endoanal US superior to a transperineal US approach? Some patients cannot tolerate anal coil insertion. In some patients, such as those with Crohn's disease, fistulas tend to extend beyond the field of view of an endoanal coil. Gray-scale US identifies fistulas as a thin hypoechoic line. Endocavitary US is more sensitive in detecting intersphincteric than transsphincteric fistulas (214). Overall, however, transperineal US in men and both endovaginal and transperineal US in women appear preferable to endoanal US when evaluating perianal inflammation. Hydrogen peroxide introduced into the fistula tract through the external opening appears of limited additional value except in assessing an internal opening (215).

Although some studies concluded that endorectal US detects more fistulas than MRI, a prospective study of MRI [1.0-T axial and coronal T2-weighted turbo spin echo (TSE) and turbo-STIR sequences] and US (10-mHz rotating endoanal probe) of patients with perianal fistulas achieved an 84% sensitivity for MRI and 60% for US, and specificities of 68% and 21%, respectively, in detecting and classifying these fistulas (216).

An MR endoanal coil was superior to a pelvic phased array coil in evaluating most fistulas, the exception being supralevator fistulas and in evaluating subcutaneous extensions where a phased array was superior (217); sagittal and coronal plane images are very helpful. MR using rectal contrast identifies more pelvic and perirectal fistulas than precontrast imaging.

As an example of the optimistic results achievable with MR, high-spatial-resolution MRI using a quadrature phased-array coil reached 100% sensitivity and 86% specificity for detecting fistulous tracks; 96% and 97%, respectively, for associated abscesses, 100% and 100%, respectively, for horseshoe fistulas, and 96% and

90%, respectively, for internal openings (218). Even when using a low field (0.1-T) MR unit, results have agreed with the final diagnosis in over 95% (219). Nevertheless, some MR studies are more pessimistic when evaluating the site and extent of a fistula; for instance, in patients with subsequently confirmed fistula-in-ano, MRI detected only 42% to 50%, depending on the radiologist's experience (220).

Genitourinary Tract Fistulas

Renocolic Fistula

Renocolic fistulas are usually secondary to renal inflammation or neoplasms. An occasional patient with xanthogranulomatous pyelonephritis and ureteric obstruction develops a renocolic fistula. An antegrade or retrograde pyelogram should identify these fistulas. Computed tomography usually reveals a complex air-fluid collection within either the kidney or the adjacent soft tissues.

Urethrorectal Fistula

Rare urethrorectal fistulas consist of fistulas communicating between the prostate or bulbomembranous urethra and rectum. Trauma from missiles is a not uncommon cause of these fistulas. A number of these patients have had prior surgery or complex anoperineal suppuration.

Detection of urethrorectal fistulas is straightforward, either via a urethrogram or a contrast enema.

Some of these fistulas close spontaneously after a more proximal-sigmoid colostomy and suprapubic cystostomy; others require surgical correction.

Colorectal Vesical Fistula

Most enterovesical fistulas are secondary to inflammatory bowel disease or diverticulitis, with an occasional one originating from a colon carcinoma, bladder carcinoma, or other neoplasms. Pneumaturia is common but not universal in patients with a colovesical fistula. At times cystitis is the primary presentation.

Most colovesical fistulas can be identified by barium enema, cystography, or cystoscopy. In some patients a one-way check valve mechanism presumably exists, and in any one patient not all three studies identify a fistula.

Figure 5.43. Rectovaginal fistula (arrow) secondary to lymphomatous infiltration.

Rectovaginal Fistula

Most rectovaginal fistulas are secondary to birth trauma, gynecologic surgery, or pelvic radiation. A rare cause is pelvic amebiasis or actinomycosis. Diverticulitis predominates as a cause of colovaginal fistulas.

Either a barium enema or vaginogram identifies these fistulas (Fig. 5.43). Pelvic MRI is useful to define involved tissue planes. T2-weighted images identify rectovaginal fistulas as hyperintense linear defects. Most internal opening can be identified.

A nitinol-silicone double-disc device was inserted transrectally into a rectovaginal fistula and the fistula occluded (221). Such an occluding device appears useful in a setting of tumor, pelvic radiation, and reluctance for repeat surgery in someone with limited life expectancy.

Other Fistulas

Some iatrogenic gastrocolic fistulas are created due to inadvertent transverse colon puncture during percutaneous gastrostomy. An occa-

sional duodenocolic fistula is secondary to colonic Crohn's disease or a neoplasm. A peptic ulcer–induced fistula to the colon is rare. Most cholecystocolic fistulas are secondary to cholecystolithiasis. Resulting inflammation and fibrosis, generally involving the hepatic flexure or proximal transverse colon, mimics the barium enema appearance of a primary colon adenocarcinoma.

One complication of interleukin-2 therapy is bowel perforation.

Pneumatosis Coli

Pneumatosis cystoides intestinalis is discussed in more detail in Chapter 4.

Pneumatosis coli represents pneumatosis cystoides intestinalis limited primarily to the colon. Similar to small bowel, pneumatosis coli can be subdivided into ischemic and non-ischemic (benign) causes. It is characterized by multiple gas-filled cysts within bowel wall. Pneumatosis most often affects the left colon; a redundant sigmoid colon is a common ancillary finding. An occasional colonic intussusception is associated with pneumatosis cystoides intestinalis.

Pneumatosis coli is readily diagnosed with conventional radiography. A barium enema or CT confirms the intramural location for these gas collections. Endosonography reveals hyperechoic collections with acoustical shadowing.

Body Packer

Smuggling of cocaine or heroin concealed in the gastrointestinal tract is not new. The drugs are typically wrapped in cellophane or condoms and swallowed. In general, rupture of a single package is above the toxic dose and is fatal. At times these packages also obstruct the bowel. Most of these "mules" are treated conservatively, although an occasional one requires surgery.

Both US and conventional abdominal radiographs readily detect swallowed drug packages. Conventional radiographs and CT identify cannabis and cocaine packages as well-marginated, rectangular, high-density structures surrounded by a gas halo, called the *double condom sign*; heroin packages are seen as poorly outlined structures resembling stool and are difficult to identify on conventional radiographs. Ultrasonography of cannabis packages reveals round hyperechoic structures.

Vascular Lesions (Bleeding)

Discussed here are those entities manifesting primarily by bleeding. Ischemic colitis has been discussed in a previous section.

The etiologies of rectal bleeding in adults are wide-ranging (Table 5.8) and differ between pediatric patients and adults; in pediatrics it is worthwhile to consider causes of rectal bleeding by age (Table 5.9).

Detection

Contrast-enhanced CT is at times worth-while in a patient with suspected lower gastrointestinal bleeding. Contrast extravasation is obviously diagnostic, but bowel wall contrast-enhancement or presence of a focal lesion also point towards a bleeding site.

Technetium-99m–red blood cell scintigraphy is often employed as a screening examination for patients with suspected colonic bleeding. Should a nuclear medicine bleeding scan be obtained and mesenteric arteriography per-

Table 5.8. Etiologies of rectal bleeding in adults

Colonic
Diverticulosis
Inflammatory bowel disease
Ischemic colitis
Infectious colitis
Neoplasms
Hemorrhoids
Angiodysplasia/arteriovenous malformations
Portal hypertension—colonic varices
Small bowel
Inflammatory bowel disease
Angiodysplasia/arteriovenous malformations
Diverticular causes
Meckel's diverticulum related
Neoplasms
Proximal to ligament of Treitz
Peptic ulcer disease
Angiodysplasia/arteriovenous malformations
Dieulafoy lesions
Portal hypertension—gastroesophageal varices

Table 5.9. Rectal bleeding in pediatric patients

Age	Common etiology	Less common etiology
Neonate (0–30 days)	Anal fissure Necrotizing enterocolitis Allergic colitis	Infectious enteritis Midgut volvulus
Infant (30 days–1 year)	Intussusception Anal fissure Allergic colitis	Meckel's diverticulum Infectious enteritis Polyp Henoch-Schönlein purpura
Child and adolescent	Meckel's diverticulum Polyp Anal fissure Infectious enteritis Inflammatory bowel disease	Henoch-Schönlein purpura Vascular malformation Coagulopathy Hemolytic-uremic syndrome

formed only if the scan is positive? The primary purpose of such a policy is to increase the percentage of positive arteriograms, yet one retrospective study concluded that a prior positive bleeding scan did not increase the odds of obtaining a positive angiogram (222), a finding at odds with a number of other studies. Thus arteriography in patients with suspected acute gastrointestinal bleeding detected bleeding in 22% of studies, but after instituting a protocol requiring positive scintigraphy before performing arteriography, the positive arteriography rate increased to 53% (223).

In patients with suspected acute lower gastrointestinal bleeding, Tc-99m–red blood cell scintigraphy achieves >80% sensitivity in detecting bleeding and in those with positive scan localizes a bleeding site in about 70%.

Colonoscopy can potentially identify a colonic bleeding site. A practical limitation exists if blood and blood clots obscure adequate visualization. Also, complete colonoscopy is necessary because in up to one third of patients a bleeding site is in the cecal region.

Therapy

After mesenteric angiography identifies a bleeding site, immediate therapeutic options include arterial embolization and infusion of vasopressin. Arterial embolization is viable therapy for most acute lower gastrointestinal bleeding. The clinical success of embolization, judged by no rebleeding, is achieved in about 90% of patients. Even hemorrhage from a large vessel can be arrested. Postembolization ischemia is rarely an issue with this technique.

One refinement is superselective microcoil embolization, with embolization performed at the vasa recta or the marginal artery of Drummond level. In one study, bleeding was arrested on a long-term basis in over 80% of patients (224). Hemostasis can be expected in all except those with a dual blood supply to the bleeding site, yet even in the latter significant reduction of bleeding is achieved. Occasional bowel ischemia, rebleeding, and even infarction are recognized complications of this procedure. At times superselective embolization includes a combination of coils, polyvinyl alcohol, and gelatin sponge particles.

Diverticular Bleeding

A typical diverticular bleed tends to be massive and arterial, and it stops spontaneously. Often little other evidence of diverticulitis is present. Past teaching was that bleeding is due to erosion of a small artery overlying the diverticulum, but whether such erosions differ from a Dieulafoy lesion is not clear.

Right-sided diverticulosis tends to present with massive rectal bleeding more often than left-sided disease, yet in general, cecal bleeding is more difficult to control than more distant bleeding.

In patients without definitive therapy, recurrent hemorrhage occurs in about 10% at 1 year.

Angiodysplasia

Among a healthy, asymptomatic population prevalence of angiodysplasia is <1%. These ectatic veins, venules, and capillaries probably develop secondary to local degeneration, especially with aging. A deficiency of collagen type IV is found in mucosal vessels in angiodysplasia. They occur in both the small and large bowel. Most, however, are smaller than 10 mm and are located in the right colon. They range from single to multiple. Most manifest in the elderly, although angiodysplastic hemorrhage does occur in young patients. Earlier reports suggested an association between angiodysplasia and aortic stenosis, but more recent studies do not confirm such a link.

Unusual associations of rectal and sigmoid colon angiodysplasia-like lesions include a 12-year-old boy with Klippel-Trenaunay-Weber syndrome who developed hematochezia (225). The presence of colon angiodysplasia, small bowel lymphoma, and duodenal carcinoid in the same patient suggests a more than fortuitous association (226).

Bleeding ranges from iron-deficiency anemia to a life-threatening acute hemorrhage.

Angiodysplasia is not detected by barium enema. Angiography and colonoscopy detect only some of these flat lesions. Most angiodysplasias are intramucosal in location, although an occasional one is deeper and thus not visible. If bleeding, scintigraphy is an appropriate first imaging modality employed.

If colonoscopy detects an incidental angiodysplasia in an otherwise asymptomatic individual, therapy probably is not necessary.

Selective mesenteric angiography reveals a tuft of abnormal vessels and an early filling vein. Superselective arterial embolization is common therapy to arrest acute bleeding from angiodysplasias. In some patients, estrogen-progesterone combination therapy has been successful in preventing rebleeding from angiodysplasias (227).

Arteriovenous Malformation

Most arteriovenous malformations are intramural in location. An occasional one has a polypoid appearance. Except for very small ones, they are detected with contrast-enhanced imaging.

Varices

Most colonic varices are associated with portal hypertension. Why only some patients develop colonic varices is not clear, although the prevalence of these varices increases in those who have had prior transection and devascularization of esophageal varices, esophageal sclerotherapy, or thrombosis of coronary and azygous drainage veins. Congenital colon varices are rare; in the absence of portal hypertension resection of such varices is curative. Varices have developed secondary to mesenteric venous obstruction and, rarely, with splenic vein thrombosis. Also rare are idiopathic colonic and mesenteric varices.

Bleeding from colorectal varices can be massive; portal hypertension needs to be excluded in these patients.

Colonic and perirectal varices can be diagnosed with contrast-enhanced CT. What is surprising is that in some patients with portal hypertension, CT detects some pararectal varices not visualized by colonoscopy and vice versa; the inferior mesenteric vein is significantly larger in patients with rectal varices than in those without.

Portal Hypertensive Colopathy

Vascular ectasia-like lesions in the colon, called portal hypertensive colopathy, develop in some patients with portal hypertension. These lesions consist of numerous irregular vessels having a hyperemic "cherry-spot" appearance.

About one third of patients with severe cirrhosis have colonic wall thickening, predominantly in the right colon (228); most patients do not have symptoms referable to the colon, and these changes presumably are related to underlying portal hypertension. Clinically these patients range from asymptomatic, to recurrent rectal bleeding, to episodes of massive hemorrhage.

Transjugular intrahepatic portosystemic shunting (TIPS) does control bleeding from portal hypertensive colopathy and, in fact, the ectasia-like colonic lesions tend to disap-

pear. Colopathy is also corrected after liver transplantation and correction of portal hypertension.

Juvenile Polyps

Juvenile polyps persist into adulthood. Occasionally such a juvenile polyp first manifests by a massive lower gastrointestinal bleed.

Dieulafoy Lesion

A small gastric mucosal defect associated with a bleeding submucosal artery is called a Dieulafoy lesion (these lesions are discussed in more detail in Chapter 2). Since their initial detection in the stomach, similar lesions have been found in the small bowel and colon. They appear to be more common in the proximal colon. They develop in both adults and children. Dieulafoy lesions occur in diverticula, where their differentiation, if any, from a typical diverticular bleed is problematic.

Dieulafoy bleeding is often massive but intermittent. Similar to gastric Dieulafoy lesions, colonoscopic sclerotherapy has successfully arrested bleeding. Selective mesenteric angiography differentiates Dieulafoy lesions from angiodysplasias—the former consists of a small bleeding artery.

Immunosuppression (AIDS)

In patients with human immunodeficiency virus infection, superimposed opportunistic infections are common. Yet not all symptoms and lesions are due to infection; some are neoplastic and others idiopathic.

Infection

Colonic histoplasmosis is not uncommon in patients with AIDS, with the most common site being the ileocecal region. Clinically, some patients develop a palpable tumor, and imaging reveals an annular constricting lesion. At times more diffuse involvement mimics ulcerative colitis. Colonoscopy in one patient revealed volcano-like ulcers and tumors; CT identified both a colon tumor and hypodense adenopathy (229); histology and biopsy cultures and lymph node aspirate revealed *Histoplasma capsulatum*, but the patient eventually developed bowel obstruction and peritonitis. At times Gomori staining of colon biopsies aids in establishing this diagnosis.

Patients with AIDS are prone to *C. difficile* infection. Among other predisposing factors in this population is the common use of antibiotics; clinically, symptoms of *C. difficile* infection in AIDS patients tend to be more severe than in non-AIDS patients.

Cytomegalovirus colitis is common in this patient population and manifests as ulcers and submucosal hemorrhage, with these ulcers ranging from aphthous to relatively deep cavities surrounded by inflammation and edema. These findings are similar to those seen in pseudomembranous colitis. In some, cytomegalovirus infection results in a focal colonic tumor. Cytomegalovirus is diagnosed by finding viral inclusion bodies in colon biopsies. These inclusions are more common in cecal biopsies rather than more distally; therefore, complete colonoscopy is necessary.

Similar to other patients, AIDS patients develop pseudomembranous colitis when treated for an infection.

It should be kept in mind that AIDS patients also develop appendicitis.

Neoplasm

Although not common, HIV infection appears to play a role in colorectal cancer development. These patients are at risk for anal squamous and cloacogenic carcinomas.

An occasional rectal Kaposi's sarcoma is successfully treated with radiation therapy.

Complications of non-Hodgkin's lymphoma in these patients include duodenocolic fistula and intussusception.

Other

Some AIDS patients develop pneumatosis coli. Usually a late finding, in most patients, it is benign and clears spontaneously. The right colon is involved more often than the left. Occasionally pneumatosis coli is associated either with intraperitoneal or retroperitoneal gas and suggests a perforation, although bowel perforation is not detected.

Prevalence of intussusception is increased in patients with AIDS-associated gastrointestinal disease. Crampy, intermittent abdominal pain is a typical presentation. Either CT or a barium enema is diagnostic.

A colitis mimicking ulcerative colitis can develop in an occasional AIDS patient with a low CD4 T-cell count.

Examination and Surgical Complications

Barium Enema

A retrospective study of over 700,000 barium enemas performed between 1992 and 1994 in the United Kingdom found an overall mortality rate of one in 56,786 (230); only three of 30 (10%) patients with bowel perforation died, compared with nine deaths among 16 (56%) patients with cardiac arrhythmia. One death was related to vaginal intubation.

In a setting of incomplete or failed sigmoidoscopy or colonoscopy, a double-contrast barium enema can be performed the same day if no biopsy or only a superficial biopsy (using small biopsy forceps) is obtained; the risk of perforation increases if biopsies are taken from diseased mucosa. A barium enema should be postponed, however, for at least 14 days if a deep biopsy is obtained. A similar delay in performing barium enema also appears warranted if a polypectomy is performed.

Focal barium extravasation, either intramural or extrinsic to bowel, results in an exuberant fibrotic reaction around barium sulfate crystals. An experimental study in rats concluded that any effect of barium sulfate on gastrointestinal tract transmural wound healing is minimal (231). At times prior focal extravasation is unsuspected; thus in one patient a tumor in the gallbladder fossa was believed to represent an advanced gallbladder cancer, but resection revealed foreign-body barium granulomas (232).

Venous barium embolization during a barium enema is a rare but highly lethal complication. Embolization can be either into systemic veins (usually from a rectal perforation) or into portal venous system.

Barium inspissation after a barium enema is rare. In most reports it is due to underlying constipation, poor radiographic technique resulting in the overfilling of a dilated, hypotonic colon, or the lack of post-enema hydration.

Colonoscopy

Colonoscopic complications consist of bleeding, sepsis, perforation, and transmural burn injuries, with the onset of symptoms occurring an average of 30 hours after colonoscopy. Bleeding is managed conservatively in approximately three quarters of these patients.

Disinfection Related

Colonoscopic cleansing is typically achieved with glutaraldehyde or hydrogen peroxide. Both agents produce tissue necrosis. Bloody diarrhea develops within a day or so after these agents contact colonic mucosa, mimicking ischemic or infectious colitis. Imaging in patients with glutaraldehyde-induced colitis reveals circumferential left-sided colonic wall thickening and heterogeneous wall contrast-enhancement; these findings resolve on follow-up. Ultrasonography also identifies colonic wall thickening, consisting of hypoechoic mucosa and hyperechoic submucosa.

An unusual colitis due to hydrogen peroxide developed while colonoscopy was still being performed; it consisted of opaque plaques or pseudomembranes, a condition called pseudolipomatosis by pathologists (233). To prevent such disinfectant colitis, the authors recommend an additional preprocedure rinse of colonoscopic channels.

Septicemia

Approximately 10% of patients develop transient bacteremia after colonoscopy. Septicemia is not common, although the risk of septicemia increases in immunocompromised patients.

Perforation

Three mechanisms are associated with colonoscopic perforations (234): (1) mechanical causes due to colonoscopic manipulation, (2) barotrauma from overinsufflation, and (3)

perforation related to therapeutic procedures. In general, perforation occurring during diagnostic colonoscopy tends to result in large lacerations; those associated with polypectomy tend to be smaller. Cecal perforations tend to be due to overinsufflation; sigmoid perforations involve mostly technical problems. Some perforations are difficult to understand. Why should a jejunal or ileal perforation develop after colonoscopy? Some perforations are not diagnosed for several days.

The appearance and sequelae of colonic perforation are myriad and are related both to the extent and site of perforation and amount of peritoneal soilage. In addition to a pneumoperitoneum, some patients develop pneumothoraces, pneumopericardium, pneumomediastinum, scrotal swelling, and even subcutaneous emphysema. A tension pneumothorax can lead to acute respiratory failure.

The current trend is toward fewer surgical interventions for colonoscopic perforations; some patients with clinically and radiographically evident perforation heal under medical management. In fact, medical therapy leads to a shorter hospitalization than with comparable surgical management. In patients believed to require surgery, either primary repair or resection and anastomosis are the procedures of choice, assuming no contamination is evident.

Other

A number of splenic ruptures have been associated with colonoscopy. Acute appendicitis developed in a 69-year-old man immediately after colonoscopy (235); no signs or symptoms of appendicitis were evident prior to colonoscopy.

Transient myocardial ischemic episodes develop during colonoscopy; these appear to be associated with tachycardia and hypoxemia.

Postresection

Mostly Rectosigmoid Complications

Although colonic ischemia and anastomotic dehiscence is not uncommon after colon surgery, rectal ischemia is rare. Rectal necrosis, however, has developed after anterior resection of a rectosigmoid carcinoma; presumably inferior mesenteric artery ligation in a setting of atherosclerosis results in an inadequate blood supply to the residual colorectum.

Extraperitoneal emphysema is not uncommon after a low anterior resection or full-thickness excision, raising the question of whether it represents benign emphysema or a postoperative leak. At times abdominal wall emphysema develops and persists for a considerable time. These entities can usually be distinguished with a contrast enema. Computed tomography findings of a leak consist of gas-fluid collections adjacent to the rectum and extending along tissue planes. With resolution of a perforation these collections should gradually diminish.

Presacral space widening is common after rectosigmoid surgery.

Hartmann's Pouch

Based on established surgical indications, either a Hartmann's pouch or a double-barrel colostomy is created to protect an anastomosis, with surgeons in the United States favoring the former. Complications related to a Hartmann's pouch include leaks, strictures, adhesions, and, on a more chronic basis, recurrent tumor and diversion colitis. A contrast study is often requested prior to colostomy takedown, which is generally several months or longer after the initial surgery. Occasional debate surfaces among radiologists about whether barium or a water-soluble agent should be used; I prefer barium because of its higher contrast and ability to detect more subtle detail, unless the study is being performed shortly after resection and the possibility of rupture and intraperitoneal spill are considerations. The presence of barium in a leak is not an issue—after all, if barium enters a sinus tract or cavity, so can infected colonic content, which produces more damage than inert barium sulfate. A more pertinent issue is that the enema balloon should not be inflated to the same degree as during a normal barium enema; these patients have decreased rectal pain sensation and, especially with the presence of a stricture, a major rectal perforation can occur.

Strictures in a Hartmann's pouch are amenable to transrectal dilation. Most small leaks heal with time, although an occasional silent leak is detected by a barium study even months later.

Stricture

Benign postoperative colonic strictures are not uncommon, most being due to ischemia. These strictures are amenable to balloon catheter dilation, either via colonoscopy or, with distal colonic and rectal strictures, simply using fluoroscopic control. A preprocedure barium enema aids in defining the site and length of a stricture. Procedure complications are rare and stricture recurrence uncommon.

An occasional ischemic stricture is treated with a self-expandable metallic prosthesis, but, in general, stricture dilation is preferred even in high-risk patients.

Postlaparoscopy

Laparoscopic resections of sigmoid diverticulitis leads to a severalfold increase in operative time over open resection but a decrease in intensive care. Length of hospital stay, complications, and operating time decrease with experience.

Abdominal wall tumor recurrence at a trocar-site scar does occur after laparoscopic carcinoma resection. This complication is rare in a laparotomy scar.

Port site hernias are an uncommon complication of laparoscopic colectomy. Superior mesenteric and portal vein thrombosis occurred after a laparoscopically assisted right hemicolectomy.

References

1. Langdon DE. Radiologic barium and colon toxicity. Am J Gastroenterol 1994;89:462.
2. Harvey CJ, Halligan S, Bartram CI, Hollings N, Sahdev A, Kingston K. Evacuation proctography: a prospective study of diagnostic and therapeutic effects. Radiology 1999;211:223–227.
3. Schoenenberger AW, Debatin JF, Guldenschuh I, Hany TF, Steiner P, Krestin GP. Dynamic MR defecography with a superconducting, open-configuration MR system. Radiology 1998;206:641–646.
4. Paetzel C, Strotzer M, Furst A, Rentsch M, Lenhart M, Feuerbach S. [Dynamic MR defecography for diagnosis of combined functional disorders of the pelvic floor in proctology.] [German] Rofo Fortschr Geb Rontgenstr Neuen Bildgeb Verfahr 2001;173:410–415.
5. Maier A, Fuchsjager M, Funovics M. [Endoanal magnetic resonance tomography in fecal incontinence.] [Review] [German] Radiologe 2000;40:465–468.
6. Marshall JB. Brown DN. Photodocumentation of total colonoscopy: how successful are endoscopists? Do reviewers agree? Gastrointest Endosc 1996;44:243–248.
7. Rex DK, Cutler CS, Lemmel GT, et al. Colonoscopic miss rates of adenomas determined by back-to-back colonoscopies. Gastroenterology 1997;112:24–28.
8. Cothren RM, Sivak MV Jr, Van Dam J, et al. Detection of dysplasia at colonoscopy using laser-induced fluorescence: a blinded study. Gastrointest Endosc 1996;44:168–176.
9. Morrin MM, Farrell RJ, Kruskal JB, Reynolds K, McGee JB, Raptopoulos V. Utility of intravenously administered contrast material at CT colonography. Radiology 2000;217:765–771.
10. Fletcher JG, Johnson CD, Welch TJ, et al. Optimization of CT colonography technique: prospective trial in 180 patients. Radiology 2000;216:704–711.
11. Kulinna C, Scheidler J, Eibel R, et al. [Diagnostic value of different rectal contrast media in the detection of colorectal diseases by multi-slice CT.] [German] Rofo Fortschr Geb Rontgenstr Neuen Bildgeb Verfahr 2002;173:749–755.
12. Morrin MM, Kruskal JB, Farrell RJ, Goldberg SN, McGee JB, Raptopoulos V. Endoluminal CT colonography after an incomplete endoscopic colonoscopy. AJR 1999;172:913–918.
13. Pickhardt PJ. Translucency rendering in 3D endoluminal CT colonography: a useful tool for increasing polyp specificity and decreasing interpretation time. AJR 2004;183:429–436.
14. McFarland EG, Brink JA, Pilgram TK, et al. Spiral CT colonography: reader agreement and diagnostic performance with two- and three-dimensional image-display techniques. Radiology 2001;218:375–383.
15. Macari M, Milano A, Lavelle M, Berman P, Megibow AJ. Comparison of time-efficient CT colonography with two- and three-dimensional colonic evaluation for detecting colorectal polyps. AJR 2000;174:1543–1549.
16. Sosna J, Morrin MM, Kruskal JB, Lavin PT, Rosen MP, Raptopoulos V. CT colonography of colorectal polyps: a metaanalysis. AJR 2003;181:1593–1598.
17. Callstrom MR, Johnson CD, Fletcher JG, et al. Computed tomography colonography without cathartic preparation: feasibility study. Radiology 2001;219:693–698.
18. Summers RM, Johnson CD, Pusanik LM, Malley JD, Youssef AM, Reed JE. Automated polyp detection at CT colonography: feasibility assessment in a human population. Radiology 2001;219:51–59.
19. Luboldt W, Mann C, Tryon CL, et al. Computer-aided diagnosis in contrast-enhanced CT colonography: an approach based on contrast. Eur Radiol 2002;12:2236–2241.
20. Zalis ME, Hahn PF, Arellano RS, Gazelle GS, Mueller PR. CT colonography with teleradiology: effect of lossy wavelet compression on polyp detection—initial observations. Radiology 2001;220:387–392.
21. Hara AK, Johnson CD, MacCarty RL, Welch TJ. Incidental extracolonic findings at CT colonography. Radiology 2000;215:353–357.
22. Luboldt W, Bauerfeind P, Wildermuth S, Marincek B, Fried M, Debatin JF. Colonic masses: detection with MR colonography. Radiology 2000;216:383–388.

23. Luboldt W, Frohlich JM, Schneider N, Weishaupt D, Landolt F, Debatin JF. MR colonography: optimized enema composition. Radiology 1999;212:265–269.
24. Luboldt W, Luz O, Vonthein R, et al. Three-dimensional double-contrast MR colonography: a display method simulating double-contrast barium enema. AJR 2001;176:930–932.
25. Chung JJ, Semelka RC, Martin DR, Marcos HB. Colon diseases: MR evaluation using combined T2–weighted single-shot echo train spin-echo and gadolinium-enhanced spoiled gradient-echo sequences. J Magn Reson Imaging 2000;12:297–305.
26. Lomas DJ, Sood RR, Graves MJ, Miller R, Hall NR, Dixon AK. Colon carcinoma: MR imaging with CO2 enema—pilot study. Radiology 2001;219:558–562.
27. Lauenstein T, Holtmann G, Schoenfelder D, Bosk S, Ruehm SG, Debatin JF. MR colonography without colonic cleansing: a new strategy to improve patient acceptance. AJR 2001;177:823–827.
28. Locher C, Duclos-Vallee JC, Rocher L, Blery M, Buffet C. [Bilateral Chilaiditi's syndrome.] [French] Presse Med 2000;29:1738.
29. Pinto A, Brunese L, Noviello D, Catalano O. [Colonic interposition between kidney and psoas muscle: anatomical variation studied with CT.] [Italian] Radiol Med 1997;94:58–60.
30. Prassopoulos P, Raissaki M, Daskalogiannaki M, Gourtsoyiannis N. Retropsoas positioned bowel: incidence and clinical relevance. J Comput Assist Tomogr 1998;22:304–307.
31. Currarino G, Coln D, Votteler T. Triad of anorectal, sacral, and presacral anomalies. AJR 1981;137:395–398.
32. Lee SC, Chun YS, Jung SE, Park KW, Kim WK. Currarino triad: anorectal malformation, sacral bony abnormality, and presacral mass—a review of 11 cases. J Pediatr Surg 1997;32:58–61.
33. Vidiscak M, Kirnak J, Smrek M. [Results of surgery in children with congenital megacolon.] [Slovak] Rozhl Chir 2001;80:197–200.
34. Bloom DA, Buonomo C, Fishman SJ, Furuta G, Nurko S. Allergic colitis: a mimic of Hirschsprung disease. Pediatr Radiol 1999;29:37–41.
35. Benya EC, Nussbaum-Blask AR, Selby DM. Colonic diverticulitis causing partial bowel obstruction in a child with cystic fibrosis. Pediatr Radiol 1997;27:918–919.
36. Binkovitz LA, Allen E, Bloom D, et al. Atypical presentation of Clostridium difficile colitis in patients with cystic fibrosis. AJR 1999;172:517–521.
37. Bru C, Sans M, Defelitto MM, et al. Hydrocolonic sonography for evaluating inflammatory bowel disease. AJR 2001;177:99–105.
38. Lee BF, Chiu NT, Wu DC, et al. Use of 99mTc (V) DMSA scintigraphy in the detection and localization of intestinal inflammation: comparison of findings and colonoscopy and biopsy. Radiology 2001;220:381–385.
39. Halme L, Edgren J, Turpeinen U, von Smitten K, Stenman UH. Urinary excretion of iohexol as a marker of disease activity in patients with inflammatory bowel disease. Scand J Gastroenterol 1997;32:148–152.
40. Lee HB, Kim JH, Yim CY, Kim DG, Ahn DS. Differences in immunophenotyping of mucosal lymphocytes between ulcerative colitis and Crohn's disease. Korean J Intern Med 1997;12:7–15.
41. Okada M, Maeda K, Yao T, et al. Right-sided ulcerative colitis. [Review] J Gastroenterol 1996;31:717–722.
42. Cammarota T, Bresso F, Sarno A, Astegiano M, Macchiarella V, Robotti D. [Abdominal pain and bowel dysfunction: the diagnostic role of ultrasonography.] [Italian] Radiol Med 2000;100:337–342.
43. Schunk K, Reiter S, Kern A, Orth T, Wanitschke R. [Hydro-MRI in inflammatory bowel diseases: a comparison with colonoscopy and histology.] [German] Rofo Fortschr Geb Rontgenstr Neuen Bildgeb Verfahr 2001;173:731–738.
44. Charron M, del Rosario FJ, Kocoshis SA. Pediatric inflammatory bowel disease: assessment with scintigraphy with 99mTc white blood cells. Radiology 1999;212:507–513.
45. Lapidus A, Bernell O, Hellers G, Lofberg R. Clinical course of colorectal Crohn's disease: a 35–year follow-up study of 507 patients. Gastroenterology 1998;114:1151–1160.
46. Nordenholtz KE, Stowe SP, Stormont JM, et al. The cause of death in inflammatory bowel disease: a comparison of death certificates and hospital charts in Rochester, New York. Am J Gastroenterol 1995;90:927–932.
47. Schunk K, Kern A, Heussel CP, et al. [Hydro-MRT with fast sequences in Crohn's disease: a comparison with fractionated gastrointestinal passage.] [German] Rofo Fortschr Geb Rontgenstr Neuen Bildgeb Verfahr 1999;170:338–346.
48. Ferguson A. Assessment and management of ulcerative colitis in children. [Review] Eur J Gastroenterol Hepatol 1997;9:858–863.
49. Raithel M, Winterkamp S, Pacurar A, Ulrich P, Hochberger J, Hahn EG. Release of mast cell tryptase from human colorectal mucosa in inflammatory bowel disease. Scand J Gastroenterol 2001;36:174–179.
50. Orholm M, Binder V, Sorensen TI, Rasmussen LP, Kyvik KO. Concordance of inflammatory bowel disease among Danish twins. Results of a nationwide study. Scand J Gastroenterol 2000;35:1075–1081.
51. Tzivras M, Souyioultzis S, Tsirantonaki M, Archimandritis A. Chronic granulocytic leukemia in a patient with ankylosing spondylitis and ulcerative colitis: an interesting association. [Review] J Clin Gastroenterol 1997;25:365–366.
52. Maconi G, Ardizzone S, Parente F, Bianchi Porro G. Ultrasonography in the evaluation of extension, activity, and follow-up of ulcerative colitis. Scand J Gastroenterol 1999;34:1103–1110.
53. Mirk P, Palazzoni G, Gimondo P. Doppler sonography of hemodynamic changes of the inferior mesenteric artery in inflammatory bowel disease: preliminary data. AJR 1999;173:381–387.
54. Guslandi M, Sorghi S, Polli D, Tittobello A. Measurement of rectal blood flow by laser Doppler flowmetry in inflammatory bowel disease. Hepatogastroenterology 1998;45:445–446.
55. Yamamoto T, Keighley MR. Proctocolectomy is associated with a higher complication rate but carries a lower recurrence rate than total colectomy and ileorectal anastomosis in Crohn colitis. Scand J Gastroenterol 1999;34:1212–1215.

56. Yamamoto T, Keighley MR. Long-term outcome of total colectomy and ileostomy for Crohn disease. Scand J Gastroenterol 1999;34:280–286.
57. Garcia Picazo D, Bermudez Rodriguez E, Moreno Resina JM. Acute cholecystitis after colectomy for ulcerative colitis. Rev Esp Enferm Dig 2000;92:392–398.
58. Schmidt CM, Horton KM, Sitzmann JV, Jones B, Bayless T. Simple radiographic evaluation of ileoanal pouch volume. Dis Colon Rectum 1996;39:66–73.
59. Aitola P, Matikainen M, Mattila J, Tomminen T, Hiltunen KM. Chronic inflammatory changes in the pouch mucosa are associated with cholangitis found on perioperative liver biopsy specimens at restorative proctocolectomy for ulcerative colitis. Scand J Gastroenterol 1998;33:289–293.
60. Libicher M, Scharf J, Wunsch A, Stern J, Dux M, Kauffmann GW. MRI of pouch-related fistulas in ulcerative colitis after restorative proctocolectomy. J Comput Assist Tomogr 1998;22:664–668.
61. Wong SK, Ho YH, Leong AP, Seow-Choen F. Clinical behavior of complicated right-sided and left-sided diverticulosis. Dis Colon Rectum 1997;40:344–348.
62. Chintapalli KN, Chopra S, Ghiatas AA, Esola CC, Fields SF, Dodd GD 3rd. Diverticulitis versus colon cancer: differentiation with helical CT findings. Radiology 1999;210:429–435.
63. Rao PM, Rhea JT. Colonic diverticulitis: evaluation of the arrowhead sign and the inflamed diverticulum for CT diagnosis. Radiology 1998;209:775–779.
64. Jang HJ, Lim HK, Lee SJ, Lee WJ, Kim EY, Kim SH. Acute diverticulitis of the cecum and ascending colon: the value of thin-section helical CT findings in excluding colonic carcinoma. AJR 2000;174:1397–1402.
65. Blakeborough A, Chapman AH, Swift S, Culpan G, Wilson D, Sheridan MB. Strictures of the sigmoid colon: barium enema evaluation. Radiology 2001;220:343–348.
66. Miller FH, Ma JJ, Scholz FJ. Imaging features of enterohemorrhagic Escherichia coli colitis. AJR 2001;177:619–623.
67. Satoh T, Sasatomi E, Wu L, Tokunaga O. Phlegmonous colitis: a specific and severe complication of chronic hepatic disease. Virchows Arch 2000;437:656–661.
68. Takahashi T, Gamboa-Dominguez A, Gomez-Mendez TJ, et al. Fulminant amebic colitis: analysis of 55 cases. Dis Colon Rectum 1997;40:1362–1367.
69. Sachdev GK, Dhol P. Colonic involvement in patients with amebic liver abscess: endoscopic findings. Gastrointest Endosc 1997;46:37–39.
70. Nagi B, Kochhar R, Bhasin DK, Singh K. Colorectal tuberculosis. [Review] Eur Radiol 2003;13:1907–1912.
71. Lee IJ, Ha HK, Park CM, et al. Abdominopelvic actinomycosis involving the gastrointestinal tract: CT features. Radiology 2001;220:76–80.
72. Uchiyama N, Ishikawa T, Miyakawa K, et al. Abdominal actinomycosis: barium enema and computed tomography findings. J Gastroenterol 1997;32:89–94.
73. Kirkpatrick ID, Greenberg HM. Evaluating the CT diagnosis of Clostridium difficile colitis: should CT guide therapy? AJR 2001;176:635–639.
74. Benoit R, Grobost O, Crepeau T. [Diaphragm-like strictures of the colon from diclofenac.] [Review] [French] Presse Med 2001;30:1102–1104.
75. Pardi DS, Tremaine WJ, Rothenberg HJ, Batts KP. Melanosis coli in inflammatory bowel disease. J Clin Gastroenterol 1998;26:167–170.
76. Nusko G, Schneider B, Schneider I, Wittekind C, Hahn EG. Anthranoid laxative use is not a risk factor for colorectal neoplasia: results of a prospective case control study. Gut 2000;46:651–655.
77. Tomas ME, Casis B, Soto S, et al. [Salmonella osteomyelitis in a patient with collagenous colitis.] [Spanish] Rev Esp Enferm Dig 1999;91:76–77.
78. De La Riva S, Betes MT, Duque JM, Angos R, Munoz Navas MA. Collagenous colitis and lymphocytic colitis: clinical and endoscopic findings. Rev Esp Enferm Dig 2000;92:86–96.
79. Bellin MF, Darchen MA, Hoang C, et al. Rectal malacoplakia in renal transplantation: MR features. J Comput Assist Tomogr 1994;18:975–978.
80. Molik KA, West KW, Rescorla FJ, Scherer LR, Engum SA, Grosfeld JL. Portal venous air: the poor prognosis persists. J Pediatr Surg 2001;36:1143–1145.
81. Patton WL, Willmann JK, Lutz AM, Rencken IO, Gooding CA. Worsening enterocolitis in neonates: diagnosis by CT examination of urine after enteral administration of iohexol. Pediatr Radiol 1999;29:95–99.
82. Balthazar EJ, Yen BC, Gordon RB. Ischemic colitis: CT evaluation of 54 cases. Radiology 1999;211:381–388.
83. Millward SF, Fortier M. Transient gastric emphysema caused by colonic infarction. AJR 2001;176:1331–1332.
84. Danse EM, Van Beers BE, Jamart J, et al. Prognosis of ischemic colitis: comparison of color Doppler sonography with early clinical and laboratory findings. AJR 2000;175:1151–1154.
85. Yao T, Iwashita A, Hoashi T, et al. Phlebosclerotic colitis: value of radiography in diagnosis—report of three cases. Radiology 2000;214:188–192.
86. Shiojima K, Mitsuhashi N, Yamakawa M, Sakurai H, Niibe H. Transrectal ultrasonography in evaluation of chronic rectal complications after radiation therapy for carcinoma of the uterine cervix. Invest Radiol 1998;33:74–79.
87. Chen JH, Lai SJ, Tsai PP, Chen YF. Localized amyloidosis mimicking carcinoma of the colon. AJR 2002;179:536–537.
88. Boudiaf M, Zidi SH, Soyer P, et al. [Primary epiploic appendicitis: CT diagnosis for conservative treatment.] [French] Presse Med 2000;29:231–236.
89. Takada A, Moriya Y, Muramatsu Y, Sagae T. A case of giant peritoneal loose bodies mimicking calcified leiomyoma originating from the rectum. Jpn J Clin Oncol 1998;28:441–442.
90. Croizet O, Moreau J, Arany Y, Delvaux M, Rumeau JL, Escourrou J. Follow-up of patients with hyperplastic polyps of the large bowel. Gastrointest Endosc 1997;46:119–123.
91. Cunnane ME, Rubesin SE, Furth EE, Levine MS, Laufer I. Small flat umbilicated tumors of the colon: radiographic and pathologic findings. AJR 2000;175:747–749.
92. Baldisserotto M, Spolidoro JV, Bahu Mda G. Graded compression sonography of the colon in the diagnosis of polyps in pediatric patients. AJR 2002;179:201–205.

93. Chiba M, Yamano H, Fujiwara K, Abe T, Iizuka M, Watanabe S. Lymph folliculitis in ulcerative colitis. Scand J Gastroenterol 2001;36:332–336.
94. Fedele L, Bianchi S, Portuese A, Borruto F, Dorta M. Transrectal ultrasonography in the assessment of rectovaginal endometriosis. Obstet Gynecol 1998;91: 444–448.
95. Manfredi R, Valentini AL. Magnetic resonance imaging of pelvic endometriosis. Rays 1998;23:702–708.
96. Smith TR, Fine SW, Jones JG. CT appearance of some colonic villous tumors. AJR 2001;177:91–93.
97. Whitelaw SC, Murday VA, Tomlinson IP, et al. Clinical and molecular features of the hereditary mixed polyposis syndrome. Gastroenterology 1997;112:327–334.
98. Bjork J, Akerbrant H, Iselius L, Alm T, Hultcrantz R. Epidemiology of familial adenomatous polyposis in Sweden: changes over time and differences in phenotype between males and females. Scand J Gastroenterol 1999;34:1230–1235.
99. Debinski HS, Love S, Spigelman AD, Phillips RK. Colorectal polyp counts and cancer risk in familial adenomatous polyposis. Gastroenterology 1996;110: 1028–1030.
100. Svab J, Peskova M, Jirasek V, Fried M, Krska Z. [Long-term results of ileo-rectal anastomosis in familial polyposis.] [Czech] Rozhl Chir 1999;78:150–153.
101. Parc YR, Olschwang S, Desaint B, Schmitt G, Parc RG, Tiret E. Familial adenomatous polyposis: prevalence of adenomas in the ileal pouch after restorative proctocolectomy. Ann Surg 2001;233:360–364.
102. Belchetz LA, Berk T, Bapat BV, Cohen Z, Gallinger S. Changing causes of mortality in patients with familial adenomatous polyposis. Dis Colon Rectum 1996;39: 384–387.
103. Suzui M, Yoshimi N, Hara A, Morishita Y, Tanaka T, Mori H. Genetic alterations in a patient with Turcot's syndrome. Pathol Int 1998;48:126–133.
104. Marsh DJ, Coulon V, Lunetta K, et al. Mutation spectrum and genotype-phenotype analyses in Cowden disease and Bannayan-Zonana syndrome, two hamartoma syndromes with germline PTEN mutation. Hum Mol Genet 1998;7:507–515.
105. Cho KC, Sundaram K, Sebastiano LS. Filiform polyposis of the small bowel in a patient with multiple hamartoma syndrome (Cowden disease). AJR 1999;173: 501–502.
106. Wada K, Asoh T, Imamura T, et al. Rectal carcinoid tumor associated with the Peutz-Jeghers syndrome. J Gastroenterol 1998;33:743–746.
107. Parnaud G, Corpet DE. [Colorectal cancer: controversial role of meat consumption.] [Review] [French] Bull Cancer 1997;84:899–911.
108. Potter MA, Cunliffe NA, Smith M, Miles RS, Flapan AD, Dunlop MG. A prospective controlled study of the association of Streptococcus bovis with colorectal carcinoma. J Clin Pathol 1998;51:473–474.
109. Toyoki Y, Satoh S, Morioka G, Asano M, Nomura K. Rectal cancer associated with acquired hypertrichosis lanuginosa as a possible cutaneous marker of internal malignancy. J Gastroenterol 1998;33: 575–577.
110. de la Taille A, Mariette C, Buisine MP, Biserte J, Triboulet JP. [Urothelial tumor and colonic cancer in the context of a syndrome of hereditary predisposition to HNPCC colonic cancer.] [French] Prog Urol 2000;10:1204–1207.
111. Gafa R, Lanza G. [Expression of protein p53 in the adenoma-colorectal carcinoma sequence.][Italian] Pathologica 1998;90:351–356.
112. Vasen HF, Sanders EA, Taal BG, et al. The risk of brain tumours in hereditary non-polyposis colorectal cancer (HNPCC). Int J Cancer 1996;65:422–425.
113. Bertario L, Russo A, Sala P, et al. Risk of colorectal cancer following colonoscopic polypectomy. Tumori 1999;85:157–162.
114. Passman MA, Pommier RF, Vetto JT. Synchronous colon primaries have the same prognosis as solitary colon cancers. [Review] Dis Colon Rectum 1996;39: 329–334.
115. Conde P, Erdozain JC, Olveira A, Herrera A, Segura JM. [A patient with five synchronous adenocarcinomas of the colon.] [Spanish] Rev Esp Enferm Dig 1998;90: 124.
116. Shida H, Ban K, Matsumoto M, et al. Asymptomatic colorectal cancer detected by screening. Dis Colon Rectum 1996;39:1130–1135.
117. Macari M, Bini EJ, Jacobs SL, et al. Significance of missed polyps at CT colonography. AJR 2004; 183:127–134.
118. Nusko G, Mansmann U, Partzsch U, et al. Invasive carcinoma in colorectal adenomas: multivariate analysis of patient and adenoma characteristics. Endoscopy 1997;29:626–631.
119. Ueyama T, Kawamoto K, Iwashita I, et al. Natural history of minute sessile colonic adenomas based on radiographic findings. Is endoscopic removal of every colonic adenoma necessary? Dis Colon Rectum 1995;38:268–272.
120. Tarraga P, Garcia-Olmo D, Celada A, Garcia-Molinero Mf, Divison JA, Casado C. Colorectal cancer screening through detection of fecal occult blood in a controlled health zone. Rev Esp Enferm Dig 1999;91:335–344.
121. Frazier AL, Colditz GA, Fuchs CS, Kuntz KM. Cost-effectiveness of screening for colorectal cancer in the general population. JAMA 2000;284:1954–1961.
122. Pariente A, Milan C, Lafon J, Faivre J. Colonoscopic screening in first-degree relatives of patients with 'sporadic' colorectal cancer: a case-control study. The Association Nationale des Gastroenterologues des Hopitaux and Registre Bourguignon des Cancers Digestifs (INSERM CRI 9505). Gastroenterology 1998;115:7–12.
123. McMahon PM, Bosch JL, Gleason S, Halpern EF, Lester JS, Gazelle GS. Cost-effectiveness of colorectal cancer screening. Radiology 2001;219:44–50.
124. Okamura S, Ohashi S, Mitake M, et al. [A case of minute IIa + IIc type early colonic cancer (5 mm in size and sm 1 in invasion depth) with metachronous liver metastasis.] [Japanese] Nippon Shokakibyo Gakkai Zasshi 1998;95:890–894.
125. Garcia-Hirschfeld Garcia J, Blanes Berenguel A, Vicioso Recio L, Marquez Moreno A, Rubio Garrido J, Matilla Vicente A. Colon cancer: p53 expression and DNA ploidy. Their relation to proximal or distal tumor site. Rev Esp Enferm Dig 1999;91:481–488.
126. Rex DK, Rahmani EY, Haseman JH, Lemmel GT, Kaster S, Buckley JS. Relative sensitivity of colonoscopy and

barium enema for detection of colorectal cancer in clinical practice. Gastroenterology 1997;112:17–23.
127. Strom E, Larsen JL. Colon cancer at barium enema examination and colonoscopy: a study from the county of Hordaland, Norway. Radiology 1999;211:211–214.
128. Hancock JH, Talbot RW. Accuracy of colonoscopy in localisation of colorectal cancer. Int J Colorectal Dis 1995;10:140–141.
129. Haseman JH, Lemmel GT, Rahmani EY, Rex DK. Failure of colonoscopy to detect colorectal cancer: evaluation of 47 cases in 20 hospitals. Gastrointest Endosc 1997;45:451–455.
130. Jang HJ, Lim HK, Park CK, Kim SH, Park JM, Choi YL. Segmental wall thickening in the colonic loop distal to colonic carcinoma at CT: importance and histopathologic correlation. Radiology 2000;216:712–717.
131. Oto A, Gelebek V, Oguz BS, et al. CT attenuation of colorectal polypoid lesions: evaluation of contrast enhancement in CT colonography. Eur Radiol 2003; 13:1657–1663.
132. Morrin MM, Farrell RJ, Kruskal JB, Reynolds K, McGee JB, Raptopoulos V. Utility of intravenously administered contrast material at CT colonography. Radiology 2000;217:765–771.
133. Yee J, McFarland E. How accurate is CT colonography? In: Dachman AH, ed. Atlas of Virtual Colonoscopy. New York: Springer, 2003:11–16.
134. Morra A, Meduri S, Ammar L, Ukmar M, Pozzi Mucelli R. [Colonoscopy with computed tomography with volume reconstruction. The results and a comparison with endoscopy and surgery.] [Italian] Radiol Med 1999;98:162–167.
135. Regge D, Galatola G, Martincich L, et al. [Use of virtual endoscopy with computerized tomography in the identification of colorectal neoplasms. Prospective study with symptomatic patients.] [Italian] Radiol Med 2000;99:449–455.
136. Yee J, Akerkar GA, Hung RK, Steinauer-Gebauer AM, Wall SD, McQuaid KR. Colorectal neoplasia: performance characteristics of CT colonography for detection in 300 patients. Radiology 2001;219:685–692.
137. Galdino GM, Yee J. Carpet lesion on CT colonography: a potential pitfall. AJR 2003;180:1332–1334.
138. Matsui T, Yao T, Yao K, et al. Natural history of superficial depressed colorectal cancer: retrospective radiographic and histologic analysis. Radiology 1996;201:226–232.
139. Sada M, Mitomi H, Igarashi M, Katsumata T, Saigenji K, Okayasu I. Cell kinetics, p53 and bcl-2 expression, and c-Ki-ras mutations in flat-elevated tubulovillous adenomas and adenocarcinomas of the colorectum: comparison with polypoid lesions. Scand J Gastroenterol 1999;34:798–807.
140. Rubio CA, Kumagai J, Kanamori T, Yanagisawa A, Nakamura K, Kato Y. Flat adenomas and flat adenocarcinomas of the colorectal mucosa in Japanese and Swedish patients. Comparative histologic study. Dis Colon Rectum 1995;38:1075–1079.
141. Watari J, Saitoh Y, Obara T, et al. Early nonpolypoid colorectal cancer: radiographic diagnosis of depth of invasion. Radiology 1997;205:67–74.
142. Kao PF, Tzen KY, Chang PL, Chang-Chien CR, Tsai MF, You DL. Diuretic renography findings in enterovesical fistula. Br J Radiol 1997;70:421–423.
143. Alcobendas F, Jorba R, Poves I, Busquets J, Engel A, Jaurrieta E. Perforated colonic cancer. Evolution and prognosis. Rev Esp Enferm Dig 2000;92:326–333.
144. Galia M, Midiri M, Carcione A, et al. [Usefulness of CT colonography in the preoperative evaluation of patients with distal occlusive colorectal carcinoma.] [Italian] Radiol Med 2001;101:235–242.
145. Fenlon HM, McAneny DB, Nunes DP, Clarke PD, Ferrucci JT. Occlusive colon carcinoma: virtual colonoscopy in the preoperative evaluation of the proximal colon. Radiology 1999;210:423–428.
146. Camunez F, Echenagusia A, Simo G, Turegano F, Vazquez J, Barreiro-Meiro I. Malignant colorectal treated by means of self-expanding metallic stents: effectiveness before surgery and in palliation. Radiology 2000;216:492–497.
147. Mainar A, De Gregorio Ariza MA, Tejero E, et al. Acute colorectal obstruction: treatment with self-expandable metallic stents before scheduled surgery—results of a multicenter study. Radiology 1999;210: 65–69.
148. Falchi M, Cecchini G, Derchi LE. [Umbilical metastasis as first sign of cecal carcinoma in a cirrhotic patient (Sister Mary Joseph nodule). Report of a case.] [Italian] Radiol Med 1999;98:94–96.
149. Osin P, Shiloni E, Pikarsky AJ, Okon E. Metastatic adenocarcinoma in a thyroid colloid nodule: a rare presentation of colon cancer. Pathology 1996;28: 236–237.
150. Sefr R, Penka I, Oliva T. [Carcinoma of the colon invading the duodenum and pancreas.] [Czech] Rozhl Chir 2000;79:112–115.
151. Zerhouni EA, Rutter C, Hamilton SR, et al. CT and MR imaging in the staging of colorectal carcinoma: report of the Radiology Diagnostic Oncology Group II. Radiology 1996;200:443–451.
152. Sitzler PJ, Seow-Choen F, Ho YH, Leong AP. Lymph node involvement and tumor depth in rectal cancers: an analysis of 805 patients. Dis Colon Rectum 1997;40:1472–1476.
153. Bipat S, Glas AS, Slors FJ, Zwinderman AH, Bossuyt PM, Stoker J. Rectal cancer: local staging and assessment of lymph node involvement with endoluminal US, CT, and MR imaging—a meta-analysis. Radiology 2004;232:773–783.
154. Civelli EM, Gallino G, Mariani L, et al. Double-contrast barium enema and computerised tomography in the pre-operative evaluation of rectal carcinoma: are they still useful diagnostic procedures? Tumori 2000;86: 389–392.
155. Palko A, Gyulai C, Fedinecz N, Balogh A, Nagy F. Water enema CT examination of rectum cancer by reduced amount of water. Rofo Fortschr Geb Rontgenstr Neuen Bildgeb Verfahr 2000;172:901–904.
156. Fuchsjager MH, Maier AG, Schima W, et al. Comparison of transrectal sonography and double-contrast MR imaging when staging rectal cancer. AJR 2003;181: 421–427.
157. Lindmark GE, Kraaz WG, Elvin PA, Glimelius BL. Rectal cancer: evaluation of staging with endosonography. Radiology 1997;204:533–538.
158. Kruskal JB, Sentovich SM, Kane RA. Staging of rectal cancer after polypectomy: usefulness of endorectal US. Radiology 1999;211:31–35.

159. Wallengren NO, Holtas S, Andren-Sandberg A, Jonsson E, Kristoffersson DT, McGill S. Rectal carcinoma: double-contrast MR imaging for preoperative staging. Radiology 2000;215:108–114.
160. Maier AG, Kersting-Sommerhoff B, Reeders JW, et al. Staging of rectal cancer by double-contrast MR imaging using the rectally administered superparamagnetic iron oxide contrast agent ferristene and IV gadodiamide injection: results of a multicenter phase II trial. J Magn Reson Imaging 2000;12:651–660.
161. Koh D-M, Brown G, Temple L, et al. Rectal Cancer: Mesorectal Lymph Nodes at MR Imaging with USPIO versus Histopathologic Findings-Initial Observations. Radiology 2004;231:91–99.
162. Urban M, Rosen HR, Holbling N, et al. MR imaging for the preoperative planning of sphincter-saving surgery for tumors of the lower third of the rectum: use of intravenous and endorectal contrast materials. Radiology 2000;214:503–508.
163. Hussain SM, Outwater EK, Siegelman ES. Mucinous versus nonmucinous rectal carcinomas: differentiation with MR imaging. Radiology 1999;213:79–85.
164. Filippone A, Ambrosini R, Fuschi M, Marinelli T, Genovesi D, Bonomo L. Preoperative T and N Staging of Colorectal Cancer: Accuracy of Contrast-enhanced Multi-Detector Row CT Colonography-Initial Experience. Radiology 2004;231:83–90.
165. Abdel-Nabi H, Doerr RJ, Lamonica DM, et al. Staging of primary colorectal carcinomas with fluorine-18 fluorodeoxyglucose whole-body PET: correlation with histopathologic and CT findings. Radiology 1998;206:755–760.
166. Paule B, Brion N. [Metastatic colorectal cancer: new therapeutics.] [Review] [French] Presse Med 2000;29:1072–1077.
167. de Vries A, Griebel J, Kremser C, et al. Monitoring of tumor microcirculation during fractionated radiation therapy in patients with rectal carcinoma: preliminary results and implications for therapy. Radiology 2000;217:385–391.
168. Delaloye AB, Delaloye B, Buchegger F, et al. Comparison of copper-67– and iodine-125–labeled anti-CEA monoclonal antibody biodistribution in patients with colorectal tumors. J Nucl Med 1997;38:847–853.
169. De Santis M, Ariosi P, Calo GF, Luppi G, Franchini M, Romagnoli R. [Antineoplastic perfusion with percutaneous stop-flow control in the treatment of advanced pelvic malignant neoplasms.] [Italian] Radiol Med 2000;100:56–61.
170. de Gregorio MA, Mainar A, Tejero E, et al. Acute colorectal obstruction: stent placement for palliative treatment—results of a multicenter study. Radiology 1998;209:117–220.
171. Laghi A, Iannaccone R, Bria E, et al. Contrast-enhanced computed tomographic colonography in the follow-up of colorectal cancer patients: a feasibility study. Eur Radiol 2003;13:883–889.
172. Schoemaker D, Black R, Giles L, Toouli J. Yearly colonoscopy, liver CT, and chest radiography do not influence 5–year survival of colorectal cancer patients. Gastroenterology 1998;114:7–14.
173. Wind P, Norklinger B, Roger V, Kahlil A, Guin E, Parc R. Long-term prognostic value of positive peritoneal washing in colon cancer. Scand J Gastroenterol 1999;34:606–610.
174. Stuckle CA, Maleszka A, Kosta P, Kirchner JK, Liermann D, Adamietz IA. [Computerized tomography evaluation of local recurrence of operated and adjuvant radiation treated rectal carcinoma. Normal and pathological changes after operation and irradiation of rectal carcinoma in 956 CT examinations.] [German] Radiologe 2001;41:491–496.
175. Even-Sapir E, Parag Y, Lerman H, et al. Detection of recurrence in patients with rectal cancer: PET/CT after abdominoperineal or anterior resection. Radiology 2004;232:815–822.
176. Kinkel K, Tardivon AA, Soyer P, et al. Dynamic contrast-enhanced subtraction versus T2–weighted spin-echo MR imaging in the follow-up of colorectal neoplasm: a prospective study of 41 patients. Radiology 1996;200:453–458.
177. Abu-Rustum N, Barakat RR, Curtin JP. Ovarian and uterine disease in women with colorectal cancer. Obstet Gynecol 1997;89:85–87.
178. Philpott GW, Schwarz SW, Anderson CJ, et al. Radioimmuno-PET- detection of colorectal carcinoma with positron-emitting copper-64–labeled monoclonal antibody. J Nucl Med 1995;36:1818–1824.
179. Olofinlade O, Adeonigbagbe O, Gualtieri N, et al. Anal carcinoma: a 15–year retrospective analysis. Scand J Gastroenterol 2000;35:1194–1199.
180. Lee HJ, Han JK, Kim TK, Kim YH, Kim KW, Choi BI. Peripheral T-cell lymphoma of the colon: double-contrast barium enema examination findings in six patients. Radiology 2001;218:751–756.
181. Kim KW, Ha HK, Kim AY, et al. Primary malignant melanoma of the rectum: CT findings in eight patients. Radiology 2004;232:181–186.
182. Krestin GP, Hauser M, Eichenberger A, Kochli OR. [Bladder and rectal infiltration by uterine carcinomas: the accuracy of CT and MRI compared to endoscopic procedures.] [German] Rofo Fortschr Geb Rontgenstr Neuen Bildgeb Verfahr 1997;167: 125–131.
183. Ha HK, Jee KR, Yu E, et al. CT features of metastatic linitis plastica to the rectum in patients with peritoneal carcinomatosis. AJR 2000;174:463–466.
184. Miyayama S, Matsui O, Kifune K, et al. Malignant colonic obstruction due to extrinsic tumor: palliative treatment with a self-expanding nitinol stent. AJR 2000;175:1631–1637.
185. Soga J. Carcinoids of the colon and ileocecal region: a statistical evaluation of 363 cases collected from the literature. J Exp Clin Cancer Res 1998;17:139–148.
186. Spread C, Berkel H, Jewell L, Jenkins H, Yakimets W. Colon carcinoid tumors. A population-based study. Dis Colon Rectum 1994;37:482–491.
187. Moore CJ, Corl FM, Fishman EK. CT of cecal volvulus: unraveling the image. AJR 2001;177:95–98.
188. Javors BR, Baker SR, Miller JA. The northern exposure sign: a newly described finding in sigmoid volvulus. AJR 1999;173:571–574.
189. Yoshikawa A, Kuramoto S, Mimura T, et al. Peutz-Jeghers syndrome manifesting complete intussusception of the appendix and associated with a focal cancer of the duodenum and a cystadenocarcinoma of the

pancreas: report of a case. Dis Colon Rectum 1998;41:517–521.
190. Fujimoto T, Fukuda T, Uetani M, et al. Unenhanced CT findings of vascular compromise in association with intussusceptions in adults. AJR 2001;176:1167–1171.
191. Hogan M, Johnson JF 3rd. Multipolypoid intussusceptum: a distinctive appearance of ileoileocolic intussusception at the ileocecal valve. Pediatr Radiol 1996;26:405–408.
192. Daneman A, Alton DJ, Lobo E, Gravett J, Kim P, Ein SH. Patterns of recurrence of intussusception in children: a 17–year review. Pediatr Radiol 1998;28:913–919.
193. Gorenstein A, Raucher A, Serour F, Witzling M, Katz R. Intussusception in children: reduction with repeated, delayed air enema. Radiology 1998;206:721–724.
194. Yoon CH, Kim HJ, Goo HW. Intussusception in children: US-guided pneumatic reduction—initial experience. Radiology 2001;218:85–88.
195. Daneman A, Alton DJ, Ein S, Wesson D, Superina R, Thorner P. Perforation during attempted intussusception reduction in children—a comparison of perforation with barium and air. Pediatr Radiol 1995;25: 81–88.
196. Walker M, Sylvain J, Stern H. Bowel obstruction in a pregnant patient with ileal pouch-anal anastomosis. [Review] Can J Surg 1997;40:471–473.
197. Polignano FM, Caradonna P, Maiorano E, Ferrarese S. Recurrence of acute colonic pseudo-obstruction in selective adrenergic dysautonomia associated with infectious toxoplasmosis. Scand J Gastroenterol 1997;32:89–94.
198. deSouza NM, Williams AD, Wilson HJ, Gilderdale DJ, Coutts GA, Black CM. Fecal incontinence in scleroderma: assessment of the anal sphincter with thin-section endoanal MR imaging. Radiology 1998;208: 529–535.
199. Kelvin FM, Hale DS, Maglinte DD, Patten BJ, Benson JT. Female pelvic organ prolapse: diagnostic contribution of dynamic cystoproctography and comparison with physical examination. AJR 1999;173:31–37.
200. Pucciani F, Rottoli ML, Bologna A, et al. Anterior rectocele and anorectal dysfunction. Int J Colorectal Dis 1998;11:1–9.
201. Kelvin FM, Hale DS, Maglinte DD, Patten BJ, Benson JT. Female pelvic organ prolapse: diagnostic contribution of dynamic cystoproctography and comparison with physical examination. AJR 1999;173:31–37.
202. Mellgren A, Lopez A, Schultz I, Anzen B. Rectocele is associated with paradoxical anal sphincter reaction. Int J Colorectal Dis 1998;13:13–16.
203. Salzano A, Grassi R, Habib I, et al. [The defecographic and clinical aspects of the solitary rectal ulcer syndrome.] [Italian] Radiol Med 1998;95:588–592.
204. Salzano A, Muto M, De Rosa A, et al. [Defecography in rectal wall prolapse conditions.] [Italian] Radiol Med 1999;97:486–490.
205. Halligan S, Malouf A, Bartram CI, Marshall M, Hollings N, Kamm MA. Predictive value of impaired evacuation at proctography in diagnosing anismus. AJR 2001;177:633–636.
206. Karoui S, Savoye-Collet C, Koning E, Leroi AM, Denis P. Prevalence of anal sphincter defects revealed by sonography in 335 incontinent patients and 115 continent patients. AJR 1999;173:389–392.
207. Stewart LK, Wilson SR. Transvaginal sonography of the anal sphincter: reliable, or not? AJR 1999;173:179–185.
208. Rociu E, Stoker J, Eijkemans MJ, Schouten WR, Lameris JS. Fecal incontinence: endoanal US versus endoanal MR imaging. Radiology 1999;212:453–458.
209. Beets-Tan RG, Morren GL, Beets GL, et al. Measurement of anal sphincter muscles: endoanal US, endoanal MR imaging, or phased-array MR imaging? A study with healthy volunteers. Radiology 2001;220: 81–89.
210. Malouf AJ, Williams AB, Halligan S, Bartram CI, Dhillon S, Kamm MA. Prospective assessment of accuracy of endoanal MR imaging and endosonography in patients with fecal incontinence. AJR 2000;175: 741–745.
211. Salzano A, De Rosa A, Amodio F, et al. [Integrated study of fecal incontinence with defecography, anal ultrasonography, perineography, and manometry.] [Italian] Radiol Med 1998;96:574–578.
212. Ellul JP, Mannion S, Khoury GA. Spontaneous rupture of the rectum with evisceration of the small intestine through the anus. Eur J Surg 1995;161:925–927.
213. Spencer JA, Chapple K, Wilson D, Ward J, Windsor AC, Ambrose NS. Outcome after surgery for perianal fistula: predictive value of MR imaging. AJR 1998;171:403–406.
214. Di Nardo R, Drudi FM, Marziale P, et al. [Role of color Doppler echography in the visualization of perianal fistulae with injections of physiologic solutions.] [Italian] Radiol Med 2000;100:235–239.
215. Sudol-Szopinska I, Jakubowski W, Szczepkowski M, Sarti D. Usefulness of hydrogen peroxide enhancement in diagnosis of anal and ano-vaginal fistulas. Eur Radiol 2003;13:1080–1084.
216. Maier AG, Funovics MA, Kreuzer SH, et al. Evaluation of perianal sepsis: comparison of anal endosonography and magnetic resonance imaging. J Magn Reson Imaging 2001;14:254–260.
217. deSouza NM, Gilderdale DJ, Coutts GA, Puni R, Steiner RE. MRI of fistula-in-ano: a comparison of endoanal coil with external phased array coil techniques. J Comput Assist Tomogr 1998;22:357–363.
218. Beets-Tan RG, Beets GL, van der Hoop AG, et al. Preoperative MR imaging of anal fistulas: Does it really help the surgeon? Radiology 2001;218:75–84.
219. Madsen SM, Myschetzky PS, Heldmann U, Rasmussen OO, Thomsen HS. Fistula in ano: evaluation with low-field magnetic resonance imaging (0.1 T). Scand J Gastroenterol 1999;34:1253–1256.
220. Scholefield JH, Berry DP, Armitage NC, Wastie ML. Magnetic resonance imaging in the management of fistula in ano. Int J Colorectal Dis 1997;12:276–279.
221. Lee BH, Choe DH, Lee JH, et al. Device for occlusion of rectovaginal fistula: clinical trials. Radiology 1997;203:65–69.
222. Pennoyer WP, Vignati PV, Cohen JL. Mesenteric angiography for lower gastrointestinal hemorrhage: are there predictors for a positive study? Dis Colon Rectum 1997;40:1014–1018.
223. Gunderman R, Leef J, Ong K, Reba R, Metz C. Scintigraphic screening prior to visceral arteriography in acute lower gastrointestinal bleeding. J Nucl Med 1998;39:1081–1083.

224. Funaki B, Kostelic JK, Lorenz J, et al. Superselective microcoil embolization of colonic hemorrhage. AJR 2001;177:829–836.
225. Duque JM, Munoz Navas M, Betes MT, Subtil JC, Angos R. [Colonic involvement in the Klippel-Trenaunay-Weber syndrome.] [Review] [Spanish] Rev Esp Enferm Dig 2000;92:44–45.
226. Gonzalez Valverde FM, Mendez Martinez M, Osma Cordoba MD, Ballester Moreno A. [Small bowel lymphoma associated to carcinoid of the duodenum and angiodysplasia of the colon.] [Spanish] Rev Esp Enferm Dig 1999;91:312–313.
227. Cacoub P, Sbai A, Benhamou Y, Godeau P, Piette JC. [Severe gastrointestinal hemorrhage secondary to diffuse angiodysplasia: efficacy of estrogen-progesterone treatment.] [French] Presse Med 2000;29: 139–141.
228. Guingrich JA, Kuhlman JE. Colonic wall thickening in patients with cirrhosis: CT findings and clinical implications. AJR 1999;172:919–924.
229. Hung CC, Wong JM, Hsueh PR, Hsieh SM, Chen MY. Intestinal obstruction and peritonitis resulting from gastrointestinal histoplasmosis in an AIDS patient. J Formos Med Assoc 1998;97:577–580.
230. Blakeborough A, Sheridan MB, Chapman AH. Complications of barium enema examinations: a survey of UK Consultant Radiologists 1992 to 1994. Clin Radiol 1997;52:142–148.
231. Shackleton KL, Stewart ET, Henderson JD Jr, Demeure MJ, Telford GL. Effect of barium sulfate on wound healing in the gastrointestinal tract of the rat. Radiology 2000;214:563–567.
232. Sasatomi E, Miyazaki K, Mori M, Satoh T, Nakano S, Tokunaga O. Polypoid adenomyoma of the gallbladder. J Gastroenterol 1997;32:704–707.
233. Ryan CK, Potter GD. Disinfectant colitis. Rinse as well as you wash. [Review] J Clin Gastroenterol 1995;21: 6–9.
234. Damore LJ 2nd, Rantis PC, Vernava AM 3rd, Longo WE. Colonoscopic perforations. Etiology, diagnosis, and management. [Review] Dis Colon Rectum 1996;39: 1308–1314.
235. Hirata K, Noguchi J, Yoshikawa I, et al. Acute appendicitis immediately after colonoscopy. Am J Gastroenterol 1996;91:2239–2240.

6

Appendix

Congenital Abnormalities

Duplication of the vermiform appendix is rare. A double appendicitis developed in a patient with appendiceal duplication (1). A rare anomalous appendiceal insertion is not at the junction of colonic taenia but more distal.

Ultrasonography (US) identifies the appendix in only a minority of patients with cystic fibrosis; the appendix is normally dilated in these patients—the appendiceal mean diameter in cystic fibrosis patients was 9.8 mm, versus a noncystic fibrosis normal control group diameter of 3.9 mm (2). A normal appendiceal wall in cystic fibrosis patients is not thickened.

Appendicitis

Clinical

Appendicitis is a common cause of an acute abdomen in the Western world but is rare in parts of Africa and Asia. Apparently appendicitis was uncommon prior to the 19th century, at which time the term *typhlitis* was applied to right lower quadrant inflammation. Finally, in 1886, Reginald Fitz (3) put this condition in a correct perspective and coined the term *appendicitis*.

A number of unusual etiologies account for appendicitis, with the final common pathway being lumen obstruction. In children, obstruction due to lymphoid hyperplasia predominates. In adults, among others causes of obstruction are primary neoplasms and metastases to the appendix (Fig. 6.1). Ingested lead shot has been found in an inflamed appendix. Patients have developed acute appendicitis immediately after colonoscopy and after trauma, although any relationship is conjecture. Although schistosomiasis is common worldwide, schistosomal appendicitis is rare. Appendicitis does occur in renal transplant patients, and the clinical differential diagnosis needs to be expanded to include complications related to the transplanted kidney.

Occasionally periappendiceal inflammation involves the right ureter and causes an unsuspected obstruction. Even bilateral ureteric obstruction and acute tubular necrosis has developed (4).

A typical scenario in appendicitis is an acute appendiceal inflammation; next an intraluminal abscess and an increase in intraluminal pressure, followed by vascular occlusion, necrosis, and eventual perforation. A time-dependent sequence is apparent during the course of appendicitis and the prevalence of acute perforation increases when the diagnosis is delayed; an increased risk of perforation becomes apparent with a delay of more than 12 hours.

Occasionally a barium enema reveals an appendiceal diverticulum (Fig. 6.2). Most of these are curiosities of no significance, but similar to diverticula at other locations, obstruction, inflammation, and resultant diverticulitis are feasible. Indeed, appendiceal

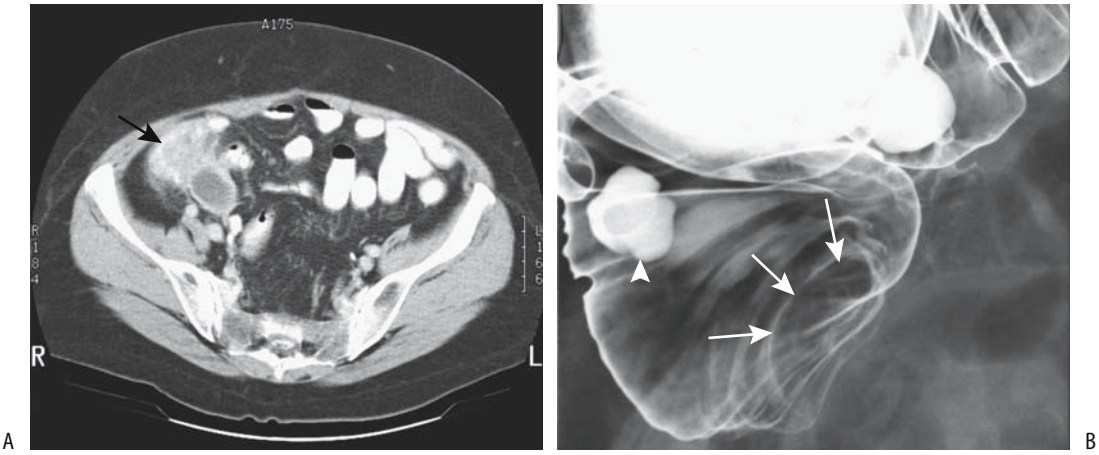

Figure 6.1. Appendicitis associated with a cecal carcinoma. A: Computed tomography (CT) identifies a soft tissue tumor indenting the cecal lumen (arrow). The fluid-filled structure adjacent to the tumor was believed to represent an appendiceal mucocele. A barium enema outlined a cecal carcinoma, confirmed by resection. (Courtesy of Patrick Fultz, M.D., University of Rochester.) B: Barium enema in another patient reveals a tumor at the cecal tip (arrows) and an incidental cecal diverticulum (arrowhead). An appendiceal phlegmon or abscess can have a similar appearance.

diverticulitis does exist, but differentiating conventional appendicitis from appendiceal diverticulitis is problematic even for a pathologist. From a clinical viewpoint both entities are similar.

Figure 6.2. Appendiceal diverticulosis.

A clinical diagnosis of appendicitis has about 20% false-positive and false-negative rates. These rates are increased in the very young and very old and in women under age 40 who have underlying gynecologic abnormalities.

Recurrence of surgically treated appendicitis is possible, presumably representing appendicitis of a residual stump. Discussions with experienced surgeons suggest that this condition is more common than the literature suggests. Recurrent appendicitis also develops in an appendiceal stump after laparoscopic appendectomy.

In most younger patients with acute appendicitis, no imaging studies are necessary. With an atypical presentation, a clinical differential diagnosis includes a number of other gastrointestinal and genitourinary conditions and can be evaluated by specific imaging tests. Mesenteritis and ileitis, regardless of etiology, are often in the differential diagnosis and are difficult to exclude. Also, in adolescent girls and women of reproductive age gynecological abnormalities need be considered and in these US should be the first imaging modality considered.

Imaging complements but does not replace clinical evaluation. A number of patients with normal imaging studies have been found to have acute appendicitis.

Diagnosis

An interesting observation in adults is that if the leukocyte count and C-reactive protein values are normal at admission and remain normal, acute appendicitis can be excluded and neither imaging nor resection is believed to be warranted (5); the authors emphasize that this finding applies only to adults, because in children with acute appendicitis both tests can be within normal limits.

Part of the problem in evaluating the efficacy of various imaging modalities is establishing a reproducible patient population. Most investigators agree that a majority of patients with suspected acute appendicitis do not need preoperative imaging, and it is this resultant patient selection, together with variations in the inherent delay in obtaining an imaging study, that introduces a bias. In addition, adults, with their more readily visualized periappendiceal fat, should not be compared to children. Even if a study does show that imaging reduces false-positive and false-negative appendectomy rates, the results should be judiciously balanced by the inherent increased delay to surgery and resultant increased risk of perforation for true-positive patients.

What is "early" appendicitis? Inflammation initially involves only the appendix, then spreads to surrounding tissues. Signs of early appendicitis are centered around an enlarged, fluid-filled appendix, which then presumably evolves into a thickened, inflamed wall, then periappendiceal inflammation, and eventually a phlegmon and abscess. The specific imaging findings are different between these categories, yet most studies lump patients into a single category and the relative mix of early and not-early appendicitis patients affects the prevalence of specific signs and study results.

Does imaging aid in the overall diagnostic accuracy in suspected acute appendicitis? Although most publications answer this question in the affirmative, an occasional dissent appears in the literature. Thus, in a controversial study of 766 consecutive patients undergoing appendectomy for suspected appendicitis at a United States university tertiary care center, neither computed tomography (CT) nor US improved diagnostic accuracy or the negative appendectomy rate (6); in fact, preoperative US delayed surgical consultation and appendectomy by 6 hours; the delay due to CT was 8 hours. A delay increases the risk of perforation with its increased morbidity. In the final analysis, whether to operate or not remains mostly a clinical decision.

Another relevant question is whether imaging has any effect on a negative appendectomy rate (normal pathologic findings). A negative appendix was found in 14% of children who underwent no imaging, 17% of those who had US (with or without CT), and only 2% of those who underwent CT only (7).

Presence of Appendicolith

Computed tomography (without enteric contrast) detects an appendicolith in about two thirds of children with appendicitis (8); for comparison, only 14% of 44 children initially suspected of appendicitis but with this diagnosis later excluded had an appendicolith. Most appendicoliths are solitary, but exceptions do occur. Some are several centimeters in diameter. Complicating the issue is that in an age-matched control population (CT obtained for trauma), 3% of children had an appendicolith. Thus in a clinical setting of suspected acute appendicitis, detection of an appendicolith is highly suggestive but not pathognomonic of appendicitis, a conclusion already established decades ago in the pre-CT era. Exceptions do occur and not all right lower quadrant calcifications are associated with appendicitis. Among other etiologies, a fecalith or ureterolith can mimic an appendicolith.

More attention needs to be placed on identifying an appendicolith than the literature suggests. A retained postappendectomy appendicolith predisposes to an abscess. Thus any preoperative imaging detection of an appendicolith should be communicated to the surgeon.

Other foreign bodies occasionally act as a nidus for appendicitis. In certain cultures lead shot appendicitis is a known entity (Fig. 6.3).

Appendiceal Gas

The earlier literature provides conflicting views about appendiceal gas; some authors suggested that gas is a normal finding; others thought gas to be a sign of appendicitis. In reality, intraluminal gas is found in both clinical settings. Computed tomography detects gas in slightly

Figure 6.3. Lead shot appendicitis. (Courtesy of Klas Mare, M.D., Göteborg, Sweden.)

over half of normal appendices; when present, it appeared as small bubbles or a tubular collection. An occasional individual has a gas–fluid level in a normal appendix. Similar findings, albeit less often, are found in patients with appendicitis (gas outside the lumen, on the other hand, is always abnormal). Ultrasound detects intraluminal gas in a majority of normal individuals and in about 15% of patients with acute appendicitis (9). Contrary to some statements in the literature, in any one patient a finding of intraluminal gas is of little diagnostic value. Gas in an appendicolith per se is of little significance. The presence of intramural or extraserosal gas generally implies a perforation.

Comparison Studies

A comparison of CT and US in suspected appendicitis is difficult to place in proper perspective. Ultrasound is rapid and requires no patient preparation, but is very operator dependent. Yet in most comparison studies CT achieves a slightly greater sensitivity and specificity than US, keeping in mind the added complexity of contrast administration (discussed below). The lack of periappendiceal fat in pediatric patients adds another variable to study comparisons, and results appear to be influenced by whether one is dealing with adults or children. Most comparison studies do not distinguish "early" or "perforated" appendicitis patients, yet disease status does influence study results. Thus US sensitivity and specificity in detecting appendicitis decrease after a perforation occurs, presumably because a decrease in appendiceal diameter makes it difficult to locate in the surrounding inflammation, and in this clinical setting CT appears to be preferred.

Unenhanced focused CT in children achieved a 97% sensitivity and 100% specificity, whereas a historical cohort of children with graded compression US reached a sensitivity of 100% and specificity of 88% (10); even with such a focused CT study, an alternate diagnosis was suggested by CT in 35% and by US in 28% of children without appendicitis.

Helical CT achieved a higher sensitivity (95% versus 78%) than graded compression US for detecting appendicitis in 386 children, adolescents, and young adults, with both techniques having similar specificity (11); of interest is that for discordant CT and US findings among these patients, CT was correct 85% of the time. In a prospective study of consecutive patients with clinical acute appendicitis, unenhanced focused single-detector helical CT and graded compression US performed in a Netherlands community teaching hospital by both body imaging radiologists and general radiology staff achieved similar accuracy for diagnosing acute appendicitis with both modalities (12): sensitivity of CT and US was 76% and 79%, respectively, and specificity was 83% and 78%.

In patients with clinically suspected acute appendicitis, unenhanced focused appendiceal CT, abdominopelvic CT, and focused appendiceal CT using colonic contrast achieved sensitivities of 78%, 72%, and 80% and specificities of 86%, 91%, and 87%, respectively (13); US without and with colonic contrast had low sensitivity (33% to 35%) but high specificity (85% to 89%), and all three CT techniques were superior to US. Another view from this study is that abdominopelvic CT provided the greatest diagnostic confidence for patients with negative findings, but focused appendiceal CT with colonic contrast provided the most confidence for patients with positive findings (13).

Finally, radiologists' diagnostic confidence appears greater with CT. Thus in children and

young adults with equivocal clinical findings for appendicitis, US was interpreted with a high or very high confidence level in only 58% of patients (14); CT was performed if US results were equivocal or appendix was not visualized (these are thus more atypical patients), yet CT was interpreted with a high or very high confidence in 92% of patients.

Conventional Radiographs

Although previously commonly obtained, conventional abdominal radiographs have been supplanted by other imaging tests. Likewise, a barium enema, although relatively accurate in detecting acute appendicitis, is rarely performed except in an older patient in whom a cecal carcinoma is suspected.

Elderly radiologists are familiar with barium retention in a normal appendix for prolonged time; if the patient develops appendicitis some time after a barium study, any residual appendiceal contrast should be placed in the proper perspective; it was situations such as this that gave rise to the surgical myth of barium-induced appendicitis.

The presence of focal adynamic ileus and mechanical ileus generally represents sequelae of a phlegmon or focal peritonitis (Fig. 6.4).

Figure 6.4. Appendicitis presenting both with adynamic ileus and small bowel obstruction.

Computed Tomography

A considerable, but often contradictory, literature discusses CT in a setting of suspected appendicitis. One should keep in mind that a number of variables affect CT study results:

1. Studies are different in pediatric patients than in adults. Children have less fat, an important component when identifying the appendix, and periappendiceal inflammation is thus less readily detected. Published CT accuracies in evaluating appendicitis are best approached by distinguishing children from adults. In younger children sedation is also an issue.
2. Should oral, rectal, or no contrast be used? Contrast does aid diagnosis, but of necessity the use of oral contrast introduces a delay in diagnosis that in certain situations is not acceptable to surgeons. Rectal contrast, administered blindly, introduces additional complexity to these studies.
3. Does intravenous contrast aid in detecting inflamed tissue or is its use superfluous in a setting of suspected appendicitis?
4. Should an abdominopelvic screening study be performed or is a study focused on the appendix using thin collimation preferred? The answer to this question is often based on whether one is dealing with a child or an adult and on overall clinical suspicion.

Evidence suggests that with unenhanced multislice CT the radiation dose can be lowered considerably without loss of diagnostic information when evaluating for appendicitis (15). Most studies agree that helical multislice CT using close collimation improves abnormality detection. In treating children, the trend is toward CT focused on the appendix rather than a general abdominopelvic scan if clinical suspicion suggests appendicitis. In adults, in whom alternate diagnoses are more common, this trend is less evident; an abdominopelvic CT scan (nonfocused scan) is more often the initial study for appendicitis, and a focused appendiceal CT study, using colonic contrast, is reserved for unusual situations. In a small minority of patients clinically suspected of having appendicitis, abnormalities are found outside the pelvis (16). The differential diagnosis often includes gynecologic abnormalities, Crohn's

disease, *Yersinia enterocolitica* infection, lymphoma, and, in adults, cecal diverticulitis and cancer.

Although intuitively obvious, one of the reasons for missing appendicitis with a focused study is if the inflamed appendix is not included in the imaged field of view. Scanning in a decubitus position is useful in some patients. In patients with clinically suspected acute appendicitis, 5-mm collimated sections through the lower abdomen and upper pelvis achieved a sensitivity of 99% and specificity of 98%, whereas 10-mm collimated sections from the diaphragm to the pubic symphysis reached a sensitivity of 82% and specificity of 95% (17); even narrower collimation is to be expected with the introduction of multislice units. In general, CT using 5-mm collimation but without oral, intravenous, or rectal contrast in adults with suspected acute appendicitis yields about 95% sensitivity and almost 100% specificity in diagnosing acute appendicitis. Even in children, focused CT achieves about 95% sensitivity and specificity (18,19).

Does intravenous, oral, and rectal contrast aid CT interpretation in suspected appendicitis? Even on such a simple topic published opinions vary. The sensitivity of detecting an inflamed appendix improves significantly with the use of intravenous (IV) contrast (20,21). The use of oral and IV contrast in children with suspected appendicitis achieved a 97% sensitivity and 93% specificity (22). Some protocols include both oral and rectal contrast. A disadvantage of oral contrast is the time involved before the contrast outlines the ileocecal region, a delay frowned upon by surgeons. A contrast enema sufficient to opacify the cecum aids in defining adjacent structures and cecal wall thickening. A contrast enema is more helpful in children, who have little abdominal fat, than in adults.

The typical criteria for a CT diagnosis of appendicitis include appendiceal wall thickening (>1 mm) or an abscess, phlegmon, or pericecal inflammation associated with appendicolith(s). An isolated appendicolith or isolated periappendiceal inflammation are secondary findings and in the absence of a thickened appendix should not be used to diagnose appendicitis. On the other hand, if the entire length of the appendix is visualized and very little or no lumen fluid is evident, no appendicolith is present, and periappendiceal fat appears normal, then appendicitis is excluded from the differential. Also, appendiceal nonvisualization on a technically correct CT scan should exclude appendicitis, keeping in mind that in some patients a phlegmon or abscess, presumably secondary to progression of inflammation, will render an appendix not visible even on narrow CT windows.

The *cecal bar sign* consists of a curved soft tissue bar separating an appendicolith from adjacent cecal contrast. Occasionally cecal contrast assumes a funnel-shaped outline, surrounded by thickened cecal wall and pointing toward the appendix, termed the *arrowhead sign*.

In any one patient the diagnosis is not always straightforward. Individually, many described signs are not pathognomonic of appendicitis and are also seen with other disorders. A normal appendix, identified by helical CT in its entire length, excludes appendicitis. An unopacified appendix >6 mm in diameter is strong presumptive evidence of appendicitis. Fat-stranding is a very sensitive but nonspecific finding in appendicitis.

Ileocolic lymph nodes tend to enlarge in appendicitis, but published detection sensitivities vary in different studies. In either case, adenopathy is found in a number of other diseases and cannot be relied on to suggest appendicitis.

Any small bowel adjacent to the appendix eventually develops a thickened wall due to inflammation or edema. Some phlegmons or abscesses are small and lie adjacent to the appendix; an occasional one extends into the pelvis and fills the pouch of Douglas. Adjacent vascular involvement ranges from mild engorgement to thrombosis.

Computed tomography in nonpregnant women clinically suspected of having either appendicitis or an acute gynecologic condition achieved 100% sensitivity and 97% specificity for diagnosing appendicitis and 87% sensitivity and 100% specificity for acute gynecologic conditions (23); CT is able to differentiate appendicitis and acute gynecologic conditions in the vast majority of women and influences both surgical and medical management in a number of them.

In summary, the use of CT, narrow collimation, and rectal contrast to opacify the cecum increases diagnostic confidence in a setting

of suspected appendicitis, especially in children. Intravenous contrast appears to be less important.

Ultrasonography

Ultrasonography in a clinical setting of suspected appendicitis has achieved mixed results, partly due to operator dependent factors. For example, appendiceal US studies performed by unsupervised technicians at night achieved a sensitivity of 26% compared with a sensitivity of 61% when studies were performed during the day by supervised technicians (24).

Some European hospitals have a policy to perform imaging, generally US, in all patients with a clinical suspicion of appendicitis (25). A further refinement is to add CT if US is equivocal. In general, US sensitivity and specificity are superior to those obtained with a clinical diagnosis only. Ultrasound allows a diagnosis of acute appendicitis in more patients more often and more quickly than is possible with clinical evaluation alone. Patients with true negative studies generally have other intestinal, mesenteric, gallbladder, or ovarian abnormalities. A number of studies show an overall sensitivity of about 85% for an US diagnosis of appendicitis. Nevertheless, to dampen some of the generally enthusiastic findings, a Danish prospective, double-blind diagnostic US study achieved poor results, reaching a sensitivity of only 49% and specificity of 88% (26). A high false negative rate US should not be used to exclude appendicitis in patients with a classic clinical presentation. Likewise, with a low clinical probability of appendicitis US is not recommended for screening because of the high false positive rate.

Visualization of a normal appendix in its entire length during US-graded compression is infrequent but when seen excludes appendicitis. A retrocecal appendix can be difficult to visualize. At times appendicitis is excluded by showing an alternative condition to account for the patient's symptomatology. It should be kept in mind, however, that appendicitis does occur synchronously with another disease having similar symptoms.

The most accurate US finding of acute appendicitis is presence of a noncompressible blind-ending tubular multilayered appendix having a maximal diameter >6 mm, a finding having a sensitivity and, in some studies, specificity in the high 90% (27). Others find a much lower specificity, primarily due to an appendiceal diameter of 6 mm or more in controls (28). One of the causes of an appendiceal diameter >6 mm in non-appendicitis patients is lymphoid hyperplasia, regardless of etiology. Other causes include excessive intraluminal content.

An appendiceal wall thickness >3 mm is generally found in acute appendicitis. The loss of appendiceal wall definition suggests ischemia or gangrene. An appendicolith appears as a bright hyperechoic structure with distal shadowing. Enlarged lymph nodes are common. Visualization of the inflamed appendix is generally accepted proof that appendicitis is present. Yet it should be realized that the appendix is also inflamed by adjacent disorders such as Crohn's disease, a tubo-ovarian abscess, colon carcinoma, and certain infections, and at times these mimic the sonographic appearance of appendicitis.

At times endovaginal US detects an appendix located in the pelvis when suprapubic US cannot locate it.

Doppler US reveals increased blood flow in the wall of an inflamed appendix. Appendiceal hyperemia is common in children with a nonperforating appendicitis but often resolves with a perforating or gangrenous appendix.

Magnetic Resonance Imaging

Magnetic resonance imaging is not commonly employed for suspected appendicitis, yet it has considerable advantages. It appears highly accurate in detecting acute appendicitis. In children with acute appendicitis, T2-weighted ultra–turbo spin echo (TSE) images revealed a markedly hyperintense region and a slightly hyperintense thickened wall, surrounded by a markedly hyperintense periappendiceal zone (29); unenhanced axial T2-weighted spin-echo imaging was the most sensitive sequence.

Peri-appendiceal inflammation appears on T1-weighted images as hypointense stranding within the hyperintense fat. Inflammatory tissue, including abscess wall, enhances postcontrast.

Scintigraphy

Scintigraphy is not commonly obtained in suspected appendicitis. Technetium-99m

(Tc-99m)–hexamethylpropyleneamine oxime (HMPAO) white blood cell scintigraphy in women with an acute abdomen, suspected of appendicitis but having atypical clinical findings, achieved a sensitivity and specificity of >90% in diagnosing appendicitis (30).

Unusual Appearance

In the majority of patients appendicitis eventually localizes in the right lower quadrant. Occasionally inflammation evolves in another location, such as in the pelvis (Fig. 6.5). Subhepatic appendicitis, at times with a fecalith, mimics acute cholecystitis. Several experienced clinicians relate encountering a gangrenous appendix in an incarcerated right inguinal hernia.

A commonly accepted dogma both in the literature and among practicing radiologists is that the presence of a contrast-filled appendix on CT excludes appendicitis. Occasionally, however, appendicitis involves only the appendiceal tip. A previous generation of radiologists practicing barium studies were taught to look for the bulbous dilatation near the tip of the appendix as a sign that the entire appendiceal lumen has been visualized; this finding is more difficult to detect with CT. Computed tomography in patients with distal appendicitis (the bulbous blind end is defined as *distal*) identifies a normal proximal appendix but does defect periappendiceal fat stranding; as expected with distal appendicitis, no abnormality is detected at the cecal base. Ultrasound can also detect distal appendicitis. Regardless of the imaging modality used, the entire appendiceal length should be studied to exclude distal appendicitis.

A right lower quadrant phlegmon or abscess is a late finding. An appendiceal abscess tends to involve adjacent bowel. Thus distal small bowel obstruction is common with neglected appendicitis. Strictures, presumably from chronic inflammation, have developed both in the ileum and sigmoid.

Appendicitis with a perforation allows appendicolith migration to unusual locations, including the pouch of Douglas; some of these calcifications are identified by postoperative CT.

In a rare presentation, scrotal US detected a hypoechoic lesion but a normal testis and epididymis in a 10-year-old boy with an inguinal hernia in the left scrotum (31); torsion was suspected, but surgery found pus in the tunica vaginalis together with surrounding inflammation. Subsequent abdominal US and MRI revealed an abscess posterior to the bladder, and laparotomy yielded a gangrenous appendix.

A rare complication of appendicitis is a vesicoappendicular fistula.

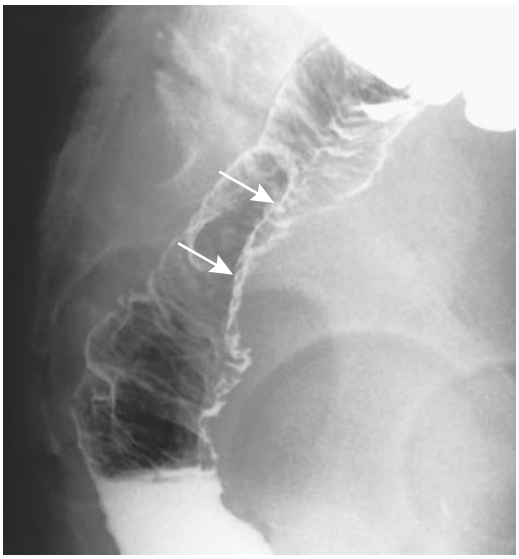

Figure 6.5. Neglected appendicitis that has evolved into a pelvic abscess. The appearance mimics a tumor in the pouch of Douglas (arrows).

Inflammatory Bowel Disease

Appendicitis appears to occur less often than expected in individuals with ulcerative colitis but roughly at the same rate as in the general population in Crohn's patients.

The clinical presentation of Crohn's disease of the appendix and typical acute appendicitis is similar. Indeed, it is conjecture whether a histologic diagnosis of *idiopathic granulomatous appendicitis* is the same entity as *Crohn's disease limited to the appendix*. Some patients with histologic acute and chronic appendicitis have granulomas but no systemic or enteric granulomatous disease. In general, the complication rate in a setting of granulomatous appendicitis is low. Some investigators suggest that if an appendectomy reveals granulomatous appen-

dicitis, further investigation is warranted to ensure that no underlying Crohn's disease exists in either the small bowel or colon. Also, presence of noncaseating granulomas is found in appendiceal sarcoidosis.

Pregnancy

Appendicitis does occur in pregnancy, during any trimester and also in the postpartum period. Maternal morbidity is essentially the same throughout the gestational period but perinatal outcome appears worse if appendicitis occurs in the second trimester. An extrauterine infection, such as appendicitis, appears to be associated with increased neonatal abnormalities.

Graded compression US is of similar value in pregnant women as in the general population.

MRI is often indicated in these patients.

Old Patients

A clinical diagnosis of appendicitis is difficult in the very young and very old (Fig. 6.6). Older patients developing acute appendicitis are considerably more likely to have a gangrenous or perforated appendix than younger patients. Among patients aged 70 to 89 years, the site of abdominal pain was atypical in half, 45% presented with bowel obstruction, a preoperative diagnosis of appendicitis was made only in half, surgery was performed within 24 hours of admission in only 40%, and appendiceal perforation occurred in 70% (32); complications developed in 70%, mostly related to perforation.

Figure 6.6. Barium enema reveals a tumor at the cecal base (arrows) in an elderly woman. A cancer was suspected but surgery revealed appendicitis.

AIDS Related

AIDS patients are prone to unusual infections. Even cytomegalovirus appendicitis can be expected in a patient with HIV infection.

Therapy

The primary purpose of early therapy of acute appendicitis is to arrest the inflammatory process prior to perforation. Mortality and morbidity rise with perforation. On the other hand, attempts to perform early appendectomy result in an increased normal appendectomy rate. An oft-repeated statement holds that an inverse relationship exists between a normal appendectomy rate and perforation rate, although the validity of such a relationship has been modified considerably by better diagnosis.

Laparoscopy

Laparoscopic appendectomy was initially greeted rather skeptically by the surgical community, yet numerous studies have concluded that, compared to open appendectomy, a laparoscopic approach leads to a shorter hospital stay. Nevertheless, a review of randomized, controlled trials of laparoscopic appendectomy in adults failed to establish superiority for the laparoscopic approach, and the authors concluded that "nothing is definitively well established" (33). The reported complication rates range from being similar for both open and laparoscopic approaches to the laparoscopic group having fewer infections and an earlier return to normal activity.

Diagnostic laparoscopy appears useful in a clinical equivocal diagnosis of appendicitis. A laparoscopic diagnosis of acute appendicitis can be immediately followed by a laparoscopic appendectomy.

Some surgeons consider acute complicated appendicitis, such as a gangrenous or perforated appendix, a relative contraindication to laparoscopic appendectomy.

Colonoscopy

Anecdotal reports describe colonoscopy both for diagnosis and therapy of unsuspected acute appendicitis. Colonoscopy reveals an inflamed appendiceal orifice. Intubation and pus aspiration are reputedly therapeutic but these patients invariably require an eventual elective appendectomy.

Other Therapy

Occasionally a patient with suspected appendicitis, especially if clinical symptoms are mild, is treated conservatively. Some of these patients then undergo an elective appendectomy.

Most periappendiceal abscesses are amenable to percutaneous drainage. Some of these can be drained using an endorectal route. Most surgeons recommend an interval appendectomy.

An incidental vaginal appendectomy can be performed in women during laparoscopic-assisted vaginal hysterectomy.

Differential Conditions

An otherwise normal appendix can be thickened by reactive inflammation due to an adjacent lesion, with the most relevant being mesenteric lymphadenitis. Complicating the issue is that lymph nodes enlarge both in appendicitis and mesenteric lymphadenitis.

Various gynecologic abnormalities, right ureter obstruction, cecal diverticulitis or cancer, and ischemia are some other conditions occasionally mimicking clinical acute appendicitis. Clinically, a rectus sheath hematoma presents similarly to appendicitis, although the correct diagnosis can be suspected either by CT or US.

Torsion of the right ovary mimics appendicitis; imaging should distinguish between these two conditions.

A cecal or appendiceal carcinoma not uncommonly manifests as appendicitis, with the clinical presentation in some patients suggesting chronic rather than acute appendicitis. Most published CT and US studies of appendicitis do not include cecal carcinoma in their alternate diagnosis groups, yet the not rare reports of cecal carcinoma mimicking CT and US findings of appendicitis are disturbing. Even in a younger adult a carcinoma often needs to be in the differential. A simple appendectomy in a setting of cecal cancer has grave consequences.

Appendiceal myeloid sarcoma in a patient with myeloid leukemia mimicked appendicitis both clinically and with CT (34). Also known as granulocytic sarcoma, myeloid sarcoma occurs in various myeloproliferative disorders, leukemia and polycythemia vera.

Thrombosis of an ovarian vein in a postpartum patient can mimic acute appendicitis both clinically and by US. Other conditions that mimic some of the imaging findings of appendicitis include Crohn's disease, tuboovarian abscess, typhlitis, cecal diverticulitis, and an adjacent neoplasm. Most often endometriosis has a different clinical presentation, but occasionally is a cause of acute appendicitis.

Chronic Appendicitis

Several recent authors have "rediscovered" the presence of recurrent episodes of abdominal pain due to appendicitis, a condition already described by Fitz in his seminal article in 1886. Many of these patients are treated conservatively, although recurrent bouts of appendicitis are common (35) (Fig. 6.7); patients with an appendiceal diameter >8 mm are more prone to develop recurrence than those with a smaller diameter. In spite of the initial clinical and imaging diagnosis of appendicitis, a basic question is often left unanswered: Did the patients indeed have appendicitis or was some other disorder responsible for the patients' symptoms?

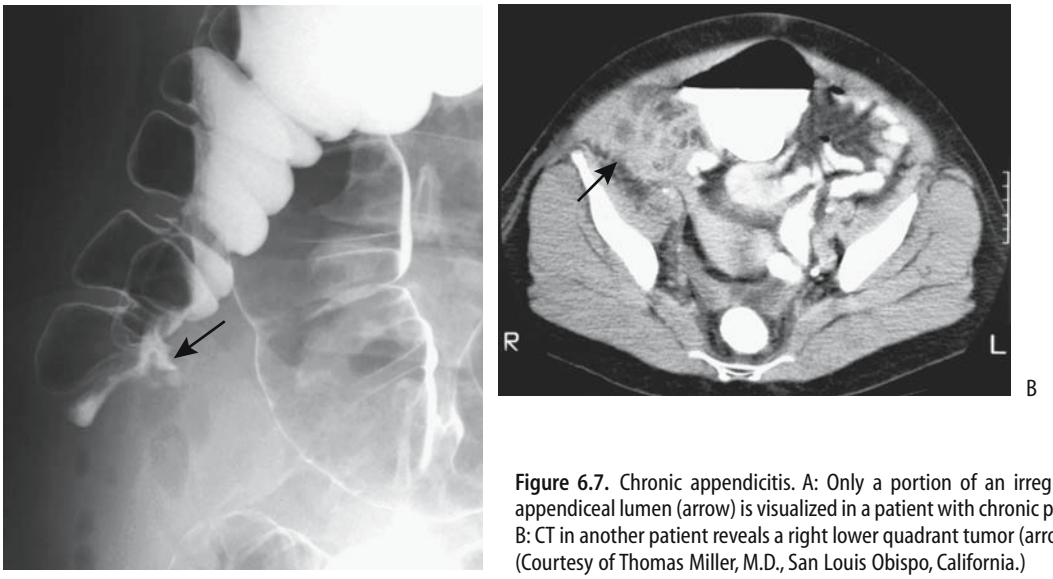

A B

Figure 6.7. Chronic appendicitis. A: Only a portion of an irregular appendiceal lumen (arrow) is visualized in a patient with chronic pain. B: CT in another patient reveals a right lower quadrant tumor (arrow). (Courtesy of Thomas Miller, M.D., San Louis Obispo, California.)

Tumors

Many appendiceal neoplasms are directly related to appendicitis, presumably by obstructing the lumen, or they are discovered incidentally by a pathologist in a resected appendix. An occasional appendiceal malignancy invades the adjacent cecum and eventually is labeled as a cecal carcinoma.

In general, the prevalence of both synchronous and metachronous colorectal neoplasms is increased in the presence of an appendiceal tumor; a study of nearly 8000 appendectomies found synchronous or metachronous colorectal cancers in 10% of patients with appendiceal carcinoids, in 33% of those with benign tumors, in 55% with secondary malignancies, and in 89% of those with primary malignancies (36).

Mucocele

A mucocele describes a grossly dilated appendiceal lumen filled with accumulated mucus. The term is descriptive in nature and does not imply a specific etiology; it is found with mucosal hyperplasia with lumen obstruction, a cystadenoma, cystadenocarcinoma, and even a mucin-producing tumor metastatic to the appendix. Some authors include the dilated appendices found normally in patients with cystic fibrosis under mucoceles, but this is not a universal practice.

Appendiceal mucoceles are associated with an increased prevalence of synchronous colon neoplasms. Thus colon tumor surveillance appears worthwhile in these patients.

An occasional mucocele is huge. Rarely, one develops postoperatively, at times even years later. Rupture of a mucocele leads to pseudomyxoma peritonei (discussed in Chapter 14). Most spontaneously rupturing mucoceles are malignant. Cecocolic intussusception by an appendiceal mucocele is very rare (37).

The barium enema appearance of a mucocele is that of a smoothly outlined mass extrinsic to the cecum in the region of the appendix. A similar finding is seen with CT (Fig. 6.8).

Ultrasonography shows an inhomogeneous tumor, often containing hyperechoic components and having posterior enhancement. Endosonography reveals a hypoechoic tumor containing hyperechoic foci. Endosonography should be able to distinguish between an appendiceal and an ovarian origin for mucoceles.

Magnetic resonance imaging identifies a cystic hypointense mass on T1- and a hyperintense mass on T2-weighted images. Their signal

Figure 6.8. Appendiceal mucocele. CT reveals a cystic structure extending inferiorly from the cecum and an abscess was suspected. Needle puncture under US guidance yielded gelatinous material. (Courtesy of Patrick Fultz, M.D., University of Rochester.)

intensity varies depending on protein content. The mucocele wall tends to be thick and enhances postcontrast.

The surgeon faces a dilemma once a mucocele is identified. If the condition is due to a simple retention cyst, an appendectomy suffices. At the other extreme, an underlying cystadenocarcinoma of the appendix requires a more extensive cancer resection.

Endometriosis

The most common site for endometriosis is the rectosigmoid, followed by the appendix and ileocecal region. Appendiceal endometriosis is usually associated with right ovarian endometriosis and is often clinically silent, being detected by the pathologist after an incidental appendectomy.

An occasional patient with appendiceal endometriosis presents with massive lower gastrointestinal bleeding or even an acute abdomen suggesting acute appendicitis. Intratumoral bleeding and necrosis presumably account for the acute presentation.

Carcinoid

A carcinoid is the most common appendiceal neoplasm. The vast majority of carcinoids are benign and, if detected incidentally in a resected appendix, are of little consequence. A rare one infiltrates the adjacent cecum and obstructs the bowel. Carcinoid induced fistulas are rare.

Somatostatin scintigraphy, performed after an incidental appendiceal carcinoid was discovered, detected focal tracer activity at the previous appendectomy site (38). No residual carcinoid was found at subsequent right hemicolectomy.

A rare and distinct entity is an adenocarcinoid, also called goblet cell carcinoid (39). These have histologic features of both a carcinoid and an adenocarcinoma and are aggressive tumors metastasizing readily. At surgery an appendiceal adenocarcinoid can mimic metastatic ovarian carcinoma.

Cystic Neoplasms

Appendiceal cystadenomas and cystadenocarcinomas typically present as soft tissue tumors extrinsic to the cecum but indenting it. The cystic nature of the tumor can be suspected from barium enema findings and confirmed either by US or CT. Occasionally mucin leaks into the surrounding soft tissues and incites inflammation and granuloma formation, at times to the point that even at surgery a carcinoma is suspected. Some appendiceal mucinous cystadenomas are associated with an elevated serum carcinoembryonic antigen (CEA) level.

Occasionally found are synchronous solid or cystic neoplasms of the ovaries and appendix. Although some authors consider them as representing two independent neoplasms, mutation analysis suggests that they are not independent but one originates from the other.

Computed tomography of primary mucinous appendiceal cystadenocarcinomas identifies not only a cystic component but also enhancing wall nodules. A gynecologic tumor is often in the differential diagnosis.

Adenoma/Adenocarcinoma

Appendiceal adenocarcinoma are uncommon. Most are not suspected preoperatively and many cancers have already metastasized at the initial presentation. Appendiceal adenocarcinomas have developed in a setting of chronic ulcerative colitis and in familial polyposis syndrome. A rare appendiceal villous adenoma caused acute appendicitis.

A necrotic appendiceal adenocarcinoma can form a fistula to adjacent structures, including bladder.

Other Tumors

A fibrous histiocytic tumor at the appendiceal tip led to appendiceal torsion (40). A hyperplastic polyp is occasionally detected in a resected appendix. Rare appendiceal ganglioneuromas and pheochromocytoma develop mostly in patients with neurofibromatosis type 1.

Metastases to the appendix are probably more common than the literature suggests, especially in a setting of carcinomatosis. A rare metastasis results in acute appendicitis. The role of appendectomy in staging and cytoreductive surgery in a setting of ovarian cancer and suspected carcinomatosis is debatable.

In spite of the rich surrounding adenopathy, lymphoma involving the appendix is rare.

Intussusception

Appendicocecal intussusception is rare. These intussusceptions range from complete to partial. Some are idiopathic, others have an underlying malignancy, endometriosis, cecal lymphangioma (41), or some other lead point.

Clinically, these intussusceptions range from acute to chronic.

The intussuscepted appendix appears as a finger-like projection in the cecal lumen. Some intussusceptions are reduced during a barium enema. Once an intussusception has progressed beyond the point of appendiceal invagination, the imaging appearance begins to mimic a cecocolic or even an ileocolic intussusception; these latter intussusceptions are discussed in Chapter 5.

Examination and Surgical Complications

Postoperative complications develop in about 10% of patients after simple acute appendicitis versus about 20% in those with gangrenous or perforated appendicitis.

Following conventional appendectomy, US identifies a seroma under the scar in about half the patients; the seroma gradually resolves. After laparoscopic appendectomy fluid collections are also relatively common even in asymptomatic patients. In the symptomatic patient these innocuous fluid collections can be difficult to distinguish from a postoperative abscess.

Even a scrotal abscess has developed after laparoscopic appendectomy.

Occasionally an incomplete appendectomy is performed. Some of these patients continue to have symptoms; in others appendicitis develops later. A postoperative appendicocutaneous fistula suggests an incomplete appendectomy or possibly retained stone.

Dropped appendicoliths are associated with necrotic appendicitis and occur more often during a laparoscopic appendectomy. Not uncommonly they result in a pelvic abscess (42).

A cecocolic intussusception develops rarely after an appendectomy.

References

1. Hennekinne S, Pessaux P, Regenet N, Fauvet R, Tuech JJ, Arnaud JP. [Double appendicitis: a rare clinical form in appendix duplication.] [French] Presse Med 2001;30:23–24.
2. Hahn H, von Kalle T, Pfadler E, Franz R, Hilz B, Farber D. [Ultrasound appendix imaging in mucoviscidosis patients.] [German] Rofo Fortschr Geb Rontgenstr Neuen Bildgeb Verfahr 1999;170:181–184.
3. Fitz RH. Perforating inflammation of the vermiform appendix, with special reference to its early diagnosis and treatment. Trans Assoc Am Physicians 1886;1: 107.
4. Tiel-van Buul MM, Aronson DC, Groothoff JW, Van Baren R, Frenkel J, Van Royen EA. The role of renal scintigraphy in the diagnosis and follow-up of unilateral ATN after complete bilateral distal ureteral obstruction as a complication of acute appendicitis. Clin Nucl Med 1998;23:141–145.
5. Grönroos JM, Grönroos P. Diagnosis of acute appendicitis. Radiology 2001;219:297–298.
6. Lee SL, Walsh AJ, Ho HS. Computed tomography and ultrasonography do not improve and may delay the diagnosis and treatment of acute appendicitis. Arch Surg 2001;136:556–562.
7. Applegate KE, Sivit CJ, Salvator AE et al. Effect of cross-sectional imaging on negative appendectomy and perforation rates in children. Radiology 2001;220:103–107.
8. Lowe LH, Penney MW, Scheker LE et al. Appendicolith revealed on CT in children with suspected appendicitis: how specific is it in the diagnosis of appendicitis? AJR 2000;175:981–984.
9. Rettenbacher T, Hollerweger A, Macheiner P, et al. Presence or absence of gas in the appendix: additional criteria to rule out or confirm acute appendicitis—evaluation with US. Radiology 2000;214(1):183–187.

10. Lowe LH, Penney MW, Stein SM, et al. Unenhanced limited CT of the abdomen in the diagnosis of appendicitis in children: comparison with sonography. AJR 2001;176:31–35.
11. Sivit CJ, Applegate KE, Stallion A, et al. Imaging evaluation of suspected appendicitis in a pediatric population: effectiveness of sonography versus CT. AJR 2000;175: 977–980.
12. Poortman P, Lohle PN, Schoemaker CM, et al. Comparison of CT and sonography in the diagnosis of acute appendicitis: a blinded prospective study. AJR 2003;181:1355–1359.
13. Wise SW, Labuski MR, Kasales CJ, et al. Comparative assessment of CT and sonographic techniques for appendiceal imaging. AJR 2001;176:933–941.
14. Pena BM, Taylor GA. Radiologists' confidence in interpretation of sonography and CT in suspected pediatric appendicitis. AJR 2000;175:71–74.
15. Keyzer C, Tack D, de Maertelae, V, Bohy P, Gevenois P, Van Gansbeke D. Acute Appendicitis: Comparison of Low-Dose and Standard-Dose Unenhanced Multi-Detector Row CT. Radiology 2004;232:164–172.
16. Kamel IR, Goldberg SN, Keogan MT, Rosen MP, Raptopoulos V. Right lower quadrant pain and suspected appendicitis: nonfocused appendiceal CT—review of 100 cases. Radiology 2000;217:159–163.
17. Weltman DI, Yu J, Krumenacker J Jr, Huang S, Moh P. Diagnosis of acute appendicitis: comparison of 5– and 10–mm CT sections in the same patient. Radiology 2000;216:172–177.
18. Sivit CJ, Dudgeon DL, Applegate KE et al. Evaluation of suspected appendicitis in children and young adults: helical CT. Radiology 2000;216:430–433.
19. Mullins ME, Kircher MF, Ryan DP, et al. Evaluation of suspected appendicitis in children using limited helical CT and colonic contrast material. AJR 2001;176:37–41.
20. Jacobs JE, Birnbaum BA, Macari M, et al. Acute appendicitis: comparison of helical CT diagnosis focused technique with oral contrast material versus nonfocused technique with oral and intravenous contrast material. Radiology 2001;220:683–690.
21. Kaiser S, Finnbogason T, Jorulf HK, Soderman E, Frenckner B. Suspected appendicitis in children: diagnosis with contrast-enhanced versus nonenhanced Helical CT. Radiology 2004;231:427–433.
22. Fefferman NR, Roche KJ, Pinkney LP, Ambrosino MM, Genieser NB. Suspected appendicitis in children: focused CT technique for evaluation. Radiology 2001;220: 691–595.
23. Rao PM, Feltmate CM, Rhea JT, Schulick AH, Novelline RA. Helical computed tomography in differentiating appendicitis and acute gynecologic conditions. Obstet Gynecol 1999;93:417–421.
24. Pohl D, Golub R, Schwartz GE, Stein HD. Appendiceal ultrasonography performed by nonradiologists: does it help in the diagnostic process? J Ultrasound Med 1998;17:217–221.
25. van Breda Vriesman AC, Kole BJ, Puylaert JB. Effect of ultrasonography and optional computed tomography on the outcome of appendectomy. Eur Radiol 2003; 13:2278–2282.
26. Jahn H, Mathiesen FK, Neckelmann K, Hovendal CP, Bellstrom T, Gottrup F. Comparison of clinical judgment and diagnostic ultrasonography in the diagnosis of acute appendicitis: experience with a score-aided diagnosis. Eur J Surg 1997;163:433–443.
27. Kessler N, Cyteval C, Gallix B, et al. Appendicitis: evaluation of sensitivity, specificity, and predictive values of US, Doppler US, and laboratory findings. Radiology 2004;230:472–478.
28. Rettenbacher T, Hollerweger A, Macheiner P, et al. Outer diameter of the vermiform appendix as a sign of acute appendicitis: evaluation at US. Radiology 2001; 218:757–762.
29. Hormann M, Paya K, Eibenberger K, et al. MR imaging in children with nonperforated acute appendicitis: value of unenhanced MR imaging in sonographically selected cases. AJR 1998;171:467–470.
30. Kao CH, Lin HT, Wang YL, Wang SJ, Liu TJ. Tc-99m HMPAO-labeled WBC scans to detect appendicitis in women. Clin Nucl Med 1996;21:768–771.
31. Yasumoto R, Kawano M, Kawanishi H, et al. Left acute scrotum associated with appendicitis. Int J Urol 1998;5: 108–110.
32. Sfairi A, Farah A, Patel JC. [Acute appendicitis in patients over 70 years of age.] [French] Presse Med 1996;25:707–710.
33. Slim K, Pezet D, Chipponi J. Laparoscopic or open appendectomy? Critical review of randomized, controlled trials. Dis Colon Rectum 1998;41:398–403.
34. Khatti S, Faria SC, Medeiros LJ, Szklaruk J. Myeloid sarcoma of the appendix mimicking acute appendicitis. AJR 2004;182:1194.
35. Cobben LP, de Van Otterloo AM, Puylaert JB. Spontaneously resolving appendicitis: frequency and natural history in 60 patients. Radiology 2000;215:349–352.
36. Connor SJ, Hanna GB, Frizelle FA. Appendiceal tumors: retrospective clinicopathologic analysis of appendiceal tumors from 7,970 appendectomies. Dis Colon Rectum 1998;41:75–80.
37. Coulier B, Pestieau S, Hamels J, Lefebvre Y. US and CT diagnosis of complete cecocolic intussusception caused by an appendiceal mucocele. Eur Radiol 2002;12: 324–328.
38. Hoegerle S, Nitzsche EU, Stumpf A, et al. Incidental appendix carcinoid. Value of somatostatin receptor imaging. Clin Nucl Med 1997;22:467–469.
39. Horiuchi S, Endo T, Shimoji H, et al. Goblet cell carcinoid of the appendix endoscopically diagnosed and examined with p53 immunostaining. J Gastroenterol 1998;33:582–587.
40. Fujishima N, Ooya M, Miura G, Yamaguchi M, Moriuti A. [A case of fibrous histiocytoma of the appendix with twisted stalk.] [Japanese] Nippon Geka Gakkai Zasshi 1998;99:865–867.
41. Wan YL, Lee TY, Hung CF, Ng KK. Ultrasound and CT findings of a cecal lymphangioma presenting with intussusception. Eur J Radiol 1998;27:77–79.
42. Kim N, Reed WP Jr, Abbas MA, Katz DS. CT identification of abscesses after dropped appendicoliths during laparoscopic appendectomy. AJR 2004;182:1203–1205.

7

Liver

Technique

Computed Tomography

In a solid organ such as the liver, computed tomography (CT) reveals characteristic attenuation alterations and morphologic changes of diffuse disorders such as cirrhosis and fatty infiltration. Similar changes are also detected with magnetic resonance imaging (MRI). Currently the primary limitation of both CT and MRI is that a number of liver disorders have overlapping imaging findings, thus limiting specificity.

The terms *helical* CT and *spiral* CT are used interchangeably. In helical CT the patient table moves at a constant speed while the x-ray tube and detectors rotate continuously, and thus scanning is in a helix rather than a circle as with conventional CT. Images obtained with helical CT do not define a specific circular body slice and are not identical to those obtained with conventional CT. There is little argument that in evaluating abdominal disease in general, and liver disorders in particular, helical CT is preferred over conventional CT.

Initial helical CT scanners could cover either large body parts or thin sections of a limited volume, but not both, a limitation largely overcome by the introduction of multidetector CT (also known as *multirow CT* and *multislice CT*) in the late 1990s. As a basic concept, multidetector CT generates more than one slice per x-ray tube rotation. Multidetector CT, with 16 detectors being readily available, 32 detectors being tested, and 64 or more detectors on the drawing boards, offers several advantages: a larger volume scanned during a given time, reduced time required to scan a given volume, narrower collimation and thus increased resolution, and shorter enhancement intervals after contrast. Multidetector helical CT allows simultaneous acquisition of multiple slices, and complex, single breath-hold techniques are thus feasible (a breath-hold is typically defined as 20 sec or less). Three-dimensional (3D) CT arteriograms without venous overlay are readily obtained by using first-pass data from a multirow detector CT scanner. One by-product of multidetector CT is a considerable increase in the number of images available for review, thus adding to study complexity. Simply decreasing the number of images evaluated is not a viable option because overlapping images at various phases of contrast flow improve disease detection.

In general, precontrast CT scanning identifies fewer liver lesions than postcontrast images. In many institutions precontrast CT is limited to specific indications such as in detecting calcifications or hemorrhage.

Correct arterial phase timing is obtained by using an initial test dose. Automatic bolus tracking initiates scanning after injection of contrast by monitoring a region-of-interest cursor placed in the abdominal aorta; a typical scenario is to set a threshold level at 100 Hounsfield units (HU) over the aortic baseline

CT level and initiate scanning about 10 seconds later. A similar approach is to start arterial phase imaging when splenic enhancement reaches a certain HU value above baseline.

On average, CT arterial phase begins to enhance about 15 to 20 seconds after the start of intravenous (IV) contrast injection, followed by portal venous enhancement about 30 seconds later and parenchyma enhancement shortly after that. Images during the arterial phase map the major hepatic artery branches, and portal phase images outline portal and hepatic venous systems. Such a biphasic or dual-phase CT technique refers to the two discrete imaging sequences obtained and not to a biphasic contrast injection. For some indications, a liver parenchyma enhancement phase, also called an equilibrium phase, obtained several minutes after the start of contrast injection, is useful.

The literature is inconsistent about defining *biphasic* and *triphasic* CT imaging. Some authors include a precontrast phase as part of these terms, but others do not. In this book a precontrast phase is not included as part of either biphasic or triphasic imaging, and the use of these terms refers to postcontrast phases only. Even here confusion exists; does "biphasic" refer to the arterial, portal venous or equilibrium phases (or any other phase for that matter)? The term *double arterial phase* imaging signifies that early and late arterial phase images are obtained during a single breath-hold study. Some use *quadruple phase to* mean that images are obtained precontrast and at three times after the start of contrast injection. No sharp boundary exists between various phases. Ideally, authors should include the specific times after the start of injection when scanning is initiated.

Computed tomography CT data are viewed either as traditional transverse images or displayed in coronal, sagittal, or 3D projections. The latter allows a direct estimate of tumor size, information at times useful to the oncologist or surgeon.

Computed Tomography Angiography

Computed tomography angiography (CTA) is a general term used in a sense similar to *conventional angiography* but is often applied to a technique of injecting IV contrast and obtaining images during the arterial phase. Use of multidetector CT is especially well suited for such vascular studies.

Computed tomography angiography can also be performed with contrast injected through a catheter advanced into a major abdominal artery; whether one obtains *CT arterial portography* or *CT hepatic arteriography* (or any other specific vessel angiography) depends on the artery used and image timing.

Computed Tomography Arterial Portography

Computed tomography arterial portography consists of angiographic placement of a catheter in the superior mesenteric artery or splenic artery, transfer of the patient to a CT suite, injection of a contrast bolus through the intraarterial catheter, followed by liver imaging during the portal venous phase. This technique maximizes attenuation differences between a neoplasm having a primarily arterial blood supply and normal liver parenchyma primarily supplied by the portal vein. It is superior to the usual intravenous contrast-enhanced CT imaging; over 80% of tumors <1 cm in diameter are imaged. It is used in some centers preoperatively for anatomic localization of lesions and in evaluating whether a patient is indeed a surgical candidate. A refinement of this technique consists of a dual-phase study: during the first phase images are obtained about 30 seconds after the start of the contrast injection, and second-phase images are obtained at 70 seconds.

In general, there is no difference in hepatic enhancement whether CT arterial portography is performed via the superior mesenteric artery or the splenic artery. In the presence of an anomalous right hepatic artery originating from the superior mesenteric artery, the catheter needs to be positioned distal to this site. Computed tomography arterial portography is of limited use in patients with portal hypertension and collateral portal blood flow away from the liver.

Altered blood flow anomalies result in a number of artifacts during arterial portography. Inhomogeneous perfusion is most common near the porta hepatis, falciform ligament, and gallbladder. Perfusion defects can either resemble a neoplasm or even mask the presence of one. A liver *zebra pattern*, consisting of alternating regions of hyper- and hypoperfusion,

is identified in some patients, regardless of whether the splenic artery or superior mesenteric artery is injected.

Computed tomography arterial portography is an invasive procedure and was more in vogue during the 1990s. It has a high sensitivity for detecting lesions but a low specificity for diagnosis due to numerous false-positive findings. Currently, it is gradually being supplanted by other advances in CT and magnetic resonance (MR) technology.

Computed Tomography Hepatic Arteriography

Computed tomography hepatic arteriography consists of contrast injected through a catheter placed in the hepatic artery and arterial phase images obtained. Tumors having primarily an arterial blood supply are thus enhanced compared to liver parenchyma, which obtains a large part of its blood supply from the portal vein. This technique is also prone to artifacts because liver parenchyma tends not to enhance homogeneously, mostly due to blood supply anomalies. These artifacts (often called pseudolesions), especially around the gallbladder fossa, can be minimized by first injecting prostaglandin into the superior mesenteric artery (1).

An additional refinement is combined CT arterial portography and CT hepatic angiography in an attempt to improve lesion detection.

Contrast Agents

A biphasic CT study typically consists of continuous IV injection of 60 to 200 mL of a contrast agent at a rate of up to 5 mL per second. In general, a uniphasic injection is superior to biphasic injection. The degree of liver enhancement depends on the amount of iodine delivered. Ionic and nonionic contrast agents provide the same degree of contrast enhancement. The nonionic agents, however, are associated with less patient discomfort, fewer motion artifacts, and fewer side effects, and are preferred over ionic agents, especially for more complex examinations such as 3D reconstruction where minimizing patient motion is paramount.

Portal venous blood flow increases after a meal. Thus an indirect method of increasing liver CT portal contrast enhancement would be to perform a study shortly after a meal, but this adds further complexity.

How common is hepatobiliary excretion of vascular contrast media? Functioning hepatocytes excrete small amounts of contrast material into the biliary system. Several-hour delayed images obtained after arterial portography result in enhancement of normal liver parenchyma; non–iodine-excreting neoplasms tend to appear hypodense. Gallbladder opacification is occasionally seen after CT angiography in patients with cirrhosis or other liver disease.

The use of iodized oil during CT is essentially limited to the study of hepatocellular carcinomas, and this topic is covered later (see Hepatocellular Carcinoma).

Ultrasonography

Conventional (Gray Scale)

Most ultrasonography (US) imaging consists of real-time, gray-scale, B-mode display, with the reflected signal amplitude displayed as a variation in brightness. This technique is referred to as gray-scale US or simply as US to distinguish it from Doppler US. The transducer is most often in contact with a patient's skin (conventional US), although it can be placed in body cavities (endoluminal US) either directly or endoscopically (endoscopic US or endosonography).

As with CT and MR, it is hoped that continued advances in US equipment design will lead to more accurate diagnoses. For instance, the introduction of tissue and contrast harmonic imaging with stimulated acoustic emission has resulted in clearer images and improved tumor detection compared to more conventional US.

One novel approach is the use of two frequencies. Preliminary data suggest that metastases have an increase in contrast-to-noise ratios at higher frequencies, in distinction to hemangiomas, which have a decreased ratio.

Intraoperative

Special transducers are available for laparoscopic US. Introduced through a 10-mm laparoscopic port, a flexible transducer tip allows contact with the curved liver surface. The often-used 7-MHz transducer provides only limited penetration of the liver; a 5-MHz transducer

gives more complete coverage of a large organ such as the liver.

However, intraoperative US does have its detractors; one study found preoperative MRI to be almost as sensitive as intraoperative US in depicting liver tumors (2); intraoperative US altered surgery in only 4% of patients.

A current limitation of laparoscopic US is the considerable time required for a complete liver scan. Nevertheless, in selected patients laparoscopic US will detect small suspicious intrahepatic tumors and, if needed, provide biopsy guidance and influence surgery.

Doppler

Doppler US is readily performed at the patient's bedside. Its primary value in the liver is in quantifying blood flow and detecting vascular lesions. Doppler US evaluates portal and hepatic venous systems for hypertension, obstruction, and presence of collaterals, and provides relative flow information in individual blood vessels. Each normal major hepatic vessel has a characteristic Doppler waveform.

Color Doppler US uses color to display a target frequency shift. Power Doppler US provides amplitude of the Doppler signal; it does not provide velocity information, but it is more sensitive in detecting flow in more structures than color Doppler US and is more sensitive and accurate in detecting tumor vascularity. One limitation of Doppler US is data reproducibility. A number of studies have documented significant interobserver and inter-equipment variability, although training does decrease the former.

Contrast Agents

Some authors use the term *ultrasound angiography* to describe contrast enhanced US.

The intravenous US contrast agent, Levovist (Schering, Berlin, Germany), consists of a suspension of micrometer-sized particles of galactose and gas bubbles. This agent passes readily through the lungs and enhances vascular signal intensity. Contrast-specific US techniques, such as phase or pulse inversion, are necessary; using this contrast agent with phase inversion harmonic mode US, normal liver parenchyma becomes hyperechoic; in most patients liver enhancement is sufficiently prolonged to allow lesion detection. Compared to conventional B-mode US, tumor conspicuity is improved and smaller tumors are detected and tumor characterization and overall diagnostic performance are significantly improved (3). Imaging can be performed during arterial (10–40 sec after injection), portal venous (50–90 sec) and late (>100 sec) phases. Late-phase uptake of Levovist differs in different types of liver tumors; malignancies are mostly hypoechoic, uptake in hemangiomas is variable, and benign tumors are mostly hyper- or isoechoic relative to liver parenchyma (4), differences aiding in separating benign tumors from malignancies.

Perflenapent emulsion (EchoGen, Sonus Pharmaceuticals, Bethell, WA), an intravascular US contrast agent, also provides liver parenchymal contrast enhancement (5).

A liver enhancing US contrast agent consists of direct injection of CO_2 into the proper hepatic artery during arteriography (6); such a technique helps detect additional liver tumors during percutaneous ethanol therapy.

Magnetic Resonance Imaging

If a prediction is to be made based on theoretical considerations, MRI appears virtually certain to achieve future status as the dominant abdominal imaging modality, especially when investigating a specific problem. It loses some of its advantages to CT if a multiorgan screening study is required. The development of open high-field strength magnets and a simpler design should make MRI more readily available. Open MRI systems have obvious advantages, but their current limitation is a low field strength. Whether imaging with 3T (tesla) units will justify their extra complexity remains to be established. New techniques are necessary with 3T imaging—tissue relaxation times differ at 3.0 T than at lower magnet strengths. Proton MR spectroscopy, including 3D MR spectroscopic imaging, shows promise but currently is mostly a research tool. Magnetic resonance spectroscopy using phosphorus 31 evaluates changes in phosphorus-containing liver metabolites and provides data on liver function. Although clinically useful in evaluating certain diseases, discussion of MR spectroscopy is beyond the scope of this work.

The discipline of MR interventional imaging is just beginning to be applied to clinical practice.

Technique

An extensive literature exists comparing various MRI sequences in their detection of specific liver abnormalities. No universal set of sequences has emerged as an optimal study for liver disease. Optimal MR sequences for liver imaging are constantly changing and are not covered in this work. New hardware and software developments lead to new optimal sequences, making it difficult to generalize about specific techniques. Differences in equipment design between various manufacturers make comparison of some sequences moot. Thus a finding that a particular set of sequences produces better resolution images or detects more focal lesions in a shorter period of time is useful information, but may not apply to other units using different imaging parameters. Even with a similar MR unit, variations in repetition time, echo time, and acquisition time change the resultant information acquired.

One limitation of liver MRI, evident mostly with older units, is motion. A major decrease in motion artifacts is achieved when the scan acquisition time is shorter than a patient's breath hold. Advances in MR coil design and the use of fast spin-echo pulse sequences designed to achieve short scan acquisition times minimize motion artifacts due to respiration and peristalsis, and yield high-resolution images.

Most liver MR studies include both T1- and T2-weighted sequences and a contrast-enhanced sequence. In general, T1 sequences provide better anatomic orientation and lesion detection, but T2 sequences are superior for lesion characterization. An occasional lesion is identified with one but not the other sequence. A hyperintense signal on T1-weighted images is not specific for any disorder and is seen with such entities as fat, proteins, blood (hematoma), melanin, and contrast agents such as gadolinium. T2-weighted sequences result in a hyperintense signal from tissue containing increased amounts of fluid and a hypointense signal from fibrotic tissue. Iron results in a very hypointense signal on T2-weighted sequences.

Fast low-angle shot (FLASH) is a type of spoiled gradient-recalled echo (GRE) technique allowing the entire liver to be covered in a single breath-hold, thus reducing motion artifacts. Blood vessels appear as a signal void. This technique is useful in dynamic contrast-enhanced imaging.

Abnormal fluid or tissue is best identified if its MR signal intensity differs as much as possible from adjacent normal tissue; to some extent these signal intensity differences can be manipulated to achieve a desired result. For example, abnormal fluid and fibrotic tissue normally have a low T1-weighted signal intensity and are thus best identified against the normally high T1-weighted signal intensity of adjacent fat. On the other hand, a hematoma, which most often has a high T1-weighted signal intensity, is better identified if, using a fat-suppression technique, fat is made to have a low T1-weighted signal intensity. Similar image manipulation is also useful with T2-weighted images.

The definition of *precontrast MRI* (occasionally called *native phase MRI*) is clear, as are *contrast-enhanced MRI* and *postcontrast MRI*. *MR angiography* (MRA) implies that images are obtained sometime after intravenous contrast injection, but a more basic definition of MRA is a study using MR images sensitive to flowing blood, and thus MRA does not necessarily require the use of a contrast agent. *Dynamic MRI* implies that serial postcontrast images are obtained during specific arterial, capillary (parenchymal), portal venous, and delayed phases, but not necessarily all phases are imaged in any one study. Some authors use the terms *dynamic MRI* and *MRA* even when only the arterial phase is imaged. In the liver, *postcontrast MR* often implies MRI during portal venous or delayed phases unless a specific other postcontrast injection phase is identified.

Intravenous contrast is used with MRI for the same reasons as with CT: it improves lesion detection and characterization compared with precontrast images. Nevertheless, many lesions <1 cm, regardless of histology, tend to have a similar MR contrast enhancement pattern. Breath-hold 3D MRA also aids lesion localization within specific liver segments.

Useful vascular contrast agents increase liver parenchyma-to-lesion signal intensity differences by their different effect on tissue proton relaxation. These differences vary with time and depend on the degree of tumor vascularity. One common technique consists of a rapid IV gadolinium contrast injection followed by several T1-weighted spoiled gradient echo (SGE) sequences, such as an arterial sequence

and a venous or interstitial sequence. Because most malignant liver neoplasms are supplied primarily by the hepatic artery, arterial (and capillary) phase images are more useful in this clinical setting than delayed images. Vessels and vascular tumors are also often best evaluated on early (capillary phase) contrast-enhanced images.

Contrast Agents

Magnetic resonance imaging contrast agents useful in the liver are classified into four broad categories:

1. Gadolinium chelates (extracellular agents)
2. Macrophage-monocytic phagocytic system agents
3. Primarily hepatobiliary agents (intracellular agents)
4. Blood-pool agents

Some contrast agents overlap between categories. For instance, primarily hepatobiliary agents have an initial extracellular distribution; gadobenate dimeglumine (Gd-BOPTA) has dual contrast agent characteristics—it is both a nonspecific and a hepatobiliary agent.

All currently available MR contrast agents shorten tissue T1 and T2 relaxation times. The paramagnetic gadolinium and manganese contrast agents primarily shorten T1 and thus increase signal intensity of normal liver parenchyma on T1-weighted images; the superparamagnetic iron oxides shorten T2 and thus decrease signal intensity on T2-weighted images. While these metal ions are efficient, they are rather toxic and are thus chelated to other small molecular weight structures such as diethylenetriamine pentaacetic acid (DTPA) to reduce their toxicity.

The above four categories can be described as follows:

1. Nonspecific extracellular gadolinium chelates are currently the most often used MR contrast agents. The gadolinium feature most useful in MRI is its T1-shortening time and thus increased signal intensity on T1-weighted images. Typically these agents are injected as a bolus and equilibrate with the extracellular (interstitial) space shortly after injection; as a result, liver lesions become isointense to liver on delayed views and thus to take full advantage of these contrast agents, dynamic imaging must be performed shortly after contrast injection (arterial phase to portal venous phase). After IV injection, their biodistribution is similar to that of iodine-containing contrast agents.

   Gadolinium chelates have a much lower adverse contrast reaction rate than iodinated contrast agents, but anaphylactic reactions and cardiopulmonary arrests, including fatal ones, do occur. These agents are excreted by glomerular filtration but at the low doses used do not manifest iodinated agent's nephrotoxicity.

2. Larger size superparamagnetic iron oxide (SPIO) particles are taken up by liver endothelial and Kupffer cells and result, among other effects, in a decrease in reticuloendothelial system (RES) enhancement on T2-weighted images. Ferumoxides is a commonly used SPIO agent consisting of a colloidal mixture of ferrous and ferric oxide. Because some well-differentiated tumors and normal liver contain RES cells and thus take up iron oxide particles, they show a considerable but similar signal loss and overall appearance, but tissues lacking RES cells, such as metastases, have little or no signal loss and thus appear hyperintense to the resultant hypointense normal RES-containing liver parenchyma. Normal liver signal intensity decreases and lesion-to-liver contrast ratio increases on T2-weighted images post-SPIO administration; as a result, not only are known tumors better identified, but, compared to unenhanced MR sequences, additional tumors are detected. These SPIO effects differ considerably among various tumors, suggesting an ability to achieve tissue characterization of different focal tumors. The SPIO enhancement is impaired in a setting of diffuse liver disease. These agents have a longer intravascular half-life than gadolinium chelates. Their role in clinical imaging is not yet fully defined, but, as mentioned, they are useful in differentiating some benign from malignant tumors. A disadvantage is that the use of SPIO is time-consuming and involves an increased rate of false positive findings.

3. Several hepatobiliary specific paramagnetic contrast agents, such as Gd-

(EOB)-DTPA and Gd-BOPTA initially act as extracellular agents and then undergo hepatocyte uptake. They are eliminated both by biliary and renal pathways. Gd-EOB-DTPA provides a biliary excretion rate of about 50% of the injected dose. Only several percent of Gd-BOPTA is taken up by hepatocytes; however, it has a high relaxivity and results in a prolonged increase in liver signal intensity. Manganese-DPDP is a hepatobiliary-specific paramagnetic contrast agent having an effect lasting for several hours. Thus delayed imaging is feasible. It also has a role in pancreatic imaging.

On T1-weighted images these agents selectively enhance both normal liver parenchyma and such hepatocyte-containing tumors as focal nodular hyperplasia, regenerative nodules, and hepatocellular adenomas and carcinomas, but show little or no enhancement of metastases or hemangiomas. One exception is metastatic neuroendocrine tumors—an occasional one will enhance with Mn-DPDP. For the vast majority of tumors, however, these hepatobiliary agents differentiate between hepatocyte-containing and nonhepatocyte-containing tumors, and thus are useful in differentiating hepatocellular carcinomas from metastases, with nonhepatocyte-origin metastases becoming more conspicuous due to the increased signal from surrounding normal liver parenchyma. Duration of liver parenchymal enhancement varies, being up to several hours for some. Both early and delayed scans are useful as these agents are excreted by the biliary tract. One use is during MR-guided thermal tumor ablation procedures when prolonged tumor visualization is desired (7); Mn-DPDP identifies more focal tumors both in cirrhotic and noncirrhotic livers than precontrast images. Excretion of manganese is decreased in a setting of biliary stasis, and thus the use of this agent in cholangiography is limited, but it appears useful for defining intrahepatic biliary anatomic variants, such as in pretransplantation liver lobe donors. Its diagnostic impact is not yet clear.

4. Ultrasmall SPIO particles, unlike most MR contrast agents, shorten both T1 and T2 relaxation times. These agents have a blood half-life measured in hours and thus appear useful as blood-pool MR contrast agents. Small iron oxide particles (<10 nm) pass through capillaries and eventually are taken up by lymph nodes and thus are also called MR lymphographic agents. Ferumoxtran consists of dextran-coated iron oxide particles about 30 nm in size. After IV injection, ferumoxtran is taken up by liver, spleen, and lymph node reticuloendothelial cells and results in a homogeneous loss of signal in these structures. In distinction to gadolinium where pre- and postcontrast images can be obtained at the same session, post-ferumoxtran scans are obtained roughly 1 day after contrast injection, and thus two scanning sessions are required.

This class of contrast agents potentially aids in differentiating highly vascular lesions, such as hemangiomas, from solid neoplasms. Traditional MRA is not feasible with these agents. Some of these blood-pool agents reduce intravascular T1 values for several hours, and thus appear useful for MR angiographic interventional procedures without the need for repeat contrast injection. They have their own problems such as superimposition of arterial and venous structures, possibly solved by more extensive 3D imaging.

Refinements in MR contrast agent use include a combination of two such agents. Thus by combining information about RES status obtained with a superparamagnetic iron oxide agent with the perfusion data of a gadolinium chelate agent, more specific information is obtained about some liver tumors than with a single agent alone.

Serum levels of patients on hemodialysis show that about 80% of gadolinium is dialyzed after the first and essentially all after the fourth dialysis; no contraindications exist to normal-dose contrast use in these patients.

Scintigraphy

The primary role of liver scintigraphy is to provide tissue characterization. Scintigraphy relies primarily on specific physiologic and biochemical properties of a lesion as compared to normal liver parenchyma. For focal liver disease

scintigraphy aids primarily in narrowing a differential diagnosis.

Radiopharmaceutical Agents

Currently two main types of radiopharmaceutical agents are used in hepatobiliary imaging; both rely on labeling with technetium-99m (Tc-99m):

1. The iminodiacetic acid (IDA) derivatives evaluate hepatocyte function and patency of the bile ducts. These lipophilic radiopharmaceuticals are extracted from blood by hepatocytes, excreted into bile, and thus outline the gallbladder and bile ducts and eventually flow into the intestine. Urinary excretion is minimal if liver function is reasonably intact. In contrast to bilirubin, the IDA compounds are excreted without being conjugated. Bilirubin, however, competes with IDA derivatives for hepatocyte receptor binding sites and excretion pathways, and there is poor image quality in a setting of hyperbilirubinemia.

   The IDA radiopharmaceuticals are useful in infants and children in evaluating neonatal jaundice, trauma, and complications developing after transplantation.
2. Colloid particles—sulfur colloid and albumin colloid—are taken up by reticuloendothelial cells, with most of these being in the liver, about 5% to 10% in the spleen, and smaller amounts in bone marrow. The particles are permanently deposited in the liver. Nonvisualization of the liver with Tc-99m–sulfur colloid scintigraphy is uncommon, occurring in severe acute hepatitis and similar diffuse parenchymal disorders.

Several additional agents are occasionally useful in liver imaging:

1. Tc-99m–labeled red blood cells study blood-pool distribution and aid in diagnosing cavernous hemangiomas.
2. After inhalation, fat-soluble xenon 133 accumulates in fatty liver tissue. Although xenon-133 scintigraphy appears theoretically worthwhile in evaluating questionable fatty infiltration, clinical application has been controversial.
3. Gallium 67 citrate is useful in abscess detection. Its value in liver abscesses is compromised by uptake in normal liver tissue. It is also taken up by some hepatocellular carcinomas, lymphomas, and metastases.
4. Normally Tc-99m–methylene diphosphonate (MDP) is used for bone scintigraphy and not liver. After IV iron therapy some patients have liver uptake of Tc-99m-MDP, presumably due to phagocytosed iron within hepatic reticuloendothelial cells.

Positron Emission Tomography

Positron emission tomography (PET) is useful for detecting early primary and metastatic liver tumors and in staging. The information obtained with PET differs from other imaging modalities: PET images metabolic activity (i.e., uptake of a specific radioisotope), rather than providing an anatomic roadmap. The primary advantage of PET is that abnormal metabolic activity is often detected before anatomic changes are evident. In clinical practice, however, PET provides complementary information to more conventional imaging.

Two types of PET-based systems are used: dedicated PET and single photon emission computed tomography (SPECT). The basic principles underlying PET and SPECT are similar: a positron emitted by a radionuclide interacts with an electron, the resultant annihilation reaction produces two 511-keV photons in opposite directions and imaging detectors placed opposite to each other then detect these photons. In a dedicated PET system the detectors are fixed in position; with SPECT the detectors rotate around the body. Positron emission tomography imaging is faster and provides higher quality images than SPECT but at considerably higher cost. Rather than being dedicated to a particular type of study, a SPECT system is also useful for other nuclear medicine imaging. Both 2D and 3D PET systems are available. Fused PET/CT units combine functional with anatomic information.

Positron emission tomography is based primarily on an increased uptake of glucose by cancer cells; thus it depends on presence of viable tumor cells. A high uptake of fluorine-18–labeled fluorodeoxyglucose (FDG) is evident in numerous neoplasms, and this agent is most

often employed clinically; PET-FDG imaging detects not only liver tumors but also tumor recurrence at primary sites. Whole-body imaging is readily performed. False-positive uptake is by brain, cardiac muscle, and inflammatory cells. FDG uptake is decreased in a setting of hyperglycemia due to competition with unlabeled glucose. FDG is excreted by kidneys and pools in the bladder, thus limiting its use in the pelvis.

For certain applications, 18F-fluoromethylcholine is more advantageous than FDG. Fluorine-18 labeled α-methyl tyrosine (FMT) is a less often employed PET tracer. Although preliminary results indicate that, compared with FDG, FMT liver uptake is less, differences in uptake between benign and malignant tumors are significantly greater with FMT-PET (8).

Monoclonal Antibody

Both preoperative and intraoperative probe scintimetry are potential monoclonal antibody techniques.

A radiotracer-labeled monoclonal antibody designed against a specific neoplasm should potentially improve tumor detection. The antibody Tc-99m–anti–carcinoembryonic antigen (CEA) is available for the study of colon cancer metastases to the liver. This antibody is also taken up by normal liver parenchyma, thus limiting tumor detection.

Angiography

Conventional angiography and digital subtraction angiography (DSA) are well-established techniques generally requiring multiple contrast injections and multiple views to outline liver vascular anatomy.

Digital rotational subtraction angiography consists of rotating an X-ray tube around the patient during contrast injection, with resulting 3D images providing easier visualization of the course and direction of major vessels and their branches than is feasible with conventional 2D imaging.

Biopsy

Most liver biopsies are performed at the bedside and do not require imaging. Whether laparoscopic liver biopsy has any advantages is uncertain, except possibly in the patient with mild-to-moderate coagulation abnormalities where a fibrin plug at the biopsy site may decrease bleeding.

Imaging is helpful when tissue from a specific focal tumor is desired. The choice of imaging used varies; US is more common in Europe and Japan, while CT is more often preferred in the United States, although considerable local variation exists.

Ultrasonography-guided liver biopsies are performed on an outpatient basis, with patients generally discharged after an observation period. These biopsies achieve a sensitivity of over 90% and specificity of 100%; false-negative results are more common in cirrhotic nodules.

Magnetic resonance–guided liver biopsies are feasible and are most useful when a tumor is identified by MRI but not CT or US or if other image-guided biopsies are incomplete. Magnetic resonance–compatible needles are available. An 18-gauge needle provides enough tissue for diagnosis with few complications. From a pathologist's viewpoint, most diagnostic dilemmas with aspiration biopsies occur with well-differentiated hepatocellular neoplasms and with rare tumors.

Transjugular or transfemoral liver biopsy is performed in a setting of coagulopathy or ascites. Use of combined fluoroscopic and US guidance during biopsy improves visualization, increases operator confidence and is advantageous in smaller patients and in children (9). Several studies have achieved a histopathologic diagnosis in over 95% using either 18- or 19-gauge transjugular biopsy needles. An occasional such biopsy contains unusual tissue, such as duodenal mucosa or renal tissue.

Wedge-shaped transient subsegmental parenchymal enhancement is occasionally found along the needle tract on postbiopsy CT; subsegmental arterioportal shunting is responsible for this finding.

Complications of transjugular liver biopsy include an occasional subcapsular hematoma, intrahepatic arteriovenous fistula, liver capsule puncture, hemobilia, and those complications related to the neck puncture site (Fig. 7.1). Complications occur both with percutaneous and laparoscopically guided liver biopsies.

Percutaneous biopsy complication rate appears to be less if US provides guidance. The presence of perihepatic ascites does not appear

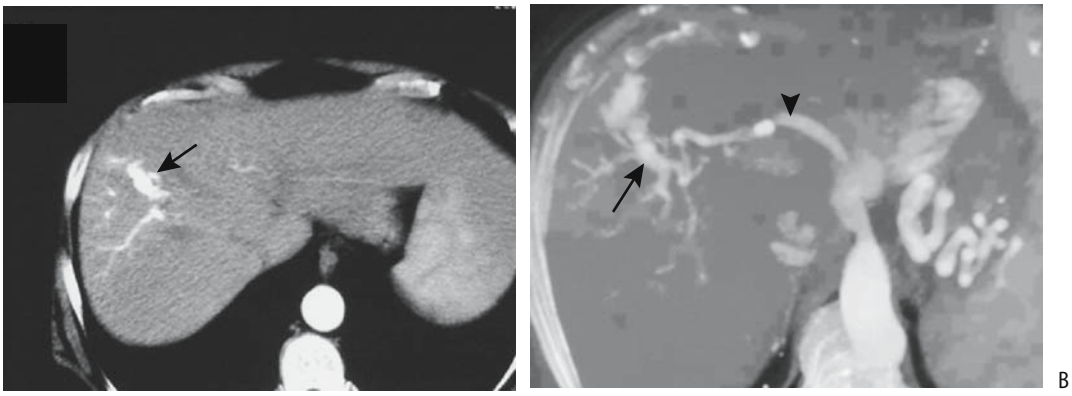

Figure 7.1. Postbiopsy arterioportal fistula. A: Computed tomography (CT) during hepatic artery phase reveals contrast in aorta and right anterior portal vein (arrow). B: Maximum intensity projection also during hepatic artery phase shows hepatic artery (arrowhead) and right portal vein branches (arrow). (*Source:* Gallego C, Velasco M, Marcuello P, Tejedor D, De Campo L, Friera A. Congenital and acquired anomalies of the portal venous system. RadioGraphics 2002;22:141–159, with permission from the Radiological Society of North America.)

to affect either major of minor complication rates. Hemobilia is not uncommon after a percutaneous biopsy, and postbiopsy hemobilia is a rare cause of pancreatitis, cholecystitis, or even portal vein thrombosis. Infective complications include a liver abscess and peritonitis.

Malignant needle tract and abdominal wall implantation are known biopsy complications, found in up to 2% of biopsies. Abdominal wall implantations have also developed after drainage of a cancer-associated abscess, transhepatic bile drainage in a setting of a hilar cholangiocarcinoma, and laparoscopic cholecystectomy in patients with unsuspected gallbladder cancer.

Congenital Abnormalities

Some congenital abnormalities manifest primarily through liver parenchymal damage while others lead to cholestasis and suggest a biliary anomaly; these latter ones are covered in Chapter 8.

Some errors of metabolism, such as hemochromatosis, manifest primarily in adulthood; they are discussed later (see Metabolic and Related Disorders).

Situs Inversus

With situs inversus, the liver is located in the left upper quadrant. It is more midline in location than usual in the heterotaxic syndromes; this includes both asplenia and polysplenia.

Although rare, hepatolithiasis can develop in a setting of situs inversus.

Lobe Atresia/Agenesis

Agenesis of the right lobe and associated portal hypertension are not common. Presumably growth arrest develops during fetal life. At times lobe agenesis is associated with other anomalies such as an ectopic gallbladder, aberrant hemidiaphragm, hammock stomach appearance, and Chilaiditi's syndrome. Congenital absence of a lobe can be associated with fibrosis.

Not all apparent absences of the right lobe are due to agenesis and agenesis of a hepatic duct should be differentiated from lobe atresia. Grossly, a similar appearance is seen in cirrhosis, malignant infiltration, or previous surgical resection. Likewise, lobar agenesis should not be confused with lobar atrophy. In lobe agenesis the right portal vein, hepatic duct, and hepatic vein are not present, but these structures are identified in an atrophied lobe (Figs. 7.2 and 7.3). Lobar atrophy is often associated with biliary obstruction. A hypoplastic right lobe can be associated with a retrohepatic gallbladder.

Accessory Lobe

Accessory liver lobes are not uncommon. Torsion of an accessory lobe can lead to

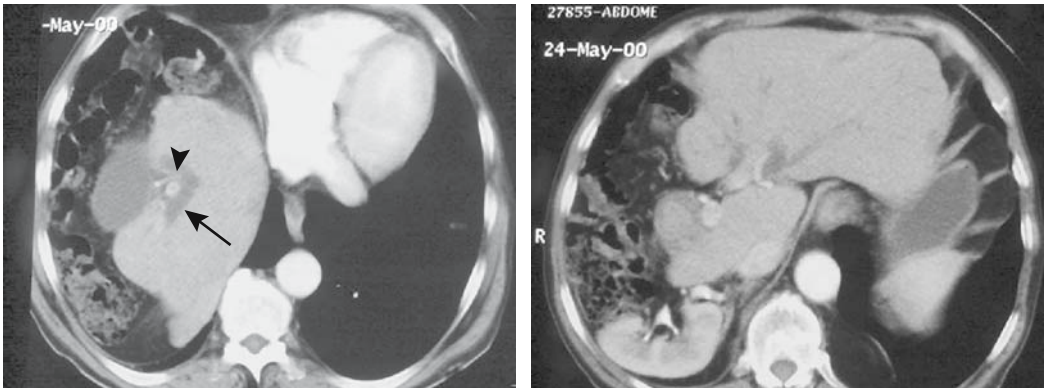

A B

Figure 7.2. Right lobe atrophy. Two views from contrast-enhanced CT reveal (A) posteriorly located gallbladder, a dilated right hepatic duct (arrow), and an atrophied right portal vein (arrowhead), and (B) left lobe hypertrophy. (*Source:* Gallego C, Velasco M, Marcuello P, Tejedor D, De Campo L, Friera A. Congenital and acquired anomalies of the portal venous system. RadioGraphics 2002;22:141–159, with permission from the Radiological Society of North America.)

volvulus and an acute abdomen, even in infants.

Glycogen Storage Disease

A number of glycogen storage diseases (GSDs) have been described, with several involved in overt liver abnormalities (Table 7.1). Some define a group of disorders that have been subsequently subdivided into subtypes. Most have an autosomal-recessive inheritance.

Type I (von Gierke's disease) is the most common and involves a defect in the microsomal glucose-6-phosphatase system, which controls glucose homeostasis. In neonates with type I disease, glycogen is deposited in hepatocytes and eventual hepatomegaly develops. Imaging reveals diffuse fatty infiltration. Some patients with type I disease develop focal nodular hyperplasia, with almost half of these patients having had a previous portacaval shunt. Surviving patients with type I (and, less often, type III)

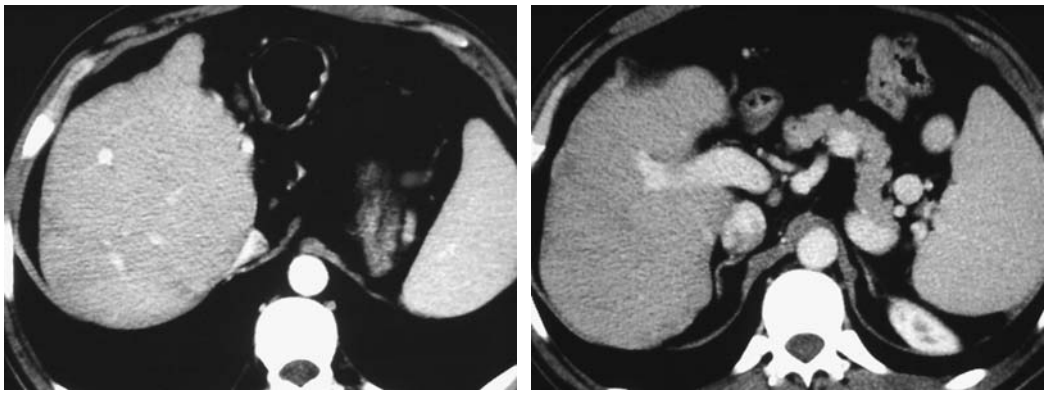

A B

Figure 7.3. Left lobe atrophy. A,B: Views from contrast-enhanced CT reveal an atrophic left portal vein and absent left lobe. (*Source:* Gallego C, Velasco M, Marcuello P, Tejedor D, De Campo L, Friera A. Congenital and acquired anomalies of the portal venous system. RadioGraphics 2002;22:141–159, with permission from the Radiological Society of North America.)

Table 7.1. Types of glycogen storage diseases

Type	Disease	Deficiency	Primary site/abnormality
I	von Gierke's	Glucose-6–phosphatase system	Liver
Ia		Glucose-6–phosphatase deficiency	Liver, kidney
Ib		Glucose-6–phosphate transport	
Ic		Pyrophosphate/phosphate transport	
II	Pompe's	Acid maltase deficiency	Myopathy
III	Forbes-Cori's	Glycogen debranching enzyme	Liver, myopathy
IV	Andersen's	Branching enzyme	Myopathy, liver
V	McArdle's	Myophosphorylase	Myopathy
VI	Hers	Hepatic phosphorylase	Liver
VII	Tarui's	Muscle phosphofructokinase	Myopathy
VIII		Phosphorylase kinase	Liver, central nervous system

disease are prone to developing hepatocellular adenomas, with an occasional one progressing to hepatocellular carcinoma; one recommendation is that serum α-fetoprotein levels and yearly US be obtained in these patients.

Some of these patients undergo a portocaval shunt. Liver transplantation is an option in some with type Ia disease. In teenagers, transplantation restores normal metabolic balance, provides a growth spurt, and improves overall quality of life; liver transplantation does not, however, prevent focal glomerulosclerosis that is part of type Ia disease.

Type IV disease usually progresses rapidly, with death before 4 years of age, although a mild variant is seen in adults as a myopathy. Some of these infants undergo liver transplantation.

Computed tomography findings in patients with glycogen storage disease vary depending on activity. Glycogen deposition leads to a hyperdense liver, although associated steatosis often modifies the appearance. Once cirrhosis and hepatosplenomegaly develop, US reveals a hyperechoic liver.

^{13}C MR spectroscopy using a whole-body MR is a noninvasive test for determining liver glycogen content.

Tyrosinemia

Tyrosinemia leads to progressive hepatocyte damage and regeneration, with surviving children developing dysplastic nodules and subsequent hepatocellular carcinoma. Imaging cannot reliably differentiate between regenerating nodules and neoplasms and, as a result, liver transplantation is recommended early in the course of this condition.

α_1-Antitrypsin Deficiency

α_1-Antitrypsin is a glycoprotein found in body fluids, serving mostly an inhibitory function. Some newborns manifest with cholestasis, which gradually clears. Some children with a homozygous deficiency develop chronic liver disease, which gradually progresses to liver failure and death, often by adolescence. Some adult cirrhotics have α_1-antitrypsin deficiency, but the relationship is unclear. Some of these patients mimic hemochromatosis patients.

α_1-ntitrypsin levels become normal after liver transplantation.

Wilson's Disease

Wilson's disease is an autosomal-recessive disorder of copper metabolism affecting approximately 5 persons per million. The primary defect is in the liver and results in copper accumulation within liver parenchyma and other structures.

A brief digression into copper metabolism is in order. Copper is found in two forms in the human body: Cu^{+} and Cu^{2+}. Cu^{+} is diamagnetic and normal amounts do not affect MR signals. Cu^{2+} is paramagnetic and decreases both T1 and T2 signals. Most normal liver copper is bound to metallothionein and is Cu^{+} and thus not paramagnetic, but evidence suggests that some oxidation to Cu^{2+} takes place, although the precise mechanisms in normal liver and tumors are poorly understood. Copper in hepatocellular carcinomas also appears to be bound to metallothionein. Distribution of copper does not correlate with intensity on T1-weighted images,

and the paramagnetic effect of divalent copper accumulation is insufficient to affect results.

Clinically, Wilson's disease is defined by several stages. First, asymptomatic copper accumulates within the liver, the liver enlarges, and steatosis develops. Next, copper is redistributed throughout the body and hepatocellular necrosis, fibrosis, and hemolysis ensue. Progression to cirrhosis leads to liver atrophy, while accumulation of copper in body tissues results in neurologic damage, at times irreversible.

Initially, either hepatic or neurologic findings tend to predominate. Fulminant hepatic failure, even in a child, is an occasional initial presentation. Copper levels in serum, urine, and liver tissue suggest the diagnosis. The ceruloplasmin level is low.

If detected sufficiently early, the use of chelating agents prevents copper overload and achieves homeostasis. When diagnosed later in its course, chelating agents may slow progression. When fulminant or advanced and the patient does not respond to conventional therapy, orthotopic liver transplantation is an option, realizing that liver transplantation only partially corrects the metabolic defect by converting a homozygous disease into a heterozygote condition.

In most Wilson's disease patients imaging studies are noncontributory. Some children with Wilson's disease and cirrhosis have marked hepatosplenomegaly and imaging evidence of portal hypertension. Although liver CT attenuation is mildly increased in many adults, sufficient overlap with normal livers makes this finding of limited use.

Imaging in one patient with Wilson's disease revealed multiple, small, enhancing nodules during the early arterial phase (10); biopsy identified dysplastic nodules.

Not all elevated hepatic copper levels in children represent Wilson's disease. An Indian childhood cirrhosis associated with excess copper ingestion exists. Excess copper ingestion in an occasional non-Indian child leads to cirrhosis, liver failure, and increased liver copper levels.

Gaucher's Disease

Gaucher's disease, an autosomal-recessive condition, is discussed in more detail in Chapter 15.

Hepatomegaly is common in patients with type 1 Gaucher's disease, at times progressing to massive hepatic fibrosis and portal hypertension. Focal intrahepatic tumors develop in some; these are hypointense on T1- and hyperintense on T2-weighted MR images.

Technetium-99m–red blood cell SPECT imaging in a patient with Gaucher's disease revealed an appearance similar to that seen with a hemangioma, believed to be secondary to focal intrahepatic extramedullary hematopoiesis (11).

Niemann-Pick Disease

Niemann-Pick disease is a metabolic disorder that progresses to cirrhosis. Some of these children develop a hepatocellular carcinoma.

Sickle Cell Disease

Although uncommon, intrahepatic cholestasis does occur in sickle cell disease. These patients develop hepatomegaly, hyperbilirubinemia, coagulopathy, and, on rare occasion, acute liver failure. Exchange transfusion appears to be effective therapy.

These patients do not have excess iron absorption, and MR does not reveal excess liver iron. After blood transfusions, however, iron in organs containing reticuloendothelial cells results in low T2 signal intensity.

Polycystic Diseases

Autosomal Dominant

Although renal involvement in patients with adult polycystic disease leads to progressive loss of renal tissue, this does not hold true in the liver; liver function tends to remain normal in most individuals until late in the disease. In distinction to autosomal-recessive congenital hepatic fibrosis, little fibrosis is evident in this entity. Of note is that in some patients adult polycystic disease mostly spares the kidneys and primarily involves the liver. In this patient population the differential diagnosis also includes rare cystic neuroendocrine or gynecologic metastases.

Dilated small bile ducts surrounded by fibrous stroma, called von Meyenburg complexes, are common in patients with adult

polycystic disease. A majority of patients with sufficient polycystic renal involvement requiring transplantation also have hepatic cysts, and in an occasional postrenal transplant patient symptomatic liver cystic disease is the primarily cause of death.

Clinical findings consist of abdominal pain, ascites, or leg edema.

Marked hepatomegaly develops, with CT showing multiple homogeneous, hypodense, variable-size cysts scattered throughout the liver (Fig. 7.4). The remaining parenchyma is compressed by these cysts, which in some patients replace most of the liver parenchyma. No wall or cyst enhancement is evident postcontrast.

As expected, these cysts are hypointense on T1- and homogeneously hyperintense on T2-weighted MR images. They do not enhance postcontrast. Intracyst hemorrhage varies their appearance even to the point of suggesting a neoplasm. An occasional patient presents with an elevated α-fetoprotein level, suggesting a hepatocellular carcinoma.

These cysts can become infected. Indium 111 leukocyte scintigraphy aids in localizing such an infected cyst.

Some of these patients develop sufficient symptoms to require surgical intervention. Either cyst fenestration or partial hepatic resection is a viable option. Aspirated fluid cytology and cyst wall biopsy to exclude a neoplasm appear reasonable prior to fenestration and fluid spread into the peritoneal cavity. Ascites is a postoperative complication of cyst fenestration. Hepatomegaly occasionally recurs.

Congenital Hepatic Fibrosis (Caroli's Disease)

The current definition of Caroli's disease is somewhat muddled. Some authors limit this term to the rare communicating biliary saccular ectasia as originally describe by Caroli (12); whereas others apply it to a broader spectrum of congenital hepatic fibrosis. Some employ *Caroli's disease* as a descriptive term and then associate it either with congenital hepatic fibrosis or infantile polycystic kidney disease. Still others use the term *Caroli's disease* to describe the rarer isolated biliary ectasia and *Caroli's syndrome* if both ectasia and hepatic fibrosis are evident.

Embryologically, intrahepatic bile ducts develop from liver progenitor cells adjacent to portal vein mesenchyme and form ductal plates, which eventually evolve into bile ducts. Lack of or disordered ductal plate remodeling leads to a number of congenital intrahepatic bile duct disorders, including congenital hepatic fibrosis. The latter represents a cholangiopathy with surrounding fibrosis. Kidney involvement is variable in these patients and ranges from renal tubular ectasia to various forms of polycystic disease, most often autosomal recessive and

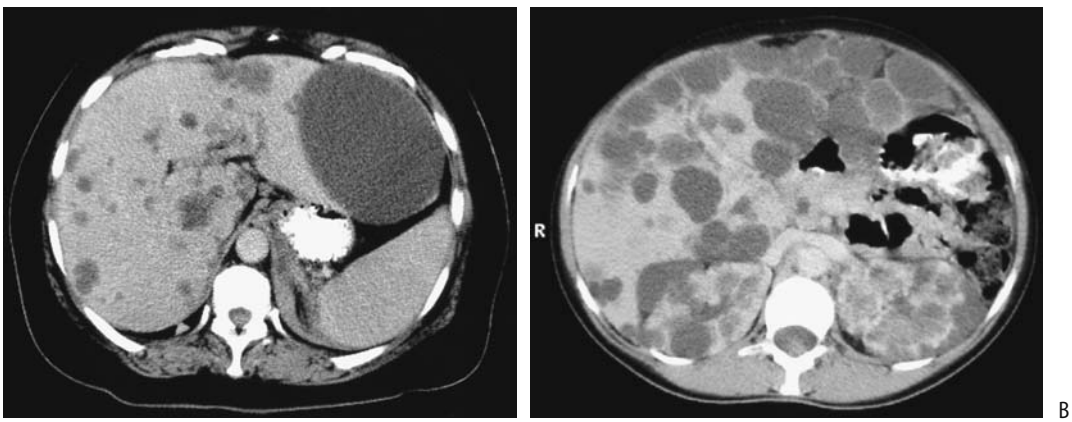

Figure 7.4. Polycystic disease. A: CT reveals numerous water-density cysts scattered throughout the liver. (Courtesy of Patrick Fultz, M.D., University of Rochester.) B: CT in another patient identifies cysts varying in size throughout the liver and kidneys. (Courtesy of Algidas Basevicius, M.D., Kaunas Medical University, Kaunas, Lithuania.)

only rarely autosomal dominant. An interesting association is Caroli's disease and occasional acute pancreatitis.

Histologically, bile ductules become ectatic but still maintain their communication with bile ducts. As an isolated finding, ectasia is found only in a minority; over time, progressive fibrosis ensues and accounts for the typical appearance of extensive periportal fibrosis and biliary dilation.

Two manifestations predominate: (1) Those patients developing extensive fibrosis early in life tend not to have prominent intrahepatic bile duct dilation. (2) Dilation is more common in those individuals who are asymptomatic until adulthood, when signs and symptoms of chronic bile stasis develop. In some of the latter patients dilated ducts predominate in one lobe. Also, in some patients Caroli's disease is associated with extrahepatic bile duct dilation, and in an occasional patient an extrahepatic choledochal cyst is the initial presentation. Calculi tend to develop either in intrahepatic cysts, in bile ducts, or both.

With severe involvement death occurs during the neonatal period from renal causes, before liver damage is evident. Some develop hepatomegaly early in life, others remain asymptomatic, and still others progress to fibrosis, liver failure, and portal hypertension; varices and hematemesis is their initial presentation. Bile stasis and infection lead to acute cholangitis, at times at an early age. Intrahepatic calculi develop in some, but the involved ducts are not obstructed. Hepatic function tends to be preserved until relatively late. Generally most of the liver is involved, although occasionally cysts are limited to one lobe; some patients have a preponderance of left lobe disease.

These patients are at increased risk of a developing hepatocellular carcinomas or cholangiocarcinomas. A not uncommon progression consists of calculi formation, pyogenic cholangitis, intrahepatic abscesses, and eventual cholangiocarcinoma.

In adults, Caroli's disease can be suspected with most imaging (Fig. 7.5). Findings include hepatomegaly, parenchymal fibrosis, numerous cysts scattered throughout the liver, or multiple cyst-like dilated bile ducts. It is necessary to show that the cysts communicate with bile ducts to distinguish this condition from autosomal-dominant polycystic disease and multiple intrahepatic abscesses. Although some intrahepatic abscesses do communicate with bile ducts, differentiation of abscesses from dilated bile ducts is generally straightforward with cholangiography.

Ultrasonography reveals extensive collaterals and a prominent periportal hyperechoic pattern, a finding also seen in other conditions. Liver parenchymal texture tends toward a heterogeneous appearance containing multiple high echoes.

With progressive fibrosis adults tend to develop portal hypertension, generally attributable to intrahepatic compression of portal vein branches by fibrosis. Doppler US findings vary depending on underlying hemodynamics. Intrinsically, the portal vein is patent, although some patients have portal vein thrombosis and cavernous transformation.

Magnetic resonance cholangiography also detects cystic intrahepatic biliary dilation.

Technetium-99m-IDA scintigraphy reveals bile stasis in cystic structures. Scintigraphy confirms that these cysts communicate with the bile ducts.

Regardless of how it is performed, cholangiography confirms the diagnosis by identifying numerous segmental dilated intrahepatic bile ducts, either saccular or fusiform in appearance.

Hereditary Hemorrhagic Telangiectasia (Osler-Weber-Rendu Disease)

Hereditary hemorrhagic telangiectasia, or *Osler-Weber-Rendu disease*, is an autosomal-dominant disorder manifesting primarily by epistaxis, yet numerous vascular malformations consisting of telangiectasias, arteriovenous fistulas, and aneurysms in the liver, spleen, and other organs often have more serious ramifications. An association of hereditary hemorrhagic telangiectasia and familial juvenile polyposis has been described in several families. Liver arteriovenous malformations are associated with fibrosis and progression to cirrhosis. High output cardiac failure, liver failure, and orthotopic liver transplantation are not uncommon. Why fibrosis and atrophy of some segments and enlargement of others develop is unknown although focal ischemia appears to play a role.

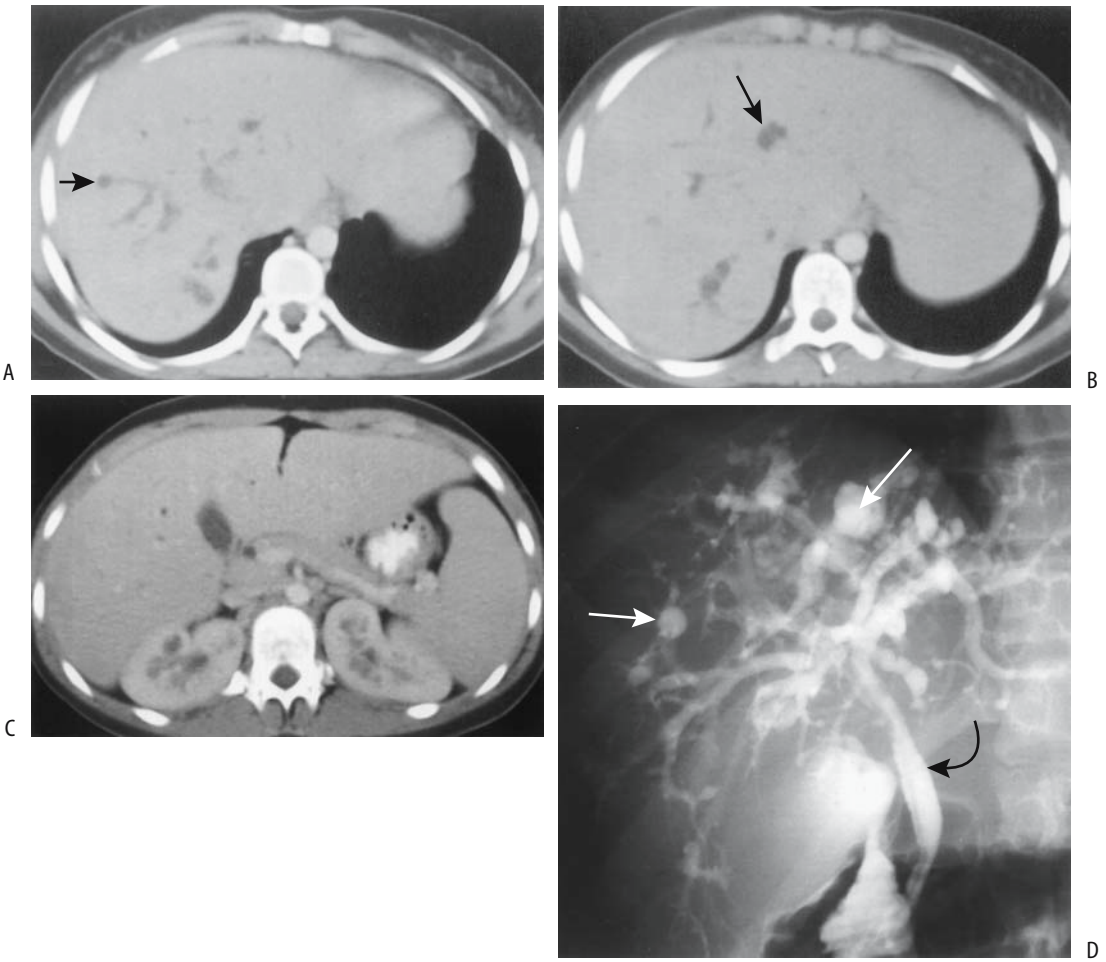

Figure 7.5. Caroli's Disease. A,B: Transverse postcontrast CT images identify round, hypodense structures (arrows) adjacent to bile ducts. C: A contrast-enhanced image shows hypodense regions in the renal medulla bilaterally. D: Endoscopic retrograde cholangiopancreatography (ERCP) identifies saccular intrahepatic cavities (arrows) communicating with bile ducts. The extrahepatic bile ducts (curved arrow) are normal. (*Source:* Fulcher AS, Turner MA, Sanyal AJ. Caroli disease and renal tubular ectasia. Radiology 2001;220:720–723, with permission from the Radiological Society of North America.)

Telangiectasia defines a collection of dilated small vessels. Dilated, tangled vascular communications are common and range from small to large confluent vascular masses. Arteriovenous communications are either to a hepatic or portal vein. Extensive arteriohepatic venous shunting leads to hepatomegaly and congestive heart failure or abdominal angina. Arterioportal shunting, on the other hand, tends to progress to portal hypertension.

In a setting of extensive vascular malformation, the hepatic artery blood flow increases and the artery and its branches dilate and become tortuous. Arterial phase and portal venous phase CT detects arteriovenous shunting, and reveals enlarged feeding vessels and tangled vessels within a malformation.

Doppler US can screen relatives of patients with hereditary hemorrhagic telangiectasia to detect intrahepatic arteriovenous shunts. Dilated vessels tend to mimic bile ducts with gray-scale US, but color Doppler US waveforms should confirm extensive shunting and suggest the diagnosis. Doppler US shows a marked increase in hepatic artery mean velocity. Enlarged hepatic veins are common. In most

patients portal venous blood velocity is unchanged compared to normals, except with an arterioportal or even portovenous shunt.

Contrast-enhanced MRI also identified shunting and simultaneous enhancement of both hepatic arteries and veins.

Angiography readily identifies multiple intrahepatic vascular malformations. The hepatic arteries have been successfully embolized in stages in symptomatic patients with hereditary hemorrhagic telangiectasia; this is not an innocuous procedure, however, and deaths from hepatic infarction and necrosis have been reported (13).

Trauma

Management Issues

Previously in a number of institutions peritoneal lavage was an initial diagnostic study performed in patients with suspected blunt abdominal trauma, and, if positive, the patient underwent laparotomy. It was difficult to evaluate outcomes of various liver injuries because investigators used their own nomenclature for liver injury. To overcome some of these problems, a liver injury classification scale was devised by the American Association for the Surgery of Trauma (Table 7.2).

Currently peritoneal lavage has been abandoned in favor of CT and a more conservative approach than used previously. Emergency CT has evolved as the first diagnostic procedure performed in trauma patients. It has led to more nonsurgical management of liver trauma, especially in hemodynamically stable patients. Even those with a moderate-to-large hemoperitoneum have been managed nonoperatively as long as the patient is hemodynamically stable. Thus some patients with grade III liver injuries are managed nonoperatively. Most blunt hepatic trauma in children is also managed conservatively without surgery; in general, the severity of injury as detected by CT does not correlate with a need for surgery.

Severe liver trauma (such as type V on the liver injury scale in Table 7.2) has a very poor prognosis. A majority of patients with grade V injuries are unstable and require laparotomy. The initial surgical concern is control of hemorrhage. One approach is percutaneous intraaortic balloon occlusion using a femoral route, followed by surgical vascular exclusion of the liver.

One complication of liver trauma is a subsequent abscess. Risk of developing an abscess is higher in patients undergoing surgery than in those managed nonoperatively. Presumably infection develops from infected bile or is spread hematogenously, with a hematoma or

Table 7.2. Surgical liver injury grading scale

Grade*	Type of injury	
I	Hematoma	Subcapsular, <10% of surface
	Laceration	Capsular, <1 cm in parenchymal depth
II	Hematoma	Subcapsular, 10–50% of surface Parenchymal, <10 cm in diameter
	Laceration	Parenchymal, 1–3 cm in parenchymal depth, <10 cm in length
III	Hematoma	Subcapsular, >50% of surface or expanding Ruptured hematoma Intraparenchymal, >10 cm or expanding
	Laceration	>3 cm in depth
IV	Laceration	25–75% of hepatic lobe (or 1–3 Couinaud segments within lobe)
V	Laceration	>75% of hepatic lobe (or >3 Couinaud segments within lobe)
	Vascular	Juxtahepatic major hepatic vein or vena cava injury
VI	Vascular	Hepatic avulsion

* Advanced one grade for multiple injuries, up to grade III.
Source: Adapted from Moore et al. (14).

necrotic liver tissue acting as a nidus. Abscess imaging is discussed in a later section; suffice it here to state that trauma-associated abscesses are readily identified by CT. The presence of gas bubbles is almost pathognomonic, although occasionally noninfected necrotic liver parenchyma secondary to ischemia has a similar appearance.

Blunt trauma is a rare cause of a major liver infarct.

Imaging

Computed tomography is the first imaging study performed in a hemodynamically stable patient suspected of blunt liver injury. A CT blunt trauma liver injury grading scale has been proposed based on CT findings (Table 7.3). Its initial function was to assess the value of CT in predicting outcome following blunt liver injury. It should be kept in mind that this CT grading scale employs different parameters than the liver injury classification scale devised by trauma surgeons; the latter is meant to help standardize surgical findings and outcomes. Also, although CT aids in establishing the scope of an initial insult and detects complications, whether a patient is explored or managed conservatively often continues to be based on clinical findings.

The most sensitive US finding in patients with liver trauma is intraabdominal free fluid; actual liver injury is detected less often. Mild parenchyma injury appears as a focal hyperechoic region.

Table 7.3. Computed tomography (CT)-based liver injury grading system

Grade	Criteria
1	Capsular avulsion Superficial laceration <1 cm Subcapsular hematoma <1 cm
2	Lacerations 1–3 cm deep Central/subcapsular hematoma 1–3 cm deep
3	Lacerations >3 cm deep Central/subcapsular hematoma >3 cm deep
4	Massive hematoma >10 cm Lobar tissue destruction/ischemia
5	Bilobar tissue destruction/ischemia

Source: Adapted from Mirvis et al. (15).

Is CT helpful in monitoring healing? In most patients routine follow-up CT does not influence subsequent treatment and often is not necessary; a need for follow-up CT should be based on the patient's clinical course.

Hemorrhage/Hematoma

A hematoma is the most common liver injury. These hematomas range from subcapsular to intraparenchymal in location. Not all are due to trauma. Common nontraumatic causes of liver hemorrhage include bleeding from a hepatic neoplasm; bleeding also occurs with hemangiomas, focal nodular hyperplasia, an occasional metastasis, the HELLP syndrome (discussed later; see Liver in Pregnancy), and such infiltrative conditions as amyloidosis.

A subcapsular hematoma tends to compress the underlying liver parenchyma, thus differentiating it from intraperitoneal fluid. An appropriately located hematoma will obstruct the intrahepatic portion of the inferior vena cava and hepatic veins and result in Budd-Chiari syndrome (discussed in Chapter 17). At times a slow bleed and resultant liver hematoma manifests by anemia.

Contrast extravasation is detected by CT if bleeding is sufficiently brisk. This extravasated contrast–blood mixture has a higher attenuation than an old hematoma, and the two are readily differentiated. If needed, transcatheter embolization is an option for hemorrhage control.

Unenhanced blood has an attenuation value of 30 HU or greater. Initially clotted blood has a CT density higher than nonclotted blood, and an acute hematoma is thus hyperdense compared to normal liver parenchyma. Some liver lacerations, however, result in a hypodense hematoma, presumably due to simultaneous leakage of bile. Postcontrast, a hematoma has a lower density than normally enhancing liver parenchyma.

Occasionally CT identifies regions of low attenuation parallel to the portal vein and its branches. Such periportal tracking of blood was initially believed to be a marker of significant liver injury, although currently most radiologists tend to ascribe periportal tracking to lymphatic distention and edema and discount its importance as a marker for significant trauma.

Its use as a guide for management decisions is controversial; whether periportal tracking is present or not has no effect on the eventual success rate of nonoperative management or on the complication rate. Such tracking usually does not signify a laceration.

The sonographic appearance of a hematoma depends on its age. Initially a hematoma is mostly hyperechoic, with some having a complex, heterogeneous appearance. With time, a hypoechoic pattern predominates as a clot lyses and eventually the hematoma becomes anechoic. A similar US pattern is found with hematomas in other solid organs.

Surgical retractors cause transient focal liver injury. Computed tomography in one patient revealed a focal, sharply marginated hypodense lesion, while MR identified a hypointense, poorly defined region on T1-weighted sequences that was heterogeneous and hyperintense on T2-weighted sequences (16).

Some traumatic liver hematomas are associated with pseudoaneurysms or arteriovenous fistulas; these should be detected by CTA and, if diagnosis is unclear, angiography.

Most subcapsular hematomas resolve within several months. Parenchymal hematomas, on the other hand, take considerably longer to resolve, probably because of their common admixture of bile.

Laceration/Rupture

Numerous nontraumatic disorders are associated with spontaneous liver rupture (Table 7.4).

Postcontrast CT reveals a liver laceration as an irregular linear or branching hypodense region surrounded by enhancing liver parenchyma (Fig. 7.6). Some of these linear lacerations mimic dilated bile ducts. Lacerations of the porta hepatis commonly involve bile ducts and major vessels. Extensive lacerations tend to radiate toward the periphery. A hemoperitoneum is common; the exception being with injury to the liver bare area (segment VII) when a hemoretroperitoneum can develop (17).

Biloma

Spontaneous perforation of an intrahepatic bile duct is uncommon. A cholangiogram, regardless of how it is performed, should reveal extravasation of contrast from the duct involved, thus establishing the diagnosis.

Table 7.4. Conditions associated with spontaneous liver rupture

Infections
Typhoid
Malaria
Nonneoplastic tumors
Hemangioma
Peliosis hepatis
Focal nodular hyperplasia
Nodular regenerative hyperplasia
Angiomyolipoma
Neoplastic tumors
Hepatic adenoma
Hepatocellular carcinoma
Metastasis
Other
HELLP syndrome
Amyloid infiltration
Polyarteritis nodosa
Ehlers-Danlos syndrome

At times differentiation among a resolving hematoma, abscess, and biloma is difficult both by CT and US. Ultrasonography simply reveals an encapsulated fluid collection. In such a scenario either scintigraphy or percutaneous aspiration of fluid is necessary to establish the diagnosis.

Magnetic resonance imaging differentiates between a simple intrahepatic biloma and

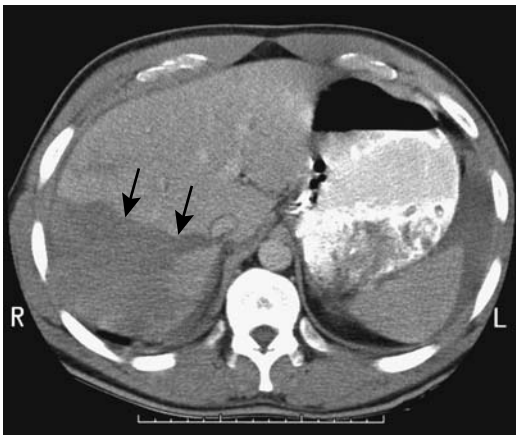

Figure 7.6. Liver laceration in a 25-year-old man (arrows). (Courtesy of Patrick Fultz, M.D., University of Rochester.)

hematoma. A biloma is hypointense on T1-weighted images and hyperintense on T2-weighted images; a hematoma is hyperintense on both T1- and T2-weighted images; in practice, blood and proteins modify the MR appearance of a biloma. Nevertheless, a differentiation is more than theoretical because most bilomas should be drained, but hematomas tend to resolve spontaneously.

Porta Hepatis Injury

Although injury to the porta hepatis region is rare, it is often lethal; intraoperative exsanguination is not an uncommon cause of death in these patients, and thus hemorrhage control is the first priority. Other associated injuries are common. Suspected bile duct injuries are identified by intraoperative cholangiography and repaired either primarily or an enteric anastomosis.

In stable patients with blunt liver injury undergoing both CT and hepatic angiography, CT was only 65% sensitive and 85% specific in detecting arterial injury (18); if in doubt, hepatic angiography is the gold standard in detecting arterial injury.

Infection/Inflammation

Abscess

Pyogenic

Clinical

A pyogenic liver abscesses is often associated with bile duct stones and duct obstruction. At times simply removing retained stones, stenting, and medical management are therapeutic.

A not uncommon etiology for multiple liver abscesses is sigmoid diverticulitis and hematogenous spread of infection to the liver. Most abdominal radiologists have encountered patients with not only multiple liver abscesses but also portal venous gas; *Bacteroides fragilis*, producing gas by fermentation, is one such responsible organism. *Chlamydia trachomatis* is a common organism found in Fitz-Hugh–Curtis syndrome. A rare liver abscess evolves with this infection. The specific diagnosis is often established by percutaneous aspiration.

An uncommon association for a liver abscess is with a silent colon adenocarcinoma.

The most common clinical presentation in patients with a pyogenic hepatic abscess is fever and leukocytosis, and less often abdominal pain, hepatomegaly, and abnormal liver tests. Jaundice and marked elevation of alkaline phosphatase are common with a biliary tract abscess origin.

The intervening liver capsule, subphrenic space, and diaphragm prevent spread of most intrahepatic abscesses into the thorax. An exception is an abscess involving the liver bare area; an occasional such abscess communicates with the mediastinum.

A liver abscess is a recognized complication of Crohn's disease. Steroids and other therapy tend to mask the presence of these abscesses. Occasionally such an abscess is the initial presentation of Crohn's disease.

Diabetes mellitus is a major predisposing factor for pyogenic liver abscesses even without a known infectious focus; gas within the abscess, detected with conventional radiography, CT, or US, is associated with a higher mortality than one without gas. Diabetes tends to predispose rupture of a pyogenic liver abscess. These patients have a high mortality even with prompt surgical cleansing of the abdominal cavity. *Klebsiella pneumoniae* is a common bacterium isolated.

Rarely, rupture of an infected gallbladder leads to a liver abscess. After percutaneous abscess drainage, contrast injected into the abscess cavity should reveal a fistulous communication with the gallbladder. A rare pyogenic liver abscess contains multiple stones and is caused by perforation of an adjacent necrotic gallbladder; these combined gallbladder and liver abscesses are notoriously difficult to evaluate adequately.

Imaging

Liver abscesses range from solitary to multiple; unilocular to multiloculated; large to small. In most instances imaging findings strongly suggest an abscess. It should be realized, however, that an occasional necrotic, or infected liver cancer presents as a hepatic abscess. These include primary liver cancer, gallbladder carcinoma, or even a metastasis. Imaging does not always differentiate a complex necrotic and

cystic cancer from a liver abscess. Likewise, a pyogenic abscess appears similar to an amebic abscess.

Only an occasional hepatic abscess contains gas.

Computed tomography shows most intrahepatic abscesses as hypodense regions but with peripheral contrast enhancement. Nevertheless, the appearance of pyogenic abscesses varies from homogeneous and hypodense to a heterogeneous solid tumor. Some abscesses incite little surrounding inflammation; others induce considerable inflammation, and postcontrast they appear target-like, with the hypodense abscess surrounded by a hyperdense rim, which in turn is surrounded by a thin hypodense periphery thought to represent liver edema. Segmental hepatic enhancement during arterial-phase CT is common, presumably caused by decreased portal flow resulting from portal tract inflammation.

Ultrasonography shows approximately two thirds of pyogenic abscesses to be hypoechoic, with the rest inhomogeneous. Anechoic abscesses are uncommon. Approximately half have a smooth wall. With progression and necrosis, abscesses tend to become more hypoechoic. The abscess wall thickens with chronicity. Gas within an abscess is hyperechoic and reveals shadowing. Contrast aided phase inversion harmonic mode US reveals rim enhancement, arteries along abscess margins and internal septa, septal enhancement, absent circulation in fluid and arterial hypervascularity surrounding the abscess (19).

Magnetic resonance imaging appearance of a liver abscess is similar to other fluid-containing lesions. Most are hypointense on T1- and hyperintense on T2-weighted images. Most abscesses tend to be better defined postcontrast and often show an immediate hyperintense enhancing rim, which persists in later phases, but the central portion, as expected, does not enhance. It should be kept in mind that many metastases also have rim enhancement. An absolute distinction between an abscess and a neoplasm is often not possible purely on MRI findings alone. An infected neoplasm complicates this issue further.

Indium 111 leukocyte scintigraphy readily detects most hepatic abscesses. An occasional abscess, however, results in a cold defect.

Normal hepatic uptake of gallium 67 makes interpretation of a Ga-67 abscess scan difficult; a Tc-99m sulfur colloid scan performed in conjunction with Ga 67 scintigraphy is helpful for interpretation.

Therapy

Although some of the smaller abscesses can be treated medically, most require either percutaneous or surgical drainage, at which time diagnostic aspiration confirms the diagnosis. In many centers surgical drainage is reserved for abscesses that cannot be adequately drained percutaneously. Percutaneous drainage using a large-caliber drainage catheter is associated with few complications and has a high success rate. Both multiloculated and multiple abscesses are drained successfully. Previously considered a lethal disease, currently abscess cure rates up to 93% are typical with percutaneous drainage. The success rate is lower in patients with an underlying malignancy. Abscesses with a biliary fistula are also drainable percutaneously. Most of the underlying fistulas resolve unless distal bile duct obstruction is present.

The major complication of percutaneous drainage is bleeding, at times massive. An occasional patient develops an empyema due to pleural puncture. Mortality associated with percutaneous abscess drainage is less than 10%.

Common dogma holds that simple percutaneous needle aspiration is not a viable therapeutic option for a pyogenic liver abscess. Yet, percutaneous needle aspiration and systemic antibiotics can be successful in healing most abscesses, realizing that about half of these abscesses require two or more sessions (20). Large gauge trocar needles and US guidance, and complete pus removal are necessary.

Currently surgical drainage or liver resection are reserved for complex abscesses, those without a safe percutaneous access route, and failed percutaneous drainages.

Amebic

Clinical

Amebic liver abscesses have a wide geographic variation. Men predominate by a ratio of about 10 : 1. In nonendemic regions a high proportion of amebiasis is found in AIDS patients.

The diagnosis is usually suspected from serologic testing. Fever, abdominal pain, and hepatomegaly are common presentations.

Independent mortality risk factors include an elevated bilirubin level, the presence of encephalopathy, the size of the abscess cavity, hypoalbuminemia, and the number of abscesses present; mortality is independent of the duration of symptoms.

Imaging

In general, imaging cannot differentiate an amebic abscess from a pyogenic abscess, and the imaging findings described above for pyogenic abscesses also apply to amebic abscesses.

Some patients develop a right pleural effusion, right basal atelectasis, a perihepatic fluid collection, or simply elevation of right hemidiaphragm. These findings occur with intra-abdominal abscesses and do not necessarily imply intrathoracic abscess spread. Nevertheless, a rare liver amebic abscess evolves into a hepatopulmonary fistula or a hepatocolic fistula, or even spreads into the mediastinum and pericardium.

In patients resistant to medical therapy, abscess communication with the bile ducts should be suspected. These patients tend to be jaundiced. A minority of amebic liver abscesses are associated with focal intrahepatic bile duct dilation, presumably secondary to obstruction.

Amebic liver abscesses range from solitary to multiple. Single abscesses tend to be more common in tropical amebiasis. A right lobe location predominates. On precontrast CT these abscesses range from iso- to hyperdense. Mother cysts tends to be hyperdense compared to daughter cysts. Secondary bacterial infection further increases the mother cyst or daughter cyst CT density. Most abscess walls enhance postcontrast. Internal septations develop in some.

Ultrasonography reveals most to have a smooth wall and a homogeneous, hypoechoic US appearance. Because of retained necrotic debris and blood, some abscesses appear solid and contain hypo- or hyperechoic internal echoes. They are surrounded by a hyperechoic wall, which in turn is surrounded by a thin peripheral halo. Some are multiseptate.

An occasional amebic liver abscess is imaged by triple-phase bone scintigraphy.

Therapy

Medical therapy of an amebic abscess is highly successful; only those not responding to medical therapy or clinically appear to be at risk of impending rupture require drainage. Nevertheless, especially with a larger abscess, faster recovery is often achieved if drug therapy is combined with image-guided percutaneous aspiration. About a third or so of these abscesses yield no *Entamoeba histolytica*. If the material obtained initially is nondiagnostic, the final aspirate should be examined because it is most often diagnostic. The aspirate usually is rather viscous, and aspiration through a large-bore catheter is helpful. Abscesses tend to recur if no drain is left in place.

Presence of a biliary fistula does not influence the cure rate for percutaneous drainage. Most biliary fistulas close spontaneously. Likewise, even with a ruptured amebic abscess percutaneous catheter drainage of extrahepatic collections appears safe and effective.

Hydatid Cyst

Clinical

Infection with *Echinococcus granulosus*, or hydatid disease, is uncommon in Northwestern Europe and North America but is endemic in the Mediterranean basin and several regions of East Africa. Dogs, ruminants, and humans constitute the infestation cycle. Most common ruminants involved are sheep and goats, although apparently camels also have a role in parts of Africa; the highest prevalence in humans is in the Turkana district of Kenya. Hydatid disease exists in cattle in West and Southern Africa but human infestation here is rare.

The most common sites of involvement are the liver and lungs, the right lobe more often than the left, adjacent to Glisson's capsule. Echinococcal cysts are slow growing and often take years to reach a large size.

Cysts contain two layers. The outer pericyst, composed of an avascular layer, is a host response to infestation. An inner endocyst, about 2 mm in thickness, is produced by the parasite and normally is adjacent to the pericyst, except when ruptured.

Although some cysts rupture spontaneously, especially when large, unrelated trauma is a not uncommon cause of cyst rupture. In a contained rupture only the endocyst ruptures, with the

pericyst remaining intact. Some cysts rupture into an adjacent bile duct or directly into the peritoneal cavity, subphrenic space, or, rarely, into the gastrointestinal tract. Communication with a gas-containing viscus leads to a gas-fluid level within the cyst. Occasional cysts have transdiaphragmatic spread to the thorax. Rupture into a blood vessel, such as a hepatic vein, is rare.

Jaundice is usually due to cyst rupture into bile ducts and intrabiliary spread of the hydatid content. The resultant obstruction is generally treated by endoscopic sphincterotomy and removal of the obstructing intrabiliary daughter cysts. Occasionally, a hydatid cyst obstructs the bile ducts close to the liver hilum simply by compression, and jaundice develops even without a biliary communication. Likewise, a hydatid cyst close to the liver hilum can lead to cavernous portal vein transformation.

In some patients hydatid cyst content in the bile ducts induces a hypersensitivity reaction, even to the point of anaphylaxis. A ruptured cyst is one cause of a relapsing generalized anaphylactic reaction, including life-threatening laryngospasm. An occasional one results in an eosinophilic cholecystitis.

The less common echinococcal infection with *Echinococcus multilocularis* is encountered in colder climates. Liver screening with US is practiced in some endemic regions, and screening appears to contribute to early detection.

A local form of aggressive hydatid disease is found in Central and South American neotropical zones. The infectious agent is *Echinococcus vogelii*, paca, and other wild rodents are intermediate hosts, and the bush dog the final host. The liver is most often involved, with metacestodes spreading into the peritoneal cavity and eventually invading other abdominal and thoracic organs. Infected patients most often present with hard, round tumors in or adjacent to the liver, hepatomegaly, increased abdominal girth, pain, and cachexia; liver involvement progresses to portal hypertension. Imaging reveals a polycystic liver disease pattern. Extensive involvement leads to numerous cysts in the liver, pancreas, spleen, and peritoneal cavity. Cyst calcifications are common.

Imaging

An imaging classification of hydatid cysts consists of the following:

Type 1: Simple unilocular cyst. Believed to be an early stage in hydatid cyst formation, these cysts are water dense on CT and anechoic on US. Cyst wall and septal enhancement is seen with CT and MR contrast, thus differentiating this entity from simple cysts.

Type 2: Cyst containing daughter cysts. Round or irregular daughter cysts are surrounded by a higher density fluid in the mother cyst.

Type 3: Dead cysts containing extensive calcifications.

Type 4: Complex cysts. These consist of superinfected cysts or ones that have ruptured. In a contained rupture imaging identifies endocyst separation from the surrounding pericyst. Bacterial superinfection implies the presence of cyst rupture.

Curvilinear cyst rim calcifications are common with *Echinococcus granulosus* infections, and a cystic pattern is detected in about half.

The CT appearance varies, although a hydatid cyst tends to have an oval and sharply defined outline. Precontrast, cysts are mostly inhomogeneous and of low density; postcontrast enhancement is inhomogeneous (Figs. 7.7 and 7.8). The sonographic appearance ranges from an anechoic cyst, mural nodules, and visualization of the endocyst, to a complex multicystic structure.

Debris either tends to be displaced toward the center of the primary cyst or is located in

Figure 7.7. Hydatid cyst. CT also identifies a soft-tissue component within the cyst (arrow). (Courtesy of Algidas Basevicius, M.D., Kaunas Medical University, Kaunas, Lithuania.)

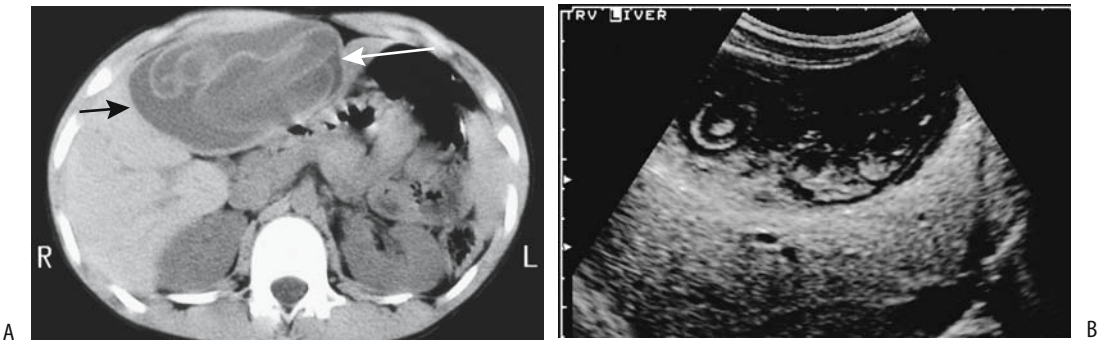

A B

Figure 7.8. Hydatid liver cyst in a 12-year-old. A: CT identifies a large cystic structure replacing most of the left lobe (arrows). A detached inner layer is seen floating in the cyst lumen. B: Ultrasonography (US) reveals an irregular cyst containing solid content (endocyst). (Courtesy of Luann Teschmacher, M.D., University of Rochester.)

the dependent portion; or, in some cysts, a fluid–fluid interface is evident. A gas–fluid level within the cyst implies communication with bile duct or viscus, although occasionally an infected, noncommunicating cyst has a gas–fluid level. Detachment of the inner layer into the cyst lumen results in a soft tissue tumor either floating or in the most dependent portion of the cyst, an appearance termed the *water lily* sign.

Daughter cysts lead to a cyst-within-a-cyst appearance. At times numerous daughter cysts result in an imaging finding of multiple small cysts in an otherwise solid-appearing tumor, an appearance mimicking a honeycomb.

Computed tomography and US often visualize intrabiliary hydatid material once biliary communication is established. Computed tomography reveals intrabiliary hydatid membrane particles as "sand"; at times the actual communication is identified. In some patients adjacent bile ducts dilate. A fat–fluid level within the cyst is a sign of biliary communication. Occasionally, hydatid material is observed in the gallbladder lumen.

A hydatid cyst sonographic classification is outlined in Table 7.5. This classification differs from the general imaging classification of hydatid cysts outlined above; it divides cystic hydatid disease into a proliferative stage and an involution stage. The US findings of types I through V represent the proliferative stage, and patients should be treated, but types VI and VII are part of disease involution and these patients do not require therapy. The cyst becomes hyperechoic as its content changes from a watery consistency to a viscid gel and the germinal layer folds within the viscid gel assume a curvilinear appearance, which no longer moves with a change in patient position.

At times endoscopic retrograde cholangiopancreatography (ERCP) is helpful, although MR cholangiography also defines bile duct involvement. Cyst communication with bile ducts, bile duct obstruction, and debris in the bile ducts can be detected (Fig. 7.9) and, at times, treated by endoscopic sphincterotomy. Extensive publications confirm that ERCP is safe in a setting of hepatic echinococcosis.

Magnetic resonance is useful in cyst characterization and in defining its relationship to the surrounding structures. Magnetic resonance imaging, MRA, and MR cholangiography should detect all hydatid cysts on both T1- and T2-weighted images and suggest a biliary communication.

Angiography is rarely performed for suspected hydatid cysts. These are avascular, often multilocular cysts.

Table 7.5. US classification of hydatid cysts

Type I:	Simple cyst
Type II:	Multiple cysts
Type III:	Cysts with detached membrane
Type IV:	Mixed cysts
Type V:	Cysts with heterogeneous echogenicity
Type VI:	Hyperechoic cysts
Type VII:	Calcified cysts

Source: Adapted from Caremani et al. (21).

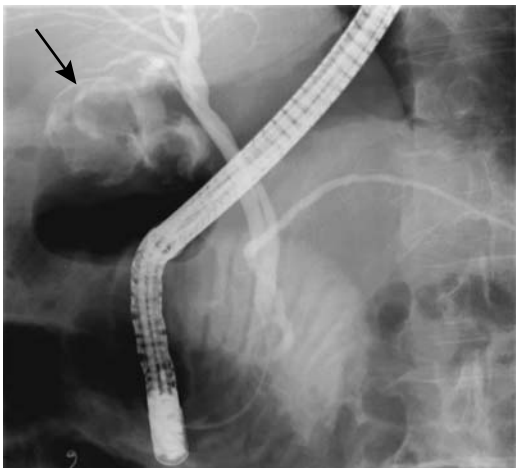

Figure 7.9. Echinococcal cyst communicating with bile ducts. Contrast partly outlines the cyst (arrow).

One should keep in mind that not all multilocular liver cysts are infectious in origin or even benign. The imaging appearances of an embryonal cell carcinoma or hepatobiliary cystadenoma mimic a hydatid cyst. With multiple hydatid cysts, liver parenchyma becomes sufficiently replaced that differentiation from polycystic disease becomes difficult.

Infection with *E. multilocularis* results in somewhat different imaging findings. Irregular, necrotic liver lesions often mimic a neoplasm (Fig. 7.10). Focal calcifications develop with both *E. multilocularis* and *E. vogelii* infections.

Biopsy/Drainage

Drainage can be both diagnostic and therapeutic. Cysts that are heavily calcified, however, are probably inactive and often are left alone.

Some biopsies are performed unintentionally without suspecting the true diagnosis and others are done on purpose. With suspicion that a lesion may indeed be hydatid in origin, the cytologist should be so informed when submitting aspirated material; in regions of low prevalence the pathologist may not consider this diagnosis. Some investigators believe that dilated pericystic bile ducts are a relative contraindication to nonsurgical treatment because of the danger of complicating biliary obstruction (22).

A number of older publications cautioned against biopsy or drainage of a hydatid cyst, although more recent experience suggests that percutaneous drainage is a relatively safe procedure. Minor allergic reactions, such as urticaria,

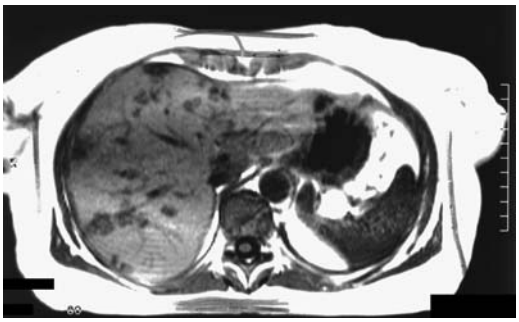

A

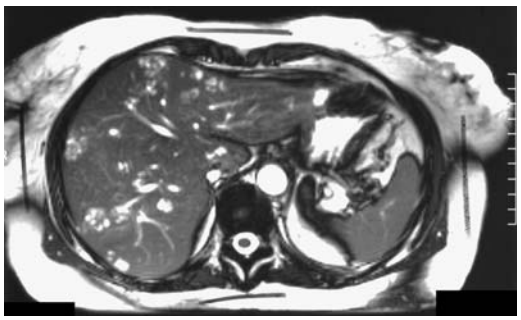

B

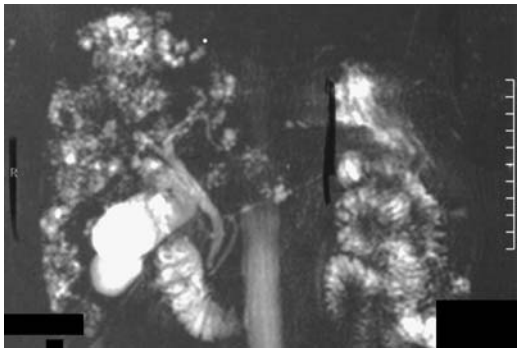

C

Figure 7.10. Echinococcus multilocularis presenting as multiple small foci scattered throughout the liver. It is hypointense on T1- (A) and hyperintense on T2-weighted magnetic resonance imaging (MRI) (B). C: Magnetic resonance cholangiopancreatography (MRCP) outlines the cysts and bile ducts. (*Source:* Burgener FA, Meyers SP, Tan RK, Zaunbauer W. Differential Diagnosis in Magnetic Resonance Imaging. Stuttgart: Thieme, 2002, with permission.)

are encountered after aspiration in an occasional patient. A rare patient develops a major reaction, including shock, and the interventional radiologist must be prepared to deal with these reactions. Fatal anaphylaxis has been reported with percutaneous therapy. Also, a possibility of seeding exists due to a spill of cyst material, although intraperitoneal leakage of cyst fluid is rare. A superimposed bacterial infection also develops occasionally.

Percutaneous

Percutaneous treatment consists either of several installations of hypertonic saline (with interval aspiration) or placement of a catheter, injection of hypertonic saline, or drainage, followed in 24 hours or later by injection of a scolicidal solution. After therapy the endocyst becomes detached and serial US shows most cysts decreasing in size and the cyst wall becoming irregular and thicker. A second drainage is necessary only if a cyst contains membranes or multiple cysts are present. Both adults and children have been treated with percutaneous drainage.

Albendazole prophylaxis is instituted and catheter drainage generally continued until drainage is <20 mL per day. Recommended imaging follow-up varies but US every month for 6 months, a control CT at 6 months, and then US and CT at yearly intervals is reasonable. The abscess cavity typically becomes obliterated within 6 months. Local recurrence is an uncommon occurrence. Another option is to treat by puncture, aspiration, injection, and reaspiration of smaller cysts and catheterization of larger cysts using hypertonic saline and absolute alcohol as cytotoxic and sclerosing agents (23).

Surgical

Surgical pericystectomy is advocated by some surgeons. Laparoscopic surgery with cyst aspiration is also performed. Hepatic resection is necessary only if multiple cysts involve the same lobe or if a cyst has essentially replaced a lobe.

Recurrent hydatid disease develops occasionally, either in the liver or other structure, even in the peritoneal cavity. Postdrainage US establishes a baseline and allows distinction of recurrence from postoperative change.

Biliary strictures develop in some patients after surgery. These strictures tend to be long, multiple, and proximal in location.

Tuberculosis

Weight loss is common in patients with hepatic tuberculosis. Not all patients with liver involvement have hepatomegaly.

Tuberculous liver infection usually presents as a diffuse process, at times called miliary; less common is a macronodular tumor, or tuberculoma, mimicking an infiltrating tumor. Computed tomography reveals a hypodense tumor that enhances less than liver parenchyma. An occasional hypodense nodule is surrounded by an enhancing rim.

Ultrasonography reveals mostly well-delineated hypoechoic tumors.

Tuberculomas are mostly hypointense on T1- and isointense on T2-weighted MR images, although considerable variation exists, ranging from hypointense to hyperintense on both T1- and T2-weighted MRI. They do not enhance post-MR contrast but some exhibit rim enhancement. The MR appearance of hepatic tuberculomas is thus not specific, being influenced by the presence of calcifications, blood, and necrosis. A biopsy is necessary for diagnosis.

Extensive multiorgan tuberculosis is illustrated by a woman with multiple calcified brain nodules and calcified hypodense tumors in the liver and spleen (24); liver tuberculomas were hypointense on T1-weighted spin-echo (SE) images and hypointense but contained a hyperintense region on T2-weighted images.

Percutaneous needle biopsy in these patients should be diagnostic. After successful antibiotic therapy the sonographic appearance should revert to that of a normal liver.

Fungal

Most fungal abscesses occur in a setting of malignancy or immunocompromise. Most of these abscesses are small and tend to be scattered throughout the liver. Each individual abscess often has an imaging appearance similar to that of a pyogenic abscess, including rim enhancement.

A biopsy, especially if obtained from the periphery of a lesion, may not provide a diagnosis.

Some of these abscesses calcify after therapy.

Candidiasis

Typically CT reveals *Candida albicans* abscesses as multiple hypodense lesions scattered throughout the liver. The appearance mimics metastases. The spleen is also often involved. A *bull's-eye* appearance to the lesion should suggest candidiasis.

The sonographic findings range from an early wheel-like appearance, to a *bull's-eye* pattern, to a homogeneously hypoechoic lesion.

Mucormycosis

Mucormycosis is an opportunistic fungal infection developing in patients with an impaired immune system or diabetes.

Mucormycosis in one patient manifested as multiple focal hypodense lesions containing centrally located vessels (25); biopsies revealed hyphae consistent with mucormycosis. Such a hypodense lesion surrounding vessels and without a mass should suggest an angioinvasive organism.

The differential includes other fungal infections, lymphoma, and *Mycobacterium tuberculosis* or *M. avium-intracellulare* infections.

Visceral Larval Migrans (Toxocariasis)

Ultrasonography in a patient with persistent eosinophilia and shown to have visceral larval migrans initially revealed a single hypoechoic lesion that progressed to multiple lesions (26); these lesions presumably represented confluent biliary granulomas. Only occasionally are larvae detected on liver biopsy. The diagnosis is confirmed with serologic testing.

Schistosomiasis

Clinical

One of the oldest diseases known, even today schistosomiasis infects a large part of the world's population. Both children and adults suffer from this infection. The primary end-organ affected depends on the river fluke involved: *Schistosoma japonicum* and *S. mekongi*, primarily Oriental in distribution, affect the liver, *S. mansoni* involves the liver and rectum, and *S. haematobium* infestation targets the urinary tract. *S. mansoni* is found in west central Africa, the Arabic peninsula, some Caribbean Islands, and the Atlantic coast of South America.

Fresh water snails serve as an intermediary host for cercariae. Humans are infected through intact skin, the cercariae migrate from peripheral venules to the lungs and heart, and reach the liver where they mature into adult worms. *S. japonicum* eggs are carried from mesenteric veins into intrahepatic portal vein terminal branches, where extensive fibrosis and a granulomatous reaction lead to presinusoidal portal hypertension.

Schistosomiasis can be divided into an acute (Katayama syndrome) and a chronic phase. Early diagnosis during the acute phase is based on clinical and laboratory data, with imaging having no direct role. Eventually these patients develop portal hypertension and esophageal varices. They have a normal hepatic venous pressure gradient due to the presinusoidal nature of their portal hypertension. Hemodynamic studies in patients with hepatic schistosomiasis reveal hyperkinetic systemic and splanchnic circulations.

Liver involvement consists of fibrosis and portal hypertension. Some patients progress to cirrhosis and liver failure. In the Middle East, cirrhosis developing in a setting of hepatic schistosomiasis should suggest superimposed hepatitis C virus infection. On the other hand, a Philippines study of prior *S. japonicum* infection found chronic viral hepatitis to be rare (27).

Patients with chronic liver schistosomiasis are at risk of developing hepatocellular carcinoma.

Imaging

Hepatosplenomegaly and lymphadenopathy are common with acute *S. mansoni* infection. Left lobe hypertrophy occurs early and is readily detected by US. On a chronic basis the porta hepatis region is usually most extensively

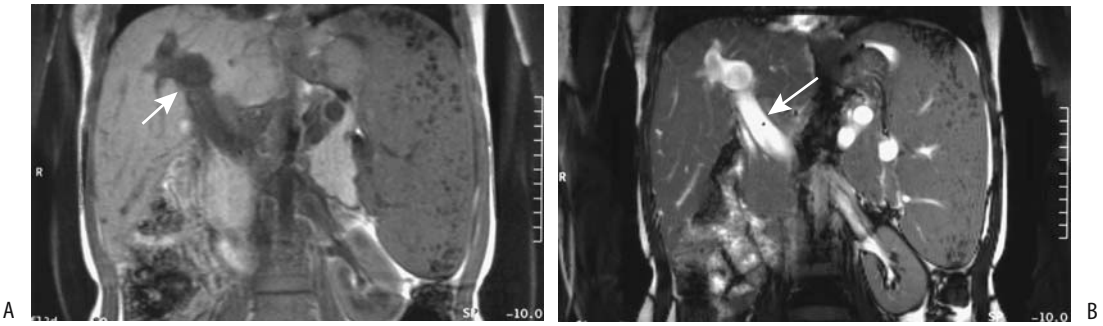

Figure 7.11. Portal hypertension induced by schistosomiasis. T1- (A) and T2-weighted (B) coronal MR images reveal a spleen larger than the normal-sized liver and a dilated portal vein (arrows). (*Source:* Burgener FA, Meyers SP, Tan RK, Zaunbauer W. Differential Diagnosis in Magnetic Resonance Imaging. Stuttgart: Thieme, 2002, with permission.)

involved, and periportal fibrosis extends intrahepatically for varying lengths. Ultrasonography rather than biopsy is often used in endemic areas to evaluate periportal fibrosis. It reveals widened hyperechoic periportal tracts, a nonspecific finding also seen in some other chronic infections. A relationship exists between the degree of periportal fibrosis as detected by US and the presence of esophageal varices.

Early in the disease MRI shows portal hypertension (Fig. 7.11); then the periportal zones become isodense on T1-weighted images and enhance with contrast. T2-weighted sequences reveal hyperintense periportal regions suggesting inflammation and edema.

Patients with *S. japonicum* infection develop almost pathognomonic *turtleback* pericapsular and parenchymal calcifications, best identified with CT; US often shows a patchy network pattern. Calcifications are uncommon with *S. mansoni* and *S. haematobium* infection.

Syphilis

The liver is commonly involved in congenital syphilis. Hepatic failure and extensive liver calcifications develop in some of these neonates.

Secondary syphilis is marked by acute hepatitis and cholestasis. Ultrasonography reveals parenchymal abnormalities due to diffuse inflammation.

Liver involvement in tertiary syphilis is rare. Multiple intrahepatic nodules mimicking metastases are found occasionally. Biopsy reveals granulomas and necrosis.

Spirochetes are identified in biopsy specimens. Pathologists have described an acquired liver deformity in end-stage tertiary syphilis known as hepar lobatum.

Actinomycosis

Liver infection by an anaerobic gram-positive bacterium of the genus *Actinomyces* is rare. No predisposing factors are found in most patients.

The diagnosis is confirmed when an *Actinomyces* species is cultured from pus aspirated from an abscess. Rather than an abscess, some patients have a more solid-appearing tumor, and a neoplasm is suspected. In particular, in a woman with a pelvic tumor and suspected liver metastases, especially if an intrauterine device is in place, biopsy should differentiate between actinomycosis and a neoplasm.

A complication of liver actinomycosis is portal vein thrombosis.

Botryomycosis

Botryomycosis, also called *bacterial pseudomycosis*, is a rare, chronic bacterial infection characterized by eosinophilic botryomycotic (bacteria-containing) granules, with gram-positive cocci and gram-negative bacilli being most often found. Clinically, the infection tends to mimic actinomycosis or some other fungal infection. Pathogenesis of this condition probably involves a symbiosis between the host and

bacteria, although the specific pathobiologic interaction is unknown.

Botryomycosis most often involves the skin and is thus familiar to dermatologists. Several patients with liver botryomycosis have been described. Most lesions consist of multiple small liver abscesses containing gram-positive microorganisms. Initial imaging often suggests a neoplasm.

Hepatitis

Imaging has a limited direct role in hepatitis, with laboratory studies and biopsy being bulwarks of diagnosis. Magnetic resonance, however, is of potential value. Among patients with proven chronic hepatitis, histopathology in about two thirds of those with patchy enhancement on early postgadolinium MRI revealed a macrophage infiltrate, hepatocyte necrosis, and steatosis (28). Prominent linear enhancement on delayed postgadolinium MRI is found with fibrosis.

Viral

An unusual cause of acute hepatitis is measles virus infection.

Viral hepatitis is common throughout the world, with the highest prevalence in East Asia. Currently viruses A through G have been identified. At least one other type of enterically transmitted hepatotropic virus probably exists. Hepatotropic viruses A through E induce hepatocellular damage either through a direct cytotoxic effect or through some yet undefined mechanisms. The common end point is hepatocellular necrosis. Co-infection is not uncommon, especially in end-stage disease.

Fat ingestion normally results in gallbladder constriction. In some patients with acute hepatitis, fat results in paradoxical gallbladder dilation, a useful imaging finding. Some patients with acute viral hepatitis present with what clinically appears to be acute cholecystitis. They recover with conservative medical management. Gallbladder US in these patients reveals considerable gallbladder wall thickening, but the gallbladder returns to normal thickness with clinical recovery.

Hepatitis A

Humans appear to be the only host for hepatitis A virus. This infection has decreased in prevalence, especially in East Asia. It is an acute infection and does not lead to a chronic carrier state. Effective immunization exists against hepatitis A virus.

Some patients with hepatitis A virus infection develop acute renal failure and nephrotic syndrome, presumably due to hepatitis A virus–triggered immune-mediated renal injury in genetically susceptible individuals. Acute viral hepatitis A can progressed to autoimmune hepatitis.

Hepatitis B

In many patients hepatitis B virus (HBV) infection is subclinical; others, however, become chronic carriers, serve as a reservoir for further spread, and develop chronic liver disease, including cirrhosis. A direct relationship exists between chronic hepatitis B infection and hepatocellular carcinoma. Thus in South African blacks, those positive for hepatitis B surface antigen had a 23-fold increased risk of developing a hepatocellular carcinoma (29); those positive for hepatitis C serology had a sevenfold increased risk, while those with both hepatitis B and C markers had a relative risk of 82. The study estimates that HBV causes about 43% of hepatocellular carcinomas in South African blacks, hepatitis C 5%, and co-infection with both 20%. Hepatitis B infection probably is a factor in China, while hepatitis C virus plays a similar role in Southern Europe and Japan. Hepatitis B virus is also suspected to have a role in other cancers.

Hepatitis B infection is transmitted vertically from mother to child. Infection in some infants progresses to fibrosis and eventual cirrhosis.

A histologic finding of hepatocyte loss, cholestasis, periportal fibrosis, and inflammation is called fibrosing cholestatic hepatitis. It is a variant of HBV infection, and affected patients have a high rate of liver failure.

Immunization against HBV is available.

Hepatitis C

Hepatitis C virus (HCV) infection is believed to cause at least 90% of previously called non-A,

non-B hepatitis. In the United States approximately 1.4% of the population is infected. Infection is acquired by either blood product transfusions or intravenous drug abuse. It is a common infection in hemophiliacs. In some patients the mode of transmission is not known. Vertical and sexual transmission is uncommon.

Hepatitis during the acute phase is invariably mild and often subclinical, but most infections become chronic. The clinical course of hepatitis C infection is unpredictable. A rough estimate of mean time between initial infection and diagnosis of chronic hepatitis is 10 years, 10 years more for cirrhosis to develop, and another 10 years before hepatocellular carcinoma is discovered, although considerable individual variation exists. Even with advanced disease, half the patients are asymptomatic. Normal biochemical tests do not exclude viral replication in anti-HCV–positive individuals. Different viral genotypes are associated with different severity of liver disease. For instance, HCV type 1b is overrepresented in patients developing cirrhosis and hepatocellular carcinoma and influences the carcinoma risk in cirrhosis.

An association exists between HCV infection and autoimmune diseases. Infection leads to autoimmune hepatitis, membranoproliferative glomerulonephritis, thyroiditis, and such skin disorders as porphyria cutanea tarda and possibly lichen planus. A relationship with Sjögren's syndrome and possibly even Behçet's syndrome is suspected. An association with Guillain-Barré syndrome (an acute demyelinating neuropathy believed to have an autoimmune basis) has been suggested. It has been implicated in periarteritis nodosa.

Unlike many other human viruses, hepatitis C virus is an RNA virus and does not appear to be integrated into host cell genome. Carcinogenesis of HCV infection is generally explained by its ability to cause hepatic inflammation, regeneration, fibrosis, and eventual cirrhosis, yet some patients appear to progress from chronic hepatitis directly to carcinoma without developing cirrhosis.

An interesting association appears to exist between HCV serology and primary hepatic lymphoma. Hepatitis C virus is both hepatotropic and lymphotropic and in some patients results in a mixed essential cryoglobulinemia, a lymphoproliferative condition that on occasion evolves into non-Hodgkin's lymphoma. The virus is detected in some lymphoma tissue. Anti–hepatitis C virus antibodies are detected in almost half of B-cell non-Hodgkin's lymphoma patients. Likewise, an occasional patient with chronic HCV infection develops reactive lymphoid hyperplasia (pseudolymphoma), with imaging suggesting a focal hepatocellular carcinoma; biopsy should be diagnostic.

Gray-scale US findings do not correlate with liver biopsy findings in patients with chronic HCV infection. Imaging does detect perihepatic lymphadenopathy, however, with number and size related to HCV activity (30). Gray-scale US can document the response to therapy. Lymph nodes appear hyperintense relative to the liver on T2-weighted MRI.

No current immunization is available against this virus. Interferon is the treatment of choice for chronic HCV infection, but relapse rate is high.

Hepatitis D

Humans are probably the only host for hepatitis D virus. Its major focus in the United States is in drug addicts. It progresses to chronic hepatitis and cirrhosis.

Hepatitis E

Hepatitis E has a worldwide distribution and is a cause of considerable morbidity and mortality in the developing world. This virus is spread through contaminated water. Infected individuals develop cholestatic jaundice, generally with few sequelae, although in pregnancy it has led to fulminant hepatic failure.

Hepatitis G

Hepatitis G virus (HGV) is a RNA virus in the family Flaviviridae and is transmitted by blood transfusion. Both acute and chronic infections occur, but its role in hepatitis is uncertain. Parenteral transmission appears common, and IV drug users, hemodialysis patients, and hemophiliacs are prone to this infection, often in association with HBV and HCV infections.

Hepatitis G virus appears to be sensitive to interferon therapy.

Epstein-Barr Virus

Infectious mononucleosis (Epstein-Barr virus infection) is a rare cause of hepatitis; it has led to fulminant hepatic failure.

Imaging

Hepatitis has no specific imaging findings, with imaging generally performed to exclude other disorders. Necrosis and regeneration on precontrast CT appear as hypodense regions. Periportal edema is seen as periportal hypodense regions on CT and hyperintense regions on T2-weighted MRI. Ultrasonography is usually normal, although at times a heterogeneous hyperechoic appearance is found.

During the initial stage of severe acute hepatitis, a transient decrease in portal blood velocity is followed by a rebound, but in chronic viral hepatitis decreased portal blood velocity correlates with the degree of fibrosis.

Fulminant Hepatic Failure/Necrosis

Clinical

Acute hepatic encephalopathy within 8 weeks of hepatocellular disease in an otherwise healthy patient is considered fulminant hepatic failure. In most patients the etiology is not known, while in others a viral infection or chemical or drug poisoning is the responsible agent. Even exertion-induced heat stroke has led to fulminant liver failure. Coagulopathy is a common feature. These patients have a high mortality rate. An uncommon cause for chronic liver failure is extensive liver involvement by a malignant vascular tumor.

Hypoglycemia is a complication of fulminant hepatic failure; causes appear multifactorial and include associated hyperinsulinemia and possible hypoglycemic agents secreted by the liver.

Therapy focuses on providing temporary liver function until subsequent resumption of regeneration. A number of artificial liver assist devices have been evaluated. Auxiliary liver transplantation, retaining the recipient liver, is one alternative. During immunosuppressive therapy, such an auxiliary liver functions normally while native liver function is almost absent; immunosuppressive therapy is withdrawn after native liver function improves, and then the graft either atrophies or is removed. Technetium-99m–mebrofenin (2,4,6-trimethyl, 5-bromo iminodiacetic acid) (BrIDA) scintigraphy can distinguish the relative function of both donor and recipient livers.

In some patients liver transplantation is the only viable option. But a word of caution is warranted prior to liver transplantation in a patient with idiopathic fulminant hepatic failure. An occasional patient with massive liver necrosis is found to have diffuse liver carcinoma. Other rare causes of acute hepatic failure are diffuse cholangiocellular carcinoma and infiltration by acute lymphoblastic leukemia.

Imaging

Iodinated contrast agents should be used with caution in these patients to prevent accentuating associated renal failure.

Fulminant liver failure results in heterogeneous CT contrast enhancement. The periportal spaces enlarge, seen as periportal low attenuation regions. This is a nonspecific finding seen also in congestion, bleeding, and tumor infiltration. Serial CT reveals that liver volume changes little in survivors, while it decreases in nonsurvivors. Poorly defined hypodense regions develop in some patients, representing regenerating nodules; they enhance to iso- or even hyperdense with contrast. An increase in, or late onset of, ascites is an ominous finding.

Necrotic liver parenchyma is hyperintense on T2-weighted SE images, whereas regeneration appears hypointense. In general, regenerating nodules have an opposite appearance to regions of necrosis.

Blood clearance and receptor indices from Tc-99m-GSA imaging of patients with fulminant hepatic failure and acute hepatitis allow distinction between the two entities (31); also, all fulminant hepatic failure survivors had receptor indices of 0.58 or more, but in five of six patients who later died, the receptor index was 0.58 or less. (The receptor index is the liver radioactivity divided by that of liver plus heart. The blood clearance index is the heart radioactivity at 15 minutes divided by that at 5 minutes after the injection.)

Serial Tc-99m-GSA scintigraphy monitors improvement; it predicts hepatic recovery

earlier than is possible with more conventional biochemical methods and provides information about both hepatic functional reserve and morphologic changes by detecting lobe enlargement or atrophy.

Serial determination of liver and spleen volumes appears related to prognosis. Thus in patients with severe acute hepatitis or with fulminant hepatic failure, a close relationship exists between survival and changing rates of liver and spleen volumes as measured by CT (32); a decrease in liver volume accompanied by a decrease in spleen volume implies a good prognosis; a decrease in liver volume without a decrease in spleen volume implies a bad prognosis.

Drug and Toxin-Related Hepatitis

Numerous antibiotics, other drugs, and chemicals result in cholestasis or, on a more chronic basis, lead to biliary obstruction. Even ecstasy, a synthetic amphetamine, has been implicated. Cholestasis, whether drug-induced or due to some other agent, is discussed later (see Metabolic and Related Disorders). The cholangitis-like appearance seen after intrahepatic artery injection of various agents, termed secondary sclerosing cholangitis, is covered in Chapter 8.

Ductular obstruction, also termed cholangiolitis or cholangiopathy, ranges from an acute condition that is reversible when the inciting agent is withdrawn to progressive damage and a picture mimicking biliary cirrhosis.

Granulomatous Hepatitis

Granulomatous hepatitis is not a specific disease but a histologic description. Although tuberculosis and sarcoidosis are commonly associated with liver granulomas, this condition also develops with a number of bacterial, fungal, and parasitic infections and a variety of drugs. An occasional lymphoma results in granulomas. A rare association exists between granulomas and Graves' hyperthyroidism. Langerhans cell granulomatosis can result in liver nodules. Chronic granulomatosis is a cause of liver failure. A diagnosis is not always clear in a setting of granulomas.

Prior infection by histoplasmosis results in calcified granulomas scattered throughout the liver and spleen. These granulomas are readily detected by CT and are similar to those seen with tuberculosis.

Autoimmune Hepatitis

Although a primary diagnosis of autoimmune hepatitis is occasionally made, similar to granulomatous hepatitis, patients with autoimmune hepatitis have elevated autoantibodies, hyperglobulinemia, an abnormal serum aminotransferase level, and no other obvious liver disease. Current evidence points to an autoimmune basis as a pathway for a number of other disorders. An overlap of autoimmune hepatitis and primary sclerosing cholangitis exists; its relationship to primary biliary cirrhosis is not clear, although in patients with findings of both autoimmune hepatitis and primary biliary cirrhosis the latter diagnosis generally prevails. Adding confusion, some overlap exists with viral hepatitis and autoimmune cholangitis. It is thus a disease of exclusion.

Autoimmune hepatitis is associated with Felty's syndrome, Sjögren's syndrome, measles, interferon therapy, gastric carcinoid, celiac disease, and some drugs. In some patients antibodies against liver cytosol appear to be a specific immunoserologic marker of autoimmune hepatitis.

No specific imaging findings mark autoimmune hepatitis. Any detected abnormalities generally point toward another specific disease.

Radiation Hepatitis

Radiation hepatitis manifests clinically as jaundice and hepatomegaly several weeks after radiation therapy. The presumed underlying mechanisms are Kupffer cell and vascular endothelial damage.

Imaging identifies the boundary between normal and irradiated liver to be sharply defined and corresponding to the radiation port, a finding not seen with overlapping ports. Once regeneration starts, the sharp boundary becomes less well defined. Radiation hepatitis is iso- to hypodense relative to normal liver on CT (Fig. 7.12). Vessels in the involved region appear normal. Postcontrast, CT appearance is inconsistent and ranges from hypo- to hyperdense.

Figure 7.12. Radiation hepatitis after prior radiation therapy for breast carcinoma. CT outlines a focal, sharply defined anterolateral defect (arrow). (Courtesy of Patrick Fultz, M.D., University of Rochester.)

The involved liver parenchyma is mostly hypoechoic on US.

Radiation hepatitis is hypointense on T1- and hyperintense on T2-weighted MR images. Anecdotal reports describe iron colloid-enhanced MRI showing decreased uptake in acute radiation-induced hepatic injury. Eventually abnormalities either resolve or the involved liver segments atrophy.

Metabolic and Related Disorders

Cholestasis

An active bile acid transport system by hepatocytes into bile canaliculi is necessary for bile acid flow. Bilirubin, various phospholipids, and other components are secreted by canaliculi, while bile duct epithelial cells secrete a bicarbonate-rich solution. A breakdown in any step of this complex chain results in cholestasis. Cholestasis, or cholestatic jaundice, is not a separate disease but a manifestation of a number of disorders discussed below.

Drug-induced cholestasis is most often due to impaired hepatocellular bile secretion. With some drugs a cholangiolitis or even a cholangitis picture predominates. Whether this condition is called hepatitis, cholestasis, or cholestatic hepatitis is a moot point. Other cholestatic conditions, including neonatal hepatitis, are discussed in Chapter 8.

Cholestasis is a manifestation of paraneoplastic syndrome in patients with malignant lymphoproliferative diseases. Extrahepatic Hodgkin's disease, renal cell carcinoma, and other cancers have been associated with cholestasis.

Acute vanishing bile duct syndrome is usually associated with drug or toxin use and is a rare cause of cholestasis. It develops mostly in adults. Rarely, cholestasis progresses to cirrhosis.

Idiopathic benign recurrent cholestasis is a rare disorder diagnosed mostly by exclusion.

Osteoporosis and osteomalacia develop in patients with chronic liver disease, especially those with chronic cholestasis.

Fatty Liver (Steatosis)

Clinical

Fatty infiltration (steatosis) ranges from diffuse to focal (Table 7.6). Drugs associated with steatosis include tetracycline and tamoxifen (used for adjuvant hormone therapy for breast cancer). Fatty liver develops in a setting of heterozygous hypobetalipoproteinemia, and this entity should be considered as a possible cause

Table 7.6. Conditions associated with fatty liver infiltration

Obesity
Hyperlipidemia
Starvation
Alcohol
Diabetes mellitus
Cystic fibrosis
Fatty liver of pregnancy
Total parenteral nutrition
Familial heterozygous hypobetalipoproteinemia
Drugs
Steroids
Certain hepatotoxins
Metabolic liver disorders
Galactosemia
Reye's syndrome
Fructose intolerance
Glycogen storage diseases

of an unexplained fatty liver. Acute fatty liver in pregnancy is discussed in a separate section.

Mild hepatic iron overload develops in some patients with nonalcoholic steatohepatitis, possibly due to the concomitant presence of the hemochromatosis gene mutation; homozygous or heterozygous mutations of this gene are common in patients with nonalcoholic steatohepatitis.

A minority of patients receiving intraperitoneal insulin during peritoneal dialysis develop subcapsular steatosis, seen with CT as subcapsular hypodense nodules or rindlike regions (33).

Steatosis generally improves once a known inciting agent is removed.

Diffuse Steatosis

Both CT and US provide qualitative rather than quantitative evidence of liver fat. Precontrast CT suggests steatosis if liver attenuation is less than the spleen; typical criteria for steatosis consist of liver attenuation 10 HU less than spleen or a liver-to-spleen ratio of <0.9. Postcontrast, the spleen is not an accurate reference standard; muscle tissue is an adequate standard only if fatty infiltration is pronounced. Contrast-enhanced CT in fatty infiltration reveals normal vessels coursing through fat, rather than being displaced as is often the case with a neoplasm.

Ultrasonography of diffuse fatty infiltration reveals a hyperechoic pattern throughout the liver, to the point of masking the normally hyperechoic portal vein wall. Kidneys have been used as a standard to establish liver echogenicity. The hepatorenal echo intensity difference is greater in fatty livers than in normal livers; a hepatorenal difference of >7 dB is a sensitive indicator of a fatty liver.

Because a normal pancreas is slightly more hyperechoic than a normal liver, it too is a useful landmark to detect increases in liver echogenicity.

Magnetic resonance spectroscopy measures the lipid volume fraction in liver steatosis. Spin-echo (SE) sequences are relatively insensitive in detecting fatty infiltration. Chemical shift imaging using in-phase and opposed-phase SGE sequences distinguishes proton signals from water and fat. Imaging with fat and water protons in-phase results in their signals being additive, while opposed-phase imaging leads to their cancellation. Thus on opposed-phase images normal liver parenchyma has an isointense signal and fat appears hypointense and these sequences are useful to detect liver fat. In-phase and opposed-phase GRE sequences provide complementary diagnostic information in the liver; in a fatty liver some focal lesions are obscured if only opposed-phase sequences are used, and for full assessment both are necessary. Fat detection is a complex MR topic, and both fat-suppressed and water-suppressed MRI have certain advantages in specific instances.

Postcontrast, simple fat deposition enhances in a similar pattern to normal liver parenchyma. Fat within abnormal tumors, on the other hand, tends to follow the underlying tumor enhancement pattern.

Focal Fatty Infiltration

Pathogenesis of focal fatty infiltration is not clear. Focal infiltration has a predilection for sites close to the falciform ligament and adjacent to gallbladder fossa. An anomalous portal venous supply, such as aberrant gastric venous drainage, is associated with focal fatty infiltrations. The importance of different insulin levels in an aberrant portal vessel as an inductor of steatosis is conjecture.

Focal fatty infiltration is segmental and often wedge-shaped in appearance; it should not be spherical in outline. As the term suggests, fat infiltrates and should not displace vessels. Rarely, focal involvement appears as multiple small lesions mimicking metastases or abscesses. Some focal infarcts have a similar appearance.

Ultrasonography of focal fatty infiltration shows a normal liver parenchyma containing fatty hyperechoic regions.

The MRI typically reveals a wedge-shaped region, hyperintense on T1-weighted images and extending to the periphery. Magnetic resonance imaging appearance is not pathognomonic; an intrahepatic cholangiocarcinoma can have a similar appearance. Post-ferumoxides, fatty infiltration is relatively high in intensity in all on T1-weighted images, with these regions ranging from hyper- to isointense on T2-weighted images (34).

Kupffer cells tend to be present in fatty infiltration, evidenced by Tc-99m–sulfur colloid uptake. A minority of focal fatty infiltrations,

however, has no colloid uptake and the appearance mimics a metastasis.

Focal Sparing

Focal regions of sparing are found in some patients with generalized fatty infiltration. Diffuse fatty infiltration with focal sparing tends to be segmental, with sparing having a predilection for segment IV and specific sites, such as subcapsular, close to the porta hepatis, and adjacent to the interlobar fissure. Efferent gallbladder blood flow plays a role in focal sparing at the gallbladder fossa. Doppler US reveals blood flow from the gallbladder in many patients with adjacent focal sparing. Thus focal sparing depends to some degree on whether the gallbladder is intact or not. In patients with fatty infiltration, gray-scale US detected focal sparing more often in patients with an intact gallbladder than in those with a prior cholecystectomy. An association exists between sparing along the posterior edge of segment IV and aberrant gastric venous drainage to this segment. A focal decrease in portal blood flow to this segment is the most likely cause of such sparing. Focal sparing of a fatty liver develops in a setting of an arterioportal shunt, presumably due to a decrease in portal blood flow.

Focal sparing is hyperdense both with pre- and postcontrast CT and appears as a hypoechoic focus with US. Difficulty arises in a fatty liver in differentiating focal sparing from neoplasms. An occasional metastasis can appear as a wedge-shaped hyperdense region on nonenhanced CT, similar to focal sparing in a fatty liver, due to focal intrahepatic portal vein obstruction.

Regions of focal sparing, representing normal liver containing reticuloendothelial cells, take up the SPIO contrast agent ferumoxides. Focal sparing thus reveals a signal loss and has a low intensity on T1- and T2-weighted images (34).

Liver metastases appear to be less common in patients with a fatty liver than in a normal liver. When present, their appearance is modified by the underlying fat (Fig. 7.13).

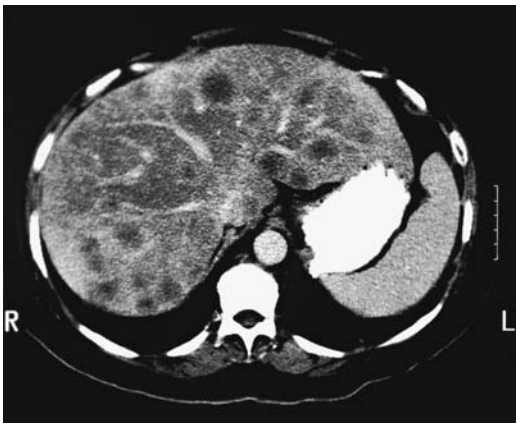

Figure 7.13. Metastatic breast carcinoma in a fatty liver. Multiple nodules are scattered throughout a heterogeneous, poorly enhancing liver. (Courtesy of Patrick Fultz, M.D., University of Rochester.)

Cirrhosis

Cirrhosis is a reaction by the liver to chronic hepatocyte injury and is often classified morphologically into micronodular and macronodular. A micronodular pattern predominates in alcohol-induced cirrhosis (also called portal or nutritional cirrhosis), while viral hepatitis generally has more of a macronodular appearance, but such a differentiation is not clear-cut, overlap exists, and with time micronodular cirrhosis tends to evolve into a mixed or macronodular appearance. So-called cardiac cirrhosis develops in some patients with chronic right-sided cardiac failure, especially in patients with constrictive pericarditis; the liver grossly mimics that seen in Laënnec's cirrhosis, except hepatic vein and sinusoidal congestion are evident. Cirrhosis due to biliary causes is discussed in later sections.

Etiologies of cirrhosis range from infectious, chemical, metabolic, and immunologic, to idiopathic. In children, causes of cirrhosis include Wilson's disease, primary Budd-Chiari syndrome, and glycogen storage disease. Cirrhosis in children is usually progressive and chronic, with attempts at regeneration resulting in a nodular and irregular liver outline.

In the Western world chronic alcoholism is the most common associated factor for cirrhosis, while in Asia chronic hepatitis predominates. Less common are hemochromatosis, chronic biliary obstruction such as Oriental cholangiohepatitis, chronic congestive failure, reaction to toxic substances such as methotrexate therapy, and idiopathic conditions such as primary biliary cirrhosis.

Table 7.7. Child-Turcotte classification of hepatic reserve

Parameter	Category A	B	C
Bilirubin (mg/dL)	<2	2–3	>3
Albumin (g/dL)	>3.5	3–3.5	<3
Ascites	None	Treatable	Refractory
Encephalopathy	None	Minimal	Severe
Muscle mass	Normal	Fair	Poor

A clinical classification of hepatic reserve is outlined in Table 7.7. In spite of new prognostic models such as the model for end-stage liver disease (MELD), short- and long-term prognostic indices (STPI and LTPI), and the Rockall score and Emory score for assessing prognosis in patients with liver disease, little evidence suggests that the long-used Child-Turcotte classification should be replaced. It is a useful guide in both a setting of portal hypertension and other conditions leading to hepatic failure; it correlates with prognosis.

Preoperative CT in patients with end-stage cirrhosis prior to liver transplantation detects enlarged lymph nodes in about half, mostly located in the porta hepatis and hepatoduodenal regions; adenopathy is most common in a setting of primary biliary cirrhosis and less common in alcohol-related cirrhosis. Histology reveals benign nodal hyperplasia.

Laënnec's Cirrhosis

The precise etiology of a shrunken liver composed of small grains, elegantly described by Laënnec in 1826, is unknown. A number of congenital and acquired conditions have cirrhosis as their final end point, but the current tendency is to distinguish them from classic Laënnec's cirrhosis on both clinical and pathologic grounds. Histologically, Laënnec's cirrhosis consists of hepatocellular necrosis, regenerating nodules, fibrosis, and steatosis, with the specific appearance in any one patient depending on the stage of disease. Superimposed inflammation is often identified. A nodular liver outline is common, with nodularity probably being secondary to both regeneration and distortion produced by fibrosis. From a clinical viewpoint, loss of liver function evolves into portal hypertension and its associated myriad complications.

For unknown reasons some patients with Laënnec's cirrhosis develop primary pulmonary hypertension. An association of cirrhosis, ascites, and pleural effusion is not uncommon. A rare cirrhotic patient develops hydrothorax with little or no evidence of ascites.

Both regenerating nodules and dysplastic nodules develop in livers involved by Laënnec's cirrhosis. These are discussed in a later section (see Nonneoplastic Tumors) because from an imaging viewpoint they are part of a differential diagnosis for focal liver tumors.

Imaging

Liver US is probably the most common screening examination performed in patients with suspected diffuse liver disease; it is also useful in routine follow-up. Nevertheless, in a setting of diffuse liver disease a strong point can be made for liver-specific contrast-enhanced MRI; if deemed necessary, a single MR study can combine unenhanced and enhanced MR to evaluate liver parenchyma, magnetic resonance cholangiopancreatography (MRCP) for bile duct visualization, and MRA to study liver vasculature.

From an imaging viewpoint, Laënnec's cirrhosis and most macronodular cirrhoses are generally treated as similar entities; with some exceptions, imaging findings tend to be similar, regardless of the inciting cause. One exception is that the caudate lobe is significantly larger, and the presence of a right posterior hepatic notch is more common in patients with alcoholic cirrhosis than in those with viral-induced cirrhosis (35).

Nevertheless, serial MR follow-up of patients with progressing viral-induced cirrhosis also shows right lobe and medial segment atrophy, correlating with clinical findings (36); in patients with stable disease the caudate lobe and lateral segment continue to increase in size.

Typical temporal findings show that initially the liver enlarges, then the right lobe and medial segment of the left lobe atrophy, and the caudate lobe and lateral segment of the left lobe become prominent, findings described years ago with rectilinear scintigraphy. This change in relative lobe size is rather specific for cirrhosis. A CT-based caudate-to-right lobe ratio of >0.65 is strong presumptive evidence for cirrhosis.

Eventually the liver shrinks. These changes are not invariable and about 25% of end-stage cirrhotic livers are normal in size. At times unusual atrophic and hypertrophic combinations lead to a bizarre appearance.

Initially CT detects a mild diffuse increase in attenuation, although more often liver attenuation remains within a normal range. Postcontrast, no significant difference in vascular enhancement and liver enhancement is evident during the arterial phase in patients with and without cirrhosis, but portal venous phase enhancement is significantly lower in cirrhotics. The liver margin varies from smooth, to nodular, to a lobular appearance.

Regeneration, fibrosis, fatty replacement, and vascular shunting lead to an inhomogeneous postcontrast CT appearance. At times thick, fibrotic bands interlace the liver. Peripherally located vessels become attenuated. Some patients develop small peribiliary cysts. More prominent collateral shunts become apparent postcontrast. Although intrahepatic arterioportal shunts are more common with hepatocellular carcinomas, they do occur in cirrhotic livers.

Mesenteric edema is common in cirrhotics; it occurs alone or in combination with omental or extraperitoneal edema. The CT appearance of mesenteric edema varies. About two thirds of patients have gastrointestinal wall thickening, and most often the jejunum and ascending colon are affected, with thickening being multisegmental, concentric, and homogeneous in appearance (37).

The CT appearance of cirrhosis is mimicked in patients undergoing systemic chemotherapy for breast cancer metastatic to the liver.

Liver outline, reflectivity, attenuation, and size are US criteria used to diagnose cirrhosis. Liver surface nodularity is recognized if ascitic fluid is identified adjacent to the liver, keeping in mind that subcapsular metastases also result in a nodular appearance. Fibrosis and fat produce a coarse, heterogeneous hyperechoic appearance. This appearance is also nonspecific and is seen in fatty infiltration and with some neoplasms, such as hepatocellular carcinoma, lymphoma, and metastases. The quadrate lobe transverse diameter (segment IV), measured on oblique subcostal US scans, was 43 mm in controls and 28 mm in cirrhotics (38). A ratio of caudal lobe width to right lobe width is another sonographic sign of cirrhosis; a cut-off value of 0.65 provides high specificity but low sensitivity. An increased ratio is also seen in other disorders. In general, the US findings of a normal liver, fatty liver, and chronic liver disease such as cirrhosis overlap somewhat, although differentiation can often be made.

In children, a Doppler US finding of portal vein velocity <20 cm/sec identified cirrhosis with a sensitivity of 83% and specificity of 100%, better than that achieved with arterioportal velocity ratios or hepatic artery visualization (39), sensitivity increased to 91% when all three signs were evaluated together.

The MRI findings are similar to those seen with CT. Magnetic resonance imaging identified hilar periportal enlargement in 98% of patients with pathologically proved early cirrhosis who did not have any other imaging findings of cirrhosis, a finding occasionally also seen in normals (40); mean hilar periportal fat thickness was significantly greater in early cirrhotics (16 ± 6 mm) than in controls (5 ± 3 mm), with the sensitivity and specificity of this finding for diagnosing cirrhosis (using a cutoff value of 10 mm) being 93% and 92%, respectively. A widened gallbladder fossa also appears to be a specific MR indicator of cirrhosis.

Fibrosis is hypointense on T1- and also hypointense on T2-weighted images, although the presence of fluid varies the T2-weighted appearance. Postcontrast, fibrosis does not enhance during the arterial phase but shows greatest enhancement during hepatic venous phase. Intervening liver parenchyma (or nodules) tends to be hypointense on T1- and hyperintense on T2-weighted images. Postcontrast parenchymal enhancement is mild in most patients; in a minority, large, irregular regions of prolonged enhancement mimic the appearance of hepatocellular carcinoma.

A MR scoring system distinguished between clinical Child-Pugh grade A cirrhosis and further severity grades with a sensitivity of 93% and specificity of 82% (41); the scoring system was based on four factors: spleen volume index, volume index of posterior + medial + lateral liver segments, the presence of ascites, and the presence of collateral vessels.

Gadolinium results in greater enhancement in cirrhotic livers than noncirrhotic ones; enhancement varied from homogeneous to heterogeneous.

The Mn-DPDP-enhanced T1-weighted GRE MRI reveals significantly less enhancement in cirrhotic than noncirrhotic livers, presumably due to extensive fibrosis. Nevertheless, lesion characterization is significantly improved in cirrhotic patients after administration of Mn-DPDP (42).

Computed tomography and MR have to a large extent replaced scintigraphy in evaluating cirrhosis. Liver reticuloendothelial function decreases in cirrhosis, leading to decreased Tc-99m sulfur colloid uptake and increased uptake by the spleen and other organs. An enlarged caudate lobe is often evident.

In vivo P-31 MR spectroscopy in cirrhotics reveals phospholipid metabolism abnormalities, although in any one patient *in vivo* findings do not necessarily mirror biopsy results.

Vascular Abnormalities

Dynamic contrast-enhanced single-section liver CT provides data for aortic, hepatic, and portal vein time-density curves, which are used to calculate liver perfusion, arterial fraction, distribution volume, and mean transit time. Hepatic perfusion parameters are significantly altered in cirrhosis and vary with the severity of disease. Patients with advanced cirrhosis tend to develop portal and mesenteric vein calcification; some portal vein calcifications are associated with portal venous thrombosis.

Portal Vein

Portal vein flow, as determined by duplex US, varies with the degree of cirrhosis. Portal vein velocity also decreases with progression of cirrhosis and is a more sensitive indicator than splenic vein velocity. Little correlation exists among portal vein flow, splenic vein flow, and extent of esophageal varices, explained, in part, by the presence of collateral circulation. The loss of reversed flow in the hepatic veins is a common finding in established cirrhosis.

Shunting

Arterioportal shunting is not uncommon in cirrhosis. These shunts vary in their CT arterial portography appearance, ranging from single to multiple and from irregular, wedge-shaped to round. The margins vary in sharpness, and contrast enhancement is apparent in some. Smaller ones undoubtedly are not identified by pre- and postcontrast imaging and blend into normal liver parenchyma. Also complicating the issue is that arterioportal fistulas develop not only in cirrhotic livers but also in superimposed hepatocellular carcinomas.

Color Doppler US is useful in indirect shunt detection; an intrahepatic arterioportal fistula should be suspected when the resistance index (RI) in one hepatic lobe is decrease at least 20% relative to the other lobe, the pulsatility index (PI) is decreased at least 30%, and portal blood flow in the lobe with decreased RI and PI is reversed (43). An actual fistula is confirmed by angiography.

More prominent arterioportal shunts are seen as hyperintense regions precontrast MR and after SPIO contrast on T2-weighted TSE images.

These patients also develop hepatic arteriosystemic venous shunting. By infusing D-sorbitol into the hepatic artery, a substance whose first-pass hepatic extraction is normally high, any resultant systemic availability reflects arteriovenous shunting. Considerable shunt variability is evident in cirrhotic patients.

In a cirrhotic liver and aberrant gastric venous drainage, the focal liver region involved by aberrant drainage is hypodense on CT, hypoechoic with US, and hyperintense on T1- and hypointense on T2-weighted MRI; as expected, this region shows early enhancement with dynamic CT and MRI.

Hepatic Veins

Abnormal hepatic vein Doppler waveforms are found in most patients with established cirrhosis, although little correlation exists between degree of liver failure and flow alterations.

Hepatic venography in patients with cirrhosis shows patchy parenchymal opacification. Visualized hepatic vein branches are distorted and compressed.

Hepatic Artery

The postprandial hepatic artery RI does not increase as much in patients with liver disease as in those with a normal liver. In particular, patients with Child-Pugh class C disease have an increase in resistance of <10% rather than >40% as found in a normal liver. This change

mirrors findings in portal blood flow discussed previously. Whether this finding in cirrhotics is due to vascular or parenchymal factors is unknown.

Complications

Neoplasm

Current knowledge suggests that a hepatocellular carcinoma developing in a setting of cirrhosis evolves from regenerating nodules to dysplastic nodules (both are discussed in a later section). These cancers tend to be insidious, multifocal, and difficult to detect by most imaging modalities. An occasional cancer is identified as a smaller nodule within a larger regenerating nodule.

Although a hepatocellular carcinoma developing in a noncirrhotic liver is often resected or treated locally, in a setting of cirrhosis liver transplantation is a more viable option. Preoperative detection of multiple cancer foci or diffuse liver involvement is generally considered a contraindication to liver transplantation because invariably metastases are present. A number of unsuspected hepatocellular carcinomas are first detected after liver transplantation.

What is the risk of harboring an unsuspected hepatocellular carcinomas in a setting of advanced cirrhosis? Data for this question are available from liver transplantation studies, but the answer varies depending on whether cirrhosis is posthepatitic or Laënnec in etiology. Unsuspected hepatocellular carcinomas were most prevalent with hepatitis B (27%) and hepatitis C (22%), less so with other etiologies of cirrhosis (44); serum α-fetoprotein levels did not suggest most small tumors.

A retrospective orthotopic cirrhotic liver transplantation study found that preoperative CT identified 61% of 18, CT during arterial portography (CTAP) 58% of 12, and MR 62% of 21 malignant tumors (45); most missed tumors were <2 cm in diameter.

Extensive fibrosis tends to mimic a neoplasm on unenhanced CT, although postcontrast CT aids in differentiating these two entities. Postcontrast MRI is also useful in differentiating between fibrosis and tumor; hepatocellular carcinomas enhance more during the arterial phase, while fibrosis enhances during the portal phase.

Ultrasonography is used as a screening test to follow patients with cirrhosis. Such a screening program performed every 6 months can lead to earlier detection of smaller, potentially curable hepatocellular carcinomas. A more basic question is whether such screening is cost-effective. For most Western patients with Child-Pugh class A cirrhosis, screening with α-fetoprotein and US every 6 months appears to provide a negligible benefit in increased life expectancy (<3 months), even when the risk of cancer is high (6% per year) (46); for some patients with a predicted cirrhosis-related survival rate above 80% at 5 years, however, screening may increase mean life expectancy by several months.

Some evidence suggests that patients with cirrhosis have an higher prevalence of extrahepatic cancers than would be expected.

Other Complications

Some patients with cirrhosis develop small peribiliary cysts adjacent to portal vein branches (peribiliary cysts are discussed later). Computed tomography reveals small periportal cysts. Ultrasonography shows these cysts as round or tubular anechoic region around major portal tracts. With time, these cysts tend to enlarge, and differentiation from bile ducts is difficult.

In general, the risk of systemic bacterial infection increases with the severity of the cirrhosis. Infection with *Vibrio parahaemolyticus* is associated with ingestion of raw seafood; in most patients this infection results in gastroenteritis, but in cirrhotic patients it has led to fatal sepsis. Spontaneous *Streptococcus bovis* bacterial peritonitis should raise suspicion for cirrhosis.

In an autopsy study, 2% of patients with viral-induced cirrhosis or subacute liver atrophy developed clinically unsuspected phlegmonous colitis (47).

Hepatorenal syndrome is a known complication of liver disease. Believed to represent a circulatory dysfunction primarily involving arterial circulation, patients with hepatorenal syndrome do not maintain a normal effective arterial blood volume. Early changes consist of renal vasoconstriction detectable by renal Doppler US. And Doppler US thus identifies cirrhotics potentially at risk for developing hepatorenal syndrome.

Endoscopic retrograde cholangiopancreatography reveals evidence of chronic pancreatitis in a minority of cirrhotics. Most of these findings are in patients with alcoholic cirrhosis.

Cirrhotics have a higher prevalence of peptic ulcer disease than the general population. *Helicobacter pylori* does not appear to play a role in these patients.

Cirrhotic patients have a significantly lower bone mineral density than controls.

Primary Biliary Cirrhosis

Clinical

Of unknown pathogenesis, primary biliary cirrhosis is probably neither autoimmune nor infectious in origin, although it is associated with autoimmune hepatitis. A strong association exists with antimitochondrial antibodies (AMAs), yet some patients are AMA negative and antinuclear antibody positive; the latter is also called autoimmune cholangitis (or cholangiopathy) rather than primary biliary cirrhosis. Whether patients with so-called autoimmune cholangitis (i.e., those with an absence of antimitochondrial antibodies) should be consigned to a separate disease entity or considered to have a variant of primary biliary cirrhosis is conjecture (autoimmune cholangitis is also discussed in Chapter 8). Few differences are evident in clinical and serologic features in AMA-negative and AMA-positive primary biliary cirrhosis patients.

A relationship exists between primary biliary cirrhosis and Sjögren's syndrome. In fact, Sjögren's syndrome is one of the most frequent extrahepatic associations of primary biliary cirrhosis, and some investigators consider that primary biliary cirrhosis is a secondary form of Sjögren's syndrome. Celiac sprue appears to be more common among patients with primary biliary cirrhosis than the general population. A rare patient also has chronic autoimmune gastritis or idiopathic thrombocytopenic purpura.

No association is believed to exist with inflammatory bowel disease, which distinguishes this condition from sclerosing cholangitis. Pregnancy probably has no effect on disease activity.

Pulmonary alveolar diffusion capacity is often impaired in these patients, although such impairment is usually asymptomatic. An association between primary biliary cirrhosis and bronchial asthma has been reported. Severe hypoxemia has developed.

Patients with primary biliary cirrhosis are believed not to be at increased risk for developing hepatocellular carcinoma. Nevertheless, hepatocellular carcinoma and even a cholangiocarcinoma does occur occasionally.

The majority of patients are middle-aged women. Typically an early prodromal stage with mild elevation of liver function tests leads to cholestasis, although some patients are symptomatic even prior to cholestasis.

Sacral insufficiency fractures have developed in women with primary biliary cirrhosis.

Pathology

Progressive destruction of intrahepatic bile ducts, surrounding inflammation, and intrahepatic bile stasis mark primary biliary cirrhosis. Liver granulomas are a characteristic feature. The granulomas are noncaseating and nonnecrotizing, consisting of epithelioid cells and occasional giant cells. These granulomas are not pathognomonic and are found in other disorders, including primary sclerosing cholangitis.

The extrahepatic bile ducts are not involved. The intrahepatic bile ducts attenuate and, with progression, become somewhat tortuous and splayed, presumably due to adjacent regenerating nodules. Histologically, the bile duct wall is not as thickened as in sclerosing cholangitis. Nodular regenerative hyperplasia is common.

Imaging

Imaging differentiation between primary biliary cirrhosis and sclerosing cholangitis is generally straightforward. A cholangiographic "pruned-tree" appearance gradually becomes evident (Fig. 7.14); the exception is in a minority of patients with sclerosing cholangitis who have involvement only of small intrahepatic ducts; a gradual obliteration of these ducts may eventually lead to an appearance mimicking primary biliary sclerosis.

Computed tomography initially detects an enlarged or normal-size liver having a smooth contour; fibrosis and regenerative nodules are evident in about one third. Varices and ascites gradually develop. With advanced disease, CT findings are similar to those seen in other types

Figure 7.14. Primary biliary cirrhosis. Only limited intrahepatic bile ducts are filled in spite of a vigorous contrast injection.

of cirrhosis, except for a higher prevalence of diffuse liver enlargement.

A MR *periportal halo sign* is helpful in identifying this entity (Fig. 7.15). This sign, consisting of a hypointense focus centered around a portal vein branch and identified either on T1- or T2-weighted images, was found in 43% of patients with primary biliary cirrhosis awaiting transplantation but in no other cirrhotic patients (48).

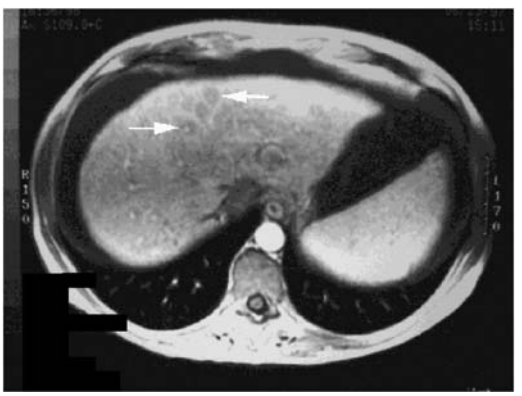

Figure 7.15. Primary biliary cirrhosis. Transverse T1-weighted MRI reveals round, hypointense lesions surrounding portal veins (arrows), a finding termed the periportal halo sign. (Courtesy of Jeffrey Wenzel, M.D., Southwest Imaging, Dallas, Texas.)

Computed tomography identifies lymphadenopathy in about 90% of patients with primary biliary cirrhosis requiring orthotopic liver transplantation (49). Adenopathy usually involves periportal and hepatoduodenal ligament nodes, and such adenopathy must be differentiated from that seen with neoplasms. A rough correlation exists between the size of the hepatoduodenal ligament lymph nodes and the degree of hepatocellular damage.

Therapy

The most common causes of death in patients with primary biliary cirrhosis are hepatic failure and gastrointestinal bleeding from varices. Currently no definitive therapy is available aside from liver transplantation. Transplantation has had a significant impact on patient survival. Nevertheless, the histologic features suggestive of recurrence develop in some transplant patients, with the recurrence rate apparently influenced by the type of immunosuppression used. During follow-up after orthotopic liver transplantation, 4% of patients developed recurrence (49).

Secondary Biliary Cirrhosis

Chronic biliary obstruction does evolve into cirrhosis. The overall appearance is similar to that seen in primary biliary cirrhosis, except for increased bile stasis and a lack of duct degeneration.

Liver involvement is uncommon in children with cystic fibrosis, but increasing survival of these patients has led to an increased number presenting with liver disease. These older children and young adults develop focal biliary cirrhosis, which eventually evolves into portal hypertension (Fig. 7.16). Some cystic fibrosis patients have undergone liver transplantation. Whether screening is useful in cystic fibrosis patients with chronic liver disease prior to developing cirrhosis remains to be established.

Fibrosis

Fibrosis is a response to a number of chronic liver insults. In some disorders fibrosis predominates with few or no parenchymal abnormalities identified.

Figure 7.16. A cirrhotic liver in a 24-year-old man with cystic fibrosis and hepatic failure. The liver has a nodular outline. Splenomegaly and vascular congestion (arrowheads) are secondary to portal hypertension. (Courtesy of Douglas S. Katz, M.D., Winthrop University Hospital, Mineola, New York.)

Ultrasonography typically reveals a hyperechoic pattern throughout a fibrotic liver. The hyperechoic changes with periportal fibrosis are seen mostly around the portal vein branches, separated from the adjacent liver parenchyma by a hypoechoic region. The underlying portal vein branches tend to be deformed.

The MRI changes of fibrosis are rather characteristic and familiar to most radiologists. SPIO-enhanced MR imaging identifies fibrosis by decreasing signal intensity from nonfibrotic regions containing Kupffer cells (50). Problems exist when fibrosis is only one part of a complex entity.

Vanishing Bile Duct Syndrome

An occasional patient with cholestasis has narrowed or small intrahepatic bile ducts (ductopenia) with no underlying disease being identified. This condition, termed vanishing bile duct syndrome, probably represents an immunologic or hypersensitive hepatotoxic reaction. Numerous drugs are associated with this condition. Pathologically, it should be suspected if absent interlobar bile ducts are found in over 50% of portal triads. Progressive cholestasis and loss of intrahepatic bile ducts in some of these patients develop to the point that a liver transplant is necessary.

Superficially, the imaging appearance of vanishing bile duct syndrome resembles diffuse intrahepatic sclerosing cholangitis.

Progressive cholestasis and the loss of intrahepatic bile ducts in some of these patients develop to the point that a liver transplant is necessary.

Iron Overload

Clinical

As a rough guide, a normal adult body contains about 4 to 5 g of iron, of which 80% is in hemoglobin, myoglobin, and iron-containing enzymes and 1 g of iron is stored. Ingested and absorbed iron is bound to transferrin and deposited in bone marrow, hepatocytes, muscle, and other tissues, but not reticuloendothelial cells; the latter derive their iron mostly from phagocytosed red blood cells. Of importance from an imaging viewpoint is that disorders associated with too much ingested iron then store the excess iron in the liver (hepatocytes) and pancreas, while iron from excess blood transfusions is stored in the liver (reticuloendothelial cells), spleen, and bone marrow. Disorders associated with excess hemolysis also lead to renal iron accumulation. Hemorrhage into tissues results in focal iron accumulation.

Iron is a hepatotoxin. Excess iron deposition in body tissues without organ damage is known as hemosiderosis. Hemochromatosis is an iron-overload disorder with structural and functional impairment of involved organs. Primary (hereditary or genetic) hemochromatosis is an inherited abnormality characterized by increased iron absorption from the gastrointestinal tract and resultant tissue iron overload. It is the most common inherited single gene disorder in those of northern European descent (51). Two point mutations in the hemochromatosis candidate gene *HFE* are known as *C282Y* and *H63D*. A diagnostic genotypic test for the *C282Y* mutation is available. Although this genetic test identifies most hemochromatosis patients, both iron-overload patients without this mutation and homozygous patients without iron overload also exist. In some patients both genetic and acquired factors play a role.

During the early latent stage of compensated hereditary hemochromatosis, aside from iron overload, only minimal hepatocyte damage is evident, but iron overload beyond a critical level

results in hepatocytic and sinusoidal cell siderosis and intracellular damage and necrosis.

Classic findings of hereditary hemochromatosis consist of bronze diabetes and an underlying cirrhosis, although currently a diagnosis is more often made at an earlier stage. Ideally, the quantity of liver iron overload is determined from a liver biopsy, but the diagnosis is often based mostly on an elevated fasting transferrin saturation level.

Hepatic iron deposition is common in thalassemia and chronic hepatitis, making differentiation between chronic hepatitis and hereditary hemochromatosis difficult. At times these disorders coexist; thus hepatitis C and hereditary hemochromatosis have led to end-stage liver disease in children. Secondary hemochromatosis develops most often in patients requiring long-term blood transfusions and those ingesting large amounts of iron. Multiple transfusions eventually lead to extensive iron overload in reticuloendothelial cells, and liver fibrosis is not a prominent feature. Bantu siderosis patients ingest large amounts of iron, which is stored mostly in reticuloendothelial cells and, to some degree, in hepatocytes.

Thalassemia patients also have increased oral iron absorption, driven not by genetic factors directly as in hereditary hemochromatosis but by increased erythroid hyperplasia. These patients initially develop liver findings similar to hereditary hemochromatosis, but additional iron overload due to transfusions modifies this appearance.

Sideroblastic anemia and erythropoiesis also result in secondary hemochromatosis, somewhat similar to transfusion overload. Hemosiderin accumulates in sideroblasts and hepatocytes, but not splenic reticuloendothelial cells. As a result, these patients have a hypointense liver and bone marrow but a close to normal appearing spleen on T1-weighted MR images. Nevertheless, some of these patients receive blood transfusions and the MR appearance can be confusing.

Untreated, patients with hereditary hemochromatosis progress to cirrhosis, congestive heart failure, and various endocrine abnormalities, including diabetes mellitus. Disease progression is gradual, findings are nonspecific, and the true cause is thus often overlooked, especially during the early phase. These patients are at increased risk of developing a hepatocellular carcinoma. A rare cholangiocarcinoma has developed in hemochromatosis, but whether this is fortuitous or not is speculation.

Imaging

A linear relationship exists between CT attenuation and liver iron content. Computed tomography sensitivity is improved by using 80 kVp instead of the usually used 120 kVp. Nevertheless, CT sensitivity in measuring liver iron is rather low, and most current research is centered on MR. When hemochromatosis is well established, the intrahepatic vessels are at a lower density than liver parenchyma; this finding is not pathognomonic, and high parenchymal attenuation is found in patients being treated with drugs such as amiodarone (amiodarone and its metabolites contain iodine and are concentrated in hepatocytes), gold therapy, prior thorium dioxide (Thorotrast) use, and occasionally in Wilson's disease.

Liver US is normal in most patients with early hemochromatosis.

Being a paramagnetic substance, iron becomes magnetized within a magnetic field, adjacent water photons lose phase coherence, and the overall effect is a hypointense MR signal. Magnetic resonance imaging in hereditary hemochromatosis reveals a decrease in liver and pancreas signal intensity on T2-weighted sequences. No such decrease in signal intensity is found in the spleen because no significant iron is deposited in the reticuloendothelial system. In iron overload due to transfusion, on the other hand, iron is deposited mostly in the reticuloendothelial cells of the spleen and liver, with relative sparing of liver hepatocytes and pancreas; as a result, a decreased signal intensity is evident on T2-weighted images of both the liver and spleen (Fig. 7.17). Initially in iron overload, signal intensity on T1-weighted images is normal but with more severe involvement a hypointense signal also becomes evident. An inverse linear relationship exists between iron concentration and signal intensity liver-to-muscle ratio. Overall, MRI detects relatively low levels of iron overload. A mathematic model is available to estimate iron concentrations from MR imaging data (52), but stringent calibration is required. Among other variables, MR field strength influences the effect of liver iron. A correlation

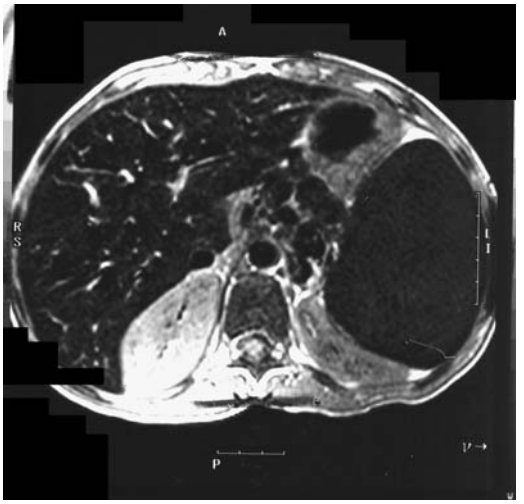

Figure 7.17. Iron overload in a 10-year-old with sickle cell disease and multiple transfusions. MR shows a markedly hypointense liver and spleen. (*Source:* Burgener FA, Meyers SP, Tan RK, Zaunbauer W. Differential Diagnosis in Magnetic Resonance Imaging. Stuttgart: Thieme, 2002, with permission.)

exists between iron concentrations obtained from percutaneous needle biopsies and a ratio of signal intensity of the liver to background noise obtained from MR sequences. Skeletal muscle T2 values are relatively constant over a wide range of iron stores and can thus be used as a reference standard. The liver-to-muscle proton density ratio correlates with hepatic iron, yet the low signal-to-noise ratios seen with high iron levels are difficult to quantitate. Although in practice MRI appears sufficiently accurate to measure liver iron concentrations, in general, qualitative results aid in establishing a diagnosis but quantitative correlation is imprecise.

Thalassemic patients without blood transfusions have an MR appearance similar to those with hereditary hemochromatosis, but after blood transfusions the picture alters, with excess iron in organs rich in reticuloendothelial cells. A multicenter MR study of thalassemia major patients suggests that the signal intensity ratio of liver-to-muscle is related to liver iron concentration (53). Hepatic 1/T2 values correlate with liver iron concentration. In general, a close correlation exists between biopsy liver iron levels and MR signal intensity.

Liver iron deposition introduces MR interpretation problems when imaging other diseases, because iron reduces parenchymal signal intensity, and some malignant foci appear more bright than usual and tend to simulate benign lesions. The reverse is also true with inflammatory conditions that increase parenchymal signal intensity.

Therapy

Hereditary hemochromatosis is often not considered in patients with end-stage liver disease because elevated iron levels are common in many other diseases. In fact, at times hemochromatosis is not even diagnosed prior to transplantation. An incidental hepatocellular carcinoma is not an uncommon finding at the time of transplantation.

These patients appear to have a higher posttransplantation mortality than patients transplanted for other causes. Also, they have increased infectious and cardiac complications.

Silicosis

Hepatosplenic silicosis also develops in patients with pulmonary silicosis. Liver biopsy in these patients reveals birefringent crystals in hyalinized nodules.

Calcified splenic nodules are detected with conventional radiography, CT, or US. Faint intrahepatic calcifications or "egg-shell" lymph node calcifications are best evaluated by CT.

Amyloidosis

Amyloidosis can be primary, secondary, or familial. In primary systemic amyloidosis, amyloid is deposited in the liver, spleen, and other structures; at times primarily liver deposits occur. A rare patient progresses to cholestasis, severe jaundice, and hepatic failure. Sinusoidal portal hypertension and spontaneous liver rupture are rare complications of primary amyloidosis.

Liver enlargement is a prominent feature in some patients. The liver is diffusely involved in both primary and secondary amyloidosis, but at times involvement is nonuniform. Hepatic and splenic calcifications are rare in primary amyloidosis. When amyloidosis is well established, noncontrast CT reveals decreased liver

parenchymal attenuation. Heterogeneous enhancement is evident postcontrast. Ultrasonography reveals a heterogeneous echo pattern.

Liver transplantation is the only effective treatment of familial amyloidosis; patients in a good nutritional state have a significantly better survival rate.

Sarcoidosis

Sarcoidosis, a granulomatous disorder of unknown etiology, is commonly diagnosed on clinical and imaging ground. The previously used Kveim test is considered too nonspecific. The angiotensin-converting enzyme (ACE) level correlates with disease activity. The lungs are primarily involved; in the abdomen, liver, spleen, and lymph nodes are most often involved, although hepatic sarcoidosis is usually asymptomatic and cholestasis infrequent.

Biopsy reveals noncaseating epithelial granulomas, often when liver function tests are still normal, but other causes of liver granulomas need be excluded, including a secondary sarcoid reaction to a neoplasm. At times histologic differentiation from sclerosing cholangitis is difficult.

Occasionally hepatic sarcoidosis progresses to cirrhosis and portal hypertension. Resultant esophageal variceal bleeding that some of these patients develop is amenable to sclerotherapy, although occasionally a shunt is necessary.

The most common CT findings of abdominal sarcoidosis are hepatosplenomegaly and diffuse adenopathy. In a minority of patients multiple hypodense nodules secondary to coalescing granulomas are found in the liver and spleen; these nodules are better identified on contrast CT. Periportal adenopathy is common and at times sufficiently extensive to result in obstructive jaundice.

Sarcoid nodules are hypointense both on T1- and T2-weighted images. They show mild, delayed contrast enhancement. The surrounding vasculature tends to be normal, thus differentiating these nodules from a malignancy. Nevertheless, the overall imaging appearance often suggests metastases, lymphoma, or even hepatic tuberculosis, especially in the uncommon patient with a normal chest radiograph.

Reticuloendothelial Failure

Hepatic reticuloendothelial failure is a poorly understood condition associated with decreased Kupffer cell function. It tends to be underdiagnosed. These patients are prone to develop infections.

Radiocolloid Tc-99m-phytate scintigraphy suggests the diagnosis; the liver is not visualized with this radiocolloid agent, but is imaged with conventional hepatobiliary agents such as Tc-99m-DTPA.

Liver in Pregnancy

Middle hepatic vein Doppler US waveform early in pregnancy has normal pulsatility, but with progression of pregnancy hepatic vein pulsatility becomes more and more flat.

Acute fatty liver occurs during pregnancy, occasionally even as early as 26 weeks, can progress to acute hepatic failure. Any transaminase elevation during pregnancy should be viewed with suspicion. A high fetal death rate is associated with acute fatty liver, but some pregnancies are managed successfully; following delivery liver function returns to normal, with only an occasionally preeclampsia persisting postpartum, liver enzymes remaining elevated, and hemolytic-uremic syndrome developing. Liver rupture is a rare complication of severe preeclampsia.

A rare complication of preeclampsia is the HELLP syndrome (hemolysis, elevated liver enzymes, and low platelets). It occurs during both pregnancy and the puerperium. Gross liver involvement ranges from subcapsular hematoma, to infarction, to small vessel occlusion, to spontaneous liver rupture.

Upper abdominal pain, nausea, and vomiting, by themselves nonspecific findings in pregnancy, are common in the HELLP syndrome. Initial clinical findings tend to suggest gallbladder disease, and US is often first performed. Although US will detect a hematoma, CT not only identifies hematomas but should also detect liver infarction or rupture, and identify any active bleeding site. Once HELLP is established, thrombocytopenia and fibrinolysis become evident and suggest the diagnosis. Liver MR spectroscopy of seven women with HELLP syndrome found relative hepatic concentrations

of phosphorus-containing metabolites and absolute concentrations of adenosine triphosphate to be similar to controls, but severe involvement results in a relative increase in phosphomonoester and an absolute decrease in hepatic adenosine triphosphate (54).

Several intrahepatic pregnancies have been described. At times CT and US identify a living fetus. Massive hemorrhage and hypovolemic shock are not uncommon presentations during the first trimester.

Tumors

A list of focal liver tumors is legion. Even such entities as focal fat and focal sparing, generally not considered as tumors, are in the imaging differential diagnosis. The simplest classification of primarily hepatocellular-origin tumors is to subdivide them into regenerative nodules (solitary necrotic nodule, focal nodular hyperplasia, nodular regenerative hyperplasia, and regenerative nodule of cirrhosis) versus dysplastic-neoplastic nodules (dysplastic nodule, adenoma, and hepatocellular carcinoma). Benign liver tumors can be divided into nonneoplastic and neoplastic (Table 7.8). With some neoplastic tumors the boundary between benign and malignant is blurred to the point that even a pathologist is hard-pressed to differentiate them. Some of the tumors developing in infants and children are unique to the pediatric patient, while others are similar to those seen in adults (Table 7.9). The most common liver malignancy in children under 3 years of age is a hepatoblastoma, while in older children a hepatocellular carcinoma is more common.

Discussion of hepatobiliary tumors is divided between this chapter and Chapter 8, but such a distinction is arbitrary. Those tumors manifesting primarily by bile duct involvement, both intrahepatic and extrahepatic, are discussed in Chapter 8. The outline adopted here is based on a broad pathologic classification modified by imaging findings. Most specialists would subdivide liver tumors based on their own viewpoint.

Detection of Focal Tumors

From an imaging viewpoint, a useful differentiation is between hypervascular and hypovascu-

Table 7.8. Benign liver tumors

	Nonneoplastic	Neoplastic
Hepatocellular origin	Fibrosing necrotic nodule Focal nodular hyperplasia Nodular regenerative hyperplasia Macroregenerative nodule and adenomatous hyperplasia Regenerating cirrhotic nodule	Hepatocellular adenoma
Cholangiocellular origin	Simple cyst Congenital hepatic fibrosis/polycystic liver disease Intrahepatic choledochal cyst	Adenoma Cystadenoma
Mesenchymal origin	Inflammatory tumor Hemangioma Peliosis hepatis "Pseudolipoma"	Hemangioendothelioma Lymphangioma Lipoma Angiomyolipoma Myelolipoma Leiomyoma Fibroma Neuroendocrine tumors
Other	Hamartoma Extramedullary hematopoiesis Intrahepatic spleen Endometrioma Teratoma	

Table 7.9. Focal Lesions in Infants and Children

- Nonneoplastic
  - Benign cysts
  - Focal nodular hyperplasia
  - Regenerating nodules
  - Focal fatty infiltration
  - Hemangioma
  - Hamartoma
  - Teratoma
- Neoplasms
  - Benign
    - Adenoma
    - Hemangioendothelioma
  - Malignant
    - Hepatoblastoma
    - Hepatocellular carcinoma
    - Metastases
    - Neuroblastoma
    - Lymphoma
    - Leukemia
    - Sarcoma
    - Rhabdomyosarcoma
    - Angiosarcoma
    - Fibrosarcoma
    - Leiomyosarcoma
  - Teratocarcinoma

lar tumors (Table 7.10) and between cystic and solid tumors. Most hepatic neoplasms are fed primarily by the hepatic artery rather than the portal vein. However, many neoplasms are better identified on portal venous phase images when normal liver parenchyma achieves maximum enhancement than during the arterial phase. A minority of tumors are hypervascular, and these are most conspicuous during the arterial phase, when greater tumor enhancement than liver parenchymal enhancement is achieved. In fact, some of these hypervascular tumors become isodense and merge into normal liver parenchyma during the portal phase. Incidentally, no universal definition exists for what constitutes a hypervascular tumor; one definition used is any tumor showing an enhancement >10 HU above that of liver parenchyma during arterial phase CT.

Arterial landmarks are better seen during the arterial phase. Likewise, parenchymal perfusion abnormalities are more often detected during the arterial phase.

Computed Tomography

The most common indication for biphasic (postcontrast arterial and portal phases) CT is to detect the usually hypervascular hepatocellular carcinomas and hypervascular metastases. Common hypervascular metastases include breast, renal cell, and thyroid carcinomas, various neuroendocrine tumors, melanoma, and most sarcomas. Diagnostic confusion stems from benign hypervascular lesions, such as focal nodular hyperplasia, adenoma, and hemangioma.

Although a majority of focal liver lesions enhance on arterial phase CT images, the pattern of enhancement often suggests a specific diagnosis (55); thus abnormal internal vessels are seen with a hepatocellular carcinoma, peripheral contrast puddles with hemangiomas, and ring-like enhancement with metastases.

Portal-phase CT images are often used when evaluating suspected hypovascular lesions, although biphasic acquisition does reveal more focal liver lesions and aids in anatomic visualization of liver vasculature.

Ultrasonography

About two thirds of liver nodules < or = 1 cm in diameter are homogeneous in appearance, and for these US cannot differentiate benign from malignant; with larger nodules, however, a heterogeneous US pattern suggests a malignancy.

Introduction of microbubble contrast agents increased both sensitivity and specificity of detecting focal liver tumors. These agents not only result in blood pool enhancement, but some also have a hepatosplenic specific late phase. Harmonic US during this late phase or stimulated acoustic emission improve detection of focal liver tumors and in some studies approach results achieved with CT (56). Thus in select patients with suspected metastases, conventional US detected 195 focal tumors, CT detected 231, and pulse inversion harmonic US using Levovist as a contrast agent detected 287 tumors, differences that are statistically significant (57); the latter technique detected the smallest lesions, which were undetected by CT and conventional US. In characterizing focal liver tumors, harmonic gray-scale US using the microbubble contrast agent perfluorocarbon is superior to conventional Doppler US (58).

Table 7.10. Differentiation between hypervascular and hypovascular liver tumors

Mostly hypervascular	Mostly hypovascular
Nonneoplastic conditions	Nonneoplastic conditions
Peliosis hepatis	Abscess[1]
Hemangioma	Granulomas
Arteriovenous malformation	Tuberculoma
Focal nodular hyperplasia	Focal fatty infiltration
Hereditary hemorrhage telangiectasia	Inflammatory (pseudo)tumor
	Nodular regenerative hyperplasia
Cystic structures	Solitary necrotic nodule
Arterial aneurysm	Mesenchymal and biliary hamartoma
Angiodysplasia	
	Cystic structures
Neoplasms	Abscess[1]
Angiomyolipoma	Simple cysts and related structures
Adenoma	Polycystic disease
Hepatocellular carcinoma	Caroli's disease
Hypervascular metastases	Hydatid cyst
Some sarcomas	Intrahepatic choledochal cyst
Neuroendocrine tumors	Biloma
Hemangioendothelioma	Hematoma
Hemangiopericytoma	Endometrioma
Adult hepatoblastoma	
	Neoplasms
	Necrotic neoplasm
	Intrahepatic cholangiocarcinoma
	Some sarcomas
	Hypovascular metastases
	Lymphoma
	Undifferentiated embryonal cell carcinoma[2]

[1] Often peripheral vascular enhancement is evident.
[2] Some have peripheral vascular enhancement.

Magnetic Resonance

When discussing MR findings, malignant tumors are best subdivided into hypervascular and hypovascular. Different imaging parameters are best suited for each category. Thus hypovascular malignancies are best detected on portal venous phase images than on other phases, and arterial phase is best for hypervascular malignancies. Only a rare focal liver tumor is detected on unenhanced images and is not visible on one of the postcontrast phases. Differential diagnosis of a detected tumor is a different topic and is discussed in the next section.

Ultrasonography reveals fat-containing tumors to be hyperechoic; T1-weighted chemical shift MRI separates these tumors from other hyperechoic tumors without fat.

Overall, postgadolinium MR detects more focal liver tumors and is markedly superior in characterizing them than postcontrast CT. A multicenter clinical study evaluating focal liver tumors concluded that significantly more and smaller tumors are detected on combined pre– and post–Gd-BOPTA images compared with precontrast images alone (59). In a cirrhotic liver, T2-weighted MRI does not provide additional diagnostic information than gadolinium enhanced MRI in detecting and characterizing tumors (60). The hepatobiliary-specific agent Gd-EOB-DTPA also detects more focal tumors than unenhanced or Gd-DTPA-enhanced images.

In tumors with low or absent reticuloendothelial tissue, the use of SPIO agents increases signal intensity between tumor and liver, and, overall, more focal liver tumors are detected than with postcontrast CT or precontrast MR. On the other hand, both normal liver and some well-differentiated tumors take up these iron oxide particles, and after contrast these tumors appear isointense and difficult to detect. Overall,

combining pre– and post–contrast-enhanced images is more accurate than the use of post-contrast MR alone.

Biopsy

In a prospective study of consecutive patients with discrete focal tumors <1 cm in diameter, found at US, biopsy achieved a sensitivity of 98% and specificity of 100% in detecting malignant tumors (61).

Differential Diagnosis of Focal Tumors

A common problem facing the radiologist is distinguishing a hemangioma or some other benign tumor from a malignancy. The problem is especially acute in a setting of a known malignancy in some other structure where the presence of liver metastases affects future patient management. The difficulty of differentiating a hemangioma from other liver tumors is evident from the extensive literature on this subject.

For incidental tumors <2 cm in size in patients with no known malignancy, about 75% are benign (62); hepatocellular carcinomas predominate among malignancies. With a history of a malignant tumor, about 50% of tumors <2 cm in size are benign.

If a hemangioma is suspected in a tumor larger than several centimeters, a useful approach is to perform Tc-99m–red blood cell SPECT scintigraphy; smaller lesions are best studied with MRI. Still, in spite of inherent limitations, CT is often employed because of ready availability. In some situations a biopsy is justified.

The following approach to evaluating focal liver tumors is adopted from the American College of Radiology Appropriateness Criteria (63):

1. Typical postcontrast CT or US benign-appearing tumor, with no history of malignancy: These are usually classified as benign. If needed, in- and out-of-phase MR should detect focal fat.
2. Typical postcontrast CT or US benign-appearing tumor, with a known history of malignancy: Similar recommendation as above, except these should be followed-up using the same imaging modality.
3. Typical postcontrast CT or US malignant tumor: Biopsy confirmation if clinically appropriate.
4. Indeterminate postcontrast CT or US tumor in an otherwise normal liver: Postcontrast MRI is often helpful with these tumors. For some tumors scintigraphy or dynamic CT is useful. If still indeterminate, biopsy should be considered.
5. Indeterminate postcontrast CT or US tumor in a cirrhotic liver: Although MRI is useful to follow these tumors, biopsy is generally needed for diagnosis.

Some very small tumors earn the sobriquet of *too small to characterize*; depending on the clinical situation, some radiologists suggest imaging follow-up.

Computed Tomography

Hemangiomas vary in their rate of contrast enhancement. Most malignant neoplasms have considerably faster enhancement, but overlap does occur with hemangiomas. The slower enhancement seen with some hemangiomas is rather characteristic but is mimicked by posttherapy metastases, although the clinical scenario should differentiate these two entities.

Arterial phase CT densities are significantly higher in focal nodular hyperplasias (mean, 118 ± 15 HU) than in hepatocellular adenomas (80 ± 10 H) (64); no significant attenuation differences were evident precontrast and during the portal venous phase.

Tumor appearance during biphasic and triphasic CT aids in differentiating between focal liver tumors. Small hemangiomas often tend to be isodense to aorta; the postcontrast CT appearance of enhancing nodules seen in larger hemangiomas is seldom found with hypervascular metastases. A homogeneous, hyperdense tumor seen during the arterial phase, combined with a hypodense tumor but continued hyperdense periphery during the parenchymal phase, suggests a carcinomas.

Inclusion of arterial and portal venous phase CT does not improve sensitivity but does improve specificity in differentiating hemangiomas from hypervascular malignancies (65).

Ultrasonography

The use of a US contrast agent aids in characterizing and differentiating some focal liver tumors. Tumor enhancement during arterial phase or reticular enhancement during parenchymal phase achieved a 92% sensitivity and 96% specificity for hepatocellular carcinoma. Ring enhancement during the arterial to portal phases or a parenchymal phase defect reached a 90% sensitivity and 95% specificity for cholangiocellular carcinoma or metastases, and puddled enhancement during the portal phase was 60% sensitive and 100% specific for a hemangioma (66). In general, postcontrast tumor flow signals (hypervascularity) favor a malignancy; lack of flow signals is more common in benign tumors but does not exclude a malignancy. A late phase hypoechoic signal favors a malignancy. Current evidence suggests that, overall, contrast enhanced US has a similar accuracy to CT in characterizing focal liver tumors.

Magnetic Resonance Imaging

T2 relaxation time is prolonged in a hemangioma because of blood stagnation. Tumor T2 relaxation times are rather specific in distinguishing a malignancy from a cavernous hemangioma or cyst. For instance, one study found T2 relaxation times for malignancies to be 92 (± 22), hemangiomas 136 (± 26) and cysts 284 (± 38) (67). In fact, if T2 relaxation times are calculated, gadolinium enhancement may not be necessary to distinguish hemangiomas from metastases (68). It should be kept in mind, however, that a rare hepatocellular carcinoma does have a prolonged T2 time. A sharp tumor margin and a tumor signal greater than or equal to that of the cerebrospinal fluid (CSF) predicts a hemangioma.

Early peripheral nodular contrast enhancement is a feature of most cavernous hemangiomas. Peak contrast enhancement occurs more than 120 seconds after contrast injection in a majority of hemangiomas, a finding uncommon with hepatocellular carcinomas, which have a much earlier peak contrast. Cysts have no contrast enhancement; most metastases show variable and moderate enhancement; peak enhancement for hypervascular metastases is generally during initial hepatic artery phase, with enhancement for hypovascular metastases peaking later.

Hypervascular tumors, similar to cavernous hemangiomas, are hyperintense on unenhanced T2-weighted MR images. A hypervascular tumor is best seen during the arterial phase. In the differential diagnosis of early enhancing tumors, however, are also some benign ones, such as focal nodular hyperplasia and adenomas. Delayed postcontrast T1-weighted SE sequences help differentiate hypervascular metastases, which range from hypo- to isointense, from hemangiomas, which remained hyperintense.

The SPIO contrast agents aid in differentiating liver nodules; normal liver parenchyma shows greatest signal loss, less so by adenomas and hemangiomas and, as expected, malignant tumors have only minimal signal loss. SPIO also improves capsule and scar detection. A tumor classification of high, iso- and low intensity on SPIO-enhanced T2-weighted and heavily T1-weighted gradient-echo images achieved a 96% diagnostic accuracy in differentiating hemangiomas, metastatic and cysts (69).

Ultrasmall superparamagnetic iron oxide particles, consisting of blood pool contrast agents, aid in differentiating highly vascular lesions, such as hemangiomas, from more solid neoplasms. The degree of enhancement on T1-weighted images and the signal intensity drop on T2-weighted images when using these contrast agents is significantly lower with malignant tumors than with hemangiomas.

Use of MnDPDP improves accuracy of differentiating a hepatocellular carcinoma from focal nodular hyperplasia and differentiating hepatocellular carcinoma from a metastasis (70), but study of this contrast agent is still in its infancy.

Nonneoplastic Tumors

The classification of nonneoplastic liver nodules is generally based on their histopathologic characteristics rather than on their etiology or imaging findings. Biliary and mesenchymal hamartomas are discussed in Chapter 8.

Some of these tumors occur singly, others tend to be multiple. Some develop preferentially in a diseased liver. Their pathogenesis is diverse and includes a vascular or hormonal imbalance,

metabolic abnormality, prior infection, and hamartomatous transformation.

Adult Cavernous Hemangioma

Clinical

Aside from congenital disorders, capillary hemangiomas (telangiectasias) are uncommon in the liver (hereditary hemorrhagic telangiectasia was discussed above; see Congenital Abnormalities).

A nonneoplastic cavernous hemangioma occurs at all ages. It is the most common liver tumor in adults. While some hemangiomas produce considerable mischief on their own, their primary importance, especially with smaller ones, lies in their imaging mimicry of metastases and hepatocellular carcinomas. They are considerably more common in women. For unknown reasons hemangiomas tend to predominate in the posterior segment of the right lobe. An occasional patient develops multiple hemangiomas, most often identified as discrete tumors. Diffuse hemangiomatosis is rare and is more often encountered in infants, where the tumor's extensive vascular shunting induces cardiac failure. Histologically, these are blood-filled, well-marginated cavities varying considerably in size and are lined by a single layer of endothelial cells. Associated fibrosis is common, and the cavities are surrounded by fibrous septa. Whether extensive fibrosis is a natural evolutionary process and represents an end-stage development is conjecture.

Most hemangiomas are asymptomatic and discovered incidentally. A minority manifest with pain. An occasional one bleeds internally or ruptures spontaneously, and the patient presents with a hemoperitoneum. Some undergo traumatic rupture, especially larger ones. Risk of malignant degeneration appears negligible.

What is the growth pattern of a liver hemangioma? Unresected hemangiomas do not always grow and do not necessarily require surgery. An US follow-up reveals that only a minority change in size: some increase, an occasional one decreases and even regresses spontaneously. A reasonable approach appears to be that if a suspected hemangioma increases in size in a setting of chronic liver disease, aspiration biopsy should be performed to exclude a malignancy.

In a setting of cirrhosis, hemangiomas tend to fibrose, and imaging diagnosis becomes more difficult. A tendency toward decreasing size is evident with progressive cirrhosis.

Giant liver cavernous hemangiomas can have unusual findings, such as portal vein obstruction due to pressure by the hemangioma, intrahepatic bile duct obstruction, or simply an elevated erythrocyte sedimentation rate (Fig. 7.18). Giant hemangiomas tend to contain a central scar.

An association between hemangiomas and Kasabach-Merritt syndrome has been described. An interesting suggestion is that this syndrome does not occur with hemangiomas and, if present, a Kaposiform hemangioendothelioma or similar tumor rather than a hemangioma should be considered.

Some hemangiomas are associated with focal nodular hyperplasia. The primary clinical significance of this association is that biopsy from such a region adjacent to a hemangioma will suggest a wrong diagnosis. A rare association of hemangiomatosis and arterioportal venous shunting appears to exist.

A rare subcapsular hemangioma is exophytic and becomes pedunculated; even a volvulus of such a pedunculated hemangioma has developed.

Figure 7.18. Angiographic appearance of large cavernous hemangioma (arrows). (Courtesy of Oscar Gutierrez, M.D., University of Chile, Santiago, Chile.)

Imaging

In a 1995 study of patients with proven cavernous hemangiomas, diagnostic sensitivity of CT angiography was 77%, US 61%, MRI 92%, and angiography 85% (71). Other studies confirm that MR detects more liver hemangiomas than other imaging modalities. Tumor detection and especially lesion characterization with T2-weighted sequences are the primary MRI advantages compared to other imaging modalities.

Iodized oil is used to characterize and follow certain focal liver lesions, especially hepatocellular carcinomas. After intraarterial injection of iodized oil, some is retained in hepatic hemangiomas, albeit inadvertently, and can be followed with subsequent CT. Serial CT shows predominantly peripheral iodized oil retention within a hemangioma; central retention is seen after injection of large amounts of oil, but retention here tends to be spotty or nodular. The oil washes out slowly but persists for at least 3 months and in some hemangiomas up to several years.

Most hemangiomas throughout the body tend to contain phleboliths, a finding not seen in liver hemangiomas. Calcifications do develop in an occasional liver hemangioma, especially in a setting of a thrombus, and tend to be most common at the tumor margin.

Postcontrast, typical liver hemangiomas reveal an irregular, nodular peripheral enhancement pattern of varying intensity and thickness during the arterial phase, contrast-enhancement from the periphery toward the center, a prolonged tumor blush, vascular lakes, and delayed contrast washout. They have well-defined borders, and smaller ones are round while larger ones tend toward an oval or lobular shape. Early more peripheral parenchymal enhancement correlates with arterioportal shunting; one study found shunting in 21% of small hemangiomas (72). Shunting is not pathognomonic of hemangiomas but is also found in a number of other entities, including hepatocellular carcinomas.

An atypical hemangioma appearance is sufficiently common that the diagnosis is not always straightforward, and considerable diagnostic uncertainty ensues. Imaging findings of some hemangiomas mimic a metastatic carcinoma, focal nodular hyperplasia, hepatic angiosarcoma, metastatic neuroendocrine tumor, or even focal intrahepatic extramedullary hematopoiesis. In particular, small hemangiomas and hypervascular metastases often have a similar imaging appearance.

Some hemangioma contains extensive fibrosis or hyalinization to the point that their vascularity is decreased considerably (compared to a more typical hemangioma). These extensively fibrotic hemangiomas tend to have an atypical imaging appearance and mimic a malignancy; typical of fibrosis, they have lower signal intensity than cerebro-spinal fluid on T2-weighted images and lack early enhancement on post-contrast MRI (Fig. 7.19). Some even have contrast enhancement from the center toward the periphery (73).

Precontrast CT and MR of some hemangiomas detect a fluid–fluid level, presumably representing blood sedimentation. Fluid–fluid levels are not specific and are seen with other lesions.

Although an imaging appearance of progressive postcontrast opacification toward the center is a characteristic hallmark of hemangiomas, this finding is not pathognomonic; an occasional hepatocellular carcinoma, cholangiocarcinoma, and metastasis have a similar finding. Likewise, early peripheral nodular enhancement is found with some focal nodular hyperplasias and vascular neoplasms.

Computed Tomography

With unenhanced CT most typical hemangiomas are hypodense to normal liver parenchyma and isodense to blood. A fibrotic component or thrombosis lowers CT density.

A typical postcontrast appearance for a hemangioma has already been described and in these CT is often very suggestive of the diagnosis. Yet CT evidence of peripheral contrast enhancement followed by progressive fill-in is found only in about two thirds; in others enhancement is either diffuse or evident only at the tumor periphery, with most of the tumor consisting of cystic cavities or scar tissue. Central scarring modifies enhancement and results in incomplete central opacification. An extensive region of hemangiomatosis reveals a honeycomb pattern. Some larger hemangiomas mimic a hypovascular metastasis, but more

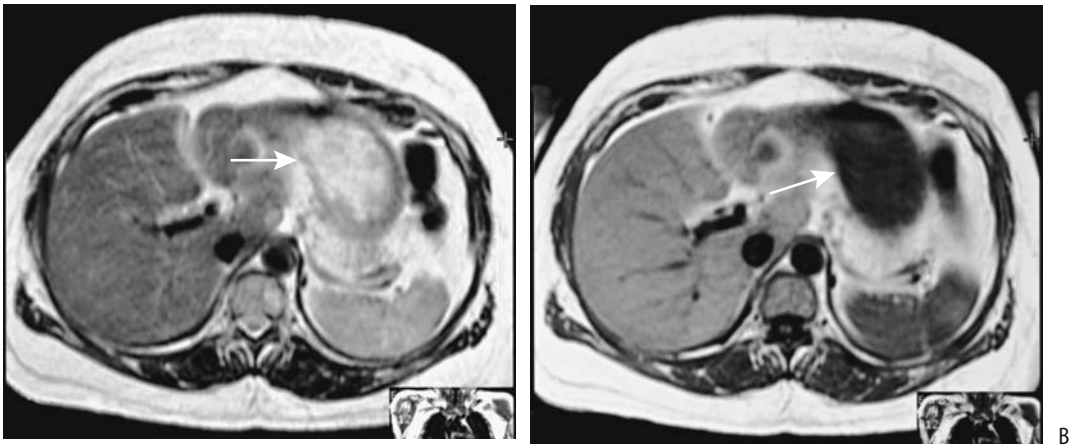

Figure 7.19. Hyalinized hemangioma. A T2-weighted fast spin echo (FSE) MRI (A) reveals a hyperintense (arrow), and a T1-weighted FSE MRI (B) reveals a hypointense (arrow) tumor. US (not shown) suggested a complex cyst. US-guided biopsy provided a diagnosis. (Courtesy of Patrick Fultz, M.D., University of Rochester.)

vascular ones suggest a hepatocellular carcinoma or a hypervascular metastasis.

Small hemangiomas, in particular, have gradual diffuse contrast enhancement. A minority of hemangiomas smaller than approximately 1 cm in diameter, however, tend to opacify with contrast rather rapidly, appear homogeneous, and mimic hypervascular malignancies; they do remain hyperdense on delayed-phase images, a finding atypical for a malignancy. Some contain small enhancing dots which persist both during arterial and portal venous phases.

Some hemangiomas are associated with arterioportal shunts. These shunts are suggested when hepatic arterial-phase CT reveals wedge-shaped or irregular homogeneous parenchymal enhancement adjacent to a hemangioma; during the portal phase this region is iso- or slightly hyperdense. These shunt are more common in rapidly enhancing hemangiomas.

Hemangiomas do develop in a fatty liver and they do enhance postcontrast, similar to those in a normal liver; the exception being that hemangiomas are hyperdense on precontrast scans compared to the hypodense fatty liver, and during the arterial phase they tend to be more isodense than usual.

Ultrasonography

The most common US appearance of a hemangioma is that of a homogeneous, well-marginated, and hyperechoic tumor. With growth, hemangiomas become heterogeneous. Less often encountered is a hyperechoic rim of varying thickness; these tend to have an isoechoic or even hypoechoic center. Some exhibit a bright hyperreflective pattern. An occasional one has increased through-transmission.

Operative or laparoscopic US detects hemangiomas as homogeneously hyperechoic tumors. Some are compressible by a probe, thus allowing differentiation from incompressible metastases.

Blood flow velocity in most hemangiomas is sufficiently slow that Doppler US is noncontributory, although occasionally a large peripheral feeding vessel is detected. Contrast-enhanced US reveals no or weak intratumoral signals with hemangiomas; a pulsatile signal or vessels within a tumor identified by Doppler US should suggest another diagnosis.

Contrast-enhanced US using pulse inversion harmonic imaging identifies a hypovascular tumor in the early arterial phase and peripheral globular enhancement in about half, especially evident in larger ones. Many hemangiomas <1 cm show either a peripheral nodular or homogeneous enhancement. Centripetal fill-in is evident in some during the late phase. Delayed washout is common (Fig. 7.20).

Most sonographically suspected hemangiomas undergo further imaging workup, although some patients at low risk for malignancy and with a typical-appearing hemangioma at US are followed with US.

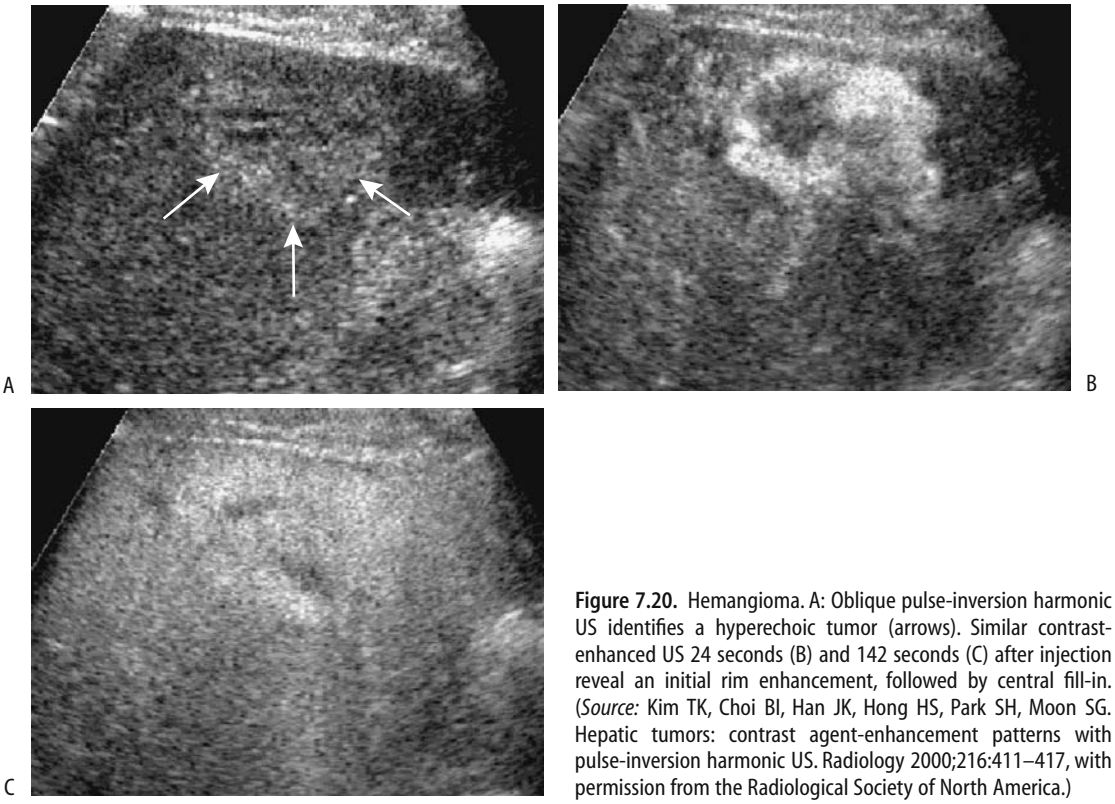

Figure 7.20. Hemangioma. A: Oblique pulse-inversion harmonic US identifies a hyperechoic tumor (arrows). Similar contrast-enhanced US 24 seconds (B) and 142 seconds (C) after injection reveal an initial rim enhancement, followed by central fill-in. (*Source:* Kim TK, Choi BI, Han JK, Hong HS, Park SH, Moon SG. Hepatic tumors: contrast agent-enhancement patterns with pulse-inversion harmonic US. Radiology 2000;216:411–417, with permission from the Radiological Society of North America.)

Magnetic Resonance

Similar to cysts and metastases, most hemangiomas appear hypointense on precontrast T1-weighted images; these sequences are thus of limited use in differentiating hemangiomas from most other tumors. Using T2-weighted fast SE sequences without fat suppression, hemangiomas are hyperintense relative to spleen (Fig. 7.21); most are homogeneous, have well-defined margins, and tend to be isointense to CSF; similar findings are found with fat suppression. Many small hemangiomas have uniform gadolinium enhancement, a pattern uncommon in larger ones which usually show peripheral nodular enhancement progressing to uniform centripetal enhancement. Large tumors tend to maintain a persistent central hypointensity. A subset of hepatic hemangiomas enhances early and diffusely and, in fact, enhances to a greater degree than most malignancies. Similar to most hemangiomas, on heavily T2-weighted images these hemangioma signal intensities and contrast-to-noise ratios are significantly greater than those of malignancies.

About 20% of hemangiomas are associated with peritumoral enhancement (74); of unknown significance, such enhancement is more common in hemangiomas with rapid

Figure 7.21. Hemangioma. T2-weighted image identifies a hyperintense tumor (arrow).

enhancement than in those with slow enhancement. Most hemangiomas increase in lesion-to-liver contrast on ferumoxides-enhanced T2-weighted MR images.

Scintigraphy

Both planar and SPECT Tc-99m–red blood cell imaging have high sensitivity and specificity in differentiating cavernous hemangiomas from other liver tumors and are often used as gold standards in comparison studies. Scintigraphy is especially useful with an atypical imaging appearance of a suspected hemangioma; SPECT detects smaller hemangiomas than planar images. Reported false positives include hepatocellular carcinoma, sarcoma, metastatic small cell lung carcinoma, and intrahepatic extramedullary hematopoiesis (11). Occasional false negatives are reported, often due to a lesion's small size.

Early perfusion phase Tc-99m–red blood cell scintigraphy shows a focal photopenic defect that gradually fills in in a centripetal manner during the blood-pool phase. A perfusion/blood-pool mismatch is the hallmark for hemangiomas. Technetium-99m–sulfur colloid and hepatobiliary scintigraphy simply reveal a filling defect. The increased activity seen on blood-pool images is absent if a thrombus has developed within a hemangioma.

If early liver images are obtained during prostate immunoscintigraphy with indium-111–labeled antibodies, a hemangioma has an appearance similar to that seen with Tc-99m–red blood cell imaging.

A marked increase in perfusion detected by scintigraphy should suggest arterioportal shunting.

Biopsy

Some radiologists hesitate to biopsy suspected hemangiomas for fear of complications, yet many have been biopsied without undue complication. This does not suggest that suspected hemangiomas should be biopsied; noninvasive protocols generally suffice for diagnosis. Rather, in an atypical and otherwise nondiagnostic suspected or even unsuspected hemangioma a biopsy can be a safe and diagnostic procedure. A bigger problem is in placing in proper perspective a biopsy that simply reveals blood cells.

Therapy

Many liver cavernous hemangiomas are managed simply by observation. Indications for surgery include an uncertain diagnosis, imaging showing enlargement, or a symptomatic tumor. An occasional one manifests acutely by bleeding or rupture, thus necessitating emergency surgery. They have been resected using a laparoscopic approach.

Palliation of symptomatic hemangiomas by transcatheter arterial embolization is an option. A rare symptomatic cavernous hemangioma is treated by radiofrequency ablation (75).

Orthotopic liver transplantation is an extreme option in patients with unresectable giant hemangiomas.

Infantile Hemangioma

Previously some hemangioendotheliomas, especially in infants, were lumped together with hemangiomas (hemangioendotheliomas are discussed later). In a setting of a vascular tumor in an infant, especially with clinical evidence of Kasabach-Merritt syndrome, a hemangioendothelioma rather than a hemangioma should be considered.

An infantile hemangioma is more common in girls and tends to be multiple. With age, these tumors tend to involute with few sequelae.

Large hemangiomas in infants are identified on T2-weighted MRI as hyperintense nodules containing fast flow and are seen as flow voids on SE images and hyperintense tumors on GRE images. One in an infant revealed an early rim enhancement after gadolinium, with progressive fill-in on delayed imaging (76). These tumors are fed by enlarged hepatic vessels; the proximal abdominal aorta is prominent, while distal to the feeding vessel takeoff it had a decreased caliber. These nodules regress after interferon-α-2a therapy and are replaced by normal-appearing liver parenchyma with no evident fat or fibrosis.

If necessary, embolization of the feeding vessels is performed to control congestive failure or treat other complications. A lobectomy is appropriate if a solitary hemangioma is confined to an anatomic lobe.

Some infants believed to have life- or function-threatening hemangiomas are treated with

radiation therapy (77); some of these infants have Kasabach-Merritt syndrome, and in these infants the hemangiomas regress and platelet counts increase after radiation therapy.

Peliosis Hepatis

Clinical

Peliosis hepatis is a rare benign disorder of unknown etiology characterized by numerous blood-filled cavities in the liver. An association exists between peliosis hepatis and some drugs, including hormones. It has regressed in extent after cessation of oral contraceptive use. It can be congenital. Other associated conditions include malignant histiocytosis, myeloid metaplasia, and hemangiosarcoma. It has developed after liver transplantation. In AIDS patients, peliosis hepatis is associated with bacillary angiomatosis. It can be subclinical and be detected incidentally, when it is a source of diagnostic confusion.

These cavities range from single to diffuse, vary in size, and are lined by endothelial cells. Hepatic insufficiency develops if enough parenchyma is replaced by these vascular spaces. Rarely, peliosis hepatis ruptures spontaneously, and an intraperitoneal hemorrhage ensues.

Imaging

Rare liver calcifications are identified in patients with peliosis hepatis.

Postcontrast CT reveals well-marginated contrast collections in the liver. Some show delayed enhancement. Occasionally some of these cystic spaces do not opacify with contrast, presumably due to thrombosis. Some tumors have gradual centripetal CT contrast enhancement, thus mimicking a hemangioma (78). These tumors are hypoechoic or even anechoic with US. They are hyperintense with all MRI sequences and enhance postcontrast.

Angiography reveals numerous vascular spaces. Typically, contrast accumulates in the late arterial phase, which becomes more distinct during the venous phase. No communication exists with the portal venous system. Early feeding arteries and draining veins are not present in peliosis hepatis.

Hepatic scintigraphy with Tc-99m–sulfur colloid or gallium is normal.

A hypervascular metastasis, hemangioma and even an abscess are occasionally included in the differential diagnosis.

Solitary (Fibrosing) Necrotic Nodule

Solitary nodules, initially described on the anterior aspect of the liver, consist of a necrotic center surrounded by a hyalinized fibrotic capsule containing elastic fibers. They are considered nonneoplastic, yet a number have been reported in patients with underlying neoplastic disease. Many are subcapsular and solitary; currently they are believed to be the final common pathway of a number of benign disorders.

They develop after microwave tissue coagulation and after various liver infections.

Focal Nodular Hyperplasia

Clinical

Focal nodular hyperplasia (FNH) is a development abnormality of unknown etiology and pathogenesis. Current thought is that it is a regenerative process; nodules appear related to a focal increase in arterial blood flow and resultant hyperplastic tissue response, and in that sense differ from adenomas, which are neoplastic. They are the second most common benign liver tumor in adults, after hemangioma. In distinction to a hepatic adenoma, FNH is not premalignant and is generally an incidental finding, but, similarly to adenomas, some of these tumors are associated with contraceptive use, and some regress after drug discontinuation. A high prevalence is found in women of childbearing age, with an occasional one encountered in infants and children.

Single nodules predominate. These are discrete tumors often having a characteristic central stellate scar containing blood vessels. Feeding vessels are of hepatic artery origin. Although vessels are prominent and the lesion contains typical hepatic structures, including hepatocytes, Kupffer cells, and proliferating bile ducts, the usual arrangement of portal tract vessels and bile ducts is not present. Histologically, anomalous arteries in fibrous septa connect to capillaries, which drain into sinusoids adjacent to fibrous septa, which in turn drain into veins located in the parenchyma.

These findings suggest a focal arteriovenous malformation with growth of surrounding parenchyma as etiology for their formation. About 80% of FNHs have a typical histologic appearance; a minority reveal prominent vessels or, interestingly, show cellular atypia to the point of suggesting an adenoma.

A core biopsy reveals deranged architecture, a finding not appreciated with cytology.

Clinically, these lesions are usually an incidental finding and rarely present with bleeding, thus distinguishing them from adenomas. Their primary significance in most patients is that they mimic a more ominous tumor. With time they can increase, decrease, or remain constant in size.

Imaging

An occasional report describes fat within or adjacent to FNH, but fat is an uncharacteristic finding. Likewise, calcifications are uncommon. These calcifications are similar in appearance to those seen in some fibrolamellar hepatocellular carcinomas.

Although the specific pattern is different, FNH has a similar appearance with various imaging modalities. Most are solitary, subcapsular in location, are often lobulated and tend to be sharply marginated. Their usual homogeneous appearance reflects a lack of hemorrhage and necrosis, except in some larger ones. Majority are <5 cm in diameter, with only a rare one being >10 cm. An occasional one is exophytic. A central hypodense region, representing a central scar with radiating fibrosis, is found in larger tumors, although a scar is generally not visible in smaller ones. Presence of a central scar is not specific for FNH and a scar is occasionally found in other tumors, such as hepatocellular carcinomas, adenomas, intrahepatic cholangiocarcinomas, and some larger hemangiomas.

With unenhanced CT these nodules tend to be homogeneous and hypo- to isodense. Precontrast FNHs tend to blend into surrounding parenchyma. Especially when small, they are identified mostly on immediate postcontrast images.

These lesions are supplied primarily by hepatic artery branches and thus arterial-phase CT reveals a transient but marked initial enhancement, which progresses to isodensity during the parenchymal (portal) phase. Multiphasic CT in patients with FNH found all tumors to be hypervascular and hyperattenuating to the liver during arterial phase, and 92% were isodense on delayed scans (79); most enhanced homogeneously, and were smooth in outline and subcapsular in location. Single-level dynamic CT during hepatic arteriography of small FNH reveals centrifugal blood flow through a fibrous scar, drainage into adjacent dilated veins and then into a hepatic sinusoid in adjacent liver tissue (80).

Ultrasonography reveals FNHs tending toward a homogeneous and isoechoic appearance and often blending into normal adjacent parenchyma, although considerable variability exists. They tend to be well marginated. A central scar is either hypoechoic or not visualized. In some, color Doppler identifies vessels radiating in a central stellate pattern; the feeding artery shows a high diastolic flow rate and has a low pulsatility index. It has a high frequency and low resistance. Contrast-enhanced US reveals intralesional flow, peripheral vascularity, and at times also a centripetal afferent vessel.

Magnetic resonance imaging appears more sensitive and specific than CT in detecting and characterizing FNH. On T1-weighted unenhanced MRI sequences, FNHs appear iso- to hypointense compared to normal liver and iso- to hyperintense on T2-weighted images (Fig. 7.22). Marked hyperintensity on T2-weighted

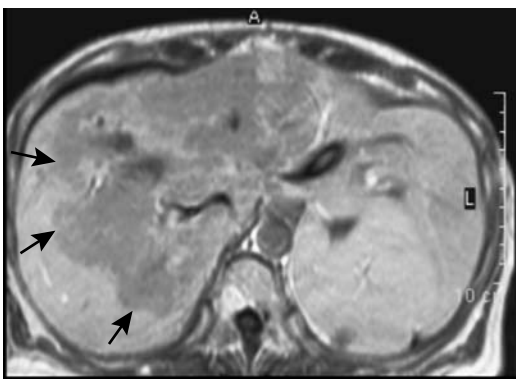

Figure 7.22. Extensive focal nodular hyperplasia. T1-weighted MRI identifies a hypointense tumor (arrows). (Courtesy of Algidas Basevicius, M.D., Kaunas Medical University, Kaunas, Lithuania.)

images is distinctly unusual and should suggest another diagnosis. A central scar, identified in over half of these tumors, tends to be hypointense on T1- and hyperintense on T2-weighted images, presumably due to prominent central vascularity. Although not encapsulated, compression of surrounding liver parenchyma often results in a hyperintense rim being evident on T2-weighted images, in distinction to the fibrotic hepatocellular carcinoma capsule which tends to be hypointense on both T1- and T2-weighted images. Here also considerable variability exists and heterogeneity and a hyperintense signal is identified in some FNH on T1-weighted images.

Postgadolinium MRI reflects their rich vascularity radiating in a stellate pattern. Similar to adenomas, an intense, uniform contrast enhancement is common during the arterial phase, becoming isodense during portal venous phase. A central scar is initially hypointense but gradually enhances on delayed images.

Because Kupffer cells are present in most FNH nodules, these tumors take up iron oxide contrast. Six FNH nodules showed a mean of 43% signal intensity loss on ferumoxides-enhanced T2-weighted images (81). A SPIO-enhanced MR detects more tumors than a precontrast MR, but little difference in signal loss exists between FNH and adenomas.

Similar to adenomas, the presence of hepatocytes within the FNH results in Mn-DPDP (mangafodipir) uptake.

Due to their Kupffer cell content, these tumors take up Tc-99m–sulfur colloid. Clearance of tracer from the tumor is delayed. A positive colloid scan is thus useful in differentiating these lesions from most hepatocellular carcinomas. A finding of decreased colloid uptake, on the other hand, is nonspecific. It should be kept in mind that some regenerating nodules, focal steatosis, and adenomas also take up sulfur colloid.

Iminodiacetic acid (IDA) hepatobiliary tracers accumulate within FNH, and most larger nodules appear as hot spots. Thus Tc-99m-IDA hepatobiliary scintigraphy shows increased tracer uptake on delayed scans in most larger tumors.

Using the hepatocyte receptor Tc-99m-neoglycoalbumin (NGA), scintigraphy showed normal to increased uptake in FNH, thus differentiating these tumors from most malignancies, which have very low to no uptake.

A characteristic arteriographic finding is a single artery feeding a hypervascular tumor that contains intense venous staining (Fig. 7.23). Although arteriography readily detects FNH, it lacks specificity in differentiating it from other focal hypervascular tumors, and angiography is rarely employed in the workup of these tumors.

The use of imaging techniques is illustrated by a report of a 17-year-old girl with a 2-cm-diameter left lobe tumor detected incidentally by US (82); CT and MRI confirmed the tumor,

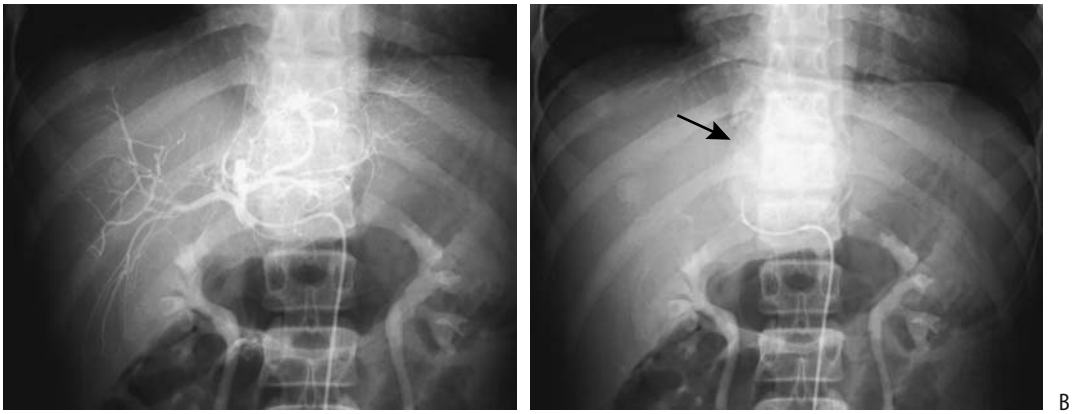

A B

Figure 7.23. Focal nodular hyperplasia in a child. Early (A) and late (B) arteriographic views illustrate delayed washout from the tumor (arrow).

and postcontrast CT and CO_2-enhanced US demonstrated early central enhancement with gradual enhancement spreading to the periphery. Color Doppler flow imaging detected a central color spot, shown by pulsed Doppler spectrum analysis to represent an artery. The lesion was not detected by hepatic arteriography. Biopsy confirmed the FNH.

In summary, no pathognomonic imaging finding exists for FNH. A fibrolamellar hepatocellular carcinoma has a very similar CT and US appearance. Likewise, overlap exists with some large hemangiomas, adenomas, and metastases. In a cancer patient findings suggesting a FNH should be confirmed by biopsy.

Nodular Regenerative Hyperplasia

Nodular regenerative hyperplasia (at times simply called *regenerative nodules*) is a specific nonneoplastic entity consisting of multiple nodules surrounded by liver atrophy. It differs from regenerating nodules seen in cirrhosis (discussed in a later section). This uncommon condition occurs in noncirrhotic livers. About half the patients have portal hypertension. The etiology is unknown, and pathogenesis appears to be multifactorial, with focal ischemia postulated by some. It is associated with collagen vascular diseases, rheumatoid arthritis, Felty's syndrome, some myeloproliferative disorders, and some drug therapy. A rare association exists with CREST syndrome (calcinosis cutis, Raynaud's phenomenon, esophageal dysfunction, sclerodactyly, and telangiectasia) and primary biliary cirrhosis.

Histologically, numerous hyperplastic nodules varying in size are diffusely scattered throughout the liver. No significant fibrosis is evident, thus distinguishing this condition from cirrhosis and focal nodular hyperplasia; the exception is if long-standing portal hypertension has developed, when fibrosis with portal venous obliteration develop; whether portal venous obliteration precedes portal hypertension or vice versa is unknown. Histologically, this condition mimics an adenoma, but the latter is usually single, while nodular regenerative hyperplasia is diffuse throughout the liver.

Computed tomography reveals multiple hypodense nodules that do not enhance postcontrast. Associated hemorrhage modifies the imaging appearance. Nodule rupture is a rare complication, with the resultant appearance mimicking an adenoma.

Ultrasonography is generally noncontributory.

The T1-weighted MR appearance is variable; most nodules are hypo- to isointense on T2-weighted images.

These regenerating nodules contain Kupffer cells and take up Tc-99m–sulfur colloid.

Inflammatory Tumor

Inflammatory tumors (*pseudotumors*) are rare in the liver. Some are discovered incidentally. Their etiology is unknown; although some probably represent an atypical inflammatory reaction to infection, others appear to be a variant of Castleman's disease (These tumors are discussed in more detail in Chapter 14). Some progress in size and are multifocal. Resection establishes the diagnosis, although at times even then a diagnosis is not definitive. At times immunohistochemistry is useful to exclude a malignancy.

Computed tomography and US usually reveal a poorly defined heterogeneous hypovascular tumor mimicking a neoplasm. Magnetic resonance contrast enhancement is variable, at times with rapid wash-out of contrast. Gadolinium enhanced gradient-echo MR of one tumor revealed an early, intense peripheral enhancement followed by homogeneous enhancement (83); no uptake was evident with ferumoxides nor mangafodipir. Some of these tumors are surrounded by a hyperintense capsule. In general, imaging suggests a malignancy.

Regenerating Nodules in Cirrhosis

Cirrhotic livers develop small nodules, called *regenerating* or *regenerative* nodules and *siderotic nodules*, histologically consisting of either foci of regeneration or dysplasia (or both), together with supporting stroma. They contain hepatocytes, bile ducts, Kupffer cells, and fibrosis, and often contain increased iron. The reason for their formation is unknown, but they appear to represent a response to growth factors. These regenerating nodules tend to be small and scattered throughout the liver.

In a broader context, regeneration is a common feature after hepatocyte damage,

regardless of etiology. Regenerative activity among liver cells and their nuclei is mild in a setting of primary biliary cirrhosis, more so in alcoholic cirrhosis, and most prominent in posthepatitic cirrhosis (HBV related); thus patients with posthepatitic cirrhosis are at greater risk for carcinoma than those with other types of cirrhosis.

Histologic differentiation of a dysplastic nodule from a regenerating nodule in a cirrhotic liver tends to be difficult from small biopsy specimens.

Neither CT nor US detects smaller nodules. Precontrast, detectable nodules are iso- to hyperdense, depending on their iron content and, in fact, are better identified precontrast than postcontrast. In distinction to most liver tumors, the blood supply to regenerating nodules is mostly portal venous, and they are thus isodense during portal phase imaging. Because of their mostly portal blood supply, these nodules do not enhance much on postcontrast arterial phase CT. In distinction to hepatocellular carcinomas, which derive most of their blood from an arterial supply, a regenerating or dysplastic nodule should be suspected if dynamic CT suggests a mostly portal venous blood supply to a nodule. One should keep in mind, however, that a dual blood supply is normal, and in actual practice this blood supply differentiation is difficult to apply to small tumors.

Computed tomography arterial portography performed prior to partial liver resection for hepatocellular carcinoma in cirrhotic patients revealed regenerative nodules as enhancing 3- to 10-mm tumors surrounded by lower density fibrous septa (84) (Fig. 7.24); CT hepatic arteriography identified regenerative nodules as nonenhancing tumors, similar in size to those seen with arterial portography, surrounded by enhancing fibrous septa. Tumor conspicuity is determined to a large degree by surrounding fibrosis. Nevertheless, CT hepatic arteriography detects more nodules and is more sensitive than CT arterial portography.

With US, regenerating nodules range from hypoechoic to hyperechoic compared to normal liver parenchyma.

Magnetic resonance imaging is more sensitive in detecting regenerating nodules than CT or US. Most regenerating nodules are iso- to hypointense on T1- and hypointense on T2-weighted images. Surrounding inflammation and fibrous septa tend to be hypointense on T1- and iso- or hyperintense on T2-weighted images. Their hypointensity on T2-weighted sequences is secondary to a paramagnetic effect from their increased iron and, in part, to surrounding fibrous septa. More complex nodules are inhomogeneous and contain discrete foci of iron (siderotic nodules), and T2-weighted MR in these reveals a hypointense focus due to the iron within a larger hyperintense iron-poor nodule.

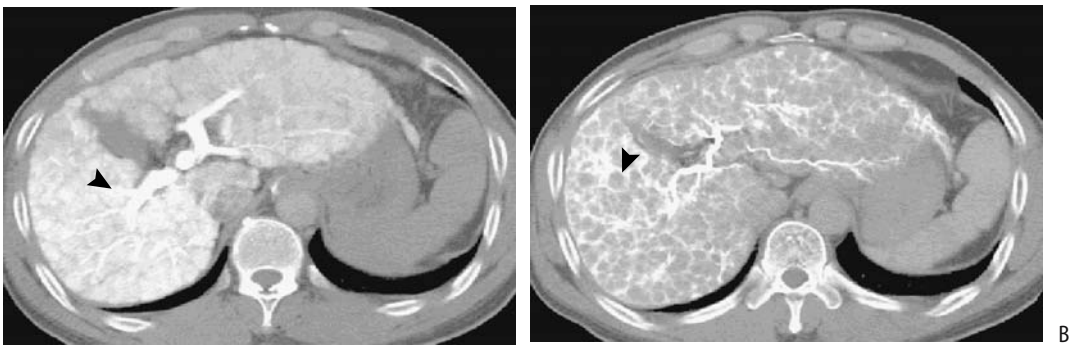

A B

Figure 7.24. Regenerating nodules in a man with cirrhosis. A: CT arterial portography shows enhancing nodules (arrowhead) in an otherwise heterogeneous liver. B: CT hepatic arteriography reveals these nodules to be poorly enhancing (arrowhead). (*Source:* Kim HC, Kim TK, Sung KB, et al. CT during hepatic arteriography and portography. RadioGraphics 2002;22:1041–1051, with permission from the Radiological Society of North America.)

Regenerating nodules enhance with MR contrast similar to liver parenchyma and thus are difficult to identify postcontrast.

An occasional regenerating nodule infarcts and resembles a hypovascular hepatocellular carcinoma or a metastasis on CT and MR imaging.

Dysplastic Nodules

The currently accepted term *dysplastic nodule* was preceded by a varied nomenclature, including *adenomatous hyperplasia*, *adenomatoid hyperplasia*, *macroregenerative nodule*, *hepatocellular pseudotumor*, and *regenerative* and *dysplastic nodules*. Whether dysplastic nodules are neoplastic or hyperplastic in origin is not settled, although a number of authors believe they represent a transition in eventual hepatocellular carcinoma development and thus should be considered premalignant, keeping in mind that some cancers appear to bypass a dysplastic stage.

A distinct nodule containing dysplastic cells without histologic evidence for malignancy is the hallmark of dysplastic nodules, although not uncommonly a pathologist identifies a small focus of hepatocellular carcinoma. From a clinical and imaging viewpoint, dysplastic nodules are often considered to represent one end of a continuous spectrum from benign to malignant tumors. Nevertheless, whether carcinogenesis involves a stepwise progression from a regenerative nodule to a dysplastic nodule and an eventual carcinoma is conjecture; some cancers appear to bypass a dysplastic stage.

Dysplastic nodules develop earlier in the course of cirrhosis in patients with chronic hepatitis than in those with an alcohol cause. Also, these nodules are more common in a setting of several congenital conditions such as α_1-antitrypsin deficiency and Wilson's disease.

Pathologists distinguish low-grade from high-grade dysplasia by the degree of cytologic atypia. Lack of invasion distinguishes high-grade dysplasia from malignancy. In distinction to hepatocellular carcinoma, immunohistochemical staining reveals no α-fetoprotein expression in dysplastic nodules. A confident diagnosis of dysplasia is problematic from a small needle biopsy, and often a resected specimen is necessary to exclude malignancy. Also, a biopsy finding of dysplasia does not exclude an adjacent malignancy.

Dynamic CT achieves a low sensitivity in detecting dysplastic nodules when subsequent orthotopic liver transplantation is used as a gold standard. Computed tomography arterial portography and CT hepatic arteriography confirm a variable and inconsistent portal and arterial blood supply (85) (Fig. 7.25).

Dysplastic nodules vary in their MR appearance, although they are rarely hyperintense on T2-weighted images, and such a finding helps differentiate them from mostly hyperintense hepatocellular carcinomas. Dysplastic nodules

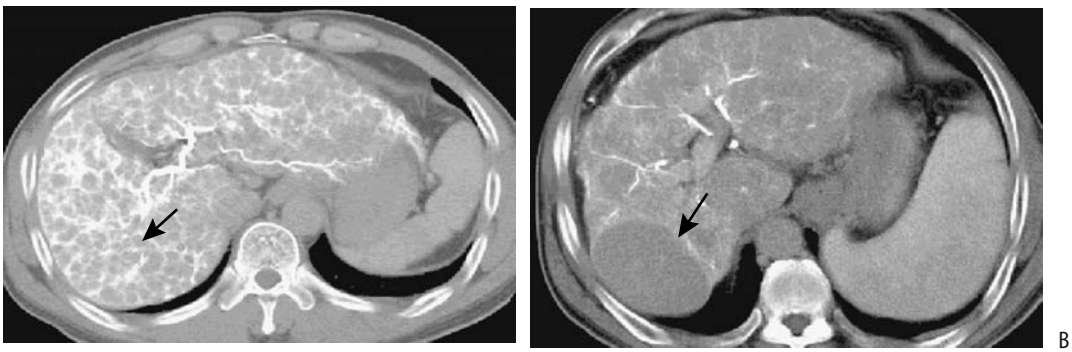

Figure 7.25. High-grade dysplastic nodules. A: CT arterial portography reveals a right lobe tumor (arrow) that is enhancing similarly to adjacent liver tissue. B: The tumor enhances less during CT hepatic arteriography than liver parenchyma. (*Source:* Kim HC, Kim TK, Sung KB, et al. CT during Hepatic Arteriography and Portography. RadioGraphics 2002;22:1041–1051, with permission from the Radiological Society of North America.)

tend to have a mostly portal venous blood supply and, in distinction to hepatocellular carcinomas, do not enhance as intensely during the arterial phase. Nevertheless, dysplastic nodules are believed to be capable of inducing angioneogenesis, and some do contain enough of an arterial blood supply to make arterial-phase differentiation difficult. A hepatocellular carcinoma developing in a dysplastic nodule tends to be hyperintense within a hypointense tumor on T2-weighted images, although the presence of cirrhosis makes MR differentiation difficult. Pretransplantation MRI in cirrhotic patients detects only a minority of dysplastic nodules.

Adding confusion to this issue, some nondysplastic nodules in cirrhotic livers are hyperintense on T1-weighted gradient-echo MRI and do not lose signal intensity on opposed-phase imaging (86); they also do not enhance during the arterial phase.

Because dysplastic nodules contain Kupffer cells, on post-SPIO contrast these nodules range from iso- to hypointense. The contrast ratios between dysplastic nodules and their surrounding liver parenchyma during SPIO-enhanced T2-weighted fast spin echo (FSE) MRI was zero or nearly zero (87); histopathologically, essentially no difference was evident in the number of Kupffer cells in these dysplastic nodules and surrounding parenchyma.

The risk of cancer in a cirrhotic liver containing dysplastic nodules makes nodule resection a rarely viable option. Liver transplantation is considered in these patients.

Extramedullary Hematopoiesis

Intrahepatic extramedullary hematopoiesis develops in some congenital hematologic disorders and hematologic malignancies. Hematopoiesis ranges from focal tumors to a rare extensive diffuse involvement. It can mimic fatty infiltration.

Intrahepatic Spleen

Splenic tissue located outside Glisson's capsule usually represents splenosis after implantation of splenic tissue due to prior splenic trauma.

Intrahepatic spleens are uncommon. Most present as a focal tumor. Splenic tissue partly embedded into liver should represent hyperplasia of congenitally ectopic splenic tissue rather than splenosis as long as it is beneath a common capsule, even in a patient postsplenectomy.

Teratoma

A teratoma is a developmental anomaly, arising from embryonal totipotential cells and containing ectoderm, mesoderm, and endoderm tissue. It is rare in the liver. It occurs primarily in infants. Some are associated with an elevated serum α-fetoprotein level and thus are confused with a hepatoblastoma.

Cystic Lesions

The differential diagnosis for an intrahepatic cyst is rather extensive. Rare cystic metastases to the liver include neuroendocrine and ovarian neoplasms. Primary cystic neoplasms are mostly of bile duct origin and are discussed in Chapter 8.

Liver and renal cysts develop in a setting of Ehlers-Danlos syndrome. The origin of some intrahepatic cysts is difficult to determine and histologic examination not only of the cyst content but also of the cyst wall is often helpful. Pathologists distinguish between true cysts (i.e., those containing an epithelial lining) and other cystic structures. A need to establish a specific diagnosis also influences therapy. Thus while percutaneous aspiration and ethanol sclerotherapy is therapeutic for some cysts, cystectomy, cyst unroofing, or fenestration provide access to a larger cyst wall specimen.

Uncomplicated cysts are hypointense on T1- and hyperintense on T2-weighted images. They do not enhance on postgadolinium arterial-phase T1-weighted SGE images; they appear hypointense during portal venous phase, and continue to maintain their lack of enhancement during the even later hepatic venous phase.

Peribiliary Cysts

Peribiliary cysts are believed to be secondary to obstruction and dilation of peribiliary glands; these cysts are distinct from congenital simple cysts. They are more common in a cirrhotic liver.

These cysts tend to be multiple, tubular, <1.5 cm in diameter, and are located either close to the hilum or along larger portal tracts. Some

enlarging cysts obstruct adjacent bile ducts. If extensive, a *string-of-beads* appearance is evident. A peribiliary cyst is also suggested if CT or US reveals water-density cysts around second- to fourth-order intrahepatic portal vein branches.

On T2-weighted MR images these cysts are similar in appearance to dilated intrahepatic bile ducts.

Simple Cysts

Simple liver cysts are common entities. They are lined by epithelium similar to that in bile ducts but they do not communicate with bile ducts. They are more common in women and increase in number with age. Some are congenital and probably originate from dilated aberrant bile ducts that did not connect with the biliary tree.

Most simple cysts are asymptomatic and are discovered as an incidental finding. An occasional one becomes huge and compresses adjacent structures. Some are complicated by bleeding or infection. Hemorrhage often leads to pain. Spontaneous rupture also occurs, at times into the peritoneal cavity.

Most simple cysts are unilocular with no internal structures. Occasionally cyst wall calcifications develop.

These cysts range in CT density between 0 and 10 HU. The cyst wall is thin or not visible, a finding not seen with most intrahepatic abscesses. A thin wall is seen, however, with cystadenomas and cystocarcinomas. A simple cyst reveals no contrast enhancement. Computed tomography of most simple cysts is diagnostic. Hemorrhage into a cyst increases the CT attenuation by 20 HU or so, seen with MRI as increased signal intensity.

Ultrasonography of a simple cyst reveals an anechoic lumen, increased through-transmission, and a thin, well-defined wall. Increased echogenicity generally is secondary to hemorrhage.

Simple cysts are very hypointense on T1- and markedly hyperintense on T2-weighted MR images, an appearance similar to a hemangioma and an occasional metastasis. Contrast-enhanced MRI distinguishes an enhancing hemangioma from a nonenhancing cyst.

Cytology, α-fetoprotein, CA 19.9, CEA, fluid culture, and lack of communication between the cyst and intrahepatic bile ducts shown by cholangiography aid in excluding other, more ominous diagnoses. Especially with hemorrhage into these cysts, the differential diagnosis includes a cystic or necrotic metastasis and a primary hepatobiliary cystic neoplasm.

Because these cysts are lined by epithelium, they recur after simple aspiration. They are amenable to laparoscopic fenestration and percutaneous ablation therapy. The simplest initial therapy for patients with symptomatic cysts is US-guided percutaneous aspiration and ethanol sclerotherapy. Few complications are encountered.

Ciliated (Foregut) Cysts

The presence of ciliated epithelium within a liver cyst should suggest a hepatic foregut cyst. These rare, congenital lesions are usually less than several centimeters in size, well defined, unilocular, isolated, and subcapsular in location. Some bulge beyond the liver outline and a thin cyst wall is evident. They tend to be hypodense on precontrast CT and hypo- to anechoic on US. They have a variable signal intensity on T1- and are strongly hyperintense on T2-weighted MR images. These cysts do not enhance postcontrast, but at times the cyst wall will enhance. They tend to be filled with bloody mucinous fluid and their hyperintensity on T1-weighted images depends on the amount of mucin and blood within the cyst.

Although a foregut cyst can be strongly suspected from its MR appearance, occasionally a cystic metastasis has a similar appearance.

Lymphangioma

The classification of lymphangiomas varies. They are related to hemangiomas in their histologic appearance and, when generalized, the term *systemic cystic angiomatosis* is often used. In the liver they range from solitary to multiple, but are rare. These cystic nonepithelial tumors are lined by endothelial cells and are filled with serous fluid or chyle. Most are solitary.

Imaging reveals complex cysts containing thin septa.

Intrahepatic Pseudocysts

Intrahepatic pseudocysts in a setting of pancreatitis are rare. Computed tomography reveals

hypodense homogeneous fluid collections, at times multiple; some obstruct a bile duct. An elevated amylase level in aspirated fluid confirms the diagnosis. If necessary, percutaneous drainage is performed.

Hepatic Artery Aneurysm

With gray-scale US, some aneurysms simulate a cyst; the two are distinguishable with Doppler US unless the aneurysm contains a thrombus.

Benign Neoplasms

The vast majority of intrahepatic tumors found to be iso- or hyperintense on T1-weighted MR sequences are of liver parenchymal origin (this finding applies only to high field strength magnets).

A common feature of benign liver neoplasms is the presence of fat within the tumor, either within hepatocytes or as discrete lipomatous tissue.

Adenoma

Clinical

A hepatocellular adenoma is a well-circumscribed, hypervascular, and usually solitary neoplasm. Most occur in women between the ages of 20 and 40 years who are on oral contraceptive therapy. In some, an adenoma regresses after cessation of therapy. Less often adenomas develop in women taking estrogen or in the presence of estrogen-producing neoplasms and in men on anabolic steroids. Adenomas do develop in infants. They are more prevalent than expected in patients with glycogen storage diseases types I and III, and in these patients multiple adenomas (adenomatosis) are encountered. An occasional one becomes pedunculated.

Some adenomas are discovered as incidental findings. Symptoms, if present, range from dull pain, to repeated episodes of severe pain due to hemorrhage into the tumor or adjacent parenchyma, to sudden onset of pain and shock due to spontaneous intraperitoneal hemorrhage. A not atypical scenario is a woman taking oral contraceptives, imaging and biopsy reveal an incidental hepatic adenoma, the tumor enlarges, and she presents with an acute abdomen due to tumor rupture and hemoperitoneum.

An adenoma has a potential for malignant transformation, although the risk of malignancy is unknown. α-Fetoprotein levels are not elevated with an adenoma; an elevated level in a setting of a known adenoma suggests carcinomatous transformation.

These tumors are supplied mostly from hepatic artery branches and an acute hemorrhage is amenable to therapeutic arterial embolization. Suspected adenomas are usually resected rather than biopsied because of possible hemorrhage and their potential for carcinomatous transformation. In addition, as discussed below, in a number of these tumors a clear-cut differentiation from hepatocellular carcinoma is not feasible by imaging alone.

Pathology

Adenomas are well-marginated, hypervascular benign neoplasms, at times containing regions of hemorrhage or necrosis. These tumors consist of hepatocytes containing increased glycogen and lipid interspersed by dilated sinusoids, but a normal acinar arrangement is missing, and supporting bile ductule and portal structures are lacking. Varying amounts of Kupffer cells are present. Only an inconstant capsule is evident, and thus hemorrhage, common with these tumors, readily spreads to surrounding liver parenchyma.

Imaging

Adenomas tend to contain fat and glycogen, with the fat being relatively uniform in distribution. Focal calcifications are identified in some. An occasional adenoma is pedunculated. In distinction to focal nodular hyperplasia, adenomas do not have a central stellate scar. The presence of a scar implies prior necrosis.

Precontrast CT reveals an iso- to hypodense tumor, the latter presumably secondary to increased fat or prior necrosis. Acute hemorrhage appears hyperdense on noncontrast CT, a condition usually found in patients with acute symptoms. Adenomas enhance during the arterial phase. Small feeding arteries accentuate an arterial phase peripheral enhancement, followed by a centripetal pattern. The lesion

becomes isodense or even hypodense on delayed images. Most adenomas are homogeneous, but larger ones tend toward heterogeneous enhancement due to hemorrhage and necrosis.

Precontrast CT detected 86% of 44 adenomas, 100% on arterial phase, 82% on portal venous phase, and 88% of 24 on delayed phase (88); contrast enhancement was homogeneous except for regions of fat, hemorrhage, and necrosis. An occasional adenoma contains calcifications.

Adenomas tend to be hyperechoic due to their fat and glycogen content. Hemorrhage also modifies their US appearance, with recent hemorrhage being hyperechoic and old blood hypoechoic, thus mimicking a cyst. Any prominent subcapsular vessels are detected by color Doppler imaging. Often the US and Doppler appearance is similar to focal nodular hyperplasia.

Some adenomas have MR characteristics departing only slightly from normal liver parenchyma, others vary in their MRI appearance and mimic other tumors, including focal nodular hyperplasia (Fig. 7.26). T1-weighted SE MRI reveals most to be hyperintense and a minority isointense or hypointense to liver parenchyma. Most are hyperintense on T2-weighted sequences; they vary in heterogeneity, presumably due to their lipid content, hemorrhage, and necrosis. The degree of T1-weighted hyperintensity is a measure of a lesion's fat content. As expected, gadolinium-enhanced MRI shows most adenomas to have early arterial enhancement, fading to become isointense during later phases.

Hemorrhage and surrounding iron deposition is evident in some adenomas. An adenoma rich in iron (called a siderotic adenoma) is hyperintense on T1-weighted images and hypointense T2-weighted images. More common are focal iron deposits, resulting in a heterogeneous MR appearance.

Three adenomas showed a mean of –7% (±24%) decrease in signal intensity on ferumoxides-enhanced T2-weighted MRI (81), presumably reflecting reticuloendothelial uptake.

The presence of hepatocytes results in tumor take-up of hepatocyte-specific scintigraphic agents such as Mn-DPDP.

Most adenomas do not have Tc-99m–sulfur colloid uptake, although a minority contain Kupffer cells. Tagged red blood cell imaging

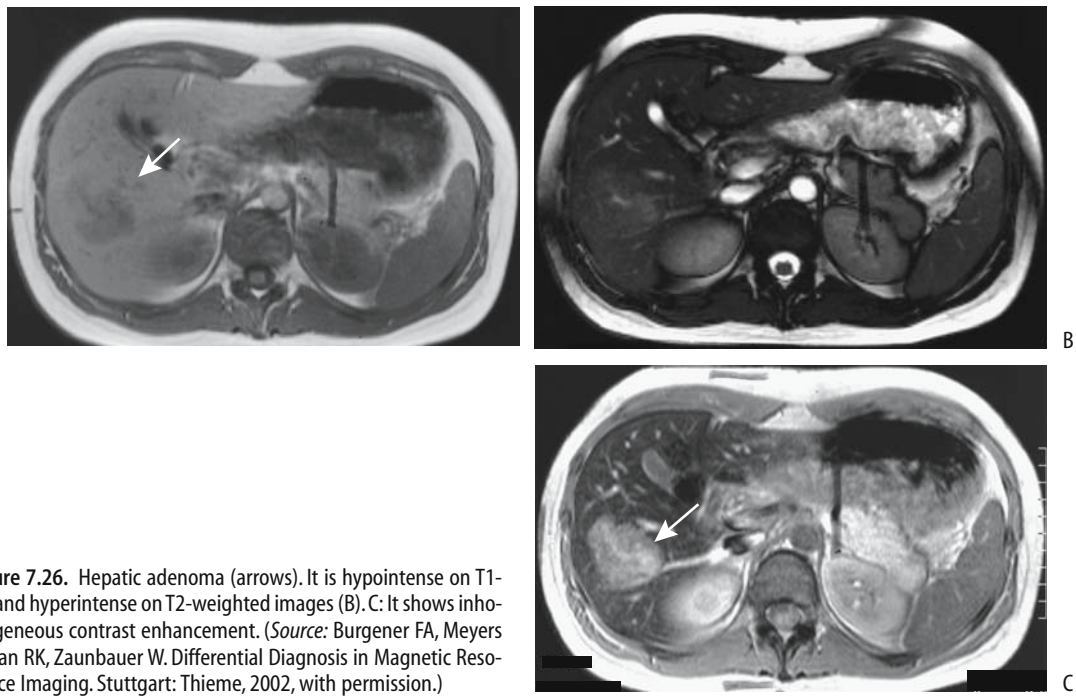

Figure 7.26. Hepatic adenoma (arrows). It is hypointense on T1- (A) and hyperintense on T2-weighted images (B). C: It shows inhomogeneous contrast enhancement. (*Source:* Burgener FA, Meyers SP, Tan RK, Zaunbauer W. Differential Diagnosis in Magnetic Resonance Imaging. Stuttgart: Thieme, 2002, with permission.)

shows early uptake and a cold defect on delayed scans.

Arteriography reveals a hypervascular tumor, at times containing hypovascular foci due to hemorrhage or necrosis. Arteriography generally does not aid in differentiating adenomas from other hepatic tumors, but arterial embolization is occasionally helpful in their preoperative management.

Many of the imaging findings of an adenoma are similar to those of a hypervascular metastasis. Imaging can usually suggest a liver adenoma, but atypical findings make differentiation from other focal tumors difficult.

Adenomatosis

Adenomas range from one, to several, to numerous scattered throughout the liver, with the latter termed adenomatosis. Adenomatosis occurs equally in both sexes and is not related to medication.

In a collection of 15 adults with >10 hepatic adenomas each and no evidence of glycogen storage disease or anabolic steroid use, 73% presented with abdominal pain, hepatomegaly was found in 67%, and abnormal liver function in 91% (89); resection showed common intratumoral hemorrhage, but only 27% evidenced clinical and imaging hemorrhage. Computed tomography and MR revealed hypervascularity in 63% and intratumoral fat in 50% of patients with CT and 80% with MR; these non–steroid-dependent adenomas grew over time, and two patients developed hepatocellular carcinomas.

Lipoma

Hepatic lipomas are rare. An association appears to exist with renal angiomyolipomas and tuberous sclerosis. An occasional patient has multiple liver lipomas.

Precontrast CT readily reveals their lipomatous nature. Postcontrast, tumor density is variable depending on the overall vascularity and the amount of other tissue present. Ultrasonography shows a hyperechoic, well-marginated tumor with posterior attenuation. It mimics focal fat or a hemangioma. A typical lipoma is hyperintense on T1-weighted images. With all sequences, including fat suppression and postcontrast, a lipoma mimics other fat-containing structures.

Occasionally seen is an encapsulated fatty nodule on the liver surface, called a pseudolipoma by some. These nodules have a fibrous capsule and contain necrotic mature fat. Computed tomography reveals subcapsular fat. Some of these tumors develop focal calcifications.

Not all lesions containing fat are lipomas. Both adenomas and angiomyolipomas contain fat. A rare hepatocellular carcinoma, especially in a setting of cirrhosis, contains sufficient fat to be detectable with imaging. A rare liver xanthoma develops in a patient with hyperlipidemia. Most myelolipomas occur in the adrenal glands; hepatic myelolipomas are rare focal, heterogeneous tumors having varied MR signal intensities, reflecting a mix of fat, marrow, and occasional calcifications.

Angiomyolipoma

A benign mixed mesenchymal tumor, an angiomyolipoma was previously classified as a hamartoma, although a rare metastasis argues for neoplastic consideration. It is a rare tumor in the liver except in patients with tuberous sclerosis who also have renal angiomyolipomas. Occasionally they are multiple. Histologically, liver angiomyolipomas are similar to those found in kidneys. Some exhibit extramedullary hematopoiesis.

The overall imaging appearance is variable depending on the amount of fat present, which ranges from minimal to mimicry of a lipoma. In fact, presence of fat is what distinguishes this tumor from other, more ominous tumors. Imaging typically reveals an inhomogeneous fatty component within a tumor.

Most liver angiomyolipomas are hypervascular.

A typical CT appearance is that of a hypodense tumor showing delayed enhancement during the portal venous phase (90); central vessels are evident in some of these tumors. They are hyperechoic by US and hyperintense on T1-weighted MRI. Fat-suppression techniques show a decreasing signal intensity.

Nevertheless, in some patients CT, US, and angiography findings are atypical and mimic focal nodular hyperplasia, hepatocellular carcinoma, or even a rare myelolipoma. Thus an occasional angiomyolipoma contains no visible

fat, US revealed these to be mainly hypoechoic, and with MR they range from hypo- to isointense on T1-weighted sequences and hyperintense on T2-weighted sequences.

Malignant Neoplasms

Hepatocellular Carcinoma

Clinical

In the United States and Western Europe the most common liver malignancy is a metastasis. In most other parts of the world hepatocellular carcinoma predominates. The incidence is gradually increasing in the United States, with a disproportionate increase in a younger patient population. While a hepatocellular carcinoma is often considered an adult tumor, it is the second most common liver malignancy in children (after hepatoblastoma).

Different presentations are seen in different countries. In North America, cirrhotic patients developing a hepatocellular carcinoma are significantly older than those without cirrhosis; survival is longer in patients without cirrhosis. Underlying chronic liver disease makes hepatocellular carcinoma detection both more difficult and also provides a clue to its presence.

Serum α-fetoprotein levels are not always elevated with these tumors, especially smaller ones, and with fibrolamellar variant carcinomas (discussed in a later section). On the other hand, diffuse hepatocellular carcinoma, infiltrating extensively, is invariably associated with high levels. Elevated α-fetoprotein levels, however, are also found in cirrhosis and some other chronic liver diseases, fulminant hepatitis, and some metastases. Hypoglycemia is common. Most often jaundice at the initial presentation is due to underlying liver failure, either secondary to parenchymal replacement by tumor or superimposed cirrhosis. Jaundice due to bile duct obstruction by tumor is unusual except late in the course. A rare hepatocellular carcinoma erodes into the bile ducts and sheds tumor fragments, and jaundice ensues secondary to tumor thrombus. This subset tends to mimic a cholangiocarcinoma in their appearance.

Most hepatocellular carcinomas are poorly differentiated and have an aggressive growth pattern. Portal vein, hepatic vein, and inferior vena cava invasion are common.

Associated Conditions

A number of underlying conditions are associated with the subsequent development of hepatocellular carcinoma (Table 7.11). Underlying chronic liver disease is common. In North America, cirrhosis is often present. In China, HBV infection in younger patients is associated with subsequent hepatocellular carcinomas without underlying cirrhosis, a finding consistent with a direct viral effect on liver cell transformation. These younger patients tend to have larger tumors than older patients, and their tumors are more advanced when first discovered. Excess liver iron also appears to predispose to cancer. In cirrhotics, risk of hepatocellular carcinoma is increased in those with iron deposits in regenerative nodules compared to those without such iron; iron in regenerative nodules tends to parallel parenchymal iron deposits.

Hepatocellular carcinomas have developed after long-term anabolic steroid administration, mostly for hematologic disorders, and in women on long-term oral contraceptives. Nevertheless, no conclusive evidence exists of a relationship between oral contraceptives and hepatocellular carcinoma. In Sweden, with

Table 7.11. Conditions associated with hepatocellular carcinoma

Mostly in adults
Viral hepatitis
Cirrhosis
Hepatic adenoma
Adenomatous hyperplasia
Hemochromatosis
Hepatotoxin exposure
Androgen use
Porphyria
Acute intermittent
Porphyria cutanea tarda
Polyvinyl chloride exposure
Diabetes mellitus
Hepatic vein thrombosis
Mostly in children
Biliary atresia
Glycogen storage disease type I
Hereditary tyrosinemia
Congenital hepatic fibrosis
α_1-Antitrypsin deficiency
Alagille syndrome

extensive oral contraceptive use, hepatocellular carcinoma incidence in women parallels that of men; on the other hand, in Japan, with negligible oral contraceptive use, incidence and mortality is gradually rising.

In cirrhotic patients, creation of a portosystemic shunt does not appear to increase risk for hepatocellular carcinoma.

Some evidence suggests that patients with chronic hepatic vein thrombosis are at risk for hepatocellular carcinoma even without any evidence for underlying cirrhosis.

An occasional patient develops a preceding paraneoplastic syndrome.

Rupture/Bleeding

A hepatocellular carcinoma is prone to spontaneous rupture and bleeding, generally into the peritoneal cavity. A rare hepatocellular carcinoma first manifests with a spontaneous rupture and the patient presents with hemoperitoneum. Some patients initially develop a subcapsular hematoma, followed by capsular rupture and hemoperitoneum. In general, larger tumors and left lobe tumors are more prone to rupture, compared to the right lobe. Peritoneal tumor spread and omental seeding are uncommon. Some tumors invade adjacent colon and result in lower gastrointestinal hemorrhage. Transcatheter selective arterial embolization can arrest such bleeding, but it is, of course only palliative.

These patients are also prone to portal hypertension, esophageal varices, and subsequent variceal bleeding. Prophylactic variceal sclerotherapy is feasible, thus decreasing the risk of subsequent variceal bleeding. Transjugular intrahepatic portosystemic shunting also helps correct portal hypertension.

Screening

In spite of its high prevalent in the Orient and Africa, with the exception of a few Asian countries few populations practice hepatocellular carcinoma screening, which is usually based on liver US and serum α-fetoprotein levels. Any patients with suspicious findings then undergo further confirmatory diagnoses. A Hong Kong US screening study of hepatitis B virus carriers with elevated α-fetoprotein levels achieved a sensitivity and specificity for hepatocellular carcinoma detection of 86% and 82%, respectively (91). Nevertheless, little evidence suggests that screening leads to any significant decrease in mortality. The few screening studies for hepatocellular carcinoma in patients with cirrhosis, generally consisting of US and serum α-fetoprotein levels every six months, have detected a cancer incidence of roughly 5% per follow-up year; yet in spite of such screening, cure rates for patients with a detected cancer amenable to definitive therapy are low and validity for screening cirrhosis patients can be questioned.

Pathology

Adenomatous hyperplasia is a poorly understood condition developing in some patients with chronic liver disease. Patients with surgically resected adenomatous hyperplasia nodules that contain cellular atypia and focal malignancy tend to develop hepatocellular carcinomas within a few years, while those with adenomatous hyperplasia but without cellular atypia do not. A sequence of regenerating nodules, adenomatous hyperplasia, and atypia appears to be a pathway for hepatocellular carcinoma development. Atypia leads to low-grade malignancy and presumably to an advanced hepatocellular carcinoma.

Whether hepatocellular carcinomas are multicentric in origin is debatable. The frequent occurrence of hepatocellular carcinomas after resection of adenomatous hyperplasia implies a multicentric origin. Direct injection of radiopaque material into resected tumor specimens shows that spread is by capsule invasion, intrahepatic invasion, and portal vein.

Small hepatocellular carcinomas tend to be of a low-grade malignancy and, in fact, macroscopic features of early hepatocellular carcinomas often resemble those of hyperplasia or adenoma rather than more advanced carcinomas. A not uncommon pattern is that of well-differentiated cells mimicking benign hepatocytes in connective tissue, factors related to patient survival; these cells became less differentiated with growth. Nevertheless, well-differentiated cancers do have a potential for metastasis.

In North America, hepatocellular carcinomas developing in a setting of cirrhosis tend to be less well-differentiated than in those without

cirrhosis and are more prone to invade the portal vein. Encapsulated tumors are more common in patients without cirrhosis.

Pathologists divide hepatocellular carcinomas into clear-cell and non–clear-cell types, but no significant prognostic differences are evident between the two.

Histologically, some metastatic carcinomas are very similar in appearance to hepatocellular carcinomas. This differentiation is especially difficult with small needle biopsy specimens; immunohistochemical staining for human albumin messenger RNA (mRNA) is helpful in some. Albumin mRNA is detected in a majority of primary and metastatic hepatocellular carcinomas, but not in nonhepatocellular tumors.

A rare extrahepatic bile duct hepatocellular carcinoma is reported. Whether these represent hepatoid differentiation of a cholangiocarcinoma or are indeed primary extrahepatic hepatocellular carcinomas is speculation. An occasional such tumor contains both hepatocyte and bile duct cell features, and an immature progenitor cell origin appears reasonable.

Because current imaging detects smaller and smaller lesions, the pathologist is now faced with the task of differentiating between low-grade malignancy and atypical hyperplasia.

Arteriovenous Shunting

Hepatocellular carcinomas are fed mostly by arterial blood, although from a hemodynamic viewpoint the situation is complex. Many of these tumors drain, in part, into a portal venule and thus mimic an arterioportal vein fistula. Shunting is more common into the portal vein than hepatic vein.

Ideally, arterioportal shunting is identified as early portal vein filling after arterial contrast injection. Shunting is often considered to be present if arterial phase CT shows wedge-shaped enhancement peripheral to a tumor and if this region becomes iso- or hyperattenuating during the portal phase. Extensive shunting leads to hepatic artery enlargement. Arterioportal shunting affects liver perfusion and decreases tumor enhancement, resulting in heterogeneous enhancement and, at times, even a hypovascular CT appearance. Such shunting is unusual with hypovascular metastases, but nontumor-associated arterioportal shunts do exist in a cirrhotic liver and can mimic a hypervascular tumor.

Arteriovenous shunting is detected with hepatic arteriography or scintigraphy by injecting Tc-99m–macroaggregated albumin (MAA) into the tumor feeding artery (angioscintigraphy). The latter technique is very sensitive in detecting small shunts. Angioscintigraphy can estimate lung shunting in patients with hepatocellular carcinomas (lung shunting is calculated as the total count over the lungs divided by the total count over both the lungs and liver) and correlates with tumor size (estimated by CT or US) and vascularity.

The presence of arteriovenous shunting has a bearing on prognosis and is considered a contraindication to arterial chemoembolization. Transcatheter arterial embolization with steel coils in some of these patients with severe arterioportal shunting results in shunt resolution and resumption of hepatopetal portal blood flow and an improved quality of life, although it has little effect on survival.

A word of caution. Non–tumor-associated arterioportal shunts do exist in a cirrhotic liver and can mimic a hypervascular tumor. Postcontrast CT reveals such nontumorous shunts as wedge-shaped and homogeneously enhancing regions, at times containing an internal linear branching pattern during the arterial phase.

Detection

Comparison Studies

The imaging technique yielding the highest tumor nodule detection rate is not established, although a trend is evident in favor of more complex contrast-enhanced MR imaging. Both superparamagnetic and hepatobiliary MR contrast agents show promise. A number of studies, mostly by Japanese investigators, show that arterial-phase MR is superior to arterial-phase CT or any other CT or MR phase in detecting and evaluating small hepatocellular carcinomas. Ferumoxides-enhanced MRI achieved a 93% sensitivity and 99% specificity in tumor detection, while combined CT arterial portography and hepatic arteriography achieved a 91% sensitivity and 94% specificity (92), and the authors suggest that MRI can replace CT for preoperative evaluation of these patients.

Tumor detection using a combined unenhanced, gadolinium-enhanced, and ferumoxides-enhanced MRI was similar to that obtained with a combined CT arterial portography and biphasic CT hepatic arteriography (93); an advantage of the MRI approach is that invasive CT angiography is not necessary.

Detection accuracy of malignant hepatic tumors (a mix of hepatocellular carcinomas and metastases) by SPIO-enhanced MR imaging is superior to unenhanced MRI and is similar to CT arterial portography (94). Relative tumor detection sensitivities depend on tumor size; CT and US detect more smaller tumors than DSA or even possibly iodized oil CT; but the latter are more sensitive with a larger tumor volume.

Magnetic resonance is probably more sensitive than CT in showing that a capsule is present and in identifying vascular involvement.

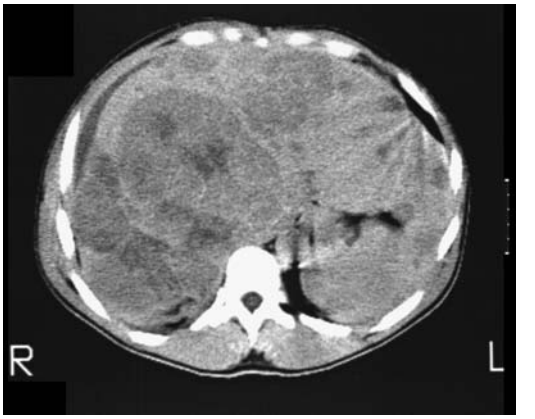

Figure 7.27. Multifocal hepatocellular carcinoma.

General Imaging Findings

A differentiation of hemangiomas from hepatocellular carcinomas (and metastases) was discussed above (see Differential Diagnosis of Focal Tumors).

About half of hepatocellular carcinomas occur as solitary, discrete tumors, with the other half consisting of several to multiple focal lesions or diffuse liver infiltration (Fig. 7.27). A rare one is extrahepatic, connected to a lobe by a pedicle. In children, signs pointing toward a hepatocellular carcinoma are the presence of underlying liver disease and significant venous invasion, findings somewhat uncommon with a hepatoblastoma. Imaging findings in children tend to mimic those seen with a hepatoblastoma (Fig. 7.28).

Most hepatocellular carcinomas are rather vascular, supplied primarily by hepatic artery branches. Vascular invasion more often involves portal vein branches rather than hepatic veins. Arterioportal shunting and hemorrhage are common. The less common well-differentiated hepatocellular carcinomas tend toward hypovascularity.

Computed tomography is not reliable in detecting bile duct invasion. Cholangiography

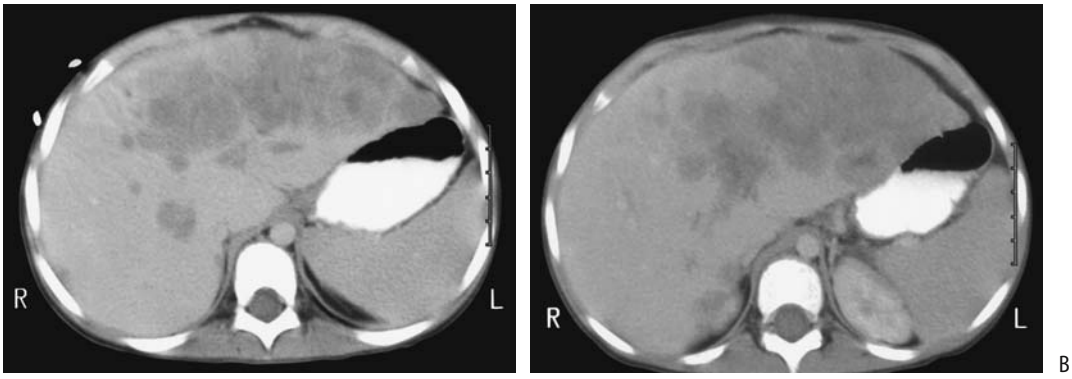

Figure 7.28. Hepatocellular carcinoma in a 5-year old girl. A,B: Arterial phase CT reveals a tumor replacing most of the left lobe and nodules scattered in the right lobe. A hepatoblastoma was in the differential diagnosis. (Courtesy of Luann Teschmacher, M.D., University of Rochester.)

can identify an intraductal tumor (Fig. 7.29), at times mimicking a stone. Also, a tumor involving the liver hilum may obstruct bile ducts and result in intrahepatic biliary dilation without direct bile duct invasion.

Aside from fibrolamellar carcinomas, gross calcifications in a hepatocellular carcinoma are uncommon. An occasional one contains a central scar, which is more often detected in a carcinoma developing in a noncirrhotic liver than in a cirrhotic liver.

Computed Tomography

A characteristic unenhanced CT appearance of hepatocellular carcinomas is that of a hypodense to isodense tumor. Some isodense tumors contain a thin hypodense rim, but the margin between tumor and adjacent parenchyma tends to be poorly defined. Typical postcontrast findings consist of marked neovascularity, enlarged feeding arteries, a dense tumor vascular blush, normal or delayed contrast washout, and arterioportal shunting. Nevertheless, considerable CT variability exists and an occasional one is even hypovascular (Fig. 7.30). Some reveal an enhancing rim during the portal phase. In general, CT contrast-enhancing regions represent viable tumor tissue, while hypodense regions are either necrotic or contain fibrosis and hemorrhage.

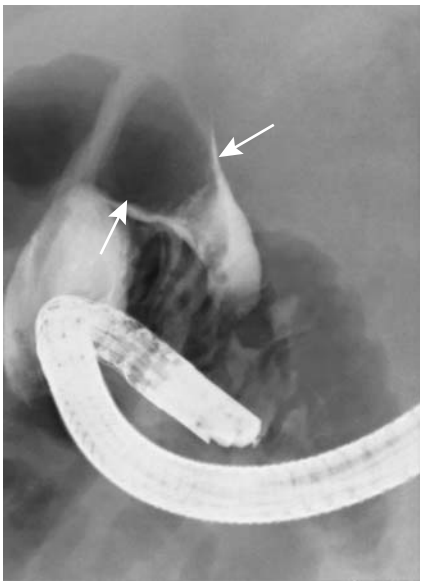

Figure 7.29. Hepatocellular carcinoma growing within hepatic duct (arrow), an uncommon presentation.

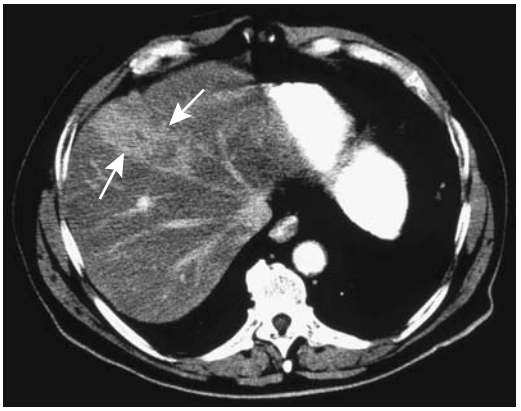

Figure 7.30. Hepatocellular carcinoma. Contrast-enhanced CT identifies a tumor replacing part of the right lobe (arrows). (Courtesy of Patrick Fultz, M.D., University of Rochester.)

What is the relative value of arterial phase, portal venous phase, and delayed phase CT in detecting these tumors? Arterial phase imaging yields the highest tumor-to-parenchyma contrast and detects more tumors than the other phases. During the arterial phase they tend toward intense homogeneous enhancement, a finding also seen with other hypervascular tumors, both benign and malignant. Larger tumors have heterogeneous arterial-phase enhancement, probably due to interspersed necrosis. Tumors missed on the arterial phase tended to be well differentiated, do not have a fibrous capsule, and are relatively hypovascular. Although different publications provide different tumor detection rates, relative tumor detection between various imaging phases is remarkably constant. A combination of arterial and portal venous phase images detects significantly more tumors than a combination of unenhanced and portal venous phase images. Any combination of two phases that includes the arterial phase is superior to a combination of portal and delayed phases. Or, for maximum tumor detection, all three phases should be obtained because a small minority of tumors are detected only on unenhanced images.

A novel technique consists of both early and late arterial-phase images obtained serially

during a single breath-hold multidetector CT study. Such double arterial-phase imaging yielded detection sensitivities of 54% for the early arterial phase, 78% for the late arterial phase, and 86% for the double arterial phase (95); the number of false-positive tumors was also reduced with double arterial-phase imaging.

The place of 3D liver CT reconstruction in evaluating hepatocellular carcinomas is not yet clear in spite of some obvious advantages. It is useful to the surgeon in defining vascular and tumor anatomy in specific segments when planning resection, yet at present 3D reconstruction is not widely practiced; considerable operator time and experience is necessary to achieve meaningful results.

One technique consists of reconstructing maximum intensity projection images of intrahepatic portal venous branches and hepatic veins, plus shaded surface display images of hepatic tumors from postcontrast CT data; when superimposed, these two sets of images provided a 3D relationship between vessels and tumors, aiding tumor localization prior to resection.

Do CT arterial portography and CT hepatic arteriography add significant information beyond what is obtained with triple-phase CT during preoperative evaluation of hepatocellular carcinomas? Adding CT arterial portography to triple-phase CT increased sensitivity from 94% to 96% and the further addition of CT hepatic arteriography increased it further to 97% (96); a disadvantage is that CT arterial portography and CT hepatic arteriography increase the false-positive rates without a corresponding gain in sensitivity.

Computed tomography hepatic arteriography aids, in part, in differentiating dysplastic nodules from hepatocellular carcinomas. Thus CT hepatic arteriography reveals that although high-grade dysplastic nodules range from hypo- to hyperdense, a majority of low-grade dysplastic nodules are isodense (97); carcinomas, on the other hand, are mostly hyperdense, especially moderately to poorly differentiated ones.

A limitation of CT hepatic arteriography is that in some patients the entire liver cannot be studied because of an aberrant blood supply; examples include the presence of an aberrant left hepatic artery originating from the left gastric artery and occlusion of a right hepatic artery; injection of contrast into the hepatic artery does not opacify these segments and thus misses tumors there.

Computed tomography arterial portography involves placing an angiographic catheter into the splenic artery or superior mesenteric artery distal to the origin of any hepatic arteries. During portal-phase imaging the normal liver is markedly enhanced, with little enhancement of neoplasms receiving their blood supply from the hepatic artery, thus accentuating contrast differences between normal parenchyma and a neoplasm. Potentially this technique allows detection of smaller tumors. Similarly to CT hepatic arteriography, CT arterial portography aids in differentiating dysplastic nodules from hepatocellular carcinomas. Thus 77% of low-grade dysplastic nodules were isodense, while only 32% of high-grade dysplastic nodules were isodense (the rest ranged from slightly to markedly hypodense) (97); all well-differentiated carcinomas ranged from slightly to markedly hypodense and moderately to poorly differentiated carcinomas all were markedly hypodense. Practical application of such CT correlation with histologic findings is yet to be established.

While CT arterial portography is rather sensitive, its specificity is rather low. Hemangiomas, focal nodular hyperplasia, regenerating nodules, and liver parenchyma being fed by aberrant vessels are detected, and in many instances these false-positive lesions cannot be distinguished from neoplasms. Follow-up double-phase CT arteriography appears useful in differentiating hepatic tumors, especially malignancies, from nonspecific perfusion abnormalities (called pseudolesions by some). These nonneoplastic perfusion abnormalities tend to be more common adjacent to the falciform ligament, gallbladder, and posterior edge of the medial segment. For unknown reasons these abnormalities occur less often adjacent to the falciform ligament in patients with cirrhosis.

Hepatocellular carcinomas not identified by CT arterial portography (i.e., false negative) tend to be central in location or associated with segmental portal vein thromboses obstructing the flow of contrast to the liver periphery.

Computed tomography arterial portography is of limited value in a setting of portal hypertension, regardless of the etiology; insufficient iodine is delivered via the portal vein to the liver to achieve adequate contrast differences for tumor visualization. Enhancement is also decreased if portosystemic shunting has developed. In these settings CT arteriography is a better choice.

Malignant tumor size tends to be overestimated with CT arterial portography. Reasons are due to parenchymal compression, portal vein obstruction, or possibly a siphoning effect by these hypervascular tumors.

Although an iodized oil CT study (also called *Lipiodol CT*) is often used as a gold standard for tumor detection, it has distinct limitations. It is generally assumed that iodized oil is retained only by malignant cells, although evidence suggests that oil is also retained by other tumors. Iodized oil can accumulate in a hemangioma. Iodized oil uptake tends to be homogeneous in tumors smaller than 2 cm in diameter, becoming inhomogeneous in larger ones, presumably secondary to necrosis.

It would be naive to think that iodized oil CT detects all tumors. Iodized oil CT appears to be a tarnished gold standard when examining tumors in explanted livers, with pretransplantation iodized oil CT sensitivity being rather low. Nevertheless, contrary to some studies, it often detects more tumors than other imaging modalities.

Occasionally spasm is encountered during arterial injection of Lipiodol, resulting in proximal Lipiodol reflux. Intraarterial buflomedil has been used to decrease arterial spasm.

Ultrasonography

Sonographic findings of hepatocellular carcinomas vary and are nonspecific. Sonography detects only a minority of hepatocellular carcinomas in patients with advanced cirrhosis, in one study identifying only 27% of tumors prior to liver transplantation (98). In the West, even small tumors range from (mostly) hypoechoic to (less often) hyperechoic, while in parts of Africa multinodular, hyperechoic tumors are more common. A thin hypoechoic rim with a hyperechoic center is evident in some; such a *target sign* is nonspecific and is also seen with metastases and some benign tumors. A complex pattern develops with growth, and these tumors range from heterogeneous, hyperechoic, hypoechoic, and nodular, to diffuse infiltration. An occasional one mimics an abscess.

Ultrasonography depicts "hemangioma-like" lesions in some cirrhotic patients (99); follow-up revealed that half were hyperechoic hepatocellular carcinomas.

Color Doppler signals are detected both at the periphery and within vascular tumors; they are detected in a majority of hepatocellular carcinomas and focal nodular hyperplasias. Power Doppler US is superior to color Doppler US in visualizing hepatocellular carcinoma blood flow and identifying tortuous intratumoral vessels. Numerous studies have confirmed that contrast-enhanced power Doppler US is superior to unenhanced power Doppler US in detecting hepatocellular carcinoma tumor vascularity. Contrast-enhanced color Doppler US of most hepatocellular carcinomas reveals intratumoral signals, afferent vessels, and peripheral vascularity.

Doppler US–generated hepatic artery velocity histograms show hepatocellular carcinoma artery flow tending toward turbulent. Occasionally color Doppler US detects reversed portal blood flow adjacent to a hepatocellular carcinoma; such flow reversal is nonspecific and is also identified with metastases, abscesses, and even subcapsular hematomas. Color Doppler US detects a feeding artery in hepatocellular carcinomas more often after contrast; a feeding artery, however, is not pathognomonic of a hepatocellular carcinoma.

Carbon dioxide–enhanced US is used to study blood flow patterns. In some hands US enhanced with intraarterial carbon dioxide microbubbles detects more hepatocellular carcinomas than contrast-enhanced CT or even iodized oil-CT. After carbon dioxide microbubble injection into the hepatic artery, real-time B-mode US will identify blood drainage into a portal vein branch through a hepatocellular carcinoma, thus confirming arterioportal shunting.

Pulse-inversion harmonic US with pre- and serial postintravenous microbubble contrast injection reveals dense tumor staining, enhancement ranging from homogeneous to

heterogeneous with rapid washout and a surrounding late pseudocapsule enhancement; centripetal fill-in, a characteristic finding with hemangiomas, is not found with these cancers (Fig. 7.31).

Using IV contrast, intermittent harmonic power Doppler US achieved a sensitivity of 93% and specificity of 100% for depicting tumor vessels and tumor stain (100). Postcontrast, conventional power Doppler US depicts significantly more signals from hepatocellular carcinomas than harmonic power Doppler US (101). On the other hand, in spite of relatively short effective enhancement duration with harmonic Doppler US, it produces fewer artifacts.

Intraoperative US detects tumors not imaged preoperatively and not localized by palpation or inspection during surgery. Not all nodules represent a malignancy. This modality thus is of value in planning specific segmental resection. In an occasional patient a planned resection based on prior CT arterial portography is modified by intraoperative US.

Magnetic Resonance Imaging

On both T1- and T2-weighted MRI, hepatocellular carcinomas range from hypointense to hyperintense compared to normal liver parenchyma. Most often, however, a hyperintense tumor on T1-weighted images suggests a hepatocellular carcinoma or a benign tumor; most metastases are hypointense. A majority of hepatocellular carcinomas are hyperintense on T2-weighted images. Small tumors tend to be iso- or somewhat hyperintense on T1- and isointense on T2-weighted images. Larger tumors tend toward heterogeneity on both T1- and T2-weighted images. Diffuse hepatocellular carcinoma infiltration ranges from subtle, often minimal precontrast findings, to a mottled hyperintense appearance on T2-weighted images; a similar heterogeneous pattern is often evident on immediate postcontrast images. A higher T1-weighted signal intensity appears related to a higher degree of tumor differentiation, more steatosis, and higher tumor copper content than surrounding liver parenchyma (102).

Chemical shift MR with both opposed-phase and in-phase FLASH imaging detects fat in a minority of hepatocellular carcinomas. T1-weighted fat-suppressed images appear superior to T1- and T2-weighted images in detecting small hepatocellular carcinomas (103).

Paramagnetic ions contributing to the MR signal include copper and iron both in the tumor and in surrounding liver parenchyma. Excess copper accumulation in some hepatocellular carcinomas may account for part of the hyperintense T1-weighted signal (103), yet the

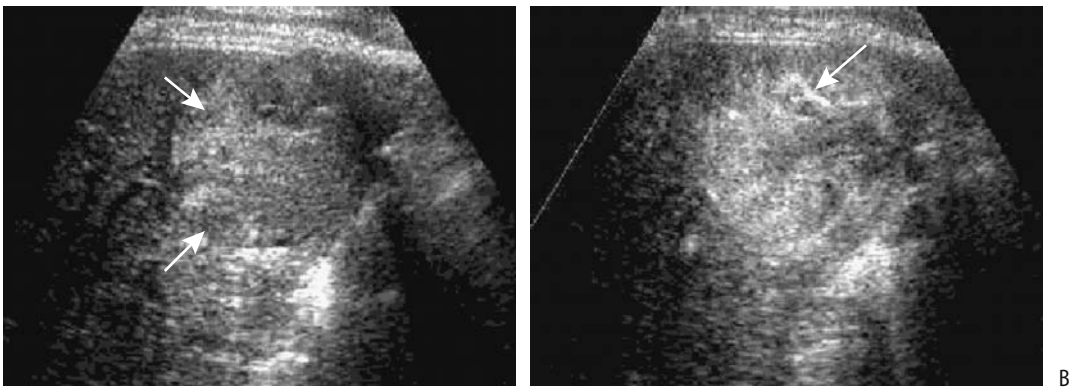

A B

Figure 7.31. Hepatocellular carcinoma. A: Oblique pulse-inversion harmonic US identifies a hyperechoic tumor (arrows). B: Similar contrast-enhanced US 33 seconds after contrast injection reveals heterogeneous tumor enhancement. The tumor contains an enhancing vessel (arrow). (*Source:* Kim TK, Choi BI, Han JK, Hong HS, Park SH, Moon SG. Hepatic tumors: contrast agent-enhancement patterns with pulse-inversion harmonic US. Radiology 2000;216:411–417, with permission from the Radiological Society of North America).

amount of divalent copper present appears to be insufficient to account for all of this signal. The often high iron content within dysplastic nodules leads to a hypointense appearance on T2-weighted images, while a carcinoma developing within this nodule will be hyperintense, an appearance of a nodule-within-nodule.

If a capsule is present, T1-weighted images reveal a hypointense rim. T2-weighted images show a capsule and surrounding structures as a double layer consisting of an inner hypointense and an outer hyperintense layer. Underlying cirrhosis influences tumor appearance and makes MR interpretation more difficult. Tumors in cirrhotic livers are smaller, less often solitary and less likely to contain a central scar.

Current evidence suggests that contrast-enhanced MRI is superior to other imaging techniques in detecting and providing a viable differential diagnosis for hepatocellular carcinomas, yet the critical evidence does not instill confidence even in MR, especially in a setting of cirrhosis. Thus pretransplantation 2D or 3D gadolinium-enhanced gradient-echo MRI using arterial, portal venous, and equilibrium phases in cirrhotic patients detected cancers only in 55% of patients shown to have cancers (104); on a lesion-by-lesion basis, MRI achieved an overall sensitivity of only 55%, missing 50% of neoplasms 1 to 2 cm in diameter and 66% of tumors <1 cm.

The most optimal type of MR contrast agent, be it a primarily hepatobiliary, superparamagnetic, or other agent, is not clear. In patients with malignant hepatic tumors (mostly hepatocellular carcinomas) gadolinium-enhanced MRI achieved greater sensitivity (81%) than ferumoxides-enhanced MR (62%) for tumor detection, but specificity was comparable (94%) (105); superiority of gadolinium was enhanced in patients with underlying cirrhosis.

Considerable MR variability in appearance is a hallmark of postcontrast hepatocellular carcinomas. For most tumors, the tumor-to-liver contrast ratio increases after intravenous gadolinium; increasing the gadolinium dose from the recommended 0.1 mL/kg of body weight does not improve the tumor-to-liver contrast.

A typical appearance of a small hypervascular hepatocellular carcinoma in cirrhosis is early but mild contrast enhancement, rapid washout and little delayed enhancement except for peritumoral coronal enhancement (106). Larger tumors have a heterogeneous pattern. The more vascular poorly differentiated hepatocellular carcinomas show marked initial enhancement, become isointense during portal venous phase and even hypointense later on. Some tumors exhibit delayed enhancement. A small minority are hypointense during the arterial phase. Also, any superimposed liver disease modifies the MRI appearance.

Lesions <1 cm and isointense on precontrast images are best identified (and often only) by their immediate homogeneous postcontrast enhancement. Of hepatocellular carcinomas < 3 cm, roughly half are detected on T1-weighted images, half on T2-weighted images and half on post-gadolinium T1-weighted images. Although some authors have published greater detection rates, relative detection pre- and postcontrast as outlined above is typical. T2-weighted image hyperintensity is related to expansive growth, peliosis, and hypervascularity, while hypointense or undetected tumors tending to be well differentiated. On postgadolinium T1-weighted images hyperintensity is related to peliosis, with undetected tumors being well differentiated and hypovascular. In general, adding dynamic imaging increases tumor detection by 20% or so over precontrast imaging.

After gadobenate dimeglumine, well-differentiated hepatocellular carcinomas tend to have a rapid increase in signal intensity during the arterial phase, while poorly differentiated carcinomas have a more delayed rise in signal intensity. Postcontrast, some hepatocellular carcinomas are surrounded by a hypointense rim on early images, with this rim enhancing later on; this enhancing rim appears to be caused by contrast draining through a (pseudo)capsule into a surrounding layer containing portal venules; arterial blood in a hepatocellular carcinoma drains into adjacent portal veins (107). Rim enhancement is evident in a majority of hepatocellular carcinomas during the portal venous phase.

Typical findings, if present, help differentiate these carcinomas from hemangiomas; the latter have early peripheral enhancement, a more marked but delayed peak enhancement, and continued delayed enhancement. Metastases tend toward peripheral enhancement, a finding lacking with hepatocellular carcinomas, which enhance throughout, albeit heterogeneously.

Superparamagnetic iron oxide contrast agents are taken up both by liver Kupffer cells and normal hepatocytes, including those in dysplastic nodules (Fig. 7.32). They accumulate in benign lesions, which thus can be differentiated from Kupffer cell-poor hepatocellular carcinomas, yet a word of caution: some uptake of SPIO is evident in well-differentiated hepatocellular carcinomas and these become isointense. As an example, during SPIO (ferumoxides)-enhanced MRI, moderately or poorly differentiated hepatocellular carcinomas had high tumor-to-liver parenchyma contrast ratios and large differences in the number of tumor-to-parenchyma Kupffer cells, while in some well-differentiated carcinomas these contrast ratios were zero or near zero (87). Although the ability to differentiate between poorly differentiated and well-differentiated hepatocellular carcinomas may appear to be an advantage, in actual practice this finding implies that well-differentiated carcinomas will either not be evident or will appear similar to benign liver tumors.

In some studies iron oxide–enhanced MRI detect more hepatocellular carcinoma nodules <10 mm in diameter than unenhanced MRI, gadolinium-enhanced MRI, or CT. In others, using different MR sequences, gadolinium-

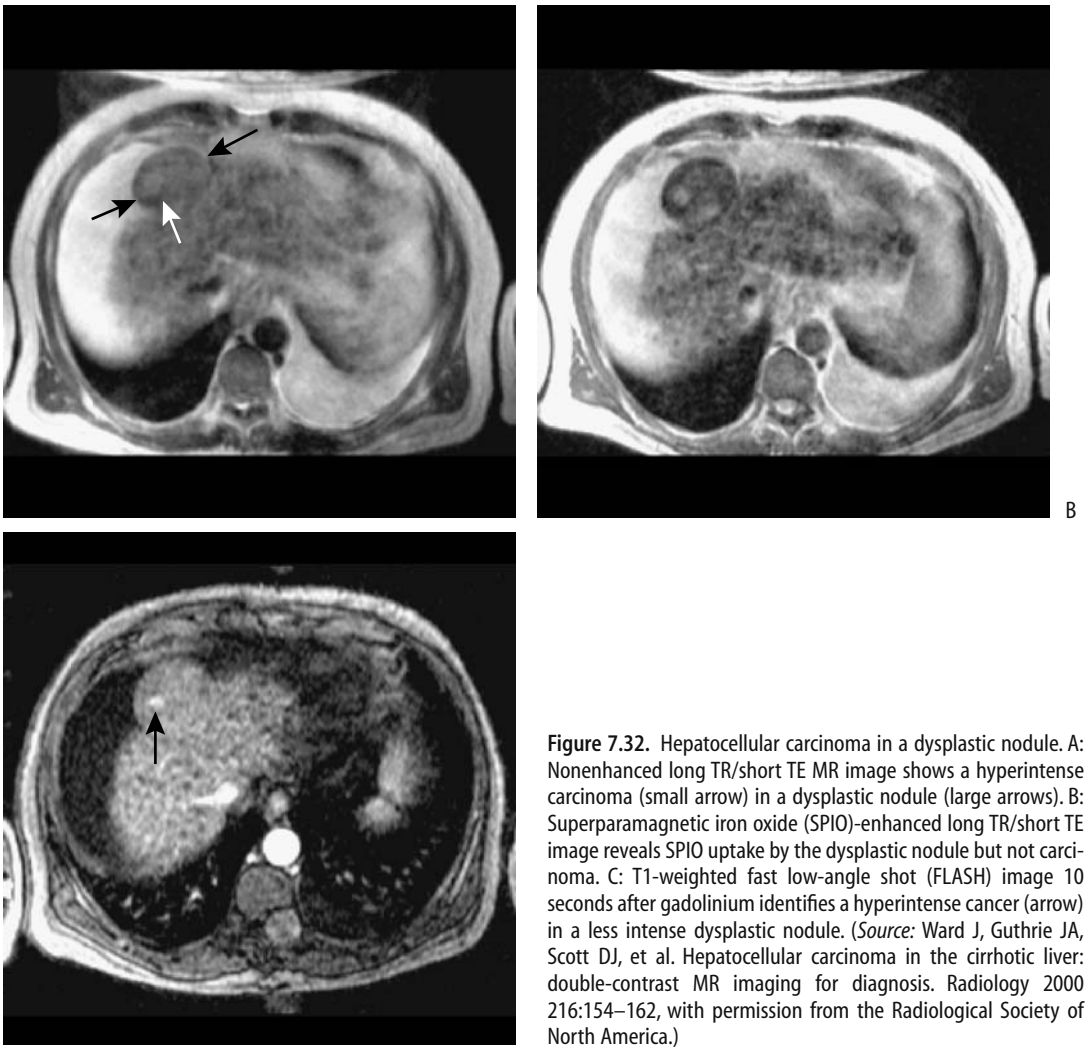

Figure 7.32. Hepatocellular carcinoma in a dysplastic nodule. A: Nonenhanced long TR/short TE MR image shows a hyperintense carcinoma (small arrow) in a dysplastic nodule (large arrows). B: Superparamagnetic iron oxide (SPIO)-enhanced long TR/short TE image reveals SPIO uptake by the dysplastic nodule but not carcinoma. C: T1-weighted fast low-angle shot (FLASH) image 10 seconds after gadolinium identifies a hyperintense cancer (arrow) in a less intense dysplastic nodule. (*Source:* Ward J, Guthrie JA, Scott DJ, et al. Hepatocellular carcinoma in the cirrhotic liver: double-contrast MR imaging for diagnosis. Radiology 2000 216:154–162, with permission from the Radiological Society of North America.)

enhanced MRI appears superior (Fig. 7.33). Such comparisons are difficult to place in a wider clinical perspective; they reflect specific MR units used and specific imaging conditions. The SPIO-enhanced hepatocellular carcinomas appear slightly bigger than on comparable gadolinium-enhanced images.

A 3D MRA rotational display, obtained from 2D TOF images using SPIO, shows their relationship to portal and hepatic veins on the same image, information useful during presurgical planning.

Chondroitin sulfate iron colloid is a potential intravenous MR contrast agent. The tumor-to-liver contrast-to-noise ratio is significantly increased after chondroitin administration, primarily in moderately to poorly differentiated hepatocellular carcinomas.

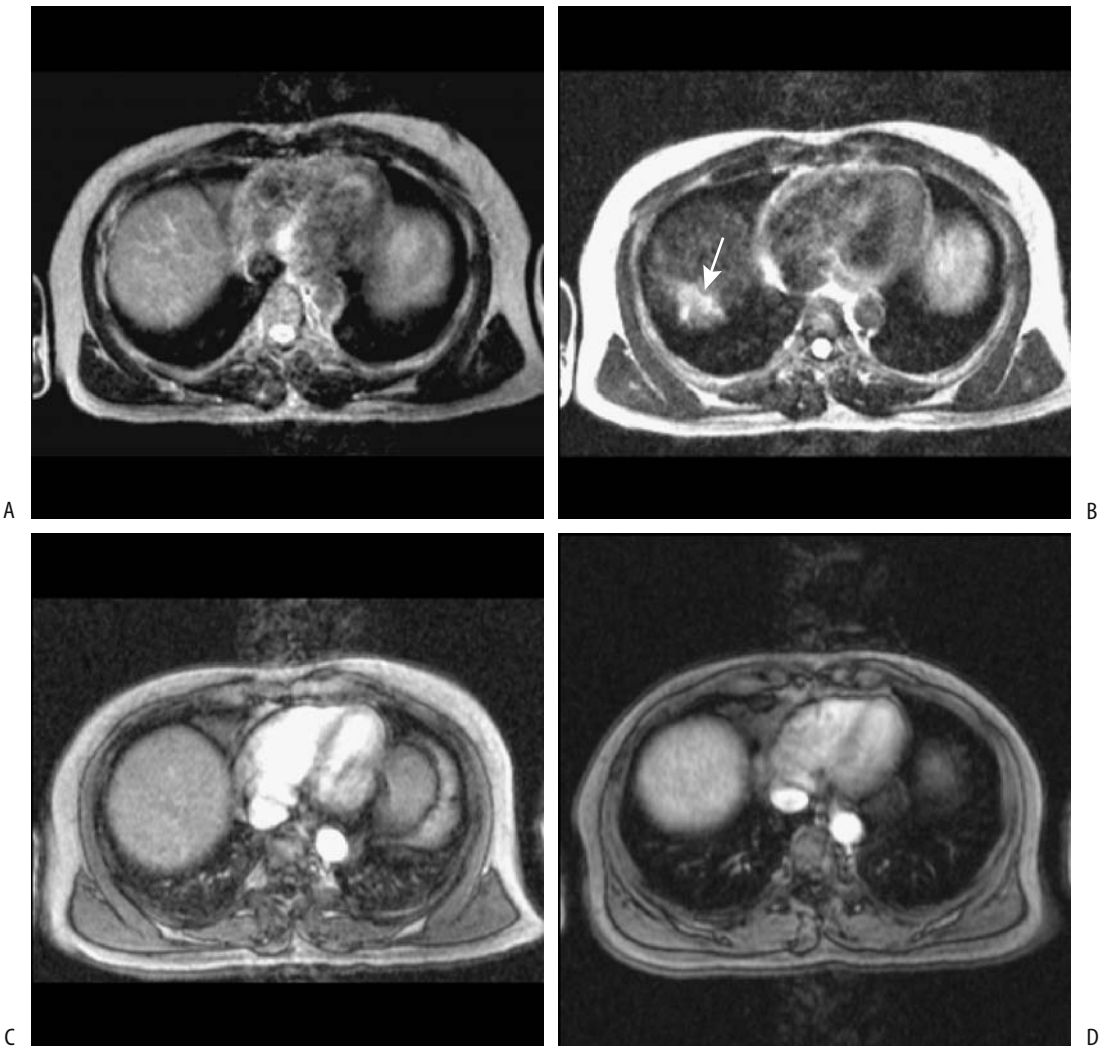

Figure 7.33. MR of a hepatocellular carcinoma in a cirrhotic liver. Nonenhanced long TR/long TE image (A), SPIO-enhanced long TR/long TE image (B), T1-weighted FLASH image 10 seconds after gadolinium (C), and T1-weighted FLASH image 40 seconds after gadolinium (D). This tumor (arrow in B) was identified only on SPIO-enhanced images. (*Source:* Ward J, Guthrie JA, Scott DJ, et al. Hepatocellular carcinoma in the cirrhotic liver: double-contrast MR imaging for diagnosis. Radiology 2000 216:154–162, with permission from the Radiological Society of North America.)

Well-differentiated hepatocellular carcinomas exhibit considerably more uptake of Mn-DPDP than poorly differentiated ones and as a result these tumors can range from hyper- to hypointense; those that become isointense are not detected with this contrast agent. In overall hepatocellular carcinoma detection Mn-DPDP appears inferior to gadolinium (108). This agent does not aid in differentiating these tumors from adenomas and focal nodular hyperplasia but does help in differentiating hepatocellular carcinomas from metastases (the latter exhibit little uptake).

Will combined use of SPIO followed by injection of a gadolinium contrast agent (called *double-contrast MRI* by some) aid carcinoma detection? Such a double-contrast study in cirrhotic patients with suspected hepatocellular carcinoma revealed that SPIO-enhanced MRI was more accurate than precontrast MRI, and double-contrast MRI was more accurate than SPIO-enhanced MRI (109). Such double MR studies are especially useful in characterizing nodules in a cirrhotic liver (110).

Scintigraphy

Some hepatocellular carcinomas have Tc-99m-IDA uptake. A not uncommon pattern is to see little or no uptake within the first hour, with the lesion subsequently filling in. In general, well-differentiated carcinomas show uptake while less differentiated ones appear cold.

Hepatocellular carcinomas show variable gallium 67 citrate uptake, a nonspecific finding; abscesses and some metastases also reveal uptake; however, in the appropriate setting such uptake should suggest a hepatocellular carcinoma.

Uptake of Tc-99m-methoxyisobutylisonitrile (MIBI) using SPECT is variable and appears related to tumor histology.

Although thallium 201 chloride is a promising tumor imaging agent, its use in the liver is limited by normal liver uptake. When sequentially combined with Tc-99m–sulfur colloid, SPECT Tl-201 images show increased activity in hepatocellular carcinomas while Tc-99m–sulfur colloid SPECT reveals photopenia at these sites.

Some neoplasms have increased FDG metabolism, and PET-FDG is useful in their detection. Most hepatocellular carcinomas have increased uptake, but a minority have uptake equal to liver and thus are not detected. FDG metabolism does not necessarily correlate with tumor differentiation. Adenomas and fibronodular hyperplasia have poor uptake.

Biopsy

A need to establish pathologic diagnosis is obvious with a suspected tumor. Percutaneous biopsy using imaging guidance usually is diagnostic. If aggressive therapy of confirmed hepatocellular carcinoma nodules is planned, knowledge of the histologic subtype may suggest a specific therapy. Thus early or sclerosing carcinomas with their limited tumor vascularity do not respond to arterial embolization. Early carcinomas tend to respond to percutaneous ethanol injection, while sclerosing types respond poorly.

Both cytology and histology can be used to diagnose these tumors. Biopsies are often performed in cirrhotic livers and results are superior when cytology and histology are combined. In general, a diagnosis can be obtained in about 90% of tumors when using an 18 gauge cutting needle and US guidance. Biopsy appears safe provided the interposing liver parenchyma is >1 cm. Postbiopsy bleeding is a recognized complication.

One biopsy complication is an intrahepatic arterioportal fistula. Postbiopsy (with a 14-gauge Thru-Cut needle) arterioportal fistulas detected by DSA can be treated with coil embolization and followed by planned chemoembolization.

Tumor spread along a needle tract after fine-needle biopsy of a hepatocellular carcinoma appears rare, with only occasional reports published.

Staging

The TNM hepatocellular carcinoma staging classification is outlined in Table 7.12. Some investigators also use a Stage 0—defined as a solitary hepatocellular carcinoma <2 cm in size in patients with compensated cirrhosis. Stage 0 is a useful concept in patients undergoing various percutaneous ablation therapies. In general, staging of these tumors is less useful than with most cancers because underlying liver function plays a major role in patient survival. Direct spread to adjacent structures is a

Table 7.12. Tumor, node, metastasis (TNM) staging of liver cancer

Primary tumor:			
Tx	Cannot be assessed		
T0	No evidence of primary tumor		
T1	Solitary tumor without vascular invasion		
T2	Solitary tumor with vascular invasion or multiple tumors, none >5 cm		
T3	Multiple tumors >5 cm or tumors involving major portal or hepatic branch		
T4	Direct invasion of adjacent organs		
Lymph node involvement:			
Nx	Regional nodes cannot be assessed		
N0	No regional nodes involved		
N1	Regional nodes involved		
Distant metastasis:			
Mx	Distant metastasis cannot be assessed		
M0	No distant metastasis		
M1	Distant metastasis		
Stage I	1	N0	M0
Stage II	T2	N0	M0
Stage IIIA	T3	N0	M0
Stage IIIB	T4	N0	M0
Stage IIIC	any T	N1	M0
Stage IV	any T	any N	M1

Source: From the AJCC Cancer Staging Manual, 6th edition (2002), published by Springer-Verlag, New York, NY, used with permission of the American Joint Committee on Cancer (AJCC), Chicago, IL.

common late finding. For example, direct invasion of the proximal transverse colon, mucosal erosion, and exsanguination are not uncommon.

Iodized oil-CT is often used as an imaging gold standard to detect additional carcinoma nodules. Its limitation has already been mentioned.

Ultrasound angiography using small CO_2 bubbles appears to aid in staging and planning therapy. Comparing helium and CO_2 bubbles injected into proper hepatic artery in patients with hepatocellular carcinoma, enhancement duration is longer with helium than with CO_2 and the degree of enhancement greater (111); helium aids in additional carcinoma nodule detection.

Hepatocellular carcinoma has a predilection for vascular invasion (Fig. 7.34). Most common is spread to the portal vein, although inferior vena caval involvement is not uncommon, an occasional one even extending intraatrially. Normally, the portal vein enhances on post-contrast MRI portal venous phase images; with invasion, the portal vein contains an intraluminal nonenhancing tumor rather than contrast-enhancing blood, although some tumor thrombi show early arterial enhancement during dual-phase CT, thus suggesting a diagnosis. The etiology of portal vein thrombosis detected in patients with a known hepatocellular carcinoma is of obvious staging importance. Not all thromboses are neoplastic in origin; the superimposed cirrhosis present in many of these patients is also associated with portal vein thrombosis. A US-guided needle biopsy of the thrombus is a viable staging technique.

Although some authors believe that metastatic hepatocellular carcinoma is rare, tumor

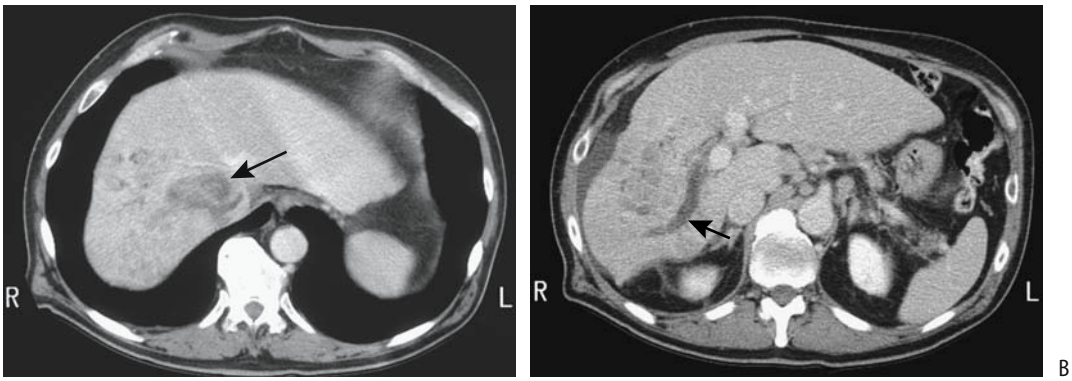

Figure 7.34. Hepatocellular carcinoma. A: More cranial CT shows an inferior vena cava thrombus (arrow). B: More caudal image reveals the tumor and a right portal vein thrombus (arrow). Adenopathy is also present. (Courtesy of Patrick Fulz, M.D., University of Rochester).

spread outside the liver is not uncommon, mostly during advanced stages. Lymphatics, lung, and skeleton are typical sites; on the other hand, biliary tract involvement is uncommon. An incidental extrahepatic tumor in a patient with stage I or II intrahepatic hepatocellular carcinoma likely is not a metastatic focus.

The uncommon intraperitoneal drop metastases range from single to multiple, but are discrete. A rare metastatic hepatocellular carcinomas causes spinal cord compression.

Therapy

If applicable, resection is the preferred therapy for liver cancers. Several other modalities have evolved as therapies for unresectable hepatocellular carcinomas (Table 7.13). Some have had limited application, while others are currently in use, especially in those parts of the world where hepatocellular carcinoma is prevalent. Conventional chemotherapy and radiation therapy have a limited role. Based on a retrospective multicenter Japanese study of patients with hepatocellular carcinoma comparing resection, transcatheter arterial chemoembolization, and percutaneous transhepatic ethanol injection, the authors recommend either resection or ethanol injection for stage I tumors < or = 3 in number and < or = 30 mm in size, ethanol injection for stage II tumors < or = 3 in number and < or = 30 mm in size and resection (if applicable) for stage I tumors >31 mm in size and regardless of number (113). Use of antiangiogenic agents to treat hepatocellular carcinomas is too new to draw any firm clinical conclusions.

Unresectable

The borderline between a resectable and an unresectable tumor varies between surgeons. Also, some hepatocellular carcinomas deemed unresectable are amenable to preoperative cytoreduction therapy to the point that it is subsequently resectable. In fact, an argument can be made that the primary role of preoperative therapy is to convert an unresectable hepatocellular carcinoma into a resectable one.

An occasional patient undergoes aggressive therapy and achieves prolonged survival even with an extensive hepatocellular carcinoma.

Resection

Preoperative localization of a focal liver lesions to a specific hepatic segment is of obvious interest to the surgeon, and therefore a need exists for imaging techniques to identify a segment in question. Two systems are in use for classifying liver lobes and segments: the Couinaud system, widely used throughout Europe and Asia, and an English system more common in Great Britain and United States (Table 7.14). The primary difference between the two systems is in nomenclature, with the Couinaud classifi-

Table 7.13. Therapy of hepatocellular carcinomas

Therapy	Approach	Action
Resection	Surgical	—
Chemoembolization	Vascular (arterial)	Ischemia
Microspheres	Vascular (arterial)	Ischemia, radiation
Ethanol	Percutaneous (injection)	Denaturation
Acetic acid	Percutaneous (injection)	Denaturation
Hot saline	Percutaneous (injection)	Hyperthermia
Radiofrequency	Percutaneous (coagulation)	Hyperthermia
Laser photocoagulation	Percutaneous (coagulation)	Hyperthermia
Microwave therapy	Percutaneous (coagulation)	Hyperthermia
Cryotherapy	Laparotomy (coagulation)	Hypothermia

Source: Adapted from D'Agostino and Solinas (112).

Table 7.14. Segmental liver anatomy

Couinaud system	English system
Dorsal sector: segment I	Caudate lobe
Left liver	Left lobe
Left paramedian sector	
Segment IV	Quadrate lobe: anterior medial segment
Segment III	Lateral segment: anterior inferior subsegment
Left lateral sector—Segment II	Lateral segment: posterior superior subsegment
Right liver	Right lobe
Right paramedian sector	
Segment V	Anterior segment: anterior inferior subsegment
Segment VIII	Anterior segment: anterior superior subsegment
Right lateral sector	
Segment VI	Posterior segment: inferior subsegment
Segment VII	Posterior segment: superior subsegment

cation dividing liver parenchyma into a left liver and a right liver, with each then being subdivided into sectors and segments. These segments are based primarily on portal vein subdivisions, their primary importance being in their anatomic use during surgical planning and resection.

Surgical resection continues to be the mainstay of therapy in patients without cirrhosis. A small solitary tumor is ideal for surgical resection. In such a setting absence of major vessel invasion or absence of intrahepatic metastases are factors affecting survival. Either a lobectomy, segmentectomy, wedge resection, or other type of resection is performed. Aggressive surgery is in vogue in some centers. A tumor thrombus in portal vein branches, hepatic veins, inferior vena cava, or bile ducts is not a contraindication to resection. In Japan, 5-year survival for patients with stage I hepatocellular carcinoma is about 70%, stage II is 50% and stage III is 30%. With recurrence, repeat surgery appears to prolong survival in some patients.

A small solitary tumor is ideal for surgical resection. In such a setting the absence of major vessel invasion or the absence of intrahepatic metastases is a factor affecting survival.

In a cirrhotic liver, postoperative residual liver function limits the extent of resection possible. Some surgeons are reluctant to perform a major hepatectomy in a setting of cirrhosis, although in some patients a partial hepatectomy in such a setting has a mortality rate close to that in patients with a normal liver. A segmentectomy is effective for small hepatocellular carcinomas and can be safely performed even in a setting of chronic liver disease. Nevertheless, postoperative hepatic decompensation is a risk in cirrhotic patients, especially those with an increased preoperative portal pressure, and some surgeons restrict resection to patients without portal hypertension. Nevertheless, highly extended resection for advanced hepatocellular carcinoma with portal vein tumor thrombi is performed in some centers.

Preoperative portal vein embolization using a percutaneous transhepatic approach is feasible. Whether such embolization aids subsequent resection is debatable.

Laparoscopic hepatic resection is feasible for a hepatocellular carcinoma.

Extracorporeal resection has been tried in patients with an otherwise inoperable liver tumor. Whether ex-vivo MRI with its high spatial resolution aids such resection is not clear.

Transplantation

In a minority of patients transplantation is an option for hepatocellular carcinomas, treating both the carcinoma and any underlying liver disease. Typical candidates are patients who should be able to tolerate major surgery, should

have at most three tumors measuring <3 cm in diameter, and should have no portal extension. Transplantation rather than resection is considered for localized tumors in a cirrhotic liver where a sizable resection risks liver failure.

Is surgical resection or transplantation preferred in a patient with cirrhosis and a hepatocellular carcinoma? Data from six French medical universities reveal an overall similar 5-year survival rate for cirrhotic patients with hepatocellular carcinomas whether treated by liver resection or transplantation (114): 31% for the resection group and 32% for the transplantation group. Among these patients the 5-year survival rate without recurrence, however, was higher in the transplantation group (60%) than in the resection group (14%).

Chemoembolization

Intraarterial embolization techniques used to treat hepatocellular carcinomas consist of inert particle embolization, a variety of embolic material containing chemotoxic agents (chemoembolization), and injection of radioactive particles (radioembolization). Of these, chemoembolization has achieved the greatest acceptance.

As minimally invasive outpatient therapy, transarterial chemoembolization offers considerable palliation for patients with unresectable hepatocellular carcinomas. Undoubtedly in the future such therapy will expand. Treatment strategies adopted probably should depend on size and tumor number. Thus percutaneous ethanol injection appears superior for a single small tumor, but intraarterial chemoembolization is superior for more or larger tumors.

Chemoembolization consists of injecting a mixture of a chemotoxic agent and also an embolic material into a tumor feeding artery (a procedure often called transcatheter arterial chemoembolization, TACE). Ethiodol (Lipiodol) is included as one of the chemoembolization ingredients for several reasons: First, this oil acts as a chemotherapeutic agent carrier. Second, because of its relatively high viscosity, it acts as a temporary embolizing agent and thus prolongs chemotherapeutic agent contact with a tumor. In addition, Ethiodol remains within tumor neovascularity much longer than in adjacent normal liver parenchyma, at times for up to 7 days (Fig. 7.35). Later, after injecting a chemotherapeutic agent, if needed, embolization of the vessel in question is performed using particulate matter.

Although mostly supplied by hepatic artery branches, an occasional parasitic blood supply is detected with these tumors. Especially with a carcinoma located ventrally beneath the diaphragm, internal mammary arteries and inferior phrenic arteries serve as feeding arteries. If necessary, Lipiodol embolization of one of these arteries can be performed.

Temporary occlusion of a draining hepatic vein may aid arterial infusion chemotherapy. Such selective hepatic vein occlusion results in a dense hepatogram, but this issue is controversial, and some investigators believe that the occlusion causes unacceptable damage to normal liver parenchyma.

Transarterial chemoembolization can be repeated several times (called *sequential chemoembolization*). Some data suggest that such sequential therapy prolongs survival compared with no therapy in those with an unresectable carcinoma. At times a port system is implanted as an aid for future hepatic artery infusion chemotherapy. An infusion pump provides ready access for follow-up CT arteriography or conventional arteriography.

The most common indication for chemoembolization is palliation. At times, reduction in tumor size allows resection or additional

Figure 7.35. CT shows residual Ethiodol retained in a multifocal hepatocellular carcinoma. (Courtesy of Patrick Fultz, M.D., University of Rochester.)

therapy, such as laser-induced thermotherapy or percutaneous ethanol injection. Initial results suggest that such a dual approach is more effective than chemoembolization alone, although survival depended considerably on the extent of underlying liver disease. With a resectable tumor, transcatheter arterial chemoembolization during the postoperative period appears to increase survival, but insufficient data are available on this subset of patients.

Portal vein thrombosis is considered a contraindication to transcatheter embolization, although embolization has been performed in patients with portal vein branch thrombosis. Arteriovenous shunting, common with hepatocellular carcinomas, is generally considered a contraindication to arterial chemoembolization. At times arteriovenous shunting, mostly arterioportal, develops during therapy. Other risk factors include coagulation abnormalities, severe portal or pulmonary hypertension, esophageal varices prone to bleeding, poor cardiovascular status, and advanced cirrhosis.

A severe postembolization syndrome and hepatic insufficiency are common complications; in general, predisposing factors—such as major portal vein obstruction, compromised hepatic reserve, biliary obstruction, excessive or nonselective iodized oil embolization—are evident in most patients with major complications. Other complications include those related to catheter placements, variceal bleeding, and severe hyperglycemia. Rare complications include carcinoma rupture after chemoembolization, adrenal hemorrhage, and acute adrenal insufficiency and ischemic cholecystitis. Procedure-related deaths have been reported. Tumor seeding along an implantable access port in the hepatic artery has developed.

Transcatheter arterial embolization affects arterial and portal perfusion hemodynamics. Arterial perfusion increases temporarily after embolization, presumably due to acute inflammation.

Biliary complications can be evaluated with Tc-99m–HIDA. Postembolization scans reveal that gallbladder filling time and contractility is worse shortly after embolization. Also, curiously, most survivors have gallbladder nonvisualization.

Transarterial chemoembolization is most effective when a tumor is limited in size and liver function is preserved. The response to chemoembolization is poor with extensive parenchymal invasion. Postprocedure survival depends on underlying liver disease (Child's class), size and number of tumors, and patient age. Patients with a predominantly hypervascular tumor respond better than those with a hypovascular tumor (115).

Published survival results vary, and a comparison of different studies using different selection criteria is difficult. Types of agents employed together with their doses and administration rates also differ and presumably influence results. In a typical study, among patients responding to therapy, survival was 90%, 67%, and 36% at 1, 2, and 3 years, respectively, while nonresponders (mostly with hypovascular tumors) achieved 70%, 17%, and 10% survival, respectively (115). Survival is better in patients with smaller tumors. Tumor decrease in size after arterial chemoembolization is of prognostic significance. Nevertheless, not all results are positive. Thus a multicenter randomized trial of patients with unresectable hepatocellular carcinoma but without severe liver disease or portal vein occlusion compared Lipiodol chemoembolization (Lipiodol, cisplatin, lecithin, and gelatin sponge injected into the hepatic artery) plus tamoxifen versus tamoxifen alone (116); although an objective response was more frequent in the Lipiodol group (24%) than in the tamoxifen group (5.5%), overall the two groups showed no difference in survival at 1 year. In a study comparing hepatic artery infusion chemotherapy versus transcatheter arterial Lipiodol chemoembolization in patients with advanced hepatocellular carcinomas, tumor response rates were significantly higher in the former group and these patients tended to have longer survival rates (117).

Some tumors are difficult to evaluate with CT after embolization due to retained iodized oil artifacts. Nevertheless, that portion of tumor retaining iodized oil after chemoembolization is typically necrotic.

Both contrast-enhanced wide-band harmonic gray-scale US and power Doppler US are used to detect tumor recurrence after chemoembolization, achieving about 90% sensitivity and specificity. Tumor vascularity detected by contrast enhanced harmonic wide-band gray-scale US after arterial chemoembolization usually implies residual tumor (118).

Postgadolinium T1-weighted MRI is reliable in evaluating chemoembolization outcome and is more accurate than precontrast MRI. Loss of enhancement postgadolinium T1-weighted images correlated with necrosis. On the other hand, focal enhancement generally signifies viable tumor.

Tc-99m-MAA SPECT angiography (hepatic arterial flow study) provides an estimate of liver vascularity and is another method of gauging the success of arterial chemoembolization.

Radioembolization

Intrahepatic artery Tc-99m-MAA injection estimates the relative tumor-to–normal parenchyma uptake of various size microspheres, including those containing therapeutic radiopharmaceutical agents. Theoretically, intraarterial infusion of microspheres containing the beta-emitter yttrium 90 selectively delivers a high radiation dose to a malignant hepatic tumor while mostly sparing adjacent normal parenchyma. One problem is that hepatocellular carcinomas have a wide tumor-to–normal parenchymal uptake ratio. Tumor vascularity, as assessed by hepatic angiography, does not predict the relative tumor-to–normal parenchyma uptake for most of these tumors.

Hepatocellular carcinomas have been embolized with iodine-131 iodized oil (radioiodinated Lipiodol) and gelatin sponges through a superselectively placed arterial catheter. Such embolization has provided long-term palliation without complications, but few conclusions can be drawn from the limited number of patients studied.

Yttrium-90 glass microspheres have also been injected percutaneously into hepatocellular carcinomas, but this technique is controversial.

Percutaneous Techniques

Hepatocellular carcinomas can be treated using a direct percutaneous approach. Such therapy can be divided into two broad categories; first, injection of chemical agents such as ethanol, acetic acid, and hot saline induce tumor coagulation necrosis. Second, thermally mediated techniques such as radiofrequency (RF) ablation, laser photocoagulation, microwave therapy, and cryotherapy result in similar tumor cell death.

Imaging provides needle and catheter insertion guidance. The introduction of open-bore MR units and nonferromagnetic instrumentation should expand interventional MR techniques.

Although comparisons of various percutaneous tumor ablation techniques are being published, they should be viewed cautiously. Type of tumor, tumor size and specific techniques used influence results. Thus a conclusion that, say, radiofrequency ablation achieves necrosis in 90% of tumors versus 80% with percutaneous ethanol injection may not be valid at other institutions.

Ethanol Injection: Percutaneous ethanol injection into unresectable hepatocellular carcinomas nodules has had wide international application, especially in patients with underlying cirrhosis, yet has been little used in the United States. Results are mostly palliative and in most patients tumors either recur or new tumors develop. Therapy is repeated with tumor recurrence, with the interval between successive treatments decreasing. A solitary nodule, pretreatment serum α-fetoprotein level <20 ng/mL, and limited cirrhosis favor longer survival. Severe complications of percutaneous ethanol injection are uncommon.

Ethanol therapy is achieved by cell membrane lysis and protein denaturation and through necrosis of vascular endothelium leading to surrounding tissue ischemia and necrosis. Absolute alcohol has a very low CT attenuation and injected alcohol can be identified on CT images. No blood flow is identified in necrotic tumors, and they are avascular at color Doppler US.

Using color Doppler US guidance, instead of injecting directly into a tumor, ethanol can be injected into a vessel supplying the tumor; limited data are available for such a technique.

Positron emission tomography performed by injecting carbon-11 ethanol via a percutaneous needle reveals high C-11 uptake in these carcinomas; no significant elimination of C-11 ethanol is evident from these tumor.

Accurate tumor localization is, of course, important. Some can be located with US. Others require CT arteriography or arterial injection of iodized oil and real-time CT fluoroscopy

during needle placement. Computed tomography fluoroscopy permits rapid assessment of needle position. Also, real-time CT fluoroscopy reconstruction evaluates ethanol distribution during injection, and the injected dose can then be modified accordingly.

Study technical variables, such as accuracy of needle placement, amount injected, and number of sessions, influence survival and make comparison of published studies difficult. Also, inhomogeneous drug distribution and dilution limit therapeutic response. Survival results are modified by tumor size and underlying liver disease. In some studies of patients with a single lesion <3 cm in diameter, the results of percutaneous ethanol injection approach those reported for resection.

Computed tomography performed shortly after ethanol injection therapy reveals an unchanged or even increased tumor diameter with a well-defined margin; necrotic tissue tends to be hypodense, while residual tumors enhance during the arterial phase, gradually becoming hypodense on later phases. These changes are less pronounced after multiple therapy sessions.

After ethanol injection, arterial phase contrast-enhanced MRI reveals increased contrast enhancement adjacent to treated tumors, presumably due to increased blood flow to surrounding tissues; similarly to US, early tumor contrast enhancement implies residual tumor.

Acetic Acid Injection: Percutaneous acetic acid injection using acid concentrations of 15% to 50% has been used for hepatocellular carcinoma nodule therapy. The number of treatment sessions needed is less with the higher concentrations, although even a 15% concentration appears adequate to successfully treat tumors. A single percutaneous injection into nodules <3.0 cm in diameter has resulted in no local recurrence of most nodules (119).

The 1-, 2-, and 3-year survival rates for patients with hypervascular hepatocellular carcinomas <3 cm in diameter treated with percutaneous acetic acid injection were 100%, 94%, and 83% (120); corresponding survival rates for those treated with transcatheter arterial embolization were 72%, 65%, and 39%, respectively. Local recurrence, as gauged by enlargement of original tumor, occurred in 3% of tumors treated with acetic acid injection and 50% of those treated by transcatheter arterial embolization.

Other Injection Techniques: Less often used is hot saline injection. Usually a larger volume of hot saline is injected than ethanol; thus fewer treatment sessions are required. Currently insufficient data exist to draw meaningful conclusions about such therapy efficacy.

Computer tomography–guided percutaneous intratumoral injection of a cisplatin/epinephrine gel (part of a clinical phase II study) in eight patients with hepatocellular carcinomas led to a local control rate of about 80% (121); a similar technique in eight patients with metastases achieved a control rate of only 38%.

Radiofrequency Coagulation: Radiofrequency ablation, laser-induced photocoagulation, and microwave therapy induce tumor thermal coagulation necrosis (thermotherapy). Radiofrequency energy is applied via shielded needle electrodes inserted into a tumor to deliver sufficient energy to induce tumor necrosis. Percutaneous needles are inserted under CT, US, or MR control. Alternate approaches are laparoscopic or laparotomic, with each one having advantages and disadvantages. Laparotomy is especially useful for tumors close to other critical organs, such as the diaphragm. The extent of ablation depends on needle tip size and energy delivered. The greatest tissue heating occurs closest to the needle tip, a disadvantage overcome by the use of continuous needle tip cooling, which results in tissue heating away from the needle.

Typically several sessions are needed for tumor ablation. Published nodule necrosis has ranged from 50% to 85% of tumors; the most sensitive sign of necrosis is lack of nodule contrast enhancement during follow-up arterial-phase CT (Fig. 7.36), with contrast-enhanced pulse inversion harmonic US and contrast-enhanced power Doppler US being less sensitive (122), although some studies suggest that contrast-enhanced, phase-inversion harmonic US is almost as accurate as CT in detecting tumor necrosis (123). Doppler US reveals a rich peripheral vascularity persisting even after successful therapy.

At times radiofrequency ablation is combined with intraarterial chemoembolization. The

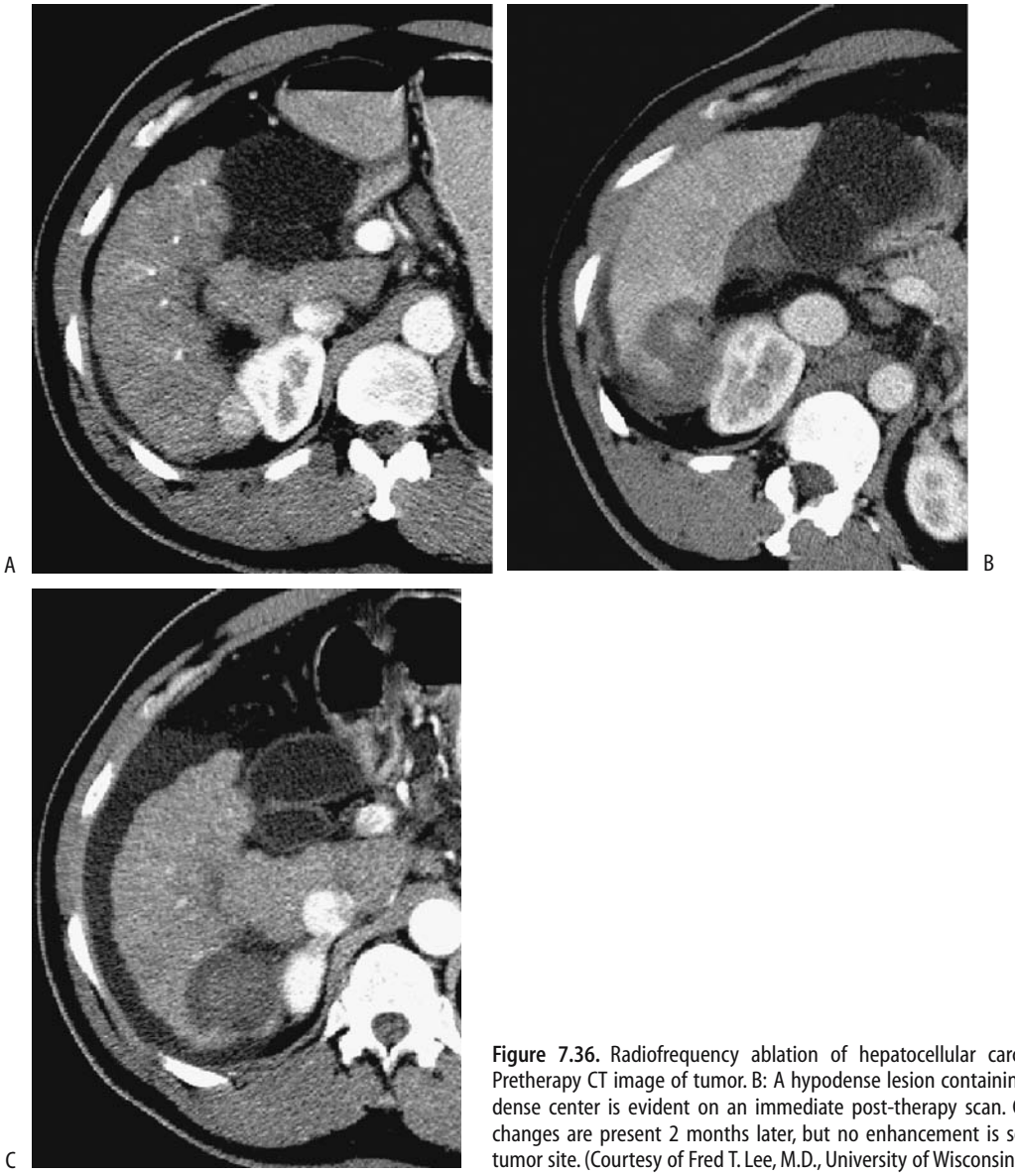

Figure 7.36. Radiofrequency ablation of hepatocellular carcinoma. A: Pretherapy CT image of tumor. B: A hypodense lesion containing a hyperdense center is evident on an immediate post-therapy scan. C: Residual changes are present 2 months later, but no enhancement is seen within tumor site. (Courtesy of Fred T. Lee, M.D., University of Wisconsin.)

combination increases extent of coagulation compared with use of radiofrequency alone [124].

Tumor necrosis is identified as a hypointense region on T2-weighted images and as a lack of enhancement on dynamic MR images. Whether the reverse is true, namely, whether residual hyperintensity on T2-weighted images and postcontrast enhancement signify residual tumor, is unclear. Appearance of new nodules signifies treatment failure, with new lesions often being more common than local recurrence.

A multicenter survey of 1139 patients by the Korean Study Group of Radiofrequency Ablation found major complications in 2.4%, with intrahepatic abscess being most common (125); one procedure-related death occurred due to peritoneal hemorrhage. Needle tract tumor seeding was reported by several institu-

tions. Whether heating surrounding tissue during needle withdrawal decreases the risk of tumor seeding remains to be established. Gastrointestinal perforation due to thermal damage is a potentially lethal complication.

Contrast-enhanced arterialphase CT reveals recurrence as a nodular, halo, or simply gross nodule enlargement pattern (126). FDG-PET/CT is also useful in evaluating therapy and following these patients after therapy.

Radiofrequency ablation has a high success rate in eliminating smaller tumors. It is effective for recurrent cancers after a partial hepatectomy. The major long term limitation to patient survival is recurrence of new cancers in these usually cirrhotic livers. Ablation can, however, serve as a bridge to liver transplantation.

Photocoagulation: Interstitial laser photocoagulation is performed by passing modified needles, under US, CT, or MR guidance, into a tumor, inserting a fiberoptic probe, and then heating the surrounding tissues using a high-power output laser generator. A wide region of necrosis is achieved with this technique. On-line MR thermometry provides control during laser ablation. Follow-up contrast-CT evaluates the degree of tumor necrosis. In general, best results are achieved with tumors <3 cm in diameter.

Using an open low field strength MR unit, lesion conspicuity and ease of puncture planning were significantly improved when the liver-specific contrast agent mangafodipir (Mn-DPDP) was used (7).

A neodymium:yttrium-aluminum-garnet (Nd:YAG) laser probe introduced with a percutaneously positioned laser application system achieved tumor necrosis with a 5-mm safety margin in 98% of 61 tumors (127); tumors up to 2 cm in diameter were treated with a single laser application. The number of needles used during therapy varies with tumor size; a single optical fiber and a single needle insertion were used in nodules < or = 2 cm, while two sessions with two laser illuminations per session were used for nodules >4 cm.

Percutaneous laser photocoagulation can be combined with other therapy, such as arterial chemoembolization; the practical advantages of such therapy are yet to be established.

Microwave Coagulation: Microwave coagulation therapy requires insertion of probes that act as antennae for externally applied microwave energy. One or more electrode is inserted into a tumor and the resultant heating leads to tumor coagulation necrosis. This technique is performed both via laparotomy and percutaneously. Superficially located hepatocellular carcinoma nodules appear most amenable to microwave therapy. Preliminary results, mostly from the Far East, appear encouraging (128).

Computer tomography shortly after microwave coagulation therapy identifies peripheral enhancement, which gradually disappears.

After microwave coagulation, MRI reveals tumors becoming more hypointense and heterogeneous on T1-weighted images and surrounded by a hyperintense rim on T2-weighted images, which enhances postgadolinium. This enhancing rim represents granulation tissue and hyperperfusing surrounding liver parenchyma. Lack of CT and MR contrast enhancement within the tumor and lack of flow signals on Doppler US imply tumor necrosis.

Complications of this technique include intratumoral hemorrhage, pleural effusion, ascites, abscess, subcapsular hematoma, portal vein thrombosis, and tumor dissemination.

Cryoablation: Cryoablation therapy, also called *cryosurgery* and *cryotherapy*, destroys tumor tissue by freezing and is used to treat both primary and metastatic tumors. Cryoablation appears to have a role in patients with multiple or advanced tumors deemed unresectable, as an adjunct to surgical resection and in patients with recurrent tumors. The size of induced freezing can be controlled, and thus precise control is feasible. Previously the relatively large size of available cryoablation probes necessitated at least a laparoscopic approach. Smaller probes are becoming available, and a percutaneous approach using imaging guidance is feasible. Liquid nitrogen is the freezing medium, although argon gas using less bulky equipment is also available.

Freezing causes ice crystals to form in tissue close to the cryoprobe. Cell death results from subsequent thawing and cell membrane rupture. Ice forms in small blood vessels slightly further from the probe and results in cell hypoxia.

Cryoablation is feasible on lesions adjacent to major blood vessels because flowing blood protects these vessels from freezing. On the other hand, a tumor edge may be incompletely frozen if the tumor abuts a blood vessel and temporary

interruption of blood flow through the vessel involved may be necessary. Cryoablation of tumors close to major bile ducts is avoided; duct wall necrosis and bile leakage are potential complications. Likewise, tumors close to the liver surface are preferentially resected rather than frozen.

Coagulation abnormalities are common after cryoablation. Over half of patients develop a reduction in platelets >50%. Possible hypothermia is a complication with prolonged therapy. Bleeding, at times massive, is believed to be due to parenchymal fragmentation secondary to freezing. A syndrome of multiorgan failure, severe coagulopathy, and disseminated intravascular coagulation has been described, called cryoshock phenomenon. A survey of centers performing hepatic cryoablation identified cryoshock in 1% of over 2000 patients, and cryoshock was believed to be responsible for some perioperative deaths (129). The procedure is not innocuous.

Intraoperative US reveals the ice ball to be hyperechoic with posterior shadowing, thus permitting control of the size of the frozen tissue. Ultrasonography shortly after freezing reveals a hypoechoic center surrounded by a hyperechoic rim, representing the interface between frozen and unfrozen tissues.

Computer tomography, US, or MRI monitors results of cryoablation. Probes and equipment designed to work with MRI should aid follow-up.

Follow-Up

Patient survival after initial tumor detection varies considerably; serum creatinine, alkaline phosphatase, and Okuda's stage are independent predictors of survival. Serum α-fetoprotein is of limited value in detecting early recurrence posthepatectomy.

Liver scintigraphy appears to have a role in detecting recurrence. Shortly after nonsurgical therapy, however, scintigraphy reveals wider tracer uptake than the actual tumor.

Recurrent tumors have been treated by carbon dioxide-enhanced US guided percutaneous ethanol injection, achieving cumulative patient survival rates of 81%, 71% and 44% for 1, 2 and 3 years, respectively (130).

Regression

An occasional hepatocellular carcinoma regresses spontaneously, a phenomenon generally associated with tumor necrosis.

Fibrolamellar Hepatocellular Carcinoma

A distinct variant is a fibrolamellar hepatocellular carcinoma. Developing in adolescents and young adults, usually it is not associated with underlying liver disease. These often large, solitary cancers tend to be well differentiated and have a good prognosis if completely resected, yet a number have already spread when first detected, with metastatic lymphadenopathy being not uncommon. In 31 patients with fibrolamellar hepatocellular carcinoma, 81% had a solitary tumor, 42% developed intrahepatic biliary obstruction, 87% had portal or hepatic vein invasion, extrahepatic grown was present in 42%, distant metastases were evident in 29%, and lymphadenopathy identified in 65% (131).

Serum α-fetoprotein levels tend to be normal in these patients. Transforming growth factor-β (TGF-β) is a pluripotent regulatory molecule present in liver but not in hepatocytes. It induces fibrosis in a number of diseases. An inverse correlation exists between TGF-β and serum α-fetoprotein levels. Although TGF-β is detected in a minority of hepatocellular carcinoma cells, it is present in a majority of fibrolamellar hepatocellular carcinomas. Nevertheless, the place of TGF-β in evaluating hepatocellular carcinomas is still unclear. TGF-β levels decrease after successful therapy.

Computed tomography shows a well-marginated, solid tumor with more uniform contrast enhancement than seen with conventional hepatocellular carcinomas. Some fibrolamellar carcinomas contain small, punctate calcifications. Central fibrosis (scar) is common, but hemorrhage and necrosis are uncommon. Arterial-phase images reveal heterogeneous enhancement with regions of hypervascularity.

Magnetic resonance imaging reveals a heterogeneous focal tumor that is hypointense on T1- and hyperintense on T2-weighted images. Intense, heterogeneous immediate postcontrast enhancement is common with these tumors

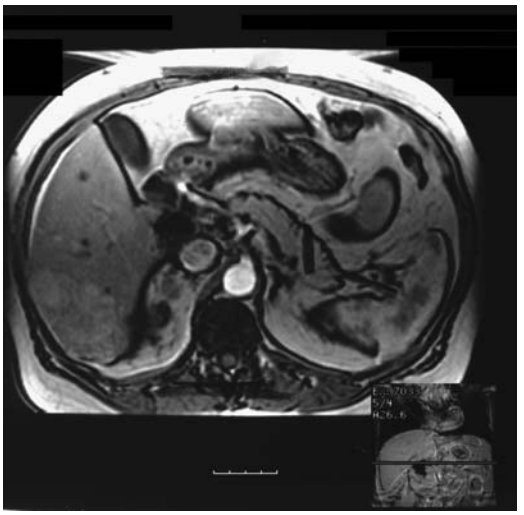

Figure 7.37. T2–weighted MRI identifies a fibrolamellar carcinoma as a slightly hyperintense right lobe tumor (arrow). It was almost isointense on T1-weighted images (not shown). (*Source:* Burgener FA, Meyers SP, Tan RK, Zaunbauer W. Differential Diagnosis in Magnetic Resonance Imaging. Stuttgart: Thieme, 2002, with permission.)

(Fig. 7.37). A central fibrous radiating scar is hypointense on both T1- and T2-weighted images, in distinction to the central scar of focal nodular hyperplasia, which is characteristically hyperintense on T2-weighted images. Also, fibrolamellar carcinoma scars are more prominent and often extend to the tumor periphery, findings not seen with FNH. The central scar enhances on delayed images in some tumors. Nevertheless, some fibrolamellar carcinomas mimic focal nodular hyperplasia.

Exceptions do occur. Some of these tumors are homogeneously hypointense on T1- and hyperintense on T2-weighted images with the central scar being markedly hyperintense on T2-weighted images, findings at variance from most fibrolamellar carcinomas.

Angiography shows these tumors to be hypervascular and contain numerous septa.

A more aggressive surgical approach than with a similar more conventional hepatocellular carcinoma appears reasonable with these tumors; even vascular reconstruction is justified.

Hepatocellular Carcinoma with Sarcomatous Changes

An occasional hepatocellular carcinoma contains a sarcomatous component, suggesting differentiation along both epithelial and mesenchymal lineages. Chondrosarcomatous differentiation and even a combination of chondrosarcomatous and osteosarcomatous components have developed, although in some of these tumors osteoclast-like giant cells probably are reactive and not neoplastic.

The diagnosis is usually made after resection.

These tumors have a poor prognosis. Some are multiple, suggesting intrahepatic metastases.

Biopsy results vary, depending on the site chosen for biopsy.

Combined Hepatocellular and Cholangiocarcinomas

Rare single tumors contain components of both hepatocellular carcinoma and cholangiocellular carcinoma. The original cell type is often conjecture. Some of these tumors presumably have one of two origins—either a double cancer or a stem cell origin, with the latter representing an intermediate type between a hepatocellular and a cholangiocarcinoma. Complicating the picture is that both a hepatocellular and a cholangiocellular carcinoma have occurred synchronously or metachronously independent of each other within the same liver; the lack of direct tumor contact, no histologic transition, and different immunohistochemical characteristics suggest separate histogenesis.

These combined tumors have one of two CT appearances: Those grossly resembling a hepatocellular carcinoma show early contrast enhancement and become hypodense during the portal venous phase, while those grossly resembling a cholangiocarcinoma reveal early peripheral contrast enhancement and contain heterogeneous hypodense regions or only central enhancement during the portal venous phase.

Adenosquamous/Squamous Carcinoma

A primary squamous liver carcinoma is rare and the is pathogenesis unknown. One hypothesis is

that the squamous cell component originates from a metaplastic transformation of adenocarcinoma cells. A number of these tumors develop in a setting of chronic infection or bile stasis. An occasional one presents as a liver abscess.

These tumors exhibit an aggressive growth pattern with early local and distant spread.

Lymphoma

Primary

Primary hepatic lymphomas are rare and their diagnosis difficult. The occasional association with hepatitis C virus has already been mentioned. Most of these tumors are non-Hodgkin's T-cell lymphomas. In distinction to secondary liver lymphomas, these usually present as a discrete tumor. Less common are primary low-grade B-cell mucosa-associated lymphoid tissue (MALT) lymphomas, which often consist of a dense portal tract lymphoid infiltrate mimicking hepatitis or a bile duct inflammatory condition.

These homogeneous lesions appear either anechoic or hypoechoic with US and mimic a cyst, although unlike a cyst they lack through-transmission. Some are surrounded by a halo. They tend to increase in size rapidly, with tumor volume doubling time being measured in days.

Most primary liver lymphomas are hypointense on T1- and hyperintense on T2-weighted images. They show heterogeneous postcontrast enhancement.

Secondary

Non-Hodgkin's lymphoma is more often focal than Hodgkin's lymphoma. Some secondary liver lymphomas infiltrate diffusely and lead to acute liver failure. Imaging tends to underdetect liver involvement. Calcifications develop in some tumors. Portal and periportal intrahepatic infiltrates compress adjacent bile ducts and are a cause of jaundice (Fig. 7.38).

Secondary lymphomas typically are hypointense on T1- and hypo- to hyperintense on T2-weighted images. Postcontrast enhancement varies considerably; tumors that are moderately hyperintense on T2-weighted images tend toward intense enhancement during early postgadolinium images, while those mildly

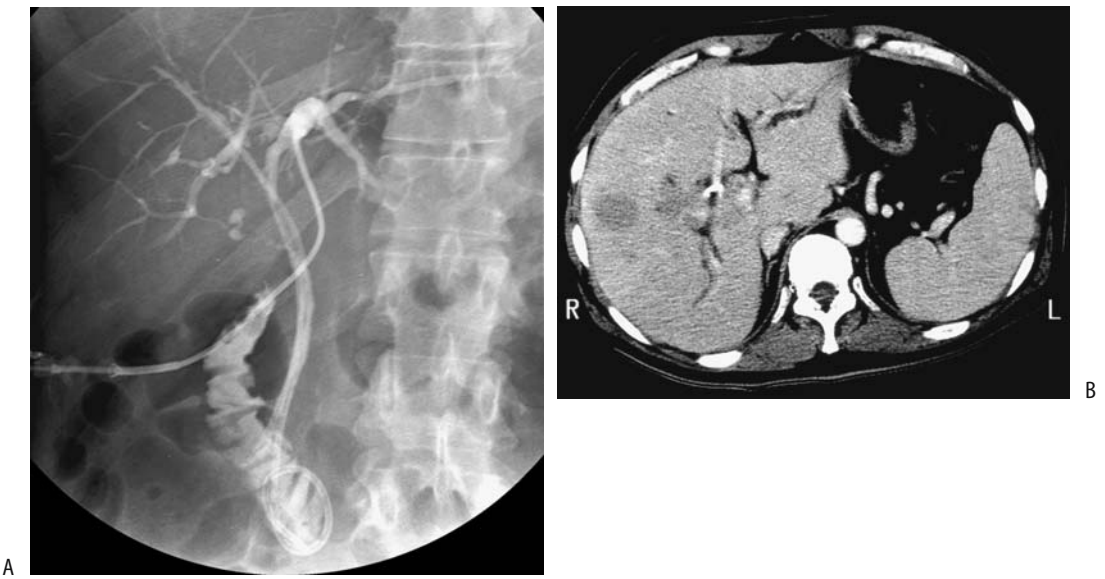

Figure 7.38. Jaundice due to liver non-Hodgkin's lymphoma. A: A cholangiogram reveals a biliary drainage catheter in place and numerous narrowed intrahepatic bile duct segments. B: A contrast-enhanced CT image shows several focal hypodense tumors. Other images identified intrahepatic tumor tracking along portal vessels. (Courtesy of Patrick Fultz, M.D., University of Rochester.)

hypo- to mildly hyperintense on T2-weighted images show only minimal early postgadolinium enhancement. Not uncommonly, immediate postcontrast images reveal a perilesional or peripheral enhancement.

Use of phosphorus MR spectra from P-31 MR spectroscopy appears potentially useful in evaluating liver involvement with lymphoma.

Most patent portal vein branches within a tumor detected by imaging imply a benign lesion, the exceptions being intrahepatic cholangiocarcinoma and lymphoma; even with periportal lymphomatous infiltration, not uncommonly patent portal vein branches are evident. Nevertheless, some primary liver lymphomas do invade the portal vein and result in tumor thrombi.

Leukemia

Leukemic infiltration of the liver ranges from focal to diffuse. At times a chronic lymphocytic leukemia transforms into a high-grade lymphoma. Some infiltrates surround portal vessels.

Hepatoblastoma

Clinical

A hepatoblastoma is the most common primary liver neoplasm in children under 3 years. These tumors occur throughout the pediatric age range, with only a rare one encountered in an adult. A male predominance is evident. It occurs in siblings. Prevalence is increased in Beckwith-Wiedemann syndrome and in hemihypertrophy. In some patients prior maternal exposure to certain drugs and chemicals appears to play a role.

A common presentation in young children is an asymptomatic abdominal mass. A large liver tumor is typical in adults. These tumors produce a number of hormones and some patients develop hypoglycemia, hypercalcemia, polycythemia, and precocious puberty in males. Most of these tumors are associated with an elevated serum α-fetoprotein level, which aids in distinguishing them from other, similar-appearing benign tumors.

This tumor probably originates from embryonal hepatic tissue and usually consists of epithelial cells or, less often, a mixture of epithelial and mesenchymal cells. The latter occasionally contains differentiated cells, such as osteoid that calcifies. These tumors readily metastasize. One of the roles of imaging is to detect metastases and determine resectability. Recurrence after therapy, including other organ involvement, is common in adults.

Imaging

A hepatoblastoma detected in an adult has no specific defining imaging findings. In children, from an imaging viewpoint a hepatoblastoma is similar in appearance to a hepatocellular carcinoma (Fig. 7.39). It readily invades adjacent vessels. When extensive, a hepatoblastoma involves almost the entire liver. Some contain both cystic and solid components. Necrosis and calcifications develop in some. An occasional one contains ossified tissue.

Precontrast CT reveals a hypodense mass. Variable contrast enhancement is seen postcontrast.

A typical US pattern is a hyperechoic lesion with poorly defined margins. The degree of echogenicity reflects hemorrhage and necrosis within the tumor.

Similarly to many other liver tumors, a hepatoblastoma is hypointense on T1- and hyperintense on T2-weighted MRI, although

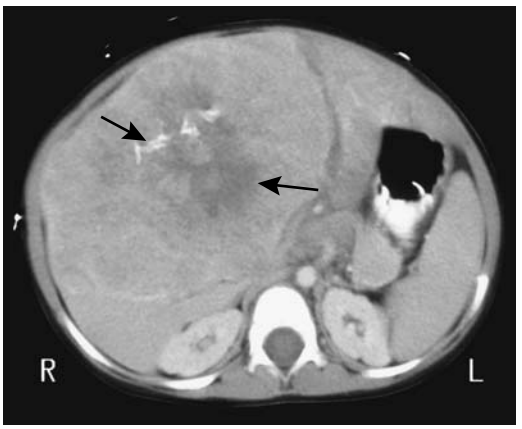

Figure 7.39. Hepatoblastoma with pulmonary metastases in a 2-year-old girl. The tumor was discovered incidentally. Contrast-enhanced CT reveals a large slightly enhancing tumor (arrows) containing central necrosis and calcifications. (Courtesy of Luann Teschmacher, M.D., University of Rochester.)

considerable heterogeneity is often evident. Magnetic resonance, especially 3D MRA, is useful in defining vascular invasion prior to partial hepatectomy.

Angiography reveals a hypervascular tumor containing neovascularity.

Occasionally a hepatoblastoma shows uptake of sulfur colloid; a hepatoblastoma, however, does not have uptake of both Tc-99m–sulfur colloid and HIDA, thus differentiating these tumors from focal nodular hyperplasia.

Sarcoma

Almost any type of sarcoma can develop in the liver, including a rare primary liver osteosarcoma.

Angiosarcoma

Hepatic angiosarcomas are rare, yet still are the most frequent primary mesenchymal liver tumor. Most develop in elderly men and most have a very poor prognosis. Metastasis is common, with survival measured in months.

A distinct association exists with prior exposure to certain chemical carcinogens, such as thorium dioxide (Thorotrast), vinyl chloride, arsenic salt therapy, cyclophosphamide treatment, and anabolic steroids. Many of these tumors, however, develop with no known predisposing factors. An angiosarcoma can be associated with disseminated intravascular coagulopathy.

Most angiosarcomas consist of multifocal but well-marginated nodules throughout the liver, seen with precontrast CT as hypodense tumors. Commonly superimposed hemorrhage modifies their imaging appearance considerably. Some display hypointense central regions on T2-weighted images and postcontrast peripheral nodular enhancement, and superficially mimic a hemangioma, but central hemorrhage is common and their heterogeneous, asymmetrical enhancement usually allows differentiation between these entities. Occasional massive tumor invasion is not detected by CT or US but is identified by MRI.

Not uncommonly, angiosarcomas are hypointense on T1- and markedly hyperintense on T2-weighted images, with hypointense septa identified on T2-weighted images; the overall appearance can mimic a cavernous hemangioma.

These tumors decrease in size after chemotherapy, gradually becoming isointense to liver and enhancing negligibly postcontrast.

Fibrosarcoma

Fibrosarcomas and its benign counterpart are rare in the liver. Solitary fibrous liver tumor in three patients, two benign and one malignant, presented as well-marginated, heterogeneously enhancing tumors (132).

Leiomyosarcoma

A primary hepatic leiomyoma or leiomyosarcoma is uncommon. Some of these patients have had another previous malignancy, and a genetic predisposition to neoplasms is postulated. Some leiomyosarcomas originate in the adjacent ligamentum teres. Most metastatic leiomyosarcomas are from the gastrointestinal tract, with an occasional one being from the uterus, vena cava, or other extraperitoneal structures.

Most patients present with right upper quadrant pain and hepatomegaly.

Imaging shows similar findings for both primary and metastatic tumors. A large, irregular tumor is common. Computed tomography appearance ranges from homogeneous with little enhancement to heterogeneous and peripheral enhancement. Some contain cystic regions. Heterogeneous contrast enhancement is common, with enhancement ranging from central to peripheral. An internal low-density region suggests fluid.

Most of these tumors are homogeneous and hypointense on T1-weighted MR images, while T2-weighted images reveal most to be sharply outlined, homogeneous, and markedly hyperintense, mimicking a hemangioma; metastases heterogeneous on T1- or T2-weighted images typically contain varying degrees of necrosis and hemorrhage (Fig. 7.40).

Percutaneous biopsy should be diagnostic of a leiomyosarcoma.

Histiocytoma

Although not uncommon in extremity soft tissues, primary malignant liver fibrous histio-

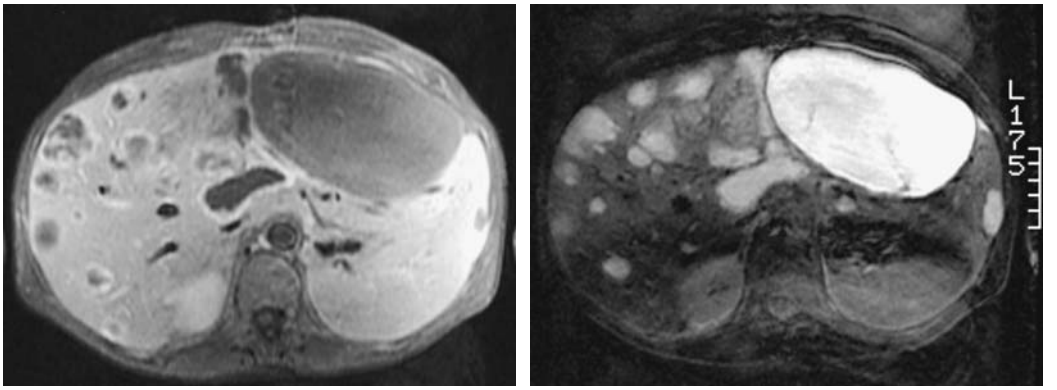

Figure 7.40. Metastatic leiomyosarcoma. A T1-weighted MRI (A) reveals multiple hypointense and a T2-weighted image (B) reveals hyperintense tumors. The patient had a primary sarcoma resected about 10 years previously. (Courtesy of Patrick Fultz, M.D., University of Rochester.)

cytoma is extremely rare. These tumors present with a palpable mass or simply with an enlarging liver. Most are large at initial presentation. Some contain calcifications.

These are poorly marginated tumors showing inhomogeneous contrast-enhancement. Their differential diagnosis includes hepatocellular carcinoma, angiosarcoma, and a hypervascular metastasis.

Undifferentiated Carcinoma/Sarcoma

Undifferentiated Embryonal Cell Carcinoma/Sarcoma

Also called *mesenchymal sarcoma*, *undifferentiated sarcoma,* and *malignant mesenchymoma*, an undifferentiated embryonal cell carcinoma is a rare, highly malignant tumor found mostly in older children and young adults. These tumors grow rapidly, patients have few symptoms, and often the first sign is an abdominal tumor.

These tumors are unique in that they are mostly solid, yet imaging often suggests the presence of a cystic component—an appearance secondary to their high water content within a myxoid stroma (Fig. 7.41). Superimposed hemorrhage and necrosis are common. Internal calcifications and a surrounding fibrous capsule are evident in some. Imaging identifies a well-encapsulated multilocular, often heterogeneous tumor. Some have peripheral contrast enhancement of a fibrous rim, with the rim being hypointense on both T1- and T2-weighted MR images.

Some appear solid at US but more cystic at CT and MRI, a finding useful in suggesting the diagnosis. T1-weighted MRI reveals a hypointense tumor, modified by scattered high signal intensities from hemorrhage, while T2-weighted MRI shows them to be mostly hyperintense. Heterogeneous, irregular enhancement, often

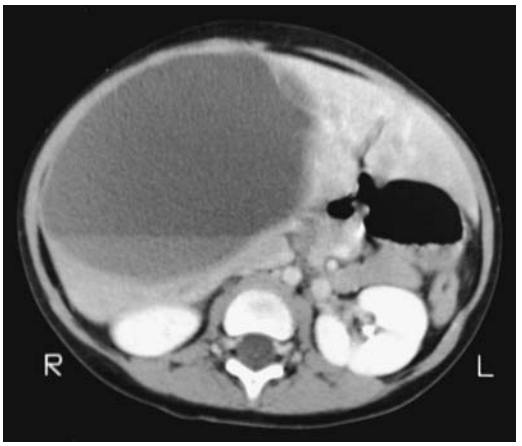

Figure 7.41. Undifferentiated embryonal sarcoma. Contrast-enhanced CT reveals a liver cyst-like tumor with a fluid–fluid level. These are mostly solid tumors, but due to their high water content CT often shows them to be of almost water density. (Courtesy of Luann Teschmacher, M.D., University of Rochester.)

more peripheral in location, is evident on postcontrast images.

Some of these tumors are initially misdiagnosed as hepatobiliary cysts, with a correct diagnosis made only after recurrence.

Undifferentiated (Rhabdoid) Tumor

A rare undifferentiated malignant primary liver tumor containing rhabdoid features develops in infants. Superficially, tumor cells resemble cells of muscle origin. Some contain neuroepithelial differentiation. The α-fetoprotein level is normal or only slightly elevated.

Metastases

Clinical

In a patient with a known nonhepatic cancer, what is the risk of a small hepatic tumor, discovered by CT, being a metastasis? A study of almost 3000 patients with cancer found small hepatic tumors (1 cm or less in diameter or too small to characterize by CT) in 13%, among these tumors interval growth was identified in 12% of patients and these tumors presumably represent metastasis (133); further analysis revealed that small hepatic tumors were metastatic in 4% of patients with lymphoma, 14% of those with colorectal carcinoma, and 22% of breast cancer patients.

Patients undergoing systemic chemotherapy for breast cancer metastatic to the liver develop an appearance similar to cirrhosis. Computed tomography reveals liver capsule retraction, an irregular lobular margin, segmental volume loss, and caudate lobe enlargement, a finding also seen in cirrhosis; retraction occurs at sites of metastases. Pathologic findings suggest regenerative nodules. An indented capsule and fibrous septa can extend into liver parenchyma, an appearance presumably due to chemotherapy-induced tumor regression followed by healing and scar formation. The overall appearance has been called *hepar lobatum,* a term of old used to describe liver syphilis.

Septicemia is a recognized presentation of an occult malignancy, especially a colorectal cancer. Likewise, some colorectal cancer liver metastases become infected and the patient presents with a liver abscess. Whether some anaerobic bacteria tend to grow selectively in tumor nodules rather than normal liver parenchyma is conjecture.

A solitary liver tumor detected synchronously with a gastric cancer is usually presumed to be a metastatic focus. In high-risk regions, such as East Asia, a concomitant hepatocellular carcinoma should also be considered in the differential diagnosis.

Detection

Most metastases have a nodular appearance and are sharply demarcated from adjacent liver parenchyma, at times by inflammation or fibrosis; diffuse tumor infiltration, as occasionally seen with primary liver carcinomas and leukemia, is unusual; extensive intrahepatic obstruction of lymphatic flow by metastases is seen on postcontrast CT as hypodense regions throughout the liver.

Calcifications develop in metastatic well-differentiated mucinous adenocarcinomas. Occasionally visible with conventional radiography, CT reveals them as fine, speckled calcifications. They are echogenic and have posterior shadowing with US.

Division between hypo- and hypervascular metastases (Table 7.15) is not absolute, and overlap occurs. Thus an occasional hypovascular lymphoma and hepatocellular carcinoma and an occasional isovascular metastasis are encountered. Breast carcinomas, in particular, although usually somewhat hypervascular, exhibit a wide range of imaging appearances. Some liver metastases, especially neuroendocrine and ovarian tumors, have a cystic component (Fig. 7.42).

Table 7.15. Vascular appearance of liver metastases

Hypovascular	Hypervascular
Colon adenocarcinoma	Renal cell carcinoma
Pancreatic adenocarcinoma	Neuroendocrine neoplasms
Gastric adenocarcinoma	Islet cell carcinoma
Transitional cell carcinoma	Carcinoid
	Malignant pheochromocytoma
	Thyroid carcinoma
	Some sarcomas
	Malignant melanoma

Figure 7.42. Multiple cystic liver metastases from a cystic pancreatic acinar carcinoma.

Comparison Studies

A number of imaging comparison studies are difficult to place in perspective because they contain an unknown number of false positive foci. In general, combining contrast enhanced CT, US and MRI allows detection of false positive tumors and distinguishing them from metastases.

A number of earlier studies concluded that MRI is superior to CT in detecting liver metastases. In particular, early postcontrast breath-hold T1-weighted and T2-weighted fat-suppressed images are very useful. Whether the introduction of multislice CT has changed these conclusions is not yet clear.

Pulse inversion harmonic US using a contrast agent identifies a similar number of metastases as helical CT (134); it detects more and smaller metastases than conventional US. In one study pulse inversion harmonic US detected 90% of metastases found on ferumoxides-enhanced MRI (135).

CT arterial portography and MRI (including arterial dominant phase, gadolinium-enhanced and spoiled gradient-echo imaging) appear similar in metastasis detection (136). Earlier studies had suggested that SPIO-enhanced MR sensitivity for metastases detection was inferior to CT arterial portography, but more recent studies show these two techniques to be similar in accuracy.

Imaging Techniques

In the United States, Canada, and parts of Europe, CT is the preferred screening modality for suspected liver metastases. In some regions US is more often performed. For hypovascular hepatic metastases, unenhanced helical CT detected 66%, arterial-dominant phase CT 74% and portal-dominant phase CT 92% of focal tumors (137); portal phase imaging depicted significantly more of these tumors than did the other two phases. Whether all three phases need be obtained for suspected hypovascular metastases continues to be debated. MRI, especially using various contrast agents, continues to gain ground.

Liver metastases range from hypoechoic to hyperechoic. In general, tumor echogenicity is related to tumor vascularity. Thus the more vascular metastatic neuroendocrine tumors tend to be hyperechoic, while less vascular metastases are more hypoechoic. No Doppler signal is observed in avascular or necrotic metastases.

Contrast-enhanced harmonic US modifies the late-phase appearance of liver parenchyma. Thus with pulse inversion harmonic US normal liver parenchyma appears hyperechoic relative to focal metastases (Fig. 7.43). Compared to unenhanced US, a contrast agent increases metastases detection sensitivity and specificity by improving metastases conspicuity. Some metastases develop a rim-like enhancement after contrast injection.

Intraoperative US is an accurate tool for detecting unsuspected metastases and is used as an aid for intraoperative biopsies and when resecting metastatic foci. Nevertheless, compared to eventual pathological study, even intraoperative US detects only about 80% of metastases. Laparoscopic US also identifies biopsy sites.

Precontrast MRI reveals most hypovascular metastases to be hypointense on T1- and isointense to slightly hyperintense on T2-weighted images, findings similar to many other liver lesions. Most metastases are poorly marginated. Nevertheless, considerable variability in appearance exists. A hyperintense T1-weighted image is seen with hemorrhage. Mucin-containing tumors also tend toward a hyperintense signal on T1-weighted images. Tumor necrosis leads to a hypointense center on T2-weighted images. Suggesting a metastasis is a

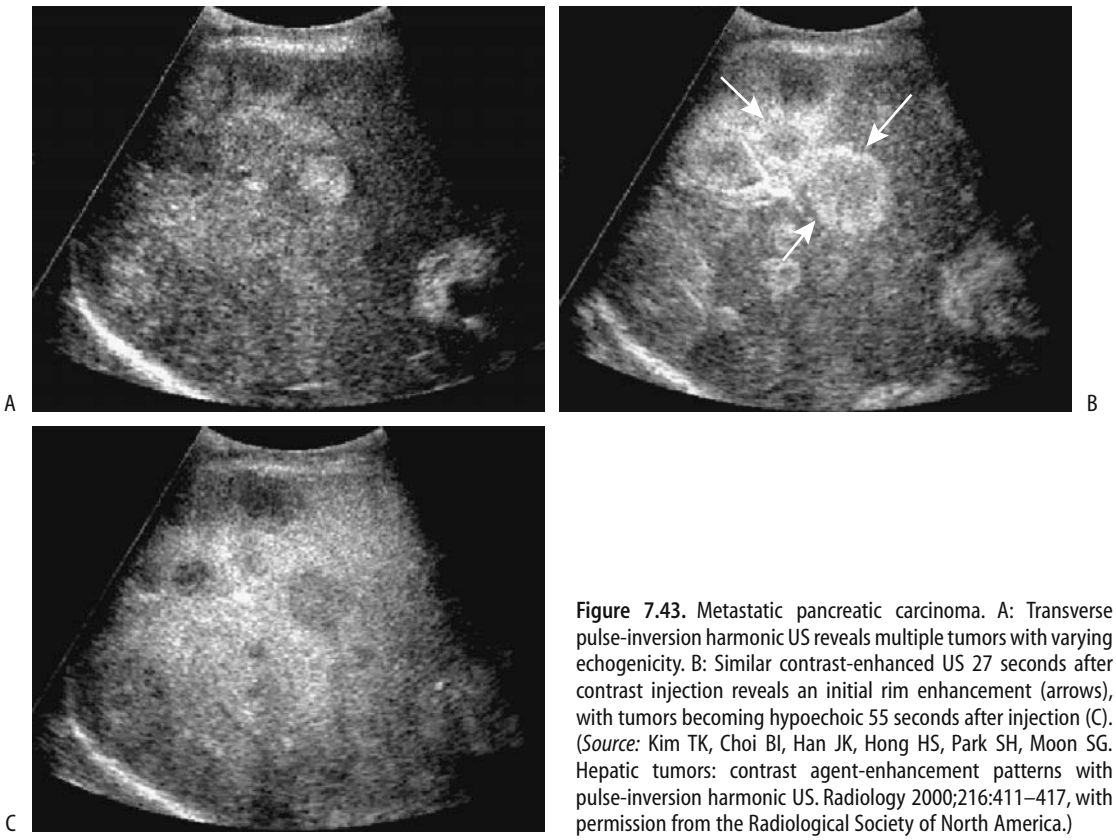

Figure 7.43. Metastatic pancreatic carcinoma. A: Transverse pulse-inversion harmonic US reveals multiple tumors with varying echogenicity. B: Similar contrast-enhanced US 27 seconds after contrast injection reveals an initial rim enhancement (arrows), with tumors becoming hypoechoic 55 seconds after injection (C). (*Source:* Kim TK, Choi BI, Han JK, Hong HS, Park SH, Moon SG. Hepatic tumors: contrast agent-enhancement patterns with pulse-inversion harmonic US. Radiology 2000;216:411–417, with permission from the Radiological Society of North America.)

heterogeneous signal intensity, an irregular margin, or a surrounding high signal intensity ring (halo). This is in distinction to hemangiomas and cysts, which tend to be more homogeneous, contain well-defined margins, and have a very high signal intensity on T2-weighted images.

Most studies suggest that gadolinium-enhanced MRI detects more metastases than unenhanced MRI. Most hypovascular metastases are best defined on portal venous phase imaging when maximum enhancement of normal liver parenchyma occurs. On immediate postcontrast images these metastases tend to mimic cysts, but delayed views reveal gradual contrast enhancement and an apparent decrease in tumor size, findings not evident with cysts.

Most metastases have a marked increase in lesion-to-liver contrast on ferumoxides-enhanced T2-weighted images (81) and this technique detects more metastatic nodules than nonenhanced MR. Similarly, mangafodipir enhanced MR also detects metastases. Nevertheless, compared to eventual pathological study, even contrast enhanced MRI misses some tumors. Pre- and serial postcontrast images provide most information.

The role of MR arterial portography is still evolving. Preliminary results using a turbo FLASH MR technique suggest that tumors >10 mm can be detected.

Somatostatin-receptor scintigraphy is useful for suspected endocrine metastases.

Fluoro-deoxy-D-glucose (FDG)-PET is evolving into a viable imaging modality for detecting liver metastases. Both adenocarcinomas and sarcomas reveal increased uptake. Preliminary evidence suggests that it rivals CT in accuracy. One should keep in mind, however, that increased uptake also occurs in some abscesses.

Radioimmunoscintigraphy with Tc-99m–labeled anti-CEA monoclonal antibody reveals uptake in some liver metastases. This study appears most useful with a rising CEA level.

Rim Enhancement

Metastases reveal varying postcontrast perilesional (rim) enhancement, best seen during the arterial phase. Some tumors compress adjacent liver parenchyma and a thick tumor border represents surrounding inflammation, desmoplastic reaction, small vessel proliferation, and eventual atrophy, although this finding explains perilesional enhancement only partly. In some tumors rim enhancement represents viable tumor surrounding a necrotic center. Aside from an abscess and an occasional hepatocellular carcinoma, few other common conditions have a similar appearance. Peripheral enhancement is also seen with cavernous hemangiomas, but their enhancement is more irregular and nodular in appearance.

Ultrasonography of some metastases reveals a hypoechoic halo or doughnut appearance, with the hypoechoic rim representing proliferating tumor cells rather than surrounding inflammation.

Similar to CT, during arterial-phase MRI, some larger hypovascular metastases reveal a peripheral enhancing rim; this enhancement gradually extends centrally, and the overall appearance superficially mimics a hemangioma. These metastases are poorly identified on capillary phase imaging. An occasional metastasis has a hypointense rim on delayed postgadolinium MRI, called the *peripheral washout sign*, described as being specific for a malignancy.

Hypovascular Metastases

Size of colorectal carcinoma metastases differ on precontrast and postcontrast CT images. Thus during tumor follow-up not only the same modality but also a similar technique should be employed.

About a third of colorectal metastases <1 cm in diameter enhance homogeneously. Larger ones tend to develop a cauliflower-like appearance and CT arteriography often detects rim enhancement. Most metastases are detected with portal-phase imaging, but arterial-phase imaging does increase tumor conspicuity and diagnostic confidence. Postcontrast CT identified 85% of tumors found at resection in patients with liver metastases from colorectal cancer and is useful in selecting patients for resection (138); false-positive findings included hemangiomas, hemorrhage, periportal fibrosis, and even normal parenchyma.

Computed tomography arterial portography is more sensitive than biphasic CT or US in detecting metastatic colorectal cancer, especially for lesions <10 mm in diameter. Sensitivities of colorectal cancer metastases detection for CT arterial portography, CT hepatic arteriography, and both procedures combined were 80%, 83%, and 87%, respectively (139); combined CT arterial portography and CT hepatic arteriography significantly improved metastases detectability, and the authors recommend both procedures for pretherapy evaluation. A practical limitation of CT arterial portography is a high false-positive rate due to perfusion anomalies and the presence of nonneoplastic hypervascular tumors. Computed tomography arterial portography also tends to overestimate tumor size.

In patients with known colorectal metastases, Regardless of tumor size, the accuracy of SPIO-enhanced T2-weighted sequences is significantly greater than with precontrast sequences (140). Also, SPIO-enhanced MR sensitivity appears to be greater than with contrast-enhanced CT.

In patients treated for colorectal cancer and suspected of harboring a recurrence, a number of studies have confirmed the superiority of FDG-PET imaging over CT; FDG-PET detects more unsuspected metastases.

Bone scintigraphy with Tc-99m–hydroxymethylene diphosphonate (HMDP) occasionally reveals ring-like tracer activity around a liver metastasis from colon carcinoma. The reason for such extraosseous radionuclide accumulation is not known.

An occasional colorectal carcinoma exhibits somatostatin receptors. The somatostatin analogue octreotide used to treat neuroendocrine tumors might be useful in this subgroup of cancers, yet little data exists on this topic.

In women with known or suspected liver metastases from breast cancer, prospectively evaluated with triple phase (precontrast, arterial phase, and portal venous phase) CT, portal venous phase is most accurate, and the routine use of precontrast and arterial phases does not appear warranted when the clinical question is simply the presence or absence of liver metastases (141).

Computed tomography and MRI detect liver metastases from cystic ovarian carcinomas either as cystic or solid tumors; as expected, the cystic components are hypodense on CT and hypointense on T1-weighted imaging and thus mimic other cystic tumors, but solid components show early peripheral globular enhancement and delayed central enhancement both on CT and MR imaging (142).

Hypervascular Metastases

Hypervascular metastases tend to be hyperintense on T2-weighted images. They are best identified on early arterial-phase postcontrast MRI when they are hyperintense to normal liver parenchyma. They reveal an immediate postcontrast peripheral enhancement, which gradually extends centripetally, followed by peripheral washout. Some are heterogeneous and some show an inconstant tumor blush. Small hypervascular metastases tend toward initial homogeneous enhancement, similar to hemangiomas, and then gradually become isointense. In general, on delayed images these metastases tend to wash out earlier than hemangiomas, although especially with smaller hypervascular metastases some imaging overlap exists with hemangiomas.

Melanoma

Melanomas range from hyper- to hypointense on both T1- and T2-weighted MRI, probably due to paramagnetic property of melanin pigmentation. Some melanomas are heterogeneous in appearance. They are hypervascular (Fig. 7.44). A combination of precontrast and portal venous-phase CT images appears as effective as arterial and portal venous-phase images in detecting metastatic melanomas (143).

Therapy

Only sparse literature discusses multimodality therapy in patients with colorectal carcinoma and unresectable liver metastases. Occasional patients undergo primary colorectal carcinoma resection and hepatic arterial infusion chemotherapy; shrinkage of liver metastases then allows hepatic lobectomy.

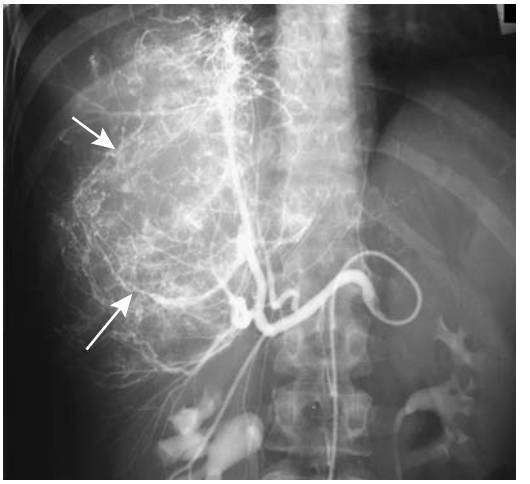

Figure 7.44. Metastatic melanoma. Angiography reveals a large confluent hypervascular tumor (arrows). (Courtesy of Oscar Gutierrez, M.D., University of Chile, Santiago, Chile.)

Antiangiogenic therapy, inhibiting endothelial growth factor activity, is still in its infancy and few conclusions can be drawn.

Resection

Liver metastases of primary tumors that normally do not drain into the portal vein are generally not considered for resection. Systemic spread of these tumors is also generally evident. Resection of liver metastases of the upper gastrointestinal tract and small bowel and of pancreatic cancers is uncommon, although an aggressive surgical approach of gastric metastases suggests improved prognosis in patients with a solitary metastasis if adequate tumor-free margins can be obtained. Few metastases are resected from a gynecologic primary. Resection of metastatic renal cell carcinoma (discussed later), Wilms' tumor, and adrenocortical carcinoma are probably still indicated. Long-term survival after hepatectomy for gallbladder carcinoma is anecdotal.

Practically, most hepatic resections are performed for metastatic colorectal and neuroendocrine tumors. With appropriate patient selection, hepatic resection of colorectal metastases to the liver can achieve 5-year survival in about one third; eventual liver failure is a common cause of death, but survival is often prolonged with resection, assuming that all metastatic foci are identified.

Intraoperative liver palpation during initial colon cancer resection continues to be a common technique of detecting liver metastases. The liver cannot be palpated during laparoscopic cancer resection, and this useful technique, generally performed during an open resection, is thus lost. Intraoperative US, either open or laparoscopic, is superior not only to preoperative US but also to surgical exploration. In some institutions results of initial intraoperative US are used to decide whether to proceed with resection, perform cryosurgery, or whether the patient is considered unsuitable for these therapies and the incision is closed. While intraoperative US provides guidance to resection and possibly reduces the number of unnecessary resections, this optimistic outlook should be balanced against available long-term evidence. The results are mixed from a number of studies about whether intraoperative liver US is useful in patients undergoing curative colorectal cancer surgery.

Intraoperative laparoscopic US is feasible as part of laparoscopic colorectal cancer resection; all liver segments can be scanned by US through a single port site. Laparoscopic US is probably more sensitive in identifying metastases than CT or preoperative US.

Surgical resection is feasible in some patients with metachronous liver metastases from renal cell carcinoma. Mean survival can be increased with such an approach, realizing that such surgery is associated with significant morbidity and mortality. Also, often multiple organ metastases are present by the time liver metastases are discovered.

An imaging study is useful shortly after resection to establish the baseline appearance. Resection margins are hyperintense on T2-weighted MRI and vary in their postcontrast enhancement. These findings gradually subside over a several-month period.

Repeat resection of recurrent hepatic metastases is mostly anecdotal but seems to occasionally improve prognosis as long as the tumor is confined to the liver.

Radiotherapy

Stereotactic irradiation of liver metastases consists of a focused radiotherapy beam delivered to a tumor with relative sparing of surrounding liver tissue. “Significantly improved survival” was achieved in 43 patients during a phase 2 trial compared to patients treated for palliation (144).

Systemic Chemotherapy

The MRI changes after systemic chemotherapy are complex and poorly understood. Some patients develop an increase in tumor signal intensity while others have a decrease.

Some evidence suggests that 18F-fluorouracil-PET of colorectal metastases is useful prior to fluorouracil chemotherapy; PET uptake by metastases predicts subsequent tumor growth rates after therapy.

Intraarterial Chemotherapy

Most clinical trials of intraarterial chemotherapy for liver metastases were performed in the late 1980s and early 1990s; most studies reported about half of patients responding, compared to 10% to 20% with systemic chemotherapy, but with little or no survival differences between the two regimens. The use of additional intraarterial agents appears to improve response, but few studies are available, so firm conclusions cannot be drawn. Currently intraarterial chemotherapy is used mostly for patients with unresectable colorectal liver metastases but without evidence of extrahepatic metastases.

An ideal intraarterial chemotherapeutic agent is extracted during its first pass through the liver. Most commonly used agents consist of 5-fluorouracil (FU) and its derivatives. A several times greater intrahepatic agent concentration is achieved with intraarterial injection compared to systemic delivery. A limiting factor for a therapeutic response is the rapid elimination of cytostatic agent from tumor cells. Another limitation is development of progressive extrahepatic tumors.

The primary toxicities of intraarterial chemotherapy are biliary and small artery intimal damage. Once damage is established, imaging findings mimic primary sclerosing cholangitis; the current data suggest that damage is primarily small vessel ischemic in nature. In one center, intrahepatic bilomas developed in almost 10% of treated patients with metastatic liver tumors (145).

Either DSA and CTA prior to each session of transcatheter arterial chemotherapy detects any underlying complications. Perfusion scintigraphy also evaluates pump function after implantation of an infusion pump. Injection of a radiotracer at a flow rate similar to that used with an infusion pump provides a distribution pattern for subsequently injected chemotherapeutic agents.

At times extrahepatic collateral vessels feed a metastasis. These collaterals can be occluded with a cyanoacrylate-Lipiodol mixture infusion into the feeding artery, performed under temporary proper hepatic artery balloon occlusion, thus improving subsequent chemotherapy.

Intraportal Chemotherapy

The rationale of portal vein infusion chemotherapy is that, compared to IV therapy, relatively high doses can be delivered to the liver.

Metastatic colorectal cancer presumably spreads to the liver via the portal venous system. With growth, these metastatic nodules are perfused primarily by arterial blood and thus most chemotherapy is via the hepatic artery route. Such delivery, however, may not reach very small metastatic nodules, and an intraportal venous infusion route appears necessary to cover these. In spite of such reasoning, cytotoxic portal vein infusion therapy has not lived up to expectations and is little practiced.

Hypoxic Perfusion

Some patients with liver metastases have been treated with hypoxic liver perfusion. The hepatic artery is occluded with a balloon catheter and perfused with saline–mitomycin C, followed by gelatin sponge embolization; any role for such a procedure in local disease control remains to be established.

Percutaneous Ethanol Injection

In distinction to hepatocellular carcinomas, liver metastases respond poorly to percutaneous ethanol injection, and such therapy currently is rarely performed, having been replaced by other percutaneous techniques.

Single-episode percutaneous ethanol injection in patients with large or multiple liver metastases, not eligible for other treatments, results in tumor necrosis in a minority of patients. Accurate tumor localization, of necessity, is vital with any percutaneous ablation technique. Fusion of CT and FDG-PET images appears useful for lesions difficult to visualize with one imaging modality alone. Also, whole-body FDG-PET imaging identifies extrahepatic metastases.

Radiofrequency Ablation

Indications and contraindications for RF tumor ablation, photocoagulation (laser-induced thermotherapy), microwave therapy, and cryoablation of metastases are similar. Small solitary metastases are ideal candidates for ablation.

Radiofrequency tumor ablation efficacy varies considerably depending on the tumor size and type. Either percutaneous or intraoperative therapy is feasible, with the latter performed in conjunction with partial hepatectomy to destroy unresectable metastases. Most percutaneous ablation is performed using US guidance, although for tumors not visualized by US, MRI guidance in an open magnet is an option (146). Focal tumors smaller than about 3 to 4 cm in diameter yield the best results. Using US guidance, 91% of 100 treated metastases (mostly colorectal) were eradicated (147); follow-up revealed tumor control to be similar for percutaneous (90%) and intraoperative ablations (94%). Among 117 treated patients estimated 1- and 3-year survival rates were 93% and 46%, respectively (148); of note is that a majority of local recurrence occurred within 1 year of therapy. After US-guided percutaneous RF ablation of breast cancer metastases, serial CT follow-up showed complete necrosis in over 90% of tumors (149); on the other hand, in a majority of these patients new metastases developed during follow-up.

Reported complications consist of subcapsular hematomas, bilioperitoneal fistulas, and abscesses. Portal vein thrombosis is more common in cirrhotic than in noncirrhotic livers. Hypertensive crises have developed. Liver insufficiency can lead to death. Similar to other procedures, new metastases rather than local recurrence often develop.

Either CT, contrast-enhanced US, or MR are used to detect residual tumors shortly after ablation (**Fig. 7.45**). Dynamic contrast enhanced MR appears to be more promising than the other modalities.

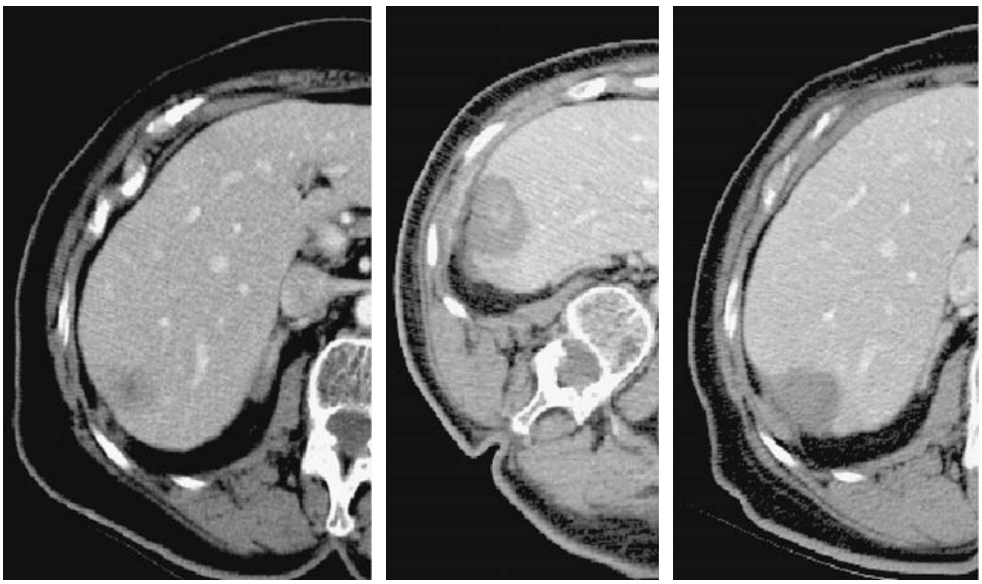

Figure 7.45. Radiofrequency ablation of metastatic colon carcinoma. Transverse CT images pretherapy (A), immediately posttherapy (B), and 4 months later (C) show progression of changes. No enhancement was evident within the lesion. (Courtesy of Fred T. Lee, M.D., University of Wisconsin.)

Results of radiofrequency ablation of colon cancer metastases approach those of resection, keeping in mind that patient selection is often not comparable for these two groups. As expected, better success is achieved with small tumors.

Photocoagulation (Thermotherapy)

Laser-induced thermotherapy using a percutaneous approach results in coagulation necrosis of metastatic nodules and adjacent liver parenchyma. Using an interventional 0.5-T MRI unit for guidance, laser irradiation with a near-infrared laser source and cooled laser light guide of 58 colorectal liver metastatic foci resulted in no residual tumor in nodules <2 cm in diameter, necrosis occurred in 71% of metastases between 2 and 3 cm, and lesser amounts in larger tumors (150). In a prospective study of patients with colorectal metastases, MR-guided laser-induced thermotherapy achieved a mean 1-year survival of 94%, 3-year survival of 56% and 5-year survival of 37% (151); to achieve these results, patient inclusion criteria consisted of the absence of extrahepatic tumor, fewer than five intrahepatic metastases, and metastases smaller than 50 mm in diameter, but included were patients with recurrent liver metastases after partial liver resection, metastases in both lobes, unresectable tumors and those patients with contraindications for surgery. Longer follow-up suggests that thermotherapy results are similar to surgical resection.

To limit arterial blood flow, degradable starch microspheres have been injected into the proper hepatic artery; whether such a technique increases percutaneous laser-induced thermotherapy effectiveness remains to be seen.

One should keep in mind that tumor volume measurements with a low field strength MR unit differ somewhat from those obtained with a 1.5-T unit. Likewise, CT volume measurements differ from MR values.

Microwave Coagulation Therapy

Currently microwave coagulation therapy of metastatic liver tumors is rarely performed. A Beijing study achieved cumulative survival rates of 91% at 1 year and 29% at 5 years, with tumor grade, number of metastases and local recurrence or new metastases each having a significant effect on survival (152).

Cryoablation

Cryoablation therapy for metastases is similar in its approach to that used for hepatocellular carcinomas (discussed above; see Hepatocellular Carcinoma). In spite of numerous cryotherapy studies published, its role in treating metastatic disease is not yet established. Should it be an alternative to surgery or is its primary role that of adjuvant therapy? In fact, whether cryotherapy has a major impact on metastatic liver disease is still debatable.

Either a percutaneous or an open surgical approach is used for cryoablation. Magnetic resonance guidance during percutaneous cryoablation identifies the tumor nodule in question and the size of the surrounding frozen liver tissue. An open MR unit reveals resultant ice balls as sharply defined expanding regions of signal loss encasing tumors; these ice balls correlate with resultant necrosis (Fig. 7.46). The mass seen immediately after therapy should be larger than the original tumor; otherwise, incompletely treatment should be suspected. Surrounding hemorrhage is common. Occasionally CT identifies gas within a tumor; it does not imply infection. In time these tumors shrink.

Thirty patients with colorectal cancer metastases confined to the liver, not deemed resectable and with <50% liver involved by tumor, underwent cryoablation followed by hepatic artery infusion chemotherapy with 5-FU, achieving a median survival of 18 months from the time of cryoablation (153); survival in this group of patients appears to be improved by such dual therapy.

Several patients undergoing synchronous hepatic cryoablation and colon cancer resection developed hepatic abscesses, although an abscess is rare after cryoablation alone.

Follow-Up

The use of bile CEA levels as early markers of occult liver metastases in patients with colorectal cancer has met with limited success; raised bile CEA occurs at initial colorectal cancer resection even without liver metastases but a raised biliary CEA level later, after the primary tumor has been resected, does predict tumor recurrence, either within the liver or at some other site. Bile sampling can be obtained by either cholangiography or, even simpler, by transhepatic gallbladder puncture.

Imaging is often used to follow the size of metastases and the response to therapy. The usefulness of a baseline posttherapy study cannot be overemphasized. In general, the same imaging modality should be used for follow-up; comparing tumor size with different imaging modalities is fraught with uncertainty. Even

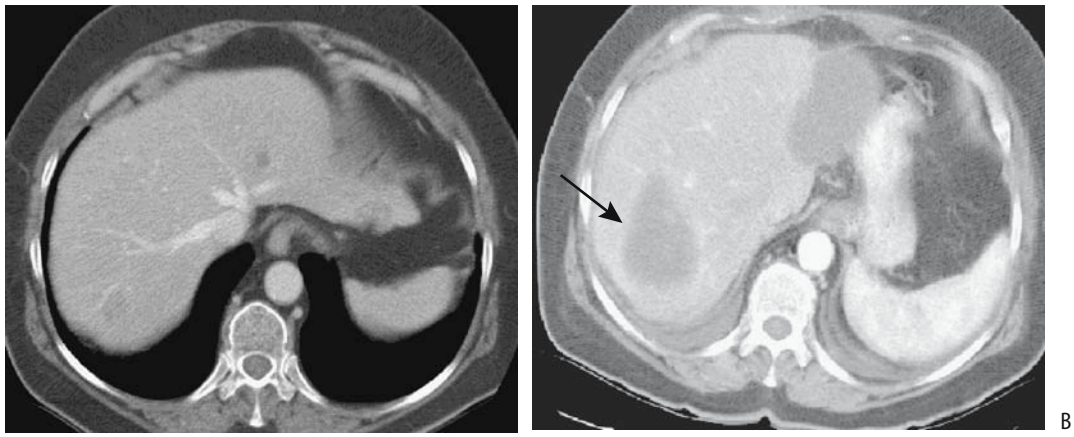

A B

Figure 7.46. Cryoablation and resection of metastatic colon carcinoma. A: Three liver lesions are present on this pretherapy image; two left lobe ones were resected and one in the right lobe was frozen. B: Postresection and postcryotherapy CT identifies a biloma/seroma at the site of left lobe resection and a residual lesion without contrast enhancement is evident at the site of right lobe cryotherapy (arrow). (Courtesy of Fred Lee, M.D., University of Wisconsin.)

CT 3D measurement of metastasis size can be used.

Magnetic resonance imaging is useful in evaluating metastases after therapy. Any viable tumor should enhance with gadolinium. Necrosis does not enhance or reveals only minimal delayed peripheral enhancement.

Some metastases undergo considerable change in their imaging features after chemotherapy; some mimic a benign lesion such as a cyst or hemangioma, while others develop such extensive fibrosis and distortion that the overall appearance mimics cirrhosis. Postcontrast MR of treated lesions tends to reveal no immediate enhancement, but fibrosis gradually becomes hyperintense on delayed images.

Other neoplasms

This section includes miscellaneous tumors not discussed previously and that are not readily classifiable either under benign or malignant categories.

Neuroendocrine Tumors

Clinical

Primary liver neuroendocrine tumors range from undifferentiated carcinomas to one with varying differentiation. The vast majority are metastatic rather than primary. Overall, they are not common.

Untreated, neuroendocrine metastases approximately double in size in 1 year. Typically, the severity of symptoms and indolent course argue for aggressive therapy.

Surgical resection is curable in some and palliative in most. Chemotherapy, somatostatin analogues, percutaneous ablation techniques and hepatic artery embolization of metastatic foci are used individually or as part of a global therapeutic approach. Long term palliation is feasible with transarterial chemoembolization but insufficient data is available to place this procedure in a proper perspective (154). The role of liver transplantation in a setting of metastatic neuroendocrine tumors is not settled. Cryoablation therapy appears useful in some of these patients. Most palliation procedures for liver neuroendocrine tumors result both in symptomatic relief and prolonged survival.

Imaging

These tumors are generally identified by contrast-enhanced imaging, with imaging-guided biopsy used to establish a specific diagnosis (Fig. 7.47).

Octreotide is a synthetic somatostatin analogue. Somatostatin receptor scintigraphy using octreotide labeled with indium 111 aids in localizing carcinoids and some other neuroendocrine tumors. Metastatic islet cell carcinomas, regardless of type, also accumulate this radiotracer as long as a tumor contains sufficient somatostatin receptors, keeping in mind that not all neuroendocrine tumors fulfill this condition. Somatostatin receptor scintigraphy is useful for several reasons: It confirms

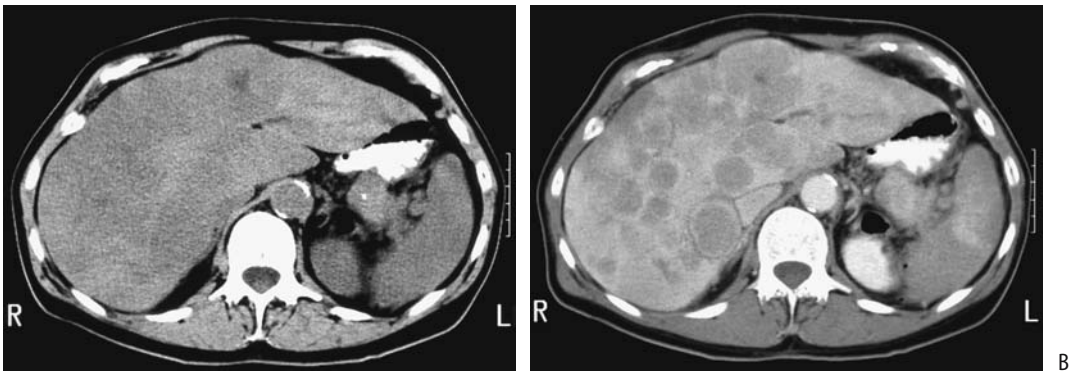

A B

Figure 7.47. Metastatic islet cell carcinoma. Precontrast (A) and contrast-enhanced (B) CTs reveal better tumor visualization after contrast. Numerous rim-enhancing nodules are scattered in the liver. (Courtesy of Patrick Fultz, M.D., University of Rochester.)

neuroendocrine liver metastases detected by other imaging and often discovers new sites. Octreotide scintigraphy also detects those tumors potentially responsive to radiolabeled octreotide therapy, but even here caution is necessary—liver, spleen, kidneys, and bladder are routinely visualized, while neuroendocrine tumors (and lymphomas) show variable uptake; therapy using somatostatin analogues may not be appropriate for all tumors accumulating In-111-DTPA-D-Phe-octreotide (In-111-pentetreotide).

Schwannoma

A primary schwannoma of the liver without associated neurofibromatosis is rare. Initially these are solid tumors, but with growth they tend to necrose and invade adjacent structures, including stomach.

Carcinoid

Most carcinoids originate in the gastrointestinal tract, with an occasional primary in some other organ, such as breast; even these metastasize to the liver. Primary liver carcinoids are rare; of interest is that the carcinoid syndrome tends not to develop in these patients. Carcinoid syndrome develops if tumor blood flow drains into the systemic venous circulation. Thus, in general, in a setting of a known primary carcinoid, the presence of carcinoid syndrome usually implies hepatic metastases, although exceptions occur and occasionally carcinoid syndrome is not evident even with widespread liver involvement.

Multiple liver foci are more common than solitary ones. Being metastatic, these carcinoids are malignant, yet specific imaging findings do not aid in differentiating between benign and malignant ones. Precontrast CT identifies carcinoid metastases as hypodense tumors, although small ones tend to be isodense. Central necrosis in larger tumors is hypodense. They enhanced during the arterial phase, with contrast enhancement then decreasing; superficially, they can mimic a hemangioma. A minority of focal carcinoids are best seen precontrast. Some are identified only on one phase.

Ultrasonography shows these tumors to range from hypo- to hyperechoic; central necrosis is anechoic. Some tumors are surrounded by a hypoechoic halo.

These tumors are hypointense on T1- and hyperintense on T2-weighted MRI; they enhance markedly during the arterial phase, less so during portal phase. A peripheral hypointense ring is seen in some of these tumors during delayed imaging, a finding also detected with some other hypervascular metastases.

Digital subtraction angiography identifies neovascularity. Larger tumors are fed by tortuous and elongated arteries. Carcinoids tend to displace and compress adjacent portal veins but not invade.

Most carcinoids contain somatostatin receptors, and octreotide scintigraphy is useful in localizing them. They are amenable to octreotide therapy.

Indium-111 pentetreotide and iodine-123–vasoactive intestinal peptide receptor imaging should suggest a carcinoid. Indium-111-pentetreotide SPECT detects more tumors than planar scans or conventional imaging.

The radiopharmaceutical metaiodobenzylguanidine (MIBG), used in the imaging and therapy of pheochromocytomas and neuroblastomas, has a limited role in imaging metastatic liver carcinoids because other imaging is more sensitive. Iodine-131-MIBG is useful, however, in treating carcinoids.

Interferon therapy has led to a clinical response, but symptoms recur after end of therapy. Embolization has had a limited application.

Gastrinoma

A rare primary liver gastrinoma has been reported.

T2-weighted sequences reveal a well-marginated, homogeneous, hyperintense tumor. Arterial phase MR sequences show larger tumors to have either homogeneous or peripheral enhancement, while smaller ones tend to be homogeneous and mimic hemangiomas. Delayed sequences show faster contrast washout than with most hemangiomas, and these sequences are most useful in differentiating metastatic gastrinomas from hemangiomas.

The intraarterial secretin test consists of sampling venous blood after secretin injection. In patients with Zollinger-Ellison syndrome, the secretin test is positive in only half or so of patients. This detection rate is less than with

other imaging available. The secretin test is useful when CT and MR are nondiagnostic.

Somatostatin receptor scintigraphy detects more gastrinoma metastases than CT, MRI, or angiography. As expected, somatostatin receptor scintigraphy does not identify hemangiomas and thus aids in this differentiation.

Indium-111-pentetreotide SPECT is becoming the imaging procedure of choice for suspected gastrinoma.

Other Tumors

Insulinomas metastatic to the liver tend to be slow growing. Either curative or palliative surgery is often considered. Chemotherapy or transcatheter arterial embolization prolongs survival. Chemical shift MR occasionally reveals a rim of steatosis surrounding metastatic insulinomas, presumably due to local insulin release (155).

Pheochromocytomas originate in a number of organs, but a liver primary is exceedingly rare.

Liver neurofibromas are rare and are associated with neurofibromatosis type 1. These tumors involve intrahepatic nerves and thus tend to have a periportal sheath-like distribution. Computed tomography reveals a hypodense infiltrating tumor mimicking lymphoma or a mesenchymal tumor.

Hemangioendothelioma

Classification of hemangioendotheliomas is confusing and still evolving. A number of vascular tumors have been called hemangioendotheliomas, including spindle cell, kaposiform, epithelioid, retiform, polymorphous, composites, and the malignant endovascular papillary angioendothelioma (Dabska's tumor). Some of these are benign vascular tumors and are angiomas, others are malignant and thus angiosarcomas, while still others classify as "borderline" malignant. Many authors simply use the term *infantile hemangioendothelioma* to designate these tumors when found in infancy and do not subdivide them further. These tumors are probably of fetal origin and tend to be multifocal. Hepatomegaly is generally present and the α-fetoprotein level is elevated, suggesting a possible hepatoblastoma.

Bilateral diffuse hepatic nodules are a common finding with hemangioendotheliomas. Tumor nodules tend to be rather uniform in size; they are hypointense on T1- and hyperintense on T2-weighted images. They enhance postcontrast.

Hemangioendotheliomas and cavernous hemangiomas have a similar CT and MRI appearance.

Some infantile hemangioendotheliomas have an early "blush" on Tc-99m–red blood cell scintigraphy.

Kaposiform Hemangioendothelioma

Kaposiform hemangioendothelioma is a more recently described entity involving multiple organs, including skin, liver, spleen, lungs, brain, and intestine. It is believed to be clinically and histologically distinct from the more typical hemangioma found in infancy. It is an aggressive, locally invasive tumor that does not metastasize. In spite of the name, this tumor, together with spindle cell hemangioendothelioma, is not associated with Kaposi's sarcoma herpesvirus (human herpesvirus 8); a polymerase test for Kaposi's sarcoma herpesvirus can be used to distinguish between Kaposi's sarcoma and other vascular tumors.

The histologic findings combine those found in a tufted angioma, lymphangioma, and Kaposi's sarcoma.

Kaposiform hemangioendotheliomas manifest somewhat later in life than infantile hemangiomas and are often associated with anemia, thrombocytopenia, and a coagulopathy (Kasabach-Merritt syndrome), and occasionally with lymphangiomatosis. Nevertheless, some of these tumors have been misdiagnosed as infantile hemangiomas. Some authors suggest that Kasabach-Merritt syndrome does not occur with hemangiomas, and if this syndrome is present a kaposiform hemangioendothelioma should be considered. Whether the occasional adult with a large so-called hemangioma and exhibiting Kasabach-Merritt syndrome actually has a hemangioendothelioma is conjecture.

Epithelioid Hemangioendothelioma

Epithelioid hemangioendotheliomas do metastasize and should be classified as malignant vascular tumors. Most occur in middle-aged

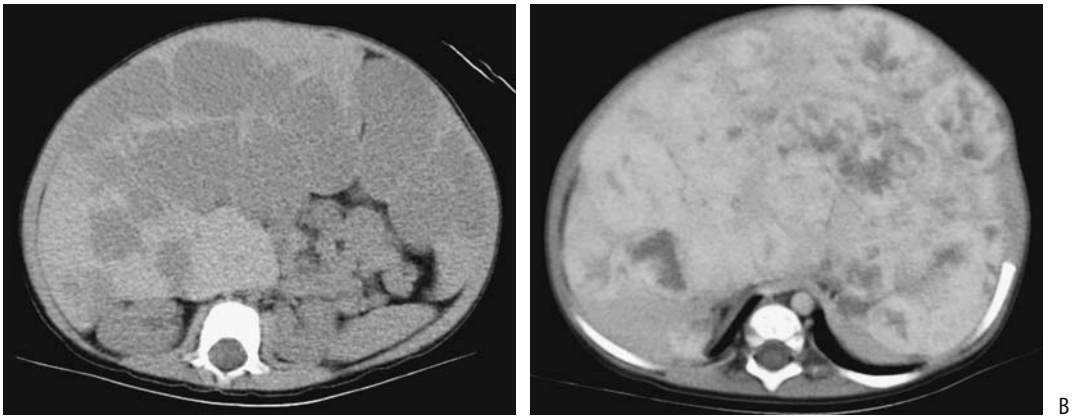

Figure 7.48. Liver hemangioendotheliosis in a 1-year-old girl. She also has skin hemangiomas and has mild congestive heart failure. A: Precontrast CT reveals an extensive blood density infiltrate involving large portions of the liver. B: Contrast-enhanced CT shows a heterogeneous tumor mostly isodense with liver. Of note is the small caliber aorta. (Courtesy of Luann Teschmacher, M.D., University of Rochester.)

women, but children are not spared. The underlying liver is usually normal.

Imaging defines the size and extent of these tumors, but their appearance often suggests a hepatocellular carcinoma. Liver biopsy is needed to establish a diagnosis. Ultrasonography is generally used to follow these lesions.

Varying degrees of mottled calcifications develop eventually.

Computed tomography reveals a hypodense tumors (Figs. 7.48 and 7.49). They tend to be hypervascular in their periphery. Contrast CT shows early peripheral enhancement followed by delayed central enhancement. Central enhancement is absent if sufficient fibrosis or thrombosis evolve. Even with extensive tumors in both lobes, the underlying hepatic vascularity tends to be normal.

These tumors are hypointense on T1- and hyperintense on T2-weighted images, although considerable variability exists.

Patients with epithelioid hemangioendotheliomas have undergone successful liver transplantation.

Other Hemangioendotheliomas

Retiform, polymorphous, and composite hemangioendotheliomas and the malignant endovascular papillary angioendothelioma usually infiltrate locally and have a high rate of local recurrence, and some will metastasize. They should be considered low-grade malignancies.

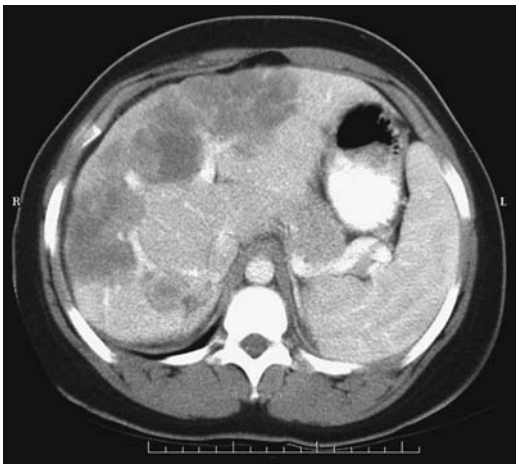

Figure 7.49. Epithelioid hemangioendothelioma in an 18-year-old woman. Contrast-enhanced CT reveals a large heterogeneous, lobulated tumor involving both right and left lobes. Some of the vessels coursing into it are attenuated. She underwent liver transplantation. (Courtesy of Patrick Fultz, M.D., University of Rochester.)

Figure 7.50. Metastatic hemangiopericytoma. She had surgery years ago for a meningeal hemangiopericytoma. A large right lobe tumor is evident. (*Source:* Cancer 1999;85(10):2245–2248. Copyright 1999 American Cancer Society. Reprinted by permission of Wiley-Liss, Inc., a subsidiary of John Wiley & Sons, Inc. Courtesy of Dr. F. Grunenberger, Hôpital de Hautepierre, Strasbourg.)

Hemangiopericytoma

The rare primary liver hemangiopericytoma occurs in both children and adults. Clinically and radiologically these tumors suggest a hemangioma or a hemangioendothelioma. Some express angiogenic factors such as fibroblast growth factor and vascular endothelial growth factor.

Occasionally detected is a metastatic hemangiopericytoma (Fig. 7.50). Some of these patients present with hypoglycemia; a history of a hemangiopericytoma resected years ago is not uncommon.

Calcification

Numerous disorders lead to increased liver parenchymal density and most are discussed in their respective sections. Not all increased density is due to calcium deposition. Increased iron stores and thorotrastosis are two such non-calcium conditions.

Whether calcifications are diffuse or focal, linear or curved, dense or barely visible allows one to narrow the differential diagnosis (Table 7.16). The patient's age, likewise, aids in differentiating diagnoses.

Table 7.16. Conditions associated with liver calcifications

- Diffuse parenchymal calcifications
  - In childhood
    - Toxoplasmosis
    - Cytomegalovirus
    - Rubella
    - Herpes simplex virus
    - Neonatal syphilitic hepatitis
  - Granulomatous hepatitis
  - Tuberculosis
  - Histoplasmosis
  - Schistosomiasis (*Schistosoma japonicum*)
  - *Pneumocystis carinii* (usually in AIDS)
  - Associated with hemo- or peritoneal dialysis
  - Amyloidosis
  - Silicosis
  - Lymphoma
  - After liver ischemia
  - Post-transplant hepatic artery thrombosis
- Focal calcifications:
  - Prior pyogenic abscess
  - Prior amebic abscess
  - Hydatid cyst
  - Primary liver tumors
    - Cavernous hemangioma
    - Focal nodular hyperplasia
    - Fibrolamellar hepatocellular carcinoma
    - Epithelioid hemangioendothelioma
  - Metastatic neoplasm
    - Mucin-producing adenocarcinoma
    - Osteogenic or chondrosarcoma
    - Some neuroendocrine tumors
  - Aneurysms
  - Intrahepatic biliary stones

Vascular Disorders

Vascular Congestion

Systemic venous engorgement, such as with congestive heart failure, constrictive pericarditis, or an episode of hypotension, leads to liver congestion, hepatomegaly, and, if severe enough, eventual liver ischemia and central lobular necrosis. Underlying liver damage is often unexpected. Shock has led to acute liver necrosis. Cirrhosis is an end point if congestion is chronic. Associated renal failure is common. These patients present with a marked increase in transaminase levels that tend to normalize rapidly. A coagulopathy with a prolonged prothrombin time is common.

Contrast-enhanced CT reveals a mottled pattern throughout the liver and delayed hepatic vein enhancement. Periportal low-attenuation nonenhancing fluid is a manifestation of venous stasis. The inferior vena cava becomes engorged and enlarges.

Enlarged hepatic veins and, at times, an enlarged inferior vena cava are gray-scale US findings of liver vascular congestion. Doppler US shows prominent portal vein pulsatility. In patients with heart failure, duplex Doppler US reveals that those with more severe left ventricular failure have a reduced portal vein pulsatility ratio; in fact, portal vein pulsatility correlates better with worsening cardiac function than vena caval or hepatic vein diameters. In chronic congestive heart failure the hepatic veins lose their triphasic contractility.

Infarction

The liver's dual blood supply makes major hepatic infarcts rare in the absence of prior surgical or radiologic intervention. Most major infarcts are encountered after liver transplantation. After a pancreaticoduodenectomy, liver infarction is more common in patients undergoing combined portal and superior mesenteric vein resection but not in those without a combined vascular resection. Liver infarcts develop in patients with vasculitides, polycythemia vera, and disseminated intravascular hypercoagulation. Sickle cell disease is associated with liver infarcts, although many of these are not detected with imaging. Blunt trauma is a rare cause of a major liver infarct. Liver infarction is a rare complication of transjugular intrahepatic portosystemic shunt (TIPS). Focal liver infarcts occur in association with diffuse or focal liver disease, often after obstruction of an intrahepatic branch of the hepatic artery. Occlusion of a portal vein branch does not result in an infarct (except in neonates). Etiology of some biopsy-confirmed focal necrosis can be identified, but in others differentiation among infection, tumor, and ischemia is not possible. Some focal infarcts evolve into focal necrosis and an abscess; others presumably heal with few sequelae.

A typical infarct appears as a well-marginated, wedge-shaped, peripheral defect; more centrally located infarcts are harder to identify. Within several days of necrosis, conventional radiography and CT detect gas bubbles in the liver, a transient finding. With a sufficient insult eventual parenchymal atrophy and scarring ensue. Some patients eventually develop diffuse liver calcifications.

Contrast-enhanced CT of an infarct reveals a hypodense region due to hypoperfusion, generally in the periphery. With hepatic artery obstruction, Doppler US identifies the lack of flow in the porta hepatis, although intrahepatic arterial flow may still exist due to collateral vessels. Occluded feeding arteries are identified in some patients.

Following abdominopelvic surgery not related to the liver, some patients develop wedge-shaped liver defects. These defects range from hypo- to hyperdense on precontrast CT. Postcontrast, these defects appear homogeneous and of higher attenuation than the surrounding liver. Of interest is that in some patients CT also detects portal vein branch clots within these defects. Follow-up CT reveals most of these defects diminishing with time, although some can persist. These postoperative defects probably represent a portal venous system thromboembolic phenomenon, and CT contrast enhancement is due to compensatory increase in hepatic arterial flow.

Postcontrast MRI reveals an infarct as a hypointense region.

Veno-Occlusive Disease

Hepatic vein obstruction is secondary to thrombosis or to such etiologies as chemotherapy or toxin ingestion. It is a rare complication of therapeutic liver radiation.

Jamaican herbal tea (*Senecio vulgaris*) drinkers are at increased risk of hepatic veno-occlusive disease. Clinically, these patients have findings similar to Budd-Chiari syndrome but imaging reveals patent major hepatic veins and inferior vena cava. Portal vein blood flow is decreased in this condition.

Budd-Chiari syndrome is discussed in Chapter 17.

Shunts

Arteriovenous

Intrahepatic arteriovenous shunting, if significant enough, leads to hepatic artery

enlargement and early venous contrast enhancement through the shunt. Early venous enhancement is also seen with some hypervascular neoplasms such as hepatocellular carcinomas. These findings are identified with postcontrast CT and arteriography.

Arterioportal

Small arterioportal venous shunts (not related to neoplasms), identified by hepatic angiography, appear as perfusion defects at CT arterial portography.

Arterial-phase dynamic MRI of small nontumorous arterioportal shunts reveal wedge-shaped, nodular, or irregular-shaped regions of contrast enhancement (156); they are not identified by unenhanced MRI. These nontumor arterioportal shunts are a cause of focal liver arterial MR hyperperfusion in a setting of normal precontrast MRI.

Liver in Idiopathic Portal Hypertension

Whether idiopathic noncirrhotic, chronic portal hypertension is one condition or a final pathway of several disorders is speculation. Histology reveals dense portal fibrosis, portal venous obliteration, and intralobular fibrosis; the appearance is similar to that found in nodular regenerative hyperplasia.

Some patients with idiopathic portal hypertension develop decreased portal venous peripheral perfusion. These regions enhance during arterial phase dynamic and are hypointense on T1- and hyperintense on T2-weighted MRI. Technetium-99m-GSA scintigraphy shows decreased accumulation, indicative of dysfunction.

Other Vascular Disorders

In patients with portal vein obstruction (in either the right or left lobe portal veins), immediate CT and MR contrast-enhanced images reveal an initial transient increase in segmental hepatic enhancement distal to the obstruction; this enhancement is secondary to increased hepatic arterial blood flow to the obstructed segment.

Hepatic sinusoidal dilatation, a rare interesting vascular condition, is associated with focal hepatocyte necrosis and intrasinusoidal fibrosis. It occurs in a setting of oral contraceptive use or pregnancy. CT reveals a poorly marginated heterogeneous hypodense region during the portal phase which gradually becomes isodense (157); T2-weighted MR identifies vessels within the lesion, an uncommon finding with a neoplasm. Delayed contrast enhancement separates this condition from peliosis hepatis, which tends to enhance early.

Vasculitides are prone to bleed, usually intrahepatic, less often intrabiliary or intraperitoneally. Some of these bleeds can be treated with transcatheter arterial embolization.

HIV/AIDS

Clinical

It is common to see hepatomegaly and splenomegaly in a setting of HIV infection. In general, low attenuation lesions in the liver should not be ascribed directly to HIV; most are secondary to another infection or a neoplasm.

Liver histology is abnormal in most autopsied HIV patients; steatosis is most common. Steatosis developing in HIV infected patients receiving antiretroviral therapy leads to hepatomegaly and is a severe and potentially fatal complication.

Imaging

Ultrasonography findings in HIV-positive patients are less specific than in the general population. In almost half of these patients US shows a diffuse hyperechoic liver, presumably secondary to steatosis.

Some opportunistic liver and splenic infections result in an US *snowstorm* appearance. Fibrosis or a fibrinous exudate probably accounts for this appearance.

Infection

Bacillary angiomatosis, a liver infection complicating AIDS, is caused by infection with *Bartonella henselae* or *B. quintana*. It mimics Kaposi's sarcoma. Computed tomography

reveals hypodense tumors that enhance postcontrast.

Pneumocystis carinii infection has led to acute hepatic failure due to *P. carinii* obstructing the hepatic sinuses and capillaries. Calcifications develop in lymph nodes, spleen, liver, and kidneys.

Liver function tests are abnormal but no specific imaging findings are seen with liver toxoplasmosis.

Immunocompromised children tend to develop multiple small liver abscesses, often fungal in origin, rather than a large drainable abscess.

Although disseminated tuberculosis is not uncommon in HIV patients, hepatic tuberculous abscesses are rare. Focal liver involvement is unusual and only an occasional AIDS patient develops liver tuberculomas.

Malignancy

An occasional hepatocellular carcinoma develops in an HIV-infected patient with no evidence of chronic liver disease or viral infection. Primary liver lymphomas also are found in HIV patients. Discrete tumors, rather than diffuse infiltration, predominate. A biopsy should be diagnostic.

Kaposi's sarcomas tend to infiltrate the portal triads.

Rare hepatic leiomyomas and leiomyosarcomas have developed in children with AIDS.

Postoperative Changes

Liver Transplantation

Pretransplant

Clinical

Children

The most common indication for orthotopic liver transplantations among 198 children was biliary atresia (42%), followed by α_1-antitrypsin deficiency (8%), Alagille's syndrome (8%), and fulminant hepatic failure (7%) (158); over half of these children were under 5 years of age. Other indications for a liver transplant in children include cryptogenic cirrhosis, and an occasional child has cystic fibrosis and resultant biliary cirrhosis. A severe organ shortage exists for children. In part, this shortage has been alleviated by using reduction hepatectomy to produce more manageable-sized liver allografts; only the left lobe or even a segment of the lobe is transplanted.

Similar to transplantation of an entire liver, infants with reduced transplants (left lateral segment or split-liver transplant grafts) also undergo a Roux-en-Y choledochojejunostomy. The vascular and biliary anatomy is different from that seen with whole liver transplantation if only a partial liver transplant is performed.

At times TIPS stabilizes an adult or child with liver failure and life-threatening variceal bleeding sufficiently to permit liver transplantation later.

In one center the 1-year actuarial survival rate in children was 80% (increasing to 88% over the last 5 study years) and for those surviving more than 1 year, the 3-, 5-, and 10-year actuarial survival rates were 95%, 93%, and 93%, respectively (158).

Adults

The most common indications for orthotopic liver transplantation in adults are cirrhosis, sclerosing cholangitis, and fulminant hepatic failure. End-stage hepatitis B cirrhosis patients were considered to be poor candidates for transplantation due to a high recurrence rate, but more recent medical therapy has led to a more favorable response. Hepatitis C virus infection recurs in most patients posttransplant and appears to be relatively benign, but the long-term sequelae are not known. In select patients transplantation is a viable option for early primary liver cancer. Prevalence of hepatocellular carcinoma is greater in a transplant recipient undergoing transplantation for cirrhosis than in the general population, with some of these cancers not detected by pretransplant imaging. Performing both CT arterioportography and DSA pretransplant achieves a sensitivity of about 85% in detecting hepatocellular carcinomas in cirrhotic livers but these tests have a relatively high false positive rate (159). Although pretransplant knowledge of an incidental neoplasm is of obvious importance, one may argue that due to the generally small size of most of these tumors the patient would still be eligible for transplantation.

Patients with primary sclerosing cholangitis who have developed a cholangiocarcinoma do

poorly after liver transplantation; the current trend is to perform liver transplantation earlier in the course of primary sclerosing cholangitis.

Spontaneous bacterial peritonitis, a complication of cirrhosis, is not a contraindication to liver transplantation provided adequate therapy for peritonitis is administered prior to transplantation.

The role of TIPS prior to transplantation is discussed in Chapter 17. The malposition of TIPS stents, however, alters and prolongs liver transplantation by interfering with cross-clamping at usual vascular sites.

Living donor transplantation involves right lobectomy or segmentectomy or left lobectomy or segmentectomy. Regeneration is a rapid process, with a transplant doubling in size within three or so weeks. Postoperative complications do occur in liver donors. Complications occur more often in right lobe than left lobe donors (160); many of these complications are amenable to interventional management, such as percutaneous drainage, bile duct dilation, arterial embolization or stent placement and resolve.

Imaging

Preoperative recipient assessment is designed to detect any anatomic variance such as portal vein patency and its major branches, and the caliber, location, and patency of the hepatic artery, hepatic veins, and inferior vena cava. Probably the most useful single imaging modality for preoperative evaluation of a potential liver transplant candidate is contrast-enhanced CT, especially multislice. This study calculates liver volume, evaluates adjacent structures, and defines underlying vascular anatomy.

Multidetector multiphase CT provide comprehensive parenchymal, vascular, and volumetric evaluation of potential living adult donors for right lobe liver transplantation. Agreement is found in donors between virtual CT right lobe volumes and graft weights obtained at surgery.

Arterial phase and portal venous phase CT with 3D volume rendering techniques can define major vessel origins, portal vein thromboses and cavernous transformation, collateral vessels, and detect unsuspected liver tumors. Such vascular information appears similar to or even superior to that obtained with DSA.

At times resection of only the left lobe or left lateral segment is performed in living donors for related transplantation, and any anatomic venous variation needs to be determined. Often US is sufficient for this task. It can identify whether the hepatic veins form a common trunk or drain separately into the inferior vena cava.

Preoperative right lobe living donor evaluation is also feasible with comprehensive abdominal T1- and T2-weighted MRI, MR cholangiography, and MR angiography; Preoperative MR evaluation in right hepatic lobe donors provides right lobe volume data similar to surgically obtained volumes, outlines intrahepatic bile duct anatomy in more patients than intraoperative cholangiography, and depicts portal veins more completely than DSA (161). Preoperative MRI findings can exclude donors, although a right hepatectomy was aborted at laparotomy in several patients because of intraoperative cholangiography findings at variance to preoperative imaging (162). A specific role for MRI is yet to be established in living donors. Of interest is a study of iodipamide enhanced multidetector CT cholangiography, showing significantly better donor biliary tract visualization than with conventional MR or mangafodipir enhanced excretory MR cholangiography (163).

Technetium-99m-GSA, binding to asialoglycoprotein liver receptors, is useful in evaluating hepatic functional reserve both prior to and after transplantation.

Is selective angiography necessary in children with end-stage liver disease who present for orthotopic liver transplantation? Such selective study does provide detailed portal vein and hepatic artery anatomy but at some risk to these children.

Intraoperative

In addition to pre- and posttransplantation evaluation, intraoperative vascular US appears useful if vascular compromise is suspected. Intraoperative US aids in establishing a liver transection line for an extended lateral segmentectomy by identifying the left medial vein.

A typical liver transplantation requires five anastomoses: four vascular ones involving the hepatic artery, portal vein, and supra- and infrahepatic inferior vena cava, and an end-to-end biliary anastomosis. A T-tube stent was often

left in place across the biliary anastomosis, although a number of surgeons have abandoned T-tube drainage to prevent bile leakage from the site. With the latter, biliary complications must be approached via ERCP. If a biliary anastomosis is not feasible, a choledochojejunostomy is created. A cholecystectomy is performed.

Posttransplant

The consequences of prolonged immunosuppressive therapy are still not completely understood.

Imaging

Computed tomography detection of focal subcapsular hepatic necrosis at some point in time is common after liver transplantation. In general, this finding is of little clinical prognostic significance, although it is associated with acute rejection.

A suprahepatic circumcaval calcification is occasionally detected by CT after transplantation. It is probably of little consequence.

Although IV Levovist in liver transplant patients results in significantly better color Doppler US arterial signals, little or no improvement is evident for the main portal vein and hepatic vein.

Magnetic resonance imaging defines hepatic venous anatomy and determines the liver volume and portal venous blood flow.

Complications

Rejection

Rejection is usually first detected roughly a week after transplantation. No specific imaging finding suggests liver rejection. During acute rejection the liver becomes edematous and intrahepatic bile ducts are compressed, resulting in incomplete filling during cholangiography (Fig. 7.51). Chronic rejection manifests by multiple bile duct strictures and a gradual and progressive reduction in number of interlobular bile ducts. In a setting of suspected rejection, imaging is used primarily to exclude biliary, vascular and other causes that clinically mimic rejection.

In some patients CT and MRI show a perivascular collar around central portal vein branches, probably secondary to impaired lymphatic drainage and resultant lymph edema.

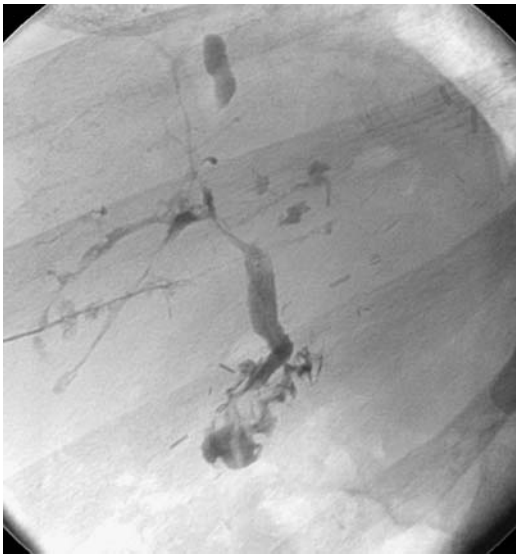

Figure 7.51. Presumed rejection of second liver in patient with autoimmune hepatitis. Numerous narrowed and dilated biliary segments are scattered throughout the liver. Ischemia can have a similar appearance. (Courtesy of David Waldman, M.D., University of Rochester.)

Doppler US changes in vessel diameter and blood flow data do not correlate consistently with acute rejection or with liver biopsy findings.

Biliary Complications

Posttransplant biliary complications encountered during the acute period consist of leakage and obstruction. Bile duct necrosis is uncommon. Strictures or stones develop on a more chronic basis.

Cholangiography, via an inserted catheter, endoscopic approach, or percutaneously, studies the suspected biliary complications (Fig. 7.52). Magnetic resonance cholangiopancreatography is evolving into a viable alternative by identifying first-order intrahepatic and extrahepatic bile ducts in over 90% of recipients. Enhancement with mangafodipir trisodium outperform conventional MR cholangiography in detecting and excluding biliary abnormalities (164).

In children, a diagnostic cholangiogram can be obtained in over 90% of attempted percutaneous transhepatic cholangiograms and a drainage catheter successfully inserted in most (165); of note is that a diagnostic cholan-

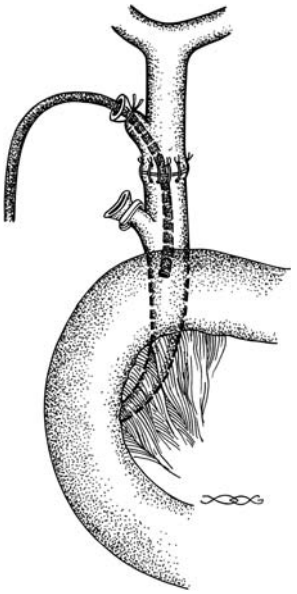

Figure 7.52. Appearance of a choledochocholedochostomy after liver transplantation. Two cystic duct stumps are evident, with a choledochal tube inserted into the proximal (transplant) one.

giogram was obtained in 92% even when intrahepatic bile ducts were not dilated.

Acute: The most common early biliary complication is biliary leakage, usually at an anastomosis. Some leaks manifest only after T-tube removal. A less common cause of bile leak is liver biopsy. Most bilomas are amenable to nonsurgical therapy, but one must ensure that a fluid collection does indeed represent bile rather than a vascular aneurysm; the latter is excluded with Doppler US.

The bile ducts receive their entire blood supply from the hepatic artery and are rather sensitive to ischemia. Thus the risk of biliary complications increases considerably with hepatic artery stenosis. Ischemic complications include leaks, strictures, and adjacent abscesses, with the most common complication being a nonanastomotic biliary stricture. In patients with complete interruption of arterial blood flow, about half also have a biliary complication.

Acute obstruction also occurs due to mechanical T-tube malposition or bile duct kinking. Partial donor cystic duct remnant obstruction and distention due to retained mucus or sludge (mucocele) occasionally compresses the adjacent hepatic duct. Ultrasonography reveals a cystic duct mucocele as an anechoic ovoid structure adjacent to bile duct. Such cystic duct mucoceles develop in a small minority of transplanted livers.

Acute biliary complications are usually evaluated by cholangiography. The role of US is controversial. In general, an abnormal US finding is predictive of biliary obstruction with a high specificity, but normal US findings do not exclude a biliary stricture or bile leakage.

Chronic: A biliary stricture is the most common long-term complication after liver transplantation. Stenoses occur most often in the recipient common bile duct, followed by the donor liver common bile duct and anastomotic site. Nonanastomotic strictures presumably are secondary to ischemia. Stones develop proximal to some stenoses.

Magnetic resonance cholangiopancreatography is a viable option in detecting late biliary complications. More invasive biliary procedures are then reserved either if MRCP does not define underlying anatomy or if interventional procedures are contemplated.

Biliary strictures are readily dilated using interventional radiology techniques. Although a success rate up to 90% can be achieved in dilating these strictures, they tend to recur. The success rate of dilating restenoses is generally lower than for an initial stenosis, and stents should be considered in this setting. Although some stents do obstruct by sludge and debris, their patency can be maintained by various interventional maneuvers.

Intrabiliary defects consist of sludge, stones, and necrotic debris.

Surprisingly, cholangitis is not common. Pancreatitis is rare.

Vascular Complications

Arteriography is the accepted gold standard in evaluating vascular complications, although both CT and US detect some complications. Multislice 3D CT angiography with volume rendering, in particular, is a promising approach in these patients. Currently, however, for suspected vascular complication Doppler US is more common than CT or MR. For therapeutic interventions an angiographic approach is necessary.

Magnetic resonance angiography is assuming a greater role in evaluating vascular anasto-

moses. 3D gadolinium-enhanced MR readily identifies vascular complications detected by angiography or surgery, in one study reaching 100% sensitivity but only 74% specificity in detecting >50% hepatic artery stenoses (166).

Arterial Complications: The most common posttransplant vascular complication is hepatic artery thrombosis. Uncorrected, in most patients thrombosis leads to fulminant sepsis, liver infarction, necrosis, and graft loss. Patients with interposition of an allogeneic iliac graft or anastomosis to an aberrant right hepatic artery appear prone to develop hepatic artery thrombosis. Thrombosis can occur early or even as late as a year after transplantation. Clinically, some but not all these patients have elevated liver transaminases, sepsis, recurrent cholangitis, or gas within the liver. Transcapsular arterial collateral vessels tend to develop after hepatic artery occlusion.

Computed tomography detects most hepatic artery thromboses. Also, CT tends to identify an irregularly shaped hypodense region both pre- and postcontrast; some of these patients develop necrosis and biliary ischemia, findings not specific for hepatic artery thrombosis but they should suggest further investigative procedures. Although some studies have shown Doppler US and CT sensitivities and specificities to be roughly comparable, one problem with US is that the hepatic artery is often incompletely visualized. The combined use of color and power Doppler US are helpful. At times the lack of hepatic artery visualization, even after Levovist injection, is due to artery occlusion. Nevertheless, some authors have expressed caution on relying on US, with false-positive or -negative results being due to rejection, recurrent hepatitis, aberrant vascular anatomy, hypotension, presence of collaterals, and other reasons.

Color Doppler US detection of transcapsular collateral flow or hepatic artery flow in the wrong direction should raise suspicion for hepatic artery thrombosis.

An occasional patient with hepatic artery thrombosis and hepatic infarction does not undergo retransplantation. Ultrasonography in these patients shows hypoechoic regions with preservation of portal tracts; these changes either resolve or progress to infarction, seen as local hyperechoic regions. Eventually these patients develop biliary strictures, bilomas, abscesses, and calcifications.

Hepatic artery stenosis tends to be more insidious than thrombosis and is most common at the anastomosis; it results in an increase in flow velocity; at times turbulent flow is detected. Abnormal Doppler US values for both resistive indexes and systolic acceleration times are more accurate predictors of stenosis than either one alone as an independent parameter. Hepatic artery stenoses, either at the anastomosis or at other sites, are amenable to percutaneous transluminal balloon angioplasty (Figs. 7.53 and 7.54). Complications of balloon angioplasty include artery spasm, pseudoaneurysm and rupture. An aortohepatic artery graft (Fig. 7.55) or

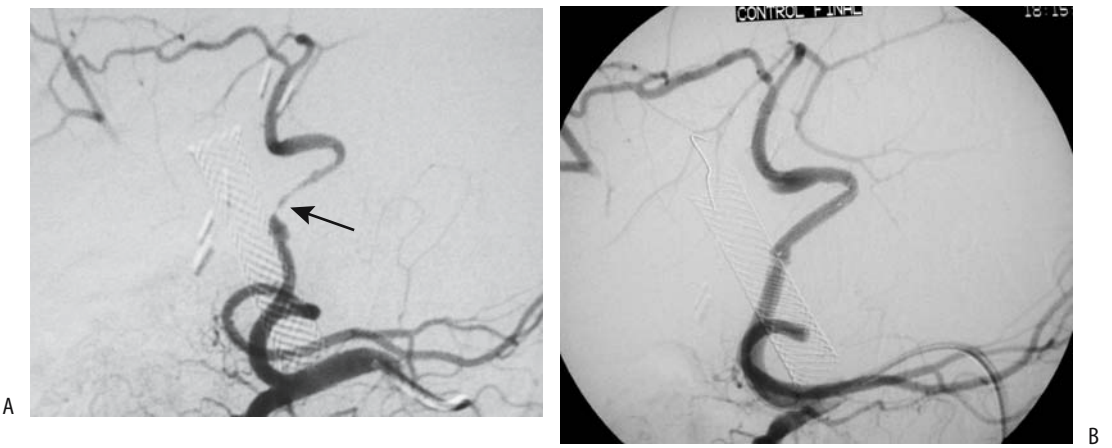

Figure 7.53. Hepatic artery stenosis in a transplanted liver. A: A stenotic (arrow) hepatic artery originates as a branch of the superior mesenteric artery. B: Hepatic artery has an essentially normal caliber after stent insertion. (Courtesy of Oscar Gutierrez, M.D., University of Chile, Santiago, Chile.)

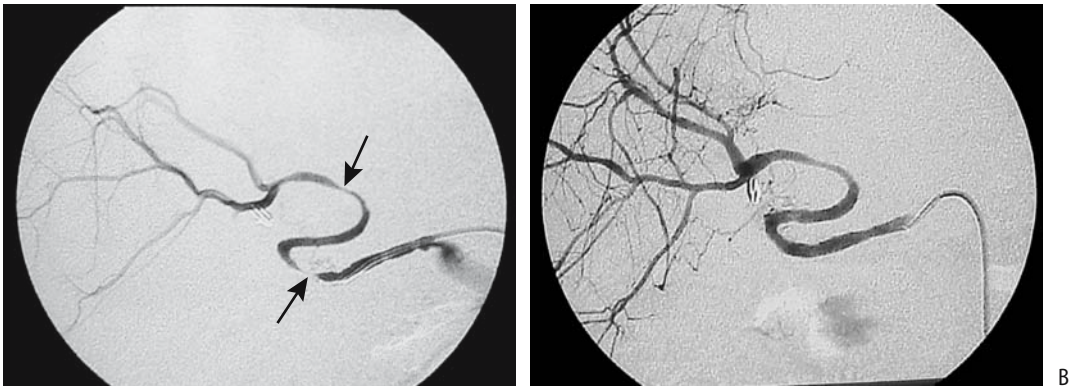

Figure 7.54. A: Multiple hepatic artery stenoses (arrows) in a transplanted liver. B: Improvement in artery caliber after angioplasty. (Courtesy of Oscar Gutierrez, M.D., University of Chile, Santiago, Chile.)

Figure 7.55. Occluded aortohepatic artery graft in a liver transplant. A: Aortogram reveals no hepatic artery flow. B: Occluded graft is partially recanalized after initial thrombolytic therapy. C: Good intrahepatic artery filling after end of thrombolytic therapy. (Courtesy of Oscar Gutierrez, M.D., University of Chile, Santiago, Chile.)

retransplantation are necessary if angioplasty is not successful. In a rare liver transplant ischemia develops secondary to an increased hepatic artery resistive index and increased splenic artery blood flow without evidence of a stenosis; some of these patients benefit from splenic artery embolization with coils.

Aneurysms occur at hepatic artery anastomoses. Aneurysm rupture leads to hemobilia, hemoperitoneum, or gastrointestinal tract bleeding. Ultrasonography reveals a cystic tumor. An aneurysm is suggested if this tumor communicates with the hepatic artery; otherwise the appearance mimics any other fluid collection. Doppler US is helpful in detecting internal blood flow, if present.

Splenic artery aneurysms are associated with portal hypertension. They are identified in about 15% of liver transplant patients.

Does hepatic arterial chemoembolization for hepatocellular carcinomas before orthotopic liver transplantation influence posttransplant hepatic arterial complications? Among 47 patients who underwent hepatic arterial chemoembolization pretransplantation, 13% developed hepatic arterial complications after transplantation (and an 8% prevalence of hepatic arterial thrombosis), while among controls 6% developed hepatic arterial complications (and 5% prevalence of hepatic arterial thrombosis) (167); the authors concluded that pretransplantation hepatic artery chemotherapy is not a risk factor for posttransplantation hepatic artery complications.

Venous Complications: The most common venous complication is portal vein thrombosis or stenosis and resultant extrahepatic portal hypertension. These patients develop ascites and variceal bleeding, at times life threatening.

The entire portal vein length needs to be visualized by real-time US to detect portal vein stenosis. Pressure gradients across a stenosis can be calculated from observed Doppler US velocities. Angiography verifies US findings. Transhepatic portal venography serves as a guide for balloon venoplasty of a stenotic segment. Occasionally an intravascular stent is necessary (Fig. 7.56). Surgical reconstruction is necessary only in a minority of these patients.

Percutaneous transhepatic balloon venoplasty was successful in 76% of children and adolescents with anastomotic portal vein stenoses in a setting of reduced-size hepatic transplantation (168); portal vein occlusion prevented portal vein access in the other 24%.

Inferior vena caval stenosis and hepatic vein stenosis is less common than portal vein involvement. It has led to Budd-Chiari syndrome. In some hands percutaneous transluminal angioplasty has had limited success, but others have found balloon angioplasty to be safe and effective in treating these chronic stenoses, and still others have achieved long-term angioplasty success only in combination with stenting (Fig. 7.57).

CT evaluates hepatic venous congestion after living donor liver transplantation; decreased contrast enhancement during CT portal venous phase correlates with severity of hepatic venous congestion and increased serum bilirubin level (169).

Postbiopsy

Complications of liver biopsy posttransplant include hemoperitoneum, hemothorax, pneumothorax, arterioportal fistula, and possible infection.

The overall prevalence of severe liver biopsy complications in posttransplant patients is similar to that found in patients without transplantation; posttransplant patients, however, are more prone to bleeding complications.

Malignancy/Lymphoproliferative Disorder

After liver transplantation and associated immunosuppression these patients are at increased risk for developing malignancies. In patients surviving more than several months posttransplantation, about 5% will develop a new tumor. Lymphoma is most common, at times being discovered within several months of transplantation. Of nonlymphoid cancers, skin cancer is the most common; other new tumors consist of a broad spectrum and include gastrointestinal adenocarcinomas, genitourinary cancers, laryngopharyngeal carcinomas, Kaposi's sarcoma, and malignant melanoma. Some of these carcinomas grow rapidly after liver transplantation.

After orthotopic liver transplantation, a hepatocellular carcinoma recurs most often in lungs or in transplanted liver; it can be single or multiple. In these immunosuppressed patients CT is

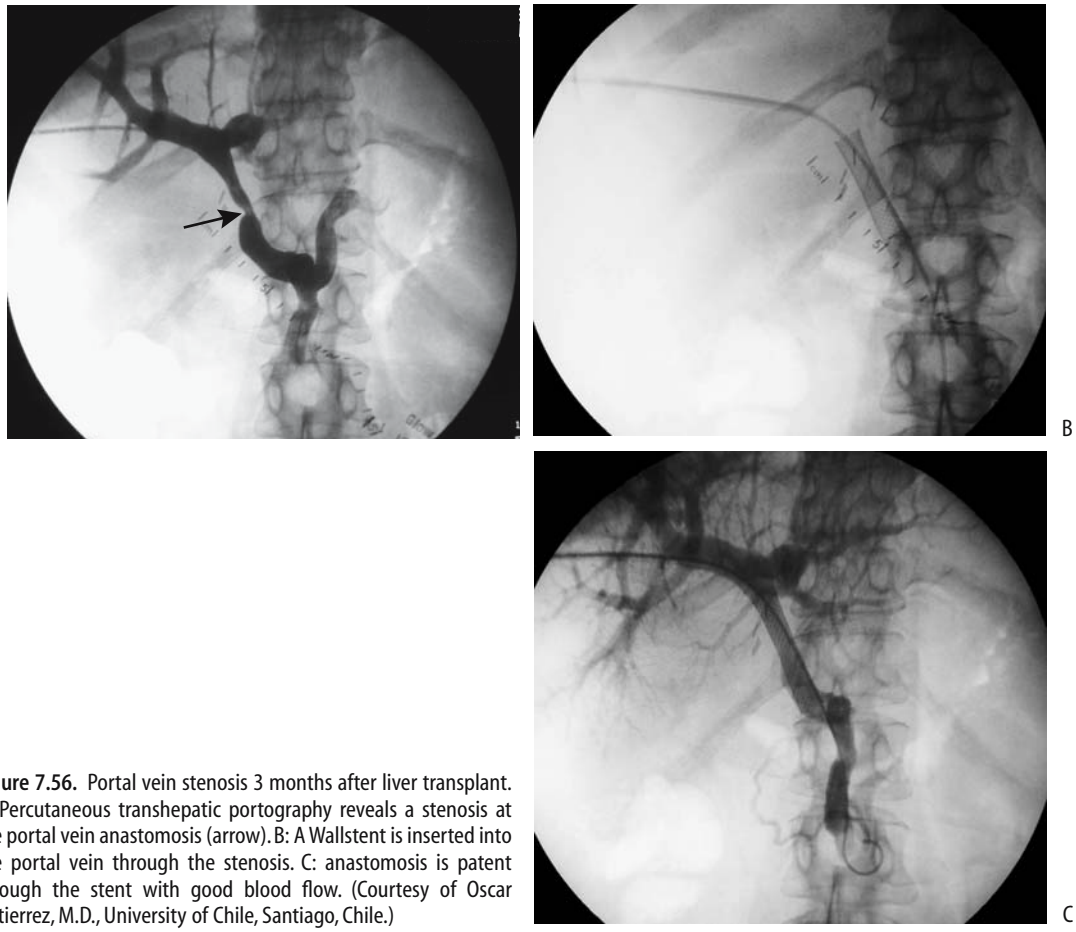

Figure 7.56. Portal vein stenosis 3 months after liver transplant. A: Percutaneous transhepatic portography reveals a stenosis at the portal vein anastomosis (arrow). B: A Wallstent is inserted into the portal vein through the stenosis. C: anastomosis is patent through the stent with good blood flow. (Courtesy of Oscar Gutierrez, M.D., University of Chile, Santiago, Chile.)

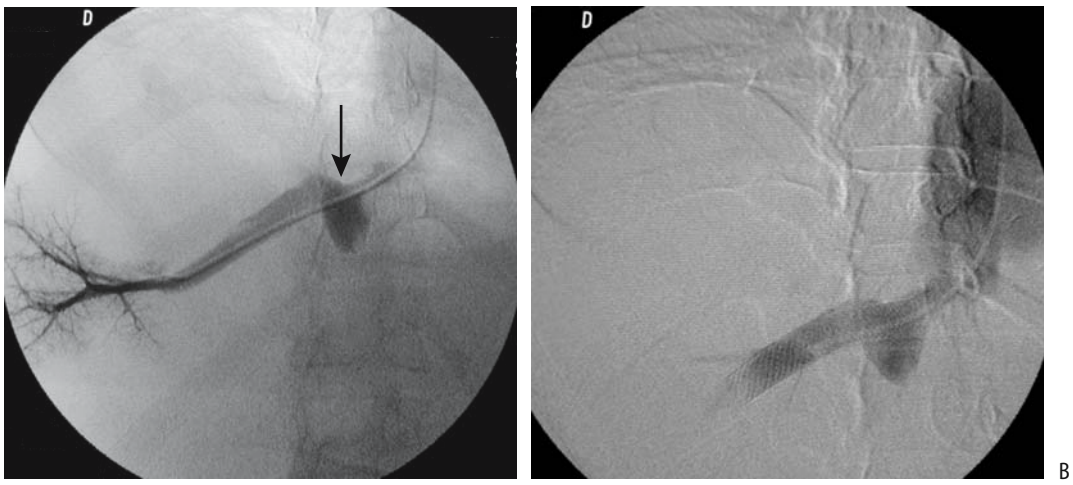

Figure 7.57. Hepatic vein stenosis in a transplanted liver. A: Hepatic venogram identifies severe stenosis at its junction with the inferior vena cava (arrow). B: Good drainage is evident after stent insertion (arrow). (Courtesy of Oscar Gutierrez, M.D., University of Chile, Santiago, Chile.)

more sensitive than serum tumor markers in detecting recurrence. Nevertheless, if a patient undergoes a liver transplant for a hepatocellular carcinoma and then develops a carcinoma in the allotransplanted liver, what is the origin of the second carcinoma? Generally recurrence of the original carcinoma is suspected, but proof can be obtained from carcinoma, transplanted liver, and recipient DNA to establish whether the carcinoma DNA is similar to or differs from the patient's and donor liver DNA.

Computed tomography abnormalities are evident in most patients with proven posttransplantation lymphoproliferative disorder, with extranodal disease being more common than splenic involvement or adenopathy (170); extranodal involvement included liver (53%), small bowel (25%), kidney (17%), mesentery (14%), and to a lesser degree adrenal glands, abdominal wall, colon, stomach, and gallbladder. A poorly marginated periportal infiltrate can encase the adjacent bile ducts and blood vessels. Serologic evidence of exposure to Epstein-Barr virus is often evident in these patients.

Other Biliary Complications

Primary biliary cirrhosis recurs in some transplanted livers. It should be kept in mind that aside for recurrence of their disease these patients also develop other, similar appearing, complications. Thus chronic graft rejection can mimic recurrence of primary biliary cirrhosis.

Postoperative immunotherapy does not suppress underlying inflammatory bowel disease; in fact, reactivation of inflammatory bowel disease and growth of colon cancer have been reported after liver transplantation.

Reported recurrence of hepatitis C infection after orthotopic liver transplantation ranges from about 60% to almost universal, with varying clinical severity. Some patients develop severe cholestatic hepatitis. The long-term sequelae of recurrent infection include scarring and progression to end-stage liver disease. Interferon antiviral therapy appears of benefit. Posttransplantation diabetes occurs more often than expected in those patients who had hepatitis C before their transplantation.

A retrospective review of 4001 of orthotopic liver transplantations found 48 bowel obstructions (171); etiology included adhesions, bowel ischemia, internal and external hernias, and volvulus. Obstructions due to internal hernias were transmesenteric or retroanastomotic and were related to choledochoenteric anastomoses. Neoplastic bowel obstruction included posttransplant lymphoproliferative disease and even an unsuspected colon carcinoma. Bowel obstruction tends to be difficult to diagnose in these patients mostly due to low suspicion and thus the lack of appropriate imaging studies.

Posttransplantation pancreatitis is uncommon.

These patients are prone to *Candida* liver abscesses, even years after liver transplantation. Hepatic abscesses are treatable by percutaneous drainage.

Pulmonary and soft tissue calcifications have developed in transplant patients with severe cytomegalovirus infection.

Gilbert's syndrome and transplantation of a liver containing an inborn error of metabolism should be suspected if unconjugated bilirubin levels remain elevated in the face of normal liver enzymes.

In Children

In children, biliary complications consisting of biliary obstruction or leak occur during the first several weeks after transplantation. Ascites is not uncommon in children after liver transplantation.

The prevalence of vascular complications appears to be greater in children than in adults. Hepatic artery thrombosis is the most serious complication in children, occurring in almost 10%; portal vein thrombosis is less common. Surgical edema has led to an increase in intraabdominal pressure to the point of hepatic artery or portal vein compression or occlusion. Various biliary complications are similar to those seen in adults.

Children are typically initially followed with daily Doppler US. As in adults, Doppler US evaluates vascular patency; a sensitivity of over 90% is achieved in showing a patent hepatic artery and portal vein. Computed tomography serves to detect suspected liver parenchymal ischemia and abscesses.

Rare posttransplant leiomyosarcomas appear to be more common in pediatric hepatic allograft patients than in adults.

Liver Cell Transplantation

Transplanted hepatocytes remain viable and function on a long-term basis. Preliminary studies suggest that such transplantation is useful for some familial hyperbilirubinemia conditions, but little clinical data is available.

Bone Marrow Transplantation

Liver veno-occlusive disease is an ominous complication after bone marrow transplantation, usually developing shortly after transplantation. Among 100 patients receiving total body irradiation or busulfan therapy followed by hematopoietic stem cell transplantation, 25% developed hepatic veno-occlusive disease and 9% died (172).

A hepatic artery resistive index below 0.55 suggests liver dysfunction in children undergoing bone marrow transplantation, but whether duplex US is sufficiently accurate in diagnosing veno-occlusive disease is not clear.

Hepatectomy/Embolization

The ability of the liver to regenerate was already known to ancient Greeks. In response to injury and influenced by a number of factors, the most important being hepatocyte growth factor, hepatocytes have an ability to divide and grow. Regeneration is a rapid process, peaking within several weeks and then gradually slowing. Such regeneration is most obvious after a partial hepatectomy, but also occurs after segmental portal vein obstruction and atrophy of involved segments. This phenomenon can be used to advantage prior to major resection by performing portal vein embolization; atrophy of embolized segments induces enlargement of remaining nondiseased segments. Such portal vein embolization is most often performed if initial residual nondiseased liver tissue is deemed to be insufficient to permit a major resection. Either a percutaneous transhepatic approach or surgical cannulation of a portal vein branch, such as the superior mesenteric vein, is used. Coils, iodized oil, and other agents serve as embolic agents. Portal blood flow to noninvolved liver, measured by Doppler US, increases markedly after embolization and then approaches baseline within 2 weeks or so; parenchymal enlargement is directly related to increased portal blood flow.

The amount of liver tissue necessary for survival after a partial hepatectomy is not established, but it varies with the degree of underlying liver disease.

Examination Complications

Vascular Procedures

Patients with atherosclerosis undergoing vascular surgery or arterial catheterization procedures are at risk for cholesterol crystal embolization. In the liver such embolization has led to focal necrosis. Usually multiple organs are involved.

Thorotrastosis

Clinical

The use of radioactive α-emitting colloid thorium dioxide (Thorotrast) as a contrast agent during the 1930s to 1950s is associated with numerous malignancies, including angiosarcoma, cholangiocarcinoma, and hepatocellular carcinoma. Synchronous cancers have developed. In addition, α-emissions cause extensive liver and spleen fibrosis and liver cirrhosis. Thorium 232 has a half-life of 1.4×10^{10} years and after intravascular injection is stored in reticuloendothelial cells.

A German Thorotrast study group was started in 1968 and includes 2326 Thorotrast patients (173); through 1999, 454 primary liver cancers have been registered, compared to three in a control group. A correlation exists between mean accumulated liver dose and risk of liver cancer, being about 600 per 10,000 persons for a liver exposure of 1 Gy.

Imaging

Thorotrast liver and spleen deposits are readily visualized with conventional radiography. Computed tomography shows Thorotrast as high-density collections in the liver, spleen, and, at

times, in lymph nodes. Ultrasonography reveals a heterogeneous echo pattern.

With MRI, the spleen contrast-to-noise ratio on T1-weighted images is lower than normal. Actual Thorotrast deposits are not seen on MRI, but MRI is useful in detecting Thorotrast-induced liver and biliary tumors.

References

1. Yamagami T, Nakamura T, Sato O, Takeuchi Y, Nishimura T. Value of intraarterial prostaglandin E(1) injection during CT hepatic arteriography. AJR 2001;177:115–119.
2. Sahani DV, Kalva SP, Tanabe KK, et al. Intraoperative US in patients undergoing surgery for liver neoplasms: comparison with MR imaging. Radiology 2004;232: 810–814.
3. Bryant TH, Blomley MJ, Albrecht T, et al. Improved characterization of liver lesions with liver-phase uptake of liver-specific microbubbles: prospective multicenter study. Radiology 2004;232:799–809.
4. Blomley MJ, Sidhu PS, Cosgrove DO, et al. Do different types of liver lesions differ in their uptake of the microbubble contrast agent SH U 508A in the late liver phase? Early experience. Radiology 2001;220:661–667.
5. Robbin ML, Eisenfeld AJ. Perflenapent emulsion: a US contrast agent for diagnostic radiology-multicenter, double-blind comparison with a placebo. EchoGen Contrast Ultrasound Study Group. Radiology 1998; 207:717–722.
6. Numata K, Tanaka K, Kiba T, et al. Nonresectable hepatocellular carcinoma: improved percutaneous ethanol injection therapy guided by CO(2)-enhanced sonography. AJR 2001;177:789–798.
7. Joarder R, de Jode M, Lamb GA, Gedroyc WM. The value of MnDPDP enhancement during MR guided laser interstitial thermoablation of liver tumors. J Magn Reson Imaging 2001;13:37–41.
8. Inoue T, Koyama K, Oriuchi N, et al. Detection of malignant tumors: whole-body PET with fluorine 18 alpha-methyl tyrosine versus FDG—preliminary study. Radiology 2001;220:54–62.
9. Habdank K, Restrepo R, Ng V, et al. Combined sonographic and fluoroscopic guidance during transjugular hepatic biopsies performed in children: a retrospective study of 74 biopsies. AJR 2003; 180:1393–1398.
10. Akhan O, Akpinar E, Oto A, et al. Unusual imaging findings in Wilson's disease. Eur Radiol 2002;12 Suppl 3:S66–69.
11. Tamm EP, Rabushka LS, Fishman EK, Hruban RH, Diehl AM, Klein A. Intrahepatic, extramedullary hematopoiesis mimicking hemangioma on technetium-99m red blood cell SPECT examination. Clin Imaging 1995;19:88–91.
12. Caroli J, Soupault R, Kossakowski J, Plocker L, Paradowska M. La dilatation polykystique congéniyale des voies biliaires intrahépatiques: essai de classification. Sem Hop 1958;34:128–135.
13. Miller FJ Jr, Whiting JH, Korzenik JR, White RI. Caution with use of hepatic embolization in the treatment of hereditary hemorrhagic telangiectasia. Radiology 1999;213:928–930.
14. Moore EE, Cogbill TH, Jurkovich GJ, Shackford SR, Malangoni MA, Champion HR. Organ injury scaling: spleen and liver (1994 revision). J Trauma 1995;38: 323–324.
15. Mirvis SE, Whitley NO, Vainwright JR, Gens DR. Blunt hepatic trauma in adults: CT-based classification and correlation with prognosis and treatment. Radiology 1989;171:27–32.
16. Earls JP, Krinsky GA, DeCorato DR. MR imaging of focal hepatic injury due to use of surgical retractors. AJR 1996;167:816–817.
17. Miele V, Andreoli C, De Cicco ML, Adami L, David V. Hemoretroperitoneum associated with liver bare area injuries: CT evaluation. Eur Radiol 2002;12:765–769.
18. Poletti PA, Mirvis SE, Shanmuganathan K, Killeen KL, Coldwell D. CT criteria for management of blunt liver trauma: correlation with angiographic and surgical findings. Radiology 2000;216:418–427.
19. Catalano O, Sandomenico F, Raso MM, Siani A. Low mechanical index contrast-enhanced sonographic findings of pyogenic hepatic abscesses. AJR 2004;182: 447–450.
20. Ch Yu S, Hg Lo R, Kan PS, Metreweli C. Pyogenic liver abscess: treatment with needle aspiration. Clin Radiol 1997;52:912–916.
21. Caremani M, Benci A, Maestrini R, Rossi G, Menchetti D. Abdominal cystic hydatid disease (CHD): classification of sonographic appearance and response to treatment. J Clin Ultrasound 1996;24:491–500.
22. Lewall DB, Nyak P. Hydatid cysts of the liver: two cautionary signs. Br J Radiol 1998;71:37–41.
23. Ustunsoz B, Akhan O, Kamiloglu MA, Somuncu I, Ugurel MS, Cetiner S. Percutaneous treatment of hydatid cysts of the liver: long-term results. AJR 1999;172:91–96.
24. Fan ZM, Zeng QY, Huo JW, et al. Macronodular multiorgans tuberculoma: CT and MR appearances. J Gastroenterol 1998;33:285–288.
25. Hagspiel KD, Kempf W, Hailemariam S, Marincek B. Mucormycosis of the liver—CT findings. AJR 1995;165: 340–342.
26. Bhatia V, Sarin SK. Hepatic visceral larva migrans: evolution of the lesion, diagnosis, and role of high-dose albendazole therapy. AJR 1994;89:624–627.
27. Kardorff R, Olveda RM, Acosta LP, et al. Hepatosplenic morbidity in schistosomiasis japonica: evaluation with Doppler sonography. Am J Trop Med Hyg 1999;60: 954–959.
28. Semelka RC, Chung JJ, Hussain SM, Marcos HB, Woosley JT. Chronic hepatitis: correlation of early patchy and late linear enhancement patterns on gadolinium-enhanced MR images with histopathology initial experience. J Magn Reson Imaging 2001;13: 385–391.
29. Kew MC, Yu MC, Kedda MA, Coppin A, Sarkin A, Hodkinson J. The relative roles of hepatitis B and C viruses in the etiology of hepatocellular carcinoma in southern African blacks. Gastroenterology 1997;112: 184–187.

30. Zhang XM, Mitchell DG, Shi H, et al. Chronic hepatitis C activity: correlation with lymphadenopathy on MR imaging. AJR 2002;179:417–422.
31. Shiomi S, Kuroki T, Kuriyama M, et al. Evaluation of fulminant hepatic failure by scintigraphy with technetium-99m-GSA. J Nucl Med 1997;38:79–82.
32. Obuchi M, Yoshiba M, Sekiyama K, et al. Serial hepatic and splenic volumetry in acute severe hepatitis. Nippon Shokakibyo Gakkai Zasshi 1999;96:147–153.
33. Khalili K, Lan FP, Hanbidge AE, Muradali D, Oreopoulos DG, Wanless IR. Hepatic subcapsular steatosis in response to intraperitoneal insulin delivery: CT findings and prevalence. AJR 2003;180:1601–1604.
34. Hirohashi S, Ueda K, Uchida H, et al. Nondiffuse fatty change of the liver: discerning pseudotumor on MR images enhanced with ferumoxides-initial observations. Radiology 2000;217:415–420.
35 Okazaki H, Ito K, Fujita T, Koike S, Takano K, Matsunaga N. Discrimination of alcoholic from virus-induced cirrhosis on MR imaging. AJR 2000;175:1677–1681.
36. Ito K, Mitchell DG, Hann HW, et al. Progressive viral-induced cirrhosis: serial MR imaging findings and clinical correlation. Radiology 1998;207:729–735.
37. Karahan OI, Dodd GD 3rd, Chintapalli KN, Rhim H, Chopra S. Gastrointestinal wall thickening in patients with cirrhosis: frequency and patterns at contrast-enhanced CT. Radiology 2000;215:103–107.
38. Lafortune M, Matricardi L, Denys A, Favret M, Dery R, Pomier-Layrargues G. Segment 4 (the quadrate lobe): a barometer of cirrhotic liver disease at US. Radiology 1998;206:157–160.
39. Tuney D, Aribal ME, Ertem D, Kotiloglu E, Pehlivanoglu E. Diagnosis of liver cirrhosis in children based on colour Doppler ultrasonography with histopathological correlation. Pediatr Radiol 1998;28:859–864.
40. Ito K, Mitchell DG, Gabata T. Enlargement of hilar periportal space: a sign of early cirrhosis at MR imaging. J Magn Reson Imaging 2000;11:136–140.
41. Ito K, Mitchell DG, Hann HW, et al. Viral-induced cirrhosis: grading of severity using MR imaging. AJR 1999;173:591–596.
42. Marti-Bonmati L, Fog AF, de Beeck BO, Kane P, Fagertun H. Safety and efficacy of Mangafodipir trisodium in patients with liver lesions and cirrhosis. Eur Radiol 2003;13:1685–1692.
43. Bolognesi M, Sacerdoti D, Bombonato G, Chiesura-Corona M, Merkel C, Gatta A. Arterioportal fistulas in patients with liver cirrhosis: usefulness of color Doppler US for screening. Radiology 2000;216: 738–743.
44. Peterson MS, Baron RL, Marsh JW Jr, Oliver JH 3rd, Confer SR, Hunt LE. Pretransplantation surveillance for possible hepatocellular carcinoma in patients with cirrhosis: epidemiology and CT-based tumor detection rate in 430 cases with surgical pathologic correlation. Radiology 2000;217:743–749.
45. Born M, Layer G, Kreft B, Schwarz N, Schild H. MRI, CT and CT arterial portography in the diagnosis of malignant liver tumors in liver cirrhosis. Rofo Fortschr Geb Rontgenstr Neuen Bildgeb Verfahr 1998;168:567–572.
46. Sarasin FP, Giostra E, Hadengue A. Cost-effectiveness of screening for detection of small hepatocellular carcinoma in Western patients with Child-Pugh class A cirrhosis. Am J Med 1996;101:422–434.
47. Satoh T, Sasatomi E, Wu L, Tokunaga O. Phlegmonous colitis: a specific and severe complication of chronic hepatic disease. Virchows Arch 2000;437: 656–661.
48. Wenzel JS, Donohoe A, Ford KL 3rd, Glastad K, Watkins D, Molmenti E. Primary biliary cirrhosis: MR imaging findings and description of MR imaging periportal halo sign. AJR 2001;176:885–889.
49. Blachar A, Federle MP, Brancatelli G. Primary biliary cirrhosis: clinical, pathologic, and helical CT findings in 53 patients. Radiology 2001;220:329–336.
50. Lucidarme O, Baleston F, Cadi M, et al. Non-invasive detection of liver fibrosis: Is superparamagnetic iron oxide particle-enhanced MR imaging a contributive technique? Eur Radiol 2003;13:467–474.
51. Brandhagen DJ, Fairbanks VF, Batts KP, Thibodeau SN. Update on hereditary hemochromatosis and the HFE gene. Mayo Clin Proc 1999;74:917–921.
52. Alustiza JM, Artetxe J, Castiella A, et al. MR quantification of hepatic iron concentration. Radiology 2004;230:479–484.
53. Midiri M, Gallo C, Finazzo M, et al. The liver in patients with beta-thalassemia major. Determination of iron levels with magnetic resonance. Radiol Med 1999;97: 60–65.
54. Magee LA, Dixon RM, Kemp GJ, Redman CW, Styles P. 31P magnetic resonance spectroscopy of the liver in HELLP syndrome. Br J Obstet Gynaecol 1999;106: 582–588.
55. Nino-Murcia M, Olcott EW, Jeffrey RB Jr, Lamm RL, Beaulieu CF, Jain KA. Focal liver lesions: pattern-based classification scheme for enhancement at arterial phase CT. Radiology 2000;215:746–751.
56. Hohmann J, Albrecht T, Hoffmann CW, Wolf KJ. Ultrasonographic detection of focal liver lesions: increased sensitivity and specificity with microbubble contrast agents. Eur J Radiol 2003;46:147–159.
57. Giovagnoni A, Martegani A, Aiani L, Ligabue G, Romagnoli R, Del Favero C. Pulse inversion ultrasonography with ultrasonography contrast media (Levovist) in the evaluation of hepatic metastasis. Radiol Med 2001;101:111–117.
58. Wilson SR, Burns PN, Muradali D, Wilson JA, Lai X. Harmonic hepatic US with microbubble contrast agent: initial experience showing improved characterization of hemangioma, hepatocellular carcinoma, and metastasis. Radiology 2000;215:153–161.
59. Petersein J, Spinazzi A, Giovagnoni A, et al. Focal liver lesions: evaluation of the efficacy of gadobenate dimeglumine in MR imaging—a multicenter phase III clinical study. Radiology 2000;215:727–736.
60. Hussain HK, Syed I, Nghiem HV, et al. T2-weighted MR imaging in the assessment of cirrhotic liver. Radiology 2004;230:637–644.
61. Yu SC, Liew CT, Lau WY, Leung TW, Metreweli C. US-guided percutaneous biopsy of small hepatic lesions. Radiology 2001;218:195–199.
62. Kreft B, Pauleit D, Bachmann R, Conrad R, Kramer A, Schild HH. Incidence and significance of small focal liver lesions in MRI. Rofo Fortschr Geb Rontgenstr Neuen Bildgeb Verfahr 2001;173:424–429.
63. Saini S, Ralls PW, Balfe DM, et al. Liver lesion characterization. ACR Appropriateness Criteria. American

College of Radiology. Radiology 2000;215(suppl):193–199.
64. Ruppert-Kohlmayr AJ, Uggowitzer MM, Kugler C, Zebedin D, Schaffler G, Ruppert GS. Focal nodular hyperplasia and hepatocellular adenoma of the liver: differentiation with multiphasic helical CT. AJR 2001;176:1493–1498.
65. Kim T, Federle MP, Baron RL, Peterson MS, Kawamori Y. Discrimination of small hepatic hemangiomas from hypervascular malignant tumors smaller than 3 cm with three-phase helical CT. Radiology 2001;219: 699–706.
66. Tanaka S, Ioka T, Oshikawa O, Hamada Y, Yoshioka F. Dynamic sonography of hepatic tumors. AJR 2001; 177:799–805.
67. Tello R, Fenlon HM, Gagliano T, deCarvalho VL, Yucel EK. Prediction rule for characterization of hepatic lesions revealed on MR imaging: estimation of malignancy. AJR 2001;176:879–884.
68. Bennett GL, Petersein A, Mayo-Smith WW, Hahn PF, Schima W, Saini S. Addition of gadolinium chelates to heavily T2–weighted MR imaging: limited role in differentiating hepatic hemangiomas from metastases. AJR 2000;174:477–485.
69. Kumano S, Murakami T, Kim T, et al. Using superparamagnetic iron oxide-enhanced MRI to differentiate metastatic hepatic tumors and nonsolid benign lesions. AJR 2003;181:1335–1339.
70. Helmberger TK, Laubenberger J, Rummeny E, et al. MRI characteristics in focal hepatic disease before and after administration of MnDPDP: discriminant analysis as a diagnostic tool. Eur Radiol 2002;12:62–70.
71. Farges O, Daradkeh S, Bismuth H. Cavernous hemangiomas of the liver: are there any indications for resection? World J Surg 1995;19:19–24.
72. Byun JH, Kim TK, Lee CW, et al. Arterioportal Shunt: Prevalence in Small Hemangiomas versus That in Hepatocellular Carcinomas 3 cm or Smaller at Two-Phase Helical CT. Radiology 2004;232:354–360.
73. Kim S, Chung JJ, Kim MJ, Park S, Lee JT, Yoo HS. Atypical inside-out pattern of hepatic hemangiomas. AJR 2000;174:1571–1574.
74. Jeong MG, Yu JS, Kim KW. Hepatic cavernous hemangioma: temporal peritumoral enhancement during multiphase dynamic MR imaging. Radiology 2000;216: 692–697.
75. Zagoria RJ, Roth TJ, Levine EA, Kavanagh PV. Radiofrequency ablation of a symptomatic hepatic cavernous hemangioma. AJR 2004;182:210–212.
76. Mortele KJ, Vanzieleghem B, Mortele B, Benoit Y, Ros PR. Solitary hepatic infantile hemangioendothelioma: dynamic gadolinium-enhanced MR imaging findings. Eur Radiol 2002;12:862–865.
77. Ogino I, Torikai K, Kobayasi S, Aida N, Hata M, Kigasawa H. Radiation therapy for life- or function-threatening infant hemangioma. Radiology 2001; 218:834–839.
78. Steinke K, Terraciano L, Wiesner W. Unusual cross-sectional imaging findings in hepatic peliosis. Eur Radiol 2003;13:1916–1919.
79. Brancatelli G, Federle MP, Grazioli L, Blachar A, Peterson MS, Thaete L. Focal nodular hyperplasia: CT findings with emphasis on multiphasic helical CT in 78 patients. Radiology 2001;219:61–68.
80. Miyayama S, Matsui O, Ueda K, et al. Hemodynamics of small hepatic focal nodular hyperplasia: evaluation with single-level dynamic CT during hepatic arteriography. AJR 2000;174:1567–1569.
81. Paley MR, Mergo PJ, Torres GM, Ros PR. Characterization of focal hepatic lesions with ferumoxides-enhanced T2-weighted MR imaging. AJR 2000;175: 159–163.
82. Nishigaki Y, Tomita E, Matsuno Y, et al. Usefulness of novel imaging modalities in diagnosis of focal nodular hyperplasia of the liver. J Gastroenterol 1997;32: 677–683.
83. Mortele KJ, Wiesner W, de Hemptinne B, Elewaut A, Praet M, Ros PR. Multifocal inflammatory pseudotumor of the liver: dynamic gadolinium-enhanced, ferumoxides-enhanced, and mangafodipir trisodium-enhanced MR imaging findings. Eur Radiol 2002;12:304–308.
84. Lim JH, Kim EY, Lee WJ, et al. Regenerative nodules in liver cirrhosis: findings at CT during arterial portography and CT hepatic arteriography with histopathologic correlation. Radiology 1999;210: 451–458.
85. Lim JH, Cho JM, Kim EY, Park CK. Dysplastic nodules in liver cirrhosis: evaluation of hemodynamics with CT during arterial portography and CT hepatic arteriography. Radiology 2000;214:869–874.
86. Krinsky GA, Israel G. Nondysplastic nodules that are hyperintense on T1-weighted gradient-echo MR imaging: frequency in cirrhotic patients undergoing transplantation. AJR 2003;180:1023–1027.
87. Lim JH, Choi D, Cho SK, et al. Conspicuity of hepatocellular nodular lesions in cirrhotic livers at ferumoxides-enhanced MR imaging: importance of Kupffer cell number. Radiology 2001;220:669–676.
88. Ichikawa T, Federle MP, Grazioli L, Nalesnik M. Hepatocellular adenoma: multiphasic CT and histopathologic findings in 25 patients. Radiology 2000;214: 861–868.
89. Grazioli L, Federle MP, Ichikawa T, Balzano E, Nalesnik M, Madariaga J. Liver adenomatosis: clinical, histopathologic, and imaging findings in 15 patients. Radiology 2000;216:395–402.
90. Yan F, Zeng M, Zhou K, et al. Hepatic angiomyolipoma: various appearances on two-phase contrast scanning of spiral CT. Eur J Radiol 2002;41:12–18.
91. Mok TS, Yu SC, Lee C, et al. False-negative rate of abdominal sonography for detecting hepatocellular carcinoma in patients with hepatitis B and elevated serum alpha-fetoprotein levels. AJR 2004;183:453–458.
92. Choi D, Kim S, Lim J, et al. Preoperative detection of hepatocellular carcinoma: ferumoxides-enhanced MR imaging versus combined helical CT during arterial portography and CT hepatic arteriography. AJR 2001; 176:475–482.
93. Kondo H, Kanematsu M, Hoshi H, et al. Preoperative detection of malignant hepatic tumors: comparison of combined methods of MR imaging with combined methods of CT. AJR 2000;174:947–954.
94. Vogl TJ, Schwarz W, Blume S, et al. Preoperative evaluation of malignant liver tumors: comparison of unenhanced and SPIO (Resovist)-enhanced MR imaging with biphasic CTAP and intraoperative US. Eur Radiol 2003;13:262–272.

95. Murakami T, Kim T, Takamura M, et al. Hypervascular hepatocellular carcinoma: detection with double arterial phase multi-detector row helical CT. Radiology 2001;218:763–767.
96. Jang HJ, Lim JH, Lee SJ, Park CK, Park HS, Do YS. Hepatocellular carcinoma: are combined CT during arterial portography and CT hepatic arteriography in addition to triple-phase helical CT all necessary for preoperative evaluation? Radiology 2000;215:373–380.
97. Hayashi M, Matsui O, Ueda K, et al. Correlation between the blood supply and grade of malignancy of hepatocellular nodules associated with liver cirrhosis: evaluation by CT during intraarterial injection of contrast medium. AJR 1999;172:969–976.
98. Liu WC, Lim JH, Park CK, et al. Poor sensitivity of sonography in detection of hepatocellular carcinoma in advanced liver cirrhosis: accuracy of pretransplantation sonography in 118 patients. Eur Radiol 2003;13: 1693–1698.
99. Caturelli E, Pompili M, Bartolucci F, et al. Hemangioma-like lesions in chronic liver disease: diagnostic evaluation in patients. Radiology 2001;220: 337–342.
100. Ding H, Kudo M, Onda H, Suetomi Y, Minami Y, Maekawa K. Hepatocellular carcinoma: depiction of tumor parenchymal flow with intermittent harmonic power Doppler US during the early arterial phase in dual-display mode. Radiology 2001;220:349–356.
101. Choi BI, Kim TK, Han JK, Kim AY, Seong CK, Park SJ. Vascularity of hepatocellular carcinoma: assessment with contrast-enhanced second-harmonic versus conventional power Doppler US. Radiology 2000;214: 381–386.
102. Ebara M, Fukuda H, Kojima Y, et al. Small hepatocellular carcinoma: relationship of signal intensity to histopathologic findings and metal content of the tumor and surrounding hepatic parenchyma. Radiology 1999;210:81–88.
103. Koushima Y, Ebara M, Fukuda H, et al. Small hepatocellular carcinoma: assessment with T1-weighted spin-echo magnetic resonance imaging with and without fat suppression. Eur J Radiol 2002;41:34–41.
104. Krinsky GA, Lee VS, Theise ND, et al. Hepatocellular carcinoma and dysplastic nodules in patients with cirrhosis: prospective diagnosis with MR imaging and explantation correlation. Radiology 2001;219:445–454.
105. Matsuo M, Kanematsu M, Itoh K, et al. Detection of malignant hepatic tumors: comparison of gadolinium- and ferumoxide-enhanced MR imaging. AJR 2001;177:637–643.
106. Ito K, Fujita T, Shimizu A, et al. Multiarterial phase dynamic MRI of small early enhancing hepatic lesions in cirrhosis or chronic hepatitis: differentiating between hypervascular hepatocellular carcinomas and pseudolesions. AJR 2004;183:699–705.
107. Itai Y. Capsule of hepatocellular carcinoma: where and how does the capsule show enhancement? Radiology 1999;210:577–579.
108. Youk JH, Lee JM, Kim CS. MRI for detection of hepatocellular carcinoma: comparison of mangafodipir trisodium and gadopentetate dimeglumine contrast agents. AJR 2004;183:1049–1054.
109. Ward J, Guthrie JA, Scott DJ, et al. Hepatocellular carcinoma in the cirrhotic liver: double-contrast MR imaging for diagnosis. Radiology 2000;216:154–162.
110. Ward J, Robinson PJ. How to detect hepatocellular carcinoma in cirrhosis. Eur Radiol 2002;12:2258–2272.
111. Nishiharu T, Yamashita Y, Arakawa A, et al. Sonographic comparison of intraarterial CO2 and helium microbubbles for detection of hepatocellular carcinoma: preliminary observations. Radiology 1998; 206:767–771.
112. D'Agostino HB, Solinas A. Percutaneous ablation therapy for hepatocellular carcinomas. AJR 1995;164: 1165–1167.
113. Ryu M, Shimamura Y, Kinoshita T, et al. Therapeutic results of resection, transcatheter arterial embolization and percutaneous transhepatic ethanol injection in 3225 patients with hepatocellular carcinoma: a retrospective multicenter study. Jpn J Clin Oncol 1997;27: 251–257.
114. Michel J, Suc B, Montpeyroux F, et al. Liver resection or transplantation for hepatocellular carcinoma? Retrospective analysis of 215 patients with cirrhosis. J Hepatol 1997;26:1274–1280.
115. Katyal S, Oliver JH, Peterson MS, Chang PJ, Baron RL, Carr BI. Prognostic significance of arterial phase CT for prediction of response to transcatheter arterial chemoembolization in unresectable hepatocellular carcinoma: a retrospective analysis. AJR 2000;175: 1665–1672.
116. Pelletier G, Ducreux M, Gay F, et al. Treatment of unresectable hepatocellular carcinoma with lipiodol chemoembolization: a multicenter randomized trial. Groupe CHC. J Hepatol 1998;29:129–134.
117. Sumie S, Yamashita F, Ando E, et al. Interventional radiology for advanced hepatocellular carcinoma: comparison of hepatic artery infusion chemotherapy and transcatheter arterial lipiodol chemoembolization. AJR 2003;181:1327–1334.
118. Morimoto M, Shirato K, Sugimori K, et al. Contrast-enhanced harmonic gray-scale sonographic-histologic correlation of the therapeutic effects of transcatheter arterial chemoembolization in patients with hepatocellular carcinoma. AJR 2003;181:65–69.
119. Liang HL, Yang CF, Pan HB, et al. Small hepatocellular carcinoma: safety and efficacy of single high-dose percutaneous acetic acid injection for treatment. Radiology 2000;214:769–774.
120. Ohnishi K, Yoshioka H, Kosaka K, et al. Treatment of hypervascular small hepatocellular carcinoma with ultrasound-guided percutaneous acetic acid injection: comparison with segmental transcatheter arterial embolization. Am J Gastroenterol 1996;91:2574–2579.
121. Engelmann K, Mack MG, Straub R, et al. CT-guided percutaneous intratumoral chemotherapy with a novel cisplatin/epinephrine injectable gel for the treatment of inoperable malignant liver tumors. Rofo Fortschr Geb Rontgenstr Neuen Bildgeb Verfahr 2000;172: 1020–1027.
122. Meloni MF, Goldberg SN, Livraghi T, et al. Hepatocellular carcinoma treated with radiofrequency ablation: comparison of pulse inversion contrast-enhanced harmonic sonography, contrast-enhanced power Doppler sonography, and helical CT. AJR 2001;177:375–380.
123. Wen YL, Kudo M, Zheng RQ, et al. Radiofrequency ablation of hepatocellular carcinoma: therapeutic

response using contrast-enhanced coded phase-inversion harmonic sonography. AJR 2003;181:57–63.
124. Kitamoto M, Imagawa M, Yamada H, et al. Radiofrequency ablation in the treatment of small hepatocellular carcinomas: comparison of the radiofrequency effect with and without chemoembolization. AJR 2003;181:997–1003.
125. Rhim H, Yoon K-H, Lee JM, Cho Y, Cho J-S, Kim SH. Major complications after radio-frequency thermal ablation of hepatic tumors: spectrum of imaging findings. Radiographics 2003;23:123–136.
126. Chopra S, Dodd GD 3rd, Chintapalli KN, Leyendecker JR, Karahan OI, Rhim H. Tumor recurrence after radiofrequency thermal ablation of hepatic tumors: spectrum of findings on dual-phase contrast-enhanced CT. AJR 2001;177:381–387.
127. Eichler K, Mack MG, Straub R, et al. Oligonodular hepatocellular carcinoma (HCC): MR-controlled laser-induced thermotherapy. Radiologe 2001;41: 915–922.
128. Dong B, Liang P, Yu X, et al. Percutaneous sonographically guided microwave coagulation therapy for hepatocellular carcinoma: results in 234 patients. AJR 2003;180:1547–1555.
129. Seifert JK, Morris DL. World survey on the complications of hepatic and prostate cryotherapy. World J Surg 1999;23:109–114.
130. Chen RC, Liao LY, Wang CS, et al. Carbon dioxide-enhanced sonographically guided percutaneous ethanol injection: treatment of patients with viable and recurrent hepatocellular carcinoma. AJR 2003;181: 1647–1652.
131. Ichikawa T, Federle MP, Grazioli L, Marsh W. Fibrolamellar hepatocellular carcinoma: pre- and posttherapy evaluation with CT and MR imaging. Radiology 2000;217:145–151.
132. Fuksbrumer MS, Klimstra D, Panicek DM. Solitary fibrous tumor of the liver: imaging findings. AJR 2000;175:1683–1687.
133. Schwartz LH, Gandras EJ, Colangelo SM, Ercolani MC, Panicek DM. Prevalence and importance of small hepatic lesions found at CT in patients with cancer. Radiology 1999;210:71–74.
134. Quaia E, Bertolotto M, Forgacs B, Rimondini A, Locatelli M, Mucelli RP. Detection of liver metastases by pulse inversion harmonic imaging during Levovist late phase: comparison with conventional ultrasound and helical CT in 160 patients. Eur Radiol 2003;13:475–483.
135. Del Frate C, Zuiani C, Londero V, et al. Comparing Levovist-enhanced pulse inversion harmonic imaging and ferumoxides-enhanced MR imaging of hepatic metastases. AJR 2003;180:1339–1346.
136. Semelka RC, Cance WG, Marcos HB, Mauro MA. Liver metastases: comparison of current MR techniques and spiral CT during arterial portography for detection in 20 surgically staged cases. Radiology 1999;213:86–91.
137. Soyer P, Poccard M, Boudiaf M, et al. Detection of Hypovascular Hepatic Metastases at Triple-Phase Helical CT: Sensitivity of Phases and Comparison with Surgical and Histopathologic Findings. Radiology 2004;231:413–420.
138. Valls C, Andia E, Sanchez A, et al. Hepatic metastases from colorectal cancer: preoperative detection and assessment of resectability with helical CT. Radiology 2001;218:55–60.
139. Inaba Y, Arai Y, Kanematsu M, et al. Revealing hepatic metastases from colorectal cancer: value of combined helical CT during arterial portography and CT hepatic arteriography with a unified CT and angiography system. AJR 2000;174:955–961.
140. Ward J, Chen F, Guthrie JA, et al. Hepatic lesion detection after superparamagnetic iron oxide enhancement: comparison of five T2–weighted sequences at 1.0 T by using alternative-free response receiver operating characteristic analysis. Radiology 2000;214:159–166.
141. Sheafor DH, Frederick MG, Paulson EK, Keogan MT, DeLong DM, Nelson RC. Comparison of unenhanced, hepatic arterial-dominant, and portal venous-dominant phase helical CT for the detection of liver metastases in women with breast carcinoma. AJR 1999;172:961–968.
142. Tang Y, Yamashita Y, Ogata I, et al. Metastatic liver tumor from cystic ovarian carcinomas: CT and MRI appearance. Radiat Med 1999;17:265–270.
143. Blake SP, Weisinger K, Atkins M, Raptopoulos V. Liver metastases from melanoma: detection with multiphasic contrast-enhanced CT. Radiology 1999;213: 92–96.
144. Herfarth KK, Debus, Lohr F, Bahner ML, Wannenmacher M. Stereotactic irradiation of liver metastases. Radiologe 2001;41:64–68.
145. Sakamoto I, Iwanaga S, Nagaoki K, et al. Intrahepatic biloma formation (bile duct necrosis) after transcatheter arterial chemoembolization. AJR 2003;181: 79–87.
146. Kelekis AD, Terraz S, Roggan A, et al. Percutaneous treatment of liver tumors with an adapted probe for cooled-tip, impedance-controlled radio-frequency ablation under open-magnet MR guidance: initial results. Eur Radiol 2003;13:1100–1105.
147. de Baere T, Elias D, Dromain C, et al. Radiofrequency ablation of 100 hepatic metastases with a mean follow-up of more than 1 year. AJR 2000;175:1619–1625.
148. Solbiati L, Livraghi T, Goldberg SN, et Percutaneous radio-frequency ablation of hepatic metastases from colorectal cancer: long-term results in 117 patients. Radiology 2001;221:159–166.
149. Livraghi T, Goldberg SN, Solbiati L, Meloni F, Ierace T, Gazelle GS. Percutaneous radio-frequency ablation of liver metastases from breast cancer: initial experience in 24 patients. Radiology 2001;220:145–149.
150. Fiedler VU, Schwarzmaier HJ, Eickmeyer F, Muller FP, Schoepp C, Verreet PR. Laser-induced interstitial thermotherapy of liver metastases in an interventional 0.5 Tesla MRI system: technique and first clinical experiences. J Magn Reson Imaging 2001;13:729–737.
151. Vogl TJ, Straub R, Eichler K, Sollner O, Mack MG. Colorectal carcinoma metastases in liver: laser-induced interstitial thermotherapy—local tumor control rate and survival data. Radiology 2004;230:450–458.
152. Liang P, Dong B, Yu X, et al. Prognostic factors for percutaneous microwave coagulation therapy of hepatic metastases. AJR 2003;181:1319–1325.
153. Stubbs RS, Alwan MH, Booth MW. Hepatic cryotherapy and subsequent hepatic arterial chemotherapy for colorectal metastases to the liver. HPB Surg 1998;11:97–104.

154. Roche A, Girish BV, de Baere T, et al. Trans-catheter arterial chemoembolization as first-line treatment for hepatic metastases from endocrine tumors. Eur Radiol 2003;13:136–140.
155. Sohn J, Siegelman E, Osiason A. Unusual patterns of hepatic steatosis caused by the local effect of insulin revealed on chemical shift MR imaging. AJR 2001;176: 471–474.
156. Yu JS, Kim KW, Jeong MG, Lee JT, Yoo HS. Nontumorous hepatic arterial-portal venous shunts: MR imaging findings. Radiology 2000;217:750–756.
157. Yang DM, Jung DH, Park CH, Kim JE, Choi SJ. Imaging findings of hepatic sinusoidal dilatation. AJR 2004;183:1075–1077.
158. Migliazza L, Lopez Santamaria M, Murcia J, et al. Long-term survival expectancy after liver transplantation in children. J Pediatr Surg 2000;35:5–8.
159. Steingruber IE, Mallouhi A, Czermak BV, et al. Pretransplantation evaluation of the cirrhotic liver with explantation correlation: accuracy of CT arterioportography and digital subtraction hepatic angiography in revealing hepatocellular carcinoma. AJR 2003; 181:99–108.
160. Lee SY, Ko GY, Gwon DI, et al. Living donor liver transplantation: complications in donors and interventional management. Radiology 2004;230:443–449.
161. Fulcher AS, Szucs RA, Bassignani MJ, Marcos A. Right lobe living donor liver transplantation: preoperative evaluation of the donor with MR imaging. AJR 2001;176:1483–1491.
162. Lee VS, Morgan GR, Teperman LW, et al. MR imaging as the sole preoperative imaging modality for right hepatectomy: a prospective study of living adult-to-adult liver donor candidates. AJR 2001;176:1475–1482.
163. Yeh BM, Breiman RS, Taouli B, Qayyum A, Roberts JP, Coakley FV. Biliary tract depiction in living potential liver donors: comparison of conventional MR, mangafodipir trisodium-enhanced excretory MR, and multidetector row CT cholangiography—initial experience. Radiology 2004;230:645–651.
164. Bridges MD, May GR, Harnois DM. Diagnosing biliary complications of orthotopic liver transplantation with mangafodipir trisodium-enhanced MR cholangiography: comparison with conventional MR cholangiography. AJR 2004;182:1497–1504.
165. Lorenz JM, Funaki B, Leef JA, Rosenblum JD, Van Ha T. Percutaneous transhepatic cholangiography and biliary drainage in pediatric liver transplant patients. AJR 2001;176:761–765.
166. Kim BS, Kim TK, Jung DJ, et al. Vascular complications after living related liver transplantation: evaluation with gadolinium-enhanced three-dimensional MR angiography. AJR 2003;181:467–474.
167. Richard HM 3rd, Silberzweig JE, Mitty HA, Lou WY, Ahn J, Cooper JM. Hepatic arterial complications in liver transplant recipients treated with pretransplantation chemoembolization for hepatocellular carcinoma. Radiology 2000;214:775–779.
168. Funaki B, Rosenblum JD, Leef JA, et al. Percutaneous treatment of portal venous stenosis in children and adolescents with segmental hepatic transplants: long-term results. Radiology 2000;215:147–151.
169. Kim BS, Kim TK, Kim JS, et al. Hepatic Venous Congestion after Living Donor Liver Transplantation with Right Lobe Graft: Two-Phase CT Findings. Radiology 2004;232:173–180.
170. Pickhardt PJ, Siegel MJ. Posttransplantation lymphoproliferative disorder of the abdomen: CT evaluation in 51 patients. Radiology 1999;213:73–78.
171. Blachar A, Federle MP. Bowel obstruction following liver transplantation: clinical and CT findings in 48 cases with emphasis on internal hernia. Radiology 2001;218:384–388.
172. Lassau N, Leclere J, Auperin A, et al. Hepatic veno-occlusive disease after myeloablative treatment and bone marrow transplantation: value of gray-scale and Doppler US in 100 patients. Radiology 1997;204: 545–552.
173. van Kaick G, Bahner ML, Liebermann D, Luhrs H, Wesch H. Thorotrast-induced liver cancer: results of the German thorotrast study. Radiologe 1999;39:643–651.

8

Gallbladder and Bile Ducts

Technique

Cholangiography

Intravenous

Although intravenous (IV) cholangiography currently is rarely performed in the United States, in some European countries and Japan it is part of a preoperative workup for suspected stones. Computed tomography (CT) drip infusion cholangiography, however, has supplanted this procedure considerably.

Endoscopic Retrograde Cholangiography

Endoscopic retrograde cholangiography (ERC) has evolved into a major diagnostic and therapeutic modality. It is a common method for performing diagnostic cholangiography, followed if necessary by sphincterotomy, biliary stone extraction, stent insertion for biliary decompression, or biopsy. Disadvantages are that it is very operator dependent, the cholangiographic image quality is often poor, and more complex therapeutic modalities are available only in certain centers. Although the final diagnosis is image based, in many institutions quality control is limited and little radiologist involvement is evident.

Cholangiography establishes the presence of a biliary obstruction. A subtle partial obstruction, however, can be missed with cholangiography, regardless of how it is performed.

Computed Tomography

Development of multislice CT has led to a major improvement in bile duct visualization. Two- and three-dimensional (3D) bile duct reconstructions can be obtained without the use of a cholangiographic agent in a majority of patients, although a biliary contrast agent does improve bile duct visualization and is often employed. Either a cholecystographic or a cholangiographic contrast agent is used, resulting in cystic duct visualization in a majority of patients. The study is performed during a single breath hold, and CT data are then reconstructed to obtain a variety of images: multiplanar reconstruction and volume rendering images. These images can then rotated and viewed from a number of directions.

Bile CT attenuation is 0 to 30 Hounsfield units (HU). Water absorption by gallbladder mucosa changes bile concentration (specific gravity) considerably. Likewise, the presence of sludge, calcium, or contrast material increases bile attenuation.

Computed tomography 10 to 12 hours after oral administration of a cholecystographic contrast agent (iopanoic acid) visualizes extrahepatic and major intrahepatic bile ducts in most individuals even after a cholecystectomy (1,2); 3D volume rendering reconstructions aid in evaluating the bile ducts, including assessing position of surgical clips in patients with postcholecystectomy syndrome.

Another approach is slow infusion of intravenous cholangiographic contrast and CT per-

formed 30 to 60 minutes after infusion. Resultant biliary images are superior to those obtained with conventional intravenous cholangiography. Such studies yield good-quality studies even in children.

Indications for CT cholangiography are still evolving. Preliminary evidence suggests that CT cholangiography is somewhat superior to MRCP in visualizing small biliary stones. The test is not useful in jaundiced patients because insufficient contrast is excreted into the bile ducts.

Magnetic Resonance

Magnetic resonance (MR) is discussed in more detail in Chapter 7. A fast spin echo (FSE) sequence separates solid from fluid-containing structures. Nonflowing fluid–filled structures such as bile ducts are hyperintense on FSE T2-weighted images, while a solid structure is hypointense. A fat-suppression technique helps accentuate bile ducts and related structures and is often employed.

Bile ranges from hypo- to hyperintense on T1-weighted sequences, approaching water intensity when dilute and becoming hyperintense when concentrated. At times a fluid–fluid layer is apparent, with the more concentrated hyperintense bile being dependent.

A potentially useful modality is intrabiliary MRI. An internal receiver coil, commercially available and used for esophageal and other internal structure MR imaging, is passed through a biliary tube into the region in question.

Magnetic resonance cholangiopancreatography is a noninvasive imaging technique of visualizing the biliary and pancreatic ducts. Resultant images are similar to those obtained with endoscopic retrograde cholangiopancreatography (ERCP), and MRCP is evolving as an alternative both to diagnostic ERCP and diagnostic percutaneous cholangiography (Fig. 8.1). An obvious sequela after introduction of MRCP has been obviation of much of diagnostic ERCP. Magnetic resonance cholangiopancreatography is feasible after a choledochojejunostomy.

Two MR approaches are feasible to visualize bile ducts: an intravenous contrast-assisted technique and a technique without contrast by using heavily T2-weighted images to make nonflowing fluid (i.e., bile) hyperintense to surrounding structures.

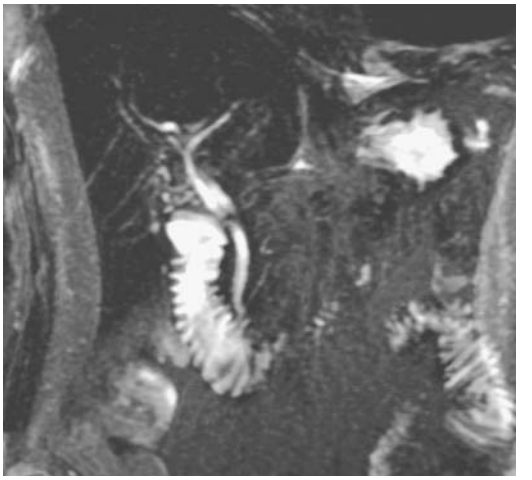

Figure 8.1. Normal magnetic resonance (MR) cholangiography in a patient with suspected pancreatitis. (Courtesy of Patrick Fultz, M.D., University of Rochester.)

A contrast-assisted technique is feasible because such IV contrast agents as manganese (II) N,N'-dipyridoxylethylenediamine-N,N'-diacetate-5,5'-bis phosphate (Mn-DPDP) and gadolinium ethoxybenzyl diethylene-triamine-pentaacetate (Gd-EOB-DTPA) are taken up by hepatocytes and excreted (secreted) into bile ducts. Using T1-weighted sequences, resultant contrast-containing bile is hyperintense, and the gallbladder and bile ducts are then visualized using 2D or 3D image manipulation techniques. The major limitation of this procedure, similar to previously popular intravenous cholangiography, is that reasonable hepatocyte function is required to accumulate enough biliary contrast to be visualized. Thus in a setting of jaundice due to bile duct obstruction and impaired hepatic function—a common scenario—this technique is unsatisfactory. On the other hand, in a postoperative patient, contrast-MRCP appears superior to noncontrast-MRCP in detecting subtle biliary leaks.

Bile ducts can be opacified if an indwelling biliary tube is in place. A simple technique is injection of dilute Gd-DTPA and the use of T1-weighted sequences. Or bile ducts can be distended with saline rather than gadolinium.

A contrast-less technique has attracted most attention and is commonly called MR cholangiopancreatography (MRCP). This technique is possible because by using heavily T2-weighted

pulse sequences, stationary fluid has a high signal intensity while surrounding soft tissues are suppressed and appear hypointense. Bile has a prolonged T2 relaxation time, compared to surrounding soft tissues, and thus on heavily T2-weighted sequences bile and pancreatic secretions are bright, surrounded by dark background tissue. Also, with heavily T2-weighted pulse sequences flowing blood has low to no signal, similar to solid structures. Thus blood vessels are not visualized with this technique.

Initial work with MRCP involved a heavily T2-weighted gradient echo sequence providing a steady state of free precession (SSFP) signals, and this technique appeared promising in the early 1990s. A limitation of this technique is the inability to visualize small fluid collections, to the point that normal bile ducts and pancreatic ducts are not seen. Another limitation is the relatively long scanning time required and the resultant motion artifacts.

A non–breath-hold heavily T2-weighted 2D FSE sequence was refined in the mid-1990s. The FSE sequences are less sensitive to motion and even nondilated ducts are routinely visualized. The 3D FSE uses thinner slices than is possible with 2D sequences, improving image quality. Other improvements include use of surface coils, a fat saturation technique, and image acquisition during quiet respiration.

Comparing 3D SSFP and 2D FSE imaging in patients with bile duct obstruction, FSE visualizes more extrahepatic and intrahepatic bile ducts than SSFP; likewise, the pancreatic duct is better seen with FSE.

The use of rapid acquisition with relaxation enhancement (RARE) and half-Fourier acquisition single-shot turbo spin echo (HASTE) techniques allows imaging during a single breath-hold. The HASTE sequence with MRCP has been refined to the point that one slice can be obtained in 2 seconds. A limitation of this technique is that slice thickness is greater than achievable with the FSE sequence. Whether better definition of selective respiratory triggered 3D turbo spin echo (TSE) outweighs the simplicity of breath-hold single-shot MRCP is not clear, but both techniques define bile ducts.

Magnetic resonance cholangiopancreatography is feasible even with a 0.2-tesla (T) unit. Fewer stones are detected with such a low field unit compared to a 1.5-T unit, but obstructive sites can be identified. A 0.5-T magnet can identify biliary obstructions and detect over 90% of stones. Acquisition times with MRCP performed using a midfield unit range up to 5 minutes or longer, depending on the resolution desired.

Some radiologists employ tap water as an oral contrast agent, but removing gastrointestinal tract fluid signals from MRCP images by using a negative oral contrast agent is preferred. Barium sulfate, iron gluconate, iron oxide agents, ferric ammonium citrate, and similar agents improve bile duct visualization.

Magnetic resonance cholangiopancreatography is technically difficult in children. However, IV sedation often suffices for MRCP, while ERCP in children requires general anesthesia. The MRCP success rates in children average about 80% to 90%, similar to those for ERCP. Non–breath-hold one-shot MRCP appears advantageous in children.

Initially, MRCP was advocated for patients with a failed ERCP. Some enthusiastic researchers have touted MRCP accuracies of 100% in identifying pancreaticobiliary disease, but in the process causing more harm than good for this procedure. Yet even more critical analyses have achieved high sensitivities and specificities. A 3D FSE technique can provide diagnostic-quality images in over 90% of patients, detecting bile duct dilation, strictures, and intraductal abnormalities. Both coronal images and 3D images rotated at different angles are useful. An axial plane tends to better outline the most distal common bile duct and pancreatic duct segments. Both dilated and nondilated extra- and main intrahepatic bile ducts are routinely imaged with MRCP. More peripheral normal side branches usually are not visualized.

In patients with suspected bile duct obstruction, MRCP initially achieved about 75% sensitivity and 75% specificity in diagnosing obstruction but did not detect stones <3 mm in diameter if the bile ducts were not dilation (3). These rather pessimistic results were later balanced by a number of more positive studies: which achieved sensitivities approaching 100% and specificities >90% in detecting biliary or pancreatic duct obstruction. In a typical study, MRCP detects all obstructions due to stones >3 mm in patients after failed or inadequate ERCP, yielding an overall sensitivity and specificity of over 95% (4).

Small calculi tend to be masked by partial volume averaging, a condition partly overcome by thinner collimation. Thin sections are also useful in evaluating strictures and bilioenteric anastomoses. The relevance of periportal edema in bile duct wall visualization is not clear.

Current indications for MRCP are an unsuccessful ERCP, a contraindication for ERCP, pregnancy, or prior anastomosis precluding ERCP access. More indications continue to be added, however, and some investigators predict that MRCP will replace ERCP for most diagnostic questions and ERCP will be relegated to a therapeutic role. The primary advantages of MR cholangiography over ERCP are its noninvasive nature, more reproducible results (i.e., less operator dependent), no sedation required, and the ability to outline ducts proximal to an obstruction. With suspected biliary obstruction, MRCP often not only confirms an obstruction but also identifies the level and suggests an etiology.

Current limitations to better MRCP duct visualization are motion artifacts, surgical clips close to the ducts, and artifacts such as air bubbles within ducts. Currently, spatial resolution of MRCP is inferior to that obtained with technically excellent ERCP, although it is probably on a par with or better than some of the suboptimally calibrated digital ERCP systems in use in a number of institutions. Spatial resolution of some MR units limits its role in characterizing bile duct stenoses and in visualizing papilla of Vater tumors. Subtle changes of sclerosing cholangitis or primary biliary cirrhosis are not evident. False-positive results, including an appearance resembling a stricture, are produced by imaging artifacts, and to minimize them optimal image manipulation is crucial.

Percutaneous Transhepatic Cholangiography

For a percutaneous approach to right lobe ducts, most radiologists use fluoroscopic guidance. If access to a left lobe duct is desired, a combination of US and fluoroscopy is convenient. Prior liver CT, especially with contrast enhancement, provides useful guidance for needle placement and subsequent biliary drainage.

Overlap of some intrahepatic ducts tends to limit their visualization. Generally by turning the patient into an oblique position duct overlap can be minimized; it is often more convenient to rotate the x-ray tube-image intensifier assembly (if feasible) rather than the patient to achieve similar results.

Operative Cholangiography

Operative cholangiography is discussed under the respective therapies in the Acute Cholecystitis section. During laparoscopic cholecystectomy, cholangiography is typically performed by cannulating the cystic duct. Gallbladder puncture and contrast injection into the gallbladder instead of cystic duct cholangiography results in worse bile duct visualization and common duct stone detection.

T-Tube Cholangiography

Placement of an intraoperative T-tube allows routine postoperative T-tube cholangiography. Commonly these patients are placed on prophylactic antibiotic therapy. Is such therapy necessary? The literature provides limited guidance. In the United States a hand-held syringe injection technique is generally used to perform T-tube cholangiography. In Europe an infusion technique is preferred.

Other Techniques

In some patients ERCP is technically not feasible. One proposed approach in such a situation is the use of endoscopic ultrasonography (US) to locate the common bile duct and guide a transduodenal aspiration needle into the duct.

Ultrasonography

Prior to laparoscopic cholecystectomy, conventional US readily detects gallstones, a gangrenous gallbladder, and abnormalities in adjacent structures. It not only determines the caliber of intra- and extrahepatic bile ducts, but also occasionally detects anomalous ducts and their insertions. Prior to initiating oral bile acid therapy, cystic duct patency can be inferred from US performed before and after a fatty meal.

In endoscopic US a transducer placed in the distal portion of the descending duodenum outlines periampullary structures and portions of the pancreatic head. The distal common bile duct and main pancreatic duct can be visual-

ized. The more superior portion of the pancreatic head, gallbladder, cystic duct, and common bile duct are studied through the duodenal bulb. Compared to conventional US, the higher frequencies used in endoscopic US provide good resolution of near objects, but more distal porta hepatis structures are poorly visualized. Also, an enlarged or calcified pancreatic head limits common bile duct visualization.

Miniaturized probes are available for endoluminal bile duct US. A probe is introduced transhepatically if a percutaneous biliary drain is in place, through a surgically inserted T-tube, or through a duodenoscope into the bile ducts. Probes 2.0 mm in diameter use a frequency of about 20 MHz, achieving a spatial resolution of <1 mm. Intraluminal, intramural, and adjacent structures are readily visualized. Such intraluminal US has limited depth penetration and should be combined with other imaging techniques for nodal and metastatic staging.

Preliminary results of 3D intraductal US are promising.

An US probe has been introduced into the gallbladder using an endoscopic transpapillary approach; a guidewire through the papilla aids probe insertion. An intraductal sonographic probe can be inserted into the gallbladder fundus in a majority of patients, but indications for this study are not clear.

Oral Cholecystography

Oral cholecystography (OCG) was the traditional imaging study for detecting gallbladder abnormalities, but with the introduction of US and scintigraphy it has almost disappeared. A nonopacified gallbladder after two consecutive contrast doses was considered evidence of gallbladder disease, assuming that extrabiliary causes for nonopacification are excluded. The earlier literature suggesting an accuracy rate for OCG of almost 100% was overoptimistic; nevertheless, OCG is accurate when stones are clearly visible in a contrast opacified gallbladder. Overall, the accuracy of OCG is probably close to 80% to 90%.

Currently the primary role for OCG is as a supplement to cholecystosonography or cholescintigraphy in those patients for whom the latter studies do not show a gallbladder abnormality in the face of strong clinical suspicion of underlying disease. In addition, in patients considered for extracorporeal gallstone lithotripsy, OCG has a role in counting the number of stones present, determining their size, and establishing cystic duct patency.

Cholangioscopy

While an endoscopic approach to the bile ducts is preferable, occasionally this technique is not feasible. Percutaneous transhepatic cholangioscopy provides biliary access and allows direct duct visualization, cholangiography, and biopsy.

Cholangioscopy can be performed for lithotripsy of biliary stones.

Scintigraphy

Magnetic resonance cholangiopancreatography and ERCP provide bile duct morphology while cholescintigraphy primarily evaluates function. These tests are thus complementary and, depending on clinical indications, at least 2 of these are often necessary for adequate biliary evaluation.

A number of iminodiacetic acid (IDA) tracer compounds are in use worldwide for cholescintigraphy, but in the United States technetium-99m-DISIDA and Tc-99m–BrIDA are available. Intravascularly, these compounds bind to albumin, are taken up by hepatocytes, are excreted into bile canaliculi, and appear in extrahepatic bile ducts 30 minutes or so after injection. In most patients small bowel activity is evident within 60 minutes.

The relative amounts of tracer flowing into the duodenum and gallbladder depend on sphincter of Oddi pressure and gallbladder tonicity. Pharmacologic agents modify flow to either the gallbladder or the duodenum. For instance, morphine sulfate induces sphincter of Oddi contraction and thus tracer flow is preferentially into the gallbladder. Likewise, IV cholecystokinin (CCK) is indicated to contract the gallbladder prior to cholescintigraphy in fasting patients and as an aid for suspected sphincter of Oddi dysfunction or acalculous cholecystitis. In a setting of a dilated duct, CCK aids in excluding an obstruction.

Cholecystokinin also provides data for measuring gallbladder ejection fraction. An ejection

fraction of <35% suggests chronic cholecystitis. Infusion over 30 or 60 minutes is required to establish reproducible results; shorter infusions lead to erratic results. One should keep in mind that a number of pharmacologic agents affect gallbladder ejection fraction; for instance, morphine decreases gallbladder ejection fraction.

It is unusual to see gallbladder uptake of bone-seeking radiopharmaceutical agents. Some patients undergoing whole-body bone scanning during chemotherapy, however, have an intense gallbladder uptake; after completion of chemotherapy, gallbladder uptake ceases. Presumably such uptake is secondary to the chemotherapy regimen employed rather than to underlying gallbladder disease.

Some patients undergoing lung perfusion studies with Tc-99m–macroaggregated albumin (MAA) have measurable gallbladder activity.

Occasionally delayed whole-body iodine 131 imaging visualizes focal radioactivity in a dilated intrahepatic duct, suggesting a metastasis; other imaging should differentiate these conditions.

Biliary Drainage

The biocompatibility of catheter material and bile mucosa is an ongoing research topic and beyond the scope of this book. The main problems encountered in clinical practice are erosions, mucosal hyperplasia, catheter encrustation, and obstruction during chronic drainage.

Biliary drainage is performed primarily to relieve an obstruction. In acute cholangitis urgent biliary drainage is generally initiated using an endoscopic approach and, if necessary, a sphincterotomy and stone extraction are performed during the same procedure. Some critically ill patients, deemed potentially unstable to be moved to a fluoroscopy suite, have had endoscopic biliary drainage performed either under sonographic guidance or blindly. Drainage through a nasobiliary catheter is preferred; the bile ducts are decompressed manually and ready catheter access allows cholangiography.

Controversy continues on the relative merits of endoscopic versus percutaneous biliary decompression for biliary obstruction. In a number of hospitals the choice depends on the relative expertise of the interventionalists and endoscopists involved and on the suspected obstruction etiology. Especially with high biliary obstructions (at porta hepatis or hepatic duct), percutaneous drainage tends to have an overall greater success rate than endoscopic drainage. Also, percutaneous biliary drainage can achieve decompression after failed endoscopic drainage, but endoscopic drainage is not often attempted after failed percutaneous drainage.

Most percutaneous biliary drainage is performed using fluoroscopic or US guidance (or both) and a right lateral approach. Left lobe biliary drainage is also feasible if a bile duct can be localized with US guidance. An open low-field strength MR unit using near real-time imaging also provides needle positioning guidance. Percutaneous biliary drainage can achieve a high success rate in patients even with nondilated bile ducts. Success rates range from 50% to 90%. Only one puncture is necessary in most patients during percutaneous transhepatic biliary drainage when color Doppler US provides guidance.

Percutaneous cholecystostomy consists of percutaneous catheter insertion into the gallbladder using imaging guidance. It is an alternative to surgical cholecystostomy, especially in high risk patients with acalculous cholecystitis.

At times biliary access is necessary in a patient after creation of a choledochojejunostomy and Roux-en-Y jejunojejunostomy and an antegrade approach is not feasible. In these patients percutaneous retrograde transjejunal cholangiography is an option, especially if the surgeon has provided superficial Roux-en-Y loop fixation. In fact, surgeons should be encouraged to perform superficial fixation of Roux-en-Y loops for biliary-enteric anastomoses to allow future access for biliary interventions.

Most duct localization is performed with an iodinated contrast agent. CO_2 cholangiography can also be performed and occasionally a duct segment not visualized with iodinated contrast is outlined by CO_2. In most studies, however, CO_2 offers little advantage.

An MRCP is feasible with a stent in place, but the results are often unsatisfactory. An indwelling polyethylene stent lumen is visible

with MRCP, but artifacts obliterate cobalt alloy and most nitinol stent lumina (5).

In a setting of distal bile duct obstruction, percutaneous biliary drainage diverts bile away from the gut. A patient's nutritional status can be improved by reintroducing this bile to the jejunum through either a nasogastric tube or a jejunal catheter passed through a gastrostomy.

Bile cytology obtained at the time of biliary drainage is a useful adjunct. In consecutive patients with presumed malignant biliary strictures undergoing percutaneous biliary drainage, single specimen bile cytology achieved a sensitivity of 15% and specificity of 100% (6); in spite of the low sensitivity, the simplicity of this procedure argues for its continued use. Bile culture is also useful during percutaneous biliary drainage. Fever, previous biliary instrumentation, and bile duct surgery are predictors of a positive bile culture, with the most common organisms being enterococcal species.

Hemobilia is a complication of percutaneous transhepatic biliary drainage. This complication is decreased if during initial needle passage the needle tract is opacified with contrast, and, if a major vascular structure communicates with this tract, it should be abandoned and another tract established.

Whether catheter tract embolization should be performed after transhepatic biliary drainage is not clear. Some interventionalists do embolize drainage tracts. Surgeons do not embolize T-tube tracts. Sufficient fibrosis ensues after long-term drainage that free peritoneal spill and peritonitis rarely are issues (except after liver transplantation). Whether embolization has any effect in a setting of distal biliary tract obstruction is arguable.

Biopsy

Fluoroscopically guided percutaneous transhepatic intraductal biopsy, usually performed as part of a percutaneous biliary drainage procedure, is useful with a suspected primary bile duct malignancy. Multiple forceps biopsies, using intraductal US guidance, achieve high tumor detection sensitivities.

Mucosal brushing is feasible either during ERCP or through a percutaneous biliary catheter. All other factors being equal, a biopsy achieves a greater sensitivity than brushings. Pain and transient hemobilia are complications.

Congenital Abnormalities

Gallbladder

Agenesis of Gallbladder

Gallbladder agenesis is rare. An absent gallbladder is found in left-sided isomerism (asplenia). Most patients with gallbladder agenesis also have an absent cystic duct, and often other gastrointestinal anomalies are evident. An association exists between gallbladder agenesis and duodenal atresia.

Some patients have symptoms clinically compatible with gallbladder disease and some even have a false-positive US study. Bile duct stones are relatively common in these patients. Gallbladder agenesis has only been diagnosed at laparoscopy for presumed cholecystitis in some of these patients.

Multiple Gallbladders

Most gallbladder duplications are discovered in a setting of either cholelithiasis or acute cholecystitis. Gallbladder duplication is more common in right-sided isomerism (polysplenia). Anecdotal reports describe not only stones in a duplicated gallbladder but also a carcinoma.

Gallbladder duplication can usually be identified with US or any type of cholangiography. Magnetic resonance imaging (MRI) is also helpful in defining the underlying anatomy. Some double gallbladders are not detected either with preoperative imaging or even during cholecystectomy and a second operation is then necessary.

Multiseptate Gallbladder

A congenital multiseptate gallbladder is rare. More common are gallbladder folds mimicking septa.

Ultrasonography should detect a multiseptate gallbladder. Endoscopic retrograde cholangiopancreatography is helpful only if sufficient

contrast fills the gallbladder to outline the septa. These patients also have impaired gallbladder function.

Ectopic Gallbladder

An abnormal gallbladder location is more common than agenesis. Congenitally lax mesenteric attachments allow gallbladder migration to unusual sites. An ectopic gallbladder can be intrahepatic, extraperitoneal, in the lesser omentum, within the falciform ligament, or in other locations. It can be located just inferior to the right hemidiaphragm. Subcutaneous gallbladder herniation through the abdominal wall is rare (7). Also rare is internal gallbladder herniation through the adjacently located foramen of Winslow and obstruction to either bile or blood flow. Some patients also have associated hepatic lobe, portal vein, and pancreaticobiliary duct anomalies.

Imaging does not identify the gallbladder in its usual position. Endoscopic retrograde cholangiopancreatography is useful in defining this condition and identifying any associated ductal anomalies prior to laparoscopic cholecystectomy.

With an intrahepatic gallbladder, Tc-99m–sulfur colloid scintigraphy reveals a focal intrahepatic defect.

Anomalous Bile Ducts

Intrahepatic bile ducts develop from liver progenitor cells in contact with portal vein mesenchyme and form ductal plates that evolve into mature ducts. Failure of evolution leads to ductal plate malformation and congenital intrahepatic bile duct disorders characterized by dilated biliary segments and surrounding fibrosis.

Considerable variation exists in intrahepatic bile duct anatomy (Fig. 8.2). A right lobe duct draining into the cystic duct, in particular, has bedeviled surgeons during apparent routine cholecystectomy.

More complex intra- and extrahepatic bile duct anomalies are rare. One rather extreme example consists of the hepatic duct draining into the gallbladder and the cystic duct then draining the entire biliary system. Some preduodenal common bile ducts are associated with a preduodenal portal vein. These and other related anomalies need to be considered to prevent bile duct injury during cholecystectomy.

Computed tomographic cholangiography detects major bile duct anomalies. Both 2D and 3D images are necessary to fully evaluate these anomalies. Whether aberrant bile ducts are better identified by CT cholangiography or MRCP is detectable; the latter images are degraded by overlapping duodenum and other ductal structures. Complicating this issue is that MRCP rather than CT cholangiography has achieved a superior role as a preferred preoperative imaging modality. What preoperative role MRCP has in alerting the surgeon to possible bile duct anomalies and thus potentially decreasing intraoperative duct injury remains to be determined.

Sphincter of Oddi Region Anomalies

Numerous anomalous biliary and pancreatic duct insertions are possible, including a long common channel (called *anomalous arrangement of the pancreaticobiliary duct* and *anomalous pancreaticobiliary ductal union* by some authors). This latter congenital variant (depending on viewpoint, considered an anomaly, maljunction, or disease) consists of pancreatic and biliary duct union outside the duodenal wall. Such a long common pancreaticobiliary channel presumably leads to pancreatic juice reflux into bile ducts. It is a common finding in patients with a choledochal cyst and gallbladder carcinoma and is also associated with gallstone-induced acute pancreatitis (discussed in Chapter 9). Several patients with an anomalous pancreaticobiliary duct junction and pancreatic carcinoma have been reported. Whether such an association is fortuitous or not is conjecture.

The prevalence of an anomalous pancreaticobiliary duct connection is unknown. Anomalous insertions are associated with dilated bile ducts (choledochal cyst), a tendency toward gallstone formation, and possibly gallbladder adenomyomatosis. Even in childhood, anomalous pancreaticobiliary ducts are associated with increased gallbladder epithelial cellular proliferation, manifesting as epithelial hyperplasia. Ultrasonography, including endoscopic US, reveals a diffuse thickened hypoechoic inner gallbladder wall layer, indicative of mucosal

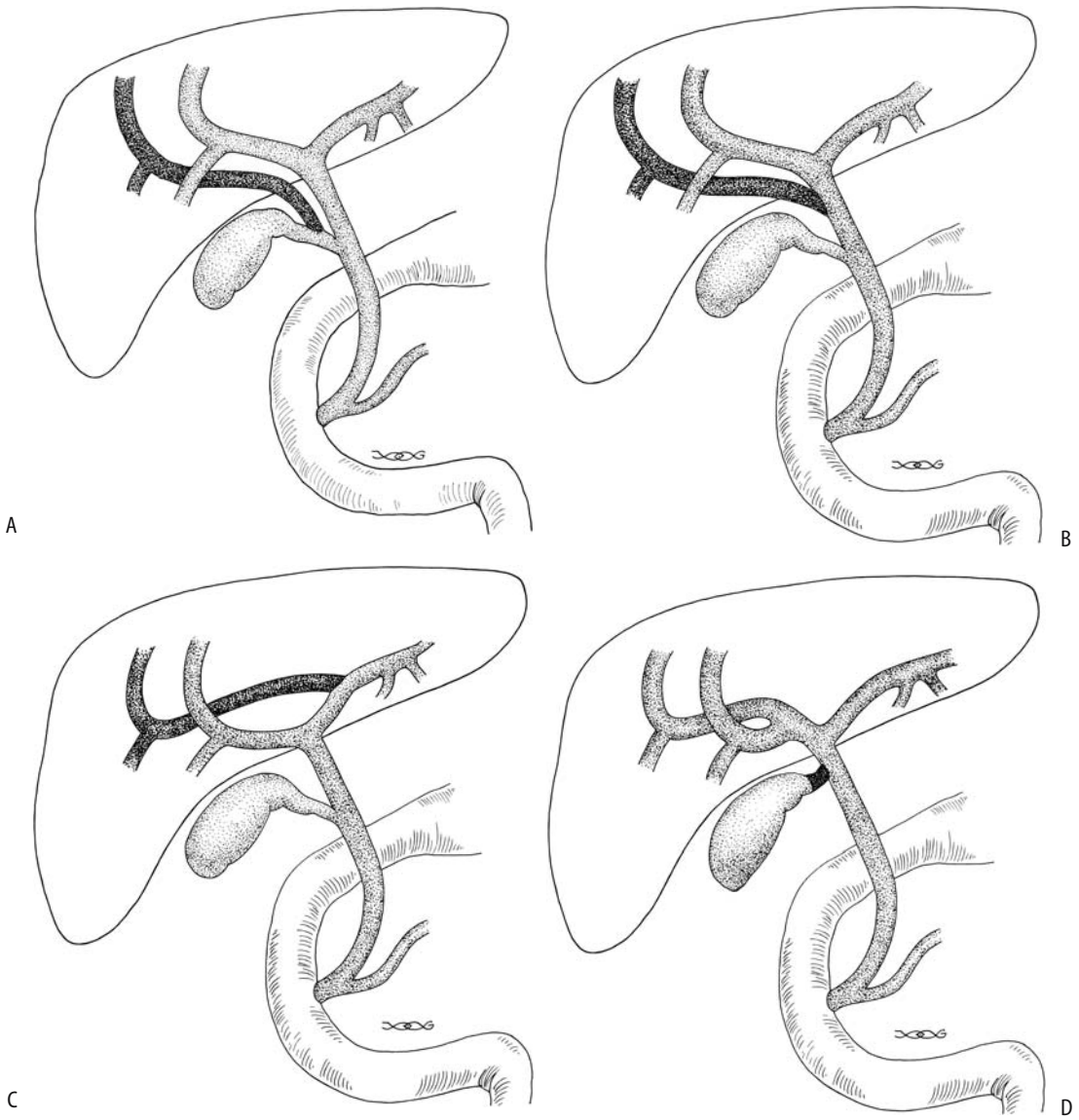

Figure 8.2. Illustration of common bile duct anomalies. A: A right lobe branch inserts into the cystic duct. B: A right lobe branch inserts into the hepatic duct. C: A right lobe duct communicates with the main left lobe duct. D: A short cystic duct inserts close to the porta hepatis and the hepatic duct is very short. In such a setting the common bile duct is readily confused with the cystic duct.

hyperplasia; this characteristic sonographic finding of gallbladder mucosal hyperplasia is found only in those who have associated anomalous pancreaticobiliary ducts. An increased risk of gallbladder cancer has been suggested in affected patients.

Computed tomographic cholangiography is useful in evaluating pancreaticobiliary duct anomalous junctions; at times pancreatic juice is identified refluxing into the bile duct. The reverse is also true—in some patients contrast refluxes from the common bile duct into the pancreatic duct.

Many of these maljunctions are readily identified with ERCP. Endoscopic US and intraductal US are helpful in defining surrounding

structures. An MRCP identifies an anomalous pancreaticobiliary duct junction in most patients, less so in children than in adults.

Regardless of whether bile ducts are dilated or not, whether a prophylactic cholecystectomy should be recommended to patients with a pancreatic or biliary maljunction because of increased gallbladder cancer risk is not clear.

Cholestatic Conditions

Especially in the very young, jaundice has a broad differential diagnosis ranging from a benign, transient event to a lethal hereditary condition. It is associated with biliary atresia, a dysplasia such as Alagille's syndrome, an acute hepatic insult such as viral hepatitis, and a choledochal cyst, and it is a manifestation of a hereditary hyperbilirubinemia. Some cholestatic conditions are a result of gene coding mutations. A number of these conditions first manifest in childhood rather than in neonates.

Neonatal Cholestasis

Clinical

The prior thinking was that a majority of neonates with persistent jaundice had either biliary atresia or sequelae of neonatal viral hepatitis. Whether these are different entities or simply different manifestations of the same condition is conjecture. Their clinical findings are indistinguishable in most neonates. Currently, other conditions have emerged in the differential diagnosis, including Alagille's syndrome. Aside from intrahepatic causes, occasional neonatal jaundice is secondary to a choledochal cyst, sepsis, hemolysis, infection, juvenile xanthogranulomatosis, or metabolic disorders such as α_1-antitrypsin deficiency, cystic fibrosis, and others.

Congenital biliary atresia ranges from a rare isolated, focal atretic segment, mostly intrahepatic atresia, to mostly extrahepatic atresia. Disrupted intrahepatic bile ducts lead to bile ductule proliferation and periportal fibrosis, with residual bile ducts replaced by fibrosis and rapid progression to cirrhosis. In a minority of neonates, extrahepatic atresia is associated with other systemic abnormalities.

Viral hepatitis can be confirmed in some neonates with clinical follow-up until jaundice resolves, although one often does not have the luxury of time. Prognosis in neonates with congenital biliary atresia is better with early intervention, generally within the first month of life.

A liver biopsy in infants with neonatal cholestasis often is not diagnostic. A high false-negative rate is evident in biliary atresia. The presence of giant cells is found in several entities.

Imaging

Most of these neonates have marked hepatomegaly and some degree of splenomegaly. With the exception of scintigraphy, most noninterventional imaging studies are of limited use in differentiating biliary atresia and neonatal hepatitis. Intrahepatic US findings are nonspecific, although if a gallbladder is identified, neonatal hepatitis is somewhat more likely. Yet about 20% of neonates with biliary atresia have an intact gallbladder, in others it is atretic or elongated. And, to add more confusion, US detected gallbladder contractions after oral feeding in 9% of 34 children with biliary atresia (8); surgery in these children revealed patency between the gallbladder and duodenum. Still, US is useful in detecting any associated cysts and other congenital anomalies, because these neonates have an increased prevalence of polysplenia, situs inversus, malrotation, and a number of vascular anomalies.

Magnetic resonance cholangiopancreatography shows promise in differentiating between biliary atresia and neonatal hepatitis by detecting extrahepatic bile ducts in the latter entity. Successful duct visualization is difficult in infants with jaundice and small ducts even when normal, but biliary atresia can be excluded if normal-appearing extrahepatic bile ducts are visualized. In some neonates and infants with biliary atresia, MRCP shows a triangular hyperintense region in the porta hepatis; histopathology reveals a cystic structure without ductal epithelium surrounded by myxoid mesenchyme and plate-like fetal bile ducts.

Technetium-99m-IDA scintigraphy differentiates among biliary atresia, neonatal hepatitis, and other causes of jaundice in most infants. If

extrahepatic biliary activity is identified, biliary atresia can be excluded with a sensitivity approaching 100%. Technetium-99m-DISIDA achieves a high sensitivity but a low specificity. Because of the low specificity, without intestinal activity this study should be considered inconclusive and both neonatal hepatitis and intrahepatic cholestasis are still in the differential diagnosis. In a review of consecutive infants from the Hospital for Sick Children in Toronto, hepatobiliary scintigraphy failed to detect biliary flow into the intestine in 62% (9); of these, 75% were shown to have extrahepatic biliary atresia, 15% neonatal hepatitis, 8% intrahepatic bile duct paucity, and 2% total parenteral nutrition-associated cholestasis. Even total parenteral nutrition-associated cholestasis is in the differential with lack of extrahepatic biliary activity. Poor versus good hepatocyte clearance cannot identify neonatal hepatitis.

Phenobarbital stimulates hepatic microsomal activity. Premedication with phenobarbital prior to scintigraphy increases the accuracy in differentiating between neonatal hepatitis and biliary atresia. Phenobarbital stimulation may not be needed when Tc-99m-BrIDA is used because this tracer undergoes greater hepatic extraction and excretion than Tc-99m-DISIDA or HIDA. Occasionally repeat scintigraphy after administering ursodeoxycholic acid changes Tc-99m-BrIDA nonexcretors with hepatitis into excretors.

An ERCP is useful in visualizing the extrahepatic bile ducts in suspected neonatal cholestasis but is technically difficult and in most centers is infrequently performed.

Therapy

In neonates and infants with biliary atresia, an intraoperative cholangiogram is usually performed to define the biliary anatomy and determine whether a primary anastomosis is feasible. In a minority the obstruction is at the common bile duct level. Even with intact main right and left hepatic ducts, quite often a Roux-en-Y hepaticojejunostomy is performed. In the absence of cholangiographically visible ducts a hepaticoportoenterostomy (Kasai procedure) is preferred.

Not all infants develop satisfactory biliary drainage following the Kasai procedure, with the success rate decreasing with age. Evidence suggests that a low hepatocellular scintigraphic extraction fraction in newborns with biliary atresia is associated with a poor postoperative prognosis (10). Incomplete drainage leads to fibrosis and eventual biliary cirrhosis and the need for liver transplantation (Fig. 8.3).

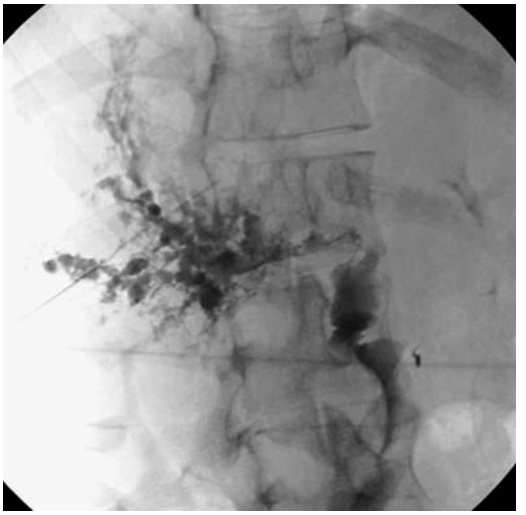

Figure 8.3. Percutaneous cholangiogram in a 17–year-old with jaundice reveals numerous cavities communicating with irregular bile ducts. He had biliary atresia as a newborn and underwent a Kasai procedure.

Hepatobiliary scintigraphy post–Kasai procedure confirms a successful anastomosis by identifying biliary drainage into the intestine.

Of Japanese patients with biliary atresia who underwent a Kasai procedure, 60% became jaundice-free (11); nevertheless, on a long-term basis portal hypertension developed in 50% of anicteric survivors, manifesting as esophageal varices or thrombocytopenia.

Alagille's Syndrome

Alagille's syndrome, or *arteriohepatic dysplasia*, is an autosomal-dominant multisystemic disorder with nearly complete penetrance and variable expression caused by a genetic defect in the short arm of chromosome 20; it results in mutations to the Jagged 1 (JAG1) protein, a ligand involved in early cell embryogenesis. A wide spectrum of JAG1 mutations includes gene deletions in a minority while most have protein

truncating, splicing, and missense mutations across the gene coding region. This multisystem anomaly leads to atypical facies, pulmonary artery stenosis, butterfly-like vertebral bodies, various cardiovascular anomalies, renal cysts, and growth and mental retardation. The primary liver abnormality consists of a paucity of intrahepatic bile ducts, with the severity varying depending on the specific JAG1 abnormality, and the resultant cholestasis manifests as neonatal jaundice. Liver biopsy tends to detect a paucity of intrahepatic bile ducts (ductopenia). Alagille's syndrome should be suspected in children with unexplained cholestasis and is confirmed by genetic analysis for mutations of the *JAG1* gene. Some of these infants progress to cirrhosis, even during childhood. Hepatocellular carcinomas have developed even in pediatric ages.

Abdominal imaging in some simply reveals hepatomegaly. The most common abnormality is a liver contour abnormality consisting of either the liver or a lobe having a spherical shape; a sulfur colloid liver–spleen radionuclide scan often shows prolonged excretion. The US findings are similar to those seen with biliary atresia.

Hepatobiliary scintigraphy in a child with Alagille's syndrome reveals hepatobiliary dysfunction, at times with foci of increased uptake due to compensatory hyperplasia in a setting of cirrhosis.

Liver transplantation is the therapy of choice in end-stage liver disease. Incidentally, the growth failure often seen in Alagille's syndrome patients is not corrected by orthotopic liver transplantation.

Familial Hyperbilirubinemias

Traditionally grouped under familial hyperbilirubinemias are nonhemolytic conditions characterized by hepatic dysfunction without gross evidence of hepatocellular injury or biliary atresia. They are subdivided into unconjugated hyperbilirubinemias consisting of Crigler-Najjar syndrome I and II and Gilbert's syndrome and conjugated hyperbilirubinemias consisting of Rotor's syndrome and Dubin-Johnson syndrome. From an imaging viewpoint these conditions are mostly curiosities, but are included because they are in the differential diagnosis of a jaundiced child.

Crigler-Najjar Syndrome

Crigler-Najjar syndrome is a rare genetic disorder inherited as autosomal dominant with variable penetrance and as an autosomal-recessive trait. It typically manifests in the pediatric age group.

This syndrome is due to a gene defect encoding bilirubin uridine diphosphate glucuronosyltransferase (UGT), which is involved in bilirubin conjugation with glucuronic acid. A number of mutations affect the coding region of this gene and lead to a decreased ability to glucuronidate bilirubin. The end result is an increase in unconjugated serum bilirubin level. Patients with this syndrome are homozygous for this defect, resulting in an abnormal form of transferase enzyme.

This syndrome is subdivided into types I and II. In type I, the absence of hepatic bilirubin glucuronyl transferase activity results in a severe unconjugated hyperbilirubinemia that invariably is fatal. In type II, a single base pair mutation results in decreased enzyme activity; in these patients this enzyme responds to phenobarbital therapy, and clinical manifestations are milder and appear similar to those found in Gilbert's syndrome.

Gilbert's Syndrome

Gilbert's syndrome, previously also known as *Meulengracht disease* in some countries, was redefined in the 1980s and today this term is applied to a chronic unconjugated hyperbilirubinemia due to increased bilirubin turnover. Using such a broad definition, this is a relatively common condition and often manifests as mild hyperbilirubinemia but no clinical illness. It is often diagnosed after puberty.

Similar to the Crigler-Najjar syndrome, a deficiency of the bilirubin uridine diphosphate (UDP)-glucuronosyltransferase gene also exists in Gilbert's syndrome. Several mutations of UGT cause mild reduction of UGT activity and mild hyperbilirubinemia. Patients with both Crigler-Najjar syndrome and Gilbert's syndrome have been described.

Gilbert's syndrome patients are at increased risk for gallstones. An association with hypertrophic pyloric stenosis has been suggested. Occasionally Gilbert's syndrome manifests first as postoperative jaundice.

Rotor's Syndrome

Cholescintigraphy does not visualize the liver, in Rotor's syndrome patients although they have persistent visualization of the cardiac blood pool and show renal excretion.

Dubin-Johnson Syndrome

Secretion of various conjugates across canalicular and other membranes is mediated by multidrug resistance protein (MRP) pumps; a defect in the *MRP2* gene, which encodes MRP2 glycoprotein in the canalicular bilirubin conjugate export pump, leads to a block in excretion of conjugated bilirubin. As a result, a conjugated hyperbilirubinemia develops but no cholestasis is evident. Histology reveals brown pigments consisting of a lipofuscin-melanin complex, mostly in centrilobular zone hepatocytes.

At times CT identifies a hyperdense liver.

Cholescintigraphy reveals poor-to-no gallbladder and bile duct activity but an intense and prolonged liver blush. Scintigraphy thus aids in differentiating Rotor's syndrome from Dubin-Johnson syndrome.

Progressive Familial Intrahepatic Cholestasis (Byler Disease)

Whether to list this condition under familial hyperbilirubinemia is a matter of definition. Undoubtedly some patients previously included under the hyperbilirubinemia conditions discussed above should be classified under progressive familial intrahepatic cholestasis. Also known as Byler disease, this condition was originally described in an Amish kindred. It is an inherited cholestatic condition having autosomal-recessive inheritance. Rather than one entity, evidence points to a group of similar genetic disorders. The same or very similar conditions exist worldwide; as an example, *cholestasis familiaris Groenlandica* is a common recessive disease in East Greenland (12). Some authors distinguish the condition found in original Amish kindred (Byler disease) from that detected in others (Byler syndrome); the genes responsible appear to be different. Two genetic types are evident (13): type 1, caused by mutations in the *FIC1* gene, coding for P-type adenosine triphosphatases (ATPases); and type 2, due to mutations in the *BSEP* gene (bile salt export pump), results in defective function of the canalicular bile salt export pump. Others describe three subtypes (14). In type 1, cholestasis presents in the neonatal period, a severe pruritus develops, histology reveals absence of ductule proliferation, and these children die due to liver failure; an inborn error in primary bile acid secretion has been suggested and a locus mapped to 18q21–q22. In type 2, pruritus does not develop, and an inborn error in primary bile acid synthesis appears to be responsible. Type 3 presents later in life, intra- and extrahepatic bile ducts are patent, often portal hypertension develops with its related complications, and liver failure ensues at a later age; an abnormal *MDR3* gene function appears to be involved. Heterozygosity in these patients appears to be associated with cholestasis of pregnancy.

Biliary diversion is often employed in these neonates with cholestasis and pruritus; liver damage is then delayed until orthotopic liver transplantation is available.

Cystic Fibrosis

The liver margin becomes irregular in cystic fibrosis patients. Postcontrast CT reveals inhomogeneous enhancement throughout the liver.

Biliary drainage is deranged in cystic fibrosis, probably due to inspissated secretions. An intrahepatic cholestasis is evident. A typical pattern is dilation of intrahepatic bile ducts, more prominent on the left, a narrowed distal common bile duct, gallbladder dysfunction, and decreased bowel transit. The bile ducts tend toward an irregular, beaded appearance; superficially the appearance can resemble sclerosing cholangitis. These patients are prone to developing gallstones.

A minority of cystic fibrosis children have abnormal liver US, with changes ranging from a diffuse hypoechoic liver with prominent portal tracks, cirrhosis, to portal hypertension (15). Portal track findings tend to be better identified with US than CT (16).

Some patients have prolonged radiotracer retention in intrahepatic ducts even with little or no biochemical evidence of liver involvement. Gallbladder nonvisualization during hepatobiliary scintigraphy in these patients has been attributed to cystic duct obstruction by viscid secretions, although a small, contracted

gallbladder is common and may account for nonvisualization even in the absence of cholecystitis.

Choledochal Cyst

Clinical

The etiology of choledochal cysts is unknown. They are usually classified under congenital cystic biliary malformations, although neonatal viral infection or a bile duct wall abnormality may be responsible. In neonates and infants some authors label this condition simply as congenital biliary dilation. The borderline between a prominent but still normal caliber duct and a choledochal cyst is a matter of definition.

A number of Western authors have commented on the rarity of choledochal cysts in their practices. These cysts are encountered more often in Asia, and most larger studies are from Asia.

A relationship between choledochal cysts and congenital hepatic fibrosis has been speculated; some neonates with choledochal cysts also have periportal fibrosis. An inconsistent association exists between a choledochal cyst and intestinal malrotation. In some adults differentiation between primary chronic dilation leading to bile stasis and stone formation and secondary dilation due to biliary stones and resultant inflammation is not possible.

In 1959, Alonso-Lej et al. (17) classified choledochal cysts into three types: I, fusiform dilation of a portion or entire extrahepatic bile duct system; II, saccular diverticular-like outpouching in extrahepatic ducts; and III, focal dilation of distal common bile duct segment (or common pancreatobiliary channel) within the wall of the duodenum. Type III is also called a choledochocele. Todani et al. (18) expanded this system in 1977 to better reflect a surgical approach. The Todani modification subdivides type I cysts into Ia, aneurysmal dilation; Ib, segmental dilation; and Ic, diffuse, cylindrical dilation; and also includes type IV cysts: IVa, multiple intra- and extrahepatic duct cysts; and IVb, multiple extrahepatic cysts only. Also added was a type V: single or multiple intrahepatic duct cysts.

The most common type of choledochal cyst is type I (Fig. 8.4). These cysts tend to be associated with biliary or sphincter of Oddi anomalies, and in these individuals reflux of pancreatic content with secondary bile duct wall inflammation and thinning appears to be a reasonable etiology for choledochal cyst formation.

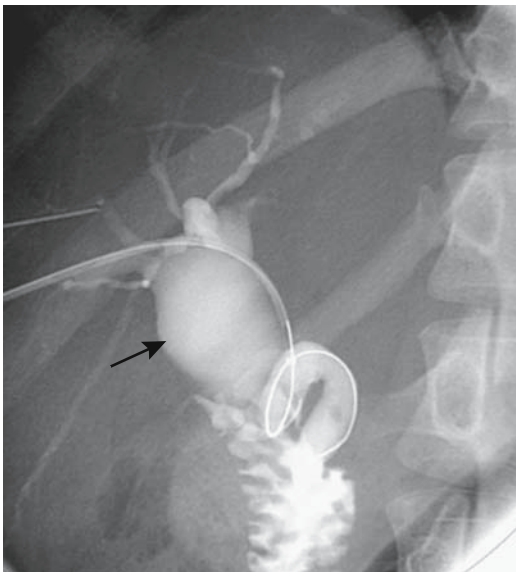

Figure 8.4. Type I choledochal cyst involving hepatic duct (arrow). (Courtesy of David Waldman, M.D., University of Rochester.)

A type II choledochal cyst is a rare congenital malformation. An occasional one presents as an adjacent tumor without an obvious bile duct communication; biliary communication presumably is obliterated due to inflammation.

No strict criteria define a type III cyst (choledochocele), and some authors include dilation of a common channel as a type of choledochocele. Using a strict definition, however, a choledochocele is probably as rare as a type II cyst. These patients are prone to choledocholithiasis. Smaller choledochoceles tend to be asymptomatic.

Among adults with choledochal cysts treated in 17 institutions of the French Associations for Surgical Research, 50% had both extra- and intrahepatic bile duct dilation and thus a Todani type IVa choledochal cyst (19); of these, nine included segmental, left lobe duct involvement, and these patients required a combined left lobectomy and extrahepatic cyst excision.

Biliary carcinoma was present in 12% of these patients.

Some authors label type V dilation of small intrahepatic radicals, as Caroli's disease (discussed later). Whether Caroli's disease is indeed a type of choledochal cyst is debatable.

Acquired dilated ducts due to prior stone disease or infection are not considered to be choledochal cysts. Even then, not all dilated ducts fit the above classification. Is a focally dilated cystic duct a choledochal cyst?

These cysts are a cause of prolonged neonatal jaundice. Others are detected in children. Only a rare choledochal cyst manifests during pregnancy. In some adults pancreatitis is their initial presentation. Their propensity to harbor a carcinoma needs to be considered when planning therapy.

The risk of biliary malignancy in a setting of a choledochal cyst increases with age, although cancers have developed in young patients. Bile stasis, irritation, possible mutagenicity of bile mixing with pancreatic secretions, and epithelial damage probably play a role in cancer development. Most tumors are adenocarcinomas but an occasional undifferentiated carcinoma, squamous cell carcinoma, or even adenoacanthoma is encountered. Gallbladder carcinomas have also been reported.

Imaging

In neonates and children, US reveals a choledochal cyst as a cystic structure in the region of the bile ducts. These dilated ducts often extend intrahepatically. The gallbladder ranges from normal in size to somewhat distended.

Traditionally, ERCP has been used to detect and evaluate choledochal cysts in adults, but CT, US, MRI, or scintigraphy is a viable alternative. Imaging reveals a fluid-filled cystic structure. Both CT cholangiography and MRCP detect choledochal cysts with roughly similar image quality and provide information comparable to ERCP; CT cholangiography appears superior to MRCP in detecting any superimposed stones, but the latter also provides information about any associated anomalous pancreaticobiliary duct junction (20) and does not require use a contrast agent. Currently, MRCP is the procedure of choice in evaluating these cysts.

A choledochocele (type III cyst) should be readily detected with MRCP or ERCP; the papilla of Vater bulges, suggesting a submucosal tumor (Fig. 8.5). Their cystic nature is also apparent by endoscopic US.

A carcinoma developing in a choledochal cyst is difficult to detect with imaging; at times a subtle focal or diffuse bile duct wall thickening suggests the diagnosis. These tumors enhance during arterial-phase CT, becoming isodense on delayed phases. Cholangiography reveals either an elevated, irregular outline, or a focal narrowing.

Hepatobiliary cholescintigraphy in patients with choledochal cysts reveals about two thirds of gallbladders nonvisualizing; resected gallbladders in some of these patients do not show evidence of cholecystitis. The diagnostic accuracy of cholescintigraphy for cholecystitis is low in patients with a choledochal cyst. With partial obstruction, scintigraphy shows tracer activity within the cyst; in general, a choledochal cyst tends to fill with radiotracer later than expected and stays filled longer. Radionuclide accumulation in the cyst but no intestinal activity is a not uncommon finding.

Therapy

No curative therapy is possible with extensive intrahepatic involvement of both lobes, aside from liver transplantation.

Figure 8.5. Choledochocele in an 85–year-old man. Contrast-enhanced computed tomography (CT) reveals a dilated distal common bile duct indenting the descending duodenum (arrow). More superior images identified a dilated gallbladder. Surprisingly, the patient was not jaundiced. (Courtesy of Patrick Fultz, M.D., University of Rochester.)

Some choledochoceles are treated by simple endoscopic unroofing. Nevertheless, because most choledochal cysts are premalignant, a simple drainage procedure is believed to be insufficient therapy in most patients. A malignancy has developed years after cystenterostomy.

Cyst excision and a hepaticojejunostomy are traditional procedures of choice, with some surgeons preferring a hepaticoantrostomy. The latter anastomosis is believed to be associated with fewer episodes of recurrent cholangitis, although postoperative cholescintigraphy does not differ significantly between the two surgical procedures and thus differences in bile stasis and reflux presumably are not a cause of the more frequent recurrent cholangitis seen after hepaticojejunostomy. An anastomotic bile duct carcinoma is a rare complication.

An unsuspected choledochal cyst is occasionally encountered during laparoscopic cholecystectomy; the underlying anatomy can be studied and a choledochocele diagnosed by either laparoscopic contact US or intraoperative cholangiography.

Findings with Tc-00m-IDA scintigraphy are similar in infants after a Roux-en-Y hepaticojejunostomy and after a hepaticoantrostomy, although the former are more prone to develop recurrent cholangitis.

Caroli's Disease

In 1958, Caroli observed numerous ectasia-like intrahepatic cysts communicating with the biliary tree (21). This disorder, as described by Caroli, is now believed to be part of the spectrum of congenital hepatic fibrosis. The latter condition is discussed in Chapter 7.

Computed tomography reveals cysts varying in size. At times a central enhancing "dot" is seen postcontrast, representing a portal vein radical, suggesting the diagnosis. With uncomplicated disease, US reveals intrahepatic anechoic cystic structures. Once sludge or stones form in these dilated segments, US identifies hyperechoic, well-marginated foci. As expected, MR reveals these cysts to be hypointense on T1- and hyperintense on T2-weighted images. Similar to CT, the central portal vein radical enhances. Occasionally MR identifies septa.

To make a diagnosis of Caroli's disease it is necessary to show that the intrahepatic "cysts" connect to bile ducts, thus distinguishing this entity from polycystic disease. Autosomal-recessive polycystic kidney disease is in the differential diagnosis of Caroli's disease. Scintigraphy in patients with polycystic kidney disease not uncommonly reveals cholestasis and intrahepatic bile duct dilation, mimicking Caroli's disease. Thus some type of cholangiogram is generally necessary to differentiate these entities.

An occasional patient is found to have localized dilation of an intrahepatic bile duct without any obstruction. Some of these ducts contain considerable mucinous material and a mucinous cystic neoplasm is often suspected, but resection reveals neither a malignancy nor fibrosis. The term *solitary cystic dilation of an intrahepatic bile duct* is used to describe this condition. The relationship of such a localised dilation to Caroli's disease is speculative.

Metachromatic Leukodystrophy

Metachromatic leukodystrophy is primarily in the domain of a neurologist, and the only purpose in mentioning it in a work on the abdomen is that an occasional patient with this lysosomal storage disorder, caused by a deficiency of the lysosomal enzyme arylsulfatase A, has an abnormal gallbladder. A diagnosis is established by detecting deficient leukocyte or fibroblast arylsulfatase A activity. A late-infancy onset is common, although atypical and late onsets have been described. Found worldwide, this condition is considerably more prevalent in certain populations, such as in the Western Navajos with an estimated carrier frequency of 1/25 to 1/50 (22).

Ultrasonography in some children with metachromatic leukodystrophy reveals a diffuse thick, hyperechoic gallbladder wall and a small lumen. A number of these children develop gallbladder papillomatosis. Because gallbladder polyposis is rare in children and has developed before neurologic symptoms of metachromatic leukodystrophy become apparent, discovery of such polyps, often made incidentally, should raise suspicion for this condition. Some children with this condition also develop gallstones. One presented with gastric outlet obstruction due to

an enlarged gallbladder, treated by percutaneous aspiration, and later developed a gallbladder carcinoma (23).

Trauma

An extrahepatic biliary injury classification scale, devised by the American Association for Surgery of Trauma, is outlined in Table 8.1.

Gallbladder

The most common gallbladder injury due to blunt trauma is contusion; perforation and avulsion are rare. Only occasionally does CT reveal gallbladder wall disruption. A hematoma is identified by CT as focal or diffuse thickening, at times mimicking cholecystitis. Pericholecystic fluid, a poorly defined gallbladder wall, a collapsed gallbladder lumen, and intraluminal blood detected by imaging in a setting of abdominal trauma should suggest gallbladder injury (Fig. 8.6).

Associated intraabdominal trauma is common, often masking underlying gallbladder perforation.

Table 8.1. Surgical biliary injury scale

Grade*	Type of injury
I	Gallbladder contusion Portal triad contusion
II	Partial gallbladder avulsion with intact cystic duct Gallbladder laceration or perforation
III	Complete gallbladder avulsion Cystic duct laceration/transection
IV	Right or left hepatic duct laceration Partial common hepatic duct laceration (≤50%) Partial common bile duct laceration (≤50%)
V	>50% transection of common hepatic duct >50% transection of common bile duct Combined right and left hepatic duct injuries Intraduodenal or intrapancreatic bile duct injury

* Advanced one grade for multiple injuries, up to grade III.
Source: Adapted from Moore et al. (24).

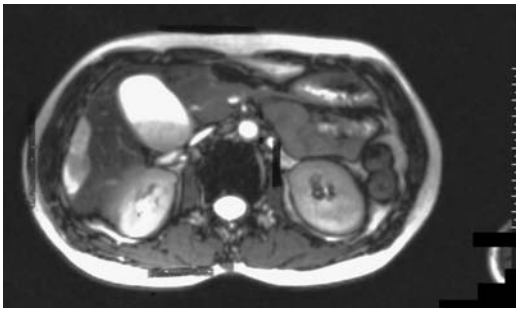

Figure 8.6. Sedimentation of blood in gallbladder on T2–weighted MR image results in a hyperintense supernatant fluid. (*Source:* Burgener FA, Meyers SP, Tan RK, Zaunbauer W. Differential Diagnosis in Magnetic Resonance Imaging. Stuttgart: Thieme, 2002, with permission.)

Bile Ducts

Spontaneous Rupture

Spontaneous bile duct perforation is uncommon and most often is associated with duct obstruction by stones. These perforations range from intrahepatic, to free intraperitoneal, to an encapsulated collection of bile. Aspirated fluid reveals a high bilirubin level. Hepatobiliary scintigraphy detects biliary ascites with a continuing leak.

A cholangiogram, whether performed percutaneously or endoscopically, should be diagnostic if the involved bile duct is visualized. These patients generally undergo surgery, although endoscopic management is also feasible.

Traumatic Bile Leakage

Biliary duct laceration and avulsion are not uncommon with blunt liver trauma. Complete transection of an intrahepatic duct is associated with liver laceration. Rupture of smaller intrahepatic ducts leads to slow bile extravasation, biloma formation tends to be delayed, and imaging findings are rather subtle. At times a subtle injury is not discovered during the initial surgery. Intrapancreatic bile duct injury, including avulsion of this biliary segment, is usually associated with pancreatic trauma. Not all bile

collections after blunt abdominal trauma represent a biloma. An intrahepatic communicating cyst or a choledochal cyst can be confused with a biloma.

Many of these patients undergo CT for suspected trauma to adjacent structures. For subtle bile leakage, however, either direct cholangiography or cholescintigraphy are the imaging modalities of choice. Major extravasation is suspected if scintigraphy reveals intraperitoneal activity greater than in the gastrointestinal tract.

Although not often performed for suspected biliary tract injury, anecdotal reports suggest that MRCP has considerable potential as an alternative to ERCP.

Obstruction

Some patients develop a biliary stricture as a delayed complication to blunt trauma. Whether these are related to a missed focal leak or ischemia is speculation. The suprapancreatic extrahepatic bile ducts are most often involved.

Infection/inflammation

Acute Cholecystitis

Clinical findings in acute cholecystitis range from mild signs and symptoms pointing to a right upper quadrant disorder to a life-threatening condition. Bacteremia is not common in acute cholecystitis; when present, however, it is associated with increased complications and a higher mortality. An occasional patient develops septic shock and dies within hours of onset of symptoms. Especially in the elderly the differential diagnosis is rather extensive.

Acute cholecystitis appears to be more common than expected after colectomy for ulcerative colitis.

Etiology

Stones

Acute calculus cholecystitis can be defined as inflammation of the gallbladder due to cystic duct obstruction by a gallstone. Infection is an integral part of this condition because without infection, instead of cholecystitis, gallbladder hydrops develops.

Infection

Mentioned here are only the more unusual infections associated with acute cholecystitis. Infection with *Ascaris lumbricoides* can result in acute cholecystitis. Ultrasonography of a worm in the gallbladder reveals an echogenic structure having nondirectional movements and containing a central anechoic tube.

Tuberculous cholecystitis is rare. The diagnosis is eventually suggested by the pathologist.

In patients with culture positive *Salmonella* enteric fever, US detected a globular, distended gallbladder in 53%, a positive sonographic Murphy's sign in 40%, pericholecystic edema or fluid in 40%, gallbladder wall thickening (>4 mm) in 34%, intraluminal echoes or sludge in 15%, intramural linear striation in 13%, and mucosal irregularity or sloughing in 6% (25).

A hepatic hydatid cyst rupturing into the gallbladder causing cystic duct obstruction and acute cholecystitis is found in endemic regions. Acute cholecystitis has been associated with *Candida albicans* infection. Even *Vibrio cholerae* infection can result in acute cholecystitis.

Other Etiologies

Occasionally acute obstructive cholecystitis is not related to obstruction by gallstones but is secondary to a cystic duct adenoma or other polyp. Anecdotal accounts describe BB shots or other missile fragments leading to acute cholecystitis. An uncommon association exists between acute cholecystitis and hemobilia.

Diagnosis

In general, initial US appears to be more productive than CT in patients with suspected acute biliary disease. Currently, CT does not have a primary role in diagnosing acute cholecystitis; although a number of CT findings have been described, most are nonspecific and some patients with acute cholecystitis have a normal-appearing gallbladder. Not uncommon is focal increased CT liver enhancement adjacent to the gallbladder bed, presumably due to increased blood flow from an inflamed gallbladder. Intra-

hepatic portal vein thrombosis is a complication in some patients with acute cholecystitis; it results in transient hyperdense regions.

Both US and cholescintigraphy achieve similar accuracies of 85% to 90% in patients with suspected acute cholecystitis, and the choice of one over the other varies in different regions of the world. Whether US or cholescintigraphy is the superior diagnostic modality in suspected acute cholecystitis is a matter of opinion. Considerable heat has been generated on this topic. Thus reputable authorities have made statements such as the following (26):

> Cholescintigraphy is generally considered to be the study of choice. . . . Although US is sometimes reflexively ordered for the diagnosis of symptomatic biliary disease, the results usually are not specific enough to make the diagnosis of acute cholecystitis.

Ultrasonography

Ideally, an US diagnosis of acute cholecystitis is made by detecting a stone obstructing the cystic duct—a rare finding. More often the sonographic signs suggesting acute cholecystitis are the presence of intraluminal gallstones, gallbladder wall thickening (at times with a three-layered wall appearance), fluid surrounding the gallbladder, and a sonographic Murphy's sign. Among 69 patients with acute abdominal pain and operated on for acute cholecystitis, preoperative US detected gallbladder wall thickening in 56%, one or more gallstones in 86%, pericholecystic fluid in 14%, gallbladder distention in 46%, and a sonographic Murphy's sign in 39% (27). Still, US results are not without controversy. In patients with right upper quadrant pain although sensitivity of a sonographic Murphy's sign is high, specificity is low due to a large number of false positives. Even if presence of gallstones, wall edema and pericholecystic fluid are included, specificity remains rather low, making Murphy's sign unreliable in distinguishing acute from chronic cholecystitis. Combined use of color velocity imaging (to determine blood flow velocity) and power Doppler US appear to improve both sensitivity and specificity, compared to gray-scale US, in detecting acute cholecystitis.

In most patients with acute cholecystitis, the gallbladder wall thickens diffusely, a nonspecific finding (Table 8.2). Patients with acute viral hepatitis not uncommonly have a cholecystitis-like clinical presentation and a markedly increased gallbladder wall thickness, as measured by US; in these patients the gallbladder wall reverts to normal once hepatitis clears.

Ultrasonography in an occasional patient with a subhepatic appendix containing an appendicolith suggests cholecystitis with a gallstone.

Occasionally color Doppler US detects gallbladder wall flow in patients with acute cholecystitis, but this is an inconsistent finding.

Magnetic Resonance Imaging

The role of MRI in suspected acute cholecystitis is still evolving. Although MRI accuracy rivals that of US, more ready availability, lower cost, and the simplicity of US ensure its continued use in most institutions.

Most publications deal primarily with T2-weighted images, which constitute a basis for MRCP. Findings of acute cholecystitis on T2-weighted sequences include the presence of gallstones, a thickened gallbladder wall, and pericholecystic fluid. Among patients with suspected acute cholecystitis, T2-weighted HASTE MRI achieved a 91% sensitivity and 79% specificity in diagnosing acute cholecystitis (28); in those patients who did have acute cholecystitis, HASTE MRI sequences detected a hyperintense pericholecystic signal in 91%, an impressive finding. Gallbladder stones were detected by HASTE MRI in 93% of patients with acute calculus cholecystitis.

Comparing MRCP and US before cholecystectomy, US was superior in evaluating gallbladder wall thickening but MRCP excelled in detecting cystic duct and gallbladder neck calculi and cystic duct obstruction (29).

Gallbladder inflammation leads to increased blood flow, resulting in increased contrast enhancement. Initial enhancement starts at the inner mucosal layer and gradually involves the entire gallbladder wall, findings detected with MR. On immediate postgadolinium images a transient increase in pericholecystic liver enhancement is common in acute cholecystitis patients.

Contrast-enhanced MRI should distinguish between gallbladder wall thickening due to acute cholecystitis and most other conditions listed in Table 8.2; aside from acute cholecysti-

Table 8.2. Causes of diffuse gallbladder wall thickening

Local conditions
Acute cholecystitis
Chronic cholecystitis
Hepatitis
Associated with portal hypertension
Portal vein thrombosis
Acute viral hepatitis
AIDS cholangitis
Systemic disorders
Hypoalbuminemia
Renal failure
Ascites
Chemotherapy
Severe congestive heart failure
Graft-versus-host disease

tis, other conditions show minimal gallbladder wall enhancement and pericholecystic liver enhancement.

Scintigraphy

Cholescintigraphy with Tc-99m-HIDA or one of the other IDA derivatives assesses gallbladder function. For this test to be valid, however, reasonably normal hepatic uptake and excretion is necessary. Cholescintigraphy results are not meaningful in a setting of severe hepatocellular dysfunction or common bile duct obstruction. The test should also be interpreted with caution after sphincterotomy because some of these patients have gallbladder nonvisualization even without acute cholecystitis. Likewise, gallbladder nonvisualization is found in patients with cystic fibrosis and in a setting of a choledochal cyst.

Several hours of fasting are normally required before cholescintigraphy is performed; otherwise, resultant gallbladder contraction prevents radiotracer and bile flow into the gallbladder, thus leading to a false-positive test. One disadvantage of cholescintigraphy is that it generally requires several hours to perform this test, a fact accentuated by ultrasonographers.

Gallbladder ejection fraction is measured during cholecystokinin cholescintigraphy and by US. In most institutions an ejection fraction of <35% is considered abnormal, although this limit varies depending on injection method used. In general, a normal gallbladder ejection fraction excludes dysfunction. Both scintigraphy and US are reproducible techniques in studying gallbladder contraction, but these two tests are not directly interchangeable.

A fatty meal induces gallbladder emptying, and, in general, a standardized liquid fatty meal results in good intraindividual reproducibility of gallbladder emptying; there is, however, considerable interindividual variability. Aside from CCK-dependent effects, other mechanisms probably are involved in gallbladder emptying. Gallbladder US in young, nulliparous women reveals fasting volume and postprandial ejection fractions to be slightly greater during the luteal phase than during the follicular phase. Gallbladder volume roughly doubles during pregnancy and then decreases postpartum. Gallbladder motility and gallbladder ejection fraction are significantly impaired in late pregnancy.

Gallbladder visualization during cholescintigraphy (or oral cholecystography) essentially excludes acute cholecystitis. Normally nonvisualization is defined as a lack of gallbladder activity up to 4 hours after radiotracer administration.

Some patients have increased tracer activity in liver parenchyma adjacent to the gallbladder—the *pericholecystic rim sign*. This activity is associated with acute cholecystitis in most but not all patients and is believed to be secondary to increased blood flow to parenchyma adjacent to an inflamed gallbladder. It is not to be confused with tracer within the gallbladder.

What is the significance of gallbladder nonvisualization but the presence of a pericholecystic rim sign? Morphine-augmentation is helpful in visualizing the gallbladder in some and thus excluding acute cholecystitis, although even then there are false-positives.

Gallbladder contractility is decreased in patients with a prior vagotomy. Likewise, the gallbladder does not contract normally in patients with achalasia or those on octreotide therapy.

Gallbladder contraction before injecting Tc-99m-IDA allows subsequent tracer material to accumulate within the gallbladder and decreases the number of false-positive results. A common drug used to stimulate gallbladder contraction is cholecystokinin-octapeptide (CCK-8). It is used selectively; for instance, in some institutions patients who have been fasting for 24 hours or longer are pretreated

with CCK while others are not. Slow infusion of a physiologic dose of CCK-8 results in more complete gallbladder emptying than a bolus injection.

If the gallbladder is not visualized in 60 to 90 minutes, often 0.04 mg/kg morphine sulfate is injected IV and additional images are obtained for 30 to 60 minutes. Intravenous morphine increases sphincter of Oddi pressure and thus bile accumulates within the gallbladder. If the gallbladder still does not visualize during morphine-augmented cholescintigraphy, in the appropriate clinical setting a diagnosis of acute cholecystitis is reasonable. If, on the other hand, the gallbladder is not visualized within an initial 90 minutes but is observed after morphine, abnormal gallbladder function should be suspected.

A variant of the above technique is to combine cholecystokinin pretreatment together with morphine augmentation. Imaging is performed in patients after Tc-99m-BrIDA until gallbladder activity is identified or up to 90 minutes postinjection; if no gallbladder is identified, a second dose of BrIDA is followed by morphine sulfate.

Gallbladder scintigraphy can be performed using indium-111–labeled autologous white blood cells. Labeled white blood cells accumulate within the gallbladder wall in acute cholecystitis. In some patients, however, delayed imaging is required, thus delaying the diagnosis.

Perforated Cholecystitis

Neglected cholecystitis evolves into gallbladder perforation. Most perforations are walled-off and result in pericholecystic fluid or a right upper quadrant abscess, a common location being between the gallbladder and adjacent liver. Free perforation into the peritoneal cavity results in bile peritonitis, while an occasional perforation into the liver evolves into a liver abscess.

Chronic perforations have evolved into a cholecystocutaneous or cholecystoenteric fistula, and even a cholecystogastric fistula (Fig. 8.7). Some cholecystoenteric fistulas are secondary to gallstones eroding into the gut (discussed in Chapter 4).

Detection of gallbladder perforation is not straightforward. Adherent omentum, fat, or adhesions often mask a recent perforation. Computed tomography visualizes only about half of gallbladder wall defects, and US even less. Pericholecystic fluid and gallbladder wall thickening are often the only pertinent imaging findings.

Gangrenous Cholecystitis

Gangrenous cholecystitis is a sequela of either calculus or acalculus cholecystitis.

Computed tomography and US reveal similar findings. The gallbladder wall is irregular and thick. Sloughed gallbladder mucosa is seen as thin intraluminal linear echoes parallel to the gallbladder wall and a striated wall edema pattern seen with US should suggest gangrenous cholecystitis. Often inflammation extends to surrounding structures. A sonographic Murphy's sign is less often elicited in these patients than with more conventional acute cholecystitis.

Color Doppler US reveals no flow within a thickened gallbladder wall in acute necrotizing cholecystitis.

Occasionally a thin rim of increased scintigraphic activity, a *rim sign*, is seen adjacent to the gallbladder fossa, a sign associated with gallbladder wall gangrene. The presence of a

Figure 8.7. Spontaneous cholecystocutaneous fistula (arrow) secondary to cystic duct obstruction by a stone.

rim sign, together with subsequent gallbladder visualization after administration of morphine, does occur with gallbladder gangrene. The rim sign should be distinguished from tracer activity in adjacent liver parenchyma.

Empyema/Abscess

Empyema, consisting of an obstructed, pus-filled gallbladder lumen, leads to marked gallbladder distention. Ultrasonography shows a markedly distended, hyperechoic sludge-containing gallbladder. Computed tomography reveals this pus-filled gallbladder content to have greater attenuation than bile. At times a frank abscess is identified (Fig. 8.8).

Laparoscopic cholecystectomy is difficult in the setting of gallbladder empyema and many of these patients undergo conventional cholecystectomy.

Emphysematous Cholecystitis

Emphysematous cholecystitis is a severe form of acute cholecystitis manifesting with gas (not air) in the gallbladder lumen, wall, bile ducts, or pericholecystic tissues, and no abnormal communication between the biliary tree and gastrointestinal tract. It develops if gas-forming bacteria predominate as the infectious organism. Diabetes mellitus is a common underlying condition. Some of these patients do not appear systemically ill, and unless imaging suggests the condition, conservative therapy may be initially initiated. Nevertheless, mortality is about 15%. Gallstones are absent in some of these patients. In some, a superimposed pneumoperitoneum suggests a perforation. Rarely, simultaneous emphysematous pyelonephritis and emphysematous cholecystitis develop.

The diagnosis is straightforward with conventional radiography and CT, revealing gas in the gallbladder lumen, wall, or pericholecystic tissues (Fig. 8.9). Ultrasono-graphy can miss emphysematous cholecystitis due to gallbladder nonvisualization; intramural gas can be confused with gas within the bowel. If the gallbladder is identified, US reveals highly reflective echoes from nondependent gallbladder wall segments. Exten-sive gas mimics gallbladder wall calcifications. Ultrasonography in one patient revealed gas bubbles rising within the gallbladder and floating to the surface, an appearance called *effervescent gallbladder* (30).

Cholescintigraphy may or may not detect cystic duct obstruction in these patients.

Although successful percutaneous gallbladder drainage has been performed in these patient, most are managed surgically.

Figure 8.8. Salmonella cholecystitis resulting in a gallbladder abscess (arrow). The abscess was drained percutaneously. (Courtesy of Georgine DeMarino, M.D., University of Iowa.)

Eosinophilic Cholecystitis

Histologically, eosinophilic cholecystitis consists of a transmural eosinophilic infiltrate. It is associated with allergic conditions, parasites, hypereosinophilic syndromes, and even with calculous acute cholecystitis. Tissue infiltration with eosinophils and eosinophilic granulomas occurs in necrotizing granulomatous vasculitis involving the gallbladder; similar features are found in allergic granulomatous angiitis of Churg and Strauss.

Therapy

In Pregnancy

Traditionally, a pregnant woman with acute cholecystitis has undergone an open cholecystectomy, although a laparoscopic cholecystectomy is feasible. If warranted, cholangiography is performed.

A pneumoperitoneum is induced during a typical laparoscopic cholecystectomy; gasless laparoscopic cholecystectomy has been performed in pregnant women.

A

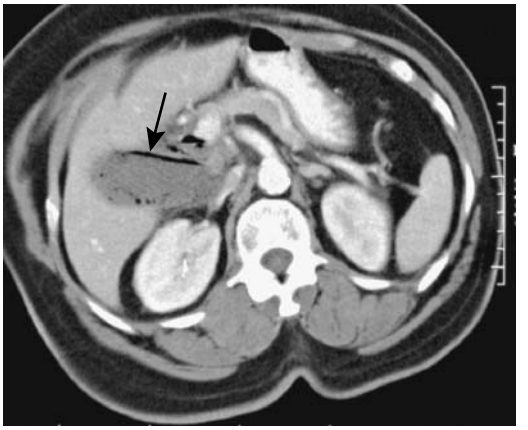

B

Figure 8.9. Emphysematous cholecystitis. Radiograph (A) and CT (B) in two different patients. Gas is present in the gallbladder wall and lumen (arrow). Pneumobilia was identified on other images.

Ultrasonography-guided percutaneous cholecystostomy may have a role in pregnancy; biliary decompression is maintained during pregnancy and an elective cholecystectomy performed after delivery.

Percutaneous Cholecystostomy/Aspiration

Does percutaneous transhepatic gallbladder drainage have a role in patients with acute suppurative cholecystitis? A common indication for percutaneous cholecystostomy is in a high surgical risk patient with suspected acute cholecystitis. Ultrasonography is commonly used for guidance. Following successful cholecystostomy most patients improve, the exception being those who have either transmural gallbladder inflammation or gangrene.

Gallbladder aspiration is an alternate procedure to percutaneous cholecystostomy in some patients. In a comparison, 82% of gallbladder aspirations and 100% of percutaneous cholecystostomies were technically successful (31); viscid sludge or pus prevented aspiration through a 21-gauge needle in some patients. Complications are more common with percutaneous cholecystostomy than aspiration. A typical scenario is US-guided percutaneous gallbladder drainage followed by laparoscopic cholecystectomy several days later, after clinical improvement. Inflammation subsides after drainage and the cystic duct often becomes patent, as shown by cholescintigraphy performed after percutaneous gallbladder drainage.

In general, for most patients with acute acalculous cholecystitis a percutaneous cholecystostomy is curative; in the presence of stones, however, a percutaneous cholecystostomy simply provides drainage and an eventual definitive procedure is necessary in most patients.

Open Cholecystectomy

This is not the place to discuss the relative merits and indications of open versus laparoscopic cholecystectomy. Rather, the emphasis here is on the role of imaging. In general, selective rather than routine intraoperative cholangiography is performed. Intraoperative fluoroscopic cholangiography is becoming more popular than static images. A fluoroscopic study can be performed faster than a comparable static study; whether the information obtained with a fluoroscopic image is sufficient is debatable. Quality control of intraoperative images remains a problem.

The indications for intraoperative cholangiography continue to be debated by surgeons. Risk factors correlating with presence of chole-

docholithiasis include history of jaundice, pancreatitis, hyperbilirubinemia and hyperamylasemia. Other criteria whether to perform intraoperative cholangiography include dilated bile ducts on preoperative US and unclear US findings.

Laparoscopic Cholecystectomy

Compared to open cholecystectomy, laparoscopic cholecystectomy requires a longer operative time, but it leads to less pain, a shorter hospitalization, and earlier recovery, and it is associated with a lower morbidity.

Cirrhosis is generally considered a relative contraindication for laparoscopic cholecystectomy.

Extensive adhesions surrounding the gallbladder make laparoscopic cholecystectomy more difficult. Neither CT nor US can reliably detect these adhesions although MRI may have a role. Nonvisualization of the gallbladder on drip infusion cholangio-graphy appears to have value in predicting extensive adhesions, but this study is rarely performed.

Imaging

Laparoscopic cholecystectomy achieves the same end result as an open cholecystectomy, yet with the former procedure surgeons generally prefer a more specific preoperative diagnosis concerning the presence or absence of bile duct stones; although these stones are readily detected by operative cholangiography, their removal during laparoscopic cholecystectomy is problematic and is one of the causes of conversion to an open cholecystectomy. The luxury of T-tube insertion if bile duct stones are detected and their later removal via the T-tube tract by interventional radiologists is not a viable option during laparoscopic cholecystectomy.

Preoperative US aids in predicting whether intraoperative difficulties are encountered. Preoperative US detection of gallbladder wall thickening was found to be the most sensitive and pericholecystic fluid the most specific indicator of a difficult laparoscopic cholecystectomy and the possible need for conversion to laparotomy (32).

Is ERC necessary prior to routine laparoscopic cholecystectomy? Prior to laparoscopic cholecystectomy, ERC not only detects bile duct stones but also outlines any anomalous biliary anatomy. If stones are found, a sphincterotomy and stone extraction are then performed. Patients having normal biliary US and normal liver function tests have a >95% negative ERC rate, and for these patients preoperatively ERC appears unnecessary. Some surgeons thus argue that endoscopic sphincterotomy prior to laparoscopic cholecystectomy should be reserved only for seriously ill patients or a suspected malignancy, because laparoscopic transcystic duct exploration can be successful in over 90% of cholecystectomies and is safe. Even if laparoscopic cystic duct exploration is not successful, then either open choledochotomy or postoperative endoscopic sphincterotomy is considered.

The role of operative cholangiography during laparoscopic cholecystectomy is not settled and depends, in part, on whether preoperative imaging is performed. Some surgeons obtain it almost routinely, while others use it selectively. The study is safe and adds little to patient morbidity, but it does prolong surgery. A learning curve exists in performing successful intraoperative cholangiography. A success rate of over 90% can be achieved. Digital C-arm fluoroscopy is a useful guide for intraoperative cholangiography. In general, laparoscopic cholangiography and, if needed, common bile duct exploration obviate a need for a later second procedure such as endoscopic sphincterotomy in patients with retained stones.

Intraoperative cholangiography detects biliary tract complications, and often conversion to an open laparotomy can be performed to repair a visualized injury. Such conversion results in earlier detection of injuries and fewer subsequent procedures to correct the injury.

Operative cholangiography performed primarily to detect bile duct stones is discussed later (see Biliary Stones).

Complications

General: Complications occur during laparoscopic cholecystectomy, with postoperative complication rates of 4% to 6% being typical. Initially, after the introduction of laparoscopic cholecystectomy, bile duct injuries were more common than during the previous open cholecystectomy era. Nevertheless, most recent

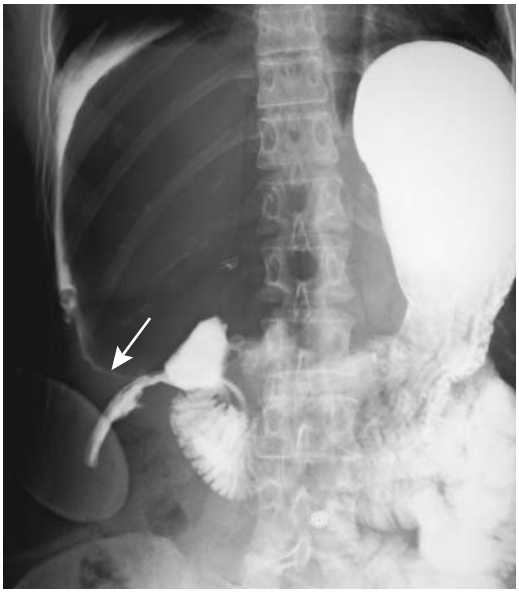

Figure 8.10. Duodenal perforation (arrow) detected 2 days after laparoscopic cholecystectomy. A water-soluble contrast agent was used to perform this study.

studies conclude that morbidity and mortality of laparoscopic cholecystectomy are lower than after an open operation. The most common complication is a bile leak, followed by retained stones, severe bleeding, subhepatic fluid or abscess, and mild pancreatitis (Fig. 8.10). A common duct stricture and retained stones are late complications, often manifesting as cholangitis rather than jaundice.

Because of ease and ready availability, conventional chest and abdomen radiographs should be obtained whenever postlaparoscopic cholecystectomy injury is suspected. They will detect pneumonia and extraluminal gas. Whether they should be followed by CT or US is debatable; either modality detects biliary obstruction and abnormal intraabdominal fluid collections. The definitive study to detect bile duct injury is cholangiography. An ERC can localize a specific site of leakage and detect any underlying strictures. If ERC is unsuccessful or if complete biliary obstruction is encountered, transhepatic cholangiography should define more proximal biliary anatomy. In general, with a major bile duct injury or stricture, percutaneous transhepatic cholangiography is of more value to the surgeon than an endoscopic approach because it defines the proximal biliary tree anatomy used for reconstruction.

In a setting of localized disruption, including a cystic duct stump leak or extravasation from ducts of Luschka, placement of a biliary stent is often therapeutic.

Bile Duct Injury: Most bile duct injuries manifest during the early postoperative period either as obstructive jaundice or a bile leak. Detection of residual stones or a clip in the bile ducts can be delayed. Most complications can be managed successfully by either ERCP or percutaneously. Biliary leaks are successfully treated by percutaneous biloma drainage combined with either endoscopic or percutaneous transhepatic biliary catheter bypass.

The Bismuth classification is used to describe major bile duct injuries (Fig. 8.11). A preoperative cholangiogram is valuable prior to bile duct injury repair. Subsequent surgical repair is more difficult and is often unsuccessful if a cholangiogram is not obtained preoperatively or the cholangiogram is incomplete.

Common sites for leakage are from a cystic duct stump or from injury to an aberrant bile

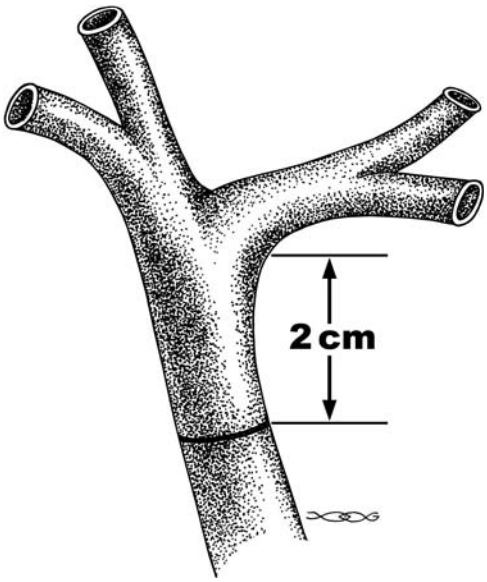

Figure 8.11. Bismuth classification of bile duct injuries. In type 1, >2 cm of hepatic duct is intact; in type 2, <2 cm remains; in type 3, little viable hepatic duct is available; and in type 4, the main right and left lobe ducts are involved.

Figure 8.12. Blown cystic duct stump (arrow). The resultant biloma was drained percutaneously.

duct (Fig. 8.12). Some patients have anomalous small right lobe ducts draining directly into the gallbladder (bile ducts of Luschka), and these are torn during a cholecystectomy. Aberrant bile duct leaks are difficult to detect because these aberrant ducts often do not opacify on operative and postoperative cholangiograms. Bile leakage also occurs with inadvertent bile duct laceration. Most bilomas form around the site of leakage; a rare one extends into the lesser sac. Typically a biloma forms within a week or so after surgery. Some bilomas are associated with jaundice. In general, only the symptomatic patient requires additional therapy.

Direct visualization of a leak is by cholangiography—directly via a T-tube, retrograde, or any other access—or indirectly by detecting a biloma with MRCP, CT cholangiography using an intravenous contrast agent, or US. Contrast enhanced MR cholangiography using Mn-DPDP or Gd-EOB-DTPA (agents taken up by hepatocytes and excreted into bile ducts) identifies bile duct leaks in these patients (33), although advantages of this technique over other methods of visualizing bile ducts are still debated. Ultrasonography reveals a biloma as a sharply marginated anechoic mass having acoustic enhancement. A hematoma or abscess is in the differential diagnosis, although the latter tends to contain a more echoic content.

Biliary scintigraphy is probably more sensitive and more specific than either CT or US in detecting a bile leak. Cholescintigraphy achieves an accuracy of mid-80% in detecting leaks, with CT and US being less sensitive. One can argue that cholescintigraphy should be the first diagnostic modality if a bile leak is suspected but in a number of centers it is relegated to a secondary role. The scintigraphic appearance of a postoperative bile leak is useful for prognosis; if most of the biliary flow is into the duodenum, a perforation will probably resolve without surgical or other intervention.

Occasionally with a small bile leak initial cholescintigraphy is normal, but repeat images obtained after IV morphine reveal a subtle leak. Also, if initial images do not identify a leak, delayed images should be obtained because some small leaks are visualized only several hours later. In spite of these techniques, bile ascites can be difficult to diagnose because of dilution. On the other hand, many small asymptomatic bile leaks are of no clinical significance.

Placement of a biliary drainage catheter, inserted either via an endoscopic approach or percutaneously, is sufficient therapy for most localized bile leaks. Endoscopists insert either an intrabiliary stent or a nasobiliary tube across a leakage site, at times adding a sphincterotomy. Endoscopic placement of a short transpapillary stent without a sphincterotomy is an effective and simple way of equalizing pressures within the bile ducts and duodenum. During percutaneous transhepatic biliary drainage, generally performed when surgical or endoscopic therapy is unsuccessful, side holes are positioned on both sides of a leak.

Among postlaparoscopic cholecystectomy patients referred for therapy of bile leaks to members of the Midwest Pancreaticobiliary Group, most common therapy consisted of sphincterotomy with stent insertion, with biliary leakage healing in 88% of patients (34); percutaneous or surgical drainage of bilomas was required in 32% of patients.

With major bile spill into the peritoneal cavity, immediate reexploration is generally indicated. Bile duct transection or other major injury is usually treated with a Roux-en-Y

hepaticojejunostomy rather than direct bile duct anastomosis; the latter is associated with subsequent stricture formation, while long-term success rates with a Roux-en-Y hepaticojejunostomy are >80%. Embolization of a biliary leakage site using a percutaneous approach is a potential therapeutic approach.

A clip placed on either the hepatic duct or the common bile duct is the most common cause of acute bile duct obstruction (Fig. 8.13). Obstruction also develops due to inadvertent bile duct cautery or fibrosis for other reasons. Hepatic duct and right hepatic duct necrosis are complications of electrocoagulation. Retained common bile duct stones also result in postoperative obstruction. Some bile duct strictures detected several months after laparoscopic cholecystectomy are associated with a traumatic neuroma, probably induced by prior bile leakage although a thermal injury during cholecystectomy and a resultant fibrous scar may predispose to traumatic neuroma formation.

Initially more proximal bile ducts do not dilate after an obstruction, and CT and US may miss a stricture; scintigraphy, on the other hand, will detect an obstruction. In the presence of a bile leak, however, lack of radionuclide activity in the intestines does not imply a more distal bile duct obstruction.

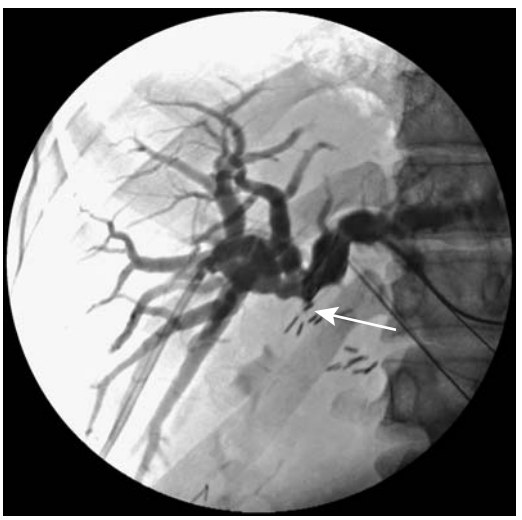

Figure 8.13. Percutaneous cholangiography in a patient with jaundice after laparoscopic cholecystectomy reveals complete hepatic duct obstruction close to the porta hepatis (arrow). Exploration revealed a metal clip obstructing the hepatic duct. (Courtesy of David Waldman, M.D., University of Rochester.)

The gold standard for detecting a bile duct obstruction is cholangiography. An MRCP is often a first choice to detect these strictures and any other related complications, such as a leak.

Percutaneous or endoscopic stricture dilation is often a viable option; results are comparable to those of surgical reconstruction. With complete obstruction, such as secondary to a clip placed on the hepatic duct, percutaneous drainage of the obstructed ducts is the initial procedure of choice. On the other hand, with a common bile duct stone or cystic duct leak, a sphincterotomy, stone extraction, and an endoprosthesis are generally preferred.

Cholelithoptysis: Stones are spilled into the peritoneal cavity more often during a laparoscopic cholecystectomy than during an open cholecystectomy. While it was initially believed that no adverse long-term complications follow cholelithoptysis, severe complications requiring a subsequent open surgical procedure have developed. Generally lavage and retrieval of as many stones as possible is attempted after such spill. In fact, open retrieval appears appropriate if several stones or a large stone are lost.

Clips have also been spilled into the peritoneal cavity; their long-term consequence is not known.

Some stones eventually become surrounded by granulation tissue. Or gallstones become encased in a pelvic tumor. Some of these patients present months or even years after a cholecystectomy with intraabdominal infection, abscess, or fistula. Gallstones spilled into the peritoneal cavity have led to bowel obstruction. Stones have eroded into the urinary bladder, eroded through the diaphragm, resulted in an empyema, and have even been expectorated.

At times the specific etiology for such a calculi-induced abscess is suggested by CT or US. Computed tomography shows a gallstone acting as a nidus for surrounding inflammation.

Incomplete Excision: During laparoscopic cholecystectomy the cystic duct is typically transected close to the gallbladder in order to decrease the risk of hepatic duct and common duct injury. This has led to an incomplete cholecystectomy and eventually recurrent cholelithiasis. A bilobed or duplicate gallbladder

is suspected if repeat surgery finds most of the gallbladder still intact in a patient with recurrent symptoms after laparoscopic cholecystectomy.

Other Complications: Tumor seeding from an unsuspected gallbladder carcinoma during cholecystectomy is discussed later in this chapter (see Gallbladder Tumors Malignant Neoplasms).

Imaging studies shortly after a cholecystectomy often detect a pneumoperitoneum. It is of little significance unless it persists.

Major infection is not common after laparoscopic cholecystectomy. Computed tomography should identify any abscesses.

Arterial trauma during surgery leads to false aneurysm formation; subsequent aneurysm rupture into a bile duct results in hemobilia, at times manifesting months after cholecystectomy. The numerous published reports attest that this is not a rare complication. The right hepatic artery is most often involved, although even a renocaval arteriovenous fistula has been reported (35). These aneurysms and hepatic artery-to-bile duct fistulas can be successfully embolized.

Unrecognized bleeding due to trocar insertion has resulted in omental or abdominal wall hematomas.

A draining umbilical sinus tract has developed at a trocar site. Small bowel has herniated through a trocar site and led to an obstruction. Unsuspected bowel injury may occur. Leakage of intestinal content into the peritoneal cavity induces a peritonitis mimicking bile peritonitis. Small bowel necrosis has been reported.

Diaphragmatic injury, even a pneumothorax, has been reported.

Underlying primary adrenal insufficiency can lead to shock, bilateral adrenal hemorrhage, and related complications after laparoscopic cholecystectomy.

Acute Acalculous Cholecystitis

Etiology

The precise etiology of acute acalculous cholecystitis is not known. The reported prevalence varies in the literature, with part of the difficulty being a lack of definition.

Bile stasis and gallbladder inflammation develop secondary to either a chemical or ischemic insult. These patients do not have cystic duct obstruction, and usually no stones are present in the gallbladder. Infection from an enteric source may play a role. Acalculous cholecystitis has occurred in association with *Vibrio cholera* infection, typhoid fever, biliary *Ascaris lumbricoides* infestation, and even *Candida* infection following cardiac transplantation.

Cholesterol crystal embolization has been implicated in patients with atherosclerotic vascular disease who develop acalculous cholecystitis. Acalculous cholecystitis develops in young immunosuppressed patients; it is associated with veno-occlusive liver disease. This condition is more common in critically ill patients, those who have had a major traumatic insult, those who are on prolonged bed rest and intensive care, or those who are debilitated.

Diagnosis

Murphy's sign is difficult to elicit both clinically and sonographically.

The sensitivity and specificity of imaging in detecting acute acalculous cholecystitis are not high. At times the diagnosis is one of exclusion. Computed tomography reveals pericholecystic inflammation, gallbladder wall thickening, and pericholecystic fluid. Gallbladder mucosa tends to enhance with contrast.

Ultrasonography findings of acalculous cholecystitis are similar to those seen with calculous cholecystitis, except for gallstones, and consist of an inconsistent Murphy's sign, gallbladder wall thickening, and pericholecystic fluid; other occasional findings include gallbladder hydrops, gallbladder sludge, and a striated gallbladder wall. These are rather nonspecific findings, especially in sick patients. Several studies have concluded that these nonspecific US findings are common in intensive care patients and that sonography is of limited value in detecting acalculous cholecystitis (36). On the other hand, acalculous cholecystitis can be excluded when gallbladder US is normal.

Scintigraphy is falsely negative in acute acalculous cholecystitis if radiotracer enters the gallbladder. A high scintigraphic false-positive rate is also found. The gallbladder does not constrict normally to stimulation by cholecystokinin in acalculous cholecystitis, although this is a nonspecific finding, common in postoperative patients.

Therapy

Acute acalculous cholecystitis is associated with high morbidity and mortality. Many patients developing acalculous cholecystitis are already at high surgical risk. Complications increase with delay in therapy. Percutaneous cholecystostomy using US guidance has evolved as the therapy of choice for these patients.

Laparoscopy has been used as a diagnostic tool for acute acalculous cholecystitis. Such diagnostic laparoscopy can be performed even at the patient's bedside.

Chronic Cholecystitis

The definition of *chronic cholecystitis* varies. On one extreme are those who consider the presence of gallbladder stones a sign of chronic cholecystitis; others limit this term to a setting of a small, thick-walled gallbladder wall containing histologic findings of chronic inflammation and fibrosis and no stones. The latter condition is also called *chronic acalculous cholecystitis*; the problem with this definition is that many gallbladders resected for other conditions in patients with no clinical evidence of disease harbor similar pathologic findings.

Actinomycosis is a rare cause of cholecystitis. Myelofibrosis has presented as chronic cholecystitis.

With the presence of gallstones and an appropriate clinical history, the diagnosis is straightforward. The issue becomes murky when gallstones are absent—a relatively common scenario in clinical practice. Considerable controversy surrounds the clinical and even pathologic diagnosis of chronic acalculous cholecystitis. In fact, some investigators question whether such a disease as chronic acalculous cholecystitis even exists or whether these patients' symptoms reflect a spectrum of disorders.

Imaging

Ultrasonography in some symptomatic patients reveals a thickened gallbladder wall and no stones, simply sludge, or stones. Without stones, whether these patients should undergo surgery is controversial; a number of postoperative patients are not relieved of their symptoms. A combined endoscopic US and stimulated biliary drainage procedure has been suggested for these patients. In patients with unremarkable transabdominal US, endoscopic US can reveal gallbladder sludge or stones, or stimulated biliary drainage is positive.

Postcontrast MRI in patients with chronic cholecystitis usually reveals a thickened gallbladder wall, with early mucosal and muscle enhancement in most; stones obviously do not enhance, and the fibrotic subserosa enhances late.

Xanthogranulomatous Cholecystitis

This chronic inflammatory condition is uncommon in the gallbladder and is analogous to xanthogranulomatous pyelonephritis. The presence of chronic infection in a setting of cholelithiasis and bile stasis presumably leads to recurrent inflammation. Also, obstruction and intramural rupture of Rokitansky-Aschoff sinuses appear to play a role. Xanthogranulomatous cholecystitis ranges from a focal condition involving only a portion of the gallbladder wall to diffuse inflammation and fibrosis extending into surrounding tissues. Intramural abscesses and inflammation are eventually replaced by lipid-filled histiocytes, round cells, and other tissue. It has developed after placement of metallic biliary stents. Histology reveals both abscesses and xanthogranulomas, seen as intramural nodules on imaging studies.

Imaging findings are nonspecific in most patients. The gallbladder wall is irregular and thickened, and it blends into adjacent liver parenchyma. Gallstones are common. Computed tomography reveals an intramural hypodense band in about one third of patients (37) or intramural hypodense nodules; similar intramural hypoechoic nodules or bands are found with US. A thickened gallbladder wall ranges from hyperechoic to isoechoic and even hypoechoic compared to liver parenchyma. Chemical shift MR is useful to detect any fat (38). Pericholecystic fluid is an inconsistent finding.

Xanthogranulomatous cholecystitis and gallbladder carcinoma tend to have a similar imaging appearance. Complicating the issue is that patients with xanthogranulomatous cholecystitis are at increased risk of developing a carcinoma. Of interest is that increased serum carbohydrate antigen 19–9 (CA 19–9) levels occur in xanthogranulomatous cholecystitis

without evidence of an underlying malignancy (39).

Percutaneous gallbladder needle biopsy is usually nondiagnostic, and histologic study of the resected gallbladder is necessary.

Laparoscopic cholecystectomy is difficult and often not successful. Extensive resection is necessary, but this carries a risk of bile duct injury. Intraoperative cholangiography is useful for guidance.

Porcelain Gallbladder

The term *porcelain gallbladder* is applied to a type of chronic cholecystitis containing a calcified gallbladder wall. The prevalence of porcelain gallbladder varies depending on the specific definition used and whether conventional radiographs or CT are employed. In a study of patients with acute abdominal pain operated on for acute cholecystitis, conventional radiography revealed linear gallbladder wall calcifications in slightly under 5% (27).

Occasionally a porcelain gallbladder and xanthogranulomatous cholecystitis coexist; a carcinoma is in the imaging differential diagnosis.

When extensive, these calcifications are detected with most imaging modalities. Still, the diagnosis is not always straightforward because large calcified confluent gallbladder stones have a similar appearance, especially with conventional radiography. In fact, large calcified stones are more common than a porcelain gallbladder.

Ultrasonography reveals a hyperechoic circular gallbladder outline with marked posterior shadowing. In some patients only part of the gallbladder wall is calcified. The sonographic findings are similar to those seen with a gallbladder filled with stones or even emphysematous cholecystitis.

Most authors agree that a porcelain gallbladder is precancerous. Therefore, even in a relatively asymptomatic patient a cholecystectomy is generally recommended. A laparoscopic cholecystectomy is feasible with a porcelain gallbladder.

Dengue Fever

Dengue hemorrhagic fever is a systemic disorder, but its severity can be gauged by using US to assess gallbladder wall thickness and the presence of intraperitoneal fluid. A prospective study in patients with mild disease found US evidence of gallbladder wall thickening in 32%, while with a more severe illness gallbladder wall thickening was seen in 95% (40); a gallbladder wall thickness ≥5 mm had a 92% specificity in identifying patients at high risk for hypovolemic shock, while a gallbladder wall thickness between 3 and 5 mm was used as a criterion for hospital admission.

Cholangitis

Acute cholangitis is caused by infection of an obstructed biliary tree, with the obstruction usually secondary to choledocholithiasis. Cholangitis is less common with a malignant obstruction. Occasionally acute cholangitis develops in a setting of bile duct sludge, with sludge presumably leading to intermittent obstruction.

An association probably exists between a peri-Vaterian diverticulum and cholangitis. The risk for cholangitis is increased if the common bile duct drains directly into the diverticulum. Distal duodenal obstruction more often results in pancreatitis rather than cholangitis (Fig. 8.14).

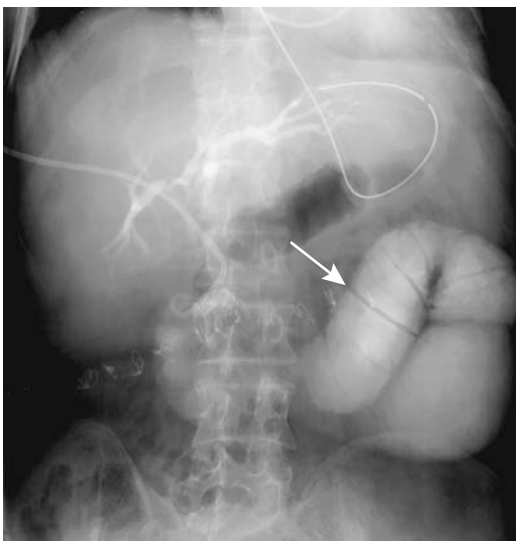

Figure 8.14. Obstructed afferent loop (arrow) causing cholangitis.

Typically eosinophilic gastroenteritis involves the stomach and small bowel, although eosinophilic cholangitis also exists. When extensive, imaging reveals marked bile duct wall thickening and lumen narrowing.

Infection

Pyogenic

Most pyogenic cholangitis develops in a setting of choledocholithiasis and, less often, strictures. An occasional patient forms recurrent stones and develops multiple episodes of ascending cholangitis. The bile ducts dilate and bile stasis is evident. Complications include liver abscess and portal vein thrombosis.

Focal or generalized bile duct dilation and strictures are the only consistent imaging finding in pyogenic cholangitis, although many of these patients also have bile duct stones and biliary obstruction. The bile duct wall is thickened and inflamed, identified by CT and MR as increased postcontrast enhancement. Often focal liver enhancement is also evident.

Computed tomography reveals liver inflammatory pseudotumors in some patients with pyogenic cholangitis, consisting of ill-defined and hypodense regions; early arterial phase images reveal nodular or wedge-shaped inhomogeneous enhancement, presumably due to chronic inflammation (41). Postcontrast, a central hypodense region is believed to represent chronic inflammation, while septa are secondary to fibroblastic proliferation (42).

An MRCP in recurrent pyogenic cholangitis is able to outline major bile ducts and thus is often superior to direct cholangiography. In one study, MRCP depicted all dilated segments, 96% of duct strictures, and 98% of segments containing calculi (43); direct cholangiography, on the other hand, depicted only about half the dilated segments, ductal strictures, and calculi.

In some institutions the initial therapy for acute cholangitis consists of antibiotics and general supportive therapy. With a poor response, especially in a high surgical risk patient, endoscopic or percutaneous biliary drainage is performed to bypass an obstruction. Others believe that early endoscopic biliary drainage is warranted in these patients, and endoscopic drainage should be performed on an urgent basis. In severe cholangitis, endoscopic biliary drainage is associated with a lower morbidity and mortality than with surgical decompression. Percutaneous transhepatic drainage or surgical drainage is a viable option if endoscopic drainage cannot be performed.

In general, prolonged interventional procedures during the acute phase are associated with increased complications. Excessive catheter manipulation should be avoided, with the aim being to place a biliary drainage catheter proximal to the obstruction.

Yearly surveillance ERCP has been proposed for patients with recurrent bile duct stones who are prone to developing episodes of acute cholangitis (44); stone removal decreases risk of cholangitis.

Hepatolithiasis (Oriental Cholangiohepatitis)

Hepatolithiasis, previously known as *Oriental cholangiohepatitis*, *recurrent pyogenic cholangitis*, and *primary intrahepatic stones*, is most often encountered in patients from East Asia, with only an occasional non-Oriental patient reported. Prevalence in East Asia varies considerably between countries. The hallmark of this condition is intrahepatic bile duct stones proximal to the confluence of right and left hepatic ducts.

The etiology of hepatolithiasis is not clear. Bile stasis and bacterial infection probably play a role. Some believe that infestation with the parasites *Clonorchis sinensis* or *Ascaris lumbricoides* results in an inflammatory reaction that starts a cycle of stasis, stone formation, and strictures, but evidence for such an association is not convincing. In Japan, a congenital basis for these strictures has been raised, with some patients having congenital common bile duct dilation.

Multiple strictures develop and calculi and debris form proximal to these strictures (Fig. 8.15). Both intra- and extrahepatic bile ducts eventually dilate, but stones form intrahepatically, more often in the left lobe rather than right lobe ducts. These stones tend to be composed of calcium bilirubinate; they tend to be soft, adhere to the duct wall, and vary in size. Their number

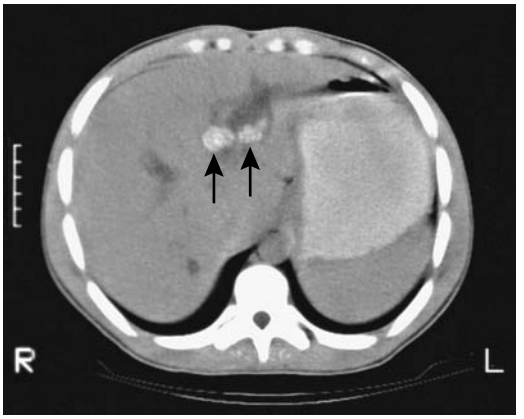

Figure 8.15. Oriental cholangiohepatitis. Computed tomography reveals stones (arrows) within dilated intrahepatic bile ducts.

ranges from several to multiple, in some patients filling most of the visualized bile ducts. In fact, often not all bile ducts are visualized by cholangiography because of segmental obstruction by stones.

This condition is progressive and not curable. Involved liver segments tend to atrophy. Untreated, recurrent cholangitis, liver abscesses, cirrhosis and eventual portal hypertension develop.

Clinically, the diagnosis is readily missed in countries with a low prevalence. Liver enzymes often are only mildly elevated, and the initial ERCP findings are subtle; early on, the extrahepatic ducts tend to appear normal, while a tight intrahepatic stricture prevents visualization of a more proximal stone in a dilated duct.

In some patients the sphincter of Oddi is destroyed, with reflux of gas and intestinal content into bile ducts. At times orally ingested contrast refluxes into the bile ducts. Stones and air bubbles can be confused with each other.

Computed tomography can suggest the diagnosis by detecting dilated intrahepatic bile ducts and stones. Once the diagnosis is suspected, ERC defines the underlying anatomy using, if necessary, a balloon catheter to dilate and obtain adequate filling of intrahepatic ducts. At times percutaneous cholangiography is necessary to outline the full extent of hepatolithiasis. Adequate antibiotic coverage is necessary for these procedures because these patients are prone to cholangitis and sepsis.

Not all strictures in oriental cholangitis are benign. These patients are at increased risk for a cholangiocarcinoma. Because of distortion and obstruction by stones, an intrahepatic cholangiocarcinoma is readily overlooked. This tumor infiltrates diffusely and mimics a benign-appearing stricture. Imaging in patients with cholangiocarcinoma in a setting of hepatolithiasis reveales irregular ductal strictures or obstruction and lobar atrophy (45); tumors and stones tend to be located in the same lobe. Some of these patients have an intraductal papillary tumor and mucin hypersecretion.

Generally, the initial therapy of these patients is surgical. Stone extraction, various biliary drainage procedures, and, at times, partial hepatectomy are performed. Liver resection is recommended by some surgeons for patients with intrahepatic segmental or subsegmental biliary stenoses. Some perform a partial left lobe resection if bilateral hepatolithiasis and strictures are found; they believe a lobectomy simplifies future treatment and may decrease complications. At times a Roux-en-Y hepaticojejunostomy is performed in order to clear stones. It is important at surgery to ensure that all stones are located and removed. Intraoperative US-guided transhepatic lithotomy is useful to detect residual stones; stones are located by US, and a surgical path is then chosen using US guidance.

A number of endoscopic and percutaneous transhepatic techniques have been developed to deal with these intrahepatic strictures and stones. At times a temporary surgical cutaneous stoma is created, allowing endoscopic access for cholangiography, stricture dilation, and stone removal. Some patients undergo exploration of extrahepatic bile ducts, any accessible stones are removed and a T-tube is inserted; using the T-tube tract for access, strictures are then dilated, stones removed, or electrohydraulic lithotripsy performed. The aim of therapy is complete stone clearance, although stone recurrence is common.

An alternative approach in some patients is percutaneous transhepatic cholangioscopy and lithotripsy. As needed, percutaneous or endoscopic stricture dilation and stone extraction are performed. Smaller intrahepatic stones can be pushed into more central ducts, while

larger stones are crushed. Stones can also be fragmented using extracorporeal shockwave lithotripsy.

Clonorchiasis

River fluke *Clonorchis sinensis* larvae migrate from the duodenum into bile ducts where they mature, preferentially residing in smaller intrahepatic ducts. With sufficient infestation, the intrahepatic bile ducts dilate, with essentially unremarkable major intra- and extrahepatic ducts. Small duct dilation is probably due to obstruction by these worms. Periductal and ductal inflammation ensue.

The initial abnormality detected by imaging is mild dilation of intrahepatic ducts. Eventually a full spectrum of oriental cholangiohepatitis develops.

Ultrasonography reveals worm aggregates as nonshadowing echogenic masses. Individual flukes are about 10 mm in length and thus considerably smaller than an *Ascaris* worm. Resultant cholangitis often leads to duct wall thickening and increased echogenicity.

Ascariasis

Ascariasis is a common helminthic infestation found worldwide, being especially prevalent in the tropics. In the United States it occurs in the deep South. The adult *Ascaris lumbricoides* worm lives in the intestinal tract where it produces few symptoms. Biliary obstruction, cholangitis, cholecystitis, pancreatitis, and an intrahepatic abscess are complications if an adult worm migrates into the bile ducts. Biliary ascariasis is more common in children than in adults. Several reports have commented on a sphincterotomy predisposing to biliary infestation.

Computed tomography identifies a worm as a hyperdense tubular structures surrounded by bile. When viewed in a transverse section, the worm has a "bull's-eye" appearance. Several worms, especially if coiled, appear as an intraluminal tumor.

Ultrasonography reveals a worm as a tubular hyperechoic structure within the bile ducts or gallbladder (Fig. 8.16). At times worm motion is identified. A long curved, tubular, nonshadowing structure containing a hypoechoic center, called the *impacted worm* sign, is occasionally identified in intrahepatic ducts; macerated round worms are seen as focal intraluminal soft tissue masses, with the US appearance mimicking a cholangiocarcinoma.

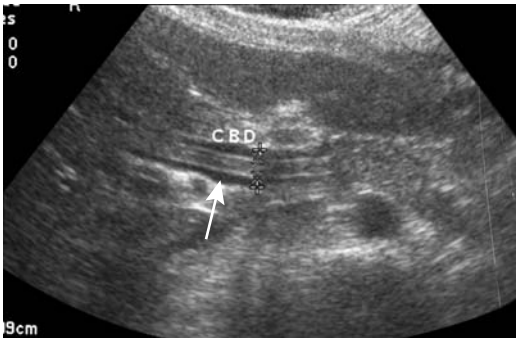

Figure 8.16. Biliary ascariasis. Ultrasonography shows a tubular hyperechoic structure (arrow) in the common bile duct. (Courtesy of Ronald O. Bude, M.D., University of Michigan.)

Magnetic resonance cholangiopancreatography has detected a hyperintense signal inside the worm digestive tract, presumably due to fluid in its gut.

The diagnosis is also established by ERC, and this technique is then used to remove the worm.

Fascioliasis

Most patients with *Fasciola hepatica* infestations have few symptoms. Occasionally bile duct involvement results in biliary colic or multiple pyogenic liver abscesses. Eosinophilia is common with acute infestation but not a chronic condition. Serologic testing is available.

Computed tomography detects hypodense foci scattered in the liver; these lesions resolve after therapy. MRI detects a hyperintense liver capsule in about half of infected patients (46); intrahepatic involvement ranges from hypointense regions on T1-weighted images and hypo- to hyperintense on T2-weighted images.

Cholangiography reveals curvilinear radiolucent defects several centimeters long within bile ducts. Rarely, fascioliasis involves the gallbladder. Superimposed biliary calculi, strictures, and regions of fusiform dilation develop with chronic infestation. Differential diagnosis of biliary fascioliasis includes sclerosing cholangitis and infection with other parasites such as

Clonorchis sinensis (flukes are smaller), *Ascaris lumbricoides* (worms are larger), or *Entamoeba histolytica*.

Endoscopic sphincterotomy and balloon extraction of parasites are feasible. An endoscopic basket can also be used to remove the worm.

Tuberculosis

Hepatic parenchymal tuberculosis is more common than bile duct involvement. Primary biliary tuberculosis is less common than periportal lymphadenitis and secondary biliary obstruction. In some patients acid-fast bacilli can be aspirated from bile during ERCP.

Actinomycosis

In distinction to pelvic involvement, biliary actinomycosis is rare.

Resection of a cystic duct remnant in an 80-year-old woman with a prior cholecystectomy and closure of a cholecystoduodenal fistula 3 years previously revealed several dense basophilic tumors containing gram-positive branching bacilli, with fluorescent-antibody staining for *Actinomyces naeslundii* (47); acid-fast bacilli staining was negative.

Primary Sclerosing Cholangitis

Clinical

Primary sclerosing cholangitis (PSC) is a chronic cholestatic disease clinically characterized by fatigue, pruritus, and jaundice. The etiology is not known. It can occur at any age, including early childhood; some of these patients have had previous neonatal jaundice.

Primary sclerosing cholangitis is a slowly progressing condition. The diagnosis is suspected by finding a cholestatic biochemical profile and confirmed by imaging of an abnormal biliary tract. In some, the disorder gradually progresses to cirrhosis and hepatic failure, and these patients are considered for liver transplantation.

An initial diagnosis of PSC during pregnancy is probably fortuitous. Liver function does not deteriorate during pregnancy, and pregnancy does not have a negative effect on PSC progression.

These patients are at increased risk of developing a cholangiocarcinoma and gallbladder adenocarcinoma.

Associated Conditions

Sclerosing cholangitis does occur as an isolated condition. More typical, especially in younger patients, is an association with inflammatory bowel disease. Liver involvement in patients with ulcerative colitis is not uncommon, although the reported prevalence varies considerably. Part of the confusion is that some patients with ulcerative colitis have nonspecific inflammation surrounding bile ducts; whether such pericholangitis is a variation of sclerosing cholangitis or a separate entity is unknown.

Sclerosing cholangitis developing in a setting of inflammatory bowel disease is still called *primary*; in spite of such an association, no evidence exists that bowel inflammation results in biliary changes. In fact, in some patients sclerosing cholangitis precedes the clinical detection of inflammatory bowel disease.

In the past, some authors excluded a diagnosis of PSC if bile duct calculi were present. Yet clinically and radiologically some patients have both sclerosing cholangitis and calculi, and bile duct calculi should be considered part of the spectrum of PSC. About 10% of PSC patients have intrahepatic bile duct calculi, and a similar number have chronic pancreatitis. An MR study of patients with PSC detected pancreatic abnormalities in 46%, consisting of a hypointense pancreas on T1-weighted images, hyperintense on T2-weighted images, decreased enhancement during the arterial phase, pancreatic enlargement, pancreatic duct narrowing, and peripancreatic edema or fluid (48).

Some patients with autoimmune hepatitis have cholestasis and bile duct strictures similar to those found in PSC. Occasionally reported are associations of PSC with thymoma and hypogammaglobulinemia, Sjögren's syndrome, Graves' hyperthyroidism, systemic lupus erythematosus, and celiac sprue. Sclerosing cholangitis has developed during interferon therapy. Whether Langerhans' cell histiocytosis, resulting in lung cysts and beaded intrahepatic ducts in infants and a rare adult, is related to PSC is

conjecture. An interesting observation is that the odds of having primary sclerosing cholangitis is significantly decreased among those who smoke (49).

Pathology

Fibro-obliterative inflammation of both intra- and extrahepatic bile ducts is a constant feature of PSC. The presence of liver noncaseating and nonnecrotizing granulomas is generally considered a feature of primary biliary cirrhosis, although similar granulomas are occasionally detected in PSC.

In Japan, eosinophilia is found in a large minority of patients with primary sclerosing cholangitis. Similarly, about a third of patients with PSC are antinuclear antibody positive.

Imaging

Both intra- and extrahepatic bile ducts are involved. In a minority of patients only intrahepatic ducts are affected (Fig. 8.17), some of the bile ducts become amputated, and the imaging appearance superficially mimics that seen with primary biliary cirrhosis. A minority of patients develop diverticular-like outpouchings (Fig. 8.18). These intramural diverticula appear as cyst-like structures within the bile wall and, if present, are almost pathognomonic of sclerosing cholangitis.

Classic findings in sclerosing cholangitis consist of multiple strictures varying in length and caliber. A beaded appearance to the bile ducts is not uncommon, with beading ranging from a fine, barely perceptible change in caliber to a coarse, undulating outline. Beading is difficult to evaluate with CT; dilated intrahepatic ducts, regardless of cause, often have an apparent beaded appearance as they course through different axial planes. Extensive hepatic fibrosis and bile duct wall thickening are common. On noncontrast CT fibrosis appears as hypoattenuating regions that become isoattenuating postcontrast. Duct wall thickening ranges from diffuse to focal.

Periportal fibrosis results in hyperechoic portal triads. Bile duct wall thickening appears variable in echogenicity with endoluminal US.

In some studies of PSC patients, MRCP has better defined intrahepatic bile ducts and identified more strictures than ERCP (50). Its noninvasive nature makes it attractive for following established disease and evaluating intrahepatic ducts not visualized by ERCP. Once PSC is well established, MRI identifies intrahepatic bile duct dilation, intrahepatic and extrahepatic bile duct stenosis, occasionally a resultant beaded appearance, and bile duct wall thickening and enhancement (51). A major function of MR is to identify underlying parenchymal damage. Magnetic resonance imaging identifies peripheral wedge-shaped hyperintense regions on T2-weighted images, regions often showing increased arterial-phase enhancement and an occasional reticular pattern (51,52). The significance of the MR parenchymal findings is not clear, and this topic is ripe for further research.

Scintigraphy confirms bile retention within bile ducts. Single photon emission computed tomography (SPECT) images reveal multiple focal regions of tracer retention due to bile stasis. In some patients an otherwise normal gallbladder fails to visualize with radiotracer.

Lymph node enlargement is not uncommon, with both porta hepatis nodes and other intraabdominal sites involved. Periportal edema is also detected.

Biliary abnormalities in most patients gradually progress over years; a more sudden change in a stricture should suggest an underlying cholangiocarcinoma. Eventually, cirrhosis and portal hypertension ensue. The right and left lobe atrophy, the caudate lobe hypertrophies, and the liver develops a prominent lobular appearance, a finding less commonly found with other causes of cirrhosis.

In spite of an occasional optimistic statement that cholangiocarcinomas can be detected in a setting of sclerosing cholangitis, not uncommonly an unsuspected cancer is first discovered by a pathologist after liver transplantation. Distortion by underlying disease makes detection of superimposed tumors difficult. Intraluminal polypoid cancers are least common in these patients; more often, a dominant stricture is found to consist of fibrosis with interspersed cancer cells. Even delayed CT contrast enhancement, a prominent feature with most cholangiocarcinomas, is often missing with these

Figure 8.17. Severe intrahepatic sclerosing cholangitis. Right lobe (A) and left lobe (B) ducts reveal numerous strictures. C: Sclerosing cholangitis in another patient involves both intra- and extrahepatic ducts (arrows). A major stricture is present at the right and left lobe junction.

cancers. Sudden, more proximal bile duct dilation should suggest a neoplastic stricture, but at that point one is already dealing with a widespread tumor.

An ERCP appearance similar to intrahepatic sclerosing cholangitis has been described with polycystic liver disease; perihilar cysts can indent bile ducts sufficiently to produce an irregular outline.

Therapy

No specific medical treatment is available for primary sclerosing cholangitis. Orthotopic liver transplantation is currently the definitive therapy. Because of the risk of developing a cholangiocarcinoma, some investigators are recommending liver transplantation earlier in the course rather than waiting until hepatic failure and cirrhosis develop. Because these patients are also at increased risk for hepatocellular carcinoma, screening for hepatocellular carcinoma as well as for cholangiocarcinoma prior to orthotopic liver transplantation appears reasonable. The prognosis is very poor if a cholangiocarcinoma is found even as an incidental finding after liver transplantation.

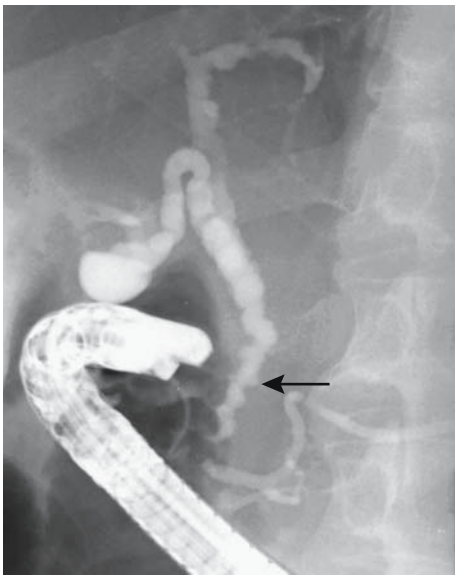

Figure 8.18. Irregular diverticular-like outpouchings (arrow) are an uncommon but characteristic finding in sclerosing cholangitis.

Endoscopic dilation of major duct stenoses is a temporizing measure in this generally progressive condition. In a minority of patients one extrahepatic bile duct stricture is responsible for most obstructive symptoms. Bile duct stricture dilation, especially surgical repair, should be approached cautiously. An occasional patient develops rapid progression of sclerosing cholangitis postoperatively; whether a fibroproliferative response is induced by duct manipulation is speculative.

A stent through a major stricture provides temporary relief in some, although stent occlusion is a common long-term complication. One variant is to provide short-term stenting; interestingly, these ducts tend to remain patent for months afterward.

Also of interest is that immunosuppression after liver transplantation does not influence inflammatory bowel disease in these patients.

Secondary Sclerosing Cholangitis

Secondary sclerosing cholangitis is associated with some infections, including HIV, bile duct ischemia, some pharmacotherapy, hepatic artery chemotherapy, and embolization and postsurgical complications. As an example, if a hydatid liver cyst communicates with the bile ducts, intracystic injection of a scolicidal solution (formaldehyde) may result in solution spread to the bile ducts and lead to secondary sclerosing cholangitis. Likewise, intraarterial infusion of chemotherapeutic agents has led to bile duct strictures; the perihilar region is most often involved, with these strictures having a smooth and symmetrical appearance.

Imaging findings of secondary sclerosing cholangitis are similar to those seen with PSC.

Autoimmune Cholangitis

Autoimmune cholangitis is a newly described entity containing features suggestive of primary biliary cirrhosis and autoimmune hepatitis; a relationship between autoimmune cholangitis and autoimmune hepatitis is not clear. Indeed, whether these should be considered separate entities or whether they simply represent specific liver pathways responding to an insult is unknown (primary biliary cirrhosis and autoimmune hepatitis are discussed in Chapter 7).

Clinically these patients have cholestasis, elevated antinuclear antibody titers, and negative antimitochondrial antibody titers, while histology reveals findings of primary biliary cirrhosis together with inflammation.

An occasional patient with Sjögren's syndrome has findings consistent with autoimmune cholangitis.

Gallbladder Tumors

Gallbladder polyps range from nonneoplastic to neoplastic, from sessile to pedunculated, from small to large. Most are several millimeters in size and are nonneoplastic. They are rare in children.

Detection

Computed Tomography

Larger gallbladder polyps are readily identified by CT. Precontrast CT reveals a majority of benign polyp to be isodense to bile and

most malignant polyps to be hyperdense. Both benign and malignant polyps enhance postcontrast and, especially for smaller ones, postcontrast imaging is necessary for their detection.

Ultrasonography

The prevalence of gallbladder polyps in diabetics and matched controls in an epidemiologic study of gallstones was 7%, with a marked male predominance (53); 90% of these polyps were <10 mm in diameter. No statistical difference in polyp prevalence was evident between diabetics and nondiabetic controls.

Conventional US readily detects gallbladder polyps. The prevalence of cancer increases directly with polyp size, and polyps >1 cm in diameter are at considerable risk for carcinoma. The vast majority of polyps <5 mm are cholesterol polyps, but an occasional cancer is <1 cm in diameter.

Endoscopic US also detects gallbladder polyps. The endoscopic US contour of a pedunculated gallbladder polyp is helpful in its differentiation; polyps having a granular contour and a foamy or globular echo pattern are mostly nonneoplastic, while a smooth, nodular, and solid appearance suggests a neoplasm.

Magnetic Resonance Imaging

A majority of polyps exhibit varying degrees of postcontrast MR enhancement, thus distinguishing them from gallstones. Cancers tend to have early and prolonged enhancement, but benign tumors vary in their washout patterns.

Nonneoplastic Tumors

Cholesterol Polyp/Cholesterolosis

Cholesterol polyps, or cholesterolosis, are the most common gallbladder polyps. The surgical literature refers to cholesterolosis as a "strawberry gallbladder." They range from solitary to multiple. Gallstones may or may not be present.

Cholesterolosis is often an incidental diagnosis, usually made by a pathologist. These polyps are not considered premalignant, although an occasional carcinoma is surrounded by glandular dysplasia and cholesterolosis; the carcinoma probably originates first and tumor epithelium then absorbed cholesterol from bile. Cholesterolosis is not part of the spectrum of acute cholecystitis. No association exists with systemic disorders such as atherosclerosis or diabetes.

Even if detected preoperatively, cholesterolosis and adenomyomatosis are not believed to be indications for cholecystectomy.

Smaller cholesterol polyps are not detected with unenhanced CT but become evident postcontrast.

Conventional US shows most larger cholesterol polyps to be pedunculated, have a granular surface, and tend toward a hypoechoic appearance, but smaller ones are mostly hyperechoic. Smaller polyps are nonmobile and adhere to the gallbladder wall, and both large and small are without acoustic shadowing. The smaller ones tend to have a smooth outline; they become irregular with growth. Endoscopic US with its higher resolution is preferred over conventional US when evaluating gallbladder polyps.

Some authors suggest that persistence of gallbladder contrast 24 hours after an oral cholecystogram is indirect evidence of cholesterolosis. No objective data support this statement, and one should not rely on this finding.

Although generally not warranted, US-guided percutaneous transhepatic needle aspiration cytology can diagnose cholesterol polyps.

Adenomyoma/Adenomyomatosis

Adenomyomatosis presents either as a focal gallbladder narrowing or as diverticular-like outpouchings, most often in the gallbladder fundus. These outpouchings, also called *cholecystitis glandularis proliferans*, are believed to represent both mucosal herniation into muscularis propria and prominent Rokitansky-Aschoff sinuses. A rare report describes a carcinoma associated with adenomyomatosis, probably being coincidental. Although somewhat controversial, in most patients adenomyomatosis is generally believed not to be associated with symptoms.

In general, an oral cholecystogram provides more information about adenomyomatosis and cholesterolosis than US but is a procedure seldom performed today. Adenomyomatosis tends to be more prominent after a fatty meal and is best seen on a post–fatty meal oral cholecystogram. A number of prior reports of gallbladder diverticula probably describe adenomyomatosis; their imaging differentiation is not clear, although some authors do attempt to differentiate between these two entities.

A typical appearance in a contrast-filled gallbladder consists of irregular diverticular-like outpouchings. When subtle, the fine granular outpouchings are difficult to identify with most current imaging techniques. At times imaging reveals a circumferential gallbladder fold resulting in an hourglass appearance (Fig. 8.19). Superficially the latter condition mimics a gallbladder septum. A rare adenomyoma appears polypoid.

Magnetic resonance RARE sequences and breath-hold are superior to other pre- and postcontrast techniques in detecting Rokitansky-Aschoff sinuses (54). Adenomyomatosis is identified as small intramural foci hypointense on T1- and hyperintense on T2-weighted images. These outpouchings should not enhance postcontrast, but adjacent gallbladder mucosa does enhance, especially if concurrent inflammation is present, and thus the occasional description of adenomyomatosis as hypointense spots in a more hyperintense gallbladder wall. Small outpouchings blend into the gallbladder wall and result in a not uncommon postcontrast appearance of homogeneous, continuous wall enhancement.

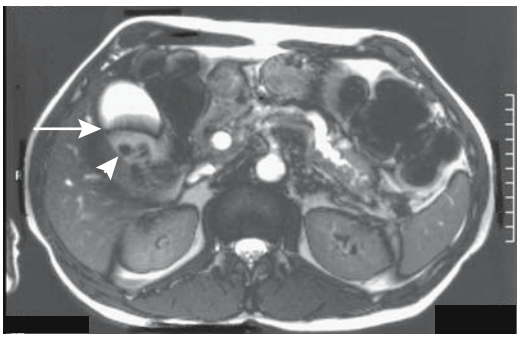

Figure 8.19. T2–weighted image of adenomyomatosis. The gallbladder contains a transverse fold (arrow) and several gallstones (arrowhead). The pancreatic and bile ducts are dilated secondary to a pancreatic cancer. (*Source:* Burgener FA, Meyers SP, Tan RK, Zaunbauer W. Differential Diagnosis in Magnetic Resonance Imaging. Stuttgart: Thieme, 2002, with permission.)

Hyperplastic/Inflammatory Polyp

Macroscopic hyperplastic polyps are uncommon, although an occasional large one is detected. Larger ones tend to enhance with contrast and angiography may even reveal neovascularity and a tumor stain.

Ectopic Tissue (Pancreatic or Gastric)

Heterotopic gastric mucosa or pancreatic tissue is occasionally found in the gallbladder. Most are polypoid, often located in the fundus. Ultrasonography reveals an echogenic polyp in the gallbladder.

Benign Neoplasms

Adenoma

Gallbladder adenomas are uncommon. Small adenomas range from pedunculated to sessile in appearance. Some adenomas are located in a region of adenomyomatous hyperplasia. An occasional gallbladder villous adenoma is not detected by transabdominal US because the gallbladder is filled with mucinous material; CT should detect these. Gallbladder adenomyomas are rare.

Malignant Neoplasms

The overwhelming majority of gallbladder malignancies are primary carcinomas, with only an occasional sarcoma, lymphoma, carcinoid, or metastasis reported.

Adenocarcinoma

Clinical

Most early gallbladder carcinomas are detected by a pathologist after cholecystectomy for cholecystitis. In spite of an occasional early

stage, even when only a microscopic carcinoma is identified, metastases often are already present. Jaundice in a setting of cancer generally implies spread to lymph nodes adjacent to extrahepatic bile ducts. An occasional gallbladder carcinoma invades the liver, necroses, and becomes infected, and the patient presents with a liver abscess.

A rare gallbladder carcinoma results in α-fetoprotein secretion. Immunostaining detects overexpression of p53 protein in most gallbladder cancers and overexpression appears directly related to increasing carcinoma grade.

Ultrasonography screening of a high-risk population is occasionally proposed to detect early gallbladder carcinomas, but such a practice is not common. Even if detected early, prognosis is generally poor.

Compared to normal ducts, patients with a congenital anomalous pancreaticobiliary junction are at increased risk for developing gallbladder cancer (sphincter of Oddi anomalies are discussed in the earlier Congenital Abnormalities section).

An association of gallbladder cancer with chronic cholecystitis is well known. Likewise, because of the high risk for cancer, detection of a porcelain gallbladder is generally deemed an indication for elective cholecystectomy. Patients with chronic *Salmonella typhi* infection are at increased risk for several hepatobiliary cancers, including gallbladder carcinoma. A possible association between actinomycosis and gallbladder carcinoma is suggested.

An increased prevalence of gallbladder carcinoma is found in a setting of sclerosing cholangitis, although the much higher risk of primary bile duct carcinoma overshadows gallbladder involvement.

Synchronous primary gallbladder and extrahepatic bile duct carcinomas are uncommon. Often differentiation of separate primaries from metastases is difficult.

Pathology

Carcinoma-in-situ implies a tumor limited to the epithelium and is usually detected by the pathologist after cholecystectomy for cholelithiasis. Most in-situ carcinomas discovered after laparoscopic cholecystectomy do not manifest lymphatic, venous, or perineural invasion and thus are potentially curable.

A diagnosis of early gallbladder carcinoma is rarely made outside of Japan. Japanese investigators divide these early tumors into superficial flat and superficial elevated types. The superficial flat carcinomas are not detected by imaging and are difficult to identify even by a pathologist. Sessile cancers are more common than pedunculated ones.

Histologic variants include papillary, mucinous, and an occasional clear cell carcinoma, although most are simply reported as adenocarcinomas. They range from well differentiated to anaplastic. A number of tumors contain more than one subtype, thus complicating the histologic subdivision. Papillary carcinomas tend to grow intraluminally, and some have a cauliflower-like appearance. Most gallbladder carcinomas, however, infiltrate early and extensively.

Detection

A number of studies confirm that a preoperative diagnosis of gallbladder cancer is achieved in only 30% to 40% of patients. In particular, stages 0 to II are diagnosed either at surgery or, more often, at histology. Imaging detection of a solitary gallstone, a gallstone elevated because of focal wall thickening, an intraluminal or invasive tumor, and discontinuity of the mucosal echo pattern suggests a carcinoma. Gallbladder wall thickening is found with both benign and malignant disease. An asymmetric or irregular wall thickening, however, is more common with a cancer. Also, a large polyp or an infiltrating tumor replacing most or all of the gallbladder lumen or invading adjacent structures suggests a cancer, regardless of whether or not gallstones are present. Nevertheless, a not uncommon scenario is a thickened gallbladder wall detected by CT or US, believed to represent chronic cholecystitis, containing a gallbladder cancer.

A necrotic, perforated gallbladder cancer mimics acute cholecystitis both clinically and by imaging. Some tumors contain hypodense regions, signifying necrosis. Viable tumor tends to enhance postcontrast. Currently the primary role of both CT and MR is in staging rather than diagnosis.

A rare mucus-secreting gallbladder carcinoma develops sufficient intratumoral calcifications to be visible by CT or even with conventional radiography.

Ultrasonography reveals either focal gallbladder wall thickening or an inhomogeneous, hyperechoic, fungating, broad-based tumor within the lumen with little acoustic shadowing. With invasion of surrounding tissues quite often the gallbladder is not recognized and US simply identifies a poorly marginated, heterogeneous mass. Associated gallstones are common. Most authors agree that endoscopic US detects more and earlier gallbladder tumor than conventional US, yet concomitant cholecystitis or stones often prevent tumor identification. Color Doppler US of a carcinoma reveals color signals both in intraluminal tumors and gallbladder wall. The presence of a high-resistance index is uncommonly detected but is suggestive of a malignancy.

Gallbladder carcinomas most often are hypointense on T1- and hyperintense on T2-weighted images. Postcontrast MRI of carcinomas reveals early and irregular enhancement, in distinction to the delayed wall enhancement found in chronic cholecystitis. The usual three-layer gallbladder wall MR appearance is destroyed by a carcinoma but tends to be preserved with inflammatory disease.

In most instances cholangiography is not helpful in detecting a gallbladder cancer because of concurrent cystic duct obstruction. Not uncommon is hepatic duct invasion due to metastasis (Fig. 8.20).

Occasionally US-guided percutaneous transhepatic fine-needle aspiration cytology from a tumor provides a diagnosis, although a malignant focus in an adenoma is readily missed.

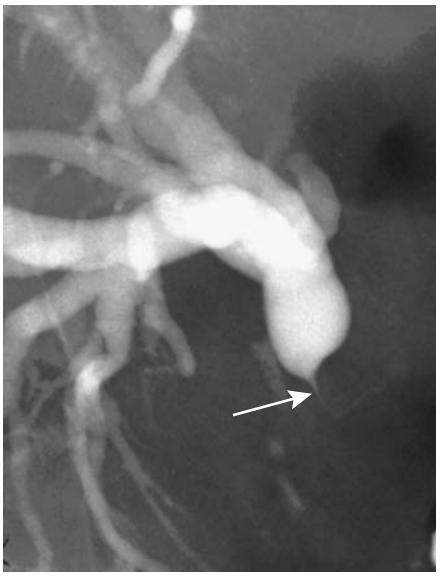

Figure 8.20. Hepatic duct obstruction (arrow) secondary to metastatic gallbladder carcinoma. Other metastases can have a similar appearance.

Staging

The tumor, node, metastasis (TNM) gallbladder cancer staging system is outlined in Table 8.3. A majority of cancers are already at an advanced stage when first discovered. A gallbladder carcinoma spreads outside the gallbladder to adjacent liver and along the cystic duct to pericholedochal and superior pancreaticoduodenal lymph nodes. Patients with T1 tumors tend not to have lymph node involvement, but a majority of those with T2–T4 tumors have lymph node metastases, with pericholedochal and cystic lymph nodes being most often involved. Involvement of multiple nodes is common.

Computer tomography is commonly used to stage gallbladder cancers, although the reported CT detection of cancer spread outside the gallbladder varied considerably (Table 8.4). Similar to a number of other tumors, CT has poor sensitivity with T1 tumors. Some studies have achieved helical CT accuracies in assessing resectability of over 90% (48), keeping in mind that resectability differs from cure. In particular, accuracy of gauging lymph node involvement is poor even with multidetector CT. Still, CT appears helpful in treatment planning. Ultrasonography is considered inadequate in staging gallbladder cancer.

Tumor spread to right and left bile duct confluence or Portal vein invasion renders a gallbladder carcinoma inoperable. In some patients percutaneous transhepatic portography and intraportal US are necessary to distinguish between vein compression and invasion.

Therapy

With the exception of carcinoma-in-situ, most gallbladder cancers discovered at surgery imply a poor prognosis. Even with an early lesion a simple cholecystectomy is not necessarily cura-

Table 8.3. Tumor, node, metastasis (TNM) staging of gallbladder tumors

Primary tumor:			
Tx	Primary tumor cannot be assessed		
T0	No evidence of primary tumor		
Tis	Carcinoma-in-situ		
T1a	Tumor invades lamina propria		
Tlb	Tumor invades muscle layer		
T2	Tumor invades perimuscular connective tissue; no extension beyond serosa or into liver		
T3	Tumor perforates serosa and/or invades liver and/or other adjacent organs		
T4	Tumor invades main portal vein or hepatic artery or multiple extrahepatic organs		
Lymph nodes:			
Nx	Regional nodes cannot be assessed		
N0	No regional lymph node metastasis		
N1	Regional lymph node metastasis		
Distant metastasis:			
Mx	Distant metastases cannot be assessed		
M0	No distant metastasis		
M1	Distant metastasis		
Tumor stages:			
Stage 0	Tis	N0	M0
Stage IA	T1	N0	M0
Stage IB	T2	N0	M0
Stage IIA	T3	N0	M0
Stage IIB	T1	N1	M0
	T2	N1	M0
	T3	N1	M0
Stage III	T4	any N	M0
Stage IV	any T	any N	M1

Source: From the AJCC Cancer Staging Manual, 6th edition (2002), published by Springer-Verlag, New York, NY, used with permission of the American Joint Committee on Cancer (AJCC), Chicago, IL.

tive; an extended cholecystectomy with lymph node dissection, at times combined with extrahepatic bile duct or hepatic resection, offers a possible cure. A 5-year survival of 10% to 15% is typical, with long-term survivors being stage I or II. Aggressive surgery appears to improve survival. A University of Bonn (Germany) study of patients undergoing curative resection, consisting of an extended cholecystectomy (cholecystectomy with lymphadenectomy and wedge hepatic resection), anatomic segmentectomy of segments IVa and V, or extended hepatectomy, achieved an actuarial 5-year survival rate of 55% (56).

Table 8.4. Helical CT detection of gallbladder carcinoma

	Sensitivity	Specificity
T1	33%	94%
T2	64–73%	80%
T3	80%	81–88%
T4	100%	95%

Source: Adapted from Yoshimitsu et al. (55).

An endoprosthesis, placed either endoscopically or percutaneously, is useful for palliation in some patients with an unresectable carcinoma.

Chemotherapy has had little impact on survival.

Metastases/Recurrence

Gallbladder carcinomas metastasize widely, even to bone. Spread to extrahepatic bile ducts, gastrointestinal tract, and adjacent structures is common. Occasionally a distant metastasis is the first clue to an underlying gallbladder carcinoma. An exceptional patient with extensive metastases, treated aggressively has prolonged survival.

More than most cancers, gallbladder carcinoma spreads readily along laparoscopic trocar sites. A number of patients have an unsuspected carcinoma first detected by a pathologist, with trocar site recurrence identified several months later. Even several recurrences have developed at laparoscopic ports (57). Peritoneal seeding also occurs, including localized seeding in the right subphrenic space.

A suspected gallbladder carcinoma probably is a contraindication to laparoscopic cholecystectomy. When a laparoscopic cholecystectomy is performed for an unsuspected carcinoma, surgical and adjuvant radiotherapy to the trocar sites appears reasonable.

Computed tomography identifies port track recurrence as a homogeneous abdominal wall tumor, often directly involving adjacent omental fat (57). Recurrences tend to enhance markedly on postcontrast CT.

Other Primary Carcinomas/Sarcomas

Both squamous and adenosquamous gallbladder carcinomas are uncommon. Often a large tumor with invasion of adjacent structures is

found at initial presentation. These tumors tend to spread widely, including hematogenously.

A gallbladder carcinosarcoma is rare. These tumors tend to be large when first detected.

Small cell carcinomas are rare tumors spreading diffusely and having a poor prognosis. Immunochemistry reveals some of these tumors to have a neuroendocrine cell origin, and presumably they are derived from intestinal metaplasia.

Lymphoma

Primary gallbladder lymphoma is sufficiently rare that only case reports exist. Computed tomography and US detects a complex tumor confined to the gallbladder. Systemic lymphoma also uncommonly involves the gallbladder.

MALT lymphomas have a propensity to involve numerous mucosal sites. Thus a 53-year-old woman with low-grade gastric mucosa-associated lymphoid tissue (MALT) lymphoma underwent a total gastrectomy, developed small bowel recurrence 18 years later, underwent chemotherapy, was in clinical remission, and then was found to have gallbladder recurrence 3 years later (58).

Melanoma

Both primary and metastatic malignant gallbladder melanomas are reported. The presence of another obvious primary site argues for a metastasis; otherwise, a distinction between primary and metastatic melanoma is difficult. Indeed, the question can be raised: Does primary gallbladder melanoma occur?

Autopsies of patients with malignant melanoma show gallbladder metastases in 15% to 20%; US reveals soft tissue tumors projecting into the lumen; an occasional one is polypoid.

Metastases to Gallbladder

Aside from melanomas, metastases to the gallbladder are not common. Renal cell carcinoma and gastric carcinoma are found occasionally. A rare metastasis appears as a polyp. An occasional metastasis presents as cholecystitis. Confusing the issue, histologic differentiation of a primary clear cell gallbladder carcinoma from a metastatic renal cell carcinoma is difficult.

Bile Duct Obstruction/Tumors

Clinical

In considering bile duct disease, the initial task is to establish whether jaundice is secondary to nonobstructive or obstructive causes. Clinical evaluation, including blood tests, makes this distinction in a majority of patients. The causes of nonobstructive jaundice range from diffuse liver disease, such as cancer, cirrhosis, and inflammation, to a congenital or metabolic condition. An occasional cause is partial distal duodenal obstruction. Once biliary obstruction is suspected, the etiology is best approached by subdividing patients by age and site of obstruction (Table 8.5). Thus a differential diagnosis can be narrowed down considerably by combining the clinical and imaging findings.

Liver function changes vary after the relief of a biliary obstruction. Aminotransferase enzymes respond differently to complete and partial decompression; after complete decompression these enzymes decline for a week or so and then remain slightly higher than normal. After partial decompression the enzyme levels continue being elevated. Serum alkaline phosphatase, γ-glutamyl transpeptidase (GGT), serum total and direct bilirubins, and serum albumin tend to decrease after both complete and partial decompression in an inconstant manner.

Detection

The borderline between a normal duct caliber and a dilated duct is one of gradation; different criteria have been established for different imaging modalities. In general, if during ERC study the extrahepatic bile duct diameter is greater than the endoscope, the ducts are probably dilated. With US, if a bile duct diameter is <40% of an adjacent portal vein branch, it probably is not dilated. When markedly dilated, bile ducts tend to assume a somewhat beaded outline.

Numerous studies have compared CT and US in their ability to identify the etiology of an obstruction, with inconclusive results. Ultrasonography appears to be more sensitive than CT in identifying carcinomas, while CT sensitivity is greater in detecting stones. Many

Table 8.5. Common etiologies of bile duct obstruction (listed by age and site of obstruction)

Site of obstruction	Newborn infant	Child to young adult	Middle age	Elderly
Intrahepatic	Biliary atresia Caroli's disease Hepatoblastoma Sarcoma[2]	Sclerosing cholangitis Caroli's disease AIDS cholangitis Hepatoblastoma HCC[1] Hamartoma Sarcoma[2]	Metastasis Cholangiocarcinoma Biliary cirrhosis HCC[1] Sclerosing cholangitis Hamartoma	Metastasis Cholangiocarcinoma HCC[1]
Hilar	Biliary atresia Sarcoma[2]	Sclerosing cholangitis AIDS cholangitis Lymphoma	Cholangiocarcinoma Metastasis HCC[1] Sclerosing cholangitis Lymphoma Sarcoidosis	Cholangiocarcinoma Metastasis HCC[1] Hepatic artery aneurysm
Suprapancreatic	Choledochal cyst Sarcoma[2]	Sclerosing cholangitis Choledochal cyst AIDS cholangitis Lymphoma	Metastasis Cholangiocarcinoma Mirizzi's syndrome Sclerosing cholangitis Iatrogenic Gallbladder carcinoma Lymphoma	Metastasis Cholangiocarcinoma Gallbladder carcinoma Mirizzi's syndrome Sclerosing cholangitis Iatrogenic Lymphoma Hepatic artery aneurysm
Intrapancreatic	Choledochal cyst Pancreatico-blastoma	Pancreatitis Choledochal cyst Stone Cystic tumors Iatrogenic	Stone Pancreatitis Cholangiocarcinoma Pancreatic carcinoma Iatrogenic	Stone Pancreatic carcinoma Cholangiocarcinoma Pancreatitis Iatrogenic
Papilla of Vater		Stone Sphincter stenosis Choledochocele	Stone Papilla carcinoma Sphincter stenosis	Stone Papilla carcinoma Sphincter stenosis

[1] HCC, hepatocellular carcinoma.
[2] Mostly embryonal rhabdomyosarcoma.

past comparisons involved nonhelical CT; undoubtedly further refinements in multislice technology and user expertise will change these results.

Computer Tomography

Initially the bile ducts are not dilated for several hours or even several days after an acute obstruction. Eventually they dilate, and CT, US, or MR should be able to locate a site of obstruction. With a distal obstruction the extrahepatic ducts dilate first, followed later by intrahepatic ducts.

Normally a fatty meal or IV cholecystokinin produces no visible change in extrahepatic bile duct caliber; increased bile production and gallbladder contraction are balanced by sphincter of Oddi relaxation. With a distal bile duct obstruction, however, these agents result in an increase in bile duct caliber proximal to the obstruction. This test is most useful with a clinically suspected biliary obstruction but is also helpful with normal or equivocal caliber extrahepatic bile ducts seen with imaging; cholangiography should, of course, detect an obstruction directly.

Ultrasonography

Ultrasonography detects most dilated bile ducts. It provides limited information in

patients with painless jaundice. It does have a role, however, as a screening test for suspected inflammation or stone disease.

In patients with bile duct strictures or filling defects undergoing intraductal US, bile cytology, and percutaneous transhepatic cholangioscopy, the sensitivity and specificity of intraductal US for diagnosing bile duct cancer were 89% and 50%, respectively (59); the sensitivity of bile cytology (64%) and transhepatic cholangioscopy (93%) increased to 96% and 100%, respectively, if results of intraductal US were included.

Cholangiography

Either percutaneous or endoscopic cholangiography readily evaluate biliary obstructions. With a complete or high-grade obstruction, a percutaneous approach rather than ERCP is preferred because it outlines ducts proximal to an obstruction used by the surgeon for reconstruction. A catheter left in place aids the surgeon in identifying the bile ducts in a surgical field often distorted by tumor or prior surgery.

In general, MR cholangiography is comparable in accuracy to ERC in detecting biliary dilation and suggesting an etiology for a stricture (60). It identifies the site of obstruction and differentiates a stone from neoplasm. It achieves sensitivities and specificities of over 90% in detecting an obstruction. In determining a cause for obstruction, in one strudy, MRCP sensitivity and specificity for choledocholithiasis were 89% and 90%, for malignant obstruction 92% and 88%, for benign stricture 63% and 90%, and for chronic pancreatitis 50% and 99% (61). In general, MRCP should detect duct dilation in all patients with clinical obstructive jaundice and depict correctly the level of obstruction in about 90%; common bile duct obstruction due to stricture and stone can be readily differentiated.

The addition of nonenhanced T1- and less heavily T2-weighted images to MRCP images improves the diagnostic accuracy of differentiating benign from malignant biliary strictures (62); gadolinium-enhanced images are useful in select patients. A cholangiocarcinoma tends to be asymmetric, have irregular margins and more often involves a longer bile duct segment than a benign stricture.

Scintigraphy

Although the extrahepatic ducts do not dilate immediately after an obstruction, HIDA scintigraphy is abnormal during this time, and no tracer activity is detected in the small bowel. Nevertheless, in a jaundiced population cholescintigraphy does not reliably differentiate between cholestasis and mechanical obstruction and is generally not employed for this purpose.

Benign Strictures

Clinical

The most common etiology for a benign biliary stricture is prior instrumentation. A stricture can develop shortly after bile duct manipulation or occur months or even years later. Rarely, the appearance mimics a web (Fig. 8.21). The most common clinical presentation is jaundice or, if only some of the intrahepatic ducts are involved, cholangitis.

Once a stricture is identified, the initial task is to exclude an underlying malignancy. A tissue diagnosis should be obtained unless the etiology of a stricture is clear. A biopsy is generally preferred over cytology. Depending on each situation, a biopsy can be obtained as part of ERCP or percutaneously using imaging guidance.

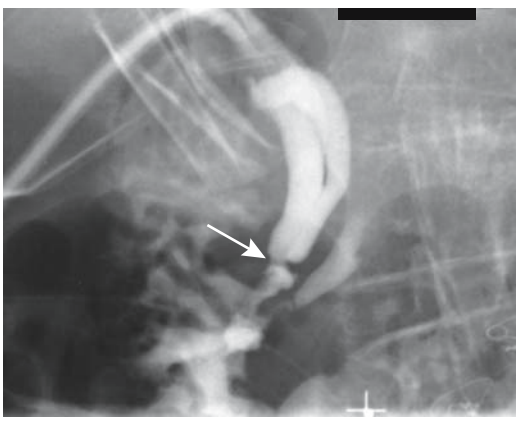

Figure 8.21. Common bile duct web (arrow). The study was performed through a biliary catheter inserted during surgery for gangrenous cholecystitis.

Sphincter of Oddi Stenosis/Dysfunction

Considerable confusion surrounds both the definition and the diagnosis of sphincter of Oddi dysfunction (dyskinesia). The true prevalence of this condition is difficult to gauge; the diagnosis is more often made in Europe than in the United States. Biliary dyskinesia, sphincter dysfunction, and even chronic acalculous cholecystitis are difficult to distinguish on clinical, imaging, and even pathologic grounds. Indeed, whether these are distinct disease entities, different manifestations of a motility disorder, or even exist at all is speculation. Some investigators include under this term all patients with biliary colic or cholestasis who do not have stones or other evidence of an anatomic obstruction proximal to the sphincter of Oddi, while others exclude those with a stricture (stenosis) at the sphincter. In a setting of biliary dilation, delayed biliary emptying of contrast, and no obvious cause of obstruction, some investigators routinely ascribe these findings to papillary stenosis or sphincter of Oddi dysfunction (or spasm), although such an approach undoubtedly includes a number of false positives.

Bile duct contrast retention at the conclusion of ERCP is used by some investigators as a sign of sphincter of Oddi dysfunction, while others rely primarily on biochemical evidence of cholestasis. Another approach is to obtain direct manometric pressure recordings of the sphincter during ERCP. Normal sphincter of Oddi pressure is 5 to 15 mm Hg above intraluminal bile or pancreatic duct pressures. Typically, basal pressure is <40 mm Hg. With sphincter of Oddi stenosis the basal pressure increases. If manometry reveals a basal sphincter pressure >40 mm Hg, even with no other evidence of stasis, a diagnosis of sphincter of Oddi dysfunction is made. Some employ flow manometry and infuse contrast under constant pressure, such as 30 cm of water; papillary stenosis is suggested if the flow rate is <12 mL/min and intraluminal pressure is >15 cm of water. Others refine this test using pharmacologic agents to relax the sphincter of Oddi. Nevertheless, a manometric study of amplitude and frequency of sphincter contractions is not always straightforward; some patients have intermittent sphincter spasm, although the basal pressure is still normal. Manometric data may not identify benign papillary stenosis. In such a setting some endoscopists perform an empiric sphincterotomy, but results are mixed.

Papilla of Vater stenosis is often ascribed to damage produced by a prior stone passing through or to instrumentation. In general, a diagnosis of papillary stenosis or dysfunction should not be made lightly, and other conditions should be sought to explain a patient's symptoms.

Therapy

Endoscopic

One indication for endoscopic sphincterotomy is stenosis of the sphincter of Oddi. Endoscopic manometry is useful to evaluate whether an endoscopic sphincterotomy has been successful. An absent choledochoduodenal pressure gradient indicates a complete sphincterotomy. Unfortunately, a high percentage of these patients restenose.

In general, significant complications occur in 5% to 10% of patients during endoscopic sphincterotomy, with bleeding being most common. Most bleeding stops spontaneously or after coagulation, although an occasional patient requires surgical control. An alternative is angiographic embolization of the bleeding site.

Pancreatitis is a known ERCP complication regardless of whether or not a sphincterotomy is performed. Some patients develop an elevation in pancreatic enzyme values but are clinically asymptomatic.

Most procedure-related perforations are extraperitoneal. Occasionally a perforation manifests only several hours after the procedure. Extraperitoneal gas can be identified either with conventional radiographs or CT. Most of these patients respond to conservative therapy. Sepsis is uncommon and patients are generally treated conservatively.

Experience with long-term stenting of benign bile duct strictures is limited. Nonmetallic stents tend to obstruct and need to be replaced periodically. Metal stents eventually become epithelialized and appear to last longer, but

some obstruct secondary to mucosal hypertrophy or calculi formation.

Surgical

Surgery for most benign bile duct strictures consists of either stricture repair alone or a choledochojejunostomy. Surgical repair of benign strictures leads to excellent or good results in over 80% of patients; the most common complication of these repairs is subsequent restricture.

The classic repair procedure for major bile duct injuries is a Roux-en-Y hepaticojejunostomy. With such an anastomosis, conventional endoscopy cannot access the anastomotic site, and either a percutaneous transhepatic approach or repeat surgery is necessary in cases of restenosis. At repeat surgery the jejunal limb going to the anastomosis is identified, an enterotomy performed, and endoscopy through the enterotomy used to diagnose and, if necessary, treat a stricture.

A biliary stricture secondary to pancreatitis generally involves a long intrapancreatic segment. An endoscopically placed stent temporarily relieves the obstruction, but these patients then require a surgical bypass. With pancreatitis limited to the head of the pancreas, a pancreaticoduodenectomy may be indicated.

Transhepatic

In some patients both endoscopic and percutaneous transhepatic therapeutic approaches are viable options. Using either technique, an appropriate-sized balloon is inserted to dilate a stricture. Prophylactic IV antibiotic therapy before and during the procedure is commonly employed. Stones encountered proximal to a stricture are either fragmented or extracted during the same procedure. Catheter stenting across the stricture provides ready future access in cases of restenosis, with the length of time a stent is left in place varying considerably among institutions.

Complications can be divided into those associated with the percutaneous procedure per se, including transhepatic access to bile ducts, and those associated with balloon dilation. They consist of septicemia, shock, significant hemorrhage, pancreatitis, and bile duct perforation.

Successful long-term patency after dilation varies considerably. In general, the restricture rate increases with time.

Phytobezoar

Phytobezoars should not collect in the bile ducts, although an occasional one does develop. Some of these form after a cholecystogastrostomy and vegetable concretions end up obstructing the extrahepatic bile ducts.

Mirizzi Syndrome

Mirizzi syndrome is produced by a gallstone impacting either in the neck of the gallbladder or within the cystic duct and secondarily obstructing the hepatic duct. The initial classification of a gallstone either simply compressing adjacent bile ducts as part of an acute episode or a cholecystocholedochal fistula forming on a chronic basis was subsequently expanded to include (63):

- Type I: hepatic duct stenosis due to a stone impacting in the cystic duct or gallbladder neck. This is the most common
- Type II: hepatic duct fistula due to a stone impacting in the cystic duct or gallbladder neck
- Type III: hepatic duct stenosis due to a stone at the duct confluence
- Type IV: hepatic duct stenosis as a complication of cholecystitis and no impacted calculus

A rationale for this classification is that the surgical approach differs in each of these four types. Thus in the presence of a cholecystocholedochal fistula (Mirizzi syndrome type II) the fistula must be repaired at surgery. A gallbladder remnant pedicle graft (choledochoplasty) can be used for repair.

Occasionally obstruction is caused by xanthogranulomatous cholecystitis, with inflammation extending to adjacent structures—whether to label such a presentation as Mirizzi syndrome is a matter of definition.

In most instances cholangiography, regardless of how it is performed, should be diagnos-

tic. Although most patients suspected of having Mirizzi syndrome undergo laparotomy, laparoscopy is also feasible in these patients. Mirizzi syndrome has also been successfully treated by extracorporeal shock-wave lithotripsy.

Extrinsic Obstruction

Vascular

Not all hilar masses represent a neoplasm. In a setting of portal vein thrombosis, large extrahepatic venous collaterals, such as cavernous transformation of the portal vein—also called bile duct varices or portal cavernoma—tend to compress and obstruct adjacent bile ducts to the point of inducing obstructive jaundice. These dilated veins mimic a neoplasm. Prolonged obstruction has led to periportal and perisinusoidal fibrosis and secondary biliary cirrhosis. At times, venous collaterals are mostly in the hepatic and common bile duct wall and result in diffuse wall thickening, mimicking both benign and malignant diseases.

A hepatic artery, gastroduodenal artery, or posterior inferior pancreaticoduodenal artery pseudoaneurysm or a pancreatic pseudocyst can also compress adjacent bile ducts and induce jaundice. Aneurysm embolization or pseudocyst aspiration should relieve obstruction.

Imaging reveals an extrinsic biliary obstruction. Cholangiography shows multiple extrinsic biliary indentations, at times serpiginous, together with proximal bile duct dilation.

Sarcoidosis

A rare cause of obstructive jaundice is hepatobiliary sarcoidosis. Most of these obstructions are secondary to enlarged sarcoidosis-involved hilar lymph nodes compressing adjacent bile ducts. In an occasional patient with sarcoidosis, cholangiography reveals findings similar to those seen with sclerosing cholangitis.

Other Obstructions

While duodenal peri-Vaterian diverticula are common, biliary obstruction by one is rare (these diverticula are discussed in Chapter 3). A food bezoar in a duodenal diverticulum or peri-Vaterian diverticulitis can result in biliary obstruction.

Almost any inflammation resulting in perihilar or superior pancreaticoduodenal adenopathy can compress adjacent bile ducts and induce obstructive jaundice. In some parts of the world tuberculous adenitis is a recognized cause. Primary retroperitoneal fibrosis can obstruct the common bile duct. A rare pancreatic hydatid cyst leads to obstructive jaundice.

Nonneoplastic Tumors

Hamartoma (von Meyenburg Complexes)

Mesenchymal and biliary hamartomas, also called *von Meyenburg complexes* and *cholangiofibromatosis*, consist of a mixture of hepatocytes, small, dilated bile ducts, and connective tissue, together with varying size cysts. These hamartomas range from solid to largely cystic circumscribed tumors, single to multiple, large or small, intrahepatic or even projecting from the liver surface. Multiple hamartomas are either uniform or random in distribution throughout the liver. A large autopsy study found these complexes in 6% of adults and 1% of children (64). They are more prevalent in polycystic kidney and liver disease.

Larger hamartomas are found mostly in young children. These cystic tumors are only mildly vascular. The α-fetoprotein level is not elevated with these tumors, helping distinguish them from hepatoblastomas.

These hamartomas are considered to be nonneoplastic developmental ductal plate malformations and are not thought to be premalignant, although a rare cholangiocarcinoma does originate in a setting of multiple bile duct hamartomas. A double cancer—a hepatocellular carcinoma and a cholangiocarcinoma—was discovered in a 74-year-old man, with the cholangiocarcinoma arising in hamartomas (65); a histologic progression from hamartomatous to adenomatous and a cholangiocarcinoma was evident.

Some of the larger hamartomas are palpable.

Computer tomography reveals small hamartomas as multiple cysts scattered throughout the liver; they tend to be irregular in shape and

do not enhance, although some are more prominent postcontrast. They do not communicate with bile ducts.

The larger ones consist of a complex mass ranging from solid to mostly cystic (Fig. 8.22). Calcifications are not common, although an occasional one does contain peripheral calcifications. They tend to be mostly hypodense on postcontrast CT, although solid components enhance with contrast. Some septa also enhance postcontrast.

Ultrasonography reveals these hamartomas to be hypoechoic. Larger ones become inhomogeneous and hyperechoic and contain acoustic shadowing.

Limited MRI of these hamartomas reveals them to be hypointense on T1- and hyperintense on T2-weighted MR images (Fig. 8.23). They are even more hyperintense on heavily T2-weighted images and are more apparent and more numerous on T2-weighted MRI and

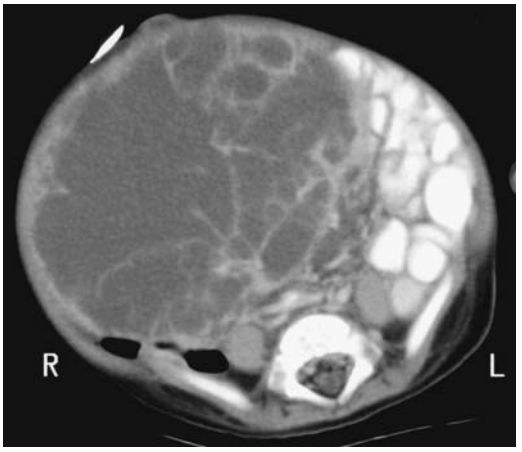

Figure 8.22. Liver mesenchymal hamartoma in an 8–month-old boy. Computed tomography shows a complex, mostly cystic tumor replacing most of an enlarged liver. Mild contrast-enhancement was evident in the solid component. (Courtesy of Luann Teschmacher, M.D., University of Rochester.)

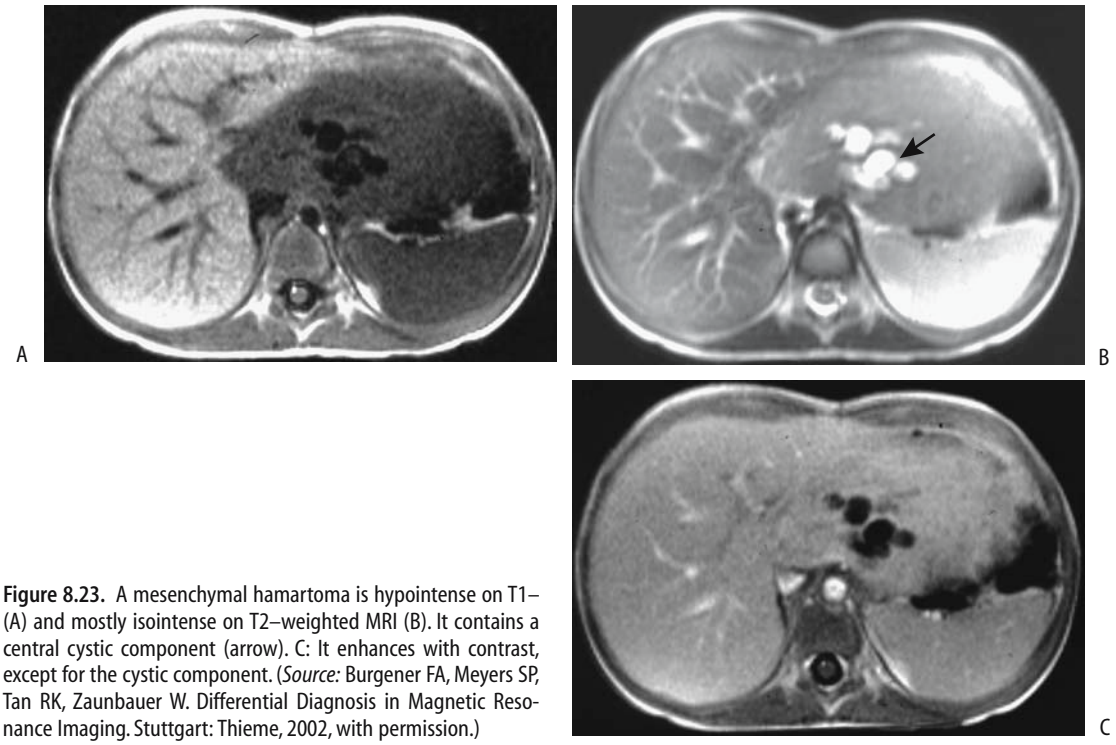

Figure 8.23. A mesenchymal hamartoma is hypointense on T1– (A) and mostly isointense on T2–weighted MRI (B). It contains a central cystic component (arrow). C: It enhances with contrast, except for the cystic component. (*Source:* Burgener FA, Meyers SP, Tan RK, Zaunbauer W. Differential Diagnosis in Magnetic Resonance Imaging. Stuttgart: Thieme, 2002, with permission.)

on MRCP than on T1-weighted images. They vary in enhancement postgadolinium, with some enhancing less than does normal liver tissue.

Angiography reveals both hypovascular and hypervascular tumors.

The imaging appearance in young children is similar to that seen with an undifferentiated embryonal cell carcinoma. In fact, some authors believe that a mesenchymal hamartoma represents a benign counterpart of an embryonal cell carcinoma.

Some intrahepatic hamartomas initially contain an enhancing rim, presumably representing compressed adjacent liver parenchyma, and superficially mimic the enhancing rim found with metastases. Hamartoma enhancement, however, does not progress centrally. The imaging differential diagnosis also includes hepatoblastoma and hepatocellular carcinoma. The presence of a cystic component in a liver tumor in children should suggest a hamartoma. Small liver cysts, not communicating with bile ducts and without renal involvement, also favor a diagnosis of hamartomas.

Fine-needle aspiration of these lesions tends to be nondiagnostic, and core biopsies are needed.

Other Nonneoplastic Tumors

Although uncommon, cholesterol polyps do develop within bile ducts.

A papilla of Vater lymphangioma is a rare cause of biliary obstruction.

Amputating neuromas develop after cholecystectomy. These are not neoplastic but rather reactive hyperplastic lesions.

Benign Neoplasms

Benign bile duct neoplasms consist roughly of an equal number of adenomas and papillomas, with other types being rare.

Adenoma/Papilloma/Papillomatosis

The terms *adenoma* and *papilloma* (and even *cholangioma*) are used loosely in the literature. Papillomatosis refers to multiple papillomas throughout the bile ducts and often also in the gallbladder. The pathologic classification of bile duct adenomas is somewhat arbitrary. While most pathologists simply classify them as tubular, papillary, or tubulopapillary, some adenomas appear to originate from peribiliary glands rather than from bile duct epithelium, and consist of a mass of disorganized but mature peribiliary gland acini and tubules, together with variable amounts of stroma, and thus should be classified as peribiliary gland hamartomas.

These tumors occur either singly or are multiple. Some secrete excessive amounts of mucus. They occur in both intra- and extrahepatic bile ducts and vary from several millimeters to several centimeters in size. Although a papilloma per se should be benign, histology often reveals cytologic atypia, and differentiation from carcinoma in situ and low-grade carcinoma is not always possible. An association exists between diffuse papillomatosis and cancer.

Most solitary adenomas appear on cholangiography simply as intraluminal polyps (Fig. 8.24). Papillary adenomas, if large enough, result in bile duct dilation due to their intralu-

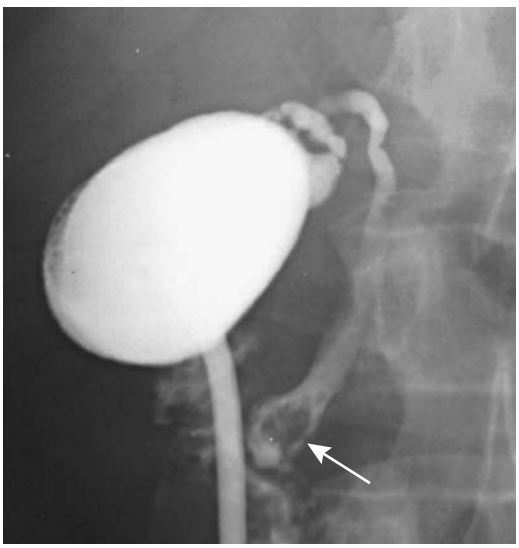

Figure 8.24. Common bile duct papilloma (arrow). Its imaging appearance is similar to a stone. (Courtesy of Daniel Wolfe, M.D., Williamsport, Pennsylvania.)

minal mass. Occasionally biliary dilation is secondary to excessive mucus secretion by these tumors, a characteristic but not pathognomonic finding. In papillomatosis the ampulla of Vater is dilated and contains mucin secretions, an appearance mimicking mucin-secreting pancreatic tumors.

Ultrasonography of papillomatosis shows small, multiple, nonshadowing, echogenic tumors adjacent to bile wall. The more proximal bile ducts tend to be dilated due to obstruction. Cholangiography reveals multiple intraluminal tumors.

These tumors enhance homogeneously after MR contrast.

The literature provides little guidance for therapy of extrahepatic papillomatosis. Some patients are managed conservatively with endoscopic follow-up.

Adenomyoma

A bile duct adenomyoma is rare. Imaging often suggests a carcinoma, and histology of a resected specimen is necessary to establish the diagnosis. Complicating this issue is the occasional benign adenomyoma undergoing malignant transformation and the patient presents with metastases.

Malignant Neoplasms

The vast majority of malignant bile duct neoplasms are adenocarcinomas (called *cholangiocellular carcinoma* and often abbreviated to *cholangiocarcinoma*) originating from biliary epithelium. Rarely seen are clear cell adenocarcinomas, mucinous adenocarcinomas, adenosquamous carcinomas, anaplastic carcinomas, squamous carcinomas, or undifferentiated carcinomas. Encountered in childhood are embryonal rhabdomyosarcomas (sarcoma botryoides).

Cholangiocellular Carcinoma

Cholangiocellular carcinoma develop throughout the bile ducts. The classification scheme adopted here divides cholangiocarcinomas into three anatomic locations: intrahepatic, hilar, and extrahepatic. These anatomic distributions reflect their somewhat different clinical presentation, differential diagnosis, and therapy. Perihilar ones are most common; resectability rate increases with a more distal location.

Clinical

A number of extrabiliary conditions are related to bile duct carcinoma (Table 8.6). Common duct stones distal to a cholangiocarcinoma are found in about 20% of patients. Coexisting gallbladder stones are common.

Cholangiocarcinomas tend to grow slowly and the initial clinical presentation with most porta hepatis and extrahepatic cholangiocarcinomas is jaundice due to major bile duct obstruction. An intrahepatic tumor only obstructs part of the bile flow, and thus jaundice is a late finding, after extensive tumor spread.

Most cholangiocarcinomas infiltrate locally and spread to adjacent lymph nodes, although distant metastasis is not uncommon late in the course. As one unusual example, metastatic cholangiocarcinoma to the testicle presented as a painless scrotal tumor (66).

Pathology

Histologically, cholangiocarcinomas range from undifferentiated to well differentiated, with the latter more common. Some are associated with an exuberant fibrotic reaction to the point that malignant cells are scant and the overall appearance mimics a benign stricture. Perineural invasion is common with proximal (towards the

Table 8.6. Conditions associated with cholangiocarcinoma

Sclerosing cholangitis
Clonorchiasis
Inflammatory bowel disease
Long-standing infectious cholangitis
Choledocholithiasis
Hepatolithiasis
Hemochromatosis
Choledochal cyst
Caroli's disease
Prior thorium dioxide (Thorotrast) use
Certain chemical exposure
Primary biliary cirrhosis (?)

liver) extrahepatic cholangiocarcinomas, but lymph node metastasis is more common with distal ones. Infiltrating tumors tend towards more frequent and extensive periductal spread than polypoid, nodular, or annular ones. Most cholangiocarcinomas are hypovascular.

A useful morphologic differentiation consists of papillary, nodular, and diffuse infiltrating types. A majority of papillary cancers are encountered in the common bile duct. Nevertheless, proximal extrahepatic cholangiocarcinomas tend to be more differentiated than more distal ones (towards the duodenum); the latter, often being moderately- to poorly-differentiated, tend towards an annular or infiltrating appearance.

Whether the rare bile duct carcinoma exhibiting adenosquamous features represents a variant of a hepatic adenosquamous carcinoma or is related to a more typical cholangiocarcinoma is conjecture.

Intrahepatic

Clinical

A peripheral (intrahepatic) cholangiocarcinoma is probably more common than reported. Many are misdiagnosed as a hepatocellular carcinoma or even a benign neoplasm. Also, not all intrahepatic tumors can be clearly categorized into distinct hepatocellular or cholangiocellular origins. Some are even misdiagnosed as metastatic adenocarcinomas. Fine-needle biopsies simply reveal adenocarcinomatous tissue, and a correct diagnosis is made in only about half of these tumors, while in others a metastatic adenocarcinoma is suggested.

Intrahepatic (peripheral) cholangiocarcinomas range from single to multicentric in origin. An occasional one grows intraluminally for varying lengths without major bile duct wall invasion. Also called a *malignant papillary neoplasm*, an intraductal component may or may not be identified by CT, depending on size (67). Diffuse infiltration predominates in others and can eventually even lead to acute hepatic failure. These intrahepatic tumors tend not to invade portal venous branches, although an occasional one invades the portal vein and leads to portal hypertension (68).

The most common presentation is abdominal pain, weight loss, and malaise. Jaundice is absent unless a tumor invades and destroys sufficient liver parenchyma. An almost constant finding is an elevated serum alkaline phosphatase level. Most of these tumors are rather invasive and often progress rapidly; an exception is with those exhibiting an intraluminal papillary growth pattern and these have a more indolent course.

Imaging

The use of earlier, less precise imaging suggested that with infiltrating tumors imaging could not suggest a specific diagnosis and that imaging findings of most intrahepatic cholangiocarcinomas were similar to those seen with a hepatocellular carcinoma or metastasis. Yet a number of findings, albeit subtle, do suggest a biliary origin. Thus considerably dilated more proximal bile ducts, due to obstruction, are found in about half of patients with an intrahepatic cholangiocarcinoma (69). A patent portal vein branch passing through a tumor is generally considered a sign of a benign lesion; an intrahepatic cholangiocarcinoma, however, often also contains a patent portal vein branch. Also, in distinction to hepatocellular carcinomas, most intrahepatic cholangiocarcinomas develop in a noncirrhotic liver. No capsule is identified. A few of these tumors develop calcifications. A minority grow primarily into the bile duct lumen. These intraluminal (papillary) intrahepatic bile duct carcinomas have rather nonspecific CT findings, but they are also associated with focal proximal intrahepatic bile duct dilation (70) (Fig. 8.25).

Cholangiography reveals obstruction and dilation of more peripheral bile ducts (Fig. 8.26). Only a rare cholangiocarcinoma infiltrates diffusely without occluding bile duct. An occasional tumor manifests with an irregular bile duct lumen, displacement, and multicentric involvement mimicking primary intrahepatic sclerosing cholangitis.

In most patients CT reveals a single, irregular, hypodense, nonencapsulated tumor of varying heterogeneity; contrast enhancement is generally evident, tending to be more pronounced in the tumor periphery, and, in fact, delayed postcontrast CT images are of value in differentiating an intrahepatic cholangiocarcinoma from a hepatocellular carcinoma. Hepatocellular carcinomas tend to have an early

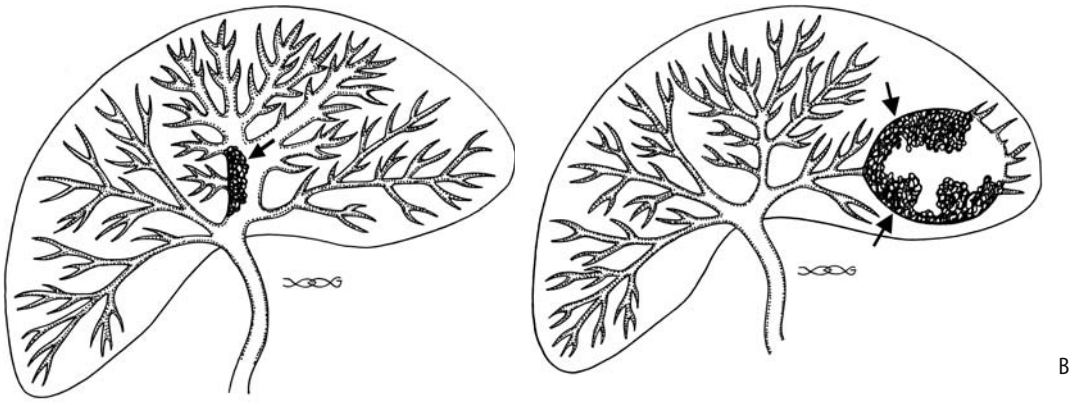

Figure 8.25. A: Diagram of intrahepatic cholangiocarcinoma (arrow) producing focal partial duct obstruction. B: A peripheral cholangiocarcinoma (arrows) has obstructed a left lobe duct resulting in a cavity mimicking an abscess.

enhancement peak followed by a gradual decrease, with the greatest tumor conspicuity during a delayed phase, several minutes after the start of contrast injection; on the other hand, with most cholangiocarcinomas the greatest conspicuity occurs during the portal venous phase, and tumor attenuation increases during the delayed phase. Such prolonged contrast retention is probably related to the fibrotic matrix associated with many cholangiocarcino-

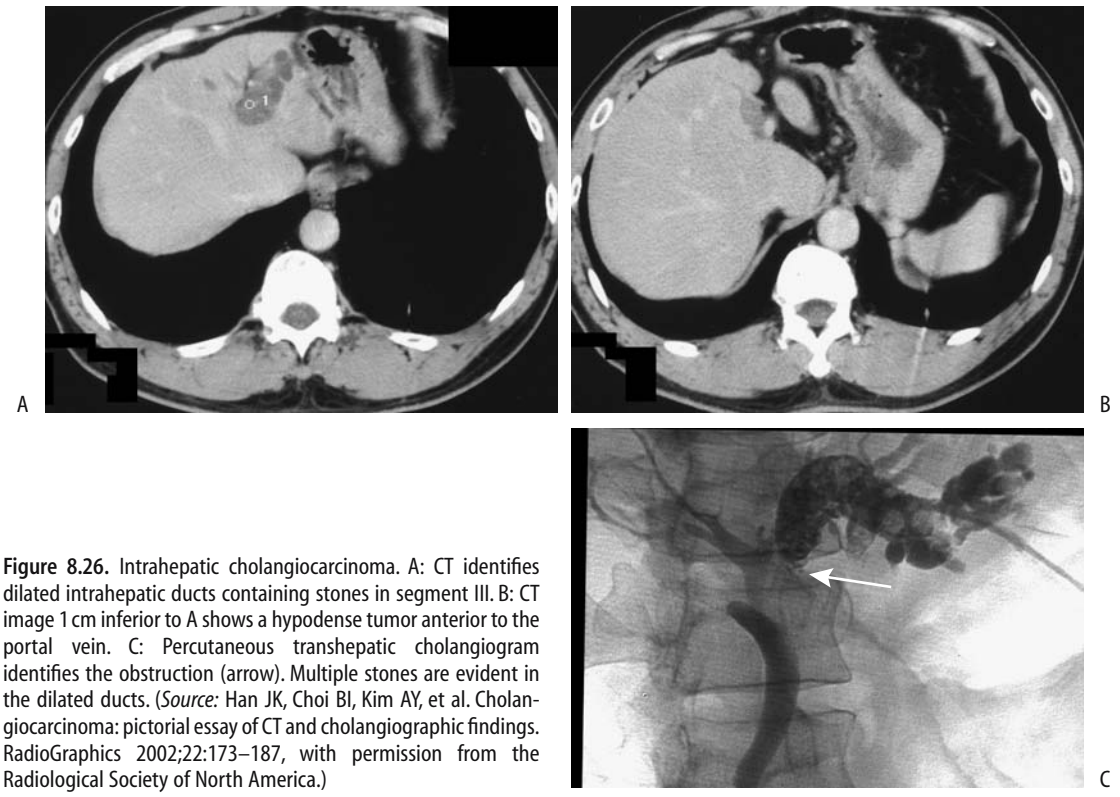

Figure 8.26. Intrahepatic cholangiocarcinoma. A: CT identifies dilated intrahepatic ducts containing stones in segment III. B: CT image 1 cm inferior to A shows a hypodense tumor anterior to the portal vein. C: Percutaneous transhepatic cholangiogram identifies the obstruction (arrow). Multiple stones are evident in the dilated ducts. (*Source:* Han JK, Choi BI, Kim AY, et al. Cholangiocarcinoma: pictorial essay of CT and cholangiographic findings. RadioGraphics 2002;22:173–187, with permission from the Radiological Society of North America.)

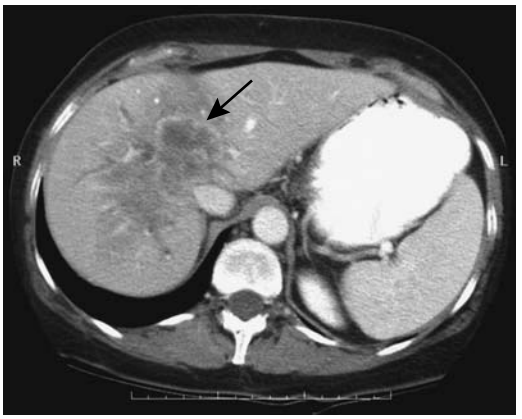

Figure 8.27. Intrahepatic cholangiocarcinoma. Contrast-enhanced CT identifies a poorly marginated tumor containing regions of necrosis (arrow). Dilated bile ducts are present in the medial segment of the left lobe and the right lobe. (Courtesy of Patrick Fultz, M.D., University of Rochester.)

mas. Exceptions, however, do occur, and a rare cholangiocarcinoma is not definable during any dynamic CT imaging phase (Fig. 8.27).

Ultrasonography reveals either a single nodule having irregular margins or additional satellite nodules. Most tumors are hypoechoic, although some contain hyperechoic regions.

Magnetic resonance imaging identifies intrahepatic cholangiocarcinomas as focal tumors, with some including a wedge-shape defect larger than the tumor itself, presumably secondary to surrounding edema and parenchymal compression, although an occasional infiltrating cholangiocarcinoma is intrinsically wedge-shaped. These tumors are mostly hypointense and occasionally isointense on T1- and variable in intensity on T2-weighted images; signal intensity on T2-weighted images depends mostly on the amount of fibrosis, necrosis, and secretions within the tumor. The occasional strongly hyperintense ones contain more secretions and necrosis. Postgadolinium enhancement varies considerably but often is progressive and moderate in extent and the intense immediate enhancement seen with many hepatocellular carcinomas is not evident. Postcontrast, some of these tumors show an enhancing rim, with progressive centrifugal filling of the tumor.

Some of these tumors encase adjacent vessels and result in focal liver atrophy and even a central scar. Central regions on T2-weighted images range from hypo- to hyperintense, with hypointensity reflecting fibrosis, a common finding with these tumors (69); postcontrast, these central hypointense regions range from homogeneous, to heterogeneous, to no enhancement, with fibrosis enhancing and necrotic regions not enhancing. None of the described findings is pathognomonic, and, with the exception of a dilated duct proximally, colorectal metastases often have a similar appearance.

Adjacent noninvolved liver parenchyma is hyperintense on T1-weighted images; the high signal intensity is not suppressed with fat saturation, and this tissue enhances postcontrast, findings probably related to fibrosis. Preliminary evidence suggests that ferumoxides improves visualization of intrahepatic cholangiocarcinomas (71).

An MRCP outlines bile ducts both proximal and distal to a tumor. Often multiple duct obstructions are detected. An MRCP can establish unresectability by showing extensive tumor spread.

Most of these tumors are hypovascular on angiography. Occasional arterioportal shunting is detected; a large tumor invades adjacent hepatic arteries and portal vein branches and can even invade the inferior vena cava. Hepatic artery invasion influences any planned resection, yet the accuracy of detecting hepatic artery invasion by CT and US is low. Multidetector CT angiography holds promise in detecting vascular invasion, but its specific role is not yet clear.

Occasionally an intrahepatic cholangiocarcinoma contains foci of sarcomatous transformation. One such cholangiocarcinoma containing malignant fibrous histiocytoma-like sarcomatous tissue was hypodense by CT; US showed a well-marginated, heterogeneous hypoechoic tumor, and MRI revealed a hypo- to isointense tumor on T1- and a heterogeneous appearance on T2-weighted images (72). The cholangiocarcinoma was hypovascular by angiography. Some of these sarcomatous tumors contain internal septa.

Therapy

Of 61 patients with an intrahepatic cholangiocarcinoma seen at the Mayo Clinic over a 31-year period, 46% underwent resection for cure

(73); survival at 3 years of those resected for cure was 60%. Survival of patients undergoing partial liver resection is significantly longer than of patients undergoing only drainage. An occasional patient survives long-term even if a tumor invades adjacent organs.

An orthotopic liver transplantation is performed in an occasional patient with a slow growing tumor, but 3-year disease-free survival after transplantation is only in the teen percents.

Arterial chemotherapy performed through an implanted port system appears to prolong survival of patients with unresectable intrahepatic cholangiocarcinomas (74).

Figure 8.28. Hilar cholangiocarcinoma (Klatskin tumor) with complete obstruction. A left duct puncture was performed and thus only the left lobe ducts are opacified.

Hilar (Klatskin Tumor)

Clinical

Carcinomas arising at or near the right and left lobe duct bifurcation were described by Klatskin in 1965, and these hilar cholangiocarcinomas often bear his name. Some authors refer to them as *central cholangiocarcinomas*. Why more cholangiocarcinomas occur at the liver hilum compared to other locations is not known. Most infiltrate diffusely and have a smooth, benign appearance, tend to spread along intrahepatic bile ducts, invade surrounding nerves and blood vessels, and produce multiple obstructions. Obstructed intrahepatic bile ducts dilate. Vascular encasement results in atrophy of involved segments. Distant metastases are uncommon.

Jaundice is the most common presentation. With asymmetrical involvement or only partial intrahepatic duct obstruction, often the only abnormality is an elevated serum alkaline phosphatase level.

Some of these patients develop segmental intrahepatic cholangitis; morbidity and mortality rates for these patients are significantly higher than for those without cholangitis. Preoperative transhepatic drainage of those intrahepatic bile ducts involved with cholangitis results in fewer complications after subsequent hepatic resection.

Imaging

Most Klatskin tumors present with diffuse infiltration and a narrowed bile duct lumen. Lumen involvement is best studied with cholangiography, either percutaneously or using an endoscopic approach. Often the right and left lobe ducts are infiltrated to the point that these ducts no longer communicate with each other (Fig. 8.28). An occasional tumor grows primarily intraductally and presents as a large expansile intraluminal mass. In general, however, although a cholangiogram can readily detect and diagnose these carcinomas, cholangiography cannot evaluate the full extent of tumor invasion.

Calcifications are uncommon in Klatskin tumors.

Unenhanced CT detects half or fewer of these hypovascular tumors. If identified, these hypo- to isodense tumors have poorly defined margins. Adjacent liver parenchyma often reveals a mottled appearance due to tumor infiltration. They are readily detected on hepatic artery dominant CT and a majority are identified on portal vein phase images. Most consist of an infiltrating stenosis; an exophytic tumor is less common and an intraluminal polyp is rare (Figs. 8.29 and 8.30).

Similar to other imaging, US reveals dilated intrahepatic bile ducts and normal caliber extrahepatic bile ducts, but the actual porta hepatis tumor typically is not identified; any visualized tumor has variable echogenicity and tends to be poorly marginated. Doppler US can evaluate portal vein involvement.

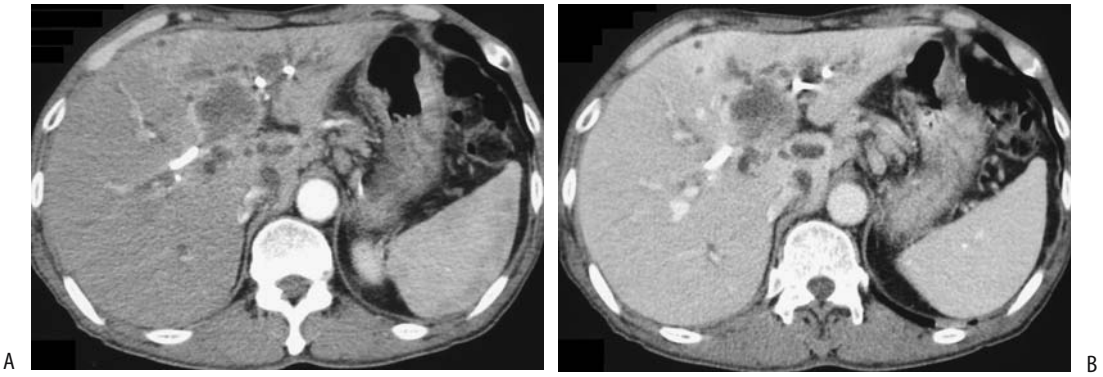

Figure 8.29. Hilar cholangiocarcinoma. Arterial- (A) and portal-phase (B) CT identifies a hypodense tumor. Catheters are in place in dilated intrahepatic ducts. (*Source:* Han JK, Choi BI, Kim AY, et al. Cholangiocarcinoma: pictorial essay of CT and cholangiographic findings. RadioGraphics 2002;22:173–187, with permission from the Radiological Society of North America.)

Magnetic resonance imaging reveals a hypointense tumor on T1- and variable intensity (mostly hyperintense) tumor on T2-weighted images, but due to their diffuse infiltration many of these tumors are difficult to detect with MR. A characteristic finding is that they enhance late with gadolinium and delayed images often show a hyperintense tumor not visible previously. Fat-suppression techniques allow easier differentiation from the often-present surrounding fat.

Although ERCP is often performed in these patients, it seldom establishes a diagnosis; full tumor extent and intrahepatic ducts generally cannot be evaluated.

Metastatic disease to the porta hepatis has a similar appearance. A metastasis should be considered if imaging reveals extensive adjacent lymph node involvement. Likewise, on occasion sclerosing cholangitis limited to the porta hepatis mimics a Klatskin tumor. Cavernous transformation of a thrombosed

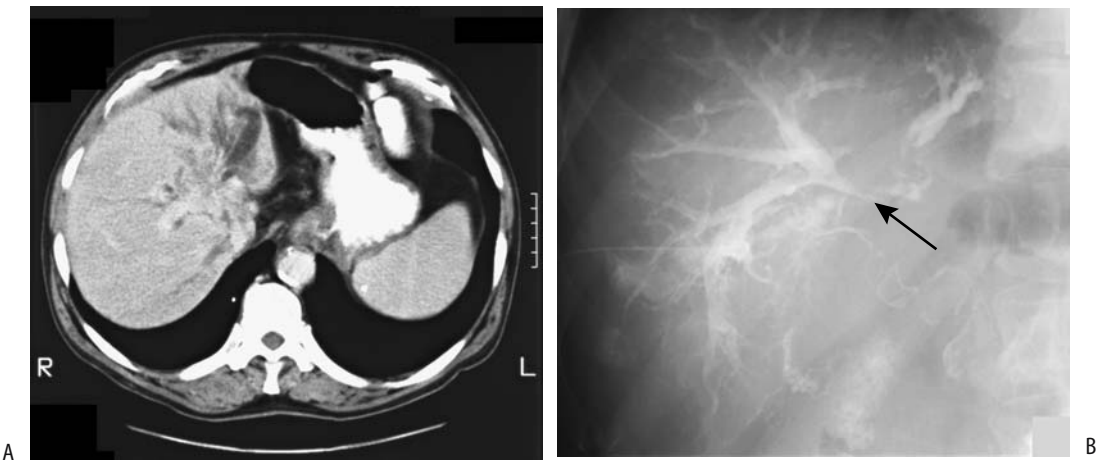

Figure 8.30. Hilar cholangiocarcinoma (Klatskin tumor). A: CT reveals dilated intrahepatic bile ducts. B: A percutaneous cholangiogram confirms obstruction at the porta hepatis (arrow). (Courtesy of Thomas Miller, M.D., San Luis Obispo, California.)

portal vein is occasionally also in the differential diagnosis.

Staging

Table 8.7 lists the TNM classification of extrahepatic bile duct tumors. Most imaging modalities tend to understage hilar adenocarcinomas; invasion of adjacent lymph nodes and liver infiltration often occur without significant imaging findings. Computed tomography is inaccurate in establishing resectability in these mostly unresectable tumors. With an extensive tumor, however, imaging studies correctly predict unresectability, and imaging thus is useful when evaluating potential resectability. If needed, intrahepatic spread is best studied with arterial portography. The primary role of angiography is to detect involvement of either the hepatic artery or the portal vein and their branches, although as already mentioned, multidetector CT angiography may supplant this role.

Percutaneous intraductal US can accurately T-stage these cholangiocarcinomas, but this technique is not widely available.

Imaging detects lobar atrophy, level of biliary obstruction, parenchymal invasion, or portal vein invasion. Both CT portography and US understage extrahepatic metastases, which are present at subsequent surgery in almost half of these patients. An MRCP is useful not only to identify an obstruction level but also as an aid in determining the extent of biliary ductal involvement and in planning drainage procedures.

Table 8.7. Tumor, node, metastasis (TNM) staging of extrahepatic bile duct tumors

Primary tumor:			
Tx	Primary tumor cannot be assessed		
T0	No evidence of primary tumor		
Tis	Carcinoma-in-situ		
T1	Tumor confined to bile duct		
T2	Tumor beyond wall of bile duct		
T3	Tumor invades liver, gallbladder, pancreas, and/or unilateral branch of portal vein		
T4	Tumor invades main portal vein, common hepatic artery, or adjacent structures		
Lymph nodes:			
Nx	Regional nodes cannot be assessed		
N0	No regional lymph node metastasis		
N1	Regional lymph node metastasis		
Distant metastasis:			
Mx	Distant metastases cannot be assessed		
M0	No distant metastasis		
M1	Distant metastasis		
Tumor stages:			
Stage 0	Tis	N0	M0
Stage IA	T1	N0	M0
Stage IB	T2	N0	M0
Stage IIA	T3	N0	M0
Stage IIB	T1	N1	M0
	T2	N1	M0
	T3	N1	M0
Stage III	T4	any N	M0
Stage IV	any T	any N	M1

Source: From the AJCC Cancer Staging Manual, 6th edition (2002), published by Springer-Verlag, New York, NY, used with permission of the American Joint Committee on Cancer (AJCC), Chicago, IL.

Therapy

Portal vein invasion and obstruction lead to parenchymal atrophy, and imaging detection of atrophy is thus presumptive evidence of such invasion. Hilar cholangiocarcinomas are generally considered unresectable in the presence of metastases, invasion of the right or left hepatic arteries or main portal vein branches, or extensive growth into adjacent liver parenchyma, although portal vein reconstruction is performed in some centers. Portal vein stent insertion is worthwhile in an occasional patient with portal vein invasion to treat portal hypertension with its associated bleeding complications.

If a hilar cholangiocarcinoma is resectable, a surgical intrahepatic anastomosis offers the hope of a cure. At times an extended right hepatectomy is necessary not only for tumor resection but also to resect undrainable segments.

A potential cure is possible with liver transplantation.

A biliary stent is left in place after resection or transplantation, providing access for follow-up cholangiography and serving as a useful landmark for follow-up imaging.

With an unresectable tumor, either percutaneous or endoscopic biliary stenting provides palliative drainage, relieves pruritus, and

improves quality of life. Percutaneous biliary drainage is technically successful in over 95% of patients. An advantage of percutaneous stenting is that access in then available to the often common associated intrahepatic obstructions. Some develop segmental obstructive cholangitis, which needs to be treated aggressively. Because these are generally slow-growing tumors, catheter drainage rather than stenting is often more appropriate. Also, in distinction to more distal bile duct stenting, endoscopic hilar stenting is more complex.

Controversy exists about whether palliative drainage should be of one or both liver lobes. A retrospective study of malignant hilar obstructions subdivided these patients into three groups (75): group A, one lobe opacified and same lobe drained; group B, both lobes opacified and both lobes drained; and group C, both lobes opacified but only one lobe drained. Among patients with more advanced lesions, median survivals of groups A, B, and C were 145, 225, and 46 days, respectively. The authors concluded that best patient survival is in those undergoing bilateral drainage and the worst survival is in those with both lobes opacified but with drainage of only one.

An extensive tumor can hinder stent insertion. At times endoscopic intraductal radiation therapy sufficiently recanalizes hilar cholangiocarcinoma strictures that a stent can be sequentially introduced. As an example of some of the therapy of unresectable hilar cholangiocarcinomas, five patients underwent percutaneous cholangiography, right and left internal biliary catheter drainage, intraductal brachytherapy using iridium 192 needles and endoprosthesis insertion, followed by external radiotherapy and chemotherapy (76); all patients had initial remission of jaundice, although eventually jaundice recurred in all and led to death, with a mean survival of 7.5 months, versus 1.75 months for 10 other unresectable patients undergoing only percutaneous drainage.

If an extensive tumor prevents stenting, a left lobe anastomoses to the stomach (hepaticogastric anastomosis) provides internal biliary diversion; fluoroscopic and endoscopic guidance are helpful.

The risk of abdominal wall tumor implantation is low after transhepatic biliary drainage in a setting of a hilar cholangiocarcinoma.

Extrahepatic

Clinical

At initial presentation not all patients with an extrahepatic cholangiocarcinoma are jaundiced and not all have abnormal liver function tests, although eventually jaundice, pruritus, and weight loss ensue.

Imaging

A typical appearance of an extrahepatic bile duct cholangiocarcinoma consists of a proximally dilated duct ending in an irregular, narrowed segment and a distal normal caliber duct. Most of these cholangiocarcinomas present as a focal stricture or a locally infiltrating tumor (Fig. 8.31). An intraluminal irregular polypoid appearance is less common. The appearance of most of these mucosa-originating cholangiocarcinoma is sufficiently different from the narrowing produced by a metastasis to adjacent lymph nodes to allow differentiation. The smoothly tapered common bile duct narrowing seen with pancreatitis likewise usually can be differentiated from an abrupt cutoff or *rat-tail*

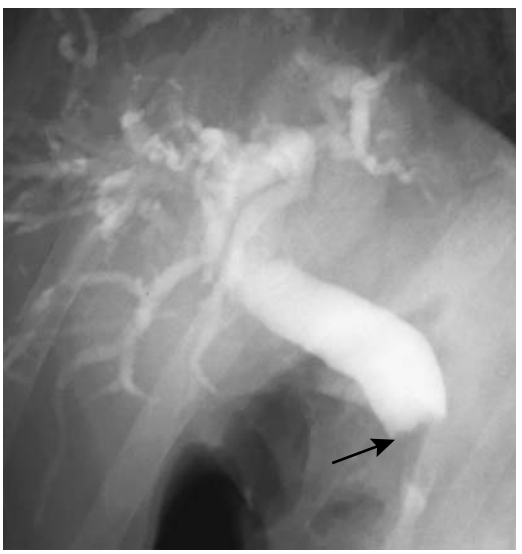

Figure 8.31. Cholangiocarcinoma obstructing mid-extrahepatic duct (arrow). The irregular proximal tumor margin argues against a pancreatic head carcinoma.

appearance characteristic of an infiltrating cholangiocarcinoma.

Endoluminal US of a malignant biliary stricture reveals asymmetrical irregular bile duct wall thickening. While such focal thickening is suggestive of a cholangiocarcinoma, it is not diagnostic.

These tumors are hypo- to isointense on T1- and iso- to mildly hyperintense on T2-weighted images. Postcontrast enhancement tends to be more pronounced during the venous phase.

A midextrahepatic cholangiocarcinoma infiltrating intramurally can spread to the gallbladder and mimic a gallbladder carcinoma. Included in the differential is also metastasis to adjacent pancreaticoduodenal lymph nodes and Mirizzi syndrome.

Staging

Patients with more distal extrahepatic cancer tend to have a better prognosis than those with more proximal ones. Over a 50% 5-year survival can be expected for patients with a resectable lower one-third bile duct tumor, at times even with positive nodes.

The pattern of lymphatic spread does vary by tumor location. Thus proximal extrahepatic cholangiocarcinomas tend to spread to common hepatic artery nodes rather than to the retropancreatic region, midextrahepatic tumors metastasize widely, including to paraaortic nodes, while distal tumors tend to involve nodes around the pancreatic head.

In patients with malignant obstruction, any hypoechoic, rounded lymph nodes or those with a conspicuous margin are generally assumed to be malignant with neural plexus invasion. CT reveals irregular masses extending medially toward the superior mesenteric and celiac arteries (77), findings presumably representing both neural invasion and desmoplastic reaction. Hepatoduodenal ligament invasion is detected by increased fat attenuation between the common bile duct and the proper hepatic artery (77).

Intraductal US has a role in staging not only cholangiocarcinomas but also other malignant biliary obstructions. Intraductal US detects adjacent pancreatic invasion. Aside from the pancreas, intraductal US is limited to hepatoduodenal ligament structures; it visualizes only a limited portal vein segment.

Percutaneous transhepatic cholangioscopy visualizes the duct mucosa and provides access for biopsies. Although biopsies do establish a diagnosis, whether staging is possible from biopsies is debatable; most biopsies are superficial and do not contain muscle or neural bundles.

Therapy

Some studies suggest that radiation therapy prolongs the survival of proximal cancer patients but has less influence on the survival of those with a more distal cancer, yet others have found that tumor location has no impact on survival.

A Whipple procedure is commonly performed for cholangiocarcinomas of the distal common bile duct.

Tumor seeding at a previous drainage site is an uncommon complication.

It is not clear what type of palliation is best with an unresectable tumor; nonoperative palliation appears to offer longer survival than surgical palliation. With stenting, patients with a distal biliary obstruction tend to survive longer and have more effective relief of jaundice than those with a more proximal obstruction. In general, endoscopic rather than percutaneous stenting is preferred for distal biliary strictures.

Intraluminal iridium-192 therapy followed by stenting appears to extend stent patency and increase survival in patients with inoperable cholangiocarcinoma. Intraluminal brachytherapy is performed using either a percutaneous transhepatic or a retrograde ERCP approach. Brachytherapy is often combined with external beam radiation therapy and chemotherapy.

In palliating malignant common bile duct obstruction, transhepatically inserted expandable metal stents appear superior to plastic stents.

Cystic Duct

A diagnosis of cystic duct carcinoma is rarely made. Undoubtedly these tumors are more common than reported, because most are indistinguishable from either a gallbladder carcinoma or carcinoma of adjacent bile ducts. These tumors are not associated with chronic chole-

cystitis and, in contradistinction to gallbladder carcinomas, are more often found in men.

Papilla of Vater Carcinoma

A carcinoma involving the papilla of Vater can originate from an adjacent duodenal mucosa, a papilla itself, a distal common bile duct, or even be pancreatic in origin. Biopsy simply reveals an adenocarcinoma. Because infiltration of surrounding structures is common, even a resected tumor often does not suggest a specific site of origin. These periampullary carcinomas are discussed in more detail in Chapter 3. Imaging findings range from a duodenal intraluminal irregular polyp, to diffuse infiltration of surrounding structures with little mass effect, to essentially a normal study with the only abnormality being common bile duct dilation (Fig. 8.32).

Magnetic resonance cholangiopancreatography has a limited role in evaluating papilla of Vater cancers; a carcinoma, benign stricture, edema from a recently passed stone, and even an impacted stone are difficult to differentiate.

Hepatocellular Carcinoma

Jaundice secondary to a hepatocellular carcinoma generally is a late finding, seen after extensive tumor infiltration throughout the liver.

An occasional hepatocellular carcinoma results in a spill of tumor debris into the bile ducts, growth as a tumor thrombus within the lumen, and, if the right and left lobe duct confluence or even the hepatic duct are involved, subsequent obstruction. Imaging reveals intraductal filling defects and proximal duct dilation. At times the bile ducts are encased by tumor. Cholangiography identifies bile duct obstruction.

A hepatocellular carcinoma is in the differential diagnosis if intrahepatic bile duct obstruction is identified and an adjacent tumor detected by CT. Magnetic resonance imaging likewise can detect an intrabiliary tumor or biliary obstruction by an adjacently located hepatocellular carcinoma.

Lymphoma/Leukemia

Primary bile duct lymphoma is very rare. It manifests as focal or diffuse bile duct wall thick-

A B

Figure 8.32. A: Obstructive jaundice caused by a poorly differentiated adenocarcinoma. A dilated common bile duct ends at the papilla (arrow). No tumor was identified either with CT or a barium study. B: Another patient with dilated bile ducts secondary to a primary papilla adenocarcinoma; imaging could not identify a tumor.

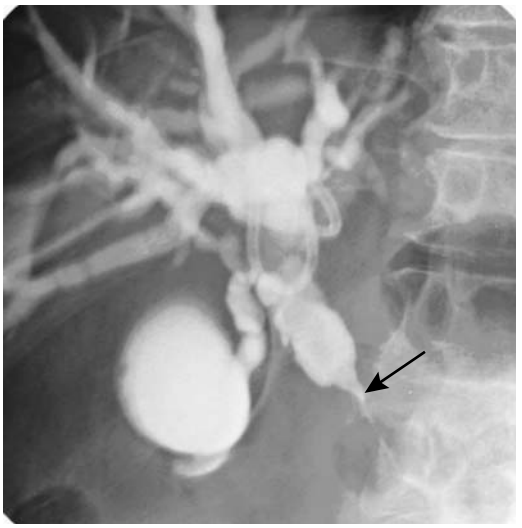

Figure 8.33. Lymphoma obstructing the hepatic duct (arrow) distal to the porta hepatis. A pancreatic head carcinoma can have a similar appearance.

ening without adenopathy; the imaging appearance mimics a cholangiocarcinoma (78). Systemic non-Hodgkin's lymphomas obstruct bile ducts by extrinsic compression from involved adjacent lymph nodes, most often in the porta hepatis (Fig. 8.33). Only rarely does a lymphoma infiltrate the bile duct wall to the point of obstruction. Thus obstructive jaundice secondary to Hodgkin's disease is rare. A rare primary hepatic B-cell lymphoma of MALT results in a periportal lymphoid infiltrate and bile duct epithelial involvement to the point of mimicking cholangitis (79).

Anecdotal reports suggest that porta hepatis lymphomas are better defined by MRI than by cholangiography, CT, or US.

Sarcoma

Biliary stromal origin neoplasms are rare. A differentiation between benign tumors and their sarcomatous counterparts is difficult at best, and from an imaging viewpoint an attempt at such distinction generally makes little sense.

The most common biliary stromal tumors are leiomyomatous in origin, with an occasional myoblastoma being reported. Hepatobiliary sarcomas, with the exception of embryonal rhabdomyosarcoma, are discussed in Chapter 7; most of these sarcomas (and their benign counterparts) are intrahepatic in location, and distinguishing whether they are of liver parenchymal or bile duct origin is not possible.

Embryonal rhabdomyosarcomas originate in bile duct submucosa, occur mostly in extrahepatic bile ducts, and are more common in young children. Histologically, they are similar to rhabdomyosarcomas (sarcoma botryoides tumors) found in the vagina and bladder. They tend to invade locally. These are aggressive tumors, and metastases are not uncommon at first presentation. Imaging reveals an intraluminal, soft tissue density, bulky tumor. Necrosis is evident within larger ones. Ultrasonography of some shows a "Swiss cheese" type of appearance. Cholangiography can be diagnostic if it shows intraluminal grape-like tumor clusters. Imaging findings are not pathognomonic; however, they are suggestive when seen in young children.

Melanoma

Primary bile duct melanoma is sufficiently rare that only a few have been reported. Most patients with metastatic melanoma have been middle-age men presenting with obstructive jaundice. Metastatic melanoma is considerably more common in the gallbladder than bile ducts.

Imaging shows dilated proximal bile ducts (Fig. 8.34). Ultrasonography identifies a hyperechoic tumor, similar to other metastases.

Metastases/Invasion to Bile Ducts

Jaundice is common in a setting of advanced gastric carcinoma. Jaundice is usually secondary to metastasis to hepatoduodenal ligament lymph nodes, with biliary obstruction being at the extrahepatic duct level (Fig. 8.35).

Jaundice in a setting of breast carcinoma is usually secondary to widespread liver metastases. In a minority of patients, similar to those with metastatic colon cancer, jaundice is due to extrahepatic intraductal metastasis or metastasis to adjacent lymph nodes (Fig. 8.36). These latter patients, with limited survival, are amenable to stenting for relief of jaundice.

Figure 8.34. Common bile duct obstruction by metastatic melanoma.

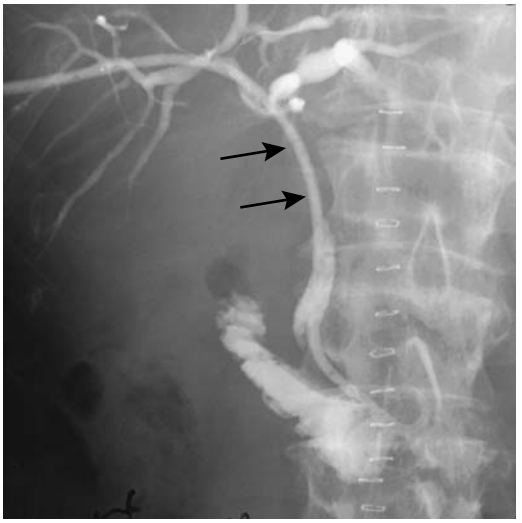

Figure 8.36. Long hepatic duct obstruction (arrows) due to an adenocarcinoma, believed to be secondary to colon cancer resected 5 years previously.

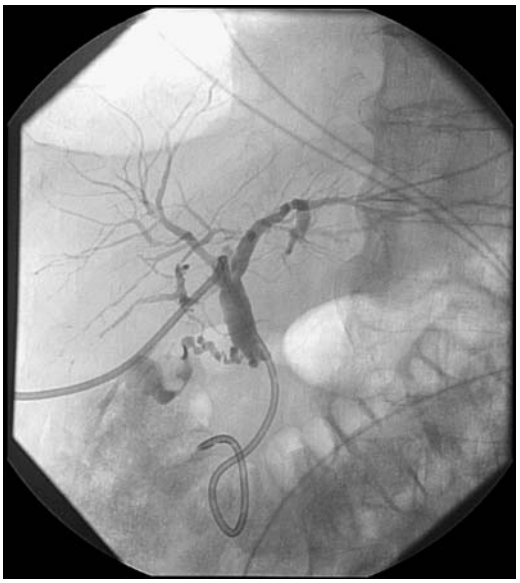

Figure 8.35. Common bile duct obstruction. This patient had colon cancer resected previously, now was believed to have metastases to the pancreaticoduodenal nodes and a bypass catheter was inserted to control jaundice. A cancer in the pancreatic head would have a similar appearance. No follow-up was available. (Courtesy of David Waldman, M.D., University of Rochester.)

Metastasis to the peripapillary region is most often due to pancreaticoduodenal node involvement and secondary obstruction of adjacent bile duct (Fig. 8.37). Rarely metastatic colon carcinoma results in focal intrahepatic bile duct dilation due to intraluminal tumor growth (80); these mimic the appearance of a cholangiocarcinoma.

Therapy of Malignant Obstruction

Preoperative Drainage

Considerable controversy exists whether preoperative percutaneous transhepatic biliary drainage in a clinical setting of obstructive jaundice has a role. Preoperative drainage is more common in Japan than in North America or Europe. On a routine basis, many United States surgeons have abandoned preoperative drainage. In general, preoperative biliary drainage is useful in malnourished patients or in those with suppurative cholangitis. Also, occasionally preoperative drainage aids the surgeon by identifying bile ducts, especially in a setting of extensive fibrosis.

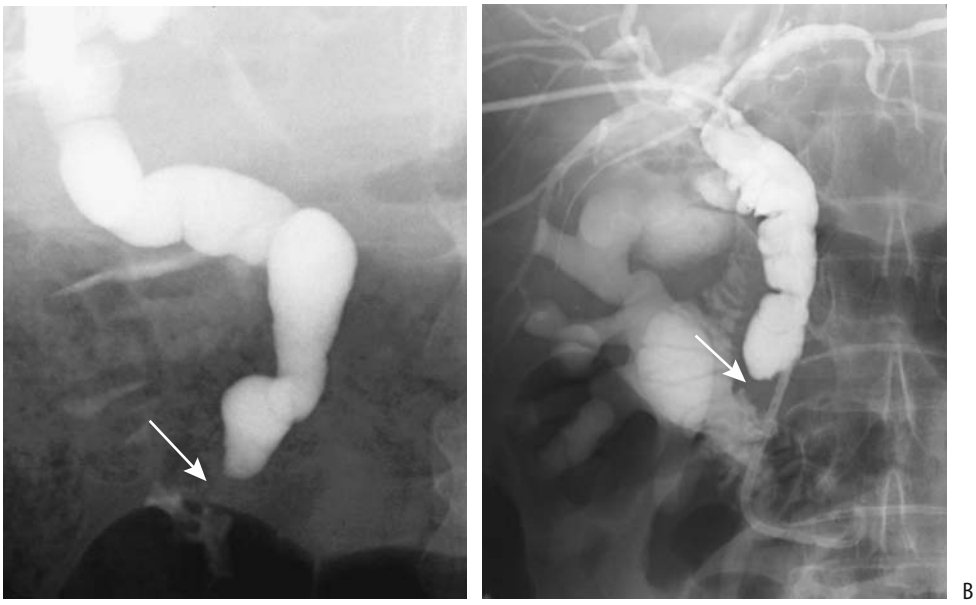

Figure 8.37. A: Obstructive jaundice caused by a metastatic colon carcinoma (arrow). The appearance is similar to a primary papilla carcinoma. B: Obstructive jaundice secondary to metastatic ovarian carcinoma.

Percutaneous biliary drainage is a technically complex procedure requiring considerable skill and is associated with specific complications. The presence of a catheter presumably promotes infection, but overt cholangitis is uncommon as long as catheter patency is ensured. Other acute complications associated with drainage include hemorrhage and sepsis. Catheter or stent obstruction and dislodgment occur as long-term complications.

Palliation

In a setting of either primary or metastatic bile duct obstruction, palliative biliary drainage, either external or internal, can be established using a surgical, percutaneous, or endoscopic route. The exception is with lymphoma, where radiotherapy has a role. Surgical biliary drainage (choledochojejunostomy) is appropriate if additional surgical procedures, such as a gastric bypass, are also deemed necessary. The choice between percutaneous or endoscopic drainage is somewhat arbitrary and often revolves around availability and patient referral. In either case, whether to stent a jaundiced patient with an inoperative cancer is individualized. With some cancers, the presence of distal metastases is a limiting factor in patient survival, rather than whether the bile ducts are obstructed or not.

Internal biliary stents provide drainage without an external drainage device. Successful jaundice palliation can be achieved using self-expandable wire mesh stents and plastic stents. Compared to surgical palliation, stenting results in similar morbidity and mortality; however, patients require a shorter hospital stay. Good palliation can be achieved in most patients.

Stent migration occurs with straight stents; migration is not common with wire meshes. Long-term complications of mesh stents include stent occlusion and cholangitis. Most stent occlusions are caused by granulation tissue, bile sludge, and tumor overgrowth rather than by ingrowth. In an uncovered stent an irregular outline develops on the inner surface due to

granulation tissue overgrowth. Overall, self-expandable endoprostheses have achieved good results and good long-term patency. Patients with a cholangiocarcinoma and gallbladder carcinoma tend to have better results than those with a pancreatic carcinoma or metastatic carcinomas.

After endoscopic plastic biliary stenting, the most common long-term complication is stent clogging. To decrease the risk of obstruction, some endoscopists institute nasobiliary drainage after stent placement.

A transjugular, transvenous approach can be used for biliary catheterization if neither an endoscopic approach nor transhepatic drainage is feasible.

Cystic Neoplasms

Discussed here are hepatobiliary cystadenomas and cystadenocarcinomas, most are biliary in origin. Other cystic, intrahepatic structures are discussed in Chapter 7.

Clinical

Little distinguishes a biliary cystadenoma from a cystadenocarcinoma either clinically or radiologically. Most arise within the liver, with only an occasional one originating from extrahepatic bile ducts. Similar tumors also arise in congenital liver cysts and in the hepatoduodenal ligament.

These rare tumors occur mostly in middle-age women. The benign variety is considered premalignant; even if resected, a high recurrence rate is evident.

Histologically, biliary cystadenomas are similar to mucinous cystic tumors found in the pancreas and ovaries. They have a fibrous capsule, internal septations, and varying degrees of nodularity, findings identified with imaging. These tumors contain nonbilious, at times mucinous, fluid. Histologically, most cystadenocarcinomas, especially mucin producing ones, are well differentiated. Pathologic differentiation of benign from malignant is rather subtle and involves gauging the degree of cellular atypia.

Some cystadenomas and carcinomas contain mesenchymal stroma. Tumors containing ovarian-type stroma appear to have a better prognosis than those that do not; imaging, however, cannot detect this type of stroma. Some patients also develop a synchronous ovarian cystadenoma or gastric carcinoma, presumably due to a common histogenetic pathway.

An occasional biliary cystadenoma grows large without producing symptoms. An abdominal mass, pain, obstructive jaundice, or even ascites are presenting findings. Some are discovered incidentally. Passage of tumor fragments from a cystadenoma communicating with bile ducts can result in biliary obstruction and obstructive jaundice.

An elevated serum tumor marker CA 19-9 is found with some, especially those containing mesenchymal stroma, but a normal serum level does not exclude a cystadenoma or cystadenocarcinoma. Carcinoembryonic antigen (CEA) and α-fetoprotein levels tend to be normal.

Differential diagnosis includes other cystic liver neoplasms, benign cysts, and, for extrahepatic lesions, pseudocysts and even gastroduodenal duplication cysts. These tumors have been mistaken for and treated as hepatic hydatid cysts.

Imaging

A cystadenoma has imaging findings similar to those of nonneoplastic hepatic cysts. Computed tomography and US show a multicystic tumor containing septations. Their appearance is rather characteristic, with both benign and malignant versions having a similar appearance, although septa without nodularity suggest a benign cystadenoma, and septations with nodularity point to a carcinoma. Computed tomography shows mostly water attenuation fluid within the cyst, although attenuation values differ depending on the amount of cholesterol, blood, and necrotic tissue present. Calcifications within either the septa or the rim are seen on rare occasion. Tumor nodules and septa enhance postcontrast.

Ultrasonography reveals an anechoic tumor, identifying internal septations in some. Hemorrhage leads to a hypoechoic appearance.

A fluid–fluid level may be present. Tumor nodules are hyperechoic. Transabdominal US differentiates only with difficulty between a solid tumor containing cystic components and a fluid collection. Both tend toward a hypoechoic appearance. Color Doppler US is useful in detecting blood flow within a malignant cystic tumor. Obviously, no flow is seen in benign fluid collections.

These tumors are hypointense on T1- and hyperintense on T2-weighted images. Mucin and hemorrhage increase their T1-weighted signal intensity. An occasional tumor is markedly hyperintense on T1- and hypointense on T2-weighted MR images, generally due to thick, proteinaceous mucinous fluid. Any septations are readily identified.

Some of these tumors communicate with the bile duct lumen, best identified with cholangiography, and bile cytology is helpful in these tumors.

Occasionally percutaneous transhepatic cholangioscopy provides a biopsy path for these tumors and defines the underlying biliary anatomy.

Mucin-Hypersecreting Tumors

So-called mucinous, ductectatic, or mucin-hypersecreting hepatobiliary cystadenomas, cystadenocarcinomas, or cholangiocarcinomas produce massive amounts of mucin within markedly dilated bile ducts. Whether these mucinous tumors are a variant of cystadenomas and cystadenocarcinomas or whether they represent a separate entity is speculation. Complicating the issue is that an occasional biliary cystadenoma secretes excess mucin and mimics an intrahepatic cyst; at times one even contains daughter cysts. The carcinomas invade hepatic parenchyma and vessels. At times widespread metastases are evident.

Their histopathologic features are similar to those of mucin-producing pancreatic duct tumors, and mucous lakes often contain adenocarcinoma cells. A frond-like papillary architecture predominates, often containing elements of dysplasia, adenoma, and carcinoma in the same tumor.

Excess mucin secretion is a rare cause of markedly dilated bile ducts distal to a tumor. Similar to their pancreatic counterparts, some result in excess mucin draining from the duodenal ampulla; or, excess mucin simply results in obstructive jaundice. An occasional tumor contain calcifications.

A rare peripheral intrahepatic tumor results in duct perforation and spill of mucin and tumor cells—a rare cause of pseudomyxoma peritonei.

Smaller tumors are not detected by imaging, and the only abnormality consists of dilated, mucin-filled ducts. Dilated bile ducts distal to the tumor are readily imaged. Cholangiography shows large intraluminal masses, a result of mucin retention. At times the duct lumen appears narrowed because only a small channel is left for bile and contrast flow. Nevertheless, every effort should be made to detect a tumor.

Mucin has a similar appearance to bile with both CT and MR, except when thick and proteinaceous, when it tends to be hyperintense on T1- and hypointense on T2-weighted MR images. Cholangiography identifies mucin as linear or elongated intraductal filling defects. These tumors are hypodense on CT and show little arterial-phase contrast enhancement; peripheral enhancement and internal septations tend to be more evident during equilibrium phase imaging (Fig. 8.38). They are hypointense on T1- and hyperintense on T2-weighted MRI.

Neuroendocrine

A bile duct granular cell tumor is rare. It is of Schwann cell origin and tends to occur at the juncture of two ducts, such as the hepatic and cystic ducts. It is most common in young women.

Cholangiography reveals a smooth stricture similar to that seen in sclerosing cholangitis. The US appearance can mimic a stone.

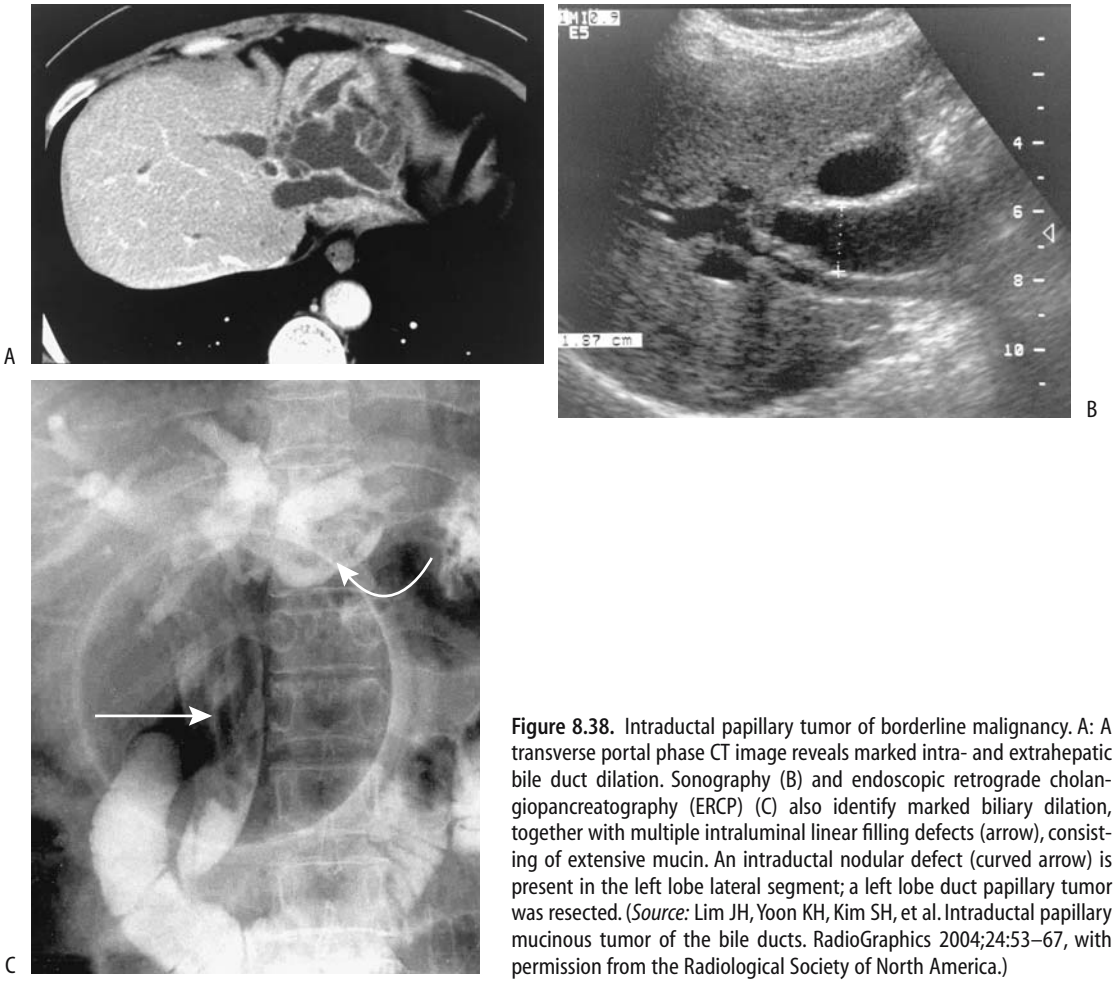

Figure 8.38. Intraductal papillary tumor of borderline malignancy. A: A transverse portal phase CT image reveals marked intra- and extrahepatic bile duct dilation. Sonography (B) and endoscopic retrograde cholangiopancreatography (ERCP) (C) also identify marked biliary dilation, together with multiple intraluminal linear filling defects (arrow), consisting of extensive mucin. An intraductal nodular defect (curved arrow) is present in the left lobe lateral segment; a left lobe duct papillary tumor was resected. (*Source:* Lim JH, Yoon KH, Kim SH, et al. Intraductal papillary mucinous tumor of the bile ducts. RadioGraphics 2004;24:53–67, with permission from the Radiological Society of North America.)

Biliary Stones

Clinical

The prevalence of gallstones varies by sex, age, and population makeup. Native Americans have an extremely high prevalence of gallstones, with most stones consisting of cholesterol. Gallstones do occur in the pediatric population.

The prevalence of both gallbladder stones and bile duct stones is greater in pregnant women than in controls. The prevalence of choledocholithiasis in pregnancy is approximately 1 in 1200 deliveries. If needed, surgical exploration is performed, although therapeutic ERC is an alternative.

Fetal cholelithiasis is very rare. Little is known about the sequelae of this poorly understood condition. Ultrasonography identifies multiple, small hyperechoic foci without distal shadowing; these clear shortly after birth.

Gallbladder volume in diabetics is larger than in controls, and they have a severalfold increased prevalence of cholesterol stones. Diabetics with autonomic neuropathy have reduced gallbladder motility, thus promoting stasis and cholesterol crystal formation. Patients with hereditary spherocytosis are at increased risk for gallstones.

Somatostatin inhibits gallbladder emptying. A somatostatinoma or therapy with somatostatin analogues is associated with an increased

risk for gallstones. Gallbladder emptying is reduced in patients with cholesterol gallstones.

Although an occasional patient has only bile duct stones and no gallbladder stones, most stones are of gallbladder origin. Primary bile duct calculi develop in a setting of strictures, cholangitis, choledochal cyst, or a congenital condition such as Caroli's disease.

A foreign body in the extrahepatic bile ducts acts as a nidus for stone formation. Case reports describe suture material and surgical clips acting as a nidus. Clip migration from its original position is occasionally diagnosed from serial conventional abdominal radiographs. Computed tomography or cholangiography confirms the diagnosis. Sphincterotomy and clip or stone extraction should be curative.

An association among initial gallstones, cholecystectomy, and subsequent development of colorectal cancer has been raised. Currently no definitive conclusions can be drawn; some studies suggest no association, other studies suggest a relationship, while still other studies suggest such an association only in women.

Gallbladder sludge probably is a factor in subsequent gallstone formation. Still, the presence of sludge is generally not believed to represent underlying gallbladder disease.

Cystic duct anatomy has been implicated in stone formation. Comparing ERC in patients with and without gallstones, stone formers have significantly longer and narrower cystic ducts than those without stones (81); also, the angle between the gallbladder and cystic duct is more acute in those with gallstones than those without.

Stone Composition

Calculi range from single to multiple, large to small, round, oval, or faceted. They contain primarily cholesterol, pigment, or a mixture of cholesterol and pigment. Pigmented stones contain a high proportion of bilirubin and tend to be considerably smaller than cholesterol stones. If a stone contains sufficient calcium to be visible with conventional radiography, it contains a predominance of pigment rather than cholesterol. Central calcifications also point toward pigment composition. In general, the composition of multiple gallstones within one gallbladder is similar, but exceptions occur.

An inverse correlation exists between CT attenuation and cholesterol content and a direct correlation among pigment contents, inorganic calcium salts, and total calcium content (82); most cholesterol stones are hypodense, but in practice many stones are mixtures. Stones containing more than about 3% calcium are hyperdense.

Oral cholecystography suggests cholesterol composition if stones are radiolucent; if multiple stones without calcification are present, they are large or have a calcified rim. Similar signs are also useful with CT to determine gallstone composition.

Only a rare stone has a specific gravity less than that of bile and thus floats in bile. Ultrasonography thus rarely detects a floating stone. On the other hand, with iodinated contrast within the gallbladder, stones composed primarily of cholesterol are buoyant. Presumably iodine increases bile-specific gravity sufficiently so that cholesterol stones float. Thus the most reliable sign of cholesterol stones with an oral cholecystogram is buoyancy. This effect of iodine upon buoyancy can also be shown with US if the examination is done after administering an appropriate oral contrast agent; with sufficient contrast in the gallbladder, cholesterol stones float.

Primary bile duct stones (i.e., stones that form in bile ducts) are pigmented.

A rare gallstone contains a drug. Specific drugs include ceftriaxone, glaphenine, and dipyridamole.

Cholecystolithiasis

Imaging

Most radiologists believe that CT is inferior to US in visualizing stones in the gallbladder. The CT appearance of a gallstone depends on its cholesterol and calcium content and ranges from that of a hypodense defect surrounded by bile, to isodense to bile and thus not visible, to an obvious calcification.

Ultrasonography should detect almost all gallbladder calculi, with detection depending on stone size rather than composition. An intraluminal, mobile, echogenic mass detected by US and associated with posterior acoustic shadowing is virtually pathognomonic for a calculus. A gallbladder filled with stones results in a hyper-

echoic tumor superficially mimicking gas-filled bowel; a porcelain gallbladder has a similar appearance. A diagnosis of stones should be made with caution in the absence of acoustic shadowing, although shadowing is absent with small calculi. Shadowing is not dependent on presence of calcifications. Sludge is mobile but generally does not have posterior shadowing. Sludge can be inhomogeneous in appearance.

Intravenous cholangiography also detects most gallbladder stones, but less than with US.

One study detected 96% of stones with 3-D fast SGE and single-shot SE MR sequences (83); a prevalent view among some MR enthusiasts is that MRI is superior to US in detecting subtle gallstones, yet the relationship between stone composition and its MR signal intensity is poorly understood. Magnetic resonance imaging reveals most gallbladder stones as round or faceted signal void (hypointense) structures on both T1- and T2 spin-echo (SE) images surrounded by the higher signal intensity bile. Some stones contain hyperintense foci on both T1- and T2-weighted sequences. An occasional stone is hyperintense on T1-weighted sequences. Stones do not enhance postcontrast, allowing differentiation from polyps.

Cholescintigraphy is insensitive in detecting gallbladder stones. Adjacent bowel compressing the gallbladder may mimic a gallstone.

Therapy

A percutaneous cholecystostomy tract can be used for gallbladder access for stone dissolution using methyl-tert-butyl ether, stone fragmentation, or stone extraction. Most of these procedures have been supplanted by laparoscopic cholecystectomy, although they still have a place in select, poor surgical risk patients.

Most medical therapies for gallstones are effective with cholesterol stones only. Therefore, prior to such therapy cholesterol stones must be distinguished from pigmented gallstones, keeping in mind that overall over 80% of radiolucent stones are composed primarily of cholesterol.

Lithotripsy

Extracorporeal shock-wave lithotripsy (ESWL) is used in select centers to shatter gallbladder stones. In general, fragments smaller than 3 mm in diameter pass spontaneously. Extracorporeal shock-wave lithotripsy achieves 65% to 85% clearance at 3 years, with success rate being inverse to stone volume and stone size. Patients with a single stone have significantly higher clearance rates and lower recurrence rates than those with multiple stones.

For stones with a CT density of <50 HU, stone clearance can be achieved in most patients, but with a density of >100 HU only a minority of patients are completely cleared. About a third of patients have posttherapy side effects such as biliary colic. Fragment impaction at the papilla of Vater can result in pancreatitis and require sphincterotomy. Complication rate increases with larger fragments.

In some centers ESWL is combined with bile acid dissolution therapy (oral ursodeoxycholic acid), although the value of adjuvant bile acid therapy is not clear.

Cholescintigraphy shows better fragment clearance associated with a higher gallbladder ejection fraction and a larger gallbladder discharge volume than in patients who retain stone fragments.

Cholecystolithotomy

High-risk patients with acute calculus cholecystitis can be treated by percutaneous cholecystostomy followed by cholecystolithotomy. After initial percutaneous gallbladder puncture and drainage, the tract is dilated and stones are extracted. Usually an interval of 4 to 6 weeks is allowed between initial gallbladder puncture and eventual dilation and stone removal to allow tract maturation. Large stones are crushed using a wire basket technique.

Cholecystolithotomy success rate of clearing gallstones is over 80%. These patients are left with an intact gallbladder and initially without gallstones. After such percutaneous stone removal, recurrent gallstones and biliary sludge are common.

Dissolution

Gallstone dissolution is feasible through direct contact with methyl-tert-butyl ether or similar substances instilled via an appropriate catheter,

and is performed in a number of European centers. Usually US is used for catheter guidance. In a multihospital European study of 803 patients, puncture was successful in 95% and in those with successful puncture stones were dissolved in 95% (84); residual sludge remained in 44% of gallbladders. The most severe complication was bile leakage in 1.6% of patients, treated with a cholecystectomy.

Once gallstones are dissolved with methyl-tert-butyl ether, patients generally undergo long-term bile acid therapy. Cessation of adjuvant bile acid therapy leads to a recurrence of stones. The 5-year stone recurrence rate is about 40% for solitary stones and 70% for multiple stones (116).

Ethyl propionate, a C5 ester, has also been used to dissolve cholesterol gallstones; clinical experience with this agent is limited.

At times an opacified rim appears in a gallstone during chemolitholysis; it consists of calcium carbonate.

Bile acid therapy is also used to dissolve gallstones. Not all gallstones, however, dissolve. Most hypodense or isodense stones respond to bile acid therapy, while those with laminated or rimmed calcifications rarely do. Thus *in vivo* CT analysis of gallstones can predict the response to bile acid therapy.

Choledocholithiasis

Biliary Colic

Biliary colic is a clinical description of the severe pain experienced by patients with biliary obstruction by stones. Sphincter of Oddi spasm also plays a role in this condition because manometry reveals significantly higher pressures during a biliary colic attack.

Gallbladder volume during biliary colic is several times greater than during the postcolic state.

Preoperative Detection

Early published sensitivities for detecting choledocholithiases with CT and transabdominal gray-scale US have been up to 90%, although most later studies report considerably lower sensitivities. Computed tomography with thin collimation and data acquisition in a single breath-hold should prevent misregistration. However, a number of bile duct stones are isodense to bile and thus not detected, a situation differing from urinary stones where even radiolucent stones are visible with CT. Specificity, however, is >90% for both CT and US. In a study of patients with suspected choledocholithiasis, the sensitivities for detecting choledocholithiasis were 65% for unenhanced CT, 92% for oral contrast-enhanced CT cholangiography (using iopanoic acid), and 96% for MRCP (85); the specificities did not differ significantly. It is because of this low CT sensitivity that unenhanced CT has never achieved the popularity it has reached with ureteral stone detection, having been supplanted initially by ERC and now by MRCP, which has a stone detection accuracy similar to that of ERC.

Although US detects only some bile duct stones, it does have a role prior to laparoscopic cholecystectomy. In a study of open cholecystectomy with routine intraoperative cholangiography for cholelithiasis, the most important preoperative predictor of bile duct stones was US detection of a dilated common bile duct (86); the authors defined three levels of risk:

1. Low: common bile duct not dilated; prevalence of bile duct stones was 1.5%
2. Moderate: dilated common bile duct but normal liver function tests; prevalence of stones was 49%
3. High: both dilated common bile duct and abnormal liver function tests; prevalence of stones was 67%

One recommendation is that ERCP should be performed if the common bile duct diameter is more than 6 to 7 mm for possible stone extraction. Yet dissenting voices are also heard. Thus among consecutive patients undergoing laparoscopic cholecystectomy in a single surgical unit, 10% had stones and almost half of patients with stones had small ducts (<6 mm as measured by preoperative US) (87); the author cautions that a preoperative US finding of a nondilated common bile duct does not imply the absence of stones.

In an occasional patient noninvasive studies are inconclusive; ERCP similarly is inconclusive or contraindicated and percutaneous cholan-

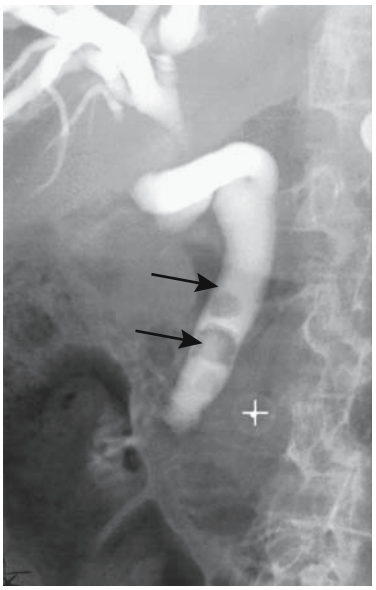

Figure 8.39. Common bile duct stones (arrows) in a jaundiced patient with dilated ducts.

giography is necessary if the diagnosis is in doubt (Fig. 8.39).

Computed Tomography

Computed tomography shows most extrahepatic bile duct calculi to be of soft tissue density; most are sharply marginated and most have a higher density than adjacent bile. An occasional obstructing stone is isodense to bile, with CT showing an abrupt termination to the column of bile; the appearance mimics that of malignancy. At times, thin collimation reveals crescent-appearing bile adjacent to a stone.

Ultrasonography

Conventional US can identify the entire common bile duct course in about 80% of patients, but detection of bile duct stones achieves only about a 60% to 70% sensitivity.

Endoscopic US achieves >90% sensitivity and almost 100% specificity in detecting bile duct stones regardless of size or bile duct caliber, and is at least as sensitive as ERC, but the need for endoscopy introduces its own complexities. Nevertheless, the complication rate for endoscopic US is significantly lower than with diagnostic ERCP.

Endoscopic US reveals bile duct stones as intraductal hyperechoic foci with, in most, acoustic shadowing. Residual debris can also be hyperechoic but typically little or no shadowing is evident.

Intraductal US has had limited application. It can detect extrahepatic bile duct stones, but its role is yet to be established.

Magnetic Resonance

Can MRI detect bile duct stones? Making study comparisons difficult is that different imaging techniques achieve different results. T2-weighted MR sequences identified stones in 78% (41), results better than with US.

Magnetic resonance cholangiopancreatography reveals choledocholithiasis better than conventional MRI, with a number of publications suggesting that detection rates are comparable to ERCP. In fact, in some studies MRCP achieves a higher sensitivity in detecting intrahepatic stones than ERCP (88). In general, MRCP sensitivities are 80% to 100% and specificities are 95% to 100% for detecting extrahepatic bile duct stones, although some studies have achieved a sensitivity of only about 60% (89). As one example, MRCP using non–breath-hold 3D fast spin echo (FSE), breath-hold single section half-Fourier RARE and breath-hold multisection half-Fourier rapid acquisition with relaxation enhancement (RARE) sequences all achieved similar sensitivities and specificities exceeding 90% in detecting bile duct stones (90). Evidence suggests that volume-rendered MRCP is superior to maximum intensity projection or thick-section MRCP for stone detection (89). Magnetic resonance cholangiopancreatography tends to be less optimal if the bile ducts are not dilated or patients cannot hold their breath during scanning. Stones not surrounded by bile, such as those close to the papilla, tend to blend into surrounding structures and even mimic a stenosis.

On T1-weighted images most stones are hyperintense to bile, while on T2-weighted images most are hypointense. Magnetic resonance cholangiopancreatography, relying on heavily T2-weighted images, reveals bile duct stones as hypointense foci within high signal intensity bile; stones as small as 2 mm in diam-

eter can be detected. One should keep in mind, however, that blood clots, gas, and polyps have a similar appearance.

Intravenous Cholangiography

Intravenous cholangiography also detects bile duct stones, and some have reported a detection rates approaching 100%. These are exceptional results. More typical is a 50% sensitivity and over 95% specificity.

Therapy

The Presurgical Patient

The imaging approach to a precholecystectomy patient suspected of harboring choledocholithiasis remains controversial. Gastroenterologists and surgeons tend to take opposite views, depending on their relative expertise. Typically, if a patient is first seen by a gastroenterologist, preoperative ERC is obtained and, if stones are identified, endoscopic sphincterotomy and stone extraction are performed. Some surgeons, on the other hand, regardless of whether an open or laparoscopic cholecystectomy is contemplated, prefer to explore extrahepatic bile ducts during surgery. Some surgeons believe that the morbidity and mortality for surgical therapy of choledocholithiasis are comparable to or lower than that with endoscopic sphincterotomy. At times a combined laparoscopic and endoscopic procedure is preferred.

One therapeutic approach with suspected biliary stones is to divide patients into low- and high-risk groups. Low-risk patients undergo endoscopic US to confirm the presence of stones, followed by surgery. High-risk patients, on the other hand, undergo ERCP and sphincterotomy. Such an approach should be modified for individual expertise; also, the availability of MRCP modifies the strategy employed.

In patients with common bile duct and hepatic duct stones, endoscopic sphincterotomy and basket extraction achieve complete stone clearance in up to 90%; adding lithotripsy raises the success rate. Small stones tend to pass spontaneously after sphincterotomy. Most stones smaller than about 1 cm can be retrieved with either a basket or a balloon. Larger stones are usually fragmented, and the fragments are then extracted. Most stones proximal to a stricture, on the other hand, are difficult to extract and the stricture must first be dilated.

Endoscopic papillary balloon dilation is performed by some endoscopists instead of a sphincterotomy; whether the risk of complications is less after balloon dilation is not clear.

Endoscopic common bile duct cannulation is often not feasible in patients with a previous Billroth II gastric resection due to an excessively long afferent loop. Nevertheless, successful ERCP has been achieved in patients with a Billroth II anastomosis and even in an occasional patient with a Roux-en-Y reconstruction. A percutaneous transhepatic approach to sphincterotomy and stone extraction is an occasional alternative.

Intraoperative Imaging

A number of patients with choledocholithiasis and failed preoperative endoscopic stone extraction undergo a conventional open cholecystectomy and common bile duct exploration. Occasionally during an open cholecystectomy a surgeon encounters a stone impacted in the distal common bile duct that cannot be removed by stone forceps, basket, or catheter. Previous surgical practice was to perform a transduodenal sphincterotomy, but some surgeons elect to leave the stone in place, insert a T-tube, and then have a radiologist extract the stone through the T-tube tract. After a T-tube is in place and the bile ducts decompressed, many of these so-called impacted stones float free. Such an approach is also feasible during laparoscopic cholecystectomy.

One approach to managing common bile duct stones is to perform endoscopic US in the operating suite before laparoscopic cholecystectomy in patients at high risk of choledocholithiasis. Ultrasonography is also feasible during laparoscopy by introducing a transducer probe through one of the trocar sites. Extrahepatic bile ducts are readily visualized, and both common bile duct and cystic duct stones are detected. The sensitivity and specificity approach 100% for stone detection; the surgical approach is then modified accordingly. In addition, intraoperative US potentially also detects gallbladder polyps and adenomyomato-

sis, although the specificity and sensitivity are not established.

Laparoscopic US can rival laparoscopic cholangiography in stone detection, although the latter procedure better defines the anatomy, and these examinations are complementary. Ultrasonography is more difficult to perform and is limited in visualizing the intrapancreatic portion of the common bile duct. Also, although laparoscopic US detects most bile duct stones, it does not detect subtle anomalous biliary ducts. A practical problem in applying published results is that technically excellent operative cholangiographic and sonographic study quality are difficult to achieve; in many institutions radiologists control neither the choice of operative radiographic equipment used nor the technical factors employed.

If during a laparoscopic cholecystectomy imaging reveals unsuspected stones, one option is to approach them with postoperative ERCP, at which time most bile ducts can be cleared of stones. On the other hand, if expertise with laparoscopic bile duct exploration is available, these patients undergo laparoscopic ductal stone clearance rather than an open procedure. The common bile duct can be explored either via a choledochotomy and T-tube insertion or through a transcystic duct choledochoscope—technically difficult procedures that prolong surgical time. In experienced hands, however, choledocholithiasis is successfully managed with primary laparoscopic choledochotomy and stone extraction. Laparoscopic transcystic common bile duct exploration or choledochotomy are easier if the cystic duct and common bile duct are dilated.

One alternative for patients with an abnormal laparoscopic cholangiogram is to thread a double-lumen catheter through the cystic duct and into the duodenum. The catheter allows postoperative cholangiography and also assists postoperative endoscopic sphincterotomy and stone extraction.

Intraoperative choledochoscopic electrohydraulic lithotripsy has been performed for a stone impacted in the distal common bile duct, but limited data are available for this procedure.

The High-Risk Patient

Extracorporeal lithotripsy is an alternative for surgically high-risk patients with choledocholithiasis. Such lithotripsy was more in vogue a number of years ago and is currently performed in only a limited number of centers, mostly in Europe. Stones are visualized by US. Complete stone clearance has been achieved in 80% to 90% of patients. Some patients require several sessions, and subsequent endoscopic fragment extraction may be necessary. One consideration is that in some patients with successful lithotripsy, stones eventually recur.

Intracorporeal contact lithotripsy using an electrohydraulic or laser lithotriptor has had limited application. Specialized equipment is required for each technique. Nevertheless, percutaneous transhepatic or retrograde cholelithotripsy is an option in some high-risk patients or with complex stones. It is performed under local anesthesia, an access tract dilated, and stones fragmented using choledochoscopic lithotripsy. Any residual fragments are removed either through a transhepatic route or endoscopically. The electrohydraulic and laser approaches have similar success rates, morbidities, and hospitalization times. An alternate technique in a patient with failed endoscopic stone therapy is percutaneous transhepatic calculi extraction using occlusion catheters and Dormia baskets (91); balloon dilation of the papilla is generally also performed. In a difficult situation, a motor-driven basket can fragment a stone. Even the Angiojet thrombectomy device has been used to clear impacted intrahepatic debris (92).

Biliary Dyskinesia

The term *biliary dyskinesia* is used to describe abnormal bile duct function when an anatomic cause has been excluded. Also called *acalculous biliary colic*, initially it was applied mostly to sphincter of Oddi spasm. A separate entity, cystic duct syndrome, has been introduced. Both represent a paradoxical response to bile flow. Thus instead of the gallbladder constricting, sphincter of Oddi dilating and bile flowing into the duodenum, the sphincter remains in spasm when cholecystokinin is injected.

Ultrasonography suggests that instead of constricting, in some patients the gallbladder initially relaxes in response to a fatty meal, followed by a marked constriction. Such

bimodal gallbladder response differs from the simple unimodal constriction of most normal gallbladders.

Cholescintigraphy is often the imaging procedure of choice in identifying these conditions. The diagnosis, however, should be made cautiously and only after excluding more obvious diagnoses.

Fistula

Cholecysto- and choledochoenteric fistulas develop primarily to the duodenum and stomach but occasionally involve small bowel and colon. About two thirds of these are choledochoduodenal, followed by cholecystoduodenal, cholecystocholedochal, and the least common being cholecystocolonic fistula; the vast majority of these fistulas are caused by biliary calculi, and a small minority are due to malignancies and, rarely, peptic ulcer disease.

Among duodenal fistulas most involve the duodenal bulb. Some of the incriminating gallstones cause gallstone ileus, although smaller gallstones pass through the gastrointestinal tract without obstructing (gallstone ileus is discussed in Chapters 3 and 4). Pneumobilia is a variable finding. Many of these patients do not have signs and symptoms of acute cholecystitis, although a past history of biliary stones or recurrent biliary tract infection is not uncommon.

A cholecystocolic fistula induces diarrhea. Cholangitis is not common. The diagnosis can be established with a barium enema, although some of these fistulas produce sufficient colonic distortion that a barium enema even suggests a colon carcinoma. Biliary scintigraphy identifies a cholecystocolic fistula by direct transverse colon visualization without significant small bowel activity.

In an occasional patient with a cholecystocutaneous fistula, gallstones pass through the fistula. At times an adjacent abscess develops. These external fistulas are best studied with fistulography. Detection of internal fistulas by imaging is problematic; the claimed detection rates with CT and MRI vary considerably.

Bronchobiliary fistulas are rare. Many of these are sequelae of prior hydatid cyst surgery; a rare one is secondary to a hepatocellular carcinoma.

Gallbladder Torsion/Volvulus

Some authors use the terms *torsion* and *volvulus* interchangeably. To maintain accuracy, *volvulus* should be reserved for gallbladder torsion with lumen obstruction.

The gallbladder fundus is encased by peritoneum, which occasionally is rather lax, thus allowing the gallbladder to twist around the elongated mesentery. A twist occludes either bile outflow, blood flow, or both, and volvulus ensues. Clinically, gallbladder volvulus mimics acute cholecystitis and is a cause of acute abdominal pain. At times gallbladder volvulus suggests acute appendicitis. Neglected gallbladder volvulus evolves to perforation, bile peritonitis, and spill of any gallstones into the peritoneal cavity. Spilled bile is often infected, thus further compounding gallbladder perforation.

Laparoscopic cholecystectomy for torsion and volvulus has been performed. Initial laparoscopic gallbladder decompression and detorsion aid subsequent cholecystectomy.

Gallbladder Hydrops

Gallbladder hydrops develops secondary to gallbladder distention due to cystic duct obstruction in the absence of infection. In some patients the gallbladder is palpable.

Vascular Lesions

Hemobilia

Hemobilia signifies hemorrhage into bile duct lumen. These patients present with upper gastrointestinal bleeding, abdominal pain is common, and, obstructive jaundice develops due to intraductal blood clots. Hemobilia originating in the gallbladder has led to malignant hypertension (93). Hemobilia is a rare cause of pancreatitis.

Causes of hemobilia are rather extensive (Table 8.8). A coagulopathy, often part of end-stage liver cirrhosis, is a somewhat neglected diagnosis of spontaneous hemobilia. An eroding umbilical venous catheter is a cause for these fistulas (Fig. 8.40). Trauma and resultant vascu-

Table 8.8. Etiologies of hemobilia

Trauma
Liver biopsy
(Pseudo)aneurysm
Hepatic artery
Cystic artery
Superior pancreaticoduodenal artery
Arterioportal fistula
Neoplasm
Hepatocellular carcinoma
Liver metastases
Gallbladder carcinoma
Vasculitis
Polyarteritis nodosa
Lupus vasculitis
Coagulopathy
Coagulopathy due to end-stage cirrhosis
Idiopathic thrombocytopenic purpura
Infection
Septic emboli
Ascariasis
Gallstone eroding into an artery
Iatrogenic

Figure 8.40. Splenic vein-to-bile duct fistula due to umbilical catheter erosion. Contrast was injected into the umbilical catheter.

lar-to-bile duct fistula are common causes of hemobilia. Even small hepatocellular carcinomas result in hemobilia. Hemobilia due to metastases, on the other hand, is uncommon.

Endoscopy detects bleeding from the ampulla of Vater.

Blood increases bile attenuation 30 to 50 HU. Blood clots form eventually and, having a higher specific gravity than bile, tend to settle into a dependent position in the gallbladder or bile ducts. Clotted blood appears as cast-like bile duct and gallbladder defects.

Ultrasonography reveals gallbladder blood clots as intraluminal masses. Blood within dilated bile ducts is hyperechoic. Aneurysms adjacent to bile ducts are detected with Doppler US; if needed, CT or selective hepatic arteriography provides confirmation.

Technetium-99m–red blood cell scintigraphy in a patient bleeding into intrahepatic bile ducts results in early gallbladder activity.

Arteriography identifies a source of uncontrolled bleeding in most patients, and transcatheter arterial embolization should arrest bleeding in most. Rarely, operative ligation of a bleeding vessel or even major liver resection is necessary.

Eventual gallbladder ischemia is a presumed common pathway for some of the cholecystitides. Ischemic cholecystitis can be induced by arterial chemoembolization of a hepatocellular carcinoma (94).

Gallbladder edema, congestion, and multiple small-vessel thrombi develop after crack cocaine use.

Bile duct ischemia is uncommon except in a setting of feeding vessel ligation or intravascular chemotherapy. Some secondary sclerosing cholangitis presumably is ischemic in origin.

Crack cocaine use leads to small-vessel thrombi, gallbladder wall edema and eventual ischemia.

Varices

Gallbladder varices develop in a setting of portal vein thrombosis. These dilated veins bypass a locally thrombosed portal vein segment and drain into intrahepatic portal vein branches. They probably do not interfere with gallbladder function. Children with portal hypertension due to extrahepatic portal vein obstruction also develop gallbladder varices.

Gallbladder varices are recognized by both CT and US, with CT arterial portography identifying communication with intrahepatic portal vein branches. Ultrasonography reveals these varices as tortuous, dilated vessels in the gallbladder wall.

Patients with portal vein cavernous transformation develop bile duct varices as part of venous collaterals; some of these varices exert sufficient pressure on the bile duct lumen to induce cholestasis. Angiography outlines the underlying vascular anatomy, and cholangiography defines these serpiginous extraluminal defects.

Pericholecystic Fluid Collections

Fluid around the gallbladder is common both in acute cholecystitis and in such conditions as pancreatitis, gallbladder torsion, ascites, adjacent abscess, and hematoma. Superficially, pericholecystic fluid mimics gallbladder wall edema, but this fluid does not enclose the entire gallbladder and does not enhance with contrast.

Immunosuppression

Acquired Immunodeficiency Syndrome

Cholecystitis

A number of opportunistic infections are implicated in acute acalculous cholecystitis in acquired immunodeficiency syndrome (AIDS) patients. Ultrasonography reveals a distended gallbladder, no calculi, and a thickened gallbladder wall—nonspecific findings.

Not all HIV-infected patients with right upper quadrant symptoms have cholecystitis. Ultrasonography in patients undergoing interleukin-2 therapy reveals gallbladder wall thickening and intramural and pericholecystic fluid (95); the severity of these findings is related to interleukin-2 dose, and both symptoms and US abnormalities resolve after the end of therapy.

Cholecystectomy in AIDS patients often does not improve symptom and is associated with a high mortality.

Cholangitis

Acquired immunodeficiency syndrome patients develop cholestatic liver enzyme abnormalities. Many of these patients have infection with an unusual organism, but some have no source for cholangitis and direct HIV infection is postulated.

Acquired immunodeficiency syndrome cholangitis, at times called *AIDS cholangiopathy* and *AIDS-related sclerosing cholangitis*, is detected with cholangiography (Fig. 8.41). Mild abnormalities found with direct cholangiography tend to be missed by other imaging modalities. Neoplastic disease, on the other hand, is better detected with CT.

Imaging reveals mild to moderate multiple strictures involving both intra- and extrahepatic bile ducts. Bile duct wall outline tends to be irregular. The overall appearance is similar to that seen in sclerosing cholangitis, although it is possible to differentiate with imaging between AIDS-associated cholangitis and primary sclerosing cholangitis; in AIDS cholangitis papillary stenosis is relatively common, and a number of these patients develop gallbladder and cystic duct involvement—findings not seen in

Figure 8.41. Acquired immunodeficiency syndrome (AIDS) cholangitis. The bile ducts contain mild strictures and a slight irregular outline is evident, findings similar to mild primary sclerosing cholangitis.

primary sclerosing cholangitis. Also, patients with AIDS cholangitis are more prone to developing superimposed pyogenic cholangitis. Considerable overlap exists between CT and cholangiographic findings.

Tumors

Children with AIDS appear to be at risk for smooth muscle neoplasms. Gallbladder leiomyomas and gallbladder Kaposi's sarcomas have been reported in HIV-infected children. Some also develop splenic artery calcifications.

Postoperative Changes

Postcholecystectomy

Does the common bile duct dilate after a cholecystectomy? One large study found that, on average, the duct did increase slightly in diameter, although some patients had no significant change (96).

Postcholecystectomy syndrome consists of recurrent biliary-like pain or dyspeptic symptoms. Some patients have sphincter of Oddi dysfunction, a dilated bile duct, or delayed biliary drainage, while others have no objective findings. An increase in bile salt concentration in fasting gastric juice occurs after cholecystectomy, suggesting that duodenogastric reflux may have a role in pathogenesis of this syndrome.

An occasional metal clip applied during cholecystectomy migrates into bile duct lumen and acts as a foreign-body nidus for gallstone formation (Fig. 8.42). Similarly, a suture thread can occasionally be identified in a postcholecystectomy bile duct stone.

Magnetic resonance cholangiopancreatography is evolving into a primary screening study for postcholecystectomy syndrome. Dilated bile ducts, strictures, retained stones, and other related abnormalities are detected. Scintigraphy often shows patent ducts but delayed biliary transit, suggesting liver dysfunction.

Figure 8.42. Metal clip encased in a stone (arrow) in a patient with a previous cholecystectomy. (Courtesy of Stephen Laucks, M.D., Hazleton, Pennsylvania.)

Sump Syndrome

Sump syndrome occurs in the presence of distal common bile duct obstruction after a side-to-side choledocho- or cholecystoduodenostomy (Fig. 8.43). Distal obstruction causes stasis and debris in the distal common bile duct stump, at times associated with cholangitis and even pancreatitis. A sphincterotomy, if feasible, should be curative. Endoscopy via the side-to-side choledocoduodenostomy or even a percutaneous transhepatic approach is occasionally helpful if transpapillary access is not possible.

This syndrome should not develop after a choledochojejunostomy or a hepaticojejunostomy.

Changes After Biliary-Enteric Anastomoses

Detection of postoperative biliary leaks is discussed in a previous section under complications of therapy for acute cholecystitis. Afferent loop obstruction is covered in Chapter 4.

A cholangiogram, regardless of how it is performed, should be diagnostic of a postoperative bilioenteric stricture (Fig. 8.44), but both ERCP and a percutaneous approach are invasive procedures. Magnetic resonance cholangiopancreatography has evolved into an accurate post-

Figure 8.43. Sump syndrome. A cholecystoduodenostomy was performed years ago. The distal bile ducts are filled with sludge (arrow).

operative imaging modality to detect these strictures, identify any residual stones, and evaluate dilated ducts. In 34 patients who underwent pancreaticobiliary ductal surgery, half-Fourier RARE MRCP achieved a 100% sensitivity and 86% to 87% specificity in detecting dilated ducts and choledochoenteric anastomotic strictures (97).

Figure 8.44. Stricture (arrow) and stones (arrowheads) after choledochojejunostomy. The patient had a prior Whipple procedure for a cholangiocarcinoma.

Rarely, cholangitis developing after a hepaticojejunostomy is secondary to reflux of intestinal content from the jejunal limb.

Endoscopic retrograde cholangiopancreatography is feasible after a choledochoduodenostomy but is precluded after a choledochojejunostomy unless the afferent limb is short. Aside from percutaneous cholangiography, MRCP is the procedure of choice to study these bile ducts.

Examination Complications

Endoscopic Retrograde Cholangiopancreatography

General

A comparison of ERCP complication rates in different centers is a complex task, and most complication studies are difficult to place in perspective. Most endoscopic complications published prior to the early 1990s were anecdotal and tended to underestimate the complications. Since then a number of large, prospective studies have established that mortality and morbidity are directly related to the patient populations studied and the presence of underlying disorders. Thus the complication rate in elderly patients with acute cholangitis is different from that encountered in elective bile duct stone removal. Complication rates for endoscopic sphincterotomy vary with operator experience, indication, amount of manipulation, and degree of duct distention. In general, sphincterotomy complications are higher when the procedure is performed for sphincter of Oddi dysfunction and lower when performed for biliary stone extraction.

Primary ERCP and sphincterotomy complications are bleeding, pancreatitis, perforation, and sepsis. Because ERCP is an endoscopic procedure, the complications of endoscopy in general also occur; these include aspiration, perforation, and the risks of sedation. Endoscopic sphincterotomy complications include intrapapillary contrast extravasation, peri-Vaterian and pericholedochal infiltration, and extraperi-

toneal contrast leakage. The latter presumably involves duodenal perforation.

Suspected post-ERCP complications are best studied with CT. Significant bleeding is an indication for arteriography and, if needed, embolization.

Pancreatitis

Although hyperamylasemia is common after ERCP, only occasionally is clinical pancreatitis evident. Nevertheless, pancreatitis is the most common complication of ERCP. A 5% risk of clinically evident pancreatitis during diagnostic ERCP and up to 10% during therapeutic procedures is probably typical for an experienced endoscopic center. Patients with a normal-caliber common bile duct appear more prone to developing pancreatitis than those with a dilated duct.

Computed tomography is not necessary with suspected mild pancreatitis. With more severe clinical signs and symptoms, CT confirms the diagnosis, identifies any necrosis, and excludes other complications. Computed tomography findings of ERCP-associated pancreatitis are similar to those seen with pancreatitis due to other causes.

Perforation

Perforations are either intra- or extraperitoneal in location; the latter is suggested if gas is identified in soft tissues around the papilla of Vater. The clinical relevance of such gas, however, is a complex issue, and soft tissue gas is detected after ERCP in some asymptomatic patients. The amount of gas, identified with CT, does not correlate with the size of a perforation. In fact, some authors do not consider isolated extraperitoneal gas to represent a perforation. At times injected contrast is identified in soft tissues and the procedure is aborted. Most extraperitoneal perforations heal spontaneously, with only a minority progressing to clinically evident infection, sepsis, and abscess.

An intraperitoneal perforation is less common and results in a pneumoperitoneum. Some of these duodenal tears are quite large. Occasionally with a large tear the endoscopist will suddenly visualize the peritoneal cavity and abort the procedure.

A guidewire or catheter readily perforates through the bile duct wall, including cystic duct. Most of these perforations close spontaneously.

Post-ERCP CT detection of an abnormal fluid collection generally implies that either percutaneous drainage or surgical correction is necessary. If the clinical or initial CT findings are ambiguous, either a contrast study or follow-up CT should clarify the cause.

A patient developing an acute abdomen after ERCP should be suspected of having either pancreatitis or a perforation. Pancreatitis generally develops several hours after a procedure, while perforations tend to manifest sooner. In most patients CT is the imaging modality of choice to distinguish between these two entities. Whether to perform a water-soluble upper gastrointestinal contrast study to detect a perforation is debatable, but probably is not necessary in most patients. Such a study should be considered only if the results will modify therapy. In a setting of a small perforation, a water-soluble contrast study shortly after ERCP often does not identify a leak, and most patients are managed conservatively.

Other Complications

Over a third of patients develop bacteremia after ERCP (98); *Escherichia coli*, *Morganella morganii*, *Staphylococcus* spp., and *Streptococcus* spp. are typical isolates. In spite of bacteremia, septicemia and clinical evidence of infection are uncommon.

Hemorrhage is a relatively common complication after endoscopic sphincterotomy, but most often is self-limiting in scope. Some bleeding can be controlled during endoscopy by sclerotherapy, cautery, epinephrine injection, or balloon tamponade, but extensive arterial bleeding requires either arteriographic embolization or surgical therapy. Hemorrhage can be delayed by 24 to 48 hours after endoscopic sphincterotomy and can be sufficiently brisk to require transfusion.

Endoscopic manipulation of benign and malignant biliary strictures is associated with few complications. Pancreatitis is a possibility. Most bleeding is treated conservatively.

A rare complication of endoscopic sphincterotomy is pneumomediastinum. Portal venous gas is also rare after ERCP and sphincterotomy; presumably intraluminal gas enters

through mucosal tears. Even fatal hepatic air embolization has developed.

Occasional unexplained prolonged cholestatic jaundice develops after ERCP; presumably it is related to the contrast agent used.

Rarely, a basketed large stone cannot be extracted. Most often such a stone is crushed or a basket wire broken and the crushed stone fragments then extracted.

Percutaneous Cholangiography

Similarly to ERCP, percutaneous transhepatic cholangiography and biliary drainage can result in bacteremia; cholangitis and septicemia are uncommon as long as adequate drainage is maintained.

Significant arterial bleeding does develop during percutaneous transhepatic biliary drainage and stenting. Arterial embolization is required in some.

Perforation of a peri-Vaterian duodenal diverticulum is a rare complication.

Poststenting

An arterioportal fistula is a complication of percutaneous biliary drainage and results in hemobilia. At times transarterial embolization is indicated.

A metallic endoprosthesis eroding through duodenal mucosa can cause bleeding or even duodenal perforation. Most stents migrating distally will pass spontaneously; several have perforated the sigmoid colon. A rare biliary stent migrates proximally into the liver and leads to an abscess.

A long-term complication of biliary stents placed for therapy of benign biliary strictures is obstruction. In one study, primary metallic stent patency decreased from 75% after 12 months to 25% after 36 months (99). Repeat stent occlusions develop due to sludge, stones, or simply mucosal hyperplasia; periodic stent replacement is necessary.

A hunting accident led to buck shot obstructing a biliary prosthesis (100).

Biopsy

Tumor seeding after percutaneous biopsy is discussed in Chapter 7.

A common complication of percutaneous liver biopsy is hemobilia.

References

1. Stabile Ianora AA, Scardapane A, Midiri M, Rotondo A, Angelelli G. [Pre- and postoperative study of the bile ducts with spiral computerized tomography.] [Italian] Radiol Med 2000;100:152–159.
2. Chopra S, Chintapalli KN, Ramakrishna K, Rhim H, Dodd GD 3rd. Helical CT cholangiography with oral cholecystographic contrast material. Radiology 2000; 214:596–601.
3. Rondeau Y, Soyer P, Meduri B, et al. [MRI cholangiography with rapid spin-echo technique: prospective evaluation of 20 patients.] [French] J Radiol 1998;79: 147–152.
4. Varghese JC, Farrell MA, Courtney G, Osborne H, Murray FE, Lee MJ. Role of MR cholangiopancreatography in patients with failed or inadequate ERCP. AJR 1999;173:1527–1533.
5. Merkle EM, Boll DT, Weidenbach H, Brambs HJ, Gabelmann A. Ability of MR cholangiography to reveal stent position and luminal diameter in patients with biliary endoprostheses: in vitro measurements and in vivo results in 30 patients. AJR 2001;176: 913–918.
6. Savader SJ, Lynch FC, Radvany MG, et al. Single-specimen bile cytology: a prospective study of 80 patients with obstructive jaundice. J Vasc Intervent Radiol 1998;9:817–821.
7. Sirikci A, Bayram M, Kervancioglu R. Incisional hernia of a normal gallbladder: sonographic and CT demonstration. Eur J Radiol 2002;41:57–59.
8. Ikeda S, Sera Y, Ohshiro H, Uchino S, Akizuki M, Kondo Y. Gallbladder contraction in biliary atresia: a pitfall of ultrasound diagnosis. Pediatr Radiol 1998;28:451–453.
9. Gilmour SM, Hershkop, M, Reifen R, Gilday D, Roberts EA. Outcome of hepatobiliary scanning in neonatal hepatitis syndrome. J Nucl Med 1997;38: 1279–1282.
10. Rossmuller B, Porn U, Schuster T, Lang T, Dresel S, Hahn K. [Prognostic value of hepatobiliary functional scintigraphy in diagnosis and after-care of biliary atresia.] [German] Rofo Fortschr Geb Rontgenstr Neuen Bildgeb Verfahr 2000;172:73–79.
11. Saeki M, Honna T, Nakano M, Kuroda T. [Portal hypertension after successful hepatic portoenterostomy in biliary atresia.] [Japanese] Nippon Geka Gakkai Zasshi 1996;97:648–652.
12. Eiberg H, Nielsen IM. Linkage of cholestasis familiaris Groenlandica/Byler-like disease to chromosome 18. Int J Circumpolar Health 2000;59:57–62.
13. Knisely AS. Progressive familial intrahepatic cholestasis: a personal perspective. Pediatr Dev Pathol 2000;3: 113–125.
14. Jacquemin E. [Progressive familial intrahepatic cholestasis and hereditary anomalies. 1. Hepatocellular metabolism of bile acids.] [French] Arch Pediatr 1998;5:45–53.

15. Patriquin H, Lenaerts C, Smith L, et al. Liver disease in children with cystic fibrosis: US-biochemical comparison in 195 patients. Radiology 1999;211:229–232.
16. Akata D, Akhan O, Ozcelik U, et al. Hepatobiliary manifestations of cystic fibrosis in children: correlation of CT and US findings. Eur J Radiol 2002;41: 26–33.
17. Alonso-Lej F, Rever WB, Pessagno DJ. Congenital choledochal cyst with a report of 2, and an analysis of 94 cases. Int Abstr Surg 1959;108:1–30.
18. Todani T, Watanabe Y, Narusue M, Tabuchi K, Okajima K. Congenital bile duct cysts: classification, operative procedures, and review of thirty-seven cases including cancer arising from choledochal cyst. Am J Surg 1977;134:263–269.
19. Lenriot JP, Gigot JF, Segol P, Fagniez PL, Fingerhut A, Adloff M. Bile duct cysts in adults: a multi-institutional retrospective study. French Associations for Surgical Research. Ann Surg 1998;228:159–166.
20. Kim MJ, Han SJ, Yoon CS, et al. Using MR cholangiopancreatography to reveal anomalous pancreaticobiliary ductal union in infants and children with choledochal cysts. AJR 2002;179:209–214.
21. Caroli J. Couinaud D. Une affection nouvelle sans doute congenitale des voies biliaires: la dilatation kystique uniobaire des canaux hepatiques. Sem Hop 1958;496: 136–142.
22. Holve S, Hu D, McCandless SE. Metachromatic leukodystrophy in the Navajo: fallout of the American-Indian wars of the nineteenth century. Am J Med Genet 2001;101:203–208.
23. Simanovsky N, Ackerman Z, Kiderman A, Fields S. Unusual gallbladder findings in two brothers with metachromatic leukodystrophy. Pediatr Radiol 1998;28:706–708.
24. Moore EE, Jurkovich GJ, Knudson MM, et al. Organ injury scaling. VI: Extrahepatic biliary, esophagus, stomach, vulva, vagina, uterus (nonpregnant), uterus (pregnant), fallopian tube, and ovary. J Trauma 1995; 39:1069–1070.
25. Shetty PB, Broome DR. Sonographic analysis of gallbladder findings in Salmonella enteric fever. J Ultrasound Med 1998;17:231–237.
26. Thrall JH, Ziessman HA. Nuclear Medicine. The Requisites. St. Louis: Mosby, 1995.
27. Pinto A, Romano S, Del Vecchio W, et al. [Personal experience in 71 consecutive patients with acute cholecystitis.] [Italian] Radiol Med 2000;99:62–67.
28. Regan F, Schaefer DC, Smith DP, Petronis JD, Bohlman ME, Magnuson TH. The diagnostic utility of HASTE MRI in the evaluation of acute cholecystitis. Half-Fourier acquisition single-shot turbo SE. J Comput Assist Tomogr 1998;22:638–642.
29. Park MS, Yu JS, Kim YH, et al. Acute cholecystitis: comparison of MR cholangiography and US. Radiology 1998;209:781–785.
30. Wu CS, Yao WJ, Hsiao CH. Effervescent gallbladder: sonographic findings in emphysematous cholecystitis. J Clin Ultrasound 1998;26:272–275.
31. Ito K, Fujita N, Noda Y, et al. Percutaneous cholecystostomy versus gallbladder aspiration for acute cholecystitis: a prospective randomized controlled trial. AJR 2004;183:193–196.
32. Dinkel HP, Kraus S, Heimbucher J, et al. Sonography for selecting candidates for laparoscopic cholecystectomy: a prospective study. AJR 2000;174:1433–1439.
33. Vitellas KM, El-Dieb A, Vaswani KK, et al. Using contrast-enhanced MR cholangiography with IV mangafodipir trisodium (Teslascan) to evaluate bile duct leaks after cholecystectomy: a prospective study of 11 patients. AJR 2002;179:409–416.
34. Ryan ME, Geenen JE, Lehman GA, et al. Endoscopic intervention for biliary leaks after laparoscopic cholecystectomy: a multicenter review. Gastrointest Endosc 1998;47:261–266.
35. Di Stasi C, Pedicelli A, Manfredi R, Sallustio G. Renocaval arteriovenous fistula as a complication of laparoscopic cholecystectomy. AJR 2001;176:261–262.
36. Boland GW, Slater G, Lu DS, Eisenberg P, Lee MJ, Mueller PR. Prevalence and significance of gallbladder abnormalities seen on sonography in intensive care unit patients. AJR 2000;174:973–977.
37. Parra JA, Acinas O, Bueno J, Guezmes A, Fernandez MA, Farinas MC. Xanthogranulomatous cholecystitis: clinical, sonographic, and CT findings in 26 patients. AJR 2000;4:979–993.
38. Hatakenaka M, Adachi T, Matsuyama A, Mori M, Yoshikawa Y. Xanthogranulomatous cholecystitis: importance of chemical-shift gradient-echo MR imaging. Eur Radiol 2003;13:2233–2235.
39. Adachi Y, Iso Y, Moriyama M, Kasai T, Hashimoto H. Increased serum CA19–9 in patients with xanthogranulomatous cholecystitis. Hepatogastroenterology 1998;45:77–80.
40. Setiawan MW, Samsi TK, Wulur H, Sugianto D, Pool TN. Dengue haemorrhagic fever: ultrasound as an aid to predict the severity of the disease. Pediatr Radiol 1998;28:1–4.
41. Arai K, Kawai K, Kohda W, Tatsu H, Matsui O, Nakahama T. Dynamic CT of acute cholangitis: early inhomogeneous enhancement of the liver. AJR 2003;181: 115–118.
42. Yoon KH, Ha HK, Lee JS, et al. Inflammatory pseudotumor of the liver in patients with recurrent pyogenic cholangitis: CT-histopathologic correlation. Radiology 1999;211:373–379.
43. Park MS, Yu JS, Kim KW, et al. Recurrent pyogenic cholangitis: comparison between MR cholangiography and direct cholangiography. Radiology 2001;220: 677–682.
44. Geenen DJ, Geenen JE, Jafri FM, et al. The role of surveillance endoscopic retrograde cholangiopancreatography in preventing episodic cholangitis in patients with recurrent common bile duct stones. Endoscopy 1998;30:18–20.
45. Sato M, Watanabe Y, Ueda S, et al. Intrahepatic cholangiocarcinoma associated with hepatolithiasis. Hepatogastroenterology 1998;45:137–144.
46. Cevikol C, Karaali K, Senol U, et al. Human fascioliasis: MR imaging findings of hepatic lesions. Eur Radiol 2003;13:141–148.
47. Ormsby AH, Bauer TW, Hall GS. Actinomycosis of the cholecystic duct: case report and review. Pathology 1998;30:65–67.
48. Ito K, Mitchell DG, Outwater EK. Pancreatic changes in primary sclerosing cholangitis: evaluation with MR imaging. AJR 1999;173:1535–1539.

49. Loftus EV Jr, Sandborn WJ, Tremaine WJ, et al. Primary sclerosing cholangitis is associated with nonsmoking: a case-control study. Gastroenterology 1996;110: 1496–1502.
50. Vitellas KM, El-Dieb A, Vaswani KK, et al. MR cholangiopancreatography in patients with primary sclerosing cholangitis: interobserver variability and comparison with endoscopic retrograde cholangiopancreatography. AJR 2002;179:399–407.
51. Ito K, Mitchell DG, Outwater EK, Blasbalg R. Primary sclerosing cholangitis: MR imaging features. AJR 1999;172:1527–1533.
52. Revelon G, Rashid A, Kawamoto S, Bluemke DA. Primary sclerosing cholangitis: MR imaging findings with pathologic correlation. AJR 1999;173:1037–1042.
53. Collett JA, Allan RB, Chisholm RJ, Wilson IR, Burt MJ, Chapman BA. Gallbladder polyps: prospective study. J Ultrasound Med 1998;17:207–211.
54. Yoshimitsu K, Honda H, Jimi M, et al. MR diagnosis of adenomyomatosis of the gallbladder and differentiation from gallbladder carcinoma: importance of showing Rokitansky-Aschoff sinuses. AJR 1999;172: 1535–1540.
55. Yoshimitsu K, Honda H, Shinozaki K, et al. Helical CT of the local spread of carcinoma of the gallbladder: evaluation according to the TNM system in patients who underwent surgical resection. AJR 2002;179: 423–428.
56. Paquet KJ. Appraisal of surgical resection of gallbladder carcinoma with special reference to hepatic resection. J Hepato Biliary Pancreatic Surg 1998;5:200–206.
57. Winston CB, Chen JW, Fong Y, Schwartz LH, Panicek DM. Recurrent gallbladder carcinoma along laparoscopic cholecystectomy port tracks: CT demonstration. Radiology 1999;212:439–444.
58. Stephen MR, Farquharson MA, Sharp RA, Jackson R. Sequential malt lymphomas of the stomach, small intestine, and gall bladder. J Clin Pathol 1998;51:77–79.
59. Tamada K, Ueno N, Tomiyama T, et al. Characterization of biliary strictures using intraductal ultrasonography: comparison with percutaneous cholangioscopic biopsy. Gastrointest Endosc 1998;47:341–349.
60. Park M-S, Kim TK, Kim KW, et al. Differentiation of extrahepatic bile duct cholangiocarcinoma from benign stricture: Findings at MRCP versus ERCP. Radiology 2004;233:234–240.
61. Alcaraz MJ, De la Morena EJ, Polo A, Ramos A, De la Cal MA, Gonzalez Mandly A. A comparative study of magnetic resonance cholangiography and direct cholangiography. Rev Esp Enferm Dig 2000;92:427–438.
62. Kim MJ, Mitchell DG, Ito K, Outwater EK. Biliary dilatation: differentiation of benign from malignant causes—value of adding conventional MR imaging to MR cholangiopancreatography. Radiology 2000;214: 173–181.
63. Nagakawa T, Ohta T, Kayahara M, et al. A new classification of Mirizzi syndrome from diagnostic and therapeutic viewpoints. Hepatogastroenterology 1997; 44:63–67.
64. Redston MS, Wanless IR. The hepatic von Meyenburg complex: prevalence and association with hepatic and renal cysts among 2843 autopsies. Mod Pathol 1996;9: 233–237.
65. Kim YW, Park YK, Park JH, et al. A case with intrahepatic double cancer: hepatocellular carcinoma and cholangiocarcinoma associated with multiple von Meyenburg complexes. Yonsei Med J 1999;40:506–509.
66. Tozawa K, Akita H, Kusada S, et al. Testicular metastases from carcinoma of the bile duct: a case report. Int J Urol 1998;5:106–107.
67. Lee JW, Han JK, Kim TK, et al. Computed tomography features of intraductal intrahepatic cholangiocarcinoma. AJR 2000;175:721–725.
68. Soyer P, Pelage JP, Zidi SH, Boudiaf M, Rymer R. Portal vein invasion by intrahepatic peripheral cholangiocarcinoma: a rare cause of portal hypertension. AJR 1998;171:1413–1414.
69. Maetani Y, Itoh K, Watanabe C, et al. MR imaging of intrahepatic cholangiocarcinoma with pathologic correlation. AJR 2001;176:1499–1507.
70. Yoon KH, Ha HK, Kim CG, et al. Malignant papillary neoplasms of the intrahepatic bile ducts: CT and histopathologic features. AJR 2000;175:1135–1139.
71. Braga HJ, Imam K, Bluemke DA. MR imaging of intrahepatic cholangiocarcinoma: use of ferumoxides for lesion localization and extension. AJR 2001;177: 111–114.
72. Matsuo S, Shinozaki T, Yamaguchi S et al. Intrahepatic cholangiocarcinoma with extensive sarcomatous change: report of a case. Surg Today 1999;29:560–563.
73. Lieser MJ, Barry MK, Rowland C, Ilstrup DM, Nagorney DM. Surgical management of intrahepatic cholangiocarcinoma: a 31–year experience. J Hepato Biliary Pancreatic Surg 1998;5:41–47.
74. Tanaka N, Yamakado K, Nakatsuka A, Fujii A, Matsumura K, Takeda K. Arterial chemoinfusion therapy through an implanted port system for patients with unresectable intrahepatic cholangiocarcinoma -initial experience. Eur J Radiol 2002;41:42–48.
75. Chang WH, Kortan P, Haber GB. Outcome in patients with bifurcation tumors who undergo unilateral versus bilateral hepatic duct drainage. Gastrointest Endosc 1998;47:354–362.
76. Golfieri R, Giampalma E, Muzzi C, et al. [Unresectable hilar cholangiocarcinoma: combined percutaneous and radiotherapeutic treatment.] [Italian] Radiol Med 2001;101:495–502.
77. Fukuda T, Iwanaga S, Sakamoto I, et al. Computed tomography of neural plexus invasion in common bile duct carcinoma. J Comput Assist Tomogr 1998;22: 351–356.
78. Lim HS, Jeong YY, Shen YL, Kang HK, Cho CK. CT and MRI findings of primary non-Hodgkin's lymphoma of the common bile duct mimicking cholangiocarcinoma. AJR 2004;182:1608–1609.
79. Maes M, Depardieu C, Dargent JL, et al. Primary low-grade B-cell lymphoma of MALT-type occurring in the liver: a study of two cases. J Hepatol 1997;27:922–927.
80. Wenzel DJ, Gaede JT, Wenzel LR. Intrabiliary colonic metastasis mimicking primary biliary neoplasia. AJR 2003;180:1029–1032.
81. Deenitchin GP, Yoshida J, Chijiiwa K, Tanaka M. Complex cystic duct is associated with cholelithiasis. HPB Surg 1998;11:33–37.
82. Garcia Molina FJ, Garcia Gil JM, Fernandez Mena J, Navarro Freire F. Computerized tomographic assess-

ment of the composition of gallstones. Rev Esp Enferm Dig 1998;90:851–862.
83. Tsai HM, Lin XZ, Chen CY, Lin PW, Lin JC. MRI of gallstones with different compositions. AJR 2004;182: 1513–1519.
84. Hellstern A, Leuschner U, Benjaminov A, et al. Dissolution of gallbladder stones with methyl tert-butyl ether and stone recurrence: a European survey. Dig Dis Sci 1998;43:911–920.
85. Soto JA, Alvarez O, Munera F, Velez SM., Valencia J, Ramirez N. Diagnosing bile duct stones: comparison of unenhanced helical CT, oral contrast-enhanced CT cholangiography, and MR cholangiography. AJR 2000; 175:1127–1134.
86. Kim KH, Kim W, Lee HI, Sung CK. Prediction of common bile duct stones: its validation in laparoscopic cholecystectomy. Hepatogastroenterology 1997;44: 1574–1579.
87. Hunt DR. Common bile duct stones in non-dilated bile ducts? An ultrasound study. Australas Radiol 1996;40: 221–222.
88. Kim TK, Kim BS, Kim JH, et al. Diagnosis of intrahepatic stones: superiority of MR cholangiopancreatography over endoscopic retrograde cholangiopancreatography. AJR 2002;179:429–434.
89. Kondo H, Kanematsu M, Shiratori Y, et al. MR cholangiography with volume rendering: receiver operating characteristic curve analysis in patients with choledocholithiasis. AJR 2001;176:1183–1189.
90. Soto JA, Barish MA, Alvarez O, Medina S. Detection of choledocholithiasis with MR cholangiography: comparison of three-dimensional fast spin-echo and single- and multisection half-Fourier rapid acquisition with relaxation enhancement sequences. Radiology 2000;215:737–745.
91. Zorger N, Manke C, Lenhart M, Volk M, Link J, Feuerbach S. [Percutaneous transpapillary extraction of biliary calculi for symptomatic choledocholithiasis after unsuccessful endoscopic treatment.] [German] Rofo Fortschr Geb Rontgenstr Neuen Bildgeb Verfahr 2001;173:92–96.
92. Loehr SP, Hamilton C, Gargan K, Gilliam J. Use of the Angiojet thrombectomy device to facilitate removal of impacted intrahepatic ductal debris. AJR 2002;179: 370–372.
93. Seguin P, Le Bouquin V, Campion JP, Malledant Y. [Hemobilia of gallbladder origin manifesting as malignant hypertension.] [French] Presse Med 1998;27:913.
94. De Diego A, Santos L, Vaquero J, et al. [Ischemic cholecystitis caused by arterial chemoembolization of hepatocellular carcinoma.] [Spanish] Rev Esp Enferm Dig 1999;91:74–75.
95. Premkumar A, Walworth CM, Vogel S, et al. Prospective sonographic evaluation of interleukin-2–induced changes in the gallbladder. Radiology 1998;206:393–396.
96. Feng BX, Song QM. Does the common bile duct dilate after cholecystectomy—sonographic evaluation in 234 patients. AJR 1995;165:859–861.
97. Tang Y, Yamashita Y, Arakawa A, et al. Pancreaticobiliary ductal system: value of half-Fourier rapid acquisition with relaxation enhancement MR cholangiopancreatography for postoperative evaluation. Radiology 2000;215:81–88.
98. Barragan Casas JM, Hernandez Hernandez JM, Garcinuno Jimenez MA, et al. Bacteremia caused by digestive system endoscopy. Rev Esp Enferm Dig 1999;91:105–116.
99. Gabelmann A, Hamid H, Brambs HJ, Rieber A. Metallic stents in benign biliary strictures: long-term effectiveness and interventional management of stent occlusion. AJR 2001;177:813–817.
100. Maroy B. [An odd hunting accident: acute obstruction of a biliary prosthesis caused by a buck shot.] [Letter] [French] Gastroenterol Clin Biol 1996;20:123.

9

Pancreas

Technique

Computed Tomography

Techniques and terminology used with computed tomography (CT) are discussed in Chapter 7. Intrapancreatic structures and peripancreatic vessels are better visualized with helical CT than with conventional CT. Multislice CT images both soft tissues and vessels and, if desired, provides three-dimensional (3D) views. Some authors use the term *pancreatic phase*, defined as 40 to 70 seconds after the start of intravenous contrast infusion.

A typical multislice CT technique consists of a biphasic (pancreatic phase and portal venous phase) thin slice study of the upper abdomen. An additional arterial phase is useful for identifying adjacent blood vessels and detecting hypervascular tumors. In general, a higher contrast dose and faster injection rate result in greater and earlier parenchymal enhancement.

Computed tomography angiography can depict secondary arterial branches such as the pancreaticoduodenal arcades and dorsal pancreatic artery. Three-dimensional volume rendering appears superior to maximum intensity projection (MIP) and shaded surface display (SSD) in evaluating these vessels (1).

Ultrasonography

The use of bowel hypotonia combined and gastroduodenal distention with water (a technique called *hydrosonography*) aids in visualizing the pancreas. After ingesting water with simethicone, followed by patient rotation, the pancreatic tail was visualized by ultrasonography (US) in 79% of patients, compared to 7% in controls (2).

Endoscopic US provides better resolution of structures in the pancreatic head than conventional US. Especially with small lesions, endoscopic US can guide percutaneous biopsy and aspiration cytology. Most endoscopic US of the pancreas is performed either transgastric or transduodenal. Color Doppler US of the pancreas is feasible using an endoscopic approach.

Intraductal US probes using up to 30-MHz transducers are being developed. A probe inserted through the ampulla into the pancreatic duct can image structures up to 20 to 30 mm in diameter. The portal vein and other adjacent larger veins are readily visualized.

Carbon dioxide bubbles mixed with heparinized saline and injected into the celiac artery are a potential intraarterial contrast agent when imaging the pancreas. Such US, termed *sonographic angiography*, appears useful when evaluating pancreatic vascularity; pancreatic ductal cancers show no or mild enhancement, while islet cell tumors and serous cystadenomas reveal strong enhancement. This specialized technique is better suited for endoscopic US rather than transabdominal US. Currently the literature on sonographic angiography is rather limited.

The pancreas can be imaged through subcostal and umbilical laparoscopic ports. A fluid-filled stomach acts as an acoustic window, although resolution of pancreatic lesions is improved by using a higher frequency transducer directly from the lesser sac.

Magnetic Resonance Imaging

Magnetic resonance (MR) techniques useful in evaluating the pancreas are T1- and T2-weighted sequences, arterial and venous phase postcontrast images, magnetic resonance cholangiopancreatography (MRCP), and magnetic resonance angiography (MRA). Fat-suppression improves image conspicuity (MRCP is discussed in more detail below; see Pancreatography). The term *hydrospiral CT* has been used for helical CT of the pancreas when using pharmacologic bowel paralysis and water distention of the stomach and duodenum.

Normal pancreas is iso- to slightly hyperintense to liver on T1-weighted images and hypointense to surrounding fat. It becomes hyperintense on T1-weighted fat-suppression images. It is iso- to hyperintense to liver on T2-weighted images. The extracellular gadolinium chelates enhance normal pancreatic parenchyma homogeneously. Because most tumor vascularity differs from normal tissue vascularity, postcontrast pancreatic-phase or equilibrium-phase imaging was initially often employed, with pancreatic ductal cancers tending to be hypointense and islet cell tumors hyperintense on these images. Currently, with further advances in technique, fat-suppressed pre- and postcontrast arterial phase T1-weighted images are commonly employed.

In normal individuals, the pancreatic arterial phase occurs at about 15 seconds from the start of contrast injection, the parenchymal phase at 25 seconds, the portal phase at 60 seconds, and the equilibrium phase at about 100 seconds. In distinction to the liver, which receives most of its blood supply from the portal vein and thus enhances maximally during the portal phase, maximal pancreatic enhancement is during the late arterial-to-pancreatic phase. After intravenous (IV) bolus of gadopentetate dimeglumine in patients with no pancreatic malignancies, the best pancreatic images are obtained 15 seconds after the arrival of contrast in the abdominal aorta (3); the peripancreatic vessels, on the other hand, are best seen at 25 seconds or later.

Short sequences that minimize artifacts are necessary in pancreatic MRI. A typical study for tumor detection consists of an oral contrast agent to outline the gastrointestinal tract and pre- and postgadolinium images. With state-of-the-art MR units, fat-suppressed, single breath-hold spoiled gradient echo (SGE) sequences are often used. Combining fat suppression and oblique imaging improves visualization of both normal pancreas and abnormalities, compared with conventional axial and axial fat-suppressed T1-weighted imaging; oral barium aids as a duodenal contrast marker in differentiating pancreatic head from adjacent bowel.

Endoscopic MRI uses an endoscope with a small radiofrequency coil attached to the tip. After endoscopic tip placement in the duodenum, the patient is placed in an MR unit and appropriate images are obtained. Preliminary results suggest that the pancreatic duct is well defined, tumors in the pancreatic head are identified, and even portal vein invasion is detected (4).

Uptake of the manganese MR contrast agent (Mn-DPDP) is evident by a normal pancreas, which becomes hyperintense on T1 postcontrast images, while signal intensity of many lesions is unchanged. As a result, lesion conspicuity is increased. Further study is needed to define the role of this contrast agent, which persists in the pancreas considerably longer than gadolinium.

Pancreatography

Endoscopic

Endoscopic retrograde pancreatography (ERP) is the current approach to direct pancreatic duct visualization.

Transgastric pancreatography using endoscopic US for guidance has been attempted. This technique has a possible role after failed endoscopic retrograde cholangiopancreatography (ERCP), although MR pancreatography appears more appropriate.

Percutaneous

One alternative is percutaneous pancreatography performed under US guidance, followed by contrast injection into the pancreatic duct under fluoroscopic control. With a previously unsuccessful ERP, this technique occasionally appears worthwhile if the pancreatic duct is dilated due to chronic pancreatitis or pancreatic carcinoma.

Computed Tomography

Similar to the bile ducts, CT multiplanar reformatted imaging using minimum intensity projections of selected tissue volume thicknesses reduces partial volume effects and makes a normal pancreatic duct visible. In particular, multiplanar images combined with 0.5-mm or thinner axial images during the arterial phase aid in evaluating the pancreatic duct (5); current techniques allows visualization of the main pancreatic duct in over 90% of patients and accessory pancreatic duct in about half, but not the side branches.

In distinction to MR pancreatography, CT pancreatography detects pancreatic calcifications.

Magnetic Resonance

Magnetic resonance cholangiopancreatography is discussed in more detail in Chapter 8. By selecting appropriate heavily weighted T2 pulse sequences, nonflowing fluid appears bright against a darker background. Magnetic resonance pancreatography relies on this property of bile and pancreatic fluid being hyperintense on T2-weighted images. The main pancreatic duct is readily identified, but normal secondary branches are visualized incompletely. Images resemble those obtained with ERCP, with a number of publications concluding that detection of pancreatic duct abnormalities is similar to ERCP. It is a noninvasive procedure, no contrast is injected into the ducts, and thus no complications are encountered. It can be performed with a mid-strength [0.5-tesla (T)] magnet. Magnetic resonance pancreatography achieves sensitivities of >80% and specificities >90% in detecting pancreatic duct stenosis, obstruction, and dilation.

Secretin stimulation of pancreatic secretions improves MR visualization of a nondilated main pancreatic duct (6); no gross improvement is evident once the pancreatic duct is dilated. Secretin stimulated MRCP can be used to measure pancreatic duct flow rates and changes in duodenal fluid volume, findings indicative of pancreatic exocrine function (7), yet whether secretin administration is of value in a setting of chronic pancreatitis as a test of pancreatic function is arguable.

Oral contrast agents such as iron gluconate, iron oxide, and barium sulfate reduce background noise and make interpretation easier.

Pancreatic duct caliber should be measured with caution on MR images; partial volume averaging of an adjacent splenic vein makes the duct appear wider with some MR sequences. If needed, T2-weighted spin-echo (SE) sequences are used to differentiate a pancreatic duct (high signal intensity fluid) from flowing blood (signal void). Magnetic resonance pancreatography overestimates duct stenoses. Secretin in a dose of 1 clinical unit/kg stimulates pancreatic exocrine secretions, distends the pancreatic duct transiently, and improves pancreatic duct visualization.

Pancreatoscopy

Instruments for direct visualization of the pancreatic duct mucosa are becoming available. Currently described are thin fiberscopes several millimeters in diameter and pancreatoscopes, which are inserted either via an ERCP cannula or are free-standing. Their primary role is in visualizing and defining lesions involving the main pancreatic duct.

Scintigraphy

2-[18F]-fluoro-deoxy-D-glucose positron emission tomography (FDG-PET) appears useful in assessing indeterminate CT findings for suspected pancreatic carcinoma. The primary future interest in PET will probably be in tumor uptake. For example, if levodopa (L-dopa) is labeled with carbon 11 in the β position, the radioactive carbon label follows L-dopa through decarboxylation to dopamine, and significant uptake occurs in a pancreatic glucagonoma and gastrinoma (8); on the other hand, with C 11 in the L-dopa carboxyl group, it is eliminated from tissue as CO_2 during decarboxylation and little C-11 uptake occurs.

Biopsy

Both solid and cystic pancreatic tumors are routinely biopsied on an outpatient basis using US guidance, the tumor etiology is established, and few complications are encountered. As an alternative, aspiration using endoscopic US as a guide achieves high diagnostic accuracy in evaluating pancreatic tumors.

The most common complication associated with fine-needle aspiration is acute pancreatitis.

The presence of a trained cytopathologist is a prerequisite to interpreting fine-needle aspiration biopsies.

Congenital Abnormalities

Several systems are in use for classifying congenital pancreatic duct anomalies. A common scheme is to subdivide anomalies into migration and fusion. The most common is fusion failure between the dorsal and ventral pancreatic ducts (pancreas divisum).

Migration variations include pancreatic rests, which are formed by incomplete migration of the prepancreatic anlage. As a result, pancreatic tissue remains in stomach wall, duodenum, and other structures. Likewise, failure of full rotation of the prepancreatic buds results in an annular pancreas.

In some patients it is difficult to predict whether a detected congenital anomaly is indeed responsible for a particular clinical problem.

Agenesis

Complete agenesis of the pancreas is incompatible with life. Partial agenesis is rare, with either the ventral or dorsal segment failing to develop. This congenital anomaly is associated with polysplenia and intrathoracic anomalies. Agenesis of the dorsal segment results in only the head of the pancreas being present; CT and MR show this segment as an oval mass. Many of these patients also have diabetes mellitus, presumably because of islet cell agenesis, which normally are predominantly located in the body and tail of the pancreas.

The uncinate process is either absent or hypoplastic in patients with intestinal nonrotation, presumably secondary to incomplete pancreatic primordial ventral bud rotation.

Pancreas Divisum

Pancreatography and immunohistochemical staining of pancreatic polypeptide identify two types of dorsal and ventral duct fusion (Fig. 9.1): (1) one-point fusion at the junction of main duct and accessory pancreatic duct, and (2) two-point fusion not only at the primary duct junction site but also at a second site. Abnormal embryologic fusion (or lack of fusion) of the ventral and dorsal primordia causes pancreas divisum.

Pancreas divisum is the most common congenital anomaly of the pancreas, with autopsy studies showing about a 6% prevalence. Some consider pancreas divisum to be an innocuous congenital variant, while others believe that it is associated with a higher prevalence of pancreatitis. The frequency of pancreas divisum in patients with pancreatitis is significantly higher than in a general population. If found in several family members, is this hereditary pancreatitis in a setting of familial pancreas divisum? Pancreatitis in this patient population often is focal and limited to a dorsal distribution. It is often technically difficult in these patients to cannulate the dorsal pancreatic duct (duct of Santorini); nevertheless, some endoscopy centers have achieved a high success rate and have become referral centers for this procedure.

Pancreas divisum does not appear to predispose to an anomalous pancreaticobiliary duct union.

Pancreas divisum is generally detected by pancreatography. At times CT identifies distinct ventral and dorsal pancreatic ducts (Fig. 9.2). Occasionally CT suggests pancreas divisum by an indistinct mass in the head of the pancreas.

An MRCP detects about half the pancreas divisum anomalies. Secretin administration appears to aid in this detection.

The prevalence of both acute relapsing pancreatitis and chronic pancreatitis appears to decrease following minor papilla sphincterotomy and resultant accessory duct decompression. At times stenting of the dorsal pancreatic duct relieves symptoms.

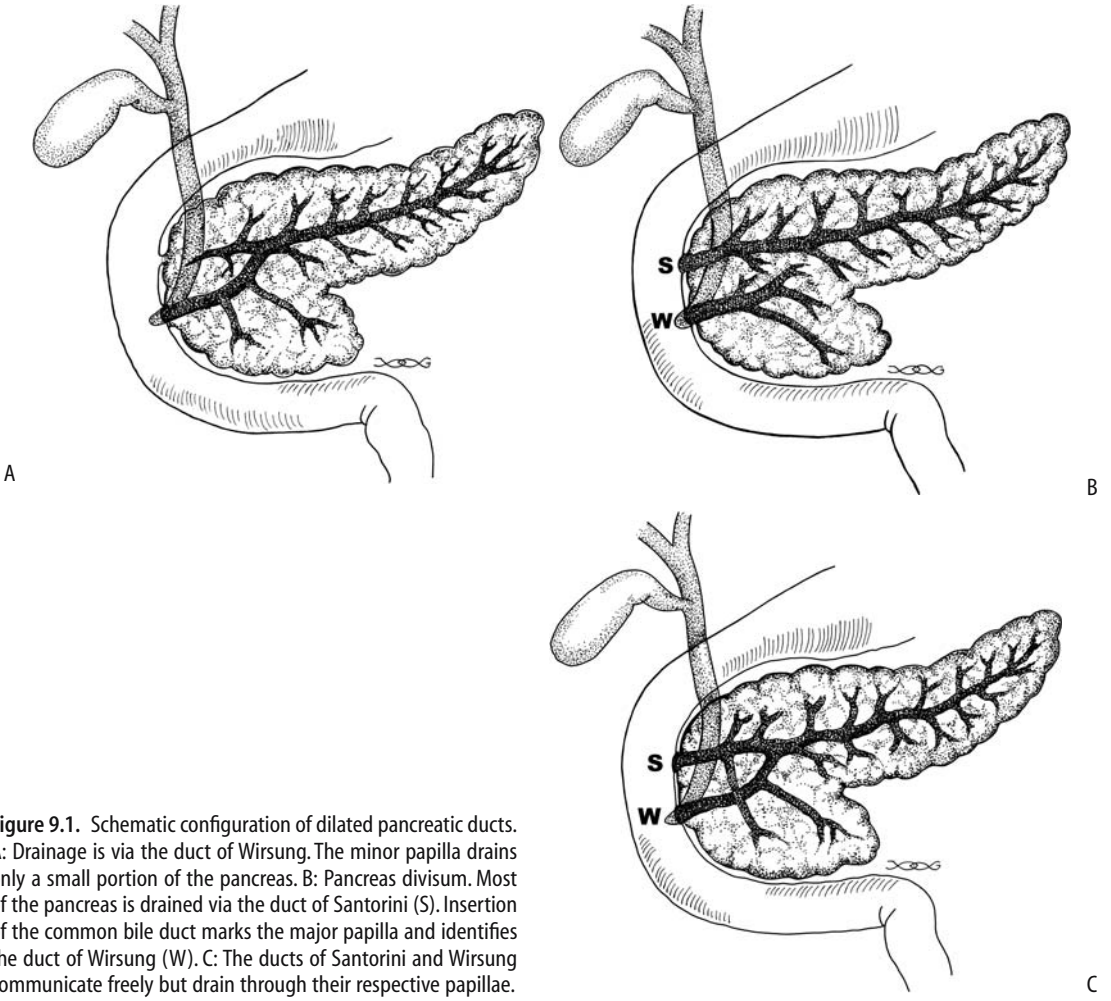

Figure 9.1. Schematic configuration of dilated pancreatic ducts. A: Drainage is via the duct of Wirsung. The minor papilla drains only a small portion of the pancreas. B: Pancreas divisum. Most of the pancreas is drained via the duct of Santorini (S). Insertion of the common bile duct marks the major papilla and identifies the duct of Wirsung (W). C: The ducts of Santorini and Wirsung communicate freely but drain through their respective papillae.

Annular Pancreas

In neonates an annular pancreas is associated with esophageal atresia, tracheoesophageal fistula, duodenal stenosis or atresia, and malrotation. Rare instances of an annular pancreas and pancreas divisum in the same patient have been reported.

Symptoms of an annular pancreas not uncommonly manifest during adulthood, the most common findings being abdominal pain, gastric outlet obstruction, pancreatitis, and a pancreatic tumor (Fig. 9.3).

In the newborn, conventional radiography of complete obstruction by an annular pancreas shows a "double-bubble" sign with no bowel gas distally. Only in a minority of older individuals does a barium study suggest annular pancreas. CT and MRCP also underdiagnose this condition. At times ERP suggests the diagnosis, although in some patients confirmation is made only at surgery. Computed tomography and MR identify the second part of the duodenum being surrounded by pancreatic tissue; at times a pancreatic duct segment is identified in the annular portion (Fig. 9.4). In some patients this circumferential duodenal narrowing is due mostly to fibrotic tissue.

A cyst developing adjacent to the duodenum in a patient with an annular pancreas and repeated attacks of pancreatitis should suggest a (pseudo)cyst.

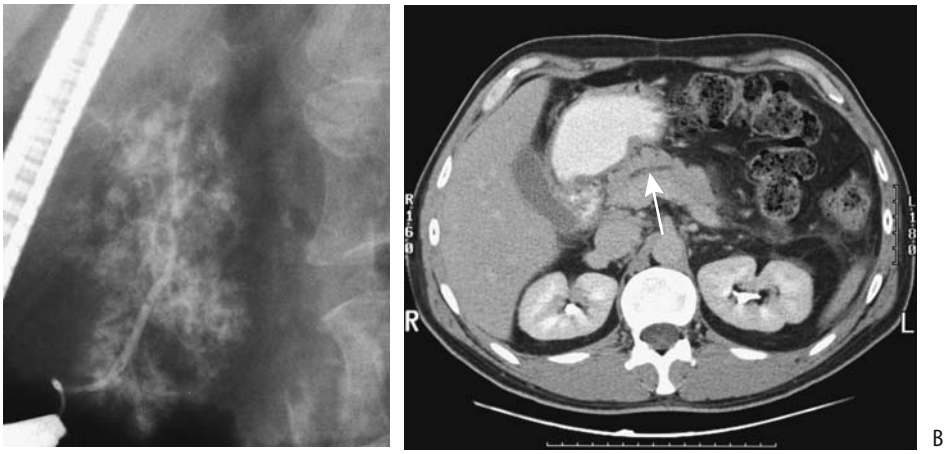

Figure 9.2. Pancreas divisum. A: Endoscopic retrograde cholangiopancreatography (ERCP) with contrast injection into the main papilla outlines only a short, narrow caliber duct of Wirsung. Parenchymal contrast is evident. B: Computed tomography (CT) identifies a dilated duct (arrow) not conforming to the usual course of the main pancreatic duct.

Ectopic Pancreas

Ectopic (heterotopic) pancreatic tissue is most often found in the gastric antrum and proximal duodenum, although it can be located anywhere in the gastrointestinal tract, including a Meckel's diverticulum.

Inflammation does develop in ectopic pancreatic tissue (called *cystic dystrophy of an ectopic pancreas* by some authors). If chronic, fibrosis and bowel stenosis ensue. Acute pancreatitis and even a (pseudo)cyst have developed in an ectopic pancreas. Similarly, this tissue is not immune to tumor formation; a car-

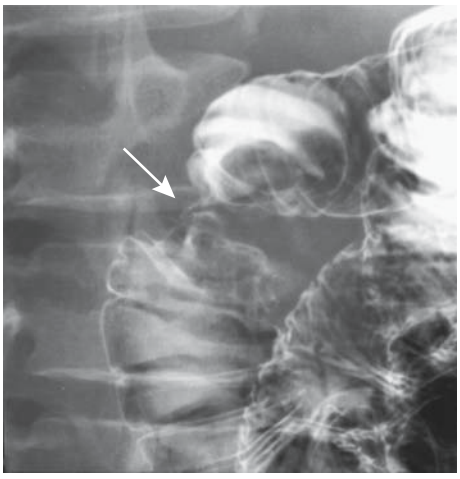

Figure 9.3. Duodenal stricture (arrow), believed to be secondary to pancreatitis in an annular pancreas.

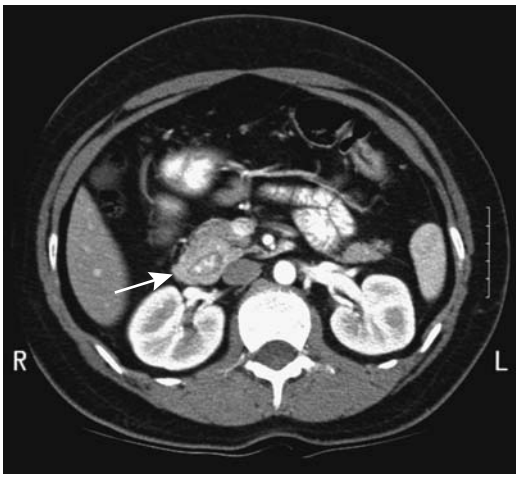

Figure 9.4. Annular pancreas. After oral and IV contrast CT shows the pancreas surrounding descending duodenum (arrow).

cinoma originated in ectopic pancreatic tissue in the esophagus, and a papillary cystic neoplasm developed in ectopic pancreatic tissue in the omentum.

Aberrant Duct Insertion

During embryonic development a network of duct branches eventually fuses and forms a primary channel. Aberrant fusion leads to a number of duplication anomalies of the pancreatic ducts and results in one or more main duct. This congenital anomaly is often associated with an apparent tumor on CT imaging.

The pancreatic duct can communicate with a duodenal duplication or even involve aberrant bile ducts and the patient presents with a periampullary cystic tumor; CT and ERCP are helpful in defining the underlying anatomy and planning surgery.

Cysts

Congenital cysts of the pancreas are either true cysts or pseudocysts. Both are rare. They range from solitary to multiple. True cysts are lined by epithelium. These cysts in neonates tend to be large and their clinical differential diagnosis often includes renal, choledochal, mesenteric, ovarian, and gastrointestinal origin cysts.

An increased prevalence of simple cysts is found in patients with polycystic kidney disease, tuberous sclerosis, and von Hippel-Lindau disease. Incidentally detected multiple pancreatic cysts, especially in a young patient without pancreatic disease, should suggest one of these entities. Patients with von Hippel-Lindau disease are also prone to developing cystic pancreatic neoplasms. In fact, in an occasional patient pancreatic lesions are the only abdominal manifestation of von Hippel-Lindau disease.

Computed tomography or MR confirms a cyst's location and its relationship to pancreatic parenchyma; imaging tends not to differentiate among congenital cysts, a cystic neoplasm, and other cystic lesion.

Precontrast CT of a lymphoepithelial cyst revealed a heterogeneous water-density tumor, with septa identified postcontrast (9); MRI showed a hypointense mass on T1- and a hyperintense mass on T2-weighted imaging, with septa identified on postgadolinium images. Endoscopic US confirmed the presence of septa and also detected fine hyperechoic structures within the cyst. A cystic neoplasm was suspected preoperatively.

Histiocytosis

Langerhans cell histiocytosis is the current term for disorders previously known as histiocytosis X. This is a rare disorder, with pancreatic involvement being even rarer.

Hereditary Pancreatic Dysfunction

Pancreatic dysfunction due to an isolated embryogenetic defect is rare. More often dysfunction is part of an inherited abnormality manifesting at multiple sites. Cystic fibrosis is an example of the latter. It is the most common cause of hereditary pancreatic dysfunction.

Cystic Fibrosis

In this autosomal-recessive disorder obstruction of small and large pancreatic ducts by thick, viscid secretions and surrounding inflammation induces fibrosis and an eventual atrophic pancreas. As a result, most patients develop exocrine pancreatic insufficiency. Acute pancreatitis is not common in cystic fibrosis patients, with some authors postulating that their pancreatic atrophy prevents a major inflammatory response.

Pathologically, parenchymal atrophy, fibrosis, and fatty infiltration are evident. In some patients fatty infiltration predominates and the pancreas appears enlarged; in others, atrophy predominates with varying degrees of fatty infiltration.

Calcifications are not common in chronic pancreatitis secondary to cystic fibrosis. When present, calcifications are scattered and not as prominent as in hereditary pancreatitis. Cysts, fatty replacement, and atrophy are detected with imaging. Once small, the pancreas may have a CT density approaching that of fat, similar to severe lipomatosis. Cysts are interspersed with segments of dilated pancreatic ducts or

they may essentially replace the pancreatic parenchyma.

Computed tomography in adolescents and adults with cystic fibrosis revealed less pancreatic tissue and more fat than in controls (10); no relationship was found between the degree of pancreatic fat and pancreatic endocrine dysfunction, but a relationship existed between the degree of fatty replacement and exocrine dysfunction.

The varied composition is reflected in the US appearance, which can range from normal to a hyperechoic pattern caused by fibrosis and fatty infiltration. In some, the pancreas blends into surrounding extraperitoneal fat and is difficult to define. Likewise, smaller cysts are not identified.

Magnetic resonance signal intensity varies depending on the degree of fatty infiltration and fibrosis present. Pancreatic T1-weighted MR in patients with cystic fibrosis reveals hyperintense signals ranging from homogeneous to a lobular outline, focal sparing, and even a normal appearance. Magnetic resonance cholangiopancreatography is useful in evaluating pancreatic duct dilation and cyst formation.

Hereditary Pancreatitis

The rare hereditary (familial) pancreatitis eventually leads to pancreatic exocrine dysfunction. It has an autosomal-dominant mode of inheritance with variable penetrance, but tends to affect only a few members of each family. This genetic defect is believed to be due to mutations in the trypsinogen gene leading to failure in inactivating prematurely activated cationic trypsin within acinar cells (11); two types are described: type I involves mutations in trypsinogen R117H and type II in trypsinogen N211. Accumulation of active trypsin mutants are believed to activate a digestive enzyme cascade process in pancreatic acinar cells, leading to autodigestion, inflammation, and acute pancreatitis. An enzymatic mutation detection method is accurate in screening individuals for known trypsinogen gene mutations.

Two types of pancreatic stones develop in this condition. Calculi in members of 10 families were composed of degraded residues of lithostathine, a pancreatic secretory protein inhibiting calcium salt crystallization (12); in one family with five affected individuals calculi were composed of >95% calcium salts.

This condition typically develops in childhood or early adolescence as acute episodes of pancreatitis, evolves into chronic pancreatitis, and gradually progresses with episodes of pancreatitis, including pseudocyst formation, to pancreatic insufficiency. An early diagnosis prior to onset of chronic pancreatitis is often not considered. Compared to patients with chronic alcoholic pancreatitis, patients with chronic hereditary pancreatitis have an earlier onset of symptoms, a delay in diagnosis, and a higher prevalence of pseudocysts, but otherwise the natural history is similar for both conditions. These patients are at increased risk for developing a pancreatic duct adenocarcinoma, the risk being approximately 50 to 60 times greater than expected (13); smoking increases this risk and lowers the age of onset by approximately 20 years.

Prominent calcifications in the pancreatic ducts are a common feature and appear similar to those seen with chronic alcoholic pancreatitis, except that this finding is almost pathognomonic of chronic hereditary pancreatitis in a young patient. A dilated pancreatic duct is also often detected.

Hereditary pancreatitis has a different clinical presentation and imaging findings, and usually is not in the differential diagnosis with cystic fibrosis.

Less Common Syndromes

The syndromes listed below are rare and have little radiologic relevance, but are occasionally raised in a differential diagnosis.

Shwachman-Diamond syndrome is a rare congenital disorder consisting of pancreatic insufficiency, growth retardation, and other abnormalities. These patients have steatorrhea, a normal sweat test, and normal intestinal mucosa. Some eventually improve their enzyme secretions and have pancreatic sufficiency. Imaging shows extensive replacement of pancreatic tissue by fat.

Pearson marrow-pancreas syndrome manifests during early infancy with failure to thrive and involves the hematopoietic system, exocrine pancreas dysfunction, and others. A primary defect involves deletions in mitochondrial DNA.

Johanson-Blizzard syndrome is an autosomal-recessive syndrome consisting of ectodermal dysplasia. Among other abnormalities, these infants develop both exocrine and endocrine pancreatic insufficiency. The primary defect is in acinar cells; at autopsy some of these infants have total absence of acini and the pancreas is replace by fat.

Histopathologically, patients with the Johanson-Blizzard syndrome and Schwachman-Diamond syndrome have preserved ductular output of fluid and electrolytes; this distinguishes them from patients with cystic fibrosis, who have a primary ductular defect.

Multiple Endocrine Neoplasia Syndromes

Multiple endocrine neoplasia (MEN) syndromes are familial autosomal-dominant disorders exhibiting incomplete penetrance and variable expression and manifesting by an increased incidence of various endocrine hyperplasias or neoplasms. They consist of synchronous or metachronous neoplastic and hyperplastic neuroendocrine tumors in several glands. These syndromes are usually divided into three types:

- Type I (Wermer's syndrome) consists of lesions in the pancreas, parathyroid, adrenal cortex, pituitary, and thyroid. Some gastric carcinoids also share a common development with enteropancreatic and parathyroid MEN-I tumors.
- Type II (Sipple's syndrome) consists of lesions in the adrenal medulla, parathyroid, and thyroid.
- Type III (multiple mucosal neuroma syndrome) consists of lesions in the adrenal medulla, thyroid, mucosal tissues, and bones.

Whether von Hippel-Lindau disease and neurofibromatosis are part of multiple endocrine neoplasia syndromes is a matter of classification.

The presence of pancreatic tumors in a patient with MEN syndrome signifies type I. The genetic defect for MEN-I appears to involve a tumor suppressor gene located in the long arm of chromosome 11. A majority of MEN-I individuals occur in familial clusters, with only an occasional sporadic one reported. Affected patients tend to have multiple organs involved, multicentric tumors within one organ are common, and complex hormone secretions are encountered. MEN-I tumors have a low but not insignificant malignant potential. Pancreatic tumors tend to be multicentric and most are hormone secreting, some being multihormonal; in fact, in the same patient different tumors often have different predominant hormonal secretions. Most common tumors are α-cell (glucagon) and β-cell (insulin) secretors. Less common are PP-cell, gastrin, and vasoactive intestinal peptide tumors. Concomitant nesidioblastosis occurs in a minority of patients. These tumors range from hyperplasia, adenoma to a carcinoma.

The majority of MEN-I patients with Zollinger-Ellison syndrome also have primary hyperparathyroidism, 30% have pituitary adenomas (about half are prolactinomas), 30% have adrenal tumors, and a smaller minority have bronchial and thymic carcinoids (14); gastrinomas tend to be multiple and often are duodenal in location. Hypercalcemia and nephrocalcinosis are common initial clinical presentations.

Because of multiplicity of tumors and their malignant potential, management of MEN-I patients with symptomatic pancreaticoduodenal tumors remains controversial. One aggressive surgical approach in a setting of hypergastrinemia and Zollinger-Ellison syndrome includes a duodenotomy, peripancreatic lymph node dissection, enucleation of pancreatic head or uncinate tumors, and a distal pancreatectomy (15); such an approach in MEN-I patients with Zollinger-Ellison syndrome resulted in 68% of patients remaining eugastrinemic during follow-up. The effect on survival of a Whipple resection is not clear.

Gastrinomas in MEN-I syndrome patients tend to be duodenal in location and difficult to locate with imaging. Some are detected only during surgical exploration by palpation, intraoperative endoscopy with transillumination, or duodenotomy.

Multiple endocrine neoplasia type II is an autosomal-dominant condition with the gene abnormality located on chromosome 10, with the responsible gene, called *RET,* being an oncogene. These patients are at sufficiently high risk for medullary thyroid carcinoma at a young age

that a thyroidectomy is considered once a diagnosis is confirmed.

One patient with MEN-II also had Hirschsprung's disease (16); aganglionosis involved the distal 5 cm of the rectum. Whether this association is fortuitous is not clear.

von Hippel-Lindau Disease

A relationship probably exists between pancreatic microcystic adenomas and von Hippel-Lindau disease; *VHL* gene alterations are detected in these tumors both in patients with von Hippel-Lindau disease and in those with sporadic microcystic adenomas. These patients are at increased risk for pancreatic and adrenal neuroendocrine tumors. A not uncommon presentation is with large liver metastases.

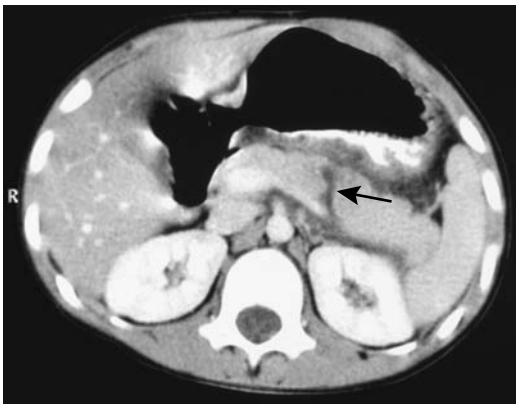

Figure 9.5. Traumatic pancreatic rupture (arrow) in a 7–year-old boy. (Courtesy of Algidas Basevicius, M.D., Kaunas Medical University, Kaunas, Lithuania.)

Trauma

A note on definition: surgeons define distal pancreas as that part containing the tail of the pancreas, while proximal means pancreatic head.

A pancreatic injury classification scale, devised by the American Association for the Surgery of Trauma, is outlined in Table 9.1. Other abdominal injuries are common in patients with pancreatic trauma. The exception is with bicycle handlebar injuries, which are a common cause of mechanical pancreatic trauma in children; these tend to produce isolated pancreatic injury and often lead to pseudocysts.

Table 9.1. Surgical pancreatic injury scale

Grade*		Type of injury
I	Hematoma	Minor contusion
	Laceration	Superficial laceration; no duct injury
II	Hematoma	Major contusion
	Laceration	Major laceration; no duct injury or tissue loss
III	Laceration	Distal transection or parenchymal injury with duct injury
IV	Laceration	Proximal transection or parenchymal injury involving ampulla
V	Laceration	Massive pancreatic head disruption

* Advanced one grade for multiple injuries, up to grade III.
Source: Modified from Moore et al. (17).

Both clinical and radiologic diagnosis of pancreatic injury is fraught with difficulty. Even in a setting of major pancreatic injury, at times initial physical findings are mild or masked by other trauma. Both CT and ERCP are often necessary to diagnose pancreatic fracture and duct disruption (Fig. 9.5). The most common site for fracture is at the pancreatic head and neck junction.

In many institutions CT is the imaging modality of choice in suspected pancreatic trauma. In both adults and children CT findings of pancreatic trauma can be subtle. At times an adjacent hematoma is the only suggestion of pancreatic injury. A pancreatic laceration, including complete transection, may not be apparent initially with CT. Therefore, with a strong suspicion for pancreatic injury and an unremarkable initial CT, a follow-up study 12 to 24 hours later is often helpful.

A CT finding of fluid (peripancreatic blood) separating the splenic artery or vein from pancreas suggests pancreatic injury. Still, such fluid may also be present in the absence of any pancreatic injury, and thus additional CT findings should be sought.

In general, CT cannot directly detect pancreatic duct injury, although a deep pancreatic laceration suggests duct disruption. Endoscopic

retrograde cholangiopancreatography is the primary study in evaluating pancreatic duct injury. Nevertheless, to better delineate pancreatic duct injury, one group of Japanese investigators performed repeat CT shortly after completing ERCP, believing that such an approach confirms ERCP findings, detects injuries not identified on ERCP, and excludes injuries in patients with equivocal ERCP (18).

Magnetic resonance pancreatography can detect complete main pancreatic duct disruption, although the literature on this topic is sparse. Current MRCP application is primarily in defining pancreatic ducts not evaluated with ERCP.

Management of children admitted with a diagnosis of pancreatic injury is individualized, keeping in mind that, in the absence of clinical deterioration or major duct injury, a more conservative therapeutic approach has evolved than practiced previously. In children with pancreatic injury a primary consideration of whether to operate or not often depends on the status of the pancreatic duct. Yet even with duct injury the trend is toward more conservative therapy. Anecdotal reports suggest that some transected pancreatic ducts recanalize spontaneously.

Duct disruption in some patients, at times involving a secondary or smaller duct, leads to pseudocyst formation. Classic therapy for traumatic pancreatic pseudocysts is cystogastrostomy or distal pancreatectomy. Children with pancreatic duct disruption and pseudocysts, however, have had successful long-term cyst catheter drainage (19).

Infection/Inflammation

Acute Pancreatitis

Classification

Acute pancreatic inflammation does not lend itself to an easy classification. Since 1963, at least four international symposia have debated this subject and proposed classifications. Among the changes adopted has been a shift in emphasis from pancreatic necrosis to presence of organ failure and inclusion of information obtained from various imaging examinations (incidentally, the terms *pancreatic necrosis* and *necrotizing pancreatitis* are used synonymously). Some of the terminology has also been redefined. There now is a distinction between an *acute fluid collection* that occurs early in acute pancreatitis and often regresses spontaneously and a *pseudocyst* that requires several weeks to form and has a distinct wall. A *pancreatic abscess* is defined as an intraabdominal collection of pus near the pancreas that contains little if any necrotic tissue. The term *infected pseudocyst* has been deleted and this entity is now considered a pancreatic abscess.

The terms *hemorrhagic pancreatitis* and *phlegmon* have also been deleted, although the wisdom in deleting the term *phlegmon* has been questioned. The primary reason for deleting *phlegmon* was its past imprecise usage. For instance, some physicians interpret phlegmon to mean a sterile process while others place it in the infectious category. Nevertheless, the vagueness of this term is useful during initial evaluation of acute pancreatitis prior to imaging studies; contrast-enhanced CT can then subdivide a *phlegmon* into interstitial versus necrotizing pancreatitis, while percutaneous aspiration can establish a *sterile* versus *infected* collection of fluid. It remains to be seen whether *phlegmon* will continue to be used in a setting of acute pancreatitis.

Etiology

Congenital Anomaly

Aberrant pancreaticobiliary duct insertions are associated with recurrent pancreatitis. Thus a pancreatic duct inserting into a communicating duodenal duplication or diverticulum and cystic duct insertion close to the ampulla have resulted in pancreatitis. Even a communicating duplication results in stasis, and, in time, calculi form within a duplication. The rare intraluminal duodenal diverticulum is also associated with acute pancreatitis.

Some patients with pancreas divisum develop pancreatitis; therapeutic options in this clinical setting are discussed in the Congenital Abnormalities section.

In the absence of more common etiologies for pancreatitis, especially in a younger patient, aberrant pancreaticobiliary duct communica-

tions and termination should be sought. An MRCP should detect any major duct anomalies and related fluid-filled structures suggesting a duplication. The inability to cannulate the main papilla during ERCP should prompt efforts to cannulate the duct of Santorini.

Bile Duct Related

Acute biliary pancreatitis appears to be more severe; more complications develop and mortality is greater in patients who have an intact gallbladder compared to those who had a previous cholecystectomy.

Choledocholithiasis is a common cause of acute pancreatitis. Although not common, gallstone pancreatitis does occur during pregnancy. Presumably a stone impacts at the ampulla of Vater, but most of these obstructions are transient and the stone passes into the duodenum. About 40% of gallstone pancreatitis recurs within 6 months, with recurrence often associated with stones in the gallbladder, and thus the rationale for performing cholecystectomy once pancreatitis is quiescent.

Clinically it is difficult to differentiate between gallstone- and non–gallstone-associated acute pancreatitis. One useful laboratory test is alanine aminotransferase (ALT) level; a greater than threefold elevation above normal has a strong positive predictive value for acute gallstone pancreatitis.

Admission plasma cholecystokinin levels in patients with gallstone pancreatitis are significantly higher than in patients with other causes of acute pancreatitis (20), although cholecystokinin levels do not correlate with serum bilirubin or pancreatic enzyme levels or severity of acute pancreatitis. Plasma cholecystokinin elevation in gallstone pancreatitis appears to be a result of a transient bile flow disturbance by stones or duct wall edema.

Hemobilia, regardless of cause, is associated with acute pancreatitis.

Anecdotal etiologies of acute pancreatitis include a bile duct suture or clip acting as a nidus, debris from a hepatocellular carcinoma rupturing into the bile ducts, and associations with primary sclerosing cholangitis and duodenal Crohn's disease. A patient with familial adenomatous polyposis with adenomas in the common bile duct developed relapsing acute pancreatitis (21).

Ethanol

Ethanol ingestion is the most common cause of acute pancreatitis in the United States.

Endoscopic Retrograde Cholangiopancreatography Induced

Endoscopic retrograde cholangiopancreatography is a not uncommon cause of subclinical or mild pancreatitis. Of more importance is that ERCP is an occasional precursor to acute necrotizing pancreatitis, especially if a sphincterotomy is performed. Among 72 consecutive patients with acute necrotizing pancreatitis requiring surgery at the Mayo Clinic, ERCP was implicated in 8% (22); of note is that on admission these post-ERCP patients had higher Acute Physiology and Chronic Health Evaluation (APACHE II) scores, more extensive pancreatic necrosis, and a higher rate of infected necrosis, and they required earlier necrosectomy and developed more enteric fistulas than similar non–ERCP-induced acute necrotizing pancreatitis patients. These post-ERCP patients had a lower mortality rate, but they were significantly younger; nevertheless, all survivors suffered long-term morbidity. The authors postulated that infection introduced during ERCP may account for some of the increased severity of pancreatitis in these patients.

A relationship appears to exist between common bile duct diameter and the subsequent risk of sphincterotomy-induced pancreatitis, with pancreatitis developing more often in patients with a nondilated bile duct.

Infection

Infectious organisms linked to pancreatitis include viral (mumps, measles, Coxsackie, hepatitis B, cytomegalovirus, varicella-zoster virus, herpes simplex virus), bacterial (mycoplasma, legionella, leptospira, salmonella), fungal (aspergillosis), and occasional parasitic infestations (toxoplasmosis, cryptosporidiosis, ascariasis) (23). Even a scorpion bite has been implicated. Acute fatal necrotizing pancreatitis has developed after liver transplantation for fulminant hepatitis B virus infection, presumably due to the hepatitis B virus.

An ascaris roundworm migrating into the pancreatic duct after sphincterotomy and pan-

creatic stent placement led to acute pancreatitis (24). These worms can be removed with a Dormia basket.

Intrabiliary rupture of a hydatid cyst and the subsequent spill of cyst contents into the bile ducts is a cause of acute pancreatitis; CT and US identify both the liver infection and bile duct debris.

Neoplasm

Pancreatic carcinomas are commonly associated with surrounding pancreatitis, although symptoms related to the cancer tend to predominate.

An occasional papilla of Vater carcinoid or a pancreatic islet cell tumor produces a pancreatic duct stricture and a clinical picture consistent with acute pancreatitis.

Drug Related

Steroids, diuretics, some antibiotics, and even cimetidine are some of the medications implicated in acute pancreatitis. Yet drug-associated pancreatitis is uncommon. Organophosphate insecticide toxicity is a rare cause of pancreatitis. Intranasal snorted heroin is associated with pancreatitis (25).

Vascular

Pancreatic ischemia is not common but does result in pancreatitis. Thus patients undergoing thoracoabdominal aortic aneurysm repair and descending thoracic aorta cross-clamping are subject to pancreatic ischemia and pancreatitis.

Cholesterol crystal embolization to the pancreas has led to necrotizing pancreatitis. Such embolization probably is more common than reported in patients with atherosclerotic vascular disease.

Other Etiologies

Rarer conditions associated with pancreatitis include the vasculitides, hyperlipidemia, ulcerative colitis, chronic renal failure, a peri-Vaterian diverticulum or neoplasm, and even a choledochal cyst. Acute pancreatitis in long-distance runners is more common in women. A rare cause of acute pancreatitis is pancreatic volvulus associated with a hiatal hernia (26). A patient with duodenal obstruction distal to the papilla occasionally presents with acute pancreatitis; more distal small bowel obstruction is not associated with pancreatitis. Thus an obstructing duodenal carcinoma distal to the papilla of Vater or even an afferent loop obstruction after a gastrectomy and Billroth II gastrojejunostomy has led to acute pancreatitis. Hypercalcemia due to hyperparathyroidism is a known cause of acute pancreatitis. Hypercalcemia secondary to a malignancy, on the other hand, seldom causes acute pancreatitis.

Clinical

Acute injury to the exocrine pancreas and resultant inflammation is the hallmark of acute pancreatitis. Usually the entire pancreas is involved. The pancreas becomes edematous and inflamed, with these changes then spreading to surrounding structures. Pancreatic enzyme release leads to tissue necrosis and hemorrhage. Pancreatic ascites is uncommon in necrotizing pancreatitis.

Typical clinical findings of acute pancreatitis are well known, but unusual presentations abound. At times acute pancreatitis initially is painless, with the patient presenting in shock or coma. Pancreatitis can mask an underlying pancreatic carcinoma. A patient with acute pancreatitis presented with symptoms referable to the scrotum (27); surgical exploration revealed fat necrosis of tunica vaginalis and spermatic cord.

A biliary etiology is most common in patients over the age of 65 years developing acute pancreatitis, and it is more likely to be necrotizing. Age in itself is not a risk factor for complications, but a relationship exists between coexistent diseases such as hypertension, diabetes, and renal failure and subsequent complications. Overall mortality is greater in the elderly.

Encephalopathy due to liver disease is well known. Less commonly encountered is encephalopathy associated with acute pancreatitis.

Traditional laboratory tests of acute pancreatitis consist of serum amylase and lipase levels. These enzyme levels do not correlate with disease severity and in some patients with acute pancreatitis are normal; a better test appears to be serum phospholipase A_2 activity, which correlates with the severity of acute pancreatitis and remains high during the severe episode

Figure 9.6. Jaundice due to pancreatitis after laparoscopic cholecystectomy. Postoperative ERCP was unsuccessful. Percutaneous transhepatic cholangiography reveals marked duct dilatation to the level of the superior pancreatic margin. Only a thin channel is evident in the intrapancreatic portion of the common bile duct (arrow). (Courtesy of David Waldman, M.D., University of Rochester.)

(28). In patients with acute pancreatitis, endotoxin in blood and peritoneal fluid is related to subsequent morbidity and mortality, suggesting that the presence of endotoxin identifies patients at high risk early in the course of acute pancreatitis (29). C-reactive protein level is a relatively accurate predictor of pancreatic necrosis.

Clinically, differential diagnoses for acute pancreatitis include bowel ischemia, perforated ulcer, and other intraabdominal catastrophes. Acute pancreatitis can be a difficult diagnosis, especially in a postoperative patient who becomes jaundiced, and more common etiologies for jaundice are generally considered (Fig. 9.6).

Imaging

Serial imaging is useful not only to follow disease progression, but also to detect complications. Once a diagnosis of acute pancreatitis is established, among other questions, imaging should address the following:

1. Is the etiology due to gallstone disease or aberrant ducts?
2. Is the disease evolving into pancreatic necrosis?
3. Is infection superimposed on pancreatic necrosis?
4. Are other sequelae developing, such as a pseudocyst?

The answers to these questions influence not only further diagnostic testing but also the choice of therapeutic modalities to be employed.

Although pancreatic necrosis can be suspected clinically, it is better identified by imaging and, at times, at surgery. Superimposed infection of necrotic tissue can also be suspected clinically, but the diagnosis is confirmed by imaging-guided percutaneous aspiration and bacteriologic sampling.

Imaging studies tend to be normal in mild pancreatitis. Generally the first abnormal finding is diffuse pancreatic enlargement. When focal, the pancreatic head is most often involved. The pancreatic outline becomes irregular. Further progression leads to necrosis, hemorrhage, and peripancreatic fluid.

Gas within the pancreas is not common in pancreatitis. Rarely, gas is seen in both pancreatic parenchyma and ducts. In general, intrapancreatic gas suggests an underlying abscess. Nevertheless, pancreatic and peripancreatic gas is found in other conditions, such as after recent laparoscopic cholecystectomy.

Pleural effusion is not an early sign of pancreatitis; generally clinical or other CT findings of severe pancreatitis occur first. The presence of a pleural effusion on admission is indicative of severe disease and has a negative prognostic value. Likewise, pancreatic necrosis is more common in patients with pulmonary infiltrates, and these patients also have a higher mortality rate.

Acute exacerbation in a setting of chronic pancreatitis may have few imaging findings. At times the presence of peripancreatic inflammation is the only finding in a patient with clinically severe acute exacerbation, although superimposed changes of chronic pancreatitis are often found.

Computed Tomography

Does administration of IV contrast media, such as during CT, worsen the outcome in acute pan-

creatitis? Using comparable clinical scores at initial diagnosis, studies tend to show that clinical pancreatitis lasts longer in patients who receive contrast as part of a CT study than those who do not, yet most of these studies are retrospective and thus have an inherent bias.

In general, CT provides better detection of peripancreatic inflammation, hemorrhage, and abscesses than US. Dynamic CT aids in defining the extent of necrosis.

The earliest CT finding is diffuse pancreatic enlargement; less often detected is focal enlargement. Computed tomography findings do not always correlate with clinical impression, and even with acute edematous pancreatitis CT can be normal. Also, imaging findings tend to lag behind clinical resolution, especially with phlegmonous pancreatitis when imaging findings can persist for months.

Inflammation evolves into an inflammatory mass, or phlegmon, which upon further damage results in pancreatic necrosis (Fig. 9.7). A phlegmon usually has a higher CT attenuation than water and is heterogeneous in appearance due to contained blood and debris. Most phlegmons exhibit poor contrast enhancement. Nonenhancing pancreatic tissue on CT is assumed to represent pancreatic necrosis (i.e., dead tissue). Nevertheless, not all nonenhancing tissue represents necrosis. At times follow-up CT reveals enhancement, indicative of viable tissue, in a region that previously did not enhance.

Surrounding tissue inflammation is common and is identified as a hazy peripancreatic thickening of fascial planes. Peripancreatic fat increases in attenuation, and these tissues reveal increased contrast enhancement. Extrapancreatic fluid collections develop with progression in severity, with fluid dissecting along tissue planes to the transverse colon, mesentery, or even spleen and left kidney. Often this fluid is not well defined, has low attenuation, tends to be poorly marginated, and consists of

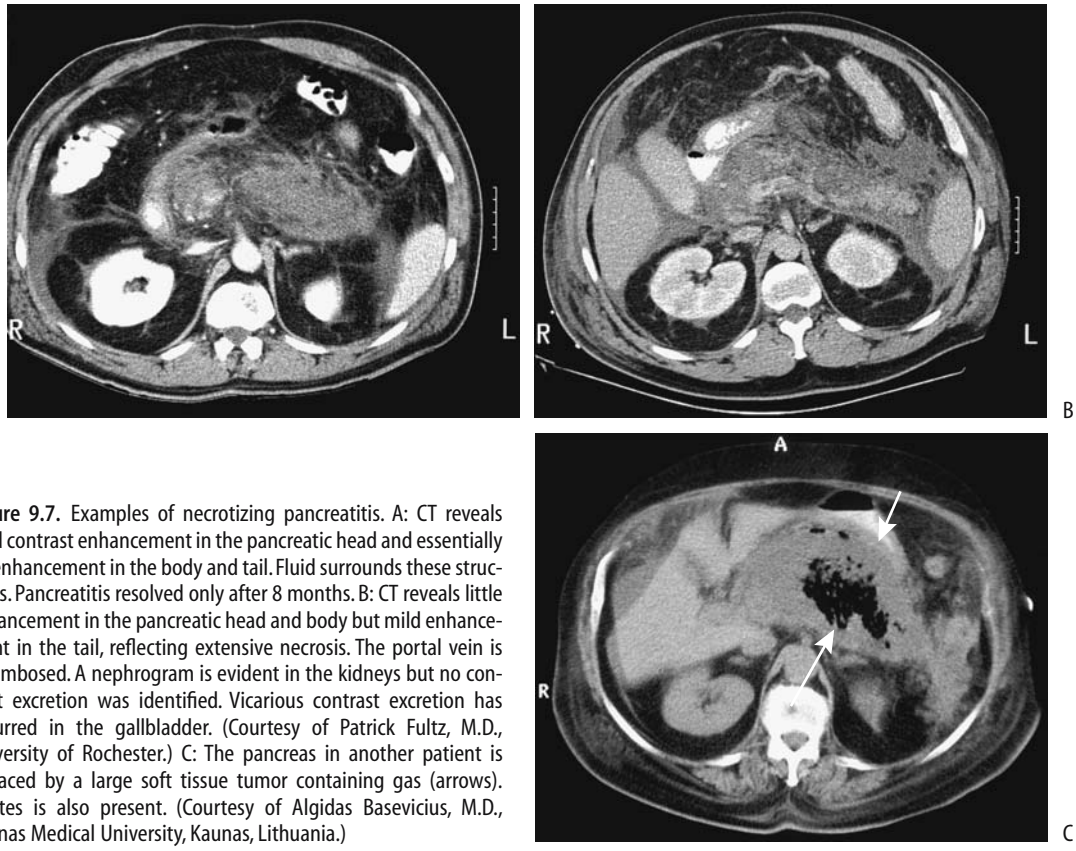

Figure 9.7. Examples of necrotizing pancreatitis. A: CT reveals mild contrast enhancement in the pancreatic head and essentially no enhancement in the body and tail. Fluid surrounds these structures. Pancreatitis resolved only after 8 months. B: CT reveals little enhancement in the pancreatic head and body but mild enhancement in the tail, reflecting extensive necrosis. The portal vein is thrombosed. A nephrogram is evident in the kidneys but no contrast excretion was identified. Vicarious contrast excretion has occurred in the gallbladder. (Courtesy of Patrick Fultz, M.D., University of Rochester.) C: The pancreas in another patient is replaced by a large soft tissue tumor containing gas (arrows). Ascites is also present. (Courtesy of Algidas Basevicius, M.D., Kaunas Medical University, Kaunas, Lithuania.)

extravasated pancreatic secretions, fat necrosis, edema, and hemorrhage. Colonic wall thickening, often first detected by CT, implies an advanced severity and increased risk for a complicated clinical course (30).

In patients with obliterated perivascular fat planes, a ratio of superior mesenteric artery diameter to superior mesenteric vein diameter is useful in differentiating pancreatitis from pancreatic carcinoma (31); a ratio greater than 1.0 suggests a malignancy.

At times pancreatitis extends to the anterior abdominal wall (Cullen's sign) or flank (Grey Turner's sign). Computed tomography findings show that anterior periumbilical extension is not directly related to extensive extraperitoneal inflammation, nor is it related to pseudocyst formation.

Ultrasonography

The role of conventional US in acute pancreatitis is limited. In most patients US can differentiate mild or edematous acute pancreatitis from severe or necrotizing pancreatitis. One established role of US is to detect whether gallstones are present.

In uncomplicated acute pancreatitis endoscopic US often (but not always) shows an enlarged pancreas; the pancreas has either normal echogenicity or is diffusely hypoechoic. Necrotizing pancreatitis presents as a focal hypoechoic tumor with or without interspersed echogenic regions. Endoscopic US can usually differentiate between edematous and necrotizing pancreatitis and will detect peripancreatic fluid, although in some patients it is difficult to detect progression to necrosis using only US criteria.

If needed, US provides guidance for percutaneous interventional procedures.

Magnetic Resonance Imaging

Whether conventional MRI offers any advantage over CT in a setting of acute pancreatitis is debatable. Viable pancreatic tissue can usually be distinguishing from necrosis with either modality. Gas and calcifications are better seen with CT.

In uncomplicated pancreatitis MRI shows a normal or diffusely enlarged pancreas. With more severe involvement the pancreas becomes hypointense on fat-suppressed T1-weighted images and is hypointense to normal liver. Decreased enhancement is evident on immediate postgadolinium images. Similar to CT, nonenhancing pancreatic tissue is assumed to represent pancreatic necrosis.

Magnetic resonance cholangiopancreatography is useful for the initial assessment of acute pancreatitis and offers a viable alternative to diagnostic ERCP in these sick patients; therapeutic ERCP can then be performed in those with a correctable abnormality detected by MRCP.

An MRCP is especially valuable in children with acute pancreatitis. Necrosis, pseudocysts, common bile duct dilation, and anomalous pancreaticobiliary ducts can be detected.

Scintigraphy

Leukocyte infiltration of the pancreas is detected by technetium-99m (Tc-99m)–hexamethylpropyleneamine oxime (hexametazime) (HMPAO) leukocyte scintigraphy. In early acute pancreatitis, positive leukocyte scintigraphy suggests a severe course, but the test is also occasionally positive in mild acute pancreatitis. Later in the course of acute pancreatitis, positive Tc-99m-HMPAO leukocyte scintigraphy suggests a superimposed infection, but here also a positive test is not synonymous with infection and is also found with milder inflammation.

Therapy

In Japan, infusion of protease inhibitors is one therapeutic modality used in acute pancreatitis (32); it is not often employed in Europe or North America.

Gallstone Pancreatitis

The evidence suggests that morbidity and mortality are decreased in patients with gallstone pancreatitis if ERCP with stone extraction is performed early in the course. An ERCP not only confirms the diagnosis, but also sphincterotomy and, if possible, extraction of any incriminating stones can be performed. This is a controversial topic; acute pancreatitis can be exacerbated by ERCP. Injection of contrast into the pancreatic duct in experimental animals

makes acute pancreatitis worse; whether such data can be extrapolated to humans is unknown.

Currently a laparoscopic surgical approach is preferred but timing is controversial. Patients with mild gallstone pancreatitis can safely undergo an operation within the first week or so, but early surgery in severe biliary pancreatitis is associated with increased mortality and morbidity. On the other hand, a prolonged time interval between onset of biliary pancreatitis and subsequent surgery risks a recurrence of pancreatitis.

A prophylactic sphincterotomy can be performed as an alternative to cholecystectomy in patients with gallstone pancreatitis who are at increased surgical risk, such as with severe cardiopulmonary, hepatic, and renal disease. Sphincterotomy decreases the risk of a new episode of acute pancreatitis, although a cholecystectomy is eventually performed in most patients with gallstone-induced pancreatitis.

Necrotizing Pancreatitis

Necrotizing pancreatitis can be defined as necrosis of pancreatic glandular tissue, surrounding fat, interstitial tissue, and associated with regions of hemorrhage. Pancreatitis due to almost any etiology can evolve into pancreatic necrosis, although in many centers pancreatitis due to a biliary etiology predominates.

Infection of necrotic pancreatic tissue is generally considered an indication for surgical debridement. Infection is most often bacterial, especially coliform in origin, but an occasional fungal infection is encountered. Mortality in severe infected pancreatic necrosis is often due to multiorgan failure.

A fluid collection can be defined as not drainable if imaging identifies solid necrotic debris >1 cm in diameter. In general, MRI appears to predict drainability better than CT or US.

Endoscopic drainage therapy is feasible in patients with extensive pancreatic necrosis. Resolution can be achieved nonoperatively in some patients by endoscopic drainage via stents and the placement of an intrapancreatic nasobiliary lavage catheter.

Another option is CT- or US-guided percutaneous catheter drainage and transcatheter debridement of infected pancreatic necrosis as the primary means of therapy. Debris is removed during multiple sessions using a combination of large-bore suction catheters, stone baskets, and large amounts of lavage fluid. Results of such drainage are mixed.

Surgeons continue to debate the merits of early versus delayed surgery in severe necrotizing pancreatitis. Some studies suggest no difference in mortality rates between early and delayed surgery (33), but other find delayed necrosectomy superior.

Major hemorrhage is a complication after surgical management of pancreatic necrosis; most often such bleeding is controlled surgically, although in selected patients angiographic therapy is useful.

Prognosis

Several studies have found no differences in clinical course and outcome when patients with acute pancreatitis are subdivided by etiology into the categories (1) alcohol, (2) gallstones, and (3) other, except that pancreatic pseudocysts develop significantly more often in alcoholics than in patients with other etiologies. Another exception to the above is with ERCP-induced acute pancreatitis (see Endoscopic Retrograde Cholangiopancreatography Induced, above). Tissue necrosis and pancreatic failure determine the mortality and morbidity of acute pancreatitis. The overall mortality rate in patients with acute necrotizing pancreatitis increases in those with infection (33).

A number of indexes have been developed to predict the severity and outcome of acute pancreatitis. Clinically, the severity of acute pancreatitis is evaluated using the Ranson prognostic factors, Glasgow, or Hong Kong criteria or the APACHE II score, while imaging relies on contrast-enhanced CT criteria or the Hill classification.

A consecutive series of patients with acute pancreatitis was used to predict the severity acute pancreatitis; the Hong Kong criteria achieved a sensitivity of 52% and specificity of 80%, the Ranson criteria values were 79% and 56%, and the Glasgow score was 83% and 60%, but the best prediction was provided by the APACHE II score (24 hours postadmission), with a sensitivity of 79% and specificity of 82% (34). While a correlation exists between clinical and imaging classifications at the two extremes

of disease, in general the clinical APACHE II score and contrast-enhanced CT criteria do not yield similar results in many of these patients; the APACHE II score appears superior to CT criteria as an indicator of disease severity.

The overall mortality in patients with severe acute pancreatitis is almost 50%.

Focal Pancreatitis

At times acute pancreatitis involves only a portion of the pancreas, with such focal pancreatitis then evolving into chronic changes limited to a segment of the pancreas. A separate description here of focal pancreatitis is not meant to imply that it is a separate disease entity; rather, its importance lies in its mimicry of pancreatic cancer.

An annular pancreas, with pancreatitis limited to the annular portion, has already been discussed. Some descending duodenal stenoses are secondary to focal pancreatitis in the annular segment.

A history of acute or chronic pancreatitis is often lacking in those with focal pancreatitis. Most often focal pancreatitis involves the pancreatic head. Computed tomography shows focal pancreatitis to be hypodense and US reveals hypoechoic tumors. It tends to be hypervascular at angiography.

Groove Pancreatitis

One form of segmental chronic pancreatitis is called "groove pancreatitis." The groove is located between the pancreatic head, the duodenum, and the common bile duct. Why focal pancreatitis should develop preferentially in this location is puzzling, although this region of the pancreas is drained by the duct of Santorini, and obstruction of this duct or aberrant ducts may play a role. Relation of this entity to focal annular pancreatitis is conjecture.

A typical appearance is a tumor simulating a pancreatic head carcinoma; differentiation between the two entities is difficult at best, and some of these patients undergo resection. Some develop a duodenal stricture.

Magnetic resonance imaging in five patients revealed a sheet-like tumor between the pancreatic head and duodenum (35); these tumors were hypointense relative to the pancreas on T1- and iso- to slightly hyperintense on T2-weighted images and had delayed contrast enhancement. Histology revealed fibrosis.

Inflammatory Pseudotumor

A number of pancreatic *inflammatory pseudotumors* have been described. Whether these should be considered a type of focal pancreatitis or as a separate entity is not clear.

Computed tomography detects an inflammatory pseudotumor of the pancreas simply as a large tumor; histology shows a mixed infiltrate of spindle cells, lymphocytes, histiocytes, and plasma cells.

Chronic Pancreatitis

Even repeat bouts of acute pancreatitis do not necessarily lead to chronic pancreatitis. In fact, clinical evidence suggests that chronic pancreatitis is a de novo condition and that acute and chronic pancreatitis should be considered separate diseases.

The most common cause of chronic pancreatitis in North America and Europe is alcohol related.

Classification

No universally acceptable classification of chronic pancreatitis exists. The diagnostic criteria of chronic pancreatitis using ERCP criteria were proposed by the Japan Pancreas Society in 1995 and are used by some. The Marseilles classification defines chronic pancreatitis as continued inflammation of the pancreas associated with irreversible damage. The pancreas may be involved focally or diffusely, and there is loss of both exocrine and endocrine function. Abdominal pain is a constant feature in the vast majority of patients.

Etiology

Many of the etiologies causing acute pancreatitis are also responsible for chronic pancreatitis. Nevertheless, some conditions lead primarily to chronic inflammation (Table 9.2). Aside from cystic fibrosis and hereditary pancreatitis (see Congenital Abnormalities), chronic pancreatitis is rare in children and adolescents. Some families with familial hyperlipidemia, cystic fibrosis,

Table 9.2. Conditions associated with chronic pancreatitis

Mostly in young patients
Hereditary (familial) pancreatitis
α_1-Antitrypsin deficiency
Familial hyperlipidemia
Cystic fibrosis
Familial hyperparathyroidism
Congenital syphilis
Idiopathic fibrosing pancreatitis of childhood
Chronic calcific pancreatitis
Tropical calcific pancreatitis
Pancreatitis in severe protein malnutrition
Infection
Viral
Tuberculous pancreatitis
Amebic pancreatitis
Schistosomiasis
Autoimmune pancreatitis
Idiopathic
Associated with Sjögren's syndrome
Associated with sarcoidosis
Sequelae of pancreatic trauma
Associated with ulcerative colitis

and hyperparathyroidism have a higher than normal prevalence of chronic pancreatitis. α_1-Antitrypsin deficiency is typically associated with pulmonary disease; in rare instances it may be associated with chronic pancreatitis.

Chronic pancreatitis has been associated with ulcerative colitis; the several reported patients suggest a possible nonfortuitous relationship between these two entities. The prevalence of chronic pancreatitis is low in primary sclerosing cholangitis, and the occasional synchronous finding is probably by chance. Some cirrhotic patients have ERCP findings consistent with chronic pancreatitis. These changes are found even in nonalcoholic cirrhotic patients.

Clinical

Idiopathic Fibrosing (Autoimmune)

A syndrome of idiopathic fibrosing pancreatitis, also called chronic relapsing pancreatitis of childhood, is a rare form of chronic pancreatitis, often developing in children and young adults. Etiology is unknown, although an autoimmune basis is postulated. Its relationship to autoimmune hepatitis, a well-established entity, is not clear.

Pain is a common feature. These patients have developed obstructive jaundice, but pancreatic insufficiency is not a prominent feature in this entity.

A curious form of chronic pancreatitis is centered on the pancreatic ducts, called *autoimmune pancreatitis*, *sclerotic pancreatitis* and *lymphoplasmacytic pancreatitis*. Whether these represent the same entity is conjecture. Imaging reveals either a focal pancreatic tumor or the entire pancreas is enlarged and is hypoechoic with US. Pancreatography in patients with autoimmune pancreatitis reveals an irregular and narrowed main pancreatic duct; some patients develop pancreatic duct obstruction. Neither pancreatic duct dilation nor calcifications develop (36). A focal pancreatic tumor, often with pancreatic duct obstruction, is not an uncommon presentation, and surgery for suspected pancreatic cancer is performed. Retroperitoneal fibrosis develops in an occasional patient (37). Resection, often for suspected pancreatic cancer, reveals pancreatic fibrosis and, at times, an eosinophilic infiltrate. Fibrosis, of course, is not limited to this condition and is common in chronic calcifying pancreatitis. Disease often recurs in the remnant pancreas. Their pancreatitis tends to respond to steroid therapy.

An autoimmune mechanism appears to be involved in Sjögren's syndrome, and the first sign of Sjögren's syndrome can be evidence of chronic pancreatitis. A not untypical scenario is the patient with a narrowed distal common bile duct believed to be neoplastic in origin, but resection reveals inflammation and fibrosis.

Chronic Obstructive

Duct obstruction with little or no evidence of stones is classified an a separate etiology for chronic pancreatitis. Yet this term is also a descriptive one representing a stage in evolution of chronic pancreatitis due to a number of etiologies, including secondary to inflammation of sphincter of Oddi, acute pancreatitis, or even a malignant tumor. Some patients diagnosed with chronic obstructive pancreatitis do develop ductal stones and, similarly, of those with chronic calcifying pancreatitis not all

have calcifications throughout their disease course.

Chronic Calcifying

Chronic calcifying pancreatitis is most often associated with chronic alcohol consumption; gallstone pancreatitis rarely progresses to calcifying pancreatitis. An exception to this is a young patient with gallstone pancreatitis and pseudocysts who eventually develops pancreatic calcification; superimposed hereditary pancreatitis may play a role in some of these patients.

The presence of pancreas divisum does not change the course of chronic calcifying pancreatitis; in these patients pancreatitis may involve only the ventral segment, only the dorsal segment, or occur throughout the pancreas; in about half of these patients detected abnormalities are segmental.

Tropical Calcific

Tropical calcific pancreatitis generally starts in childhood. The etiology is not known, although these patients tend to have underlying nutritional deficiencies.

Tuberculous

Isolated tuberculous pancreatitis or a pancreatic abscess are rare. This entity is more often seen in association with lung tuberculosis.

Peripancreatic and mesenteric lymph nodes are often also enlarged, bowel wall is thickened, and ascites is present. Some patients have hepatosplenic involvement and splenic vein thrombosis. Tuberculous pancreatitis presents as a pancreatic tumor, at times containing cystic components, and tends to mimic a primary pancreatic neoplasm, including an appearance of vascular invasion. Some patients undergo laparotomy for suspected cancer. Attempted resection risks formation of a pancreatic fistula and miliary peritoneal dissemination.

Focal tuberculomas are hypodense on CT. US shows inhomogeneous hypoechoic tumors within the pancreas. A cystic component may be evident. Endoscopic US is often compatible with a cystic pancreatic neoplasm.

Even ERCP reveals a stricture, and pancreatic duct displacement can mimic a neoplasm.

Other Etiologies

Eosinophilic pancreatitis is a rare entity of unknown etiology. It mimics a pancreatic neoplasm. An 18-year-old man presented with obstructive jaundice, epigastric pain, and weight loss, endoscopic US detected a small round, hypoechoic tumor in the head of the pancreas, an endocrine tumor was suspected, and a duodenopancreatectomy performed (38). An ERP in another man with weight loss and obstructive jaundice identified a narrow, smooth main pancreatic duct and a tight common bile duct stenosis (38). Both patients were eventually diagnosed with eosinophilic pancreatitis.

Hydatid disease of the liver as a cause of pancreatitis has been mentioned above (see Acute Pancreatitis). Direct pancreatic involvement is rare. These cystic lesions tend to be misdiagnosed as pseudocysts and ascribed to pancreatitis or trauma. About half of the cysts occur in the head of the pancreas, a somewhat uncommon location for pseudocysts. Calcifications may develop.

Pancreatic inflammation and fibrosis develop in congenital syphilis.

In the Middle East, schistosomiasis (due to *Schistosoma mansoni* and *Schistosoma haematobium*) leads not only to hepatobiliary but also to pancreatic calcifications.

A hydatid cyst in the head of the pancreas can result in obstructive jaundice.

Malignant Potential

Although pancreatic cancer is often associated with surrounding pancreatitis, the risk of carcinoma developing in a setting of chronic pancreatitis is not known. Histology in patients with advanced chronic pancreatitis revealed duct epithelial hyperplasia in 31%, focal squamous metaplasia in 21%, cellular dysplasia in 8%, and dysplastic acinar nodules in 21% (39); overall, extensive pancreatic fibrosis was associated with epithelial anomalies in 66% of patients.

Pathology

Acinar atrophy, acinar dilation, and intralobular fibrosis are typical histologic findings, although a diagnosis of chronic pancreatitis is not always straightforward, even for pathologists.

Autopsies in patients with chronic alcohol abuse reveal two distinct pathologic patterns of fibrosis: either perilobular or intralobular, suggesting different etiologic factors (40). The perilobular type is irregular, occasionally patchy, and when advanced extended into intralobular regions to the point of completely replacing pancreatic tissue by fibrosis. Intralobular fibrosis, on the other hand, is uniform in distribution. Such ancillary findings as protein plugs, pancreatic duct hyperplasia and stones, extensive intra- and peripancreatic fibrosis, splenic vein and bile duct involvement, and pseudocyst formation are more common with perilobular fibrosis. Associated liver cirrhosis is greater with intralobular fibrosis.

Imaging

The imaging differential of chronic pancreatitis includes changes found in the elderly; one should keep in mind that some degree of pancreatic atrophy and scaring and dilation of pancreatic ducts occur in elderly patients with no previous history of pancreatitis. Also, residual duct scarring after a bout of severe acute pancreatitis is not a sign of chronic pancreatitis.

In a setting of chronic pancreatitis the gland atrophies, pancreatic ducts dilate, and stasis of pancreatic secretions occurs, even without obstruction. The etiology for such stasis and duct dilation is incompletely understood, but includes chronic duct wall inflammation, dilation of capillaries, and loss of duct epithelium; duct obstruction results in reflux of luminal content into extracellular space. A tortuous and beaded duct appearance is common.

Endoscopic US is considerably more sensitive than abdominal US in diagnosing chronic pancreatitis. Sensitivity for ERCP is only about 75%, but specificity approaches 100%. Whether CT or MRI is more sensitive in detecting early changes of chronic pancreatitis is arguable; CT detects subtle calcifications better, but MRI is better at identifying fibrosis.

Computed Tomography

A CT finding of focal pancreatic enlargement often raises the possibility of a pancreatic malignancy. Pancreatic duct dilation is nonspecific and is found in pancreatitis or malignancy, or is a normal finding in the aged.

Ultrasonography

Sonographic pancreatic texture in chronic pancreatitis ranges from hypoechoic to hyperechoic, with the latter representing calcifications.

A controversy in endoscopic circles is whether in chronic pancreatitis endoscopic US is preferred over ERCP. Abnormal findings may be detected earlier with endoscopic US than with ERCP. In a setting of chronic pancreatitis, endoscopic US and ERCP show good correlation in measuring the size of the duct of Wirsung. Duct dimensions on ERCP tend to be larger than those obtained with other imaging modalities because of x-ray magnification and distention with contrast. Endoscopic US reveals dilatation of the main pancreatic duct, heterogeneous echogenicity of the pancreatic parenchyma, and small cysts. Endoscopic US detects pseudocysts and occasionally may suggest a superimposed pancreatic carcinoma.

Magnetic Resonance Imaging

Atrophy, a heterogeneous appearance, and a dilated pancreatic duct are common MR findings in chronic pancreatitis. Fibrosis tends to decrease the signal intensity on T1-weighted fat-suppression images. Decreased heterogenous arterial phase contrast enhancement is common; nevertheless, gadolinium enhanced MRI in patients with chronic pancreatitis and pancreatic carcinoma can show similar abnormal pancreatic enhancement in both entities. The two cannot be distinguished based on degree and time of enhancement (41).

Magnetic resonance cholangiopancreatography tends to overestimate pancreatic duct stenosis and underestimate the dilation of secondary branches and filling defects in the pancreatic duct (42), but it is superior to ERCP in depicting that part of the pancreas distal to an obstruction.

Pancreatography

Pancreatography findings in patients with chronic pancreatitis and an inflammatory tumor range from a smooth or irregular stenosis, to obstruction or a patent duct; the length of

stenosis varies. The pancreatic duct distal to the tumor is dilated in about three fourths of patients. Irregular dilation of secondary pancreatic ducts develops throughout the pancreas in some patients with diffuse mild chronic pancreatitis. When localized, similar changes are also found with neoplasms or simply reflect changes seen with age.

The secretin-pancreozymin test and ERCP concur in most patients with chronic pancreatitis. A majority of patients with an abnormal ERCP but normal secretin-pancreozymin test have a prior history of acute pancreatitis, but no clinical or laboratory evidence of chronic pancreatitis. Thus both tests complement each other when chronic pancreatitis is suspected because ERCP tends to overdiagnose this condition. Secretin-stimulated MRP in patients with chronic pancreatitis visualizes more pancreatic duct segments and secondary ducts and more stenoses and intraluminal defects than presecretin (43). At times acinar filling develops postsecretin in chronic pancreatitis. This test also aids in assessing pancreatic exocrine function. Thus reduced duodenal filling postsecretin in patients with chronic pancreatitis achieved a 72% sensitivity and 87% specificity in detecting decreased function (44).

Calcifications

The only reliable and almost pathognomonic imaging finding of chronic pancreatitis is pancreatic calcifications, readily identified by both CT and conventional radiography (Fig. 9.8). A majority of these calcifications are intraductal in location, in either the main duct or side branches. These calcifications are multiple and vary in size. They may be limited to a portion of the pancreas or be scattered throughout. With time, these calcifications remain static or increase in extent, although in an occasional patient they may decrease. The extent of calcification has a poor correlation with the degree of pancreatic exocrine dysfunction.

Occasionally similar calcifications develop in severe protein malnutrition. Pancreatic parenchymal calcifications may also develop after direct trauma to the pancreas and possibly after ischemia. Biliary and pancreatic calcifications have been reported in schistosomiasis.

It has been observed that patients with chronic pancreatitis have a higher prevalence of aortic calcification than a control population (45).

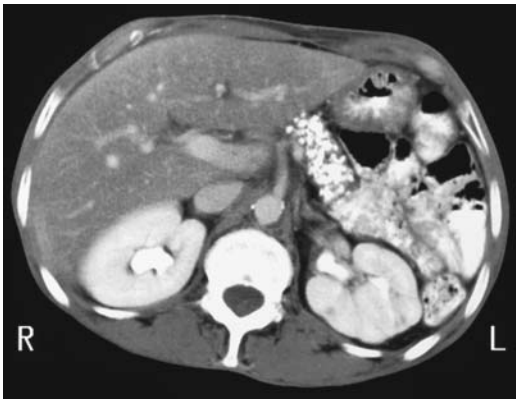

Figure 9.8. Chronic pancreatitis. Computed tomography reveals extensive calcifications that have replaced most of the pancreatic parenchyma. (Courtesy of Patrick Fultz, M.D., University of Rochester.)

Therapy

Most therapy in chronic pancreatitis revolves around attempts to control pain. Confounding treatment is that pain disappears spontaneously in some of these patients.

Endoscopic

One source of pain in these patients is increased pancreatic duct pressure. Endoscopic sphincterotomy or main pancreatic duct stenting reduces this pressure, and these patients have rapid pain resolution; in many of these patients such therapy is only temporary, however, and they will need to undergo more definitive procedures. A stent can be inserted in most patients even with pancreatic duct disruption. With a stricture or stone distal to the disruption and pseudocyst formation, a cystoenterostomy (either gastric or duodenal) is also necessary.

Endoscopic catheter and balloon techniques have evolved to the point that a number of main pancreatic duct concretions can be removed; currently this is not possible with calculi located in secondary branches. Therefore, if stone therapy is contemplated, it is useful

to know a specific concretion location. This information can be provided by CT and subsequent 3D reconstruction.

Two patients with chronic pancreatitis and multiple calcifications in the main and accessory pancreatic ducts underwent intraductal infusion of citrates through a nasopancreatic catheter (46); the stones fragmented and dissolved.

Extracorporeal Shock-Wave Lithotripsy

Extracorporeal shock-wave lithotripsy (ESWL) is viable initial therapy in patients with chronic pancreatitis and stones in the main pancreatic duct unretrievable by ERCP. Published results are encouraging. Stones are disintegrated and complete stone clearance obtained in 75% to 80% of patients. A combined endoscopic-ESWL approach is often used. Clinical pancreatitis is rare after ESWL therapy. Not all patients are cured of their pain, and some eventually required a Whipple or Puestow procedure for relief of symptoms or persistent obstruction.

Surgical

Partial common bile duct obstruction is common in chronic pancreatitis. Without relief of obstruction, these surgical high-risk patients progress to cholangitis and cirrhosis. Biliary imaging provides a road map for surgical planning. Common surgical procedures to relieve intrapancreatic biliary obstruction are choledochoduodenostomy or choledochojejunostomy.

A Puestow procedure consists of a lateral side-to-side pancreaticojejunostomy, useful to decompress a dilated pancreatic duct (Fig. 9.9). If no pancreatic tissue is resected, little change in existing endocrine or exocrine function should be evident. Computed tomography identifies most of these pancreaticojejunal anastomoses located anterior to the pancreatic body or tail; fluid, gas, or oral contrast is evident next to the anastomosis in some. Such fluid or gas either close to the anastomosis or in an adjacent Roux-en-Y loop should not be confused with an abscess. Complications of a Puestow procedure include fluid collections, abscess, pseudocyst, hematoma, and small-bowel or Roux-en-Y obstruction.

Partial pancreatic resection is considered for a failed pancreaticojejunostomy, localized disease, or if the pancreatic duct is not dilated. With resection of pancreatic head and duodenum (Whipple procedure), a Roux-en-Y is performed and the common bile duct and residual pancreatic duct anastomosed to the jejunum. A complication after this operation is breakdown at the pancreaticojejunostomy. As a result, pancreatic duct anastomosis into the stomach has become common; an anastomotic breakdown here is less likely. A duodenum-preserving pancreatic head resection together with a pancreaticogastric or pancreaticojejunal anastomosis is a viable alternative in some centers (Fig. 9.10).

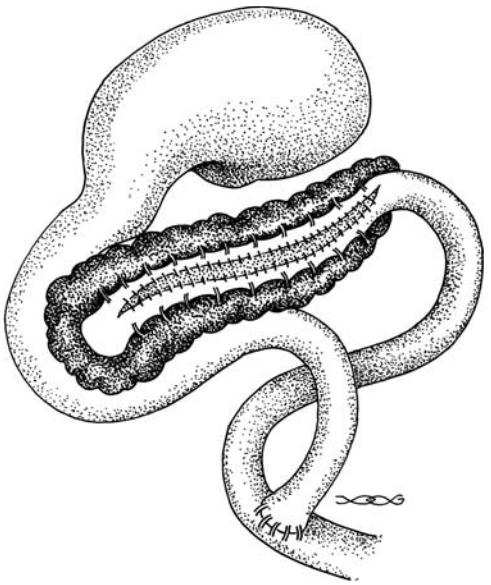

Figure 9.9. Appearance of a lateral side-to-side pancreaticojejunostomy (Puestow procedure).

A distal pancreatectomy is performed if disease is limited to the body or tail of the pancreas. Patients undergoing a distal pancreatectomy have a better outcome than those with a pancreaticoduodenectomy or pancreaticojejunostomy).

Complications of Pancreatitis

Pancreatic necrosis and infection were discussed in a previous section. The complications covered here include pancreatic and gastrointestinal fistulas, pseudocysts, and changes involving other structures.

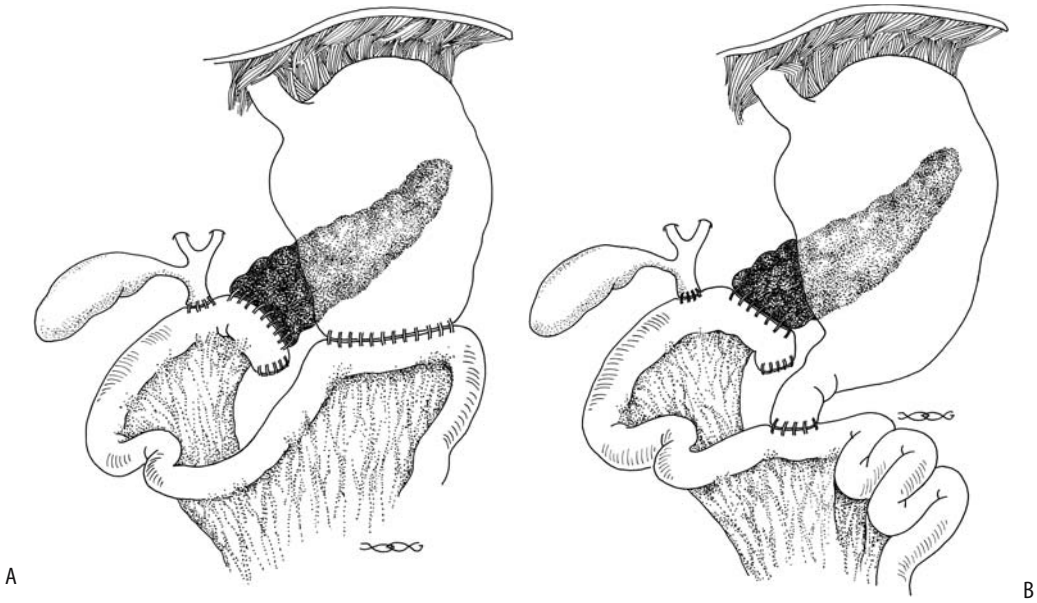

Figure 9.10. Schematic of a pancreaticoduodenectomy (Whipple procedure). A: A pancreaticojejunostomy is proximal to the choledochojejunostomy and a gastrojejunostomy is more distal. B: A similar procedure to that in part A, except that a pylorus-sparing duodenojejunostomy is substituted for the gastrojejunostomy. The biliary anastomosis can be studied via a T-tube and the gastric anastomosis with oral contrast, but the pancreaticojejunostomy is not readily accessible. Indirect evidence of a breakdown of this anastomosis is provided by CT detection of an abscess in this region. In place of a pancreaticojejunostomy some surgeons perform a pancreaticogastrostomy.

Fistulas

Pancreatic duct disruption leads to an undrained collection and pseudocyst formation; in a similar setting a pancreatic fistula forms after necrosectomy and external drainage. In general, the mortality rate is higher with a gastrointestinal fistula as compared to a pancreatic fistula or pseudocyst. A persistent pancreatocutaneous fistula develops in about half of patients after percutaneous drainage of pancreatic fluid collections (47); whether a fistula develops or not appears related primarily to the severity of pancreatitis rather than to its cause. A pancreaticopleural fistula is rare.

An occasional pancreatic duct fistula is visualized by ERCP. Some of these fistulas are also identified by CT and US. Biliary scintigraphy appears worthwhile with a suspected biliary fistula developing in a setting of chronic pancreatitis.

Anecdotal reports describe fibrin glue being used to successfully occlude these fistulas.

Pseudocyst

Clinical

Pancreatic pseudocysts develop in both acute and chronic pancreatitis. It takes 4 to 6 weeks for a pseudocyst to "mature" and form into a well-defined structure with an identifiable wall. These cysts can be classified as intrapancreatic or extrapancreatic in location; the location is best defined with CT. A mature cyst may or may not communicate with the pancreatic ductal system; such communication is best established with ERCP. Noncommunicating cysts are probably secondary to necrotic liquefaction of pancreatic tissue or prior limited communication with pancreatic ducts. In chronic pancreatitis the cysts generally communicate with ducts and tend to be associated with main pancreatic duct obstruction.

Although the most common site for pseudocysts is around the tail of the pancreas, they have been reported in almost any location in the

abdomen and occasionally even in the chest. Pseudocysts have developed in intrahepatic and intrasplenic locations. They have involved both the right and left liver lobes. A pseudocyst originating from the tail of the pancreas has extended into the left renal space and has mimicked a renal cyst on CT.

Pseudocysts vary considerably in size. Most small pseudocysts resolve spontaneously. The wall of some chronic pseudocysts calcifies. Pseudocyst content amylase and lipase levels do not correlate with exocrine pancreatic function, and cyst enzyme levels vary considerably between consecutive punctures of the same cyst; with noncommunicating cysts the pseudocyst content differs from pancreatic juice.

Diagnosis

Computed tomography of an uncomplicated pseudocyst shows fluid of near-water density. Either hemorrhage or infection increases attenuation. Pseudocysts have smooth margins (Fig. 9.11).

An uncomplicated pseudocyst is anechoic, but hemorrhage, debris, or infection produces a heterogeneous complex echo pattern. Blood clots appear as a solid component.

An MRCP readily detects these cystic structures. Communication with pancreatic ducts is not as readily apparent as with ERCP.

It is worthwhile to emphasize that not all pancreatic cysts are pseudocysts. Cystic pancreatic neoplasms and true cysts are also in the differential diagnosis. About three quarters or more of all pancreatic cysts are pseudocysts secondary to pancreatitis, with the others being primarily neoplastic. Complicating the issue is that some pancreatic neoplasms are associated with pancreatitis. It is essential to differentiate among a pseudocyst, a neoplastic cyst, and other nonneoplastic cysts. A number of reports describe what initially appears to be a pseudocyst, which is treated by a cystenterostomy, with subsequent dire consequences. Even a gastric duplication has been misdiagnosed as a pancreatic pseudocyst. A cystic neoplasm should be considered especially in patients without a history or risk factors for pancreatitis.

A reverse misdiagnosis can also occur. Thus imaging in a 37-year-old asymptomatic man being investigated for hypertension detected two small cysts and a larger unilocular cyst containing a mural nodule in the pancreas; ERCP showed communication of the pancreatic duct with a cyst but no ductal changes, suggesting chronic pancreatitis was evident and a tentative diagnosis of a malignant mucinous cystic neoplasms was made (48). Intraoperative frozen section of the cyst wall revealed a pseudocyst, with mural nodules representing sludge within the pseudocyst.

A cystic pancreatic neoplasm and a pseudocyst have a similar US appearance. Serial US, especially if obtained early in the formation of a pseudocyst, aids in differentiating between these two. When small, an aneurysm is also in the US differential diagnosis; Doppler US should differentiate these.

The relative MR signal intensity on T1-weighted images of pseudocysts, other benign cysts, and cystic neoplasms overlaps. Other rare cystic nonneoplastic pancreatic lesions include retention cysts and simple cysts.

Figure 9.11. Pseudocyst in pancreatic head, an unusual location (arrow). (Courtesy of Patrick Fulz, M.D., University of Rochester.)

Pseudocyst Complications

A pseudocyst can rupture into any adjacent structure. Spontaneous rupture into surrounding structures results in surrounding inflammation and possible sinus tracts between the pseudocyst and duodenum. Perforation can occurred into the colon. A pseudocyst can erode into the portal vein, with embolization of pseudocyst content into the intrahepatic portal vein branches. Rupture into the peritoneal cavity results in acute peritonitis. Differentiation from infected pancreatic ascites is difficult.

Prevalence of pseudoaneurysms in pancreatitis patients is difficult to gauge but probably is around 10%. Many of the smaller ones remain silent unless rupture occurs or they are discovered with an imaging study. Spontaneous arterial hemorrhage associated with a pseudocyst is not uncommon. The involved vessel becomes dilated (pseudoaneurysm formation) and ruptures. Bleeding is into the pseudocyst, intraperitoneal, into the gastrointestinal tract, through the papilla of Vater (hemosuccus pancreaticus), or into any structure surrounding the cyst. Bleeding is generally from one of the peripancreatic arteries (49), although any nearby artery, including the splenic artery and even the middle colic artery, can be involved. Bleeding ranges from slow to massive to the point of exsanguination.

Contrast-enhanced CT should detect high attenuation blood within a pseudoaneurysm. During an acute bleed CT may detect extravasating contrast.

Ultrasonography identifies an aneurysm as a cyst, often with an adjacent crescent rim. Doppler US should detect blood flow and allows differentiation of a pseudoaneurysm from a pseudocyst or other fluid collection.

Angiography allows transcatheter embolization of the feeding vessel. Although embolization arrests most acute bleeding, it may recur and require reembolization. Steel coil embolization is more successful than Gelfoam embolization. Unsuccessful bleeding artery embolization usually necessitates a pancreatectomy (49).

Infection turns a pseudocyst into an abscess. Differentiation of a noninfected from an infected pseudocyst is an art and relies on clinical and imaging findings. Positive Tc-99m-HMPAO leukocyte scintigraphy suggests a pancreatic abscess; on the other hand, a normal scintigram points toward a noninfected pseudocyst.

A pseudocyst may obstruct any adjacent hollow viscus. Thus with bile duct compression patients develop obstructive jaundice. A rare large pseudocyst results in gastric or small bowel obstruction.

Pseudocyst Therapy

Pseudocysts are treated by a number of percutaneous (repeat cyst aspiration, external catheter drainage, transgastric catheter drainage), endoscopic (transgastric catheter, transampillary stenting, insertion of nasocystic drainage catheter), and surgical procedures. Internal drainage to the stomach or bowel has varying degrees of success. The type and degree of aggressive intervention varies depending on the expertise of the physicians involved and the traditions of the institution. Overall, a trend has been away from open surgical drainage to nonsurgical intervention. Simple aspiration has a high recurrence rate and is not often performed. Percutaneous catheter drainage has a recurrence rate similar to surgical internal drainage, but is associated with fewer complications. A percutaneous transgastric approach, with resultant internal drainage into the stomach, is used in a number of institutions with good results and a low recurrence rate. A percutaneous catheter allows serial study of cyst size and any pancreatic duct communication. A double-mushroom stent has been described to provide internal drainage into the stomach (percutaneous cystogastrostomy), thus avoiding an external catheter. Recurrence of a pseudocyst should suggest a persistent or recurrent pancreatic duct obstruction by a stone.

Endoscopic drainage of pancreatic pseudocysts is performed in some centers. Endoscopic US prior to the procedure detects any interposed larger vessels (including varices) and aids in establishing the best site for drainage. A pancreaticoportal fistula is a complication after an endoscopic cystogastrostomy (50).

In general, a high-resolution imaging study aimed at detecting any associated pseudoaneurysm is performed prior to pseudocyst drainage. If a pseudoaneurysm is detected, angiography allows confirmation and embolization.

Intrasplenic pseudocysts have been drained percutaneously. A percutaneous paraspinal, extrapleural CT-guided approach was used to drain a mediastinal pseudocyst (51).

Abscess

Some pancreatic phlegmons evolve into an abscess. A pseudocyst can become infected. The infecting agent usually is bacterial, with only an occasional one being fungal. *Klebsiella* sp., *Escherichia coli*, and *Staphylococcus aureus* predominate, and most infections contain only one organism.

The presence of gas suggests an abscess, but not all abscesses contain gas. Gas is also found secondary to an infection of necrotic pancreatic tissue with gas-forming organisms, so-called gas gangrene. An enteric communication also leads to intrapancreatic gas collections.

Computed tomography and MR show a pancreatic abscess as a thick-walled cavity containing low-attenuation fluid (Fig. 9.12). Adjacent pancreatic parenchyma usually enhances with contrast. Infected necrotic tissue, on the other hand, consists of nonenhancing or poorly enhancing liquefied pancreatic tissue.

Ultrasonography shows a pancreatic abscess as a thick-walled hypoechoic cavity. US cannot distinguish whether a focus of necrotic tissue is infected or not. Similarly, US cannot determine whether a pseudocyst is infected or not.

Percutaneous needle aspiration using imaging guidance should detect pancreatic infection. Established abscesses are amenable to percutaneous catheter drainage; necrosis, on the other hand, whether infected or not, generally requires surgical debridement.

Gastrointestinal Tract

Severe ileus is common but generally clears as pancreatitis improves.

Duodenal obstruction is a known complication of pancreatitis, with the diagnosis generally suspected clinically. An oral barium study is diagnostic. Obstruction in a setting of acute pancreatitis often clears spontaneously, but fibrosis developing in chronic pancreatitis usually requires surgical correction. No one surgical procedure is applicable in all patients, with the myriad procedures performed reflecting concomitant common bile duct and pancreatic duct obstruction in some of these patients.

Transverse colon involvement in necrotizing pancreatitis is rare but is associated with colon necrosis, perforation, and peritonitis. The sequelae also include colon stenosis.

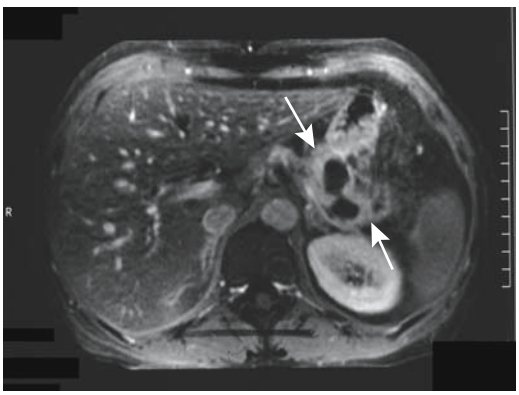

Figure 9.12. Abscess involving pancreatic tail. Contrast-enhanced magnetic resonance imaging (MRI) identifies a peripheral enhancing rim (arrows) containing nonenhancing components. (*Source:* From Burgener FA, Meyers SP, Tan RK, Zaunbauer W. Differential Diagnosis in Magnetic Resonance Imaging. Stuttgart: Thieme, 2002, with permission.)

Biliary

Occasionally severe acute necrotizing pancreatitis results not only in biliary obstruction but also in a bile duct leak or even necrosis of the adjacent common bile duct. Percutaneous biliary drainage provides temporary relief, with definitive surgical correction performed, as necessary, after pancreatitis subsides.

Fasting and postprandial gallbladder volumes are increased above normal, and gallbladder contraction is reduced in patients with chronic pancreatitis, possibly due to decreased cholecystokinin secretion.

Spleen

Splenic complications of pancreatitis are not common but include splenic infarct, subcapsular hematoma, and abscess. The absence of CT contrast enhancement of splenic parenchyma suggests a splenic infarction. A pseudocyst in the tail of the pancreas and splenic vein thrombosis led to splenic rupture (52).

Vascular

Disseminated intravascular coagulopathy is common in acute pancreatitis. Peripancreatic hematomas develop in some patients, including duodenal intramural hematomas.

Splenic vein, portal vein, or superior mesenteric vein thromboses complicate acute and chronic pancreatitis. Often such thrombosis is asymptomatic, and extensive collateral vessels are a first manifestation. Some of these patients develop gastric varices; esophageal varices are not common. Because collateral vessels bypass thrombosed veins and the intrahepatic vascu-

larity is intact, these patients tend not to develop variceal bleeding to the extent seen in patients with hepatic cirrhosis. Acute mesenteric vein thrombosis can lead to small bowel infarction. Some of these thrombi are reversible and follow-up CT identifies resolution after pancreatitis clears.

A thrombus can be detected with most imaging. Computed tomography shows a hypodense splenic vein and a normal portal vein. Gray-scale US reveals an echogenic intraluminal thrombus.

Other Complications

An occasional patient develops pleural effusion and even pericardial effusion during acute pancreatitis. Even cardiorespiratory arrest has developed secondary to chylous cardiac tamponade.

At times pancreatitis involves the peripancreatic tissues to the point of obliterating the perivascular fat planes, and imaging suggests an infiltrating carcinoma.

The development of acute renal failure in acute pancreatitis is associated with a high mortality.

Pancreatic ascites is a result of pancreatic duct disruption; it is more common in chronic than acute pancreatitis; at times massive chylous ascites develops months after onset of pancreatitis.

Intraosseous fat necrosis is a rare complication of pancreatitis (53). Most unusual was a patient with acute pancreatitis developing splenic vein thrombosis, splenic infarction, and spinal cord infarction resulting in paraplegia (54).

Dengue Hemorrhagic Fever

Epigastric pain is common in dengue hemorrhagic fever. The diagnosis is established by serologic examination and viral isolation.

Ultrasonography in children with dengue detected an enlarged pancreas in 29%, with the prevalence increasing in those with severe disease (55); relative to the liver, the pancreas was isoechoic in 69%, with the rest being either hyper- or hypoechoic. Elevated serum amylase and lipase levels were common in those with severe disease and an enlarged pancreas.

Leptospirosis

Leptospirosis rarely presents with pancreatitis. In a rare patient infection with *Leptospira icterohaemorrhagiae* mimics pancreatitis.

Clonorchis Infestation

Computed tomography identifies small pancreatic cysts in patients with pancreatitis associated with *Clonorchis sinensis* infestation (56).

Lipomatosis

Increased pancreatic fat (called *lipomatous pseudohypertrophy* by some authors) develops in obesity, chronic pancreatitis, diabetes mellitus, cystic fibrosis and other hereditary dysfunctions, long-term steroid therapy, and some viral infections. Occasionally fatty replacement is associated with a pancreatic mesenchymal neoplasm. In a rare patient lipomatosis is idiopathic. The pancreas becomes enlarged secondary to diffuse fatty infiltration. The exocrine glandular tissue is atrophic, but the islets of Langerhans tend to be preserved.

Lipomatosis is readily detected with imaging (Fig. 9.13).

Similar to the liver, focal fatty masses also develop in the pancreas. These lesions generally

Figure 9.13. Fat infiltration of pancreas associated with obesity, detected on contrast-enhanced CT. Similar changes are found in cystic fibrosis patients. (Courtesy of Douglas Katz, M.D., Winthrop University, Mineolar, New York.)

are well defined; CT shows these tumors to have the same density as peripancreatic fat. With US, they range from hypoechoic to hyperechoic.

Iron Deposition

In patients with hemochromatosis, iron is deposited not only in the liver but also in pancreatic parenchyma, and these patients develop diabetes mellitus and exocrine abnormalities. With sufficient iron deposition, MRI reveals a hypointense pancreas on T2-weighted images.

Compared to the liver, the pancreas contains limited reticuloendothelial tissue. In distinction to the liver and spleen, after blood transfusions MR reveals little pancreatic change, except that after repeated transfusions and reticuloendothelial saturation iron is deposited in pancreatic parenchymal cells, and these patients develop both endocrine and exocrine abnormalities.

Among 20 patients with transfusion-dependent β-thalassemia major, pancreas-to-fat signal intensity ratio was decreased in 85% and increased in 15% on SE T1- and fast spin echo (FSE) T2-weighted images (compared with controls) (57); a significant correlation existed between increased pancreas-to-fat signal intensity ratios and decreased serum trypsin levels and a decreased pancreas-to-fat signal intensity ratio and increased serum ferritin levels.

Amyloidosis

Primary amyloidosis of the pancreas is rare. More common is pancreatic involvement in a setting of systemic amyloidosis.

Sarcoidosis

Even with systemic sarcoidosis, pancreatic involvement is rare. In fact, most patients with pancreatic sarcoidosis have no antecedent history of sarcoidosis. The clinical presentation can mimic pancreatitis or a pancreatic malignancy, and can include jaundice. Idiopathic chronic pancreatitis can manifest at the same time as generalized sarcoidosis.

The diagnosis can be suspected if biopsies reveal noncaseating epithelioid granulomas, keeping in mind that granulomas are found as a reaction to fungi, tuberculosis, some cancers, and foreign substances. Sarcoid infiltration leads to extrinsic narrowing of the distal common bile duct or pancreatic duct.

Tumors

Differential Diagnosis of Focal Tumors

Benign focal pancreatic tumors can be divided into nonneoplastic and neoplastic (Table 9.3). Considerable overlap exists in the imaging differential diagnosis of these tumors, especially for the cystic varieties, and preoperative differentiation between a pancreatic malignancy and a benign condition continues to pose a dilemma. Most pancreatic surgeons have encountered the patient with a pancreatic tumor who undergoes a laparotomy or even resection for a suspected malignancy only to discover that the condition is benign.

Most pancreatic fibrosis involves the entire pancreas; when focal, neither CT nor US nor MR readily differentiates focal chronic pancreatitis from a malignancy (58).

Nonneoplastic

Lymphoepithelial Cyst

Pancreatic lymphoepithelial cysts are rare. These cysts are lined by squamous epithelium

Table 9.3. Benign focal tumors of the pancreas

Nonneoplastic	Neoplastic
Mostly solid:	
Hemangioma	Papilloma
Teratoma	Adenoma
Extramedullary hematopoiesis	Solid neuroendocrine tumors
Accessory spleen	Giant cell tumor
	Paraganglioma
	Solid mesenchymal neoplasms
Mostly cystic:	
Pseudocyst	Microcystic adenoma
Abscess	Mucinous cystic adenoma
Cystic teratoma	Cystic neuroendocrine tumor
Epithelial cyst	Papillary cystic adenoma
Lymphangioma	Cystic mesenchymal neoplasms
Aneurysm	Hemangiopericytoma

and are surrounded by lymphoid tissue. They occur throughout the pancreas and some are even exophytic in location. Their etiology is not known.

The imaging findings of these nonneoplastic cystic tumors are similar to those seen with a mucinous cystic pancreatic neoplasm. Imaging of a pancreatic lymphoepithelial cyst reveals a heterogeneous water-density tumor, often containing septa. Endoscopic US is useful to confirm the presence of septa, a somewhat nonspecific finding. In two lymphoepithelial cysts a lipid component was detected by CT and MRI (59). Some have multiple cystic regions and rim calcifications. With most of these cysts a diagnosis is established only after resection.

Lymphangioma

Pancreatic lymphangiomas are rare. These usually multilocular cystic nonepithelial tumors are lined by endothelial cells and are filled with serous fluid or chyle. Ten of these tumors, in patients ranging in age from 2 to 61 years at initial presentation, were collected by the Endocrine Pathology Registry of the Armed Forces Institute of Pathology (60); six were in the tail of the pancreas.

Computed tomography of two lymphangiomas revealed complex cysts containing septa and thin and regular walls, some calcified (61).

Other Tumors

A rare intrapancreatic accessory spleen has been described. These are hypervascular on CT and isointense to the spleen on MRI. At times scintigraphy is useful to confirm activity.

An inflammatory pseudotumor is more common in the liver than in the pancreas. Imaging of these solid tumors reveals findings similar to a malignancy (62); a histopathologic study is necessary for diagnosis.

Benign Neoplasms

Other benign pancreatic neoplasms are discussed in a later sections (see Cystic Neoplasms, and Neuroendocrine (Islet Cell) Tumors).

Papilloma/Papillomatosis

Not all solid pancreatic tumors are malignant. A papilloma can be quite large. The diagnosis is established by fine-needle aspiration cytology. Diffuse papillomatosis may involve both the pancreatic ducts and bile ducts.

Adenoma

An intraductal adenoma is rare. These are premalignant tumors and some already contain a carcinoma in situ. Even small adenomas in the main pancreatic duct can be associated with acute pancreatitis.

Benign Stromal Tumors

Stromal (mesenchymal) tumors are very rare in the pancreas. Benign varieties include fibroma, fibromyoma, lipoma, lymphangioma, hemangioma, schwannoma, and leiomyoma. They range from solid to cystic in appearance.

Fat-containing pancreatic tumors consist of focal fatty deposits, lipoma, liposarcoma, and a mixed mesenchymal tumor such as a fibrolipoma or cystic teratoma. Although fatty infiltration of the pancreas is common, a lipoma is rare. A lipoma is identified by CT as a well-defined, focal, homogeneous tumor ranging in density from −80 to −120 HU and no contrast enhancement. An MRI reveals similar findings. Ultrasonography shows a solid hypoechoic tumor. Favoring a lipoma is a homogeneous tumor containing a well-defined margin. Lipomatosis is more diffuse in extent. Focal lipomatosis lacks a surrounding capsule but otherwise is similar to a lipoma.

Malignant Neoplasms

Adenocarcinoma

Clinical

General

Adenocarcinoma of the pancreas is the fourth leading cause of cancer death in the United States and the incidence continues to increase in the Western world. It is more common in males. Typically, the cancer is discovered when it has already spread extensively.

About two thirds of pancreatic carcinomas originate in the head of the pancreas. Jaundice is typically the initial presentation, and an enlarged, nontender gallbladder is often palpable (Courvoisier gallbladder). Occasionally, however, even a large pancreatic head tumor will not obstruct bile ducts. Duodenal obstruction initially is uncommon with a pancreatic head carcinoma, the exception being with a cancer developing in an annular pancreas, where duodenal obstruction is due directly to the cancer or, if the cancer develops in the adjacent pancreatic head, the obstruction is due to the surrounding pancreatitis. Pancreatic body and tail carcinomas present with pain and weight loss and generally extensive local invasion and metastases are already present when the tumor is first discovered.

Dull, almost constant visceral pain due to neural invasion is characteristic for these tumors. Malabsorption, steatorrhea, and weight loss ensue. Diabetes mellitus is quite common, but its etiology is puzzling. Pancreatic cancer patients show increased peripheral tissue resistance to insulin. Diabetes is an early manifestation, and long-standing diabetics are also at increased risk for pancreatic cancer.

Surrounding focal pancreatitis is common, possibly a result of duct obstruction and rupture. An occasional patient presents with pancreatitis, even with acute recurrent pancreatitis.

An association exists between deep venous thrombosis, pulmonary emboli, and pancreatic cancer. Date from the Danish Cancer Registry yields a cancer incidence ratio of 1.3 in these patients, but the risk is elevated only during the first 6 months and then declines to slightly above 1.0 at 1 year after thrombosis (63); of note is that distant metastases were already present in 40% of patients with a cancer detected within 1 year of thromboembolism.

Various paraneoplastic syndromes are more common with an acinar cell origin carcinoma. An occasional pancreatic carcinoma is preceded by seborrheic keratosis (Leser-Trelat sign); skin lesions tend to diminish after resection, but progress with tumor recurrence.

Etiology

Several risk factors are identified for pancreatic carcinoma. The relative risk of developing pancreatic cancer is about six times greater in patients who have had previous pancreatitis, with this risk beginning to increase 5 or more years after a diagnosis of pancreatitis is established. This risk appears to be independent of sex, country, and type of pancreatitis.

The initial data pointed to an association with cigarette smoking and coffee, but a Health Professionals Follow-Up Study and the Nurses' Health Study, consisting of nearly two million person-years of follow-up and 288 pancreatic cancers, concluded that neither coffee nor alcohol increases the risk for pancreatic cancer (64). Likewise, if an association with a previous cholecystectomy exists, it is a modest one at best. An increased prevalence of gallstones, however, is found in those with pancreatic cancer.

In rare families an autosomal-dominant predilection for pancreatic cancer appears to exist.

With an increase in life expectancy in patients with Hodgkin's disease after chemotherapy and radiation, the development of a second malignancy is a well-recognized entity. Among these are reports of pancreatic cancer.

An increased risk of pancreatic cancer appears to exist in patients with cystic fibrosis.

Patients with von Recklinghausen's disease are more prone to developing neuroendocrine pancreatic neoplasms than the average population, but not those of ductal origin.

Screening

Screening for pancreatic cancer is not widely practiced, and most tumors are not detected at an early tumor stage. Nevertheless, an abdominal US screening program in Japan achieved impressive results for detecting pancreatic cancer, reaching a sensitivity and specificity of 98% and 96%, respectively (65).

Ideally, screening should detect a potentially curable cancer. A definition of high-risk groups is still evolving. Detection of K-*ras* mutations in endoscopically obtained pancreatic juice is applicable only to a high-risk group. Current technology suggests CT or US as a screening tool and, if either modality suggests a pancreatic carcinoma, then endoscopic US or MRCP should be done.

Serum Markers

A number of tumor markers are available. Their current major diagnostic limitation is a lack of tumor specificity and, to a lesser extent, low sensitivity in detecting a pancreatic carcinoma.

Serum levels of CA 19-9 appear useful in discriminating pancreatic cancer from benign disease, predicting resectability, survival rate after surgery, and as a marker for recurrence. The sensitivity of CA 19-9 levels in discriminating between benign and malignant disease was 85% (66); patients with a resectable tumor had CA 19-9 levels significantly lower than those with an unresectable tumor. After tumor resection, survival for those with CA 19-9 levels returning to normal was significantly longer than for those with CA 19-9 levels not normalizing. A majority of postoperative patients developing a recurrence have increased CA 19-9 levels. Nevertheless, false-positive CA 19-9 levels occur in pancreatitis, and the specificity of this test is low.

Pathology

Pancreatic adenocarcinomas are very aggressive tumors, and at the initial diagnosis either intrapancreatic metastases or multicentric tumor origin is common. A capsule is not evident. Often a desmoplastic reaction surrounds a tumor, making it appear larger. Either the main pancreatic duct or one of its secondary branches becomes obstructed early in the course, leading to duct dilation. A prominent histologic finding is early and extensive perineural invasion, believed to account for the persistent and severe pain associated with these tumors. Vascular invasion and spread to adjacent lymph nodes is also an early finding.

Most pancreatic adenocarcinomas arise from pancreatic duct epithelium. A spectrum of changes ranging from ductal hyperplasia to carcinoma in situ are identified. Cancer variants include giant cell carcinoma, acinar cell adenocarcinoma, adenosquamous carcinoma, mucinous-type carcinoma, and probably some of the cystadenocarcinomas. A need for histopathologic diagnosis exists because about 10% of suspected pancreatic carcinomas are either not of ductal origin or not even malignant. Thus either a needle biopsy (or even cytology) or surgical biopsy is necessary.

Instead of ductal origin, an occasional neoplasm originates from pancreatic acinar cells; these include acinar cell adenocarcinomas and cystadenocarcinomas. An acinar cell adenocarcinoma is more common in elderly men and has an even worse prognosis than ductal ones. At initial presentation these tumors tend to be large and partly necrotic. For unknown reasons an occasional one is associated with subcutaneous fat necrosis. A rare carcinoma has both acinar and endocrine components.

Pancreatic adenocarcinoma in children is either ductal or acinar in origin. Early metastasis is common.

These carcinomas involve activation of the Ki-*ras* oncogene, inactivation or mutation of the *p53* tumor-suppressor gene, and dysregulation of growth factors. Additional tumor-suppression genes have been identified. Mutations in the *p53* tumor-suppressor gene are present in up to 60% of solid pancreatic carcinomas. Pancreatic adenocarcinomas DNA also yield Ki-*ras* mutations in most patients (67). Ki-*ras* and *p53* mutations are also identified in pancreatic juice from these patients, and such study may have a future role in early pancreatic cancer detection.

Early Cancer

No consensus exists for defining an early pancreatic cancer. Ideally, these should be cancers limited to duct epithelium. Follow-up of patients with tumor limited to the duct epithelium reveals a high 5-year survival rate (68), but these tumors are rarely detected.

A review of small pancreatic cancers <2 cm or stage I cancers (pooled from 15 publications) found 42% to be stage I and 58% to have no lymph node metastasis, and in almost all reports the 5-year postoperative survival rate was <50% (69); among pancreatic cancers 1 cm or less (pooled from three publications), 85% to 100% were stage I and the 5-year postoperative survival rate was 78% to 100%. Patients with 12 carcinoma-in-situ and intraductal carcinomas (pooled from four publications) were all stage I and were alive with no evidence of tumor recurrence for varying lengths of time. Based on these results, the authors propose that either pancreatic cancers <1 cm or in-situ and intraductal cancers with minimal invasion be defined as early pancreatic cancers.

The problem of defining early cancer is illustrated by a 63-year-old man who had a CT for follow-up of rectal cancer, which revealed a pancreatic cyst in the head of the pancreas; ERP showed a narrowed main pancreatic duct in the body, and MRCP identified dilated ducts draining this region (70). Cancer cells were obtained by brushing cytology, and a total pancreatectomy was performed. Two sites of invasive carcinoma were identified in the neck and body, and there were multiple foci of severe dysplasia in the body of the pancreas, with some foci containing carcinoma in situ. The cystic tumor was an intraductal papillary adenoma.

Detection

Some pancreatic cancers are associated with pancreatic stones. In most of these patients pancreatic calcifications precede the cancer and are findings of superimposed chronic pancreatitis, while in a minority stones form in dilated pancreatic ducts and cysts upstream from a cancer.

Comparison Studies

In most hands a CT diagnosis of pancreatic carcinoma is more reliable than its transabdominal sonographic counterpart. Earlier studies showed endoscopic US superior to nonhelical CT, but comparing CT with endoscopic US in detecting pancreatic carcinomas, both techniques identified a pancreatic tumor equally well, although in the diagnosis of malignancy CT appears superior. No consensus exists between the relative accuracies of CT and ERP. Most publications agree that for pancreatic cancer detection, intraductal US, a technically difficult and not readily available study, is currently superior to other imaging, especially for cancers smaller than 2 cm in diameter.

In consecutive patients suspected of having a focal pancreatic lesion (mostly adenocarcinomas), triphasic CT detected 88%, precontrast MRI 91%, and post-mangafodipir MRI 93% (71); use of mangafodipir did not significantly improve detection. Another study of thin-section CT and MRI (precontrast and post-oral and IV contrast) revealed no statistically significant differences in detecting pancreatic neoplasms (72).

General Imaging Findings

A majority of pancreatic cancers present as focal tumors and thus only a portion of the pancreas is enlarged. It is the less common infiltrative variety that is difficult to identify. At times the only imaging finding is a subtle alteration in pancreatic gland outline. Especially when a tumor originates from the uncinate process, this finding is difficult to differentiate from normal, keeping in mind that a pancreatic gland contour abnormality may be a normal variant, especially in the elderly. Distortion due to associated atrophy or pancreatitis is common.

Pancreatic head cancers tend to obstruct both the pancreatic and common bile ducts (Fig. 9.14). If obstructed, the pancreatic duct dilates; duct dilation upstream of the tumor is occasionally the only finding detected by imaging, a finding also seen in chronic pancreatitis (Fig. 9.15). An abrupt duct obstruction should raise suspicion for an underlying neoplasm; this finding is more common with a neoplasm than with chronic pancreatitis, where the entire pancreatic duct tends to be dilated. Even detection of a focal tumor is not pathognomonic; focal pancreatitis may have similar imaging findings.

Most pancreatic cancers develop in a setting of a grossly normal pancreas, but with growth, surrounding pancreatitis is common and tends

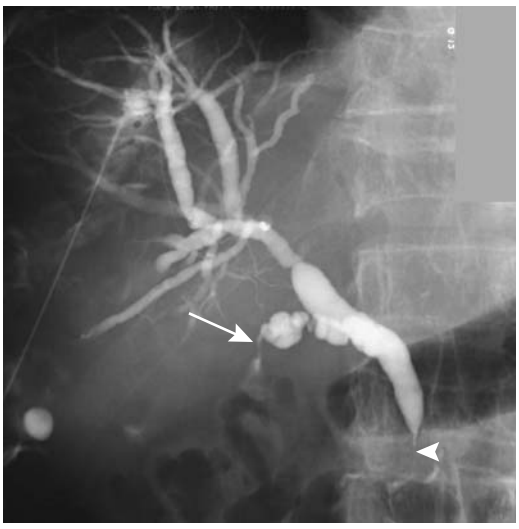

Figure 9.14. An adenocarcinoma, probably of pancreatic origin, obstructs the common bile duct (arrowhead). The cystic duct is also infiltrated (arrow).

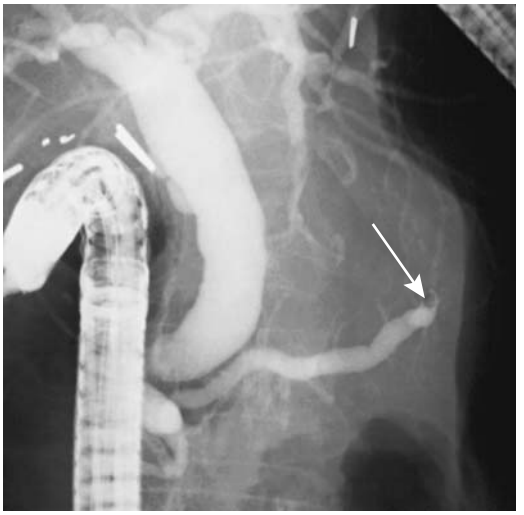

Figure 9.15. The pancreatic duct is obstructed (arrow) by a carcinoma in the pancreatic body.

to obscure a tumor. The overall appearance is often also complicated by superimposed gland atrophy. At times a carcinoma in the body or tail is sufficiently large at initial presentation that it appears as an obvious necrotic tumor (Fig. 9.16).

Computed Tomography

Computed tomography became a primary modality for pancreatic carcinoma detection early in its development. Throughout this era it was plagued by both false-negative and false-positive studies, although with equipment and software improvements both have decreased considerably. Thin-section CT, bowel distention by oral tap water, and individually determined time-to-peak contrast are some of the technical refinements applied. Current multislice CT use in pancreatic cancer detection consists primarily of arterial and portal venous images, keeping in mind that various MR techniques are making strong inroads.

Precontrast, a majority of pancreatic adenocarcinomas are detected by CT as hypo- to isodense tumors, with only about half being recognized as a discrete tumor. At times only pancreatic duct dilation is evident.

The literature is undecided about whether arterial-, parenchymal-, and venous-phase scans are necessary for tumor detection. Some investigators suggest that venous-phase scans suffice. Although some studies found no difference in tumor attenuation between arterial-phase and venous-phase CT others suggest mean tumor-to-pancreas contrast differences to be significantly greater at 40 to 70 seconds (pancreatic phase) (57–67 HU) than at 70 to 100 seconds (portal vein phase) (35–39 HU) (73). Both greater pancreatic tissue enhancement and lower tumor enhancement were evident during the earlier time frames. Surrounding vascular structures are also better opacified during earlier phase. Tumor CT density does vary, however, with delayed enhancement seen in some small lesions (Fig. 9.17). Isodense regions on both early- and late-phase postcontrast CT contain either increased tumor cellularity or a mix of acinar tissue and tumor cells; hypodense regions on early-phase images and iso- or hyperdense on late-phase images consist mostly of dense fibrosis. Hypodense regions on both early- and late-phase images and unenhanced regions represent mostly mucin or necrosis.

Postcontrast multidetector row CT shows that maximal tumor-to-parenchyma attenuation differences are equivalent during the parenchymal phase and portal venous phase, but in both phases are greater than during the arterial phase (74); subjectively, tumor conspicuity is similar during parenchymal and portal venous phases. It is this marked enhancement of normal pancreatic parenchyma during the parenchymal

Figure 9.16. Carcinoma body of pancreas. Computed tomography reveals a large necrotic tumor (arrow).

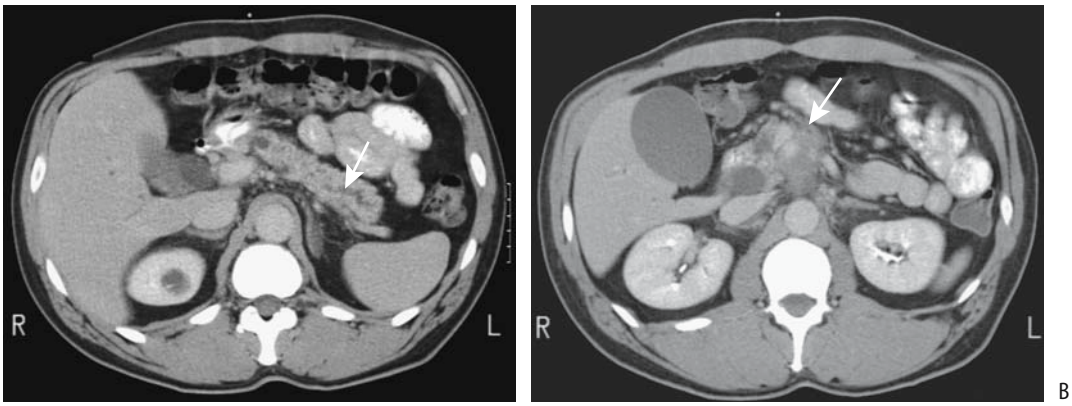

Figure 9.17. Pancreatic head carcinoma. A: Contrast-enhanced CT reveals a dilated pancreatic duct (arrow). B: An image slightly inferior also identifies a poorly enhancing tumor in the pancreatic head (arrow). (Courtesy of Patrick Fultz, M.D., University of Rochester.)

phase that provides increased detection of these hypovascular neoplasms (compared with conventional CT).

Thin-section CT outlines peripancreatic venous anatomy and detects major variations. Helical CT visualizes normal inferior pancreaticoduodenal veins in up to half of studies (75); these vessels dilate when a tumor invades the superior mesenteric vein or portal vein. Inferior pancreaticoduodenal vein invasion leads to dilation of other peripancreatic veins, such as superior pancreaticoduodenal veins and gastrocolic vein, and generally signifies tumor invasion of the third duodenal segment.

Computed tomography arteriography in 36 patients with pancreaticoduodenal tumors concluded that tumor conspicuity was not superior to that obtained with conventional IV contrast injection, except in patients with cystic tumors (76).

Ultrasonography

Based on data from the Swedish Death and Cancer Registries, a clinical diagnosis of tumor in the pancreatic region confirmed within 1 year after a US study in 140 of patients achieved an US sensitivity of tumor detection of 89% and specificity of 99%, and the authors concluded that US is a viable primary diagnostic study in patients with suspected pancreatic tumors (77).

Gray-scale US shows most pancreatic carcinomas to be hypoechoic or heterogeneous to adjacent normal parenchyma. In the aged, part of the pancreas is often hypoechoic, especially the uncinate process, making differentiation between normal and carcinoma difficult. The use of bowel hypotonia combined with gastroduodenal distention with water aids both tumor detection and in assessing resectability. Calcifications, if present, are limited to the periphery of the hypoechoic masses and most often are sequelae of prior chronic pancreatitis.

Color Doppler aids in establishing unresectability by detecting vascular occlusion and circumferential vessel encasement.

Endoscopic and intraductal US detect considerably more tumors than conventional US.

Magnetic Resonance Imaging

On T1-weighted fat-suppressed MRI, carcinomas appear as hypointense tumors having an intensity similar to the spleen. If a pancreatic head carcinoma is associated with atrophy of the body and tail, the latter also are hypointense on T1-weighted images. Signal intensity varies on T2-weighted images and these images are of limited use.

Optimal MR sequences to detect a subtle tumor are still evolving. Dynamic MR and fat-suppression are more useful than conventional SE imaging. Due to their relative hypovascularity, most pancreatic carcinomas are hypointense to normal pancreatic tissue on immediate post-contrast images and variable in appearance on

more delayed images. Normal pancreas achieves maximum MR enhancement during the arterial phase, and images at this time generally are best at maximizing the intensity differences between normal pancreas and a carcinoma. This technique is most useful for small cancers that do not produce a contour abnormality. A hyperintense ring often surrounds the cancer postcontrast, probably representing compressed adjacent pancreatic parenchyma and surrounding inflammation.

The MRCP results are similar to ERCP in detecting pancreatic cancer, but an advantage of MRCP is that it can be combined with other MRI to provide additional information. Thus in 52 patients with suspected pancreatic cancer, the accuracy of MRCP alone was 80% and of ERCP 85%, but combined MRI and MRCP achieved an accuracy of 88% (78).

An MRCP detected an obstruction or irregular stenosis in 96% of 129 patients with a pancreatic carcinoma, while a majority of inflammatory pancreatic tumors had a nonobstructed duct (79). Nevertheless, MR differentiation between a pancreatic carcinoma and chronic pancreatitis is not possible in a minority of patients.

Scintigraphy

No ideal radiopharmaceutical agent is available for pancreatic imaging. Some techniques, however, are promising. Thallium-201-chloride single photon emission computed tomography (SPECT) shows positive uptake in pancreatic cancers. Uptake of this agent is also evident in some patients with chronic pancreatitis.

Focal FDG-PET uptake is seen in pancreatic carcinomas, with several studies achieving sensitivities and specificities in the 80% range. Typically, FDG-PET is considered positive if pancreatic activity exceeds background and negative if activity is less than or equal to background activity. Unfortunately, focal FDG-PET uptake is also found with benign tumors and pancreatic inflammation. Also, the accuracy of FDG-PET scintigraphy is dependent on serum glucose levels.

Iodine 123 vasoactive intestinal peptide (VIP) binds to pancreatic tumor cells and has an affinity for pancreatic cancer. In one study primary pancreatic tumors were visualized by this test in 90% of patients if disease was confined to the pancreas and in 32% of patients if regional or liver metastases were present (80).

Percutaneous Transhepatic Cholangiography

Percutaneous transhepatic cholangiography (PTC) usually can suggest a carcinoma in the head of the pancreas. In most institutions, however, ERCP is the procedure performed. In a setting of a failed ERCP, percutaneous cholangiography is a viable alternative.

Endoscopic Retrograde Cholangiopancreatography

Endoscopic retrograde cholangiopancreatography not only provides imaging of both the pancreatic and biliary ducts, but also in a setting of suspected malignancy ERCP can obtain brush cytology and thus detect carcinoma in situ and marked atypia. The role of screening high-risk patients with cytology is yet to be established.

Biopsy

If CT or US suggests a pancreatic tumor, these modalities are useful in guiding fine-needle aspiration. Accuracy of a percutaneous pancreatic biopsy has ranged up to 90%, although it is lower in most studies. A positive biopsy or cytology is generally diagnostic of a pancreatic carcinoma. A negative biopsy, however, does not exclude a cancer. In a setting of imaging suspicion for a cancer, some studies report about half of patients with an atypical cell or negative biopsy are eventually confirmed as malignant. This points to some of the problems encountered with biopsies.

Groove carcinoma. A carcinoma originating in the groove between the duodenum and pancreatic head is called a *groove carcinoma* by some authors. Whether all of these are indeed pancreatic in origin or whether some originate from the papilla of Vater or even distal common bile duct is conjecture.

Imaging reveals sheet-like tumor within this groove (81). These tumors tend to be hypointense on T1-weighted images and hyperintense on T2-weighted MR images. Most are

hypovascular on early arterial phase and show delayed enhancement during a late phase. Narrowing of the intrapancreatic common bile duct is a common feature. Peripancreatic and adjacent duodenal wall invasion is also common at initial presentation, making resection difficult. The imaging findings resemble those of duodenal carcinoma, metastasis to pancreaticoduodenal lymph nodes or even groove pancreatitis.

Staging/Resectability

Although a Union Internationale Contre le Cancer tumor, node, metastasis (TNM) staging system exists for pancreatic cancer (Table 9.4), the staging of resected cancers is probably of little clinical relevance; some might consider such an approach too pessimistic given the gradual improvement, albeit slow, in postoperative survival. The current emphasis is primarily on detecting unresectability. In general, imaging is considerably more accurate in detecting unresectability than in establishing that a pancreatic carcinoma is indeed resectable. In analyzing the data one should keep in mind that resectability is defined differently by various surgeons and the definition has become more liberal with time. Also, with pancreatic cancers resectability is not the same as cure.

Table 9.4. Tumor, node, metastasis (TNM) staging of exocrine pancreatic tumors

Primary tumor:	
Tx	Primary tumor cannot be assessed
T0	No evidence of primary tumor
T1	Tumor limited to the pancreas 2 cm or less in greatest dimension
T2	Tumor limited to the pancreas more than 2 cm in greatest dimension
T3	Tumor extends beyond pancreas, but without involving celiac axis or superior mesenteric artery
T4	Tumor involves celiac axis or superior mesenteric artery
Lymph nodes:	
Nx	Regional lymph nodes cannot be assessed
N0	No regional lymph node metastasis
Nla	Regional lymph node metastasis to a single lymph node
N1b	Regional lymph node metastasis to multiple lymph nodes
Distant metastasis:	
Mx	Presence of distant metastasis cannot be assessed
M0	No distant metastasis
M1	Distant metastasis

Tumor stages: (check)			
Stage IA	TI	N0	M0
Stage IB	T2	N0	M0
Stage IIA	T3	N0	M0
Stage IIB	T1–3	N1	M0
Stage III	T4	any N	M0
Stage IV	any T	any N	M1

Source: From the AJCC Cancer Staging Manual, 6th edition (2002), published by Springer-Verlag, New York, NY, used with permission of the American Joint Committee on Cancer (AJCC), Chicago, IL.

Even in a setting of widespread lymph nodes metastases, the lymph nodes often are normal in size. Similarly, enlarged nodes in some patients simply represent associated inflammation. The issue is actually more complex; thus an immunohistochemical antiepithelial monoclonal antibody test revealed tumor cells in 43% of lymph nodes that histopathologically did not contain tumor (82); of note is that 75% of patients staged pN0 had these cells. Using multivariate Cox's regression analysis, the authors found that the presence of these cells in otherwise histologically tumor-free lymph nodes represents an independent prognostic factor for both reduced relapse-free survival and overall survival, and suggest that staging include immunohistochemical testing (82); patients with minimal residual tumor could then be selected for additional therapy.

Another complicating factor is that pancreatic adenocarcinoma cells frequently bypass initial draining lymph nodes and become established in secondary sites, and small tumors are not uncommonly associated with remote metastases. Cancers of the body and tail are prone to peritoneal and hematogenous spread more often than cancers of the head of the pancreas. Ascites in a patient with known pancreatic cancer generally implies peritoneal spread even in the face of normal imaging.

Arterial occlusion is generally a relatively late finding.

Comparison Studies

In patients with known or suspected pancreatic carcinoma, introduction of helical CT led to a greater sensitivity in establishing resectability with this modality than with MRI, although further advances in MR since then suggest that

MR is superior. A study in 1999 found that MRI was significantly better than CT in assessing resectability (83). Compared with CT, mangafodipir enhanced MR appears superior in evaluating resectability and provides better detection of small metastases (84). Useful MR sequences include FSE, fat-suppression, T1-weighted breath-hold gradient-echo FLASH and pre- and postcontrast. Nevertheless, current multislice CT achieves a diagnosis of unresectability with a sensitivity of about 95% and specificity of 85% (85), impressive results.

In detecting vascular involvement, CT appears superior to endoscopic US. Postcontrast thin-section CT appears superior to breath-hold postcontrast MRI in detecting peripancreatic vein, portal vein, or peripancreatic arterial invasion (86). Color Doppler US detection of portal vein invasion appears to be similar to that seen with CT and angiography.

Computed Tomography

Traditionally, angiography was performed to assess vascular encasement, although currently CT is preferred. More recently, CT arterial portography has been suggested as being superior even to angiography in detecting encasement but is not widely employed.

Preoperative optimized thin slice CT achieves a sensitivity of about 90% in predicting unresectability and a similar or better sensitivity and specificity in assessing resectability. The current major limitation of CT consists of undetected small metastases to the liver and peritoneum (87). CT arterial portography has been suggested as being superior even to angiography in detecting encasement but is not widely employed.

Postcontrast early-phase and late-phase CTs study different entities. Arterial-phase CT detects arterial encasement, while portal phase is useful in determining portal vein and superior mesenteric vein involvement. Retroperitoneal invasion is better evaluated on early-phase CT. Reconstructed 3D arterial phase data are helpful if arterial encasement is suspected. At times arterial invasion is seen simply as vessel wall thickening. Most major vascular involvement involves the portal vein and superior mesenteric vein, although narrowing can be due to either simply extrinsic impression or direct tumor invasion. Using thin-section contrast-enhanced CT, if a fat plane or pancreatic parenchymal tissue can be identified between a tumor and adjacent vessels, the tumor is resectable without venous resection being necessary; complicating matters, some veins adjacent to the pancreas are not surrounded by fat and their encasement is difficult to detect. In general, upstream dilation of small peripancreatic veins implies unresectability. Tumor encasement of adjacent vessels implies vascular invasion and generally connotes an inability to resect with negative surgical margins. The degree of circumferential peripancreatic vein encasement by a tumor, as shown by thin-section pancreatic-phase CT, aids in predicting which patients have unresectable tumors (88). Another sign suggesting unresectability is a tethered, teardrop-shaped superior mesenteric vein (teardrop sign) (89); together with other findings, the presence of a teardrop-shaped superior mesenteric vein increases sensitivity in detecting unresectability. Splanchnic venous invasion results in a delay in contrast washout from the small bowel; these patients have increased small bowel wall enhancement and a decrease in portal vein enhancement compared to those without invasion.

Multiplanar and 3D volume-rendered CT techniques show promise in detecting vascular involvement, although considerable intra- and interobserver variability in tumor grading exists, and these techniques are best used together with axial images (90).

Infiltration of adjacent organs or adenopathy implies unresectability, keeping in mind that even an optimal CT technique is inherently limited in detecting lymphatic involvement unless a node is enlarged or contains a contour abnormality. Computed tomography detects only about half of nodal involvement, while detecting liver metastases in 75% of patients (91).

Ultrasonography

Endoscopic US aids in staging these tumors. Endoscopic US suggests portal vein invasion if an irregular venous wall outline, loss of wall interface and proximity of tumor are detected. Limitations of this technique include an inability to assess direct tumor invasion into the mesocolon and an inability to evaluate the effect of peritumoral pancreatitis. Likewise, similar to

other imaging modalities, although endoscopic US detects lymph node enlargement, metastases cannot be differentiated from benign lymphadenopathy.

Is color Doppler US useful for detecting vascular involvement? Changes in portal vein blood flow velocity are seen with tumor compression or invasion. Resectability is suggested by lack of tumor contact with major vessels as detected by Doppler US. Likewise, vessel encasement signifies unresectability. Problems are encountered in those patients with contact but no encasement between tumor and vessel, and the Doppler US results are mixed in suggesting resectable.

The value of laparoscopic US in staging pancreatic cancers is still uncertain. At times laparoscopic US detects liver metastases not seen by other imaging modalities.

Intraportal endovascular US is feasible intraoperatively via the superior mesenteric vein or preoperatively via a percutaneous transhepatic approach. Sensitivities and specificities >90% can be achieved in detecting portal vein invasion, and in select individuals such an approach is potentially useful. Portal vein invasion is implied by obliteration of the portal vein echogenic outline. Such an endovascular approach has also been suggested for detecting adjacent extrapancreatic nerve plexus invasion (92).

Magnetic Resonance Imaging

Magnetic resonance studies available to evaluate and stage pancreatic cancer include breath-hold T1- and T2-weighted sequences, MRCP, and breath-hold MRI using gadolinium and mangafodipir contrast, at times in a 3D presentation. Such an approach provides multiple specific MR examinations, all obtained as part of one study. Similar to other applications, MRI preoperative staging depends on the magnet field strength and scanning parameters used. Evolving study parameters make predictions for optimal tumor staging techniques unpredictable. Different techniques appear advantageous for gauging vascular invasion and detecting adenopathy. One MR indication appears to be in patients with inconclusive CT, especially those with a CT finding of an indeterminate pancreatic head enlargement.

Both pre- and postcontrast MRI is useful in staging. Precontrast T1-weighted images are useful in evaluating peripancreatic tumor extension, but tissue planes between tumor and peripancreatic fat are not as well seen postcontrast; on the other hand, tumor margins and surrounding vasculature are better identified on postcontrast images (Fig. 9.18). Due to fibrosis, MRI tends to overestimate vascular invasion.

A combination of conventional MR, 3D MRCP, and venous and arterial MRA both detect a cancer and can suggest unresectability due to vascular invasion and identify any bile duct or pancreatic duct obstruction.

Angiography

Currently arteriography is little used for staging pancreatic cancer. Angiography tends to overestimate tumor invasion.

Theoretically, percutaneous transhepatic portography and intravascular US hold promise in evaluating portal and superior mesenteric vein involvement by tumor, but preliminary results reveal high false positive and negative rates (93); also, these procedures are not without significant complications.

Therapy

Therapy for pancreatic ductal adenocarcinoma can be divided into attempted cure and palliation.

Resection

Some of the reported survival rates after resection of pancreatic carcinoma are rather optimistic and need to be placed in a proper perspective. Little consistency in reporting survivors is evident in the literature, reported patient selection bias exists and some studies do not exclude cystic and neuroendocrine tumors with their more favorable survival. In particular, 5-year survival rates of about 30% after resection should be viewed critically. The overall survival rate is probably <1% and, in spite of some reports, resection does not have any discernible impact on patient survival.

The pros and cons of preoperative biliary drainage in a setting of obstructive jaundice are discussed in Chapter 8.

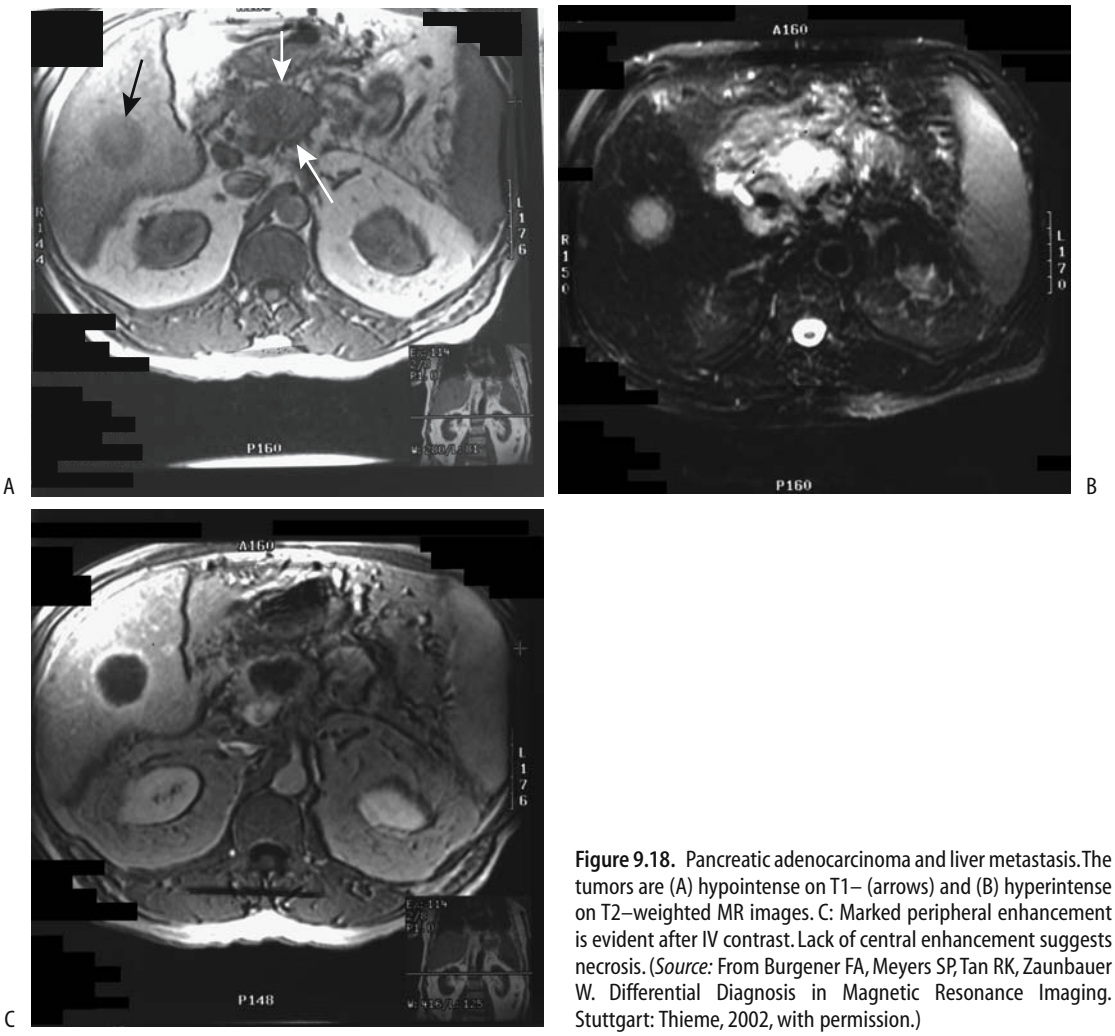

Figure 9.18. Pancreatic adenocarcinoma and liver metastasis. The tumors are (A) hypointense on T1– (arrows) and (B) hyperintense on T2–weighted MR images. C: Marked peripheral enhancement is evident after IV contrast. Lack of central enhancement suggests necrosis. (*Source:* From Burgener FA, Meyers SP, Tan RK, Zaunbauer W. Differential Diagnosis in Magnetic Resonance Imaging. Stuttgart: Thieme, 2002, with permission.)

Pancreaticoduodenectomy (Whipple procedure) is performed for cure in selected patients with a carcinoma in the head of the pancreas. Even the presence of lymph nodes metastases is no longer considered a contraindication to resection by some surgeons. The postoperative survival in patients with extrapancreatic neural plexus involvement is significantly lower than in those without such involvement.

The immediate surgical mortality and morbidity rates have been decreasing, and some surgeons are performing more radical operations. In addition to a Whipple procedure, some surgeons are dissecting lymph nodes and excising retroperitoneal nerves. If necessary, portal vein resection and even resection of adjacent arteries are performed. Such aggressive surgical approaches appear to prolong survival.

The Whipple procedure consists of resection of the head of the pancreas, adjacent duodenum and gastric antrum, and three anastomoses—choledochojejunostomy (or hepaticojejunostomy), pancreaticojejunostomy (or pancreaticogastrostomy), and a gastrojejunostomy. Any one of these may leak, although the pancreaticojejunostomy site is more prone to disruption than other anastomoses and thus some surgeons prefer a pancreaticogastrostomy. Others disagree and believe that the risk of fistula formation is comparable with the two anastomoses (144). Also, some surgeons prefer to leave the

antrum intact and perform a duodenojejunostomy, a variant known as a pylorus-preserving Whipple procedure.

Complications encountered after a Whipple procedure include adjacent abscess formation, breakdown at one of the anastomoses with fistula formation, gastric outlet obstruction, and pancreatitis. A pancreatic fistula typically manifests as prolonged pancreatic fluid drainage from one of the drain sites, and in this setting it is worthwhile performing fistulography using one of the surgical drains close to the pancreatic anastomosis. The pancreaticojejunostomy cannot be readily imaged directly. Most pancreatic fistulas tend to close spontaneously. Less common, and less serious, is leakage at a choledochoenteric site. Of note is that bile leakage usually also occurs in those patients who have pancreatic leakage. Delayed gastric emptying is a common finding after a pylorus-preserving pancreaticoduodenectomy. Imaging should detect most complications. Delayed gastric emptying tends to resolve within several months. In a number of patients diabetes appears or deteriorates after surgery.

A postoperative T-tube cholangiogram evaluates the bilioenteric anastomosis while a contrast upper gastrointestinal examination detects enteric perforation and gastric outlet obstruction. Computed tomography is generally the procedure of choice for a suspected postoperative abscess; also, postoperative distortion and fibrosis make later CT interpretation difficult and a baseline study is thus very helpful.

Computed tomography commonly detects small fluid collections in the surgical field. Most of these resolve spontaneously and do not require aspiration unless an infected site is suspected.

Chemotherapy/Radiotherapy

In a setting of unresectable pancreatic cancer, chemotherapy is rarely employed, although an occasional prolonged survival has been reported. Some of these tumors shrink after chemotherapy or radiotherapy, although tumor size is difficult to measure with imaging.

Preliminary results with immunochemotherapy combined with resection show a higher response rate than to surgery alone.

Pancreatic adenocarcinomas are relatively radioresistant, and a dose of >50 Gy is necessary, resulting in high morbidity with external beam radiotherapy. High-dose intraoperative radiotherapy provides palliative pain relief, but a high prevalence of distant metastases in most patients precludes a cure even in patients with a curative resection.

Median survival for patients with unresectable pancreatic adenocarcinoma treated with neutron irradiation was 6 months, while median survival for patients with neutron irradiation plus chemotherapy was 9 months (94); actuarial survival rates at 3 years were 0 and 7%, respectively, and the authors concluded that neutron irradiation obliterates pancreatic cancer at the primary site but does not change long-term survival.

Palliation

Either early or late biliary obstruction is a common feature of most pancreatic head carcinomas. Therefore, if the cancer is deemed unresectable, surgical palliation consisting of a bilioenteric anastomosis and a gastric bypass (gastrojejunostomy) is performed by some surgeons, although high morbidity and often a lack of life prolongation make such an approach questionable. With no surgery planned, either percutaneous or endoscopic stenting is an alternative (Fig. 9.19). Stenting can control jaundice, but it should be kept in mind that, in

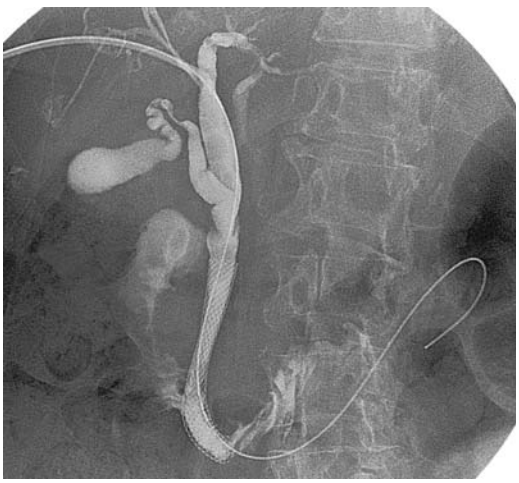

Figure 9.19. Biliary stent in a patient with pancreatic carcinoma. (Courtesy of David Waldman, M.D., University of Rochester.)

general, jaundice per se is not an indication for therapy; uncontrolled pruritus is. Generally endoscopic biliary drainage is performed if the intrapancreatic portion of the bile duct is obstructed. A percutaneous approach is available with endoscopic failure or a more proximal obstruction.

An unresectable pancreatic head carcinoma tends to invade and eventually obstruct the duodenum. Relative merits of palliation versus resection are still debated. Some of these duodenal obstructions can be palliated with self-expandable duodenal endoprostheses; the commonly associated bile duct obstruction must also be addressed. Patients undergoing operative palliation for unresected ductal adenocarcinoma achieve a one-year survival of about 20%; to put this in perspective, the operative mortality rate after either resection or palliative bypass can be >10% and the relative merits of palliation versus resection are still debated.

Pancreatic carcinomas tend to invade the adjacent portal vein and lead to portal hypertension, with its associated complications. Stents placed across stenotic or occluded veins during percutaneous transhepatic portography led to a decrease in mean portal venous pressure (95); stent patency was considerably greater in patients without splanchnic venous invasion than in those with splanchnic involvement.

Moderate to severe pain is a common feature of a pancreatic carcinoma. If medical management of pain is insufficient, percutaneous celiac axis plexus blockade should be considered.

Metastasis

Hepatic metastases are common in patients with pancreatic ductal carcinoma; normally pancreatic veins drain into the portal vein, and this would explain why the liver is the most common site for metastasis. In a minority of patients pulmonary metastases and other hematogenous metastases are found without hepatic metastases. The reasons for such occasional odd metastatic distribution are speculative, but possibly include hepatofugal portosystemic shunting. Practically, pancreatic metastases occur throughout the body. An occasional cutaneous metastasis is encountered, most often at the umbilicus, and a metastatic skin lesion has been a first manifestation of pancreatic cancer.

In patients with pancreatic cancer who had no distant metastases at surgery, follow-up CT and autopsy revealed that 60% developed local recurrence, 52% liver metastases, and 32% both (96).

Other Carcinomas

Encountered occasionally are poorly differentiated carcinomas that defy classification. Their imaging findings vary. Some even mimic a pancreatic neuroendocrine tumor.

Adenosquamous Carcinoma

Adenosquamous and squamous carcinomas are rare in the pancreas. Clinically they behave similarly to a ductal adenocarcinoma. An adenosquamous or squamous carcinoma typically presents as a large, cystic tumor. Multiple calcifications have developed. Computed tomography reveals contrast enhancement, and, overall, imaging suggests a mucinous cystadenocarcinoma. Thus a typical appearance is a hypodense, fluid-filled tumor surrounded by calcifications.

Small Cell Carcinoma

Although the rare pancreatic small cell carcinoma has a poor prognosis, its importance lies in its favorable response to chemotherapy. Some small cell carcinomas are cystic and contain a hypervascular rim; late-phase contrast CT reveals tumor staining. US reveals the cystic regions, consisting of necrotic tumor and hemorrhage, to be mostly hypoechoic. Imaging findings suggest a hypervascular pancreatic tumor.

Pleomorphic Carcinoma (Sarcomatoid Carcinoma)

A pancreatic giant cell carcinoma, also known as sarcomatoid carcinoma or pleomorphic carcinoma, is a rare, highly aggressive variant having characteristic histologic features. In distinction to a more common carcinoma, the giant cell variety often results in massive lym-

phadenopathy and extensive liver involvement. Its relationship to more common adenocarcinomas is not known. These tumors have a poor prognosis.

These tumors have a sarcoma-like growth pattern and contain mono- and multinucleated tumor giant cells. Necrosis and hemorrhage are common. Immunohistochemical study of a mixed pancreatic giant cell tumor revealed osteoclastic and pleomorphic type giant cells together with ductal adenocarcinoma (97); the authors believe this tumor is a carcinosarcoma-like neoplasm containing both epithelial and mesenchymal components.

Imaging usually shows a large, well-marginated, and hypervascular tumor.

Hepatoid Carcinoma

A hepatoid carcinoma, consisting of histologic evidence of hepatocytic differentiation, bile production, and elevated α-fetoprotein levels, is rare in the pancreas. One was part of an islet cell glucagonoma, while another one was part of a pancreatic duct carcinoma (98).

Pancreaticoblastoma

A pancreaticoblastoma is a tumor of childhood, only rarely detected in adults. In children, most pancreatic neoplasms are of acinar origin, rather than ductal as in adults. In distinction to children, prognosis is poor in affected adults, but even in children some of these tumors are aggressive, invade adjacent vessels, infiltrate surrounding structures, and metastasize (99).

A pancreaticoblastoma has a distinct histologic appearance. Both solid and cystic components are common. Hemorrhage, necrosis, and calcification develop in some. These tumors are rather complex and at times both neuroendocrine and mesenchymal cells are present. Some consist of tubular gland-like structures, squamoid components and small round cells, with the latter suggesting neuroendocrine cells having an origin from primitive multipotential stem cells with exocrine and neuroendocrine differentiation.

Most pancreaticoblastomas are located in the head of the pancreas and are large at the initial presentation. Some are associated with elevated serum α-fetoprotein level. They usually metastasize to liver.

Computed tomography in 10 patients (age range, 2 to 20 years) with pancreaticoblastomas identified heterogeneous (nine of 10) enhancing (10 of 10) tumors with well-defined margins (nine of 10) (100); two contained calcifications. An MRI of three of these tumors revealed hypo- to isointense signal on T1- and hyperintense signal on T2-weighted images. Postcontrast, some of these tumors are multiloculated and contain septations. Ultrasonography reveals a mixed hyperechoic solid tumor.

Lymphoma/Leukemia

Both lymphoma and leukemia involve the pancreas, and either a localized tumor or a diffusely enlarged pancreas is evident to the point of obstructive jaundice. Rarely, lymphoma is confined to the pancreas and a pancreatic malignancy and pancreatitis are then in the differential diagnosis. In particular, pancreatic lymphoma mimics atypical chronic pancreatitis, such as autoimmune pancreatitis. While a positive percutaneous biopsy in these patients establishes the diagnosis, a negative biopsy is nondiagnostic; also, a biopsy is usually not performed in patients with clinically suspected pancreatitis.

Computed tomography in pancreatic non-Hodgkin's lymphoma reveals a homogeneous hypodense pattern with mild contrast enhancement (61); necrosis or calcifications are not evident in either the diffuse or nodular forms. Adjacent lymph nodes may or may not be involved. A characteristic of primary pancreatic lymphoma is that, even when extensive, it tends not to obstruct the pancreatic duct, and thus ductal dilation is not present (101); this is in distinction to the more common adenocarcinomas, which commonly obstruct the pancreatic duct.

Adult T-cell leukemic infiltration led to a diffusely swollen pancreatic body and tail, identified by CT and US (102); a biopsy confirmed leukemic infiltration, and a Southern blot analysis revealed human T-cell lymphotropic virus type I (HTLV-I) proviral DNA both in pancreas and peripheral blood.

Plasmacytoma

Major pancreatic involvement with multiple myeloma is uncommon. Multiple myeloma pre-

senting as a pancreatic tumor and causing jaundice is rare, with pancreatic involvement often being a preterminal event. Computed tomography identifies a homogeneous solid tumor; the appearance mimics lymphoma. In some patients even a biopsy can confuse multiple myeloma with lymphoma.

Sarcoma

Primary sarcomas are rarely encountered in the pancreas. They tend to be rather aggressive. A differential problem is to exclude pancreatic invasion by mesenchymal tumors originating in other extraperitoneal structures.

A rare primary pancreatic malignant fibrous histiocytoma (103) and malignant mesothelioma (104) have been reported. Computed tomography and US simply detect a large tumor. About 70% of malignant fibrous histiocytomas have alterations in the *p53* tumor-suppressor gene, a finding generally associated with a poor prognosis.

A pancreatic undifferentiated (anaplastic) carcinoma was associated with a sarcomatous spindle cell component and a cyst composed of epithelial tumor cells (105); metastases were present in the liver and lymph nodes.

Metastases to Pancreas

A number of distant sources, including hepatocellular, lung, breast carcinoma, melanoma, and osteosarcoma metastasize to the pancreas. Probably most common is a renal cell carcinoma, at times being a solitary focus. The time interval between nephrectomy and detection of a pancreatic metastasis can be years.

Even if detected by imaging, most pancreatic metastases cause few symptoms and are overshadowed by symptoms referable to the primary tumor or other metastatic sites. Endoscopic US identifies most metastases as hypo- to isoechoic to pancreatic parenchyma, homogeneous, round, and well circumscribed—an appearance different from that seen with most primary pancreatic carcinomas; only an occasional metastasis has a heterogeneous appearance and indistinct margins mimicking a primary pancreatic carcinoma or focal pancreatitis.

In general, the CT and MR appearance of a pancreatic metastasis parallels that seen with the primary tumor. Renal metastases range from solitary to multiple tumors or diffuse pancreatic enlargement. Thin-section three-phase postcontrast CT of nine patients with metastatic renal cell carcinoma revealed conspicuous early enhancement (106). They are hypointense compared to the normal pancreas on T1- and hyperintense on T2-weighted images. Smaller metastases show immediate postcontrast images enhancement and larger ones have rim enhancement.

A metastasis rather than a primary tumor should be suspected in a patient with a known malignancy and a new solitary pancreatic tumor. Nevertheless, most of these patients require a biopsy for confirmation.

Cystic Neoplasms

Clinical

The most common cystic pancreatic lesions are pseudocysts, followed by cystic neoplasms and true pancreatic cysts. Rarer causes of pancreatic cysts include a cystic teratoma, lymphoepithelial cyst, and a cystic lymphangioma. The importance of cystic pancreatic neoplasms lies in their considerably better prognosis compared to that of adenocarcinomas. Nevertheless, more than one cystic tumor has been either drained or anastomosed to the stomach in a mistaken belief that it represents a pseudocyst, often with dire consequences.

The current classification of cystic pancreatic neoplasms is somewhat arbitrary. Overall, only a minority of cystic neoplasms are malignant. Undoubtedly an occasional cystic endocrine carcinoma is misclassified among these tumors. Pathologists generally differentiate these neoplasms along immunohistochemical lines. Some have questioned whether these tumors are indeed a separate definable entity and believe that most should be classified among more conventional glandular and acinar origin neoplasms. Most of these neoplasms are divided into two basic types: microcystic adenomas (previously called serous cystadenomas) and mucinous cystic (or macrocystic) neoplasms. The distinction is important, because the former are benign while the latter include both mucinous cystadenomas and cystadenocarcinomas.

A familial association between autosomal-dominant polycystic kidney disease and cystadenocarcinoma of the pancreas and liver was reported in one family (107).

Most patients with cystic pancreatic neoplasms have abdominal pain. Weight loss, jaundice, and an abdominal tumor, at times large, are the presenting clinical findings, although some tumors are discovered in an asymptomatic patient. Complications encountered include obstruction of adjacent gastrointestinal structures, perforation, and hemorrhage.

Cyst fluid analysis aids in differentiating pseudocysts from neoplasms (Table 9.5). Amylase level was >16,000 international units (IU) per milliliter in 13 out of 14 pseudocysts and <83 IU/mL in seven of eight cystic neoplasms (108). In general, a pancreatic cyst associated with an elevated serum CA 19-9 level or elevated CA 72-4 cyst fluid level should be considered a neoplasm. Positive cytology is diagnostic.

Table 9.5. Pancreatic cyst fluid analysis

Carcinoembryonic antigen (CEA) levels
High in mucinous cystadenomas and cystadenocarcinomas
Low in pseudocysts and serous cystadenomas
CA 19–9 tumor marker values
High in ductal carcinomas and mucinous cystic neoplasms
Low in pseudocysts
Variable in serous cystadenomas
CA 72–4 tumor marker values
High in mucinous cystic neoplasms
Low in pseudocysts
CA 125 tumor marker values
High in mucinous adenocarcinomas
Low in pseudocysts
Variable in serous and mucinous cystadenomas
Fluid amylase and lipase levels
Generally high in pseudocysts
Low in cystic tumors
Cyst fluid relative viscosity
High in mucinous tumors
Low in pseudocysts and serous cystadenomas
Cytology
About 50% sensitivity in detecting malignant cysts

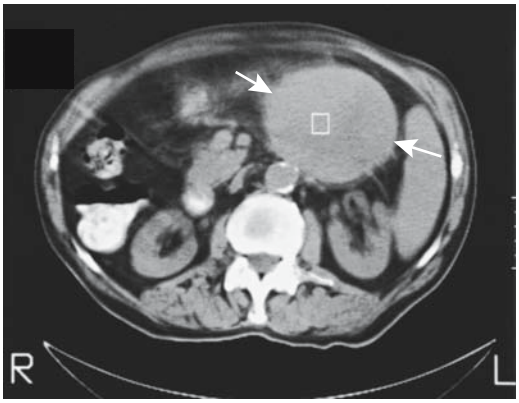

Figure 9.20. Cystic pancreatic acinar carcinoma, with most of the tumor located adjacent to pancreas (arrows).

Imaging

A majority of cystic neoplasms are either partially or almost completely cystic, yet even in the latter most but not all have a solid component, a finding not present in a pseudocyst. A minority communicate with the pancreatic ducts. An occasional one develops a pancreaticoenteric fistula.

Computed tomography is often the diagnostic modality of choice in preoperative evaluation of these cystic tumors, yet the published results provide limited guidance. Imaging appears rather limited in distinguishing among a microcystic adenoma, a mucinous cystadenoma, and a mucinous cystadenocarcinoma (Fig. 9.20). On the other hand, the presence of cysts <2 cm points toward a serous tumor, and peripheral tumoral calcifications are associated with mucinous tumors (109).

These tumors are readily misdiagnosed as pseudocysts by both CT and conventional US, and less so by endoscopic US. Endoscopic US of 52 pancreatic solitary cystic tumors, consisting of benign and malignant cystic neoplasms and nonneoplastic cysts, found that all neoplasms have a thick wall, tumor protrudes into the cysts, any septa present are thick, or the cysts are small (110); nonneoplastic cysts, on the other hand, contain thin septa or the cysts are simple.

Magnetic resonance signal intensity is of limited use in distinguishing among various cystic neoplasms, which are hypointense on T1- and hyperintense on T2-weighted images. They show little or no postcontrast enhancement.

Microcystic (Serous) Neoplasm

Clinical

Microcystic neoplasms invariably are benign, with only a few malignant ones reported. In distinction with their mucinous counterpart, microcystic adenomas are not considered premalignant, with rare exceptions. Most of these tumors, also called serous cystadenomas, are well encapsulated and nodular and contain numerous small cysts and septa. The cysts are filled with serous fluid and contain little mucin.

Some authors believe the term *microcystic* serous adenoma is too limiting and that a macrocystic variant of the same neoplasm exists; the term *serous cystadenoma* is thus used for both morphologic variants. Nevertheless, the term *macrocystic serous tumor* is useful; these tumors are often misdiagnosed as either mucinous cystic neoplasms or pseudocysts. In fact, some tumors are misclassified even with intraoperative frozen section. Serum tumor markers with macrocystic serous tumors tend to be normal, although CA 125 and CA 19-9 are elevated in the cyst fluid in some of these tumors (111). The macrocystic variant of serous adenoma consists of a small uni- or bilocular cyst containing a thin wall without any mural nodules (112); these are indistinguishable from mucinous cystic tumors.

A rare variant is a histologically solid serous cystadenoma with cytologic, histochemical, and immunohistochemical features indistinguishable from a typical serous cystadenoma. Whether such a pancreatic tumor is a separate pathologic entity is debatable.

Symptomatic patients tend to have a large tumor, with symptoms presumably due to compression of adjacent structures. Smaller tumors often are detected incidentally. An occasional microcystic adenoma having a sponge-like consistency will almost entirely replace the pancreas.

Imaging

A majority of microcystic (serous) neoplasms contain many small cysts, a minority consist of larger cysts (macrolacunar) and a minority are mixed; imaging can suggest the diagnosis in a majority of the small and mixed cystic variety, but the larger cystic tumors are indistinguishable from other pancreatic cysts by either CT (Fig. 9.21) or MR (Fig. 9.22).

Some of these tumors containing small cysts have a "honeycomb" appearance on imaging. At times the cysts are sufficiently small to suggest a solid tumor (Fig. 9.23). A central scar with radiating septa is evident in some, and occasionally sunburst-like calcifications are detected in the central scar. In some, thin septations enhance on immediate postcontrast images. Any solid component also enhances.

Even when large, these benign tumors tend not to obstruct the pancreatic duct. Also, only a small minority of serous cystadenomas communicate with the pancreatic duct. An occasional microcystic adenoma is sufficiently large to compress and occlude the splenic vein, resulting in hepatopetal collaterals via gastric fundal varices.

Mucinous Cystic Neoplasms

Clinical

A distinction is often made between mucinous cystic neoplasms and intraductal mucinous tumors—a tenuous and somewhat arbitrary differentiation based more on clinical and radiologic findings and tumor location than on pathologic grounds (113). From a simplistic viewpoint, mucinous cystic neoplasms do not communicate with the pancreatic ducts while intraductal mucinous tumors do communicate. Yet even this definition is not satisfactory. Most mucinous cystic neoplasms consist of a cystic septa-containing tumor and no pancreatic duct dilation unless obstructed by the tumor, while intraductal papillary mucinous tumors are small and lobulated—assuming they are visualized at all—and a major finding with them is a dilated main or branch pancreatic duct containing exuberant mucus.

Mucinous cystic neoplasms of the pancreas range from benign (cystadenoma) to malignant (cystadenocarcinoma), with an occasional tumor labeled borderline malignant. A cystadenoma is considered to be premalignant. These tumors range from unilocular to multilocular and their size varies considerably; their cavities are filled with mucin. Pancreatic body and tail are preferred sites. The malignant variety quite often obstructs the pancreatic duct. Tumor aspiration usually simply reveals mucin. A pre-

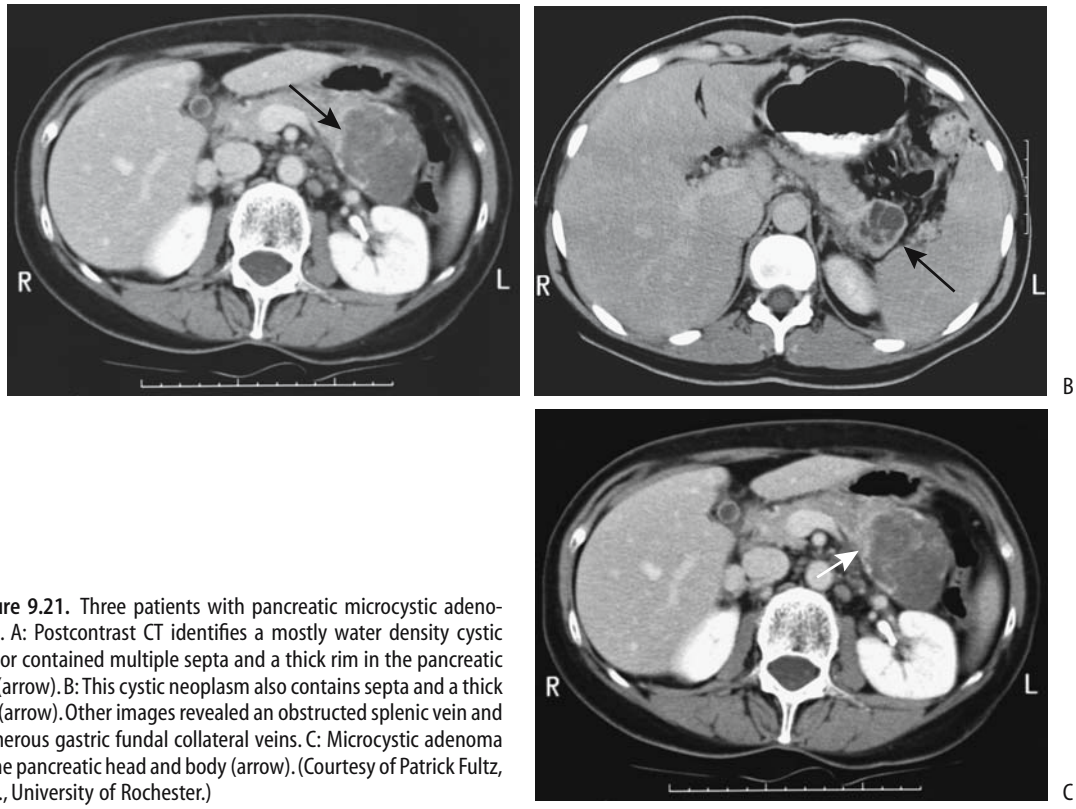

Figure 9.21. Three patients with pancreatic microcystic adenomas. A: Postcontrast CT identifies a mostly water density cystic tumor contained multiple septa and a thick rim in the pancreatic tail (arrow). B: This cystic neoplasm also contains septa and a thick rim (arrow). Other images revealed an obstructed splenic vein and numerous gastric fundal collateral veins. C: Microcystic adenoma in the pancreatic head and body (arrow). (Courtesy of Patrick Fultz, M.D., University of Rochester.)

ponderance of these neoplasms occurs in middle-aged women.

A not uncommon occurrence is a cystadenocarcinoma initially misdiagnosed as a pseudocyst and the cyst then marsupialized to the stomach (Fig. 9.24); the tumors true nature is realized only later when liver metastases are detected.

A review of patients with this tumor revealed an overall 5-year survival rate for resectable

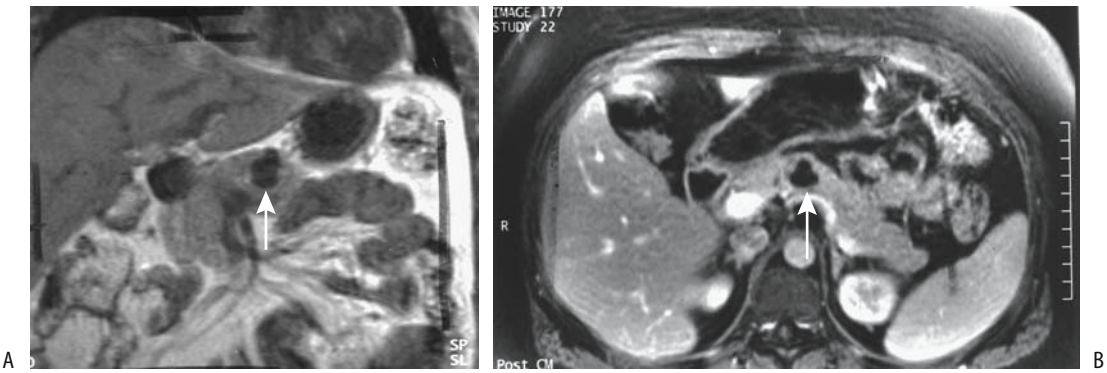

Figure 9.22. Microcystic adenoma. A: Coronal T1-weighted MR image reveals a pancreatic cyst (arrows). B: It does not enhance after contrast (arrow). (*Source:* From Burgener FA, Meyers SP, Tan RK, Zaunbauer W. Differential Diagnosis in Magnetic Resonance Imaging. Stuttgart: Thieme, 2002, with permission.)

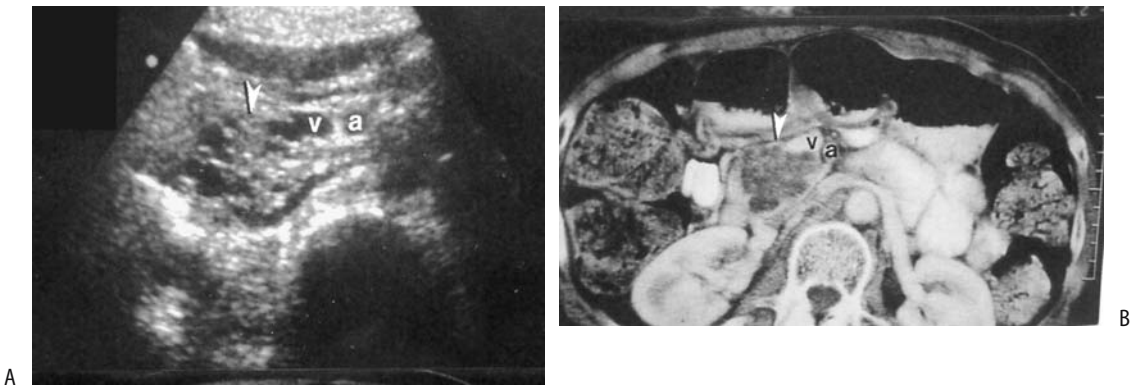

Figure 9.23. Microcystic adenoma. Transverse US (A) and CT (B) identify a tumor in the pancreatic head (arrowhead) (a, superior mesenteric artery; v, vein). (*Source:* From Yeh HC, Stancato-Pasik A, Shapiro RS. Microcystic features at US: a nonspecific sign for microcystic adenomas of the pancreas. RadioGraphics 2001;21:1455–1461, with permission from the Radiological Society of North America.)

ones of 83%, and for those with infiltration limited to the pancreatic parenchyma, 74%; but this survival rate is only 28% if infiltration extends to other organs (114).

Imaging

Imaging reveals one or more cysts; typically these cysts are fewer but larger than seen with serous tumors (Fig. 9.25). Ultrasonography reveals a unilocular or, more often, a multilocular anechoic tumor, with tumor excrescences and debris modifying this appearance. Endoscopic US better evaluates their complex structure. Thus the number of cysts and cyst size are useful criteria in differentiating between the microcystic (serous) and macrocystic (mucinous) tumors. Using criteria that a mucinous-cystic neoplasm should contain fewer than six cysts having a diameter of >2 cm, out of 17 mucinous cystadenomas and cystadenocarcinomas US correctly diagnosed 88% (115).

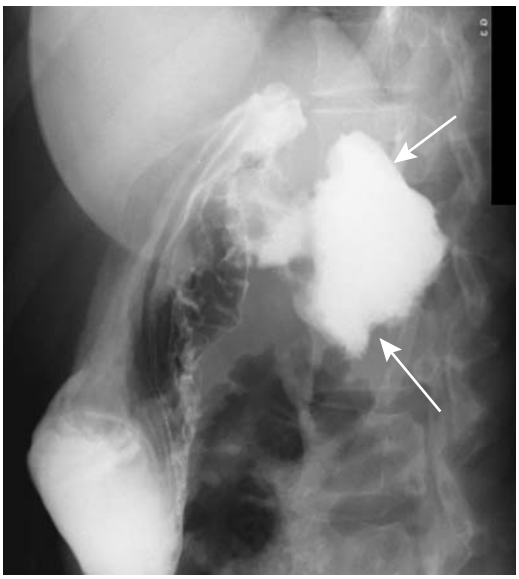

Figure 9.24. Pancreatic cystadenoma (arrows) communicating with stomach. This patient was believed to have a pseudocyst, which was anastomosed to the stomach.

Soft tissue nodules project into some of these cysts. Septations tend to be thicker than those seen with microcystic neoplasms. An occasional tumor develops calcifications that are seen with both benign and malignant tumors. Local invasion is evident with some carcinomas. Occasionally these tumors are first detected through liver metastases. Thus a large calcified tumor in the body and tail occasionally manifests its malignant nature with multiple liver tumors.

An MRI identifies multilocular or unilocular cysts having a relatively thick wall (Fig. 9.26). The cysts tend toward hyperintensity on T1-weighted sequences, presumably due to their high mucin content, and are, as expected for nonflowing fluid, hyperintense on T2-weighted images. Those tumors containing more mucin have a higher MR T1-weighted signal intensity than those containing more watery fluid; tumors containing gelatinous mucin tend to be

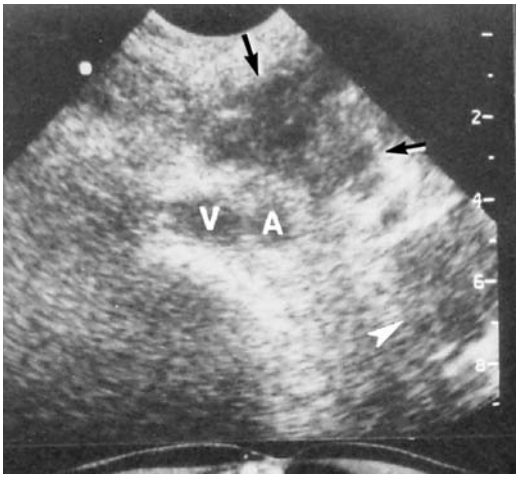

A

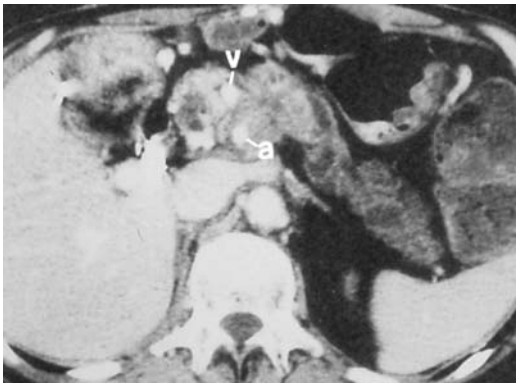

B

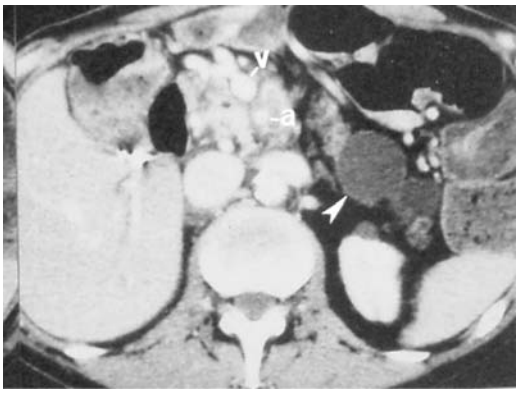

C

Figure 9.25. Mucinous cystadenoma. A: Transverse US identifies multiple pancreatic cysts (arrow), including one in the tail (arrowhead) (A, aorta; V, vena cava). B: CT reveals superior mesenteric artery (a) and vein (v) encased by tumor. C: A scan inferior to that in part B identifies a pancreatic tail cyst (arrowhead) (a, aorta; v, vena cava). (*Source:* From Yeh HC, Stancato-Pasik A, Shapiro RS. Microcystic features at US: a nonspecific sign for microcystic adenomas of the pancreas. RadioGraphics 2001;21:1455–1461, with permission from the Radiological Society of North America.)

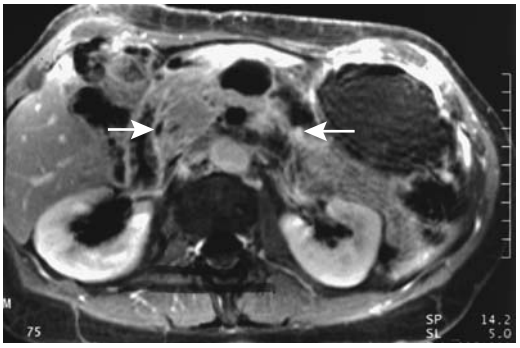

A

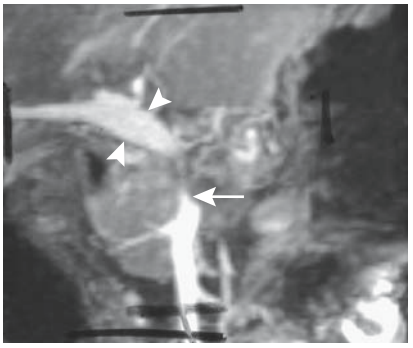

B

Figure 9.26. Mucinous cystic adenocarcinoma. A: A contrast-enhanced MRI reveals a tumor containing solid and cystic components (arrows). B: Magnetic resonance angiography (MRA) identifies a narrowed superior mesenteric vein (arrow), patent portal vein (arrowheads) and nonvisualization of an occluded splenic vein. (*Source:* From Burgener FA, Meyers SP, Tan RK, Zaunbauer W. Differential Diagnosis in Magnetic Resonance Imaging. Stuttgart: Thieme, 2002, with permission.)

malignant, while those containing more watery fluid tend to be benign. The cysts do not enhance postcontrast.

Benign and malignant tumor varieties have a similar imaging appearance, although thick septa and nodularity point toward malignancy. Invasion of adjoining structures or metastasis signifies malignancy.

An FDG-PET detected only 59% of 22 mucinous carcinomas, with an inverse correlation with the amount of tumor mucin (116).

Intraductal Mucin-Producing Tumors

Clinical

One uncommon type of a mucinous tumor originates from the pancreatic ducts. These tumors have been called *mucinous ductal ectasia*, *duct ectatic mucinous cystic tumor*, *intraductal hypersecreting neoplasm*, *mucin-hypersecreting*, *ductal papillary adenoma* or *adenocarcinoma*, *intraductal adenomatosis*, *intraductal papillary mucinous tumor*, *diffuse papillomatosis,* and the currently generally preferred term of *intraductal mucin-producing tumor*. As already noted, most authors differentiate them from mucinous-cystic neoplasms discussed in the previous section. Whether these intraductal papillary mucinous tumors are a variant of pancreatic mucin-producing cystic neoplasms or a separate entity is conjecture (Fig. 9.27). Likewise, a relationship of these tumors to papillary cystic (embryonal) neoplasms (discussed in a later section) is not clear.

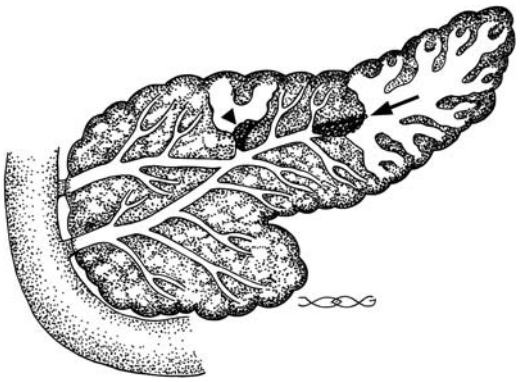

Figure 9.27. Illustration of an intraductal mucin-producing tumor obstructing the main pancreatic duct (arrow) and a secondary branch (arrowhead). In both instances obstruction results in dilated ducts. The ducts of Santorini and Wirsung are shown to be communicating.

A slight male predominance was evident among 22 patients at the Endocrine Tumor Registry of the Armed Forces Institute of Pathology, with a mean age at presentation of 64 years (117), findings in distinction to mucinous-cystic neoplasms, which occur mostly in middle-aged women. Pain is a common presentation, often suggesting pancreatitis. Complicating the issue, associated pancreatitis is common. Up to one third of these patients develop diabetes.

Anecdotal reports describe a second pancreatic primary tumor or even a hilar cholangiocarcinoma.

An intraductal papillary mucinous tumor is a rare cause of pseudomyxoma peritonei (118).

In the Armed Forces Institute of Pathology study, only two of 22 patients died of this disease (117); aside from three operative deaths and three deaths from other causes, the remaining patients were alive without evidence of disease an average of 58 months after presentation. Patients with an exclusively intraductal tumor do well after resection, but those with an invasive adenocarcinoma have a poor prognosis. Patients with mucus-filled dilated ducts but without a detectable tumor have had endoscopic sphincterotomy to relieve pain and then were followed by imaging, but in view of the uncertainty for malignancy, even with a biopsy in hand, many of these tumors are resected with a wide margin, at times consisting of a pancreaticoduodenectomy. If they are not corrected, eventual pancreatic atrophy of the obstructed segments ensues.

Pathologic Findings

Not all of these tumors are neoplastic in origin. Histologically, these tumors range from hyperplasia, dysplasia, and adenoma, to mucin-hypersecreting carcinoma and various intermediate combinations. A villous structure is common. Papillae lined by columnar epithelium contain varying degrees of epithelial dysplasia, often with an adjacent adenocarcinoma. A benign tumor probably is at risk of malignant transformation. Histologically, these tumors share a number of characteristics with colorectal villous adenomas.

Some of these tumors are positive for p53 protein and K-*ras* mutations. *p53* overexpression increases with tumor grade, which is in distinction to solid pancreatic cancers, which exhibit no change for tumor grade. Alterations of these two genes occur in hyperplasia, dysplasia, and carcinomas, and presumably represent early changes in tumor evolution.

The benign variety tend to communicate with secondary branches, while malignant ones more often involve the main pancreatic duct, but a distinction between benign and malignant tumors is difficult at best. Most of these tumors are small, grow slowly, and produce exuberant mucus. Serum tumor markers do not aid in differentiating benign from malignant tumors.

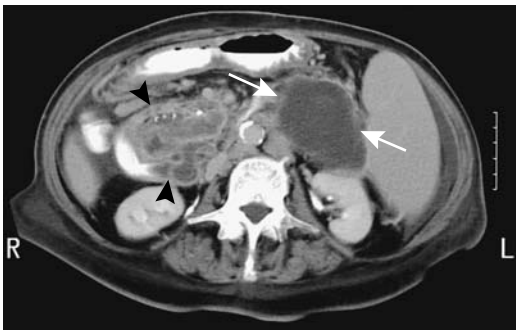

Figure 9.28. Pancreatitis, pseudocyst (arrows) and probable mucinous cystic pancreatic head tumor (arrowheads) in an 83-year-old woman. Calcifications are present within the tumor. The pancreatic duct is dilated and the tumor prolapses into the duodenum. ERCP also identified a prolapsing papilla. No biopsy or resection were performed. (Courtesy of Patrick Fultz, M.D., University of Rochester.)

Imaging

The hallmark of these tumors is a dilated pancreatic duct and increased amounts of intraluminal mucin; the tumor either fills the duct lumen or, less often, lines the lumen. A location in the head of the pancreas is most common (117). With tumors originating in the main pancreatic duct, this duct is considerably more dilated with malignant tumors (119); segmental dilation is common with benign tumors. Even with a tumor located in a secondary duct, the main pancreatic duct often dilates due to excess mucus and resultant obstruction, although dilation generally is less than with main duct tumors. With some, endoscopy reveals viscid mucin draining from a patulous ampulla in a bulging papilla of Vater (Fig. 9.28). During ERCP an intraductal tumor is often too small to be visualized directly or is obscured by adjacent thick mucus, although fixed filling defects should suggest a malignant tumor.

Computed tomography signs of malignancy are the presence of a solid tumor, a main pancreatic duct diameter >10 mm, a diffuse or multifocal tumor, and calcified intraluminal contents (120); of note is that in some of these patients, the CT-histopathologic correlation of duct involvement, lesion location, and presence of malignancy is poor. Computed tomography reveals frond-like projections in an occasional tumor. Larger tumors are detected with both thin-section CT (121) and MRCP (122). At times intraductal content contains calcifications.

Intraductal US, using a frequency of 20 or 30 mHz, aids in outlining tumor extent and parenchymal invasion. In branch duct tumors intraductal US appears superior to endoscopic US in identifying mural nodules.

Magnetic resonance cholangiopancreatography is evolving as the imaging procedure of choice to evaluate these tumors, at times providing more information than does ERCP (Fig. 9.29). An MRCP detects dilated main and secondary ducts better than ERCP (123); intraluminal nodules, on the other hand, are often better defined by ERCP. Pancreatography reveals duct dilation, often with numerous noncalcified intraluminal filling defects or obstruction and excess mucus. The ducts tend to be blocked to retrograde flow of contrast.

Imaging differential diagnosis includes chronic pancreatitis, other cystic neoplasms, or even pancreatic duct obstruction and secondary dilation due to a stone or adenocarcinoma. Likewise, although CT, US, and pancreatography can suggest a diagnosis of an intraductal tumor, imaging cannot reliably differentiate malignant from benign tumors. A large tumor and involvement of pancreatic parenchyma suggest a malignancy. Also, excrescent nodules are more common with a malignancy.

Oncocytic Tumors

A pancreatic intraductal oncocytic papillary neoplasm consists of mucin-filled cysts con-

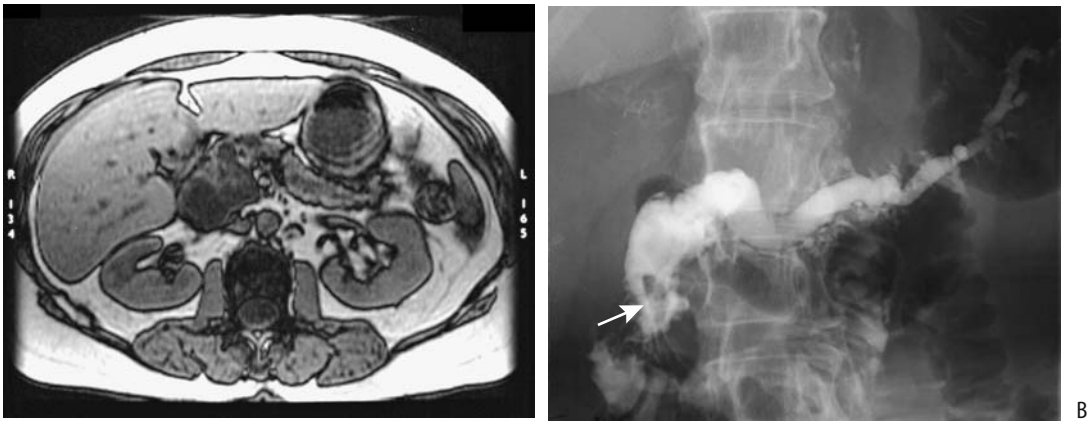

Figure 9.29. Intraductal papillary mucinous tumor of pancreas. MR (A) and ERCP (B) identify a dilated and obstructed pancreatic duct and an intraluminal tumor component (arrow). (Courtesy of Temil Tirkes, M.D., University of Pennsylvania.)

taining nodular papillary outpouchings. Some of these tumors communicate with dilated pancreatic ducts. The cysts probably represent dilated ducts. The papillary component consists of a fibrovascular core lined by stratified oncocytic cells. Although these tumors are intraductal, some become invasive.

Whether these tumors represent a separate entity, are part of the spectrum of intraductal mucinous tumors, or are papillary cystic neoplasms is conjecture.

Papillary Cystic Neoplasms (Embryonic Tumor)

The classification and terminology of papillary cystic neoplasms of the pancreas is still evolving. These tumors are also called *solid and papillary epithelial neoplasms*, *solid and cystic tumors of the pancreas,* and *Frantz's tumors* in some European literature. In the older literature a number of these tumors were labeled as nonfunctioning islet cell tumors, and the differences between these two entities are not clear. Some postulate that these papillary cystic neoplasms originate from pleuropotential embryonic stem cells, and thus the term *pancreatic embryonic tumor* is preferred by some.

Most papillary cystic tumors of the pancreas occur in young women, with an occasional one encountered in a teenager. Most of these tumors are large, well circumscribed, and locally invasive. They are considered either benign or low-grade malignant. Aggressive ones tend to be larger and have a thicker capsule. Of interest is that a number of these patients developing metastases, including peritoneal carcinomatosis, had prior trauma (124).

In 53 women and three men (mean age at diagnosis, 25 years) with proven papillary cystic neoplasms of the pancreas, the mean tumor diameter was 9.0 cm; they were located in the tail ($n = 30$), head ($n = 18$), and body ($n = 8$); and all tumors contained either hemorrhage or cystic degeneration, ranging from solid friable tumor to gelatinous or cystic regions (125). All tumors were encapsulated, and a minority contained calcifications or fluid-debris levels.

Pathologists have difficulty in discriminating between papillary cystic tumors and nonfunctioning endocrine tumors. Histology of a papillary cystic tumor reveals small, eosinophilic tumor cells often arranged in rosettes; these tumor cells tend to be immunohistochemically positive for somatostatin, α-1 antitrypsin, neuron-specific enolase and synaptophysin. Some contain immature neurosecretory granules.

The most common imaging appearance is a mixture of solid and cystic components in a tumor surrounded by a thick capsule. An occasional one appears solid. The cystic component ranges from barely identifiable to the tumor resembling a pseudocyst. Hemorrhage and necrosis are common and blood and debris in

the cystic component increase CT density levels. Computed tomography reveals the capsule as a hypodense structure enhancing with contrast. Calcifications develop within a fibrous capsule or solid tumor component in some. Extracapsular spread is unusual.

Magnetic resonance imaging reveals the solid component to be isointense or even hypointense on T1- and hyperintense on T2-weighted images. Hemorrhage is common and results in a hyperintense T1-weighted image. The solid component enhances postcontrast.

Angiography identifies either a hypovascular or avascular tumor, thus differentiating these tumors from nonfunctioning islet cell tumors, which tend to be hypervascular.

Imaging can distinguish these tumors from ductal pancreatic adenocarcinomas; the latter typically are more invasive. Serous and mucinous cystadenomas and carcinomas usually do not have a solid tumor component to the extent seen with papillary cystic neoplasms.

A percutaneous biopsy is usually superfluous because most of these tumors are resected. In fact, it has been stated that "tumor biopsies . . . should never be performed" because of possible spread by trauma (124).

Other Tumors

A hemangiopericytoma is rare in any location. Its malignant propensity varies considerably and, in general, malignancy is established by detecting metastases. Intraabdominal hemangiopericytomas tend to be very aggressive.

Ultrasonography and CT typically reveal a cystic tumor.

A cystic teratoma of the pancreas contained multiple calcifications, mucin, and lipid components (61).

Neuroendocrine (Islet Cell) Tumors

Clinical

Pancreatic neuroendocrine tumors are often also called islet of Langerhans tumors, although a number originate at other sites. Most share certain cytochemical characteristics and have been labeled as *APUDomas* (amine precursor uptake and decarboxylation), although currently most authors prefer the term *neuroendocrine tumors*. These tumors are not confined to the pancreas but also include pituitary gland adenomas, adrenal gland pheochromocytomas and neuroblastomas, medullary thyroid carcinomas, and carcinoid tumors in the gastrointestinal tract and lung.

About half of these tumors produce a number of hormones and occasionally even switch secretion to a different hormone. Rare functioning endocrine tumors include calcitoninoma (126), ACTHoma (adrenocorticotropic hormone), and neurotensinoma. The activity of one hormone generally predominates, and these tumors are classified based on the predominant hormone detected. Some are clinically silent and are discovered incidentally, and some are associated with hypercalcemia. In general, with the exception of insulinomas, most are malignant and are highly vascular.

The presence of calcitonin secretion does not necessarily imply a calcitoninoma and is occasionally found in a nonfunctioning endocrine tumor. Calcitonin secretion often implies malignancy, and many such tumors already have metastasized; calcitonin secretion should be suspected in patients with a neuroendocrine tumor and diarrhea that cannot be otherwise explained.

Although uncommon, the first evidence of an islet cell tumor can be acute pancreatitis, either associated with duct obstruction or due to other reasons.

A carcinoid, pheochromocytoma, islet cell tumor, Merkel cell carcinoma, and other neuroendocrine tumors often contain vasoactive intestine polypeptide (VIP), somatostatin, and other receptors. Therapy with somatostatin analogues in these patients reduces hormonal hypersecretion. This in turn helps control flushing attacks, diarrhea, hypoglycemia, and electrolyte abnormalities that patients with carcinoid tumors and other islet cell tumors are prone to developing.

Detection of a neuroendocrine pancreatic tumor in association with another tumor, especially a neural one, should suggest von Hippel-Lindau disease.

Imaging

Depending on the type of neuroendocrine tumor suspected, preoperative localization may include CT, MRI, radionuclide scanning, angiography, and venous blood sampling. During

surgical exploration, intraoperative US is useful in detecting occult tumors and in defining underlying anatomy. Whether enucleation is performed or resection is required often depends on the tumor's proximity to the pancreatic duct; intraoperative US can provide this information. A high-frequency transducer is essential for detecting and evaluating these small tumors.

Most of these tumors are hypervascular. Larger tumors are more prone to calcify (Fig. 9.30). Insulinomas tend to be more homogeneous in appearance, while non–insulin-producing tumors are more cystic or necrotic. Only an occasional one obstructs the pancreatic duct, results in vascular encasement, or leads to portal vein thrombosis, findings common with ductal carcinomas.

More islet cell tumors are detected with biphase CT than conventional CT. Tumors several millimeters in diameter can be detected. Most are detected during the arterial phase, although some are identified only during the venous phase. Computed tomographic arteriography with contrast injected through a celiac artery catheter is occasionally helpful when searching for these small hypervascular tumors.

Gray-scale US shows most islet cell tumors to be well-marginated and hypo- to isoechoic. Some are detected only with intraoperative or endoscopic US. An intraductal high-frequency transducer is useful in detecting tumors adjacent to the duct.

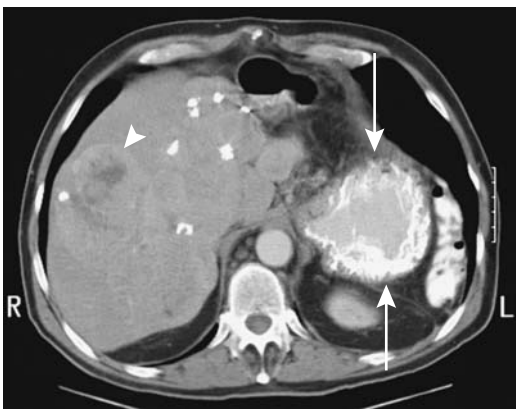

Figure 9.30. Metastatic islet cell carcinoma. Computed tomography reveals a calcified tumor in the pancreatic tail (arrows) and a liver metastasis (arrowhead). The patient has had a previous left hepatectomy. (Courtesy of Patrick Fultz, M.D., University of Rochester.)

Contrary to some earlier studies suggesting that MR is superior to CT, a later study found biphasic CT and MRI similar in detecting these tumors (127). Another study of 28 patients with clinically suspected functional islet cell tumors achieved even better MRI results, reaching a sensitivity of 85% and specificity of 100% in tumor detection (128). Most of these tumors are hypointense on T1- and hyperintense on fat-suppressed T2-weighted images. They enhance more than surrounding normal pancreatic parenchyma early after contrast injection and gradually become isointense (129). Except for gastrinomas, enhancement is either uniformly homogeneous or heterogeneous. Magnetic resonance features distinguishing these tumors from pancreatic ductal adenocarcinomas are their hyperintense signal on T2-weighted images, early postcontrast enhancement, and, for many of the malignant ones, hypervascular liver metastases. A number exhibit a ring-like enhancement immediately postcontrast. Nevertheless, the occasional poorly differentiated ones and those inciting a desmoplastic reaction tend to be isointense on T2-weighted images, show little postcontrast enhancement, and mimic ductal adenocarcinomas.

An occasional islet cell tumor results in a main pancreatic duct stricture.

Portal venous sampling is performed using a transhepatic approach. The technique is insensitive when multiple tumors are present.

Except for insulinomas, most neuroendocrine tumors contain varying amounts of somatostatin receptors, which bind somatostatin analogues. Whole-body imaging using a somatostatin analogue (indium-111–diethylenetriamine pentaacetic acid (DTPA)–octreotide, Octreoscan), also known as *somatostatin receptor scintigraphy*, is useful in localizing these tumors. Results in primary tumor detection are variable, but in a setting of positive laboratory tests but negative imaging this test appears worthwhile. It has a role in detecting tumor recurrence and metastases. Also, tumors found to be somatostatin receptor positive respond to somatostatin analogue therapy.

An ectopic thyroid mimicked a pancreatic tumor (130).

Numerous endocrine tumors have been biopsied without complication. Nevertheless, a functioning endocrine tumor should be approached with caution because of possible excess hormone release.

Hyperinsulinoma Conditions

The most common but not the only etiology of recurrent severe hypoglycemia in an adult is an insulinoma. Less common is nesidioblastosis and neoplasms producing insulin-like growth factor. Thus an occasional patient with a hemangiopericytoma presents with hypoglycemia; a history of a hemangiopericytoma resected previously is not uncommon. Generally not appreciated is that a large nonpancreatic leiomyosarcoma may mimic clinical findings of an insulinoma, including severe hypoglycemia. Even a bowel adenocarcinoma with liver metastases can have hypoglycemia induced by tumor insulin-like growth factor production. Occasionally encountered is hypoglycemia developing in a patient with renal failure or fulminant hepatic failure.

Insulinoma

The most common islet cell endocrine tumor is an insulinoma. A Japanese literature search of over 1000 patients with insulinoma or hypoglycemic syndrome revealed that 81% of these tumors were 20 mm or smaller (131). About 90% are benign and most tend to be solitary, solid, and homogeneous. Multiple insulinomas should suggest MEN-I syndrome. Primary extrapancreatic insulinomas are rare. Cystic insulinomas are uncommon. Histologically, an insulinoma mimics normal islet cells. It is difficult to tell with some whether indeed it is a neoplasm or simply represents hyperplasia.

Autonomous insulin synthesis and secretion are the hallmark of an insulinoma even in a setting of low blood glucose levels, leading to further hypoglycemia and resultant clinical findings.

Most insulinomas are small and are difficult to detect with imaging. Conventional CT, gray-scale US, and MRI are of limited value. In one study, combined dual-phase thin-section multidetector CT and endoscopic US achieved a diagnostic sensitivity of 100% in detecting these tumors (132). Endoscopic US appears to be somewhat more sensitive in detecting insulinomas in the pancreatic head and less sensitive in the pancreatic tail. Nevertheless, some tumors are found only by the surgeon or by intraoperative US; some surgeons opine that detection of an insulinoma does not require extensive preoperative localization.

A rare insulinoma is hyperdense to normal pancreatic parenchyma on precontrast CT. An early arterial phase and pancreatic phase appears best in detecting these tumors (133). Postcontrast CT ring-like enhancement progressing into homogeneous tumor enhancement is seen in about half of these tumors.

The uncommon malignant insulinoma is a highly vascular tumor in the pancreatic tail often detected from liver metastases; liver venous sampling after arterial stimulation with calcium confirms insulin secretion. In some, serum levels of α-fetoprotein and trypsin are markedly elevated.

Intraoperative US is very helpful in localizing these tumors and in defining adjacent structures.

Magnetic resonance imaging localizes some pancreatic insulinomas. They are hypointense on T1- and hyperintense on T2-weighted sequences and are homogeneously hyperintense on postcontrast images.

While not usually performed, indium-111–octreotide scintigraphy does, at times, localize an insulinoma.

Insulin venous sampling is useful in detecting insulinomas not detected by other imaging modalities. Calcium gluconate is injected directly into the gastroduodenal, splenic, and superior mesenteric arteries, followed by venous sampling. Injection into an artery supplying an insulinoma results in a marked increase in the draining vein insulin level. An insulin increase post–calcium infusion of at least 100% above basal levels is considered abnormal. Such an approach obviates the need for transhepatic portal venous sampling and is simpler. This test is also useful for suspected hepatic metastases; no increase in insulin concentration in hepatic venous blood after intraarterial calcium stimulation makes insulinoma liver metastases unlikely. Nevertheless, this test should be interpreted with caution, because an injection into an artery not supplying a tumor may also increase venous insulin levels, possibly by the influx of

calcium into a tumor via intrapancreatic anastomoses.

Nesidioblastosis

Nesidioblastosis, also called *noninsulinoma pancreatogenous hypoglycemic syndrome* and other similar names, is a rare condition consisting of islet hyperplasia and β-cell hyperfunction. This is a nonneoplastic condition but is discussed here because it is in the differential of a suspected insulinoma. Also, occasionally nesidioblastosis coexists with an insulinoma (131).

Nesidioblastosis is a well-recognized entity in neonates but also occasionally develops in adults. It may be part of MEN-I syndrome. Familial nesidioblastosis occurs in neonates.

These patients present with hyperinsulinemic hypoglycemia, but a prolonged fast tends to be normal. An insulinoma is usually suspected, but preoperative localization, operative exploration, and intraoperative US do not detect a tumor. At times a blind distal pancreatectomy is performed. The diagnosis is made by the pathologist finding nesidioblasts and islet cell hyperplasia in a resected specimen. Also, the islets are structurally abnormal. A defect in insulin gene regulation appears involved in these patients.

Portal venous sampling in some of these patients shows a gradient in insulin concentration, and a misdiagnosis of insulinoma is thus made. These patients have a positive selective arterial calcium stimulation test indicative of pancreatic β-cell hyperfunction (there is an increase in plasma insulin level when calcium is injected into the arteries supplying the pancreas) (134).

In neonates, a >95% pancreatectomy is performed for persistent hyperinsulinemic hypoglycemia due to nesidioblastosis and failed medical management. At times only that portion of the gland lying between the common bile duct and duodenum and a small rim of pancreas along the duodenal sweep are not resected; still, in about one third of children with such a resection, hyperinsulinemia and hypoglycemia recur and a near-total pancreatic resection is then necessary. Of interest is that partial pancreatic regrowth develops in some of these ueouates. On a long-term basis, over two thirds of these children with a 95% pancreatectomy develop diabetes.

Gastrinoma

Clinical

The Zollinger-Ellison syndrome is caused by a gastrin-secreting tumor. Most gastrinomas are malignant. About 25% of gastrinomas occur in a setting of MEN-I syndrome and a patient presenting with a gastrinoma probably should be investigated for this syndrome. Gastrinomas tend to be multiple when part of MEN-I syndrome. The risk of gastrinoma malignancy, growth rates, and high prevalence in the duodenum seen in MEN-I patients cannot be extrapolated to patients with isolated gastrinomas. Even with liver metastases these tumors grow slowly, and prolonged survival is feasible.

Some of these tumors are extrapancreatic in location (duodenal gastrinomas are discussed in Chapter 3). Occasionally a small gastrinoma is discovered in a lymph node; most of these are metastatic foci, although a rare one is believed to represent a primary tumor and excision of that lymph node should be curative. With such a scenario a search for a primary gastrinomas should, of course, be performed.

A review of patients with gastrinoma/Zollinger-Ellison syndrome found that a correct preoperative diagnosis is made in about half of these patients, and about half of these tumors are <20 mm in diameter (135); although about 40% had metastases, the 10-year survival rate was 64%.

These patients develop recurrent, multiple ulcers in atypical locations. They have basal gastric acid hypersecretion and a markedly elevated fasting serum gastrin level, with values considerably greater than seen after a truncal vagotomy or proximal gastric vagotomy.

In the absence of metastases, unless surgery is contraindicated, even with negative preoperative imaging studies these patients probably should undergo exploratory laparotomy, with the aim of a curative resection. Previously, if excision was not feasible, a total gastrectomy was performed for symptom control; today total gastrectomy is rarely performed and in most patients gastric acid hypersecretion is managed with H2 receptor antagonists. Thus with suspected liver metastases a biopsy establishes the

diagnosis and these patients are then treated medically.

Many of these tumors contain somatostatin receptors, and somatostatin analogues are potential therapeutic agents. Using an autoradiography technique, both pancreatic carcinomas and gastrinomas expressed specific somatostatin receptors (136); in gastrinomas, octreotide inhibited iodine-125–somatostatin-28 binding similar to somatostatin-28, but little competitive binding of I-125–somatostatin-28 was evident in carcinomas, suggesting that somatostatin receptors in gastrinomas differ from those in carcinomas.

Imaging

A barium study detects gastritis, often severe, and peptic ulcer disease, especially in postbulbar regions. Hyperacidity is also associated with reflux esophagitis in many of these patients.

The imaging procedures useful in detecting a gastrinoma include CT, endoscopic US, MRI, indium-111–octreotide scintigraphy, and selective arterial secretin injection, with the initial study of choice often being octreotide scintigraphy. Still, only approximately half of gastrinomas are detected with these studies (Fig. 9.31).

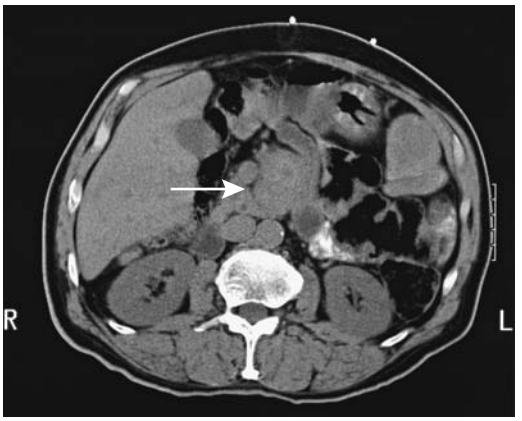

Figure 9.31. Gastrinoma in a 75-year-old man. Transverse precontrast CT identifies enlargement of the pancreatic head (arrow). Initially believed to represent a pancreatic carcinoma, biopsy suggested a gastrinoma. (Courtesy of Patrick Fultz, M.D., University of Rochester.)

In patients with Zollinger-Ellison syndrome, duodenal, lymph node, and pancreatic gastrinomas were eventually found in 42%, 38%, and 17% of patients, respectively (137). Of these tumors, endoscopic US detected 50% of duodenal wall tumors while conventional endoscopy detected 40%. Endoscopic US detected 75% of pancreatic tumors while CT detected 25%; endoscopic US detected 62% of lymph node tumors while CT detected none. The authors concluded that endoscopic US is the imaging technique of choice for preoperative imaging of gastrinomas. At times intraoperative US is necessary in locating small gastrinomas.

Similar to other solid pancreatic tumors, gastrinomas are hypointense on T1- and hyperintense on T2-weighted fat-suppressed MRI. In distinction to most other neuroendocrine tumors, gastrinomas enhance postcontrast in a ring pattern (129). Such ring-like enhancement is also seen in liver metastases; this finding is not specific for gastrinomas but is also occasionally found with other neuroendocrine tumors. An occasional cystic component is detected in a gastrinoma.

Indium-111–pentetreotide scintigraphy is probably superior to CT in localizing gastrinomas; scintigraphy can detect duodenal tumors several millimeters in size. Nevertheless, In-111–pentetreotide is not foolproof. In a patient with a previous partial pancreatectomy and splenectomy and now presenting with Zollinger-Ellison syndrome, In-111–pentetreotide scintigraphy revealed nodular increased uptake in an accessory spleen (138).

Glucagonoma

Pancreatic glucagonomas are uncommon. These are slow-growing tumors, most are malignant, and metastases are often present at initial detection.

Glucagonomas result in elevated serum glucagon levels. These are complex tumors, however, and patients often have increased gastrin levels, VIP, serotonin, insulin, human pancreatic polypeptide, calcitonin, and adrenocorticotropic hormone; metastases are common at initial presentation.

The glucagonoma syndrome consists of weight loss, necrolytic migratory erythema, dia-

betes mellitus, stomatitis, and diarrhea. In a number of patients a specific erythematous rash suggests the diagnosis.

Contrast-enhanced CT should detect larger tumors. Similar to other solid pancreatic tumors, glucagonoma are hypointense on T1- and hyperintense on T2-weighted MRI. Postcontrast, most reveal early diffuse, heterogeneous enhancement.

Glucagonomas metastasize readily. Still, in spite of liver metastases, prolonged survival is possible through judicious surgery, hepatic artery tumor embolization, and somatostatin analogue therapy.

Somatostatinoma

Most somatostatinomas occur in the pancreas or duodenum and most are malignant. High plasma somatostatin levels are found in some patients. Metastases are common at initial presentation. These patients have elevation of fasting plasma somatostatin levels. Any clinical hormonal effect depends on other peptides being secreted in addition to somatostatin, although somatostatin does tend to inhibit the release of other hormones.

No specific imaging findings exist for smaller tumors. Larger somatostatinomas are hypointense on T1- and hyperintense on T2-weighted MRI. Postcontrast, most exhibit early diffuse, heterogeneous enhancement.

Abnormal In-111–pentetreotide uptake occurs with some somatostatinomas.

Vasoactive Intestinal Peptide Tumors

Vasoactive intestine polypeptide–secreting tumors (*VIPomas*, *Verner-Morrison syndrome*) are associated with increased plasma vasoactive intestinal polypeptide levels, although elevation can be episodic. These tumors tend to be solitary and have a predilection for the pancreatic tail.

A review yielded 241 patients with VIPomas, with 74% being intrapancreatic and 26% extrapancreatic in origin (139); among extrapancreatic ones, 23% were nonneurogenic in origin. About two thirds of pancreatic VIPomas were malignant versus one third of extrapancreatic tumors. Of necessity, the definition of a VIPoma overlaps with some other tumors, and the above review includes such extrapancreatic neurogenic tumors as ganglioneuromas, ganglioneuroblastomas, and neuroblastomas. An occasional VIPoma contains large amounts of amyloid.

The classic clinical findings are secretory diarrhea, hypokalemia, hypochlorhydria, and metabolic acidosis. Metastasis is not uncommon at first presentation.

VIPomas are hypointense on T1- and hyperintense on T2-weighted MRI. Postcontrast, most have early diffuse, heterogeneous enhancement. Some metastases show intense peripheral enhancement on immediate postcontrast SGE images.

One tumor, not detected by other imaging or by radiolabeled octreotide, was localized in the pancreatic tail by I-123–VIP (140).

Carcinoid'

Pancreatic carcinoids are rare; most are malignant, and metastasis at time of diagnosis is common. In the literature, the terms *serotonin-producing tumor of the pancreas* and *pancreatic serotoninoma* are also used to designate these tumors.

The carcinoid syndrome is absent unless liver metastasis is present. A diagnosis of pancreatic carcinoid is made if a pancreatic tumor is associated with elevated serum 5-hydroxytryptamine (serotonin) levels or elevated urine 5-hydroxyindole acetic acid (5-HIAA) levels. Ideally, serotonin is isolated in tumor tissue, and no other dominant hormone is detected. Positive silver staining in tumor cells is suggestive of a carcinoid but is not as specific as a serotonin assay. Some pancreatic neuroendocrine tumors labeled as being nonfunctioning (discussed below) probably represent carcinoids with low levels of serotonin production.

Carcinoids are hypointense on T1- and hyperintense on T2-weighted images. A heterogeneous enhancement is evident on immediate postcontrast images.

Paraganglioma

Pancreatic paragangliomas are rare. Some secrete somatostatin and other hormones. An occasional one is discovered only after it has metastasized.

Schwannoma

Pancreatic schwannomas range from benign to malignant, solid to cystic. Most are solitary, except in a setting of von Recklinghausen's disease. A schwannoma originating close to the celiac axis can be misdiagnosed as an intrapancreatic neoplasm.

Schwannomas tend to be sharply marginated. Some mimic a pseudocyst. Computed tomography reveals an inhomogeneous appearance and some contain septa. They have a variable CT appearance, ranging from iso- to hypodense (61); they enhance with contrast. Some contain a necrotic center. They are hypointense on T1- and hyperintense on T2-weighted MR sequences.

Neurofibroma

Computed tomography of a plexiform neurofibroma revealed a near-water homogeneous density, mild contrast enhancement, and an infiltrating appearance (61).

Nonfunctioning Islet Cell Tumor

Islet cell tumors not associated with clinically detectable hormone production are called nonfunctioning. Some do secrete a polypeptide, but are still considered nonfunctioning if the patient is asymptomatic. Differentiation between functioning and nonfunctioning is not straightforward. At times a primary islet cell carcinoma is nonfunctioning and is resected, but later metastases develop a de novo capacity to secrete hormones.

The controversy in differentiating these tumors from papillary cystic neoplasms has already been mentioned. Focal lymphoma is also in the differential of an occasional solid nonfunctioning neuroendocrine tumor.

Most of these tumors are slow-growing. Smaller tumors tend to be benign, but most tumors >5 cm are malignant (141). Aside from incidentally discovered ones, these tumors tend to be large when first detected and metastases are often evident. Incidentally, malignancy cannot be established by histology, and evidence of either metastases or local invasion is the criterion used.

A rare nonfunctioning malignant islet cell tumor contains eggshell calcifications.

Postcontrast CT shows better tumor conspicuity during the arterial phase than portal venous phase (142); the arterial phase also detects more liver metastases than the portal phase. On the other hand, venous encasement by tumor is better identified during the portal venous phase.

Computed tomography typically shows a large, hypervascular tumor (141). Some tumors contain cystic regions and punctate calcifications, an appearance that distinguishes them from ductal adenocarcinomas. The larger ones tend toward necrosis. A heterogeneous CT contrast enhancement pattern is common.

A correct preoperative diagnosis is not common. Both a primary tumor and metastases tend to respond to chemotherapy. Their better prognosis makes it important to distinguish these tumors from the more common pancreatic ductal adenocarcinomas.

Pancreas in Diabetes Mellitus

Postmortem pancreatic angiography in non–insulin-dependent diabetics revealed that 58% of diabetics and 20% of controls showed one or more of the following (143): >50% celiac or splenic artery stenosis, two or more irregular intrapancreatic branches, or decreased vascularity in the body and tail—segments responsible for most insulin secretion.

Insulin-dependent type 1 diabetes is caused by autoimmune destruction of insulin-producing β-cells. If diabetes is identified early enough, some of these patients still have functioning residual β-cells and benefit from adjuvant immunotherapy to protect remaining β-cell function.

Technetium-99m–human polyclonal immunoglobulin (HIG) scintigraphy in nearly half of newly diagnosed type 1 diabetics shows a significant accumulation of radiolabeled HIG in the pancreas (144); thus HIG scintigraphy, performed at the time of diabetes onset identifies a subset of patients who appear to benefit from adjuvant immunotherapy.

Some diabetics also have an abnormal exocrine pancreas. Endoscopic retrograde pancreatography reveals pancreatic duct abnormalities consisting of dilation, stenosis, tortuosity, obstruction, or calculi.

In pediatric patients with insulin-dependent diabetes mellitus, US reveals an inverse relationship between pancreatic size and the duration of diabetes (145); the pancreas was larger in children aged 3 to 7 years who had diabetes for 2 years or less than in older children who had had diabetes for >5 years. In children, diabetes thus appears to affect pancreatic growth.

Vascular Lesions

Hemosuccus pancreaticus, also called *wirsungorrhagia* in some of the French literature, signifies hemorrhage into the pancreatic duct. It is rarely detected.

Bleeding from the ampulla is either from the pancreatic or bile ducts. At times angiography is useful in locating and embolizing a specific site of bleeding. Most pancreatic bleeding is secondary to chronic pancreatitis.

Aneurysms or pseudoaneurysms of a pancreatic artery are rare in the absence of pancreatitis. Bleeding pseudoaneurysms in a setting of pancreatitis have already been discussed. These aneurysms are a cause of massive blood loss, even exsanguination. Aside from bleeding, a rare pseudoaneurysm results in bile duct obstruction due to compression.

Arteriovenous malformations are rare in the pancreas but are a cause of bleeding. Endoscopic Doppler US revealed a pulsatile waveform in one pancreatic malformation adjacent to the duodenum (146); arteriography confirmed an extensive vascular network. Resection of pancreatic head arteriovenous malformations is difficult; some of these patients require a Whipple procedure to control bleeding. Radiation therapy is an option for larger arteriovenous malformation (147).

Immunosuppression

Acquired immunodeficiency syndrome patients have developed non-Hodgkin's lymphomas located primarily in the pancreas; imaging reveals diffuse infiltration. A percutaneous CT-guided needle biopsy should be diagnosis.

Unusual infections abound. In one patient, AIDS initially manifested as a tuberculous pancreatic abscess (148).

Bile duct abnormalities are well described in AIDS patients, but pancreatic duct changes are less well known. Over half have pancreatographic abnormalities consisting of dilation, an irregular contour to the main and secondary ducts, and main duct stenosis. Most patients with pancreatic duct abnormalities also have AIDS-related cholangitis.

Drug-induced pancreatitis develops in AIDS patients. Dideoxyinosine is an antiretroviral agent used to treat HIV infection; both pseudocyst formation and relapse of pancreatitis are associated with this drug.

Total amylase is of limited value in identifying pancreatic disease in HIV-infected patients; 28% of ambulant HIV-positive males had elevated total amylase values; however, almost half of these were due to an increased salivary fraction (149).

Postoperative Changes

Transplantation

Indications

A pancreatic transplantation is indicated in a patient with insulin-dependent diabetes mellitus who also requires a renal transplant, with both organs being transplanted at the same time. An isolated pancreatic transplant is performed in patients who already have a functioning renal transplant or in those with diabetic complications who do not have gross nephropathy. If transplantation is successful, the patient no longer depends on external insulin but has hyperinsulinemia and remains on chronic immunosuppressive therapy.

Pretransplant cardiac function is generally obtained; stress thallium scintigraphy is typical, with more invasive cardiac imaging reserved for specific situations.

Initially the transplanted pancreas and attached duodenum were placed in the right iliac fossa, and a side-to-side duodenovesical anastomosis was performed. Arterial supply to the donor pancreas is from the recipient common iliac artery, and venous drainage is to the common or external iliac vein. A simultaneously transplanted kidney is placed in the left iliac fossa. An alternate approach is primary enteric drainage. The native pancreas is not

resected. Such a transplant results in two nonphysiologic events: (1) Pancreatic endocrine secretions are into the systemic circulation, bypassing the liver, and they lead to hyperinsulinemia. (2) Exocrine secretions into the bladder result in inflammation, infection with possible pancreatitis, and a metabolic acidosis. To overcome these problems a revised procedure was subsequently adopted by some centers: The donor duodenum is anastomosed to a jejunal loop and pancreatic venous drainage is to the recipient portal venous system.

Following total or subtotal pancreatectomy for chronic pancreatitis, pancreatic islet autotransplantation by intraportal infusion of pancreatic tissue leads to approximately half of these patients becoming insulin independent. Clinical pancreatic islet transplantation, however, is still in its infancy.

Results

Overall results among 500 simultaneous pancreas-kidney transplants at the University of Wisconsin through October 1997, are as follows (150): patient survival at 1, 5, and 10 years was 96%, 89%, and 76%; kidney function, 89%, 80%, and 67%; and pancreas function, 87%, 78%, and 67%. Since June 1995, 1-year survival rates are as follows: patient, 98%; kidney, 94%; and pancreas, 93%. Conversion from bladder drainage to enteric drainage was required in 24% of patients, with primary indications for enteric conversion being leak in 14%, urethritis and extravasation in 7%, and chronic hematuria in 3% of patients.

Pancreatic allograft excretion and perfusion can be studied with secretin-augmented MR pancreatography and dynamic contrast enhanced MRI. Patients with a normally functioning graft produced 236 ml (s. d. +/– 104) of pancreatic juice and those with dysfunctional grafts produced only 42 ml (+/– 25) (151).

Thallium-201 scintigraphy provides static images of the transplanted pancreas. Technetium-99m–sestamibi scintigraphy provides both dynamic and static images, in some patients being superior to thallium-201 studies.

Complications

Rejection ranges up to 9% at 1 year. Other complications are only slightly less common, with vascular thrombosis leading the list. Unlike renal transplant failure, pancreas transplant failure is more covert. Rejection, however, often involves both kidney and pancreas. The degree of parenchymal enhancement at dynamic contrast-enhanced MRI appears useful in detecting acute transplant rejection. Dynamic contrast-enhanced gradient-recalled echo (GRE) MR studies showed a mean parenchymal enhancement of 106% in patients with no biopsy evidence of rejection, 66% in those with mild, 62% in those with moderate, and 57% in those with severe acute rejection (152); infarcted transplants revealed parenchymal enhancement of 3% and could thus be readily identified. Overlap existed, however, between some patients in the normal and rejection groups, and a biopsy is still necessary in some.

Biopsy is performed either percutaneously or cystoscopically through the duodenal anastomosis. With the latter, an US-guided and cystoscopically directed approach appears advantageous. CT- or US-guided core biopsies of pancreas grafts are satisfactory in most patients. The most common biopsy complication is self-limited bleeding from a biopsy site; less often encountered are major bleeding and asymptomatic hyperamylasemia.

Posttransplant CT is indicated in patients with fever, elevated serum amylase levels, and suspected fluid collections.

Ultrasonography of a transplanted pancreas is more difficult than of a kidney. Especially if enteric rather than bladder drainage is created, superimposed bowel and an indistinct margin make organ identification difficult. Fluid collections can be detected but their clinical significance is difficult to assess in the postoperative period. Neither absolute resistive indexes, obtained from US data, nor changes in resistive indexes correlate with acute rejection. Doppler US is useful, however, in detecting vascular thromboses and strictures.

Urologic complications are not uncommon with duodenum anastomosed to the urinary bladder and exocrine pancreatic secretions thus draining into the bladder. Complications of kidney-pancreas transplantations include urinary tract infections, hematuria, leaking duodenovesical anastomosis, and ureteral and urethral abnormalities. The most common postsurgical complication is a leak at the duodenovesical anastomosis, resulting in accumulation

of peritoneal fluid. A radionuclide cystogram confirms a communication between the bladder and peritoneal cavity. The duodenovesical anastomosis can also be evaluated by conventional cystography or CT cystography. Computed tomography cystography should be performed both with the bladder distended and after voiding; at times full distention will not detect a leak that is evident after voiding.

Urethral stricture and urethral disruption are complications of pancreatic transplantation in male patients; extravasation occurs at either the bulbar urethra or the bulbomembranous junction.

Magnetic resonance angiography is useful in detecting vascular complications. The absence of flow, vascular thrombosis, rejection, and infarction are detected. An MRA should detect almost all acute vascular compromise. Postcontrast 3D MR after kidney-pancreas transplantation readily detects larger transplanted arteries, seen as hyperintense structures, but transplanted venous vessels are less often identified. Gadolinium-enhanced 3D MRI in five patients with venous thrombosis and occlusion revealed serpentine voids within graft parenchyma or at the venous anastomosis during venous-phase imaging (153); the lack of graft enhancement or heterogeneous enhancement corresponded to gland necrosis, confirmed at pancreatectomy.

Allograft pancreatitis is relatively common. Other complications include fistulas and infection. Some patients develop hypoglycemia, at times years later.

Follow-up of patients with uremia and type 1 diabetes after a kidney-pancreas transplant and similar patients after kidney-only transplantation revealed that the double transplant patients were at lower risk for atherosclerosis than kidney-only transplant patients (154). Nevertheless, underlying atherosclerosis unrelated to transplantation is common in these patients.

Postpancreatic transplantation lymphoproliferative disorders manifest by diffuse allograft enlargement, an imaging appearance similar to that seen with transplant rejection or acute pancreatitis (155).

Resection

Traditionally, a Whipple procedure was performed when resecting the pancreatic head, which involves a pancreaticoduodenectomy and includes segments of extrahepatic bile ducts and pancreatic duct. The high mortality associated with a Whipple procedure a generation ago has dropped markedly and this procedure is now also being performed for some patients with chronic pancreatitis. Currently some surgeons are resecting only the pancreatic head and preserving the adjacent duodenum, the common bile duct, and the papilla of Vater. An end-to-end anastomosis is performed to connect the pancreatic duct to the intestinal tract.

After a pylorus-preserving pancreaticoduodenectomy, most patients have abnormal pyloric function (156); alkaline reflux is common and some patients develop gastritis.

Total pancreatectomy is rarely performed; in a setting of pancreatic cancer; it has not led to increased survival but does introduce major endocrine management problems.

One complication of a pancreaticoduodenectomy with portal and superior mesenteric vein resection is localized liver infarction. Computed tomography should detect most of these complications. A distinctly unusual occurrence after a Whipple procedure was rectal evacuation of a portal vein graft (157); presumably the underlying cause was graft infection.

Examination Complications

Laparoscopy

Laparoscopy has a limited role in pancreatic disease. Port site seeding after laparoscopic staging of a pancreatic carcinoma is a complication.

Endoscopic Retrograde Cholangiopancreatography

The major complication of ERP and endoscopic sphincterotomy is pancreatitis, at times life-threatening and resulting in massive peripancreatic necrosis. The risk of such pancreatitis is difficult to gauge. In a 1-year prospective study of 430 consecutive ERCP examinations in a single center, pancreatitis developed in 3% of patients (158); hyperamylasemia occurred in 8%. Both pancreatitis and hyperamylasemia are more common after difficult procedures. Over-

injection of contrast is probably one of the causes. The high osmolality and ionic nature of iodinated contrast agents may play a role, although some studies suggest that the use of nonionic contrast agents does not decrease the risk of postprocedure pancreatitis. Some of the risk factors associated with postprocedure pancreatitis include the presence of prior or current pancreatitis, pancreatic duct stricture, and sphincter of Oddi abnormalities. Curiously, endoscopic sphincterotomy performed in a setting of nondilated bile ducts is also associated with an increased risk of pancreatitis. A direct correlation exists between postprocedure pancreatitis and number of pancreatic duct injections; also, those with difficult common bile duct cannulations are more to develop pancreatitis.

Computed tomography performed after ERCP papillotomy occasionally detects a pancreatic "tumor" (159).

Technetium-99m–HMPAO leucocyte scintigraphy has been disappointing in detecting mild acute pancreatitis after ERCP.

Biopsy

Pancreatitis, with fatal outcome, has followed percutaneous pancreatic biopsy. Needle tract tumor seeding is a complication. Whether there is an increased risk of seeding with the use of larger needles is conjecture.

In addition to percutaneous pancreatic biopsy, US-guided laparoscopic biopsy of the pancreas can be performed. Port site seeding after laparoscopic carcinoma biopsy has occurred.

References

1. Hong KC, Freeny PC. Pancreaticoduodenal arcades and dorsal pancreatic artery: comparison of CT angiography with three-dimensional volume rendering, maximum intensity projection, and shaded-surface display. AJR 1999;172:925–931.
2. Abu-Yousef MM, El-Zein Y. Improved US visualization of the pancreatic tail with simethicone, water, and patient rotation. Radiology 2000;217:780–785.
3. Kanematsu M, Shiratori Y, Hoshi H, Kondo H, Matsuo M, Moriwaki H. Pancreas and peripancreatic vessels: effect of imaging delay on gadolinium enhancement at dynamic gradient-recalled-echo MR imaging. Radiology 2000;215:95–102.
4. Inui K, Nakazawa S, Yoshino J, Ukai H. Endoscopic MRI. [Review] Pancreas 1998;16:413–417.
5. Itoh S, Ikeda M, Ota T, Satake H, Takai K, Ishigaki T. Assessment of the pancreatic and intrapancreatic bile ducts using 0.5-mm collimation and multiplanar reformatted images in multislice CT. Eur Radiol 2003;13:277–285.
6. Helmberger H, Hellerhoff K, Rull T, Brandt C, Gerhardt P. [Functional MR-pancreatography with secretin. A comparison of imaging quality and diagnostic value.] [German] Rofo Fortschr Geb Rontgenstr Neuen Bildgeb Verfahr 2000;172:367–373.
7. Punwani S, Gillams AR, Lees WR. Non-invasive quantification of pancreatic exocrine function using secretin-stimulated MRCP. Eur Radiol 2003;13: 273–276.
8. Bergstrom M, Eriksson B, Oberg K, et al. In vivo demonstration of enzyme activity in endocrine pancreatic tumors: decarboxylation of carbon-11-DOPA to carbon-11-dopamine. J Nucl Med 1996;37:32–37.
9. Kazumori H, Sizuku T, Ueki T, Uchida Y, Yamamoto S. Lymphoepithelial cyst of the pancreas. J Gastroenterol 1997;32:700–703.
10. Soyer P, Spelle L, Pelage JP, et al. Cystic fibrosis in adolescents and adults: fatty replacement of the pancreas—CT evaluation and functional correlation. Radiology 1999;210:611–615.
11. Gates LK Jr, Ulrich CD 2nd, Whitcomb DC. Hereditary pancreatitis. Gene defects and their implications. [Review] Surg Clin North Am 1999;79:711–722.
12. Sarles H, Camarena J, Bernard JP, Sahel J, Laugier R. Two forms of hereditary chronic pancreatitis. Pancreas 1996;12:138–141.
13. Lowenfels AB, Maisonneuve P, Whitcomb DC. Risk factors for cancer in hereditary pancreatitis. International Hereditary Pancreatitis Study Group. Med Clin North Am 2000;84:565–573.
14. Mignon M, Cadiot G. Diagnostic and therapeutic criteria in patients with Zollinger-Ellison syndrome and multiple endocrine neoplasia type 1. [Review] J Intern Med 1998;243:489–494.
15. Thompson NW. Current concepts in the surgical management of multiple endocrine neoplasia type 1 pancreatic-duodenal disease. Results in the treatment of 40 patients with Zollinger-Ellison syndrome, hypoglycaemia or both. J Intern Med 1998;243:495–500.
16. Romeo G, Ceccherini I, Celli J, et al. Association of multiple endocrine neoplasia type 2 and Hirschsprung disease. J Intern Med 1998;243:515–520.
17. Moore EE, Cogbill TH, Malangoni MA, et al. Organ injury scaling. [Review] Surg Clin North Am 1995; 75:293–303.
18. Takishima T, Horiike S, Sugimoto K, et al. Role of repeat computed tomography after emergency endoscopic retrograde pancreatography in the diagnosis of traumatic injury to pancreatic ducts. J Trauma 1996;40: 253–257.
19. Lucaya J, Vazquez E, Caballero F, Chait PG, Daneman A, Wesson D. Non-operative management of traumatic pancreatic pseudocysts associated with pancreatic duct laceration in children. Pediatr Radiol 1998;28: 5–8.
20. Shirohara H, Otsuki M. Plasma cholecystokinin levels in acute pancreatitis. Pancreas 1997;14:249–254.

21. Futami H, Furuta T, Hanai H, Nakamura S, Baba S, Kaneko E. Adenoma of the common human bile duct in Gardner's syndrome may cause relapsing acute pancreatitis. J Gastroenterol 1997;32:558–561.
22. Fung AS, Tsiotos GG, Sarr MG. ERCP-induced acute necrotizing pancreatitis: is it a more severe disease? Pancreas 1997;15:217–221.
23. Parenti DM, Steinberg W, Kang P. Infectious causes of acute pancreatitis. [Review] Pancreas 1996;13:356–371.
24. Guelrud M, Herrera I. Acute pancreatitis due to pancreatic duct Ascaris migration after pancreatic sphincterotomy and pancreatic stent placement. Endoscopy 1997;29:S53.
25. Mitterhofer AP, Antonelli M, Genuini I, Bertazzoni G. High-dose intranasal snorted heroin: a new cause of pancreatitis. Pancreas 1998;17:213–215.
26. Chevallier P, Peten E, Pellegrino C, Souci J, Motamedi JP, Padovani B. Hiatal hernia with pancreatic volvulus: a rare cause of acute pancreatitis. AJR 2001;177: 373–374.
27. Lin YL, Lin MT, Huang GT, et al. Acute pancreatitis masquerading as testicular torsion. Am J Emerg Med 1996;14:654–655.
28. Makela A, Kuusi T, Schroder T. Serum phospholipase A2, amylase, lipase, and urinary amylase activities in relation to the severity of acute pancreatitis. Eur J Surg 1997;163:915–922.
29. Wig JD, Kochhar R, Ray JD, Krishna Rao DV, Gupta NM, Ganguly NK. Endotoxemia predicts outcome in acute pancreatitis. J Clin Gastroenterol 1998;26: 121–124.
30. Wiesner W, Studler U, Kocher T, Degen L, Buitrago-Tellez CH, Steinbrich W. Colonic involvement in non-necrotizing acute pancreatitis: correlation of CT findings with the clinical course of affected patients. Eur Radiol 2003;13:897–902.
31. Elmas N, Oran I, Oyar O, Ozer H. A new criterion in differentiation of pancreatitis and pancreatic carcinoma: artery-to-vein ratio using the superior mesenteric vessels. Abdom Imaging 1996;21:331–333.
32. Watanabe S. Acute pancreatitis: overview of medical aspects. [Review] Pancreas 1998;16:307–311.
33. Takeda K, Matsuno S, Sunamura M, Kobari M. Surgical aspects and management of acute necrotizing pancreatitis: recent results of a cooperative national survey in Japan. Pancreas 1998;16:316–322.
34. Heath DI, Meng WC, Anderson JH, Leung KL, Lau WY, Li AK. Failure of the Hong Kong criteria to predict the severity of acute pancreatitis. Int J Pancreatol 1997;22:201–206.
35. Irie H, Honda H, Kuroiwa T, et al. MRI of groove pancreatitis. J Comput Assist Tomogr 1998;22:651–655.
36. Kawamoto S, Siegelman SS, Hruban RH, Fishman EK. Lymphoplasmacytic sclerosing pancreatitis with obstructive jaundice: CT and pathology features. AJR 2004;183:915–921.
37. Fukukura Y, Fujiyoshi F, Nakamura F, Hamada H, Nakajo M. Autoimmune pancreatitis associated with idiopathic retroperitoneal fibrosis. AJR 2003;181:993–995.
38. Barthet M, Hastier P, Buckley MJ, et al. Eosinophilic pancreatitis mimicking pancreatic neoplasia: EUS and ERCP findings—is nonsurgical diagnosis possible? Pancreas 1998;17:419–422.
39. Cylwik B, Nowak HF, Puchalski Z, Barczyk J. Epithelial anomalies in chronic pancreatitis as a risk factor of pancreatic cancer. Hepatogastroenterology 1998;45: 528–532.
40. Suda K, Takase M, Takei K, Nakamura T, Akai J, Nakamura T. Histopathologic study of coexistent pathologic states in pancreatic fibrosis in patients with chronic alcohol abuse: two distinct pathologic fibrosis entities with different mechanisms. Pancreas 1996; 12:369–372.
41. Johnson PT, Outwater EK. Pancreatic carcinoma versus chronic pancreatitis: dynamic MR imaging. Radiology 1999;212:213–218.
42. Ueno E, Takada Y, Yoshida I, Toda J, Sugiura T, Toki F. Pancreatic diseases: evaluation with MR cholangiopancreatography. Pancreas 1998;16:418–426.
43. Manfredi R, Costamagna G, Brizi MG, et al. Severe chronic pancreatitis versus suspected pancreatic disease: dynamic MR cholangiopancreatography after secretin stimulation. Radiology 2000;214:849–855.
44. Cappeliez O, Delhaye M, Deviere J, et al. Chronic pancreatitis: evaluation of pancreatic exocrine function with MR pancreatography after secretin stimulation. Radiology 2000;215:358–364.
45. Gullo L, Tassoni U, Mazzoni G, Stefanini F. Increased prevalence of aortic calcification in chronic pancreatitis. Am J Gastroenterol 1996;91:759–761.
46. Guitron A, Gonzalez-Loya H, Barinagarrementeria R, Sarol JC, Adalid R, Rodriguez-Delgado J. Dissolution of pancreatic lithiasis by direct citrate application into the pancreatic duct in two patients with chronic idiopathic pancreatitis. Dig Dis 1997;15:120–123.
47. Fotoohi M, D'Agostino HB, Wollman B, Chon K, Shahrokni S, van Sonnenberg E. Persistent pancreatocutaneous fistula after percutaneous drainage of pancreatic fluid collections: role of cause and severity of pancreatitis. Radiology 1999;213:573–578.
48. Kuba H, Yamaguchi K, Shimizu S, et al. Chronic asymptomatic pseudocyst with sludge aggregates masquerading as mucinous cystic neoplasm of the pancreas. J Gastroenterol 1998;33:766–769.
49. Masatsugu T, Yamaguchi K, Yokohata K, Mizumoto K, Chijiiwa K, Tanaka M. Hemorrhagic pseudocyst and pseudocyst with pseudoaneurysm successfully treated by pancreatectomy: report of three cases. J Hepato Biliary Pancreatic Surg 2000;7:432–437.
50. Hastier P, Buckley MJ, Dumas R, et al. Pancreaticoportal fistula after endoscopic cystogastrostomy in chronic calcifying pancreatitis. Pancreas 1998;17: 208–210.
51. Aabakken L, Chittom P, McKay DC, Uflacker R, Wilson FA. Percutaneous drainage of a mediastinal pancreatic pseudocyst: a paraspinal, extrapleural CT-guided approach. J Vasc Interv Radiol 1997;8:283–285.
52. Garre Sanchez MC, Garcia Munoz P, Torrella Cortes E, Alberca de las Parras F, Guillen Pardo B, Lopez Alanis A. [Splenic rupture in acute pancreatitis.] [Spanish] Gastroenterol Hepatol 1996;19:462–463.
53. Karasick D, Schweitzer ME. Case 4: intraosseous fat necrosis associated with pancreatitis. Radiology 1998;209:521–524.
54. Wei SC, Kao JH, Lee WY, Lin JT, Wang TH. Acute pancreatitis complicated by infarction of the spleen

and spinal cord. J Formos Med Assoc 1997;96:754–757.
55. Setiawan MW, Samsi TK, Wulur H, Sugianto D, Pool TN. Epigastric pain and sonographic assessment of the pancreas in dengue hemorrhagic fever. J Clin Ultrasound 1998;26:257–259.
56. Kim YH. Pancreatitis in association with Clonorchis sinensis infestation: CT evaluation. AJR 1999;172: 1293–1296.
57. Midiri M, Lo Casto A, Sparacia G, et al. Magnetic resonance imaging of pancreatic changes in patients with transfusion-dependent beta-thalassemia major. AJR 1999;173:187–192.
58. Kim T, Murakami T, Takamura M, et al. Pancreatic mass due to chronic pancreatitis: correlation of CT and MR imaging features with pathologic findings. AJR 2001;177:367–371.
59. Fukukura Y, Inoue H, Miyazono N, et al. Lymphoepithelial cysts of the pancreas: demonstration of lipid component using CT and MRI. [Review] J Comput Assist Tomogr 1998;22:311–313.
60. Paal E, Thompson LD, Heffess CS. A clinicopathologic and immunohistochemical study of ten pancreatic lymphangiomas and a review of the literature. Cancer 1998;82:2150–2158.
61. Ferrozzi F, Cusmano F, Zuccoli G, Tognini G, Bassi S, Gabrielli M. [Mesenchymal tumors of the pancreas: computed tomography patterns.] [Italian] Radiol Med 1999;98:295–299.
62. Voss SD, Kruskal JB, Kane RA. Chronic inflammatory pseudotumor arising in the hepatobiliary-pancreatic system: progressive multisystemic organ involvement in four patients. AJR 1999;173:1049–1054.
63. Sorensen HT, Mellemkjaer L, Steffensen FH, Olsen JH, Nielsen GL. The risk of a diagnosis of cancer after primary deep venous thrombosis or pulmonary embolism. N Engl J Med 1998;338:1169–1173.
64. Michaud DS, Giovannucci E, Willett WC, Colditz GA, Fuchs CS. Coffee and alcohol consumption and the risk of pancreatic cancer in two prospective United States cohorts. Cancer Epidemiol Biomarkers Prev 2001;10: 429–437.
65. Tanaka S, Kitamra T, Yamamoto K, et al. Evaluation of routine sonography for early detection of pancreatic cancer. Jpn J Clin Oncol 1996;26:422–427.
66. Safi F, Schlosser W, Falkenreck S, Beger HG. Prognostic value of CA 19–9 serum course in pancreatic cancer. Hepatogastroenterology 1998;45:253–259.
67. Kondoh S, Kaino M, Okita S, Ryozawa S, Akiyama T, Okita K. Detection of Ki-ras and p53 gene mutations in tissue and pancreatic juice from pancreatic adenocarcinomas. J Gastroenterol 1998;33:390–396.
68. Ariyama J, Suyama M, Satoh K, Sai J. Imaging of small pancreatic ductal adenocarcinoma. [Review] Pancreas 1998;16:396–401.
69. Tsunoda T, Yamamoto Y, Kimoto M, et al. Staging and treatment for patients with pancreatic cancer. How small is an early pancreatic cancer? J Hepato Biliary Pancreatic Surg 1998;5:128–132.
70. Yokohata K, Shirahane K, Yonemasu H, et al. Focal ductal branch dilatation on magnetic resonance cholangiopancreatography: a hint for early diagnosis of pancreatic carcinoma. Scand J Gastroenterol 2000; 35:1229–1232.
71. Romijn MG, Stoker J, van Eijck CH, van Muiswinkel JM, Torres CG, Lameris JS. MRI with mangafodipir trisodium in the detection and staging of pancreatic cancer. J Magn Reson Imaging 2000;12:261–268.
72. Fink C, Grenacher L, Hansmann HJ, et al. [Prospective study to compare high-resolution computed tomography and magnetic resonance imaging in the detection of pancreatic neoplasms: use of intravenous and oral MR contrast media.] [German] Rofo Fortschr Geb Rontgenstr Neuen Bildgeb Verfahr 2001;173:724–730.
73. Boland GW, O'Malley ME, Saez M, Fernandez-del-Castillo C, Warshaw AL, Mueller PR. Pancreatic-phase versus portal vein-phase helical CT of the pancreas: optimal temporal window for evaluation of pancreatic adenocarcinoma. AJR 1999;172:605–608.
74. McNulty NJ, Francis IR, Platt JF, Cohan RH, Korobkin M, Gebremariam A. Multi-detector row helical CT of the pancreas: effect of contrast-enhanced multiphasic imaging on enhancement of the pancreas, peripancreatic vasculature, and pancreatic adenocarcinoma. Radiology 2001;220:97–102.
75. Yamada Y, Mori H, Kiyosue H, Matsumoto S, Hori Y, Maeda T. Computed tomography assessment of the inferior peripancreatic veins: clinical significance. AJR 2000;174:677–684.
76. Furukawa H, Iwata R, Moriyama N, Kosuge T. Selective intraarterial contrast-enhanced CT of pancreaticoduodenal tumors: early clinical experience in evaluating blood supply and detectability. AJR 2000;75:91–97.
77. Karlson BM, Ekbom A, Lindgren PG, Kallskog V, Rastad J. Abdominal US for diagnosis of pancreatic tumor: prospective cohort analysis. Radiology 1999;213:107–111.
78. Diehl SJ, Lehmann KJ, Gaa J, Meier-Willersen HJ, Wendl K, Georgi M. [The value of magnetic resonance tomography (MRT), magnetic resonance cholangiopancreatography (MRCP) and endoscopic retrograde cholangiopancreatography (ERCP) in the diagnosis of pancreatic tumors.] [German] Rofo Fortschr Geb Rontgenstr Neuen Bildgeb Verfahr 1999; 170:463–469.
79. Ichikawa T, Sou H, Araki T, et al. Duct-penetrating sign at MRCP: usefulness for differentiating inflammatory pancreatic mass from pancreatic carcinomas. Radiology 2001;221:107–116.
80. Raderer M, Kurtaran A, Yang Q, et al. Iodine-123–vasoactive intestinal peptide receptor scanning in patients with pancreatic cancer. J Nucl Med 1998;39:1570–1575.
81. Gabata T, Kadoya M, Terayama N, Sanada J, Kobayashi S, Matsui O. Groove pancreatic carcinomas: radiological and pathological findings. Eur Radiol 2003;13: 1679–1684.
82. Hosch SB, Knoefel WT, Metz S, et al. Early lymphatic tumor cell dissemination in pancreatic cancer: frequency and prognostic significance. Pancreas 1997; 15:154–159.
83. Sheridan MB, Ward J, Guthrie JA, et al. Dynamic contrast-enhanced MR imaging and dual-phase helical CT in the preoperative assessment of suspected pancreatic cancer: a comparative study with receiver operating characteristic analysis. AJR 1999;173:583–590.
84. Schima W, Fugger R, Schober E, et al. Diagnosis and staging of pancreatic cancer: comparison of man-

gafodipir trisodium-enhanced MR imaging and contrast-enhanced helical hydro-CT. AJR 2002;179: 717–724.
85. Catalano C, Laghi A, Fraioli F, et al. Pancreatic carcinoma: the role of high-resolution multislice spiral CT in the diagnosis and assessment of resectability. Eur Radiol 2003;13:149–156.
86. Nishiharu T, Yamashita Y, Abe Y, et al. Local extension of pancreatic carcinoma: assessment with thin-section helical CT versus with breath-hold fast MR imaging—ROC analysis. Radiology 1999;212:445–452.
87. Vargas R, Nino-Murcia M, Trueblood W, Jeffrey RB Jr. MDCT in Pancreatic adenocarcinoma: prediction of vascular invasion and resectability using a multiphasic technique with curved planar reformations. AJR 2004;182:419–425.
88. O'Malley ME, Boland GW, Wood BJ, Fernandez-del Castillo C, Warshaw AL, Mueller PR. Adenocarcinoma of the head of the pancreas: determination of surgical unresectability with thin-section pancreatic-phase helical CT. AJR 1999;173:1513–1518.
89. Hough TJ, Raptopoulos V, Siewert B, Matthews JB. Teardrop superior mesenteric vein: CT sign for unresectable carcinoma of the pancreas. AJR 1999;173: 1509–1512.
90. Baek SY, Sheafor DH, Keogan MT, DeLong DM, Nelson RC. Two-dimensional multiplanar and three-dimensional volume-rendered vascular CT in pancreatic carcinoma: interobserver agreement and comparison with standard helical techniques. AJR 2001;176: 1467–1473.
91. Diehl SJ, Lehmann KJ, Sadick M, Lachmann R, Georgi M. Pancreatic cancer: value of dual-phase helical CT in assessing resectability. Radiology 1998; 206:373–378.
92. Kaneko T, Nakao A, Inoue S, et al. Extrapancreatic nerve plexus invasion by carcinoma of the head of the pancreas. Diagnosis with intraportal endovascular ultrasonography. Int J Pancreatol 1996;19:1–7.
93. Hannesson PH, Lundstedt C, Dawiskiba S, Stridbeck H, Ihse I. Transhepatic intravascular ultrasound for evaluation of portal venous involvement in patients with cancer of the pancreatic head region. Eur Radiol 2002;12:1150–1154.
94. Cohen L, Hendrickson FR, Lennox AJ, Kroc TK, Hatcher MA, Bennett BR. Pancreatic cancer: treatment with neutron irradiation alone and with chemotherapy. Radiology 1996;200:627–630.
95. Yamakado K, Nakatsuka A, Tanaka N, et al. Portal venous stent placement in patients with pancreatic and biliary neoplasms invading portal veins and causing portal hypertension: initial experience. Radiology 2001;220:150–156.
96. Hishinuma S, Ogata Y, Matsui J, Ozawa I. Results of surgery and adjuvant radiotherapy for pancreatic cancer. J Hepato Biliary Pancreatic Surg 1998;5: 143–150.
97. Watanabe M, Miura H, Inoue H. Et al. Mixed osteoclastic/pleomorphic-type giant cell tumor of the pancreas with ductal adenocarcinoma: histochemical and immunohistochemical study with review of the literature. [Review] Pancreas 1997;15:201–208.
98. Paner GP, Thompson KS, Reyes CV. Hepatoid carcinoma of the pancreas. Cancer 2000;88:1582–1589.
99. Gupta AK, Mitra DK, Berry M, Dinda AK, Bhatnagar V. Sonography and CT of pancreatoblastoma in children. AJR 2000;174:1639–1641.
100. Montemarano H, Lonergan GJ, Bulas DI, Selby DM. Pancreatoblastoma: imaging findings in 10 patients and review of the literature. [Review] Radiology 2000;214:476–482.
101. Merkle EM, Bender GN, Brambs HJ. Imaging findings in pancreatic lymphoma: differential aspects. AJR 2000;174:671–675.
102. Mizumoto K, Suehara N, Ohuchida J, et al. Pancreatic tumor formed by infiltration of adult T-cell leukemia cells. Int J Pancreatol 1997;21:253–257.
103. Bastian D, Ramaswamy A, Barth PJ, Gerdes B, Ernst M, Bartsch D. Malignant fibrous histiocytoma of the pancreas: a case report with genetic analysis. [Review] Cancer 1999;85:2352–2358.
104. Luttges J, Pierre E, Zamboni G, et al. [Malignant non-epithelial tumors of the pancreas.] [German] Pathologe 1997;18:233–237.
105. Motoo Y, Kawashima A, Watanabe H, Su SB, Okai T, Sawabu N. Undifferentiated (anaplastic) carcinoma of the pancreas showing sarcomatous change and neoplastic cyst formation. Int J Pancreatol 1997;21: 243–248.
106. Ng CS, Loyer EM, Iyer RB, David CL, DuBrow RA, Charnsangavej C. Metastases to the pancreas from renal cell carcinoma: findings on three-phase contrast-enhanced helical CT. AJR 1999;172:1555–1559.
107. Niv Y, Turani C, Kahan E, Fraser GM. Association between pancreatic cystadenocarcinoma, malignant liver cysts, and polycystic disease of the kidney. Gastroenterology 1997;112:2104–2107.
108. Sand JA, Hyoty MK, Mattila J, Dagorn JC, Nordback IH. Clinical assessment compared with cyst fluid analysis in the differential diagnosis of cystic lesions in the pancreas. Surgery 1996;119:275–280.
109. Curry CA, Eng J, Horton KM, et al. Computed tomography of primary cystic pancreatic neoplasms: can CT be used for patient triage and treatment? AJR 2000; 175:99–103.
110. Koito K, Namieno T, Nagakawa T, Shyonai T, Hirokawa N, Morita K. Solitary cystic tumor of the pancreas: EUS-pathologic correlation. Gastrointest Endosc 1997;45:268–276.
111. Sperti C, Pasquali C, Perasole A, Liessi G, Pedrazzoli S. Macrocystic serous cystadenoma of the pancreas: clinicopathologic features in seven cases. Int J Pancreatol 2000;28:1–7.
112. Khurana B, Mortele KJ, Glickman J, Silverman SG, Ros PR. Macrocystic serous adenoma of the pancreas: radiologic-pathologic correlation. AJR 2003;181:119–123.
113. Fukushima N, Mukai K. Pancreatic neoplasms with abundant mucus production: emphasis on intraductal papillary-mucinous tumors and mucinous cystic tumors. [Review] Adv Anat Pathol 1999;6:65–77.
114. Kimura W, Kuroda A, Makuuchi M. Problems in the diagnosis and treatment of a so-called mucin-producing tumor of the pancreas. [Review] Pancreas 1998;16:363–369.
115. Torresan F, Casadei R, Solmi L, Marrano D, Gandolfi L. The role of ultrasound in the differential diagnosis of

serous and mucinous cystic tumours of the pancreas. Eur J Gastroenterol Hepatol 1997;9:169–172.
116. Berger KL, Nicholson SA, Dehdashti F, Siegel BA. FDG PET evaluation of mucinous neoplasms: correlation of FDG uptake with histopathologic features. AJR 2000;174:1005–1008.
117. Paal E, Thompson LD, Przygodzki RM, Bratthauer GL, Heffess CS. A clinicopathologic and immunohistochemical study of 22 intraductal papillary mucinous neoplasms of the pancreas, with a review of the literature. [Review] Mod Pathol 1999;12:518–528.
118. Zanelli M, Casadei R, Santini D, et al. Pseudomyxoma peritonei associated with intraductal papillary-mucinous neoplasm of the pancreas. Pancreas 1998; 17:100–102.
119. Irie H, Honda H, Aibe H, et al. Magnetic resonance cholangiopancreatographic differentiation of benign and malignant intraductal mucin-producing tumors of the pancreas. AJR 2000;174:1403–1408.
120. Taouli B, Vilgrain V, Vullierme MP, et al. Intraductal papillary mucinous tumors of the pancreas: helical CT with histopathologic correlation. Radiology 2000; 217:757–764.
121. Fukukura Y, Fujiyoshi F, Sasaki M, Inoue H, Yonezawa S, Nakajo M. Intraductal papillary mucinous tumors of the pancreas: thin-section helical CT findings. AJR 2000;174:441–447.
122. Onaya H, Itai Y, Niitsu M, Chiba T, Michishita N, Saida Y. Ductectatic mucinous cystic neoplasms of the pancreas: evaluation with MR cholangiopancreatography. AJR 1998;171:171–177.
123. Koito K, Namieno T, Ichimura T, et al. Mucin-producing pancreatic tumors: comparison of MR cholangiopancreatography with endoscopic retrograde cholangiopancreatography. Radiology 1998;208: 231–237.
124. Levy P, Bougaran J, Gayet B. [Diffuse peritoneal carcinosis of pseudo-papillary and solid tumor of the pancreas. Role of abdominal injury.] [Review] [French] Gastroenterol Clin Biol 1997;21:789–793.
125. Buetow PC, Buck JL, Pantongrag-Brown L, Beck KG, Ros PR, Adair CF. Solid and papillary epithelial neoplasm of the pancreas: imaging-pathologic correlation on 56 cases. Radiology 1996;199:707–711.
126. Kaassis M, Duquenne M, Croue A, Ronceray J, Rohmer V, Bigorgne JC. [Calcitonin-secreting neuroendocrine carcinoma of the pancreas with splenic invasion and paraneoplastic hypercalcemia.] [French] Presse Med 2001;30:24.
127. Ichikawa T, Peterson MS, Federle MP, et al. Islet cell tumor of the pancreas: biphasic CT versus MR imaging in tumor detection. Radiology 2000;216:163–171.
128. Thoeni RF, Mueller-Lisse UG, Chan R, Do NK, Shyn PB. Detection of small, functional islet cell tumors in the pancreas: selection of MR imaging sequences for optimal sensitivity. Radiology 2000;214:483–490.
129. Semelka RC, Custodio CM, Cem Balci N, Woosley JT. Neuroendocrine tumors of the pancreas: spectrum of appearances on MRI. J Magn Reson Imaging 2000; 11:141–148.
130. Seelig MH, Schonleben K. Intra-abdominal ectopic thyroid presenting as a pancreatic tumour. [Review] Eur J Surg 1997;163:549–551.
131. Soga J, Yakuwa Y, Osaka M. Insulinoma/hypoglycemic syndrome: a statistical evaluation of 1085 reported cases of a Japanese series. J Exp Clin Cancer Res 1998;17:379–388.
132. Gouya H, Vignaux O, Augui J, et al. CT, endoscopic sonography, and a combined protocol for preoperative evaluation of pancreatic insulinomas. AJR 2003;181: 987–992.
133. Fidler JL, Fletcher JG, Reading CC, et al. Preoperative detection of pancreatic insulinomas on multiphasic helical CT. AJR 2003;181:775–780.
134. Service FJ, Natt N, Thompson GB, et al. Noninsulinoma pancreatogenous hypoglycemia: a novel syndrome of hyperinsulinemic hypoglycemia in adults independent of mutations in Kir6.2 and SUR1 genes. J Clin Endocrinol Metab 1999;84:1582–1589.
135. Soga J, Yakuwa Y. The gastrinoma/Zollinger-Ellison syndrome: statistical evaluation of a Japanese series of 359 cases. J Hepato Biliary Pancreatic Surg 1009;5: 77–85.
136. Tang C, Biemond I, Verspaget HW, Offerhaus GJ, Lamers CB. Expression of somatostatin receptors in human pancreatic tumor. Pancreas 1998;17:80–84.
137. Ruszniewski P, Amouyal P, Amouyal G, et al. Localization of gastrinomas by endoscopic ultrasonography in patients with Zollinger-Ellison syndrome. Surgery 1995;117:629–635.
138. Lebtahi R, Cadiot G, Marmuse JP, et al. False-positive somatostatin receptor scintigraphy due to an accessory spleen. J Nucl Med 1997;38:1979–1981.
139. Soga J, Yakuwa Y. Vipoma/diarrheogenic syndrome: a statistical evaluation of 241 reported cases. J Exp Clin Cancer Res 1998;17:389–400.
140. Virgolini I, Kurtaran A, Leimer M, et al. Location of a VIPoma by iodine-123–vasoactive intestinal peptide scintigraphy. J Nucl Med 1998;39:1575–1579.
141. Furukawa H, Mukai K, Kosuge T, et al. Nonfunctioning islet cell tumors of the pancreas: clinical, imaging and pathological aspects in 16 patients. Jpn J Clin Oncol 1998;28:255–261.
142. Stafford-Johnson DB, Francis IR, Eckhauser FE, Knol JA, Chang AE. Dual-phase helical CT of nonfunctioning islet cell tumors. J Comput Assist Tomogr 1998; 22:335–339.
143. Kauppila LI, Hekali P, Penttila A. Postmortem pancreatic angiography in 45 subjects with non-insulin-dependent diabetes mellitus and 51 controls. Pancreas 1998;16:60–65.
144. Barone R, Procaccini E, Chianelli M, et al. Prognostic relevance of pancreatic uptake of technetium-99m labelled human polyclonal immunoglobulins in patients with type 1 diabetes. Eur J Nucl Med 1998; 25:503–508.
145. Altobelli E, Blasetti A, Verrotti A, Di Giandomenico V, Bonomo L, Chiarelli F. Size of pancreas in children and adolescents with type I (insulin-dependent) diabetes. J Clin Ultrasound 1998;26:391–395.
146. Tano S, Ueno N, Ueno T, Wada S, Aizawa T, Kimura K. Pancreatic arteriovenous malformation with duodenal ulcer. Demonstration by color Doppler ultrasonography. Dig Dis Sci 1996;41:1232–1237.
147. Sato M, Kishi K, Shirai S, et al. Radiation therapy for a massive arteriovenous malformation of the pancreas. AJR 2003;181:1627–1628.

148. Molina M, Ortega G, Redondo C, Galera C, Perez Lujan YR. [Tuberculous abscess of the pancreas as initial manifestation of AIDS.] [Spanish] Gastroenterol Hepatol 1997;20:165–166.
149. Hancock MR, Smith NA, Hawkins DA, Gazzard B, Ball SG. Biochemical assessment of pancreatic disease in human immunodeficiency virus infected men. J Clin Pathol 1997;50:674–676.
150. Sollinger HW, Odorico JS, Knechtle SJ, D'Alessandro AM, Kalayoglu M, Pirsch JD. Experience with 500 simultaneous pancreas-kidney transplants. Ann Surg 1998;228:284–296.
151. Heverhagen JT, Wagner HJ, Ebel H, Levine AL, Klose KJ, Hellinger A. Pancreatic transplants: noninvasive evaluation with secretin-augmented MR pancreatography and MR perfusion measurements—preliminary results. Radiology 2004;233:273–280.
152. Krebs TL, Daly B, Wong-You-Cheong JJ, Carroll K, Bartlett ST. Acute pancreatic transplant rejection: evaluation with dynamic contrast-enhanced MR imaging compared with histopathologic analysis. Radiology 1999;210:437–442.
153. Eubank WB, Schmiedl UP, Levy AE, Marsh CL. Venous thrombosis and occlusion after pancreas transplantation: evaluation with breath-hold gadolinium-enhanced three-dimensional MR imaging. AJR 2000;175: 381–385.
154. Fiorina P, La Rocca E, Venturini M, et al. Effects of kidney-pancreas transplantation on atherosclerotic risk factors and endothelial function in patients with uremia and type 1 diabetes. Diabetes 2001;50:496–501.
155. Meador TL, Krebs TL, Cheong JJ, Daly B, Keay S, Bartlett S. Imaging features of posttransplantation lymphoproliferative disorder in pancreas transplant recipients. AJR 2000;174:121–124.
156. Lupo LG, Pannarale OC, Altomare DF, et al. Is pyloric function preserved in pylorus-preserving pancreaticoduodenectomy? Eur J Surg 1998;164:127–132.
157. Aldrighetti L, Ferla G. Portal vein graft rectal evacuation after Whipple procedure. The Fabrizio's disease. Hepatogastroenterology 1996;43:1638–1639.
158. Dickinson RJ, Davies S. Post-ERCP pancreatitis and hyperamylasaemia: the role of operative and patient factors. Eur J Gastroenterol Hepatol 1998;10:423–428.
159. Hans de Vries J, Duijm LE, Dekker W, Guit GL, Ferwerda J, Scholten ET. Computed tomography before and after ERCP: detection of pancreatic pseudotumor, asymptomatic retroperitoneal perforation, and duodenal diverticulum. Gastrointest Endosc 1997;45: 231–235.

Part II

Genitourinary System

10

Kidneys and Ureters

Technique

Conventional Radiography and Urography

Indications for intravenous (IV) pyelography (the term *IV urography* is used by some) have decreased considerably, but this examination is still indicated if pyelocalyceal visualization is needed. Small transitional cell carcinomas, pyeloureteritis cystica, medullary sponge kidney, and papillary necrosis continue to be best identified with IV urography. A current major indication for IV urography is in investigating hematuria in adults, although here computed tomographic urography combined with cystoscopy are making inroads, and magnetic resonance (MR) is not far behind.

Intravenous urography is insensitive in detecting small renal parenchymal tumors. Thus about one third of tumors <3 cm in diameter are not detected. Even with larger tumors urography is generally insensitive in differentiating benign from malignant tumors. This test, however, does provide information on renal function and gross anatomy, and it aids in evaluating disorders of the collective systems. It tends to be somewhat inferior in infants compared to older children.

Retrograde ureteropyelography has a role if insufficient contrast is excreted during an IV urogram. For suspected obstruction, however, currently noncontrast computed tomography (CT) is considered to be superior.

Computed Tomography

The introduction of multislice helical CT has had a major impact on uroradiology. Multislice CT allows imaging during specific contrast opacification phases. Depending on the study indication, the CT protocol used can be modified accordingly. Thus suspected acute urinary obstruction by a stone is studied without contrast, in the workup of hypertension and suspected renal artery stenosis emphasis is on arterial phase images, while some infections are detected only during later phases; small renal tumors are readily imaged in a breathhold; potential living renal donor evaluation is simplified and therapy aided by three-dimensional (3D) imaging. Using a two-bolus technique both a nephrogenic and excretory phases can be obtained with one scan, although such a protocol tends not to visualize all of the ureters completely.

Are screening serum creatinine levels necessary prior to contrast CT studies? Only 3% of over 2000 consecutive outpatients undergoing contrast-enhanced CT had elevated serum creatinine levels, and risk factors were identified in a majority of these (1); screening for risk factors appears adequate in this patient population.

Renal opacification can be divided into three phases: first is an early vascular or bolus phase, then a nephrogram phase (consisting of a nephrogram), followed by a pyelogram or equilibrium (delayed) phase. A corticomedullary phase, providing maximum differen-

tiation between renal cortex and medulla, occurs during the early phase. Whether a corticomedullary phase or a later nephrogram phase should be used for subtle tumor detection is debatable, although some evidence suggests that the nephrogram phase is superior. Both neoplasms and normal renal parenchyma enhance significantly more during the nephrogram phase than during the corticomedullary phase. In general, more tumors <3 cm in diameter are detected on the nephrogram phase than on the corticomedullary phase. The onset of a nephrogram phase varies among patients and technique used; a faster injection rate results in an earlier onset—roughly 100 seconds at 2 mL/sec and 90 seconds at 3 mL/sec. The corticomedullary phase is more useful, however, for detection of such conditions as an aneurysm, arteriovenous malformation, or fistula, and in evaluating tumor vascularity. Also, the earlier phase is more advantageous if optimal liver and other abdominal structure visualization is required. Renal tumors tend to be detected with greater confidence on delayed images than on early-phase images. One solution is to obtain images during both phases (corticomedullary and nephrogram), but whether the extra complexity and cost justify such an approach for a limited gain is not clear; a decision based on individual indications appears reasonable.

Renal CT performed shortly after excretory urography—called CT urography—is a variation of delayed-phase CT combining high spacial resolution of conventional filming with high contrast resolution of CT. Even pyelovenous backflow can be identified on CT urography (2). Only about half of renal parenchymal tumors identified on CT are detected on the previous excretory urogram, but such a combination study tends to increase the clinicians' confidence in some findings. A variant of this technique is to obtain delayed postcontrast coronal images or a delayed CT scout image. Validity of these various combined procedures in evaluating hematuria is yet to be established in larger studies.

Furosemide-enhanced CT urography, obtained 10 minutes after contrast agent injection, outlines pelvicaliceal structures and identifies calculi inside opacified urine and differentiates them from phleboliths (3).

Three-dimensional CT imaging techniques are useful both in evaluating suspected tumors and in planning a partial nephrectomy, such as orientation of blood vessels to a tumor or other structure. One should not rely only on 3D images, however, because to an experienced eye axial and coronal images provide more detailed information, especially about small vessels that tend to be overlooked on 3D images.

In a patient with microscopic hematuria and a normal excretory urogram, should CT or ultrasonography (US) be performed next? Although this topic generated considerable controversy in the 1990s, currently many investigators believe that CT detects more tumors overall, especially smaller ones. In fact, a more pertinent current question is whether CT or MR is indicated as a primary imaging modality in such a clinical setting.

Ultrasonography

Renal cortex is isoechoic to liver, and the centrally located renal sinus is hyperechoic to surrounding renal parenchyma.

Similar to other structures, use of an intravascular US contrast agent (such as Levovist; Schering AG, Berlin, Germany) enhances vascular signals and makes vascularity more evident. Diagnostic accuracy is improved, especially for hyperechoic tumors and complex cysts.

Doppler US provides data for the intrarenal arterial blood flow resistive index (RI) and pulsatility index (PI). These indices increase with age, acute obstructive uropathy, use of certain drugs, and in some nephropathies.

Endoluminal US using a high-frequency transducer housed in a catheter and advanced endoscopically into a ureter is moving from research into clinical practice. Potentially, the information obtained helps guide biopsy and laser therapy and defines vessels adjacent to a ureter.

Magnetic Resonance Imaging

Currently for most suspected renal conditions CT is performed rather than magnetic resonance imaging (MRI), but MRI is used in a setting of contrast allergy or renal failure, and for studying some complex masses. It is also useful in evaluating venous thrombosis in a setting of renal carcinoma. It provides both spatial resolution and information on renal

function and potentially is more useful than either CT or nuclear medicine. Magnetic resonance applications range from multiphase 3D magnetic resonance angiography (MRA) to evaluate renal artery stenosis and renal perfusion abnormalities, MR nephrography, and MR urography of the renal collecting systems (especially useful in posttransplant complications). Potentially, a single MR study evaluates renovascular disease, assesses renal function, detects renal tumors, and identifies urinary tract abnormalities, all without radiation exposure. More often, however, the specific MR sequences best suited for each application are selected.

Conventional

As with CT, several distinct phases—cortical, medullary, and pyelocaliceal—are evident after IV paramagnetic gadolinium contrast injection. Some investigators add an intermediate corticomedullary junction phase. Magnetic resonance signal intensity normally decreases in the pyelocaliceal phase due to contrast agent concentration. When searching for small renal tumors, use of a body phased-array coil in combination with fast low-angle shot (FLASH) and fat suppression pre- and postcontrast thin-section MR allow imaging in single breath-holds. Sagittal and coronal plane images improve evaluation.

Both T1- and T2-weighted sequences are useful with contrast-enhanced MRI to evaluate renal blood flow and renal function. During the early phase, a renal cortex signal increase in T1-weighted sequences is matched by a similar signal decrease in T2-weighted sequences; during later phases, however, T2-weighted sequence signal intensity in the medulla decreases markedly. Thus renal cortical blood flow can be evaluated with either sequence, but T2-weighted sequences appear more useful in evaluating renal medulla. Presumably increased amounts of contrast in renal tubules account for the medullary decreased signal intensity during later phase T2-weighted sequences.

Serial dynamic MR gradient echo imaging using a low contrast dose can be used to obtain an intensity-time curve, similar to radionuclide renography. This technique allows assessment of split renal function and urinary excretory status and is an alternative to radionuclide renography. Preliminary studies suggest that good correlation exists between MR renography and radionuclide renography results (4).

A general disadvantage of MR in children, especially younger ones, is the need for sedation. A relative disadvantage in certain renal applications is its poor sensitivity in detecting calcifications.

Surprisingly, diagnostic accuracy in patients with a clinical suspicion for renal tumor was comparable when studies were performed using either a low field [0.2 tesla (T)] or a high field (1.5 T) magnet, although the signal-to-noise and contrast-to-noise ratios were significantly worse at low field strength (5).

Gadolinium diethylenetriamine pentaacetic acid (Gd-DTPA) is an ionic agent. A nonionic version is also available in some countries. No significant differences exist in either signal intensity or function between these two agents.

Magnetic Resonance Urography

Magnetic resonance urography both without and with contrast agents is evolving into viable alternative studies in select patients. No consensus is yet apparent on which specific MR sequences constitute MR urography. A more basic question concerns the role of MR urography: Does it have any advantages over conventional or CT urography?

A heavily T2-weighted sequence consisting of rapid acquisition of images obtained in less than 30 seconds with a relaxation enhancement technique results in solid organs and flowing fluid being hypointense, and stationary fluid, such as urine in collecting systems and ureters, being hyperintense; the entire urinary tract is visualized on one image without use of contrast (this technique is also called MR pyelography). The urinary tract is depicted even with nonfunctioning kidneys. A reconstructed 3D image provides an overall view. Magnetic resonance spatial resolution is superior to that of US. A current limitation of MR urography is that with the present MR units small calculi are poorly imaged.

A breath-hold 1.5 T MR half-Fourier acquisition single-shot turbo spin echo (HASTE) sequence visualizes renal collecting systems and ureters similarly to excretory urography. The HASTE sequences can be used to acquire images in the axial, sagittal, or coronal planes. These MR urography sequences outline non-

functioning urinary tracts that cannot be visualized with excretory urography and identifies level of obstruction without the use of contrast agents. This technique is advantageous in evaluating hydronephrosis during pregnancy, but future indications will undoubtedly expand.

Gadolinium chelates are filtered by renal glomeruli and excreted. One should keep in mind that dilute gadolinium is hyperintense on T1-weighted images, but when concentrated it induces a signal loss and becomes hypointense. Also, if one is performing CT shortly afterward, renal excretion of gadolinium can mimic a calculus on noncontrast CT (6).

Breath-hold 3D MR urography using fast gradient echo performed 5 to 10 minutes after injecting only several mL of Gd-DTPA visualizes the urinary tracts as hyperintense structures (7); urinary tract detection was superior to that obtained with a heavily T2-weighted sequence.

The ureters can thus be studied either with nonenhanced T2-weighted TSE imaging or gadolinium enhanced T1-weighted sequences. A preliminary study comparing these two sequences in infants and children found that although the ureters were more often better visualized with the gadolinium enhanced sequences, the two sequences are complementary (8). MR urography is feasible in young infants using only oral sedation. MR urography appears useful in patients with an ileal neobladder. Although the nonenhanced T2-weighted sequences can detect a point of ureteric obstruction, they do not readily establish an etiology—generally additional MR sequences are required.

Several paramagnetic contrast agents initially designed primarily for hepatobiliary applications, such as Gd-ethoxybenzyl (EOB)-DTPA and Gd–benzyloxypropionic-tetraacetate (BOPTA) initially function as extracellular agents and are then eliminated via biliary and renal pathways. Thus MR urography using Gd-BOPTA–enhanced breath-hold 3D FLASH sequences was comparable to conventional excretory urography (9); caliceal fornices were better visualized with conventional urography, but MR urography was superior in the distal ureters and the bladder, and in evaluating obstructive causes.

A further refinement is the use of a diuretic agent. Even a nondilated urinary tract is visualized.

Several virtual endoscopy techniques are feasible. Using surface-rendering techniques, unenhanced MR urography data can be presented in a virtual endoscopy format (10). Virtual endoscopy of the upper urinary tract can be reconstructed from T1-weighted 3D gradient-echo sequences obtained after urinary tract enhancement by IV gadolinium. Such a technique provides an endoluminal view of the calices, ureters, and ureteral orifices.

Scintigraphy

With its low radiation burden, renal scintigraphy is commonly used for initial evaluation and follow-up in children. Its main advantage over other imaging modalities is that to some degree function can be quantified.

Plasma clearance methods estimate overall renal function. Scintigraphy provides an estimate of each kidney function and detects gross structural defects. Currently scintigraphy is used to evaluate renal vascular hypertension, renal function after transplantation, suspected infection, and, occasionally, obstructive nephropathy.

Radiopharmaceutical agents useful in renal scintigraphy include the following:

Technetium-99m (Tc-99m)-mercaptoacetylglycilglycilglycine (MAG3) is an all-purpose renal agent. It is cleared by tubular secretion and is useful in flow and function studies. Effective renal plasma flow can be calculated with this radiotracer. It has a role in diuresis renography in neonates and infants. This compound is excreted vicariously by the liver and is then detected in the gallbladder. In imaging renal allografts, Tc-99m-MAG3 results in better image quality than Tc-99m-DTPA.

Tc-99m–L,L-ethylenedicysteine (L,L-EC) is a newer renal tubular tracer used as an alternative to Tc-99m-MAG3. It has similar excretion characteristics but higher plasma clearance than MAG3. It is also used to obtain the effective renal plasma flow rate. In patients with chronic renal failure, image quality is similar to that of Tc-99m-MAG3.

Tc-99m-DTPA is filtered by glomeruli and the glomerular filtration rate can be calculated.

Scintigraphy outlines renal and collecting system anatomy.

Tc-99m–2,3-dimercaptosuccinic acid (DMSA) binds to proximal tubules and results in prolonged renal retention. Its use in planar imaging allows evaluation of focal functional disorders and gross parenchymal damage. In children, planar Tc-99m-DMSA is useful in estimating renal function. Single photon emission computed tomography (SPECT) Tc-99m-DMSA scintigraphy is more effective than planar in detecting renal cortical defects.

Tc-99m-glucoheptonate is also used as a renal imaging agent. Neither glucoheptonate nor DMSA is taken up by renal cysts or neoplasms, and these appear as defects.

Iodine-131–ortho-iodohippurate (OIH) is an older agent that has been replaced to a large degree by Tc-99m-MAG3.

Carbon-11 acetate positron emission tomography (PET) imaging reveals prompt renal uptake even in a setting of reduced renal function.

Biopsy

Image-guided percutaneous renal biopsy is useful in obtaining tissue from suspected small lesions, and at times such a biopsy replaces surgical exploration. Most biopsies differentiate between benign and malignant disease and between primary renal cell carcinoma and metastatic disease, or they confirm renal involvement by lymphoma. If needed, several biopsies are obtained at the same time. Computed tomography or US–guided 18-gauge needle biopsies provide adequate biopsy material for analysis in most patients. Negative percutaneous biopsy results in small (<3 cm) and large (>6 cm) tumors, however, should be viewed with caution (11). Renal biopsy with an automated device using a 14-gauge needle in renal allografts and native kidneys has a >95% tissue recovery rate, but is associated with a serious complication rate of about 3% (12), including death, loss of renal allograft, major hemorrhage (requiring blood transfusion) and creation of an arteriovenous fistula.

In patients at high risk, a transfemoral vein biopsy using flexible forceps is an alternative approach.

Tissue cores adequate for histopathologic diagnosis were obtained in 98% of both transjugular renal biopsies and percutaneous renal biopsies (13); transjugular renal biopsies are an option in patients with contraindications or failure of percutaneous biopsy and in those requiring multiorgan biopsies.

Percutaneous Nephrostomy/Stenting

Percutaneous nephrostomy is commonly performed for emergency decompression of an obstructed urinary system. It is an integral part of several interventional procedures such as percutaneous nephrolithotomy, ureteral stenting, and dilation. It is feasible in children and adolescents on an outpatient basis; one study excluded outpatient nephrostomies in a setting of infection, stone therapy, solitary kidney with renal failure, and similar reasons (14). A puncture success rate of almost 100% is common. At times a nephrostomy is necessary with a nondilated system, such as a ureteral leak or fistula; fluoroscopy or US-guided injection of air or carbon dioxide into nondependent calyces aids catheter insertion (15).

Double-J stents are commonly used to treat ureteral obstruction. These stents are inserted retrograde by an urologist or antegrade by an interventional radiologist. At times a guidewire passes through an obstruction but the catheter fails to do so; a combined retrograde and antegrade approach may then be successful.

Both self-expandable and balloon expandable metallic stents are used for palliation of malignant ureteral obstruction.

Complications of percutaneous nephrostomy tube placement include hemorrhage requiring transfusion, a complication minimized by maintaining a platelet count above 100,000/mm^3. Inadvertent enteric puncture occurs occasionally. Long-term obstructions include urothelial hyperplastic reaction and tumor ingrowth or invasion of one stent end.

In a setting of unresectable pelvic cancer or radiation or both, a permanent percutaneous nephrostomy is often an option for a variety of conditions, including unresectable pelvic fistulas and incontinence. Many of these patients already have distal urinary tract obstruction. If not, ureteral occlusion is achieved using a

percutaneous approach and a permanent external diversion is then provided. Complications include nephrostomy catheter occlusion and retrograde coil migration into the renal pelvis.

Congenital Abnormalities

Screening for Congenital Abnormalities

Ultrasonography screening for congenital genitourinary abnormalities is a simple procedure but it is rarely performed during a routine health check-up. Major anomalies can be expected in under 1% of infants, including unilateral renal agenesis, vesiculoureteral reflux, hydronephrosis or megaureter, horseshoe kidney and ureterocele.

Fetal MRI can evaluate for oligohydramnios or anhydramnios and congenital genitourinary anomalies (16). It is currently underused.

Renal Agenesis

Renal malformation includes the absence of renal tissue (aplasia) or the presence of undifferentiated renal tissue (dysplasia). Bilateral renal agenesis is incompatible with life; many of these babies are stillborn and tend to have a characteristic oligohydramnios-induced Potter facies and numerous other anomalies (Potter sequence). Incidentally, Potter sequence is also seen with bilateral renal hypodysplasia, severe obstructive uropathy, and polycystic kidney disease, but an occasional such baby survives. Although sporadic, agenesis is more common in males, and a familial pattern is identified in about one third of patients. In a broader context, renal agenesis is lumped together with dysgenesis and it is called hereditary renal adysplasia (multicystic dysplasia is discussed in a later section).

Unilateral renal agenesis is relatively common (about one in 1000 births), with the single kidney compensating through hypertrophy. In some individuals renal agenesis is the end result of an involuted multicystic dysplastic kidney. Renal agenesis is associated with an ipsilateral seminal vesicle cyst and ipsilateral ovarian dysplasia. Bladder duplication is also occasionally found with renal agenesis.

The rare unipapillary kidney has a solitary calyx and papilla. It is more common on the left side. Almost always other abnormalities are present, including megaureter, ectopic ureter with vesicoureteral reflux, and renal agenesis on the contralateral side.

Imaging of renal agenesis reveals an empty renal fossa; keep in mind that an ectopic kidney also presents with an empty renal fossa. Prevalence of ipsilateral adrenal gland absence is slightly greater with renal agenesis than in the general population; when present, the ipsilateral adrenal gland tends to be more elongated than usual. On the left side the colon splenic flexure tends to fill an empty renal fossa.

A congenitally solitary kidney is about 1.8 times heavier than a normal kidney. The diameter of its glomeruli and convoluted tubules are similar to that of a control, but a solitary kidney contains twice as many glomeruli. The congenital solitary kidney is thus hyperplastic and not hypertrophic.

The imaging approach in a child with a suspected single kidney is not clear; a point can be made for initial US followed by MR urography. Children with unilateral agenesis are prone to vesicoureteral reflux on the contralateral side, with reflux being detected in over one third. A voiding cystourethrogram is thus recommended even if neither infection nor hydronephrosis is evident.

Hypoplasia

Simple hypoplasia implies a small but otherwise normal kidney. It is a rare anomaly. The number of calyces tends to be reduced. Focal hypoplasia entails a reduction in the number of calyces and associated renal parenchyma. Some patients have a small kidney that also has segmental parenchymal thinning and an associated dilated collecting system in this region; the appearance mimics that of chronic pyelonephritis.

In the rare oligonephronic hypoplasia, the kidneys are small and contain only one or two calyces.

Duplicated Collecting System

Duplication anomalies range from a bifid collecting system to duplication of both kidney and ureter. Most duplications are unilateral; if bilat-

eral, they tend to be asymmetrical. A duplication is considered incomplete if the two ureters join before inserting at one bladder orifice. In a complete duplication both ureters insert separately. Duplications are familial and are more common in women. In most patients a functioning duplicated system is a curiosity, and whether to consider an otherwise unremarkable duplicated system as part of a normal spectrum is a matter of opinion.

Partial duplications have a Y configuration. Much rarer are inverted-Y partial ureteral duplications, with the two duplicated lower ureteral segments inserting either in an orthotopic or ectopic location. Perhaps rarest of all is ureteral duplication with blind superior and inferior ends (17).

Duplications are difficult to detect on precontrast axial CT. Postcontrast visualization of two ureters provides a clue to the presence of a duplication. Postcontrast CT coronal views and conventional radiographs offer another clue: the uppermost lower pole calyx (which is generally the kidney's middle calyx) is located more lateral than expected, and as a result the kidney axis is more vertical than expected. Considerable calyceal distortion occurs with grade 5 reflux, and counting the number of calyces is an unreliable way to detect a duplication.

Neither US nor scintigraphy has sufficient resolution to reliably detect most duplications. Magnetic resonance coronal views are useful in a setting of poor renal function; thus T2-weighted images reveal fluid-filled upper and lower pole structures.

With a complete duplication the lower renal pole is generally larger and its draining ureter inserts in a normal position at the bladder trigone. The upper pole ureter inserts abnormally in a more caudal position in the bladder, urethra, or adjacent structures. A ureterocele is a common associated anomaly. The upper pole ureter obstructs more often than the lower pole ureter; most obstructions are in the distal portion of the ureter, although at times an obstruction occurs at the ureteropelvic junction and involves either ureteral segment. Similar to a normal system, a transitional cell carcinoma can develop in a completely duplicated collecting system, leading to a complex imaging appearance.

Therapy for obstruction or reflux of a single ureter in a duplicated system is common sheath reimplantation, with some surgeons performing an ipsilateral ureteroureterostomy.

Ectopia

Kidneys

Ectopia means an abnormal location for a structure. Ectopic kidneys range in location anywhere from just inferior to the diaphragm to the pelvis. A rare renal ectopia is intrathoracic; these are more common on the left and in males. The lack of imaging detection of a kidney in its usual location should not be assumed to represent agenesis; the entire abdomen needs to be scanned for an ectopic kidney, which at times is small and poorly functioning.

Malrotation of a normally positioned kidney is generally a curiosity of little significance.

An ectopic kidney undergoes incomplete rotation around its axis (it is thus malrotated), and the renal pelvis tends to face more anterior than usual. The renal collecting system does not drain as readily as in a normally situated kidney, relative stasis ensues, and thus an increased prevalence of stone formation is found in these kidneys. Ureteropelvic junction obstruction is also relatively common. These kidneys tend to be dysplastic and some are associated with other malformations.

In renal ectopia the ureter length is appropriate for kidney position; in renal ptosis the ureter appears more tortuous and is more appropriate to a normally positioned kidney.

A normal US renal sinus echo complex is absent in two thirds of ectopic kidneys, while in the other one third it is eccentric in location.

Crossed Ectopia

In crossed renal ectopia both kidneys are on one side of the abdomen. They are usually partly fused and the ectopic kidney malrotated. The ureter from the ectopic lower kidney crosses the midline and usually inserts in its normal position. Such crossed fused renal ectopia is an uncommon congenital anomaly generally of little or no clinical significance. In some, however, renal ectopia is associated with other congenital abnormalities, including ectopic ureteral insertion.

Ultrasonography of crossed fused renal ectopia identifies an empty renal fossa and a

distorted, enlarged kidney with a duplicated renal sinus. At times the ectopic kidney is difficult to identify with US due to malrotation.

Technetium-99m-DMSA shows an empty renal fossa and outlines the functional status of an ectopic kidney.

Horseshoe Kidney

A horseshoe kidney is a type of ectopia consisting of partial fusion of the two kidneys occurring in about 0.25% of the population. The lower poles of both kidneys extend more medially than usual and either have fused renal parenchyma or are connected by fibrosis. Fusion is anterior to the aorta, and the kidneys tend to be more inferior in location than usual. Each kidney has its own collecting system. Often multiple and complex renal arteries are present. Rarely, associated inferior vena cava anomalies or a retrocaval ureter are also present.

Neoplasms do develop in a horseshoe kidney, probably at the same incidence as in normal kidneys although transitional cell carcinomas occur somewhat more often than expected. The diagnosis of a transitional cell carcinoma is generally made at an advanced stage in these patients. Patients with a horseshoe kidney also appear more prone to developing a primary carcinoid tumor.

Urolithiasis developing in patients with a horseshoe kidney is treated with either percutaneous nephrolithotomy or extracorporeal shock-wave lithotripsy (ESWL), similarly to those in patients with normal kidneys.

A bone scan in a patient with a horseshoe kidney can mimic bone metastases. An apparent horseshoe kidney (pseudo–horseshoe kidneys) is seen in patients with spina bifida; gibbus deformity causes lower renal pole medial migration. In these patients, however, the prevalence of true horseshoe kidneys is also somewhat increased.

Ureters

Ureteral Bud Remnants

A ureteral bud remnant associated with renal agenesis or dysplasia is usually identified with a retrograde study, provided reflux exists. In the absence of reflux or with an ectopic insertion, detection is difficult at best. At times an ectopic insertion is suggested indirectly by severely deformed adjacent structures.

Ectopia

A right retrocaval ureter passes posterior to the vena cava and courses inferiorly in a more medial position than usual. Most patients with a retrocaval ureter are asymptomatic, and this condition is discovered incidentally during either urography or CT. A rare anomaly is a left retrocaval ureter associated with a left inferior vena cava.

Ectopic insertion of a single ureter is into any adjacent structure proximal to the external urethral sphincter. It occurs more often in males and occasionally is associated with prostatitis or epididymitis. Some are associated with other anomalies, such as a crossed single ectopic ureterocele. The kidney drained by such an ectopic ureter tends to be dysplastic.

An ectopic duplicated ureter is more common in females and is more often on the left. The ectopic ureter usually drains the upper pole of a duplex kidney and tends to insert into the urethra distal to the urethral sphincter, thus accounting for urinary incontinence. Occasionally found are intraprostatic and vaginal ectopic insertions.

Even if the distal end of an ectopic ureter is not stenotic, a low-inserting ectopic ureter can be obstructed by an adjacent urethral sphincter. Huge ureters terminating in the posterior urethra are occasionally found.

Detecting most ectopic ureters with imaging should be straightforward, yet delayed detection of an infrasphincteric ectopic ureter is not uncommon, especially in girls. Delayed, inappropriate and misleading imaging contribute to this problem. Technically excellent excretory urography is generally diagnostic, although problems occur with a ureter draining a dysplastic kidney. Contrast enhanced CT or 99mTc-DMSA scintigraphy aid detection of an ectopic insertion if a dysplastic kidney is present.

With a sufficiently small and poorly functioning renal segment, an occult ectopic ureter and its insertion can be difficult to visualize with imaging. Problems also arise with unusual insertions and with a poorly functioning kidney. Some insertions are only

transiently visible on one of several imaging studies. Vaginography defines the insertion of some ectopic vaginal ureters because these ureters tend to reflux. Occasionally MRI is useful, such as with an ectopic ureter from a poorly functioning upper pole duplicated kidney that is not detected with IV pyelography and US.

A triple ureter, with an ectopic opening into the vagina has been described (18).

Ectopic ureteroceles are discussed in Chapter 11.

Nephroptosis

One can be criticized for including nephroptosis, or floating kidney, as an abnormality. Older physicians are undoubtedly familiar with this condition and the resultant attempts to cure it by nephropexy, a procedure that is considerably less common today. Recently, however, a few reports have described laparoscopic nephropexy as therapy for symptomatic nephroptosis, and this procedure is again somewhat in vogue.

Occasionally nephroptosis is a cause of chronic ureteral obstruction and associated symptomatology.

Multicystic Dysplasia

Clinical

Fetal kidney nephrons form from fetal metanephric blastema surrounding the ureteral bud. This fetal blastema normally matures during gestation, but occasionally some persists after birth as nephrogenic rests. These nephrogenic rests are associated with an increased risk of multicystic dysplasia, multilocular cystic nephroma, and Wilms' tumors. They are more common in several syndromes, such as Beckwith-Wiedemann syndrome (discussed in a later section), hemihypertrophy, and sporadic aniridia; children with these syndromes should be screened for Wilms' tumors.

Complete multicystic dysplasia (also called *multicystic kidney*, *renal dysplasia,* and *renal dysgenesis*) is found only unilaterally—complete bilateral involvement is incompatible with life. Depending on the extent of involvement, dysplasia is limited to the infundibula, renal pelvis, and proximal ureter, or it involves a kidney to the point that dilated calyces appear as intrarenal cysts. Segmental multicystic dysplasia occurs in a setting of a duplex collecting system. At times a hypoplastic renal artery is identified.

Most often multicystic dysplasia is detected as an abdominal tumor in infancy. Some older patients present with ureteropelvic junction obstruction. The condition is discovered in an occasional adult as an incidental finding.

A variant of multicystic dysplasia includes an associated hydronephrosis, with renal cysts communicating with the renal pelvis. This condition presumably develops from incomplete ureteral obstruction. Often some renal function is evident.

Among term neonates and infants with unilateral multicystic dysplastic kidneys, in those with no vesicoureteral reflux the contralateral kidney was more than 1 standard deviation longer than the mean for age in 54% (19). Contralateral vesicoureteral reflux is detected in 15% to 25% of children with a newly diagnosed multicystic kidney, and these refluxing kidneys are significantly shorter than nonrefluxing ones. Other anomalies include ectopic ureters, ureterocele, bladder diverticula, and urethral duplication. An association exists among renal dysplasia, Gartner's duct cyst, and ipsilateral müllerian duct obstruction. An investigation for lower urinary tract abnormalities is thus in order in these infants. Extraurinary anomalies include bowel malrotation and congenital cardiomyopathy.

Renal malignancy is rare in multicystic dysplasia, and current opinion is that this condition is not premalignant, although the kidney appears prone to nodular renal blastema and reports suggest that renal cell carcinoma, Wilms' tumor, and even mesothelioma appear to be more common than by chance alone. Complicating the issue is that occasionally other lesions, including tumors are misdiagnosed as multicystic dysplasia.

The current trend is to follow segmental multicystic kidneys nonoperatively because these cysts tend to involute and the kidney decreases in size. With age, some patients develop extensive calcifications. At times by adulthood only a cystic remnant with a calcified rim is apparent.

Figure 10.1. Right multicystic dysplastic kidney. Noncontrast computed tomography (CT) identifies a small, irregular right kidney (arrow). (Courtesy of Nancy Curry, M.D., Medical University of South Carolina.)

Imaging

A voiding cystourethrogram and renal US appear appropriate in newborns with suspected multicystic kidney disease to confirm the diagnosis and detect any associated anomalies. The grape-like intrarenal cysts do not communicate with the ureter. Little normal renal parenchyma is detected in the involved kidney (Fig. 10.1). A characteristic finding is a club-like deformity of a rudimentary ureter. A small dysplastic kidney is more echogenic than a normal kidney; the US differential diagnosis also includes hydronephrosis due to other etiologies.

Occasionally during renal scintigraphy a multicystic dysplastic kidney accumulates a radiopharmaceutical agent; such uptake correlates with the presence of mature renal cortical tissue in the diseased kidney.

Tc-99m-DMSA renal uptake is decreased in the contralateral kidney in a majority of patients with a multicystic kidney, reflecting tubular and glomerular damage.

Polycystic Disease

Autosomal Dominant

Clinical

Autosomal-dominant polycystic disease, also called *adult polycystic kidney disease* and *Potter type III*, is the most common hereditary renal disorder. It is not a simple entity; no family history of renal disease is obtained in about half the patients, and variable penetrance and expressivity are apparent. Many of these patients develop hypertension. Renal failure is a late finding. These patients are also prone to developing aortic and cerebral aneurysms with their related complications.

A rare disorder called oral-facial-digital syndrome type 1 includes polycystic kidney disease as one component. The syndrome is X-linked, with affected males dying before birth. Although renal findings resemble autosomal polycystic disease and a dominant inheritance pattern is evident, histopathology reveals mostly glomerular cysts (20).

There are two subtypes of autosomal-dominant polycystic disease. Polycystic kidney disease type 2 (PKD2) has a milder clinical phenotype than PKD1; the median age at death or onset of end-stage renal disease is 53 years for individuals with PKD1 and 69 years for those with PKD2 (21). About half of these patients also develop liver cysts; far fewer develop pancreatic or splenic cysts or even adrenal cysts. A rare patient also has Caroli's disease, but this association is less common than with autosomal-recessive polycystic disease. Polycystic kidney disease can develop in a horseshoe kidney. Histologically, cystic changes occur both in nephrons and collecting ducts. Eventually multiple cysts of varying size are found in both the renal cortex and the medulla. Subcapsular cysts also develop.

Abdominal pain is a common presentation. Many patients develop hypertension. An occasional cyst rupture into the collecting system leads to hematuria. Enlarged kidneys are palpable in some individuals. Renal stones with their related complications are more prevalent than in the general population. Eventually renal failure ensues. The rare emphysematous pyelonephritis is probably due to superimposed infection rather than polycystic disease. Likewise, renal cell carcinoma developing in a setting of polycystic disease is probably fortuitous.

Typically few cysts are detected early in life, but gradually multiple bilateral cysts enlarge and interstitial fibrosis develops with loss of normal renal tissue. Not uncommonly progressive worsening of renal function manifests in early adulthood. The cysts compress and distort adjacent calyces and eventually little renal

parenchyma is detected. Why the loss of normal renal tissue is part of this condition is puzzling. Still, the kidneys are larger than normal.

Several criteria are used to identify patients at risk for developing adult polycystic kidney disease. One scheme is that the presence of at least two renal cysts (either unilateral or bilateral) in individuals at risk and younger than 30 years is regarded as sufficient to establish the diagnosis; in those 30 to 59 years of age at least two cysts in each kidney and in those above 60 years of age at least four cysts in each kidney are required. Ultrasonography can be used to screen for these cysts.

Imaging

Initially cysts are small, but eventually imaging identifies bilateral enlarged kidneys, at times markedly asymmetrical, and containing multiple cysts. The cysts vary in size and distort surrounding parenchyma. Computed tomography shows most cysts to resemble simple cysts, although hemorrhage into cysts is common and these are hyperdense to water (Fig. 10.2). Some have a fluid–fluid level or even appear as a solid tumor. Renal calcifications are generally secondary to calculi, prior hemorrhage into a cyst, or cyst wall calcifications.

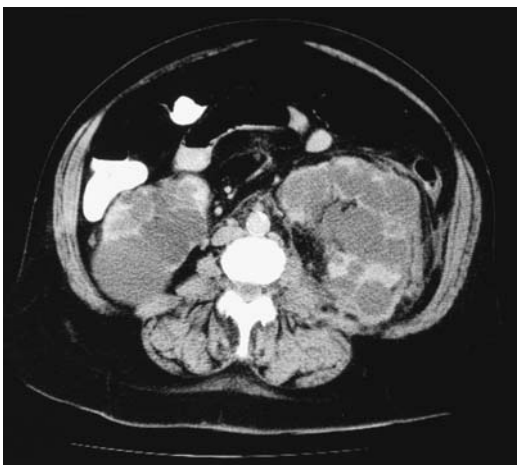

Figure 10.2. Polycystic disease. Transverse CT image through the kidneys reveals numerous cysts varying in size. Little renal parenchyma is left. (Courtesy of Patrick Fultz, M.D., University of Rochester.)

Computed tomography or MR is useful to evaluate for any associated liver disease.

The sensitivity of renal US in individuals under 30 years of age at risk for autosomal-dominant polycystic kidney disease was 95% for those with PKD1 but only 67% for those with PKD2, but US sensitivity for either PKD type in individuals aged 30 years or older was 100% (22); DNA genetic linkage analysis was the gold standard.

These cysts vary from hypo- to hyperintense both with T1- and T2-weighted images, presumably due to prior hemorrhage (Fig. 10.3). A fluid-fluid level is identified in some.

Therapy

Follow-up of these patients is generally by US. Computed tomography is useful to evaluate for a suspected complication. Intravenous urography has no role in follow-up.

Open transperitoneal bilateral renal cyst reduction surgery is an option in symptomatic patients; one advantage of this approach is that any liver cysts are also amenable to therapy. Laparoscopic cyst unroofing (decortication or marsupialization) for relief of pain is also an option; intraoperative US aids cyst detection during the laparoscopic procedure. Some of these patients require repeat cyst unroofing before pain relief is achieved.

A number of these patients eventually undergo renal transplantation. Some surgeons recommend nephrectomy prior to renal transplantation, although others disagree and reserve nephrectomy for those with intracystic hemorrhage, significant hematuria, pyonephrosis, or other complications.

Autosomal Recessive

Also known as *Potter type I* and *infantile polycystic disease*, the autosomal-recessive form of polycystic kidney disease manifests early in life. The underlying defect is renal tubular ectasia. The nephrons are normal. Expressivity varies, with some patients not surviving beyond the neonatal period. Those with milder renal involvement survive longer and develop hepatobiliary fibrosis and dilated bile ducts. Thus the severe form detected in infancy results primarily in renal involvement, called infantile polycystic disease, while in older children liver

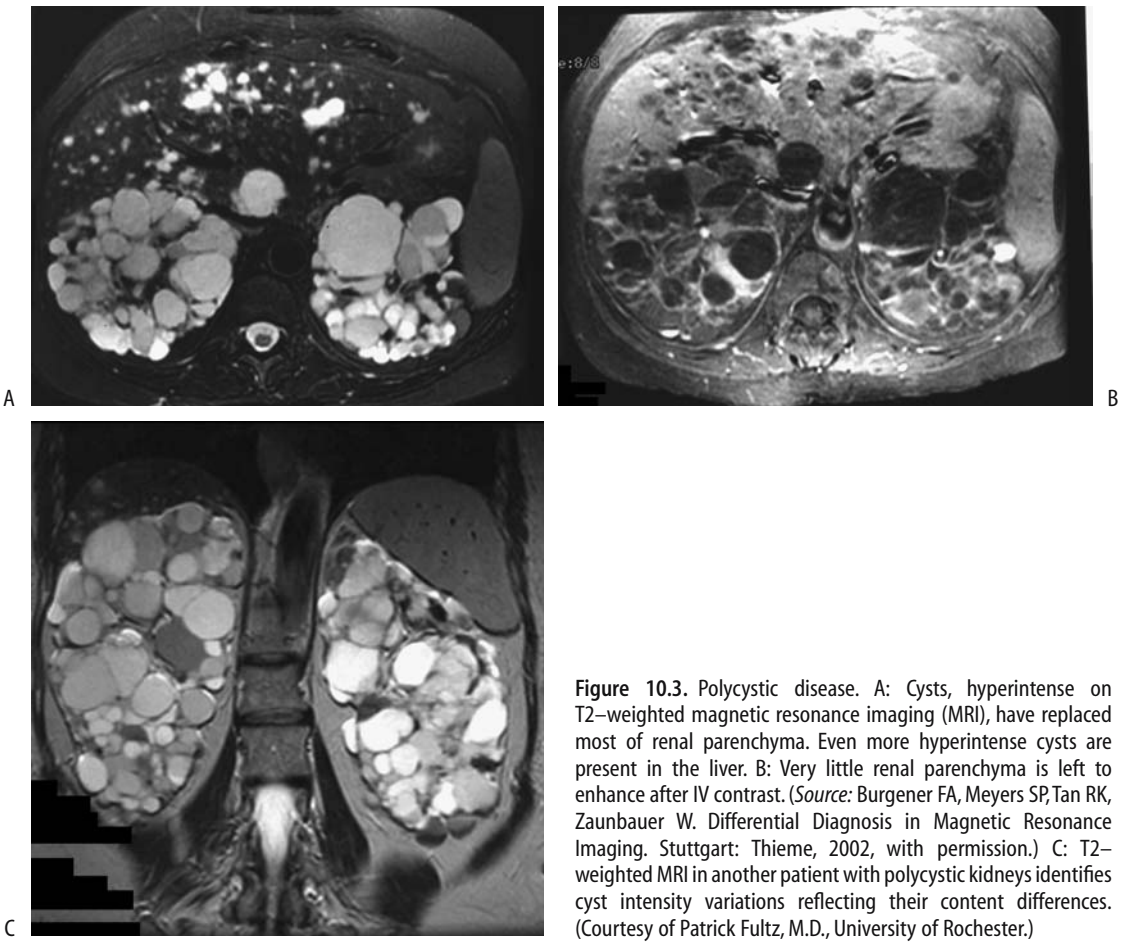

Figure 10.3. Polycystic disease. A: Cysts, hyperintense on T2–weighted magnetic resonance imaging (MRI), have replaced most of renal parenchyma. Even more hyperintense cysts are present in the liver. B: Very little renal parenchyma is left to enhance after IV contrast. (*Source:* Burgener FA, Meyers SP, Tan RK, Zaunbauer W. Differential Diagnosis in Magnetic Resonance Imaging. Stuttgart: Thieme, 2002, with permission.) C: T2–weighted MRI in another patient with polycystic kidneys identifies cyst intensity variations reflecting their content differences. (Courtesy of Patrick Fultz, M.D., University of Rochester.)

changes predominate and this entity is labeled *juvenile form* or *congenital hepatic fibrosis* (see Caroli's disease, discussed in Chapter 7). Yet whether autosomal-recessive polycystic kidney disease and congenital hepatic fibrosis are indeed the same entity but with different manifestations is not clear. Some adults with autosomal-dominant polycystic disease and those with multicystic dysplasia also develop similar hepatic fibrosis.

In the infantile form numerous small cysts (several millimeter range) develop throughout, the kidneys are markedly enlarged, poor function is evident early on, and renal failure gradually ensues.

Computed tomography reveals renal cysts to be near water density unless superimposed bleeding occurs. Magnetic resonance imaging identifies similar findings. Both CT and MRI also help detect any hepatic fibrosis and dilated bile ducts.

Ultrasonography in the infantile form shows bilaterally enlarged and diffusely hyperechoic kidneys, a pattern that in these infants strongly suggests the diagnosis. High-resolution US reveals dilated ectatic tubules arranged radially perpendicular to renal capsule, with the peripheral renal cortex initially not involved because it normally does not contain collecting ducts.

In surviving infants (presumably those having the juvenile form), the initial abnormalities tend to be limited to the kidneys, but gradually the disease focus shifts as hepatic damage leads to portal hypertension and its sequelae. Serial US in the juvenile form reveals that initially enlarged kidneys either shrink in

size or remain stable with age; renal echogenicity approaches that seen in patients with autosomal-dominant polycystic kidney disease but without marked kidney enlargement.

Alport's Syndrome

Alport's syndrome is an inherited, degenerative disorder involving basement membrane collagen that lacks Goodpasture antigen. Both sex-linked dominant and autosomal-recessive forms are described. Electron microscopy–observed anomalies are almost specific for this syndrome. It is linked to Goodpasture's disease, an uncommon autoimmune condition also showing a similar basement membrane collagen abnormality. In a broader context, this syndrome is linked to antiglomerular basement membrane disease and thin basement membrane disease, both diseases being more common than Alport's syndrome.

Symptoms start in childhood. Hematuria and proteinuria eventually progress to renal failure.

Imaging identifies small, smooth kidneys with poor function.

Alagille's Syndrome

Alagille's syndrome, or arteriohepatic dysplasia, is discussed in more detail in Chapter 8. These patients also develop tubulointerstitial nephritis and renal tubular acidosis. An occasional manifestation is resultant renovascular hypertension.

Angiography reveals uni- or bilateral renal artery stenoses and abnormalities in the aorta and celiac superior mesenteric and subclavian arteries. Some patients develop bilateral renal cysts and aortic wall calcifications at an early age.

Glomerulocystic Disease

Both sporadic and familial glomerulocystic disease develop. The hallmark of this disease is dilation of Bowman's space and proximal convoluted tubules. Numerous glomerular cysts develop but without dysplasia. Affected infants have enlarged kidneys. Liver cysts may be present.

Glomerulocystic disease associated with either hypoplastic or normal-sized kidneys is found in older children and adults and probably represents an acquired type of glomerulocystic disease. Whether this is the same entity seen in infants is conjecture. In fact, glomerulocystic disease is probably much more common than the relatively small number of published cases suggest; in adults it may be asymptomatic and only becomes symptomatic when another condition, such as lupus glomerulonephropathy or hemolytic-uremic syndrome, is superimposed.

The diagnosis is suggested by renal biopsy, although histopathology is not always straightforward. In addition to glomerulocystic kidney disease, renal cysts are found in autosomal-recessive polycystic kidney disease, autosomal-dominant polycystic kidney disease, and diffuse cystic dysplasia.

In the neonate, both polycystic diseases and glomerulocystic disease result in bilaterally enlarged hyperechoic kidneys. High-resolution US detects small, isolated cysts in a hyperechoic renal cortex, with these cysts usually being smaller than those found in typical autosomal-dominant polycystic kidney disease. Also, these cysts extend to the periphery, but no cysts are seen in renal medulla, which distinguishes this condition from both autosomal-recessive and -dominant polycystic diseases.

Medullary Cystic Disease

Renal medullary cystic disease consists of a spectrum of abnormalities eventually leading to renal failure. These patients have progressive renal tubular atrophy. Two forms are described: a juvenile form (also called *juvenile nephronophthisis*) inherited as an autosomal-recessive trait manifesting in childhood, and an adult form inherited as an autosomal-dominant trait. A tubulointerstitial nephritis develops in both forms. Gross medullary cysts are found in the adult form, while smaller cysts develop in the juvenile form.

In the juvenile form US reveals increased echogenicity secondary to the small cysts. The corticomedullary junction is poorly differentiated. Urography shows decreased contrast excretion, and pyelography identifies tubular ectasia. Renal size tends to decrease with disease progression, and corticomedullary cysts became evident. These cysts are better defined with CT and MRI than with US.

Because US abnormalities appear before clinical symptoms or signs are evident, US is useful in screening suspected families.

Biopsy suggests the diagnosis.

Familial Glomerulosclerosis (Familial Nephrotic Syndrome)

In the nail-patella syndrome, nail and skeletal abnormalities are associated with a nephropathy. Renal biopsy reveals glomerulosclerosis, and electron microscopy identifies massive fibrillar collagen within a mesangial matrix and basement membrane, a hallmark of this condition. Similar changes are also found in some patients with proteinuria and hematuria but without other stigmata of nail-patella syndrome. These patients have mild proteinuria early in life, and nephrotic syndrome becomes apparent during the second or third decade.

Tuberous Sclerosis

Tuberous sclerosis, or *Bourneville-Pringle disease*, is a neurocutaneous disorder having an autosomal-dominant inheritance, although spontaneous mutations also occur. Mental retardation and seizures are part of multiorgan involvement and renal lesions are common, consisting mostly of angiomyolipomas and cysts. Prevalence of lymphangioleiomyomatosis is also increased in tuberous sclerosis. Imaging in affected individuals begins to identify renal lesion during early childhood and most individuals have developed renal tumors by late childhood. Most common are angiomyolipomas, followed by simple renal cysts.

An occasional cyst disappears during follow-up but angiomyolipomas do not. Although generally believed that these patients are not at increased risk for renal cell carcinomas, anecdotal reports of renal malignancies abound.

An occasional patient has multiple cysts to the point of mimicking polycystic disease. Angiomyolipomas are prone to bleeding and forming hematomas. Eventually renal insufficiency and renal failure ensue if sufficient parenchyma is replaced by cysts and tumors. A rare first presentation is an elderly patient with gradual renal failure and imaging detecting marked bilateral renal parenchymal distortion due to multiple cysts and angiomyolipomas.

Von Hippel-Lindau Disease

Von Hippel-Lindau disease is a hereditary cancer syndrome caused by mutations of the *VHL* tumor-suppressor gene, which is located on the short arm of chromosome 3. The *VHL* gene produces a tumor-suppressor protein, called pVHL, which plays a role in angiogenesis, cell cycle regulation, and other functions, and regulates both growth and differentiation of kidney cells. Mutations of the *VHL* gene are also found in mesotheliomas and small cell lung carcinomas. Nevertheless, the etiology of von Hippel-Lindau disease appears to be more complex than currently apparent because a germ cell mutation is identified only in 70% of affected patients. Also, systematic investigation of families of involved individuals often detects additional silent tumors.

This autosomal-dominant disease has age-related penetrance of close to 100% at age 60 years. Affected individuals develop central nervous system hemangioblastomas, retinal angiomas, pancreatic cysts and islet cell tumors, adrenal pheochromocytomas and paragangliomas, epididymal cystadenomas, and in the kidneys cysts and clear cell carcinomas. Only a subgroup of these patients is at increased risk for developing a pheochromocytoma. Thus these patients are subdivided into type I (without pheochromocytoma) and type II (with pheochromocytoma).

Renal cysts are often multifocal and bilateral and are predominantly cortical in location. They do not progress to renal failure. There is, however, an increased prevalence of neoplasms in these cyst-containing kidneys. Multicentric renal cell carcinomas are common, at times bilaterally.

Among patients with von Hippel-Lindau disease having renal cell carcinomas, cancers occur 25 years earlier, are more often associated with renal cysts, and tend to be multifocal and bilateral, but have a lower grade histology and better 10-year survival than unselected patients with renal cell carcinoma (23); metastases occurred in von Hippel-Lindau disease patients only when tumors were >7 cm in diameter. These tumors tend to be encased by a fibrous capsule.

The treatment of cysts and tumors in this disease has become rather conservative and differs from conventional therapy. Many asymp-

tomatic lesions are observed rather than resected, and CT, US, and MRI are used for screening, follow-up of known lesions, and overall management of these patients, keeping in mind that CT and especially US miss small tumors in these patients. A renal carcinoma is resected only when it has grown to a certain size. Over the last several decades surgery in these patients has evolved from radical nephrectomy to a nephron-sparing operation. A radical nephrectomy is reserved for larger or more numerous tumors; follow-up consists of CT, chest radiography, and renal function tests every 6 months.

These patients develop end-stage renal failure both from surgical therapy and from tumor growth. Theoretically, transplantation with its associated immunosuppression may predispose to tumor recurrence, but in practice this does not occur.

Sickle Cell Disease

The primary kidney abnormality in sickle cell disease is small vessel involvement leading to renal function impairment. The hemolysis these patients experience also results in glomerular hemoglobin deposition. Findings in other organs, primarily spleen, are common. Patients with heterozygous or homozygous sickle cell disease develop enlarged kidneys, focal infarcts, cortical necrosis, and progressive renal insufficiency.

Most teenagers with sickle cell disease have a normal renal US appearance, gradually developing either a focal or a diffuse increase in reflectivity in the renal medulla or throughout the kidney, changes similar to those seen in early nephrocalcinosis. Both RI and PI are increased, with findings directly related to disease severity.

With iron deposition, MR reveals hypointense signals from renal cortices on both T1- and T2-weighted images.

Hemophilia

Ultrasonography in hemophilia type A patients identifies smaller than usual kidneys and dilated calyces and renal pelves, at times containing blood clots. Calculi are common. The overall appearance mimics that seen in chronic pyelonephritis.

Adjacent hematomas are secondary to retroperitoneal bleeding.

Beckwith-Wiedemann Syndrome

Beckwith-Wiedemann syndrome is a congenital overgrowth syndrome with a high sporadic occurrence, manifesting variable expressivity. There is a Beckwith-Wiedemann registry at the National Cancer Institute. Common abnormalities include macroglossia, abdominal wall defect, large birth weight, nephromegaly, and less often hemihypertrophy.

Affected children are prone to developing childhood solid tumors, including Wilms' tumor, adrenocortical carcinoma, and hepatoblastoma. An occasional child has a sarcoma or renal cell carcinoma. One should keep in mind, however, that not all renal tumors in these patients are malignant. Benign renal abnormalities, consisting of renal cysts, caliceal diverticula, hydronephrosis, and nephrolithiasis, occur in approximately 25% of these patients; most patients are asymptomatic.

Bartter's Syndrome

The rare Bartter's syndrome leads to hypokalemia and increased plasma renin and angiotensin II levels. It should be suspected in a child with nephrocalcinosis and a history of polyhydramnios and premature delivery.

Renal US findings vary; US tends to reveal hyperechoic pyramids or diffuse hyperechoic kidneys.

Baseline scintigraphy in one patient was normal, but pharmacologic blockade of the renin-angiotensin system with captopril revealed a bilateral increase of parenchymal transit time, time to maximum activity, and retained cortical activity (24); the authors suggest captopril renography for differentiating Bartter's syndrome from other causes of hypokalemia.

Tyrosinemia

A deficiency of fumarylacetoacetate hydrolase leads to tyrosinemia, an autosomal-recessive

disorder especially prevalent in the province of Quebec. Children with this lethal disease develop central nervous system and liver abnormalities early in life. Renal function is often impaired.

Computed tomography and US in 32 children with tyrosinemia undergoing liver transplantation revealed enlarged kidneys in 47%, a hyperechoic appearance in 47%, nephrocalcinosis in 16%, and delayed contrast excretion in 64% (25); liver transplantation improved renal function in about half of these children, but enlarged kidneys and a hyperechoic appearance persisted.

Congenital Hydronephrosis and Hydroureter

Many infants with hydronephrosis also have renal tubular dysfunction, with renal tubular acidosis being most common. Hydronephrosis is readily diagnosed by most imaging modalities.

A congenital urinary tract obstruction evolves while a fetal kidney is still developing. The sequelae of a congenital obstruction thus result in findings that tend to be different from those seen with an obstruction developing later in life.

In newborns with unilateral hydronephrosis, the contralateral kidney ranges from larger than normal, to normal in size, to small, and such findings should be interpreted cautiously. Distinguishing obstructive from nonobstructive hydronephrosis in neonates can be difficult. Without an obvious obstructive site, some of these neonates are followed medically until they grow.

At times with known prenatal hydronephrosis, renal US performed immediately after birth is falsely negative for hydronephrosis, probably due to oliguria. Cystourethrography appears indicated in these children because of an increased risk for vesicoureteral reflux.

The term *megacystis-megaureter* is descriptive and is most often applied to uncorrected vesicoureteral reflux and resultant dilation. In this sense it can be either congenital or acquired. Whether it represents a sequela of uncorrected massive chronic reflux or is a residue of a congenital hydroureter is conjecture. Megacystis-megaureter can be extreme to the point that one or both ureters dilate massively. The bladder also enlarges.

Ureteroceles are discussed in Chapter 11.

Megacalyces

An infant or adult occasionally has calyceal dilation without concomitant renal pelvis dilation and without underlying obstruction. Whether this condition, also called *Puigvert's disease*, is congenital or acquired is conjecture. Medullary pyramids are thinned and as a result the calyces have a straight or even convex outline rather than their usual concave shape. The number of calyces tends to be increased and they have a polygonal shape. The renal pelvis is not dilated and renal function is normal. Megacalyces is associated with increased stone formation.

Intravenous urography defines the condition and excludes an obstruction.

Ureteropelvic Junction Obstruction

The most common congenital urinary tract obstruction is at the ureteropelvic junction. A ureteropelvic junction stricture in the very young may represent a mild form of multicystic dysplasia. It is not common.

Midureteral Obstruction

A congenital midureteral obstruction is rare, with some of these strictures being classified as ureteropelvic junction strictures. A rare association exists between ureteral valves and ureteral strictures. Congenital adynamic midureteral segments are rare. Resection reveals muscular disarray but a patent ureter lumen.

Primary Megaureter

In congenital or primary megaureter a short nonperistaltic distal ureteral segment results in functional obstruction, while the more proximal ureter dilates and does have peristalsis. Etiology for the nonperistaltic segment is unknown but, unlike rectal aganglionosis, ganglion cells are present in this segment. Some authors subdivide primary megaureter into the following categories: (1) obstructive, (2) refluxing, and (3) nonobstructive and nonrefluxing. The degree of obstruction varies, and calyces are not dilated when obstruction is mild. The condition is more

often detected in children than adults and is more common on the left side. In some, ureteral dilation does not progress with age and may even improve. A rare patient first presents with a ureteral stone in a megaureter and an already nonfunctional kidney.

Differential diagnosis includes ureteral dilation secondary to reflux (megacystis-megaureter) and distal anatomic ureteral obstruction. Generally the distal ureter is not narrowed in a setting of reflux. At times a retrograde study is necessary to exclude anatomic obstruction.

Trauma

A renal injury classification scale, devised by the American Association for the Surgery of Trauma, is outlined in Table 10.1. New classifications of renal trauma continue to be devised, indicating that there are perceived limitations of the prior systems. Radiologic classifications have also been published.

In a setting of abdominal trauma, clinical evaluation of genitourinary trauma is notoriously difficult. As a result, at least in the United States, trauma physicians are rather generous in obtaining screening imaging studies in these patients, thus achieving a low yield for positive studies.

Penetrating Injuries

Intravenous urography is insensitive in evaluating renal damage from a penetrating injury, and, if stable, these patients generally undergo CT. Kidney damage due to anterior abdominal gunshot and knife wounds invariably also involves intraperitoneal structures, and most of these patients are explored. As a result, some surgeons argue against a need for any preoperative abdominal imaging studies. Flank or posterior stab wounds, on the other hand, are often evaluated with contrast-enhanced CT and the results are used to guide therapy.

Blunt Trauma

Clinical

Blunt renal injuries consist of contusion, laceration, rupture, and injury to the renal pedicle. Ureter rupture due to blunt trauma is rare. Most ureteral injury is from gunshot and stab wounds.

Renal trauma should be suspected in a setting of shock, hematuria, or adjacent fractures. Several studies have correlated the lack of hematuria with absence of major urinary tract injury, yet occasional patients without hematuria do have urinary tract injury, especially to the renal pedicle and ureter, and the degree of hematuria does not correlate with the extent of the injury eventually detected. Even a major ureteral laceration does not lead to hematuria in about one third of patients. Leakage from the urinary tract results in an accumulation of urine and either a urinoma or urinary ascites ensue.

The presence of hematuria, on the other hand, is generally investigated further with imaging studies. Often not only is urinary tract

Table 10.1. Surgical renal injury scale

Grade*	Type of injury	
I	Contusion	Hematuria with normal urologic studies
	Hematoma	Subcapsular, nonexpanding
II	Hematoma	Perirenal, nonexpanding
	Laceration	Parenchymal, <1 cm, without urinary extravasation
III	Laceration	Parenchymal, >1 cm, without urinary extravasation
IV	Laceration	Extending through cortex, medulla and collecting system
	Vascular	Main renal artery or vein injury with contained hemorrhage
V	Laceration	Shattered kidney
	Vascular	Hilar avulsion with devascularized kidney

* Advanced one grade for multiple injuries, up to grade III.
Source: Modified from Moore et al. (26).

injury present but also multiorgan damage. Incidentally, not all red urine represents blood. Porphyrins and certain drugs and foods lead to red-colored urine. About 15% of the population has a genetic predisposition to beeturia, due to the betalaine red pigment found in beet root.

In children, the kidney is the most common organ injured in blunt abdominal trauma. Complicating the issue is that congenital malformations need be considered. Thus underlying hydronephrosis or even an extrarenal pelvis predisposes to a laceration or avulsion.

A rare cause of nontraumatic ureteral hematoma is overcoagulation.

Imaging

Intravenous urography is no longer the primary imaging modality for renal trauma, having been supplanted by CT, which also evaluates other intraabdominal structures. If CT is not readily available, urography is an alternate for evaluating the upper urinary system. A normal IV urogram essentially excludes major renal and ureteral injury, although rare instances of severe renal laceration have not been detected with an urogram.

Limited urography, consisting of a scout radiograph, a radiograph shortly after contrast injection, and perhaps another one in 5 minutes or so (called "one-shot urography" by some clinicians) is a fast study to assess gross renal function and establish that there are indeed two kidneys in an unstable patient, but it is inadequate to assess for underlying renal trauma and should be discouraged in stable patients. It is a useful study in unstable patients who then undergo immediate exploration; their renal status is determined intraoperatively.

Many trauma patients have multiple injuries and, in the United States and some other countries, if they are hemodynamically stable, contrast-enhanced helical CT has become the screening tool of choice. Precontrast images are generally not obtained. An early-phase CT evaluates the renal pedicle and overall vascularity, a parenchymal-phase CT detects renal lacerations, and a delayed-phase CT provides information about contrast excretion and possible extravasation (Fig. 10.4). Such a technique also evaluates injury to the liver, spleen, pancreas, and adjacent structures. In particular, one should not rely on early-phase images to exclude collecting system injury with contrast extravasation; delayed scans are necessary. At times delayed serial postcontrast views reveal an increasing CT density or MR signal intensity in adjacent fluid, confirming extravasation.

In some countries US is the primary imaging modality in evaluating renal trauma. Ultra-

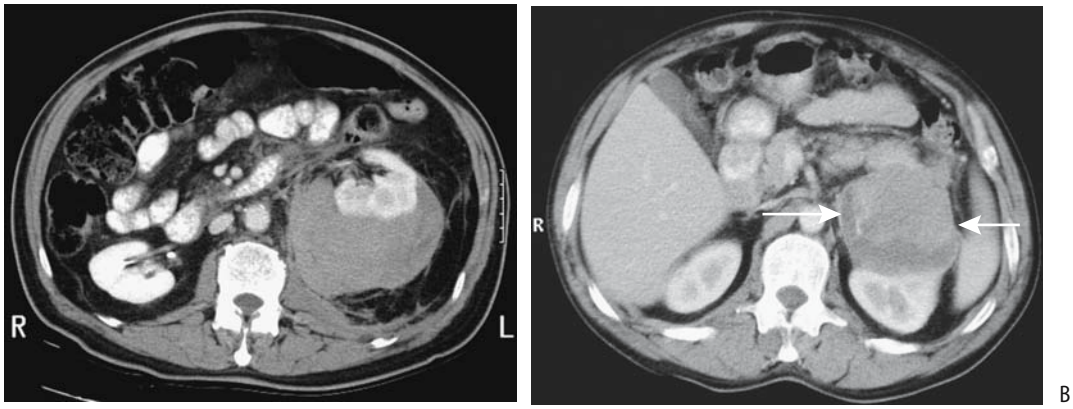

A B

Figure 10.4. Perirenal hematoma. A: CT identifies left perirenal fluid in a man who fell down stairs. (Courtesy of Patrick Fultz, M.D., University of Rochester.) B: Contrast-enhanced CT in another patient reveals a focal fluid collection anterior to the left kidney (arrows). (Courtesy of Algidas Basevicius, M.D., Kaunas Medical University, Kaunas, Lithuania.)

sonography can detect major vascular injury, renal fracture, or gross extravasation. It is a common modality in children. Nevertheless, accuracy of US appears to be less than with CT and even iv urography.

Currently MRI is not the initial imaging modality in suspected renal trauma, with availability, cost, and imaging time delays being some of the factors involved. Nevertheless, MRI complements CT in some trauma patients, especially those with equivocal CT findings, those who need repeat imaging studies, and those with an iodine allergy.

Ureteropelvic junction avulsion consists of complete ureteral transection, and thus no contrast is identified in the distal ureter, but contrast extravasation is evident, often perirenal in location. Although ureter nonvisualization is at times even a normal finding, in the appropriate clinical setting such a finding suggests avulsion, and a more specific study of ureter integrity, such as retrograde pyelography, should be considered. Both contrast extravasation and contrast in the ureter distally signify an ureteropelvic junction laceration. These findings are detected with both urography and postcontrast CT, but in any one patient the differentiation between avulsion and laceration can be difficult. Differentiation between avulsion and laceration has therapeutic implications because the latter is often managed conservatively.

At times a preexisting abnormality alters an otherwise more typical appearance of renal trauma. A renal cyst is prone to rupturing during blunt abdominal trauma, and the patient develops either hematuria or retroperitoneal hemorrhage. Such trauma-induced rupture of a renal cyst modifies the appearance of an associated hematoma. Ultrasonography identifies an acute hematoma as an isoechoic or hyperechoic tumor mimicking a neoplasm; it becomes more heterogeneous during resolution.

Renal scintigraphy has a role in detecting urinary leaks in patients with a contraindication to IV contrast. It is also often employed in renal transplant patients.

Vascular Injury

Renal pedicle injury consists of renal artery or major vein laceration, avulsion, or thrombosis.

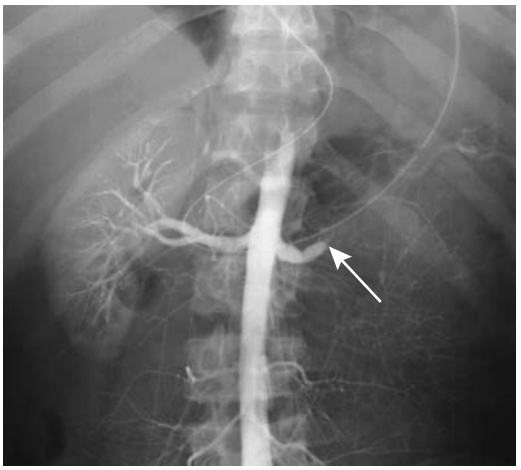

Figure 10.5. Aortography in this patient after a motorcycle accident reveals complete left renal artery occlusion (arrow) due to a subintimal tear. No renal function was evident. No extravasation was seen. (Courtesy of David Waldman, M.D., University of Rochester.)

An associated extraperitoneal hematoma is common. In some centers angiography is the imaging modality of choice with suspected renal pedicle injury; in others CT is preferred (Fig. 10.5). The lack of contrast enhancement of renal parenchyma is a hallmark of pedicle injury, a finding that is not always reliable. Some patients have partial parenchymal enhancement in spite of main renal artery and vein disruption, at times due to an intact accessory renal artery, extensive capsular collaterals or even flow being maintained by an adjacent hematoma. Computed tomographic detection of an extensive extraperitoneal hematoma is common with a pedicle injury.

An arterial intimal tear can initially lead to an intimal flap and evolve into a thrombus. Extensive involvement results in a lack of perfusion and excretion by the kidney involved, although distal ischemia is usually segmental rather than the entire kidney being involved. Occlusion of the main renal artery or of a main branch is equally well seen either by contrast-enhanced helical CT or angiography in most, but not all, patients. Occasionally helical CT identifies an

abrupt cut-off to the renal artery. Contrast-enhanced helical CT should also detect any pseudoaneurysms.

Retrograde flow of IV contrast into the renal vein suggests renal artery obstruction.

Avulsion results in renal infarction. A hematoma surrounds the site of rupture and at times a postcontrast study detects contrast extravasation. Renal artery thrombosis or renal pedicle avulsion should be suspected with postcontrast nonvisualization of a kidney, although an absent kidney, vascular spasm, or simply an ectopic kidney outside the imaged field results in similar findings.

Ultrasonography of some renal pedicle ruptures is initially noncontributory, and either CT or renal arteriography is required to exclude major pedicle injury.

Occasionally occult renal injury results in posttraumatic arterial hypertension. Whether computed tomography angiography (CTA) or arteriography should be performed is debatable, although arteriography is considered to be the gold standard. Renal artery or major branch laceration or intrarenal artery constriction is detected in some of these patients.

Renal vein thrombosis results in an enlarged kidney and a delayed and diminished nephrogram. Renal vein laceration leads to a perinephric hematoma that tends to mask the seriousness of an underlying vascular injury. Quite often CT suggests a laceration only indirectly if a follow-up scan reveals an increasing perinephric hematoma.

Therapy

A rather conservative therapeutic approach is evolving for CT-detected renal trauma in stable patients. For similar injuries some urologists favor exploration while others manage them conservatively as long as the patient is hemodynamically stable. When contemplating nephrectomy versus conservative therapy of a damaged kidney, a postcontrast CT finding of enhancing parenchymal rim, even if thin, and excretion of contrast into calyces should suggest a more conservative approach. Percutaneous interventional techniques suffice for some complications. With continued bleeding, after diagnostic angiography establishes a site of hemorrhage in patients with traumatic kidney injury, transarterial superselective embolization should stop the bleeding in most patients. Most localized extravasations resolve spontaneously. On the other hand, patients with renal pedicle trauma require prompt revascularization to avoid future kidney loss.

Most unrecognized complications manifest within the first 4 weeks of injury; the exceptions are hypertension, hydronephrosis due to partial obstruction, infected urinoma, and pyelonephritis. A devitalized kidney segment predisposes to subsequent infection.

Injuries to the main renal artery are treated either by surgical revascularization or conservatively. Percutaneous insertion of an endovascular stent suffices for some vascular injuries. Posttherapy hypertension can be due to either an initial injury or a therapy complication.

Posttherapy renal function can be confirmed by scintigraphy.

Small or Large Kidney(s)

At times imaging reveals a kidney that is smaller or larger than normal. Some of the conditions associated with smaller than normal kidneys having a smooth outline are listed in Table 10.2. It is difficult in an older patient to determine if a small kidney is secondary to congenital hypoplasia or dysplasia or is due to an acquired condition such as ischemia or infection.

Hypotension results in an increasingly dense and persisting bilateral nephrogram postcontrast in kidneys that appear smaller than usual. A similar but unilateral nephrogram occurs with urinary tract obstruction and acute renal vein thrombosis.

Conditions leading to an enlarged kidney are limited (Table 10.3). Diffuse tumor infiltration results in a poorly defined border between tumor and normal parenchyma, making detection difficult. A reniform shape is generally preserved. In children, the most common cause of bilateral enlarged kidneys is leukemic infiltration.

Table 10.2. Conditions associated with a small, smooth kidney(s)

- Congenital causes
  - Dysplasia
  - Hypoplasia
  - Prune belly syndrome (Eagle-Barrett syndrome)
  - Laurence-Moon-Biedl syndrome (?)
  - Sequelae of multicystic dysplasia
  - Alport's syndrome
- Infection/inflammation
  - Chronic pyelonephritis
  - Chronic glomerulonephritis
  - Post-infection or obstruction
- Radiation (late)
- Papillary or cortical necrosis
- Medullary cystic disease
- Amyloidosis (late stage)
- Lead poisoning
- Hemophilia
- Chronic vesicoureteral reflux
- Diabetes (late stage)
- Collagen vascular disorders
- Vascular causes
  - Associated with hypertension
    - Renal artery stenosis
    - Nephroptosis
    - Dissection
  - Ischemia
    - Arterial
      - Emboli
      - Thrombosis
    - Chronic renal vein thrombosis
  - Hypotension
  - Nephrosclerosis

Infection/Inflammation

Acute Pyelonephritis

There is no uniform agreement on how to describe an acute bacterial infection of the kidney. Such terms as *acute pyelonephritis*, *acute bacterial nephritis*, *lobar nephritis*, and *lobar nephronia* abound in the literature and are often applied haphazardly. In addition, some patients have a pyelitis only, with relative parenchymal sparing. The Society of Uroradiology has recommended that the term *acute pyelonephritis* be adopted for this condition and this term is used here. Two complementary but distinct definitions are available for acute pyelonephritis: a clinical one and a pathologic finding.

Most acute pyelonephritis is secondary to an ascending infection. The less common hematogenous source of acute pyelonephritis often results in a different appearance from that seen in a setting of reflux; the inflammation initially is not lobar in distribution; rather, multiple foci of involvement predominate in the renal periphery. Eventually, however, most inflammations become confluent, and their appearance is similar regardless of origin.

Pathologically, a focal involved segment is sharply demarcated from adjacent normal parenchyma. In some, tissue necrosis progresses to frank abscess and, with a severe-enough inflammation, the extrarenal space becomes involved.

Table 10.3. Enlarged kidney(s)

- Congenital causes
  - Dysplasia
  - (Poly)cystic disease
  - Hemihypertrophy
- Trauma
- Urinary obstruction
- Infection/inflammation
  - Acute pyelonephritis
  - Acute glomerulonephritis
  - Acute interstitial nephritis
  - Abscess
  - Chronic infection
- Diffuse infiltration
  - Neoplasia
  - Amyloidosis (initially)
  - Sarcoidosis
- Lymphangiectasia
- Acute tubular necrosis
- Diabetes (initially)
- Nephrotic syndrome
- Vascular causes
  - Acute renal vein occlusion
  - Hemolytic-uremic syndrome
  - Sickle cell disease
- Transplanted kidney

Most treated acute pyelonephritis leads to no sequelae. A minority of patients develop cortical scarring, which is detectable with scintigraphy or urography. Renal insufficiency is rare; perhaps more common is renal hypertension.

Children

Clinical

Especially in children, it is reasonable to ascribe acute pyelonephritis to vesicoureteral reflux and retrograde introduction of bacteria. The problem is that in children with acute pyelonephritis only about half are shown to have reflux, while reflux is even less common in adults. Both vesicoureteral reflux frequency and grade progressively decrease with age.

End-stage renal disease secondary to postinfectious nephropathy probably occurs only after pyelonephritis, rather than after such urinary tract infections as cystitis. There is thus a need for a reliable test to detect pyelonephritis, especially in young children where a clinical diagnosis is difficult.

Because congenital urinary tract anomalies are not uncommon in children with a urinary tract infection, the underlying anatomy needs to be studied. Especially in young children, vesicoureteral reflux is common in association with acute pyelonephritis, and thus voiding cystourethrography (or in some centers radionuclide cystography) appears reasonable. After the age of 9 to 10 years or so, reflux in association with acute pyelonephritis is sufficiently uncommon that a need for voiding cystourethrography is individualized.

Imaging

Neither an IV urogram nor US is sufficiently sensitive to serve as a screening test for pyelonephritis in children. Most urograms during an acute attack are normal. In some children considerable time elapses before sufficient renal damage develops to be visible with urography. In a minority, the involved kidney is enlarged and a delay and decreased contrast concentration are evident. The affected kidney returns to normal size in a week or so after the start of treatment. Urography is normally performed primarily to detect other associated conditions, such as obstruction. Computed tomography is also normal in a minority of these children.

Ultrasonography reveals a hyperechoic renal sinus in some children with in acute pyelonephritis (27), yet both US and power Doppler US findings range from normal to focal or multifocal defects, and normal US does not exclude parenchymal damage; even Doppler US underestimates the extent of involvement.

In children, Tc-99m-DMSA scintigraphy is more sensitive in detecting pyelonephritis than is US or IV urography and appears to be even more sensitive than CT and is preferred in detecting and following renal damage due to acute urinary tract infection. While planar DMSA scintigraphy does detect renal cortical defects, DMSA-SPECT detects more and is preferred. Tc-99m-DMSA scintigraphy reveals parenchymal findings suggestive of pyelonephritis in a majority. In some, DMSA scintigraphy simply shows swollen kidneys, with swelling obscuring the focal defects. Nevertheless, although a high sensitivity is achieved in detecting pyelonephritic cortical damage, scintigraphy cannot exclude the diagnosis.

Tc-99m-MAG3 and Tc-99m-glucoheptonate are also used to evaluate pyelonephritis in children. Using a mild (grade 1), moderate (grade 2), and marked (grade 3) scale to grade the severity of decreased radionuclide localization, MAG3 studies were able to detect 79% of grade 2 and 96% of grade 3 cortical lesions but only 59% of grade 1 lesions compared with Tc-99m-glucoheptonate scans (28).

In a study of children with fever-producing urinary tract infection, gadolinium-enhanced MRI detected more pyelonephritic foci than Tc-99m-DMSA cortical scintigraphy (29). The role of MR in this setting is still evolving.

Adults

Clinical

An unusual organisms, *Mycoplasma hominis*, is occasionally implicated in acute pyelonephritis. It should be considered if the patient does not improve with conventional antibiotic therapy and no organism is identified; special urine cultures are necessary to grow this organism.

Renal vein thrombosis, a common complication of acute pyelonephritis in the preantibiotic era, currently is rarely encountered.

One approach is to treat patients with suspected uncomplicated acute pyelonephritis medically for 72 hours, and limit imaging only to those who do not respond or respond poorly. Diabetics and other high-risk patients should undergo imaging early in the course of infection.

Imaging

Imaging has a limited role during most episodes of clinical acute pyelonephritis in adults; in many patients no imaging abnormality is found, yet imaging is often obtained—not to detect infection, but rather in a search for underlying congenital abnormalities that predispose to infection and detect any obstruction, stasis, calculi, or focus of infection.

Intravenous urography appears indicated in diabetics, patients not responding to antibiotics within 72 hours, and in a setting of an unusual organism. Suspected progression to an abscess or other complication warrants CT. A percutaneous nephrostomy is indicated with the presence of an obstructed collecting system.

The kidneys increase in size during acute pyelonephritis. In some adults focal swelling and decreased attenuation persists for months. If pyelonephritis is severe enough, both in children and adults the final end point is focal scarring of the affected lobe.

Mild acute pyelonephritis does not result in any specific CT findings. Either focal swelling or enlargement of the entire kidney develops with more severe involvement. Precontrast images occasionally show hypodense or hyperdense regions compared to normal parenchyma, with increased attenuation probably representing focal hemorrhage. Postcontrast CT in some patients reveals perfusion defects extending from the papilla to the periphery. At times the involved parenchyma exhibits near-water density, or delayed postcontrast scans show enhancement of involved segments.

Computed tomography detects postcontrast renal perfusion defects in up to two thirds of patients with acute pyelonephritis, depending on the severity of infection. These defects range from unilateral to multifocal and bilateral. The temporal findings are not constant and can change rapidly. Thus a hypodense heterogeneous region can evolve into a streaky, hyperdense appearance. In general, the CT findings do not change clinical management. Perinephric inflammation is evident with some infections, and CT reveals thickening of Gerota's fascia and stranding in the perinephric fat.

With a hematogenous origin, instead of wedge-shaped defects, more numerous rounded low-attenuation parenchymal defects predominate. An occasional patient develops a focal intraparenchymal homogeneous tumor mimicking a neoplasm without other parenchymal or perirenal abnormalities.

Ultrasonography identifies hydronephrosis, but is relatively insensitive in detecting renal parenchymal inflammation. A majority of pyelonephritic kidneys appear normal. With a severe inflammation, US identifies hypo- to isoechoic and occasionally even hyperechoic regions. The latter presumably represent hemorrhage. Compared to transabdominal US, Doppler US appears to improve the detection of acute pyelonephritis, although it probably is not as sensitive as CT.

Because of cost and restricted availability, MRI currently plays a limited role in most patients with suspected acute pyelonephritis. During an acute attack the kidney is hypointense on T1- and hyperintense on T2-weighted images.

Tc-99m-DMSA renal scintigraphy either reveals a normal scan or identifies cortical defects; in a setting of acute pyelonephritis, scintigraphy appears to be more sensitive than IV urography or US.

Emphysematous Pyelonephritis

Clinical

Emphysematous pyelonephritis is not a separate entity, but a severe type of necrotizing pyelonephritis. The criteria for defining this condition are not settled; some authors define emphysematous pyelonephritis only if gas is found within renal parenchyma, while others expand the definition and include gas not only within the parenchyma but also in the excretory system and perirenal spaces. Emphysematous pyelonephritis should be differentiated from emphysematous pyelitis; the latter is a generally benign condition consisting of gas in the urinary collecting system.

Emphysematous pyelonephritis develops mostly in diabetic patients, both insulin and non–insulin dependent. Concomitant urinary obstruction is more common in nondiabetics. It is a rapidly progressive, life-threatening infection associated with gas-forming coliform bacteria such as *Escherichia coli* and others. It is almost always unilateral. The simultaneous occurrence of emphysematous pyelonephritis and emphysematous cholecystitis is rare.

Gas is located in the renal parenchyma, perirenal tissues, and at times the collecting system.

Imaging

In spite of some authors' opinion that a diagnosis of emphysematous pyelonephritis should be made by CT, quite often conventional radiography is sufficient to detect this condition. Thus in patients with emphysematous pyelonephritis diagnosed by CT, abnormal gas was identified with conventional radiography in 66% and US in 88% (30). When localized, emphysematous pyelonephritis can mimic an abscess (Fig. 10.6).

Emphysematous pyelonephritis generally is not associated with ureteral obstruction.

The imaging appearance of emphysematous pyelonephritis consists of either parenchymal destruction with absence of fluid or the presence of streaky or mottled gas, or it contains either renal or perirenal fluid and bubbly or loculated gas or collecting system gas. Such differentiation appears to be of prognostic importance because the former patients have a more fulminant course.

Therapy

Although some of these patients respond to medical management, many undergo a nephrectomy. Some have been successfully treated with imaging-guided percutaneous drainage, but such drainage is not feasible with diffuse involvement. Some drained patients subsequently require elective nephrectomy for adequate therapy.

The serum creatinine level is the most reliable predictor of outcome. Affected kidneys tend to recover function after medical therapy, although many of these patients with underlying diabetes already suffer from chronic renal failure.

Abscess

The term *renal carbuncle* is used by some radiologists; it has no specific imaging definition and some use it as a synonym for renal abscess. The term is probably best avoided in describing imaging findings.

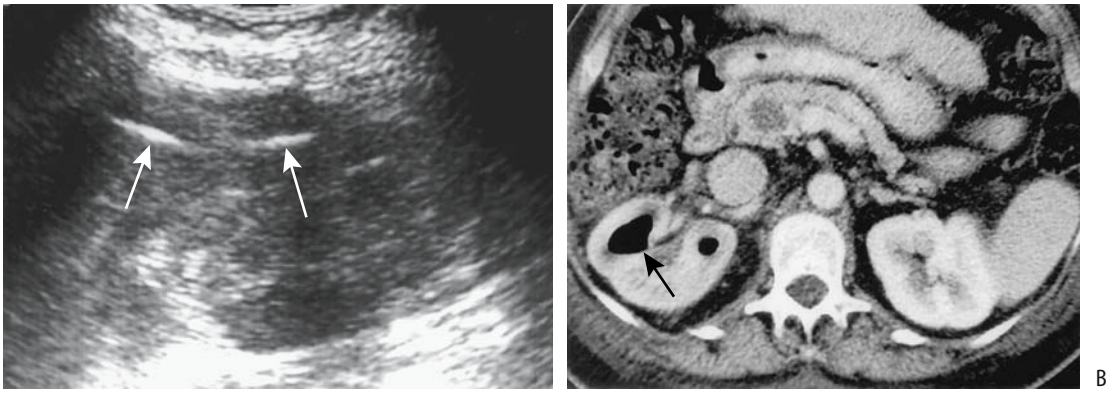

Figure 10.6. Emphysematous pyelitis. A: Ultrasonography in a woman with cirrhosis and portal hypertension reveals hyperechoic structures with distal shadowing (arrows) in the right kidney. B: Transverse postcontrast CT identifies a gas-fluid level in a dilated calix (arrow). Follow-up CT 3 weeks after therapy revealed a normal appearing right kidney. (*Source:* Roy C, Pfleger DD, Tuchmann C, Lang HH, Saussine CC, Jacqmin D. Emphysematous pyelitis: findings in five patients. Radiology 2001;218:647–650, with permission from the Radiological Society of North America.)

At times acute pyelonephritis progresses to scattered small abscesses, which eventually coalesce into a gross abscess. The involved kidney is often enlarged. An abscess tends to be sharply marginated and has a rim of contrast enhancement. A subcapsular abscess displaces and compresses the adjacent renal parenchyma. Gas within an abscess is not common. Some renal abscesses are associated with extrarenal abscesses in adjacent structures.

In general, CT detects renal and extrarenal abscesses better than US (Fig. 10.7). Still, US detects the larger abscesses and often is more readily available in monitoring resolution. Ultrasonography of an abscess identifies a complex, thick-walled, cystic, fluid-containing mass. Abscesses tend to be hypoechoic or anechoic. With maturity the abscess outline becomes better defined.

Gadolinium-enhanced MRI reveals renal abscesses as heterogeneous hypointense tumors; perinephric inflammatory stranding is common. The MRI findings are similar to those seen with contrast-enhanced CT, and in patients who should not receive iodinated contrast, MRI is a viable alternative.

An abnormal scintigram showing photopenic regions in the kidney is nonspecific and does not differentiate between inflammation and abscess.

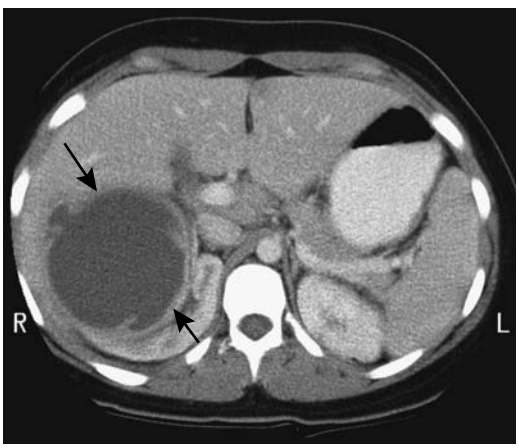

Figure 10.7. Right renal abscess. Contrast-enhanced CT reveals a huge fluid-filled structure at the superior pole of the right kidney (arrows). It was drained percutaneously. (Courtesy of Patrick Fultz, M.D., University of Rochester.)

The imaging differential for most intrarenal abscesses includes a hemorrhagic or infected cyst and a cystic neoplasm.

Pyonephrosis

Pyonephrosis defines an obstructed and infected renal collecting system. Invariably renal parenchymal damage due to acute pyelonephritis is also present. Clinically these patients range from being asymptomatic to being in septic shock. Stones account for most distal obstructions. Pyonephrosis is not clinically evident in some and only an obstructed urinary tract is suspected until aspiration provides the diagnosis.

In a rare patient infection leads to gas within the excretory system, called *emphysematous pyelitis*. This condition must be differentiated from bladder reflux, recent instrumentation, or a bowel fistula, conditions that can also introduce gas into the renal excretory system.

The affected kidney usually shows little or no function. Urine in pyonephrosis tends to have increased CT attenuation. At times gray-scale US detects hyperechoic debris or gas, although in many patients only hydronephrosis is found.

An occasional pyonephrosis ruptures and results in a perinephric abscess. Even rarer is for such rupture to result in generalized peritonitis.

Fungal Infection

Urinary fungal infections are encountered with increasing frequency both because of the wider use of broad-spectrum antibiotics and an increasing number of immunocompromised patients. The most common organism is *Candida albicans*, followed by *Torulopsis glabrata*. Some fungal infections develop bilaterally.

Most renal candidiasis occurs in a setting of systemic involvement. Typically numerous abscesses are scattered throughout the kidneys, similar to bacterial infections. Occasionally collecting system involvement results in a fungus ball, an appearance similar to an intraluminal tumor, but a fungus ball moves with a change in patient position and can even obstruct outflow. Fungus balls tend to be heterogeneous and hypodense, with no contrast enhancement, while US reveals a hyperechoic tumor with no posterior acoustic shadowing (31).

Tuberculosis

Most urinary tuberculosis is due to hematogenous spread. At times the primary site is not identified, although active or inactive lung disease is found in a majority. Although initially both kidneys are infected, disease often progresses unilaterally.

Among 57 patients with urogenital tuberculosis, fever, anorexia, and weight loss were evident only in 11%, 16% had an isolated genital lesion, and, surprisingly, 14% presented with renal failure (32); bacilluria was identified only in 5%. These patients have a sterile pyuria, microscopic hematuria, and an acidic urine. The diagnosis is confirmed by urine culture, a procedure taking up to 4 weeks. At times US-guided aspiration is helpful in establishing the diagnosis. A polymerase chain reaction to detect mycobacterial DNA has a high sensitivity and establishes the diagnosis.

Urography was abnormal in 80% of affected individuals, with the most frequent abnormality being a nonfunctioning silent kidney found in 40% (32).

Focal infections, or tuberculomas, develop initially. Tuberculomas tend to be hypointense on both T1- and T2-weighted MRI, provided they contain no calcifications, hemorrhage, or fibrosis. These either resolve spontaneously or enlarge, become necrotic, and communicate with the collecting system, spreading infection distally. Imaging at this stage reveals irregular, necrotic, and moth-eaten papilla, at times mimicking papillary necrosis due to other causes. Some calyces become obstructed due to infundibular stenosis. Strictures range in location from calyces to ureters, leading to obstruction and further damage. Cortical scarring, calyceal distortion, and strictures with caliectasis develop. In some, CT simply identifies small hypodense tumors along the renal cortex (33). Ulcerations, abscesses, and fibrosis dominate the late stages of infection. Extension of infection outside the kidney leads to perinephric abscesses. Calcifications vary from curvilinear to diffuse, from homogeneous to granular. If neglected, eventually the small, calcified kidney loses all function.

Ureteral involvement results in a shaggy, irregular lumen. A dilated ureter ensues with ureterovesical junction obstruction. In time, the ureter wall thickens, ulcers develop, and extensive fibrosis leads to foreshortening. Ureteral calcifications are uncommon, thus aiding in distinguishing tuberculosis from the more common ureteral calcifications found in schistosomiasis.

Some patients with bladder trigone involvement develop upper tract obstruction and eventually renal function is lost even if the obstruction is relieved by stenting or a percutaneous nephrostomy; a kidney can deteriorate from an acceptable pretherapy glomerular filtration rate to becoming nonfunctional after relief of an obstruction. Predictors of renal recovery after diversion are an adequate residual renal cortex and a glomerular filtration rate of >15 mL/min.

At the more advanced stages CT and urography should suggest the diagnosis. In some patients xanthogranulomatous pyelonephritis is in the differential. At times a tuberculous kidney develops a fistula to an adjacent organ.

Schistosomiasis

Schistosomiasis generally affects the lower portion of both ureters. Involvement is usually bilateral and results in stenosis and a thickened ureteral wall. Often multiple strictures are evident and proximal ureteral dilation develops. Early in the course a contrast study often reveals soft tissue polyps. Calcifications develop with chronic infection and have a characteristic linear appearance; a diagnosis of schistosomiasis can be strongly suggested if such calcifications are seen in a young adult from endemic regions.

Curiously, in distinction to bladder involvement, ureteral schistosomiasis is not associated with a high risk of ureter cancer.

Echinococcal Cyst

Although uncommon, hydatid cysts do occur in the kidneys, with *Echinococcus granulosus* being more common than *Echinococcus multilocularis*. In rare instances renal cysts develop bilaterally. Ureteral cysts are rare. No age group is immune, including children.

Patients are often asymptomatic until the pressure on an adjacent structure or cyst rupture develops. Rupture into a collecting system leads to hydatiduria and possible renal colic due to cyst debris.

Figure 10.8. Primary renal hydatid disease. Unenhanced CT reveals a hypodense tumor in the left kidney. Peripheral daughter cysts and calcifications are evident. (*Source:* Polat P, Kantarci M, Alper F, Suma S, Koruyucu MB, Okur A. Hydatid disease from head to toe. RadioGraphics 2003;23:475–494, with permission from the Radiological Society of North America.)

Extensive cyst wall calcifications are common. A typical appearance is a calcified tumor compressing the pelvicalyceal system or ureter, at times identified even with conventional radiography. Similar to the liver, some cysts contain mural nodules (Fig. 10.8). The presence of a solid component within a cyst mimics a renal cell carcinoma. At times "sand" is detected in the dependent portion of a cyst. Daughter cysts lead to a multiloculated appearance. In time, calcified daughter cysts result in a cysts-within-a-cyst appearance, a finding suggesting the diagnosis.

Most hydatid cysts have mixed echogenicity on US.

As in the liver, percutaneous drainage of renal hydatid cysts is a therapeutic option.

Brucellosis

Brucellosis is rare in the kidney. These infections range from acute focal brucella nephritis, to a focal brucelloma, to diffuse. All ages are affected.

Actinomycosis

Renal actinomycosis is readily confused with a malignancy, leading to a nephrectomy. Percutaneous needle aspiration tends to be nondiagnostic. Some patients require several explorations and numerous intraoperative biopsies to establish a correct diagnosis.

Similar to other sites, renal actinomycosis often progresses to extensive fistulas, including renoenteric fistulas. This chronic infection is a cause of retroperitoneal fibrosis and obstructive uropathy.

Botryomycosis

Botryomycosis, or a chronic bacterial infection consisting histologically of abscesses containing bacteria-bearing granules, is rare in the kidney. Most often *Staphylococcus aureus* is involved. The imaging appearance in some patients mimics a renal cell carcinoma. The diagnosis consists of detecting aggregates of organisms in sulfur-like granules within an abscess or urine. These granules should not be confused with actinomycosis.

Leishmaniasis

Infestation with protozoan parasites of the genus *Leishmania* ranges from cutaneous lesions to fatal systemic involvement. In southern France, *Leishmania infantum* is endemic, is carried by sand flies, and causes infantile leishmaniasis (Mediterranean visceral leishmaniasis).

Leishmaniasis of the genitourinary tract is rare. Its imaging appearance mimics pyonephrosis caused by more common organisms.

Filariasis

Chyluria, or white urine, is a complication of filarial infection, found most often in tropical regions. It is probably due to focal lymphatic rupture into collecting systems. In temperate climates chyluria is due to retroperitoneal malignancy, trauma, or chronic infection resulting in lymphatic obstruction.

Pedal lymphoscintigraphy using Tc-99m–sulfur colloid detects retrograde lymph flow into the kidneys.

Chyluria due to filariasis was successfully treated by endoscopic coagulation of suspected rupture sites, most often in a caliceal fornix (34).

Viral Infection

Hantavirus infection leads to an interstitial hemorrhagic nephritis, occasionally progressing to acute tubular necrosis (discussed in a later section). Some evidence suggests that *Hantavirus* infection is a risk factor for subsequent renal hypertension.

Chronic Pyelonephritis (Nephropathy)

Chronic pyelonephritis is not a single disease but rather a convenient description of a number of related entities. Pathologists tend to subdivide chronic pyelonephritis into interstitial and granulomatous varieties, with the latter including such entities as xanthogranulomatous pyelonephritis, malacoplakia, and renal tuberculosis.

An association between vesicoureteral reflux, urinary tract infection, and subsequent renal damage is well known, with such terms as *reflux nephropathy* and *postinfectious nephropathy* applied to this condition. If unchecked, renal injury has the potential to progress to overt end-stage renal failure.

Vesicoureteral reflux in children progressing to intrarenal reflux leads to renal damage (intrarenal reflux implies reflux into ducts of Bellini). Reflux into collecting tubules is more common in compound papillae, which in turn are more often located in the renal poles. Thus intrarenal reflux and clinical chronic pyelonephritis progress to loss of renal parenchyma, typically at the renal poles, manifesting with imaging as renal scarring. Scarring results in inhomogeneous contrast enhancement and is also detected with DMSA scintigraphy. With progression, scarring eventually evolves into small, lobulated kidneys, distorted and clubbed calyces, and renal cortical juxtapapillary scarring, findings that are readily detected, although whether a small kidney is secondary to chronic damage due to vesicoureteral reflux or whether it represents congenital renal hypoplasia cannot be ascertained.

With enough loss of renal function, a noninvolved contralateral kidney becomes hypertrophic. At times normal residual parenchyma in a focally diseased kidney also undergoes compensatory hypertrophy.

Problems arise in detecting progression of renal damage. Neither IV urography nor US nor scintigraphy provides an accurate quantitative assessment of residual normal renal tissue. Computed tomography and probably MR can measure remaining renal parenchymal volume and thus provide prognostic data.

Xanthogranulomatous Pyelonephritis

Xanthogranulomatous pyelonephritis is an atypical, chronic renal inflammation often progressing to parenchymal destruction. It ranges from focal, where it mimics a neoplasm, to diffuse, but bilateral involvement is uncommon. With some, fistulas develop into surrounding structures, including the colon (35). It can evolve into an adjoining abscess. The involved kidney enlarges and either functions poorly or is nonfunctioning. Women are more often affected; it occurs in children, where this diagnosis is often not considered. In fact, in children xanthogranulomatous pyelonephritis and resultant end-stage pyelonephritis are not uncommon causes for a nephrectomy.

Histology reveals an inflammatory infiltrate containing large lipid-filled macrophages (xanthoma cells), fibrosis, and fat necrosis if the perirenal fat is involved. An uncommon association is with an underlying malignancy.

A common clinical presentation is anemia, leukocytosis, and flank pain. A majority of patients have urinary obstruction due to nephrolithiasis, at times even a staghorn calculus. Urography and US reveal calculi, hydronephrosis, or a renal tumor, findings that are nonspecific. Computed tomography findings include renal enlargement, usually the presence of a calculus, scattered hypodense regions representing obstructed calyces and other fluid-filled cavities, and, at times, extrarenal phlegmon extension. Chemical-shift MR aids in detecting fat. The kidney does not function with diffuse involvement. Inflamed tissue surrounding a cavity often enhances with contrast. An occasional fistula develops, including a renocolic fistula.

A minority of patients present with a tumoral form mimicking renal carcinoma, with imaging often suggesting a neoplasm, and even producing a vena cava thrombus. A biopsy is often nec-

essary to establish a diagnosis. In general, many of these patients eventually undergo a nephrectomy. There can be, however, total renal recovery on antibiotic therapy alone.

Malacoplakia

Malacoplakia is an uncommon chronic inflammatory condition (chronic tubulointerstitial nephritis) characterized by round intra- and extracellular inclusions known as Michaelis-Gutmann bodies. Histology reveals large, foamy, granular macrophages with eccentric nuclei and prominent nucleoli containing laminated inclusions. Macrophage dysfunction appears to be the underlying pathogenesis. Its relationship to xanthogranulomatous pyelonephritis remains conjecture.

Malacoplakia affects a number of organs, with the urinary tract being the most common site. It develops in debilitated and immunocompromised patients. Some patients have had renal transplants. It is more common in women. Ureteral involvement is less common than renal. Occasionally it develops bilaterally. Recurrent *E. coli* infection is often detected. Inflammation tends to spread to adjacent structures. Needle biopsy is often diagnostic.

Contrast CT identifies variable enhancement of a soft tissue or partly cystic tumor or multiple tumors. Calcifications are not a feature of this condition. Hydronephrosis develops with extensive ureteral involvement.

Gallium-67-citrate scintigraphy reveals renal uptake; serial Ga-67 scanning identifies decreased uptake or complete resolution after antibiotic therapy, and this test appears useful in establishing an end point to therapy.

When extensive, malacoplakia mimics a neoplasm, inflammation, or even ureteritis cystica. An occasional scenario is that imaging detects a ureteral tumor, a carcinoma is suspected, and a nephroureterectomy is performed; malacoplakia is diagnosed only on histologic examination of the resected specimen.

Erdheim-Chester Disease

Erdheim-Chester disease, an uncommon systemic histiocytosis, is discussed in more detail in Chapter 14. Although retroperitoneal involvement is common, perirenal complications are unusual and often consist of ureteral obstruction. Because tissue manipulation tends to exaggerate fibrosis, surgery should be avoided in these patients and obstruction treated with an endoprosthesis, if possible.

One patient with long-standing extraperitoneal Erdheim-Chester disease developed renal arteries stenosis, bilateral ureteral stenosis, and an adhesive capsulitis (36).

Sjögren's Syndrome

Renal involvement is subclinical in many Sjögren's patients. Yet the reverse is also true; at times renal involvement, including severe hypokalemia, is the initial manifestation of Sjögren's syndrome. When present, it most often manifests as a tubulointerstitial nephritis or renal tubular acidosis and stone disease, including nephrolithiasis and nephrocalcinosis.

An inflammatory tumor develops occasionally. These tumors tend to be heterogeneous and hypodense with CT and hyperechoic with US. Differential diagnosis for such a tumor includes infection, infarction, and a malignancy.

Sinus Lipomatosis

At times a portion or almost the entire kidney is replaced by fat, most often unilaterally, called *replacement lipomatosis*. Rarely, perirenal or even periureteral tissues are also involved. Many of these patients have a long history of chronic infection, calculi, and renal atrophy. An obstructing calculus is identified in some, and these kidneys often have decreased function or are nonfunctioning. Xanthogranulomatous pyelonephritis, in particular, is often associated with lipomatosis, yet these are two distinct entities. Little evidence suggests a neoplastic association.

Histology reveals renal parenchymal atrophy and extensive replacement lipomatosis, in distinction to the large lipid-filled infiltrating macrophages found in xanthogranulomatous pyelonephritis

The involved kidney enlarges. Renal sinus fat is exaggerated and replaces atrophied parenchyma. This extensive fat deposition is identified by CT and US and aids in differentiating replacement lipomatosis from the infiltrative xanthogranulomatous pyelonephritis. At times the overall appearance suggests a fat-

containing neoplasm, but the latter generally results in little parenchymal atrophy.

Tumors

The Indeterminate Renal Tumor

Wide use of imaging techniques has led to a rise in the number of incidentally detected renal tumors. Although many are not associated with any clinical signs and symptoms and although most are shown to be simple renal cysts, a number are neoplastic and thus present a diagnostic dilemma. Imaging classification of some of these is straightforward, but others are indeterminate in their appearance. In particular, tumors <1 cm in diameter are difficult to characterize by imaging, and the literature provides little guidance about their management. Initial annual imaging appears reasonable to establish whether growth occurs, but such an approach is based more on intuition than on any hard data. In the very young, the very old, and those with a limited life expectancy, an argument can be made for watchful waiting. Imaging and possible therapy of a small indeterminate renal tumor in a young adult poses a dilemma; if US is nondiagnostic for a simple cyst, an argument can be made for CT follow-up and resection only if it grows.

In general, CT and MR can readily distinguish between a benign cyst and a malignancy. More problematic is differentiating solid tumors—a renal cell adenoma, carcinoma, oncocytoma, metastasis, lymphoma, and other less common tumors tend to have a similar appearance. The differential diagnosis often also includes inflammatory conditions, some hemorrhagic or infected renal cysts, abscesses, and some vascular abnormalities. Imaging often cannot reliably distinguish between these conditions, with the exception of angiomyolipomas. A small but heterogeneous tumor generally represents a cancer, keeping in mind that CT shows some cancers to be homogeneous. At times CT suggests focal inflammation in a solid tumor by detecting peripheral rim contrast enhancement. Perinephric infiltration is found with both inflammatory conditions and lymphomas.

Most cancers tend to be hypoechoic on US; hyperechoic tumors range from angiomyolipomas, some cancers and an occasional adenoma. Hypervascular tumors are generally cancers but hypovascular tumors include cancers, adenomas, angiomyolipomas and even an occasional hemorrhagic cyst.

Phase-inversion tissue harmonic imaging is superior to B-mode US in study of focal kidney lesions (37); it achieves greater image quality, lesion conspicuity and better fluid-solid differentiation than B-mode US.

A renal tumor believed to contain a cystic component is best approached with US; many of these are identified as simple cysts. Complex cysts, however, are indeterminate with US and require further evaluation. Contrast CT, and lately MRI, are preferred for a tumor containing a solid component. If needed, scintigraphy using a cortical imaging agent distinguishes functioning renal tissue from nonfunctioning neoplasms. If the tumor is still indeterminate, biopsy provides a histopathologic diagnosis for most but not all solid tumors, although with current imaging few indeterminate renal tumors need a biopsy.

Among renal tumors suspicious for being malignant on CT, a majority appear heterogeneous on T2-weighted images and enhance on dynamic MRI. An occasional one does not enhance, primarily due to hemorrhage, but even these tend to be heterogeneous on T2-weighted images (38).

The role of 2-[18F]-fluoro-deoxy-D-glucose (FDG)-PET in evaluating indeterminate renal cysts is not defined, and currently insufficient evidence exists to suggest it for the study of indeterminate renal tumors.

Nonneoplastic

Ectopic Splenic Tissue

Ectopic splenic tissue within the kidney can mimic a solid tumor. A radionuclide spleen scan should suggest the diagnosis.

Lobar Dysmorphism

Renal lobar dysmorphism is a normal developmental variant that simulates a renal tumor. Some are detected incidentally by imaging. They range from intrarenal to peripelvic in location. Contrast CT can suggest the diagnosis; during the corticomedullary phase the oval-shaped lobar dysmorphism is detected in the perihilar

medulla, while the nephrogram phase reveals accumulation of contrast within pyramids.

Inflammatory Pseudotumor

Inflammatory pseudotumors, of controversial pathogenesis, are rare in the kidneys or ureters (this condition is discussed in Chapter 14). Imaging identifies a soft tissue tumor.

Rosai-Dorfman Disease (Sinus Histiocytosis)

A rare benign entity first described in 1969, Rosai-Dorfman disease consists of sinus histiocytosis with massive lymphadenopathy, although several patients with bilateral renal infiltration by inflammatory cells, including histiocytes, and without adenopathy, have been described.

Ultrasonography in one patient revealed large, heterogeneous hypoechoic renal tumors containing calcifications (39); postcontrast CT showed less homogeneous tumor enhancement than renal parenchyma and no invasion, but collecting system distortion was evident.

Hamartoma

A cystic hamartoma of the renal pelvis is a rare tumor consisting of fibroblasts, smooth muscle, and epithelial tissue. Some mesoblastic nephromas reported in the literature may represent cystic hamartomas. These cystic tumors develop adjacent to the renal pelvis and are detected by most imaging.

Angiomyolipomas are discussed later in this chapter (see Mesenchymal Neoplasms).

Fibroepithelial Polyp

The benign fibroepithelial polyp contains epithelium and stromal tissue. Whether these polyps represent a hamartoma or are part of a reactive postinflammatory process is debatable. Most occur in the renal pelvis. Some develop a thick stalk covered by normal overlying transitional epithelium. Anecdotal reports describe multiple ureteral fibroepithelial polyps. They should be differentiated from papillomas, which are neoplastic in origin. They are rare in children.

Clinically, these polyps bleed or the patient presents with pain due to obstruction.

Intravenous urography and CT identify an intraluminal polyp. Some of these tumors are rather large and fill almost the entire renal pelvis. These polyps are a cause of ureter obstruction and the resultant hydronephrosis. An occasional one is cystic and contains septa.

Ureteral fibroepithelial polyps tend to mimic transitional cell carcinoma. The radiographic and ureteroscopic appearance of a ureteral rhabdomyosarcoma suggested a benign fibroepithelial polyp (40).

Vascular Tumors

Arteriovenous Malformation

Arteriovenous malformations develop in both the kidneys and the ureters. They are a cause of hematuria, which at times is massive.

Imaging findings of some renal arteriovenous malformations are similar to those of renal cell carcinomas. Some renal arteriovenous malformations are misdiagnosed with CT as a solid tumor, suggesting a malignancy.

Hematuria due to an arteriovenous malformation can generally be controlled by transarterial embolization and ablation; hematuria can recur and these malformations are amenable to retreatment; complications include varying degrees of renal infarction, pulmonary embolism, and renin-dependent hypertension.

Hemangioma

Most renal hemangiomas occur as part of Sturge-Weber syndrome or Klippel-Trénaunay syndrome. They are not common. Both capillary and cavernous varieties occur, but cavernous ones are more common. Most renal hemangiomas are discovered incidentally, with an occasional one manifesting by bleeding.

Imaging usually suggests a solid renal tumor similar to a renal cell carcinoma. An occasional one occurs at the renal hilum or even renal capsule.

Papillary Endothelial Hyperplasia

Precontrast CT of renal intravascular papillary endothelial hyperplasia (*Masson's tumor*) revealed a 3-cm perirenal hypodense tumor, while dynamic CT identified peripheral enhancement during an early phase and homoge-

neous enhancement during delayed phase (41); the appearance mimicked a hemangioma.

Cystic Nonneoplastic Conditions

Classification

Some of the renal tumors having a cystic component detected with imaging are listed in Table 10.4. Discussed in this section are the more common cystic renal conditions. Cystic hamartomas have already been mentioned. Various cystic neoplasms are covered later in their respective sections.

The Bosniak system of classifying cystic renal masses is based on their CT appearance (Table 10.5). It is of practical use. Cysts in category II contain one to two thin septa; if in doubt, a category III cyst should be considered, which has a more complex gradation, is indeterminate, and many need a histologic diagnosis. About half or so of category III cysts are malignant. Solid nodules in a cyst (category IV cyst) enhancing with contrast imply a malignancy. Aspiration is indicated of cysts in category IV, and if the aspirate is bloody a neoplasm is likely. A chronic renal abscess is in the differential for a category IV cyst. A study of patients with cystic renal tumors from two teaching institutions found that all resected Bosniak category I and II tumors were benign and category IV tumors were malignant (43); on the other hand, 59% of category III tumors were malignant.

Table 10.4. Renal cystic tumors

Simple cyst
Complex cyst
Hemorrhagic cyst
Infected cyst
Dialysis acquired cysts
Congenital cystic disorders
Multicystic dysplasia
Autosomal dominant polycystic disease
Autosomal recessive polycystic disease
Glomerulocystic disease
von Hippel-Lindau disease
Tuberous sclerosis
Ehlers-Danlos syndrome
Congenital megacalyces
Focal hydronephrosis
Calyceal diverticulum
Pyelogenic cyst
Urinoma
Infection/inflammation
Papillary necrosis
Cystic renal pelvis hamartoma
Cystic neoplasms
Multilocular cystic nephroma
Cystic carcinoma
Vascular causes
Aneurysm
Renal vein varices
Arteriovenous malformations
Hematoma
Hemangioma

Table 10.5. Bosniak system of classifying cystic renal masses

Category I	Simple cyst
Category II	Mildly complicated but clearly benign Thin septa, few calcifications
Category III	More complicated cyst—indeterminate, need histological diagnosis Thicker septa, multilocular, increased density, more calcifications
Category IV	Cystic neoplasm Thick walls, enhancing soft-tissue component

Source: Adapted from Bosniak (42).

The Bosniak classification does have limitations; some minimally complex cystic renal tumors contain malignant cells; some malignant tumors in categories II and III have contrast enhancement of less than 10 HU. In general, category II cysts are better evaluated with CT than US. Magnetic resonance imaging and renal angiography have a role in defining Bosniak category II and III cysts, but even here diagnostic confidence is at times difficult, especially with smaller cystic tumors.

The Bosniak classification has been applied using MR imaging criteria. In general, CT and MR imaging findings are similar, but in some cysts MR depicts additional septa, thicker cyst wall and septa, or different enhancement patterns, resulting in upgrading of the Bosniak classification (44).

A primary imaging function both for cysts and solid tumors is to differentiate intrarenal

from extrarenal ones, a task not always possible. Capsular tumors are one example, yet at times even a retroperitoneal lesion adjacent to the kidney mimics an intrarenal neoplasm. A rare mucinous cystadenoma originating in retroperitoneal tissues can suggest a renal cyst.

Simple Cyst

Clinical

Simple renal cysts are present in about 10% of the population. They are not common in children but increase in size and number with age. Their pathogenesis is unknown. Most simple cysts are solitary, unilocular, and located in the cortex, with the more central ones known as parapelvic cysts. Perinephric cysts are those located beneath the renal capsule. The terms *parapelvic* and *perinephric* cyst are useful to describe a cyst's location. Exoparenchymal cysts are larger and have a greater tendency to increase in size than endoparenchymal cysts.

Most simple cysts are detected incidentally. Some larger ones are associated with hematuria or flank pain.

Imaging

A simple cyst should have a sharp, well-defined margin at its interface with normal renal parenchyma. Simple cysts do not have thick walls or prominent septa. Likewise, no associated soft tissue mass should be present. Many of these cysts are defined by US, but any suggestion of an associated solid component or wall thickening requires CT, or, in some instances a biopsy. Some benign cysts have thin, linear calcifications corresponding to the cyst wall or septa. Any mottled or amorphous calcifications should be viewed with suspicion. Septa in a benign cyst should be uniformly thin.

Computed tomography attenuation of a simple cyst should be that of water. A density greater than 10 HU suggests a complex cyst. Higher densities are seen with hemorrhage into a simple cyst. Infection results in a thickened wall. Compared to an unenhanced density, the attenuation coefficient of a cyst should increase by no more than 10 HU during the corticomedullary and parenchymal phases (45). Any greater enhancement or nodularity should raise suspicion for a malignancy. However, a caveat is in order: a renal cyst attenuation increase up to about 10 HU postcontrast is often due to an artifact from surrounding parenchymal enhancement (46).

With gray-scale US a simple cyst should show an anechoic lumen, well-defined walls, acoustic enhancement posterior to the cyst, and no associated nodularity or wall thickening. Thin septa may be identified, findings often not seen with CT.

The differential diagnosis for a "simple cyst" detected by gray-scale US includes an obstructed calyx, calyceal diverticulum, papillary necrosis, an aneurysm, and a vascular tumor. A pseudoaneurysm mimics a cyst on gray-scale US, and Doppler US is necessary to differentiate between them; Doppler US shows no flow, thus excluding a vascular lesion (except a thrombosed one).

Similar to other nonflowing fluid of water density, a simple cyst is hypointense or almost has a signal void on T1- and is hyperintense on T2-weighted MRI. It does not enhance postcontrast. The cyst wall should be imperceptible; otherwise a more complex cyst etiology should be suggested.

Therapy

A high recurrence rate is common after aspiration of a simple cyst. Typical therapy consists of percutaneous injection of a sclerosing agent, with repeat injection if a cyst recurs. Use of 95% to 98% alcohol is effective and leads to complete regression of most cysts, except those >10 cm in diameter. One technique consists of catheter insertion under US control, cyst drainage and sampling for bacteriologic and cytologic study, cyst opacification with contrast, instillation of roughly half the cyst volume of ethanol, and clamping for 20 minutes. Some authors prefer two sequential sclerosing agent injections over a 48-hour period. Local infiltration or intravascular injection results in lysis of cell membrane, protein denaturation, local vascular occlusion, and cell death.

Laparoscopic decortication of simple renal cysts is effective therapy for pain relief. Such therapy must be limited to Bosniak categories I and II cysts with their low risk for cancer.

In an occasional hypertensive patient, drainage of a simple cyst corrects hypertension; rather than ascribe hypertension directly to the

cyst, it is more likely that the cyst had compressed and narrowed an adjacent renal artery.

Parapelvic Cyst

Radiologists describe a cyst located in the renal sinus region, adjacent to renal pelvis, as a *renal sinus cyst* or *parapelvic cyst*. Most are simple cysts. Many of these cysts presumably form by prior urine extravasation or are embryologic lymphocysts. Most are detected as an incidental finding, but an occasional one compresses the adjacent renal pelvis sufficiently to produce some degree of obstruction. They vary in size, and range from solitary to multiple and unilateral to bilateral.

These cysts mimic a portion of the renal collecting system on precontrast imaging and do not enhance on postcontrast CT. Delayed images postcontrast identify the lack of communication with the urinary collecting system. At times US confuses a parapelvic cyst with hydronephrosis. An occasional one suggests a cystic neoplasm.

Complex Cyst

While a complex cyst is a pathologic entity, radiologists use the term in a descriptive sense for a cyst containing blood, septa, a thick wall, or calcifications. Complex cysts have thicker walls than simple cysts, better defined septations, a suggestion of nodularity, and calcifications may develop, or they do not contain clear fluid. Occasionally a fluid–fluid level develops in a cyst after a recent hemorrhage. Differentiation from a simple cyst is one of gradation. Thus bleeding or infection in a simple cyst changes cyst fluid composition and leads to wall thickening. From an imaging viewpoint, the major importance of a complex cyst is its mimicry of a malignant cyst.

The risk of a complex cyst being malignant increases with imaging findings of more complex structures; thus discrete cyst wall thickening, irregular septations, or any nodularity points toward a cystic malignancy, and aspiration of such a cyst serves little purpose; even if a benign aspirate is obtained, such a cyst should be assumed to contain a malignant component.

Increased fluid echogenicity is generally secondary to blood or infection.

Delayed postcontrast CT is occasionally helpful in differentiating a homogeneous complex renal cyst from a neoplasm; those showing no change in attenuation between initial postcontrast and delayed CT are most consistent with a cyst, but cysts showing an attenuation decrease suggest presence of vascularity (47).

Pre- and postcontrast MR is helpful in evaluating complex cysts, although the MR appearance of benign and malignant complex cysts overlaps. Cyst content varies considerably in intensity on precontrast T1- and T2-weighted images due to different protein concentrations, but cyst content should not enhance postcontrast. In particular, a complex cysts containing a heterogeneous MR fluid signal intensity should be viewed with suspicion for a malignancy. Cysts with an irregular, thick cyst wall or mural nodules tend to be malignant.

An occasional cyst is more dense than renal parenchyma on precontrast CT. These hyperdense cysts contain old blood, milk of calcium, or a similar component. In fact, a cyst may not be suspected because of the hyperdense CT appearance; US should reveal their cystic nature. These cysts may contain internal echoes. While some of these cysts may be followed serially, an occasional cystic renal carcinoma also has a hyperdense CT appearance.

Infected Cyst

An infected cyst often develops a discrete, thickened wall. Gas or debris is part of the cyst content in some. Septations develop in both infected and hemorrhagic cysts.

Most suspected infected cysts are drained both for therapy and to exclude an underlying malignancy.

Hemorrhagic Cyst

In adults, hemorrhage into a benign renal cyst is relatively common. It is rare in children. Nevertheless, caution is required in ascribing hemorrhage to an underlying benign cyst; hemorrhage also occurs into renal cell carcinomas, especially in patients with renal failure.

Computed tomography of a hemorrhagic cyst reveals a hyperdense cyst. Cyst content does not enhance postcontrast. Gray-scale US

shows increased internal echoes. If followed serially, findings should regress with time. In an occasional hemorrhagic cyst both CT and US suggest a solid tumor, and these cysts are generally resected.

T2-weighted MRI within days of hemorrhage into a cyst reveals a hypointense signal. Later, hemorrhage results in a hyperintense signal on both T1- and T2-weighted images. Some hemorrhagic cysts contain a fluid–fluid level. A benign cyst should have a very thin wall.

Lymphangiectasia

Renal lymphangiectasia (also called *lymphangiomatosis* and *lymphangiomas* when cystic) is considered to be a lymphatic developmental malformation, although some authors believe inflammation and lymphatic blockage are inciting factors while still others classify it as a mesenchymal neoplasm. A rare familial association is described. These cysts are lined by endothelial cells. They are rare in the kidneys. Most affected patients are asymptomatic, but pain or hematuria is an occasional presentation. A rare association is with renal vein thrombosis.

Detected mostly in children and young adults, renal lymphangiectasia is one of the causes of an enlarged kidney. Lymphangiomas appear as multicystic tumors, peripelvic or perinephric in location. Rather than being cystic, at times diffuse perinephric fluid is identified. This fluid is close to water density, except if tainted by hemorrhage. Aside for an often more peripheral location and perinephric fluid, imaging findings tend to mimic multilocular cysts found in more common disorders.

In some, lymphangiectasia is associated with a preserved rim of renal cortex and decreased medullary attenuation. Ultrasonography reveals a hyperechoic kidney. Computed tomography and US findings suggest the diagnosis (Fig. 10.9). Aspiration of chyle from perinephric fluid should be diagnostic.

Localized Cystic Disease

Localized cystic disease of the kidney is a descriptive term for a condition that cannot be readily classified. These patients had unilateral multiple cysts varying in size, separated by normal renal parenchyma, and contained in a larger nonneoplastic tumor (48). No family history of autosomal-dominant polycystic kidney disease is found. Hematuria or flank pain is a usual presenting symptom. Imaging reveals one or several cysts in a larger tumor, at times suggesting a cystic neoplasm.

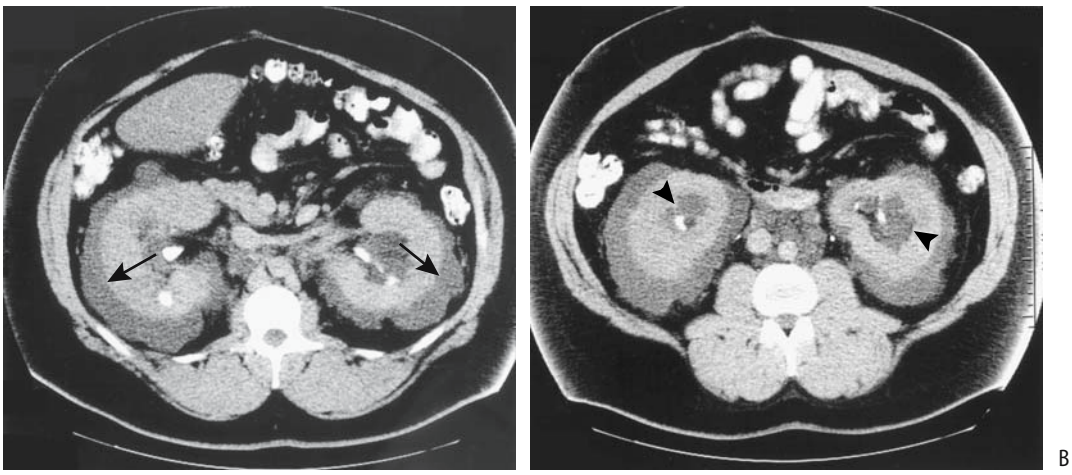

A B

Figure 10.9. Renal lymphangiectasia. A,B: Transverse contrast-enhanced CT images show bilateral perirenal fluid (arrows), peripelvic fluid (arrowheads), and fluid around great vessels. Attenuation of the perinephric collections is less than 10 HU (*Source:* Ramseyer LT. Case 34: renal lymphangiectasia. Radiology 2001;219:442–444, with permission from the Radiological Society of North America.)

Renal Cell Adenoma and Adenocarcinoma

Throughout this book most benign and malignant neoplasms are discussed as separate entities, but such differentiation is impractical with renal cell adenomas and carcinomas. Whether a renal adenoma is a separate and distinct entity or whether it is a premalignant version of a renal cell carcinoma is debatable. Indeed, pathologic criteria defining a renal cell adenoma are not clear and while clinically a distinction is obviously desirable, both pathologically and radiologically the boundaries between renal cell adenomas and adenocarcinomas are blurred. Tumors smaller than about 3 cm tend not to metastasize, and some investigators believe these represent mostly adenomas. From an imaging viewpoint it appears best to discuss these tumors as part of a spectrum.

The term *hypernephroma* is often used synonymously for a renal adenocarcinoma. An older term, *Grawitz tumor*, is rarely encountered.

Classification

One practical classification of renal cell adenomas and carcinomas is based on their primary morphological features (49):

1. Clear cell type carcinomas
2. Chromophil (papillary) adenomas and carcinomas
3. Chromophobe adenomas and carcinomas
4. Duct of Bellini carcinomas
5. Oncocytic adenomas (oncocytoma)
6. Metanephroid adenomas
7. Transitional cell carcinomas
8. Neuroendocrine carcinomas

Tumors originating from proximal tubules (clear cell and chromophilic cell types) make up approximately 85% of renal cancers (49); tumors from connecting tubules and ducts (chromophobic, ducts of Bellini, and oncocytic) make up about 11%. Others are rare.

Collecting duct carcinomas occur in a wide age range and are more common in males. They are centered in the renal medulla but infiltrate extensively, and many patients already have metastases at initial presentation. Classification of these carcinomas is incomplete. Renal medullary carcinomas associated with sickle cell trait (discussed later) are also collecting duct neoplasms.

One limitation of a morphologic classification as outlined above is the heterogeneity of some of these tumors. To overcome this, the Heidelberg Classification of Renal Cell Tumors was developed in 1996, based on tumor genetic properties correlated with their histologic findings (50); this classification subdivides renal cell tumors into benign and malignant parenchymal neoplasms. Benign tumors are further classified into metanephric adenomas and adenofibromas, papillary renal cell adenomas, and oncocytomas. Malignant tumors are classified into conventional renal cell adenocarcinoma, papillary (chromophil) renal cell carcinoma, chromophobe renal cell carcinoma, and collecting duct carcinomas. Some of these tumors cannot be readily classified. Others represent separate entities.

At times helical CT findings can suggest a particular subtype. Clear cell carcinomas have greater contrast enhancement than chromophil (papillary), chromophobe and duct of Bellini carcinomas (51); chromophobe carcinomas tend to have homogeneous contrast enhancement. Calcifications are more common in chromophil and chromophobe carcinomas than in other types. The latter tend not to invade venous structures.

Clinical Aspects

General

Discussed in the next few sections are the clinical, imaging, and therapeutic aspects of the most common type of renal cell carcinoma, namely clear cell adenocarcinomas. Cystic carcinomas, chromophil carcinomas, and others are covered in later sections.

No specific serum markers are available for renal cell carcinomas. Renal cell carcinomas do not produce α-fetoprotein, with an occasional exception. Although of limited sensitivity and specificity, a radioimmunoassay of tumor-associated trypsin inhibitor appears promising.

Renal cell carcinomas are not common in children; their prevalence increases with age. When detected in childhood, these tumors tend

to be at an advanced stage. Yet prognosis appears favorable even at this stage.

Hematuria is still the primary presentation for about 60% of these tumors; a minority present with systemic symptoms or a paraneoplastic syndrome. Flank pain or a palpable mass is found in a minority.

Paraneoplastic Syndrome and Systemic Manifestations

Renal cell carcinoma is associated with several paraneoplastic manifestations. A nephrogenic liver dysfunction syndrome without jaundice (*Stauffer's syndrome*) or cholestatic jaundice develops in some patients.

Some renal cell carcinomas produce hormones that have their own manifestations. These include renin (hypertension), parathormone (hypercalcemia), erythropoietin (erythrocytosis), gonadotropin (gynecomastia), and adrenocorticotrophic hormone (Cushing's syndrome). Hyperglycemia is rare. Hypercalcemia occurs in a number of clinical settings, including such malignancies as lung, breast, ovary, squamous cell, and renal, and some hematologic cancers. Hypercalcemia is rare with other genitourinary malignancies.

Some patients with proven renal cell carcinoma and without an obvious cause of serum alkaline phosphatase elevation, such as metastases or other liver or bone diseases or pregnancy, have an elevated phosphatase level, probably due to a paraneoplastic syndrome. In some patients alkaline phosphatase normalizes after nephrectomy, and metastases develop later without phosphatase elevation.

Etiology

Several syndromes are associated with familial renal cell carcinomas, with the best known being von Hippel-Lindau disease. Renal cell carcinomas in this disease tend to be multicentric and bilateral.

Hereditary papillary renal cell carcinoma is probably in a distinct class of inherited malignancies. Germline missense mutations, allelic losses and duplications of certain chromosomes, and mutation of the *VHL* gene occur in some renal cell carcinomas. Involved individuals appear to exhibit an autosomal-dominant transmission with reduced penetrance. A number of these hereditary renal cell cancers are detected incidentally in asymptomatic individuals. Currently a patient presenting with bilateral, multiple, or an early onset of renal cancer should be investigated for von Hippel-Lindau disease and possibly other syndromes. Birt-Hogg-Dubé syndrome, probably familiar only to dermatologists, appears to be associated with familial renal tumors, including oncocytomas and papillary renal cell carcinomas (52).

Patients in chronic renal failure undergoing dialysis who then develop acquired cystic kidney disease are at increased risk of developing renal cell carcinomas. These cancers tend to be hypovascular and difficult to detect early in their course.

Exposure to certain chemicals increases the risk of developing renal cell carcinoma. Thus long-term exposure to trichloroethylene, an industrial solvent, leads to an increased incidence of these tumors. Patients exposed to high and cumulative doses of this solvent have mutations in the *VHL* gene. An association exists between the number of mutations and the severity of exposure to this solvent (53); the mutations are often multiple and show a loss of heterozygosity.

Radiation therapy–induced renal cell carcinoma is rare. In the few reported patients, radiotherapy occurred several decades earlier.

With the increased survival seen after therapy for childhood neuroblastomas, these patients appear to be at increased risk for subsequent renal cell carcinoma.

Associated Conditions

A synchronous second primary is uncommon, with anecdotal reports describing double primary tumors of the kidney and ovary. A higher than expected synchronous association appears to exist between renal cell carcinoma and non-Hodgkin's lymphoma. A greater than expected risk of a metachronous second primary also exists in these patients, with the most frequent second neoplasm being in the gastrointestinal tract.

Renal cell carcinoma is association with renal cystic diseases, including simple renal cysts, acquired cystic diseases of the kidney, multilo-

cular cysts, and occasionally even polycystic kidney disease.

Incidental Tumor

Most studies suggest that incidentally discovered renal cell carcinomas tend to be smaller, are more often localized to the kidney, show less vascular invasion, and are of a lower tumor stage, and these patients have greater survival compared to a symptomatic tumor. Some studies suggest, however, that no prognostic differences exist for the same tumor stage. Practically, numerous exceptions exist and it is difficult to generalize.

Over the last several decades the number of incidental renal cell carcinomas detected has increased considerably, while deaths from renal cancer have decreased. A kidney-sparing operation is now much more often feasible than in the past. Of interest is that the examination most responsible for discovering an incidental tumor is US.

Multicentric Tumors

Renal cell adenomas and carcinomas occur bilaterally and are often multicentric (Fig. 10.10). Multiple synchronous renal cell carcinomas occur in von Hippel-Lindau disease and the acquired cystic conditions developing in end-stage renal disease. The reported prevalence of multicentricity varies, ranging from 10% to almost 50%. Whether a relationship exists between multicentricity and the size or stage of a primary tumor is not clear, realizing that whether a partial or total nephrectomy is performed is often based on the size of the carcinoma.

A rare patient is found to have multiple renal cell adenomas or adenomatosis. This condition is more common in a setting of end-stage renal disease.

Growth

Renal cell carcinomas tend to be relatively slow-growing tumors. Typical tumor volume doubling time is over 1 year; on the other hand, metastases grow considerably faster, and the microenvironment appears to play a role in their growth rate. Because of their slow growth, watchful waiting appears appropriate for some of these patients. Nevertheless, tumor size is related both to tumor stage and survival, with larger tumors generally being of an increased stage and associated with a worse prognosis; keep in mind that some very large renal cell carcinomas tend to have a favorable prognosis.

Rare spontaneous regression of a renal cell adenocarcinoma is reported. Most contain calcifications or a cystic, necrotic cavity and few viable carcinoma cells.

Screening

Several sonographic screening studies have eventually led to a renal cell carcinoma diagnosis in <0.2% of healthy adults. Most detected hyperechoic renal tumors are angiomyolipomas, with others being some other tumor, a cyst, or simply a normal variant.

Pathologic Study

Renal adenomas are defined as those having a low nuclear grade tubulopapillary histology, and <5 mm in diameter (54); most are located in the cortex and have a discrete border. Autopsy studies commonly identify what appear to be cortical adenomas. Pathologists use the term *renal cortical neoplasm of low malignant potential* for similar low-grade histology but slightly larger tumors (54).

Renal cell carcinomas show considerable histologic variability. Many adenocarcinomas have varying degrees of tubular differentiation. Some are difficult to classify. Some require immunohistochemical staining and electron microscopy for adequate evaluation.

One grading scheme consists of applying the worst grade that occupies more than 10% of a tumor; the presence of a higher grade, the number of satellite tumors, and vein invasion are directly proportional to tumor size. Thus small carcinomas tend to contain more grade 1 carcinomas, with their frequency decreasing with increasing tumor diameter as grade 3 cancers increase in frequency; venous involvement and risk of metastases also correlates directly with tumor size. Multifocal carcinomas are also more prevalent in larger tumors. Necrosis, hemorrhage, and cystic degeneration are common in larger cancers. They invade locally, spread to regional lymph nodes, and metastasize mostly hematogenously.

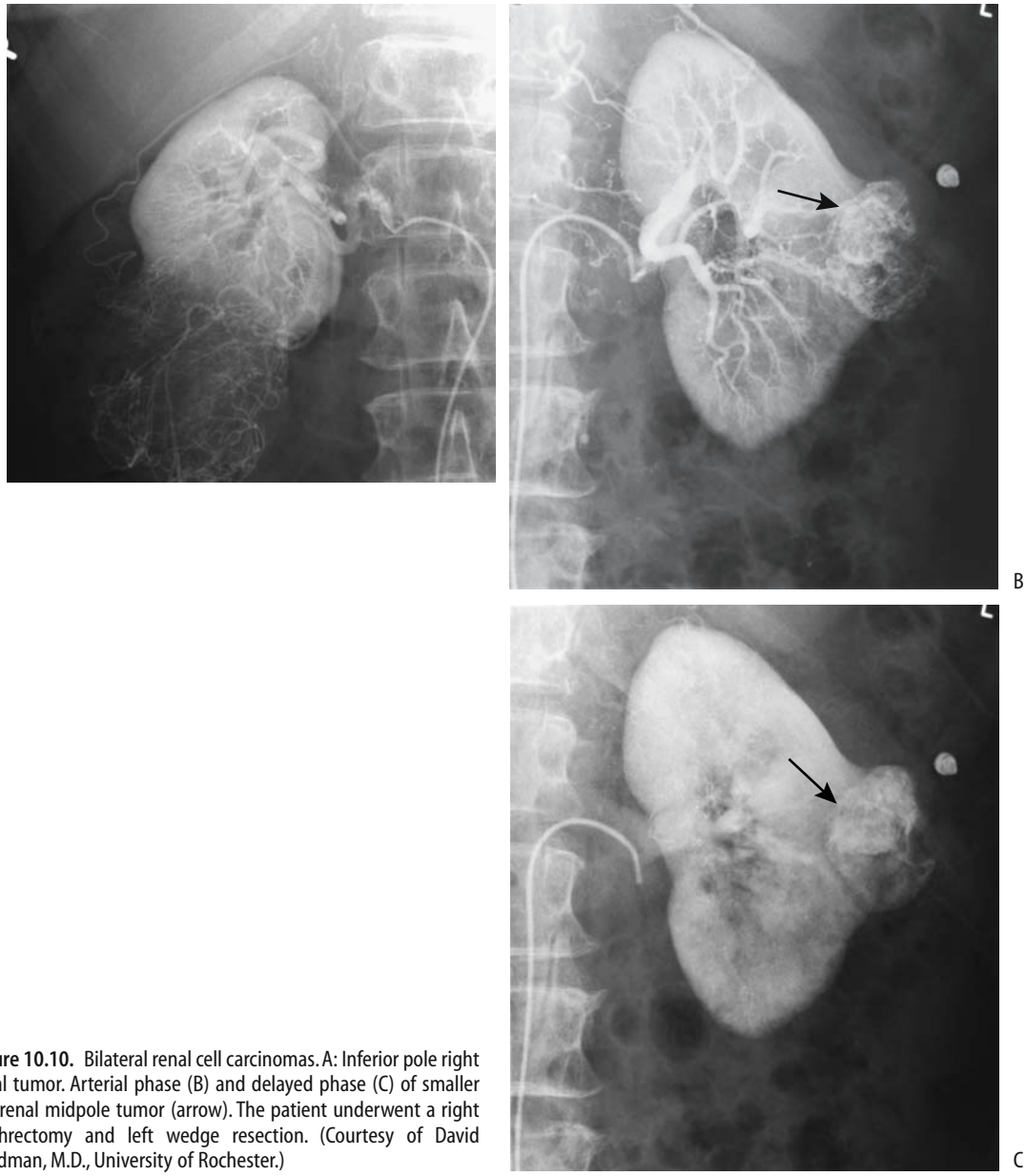

Figure 10.10. Bilateral renal cell carcinomas. A: Inferior pole right renal tumor. Arterial phase (B) and delayed phase (C) of smaller left renal midpole tumor (arrow). The patient underwent a right nephrectomy and left wedge resection. (Courtesy of David Waldman, M.D., University of Rochester.)

Some renal cell carcinomas contain intracellular lipid and glycogen; the clear cell appearance of chromophobe carcinomas is due in large part to such lipid content. In fact, fat staining for intracellular lipid is an established technique to identify renal cell carcinomas in urine cytology specimens. This lipid is rarely detected by CT, but needs to be taken into account with more sensitive MR studies.

Detection

One problem in comparing results from different studies is that often renal cell carcinomas are not subclassified into subtypes, yet the subtype affects not only its imaging appearance but also the prognosis. For instance, the MR appearance of most clear cell carcinomas is different from that of papillary cell carcinomas. And not all of

these tumors are malignant, thus affecting prognostic considerations.

Although hematuria has numerous causes, generally a neoplasm needs to be excluded and both upper and lower urinary tracts must be studied. Traditionally, IV urography was the initial study for the upper urinary tracts but it has been supplanted in some institutions by US, although the documentation for such a change is rather weak. In either case, if one study is negative and a bladder tumor has been excluded, then the other study is indicated. Some investigators believe that with a negative first study, CT should be the second study, but here also firm evidence is lacking. With an ambiguous first study, on the other hand, CT seems reasonable.

A minority of renal cell carcinomas contain calcifications, with the prevalence increasing with tumor size. Calcifications range from punctate to linear and are located either in the center or on the periphery. Peripheral calcifications are seen more often in association with cysts but do occur in cystic adenocarcinomas. Calcifications are less common in most other solid renal tumors, and detection of calcifications makes a renal cell carcinoma more likely.

Renal function tends to be preserved except with very extensive tumors. Lack of function should suggest renal vein thrombosis.

Using current imaging techniques, in general, any solid non–fat-containing renal tumor should be considered malignant. Adenomas have a similar imaging appearance to that of carcinomas (Fig. 10.11). Serial follow-up is problematic because some renal cell carcinomas show little or no size change over a year or more. Renal cell cancers tend to be larger, are more round and more encapsulated than metastases. Enlarged perirenal lymph nodes, on the other hand, are more common with metastases.

Ultrasonography is generally the first imaging test obtained in children with a palpable abdominal tumor. Except for a suspected cystic tumor, either contrast CT or MRA is obtained next.

Computed Tomography

Computed tomography is considered to be accurate in detecting renal tumors. Some studies have reported CT sensitivities and specificities >98% in detecting these tumors, but enthusiasm for these high percentages should be tempered by an inherent build-in patient selection bias. Detection varies with tumor size, with a majority of tumors <5 mm not detected.

Because most renal cell carcinomas originate from the cortex, a renal contour bulge is common. On precontrast CT most small tumors are isodense to renal parenchyma. Larger tumors tend to necrose and bleed and are heterogeneous in appearance. Postcontrast, carcinomas exhibit variable CT enhancement,

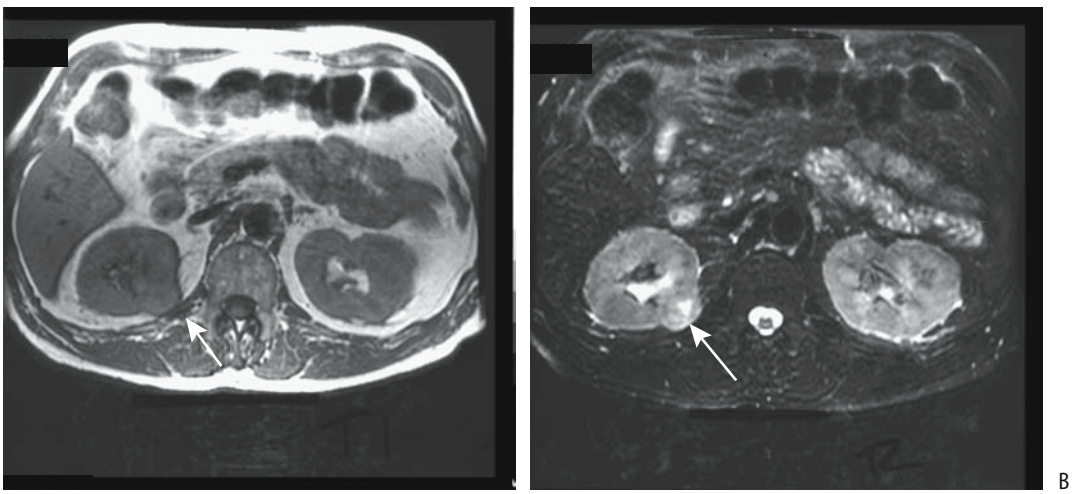

A B

Figure 10.11. A renal adenoma (arrows) is isointense on T1- (A) and T2- (B) weighted MR images. (*Source:* Burgener FA, Meyers SP, Tan RK, Zaunbauer W. Differential Diagnosis in Magnetic Resonance Imaging. Stuttgart: Thieme, 2002, with permission.)

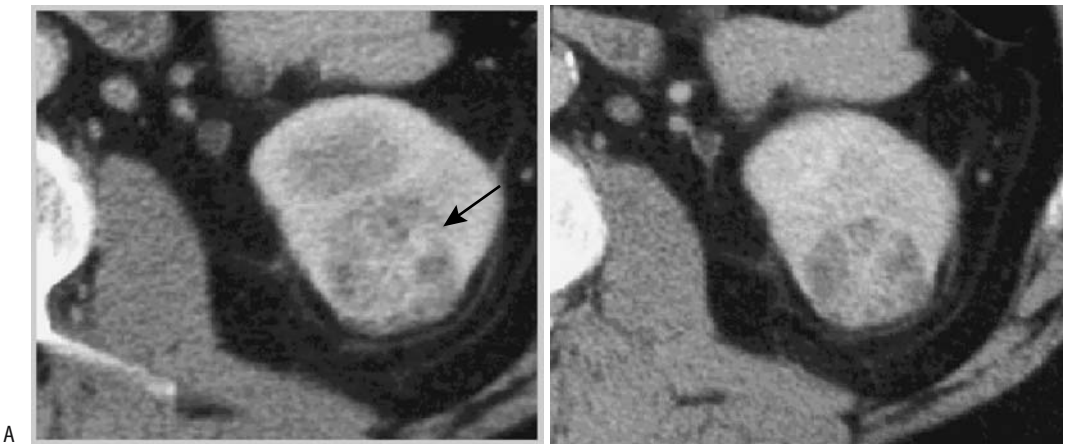

Figure 10.12. Clear cell renal cell carcinoma. A: Corticomedullary phase CT shows a heterogeneously enhancing tumor (arrow.) B: Nephrographic phase CT better defines tumor. (*Source:* Szolar DH, Kammerhuber F, Altziebler S, et al. Multiphasic helical CT of the kidney: increased conspicuity for detection and characterization of small (<3 cm) renal masses. Radiology 1997;202:211–217, with permission from the Radiological Society of North America.)

generally less than normal renal parenchyma (Figs. 10.12 and 10.13). Small tumors tend to have homogeneous contrast enhancement, while larger ones are heterogeneous. A nonenhancing central scar surrounded by an irregular enhancing rim is found in some. Larger tumors tend to have an indistinct margin between the tumor and the adjacent normal parenchyma. A not uncommon appearance for a renal carcinoma at initial presentation is that of a large hypervascular tumor having inhomogeneous contrast enhancement.

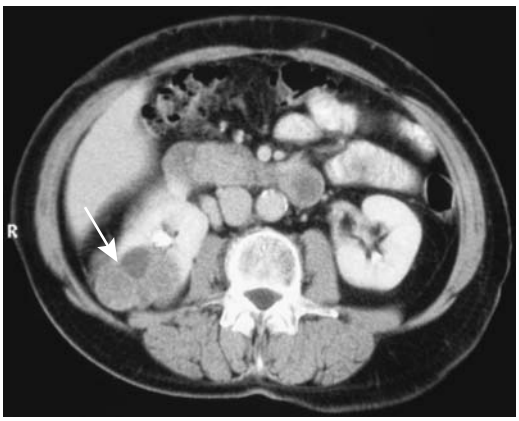

Figure 10.13. Right renal cell carcinoma. Computed tomography identifies a poorly enhancing tumor (arrow). (Courtesy of Algidas Basevicius, M.D., Kaunas Medical University, Kaunas, Lithuania.)

Computed tomography often detects collateral renal capsular veins, and at times even gonadal vein collaterals. These collateral veins are a manifestation of the extensive high-flow state and arteriovenous shunting present in many of these highly vascular tumors; they tend to be more prominent with larger tumors. An arteriovenous fistula is detected in some cancers.

A common assumption is that radiographically visible fat does not occur in a renal cell carcinoma, and the presence of fat, if detected by CT, essentially excludes a carcinoma. Yet exceptions do occur. Some renal cell carcinomas encase adjacent fat. Metaplasia within a necrotic tumor results in fat. The presence of fat is even more relevant with MR studies (discussed later).

Ultrasonography

Renal cell carcinomas range from hypoechoic to hyperechoic compared to normal renal parenchyma. Acoustic shadowing is not found. Smaller tumors tend toward a hyperechoic appearance, and US cannot differentiate small renal cell carcinomas from angiomyolipomas. An anechoic or hypoechoic rim is detected in a minority of solid renal cell carcinomas, a finding not seen with angiomyolipomas. Con-

trast enhanced second harmonic US detected a rim of perilesional enhancement, mostly in the tardive phase, in 86% of renal cell carcinomas but not in noncarcinomas (55).

Doppler US detection of blood flow within a cyst suggests a malignancy. Hypervascularity, intratumoral high flow arterial signals, and a high pulsatility index within a complex cyst also suggest a malignancy. Some inflammatory tumors, however, have similar findings; also, hypovascular malignancies will be missed. In particular, small tumors are difficult to characterize.

Magnetic Resonance

Magnetic resonance is useful in renal cancer detection and preoperative evaluation when other imaging modalities are limited by artifacts or the use of iodinated contrast agents is contraindicated. Current MRI techniques achieve accuracies in renal tumor detection and characterization similar to those of CT.

Small renal cell carcinomas tend to be hypo- to isointense on T1-weighted MR images and iso- to hyperintense on T2-weighted images; regions of high signal intensity on precontrast T1-weighted images represent intratumoral hemorrhage, while hypointensity on T2-weighted image is caused by hemosiderin, hemorrhage, or necrosis. Considerable intensity variation exists, however, and some small tumors are missed on noncontrast images (Figs. 10.14 and 10.15). Larger tumors tend toward a heterogeneous appearance. The use of gadolinium improves tumor detection and characterization. Postcontrast, carcinomas <3 cm in diameter range from hypervascular (enhancement greater than that of renal cortex) to hypovascular (56), while those >3 cm tend more toward hypovascularity.

Some renal cell carcinomas contain sufficient fat that they undergo a loss of signal intensity on chemical shift opposed-phase MRI (Figs. 10.16 and Fig. 10.17); generally insufficient fat is present to be detected by CT. Magnetic resonance findings in these tumors overlap those seen with little or no fat-containing angiomyolipomas, and thus the dictum that renal cell adenocarcinomas rarely contain fat should be modified when applied to MR. These intracellular lipid-containing carcinomas are mostly chromophobe (clear cell) carcinomas, and thus chemical shift imaging tends to differentiate them from other renal cell carcinomas. Chemical shift gradient-echo MRI reveals a significantly higher signal loss in clear cell carcinomas compared to non–clear cell carcinomas (57); a significant correlation exists between specimen fat staining and signal loss. Signal intensity loss on opposed phase images is not seen with all clear cell carcinomas and even in

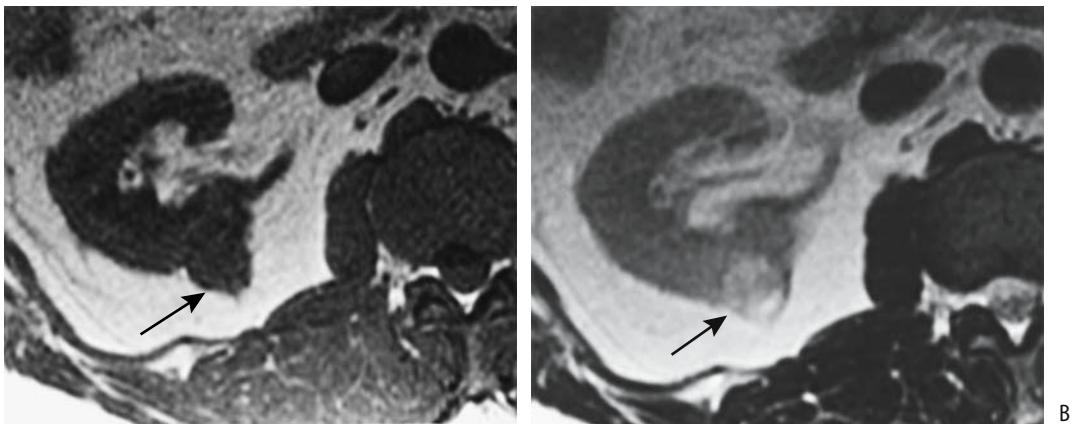

A B

Figure 10.14. Small alveolar renal cell carcinoma in posterior aspect of right kidney (arrows). The tumor is isointense on T1-weighted (A) and hyperintense on T2-weighted (B) MRI. (*Source:* Shinmoto H, Yuasa Y, Tanimoto A, et al. Small renal cell carcinoma: MRI with pathologic correlation. J Magn Reson Imaging 1998;8:690–694, with permission of Wiley-Liss, a subsidiary of John Wiley & Sons.)

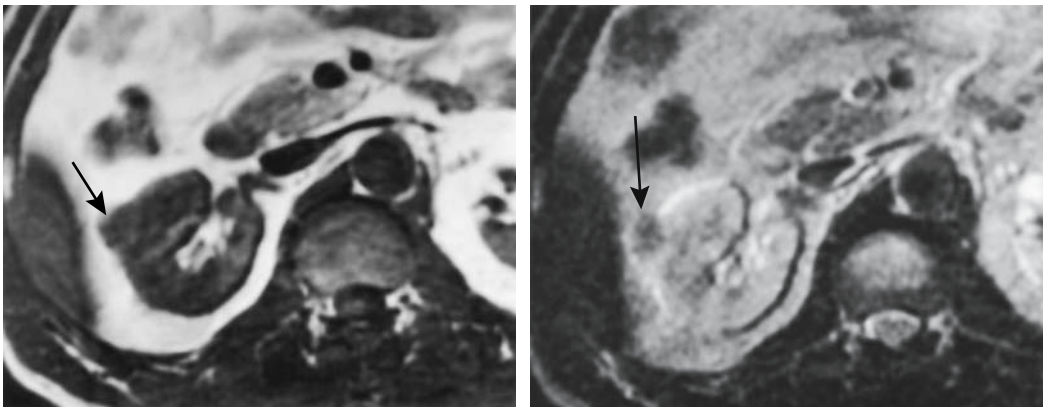

Figure 10.15. Small papillary renal cell carcinoma (arrows). The tumor is somewhat isointense on T1-weighted (A) and hypointense on T2-weighted (B) MRI. (*Source:* Shinmoto H, Yuasa Y, Tanimoto A, et al. Small renal cell carcinoma: MRI with pathologic correlation. J Magn Reson Imaging 1998;8:690–694, with permission of Wiley-Liss, a subsidiary of John Wiley & Sons.)

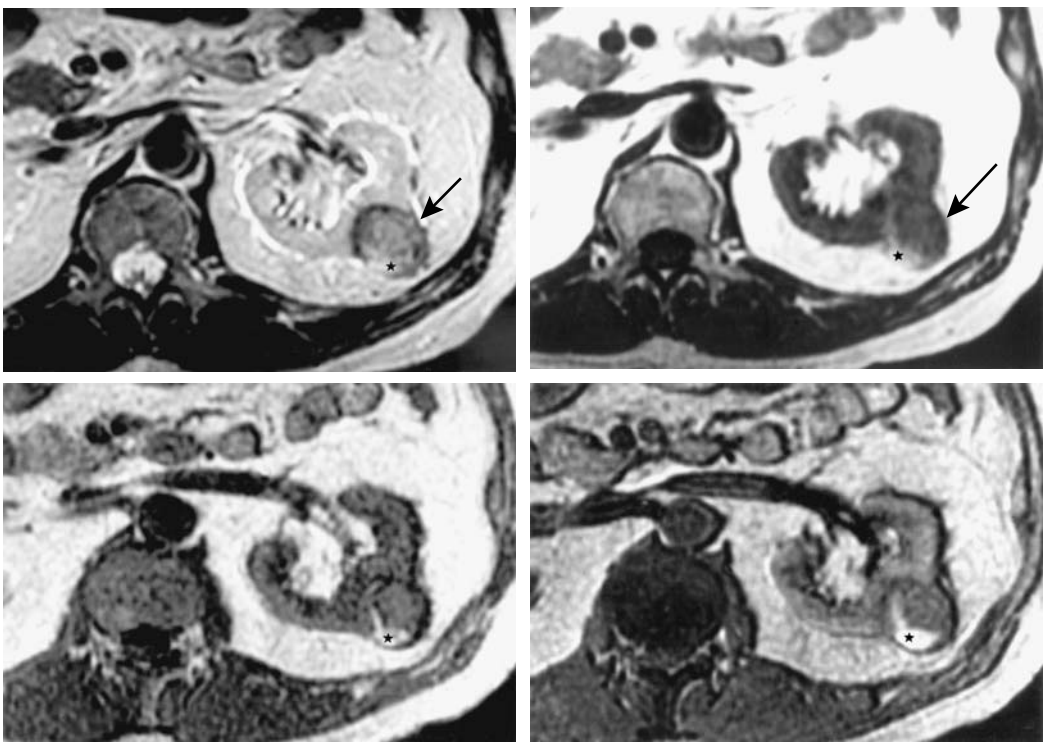

Figure 10.16. Magnetic resonance fat detection in clear cell renal cell carcinoma. T2-weighted fast spin echo (FSE) (A) and T1-weighted spin echo images (B) identify this tumor (arrow). In-phase (C) and out-of-phase (D) chemical shift gradient echo images show that it has a lower signal intensity on out-of-phase imaging. Chemical shift imaging helps identify fat within clear cell carcinomas, which differentiates these tumors from other carcinomas (*Source:* Yoshimitsu K, Honda H, Kuroiwa T, et al. Magnetic resonance detection of cytoplasmic fat in clear cell renal cell carcinoma utilizing chemical shift gradient-echo imaging. J Magn Reson Imaging 1999;9:579–585, with permission of Wiley-Liss, a subsidiary of John Wiley & Sons.)

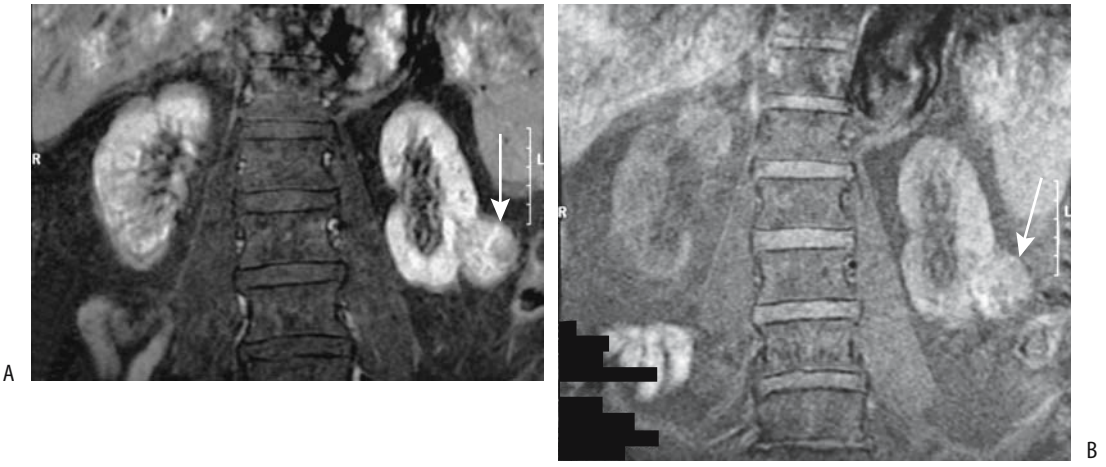

Figure 10.17. Left renal cell carcinoma. Pre- (A) and postcontrast (B) T1-weighted coronal MR images using fat suppression reveal a heterogeneous renal tumor (arrow). (Courtesy of Patrick Fultz, M.D., University of Rochester.)

any one tumor is not uniform, resulting in a heterogeneous appearance. Also regions of tumor necrosis do not lead to a signal loss.

Scintigraphy

Bone scintigraphy can be positive in a hypervascular clear cell renal neoplasm.

An FDG-PET scan detects most but not all renal cell carcinomas. Angiomyolipomas and some other tumors result in false-positive findings, and in renal cancer detection PET offers no significant advantage over other imaging modalities. Positron emission tomography depicts solid renal neoplasms as regions of increased uptake and cysts are seen as photopenic regions.

Biopsy

In most instances a renal cell carcinoma is diagnosed with imaging, and a biopsy or aspiration cytology is not obtained prior to surgery. Even tumors with an atypical imaging appearance are generally investigated surgically. In particular for small, discrete lesions, the efficacy of aspiration cytology in determining tumor pathology is limited and has led to complications.

Currently the primary role for aspiration cytology is in a nonoperable patient where a tissue diagnosis needs to be established prior to alternative therapy or if metastases or lymphoma are suspected.

Staging

General

Stage is the most important prognostic factor in renal cell carcinoma patients. Two classification systems are in use for staging renal cell carcinomas: Robson staging system, more popular in the United States and somewhat simpler to use; and the tumor, node, metastasis (TNM) system (Table 10.6). Both suffer limitations to staging accuracy and both tend to understage more often than overstage.

Lymphatic spread of renal cell carcinoma during initial detection is about 10% or less; most affected patients have advanced stage disease, distant metastases, a large tumor, and poor survival.

Imaging

Either a chest radiograph or chest CT is helpful in a search for metastases, although which of these two is preferred is debatable.

Currently helical CT is the primary staging modality used. How reliable is CT in staging renal cell carcinoma? A number of studies suggest that overall T-staging accuracy is only about 60% (58). Although of prognostic importance, the low CT sensitivity and specificity in detecting fat invasion is not crucial because perinephric fat is also resected during a nephrectomy for cancer and imaging detection of

Table 10.6. Tumor, node, metastasis (TNM) classification of primary renal cell carcinoma

Primary tumor:			
Tx	Primary tumor cannot be assessed		
T0	No evidence of primary tumor		
T1a	Tumor 4 cm or less in greatest dimension limited to kidney		
T1b	Tumor more than 4 cm but less than 7 cm in greatest dimension limited to kidney		
T2	Tumor more than 7 cm in greatest dimension limited to kidney.		
T3a	Tumor invades adrenal gland or perinephric tissues but not beyond Gerota's fascia		
T3b	Tumor invades renal vein or vena cava below diaphragm		
T3c	Tumor grossly extends into vena cava above diaphragm or invades wall of vena cava		
T4	Tumor invades beyond Gerota's fascia.		
Lymph nodes:			
Nx	Regional lymph nodes cannot be assessed.		
N0	No regional lymph node metastasis.		
N1	Metastasis in a single lymph node		
N2	Metastasis in more than one regional node		
Distant metastasis:			
Mx	Distant metastasis cannot be assessed		
M0	No distant metastasis		
M1	Distant metastasis		
Tumor stages:			
Stage I	T1	N0	M0
Stage II	T2	N0	M0
Stage III	T1	N1	M0
	T2	N1	M0
	T3	N0	M0
	T3	N1	M0
Stage IV	T4	N0	M0
	T4	N1	M0
	any T	N2	M0
	any T	any N	M1

Note: Above classification applies to clear cell renal carcinoma, papillary renal carcinoma, chromophobe renal carcinoma, and collecting duct renal carcinoma.
Source: From the AJCC Cancer Staging Manual, 6th edition (2002), published by Springer-Verlag, New York, NY, used with permission of the American Joint Committee on Cancer (AJCC), Chicago, IL.

perinephric fat invasion does not influence surgery.

Dynamic MRA is an alternate in place of CT in a setting of severe renal dysfunction, extensive polycystic kidney disease, or a contraindication to iodinated contrast media. Potentially, MR could replace CT in staging these tumors. Compared to surgical and pathologic staging, MRI using T1-, T2-weighted, gadolinium enhanced and time-of-flight sequences achieved good T and M staging, but was poor for N staging (59); MRI can readily assess venous invasion.

Both CT and MR detect adenopathy but cannot determine whether an enlarged node is secondary to inflammation or tumor. Some authors believe that CT staging accuracy for lymphadenopathy is close to chance (58). The role of MR in evaluating adenopathy and metastases continues to expand. Ultrasonography appears inferior in adenopathy detection.

A reasonable preoperative staging strategy in the occasional pregnant woman developing a malignant renal tumor consists of abdominal US and MRI to define local tumor extension and a chest radiograph to detect pulmonary metastases.

Either CT or MR is used to detect adjacent organ invasion. Bone scintigraphy has a limited role in initial tumor staging unless clinical or laboratory evidence suggests bone involvement.

Vascular Invasion

Even small carcinomas tend to invade adjacent renal vein branches, but extension as a tumor thrombus into the renal vein and inferior vena cava is uncommon for small tumors; the risk of invasion increases with tumor size, and venous extension to the right atrium is not uncommon with large tumors (Figs. 10.18 and 10.19). Obviously, detecting venous extension is important in planning resection. Imaging should also detect any anomalous vascularity. Angiography currently does not have a role in the staging of renal cell carcinomas but is occasionally performed to define blood supply and as a prelude to preoperative embolization (Fig. 10.20). Contrast CT and MRA have supplanted angiography's role both in a search for renal vein invasion and in providing a vascular road map for the surgeon (Fig. 10.21).

Even small vessel invasion affects prognosis. One of the reasons is that a tumor thrombus contains more dividing cells than a primary tumor, that is, a tumor thrombus has a shorter tumor doubling time and thus is more aggressive, a conclusion reached by comparing the proliferation index of primary renal cell carcinomas and their corresponding neoplastic thrombi (60). Patients with renal cell carcinomas exhibiting micro- or macrovascular

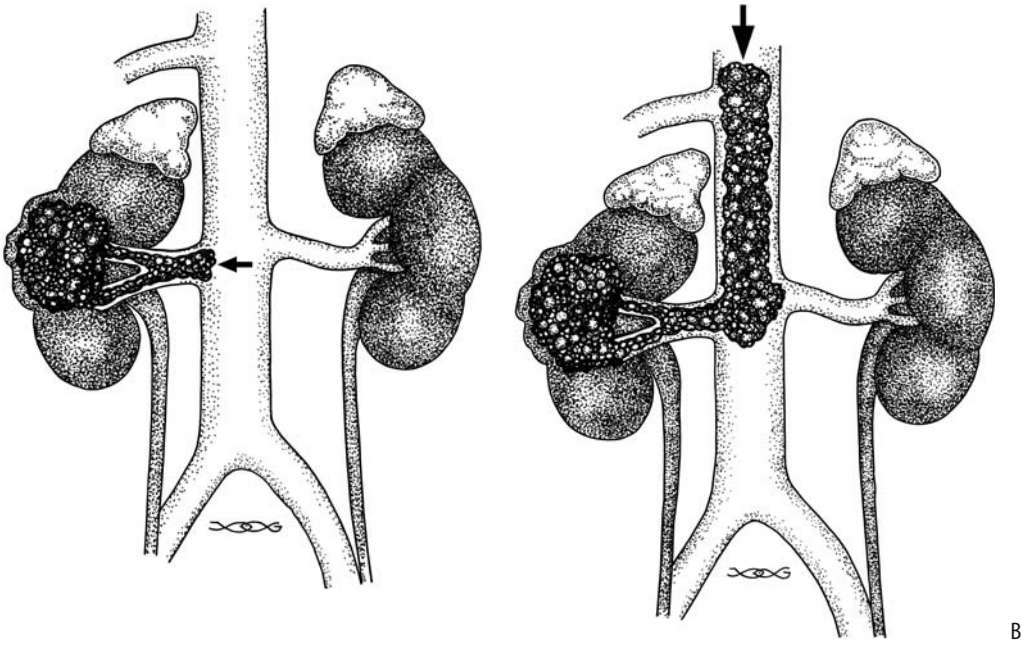

Figure 10.18. Venous extension of renal cell carcinoma. A: A cancer has invaded the renal vein to the level of inferior vena cava (arrow). B: With further growth, the cancer now extends above one of the hepatic veins (arrow).

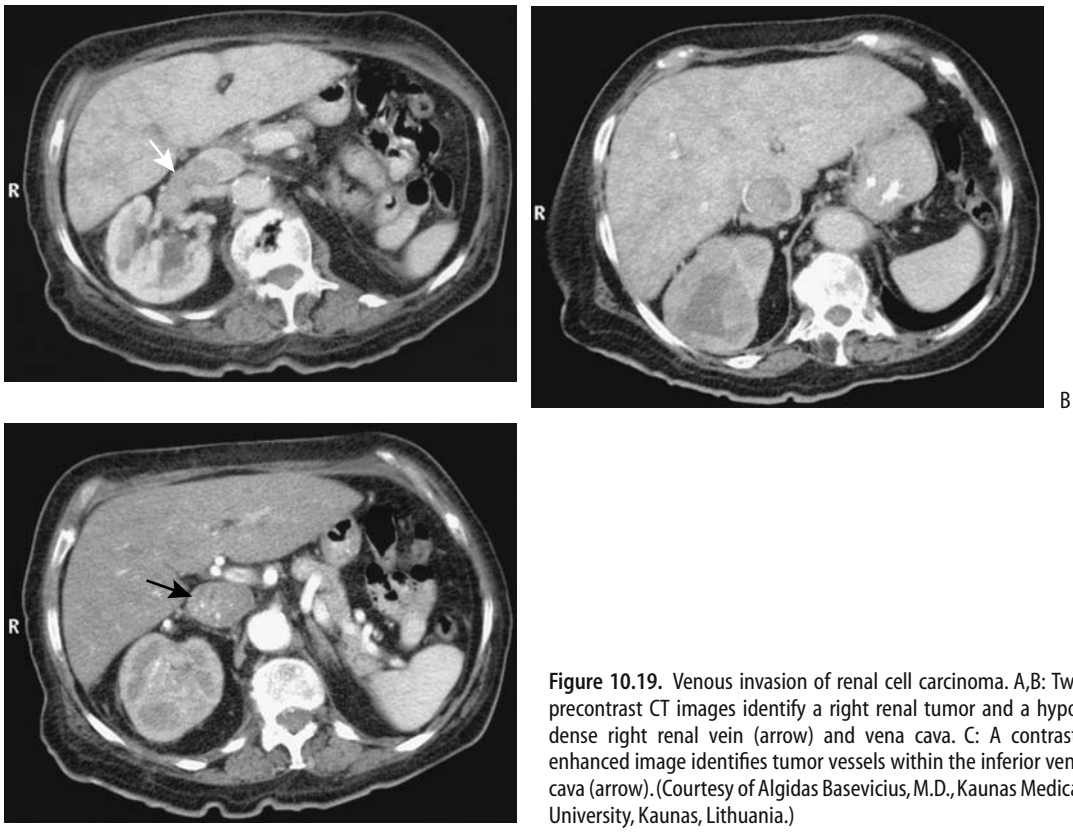

Figure 10.19. Venous invasion of renal cell carcinoma. A,B: Two precontrast CT images identify a right renal tumor and a hypodense right renal vein (arrow) and vena cava. C: A contrast-enhanced image identifies tumor vessels within the inferior vena cava (arrow). (Courtesy of Algidas Basevicius, M.D., Kaunas Medical University, Kaunas, Lithuania.)

Figure 10.20. Right renal cell carcinoma. Contrast filling and stretching of intrarenal vessels in a vascular tumor are evident. Metastases were also detected. (Courtesy of David Waldman, M.D., University of Rochester.)

invasion have a significantly worse prognosis than those without such invasion; prognosis also varies with the extent of vascular invasion. Detection of small vessel invasion is beyond the resolution of the current imaging modalities.

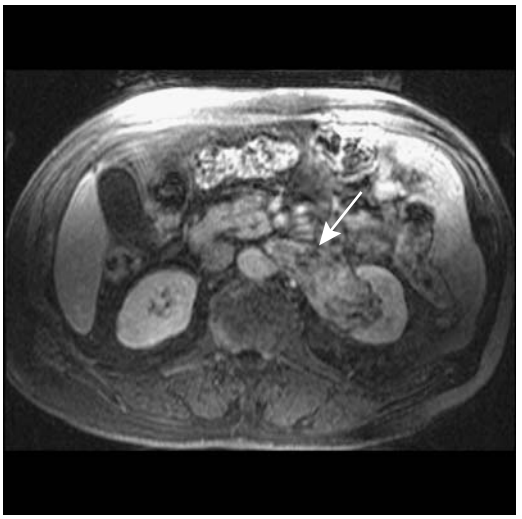

Figure 10.21. Transverse MR image reveals a left renal cell carcinoma with renal vein invasion (arrow). (Courtesy of Brian R. Herts, M.D., Cleveland Clinic Foundation.)

Figure 10.22. Coronal MR image identifies an intraluminal inferior vena cava filling defect defect (arrow) in a patient with a left renal cell carcinoma. (Courtesy of Brian R. Herts, M.D., Cleveland Clinic Foundation.)

Imaging can determine whether the inferior vena cava is simply compressed by an extrinsic tumor or whether a tumor extends intraluminally (Fig. 10.22). The extent of inferior vena caval involvement determines the type and complexity of the resection. To reduce blood loss, surgery in a setting of inferior vena cava invasion necessitates either direct caval clamping or the use of cardiopulmonary bypass. Imaging should thus identify whether a thrombus barely involves the vena cava, remains below most inferior hepatic veins, terminates between the hepatic veins and the diaphragm, or extends above the diaphragm and possibly into the right atrium. Contrast-enhanced imaging differentiates between a bland thrombus and a tumor thrombus. Invasion of the caval wall, although not common, is difficult to determine with imaging, which is unfortunate because invasion necessitates partial vena caval resection. MR is superior to both CT and US in detecting inferior vena cava tumor thrombi, although technically good CT is often adequate. CT tends not to identify the cephalad extent of a tumor thrombus.

Preoperative helical CT detects renal vein invasion with a sensitivity of >80% and a

specificity approaching 100%; reported sensitivity varies depending on whether small intrarenal venous thrombi are considered or not. False-positive results occur due to unopacified blood producing a flow void artifacts. Magnetic resonance imaging should detect all distal renal vein involvement; cavography should be considered if neither CT nor MR is satisfactory.

Ultrasonography identifies tumor venous extension as renal vein or inferior vena cava distention by echogenic material and decreased or absent flow in this segment, as detected by Doppler US. Tumors limited to the intrarenal veins account for some false-positive results. The current role of color Doppler US in detecting tumor venous extension appears to be in those patients with an incomplete or equivocal CT examination and unavailability of MR.

With a suspected carcinoma invading the inferior vena cava and possibly extending into the right atrium, transesophageal echocardiography is useful to establish the cephalad extent of a cavoatrial tumor and aid surgical management.

If needed, intraoperative US defines the extent of vena caval invasion. Ultrasonography may aid instrument placement and decrease the risk of tumor thrombus dislodgment.

Therapy

Controversy surrounds the therapy of small (<2 cm) renal cell tumors of low malignant potential. In most patients these tumors are resected (often with a nephron-sparing resection), but in a high surgical risk patient an argument can be made for CT follow-up and resection only if tumor growth ensues. Conventional chemotherapy and radiotherapy are largely ineffective for renal cell carcinomas.

Medical Therapy

Interleukin-2 is a T-cell growth factor that also enhances natural killer cell function. Its preliminary use suggests a role in metastatic renal cell carcinoma. The response appears to be greater for metastatic foci rather than for the primary renal tumor, with an objective response rate of about 15% to 30% of patients. Tumor regression is achieved in up to one third of patients, with a complete response in an occasional one. Interleukin-2 was approved by the Food and Drug Administration in 1992 for treatment of metastatic renal cell carcinoma. The response to interleukin-2 therapy is difficult to evaluate with imaging due to residual deformity. 2-[18F]-fluoro-deoxy-D-glucose—PET imaging appears useful in these patients, but if interleukin-2 therapy is contemplated, a pretherapy scan aids in establishing a baseline.

Interferons, produced by the body in response to viral infections, also have an antitumor effect due to direct cytotoxicity and activation of a number of immunologic pathways. Both recombinant α-interferon and γ-interferon, at times combined, have been used to treat metastatic renal cell carcinoma, although little data is available on the effect of interferon therapy on survival in patients with inoperable renal cell carcinoma. Preliminary results suggest prolonged survival in interferon-treated patients.

Cimetidine blocks histamine-mediated activation of suppressor T-cells and appears to have antitumor immune properties. Anecdotal reports suggest a response in some patients treated with cimetidine for metastatic renal cell carcinoma.

Resection

Refinements in surgical technique have led to more conservative surgery such as enucleation and heminephrectomy. Current experience suggests that in selected patients conservative surgery is as effective as radical surgery. With an increasing number of small tumors detected incidentally, conservative (nephron sparing) surgery achieves good long-term results. Complicating the issue, however, is multicentricity of some small tumors. Also, an invasive growth pattern, high-grade nuclear atypia, and Bellini duct carcinomas are associated with a poor prognosis. Some surgeons believe that even with a localized renal cell carcinoma radical nephrectomy has a role; it has low morbidity, excellent local tumor control, and high survival. These surgeons maintain that for patients with a normally functioning contralateral kidney, no convincing evidence exists to justify a nephron-sparing operation on a routine basis. Nevertheless, laparoscopic wedge resection of smaller renal carcinomas is successfully performed. One indication for nephron-sparing

surgery is bilateral renal cell carcinomas. Because of its high spatial resolution, intraoperative US is very useful in such a setting to better define indeterminate lesions, revealing more extensive or satellite lesions and establishing tumor margins. Intraoperative US and frozen section biopsy may spare the patient a nephrectomy.

Successful tumor enucleation implies that a tumor has a discrete border (i.e., has a pseudocapsule). Such a pseudocapsule is best defined by T2-weighted MRI and dynamic T1-weighted MRI.

Lymphadenectomy is indicated for patients with enlarged lymph nodes or a large tumor but without distant metastases and, in general, those tumors believed to be curable. On the other hand, the vast majority of patients with lymph node involvement already have additional, mostly multifocal metastases, and thus extensive lymph node dissection on a routine basis as part of a radical nephrectomy appears to have a limited effect on survival (node dissection is useful, however, for staging).

Similar to other malignancies, a postoperative imaging study is useful in establishing a baseline for detecting future tumor recurrence. Invariably, the underlying anatomy is distorted at surgery. At times imaging after a nephron-sparing operation reveals a *pseudotumor*; these tumors have round contours and enhance with contrast, resolving eventually except for a small cortical scar.

An occasional solitary metastasis is resected. Pulmonary resection for metastatic renal cell carcinoma is viable therapy for some selected slow-growing tumors.

Tumor Embolization

Need for a definitive diagnosis prior to tumor embolization or ablation therapy is obvious, yet a number of benign tumors have undergone needless therapy before a diagnosis is established. This problem appears more acute in the kidney than the liver and often revolves around nonfat-containing angiomyolipomas.

Tumor embolization is performed both as a stand-alone procedure and preoperatively. Embolization of extensive renal cell carcinomas decreases blood loss and simplifies surgery (Figs. 10.23 and 10.24). Some patients develop spontaneous renal vein-to–portal vein anastomoses, and such anastomoses need be considered prior to embolization. Aside from embolization, selective angiography aids in planning a nephron-sparing operation.

Embolization in a setting of tumor thrombus in the renal vein or inferior vena cava carries a potential risk of distal tumor embolization. A

A B

Figure 10.23. Hypervascular renal cell carcinoma. A: Arteriography reveals a right renal tumor (arrows). B: Successful embolization of the major artery feeding this tumor was performed. (Courtesy of David Waldman, M.D., University of Rochester.)

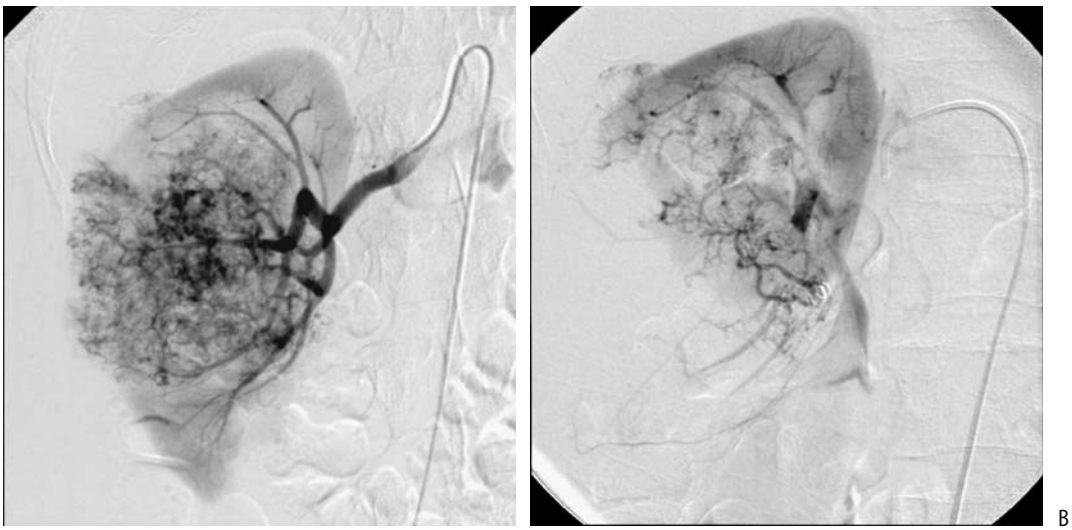

Figure 10.24. Embolization of right renal cell carcinoma. Images before (A) and after (B) renal artery spring coil embolization prior to surgery. A considerable decrease in tumor vascularity is evident, but some feeding vessels still remain. (Courtesy of David Waldman, M.D., University of Rochester.)

suprarenal inferior vena cava filter minimizes this risk.

A major role for tumor embolization is palliation of hemorrhage or pain in inoperable patients. Superselective embolization of inoperable renal tumors is occasionally performed in patients with a solitary kidney; insufficient data preclude drawing any firm conclusions about the validity of such an approach.

Other Ablation Therapy

Laparoscopic cryoablation of small renal tumors is feasible (61); the efficacy of such therapy is incompletely studied.

Percutaneous injection or coagulation therapy of renal neoplasms has lagged similar counterparts in the liver. More than in most other organs, renal neoplasm therapy has remained in the province of the urologist and generally intraoperative US guidance is used.

Feasibility of percutaneous image guided radiofrequency ablation of renal cell carcinomas has been established in poor surgical risk patients (62). Interactive MR image guided radiofrequency interstitial thermal ablation of renal cell carcinomas is a new field. A low field strength unit monitors until the tumor is replaced by a hypointense zone, identified on T2-weighted images acquired intermittently during ablation. Preliminary results are encouraging (63). One reported complication is skin metastasis at the electrode insertion site. Isolated local recurrences after radical nephrectomy are also amenable to radiofrequency ablation (64). Contrast enhanced CT immediately after ablation detects residual viable tumor. US identifies a hyperechoic interface at the junction of normal renal parenchyma and frozen tissue.

Therapy for Bilateral Tumors

Conservative surgery, such as heminephrectomies, is the initial consideration for bilateral and synchronous renal cell carcinomas. Occasionally bilateral nephrectomy and chronic dialysis is the only viable option, in which case renal transplantation should be considered.

Recurrence/Follow-Up

Renal carcinoma metastases more often are of a higher grade of malignancy than the primary rather than of a lower grade. Thus prognosis in patients with metastatic disease is based both

on primary tumor grade and on that of the metastases.

A small tumor detected on a postcancer resection imaging study is generally considered to be a recurrence or a new cancer (assuming it was not evident on preresection imaging). The presence of small synchronous renal cell carcinomas and an increased prevalence of metachronous cancers suggest that serial imaging surveillance, possibly on an annual basis, of residual ipsilateral renal tissue (if any) and the contralateral kidney is indicated.

Initially most lung metastases are asymptomatic and are detected by screening. Bone metastases, on the other hand, become symptomatic early on. Chest follow-up is with either chest radiograph or CT, with proponents advocating either one or the other. Certainly CT is more sensitive in detecting metastases both in the chest and adjacent bones (assuming bone windows are used) and more often detects the rare solitary and resectable lung metastasis. On the other hand, CT also detects benign incidental nodules, often leading to unnecessary biopsy.

Currently CT is the study of choice to detect abdominal recurrence. Ultrasonography is less sensitive than CT. Magnetic resonance imaging is rarely employed for primary screening, although preliminary evidence suggests that it is equal, if not superior, to CT in tumor detection. It has a role in select patients, such as those with an iodine allergy. Nuclear scintigraphy requires separate scanning for bone, liver-spleen, etc. Nuclear scintigraphy is currently the examination of choice in detecting bone metastases, but whether serial scans are beneficial in the absence of bone symptoms is debatable, and they are not often employed.

Rarely, a metastasis regresses spontaneously. Thus spontaneous regression of pulmonary metastases does occur. One should realize, however, that not all lung tumors in a patient with known renal cell carcinoma are metastases.

Prognosis

Based on tumor recurrence patterns, one recommended follow-up schedule is based on tumor stage: patients with stage T1 carcinoma are evaluated yearly clinically, those with stage T2 disease also have an annual chest radiograph and abdominal CT every 2 years, while those with stage T3 disease undergo abdominal CT every 6 months for the first 2 years (65).

A nephrectomy in the presence of metastases is often justified as an attempt to prolong life or improve quality of life. A cure even after resection of a solitary metastasis is not common.

Sites of Metastases

Renal cell carcinoma is unpredictable in its spread, and metastases develop to unusual sites. Most common are metastases to the lungs and bone. Metastasis to the pancreas is not rare, in spite of statements to the contrary by some authors. Some metastases are already evident at the time of initial cancer diagnosis; in fact an occasional metastasis is detected and resected even before the primary tumor site is discovered.

Spread to the adrenal glands is by either direct extension or metastasis. Direct adrenal invasion is uncommon by a superior pole tumor less than several centimeters in diameter. Some of these metastases are from a contralateral kidney, presumably hematogenous in nature.

Unlike transitional cell carcinomas, metastasis along the ipsilateral ureteral stump following a previous radical nephrectomy is rare for renal cell carcinomas.

Resection of liver metastasis is often feasible, especially with a single focus, with prolongation of survival but at a cost of a high mortality rate.

Late Recurrence

Late recurrence is arbitrarily defined as 10 years or longer postnephrectomy. Tumor recurrence years after initial therapy suggests that use of a 5-year survival time frame is too short for this tumor. Renal cell carcinoma can recur years after nephrectomy. Anecdotal reports abound of pulmonary, pancreatic, and other metastases developing many years after nephrectomy. In general, prognosis is better in those with late rather than early recurrence.

Cystic Carcinomas

About 10% of all renal cell carcinomas are cystic. Complicating the picture is that more often a solid renal cell carcinoma is associated with an incidental cyst close by, such as a simple

cyst or acquired cystic disease of the kidney. The solid component of most cystic carcinomas is located close to underlying renal parenchyma. Rarely, a carcinoma arises from the outer surface of what appears to be a simple cyst.

Cystic carcinomas are classified into several patterns: multilocular, unilocular, necrotic, and those originating in the wall of a simple cyst; histopathologically, multilocular carcinomas can be divided into macrocystic and microcystic. Macrocystic tumors appear multilocular on US and contrast-enhanced CT; angiography reveals neovascularity in most tumors. When first detected, most multilocular cystic renal cell carcinomas already have a significant cystic component. When small, however, imaging shows them to be solid, although histology of resected specimens does reveal a microcystic component. On precontrast CT, microcystic tumors range from hypodense to hyperdense depending on the amount of hemorrhage. They exhibit slight CT contrast enhancement, are hyperechoic, and do not appear cystic on US; MRI reveals high signal intensities on both T1- and T2-weighted images, and dynamic enhancement shows an irregular contrast enhancement pattern. Angiography of these small tumors typically shows little evidence of neovascularity.

Unilocular carcinomas consist of a cystic tumor containing either an irregular wall or mural nodules, detected by contrast-enhanced CT and US. Necrotic tumors range from anechoic to varying echogenicity, while their CT appearance varied from cystic with mural nodules to an irregular tumor. Neovascularity is common in viable tumor surrounding necrotic regions.

US using Levovist enhanced pulse inversion harmonic imaging shows that the thick wall of both cystic renal cell carcinomas and complex inflammatory cysts has intense contrast enhancement during the arterial phase (66).

Larger cystic renal cell carcinomas tend to have a complex cystic imaging appearance. In general, a cyst with a thick or irregular wall, prominent septa, wall calcifications, septations, or associated with an adjacent soft tissue component suggests a malignancy. Nevertheless, overlap occurs between benign complex cysts and cystic malignancies, and tumor identification is difficult. Temporal changes occur in some of these tumors. As an example, a simple renal cyst was resected; 1 year later numerous cysts encased the kidney, with cyst walls lined by a single layer of cuboidal epithelium (67). The degree of differentiation argued against a carcinoma and suggested a cystic mesothelioma, cystic lymphangioma, or even a multicystic dysplastic kidney, yet the tumor recurred repeatedly, invaded bowel, and became almost solid.

Aspiration cytology tends to be negative with cystic neoplasms, and a negative aspirate is of limited significance. A number of cystic carcinomas yield clear fluid, but this finding cannot be relied on. Comparing fluid aspirated from benign renal cysts and cysts containing a carcinoma, interleukin-6, basic fibroblast growth factor concentrations, and epidermal growth factor levels tend to be higher in malignant cysts.

Laparoscopic biopsy, followed by open resection is an option for complex cysts suspicious for cancer.

Prognosis is similar both for solid and cystic carcinomas.

Chromophil (Papillary) Adenoma and Carcinoma

Renal papillary adenomas are common renal epithelial neoplasms; most are in the several millimeter size range. Papillary renal cell carcinoma is the second most common carcinoma of the renal tubules. These neoplasms manifest an adenoma-to-carcinoma evolution, and a continuous tumor spectrum ranging from papillary adenoma to papillary carcinoma is encountered. Synchronous papillary renal adenomas and carcinomas occur. Several families of a hereditary papillary renal cancer syndrome are reported.

These tumors tend to be multifocal and bilateral. They have specific immunohistochemical and genetic features distinct from other renal carcinomas.

Detected papillary renal cell carcinomas tend to be large, well-defined, and relatively hypovascular, and tend to enhance less with CT contrast than do clear cell tumors. Some exhibit occasional short intratumoral contrast-related stranding. Computed tomography revealed nine of 10 papillary renal cell carcinomas to be rounded, well-circumscribed, and sharply mar-

ginated tumors containing central hypodense regions representing necrosis, surrounded by viable tumor seen as contrast-enhancing serpiginous tissue (68). An occasional cystic tumor contains multiple nodules. Some are associated with cholesterol necrosis and these tumors mimic an angiomyolipoma (69).

Although US detects fewer papillary tumors than CT, it aids in evaluating any cystic component.

Papillary renal tumors tend to be hypointense on T2-weighted images, often due to hemosiderin, hemorrhage, and necrosis, although hypointensity in some appears to be intrinsic to the papillary component.

These tumors often pose a diagnostic dilemma because of their benign appearance.

Chromophobe Carcinoma

A chromophobe renal carcinoma is considered a subtype of renal cell carcinoma exhibiting a low chromosome number. Histology reveals a mix of clear cells containing lipid and glycogen and eosinophilic cells.

These carcinomas occur in childhood. Prognosis is considerably better than with conventional renal cell carcinomas.

These tumors range from hypovascular to avascular. A minority of chromophobe carcinomas contain a central scar.

Duct of Bellini Carcinoma

Carcinoma of ducts of Bellini, or collecting duct carcinoma, originates from ducts of Bellini epithelium in the distal tubules located in the renal medulla. The prevalence is about 1% of all renal carcinomas.

Whether this tumor should be classified as a separate carcinoma or is a variant of a renal cell carcinoma is not clear. Histologic differentiation from a more common renal cell carcinoma is difficult, although morphologically, immunochemically, and cytogenetically it can be defined as a separate entity. Chromosome analysis suggests that molecular development of this neoplasm is different from that of a more common renal cell carcinoma. Specific tumor-suppressor genes appear to be involved in its pathogenesis. Embryologically, collecting ducts originate from the wolffian duct system, similar to renal calyces and ureters, and a point can thus be made of a relationship of this tumor with transitional cell carcinomas.

This rare, aggressive neoplasm manifests in a younger population than the more common clear cell carcinoma. It develops in children. Hematuria is a common presentation. Some patients have positive urine cytology. It is not uncommon to find metastases at the time of first presentation.

Because duct of Bellini carcinomas originate predominantly centrally in the medulla, they tend not to deform the renal outline, a finding distinguishing these tumors from more common renal cell carcinomas. Imaging shows a solid, hypodense, and hypovascular or even avascular renal tumor with limited contrast enhancement. They tend to protrude into the central sinuses.

Oncocytoma

Clinical

Some authors classify oncocytomas as a type of renal adenoma. Epithelial oncocytes have a granular eosinophilic cytoplasm rich in mitochondria. These cells are not limited to oncocytomas but are also found in granular cell carcinomas (oncocytic adenocarcinomas) and some clear cell adenocarcinomas. Oncocytomas occur in several organs, but most often are found in kidneys. Mitochondrial DNA analysis suggests that a specific mitochondrial DNA alteration is responsible for oncocytomas.

Renal oncocytomas are more common in some families. These tumors are often detected incidentally in asymptomatic individuals; some are multiple and bilateral, with a rare patient having hundreds of nodules scattered throughout both kidneys.

Renal oncocytomas are probably benign tumors consisting primarily of oncocytic cells. They appear to originate from the cortical part of collecting tubules. Their prevalence is difficult to gauge because some have been misclassified as renal cell carcinomas or chromophobe carcinomas. Especially in the older literature an occasional one has been reported to metastasize, but whether these are misclassified is difficult to gauge.

Percutaneous biopsy or cytology tends to be misleading because some oncocytomas mimic a granular renal cell carcinoma. On the other

hand, a biopsy or aspiration cytology from a region rich in oncocytes may not detect an adjacent focus of carcinoma unless extensive sampling is performed. Pathologically, a diagnosis of an oncocytoma is one of exclusion by eliminating other, more ominous, tumors.

An occasional renal oncocytoma ruptures. Adjacent fat next to such a ruptured oncocytoma can mimic an angiomyolipoma.

Imaging

Oncocytomas are solid, homogeneous, well-marginated, and often large tumors. They have no specific imaging findings; CT, US, and MR simply reveal a solid, well-marginated tumor. Especially when small, their imaging appearance is indistinguishable from that of renal cell carcinomas. In distinction to renal adenocarcinomas, necrosis and hemorrhage are not common, although larger oncocytomas tend to contain a central stellate scar that mimics the necrosis seen in a renal cell carcinoma. Cystic changes and calcifications are rare. They tend to be somewhat hypervascular. In general, imaging can suggest an oncocytoma but will not differentiate it from a renal adenocarcinoma.

Oncocytomas are hypointense on T1-weighted MR images but vary in intensity on T2-weighted images. About half have a well-defined capsule. Post-MR contrast a minority of oncocytomas reveal a "spoke-wheel" enhancement pattern. These MR findings do not exclude a renal cell carcinoma.

Urothelial Tumors

Papilloma

Papillomas are transitional cell epithelial tumors that are difficult to classify. Histologically, differentiation from a low-grade transitional cell carcinoma is difficult, and controversy exists about whether they are indeed a separate benign entity or whether they represent a spectrum of transitional cell carcinomas. They are rare in the upper urinary tract. A male predominance is evident.

The even rarer upper urinary tract inverted papillomas are of uncertain malignant potential. Etiology of this proliferative tumor is unknown, and histopathologic diagnosis difficult. Of note is that some inverted papillomas precede, are synchronous with, or are metachronous with a malignant urothelial tumor, and thus the discovery of one requires a search for other urinary tract tumors.

The imaging appearance of papillomas is similar to that of other urothelial neoplasms. They range from sessile to pedunculated. The differential diagnosis includes transitional cell carcinoma, blood clots, a fungus ball, calculi, fibroepithelial polyp, and malacoplakia.

Local excision appears sufficient for these tumors.

Transitional Cell Carcinoma

Clinical

Urothelial origin malignant neoplasms include transitional cell carcinoma, squamous cell carcinoma, and adenocarcinoma. Of these, transitional cell carcinomas predominate and, after renal cell adenocarcinomas, represent the second most common renal neoplasm in adults. A minority contain a squamous cell metaplasia component. A rare transitional cell carcinoma contains a sarcomatoid component. Data from the Dutch hereditary nonpolyposis colorectal cancer registry suggest that patients with hereditary nonpolyposis colorectal cancer are at an increased risk of developing upper urinary tract transitional cell carcinomas (70).

Among transitional cell carcinomas originating in renal collecting systems, roughly one quarter are in an upper calyx, one quarter in a lower calyx, one quarter in renal pelvis, about 5% in a middle calyx and the rest are more extensive; in the ureters, slightly under 10% are in the upper segment, 20% in the middle, slightly under 50% in the lower segment, and 20% in the distal ureteral. A rare patient has the entire ureter affected. A number of reports describe a ureteral stump transitional cell carcinoma developing years after a nephrectomy for a benign or malignant condition.

The most common clinical finding with these tumors is intermittent hematuria, followed by flank pain. Ureteral obstruction and a nonfunctioning kidney develop eventually and thus a need for retrograde pyelography. A rare obstruction leads to ureteral rupture.

While positive cytology is obviously diagnostic, negative cytology does not exclude a transitional cell carcinoma. Especially with intrarenal

tumor, washings tend to be nondiagnostic. Also, positive cytology does not identify the site of origin.

Imaging

Transitional cell carcinomas range from polypoid, to nodular, to flat. Some polypoid ones are on a stalk; these tend to be low grade and are often associated with adjacent ureter dilation, but differentiation from a stone is difficult in some patients, even with retrograde pyelography. The flat type, often containing squamous cell carcinoma components, tends to infiltrate, has little if any intraluminal component, and usually is of a higher grade malignancy; as expected, this type is more difficult to detect. If extensive, a more proximal infiltrating one will obstruct ("amputate") a calyx. Calcifications are rare.

When large, these tumors infiltrate extensively and mimic a renal cell carcinoma, although, being centrally located, they are less prone to producing a renal contour abnormality. Some intrarenal transitional cell carcinomas are highly invasive, become necrotic, and involve a large portion if not the entire kidney. Only a rare transitional cell carcinoma extends into the vena cava as a tumor thrombus.

Being urothelial in origin, pyelography (IV, retrograde or antegrade) should have a high tumor detection rate, even higher than with CT and gray-scale US. A major limitation of IV pyelography is the lack of sufficient contrast opacification.

Computed tomography identifies a transitional cell carcinoma as a soft tissue density tumor adjacent to water density urine. It is isodense to renal parenchyma. Its density is lower than that of blood clots. Computed tomography identifies a cystic component in a minority. These tumors enhance slightly after contrast, although enhancement is less than that of renal parenchyma. At times a lucent stone is in the differential diagnosis, but CT should differentiate even a uric acid stone, which is denser than a transitional cell carcinoma.

Computed tomography is used in staging transitional cell carcinomas, although the type of staging criteria used and the presence of hydronephrosis influence staging accuracy. While CT detects invasion of adjacent structures and distant metastases, it is limited in differentiating a superficial tumor from one invading muscle layers or renal pelvis. Proximal hydronephrosis tends to result in overstaging; CT sensitivity and specificity is considerably greater in assessing renal parenchymal invasion than in detecting ureteral or perirenal fat invasion. Staging accuracy is improved by decreasing CT thicknesses through the tumor.

If sufficiently large, US shows these tumors to be hyperechoic to renal parenchyma.

Endoluminal US holds promise; tumor location, size, and staging can be studied with this technique.

These tumors are hypointense on T2-weighted MRI. Some of these hypovascular carcinomas enhance considerably with contrast MRI.

Therapy/Survival

Upper tract carcinoma in situ is occasionally treated by bacillus Calmette-Guérin instillation; although normalization of urinary cytology is reported, only limited studies are available.

Ureteroscopic biopsy and cytology are helpful in defining and grading these tumors. Tumor stage and grade are interrelated and have prognostic significance; most tumors with a low or moderate grade are at a low stage and those with a high grade are at a stage T2 or T3.

Among Japanese patients with renal pelvic or ureteral cancer who underwent lymph node dissection, no lymph node involvement was found in about two thirds (71). The 5-year survival rate was 79% for pN0, decreasing to 12% for pN1, 20% for pN2, and 0% for pN3. These are somewhat biased statistics because only patients selected for lymph node dissection are included.

Because of these tumors synchronous and metachronous potential, a nephroureterectomy is generally performed. A search for associated bladder cancers is also warranted. Close follow-up is necessary for metachronous tumors, especially during the first several years after initial surgery.

Nephrogenic Metaplasia/ Adenoma/Adenocarcinoma

Nephrogenic metaplasia, or nephrogenic adenoma, is a rare, benign urothelial condition histologically consisting of glandular structures. This condition is more common in the

bladder but occasionally is detected in the ureters or renal collecting systems. Most metaplasias are associated with chronic infection, and the pathogenesis presumably includes metaplasia in response to a prior inflammation or trauma. Some tumor cells show severe nuclear atypia and staining for anti-p53, suggesting that p53 has a role in adenoma-to-adenocarcinoma transformation of these tumors. A rare adenoma is cystic.

Although nephrogenic metaplasia is considered to be a benign condition, a rare primary nephrogenic (urothelial) adenocarcinoma is reported, at times consisting of nephrolithiasis, nuclear atypia suggesting a malignancy, a tubulovillous adenoma, and intestinal metaplasia in adjacent epithelium. A typical scenario consists of urography in a patient with pain and hematuria revealing a ureteral tumor, a biopsy identifies nephrogenic metaplasia, and this segment is resected.

Although resection should be curative, recurrence is not uncommon. Whether recurrence is due to incomplete resection or a new focus from diseased urothelium is often unknown.

Squamous Cell Carcinoma

Squamous metaplasia (also known as *keratinizing* and *desquamating malpighian metaplasia*) and subsequent squamous cell carcinoma develop in a setting of chronic urolithiasis or infection. Upper tract infection with *Schistosoma hematobium* is associated with this tumor.

No distinguishing imaging characteristics identify squamous cell metaplasia. At best, it appears as a polyp, often in the renal pelvis. It is diagnosed either from a biopsy specimen or on histologic study after nephroureterectomy.

These carcinomas range from flat, ulcerated plaques to large, bulky renal pelvis tumors. They have a tendency for intramural growth. Associated stones and xanthogranulomatous pyelonephritis make detection difficult. At times their imaging appearance mimics a transitional cell carcinoma. Both local spread and metastasis are common at the initial presentation. As an example, a man with a destroyed and painful kidney containing a staghorn calculus and believed to contain pyonephrosis underwent nephrectomy (72); a renal pelvis squamous cell carcinoma had invaded the kidney and psoas muscle.

Sarcomatoid Carcinoma

Sarcomatoid carcinomas contain elements of adenocarcinoma, transitional cell carcinoma, and sarcoma. Some of these carcinomas are related to prior radiation therapy to other organs. About 5% of renal cancers are histologically sarcomatoid in nature. Survival of patients with these cancers is measured in months.

Imaging findings of most sarcomatoid carcinomas are similar to the more common renal adenocarcinomas.

Medullary Carcinoma

Renal medullary carcinoma is a rare collecting duct neoplasm affecting teenagers and young adults with sickle cell trait or hemoglobin SC disease. Presumably an unidentified genetic component is a factor in its pathogenesis. The tumor has a distinctive microscopic appearance consisting of a diffuse and glandular growth pattern, an inflammatory infiltrate, and the presence of rhabdoid/plasmacytoid cells or even sarcomatoid cells.

This entity should be considered in a young patient with sickle cell trait or hemoglobin SC disease who develops hematuria. Distant metastasis at the initial presentation is not uncommon. These tumors are centrally located and infiltrate the renal parenchyma and renal sinus; occasionally a necrotic tumor communicates with the collecting system. They show heterogeneous contrast enhancement, presumably due to necrosis. Venous invasion and nodal metastases are common.

This is an aggressive malignant neoplasm having a poor prognosis. The interval from diagnosis to death averages only several months; no objective response is seen to chemo- and immunotherapies.

Other Renal Epithelial Tumors

A number of mostly cystic renal neoplasms cause considerable confusion and defy ready classification. The traditional method is to divide them into benign (metanephric adenoma, multilocular cystic nephroma, nephronogenic nephroma, and congenital mesoblastic nephroma) and malignant (Wilms' tumor, atypical mesoblastic nephroma, and cystic partially differentiated nephroblastoma) neo-

plasms, although some defy discrete classification. From a radiologic perspective it appears more appropriate to classify them into solid and cystic neoplasms and then subdivide by patient age (Table 10.7). In addition to the neoplasms listed in the table, a multicystic dysplastic kidney and segmental multicystic dysplasia in a duplicated renal collecting system are also in the differential diagnosis.

An association of fetal nephrogenic rests and multicystic dysplasia has already been discussed. Nephrogenic tissue is also associated with some neoplasms; benign ones include multilocular cystic nephroma and nephrogenic nephroma, and the malignant ones are Wilms' tumor and mesoblastic nephroma. And then there is cystic partially differentiated nephroblastoma (discussed below); pathologists usually classify it as a separate entity, but strong evidence for this is lacking.

Wilms' Tumor (Nephroblastoma)

Nephroblastomatosis

Persistence of renal blastema tissue in a neonate is known as nephroblastomatosis. While immature metanephric tissue (nephrogenic rests) found in nephroblastomatosis is not intrinsically neoplastic, it is believed to be able to undergo neoplastic change, and nephroblastomatosis is probably a precursor of Wilms' tumors, or at least some of them. If one resected kidney contains metanephric tissue, the contralateral kidney is at increased risk of containing a Wilms' tumor. Persistent metanephric tissue is found in a number of syndromes, including Beckwith-Wiedemann syndrome (discussed earlier; see Congenital Abnormalities, above), Denys-Drash syndrome (gonadal dysgenesis, nephropathy, and renal failure), Perlman syndrome, hemihypertrophy, neurofibromatosis, and sporadic aniridia. Early and often bilateral Wilms' tumors develop in patients with these syndromes.

Denys-Drash syndrome is caused by a mutation in the *WT1* gene on chromosome 11p13, a tumor-suppressor gene. It is highly expressed during genital and renal development. Wilms' tumors in this syndrome are derived from cells homozygous for this mutation.

A kidney diffusely affected with nephroblastomatosis is enlarged and has a plaque-like or lobular outline. Imaging shows a subcapsular tumor or tumors. Data from the German Nephroblastoma Study Group identified nephrogenic rests as multinodular, peripheral cortical lesions, with diffuse extension being less common (73); the rests were homogeneous and hypodense, hypoechoic, and hypointense on both T1- and T2-weighted images and were best seen with postcontrast CT and T1-weighted MRI. They enhance less post–CT contrast than do renal parenchyma. Lesions <1 cm were rarely identified by US. Overall, homogeneity was the most reliable criterion in differentiating nephrogenic rests from Wilms' tumors.

Table 10.7. Classification of primary renal neoplasms (by age and solid versus cystic)

Age	Mostly solid	Mostly cystic
Neonates	Mesoblastic nephroma	Cystic mesoblastic nephroma
Children	Wilms' tumor (nephroblastoma) Mesoblastic nephroma Metanephric adenoma Chromophobe carcinoma Duct of Bellini carcinoma	Cystic Wilms' tumor Multilocular cystic nephroma Cystic partially differentiated nephroblastoma Cystic clear cell sarcoma Cystic mesoblastic nephroma Cystic renal cell carcinoma
Adults	Renal cell carcinoma Wilms' tumor (rare) Mesoblastic nephroma (rare) Metanephric adenoma Chromophobe carcinoma Duct of Bellini carcinoma Oncocytoma	Multilocular cystic nephroma Cystic renal cell carcinoma Cystic partially differentiated nephroblastoma Cystic Wilms' tumor (rare)

Children

Clinical

A Wilms' tumor, or nephroblastoma, is the most common solid abdominal malignancy in childhood. The vast majority originate in the kidneys, with only an occasional one developing in other extraperitoneal structures, presumably from retained mesonephric tissue. Some are bilateral, with most of these being synchronous rather than metachronous. An occasional Wilms' tumor first manifests as pulmonary metastases. It is rare in the neonate; nevertheless, synchronous bilateral Wilms' tumors in neonates are described. A majority are detected in children below the age of 5 years.

An occasional Wilms' tumor is familial. Children with hemihypertrophy are at an increased risk of having Wilms' tumor; the risk is about 5%, and these children should undergo serial surveys up to about the age of 8 years. The prevalence of Wilms' tumors is considerably higher in children with aniridia, who should also undergo serial surveillance. An occasional Wilms' tumor develops in a setting of cryptorchidism. A number of chromosome abnormalities are evident in some of these patients, including a Wilms' tumor-suppressor gene at 11p13.

A minority of these tumors contain bone, cartilage, fat, or other atypical tissue. Some investigators label these as "teratoid Wilms'" tumors. Some such teratoid Wilms' tumors contain a cystic component.

A palpable abdominal tumor is a common presentation. Bleeding develops in some tumors and they enlarge suddenly due to hemorrhage. A hematoma or urinoma is not an uncommon association. Renin is produced by a minority and these children develop hypertension.

These tumors spread hematogenously to lungs, liver, bone, and other organs. The overall prognosis (long-term cure) in children with Wilms' tumors is approximately 80%.

Ultrasonography-guided needle biopsies of pediatric renal tumors, including Wilms' tumors, have been safely performed, although the technique is controversial.

Imaging

Typically, when first detected these are large, round, soft tissue tumors infiltrating and distorting adjacent renal parenchyma (Fig. 10.25). Some are mostly exophytic. Necrosis is common. An occasional Wilms' tumor contains fat or calcifications, although in general calcifications in a juxtarenal tumor in a child should suggest a neuroblastoma.

Figure 10.25. Anaplastic Wilms' tumor in a 6-year-old with a palpable abdominal tumor. Computed tomography identifies a left renal tumor deviating the kidney anterior and medial. A claw sign suggests the diagnosis. Adenopathy is also present. Other studies detected pulmonary metastases. (Courtesy of Luann Teschmacher, M.D., University of Rochester.)

Postcontrast CT and nonenhanced MRI appear equally accurate in establishing size and tumor origin, although both are inaccurate in staging. Ultrasonography can assess tumor size but not origin. Ultrasonography most often identifies a large, well-marginated tumor of heterogeneous, increased echogenicity due to necrosis and hemorrhage. Possible renal vein and inferior vena caval invasion is evaluated with Doppler US.

Magnetic resonance typically reveals these tumor to be hypointense on T1- and hyperintense on T2-weighted images. Larger ones often contain blood and are heterogeneous in appearance. Their postcontrast enhancement is variable.

Renal vein invasion is common, and some extend into the inferior vena cava; and an occasional one even grows into the right atrium (Fig. 10.26). A tumor thrombus extending into the left renal vein can obstruct the gonadal vein and result in a varicocele. Ultrasonography should identify most such tumor extensions. Aortic encasement is uncommon. These tumors also grow into the calyces and adjacent ureter.

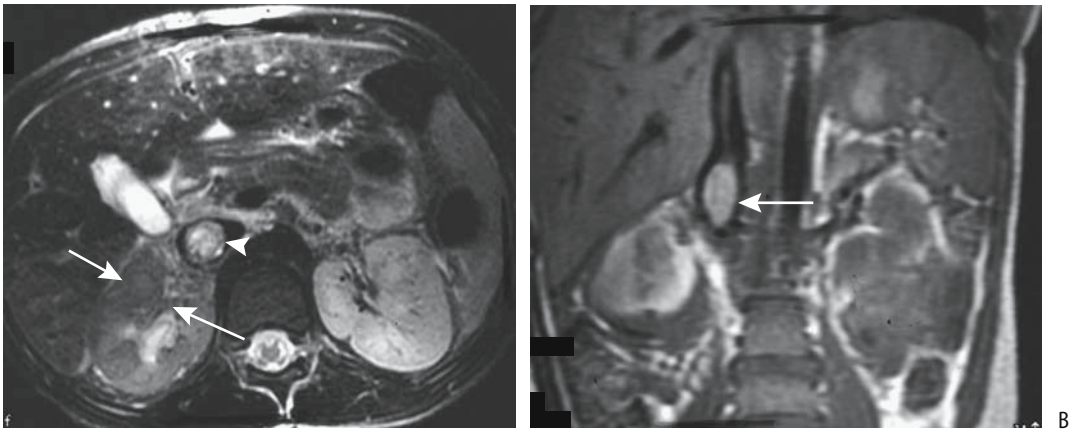

Figure 10.26. Wilms' tumor. A: T2–weighted transverse MR image identifies a right renal tumor (arrows) with extension into the renal vein (arrowhead). B: Coronal T1-weighted image shows tumor extension into the vena cava (arrow). (*Source:* Burgener FA, Meyers SP, Tan RK, Zaunbauer W. Differential Diagnosis in Magnetic Resonance Imaging. Stuttgart: Thieme, 2002, with permission.)

A rare one even extends intraluminally in the ureter.

A rare Wilms' tumor is multicystic and mimics a multilocular cystic nephroma or benign renal cystic disease. Likewise, differentiation from a neuroblastoma can be difficult, although a neuroblastoma tends to be ill-defined and more heterogeneous in appearance. Also, a neuroblastoma tends to metastasize early and extensively. Superficially, a Wilms' tumor can be confused with xanthogranulomatous pyelonephritis.

Therapy and Outcome

Bilateral Wilms' tumors present a therapeutic dilemma. Conservative surgical therapy with initial biopsy followed by chemotherapy and delayed tumor resection in children with bilateral Wilms' tumors in the United Kingdom Children's Cancer Study Group resulted in a mean preserved renal mass of 45%, but initial surgical resection followed by chemotherapy left a renal mass of 35% (74); children in both groups had similar survival and similar renal function.

Imaging after chemotherapy usually identifies necrosis, hemorrhage and calcifications. In one child CT after chemotherapy showed an increase in tumor size and extensive fatty infiltration (75); resection revealed no residual blastema.

Follow-up of the remaining kidney in children after unilateral nephrectomy for Wilms' tumor reveals that only half develop renal hypertrophy.

Adults

A Wilms' tumor is rare in adults. Histologically, these tumors are similar to the ones seen in children, and the therapy likewise is similar, but these tumors grow rapidly and prognosis is worse than in children, possibly due to their more advanced presentation. Even extrarenal Wilms' tumors have developed in adults (76).

A typical Wilms' tumor in an adult consists of a complex mass often containing a cystic component. These tend to be large, hypovascular and multilocular tumors containing a limited solid component. The differential includes a cystic carcinoma and a multilocular cystic nephroma.

Multilocular Cystic Nephroma/Cystic Partially Differentiated Nephroblastoma

Clinical

These tumors consist of a mixture of epithelial and mesenchymal components. In the past, a multilocular cystic nephroma, also called *multicystic nephroma*, *cystic lymphangioma*, and

multilocular cyst, was considered a hamartoma, although the current thinking leans toward a neoplastic origin. Some authors classify multilocular cystic nephroma and cystic partially differentiated nephroblastoma in young children as one entity and believe that they represent cystic Wilms' tumors having little potential for invasion or metastasis (77); in adults, however, these authors believe that multilocular cystic nephroma is a separate benign entity independent of Wilms' tumor, although a rare one does undergo malignant transformation and develops into a carcinoma or sarcoma. In one adult, a cystic partially differentiated nephroblastoma exhibited cell maturation intermediate between a multilocular cystic nephroma and a Wilms' tumor (78).

A similar condition is found in some infants with other gastrointestinal and skeletal abnormalities, including visceromegaly (Perlman syndrome), an autosomal-recessive condition.

In children (mostly young boys) a multilocular cystic nephroma is radiographically and grossly indistinguishable from a cystic partially differentiated nephroblastoma. Both are cystic thin-walled tumors containing multiple septations surrounded by a fibrous capsule. These tumors differ histologically in that a multilocular cystic nephroma is composed of mature differentiated tissue and does not contain blastemal elements, while septa in a cystic partially differentiated nephroblastoma do contain embryonal cells. Calcifications are uncommon in children.

Imaging

Imaging detects both of these cystic tumors but cannot differentiate between them. Their appearance is similar to other cystic tumors. They occur unilaterally. In children, the numerous small cysts can appear solid, and imaging findings resemble a Wilms' tumor. In adults (mostly women), imaging and even aspiration biopsy findings mimic a cystic renal cell carcinoma, although these tumors are not related.

Computed tomography reveals multilocular cystic nephromas to be homogeneous, multicystic tumors containing thin septa without a solid components; for some reason a lower pole location predominates. The cystic component does not enhance with contrast. Their hallmark is that septa tend to be their only prominent solid component, and the presence of a solid component should suggest either malignant transformation or another diagnosis.

Magnetic resonance imaging of a multilocular cystic nephroma reveals a complex solitary renal cystic tumor often protruding into the renal collecting system and containing thin septa, with the cystic component varying from hypo- to hyperintense on T1-weighted images. Any solid component and septa enhance postcontrast in all cases.

Nephrectomy in a patient with a multilocular cystic nephroma should be curative. With a cystic partially differentiated nephroblastoma, however, some tumors recur locally.

Metanephric (Embryonal) Adenoma

A curious tumor composed of small tubular, papillary, and glomeruloid structures and consisting of proliferating primitive epithelial cells mimicking an embryonal nephron was first described in 1980 and called a *nephronogenic nephroma* (79). Later, a similar benign mixed epithelial and mesenchymal renal tumor was termed an *embryonal adenoma*. Since then, a number of reports have used the term *metanephric adenoma*. Whether this tumor represents a benign counterpart of Wilms' tumor is conjecture. Metanephric adenomas and metanephric adenofibromas (discussed below) are closely related neoplasms. In either case, a renal metanephric adenoma is a distinctive renal cortical neoplasm usually classified among nephroblastic tumors. Its histologic appearance is similar to that of metanephric hamartomas found in nephroblastomatosis. In spite of a morphologic similarity to Wilms' tumor, genetics suggest a relationship to papillary adenomas and papillary renal cell carcinomas.

These tumors consist of differentiated cells containing few or absent mitoses; tubules and glomeruli are often identified. Its metanephric (embryonic) architectural and cytologic appearance is characteristic, although pathologic study of some tumors suggests a malignancy. Needle biopsy and aspiration cytology specimens have been misdiagnosed as Wilms' tumor. The reverse is also true: a renal cell carcinoma and a metastasis from a poorly differentiated thyroid carcinoma can be misdiagnosed as metanephric adenomas. Most authors

consider these tumors to be benign, although a metanephric adenoma in a 7-year-old girl metastasized to lymph nodes (80).

There are two age peaks; half occur in children and the other half mostly in women in their 50s. Most tumors are discovered incidentally, with only a minority of patients having pain, hematuria, or a palpable tumor. Polycythemia and acquired von Willebrand's disease develop in some patients. An association of a metanephric adenoma with embryonal hyperplasia of Bowman's capsular epithelium was reported in a 9-year-old boy on peritoneal dialysis (81).

Metanephric adenomas are well-circumscribed, unencapsulated tumors varying in size. Some contain fibrosis and calcifications. Computed tomography, US, and MRI usually reveal a solid tumor with occasional necrosis and cystic degeneration, suggestive of a hypovascular renal cell carcinoma. They are iso- to hyperdense on CT. They range from hypo- to hyperechoic on US.

Simple resection is curative in almost all patients.

Metanephric (Nephrogenic) Adenofibroma

The histology of metanephric adenofibromas (previously also called nephrogenic adenofibromas) reveals a proliferation of spindle cells, similar to what is found in congenital mesoblastic nephroma, encasing nodules of embryonal epithelium similar to the nephroblastomatosis associated with Wilms' tumor; it is thus not surprising that these tumors have been misdiagnosed as Wilms' tumors and mesoblastic nephromas.

These are childhood tumors. A not uncommon presentation is hematuria, hypertension, or polycythemia.

Metanephric Stromal Tumor

A metanephric stromal tumor is a renal medullary spindle cell (fibrous) tumor containing smooth-walled cysts that entrap native kidney tissue. Although such a description suggests that it should be classified under mesenchymal tumors, it is histologically identical to the stromal component of metanephric adenofibroma and is discussed with the latter entity (see above).

Histology reveals onion-skin cuffing around entrapped renal tubules, heterologous glial or cartilage differentiation, and vascular changes consisting of angiodysplasia of entrapped arterioles and juxtaglomerular cell hyperplasia of entrapped glomeruli (82).

The mean age of 31 patients with a metanephric stromal tumors was 2 years; most tumors presented as an abdominal tumor (82); they did not metastasize. The differential diagnosis includes renal clear cell sarcoma.

Mesoblastic Nephroma (Bolande's Tumor)

Infants

Congenital mesoblastic nephroma, at times called *congenital Wilms' tumor*, comprises about half of renal tumors encountered during the neonatal period. Most occur within the first month of life, and their prevalence decreases during childhood. They present as a large abdominal tumor. The prognosis depends on the infant's age, being best for tumors discovered early in life.

Earlier publications considered mesoblastic nephromas to be a benign neoplasm, possibly even hamartomatous in origin. In fact, the favorable prognosis of Wilms' tumors in neonates reported previously is suspect because many of these were probably mesoblastic nephromas rather than Wilms' tumors.

The morphologic and cytogenetic evidence suggests a relationship between congenital mesoblastic nephromas and infantile fibrosarcomas. Not only are these tumors similar histologically, but also both are associated with similar chromosome polysomies and they may represent a single entity. Congenital mesoblastic nephromas and Wilms' tumors also appear to share common genetic pathways and abnormalities.

Mesoblastic nephromas are mostly solid tumors which usually follow a benign course but tend to invade adjacent structures. Some authors subdivide these tumors into congenital and atypical, with the latter including aggressive and potentially malignant variants. The aggressive variety tends to recur or metastasize. A rare aggressive mesoblastic nephroma ruptures spontaneously.

Imaging reveals a solid, homogeneous, usually large tumor. Hemorrhage and necrosis

develop in the aggressive and malignant variants, although cystic degeneration is not common. Their imaging appearance mimics a Wilms' tumor.

Some mesoblastic nephromas show uptake of Tc-99m-DMSA.

Adults

The rare similar adult renal tumor consisting of epithelial and stromal tissue is probably a different entity than the pediatric variety. Immunohistochemistry and electron microscopy aid in identifying this tumor. Some mesoblastic nephromas in adults may represent cystic hamartomas. An adult mesoblastic nephroma can grow either intra- or predominantly extrarenal, at times even mimicking an adrenal tumor.

Lymphoma/Leukemia

Clinical

True lymphatics are not present in the kidneys and primary renal lymphoma is rare. Secondary involvement is either via contiguous spread from perirenal disease or from hematogenous dissemination. Involvement with non-Hodgkin's lymphoma is considerably more common than Hodgkin's lymphoma. Kidneys of immune-deficient patients are more prone to involvement by lymphoma. Infiltration is usually bilateral.

Lymphoma involvement in other locations tends to dominate the clinical findings. Most renal involvement does not lead to symptoms until late in the course. A rare presentation is acute renal failure.

A granulocytic sarcoma (also called a chloroma) develops in a minority of patients after therapy for some leukemias. These solid renal tumors are hypointense on T1- and hyperintense on T2-weighted images. They show little contrast enhancement.

Imaging

Imaging detects only a minority of lymphomatous renal involvement. No typical pattern predominates, and renal lymphoma ranges from solitary to multiple tumors, diffuse infiltration, or invasion from adjacent structures. Even perirenal involvement varies considerably from focal tumors to plaque-like infiltration. Retroperitoneal lymphoma generally invades the kidneys through renal sinuses, and thus the renal medulla is more often involved than the cortex.

Necrosis is uncommon in renal lymphomas, even when large. Likewise, lymphoma rarely results in a vascular tumor thrombus.

Computed tomography findings in the rare primary non-Hodgkin's renal lymphoma range from a single nodule, multiple nodules, and diffuse infiltration, to a lymphomatous mass encasing the kidney. Lymphomatous foci are homogeneous and mostly slightly hyperdense to isodense on precontrast CT and do not enhance as much as normal renal parenchyma postcontrast. Focal tumors maintain a discrete margin. Diffuse infiltration results in an overall renal structure disorganization. A not unusual appearance is renal invasion by retroperitoneal lymphoma, but the lack of adjacent adenopathy is unreliable in excluding lymphoma. While CT allows evaluation of the site and size of involvement, it cannot establish a diagnosis; similar findings are seen with a renal cell carcinoma, transitional cell carcinoma, metastatic disease, or even some chronic inflammatory conditions.

Two sonographic patterns are evident: either a bilateral nodular infiltrate or diffuse renal enlargement with loss of differentiation between renal sinus echoes and parenchyma. The typical infiltration is hypoechoic, but at times homogeneous involvement results in an anechoic pattern mimicking a cyst.

Magnetic resonance imaging shows iso- or slight hypointense tumors on T1- and hypointense tumors on T2-weighted images. Postcontrast lymphomas show minimal tumor enhancement, in distinction to renal cell carcinomas where early enhancement is common. Whether CT or MR is superior in identifying and defining lymphomatous involvement is not clear. Ureteral involvement consists either of encasement or displacement by an adjacent lymphomatous focus.

Leukemic involvement results in symmetrically enlarged kidneys and compressed collecting systems.

Multiple Myeloma

Renal histology in patients with myeloma nephropathy revealed 14% with tubulointerstitial nephritis, 11% with amyloidosis, 7% with acute tubular necrosis, and 4% each with nodular glomerulosclerosis and plasma cell infiltration (83); at times renal biopsy pro-vides the first clue to a diagnosis of myeloma by identifying myeloma cast nephropathy.

Tubular precipitation of Bence-Jones proteins is a cause of renal failure in multiple myeloma patients. Haphazard IV contrast injection is a cause of such precipitation, but with preplanning and adequate hydration a number of these patients have undergone contrast studies without complication.

Resorption of calcium from bone and the resultant hypercalcemia lead to nephrocalcinosis. The kidneys enlarge, and the collecting systems are compressed. These patients are also prone to developing uric acid calculi.

Unexplained renal failure in a patient even with absent skeletal lesions can still be due to multiple myeloma.

Mesenchymal Neoplasms

Angiomyolipoma

Clinical

Classification of angiomyolipomas has evolved from their being considered hamartomas to benign neoplasms, although a rare one does undergo sarcomatous transformation and a propensity to metastasize. Even the usually benign variety tends to be locally aggressive and produces considerable mischief. In some studies 20% to 50% are detected in tuberous sclerosis patients, where they tend to be multiple and bilateral. Angiomyolipomas are associated to a lesser degree with von Recklinghausen's disease, von Hippel-Lindau disease, and adult polycystic disease, and are found in about half of patients with pulmonary lymphangiomyomatosis. In general, a finding of multiple angiomyolipomas should suggest tuberous sclerosis (Fig. 10.27). In tuberous sclerosis, angiomyolipomas occur earlier in life than sporadic ones, and most are discovered incidentally. An occasional tuberous sclerosis patient develops bilateral renal angiomyolipomas, pulmonary lymphangioleiomyomatosis, and tumors at other sites, but in general extrarenal angiomyolipomas are rare.

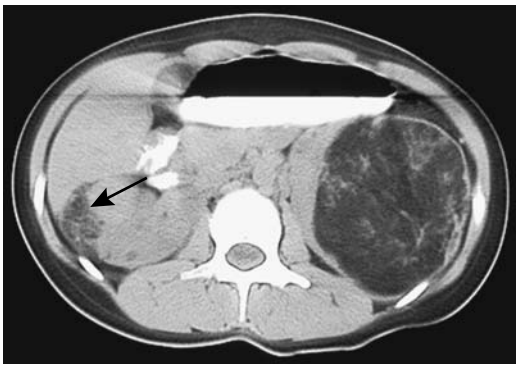

Figure 10.27. Renal angiomyolipomas in a 17-year-old with tuberous sclerosis. The left fat-containing tumor is obvious. A smaller angiomyolipoma is also present in the right kidney (arrow). (Courtesy of Luann Teschmacher, M.D., University of Rochester.)

These tumors develop in the renal capsule, cortex, and medulla. Histologically they are composed of haphazardly arranged blood vessels, disorganized smooth muscle fibers, and varying amounts of fat. Some contain sheets of epithelioid cells, suggesting a malignancy. Those without fat mimic a leiomyoma. Histologically, no sarcomatous transformation should be evident in either the leiomyomatous or lipomatous components.

Serial CT and US provide a measure of renal angiomyolipoma growth rates. The mean growth rate of isolated tumors is about 5% per year, being considerably more in those with tuberous sclerosis. No correlation exists between the amount of fat in a tumor and its growth rate. Growth tends to be unpredictable. Some tumors are stable for years and then undergo a fast increase in size, followed by another period of quiescence. Rapid growth occasionally occurs in pregnancy, suggesting that hormones play a role in their growth. An occasional angiomyolipoma is huge at initial presentation.

Spontaneous, solitary tumors are most common in middle-aged women and are rare in children. Pain, a palpable tumor, or hematuria is a common presentation, although many of these tumors are asymptomatic.

Pathologists describe a rare epithelioid angiomyolipoma as a separate entity. It tends to mimic renal cell carcinoma; it contains regions of hemorrhage and necrosis. Fatty tissue is not identified.

The rare liposarcoma is indistinguishable with imaging from an angiomyolipoma. This problem is especially pertinent when an incidental renal angiomyolipoma is detected in the work-up of another carcinoma and a metastatic liposarcoma is suspected.

Imaging

Angiomyolipomas are diagnosed with CT, US, or MR (Figs. 10.28 and 10.29); most contain sufficient focal fat to be identified with CT, appear as homogeneous and hyperechoic tumors containing smooth margins with US, and have hyperintense signals on T1- and hypointense signals on T2-weighted MRI.

Focal fat is also found in lipomas and some liposarcomas, but these tumors are rare in the kidneys. Clear cell renal cell carcinomas contain intracellular lipid and glycogen, which is detectable with chemical shift MR, but this fat is diffuse. Focal regions of fat are rare in renal cell carcinomas.

Calcifications are not a feature of angiomyolipomas except secondary to hemorrhage. Even when associated with fat, calcifications should suggest a carcinoma.

Diagnostic difficulty occurs when a tumor is small or contains very little fat. Conventional CT may not detect fat in tumors smaller than several centimeters in size. Multislice helical CT is more sensitive and is preferred for small lesions. These low-fat tumors are homogeneously hyperdense on unenhanced CT, show homogeneous postcontrast CT enhancement, and are isoechoic on US. Recent hemorrhage tends to mask any fatty component. Occasionally in such tumors a small amount of fat is detected with chemical shift MRI but not CT; in these, a renal cell carcinoma is in the differential diagnosis.

The diagnosis appears more difficult in children. Some of these tumors in children contain little fat and imaging simply identifies a large renal tumor. Even a fine needle biopsy may be misleading and a Wilms' tumor initially suspected. The reverse is also true; US detection of a hyperechoic tumor in a child with von Hippel-Lindau disease suggests an angiomyolipoma, yet an occasional such tumor is a renal cell carcinoma.

A CT diagnosis is straightforward with most angiomyolipomas. Fat intermixed with other tissue detected on thin-section nonenhanced CT is strong presumptive evidence for an

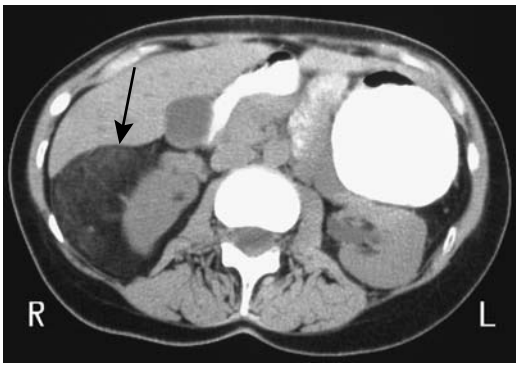

A

B

Figure 10.28. Right renal angiomyolipoma. A: CT identifies a fat-containing tumor in the superior renal pole (arrow). B: Selective angiography shows a poorly vascular tumor that was subsequently embolized. (Courtesy of David Waldman, M.D., University of Rochester.)

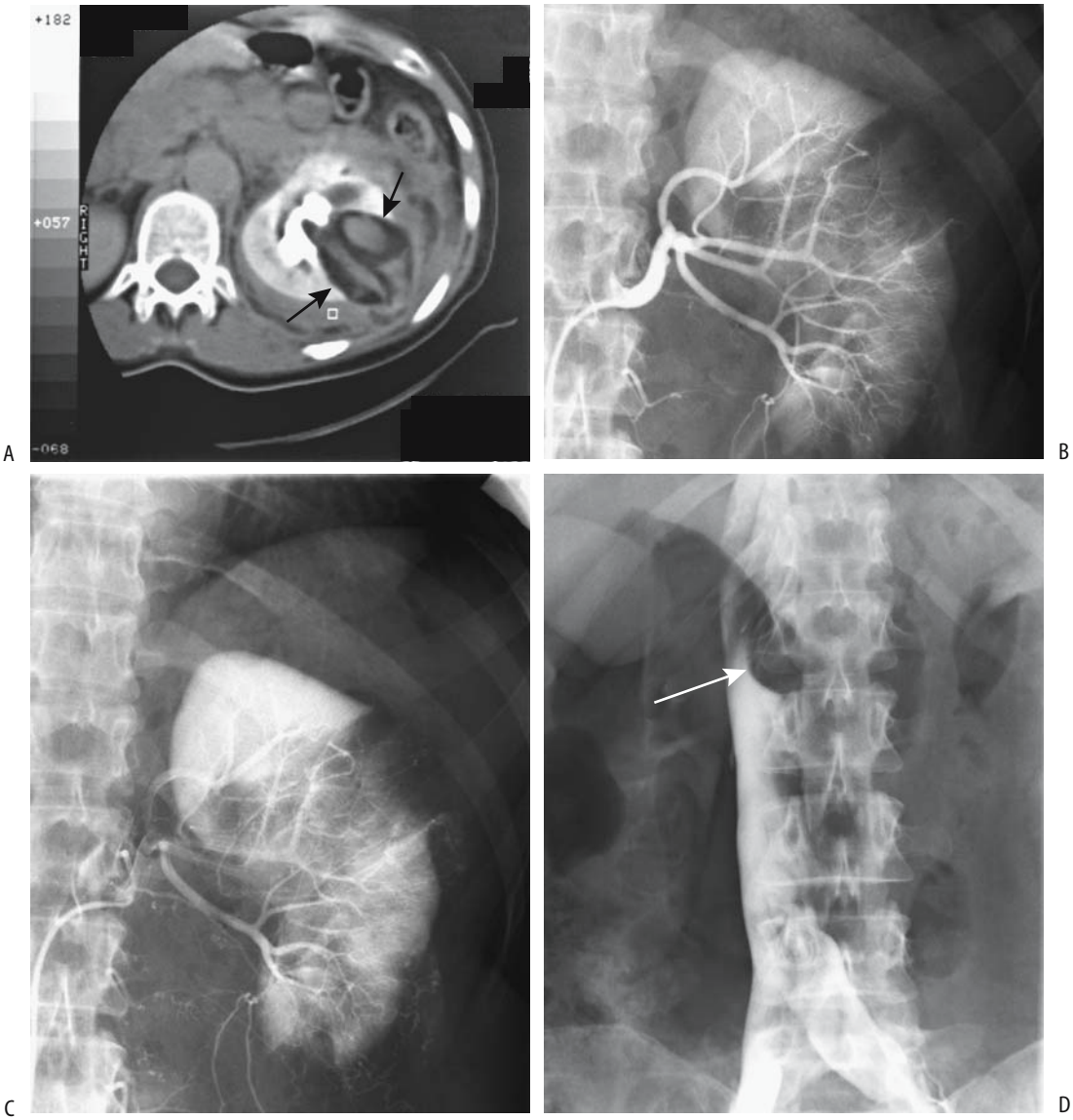

Figure 10.29. Angiomyolipoma with a retroperitoneal bleed. A: CT reveals a fat-containing left renal tumor (arrows). Arterial-phase (B) and delayed-phase (C) arteriography also identify the tumor but did not detect a site of bleeding. D: An inferior vena cavagram study reveals caval compression from the left side by the extensive retroperitoneal bleeding (arrow). (Courtesy of Oscar Gutierrez, M.D., University of Chile, Santiago, Chile.)

angiomyolipoma. Precontrast CT should be used; postcontrast enhancement may increase the density to the level of water. Angiomyolipomas tend to be well marginated but do not have a capsule. Cystic regions are not common. Larger tumors often extend outside the kidney. With an atypical CT appearance aspiration biopsy or cytology should provide a definitive diagnosis.

A typical sonographic appearance of an angiomyolipoma is that of a well-circumscribed, homogeneous, hyperechoic tumor.

Shadowing is detected in some, a finding unusual for a carcinoma. Because many small renal cell carcinomas are also hyperechoic, it is necessary to confirm US findings with other imaging. In some instances, however, a homogeneously hyperechoic lesion is accepted without confirmation as a probable angiomyolipoma, especially in patients under the age of 50 and with a tumor smaller than 15 mm or possibly 10 mm in diameter. In some patients with tuberous sclerosis and a confluence of multiple angiomyolipomas, US simply reveals diffusely increased echogenicity in markedly enlarged kidneys.

Ultrasonography frequency-dependent attenuation is potentially useful in differentiating renal cell carcinomas from angiomyolipomas. Frequency-dependent attenuation values of renal cell carcinomas are significantly lower than those of angiomyolipomas. Some overlap does exist, and the practical application of this technique remains to be established.

The fat component even in small tumors is identified by fat-suppressed T1-weighted MRI. Fat in these tumors tends to be scattered throughout the lesion. Opposed phase MRI alone, being sensitive even to intracytoplasmic lipid found in some renal cell carcinomas, is inappropriate to evaluate the gross fat in angiomyolipomas and differentiate them from carcinomas. Magnetic resonance imaging can reliably identify small (<1.5 cm) angiomyolipomas using a combination of sequences. Thus in-phase sequences show them to be minimally or moderately hyperintense relative to the renal cortex, and fat-suppressed sequences reveal a loss of signal intensity (84). Some tumors are difficult to identify due to limited signal differences or breathing artifacts.

Complications

Complications include compression of adjacent calyces and intratumoral, subcapsular, perirenal, or pararenal bleeding and hematoma (Fig. 10.30). These tumors undergo cystic degeneration. Spontaneous rupture is not uncommon and an angiomyolipoma should be high in the differential for the patient presenting with spontaneous rupture and bleeding of a renal tumor.

Extrarenal extension into the perirenal fat and lymph nodes is common, and these enlarged pararenal lymph nodes cause additional diagnostic and therapeutic dilemmas. Computed tomography shows these enlarged lymph nodes to be of soft tissue density, although an occasional one contains fat.

Extension into a renal vein and inferior vena cava as a tumor thrombus represents an additional complication. Computed tomography can occasionally detect fat within a thrombus. Renal vein involvement is more common on the right and does not necessarily imply malig-

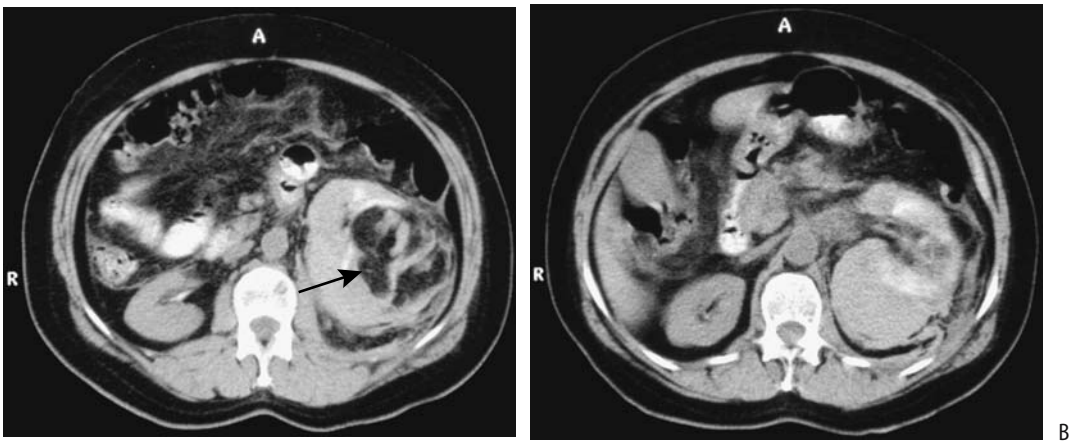

Figure 10.30. Bleeding left renal angiomyolipoma. Noncontrast CT reveals a fat-containing left renal tumor (A, arrow), surrounded by a well-marginated infiltrate having a CT density similar to aorta (B). (Courtesy of Algidas Basevicius, M.D., Kaunas Medical University, Kaunas, Lithuania.)

nant transformation. Complicating matters, an occasional one is associated with a renal cell carcinoma.

Therapy

Many of these tumors are still treated with a nephrectomy, although a trend is toward a more conservative approach—partial nephrectomy or enucleation is feasible in some patients. Incomplete tumor excision, however, leads to recurrence, often rapidly.

In patients with tuberous sclerosis, embolization is effective in long-term management of hemorrhage; most of these patients require several embolization sessions. If needed, a partial nephrectomy is then performed.

Symptomatic renal angiomyolipomas have been embolized with a mixture of iodized oil and absolute ethanol (85); some tumors decrease in size and others do not change, but most patients remain asymptomatic (except with incomplete embolization). Follow-up after embolization reveals that it is the angiomyogenic components that disappear, while fatty tissue undergoes liquefactive necrosis.

Lymphangiomyoma

Lymphangiomyomas, considered to be hamartomas rather than neoplasms by some authors, are discussed in more detail in Chapter 14. Lymphangiomyomas are related to angiomyolipomas and are occasionally associated with an angiomyolipoma; they are also suspected of being a manifestation of tuberous sclerosis.

One cause of chyluria is renal or retroperitoneal lymphangioleiomyomatosis.

These are cystic, hypervascular lesions, readily confused with renal cell carcinomas.

Leiomyomatous Neoplasms

Leiomyosarcomas account for half or more of the rare renal sarcomas. Even after resection, differentiation between a leiomyoma and its malignant counterpart is difficult. These tumors originate mostly from blood vessels, although some of the reported renal leiomyomas probably represent atypical angiomyolipomas.

Most benign leiomyomatous tumors are solid and well marginated, but degeneration leads to a cystic appearance. An occasional one contains calcifications. Computed tomography and US reveal a heterogeneous and hypoechoic tumor.

Imaging shows most sarcomas as large, invasive, necrotic tumors. They tend to mimic a large renal cell carcinoma. Poorly defined calcifications are seen in a minority. Metastases at initial presentation are common.

Angiomatous Neoplasms

A primary renal angiosarcoma is very rare, with only case reports described. They are also known as a *malignant hemangioendothelioma*, *hemangioendothelial sarcoma*, and *vascular sarcoma* and appear as single or multiple tumors. They arise from blood vessel endothelial cells. Hemorrhage is a common presentation. Some contain fat cells suggesting an angiomyolipoma.

An epithelioid angiosarcoma is a very aggressive tumor mimicking a primary epithelial tumor.

Clear Cell Sarcoma

Clear cell sarcomas are rare tumors found in younger children. Initially thought to be a variant of Wilms' tumor, this tumor has distinct immunohistochemical and flow cytometric findings differing from Wilms' tumors. Its relationship to mesoblastic nephroma is not clear. Clear cell sarcomas exhibit p53 protein nuclear immunopositivity, suggesting alterations in the *p53* tumor-suppressor gene.

The imaging findings of clear cell sarcomas are similar to those of a Wilms' tumor, with differentiation made by histology.

This is an aggressive tumor having a poor prognosis and a predilection for bone metastasis.

Ossifying Renal Tumor of Infancy

The few reported ossifying renal tumors of infancy occurred in infants under the age of 14 months. They appear to be benign. These tumors contain varying proportions of osteoid, osteoblastic cells, and spindle cells. Whether the osteoid component represents a form of urothelial transformation is speculation. The proportion of osteoid and the degree of osseous maturation increases with age.

Gross hematuria is the most common presentation. An occasional infant presents with a palpable abdominal mass.

Typically these tumors are attached to a renal papilla and present as a pelvicalyceal system tumor. Some resemble a staghorn calculus.

Osteogenic Sarcoma

A primary renal osteogenic sarcoma is very rare and should be distinguished from a sarcomatoid variant of renal cell carcinoma with osteoid formation. Whether these tumors represent a sarcomatous version of an angiomyolipoma is speculation.

Patients with a primary renal osteogenic sarcoma have elevated serum alkaline phosphatase levels but no underlying bone disease.

These tumors contain calcifications. A "sunburst" type of calcification, if present, should suggest the diagnosis. The differential diagnosis for a calcified renal tumor includes a calcified inflammatory tumor, renal cell carcinoma, and a metastatic or invading osteogenic sarcoma.

Histiocytoma

A majority of renal histiocytomas are malignant. A renal capsule origin is common. A review of 44 malignant renal fibrous histiocytomas found an average patient age of 58 years, no sex predilection, and two thirds of tumors involving the left kidney (86). Symptoms tend to be few, and a late presentation is common. Sudden flank pain suggests spontaneous tumor rupture.

Imaging reveals a solid tumor tending to be hypodense on CT, hypoechoic on US, and hypovascular on angiography (86). A correct preoperative diagnosis is not common, with renal cell carcinoma or oncocytoma often being suspected.

These tumors have a poor prognosis. Metastases and local recurrence after resection are common.

Reninoma (Juxtaglomerular Tumor)

These rare renin-secreting tumors, known as *reninomas* and *juxtaglomerular cell tumors*, occur both in children and adults and are more common in females. Their primary importance is their renin production and resultant hypertension, which can be severe, often associated with hypokalemia and hyperaldosteronism. An occasional incidentally discovered reninoma is nonfunctioning. As its name implies, these tumors originate from juxtaglomerular cells. Whether they are hamartomas or neoplasms is not established. They are benign. Histologically, some of these tumors mimic a hemangiopericytoma, with the latter tumor occasionally also resulting in hypertension.

These are solid, hypovascular tumors on CT and hyperechoic on US. Most reninomas are smaller than 2 to 3 cm in diameter. Even if a reninoma is too small to be detected with imaging, with strong clinical suspicion renal vein catheterization and renin-level sampling should suggest a tumor site. It should be kept in mind, however, that some renal cell carcinomas and other renal tumors on occasion also produce renin.

Resection leads to a marked drop in blood pressure in most but not all patients, with the latter presumably having a residual angiopathy.

Hemangiopericytoma

Hemangiopericytomas are rare in the kidneys. An occasional one leads to hypertension. These are well-marginated, solid, hypovascular renal sinus tumors involving the renal hilum to the point of suggesting a renal pelvis transitional cell carcinoma. Some are large at the initial presentation, compressing the renal pelvis and causing hydronephrosis and parenchymal atrophy.

Needle aspiration cytology may suggest the diagnosis, although the appearance is similar to that seen with other spindle cell tumors. Immunohistochemistry is helpful.

Renal Capsule Neoplasms

Neoplasms originating from the renal capsule are not common. They represent a spectrum of mesenchymal origin, with some earlier authors simply referring to them as *capsulomas*. They include a histiocytoma, solitary fibrous tumor, leiomyoma, lipoma, and even an angiomyolipoma, the latter a rare site for this tumor. Differentiating capsular from renal and extraperitoneal origin tumors is often difficult, especially with larger ones. Identifying a capsular artery by angiography as a primary tumor

feeding artery is helpful. Depending on the type of tumor, the adjacent renal parenchyma is either compressed or invaded. Often a renal cell carcinoma or oncocytoma is suspected.

Multiple renal capsular leiomyomas have been reported.

Other Tumors

Although a renomedullary interstitial tumor (previously called *medullary fibroma*) is detected in 26% to 41% of autopsies (87), the majority are only several millimeters in diameter and not detected by imaging. One did not enhance by CT, was hypointense both on T1- and T2-weighted images, and arteriography revealed no neovascularity (87).

A normal kidney does not contain fat, and only limited case reports of renal lipomas are published. They predominate in women.

Metastases

Renal

Metastases to the kidneys are common, with multiple foci and bilateral involvement typical. Problems arise when there is a single renal tumor in a patient with a history of a malignancy. Is this an isolated metastasis or a second primary, such as a renal cell carcinoma? Occasionally even an abscess mimics a neoplasm. The distinction influences subsequent patient management, and in such a scenario a renal biopsy is often necessary.

Most renal malignant melanomas represent metastases, but a rare melanoma believed to be primary to the kidney has been reported (88).

Symptoms related to a primary tumor often overshadow those due to renal involvement. A patient occasionally presents with acute renal failure due to diffuse metastases, but more common are silent metastases. Hematuria and proteinuria develop eventually but renal function tends to be preserved until a marked tumor load develops. In a number of these patients a search for renal metastases is more an academic exercise than a practical endeavor.

Many renal metastases have a CT, US, and MRI appearance similar to that of renal cell carcinoma or lymphoma, although metastases tend to be small, multiple, and not deform the renal outline. A renal tumor in a patient with widespread metastases is most likely metastatic. Computed tomography often reveals smaller and more numerous metastases than US; most are hypodense and inhomogeneous on precontrast CT, while postcontrast CT reveals most to have inhomogeneous enhancement. Most enhance less than normal renal parenchyma. Metastatic thyroid carcinomas, on the other hand, tend to be hyperdense and have variable contrast enhancement. Renal vein invasion is rare with metastatic disease.

The sonographic appearance of metastases varies; they range considerably in their homogeneity. Most are hypoechoic, although some, such as thyroid carcinomas, are hyperechoic or even isoechoic.

Metastasis from a hepatocellular carcinoma tends to mimic a renal cell carcinoma with both imaging and even needle biopsy.

A metastatic ovarian or appendiceal cystadenocarcinoma presents as a cystic tumor.

Ureteral

Metastases to the ureter can generally be divided into those from a pelvic cancer and those extrapelvic in origin.

A carcinoma metastatic to the periureteral region obstructs the ureter and the patient presents with flank pain and urinary tract infection. One conservative approach in patients with metastatic disease is US to monitor for hydronephrosis.

Drainage of ureteral obstruction due to pelvic or extrapelvic cancer with double-J catheters has a relatively high success rate; if necessary, a percutaneous nephrostomy is performed.

Self-expandable Wallstents have had limited acceptance in bypassing malignant ureteral obstructions. Patient survival is generally related to the primary tumor and not to stent placement.

Rhabdoid Tumor

Malignant rhabdoid tumors were initially thought to be a variant of Wilms' tumor but currently are believed to represent a distinct clinicopathologic entity. An occasional rhabdoid tumor develops at an extrarenal site. In the kidney it is a highly malignant neoplasm occurring most often in infants, less often in young

children. Curiously, about half of these tumors have an associated primary or metastatic central nervous system tumor.

This is a solid renal hilum tumor. A CT finding of a heterogeneous tumor, together with a peripheral eccentric crescent having an attenuation of fluid, representing subcapsular hemorrhage or peripheral tumor necrosis adjacent to tumor lobules, is common with these tumors. Some contain calcifications outlining tumor lobules. These findings are not pathognomonic, however, and are seen with other renal neoplasms in children. A Wilms' tumor is generally in the differential diagnosis—the distinction is important because of the considerably better prognosis with a Wilms' tumor.

Small Cell Carcinoma

The descriptive term *small cell tumor* is applied to a group of neoplasms having similar morphologic characteristics. These include lymphomas and various neuroendocrine carcinomas. Nonneuroendocrine small cell carcinomas, also called *nonfunctioning neuroendocrine carcinomas* or simply *small cell carcinomas*, are very rare in the kidneys and ureters. Some contain hyperchromatic small cells with neurosecretory granules. Others combine features with a transitional cell carcinoma, and still others exhibit adenomatous or squamous differentiation.

These are very malignant tumors with metastases common at the initial presentation. Often metastases are discovered first.

Neuroendocrine Tumors

An occasional malignant primitive renal neuroectodermal tumor is encountered that cannot be readily classified.

A possible relationship between H2 receptor antagonist therapy and neuroendocrine carcinomas is suggested.

Neuroblastoma

Most neuroblastomas originate in the adrenal glands (discussed in Chapter 16). They occur primarily in the young and often are in the differential diagnosis of a renal or suprarenal tumor.

Neurilemoma (Schwannoma)

A neurilemoma originates from neural Schwann cells and is rare in the kidneys. It has no specific imaging findings. Some extraperitoneal ones simply surround and obstruct the ureter or ureteropelvic junction.

Wide excision is the treatment of choice, because up to one third are malignant. They can recur locally or metastasize.

Carcinoid Tumor

Primary renal carcinoid tumors are rare. These tend to be solid, with an occasional one containing calcifications. An occasional one originates from a cyst wall. For some reason renal carcinoids are more common in horseshoe kidneys (89), developing even in a horseshoe kidney isthmus.

Some larger carcinoids undergo hemorrhagic necrosis.

Dilated Urinary Tract

Renal collecting system dilation, or hydronephrosis, can be secondary to obstruction or functional in nature. Hydronephrosis varies from barely discernible to gigantic. At times huge hydronephrosis displaces the kidney away from its usual location. Complicating the issue, an occasional patient has intermittent hydronephrosis and, when asymptomatic, IV urography or US reveal only mild renal pelvic dilatation at best. These patients should thus be studied when symptomatic.

Urinary Obstruction

General

The etiologies for urinary tract obstruction range from intrinsic to the urinary tract to extrinsic, benign conditions to a malignancy. Some unilateral urinary obstructions are insidious, and renal function is lost before damage is clinically suspected. As an example, in a patient with terminal ileal Crohn's disease, a surrounding inflammatory mass (phlegmon) can involve and obstruct the right ureter and lead to irreversible loss of renal function before damage is detected.

In general, with unilateral ureteral obstruction at an early age, ipsilateral kidney growth is impaired while the contralateral kidney undergoes compensatory growth. This association of ureteral obstruction and subsequent renal growth retardation is probably mediated by complex regulation of cell proliferation, destruction, and other factors.

Urinary perforation proximal to an obstruction is generally secondary to an acute obstruction, typically a stone. An occasional neoplasm, such as a transitional cell carcinoma, not only obstructs the urinary tract but also weakens the ureteral wall sufficiently to produce rupture, but the tumor then continues to grow in the perirenal urinoma. Resultant extensive deformity makes tumor identification difficult.

Imaging

Most imaging of suspected obstruction is straightforward. A contrast study of an acute obstruction shows a persistent unilateral nephrogram and delayed collecting system filling. It should be kept in mind that these findings are not pathognomonic for urinary tract obstruction, and similar changes may be seen with vascular obstruction, a vasculitis, infection, and a number of other causes of renal failure, including acute glomerulonephritis and acute tubular necrosis.

Normally a pyelogram persists for a short period of time after IV contrast. With obstruction, a pyelogram can persist for hours. A pyelogram occasionally persists for weeks if the ureter is encased by tumor, and the lymphatics are an obstruction.

Occasionally urinary tract obstruction cannot be readily distinguished from nonobstructive hydroureteronephrosis. In such a setting the Whitaker perfusion test still has a role. This is an invasive test requiring percutaneous renal pelvis puncture, bladder catheterization, and measurement of pressure differences between the two sites during contrast infusion.

A prominent extrarenal pelvis detected with CT is differentiated from hydronephrosis by evaluating the superior and inferior pole collecting systems; calyces are not dilated in the presence of a simple extrarenal pelvis. Computed tomography readily identifies a dilated ureter, keeping in mind that on occasion a dilated gonadal vein mimics the appearance of a dilated ureter.

In a majority of patients with acute renal obstruction, unenhanced helical CT reveals that an obstructed kidney is less dense than the contralateral unobstructed kidney (90); this difference is visually detected and constitutes a secondary sign for acute obstruction.

Gray-scale US readily detects moderate hydronephrosis as an anechoic region conforming to the renal collecting system. Mild hydronephrosis can be confused with prominent renal veins; Doppler US is helpful in this setting. Determining whether hydronephrosis is indeed secondary to urinary tract obstruction is more problematic. Also, the etiology of an obstruction may not be evident with US.

Gray-scale US is reasonable in monitoring residual postoperative urinary tract dilation in children. Normally infundibular and ureteral dilation decrease gradually after surgery. In children, US findings pointing to obstruction include a hyperechoic renal appearance, a parenchymal rim of 5 mm or less, contralateral hypertrophy, a resistive index (RI) of 1.10 or greater, an RI difference with diuresis of 70% or greater, a ureter diameter 10 mm or greater, and an aperistaltic ureter (91); how practical these findings are in differentiating obstructive from nonobstructive hydronephrosis is not clear.

Resistance to renal arterial blood flow (RI), as measured with renal Doppler US, is increased in most acute obstructive uropathies. With unilateral obstruction, RI and the pulsatility index (PI) are greater in the obstructed kidney than a contralateral kidney, keeping in mind that RI increases with age and some nephropathies. The published RI sensitivities in detecting an acute urinary obstruction depend on accepted RI cutoff values, but even then they vary considerably, and some authors have concluded that RI values are not useful enough to detect acute urinary tract obstruction.

Occasionally endorectal or endovaginal 3D US is helpful with suspected distal ureteral or ureterovesical junction obstruction. Normal ureters have forceful ureteral jets. Initially after stenting, ureters have passive flow, with peristaltic activity only gradually becoming evident; Doppler US is not reliable in diagnosing an obstruction in a stented ureter.

A respiratory-triggered 3D fast spin-echo MR technique can detect urinary tract dilation

without the use of IV contrast. Comparing breath-hold heavily T2-weighted sequences (thin-slice HASTE) with gadolinium-enhanced 3D FLASH MR sequences in patients with acute flank pain, both MR urography techniques were comparable in detecting obstruction (92); however, 3D FLASH was superior for stone detection, reaching a sensitivity of 96% to 100% and specificity of 100% compared with a sensitivity of 54% to 58% and specificity of 100% for HASTE T2-weighted sequences. For the best results, both sequences are recommended in patients with acute flank pain.

Perirenal fluid is common in acutely obstructed kidneys but generally not present with a chronic obstruction. The HASTE MR urography, which identifies not only ureteral obstruction but also presence of any perirenal fluid, detects a high perirenal signal in most patients with acute ureteric obstruction and is thus useful in differentiating acute from chronic obstruction.

Radionuclide renography also identifies most ureteral obstruction if renal function is adequate, but does not provide anatomic detail. Either Tc-99m-DTPA or Tc-99m-MAG3 is commonly used. Radiotracer stasis is evident in a dilated system, be it obstructed or not. In the absence of obstruction, vigorous hydration or the use of a diuretic result in a washout, but an obstruction leads to prolonged retention. Comparing furosemide injected 20 minutes after renography versus furosemide injected 15 minutes before renography in children, the earlier furosemide injection revealed seven times more obstructions than the later injection (93).

Obstruction by Stones (Renal Colic)

Clinical

Acute flank pain and hematuria are typical presentations in patients with acute obstruction. About 85% of these patients have hematuria. An obstruction induces prostaglandin secretion, which increases renal blood flow and glomerular filtration rate and results in renal colic. Nevertheless, a clinical diagnosis of obstruction is not straightforward and is accurate in only about half of the patients.

Although a stone can obstruct anywhere in the ureter, the most common site is at the ureterovesical junction, followed by a site just distal to the ureteropelvic junction and midureter at the iliac vessel level.

One complication among patients with a chronically impacted ureteral stone is a stricture; a previous ureteral perforation at the site of a stone appears to be a risk factor for stricture.

Not all flank pain is due to renal colic. Among less common causes mimicking the flank pain of renal colic are ovarian vein thrombophlebitis. Acute renal artery obstruction can mimic renal colic pain. A unique cause of renal colic was a bird shot calculus after a gunshot wound to the abdomen (94).

Imaging

Considerable literature analyzed the role of conventional radiography and US in patients with flank pain believed to be renal colic in origin, with conventional teaching being that about 80% of ureteral stones contain sufficient calcium to be radiopaque and thus could be identified with conventional radiography. Some studies reported a sensitivity and specificity of over 90% in detecting a calculus, especially if conventional radiography and US are combined. More critical studies, however, do not achieve such optimistic results. In some studies conventional radiographs could detect ureteral calculi with a sensitivity of <50%. A prospective study of patients with renal colic achieved US sensitivity of only 61% in detecting ureteral calculi, while CT sensitivity was 96% (95). Incidentally, conventional abdominal radiography and CT scout radiography have different resolution; thus abdominal radiography revealed 60% and CT scout radiography only 47% of ureteral calculi (96). Digital abdominal radiography identifies most urinary tract calculi >5 mm and those calculi having a CT attenuation of >300 HU (97). Stone visualization can be enhanced on a CT scout view by a low kilovoltage setting.

Traditionally, IV urography was performed for suspected renal colic, but it has been supplanted to a large extent by noncontrast CT. That noncontrast CT is as effective as or better than IV urography in identifying ureteral calculi and equally effective in determining the presence or absence of ureteral obstruction has been confirmed by numerous studies. Helical CT also

provides such accessory signs as periureteral and perirenal fat infiltration and ureteral edema, and, in fact, achieves greater detection of renal and ureteral calculi in patients with acute flank pain than IV urography. Most helical CT studies report sensitivities and specificities in the high 90% for detecting obstructing ureteral calculi. Also, in the absence of urolithiasis an alternative diagnoses can often be established. As a result, in a number of countries, including the United States, noncontrast helical CT is preferred; in other countries, such as France, US has a more prominent role.

One side effect of clinicians becoming more comfortable with unenhanced helical CT in a setting of suspected acute urinary tract obstruction is that the indications for this technique are being arbitrarily expanded. As a result, the number of stones being detected is decreasing and the number of other diagnoses is increasing, a trend bound to continue. Given such expanded indications, an argument can be made for adding a contrast-enhanced CT study if the initial unenhanced CT is negative for obstruction by stones, yet little published data supports such an approach.

Phleboliths are in the differential diagnosis of pelvic calcifications. Most phleboliths are round and on conventional abdominal radiographs often have a radiolucent center, a finding identified with CT in about 10%. Their size and appearance varies and no pathognomonic sign differentiates ureteral stones from phleboliths aside from establishing ureteral continuity for a stone. Especially difficult with noncontrast CT is distinguishing pelvic phleboliths from minimally obstructing distal ureteral calculi, at times leading to unnecessary retrograde urography. Many ureteral stones are surrounded by a soft tissue rim (*soft tissue rim sign*), representing ureteral wall and possible edema, although an occasional phlebolith also has a soft tissue rim. Surrounding edema is less evident in patients with chronic renal failure.

An eccentric, tapering soft tissue density pelvic vein adjacent to a calcification identifies a phlebolith (*comet sign* or *tail sign*); this appearance also is not pathognomonic and a curvilinear nondilated ureter can mimic this appearance. Prevalence of the comet sign varies—some studies find it only in a minority of phlebolith while others believe it is present in a majority.

A passed stone is occasionally detected in the bladder. Secondary signs of prior obstruction, namely, a surrounding soft tissue rim without evidence of a ureteral stone, are often still evident.

A caveat is in order for the patient with clinically suspected obstruction due to a renal stone but a normal unenhanced CT study. Renal ischemia secondary to renal artery obstruction is in the differential diagnosis and will not be detected with precontrast CT. Also, a rare renal carcinoma, not evident on precontrast CT, first presents with flank pain (98), and thus postcontrast CT is necessary in these patients. Alternatively, Doppler US should detect major renal ischemia.

Once a site of obstruction is identified, narrow collimation scanning of the region in question often identifies an etiology. Calculi as small as 1 mm in diameter are detected. Secondary signs of obstruction consist of hydroureter, perinephric and periureteral stranding, ureterovesical junction edema, hydronephrosis, and renal enlargement; keep in mind that calyces are not unduly dilated and little perinephric stranding is evident early in an obstruction or with an incomplete obstruction. In general, the extent of perinephric edema correlates with the degree of ureteral obstruction. Although an indirect sign, attenuation difference between kidneys greater than or equal to 5.0 on unenhanced helical CT achieved a 60% sensitivity and 100% specificity in detecting ureteral obstruction (99).

Whether a stone is impacted at the ureterovesical junction or is already in the bladder can be difficult to determine for stones located close to the ureterovesical junction. If the diagnosis is uncertain with the patient imaged in the supine position, a prone position image will usually distinguish between these entities.

Color Doppler US in patients with complete ureteral obstruction by a stone revealed the absence of a normally present ureterovesical jet; with incomplete obstruction the jet tended to be continuous but decreased in volume and intensity. Also, a distal ureteral stone diverts the jet orientation from its usual anteromedial direction. These findings are indirect evidence for a ureteral stone.

Contrast enhanced MRI can also suggest an obstructed ureter. Defining renal transit time as

the time interval between contrast appearance in the kidney and in the ureter at or below the lower pole level, a time >490 sec suggests an obstructed ureter (100); a normal transit time is <245 sec.

Therapy

The degree of obstruction, the stone location, and the underlying renal function are not major issues during initial therapy of patients with acute ureteral stone obstruction. More relevant is whether CT can predict which stones will pass spontaneously. In patients with a single stone, the mean stone diameter in those with spontaneous stone passage was 2.9 mm and in those with failed conservative therapy 7.8 mm (101); also, perinephric fat stranding and perinephric fluid collections were significantly higher in patients with spontaneous stone passage.

The usual options for obstruction and infection due to ureteral calculi are percutaneous nephrostomy or retrograde ureteral catheterization with drainage. Both procedures relieved an obstruction and infection; the choice depends on procedure availability and cost.

Ureteropelvic Junction Obstruction

Clinical

Ureteropelvic junction obstruction is more common on the left side. Depending on chronicity, the resultant distention ranges from an almost-normal mild renal pelvis prominence to severe hydronephrosis. Likewise, patients can be asymptomatic or have a palpable mass, with the later more common in infants.

Both intrinsic and extrinsic obstructions develop at the ureteropelvic junction. Intrinsic obstructions include congenital strictures, ischemic strictures, fibrosis, redundant mucosa, ureteral kinks, or even a peristaltic abnormality. With some apparent strictures no underlying abnormality is found. Extrinsic obstructions include fibrosis and compression by adjacent blood vessels; the latter are usually incidental findings, although an occasional crossing renal vessel leads to intermittent ureteral obstruction.

Most mild ureteropelvic junction obstructions remain stable for prolonged periods of time. An occasional one resolves spontaneously while some evolve into renal damage. If stable, US is useful in following this condition every 6 months or so.

Imaging

Urography readily detects a ureteropelvic junction obstruction. Some have suggested that US overdiagnoses this condition, although others disagree and believe that US allows the detection of an obstruction at an earlier age.

Computed tomography angiography of patients with symptomatic ureteropelvic junction obstruction should achieve near 100% seusitivity and specificity in detecting crossing arteries. These vessels are either posterior or anterior to the ureter. Axial CT generally is sufficient, although 3D reconstruction provides better spatial orientation of the surrounding structures.

Nonenhanced color Doppler US detected only 65% of crossing vessels in patients with ureteropelvic junction obstruction, while contrast-enhanced Doppler US detected 96% (102). Doppler US proponents thus maintain that their detection results are equivalent to those achieved by CT.

Occasionally an infant with a ureteropelvic junction obstruction has such large renal pelves that they extend almost to the bladder. In such a setting US may suggest an incorrect diagnosis of ureterovesical junction obstruction. Likewise, occasionally vesicoureteral reflux mimics a ureteropelvic junction obstruction.

Patients with an unilateral ureteropelvic junction obstruction have increased differential function as shown with DTPA scintigraphy, possibly due to compensatory hyperfunction.

Therapy and Outcome

Over half of neonates with unilateral hydronephrosis detected by pre- and postnatal US and followed with sequential nuclear renograms eventually revert to normal renal function and washout; those with poor or worsening kidney function and drainage require pyeloplasty.

Adjacent arteries are a relative contraindication to endopyelotomy, and recognition of crossing vessels is of prognostic value for successful endopyelotomy. Nevertheless, the need for preoperative imaging has been questioned

and successful endopyelotomy has been performed in patients with ureteropelvic junction obstruction who had CT evidence of crossing vessels.

Children with unilateral ureteropelvic junction obstruction have not only impaired renal function but also delayed body growth. Longstanding dilation often persists after pyeloplasty, but renal function improves, mostly in younger children. Improvement is slow—only in a minority during the first 6 months, but a majority of the patients improve within 2 years. Long-term follow-up of retrograde balloon dilatation of ureteropelvic junction stenosis reveals variable results; some patients had persistent residual stenosis, but in a few the procedure led to complete ureteropelvic junction obstruction requiring surgical correction.

Ureteral Obstruction

Strictures

The etiologies of a benign ureteral stricture are listed in Table 10.8. Ureteral ischemia is a not uncommon cause of ureteral stricture. Most benign strictures involve a short segment, although an occasional one extends for considerable length.

Benign ureteral strictures are dilated using either an antegrade or retrograde approach. Success depends not only on the underlying etiology and the length of a stricture but also on relative operator expertise. Balloon dilation using a percutaneous approach has become popular, including dilation of restenosis, although overall the long results of percutaneous dilation have been poor and, at times, even multiple dilations do not achieve ureteral patency.

A rare cause of bilateral ureteral obstruction and hydronephrosis is retroperitoneal systemic sclerosis.

Table 10.8. Etiologies of benign ureteral strictures (from more common to less common)

Ureteral stones
Ischemia
Thromboemboli
Vascular reconstructive surgery
Sequelae to adjacent organ resection
Polyarteritis nodosa
Trauma
Adjacent Crohn's disease
Infection
Tuberculosis
Bilharziasis
Retroperitoneal fibrosis
Idiopathic

Extrinsic

Ureteral metastases have already been discussed. Occasionally inflammation surrounding an abdominal aortic aneurysm entraps one or both ureters and results in obstruction. Similarly, extrinsic ureteral compression and obstruction occurs with abdominal fibromatosis due to several disorders.

Aberrant arteries may compress a ureter, leading to varying degrees of obstruction. As already mentioned, the most common location is at the ureteropelvic junction, but it can occur anywhere along the ureter.

Ureteral obstruction develops secondary to an adjacent neoplasm, perforated appendiceal abscess, and an adjacent hematoma. An ileocecal phlegmon in Crohn's disease not uncommonly obstructs the right ureter, but rarely the left. Extensive periureteral venous collaterals due to a thrombosed or absent infrarenal vena cava can result in ureteral obstruction. Anecdotal reports describe an infected urachal cyst, uterine prolapse, and even methacrylate migrating into the pelvic cavity after hip arthroplasty, resulting in ureteral obstruction. Castleman's disease can present as a recurrent tumor, detected by imaging (103).

Placement of metallic stents in ureters obstructed by an extrinsic tumor, such as an extensive gynecologic cancer, is effective in maintaining renal function during chemotherapy or radiation therapy. If necessary, these stents can be augmented by cystoscopically inserted temporary J endostents. Renal RI, obtained from Doppler US data, was found useful in following patients with unilateral extrinsic ureteral obstruction after therapy with double-J ureteral stents (104).

Retrocaval Ureter

A retrocaval ureter represents an anomalous vena caval development with persistence of the ventral vasculature. A retroiliac ureter is rare. The clinical significance of a retrocaval ureter depends on the degree of obstruction. Urography suggests the diagnosis. Contrast-enhanced CT should be diagnostic.

Reanastomosis using a laparoscopic approach is a viable option.

Ovarian Vein Syndrome

Ovarian vein syndrome consists of ureter compression between the external iliac artery and a dilated ovarian vein. It is more common on the right. Occasionally a thrombosed right ovarian vein produces a distinct impression on the ureter, although obstruction is rare.

A similar syndrome on the left side is due to ureter compression between a dilated ovarian vein and the psoas muscle.

Endometriosis

Ureteral endometriosis is generally part of diffuse pelvic involvement. Both focal and diffuse disease lead to ureteral obstruction, generally in the distal ureter. It can be silent and progress to loss of renal function. At times both ureters are involved.

A typical appearance is that of a focal or long infiltrating-appearing ureteral stricture, similar to encasement by extrinsic fibrosis or tumor. Retroperitoneal fibrosis has a similar appearance but the two conditions have different clinical presentations.

Hernia

Ureteral herniation is a rare cause of ureteral obstruction. Possible herniation sites include inguinal, femoral, and sciatic hernias. A number of these obstructions are chronic, manifesting by more proximal hydronephrosis.

Any imaging modality visualizing the ureter should detect such a hernia.

Other Obstructions

Ureteral polyps are not common. Occasionally such a polyp intussuscepts and results in an acute obstruction.

Antegrade ureteral intussusception can develop after antegrade instrumentation. Intussusception can be related to an indwelling endoprosthesis.

A cholesteatoma in the midportion of the left ureter led to obstruction and hydronephrosis (105).

Rarely, polyarteritis nodosa is associated with ureteral obstructions, presumably due to a periureteral vessel vasculitis.

During Pregnancy

Proximal ureters dilate during pregnancy due to extrinsic compression, although hormonal factors may also play a role. At times dilation is asymmetrical and a superimposed ureteral calculus is suspected. Dilation gradually resolves after delivery.

With suspected obstruction during pregnancy US evaluates hydronephrosis and at times suggests an etiology. Ureteral jets identified at color Doppler US imply lack of obstruction at the ureterovesicular junction. Occasionally late in a pregnancy no ureteral jet is identified in the absence of obstruction; turning the patient to a contralateral decubitus position generally restores this sign.

Spontaneous urinary tract rupture during pregnancy is rare and generally occurs in a setting of a diseased kidney. Rupture is either in the collecting systems or it involves the kidney parenchyma. Most ruptures occur in the second or third trimester.

If relief of an obstruction is believed necessary, a percutaneous nephrostomy rather than surgical decompression should be considered. Many women with symptomatic acute hydronephrosis are managed with ureteral stenting.

Diabetes Insipidus

Nephrogenic diabetes insipidus is a cause of nonobstructive urinary tract dilatation.

Reflux

Clinical

Vesicoureteral reflux is abnormal. A number of investigators ascribe most reflux to an abnormal ureterovesical junction, although morphologi-

cally this junction is indistinguishable from those without reflux. Nerve density and distribution are similar. Especially in male infants, vesicoureteral reflux tends to be associated with abnormal voiding urodynamics, such as a small voided volume, inadequate voiding dynamics, markedly dyssynergy, and an obstructive pattern. In males an association exists between reflux and a simultaneous increase in detrusor pressure. A familial tendency to vesicoureteral reflux exists.

In children, vesicoureteral reflux is associated with urinary tract infection and impaired growth, although whether reflux per se or the often commonly associated renal tubular acidosis is responsible for growth failure is not clear. Although both reflux frequency and grade tend to decrease with age, reflux remains a common cause of end-stage renal failure requiring renal transplantation. Some of these children also develop hypertension or urinary infections and thus may also require bilateral nephrectomies of the native kidneys.

Reflux tends to be intermittent, and the time to resolution varies widely.

A ureter inserting into a diverticulum is at an increased risk of vesicoureteral reflux. Patients with renal dysplasia are also at an increased risk for reflux, although whether dysplasia is secondary to reflux is not clear.

Screening

In view of renal parenchymal damage associated with vesicoureteral reflux, should US screening for reflux be instituted early in life? Several studies have found that even using a meticulous technique, prenatal and neonatal US achieves a low sensitivity for detecting vesicoureteral reflux. In children, often major renal damage has already occurred when an acute urinary tract infection or a megaureter becomes evident. One proposal is to perform cystography in those at risk for reflux, such as newborns with pyelocaliceal dilation and in siblings of those treated for vesicoureteral reflux, yet such an approach also misses some infants with reflux.

Detection

A search for reflux appears appropriate in infants with a urinary tract infection. Although often called screening, in a pure sense this is no longer screening but an attempt to detect reflux in a symptomatic patient. Young boys probably should also be studied if they develop an infection because of the relatively high prevalence of posterior urethral valves. Screening of girls with a first infection is somewhat controversial, but a general trend toward earlier study is evolving. In women a search for reflux is appropriate for recurrent infection.

The two primary examinations used to detect vesicoureteral reflux are fluoroscopic voiding cystourethrography and radionuclide cystography, with some centers also having introduced contrast enhanced voiding urosonography. Each study has its proponents. Scintigraphy has a lower radiation dose but also provides fewer anatomic details. One approach is to use voiding cystourethrography in boys, who are more prone to have other underlying anatomic abnormalities such as urethral valves, and radionuclide cystography is girls, in whom anatomic abnormalities are uncommon. Because of its low radiation dose, radionuclide cystography is useful as a follow-up examination, but the lack of anatomic detail limits it as a first study.

A number of vesicoureteral reflux grading systems have been proposed. One classification, based on the results of voiding cystourethrography, is outlined in Table 10.9. Reflux can be missed with incomplete bladder distention. At times reflux is observed only after several episodes of bladder filling to capacity and having the patient void. If reflux is detected during a voiding cystourethrogram, the study should be modified so the degree of calyceal and ureteral dilation can be evaluated and any

Table 10.9. Classification of vesicoureteral reflux

Grade	Description
I	Reflux into ureter
II	Reflux into collecting system, without dilation and with normal calyceal fornices
III	Reflux into collecting system, with mild to moderate ureter dilation and mild dilation of renal pelvis
IV	Moderate ureter and renal pelvis dilation, obliteration of forniceal angle but papillary outline is preserved
V	Severe ureter, renal pelvis and caliceal dilation, papillary outline not preserved

underlying obstruction detected. Often a duplicated collecting system can be suspected from this examination.

What is the role of US in detecting reflux? Intermittent renal collecting system dilation and contraction during real-time renal US is an indirect sign of vesicoureteral reflux (106). Likewise, renal pelvis dilation during bladder contractions points to reflux, yet a large minority of children with negative renal US have reflux at voiding cystourethrography.

In spite of some rather optimistic claims, it is still difficult to gauge the accuracy of intravesical contrast enhanced voiding US in detecting and grading vesicoureteral reflux in children. Although presence of microbubbles in the ureters or renal pelves does signify reflux, in one study 38% of such reflux was graded either lower or higher than with voiding cystourethrography (107). Additional work is necessary to place contrast enhanced voiding US in a proper clinical perspective.

An occasional author suggests air as a US bladder contrast agent; although uncommon, intravasation of an instilled contrast agent does occur, especially with the distention pressures generally employed to detect reflux, and air thus cannot be recommended.

Mild renal pelvic dilation detected at renal US is not a reliable sign of vesicoureteral reflux. An increase in renal pelvic size on postvoid US also does not signify vesicoureteral reflux.

Upper urinary tract wall thickening in children occurs secondarily to urinary tract infection, chronic obstruction, and chronic vesicoureteral reflux. Thus voiding cystourethrography appears reasonable to evaluate for reflux in these children if US detects upper urinary tract wall thickening.

Radionuclide cystography is performed with Tc-99m–sulfur colloid (it is not absorbed from the bladder). Reflux is detected as any activity superior to the bladder. A reflux grading system of *mild*, *moderate* and *severe* is generally employed. This radionuclide test provides grossly similar information to a voiding cystourethrogram regarding reflux, although continuous monitoring during scintigraphy may better detect intermittent reflux. Its disadvantage is a poorer spatial resolution. At times vesicoureteral reflux is not evident during an initial fluoroscopic or scintigraphic study, but reflux becomes apparent during a second cycle of bladder filling. When to perform such a second cycle is not clear; a positive study is more common in patients strongly suspected of having reflux.

The SPECT Tc-99m-DMSA is a noninvasive test useful in assessing functional kidney impairment in children due to pyelonephritis or in those with vesicoureteral reflux.

Therapy

Due to increased pre- and postnatal US screening, more infants with vesicoureteral reflux are being detected. Reflux is being managed both medically and surgically. Endoscopic therapy consists of injecting polytetrafluoroethylene (Teflon) or polydimethylsiloxane (Macroplastique). Resection after the failure of endoscopic therapy reveals that both substances induce an inflammatory giant cell macrophage reaction, new vessel formation, and fibrosis (108).

Among 302 children under 11 years of age with urinary tract infection and grade III or IV vesicoureteral reflux enrolled in the European branch of the International Reflux Study in Children group and randomly assigned to surgical or medical therapy, follow-up for 10 years with serial IV urography revealed no significant difference in mean renal growth between the two groups (109). Debate continues, however, about the relative merits of conservative versus surgical therapy.

Conventional Surgery

The classic surgical therapy for vesicoureteral reflux is ureteral reimplantation. Infants with reflux typically undergo surgical correction at about the age of 6 months, although in a setting of hydronephrosis or renal damage correction as early as 1 month of age is performed. In some surgical centers a very high success rate in correcting reflux is achieved.

A minority of patients with unilateral vesicoureteral reflux treated by reimplantation develop postoperative contralateral vesicoureteral reflux; most such reflux resolved spontaneously. Although it is tempting to attribute any new contralateral reflux to the surgical procedure, one should keep in mind that new reflux develops in some children.

In some children with persistent vesicoureteral reflux after ureteral reimplantation, subsequent endoscopic subureteral Teflon injection corrects the reflux in most.

Injection Therapy

Subureteral collagen or polytetrafluoroethylene (Teflon) injection is an alternative therapy to surgical ureteral reimplantation and it corrects reflux in about 80% of patients. In children with neurogenic bladder dysfunction and vesicoureteral reflux, success rates are greater after ureteroneocystostomy than after subureteral Teflon injection, yet the latter procedure is often employed in managing reflux because of relative procedure simplicity and ability, if necessary, to perform secondary reimplantation. The operative cost is considerably less than that for reimplantation, and morbidity is minimal.

Results of endoscopic collagen injection in treating children with reflux into a totally duplicated ureter system were disappointing; eventually many of these children require surgical correction.

Among infants and children with posterior urethral valves and vesicoureteral reflux, reflux resolves in only a minority. Most require correction.

Ultrasonography shows collagen to be hyperechoic compared to the bladder wall shortly after endoscopic subureteral injection, and it gradually becomes isoechoic. On a long-term basis US does not detect some residual periureteral Teflon.

Diverticula

Calyceal

Calyceal diverticula are lined by transitional epithelium and communicate with an adjacent calyx. They can be located anywhere in the collecting system, although upper and lower pole fornices predominate. Their pathogenesis is unknown. Most are incidental findings. An occasional one becomes obstructed or is a site for stone formation and a nidus for infection.

Many of these diverticula have a typical radiographic appearance. They communicate with an adjacent calyx; thus postcontrast they opacify only after contrast enters the involved calyx, differentiating them from papillary necrosis, which, being in continuity with tubules of Bellini, opacifies before the involved calyx. Some contain debris or stones. Delayed contrast filling is evident with some.

A cyst communicating with a calyx is a nonspecific finding: a pyelogenic cyst or any inflammatory or neoplastic tumor can rupture into a calyx. Radiographically, an abscess that has drained into an adjacent calyx has a similar appearance.

Percutaneous calyceal diverticulectomy (most with stones) consists of stone removal and diverticular neck incision or dilation and diverticular wall fulguration.

Ureteral

The pathogenesis of ureteral diverticula is not clear. Some authors refer to them as pseudodiverticula. They are usually detected during high-quality urography or retrograde pyelography and appear as small ureteral outpouchings. They occur primarily in the upper one third of the ureter and generally are multiple and often bilateral.

Associated urinary tract abnormalities are common, ranging from bladder outlet obstruction, to neoplasms, to renal stones and others.

Calcifications

Urolithiasis

Clinical

Urolithiasis means a calculus within the urinary tract. Renal (nephrolithiasis) and ureteral calculi predominate in developed countries, while bladder calcifications are more common in underdeveloped parts of the world. Stones range from small to large. Most radiologists have encountered a giant staghorn calculus; these have a complex composition. An underlying urinary tract infection is common.

Most patients with nonobstructing stones are asymptomatic, although an occasional stone results in hematuria or infection.

In general, about one third of patients with a first renal stone develop a recurrence within 5 years. These patients are usually investigated for an underlying cause, such as primary hyperparathyroidism, renal tubular acidosis, urinary tract infection, and cystinuria. Urography, lately supplanted by noncontrast CT, is often included in the workup. Stone analysis often guides further studies.

A study based on data from the Swedish Inpatient Register and Swedish Cancer Registry followed over 61,000 patients hospitalized for renal or ureter stones and concluded that although these patients are not at risk for developing a future renal cell cancer, they are at increased risk for renal pelvis, ureter, and bladder cancer (110); chronic irritation and infection appear to play a role because tumors tended to develop on the same side as stones.

Associated Conditions

Epidemiologic studies have established an association between arterial hypertension and renal stone disease. Alterations in calcium metabolism play a role in both entities.

Over 5% of cystic fibrosis patients older than 15 years have had urolithiasis in the past.

Renal stone disease is induced by some drugs. In France, the most common drugs involved are calcium and vitamin D supplements and long-term therapy with carbonic anhydrase inhibitors (111). Furosemide therapy of premature neonates for hyaline membrane disease is associated with urolithiasis.

Occasionally reported is heterotopic ossification within a renal stone. A suture retained in the renal pelvis from prior surgery can act as a nidus for subsequent calcification.

Patients with primary hyperparathyroidism have an increased prevalence of renal stones, but only a small percentage of patients with idiopathic stones are hyperparathyroid. A metabolic defect is detected in about half of patients who develop calcium stones.

Calcium containing stones consist of calcium oxalate and calcium phosphate. Less common are magnesium ammonium phosphate (struvite) stones. Calcium oxalate stones are associated with certain blood groups. The prevalence of these stones in patients with blood group O is several times greater than in patients with blood group A.

Patients with gout, Crohn's disease involving the small bowel, and some myeloproliferative disorders have an increased prevalence of uric acid stones. Pure uric acid stones are lucent.

Cystine stones develop in a setting of cystinuria, a rare autosomal-recessive disorder. These stones form in the first and second decades of life, while uric acid stones form in older patients. Cystine stones are only slightly radiopaque and range from small to large. Recurrent stones are common, and lifetime surveillance is necessary in affected individuals.

Patients with struvite stones are prone to persistent infections.

Imaging

Imaging of suspected urinary obstruction is discussed in the previous Dilated Urinary Tract section.

Unenhanced CT readily identifies ureteral stones; keep in mind that with the use of wide collimation some smaller stones, especially uric acid stones, are insufficiently dense to be detected. Narrow collimation is thus necessary. At 1-mm collimation, stones can be grouped by attenuation: uric acid (least dense), cystine and struvite, calcium oxalate monohydrate, and brushite and hydroxyapatite (most dense) (112). In vitro CT using HU measurements of chemically pure stones identified the chemical composition of uric acid, struvite, and calcium oxalate stones, but could not differentiate calcium oxalate from brushite stones and struvite from cystine stones (113); the use of dual CT kilovoltage aids differentiation.

The sonographic appearance of a calculus reflects its size rather than its internal composition. Calculi are hyperechoic and, aside from small ones, have posterior acoustic shadowing (Fig. 10.31). Ultrasonography is insensitive in measuring stone size. Ultrasonography is better in detecting renal calculi than ureteral calculi. In women, transvaginal US can detect stones in the distal ureter, and this modality should be considered in the pregnant patient.

An interesting stone finding consists of a "twinkling" artifact detected by color and power Doppler US (114); this phenomenon appears as a rapidly changing color complex located behind a stone, similar to a comet's tail. It aids in stone detection. Also, a twinkling artifact depends, in part, on stone composition. Thus it

Figure 10.31. Right renal nephrocalcinosis in a child. Longitudinal US scan identifies numerous discrete hyperechoic foci in the kidney. (Courtesy of Luann Teschmacher, M.D., University of Rochester.)

is present with calcium oxalate dihydrate and calcium phosphate stones, but it is absent with calcium oxalate monohydrate and urate stones (115).

Magnetic resonance reveals a stone as a signal void, regardless of stone composition. T2-weighted MRI (MR urography) identifies hyperintense urine, at times in a dilated ureter, and a hypointense or signal void stone at the site of obstruction. A blood clot also results in a hypointense signal.

Conventional radiographs are often employed in follow-up of known stones; stones detected only with helical CT should be followed with that imaging modality. Helical CT allows 3D reconstruction of stone shape, number, and size. The role of helical CT in lithotripsy planning is still evolving.

Therapy

The ideal goal of therapy is to eliminate all fragments. One proposed stone management strategy consists of surveillance for asymptomatic caliceal stones <5 mm in diameter; symptomatic stones <20 mm in diameter are treated with ESWL, while a combination of percutaneous nephrolithotomy and ESWL is used for stones >20 mm in diameter (116); stones resistant to ESWL, such as cystine stones, often require percutaneous nephrolithotomy or ureterorenoscopic endocorporeal lithotripsy.

Extracorporeal Shock-Wave Lithotripsy

Extracorporeal shock-wave lithotripsy (ESWL) is now the treatment of choice for most larger renal or ureteral calculi. Both US and fluoroscopic guidance are employed. Occasionally IV contrast is necessary to define a stone. Large stones are often approached by both ESWL and percutaneous nephrolithotomy, while patients with an underlying congenital anomaly tend to undergo surgical reconstruction and stone clearance.

Extracorporeal shock-wave lithotripsy is used to treat patients with urolithiasis in a solitary kidney and patients with calculi in anomalous kidneys. An increased risk exists with a solitary kidney, because a subcapsular hematoma after ESWL in a solitary kidney can result in acute renal failure. Extracorporeal shock-wave lithotripsy is performed in children; although the procedure is similar to that in adults, some issues, such as sedation, are more pertinent to children.

The overall success rate for lithotripsy is about 80%, although the rate varies among institutions and with stone size and composition. An ESWL study found that 95% of calculi <15 mm in maximum length were successfully disintegrated, while only 8% of those >25 mm in length were disintegrated (117); for calculi between 15 and 25 mm, however, instead of maximum length, volume was a better indicator, with 90% of calculi <6 cm^3 successfully disintegrated, while none >6 cm^3 were disintegrated. Spiculated, low-density stones are cleared more readily than smooth, dense stones. Peak shock wave pressure generated by many ESWL units at the focus is between 80 and 120 MPa, and, in theory, the peak pressure required to disintegrate a 6-cm^3 calculus was calculated to be approximately 80 MPa (117).

Technetium-99m-DMSA scintigraphy performed the day before and at least 6 months after ESWL in children did not identify any significant parenchymal lesions (118); stone fragmentation or elimination was achieved in 90% of these children. Likewise, no blood pressure or renal function changes were evident.

In patients who become stone free after ESWL, the ipsilateral typical recurrence-free rates are about 95% and 65% after 1 and 5 years, respectively, and vary depending on the therapy for any underlying lithogenesis.

Morbid obesity makes ESWL difficult. Patients with a bleeding diathesis require adequate perilithotripsy therapy. The literature suggests that lithotripsy is feasible in patients with calcified aneurysms and cardiac pacemakers, but it requires close monitoring. Pregnancy is generally considered a contraindication to ESWL.

Patients with a pheochromocytoma have had severe reactions while undergoing ESWL.

Less than 1% of patients develop a hematoma; preexisting hypertension is a risk factor for perinephric or subcapsular hematoma. These hematomas can be diagnosed by US and most are managed conservatively. An occasional patient with a perirenal hematoma manifests hypertension, generally transient; a rare patient develops permanent hypertension as a late finding; a temporal relationship to previous lithotripsy is difficult to establish; some of these patients have had decreased renal function prior to lithotripsy.

Fever suggesting postprocedure obstruction is approached with urinary tract drainage and possible ureteroscopy. Drainage catheters are inserted to bypass a heavy stone load. Few complications are associated with these ureteral catheters, although encrustation becomes a problem in catheters retained longer than about 6 weeks.

A resultant fibrous scar, detected by imaging, is presumptive evidence for renal parenchymal damage during lithotripsy. Posttherapy Tc-99m-DMSA scintigraphy should detect any acquired parenchymal scars after ESWL. Anecdotal complications include renal laceration, small bowel perforation, splenic rupture, and even abdominal aortic rupture.

Ureteroscopy

Using an ureteroscopic approach, therapy options for ureteral stones include laser or electrohydraulic lithotripsy or simply the use of endoscopic baskets and similar grasping tools. Even intrarenal calculi are amenable to such therapy.

Ureteroscopy is more successful than ESWL for larger calculi. One option is ureteroscopic laser lithotripsy. Lithotripsy stone fragmentation is more successful in lower ureteral stones than in upper ureteral stones. Stone fragmentation by holmium:yttrium-aluminum-garnet (Ho:YAG) lithotripsy is primarily due to photothermal chemical decomposition rather than to photomechanical or photoacoustical fragmentation (119); thus calcium carbonate was found in samples composed of calcium oxalate calculi, calcium pyrophosphate in calcium hydrogen phosphate stones, free sulfur, and cysteine in cystine stones and cyanide in uric acid calculi.

Percutaneous Nephrolithotomy

In a retrospective study of lower pole stones 10 to 20 mm in size, a stone-free status was achieved in 44% of patients with ESWL and 72% with percutaneous nephrolithotomy (120); the difference in success rate was less significant for smaller stones. On the other hand, morbidity was higher with the nephrolithotomy technique.

Severe hemorrhage developed in 2% of patients after percutaneous nephrolithotomy (121); renal arteriography revealed a mix of arteriovenous fistulas, false aneurysms, and arteriolar injuries, all successfully treated by embolization.

Staghorn Calculi

Staghorn calculi are usually treated by either ESWL or surgery, but the optimal therapy is still controversial. Lithotripsy alone is effective in about 50% of the patients.

Ultrasonography guidance is an option for percutaneous lithotomy, but the entire stone burden is removed only in a minority of patients; others require either lithotripsy or surgery.

Fiberoptic transurethral nephrolithotripsy has been combined with ESWL to treat staghorn calculi. The stones are initially disintegrated by nephrolithotripsy, and ESWL is then performed for residual fragments.

Nephrocalcinosis

Nephrocalcinosis designates renal parenchymal calcifications. These calcifications range from discrete to diffuse and tend to be bilateral. Nephrocalcinosis can be further subdivided by location—cortex or medulla. In either site calcifications can be dystrophic or metastatic. Dystrophic calcifications (those in abnormal tissue) develop at sites of ischemic, necrotic, or infected tissue, while metastatic nephrocalcinosis develop in normal tissue.

Medullary nephrocalcinosis tends to be bilateral and symmetrical. It has developed in a setting of vesicoureteral reflux, presumably related to urine stasis in collecting tubules.

Precontrast CT in medullary nephrocalcinosis reveals multiple medullary calcifications. Some mimic nephrolithiasis.

Ultrasonography appears to be reliable in grading nephrocalcinosis, although reliability in assessing change between examinations is only fair. Ultrasonography in primarily medullary nephrocalcinosis reveals hyperechoic medullary pyramids. Posterior shadowing develops only when the condition is advanced. Ultrasonography findings may precede the development of visible calcifications seen with conventional radiography.

Sarcoidosis

Sarcoidosis typically involves lungs, skin, and, at times, eyes. In a setting of sarcoidosis about 25% of patients develop hypercalciuria and 15% urinary lithiasis. A rare manifestation of renal sarcoidosis is focal granulomatous interstitial nephritis (122), with secondary ectopic calcitriol secretion by the granulomas and resultant nephrocalcinosis.

Rarery, ureteral infiltration by sarcoidosis leads to obstruction and hydronephrosis.

Calcifications in Cysts

An occasional benign cyst contains thin, curvilinear calcifications, probably induced by prior hemorrhage or infection. Any amorphous calcifications should raise suspicion for a neoplasm.

Hyperoxaluria

One of the conditions resulting in diffuse cortical calcifications is oxalosis. When extensive, these calcifications can be identified with conventional radiography.

Gas in the Parenchyma or Collecting System

Gas in the renal parenchyma or collecting system can be secondary to a fistula, abscess, or emphysematous pyelonephritis.

A spontaneous nephrocutaneous or nephroenteric fistula is rare and is usually associated with a staghorn calculus and obstruction. A fistula can be secondary to an extrinsic infection or, less likely, a neoplasm.

Computed tomography shows gas-fluid collections within the kidney, perinephric inflammatory changes, and, at times, extension of renal contrast outside the collecting system. Neither an antegrade nor a retrograde pyelogram may define a renal fistula.

Antegrade stent insertion is the primary therapy of choice for an enteroureteral fistula. If the antegrade approach fails, a cystoscopic retrograde approach will generally also fail. In some patients combining an antegrade with a retrograde approach succeeds in stent placement.

Renal Failure/Insufficiency

Clinical

Differentiation of renal failure from renal insufficiency depends on the degree of loss in renal function, with the final end point of renal failure being end-stage renal disease. The etiologies of renal failure are complex, varied, and often interrelated; some are listed in Table 10.10. Differentiation into acute and chronic renal failure aids in clinical management. A subdivision into prerenal, renal, and postrenal etiologies is helpful. Diabetes mellitus is the most common cause of chronic renal failure in adults. Vesicoureteral reflux is probably the commonest cause of end-stage renal failure in children. Most patients with glomerular kidney disorders have a progressive loss of renal function, with eventual histologic evidence of glomerulosclerosis and tubulointerstitial fibrosis. Presumably such fibrosis is not the initiating factor in renal failure but represents a final pathway.

Urinary tract obstruction is an uncommon cause of renal failure, except in individuals with a single kidney, where it can lead to either acute or chronic renal failure. Ultrasonography readily detects hydronephrosis and can steer the further workup, but keep in mind that an occasional obstructed urinary system does not lead to hydronephrosis. Intravenous urography is not indicated in acute renal failure even with a suspected urinary obstruction.

Table 10.10. Conditions associated with renal failure

Vascular causes (hypoperfusion) Bilateral renal artery occlusion/stenosis Shock Hypertensive nephropathy Other causes for ischemia	Rhabdomyolysis
Diabetic nephropathy	Pregnancy-related
Vesicoureteral reflux	Nephrotic syndrome
Urinary obstruction Stones Benign strictures Malignant obstruction	Membranous nephropathy
Urinary infection	Glomerulonephritis (acute or chronic)
Papillary or cortical necrosis	Hemolytic-uremic syndrome
Acute tubular necrosis	Cirrhosis/hepatorenal syndrome
Acute interstitial nephritis	Congenital medullary cystic disease
Drug or poison induced	Polycystic kidney disease Autosomal dominant Autosomal recessive
Tubulointerstitial nephritis	Alport's syndrome
Multiple myeloma	Chronic tubular dysfunction Renal tubular acidosis Fanconi's syndrome Cystinosis

Upper gastrointestinal symptoms are common in patients with chronic renal failure. Most patients with chronic renal failure have an abnormal radionuclide solid meal gastric emptying time. Renal failure patients developing upper gastrointestinal bleeding should be suspected of erosive gastritis, erosive esophagitis, and gastric ulcer.

An occasional patient with renal failure develops spontaneous hypoglycemia.

The following discussion of renal failure causes is subdivided only approximately and overlap exists. For instance, hypoperfusion (shock) due to trauma is a cause of acute prerenal failure but can also lead to acute tubular necrosis.

Imaging

Renal failure often has no characteristic imaging characteristics per se, but certain findings are useful. The kidneys tend to increase in size in patients with acute renal failure, an increase measurable with US. Chronic renal failure, on the other hand, results in small, hyperechoic kidneys due to underlying sclerosis and fibrosis. Ultrasonography identified an extracapsular hypoechoic rim, called the *kidney sweat sign*, in 14% of 330 patients with renal failure (123); this finding occurs bilateral. Magnetic resonance imaging reveals a loss of corticomedullary interface in a setting of renal insufficiency due to a variety of conditions. The primary role of imaging is to exclude obstruction and detect hydronephrosis, calculi, and location and size of the kidneys. Depending on the information needed, US or scintigraphy is sufficient in some patients, while in others noncontrast CT is necessary. In some patients with renal failure a contrast study is necessary to exclude a vascular etiology.

Magnetic resonance imaging measurement of mean cortical thickness in patients with glomerular disease differs significantly from that in patients with normal kidneys and those with other renal parenchymal disorders. The normal postcontrast pyelocaliceal phase MR signal intensity decrease is lacking in renal insufficiency patients; this change is due to the reduced renal concentrating ability in these patients. Also, a minority of patients with renal disease have diffuse medullary hyperintensity on delayed postcontrast images.

Serum creatinine level is only a crude estimate of renal function; creatinine clearance is a better test, although it is of limited use in a

setting of acute renal failure. Newer methods of estimating glomerular filtration rate include plasma clearance of small amounts of iohexol, a nonionic contrast agent. A correlation exists between renal clearance of inulin and iohexol in patients with moderate to severe renal failure. Doppler US appears useful in following acute renal failure; recovery of renal function is associated with a progressive drop in resistive index.

The normal postintravenous contrast pyelocaliceal phase MR signal intensity decrease is lacking in renal insufficiency patients; this change is due to the reduced renal concentrating ability in these patients.

Vascular Causes

A common cause of acute prerenal failure is hypoperfusion due to either cardiac failure or hypovolemia; the latter condition is detected with a fluid-load challenge. Bilateral renal artery or vein occlusion, although rare, also leads to renal hypoperfusion, with a lack of response to a fluid load. Vascular occlusion in a solitary kidney is perhaps a more common cause of acute failure than bilateral vascular involvement; US should exclude this finding.

Atherosclerotic vascular disease or small vessel disease such as cholesterol crystal embolization have led to acute renal failure. Drug-induced vasomotor disorders also play a role. Bilateral vasculitis leading to renal artery obstruction and small vessel disease are less common causes of acute renal failure.

Hypertensive nephropathy and related renal artery stenosis are common causes of chronic renal failure. The latter is discussed in Chapter 17.

Acute Tubular Necrosis

Acute tubular necrosis is a common cause of acute renal failure and associated high morbidity and mortality. The causes of acute tubular necrosis include nephrotoxic, ischemic, hypotensive, and other factors. It occurs after bilateral ureteral obstruction due to any cause. The evidence suggests that it is induced by tubular damage and tubular obstruction, although a role for renin is also suggested. Included among nephrotoxic agents are the following:

1. Iodinated radiographic contrast agents. The risk of nephrotoxicity is increased in a setting of impaired renal function.
2. Viper venom is mainly hemotoxic and causes coagulation abnormalities, but about one third of patients after systemic envenomation have renal involvement; renal biopsy in those with severe renal dysfunction reveals acute tubular necrosis.
3. Overexposure to aliphatic hydrocarbons present in diesel fuels and solvents.
4. A nephropathy due to *Amanita phalloides* exposure.

Clinically, acute tubular necrosis is mimicked by bilateral renal artery occlusion or severe stenosis, and these conditions should be excluded. Ultrasonography identifies normal kidneys in a setting of acute tubular necrosis. Doppler US, however, reveals an increased RI in most of these patients. Scintigraphy with Tc-99m-DTPA or Tc-99m-MAG3 is useful in these patients to confirm the presence of acute tubular necrosis and exclude renal vascular occlusion; parenchymal activity without excretion suggests acute tubular necrosis.

Intravenous contrast in patients with acute tubular necrosis shows a dense, persisting nephrogram with little or no excretion of contrast from enlarged kidneys. Contrast can persist in renal parenchyma for a prolonged time.

Acute Cortical Necrosis

The etiology of acute cortical necrosis is usually multifactorial. Prior to 1980, obstetrical causes were common; since then sepsis, dehydration, drugs (discussed in the next section), and, in India, snake bite predominate. Shock and transfusion reaction have been implicated. Urinary obstruction is occasionally implicated. Chronic pyelonephritis, diabetes, and hypotension probably also play a role in this condition.

The underlying abnormality is cortical ischemia with relative sparing of medulla. Peripheral cortical regions remain viable due to intact capsular vessels. Initially involved kidneys enlarge but on a chronic basis shrink in size.

Acute cortical necrosis can be unilateral or bilateral. The papillae cavitate, and communi-

cate with an adjacent calyx, and the sloughing of papillae leads to calyceal clubbing. In time, linear cortical calcifications develop.

A diagnosis of acute cortical necrosis is most often suggested by IV urography or postcontrast CT. It can be detected by renal arteriography; the renal cortex does not enhance after contrast injection while the medulla enhances. No contrast excretion is evident from abnormal papillae. Magnetic resonance reveals a hypointense cortex on T2-weighted images.

Drug Induced

Renal toxicity is ascribed to numerous drugs, with some being anecdotal reports with little proof. An increased risk of nephrotoxicity due to long-term analgesic exposure is suggested by a number of studies. Yet one review concluded that although excessive use of phenacetin-containing analgesics probably does cause renal papillary necrosis and interstitial nephritis, no convincing epidemiologic evidence exists that non–phenacetin-containing analgesics (such as acetaminophen and aspirin) or nonsteroidal antiinflammatory drugs (NSAIDs) cause renal damage (124). Nevertheless, the literature contains numerous reports of an increased risk of nephrotoxicity from NSAIDs due to dehydration, hypotension and resultant renal hypoperfusion, congestive heart failure, and underlying renal failure. The NSAIDs appear to inhibit renal synthesis of prostaglandins. Normally in low perfusion states the vasodilator prostaglandins help prevent vasoconstriction and maintain renal blood flow, and in this setting the inhibition of prostaglandin production leads to renal failure and fluid retention.

Other believed associations with NSAIDs include acute tubulointerstitial nephritis, papillary necrosis, and nephrotic syndrome.

Patients with analgesic nephropathy lose renal volume bilaterally, and the kidneys develop an irregular outline. Papillary calcifications are common. Even in the early stages of analgesic nephropathy, CT detects papillary calcifications with a high sensitivity, and CT is superior in detecting calcifications to US and conventional radiography.

Even mannitol has led to acute anuric renal failure in a setting of chronic renal failure due to diabetic nephropathy.

Acute Interstitial Nephritis

Acute interstitial nephritis is believed to represent an acute hypersensitivity reaction, most often secondary to drugs, including NSAIDs. Abnormal leakage from glomerular capillaries and an interstitial infiltrate lead to nephrotic syndrome and eventual renal failure. In general, renal failure resolves after withdrawal of the offending agent, although deaths are reported.

Prolonged renal failure developed in an adult with Henoch-Schönlein purpura after an episode of macroscopic hematuria (125); histology revealed findings of tubulointerstitial nephritis. Some infections are associated with acute interstitial nephritis.

The kidneys enlarge during the acute phase. Delayed postcontrast CT reveals corticomedullary contrast enhancement due to vascular and tubular stasis. Ultrasonography detects diffusely hyperechoic cortices. The kidneys gradually decrease in size as the condition clears.

Chronic Tubular Dysfunction Disorders

Damage to renal tubules often also involves adjacent interstitial tissue and vice versa. The major factor in renal failure, however, is tubular damage. From a prognostic viewpoint, tubular injury progressing to tubular atrophy leads to a permanent loss of renal function.

Renal Tubular Acidosis

The term *renal tubular acidosis* describes several tubular transport disorders. Traditionally, it is subdivided into proximal and distal types based on which nephron segment is involved, although such an approach is an oversimplification of the underlying pathophysiology:

- Type I: defect in hydrogen ion secretion (distal renal tubular acidosis)
- Type II: defect involving bicarbonate reabsorption (proximal renal tubular acidosis)
- Type III: defects in both distal and proximal renal tubules

Type IV: aldosterone deficiency and resistance to aldosterone result in a hyperkalemic renal tubular acidosis

In general, renal tubular acidosis in childhood has a congenital etiology, while in adults acidosis tends to be secondary to another condition. The prevalence of renal cysts appears increased in type I renal tubular acidosis.

Some children with vesicoureteral reflux also have renal tubular acidosis; growth failure in these children probably is due to the renal tubular acidosis.

Patients with type I disease develop nephrocalcinosis. Aside from detecting nephrolithiasis and nephrocalcinosis and excluding other conditions, imaging has a limited role in these disorders.

Renal tubular acidosis and decreased renal function result in decreased renal accumulation of Tc-99m-DMSA and increased background activity. Such a renal pattern should lead to a search for an underlying defect.

Cystinosis

Nephropathic cystinosis results in renal tubular acidosis.

The importance of detecting nephropathic cystinosis lies in that effective therapy exists for cystine accumulation.

Tubulointerstitial Nephritis

Medullary cystic disease, a type of tubulointerstitial nephritis, was discussed earlier (see Congenital Abnormalities).

Etiology of renal tubulointerstitial fibrosis is unknown, although two peptides—transforming growth factor-β (TGF-β) and angiotensin II—appear to play a role. Also, both interstitial fibroblasts and renal tubular epithelium are involved in formation of an extracellular matrix. Initially affected patients tend to be asymptomatic, and the condition is often discovered only when advanced.

Infection

Among unusual infections, Legionnaire's disease has led to acute renal failure. Rocky Mountain spotted fever, due to infection with *Rickettsia rickettsii*, is associated with acute renal failure; infected patients developing acute renal failure have a high mortality. Severe leptospirosis and severe malaria have led to acute renal failure.

Reversible acute oliguric renal failure is a rare complication of nonfulminant hepatitis A infection in some patients.

Rhabdomyolysis

Rhabdomyolysis typically develops secondary to muscle compression, epilepsy, infection, ischemia, heat stroke, or trauma, and results in acute renal failure. Occasionally nontraumatic rhabdomyolysis develops in a setting of diabetic ketoacidosis. Presumably increased myoglobin levels are responsible for renal damage in this condition; myoglobin is a nephrotoxin.

In Pregnancy

Septic abortion used to be the main cause of renal failure in pregnancy; currently preeclampsia and eclampsia are more common factors. In some women renal failure is multifactorial; thus chronic hypertension or acute pyelonephritis in a setting of preeclampsia should be considered. Occasionally idiopathic postpartum renal failure develops. Chronic renal failure ensues in some patients.

A rare complication is HELLP syndrome (hemolysis, elevated liver enzymes, and low platelets) occurring during both pregnancy and puerperium. A major complication of this syndrome is acute renal failure. In a pregnancy-related acute renal failure study, HELLP syndrome accounted for 36%, postpartum hemorrhage for 26%, preeclampsia/eclampsia for 15%, and abruptio placenta for 10% (126).

Hemolytic-uremic syndrome is a rare complication developing in pregnancy and postpartum.

Diabetic Nephropathy

The most common cause of chronic renal failure is diabetes mellitus. One should keep in mind, however, that diabetic patients also develop renal stones, reflux, and infections, and in these patients voiding cystourethrography, urodynamic studies, and at times retrograde pyelography are indicated to exclude related conditions.

Initially the kidneys enlarge, but with time shrink in size. A glomerulosclerosis ensues and eventually nephrotic syndrome and end-stage renal failure develop.

Pre- and postcontrast helical CT in type 2 diabetic patients reveal that both axial renal diameters and arterial-phase cortical density are less in those with a nephropathy than in nonnephropathic diabetics and controls (127); these changes are related to the duration of disease.

Once nephropathy is well established, US identifies hyperechoic cortices. In patients with insulin-dependent diabetes mellitus but normal creatinine and blood urea nitrogen levels, Doppler US–derived renal interlobar artery RI is not sensitive enough in screening for glomerular hyperfiltration.

Glomerulonephritis

The subtypes of glomerulonephritis include membranous, immunoglobulin A (IgA)-related, vasculitis, and idiopathic. Systemic diseases associated with glomerulonephritis include a number of infections, polyarteritis nodosa, systemic lupus erythematosus, and Wegener's granulomatosis. A minority of cirrhotic patients have glomerulonephritis ranging from membranoproliferative to focal segmental and membranous. An infected ventriculoatrial shunt can lead to glomerulonephritis, a condition known as shunt nephritis. Even an occasional patient with inflammatory bowel disease develops proteinuria due to membranous glomerulonephritis. Glomerulonephritis and nephrotic syndrome are associated with solid neoplasm paraneoplastic syndromes. Histopathology typically reveals membranous glomerulonephritis. Proteinuria generally clears after tumor resection.

Renal enlargement is common in acute glomerulonephritis. Renal echogenicity varies, but often is greater than in the adjacent liver. Echogenicity decreases with clinical improvement.

Chronic glomerulonephritis leads to a gradual loss of renal parenchyma. Only a faint but persisting nephrogram is identified post–contrast injection. Eventually the kidneys become small, smooth, and hyperechoic, similar to other end-stage renal disease.

Color Doppler US is helpful in distinguishing glomerular nephropathy and disorders of vascular origin. The resistive index is related more to the site of disease than to the degree of renal failure. A normal RI is found in most patients with glomerulonephrosis, while patients with tubulointerstitial or vascular nephrosis have an increased resistive index.

Absent parenchymal uptake during scintigraphy with Tc-99m-MAG3 suggests acute glomerulonephritis.

Patients with newly discovered glomerulonephritis probably should undergo chest radiography not only to detect evidence of cardiac failure and effusions but also to establish a baseline appearance.

Focal Segmental Glomerulosclerosis

Focal segmental glomerulosclerosis is a syndrome resulting in chronic, progressive renal fibrosis. It is a common cause of renal disease. Histology reveals sclerosis of some but not all glomeruli (hence the name). It does not appear to be an immune response. Most authors subdivide it into a primary form, with no discernible cause, and a secondary form associated with a number of diseases, including diabetes, analgesic abuse, reflux nephropathy, a rejection phenomenon, HIV-associated nephropathy, and, in some patients, renovascular hypertension. Collapsing glomerulopathy is a variant of focal segmental glomerulosclerosis manifesting by the collapse of glomerular capillaries, marked podocyte enlargement, and associated tubulointerstitial disease.

Clinically this entity manifests as nephrotic syndrome and leads to progressive renal failure. It develops both in children and adults.

Imaging plays a role mostly in detecting damage due to secondary causes. A hypertensive patient developed unilateral focal segmental glomerulosclerosis associated with contralateral renal artery stenosis (128); the contralateral kidney presumably was spared glomerulosclerosis by the renal artery stenosis. The patient's renal insufficiency resolved after renal artery stenosis repair, suggesting renovascular hypertension as the primary cause for focal segmental glomerulosclerosis.

Therapy of any underlying condition is generally instituted. Corticosteroids are often used to treat patients with idiopathic focal segmental glomerulosclerosis, despite a lack of evidence for such therapy. The eventual therapy is renal

transplantation. Focal segmental glomerulosclerosis patients who receive a cadaveric transplant have a significantly higher graft loss rate than those with a human leukocyte antigen (HLA)-identical living-related transplant.

Hemolytic-Uremic Syndrome

A number of bacterial and viral infections are associated with hemolytic-uremic syndrome. Thus enterohemorrhagic *E. coli* infection causes both hemorrhagic colitis and hemolytic-uremic syndrome. Some patients recover with medical therapy, including hemodialysis. In children, *E. coli*–induced hemolytic-uremic syndrome and resultant renal failure are common factors leading to kidney transplantation.

Scleroderma renal crisis is a rare cause of acute renal failure due to microvascular disease and other factors.

Doppler US reveals an increase both in RI and PI. Renal artery flow is decreased. Renal volume is increased.

Cirrhosis/Hepatorenal Syndrome

Increased renal vascular resistance (RI) develops in patients with progressive cirrhosis. Even in patients with Child's class A cirrhosis without ascites, renal RI is increased (>0.7) in about a third of patients (129). A greater increase in both RI and PI occurs in those with Child's B and C cirrhosis. On the other hand, 99mTc-DTPA renography identifies a reduced glomerular filtration rate only in more advanced cirrhosis and Doppler US detects earlier than renography those cirrhotic patients at higher risk of developing renal failure.

Hepatorenal syndrome consists of renal failure in association with severe liver disease. The mortality rate is high once this syndrome is established.

Post–Bone Marrow Transplantation

Acute renal failure is a recognized complication after bone marrow transplantation. On an acute basis tumor lysis syndrome and marrow-infusion–associated toxicities occur. Veno-occlusive disease leading to hepatorenal-like syndrome occurs within about 1 month and is a common cause of acute renal failure. Late failure includes bone marrow transplantation–associated nephropathy and cyclosporine nephrotoxicity. These patients also develop sepsis, hypotension, and other related complications, and often renal failure is multifactorial.

Nephrotic Syndrome

Nephrotic syndrome is an end-stage condition induced by a number of entities. Clinically it manifests by hypoproteinemia, proteinuria, and hypercholesterolemia.

Nephrotic syndrome is an occasional manifestation of neoplastic disease. Patients with thymoma are prone to developing a nephrotic syndrome, ranging from minimal histologic change in some to focal segmental glomerulonephritis, proliferative glomerulonephritis, and membranous glomerulopathy. Such diverse conditions as systemic amyloidosis, lupus erythematosus, and renal vein thrombosis can manifest as nephrotic syndrome. Some patients with renal vein thrombosis are asymptomatic, with imaging offering a clue to the underlying condition; the involved renal vein is widened by a thrombus and the affected kidney is enlarged.

Patients with nephrotic syndrome undergoing bicarbonate hemodialysis have developed extensive metastatic calcifications throughout the body. These calcifications are detected by scintigraphy.

Miscellaneous Conditions

Medullary Sponge Kidney

Medullary sponge kidney, or *tubular ectasia*, refers to cystic collecting tubule dilation (ducts of Bellini) and is believed to be a congenital disorder, although usually manifesting in adulthood. It ranges from focal to generalized. In a minority of patients it is associated with calcifications within collecting tubules.

Tubular ectasia is the early hallmark of this condition, identified by IV urography as contrast-filled streaks opacifying renal pyramids before or simultaneously as adjacent calyces (Fig. 10.32). A clear border tends to be preserved between the abnormally opacified papillae and calyces. At times faint calcifications develop. This condition should be differentiated from a normal postcontrast papillary blush, seen as a

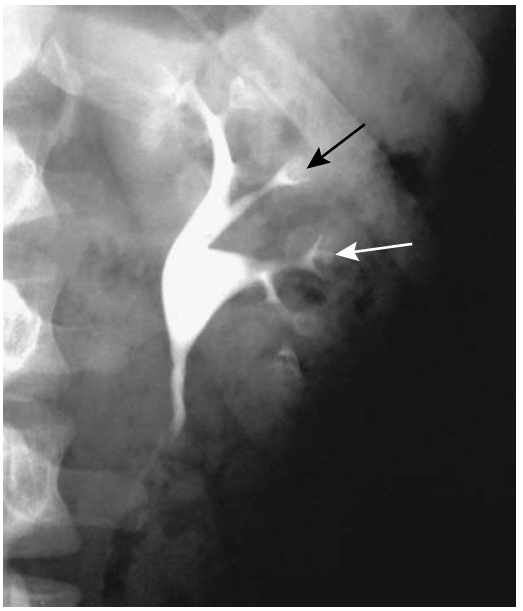

Figure 10.32. Renal tubular ectasia is identified as barely perceptible streaks of contrast (arrows) in the papillary regions during an IV urogram.

homogeneous papillary enhancement. Some authors use the term *benign tubular ectasia* to designate early findings and to differentiate them from more advanced medullary sponge kidney, but whether such early findings indeed are part of a spectrum of medullary sponge kidney is not clear.

Occasionally similar findings are detected with CT and MR. Ultrasonography shows increased echogenicity if renal pyramid calcifications have developed.

Papillary Necrosis

The term *papillary necrosis* describes specific damage to the papilla detected by imaging. Common conditions associated with papillary necrosis include analgesic and NSAID abuse, diabetes mellitus, some infections, and sickle cell anemia. The final pathway probably is ischemia. Findings develop either acutely or on a chronic, indolent basis.

Imaging findings tend to be rather specific and are best seen with IV pyelography: papillary erosions, necrosis, sloughing, and eventual passage of necrotic debris distally, with an eventual residual blunted calyx (Fig. 10.33). Calcifications develop in the papillary region. Either a portion or the entire papilla is involved; necrosis involves either one or several papilla; it is either unilateral or bilateral.

Papillary necrosis should be differentiated from medullary sponge kidney.

Radiation Nephritis

Damage occurs directly to the renal tubules and glomeruli and is due to radiation vasculitis. Some patients develop renal failure or hypertension.

A sufficient radiation dose results in a shrunken kidney. The renal outline becomes irregular. Damage is limited to the radiation port.

Amyloidosis

Both primary and secondary amyloidosis affect the kidneys. Affected patients are prone to developing renal vein thrombosis, and the sudden onset of nephrotic syndrome should suggest this diagnosis. Renal failure is common in patients with extensive renal amyloidosis.

Benign lymph node hyperplasia (Castleman's disease) is associated with renal amyloidosis. Occasionally a patient with Crohn's disease and renal amyloidosis develops nephrotic syndrome.

Initially the kidneys enlarge, but in time cortical atrophy ensues and the kidneys shrink. Focal amyloid infiltration mimics a neoplasm. Occasionally scattered, amorphous calcifications develop. At times US reveals a prominent medulla and a hyperechoic renal parenchyma.

Lupus Nephritis

Lupus nephritis is a manifestation of systemic lupus erythematosus. These patients develop a nonspecific sclerotic change and immunoglobulin deposition within glomerular small arterioles and capillaries. A patient with lupus erythematosus who develops a nephrotic syndrome should be investigated for renal vein thrombosis.

Renal Doppler US is useful in these patients. A normal RI predicts a better renal outcome regardless of creatinine level.

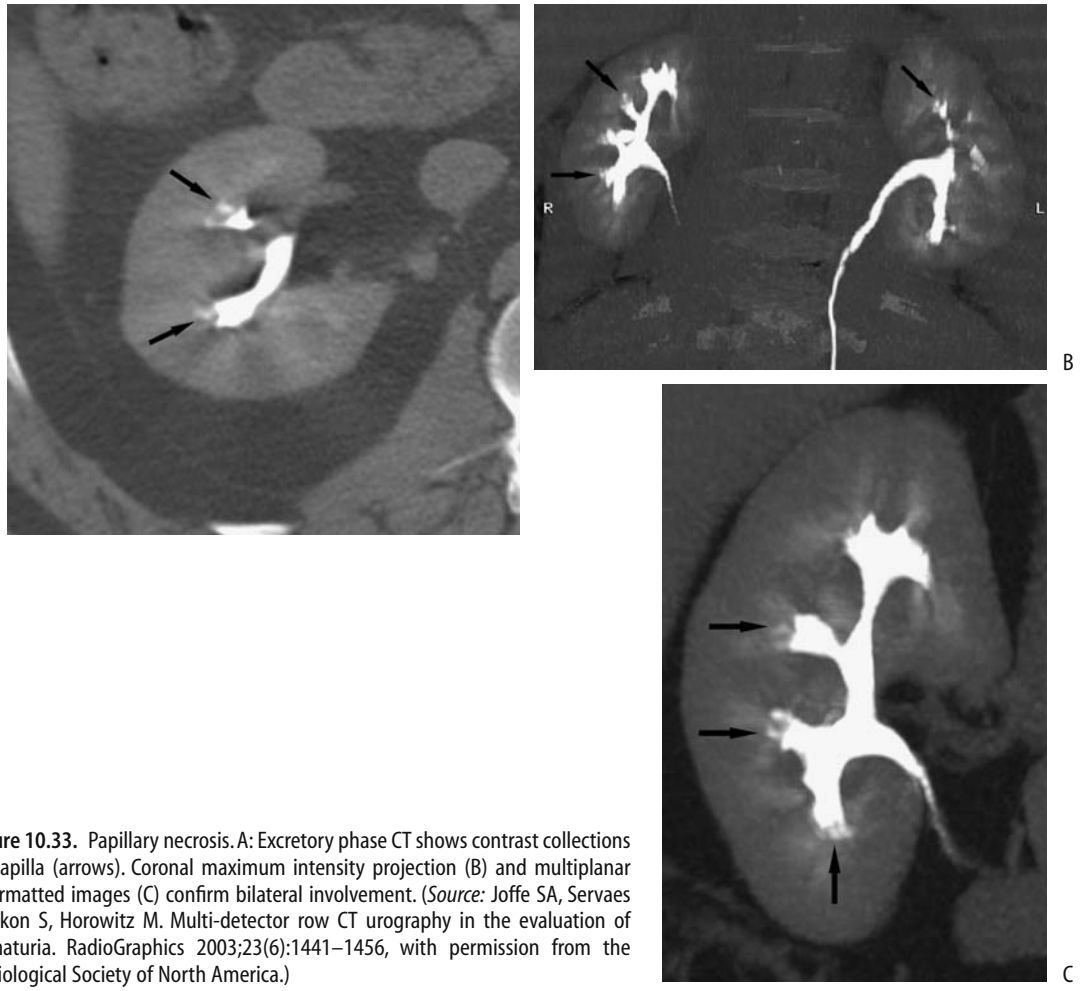

Figure 10.33. Papillary necrosis. A: Excretory phase CT shows contrast collections in papilla (arrows). Coronal maximum intensity projection (B) and multiplanar reformatted images (C) confirm bilateral involvement. (*Source:* Joffe SA, Servaes S, Okon S, Horowitz M. Multi-detector row CT urography in the evaluation of hematuria. RadioGraphics 2003;23(6):1441–1456, with permission from the Radiological Society of North America.)

Pseudoxanthoma Elasticum

Ultrasonography in pseudoxanthoma elasticum reveals highly reflective foci in the renal parenchyma. While this finding is suggestive of pseudoxanthoma elasticum, it is not pathognomonic and is also found in other conditions.

Intravascular Hemolysis

Hemoglobin from intravascular hemolysis is bound to plasma proteins and metabolized by the liver. Excess unbound hemoglobin is filtered by the kidney, some is excreted, and some is reabsorbed by tubules and stored in the renal cortex. Thus conditions associated with intravascular hemolysis and the resultant renal cortical iron storage produce a hypointense cortical signal on T2-weighted MRI.

Dialysis-Associated Findings

Using typical doses of gadolinium contrastagents in dialysis patients, 79% of the contrast agent was dialyzed after the first dialysis and

99.6% after the fourth (130); the authors conclude that being on hemodialysis is not a contraindication for the use of these contrast agents.

Dialysis-Acquired Cysts

A better name for this condition is *acquired cystic disease of the kidney* because the onset of cysts begins in patients with chronic renal failure even before dialysis is started. A common condition in patients with end-stage renal disease undergoing long-term hemo- or peritoneal dialysis, cyst prevalence increases with duration of dialysis. Why these cysts form is not known, but they tend to involute after renal transplantation. Some of these cysts from dialysis patients are lined with cuboidal epithelium.

Most patients with these cysts are asymptomatic. Pain and hematuria are mostly due to cyst rupture and bleeding.

Imaging of these often small, distorted native kidneys is difficult, especially with US. Computed tomography using IV contrast is feasible if the patient is on dialysis. These patients are at increased risk of developing renal cell carcinoma, and any contrast enhancement suggests a malignancy. Imaging detects numerous cortical cysts in a small kidney. Intracystic hemorrhage and its sequelae tend to mimic a neoplasm. Cyst wall calcifications develop, presumably from prior hemorrhage, but limited urinary output makes kidney stones uncommon.

Magnetic resonance imaging is an alternative imaging modality. The content of some cysts is hyperintense on T1-weighted MRI due to past hemorrhage. No enhancement is evident post–MR contrast, thus differentiating these cysts from neoplasms.

Eventually the imaging appearance approaches that seen with autosomal-dominant polycystic disease, but unlike polycystic disease these patients do not develop cysts in other organs.

Malignancies

Long-term dialysis is associated with several benign and malignant renal neoplasms, occasionally developing even in children. Some malignant-appearing tumors histologically exhibit growth patterns suggesting a benign tumor, including renal cell carcinomas and urothelial carcinomas. Some surveys suggest that especially young patients undergoing prolonged dialysis who develop renal cysts are prone to renal cell carcinomas and they should undergo regular screening by imaging.

Early postcontrast helical CT achieved a 96% sensitivity and 95% specificity in detecting a carcinoma in chronic hemodialysis patients, while delayed images had an 83% sensitivity and 94% specificity (131); early postcontrast images revealed significant enhancement differences between carcinoma and adjacent renal parenchyma, a finding not seen on delayed images.

Other Findings

Urinary stones are uncommon in native kidneys in these patients, presumably due to their decreased urine production, but renal calcifications are common.

On rare occasions emphysematous pyelonephritis develops in a nonfunctioning renal allograft of a diabetic patient.

Mesenteric ischemia appears to be more common than expected in patients with end-stage renal disease.

Pyeloureteritis Cystica

Of unknown etiology but probably due to degeneration, pyeloureteritis cystica consists of numerous fluid-filled cysts in the collecting system or ureter wall. Associated chronic infection is common. It is not premalignant. The condition is generally detected incidentally.

Imaging shows multiple small, uniform size, and round soft-tissue tumors in a ureter or renal pelvis (Fig. 10.34). Occasionally malacoplakia is in the differential diagnosis, but tumors in the latter condition tend to be more irregular in outline and the involved ureter somewhat dilated—findings not seen in pyeloureteritis cystica. Ureteral varices tend to be more serpiginous in appearance.

Figure 10.34. Ureteritis cystica.

Perinephric Conditions

Thickening

The right anterior extrarenal space extends from the perirenal fascia to the liver capsule. Conditions that widen this space and are hyperechoic include acute inflammatory conditions such as pancreatitis, appendicitis, acute cholangitis, adjacent abscess, ischemic bowel disease, and even a penetrating ulcer. An increased width with normal echogenicity is seen with chronic inflammation, peritoneal metastases, previous surgery, and steroid therapy. Left perirenal fat necrosis develops with severe pancreatitis; CT and MR reveal a fat-containing infiltrate mimicking a retroperitoneal tumor, but associated pancreatic findings should suggest the correct diagnosis.

Urinomas and lymphoceles are discussed in Chapter 14.

Hematoma

Spontaneous nontraumatic subcapsular or perirenal hemorrhage, also called *Wunderlich syndrome*, is not common. Clinically, an underlying neoplasm or bleeding diathesis needs to be excluded, although occasionally polycystic kidneys, a vasculitis, glomerulonephritis, or pyelonephritis is responsible.

Computed tomography or angiography should suggest an etiology for most of these hematomas. Acute hemorrhage may hide an underlying neoplasm, and some of these patients require exploration or follow-up study after the hematoma resolves.

Abscess

Most perinephric abscesses are associated with renal or adjacent organ infection. Some abscesses are confined by Gerota's fascia, while others extend into the adjacent retroperitoneal structures.

Most of these abscesses are readily detected with imaging. An occasional perinephric abscess mimics a neoplasm.

Ultrasonography of a perinephric abscess often reveals a complex fluid collection. These abscesses can be successfully drained during laparoscopy, although many are drained percutaneously.

Tumors

Similarly to infection, tumors spread readily in the perirenal space. Most primary tumors are of mesenchymal origin. Lymphoma either involves this space diffusely, with little displacement of adjacent structures, or develops in a nodular pattern. A similar diffuse involvement is also occasionally found with metastatic melanoma. Differentiation from an adrenal tumor can be difficult.

A diagnosis of perirenal lymphoma is not always straightforward; at times even a needle biopsy is not diagnostic.

Vascular Disorders

Arteriovenous malformations and hemangiomas were discussed earlier (see Vascular Tumors).

Ischemia

One result of renal ischemia is renovascular hypertension (discussed in Chapter 17), but in some patients ischemia manifests primarily as renal failure (also called *ischemic nephropathy*). Also, renal artery stenosis is but one etiology of renal ischemia, with other etiologies being vessel compression by extrinsic tumors, artery thrombosis, emboli, vasculitides, and venous occlusions. Major renal vein obstruction eventually leads to the ischemia–renal failure cycle but not to hypertension. In addition, renal vein obstruction has different imaging manifestations.

Renal ischemia is incompletely understood. Normal kidneys receive more blood than necessary for functioning and tolerate considerable underperfusion as long as systolic blood pressure is above 70 or 80 mm Hg or so. Ischemia is less common in a setting of fibromuscular dysplasia than with atherosclerotic disease.

A sufficient decrease in renal blood supply, regardless of etiology, will evolve into renal infarction. Acute infarction has developed in Behçet's disease, primary renal artery dissection or thrombosis, cocaine abuse, and a subcapsular hematoma secondary to metastasis to the kidney, and has even been idiopathic. In a setting of renal artery stenosis, acute renal failure has developed after some medications, including diuretics and other antihypertensive drugs.

Clinically, acute nontraumatic renal artery thrombosis and resultant ischemia typically manifest by sudden onset of flank pain. On a more chronic basis decreased arterial flow is less symptomatic, and some of these patients simply develop a small, nonfunctioning kidney.

The onset of flank pain due to acute renal ischemia/infarction mimics that of renal colic. Among 300 patients admitted with renal colic, renal parenchymal infarction was eventually diagnosed in three patients (132).

Intravenous urography of acute renal artery obstruction reveals a nonfunctioning but normal-sized kidney. Ultrasonography also shows a normal kidney. No major renal blood flow is identified with Doppler US. In such a clinical setting postcontrast helical CT or angiography simply confirms the diagnosis.

Computed tomography performed without contrast in a search for calculi will miss renal arterial ischemia. Thus in such a clinical scenario, if nonenhanced CT does not reveal an abnormality to explain the patient's clinical findings, a postcontrast CT is indicated to evaluate for a possible renal infarct.

Postcontrast CT of a total infarct shows a hypodense, nonfunctioning kidney. Prominent capsular collaterals, called the *cortical rim sign*, often lead to surrounding vascular enhancement. A focal infarction appears as a wedge-shaped region of decreased or absent contrast enhancement with sharply defined margins, most often extending to the capsule. Ultrasonography reveals a wedge-shaped hypoechoic region. Eventually the involved parenchyma atrophies, a scar forms, and an irregular renal outline remains as evidence of prior infarction.

Early intraarterial fibrinolysis therapy is indicated if recovery is anticipated. Renal ischemic due to renal artery stenosis is treatable by angioplasty (discussed in Chapter 17).

Nephrosclerosis

Arteriolar spasm, endothelial spasm, muscle hypertrophy, and eventual fibrosis develop in hypertension-induced nephrosclerosis. The final pathway is renal ischemia. Proteinuria is common. If untreated, renal failure ensues. The kidneys gradually shrink and cortical thinning becomes evident. Calyces are not affected.

Immunosuppression/Acquired Immunodeficiency Syndrome

General

Renal abnormalities are common in HIV-infected patients. Ultrasoaography findings cousist of enlarged kidneys, decreased corticomedullary definition, decreased renal sinus fat, and a heterogeneous parenchyma, some with hyperechoic striations (133). In general, increased renal insufficiency in AIDS patients is associated with pelvocalyceal thickening and a hyperechoic appearance.

Cerebral toxoplasmosis in AIDS patients is treated with sulfadiazine, which is associated with acute renal failure due to sulfadiazine-induced crystalluria. Ultrasonography findings consist of hyperechoic foci in renal parenchyma and hyperechoic debris in collecting systems.

Stones and hydronephrosis also develop in these patients.

The HIV-infected patients on indinavir sulfate therapy, a protease inhibitor used to treat HIV infection, develop ureteral obstruction due to nonopaque indinavir crystals.

An occasional AIDS patient develops a spontaneous perinephric hematoma.

Infection

Similar to other sites, renal infection with *Pneumocystis carinii*, aspergillus abscess, cytomegalovirus, and other unusual organisms develop in these patients. Some of these infections eventually evolve into multiple, punctate parenchymal calcifications. Focal mucormycosis mimics a renal neoplasm.

Tumor

Simple renal cysts are considerably more prevalent in children with AIDS that in normal children.

Renal involvement with lymphoma is common in AIDS. Even rarer lymphomas develop, such as a non-Hodgkin's angiocentric renal lymphoma, which shows a propensity to invade and destroy small vessels.

Renal leiomyosarcomas develop in HIV-infected patients, including children.

Postoperative Changes

Kidney Transplantation

An uncommon indication for renal transplantation is bilateral, and synchronous renal cell cancers requiring bilateral nephrectomies. These patients undergo bilateral nephrectomies, a waiting period of several years on dialysis follows, and then they undergo renal transplantation. Such an approach is undoubtedly uncommon; most patients with early and low-grade renal cell carcinomas undergo partial nephrectomies.

An occasional patient receives both a kidney and a pancreas transplant; the consequences of the transplanted pancreas, with its exocrine secretions draining into the bladder, are discussed in Chapter 9. For a number of indications rare patients have also received both kidney and bone marrow transplantation; these dual transplants are not discussed in this book.

Pretransplant Donor Evaluation

Preoperative donor kidney evaluation is performed to detect accessory renal arteries and other anomalies. In a setting of multiple renal arteries, donor renal artery reconstruction rather than ligation preserves renal mass. Although generally not affecting gross renal function, ligation of accessory renal arteries tends to be associated with focal renal infarction.

Horseshoe kidneys are used for transplantation. When possible, a horseshoe kidney is divided at the isthmus and the halves are transplanted into two recipients. Part of a living donor horseshoe kidney can be used.

Traditionally, renal vasculature was evaluated with angiography, a role partially supplanted by CT and now by MRA. Intraarterial DSA achieves over 95% sensitivity and specificity in detecting accessory renal arteries in kidney donors. Other abnormalities detected by arteriography include fibromuscular dysplasia and atherosclerosis, findings often affecting planned surgery.

Preoperative CT and MRA in living renal donors detect essentially the same number of renal arteries, with disagreement primarily among several-millimeter-diameter accessory vessels (134). Multislice helical CT with transverse, coronal, and 3D reconstructions detects most accessory arteries and early branching and defines other relevant anatomy, but these are rather technically complex studies requiring close attention to detail.

Gadolinium enhanced MRA correctly identifies the arterial supply to native kidneys (including accessory renal arteries), most proximal arterial branches and some anomalous draining renal veins (135,136). Addition of MIP, volume rendering and SSD algorithms may improve image presentation, but they do not improve accuracy. MRA can also evaluate renal size and fetal lobulations without the potential angiography complications. Reported sensitivities of detecting accessory renal arteries range from 75% to 100%, with the latter being rather optimistic. Also the ability of MRA to detect fibromuscular dysplasia is not established.

Reported Doppler US sensitivities in detecting accessory renal arteries range up to 100%,

but these studies are plagued by low specificities.

MR urography can potentially detect urinary collecting system abnormalities in living renal donors. Whether the technique is sufficiently accurate in actual practice to detect ureteric duplications and other relevant anomalies is not clear.

Transplantation

Whether a voiding cystourethrogram is performed in transplant recipients prior to renal transplantation varies between institutions. Some believe this study adds little value.

Some children requiring renal transplantation also have bladder dysfunction, such as posterior urethral valves, a neurogenic bladder, or vesicoureteral reflux, and augmentation cystoplasty is added either before or after transplantation.

With the exception of small children, the transplanted kidney is nearly always placed in the iliac fossa, extraperitoneal in location. Here the kidney is close to major vessels and bladder and is supported by surrounding structures. A side-to-end arterial anastomosis goes to the external iliac artery and an end-to-side venous anastomosis goes to the external iliac vein. The left iliac fossa is used if a second transplantation is necessary; third transplantations are high in the right iliac fossa.

Renal transplantation is feasible in patients infected with *Schistosoma haematobium*. Pretransplant antischistosomal chemotherapy controls posttransplant schistosomal infection; the increased risk for bladder cancer in these patients justifies close follow-up.

Posttransplant Evaluation

Clinical

Rough data from several sources suggest that first-year posttransplant mortality is about 4%, mostly due to infection; transplanted kidney loss ranges from 5% to 10%, mostly due to rejection, with a subsequent graft loss of about 5% per year. The half-life of transplanted kidneys varies widely, depending on donor compatibility and whether a living donor kidney or a cadaver kidney is used.

The most common direct surgical complication is ureteral obstruction. Other complications include ureteral or bladder fistulas, bladder outflow obstruction, ureteral stones, and lymphoceles. Transplantation complications can be divided into early and late. Early ones include rejection, urine leaks, and obstruction. The major late complication is renal artery stenosis.

Posttransplant drug therapy can result in hypersplenism and portal hypertension; these patients present with splenomegaly and thrombocytopenia.

Imaging

Because most transplanted kidneys are located rather superficially, gray-scale US can be performed with a higher resolution transducer than usual. As a result, better anatomic detail is achieved than is possible with a native kidney.

Regions of decreased color on color Doppler US scans in a transplanted kidney appear to be related to focal perfusion abnormalities. Such focal hypoperfusion regions include infections, arteriovenous fistulas, a kinked artery, and severed accessory arteries.

A color Doppler US finding of a significant decrease in interlobar artery blood flow, but with no flow changes in segmental arteries, suggests acute rejection. Decreased interlobar artery blood flow is also found in renal artery stenosis and interstitial edema.

One subset of patients consists of those with an oligoanuric allograft suspected to be due to either severe rejection or renal artery or vein thrombosis. Both Tc-99m-DTPA scintigraphy and color Duplex US can differentiate minimal and not perfused renal allografts.

Contrast-enhanced MRI can differentiate between graft kidneys with normal function, mild dysfunction, and severe dysfunction. Magnetic resonance imaging in transplant patients with normal renal function typically shows an expected postcontrast increase in signal intensity of the renal cortex and medulla, followed by a signal intensity decrease in the medulla. Patients with acute allograft rejection have less postcontrast increase in cortical signal intensity than those with normal allografts. Magnetic resonance imaging cannot, however, differentiate between normal, acute rejection and acute tubular necrosis, but MRA can evaluate renal artery anatomy (Fig. 10.35).

Scintigraphy evaluates function in a transplanted kidney. A Tc-99m-MAG3 renogram

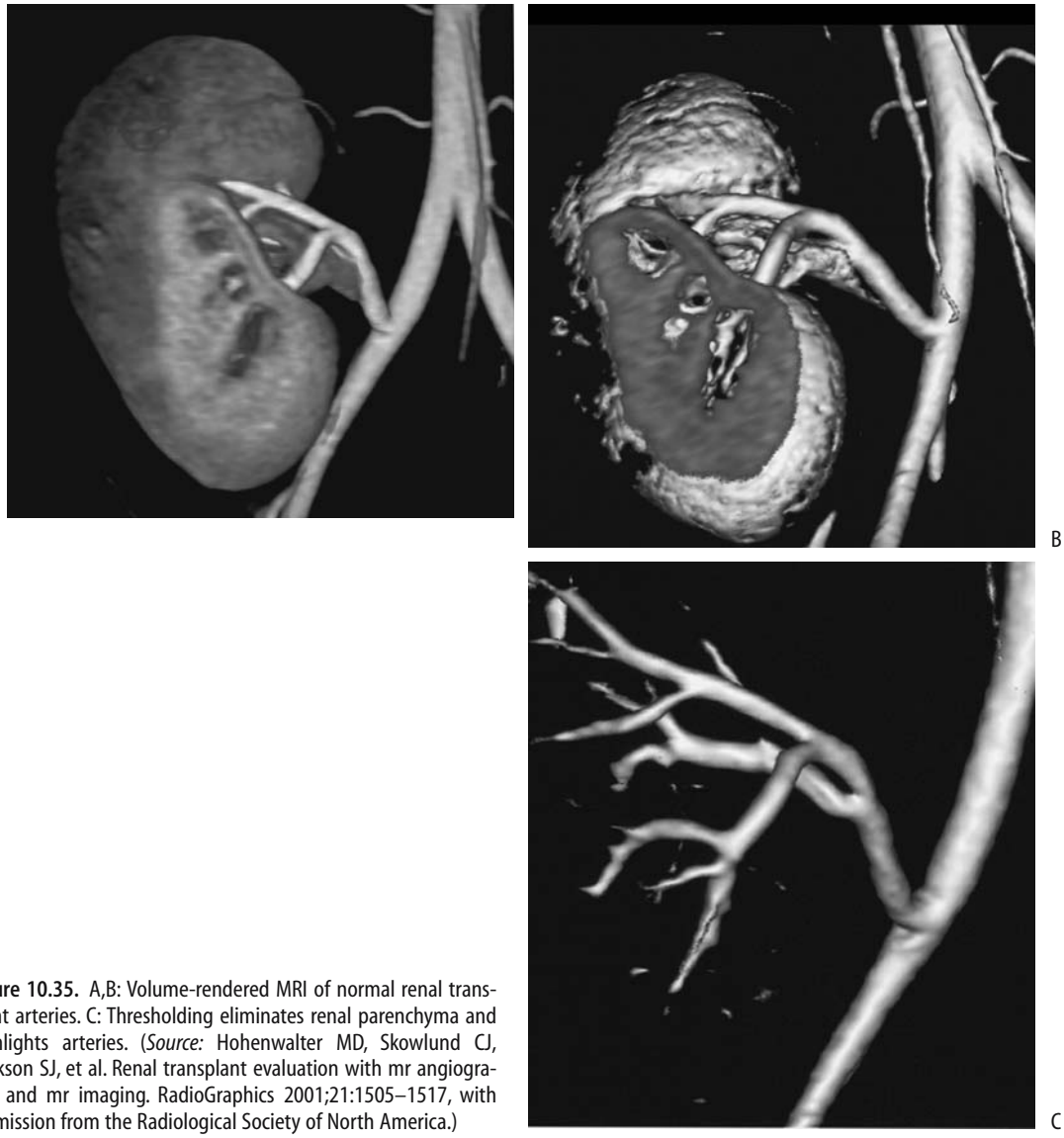

Figure 10.35. A,B: Volume-rendered MRI of normal renal transplant arteries. C: Thresholding eliminates renal parenchyma and highlights arteries. (*Source:* Hohenwalter MD, Skowlund CJ, Erickson SJ, et al. Renal transplant evaluation with mr angiography and mr imaging. RadioGraphics 2001;21:1505–1517, with permission from the Radiological Society of North America.)

appears useful in determining renal transplant prognosis during the postoperative period. Initial tracer uptake is decreased or absent with transplant dysfunctions such as acute tubular necrosis, acute rejection, and an obstruction than in normally functioning ones. A focal photopenic defect in a renal transplant suggests tubular injury. Similarly, Tc-99m-MAG3 transit time is prolonged in obstructive kidneys.

Postural drainage stasis occasionally develops in a transplanted kidney. Postural stasis can be evaluated by varying the patient position during Tc-99m-MAG3 imaging.

Carbon dioxide angiography is feasible in a transplanted kidney. Major stenoses, arteriovenous shunting, and diffuse arterial disease can be evaluated (137), although insufficient data preclude establishing a specific role to this modality.

Rejection

Differentiation between acute tubular necrosis and acute rejection is of obvious importance, but imaging provides only limited assistance, and a biopsy is generally necessary to evaluate graft dysfunction and distinguish between these two. Biopsy complication rates are low, although bleeding, pseudoaneurysm formation, or an arteriovenous fistula do form if an adjacent artery or vein is injured.

Acute tubular necrosis is due to transplantation-associated ischemia and occurs within a day or so. Acute rejection occurs from the time of surgery to several months after transplantation. Rejection leads to renal swelling, a finding seen with other complications. Viral infections are often in the differential diagnosis; some, such as Epstein-Barr viral infections, are associated with lymphoproliferative disorders and are detected with a polymerase chain reaction.

Doppler US appears helpful in monitoring rejection. The pulsatility index, which is dependent on flow resistance, increases with rejection and in some hands when combined with peak arterial systolic velocity and acceleration index achieves a high sensitivity and specificity in differentiating a normally functioning transplant from a hypofunctioning one. Others, however, find that Doppler US cortical vascularity data do not correlate with rejection, and even severe transplant rejection can be associated with normal vascularity (138). In children with chronic rejection, power Doppler US using a high-frequency and high-resolution transducer (13 MHz) found irregular and narrow interlobular vessels, in distinction to children with chronic rejection who have a palisade-like appearance (139); the authors ascribe their results to use of a high-frequency transducer, which was possible because of decreased tissue thickness in children.

Postcontrast MRI holds promise in differentiating transplant rejection from acute tubular necrosis. Magnetic resonance signal intensity data after contrast injection shows that in patients with transplant rejection the time to peak intensity in the renal cortex and medulla are longer than in patients with normal grafts; in patients with acute tubular necrosis, on the other hand, renal cortex and medulla times are similar to normal.

Using surface coils, adiabatic excitation pulses and in vivo phosphorus MR spectroscopy, phosphorus-31 MR spectroscopy appears to have a role in detecting and possibly differentiating rejection and acute tubular necrosis. Patients with rejected kidneys have a higher inorganic phosphate-to–α-adenosine triphosphate ratio than controls and a reduced pH (140). Rejection and tubular necrosis could be differentiated from each other by pH. These findings need to be placed in a larger clinical perspective.

Scintigraphy in acute rejection reveals decreased perfusion, a finding also seen in other complications. An initial study shortly after the transplant is useful in establishing a baseline.

Xenon-CT is used to study cerebral perfusion; it can also measure regional blood flow in a transplanted kidney. Although differences in perfusion exist between normal kidney medulla and cortex, these perfusion differences are less evident in patients with chronic rejection.

Vascular Complications

Arterial Stenosis

Posttransplantation hypertension is common. In about one third or so of these hypertensive patients their hypertension is related to renal artery stenosis. The prevalence of renal artery stenosis is more common in cadaveric donor kidneys compared to living donor kidneys. This stenosis-associated hypertension can be treated medically, by angioplasty, or by surgical revascularization.

Stenoses occur at the anastomosis, distal to the anastomosis (donor artery), or, least common, proximal to the anastomosis in the recipient's artery (Fig. 10.36). Stenosis may be related to surgery or may be part of rejection. It can recur after angioplasty.

Acceleration time, obtained with Doppler US, is prolonged with a significant proximal arterial stenosis, although the clinical accuracy in detecting arterial stenosis varies depending on the assumed threshold. Another measure is transplant artery peak systolic velocity, but here also results have been inconsistent. Peak systolic velocity varies considerably even without a stenosis, although use of the iliac artery as a standard is helpful.

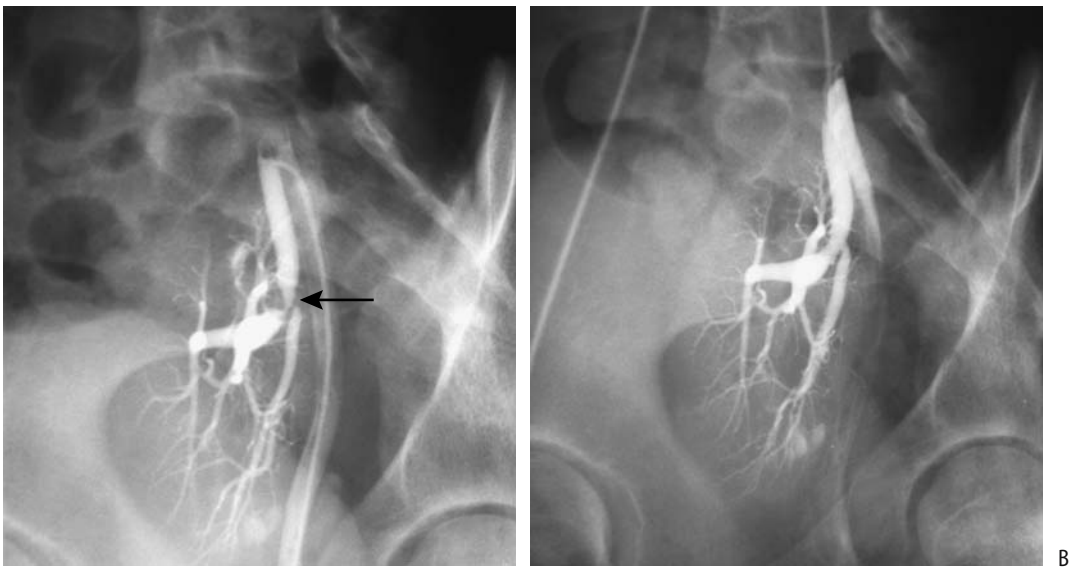

Figure 10.36. Renal artery stenosis in a transplanted kidney. A: Initial arteriogram reveals a tight stricture (arrow). B: Lumen is patent after dilation. (Courtesy of Oscar Gutierrez, M.D., University of Chile, Santiago, Chile.)

Magnetic resonance indications in suspected renal artery stenosis continue to increase and gadolinium-enhanced MRA is assuming a major role in detecting transplanted renal artery stenosis, in some studies achieving sensitivities of >85% and specificities approaching 100% and in some patients even being superior to DSA. Depending on the sequences adopted and the type of reconstruction, transplant artery stenoses, renal vein thromboses, extrinsic compression, and perfusion deficits are identified with varying degrees of accuracy (Fig. 10.37). The relative roles for color Doppler US and MRA are not settled, but MRA appears to slightly overestimate renal artery stenosis while color Doppler US is more prone toward false-positive results.

Posttransplant renal artery stenosis is amenable to percutaneous transluminal angioplasty, and in a number of institutions angioplasty is the procedure of choice for this complication. In experienced hands complication rates are low. Surgical revascularization is indicated if angioplasty is unsuccessful, although a restenosis after angioplasty can be treated with an endoluminal stent placed across the site of restenosis.

Arterial Thrombosis

The etiologies of renal artery thrombosis occurring shortly after transplantation include hypotension, renal artery stenosis, graft rejection with extensive arteriolar occlusions, and retrograde renal artery thrombosis, or it may be related to the surgical procedure.

Neither arterial nor venous flow is detected with Doppler US distal to a complete occlusion.

Vein Occlusion

The consequences of renal vein thrombosis are similar to those of renal artery thrombosis because the transplanted kidney has no additional collateral veins.

In the absence of proximal renal artery stenosis, Doppler US findings suggestive of partial venous occlusion after transplantation include the presence of small amplitude arterial waveforms but with diastolic flow still present; with complete renal vein obstruction no venous flow is evident and diastolic flow in the renal artery is reversed.

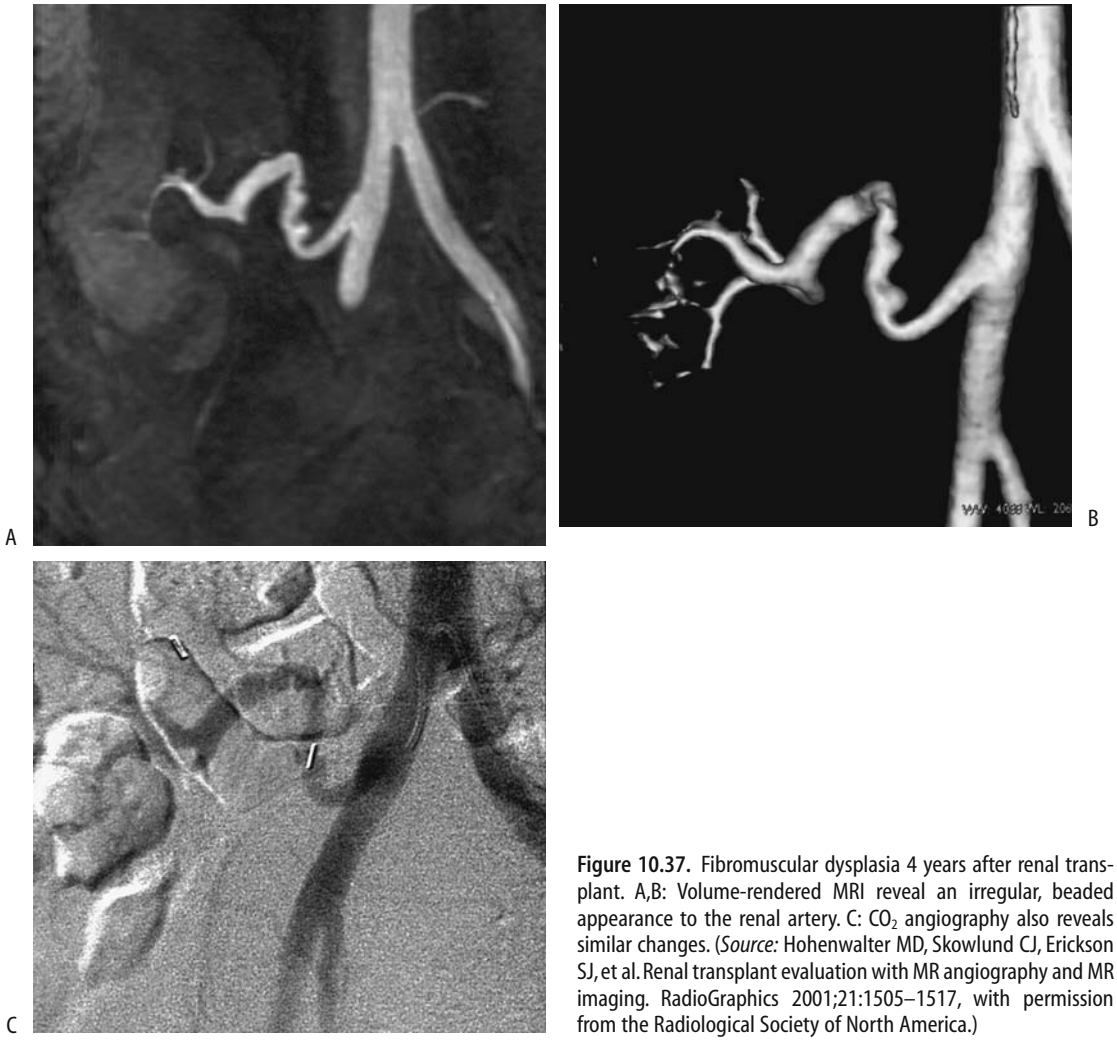

Figure 10.37. Fibromuscular dysplasia 4 years after renal transplant. A,B: Volume-rendered MRI reveal an irregular, beaded appearance to the renal artery. C: CO_2 angiography also reveals similar changes. (*Source:* Hohenwalter MD, Skowlund CJ, Erickson SJ, et al. Renal transplant evaluation with MR angiography and MR imaging. RadioGraphics 2001;21:1505–1517, with permission from the Radiological Society of North America.)

Vascular Fistula

The gold standard in detecting vascular fistulas is arteriography. Doppler US detects only some of these fistulas and early-phase contrast CT should be considered in a setting of normal Doppler US but clinical suspicion of a fistula. These fistulas are successfully occluded with transcatheter embolization; nevertheless, the complication rate is high even after successful embolization and includes renal artery occlusion and major hemorrhage necessitating a nephrectomy.

Ureter Complications

Renal pelvic and ureteral complications develop in roughly 10% to 15% of patients undergoing renal transplantation and include obstruction, necrosis, and urinary fistula. They are more common in a setting of multiple donor kidney renal arteries. Urinary obstruction occurs roughly equally in living-related donors and cadaveric donors, but leakage is more common in living donors. Ureter complications are managed with a percutaneous nephrostomy, transurethral bladder drainage, or drainage of fluid collections.

Magnetic resonance imaging appears to have a role in evaluating posttransplant ureter complications. Similar to the bile ducts, MR images mimicking conventional urography are feasible. In patients with suspected urologic abnormalities, MR urography identifies dilated renal pelves and detects ureteral leaks and obstructions.

Ureteral obstruction develops secondary to postoperative edema, anastomotic stricture, kinking or compression by an extrinsic urinoma, hematoma, or lymphocele (Fig. 10.38). The ureteroneocystostomy is the most common site of obstructions. A ureter can be trapped in an obturator hernia. Because of denervation, posttransplant patients manifest obstruction simply by worsening renal function. With a stenosis, US or scintigraphy should detect any underlying hydronephrosis, but keep in mind that dilation is not always secondary to an obstruction.

Posttransplant ureteral obstructions are treated with ureteral balloon dilation and antegrade placement of nephroureteral stents; about two thirds of those with early obstruction are treated successfully, but the success rate decreases in those with late obstruction. Obstruction can also be relieved with a percutaneous nephrostomy. Only a minority of patients eventually require open surgery. In general, the survival of a renal graft in patients who develop ureteral stenoses or fistulas is shorter than in those without these complications.

Most urinary extravasations occur at the ureteral anastomosis and result in a urinoma (Figs. 10.39 and 10.40). Some leaks are secondary to ureteral necrosis, presumably ischemic in origin, and are difficult to treat.

Ultrasonography detects most urinomas. Scintigraphy during the acute time period shows radiotracer activity in the urinoma.

A posttransplant leak is approached with a percutaneous nephrostomy and antegrade placement of a nephroureteral stent; leaks that do not heal require surgical repair.

Ureteral complications requiring reconstruction range from complete ureteral necrosis to long or multiple ureteral strictures. Most often with ureteral necrosis a part of the bladder is used as a substitute, although an artificial ureter has also been successfully employed.

Fluid Collections

Postoperative fluid collections are common and range from hematoma, seroma, urinoma, and lymphocele, to an abscess. Most small hematomas and lymphoceles resolve spontaneously.

Many of these fluid collections have a similar gray-scale US appearance, and fluid aspiration

Figure 10.38. Percutaneous nephrostogram of a transplanted kidney with an obstructed ureter. A: A proximal leak is evident (arrow) in a more distally obstructed ureter. B: A catheter has been advanced through the obstruction. (Courtesy of David Waldman, M.D., University of Rochester.)

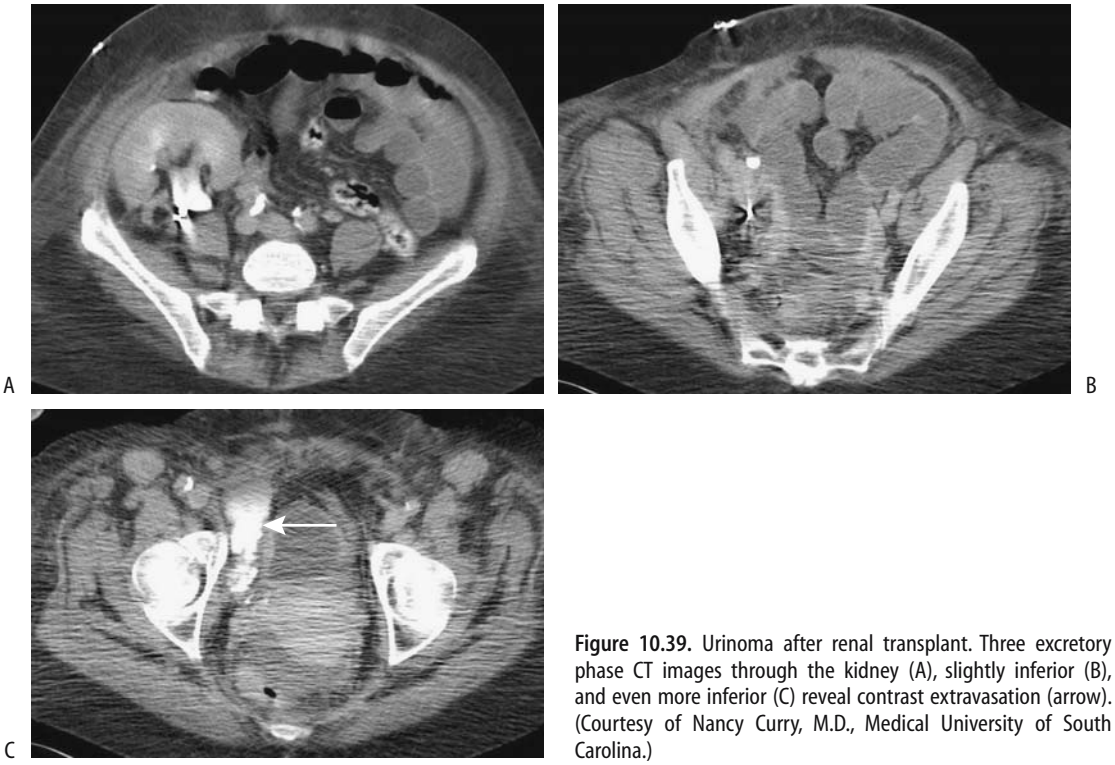

Figure 10.39. Urinoma after renal transplant. Three excretory phase CT images through the kidney (A), slightly inferior (B), and even more inferior (C) reveal contrast extravasation (arrow). (Courtesy of Nancy Curry, M.D., Medical University of South Carolina.)

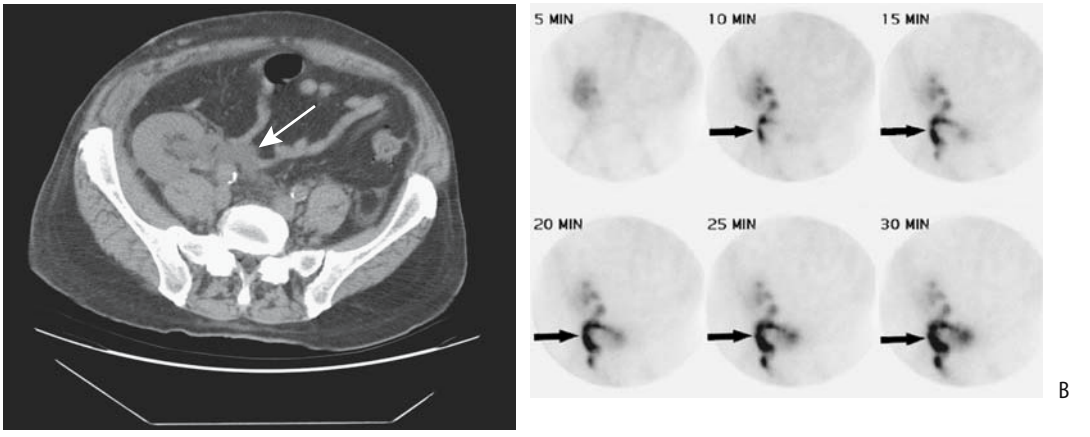

Figure 10.40. Urine leak after renal transplantation 1 week earlier. A: CT shows a fluid collection medial to the ureteropelvic junction (arrow). B: Dynamic renal scintigraphy using Tc-99m-DMSA identifies progressive tracer accumulation in this region (arrows). (*Source:* Titton R, Gervais DA, Hahn PF, Harisinghani MG, Arellano RS, Mueller PR. Urine leaks and urinomas: diagnosis and imaging-guided intervention. RadioGraphics 2003;23:1133–1147, with permission from the Radiological Society of North America.)

is necessary to differentiate between them. A hematoma initially is hyperechoic, but gradually becomes hypoechoic and eventually anechoic.

A seroma, urinoma, and lymphocele are all hypointense on T1- and hyperintense on T2-weighted MRI. Significant urinomas usually require reoperation.

Lymphoceles develop from the disruption of pelvic lymphatics. They tend to become multiseptated. Therapy of these posttransplant lymphoceles includes open or laparoscopic marsupialization, percutaneous drainage, and percutaneous injection of a sclerotic agent. External drainage has a high failure rate, but percutaneous sclerotherapy using a povidone-iodine agent is a simple technique and has had considerable application; recurrent lymphoceles can be retreated percutaneously. Laparoscopic marsupialization with internal drainage is feasible, and effective therapy for posttransplant lymphoceles but is more invasive. Intraoperative US guidance is often helpful.

Stones

The frequency of urinary calculi in a transplanted kidney ranges up to 3%, a prevalence greater than in the general population. About half of these stones are composed of urate. Not all filling defects are stones. Blood clots, fungus balls, or sloughed papillae are also encountered.

Lymphoproliferative Disorder/Neoplasms

Renal transplant patients are immunosuppressed and, not surprisingly, are at an increased risk of developing neoplasms. Epstein-Barr virus infection is believed to be responsible for most of this increased risk. To put this issue in perspective, approximately 1% of renal transplant patients develop a lymphoproliferative disorder, considerably more than the general population. A retrospective Italian study found 15 cancers in 11 posttransplant patients, including skin cancers, Kaposi's sarcomas, renal carcinomas, transitional cell carcinoma, and even colon cancer (141); the mean time of immunosuppression until tumor detection was 45 months, and, surprisingly, no lymphomas or female genital tract cancers were found.

Over the years, the sites of lymphoproliferative disorder involvement in renal transplant patients have changed considerably; central nervous system involvement predominated initially, during the cyclosporine era thoracic and abdominal sites were more common, while isolated involvement of the transplanted kidney is now more evident. Currently lymphoproliferative disorders most often present as solitary or multiple tumors, often limited either to the allograft or allograft hilum (142); most are extranodal in location. Newer immunosuppression agents are evolving, and the type of neoplasms encountered in different studies reflects, in part, the immunosuppressive approach used.

Lymphoproliferation ranges from a nonspecific mild adenopathy to malignant lymphoma. B-cell non-Hodgkin's lymphoma is most common, but other lymphomas are also encountered. In general, these lymphomas tend to be more aggressive than their counterparts in nonimmunosuppressed individuals.

Transplant patients develop renal cell carcinomas in the native kidneys and in the renal allograft and ovarian carcinomas. No significant relationship exists between the prevalence of renal cell carcinoma and the presence of acquired cystic kidney disease, patient age, type and duration of dialysis, or drugs used. Screening of the native kidneys appears reasonable in patients undergoing US of a renal allograft.

Those Australian and New Zealand Dialysis and Transplant Registry patients who had renal transplantation as a result of analgesic nephropathy were found to be at an increased risk of developing posttransplant transitional cell carcinomas of the upper urinary tracts compared to patients undergoing transplantation for other causes of renal failure (143); their tumors tend to be of a higher grade and stage, and they have a worse outcome than do other transplant patients. Screening with urinalysis and voided urine cytology does not appear to be reliable in detecting upper renal tract malignancies. Annual cystoscopy and retrograde ureteral catheterization with washings, brushings, and radiologic imaging were advocated in these patients. The patients should also be screened before transplantation.

Both bladder nephrogenic metaplasia and nephrogenic adenomas develop in these patients; these benign tumors, considered to be without malignant potential, have a relatively high relapse rate. Their long-term course in

these immunosuppressed patients is not clear.

The prevalence of cutaneous squamous cell carcinoma, basal cell carcinoma, cutaneous malignant fibrous histiocytoma, atypical fibroxanthoma, and Kaposi's sarcoma is increased considerably over a control population. Among other tumors, basal cell epithelioma of the scalp, gastric adenocarcinoma, central nervous system lymphoma, breast carcinoma, and adenocarcinoma of the colon have been reported.

An annual abdominal US appears to have a role in detecting some neoplasms in asymptomatic renal allograft recipients. One should keep in mind, however, that US does not detect smaller tumors. Some evidence suggests that MR is superior in detecting lymphoproliferative disorders. Lymphomas appear as soft tissue tumors isodense to soft tissue on CT and hypodense postcontrast, iso- or hypoechoic with US, and hypo- to isointense on T1- and hypointense on T2-weighted MRI and show minimal contrast enhancement. They are located in either renal parenchyma or renal hilum; at the latter location encasement of hilar vessels or excretory tract compression and obstruction is common. In the absence of therapy, calcifications suggest necrosis.

Infection

Bacterial allograft pyelonephritis leads to acute renal failure. Some patients also have superimposed acute rejection. Viral infections, such as with cytomegalovirus, are also associated with rejection. Therefore, in these patients both imaging and graft biopsy are necessary. A relationship between urinary tract infection and chronic rejection has been raised.

Especially in children, vesicoureteral reflux is a risk factor for pyelonephritis and graft dysfunction. Comparing voiding cystourethrography and contrast enhanced voiding US in adults with transplanted kidneys and suspected of reflux, US sensitivity and specificity for detecting reflux were 93% and 95%, respectively (144); agreement between the two studies was 95%. An antireflux reimplantation procedure is helpful in some of these children.

Tuberculous nephropathy is uncommon in renal transplant patients, even if they have had chest tuberculosis preoperatively (145). Some of these patients develop acute rejection and undergo steroid therapy. Also, a normal graft function does not exclude tuberculous infection.

Failed Transplant

Failed renal allografts are usually left in situ and the patient then undergoes either dialysis or retransplantation. Most of these failed kidneys are asymptomatic and gradually shrink in size, and a number eventually calcify. Some develop fatty infiltration and become hydronephrotic, findings detectable with imaging. Acute enlargement of a failed transplant should suggest an infarct and hemorrhage.

Other Complications

Torsion of an intraperitoneal renal transplant should be suspected if abnormal perfusion is associated with a change in renal axis.

Occasionally acute tubular necrosis develops in a newly transplanted allograft kidney following unrelated surgery; Tc-99m-MAG3 scintigraphy detects focal acute tubular necrosis.

Not all pain in these patients is related to a transplant; right lower quadrant pain in renal transplant patients can be secondary to acute appendicitis and related conditions.

Post–Bone Marrow Transplant

Acute renal failure developed in roughly 25% of bone marrow transplant patients, most often occurring during the first month after transplantation. This complication occurs primarily in allogenic bone marrow transplantation. The etiologies for such failure tend to be multifactorial and include nephrotoxicity, liver veno-occlusive disease, and others.

Nephrectomy

An arteriovenous fistula of the renal pedicle is a rare complication of nephrectomy, at times developing years after a nephrectomy. Turbulent blood flow in the fistula often results in a bruit. With time, the artery feeding a fistula and draining vein dilate and collateral vessels develop. Doppler US should detect these fistulas.

Conduits

An ileal conduit is formed after a cystectomy. A not uncommon complication is an ureteroileal stricture. These strictures are amenable to dilation with a balloon catheter, followed by stenting with a double-J stent, with good results. Stents can be inserted through urinary diversion stomas.

Major ureteroileal reflux of a Kock pouch is an occasional complication, and these patients undergo an antireflux ureteroileal implantation. Follow-up of these patients is with a retrograde study to detect any reflux.

An adenocarcinoma within an ileal conduit is a recognized but rare complication years later.

If necessary, a ureteral defect is replaced by an interposed ileal loop (ureteroileoplasty), thus preserving ureter continuity. Several studies suggest that such ileal interposition is a safe and effective procedure.

Some of the complications encountered after ureterosigmoidostomy are pyelonephritis, hyperchloremic metabolic acidosis, incontinence, and a late development of anastomotic colon carcinoma.

A patient with a ureterocutaneostomy developed a squamous cell carcinoma at the stomal site; presumably chronic infection and irritation of the indwelling catheter were factors in carcinoma formation.

Examination and Surgical Complications

Biopsy

Needle tract seeding after percutaneous biopsy occurs with numerous neoplasms, including even a Wilms' tumor, and some investigators do not perform pretreatment needle biopsies of renal tumors in children for fear of needle tract tumor seeding.

More hemorrhage, arteriovenous and arteriocaliceal fistulas, and other complications are encountered when renal biopsy is performed with a 14-gauge needle rather than when an 18-gauge needle is used. Also, percutaneous renal biopsy can lead to a subcapsular hematoma and hypertension.

An arteriovenous fistula is probably more common than suspected after a renal biopsy. Fistulas also develop secondary to renal surgery. Some fistulas manifest with hematuria (Fig. 10.41), but many patients are asymptomatic. A rare fistula leads to renal ischemia or even hypertension. Some are associated with a pseudoaneurysm.

Color Doppler US readily detects these fistulas and is useful in follow-up. Eventually, most fistulas tend to resolve. If needed, a fistula is treated by superselective angiographic embolization, including transcatheter coil occlusion. Usually such embolization results in limited renal parenchymal loss. Postocclusion hypertension is uncommon.

Catheter and Stent Related

Minor complications of ureteral catheters and stents include hematuria, dysuria, frequency, and flank and suprapubic pain. Major complications encountered are initial catheter malposition, obstruction, stent migration or fracture, necrosis, erosion into adjacent structures, and ureterovascular fistula. Some stents break spontaneously; others are associated with stone formation. A broken stent usually can be removed either by ureteroscopy or by using a percutaneous approach. An uncommon complication is a knot forming in a ureteral catheter. A stiff guidewire advanced through the catheter lumen aids in untying such a knot. Rarer complications include a pelvic abscess and even septic hip arthritis. Blood clots and debris can obstruct the lumen, although flow is often both inside and around a stent. The risk of obstruction is decreased by using a large-bore catheter. Being foreign bodies, they lead to urinary infection and encrustation (Fig. 10.42). Encrustation is minimized by high fluid intake, treating infections vigorously, and routine catheter exchange. Both proximal and distal J-loops minimize but do not prevent stent migration either proximally or distally. Because stents are radiopaque, their position is generally verified with conventional radiography. Computed tomography establishes catheter patency indirectly by revealing an interval decrease in hydronephrosis. If necessary, a voiding cystogram establishes patency because most catheters will reflux. Other tests of catheter

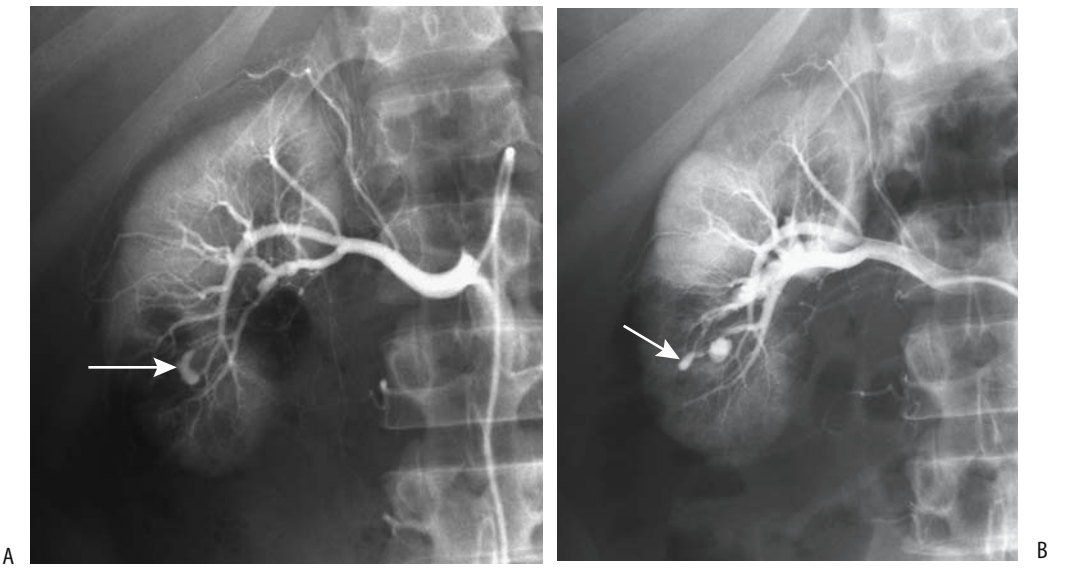

Figure 10.41. Hematuria after renal biopsy led to an arteriogram. Early (A) and late (B) arterial phase renal arteriograms reveal contrast extravasation (arrow). Early venous filling was evident on other films. He underwent successful Gelfoam and Ivalon embolization. (Courtesy of Oscar Gutierrez, M.D., University of Chile, Santiago, Chile.)

Figure 10.42. Ureteral stent encrustation. A: A conventional radiograph shows a right ureteral stent with radiopaque encrustation both proximally and distally. B: A urogram reveals ureteropelvic obstruction due to the proximal encrustation. Several cystoscopic attempts were necessary to treat the vesical encrustations. Renal encrustations were treat percutaneously and eventually the stent was successfully removed. (*Source:* Dyer RB, Chen MY, Zagoria RJ, Regan JD, Hood CG, Kavanagh PV. Complications of ureteral stent placement. RadioGraphics 2002;22:1005–1022, with permission from the Radiological Society of North America.)

patency include Doppler US detection of urinary jets and measurement of the resistance index with Doppler US. Nuclear renography, often combined with a diuretic agent, evaluates patency in an appropriate clinical setting.

Because urethral catheters positioned with a distal tip in the bladder result in reflux, their use is inappropriate if additional reflux is detrimental.

Stent erosion into an adjacent vessel is favored by ischemia—often due to either prior radiation therapy or extensive surgery.

Most ureteral stents are retrieved cystoscopically. Occasionally it is necessary to retrieve a stent using a percutaneous fluoroscopic approach. Some stents remain in place for a number of years and become encrusted. The initial approach to such a chronic stent should be an IV urogram to evaluate renal function and identify any obstruction. With no significant encrustation, stent extraction under fluoroscopic control is generally successful. With encrustation, ESWL can be successful. With a fixed proximal J-curved stent percutaneous removal may be successful.

Vascular Complications

Significant hematuria occasionally develops after an invasive percutaneous renal procedure. Angiography should detect any underlying vascular injury and, if necessary, transarterial embolization with Gelfoam, steel coils, or other material performed.

A rare complication of renal angioplasty is acute pulmonary edema.

Nephrectomy

Either a transabdominal or retroperitoneal approach is used during laparoscopic radical nephrectomy. The incidence of complications and the need for conversion to open surgery decreases with experience. These complications range from access site complications, such as hernia formation and hematoma, to vascular injury, splenic laceration, adrenal injury, and pneumothorax.

Computed tomography reliably identifies postoperative bleeding, urinary leak, or obstruction in these patients.

Nephrostomy

The most common indication for percutaneous nephrostomy is renal collecting system obstruction; an occasional nephrostomy is performed to bypass a ureteral fistula. These common procedures are associated with few serious complications. Transient hematuria is common after the procedure. Occasional hemorrhage requires transfusion. Rare complications include gallbladder puncture and peritonitis and air embolism.

While palliative percutaneous nephrostomy does decompress a more distal malignant obstruction, whether it improves quality of life in patients with an unresectable cancer is another question.

Related to Other Abdominopelvic Surgery

One complication of gynecologic surgery is iatrogenic ureteral injury. The risk of ureteral injury is about 10 times greater during an abdominal hysterectomy than during vaginal surgery; some of these injuries are relatively asymptomatic and lead to a silent kidney loss.

A rare complication is a bladder or ureteroacetabular fistula, often a result of extensive pelvic surgery.

An occasional surgical scar shows uptake of Tc-99m–methylene diphosphonate (MDP).

Ureteroscopy

Possible complications of ureteroscopic calculi removal are perforation, stricture, and even ureter avulsion. Avulsion of the lumbar ureter is related to both ureteroscope and Dormia catheter manipulation. During an iatrogenic ureteral perforation a calculus can be pushed into the retroperitoneum alongside the ureter. Such paraureteral calculi should not result in a subsequent stricture.

Contrast Nephropathy

According to the Contrast Media Safety Committee of The European Society of Urogenital Radiology, hemodialysis and peritoneal dialysis

remove both iodinated and gadolinium contrast agents (146); several hemodialysis sessions or several weeks of continuous ambulatory dialysis are necessary to removal all contrast. It should be noted, however, that hemodialysis does not protect poorly functioning kidneys against contrast induced nephrotoxicity.

Contrast-associated nephropathy is a poorly understood and generally unpredictable phenomenon. Its prevalence is increased in patients with diabetic nephropathy. Also, elderly patients and those who are azotemic, hypertensive, dehydrated, or have hyperuricemia are at increased risk of developing contrast nephropathy. High blood urea nitrogen and high creatinine levels are additional risk factors.

Creatinine clearance is generally employed to monitor changes in renal function due to suspected contrast nephropathy, although the primary effect of contrast agents is on renal tubules rather than glomerular function. In either case, most changes are mild and reversible and do not need therapy.

Occasionally prolonged renal cortical contrast retention is evident after vascular contrast injection. While retention can be seen in such conditions as hypotension, in some patients retention persists for several days or even longer in the absence of any known underlying abnormality. Computed tomography performed hours after angiography identifies renal cortical contrast in a minority of patients; these patients are at an increased risk, albeit low, of contrast-associated nephropathy. The large contrast volumes used correlate with contrast retention and nephropathy.

Hydration prior to contrast injection is effective in decreasing the risk of contrast nephropathy. The use of low osmolar contrast agents also lessens the prevalence of contrast nephropathy. Preliminary results suggest that prophylactic prostaglandin E_1 may have a role in patients at risk.

A neutral gadolinium chelate (gadobutrol), injected IV at doses of either 0.1 or 0.3 mmol per kg of body weight in patients with marginal excretory function (creatinine clearance <30 mL/min), did not affect renal function and thus appears to be a safe MR contrast agent even in patients with impaired renal function (147); hydration, treatment with diuretics, and hemodialysis are not required after the use of this contrast agent. Yet gadolinium contrast agents are not completely innocuous, and occasional reports describe acute renal failure after their use. Several reports describe use of gadolinium-based contrast agents for CT imaging in patients with renal insufficiency or prior severe reaction to an iodinated agent. In fact, the toxicity of gadolinium agents, at doses achieving equivalent x-ray stopping power, is greater than that of nonionic iodinated agents. This is in distinction to the use of approved lower gadolinium doses during MRI, which are insufficient for useful x-ray contrast, and which have negligible nephrotoxicity. The European Society of Urogenital Radiology position is that gadolinium-based contrast agents are more nephrotoxic than iodinated contrast agents in equivalent x-ray attenuation doses and use of gadolinium contrast agents for angiography or CT is not recommended.

References

1. Tippins RB, Torres WE, Baumgartner BR, Baumgarten DA. Are screening serum creatinine levels necessary prior to outpatient CT examinations? Radiology 2000;216:481–484.
2. Nemeth AJ, Patel SK. Pyelovenous backflow seen on CT urography. AJR 2004;182:532–533.
3. Nolte-Ernsting CC, Wildberger JE, Borchers H, Schmitz-Rode T, Gunther RW. Multi-slice CT urography after diuretic injection: initial results. Rofo Fortschr Geb Rontgenstr Neuen Bildgeb Verfahr 2001;173:176–180.
4. Teh HS, Ang ES, Wong WC, et al. MR renography using a dynamic gradient-echo sequence and low-dose gadopentetate dimeglumine as an alternative to radionuclide renography. AJR 2003;181:441–450.
5. Gehl HB, Lorch H, Amblank OB, Engerhoff B, Weiss HD. [Comparative magnetic resonance imaging of renal space-occupying lesions with a high and low field MRI system.] [German] Rofo Fortschr Geb Rontgenstr Neuen Bildgeb Verfahr 1998;169:484–489.
6. Donnelly LF, Nelson RC. Renal excretion of gadolinium mimicking calculi on non-contrast CT. Pediatr Radiol 1998;28:417.
7. Obuchi M, Takahara T, Takahashi M, et al. [Breath-hold 3D MR urography with 2 ml Gd-DTPA injection.] [Japanese] Nippon Igaku Hoshasen Gakkai Zasshi 1998;58:163–165.
8. Borthne AS, Pierre-Jerome C, Gjesdal KI, Storaas T, Courivaud F, Eriksen M. Pediatric excretory MR urography: comparative study of enhanced and non-enhanced techniques. Eur Radiol 2003;13:1423–1427.
9. Allkemper T, Tombach B, Heindel W. [Gd-BOPTA enhanced excretory MR urography without administration of diuretics.] [German] Rofo Fortschr Geb Rontgenstr Neuen Bildgeb Verfahr 2001;173:115–120.

10. Neri E, Boraschi P, Caramella D, et al. Magnetic resonance virtual endoscopy of the upper urinary tract. AJR 2000;175:1697–1702.
11. Rybicki FJ, Shu KM, Cibas ES, Fielding JR, vanSonnenberg E, Silverman SG. Percutaneous biopsy of renal masses: sensitivity and negative predictive value stratified by clinical setting and size of masses. AJR 2003;180:1281–1287.
12. Preda A, Van Dijk LC, Van Oostaijen JA, Pattynama PM. Complication rate and diagnostic yield of 515 consecutive ultrasound-guided biopsies of renal allografts and native kidneys using a 14-gauge Biopty gun. Eur Radiol 2003;13:527–530.
13. Cluzel P, Martinez F, Bellin MF, et al. Transjugular versus percutaneous renal biopsy for the diagnosis of parenchymal disease: comparison of sampling effectiveness and complications. Radiology 2000;215: 689–693.
14. Hogan MJ, Coley BD, Jayanthi VR, Shiels WE, Koff SA. Percutaneous nephrostomy in children and adolescents: outpatient management. Radiology 2001;218: 207–210.
15. Patel U, Hussain FF. Percutaneous nephrostomy of nondilated renal collecting systems with fluoroscopic guidance: technique and results. Radiology 2004;233: 226–233.
16. Caire JT, Ramus RM, Magee KP, Fullington BK, Ewalt DH, Twickler DM. MRI of fetal genitourinary anomalies. AJR 2003;181:1381–1385.
17. Choi JY, Kim SH, Kim SH. Double-blind ureteral duplication: report of two cases. Eur Radiol 2002;12 Suppl 3:S136–139.
18. Wikstrom M, Hauger W, Sinagowitz E. [A triple ureter with an ectopic opening into the vagina.] [Review] [German] Rofo Fortschr Geb Rontgenstr Neuen Bildgeb Verfahr 1999;171:497–498.
19. Zerin JM, Leiser J. The impact of vesicoureteral reflux on contralateral renal length in infants with multicystic dysplastic kidney. Pediatr Radiol 1998;28:683–686.
20. Feather SA, Winyard PJ, Dodd S, Woolf AS. Oral-facial-digital syndrome type 1 is another dominant polycystic kidney disease: clinical, radiological and histopathological features of a new kindred. Nephrol Dial Transplant 1997;12:1354–1361.
21. Hateboer N, v Dijk MA, Bogdanova N, et al. Comparison of phenotypes of polycystic kidney disease types 1 and 2. European PKD1–PKD2 Study Group. Lancet 1999;353:103–107.
22. Nicolau C, Torra R, Badenas C, et al. Autosomal dominant polycystic kidney disease types 1 and 2: assessment of US sensitivity for diagnosis. Radiology 1999; 213:273–276.
23. Neumann HP, Bender BU, Berger DP, et al. Prevalence, morphology and biology of renal cell carcinoma in von Hippel-Lindau disease compared to sporadic renal cell carcinoma. J Urol 1998;160:1248–1254.
24. Dondi M, Fanti S, Monetti N. Bartter's syndrome: renal scintigraphic appearance after captopril administration. J Nucl Med 1996;37:1688–1690.
25. Forget S, Patriquin HB, Dubois J, et al. The kidney in children with tyrosinemia: sonographic, CT and biochemical findings. Pediatr Radiol 1999;29:104–108.
26. Moore EE, Cogbill TH, Malangoni MA, et al. Organ injury scaling. [Review] Surg Clin North Am 1995; 75:293–303.
27. Dacher JN, Avni F, Francois A, et al. Renal sinus hyperechogenicity in acute pyelonephritis: description and pathological correlation. Pediatr Radiol 1999;29:179–182.
28. Laguna R, Silva F, Orduna E, Conway JJ, Weiss S, Calderon C. Technetium-99m-MAG3 in early identification of pyelonephritis in children. J Nucl Med 1998; 39:1254–1257.
29. Lonergan GJ, Pennington DJ, Morrison JC, Haws RM, Grimley MS, Kao TC. Childhood pyelonephritis: comparison of gadolinium-enhanced MR imaging and renal cortical scintigraphy for diagnosis. Radiology 1998;207:377–384.
30. Kuo YT, Chen MT, Liu GC, Huang CN, Huang CL, Huang CH. Emphysematous pyelonephritis: imaging diagnosis and follow-up. Kao-Hsiung I Chih 1999;15: 159–170.
31. el Fakir Y, Kabbaj N, Dafiri R, Imani F. [Imaging of urinary Candida bezoars.] [French] Prog Urol 1999;9:513–517.
32. el Khader K, Lrhorfi MH, el Fassi J, Tazi K, Hachimi M, Lakrissa A. [Urogenital tuberculosis. Experience in 10 years.] [French] Prog Urol 2001;11:62–67.
33. Kirchner TH, Kirchner J, Jacobi V. [Renal parenchymal defects as signs of renal tuberculosis.] [German] Rontgenpraxis 2000;52:332–234.
34. Yagi S, Goto T, Kawamoto K, et al. Endoscopic treatment of refractory filarial chyluria: a preliminary report. J Urol 1998;159:1615–1618.
35. Weber MA, Wasser K, Schwenger V, Hallscheidt P, Nahm AM, Delorme S. [Palpable resistance in the right renal area. Xanthogranulomatous pyelonephritis with fistulization in the colon ascendens and M. psoas major.] [German] Radiologe 2002;42:46–50.
36. Leluc O, Andre M, Marciano S, Lafforgue P, Rossi D, Bartoli J. [Retroperitoneal complications of Erdheim-Chester disease.] [French] J Radiol 2001;82:580–582.
37. Schmidt T, Hohl C, Haage P, et al. Diagnostic accuracy of phase-inversion tissue harmonic imaging versus fundamental B-mode sonography in the evaluation of focal lesions of the kidney. AJR 2003;180:1639–1647.
38. Tello R, Davison BD, O'Malley M, et al. Magnetic resonance imaging of renal masses interpreted on CT to be suspicious. AJR 2000;174:1017–1022.
39. Bain ES, Kinney TB, Gooding JM, Casola G, Ysrael MZ. Sinus histiocytosis with massive lymphadenopathy (Rosai-Dorfman disease): a rare cause of bilateral renal masses. AJR 1999;172:995–996.
40. Townsend MF 3rd, Gal AA, Thoms WW, Newman JL, Eble JN, Graham SD Jr. Ureteral rhabdomyosarcoma. Urology 1999(online);54:561.
41. Johraku A, Miyanaga N, Sekido N, et al. A case of intravascular papillary endothelial hyperplasia (Masson's tumor) arising from renal sinus. Jpn J Clin Oncol 1997;27:433–436.
42. Bosniak MA. The use of the Bosniak classification system for renal cysts and cystic tumors. J Urol 1997;157:1852–1853.
43. Curry NS, Cochran ST, Bissada NK. Cystic renal masses: accurate Bosniak classification requires adequate renal CT. AJR 2000;175:339–342.

44. Israel GM, Hindman N, Bosniak MA. Evaluation of cystic renal masses: comparison of CT and MR imaging by using the Bosniak classification system. Radiology 2004;231:365–371.
45. Chung EP, Herts BR, Linnell G, et al. Analysis of changes in attenuation of proven renal cysts on different scanning phases of triphasic MDCT. AJR 2004;182:405–410.
46. Bae KT, Heiken JP, Siegel CL, Bennett HF. Renal cysts: is attenuation artifactually increased on contrast-enhanced CT images? Radiology 2000;216:792–796.
47. Macari M, Bosniak MA. Delayed CT to evaluate renal masses incidentally discovered at contrast-enhanced CT: demonstration of vascularity with de-enhancement. Radiology 1999;213:674–680.
48. Slywotzky CM, Bosniak MA. Localized cystic disease of the kidney. AJR 2001;176:843–849.
49. Storkel S, van den Berg E. Morphological classification of renal cancer. World J Urol 1995;13:153–158.
50. Kovacs G, Akhtar M, Beckwith BJ, et al. The Heidelberg classification of renal cell tumours. [Review] J Pathol 1997;83:131–133.
51. Kim JK, Kim TK, Ahn HJ, Kim CS, Kim KR, Cho KS. Differentiation of subtypes of renal cell carcinoma on helical CT scans. AJR 2002;178:1499–1506.
52. Toro JR, Glenn G, Duray P, et al. Birt-Hogg-Dube syndrome: a novel marker of kidney neoplasia. Arch Dermatol 1999;135:1195–1202.
53. Brauch H, Weirich G, Hornauer MA, Storkel S, Wohl T, Bruning T. Trichloroethylene exposure and specific somatic mutations in patients with renal cell carcinoma. J Nat Cancer Inst 1999;91:854–661.
54. Ligato S, Ro JY, Tamboli P, Amin MB, Ayala AG. Benign tumors and tumor-like lesions of the adult kidney. Part I: Benign renal epithelial neoplasms. Adv Anat Pathol 1999;6:1–11.
55. Ascenti G, Gaeta M, Magno C, et al. Contrast-enhanced second-harmonic sonography in the detection of pseudocapsule in renal cell carcinoma. AJR 2004;182: 1525–1530.
56. Scialpi M, Di Maggio A, Midiri M, Loperfido A, Angelelli G, Rotondo A. Small renal masses: assessment of lesion characterization and vascularity on dynamic contrast-enhanced MR imaging with fat suppression. AJR 2000;175:751–757.
57. Yoshimitsu K, Honda H, Kuroiwa T, et al. Magnetic resonance detection of cytoplasmic fat in clear cell renal cell carcinoma utilizing chemical shift gradient-echo imaging. J Magn Reson Imaging 1999;9:579–585.
58. Schubert RA, Schleicher C, Mentzel HJ, Wunderlich H, Schubert J, Kaiser WA. [The observed and chance-corrected agreement of the computed tomographic and histological staging results in renal-cell carcinoma.] [German] Rofo Fortschr Geb Rontgenstr Neuen Bildgeb Verfahr 1999;170:358–364.
59. Ergen FB, Hussain HK, Caoili EM, et al. MRI for preoperative staging of renal cell carcinoma using the 1997 TNM classification: comparison with surgical and pathologic staging. AJR 2004;182:217–225.
60. Lebret T, Becette V, Colau A, et al. [Study of the Ki-67 antibody immunolabeling of renal adenocarcinomas with or without renal vein thrombosis.] [French] Prog Urol 1999;9:649–654.
61. Remer EM, Weinberg EJ, Oto A, O'Malley CM, Gill IS. Magnetic resonance imaging of the kidneys after laparoscopic cryoablation. AJR 2000;174:635–640.
62. Mayo-Smith WW, Dupuy DE, Parikh PM, Pezzullo JA, Cronan JJ. Imaging-guided percutaneous radiofrequency ablation of solid renal masses: techniques and outcomes of 38 treatment sessions in 32 consecutive patients. AJR 2003;180:1503–1508.
63. Lewin JS, Nour SG, Connell CF, et al. Phase II clinical trial of interactive MR imaging-guided interstitial radiofrequency thermal ablation of primary kidney tumors: initial experience. Radiology 2004;232:835–845.
64. McLaughlin CA, Chen MY, Torti FM, Hall MC, Zagoria RJ. Radiofrequency ablation of isolated local recurrence of renal cell carcinoma after radical nephrectomy. AJR 2003;181:93–94.
65. Hafez KS, Novick AC, Campbell SC. Patterns of tumor recurrence and guidelines for followup after nephron sparing surgery for sporadic renal cell carcinoma. J Urol 1997;157:2067–2070.
66. Quaia E, Siracusano S, Bertolotto M, Monduzzi M, Mucelli RP. Characterization of renal tumours with pulse inversion harmonic imaging by intermittent high mechanical index technique: initial results. Eur Radiol 2003;13:1402–1412.
67. Shishikura Y, Furusato M, Aizawa S. Cystic renal cell carcinoma: arose as a simple cyst, recurred repeatedly as a multicystic mass and finally presented as a solid mass. Pathol Int 1998;48:623–628.
68. Mahnken AH, Wildberger JE, Bergmann F, Fuzesi L, Adam G, Gunther R. [Papillary renal cell carcinoma: comparison of CT and gross morphology.] [German] Rofo Fortschr Geb Rontgenstr Neuen Bildgeb Verfahr 2000;172:1011–1015.
69. Lesavre A, Correas JM, Merran S, Grenier N, Vieillefond A, Helenon O. CT of papillary renal cell carcinomas with cholesterol necrosis mimicking angiomyolipomas. AJR 2003;181:143–145.
70. Sijmons RH, Kiemeney LA, Witjes JA, Vasen HF. Urinary tract cancer and hereditary nonpolyposis colorectal cancer: risks and screening options. J Urol 1998;160:466–470.
71. Kitamura Y, Watanabe M, Komatsubara S, Sakata Y, Miyajima N. [Regional lymph node metastasis in renal pelvic or ureteral cancer.] [Japanese] Nippon Hinyokika Gakkai Zasshi 1998;89:522–528.
72. Van Glabeke E, Chartier-Kastler E, Delcourt A, Cluzel P, Bruel S, Richard F. [Epidermoid cancer of the kidney pelvis.] [French] Prog Urol 2000;10:1200–1203.
73. Rohrschneider WK, Weirich A, Rieden K, Darge K, Troger J, Graf N. US, CT and MR imaging characteristics of nephroblastomatosis. Pediatr Radiol 1998;28: 435–443.
74. Kumar R, Fitzgerald R, Breatnach F. Conservative surgical management of bilateral Wilms tumor: results of the United Kingdom Children's Cancer Study Group. J Urol 1998;160:1450–1453.
75. Jeanes AC, Beese RC, McHugh K, Ramsay AD. Fatty degeneration in a Wilms' tumour after chemotherapy. Eur Radiol 2002;12 Suppl 3:S149–151.

76. Isaac MA, Vijayalakshmi S, Madhu CS, Bosincu L, Nogales FF. Pure cystic nephroblastoma of the ovary with a review of extrarenal Wilms' tumors. [Review] Hum Pathol 2000;31:761–764.
77. Eble JN, Bonsib SM. Extensively cystic renal neoplasms: cystic nephroma, cystic partially differentiated nephroblastoma, multilocular cystic renal cell carcinoma, and cystic hamartoma of renal pelvis. [Review] Semin Diagn Pathol 1998;15:2–20.
78. Nagao T, Sugano I, Ishida Y, et al. Cystic partially differentiated nephroblastoma in an adult: an immunohistochemical, lectin histochemical and ultrastructural study. Histopathology 1999;35:65–73.
79. Pages A, Granier M. [Nephronogenic nephroma (author's transl).] [French] Arch Anat Cytol Pathol 1980;28:99–103.
80. Renshaw AA, Freyer DR, Hammers YA. Metastatic metanephric adenoma in a child. Am J Surg Pathol 2000;24:570–574.
81. Keshani de Silva V, Tobias V, Kainer G, Beckwith B. Metanephric adenoma with embryonal hyperplasia of Bowman's capsular epithelium: previously unreported association. Pediatr Dev Pathol 2000;3:472–478.
82. Argani P, Beckwith JB. Metanephric stromal tumor: report of 31 cases of a distinctive pediatric renal neoplasm. Am J Surg Pathol 2000;24:917–926.
83. Sakhuja V, Jha V, Varma S, et al. Renal involvement in multiple myeloma: a 10–year study. Ren Fail 2000;22: 465–477.
84. Burdeny DA, Semelka RC, Kelekis NL, Reinhold C, Ascher SM. Small (<1.5 cm) angiomyolipomas of the kidney: characterization by the combined use of in-phase and fat-attenuated MR techniques. Magn Reson Imaging 1997;15:141–145.
85. Lee W, Kim TS, Chung JW, Han JK, Kim SH, Park JH. Renal angiomyolipoma: embolotherapy with a mixture of alcohol and iodized oil. J Vasc Interv Radiol 1998;9: 255–261.
86. Haddad FS, de la Vega DJ, DuBose Dent E Jr, Shippel RM. Renal fibrohistiocytic sarcoma. Three cases and a review of the literature. [Review] J Med Liban 1998;46: 335–342.
87. Tsurukawa H, Iuchi H, Osanai H, et al. [Renomedullary interstitial cell tumor: a case report.] [Review] [Japanese] Nippon Hinyokika Gakkai Zasshi 2000;91: 37–40.
88. Tajima K, Saito K, Umeda Y, Murata T, Satani H. Malignant melanoma of the kidney presenting as a primary tumor. Int J Urol 1997;4:94–96.
89. Soulie M, Escourrou G, Vazzoler N, et al. [Primary carcinoid tumor and horseshoe kidney: potential association.] [French] Prog Urol 2001;11:301–303.
90. Georgiades CS, Moore CJ, Smith DP. Differences of renal parenchymal attenuation for acutely obstructed and unobstructed kidneys on unenhanced helical CT: a useful secondary sign? AJR 2001;76:965–968.
91. Garcia-Pena BM, Keller MS, Schwartz DS, Korsvik HE, Weiss RM. The ultrasonographic differentiation of obstructive versus nonobstructive hydronephrosis in children: a multivariate scoring system. J Urol 1997; 158:560–565.
92. Sudah M, Vanninen R, Partanen K, Heino A, Vainio P, Ala-Opas M. Magnetic resonance urography in evaluation of acute flank pain: T2–weighted sequences and gadolinium-enhanced three-dimensional FLASH compared with urography AJR 2001;176:105–112.
93. Foda MM, Gatfield CT, Matzinger M, et al. A prospective randomized trial comparing 2 diuresis renography techniques for evaluation of suspected upper urinary tract obstruction in children. J Urol 1998;159:1691–1693.
94. Harrington TG, Kandel LB. Renal colic following a gunshot wound to the abdomen: the birdshot calculus. J Urol 1997;157:1351–1352.
95. Sheafor DH, Hertzberg BS, Freed KS, et al. Nonenhanced helical CT and US in the emergency evaluation of patients with renal colic: prospective com-parison. Radiology 2000;217:792–797.
96. Assi Z, Platt JF, Francis IR, Cohan RH, Korobkin M. Sensitivity of CT scout radiography and abdominal radiography for revealing ureteral calculi on helical CT: implications for radiologic follow-up. AJR 2000;175:333–337.
97. Zagoria RJ, Khatod EG, Chen MY. Abdominal radiography after CT reveals urinary calculi: a method to predict usefulness of abdominal radiography on the basis of size and CT attenuation of calculi. AJR 2001;176:1117–1122.
98. Chong WK, Wysoki M, Heller LG, Zegel HG. Renal carcinoma presenting with flank pain: a potential drawback of unenhanced CT. AJR 2000;174:667–669.
99. Goldman SM, Faintuch S, Ajzen SA, et al. Diagnostic value of attenuation measurements of the kidney on unenhanced helical CT of obstructive ureterolithiasis. AJR 2004;182:1251–1254.
100. Jones RA, Perez-Brayfield MR, Kirsch AJ, Grattan-Smith JD. Renal transit time with MR urography in children. Radiology 2004;233:41–50.
101. Takahashi N, Kawashima A, Ernst RD, et al. Ureterolithiasis: can clinical outcome be predicted with unenhanced helical CT? Radiology 1998;208: 97–102.
102. Frauscher F, Janetschek G, Helweg G, Strasser H, Bartsch G, zur Nedden D. Crossing vessels at the ureteropelvic junction: detection with contrast-enhanced color Doppler imaging. Radiology 1999;210: 727–731.
103. Nishie A, Yoshimitsu K, Irie H, et al. Radiologic features of Castleman's disease occupying the renal sinus. AJR 2003;181:1037–1040.
104. Geavlete P, Georgescu D, Nita G, Cauni V. [Doppler ultrasonography in the function assessment of double J ureteral endoprosthesis in patients with extrinsic ureteral obstruction.] [French] Prog Urol 2001;11: 22–28.
105. Sugamoto T, Yokoyama M, Nishio S, Takeuchi M. Cholesteatoma of the ureter: a case report. [Review] Int J Urol 1997;4:621–622.
106. Weinberg B, Yeung N. Sonographic sign of intermittent dilatation of the renal collecting system in 10 patients with vesicoureteral reflux. J Clin Ultrasound 1998;26: 65–68.
107. Darge K, Troeger J. Vesicoureteral reflux grading in contrast-enhanced voiding urosonography. Eur J Radiol 2002;43:122–128.
108. Bertschy C, Aubert D, Piolat C, Billerey C. [Ureterovesical implantation after failure of endoscopic treatment of reflux: anatomical and histological study of 61

resection specimens from 40 children.] [French] Prog Urol 2001;11:113–117.
109. Olbing H, Hirche H, Koskimies O, et al. Renal growth in children with severe vesicoureteral reflux: 10-year prospective study of medical and surgical treatment: the International Reflux Study in Children (European branch).] Radiology 2000;216:731–737.
110. Chow WH, Lindblad P, Gridley G, et al. Risk of urinary tract cancers following kidney or ureter stones. J Nat Cancer Inst 1997;89:1453–1457.
111. Daudon M. [Drug-induced urinary calculi in 1999.] [Review] [French] Prog Urol 1999;9:1023–1033.
112. Saw KC, McAteer JA, Monga AG, Chua GT, Lingeman JE, Williams JC Jr. Helical CT of urinary calculi: effect of stone composition, stone size, and scan collimation. AJR 2000;175:329–332.
113. Mostafavi MR, Ernst RD, Saltzman B. Accurate determination of chemical composition of urinary calculi by spiral computerized tomography. J Urol 1998;159: 673–675.
114. Lee JY, Kim SH, Cho JY, Han D. Color and power Doppler twinkling artifacts from urinary stones: clinical observations and phantom studies. AJR 2001;176: 1441–1445.
115. Chelfouh N, Grenier N, Higueret D, et al. Characterization of urinary calculi: in vitro study of "twinkling artifact" revealed by color-flow sonography. AJR 1998;171: 1055–1060.
116. Dore B. [Management of renal calix calculosis.] [Review] [French] Presse Med 1999;28:2181–2188.
117. Soh J. [The maximum volume of urinary calculi to be disintegrated by ESWL.] [Japanese] Nippon Hinyokika Gakkai Zasshi 1998;89:23–28.
118. Traxer O, Lottmann H, Archambaud F, Helal B, Mercier Pageyral B. [Long-term evaluation with DMSA-Tc 99m scintigraphy of renal parenchymal involvement in children after shockwave extracorporeal lithotripsy.] [French] Prog Urol 1998;8:502–506.
119. Chan KF, Vassar GJ, Pfefer TJ, et al. Holmium:YAG laser lithotripsy: a dominant photothermal ablative mechanism with chemical decomposition of urinary calculi. Lasers Surg Med 1999;25:22–37.
120. Havel D, Saussine C, Fath C, Lang H, Faure F, Jacqmin D. Single stones of the lower pole of the kidney. Comparative results of extracorporeal shock wave lithotripsy and percutaneous nephrolithotomy. Eur Urol 1998;33:396–400.
121. Gremmo E, Ballanger P, Dore B, Aubert J. [Hemorrhagic complications during percutaneous nephrolithotomy. Retrospective studies of 772 cases.] [French] Prog Urol 1999;9:460–463.
122. Schillinger F, Delclaux B, Milcent T, et al. [Renal sarcoidosis with a pseudotumoral pyelic localization.] [French] Presse Med 1999;28:683–685.
123. Yassa NA, Peng M, Ralls PW. Perirenal lucency ("kidney sweat"): a new sign of renal failure. AJR 1999;173:1075–1077.
124. Delzell E, Shapiro S. A review of epidemiologic studies of nonnarcotic analgesics and chronic renal disease. [Review] Medicine 1998;77:102–121.
125. Michail S, Stathakis C, Nakopoulou L, et al. Acute renal failure in an adult patient with Henoch-Schoenlein purpura after episode of macroscopic hematuria. Ren Fail 1999;21:107–111.
126. Selcuk NY, Odabas AR, Cetinkaya R, Tonbul HZ, San A. Outcome of pregnancies with HELLP syndrome complicated by acute renal failure (1989–1999). Ren Fail 2000;22:319–327.
127. Angelelli G, Stabile Ianora AA, Scardapane A, Rotondo A. [Computerized tomography in the study of the diabetic kidney.] [Italian] Radiol Med 2000;99:72–80.
128. Johnston RJ, Alkhunaizi AM. Unilateral focal segmental glomerulosclerosis with contralateral sparing on the side of renal artery stenosis. AJR 1999;172:35–37.
129. Colli A, Fraquelli M, Pometta R, Cocciolo M, Visentin S, Conte D. Renovascular impedance and esophageal varices in patients with Child-Pugh class A cirrhosis. Radiology 2001;219:712–715.
130. Katagiri K, Okada S, Kumazaki T, Tsuboi N. [Clearance of gadolinium contrast agent by hemodialysis: in vitro and clinical studies.] [Japanese] Nippon Igaku Hoshasen Gakkai Zasshi 1998;58:739–744.
131. Takebayashi S, Hidai H, Chiba T, Takagi H, Koike S, Matsubara S. Using helical CT to evaluate renal cell carcinoma in patients undergoing hemodialysis: value of early enhanced images. AJR 1999;172:429–433.
132. Vidart A, Pfister C, Bugel H, Savoye-Collet C, Thoumas D, Grise P. [Role of helical tomodensitometry in the early diagnosis of renal infarction.] [French] Prog Urol 2001; 11:217–221.
133. Di Fiori JL, Rodrigue D, Kaptein EM, Ralls PW. Diagnostic sonography of HIV-associated nephropathy: new observations and clinical correlation. AJR 1998;171:713–716.
134. Rankin SC, Jan W, Koffman CG. Noninvasive imaging of living related kidney donors: evaluation with CT angiography and gadolinium-enhanced MR angiography. AJR 2001;177:349–355.
135. Fink C, Hallscheidt PJ, Hosch WP, et al. Preoperative evaluation of living renal donors: value of contrast-enhanced 3D magnetic resonance angiography and comparison of three rendering algorithms. Eur Radiol 2003;13:794–801.
136. Jha RC, Korangy SJ, Ascher SM, Takahama J, Kuo PC, Johnson LB. MR angiography and preoperative evaluation for laparoscopic donor nephrectomy. AJR 2002; 178:1489–1495.
137. Moresco KP, Patel NH, Namyslowski Y, Shah H, Johnson MS, Trerotola SO. Carbon dioxide angiography of the transplanted kidney: technical considerations and imaging findings. AJR 1998;171:1271–1276.
138. Hilborn MD, Bude RO, Murphy KJ, Platt JF, Rubin JM. Renal transplant evaluation with power Doppler sonography. Br J Radiol 1997;70:39–42.
139. Amodio F, Rossi E, Carbone M, et al. [Echographic study with high-frequency and high-spatial resolution transducer in the evaluation of renal transplant in pediatric age.] [Italian] Radiol Med 2000;99:68–71.
140. Heindel W, Kugel H, Wenzel F, Stippel D, Schmidt R, Lackner K. Localized 31P MR spectroscopy of the transplanted human kidney in situ shows altered metabolism in rejection and acute tubular necrosis. J Magn Reson Imaging 1997;7:858–864.
141. Capocasale E, Bignardi L, Adorni A, D'Errico G, Viola V, Botta GC. [Neoplasms and kidney transplantation.

Case contribution.] [Italian] Minerva Urol Nefrol 1998;50:127–131.
142. Lopez-Ben R, Smith JK, Kew CE 2nd, Kenney PJ, Julian BA, Robbin ML. Focal posttransplantation lymphoproliferative disorder at the renal allograft hilum. AJR 2000;175:1417–1422.
143. Swindle P, Falk M, Rigby R, Petrie J, Hawley C, Nicol D. Transitional cell carcinoma in renal transplant recipients: the influence of compound analgesics. Br J Urol 1998;81:229–233.
144. Valentini AL, De Gaetano AM, Minordi LM, et al. Contrast-enhanced voiding US for grading of reflux in adult patients prior to antireflux ureteral implantation. Radiology 2004;233:35–39.
145. Lezaic V, Radivojevic R, Radosavljevic G, et al. Does tuberculosis after kidney transplantation follow the trend of tuberculosis in general population? Ren Fail 2001;23:97–106.
146. Morcos SK, Thomsen HS, Webb JA, et al. Dialysis and contrast media. Eur Radiol 2002;12:3026–3030.
147. Tombach B, Bremer C, Reimer P, et al. Renal tolerance of a neutral gadolinium chelate (gadobutrol) in patients with chronic renal failure: results of a randomized study. Radiology 2001;218:651–657.

11

Bladder

Technique

Conventional Cystography

Cystography is a well-established technique in evaluating the bladder lumen and providing access for biopsies. It is often used as a gold standard when evaluating other imaging procedures. Cystography as used here implies conventional cystography, which consists of lumen distention with a contrast agent introduced via a catheter and appropriate filming. Cystography is also feasible using computed tomography (CT), ultrasonography (US), magnetic resonance (MR), and radionuclide techniques.

Voiding cystourethrography continues to be the gold standard for imaging evaluation children with urinary tract infection, male urethra, functional bladder conditions and in detecting vesicoureteral reflux. Although radionuclide and contrast enhanced US cystography have a role in screening and follow-up of established conditions, most initial evaluation of function and anatomy appears best served by voiding cystourethrography.

Computed Tomography

A typical CT cystography technique consists of contiguous 5-mm axial scans after bladder distention with a 4% iodinated solution as a positive contrast agent. Air or carbon dioxide is occasionally used for bladder distention, but a potential complication of air is air embolism. Imaging in both the supine and prone positions is necessary when using gas to detect tumors otherwise covered with fluid.

Similar to CT colonoscopy, CT cystoscopy (also called *virtual cystoscopy*) is feasible with a contrast filled bladder. Computed tomography cystoscopy is an alternate procedure in patients with urethral strictures who cannot undergo conventional cystoscopy or cystography but indications are expanding and some enthusiasts believe it will replace a large part of conventional cystoscopy. Three-dimensional (3D) CT cystography using perspective volume rendering and a shaded-surface 3D outline evaluates tumor size and shape and provides information about its relationship to adjoining mucosa. With current techniques, however, endoscopic cystoscopy has better spatial resolution in detecting small bladder tumors; thus CT cystoscopy detected 90% of bladder tumors, with all undetected tumors being <5 mm in diameter (1); transverse and virtual images are complementary—some small tumors are identified only on virtual images but bladder wall thickening is more apparent on transverse images.

Flow of opacified urine into the bladder during contrast-enhanced CT results in intraluminal artifacts due to incomplete mixing. If necessary, delayed bladder images should be obtained to eliminate these artifacts.

Ultrasonography

Bladder US is performed using a transabdominal, endorectal, endovaginal, or endourethral approach. Color Doppler US detects ureteral jets and with unilateral ureteral obstruction, Doppler US reveals asymmetry to these ureteral jets. The presence of normal ureteral jets excludes significant obstruction.

Intravesical instillation of an US contrast agent aids detection of certain abnormalities, such as vesicoureteral reflux. A galactose-based microbubble contrast agent, Levovist, is typically employed. Contrast duration for this agent varies when mixed with normal saline. A high concentration of dissolved oxygen in normal saline appears to prevent diffusion of gas from the microbubbles into the solution and as a result contrast duration is longer than with use of a low oxygen concentration solution, such as is found in vacuum sealed containers (2).

Magnetic Resonance Imaging

On T1-weighted images urine is homogeneously hypointense and blends into the bladder wall. On T2-weighted images urine is hyperintense while bladder wall muscle layers remain hypointense and the two can be differentiated from each other. Immediate postcontrast images reveal little or no urine enhancement, but with renal excretion urine becomes hyperintense on delayed images.

Bladder instillation of a superparamagnetic iron oxide contrast agent aids in evaluating intraluminal extension of bladder tumors. High-resolution T2-weighted turbo spin echo (TSE) sequences detect tumors as small as 4 mm and estimate the depth of infiltration by identifying inner and outer bladder wall margins (3); this technique, however, does not readily identify different bladder wall layers.

Magnetic resonance (MR) cystoscopy is based on principles similar to CT cystoscopy. After filling the bladder with a negative contrast agent and using a heavily T2-weighted sequence such as half-Fourier acquisition single-shot turbo spin echo (HASTE), axial and virtual cystoscopic images achieved a sensitivity of about 90% in detecting tumors <1 cm and 100% for tumors 1 cm or larger (4), results not differing statistically from CT cystoscopy or conventional cystoscopy.

Virtual MR cystoscopy without bladder filling with contrast or use of IV contrast is also feasible; tumors >1 cm are readily detected (5). The role of such a contrast-less MR study in screening and diagnosis remains to be established.

Scintigraphy

Radionuclide cystography is less often performed than conventional cystography because of its poorer spatial resolution. Technetium-99m (Tc-99m)–sulfur colloid is not absorbed from the bladder and is thus employed. Indirect radionuclide cystography using Tc-99m-mercaptoacetylglycilglycilglycine (MAG3) may be sufficient for some indications.

Congenital Abnormalities

Agenesis

Bladder agenesis is very rare and is usually associated with other major anomalies. Most affected neonates are stillborn.

Duplication

Bladder duplication is rare. With complete duplication each kidney and ureter drains into its separate bladder, which then drains by separate urethras. Some duplications are incomplete and the two bladders communicate through an isthmus. Some bladders only appear duplicated because of an internal septum. An “hourglass” bladder or a large diverticulum arising from the dome of the bladder also mimics an incomplete duplication.

Cystography readily detects a bladder duplication.

A rare bladder duplication is associated with exstrophy, epispadias, and other abnormalities.

Cloacal Exstrophy

Various gradations in failure of fusion of the inferior abdominal wall range from an omphalocele, to cloacal (bladder) exstrophy, to epispadias. This condition is more common in males. In some, the anterior abdominal muscles and anterior bladder wall are absent.

Cloacal exstrophy is associated with an omphalocele, imperforate anus, exstrophy of

two hemibladders, and an everted cecum between which lie the hemibladders. Epispadias is part of an exstrophy abnormality. Cryptorchidism and an umbilical hernia are common. Extensive bowel anomalies include a blind-ending hindgut and an omphalocele. The terminal ileum may prolapse out of the cecum. Spinal anomalies are common and the spinal cord is tethered. An association exists between bladder exstrophy and subsequent development of a bladder malignancy.

Conventional radiographs reveal symphysis pubis widening. Such widening is not pathognomonic for cloacal exstrophy but is also found in cloacal malformation, epispadias, and other hindgut malformations. In exstrophy the iliac bones are rotated laterally.

Surgical treatment of these patients is complex and includes closure of an omphalocele, separation of the gastrointestinal tract from hemibladders, and creation of a single bladder. A bladder continence mechanism needs to be created. Lastly, if possible, a colon pull-through is performed.

Previous therapy for cloacal exstrophy was cystectomy and ureterosigmoidostomy. A number of complications develop with this procedure, including urinary infections and renal damage, with the major long-term complication being development of rectosigmoid adenocarcinoma. The risk of carcinoma is much less after creation of a urinary colonic conduit than with a simple ureteral sigmoidostomy.

Serial renal US is worthwhile in these patients to assess renal status and check for development of hydronephrosis. Renal ectopia is common. These patients are prone to reflux.

A cloacal malformation is a different entity, occurs only in girls, and is not related to cloacal exstrophy; it is discussed in Chapter 12.

Ureterocele

Clinical

A ureterocele is a congenital anomaly consisting of a dilated intramural ureteral segment. It is associated with urinary retention and infection. Ureteroceles are mostly a pediatric diagnosis but they occasionally first manifest in adulthood. They are classified into simple and ectopic, depending on the distal orifice. About 10% are bilateral. Some authors suggest that siblings of children with ureteroceles be screened for urogenital abnormalities.

Ectopic ureteroceles are often part of a duplicated renal collecting systems, with most terminating a ureter draining the upper renal pole. They are more common in girls and are a common cause of bladder obstruction in girls. An extreme example consists of bilateral ureteroceles and bilateral duplex systems. An ectopic ureterocele does occur in patients with a single kidney or a horseshoe kidney.

An ectopic ureterocele can distort an adjacent normally located ureterovesical junction to the point of inducing reflux. A rare ureterocele prolapses and even strangulates. Or occasionally a simple ureterocele even prolapses into the urethra and leads to bladder outlet obstruction. Bladder outlet obstruction can also be due to a simple ureterocele if it is large enough.

If necessary, a ureterocele is treated by endoscopic ureterocele incision; the success rate is lower with ectopic ureteroceles. Vesicoureteral reflux develops after such endoscopic incision in about half the patients, with reflux being more common with an ectopic ureterocele.

Imaging

Intravenous urography of a simple ureterocele is usually diagnostic. A ureterocele is seen as a cyst-like dilation of the distal ureter protruding into the bladder lumen; the ureterocele wall appears as a thin radiolucent line, although infection or stasis results in thickening. The typical "cobra-head" appearance is familiar to most radiologists. At times urography simply reveals a large radiolucent tumor in the bladder in association with nonvisualization of the ipsilateral kidney upper pole.

A cystogram detects a ureterocele, provided instilled contrast does not efface or obscure it. Serial visualization during bladder filling and voiding is helpful.

Computed tomography of a ureterocele reveals a well-marginated soft tissue tumor at the ureteral insertion (Fig. 11.1). A simple ureterocele is seen on US as a thin-walled, fluid-filled structure at the trigone.

Occasionally a diminutive renal upper pole is drained by a small duplicated ureter that terminates in a relatively large ureterocele. This condition, called ureterocele disproportion, is

Figure 11.1. Ureterocele. Excretory phase three-dimensional (3D) computed tomography (CT) reconstruction identifies hydronephrosis, hydroureter, and a ureterocele (arrow). (*Source:* Joffe SA, Servaes S, Okon S, Horowitz M. Multi-detector row CT urography in the evaluation of hematuria. RadioGraphics 2003;23(6):1441–1456, with permission from the Radiological Society of North America.)

difficult to diagnose with most imaging modalities.

Some ureteral duplications and ectopic ureteroceles are associated with ureteral obstruction, marked hydronephrosis, and dilation of the involved ureter to the point that adjacent nonobstructed collecting systems are displaced inferiorly. The reverse can also occur—occasionally an obstructed normal ureter mimics the appearance of a ureterocele.

Stones develop in some ureteroceles.

The term *ureterocele eversion* describes a ureterocele that everts or intussuscepts retrograde into the ureter during voiding cystourethrography. Radiographically, the outpouching can appear similar to a paraureteral bladder diverticulum. At times fluoroscopy aids in detecting these eversions.

Urachal Abnormalities

The urachus, or median umbilical ligament, is a residual fibromuscular cord located in the midline extending from the anterior superior bladder wall to the umbilicus. This embryonic communication normally closes before birth, but patency after birth results in luminal communication between the bladder and the umbilicus. Partial obliteration leads to a blind ending sinus at the umbilical end, or, with failure of the bladder end to close, a sinus communicates with the bladder (*vesicourachal diverticulum*). A urachal cyst (*omphalovesical cyst*) represents a cavity in the urachus with both the bladder and umbilical ends closed. In children with urachal abnormalities, urachal sinuses and cysts predominate, with a patent urachus and a urachal diverticulum being less common.

Ultrasonography identifies a midline mass between the rectus abdominis muscle and the superior-anterior bladder wall, representing a urachal remnant, in about one third of young adults. A majority of these urachal remnants are nodular, with a minority being tubular in shape. Their prevalence decreases with age, presumably due to involution. In most people a urachal remnant is a normal variant. Occasionally one manifests by hematuria and is resected.

Fistula and Sinus Tract

Urachal anomalies are more common in males. The prevalence of vesicourachal fistulas is increased in the prune belly syndrome. A patent urachus is also associated with urethral obstruction, such as posterior urethral valves or urethral atresia.

The presence of a patent urachus is generally suspected in the neonate and is best established by direct contrast injection into the umbilical opening. A voiding cystourethrogram also detects patency, provided the images are obtained with the infant in a lateral projection. At times an almost patent urachus is initially asymptomatic but manifests later in life when a bladder outlet obstruction develops.

A vesicourachal diverticulum is a midline outpouching extending from the superior-anterior bladder wall. Most are discovered incidentally. Occasionally stasis results in recurrent urinary tract infection and stone formation. Cancer originating in a vesicourachal diverticulum is an uncommon occurrence developing in adults.

A vesicourachal diverticulum can be suggested by CT, US, or MRI by detecting a bladder outpouching in the appropriate location.

Infection

Infection leads to a pyourachus, located in the midline, deep to the rectus abdominis muscle.

Imaging reveals a fluid-filled midline cavity close to the anterior bladder wall. When infected, the cyst in effect becomes an abscess and the cyst wall gradually thickens. A characteristic CT finding of a pyourachus is a conical-shaped structure extending from the umbilicus to the bladder dome. Inflammatory changes in adjacent subcutaneous tissues, the rectus abdominis muscle, and mesenteric fat surround the infected urachus. Chronic infection results in a thickened cyst wall.

An infected urachal cyst can be drained percutaneously, although this is generally a temporary measure because of an increased reinfection rate. For these reasons most urachal cysts are resected. Also, if an infected urachal cyst is suspected in an adult, a necrotic (or infected) carcinoma should be in the differential diagnosis.

Cyst/Neoplasm

Some urachal cysts remain asymptomatic, and others serve as a nidus for infection, while a neoplasm develops in an occasional one. Some urachal cysts gradually enlarge. In general, if US or other imaging shows a midline cystic structure between the umbilicus and bladder not related to bowel, an urachal cyst should be suspected.

Occasionally dystrophic calcifications or osseous metaplasia develop in an urachal cyst wall. Metaplasia of urachal transitional epithelium can evolve into an adenoma and carcinoma. A majority of these carcinomas are adenocarcinomas, with an occasional transitional cell carcinoma, squamous cell carcinoma, sarcoma, or even a small cell carcinoma. In general, most carcinomas are detected late when the tumor has already spread. A not uncommon presentation is a suprapubic tumor, hematuria, mucusuria, pain, or discharge from the umbilicus. An occasional urachal adenocarcinoma metastasizes (6); a urachal mucinous carcinoma is a less common cause of pseudomyxoma peritonei.

Imaging reveals a tumor involving the bladder apex, mostly extravesical in location and often growing along the urachus. Primary bladder carcinomas tend not to have these findings. Some mucin-producing urachal adenocarcinomas develop psammomatous calcifications, findings readily detected by CT. These mucinous adenocarcinomas can be solid, cystic, or mixed.

Ultrasonography should readily detect urachal cysts. If needed, CT confirms the diagnosis. Doppler US of an urachus adenocarcinoma revealed neovascularity and a low resistive index in the tumor (7).

Trauma

Spontaneous bladder rupture in the absence of trauma is rare but has occurred in a setting of previous radiation therapy, surgery, infection, or is idiopathic. Contrast extravasation may occur during voiding cystourethrography performed in a patient with an unused bladder. Most of these extravasations are self-limiting.

The risk of bladder rupture increases with bladder distention. Perforation of an empty bladder is generally associated with a penetrating injury, either extrinsic or a bone fragment.

After blunt pelvic trauma or in a setting of pelvic fractures, bladder or urethral injury is suggested by hematuria or inability to urinate. A small minority of patients with bladder rupture have only microscopic hematuria. A direct association exists between gross hematuria and bladder perforation, most being extraperitoneal, less often intraperitoneal, and least common being both intra- and extraperitoneal. Pelvic fractures are present in a majority of patients with bladder perforation.

A retrograde urethrogram is generally obtained to exclude urethral injury, followed by a cystogram. At times extraperitoneal contrast extravasation is only seen on postdrainage radiographs. A cystogram should detect not only bladder rupture but also determine whether the rupture is intra- or extraperitoneal (Fig. 11.2). During the cystogram an attempt should be made to identify a site of perforation. Subtle intraperitoneal leaks are difficult to

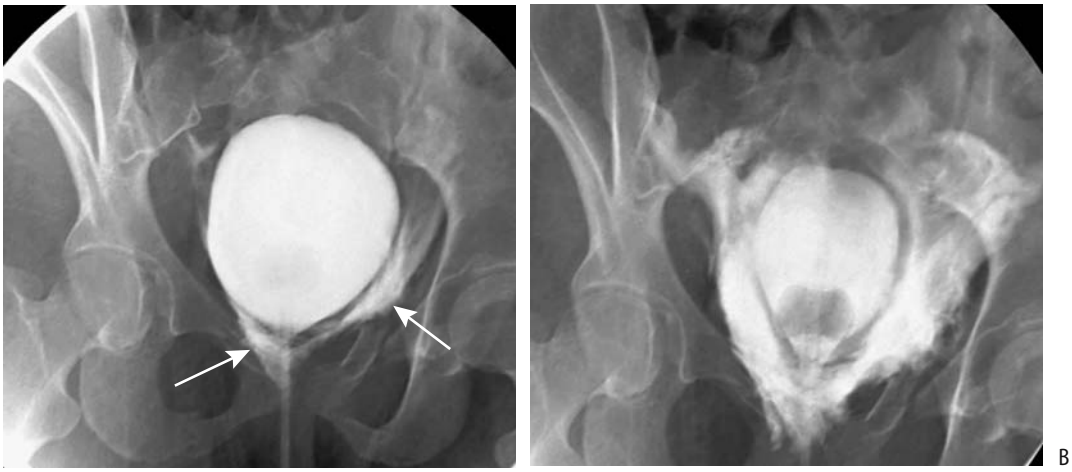

Figure 11.2. Bladder perforation. Early bladder filling (A) and after partial drainage (B) views during a cystogram indentify contrast extravasation from the bladder base (arrows).

detect; the diagnosis is generally made by seeing contrast outline the loops of the bowel. Occasionally contrast absorbed from the peritoneal cavity and excreted by kidneys provides a clue to an intraperitoneal leak and thus a radiograph over the kidneys after a cystogram is useful.

Intravenous urography is inadequate to evaluate bladder trauma. Likewise, US is not a substitute for a cystogram in a setting of trauma, although US may detect a hematoma or fluid in the peritoneal cavity. Magnetic resonance is generally precluded during the immediate post-trauma period by monitoring logistics in a strong magnetic field.

Many of these trauma patients undergo contrast CT to evaluate for pelvic and abdominal trauma. The presence of pelvic fractures and pelvic fluid is associated with bladder rupture, but a bladder perforation cannot be excluded on this study without full bladder distension. In some centers CT cystography, performed after retrograde instillation of contrast, has replaced conventional cystography. Another option is to clamp the patient's Foley catheter prior to scanning and add a 5-minute or so delay after intravenous (IV) contrast injection to allow for bladder distention. Thin, contiguous slices through the bladder are necessary for this study. Preliminary evidence suggests that CT cystography achieves similar accuracy to that of conventional cystography (8), but the practical choice between these two studies is not settled. Also, extravasated contrast detected on a CT cystogram performed after IV contrast injection does not necessarily represents bladder rupture—renal injury can lead to similar findings.

Whether children with pelvic trauma should first undergo a cystogram or CT is debatable, and the role of a CT cystogram in children is not clear.

Extraperitoneal urine and contrast extravasation is into the prevesical space of Retzius; fluid can dissect along the tissue fascial planes and extend into the scrotum or dissect laterally into the hip, resulting in such curiosities as a hip arthrogram becaming evident due to extraperitoneal bladder rupture and an acetabular fracture.

In general, extraperitoneal bladder rupture is managed by catheter drainage, while intraperitoneal rupture is explored surgically. Most extraperitoneal bladder ruptures resolve without surgery. The key to successful management is continuous bladder drainage.

Shotgun pellets have passed spontaneously during voiding.

Wall Thickening

Infection/Inflammation

Cystitis

General Imaging Findings

Lower urinary tract infection is considerably more common in women than men. Most attacks clear with antibiotic therapy and recur only in a minority. Imaging is generally reserved for those women not responding to antibiotics, frequent reinfections, atypical presentation, or known risk factors, including hematuria, suspected upper urinary tract infection, past history of stones, infection, or reflux.

If imaging is deemed necessary for suspected upper tract involvement, IV urography is generally the first preferred test. A minority of authors recommend a conventional radiograph combined with US. Some bladder abnormalities are detected on an IV urogram, although voiding cystography provides more information, including the presence of vesicoureteral reflux. Urethral diverticula are also detected with voiding cystography, although at times a specific double-balloon urethrogram and other studies are necessary for their detection (urethral diverticula are discussed in Chapter 12).

While mild cystitis has no abnormal radiographic findings, with progressively more severe involvement focal mural thickening evolves, intraluminal tumors may develop, and occasionally an irregular outline become evident. Initially bladder capacity tends to be normal, but with progressive inflammation the lumen contracts.

In adults, the presence of bladder wall thickening and irregularity can be secondary to either inflammation or neoplasm, and in many patients a biopsy is necessary to narrow the diagnosis. Not all bladder polyps are neoplastic; occasionally cystitis results in inflammatory polyps. These inflammatory tumors can be differentiated from other spindle cell proliferations by immunohistochemical means.

Most so-called congenital hourglass bladders are found in adult males and are associated with bladder inflammation. Imaging simply reveals an hourglass outline.

T1-weighted MRI reveals two distinct layers in a cystitis-thickened bladder wall: a hyperintense inner and an isointense outer layer. T2-weighted MRI reveals four distinct layers: (1) hypointense inner epithelium, (2) hyperintense lamina propria, (3) hypointense muscle layer, and (4) isointense outer layer representing muscle and connective tissue.

Interstitial Cystitis

Interstitial cystitis is more of a syndrome than a specific disease. Etiology is unknown but is often multifactorial in origin. *Helicobacter pylori* probably is not a cause of this condition. A relationship has been suggested between interstitial cystitis and collagenous colitis. The vast majority affected are women.

Interstitial cystitis is a severe and debilitating bladder disorder manifesting by pelvic pain and urinary frequency. No diagnostic test is available for this condition and it is diagnosed by exclusion. Urodynamic studies, including a voiding cystourethrogram, are necessary to exclude other conditions. Thus in patients initially believed to have interstitial cystitis, urethral abnormalities such as periurethral fibrosis, urethral diverticula, and chronic urethritis are common; eventually only four of 23 patients in one study were believed to suffer from interstitial cystitis (9).

Therapy is difficult. Some women with intractable interstitial cystitis undergo enterocystoplasty, but even some of these continue being symptomatic. Some require an ileal loop diversion. Of interest is that some subsequent ileal loop biopsies also show histologic changes of interstitial cystitis. Intravesical bacillus Calmette-Guérin (BCG) therapy has led to improvement in some patients (10).

An anterior vaginal hernia (enterocele) developed in 11% of women who underwent cystectomy and urethrectomy for intractable interstitial cystitis (11); clinically, these hernias mimic a midline cystocele except they contain bowel.

Hemorrhagic Cystitis

In some patients hemorrhagic cystitis and interstitial nephritis are associated with the use of nonsteroidal antiinflammatory drugs (NSAIDs). Cyclophosphamide therapy is also implicated, at times resulting in massive bleeding. Radiation cystitis, secondary to pelvic radiation therapy, also manifests as hemorrhagic

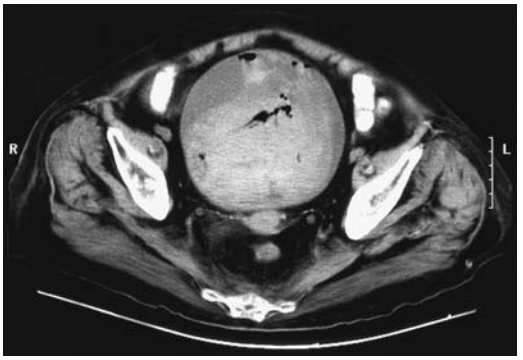

Figure 11.3. Hemorrhagic cystitis due to Cytoxan therapy. Computed tomography reveals a thick-walled bladder containing blood clots, debris, and gas. (Courtesy of Patrick Fultz, M.D., University of Rochester.)

cystitis. Bladder wall edema and inflammation resolves in some patients, while in others it progresses to a small, shrunken bladder. Of interest is that hyperbaric oxygen therapy appears helpful in radiation cystitis (12); hematuria subsides and symptoms improve.

The CT and MR appearance of hemorrhagic cystitis varies depending on timing (Fig. 11.3). Active and very recent bleeding has T1- and T2-weighted imaging characteristics of fluid. Slightly older blood becomes hyperintense on T1- and hypointense on T2-weighted images, findings reflecting intracellular methemoglobin due to subacute intramural hemorrhage.

Eosinophilic Cystitis

Eosinophilic cystitis is a histologic diagnosis characterized by massive eosinophilic infiltration. Etiology in most patients is unknown, although remission in some patients undergoing steroid therapy suggests an allergic condition. One should keep in mind, however, that occasionally a chronic infection results in eosinophilic cystitis. Partial cystectomy and a pseudoneoplastic condition or reaction to suture material can also lead to eosinophilic cystitis.

Eosinophilic cystitis can be subdivided into three clinical entities having different presentations and treatments (13):

Group I consists of young adults and children with a background of atopy or parasitic infestation who have micturition difficulties or hematuria. They respond to steroids.

Group II consists mostly of middle-aged women with chronic, recurrent cystopathy. They respond poorly to therapy.

Group III consists of elderly patients with chronic bladder irritation or other type of injury. They usually do not require therapy.

Some of these patients have eosinophilia and eosinophiluria. A minority progress to fibrosis and a small, retracted bladder, similar to that seen with interstitial or tuberculous cystitis. Ureteral involvement and hydronephrosis necessitate surgery.

Imaging findings in eosinophilic cystitis are nonspecific. Some patients develop an intraluminal tumor. Spontaneous bladder rupture is a rare complication of eosinophilic cystitis.

Emphysematous Cystitis

Emphysematous cystitis almost always implies infection, with the most common infection being due to *Escherichia coli*. Many of these patients are diabetics. Occasionally emphysematous pyelonephritis coexists with emphysematous cystitis. Some of these patients have gas in the bladder and develop pneumaturia, thus suggesting an enterovesical fistula. Untreated, the condition evolves into bladder gangrene.

Cystoscopy reveals bladder mucosal vesicles.

Computed tomography readily detects emphysematous cystitis or emphysematous pyelonephritis. Conventional radiographs may miss small amounts of intraluminal air unless films with a horizontal x-ray beam are obtained. Ultrasonography reveals a thickened hyperechoic bladder wall and acoustic shadowing within the lumen.

Fungal Cystitis

Fungal infection of the lower urinary tract is seen in patients with a neurogenic bladder, prolonged antibiotic therapy, or prolonged use of an indwelling catheter. Occasionally the condition evolves into emphysematous cystitis, especially in diabetics.

When extensive, *Candida* cystitis results in a "fungus ball," which on rare occasion can result in bladder outlet obstruction.

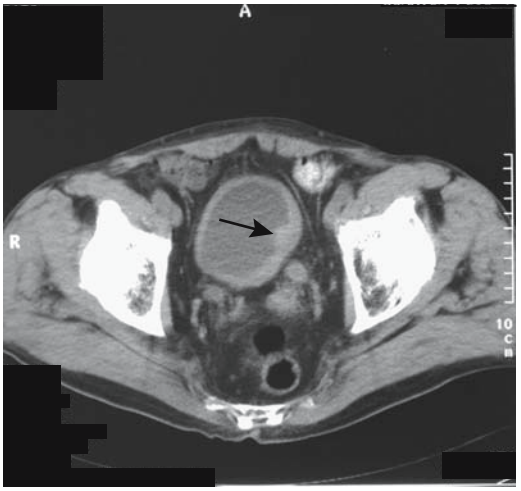

Figure 11.4. Bladder tuberculosis in a patient with previous renal tuberculosis. Computed tomography shows a thick walled shrunken bladder and a nodule projecting from the wall (arrows). The ureters are dilated. (Courtesy of Egle Jonaitiene, M.D., Kaunas Medical University, Kaunas, Lithuania.)

Tuberculous Cystitis

Bladder tuberculosis is usually associated with renal involvement. This chronic infection results in an interstitial cystitis and an eventual spastic, small capacity, thick-walled bladder. Clinical presentation tends to mimic interstitial cystitis. A rare tuberculous cystitis results in a spontaneous bladder perforation.

Cystography reveals a polypoid bladder outline, ulcerations, and infiltration of the ureterovesical junctions, with the latter evolving into ureteral obstruction or vesicoureteral reflux. Calcifications develop in some bladders but are not commonly detected with conventional radiography. Any intraluminal septations are best seen with either CT or US. Extensive granulomas result in a polypoid appearance. The overall appearance mimics a malignancy (Fig. 11.4).

Schistosomal Cystitis

Schistosomiasis (*bilharziasis*) is endemic in Africa and western Asia, and infection occurs by contact with water containing cercariae emitted from snails. *Schistosoma haematobium* develops in portal veins and migrates against the blood flow in the portal vein, the inferior mesenteric vein, and probably from hemorrhoidal veins into bladder veins, where adults deposit eggs. The eggs then pass through the bladder wall and are eliminated in urine.

Initially involved are bladder trigone and adjacent ureteral segments, distinguishing schistosomiasis from tuberculosis; the kidneys are primarily involved with the latter, and the ureters are secondarily affected.

Hematuria is a typical and often the only clinical presentation. Neither urinary tract infections nor urinary stones are more common than in the general population.

The bladder wall gradually assumes an irregular outline and hydroureters develop. At times a biopsy yields eosinophilic cystitis. Some patients develop granulomatous bladder polyps. Fibrosis and hyperplastic changes evolve into squamous metaplasia, predisposing these patients to subsequent carcinoma. An early onset of chromosomal aberration is found even in histologically benign-appearing mucosa. Carcinomas in bilharziasis are common and occur at a relatively early age. Tumors range from nodular to infiltrating.

A classic conventional radiographic finding of bladder schistosomiasis is bladder wall calcification, and in endemic areas in the appropriate clinical setting, little else is in the differential diagnosis. These calcifications are better defined with CT. They range from being barely visible, to those having a thin, rim-like appearance, to marked calcification of the entire bladder wall. Ureteral calcifications appear as distal ureteral linear, parallel lines mimicking vascular calcifications.

Urography reveals thickened folds and a shrunken bladder lumen. An enlarged prostate elevating the bladder base is common. In some countries the ready availability of US has made this modality the imaging choice in following these patients.

Actinomycosal Cystitis

Bladder actinomycosis is uncommon. Infected individuals tend to develop extensive fistulas and fibrosis; at times the appearance mimics that of a bladder tumor.

Granulomatous Cystitis

A granulomatous cystitis, often seen in children, is part of eosinophilic cystitis and is often

considered to be an immunologic disorder, although a number of these children probably suffer from chronic granulomatous disease, an inherited disease characterized by recurrent bacterial or fungal infections. These children present with hematuria, urgency, and dysuria. They develop chronic bladder tumors mimicking neoplasms.

Crohn's Disease

Cystitis in Crohn's patients most often is secondary to an adjacent phlegmon or an enterovesical fistula. A rare patient presents with gross hematuria.

Malacoplakia

Malacoplakia is a granulomatous inflammatory reaction characterized by bladder wall thickening, at times involving adjacent structures. Pathogenesis is unknown, although many of these patients have other underlying systemic disorders.

Infection by urea splitting organisms results in deposition of inorganic salts and an alkaline encrusted cystitis. These encrustations are associated with malacoplakia, although the relationship between alkaline encrusted cystitis and malacoplakia is incompletely understood. Both malacoplakia and primary squamous cell carcinoma have developed in chronic cystitis.

Imaging reveals one or more intraluminal sessile nodules varying in size, occasionally leading to vesicoureteral junction stenosis and hydronephrosis.

If diffuse, cystitis cystica is in the imaging differential diagnosis.

Ischemia

Bladder overdistention can lead to ischemia and eventual gangrene. The mucosa is most sensitive to ischemia and occasionally a necrotic mucosa will slough; eventually the mucosa will regenerate.

Bladder infarction develops with bladder strangulated in an inguinal hernia.

Behçet's Syndrome

Urinary tract involvement in Behçet's syndrome can lead to recurrent cystitis, urethritis, or epididymitis. Extensive fistulas are not common; if present, actinomycosis or Crohn's disease is more likely.

Radiation

Acute radiation cystitis starts 4 to 6 weeks after therapy and presents as a hemorrhagic cystitis. Imaging reveals edema and a nodular outline. Postcontrast MRI reveals an enhancing bladder wall; the appearance is similar to that of other causes of cystitis and to some neoplastic infiltrations.

Chronic cystitis develops months or years later and results in a scarred, fibrotic bladder wall with a small shrunken lumen. In general, imaging during the chronic stage is nonspecific. Radiation cystitis is one cause of a nonfunctioning hypertonic bladder.

Occasionally a vesical fistula develops secondary to radiation therapy.

Amyloidosis

Primary bladder amyloidosis is rare; more often encountered is secondary bladder amyloidosis, both presenting with hematuria. The diagnosis is made by histologic examination. Once detected, systemic amyloidosis or a malignant lymphoproliferative disorder should be excluded.

Amyloid infiltration results in a thickened, somewhat irregular bladder wall, and the imaging appearance mimics that of an infiltrating neoplasm. Magnetic resonance imaging reveals amyloid infiltration as a hypointense region on T2-weighted images (compared to a normal bladder wall).

Systemic Sclerosis

Lower urinary tract involvement with systemic sclerosis is not common. Bladder involvement results in varying degrees of wall fibrosis. While autonomic dysfunction is common, urodynamic abnormalities are not.

Tumors

Nonneoplastic Tumors

Interureteric Ridge Edema

Interureteric ridge edema is related to trauma or acute distal ureteral obstruction. It is best

identified with the bladder either partially filled or almost empty.

Cystitis Cystica (Cystitis Glandularis)

A condition of unknown etiology, cystitis cystica is associated with chronic urinary tract infection. Histology reveals marked mucosal thickening, lymphatic obstruction, bladder wall edema, and intramural cysts.

Cystitis glandularis is probably a more severe form of cystitis cystica. Pathologically, considerable difficulty can be encountered in distinguishing cystitis glandularis from an adenocarcinoma, and anecdotal reports describe partial cystectomy performed because of an erroneous diagnosis of adenocarcinoma. Confusing the picture further is the occasional patient with cystitis glandularis who subsequently develops an adenocarcinoma, presumably due to the persistence of chronic irritation. At times cystitis glandularis and pelvic lipomatosis coexist.

A cystogram reveals large nodules or even a single confluent infiltrating tumor, often at the bladder base; the imaging appearance is very similar to that of a neoplasm, although the presence of several smooth bladder base nodules should suggest cystitis cystica. Both CT and US show irregular regions of bladder wall thickening in association with intraluminal tumors. Trigone involvement leads to ureter obstruction.

Hemangioma

Bladder hemangiomas are not common. They occur in all age groups but are more prevalent in children and young adults. Especially in children, they manifest with hematuria.

Hemangiomas range from a focal, sessile tumor to a diffuse intramural infiltration. Some are multiple. Similar to hemangiomas at other sites, MR shows them to be hypointense on T1- and hyperintense on T2-weighted images.

The role of selective arterial embolization is not well established for these rare tumors.

Pseudosarcoma

A fibroblastic proliferation of unknown etiology, called a *pseudosarcomatous myofibroblastic (fibromyxoid) tumor* or *inflammatory pseudotumor*, develops in a number of organs, including the bladder. This tumor has some characteristics of a desmoid tumor; indeed, whether these are all the same entity is conjecture. It occurs in both children and adults. It is not associated with prior trauma. Some patients present with hematuria or progressive anemia. Associated pain suggests a hematoma or even intraperitoneal hemorrhage.

The bladder wall and, at times, surrounding tissues are infiltrated by a tumor superficially resembling a sarcoma. These are highly vascular myxoid stroma tumors showing both early and delayed CT contrast enhancement. In children, both clinically and radiologically this tumor has been mistaken for an embryonal rhabdomyosarcoma or some other type of sarcoma. The diagnosis is established by histology; no cytologic atypia or increase in number of mitoses should be evident. Immunohistochemistry reveals myofibroblast proliferation. Immunoreactivity with vimentin is positive in some patients.

Condyloma

A bladder condyloma is rare. These tumors are induced by human papilloma virus infection, result in a proliferation of squamous epithelium, and are associated with an increased risk of malignancy.

A cystogram reveals one or more intraluminal tumor. Imaging identifies an irregular bladder wall thickening and, in fact, a large condyloma mimics a neoplasm.

Endometriosis

Bladder endometriosis is rare. Most often it is contiguous with an extrinsic endometrioma and presents as an infiltrating tumor at the bladder dome. Several reports describe malignant transformation in bladder endometriosis; most often these are clear cell adenocarcinomas.

Some women with bladder endometriosis develop dysuria and hypogastric pain. Bladder and ureteral endometriosis was associated with recurrent acute pyelonephritis (14).

Computed tomography or MR should define the often present extrinsic soft tissue component (Fig. 11.5). Nevertheless, a neoplasm cannot be excluded from the imaging appearance.

Figure 11.5. Bladder endometriosis. Computed tomography identifies an irregular intramural tumor posterior and to the left of the bladder (arrow). The appearance mimics a neoplasm. (Courtesy of Patrick Fultz, M.D., University of Rochester.)

Benign Neoplasms

Papilloma

A papilloma consists of a fibrovascular bundle covered by either transitional or squamous cells. As discussed in Chapter 10, papilloma etiology is unknown and their histopathologic diagnosis difficult.

A type of transitional cell papilloma is the inverted papilloma, found throughout the urothelial tract, but most often in the bladder. An initial diagnosis of an inverted papilloma should be made with care; papillomas mimic and are readily misdiagnosed as transitional cell carcinomas. These tumors are believed to be related to human papillomavirus type 18 infection, chronic irritation, and subsequent metaplasia. An occasional one is associated with a more proximal urothelial carcinoma or a superficial bladder tumor.

A typical papilloma appearance is that of an isolated, endophytic tumor. On immediate postcontrast MRI papillomas appear as enhancing polyps arising from a less enhancing bladder wall and surrounded by intraluminal signal-void urine.

Leiomyoma

Bladder leiomyomas are the most common benign bladder neoplasm but still represent less than 1% of all bladder tumors. They are detected in a younger patient age group than are carcinomas.

Many of these patients are asymptomatic, and these tumors are detected incidentally. Some manifest with hematuria, and less often bladder outlet obstruction or ureteral obstruction.

Intraluminal growth is most common; a minority grow extravesically, while a dumbbell appearance is relatively rare. Some extravesical leiomyomas reach a large size before being detected.

A cystogram reveals leiomyomas as smooth, sessile tumors. Magnetic resonance typically identifies a well-marginated tumor having an intermediate signal intensity on T1- and intermediate-to-hypointense signal on T2-weighted images. Leiomyomas exhibit variable MR contrast enhancement. Tumor degeneration leads to a varied appearance.

An imaging-guided suprapubic biopsy can often establish the diagnosis, although most of these tumors are resected.

Nephrogenic Metaplasia/Adenoma

Nephrogenic metaplasia is a rare condition occurring throughout the urothelium but most often involving the bladder. The pathogenesis is unknown, but prior stone disease or some type of trauma appears to be the predisposing factor. Whether the occasionally reported nephrogenic adenoma simply represents further cell differentiation or is the same entity is speculation.

Nephrogenic adenomas occur in the bladder, bulbar urethra, urethral diverticula, and prostatic urethra. Most are discovered incidentally. A history of prior instrumentation or inflammation is not uncommon; these adenomas probably represent a metaplastic response to prior urothelial trauma. Select examples include a 4-year-old girl with a bladder nephrogenic adenoma (15); she had a ureterocele resection and bilateral ureter reimplantations at 3 months of age. Cystoscopy in a 76-year-old man revealed a papillary nephrogenic adenoma (16); he had received intravesical BCG therapy for recurrent bladder transitional cell carcinoma.

Most of these adenomas are polypoid, and imaging simply reveals a sessile tumor, although some are flat.

Recurrence is common after resection, but most authors agree that little risk of malignant transformation exists; nevertheless, some

nephrogenic metaplasias and adenomas are associated with bladder cancer. A rare report describes a bladder villous adenoma, at times with foci of adenocarcinoma.

Malignant Neoplasms

Transitional Cell Carcinoma

Clinical Aspects

Primary bladder cancer is three times more common in men than women and more common in whites than blacks. In the West, most bladder cancers are transitional cell carcinomas. They range from carcinoma in situ to diffuse infiltration and metastasis. Adenocarcinoma and squamous cell carcinoma are considerably less common and tend to occur in certain settings, discussed later.

Epithelial origin bladder neoplasms are uncommon in the second decade of life and rare in the first. Most bladder neoplasms at these ages are of mesodermal origin. Some studies suggest that patients under 40 years of age with bladder transitional cell carcinoma have a lower recurrence rate and a better prognosis compared to older patients, but other studies conclude that the prognosis depends primarily on tumor stage and is not correlated with age. In children, transitional cell carcinomas tend to be low grade and have a low recurrence rate.

The most common clinical presentation is painless hematuria, ranging from gross to microscopic and often intermittent. Ureteral obstruction due to an adjacent cancer is often silent. Spontaneous perforation of a bladder carcinoma is a curiosity. An occasional bladder cancer manifests first via spread to other structures, at times to unusual sites.

The Leser-Trelat sign consists of an association of multiple seborrheic keratoses with an internal malignancy. It occurs with transitional cell bladder carcinomas.

Etiology

A familial form of bladder transitional cell carcinoma exists, with two genetic patterns: a minor autosomal-dominant pattern and a more common multifactorial pattern involving both genetic and environmental factors. Some papillary and invasive tumors harbor a chromosome 9 allelic loss, while others contain a *p53* gene mutation without alterations of chromosome 9. Immunohistochemical study of bladder tumors in patients younger than 30 years reveals *p53* gene product overexpression in a majority (17); aneuploidy of chromosome 17 is common. The *p53* gene mutations are associated with high-grade, high-stage urothelial cancers, and these gene mutations suggest a monoclonal origin for multicentric cancers. An extremely early age at onset, in particular, should suggest a genetic factor.

Infection, the presence of stones, smoking, various direct-acting chemicals, and a number of environmental factors are associated with these cancers. Carcinogenic chemicals implicated include benzidine and 4-aminobiphenyl; cyclophosphamide also appears to increase the risk of bladder cancer. Some affected individuals are infected with human type 18 papillomavirus.

Bladder carcinoma is the most common malignancy in those parts of the Middle East and Africa where schistosomiasis is endemic. The specific relationship is not clear, but *N*-nitrosamine compounds appear involved because urine levels of these compounds are increased in patients with schistosomiasis-associated bladder cancer.

Associated Conditions

In patients with renal pelvis and ureteral transitional cell carcinomas, almost half have synchronous or will develop metachronous bladder tumors, and these patients should undergo regular cytologic evaluation and radiologic screening for a prolonged time period in order to detect these associated bladder carcinomas. On the other hand, only in a small minority does a bladder tumor antedate an upper tract tumor, and in these patients the primary bladder tumor tends to be multifocal. Whether patients with a bladder cancer should undergo regular upper urinary tract follow-up is not clear from the literature, although among patients with stages Ta, T1, and Tis bladder tumors entered in a prospective trial of BCG therapy and followed for 15 years or longer, 21% developed upper tract tumors (18); some of these tumors occurred between 10 and 15 years later, and thus these patients need lifelong follow-up. Intravenous urography is useful for screening upper urinary tracts; retrograde pyelography provides

alternate visualization if IV urography is inconclusive. Some investigators, on the other hand, believe that IV urography at the initial diagnosis of bladder cancer is unnecessary because of a low upper urinary tract tumor detection rate with urography.

In patients with a prostate or bladder cancer, the risk of having or developing the other cancer is considerably greater than expected. Patients with a bladder carcinoma are also at increased risk for renal cell carcinomas and bronchopulmonary carcinoma.

Pathology

Histologically, a diagnosis of transitional cell carcinoma is not always straightforward. Mimicry by benign cystitis glandularis has already been mentioned. The reverse is also true; even an invasive bladder transitional carcinoma can be composed of cells and glands having relatively bland cytologic features suggesting a benign condition.

Metaplastic changes, at times extensive, are often observed in a setting of a bladder cancer. Epithelial dysplasia is found in most resected bladders with a bladder cancer. Incidental carcinoma in situ is also common, and up to one third of cancers are multifocal. An occasional bladder carcinoma exhibits osseous or cartilaginous metaplasia or osteoclast-like giant cells.

The World Health Organization grading system for transitional cell carcinomas consists of grade I lesions, which are low grade (well-differentiated), and grade III lesions, which are poorly differentiated. Grade II lesions are intermediate. Grade I tumors rarely invade, and the vast majority of invasive tumors are grade III.

Detection

Urinary cytology detects low-grade bladder cancers with about 50% sensitivity, although currently the diagnosis is generally established by cystoscopy and biopsy. Bladder wash cytology at the time of cystoscopy also aids in diagnosis.

Proposed tests to detect urothelial neoplasms include tumor antigen, fibrin/fibrinogen degradation products, and nuclear matrix protein (NMP-22); these require further study to establish their place in cancer detection.

Bladder transitional cell carcinomas range from exophytic (papillary) to infiltrating or a combination of both. Exophytic tumors are either polypoid or frond-like. Demonstration of intraluminal extension, although helpful in localizing a tumor, does not aid tumor staging. A carcinoma can originate in a bladder diverticulum.

Computed tomography identifies a soft tissue tumor arising from the bladder wall (Fig. 11.6). Depending on growth, these tumors range from a sessile polyp to bladder wall thickening. The least common is a pedunculated polyp. Tumors at the bladder dome or trigone are poorly imaged with CT, the limitation being the axial slices used. Because of partial volume averaging, these lesions tend to blend into the bladder wall and surrounding structures. Likewise, tumors at the bladder base tend to blend into the prostate. In general, CT misses lesions smaller than about 1 to 2 cm in diameter. Computed tomography also cannot distinguish adherent blood clots from a tumor. Coronal views are often helpful.

Contrast enhanced multidetector CT reveals bladder cancers enhancing more than the surrounding bladder wall, best seen on 60–80 sec delayed scans (19); tumors <4 cm in diameter tend to have homogeneous enhancement, larger ones become more heterogeneous. A urine distended bladder aids tumor detection.

Computer tomography cystoscopy, with the bladder opacified with contrast, can also detect

Figure 11.6. Bladder transitional cell carcinoma. Excretory phase CT identifies a right bladder tumor (arrow). The bladder base tumor (arrowheads) is due to prostatic enlargement. (*Source:* Joffe SA, Servaes S, Okon S, Horowitz M. Multi-detector row CT urography in the evaluation of hematuria. RadioGraphics 2003;23(6):1441–1456, with permission from the Radiological Society of North America.)

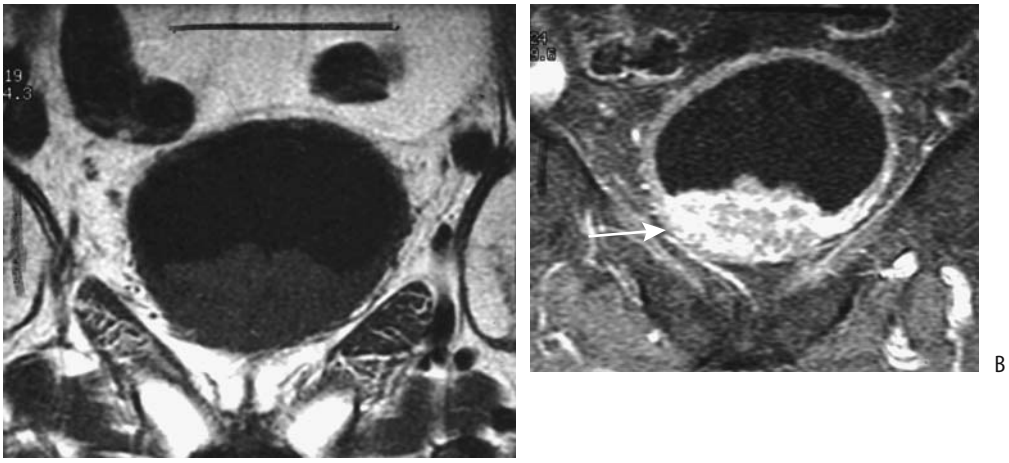

Figure 11.7. Bladder carcinoma. Coronal T1–weighted (A) and contrast-enhanced (B) MR images reveal a mostly intraluminal, heterogeneous tumor (arrow). (*Source:* Burgener FA, Meyers SP, Tan RK, Zaunbauer W. Differential diagnosis in magnetic resonance imaging. Stuttgart: Thieme, 2002, with permission.)

bladder cancer, with undetected tumors generally being <5 mm in diameter. One study, however, identified 88% of tumors <5 mm (20). Transverse and virtual cystoscopy images are complimentary—some small tumors are identified only on virtual images but bladder wall thickening is more apparent on transverse images. Computer tomography 3D cystography using perspective volume rendering and a shaded-surface 3D outline evaluates tumor size and shape and provides information about its relationship to adjoining mucosa. With current techniques, however, endoscopic cystoscopy has better spatial resolution in detecting small bladder tumors.

A typical US appearance of a transitional cell carcinoma is that of a hypoechoic tumor. The findings are nonspecific. Bladder tumors can be evaluated with endourethral US. The major limitation of intravesical US is the inability to differentiate among neoplasms, inflammation, and bladder wall hypertrophy due to other factors. Likewise, intravesical US is limited in evaluating deep invasion.

These carcinomas have a T1-weighted signal intensity similar to that of muscle (Fig. 11.7). T2-weighted images reveal a higher signal intensity than normal bladder wall or fibrosis. Tumor detection is superior with postcontrast images, although one should keep in mind that both cystitis and tumors exhibit early MR contrast enhancement.

Superficial tumor calcifications are usually secondary to calcium salt deposition. More central calcifications develop secondary to tumor necrosis, although such calcifications are also seen in carcinosarcomas containing osseous metaplasia or an osteosarcoma component.

One bladder transitional cell carcinoma showed intense uptake of Tc-99m–hydroxymethylene diphosphonate (HMDP) during bone scintigraphy (21); uptake corresponded to a bladder tumor containing punctate and curvilinear calcifications identified by CT, and chemisorption of urinary Tc-99m-HMDP excretion probably accounted for the uptake.

A biopsy is necessary to establish the diagnosis; both benign and malignant tumors and some nonneoplastic conditions overlap in their imaging appearance. Cystoscopic tumor detection specificity and sensitivity are improved by using laser-induced autofluorescence spectra for guidance of suspicious lesions that are otherwise difficult to detect.

Staging

The Union Internationale Contre le Cancer (UICC) and American Joint Committee on Cancer (AJCC) both use the tumor, node, metastasis (TNM) staging system for bladder cancers (Table 11.1). This system differentiates superficial from infiltrating tumors. The TNM

Table 11.1. Tumor, node, metastasis (TNM) staging of bladder cancer

Primary tumor:			
Tx	Primary tumor cannot be assessed		
T0	No evidence of primary tumor		
Ta	Non-invasive papillary carcinoma		
Tis	Carcinoma in situ		
T1	Tumor invades subepithelial connective tissue		
T2a	Tumor invades superficial muscle		
T2b	Tumor invades deep muscle		
T3	Tumor invades perivesical tissue		
T4a	Tumor invades prostate, uterus, vagina		
T4b	Tumor invades pelvic wall, abdominal wall		
Lymph nodes:			
Nx	Regional nodes cannot be assessed		
N0	No regional lymph node metastasis		
N1	Metastasis to single lymph node 2 cm or less in greatest dimension		
N2	Metastasis to single lymph node larger than 2 cm but not more than 3 cm		
N3	Metastasis in a lymph node more than 3 cm in greatest dimension		
Distant metastasis:			
Mx	Distant metastases cannot be assessed		
M0	No distant metastasis		
M1	Distant metastasis		
Tumor stages:			
Stage 0a	Ta	N0	M0
Stage 0is	Tis	N0	M0
Stage I	T1	N0	M0
Stage II	T2a	N0	M0
	T2b	N0	M0
Stage III	T3	N0	M0
	T4a	N0	M0
Stage IV	T4b	N0	M0
	any T	N1	M0
	any T	N2	M0
	any T	N3	M0
	any T	any N	M1

Source: From the AJCC Cancer Staging Manual, 6th edition (2002), published by Springer-Verlag, New York, NY, used with permission of the American Joint Committee on Cancer (AJCC), Chicago, IL.

system is used for both pretherapy staging and postresection staging (pathologic staging). Tumor stage is the most important predictive prognosis factor. The presence of bilateral ureteral obstruction affects the prognosis. Over 90% of patients with bilateral obstruction have extravesical extension of their cancer, but among those with unilateral obstruction a third have disease confined to the bladder, at times with the cancer even limited to the bladder mucosa (22). In patients with a bladder cancer, the presence or absence of accompanying carcinoma in situ or epithelial dysplasia does not seem to influence survival significantly.

Recent cystoscopic biopsy leads to confusion because of edema and interferes with accurate tumor staging, and it is reasonable to delay a staging imaging study for several weeks after biopsy.

For superficial bladder tumors clinical staging (cystoscopy and biopsy) appears superior to MRI, but MRI is better than clinical staging for more infiltrating tumors.

Currently CT is not sufficiently accurate in staging bladder tumors ranging from carcinoma in situ through tumors invading deep muscle. Because no definite fat planes exist between bladder and adjacent posterior structures, CT cannot readily define the invasion of these structures (Figs. 11.8 and 11.9). Seminal vesicles have a CT soft tissue density whether invaded or not; an exception is the seminal vesicle anterior surfaces, where fat angle obliteration between the seminal vesicle anterior surface and posterior bladder wall implies tumor invasion. Computed tomography is more accurate with more advanced tumors. Computed tomography does evaluate for metastases. Overall CT staging accuracy is only 30% to 40% and CT changes management in only few patients.

Figure 11.8. Invasive bladder carcinoma. Computed tomography identifies an infiltrating tumor in the left posterior bladder wall. It was inseparable from the uterus and sigmoid colon but invasion could not be determined. (Courtesy of Patrick Fultz, M.D., University of Rochester.)

Transabdominal US is seldom used to stage bladder cancers, having been replaced by more accurate imaging modalities. Endorectal US also has a low accuracy, but endourethral US shows promise in local staging of these tumors, especially for those limited to the bladder wall. Endourethral US is useful in detecting tumors in bladder diverticula.

Although color Doppler US detects some vascularity in transitional cell carcinomas, the Doppler findings are not helpful in evaluating tumor grade or stage, although in general, larger and higher-grade tumors tend to be more vascular.

Magnetic resonance imaging has the potential for accurate bladder tumor staging, although both CT and MR tend to overstage more often than understage. The use of surface coils leads to better image quality than does the use of body coils. Endorectal coils improve visualization of the bladder base and dorsal structures but are of limited use for the rest of the bladder. T1-weighted images provide good contrast between hyperintense perivesical fat and isointense bladder wall, and detects perivesical fat invasion, spread to lymph nodes, and bone marrow metastases; the latter are identified against the hyperintense normal marrow. T2-weighted images evaluate bladder wall infiltration and prostatic and adjacent structure invasion, although differentiation between tumor and edema is difficult. Using early-phase contrast enhancement, MRI achieves relatively high staging accuracy, especially in differentiating between superficial tumors and those invading muscle. Magnetic resonance appears especially useful in evaluating depth of bladder wall invasion. It thus appears reasonable to perform MRI before resection. Postcontrast MR reveals early tumor enhancement and appears more sensitive and specific than precontrast imaging. Bladder cancers begin to enhance several seconds after the start of arterial enhancement, which is earlier than most other structures.

When staging for lymph node involvement, CT and conventional MRI appear comparable. The accuracy of MRI is very technique dependent, and the results obtained with a specific technique do not apply to all MR scanners and techniques. Lymph nodes have longer T1 relaxation times than fat and thus T1-weighted images are useful in distinguishing nodes from adjacent pelvic fat, although subtle findings are better defined with postcontrast fat-suppressed images. Separating adjacent skeletal muscle from nodes, on the other hand, is easier on T2-weighted images, and thus several sequences are usually employed. In either case, CT and MRI simply detect whether a lymph node is enlarged or not but cannot detect whether it is infiltrated by tumor or enlarged secondary to a benign cause.

Bladder cancers spread to the lungs; chest radiography is a simple screening test, at times supplemented by chest CT. Bone scintigraphy is

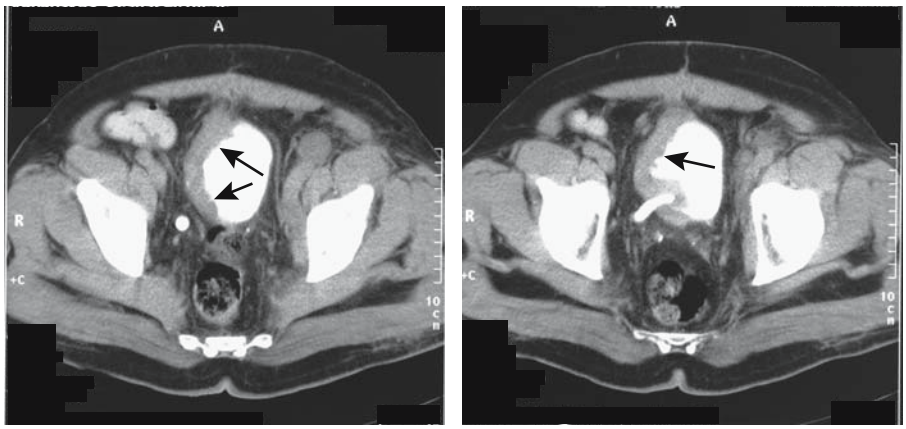

A B

Figure 11.9. Invasive bladder carcinoma. More superior (A) and inferior (B) transverse pelvic CT images show marked right-sided bladder wall thickening (arrows). Reflux into the right ureter is evident. The cancer is extending almost to the anterior abdominal wall. (Courtesy of Egle Jonaitiene, M.D., Kaunas Medical University, Kaunas, Lithuania.)

not commonly obtained at initial staging unless symptoms suggest bone metastases.

Attempts have been made to evaluate bladder cancers with positron emission tomography (PET) using both 2-[18F]-fluoro-deoxy-D-glucose (FDG) and other compounds, but the results for local tumor spread are not superior to those of more traditional imaging. Urinary excretion of FDG limits tumor identification from the surrounding activity. For detecting lymph node involvement, however, PET-FDG in patients with bladder neck carcinoma achieved a 67% sensitivity and 86% specificity (23); these results appear superior to those obtained with CT or MRI studies.

Therapy

Therapy of a bleeding, nonresectable bladder cancer is difficult. One approach is intraarterial chemoperfusion with mitoxantrone, which in one study controlled hemorrhage in 14 of 15 patients (24). In patients with life-threatening bleeding, intraarterial embolization is the procedure of choice.

Resection: Resection ranges from local excision, to segmental resection, to radical cystectomy. The surgical therapy adopted depends on the extent of tumor and varies for superficial disease and muscle-invasive disease. Noninvasive, low-grade cancers are often fulgurated. The 5-year survival for patients with treated bladder carcinoma-in-situ is about 90%. Stage Ta and some T1 cancers are resected transurethrally. Nevertheless, because of a high rate of recurrence even with these tumors, additional therapy is often instituted; surveillance cystoscopy results in an excellent 5-year survival. Dysplasia or a multicentric cancer requires resection. T1 disease, by definition, signifies lamina propria invasion but is still considered superficial; if treated by focal resection, recurrence eventually develops in almost half of these patients and the surgeon is faced with a dilemma in these patients between focal resection and a cystectomy.

In the United States, therapy for stage T2 to T4 bladder cancer is generally a total cystoprostatectomy. Two types of ileal conduits are constructed after bladder resection: a stomal noncontinent ileal diversion or a continent urinary reservoir anastomosed to either the urethra or a cutaneous stoma requiring intermittent catheterization (Kock pouch). The ureters are anastomosed to the neobladder. In some countries radiotherapy is preferred initially. Some stage pT2 bladder transitional cell carcinomas are treated by conservative surgery and iridium-192 brachytherapy.

Urinary tract diversion into the sigmoid colon was the initial anastomosis performed after a cystectomy until this operation was superseded by the use of various ileal conduits. A ureterosigmoidostomy is still encountered in the follow-up of previously operated patients. The complications of such diversion includes septic reflux, anastomotic stenosis, and hyperchloremic metabolic acidosis.

A study of patients undergoing cystectomy for bladder cancer found the 5-year survival for those with tumors confined to the bladder (<T3) to be 79%, but in patients with tumor spread beyond the bladder (>T3) survival was only 28% (25); from a lymph node viewpoint, 5-year survival for those with N0, N1, and N2–3 nodes was 64%, 48% and 14%, respectively.

Cystectomy is generally not considered for tumors extending beyond the bladder wall. Prostatic involvement is common with invasive transitional cell bladder cancers. Transitional cell carcinoma has a tendency to invade the prostatic urethra, and such invasion has a poor prognosis. Also, intravesical chemotherapy is ineffective in the prostatic urethra.

Bacillus Calmette-Guérin: Besides surgery, chemotherapy and immunotherapy with BCG are used to treat superficial bladder cancer. After the initial resection of a superficial transitional cell carcinoma, the risk of a subsequent tumor is decreased by adding either intravesical adjuvant chemotherapy or BCG immunotherapy. Some long-term studies of intravesical chemotherapy, however, reveal a limited decrease in tumor recurrence, and the use of routine prophylactic intravesical chemotherapy is questioned. BCG, on the other hand, is an effective intravesical agent in the prophylaxis and therapy of superficial transitional cell carcinoma; nevertheless, the use of BCG for Ta and T1 cancers varies considerably.

Bacillus Calmette-Guérin is a potent immune stimulant and exerts a direct toxic effect. Intravesical instillation leads to an inflammatory and immune cell infiltration into bladder lamina propria. The use of BCG prophylaxis results in less tumor recurrence than with surgical tumor

resection. Therapy with BCG in patients with primary bladder carcinoma-in-situ leads to complete response in a majority of patients. It appears to delay progression and the need for cystectomy in high-risk patients—those with dysplasia, carcinoma in situ, and multiple primary tumors. Low-dose BCG therapy in high-risk patients with stage T1, grade 3 bladder tumors combined with transurethral tumor resection resulted in 80% of patients responding to BCG instillation (26).

Among patients with pTa or pT1 bladder tumors treated by transurethral resection and intravesical BCG with 2 years of maintenance therapy, 62% of patients were recurrence-free at 48 months (27); a similar group of patients treated by transurethral resection alone and a group treated with transurethral resection and mitomycin C achieved recurrence-free results in 18% and 38% of patients, respectively. At 42 months, 11% of pT1 tumors treated with BCG had progressed to invasive carcinoma, compared to 25% of those treated by transurethral resection alone and 21% of those treated with transurethral resection and mitomycin C (27).

In a minority of patients BCG instillation results in toxicity, and a number of complications develop. In addition to the sequelae of tuberculous infection, tuberculous lymphadenitis leads to tumor overstaging. Bacillus Calmette-Guérin therapy for superficial bladder tumor led to epididymitis and epididymal abscess requiring an orchidectomy (28). Tuberculous enteritis (29) and mycotic aneurysms (30) have developed. In France, BCG Pasteur strain was used previously, more recently being supplanted by the Connaught (Toronto) strain. Toxicity appears similar for the two strains (31).

Ultrasonography after BCG therapy reveals hypoechoic foci in the prostate transition zone, representing necrotizing granulomas; confusing the issue is that bladder carcinoma invading the prostate also appears hypoechoic, and thus biopsies of these lesions are indicated.

Other Therapy: Some advanced bladder cancers are treated with radiotherapy and chemotherapy. Computed tomographic cystography commonly identifies bladder wall thickening at a tumor site after radiotherapy and chemotherapy due to a granulomatous reaction even without tumor recurrence. Magnetic resonance angiography (MRA) appears useful in evaluating the chemotherapy response in patients with advanced bladder cancer. Using persisting early contrast enhancement as a criterion, MRA achieves high sensitivity and specificity in distinguishing responders from nonresponders.

Superficial bladder tumors have been treated cystoscopically by injecting ethanol through a needle into the tumor base. Photodynamic therapy for small papillary bladder cancers achieves a response.

Interferon-α appears useful in carcinoma in situ and primary and recurrent papillary transitional cell carcinomas, although the response and relapse rates are inferior to those of BCG. Intravesical recombinant interferon-α therapy also appears useful in patients not responding or refractory to BCG therapy. Interleukin-2 is a potential agent in bladder cancer therapy. Even garlic appears to inhibit cancer cell growth and protects against suppression of immunity by chemotherapy (32).

Microwave-induced hyperthermia is occasionally mentioned for recurrent superficial bladder tumors not amenable to transurethral resection.

Metastasis/Recurrence

Clinical: After resection of one tumor, whether a new bladder tumor represents a recurrence or a new metachronous tumor is often unclear. Findings of distinct foci of synchronous carcinoma or carcinoma in situ argue for separate tumors. On the other hand, the increased risk for subsequent bladder cancers after an upper tract transitional cell carcinoma and lower risk of upper tract tumors after an initial bladder cancers argues for tumor dissemination.

Most recurrence of bladder carcinoma is detected within several years of initial surgery, with risk gradually tapering thereafter, although occasional metastases are detected a decade or longer after cystectomy. Most bladder cancers spread locally. Urethral recurrence after cystoprostatectomy occurs in about 5% of patients. Following cystectomy, recurrence within an ileal conduit is uncommon. Some tumors recur in regional lymph nodes, and distant metastases eventually develop in up to one third. Distal metastases are most common to the lungs, and then to the lymph nodes, bone, and liver. Rarer sites include malignant pericardial

effusion and brain metastases. The gastrointestinal tract is rarely involved, with an occasional recurrence presenting as an annular rectal tumor. An uncommon cancer spreads intraperitoneally and results in ascites and peritoneal carcinomatosis. If possible, a site of tumor origin should be determined because transitional cell bladder carcinomas have a worse prognosis than similar spread from the ovaries.

Surveillance: Cystoscopy and urine cytology are traditional surveillance examinations in the follow-up of bladder cancer; keep in mind that although urine cytology sensitivity is only about 30% to 50%, its specificity approaches 100%. Several other tests, including bladder tumor antigen, fibrin/fibrinogen degradation products, and nuclear matrix protein tests, are in use to a varying degree in different countries. The published evidence suggests that some of them even surpass cytology in detecting recurrence, but their role in routine follow-up is not clearly established and they are often employed as ancillary tests.

The postoperative imaging approach varies depending on the type of resection (if any). For most superficial bladder cancers no imaging follow-up is necessary unless additional risk factors are present: tumor >3 cm, several tumor foci, higher than grade I tumor, or the presence of additional foci of dysplasia.

Follow-up imaging of invasive transitional cell carcinomas consists of CT, chest radiography, IV urography, and, in some centers, US. The role of MRI is still evolving. Computed tomography is recommended every 3 to 6 months initially. Because therapy causes considerable distortion, an initial posttherapy CT study is especially valuable to establish a baseline. Posttherapy edema, fibrosis, and tumor recurrence have a similar CT appearance. Edema is identified as a diffuse increase in perivesical fat density. One recommendation after successful bladder cancer therapy is that these patients be followed with an IV urogram or similar imaging study to assess for upper urinary tract cancer, on the average every 1 to 2 years, although some believe that subsequent studies should be tailored to the clinical findings.

The evidence is accumulating that MRI is more accurate than CT in detecting bladder cancer recurrences, and a gradual shift toward MR studies is evident. No firm guidelines are established. T2-weighted images are useful in differentiating late recurrence (iso- to hyperintense) from residual fibrosis (hypointense). Within 6 to 12 months after therapy, however, these differences cannot be reliably differentiated.

The use of US for postoperative surveillance of bladder cancers is occasionally suggested, but a low sensitivity limits its use.

Adenocarcinoma

Bladder adenocarcinomas are not common. Many are primarily urachal in origin, involve the bladder dome, and are not of direct bladder origin, but a bladder carcinoma is in the differential diagnosis. An occasional bladder adenocarcinoma is associated with long-standing irritation and has developed in a defunctionalized bladder. A rare bladder adenocarcinoma is a consequence of bladder endometriosis.

A signet-ring cell adenocarcinoma or linitis plastica of the bladder is a highly malignant tumor having a poor prognosis. Most of these tumors contain signet-ring cells mixed with gland and papillary structures, at times even foci of transitional cell carcinoma. Compounding the issue is that a gastrointestinal or prostatic metastasis is often in the differential diagnosis, and thus a search for another primary is often necessary. A typical imaging appearance of a signet-ring cell adenocarcinoma is diffuse bladder wall invasion without a significant intraluminal component.

A hepatoid adenocarcinoma, representing extrahepatic hepatocellular differentiation, is a rare variant in the bladder; some of these tumors produce α-fetoprotein.

Squamous Cell Carcinoma

In most countries bladder squamous cell carcinomas represents only several percent of all primary bladder cancers, but in schistosomiasis-endemic countries a squamous cell carcinoma is the most common primary bladder cancer. In North America and Europe a squamous cell carcinoma is more common in bladder diverticula and is often associated with chronic bladder inflammation, such as long-standing bladder calculi or the presence of indwelling catheters.

A verrucoid carcinoma is a descriptive term for a squamous cell carcinoma having a frond-like pattern.

Computed tomography of primary squamous cell carcinoma often shows a predominantly extraluminal tumor component with invasion into adjacent structures, although some are predominantly intraluminal.

Lymphoma

Primary non-Hodgkin's lymphoma of the bladder is rare. Hematuria is the most common presentation, although prostatic involvement results in outlet obstruction. An occasional primary bladder lymphoma presents as a large pelvic tumor. Diffuse lymphomatous involvement simply thickens the bladder wall.

Magnetic resonance signal intensities from lymphoma-involved bladder are similar to those from adjacent lymphomatous lymph nodes.

An enterovesical fistula secondary to a non-Hodgkin's lymphoma is a rare complication.

Sarcoma

In adults, nonepithelial bladder malignancies include leiomyosarcoma and rhabdomyosarcoma; both are rare. These are aggressive, rapidly growing tumors with early local invasion. Rhabdomyosarcomas occur in both the bladder and the prostate. A biopsy should establish the diagnosis.

Imaging features for most sarcomas overlap. Extensive cystitis, lymphoma, and other tumors have a similar appearance. Ultrasonography reveals a large heterogeneous tumor. Doppler US typically detects nonpulsatile low velocity flow.

Sarcoma botryoides is a rhabdomyosarcoma originating in hollow organs and growing primarily intraluminally in grape-like clusters. A rare one arises from the bladder wall (Fig. 11.10).

Most bladder tumors in younger children are rhabdomyosarcomas. They are more common in boys. They tend to occur at the trigone or posterior bladder wall and either infiltrate or grow intraluminally as a lobular, irregular bladder tumor. Superficially, an intraluminal tumor tends to mimic blood clots. Some of these tumors prolapse into the urethra and obstruct. Those originating at the bladder dome can grow intraabdominally; determining the site of origin for some of these is difficult.

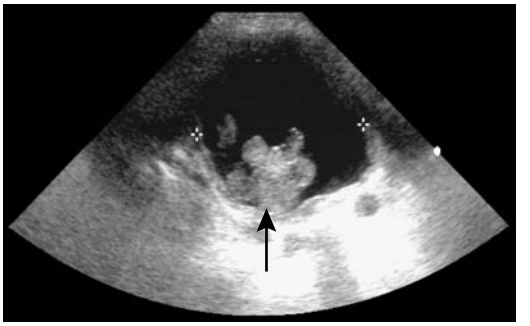

Figure 11.10. Bladder rhabdomyosarcoma in a teenage boy with hematuria. US reveals a polypoid intraluminal tumor (arrow). (Courtesy of Luann Teschmacher, M.D., University of Rochester.)

The rare bladder malignant histiocytoma and histiocytofibroma are aggressive sarcomas, at times associated with a hematologic malignancy.

Carcinosarcoma and Sarcomatoid Carcinoma

Some bladder carcinomas contain a prominent spindle cell component and are known as sarcomatoid carcinomas. Whether these are distinct from carcinosarcomas is debated in the pathologic literature (purists argue for distinct tumors). Other terms for these tumors are *malignant mixed mesodermal tumor* and *metaplastic carcinoma*. Whether this neoplasm is secondary to collision of two tumors or whether it represents separate differentiation from a single source is speculation.

The clinical presentation is similar to that of the more typical transitional cell carcinoma.

Among 15 patients with bladder carcinosarcoma seen at the Mayo Clinic, the most common carcinomatous component was a urothelial carcinoma, less often squamous cell carcinoma or small cell carcinoma, while the sarcomatous component consisted of chondrosarcoma, leiomyosarcoma, malignant fibrous histiocytoma, and other types (33); during the same time frame 26 patients were diagnosed with a sarcomatoid carcinoma, with the tumor consisting primarily of an urothelial carcinoma.

A rare sarcomatoid carcinoma originates in a bladder diverticulum.

Both carcinosarcoma and sarcomatoid carcinoma are highly aggressive tumors having a similar outcome regardless of histologic findings and treatment. These tumors metastasize readily and mimic other neoplasms, including lymphoma. They have no characteristic imaging findings. Most are large, solid, exophytic tumors when first detected. Some bladder carcinosarcomas contain calcifications and even osseous metaplasia. The diagnosis is suggested by immunohistochemistry.

Metastases/Invasion

Invasion from an adjacent cancer is more common than metastasis to the bladder. Thus prostatic carcinoma, gynecologic malignancies, rectal and even an appendiceal carcinoma readily invade the bladder. Some of these extrinsic tumors mimic a primary bladder carcinoma.

Coincident upper tract transitional cell carcinomas and bladder cancers have already been discussed. An occasional upper tract cancer, however, metastasizes to the bladder and is not a second primary, although differentiation of these is difficult. An occasional renal cell carcinoma metastasis to the ureteral stump and bladder is detected after a nephrectomy.

Only a few metastatic melanomas to the bladder have been reported.

Local invasion is from the outer wall inward; thus cystoscopy will not detect early invasion. Computed tomography and MR evidence of an asymmetric bladder wall thickening and increased MR signal intensity of the involved bladder wall segment are signs of invasion. Eventual intraluminal extension is evident.

Small Cell Carcinoma

The rare bladder small cell carcinoma appears to be less aggressive than a similar lung carcinoma. One should keep in mind that neuroendocrine tumors also have a small cell appearance but are characterized by their immunohistochemical properties; in some publications a distinction between small cell carcinomas and some neuroendocrine tumors is blurred. Histologically, these tumors also tend to mimic lymphoma. Occasionally bladder metastases from lung cancer has a similar appearance. Imaging simply reveals a solid tumor.

Most of these tumors result in hematuria. Adding chemotherapy to radical surgery appears to improve survival.

Neuroendocrine Tumors

The bladder trigone contains cells of neural crest origin.

Neurofibroma

The most common genitourinary involvement by neurofibromatosis is in the bladder. Although an occasional single neurofibroma is detected, more often these tumors are part of neurofibromatosis type I. Only a rare bladder neurofibroma is malignant. A trigone neurofibroma can obstruct an adjacent ureter.

These tumors range from a focal, well-marginated one to diffuse infiltration by a plexiform neurofibroma. Some neurofibromas have an imaging appearance similar to that of bladder leiomyomas, although neurofibromas often are more hyperintense on T2-weighted images than leiomyomas.

Paraganglioma (Pheochromocytoma)

Paragangliomas are uncommon catecholamine-producing tumors originating from chromaffin cells in the bladder paraganglion system. They can be multicentric. The most common location is in the trigone, followed by the bladder dome. Only an occasional one is malignant.

Hematuria is common. Some patients develop atypical hypertension, including palpitations, excessive sweating, paroxysmal hypertension, or even a hypertensive crisis during micturition due to release of epinephrine or norepinephrine.

Similar to other sites, bladder paragangliomas are solid, hypervascular tumors readily detected by CT and angiography. At times selective venous blood sampling is helpful in localizing these tumors. An occasional paraganglioma contains curvilinear calcification. Ultrasonography shows a solid, echogenic mass containing low-impedance flow. These tumors are interme-

diate to hypointense on T1- and hyperintense on T2-weighted MR images.

Long-term follow-up is necessary after resection of these tumors because recurrences or metastases can develop years later.

Intraluminal Mass

Causes of intraluminal bladder masses not attached to the bladder wall include blood clots, stones, fungus balls, and foreign bodies/bezoars.

Bladder calculi either form in the kidney and migrate to the bladder, or form de novo in the bladder. In certain parts of Asia and Africa bladder stones develop in children, called endemic bladder stones. Primary bladder calculi develop in a setting of stasis or the presence of a foreign body. Most small stones are mobile, with an occasional one adhering to the bladder wall due to adjacent inflammation. Thickening of the bladder wall is common. Stasis in an hourglass bladder incarcerated within a hernia has led to stone formation.

Occasionally giant bladder calculi fill almost the entire bladder lumen. Most of these stones contain calcium and are relatively radiopaque.

Bladder and urethral stones can be treated by ultrasonic lithotripsy, using either a transurethral or a percutaneous cystolithotripsy approach.

The most common entry site for bladder foreign bodies is through the urethra, with the foreign body being either self-introduced or introduced during a transurethral surgical procedure. Items mentioned in the literature range from bizarre household products to various surgical instruments. A second access route is during laparotomy or laparoscopic procedures. Least common are foreign bodies migrating from a site outside the bladder; these include such foreign bodies as synthetic gum used to protect a surgical ureterostomy and an intrauterine device migrating into the bladder lumen. Shotgun pellets have been passed spontaneously during voiding.

Clinical presentations range from recurrent infections to acute obstruction, depending on the type and location of a foreign body.

Dilation/Obstruction

Bladder outlet and urethral obstruction is discussed in Chapters 12 and 13.

Prolonged bladder outlet obstruction does lead to renal failure. An overdistended bladder resulted in bilateral iliac vein obstruction and bilateral urinary obstruction, and led to a pulmonary embolus (34).

Occasionally a patient with urinary retention has no anatomic obstruction, but "functional" bladder neck obstruction is believed to be responsible. Some of these patients with functional obstruction have normal cystourethrography and retrograde urethrography. The external sphincter opens during voiding but the bladder neck relaxes either intermittently or inadequately.

Neurogenic Bladder

Normal bladder intraluminal pressure is less than 10 to 15 cm of water. In general, a chronic constant pressure of greater than about 40 cm of water leads to bladder wall thickening, trabeculations, and outpouchings.

Bladder dysfunction is classified into an uninhibited neurogenic bladder, hyperreflexive detrusor (reflex neurogenic, contractile bladder), areflexic detrusor (autonomous neurogenic, flaccid bladder), and sensory or motor paralysis (Table 11.2).

In an uninhibited neurogenic bladder voluntary external sphincter contraction prevents voiding during uninhibited voiding. As a result, the posterior urethra is dilated to the external sphincter level and the imaging appearance is similar to a spinning top. These findings occur in infants with an immature bladder and adults with a cerebral cortical lesion (stroke, brain tumor). In infants the imaging appearance tends to be similar to that seen with posterior urethral valves.

Patients with a lesion above the lower lumbar level have detrusor hyperreflexia and develop a trabeculated thick-walled bladder. Such a hyperreflexive detrusor is found in patients with multiple sclerosis and lesions inducing spinal cord damage (trauma, tumor, syringomyelia). A large postvoid residue is common.

Table 11.2. Summary of neurogenic bladder dysfunction

Type	Bladder sensation	Initiate voiding	Inhibit voiding	Bladder capacity	Uninhibited bladder contraction	External sphincter dyssynergia	Bladder contour
Uninhibited neurogenic	+	+	−	↓	+	±	Smooth or trabeculated
Reflex neurogenic	−	−	−	↓	+	+	Trabeculated
Autonomous neurogenic	−	−	−	↑	−	+	Smooth or trabeculated
Sensory paralytic	−	+	+	↑↑	−	−	Smooth
Motor paralytic	+	−	−	↑	−	±	Smooth

Bladder contractions result in bladder neck opening, but the striated external sphincter does not open and thus bladder pressure increases. Associated vesicoureteral reflux is common in these patients, and if not corrected often results in loss of renal function.

Lower motor neuron involvement leads to detrusor areflexia. These patients develop a large, thin-walled bladder. No detrusor contractions are evident with an areflexic detrusor. The bladder neck remains open, external sphincter does not constrict normally, and these patients are incontinent.

Additional variants of a neurogenic bladder include sensory and motor paralysis. The former is most often found in diabetics. An association exists between gastroparesis and bladder dysfunction; patients with both idiopathic gastroparesis and diabetic gastroparesis are affected. Presumably a similar autonomic neuropathy is responsible for both gastric and bladder involvement.

Motor paralysis develops in some multiple sclerosis and polio patients. Urinary incontinence and retention are common problems in multiple sclerosis, often presenting a complex appearance. A majority of multiple sclerosis patients have detrusor hyperreflexia and a minority areflexia; these patients also develop bladder diverticula, urinary infection, hydronephrosis, and reflux.

Voiding dysfunction develops in patients with lumbar spinal stenosis. Dysfunction improves in some after a decompressive laminectomy, but others continue with a poor outcome.

A neurogenic bladder has been reported in Wolfram's syndrome (diabetes insipidus, diabetes mellitus, optic atrophy, and deafness) (35).

Autonomic dysreflexia, encountered in patients with a neurogenic bladder and similar conditions, is discussed later (see Examination Complications).

Calcifications

Bladder lumen calcifications consist of calculi and foreign bodies. Bladder wall calcifications include infections (schistosomiasis and tuberculosis), neoplasms, therapy related (radiation, chemo-, and immunotherapy, cyclophosphamide, BCG, thiotepa, and mitomycin C), phleboliths, arteriosclerosis, alkaline cystitis, and amyloidosis. Some calcifications are readily apparent with conventional radiography while others are detected only with a higher radiographic contrast imaging modality such as CT.

Fistula

Vesicovaginal

Common causes of vesicovaginal fistulas are prior gynecologic procedure, such as hysterectomy, and, in rural North Africa, obstetrical trauma (36). Less common etiologies include adjacent neoplasms and radiation therapy.

Cystography is the procedure of choice to detect these fistulas. A vaginogram is less often

diagnostic. In distinction to enterovesical fistulas, the presence of gas within the bladder is uncommon with a vesicovaginal fistula.

Enterovesical

The most common cause of enterovesical fistulas in adults is sigmoid diverticulitis. Less often encountered are colon and bladder malignancies, Crohn's disease, pelvic radiation, trauma, and infection by actinomycosis, tuberculosis, lymphogranuloma venereum, or an adjacent abscess, such as neglected appendicitis.

Indirect signs of a fistula include gas within the bladder and an irregular outline to the bladder wall. With some fistulas cystoscopy is noncontributory.

A suspected fistula is studied by cystography or barium enema; either study demonstrates most fistulas, although occasionally only one or the other outlines a fistula. A rare clinically suspected fistula is not detected with imaging; some of these become evident a week or so later. As a last resort, the Bourne test should be considered; following a nondiagnostic barium enema, a horizontal x-ray beam radiograph is obtained of a centrifuged urine sample. The sample may contain sufficient barium to be visible on the radiograph. The need for a Bourne test is rare and it is now mostly of historical interest.

Computed tomography and MRI outline some bladder fistulas. Gadolinium-enhanced T1-weighted MR images are superior in showing a fistula compared to precontrast images. If a fistula is accessible, contrast injection into the fistula and fistulography or MRI should define it.

Occasionally Tc-99m–diethylenetriamine pentaacetic acid (DTPA) renography shows radioactivity in the sigmoid colon with an enterovesical fistula.

Uterovesical

These fistulas are rare. In a collection of five uterovesical fistulas all were secondary to a prior cesarean section and all presented with intermittent hematuria (37); hysterosalpingography revealed some of these fistulas. In another collection of 10 such fistulas, 60% were secondary to cesarian section and 40% to prior abnormal delivery (38). Not all manifest with vaginal urinary leakage; an occasional one results in hematuria.

Diverticula

Bladder diverticula form when mucosa herniates through overlying muscle. A purist would thus describe them as *pseudodiverticula*, a term not generally used. Some diverticula have smooth muscle fibers within the wall. Fibrosis develops in some secondary to chronic inflammation. Diverticula may be single or multiple, small or large. Most diverticula have a wide neck. At times a diverticulum is larger than the remainder of the bladder. Very large diverticula tend to have a relatively smooth outline.

Diverticula may be primary developmental in origin or acquired secondary to another abnormality. An increased prevalence occurs in patients with Ehlers-Danlos syndrome and prune belly syndrome. They develop because of outflow obstruction, stasis, or prior surgery. An occasional one is associated with urinary retention or undergoes spontaneous rupture.

Diverticula close to the ureterovesical junction were described by Hutch in patients with a neuropathic bladder. These diverticula are believed to develop due to weakening of the detrusor muscle in this region and are associated with vesicoureteral reflux. If the ureter inserts into a diverticulum, the appearance mimics a ureterocele. Or, a Hutch diverticulum simply obstructs an adjacent ureter by its bulk.

A bladder diverticulum can be diagnosed by US if a communication with the main bladder lumen can be identified. Ultrasonography reveals an occasional bladder diverticulum as a complex pelvic tumor apparently separated from the bladder, leading to diagnostic confusion.

Endoscopic therapy of bladder diverticula has been performed with varying success.

The prevalence of neoplasms within a bladder diverticulum is greater than in a normal bladder, probably because of chronic inflammation and stasis. The most common neoplasm is a transitional cell carcinoma. Occasionally a sarcoma, squamous cell carcinoma, or even an adenocarcinoma develops in a diverticulum.

Most malignancies are detected late and are associated with a poor prognosis.

Ultrasonography reveals a diverticular neoplasm as an intraluminal, hyperechoic, nonshadowing tumor that does not change with a change in patient position. A cystogram may not detect the diverticulum, and a diverticular tumor is thus missed. Computed tomography and MRI outline an intraluminal soft tissue tumor. An MRI in oblique planes can identify the diverticular neck and establish that a tumor is indeed within the diverticulum. Localized tumor infiltration is seen as focal diverticular wall thickening. Occasionally associated calcifications are detected.

Herniation

Clinical

A *cystocele* is a bladder hernia, although many authors use this term in a narrower sense to describe bladder prolapse into the vagina. In women, a common type of cystocele consists of an abnormal bulge by the bladder into the anterior vaginal wall due to weakness in the pubocervical fascia. The appearance of such a cystocele, with bladder outline below the symphysis pubis, is familiar to most radiologists. These cystoceles become more prominent with the patient upright. Many are associated with generalized pelvic floor laxity and stress incontinence (incontinence is discussed in the next section).

In men, a common site for bladder hernias is into the inguinal canal; in women, femoral canal hernias are more common. In men most inguinal hernias are direct and more often on the right.

Unless large or obstructed, most bladder hernias are asymptomatic. Some men have two-phase micturition that improves when pressure is exerted on the scrotum. Clinically, some men with a bladder hernia are suspected of prostatism but no bladder outlet obstruction is found. Complications include bladder incarceration or even infarction in a strangulated hernia. A massive inguinoscrotal bladder hernia can lead to acute renal insufficiency.

Complete bladder inversion through the urethra is very rare (39); a cystogram through an orifice posterior to the extruded mass yielded a bladder volume of 20 mL.

Imaging

A bladder groin hernia, regardless of type, is identified by IV urography or cystography; in some patients a hernia becomes evident only when they are upright or prone, or if a delayed radiograph is obtained. With suspicion of a bladder groin hernia, video urodynamic imaging with the patient standing is helpful. The presence of lateral displacement of the distal ureter, a small visualized bladder volume, and incomplete bladder base visualization suggest a bladder hernia. Most appear as wide-mouthed bladder protrusions into the inguinal region. Bilateral inguinal bladder hernias are not uncommon.

Technetium-99m–methylene diphosphonate (MDP) bone scintigraphy detects a bladder groin hernia through increased inguinal region activity that changes with a change in patient position. Bone scintigraphy will also detect bladder herniation into the scrotum.

Incontinence

Urinary incontinence is considerably more common in women, and most incontinence classifications pertain to women.

Women

Clinical

Urinary incontinence is related to pelvic organ prolapse and other pelvic floor abnormalities and is discussed in more detail in Chapter 12. In young girls presenting with incontinence, an ectopic ureter inserting below the urethral sphincter or even into the vagina should be suspected.

Urinary incontinence is traditionally divided into three subtypes: stress, urge, and mixed. Stress incontinence occurs in a setting of increased intraabdominal pressure and insufficient urethral resistance. Urge incontinence consists of an inability to inhibit bladder contractions. At times urge incontinence is precipitated by coughing or straining and the two

types of incontinence overlap. Mixed incontinence is common and probably consists of several variants. Most classifications are based on stress incontinence, although some women with urge incontinence or a mixed type are also undoubtedly included. One classification sof stress urinary incontinence is based on endorectal US findings of urethral hypermobility, bladder neck incompetence, intrinsic urethral sphincter incompetence, and whether a cystocele is present or not. At times the urethral sphincter does not function normally because of prior surgery and fibrosis or a spinal cord lesion.

Urethral hypermobility results in an excessive change in urethral axis with straining and leads to urinary incontinence. Senior radiologists probably remember performing chain cystograms to help detect stress incontinence, a study that has been supplanted by newer imaging modalities.

Imaging

Voiding cystourethrography (VCUG) has been used to evaluate stress incontinence, yet this examination appears to be of limited value. It detects less than two-thirds of stress incontinence; false positives include women with detrusor instability and urge incontinence. Previously taught measurements of posterior vesicourethral angle change, urethral descent, urethral inclination and presence of a urethrocele on straining, detected on a VCUG, have been questioned in their ability to predict stress incontinence, yet some of these findings are now being resurrected with MRI studies.

Perineal US can be performed after injecting a hyperechoic contrast agent transurethrally. With the patient upright, contrast outlines the inferior part of the bladder. Stress incontinence is associated with the presence of a cystocele, a funnel-like opening of the proximal urethra, an increase in the retrovesical angle, and bladder neck descent. By evaluating bladder neck mobility relative to the symphysis pubis, perineal US achieved a sensitivity of only 78% and a specificity of 77% in detecting stress incontinence (40), and the authors concluded that perineal US is not sensitive enough to be used for predicting stress incontinence. Nevertheless, perineal US appears superior to the lateral view chain urethrogram if bladder neck mobility is studied during a Valsalva maneuver.

Depth and width of proximal urethral dilation during coughing and Valsalva maneuver are readily assessed by perineal US. Bladder neck descent occurs both in continent and incontinent women. The urethra dilates during coughing and Valsalva maneuver both in incontinent and some continent women and dilation *per se* does not imply incontinence.

An alternative technique is endorectal US in a standing position, the bladder filled with saline, and the test performed at rest and during a Valsalva maneuver; those with stress incontinence have a larger pubovesical angle during both resting and straining than controls; however, considerable overlap exists. Endorectal US shows the midurethral cross-sectional area to be significantly smaller in women with stress incontinence than in those without, a difference due to a significantly smaller peripheral striated muscle component in those with stress incontinence (41); this peripheral striated muscle surrounded the urethra completely in 36% of women without stress incontinence, but only in 5% of those with severe incontinence. The urethropelvic ligament thickness was significantly thinner in those with stress incontinence. The clinical application of these findings in formulating therapy remains to be established.

Endovaginal US measures the distance from the bladder neck to the symphysis pubis. Various displacement criteria with and without stress have been suggested to detect urinary stress incontinence, none achieving popularity.

Magnetic resonance imaging is acquiring a primary role in evaluating stress incontinence, although technical limitations exist with horizontal bore MR units; ideally, the study should be performed with the patient in the upright position. Sagittal T2-weighted MRI identifies a cystocele as a posteriorly bulging bladder into the vagina. High resolution endovaginal MR provides detailed dynamic pelvic floor visualization during straining when using T2-weighted single-shot fast spin echo (FSE) sequences without contrast. Levator ani thinning is associated with stress urine incontinence (42). Varying degrees of protrusion, including prolapse, are identified. Stress incontinence is associated with a greater vesicourethral angle and larger retropubic space than found in continent women. Both bladder floor descent and

cervical descent is greater in incontinent than in nulliparous women, but symptoms do not always correlate with the amplitude of bladder floor descent (43).

Therapy

A vesicourethropexy (Marshall-Marchetti operation) has a high early postoperative success rate, which decreases with time. Postoperative imaging identifies an elevated bladder base. A similar bladder elevation is also occasionally seen due to large degenerative bony spurs at the symphysis pubis.

A number of bulking agents, including autologous fat, polytetrafluoroethylene, and bovine collagen have been injected to treat stress incontinence but most are associated with either side effects or limited long-term results. Periurethral collagen (glutaraldehyde crosslinked bovine collagen) injection has become popular therapy for symptomatic urinary stress incontinence since gaining United States Food and Drug Administration approval. The agent is injected under local anesthesia. It appears to be biocompatible with little evidence of a foreign-body or immunologic reaction. Collagen is partially reabsorbed within several years. A follow-up of 24 months after periurethral collagen injection in women with severe urinary incontinence resulted in a continent rate of 33%, with 39% improved and 28% considered to be failures (44). Complications include urinary urgency and incontinence, at times irreversible, hematuria, and urinary retention. Urinary tract infection after collagen injection is uncommon.

Comparing posttherapy transvesical and endovaginal US, the endovaginal approach reveals collagen in more patients; collagen is identified as circumscribed masses at the bladder base having varying echogenicity. Magnetic resonance imaging identifies collagen as hyperintense foci within the urethral wall; neither visualized collagen volume nor its position are related to clinical outcome.

Periurethral silicone implants in women with intrinsic sphincter deficiency resulted in a subjective success rate of 80% at 6 weeks and 60% at 1 year (45).

Implantable microballoons have also been used as therapy for female urinary incontinence. These consist of self-detachable crosslinked silicone balloons and a biocompatible filler material. This technique is most effective in treating intrinsic sphincter deficiency.

Men

Continence after prostatectomy is maintained by an intact sphincter. Urinary stress incontinence after prostatectomy is generally due to sphincter dysfunction, such as scarring or decreased contractions, findings evaluated with endourethral US.

Transurethral collagen injection is used to treat urinary incontinence after radical prostatectomy. Collagen injection in men with incontinence result in a low continence rate: 20% to 24% in several studies; the success of the cure by collagen injection is influenced by the severity of the pretreatment incontinence, detrusor overactivity, and other factors. Endorectal US in men after collagen injection reveals hypoechoic masses adjacent to the bladder.

Children

Urinary incontinence is a common pediatric urologic problem. In infants the reflex-controlled bladder matures to normal bladder function during the first several years of life as the bladder sphincter grows and central nervous control of micturition matures. Sufficient anatomic maturation is necessary before neurologic control is established.

Collagen injection for incontinence has achieved mixed results in children. One study reported that 5% of children became continent and 25% improved, and the authors questioned the high collagen injection cure rates previously reported for urinary incontinence in children (46).

Immunosuppression

Acute hemorrhagic cystitis is occasionally reported after a kidney transplant, probably due to an adenovirus infection.

Immunosuppressed renal transplant patients are more prone to developing a bladder lymphoma than the general population.

Postoperative Changes

Bladder Augmentation

Enterocystoplasty, or bladder augmentation, increases bladder capacity in patients with a small bladder volume. Usually a loop of small bowel is used (ileocystoplasty), but sigmoidocystoplasty is also employed. Gastrocystoplasty, ureterocystoplasty, and seromuscular augmentation are less common techniques, with various artificial materials still in the realm of experimentation.

Especially with a neurogenic bladder, enterocystoplasty leads to a decrease in intravesical pressure and less vesicoureteral reflux. This procedure is also performed in children with renal transplantation who have bladder dysfunction.

Some patients develop bowel dysfunction after enterocystoplasty; for unknown reasons such dysfunction appears to be more prevalent after enterocystoplasty performed for detrusor instability.

An occasional neoplasm develops years after enterocystoplasty. A tubulovillous adenoma was found in the cecal segment after a cecocystoplasty. Anecdotal reports describe ileal adenocarcinomas and even squamous cell carcinoma in an augmentation, at times decades later. An occasional such cancer is discovered during investigation of an elevated carcinoembryonic antigen (CEA) level.

Continent Urinary Diversion (Pouch)

A continent urinary diversion results in a cutaneous stoma and avoids an external device. Intermittent catheterization is required with these pouches. The Koch pouch consists of an ileourethral reservoir. Transection of the ileal antimesenteric border and folding of the ileal segments abolishes peristalsis, which would result in incontinence. The Mainz pouch consists of a low-pressure rectosigmoid reservoir. The bowel is opened along its antimesenteric border and a side-to-side anastomosis is performed. The Indiana pouch uses an isolated right colon as a reservoir, the ileocecal valve as a continent mechanism, and terminal ileum as a conduit. A risk of malignancy in the colon reservoir exists, but this risk is less than in previously used ureterosigmoidostomy where fecal and urinary systems were combined.

The appendix is occasionally used as a urinary conduit or an outlet during urinary reconstruction for a continent reservoir. Even a Meckel's diverticulum has been used as a continence mechanism.

Ureteroenteric anastomotic strictures after an ileal conduit urinary diversion have been successfully treated with expandable metallic stents.

An occasional neoplasm has developed in a continent ileostomy but the incidence of these is low.

Orthotopic Bladder Reconstruction

Orthotopic bladder reconstruction is performed for muscle invasive bladder cancer, provided the prostate and urethra are not involved. After cystectomy either a colon segment or, more often, an ileum is used as a bladder substitute and anastomosed to the urethra. This procedure is an alternative to a cutaneous urinary diversion. Two currently used procedures are the Hautmann and Studer modifications. These neoileal bladder replacements use an ileal segment and provide an antireflux mechanism.

The Hautmann ileal neobladder consists of a detubularized, low-pressure, high-capacity reservoir constructed from ileum, without valves, and anastomosed to the urethra. Urodynamic imaging shows this neobladder to have a capacity similar to that of a normal bladder, a pressure of <30 cm water, and no reflux. Initially the prostatic urethra was resected to establish a safe resection margin, and this operation was performed only in men. Currently, however, both a radical cystectomy and a bladder neck-sparing cystectomy, together with an orthotopic ileal neobladder anastomosed to the proximal urethra, are also performed in women (47); the position of the urethral resection line does affect the incontinence rate and the need for intermittent catheterization. Continence is achieved by most men and women.

Neobladder-related complications include abscess, urinary leakage or fistula, ureteral and urethroileal stenosis, and venous thrombosis. An occasional patient develops calculi. Fistulas

are mostly a complication of combined irradiation and orthotopic bladder replacement.

Postoperative upper tract surveillance is with IV urography, CT, and renal US. Postcontrast MRI should reveal normal renal enhancement and visualize the neobladder. Also, MRI provides renal function data similar to that obtained with scintigraphy. Dynamic digital urography using serial image acquisition after bolus contrast injection is a novel way of studying orthotopic ileal neobladders (48), but this technique is not widely practiced.

Postoperative surgical anatomy after orthotopic bladder reconstruction can be evaluated with 3D CT (virtual endoscopy); while such imaging is useful if reoperation is required, its need on a routine basis is not established.

Postoperative Complications

Urinary tract damage occurring during various gynecologic laparoscopic procedures includes bladder perforation, ureteral injury, and bladder fistula. The prevalence of these complications after major laparoscopic gynecologic surgery is probably similar to that seen after standard surgery.

Leak

Anastomotic leakage is a recognized complication of urinary tract reconstructive surgery (Fig. 11.11). The most common site is at the urethroenteric anastomosis. A majority of leaks are extraperitoneal in location; it is the intraperitoneal pouch leaks that are more difficult to detect with imaging. A number of leaks are delayed.

Catheter drainage or stenting as appropriate is therapeutic for most leaks.

Stones/Stricture

Patients with an enterocystoplasty or continent diversion are at risk for stone formation and ureterointestinal stricture. Patients with a continent diversion are more prone to developing stones than those with an augmentation or a substitution cystoplasty.

Surgical treatment of ureterointestinal strictures consists of open ureteral reimplantation. Percutaneous antegrade dilation is a viable alternative in some patients, but is plagued by a low success rate and recurrent restenosis.

Dilated ureters are common in patients with a neobladder, and it is difficult to differentiate between partial obstruction and dilation due to reflux and other causes. An IV urogram with furosemide is occasionally helpful in such a situation. Furosemide normally results in good contrast flow distally once renal pelves are opacified; on the other hand, increased renal pelvis and caliceal dilation and the lack of contrast washout during such diuresis imply an obstruction.

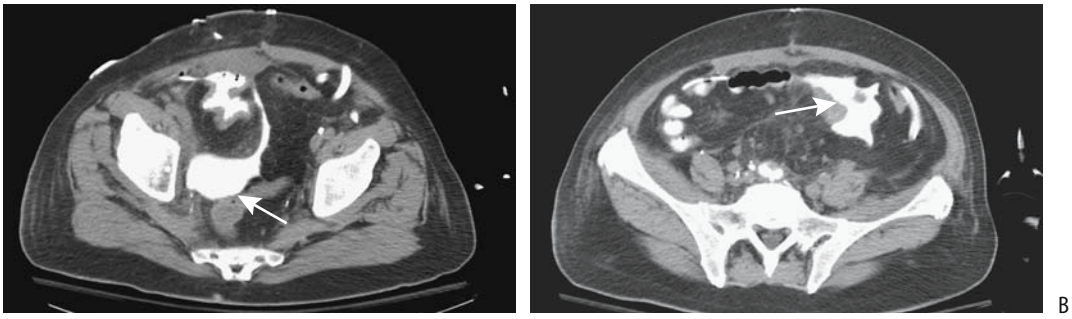

A B

Figure 11.11. Bladder leak after subtotal cystectomy and neobladder formation. A: CT cystogram identifies contrast in the bladder and extravasation posteriorly (arrow). B: Extravasation also extends to the left, adjacent to bowel (arrow). (*Source:* Titton R, Gervais DA, Hahn PF, Harisinghani MG, Arellano RS, Mueller PR. Urine leaks and urinomas: diagnosis and imaging-guided intervention. RadioGraphics 2003;23:1133–1147, with permission from the Radiological Society of North America.)

Malignancy

A low but increased risk of cancer exists after various uroenteric anastomoses, generally beginning a decade or more after surgery. These range from adenocarcinoma to transitional cell carcinoma and squamous cell carcinoma. A reasonable approach is to recommend routine annual surveillance beginning about 10 years after the initial surgery.

Other Complications

An ileoileal intussusception is an uncommon complication of bladder augmentation. Computed tomography and MR should detect this complication.

An autostapler is often used when bowel is interposed in the urinary tract, with the metallic staples buried beneath the intestinal mucosa. A staple expressed into the bladder lumen acts as a nidus for subsequent stone formation.

An occasional patient with portal hypertension develops massive bleeding from ileal conduit peristomal varices; such bleeding can be controlled with transjugular intrahepatic portosystemic shunt (TIPS).

Examination Complications

Cystography

Rupture/Extravasation

Extravasation of contrast or even frank perforation is one of the complications of cystography. Typically a tear occurs during filling of an unused or partially used bladder. Patients with chronic renal failure appear to be at increased risk. Although rare, an indwelling catheter is associated with a bladder perforation; occasionally a Foley catheter occludes the bladder outlet and results in greater pressures than normal. Nevertheless, extravasation also occurs in patients with no known underlying risk factors. The most common site is lateral to the trigone, close to the ureteral insertion.

Some patients develop intramural intravasation, while others have frank bladder wall rupture. Many of these patients remain asymptomatic. Cystoscopic findings range from isolated mucosal tears and diffuse mucosal hemorrhage to frank rupture.

Many extravasations resolve without therapy, aside from maintaining a low luminal pressure.

Autonomic Dysreflexia

In patients with previous spinal cord injury, imaging studies leading to bladder or colonic distention should be approached cautiously. Autonomic dysreflexia is caused by spinal cord lesions above the T6 level. It is not an uncommon complication in patients with a cord lesion who are undergoing manipulative urologic procedures such as cystography or voiding cystourethrography. It is also occasionally encountered with a barium enema or similar procedures. It is induced by overstimulation of α-adrenergic fibers in the bladder neck. With a rise in intravesical pressure the bladder neck is stretched and α-adrenergic receptors excrete norepinephrine. Elevated circulating norepinephrine level leads to peripheral arterial constriction and hypertension. Normally this peripheral arterial constriction is countered by splanchnic vessel dilation, but with a spinal cord lesion above T6 no reflex portal vessel dilation occurs. The resultant hypertension stimulates the carotid sinus, and aortic arch baroreceptors which result in bradycardia and vasodilation above the cord injury level. Impulses originating from stretched bladder or colon afferent sensory nerve endings ascend to the point of spinal cord injury and initiate the release of sympathetic motor impulses in efferent tracts, leading to sympathetic hyperreflexia and spasm and vasoconstriction below the level of injury. Clinically, both systolic and diastolic hypertension, bradycardia, nausea, abdominal pain and redness, and profuse sweating of the head and neck develop. It can be life-threatening.

In patients with a spinal cord lesion, constant blood pressure monitoring should be considered during manipulative radiologic procedures so that the onset of this syndrome is detected in its early phase; generally terminating the procedure and bladder drainage resolves the hypertension. Therapy of autonomic dysreflexia differs from treatment of typical contrast reactions; namely, treatment is to remove the inciting cause and treat the hypertension, if still present. Occasionally hypertension persists even when the inciting stimulus is removed, and fast-acting antihypertensive therapy may be necessary. If needed, patients at risk for auto-

nomic dysreflexia can be premedicated with α-blocking agents prior to the procedure.

Catheter Related

The balloon of a chronic indwelling catheter may not deflate. An attempt at bursting the balloon should minimize the possibility of leaving any catheter fragments in the bladder. An in vitro study comparing the results of a needle technique, overinflation, instillation of ether, and using a stylet through the inflation channel found that a needle technique achieved the best results with the fewest fragments (49).

A knot can form during catheterization of a continent stoma and lead to acute urinary retention. Similar catheter knotting within the bladder is a complication of cystourethrography; some of these knots can be untied using a stiff guidewire.

References

1. Song JH, Francis IR, Platt JF, et al. Bladder tumor detection at virtual cystoscopy. Radiology 2001;218:95–100.
2. Darge K, Bruchelt W, Roessling G, Troeger J. Interaction of normal saline solution with ultrasound contrast medium: significant implication for sonographic diagnosis of vesicoureteral reflux. Eur Radiol 2003;13:213–218.
3. Beyersdorff D, Taupitz M, Giessing M, et al. [The staging of bladder tumors in MRT: the value of the intravesical application of an iron oxide-containing contrast medium in combination with high-resolution T2-weighted imaging.] [German] Rofo Fortschr Geb Rontgenstr Neuen Bildgeb 2000;172:504–508.
4. Bernhardt TM, Schmidl H, Philipp C, Allhoff EP, Rapp-Bernhardt U. Diagnostic potential of virtual cystoscopy of the bladder: MRI vs CT. Preliminary report. Eur Radiol 2003;13:305–312.
5. Lammle M, Beer A, Settles M, Hannig C, Schwaibold H, Drews C. Reliability of MR imaging-based virtual cystoscopy in the diagnosis of cancer of the urinary bladder. AJR 2002;178:1483–1488.
6. Yanagisawa S, Fujinaga Y, Kadoya M. Urachal mucinous cystadenocarcinoma with a cystic ovarian metastasis. AJR 2003;180:1183–1184.
7. Oyar O, Yesildag A, Gulsoy UK, Perk H. The image of urachus adenocarcinoma on Doppler ultrasonography. Eur J Radiol 2002;44:48–51.
8. Peng MY, Parisky YR, Cornwell EE 3rd, Radin R, Bragin S. Computed tomography cystography versus conventional cystography in evaluation of bladder injury. AJR 1999;173:1269–1272.
9. Lemack GE, Zimmern PE. [Interstitial cystitis: reevaluation of patients who do not respond to standard treatments.] [French] Prog Urol 2001;11:239–244.
10. Peters KM, Diokno AC, Steinert BW, Gonzalez JA. The efficacy of intravesical bacillus Calmette-Guerin in the treatment of interstitial cystitis: long-term followup. J Urol 1998;159:1483–1486.
11. Anderson J, Carrion R, Ordorica R, Hoffman M, Arango H, Lockhart JL. Anterior enterocele following cystectomy for intractable interstitial cystitis. J Urol 1998;159:1868–1870.
12. Miyazato T, Yusa T, Onaga T, et al. [Hyperbaric oxygen therapy for radiation-induced hemorrhagic cystitis.] [Japanese] Nippon Hinyokika Gakkai Zasshi 1998;89:552–556.
13. Server Pastor G, Lopez Cubillana P, Garcia Hernandez JA, Hita Rosino E, Asensio Egea L, Rigabert Montiel M. [Eosinophilic cystitis: a single anatomopathologic entity and three different presentation forms. Proposed classification.] [Review] [Spanish] Actas Urol Esp 1996;20:155–161.
14. Parant O, Soulie M, Tollon C, Monrozies X. [Ureteral and vesicular endometriosis: case report.] [French] Prog Urol 1999;9:522–527.
15. Jequier S, Bugmann P, Brundler MA. Nephrogenic adenoma of the bladder: ultrasound demonstration. A case report. Pediatr Radiol 1999;29:185–187.
16. Oyama N, Tanase K, Akino H, Mori H, Kanamaru H, Okada K. Nephrogenic adenoma in a patient with transitional cell carcinoma of the bladder receiving intravesical bacillus Calmette-Guerin. [Review] Int J Urol 1998;5:185–187.
17. Linn JF, Sesterhenn I, Mostofi FK, Schoenberg M. The molecular characteristics of bladder cancer in young patients. J Urol 1998;159:1493–1496.
18. Herr HW, Cookson MS, Soloway SM. Upper tract tumors in patients with primary bladder cancer followed for 15 years. J Urol 1996;156:1286–1287.
19. Kim JK, Park SY, Ahn HJ, Kim CS, Cho KS. Bladder cancer: analysis of multi-detector row helical CT enhancement pattern and accuracy in tumor detection and perivesical staging. Radiology 2004;231:725–731.
20. Kim JK, Ahn JH, Park T, Ahn HJ, Kim CS, Cho KS. Virtual cystoscopy of the contrast material-filled bladder in patients with gross hematuria. AJR 2002;179:763–768.
21. Taniguchi M, Tatsuta N, Yokota H, et al. Incrustation and uptake of skeletal imaging agent in transitional cell carcinoma. J Nucl Med 1997;38:1206–1207.
22. Haleblian GE, Skinner EC, Dickinson MG, Lieskovsky G, Boyd SD, Skinner DG. Hydronephrosis as a prognostic indicator in bladder cancer patients. J Urol 1998;160:2011–20144.
23. Bachor R, Kotzerke J, Reske SN, Hautmann R. [Lymph node staging of bladder neck carcinoma with positron emission tomography.] [German] Urologe A 1999;38:46–50.
24. Textor HJ, Wilhelm K, Strunk H, Layer G, Dolitzsch C, Schild HH. [Locoregional chemoperfusion with mitoxantrone for palliative therapy in bleeding bladder cancer compared with embolization.] [German] Rofo Fortschr Geb Rontgenstr Neuen Bildgeb Verfahr 2000;172:462–466.
25. Lebret T, Herve JM, Yonneau L, et al. [Study of survival after cystectomy for bladder cancer. Report of 504 cases.] [French] Prog Urol 2000;10:553–560.
26. Lebret T, Gaudez F, Herve JM, Barre P, Lugagne PM, Botto H. Low-dose BCG instillations in the treatment of

stage T1 grade 3 bladder tumours: recurrence, progression and success. Eur Urol 1998;34:67–72.
27. Ayed M, Ben Hassine L, Ben Slama R, et al. [Results of BCG in the treatment of pTa and pT1 bladder tumors. Evaluation of a long protocol using 75 mg of Pasteur strain BCG.] [French] Prog Urol 1998;8:206–210.
28. Sebe P, Haab F, Nouri M, Tligui M, Gattegno B, Thibault P. [Epididymal gaseous abscess after BCG treatment.] [French] Prog Urol 2000;10:99–100.
29. Nemoto R, Nakamura I, Honjyo I, Takahashi M, Abe C. Tuberculous enteritis after intravesical bacillus Calmette-Guerin therapy: a case of mistaken identity. J Urol 1998;159:2091–2092.
30. Damm O, Briheim G, Hagstrom T, Jonsson B, Skau T. Ruptured mycotic aneurysm of the abdominal aorta: a serious complication of intravesical instillation bacillus Calmette-Guerin therapy. J Urol 1998;159:984.
31. Champetier D, Valignat C, Lopez JG, Ruffion A, Devonec M, Perrin P. [Intravesical BCG-therapy: comparison of side effects of Connaught (Toronto) and Pasteur (Paris) strains.] [French] Prog Urol 2000;10:542–547.
32. Lamm DL, Riggs DR. The potential application of Allium sativum (garlic) for the treatment of bladder cancer. [Review] Urol Clin North Am 2000;27:157–162.
33. Lopez-Beltran A, Pacelli A, Rothenberg HJ, et al. Carcinosarcoma and sarcomatoid carcinoma of the bladder: clinicopathological study of 41 cases. J Urol 1998;159: 1497–1503.
34. Sousa Escandon MA, Alejandro M, Garcia Figueiras R, et al. [Pulmonary thromboembolism after chronic bladder distention.] [Review] [French] Prog Urol 2001;11:323–326.
35. Monllor Gisbert J, Tano Pino F, Rodriguez Arteaga P, Galbis Palau F. [Urologic manifestations in Wolfram's syndrome.] [Spanish] Actas Urol Esp 1996;20:474–477.
36. Moudouni S, Nouri M, Koutani A, Ibn Attya A, Hachimi M, Lakrissa A. [Obstetrical vesico-vaginal fistula. Report of 114 cases.] [French] Prog Urol 2001;11:103–108.
37. Sylla C, Fall PA, Diallo AB, et al. [Vesico-uterine fistulae. Report of 5 cases.] [French] Prog Urol 2000;10:634–637.
38. Tazi K, el Fassi J, Karmouni T, et al. [Vesico-uterine fistula. Report of 10 cases.] [French] Prog Urol 2000;10: 1173–1176.
39. Takahashi E, Nakajima F, Taoka Y, et al. [A case report of complete inversion of the bladder in an old woman.] [Japanese] Nippon Hinyokika Gakkai Zasshi 1998;89: 975–978.
40. Chen GD, Su TH, Lin LY. Applicability of perineal sonography in anatomical evaluation of bladder neck in women with and without genuine stress incontinence. J Clin Ultrasound 1997;25:189–194.
41. Kuo HC. Transrectal sonographic investigation of urethral and paraurethral structures in women with stress urinary incontinence. J Ultrasound Med 1998;17:311–320.
42. Stoker J, Rociu E, Bosch JL. High-resolution endovaginal MR imaging in stress urinary incontinence. Eur Radiol 2003;13:2031–2037.
43. Unterweger M, Marincek B, Gottstein-Aalame N, et al. Ultrafast MR imaging of the pelvic floor. AJR 2001;176: 959–963.
44. Game X, Malavaud B, Mouzin M, Rischmann P, Sarramon JP. [Periurethral collagen injections: results after 2 years in 25 patients with severe urinary incontinence.] [French] Prog Urol 2001;11:283–287.
45. Hidar S, Attyaoui F, de Leval J. [Periurethral injection of silicone microparticles in the treatment of sphincter deficiency urinary incontinence.] [French] Prog Urol 2000;10:219–223.
46. Sundaram CP, Reinberg Y, Aliabadi HA. Failure to obtain durable results with collagen implantation in children with urinary incontinence. J Urol 1997;157:2306–2307.
47. Hautmann RE, de Petriconi R, Kleinschmidt K, Gottfried HW, Gschwend JE. Orthotopic ileal neobladder in females: impact of the urethral resection line on functional results. Int Urogynecol J Pelvic Floor Dysfunct 2000;11:224–229.
48. Sardanelli F, Zandrino F, De Cicco E, Iozzelli A, De Caro G, Pacella M. [An evaluation of orthotopic ileal neobladders by dynamic digital urography.] [Italian] Radiol Med 2000;100:37–41.
49. Gulmez I, Ekmekcioglu O, Karacagil M. A comparison of various methods to burst Foley catheter balloons and the risk of free-fragment formation. Br J Urol 1996;77:716–718.

12

Female Reproductive Organs

Technique

Hysterosalpingography

Conventional

The gold standard in evaluating tubal patency is laparoscopy, although in many institutions hysterosalpingography is commonly used. In developed countries hysterosalpingography is performed with fluoroscopic visualization; in others, where fluoroscopic equipment often does not exist, a delayed anteroposterior image after contrast instillation is an alternative.

The primary application of hysterosalpingography is in evaluating infertility. This examination is readily performed by most radiologists, does not require anesthesia, and side effects and complications are uncommon, with the major complication being pelvic infection. The indications for this examination have decreased considerably, and the current major indication is to determine whether fallopian tubes are patent or not. It has been supplanted by magnetic resonance (MR) in evaluating most müllerian duct anomalies. This examination does not evaluate well the fimbriated fallopian tube ends and external structures. A lack of intraperitoneal contrast spill does not establish tubal obstruction; spasm, mucous plugs, and technical factors in performing the study also result in nonspillage. Thus in one study only 84% of the nonpatent tubes at hysterosalpingography were obstructed at perioperative salpingoscopy (1).

A number of studies have commented on an increased pregnancy rate after hysterosalpingography. The choice of a water-soluble versus an oil-soluble contrast agent in performing hysterosalpingography does not affect the subsequent rate of term pregnancy (2).

Other Imaging Techniques

Selective catheterization of the fallopian tubes (selective salpingography) is useful if hysterosalpingography reveals a blocked tube and further intervention is contemplated. If needed, a guide wire is inserted through the tube and a catheter is advanced into the tube. At times a fallopian tube believed to be obstructed will be shown to be patent with this technique.

Endovaginal ultrasonography (US) during air and saline instillation into the uterus also evaluates tubal patency (variously called *sonosalpingography*, *hysterosalpingosonography*, and similar names). The use of B-mode US and Doppler US to assess tubal flow of a contrast agent and thus establish tubal patency have been proposed, but with limited success.

A liquid containing air bubbles, such as agitated saline or one containing human serum albumen, can be used as a contrast agent during sonographic hysterosalpingography. Fluid and air bubbles are seen in the cul-de-sac if the fallopian tubes are patent. These procedures are similar to hysterosalpingography except that endovaginal US is used.

In a woman with a contraindication to iodine-based contrast, tubal patency can be established by magnetic resonance imaging (MRI) after infusing gadolinium–diethylenetriamine pentaacetic acid (Gd-DTPA); the presence of contrast material in the peritoneal cavity implies tubal patency.

Anecdotal hysterosalpingoscintigraphy using technetium-99m (Tc-99m)–macroaggregated albumin (MAA) has been reported.

Computed Tomography

Pelvic CT is commonly used to evaluate gynecologic disease. Computed tomography is especially useful in staging malignancies. An occasional false-positive diagnosis of malignancy does occur, and among other entities it includes pelvic actinomycosis, chronic appendicitis, and even an ectopic pregnancy.

Ultrasonography

A number of terms describe US of the female pelvic structures: s*onography*, *sonohysterography*, *hysterosonography*, *vaginosonography*, *transvaginal echography*, and other similar terms are used. Saline may or may not be instilled into the uterine cavity prior to scanning. The examination is performed either using a transabdominal approach or the probe is positioned in the vagina, uterus, or rectum. Ultrasonography during surgery uses a sterile intraabdominal probe.

For consistency, the terms *transabdominal*, *endovaginal*, and *endorectal US* are used here. Whenever intrauterine saline is instilled it is specifically mentioned. Unless Doppler is mentioned, the examination involves conventional US.

Intraoperative US is useful in guiding difficult dilation and curettage (D&C). Endovaginal sonohysterography aids some operative intrauterine biopsies and resections, although its effectiveness compared to hysteroscopy is not known.

Transabdominal US provides a general overview of the pelvis. It is limited in obese patients. Endovaginal US allows the use of higher frequency transducers and thus has better resolution than a transabdominal approach, but it has a limited field of view, especially of large tumors. The two studies are therefore complementary and at times both need to be performed.

Endovaginal US is generally considered more specific in detecting adnexal and ovarian disorders than transabdominal US. In women with postmenopausal bleeding, endovaginal US improves clinical diagnostic accuracy and the certainty of diagnosis. Both conventional and Doppler US are feasible. No definite contraindication to endovaginal US exists. A three-dimensional (3D) endovaginal US technique is employed in some centers; whether it provides any advantage over the current 2D techniques remains to be established.

The terms *sonohysterography* and *hysterosonography* are generally used to indicate that the uterine cavity has been distended with fluid, usually sterile saline. It then should be qualified whether the examination is performed transabdominally or endovaginally. Sterile saline injected into the uterine cavity acts as a sonographic window for endovaginal US. Such scanning achieves higher resolution than is obtainable with conventional endovaginal US. A number of publications have reported sensitivities and specificities of over 95% for this technique in detecting intracavitary lesions, and this technique has gained wide acceptance. Yet a word of caution is in order about this procedure: A risk of intraperitoneal malignant cell dissemination exists in a setting of endometrial cancer. In an elegant study of infusion sonohysterography using 10 to 20 mL of saline performed when the abdomen was open but prior to the start of a surgical procedure, fluid spilled from the fallopian tubes was shown to contain malignant cells (3). Whether the use of sterile water rather than saline to lyse free tumor cells is helpful remains to be established.

Intrauterine US has a higher sensitivity and specificity than an endovaginal approach in detecting uterine abnormalities. Some authors have suggested that intrauterine US might replace hysterosalpingography for uterine study. This may be so, although part of the reason may be the poor study quality of much of hysterosalpingography, especially with digital filming—gross contrast-filled uterine images provide no intrauterine details.

The indications for intrauterine US are not yet settled, but it appears to have a role between that of hysterosalpingography and hysteroscopy.

Endovaginal Doppler US measures blood flow velocity in uterine arteries and both a resistive index (RI) and pulsatility index (PI) are readily calculated. From a simplistic viewpoint, flow with a high PI is common with a benign tumor, while a low PI value suggests a malignancy. These indices are used together with other imaging findings.

The uterine arteries are assessed using a transperineal approach. No significant differences in PI should be detected between the transperineal and endovaginal routes. Likewise, no differences should be evident between endovaginal color Doppler imaging and color Doppler energy in assessing ovarian blood flow or detecting tumors.

Few studies have evaluated the role of laparoscopic US. In women undergoing both endovaginal US and laparoscopic US, the latter revealed additional morphologic detail, better defined the adnexal masses, and detected more adnexal lesions than endovaginal US (4).

Magnetic Resonance Imaging

Magnetic resonance has evolved into the imaging modality of choice for the study of the female pelvis. The relatively high cost of MRI is generally cited as the reason it is currently not used more often as a screening examination. Nevertheless, a number of studies have concluded that MRI is superior to CT and US in evaluating neoplasms and other gynecologic conditions, and future MR application in gynecologic disorders will undoubtedly increase. Magnetic resonance imaging is useful in women with primary amenorrhea both to detect congenital anomalies and as an aid for surgical planning. It provides the best results if the protocol is tailored to a specific question to be answered. Aside from possible screening, the trend is away from set generalized protocols. Endovaginal and endorectal coils are used only if advantageous for a specific question. Coronal T2-weighted images are very useful, especially in uterine evaluation. In particular for cystic lesions, fluid signal intensity is often expressed relative to the signal intensity of urine.

Magnetic resonance hysterography using saline injection has been proposed, but similar to US, a possibility of intraperitoneal malignant cell dissemination exists in a setting of endometrial cancer.

One limitation of pelvic MRI is the lack of contrast differentiation between bowel and adjacent soft tissue structures. Prior administration of an oral contrast agent is helpful. Positive oral contrast agents are commonly used, although a negative agent tends to identify bowel wall and adjacent structures better. A suspension of superparamagnetic iron oxide particles (a negative oral contrast agent) shows promise in differentiating bowel loops from adjacent structures. Intravenous contrast-enhanced MRI visualizes normal ovarian and uterine anatomy. The uterus normally enhances several seconds before the cervix. Some studies suggest that T2-weighted images are superior to postcontrast T1-weighted images in evaluating both normal and abnormal pelvic structures, although most investigators believe that contrast-enhanced MRI is superior to precontrast MR in characterizing and differentiating pelvic tumors.

Magnetically labeled water perfusion imaging is a possible noncontrast technique for evaluating uterine blood flow. The use of short inversion delay times reveals the uterine artery dividing into its branches (5); longer inversion delay times reveal intracervical branching, followed by tissue enhancement.

Proton MR spectroscopy, although in clinical use in evaluating brain tumors, is rarely employed in gynecologic practice. This spectroscopic technique detects tumor metabolites, provided that a tumor is sufficiently large to be imaged. Single-voxel proton MR spectroscopy of pelvic tumors identifies a characteristic lactate signal in both malignant and some benign tumors (6); a signal from choline-containing compounds was detected only in solid tumors. The presence of lactate signifies anaerobic glycolysis. A high lipid peak is evident in tumors containing a high fat content, such as dermoid cysts.

Scintigraphy

Pelvic scintigraphy occasionally detects a hypervascular uterus. In general, such a blush represents increased uterine vascularity during the secretory and menstrual phases; a similar

blush during earlier phases should be considered abnormal.

Carbon-11-methionine is used as a positron emission tomography (PET) tracer. Preliminary studies suggest that benign or borderline malignant ovarian neoplasms do not accumulate C-11-methionine while carcinomas evidence significant uptake; in some patients this study thus appears useful in differentiating benign from malignant ovarian neoplasms.

Malignant ovarian tumors show 2-[18F]-fluoro-deoxy-D-glucose (FDG)-PET uptake. The limitations are that inflammatory processes and endometrial and follicular cysts also have an affinity for FDG, while borderline carcinomas tend to be false negative. Intrauterine accumulation of this agent occurs during menstruation. In general, FDG-PET is more helpful in detecting recurrent ovarian carcinoma.

Radioimmunoscintigraphy has a role in detecting the spread of ovarian cancer. A common agent used is indium-111–satumomab pendetide (OncoScint)-labeled antibody to tumor-associated antigen.

Biopsy

Endovaginal US-guided biopsy and drainage are established diagnostic and therapeutic procedures. Most complications are self-limiting and consist of infection and hemorrhage.

Congenital Abnormalities

Müllerian Duct Anomalies

Bilateral fallopian tubes develop from Müllerian (paramesonephric) ducts, with the fused caudal ductal segments forming the uterus, cervix, and upper part of vagina. The lack of development or a müllerian duct fusion defect results in a specific developmental abnormality. Several müllerian duct anomaly classifications have been proposed; the one used here is a classification proposed by Buttram and Gibbons in 1979, and adopted by others since then (Table 12.1).

Congenital uterine malformations include agenesis, unicornuate, bicornuate, and septate uterus. The prevalence of these malformations is <5%. Most affected women are not at an increased risk for sterility; however, they have a higher rate of spontaneous abortion and premature births compared to those with a normal uterus. Also, these women are at an increased risk for urinary tract abnormalities, including renal agenesis.

Table 12.1. Müllerian duct abnormality classification

- I. Segmental müllerian agenesis or hypoplasia
  - A. Vaginal
  - B. Cervical
  - C. Fundal
  - D. Tubal
  - E. Combined
- II. Unicornuate
  - A. With rudimentary horn
    - With endometrial cavity
      - Communicating
      - Noncommunicating
    - Without endometrial cavity
  - B. Without rudimentary horn
- III. Didelphys
- IV. Bicornuate
  - A. Complete
  - B. Partial
  - C. Arcuate
- V. Septate
  - A. Complete
  - B. Incomplete
- VI. DES related

Source: Adapted from Buttram and Gibbons (7).

Imaging

Congenital uterine malformations are commonly studied with hysterosalpingography, although US is often the first imaging modality employed and is believed by some to be more sensitive. Three-dimensional US is useful in the study of müllerian duct abnormalities, achieving a sensitivity and specificity of close to 100% in defining these abnormalities. Nevertheless, MRI has evolved as the preferred imaging modality in evaluating suspected müllerian duct abnormalities. In particular, MRI is useful in differentiating a bicornuate uterus from a septate uterus. It aids in locating gonadal tissue

not visualized by US and is useful in identifying ambiguous genitalia.

Coronal T2-weighted MR images of the uterus are easier to interpret if their oblique axis is placed parallel to the endometrial canal. The degree of obliquity can be estimated from sagittal images.

Prior surgery makes interpretation of imaging findings more difficult; this is especially true with MRI.

Agenesis/Hypoplasia

The Mayer-Rokitansky-Küster-Hauser (MRKH) syndrome consists of congenital absence of the vagina and uterus and represents complete cessation of müllerian duct development; this syndrome is believed to be due to a deficiency of estrogen and other receptors. Ovarian neoplasms develop in young girls in association with this syndrome.

Some authors divide this syndrome into a typical or isolated form, consisting of symmetrical nonfunctioning muscular buds (müllerian duct remnants) and normal fallopian tubes, and an atypical, more generalized form consisting of aplasia of one or both buds and with or without fallopian tube dysplasia. Some duct remnants are cystic. Differentiation between the two forms is made on the basis of laparoscopic findings, although MRI can often suggests a diagnosis. The atypical form is associated with skeletal, renal, and ovarian abnormalities. Lack of adequate müllerian duct development leads to vaginal agenesis; with a functioning uterine anlage, MRKH syndrome results in hematometra. With a laparoscopic finding of an atypical MRKH syndrome, appropriate imaging is reasonable, often beginning with MR (Fig. 12.1).

A complex of renal dysgenesis, Gartner's duct cyst, and ipsilateral müllerian duct obstruction in 10 girls resulted in a dilated Gartner's duct protruding into the bladder and presenting as a ureterocele in some and extending posterior to the bladder in others (8); all had unilateral müllerian duct obstruction.

Agenesis of a portion of the müllerian ducts and congenital absence of the uterus and vagina is also found in male pseudohermaphrodites. Occasionally genitography is helpful in defining the underlying anatomy.

The appearance of a hypoplastic uterus is that of a normal uterus except for a smaller size. This condition is not common. A small uterus is also seen in such conditions as prior diethylstilbestrol (DES) exposure.

Isolated fallopian tube agenesis is rare and is associated with maldevelopment of mesonephric and paramesonephric ducts, possibly on an ischemic basis. Hysterosalpingography simply reveals fallopian tube nonfilling. Tubal obstruction due to other causes, including prior fallopian tube torsion causing hemorrhage and eventual reabsorption, must be excluded.

Unicornuate Uterus

Abnormal unilateral development of one of the Müllerian ducts results in an unicornuate uterus. These women have a high prevalence of associated urinary tract abnormalities, including an ectopic kidney, renal agenesis, double renal pelvis, horseshoe kidney, and medullary sponge kidney. They also suffer from a high spontaneous abortion rate and a high rate of ovum implantation in a rudimentary horn and subsequent rupture during pregnancy.

Hysterosalpingography reveals a fusiform-shaped uterus tapering to its connection with the single fallopian tube. The uterus is displaced toward the side of the functioning tube. When performing this study, one must be careful not to confuse a bicornuate or septate uterus with a unicornuate one. Even if hysterosalpingography does demonstrate what appears to be a unicornuate uterus, a contralateral noncommunicating uterine horn may still be present but simply not communicate with the main uterine cavity, a finding not detected with hysterosalpingography. Such a rudimentary noncommunicating horn is detected by CT, US, or MRI, although US may be nonspecific, defining only a single cavity but without providing sufficient detail. Magnetic resonance imaging is the procedure of choice to provide both uterine and adnexal region anatomic details.

A pregnancy in a noncommunicating rudimentary horn is associated with a high rate of perforation and thus, if detected, resection of this cavity is generally performed. Such a cavity also predisposes to endometriosis, presumably due to retrograde expulsion of menstrual products.

Figure 12.1. Uterine agenesis (Mayer-Rokitansky-Küster-Hauser syndrome.] A: Sagittal T2-weighted image shows absence of uterus and vagina. B: Coronal image confirms left renal agenesis. (*Source:* Imaoka I, Wada A, Matsuo M, Yoshida M, Kitagaki H, Sugimura K. MR imaging of disorders associated with female infertility: use in diagnosis, treatment, and management. RadioGraphics 2003;23:1401–1421, with permission from the Radiological Society of North America.)

Didelphys

A didelphic uterus results from fusion failure of müllerian duct caudal segments (Fig. 12.2). In complete didelphys each uterine cavity has a separate cervix and a variable septum is present in the vagina (Figs. 12.3 and 12.4). Some women also have associated renal agenesis, dysplasia, or hypoplasia, and an ectopic ureter to Gartner's duct cysts. A duplicated uterus can be occluded unilaterally. Girls with unilateral occlusion of a duplicated uterus develop hydrocolpos, hydrometrocolpos, hematometrocolpos, and hematosalpinx.

During hysterosalpingography uterus didelphys is confused with a unicornuate uterus if only one of the uterine cavities is injected with contrast. Magnetic resonance imaging is the examination of choice in defining these abnormalities and providing preoperative guidance (Figs. 12.5 and 12.6). It should be noted that a congenital anomaly of cloacal exstrophy is also associated with two vaginas and hemiuteri.

Bicornuate

It is necessary to differentiate between a bicornuate and a septate uterus because of the differences in pregnancy outcome and because therapeutic approaches for these two conditions are different. A bicornuate uterus tends to be associated with a normal pregnancy while abortion rates with a septate uterus are about double that of a bicornuate uterus.

Obstruction of one uterine horn leads to a unilateral hematometra. A variant is a partial vaginal septum and resultant hematometrocolpos. Complicating the diagnosis is that an occasional bicornuate uterus reveals unilateral intermittent occlusion.

During hysterosalpingography a bicornuate uterus resembles a septate uterus. It is also similar to uterus didelphys, except that a bicornuate uterus has only one cervical os. Measurement of the angle of divergence between the two uterine cavities during hysterosalpingography has been used in an attempt to differentiate between a bicornuate and a septate uterus. A

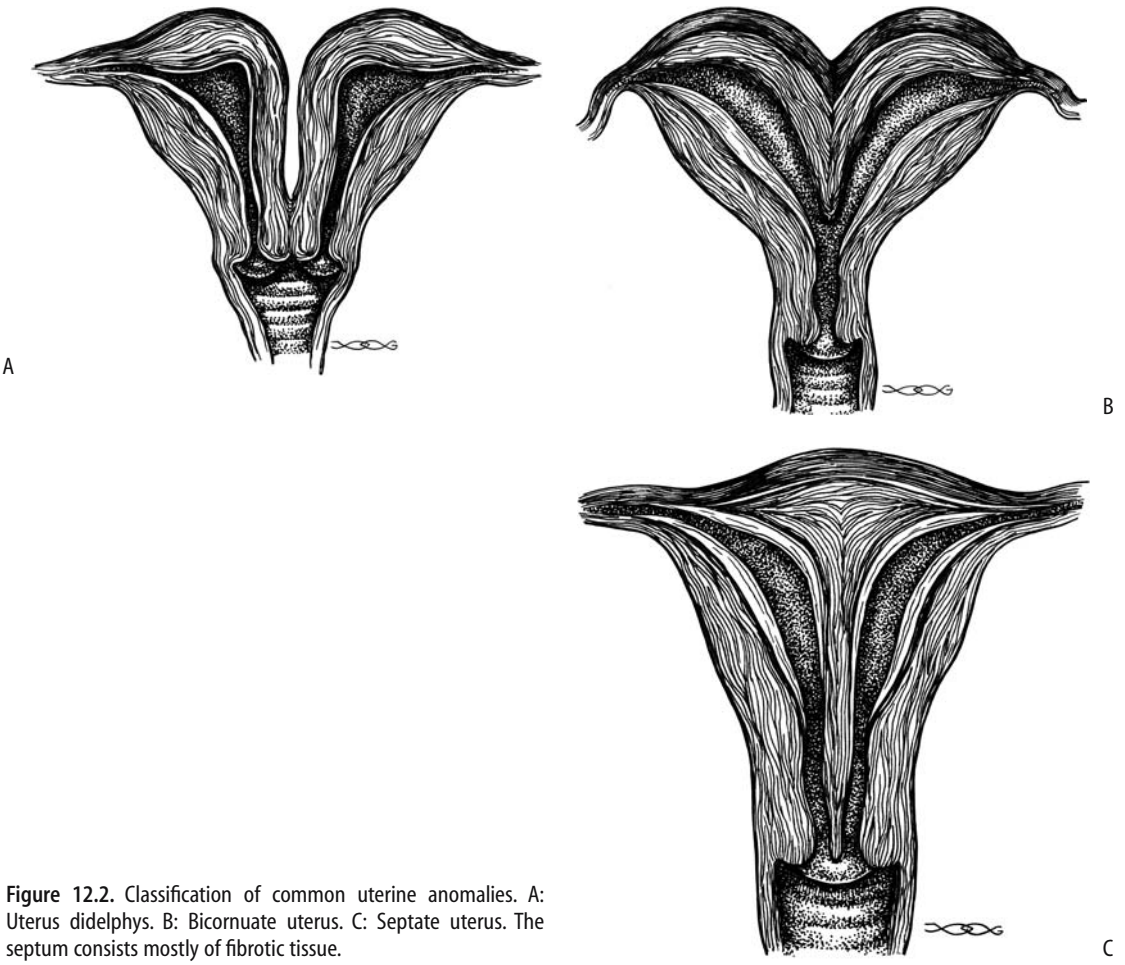

Figure 12.2. Classification of common uterine anomalies. A: Uterus didelphys. B: Bicornuate uterus. C: Septate uterus. The septum consists mostly of fibrotic tissue.

septate uterus is suggested with an angle less than 75 degrees, while with an increased angle a bicornuate uterus is more likely. Nevertheless, considerable overlap exists between these two conditions; MR provides better differentiation. Magnetic resonance imaging has a sensitivity and specificity similar to those of laparoscopy in this differential and is currently the preferred procedure (Fig. 12.7).

Magnetic resonance imaging defines both the outer and inner uterine contours, and it is the external contour that is most useful in differentiating a bicornuate from a septate uterus. The external fundal outline is convex outward in the normal uterus, or it is flat, or it has a short indentation in a septate uterus, and it is deeply indented (fundal notch) in a bicornuate uterus, an abnormality that cannot be detected by hysterosalpingography. The intercornual distance (maximal lateral extent between the high signal endometrium) is normal in a septate uterus and is increased in a bicornuate uterus.

An arcuate uterus should be considered to represent either a mild form of bicornuate uterus or a normal variant. It is usually associated with normal term gestation.

Septate

A septate uterus occurs when the septum of the fused müllerian ducts fails to absorb. The residual septum ranges from complete to partial and consists of fibrous tissue, myometrium, or both. Because the müllerian ducts have already fused, the external uterine surface is normal, distin-

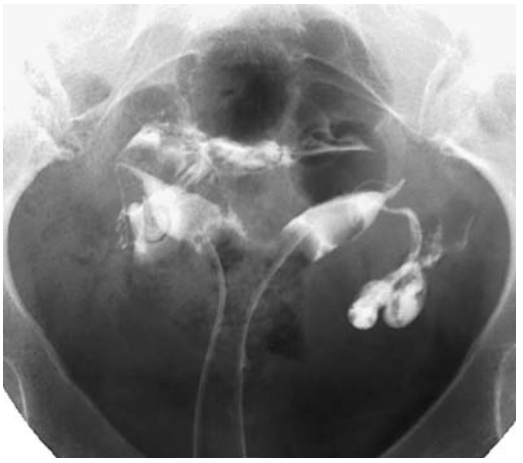

Figure 12.3. Uterus didelphys. Two uterine cavities are evident. The patient had a previous vaginal septum resected.

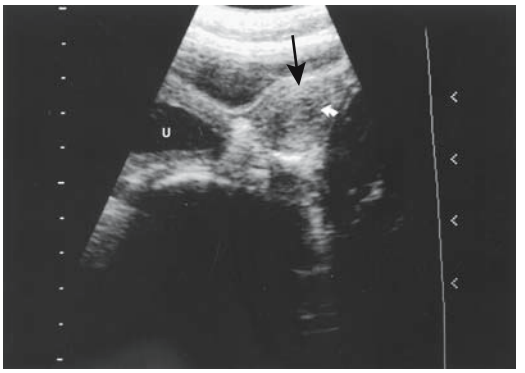

A

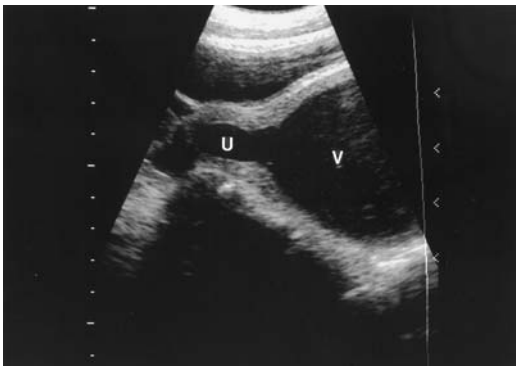

B

C

Figure 12.4. Duplicated uterus with an obstructed hemivagina in a 12-year-old girl. A: Transverse ultrasonography (US) scan identifies a dilated right uterus (u) and a normal left uterus (curved arrow). B: A dilated uterine cavity (u) and distended vagina (v) are identified by longitudinal US of the obstructed right side. C: An endometrial cyst (c) is also present adjacent to the right ovary. (*Source:* Garel L, Dubois J, Grignon A, Filiatrault D, Vliet GV. Ultrasonography of the pediatric female pelvis: a clinical perspective. Radiographics 2001;21: 1393–1407, with permission from the Radiological Society of North America.)

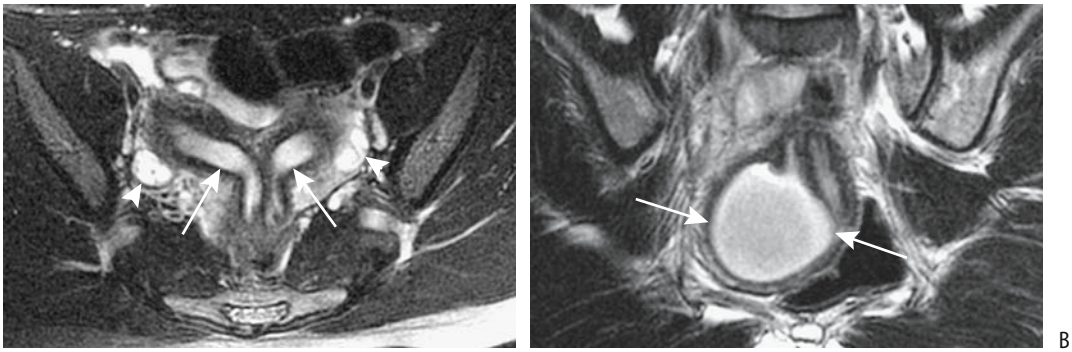

Figure 12.5. Uterus didelphys with obstructed hemivagina. A: Transverse T2-weighted MRI identifies two uteri (arrows), two cervices, and both ovaries (arrowheads.] B: Coronal T2-weighted image shows a hematocele (arrows) due to an obstructed right hemivagina. (*Source:* Imaoka I, Kitagaki H, Sugimura K. MR imaging associated with female infertility. Nichi-Doku Iho 2000;45:440–450, with permission from Nihon Schering K. K.)

guishing this abnormality from a bicornuate uterus.

Magnetic resonance imaging is helpful in identifying this condition (Figs. 12.8 and 12.9). Nevertheless, both US and MRI most often misdiagnose a septate uterus as either a normal or bicornuate uterus. The MR septal signal intensity varies depending on its composition and often is not a reliable indicator in differentiating a septate from a bicornuate uterus; on T2-weighted images a fibrous septum is seen as a hypointense region, while a myometrial septum has a signal intensity similar to myometrium.

Generally hysteroscopic metroplasty is performed for a septate uterus, with preservation of future vaginal delivery.

Diethylstilbestrol-Related Abnormalities

Patients who have been exposed in utero to DES develop a number of gynecologic abnormalities, including cervical stenosis, various uterine

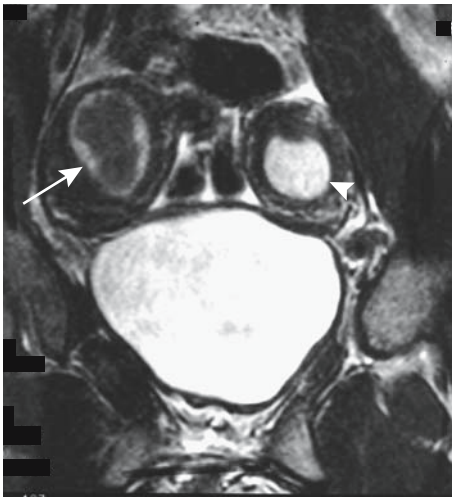

Figure 12.6. Didelphys in a 13-year-old. Right uterus (arrow) is hypointense due to blood and left uterus (arrowhead) hyperintense due to fluid and secretions. (*Source:* Burgener FA, Meyers SP, Tan RK, Zaunbauer W. Differential Diagnosis in Magnetic Resonance Imaging. Stuttgart: Thieme, 2002, with permission.)

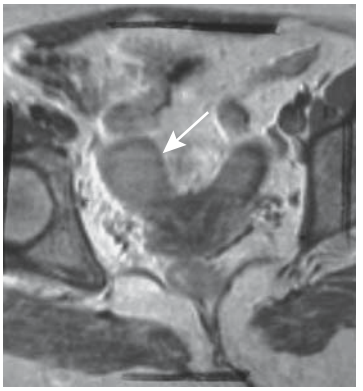

Figure 12.7. Endometrial carcinoma in a bicornate uterus. A transverse oblique MR image identifies an intrauterine tumor (arrow). (*Source:* Burgener FA, Meyers SP, Tan RK, Zaunbauer W. Differential Diagnosis in Magnetic Resonance Imaging. Stuttgart: Thieme, 2002, with permission.)

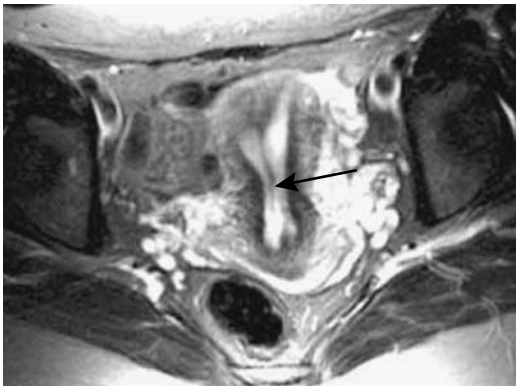

Figure 12.8. Septate uterus. Transverse T2–weighted image identifies a septum in the uterine cavity (arrow). The external uterine outline is normal. (*Source:* Imaoka I, Kitagaki H, Sugimura K. MR imaging associated with female infertility. Nichi-Doku Iho 2000;45:440–450, with permission from Nihon Schering K. K.)

development abnormalities, and distorted fallopian tubes. Clinically, DES exposure is associated with subsequent infertility and ectopic pregnancies.

Hysterosalpingography in these patients shows a narrow irregular cervix and a small irregular uterine cavity. The uterus may have a T-shape. Currently hysterosalpingography is the preferred imaging modality in evaluating DES-related abnormalities.

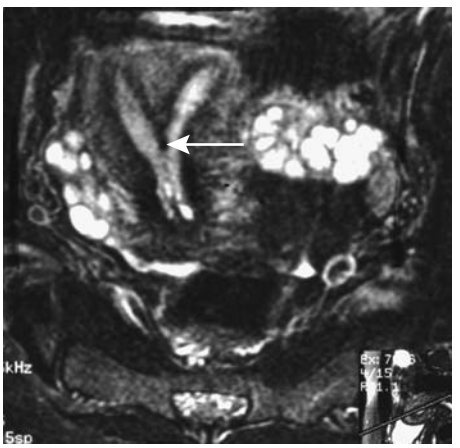

Figure 12.9. Septate uterus (arrow) identified on T2-weighted transverse oblique MR image. (*Source:* Burgener FA, Meyers SP, Tan RK, Zaunbauer W. Differential Diagnosis in Magnetic Resonance Imaging. Stuttgart: Thieme, 2002, with permission.)

Sex Differentiation Abnormalities

These abnormalities are usually subdivided into genetic disorders, gonadal disorders, and phenotypic sex differentiation disorders. Unless testicular tissue is present, a fetus develops into a female or a variant of a female. Genetic and hormonal evaluations are needed to define the underlying abnormalities in many of these infants and imaging has a limited role. Ultrasonography is helpful in outlining internal genital anatomy, although MRI provides better resolution.

Gonadal Disorders

Gonadal disorders include true hermaphroditism and gonadal dysgenesis (*Turner's syndrome*). Both ovarian and testicular tissue is present in true hermaphrodites. For instance, an ovotestis can contain spermatogenesis in testicular tissue.

Patients with Turner's syndrome have their gonads replaced by connective tissue. The incidence of malignancy is increased in this tissue.

Phenotypic Differentiation Disorders

Phenotypic abnormalities develop in a setting of several endocrine disturbances. Female pseudohermaphrodites have a normal female XX karyotype and normal internal female genitalia, but have virilizing external genitalia due to excess androgen from a number of sources. The most common etiology is congenital adrenal hyperplasia. Ultrasonography or MRI should confirm normal internal genitalia.

Male pseudohermaphrodites have a normal male XY karyotype, and testicular tissue is present, but the internal or external genitalia is ambiguous. Imaging should exclude the presence of ovaries and uterus.

Testicular feminization is a rare sex-linked disorder caused by androgen receptor gene mutations. Peripheral insensitivity to androgen leads to female external genitalia, undeveloped müllerian duct structures, androgen-producing testes, and a male genotype. As a result, the proximal third of the vagina, cervix, uterus, and fallopian tubes are either absent or rudimentary. The sexual orientation is female. Testes are undescended. Ultrasonography identifies a blind-ending vagina and no uterus or adnexal

structures; MRI also diagnoses uterine agenesis and detects undescended testes, often within or just below the inguinal canal; the testes are smaller and more hypointense than normal on T1-weighted images and isointense on T2-weighted images.

Testicular feminization should be suspected in girls having ambiguous genitalia and an inguinal hernia. Later these patients have primary amenorrhea. In distinction to male cryptorchidism, the incidence of testicular neoplasms in patients with testicular feminization begins to increase only after the age of 30 years. Thus in the complete form of testicular feminization gonadectomy can be delayed.

Cloacal Malformation

In a cloacal malformation the rectal, urinary, and genital tracts communicate and exit through a common perineal opening, or cloaca. This rare anomaly occurs only in girls, develops early in the embryo, and varies in appearance depending on how the connecting tracts join.

A diverting colostomy is generally performed initially. A contrast study of the cloaca helps define the underlying anatomy. Using this study as a guide, a catheter can be advanced into the bladder and a cystogram performed. Injection into the distal limb of the colostomy should define the rectal communication.

Diastasis of the symphysis pubis is common in these girls. Sacral and spinal chord abnormalities are common.

McCune-Albright Syndrome

A combination of café-au-lait spots, fibrous dysplasia, and precocious puberty is found in McCune-Albright syndrome. Ovarian follicular cysts are a common finding.

Vagina and Urethra

Gartner's duct cysts originate from mesonephric (wolffian) duct remnants that fail to reabsorb. Most occur parallel and anterolateral to the vagina and are small and asymptomatic, although occasionally a large cyst is encountered. An occasional one visualizes during hysterosalpingography if it communicates with the uterus.

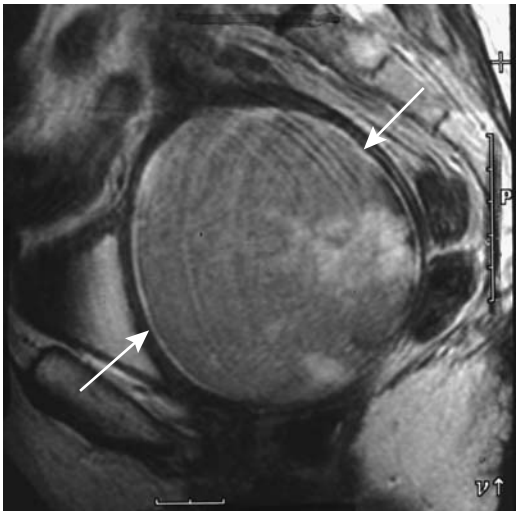

Figure 12.10. Pyometra secondary to an obstructed cervix. Sagittal T2-weighted MR image reveals a greatly distended uterus (arrows). Blood and debris account for the slightly hyperintense appearance. (*Source:* Burgener FA, Meyers SP, Tan RK, Zaunbauer W. Differential Diagnosis in Magnetic Resonance Imaging. Stuttgart: Thieme, 2002, with permission.)

Vaginal obstruction results in hemato (metro)colpos or hydrocolpos. At times the obstruction evolves into a large pelvic soft tissue tumor, evident both clinically and with imaging. Obstructions range from imperforate hymen to a vaginal septum. With hematometra, cervical dysgenesis is also in the differential. Both US and MR are useful in detecting these abnormalities (Fig. 12.10). Endorectal US is a viable alternate for suspected vaginal abnormalities if endovaginal US is not feasible. Transperineal US should detect a vaginal septum.

Magnetic resonance imaging of hematocolpos reveals a high signal intensity blood collection on both T1- and T2-weighted images and helps establish whether the distention extends into the fallopian tubes.

Congenital urethral valves are rare in female infants, with most distal urethral obstructions being secondary to a mucous membrane. Urethral duplication is also rare.

Trauma

Blunt abdominal trauma results in uterine rupture, especially during pregnancy. Most are seat-belt injuries; traumatic rupture involves the

fundus, and fetus and placenta extrude into the maternal abdomen. Uterine rupture during the second or third trimester of pregnancy should be diagnostic with US; an empty uterus is identified. Computed tomography can also detect uterine rupture and an intraabdominal fetus.

Uterine rupture during labor is associated with prior hysteroscopy, prior repeated curettage, and perforation. Spontaneous uterine rupture during pregnancy is a complication of Ehlers-Danlos syndrome type IV.

Urethral rupture due to pelvic fracture is rare in women (9). If present, an associated vaginal tear is often also found.

Ultrasonography can detect vaginal foreign bodies in young girls. The echogenicity and acoustic shadowing of a foreign body varies. At times US detects an indentation of the posterior bladder wall.

Acute Gynecologic Conditions

Imaging of acute gynecologic conditions are discussed in more detail in their respective sections in this chapter. Not uncommonly these conditions are in a differential diagnosis of an acute abdomen (discussed in Chapter 14).

Computed tomography in 100 consecutive nonpregnant women suspected of having appendicitis or an acute gynecologic condition achieved a 100% sensitivity and 97% specificity in diagnosing appendicitis and 87% sensitivity and 100% specificity for acute gynecologic condition (10).

Torsion

Ovary

Clinical

Torsion, or a twist of the ovary around its pedicle, leads to venous stasis, edema, and eventual ischemia. Although isolated ovarian torsion does occur, usually it is associated with fallopian tube torsion. It can occur during pregnancy. An ovarian cyst or other tumor, regardless of etiology, predisposes to torsion (gynecologists and urologists prefer the terms *severe torsion* or even simply *torsion* to what gastroenterologists would label as *volvulus* for an equivalent condition in the gut).

Ovarian torsion occurs most often in girls and young women but has developed in neonates. Depending on the degree of twist, the onset of pain ranges from gradual to sudden. Severe pain is a common presentation of complete torsion. Clinically, acute right ovarian torsion mimics appendicitis. A not uncommon scenario consists of acute appendicitis being suspected in a young girl, but subsequent laparotomy detects a torsed and necrotic ovary.

Chronic partial ovarian torsion is rare. Intermittent venous obstruction and edema result in massive ovarian enlargement.

Neglected amputated ovaries secondary to ovarian torsion can evolve into calcified cystic tumors which became attached to adjacent structures by a pedicle containing vessels.

Salpingo-oophorectomy is often performed for ovarian torsion. Occasionally prophylactic oophoropexy or even laparoscopic shortening of the uteroovarian ligament is feasible for intermittent torsion.

Imaging

Imaging shows a large, irregular adnexal tumor ranging from solid to thick-walled and cystic (Figs. 12.11 and 12.12). Any cystic component,

Figure 12.11. Ovarian torsion in an 11-year-old girl with pelvic pain. Computed tomography reveals a retrovesical tumor. Normal gynecological structures were not identified. An appendiceal abscess was initially suspected. (Courtesy of Luann Teschmacher, M.D., University of Rochester.)

when present, represents engorged follicles. Some hemorrhage is common and, if untreated, eventual necrosis ensues.

Echogenicity of a torsed ovary varies considerably. A US finding of a twisted vascular pedicle is suggestive of ovarian torsion but this is not always present. Doppler US suggests the degree of viability of a torsed ovary. With a nonviable ovary, Doppler US shows absent arterial and venous flow centrally, low-velocity arterial flow in the periphery, or absent or even reversed diastolic arterial flow. The lack of blood flow within a twisted vascular pedicle implies a nonviable ovary. The presence of internal arterial flow has prognostic implications because some of these can be treated successfully with laparoscopic untwisting.

Occasionally US detects an engorged fallopian tube. Cul-de-sac fluid is a common but nonspecific finding. Ultrasonography is not foolproof, however. Transabdominal US in two girls with abdominal cysts revealed a "double wall" sign, and duplication cysts were diagnosed (11); surgery revealed ovarian cysts, torsion, and hemorrhage within the cyst wall.

In addition to detecting engorged blood vessels in ovarian torsion, MR often also detects uterine deviation to the twisted side. The lack of CT or MRI contrast enhancement of the involved ovary signifies arterial compromise. The wall of any associated cystic tumor is edematous and thickened. Any superimposed hemorrhage modifies the imaging appearance.

A rare finding with torsion involving an ovarian tumor is presence of intravascular gas within the tumor. This gas probably represents oxygen released from trapped oxyhemoglobin.

Fallopian Tube

Isolated fallopian tube torsion can develop in the absence of prior surgery or infection, but it is rare. Prior adhesions, inflammation, or ovarian disease predisposes to torsion. Possible congenital associations include a long mesosalpinx or mesovarium. Clinically, these patients have severe lower abdominal pain and signs of peritoneal inflammation.

Ultrasonography reveals an adnexal tumor and also a hydrosalpinx.

Uterus

Uterine torsion consists of the long uterine axis being rotated more than 45 degrees. Some of these torsions involve a uterine myoma.

Torsed uterine leiomyomas tend to be hyperintense on T2-weighted MRI once ischemia develops.

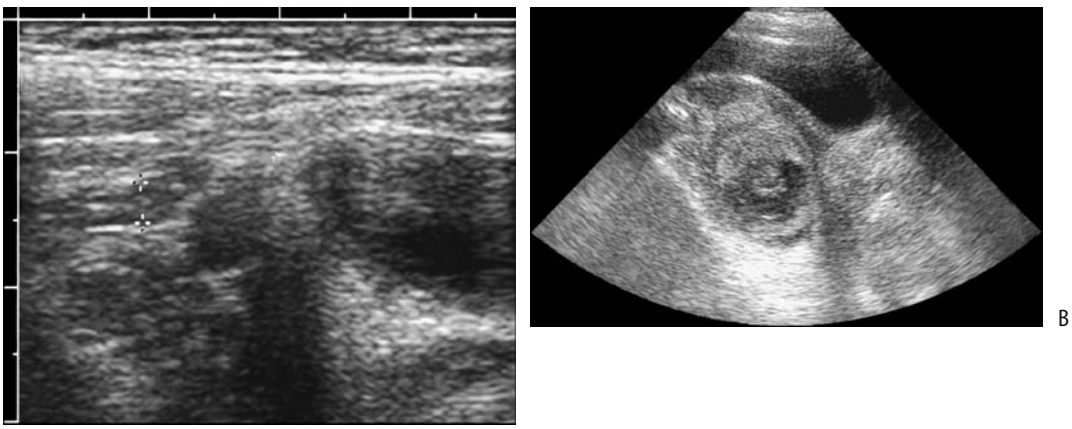

Figure 12.12. Ovarian torsion. A: US in a young girl with suspected appendicitis identified a normal appendix (cursors). B: Further pelvic US detected a tumor in the pouch of Douglas and cul-de-sac. Surgery revealed a left fallopian tube and ovary torsed 720 degrees. (Courtesy of Luann Teschmacher, M.D., University of Rochester.)

Infection/Inflammation

Pelvic Inflammatory Disease

Pelvic inflammatory disease (PID) is most often bacterial in origin and most often bilateral. Clinically, it mimics an acute abdomen and suggests appendicitis or bowel perforation. Acute salpingitis typically manifests as a pyosalpinx or hydrosalpinx. The infection spreads and evolves into either peritonitis or a tubo-ovarian abscess. Peritonitis ranges from diffuse to focal, occasionally localizing around the liver (Fitz-Hugh Curtis syndrome is discussed in Chapter 14). Gonococcal ovarian infection is rare. The clinical presentation is nonspecific.

Hysterosalpingography is contraindicated during suspected acute salpingitis. Endovaginal US often identifies free fluid in the cul-de-sac but endovaginal US has a low sensitivity in identifying fallopian tube intraluminal fluid or even a developing tuboovarian abscessees. Either CT, US, or MRI should detect a tuboovarian abscess or hydrosalpinx once it is established. A hydrosalpinx is common, usually bilaterally. Superficially, the imaging appearance of a pyosalpinx or hydrosalpinx mimics a dilated loop of bowel. The wall of a pyosalpinx tends to enhance considerably with contrast. Endovaginal Doppler US reveals a low resistive index in presence of severe infection.

Magnetic resonance imaging is not often performed for suspected PID but it has considerable potential. MRI findings include a fluid-filled tube, pyosalpinx, tubo-ovarian abscess, polycystic-appearing ovaries, and pelvic fluid. In one study, MRI sensitivity in detecting PID was 95% and specificity 89% and, for comparison, endovaginal US sensitivity was 81% and specificity 78% (12).

One sequela of scarring during healing is tubal obstruction and resultant hydrosalpinx formation.

Abscess

Among less common causes of a tubo-ovarian abscess is endovaginal oocyte retrieval for in vitro fertilization. Clinically, these patients present with pain and often a palpable tumor.

The CT and US findings of a tubo-ovarian abscess, regardless of cause, are similar to those of other intraabdominal abscesses. Often an abscess consists of a complex, thick-walled, cystic adnexal tumor having no specific characteristics. Some abscesses are associated with a hydrosalpinx. The presence of gas, although uncommon, is almost pathognomonic of an abscess. Most of these abscesses form discrete tumors, with an occasional one being diffuse and having an appearance similar to focal peritonitis.

Ovarian abscesses range from hypointense to hyperintense on T1-weighted images. A thin hyperintense rim is common. Most abscesses are hyperintense on T2-weighted images. Many contain linear stranding.

Some of these abscesses obstruct an adjacent ureter, and imaging should thus also evaluate for any hydroureter. The presence of adenopathy is variable.

The imaging appearances of a tubo-ovarian abscess and a necrotic tumor overlap. The differential often also includes an appendiceal or Crohn's abscess.

Pelvic abscesses are drainable using an endovaginal US-guided trocar and catheters (13).

Tuberculosis

Adnexal involvement with tuberculosis is uncommon. A typical pattern of spread in affected individuals is from fallopian tubes to the uterus, with resultant infertility.

Tubal calcifications develop with tuberculous involvement. These are seen as linear or somewhat nodular calcifications along the fallopian tubes. Generally both tubes are involved. The presence of such calcifications, regardless of how they are detected, should suggest tuberculosis.

Hysterosalpingography identifies fallopian tube occlusion or narrowing, with the tube lumen having an irregular, beaded appearance. Outpouchings tend to mimic salpingitis isthmica nodosa. Any contrast spilled from the fimbriated tubal ends is loculated. A hydrosalpinx develops in some. Extensive fistulas are not common. Endovaginal US reveals fallopian tube wall thickening. Any hydrosalpinx is readily detected.

Uterine involvement leads to synechiae varying in size and extent; these synechiae can

be identified if intrauterine fluid is instilled. An eventual decrease or even obliteration of the uterine cavity ensues. Endovaginal US reveals a thickened and inhomogeneous endometrium. Occasionally endometrial aspiration biopsy in a woman with bleeding yields necrotic debris with focal granulomas and even acid-fast bacilli.

Cervical tuberculosis can mimic a carcinoma; a biopsy should be diagnostic.

Actinomycosis

Pelvic actinomycosis is a chronic infection with the anaerobic gram-positive bacteria *Actinomyces israelii*. This commensal is found in normal body cavities; its growth is promoted by the presence of an intrauterine device. When invasive, it causes a chronic, indolent infection consisting of a soft tissue tumor mimicking a neoplasm. Histology identifies characteristic actinomyces granules.

The imaging findings are often more extensive than the symptoms suggest. A characteristic of this infection is extensive fistulization extending into surrounding structures. Occasionally one of the ureters becomes obstructed.

Two examples serve to illustrate the great mimicry of this infection: Pelvic actinomycosis with secondary liver involvement in a 50-year-old woman initially suggested a pelvic neoplasm with liver metastases (14). Computed tomography and US in a 37-year-old nulliparous woman with an intrauterine device revealed a large right adnexal mass adherent to the uterus and compressing the bladder, a preoperative diagnosis of ovarian cancer was made, and she underwent bilateral salpingo-oophorectomy and total abdominal hysterectomy (15); the resected specimen revealed actinomycosis.

Endometritis/Cervicitis

Among rarer causes of endometritis is infection with *Trichinella spiralis*, at times resulting in small calcifications with trichinella infiltrating the basal endometrium. A rare endometritis evolves into pyometra, perforation, and an acute abdomen.

Most syphilitic cervicitis is evident both clinically and pathologically. Rarely, syphilis presents with a cervical tumor mimicking a carcinoma.

Rarer Infections

Especially in the tropics, colorectal amebiasis can evolve into an amebic rectovaginal fistula. These fistulas heal after definitive therapy.

In endemic areas fallopian tube involvement with *Schistosoma haematobium* infection should be considered. Infected patients have an increased incidence of ectopic pregnancies and eventually develop infertility. Schistosoma eggs are found in the fallopian tubes, resulting in hydrosalpinx and PID.

Ovarian echinococcal infection is rare even in endemic regions, although adnexal involvement is not. Imaging reveals a pelvic cyst, with some cysts containing internal septa or even having an onion skin appearance. With active disease, color Doppler reveals increased peripheral vascularity. In endemic regions a check for hydatid serology appears reasonable.

Salpingitis Isthmica Nodosa

Salpingitis isthmica nodosa is an inflammatory disorder affecting the fallopian tubes and associated with infertility and an increased risk of ectopic pregnancy.

Hysterosalpingography reveals multiple diverticulum-like outpouchings adjacent to the tubal lumen, most often in the proximal isthmic portion of the tube, with the distal isthmus and tubal segments adjacent to uterine cornua less often involved. Fallopian tubes tend to be more convoluted than usual, a difficult subjective finding. Associated hydrosalpinx and tubal occlusion are common. Selective salpingography establishes whether fallopian tubes are patent.

Uterine Synechiae

Intrauterine adhesions, or synechiae, range from focal to diffuse involvement of the uterine cavity. Synechiae are associated with infertility (*Asherman's syndrome*). Most common causes

of Asherman's syndrome are postpartum uterine surgery and termination of pregnancy. Rare causes include infections such as tuberculosis and even schistosomiasis.

Hysterosalpingography identifies synechiae as irregular fixed filling defects within the uterine cavity. A severity grading system is reported (Table 12.2), although the hysterographic findings do not always reflect the hysteroscopic appearance. Most synechiae can be differentiated from polyps because the latter have a smooth round or oval configuration and synechiae are irregular in outline. Occasionally extensive adhesions obliterate the endometrial cavity to the point of preventing filling during hysterosalpingography.

Synechiae are identified with endovaginal US. Sonohysterography reveals synechiae as bridging bands in the fluid-distended uterine cavity.

The fibrous synechiae have a low signal intensity on T2-weighted MRI and are not visualized directly, but MRI is useful in evaluating the uterine cavity above adhesions for the presence of endometrial tissue. A normal endometrium and endometrium-to-myometrium junctional zone are absent on T2-weighted MRI in women with severe Asherman's syndrome.

Operative hysteroscopy consisting of the surgical division of synechiae is the therapy of choice. Video-enhanced endoscopic hysteroscopy is further aided by intraoperative US; such US allows hysteroscopic lysis of adhesions at equivalent distances from the uterine wall, especially in the uterine cornua.

Table 12.2. Hysterographic classification of Asherman's syndrome

Grade	Description
1	Single uterine defect less than one tenth of uterus in size
2	One or more defects occupying less than one fifth of uterus No gross uterine cavity deformity
3	About one third of uterus involved Uterine cavity deformed by adhesions
4	All or most of uterus involved Severe deformity

Source: Adapted from Dykes et al. (16).

An endometrial carcinoma can develop in a setting of intrauterine synechiae.

Pregnancy Related

Normal Pregnancy

Hysterosalpingography is contraindicated during pregnancy. If performed, it reveals an early intrauterine pregnancy as a small sessile tumor.

Ultrasonography

The ability of US to visualize normal ovaries decreases from the first trimester to the second and from the second trimester to the third.

Early US signs of an intrauterine pregnancy include a *chorionic rim sign*, consisting of a hyperechoic rim around an intrauterine fluid collection, and the presence of a double decidual sac. Sensitivities of these two signs for an intrauterine pregnancy are about 60–80%, and specificity approaches 100%.

Endovaginal US can assess the corpus luteum during early pregnancy. Corpus luteum ranges from macrocystic, to microcystic, to noncystic. No correlation exists between corpus luteum size and pregnancy failure, although a decrease in volume between two examinations is associated with a greater risk of nonviable outcome.

A hyperechoic, thick-walled sac within a thickened endometrium suggests an intrauterine pregnancy, although it is insensitive in detecting an early pregnancy. With a positive pregnancy test and endovaginal US evidence of intrauterine fluid but without an embryo or yolk sac, follow-up US is necessary.

Doppler US of the uterine arteries can be obtained by either endovaginal and transabdominal techniques. During early pregnancy, the intrauterine arterial peak systolic velocity and resistive index values recorded transabdominally are lower than the endovaginal ones, but after 28 weeks of gestation the differences narrow.

An abnormal uteroplacental circulation, detected by Doppler US, suggests a spontaneous preterm delivery. An abnormal color Doppler

study of a viable early pregnancy is associated with an increased risk of miscarriage. A uterine artery systolic/diastolic ratio significantly higher than normal later in pregnancy is often found with preterm delivery.

Transperineal US is often used to monitor cervical effacement at the start of labor. Ultrasonography reveals progressive cervical canal shortening and the opening of a funnel-shaped internal os, which gradually extends to the lower cervix and leads to effacement.

Magnetic Resonance Imaging

Magnetic resonance imaging offers a number of advantages in the pregnant patient and fetus. It is used for pelvimetry, because aside from the lack of ionizing radiation, MRI readily outlines the maternal bony pelvis and related soft tissues together with the fetus. A number of MR pelvimetry techniques have been described, most having the goal of decreasing image acquisition time.

Magnetic resonance is a viable alternative for differentiating hydronephrosis of pregnancy from hydronephrosis due to an obstructing stone. Only limited studies are available on the use of gadolinium in pregnancy. Current evidence points to no obvious harm.

Ectopic Pregnancy

An ectopic pregnancy implants either within the fallopian tube or in other locations in the pelvis or abdomen. Intraabdominal pregnancy is discussed in Chapter 14.

Etiology for ectopic implantation is unknown. Previous infection appears to play a role. Women on progestin-only pills are more prone to extrauterine pregnancies than those on combined oral therapy.

A human chorionic gonadotropin (hCG) of >2000 mIU/mL and no US evidence of an intrauterine pregnancy is suggestive of an ectopic pregnancy, although some of these women do have a normal pregnancy. In early pregnancy small amounts of intrauterine fluid detected by US should be interpreted with caution; it is found with both an intrauterine and an ectopic pregnancy.

Some ectopic pregnancies resolve spontaneously. A longer time from the last menstrual period, decreasing β-hCG levels, the absence of gestational sac, and a high ectopic pregnancy resistive index are predictors of spontaneous resolution (17).

Tubal

Clinical

Tubal rupture due to an ectopic tubal pregnancy is treated by salpingectomy. On the other hand, an ectopic tubal pregnancy detected prior to tubal rupture is amenable to laparoscopic microsurgery or other therapy.

An ectopic pregnancy manifests as pain, vaginal bleeding, and an adnexal mass. These findings are nonspecific and are found in a number of other conditions both in the pregnant and nonpregnant woman. A pregnancy test differentiates between these two groups. A tubal pregnancy results in hemosalpinx, bloody ascites, and a complex adnexal mass, findings identified by imaging with varying success rates. A bilateral tubal ectopic pregnancy is extremely rare.

A ruptured ovarian neoplasm in a pregnant woman mimics a ruptured ectopic pregnancy.

Imaging

Transabdominal US is generally performed as an initial examination for a suspected ectopic pregnancy. With a positive pregnancy test, the primary role of US is to detect an intrauterine pregnancy. The significance of not detecting an intrauterine pregnancy is limited, although an ectopic pregnancy is then considered. A definite diagnosis of an ectopic pregnancy is sonographic detection of a live embryo in an extrauterine location, a finding not often made.

Endovaginal US provides additional information in a setting of both an ectopic pregnancy and an intrauterine pregnancy. It is possible to detect an intrauterine pregnancy within several weeks after conception. The *intradecidual sign* consists of a hyperechoic endometrial region in the thickened decidua. This sign, in those with a β-hCG level >2000 mIU/ml, achieved a sensitivity of 88% for diagnosing an intrauterine pregnancy (18). In a typical clinical setting sonographic evidence of an intrauterine

pregnancy essentially excludes an ectopic pregnancy (see Heterotopic Pregnancy, below). An ectopic pregnancy can be missed with endovaginal US, and some practices perform both transabdominal US for an overview and endovaginal US for its higher resolution; occasionally an ectopic pregnancy is detected with transabdominal US but not endovaginal US.

The ovary is a useful landmark when searching for an ectopic pregnancy. With endovaginal US an ectopic tubal pregnancy appears as a ring-like tumor having an anechoic center and a hyperechoic periphery—an *adnexal ring sign*. Although often sought, this sign is not pathognomonic for an ectopic pregnancy. In some patients with a subsequently proven ectopic pregnancy, US will not detect any adnexal tumor or tubal ring. The reverse is also true, namely, the sonographic findings of an ectopic pregnancy can be mimicked by other conditions, for instance, a ruptured ovarian hemorrhagic cyst (19). The presence of intrauterine fluid does not exclude an ectopic pregnancy because such a pregnancy may be associated with a pseudosac.

Published sensitivities and specificities of US in detecting an ectopic pregnancy vary depending on specific criteria used. In general, with a positive pregnancy test and no detectable intrauterine pregnancy, the presence of fallopian tube rings or extraovarian complex tumors has a high specificity and sensitivity for a tubal pregnancy.

In symptomatic pregnant women, an US three-layer endometrial appearance has been described in some women with ectopic pregnancy, but this sign is also seen in other conditions. Small endometrial decidual cysts are also identified in some ectopic pregnancies, but their significance is questionable.

Color Doppler US is believed to add little to a diagnosis of an ectopic pregnancy. Nevertheless, only an occasional ectopic pregnancy has arterial endometrial blood flow, and the presence of endometrial arterial blood flow aids in excluding an ectopic pregnancy.

In general, the presence of an adnexal tumor or intraperitoneal fluid should not be used as a criterion for diagnosing tubal rupture. With a distended tube, blood and an amniotic sac of a tubal pregnancy have different MR signal intensities; bloody ascitic fluid has varying hyperintensity on T1-weighted MR images. An adnexal tumor has a complex signal intensity on both T1- and T2-weighted images.

The therapy of an ectopic pregnancy generally is surgical. As alternate therapy, tubal pregnancies can be managed with local methotrexate injection using abdominal or endovaginal US for guidance. Nevertheless, methotrexate therapy has its own complications, including an acute abdomen and bleeding. Of interest is that hysterosalpingography after methotrexate therapy shows bilateral tubal patency in some of these women.

Cornual

A cornual ectopic pregnancy is rare, occurring in about 2% to 4% of all ectopic pregnancies. Rupture at the implantation site occurs at an advanced gestational age, and resultant severe bleeding is associated with increased maternal morbidity and mortality.

A cornual pregnancy has been successfully treated with methotrexate injection; US and laparoscopy are used for guidance.

Ovarian

An intraovarian ectopic pregnancy is rare. Surgical findings range from a hematoma, to an ovum, to placenta and fetus. Most often implantation is superficial and the ovary can be preserved.

Ultrasonography usually shows a complex nonspecific tumor. Some of these consist of a double hyperechoic structure surrounding a hypoechoic region. Endovaginal US aids in localization.

In the rare combined intrauterine and ovarian pregnancy, the ovarian pregnancy consists of a rapidly growing adnexal tumor and intraperitoneal hemorrhage, and it is not surprising that US cannot distinguish between an intraovarian pregnancy and an ovarian cancer.

Cervical

It has been said (20):

> The majority of obstetricians will never see a cervical pregnancy; the minority who has to treat this pathology wishes to have never seen one.

In one pregnant woman with painless bleeding, US identified no embryonal structures, a retained miscarriage was presumed, and during cervical dilation uncontrollable hemorrhage ensued (20); a total hysterectomy was performed.

Ultrasonography can suggest a cervical pregnancy. However, cervical abortion and even gestational trophoblastic disease occasionally has similar US findings.

Magnetic resonance imaging in women with a cervical pregnancy revealed a poorly marginated heterogeneous tumor that was hyperintense on T1-weighted images (21); it contains markedly enhancing solid components and is surrounded by peripheral enhancement. Postcontrast MR can evaluate the trophoblast blood supply prior to therapy.

Heterotopic Pregnancy

A heterotopic pregnancy consists of both an intrauterine and extrauterine pregnancy. It is a rare entity. The incidence of a heterotopic pregnancy increases in women who have undergone assisted reproduction. The condition can be suspected with endovaginal US by detecting both pregnancies. At times a salpingectomy is feasible on the extrauterine pregnancy, and the intrauterine pregnancy continued to term.

Uterine Rupture

Uterine rupture during labor is not common in the West. It is associated with prior uterine scarring and carries a high fetal death rate. The rare spontaneous rupture of an unscarred uterus occurs mostly in older, multiparous women.

Uterine Dehiscence

Complete uterine dehiscence after cesarean section consists of transmural disruption, while partial dehiscence involves disruption only of the endometrial or serosal layer. Occasionally an anteriorly placed placenta beneath the uterine scar masks dehiscence. In general, CT is unreliable in detecting dehiscence, but preliminary studies suggest that MRI is useful.

Ultrasonography appears useful in assessing the risk of rupture during subsequent pregnancies in women with previous cesarean section. The risk of rupture or dehiscence is related to the thickness of the lower uterine segment and in pregnant women with a previous cesarean section, preoperative US can measure this lower uterine segments. Resultant sensitivity and specificity in predicting dehiscence will vary depending on the assumed lower uterine segment cut-off thickness.

Preliminary study suggests that MRI is useful in detecting uterine dehiscence.

Preeclampsia and Related Conditions

Preeclampsia is characterized by hypertension and proteinuria. Edema develops in some of these women. Preeclampsia leads to multiorgan damage, including placenta, liver, kidneys, and brain; it can lead to eclampsia, and is the primary cause of maternal death in a number of countries.

In women with pregnancy-induced hypertension the HELLP syndrome (consisting of hemolysis, elevated liver enzymes, and low platelets) is a life-threatening, severe complication associated with preeclampsia and eclampsia, but it has also developed after delivery. Pathogenesis appears multifactorial and probably involves genetic and immunologic factors. The coagulation system is activated, and endothelial dysfunction becomes evident, with fibrin deposition in vessels and liver sinusoids. Thrombocytopenia and fibrinolysis ensue with vascular thromboses and emboli. The HELLP syndrome has led to intracerebral hemorrhage and death. Cardiopulmonary and renal complications develop, and these women are at risk of acute renal failure and spontaneous liver rupture with its associated high maternal and fetal mortality. This syndrome is usually treated by prompt delivery.

Ophthalmic artery pulsatility and resistivity indices, measured with Doppler US, decrease in preeclamptic women (compared to normotensive gravid women) (22); these indices increase with progression to severe preeclampsia, suggesting that early vasodilation and late vasospasm are part of the spectrum of preeclampsia.

Doppler US of the umbilical and uterine arteries is useful in preeclamptic women and those with HELLP syndrome. Impaired placen-

tal hemodynamics is common, with one study finding blood flow restriction in at least one uterine artery in a majority of women (23). Women with an abnormal Doppler study before delivery have significantly higher blood pressures than those with a normal predelivery study; likewise, abnormal Doppler US is associated with an increased number of perinatal deaths and significantly higher fetal distress as compared to a normal Doppler study.

Placenta

Dynamic MR reveals early placental enhancement; it has heterogeneous enhancement during the second trimester and evolving into enhanced lobules during the third trimester; normal placental enhancement precedes myometrial en-hancement and it can be differentiated from myometrium.

A placental maturity classification was developed in 1979, based on US findings of placental texture (24); this classification, using a grading scale from 0 to 3, correlates with fetal pulmonic maturity as determined by the lecithin-sphingomyelin ratio. Those with premature placental aging are at increased risk of perinatal complications such as hypertension, oligohydramnios, and delayed intrauterine growth.

A relationship exists between smoking and placental calcifications.

Transabdominal US should detect most placenta previa, with only occasional transperineal or endovaginal US necessary. An MRI can provide substantially similar information, but at the expense of substituting a more complex study for a simpler one.

Placenta membranacea or placenta diffusa results when chorion fails to differentiate. It is associated with bleeding, abortion, and fetal death. Ultrasonography in placenta membranacea reveals total placenta previa covering the uterine wall and containing numerous lacuna.

With placenta increta, chorionic villi invade the myometrium while placenta percreta signifies that the villi penetrated through the myometrium. Both evolve in a setting of uterine scarring such as prior cesarean section, D&C, and other causes. An association exists with placenta previa. Placenta percreta can lead to uterine rupture and an acute abdomen.

Ultrasonography suggests placenta accreta by detecting the absence of the typically visualized retroplacental sonolucent space. Doppler US in placenta percreta reveals placental extension into the myometrium and increased blood flow through the myometrium. Gadolinium-enhanced MRI also differentiates placenta accreta from placenta percreta.

The resultant bleeding with abnormal placentation can be massive and a total hysterectomy required for bleeding control. Hypogastric artery balloon occlusion in several women with abnormal placentation, performed after cesarean delivery but prior to hysterectomy and hypogastric artery ligation, was effective in decreasing blood loss (25).

Placental nontrophoblastic tumors include chorioangioma and teratoma. These tumors are benign and often overlooked, but multiple placental chorioangiomas lead to fetal cardiac failure or anemia. Their presence can be suggested by US.

Antepartum Bleeding

Discussed here are only some of the more unusual causes of pregnancy-related bleeding. Premature delivery and various placental abnormalities, discussed above, are common causes. Most first trimester bleeding is associated with either an ectopic pregnancy or partial placental separation from its myometrial implantation (separation occurring before the 20th week of pregnancy is called abortion and separation after the 20th week *abruptio placentae*). Common causes of bleeding during the last half of pregnancy are placenta previa (low placental implantation) and abruptio placentae.

Transabdominal US may not detect a cause for first trimester bleeding, and in these women endovaginal US, with its better resolution, is more helpful. If detected, a subchorionic hematoma has a crescent appearance elevating the chorionic membrane. Ultrasonography establishes whether a normal-appearing gestational sac is visible. A clot secondary to abruptio placentae often has a similar transabdominal US appearance to normal placenta and thus normal US does not exclude abruptio. At times only an abnormally thick placenta is detected.

Most intraamniotic bleeding is secondary to trauma. It is common after amniocentesis. A rare cause of third trimester bleeding is cervical varices.

Postpartum Bleeding

Retained intrauterine placental tissue postpartum or postabortion is termed a placental polyp. It is associated with massive bleeding, at times months or even years after delivery. Ultrasonography after delivery has low sensitivity in detecting retained trophoblastic tissue; if detected, this tissue appears as a heterogenous, hyperechoic tumor. At times retained fluid is evident. Sonohysterography detects free-floating endometrial tissue, yet the role of endovaginal sonohysterography is not clear in this setting, although it is more sensitive than endovaginal US; it should decrease the number of curettages in women with bleeding.

Magnetic resonance imaging reveals most placental polyps as pedunculated intrauterine tumors. They are hyperintense on T2-weighted images, with blood often surrounding them. Postcontrast, these polyps enhance more than myometrium and appear as a high signal intensity uterine cavity tumor.

Bleeding postpartum is generally managed medically. At times hysterectomy is necessary for unresponsive major bleeding, but arterial embolization should be considered in intractable postpartum bleeding not controlled with vaginal packing and uterotonic drugs. In these patients angiography is useful not only to identify a bleeding site but also to act as a guide for selective embolization of the vessel involved. Embolization controls both immediate and delayed bleeding. Generally multiple arteries are embolized, including uterine, vaginal, ovarian arteries or even a division of the internal iliac arteries. Few complications are encountered with uterine artery embolization, and normal menses resumes in almost all women with obstetric hemorrhage who undergo selective uterine artery embolization (26).

It takes about 7 weeks for the postpartum uterus to involute to its baseline.

The differential diagnosis of a placental polyp includes a choriocarcinoma, although the latter is associated with elevated serum β-hCG levels. A leiomyoma has variable signal intensities. Gestational trophoblastic disease and a uterine arteriovenous malformation are also in the differential.

A rare cause of late postpartum hemorrhage after cesarean section is an aneurysm bleeding into the uterus; angiography not only is diagnostic but also permits therapeutic embolization.

Gestational Trophoblastic Disease

Gestational trophoblastic diseases include a spectrum of disorders ranging from hydatidiform mole (molar pregnancy) to a choriocarcinoma and the rare placental site trophoblastic tumor. They originate from trophoblastic tissue and are believed to be due to abnormal fertilization. Most are located in the uterus, although an ectopic one originates in the ovary and other sites of an ectopic pregnancy.

Hydatidiform Mole

A hydatidiform mole is not a neoplasm, although an occasional one progresses to a persistent trophoblastic neoplasm (see below). A mole can be complete or partial.

A complete molar pregnancy develops when a normal sperm fertilizes an aberrant ovum containing abnormal maternal chromosomes. No viable fetus develops. The placenta contains abnormal chorionic villi and excessive trophoblastic proliferation, with the latter leading to elevated serum β-hCG levels. Following evacuation of a mole, β-hCG levels should gradually return to normal; otherwise continued trophoblastic disease should be suspected.

A partial mole contains a fetus, although usually an abnormal one. A hydatidiform mole can coexist with viable multiple pregnancies. The risk of molar pregnancy is increased at the extremes of reproductive life and in those with a prior mole.

Bleeding and a uterus larger than expected are the most common presentation. Preeclampsia is not uncommon. With current management nearly all of these patients can be cured.

A hydatidiform mole distends the uterine cavity but does not invade the myometrium. Computed tomography reveals a hypervascular tumor, at times containing cystic regions. Either

a diffusely enlarged uterus or a focal tumor is evident. A site of tumor origin needs to be established; at times a sonographically suspected mole turns out to be a mucoid ovarian cyst or even an endometrial carcinoma.

Among 74 women from the New England Trophoblastic Disease Center, US diagnosed a complete hydatid mole in only 10% of patients before the onset of symptoms (27). Ultrasonography of a hydatidiform mole identifies multiple anechoic regions, although this finding is seen only in about 80% of confirmed moles; a fetus is not detected unless a twin pregnancy is present. A partial mole is often not detected.

Magnetic resonance imaging reveals either diffuse uterine enlargement or a focal tumor, loss of normal zonal anatomy, and abnormal uterine vascularity.

Persistent Trophoblastic Neoplasia

Classified under persistent trophoblastic neoplasia complex are invasive mole, choriocarcinoma, and placental site trophoblastic neoplasm. The staging of gestational trophoblastic tumors is outlined in Table 12.3.

Invasive Mole

The presence of chorionic villi and trophoblastic proliferation in the myometrium constitutes an invasive mole. At times invasion is beyond the uterus and is embolic at distant sites. Some moles lead to severe hemorrhage.

Choriocarcinoma

A rare molar pregnancy evolves into a choriocarcinoma (nongestational ovarian choriocarcinoma is discussed later; see Malignant Germ Cell Tumor). Some choriocarcinomas are not preceded by a molar pregnancy but follow a term pregnancy. A choriocarcinoma developing after a full-term pregnancy often has a poor prognosis. A very rare choriocarcinoma develops independently of gestation; it consists of invasive trophoblastic proliferation and lack of formed villi. A gestational choriocarcinoma together with a viable pregnancy is even rarer. Rare infant–mother choriocarcinomas are reported.

Gestational choriocarcinomas invade the myometrium and spread hematogenously. Some first present as a metastasis, including to brain,

Table 12.3. Tumor, node, metastasis (TNM) staging of gestational trophoblastic tumors

FIGO stage	TNM stage			
	Primary tumor:			
	Tx	Primary tumor cannot be assessed		
	T0	No evidence of primary tumor		
	Tis	Carcinoma-in-situ		
I	T1	Tumor confined to uterus		
II	T2	Tumor extends to other structures		
	Distant metastasis:			
	Mx	Distant metastases cannot be assessed		
	M0	No distant metastasis		
III	M1a	Lung metastasis		
IV	M1b	Any other metastases		
TNM tumor stages:				
Stage IA	T1	M0	Low risk	
Stage IB	T1	M0	High risk	
Stage IIA	T2	M0	Low risk	
Stage IIB	T2	M0	High risk	
Stage IIIA	any T	M1a	Low risk	
Stage IIIB	any T	M1a	High risk	
Stage IVA	any T	M1b	Low risk	
Stage IVB	any T	M1b	High risk	
Risk factors	0	1	2	4
Age	<40	≥40		
Antecedent pregnancy	Hydatid mole	Abortion	Term pregnancy	—
Interval from pregnancy (months)	<4	4–<7	7–12	>12
hCG (IU/mL)	$<10^3$	$\geq 10^3$–$<10^4$	10^4–$<10^5$	$\geq 10^5$
Tumor size (incl. uterus)	<3 cm	3–<5 cm	≥5 cm	—
Site of metastases	Lung	Spleen Kidney	Gastrointestinal tract	Brain Liver
Number of metastases	—	1–4	5–8	>8

Low risk: seven or fewer risk factors.
High risk: eight or more risk factors.
FIGO, Federation Internationale de Gynecologie et Obstetrique (International Federation of Gynecology and Obstetrics); hCG, human chorionic gonadotropin.
Source: From the AJCC Cancer Staging Manual, 6th edition (2002), published by Springer-Verlag, New York, NY, used with permission of the American Joint Committee on Cancer (AJCC), Chicago, IL.

yet even brain metastatic is curable in about 50% with chemotherapy and irradiation.

The role of imaging is to detect local and distal spread. Myometrial invasion is identified as small, mostly hyperechoic nodules, better seen with endovaginal than transabdominal US. At times Doppler US detects diffuse myometrial invasion by identifying hypervascularity and low-impedance blood flow. Coronal MR is useful to identify the nodules' location. Distal spread is evaluated by head CT, chest radiographs, and other appropriate imaging.

Placental Site Trophoblastic Neoplasm

A placental site trophoblastic neoplasm readily infiltrates the myometrium and leads to vascular dilation, visualized by Doppler US as cystic spaces representing blood vessels. The role of MR in this condition is speculative, although a tumor and myometrial invasion can be identified.

With failed initial systemic chemotherapy for metastatic trophoblastic neoplasm, selective chemoembolization is occasionally successful.

Ovarian Hyperstimulation Syndrome

Ovarian hyperstimulation syndrome develops if the ovaries are overstimulated by either medication or idiopathic. Fertility medications stimulate follicle maturation and result in multiple large follicles. Some of these ovaries enlarge to the point that they are palpable. They are readily detected by transabdominal US. Sufficient fluid transudation from follicles manifests as ascites. Pregnancy makes the syndrome worse. It is a potentially life-threatening complication.

The ovarian hyperstimulation syndrome develops during assisted reproduction; elevated serum estradiol levels and retrieved oocyte numbers suggest the ovarian hyperstimulation syndrome, but neither parameter by itself is pathognomonic.

Infertility-Related Conditions

Ovarian causes of infertility include anovulation due to follicular atresia or polycystic disease, empty follicle or unruptured follicle syndromes, chronic anovulation, and ovarian endometriosis. Serum hormone levels and US during ovarian cycles identify some of these causes. Impaired uterine blood perfusion can also result in infertility. Aspirin improves uterine perfusion in those women found to have impaired perfusion during their menstrual cycles, as detected with Doppler US.

Ectopic pregnancies do develop after in vitro fertilization. Fallopian tube disease appears to be the main risk factor for ectopic pregnancy after in vitro fertilization.

Use of US-guidance for embryo transfer appears to improve pregnancy rates by optimizing placement of embryos. Implantation rates with US guidance were 29% versus 18% without US-guidance, while the corresponding pregnancy rates in cycles with easy transfers were 63% versus 36% (28).

Sonohysterography combined either with sonosalpingography or sonohysterosalpingography in infertile women achieved a diagnostic accuracy of 98% in detecting submucosal fibroids, 96% for polyps, and 81% for synechiae (29); tubal patency was correctly assessed in 79% with a saline solution and in 92% when using a contrast agent.

Tumors

Differential Diagnosis of Adnexal Tumors

After detecting an adnexal tumor, the primary tasks of imaging are to establish its site of origin and then determine whether it is cystic or solid.

Considerable controversy ensued in the 1990s about whether endovaginal US or MRI was the preferred initial imaging modality in evaluating adnexal tumors. As an example, in women with adnexal tumors, endovaginal US was found superior for simple cysts, hemorrhagic cysts, endometriomas, and ovarian carcinomas; MRI was found superior for dermoids; and both were equally effective for pedunculated fibroids (30). Further advances in equipment and software have rendered many of these and similar conclusions obsolete.

In general, endovaginal US findings are more accurate than those obtained with transabdominal US, although the latter provides a wider overall view. Doppler US is more sensitive in

women with adnexal tumors than gray-scale US; malignant tumors tend to be vascular and have a lower PI and RI than benign neoplasms and inflammatory tumors, yet sufficient overlap exists to make this Doppler US finding of limited clinical use. Serum CA 125 levels achieve high specificity in differentiating malignant from benign tumors.

The prevalence of malignancy in adnexal tumors is considerably greater in postmenopausal women than in premenopausal. Benign versus malignant differentiation of any one adnexal tumor with imaging is imprecise. Many benign and malignant tumors contain a cystic component. As a rough initial differentiation, a completely cystic tumor is most likely benign, while the presence of a solid component raises the possibility of a malignancy. In fact, the most significant US criterion for malignancy is presence of a solid component and ascites. Necrosis in a solid tumor and nodules in a cystic tumor detected with postcontrast MRI suggest a malignancy (31).

Endovaginal US of adnexal tumors achieves a high sensitivity but low specificity for identifying solid tissue within a partly cystic tumor, with false-positive US results being due to the presence of blood and other debris. Postcontrast MRI, on the other hand, differentiates between tumor and blood and achieves high sensitivity and specificity.

The differential diagnosis of adnexal tumors is best approached by subdividing into those found in premenopausal and postmenopausal women. Adnexal tumors during pregnancy were discussed in a previous section.

Premenopausal

A majority of adnexal tumors in premenopausal women are benign. Simple cysts, in particular, are benign and often resolve. The differential includes inflammatory tumors, ectopic pregnancy, functional cysts, and (benign and malignant) neoplasms (Table 12.4). An imaging finding of a cystic component includes in the differential a nonneoplastic cyst, most often a functional cyst, and a cystic neoplasm. Follicular cysts are the most common functional cyst, and most resolve within several months. Benign complex cysts include hemorrhagic cysts and endometriomas. A mature cystic teratoma is also in the differential diagnosis of cystic neoplasms in a premenopausal woman.

Ovarian tumors in girls tend to be large when first detected; an exception is with tumors having endocrine activity.

A follow-up US study in about 6 weeks appears reasonable for a complex adnexal cystic tumor detected by US in a premenopausal woman; if unchanged in size or larger, exploration is indicated.

Cystic malignant neoplasms have thick septa and varying amounts of a solid component, findings lacking in most benign tumors. Also, Doppler US reveals increased blood flow and lower pulsatility and resistance indexes in malignant neoplasms.

Table 12.4. Differential diagnosis of adnexal tumors in premenopausal women

Tumor type	Comment
Inflammatory tumors	Tend to be complex cystic and solid, often tender
Ectopic pregnancy	
Cystic	
Functional cysts	
Follicular cysts	Most common functional cyst
Corpus luteum cyst	
Theca lutein cyst	Occurs in molar pregnancy and hyperstimulation syndrome
Mature cystic teratoma	A common cystic neoplasm, especially in younger women
Serous and mucinous neoplasm	Benign ones appear as simple cysts, often lacking septa Malignant ones have thick septa and solid components
Solid	
Benign neoplasm	
Malignant neoplasm	
Germ cell tumors	Ovarian neoplasms in childhood tend to be of germ cell origin

Postmenopausal

An adnexal tumor in a postmenopausal woman is generally considered to be malignant until proven otherwise and resection is warranted, especially if associated with an elevated CA-125 level.

Ultrasonography detection of a simple cyst-like tumor in a postmenopausal woman raises a management dilemma. While most of these cysts are benign, an occasional one is malignant. One option is to follow smaller cysts (about 5 cm or less in diameter) with serial imaging and resect those showing any evidence of enlargement. Larger ones generally are resected. A complex cyst or solid tumor detected by US is assumed to be malignant; preoperative CT (or, perhaps even more appropriate, MRI) is useful for staging.

With a known previous nongynecologic malignancy, differential diagnosis of an adnexal tumor also includes a metastasis. Among women with breast cancer and US-detected adnexal tumors, histopathologic study revealed 74% to have benign adnexal disease and 26% malignant—of the latter half were primary ovarian cancers and half breast metastases (32). Similarly, with a history of colorectal carcinoma and a new adnexal tumor, a majority of these tumors are metastatic colon cancers rather than primary ovarian neoplasms.

What imaging tests are appropriate in a woman with a clinically asymptomatic suspicious adnexal mass detected by screening US? Endovaginal US, MRI, and PET achieved sensitivities of 92%, 83%, and 58%, respectively, and specificities of 59%, 84%, 78%, respectively, in tumor characterization (33); MRI using contrast-enhanced fat-saturated T1-weighted sequences was especially useful with dermoid cysts and endometrial cysts, but all three modalities revealed uncertainty with borderline tumors. The high sensitivity of endovaginal US argues for this modality as the next test in this clinical setting.

Major MRI findings pointing towards malignancy are ascites and nodules on the wall and septum of a cystic tumor (34); other features associated with malignancy include a part solid-part cystic tumor, irregular tumor wall, a large tumor and early contrast enhancement.

Some tumors are difficult to differentiate between an ovarian and a subserosal uterine origin. Presence of an ovarian vascular pedicle for a tumor, detected with helical CT, confirms an ovarian origin with a high degree of sensitivity (35).

Endometriosis

Clinical

Endometrial tissue in an ectopic location outside the uterus, called endometriosis, and involving ovaries, fallopian tubes, and adjacent structures is discussed here. Endometriosis at more distal sites is discussed in each corresponding chapter. Endometrial tissue invading the uterine myometrium is known as adenomyosis and is covered later in this chapter. Some authors label uterine endometrial tissue as *endometriosis interna* and endometrium outside the uterus as *endometriosis externa*, or simply as *pelvic endometriosis.* Endometriosis often involves multiple pelvic sites, presenting as adnexal tumors.

Although several pathogenetic mechanisms have been proposed, transtubal retrograde dissemination appears to be the most likely mechanism in a majority of women; an increased prevalence occurs in a setting of obstructed normal menstrual outflow. Vascular, lymphatic, and mechanical spread during surgery probably also play an occasional role. Endometriosis has developed in a surgical scar, especially after a cesarean section or hysterectomy. It is estrogen dependent. In the absence of hormone replacement therapy and obesity, symptomatic endometriosis is rare in postmenopausal women. The immunologic factors involved in endometriosis constitute an active research field.

The prevalence of endometriosis is about 10% to 20% in menstruating women. It ranges from diffuse to focal, with the latter known as an endometrioma, and can develop anywhere in the abdomen, including abdominal wall, inguinal canal, umbilicus, or surgical scar. Endometriosis of the mesentery, omentum, or bowel wall is less common than peritoneal involvement. Prevalence of endometriosis is increased in women with a cystic mesothelioma and in a setting of disseminated leiomyomatosis. Endometriosis is one of the causes of bloody ascites, in an occasional patient evolves in peritonitis and eventually evolves into scarring. A

rare endometrioid carcinoma develops at a scar endometriosis site. Ectopic endometrial tissue bleeds during menses, is surrounded by inflammation, and eventually fibrosis develops. Pain and infertility are the most common presentations. Nevertheless, symptoms are not always cyclic and often are nonspecific. In fact, an incidentally detected focus of extrauterine endometrial tissue in an otherwise asymptomatic and fertile woman is not uncommon.

Traditionally, laparoscopy is the primary study in patients with suspected endometriosis, being supplanted in a number of institutions by MR as the initial study, which also serves as a guide to subsequent laparoscopy and histologic confirmation.

Percutaneous endometrioma aspiration results in a high recurrence rate. Whether the use of hormonal suppression therapy decreases recurrence is conjecture.

Imaging

Imaging reveals endometriosis as one or multiple thick-walled cystic tumors. An occasional one is solid. Surrounding fibrosis is common and with long-standing disease extensive pelvic distortion is evident, at times mimicking widespread metastases (Fig. 12.13). Intraperitoneal endometriosis most often consists of solid or partly cystic tumors, at times mimicking metastasis. The cystic component is partly filled with blood products; their CT density ranges from water to soft tissue. Blood clots, generally adjacent to the wall of a cyst, are hyperdense. Fallopian tubes involved by endometriosis have an irregular, beaded appearance on hysterosalpingography.

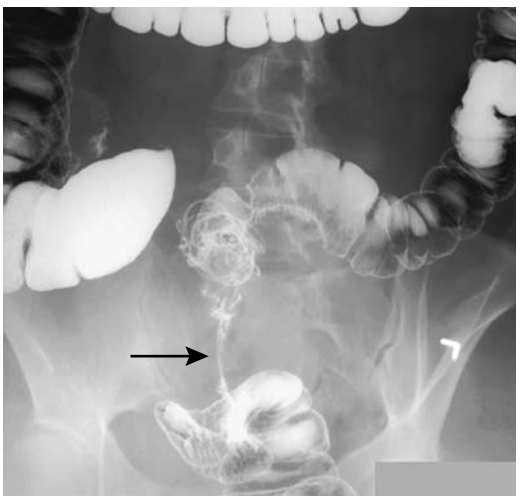

Figure 12.13. Severe endometriosis resulting in a frozen pelvis. Barium enema reveals a long rectal stricture (arrow). The sigmoid colon is also infiltrated.

An endovaginal approach is preferred with US. These tumors' echogenicity spectrum reflects their varied cystic-to-solid appearance. The solid component in larger tumors often appears nodular. A homogeneous hypoechoic cyst containing low-level echoes is a common finding; at times septations and a multilocular appearance are evident. No specific US features point toward an endometrioma, but in an adnexal tumor with these findings an endometrioma is suggested if neoplastic features can be excluded. Endovaginal US sensitivity and specificity of about 90% can be expected in suggesting an endometrioma. Color and pulsed Doppler US provides limited additional information except for excluding blood flow within cystic regions.

The reported endorectal US sensitivity and specificity percents are in the high 90s for detecting rectovaginal endometriosis (36); the sensitivity for uterosacral ligament infiltration is about 80%, perhaps reflecting the greater distances involved, but the specificity percents remain in the high 90s.

Magnetic resonance is the imaging procedure of choice in detecting and defining subtle endometrial implants; fat suppression aids in visualizing small implants, being especially useful for implants <5 mm. Sensitivity and specificity of MRI in detecting pelvic endometriosis are >90% (37). Although MR findings vary considerably, MR will often differentiate an endometrioma from other adnexal tumors. With conventional MRI small implants have an appearance similar to fat—hyperintense on T1- and hypointense on T2-weighted images relative to myometrium, often being homogeneous when small. Some foci appear as small cystic tumors. Endometrioma fluid due to a prior bleed is hyperintense on both T1- and T2-weighted images. Recent bleeding is hypointense and the overall appearance thus can vary considerably. Solid nodules enhance postgadolinium. In general, hyperintense fluid on T1-weighted MRI in dilated fallopian tubes suggests pelvic endometriosis.

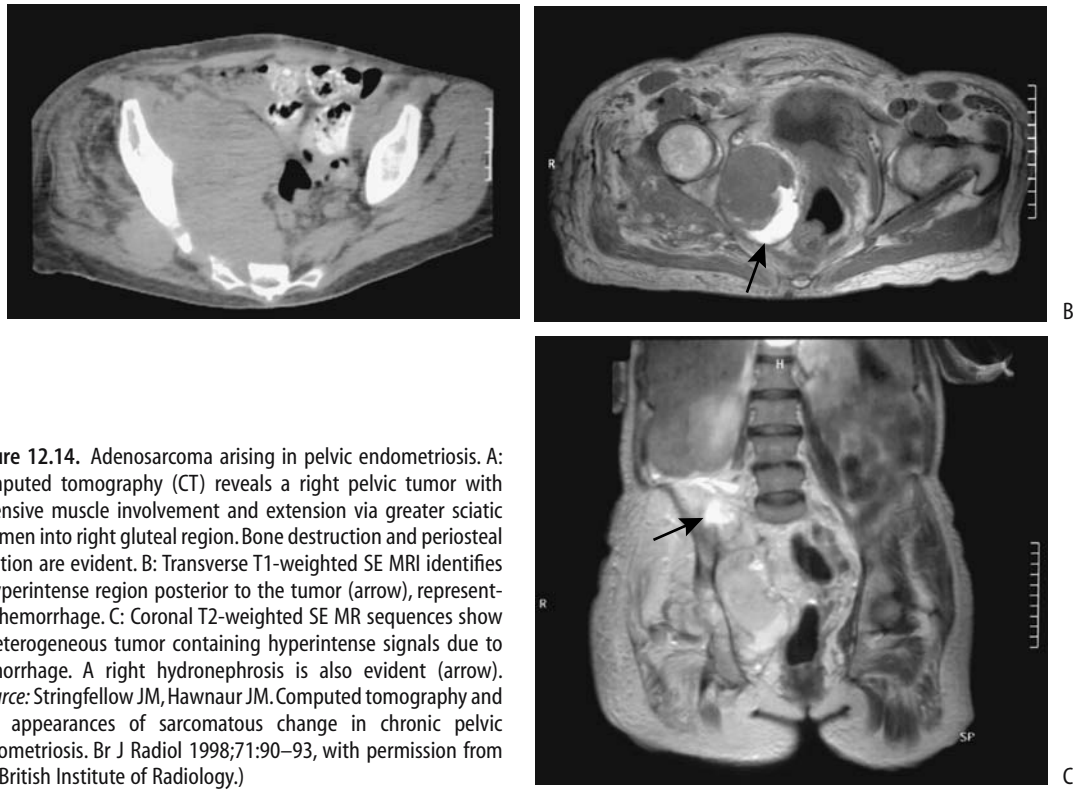

Figure 12.14. Adenosarcoma arising in pelvic endometriosis. A: Computed tomography (CT) reveals a right pelvic tumor with extensive muscle involvement and extension via greater sciatic foramen into right gluteal region. Bone destruction and periosteal reaction are evident. B: Transverse T1-weighted SE MRI identifies a hyperintense region posterior to the tumor (arrow), representing hemorrhage. C: Coronal T2-weighted SE MR sequences show a heterogeneous tumor containing hyperintense signals due to hemorrhage. A right hydronephrosis is also evident (arrow). (*Source:* Stringfellow JM, Hawnaur JM. Computed tomography and MRI appearances of sarcomatous change in chronic pelvic endometriosis. Br J Radiol 1998;71:90–93, with permission from the British Institute of Radiology.)

In general, the imaging appearance of an endometrioma tends to mimic a cystic ovarian neoplasm, a dermoid cyst, or a hemorrhagic ovarian cyst. Imaging is useful in guiding a diagnostic biopsy.

Complications

Rupture of an ovarian endometrioma results in a chemical peritonitis and an acute abdomen. Although rare, rupture can occur during pregnancy.

An enlarging endometrioma raises suspicion for malignancy, with the most common malignancy developing in extraovarian endometriosis being an adenocarcinoma. Unopposed estrogen stimulation appears to play a role in the development of these malignancies. The MR detection of contrast-enhancing mural nodules suggests a malignant endometrioma (38); nodule enhancement is easier to identify on subtraction images. One should keep in mind, however, that ovarian endometriomas enlarge and form decidua during pregnancy, changes probably induced by progesterone.

An occasional sarcoma or primary squamous cell carcinoma develops in a region of endometriosis (Fig. 12.14). Image-guided biopsies of pelvic endometriosis should not be relied upon to exclude a malignancy because they may simply yield endometrial tissue.

Ovary and Adnexa

Discussed here are a diverse group of ovarian neoplasms and related tumor-like conditions, such as various ovarian and paraovarian cysts. Fallopian tube neoplasms are covered in a later section.

Ovarian neopasms are a diverse group and are usually subdivided into those having a stromal cell, germ cell, and epithelial cell origin. Both benign and malignant neoplasms originate from all three cell types. Some of these neoplasms cannot be subdivided simply into benign and malignant varieties and a borderline

(or low malignant potential) tumor category is used by pathologists. Germ cell origin neoplasms are more common in younger women, while epithelial origin neoplasms predominate in postmenopausal women. Mature cystic teratomas predominate among ovarian tumors found in girls under the age of 15 years.

Benign Tumors

A number of benign ovarian and other adnexal tumors are treated with laparoscopic surgery. The major limitation of a laparoscopic approach is the inability to definitely confirm the benignity of the lesion in question. It is not rare to have an initial laparoscopic diagnosis and begin treatment of what is thought to be benign disease, but subsequently discover that the condition is indeed malignant.

Granuloma

Ovarian granulomas are most often a result of an inflammatory reaction—typically a result of a foreign body reaction to suture material introduced at previous surgery. Other causes include infections such as a bacterial tubo-ovarian abscess or tuberculosis, endometriosis, Crohn's disease, previous diathermy or a necrotizing reaction to previous surgery. Some are idiopathic.

Sex Cord–Stromal Tumors

These tumors originate from sex cords and mesenchymal tissue. Most are benign. They are rare in young women and most occur in the postmenopausal age group. Some produce estrogen and/or androgen with their resultant clinical manifestations.

A variant of a sex cord tumor is one containing annular tubules, with the predominant component being intermediate between a granulosa cell tumor and a Sertoli cell tumor. Of interest is that some of these tumors are associated with Peutz-Jeghers syndrome.

Fibroma/Thecoma

Both of these solid tumors originate from ovarian stroma. Their pathologic appearance is similar and a tumor is often classified depending on the preponderance of thecal cells or fibrous tissue.

Thecomas occur mostly in middle-aged and older women and constitute less than 5% of all ovarian neoplasms. They are rare in prepubertal girls. Most are benign and 90% are unilateral. They tend to be associated with excess estrogen production, a finding not seen with fibromas. Also, some thecomas are associated with endometrial hyperplasia and endometrial carcinoma. An interesting association exists between luteinized thecomas and sclerosing peritonitis. Some of these present with an acute abdomen.

Ovarian fibromas are most common in middle age. Most are asymptomatic but an occasional fibroma is a component of Meigs' syndrome. An increased incidence occurs in some families and in Gorlin's syndrome (*basal cell nevus syndrome*). Ascites is common with larger fibromas and thecomas.

The imaging appearance of fibromas and thecomas is similar. Computed tomography shows most tumors to be solid and homogeneous, but they tend to become inhomogeneous when large. Some develop calcifications. The more homogeneous tumors are hypoechoic by US. The CT and US differential diagnosis includes other solid extraperitoneal tumors such as a teratoma and lymphoma. Fibromas, thecomas, and Brenner tumors have similar imaging and operative findings.

These tumors are hypointense on both T1- and T2-weighted MRI, a rather specific appearance differing from that of most other solid ovarian tumors. Degeneration within larger tumors tends to produce a heterogeneous and cystic appearance. Their contrast enhancement varies considerably. Because their appearance is similar to that of uterine fibroids, the tumor origin needs to be established to differentiate these entities.

The MRI appearance of the rare ovarian leiomyoma is similar.

Granulosa Cell Tumor

Granulosa cell tumors are benign tumors found mostly in postmenopausal women. Some produce excess estrogen and, if it is uncorrected, these women are prone to develop endometrial carcinoma. Serum tumor markers tend to be normal. A rare variant is found in the pediatric age and younger women, where some

of these tumors manifest due to their estrogen or androgen production.

Smaller tumors are solid, but a cystic component often develops with growth, and as a result the imaging findings of larger ones tend to mimic those of cystadenomas. Their imaging appearance ranges from unilocular to multilocular cystic, thick- to thin-walled, and homogeneously to heterogeneously solid (39). Bleeding, infarction, and tumor degeneration contribute to their heterogeneous appearance.

Magnetic resonance imaging reveals solid tumors with a variable cystic component and intratumoral hemorrhage; the solid component enhances postcontrast. The uterus is often enlarged, and endometrial thickening is evident (Fig. 12.15).

These tumors tend to recur years after an apparent cure, and thus long-term follow-up is necessary after initial therapy.

Sertoli-Leydig Cell Tumor

This rare tumor occurs mostly in girls and young women, occasionally bilaterally. Some are associated with elevated serum α-fetoprotein levels. These tumors produce androgen and other hormones, and some women develop masculinization. An occasional one produces renin and is a cause of hypertension. In distinction to other sex cord tumors, a number of Sertoli-Leydig tumors are malignant, at times even being poorly differentiated.

The imaging appearance is similar to granulosa cell tumors. Some small Leydig cell tumors are not detected by US in spite of high plasma testosterone levels and virilization.

Cystic Tumors

Clinical

Benign ovarian cysts range from incidental simple cysts, to functional cysts, to a cyst manifesting by its neoplastic nature. The terms *simple cyst* and *functional cyst* are often used interchangeably and generally imply a follicular cyst.

Doppler US follow-up in premenopausal women with adnexal cysts reveals that about one third regress spontaneously and thus

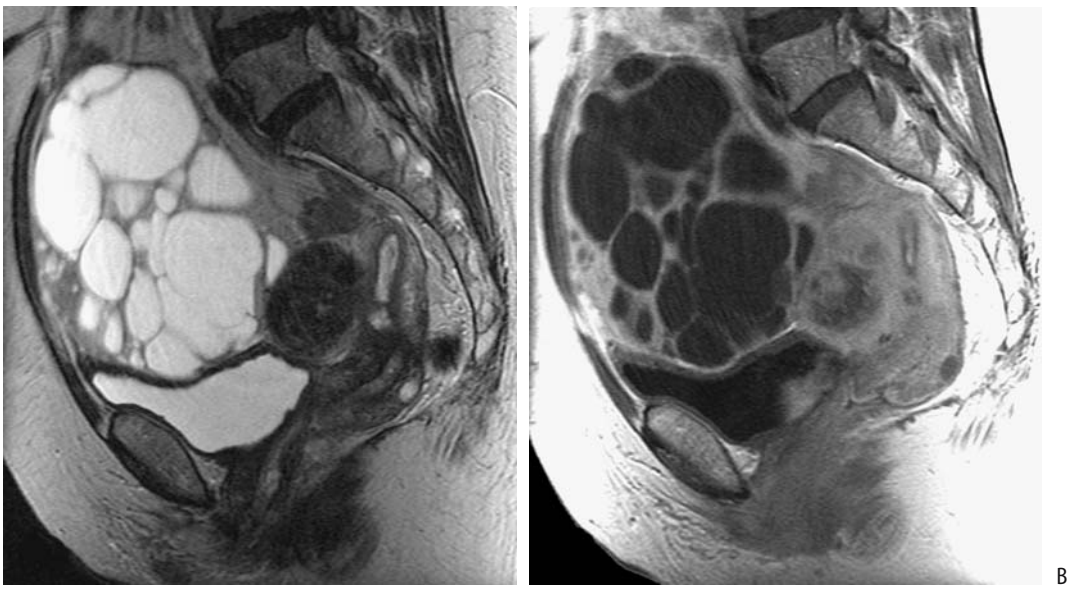

Figure 12.15. Granulosa cell tumor in a woman with bleeding and elevated estradiol level. A: Sagittal T2-weighted magnetic resonance (MR) identifies a multicystic tumor anterior to the uterus. The uterus is enlarged, has thickened endometrium, and contains a leiomyoma. B: Sagittal post-contrast T1-weighted image reveals enhancing tumor wall and septa. (*Source:* Kido A, Togashi K, Koyama T, Yamaoka T, Fujiwara T, Fujii S. Diffusely enlarged uterus: evaluation with MR imaging. RadioGraphics 2003;23:1423–1439, with permission from the Radiological Society of North America.)

are simple (functional) cysts. Ultrasonography cannot differentiate between cysts that will regress and those that will not.

Small, thin-walled, anechoic, nonpalpable ovarian cysts detected by US present a dilemma. What is the malignant potential of these small cysts in a postmenopausal woman? Follow-up US reveals that most of these cysts remain stable, with an occasional one even resolving. The risk of malignancy appears sufficiently low that follow-up with US of stable cysts appears reasonable, assuming there is no family history of ovarian, breast, or colon cancer. The CA-125 antigen serum level should also remain low.

A US pelvic cancer screening program of postmenopausal women defined a simple cyst as an anechoic cyst <5 cm in diameter having a morphologic appearance of a typical benign cyst (smooth, aseptate, hypoechoic) (40); women with a cyst were followed at 3- to 6-month intervals and evaluated for possible surgical intervention. Of these simple cysts, 23% resolved spontaneously and 59% persisted (other women were lost to follow-up). No malignancy was identified in women with a persistent cyst who underwent surgery. Of interest, a woman with congenital hypothyroidism had bilateral multicystic ovaries (41); the cysts disappeared after thyroid hormone therapy.

Follicular (Simple) Cysts

The prevalence of simple cysts is <10% in postmenopausal women. Imaging identifies the presence of a cyst, although most functional cysts have a similar appearance. If multiple, these cysts tend to vary in size, in distinction to polycystic disease where cysts tend to be small and about the same size.

Most follicular cysts are under hormonal influence and result from a failure to ovulate or involute. They are benign, most are small, and most regress following a menstrual cycle. Those cysts that do not regress are not under hormonal control and some other tumor, either benign or malignant, is often considered. Follicular cysts are found in McCune-Albright syndrome.

At times US in neonates, infants and young children with a lower abdominal cystic tumor detects a small cyst along the wall of a cystic tumor (called a *daughter cyst sign*); these daughter cysts, pathologically identified as ovarian follicles, occur in ovarian cysts but not in cysts of other etiologies (42).

Simple ovarian cysts have an appearance similar to that of cysts elsewhere; namely, they are entirely cystic, smooth-walled, and homogeneous, and they contain no internal debris. Any septa are thin and smooth. Doppler US reveals no internal vessels. Simple cysts are hypointense on T1- and hyperintense on T2-weighted MRI.

Ultrasonography reveals a fluid-filled thin-walled structure. Uncomplicated cysts are hypointense on T1- and hyperintense on T2-weighted images. Blood and other debris within the cyst modify their appearance. Due to a surrounding theca and stromal reaction, functional cysts tend to have hypointense rims on T2-weighted images.

Ultrasonography is useful in correlating cyst regression with menstrual cycle.

Some ovarian cysts have thick walls, contain septa, and have internal echoes; in these, US does not differentiate between solid and cystic tumors.

Depending on imaging appearance, the differential diagnosis of an ovarian cyst includes a simple cyst, hemorrhagic cyst, endometrioma, dermoid cyst, and other neoplasms, both benign and malignant. At times, even an appendiceal abscess located in the pelvis is in the differential.

Ultrasound-guided percutaneous aspiration of a simple ovarian cyst is a straightforward procedure associated with few complications. Nevertheless, this is a controversial topic and therapy of these cysts is not settled. Authors discouraging aspiration point to a high cyst recurrence rare (cysts recur in about half or slightly more instances), sampling errors encountered with complex cysts, and possible needle tract seeding by malignant cells. On the other hand, numerous studies have established the relative safety and effectiveness of percutaneous aspiration of preselected cysts. Especially in high surgical risk women, US-guided aspiration of benign-appearing ovarian cysts appears worthwhile to evaluate for malignant potential. If needed, recurrent cysts can be resected, but cysts several cm in diameter are followed. In general, a high concentration of estradiol in

aspirated fluid predicts a low cyst recurrence rate.

Corpus Luteum Cysts

Corpus luteum cysts are associated with pain, and they may rupture and bleed. They tend to be unilateral and are larger than follicular cysts.

The cyst wall of corpus luteum cyst is thicker and more nodular than a simple cyst. The wall enhances post–MR contrast. Also, bleeding modifies cyst content. The overall appearance of some of these cysts overlaps with endometriomas and cystic ovarian malignancies.

Theca-Lutein Cysts

Theca lutein cysts are associated with pregnancy, tend to be large, and occur bilaterally. Multiple theca-lutein cysts develop in ovarian hyperstimulation syndrome during therapy for infertility and in association with gestational trophoblastic disease, resulting in gross ovarian enlargement. In fact, in the appropriate setting the presence of theca-lutein cysts and an endometrial tumor should suggest gestational trophoblastic disease.

Some of these cysts manifest by rupture and bleeding. Ascites is evident in some women.

Ultrasonography reveals a smooth-walled cyst, with no blood flow to the cyst identified by Doppler US. The cysts' MR appearance varies considerably.

Hemorrhagic Cyst

A hemorrhagic cyst is a descriptive term for a ruptured corpus luteum cyst or follicular cyst that bleeds internally and contains blood. Sudden onset of midcycle pain is a common presentation. These cysts tend to resolve within several menstrual cycles. Their size varies considerably.

Ultrasonography of these cysts ranges from hypo- to hyperechoic, varying considerably depending on the age of hemorrhage. Some are associated with peritoneal fluid. An occasional one is thick-walled and mimics the adnexal ring sign of an ectopic pregnancy (19); a key difference is that a ring sign with a hemorrhagic cyst is intraovarian, while with an adnexal pregnancy it is extraovarian.

Bleeding into a cyst increases the usually low signal intensity on T1-weighted MRI, and many of these cysts appear hyperintense both on T1- and T2-weighted images.

The overall appearance of some hemorrhagic cysts mimics a ruptured ectopic pregnancy with its surrounding blood.

Paraovarian and Paratubal Cysts

Some of these cysts are located within the broad ligament. A paraovarian cyst should be suspected if US detects a separate and normal ipsilateral ovary, although this diagnosis is not often made. Paraovarian cysts tend to be misdiagnosed as ovarian cysts, while paratubal cysts are not detected due to their small size.

Peritoneal inclusion cysts are in the differential diagnosis. These cysts are discussed in Chapter 14.

Mature Cystic Teratoma/Dermoid Cyst

Clinical: Mature cystic teratomas, also called dermoid cysts, are the most common neoplasms of germ cell origin. They are almost always benign, in distinction to other malignant germ cell tumors (discussed later). These tumors are composed of all three germ cell layers, although ectodermal components tend to predominate.

About 10% of cystic teratomas develop bilaterally. They grow slowly, and are found in pediatric and postmenopausal age groups, but are most common in young women. They are the most common ovarian tumor in pediatrics. They are slow-growing tumors and most tend to be asymptomatic, but they are also prone to torsion, rupture, and malignant degeneration; therefore, surgical resection is usually considered when discovered.

These cysts tend to be unilocular, and septations are present in some; the cysts are lined by squamous epithelium and contain sebaceous material; only a rare teratoma consists of a mostly solid tumor.

Most mature cystic teratomas undergo surgical resection and thus image-guided biopsy is moot.

Imaging: Fat detected by imaging within an ovarian tumor should suggest a mature teratoma. Magnetic resonance imaging identifies fat in about 90% of ovarian teratomas. Fat

is mostly in the cystic cavity, occasionally in the cyst wall. Fat is associated with sebaceous glands, which are prominent in most dermoids. The MR appearance of teratomas without fat is similar to that of other cystic ovarian tumors.

Some teratomas contain a fluid (fat)-fluid level, debris, or calcifications, findings identified by CT or MRI and, at times, with conventional radiography (Fig. 12.16). Calcifications, including teeth, generally in an associated soft tissue nodule, are characteristic of a mature cystic teratoma.

A teratoma typically has a cystic component and contains focal or diffuse regions of increased echogenicity consisting of hyperechoic lines and nodules, with the latter representing a dermoid plug consisting of fat (sebum), hair, or calcifications. An acute bleed into a simple cyst may be sufficiently hyperechoic to mimic a dermoid plug; a follow-up examination should differentiate these two. A cystic teratoma can also mimic loops of bowel with US and be overlooked.

Doppler US detects blood flow only in a minority of dermoid cysts, and only from peripheral tissue surrounding the tumor (but see below for struma ovarii tumors).

On T1-weighted MRI fatty regions are hyperintense, while calcifications and fibrosis are hypointense. Similar to US, MRI using T1- and T2-weighted sequences cannot readily differentiate teratomas and cystic hemorrhagic tumors; the use of fat-saturation sequences increases tumor characterization considerably.

Mature cystic teratomas without fatty fluid (sebum) have an atypical MR appearance. They are hypointense on T1- and hyperintense on T2-weighted images, consistent with fluid in the cyst. They show heterogeneous postcontrast enhancement, yet even in these teratomas MRI often identifies fat as focal hyperintense regions in the cyst wall.

The rare solid mature teratoma has an imaging appearance similar to an immature teratoma (Fig. 12.17). A biopsy diagnosis of a solid mature teratoma should be made with caution because many immature teratomas also contain histologically mature-appearing tissue.

Occasionally a leiomyoma contains calcifications or fat and the CT and US appearance mimics a cystic teratoma. A perforated appendix with a stone can have a similar echogenic appearance. On the other hand, chemical shift gradient echo MRI differentiates cystic teratomas from endometriomas.

Complications: Cystic teratoma complications include bleeding, perforation (rupture), malignant degeneration, and, rarely, torsion. The fatty component tends to be preserved after torsion (imaging findings of ovarian torsion were discussed earlier).

Perforation of a cystic teratoma ranges from gradual leakage leading to a granulomatous peritonitis or ascites to sudden rupture and an acute abdomen. Spill of cyst content, resultant

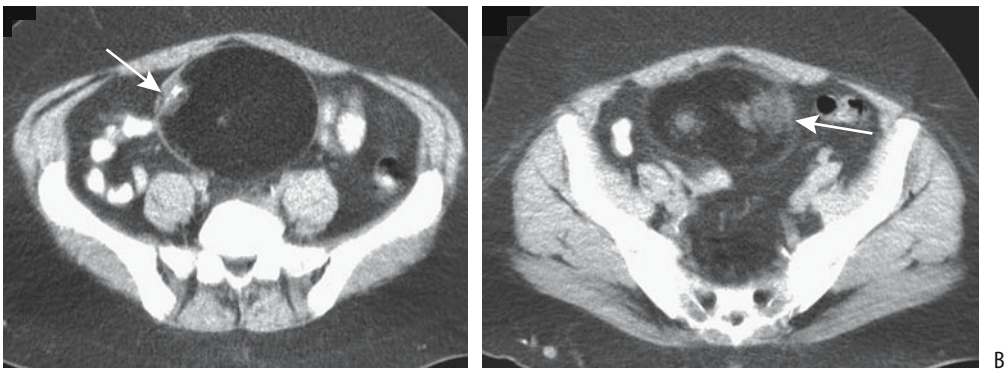

A B

Figure 12.16. Cystic teratoma. A: CT detects a large, midline mostly fat density tumor containing a bone fragment (arrow) and encased by a thin capsule. B: A slightly more inferior image identifies soft tissue nodules (arrow). (Courtesy of Egle Jonaitiene, M.D., Kaunas Medical University, Kaunas, Lithuania.)

Figure 12.17. Mature ovarian teratoma in a 2-year-old girl. Transverse US scan reveals a solid retrovesical tumor with echogenic shadowing (arrow). (*Source:* Garel L, Dubois J, Grignon A, Filiatrault D, Vliet GV. Ultrasonography of the pediatric female pelvis: a clinical perspective. Radiographics 2001;21:1393–1407, with permission from the Radiological Society of North America.)

chemical peritonitis, and ascites are identified with postcontrast T1-weighted MRI. The resultant appearance can mimic carcinomatosis or chronic peritonitis.

Immature teratomas are malignant and are discussed in a later section. Mature teratomas do not evolve into immature teratomas; thus the occasional malignancy in a mature cystic teratoma represents a *de novo* malignant transformation, generally a squamous cell carcinoma, less often an adenocarcinoma, and a rare one believed to be of thyroid origin. Sarcomas are least common; some of these are part of a carcinosarcoma and occur in association with a squamous carcinoma or, very rarely, an adenocarcinoma. Most malignancies occur in postmenopausal women. The time to malignant degeneration varies, at times being decades after initial diagnosis. A rare woman first presents with metastases, later shown to be from a primary small cell carcinoma arising in an ovarian mature cystic teratoma. Interestingly, some younger women developing ovarian mucinous tumors are found to also have a teratoma, an association greater than by chance.

A prominent soft tissue component in a cystic teratoma, detected by any imaging modality, should raise suspicion of a malignancy. These tumors spread by transmural invasion and thus differ from primary epithelial cancers. MRI of some of these tumors thus reveals not only a solid component, but also transmural and surrounding structure invasion. At times a solid lobulated tumor extends into surrounding fat The malignant component enhances postcontrast. Some dermoid/carcinoma tumors are huge and consist of mural intracavitary nodules containing regions of necrosis and hemorrhage. A retrospective study of women with squamous cell carcinoma in an ovarian mature cystic teratoma, treated by the Tokai Ovarian Tumor Study Group, revealed a 5-year survival of 95% for those with stage I and 80% for stage II, but 12 of 13 patients with stage III died within 20 months (43).

Struma Ovarii

Struma ovarii is an uncommon, usually benign ovarian neoplasm, with only rare malignant ones reported. Most investigators classify struma ovarii as a mature cystic teratoma variant containing predominantly or exclusively one tissue, namely thyroid. These tumors occur unilaterally in adult women. An occasional one is associated with a mature cystic teratoma. Most are not hormonally active.

Histologically, these tumors contain varying-size cysts separated by fibrous septa. The hallmark of this tumor is the presence of thyroid follicles, albeit at times scant in nature. The correct diagnosis is readily overlooked if only a few thyroid follicles are identified. Immunohistochemical staining for thyroglobulin is helpful if the diagnosis is in doubt. A histologic diagnosis of malignancy is difficult with these tumors, especially in a setting of a well-differentiated follicular stroma.

Imaging reveals both cystic and solid components; even nonfunctional struma ovarii can show iodine-123 uptake by the tumor. In distinction to mature cystic teratomas, struma ovarii do not contain fat and the cystic spaces are filled with a gelatinous colloid material. Ultrasonography typically identifies a complex solid and cystic tumor. Doppler US detects blood flow not only in the capsule but also within the solid component. Detection of flow within an apparent cystic teratoma should thus suggest struma ovarii.

Magnetic resonance imaging of struma ovarii tumors reveals complex solid and cystic components. The cyst fluid varies from hypointense

to hyperintense both on T1- and T2-weighted images, presumably secondary to hemorrhage and possibly due to viscous proteinaceous material. Solid components are intermediate in signal intensity on T1- and hyperintense on T2-weighed images; postcontrast, solid components reveal an intense contrast enhancement. These tumors thus mimic a malignancy.

Polycystic Disease (Stein-Leventhal Syndrome)

Polycystic ovarian disease (Stein-Leventhal syndrome) consists of oligomenorrhea, anovulation, hyperandrogenism, and obesity in a setting of enlarged, polycystic ovaries. Serum luteinizing hormone levels are increased and follicle-stimulating hormone levels are decreased. Infertility is common. The clinical presentation varies, however, some women have a normal menstrual cycle and some with imaging-confirmed polycystic ovarian disease have no clinical or endocrinologic findings. It is this latter finding that suggests that the presence of multiple peripheral ovarian cysts detected by imaging is not pathognomonic for polycystic ovarian disease.

Computed tomography detects enlarged ovaries containing numerous small cysts, generally uniform in size. In some women the cysts are sufficiently small, making their identification difficult. The cysts are close to water density. Hemorrhage is rare.

The diagnosis can be suggested by US. Ovaries tend to be more round rather than oval in configuration, and are markedly asymmetrical in about half of the women. In general, the ovaries are enlarged, although they overlap both in ovarian volume and number of follicles exists. Multiple peripheral cysts, at times with hyperechoic stroma, are detected with US in some but not all affected women.

Magnetic resonance reveals a hypointense signal from these cysts on T1- and hyperintense signal on T2-weighted images.

Primary Epithelial Neoplasms

A majority of ovarian neoplasms are of epithelial origin, with adenocarcinoma being more common than adenoma. Especially when discussing malignant ovarian neoplasms, some authors lump epithelial, germ cell, and stromal tumors together and treat them as a single entity. Some ovarian tumors, such as poorly differentiated carcinomas, defy subdivision.

The most common ovarian epithelial malignancy is a serous cystadenocarcinoma, followed by mucinous cystadenocarcinoma, then endometrioid carcinoma, clear cell carcinoma, and the least common being poorly differentiated carcinomas. Only rarely encountered are small cell carcinomas and squamous cell carcinomas.

Primary ovarian adenomas and adenocarcinomas are discussed together; the initial clinical approach is similar for both and many of the imaging findings overlap.

Serous and Mucinous Adenoma and Adenocarcinoma

While ovarian cancer is less common than uterine or cervical cancer, it results in a higher mortality rate. The risk of developing an ovarian cancer is associated with older age, nulliparity, and a family history of ovarian cancer. Because of few initial symptoms, a late diagnosis (stage III or IV) for ovarian carcinoma is common and mortality has decreased little during the last several decades.

The prevalence of mucinous versus serous cystadenocarcinomas is age dependent; in women under the age of 40, most are mucinous while over the age of 40 most are serous. Younger women developing a malignant epithelial ovarian tumor are more likely to have a borderline and early-stage tumor than are older women; also, the 5-year survival rate is significantly better in younger patients.

Migratory thrombophlebitis is a known complication of a number of internal malignancies, including ovarian cancers (Fig. 12.18). Thrombocytosis and venous thrombosis is significantly more prevalent in patients with ovarian epithelial carcinoma than in those with benign cysts or controls.

Genetics: About 95% of ovarian cancer is sporadic. Yet epithelial ovarian cancers occur in certain families and an autosomal dominant transmission is evident. Cancers in these families occur at a younger age than the general population and daughters of mothers with ovarian

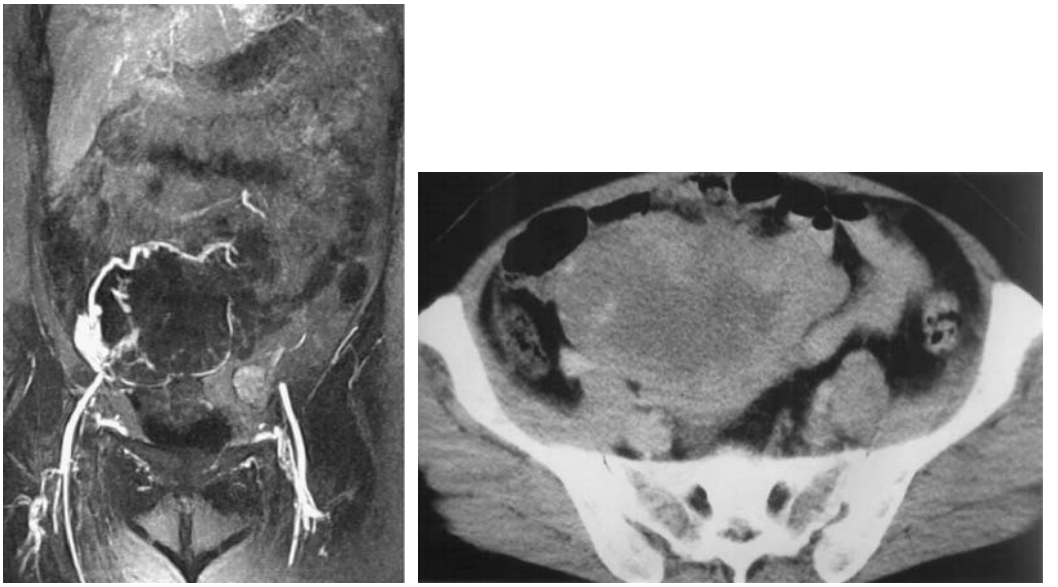

Figure 12.18. Deep venous thrombosis associated with ovarian cancer. A: Extensive pelvic venous occlusions are present. B: Contrast-enhanced CT identifies an enhancing pelvic tumor containing central necrosis. (*Source:* Sandstede JJW, Krause U, Pabst T, et al. Deep venous thrombosis and consecutive pulmonary embolism as the first sign of an ovarian cancer. J Magn Reson Imaging 2000;12:497–500, with permission from Wiley-Liss, a subsidiary of John Wiley & Sons.)

cancers develop their ovarian cancer at a significantly younger age than their mothers. Several distinct cancer syndromes have been described: hereditary site-specific ovarian cancer, hereditary breast–ovarian cancer syndrome, and as part of a nonpolyposis colorectal cancer syndrome (Lynch syndrome II). Mutations in the *BRCA1* tumor suppressor gene, located on chromosome 17q21, are responsible for most cases of inherited predisposition to breast and ovarian cancer, followed by mutation of the *BRCA2* tumor-suppressor gene.

Some sporadic ovarian cancers have mutations in the *p53* tumor-suppressor gene. Invasive serous and undifferentiated ovarian carcinomas reveal *p53* mutations and loss of genetic material in chromosome 17 and other chromosomal complexes, findings uncommon in mucinous and endometrioid carcinomas (44). *KRAS* mutations are found in up to half of mucinous ovarian carcinomas and mucinous borderline malignant tumors (44). Also, p53 protein accumulates similarly in both mucinous cystadenocarcinomas and borderline malignant mucinous tumors, and in the latter tumors it can also be identified in morphologically benign tumor regions.

Associated Conditions: Women with a primary ovarian or uterine carcinoma are at increased risk of developing a second primary malignancy of the colon, breast, uterus, and other organs. This increased risk is explained, in part, by the therapy of the primary malignancy, although undoubtedly such factors as heredity and hormones also play a role. Most of these second primary tumors are detected by symptoms from the second tumor and not follow-up of the primary cancer.

The dominantly inherited Li-Fraumeni syndrome consists of a genetic predisposition to sarcomas, breast carcinomas, ovarian neoplasms, and other tumors. Members of Li-Fraumeni syndrome families also are at risk of developing multiple primary cancers, with the highest risk being in those who survive childhood cancer (45); about 50% of these families have germline mutations of tumor-suppressor gene *p53*.

A rare ovarian adenocarcinoma develops years after tamoxifen therapy.

Screening: Currently no consensus exists regarding screening for ovarian carcinoma, although several studies suggest that transabdominal US has a moderate sensitivity in detecting ovarian cancer. Endovaginal US identifies most normal-to-atrophic ovaries in postmenopausal women, and even in those with nonvisualized ovaries an assumption of no tumor can be made. Adding Doppler US improves the tumor detection rate. Both endovaginal US and Doppler US suffer from a high false-positive rate and thus a low specificity. Nevertheless, screening US is not universally recommended, but it probably is of value in those with a family history of ovarian cancer.

Neither CT nor MRI is indicated for screening ovarian cancer.

In some women, but probably only in a minority with stage I tumors, elevated serum CA-125 levels are detected prior to the cancer being clinically evident. Ovarian cancer syndrome families have been screened with serum CA 125 and endovaginal US, with mixed results. Serum CA 125 is a glycoprotein tumor marker; elevated levels are also found in a number of other malignancies, including breast, endometrium, colon, pancreas, and some nonmalignant conditions, such as endometriosis, PID, pregnancy, uterine leiomyomas, and some liver disorders. CA-125 levels fluctuate during the menstrual cycle. It is insensitive with mucinous cancers. Its current major use is in following response to therapy and evaluating recurrence.

Pathologic Study

Ovarian epithelial neoplasms range from adenomas to adenocarcinomas, either serous or mucinous. A cystic structure is quite common. Overall, the serous variety predominates, and serous cystadenomas are slightly more common than serous cystadenocarcinomas. Some carcinomas are associated with an underlying ovarian abnormality, such as a complex cyst. Especially with the mucinous variety, a tumor may show considerable histopathologic variability and contain both benign and malignant components.

The best prognosis is with mucinous and endometrioid carcinomas, while a poorly differentiated carcinoma has the worst prognosis. With ovarian cystadenocarcinomas a better prognosis is associated with normotypic tumors, those having a mostly cystic content, a mononuclear infiltrate, limited histologic atypia, and no invasion.

Human papilloma virus RNA is detected in some ovarian carcinomas, although the biologic significance of this finding is not clear.

Most serous adenomas are unilocular and lined by a single cell layer, with a minority having solid papillary projections or a fibrous component. They vary in size considerably. About half of serous adenocarcinomas develop bilaterally. Serous adenomas, on the other hand, tend to occur unilaterally. Some consist mostly of an adenomatous component but contain foci of borderline or carcinomatous cells, thus suggesting a counterpart to the large bowel adenoma-carcinoma sequence—a controversial topic among pathologists. Serous ovarian carcinomas contain solid regions of tumor and varying amounts of necrosis and hemorrhage. Grade 1 tumors have a fine papillary structure, while grade 3 tumors consist of sheets of undifferentiated cells. In general, the less differentiated tumors are more prone to hemorrhage, necrosis, and increased solid components.

Primary ovarian serous carcinomas are histologically identical to the rare primary peritoneal papillary serous carcinoma. These serous tumors presumably have a multifocal origin. Confusion between these two entities abounds in a setting of a serous carcinoma discovered in the peritoneal cavity—is it a metastatic ovarian or a primary peritoneal tumor? The practical significance of such a differentiation is in the better prognosis with a primary peritoneal tumor.

A majority of mucinous ovarian tumors are benign. Both benign and malignant mucinous neoplasms are more common unilaterally. These tumors tend to be multilocular and an occasional one is huge. Similar to their serous counterpart, the cystic component of benign ones tends to be lined by a single cell layer, while the carcinomatous ones contain more solid components. More malignant ones often have less mucin and resemble other solid epithelial carcinomas.

The term *borderline malignant tumor* of the ovary (also known as *low malignant potential tumor*) designates a slow-growing epithelial tumor having a low potential for invasion or metastasis. These tumors are considered by some to be a distinct histologic and clinical entity, although aside from a better prognosis than with a more typical ovarian carcinoma, nothing suggests that they represent a separate entity. They can be either serous or mucinous. The Federation Internationale de Gynecologie et Obstetrique (International Federation of Gynecology and Obstetrics) (FIGO) and World Health Organization (WHO) use stromal invasion, defined as destructive infiltrative growth, to differentiate between a serous borderline tumor and an invasive carcinoma. These borderline malignant tumors have a better prognosis than more malignant ones, most are FIGO stage 1 at initial diagnosis. Similar to benign tumors, if stage 1 borderline malignant tumors are completely resected, further imaging is of limited use; on the other hand, with a more advanced stage, baseline posttherapy CT or MRI are appropriate.

Evidence suggests that ovarian mucinous borderline tumors can be subdivided into two distinct subtypes: intestinal and müllerian. Histology of the intestinal subtype reveals intestinal differentiation, while müllerian ones contain no such differentiation. Intestinal subtype is more likely to be a higher stage than the müllerian subtype.

An intermediate category, or micropapillary serous carcinoma, does not manifest a destructive infiltrative growth pattern but behaves as a low-grade invasive carcinoma.

Detection

The role of imaging in women with a suspected or palpable abnormal pelvic tumor of indeterminate origin is to determine the site of origin for that mass and aid in establishing whether it is benign or malignant. No consensus exists about the initial imaging modality to be used. Transabdominal US is often the first imaging study performed, although endovaginal US is preferred by some. At times both are performed. Computed tomography also plays a role, with MRI gaining credence in some centers as the imaging modality of choice. Nevertheless, in many centers most ovarian carcinomas present in an advanced stage and are detected on physical examination, with perhaps US being performed prior to exploratory laparotomy. At surgery the diagnosis is confirmed, the tumor is staged, and, as appropriate, it is either resected or debulked.

Calcifications in ovarian adenomas and adenocarcinomas have a fine, amorphous pattern and are scattered throughout the tumor. Some calcifications are sufficiently fine that they are identified as a diffuse increase in density throughout the tumor. In general, these calcifications suggest a serous tumor, in distinction to the coarser calcifications seen with mature teratomas.

These tumors range from solid to mostly cystic. Imaging shows most tumors as large, thin- or thick-walled, unilocular or multilocular cysts containing nodules varying in size. Overall, mucinous tumors tend to be larger than their serous counterparts.

The most common appearance of a serous cystadenoma is that of a thin-walled unilocular cyst. Intracystic papillary projections are found in some, but their presence should raise suspicion for a carcinoma. The unilocular and thin-walled ones tend to mimic a functional cyst, and a diagnosis of ovarian carcinoma is not always straightforward.

Most mucinous cystadenomas and cystadenocarcinomas are multilocular. Thick septations, nodules, and intratumoral hemorrhage suggest a carcinoma. Nevertheless, considerable overlap exists in the imaging findings between benign and corresponding malignant neoplasms. The findings suggesting a malignancy include a prominent solid component, thickened tumor wall or septa, nodularity, and tumor necrosis. Tumor spread to peritoneum or other adjacent structures is more common with a malignant tumor than with benign disease, but overlap exists. Also, larger fluid collections are associated with malignancy.

The CT density of serous tumors is close to that of water, while mucinous ones approach soft tissue density. Septal thickness varies considerably.

Transabdominal US detects most larger ovarian carcinomas simply as abnormal cystic tumors, with cyst echogenicity varying depending on cyst content. Ultrasonography results are operator and equipment dependent. Attempts to differentiate benign from malignant neoplasms

using morphologic findings have not achieved wide acceptance, although the presence of a solid component suggests a malignant tumor. Adding complexity to the issue are borderline tumors that cannot be reliably differentiated from either benign or malignant tumors by their imaging characteristics or their RI and PI values.

Can endovaginal color Doppler US differentiate benign and malignant ovarian and tubal tumors? In general, a low tumor marker CA 125 and Doppler US evidence of a lack of tumor blood flow exclude ovarian malignancy. Centrally located blood vessels are more common with malignant tumors, but even if no flow is detected by color Doppler US an ovarian malignancy cannot be excluded. In general, while PI and RI tend to be lower for malignant ovarian tumors, the values overlap and it seems reasonable to conclude that neither index is sufficiently reliable to be used in differentiating benign from malignant ovarian tumors. A diastolic notch is found in many benign tumors but is uncommon in malignant tumors. No single Doppler US criterion can differentiate between benign and malignant tumors, although a combination of the above findings is useful. By combining the results of endovaginal US and Doppler US, a sensitivity of over 90% is achieved by some operators in suggesting malignancy. In general, the diagnostic accuracy of endovaginal US is significantly greater in premenopausal than in postmenopausal women.

Magnetic resonance signal intensity of mucinous cystadenomas and cystadenocarcinomas varies considerably depending on the amount of mucin and blood. Fluid in serous cystadenomas has characteristics of water on all MR sequences, except when modified by hemorrhage.

Larger papillary projections in epithelial ovarian neoplasms have a distinctive fibrous stalk terminating in papillae containing signal intensities similar to fluid on T2-weighted images; smaller papillae are isointense signal on T2-weighted images. Papillae enhance post–MR contrast.

Endometrioid Neoplasms

Endometrioid ovarian neoplasms often arise in a setting of endometriosis and most are malignant. Almost one third of these women also have an endometrial adenocarcinoma. An association between ovarian endometrioid carcinoma and long-term tamoxifen use has been suggested.

Histologically, an endometrioid adenocarcinoma is difficult to differentiate from a carcinoma arising adjacent to a region of endometriosis. Some endometrioid carcinomas contain a squamous carcinoma component or a clear cell carcinoma. An occasional endometrioid tumor contains a yolk sac tumor component; these are aggressive tumors having a poor prognosis. A rare well-differentiated endometrioid adenocarcinoma is associated with elevated serum α-fetoprotein levels.

The imaging appearance of most endometrioid carcinomas is similar to that of serous and mucinous ovarian adenocarcinomas. Occasionally an endometrioid carcinoma has a more solid component, probably related to necrosis. In distinction to serous and mucinous tumors, papillary projections are uncommon in endometrioid carcinomas.

Five-year survival of women with an ovarian endometrioid carcinoma is similar to those with a serous carcinoma.

Clear Cell Carcinoma

Clear cell carcinomas invade locally but have a better prognosis than their serous and mucinous counterparts (in distinction to uterine endometrial clear cell adenocarcinomas, which have a worse prognosis than non–clear cell endometrial carcinomas). A solid component, including nodules in a unilocular cyst is a common imaging appearance for these ovarian tumors. They tend to mimic serous cystadenocarcinomas in their imaging appearance.

Staging

Tumor stage is the major prognostic factor with ovarian epithelial cancers. The FIGO and TNM ovarian cancer staging systems are outlined in Table 12.5.

Ovarian malignancies tend to be initially diagnosed and staged during exploratory laparotomy. Evaluation under general anesthesia is relatively accurate for localized tumors,

Table 12.5. FIGO and TNM staging of ovarian tumors

FIGO stage	TNM stage	
Primary tumor:		
	Tx	Primary tumor cannot be assessed
	T0	No evidence of primary tumor
IA	T1a	Tumor limited to one ovary; capsule intact, no tumor on ovarian surface; no malignant cells in ascites or peritoneal washings
IB	T1b	Tumor limited to both ovaries; capsules intact, no tumor on ovarian surface; no malignant cells in ascites or peritoneal washings
IC	T1c	Turner limited to one or both ovaries with any of the following: capsule ruptured, tumor on ovarian surface, malignant cells in ascites or peritoneal washings
IIA	T2a	Extension and/or implants on uterus and/or tube(s); no malignant cells in ascites or peritoneal washings
IIB	T2b	Extension to other pelvic tissues; no malignant cells in ascites or peritonea washings
IIC	T2c	Pelvic extension (2a or 2b) with malignant cells in ascites or peritoneal washings
IIIA	T3a	Microscopic peritoneal metastasis beyond pelvis
IIIB	T3b	Macroscopic peritoneal metastasis beyond pelvis 2 cm or less in greatest dimension
IIIC	T3c	Peritoneal metastasis beyond pelvis more than 2 cm in greatest dimension and/or regional lymph node metastasis
	Lymph nodes:	
	Nx	Regional nodes cannot be assessed
	N0	No regional lymph node metastasis
IIIC	N1	Regional lymph node metastasis
	Distant metastasis:	
	Mx	Distant metastases cannot be assessed
	M0	No distant metastasis
IV	M1	Distant metastasis (excludes peritoneal metastasis)

TNM pathologic classification:

Stage grouping:			
Stage IA	Tla	N0	M0
Stage IB	Tlb	N0	M0
Stage IC	Tlc	N0	M0
Stage IIA	T2a	N0	M0
Stage IIB	T2b	N0	M0
Stage IIC	T2c	N0	M0
Stage IIIA	T3a	N0	M0
Stage IIIB	T3b	N0	M0
Stage IIIC	T3c	N0	M0
	any T	N1	M0
Stage IV	any T	any N	M1

Note: Presence of ascites does not affect staging unless malignant cells are present.
Source: From the AJCC Cancer Staging Manual, 6th edition (2002), published by Springer-Verlag, New York, NY, used with permission of the American Joint Committee on Cancer (AJCC), Chicago, IL.

but is insensitive for more advanced lesions; extensive adnexal infiltration and lymphatic involvement are difficult to stage accurately. Complete staging includes hysterosalpingo-oophorectomy, para-aortic and retroperitoneal lymph node biopsy, omentectomy, peritoneal biopsy, and peritoneal washings.

Ovarian adenocarcinomas spread primarily to the peritoneal cavity, followed by adjacent structures and lymph nodes. The serous variety involves lymphatics more often than its mucinous counterpart. Hematogenous spread is a late occurrence. Peritoneal involvement, or pseudomyxoma peritonei, is more common with a mucinous carcinoma.

Chest radiography continues to be used to stage these tumors. Intravenous urography is rarely employed for staging. A barium enema is useful with the larger tumors to gauge colorectal invasion and with suspicion that an ovarian tumor may represent a colorectal metastasis rather than a primary tumor. In a number

of institutions colonoscopy is used instead, although little evidence exists that it is superior to a barium enema.

An overall staging accuracy appears similar for CT and MRI; neither imaging modality detects small mesenteric or small bowel implants. A CT limitation is its inability to detect subtle bowel serosal involvement and early peritoneal spread. Magnetic resonance imaging probably has similar limitations, but the evidence for this is not clear. Somewhat better results are obtained in staging advanced ovarian cancer; The Radiological Diagnostic Oncology Group reported a 92% CT sensitivity, 95% for MRI, and 69% for US in detecting peritoneal metastases (46); both CT and MRI were especially useful in subdiaphragmatic spaces and hepatic surfaces. Preoperative evaluation of pelvic and paraaortic lymph node metastases has a low sensitivity but high specificity, a consequence of assuming that lymph nodes above a certain size (typically 1.5 cm or larger) are involved by metastases. With these criteria, the detection of para-aortic lymph node metastases is greater than that for pelvic node involvement. One study achieved a MRI sensitivity of only 28% for pelvic lymph node involvement (47), a not untypical result. Complicating nodal analysis is that some women have positive paraaortic nodes but no pelvic node involvement; para-aortic node metastasis presumably occurs both by spread from pelvic nodes and directly.

Magnetic resonance imaging achieved a sensitivity of 73–77% for detecting bowel and mesentery spread, considerably better than for omental (38%) and lesser sac (43%) involvement (47). Carcinomatosis is detected with about a 90% sensitivity and specificity.

Addition of FDG-PET to CT increases accuracy of staging ovarian cancer considerably (48) and these dual modalities will undoubtedly be employed more often in the future.

Therapy

The current therapy for large, bulky ovarian carcinomas is cytoreductive surgery followed by chemotherapy. Such an approach is often not curative but does result in clinical remission and prolongs survival. Computed tomography aids in identifying those women who will not benefit from cytoreductive surgery.

Incidentally, postcontrast CT identified ovarian vein thrombosis in 80% of women after abdominal hysterectomy and bilateral salpingo-oophorectomy (49); no clinical thrombophlebitis was evident.

Follow-up/Metastasis

Follow-up of a woman with a previous ovarian carcinoma includes a physical examination, serum CA-125 levels, and imaging. CA 125 is useful in detecting recurrence of most (but not mucinous) ovarian carcinomas.

A longitudinal study in women with treated ovarian cancer found contrast-enhanced MRI to have a sensitivity of 91% and specificity of 87% in detecting residual tumor—results superior to serum CA-125 level and physical examination (50). Nevertheless, CT has a limited role in routine follow-up after carcinoma resection. Because of a high false negative recurrence rate, a normal CT scan is of limited use, realizing that a true positive study can save reexploration. On the other hand, in women with suspected or known recurrent ovarian cancer who are considered for secondary cytoreductive surgery, CT aids in differentiating between those amenable to debulking and those with an nonresectable tumor (51); hydronephrosis and pelvic sidewall invasion were findings pointing to tumor nonresectability. In some institutions a second-look laparotomy is preferred as a viable follow-up procedure.

Some investigators find that conventional imaging sensitivity and specificity are improved considerably by also performing whole-body FDG-PET (52), results difficult to place in perspective because other studies have found that FDG-PET does not improve the overall diagnostic accuracy in detecting recurrent ovarian carcinoma (compared with CT), especially for small tumor recurrences (53). It does have a role in women with inconclusive other imaging.

Magnetic resonance imaging is useful prior to reexploration in women with surgically staged ovarian cancer. Although MRI misses small implants, it does detect larger ones. Either a hyperintense abnormal structure on T2-weighted spin-echo (SE) images or early contrast enhancement on dynamic subtraction images suggests a recurrent tumor. Postopera-

tive fibrosis is hypointense on both T1- and T2-weighted MRI, and thus MRI should allow differentiation of fibrosis from recurrent tumor. Postoperative distortion, however, often results in a complex picture. Dynamic postcontrast subtraction MRI appears more accurate than precontrast imaging in differentiating fibrosis from recurrent tumor, although both sequences are often obtained.

In a prospective, blinded study of women with ovarian carcinoma, normal CA-125 levels, and no clinical evidence of disease after primary cytoreductive surgery and cytotoxic chemotherapy, immunoscintigraphy using indium-satumomab pendetide detected disease in all women with histologically proven tumor at reassessment laparotomy (54).

After the initial curative therapy, distant metastases are more common than local spread. Metastasis to the peritoneal cavity or even the stomach is not uncommon even with normal-sized preoperative ovaries.

Lymphatic spread is common. Enlarged paracardiac lymph nodes, detected by CT, represent a significant adverse prognostic factor.

Peritoneal involvement can be followed with peritoneal washings, which are often positive prior to imaging detection. Cul-de-sac aspiration cytology is useful in detecting tumor recurrence; it can be the only indication of recurrence. If needed, an implanted reservoir provides peritoneal washings for cytology at set intervals. Paracentesis and laparoscopy are not without risk, however; abdominal wall metastases develop in a minority of women at laparoscopic or paracentesis sites. Most of these metastases occur in a setting of FIGO stages IIIC to IV.

Metastasis to the liver as the first site is unusual, although eventual liver involvement, detected at autopsy, is relatively common. Abdominal or pelvic recurrence usually precedes lung metastases, but lung metastases, in the absence of disease in the abdomen and pelvis, occurs in 3% to 5% of women (55,56), and those with chest involvement usually also have elevated serum tumor markers.

Ovarian carcinoma metastasizes to the central nervous system. Most of these are serous cystadenocarcinomas. Unusual sites for metastases include axillary lymph nodes, inferior vena cava, breast, and bone.

Squamous Cell Carcinoma

Most primary ovarian squamous cell carcinomas are part of a dermoid cyst or associated with endometriosis, although an isolated squamous cell carcinoma also occurs. Some are associated with a cervical neoplasm. Human papilloma virus is identified in some of these tumors.

Ovarian squamous cell carcinomas tend to be solid except for regions of necrosis.

Brenner (Transitional Cell) Tumor

Brenner tumors, or transitional cell tumors, are of epithelial-stromal origin. Their appearance is similar to transitional cell uroepithelium, most are considered benign, but an occasional one is of low malignancy or even represents a transitional cell carcinoma. Some are associated with mucinous ovarian neoplasms. Occasionally found are bilateral Brenner tumors.

Imaging reveals most to be solid tumors, at times quite large. Extensive calcifications are a characteristic finding. A cystic component found in some of these tumors probably represents another cystic neoplasm.

These tumors tend to be hypointense on both T1- and T2-weighted MRI and thus appear similar to an ovarian fibroma or uterine leiomyoma.

Psammoma Tumors

Psammoma ovarian carcinomas tend to be of low malignancy, comparable to borderline-malignant ovarian tumors. Some contain extensive calcifications and can mimic a leiomyoma.

Sarcoma

Primary ovarian sarcomas are rare. Most are mixed müllerian tumors and include such components as endometrioid stromal sarcoma, rhabdomyosarcoma, or even a chondrosarcoma or adenocarcinoma. These tend to be rather aggressive tumors. A primary ovarian leiomyosarcoma developed in an adolescent who had prior radiation therapy for a medulloblastoma (57).

An ovarian fibrosarcoma contains solid, CT contrast-enhancing regions and a cystic component consisting of hemorrhage, degeneration,

and necrosis. Fibrosis is not a prominent feature with these tumors and MR is nonspecific.

Similar to other sites, a primary ovarian angiosarcoma is a solid tumor usually containing multiple necrotic and hemorrhagic foci.

Malignant Germ Cell Tumor

Malignant ovarian germ cell tumors account for 2% to 5% of all ovarian cancers. Age at presentation is considerably younger than with epithelial carcinomas. These tumors are mostly solid, heterogeneous, tend to necrose with growth, and develop amorphous calcifications (Fig. 12.19). Any septa present tend to be thick.

Generally a biopsy is necessary for diagnosis.

2-[18F]-fluoro-deoxy-D-glucose–PET in women after therapy reveals residual viable tumors to have an intense FDG uptake, allowing differentiation from mature teratomas, necrosis, or scar (58).

Dysgerminoma

Dysgerminomas are malignant, undifferentiated germ cell tumors. They represent the female counterpart to testicular seminomas. They occur almost always in adolescents and young women; some develop during pregnancy and some are bilateral. Increased prevalence is found in gonadal dysgenesis.

Some dysgerminomas result in hypercalcemia, leading to renal medullary calcinosis and vascular calcifications. A minority contain syncytiotrophoblasts and result in elevated β-hCG levels, but the α-fetoprotein levels are normal. As an example, a dysgerminoma with syncytiotrophoblastic giant cells was found in an 18-year-old phenotypic woman with 46,XX gonadal dysgenesis (59).

Lymph node involvement and intraperitoneal tumor nodules are common, with the nodules generally being small and few in number, but ascitic fluid cytology is positive in over half.

Imaging reveals a solid, multilobulated tumor. Internal fibrovascular septa are common. At times color Doppler US reveals prominent flow within septa.

These tumors are radiosensitive.

Immature Teratoma

Immature teratomas are rare, malignant germ cell origin neoplasms found mostly in girls and young women. These are rapidly growing, mostly solid tumors. Similar to their benign counterpart (mature cystic teratoma), they contain tissue from all three germ cell layers, but some of this tissue is immature or embryonic in origin. Some contain yolk sac tumor elements, and this component presumably accounts for the occasionally elevated serum α-fetoprotein levels. Any cystic component contains fluid ranging from water density to blood or sebaceous material (Fig. 12.20). Some immature

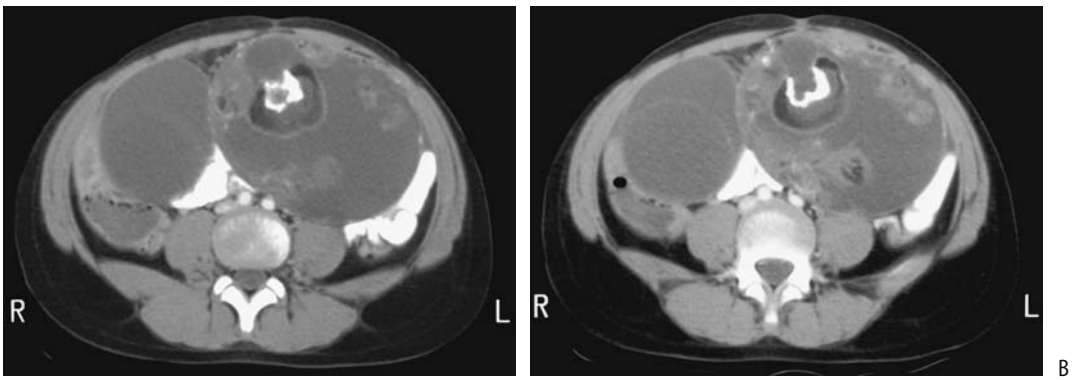

A B

Figure 12.19. Ovarian germ cell tumor with crossover syndrome in a 7-year-old girl with pain and precocious puberty. A,B: Two CT images show bilateral complex, cystic ovarian tumors with left one containing calcifications. The right ovary was stimulated by the left ovarian tumor. (Courtesy of Luann Teschmacher, M.D., University of Rochester.)

Figure 12.20. Longitudinal US scan in an 8-year-old girl reveals a cystic tumor containing mural nodules. It was an immature ovarian teratoma. (*Source:* Garel L, Dubois J, Grignon A, Filiatrault D, Vliet GV. Ultrasonography of the pediatric female pelvis: a clinical perspective. Radiographics 2001;21:1393–1407, with permission from the Radiological Society of North America.)

teratomas are associated with an ipsilateral mature teratoma.

At initial presentation most immature teratomas are larger than mature teratomas. Solid, irregular components predominate. Many contain amorphous calcifications and often also fat and old blood. Peritoneal spread is common.

MRI reveals solid tumors containing numerous cysts and punctate foci of fat (60); the solid components are heterogeneous on T2-weighted images. Cysts tend to contain simple fluid, in distinction to the sebaceous fluid in most mature cystic teratomas. Presence of ascites suggests peritoneal spread.

After chemotherapy some immature teratomas undergo maturation and resemble mature teratomas.

Embryonal Cell Carcinoma

A pure embryonal cell carcinoma is rare. More often it is part of another tumor. It is associated with elevated serum α-fetoprotein and β-hCG levels. It is the female equivalent of male testicular carcinomas.

In the appropriate clinical setting this tumor and choriocarcinoma result in precocious puberty.

Yolk Sac (Endodermal Sinus) Tumor

A yolk sac tumor, or endodermal sinus tumor, occurs mostly in girls and young women. It is a highly malignant ovarian and occasionally vaginal tumor. These tumors are believed to originate from an embryonal carcinoma differentiating into yolk sac structures. They are associated with contralateral or ipsilateral ovarian mature cystic teratomas. Yolk sac tumors are characterized by their rapid growth, early metastasis, and rapid recurrence following therapy. Abdominal pain and a palpable mass are typical presentations.

Computed tomography reveals yolk sac tumors to be complex, having a heterogeneous appearance, with hemorrhage and necrosis often present. They range from predominantly cystic to solid. Ultrasonography findings vary from hypoechoic to hyperechoic. They reveal marked MR contrast enhancement; FDG-PET identifies a metabolically active tumor.

The imaging differential diagnosis includes a tubo-ovarian or appendiceal abscess and other ovarian cysts and neoplasms.

These tumors tend to result in an elevated serum α-fetoprotein level; thus if imaging reveals a complex, mostly cystic pelvic mass in a young woman, it seems reasonable to obtain serum α-fetoprotein level. Also, the serum α-fetoprotein level is useful in gauging the response to therapy. Surgery combined with chemotherapy achieves a high survival if the tumor is limited to the ovary.

Hepatoid Carcinoma

Primary ovarian hepatoid tumors histologically resemble hepatocellular carcinomas, although they are a variant of a yolk sac tumor. These rare, aggressive tumors found in young women tend to be large at initial presentation. Admixed yolk sac tumors are common, but if the tumor is primarily hepatoid, a metastatic hepatocellular carcinoma is in the differential. Some are associated with elevated serum α-fetoprotein levels.

Choriocarcinoma

Similar to embryonal cell carcinomas, pure primary ovarian choriocarcinomas are rare and

most are mixed with other germ cell elements. The primary form has one of two origins: in association with an ovarian pregnancy and nongestationally as a primary germ cell tumor that differentiates to trophoblastic structures. Some of these tumors result in an elevated serum β-hCG level.

Imaging has a limited role in evaluating these tumors. These are solid and cystic highly vascular tumors. Larger ones become necrotic and bleed.

Metastases to Ovary

Metastases to the ovaries originate both from gynecologic and nongynecologic sites. Among nongynecologic tumors, breast and gastrointestinal tract cancers predominate. Some authors believe that a hallmark of metastases is bilateral ovarian involvement, although a multiinstitutional Radiology Diagnostic Oncology Group study of women with primary ovarian carcinoma and with a secondary ovarian neoplasm found that neither a predominately solid appearance nor bilaterality was significantly different between these two neoplasm groups (61). Some tumors metastatic to the ovary mimic a primary ovarian malignancy. At times a site of tumor origin cannot be established in the face of a widespread tumor spread.

Premenopausal ovaries appear to be more prone to developing metastases, probably because of their increased vascularity compared to postmenopausal ovaries.

Krukenberg Tumor

The definition of a Krukenberg tumor has undergone a change since the original definition of a gastric adenocarcinoma metastasizing to either one or both ovaries; presumably this condition represents drop metastases in the peritoneal cavity.

Currently many pathologists use the term *Krukenberg tumor* to describe a malignant mucinous signet-ring carcinoma located in the ovaries. Tumor primaries include the gastrointestinal tract, biliary tract, pancreas, and breast. A rare androgen-secreting Krukenberg tumor is encountered. Krukenberg tumors have been reported both in young women and in a setting of pregnancy. Surprisingly, a palliative oophorectomy and partial gastrectomy has led to long survival or even cure.

These tumors range from mostly solid and mostly cystic to entirely cystic. The cyst walls tend to exhibit strong CT contrast enhancement. Typically, MRI reveals a sharp tumor outline. Occasionally some of the more cystic tumors contain septations. A hypointense solid component on T2-weighted images is common with Krukenberg tumors, a nonspecific finding also seen with primary ovarian neoplasms. However, the presence of such a hypointense component, especially with bilateral ovarian tumors, should suggest a Krukenberg tumor. Some of these tumors contain fat, which is hyperintense on T1-weighted images and exhibits a decrease in signal intensity on fat-saturated, T1-weighted images (62).

Mesothelioma

An occasional malignant mesothelioma is confined to one or both ovaries and presumably represents an ovarian primary. More often, however, ovarian involvement occurs in a setting of widespread peritoneal seeding, and tumor origin cannot be determined. In addition, the histologic appearance of mesotheliomas varies considerably, and many of these tumors are either initially misdiagnosed by the pathologist or the diagnosis is uncertain.

These women do not have a history of asbestos exposure.

Most of these tumors are solid and of soft tissue density, with only an occasional one having a cystic component (Fig. 12.21).

Other Metastases

Colorectal carcinoma metastasis to the ovaries as initial presentation is uncommon. The exception is in adolescent girls, when colorectal carcinoma has an increased propensity to metastasize to the ovaries; these metastases range from solid to multilocular and mimic a primary ovarian neoplasm.

A uterine endometrial carcinoma does metastasize to the ovaries; often it is not possible to differentiate it from a primary ovarian endometrioid carcinoma.

One woman with an intraoperative diagnosis of disseminated ovarian carcinoma was found

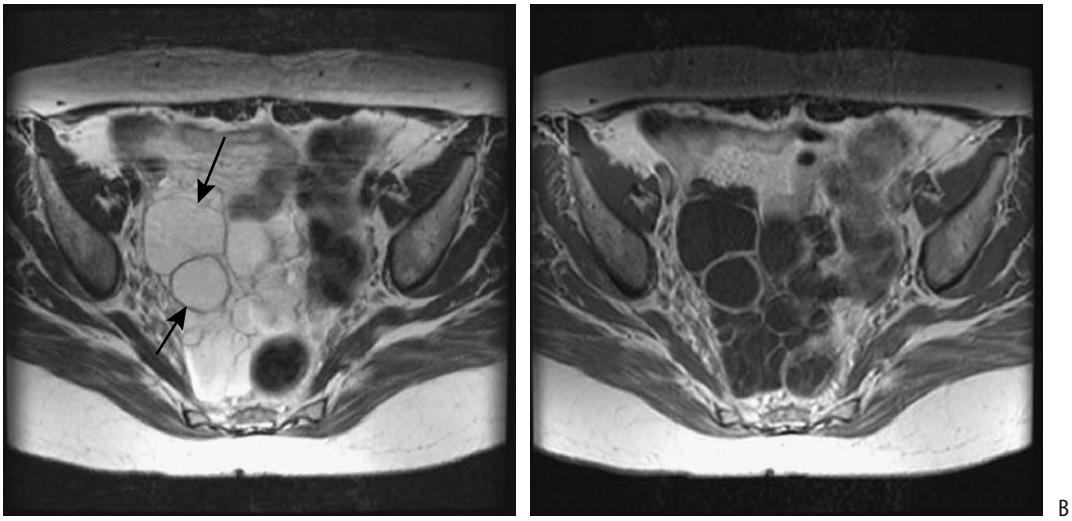

Figure 12.21. Multicystic mesothelioma. A: Transverse fast spin echo (FSE) T2-weighted MR image shows a pelvic tumor containing a hyperintense signal (arrows). B: Contrast-enhanced T1-weighted image reveals enhancement only in the solid component and septa of this multicystic tumor. (*Source:* Szklaruk J, Tamm EP, Choi H, Varavithya V. MR imaging of common and uncommon large pelvic masses. RadioGraphics 2003;23:403–424, with permission from the Radiological Society of North America.)

to have a metastatic adenocarcinoid, believed to be primary in the appendix (63).

Metastatic carcinoids, and the difficulty in distinguishing a metastasis from a primary ovarian carcinoid, are discussed below (see Carcinoid).

Magnetic resonance imaging of the rare metastatic malignant melanoma reveals a hyperintense signal on T1-weighted images. This finding is not seen with the even rarer amelanotic melanoma.

Lymphoma/leukemia

Primary ovarian lymphoma is rare. Ovariectomy is curative in this setting. More often, generalized non-Hodgkin's lymphoma involves bilateral ovaries, usually diffusely. Ascites is uncommon.

Computed tomography in women with ovarian lymphoma revealed well-marginated, often bilateral, hypodense tumors showing only mild contrast enhancement. Ultrasonography reveals solid, mostly homogeneous and hypoechoic tumors, and color Doppler US identifies mild vascularity. Magnetic resonance imaging detects homogeneous tumors moderately hypointense on T1- and slightly hyperintense on T2-weighted images, with only occasional contrast enhancement. Extensive associated lymph node enlargement should suggest the diagnosis. Little contrast enhancement, lack of a cystic or necrotic component, and no ascites argues against a primary ovarian epithelial neoplasm. An ovarian lymphoma can be associated with small peripheral cysts which represent ovarian follicles.

Leukemic infiltration of the ovaries does develop but generally systemic findings predominate.

Small Cell Carcinoma

The term *ovarian small cell carcinoma* is a descriptive one and includes several different tumor lineages. Some ovarian carcinomas are poorly differentiated and are difficult to categorize, and the occasional primary ovarian tumor resembling a lung small cell carcinoma falls in this category. Bilateral tumors are not uncommon. Some also contain a component of another tumor type, such as an endometrioid carci-

noma, or exhibit squamous differentiation. Some small cell carcinomas are associated with hypercalcemia; these occur mostly in girls and young women and have a poor prognosis.

Histologically, these tumors consist of diffuse sheets of small cells and a follicle-like component.

Carcinoid

Primary ovarian carcinoids are rare. Their classification is uncertain, but as mentioned earlier the current thinking is that they represent a teratoma; a worldwide registry of 329 women with ovarian carcinoids found 57% associated with a cystic teratoma or dermoid (64). Differences in carcinoid characteristics in these two groups are outlined in Table 12.6. Pathologists include strumal and mucinous varieties as subtypes of carcinoid tumor. A majority have a benign course.

Metastatic carcinoids to the ovary are more common than primary ones. At times differentiation between a metastasis and primary carcinoid is not possible; the lack of an identifiable nonovarian primary source does not exclude metastases. Some authors assume that bilateral ovarian carcinoids represent metastases rather than a primary ovarian origin, although exceptions probably occur.

Most ovarian carcinoids develop in postmenopausal women. The carcinoid syndrome is found only in a minority and appears related to tumor size.

Carcinoids are solid tumors, and their imaging appearance is similar to that of other solid ovarian neoplasms.

Excellent survival follows resection if the tumor is confined to one ovary.

Primary Ovarian Neuroendocrine Tumors

Primary ovarian neuroendocrine tumors are sufficiently rare to be almost ignored by most authors. They are difficult to classify but probably belong in the teratoma group. Histologically they can be subdivided into differentiated, primitive and anaplastic. They range from cystic to solid, and benign to wildly malignant.

Three histologic types are identified: differentiated, primitive, and anaplastic. Some resemble a medulloepithelioma, ependymoma, neuroblastoma, or medulloblastoma. The anaplastic ones can resemble a glioblastoma. Some contain foci of a mature cystic teratoma.

Renin Secreting Tumor

The rare ovarian renin secreting tumor can result in erythropoietin production and polycythemia. An occasional one results in elevated testosterone levels and virilization. Imaging identifies a solid ovarian tumor.

Meigs' Syndrome

Meigs' syndrome is an association of an ovarian tumor with ascites and pleural effusion but no tumor spread. The ovarian tumors range from benign to malignant. Occasionally a nonovarian tumor, such as a fallopian adenocarcinoma, is the underlying cause. Serum CA-125 levels are elevated and often the pleural fluid CA-125 level is also markedly elevated. Pathophysiology of the pleural effusion is not clear.

Table 12.6. Comparison of ovarian carcinoids with and without cystic teratoma/dermoid tumors

	With cystic teratoma/dermoid	Without cystic teratoma/dermoid
Number of carcinoid tumors	189 (57%)	140 (43%)
Average tumor size	45 mm	90 mm*
Rate of metastases	6%	22%*
Rate of liver spread	2%	15%*
Prevalence of carcinoid syndrome	14%	23%*
Five-year survival	94%	84%*

* Statistically significant differences between two groups.
Source: Adapted from Soga et al. (64).

This syndrome should be suspected in a setting of an ovarian tumor, ascites and pleural effusion, elevated CA-125 level, negative fluid cytology, and if imaging detects no peritoneal implants.

Ascites and pleural effusion clear after resection of the underlying tumor.

Fallopian Tube and Broad Ligament Neoplasms

Fallopian tube epithelial carcinomas include serous, mucinous, clear cell, endometrioid, and even a rare squamous cell carcinoma. A borderline papillary serous tumor, similar in appearance to its counterpart in the ovary, also occurs. Mesenchymal and mixed epithelial-mesenchymal neoplasms are rare. The most common fallopian tube malignancy is a serous adenocarcinoma. An occasional one develops bilaterally. Still, a fallopian tube carcinoma is the least common primary malignancy of the gynecologic organs.

Fallopian tube cancers are small, solid, and lobulated tumors having a CT soft tissue density and enhancing less than myometrium. They tend to be hypointense on T1- and homogeneously hyperintense on T2-weighted images (Fig. 12.22). Some are surrounded by fluid.

Table 12.7 lists both the FIGO and TNM staging systems for fallopian tube tumors. Published 5-year survival rates vary considerably, but range from 80% to 90% for stage I, dropping to about 20% for stages III.

Primary broad ligament neoplasms are rare. The most common one is a leiomyoma, with its malignant counterpart, leiomyosarcoma, being extremely rare. A rare granulosa cell tumor originates in the broad ligament. Broad ligament cystadenomas and carcinomas develop in a setting of von Hippel-Lindau disease; these tumors are similar in histologic appearance to the epididymal tumors found in men with von Hippel-Lindau disease.

A correct preoperative diagnosis is not common for fallopian tube and broad ligament neoplasms. Imaging simply reveals an adnexal tumor, often containing complex cystic and solid components. Some patients have an elevated CA-125 level, but the nonspecific nature of this marker precludes its use in diagnosis; it is more suitable for follow-up after surgery.

Figure 12.22. Fallopian tube adenocarcinoma in a 76-year-old woman. A: Sagittal FSE T2–weighted MR image identifies a pelvic mass containing heterogeneous signal intensity. This tumor was in the cul-de-sac, compressed the rectosigmoid colon, and was adherent to small bowel. B: Transverse postcontrast T1-weighted MR image shows peripheral tumor enhancement with extensive non-enhancing regions of necrosis. (*Source:* Szklaruk J, Tamm EP, Choi H, Varavithya V. MR imaging of common and uncommon large pelvic masses. RadioGraphics 2003;23:403–424, with permission from the Radiological Society of North America.)

Table 12.7. TNM staging of fallopian tube tumors

FIGO stage	TNM stage			
	Primary tumor:			
	Tx	Primary tumor cannot be assessed		
	T0	No evidence of primary tumor		
	Tis	Carcinoma-in-situ		
IA	T1a	Tumor limited to one tube without serosal penetration		
IB	T1b	Tumor limited to both tubes without serosal penetration		
IC	T1c	Tumor limited to one or both tubes with extension through tubal serosa		
IIA	T2a	Extension or metastasis to uterus and/or ovaries		
IIB	T2b	Extension to other pelvic structures		
IIC	T2c	Extension to pelvis with malignant cells in ascites or peritoneal washings		
IIIA	T3a	Microscopic peritoneal metastases outside pelvis		
IIIB	T3b	Macroscopic metastases less than 2 cm in diameter		
IIIC	T3c	Peritoneal metastases greater than 2 cm in diameter		
	Lymph nodes:			
	Nx	Regional nodes cannot be assessed		
	N0	No regional lymph node metastasis		
IIIC	N1	Regional lymph node metastasis		
	Distant metastasis:			
	Mx	Distant metastases cannot be assessed		
	M0	No distant metastasis		
IV	M1	Distant metastasis		
TNM tumor stages:				
Stage 0is		Tis	N0	M0
Stage IA		T1a	N0	M0
Stabe IB		T1b	N0	M0
Stage IC		T1c	N0	M0
Stage IIA		T2a	N0	M0
Stage IIB		T2b	N0	M0
Stage IIC		T2c	N0	M0
Stage IIIA		T3a	N0	M0
Stage IIIB		T3b	N0	M0
Stage IIIC		T3c	N0	M0
		any T	N1	M0
Stage IV		any T	any N	M1

Note: Both the Federation Internationale de Gynecologie et d'Obstetrique (FIGO) and TNM systems are included for comparison.
Source: From the AJCC Cancer Staging Manual, 6th edition (2002), published by Springer-Verlag, New York, NY, used with permission of the American Joint Committee on Cancer (AJCC), Chicago, IL.

The spread of fallopian tube carcinomas is primarily to the peritoneum, ovaries, and uterus. Intravascular spread via the inferior vena cava is rare.

Uterus

Endometrial Atrophy and Hyperplasia

Unopposed endometrial stimulation by estrogen leads to a greater than normal proliferation of endometrial glands and endometrial thickening. This condition develops in premenopausal women with polycystic disease, obesity, and estrogen-producing ovarian tumors. In postmenopausal women it is most often secondary to hormone therapy with unopposed estrogen.

Ultrasonography outlines the endometrium and measures its thickness, but cannot differentiate between a normal endometrium, hyperplasia, or a carcinoma. Small endometrial cysts are found both in atrophy and hyperplasia and in benign and malignant conditions. Most imaging studies have thus relied on evaluating a relationship between endometrial thickness and the presence of endometrial disease. Endometrial thickness measured by endovaginal US is greater than that obtained with a transabdominal approach, and measurements obtained with these two modalities are not directly comparable. Intra- and interobserver agreement of endovaginal US endometrial thickness measurements is relatively good, but a measurement close to any cutoff value should be interpreted with caution, especially if such a measurement affects clinical management.

A thin endometrium or smooth endometrial thickening detected by endovaginal hysterosonography suggests a benign condition. The presence of any irregular endometrial thickening or an inhomogeneous nodularity suggests a malignancy.

Precontrast MR cannot differentiate endometrial thickening from uterine secretions. Both are hypointense on T1-weighted images and hyperintense on T2-weighted images. Postcontrast, however, the endometrium enhances while secretions do not. Blood in the endometrial cavity can be differentiated on precontrast images; blood is hyperintense on T1-weighted images.

The use of oral contraceptives results in a gradual decrease in uterine size; the endometrium thins and shows little variation with menstrual cycle.

In postmenopausal women the endometrium is atrophic, and a thickened endometrium is presumptive evidence of a cancer; keep in mind that thickness measurements for hyperplasia and carcinoma overlap. Endovaginal US readily measures endometrial thickness. One problem is that the measured maximal endometrial thickness in postmenopausal women with endometrial atrophy and no abnormality varies considerably, ranging from 1.5 to 6 mm in various studies. The cutoff value below which the endometrium is considered normal is somewhat arbitrary, and resultant sensitivities and specificities of detecting endometrial disease vary, depending on the assumed endometrial normal cutoff thickness. A lower assumed limit for normal thickness increases confidence in a conclusion that no cancer is present and curettage can be avoided. A higher assumed limit decreases the number of false positives and thus increases specificity, but at the expense of sensitivity. As an example, the sensitivity of endovaginal US in detecting endometrial disease is about 95% to 98% when a maximum normal endometrial thickness of 2 mm is assumed, but decreases to about 80% if a 4 mm cutoff is adopted. A typical study conclusion is that postmenopausal women with an endometrial thickness >4 mm or some other similar limit need further study. Most cancers encountered in postmenopausal women are associated with an endovaginal US measured endometrial thickness of about 10 mm or more, but it is the smaller cancers and thinner endometria that are problematic.

To place this problem in another perspective, no subsequent abnormalities are detected in postmenopausal women if the endometrial thickness is <3 mm or so; an endometrial thickness of >10 mm is associated with hyperplasia, polyps, and carcinoma. The difficulty is in the intermediate group, which consists of a third or more of women with bleeding. Further guidance is provided in these women if endovaginal US detects a hypoechoic signal and a central echo between symmetrical endometrial surfaces—findings associated with no significant abnormality—while heterogeneity and a hyperechoic signal suggests an abnormality.

Some studies suggest that endovaginal US in women with irregular bleedings is as effective as D&C in detecting endometrial abnormalities (65), although it has a low specificity in detecting endometrial abnormalities, limiting its use in this patient population. In spite of these limitations, endovaginal US has evolved into a screening test for endometrial cancer, similar to the Papanicolaou screening test for cervical cancer. One should keep in mind, however, the occasional reported malignancy with an endometrial thickness of <3 mm.

Sonohysterography provides additional information. Among asymptomatic postmenopausal women evaluated with sonohysterography followed by endometrial biopsy before initiating hormone replacement therapy, hyperplasia was discovered in 23% of those with an endometrial thickness >5 mm and in none with an endometrial thickness of ≤5 mm (66); sonohysterography also detected other intrauterine abnormalities in 37% of women with an endometrial thickness of ≤5 mm and in 64% of those with an endometrial thickness >5 mm. The authors concluded that while an endometrial thickness of ≤5 mm does exclude hyperplasia, it does not exclude other intrauterine abnormalities.

In a postmenopausal woman occasionally US identifies endometrial fluid and a thin endometrium. Although such fluid is usually benign, in rare instances it is associated with a carcinoma. Intrauterine US using a high-frequency probe potentially evaluates myometrial invasion by an endometrial carcinoma.

Magnetic resonance reveals endometrial hyperplasia as diffuse endometrial thickening, best seen with T2-weighted imaging.

Endometrial Ossification

A rare premenopausal and even rarer postmenopausal woman develops endometrial ossifications. Endovaginal US in a 62-year-old woman revealed a hyperechoic region in the uterine cavity, suggesting an intrauterine foreign body (67); histology of endometrial curettage showed mature bone and a neutrophilic infiltrate with no evidence of malignancy.

Pathologically, endometrial ossification should not be confused with a müllerian adenosarcoma.

Benign Tumors

Endometrial Polyps

While the term *endometrial polyp* is a descriptive one, it is generally used to describe a focus of localized intraluminal endometrial hyperplasia. It is analogous to hyperplastic polyps found in the large bowel. Clinically, these polyps range from an incidental finding, a cause for bleeding, or are associated with infertility. They range from sessile to pedunculated, single or multiple, solid or containing cysts. Most are focal, with an occasional one extending diffusely for varying lengths. Endometrial polyps are more prevalent among women with a cervical polyp compared to those without a cervical polyp.

These polyps can be detected with hysterosalpingography. Ultrasonography reveals a focal homogeneous hyperechoic tumor outlined by smooth borders; at times a stalk is seen. Endovaginal sonohysterography (i.e., uterus distended with fluid) aids in their detection and generally allows differentiation of endometrial origin polyps and more deeply placed leiomyomata, although one should keep in mind that an occasional leiomyoma is pedunculated.

T2-weighted MRI reveals endometrial polyps as hypo- to isointense tumors compared to normal endometrium. They enhance postcontrast. Most authors believe that MRI is not sensitive enough to reliably distinguish a benign polyp from a malignancy. Nevertheless, T2-weighted fast spin echo FSE sequences in women with surgically proved endometrial polyps or carcinomas found that a central fibrous core (suggested by a hypointense signal) and intratumoral cysts (suggested by a hyperintense signal) were more common in endometrial polyps than in carcinomas, while myometrial invasion and necrosis were signs of a carcinoma (68); overall, a mean sensitivity of 79% and specificity of 89% were achieved in diagnosing a carcinoma.

Adenomyosis

Endometrial tissue within the myometrium is adenomyosis. The etiology is unknown. Most often adenomyosis is diffuse, although it also occurs focally and is then known as an adenomyoma. It consists of a focal aggregate of endometrial tissue and smooth muscle within the myometrium and has a discrete margin. An occasional one extends into the cervix. It is a common condition that prior to the US and MRI era was diagnosed primarily after hysterectomy.

Presenting symptoms with adenomyosis and adenomyoma tend to be nonspecific and mimic other disorders, including leiomyomatosis. An adenomyoma is an occasional source of bleeding. Adenomyosis does not respond to hormone stimulation.

Hysterosalpingography reveals single or multiple diverticular-like outpouchings extending into the uterine wall. Not all such outpouchings represents adenomyosis; many outpouchings are due to dilated glands or have other etiologies.

The uterus enlarges in diffuse adenomyosis. Although US and MR appearances of diffuse adenomyosis are usually characteristic, an adenomyoma occasionally appears similar to a small leiomyoma. Endovaginal US, with its better resolution, does detect adenomyosis. Published endovaginal US sensitivities in diagnosing adenomyosis or adenomyomas are in the 80% range and specificity percents in the high 80s to low 90s range.

Endovaginal US criteria of adenomyomas consist of poorly defined heterogeneous, hypo-, and hyperechoic subendometrial nodules containing small anechoic lakes and an asymmetric myometrial thickness. Although small myometrial cysts are common in adenomyosis, some cysts are congenital in origin and others are found in such disorders as leiomyomas. A false-positive diagnosis occurs secondary to vascular calcifications or muscle hypertrophy.

Endovaginal US and MRI have similar accuracies in detecting uterine adenomyosis. Magnetic resonance imaging is useful during pregnancy. Diffuse involvement typically reveals widening of the hypointense junctional zone on T2-weighted images, while cystic regions appear hyperintense. An MR junctional zone thickness of ≥12 mm appears reasonable in suggesting adenomyosis. The thickened hypointense junctional zone often has an irregular appearance due to smooth muscle hypertrophy surrounding endometrial glands.

Magnetic resonance identifies focal adenomyomas as poorly marginated hypointense regions within the myometrium (Fig. 12.23). Some adenomyomas enhance with contrast, but their appearance is not specific. Polypoid ade-

Figure 12.23. Adenomyosis. Sagittal T2-weighted image identifies an enlarged uterus containing multiple hyperintense myometrial foci (arrowheads). (*Source:* Imaoka I, Wada A, Matsuo M, Yoshida M, Kitagaki H, Sugimura K. MR imaging of disorders associated with female infertility: use in diagnosis, treatment, and management. RadioGraphics 2003;23:1401–1421, with permission from the Radiological Society of North America.)

nomyomas have a T2-weighted tumor signal intensity similar to that of adenomyosis. Adenomyotic cysts are filled with heterogeneous, often hyperintense fluid on T1-weighted images; some have a hypointense rim on T2-weighted images.

Uterine artery embolization is alternate therapy for women with menorrhagia due to adenomyosis. Studies suggest an improvement in symptoms and quality of life (69). Contrast enhanced MRI after uterine artery embolization reveals adenomyosis devascularization (70).

Leiomyomatous Tumors

Clinical

Uterine leiomyomas, also called *fibroids* and *myomas*, are well-marginated tumors consisting of smooth muscle and fibrous connective tissue. They do not have a true capsule. A familial predisposition exists to uterine leiomyomas. Their prevalence increases with age and they are more common in black than in white women.

Leiomyoma growth is variable and unpredictable. Increased tumor vascularity appears to predispose to growth; a leiomyoma with a detectable feeding artery is more prone to increase in volume than one without an identifiable feeding artery (71). With growth, ischemia leads to necrosis, hemorrhage, fibrosis, and calcification. Leiomyomas often grow during pregnancy; growth tends to be greatest during the first trimester. Following pregnancy, some myomas revert to their prepregnancy size. Some decrease in size after discontinuation of oral contraceptives.

Leiomyomas range in location from intraluminal, to intramural, to subserosal, some even being pedunculated. Intramural ones are confined to myometrium, submucosal tumors extend into the uterine cavity, and subserosal ones extend from the outer margin (exophytic). Intramural leiomyomas are the most common but the least often symptomatic. Larger myomas distort the uterine cavity but tend not to interfere with pregnancy unless they are located in the lower uterine segment or cervix. A submucosal location is the least common, but these are most often symptomatic, resulting in dysmenorrhea and infertility. An occasional pedunculated submucosal leiomyoma protrudes into the cervix. Some subserosal leiomyomas become pedunculated and mimic an extrauterine tumor or extend laterally into the broad ligament and mimics an ovarian tumor.

Lipoleiomyoma

Fat is normally not present in the myometrium, but is occasionally found in regions of degeneration or metaplasia. Fat is also detected in some leiomyomas, and pathologists label these mesenchymal neoplasms lipoleiomyomas. They constitute about 1% of all leiomyomas. Some pathologists believe that uterine lipoleiomyomatous tumors do not constitute a single entity but represent two distinct neoplasms: lipoleiomyoma and angiolipoleiomyoma. The former probably originates from lipomatous metaplasia within a leiomyoma, while the latter is analogous to a renal angiomyolipoma.

Magnetic resonance findings of uterine lipoleiomyomas vary considerably depending

on predominant tumor composition; some are even hyperintense on T2-weighted images.

Imaging

Intramural myomas are usually evaluated by transabdominal US and occasionally by endovaginal US, MRI, and hysteroscopy. Their follow-up is with US, although if a uterine-sparing myomectomy is contemplated and number and specific location of these myomas is needed, greater accuracy and sensitivity of MRI is advantageous.

Larger leiomyomas calcify and have a characteristic conventional radiographic appearance familiar to most radiologists.

Computed tomography shows a homogeneous, lobular uterine tumor, with any necrotic regions appearing hypodense. Aside from necrosis, most myomas enhance with contrast similar to normal myometrium, while most carcinomas are hypodense, although overlap exists (Fig. 12.24). Submucosal myomas growing into the uterine lumen tend to have a complex appearance, contain a hypervascular component, and at times mimic a carcinoma or sarcoma.

In women with uterine tumors, endovaginal US achieves a sensitivity of 90% to 95% in diagnosing leiomyomas. Specificity varies considerably, depending on false-positive rate. Although endovaginal US is more accurate than transabdominal US in a number of conditions, this may not be true for leiomyomas, especially those originating from the fundus and transabdominal US is indicated.

The sonographic diagnosis of most uterine myomas is straightforward. Most appear as

Figure 12.24. A large degenerative uterine leiomyoma extends from the pelvis into the abdomen. A,B: CT identifies a heterogeneous, cyst-containing, poorly enhancing tumor displacing bowel. C: A more inferior image identifies a smaller myoma anteriorly (arrow). In spite of extensive degeneration, only minimal tumor calcifications were evident. (Courtesy of Egle Jonaitiene, M.D., Kaunas Medical University, Kaunas, Lithuania.)

hypoechoic solid tumors having discrete margins. With cystic degeneration, especially in the submucosa, US reveals a "honeycomb" pattern mimicking endometrial hyperplasia. Some leiomyomas produce discrete acoustic shadowing with both transabdominal and endovaginal US (72). This shadowing originates from fibroid, muscle, and connective tissue transitional zones. Central hypoechoic foci and no detectable Doppler blood flow in some exophytic leiomyomas presumably represent necrosis.

Endovaginal color Doppler US provides myoma blood flow data. Intratumoral blood flow has a negative correlation with myoma size. Some myomas have PI values <1.0, similar to some malignancies. In general, neither PI nor RI can differentiate a myomatous from a nonmyomatous uterus.

Magnetic resonance imaging appears superior to US in detecting and localizing leiomyomas and establishing their relationship to the uterus. Nondegenerated leiomyomas are isointense to hypointense on T1- and also hypointense on T2-weighted images. Tumor margin is usually well defined, with an occasional hyperintense rim identified on T2-weighted images. Degeneration results in a variable appearance, with hemorrhage having a higher signal intensity on T1-weighted images and cystic degeneration being hypointense on T1- and hyperintense on T2-weighted images. Cystic regions do not enhance after intravenous (IV) contrast. Some initially nonenhancing regions postcontrast do eventually enhance on delayed images, probably due to vascular insufficiency. If needed, different imaging planes are useful to show that a pedunculated leiomyoma connects to the uterus.

Flow voids are detected by MRI between the uterus and some larger leiomyomas (73); pathologically, these flow voids are believed to represent dilated feeding arteries located outside of the leiomyoma.

The ovaries should be identified if a suspected leiomyoma has an atypical appearance or location. If the tumor cannot be separated from the ovaries, an ovarian fibroma/thecoma is in the MR differential diagnosis.

Complications

Clinically, some degenerated uterine leiomyomas mimic acute appendicitis; US aids in differentiating between these two conditions. Torsion, most often with a pedunculated subserosal leiomyoma, and hemorrhagic infarct of a leiomyoma lead to ischemia and an acute abdomen. Magnetic resonance imaging identifies a hyperintense rim on T1- and a hypointense rim on T2-weighted images, probably representing dilated blood vessels at the periphery.

Occasionally a large leiomyoma results in urinary retention. Similarly, a more posterior one can compress the rectum and result in constipation. A myomatous uterus compressing pelvic veins can induce pelvic vein thrombosis.

A leiomyosarcoma develops de novo either from smooth muscle cells or from sarcomatoid degeneration of a leiomyoma; the latter is rare but should be suspected if a myoma increases rapidly in size.

A rare uterine leiomyomatosis extends into the vena cava and even intracardiac.

Therapy

Medical therapy of fibroids ranges from nonsteroidal antiinflammatory drugs (NSAIDs) to hormonal therapy. Tumors do shrink in size but generally regrow after cessation of therapy.

Surgical options range from hysterectomy to myomectomy, including laparoscopic and hysteroscopic approaches.

Since the initial description in 1995 of selective arterial embolization of myomas with Ivalon particles (74), uterine artery embolization has evolved as viable therapy for symptomatic myomas. Considerable literature confirms that it is a less invasive and is safer in women with symptomatic leiomyomas than a myomectomy (75). Myoma feeding arteries are endarteries, while the myometrium is supplied by a collateral network. Thus myometrial vascularity tends to be preserved even in the face of myoma ischemia and necrosis. Presence of adenomyosis is not a contraindication to uterine artery embolization because similar therapy is also beneficial in women with adenomyosis. Postprocedure MR suggests that successful embolization results in hemorrhagic infarction (Fig. 12.25). Most investigators embolize polyvinyl alcohol particles, although gelatin microspheres, used in neuroradiology, appear promising. Most embolizations are bilateral; bilateral uterine artery embolization

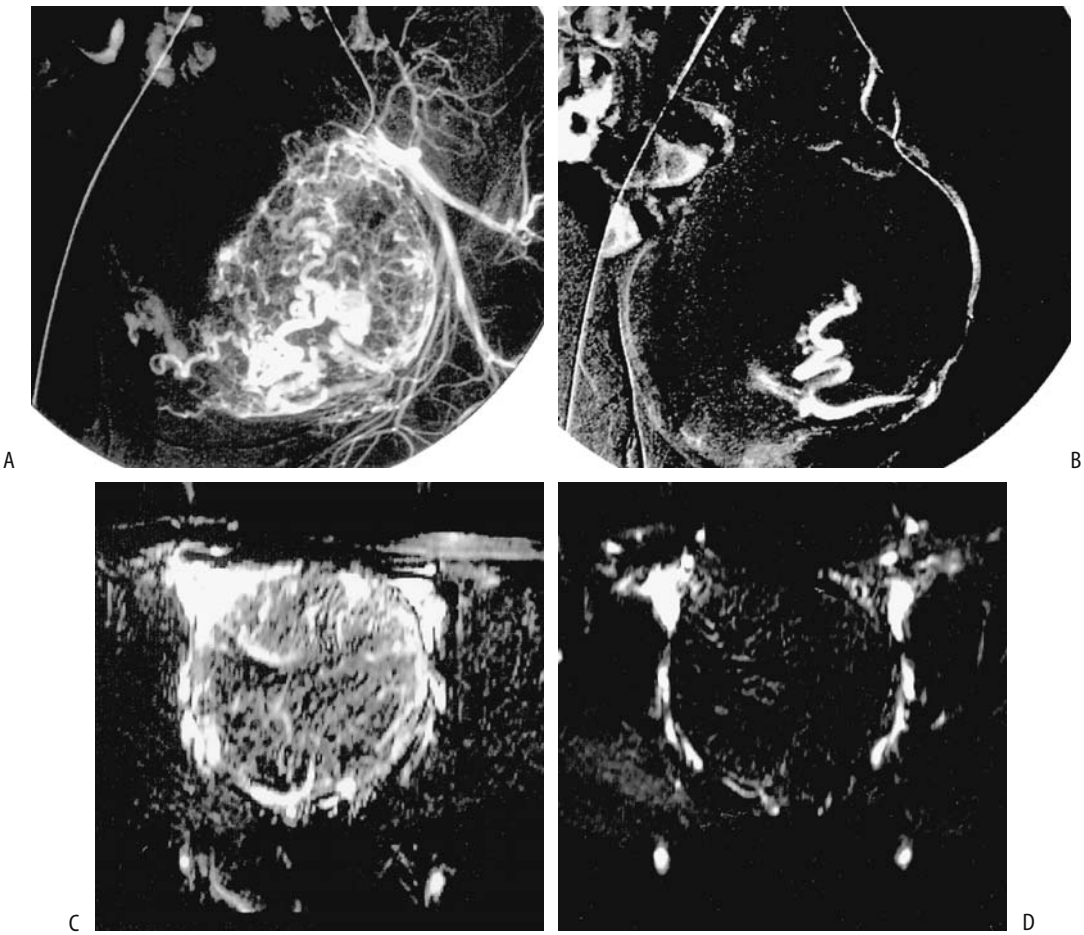

Figure 12.25. Uterine fibroid embolization. Shown are arteriograms before (A) and at the end of uterine fibroid embolization (B) and corresponding MR images before (C) and 1 day after embolization (D). MR images were obtained with an extraslice spin tagging technique, which evaluates tumor perfusion and tumor volume without the use of contrast. Serial posttherapy MR images revealed a decrease in original tumor size. (*Source:* Hagspiel KD, Matsumoto AH, Berr SS. Uterine fibroid embolization: assessment of treatment response using perfusion-weighted extraslice spin tagging (EST) magnetic resonance imaging. J Magn Reson Imaging 2001;13:982–986, with permission from Wiley-Liss, a subsidiary of John Wiley & Sons.)

can be performed using a single femoral approach.

First-pass postcontrast MRI can monitor uterine perfusion after fibroid embolization (76). The clinical utility of such monitoring is not clear. Arterial spin tagging MRI assesses uterine fibroid perfusion before and after arterial embolization (77); this technique provides an estimate of tumor volume and perfusion changes after embolization.

Reported symptomatic improvement ranges from 80% to 85%, results similar to those obtained with myomectomy. Pain and fever are common after the procedure. An occasional postprocedure infection requires hysterectomy. Sloughed fibroids (78), uterine necrosis (79) and even death secondary to overwhelming sepsis after embolization have been reported (80). Uterine artery embolization can lead to loss of ovarian arterial perfusion, but US reveals that most women reestablish perfusion and do not develop ovarian failure (81). Amenorrhea develops in a minority. On the other hand, embolization avoids surgery in most patients, and

menstrual periods return to normal in menorrhagic women. Full-term pregnancy has occurred after embolization.

Postprocedure imaging follow-up, if deemed necessary, consists of measuring decrease in myoma volume, uterine volume, or change in uterine blood flow. All require that a similar preprocedure imaging study be available. A marked reduction in fibroid volume occurs after successful embolization, with mean myoma volume continuing to decrease for a number of months. Follow-up US shows about a 50% eventual reduction in uterine volume. Serial gadolinium-enhanced MRI reveals that completely infarcted uterine fibroids eventually decrease in size considerably, but partially infarcted ones can regrow and result in recurrent symptoms (82). Interestingly, a preembolization high signal intensity on T1-weighted images predicted a poor response and a high signal intensity on T2-weighted images a good response, but the degree of contrast enhancement did not correlate with myoma volume reduction (83).

Another therapeutic option is laser ablation of uterine fibroids using an open MR scanner for needle guidance. One study achieved a mean fibroid volume decrease of 38% at 3 months (84); a percutaneous approach under local anesthetic was used.

Neither US nor MRI differentiates between a leiomyoma and a leiomyosarcoma, and one concern is embolizing a leiomyosarcoma. A biopsy is generally not helpful. A rationale for continuing to perform embolization is the very low prevalence of sarcomatous degeneration, but a sarcoma is in the differential diagnosis if a tumor continues to grow after embolization; sarcomas tend to develop an extensive parasitic blood supply (85).

Lipoma

Lipomatous uterine tumors include pure lipomas, fibrolipomyomas, and lipoleiomyomas (discussed previously). These tumors are not common. With some, a correct preoperative diagnosis can be suggested by imaging. Differentiation between a lipomatous uterine tumor and an ovarian dermoid has clinical significance, because most lipomatous tumors can be observed. A dermoid, on the other hand, is associated with more complications and is usually resected. The boundaries and origin of a large lipomatous tumor are difficult to establish with endovaginal US; therefore, in this setting transabdominal US with its better global definition is worthwhile.

Ultrasonography shows a homogeneous, hyperechoic tumor, similar to a dermoid. Doppler US reveals lack of blood flow. To differentiate between the two, a tumor site of origin needs to be established; a lipomatous tumor originates from uterine myometrium, while most dermoids are ovarian in origin.

Hemangiopericytoma

Uterine hemangiopericytomas are rare. They are readily confused with a highly vascular leiomyoma or leiomyosarcoma. There is no specific imaging finding for these tumors.

Adenomatoid Tumor/Benign Mesothelioma

These are rare, benign tumors usually presenting as a focal mass. An occasional one infiltrates the myometrium diffusely.

Cervical Cysts

Nabothian cysts, or inclusion cysts, of the cervix are common. They vary in size considerably. Although most are incidental findings, the larger ones and multiple cysts tend to enlarge the cervix.

T2-weighted MR images reveal a hyperintense signal, reflecting the cystic nature of these lesions. They are sharply marginated and do not enhance postcontrast.

Hydrometrocolpos

Hydrometrocolpos means a nonsanguineous fluid-filled uterus and vagina. The most common cause is an imperforate hymen, although it may also be secondary to undetected vaginal atresia. Hydrometra and hematometra occur with cervical obstruction. A unilateral hydro- or hematometrocolpos develops in a bicornuate uterus with an obstructing partial vaginal septum.

Ultrasonography of hydrometrocolpos reveals a cystic, anechoic structure. Residual

blood products lead to an increase in echogenicity.

Pyometra

The imaging findings of pus in the uterine cavity, or pyometra, are similar to those seen with hydrometra or hematometra.

Malignant Tumors of the Uterus and Cervix

A majority of endometrial malignancies are adenocarcinomas. Less common are adenoacanthomas, transitional cell carcinomas, adenosquamous carcinomas, and squamous carcinomas.

Adenocarcinoma

Clinical

The most frequent gynecologic malignancy in women is an endometrial adenocarcinoma. Initially detected tumors are mostly stages I and II. Overall, they are associated with a relatively good prognosis, with a 5-year disease-free survival being over 80%. Most develop in postmenopausal women. Premenopausal women with these tumors are prone to develop synchronous ovarian malignancies.

An association between human papilloma virus (HPV) infection and ovarian and endometrial carcinomas is controversial. Some studies point to only a limited association, while others have found HPV sequences in roughly half of ovarian carcinomas and some endometrial carcinomas. The biologic significance of such infection is yet to be determined.

Conditions believed to be risk factors for endometrial carcinoma include those that result in unopposed endometrial stimulation by estrogen and include obesity, hypertension, diabetes mellitus, polycystic disease (Stein-Leventhal syndrome), long-standing estrogen use, and functioning granulosa cell tumors and thecomas. In premenopausal women some forms of endometrial hyperplasia evolve into an adenocarcinoma. On rare occasion an endometrial adenocarcinoma develops in a setting of an intrauterine pregnancy. In postmenopausal women, unopposed estrogen replacement therapy is associated with these tumors. An estrogen antagonist, tamoxifen, is used for adjuvant therapy of breast cancer. Tamoxifen has an estrogenic effect on the endometrium, and therapy increases the risk of endometrial carcinoma, endometrial polyps, and cystic hyperplasia.

Even if an endometrial cancer shows no myometrial invasion, hysterectomy does not necessarily result in cure; recurrence, peritoneal dissemination, and lymph node metastases are possible due to earlier spread.

With growth, some endometrial carcinomas obstruct the cervix and result in hydrometra or hematometra.

Screening for endometrial cancer consists mostly of measuring endometrial thickness with endovaginal US, especially in postmenopausal women (discussed in a previous section).

Pathologic Study

Common endometrial adenocarcinomas predominate. Less often found are papillary, serous, mucinous, and clear-cell adenocarcinomas. A rare oxyphilic cell variant of endometrioid adenocarcinoma is believed to represent an early stage of adenocarcinoma. The rare hepatoid adenocarcinoma is discussed in a later section.

Detection

The diagnostic approach to a woman with postmenopausal bleeding and suspected endometrial carcinoma consists of endometrial and endocervical curettage performed under anesthesia, often on an outpatient basis. A hysteroscopic approach is used if the above procedure is unsatisfactory.

Hysterosalpingography is rarely performed for suspected endometrial carcinoma. The incidentally detected carcinoma appears as a single or multiple irregular tumor extending into the uterine cavity.

Computed tomography reveals an endometrial carcinoma either as a focal or diffuse uterine wall thickening. These cancers show less contrast enhancement than normal myometrium or cervix. Cervical canal obstruction is inferred by detecting intraluminal fluid, although obstruction may be due to benign

causes. Some of these cancers are mostly exophytic and are seen as an intraluminal uterine soft tissue tumor, at times having a cystic appearance.

Most authorities agree that endovaginal US is superior to transabdominal US in detecting endometrial neoplasms. Although endovaginal US does detect many endometrial cancers with reasonable certainty, detection of subtle cancers revolves around measurement of a thickened endometrium, adjusted for age and possible hormone therapy (discussed earlier; see Endometrial Atrophy and Hyperplasia).

Blood flow through an endometrial cancer can be measured with endovaginal color Doppler US, but intratumoral blood flow analysis does not predict either tumor stage or provide a histologic diagnosis and, in fact, does not discriminate between benign and malignant endometrium.

The MRI findings of benign endometrial disease and carcinoma overlap somewhat (staging is discussed in the next section) (Fig. 12.26). Because T2-weighted images identify uterine zonal anatomy, they are useful both in detecting and staging endometrial cancers. These tumors tend to be isointense to normal endometrium, and thus smaller cancers blend in with the endometrium. With growth, the endometrium widens, a nonspecific finding.

Staging

Clinical: Imaging findings of endometrial carcinoma need to be placed in a surgical perspective. Clinical staging of endometrial carcinoma is sufficiently inaccurate that FIGO recommends surgical staging (FIGO and TNM staging is given in Table 12.8). Currently most surgeons stage endometrial carcinoma at surgery and modify the resultant therapeutic approach accordingly. In a high surgical risk woman or with suspected advanced disease, however, imaging does provide additional information prior to therapy.

Histologic grade and stage establish the prognosis. Prognosis is significantly worse with clear cell adenocarcinomas and mixed endometrial–clear cell types compared with more typical endometrial carcinoma.

The depth of myometrial invasion is of prognostic significance. Many surgeons use an intraoperative visual estimate of myometrial invasion as a guide to surgical aggressiveness in staging these tumors. A 50% depth of invasion is often used to differentiate lower risk from higher risk patients, and a number of imaging efficacy studies have also adopted a 50% myometrial invasion guideline.

In a setting of coexistent adenomyosis and endometrial cancer, depth of myometrial invasion is better defined by contrast enhanced

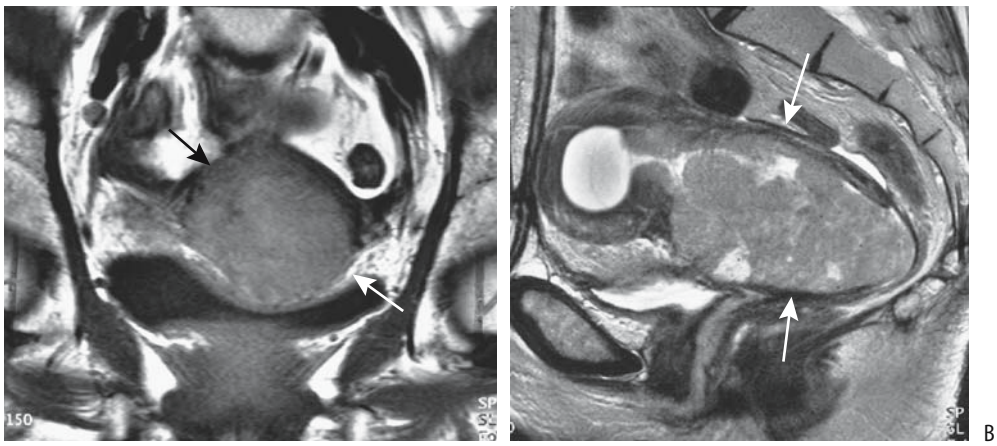

A B

Figure 12.26. Endometrial carcinoma. A: Coronal T1-weighted MR image reveals a uterine tumor (arrows). B: Sagittal contrast-enhanced image better identifies tumor size (arrows), including fluid in an obstructed fundus (arrowheads). (*Source:* Burgener FA, Meyers SP, Tan RK, Zaunbauer W. Differential Diagnosis in Magnetic Resonance Imaging. Stuttgart: Thieme, 2002, with permission.)

Table 12.8. TNM Staging of corpus uteri tumors

FIGO stage	TNM stage			
	Primary tumor:			
	Tx	Primary tumor cannot be assessed		
	T0	No evidence of primary tumor		
	Tis	Carcinoma-in-situ		
IA	T1a	Tumor limited to endometrium		
IB	T1b	Tumor invades less than half of myometrium		
IC	T1c	Tumor invades one half or more of myometrium		
IIA	T2a	Tumor limited to glandular epithelium of endocervix		
IIB	T2b	Invasion of stromal connective tissue in cervix		
IIIA	T3a	Tumor involves serosa and/or adnexa without cancer cells in ascites or peritoneal washings		
IIIB	T3b	Tumor involves vagina		
IVA	T4	Tumor invades bladder and/or bowel mucosa		
	Lymph nodes:			
	Nx	Regional nodes cannot be assessed		
	N0	No regional lymph node metastasis		
IIIC	N1	Metastasis to pelvis and/or para-aortic nodes		
	Distant metastasis:			
	Mx	Distant metastases cannot be assessed		
	M0	No distant metastasis		
IVB	M1	Distant metastasis		
TNM tumor stages:				
Stage 0is	Tis		N0	M0
Stage IA	T1a		N0	M0
Stage IB	T1b		N0	M0
Stage IC	T1c		N0	M0
Stage IIA	T2a		N0	M0
Stage IIB	T2b		N0	M0
Stage IIIA	T3a		N0	M0
Stage IIIB	T3b		N0	M0
Stage IIIC	T1		N1	M0
	T2		N1	M0
	T3		N1	M0
Stage IVA	T4		any N	M0
Stage IVB	any T		any N	M1

Source: From the AJCC Cancer Staging Manual, 6th edition (2002), published by Springer-Verlag, New York, NY, used with permission of the American Joint Committee on Cancer (AJCC), Chicago, IL.

dynamic T1-weighted MR imaging than by precontrast images (86).

An elevated preoperative CA-125 level is predictive of poor survival.

Imaging: Whether CT or endovaginal US is superior in gauging the depth of myometrial invasion is debatable. Initial reports suggested a similar accuracy for both CT and MRI in detecting cervical extension, although the junction between the uterus and cervix is not clearly identified by CT. A later helical CT study achieved a sensitivity of 83% and specificity of only 42% for detecting deep myometrial invasion and a sensitivity of 25% and specificity of 70% for cervical involvement (87), findings considerably worse than with MRI. The relatively poor CT soft tissue contrast (compared to MR) limits CT use in early staging but it is useful in advanced tumor stages.

Transabdominal US has a limited role in staging. On the other hand, endovaginal US is widely employed, achieving sensitivities of 65% to 90% in differentiating absent or superficial myometrial invasion from deep invasion (where deep invasion is generally defined as >50% myometrial involvement). Ultrasonography both overestimates and underestimates invasion; false positives include the presence of other uterine disease, including polyps.

In many institutions MRI has evolved into a leading role in staging endometrial carcinoma. Reported MR sensitivity and specificity in assessing myometrial infiltration are 87% and 91%, for cervical infiltration 80% and 96%, but for lymph node involvement only 50% and 95%, respectively (88). In assessing myometrial invasion postcontrast MRI is significantly better than nonenhanced MR. T2-weighted FSE and dynamic T1-weighted images are preferred, with parasagittal and coronal imaging assessing cervical and myometrial invasion. Overall, postcontrast MR staging accuracy is about 90%.

Disruption of the hypointense junctional zone by a hyperintense tumor, identified on T2-weighted images, implies myometrial invasion, although the junctional zone is not always identified in postmenopausal women. Magnetic resonance imaging staging is degraded by the presence of benign endometrial disease such as endometritis. Most endometrial carcinomas have less MR contrast enhancement than adjacent normal myometrium, with some exceptions. A tumor signal intensity in the outer half

of the myometrium signifies deep myometrial invasion, while disruption of the outer myometrial stripe is found with tumor extending beyond myometrium. Early, dynamic MRI is especially helpful in gauging myometrial invasion; it is more accurate than contrast-enhanced T1-weighted imaging or conventional T2-weighted imaging.

Focal disruption of the entire myometrial thickness implies serosal invasion. It is in detecting serosal invasion that MR achieves its lowest sensitivity, with false-positive results occurring mostly when the myometrium is <5 mm thick. Magnetic resonance imaging achieves an accuracy of about 90% in detecting cervical invasion. Normally the cervical epithelium is hyperintense on postcontrast images; continuous cervical epithelial enhancement on dynamic sequences aids in excluding cervical invasion (89). Compared to cervical squamous cell carcinomas, MRI of adenocarcinomas invading the cervix reveals a larger tumor and less overall tumor contrast enhancement but show greater enhancement at the tumor periphery compared to patients with a cervical squamous carcinoma. Occasionally a cancer has a polyp-like appearance in the cervical canal without invading cervical epithelium.

Computed tomography and MRI are similar in detecting nodal involvement, and both are superior to US. Both CT and MRI simply detect lymph node enlargement rather than identify direct tumor involvement.

Intraperitoneal metastases consist of solid or cystic tumors. Ascites is common. Small intraperitoneal tumor foci, however, are readily missed with imaging.

Bladder or rectal invasion is seen as an asymmetric wall thickening, with tumor at times extending intraluminally. A hyperintense bladder or rectal wall segment suggests invasion.

A chest radiograph aids in assessing lung involvement.

Recurrence/Metastasis

Metastasis to bone by endometrial carcinoma is unusual, although an occasional isolated, solitary bone metastasis is detected even before the primary tumor. An occasional metastasis is to the umbilicus (umbilical metastases of an abdominal cancer are also called Sister Mary Joseph nodes). Malignant pericardial effusion and brain metastases are rare.

A complication of locally advanced cervical carcinomas is uncontrolled hemorrhage. Embolization of the bleeding site is a therapeutic option.

Other Carcinomas

Only a limited number of endometrial transitional cell carcinomas have been reported. They have no distinguishing imaging findings.

A primary endometrial squamous cell carcinoma is rare. No specific imaging findings are available. In fact, even curettage specimens may not be diagnostic, revealing only differentiated squamous epithelium.

Several hepatoid adenocarcinomas have been described in the uterus, where they are considerably less common than in the ovaries. An endometrial hepatoid adenocarcinoma should be suspected if α-fetoprotein levels are elevated with a suspected endometrial carcinoma.

Sarcoma

Sarcomas represent 3% to 5% of all uterine malignancies. Leiomyosarcomas and stromal sarcomas are most common, with mixed müllerian sarcomas and rhabdomyosarcomas being occasionally encountered.

Most sarcomas are large at initial detection and imaging simply detects a large, irregular, necrotic tumor. Often the uterine outline is difficult to identify.

Stromal Sarcoma

Histologically an endometrial stromal sarcoma reveals intramural nests of endometrial stromal cells without endometrial glands. Most often originating from the endometrium, an occasional one arises from adenomyosis or endometriosis. A minority of these sarcomas are associated with antecedent pelvic radiation therapy. Anecdotal reports describe various uterine sarcomas developing years after tamoxifen therapy for breast cancer. Some exhibit complex histology and contain ovarian sex cord-like structures. Smaller ones tend to be confused histologically with adenomyomatosis containing few glands; imaging has a limited

role in differentiating between these two conditions. Also, uterine leiomyosarcomas have a similar imaging appearance.

Imaging reveals a complex cystic tumor within the myometrium. The solid component enhances with contrast. T2-weighted MRI of patients with endometrial stromal sarcoma reveals hypointense bands within regions of myometrial involvement, with pathologic study identifying these bands as preserved myometrium (90); these sarcomas tend to spread along vessels.

Leiomyosarcoma

Many uterine leiomyosarcomas are an unexpected finding after a hysterectomy for uterine fibromyomas. They have a poor prognosis, except for the occasional small, noninfiltrating tumor exhibiting little mitotic activity. Occasionally lung metastases regress after oophorectomy, presumably due to the lack of further ovarian hormone stimulation.

Ultrasonography findings are similar to those seen with a leiomyoma, except these tumors tend to have a more heterogeneous pattern with hyperechoic and anechoic regions and with cystic degeneration. Endovaginal color Doppler US reveals abnormal tumor vessels within sarcomas, a finding seen only in a minority of leiomyomas.

The MRI findings of most sarcomas are similar to those seen with a large leiomyoma. These tumors have a heterogeneous MR signal intensity.

Metastases developing after a hysterectomy for leiomyoma imply a missed low-grade leiomyosarcoma.

Mixed Müllerian Tumors (Carcinosarcomas)

Mixed müllerian tumors, also called *carcinosarcomas* and *müllerian adenosarcomas*, commonly have a benign, at times pedunculated appearance. In some immunohistochemical staining reveals estrogen and progesterone hormone receptors. A rare one produces α-fetoprotein. The relationship of such a tumor with hepatoid carcinomas (discussed previously) is conjecture. A cystic carcinosarcoma is rare.

Dynamic MRI of four revealed focal early and persistent enhancement, similar to the myometrium, mixed with regions of delayed enhancement (91); histology of the early enhancing component revealed mostly sarcomatous tissue containing prominent vascularity.

Rhabdomyosarcoma (Botryoides)

Sarcoma botryoides (*embryonal rhabdomyosarcoma*) typically occurs in the pediatric age group and is rare in an adult. In infants it usually involves the vagina and spreads by direct invasion and lymphatics, while in older girls a cervical origin is more common. These are soft tissue tumors. Necrosis and calcifications develop in some. They exhibit heterogeneous contrast enhancement.

Lymphoma

Primary malignant non-Hodgkin's lymphoma of the uterus is rare. Cervical lymphoma is difficult to diagnose because the lymphomatous infiltrate often mimics an inflammatory condition (Fig. 12.27). MRI of one primary cervical lymphoma revealed sparing of mucosa, most of stroma and uterine junctional zone, differentiating this condition from a carcinoma (92).

Secondary uterine involvement is common in the late stages of systemic lymphoma.

Cervical Carcinoma

Clinical

The current evidence suggests that HPV plays a role in cervical cancer. The HPV DNA is present in most cervical cancers. Immunosuppression and smoking are also risk factors for cervical cancer.

Most cervical carcinomas arise at the squamocolumnar junction. In younger women this junction tends to be located on the ectocervix, but with age evolves into the endocervical canal. These cancers range from adenocarcinomas and adenosquamous carcinomas to squamous cell carcinomas. A rare cervical adenocarcinoma contains other carcinomatous tissue; thus both choriocarcinomatous and hepatoid differentiation have developed, probably either from aberrant differentiation or neometaplasia of underlying epithelial cells.

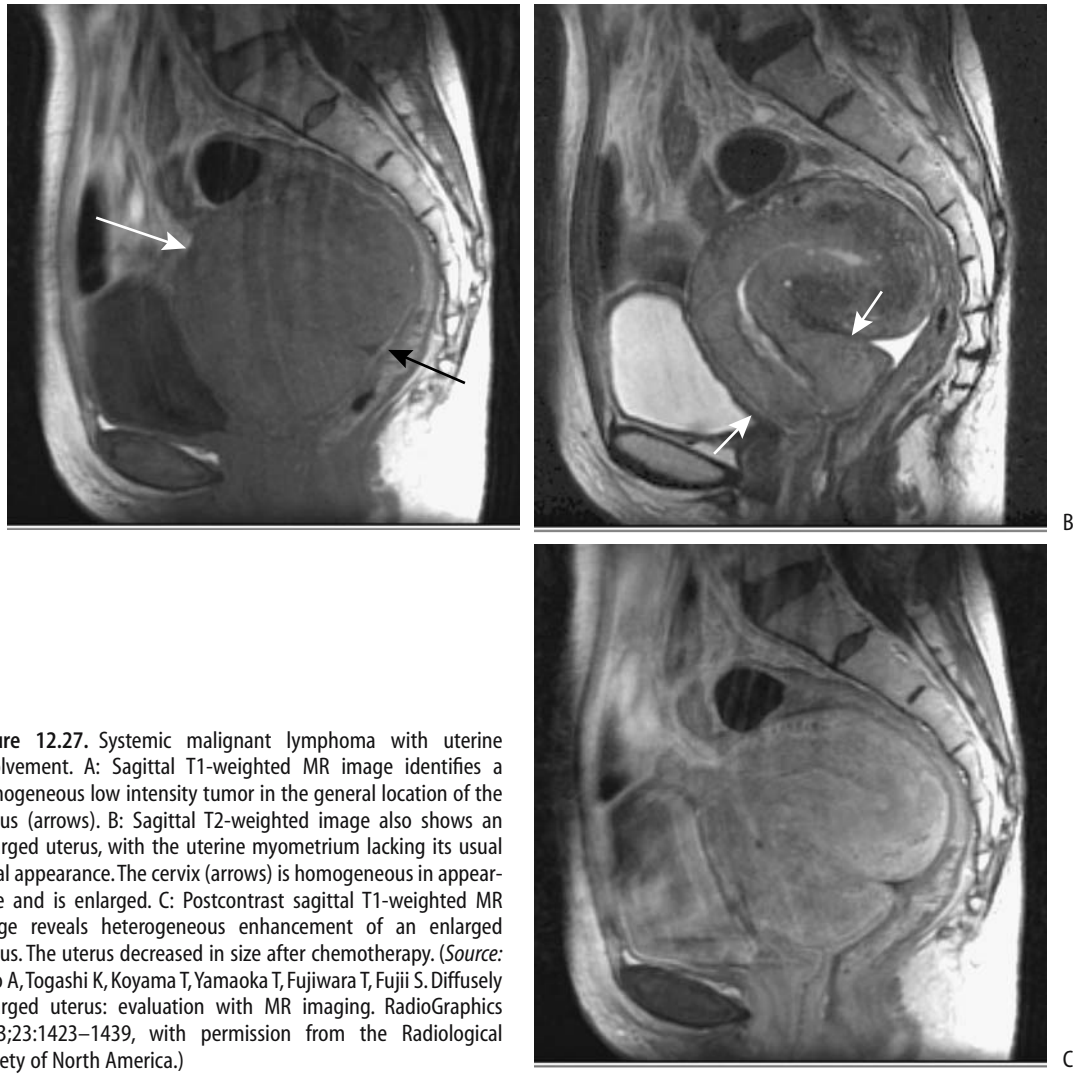

Figure 12.27. Systemic malignant lymphoma with uterine involvement. A: Sagittal T1-weighted MR image identifies a homogeneous low intensity tumor in the general location of the uterus (arrows). B: Sagittal T2-weighted image also shows an enlarged uterus, with the uterine myometrium lacking its usual zonal appearance. The cervix (arrows) is homogeneous in appearance and is enlarged. C: Postcontrast sagittal T1-weighted MR image reveals heterogeneous enhancement of an enlarged uterus. The uterus decreased in size after chemotherapy. (*Source:* Kido A, Togashi K, Koyama T, Yamaoka T, Fujiwara T, Fujii S. Diffusely enlarged uterus: evaluation with MR imaging. RadioGraphics 2003;23:1423–1439, with permission from the Radiological Society of North America.)

Neuroendocrine differentiation is evident in some, especially those with glandular differentiation.

Screening is with Papanicolaou smears. This is not a foolproof test, and both false-positive and false-negative results occur. A Papanicolaou smear tends not to detect small-cell carcinomas; immunohistologic staining is helpful with these. Overall, small cell cervical carcinomas have a poor prognosis.

Screening for cervical carcinoma is not practiced universally. A mass screening program was started in Finland in the mid-1960s. During the initial screening years the mean incidence of cervical carcinoma was 15 per 100,000 patient-years, while in 1991 it had decreased to 3 (93); mortality rate also decreased proportionally. The decrease was primarily in squamous cell carcinomas rather than in adenocarcinomas.

Detection

Imaging does not have a primary role in cervical carcinoma detection.

Carcinomas in the ectocervix tend to be polypoid and extend into the vagina. Endocervical cancers, on the other hand, infiltrate adjacent soft tissues. Fluid accumulates in the

uterine cavity with cervical canal obstruction. It is unusual to find a cervical carcinoma invading the endometrium, although an occasional one extends into myometrium. Because these tumors are centered in the cervix, most can be differentiated from endometrial carcinomas, which are centered in the endometrium. Computed tomography detects a cervical carcinoma as a soft tissue tumor either in the ecto- or endocervix. These tumors enhance less with contrast than do the surrounding soft tissues.

Endorectal US reveals cervical carcinomas as poorly defined tumors having indistinct margins in an enlarged cervix, ranging from hypoechoic to isoechoic relative to normal uterine tissue. Endovaginal color Doppler US of uterine arteries reveals a RI and PI significantly lower than normal.

In consecutive women, using a 0.5 tesla (T) unit, endovaginal MRI provided more information with stage I cervical carcinoma than an external phased array coil MR technique (94); endovaginal MR sensitivity was 96% and specificity 70% for tumor detection, while the external coil technique sensitivity was only 54% but at a higher specificity of 84%. The authors believe that the higher specificity with the external coil technique was because small abnormalities were seldom identified.

Magnetic resonance imaging reveals a cervical tumor isointense to muscle on T1- and hyperintense on T2-weighted images (Fig. 12.28). Most tumors are better defined on T2-weighted images, although smaller ones enhance with contrast and tend to be best seen postcontrast. Contrast enhancement occurs slightly earlier in a carcinoma than in normal cervical tissue. Postcontrast images occasionally show a hyperintense rim.

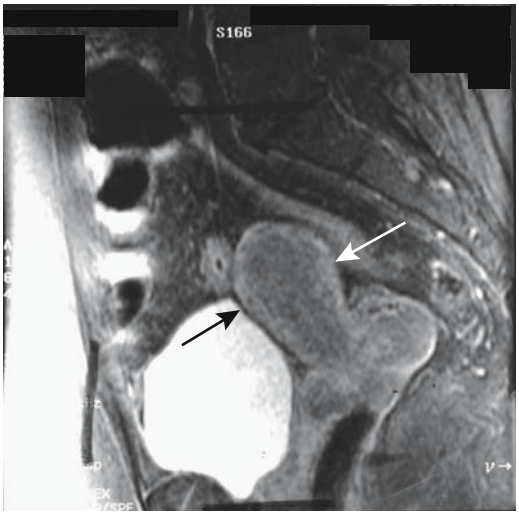

Figure 12.28. Cervical carcinoma. Contrast-enhanced sagittal MR image identifies a cervical tumor (arrows) having similar enhancement to uterus. (*Source:* Burgener FA, Meyers SP, Tan RK, Zaunbauer W. Differential Diagnosis in Magnetic Resonance Imaging. Stuttgart: Thieme, 2002, with permission.)

Staging

Clinical Staging: Initially cervical carcinoma spreads by direct extension into surrounding tissues. Pelvic lymph node involvement is common, with subsequent spread to para-aortic nodes. Hematogenous metastases are generally a late finding. Metastases have occurred in an episiotomy scar, scalene lymph nodes, pericardium, brain, and leptomeninges.

Clinical staging guidelines of cervical carcinoma by FIGO include chest radiography, barium enema, and IV urography, but do not include CT, US, or MRI findings (Table 12.9). A number of investigators have empirically modified the FIGO staging classification to

Table 12.9. Staging of cervical tumors

FIGO stage	TNM stage	
	Primary tumor:	
	Tx	Primary tumor cannot be assessed
	T0	No evidence of primary tumor
	Tis	Carcinoma-in-situ
IA	T1a	Invasive carcinoma diagnosed at microscopy
IB	T1b	Clinically visible lesion
IIA	T2a	No parametrial invasion
IIB	T2b	Parametrial invasion
IIIA	T3a	Tumor involves lower one-third of vagina
IIIB	T3b	Tumor extends to pelvic wall and/or or hydronephrosis
IVA	T4	Tumor invades bladder mucosa or rectum and/or extends beyond true pelvis

Source: From the AJCC Cancer Staging Manual, 6th edition (2002), published by Springer-Verlag, New York, NY, used with permission of the American Joint Committee on Cancer (AJCC), Chicago, IL.

include imaging, especially MRI. The latter offers additional data on stromal invasion and lymph node involvement. Postcontrast MRI, in particular, appears very useful. In a number of practices, a barium enema and IV urography are no longer obtained in staging these tumors. Ultrasonography, including endovaginal US, has achieved only limited acceptance.

Clinical FIGO staging is somewhat inaccurate, especially with nodal involvement and advanced stages, more often underestimating rather than overestimating tumor spread. In fact, lymph node involvement is not assessed in clinical FIGO staging. Nevertheless, clinical FIGO staging is the primary factor guiding treatment decisions. Imaging also has limitations, as discussed below; nevertheless, imaging is widely employed for both prognosis and therapeutic decisions.

General Imaging Findings: Relative imaging accuracy in staging early cervical carcinoma is not settled. Computed tomography has low staging accuracy. It cannot evaluate size or stromal invasion because it does not differentiate tumor from surrounding normal cervical tissue. Parametrial invasion is difficult to define. Computed tomography is useful, however, in suspected advanced disease, and CT detects ureteral invasion and the resultant hydronephrosis as well as rectosigmoid invasion. Comparison studies of CT versus MRI show MRI to be superior in staging these tumors (95) and, in general, CT has been largely supplanted by MRI (Fig. 12.29). Both sagittal and coronal views are useful.

Endovaginal Doppler US in women with locally advanced cervical carcinoma reveals significantly lower RI and PI values for the uterine arteries than in healthy women; no differences exist between tumor stages, and this information appears of limited use in staging.

In distinction to some other tumors, dynamic contrast enhanced MR of cervical carcinomas does not aid in treatment decisions in those considered for radical hysterectomy (96). T2-weighted sequences appear superior to contrast enhanced and fat-suppressed images. A phased array coil and a body coil achieve similar accuracies in local staging of invasive cervical cancer.

T2-weighted MRI reveals a hyperintense cervical tumor with an adjacent hypointense stromal ring (assuming the tumor is sufficiently large to be visible). Preservation of this hypointense stroma surrounding the tumor on T2-weighted images argues against parametrial invasion. Stromal disruption without visible parametrial tumor invasion is often considered an indeterminate finding, although the extent of stromal invasion detected varies on the sequences used. Magnetic resonance imaging can correctly predict myometrial invasion and identify cancer extension in relation to the internal os (97).

Regions of increased MR contrast enhancement consist mainly of cancer cell fascicles, while poorly enhancing regions are composed mostly of fibrous tissue containing scattered cancer cells (98) (Fig. 12.30). Contrast-enhanced dynamic MRI assesses tumor angiogenesis and appears to have prognostic significance. MR time versus signal-intensity curves of tumor contrast enhancement reveals that high-grade tumors have earlier MR contrast enhancement than lower grade ones, presumably due to their increased vascularity (99).

Vaginal invasion is usually evaluated clinically. Early vaginal invasion is difficult to detect with MRI, although MRI aids in detecting forniceal invasion. Rectal or bladder wall invasion is identified either on T2-weighted images or postcontrast. Magnetic resonance imaging suggests bladder invasion if an irregular bladder wall outline is evident or tumors protrude into the lumen.

Lymph Node Involvement: The ability to detect pelvic lymph node metastases is of obvious importance for staging gynecologic cancers, yet a high false-negative rate is evident with all imaging modalities. Thus in patients with various gynecologic cancers, the sensitivities were CT, 48%; MRI, 54%; and PET, 24% (100). The specificities, as expected, were high: CT, 97%; MRI, 91%; and PET, 77%. Other studies have achieved higher CT and MRI sensitivities (101), but otherwise these findings are typical. The poor PET results are due primarily to urinary FDG making the evaluation of pelvic lymph nodes difficult. A typical imaging definition of a metastatic node is a rounded soft tissue structure >10 mm in diameter or a node containing central necrosis. Central necrosis had a positive

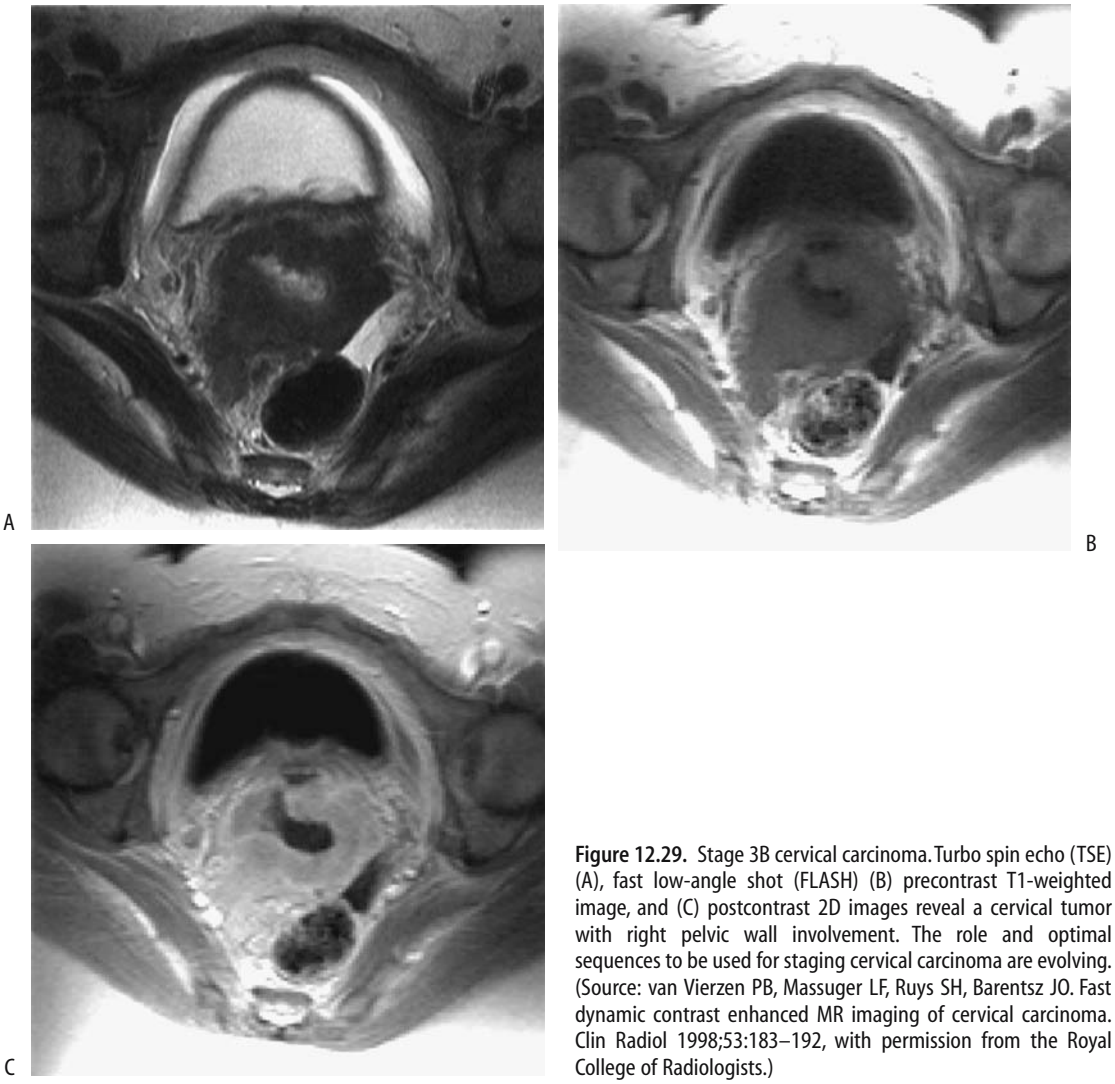

Figure 12.29. Stage 3B cervical carcinoma. Turbo spin echo (TSE) (A), fast low-angle shot (FLASH) (B) precontrast T1-weighted image, and (C) postcontrast 2D images reveal a cervical tumor with right pelvic wall involvement. The role and optimal sequences to be used for staging cervical carcinoma are evolving. (Source: van Vierzen PB, Massuger LF, Ruys SH, Barentsz JO. Fast dynamic contrast enhanced MR imaging of cervical carcinoma. Clin Radiol 1998;53:183–192, with permission from the Royal College of Radiologists.)

predictive value of 100% in detecting metastasis but is not common. Changing a metastatic node size criterion influences the sensitivity and specificity.

Lymphangiography, CT, and MRI are grossly similar in their ability to detect lymph node metastasis from invasive cervical cancer; because CT and MRI are less invasive, they are preferred. Abdominal US yield in detecting lymph node metastasis is low, so it has a limited role. Even intraoperative laparoscopic US of pelvic lymph nodes detects only slightly more than half of metastatic nodes.

Therapy

Therapy of premalignant cervical lesions includes cryotherapy, laser vaporization, and excision.

Therapy for invasive cervical carcinoma is generally surgical, except with extensive invasion to surrounding structures when radiation therapy is employed. Radiation therapy is also an option in those with pelvic recurrence after initial surgery. Occasionally long survival is achieved with radiotherapy for an unresectable cervical carcinoma. Adding chemotherapy improves prognosis in some.

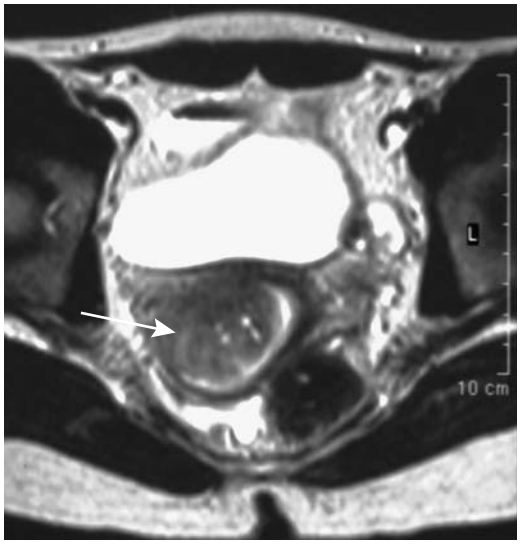

A

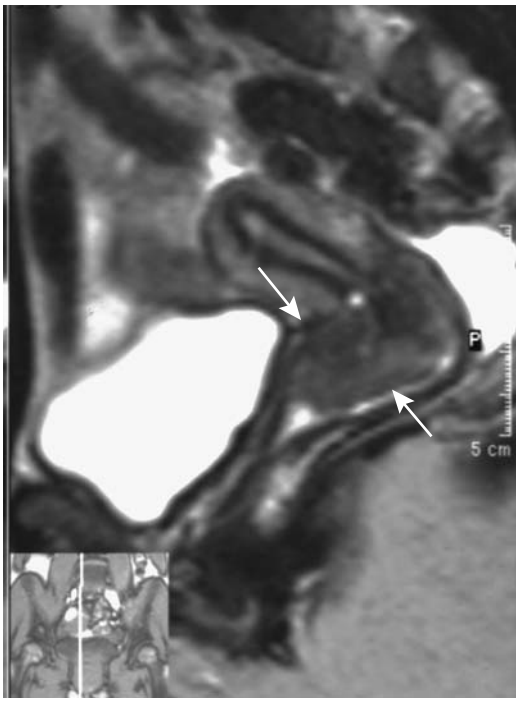

B

Figure 12.30. Cervical carcinoma. Transverse (A) and sagittal (B) MR images reveal a tumor infiltrating the uterine cervix (arrows). Right parametrial and myometrial invasion were suspected. (Courtesy of Egle Jonaitiene, M.D., Kaunas Medical University, Kaunas, Lithuania.)

Clinical stages IB and IIA are treated either by radical hysterectomy and pelvic lymphadenopathy or radiation therapy, depending on tumor size, while stages IIB and higher are in the province of radiation and chemotherapy. Thus a finding of parametrial invasion (stage IIB) affects the therapeutic options.

Local tumor control with radiation therapy depends on the site and the size of the recurrence, the type of therapy, and the dose used. Survival for those with central recurrence is longer than for those with pelvic wall recurrence.

Follow-Up

Surgery and radiation distort the subsequent imaging appearance, and follow-up is simplified if a posttherapy baseline study is obtained. Women who undergo laparotomy before radiotherapy appear to be at increased risk of developing small bowel obstruction.

Only a few studies discuss whether CT or MR is preferred for follow-up, although, similar to other pelvic tumors, a trend appears toward greater MR use, as it appears to be better able to differentiate between fibrosis and recurrence. Recurrence is either central around the cervix after radiotherapy, or at the vaginal cuff after hysterectomy, or at the pelvic side walls.

Magnetic resonance imaging estimates tumor size rather accurately, and when performed before and after chemotherapy it aids in evaluating tumor response. Initially both tumor recurrence and changes secondary to surgery and radiation are hypointense on T1- and hyperintense on T2-weighted MRI, but on a longer term basis (about 1 year or so) fibrosis also becomes hypointense on T2-weighted images. Actual results are more complex, because after radiotherapy local tumor recurrence tends to have a heterogeneous T2-weighted signal, with inflammation during the early posttherapy period being hyperintense. Later, cancer, degeneration, and necrosis are hyperintense, while fibrosis and granulation are hypointense. Magnetic resonance imaging after radiation therapy achieves a lower specificity in detecting tumor recurrence during the first 6 months after start of radiation therapy, but later sensitivity increases.

Local spread eventually encases and eventually obstructs the ureters. Metallic stents, at times augmented by J-endostents, are useful to maintain ureteral patency.

Adenoma Malignum

Adenoma malignum (minimal deviation adenocarcinoma) of the uterine cervix is a rare neoplasm suggested by cytologic atypia but not detected by cervical biopsy or Papanicolaou smears. Most authors separate it from the more conventional cervical adenocarcinoma. Pathologically, it tends to have a benign, cystic appearance and mimics endocervical glandular hyperplasia or cervical nabothian cysts, which are filled with mucus. This tumor has a poor prognosis. It tends to spread to the peritoneal cavity early in its course and is relatively resistant to radiotherapy and chemotherapy. Interestingly, this tumor often develops in patients with Peutz-Jeghers syndrome.

Endovaginal Doppler US showed extensive small vessels surrounding one such cystic tumor (102).

Magnetic resonance reveals multiple cysts deep in the cervical stroma. T1-weighted images shows them to be either isointense or slightly hyperintense relative to uterus and markedly hyperintense on T2-weighted images. These tumors contain solid components, with both the cystic and solid portions best identified on postcontrast images.

Whether MR can differentiate adenoma malignum from more benign cervical cystic lesions is debatable.

Other Cervical Tumors

An adenosarcoma is a rare tumor, most often occurring as a polyp in the endometrial cavity. Less often it originates in the cervix, mimics a benign cervical polyp, and is resected, and only histology identifies both he benign epithelial cells and the sarcomatous stroma.

A rare cervical neoplasm differentiates into a small cell neuroendocrine carcinoma. Lymph node metastases are common.

Vaginal Tumors

Many primary vaginal neoplasms are epidermoid in origin. They tend to have a polypoid or superficial ulcerating appearance, and most occur in the upper half of the vagina.

Carcinoma

A clear cell carcinoma of the vagina is associated with past exposure to diethylstilbestrol (DES). These tumors range from polypoid to infiltrating. Radiology has a limited role in their diagnosis but MR is useful in gauging spread.

Sarcoma

Vaginal rhabdomyosarcomas are found almost exclusively in young children, with only a few reported in postmenopausal women. Imaging is limited in their evaluation, except in outlining surrounding anatomy. Ultrasonography reveals a solid, mostly hypoechoic tumor.

An angiosarcoma infiltrates the surrounding soft tissues. These highly vascular tumors often are amenable to preoperative angiographic embolization.

Melanoma

Primary vaginal melanoma is rare. Most develop in postmenopausal women and occur in the lower third of the vagina. A bleeding exophytic tumor is not uncommon. Primary melanomas tend to infiltrate early, often involve the lymphatics, and have a poor prognosis. Melanoma metastasis to the vagina is also rare.

Fat-saturated T1-weighted MRI appears more useful than more conventional sequences in establishing the extent of tumor spread.

Metastasis/Invasion

Occasionally a mole invades the vagina. Women with these hypervascular tumors are at significant risk for major hemorrhage. Selective angiography with embolization can be lifesaving.

Paravaginal Cysts

Paravaginal cysts can be either inflammatory or developmental in origin (Table 12.10). They tend to be well defined and ovoid in shape. Their content of clear fluid, pus, or blood determines their imaging characteristics. Similar to other simple cysts, most paravaginal cysts are

Table 12.10. Paravaginal cysts

Inflammatory
Bartholin's gland cyst
Epithelial inclusion cyst
Mucous cyst
Developmental
Urogenital sinus cyst
Mesonephric cyst
Wolffian duct
Gartner's duct
Paramesonephric cyst
(Urethral diverticulum)

hypointense on T1- and hyperintense on T2-weighted MRI. Some have a fluid–fluid level; the dependent fluid is hypointense and the nondependent fluid hyperintense on T2-weighted images. These cysts show no contrast enhancement; the presence of a solid component or any enhancement should suggest a neoplasm.

Urethral Tumors

Most nephrogenic adenomas originate in the urinary bladder, with only an occasional one originating in the urethra or even in a urethral diverticulum. Most mimic other anterior vaginal wall tumors. Magnetic resonance imaging is useful in defining their extent.

An inverted papilloma of the female urethra is rare.

Primary urethral melanomas usually involve the distal portion. Most tend to be polypoid (103). Most of these tumors contain melanin, although prominent melanin is found only in a minority.

Urethral leiomyomas are very rare. Initial presentation is either acute urinary retention or hematuria, with an occasional stress incontinence.

The proximal one third of the female urethra is lined by transitional epithelium, and thus most proximal urethral carcinomas are transitional cell carcinomas, while distal ones tend toward adenocarcinomas. At initial presentation most have already spread to periurethral tissues and have a poor prognosis. Urethral carcinomas typically manifest with acute urinary retention. Lymph node metastasis is not uncommon at initial presentation. Computed tomography and MR reveal a well-marginated tumor with peripheral enhancement. The bladder base becomes elevated.

The rare periurethral sarcoma or carcinosarcoma also presents with acute urinary retention; imaging should suggest a urethral tumor.

Obstruction

Fallopian Tubes

The most common etiology for fallopian tube obstruction is pelvic inflammatory disease (discussed earlier in this chapter).

Hysterosalpingography is generally considered to be the gold standard in detecting fallopian tube occlusion in infertile patients. False-positive diagnoses of obstruction are caused by inspissated mucus, tubal diverticula in the distal ampulla in otherwise patent tubes, or insufficient pressure during contrast injection.

Hydrosalpinx

Fallopian tube obstruction due to any cause can result in a hydrosalpinx. Some patients undergoing in-vitro fertilization develop a hydrosalpinx, believed to be secondary both to an obstruction and increased secretions due to hormonal stimulation. The hydrosalpinx can be followed to resolution with serial US.

Magnetic resonance imaging identifies most dilated fallopian tubes and differentiates them from other adnexal tumors.

A primary megaureter can mimic a hydrosalpinx on US.

Recanalization

With lack of contrast spill into the peritoneal cavity during hysterosalpingography, selective salpingography differentiates between spasm and anatomic obstruction, and, if necessary, fallopian tube recanalization clears an obstruction (104); successful recanalization can be achieved in most women. On a long-term basis a number of these women again develop tubal obstruction.

Occlusion (Sterilization)

Most sterilization procedures belong in the realm of the obstetrician/gynecologist. The role of fallopian tubal occlusion with n-butyl-2-cyanoacrylate is not yet clear.

Cervix

Benign cervical stenosis is an occasional cause of infertility. It is often suspected when difficulty cannulating the cervical canal is encountered. Therapy consists of cannulating the cervix under fluoroscopic guidance and dilating the endocervical canal with balloon catheters or dilators.

Urethra

Bladder outlet obstruction is rare in women. Many of these women have had prior pelvic surgery. An occasional urethral neoplasm is a cause for obstruction.

Diverticula

Fallopian Tube

Salpingitis isthmica nodosa, or diverticulosis, is associated with pelvic inflammatory disease. Mucosal proliferation extends into the muscle layers, and the fallopian tube wall thickens. Infertility is common. An increased risk of ectopic pregnancy is associated with this condition.

Hysterosalpingography reveals diverticulum-like outpouchings in one or both fallopian tubes. These outpouchings range from solitary to multiple. The fallopian tubes tend to be dilated or obstructed, and a diverticulum can mimic distal tubal occlusion.

Fallopian tube recanalization is possible in salpingitis isthmica nodosa and may allow future intrauterine pregnancy.

Urethral

Incontinence and voiding dysfunction, regardless of cause, are discussed in Chapter 11.

Believed to represent sequelae of prior infected, obstructed, and ruptured periurethral glands, most urethral diverticula in women are acquired. Some authors differentiate a true diverticulum from a pseudodiverticulum, with the latter representing mucosal herniation through a periurethral fascial defect. Occasionally multiple, they are periurethral in location, and are most common along the posterolateral wall in the distal two thirds of the urethra.

These diverticula fill during voiding and then empty intermittently. Some larger ones are palpable. The differential diagnosis of a palpable periurethral soft tissue tumor includes a diverticulum, a periurethral cyst, and a soft tissue neoplasm.

Periurethral glands and ducts empty close to the urethral meatus, with the largest ones called Skene's ducts. A Skene's duct cyst, a consequence of either a congenital abnormality or a chronic inflammation, is palpable along the anterior vaginal wall. These cysts do not communicate with the urethral lumen, and a urethrogram thus differentiates them from diverticula. Also, MR identifies not only a cystic structure but also a solid, enhancing glandular component.

Adenomas and adenocarcinomas originate in urethral diverticula and paraurethral ducts near the urethral lumen. These are difficult to diagnose.

A radiopaque or lucent calculus forms in some of these diverticula secondary to stasis; it needs to be differentiated from a malignancy, generally an adenocarcinoma.

Urethral diverticula are studied with voiding cystourethrography, double-balloon urethrography, and US using an endovaginal, endorectal, or transperineal approach. False-negative results occur with all of these procedures. Voiding cystourethrography visualized only about three quarters of these diverticula, but due to its simplicity it is often the first test obtained. Urethroscopy has a low yield rate. Traditionally the double-balloon urethrogram has been the procedure of choice, although current US accuracy approaches that of a double-balloon study. Magnetic resonance occasionally aids in establishing the relationship of a diverticulum to the urethra and in evaluating other etiologies of a palpable tumor in this location. Video urodynamic studies reveal stress incontinence in some of these women, and then both a diverticulectomy and an anti-incontinence procedure are necessary.

Either endovaginal or endorectal US provides useful information about the shape, volume,

and content of a diverticulum, and about its relationship to the urethra. An endoluminal catheter-based US transducer identifies a diverticulum and aids in evaluating any periurethral inflammation and diverticular wall thickness.

Although currently not often used, MRI both detects these diverticula and outlines the surrounding structures. No bladder catheterization is required. Diverticula are hypointense on T1- and hyperintense on T2-weighted images. Currently MR has a role in women with a clinical suspicion of a diverticulum but negative double-balloon urethrography or US study; keep in mind that false-negative studies also occur with MR.

A rare diverticulum recurs postoperatively (105).

Fistulas

The role of imaging is to define the fistulous communications. External fistulas are best studied with fistulography. Magnetic resonance imaging appears superior to other imaging modalities in detecting and outlining the extent of vaginal and uterine fistulas.

An enterouterine fistula is rare. Most are secondary to neoplasms; these do not heal if tumor has grown into the fistula.

Vesicouterine fistulas tend to be secondary to prior cesarean section or abnormal delivery (106); urinary leakage from the vagina or cyclic hematuria is typical presentations. These fistulas are better identified with a cystogram than IV urography; hysterosalpingography also has a high yield rate, provided the study is of high quality.

Most vaginal fistulas are recto- or colovaginal, urethrovaginal, cervicovaginal, or vesicovaginal, with the latter being most common. Most are related to pregnancy or prior hysterectomy. Malignancy, radiation therapy, diverticulitis, inflammatory bowel disease, and even Behçet's syndrome are less common associated conditions.

Simple urovaginal fistulas extend to the bladder, urethra, or ureter; they are complex if more than two organs are involved. Most of these fistulas are symptomatic.

With a suspected vaginal fistula, vaginography using a water-soluble contrast agent should outline it. A barium enema is an alternative with a suspected colo- or rectovaginal fistula. Some authors have had better success in detecting a fistula with vaginography than with barium enema, although the results depend considerably on the technique of examination and attention to detail. Over the years I have had more success with a barium enema than with vaginography. If either method does not outline a fistula, then the other should be performed.

A rectovaginal fistula-occluding device, containing a nitinol wire and designed for endorectal insertion, successfully occluded several fistulas associated with pelvic irradiation or surgery (107).

Prolapse and Pelvic Floor Abnormalities

Discussed here is pelvic floor prolapse in a global context only. Cystoceles and urinary incontinence are covered in more detail in Chapter 11, while rectal prolapse is discussed in Chapter 5. The two primary imaging studies used are MR and cystocolpoproctography (or specific components of the latter, such as proctography). Functional MRI is gradually replacing proctography in women suspected pelvic floor dysfunction and pelvic prolapse. Rectal and vaginal opacification (either with water or an enteral MR contrast agent) aids in establishing reference organ positions both at rest and during straining. A high field strength MR magnet using fast gradient echo sequences and an endovaginal coil provides pelvic floor images during relaxation and straining. Sagittal images are most often employed using a pubococcygeal reference line. At times 3D images are useful but they are not essential.

Normally pelvic organs do not descend below a pubococcygeal reference line on straining, and the pelvic floor muscles do not change their position (Fig. 12.31). Normal pelvic organ position is defined in reference to this line, but no universal criteria exist defining the borderland of prolapse. Complex organ prolapse is more common than individual prolapse; at times a cystocele or an enterocele is masked by a rectocele.

Pelvic prolapse is the displacement of pelvic structures due to an endopelvic fascia weakness. To illustrate the often complex interrelated

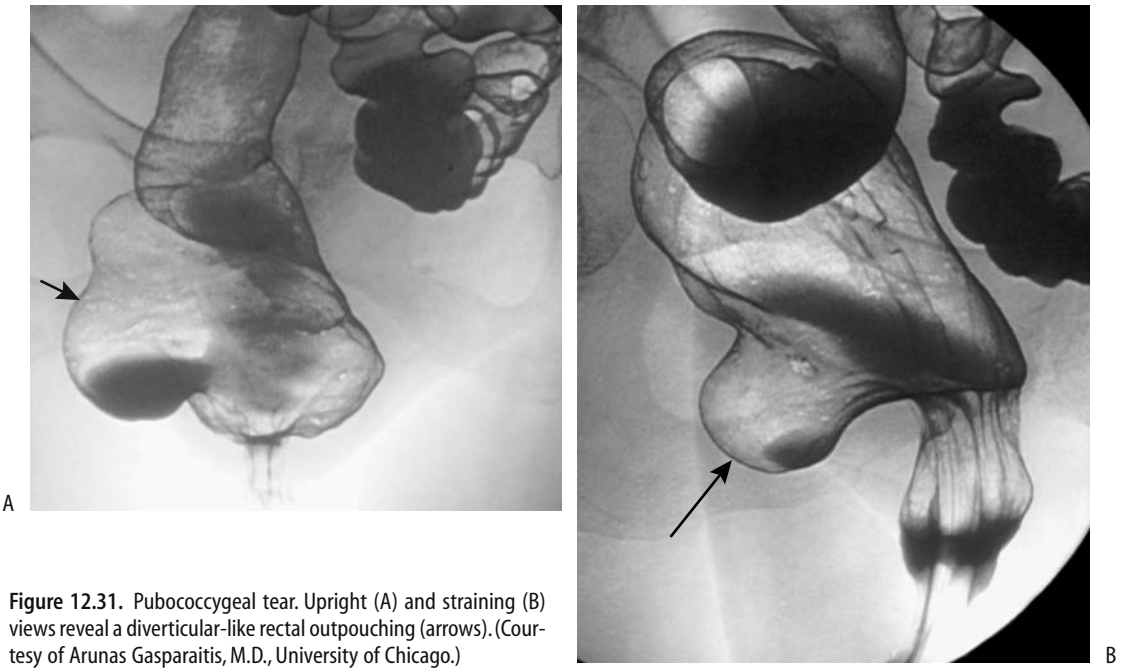

Figure 12.31. Pubococcygeal tear. Upright (A) and straining (B) views reveal a diverticular-like rectal outpouching (arrows). (Courtesy of Arunas Gasparaitis, M.D., University of Chicago.)

abnormalities found with lax pelvic organs and pelvic floor muscles, in 15 patients with constipation, a single sagittal section with T2-weighted gradient echo sequence and dynamic MRI identified rectal prolapse ($n = 5$), an anterior rectocele ($n = 8$), pelvic floor descent ($n = 5$), enterocele ($n = 2$) and anorectal dyscoordination ($n = 3$) (108); in 15 patients with incontinence, such a dynamic MR study detected an anterior rectocele ($n = 10$), pelvic floor descent ($n = 11$), enterocele ($n = 2$), rectal prolapse ($n = 1$), and puborectalis insufficiency ($n = 1$). Triphasic dynamic MRI and triphasic fluoroscopic cystocolpoproctography using similar amounts of contrast to opacify the bladder, vagina, and rectum achieves similar results (109); although cystoceles and enteroceles tend to be underestimated by MR, pelvic organs and pelvic floor muscles are better identified with this modality. Also, cystoproctography does not reveal peritoneoceles.

From an imaging viewpoint, the pelvic floor can be subdivided into an anterior compartment where urethroceles and cystoceles develop, a middle compartment for uterine prolapse and enteroceles, and a posterior compartment for rectoceles (110); clinical and imaging findings do not, however, always provide similar results, and the role of imaging is not settled. Dynamic cystoproctography reveals that over 90% of women with pelvic floor dysfunction have abnormalities in all three compartments (111); for example, among women with middle compartment (genital) symptoms, 91% had cystoceles, 56% a hypermobile bladder neck, 82% rectoceles, 58% enteroceles, 11% sigmoidoceles, 20% rectoanal intussusception, and 16% anal incontinence. Most rectoceles and cystoceles detected by cystoproctography are also evident on physical examination; the correlation between imaging and physical examination for enteroceles and sigmoidoceles is poor.

Not all widening of the rectovaginal space on straining is due to a rectocele. A peritoneocele should be suspected in women with unexplained widening. Less often is bowel present in this space.

Vaginal vault or cervical prolapse leads to vaginal mucosal eversion. Complete uterine prolapse is called procidentia. Sagittal T2-weighted MR images identify not only prolapsing gynecologic structures, but also any associated bladder or bowel prolapse.

Rarely, the uterus and ovary herniate into an inguinal hernia.

Pneumatosis

Pneumatosis of gynecologic organs is rare. If present, infection with a gas-forming organism or tissue necrosis should be suspected.

Imaging occasionally detects vaginitis emphysematosa, consisting of gas-filled cysts in the vaginal wall (112); this is a benign and self-limiting condition.

Vascular Lesions

Ovarian vein syndrome is discussed in Chapter 10. It usually occurs on the right and is due to compression of the ureter between the external iliac artery and a dilated ovarian vein. Left ovarian vein syndrome is due to ureteric compression between a dilated ovarian vein and the psoas muscle.

Bleeding

Postpartum bleeding was discussed earlier (see Pregnancy Related).

The most common causes of prepubertal vaginal bleeding consist of vaginal foreign bodies, precocious puberty, or tumors such as vaginal rhabdomyosarcoma or hemangioma.

In women with postmenopausal bleeding, US is a useful first step; a combination of endovaginal US without and with saline instilled into the uterus (endovaginal hysterosonography) is often more useful than either study alone. Both US studies achieve higher sensitivities in locating a bleeding site than does a diagnostic hysteroscopy.

Advanced pelvic malignancies not uncommonly result in major bleeding. In many of these women a diagnosis is already established, and surgery is not a viable option. Transcatheter embolization arrests bleeding in a majority of these women.

Ovarian Varicocele/Pelvic Congestion Syndrome

Ovarian and broad ligament varicoceles, or varices, develop most often due to ovarian vein incontinence and result in pelvic congestion. Secondary causes include inferior vena caval obstruction, portal hypertension, and other etiologies for increased blood flow in this region, such as an extensive vascular malformation.

Chronic pelvic pain is the most common presentation in these mostly multiparous women.

Imaging reveals serpentine paraovarian structures that enhance postcontrast. Unfortunately, it is difficult to place dilated ovarian veins in a proper perspective. Thus defining an incompetent and dilated ovarian vein as one measuring 7 mm or greater, arterial phase helical CT found that 47% of asymptomatic women renal donors had dilated ovarian veins, more often on the left but bilateral in some women (113), a finding questioning the relevance of dilated ovarian veins. Others have found a 10% prevalence of ovarian varices in the general population, with slightly more than half of these having pelvic congestion syndrome and thus possibly benefitting from ovarian vein embolization or ligation (114).

Most of these varicoceles are treated surgically. A percutaneous approach using a sclerosing agent has been employed successfully. Although embolization achieves a high initial technical success rate, complete relief of pain is variable.

Ovarian Vein Thrombophlebitis/Thrombosis

Most often ovarian vein thrombosis is detected postpartum, yet imaging has detected thrombosis in a variety of other settings, some associated with symptoms, others incidentally. In some women postpartum ovarian vein thrombosis is a sequela of infection. As already mentioned, ovarian vein thrombosis is a common incidental finding in women who have had a hysterectomy and bilateral salpingo-oophorectomy (49). Occasionally pelvic vein thrombosis develops in association with large uterine fibroids. A clinical diagnosis of ovarian vein thrombosis with its associated therapeutic implications should not be made lightly or based on imaging findings alone.

The right vein is affected more often. Some thrombi extend into the inferior vena cava. Clin-

ically, these patients are febrile and an infection is usually suspected. Puerperal ovarian vein thrombophlebitis can mimic renal colic and acute appendicitis. Pulmonary emboli are occasionally an early manifestation.

The diagnosis is suggested by CT, Doppler US, or MRI. A word of caution: at times early-phase postcontrast helical CT reveals retrograde flow in a normal ovarian vein. Therefore, asymmetric ovarian vein density during early-phase helical CT should not be misdiagnosed as a sign of ovarian vein thrombosis. Also, MR angiography shows absent flow in some ovarian veins even if they are patent, but MRI should detect vessel patency.

Ultrasonography reveals a tubular soft tissue tumor in the pelvis, at times extending to the inferior vena cava. A thrombus ranges from hypo- to hyperechoic. Adjacent inflammation is common, and right-sided ovarian vein thrombosis can suggest acute appendicitis. Ultrasonography should detect any ureteral involvement. Ultrasonography also can monitor the response to anticoagulant therapy.

Hemangioma

Ovarian hemangiomas are rare. Magnetic resonance imaging can suggest the diagnosis.

Uterine hemangiomas are also rare. Some of these contain punctate calcifications, aiding identification. Ultrasonography identified extensive uterine hemangiomatosis in a pregnant woman with Klippel-Trenaunay-Weber syndrome (115). Hemangiomas are homogeneous and hyperintense on T2-weighted images, thus distinguishing them from the more common hypointense myomas (Fig. 12.32).

Arteriovenous Malformations

Gynecologic arteriovenous malformations are uncommon but are one of the causes of uterine arteriovenous shunting. Past nomenclature used for these tumors included *circoid aneurysm* and *arteriovenous aneurysm* or *fistula*. They have been miscalled *angiomas* and *cavernous hemangiomas*. These malformations contain proliferating vascular channels, often

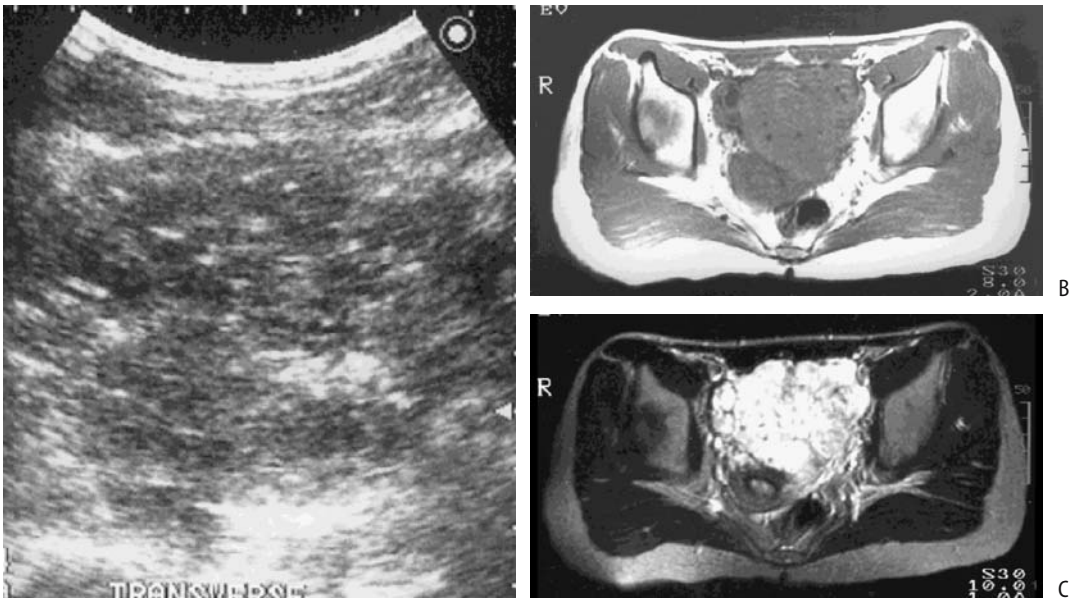

Figure 12.32. Uterine cavernous hemangioma. A: US reveals a pelvic tumor. Doppler (not shown) did not detect blood flow. T1- (B) and T2- (C) weighted MR images confirms a pelvic tumor which was located posterior to the bladder. (Courtesy of Takao Kobayashi, M.D., Shinshu University, Nagano prefecture, Japan.)

small and capillary-like in appearance. Most of these malformations are believed to be congenital in origin. Most develop in the myometrium.

Metrorrhagia is a common presentation. It is more common in premenopausal women. Uncontrolled bleeding after dilation and curettage should suggest an arteriovenous malformation, a (pseudo)aneurysm, an arteriovenous fistula, or a large vessel trauma.

Gray-scale US in women with uterine arteriovenous malformations is nonspecific, revealing subtle inhomogeneous myometrial tubular structures. Doppler US detects low-resistence flow and signals with flow reversals, suggesting arteriovenous shunting (Fig. 12.33).

Magnetic resonance imaging detects an arteriovenous malformation as a focal uterine tumor containing disrupted junctional zones and, if the tumor is large enough, prominent parametrial blood vessels. Flowing blood in these malformations presents as a serpiginous signal void on both T1- and T2-weighted MRI, while stasis results in a hyperintense signal on T2-weighted images. A malformation enhances on postcontrast images, similar to blood vessels. Magnetic resonance angiography shows tortuous, coiled vessels in the pelvis.

Only a few vaginal arteriovenous malformations have been described. These lesions can be suspected with Doppler US, CT, and MRI. They are hypointense on T1- and hyperintense on T2-weighted images; contrast-enhanced T1-weighted images reveal paradoxical flow-related enhancement in some, possibly caused by turbulent blood flow.

Traditional therapy of massive uncontrolled bleeding was uterine artery ligation or hysterectomy. Pelvic arteriography is diagnostic and also provides access for transcatheter embolization for these often surgically difficult to resect tumors. Selective transcatheter arterial embolization of uterine arteriovenous malformations and other similar vascular abnormalities tends to preserve reproductive capacity.

Uterine Artery Aneurysms

Uterine true aneurysms are rare. (Pseudo)-aneurysms are more common and are a cause of massive bleeding (Fig. 12.34).

Gray-scale US reveals a pulsating, hypo- or anechoic structure. True fusiform aneurysms contain an arterial flow pattern. Color and duplex Doppler US identify (pseudo)aneurysms

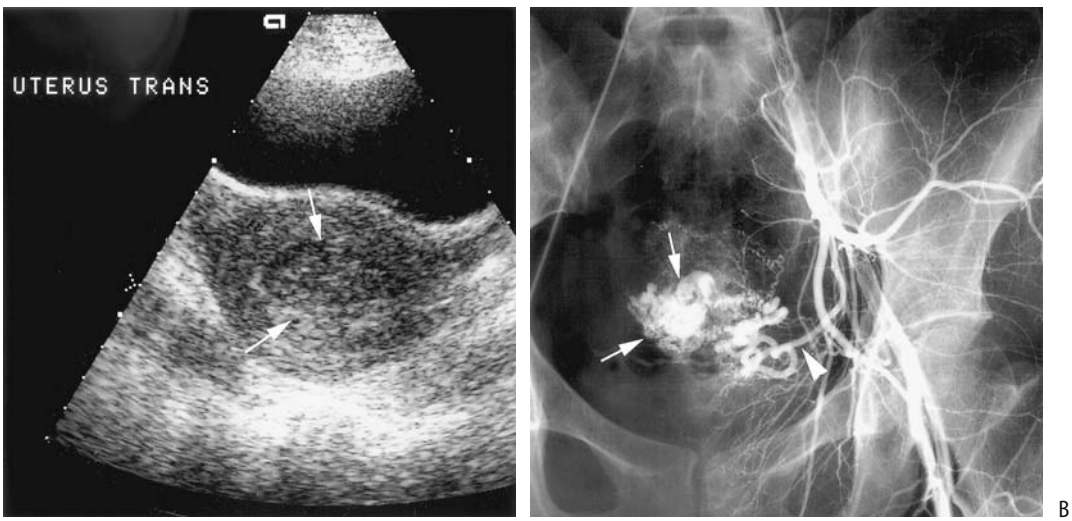

A B

Figure 12.33. Uterine arteriovenous malformation resulting in vaginal bleeding after dilation and curettage (D&C). A: Transverse gray-scale US reveals a subtle heterogenous appearance on the left side of the uterus (arrows). Color Doppler US revealed increased blood flow in this region (not shown). B: Arteriography identifies a collection of vessels (arrows) supplied by the left uterine artery (arrowhead); it was embolized with coils. (*Source:* Kwon JH, Kim GS. Obstetric iatrogenic arterial injuries of the uterus. Radiographics 2002;22:35–46, with permission from the Radiological Society of North America.)

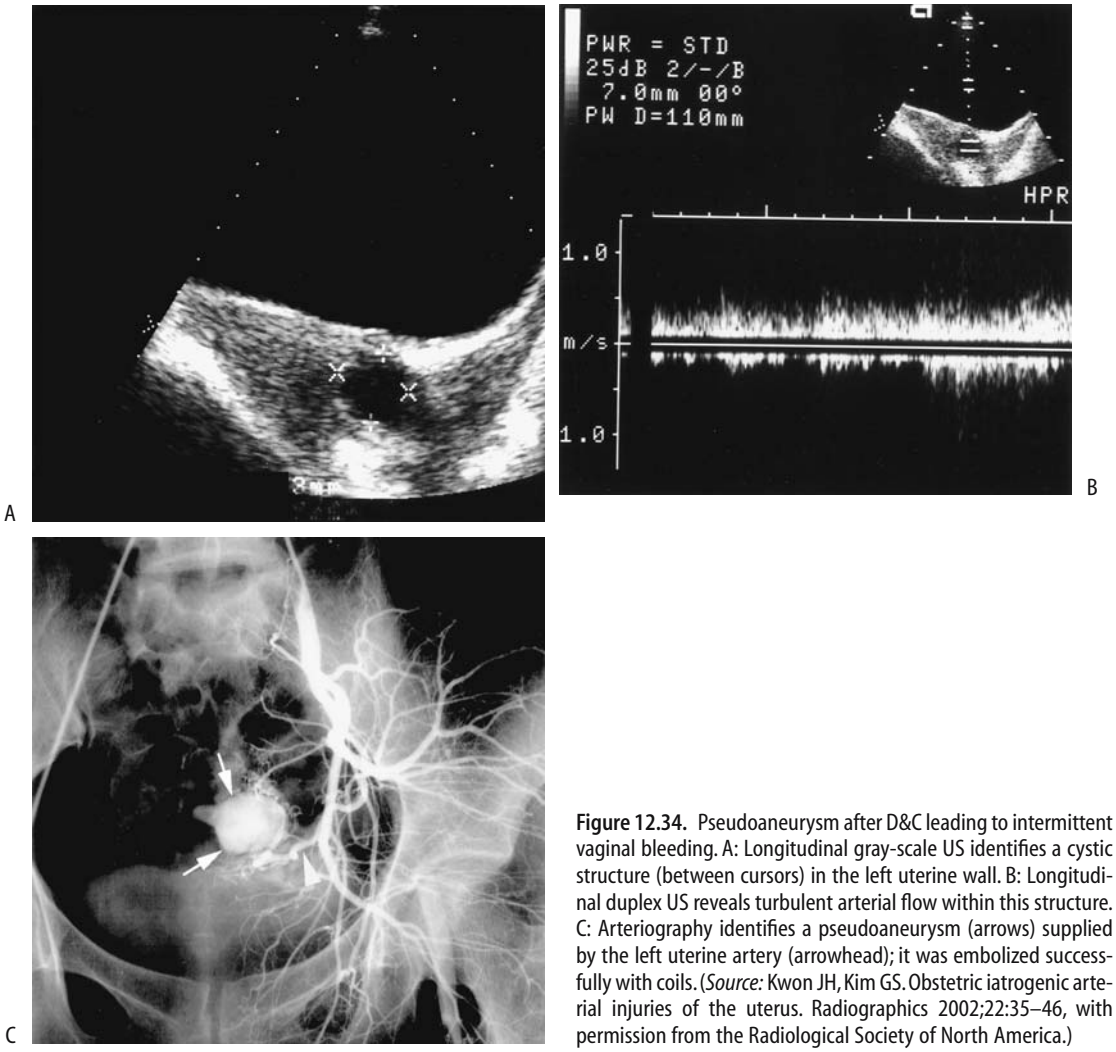

Figure 12.34. Pseudoaneurysm after D&C leading to intermittent vaginal bleeding. A: Longitudinal gray-scale US identifies a cystic structure (between cursors) in the left uterine wall. B: Longitudinal duplex US reveals turbulent arterial flow within this structure. C: Arteriography identifies a pseudoaneurysm (arrows) supplied by the left uterine artery (arrowhead); it was embolized successfully with coils. (*Source:* Kwon JH, Kim GS. Obstetric iatrogenic arterial injuries of the uterus. Radiographics 2002;22:35–46, with permission from the Radiological Society of North America.)

as cystic structures containing swirling fluid, similar to saccular aneurysms.

Immunosuppression

An association exists between cervical condyloma, dysplasia, and HIV infection. Acquired immunodeficiency syndrome (AIDS) patients have an increased prevalence of cervical cancer (compared to general population). In fact, based on data from the New York City Department of Health, the most common AIDS-related malignancy in women is cervical cancer (55%), followed by lymphoma (29%) and Kaposi sarcoma (16%) (116); in some women cervical cancer is the initial AIDS-defining illness.

Although non-Hodgkin's lymphomas are relatively common in AIDS patients, ovarian involvement is rare. An occasional disseminated Burkitt's lymphoma involves the ovaries.

Posttherapy

Post–Hormone Therapy

Postmenopausal women are placed on estrogen therapy to lessen the osteoporosis or control ovarian atrophy. Because of an increased risk of endometrial hyperplasia and carcinoma with estrogen therapy alone, various regimens of progesterone are often added.

Endovaginal US in asymptomatic postmenopausal women after the initiation of hormone replacement therapy reveals an increased endometrial thickness after the start of therapy. Sequential hormone therapy leads to changes similar to a premenopausal endometrium. Endometrial thickness measured with endovaginal US in healthy women in physiologic menopause was 3.5 mm, increasing to 5.7 mm after estrogen therapy alone (117); after adding progestin, endometrial thickness measured 6.0 mm. Endovaginal color Doppler US reveals that uterine artery PI and RI decrease during the first month of therapy.

Uterine artery pulsatility index in postmenopausal women receiving hormone replacement treatment tends to decrease, presumably due to increased uterine vascularity.

Some women develop vaginal bleeding while on hormonal therapy. Ultrasonography measurement of endometrial thickness does not select those who will bleed.

Postchemotherapy Changes

Tamoxifen citrate is a nonsteroidal antiestrogen agent binding to estrogen receptors and is used in breast cancer therapy. One of the side effects of tamoxifen is endometrial and myometrial stimulation and its use is associated with endometrial hyperplasia, polyps, and carcinomas. Fibromyomas also grow.

Endovaginal US found 69% of postmenopausal women treated with adjuvant tamoxifen to have an endometrial thickness >2.5 mm (118). One recommendation is that an endometrial thickness of 6 mm be considered a cutoff for endovaginal US in asymptomatic postmenopausal women receiving tamoxifen. A thickened, irregular, and hyperechoic endometrium containing small cysts or a homogeneous appearance is typical. Endovaginal US using intrauterine saline as a contrast agent (hysterosonography) is more specific but not significantly more sensitive than endovaginal US in detecting endometrial abnormalities (119,120). Tamoxifen polyps tend to be larger than typical polyps and are composed of cystic glandular dilation, epithelial metaplasia, and periglandular stromal condensation (121). These polyps range from sessile to pedunculated and appear as a hyperechoic, smoothly marginated tumor. Some contain cysts. An irregular polyp outline or endometrial thickening should raise suspicion for a carcinoma.

Magnetic resonance imaging identifies two patterns in postmenopausal women with breast cancer receiving tamoxifen therapy (122):

1. A homogeneous hyperintense endometrium on T2-weighted images, postcontrast enhancement of the endometrial-myometrial junction, and a lumen signal void. Histopathology in two thirds of these women revealed either atrophic or proliferative endometria.
2. A heterogeneous endometrium on T2-weighted images, postcontrast enhancement of the endometrial-myometrial junction, and lattice-like lumen enhancement, with most of these women having polyps.

Chemotherapy for breast cancer results in a loss of uterine volume, measurable with serial imaging.

Some investigators advocate routine US and endometrial biopsy even in asymptomatic women receiving tamoxifen. Hysteroscopy is used to resect any visualized polyps, and endometrial curettage evaluates abnormal endometrial thickening. An American College of Obstetricians and Gynecologists recommendation for women with breast cancer being treated with tamoxifen is to discontinue therapy if atypical hyperplasia is detected (121); a hysterectomy should be considered if further tamoxifen therapy is deemed necessary.

Postoperative Changes

One of the complications encountered with gynecologic surgery is ureteral damage. If damage is suspected, postoperative color Doppler US detection of ureteral jets is worth-

while, keeping in mind that it takes longer to visualize bilateral ureteral jets immediately after surgery.

Postlaparoscopy

The most common complication after laparoscopic gynecologic surgery is an incisional hernia. Omental herniation can occur through a trocar incision site.

Postoophorectomy

Occasionally ovarian remnants are left behind unintentionally after an oophorectomy. Some of these remnants are functional and lead to symptoms. Ultrasonography in women with ovarian remnants reveals a range from simple cysts, multiple septations, and presumed residual ovarian tissue with arterial and venous flow; aspiration of ovarian remnants provides symptomatic relief. Thus a US finding of a cystic or multiseptated pelvic mass containing a rim of vascular solid tissue, detected postoophorectomy, should raise the possibility of an ovarian remnant.

Poststerilization

Tubal sterilization is performed by ligation, occlusion with a clip or band, or by partial fallopian tube resection. Most of these obstructions are in the tube midportion and a postprocedure hysterosalpingogram reveals partial fallopian tube visualization.

Transcervical fallopian tube recanalization is achievable in most women. A successful pregnancy following recanalization, on the other hand, occurs in less than half. One complication of tubal recanalization is tubal perforation, usually associated with few, if any, sequelae.

Posthysterectomy

Hysterectomy-associated complications include pelvic abscess and injury to adjacent structures.

Endovaginal US commonly reveals pelvic fluid collections during the first postoperative week; these fluid collections gradually resolve and do not imply a postoperative complication. Thus even complex fluid collections in a woman after hysterectomy do not necessitate antibiotic therapy or surgical drainage.

Imaging of the vaginal cuff shows a symmetric or slightly asymmetric soft tissue tumor, usually surrounded by fat. Sagittal US reveals the vaginal cuff as a hypoechoic linear structure with a thin central echogenic line. Unfortunately, a postoperative hematoma, seroma, abscess, or lymphocele also has a similar appearance, thus making detection of complications difficult. The presence of gas bubbles raises suspicion of an abscess.

Postoperative fibrosis is common. In general, MRI is superior to CT in detecting tumor recurrence, because MRI allows a distinction between fibrosis and tumor; fibrosis has a low signal intensity on T2-weighted images, while tumor has a high signal intensity.

Post-Laser Ablation of Endometrium

Laser endometrial ablation is performed to control symptomatic heavy, painful menses. Magnetic resonance imaging immediately after therapy reveals an increase in uterine volume due to endometrial swelling.

Intrauterine Device Complications

An occasional intrauterine device migrates into the peritoneal cavity. Imaging or laparoscopy should localize it. One, inserted 4 years previously, migrated into the bladder and led to recurrent urinary tract infections (123); it was detected by US, conventional radiographs, and cystoscopy. These migrating devices tend to become surrounded by adhesions and thus are difficult to remove.

An intrauterine device was inserted through the urethra into the bladder (124); it could not be removed by transurethral endoscopy and required surgery.

Postradiation Therapy

Interstitial edema and inflammation of involved tissues develop shortly after radiation therapy. Magnetic resonance imaging during this phase reveals a hyperintense signal on T2-weighted

images. Once fibrosis develops, after about 1 year, a hypointense signal predominates from the involved tissue and little postcontrast enhancement is evident.

Girls with Wilms' tumors who underwent whole abdomen radiotherapy were later found to have primary ovarian failure (125); US revealed their ovaries to be undetected or small and their uteri to be abnormally small in spite of hormone replacement therapy. Ultrasonography in those who underwent hemiabdomen radiotherapy identified normal gonadotropin levels and a normal-sized uterus, but the ovary on the radiotherapy side was not seen or was small in half of the patients (125).

Chronic radiation changes consist primarily of fibrosis. Magnetic resonance imaging shows a low signal intensity on T2-weighted images. Postcontrast MR reveals tissue enhancement even during the chronic phase.

Examination and Surgical Complications

Hysterosalpingography

Intravasation and subsequent embolization into the lungs are known complications of hysterosalpingography. The previously used oil-based media probably were less painful, but a number of embolization-associated deaths were reported. Therefore, most radiologists currently use water-soluble agents.

Tumor Seeding

Pelviscopic excision of malignant gynecologic tumors potentially disseminates malignant cells to surrounding structures. Localized tumor seeding or tumor dissemination develops intraperitoneally and at trocar sites after laparoscopic tumor resection. Most of these metastases are in patients with FIGO stages IIIC to IV, although even an ovarian mature cystic teratoma containing a focus of carcinoma poses a risk. Seeding occurs not only from malignant tumors; thus during laparoscopic myomectomy fragments of uterine leiomyomas were inadvertently implanted and grew in abdominal-wall incisions.

References

1. Valentini AL, Muzii L, Marana R, et al. Fallopian tube disease: the cobblestone pattern as a radiographic sign. Radiology 2000;217:521–525.
2. Spring DB, Barkan HE, Pruyn SC. Potential therapeutic effects of contrast materials in hysterosalpingography: a prospective randomized clinical trial. Kaiser Permanente Infertility Work Group. Radiology 2000; 214:53–57.
3. Alcazar JL, Errasti T, Zornoza A. Saline infusion sonohysterography in endometrial cancer: assessment of malignant cells dissemination risk. Acta Obstet Gynecol Scand 2000;79:321–322.
4. Yang WT, Yuen PM, Ho SS, Leung TN, Metreweli C. Intraoperative laparoscopic sonography for improved preoperative sonographic pathologic characterization of adnexal masses. J Ultrasound Med 1998; 17:53–61.
5. Hawighorst H, Bock M, Knopp MV, et al. Magnetically labeled water perfusion imaging of the uterine arteries and of normal and malignant cervical tissue: initial experiences. Magn Reson Imaging 1998;16:225–234.
6. Okada T, Harada M, Matsuzaki K, Nishitani H, Aono T. Evaluation of female intrapelvic tumors by clinical proton MR spectroscopy. J Magn Reson Imaging 2001;13:912–917.
7. Buttram VC Jr, Gibbons WE. Müllerian anomalies: a proposed classification (an analysis of 144 cases). Fertil Steril 1979;32:40–46.
8. Sheih CP, Li YW, Liao YJ, Huang TS, Kao SP, Chen WJ. Diagnosing the combination of renal dysgenesis, Gartner's duct cyst and ipsilateral mullerian duct obstruction. J Urol 1998;159:217–221.
9. Mevel O, Tahan H, Michel F. [Rupture of the female urethra in pelvic fractures: report of 2 cases.] [French] Prog Urol 2000;10:1212–1216.
10. Rao PM, Feltmate CM, Rhea JT, Schulick AH, Novelline RA. Helical computed tomography in differentiating appendicitis and acute gynecologic conditions. Obstet Gynecol 1999;93:417–421.
11. Godfrey H, Abernethy L, Boothroyd A. Torsion of an ovarian cyst mimicking enteric duplication cyst on transabdominal ultrasound: two cases. Pediatr Radiol 1998;28:171–173.
12. Tukeva TA, Aronen HJ, Karjalainen PT, Molander P, Paavonen T, Paavonen J. MR imaging in pelvic inflammatory disease: comparison with laparoscopy and US. Radiology 1999;210:209–216.
13. Varghese JC, O'Neill MJ, Gervais DA, Boland GW, Mueller PR. Transvaginal catheter drainage of tuboovarian abscess using the trocar method: technique and literature review. [Review] AJR 2001;177: 139–144.
14. Reyal F, Grynberg H, Sibony O, et al. [Pelvic actinomycosis: a case with secondary localization in the liver.] [French] Presse Med 1999;28:2098–2099.
15. Kirova YM, Feuilhade F, Belda-Lefrere MA, Le Bourgeois JP. Intrauterine device—associated pelvic actinomycosis: a rare disease mimicking advanced ovarian cancer: a case report. Eur J Gynaecol Oncol 1997;18:502–503.

16. Dykes TA, Isler RJ, McLean AC. MR imaging of Asherman syndrome: total endometrial obliteration. J Comput Assist Tomogr 1991;15:858–860.
17. Atri M, Chow CM, Kintzen G, et al. Expectant treatment of ectopic pregnancies: clinical and sonographic predictors. AJR 2001;176:123–127.
18. Chiang G, Levine D, Swire M, McNamara A, Mehta T. The intradecidual sign: is it reliable for diagnosis of early intrauterine pregnancy? AJR 2004;183:725–731.
19. Hertzberg BS, Kliewer MA, Bowie JD. Adnexal ring sign and hemoperitoneum caused by hemorrhagic ovarian cyst: pitfall in the sonographic diagnosis of ectopic pregnancy. AJR 1999;173:1301–1302.
20. Giambanco L, Chianchiano N, Palmeri V, Catalano G. [Cervical pregnancy: an obstetric emergency. A clinical case.] [Italian] Minerva Ginecol 1998;50: 321–324.
21. Jung SE, Byun JY, Lee JM, Choi BG, Hahn ST. Characteristic MR findings of cervical pregnancy. J Magn Reson Imaging 2001;13:918–922.
22. Ayaz T, Akansel G, Hayirlioglu A, Arslan A, Suer N, Kuru I. Ophthalmic artery color Doppler ultrasonography in mild-to-moderate preeclampsia. Eur J Radiol 2003;46:244–249.
23. Joern H, Funk A, Rath W. Doppler sonographic findings for hypertension in pregnancy and HELLP syndrome. J Perinat Med 1999;27:388–394.
24. Grannum PA, Berkowitz RL, Hobbins JC. The ultrasonic changes in the maturing placenta and their relation to fetal pulmonic maturity. Am J Obstet Gynecol 1979;133:915–922.
25. Kidney DD, Nguyen AM, Ahdoot D, Bickmore D, Deutsch LS, Majors C. Prophylactic perioperative hypogastric artery balloon occlusion in abnormal placentation. AJR 2001;176:1521–1524.
26. Deux JF, Bazot M, Le Blanche AF, et al. Is selective embolization of uterine arteries a safe alternative to hysterectomy in patients with postpartum hemorrhage? AJR 2001;177:145–149.
27. Soto-Wright V, Bernstein M, Goldstein DP, Berkowitz RS. The changing clinical presentation of complete molar pregnancy. Obstet Gynecol 1995;86:775–779.
28. Lindheim SR, Cohen MA, Sauer MV. Ultrasound guided embryo transfer significantly improves pregnancy rates in women undergoing oocyte donation. Int J Gynaecol Obstet 1999;66:281–284.
29. Fleischer AC, Vasquez JM, Cullinan JA, Eisenberg E. Sonohysterography combined with sonosalpingography: correlation with endoscopic findings in infertility patients. J Ultrasound Med 1997;16:381–384.
30. Jain KA, Friedman DL, Pettinger TW, Alagappan R, Jeffrey RB Jr, Sommer FG. Adnexal masses: comparison of specificity of endovaginal US and pelvic MR imaging. Radiology 1993;186:697–704.
31. Hricak H, Chen M, Coakley FV, et al. Complex adnexal masses: detection and characterization with MR imaging—multivariate analysis. Radiology 2000;214: 39–46.
32. Hann LE, Lui DM, Shi W, Bach AM, Selland DL, Castiel M. Adnexal masses in women with breast cancer: US findings with clinical and histopathologic correlation. Radiology 2000;216:242–247.
33. Rieber A, Nussle K, Stohr I, et al. Preoperative diagnosis of ovarian tumors with MR imaging: comparison with transvaginal sonography, positron emission tomography, and histologic findings. AJR 2001;177: 123–129.
34. Sohaib SA, Sahdev A, Van Trappen P, Jacobs IJ, Reznek RH. Characterization of adnexal mass lesions on MR imaging. AJR 2003;180:1297–1304.
35. Lee JH, Jeong YK, Park JK, Hwang JC. "Ovarian vascular pedicle" sign revealing organ of origin of a pelvic mass lesion on helical CT. AJR 2003;181:131–137.
36. Fedele L, Bianchi S, Portuese A, Borruto F, Dorta M. Transrectal ultrasonography in the assessment of rectovaginal endometriosis. Obstet Gynecol 1998;91:444–448.
37. Bazot M, Darai E, Hourani R, et al. Deep pelvic endometriosis: MR imaging for diagnosis and prediction of extension of disease. Radiology 2004;232:379–389.
38. Tanaka YO, Yoshizako T, Nishida M, Yamaguchi M, Sugimura K, Itai Y. Ovarian carcinoma in patients with endometriosis: MR imaging findings. AJR 2000;175: 1423–1430.
39. Ko SF, Wan YL, Ng SH, et al. Adult ovarian granulosa cell tumors: spectrum of sonographic and CT findings with pathologic correlation. AJR 1999;172:1227–1233.
40. Conway C, Zalud I, Dilena M, et al. Simple cyst in the postmenopausal patient: detection and management. J Ultrasound Med 1998;17:369–372.
41. Chen CH, Tiu CM, Chou YH, Chen WY, Hwang B, Niu DM. Congenital hypothyroidism with multiple ovarian cysts. Eur J Pediatr 1999;158:851–852.
42. Lee HJ, Woo SK, Kim JS, Suh SJ. "Daughter cyst" sign: a sonographic finding of ovarian cyst in neonates, infants, and young children. AJR 2000;174:1013–1015.
43. Kikkawa F, Ishikawa H, Tamakoshi K, Nawa A, Suganuma N, Tomoda Y. Squamous cell carcinoma arising from mature cystic teratoma of the ovary: a clinicopathologic analysis. Obstet Gynecol 1997;89: 1017–1022.
44. Diebold J. [Molecular genetics of epithelial ovarian neoplasms: correlations with phenotype and biological behavior.] [Review] [German] Pathologe 1998;19: 95–103.
45. Hisada M, Garber JE, Fung CY, Fraumeni JF Jr, Li FP. Multiple primary cancers in families with Li-Fraumeni syndrome. J Natl Cancer Inst 1998;90:606–611.
46. Tempany CM, Zou KH, Silverman SG, Brown DL, Kurtz AB, McNeil BJ. Staging of advanced ovarian cancer: comparison of imaging modalities—report from the Radiological Diagnostic Oncology Group. Radiology 2000;215:761–767.
47. Ricke J, Sehouli J, Hach C, Hanninen EL, Lichtenegger W, Felix R. Prospective evaluation of contrast-enhanced MRI in the depiction of peritoneal spread in primary or recurrent ovarian cancer. Eur Radiol 2003;13:943–949.
48. Yoshida Y, Kurokawa T, Kawahara K, et al. Incremental benefits of FDG positron emission tomography over CT alone for the preoperative staging of ovarian cancer. AJR 2004;182:227–233.
49. Yassa NA, Ryst E. Ovarian vein thrombosis: a common incidental finding in patients who have undergone total abdominal hysterectomy and bilateral salpingo-oophorectomy with retroperitoneal lymph node dissection. AJR 1999;172:45–47.

50. Low RN, Saleh F, Song SY, et al. Treated ovarian cancer: comparison of MR imaging with serum CA-125 level and physical examination—a longitudinal study. Radiology 1999;211:519–528.
51. Funt SA, Hricak H, Abu-Rustum N, Mazumdar M, Felderman H, Chi DS. Role of CT in the management of recurrent ovarian cancer. AJR 2004;182:393–398.
52. Nakamoto Y, Saga T, Ishimori T, et al. Clinical value of positron emission tomography with FDG for recurrent ovarian cancer. AJR 2001;176:1449–1454.
53. Cho SM, Ha HK, Byun JY, et al. Usefulness of FDG PET for assessment of early recurrent epithelial ovarian cancer. AJR 2002;179:391–395.
54. Method MW, Serafini AN, Averette HE, Rodriguez M, Penalver MA, Sevin BU. The role of radioimmunoscintigraphy and computed tomography scan prior to reassessment laparotomy of patients with ovarian carcinoma. A preliminary report. Cancer 1996;77:2286–2293.
55. Sella T, Rosenbaum E, Edelmann DZ, Agid R, Bloom AI, Libson E. Value of chest CT scans in routine ovarian carcinoma follow-up. AJR 2001;177:857–859.
56. Dachman AH, Visweswaran A, Battula R, Jameel S, Waggoner SE. Role of chest CT in the follow-up of ovarian adenocarcinoma. AJR 2001;176:701–705.
57. O'Sullivan SG, Das Narla L, Ferraro E. Primary ovarian leiomyosarcoma in an adolescent following radiation for medulloblastoma. Pediatr Radiol 1998;28:468–470.
58. Sugawara Y, Zasadny KR, Grossman HB, Francis IR, Clarke MF, Wahl RL. Germ cell tumor: differentiation of viable tumor, mature teratoma, and necrotic tissue with FDG PET and kinetic modeling. Radiology 1999;211:249–256.
59. Morimura Y, Nishiyama H, Yanagida K, Sato A. Dysgerminoma with syncytiotrophoblastic giant cells arising from 46,XX pure gonadal dysgenesis. Obstet Gynecol 1998;92:654–656.
60. Yamaoka T, Togashi K, Koyama T, et al. Immature teratoma of the ovary: correlation of MR imaging and pathologic findings. Eur Radiol 2003;13:313–319.
61. Brown DL, Zou KH, Tempany CM, et al. Primary versus secondary ovarian malignancy: imaging findings of adnexal masses in the Radiology Diagnostic Oncology Group Study. Radiology 2001;219:213–218.
62. Jeong YY, Kang HK, Seo JJ, Nam JH. Luteinized fat in Krukenberg tumor: MR findings. Eur Radiol 2002;12 Suppl 3:S130–132.
63. Tjalma WA, Schatteman E, Goovaerts G, Verkinderen L, Van-den Borre F, Keersmaekers G. Adenocarcinoid of the appendix presenting as a disseminated ovarian carcinoma: report of a case. Surg Today 2000;30:78–81.
64. Soga J, Osaka M, Yakuwa Y. Carcinoids of the ovary: an analysis of 329 reported cases. J Exp Clin Cancer Res 2000;19:271–280.
65. Bakos O, Heimer G. Transvaginal ultrasonographic evaluation of the endometrium related to the histological findings in pre- and perimenopausal women. Gynecol Obstet Invest 1998;45:199–204.
66. Cohen MA, Sauer MV, Keltz M, Lindheim SR. Utilizing routine sonohysterography to detect intrauterine pathology before initiating hormone replacement therapy. Menopause 1999;6:68–70.
67. Shimizu M, Nakayama M. Endometrial ossification in a postmenopausal woman. J Clin Pathol 1997;50:171–172.
68. Grasel RP, Outwater EK, Siegelman ES, Capuzzi D, Parker L, Hussain SM. Endometrial polyps: MR imaging features and distinction from endometrial carcinoma. Radiology 2000;214:47–52.
69. Siskin GP, Tublin ME, Stainken BF, Dowling K, Dolen EG. Uterine artery embolization for the treatment of adenomyosis: clinical response and evaluation with MR imaging. AJR 2001;177:297–302.
70. Jha RC, Takahama J, Imaoka I, et al. Adenomyosis: MRI of the uterus treated with uterine artery embolization. AJR 2003;181:851–856.
71. Tsuda H, Kawabata M, Nakamoto O, Yamamoto K. Clinical predictors in the natural history of uterine leiomyoma: preliminary study. J Ultrasound Med 1998;17:17–20.
72. Caoili EM, Hertzberg BS, Kliewer MA, DeLong D, Bowie JD. Refractory shadowing from pelvic masses on sonography: a useful diagnostic sign for uterine leiomyomas. AJR 2000;174:97–101.
73. Torashima M, Yamashita Y, Matsuno Y, et al. The value of detection of flow voids between the uterus and the leiomyoma with MRI. J Magn Reson Imaging 1998;8:427–431.
74. Ravina JH, Herbreteau D, Ciraru-Vigneron N, et al. Arterial embolisation to treat uterine myomata. Lancet 1995;346:671–672.
75. Razavi MK, Hwang G, Jahed A, Modanloo S, Chen B. Abdominal myomectomy versus uterine fibroid embolization in the treatment of symptomatic uterine leiomyomas. AJR 2003;180:1571–1575.
76. Li W, Brophy DP, Chen Q, Edelman RR, Prasad PV. Semiquantitative assessment of uterine perfusion using first pass dynamic contrast-enhanced MR imaging for patients treated with uterine fibroid embolization. J Magn Reson Imaging 2000;12:1004–1008.
77. Hagspiel KD, Matsumoto AH, Berr SS. Uterine fibroid embolization: assessment of treatment response using perfusion-weighted extraslice spin tagging (EST) magnetic resonance imaging. J Magn Reson Imaging 2001;13:982–986.
78. Katsumori T, Nakajima K, Mihara T. Is a large fibroid a high-risk factor for uterine artery embolization? AJR 2003;181:1309–1314.
79. Gabriel H, Pinto CM, Kumar M, et al. MRI detection of uterine necrosis after uterine artery embolization for fibroids. AJR 2004;183:733–736.
80. Vashisht A, Studd JW, Carey AH, et al. Fibroid embolisation: a technique not without significant complications. Br J Obstet Gynaecol 2000;107:1166–1170.
81. Ryu RK, Siddiqi A, Omary RA, et al. Sonography of delayed effects of uterine artery embolization on ovarian arterial perfusion and function. AJR 2003;181:89–92.
82. Pelage JP, Guaou NG, Jha RC, Ascher SM, Spies JB. Uterine fibroid tumors: long-term MR imaging outcome after embolization. Radiology 2004;230:803–809.
83. Burn PR, McCall JM, Chinn RJ, Vashisht A, Smith JR, Healy JC. Uterine fibroleiomyoma: MR imaging

appearances before and after embolization of uterine arteries. Radiology 2000;214:729–734.
84. Law P, Gedroyc WM, Regan L. Magnetic resonance-guided percutaneous laser ablation of uterine fibroids. J Magn Reson Imaging 2000;12:565–570.
85. Common AA, Mocarski EJ, Kolin A, Pron G, Soucie J. Therapeutic failure of uterine fibroid embolization caused by underlying leiomyosarcoma. J Vasc Interv Radiol 2001;12:1449–1452.
86. Utsunomiya D, Notsute S, Hayashida Y, et al. Endometrial carcinoma in adenomyosis: assessment of myometrial invasion on T2-weighted spin-echo and gadolinium-enhanced T1-weighted images. AJR 2004; 182:399–404.
87. Hardesty LA, Sumkin JH, Hakim C, Johns C, Nath M. The ability of helical CT to preoperatively stage endometrial carcinoma. AJR 2001;176:603–606.
88. Manfredi R, Mirk P, Maresca G, et al. Local-regional staging of endometrial carcinoma: role of MR imaging in surgical planning. Radiology 2004;231:372–378.
89. Seki H, Takano T, Sakai K. Value of dynamic MR imaging in assessing endometrial carcinoma involvement of the cervix. AJR 2000;175:171–176.
90. Koyama T, Togashi K, Konishi I, et al. MR imaging of endometrial stromal sarcoma: correlation with pathologic findings. AJR 1999;173:767–772.
91. Ohguri T, Aoki T, Watanabe H, et al. MRI findings including gadolinium-enhanced dynamic studies of malignant, mixed mesodermal tumors of the uterus: differentiation from endometrial carcinomas. Eur Radiol 2002;12:2737–2742.
92. Marin C, Seoane JM, Sanchez M, Ruiz Y, Garcia JA. Magnetic resonance imaging of primary lymphoma of the cervix. Eur Radiol 2002;12:1541–1545.
93. Nieminen P, Kallio M, Hakama M. The effect of mass screening on incidence and mortality of squamous and adenocarcinoma of cervix uteri. Obstet Gynecol 1995;85:1017–1021.
94. deSouza NM, Whittle M, Williams AD, et al. Magnetic resonance imaging of the primary site in stage I cervical carcinoma: a comparison of endovaginal coil with external phased array coil techniques at 0.5 T. J Magn Reson Imaging 2000;12:1020–1026.
95. Ozsarlak O, Tjalma W, Schepens E, et al. The correlation of preoperative CT, MR imaging, and clinical staging (FIGO) with histopathology findings in primary cervical carcinoma. Eur Radiol 2003;13: 2338–235.
96. Postema S, Pattynama PM, van Rijswijk CS, Trimbos JB. Cervical carcinoma: can dynamic contrast-enhanced MR imaging help predict tumor aggressiveness? Radiology 1999;210:217–220.
97. Peppercorn PD, Jeyarajah AR, Woolas R, et al. Role of MR imaging in the selection of patients with early cervical carcinoma for fertility-preserving surgery: initial experience. Radiology 1999;212:395–399.
98. Yamashita Y, Baba T, Baba Y, et al. Dynamic contrast-enhanced MR imaging of uterine cervical cancer: pharmacokinetic analysis with histopathologic correlation and its importance in predicting the outcome of radiation therapy. Radiology 2000;216: 803–809.
99. Boss EA, Massuger LF, Pop LA, et al. Post-radiotherapy contrast enhancement changes in fast dynamic MRI of cervical carcinoma. J Magn Reson Imaging 2001;13: 600–606.
100. Williams AD, Cousins C, Soutter WP, et al. Detection of pelvic lymph node metastases in gynecologic malignancy: a comparison of CT, MR imaging, and positron emission tomography. AJR 2001;177:343–348.
101. Yang WT, Lam WW, Yu MY, Cheung TH, Metreweli C. Comparison of dynamic helical CT and dynamic MR imaging in the evaluation of pelvic lymph nodes in cervical carcinoma. AJR 2000;175:759–766.
102. Umesaki N, Nakai Y, Honda K, et al. Power Doppler findings of adenoma malignum of uterine cervix. Gynecol Obstet Invest 1998;45:213–216.
103. Oliva E, Quinn TR, Amin MB, et al. Primary malignant melanoma of the urethra: a clinicopathologic analysis of 15 cases. Am J Surg Pathol 2000;24:785–796.
104. Thurmond AS, Machan LS, Maubon AJ, et al. A review of selective salpingography and fallopian tube catheterization. Radiographics 2000;20:1759–1768.
105. el Khader K, Ouali M, Nouri M, Koutani A, Hachimi M, Lakrissa A. [Urethral diverticulosis in women. Analysis of 15 cases.] [French] Prog Urol 2001;11: 97–102.
106. Tazi K, el Fassi J, Karmouni T, et al. [Vesico-uterine fistula. Report of 10 cases.] [French] Prog Urol 2000;10: 1173–1176.
107. Lee BH, Choe DH, Lee JH, et al. Device for occlusion of rectovaginal fistula: clinical trials. Radiology 1997;203: 65–69.
108. Paetzel C, Strotzer M, Furst A, Rentsch M, Lenhart M, Feuerbach S. [Dynamic MR defecography for diagnosis of combined functional disorders of the pelvic floor in proctology.] [German] Rofo Fortschr Geb Rontgenstr Neuen Bildgeb Verfahr 2001;173:410–415.
109. Kelvin FM, Maglinte DD, Hale DS, Benson JT. Female pelvic organ prolapse: a comparison of triphasic dynamic MR imaging and triphasic fluoroscopic cystocolpoproctography. AJR 2000;174:81–88.
110. Anthuber C, Lienemann A. [Morphological and functional pelvic floor disorders from the gynecological viewpoint.] [Review] [German] Radiologe 2000;40: 437–445.
111. Maglinte DD, Kelvin FM, Fitzgerald K, Hale DS, Benson JT. Association of compartment defects in pelvic floor dysfunction. AJR 1999;172:439–444.
112. Leder RA, Paulson EK. Vaginitis emphysematosa: CT and review of the literature. AJR 2001;176:623–625.
113. Rozenblit AM, Ricci ZJ, Tuvia J, Amis ES Jr. Incompetent and dilated ovarian veins: a common CT finding in asymptomatic parous women. AJR 2001;176: 119–122.
114. Belenky A, Bartal G, Atar E, Cohen M, Bachar GN. Ovarian varices in healthy female kidney donors: incidence, morbidity, and clinical outcome. AJR 2002; 179:625–627.
115. Richards DS, Cruz AC. Sonographic demonstration of widespread uterine angiomatosis in a pregnant patient with Klippel-Trenaunay-Weber syndrome. J Ultrasound Med 1997;16:631–633.
116. Maiman M, Fruchter RG, Clark M, Arrastia CD, Matthews R, Gates EJ. Cervical cancer as an AIDS-defining illness. Obstet Gynecol 1997;89:76–80.
117. Berardesca C, Chiechi LM, Caradonna F, Loizzi V, Loizzi P. [Ultrasonic evaluation of endometrial changes

induced by cyclic sequential hormone substitution therapy.] [Italian] Minerva Ginecol 1998;50:503–505.
118. Tesoro MR, Borgida AF, MacLaurin NA, Asuncion CM. Transvaginal endometrial sonography in postmenopausal women taking tamoxifen. Obstet Gynecol 1999;93:363–366.
119. Hann LE, Gretz EM, Bach AM, Francis SM. Sonohysterography for evaluation of the endometrium in women treated with tamoxifen. AJR 2001;177:337–342.
120. Fong K, Kung R, Lytwyn A, et al. Endometrial evaluation with transvaginal US and hysterosonography in asymptomatic postmenopausal women with breast cancer receiving tamoxifen. Radiology 2001;220:765–773.
121. Ascher SM, Imaoka I, Lage JM. Tamoxifen-induced uterine abnormalities: the role of imaging. [Review] Radiology 2000;214:29–38.
122. Ascher SM, Johnson JC, Barnes WA, Bae CJ, Patt RH, Zeman RK. MR imaging appearance of the uterus in postmenopausal women receiving tamoxifen therapy for breast cancer: histopathologic correlation. Radiology 1996;200:105–110.
123. Ndoye A, Ba M, Fall PA, Sylla C, Gueye DM, Diagne BA. [Migration of an intrauterine device to the bladder.] [French] Prog Urol 2000;10:295–297.
124. Hernandez-Valencia M, Carrillo Pacheco A. [Intravesical translocation of an intrauterine device, report of a case.] [Spanish] Ginecol Obstet Mex 1998;66: 290–292.
125. Nussbaum Blask AR, Nicholson HS, Markle BM, Wechsler-Jentzch K, O'Donnell R, Byrne J. Sonographic detection of uterine and ovarian abnormalities in female survivors of Wilms' tumor treated with radiotherapy. AJR 1999;172:759–763.

13

Male Reproductive Organs

Technique

Ultrasonography

Ultrasonography (US) has become the modality of choice for scrotal imaging. It can differentiate intra- from extratesticular tumors with a sensitivity of over 95%. The specificity, however, is considerably lower. Transducers using 10-MHz provide detailed resolution, although with scrotal swelling a lower frequency is necessary for full coverage.

Seminal vesicles and surrounding structures are readily studied with endorectal US. Three-dimensional (3D) endorectal US outlines the prostate in three planes and aids the study of transition zone hyperplasia; the central zone and enlarged transition zones are best identified using a coronal plane.

Transabdominal gray-scale US has a limited role in evaluating the prostate; the gland is located too far posteriorly and is too small for detailed study. An endorectal US approach is preferred.

Variability in interpreting endorectal US prostate images is a concern. Even well-trained physicians differ both in describing findings of random videotaped images of the prostate and in deciding whether to biopsy.

Transperineal US during contrast enhanced voiding urosonography has been proposed in children (1). Posterior urethral valves can be detected with this technique but further work is necessary to establish its clinical relevance.

Magnetic Resonance Imaging

Magnetic resonance imaging (MRI) of the scrotum is still evolving. Especially in children, with an equivocal US study MRI may obviate the need for exploratory surgery. In addition, new applications being reported suggest that MRI will evolve into the primary imaging modality of the testes.

Endorectal surface coils allow prostate zonal study. The prostatic capsule, neurovascular bundles, vas deferens, and seminal vesicles are readily studied.

T1-weighted magnetic resonance (MR) images outline the prostatic margin with surrounding fat, although the internal prostate zonal architecture is not defined. T2-weighted images show a hyperintense peripheral zone and a heterogeneous more hypointense central and transition zones. An endorectal coil improves spatial resolution. Postgadolinium T1-weighted images reveal less peripheral zone enhancement than central zone.

Magnetic resonance voiding cystourethrography is feasible after gadolinium-enhanced excretory MR urography. Magnetic resonance fluoroscopy using a T1-weighted gradient echo sequence provides real-time urethral imaging during voiding. Both sonourethrography and MR imaging of the anterior urethra are feasible, with the urethral lumen distended with saline. Both modalities provide information about periurethral tissues.

Urethrography

At times urethral catheterization is difficult or even impossible. In such a setting, advancing a urethral catheter over a hydrophilic guidewire is helpful. Ultrasonography has been used instead of a retrograde urethrogram to visualize the urethra; US can provide a 3D view of the urethra.

Urethrography is performed using an iodinated contrast agent. Occasionally reported is use of undiluted gadolinium diethylenetriamine-pentaacetate (Gd-DTPA) in someone with a severe reaction to iodine-containing contrast, achieving good radiographic contrast, but such use should be balanced against the greater toxicity of gadolinium contrast compared to iodinated contrast.

Cavernosography

Cavernosography, performed by direct contrast injection into the corpora cavernosa, provides cavernous arterial systolic occlusion pressure. Vasodilators aid in interpreting these studies. This study currently is rarely performed, having been supplanted by US and clinical evaluation using erection-enhancing pharmacologic agents.

Color duplex Doppler US is considerably simpler than cavernosography and measures peak velocity flow, which correlates with cavernous arterial systolic occlusion pressure; peak velocity flow measurement represents a noninvasive evaluation of corporeal artery function.

Vesiculography (Vasography)

Seminal vesicle, vas deferens, and ejaculatory duct patency is established by vesiculography, performed by cannulating and injecting contrast into the vas deferens. Surgical cannulation is often employed, although endorectal US-guided seminal vesiculography is feasible. If endorectal US identifies dilated seminal vesicles or midline cysts, US-guided seminal tract puncture and contrast injection allows radiographic visualization of these structures. Injecting a mixture of contrast agent and indigo-carmine dye is useful if identification of these structures is desired during subsequent surgery.

Scintigraphy

Monoclonal antibody radioimmunoscintigraphy with indium-111–capromab pendetide is promising in men with prostate cancer, both to detect initial lymph node involvement and in those with suspected recurrent or residual disease after prostatectomy. This murine-derived antibody is believed to act against the intracellular domain of prostate-specific membrane antigen, a glycoprotein expressed by prostate epithelial cells.

Testicular scanning is performed with technetium-99m (Tc-99m)-pertechnetate. This radiotracer establishes a blood flow pattern.

Biopsy

Traditional prostate biopsy is performed using a digital rectal examination for guidance, with a needle being inserted either transperineally or transrectally. Currently an endorectal US-guided approach is commonly employed, using a needle up to 18-gauge for core biopsies. If a tumor can be palpated or localized by US, a direct biopsy is obtained, but, as will be discussed later, US-guided multisextant biopsies are often preferred. Endorectal US-guided prostatic nerve blockade increases patient comfort prior to systematic needle biopsy of the prostate.

A transrectal US-guided prostate biopsy is quite safe. Of necessity, a transrectal biopsy approach is through a nonsterile field, but postprocedure infections are surprisingly few.

An MRI-guided prostate biopsy is also feasible, mostly using an open magnet.

Congenital Abnormalities

Prostate

Two types of prostatic ectopia are possible, developing from either urogenital sinus or mesonephric structures. Ectopic prostatic tissue has been found along the lateral rectal wall.

Müllerian remnants, including utricular cysts, coexist with hypospadias.

Wolffian Duct Structures

Failure of seminal vesicle buds to develop results in absent seminal vesicles. Some individ-

uals also have ureteric bud failure, leading to an absent ipsilateral ureter and kidney. Thus detection of a seminal vesicle cyst or similar anomaly should lead to a renal study to exclude associated renal agenesis. Most seminal vesicle cysts are congenital; they are discussed later (see Wolffian duct structures).

Congenital bilateral vas deferens absence is a cause of azoospermia. This condition is detected with rectal US.

An ectopic ejaculatory duct insertion is rare.

Persistent Müllerian Duct Syndrome

Normally in a male fetus antimüllerian hormone causes müllerian duct regression. Absence or lack of function of this hormone results in a uterus and fallopian tubes being present in a phenotypically normal male, a condition called persistent müllerian duct syndrome. Two types exist: in the male type, one testis descends normally but the uterus and fallopian tubes are in or close to the inguinal canal, while in the female type bilateral cryptorchidism is evident and testes are located in the broad ligament and the uterus is in the pelvis. Simple cryptorchidism is generally suspected preoperatively because male external genitalia are otherwise normal.

Imaging findings are confusing if the diagnosis is not suspected. Computed tomography (CT) and MR identify a uterus and fallopian tubes as tubular structures posterior to the bladder, and testes located close to where ovaries are normally found in a phenotypically normal male. Testicular atrophy develops in older individuals, making further identification difficult. Similar to other males with cryptorchidism, these individuals are prone to developing testicular cancer.

Urethra

Duplication

Urethral duplication is rare. Most are located in the midline and lie in a dorsal-to-ventral direction. Duplications range from complete to incomplete, and the duplicated urethra originates either from the bladder or a normal urethra. An accessory urethral termination ranges from an epispadial to a hypospadial location. Some duplications are associated with renal and multisystem abnormalities. Pubic bones tend to be abnormally separated with epispadial duplications.

A congenital urethroperineal fistula is a separate entity distinct from a duplication. Boys with a congenital urethroperineal fistula have normal micturition. An extreme hypospadial urethral duplication mimics a congenital urethroperineal fistula. In general, in a duplication the ventral urethra is the more functional channel, while with a fistula the dorsal channel is usually the primary one.

Cystography defines the underlying anatomy prior to surgical correction. For complete evaluation of a duplicated system, both a voiding cystourethrogram and a retrograde urethrogram are obtained.

Valves

Posterior valves

The most common cause of urethral obstruction in male infants is the presence of congenital posterior urethral valves. Obstruction varies in gradation. At times mild obstruction is not discovered until adolescence or even later. Some of these infants develop marked hydronephrosis and renal failure before the condition is detected. These valves are usually classified into three type:

- Type I valves are folds extending from the verumontanum to the anterolateral urethral wall. These are most common.
- Type II valves also arise from the verumontanum but extend proximally into the bladder neck. These valves tend to be of limited significance and probably are acquired rather than congenital in origin.
- Type III valves consist of a prominent urogenital membrane with a central opening distal to the verumontanum. They are rare.

A syndrome exists of posterior urethral valves, persistent unilateral reflux, and unilateral renal dysplasia even to the point of nonfunction. A majority of infants and children with posterior urethral valves have vesicoureteral reflux, which often does not resolve after valve ablation. Long-term follow-up is thus required. Some of these infants also have impaired bladder compliance and detrusor instability, and these findings persist after valve

Figure 13.1. Posterior urethral valves in an 11-year-old. The prostatic urethra is dilated and has a "spinning-top" configuration.

ablation; in addition to voiding cystourethrography, postoperative urodynamic studies are often helpful.

After birth, a voiding cystourethrogram should be diagnostic for posterior urethral valves (Fig. 13.1). Catheterization is easy in those with type 1 valves, but may not be possible with type 3 valves, depending on the central opening. The prostatic and membranous urethra are dilated, with an abrupt transition in caliber at the valve site. At times the valves are identified.

In many infants US detects a dilated posterior urethra during voiding and bilateral hydronephrosis (Fig. 13.2). Vesicoureteral reflux and hydronephrosis is associated with a dysplastic kidney in some. A thick, trabeculated bladder wall and diverticula develop eventually. Severe obstruction in a neonate can result in calyceal perforation and urinary ascites.

A retrograde urethrogram is not appropriate for detecting these valves; they tend to be effaced against the urethral wall, and obstruction is not detected. A voiding cystourethrogram is the examination of choice. In a search for posterior urethral valves, some radiologists remove the catheter while others leave it in place. Some believe that a catheter can obscure the valves.

Voiding cystourethrography in boys with severe posterior urethral valves identifies a trabeculated bladder body and smooth bladder base; bladder base trabeculations do not develop. A trabeculated bladder body evolves as a result of contractions due to parasympathetic (cholinergic) stimulation during voiding, while the bladder base relaxes due to sympathetic (adrenergic) stimulation and thus remains smooth.

Indications for percutaneous nephrostomy in neonates with posterior urethral valves include renal failure, severe infection, and, at times, evaluation of a dilated collecting system. Such diversion, however, is not without its own problems. Even if a proximal urinary tract diversion is performed, many neonafes tend to continue losing renal function. Diversion also results in a defunctionalized bladder and loss of bladder compliance. In general, primary valve ablation performed in infants prior to age 1 year results in better recovery of bladder function than those treated with urinary diversion, realizing that in some of these infants neither procedure halts progression of renal insufficiency.

Results of renal transplantation in children with end stage renal disease due to posterior urethral valves are similar to those obtained in children with nonobstructive renal disease. In either case, probably all children with contemplated renal transplantation should be studied for the presence of congenital posterior urethral valves; the presence of these valves has a role in graft function deterioration.

Anterior Valves

True anterior urethral valves are rare, with most believed to represent a fold that is part of a urethral diverticulum. Some of these valves are detected investigating prenatal hydronephrosis, while others manifest by voiding dysfunction later in life. Bladder rupture can develop in a neonate with anterior urethral valves.

A voiding cystourethrogram should detect these valves, although their imaging appearance is very similar to that of an anterior urethral diverticulum.

Stricture

Urethral strictures are distinct from posterior or anterior urethral valves. Identical congenital urethral strictures occasionally develop in relatives.

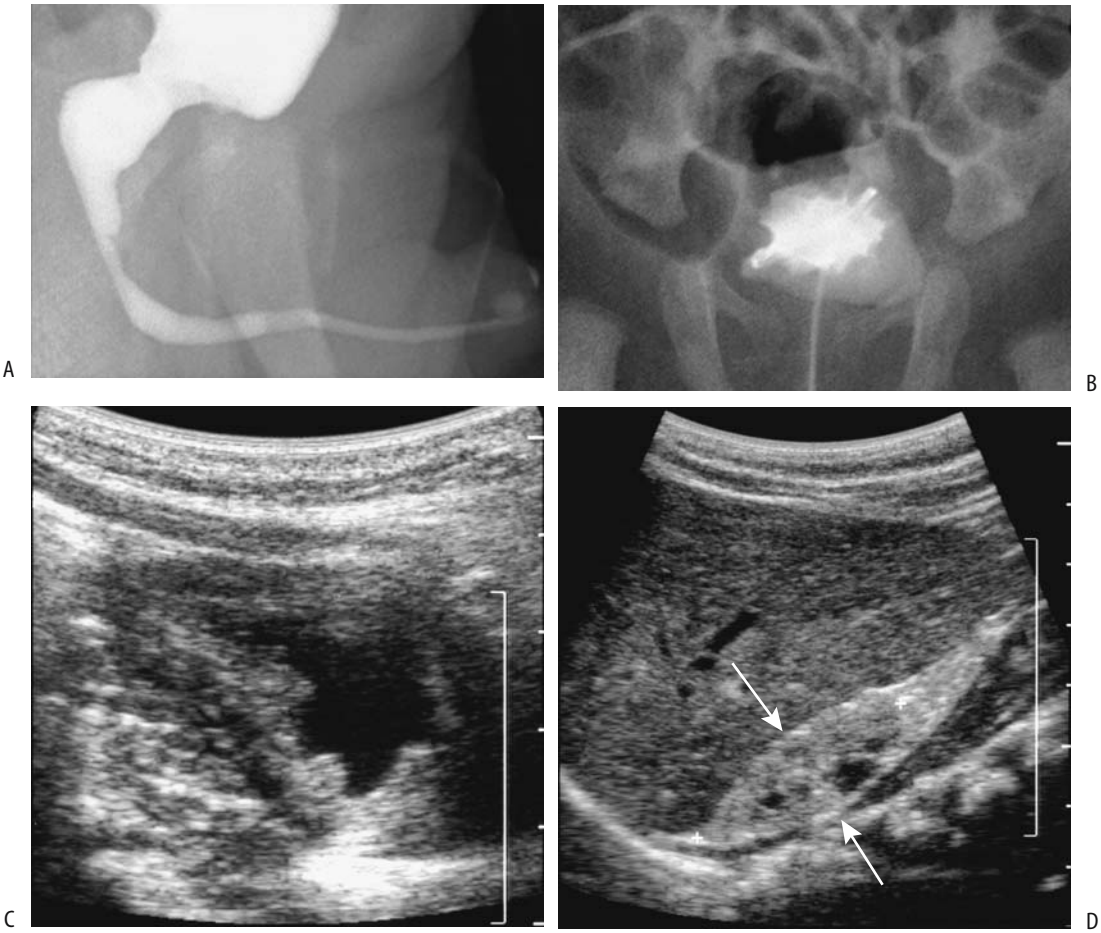

Figure 13.2. Posterior urethral valves in a 4-week-old infant with failure to thrive. A: A voiding cystourethrogram reveals a dilated proximal urethra. B: A cystogram identifies marked bladder trabeculations. C: Ultrasonography (US) confirms bladder wall thickening. D: Renal US reveals a shrunken, hyperechoic, dysplastic kidney (arrows) containing several cysts. (Courtesy of Luann Teschmacher, M.D., University of Rochester.)

Diverticulum

A congenital urethral diverticulum originates from the anterior urethra and is associated with urethral obstruction. These diverticula have either a saccular appearance (and originate from the ventral urethral wall) or are diffuse (megalourethra).

A saccular diverticulum is a ventral outpouching in the midurethra; it is rare in the bulbous urethra, in which case cystic dilation of Cowper's gland duct should be suspected. It contains a valve-like deformity in its distal end; as the diverticulum fills with urine, the distal end is elevated into the urethra and limits flow. Clinically, a saccular diverticulum should be suspected with intermittent urinary obstruction swelling of the penis.

A voiding cystourethrogram should detect an abnormality but may not differentiate a diverticulum from anterior urethral valves.

Hypospadias

Hypospadias consists of an abnormal ventral urethral termination due to failure of urogenital fold fusion. Varying degrees of malposition are possible; at times a urethra even terminates in the perineum. The utricle tends to be

enlarged, with its size having a direct relationship to severity of hypospadias.

About 10% of boys with hypospadias have a familial history and have associated cryptorchidism; renal abnormalities are uncommon. A distal urethral malignancy occasionally develops in men with congenital hypospadias.

A voiding cystourethrogram aids in defining underlying anatomy.

Epispadias

Epispadias is part of the spectrum of pelvic abdominal wall failure-to-fuse anomalies. Failure of dorsal urethral closure results in epispadias. Various gradations occur ranging from failure of bladder neck closure to a defect in the distal urethra. The urethral sphincter is underdeveloped, and these boys have incontinence.

A blind epispadial sinus, or congenital prepubic sinus, is a congenital accessory urethra that does not communicate with the bladder. The underlying anatomy can be outlined with a fistulogram.

Megalourethra

Urethrography in a male infant with a megalourethra revealed crescent-shaped anterior urethral dilatation (2); associated abnormalities included prune-belly syndrome, absent corpus spongiosum, and bilateral undescended testes.

Testes

Anorchia/Cryptorchidism

Clinical

Scrotal agenesis is very rare. Among boys with a clinically impalpable testis, about one-fifth have an absent testis (anorchia) and the rest cryptorchidism. A minority of boys with anorchia have complete testicular agenesis along with epididymis and vas deferens, but a majority have blind-ending cord structures—also called a vanishing testis. The blind-ending cord in these boys with a vanishing testis terminates mostly in the inguinal canal, with a minority intraabdominally, in the superficial inguinal ring, or, least common, in the scrotum. Yet the diagnosis of agenesis is imprecise; some individuals who have negative inguinal canal, and scrotal exploration have later developed an intraabdominal seminoma, presumably from an overlooked intraabdominal testis.

Cryptorchidism is more common than anorchia. Pathogenesis of cryptorchidism is unclear; it is probably part of an embryogenetic defect. These infants are also prone to develop renal agenesis, ureteral duplication and seminal vessel abnormalities. Normally at birth the testes are already descended into the scrotum. With clinical suspicion of an undescended testes, the primary question is: What is the location of the testis? Clinically, these infants can be subdivided into those with a nonpalpable testis and those with a palpable testis in an abnormal location. About 25% have a nonpalpable testis located in the abdomen or inguinal canal (and occasionally even distal to the external inguinal ring), while a palpable testis ranges in location from the inguinal canal, inguinal pouch, and high scrotal position, to even an unusual ectopic position. In most babies with cryptorchidism the testis descends shortly after birth, but an undescended testis persisting beyond the age of 1 year generally will not change position. By puberty, an undescended testis degenerates and has a low spermatogenesis rate.

A high scrotal testis is one located below the external inguinal canal; it can be manipulated to the upper scrotum, but then ascends. Some consider it to represent the mildest form of an undescended testis. A high scrotal testis tends to be smaller than the contralateral one. These boys have a higher prevalence of testicular torsion.

A nonpalpable testis is more common on the left side.

Bilateral cryptorchidism is found in about half of adults with Noonan's syndrome. A high prevalence of undescended testis is found in Down syndrome. Premature infants are somewhat prone to having cryptorchidism. An association exists between cryptorchidism and epididymal abnormalities.

An undescended testis is prone to developing a malignancy, with the most common tumors being a seminoma and embryonal cell carcinoma. Metachronous tumors occur with bilateral cryptorchidism. The risk of malignancy increases even after orchiopexy, to the point that some surgeons advocate orchidectomy

for postpubertal cryptorchid males. As an example of the risk for cancer, a 26-year-old man with Noonan's syndrome had had bilateral orchiopexy for undescended testicles at 12 years of age, and now US confirmed a right testicular solid tumor and CT identified retroperitoneal adenopathy (3); orchiectomy revealed findings consistent with a seminoma.

Postpubertal males with cryptorchidism rarely have normal spermatogenesis; maturation arrest and seminiferous tubular atrophy are common. Bilateral dysgenesis is evident even with unilateral cryptorchidism because the risk of malignancy is also increased in the contralateral normally located testis and some investigators suggest a post-pubertal biopsy for carcinoma-in-situ.

Transverse testicular ectopia, consisting of an abnormal testicular descent resulting in a unilateral location of both testes, is extremely rare. It is usually associated with an inguinal hernia. The spermatic cord of the ectopic testis originates from its correct site. In such a situation, one testis is in the inguinal region and another in the ipsilateral scrotum.

An undescended testis can develop torsion later in life; an underlying neoplasm is associated with such torsion.

Imaging

Individuals operated on previously for cryptorchidism tend to develop microlithiasis (4); annual US surveillance is recommended for these patients with microlithiases.

Because of ease and ready availability, US is the current primary imaging modality in evaluating cryptorchidism. Ultrasonography correctly identifies over 90% of inguinal testes but only a minority of atrophic inguinal testes. Ultrasonography has a low yield if no testis is palpable or is intraabdominal in location or in those with an associated inguinal hernia. MRI should be considered for these infants.

Ultrasonography identifies an undescended testis as a smooth oval structure that is usually smaller than a normal testis. An enlarged lymph node has a similar appearance, and visualization of a linear echogenic mediastinum testis is helpful in differentiating between these two structures.

Computed tomography is limited in this condition. Especially in children, the lack of surrounding fat makes testis detection difficult.

Magnetic resonance imaging is evolving as the preferred imaging modality for an undescended testis and its role will undoubtedly increase in the future. It localizes most undescended testes, including those in the abdomen. A current reasonable approach is to add either MR or US if the first study is inconclusive. A testis is hypointense on T1- and hyperintense on T2-weighted signal intensity, although the T2-weighted signal intensity is lower than usual with an atrophic or fibrotic testis. Most undescended testes are perivesical in location, with an occasional one outside the pelvis.

One promising technique is MR venography; imaging at various delayed venous phases after gadolinium infusion detects the contrast-enhanced pampiniform venous plexus. This technique detected testes not identified with more conventional MRI (5).

Spermatic arteriography has been supplanted by noninvasive imaging.

Thermography has been suggested as an aid in detecting an undescended testis but is of limited use with an abdominal testis. It appears to have a role if a high undescended testis is suspected but is not palpable and not detected by US.

Therapy

In the past, therapy for an undescended testis included surgical exploration, supplanted later by subumbilical laparoscopy, and, more recently, transinguinal laparoscopy. One approach for a nonpalpable testis is initial abdominal laparoscopy; if vas deferens or spermatic vessels enter the internal inguinal ring, surgical exploration of the inguinal canal is performed, but if both vas deferens and spermatic vessels are absent or end blindly intraabdominally, a diagnosis of anorchia or vanishing testis is presumed.

Residual testicular and epididymal abnormalities persist in adults who are treated for an undescended testis in childhood. The cryptorchid testis is smaller in adults treated surgically when they were children. The fertility rate of adult men who underwent surgical correction of bilateral cryptorchidism as children is markedly reduced compared to those who had unilateral cryptorchidism; the resultant fertility

is independent of surgical timing. These adults tend to have an abnormal US echo pattern in the involved testes.

Polyorchidism

Polyorchidism is uncommon. It is a result of transverse division of the embryonic genital ridge. Bilateral polyorchidism is extremely rare.

These boys are at an increased risk for cryptorchidism, inguinal hernia, and testicular malignancy, at times uncommon ones such as a rete testis adenoma and an embryonal carcinoma.

An occasional polyorchid testis is detected by US.

Dysplasia

Cystic dysplasia is a rare congenital nonneoplastic condition resulting in multiple cysts in the mediastinum testes. The defect probably represents a lack of connection between rete testis tubules and efferent ductules.

Rete testis cystic dysplasia presents as a scrotal or abdominal tumor. Ipsilateral renal agenesis is found in some individuals, and whenever cystic dysplasia is detected, ipsilateral renal agenesis should be excluded. Other associated lesions include multicystic dysplastic kidney, duplication anomalies, and cryptorchidism. Multicystic epididymides and seminal vesicles have developed in association with polycystic renal disease.

Ultrasonography reveals multiple small cysts. The appearance is similar to that seen with a teratoma or even testicular microlithiasis.

Vas Deferens

Wolffian duct structures include the epididymis, vas deferens, seminal vesicles, and ejaculatory ducts. Malformations of these structures consist of cysts, agenesis, and partial atresia; an occasional one is associated with renal agenesis. Congenital absence of the vas deferens can be either bilateral or unilateral. In some, unilateral vas deferens agenesis is associated with unilateral renal agenesis (bilateral renal agenesis is incompatible with life), and a finding of vas deferens agenesis should lead to a renal study. Those with congenital unilateral vas deferens absence and infertility often have anomalies in the contralateral testes. An association exists between the absence of a vas deferens and cystic fibrosis; in fact, congenital bilateral vas deferens absence probably is a mild form of cystic fibrosis.

Four patterns were identified among men with vas deferens agenesis (6): bilateral agenesis (64%), bilateral agenesis associated with unilateral renal agenesis (3%), unilateral agenesis (15%), and unilateral agenesis with unilateral renal agenesis (18%). A cystic fibrosis mutation was detected in 64% of men with bilateral agenesis but in none with unilateral agenesis, and the latter condition thus presumably is due to a different pathogenetic pathway.

The absence of vas deferens is identified by endorectal US.

Other anomalies include an ectopic vas deferens and vas deferens duplications.

Abnormal wolffian duct development can result in an ectopic vas deferens insertion into the posterior bladder wall.

Splenogonadal Fusion

An unusual cause of a scrotal mass in boys is splenogonadal fusion. In this congenital entity, splenic tissue is located in the epididymis, tunica albuginea, or along the spermatic cord, almost always on the left side. Although usually found as a discrete tumor, occasionally varying amounts of splenic tissue extend from the splenic hilum inferiorly. Such continuous splenic tissue is associated with other systemic anomalies.

Many of these discrete splenic tumors are initially thought to represent a neoplasm. Consideration of splenogonadal fusion is important because at times a surgeon is able to dissect splenic tissue off the tunica albuginea.

Adrenal Rests

Testicular epididymal and adjacent structure adrenal rests derive from aberrant adrenal cortical tissue migrating into these structures during fetal development. Incidental adrenal rests are most common in newborns but generally involute with age. Hyperplasia of these adrenal rests leads to either focal tumors or diffuse testicular enlargement. In fact, a testicu-

lar tumor in a male with congenital adrenal hyperplasia most often represents testicular adrenal rests. These testicular rests can change in size, at times rapidly. Most symptomatic ones are discovered in the pediatric age group, at times associated with precocious puberty. These solid, multiple, and usually bilateral tumors are believed to develop secondary to elevated adrenocorticotropic hormone (ACTH) levels and are also found in Addison's disease and Cushing's syndrome. A rare such adrenal rest develops a malignancy.

Most are located adjacent to the mediastinum testis. US reveals these predominantly intratesticular, often multiple, bilateral tumors to be mostly hypoechoic when small but often contain hyperechoic regions with growth (7); with color Doppler US they range from hypervascular, isovascular, to hypovascular relative to normal testis. Some contain a spoke-wheel pattern of converging vessels. They are isointense on T1- and hypointense on T2-weighted MR images, tumor margins are well-defined and most show contrast enhancement (7). Their appearance suggests a neoplasm. With the presence of adrenal hyperplasia, whether these tumors should be investigated for a possible underlying malignancy remains an individual clinical decision.

Ultrasonography and MRI appear similar in detecting intratesticular adrenal rest tissue (8); MR showed 71% of testicular adrenal rests to be isointense and 29% slightly hyperintense to normal testicular tissue on T1-weighted images; all were hypointense on T2-weighted images, and 85% enhanced diffusely postcontrast.

At times testicular vein sampling reveals elevated cortisol levels (compared with peripheral blood).

These tumors regress with glucocorticoid therapy.

Trauma

Urethra

Anterior pelvic arch fractures are usually associated with membranous urethral injury, while straddle injuries tend to involve the bulbous urethra. Associated bladder injury should also be suspected. A retrograde urethrogram should be obtained with any suspected urethral injury.

Table 13.1. Classification of blunt urethral trauma

Type I:	Posterior urethra intact but stretched
Type II:	Partial or complete posterior injury with tear of membranous urethra above urogenital diaphragm
Type III:	Partial or complete combined anterior/posterior urethral injury with urogenital diaphragm disruption
Type IV:	Bladder neck injury with extension into urethra
IVA:	Injury to base of bladder with periurethral extravasation simulating a true type IV injury
Type V:	Partial or complete anterior urethral injury

Source: Adapted from Goldman et al. (9).

Urethral trauma ranges from incomplete to complete rupture. Blind bladder catheterization should be discouraged in such a setting to avoid converting a partial tear into complete rupture. A classification of injury to the anterior and posterior urethra is outlined in Table 13.1. Type IV injury is least common. A retrograde urethrogram should be diagnostic for a tear.

Although CT is not directly employed for urethral trauma, it is often obtained to evaluate pelvic structures, and it does provide indirect evidence of urethral injury. With type I injury the prostate is elevated, type II is associated with contrast extravasation above the urogenital diaphragm, and type III is associated with extravasation below the urogenital diaphragm. An MRI can establish the length of urethral injury and any prostatic displacement. The sequelae of urethral injury are stricture, impotence, and incontinence, the latter due to prior sphincter injury. Future impotence is suggested if MRI detects avulsion of the corpus cavernosum, separation of the corporeal body, and superior or lateral prostatic displacement. With both corpus cavernosum avulsion and prostatic displacement, the probability of permanent impotence is over 90%.

Strictures in boys with posttraumatic urethral disruption are almost always inferior to the verumontanum; stricture length tends to be overestimated during urethrography due to incomplete filling.

Smaller, less fibrous posttraumatic rectourethral fistulas tend to heal spontaneously after a double diversion; others require recon-

struction. A urethral stricture is a potential postreconstruction complication.

Penis

The most common conditions resulting in priapism due to trauma are an intracavernosal arteriovenous fistula, a pseudoaneurysm, or asymmetric cavernosal arterial blood flow. These fistulas can be detected by selective angiography, and subsequent embolization can be therapeutic. The embolic materials used are autologous blood clots, *N*-butyl-cyanoacrylate, and others.

With suspected penile fracture some surgeons operate without any diagnostic imaging being performed, with imaging requested primarily for equivocal clinical findings. In this setting, however, traumatic rupture of the corpus cavernosum is not uncommon and some investigators believe that preoperative cavernosography should be performed and therapy modified accordingly. A corpus cavernosum tear is identified as contrast extravasation during cavernosography. Most corpora cavernosa ruptures are proximal, the vast majority being unilateral; associated complete urethral rupture is rare.

Mostly anecdotal reports suggest that MRI is superior to US in identifying corpus cavernosum rupture; the role of MR will undoubtedly expand. MRI detects corpus cavernosum rupture as a discontinuity in the hypointense tunica albuginea (10); associated subcutaneous haematoma were identified both on T1- and T2-weighted images, but corpus cavernosum haematomas were better seen on contrast enhanced T1-weighted images.

Follow-up MRI after surgical repair reveals a hyperintense signal at the tunical suture site on precontrast T1-weighted images, enhancing with contrast (10); the tear site gradually recovered its hypointensity on spin echo sequences.

Scrotum and Testes

A painful, ecchymotic scrotum is common after scrotal trauma. Preoperative US is useful in suspected testicular rupture. Still, both false-positive and false-negative findings occur. For instance, fracture of the tunica albuginea can be missed with US. Ultrasonography cannot provide an accurate diagnosis of rupture. On the other hand, if US is abnormal, even if the findings are nonspecific, testicular rupture should be suspected. Ultrasonography reveals testicular rupture as regions of heterogeneous echogenicity and loss of normal contour. Only occasional fracture planes are identified by US.

An intratesticular pseudoaneurysm developed after blunt trauma (11).

Traumatic dislocation of the testis is rare and most are inguinal in location. Associated spermatic cord injury is also often present. Imaging is helpful in guiding surgical correction.

Among mountain bikers (with less than half being symptomatic), 94% had abnormal scrotal US, consisting of scrotal calculi (81%), epididymal cysts (46%), epididymal calcifications (40%), testicular calcifications (32%), hydroceles (28%), varicoceles (11%), and testicular microlithiasis (1%) (12).

Prostate and Adjacent Structures

Hyperplasia/Hypertrophy

Clinical

Benign prostatic hyperplasia (BPH), also called *benign hypertrophy*, *adenomatous hypertrophy*, or simply *adenoma*, increases with age. Some physicians use this term to describe a symptom complex rather than use it as an anatomic entity. The term *lower urinary tract symptoms* is used by some for this broad clinical entity.

The prevalence varies among racial and ethnic groups; it is considerably less common among Japanese men than among Caucasians. Estrogen has a role in its development. Serum beta-carotene and smoking appear to be risk factors for BPH. Familial BPH does exist.

Most benign hyperplasia occurs in the transition zone and only occasionally in the periurethral glandular zone. Some enlarged glands contain cysts, calcifications, or even regions of hemorrhage. Little correlation is apparent between prostatic calcifications and the extent of hyperplasia. Likewise, endorectal US measurements of prostate size or transition zone volume do not relate to the degree of bladder outlet obstruction. Also, the volume of residual

urine correlates poorly with prostate size and flow rate. Prostatic capsule rigidity may play a role in benign hyperplasia. Prostatic innervation also appears to be a factor, because α-adrenergic receptor blocking agents lower resistance to flow in those with an enlarged prostate. On the other hand, in a setting of benign hyperplasia ischemia does not appear to be a factor in bladder outlet obstruction.

Occasionally a prostatic biopsy suggests a low-grade adenocarcinoma, which actually represents hyperplasia of verumontanum mucosal glands.

At times voiding cystourethrography shows a smooth posterior impression at the bladder neck. If this impression is only several millimeters in length, it probably should be considered within the normal range. When enlarged, it is called median lobe hyperplasia and is produced by periurethral gland hyperplasia. Such hyperplasia occurs in men with spinal cord injury and in those who have undergone numerous catheterizations.

Occasionally an inguinal cystocele mimics clinical findings of prostatic enlargement but without actual evidence of bladder outlet obstruction. Also, not all prostatic enlargement is secondary to hyperplasia or neoplasm; in some parts of the world bladder schistosomiasis is a cause of prostatic enlargement.

Imaging

Does intravenous (IV) urography have a continued role in men with prostatism? In a large minority of patients with prostatism, IV urography reveals excretory system dilation, calculi, an unexpected congenital anomaly, or other abnormality. Voiding cystourethrography adds little to the diagnosis, except perhaps in younger men in a search for alternate diagnoses for urethral obstruction. Prostate size cannot be evaluated with this examination.

Computed tomography reveals prostatic hypertrophy as a smooth homogeneous, but CT is not indicated for simple benign prostatism. Computed tomography attenuation values are similar for benign disease and a malignancy.

Bladder wall thickening is common with bladder outlet obstruction. To obtain reproducible US results, bladder wall thickness should be measured after bladder filling with a standardized amount of fluid—about 150 mL. Not all bladder wall thickening is due to bladder outlet obstruction.

The sonographic appearance varies from a fine to a rough pattern or a combination, and hypoechoic to hyperechoic. Echogenicity in any one patient is due to a mix of complex hyperplastic glands and a cystic atrophic component. Nodules are detected in some glands. Any calcifications present appear hyperechoic. At times the central and peripheral gland portions appear to be separated.

Prostatic size estimates are of less importance in BPH than with a suspected cancer. In addition, a "gold standard" is more difficult to establish than with a radical prostatectomy for cancer. Studies suggest that endorectal US and MRI measurements of prostatic hyperplasia are similar, although endorectal US may underestimate prostatic weight. Gross prostate size estimates, however, are useful; transurethral resection is more difficult with a very large gland.

Magnetic resonance imaging reveals BPH to be hypointense on T1- and heterogeneous and mildly hyperintense on T2-weighted images (Fig. 13.3).

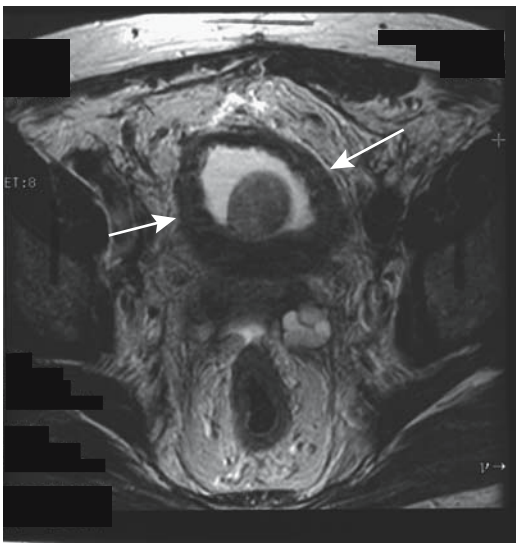

Figure 13.3. Benign prostatic hypertrophy, bladder outlet obstruction, and thick bladder wall (arrows), detected on T2-weighted magnetic resonance (MR) image. (*Source:* Burgener FA, Meyers SP, Tan RK, Zaunbauer W. Differential Diagnosis in Magnetic Resonance Imaging. Stuttgart: Thieme, 2002, with permission.)

Therapy

Resection

Currently surgical resection is the gold standard in treating BPH, most often using a transurethral approach. Post-resection MRI reveals degenerative changes near the prostate surface and shrinkage of the prostatic capsule. A dilated prostatic urethra is readily identified.

A complication of a radical retropubic prostatectomy is an inguinal hernia. Most of these hernias are indirect. Fistulas are uncommon; with surgery being close to the symphysis pubis, an occasional fistula leads to osteitis pubis.

Bladder hypertrophy due to obstruction by BPH is to a large extent reversible after surgical relief, except in those with irreversible degenerative changes.

Nonsurgical

The natural progression of BPH suggests that in many men an initial decision to prescribe no therapy is a viable option; symptoms in most men do not progress. In some, α-adrenergic-blocker therapy and 5α-reductase inhibitor therapy are helpful.

Although a number of nonsurgical techniques, such as laser therapy, microwave thermotherapy, and others have been tried, thermal ablation is currently the only viable alternative to surgery, achieving similar results. Balloon dilation has been disappointing.

Laser Therapy

Laser ablation thermotherapy leads to coagulation necrosis, with eventual reepithelialization. In theory, laser coagulation shrinks the prostate by inducing prostatic necrosis without injury to the urethra or surrounding tissues. Currently, results from US-guided laser-induced transurethral thermal therapy appear inferior to those obtained with transurethral resection. One disadvantage of laser therapy is that no tissue is obtained and it takes longer to attain symptomatic improvement compared to transurethral resection. Prostatic volume initially is not reduced, and postprocedure urinary retention is common. Laser therapy, however, is still a new technique, and further advances are to be expected.

Few complications are encountered and symptoms eventually improve in most. Rarely, the loss of ejaculation, epididymitis, or an abscess develops. Urethral stricture is a late complication.

Magnetic resonance imaging detects prostate changes during and after laser-induced thermotherapy. Repetitive T2-weighted fast spin echo (FSE) MRI during coagulative laser thermotherapy revealed persistent hypointense regions, presumably representing coagulation necrosis. These regions increase in size during therapy. The prostate remains enlarged shortly after treatment, and contains poorly defined hypointense regions surrounding the urethra; with time, the prostate gland returns to its preoperative size.

Central coagulation necrosis is seen as a hypointense region surrounded by a hyperintense rim. The prostate increases in size, presumably due to edema; edema is evident in the surrounding tissues and the presacral space thickens. Subtracting postprocedure laser-induced lesion volume (obtained via MR planimetry) from preprocedure volume predicts prostatic volumes at late follow-up (13), although transitional zone volume was underestimated and peripheral zone volume was overestimated.

Microwave Ablation

Transurethral microwave thermotherapy is a potential outpatient procedure requiring little or no anesthesia. A temperature ≥60°C results in coagulation and tissue necrosis. Tissue vaporization ensues if the temperature is >100°C. Use of higher energy levels improves results but at the expense of increased morbidity.

Symptomatic improvement is achieved in about half of men treated with microwave thermotherapy. Imaging findings are inconstant. Magnetic resonance imaging detects prostatic urethral widening. Necrosis is an inconstant finding. Findings on voiding cystourethrography and retrograde urethrography before and after transurethral microwave therapy do not correlate with subjective improvement. The transition zone volume, obtained from pretreatment endorectal US, appears to relate to long-term microwave thermotherapy efficacy.

Other Therapy

Self-expanding endourethral stents have been used to treat bladder outlet obstruction due to prostatic hyperplasia; still, urethral stents have had limited success, with some stents dislodge or become encrusted.

Preliminary results using an electrosurgical generator for transurethral prostatic electrovaporization are encouraging. Postoperative urine incontinence is a potential complication.

High-intensity focused ultrasound therapy is still experimental.

Infection/Inflammation

Prostatitis

Prostatitis can be either acute or chronic. At times a specific pathogen is detected; if not, the clinical symptoms are often ascribed to prostatodynia, a previously poorly defined condition. In this work prostatodynia is used to designate pelvic venous congestion and is discussed later (see Vascular Abnormalities).

Granulomatous prostatitis is a histologic diagnosis. Common causes are prior prostatic surgery and prostatic needle biopsy. Occasionally prostatic granulomas develop in a setting of prior bacillus Calmette-Guérin therapy.

Ultrasonography reveals a complex pattern in prostatitis. At times prostatic nodules are present. In a normal gland Doppler US using a coronal plane reveals capsular and parenchymal arteries radiating symmetrically. These arteries become more prominent in acute prostatitis.

Ejaculatory duct calcifications develop in chronic prostatitis.

Early prostatic cancer and prostatitis are difficult to differentiate with current imaging. Of interest is that in some patients with prostatitis MR spectroscopy detects an elevated choline peak and reduced or no citrate, findings mimicking those of cancer (14).

Abscess

Predisposing factors for periprostatic or prostatic abscesses are diabetes mellitus, urethral catheterization or manipulation, and an immunocompromised status. Most abscesses are infected, with only an occasional sterile abscess encountered. Any portion of the prostate can be involved, and an abscess may or may not communicate with the urethra. Some prostatic abscesses result in bladder outlet obstruction.

A prostatic abscess is detected either by CT or endorectal US. Typically US reveals hypoechoic or anechoic regions with internal echoes, suggesting fluid-filled structures containing septations. Some mimic loculated cystic prostatic tumor.

Once diagnosed, a prostatic abscess can be drained using endorectal US guidance, and a perineal or transurethral drainage approach can be used.

Tuberculosis

Tuberculosis either is primarily genital in origin and involves the seminal vesicles, prostate, and adjacent structures, or these structures are involved by extension from the kidneys. An occasional tuberculous prostatitis is associated with intravesical carcinoma therapy with bacillus Calmette-Guérin.

Tuberculosis results in prostatic inflammation, enlargement, necrosis, or abscess. Cystography reveals prostatic enlargement simply as bladder base elevation. Urethrography identifies any urethral stricture or fistula to adjacent structures. Endorectal US reveals prostatic enlargement with multiple hypoechoic foci within the gland, usually anteriorly in the transition zone, representing necrotizing granulomas. Eventually these granulomas calcify.

In some men seminal vesicle and vas deferens calcifications are the only imaging abnormality. Vas deferens calcifications are either intramural or intraluminal in location, and the appearance mimics findings seen with diabetes mellitus.

Computed tomography reveals inflammation of the surrounding structures, including perivesical fat stranding.

Other infections

The seminal vesicles dilate and calcify secondary to schistosomal involvement. At times the ejaculatory ducts also dilate. Schistosomiasis induces prostatic retention cyst formation and eventual prostatic enlargement and calcifications.

Ultrasonography detects hyperechoic prostatic foci. Seminal vesiculography outlines the dilated lumen and irregular border. After therapy the prostate decreases in size and the hyperechoic foci become less evident. Some investigators believe that calcifications also diminish.

In endemic regions the presence of typical calcifications is presumptive evidence for schistosomiasis.

Prostatic aspergillosis is rare in a immunocompetent patient. It is associated with recurrent urinary tract infections.

Brucellar prostatitis is rare even in brucellosis-endemic regions, such as certain provinces of Spain. Ultrasonography is useful to follow therapy.

Malacoplakia

Prostatic malacoplakia is a granulomatous inflammatory disorder, presumably being a variant of chronic granulomatous prostatitis. Prostatic malacoplakia can form fistulas to adjacent structures. It often mimics a malignancy and some affected men have undergone a radical prostatectomy for suspected carcinoma.

Past urinary tract infections are a common precedent.

Ultrasonography revealed a hypoechoic peripheral zone tumor in three men with prostatic malacoplakia (15).

A biopsy should provide the diagnosis by detecting Michaelis-Gutmann bodies, although even a biopsy can be misdiagnosed as a carcinoma.

Tumors

Sclerosing Adenosis

Sclerosing adenosis usually develops in a setting of prostatic gland hyperplasia. Even histologically, this entity is difficult to differentiate from a well-differentiated adenocarcinoma.

Prostatic and Müllerian Cysts

Prostatic cysts are uncommon. Embryologically, many of these cysts represent either an enlarged prostatic utricle or a cystic müllerian duct; both tend to be located close to the midline, which helps differentiate them from the more laterally located seminal vesicle and ejaculatory duct cysts. Müllerian duct cysts tend to project somewhat lateral to the midline, while utricle cysts are midline structures; müllerian duct cysts tend to be larger and extend further superiorly, while utricle cysts tend to be small. However, considerable overlap exists and these cysts cannot be readily differentiated from each other. A rare müllerian duct cyst is associated with prostatitis.

A dilated utricle is associated with hypospadias and testicular abnormalities. Some utricle cysts lead to dysuria. They vary in size. Urography and US simply detect a retrovesical cyst.

An occasional midline prostatic cyst is a cystadenoma or a simple cyst, but not all prostatic cysts are benign. A rare one is a prostatic cystic adenocarcinoma, often in a young man.

Clinically most prostatic cysts are asymptomatic, although an occasional larger one leads to bladder outlet obstruction or becomes infected.

Magnetic resonance reveals prostatic cysts similar to other fluid-filled structures; namely, they are hypointense on T1- and hyperintense on T2-weighted images. Blood and other fluid modify these findings.

Prostatic cysts are amenable to transrectal puncture and drainage under US guidance. A müllerian duct cyst causing ejaculatory duct obstruction was drained transurethrally using US guidance (16).

Benign Neoplasm

Benign prostatic neoplasms are almost nonexistent, and most reported ones are anecdotal. No imaging features differentiate them from malignancies.

A schwannoma within the prostate ranges from a focal tumor to an enlarged prostate. Transrectal US identified one as a hypoechoic nodule in the periphery (17); specific diagnosis could be established only by biopsy.

Prostate involvement in neurofibromatosis is rare. Endorectal coil MR localizes and provides guidance for biopsy of suspicious tumors.

Prostate Carcinoma

Primary

Clinical Aspects

General: In the West, prostatic cancer is the most commonly diagnosed cancer in men. For

unknown reasons, the relative incidence appears to be increasing in both Europe and North America. Only part of this increase is explained by improved diagnosis. One factor influencing results is that the number of prostate T1a–b cancers has declined considerably, with the decline probably due to less frequent use of surgical prostatectomy for treating BPH. At least in the United States a rise and fall in prostate cancer detection rates occurred in the 1990s, believed by some to represent primarily a removal of previously undetected T2 cancers from the prostate cancer pool due to improved screening, leaving behind mostly undetected T1c cancers as a residual reservoir (18). Among men treated with a radical prostatectomy for clinical stages T1c to T2c from 1988 to 1996, T1c cancers increased from 10% in 1988 to 73% in 1996, cancers confined to the prostate increased from 40% to 75%, and transition zone cancers increased from 10% to 21% (18); on the other hand, seminal vesicle invasion decreased from 18% to 5%, positive surgical margins decreased from 30% to 14%, and the mean patient age decreased from 65 to 62 years.

Unlike many other cancers, prostate cancer has a wide spectrum of activity, and a number of these cancers do not result in serious morbidity and mortality. Especially well-differentiated ones tend to be quiescent for considerable time, although the current concept is that prostatic cancers progress. Some investigators assume a simplistic division of prostatic cancers into indolent ones that are unlikely to progress and those that result in extensive morbidity and mortality. Probably a more realistic assumption is a continuous spectrum containing two peaks. Thus although prostate cancer is quite common in elderly men, it is difficult to predict in any one individual whether the cancer will progress or not. Extrapolating findings from an autopsy study of prostates containing a clinically undetected carcinoma, carcinomas remaining clinically insignificant throughout life tend to have long doubling time, while those that become clinically significant are likely to have doubling times of several years or less; thus knowledge of a tumor doubling time in an elderly patient could provide clinical guidance.

In men at a mean age of 64 years, the Association Française d'Urologie estimates a 43% histologic prevalence of prostate cancer and that it takes about 12 years for a 0.5-cc cancer to reach a volume of 4 cc, a size associated with the risk of distant metastases (19); without therapy, a localized cancer diagnosed before age of 65 years results in a survival of less than 30%. Complicating matters, even with therapy prostate cancer diagnosed before the age of 50 years is associated with <50% survival at 5 years; many of these men already have metastases at initial diagnosis.

Most prostatic carcinomas originate in the prostatic gland periphery. With growth, the tumor invades the surrounding structures, including the rectum. Thus occasionally an invasive prostatic carcinoma presents with rectal bleeding.

One patient with prostate cancer developed disseminated intravascular coagulopathy (20); the authors postulated the release of procoagulation substances during diagnostic or therapeutic procedures.

Etiology: A study combining data from several French urologic centers concluded that clusters in families (familial) account for 15% to 25% of prostate cancers and hereditary forms were evident in 5% to 10% (21). In addition to such an inherited trait, having an autosomal-dominant mode with variable penetrance, environmental factors also have a role, and in some of these men a purely environmental influence is evident. Carriers of a germline mutations in the *BRCA1* gene on chromosome 17q appear at increased risk for prostate cancer. In general, a hereditary influence is more evident in those who develop prostate cancer at a younger age. No major pathologic differences exist between the hereditary and sporadic forms of cancer.

Applying familial cancer data to clinical practice, the Association Française d'Urologie estimates that, compared to the general population, a family history (first-degree relative) of prostate cancer is associated with a two- to threefold increased risk of prostatic cancer (19); such a familial association thus defines a high-risk group for screening.

Schistosomiasis is associated with bladder, rectal, and renal cancers. No definite association with prostate cancer is established, although prostate cancer is occasionally reported in young men with schistosomiasis.

Although adenomatous hyperplasia appears intermediate between BPH and a well-differentiated carcinoma, suggesting that it is a

possible precursor for carcinomas arising in the transition zone, BPH is not considered to be a precursor to prostatic cancer. Likewise, in spite of some earlier reports, no definite association exists between prior vasectomy and prostate cancer.

Screening: Screening for prostatic cancer is controversial. In the United States and some European countries routine physical examination of men at risk (generally considered to be those over age 50 years) include a digital rectal examination and determination of serum prostate-specific antigen (PSA) level. In some countries PSA testing is not routinely performed, the reasoning being that its use in screening results in overdiagnosis and overtreatment. Also, some believe that no firm evidence exists that early diagnosis decreases mortality. In addition, because of the prolonged time course of prostatic cancer growth in some men, whether cure in the higher surgical risk group really represents the best option is also questioned. Some physicians believe that PSA testing is not usually indicated in men over about 70 years unless digital examination suggests prostatic disease; another viewpoint is that in those with a life expectancy greater than of 10 to 15 years an elevated PSA level is an indication for US and biopsy. Nevertheless, in countries with extensive screening, evidence suggests that an earlier diagnosis has an impact on this cancer, and the number of men seen with advanced disease decreases.

In the United States, the recommended frequency for PSA screening for prostate cancer is every year, although an optimal interval has not been established. A Rotterdam study, in which 4133 men, aged 55 to 75 years, underwent PSA screening initially, again 4 years later in over half the subjects, and, when indicated, a needle biopsy was performed, found that initially 36% of the cancers detected had a Gleason score of 7 or higher but only 16% of those detected 4 years later had such an elevated score (22); initially 25% of the cancers detected had adverse prognostic features, but only 6% of those detected 4 years later did, and the authors concluded that most large prostate cancers are detected by PSA screening and, among these men, a screening interval of 4 years appears to be short enough to prevent large tumors from developing.

A serum PSA level of up to 4 nanograms per milliliter is commonly assumed to be within the normal range, although this level is arbitrary, and a number of men with a lower PSA level have developed prostatic cancer. Of interest is that many of these tumors are also not detected by endorectal US and digital rectal examination.

The production of PSA is influenced by androgen levels, and those taking drugs for androgen suppression have low PSA levels even in the presence of a prostatic carcinoma. False serum positive PSA levels are uncommon when using a monoclonal assay. The PSA levels are elevated in some men with urinary tract infection but decline as infection clears; this marker thus appears useful in following infection progression. The PSA level is also increased with some nonprostatic neoplasms, including some lymphomas.

A digital rectal screening examination detects two thirds to three quarters of prostatic cancers. In general, the sensitivity of the PSA assay is higher than either digital rectal examination or endorectal US. When combining serum PSA levels and digital rectal examinations for screening, some cancers are detected because of an elevated PSA level only. A high proportion of these men will have a nonpalpable prostate cancer, and endorectal US is appropriate in this population.

About 40% to 50% of hypoechoic foci identified by endorectal US are cancerous. These percentages can be improved; thus a majority of hypoechoic foci in men with a PSA >10 ng/mL are positive for cancer, but in those with a PSA ≤4 ng/mL only a small minority are positive.

What is the effect of instituting PSA screening and sextant biopsies on prostate cancer detection? From serum stored in Göteborg, Sweden, in 1980, PSA was analyzed for 658 men born in 1913 with no previously known prostate cancer (23); among those found to have a PSA level of >3 ng/mL, the mean time from increased PSA to an eventual clinical diagnosis of prostate cancer was 7 years. Thus screening 67-year-old men should lead to cancer detection and treatment a mean of 7 years before clinical symptoms develop.

In summary, in asymptomatic men a screening digital rectal examination together with a

serum PSA level detects more prostate cancer and at an earlier stage than a digital rectal examination alone. Currently endorectal US is not sufficiently sensitive and specific to be used for routine screening for prostate cancer. Nevertheless, a basic question remains: Are the additional cancers detected with a screening program mostly latent ones of limited future significance or do they represent those that will progress and, if untreated, metastasize?

A number of PSA-related tests have been investigated: serum PSA level, age-adjusted PSA level, PSA density, PSA velocity and a ratio of free-to-total PSA. In blood, PSA is either free or bound to proteins. PSA associated with prostate cancer tends to be more protein-bound and thus the ratio of free-to-bound PSA appears of some value in estimating cancer risk. A PSA age-corrected level is often used in screening programs. The rationale is that it will detect younger patients with potentially curable prostate cancer and identify those older patients not requiring additional tests.

The ratio of free to total PSA varies with prostate volume, but this ratio is of limited use in differentiating benign from malignant disease. It appears to have a role with a serum total PSA level between 4 and 10 ng/mL, and some authors suggest the use of this ratio in men with a total PSA level between these levels as an indicator of whether to biopsy or not, yet the cutoff ratio used influences the resultant sensitivity and specificity. The specificity can be improved, but at decreased sensitivity (i.e., fewer cancers detected). Currently this ratio is not commonly employed as an initial guide about whether to biopsy.

Serum PSA levels increase with prostate volume. Thus rather than relying on an absolute serum value, a PSA density value appears useful, defined as serum PSA level divided by prostatic gland volume as measured by rectal US and expressed in nanograms per milliliter per milliliter of tissue. Theoretically, PSA density compensates for the gradual increase in PSA level due to gland growth with age. A PSA density value is most useful in men with a normal digital rectal examination and a PSA level between 4 and 10 ng/mL, although some authors deem such density measurements unreliable. In men with a PSA level >10 ng/mL, the PSA density is of even less significance.

A variant of the above is to use the PSA value adjusted for prostate transitional zone volume. This PSA transition zone density is obtained by dividing the PSA value by the transition zone volume. A change in PSA blood level over time is known as PSA velocity and is expressed as a PSA increase per year. Although men with BPH also have an increase in PSA level with age, those with cancer have a more logarithmic increase. The PSA velocity is of less use in patients with an elevated PSA level and negative biopsy.

Pathologic Study

Adenocarcinoma accounts for about 95% of all prostatic malignancies. Mucinous adenocarcinomas of the prostate are uncommon, and their prognosis is worse than that of a more typical adenocarcinoma. A rare papillary cyst-adenocarcinoma has been reported; cyst aspiration yields a very high PSA level. An adenoid cystic carcinoma is a variant of a prostatic adenocarcinoma; some of these are associated with a normal PSA level even in the face of spread.

Of the rest, transitional cell carcinoma predominates, followed by an occasional squamous cell carcinoma, small cell carcinoma, sarcoma, and metastasis to the prostate. Primary squamous cell carcinomas and sarcomatoid carcinoma have developed in previously treated adenocarcinomas, although a sarcomatoid carcinoma can originate de novo (24). A rare prostatic carcinoma contains endometrioid features; both PSA and CEA levels tend to be elevated. These are rather aggressive cancers. A curiosity is one malignancy metastasizing to another malignancy. Thus prostate carcinomas have metastasized to renal cell carcinomas.

Occasionally a biopsy reveals prostatic intraepithelial neoplasia without an adenocarcinoma. This neoplasia, considered a precursor of prostate cancer, is subdivided into high grade and low grade; high-grade intraepithelial neoplasia is believed to be premalignant and a strong predictor of later cancer, while the low-grade variety tends to behave like BPH and is associated with a low risk of carcinoma. Abnormal growth factor receptors and general genetic instability are associated findings with prostatic intraepithelial neoplasia. A biopsy finding of

high-grade intraepithelial neoplasia without evidence of a carcinoma generally should be followed by additional biopsies. One should also keep in mind that some prostatic intraepithelial neoplasias are difficult to differentiate from cancers based on cytologic material.

A finding of neuroendocrine tumor cells is not uncommon in prostate cancers and presumably reflects different stem cell evolution. In distinction to androgen-responsive prostate cancer cells, these neuroendocrine tumor cells lack androgen receptors and are androgen insensitive.

Prostate carcinomas are graded using either the Gleason or World Health Organization (WHO) grading systems (with nucleolar subgrading). In the United States the Gleason grading system is more widely used. At least for relatively advanced primary tumors the Gleason grading system appears superior in predicting prognosis than the WHO grading system (25).

In the Gleason system the tumor glandular pattern is evaluated and the two most common patterns graded from 1 to 5. These primary and secondary patterns are then combined to obtain a Gleason score. A score of 2 signifies a well-differentiated tumor and 10 is a highly malignant one. In general, a biopsy Gleason score correlates with resected prostate specimen Gleason score. Paired biopsies and prostatectomy specimens from clinically localized prostate cancers revealed exact score agreement in 57% and a difference of ±1 unit in 92% of the paired samples and predicted tumor stage (26); with minimal tumor size on a biopsy, however, the Gleason score does not predict tumor stage.

A less often used grading system is based on an estimate of mean nuclear volume, developed by Gunderson and Jensen. In some hands this system is prognostically superior to the Gleason system.

Cytometry of the DNA is useful in some patients. Thus a finding of a constant diploid and tetraploid pattern with DNA cytometry identifies those who are at little or no significant risk of tumor progression even without therapy (27); men with a DNA tetraploid histogram may deteriorate with hormonal therapy. A DNA aneuploid pattern suggests that a cancer may not respond to hormonal therapy.

A xanthoma is a localized collection of cholesterol-filled histiocytes. Most are idiopathic, although some develop in a setting of hyperlipidemia. Their importance is that occasionally a xanthoma biopsy suggests a carcinoma; confusing the issue, xanthomas have been reported adjacent to foci of adenocarcinoma. A foamy gland carcinoma contains xanthomatous cytoplasm but lacks the nuclear enlargement and prominent nucleoli associated with a carcinoma.

Detection

Currently the most common initiator for a search for prostate carcinoma is a screening finding of an elevated PSA level. Examinations used in prostate cancer detection include digital rectal examination, endorectal US, MRI, and US-guided transrectal biopsy. Each of these procedures has its limitations. In general, the detection rate for prostate carcinoma increases when these procedures are used in combination.

Computed Tomography: Nonhelical CT detects an enlarged gland but cannot distinguish between BPH and a neoplasm. Carcinoma is suggested only by an irregular contour outline. Helical CT, on the other hand, identified cancer in 88% of patients as peripheral zone regions of contrast enhancement (28); transitional zone cancers, on the other hand, appear similar to benign nodules.

Ultrasonography: Most peripheral zone carcinomas are hypoechoic, a nonspecific finding because a number of benign conditions are also hypoechoic. If a tumor is hypoechoic and also palpable, the probability of carcinoma is about 75%. Hyperechoic prostatic cancers are less common. They tend to be large when first detected. The least common are isoechoic ones. Common US criteria used to suggest a prostate cancer are the presence of a peripheral zone hypoechoic nodule, peripheral zone inhomogeneity, and loss of zonal architecture.

Adenocarcinomas originating in the transition zone are usually not detected with US.

Endorectal US provides more information than a transabdominal approach. Nevertheless, to put US in perspective, based on data from sextant biopsies, in one study overall agreement

between gray-scale and Doppler US findings and biopsy results were minimally superior to chance, and the authors concluded that sextant biopsies are still necessary (29). A number of controlled studies suggest that gray-scale US detects about half or less of prostatic cancers. One study found that endorectal gray-scale US detected less than half of 190 subsequently found cancers (30); targeted biopsies detected 57% of these cancers, with the rest detected by sextant biopsies, and the authors concluded that targeted biopsies should be accompanied by sextant biopsies. Although sensitivity and specificity obtained with US is disappointing, US has an established role in biopsy guidance and a potential future role in evaluating tumor blood supply and possibly assessing temperature distribution during some therapeutic heat applications.

Preliminary studies suggest that contrast-enhanced US aids cancer detection. Using biopsy sites showing prostate cancers as a gold standard, gray-scale and Doppler US sensitivity of cancer detection increased from 38% precontrast to 65% postcontrast, but the specificity was unchanged (31). Endorectal US and color Doppler US achieved a 78% sensitivity in detecting proven prostate carcinomas (32); use of a contrast agent (Levovist) improved the sensitivity significantly to 93%. Of interest is that post-Levovist, most of the cancers appeared avascular within a strongly enhancing peripheral gland.

Most malignant tumors are associated with angiogenesis and increased blood velocity through these vessels. Although color Doppler US detects such increased velocity, small neoplasms are missed. Also, some infiltrating cancers are isovascular and isoechoic. Some studies suggest a positive correlation between tumor blood supply and Gleason score. One should keep in mind that some benign lesions also have increased flow.

Magnetic Resonance Imaging: Of all imaging modalities, MRI shows the greatest potential in detecting prostatic carcinomas. It is performed with either a body coil or, preferably, an endorectal coil. Compared to histopathological results in consecutive patients with prostate cancer, endorectal coil MRI cancer detection rate for tumors <5 mm was only 5% but increased to 89% for tumors >10 mm (33). MRI using endorectal and pelvic phased-array coils detects more prostate cancers than digital rectal examination or endorectal US; predicted tumor volume obtained from MRI correlates with resected tumor volume.

On T2-weighted images a prostatic carcinoma typically is hypointense relative to the higher intensity normal peripheral zone. Nevertheless, a hypointense peripheral zone is not pathognomonic for a prostatic cancer; prostatitis, benign prostatic hyperplasia, or an infarct can have a similar appearance. A wedge shape and diffuse extension without mass in a hypointense peripheral zone suggest benignity, while a large size is associated with malignancy (34). Cancers in the central and transitional zones are difficult to identify with MRI; when large, they tend to disrupt the normal gland architecture. On gadolinium enhanced images the normal prostate enhances more in the central zone than peripheral zone; a carcinoma, on the other hand, ranges from enhancing more than the normal peripheral zone, to about the same enhancement and occasionally even less than peripheral zone and gadolinium-enhanced images do not appear reliable in MR imaging of prostatic carcinoma. Overlap also exists with hyperplasia. Dynamic contrast enhanced images may, however, provide better tumor definition by outlining tumor margins more clearly than with unenhanced images. Currently gadolinium is not routinely employed in evaluating prostatic carcinomas.

Dynamic contrast-enhanced images, on the other hand, may provide better tumor definition by outlining tumor margins more clearly than with unenhanced images. Currently gadolinium is not routinely employed in evaluating prostatic carcinomas.

^{1}H–MR spectroscopy reveals a correlation between water T2-relaxation time and tissue citrate concentration. Endorectal ^{1}H–MR spectroscopy detects metabolic differences between normal prostatic tissue, benign disease, and cancer, and thus potentially can differentiate benign from malignant disease. Significantly higher choline levels and significantly lower citrate levels are found in cancer tissue compared with BPH and normal tissue. Men with cancer have a significantly lower citrate-to-choline ratio than those with BPH. A present limitation in differentiating tumors is MR

spatial resolution. MR spectroscopy appears to be useful in a setting of negative biopsy and a rising PSA level. Also, with extensive postbiopsy distortion, such as hemorrhage, adding MR spectroscopic imaging to MR imaging improves prostate cancer detection rates; cancer is identified at MR spectroscopic imaging by an elevated metabolite ratio above normal.

Adding 3D proton MR spectroscopic imaging to MRI improves prostate cancer detection and localization compared to the use of MRI alone (35).

Scintigraphy: Attempts have been made to differentiate BPH and prostate cancer with 2-[18F]-fluoro-deoxy-D-glucose positron emission tomography (FDG-PET), but results are unreliable. Regions of high tumor uptake blend with radioactivity in urine and measures should be taken to eliminate the latter. Likewise, PET is not as sensitive as bone scintigraphy in detecting bone metastases. On the other hand, prostate cancers have an increased uptake of choline, which is needed for phosphatidylcholine synthesis, a cell membrane phospholipid. Positron emission tomography after IV carbon-11-choline in men with prostate cancer reveals marked tumor uptake and negligible urine radioactivity. Occasionally a positive choline scan detects a tumor in the face of a negative PET-FDG scan (36).

Radioimmunoscintigraphy using Tc-99m-labeled monoclonal antibody (CYT-351) against a membrane antigen in men with suspected prostatic malignancy shows potential in imaging both the primary site and metastatic foci.

Biopsy: Six sextant core needle biopsies represent the current standard in detecting stage T1c and T2 prostate cancer. Ultrasonography guidance using an endorectal approach and an automated biopsy gun are some of the refinements available. More extensive biopsies are obtained from sonographically detected hypoechoic regions. Combining the two techniques yields a higher positive rate than with either one alone. Using a sextant biopsy pattern, cancer detection rates appear higher if the prostate is small; a greater sampling error is probably introduced with a large prostate, and thus more samples are needed with a large gland. The positive yield of systematic six-sector biopsy decreases when the prostate gland volume is enlarged. In men with a clinical suspicion of prostate cancer, a correlation exists between serum PSA level and a likelihood of obtaining a positive biopsy.

Aspiration cytology rather than core biopsy is also feasible, although aspiration cytology detects somewhat fewer cancers than a needle biopsy and appears to be an inadequate screening modality for occult carcinomas in a setting of a normal digital rectal examination and normal acid phosphatase level. An advantage of a core needle biopsy is that with sufficient carcinoma tissue in the biopsy, grading is similar to that obtained from prostatectomy tissue, because most prostatic cancers tend to be highly malignant.

Prostatic cancer detection is improved if instead of six biopsies, additional US-guided transrectal prostatic biopsies are obtained. Thus 10 instead of six biopsies increases cancer detection several percentages, with a greatest improvement found in those with a small cancer. An increased number of biopsies should be balanced, however, against an increased risk for complications.

Although some studies suggest that US-guided transrectal biopsy results are similar to those obtained with finger-guided transperineal biopsy (37), most authors consider the transperineal approach to be less reliable and use it when a transrectal approach is contraindicated. Biopsy sensitivity is superior when using US guidance versus digital rectal guidance, and, in fact, often a primary use of endorectal US is in directing a biopsy needle into suspicious regions.

Instead of endorectal US, endourethral US guidance is an alternative for transperineal prostate biopsies; this approach provides biopsy guidance for those men who had a previous rectal resection.

Endorectal MR is potentially useful both to identify tumor sites and as a guide for prostatic biopsy, replacing US.

Few major but frequent minor complications are encountered after transrectal prostatic biopsy. The most common complication is persistent hematuria; infectious complications are rare. Postbiopsy hemorrhage affects MR spectroscopy by hiding metabolic peaks and this test should be performed prior to biopsy or at least a month later.

What should be suggested in a setting of an elevated PSA level or an abnormal digital rectal

examination but negative transrectal US-guided biopsies? Several studies suggest that among this subset of men a repeat biopsy within 6 weeks to 6 months will be positive in 10% to 50%. The chance of a second biopsy being positive increases if the serum PSA level is >10 ng/mL or if premalignant changes are detected on the initial biopsy. A negative sextant biopsy thus does not exclude a tumor and is of limited prognostic value. Also, prior hormone therapy influences biopsy results; some men who undergo hormone therapy have sparse tumor cells.

Staging

Whether a cancer is confined to the prostate or extends beyond the prostatic capsule is of obvious importance because it influences whether a prostatectomy or nonsurgical therapy is considered. A cancer growing beyond the prostate most often is in the posterolateral portion of the gland. At times a sharp beak extending from the prostate at this location is identified, representing tumor penetration through the capsule. The capsule itself is not identified. A bulging prostate capsule is suggestive but not diagnostic of extension beyond the capsule.

Table 13.2 outlines the tumor, node, metastasis (TNM) clinical staging system. Although a biopsy specimen Gleason score and digital rectal examination are relatively reliable in predicting tumor stage, the initial serum PSA level has evolved to be of greatest prognostic significance. It not only correlates directly with the probability of extracapsular tumor spread, but also is a predictor of treatment failure.

Prostate-Specific Antigen Level: In some institutions prostate cancer staging consists of a digital rectal examination, measurement of serum tumor markers, and a radionuclide bone scan, with CT or MRI performed only as needed. Others do not obtain bone scans and skeletal radiography in the routine staging of prostatic carcinoma, believing that these studies are useful primarily with clinical suspicion of bone involvement or if the PSA level is elevated (bone metastases are discussed later; see Distal Spread).

Prostate volume can be calculated from US data and density of serum PSA relative to total prostate volume or transition zone volume then obtained. The PSA density appears useful in men with prostate cancer and PSA levels of 4 to 10 ng/mL. In suggesting extracapsular invasion, PSA density values calculated using the transitional zone volume appear superior to PSA den-

Table 13.2. Tumor, node, metastasis (TNM) staging (clinical) of prostate tumors

Primary tumor:	
Tx	Primary tumor cannot be assessed
T0	No evidence of primary tumor
Tis	Carcinoma in situ
T1a	Tumor incidental histology in 5% or less of tissue resected
T1b	Tumor incidental histology in greater than 5% of tissue resected
T1c	Tumor identified by needle biopsy
T2a	Tumor involves one-half of one lobe or less
T2b	Tumor involves more than one-half of one lobe but not both lobes
T2c	Tumor involves both lobes
T3a	Tumor extends through capsule
T3b	Tumor invades seminal vesicles
T4	Tumor is fixed or invades adjacent structures

Lymph nodes:	
Nx	Regional nodes cannot be assessed
N0	No regional lymph node metastasis
N1	Metastasis to regional lymph nodes

Distant metastasis:	
Mx	Distant metastases cannot be assessed
M0	No distant metastasis
M1a	Nonregional lymph nodes involved
M1b	Bone metastasis
M1c	Other sites involved

Tumor stages:				
Stage I	T1a	N0	M0	G1
Stage II	T1a	N0	M0	G2, 3–4
	T1b	N0	M0	any G
	T1c	N0	M0	any G
	T2	N0	M0	any G
Stage III	T3	N0	M0	any G
Stage IV	T4	N0	M0	any G
	any T	N1	M0	any G
	any T	any N	M1	any G

G: Gleason score	
Gx	Grade cannot be assessed
G1	Well-differentiated tumor (Gleason 2–4)
G2	Moderately differentiated (Gleason 5–6)
G3–4	Poorly differentiated/undifferentiated (Gleason 7–10)

Source: From the AJCC Cancer Staging Manual, 6th edition (2002), published by Springer-Verlag, New York, NY, used with permission of the American Joint Committee on Cancer (AJCC), Chicago, IL.

sities obtained from total prostate volume. The results depend on the ability to obtain accurate sonographic total prostate and transitional zone volumes.

Local Extension: Differentiation of intraprostatic tumor (pT2) from extraprostatic spread (pT3) has both prognostic and therapeutic implications, yet this differentiation is often made mostly on indirect evidence. Thus a Gleason score >7, perineural invasion, and most biopsies being positive argue for extraprostatic spread, while a low Gleason score or only one out of six positive biopsies suggest an intraprostatic tumor. A rough estimate of cancer spread can be based on the serum PSA level. In one study of men with prostate-confined tumors (pT2N0), mean total PSA was 7 ng/ml, while in those with extracapsular spread (pT3pN0/N+) it was 10 ng/ml (38)]; the free/total PSA ratios were not significant. A PSA level >20 ng/ml has a specificity of almost 100% in predicting extracapsular spread. Similarly, significant differences are evident in serum PSA levels between all T stages and metastases.

Study comparisons of tumor extension should be viewed critically; some authors use microscopic capsular penetration as detected by histology as their gold standard, while others rely on macroscopic criteria. Imaging detects gross morphological changes, thus its accuracy is limited in evaluating a disease notorious for microscopic tumor spread.

Computed tomography has a relatively low accuracy in staging local tumor extension; capsule penetration is difficult to detect (Fig. 13.4). Even invasion of seminal vesicles or lymph nodes correlates poorly with subsequent postoperative staging. In general, with a newly diagnosed, untreated prostate cancer and a serum PSA level of <20 ng/mL, the likelihood of an abnormal CT finding is extremely low. Most published studies were done prior to the intro-

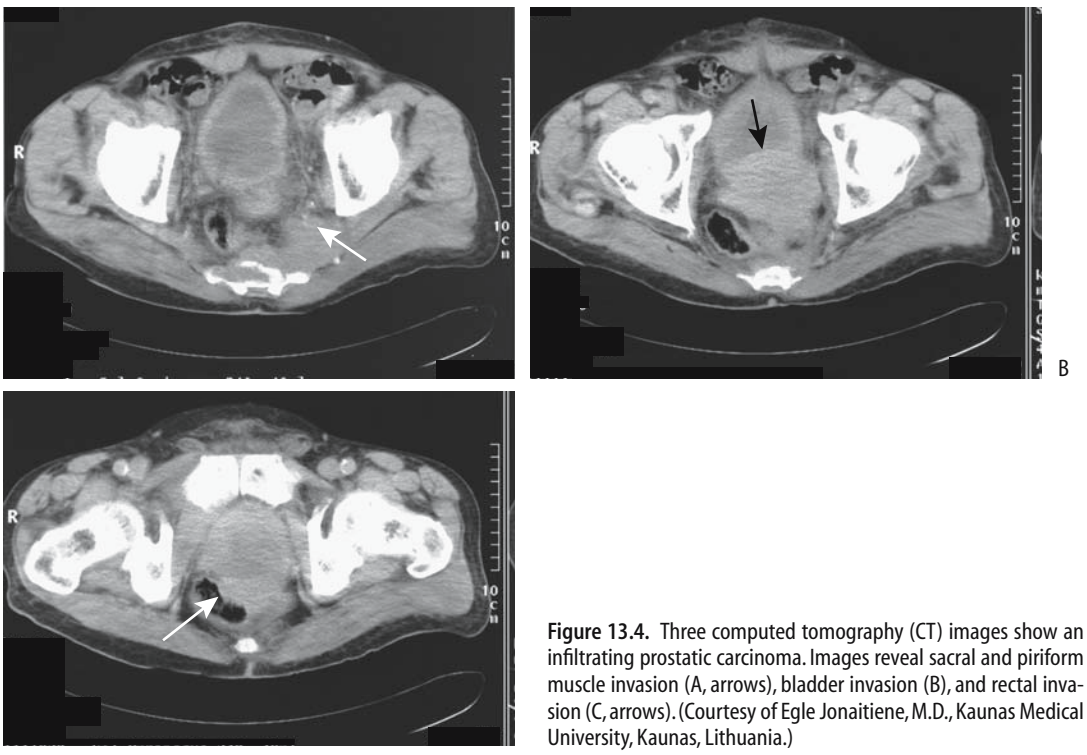

Figure 13.4. Three computed tomography (CT) images show an infiltrating prostatic carcinoma. Images reveal sacral and piriform muscle invasion (A, arrows), bladder invasion (B), and rectal invasion (C, arrows). (Courtesy of Egle Jonaitiene, M.D., Kaunas Medical University, Kaunas, Lithuania.)

duction of multislice CT, and the impact of this modality on prostate cancer staging remains to be established.

In men selected for radiation therapy, contrast-enhanced abdominal and pelvic CT provide a low yield, and the need for this study, aside for treatment-planning CT, is questioned (39).

Although rather optimistic endorectal US staging results have been published, overall this modality has not lived up to expectations. Prospective studies suggest that endorectal US is no better than digital rectal examination in detecting extracapsular spread. In general, endorectal US does not detect about 25% of tumors and is not reliable in establishing extracapsular spread. Occasionally extraprostatic extension can be suggested if US can establish tumor contact with the prostate capsule.

Published reports of MRI staging of prostatic cancer should be interpreted with caution because study quality varies considerably among institutions, and interreader differences in interpretation exist. Thus among consecutive patients with MR studies read twice by two radiologists in random order, intraobserver and interobserver agreement ranged from fair to good (33). Published MR staging accuracies for local extension vary considerably. Sensitivities of capsular penetration range from 15% to 85% and seminal vesicle invasion from 25%; published specificities have a similar wide variability. Conclusions range from MR being better than US to endorectal coil MRI having insufficient staging accuracy to influence treatment planning. Some studies suggest that cancer detection rates improve with contrast enhancement, while others do not (40). In general, use of an endorectal coil, a breath hold technique and multiple imaging planes aid staging. A multivariate analysis concluded that adding endorectal MR imaging findings to serum PSA levels and percent of cancer in core biopsies improved prediction of extracapsular invasion (41). Use of a 3T magnet improves staging accuracy but further work is needed.

An MR finding of rectoprostatic angle obliteration and neurovascular bundle asymmetry are predictive of extracapsular extension. Macroscopic capsular penetration is identified as capsular discontinuity and invasion of adjacent adipose tissue. One should keep in mind, however, that a prior biopsy can also result in capsular irregularity without tumor invasion (42). Tumor spread to seminal vesicles is seen on T2-weighted MR images as a low signal intensity region replacing part of a seminal vesicle. Infiltration can be either unilateral or bilateral. An early finding is thickening of seminal vesicle tubules. Asymmetrical seminal vesicle enlargement should raise suspicion for tumor involvement. With diffuse tumor spread to the seminal vesicles the appearance mimics that of an inflammatory condition.

Stage of seminal vesicle invasion is predictive of postoperative disease progression. To some degree the number and site of positive prostatic sextant biopsies correlate with seminal vesicle invasion; seminal vesicle infiltration correlates with the presence of positive basal prostatic biopsies. Seminal vesicles are amenable to direct biopsy using US guidance. Most of these biopsies are performed lateral to the prostate, in the medial third of the seminal vesicle. A negative biopsy does not exclude tumor spread to the seminal vesicle, with eventual histology identifying seminal vesicle invasion in up to one third of men with negative biopsies, and such biopsies contribute little to staging.

Seminal vesicles invasion ranges from proximal part involvement to extension to the free end, with the latter signifying a worse prognosis. Thus a biopsy identifying invasion to the free end influences the prognosis after radical prostatectomy.

Lymph Node Involvement: Lymph node involvement with prostatic cancer is of prognostic significance. Even microscopic spread is associated with a poor prognosis. Currently the only reliable means of detecting early nodal involvement is either resection or biopsy, although a high Gleason score or a PSA >20 ng/mL implies an increased risk of node involvement.

The current therapy of most biopsy-proven prostatic carcinomas is radical prostatectomy. On the other hand, a radical prostatectomy by itself is not warranted if nodal metastases are present. Therefore, detection of lymph node metastasis is crucial, and pelvic lymph node dissection is used to stage these cancers. In such a setting the preoperative ability of imaging to assess lymph node disease is important. Image-guided fine-needle aspiration biopsy (actually, cytology) of pelvic and para-aortic nodes

appears worthwhile if suspicious nodes are identified.

Preoperative imaging tends to underestimate the degree of lymph node involvement. Routine use of cross-sectional imaging (CT or MRI) to determine whether pelvic lymph node metastases are evident is controversial, yields a low accuracy, and is probably not justified; in select men at high risk for nodal metastasis, however, such as with an elevated PSA level, it appears cost-effective, keeping in mind that CT provides only indirect evidence of nodal involvement, namely, enlarged nodes. Generally 1 cm is used as a border between normal and abnormal nodes. Computed tomography sensitivity can be improved if a smaller limit is selected, but at the expense of worse specificity. Computed tomography–guided node biopsy can then be considered, although localization problems arise with smaller nodes.

Currently the primary MRI criterion useful in identifying lymph node metastasis is node size. Ferumoxtran-enhanced MRI detection of metastasis to normal-sized pelvic lymph nodes needs further study.

At times a diagnosis is not straightforward even with generalized lymphadenopathy; a lymphoma can be suspected if adenopathy is detected prior to the prostate cancer. These men generally undergo node biopsies, which reveal an adenocarcinoma, leading to a workup for a primary site.

Detection of pelvic lymph node metastases with FDG-PET is limited because of superimposed bladder tracer activity.

Radioimmunoscintigraphy with indium-111–capromab pendetide achieve sensitivities and specificities for pelvic lymph node metastases superior to most other imaging studies. Also, capromab specificity can be improved further by combining results with pelvic CT and MRI (43).

The efficacy of lymphangiography in assessing lymph node involvement is low, even when combined with CT or biopsy, and currently lymphangiography is rarely performed for this indication, having been supplanted by newer imaging modalities.

Men with localized prostate cancer who undergo endorectal US with systematic sextant biopsies can be divided into three groups (Table 13.3); those meeting group III criteria should undergo pelvic lymphadenectomy (44). A positive seminal vesicle biopsy is also a predictor of pelvic lymph node metastases; perineural invasion is an independent predictor.

Distal Spread: Using systematic six-sextant prostatic biopsy as a guide, a significant relationship exists between the number of positive biopsy cores and bone metastasis. With a newly diagnosed prostate cancer and a PSA level of <10 ng/mL, the probability of detecting bone metastases with a bone scan is probably <1%, and a bone scan thus appears unnecessary if no clinical signs of bone involvement are evident. Yet the PSA level is somewhat limited in discriminating between those with and those without bone metastases, and some authors have questioned whether a staging radionuclide bone scan can indeed be omitted in those with a serum PSA level of <10 ng/mL. Yet among men with a localized prostate cancer and a PSA level of <20 ng/mL, 3% had bone metastases (45); the authors concluded that bone scintigraphy is necessary when staging these tumors. Others disagree. One should keep in mind that bone metastases occur in some men after therapy of a primary tumor even with an initially negative

Table 13.3. Results of pelvic lymphadenectomy in 130 men with localized prostate cancer

	Preoperative findings	Lymphadenectomy results*
Group I	Negative basal biopsies, and clinical stage T2 (irrespective of PSA)	All had negative lymph nodes
Group II	Positive basal biopsy, and clinical stage T2, and PSA <10 ng/mL	All but one were lymph node negative
Group III	Positive basal biopsy, and/or clinical stage T3, and/or PSA >10 ng/mL	17 of 18 with positive nodes were in this group

*Radical prostatectomy and pelvic lymphadenectomy revealed that 18 of the 130 patients had positive pelvic lymph nodes.
PSA, prostate-specific antigen.
Source: Adapted from Dunzinger et al. (44).

bone scan and a question arises whether metastatic cancer cells were already present at the time of initial therapy but were undetected by a bone scan? Bone marrow aspirates from men with no evidence of metastatic disease suggests that some already have micrometastases.

Bone scintigraphy is the current procedure of choice to detect bone metastases. Positive bone scintigraphy should be correlated with appropriate bone radiographs to exclude degenerative changes as a cause for a positive uptake; bone radiography per se is insensitive in detecting early bone metastases.

Magnetic resonance imaging using short T1 sequences is becoming a viable alterative to bone scintigraphy. Currently, MR is employed in evaluating inconclusive bone scans, although the evidence suggests that it is more sensitive than scintigraphy in detecting bone metastases. Bone radiographs are less sensitive but are of use as an aid in detecting false-positive scintigraphy due to degenerative disease. 2-[18F]-fluoro-deoxy-D-glucose PET is less sensitive than scintigraphy in detecting bone metastases. Further imaging studies are generally pointless once bone metastases are detected.

A solitary metastasis to the peripheral skeleton is relatively uncommon, but at times has an atypical appearance.

Lung metastases are a late event, and thus chest radiographs are not indicated during the initial follow-up.

Prostatic cancer metastasis to the ureter, either via lymphatics or hematogenously, can manifest as renal colic. Ureteral obstruction secondary to metastatic prostate adenocarcinoma is amenable to balloon dilation and subsequent antegrade Wallstent insertion.

Penile metastasis from prostate cancer is rare. Some of these appear to be related to prior urethral catheterization, and transurethral prostatectomy.

Therapy

Current therapy consists of surgery in its various modifications, radiotherapy, androgen-deprivation therapy, or simply a wait-and-see approach.

Surgery is the accepted therapy for newly diagnosed prostate cancer in many centers, especially in the United States. A not uncommon scenario for low-grade and localized tumors is staging lymphadenectomy, and if frozen section reveals these to be not involved, proceeding to radical prostatectomy.

Given the low inherent mortality associated with a number of these cancers, however, conservative management, especially in frail and elderly men, continues to be employed, and androgen-deprivation therapy is more often employed in these men, especially outside the United States. The boundary between surgery and conservative management is a controversial topic but with time is gradually tilting more toward surgery, given the more frequent detection of early cancers and resultant low surgical morbidity and mortality.

The presence of tumor spread beyond the prostatic capsule generally reflects a change from surgery to radiotherapy, although no precise changeover point is defined. Prostatectomy and either lymph node resection or radiotherapy for nodal metastasis result in a high rate of recurrence. Androgen-deprivation therapy is considered with lymph node involvement.

Radical prostatectomy is generally considered the gold standard in treating localized prostate cancer. Yet a number of these prostatectomies, performed for stage T1c disease, reveal potentially insignificant tumors. Although the term *insignificant* in this context is difficult to define, a typical definition consists of a cancer confined to the prostate, a tumor volume <0.5 cc, and a Gleason score of <7 (46). Relatively clear indications exist for radical prostatectomy, yet considerable variations in surgical practice exist, even in the same country. Thus a 2001 survey in France found that the probability of being treated by radical prostatectomy was three times higher in one department compared to others and 2.6 times higher in private practices (47). Such variability introduces another variable when analyzing survival data.

A laparoscopic radical prostatectomy is feasible, with reported outcomes similar to those of a conventional retropubic approach.

Intraoperative endorectal US during radical retropubic prostatectomy is helpful in identifying the urethral division site but is not commonly employed.

Complications after a radical prostatectomy include rectal injury, abscess, major hemorrhage, anastomotic urinary leakage, anastomotic stricture, and lymphocele formation.

Cystography is commonly obtained a week or so after radical prostatectomy to assess the vesicourethral anastomosis. If extravasation is detected, as long as a catheter is left in place until healing, the extravasation does not influence subsequent stricture formation. Another approach is simply to keep the catheter in place for 14 to 21 days, without cystographic confirmation of anastomotic integrity. Computed tomography after a radical prostatectomy often reveals a complete or incomplete transverse bar of soft tissue in the rectovesical space. This is a normal postoperative finding.

After a radical prostatectomy the bladder neck widens and assumes a funnel-shaped appearance. This defect is readily identified with endorectal US and cystography. Ultrasonography also reveals a hypoechoic tumor surrounding the vesicourethral anastomosis and indenting the bladder anterior wall. Eventual fibrosis results in a hypointense signal on T2-weighted MR images.

Radiotherapy: Radiotherapy has a role in treating pelvis-confined prostate cancer. External radiotherapy combined with hormone therapy in men with cT2 prostatic adenocarcinoma achieved a 100% overall 5-year survival. Even with incurable prostate cancer, radiotherapy delays tumor regrowth and achieves a several-year delay in tumor progression in most men. In men with clinically localized prostate cancer, progression-free and overall survival rates are significantly improved if androgen ablation is added to radiotherapy.

Follow-up of patients after radiotherapy consists of digital rectal examination and PSA level. Serum PSA decreases but it does not drop to undetectable levels as occurs after resection. A rising PSA signifies tumor growth and should prompt bone scintigraphy. If scintigraphy is positive, no further workup is needed. Magnetic resonance imaging has a role in a setting of a negative or indeterminate bone scan and a rising PSA level.

Hematochezia is common after prostate radiation therapy. One should not ascribe all bleeding to such therapy; some men have concomitant bowel disease, including colon cancer.

Brachytherapy is potentially curative for either initial or recurrent localized prostatic cancer. Computed tomography– or transrectal US-guided implants consist either of palladium 103 or iodine 125, at times supplemented with external beam radiotherapy. A urethrorectal fistula developed in 1% of men undergoing brachytherapy (48); interestingly, all fistulas were in those who also had anterior rectal biopsy adjacent to the prostate.

Coronal T2-weighted endorectal MRI in 35 consecutive patients after brachytherapy for prostate cancer reveals a diffuse hypointense signal and indistinct zonal anatomy (49); both intra- and extraprostatic seeds can be identified. Endorectal MRI evaluates both seed distribution and brachytherapy-related changes. Recurrent cancer has early contrast enhancement on dynamic MRI; focal peripheral zone early enhancement greater than in the central zone suggests recurrence.

Cryoablation: Transperineal percutaneous cryoablation using endorectal US-guidance has received considerable interest in treating localized prostate cancer; preliminary studies are encouraging. Posttherapy PSA levels are of prognostic significance; those with a PSA level >0.5 ng/mL are likely to have residual disease.

Salvage cryoablation is occasionally performed in men with locally recurrent prostate cancer after radiation, hormonal therapy, or systemic chemotherapy. This procedure is associated with significant morbidity, including urinary incontinence, obstruction, and impotence.

A cryoshock phenomenon consisting of multiorgan failure, severe coagulopathy, and disseminated intravascular coagulation has been described after liver cryotherapy. A multiinstitution questionnaire identified two instances of cryoshock after prostatic cryoablation (out of 5432 patients) (50). An uncommon complication after cryoablation is necrosis of the symphysis pubis.

Endorectal US 3D prostate images are used by some investigators for probe placement and monitoring during cryoablation, realizing that in this setting endorectal US achieves a low sensitivity in detecting residual prostate carcinoma and is not reliable for this indication.

Magnetic resonance imaging after cryoablation reveals liquefactive necrosis in the prostate bed and a decrease in prostate volume with loss of zone differentiation. Necrotic regions appear as a signal void on postcontrast MRI. A thick

capsule surrounds the gland postablation. Magnetic resonance does not differentiate cryosurgery-induced changes from recurrent tumor, and a baseline posttherapy study is thus very useful.

Magnetic resonance spectroscopy after cryosurgery reveals that necrotic tissue does not contain any observable choline or citrate and MR spectroscopy thus is useful to gauge success of therapy.

Prominent uptake of Tc-99m–methylene diphosphonate (MDP) is evident within the prostate bed after cryoablation, presumably due to neovascular hyperemia.

Other Therapy: During percutaneous radiofrequency (RF) ablation of prostate cancer, RF energy is delivered through needle electrodes inserted transperineally using endorectal US guidance. Preliminary results appear promising. Extensive coagulation necrosis develops in involved tissues.

Magnetic resonance imaging can monitor percutaneous interstitial microwave thermoablation (51); MRI-derived temperatures reflected tissue temperatures.

Therapy with transrectal high-intensity focused ultrasound is feasible, but the role of such therapy is not clear. Among men with clinical stage T1 or T2 prostatic cancer, not eligible for a radical prostatectomy, treated by transrectal high-intensity focused ultrasound, negative follow-up biopsies were obtained in 61% (52); of concern are the complications—rectourethral fistulas, rectal burns, urinary retention, severe incontinence, bladder neck scleroses, and urinary tract infection.

A permanent metal stent can be inserted in high surgical risk men with bladder outlet obstruction.

Leuprolide, an agonist of luteinizing hormone–releasing hormone, and flutamide, an antiandrogen, are some of the agents used for androgen-deprivation therapy of localized prostate cancer. These agents result in gland shrinkage and decrease of high-grade intraepithelial tumors, but invariably residual tumor remains. After androgen-deprivation therapy, MR shows tumor volume and signal intensity decreasing, together with a reduction in tumor permeability as measured by contrast enhancement parameters (53); one effect is poorer tumor visualization. One should keep in mind that androgen-deprivation therapy tends to suppress serum PSA levels, and these levels thus may not accurately reflect disease activity, although a rising level warrants further study.

Outcome/Follow-Up

Clinical: Especially in elderly and high-risk men, some small prostate cancers are treated conservatively. Such an approach requires caution because many of these men will eventually die of their prostatic cancers. Thus a retrospective study of men with a known diagnosis of prostate cancer who died in Göteborg, Sweden, during a specific time period, and who underwent hormonal therapy, found that among those who survived at least 10 years, the mortality rate due to prostate cancer was 63% and this mortality increased steadily over time (54); even among those in stage M0 at initial diagnosis, 50% died of prostate cancer.

The 5-year survival rate for those with pathologic stage III or higher tumors, treated by radical prostatectomy and adjuvant hormone and radiation therapy, is over 80%. Life expectancy is unpredictable in some men even with metastases. Thus some men with metastatic prostate cancer survive for more than 5 years; size and primary tumor differentiation are prognostic survival factors. Nevertheless, even with prostatectomy specimen Gleason score 8 to 10 tumors, a preoperative serum PSA level ≤10 ng/mL and organ-confined disease are significant predictors of achieving prolonged disease-free survival (55).

Serum PSA levels and a digital rectal examination are used for follow-up to detect recurrence after therapy. After a radical prostatectomy serum PSA levels should be undetectable within several weeks unless residual disease is present. Any subsequent detectable level implies relapse. Yet follow-up of men after a radical retropubic prostatectomy for clinically localized (≤T2) disease who then had an elevated postoperative PSA level revealed that 94% of these men had no evidence of metastatic disease (based on a bone scan) 5 years from the time of PSA elevation, and 91% had no such evidence at 10 years (56).

Initially during radiotherapy serum PSA increases (57), then decreases but does not drop to undetectable levels as found after resection. Follow-up of these patients consists of digital

rectal examination and monitoring PSA levels. A rising PSA should prompt bone scintigraphy. If scintigraphy is positive, no further workup is needed. Magnetic resonance imaging has a role in a setting of an indeterminate bone scan. A rising PSA level and negative bone scintigraphy suggests local recurrence and transrectal US-guided biopsy and CT or MR for adenopathy appear appropriate.

In men with inoperable prostate cancer, radionuclide bone scans, serum PSA, and serum prostatic acid phosphatase levels monitor progression, although some investigators believe that serum PSA level by itself is sufficient to follow disease progression. Men with untreated prostatic cancer or those refractory to endocrine therapy have an exponential increase both in PSA level and in prostatic acid phosphatase level; tumor marker doubling time is a useful guide in estimating cancer growth rates and in determining prognosis after relapse.

Urinary PSA levels are not useful for post-therapy follow-up because PSA is also secreted by periurethral glands.

Imaging: Postoperative recurrence is either local or metastatic. Computed tomography sensitivity in detecting local recurrence is low, with postoperative deformity making evaluation difficult. Endorectal US is more sensitive but less specific than digital rectal examination for detecting local recurrence although both provide only limited information (58). Adding Doppler US improves both sensitivity and specificity. With an elevated serum PSA level and a negative bone scan, US-guided prostate fossa biopsies should be considered, especially of any hypoechoic foci detected by endorectal US. Negative biopsies, however, are of limited significance.

For detecting local recurrence, an endorectal coil MRI study is superior to a body coil MRI study. Endorectal surface coil MRI sensitivities and specificities close to 100% have been enthusiastically reported in detecting local recurrence and some authors believe that endorectal MRI has a place in those who have had a prostatectomy and local recurrence is suspected (59). Nevertheless, one study found poor accuracy, and solid tumor foci were detected only if they were >1 cm in diameter, while diffuse tumor infiltration was not detected (60). The authors also found that contrast-enhancement provided no additional information, and they concluded that in this setting MRI cannot replace follow-up biopsy. When seen, recurrence is identified as a soft tissue tumor in the prostatic bed, which is hypo- to isointense on T1- and hyperintense on T2-weighted images. A fibrotic peripheral zone is hypointense.

Monoclonal antibody radioimmunoscintigraphy with In-111–capromab pendetide shows promise in detecting occult recurrence. This antibody conjugate localizes to a glycoprotein found primarily on prostate tissue cell membranes. In men with an elevated serum PSA at least 3 months after therapy, monoclonal antibody imaging was superior to PET scanning in identifying recurrent cancer; most common sites of recurrence are prostatic fossa and lymph nodes.

Small Cell/Anaplastic Carcinoma

A nondifferentiated small cell prostatic carcinoma is rare. These are aggressive tumors associated with a poor prognosis. These tumors often exhibit morphologic and functional neuroendocrine characteristics. Superficially, some mimic a lymphoma. The CEA levels tend to be normal.

Computed tomography often detects metastatic disease in men presenting with an anaplastic prostate carcinoma; bone metastases are associated with a more modest PSA level compared to a typical prostatic carcinoma.

Lymphoma/leukemia

Primary non-Hodgkin's lymphoma of the prostate is rare. Clinically, these lymphomas can mimic acute prostatitis.

Secondary hematologic malignancies involving the prostate and adjacent lymph nodes range from chronic lymphocytic leukemia to lymphoma. Transrectal US–guided prostate biopsies should be diagnostic.

An occasional outlet obstruction is the first manifestation of a leukemic or lymphomatous prostatic infiltrate.

Mesenchymal Neoplasms

Prostatic leiomyomas are rare. These tumors can be quite large and imaging findings nonspecific. A diagnosis is established with a biopsy.

Of clinical importance are postoperative spindle cell nodules and pseudosarcomatous fibromyxoid tumors; pathologically, these tumors may be misidentified as sarcomas.

Most prostatic sarcomas occur in children under 10 years of age, thus allowing differentiation from carcinoma. Most of these are rhabdomyosarcomas. In adults about 25% of prostatic sarcomas are leiomyosarcomas. Previous pelvic radiation, such as for a seminoma, is occasionally associated with a prostate sarcoma. These tumors tend to be large at initial presentation.

Ultrasonography identifies most prostatic sarcomas as heterogeneous tumors having decreased attenuation, probably due to focal necrosis.

These sarcomas are hyperintense on T2-weighted MRI, with the surrounding fibrosis being hypointense.

Wolffian Duct Structures

Endorectal US appears to be a reasonable first study in evaluating the distal male reproductive tract for potentially correctable causes of infertility. Cysts and duct obstructions are detected.

Seminal Vesicle Disorders

Seminal vesicle cysts can be either congenital or acquired. They are located posterolateral to the bladder in the general location of the seminal vesicles. An occasional one is more midline in location and inhomogeneous in appearance. Most cysts are unilateral and more frequent on the right side. A cyst can obstruct an adjacent seminal vesicle. A rare cyst is huge. Most of these cysts are discovered incidentally. An association exists between seminal vesicle cysts and absence or dysplasia of the ipsilateral kidney. An ectopic ureteral insertion into the seminal vesicle is found in some of these patients; the presence of a seminal vesicle cyst thus warrants further imaging; both structures originate from a common embryologic mesonephric duct.

Multiple, bilateral seminal vesicle cysts develop in men with autosomal-dominant polycystic kidney disease.

Computed tomography density tends to be >40 Hounsfield units (HU) in seminal vesicle cysts. Endorectal US readily identifies these retrovesically located cysts. Magnetic resonance imaging is also very useful in detecting seminal vesicle cysts, which are hyperintense on both T1- and T2-weighted images.

Transperineal puncture under endorectal US guidance fills a cyst with contrast and establishes the diagnosis. Most seminal vesicle cysts are resected; a minority undergo transurethral marsupialization using endorectal US guidance.

In temperate climates the most common cause of seminal vesicle calcifications is diabetes mellitus. Schistosomal calcifications are encountered in the Near East. Less often calcifications are secondary to tuberculosis. Seminal vesicle calculi are associated with painful ejaculation. Endorectal US detects duct obstruction by stones or fibrosis. Calcifications are hypointense on both T1- and T2-weighted MRI.

Seminal vesicle hydatid cysts are rare. CT reveals thin wall water-density cysts (61); some also develop daughter cysts. An infected cyst can evolve into an abscess. These abscesses can be drained percutaneously.

An infected cyst can evolve into an abscess. These abscesses can be drained percutaneously.

Most seminal vesicle neoplasms are reported anecdotally. A rare cystadenoma mimics a cyst.

Rarely, amyloidosis infiltrates the seminal vesicles.

Ejaculatory Duct Disorders

An ejaculatory duct cyst adjacent to the duct can occlude the duct lumen. Some of these cysts are associated with infertility. These cysts are identified and treated using endorectal US guidance. Their aspirate contains spermatozoa, thus distinguishing these cysts from müllerian duct cysts.

Occasionally identified is urethroseminal reflux into the ejaculatory ducts.

Endorectal US–guided opacification of the seminal tracts with contrast is useful in men with suspected ejaculatory duct obstruction and dilated seminal vesicles. Most ejaculatory duct obstructions are bilateral.

Hemospermia

Causes of hemospermia include prostatitis, seminal vesicle or ejaculatory duct calcifications, cysts, and vascular anomalies. End-

orectal gray-scale and Doppler US determine the cause of hemospermia in most in men. Detected are periurethral calcifications, prostatic inflammation, seminal vesicle ectasia, and various cysts. Magnetic resonance using an endorectal coil is probably more sensitive. Hyperintense seminal vesicles on T1-weighted images suggest hemorrhage, and hypointense ones both on T1- and T2-weighted images consist of fibrosis due to chronic inflammation.

Penis

Urethra

Extravasation/Fistula

Unusual causes of anterior urethral fistulas are involvement by Crohn's disease and infection by tuberculosis and schistosomiasis. An occasional primary adenocarcinoma originates in a urethrorectal fistula.

Most catheters inserted through a urethral perforation are readily apparent on a contrast study. A urethroscrotal fistula leads to massive scrotal enlargement. These are readily apparent with imaging; bone scintigraphy reveals an appearance similar to a scrotal bladder.

Obstruction

In adult men the most common cause of bladder outlet obstruction is BPH. Less common are prostate, bladder and related structure neoplasms, inflammation, urethral strictures, and a neurogenic bladder. Urethral valves as a cause of obstruction are of more importance in the pediatric age group.

Stricture

Distal to the prostate, the most frequent acquired abnormality of the male urethra is a benign urethral stricture. An uncorrected stricture eventually leads to hydronephrosis, chronic pyelonephritis, vesicoureteral reflux, and renal failure. These complications often are irreversible.

A rare cause of urethral obstruction is primary amyloidosis of the penile urethra these strictures are amenable to urethral dilation.

Urethral strictures are studied by a retrograde urethrogram. Ultrasonography (also called sonourethrography) also appears to have a role. Sonourethrography evaluates both length and severity of a stricture. It visualizes not only strictures but also associated corpus spongiosum fibrosis which ranges from iso- to hyperechoic to the corpus spongiosum.

With recurrent posterior (bulbar) urethral strictures, initial balloon angioplasty followed by insertion of an expandable metallic stent appears worthwhile; short-term results are satisfactory, but some men develop an exuberant fibrotic reaction requiring either a urethrotomy or urethroplasty.

A bioabsorbable self-expandable reinforced poly-l-lactic acid spiral stent shows promise. Inserted immediately after urethrotomy in men with recurrent urethral strictures, all but one stent was epithelialized at 6 months and degraded in all at 12 months (62).

Urethral Valves

Posterior urethral valves were discussed earlier (see Congenital). Anterior urethral valves rarely result in obstruction. Similar to posterior urethral valves, they are usually detected with a voiding cystourethrogram.

Calculi

Urethral calculi are either primary or secondary. Primary calculi develop in a diverticulum, proximal to a stricture, or in the presence of a foreign body. Secondary calculi pass from the bladder.

Urethral calculi are best detected by conventional radiography; they can be missed during a contrast study if only contrast-filled images are obtained.

Verumontanum Hyperplasia

Hyperplasia of verumontanum mucosal glands is a rare cause of urethral obstruction. Occasionally a prostatic biopsy suggests a low grade adenocarcinoma, but in reality it represents hyperplasia of verumontanum mucosal glands.

Functional Obstruction

The clinical role of endorectal US while voiding is yet to be established. It has been used to study suspected dysfunctional voiding when more obvious causes are excluded; voiding US detects

abnormal motion of the posterior urethra during voiding.

Occasionally voiding cystourethrography detects extreme posterior urethral ballooning and a disproportionate caliber between the posterior and penile urethra; in some individuals a kink is identified between the two segments, but in others no obvious obstruction is identified.

Diverticulum

Urethral diverticula are rare in males. Congenital ones predominate in young boys, while in adults most are secondary either to previous trauma or an adjacent abscess rupturing into the urethra. Urethral diverticula develop in men with spinal cord injuries. Stones tend to form within these diverticula, presumably due to stasis. Diverticula close to the fossa navicularis are associated with meatal stenosis.

Neoplasms, including a nephrogenic adenoma, can develop in an urethral diverticulum.

Diverticula are detected by US, CT, and MRI. More proximal ones mimic a müllerian duct cyst or a dilated utricle and are midline in position. These outpouchings are readily identified with a voiding cystourethrogram, which reveals a diverticulum filling and compressing the urethra during voiding and then emptying at the end of micturition. Differentiation from an anterior urethral valve is difficult in some individuals; keep in mind that the pathogenesis of some urethral diverticula and anterior urethral valves appears similar.

Tumors

Urethral

Polyps in the male urethra are rare; most are not neoplastic and tend to occur in the posterior urethra. Some fibroepithelial polyps are pedunculated and at times reflux into the bladder at rest. Schistosomiasis also results in urethral polyps. Obstruction is the most common presentation.

Either a voiding cystourethrogram or retrograde urethrogram should detect a polyp. The differential diagnosis for a polyp detected with a urethrogram includes an ectopic ureterocele; US should differentiate between these two conditions because a polyp is hyperechoic while a ureterocele is anechoic.

Condyloma acuminata is seen as multiple intraluminal urethral tumors. They tend to have a shaggy, irregular appearance.

A urethral hemangioma is a benign vascular tumor. Hematuria is a typical presentation. At times postejaculation hematuria or clot-induced urinary retention develops. Treatment is surgical, although depending on the size and number of lesions, selective arterial embolization may be worthwhile.

Primary urethral adenomas and carcinomas are uncommon. They tend to evolve in a setting of superimposed chronic disease. The histology of these tumors varies; posterior urethral cancers tend to be transitional cell carcinomas, anterior urethral ones often are squamous cell carcinomas, and Cowper's or Littre's gland tumors are adenocarcinomas. A rare transitional cell carcinomas develops in the fossa navicularis; some of these are associated with synchronous or metachronous more proximal transitional cell carcinomas. An occasional adenocarcinoma in situ is detected in a villous adenoma. Chronic strictures predispose to cancer, generally a squamous cell carcinoma; these cancers tend to be irregular in outline. The rare urethral epidermoid carcinoma is also associated with a prior urethral stricture and related complications.

Smaller transitional cell carcinomas often present as intraluminal urethral nodules; with growth they infiltrate the adjacent structures. A rare transitional cell carcinoma is occasionally detected in the fossa navicularis. Squamous cell carcinomas infiltrate and often ulcerate. At times a blood clot mimics a malignancy, although blood clots tend to be more irregular and elongated in appearance. Sinus tracts developing in some cancers mask the underlying tumor, which is often detected by finding marked progression between examinations.

Primary malignant melanoma is more common in the distal urethra and tends to be polypoid in appearance. The histopathology is similar to that of melanomas at other sites. Occasionally confusing the pathologic diagnosis is an amelanotic appearance. An occasional one mimics a urethral carcinoma.

Non-Hodgkin's lymphoma involving the urethra is rare. Urethral obstruction is a typical presentation.

Prior hypospadias repair and urethral reconstruction using bladder mucosa, appears to predispose to urethral nephrogenic adenoma formation either at the anastomosis or the graft. Their gross appearance mimicks a carcinoma.

Nonurethral

A corpus cavernosum hemangioma is rare. Some of these have an atypical appearance, are inhomogeneous and even MRI does not distinguish between benign and malignant disease.

A squamous cell carcinoma is the most common penile tumor. Phimosis or human papilloma virus infection are often present. Nodal metastases are common at initial presentation. Tumor stage, lymph node metastasis, and tumor differentiation are independent prognostic factors for survival. Computed tomography often detects inguinal adenopathy at initial presentation, but it should be kept in mind that inflammatory causes for adenopathy are common. Magnetic resonance T2-weighted images are more useful than T1 images in evaluating penile cancers.

Metastases to the penis are uncommon. Among other tumors, prostatic carcinoma has metastasized to the penis. Magnetic resonance imaging is helpful in establishing the extent of invasion.

Cowper's Glands

Paired Cowper's glands and ducts are located along the ventral surface of the bulbous urethra. Not uncommonly these ducts fill during an urethrogram or, rarely, on IV urography after voiding. Normal ducts are readily differentiated from fistulas and contrast extravasation.

Duct obstruction results in a retention cyst, which, if large enough, produces a soft tissue impression along the ventral surface during voiding cystourethrography. An occasional one enlarges sufficiently to obstruct the urethra. These glands are also occasionally involved by neoplasms, infection, or stones.

Priapism

Priapism is a sustained erection caused by an abnormal process. It can be partial. In adults, most are idiopathic, with an occasional one a direct result of trauma or a posttraumatic arteriovenous fistula. Rarely, priapism is associated with drug therapy, thromboemboli, sickle cell disease, malignant infiltration of surrounding structures, an adjacent abscess, or a neurologic condition. In pediatrics, aside from trauma, priapism is most often secondary to sickle cell disease or a hematologic malignancy.

Priapism is classifications into low-flow (venous) and high-flow (arterial) states. The low-flow or ischemic type occurs with perineal trauma–induced venous thrombosis, hematoma, or edema of adjacent tissue. The resultant vascular stasis within the corpora leads to a delay in penile venous drainage. High-flow priapism is due to persistent blood inflow, such as with a cavernosal artery laceration (arteriocavernosal fistula).

Doppler US aids in distinguishing the two types of priapism. Arteriosinusoidal fistulas result in pulsatile, high-flow corpora cavernosa signals. Perineal duplex Doppler US achieves almost 100% sensitivity in detecting high-flow arterial priapism, but false positives do occur and limit the specificity.

In low-flow priapism, pudendal arteriography opacifies the dorsal and bulbar arteries, but not cavernosal arteries because of decreased inflow and stasis.

In selected individuals both CT and US are useful in excluding an underlying neoplasm or abscess as the etiology for the priapism.

High-flow priapism, generally related to trauma, can be treated with selective bulbocavernosal artery embolization.

Peyronie's Disease

Peyronie's disease consists of excessive fibrosis and plaques in the sheath covering the corpora cavernosa. It is probably caused by a vasculitis or inflammation. Calcified plaques develop eventually, and if sufficiently extensive, they are visible with conventional radiography. Soft tissue radiography using a mammography technique detects calcifications but does not detect plaques without calcification. Calcifications are also detected with US and CT.

Palpation and US are the examinations of choice in detecting plaques. Plaques vary in size from less than 1 cm to several cm in length and from 2 to 4 mm in thickness. Ultrasonography reveals more extensive plaques than does clini-

cal evaluation. Ultrasonography detects tunica albuginea thickening. Some investigators consider inflammation to be present if hypoechoic foci are identified around a central hyperechoic region.

Doppler US after intracavernosal papaverine injection in these patients reveals decreased peak systolic flow velocity and increased end diastolic flow velocity. Contrast enhanced color and power Doppler US identifies vascularity around plaques in about one-third of patients with established Peyronie's disease. Doppler US shows that penile cavernosal-spongiosal communications near plaques remain patent with low resistance flow, providing a pathway for blood leakage (63); these findings are difficult to place in proper perspective.

Whether MRI detects more plaques than does US is debatable. Some plaques show postcontrast enhancement, suggesting active inflammation, and MR appears superior in monitoring the progression of the inflammation.

Peyronie's disease has been treated with local injection of interferon-alfa-2b into plaques. Noncalcified plaques respond best. Extracorporeal shock-wave lithotripsy (ESWL) has been used to treat symptomatic plaques believed to be of recent origin. The preliminary results appear encouraging (64).

Impotence

Vascular causes of impotence are most common, followed by diabetes mellitus and others. Vasculogenic impotence is usually divided into insufficient arterial inflow (arteriogenic) and excessive venous leakage (venogenic).

Arteriogenic

Internal iliac arteriography has been considered the gold standard in detecting arteriogenic impotence, and although numerous studies over the years have established its usefulness, it is little used today. An erection developing after intracavernosal injection of papaverine is presumed to be evidence that the arterial and venous pathways are intact. Following papaverine injection, diabetic individuals have a significantly lower cavernosal artery peak blood flow velocity than do nondiabetics.

Color Doppler US evaluates arteriogenic impotence by measuring peak systolic velocity and systolic rise time of deep arteries supplying the corpora cavernosa. Following papaverine injection, a systolic rise time of 110 msec or greater appears to be a good discriminant for arterial disease. A peak systolic velocity in the cavernosal arteries of greater than 25 to 30 cm/sec is a normal response to papaverine or prostaglandin B_1 injection. These values should be accepted with caution because they are lower if penile arterial communications exist. Marked differences in velocity between the two cavernosal arteries suggest unilateral disease. Reversal of systolic flow implies proximal penile artery obstruction.

Extensive vascular connections exist between the penile dorsal artery and cavernous arteries, but the dorsal artery function in impotence is not clear. Normally dorsal artery color Doppler US reveals an increase both in systolic and diastolic velocities after intracavernous papaverine injection. Flow is decreased or even absent in the dorsal artery in men with arteriogenic impotence.

Venogenic

The gold standard in diagnosing venogenic impotence is pharmacologically aided cavernosometry and cavernosography. Role of color Doppler US after cavernosal papaverine injection in diagnosing venous dysfunction is not clear; published sensitivities have ranged from 50% to 100% in detecting venous dysfunction.

The cavernous artery resistance index (RI) is obtained from Doppler US data by:

$$RI = (\text{peak systolic velocity} - \text{end diastolic velocity})/\text{peak systolic velocity}$$

After intracavernous injection of prostaglandin, Doppler US in men with suspected venogenic impotence found RI values in those with corporal leakages to be significantly lower than in those with previously normal cavernosometry and cavernosography, although some overlap exists (65); men with an RI >0.9 were not venogenic impotent and those with an RI <0.75 had corporal leakages, while in those with an RI between 0.75 and 0.9, cavernosometry and cavernosography were necessary for diagnosis.

Thrombophlebitis

Anecdotal reports of thrombophlebitis of the penile superficial dorsal vein have been reported. Etiologies include trauma associated with sexual intercourse, penile strangulation, penile injection, infection, neoplasms, and prior surgery.

Scrotum and Spermatic Cord

Acute Scrotum

Acute onset of scrotal swelling and pain should be approached as an emergency. The most common etiologies are testicular torsion, testicular appendage torsion, acute epididymitis, acute epididymo-orchitis, and trauma. Less common are vasculitis, hematoma, and a strangulated hernia. Both a perforated appendicitis and laparoscopic appendectomy can result in an abscess, even in the scrotum. Some of these conditions mimic testicular torsion on scrotal US. Testicular torsion is most common in infants under 1 year, while in older individuals testicular appendage torsion predominates. Epididymoorchitis increases in frequency with age. A differential diagnosis based on age should be used with caution, however, because considerable overlap exists.

Especially in pediatric patients, Doppler US is often the study of choice to differentiate conditions associated with decreased blood flow, such as torsion, from inflammatory disorders where blood flow is often increased. Scrotal scintigraphy is also sensitive in differentiating ischemic conditions from inflammation, realizing that a choice of imaging modality is often based on relative availability and local expertise.

Dynamic contrast-enhanced subtraction MRI evaluates testicular perfusion and relies more on functional rather than anatomic criteria. Dynamic MRI has better spatial resolution than scintigraphy. It aids in differentiating testicular from extratesticular disorders. One limitation is the need for sedation for younger boys.

Testicular Torsion

Testicular torsion (or spermatic cord torsion) occurs at all ages of childhood, but with two peaks: one in newborns where presumably it represents continued evolution of an intrauterine condition, and another during puberty and adolescence. It is uncommon after the age of 35 years.

Newborn

Spermatic cord torsion occurs both prenatally and postnatally. In the newborn, torsion manifests as a testicular tumor. Occasionally a neonate is found with bilateral testicular torsion.

Gray-scale US shows an enlarged testis. A hydrocele is present in some. Color Doppler US is useful in detecting testicular torsion, although the small testicular size in newborns makes evaluation difficult; intratesticular blood flow is lacking on the affected side and normal on the contralateral side.

Delayed therapy or tight torsion consisting of several turns is associated with a poor prognosis. Yet a case can be made for conserving even a necrotic testes found at surgery; some partially necrotic testes retain normal long-term function.

Children and Adults

Clinical

Testicular torsion occurs primarily in postpuberty boys and young men. Torsion of the testicular appendage should be suspected in younger boys. Simultaneous bilateral testicular torsion has been reported. The incidence of torsion increases after orchiopexy for an undescended testis.

Torsion is treated as an emergency. Torsion obstructs venous blood flow and leads to congestion, swelling, hemorrhage, and eventual ischemia. The time frame for ischemia to develop varies depending on the degree of torsion and the resultant vascular obstruction. A delay of 6 to 12 hours increases testicular loss rate considerably. Without therapy, torsion eventually progresses to testicular atrophy.

Nausea and vomiting are common in boys with testicular torsion, findings uncommon in those with testicular appendage torsion or those with epididymoorchitis. Some surgeons consider that older boys with acute scrotal pain less

than 12 hours in duration, especially if associated with nausea or vomiting, have testicular torsion, imaging is not necessary and exploration is performed. Although currently diagnostic imaging prior to surgical correction is often performed, an occasional publication still maintains (66):

> . . . physical examination is sufficient to manage patients with torsion of the spermatic cord.

In view of more recent sonographic refinements, some institutions have modified their previous policy of surgical intervention for all those with an acute scrotum; one approach is to operate when a surgeon has a high degree of suspicion for torsion and perform emergency Doppler US in the rest; those having a normal or increased testicular blood flow are presumed not to have testicular torsion and are treated medically. Such an approach assumes ready availability, on an emergency basis, of experienced sonographic personnel and equipment.

Intermittent testicular torsion results in recurrent testicular pain that remits either spontaneously or after self-manipulation. Imaging is often noncontributory in this condition. In one such 12-year-old, color Doppler detected bilateral flow but pulsed Doppler revealed asymmetric high-impedance flow with an increased resistive index on the involved side (67).

Imaging

With testicular torsion, gray-scale US shows testicular enlargement, varying testicular echogenicity, and often a hydrocele. At times US also detects any related complications requiring surgical intervention. When performed for testicular torsion, a US finding of an inhomogeneous or hypoechoic testis suggests a nonviable testis, and a normal homogeneous, isoechoic appearance suggests a viable testis. Nevertheless, these findings are often not clearly identified; overlap exists, and gray-scale US alone often cannot be relied on during the immediate decision-making time frame.

The primary role of color Doppler US is to differentiate acute testicular torsion from other acute conditions such as acute epididymitis, sequelae of trauma, or a neoplasm. Ideally, normal blood flow and a cord compression test should exclude torsion in most individuals.

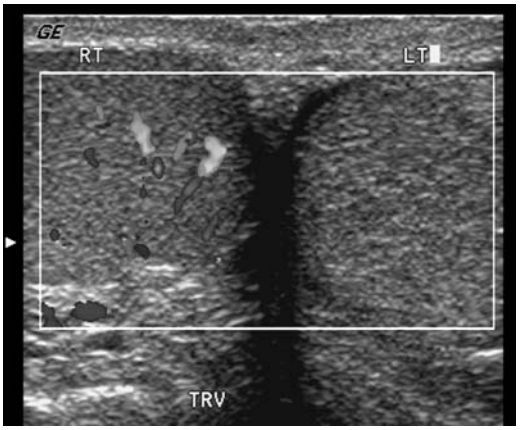

Figure 13.5. Testicular torsion. Transverse Doppler image of both testes shows completely absent flow to left testis. (Courtesy of Deborah Rubens MD, University of Rochester.)

Torsion results in no perfusion and thus no Doppler signal on the affected side (Fig. 13.5). A potential pitfall in a Doppler US diagnosis of testicular torsion includes the occasional spontaneous testicular detorsion; Doppler US reveals normal or even increased testicular blood flow with detorsion. In some studies, Doppler US reaches a sensitivity and specificity of >90% in detecting testicular torsion, although in one study Doppler US identified no blood flow in the symptomatic testis in 61% of individuals with proven testicular torsion, but in the other 39% Doppler US was unreliable (intratesticular perfusion was present or no signal was obtained in either testis) (68); in all individuals with testicular torsion, however, high-resolution US detected a spiral twist of the spermatic cord at the external inguinal canal. A twisted spermatic cord in the scrotum is identified as a round or oval extratesticular mass connecting superiorly with a normal inguinal cord.

Nevertheless, imaging and diagnostic problems remain. One should keep in mind that Doppler US also detects the lack of perfusion in some normal prepubertal testes. At times Doppler US identifies blood flow in a setting of partial necrosis. Operator experience, use of appropriate Doppler US equipment, and knowledge of study limitations play a role.

An MRI of testicular torsion shows a twisting spermatic cord, described as a whirlpool

appearance. The twist has a hypointense signal. Currently, however, MRI is limited in evaluating torsion, often due to logistic problems.

Considerable literature exists for radionuclide scrotal imaging with Tc-99m-pertechnetate for suspected testicular torsion, although this examination has been supplanted by Doppler US in some institutions. Among individuals presenting with acute scrotal pain, published scintigraphy specificities and sensitivities approach 100% in detecting testicular torsion. A photopenic region in the hemiscrotum is compatible with testicular torsion, although cysts such as hydroceles and spermatoceles are also photopenic, and care is necessary to distinguish these entities. An inguinal testis needs to be excluded. Also, early torsion may not show asymmetry.

Color Doppler US and scintigraphy achieved similar statistical significance in detecting testicular torsion in boys with acute scrotal symptoms and clinically equivocal clinical presentations, except that scintigraphic specificity was greater (69); scintigraphy appears to prevent unnecessary surgery in some of those with equivocal findings on Doppler US. Which modality to employ often evolves into relative imaging availability for this acute condition.

Testicular Appendage Torsion

A distinction of testicular torsion and torsion of the testicular appendages is of clinical importance because the latter does not require emergency surgery.

Ultrasonography of appendix testis torsion shows an enlarged, homogeneous appendix testis medial or posterior to the head of the epididymis; some US scans reveal varying echogenicity. A hydrocele may be identified. Scrotal wall thickening and an enlarged epididymis head can develop. Color Doppler US reveals normal or increased flow, a finding that usually excludes testicular torsion.

A scintigraphy finding of a normal radionuclide angiogram and a localized focus of increased tracer activity suggest testicular appendage torsion, but keep in mind that increased tracer uptake is not present during the first several hours after onset of symptoms and radionuclide scrotal imaging may be falsely negative for testicular appendage torsion during this time.

Infection/Inflammation

Epididymitis

Acute

Acute epididymitis is the most common cause of acute scrotal pain and swelling in teenagers and young men. It is usually due to retrograde spread of infection from either the bladder or prostate, and it tends to be unilateral. Most acute scrotal infections originate in the epididymis rather than the testis and result in isolated epididymal involvement (epididymitis). Less common is both epididymal and testicular involvement (epididymo-orchitis). Especially in infants and children, associated congenital anomalies are common and they should undergo full urologic evaluation.

Amiodarone, an antiarrhythmic agent, induces a sterile epididymitis; it is treated by lowering the drug dosage. Hemorrhagic epididymitis occurs in Henoch-Schönlein purpura. Acute unilateral epididymitis with an abscess developed in a patient after bacillus Calmette-Guérin therapy for superficial bladder cancer (70).

Acute testicular segmental infarction is a complication of epididymitis (Fig. 13.6). In addition to findings of epididymitis, gray-scale US reveals a testicular infarct as a discrete hypoechoic testicular tumor that has little or no flow detected with color Doppler US. An occa-

Figure 13.6. Magnetic resonance imaging of segmental testicular infarction (arrow). [Courtesy of Gabriel Fernández, M.D., Vigo (Pontevedra), Spain.]

sional epididymitis evolves into an epididymal abscess.

Spermatic cord vascularity is increased in acute epididymitis, while testicular blood flow is normal or increased. This increased cord vascularity helps differentiate acute epididymitis from torsion, which has a similar clinical presentation but decreased spermatic cord vascularity.

High-resolution gray-scale US most often reveals an enlarged hypoechoic epididymis. A hydrocele is apparent in some. The testis is also abnormal with an associated orchitis (epididymo-orchitis). With epididymal hemorrhage the epididymis assumes a heterogeneous appearance. Still, some individuals with acute epididymitis have a normal gray-scale US examination and only Doppler US is abnormal. Doppler US detects epididymal hyperperfusion in epididymitis and establishes testicular peak systolic blood velocities in the right and left side (Fig. 13.7). Peak systolic velocity is increased in acute orchitis and epididymitis.

T2-weighted MR signal intensity ranges from hyper- to hypointense with acute epididymitis. Use of IV contrast enhancement aids in accentuating changes bilaterally.

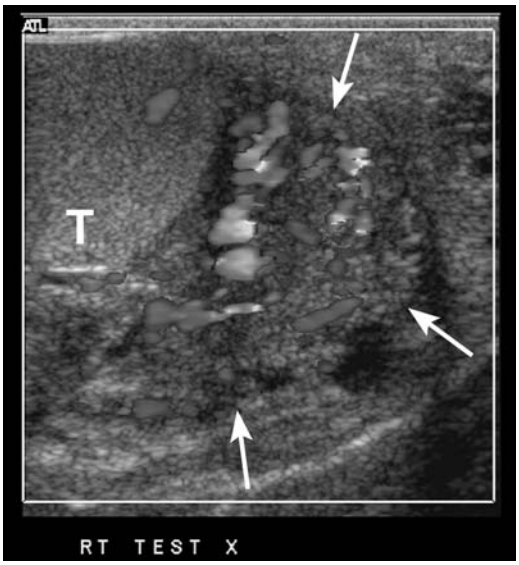

Figure 13.7. Epididymitis. Transverse Doppler image of right testis and epididymis shows enlarged hypervascular epididymis (arrows) compared to testis (T). (Courtesy of Deborah Rubens MD, University of Rochester.)

Testicular scintigraphy with Tc-99m-pertechnetate discloses varying blood flow patterns. Inflammation results in hyperemia, and any asymmetry should be viewed as abnormal.

In general, an enlarged epididymis and a testicular tumor point to infection rather than neoplasia; most often orchitis extends from epididymitis, while testicular neoplasms involve the epididymis mostly during their later stages. Likewise, scrotal skin thickening and a hydrocele suggest infection.

Chronic

Occasionally acute epididymitis evolves into chronic inflammation and a painless tumor indistinguishable from other scrotal tumors. At times chronic epididymitis leads to fibrosis and an enlarged epididymis having a heterogeneous echo appearance. Other complications of epididymitis include abscess, pyocele, and infarct.

Epididymal tuberculosis has developed into a hard, nontender tumor, at times containing calcifications. Testicular involvement is common. Chlamydial epididymitis has also presented as a solid scrotal tumor. Occasionally encountered is an epididymal Candida abscess. Leukemic infiltration can mimic epididymo-orchitis.

Involvement by Behçet's disease led to recurrent epididymo-orchitis (71).

Orchitis

Most episodes of orchitis result from extensions of acute epididymitis. In isolated orchitis a viral infection, such as mumps, should be suspected. Neglected testicular torsion or an infected neoplasm are less common causes of orchitis and possible abscess.

An early US finding of orchitis is increased vascularity in the inflamed testis. With progression, the testis enlarges, becomes hypoechoic, and is covered by a thickened, echogenic tunica albuginea. Ultrasonography of focal orchitis shows a mixed or hypoechoic tumor mimicking a neoplasm. A focal region of hypervascularity detected by Doppler US may represent either inflammation or a neoplasm; follow-up US of an inflammation should show return to normal.

Magnetic resonance imaging shows either a focal region or a diffuse heterogeneous decrease in signal intensity on T2-weighted images.

Technetium-99m-pertechnetate scintigraphy of an inguinal hernia can mimic the appearance of orchitis.

Severe infection evolves into suppuration, abscess, or testicular infarction. In general, the imaging findings of a testicular abscess are similar to those of a neoplasm. Often clinical findings and response to therapy distinguish these conditions.

Granulomatous Epididymo-Orchitis

Grouped under granulomatous epididymo-orchitis are tuberculosis, brucellosis, syphilis, some fungi, and a rare idiopathic inflammation. From a clinical viewpoint little purpose is served in attempting to differentiate epididymal involvement from orchitis or the more common epididymo-orchitis.

Tuberculosis

Scrotal tuberculosis develops from either hematogenous spread or extension from prostate and seminal vesicle infection. Initial involvement is generally an epididymitis, extending to an epididymo-orchitis and occasionally orchitis, most often unilateral. A common clinical presentation consists of a painless chronic epididymal nodule, and the presence of such a nodule, especially in a setting of infertility, should suggest tuberculous epididymitis. A neoplasm is often in the differential diagnosis of a tuberculoma. An occasional tuberculoma arises as an asymptomatic inguinal spermatic cord nodule. A tubercular pyocele tends to be more heterogeneous than a typical abscess. Some contain internal septations.

Epididymal involvement ranges from nodular to diffuse. A heterogeneous, hypoechoic pattern is most common, followed by a mixed pattern, with a hyperechoic pattern being the least common. Most other infections result in a homogeneous US appearance, and thus an enlarged heterogeneous epididymis should suggest tuberculosis. Testicular involvement ranges from an enlarged hypoechoic testis, to a hypoechoic focus, to multiple small hypoechoic nodules in an enlarged testis. A hydrocele is common. Sinus tracts and calcifications occasionally develop.

Brucellosis

Brucellosis is implicated in 10% to 15% of men with epididymo-orchitis in brucellosis endemic regions of Turkey and Spain. Most involvement is unilateral and ranges from heterogeneous epididymis, to diffuse orchitis, to focal hypoechoic testicular tumors. Doppler US detects increased vascularity. Scrotal wall and tunica albuginea thickening, and a hydrocele are associate findings.

Idiopathic Granulomatous

Idiopathic granulomatous orchitis is a rare inflammatory condition, possibly due to sperm extravasation and resultant reaction. It is rarely bilateral. Imaging findings tend to mimic a testicular cancer. Ultrasonography reveals a solid testicular mass. Calcifications develop within some of these tumors. The diagnosis is usually made after orchiectomy.

Filariasis

Infection with *Wuchereria bancrofti* (filariasis) is common in some parts of the tropics. Microfilariae from the blood are ingested by mosquitoes, and with further development they eventually evolve into larvae, which are then injected into humans. The nematode resides in human lymphatics, where it incites a lymphangitis and eventual lymphatic obstruction. Occasionally dead nematodes calcify, and imaging reveals small thin, linear strands.

Not all lymphedema is on an infective basis. Occasionally seen is congenital lymphedema. It also develops after surgical dissection and due to lymphatic obstruction by tumors.

Lymphatic obstruction leads to dilated, thin-walled, fluid-filled structures. At times a superimposed bacterial infection develops. Lymphatic rupture leads to lymphoceles, while lymphatic sinuses drain into surrounding tissues, some even forming external sinuses. Eventually extravasated lymph, resultant fibrosis, and other reactive changes lead to a hard, thickened infiltrate mimicking a neoplasm.

Filarial epididymo-orchitis and spermatic cord lymphadenitis are often bilateral. Initially

the involved spermatic cord enlarges and has a homogeneous, hypoechoic US appearance. Ultrasonography detects dilated lymphatics even in those patients who are still asymptomatic. Associated hydroceles initially are anechoic, but with fibrosis and debris result in a more heterogeneous appearance and tend to mimic a pyocele. At this stage calcified granulomas and surrounding capsular calcifications are common.

Other Infections

Amebiasis involving the scrotum is rare. A hydatid cyst can develop in an undescended testes.

Similar to epididymitis, fungal orchitis is typically encountered in debilitated or diabetic patients. Even scrotal aspergillosis has developed.

Mumps orchitis is not common but should be suspected with a preceding parotitis. These individuals have marked scrotal swelling, fever, and significantly elevated serum C-reactive protein levels.

Some instances of mumps orchitis progress to testicular atrophy.

Fournier's Gangrene

A necrotizing fasciitis, known as *genitoperineal gangrene*, *perineoscrotal gangrene*, *necrotizing fasciitis*, or *Fournier's gangrene*, is a fulminant infective obliterative endarteritis involving the perineum and external genitalia and resulting in progressive necrosis and systemic sepsis. Named after the French dermatologist who first described it in 1883, some authors limit the use of the term *Fournier's gangrene* only to a primary infection and not to the more common secondary infections of the genitalia or perineum. Men are primarily affected. A urethral or anorectal source is found in about half; in the other half no cause is identified. Debilitated and diabetic individuals are more often affected, with Fournier's gangrene occasionally being the initial clinical manifestation of unsuspected diabetes.

Conventional radiography and CT identify subcutaneous emphysema in about half of these individuals. Asymmetric fascial thickening and fat stranding are common imaging findings, occasionally seen even before subcutaneous emphysema is apparent, and these findings should suggest Fournier's gangrene. The differential diagnosis includes a scrotal abscess and extension of gas from a more superiorly located source, such as diverticulitis. At times Fournier's gangrene coexists with an abscess.

These patients represent urologic emergencies. Debridement, antibiotics, and hyperbaric oxygen are the current therapies employed. Mortality remains high despite broad-spectrum antibiotics and aggressive surgical debridement.

Granuloma

Some solid, painful epididymal or vas deferens tumors represent granulomas. A number of these have developed after vasectomy and probably are a tissue reaction to sperm extravasation into surrounding tissues; an occasional one is caused by a foreign-body reaction. Ultrasonography reveals these granulomas to be solid and either iso- or hypoechoic. An occasional one eventually calcifies. Some enhance on postcontrast MRI.

Malacoplakia

Malakoplakia of the testis is rare. Occasionally it manifests as painless testicular enlargement. Some men have had a preceding urinary tract bacterial infection.

A testicular cancer is often suspected.

Sarcoidosis

Even in a setting of systemic sarcoidosis, genital involvement is uncommon, although sarcoidosis and inflammatory nodules have presented as extratesticular scrotal tumors. The epididymis tends to be involved more often than the testis. Some affected individuals develop signs and symptoms mimicking epididymitis. A painless tumor develops in others.

Imaging findings are similar to those seen with epididymitis or a testicular neoplasm.

Tumors

Clinical

An extensive differential diagnosis exists for the infant or boy presenting with a scrotal tumor

Table 13.4. Etiology of a painless scrotal tumor in the pediatric age group

Testicular
Neoplasm
Cyst
Congenital malformation
Posttraumatic
Infection/inflammation
Extratesticular
Neoplasm
Cyst
Hematocele
Infection/inflammation
Pachyvaginalitis testis
Sebaceous cyst
Splenogonadal fusion

Source: Adapted from Aragona et al. (72).

(Table 13.4); two peak age groups exist: 0 to 1 year and 13 to 14 years. In adults, most intratesticular tumors are malignant, while most extratesticular tumors tend to be benign.

The most often encountered epididymal tumors are adenomatoid tumors, leiomyomas, and cystadenomas. Men with von Hippel-Lindau disease are at increased risk for epididymal cystadenomas, similar to the increased incidence of broad ligament cystadenomas found in women with this disease. Anyone presenting with bilateral epididymal cystadenomas should be investigated for this disease.

Imaging

Testicular US readily differentiates intratesticular from extratesticular tumors. In further differentiating between benign and malignant tumors in pediatrics, the imaging modality chosen is often US, but the literature provides conflicting data; some authors achieve sensitivities and specificities over 90% in detecting testicular malignancies, but others find poor specificity and believe that the role of US is limited in this differential.

Currently MRI is limited in differentiating among various scrotal tumors.

Cystic Nonneoplastic Conditions

Cysts originate in the epididymis, spermatic cord, tunica vaginalis, and tunica albuginea (Table 13.5). Most are of unknown etiology. One of the tasks of US is to differentiate between intratesticular and extratesticular cysts. The latter are more common.

Testicular Fluid

In addition to the differential diagnoses listed in Table 13.5, fluid is also present in dermoid cysts and mature teratomas with a cystic component, although often these latter have an associated soft tissue component. These cysts vary in size up to several centimeters in diameter. They are smooth and homogeneous in appearance.

Not all testicular cysts are benign. Some testicular neoplasms develop cystic components. In general, a simple, nonpalpable intratesticular cyst is usually followed clinically. If, on the other hand, US detects a solid component, there is internal echogenicity, septa are present, or if a thick cyst wall is detected, a malignancy is more likely.

Simple Testicular Cyst

Simple intratesticular cysts tend to be small and are filled with serous fluid. Ultrasonography

Table 13.5. Scrotal cystic structures

Intratesticular
Testicular neoplasm containing cysts
Simple testicular cyst
Tunica albuginea cyst
Epidermoid cyst
Rete testis dilatation
Abscess
Cystic dysplasia
Extratesticular
Spermatocele
Epididymal cyst
Hydrocele
Hematocele
Cystocele
Lymphocele
Lymphangioma
Epididymal papillary cystadenoma
Abscess
Pyocele
Amebiasis
Vascular
Varicocele
Hemangioma
Arteriovenous malformation

detects many simple testicular cysts and also aids in differentiating a simple cyst from a neoplasm. These cysts are anechoic, and they have a thin wall and no solid component.

A simple testicular cyst is hypointense on T1- and hyperintense on T2-weighted images. The high T2-weighted signal intensity makes some of these cysts isointense to normal surrounding parenchyma.

Typically these cysts are excised without performing an orchidectomy.

Tunica Albuginea Cyst

Tunica albuginea cysts develop within the tunica. Most are small and solitary, and are discovered incidentally. Some are palpable. They contain either serous fluid or blood.

At times due to prior trauma, tunica vaginalis cysts develop between the visceral portion of the tunica vaginalis and the tunica albuginea. Some indent the testis, thus aiding in distinguishing them from a hydrocele.

Ultrasonography suggests a benign cyst if it is unilocular. If the cyst is multilocular and complex, a malignancy is in the differential. Ultrasonography cannot differentiate between tunica albuginea cysts and tunica vaginalis cysts.

Epidermoid Cyst

Epidermoid cysts are believed to be of germ cell origin, possibly representing a teratoma variant differentiating along ectodermal lines. They are benign, occur at any age, and can be bilateral and large. Clinically, they tend to be detected as painless testicular tumors. Some epidermoid cysts are extratesticular in location.

Because these cysts contain cholesterol crystals and other residual debris, US reveals a hypoechoic, well-marginated tumor with a hyperechoic wall. Some have a laminated or concentric ring-like alternating hypo- and hyperechoic appearance (73), and some contain calcifications.

Magnetic resonance imaging of a scrotal epidermoid cyst tends to show similar findings to those of an intracranial epidermoid cyst; namely, most are hypointense on T1- and hyperintense on T2-weighted images. Some have a peripheral hypointense region on both T1- and T2-weighted images, giving them a *bull's-eye* or *onion ring* appearance.

These are avascular tumors; Doppler US reveals no flow, and they do not enhance post-contrast MR (73).

Although epidermoid cysts can be treated by simple enucleation, with a newly discovered tumor the differential diagnosis often includes a teratoma or a malignancy; imaging cannot differentiate between these entities, and histologic study of surrounding tissue is necessary.

Rete Testis Dilatation (Tubular Ectasia)

Some men develop dilation and possible cysts in the rete testis, at times bilaterally. Most men with this benign condition are over 55 years old, with only a rare case reported in a child; in the latter this condition can be associated with other congenital urinary anomalies and an embryonic malformation is the most likely cause.

Physical examination detects a scrotal tumor typical of a spermatocele.

Ultrasonography reveals a testicular tumor containing multiple small spherical or tubular anechoic or hypoechoic structures with coarse internal echoes without an associated solid component. Cysts, if present, are located in the periphery, in the region of the mediastinum testis. Coexisting epididymal cysts, epididymitis, and spermatoceles are often present. The US appearance, location, and frequently coexisting epididymal abnormality suggest that this condition represents rete testis dilation, probably in association with epididymal obstruction. The rare rete testis adenocarcinoma probably has a similar appearance. Cystic dysplasia of the testis also has a similar US appearance, although cystic dysplasia occurs mostly in children. Dilation of the rete testis is differentiated from a varicocele by the lack of flow, shown by Doppler US.

Magnetic resonance imaging also detects these tumors. They are hypointense on T1- and iso- to hyperintense on T2-weighted images, in distinction to most testicular tumors, which are hypointense on T2 weighted images. They do not enhance after IV gadolinium.

In some men this condition can be differentiated from a testicular neoplasm on the basis of clinical, US, and MRI findings, and orchiectomy is not necessary to establish the diagnosis.

Extratesticular Fluid

Bowel in an inguinal hernia can mimic the cystic structures outlined below. Bowel is identified with US by peristalsis. Some bowel in a hernia can often be reduced manually.

An epidermal scrotal inclusion cyst, cutaneous in location, is probably due to abnormal embryonal closure of the median raphe. These cysts range from cystic to mostly solid structures, most are hypoechoic but their echogenicity varies considerably.

Spermatocele

The seminiferous tubules merge and connect with tubuli recti, which then enter the mediastinum testis and form the rete testis. Efferent ductules from the rete testis form the head of the epididymis. Dilation of the efferent ductules within the epididymis is believed to result in spermatoceles and epididymal cysts. Spermatoceles are filled with thick, debris-laden fluid.

Ultrasonography reveals spermatoceles as unilocular or multilocular epididymal cysts. Debris within the spermatocele usually makes it hyperechoic. Uncommonly, a spermatocele has an appearance of a solid tumor. Sonographically spermatoceles, hydroceles, and epididymal cysts have a similar appearance. Their MRI appearance varies depending on fluid content.

Epididymal Cyst

Epididymal cysts are common; some are multiple and often are an incidental finding. Their etiology is unknown, but they appear to be congenital in nature. Some adolescents present with an uncomfortable scrotal tumor.

These serous fluid-filled cysts have a typical imaging appearance of an epididymal cyst as described above.

Symptomatic epididymal cysts and hydroceles are treated either surgically or with sclerotherapy. Multiple sclerotherapy treatments achieve a high success rate.

Hydrocele

Increased serous fluid in the tunica vaginalis sac represents a hydrocele. It is either congenital and is detected early in life or develops later and manifests as painless scrotal swelling. The scrotum is most often involved, although occasionally a focal hydrocele develops in the spermatic cord.

The processus vaginalis is an inferior outpouching of the peritoneal cavity. Failure of the tunica vaginalis to close off from the peritoneal cavity results in communication between these two structures and fluid accumulates. Partial closure results in a cyst-like structure within the spermatic cord. Spermatic cord hydroceles present as firm inguinal tumors; US identifies a focal, anechoic, and avascular tumor superior to and separate from the testicle.

Abdominoscrotal hydroceles are rare; even rarer are bilateral ones. Most occur in the pediatric age group, enlarge rapidly, and tend to be quite large at initial presentation. Most congenital hydroceles in neonates resolve spontaneously and do not require imaging studies. If a hydrocele does not resolve and therapy is contemplated, imaging helps define the underlying anatomy and detects whether a hydrocele extends into the pelvis.

In a rare newborn a meconium-hydrocele results in an acute scrotum.

Most acquired hydroceles are idiopathic or related to trauma. Some are associated with an underlying disorder such as epididymitis, orchitis, trauma, torsion, or even a neoplasm. In particular, a small hydrocele should raise suspicion of an underlying neoplasm. Most are unilocular, although an occasional multilocular one is encountered. Calculi within hydroceles are not uncommon; US reveals hyperechoic, movable foci in the fluid. Multiple calcifications within a hydrocele should raise suspicion of tuberculosis.

Either US or MRI can be used to evaluate hydroceles, which tend to be mostly anechoic by US and provide an acoustic window for evaluating the underlying testis. Less common is a hyperechoic hydrocele, due to the presence of cholesterol crystals. Hydroceles are homogeneous and hypointense on T1- and hyperintense on T2-weighted images, characteristic of fluid. Occasionally septations are identified within a hydrocele, although prominent septations should suggest a hematocele or pyocele.

A rare hydrocele becomes infected and is a surgical emergency.

After aspirating all fluid, some sclerotherapies have resulted in hydrocele disappearance. On the other hand, an attempt to treat testicular hydroceles by aspiration and injection of a two component fibrin glue consisting of fibrinogen and human thrombin led to hydrocele recurrences (74).

Hematocele

A hematocele consists of blood within a tunica vaginalis sac (i.e., a hydrocele with blood), while a hematoma is blood within the wall. Most hematoceles are traumatic in origin, with a minority due to neoplasm or a bleeding dyscrasia. Clinically, a hematocele presents as a firm, painful mass that does not transilluminate. An acute hematocele is often associated with testicular rupture. An occasional scrotal hematoma in neonates is associated with adrenal hemorrhage.

Initially US shows a hematocele to be mostly anechoic; with time it evolves into a hyperechoic structure and eventually develops a capsule, septations, and even calcifications; at this stage US of a hydrocele, pyocele, and hematocele reveals similar findings.

During the subacute phase, blood within a hematocele is hyperintense both on T1- and T2-weighted MRI.

Pyocele

A pyocele consists of pus in the tunica vaginalis, generally secondary to an epididymo-orchitis or rupture of a testicular abscess. A scrotal pyocele can be a sequela of bacterial peritonitis, presumably secondary to a peritoneal communication.

A hematocele and a pyocele have a similar initial US appearance, although an enlarged epididymis or testis is more common with a pyocele. Some pyoceles develop internal septa.

Cystocele

A scrotal cystocele is in the differential diagnosis of a fluid-filled scrotal structure. A cystocele should empty with voiding. At times US does not identify the actual connection between a cystocele and bladder.

Lymphocele

Representing an accumulation of lymph in a cystic structure, most scrotal lymphoceles (lymphocysts) develop after pelvic surgery. It can be difficult to differentiate a lymphocele from other cystic abnormalities.

A hydrocele, cystocele, and a lymphocele have similar US appearances, although the presence of septations suggests the latter. With a nondiagnostic fluid aspirate, a Tc-99m albumin colloid lymphogram may visualize pelvic lymphatic channels and eventual pooling of activity within a scrotal lymphocele.

Lymphangioma

A lymphangioma is a tumor of lymphatic channels, often greatly dilated, and lined by endothelial cells. A chronic painless scrotal swelling is the most common presentation. Lymphangiomas range from solid, cystic, to mixed multilocular ones and are a sequella of congenital lymphatic obstruction. Ultrasonography reveals a complex, septated cystic tumor with a normal testis and cord in most. Their US appearance is similar to a hematocele or a pyocele. At times US suggests multiple cystic tumors adjacent to the testis. Yet a correct preoperative diagnosis is difficult and the differential ranges from hernias to various scrotal cysts. Some lymphangiomas extend into the perineum, inguinal region, pelvis and retroperitoneum. They recur after incomplete excision.

Arteriovenous Malformation

A scrotal arteriovenous malformation is either congenital or traumatic in origin.

Doppler US of an arteriovenous malformation reveals a high-velocity waveform; it can thus be differentiated from a varicocele. Magnetic resonance imaging outlines the extent of the lesion and detects fast flow within the visualized vessels.

Testicular Tumors

Considerable variability exists in classifying testicular tumors. Most authors employ a histologic classification, and one such modified scheme is used here, although from an imaging viewpoint it is not ideal.

Testicular cancer is the most common malignancy of young men. With adequate therapy a 5-year survival of over 90% is achieved. Cancer prevalence is considerably higher in the white population of America and Europe compared to Asia and Africa, and the prevalence is increasing in Western Europe. Testicular tumors are rare in related family members. Those who have had one testicular cancer are at a considerably higher lifetime risk of developing another testicular cancer, either synchronously or metachronously. An increased risk, including bilateral tumors, exists in a setting of cryptorchidism. Testicular carcinomas develop in a setting of known testicular microlithiasis (discussed later; see Calcifications).

Typically a testicular neoplasm first manifests as a painless unilateral nodule. In general, a solid intratesticular tumor is considered to be malignant until proven otherwise.

Most testicular neoplasms are treated by orchiectomy. In a solitary testis an organ-preserving resection is often appropriate. The potential role of such therapy as transcutaneous high-intensity focused ultrasound as an alternate to organ-preserving surgery is not clear.

The rare gonadoblastoma contains elements of germ cells and stromal tissue. Most are limited to patients with intersex syndromes.

Germ Cell Tumors

Clinical

Over 90% of testicular neoplasms are of germ cell origin, and in adults almost half of all germ cell tumors are seminomatous in origin. Seminomatous tissue is also often present in mixed germ cell tumors. The prevalence of germ cell tumors is approximately 4 per 100,000. The main reason to differentiate germ cell neoplasms as seminomas and nonseminomas is that they are treated differently. Germ cell tumors are not common in the pediatric age group.

An association appears to exist between prior infection by Epstein-Barr virus and subsequent development of seminomas and embryonal carcinomas. Patients with Down syndrome are at a slightly increased risk for testicular cancer; presumably the multiorgan malformations found in trisomy 21 also affect gonads.

Although not common, testicular germ cell tumors do occur bilaterally and are either synchronous or metachronous in origin. Men with a testicular cancer who have an atrophic contralateral testis and those presenting at age 30 years or younger are at increased risk for a second germ cell tumor in the contralateral testis.

An association exists between membranous glomerulonephritis and a seminoma, presumably representing a manifestation of paraneoplastic syndrome. Gynecomastia develops in a minority of males both with seminoma and nonseminoma and, in a young adult, should lead to a further workup.

Occasionally a testicular tumor first manifests through metastases, with the primary tumor not palpable, and initially the metastasis is believed to represent an extraperitoneal extragonadal germ cell tumor. Ultrasonography detects some of the underlying silent primary tumors, although a rare primary testicular tumor regresses to the point that only a scar remains. An occasional primary testicular site is detected only years later (called burned-out cancer). Testicular US reveals such a burned-out testicular tumor as a hyperechoic region. Some of these men have undergone chemotherapy, retroperitoneal lymph node dissection, and an ipsilateral orchiectomy, with pathologic examination simply revealing a testicular scar; the hyperechoic focus seen with US probably represents the remains of such a burned-out neoplasm. The etiology of this phenomenon is unknown, although ischemic or immunologic factors are probably involved.

Complicating this issue is that not all germ cell tumors occur only in the testes. For instance, Klinefelter's syndrome patients have an increased prevalence of extragonadal germ cell tumors.

Among more bizarre tumors were simultaneous germ cell and stromal tumors in the same testis in a 24-year-old man (75); the tumor contained seminoma, embryonal carcinoma, choriocarcinoma, and Leydig cell tumor components.

Doubling rate for many germ cell tumors is measured in days.

Detection

High-resolution US should detect most germ cell tumors. These tumors are mostly hypoechoic to normal testicular parenchyma. In general, although many hyperechoic testicular

tumors are benign, their US appearance alone cannot be used to exclude a malignancy. Most testicular neoplasms are hypervascular. Doppler US has played a limited role in evaluating these tumors.

A diagnosis of germ cell tumor is typically established by radical inguinal orchiectomy.

Staging

A number of staging systems are in use for seminomas and nonseminomatous germ cell tumors, but the TNM staging system is common (Table 13.6). Most seminomas spread via lymphatics, while nonseminomatous teratomas and

Table 13.6. Tumor, node, metastasis (TNM) staging systems of testicular tumors

(Extent of primary tumor is classified after radical orchiectomy)

Primary tumor:

Tx	Primary tumor cannot be assessed
T0	No evidence of primary tumor
Tis	Intratubular germ cell neoplasia (carcinoma in situ)
TI	Tumor limited to testis and epididymis without vascular/lymphatic invasion; tumor may invade into tunica albuginea but not tunica vaginalis
T2	Tumor limited to testis and epididymis with vascular/lymphatic invasion, or tumor extending through tunica albuginea with involvement of tunica vaginalis
T3	Tumor invades spermatic cord with or without vascular/lymphatic invasion
T4	Tumor invades scrotum with or without vascular/lymphatic invasion

Lymph nodes (clinical):

Nx	Regional lymph nodes cannot be assessed
N0	No regional lymph node metastasis
N1	Metastasis with lymph node mass 2 cm or less in greatest dimension; or multiple lymph nodes, none more than 2 cm in greatest dimension
N2	Metastasis with lymph node mass, more than 2 cm but not more than 5 cm in greatest dimension; or multiple lymph nodes, any one mass greater than 2 cm but not more than 5 cm in greatest dimension
N3	Metastasis with lymph node mass more than 5 cm in greatest dimension

Lymph nodes (pathologic):

Nx	Regional lymph nodes cannot be assessed
N0	No regional lymph node metastasis
N1	Metastasis with lymph node mass 2 cm or less in greatest dimension and less than or equal to 5 nodes positive, none more than 2 cm in greatest dimension
N2	Metastasis with lymph node mass more than 2 cm but not more than 5 cm in greatest dimension; or more than 5 nodes positive, none more than 5 cm; or evidence of extranodal extension of tumor
N3	Metastasis with a lymph node mass more than 5 cm in greatest dimension

Distant metastasis:

Mx	Distant metastasis cannot be assessed
M0	No distant metastasis
M1a	Nonregional nodal or pulmonary metastasis
M1b	Distant metastasis other than to nonregional lymph nodes and lungs

Serum tumor markers:

Sx	Marker studies not available or not performed
S0	Marker study levels within normal limits
S1	LDH $<1.5 \times$ N and hCG (mIU/mL) <5000 and AFP (ng/mL) <1000
S2	LDH $1.5–10 \times$ N or hCG (mIU/mL) 5000–50,000 or AFP (ng/mL) 1000–10,000
S3	LDH $>10 \times$ N or hCG (mlu/mL) >50,000 or AFP (ng/mL) >10,000

Tumor stages:

Stage 0	Tis	N0	M0	S0
Stage IA	T1	N0	M0	S0
Stage IB	T2	N0	M0	S0
	T3	N0	M0	S0
	T4	N0	M0	S0
Stage IC	any T	N0	M0	S1–3
Stage IIA	any T	N1	M0	S0
	any T	N1	M0	S1
Stage IIB	any T	N2	M0	S0
	any T	N2	M0	S1
Stage IIC	any T	N3	M0	S0
	any T	N3	M0	S1
Stage IIIA	any T	any N	M1a	S0
	any T	any N	M1a	S1
Stage IIIB	any T	N1–3	M0	S2
	any T	any N	M1a	S2
Stage IIIC	any T	N1–3	M0	S3
	any T	any N	M1a	S3
	any T	any N	M1b	any S

Serum tumor maker abbreviations: AFP, α-fetoprotein; hCG, human chorionic gonadotropin; N, upper limit of normal for lactate dehydrogenase (LDH) assay; mIU, milli International units.

Source: From the AJCC Cancer Staging Manual, 6th edition (2002), published by Springer-Verlag, New York, NY, used with permission of the American Joint Committee on Cancer (AJCC), Chicago, IL.

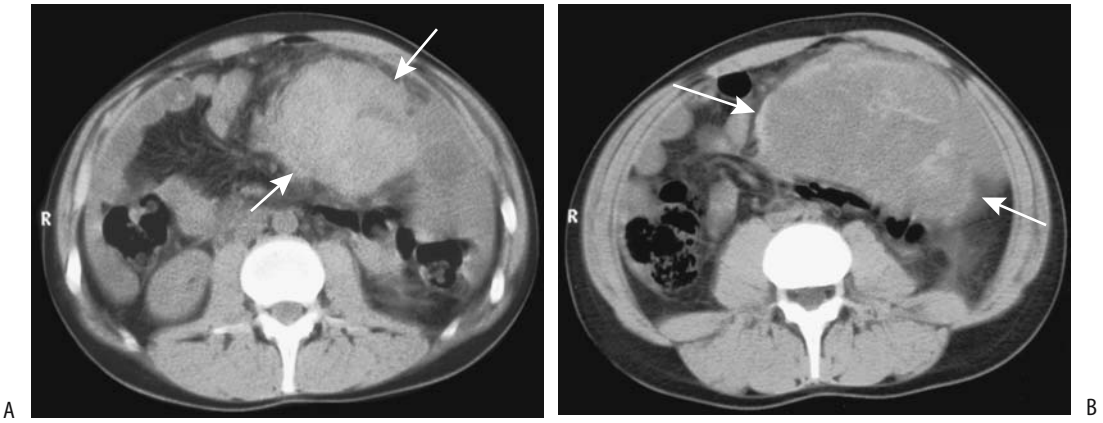

Figure 13.8. Metastatic seminoma. A,B: Two CT images identify a large, poorly marginated intraabdominal tumor (arrows). Extensive peritoneal involvement, including ascites, was also evident. (Courtesy of Algidas Basevicius, M.D., Kaunas Medical University, Kaunas, Lithuania.)

choriocarcinomas more often spread primarily hematogenously. Thus lung metastases are more common with nonseminomas, but retroperitoneal, mediastinal, and neck involvement is more common with seminomas (Fig. 13.8).

Testicular lymphatics drain alongside the testicular arteries and veins into nodes close to the renal hila and eventually into para-aortic nodes. Left sentinel nodes are located close to the renal hilum; on the right these nodes are paracaval in location, inferior to the renal vessels. Tumors involving the epididymis drain into the iliac nodes. Right-sided tumors tend to spread more often to the left para-aortic nodes than vice versa. Drainage occurs to other sites, such as to inguinal and iliac nodes, if the usual lymphatic drainage pathways become obstructed.

With metastasis, left renal vein and inferior vena caval invasion are not uncommon and are detected by imaging (Fig. 13.9). An endovascular biopsy is diagnostic. These tumors can result in a life-threatening malignant pulmonary embolus.

The results of a prospective multicenter study of extraperitoneal lymph node involvement by testicular tumors are listed in Table 13.7. Although this study is now dated, it does provide relative sensitivities of various tests. Nodal involvement by tumor is not identified by CT directly; rather, enlarged lymph nodes in the presence of known tumor suggest metastases. In general, as the diameter of a lymph node increases, the likelihood of metastasis increases almost continuously. Ultrasonography is not accurate in detecting extraperitoneal lymph node involvement.

When associated with germ cell tumors, laminar calcifications suggest extension beyond the tunica albuginea (77). An occasional "burned-out" germ cell tumor develops curvilinear calcifications, similar to those seen with a Sertoli cell tumor.

Currently chest and abdominopelvic CT are part of staging these tumors. A negative study, however, has limited significance. Imaging cannot differentiate reliably between stage I (tumor confined to testis) and stage II (spread to regional nodes), and thus retroperitoneal lymph node dissection is necessary.

Magnetic resonance imaging has a limited role in the staging of germ cell tumors. Tumor signal intensity is similar to that of normal tunica albuginea, and invasion cannot be readily determined. In evaluating extraperitoneal lymph node invasion, MRI is similar to CT; namely, lymph node size is used as the primary criterion.

Preliminary studies suggest that FDG-PET appears to have a role in staging metastatic testicular germ cell tumors by detecting increased carbohydrate metabolism of malig-

Figure 13.9. Metastatic testicular carcinoma. Inferior vena cavagram reveals a tumor thrombi in the inferior vena cava (arrows) and occlusion of the left common iliac vein. Retroperitoneal adenopathy and lung metastases were also present. (Courtesy of David Waldman, M.D., University of Rochester.)

nant cells. Both primary seminomas and malignant teratomas reveal avid uptake. Normal tissue uptake is found in differentiated teratomas and in necrotic tissue.

L-(1–11C)tyrosine PET imaging in men with retroperitoneal metastatic nonseminoma testicular germ cell tumors did not detect most tumors (78); in fact, even with large, inhomogeneous tumors identified by CT, PET revealed decreased uptake at the site.

Table 13.7. Retroperitoneal lymph node involvement by testicular tumors*

	Sensitivity (%)	Specificity (%)
Bipedal lymphography	71	60
Computed tomography	41	94
Abdominal ultrasonography	31	87
α-fetoprotein/human chorionic gonadotropin	37	93
All modalities combined	88	48

*Final diagnosis was based on histology of resected retroperitoneal lymph nodes.
Source: Adapted from Bussar-Maatz and Weissbach (76).

Lymphography has been used in the past to evaluate extraperitoneal lymph node involvement. With advances in CT, however, lymphography currently is rarely employed for this purpose; CT, especially multislice, provides additional information about tumor invasion.

Follow-Up

The current primary role of FDG-PET is in men with elevated serum tumor markers and no tumor identified by conventional imaging; keep in mind that FDG-PET is also positive in a setting of postoperative inflammation (79). False-negative studies also occur. The FDG-PET scans are more accurate than CT in detecting residual tumor when performed several weeks or later after chemotherapy.

In evaluating local recurrence after orchiectomy for testicular neoplasms, 67% of US-detected focal tumors and 27% of heterogeneous changes consisted of cancer (80).

Seminoma

Seminoma is the most common germ cell tumor. Histologically, most seminomas are solid tumors composed of sheets of uniform large tumor cells having an overall superimposed fibrous structure, with an anaplastic appearance found in a minority. Some contain a lymphocytic infiltrate. These tumors vary from a small nodule to diffuse infiltration and testicular enlargement. An occasional one is associated with testicular microlithiasis.

Peak incidence occurs in the fourth and fifth decades of life. It is rare under the age of 10 years and over the age of 60 years. A minority of patients have detectable tumor markers β-human chorionic gonadotropin (β-hCG), lactate dehydrogenase, and placental alkaline phosphatase. In most patients with a seminoma at least one of these three markers is elevated. Elevated serum lactate dehydrogenase levels correlate with seminoma invasive status, metastatic status, and poor outcome, while serum β-hCG levels correlate only with metastatic status; most seminomas produce small amounts of hCG, and an elevated serum level reflects an increase in tumor volume and thus suggests metastases. Placental alkaline phosphatase has the highest

sensitivity for detecting metastatic disease. A pure seminoma does not result in elevated α-fetoprotein levels, and the presence of this tumor marker should suggest a nonseminomatous or mixed tumor.

Some of these tumors first manifest by their metastases. The anaplastic variety appears to be more aggressive than a more typical seminoma.

Ultrasonography reveals most seminomas as focal, solid, and well-circumscribed hypoechoic tumors. Most other germ cell tumors do not have a clearly defined tumor margin. A minority of seminomas contain hypoechoic regions. Cystic or hyperechoic regions are not seen and, if present, should suggest another diagnosis. Larger tumors tend to be hypervascular, a finding evident with Doppler US (Fig. 13.10).

Seminomas are isointense to normal tissue on T1- and mostly hypointense and relatively homogeneous on T2-weighted MR images. They tend to be homogeneous, and regions of increased signal intensity presumably represent either bleeding or calcifications. They enhance less than normal testicular tissue.

Initial seminoma therapy is orchidectomy. Radiotherapy and chemotherapy for postorchidectomy relapse of stage I and IIA disease achieves long-term cure rates of 85% or more; relapse-free rates are predicted by tumor size, age, and small vessel invasion.

Seminoma patients require long-term posttherapy follow-up, including a search for radiotherapy-related secondary cancers years later. Thus a review of men treated at the Institut Claudius Regaud for stages I and II testicular seminoma found an overall second nongerm cell cancer in 11% (81); the Standardized Incidence Ratio was significantly increased in men treated with supra- plus infradiaphragmatic radiation, but not in those treated with infradiaphragmatic radiation only. Also, the incidence of second cancers increased with the duration of follow-up.

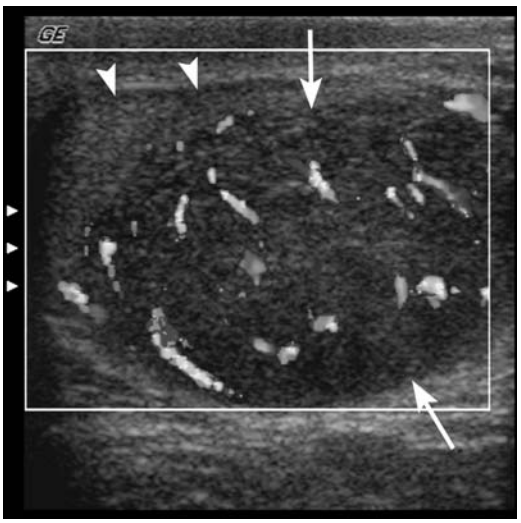

Figure 13.10. Testicular seminoma. Transverse Doppler image of the left testis. Note hypervascular hypoechoic mass (arrows) occupying most of the testis. Residular normal testicular tissue is present anteriorly (arrowhead). (Courtesy of Deborah Rubens MD, University of Rochester.)

Spermatocytic Seminoma

Whether a spermatocytic seminoma is a variant of a seminoma or a separate entity is debatable. Histologically, cells resemble maturing spermatogonia. This is a rare testicular neoplasm occurring only in adults and developing only in descended testes. The vast majority are benign, although an occasional one is associated with a testicular sarcoma.

Nonseminoma

In the United States, embryonal cell carcinoma, yolk sac tumor, teratoma, and choriocarcinoma are considered nonseminomatous germ cell tumors. British authors prefer to lump nonseminomatous germ cell tumors under malignant teratomas. A number of these tumors contain more than one cell type and these are known as mixed germ cell tumors. Histologically, nonseminomatous germ cell tumors have a heterogeneous appearance. They are prone to hemorrhage and necrosis. An elevated serum α-fetoprotein level should suggest a nonseminoma.

Magnetic resonance imaging reveals most of these tumors to be more heterogeneous than seminomas with all sequences. They contain regions of high and low signal intensity both with T1- and T2-weighted images. Because of their MRI heterogeneity, most, but not all, of these tumors can be differentiated from seminomatous tumors.

Embryonal Cell Carcinoma: An embryonal cell carcinoma is a highly malignant undifferentiated tumor occurring either by itself or as part of a mixed germ cell tumor. A rare embryonal cell carcinoma undergoes differentiation to a peripheral neurectodermal tumor. These tumors occur after puberty, with a peak in young men. They invade readily. Metastases are common at the time of initial diagnosis. Embryonal cell carcinomas are associated with elevated α-fetoprotein levels and about half have elevated β-hCG levels.

Ultrasonography can reveal cysts, calcifications, or areas of hemorrhage. These tumors tend to be hypoechoic.

Yolk Sac Tumors: A yolk sac tumor, or endodermal sinus tumor, predominates in childhood, representing an embryonal adenocarcinoma of the prepubertal testis. It is the most common testicular neoplasm in infants. In adult men this tumor tends to be part of a mixed germ cell tumor. An occasional one occurs in other body parts. Most infants with a yolk sac tumor have elevated α-fetoprotein levels.

A yolk sac tumor occasionally is associated with testicular microlithiasis. The US appearance varies from heterogeneous to homogeneous. Some tumors contain cystic regions. This tumor is not as well marginated as a seminoma and tends to invade adjacent structures.

Teratoma: Primary testicular teratomas contain several germ cell layers and are classified into mature and immature types, with the latter (*teratocarcinoma*, *teratosarcoma*, or *teratoma with malignant transformation*) containing undifferentiated tissue from germ cell layers and having undergone malignant transformation.

Teratomas have two peak incidences: one in infancy and early childhood and another in young men. In the very young they tend to be mature and benign. About half of prepubertal boys with a testicular teratoma have an elevated α-fetoprotein level. Most postpubertal teratomas are malignant. Of interest is that any element in a teratoma can metastasize. A majority of malignant testicular teratomas present with metastatic disease. Occasionally a metastasis contains other subtypes of nonseminomatous germ cell tumors, such as a sarcoma, adenocarcinoma, or even a neuroectodermal tumor.

Pretherapy, most teratomas have an inhomogeneous appearance and contain both solid and cystic components. A cystic region should not be confused with a benign cyst. Some contain calcifications; the presence of bone or cartilage indicates maturity. A capsule is seen as a hypointense band in the periphery. A PET scan suggests a malignant teratoma in presence of increased tumor uptake.

Choriocarcinoma: A choriocarcinoma is the least common testicular malignancy. Histologically, this tumor contains two cell types: syncytiotrophoblasts and cytotrophoblasts. Most choriocarcinomas are part of a mixed germ cell tumor. An occasional choriocarcinoma is extraperitoneal in origin.

This is a highly malignant tumor occurring mostly in the second and third decades of life. Metastasis is via both lymphatic and hematogenous routes, and at times metastases manifest before a primary tumor is detected. These tumors are associated with elevated β-hCG levels produced by syncytiotrophoblasts; α-fetoprotein levels are not elevated in pure choriocarcinomas.

Hemorrhage and necrosis are common imaging findings.

Mixed Germ Cell Tumor: A mixed germ cell tumor contains several germ cell elements, with the most common combination being an embryonal cell carcinoma and teratoma elements (teratocarcinoma). The embryonal carcinomatous component often represents more than 50% of the tumor mass. These tumors often contain both solid and cystic components and have an overall inhomogeneous appearance.

A gonadoblastoma consists of a mixture of a germ cell tumor and a stromal tumor. Most occur in a setting of cryptorchidism and other congenital abnormalities.

Only about half of mixed germ cell tumors have a homogeneous appearance; many contain cystic degeneration, hemorrhage, or necrosis, and, as a result, the US appearance varies considerably. An imaging appearance of a necrotic tumor containing multilocular cysts is common.

An FDG-PET scan of retroperitoneal metastases often reveals heterogeneous, increased glucose metabolism prior to chemotherapy, reverting to normal FDG uptake after chemotherapy.

Therapy/Follow-Up of Nonseminomas: Chemotherapy is curative in most individuals with nonseminomatous tumors.

Imaging studies generally do not play a major role in the follow-up of nonseminoma and mixed germ cell tumors because adequate serum markers are available (α-fetoprotein and β-hCG). Persistent elevation of tumor markers after orchidectomy suggests residual tumor. Although increased levels usually signify tumor progression, they are not specific to tumor type. Elevated α-fetoprotein levels occur with hepatocellular carcinomas, some gastrointestinal neoplasms, bronchial carcinomas, and some benign liver disorders, while β-hCG levels are elevated with some gastrointestinal, liver, pancreatic, and urogenital neoplasms. At times elevated β-hCG levels result in gynecomastia. Negative tumor marker levels are of less significance and are seen even with metastatic disease.

Imaging is useful after orchidectomy primarily to detect metastases. A tumor developing after chemotherapy is not necessarily a recurrence; some of these are mature teratomas. Computed tomography is often employed to detect residual tumor after chemotherapy of relapsing nonseminomatous testicular tumors. Among men treated by salvage chemotherapy, CT does not reliably differentiate tumor, scarring, and necrosis (82); CT does, however, provide guidance for lymphadenectomy, which is often considered.

Among men with clinical stage I (T1) nonseminomatous germ cell testicular tumors treated by orchiectomy alone, 74% remained disease-free when followed for a median of 11 years (83); relapses are mostly in those with predominantly embryonal carcinomas and tumors showing vascular invasion, and the authors suggest management by surveillance alone after orchiectomy in this select population with clinical stage I tumors, normal serum markers, and neither predominant embryonal carcinoma nor vascular invasion.

The growing teratoma syndrome is applied to nonseminoma testicular germ cell tumors, which, after chemotherapy, continue to enlarge in a setting of normal tumor markers. Residual tumor resection is associated with a good prognosis. Nevertheless, this issue is complex, illustrated by the following: An orchiectomy in a 21-year-old man with a left testicular tumor and extraperitoneal lymph node metastases revealed a mixed germ cell tumor containing immature teratoma, embryonal carcinoma, and seminoma components (84); after chemotherapy, α-fetoprotein levels declined, but over the next 8 years he underwent several paraaortic tumor resections for enlarged nodes, with the last one yielding adenocarcinoma within parts of a mature teratoma. The authors concluded that the malignant potential of these tumors cannot be evaluated from its maturation and any residual tumor should be resected.

Among extraperitoneal tumors detected by CT after chemotherapy for nonseminomatous testicular cancers, at resection 47% consisted of benign tissue and 53% were either mature teratomas or residual cancer (85); a small residual tumor size and reduction in size after chemotherapy are predictors of benign histology.

An occasional man successfully treated for a nonseminomatous germ cell tumor develops lymphoma years later.

Sex Cord and Stromal Tumors

The nongerm cell tumors include Leydig cell tumor, Sertoli cell tumor, and granulosa cell tumor. Most are benign. Combinations of several of these tumors also occur; these are simply called stromal tumors. Hormone secretion is common.

Leydig Cell Tumors.

Stromal (interstitial) Leydig cells produce androgen necessary for spermatogenesis. A Leydig cell tumor is the most common stromal tumor. It is a tumor of adults, with only a minority developing prepuberty. In the elderly these tumors tend toward malignancy, with the more malignant ones becoming hemorrhagic and necrotic. In some adults, only metastasis establishes their malignant nature.

A common presentation is a painless tumor or testicular enlargement. Some young boys develop precocious puberty, while young men tend towards gynecomastia and infertility. Serum testosterone levels are normal or low. An occasional malignant Leydig cell tumor is associated with high progesterone levels. A Leydig cell tumor can develop in a cryptorchid testis.

Leydig cell tumors are well marginated, encapsulated, solid, and relatively homoge-

neous, although some larger ones develop cysts and necrosis. Most are similar in appearance to germ cell tumors. Ultrasonography findings vary and range from hypo- to hyperechoic. They tend to be isointense on T1- and hypointense on T2-weighted images, an appearance similar to germ cell tumors (Fig. 13.11). Some malignant Leydig cell tumors have foci of increased signal intensity both on T1- and T2-weighted images, thus mimicking nonseminomatous germ cell tumors.

Sertoli Cell Tumors

Sertoli cells line the tubule basement membrane. Most Sertoli cell tumors are benign. Their prevalence is increased in tuberous sclerosis and Peutz-Jeghers syndrome. Some of these tumors calcify and some are bilateral.

One variant is a large-cell calcifying Sertoli cell tumor found mostly in boys. Usually benign, it has distinctive microscopic features and contains multifocal and curvilinear calcifications identifiable by imaging. This tumor is one of the components in Carney's complex (which includes cardiac and skin myxomas, myxoid mammary fibroadenomas, skin pigmentation, adrenocortical abnormalities, pituitary adenoma, and testicular tumors such as large-cell calcifying Sertoli cell tumor).

Granulosa Cell Tumor

Granulosa cell and theca tumors are rare in males. Two peaks occur: one during the first month of life and the other one in late adulthood. Their imaging appearance is similar to that of other stromal tumors.

Carcinoid

A primary testicular carcinoid is exceedingly rare. Carcinoid metastases to testes are more common.

Metastatic to Testes

Metastatic spread to the scrotum is by spermatic cord, lymphatics, or, least often, via a hematoge-

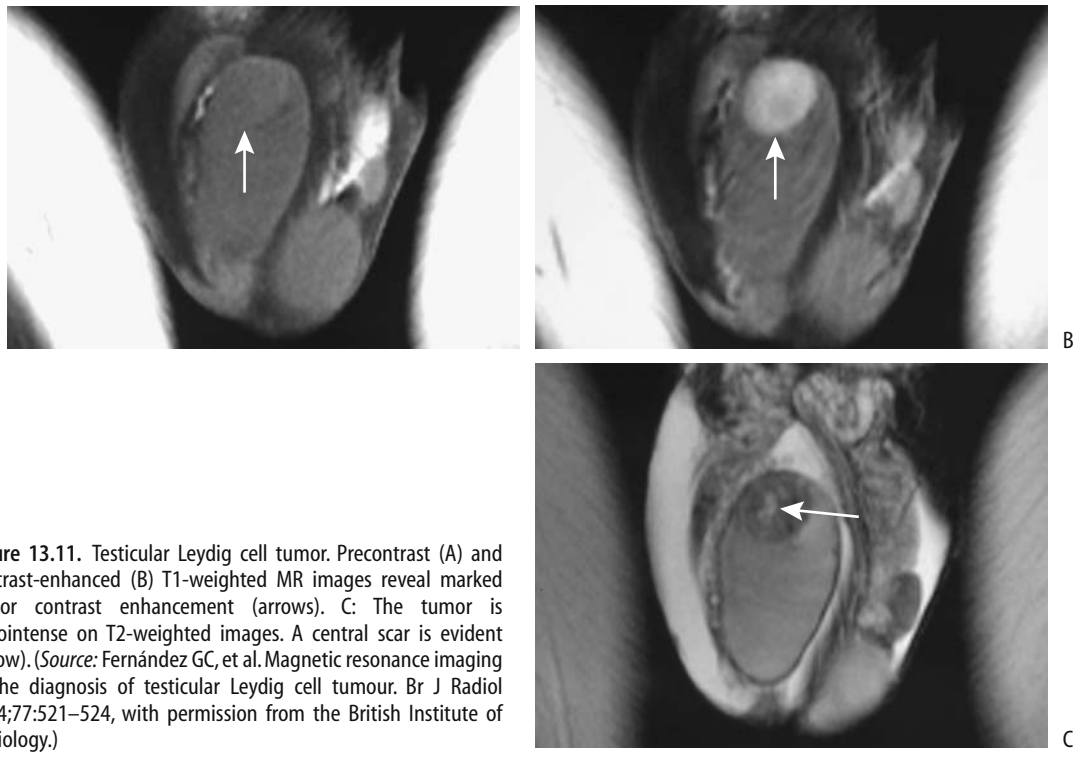

Figure 13.11. Testicular Leydig cell tumor. Precontrast (A) and contrast-enhanced (B) T1-weighted MR images reveal marked tumor contrast enhancement (arrows). C: The tumor is hypointense on T2-weighted images. A central scar is evident (arrow). (*Source:* Fernández GC, et al. Magnetic resonance imaging in the diagnosis of testicular Leydig cell tumour. Br J Radiol 2004;77:521–524, with permission from the British Institute of Radiology.)

nous route. Overall, metastases to the testes are uncommon. Prostatic, appendiceal or colonic signet ring carcinomas and a rare renal cell carcinoma have spread via the spermatic cord. Anecdotal metastatic bile duct carcinomas are reported.

Metastases tend to be multiple. Ultrasonography reveals variable echogenicity.

Lymphoma/Leukemia

Primary testicular lymphoma occurs in all age groups but is not common. In distinction to other testicular tumors, secondary lymphoma occurs in older men; lymphoma should be considered if an elderly man develops a testicular tumor. Almost all secondary malignant lymphomas are non-Hodgkin's B-cell lymphomas. In an occasional patient testicular lymphoma is a first manifestation for this tumor.

Lymphomas and leukemic involvement tend to be bilateral. They range from focal to diffuse infiltration. Ultrasonography reveals a hypoechoic, homogeneous focal or diffuse tumor, similar to germ cell tumors. Associated adenopathy is common, and the epididymis and spermatic cord are also often involved.

Lymphomas tend to be hypointense relative to hydrocele fluid on MR. Similar to lymphomas elsewhere, a homogeneous appearance is common.

Testicular involvement in leukemia is common, especially during recurrence. During remission leukemic cells may persist in the testis in spite of adequate chemotherapy. Leukemia manifests as testicular enlargement. Imaging reveals diffuse infiltration, similar to primary tumors.

Myeloma

A testicular plasmacytoma is rare. It is more common to find testicular infiltration as part of multiple myeloma.

Hemangioma

Both testicular and extratesticular cavernous hemangiomas are rare, and only anecdotal reports exist. Most are detected as palpable nodules and a malignancy is suspected clinically. Hemangiomas have similar imaging findings to the unrelated rare paratesticular epithelioid hemangioendothelioma; it has a good prognosis.

Ultrasonography of hemangiomas ranges from nondiagnostic to a heterogeneous tumor replacing parenchyma. Most are hypoechoic, but their echogenicity varies. Some hemangiomas contain calcifications. Color Doppler US of one revealed intense flow in the tumor and normal flow in the surrounding parenchyma (86). Ultrasonography of extratesticular hemangiomas tends to suggest a varicocele.

These hemangiomas are slightly hyperintense on T1- and markedly hyperintense on T2-weighted images. Any thrombi appear as signal voids.

Extratesticular Tumors

Ultrasonography can differentiate most testicular from extratesticular tumors. Whether an extratesticular tumor originates from the epididymis is more problematic. Ultrasonography cannot differentiate the considerably more common benign extratesticular tumors from a malignant one.

Mesenchymal Tumors

Lumped under this heading are mesothelioma-origin tumors, various sarcomas, and their benign counterparts. Most originate in the spermatic cord or epididymis. Some undoubtedly are a component of a teratoma.

Over 90% of spermatic cord neoplasms are of mesenchymal origin.

Adenomatoid Tumor/Nonpapillary Benign Mesothelioma

The most common benign neoplasm involving epididymis is an adenomatoid tumor, also known as a *nonpapillary benign mesothelioma*. A rare adenomatoid tumor originates in the testis or spermatic cord. Immunohistochemical study suggests a mesothelial cell origin (87). Occurring in adults, these slow-growing tumors are most common in young men; many are asymptomatic.

These tumors vary in their imaging appearance. Most are solid and well marginated, but an occasional one is predominantly cystic. Varying amounts of fibrosis are common. They range from hyper- to mostly isoechoic in appearance.

Some invade adjacent testis and mimic a carcinoma, although testicular malignancies do not typically have an isoechoic appearance.

Malignant Mesothelioma

Malignant mesotheliomas of the tunica vaginalis are uncommon, affecting men over age 50 years. Anecdotal synchronous bilateral malignant mesotheliomas are reported. An association exists with prior asbestos exposure. These tumors range from an aggressive course to more indolent ones. Histologic differentiation from a benign adenomatoid tumor is difficult.

These are solid, nodular tumors. They spread primarily via lymphatics; one of the few remaining indications for a lymphogram is in the workup of a malignant mesothelioma.

Complete tumor excision should be curative.

Benign Mesenchymal Tumors

Lipomas are common extratesticular and spermatic cord tumor. Some of these tumors are complex, containing other mesenchymal tissue. Occurring over a wide age range, many are discovered incidentally.

A lipoma appears as fat density on CT and as a hyperechoic tumor on US. Magnetic resonance reveals a relatively homogeneous hyperintense tumor on T1-weighted images; some lipomas are hyperintense to fat on T2-weighted images.

A rare scrotal tumor of unknown etiology consists primarily of fibrosis and is nonneoplastic in origin. Most of these fibromas are hyperechoic on US. Some have a striated appearance. Magnetic resonance reveals a hypointense tumor on T1- and an inhomogeneous hypointense tumor on T2-weighted images. They tend to have inhomogeneous contrast enhancement.

Aggressive fibromatosis (desmoid tumor) of the spermatic cord is rare; histologically these tumors are similar to other desmoid tumors found in the abdomen and are associated with Gardner's syndrome. These tumors recur following local excision.

Sarcoma

Paratesticular rhabdomyosarcomas occur in infants and children, while leiomyosarcomas are more common in adults. Rhabdomyosarcomas are mostly solid and occasionally partly cystic, and mimic benign neoplasms. A rhabdomyosarcoma should be considered in children with a paratesticular cystic tumor containing a solid component. Some of these tumors are associated with a hydrocele.

The rare liposarcoma is most common in the spermatic cord (88); some are associated with surrounded inflammation and fibrosis.

The term *malignant mesenchymoma* appears appropriate for some of these tumors; an occasional one contains such elements as a liposarcoma, chondrosarcoma, and even osteosarcoma.

With most of these tumors preoperative imaging discloses a nonspecific intrascrotal, paratesticular tumor. Ultrasonography and MR reveal a homogeneous tumor indistinguishable but separate from a normal testis. A similar appearance is seen with benign mesenchymal tumors, which, statistically, are more common in this location.

A rare paratesticular tumor is reactive pseudosarcomatous myofibroblastic proliferation (proliferative funiculitis). It is of unknown etiology, although prior trauma appears to be a factor.

Adenoma

Histologically, an adenoma is similar to a well-differentiated renal cell carcinoma and a multicystic papillary adenocarcinoma of the rete testis, thus metastasis is in the differential diagnosis. This tumor is associated with von Hippel-Lindau disease, at times occurring bilaterally. In the presence of other, more ominous systemic tumors found in von Hippel-Lindau disease, most of these cystadenomas are asymptomatic.

These adenomas range from solid to mostly cystic with papillary soft tissue projections.

Metastasis

Detection of an epithelial malignant neoplasm in the spermatic cord most often represents a metastasis. Even in an asymptomatic patient, a search for a primary site is warranted. A spermatic cord adenocarcinoma is occasionally a first manifestation of a silent colon cancer.

Calcifications

Testicular

The term *microlithiasis* implies microscopic calcifications that should not be visible with imaging, but this term has become ingrained in medical and radiologic usage for the faint, barely perceptible calcifications detected with high-resolution imaging and is used in this context here. Pathologically, these calcifications either consist of amorphous calcific debris or, more often, are laminated (77); most are multiple. They appear to represent a defect in Sertoli cell phagocytosis of tubular debris. The prevalence of testicular microlithiasis in a population referred for scrotal US was <1% (89).

Testicular calcifications occur in a number of benign conditions and malignancies, in boys and in adults (Table 13.8). In some individuals microlithiasis is discovered as an incidental finding. The relative risk of a concurrent tumor being present is about 22-fold compared to controls (89). Some calcifications are premalignant; neoplasms developing later in some of these individuals, with time interval between discovery of microlithiasis and subsequent neoplasm detection ranging up to a decade.

Table 13.8. Conditions associated with testicular calcifications

Idiopathic
Cryptorchidism
Klinefelter's syndrome
Down syndrome
Infection/inflammation
Tuberculosis
Filariasis
Granulomatous orchitis
Sarcoidosis
Neoplasms
In association with pulmonary microlithiasis
Epidermoid cysts
Ischemia
Trauma
Prior testicular torsion
Vasculitis
Hematoma
Infertility

Typically, US reveals testicular microlithiasis as numerous diffuse, small, nonshadowing hyperechoic foci throughout the parenchyma. A tendency toward a peripheral location is evident with some. Any clustering of calcifications should suggest a malignancy.

Although the approach to incidentally discovered microlithiasis varies, an initial clinical evaluation for a silent malignancy, including CT of the chest and abdomen, appears reasonable. Some investigators follow these patients with serial imaging and tumor markers (α-fetoprotein and β-hCG), although sufficient data are not available to provide firm recommendations.

Extratesticular

Prostatic calcifications are common. Occasionally during a bone scan uptake of Tc-99m-MDP, radiotracer is detected around prostatic calcifications; presumably this tissue is metabolically active.

Calcifications develop in some extratesticular benign tumors. The sequela of a hematocele has already been mentioned. Some calcifications are loose in the tunica vaginalis sac; the literature refers to these as scrotal pearls. An occasional such calcification floats in a hydrocele.

Vascular Abnormalities

Varicocele (Spermatic Vein)

Clinical

A varicocele consists of either a single enlarged vein or several freely communicating veins containing incompetent valves. The primary importance of a varicocele is its association with infertility and testicular hypotrophy, although at times a varicocele leads to pain. Only a minority of men with a varicocele are infertile, however, and it is not possible to predict among teenagers with a newly discovered varicocele who will become infertile.

In younger men most varicoceles are idiopathic, but a secondary cause is more common in older individuals. At times an extrinsic tumor, such as a left-sided renal cell carcinoma, compresses or occludes the testicular vein and

first manifests as a left varicocele. Rarer conditions include hydronephrosis and malignant lymphadenopathy adjacent to the veins.

Varicocele prevalence gradually increases in teenagers, reaching adult levels at about the age of 18 years. In the pediatric age group a varicocele is often associated with a small testis. Testicular growth can be expected after therapy. In infertile men with varicoceles both testicles tend to be atrophic, and sperm motility is low. Correction of a varicocele in an adult often produces poor results, thus the emphasis on early detection.

Varicoceles are more common on the left, although in infertile men varicoceles are most often bilateral. A large study found 87% of individuals to have left varicoceles only, 2% right varicoceles, and 11% bilateral varicoceles (90). The more common left varicocele typically drains into the left renal vein. With an isolated right varicocele, compression of the right spermatic vein by an extrinsic tumor should be considered. Most right varicoceles join the inferior vena cava just inferior to the right renal vein, but aberrant drainage pathways are not uncommon; communication with the paravertebral veins or portal venous system, especially left colic vein, is found in a minority (91). Detection of these alternate pathways aids in reducing recurrence after therapy. A minority of varicoceles are intratesticular in location.

Idiopathic thrombosis of a varicocele is rare (92); clinically, on an acute basis it mimics a strangulated inguinal hernia or testicular torsion.

Imaging

Gray-scale US reveals most varicoceles as dilated, tubular blood-filled structures. Venography identifies testicular (internal spermatic) vein insufficiency by showing reflux of contrast from the left renal vein into the testicular vein and pampiniform plexus.

The internal spermatic vein becomes palpable at a diameter of about 3 to 3.5 mm and Doppler US detects reversal of venous blood flow in veins wider than about 3.5 mm, realizing that clinical and US diagnoses of a varicocele do not always agree. Although Doppler US does detect a subclinical varicocele, its sensitivity probably is less than that of venography. Also, the borderland between normal diameter and a varicocele is not clearly defined. Does venous reflux always signify a varicocele?

A rare varicocele is intratesticular and simply represents a dilated intratesticular vein. These intratesticular varicoceles range from bilateral to unilateral, and about half are not associated with an extratesticular varicocele. Ultrasonography detects these varicoceles as dilated serpiginous intratesticular veins close to the mediastinum testis. Doppler US confirms a low-flow state, which varies with the Valsalva maneuver. Care is necessary with US to differentiate between an intratesticular varicocele and tubular ectasia.

Magnetic resonance imaging of an intratesticular varicocele reveals a tortuous tubular structure hypointense on T1- and T2-weighted images; it had the same signal intensity as testicular parenchyma. The more common extratesticular varicoceles have a serpiginous course and a varied signal intensity, depending on flow. They enhance on immediate postcontrast images.

Scintigraphy is not commonly used to evaluate varicoceles. Occasionally detected is retrograde blood flow in the internal spermatic vein. Relative blood-pool activity in each hemiscrotum appears to correlate with the presence of a palpable varicocele, but the relevance of such scintigraphy is not established.

Venography not only detects a varicocele but also is used for therapy. Detachable balloons, coils, and a number of foreign materials have been tried with varying success rates.

During a Valsalva maneuver while upright, infrared thermometry reveals an increase in scrotal temperature in those with a varicocele; after internal spermatic vein ligation, the scrotal temperature decreases to that of controls.

Therapy

Considerable evidence suggests that early varicocele treatment in pubertal boys prevents testicular growth arrest. Even in adolescents with grade 2 or 3 varicoceles, within a year of varicocele repair the involved testis increases in size. The goal of therapy in individuals with infertility is to improve sperm density and sperm motility. Varicocelectomy even of a unilateral varicocele results in an improvement.

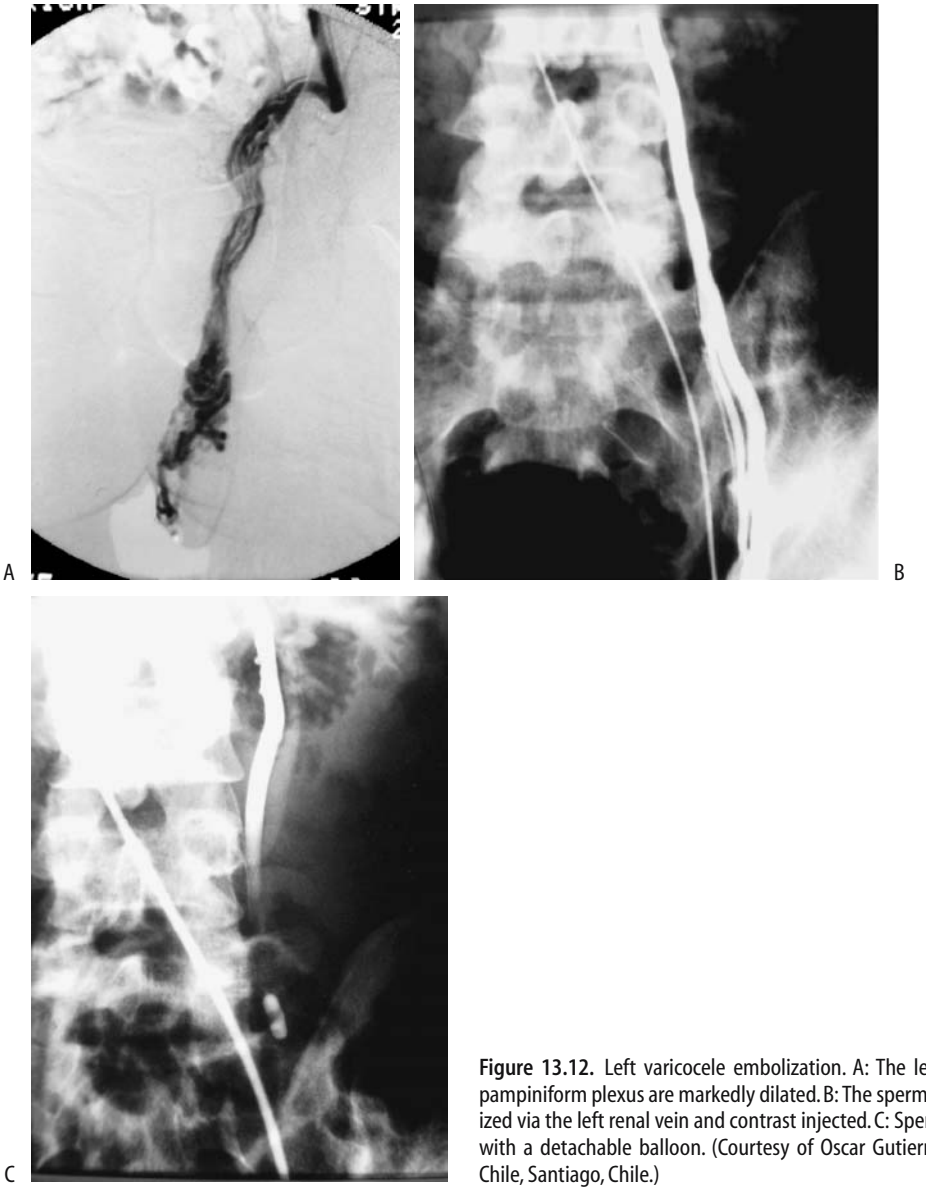

Figure 13.12. Left varicocele embolization. A: The left spermatic vein and pampiniform plexus are markedly dilated. B: The spermatic vein was catheterized via the left renal vein and contrast injected. C: Spermatic vein is occluded with a detachable balloon. (Courtesy of Oscar Gutierrez, M.D., University of Chile, Santiago, Chile.)

Prior to therapy, it appears worthwhile to ensure that the underlying kidney is normal. Traditional therapy of a varicocele is open extraperitoneal repair. Recurrence is greater with spermatic vein ligation, but the risk of major complications, including testicular ischemia and hydrocele, increases with spermatic cord venous channel ligation. Currently percutaneous embolization using either stainless steel occluding spring coils or sclerotherapy is more common. Alternative therapy consists of detachable embolization balloons and laparoscopic varicocelectomy (Fig. 13.12). Initial spermatic vein phlebography helps establish underlying anatomic variants Current evidence suggests that in infertile men no significant difference in outcome exists between surgical ligation and percutaneous embolization.

A long-term study of almost 1500 patients with varicoceles using basilic vein access achieved a success rate of 82% for sclerotherapy and 84% for a combination of sclerotherapy and embolization (90); therapy could not be performed in 7% of patients due to basilic vein spasm, catheterization difficulties, or anatomic variation. Some published successful percutaneous varicocele treatment rates are >90%.

Persisting or recurrent varicoceles are generally due to collateral vessels. A combination of endovascular occlusive metal coils—which is comparable with surgical ligation, and a sclerosing agent—which diffuses and scleroses collateral veins and thus decreases recurrence, appears superior to separate use of these agents. Others embolize silicone or latex balloons combined with a sclerosing agent.

An intratesticular varicocele was treated by transcatheter embolization of the spermatic vein (93).

Is an intraoperative postligation venogram necessary during varicocelectomy to confirm the completeness of varicocele ligation? Among boys with postoperative recurrent varicoceles, the presence of patent collateral veins missed at initial surgical ligation caused recurrence in 68%, ineffective vein ligation in 27%, and incompetence of extrafunicular plexus in 5% (94); missed collateral veins were due to the presence of either a double or triple spermatic vein, venous bridges across the surgical ligation, or extraperitoneal anastomoses. A minority of individuals have anastomoses with the portal or systemic veins—among others, with the left colic vein, paravertebral venous plexus, inferior mesenteric veins, and splenic veins (91). Following surgical correction, recurrence usually consists of collateral vessels running parallel to the original varicocele. Knowledge of underlying anastomoses is necessary to prevent recurrence after therapy.

Instead of a venogram, some surgeons use Doppler US to identify accessory spermatic veins and evaluate surgical results.

Prostatodynia (Pelvic Venous Congestion)

Prostatodynia signifies pain referable to the prostate. The relationship between prostatitis and prostatodynia is murky, and the latter term is occasionally used to describe clinically atypical prostatitis. Prostatodynia is a clinical diagnosis while pelvic venous congestion is an objective finding based on imaging data. Although many men with prostatodynia do have pelvic venous congestion, these terms are not synonymous.

Endorectal US and transperineal color Doppler US detects intrapelvic venous congestion. Typical 3D MR venography findings of pelvic venous congestion consist of dilated and often thickened prostatic capsular veins, pudendal plexus, and the plexus posterior to the bladder. Three-dimensional MR images provide a global view.

Ischemia

The most common cause of testicular ischemia and atrophy is testicular torsion (discussed earlier; see Testicular Torsion). Penile gangrene and necrosis develop in patients with chronic renal failure; presumably gangrene is ischemic in nature due to progressive vascular calcifications (calciphylaxis) induced by secondary hyperparathyroidism developing with chronic renal failure. Other causes include infection, trauma, and some vasculitides, such as polyarteritis nodosa. Emphysematous infarction is a complication of epididymo-orchitis. Testicular infarction develops in sickle cell disease. A relatively new diagnosis is segmental testicular infarction; MR appears to be the imaging modality of choice for this condition, which is treated with watchful waiting and which reveals eventual partial or complete revascularization (95,96). Penile necrosis has been reported after coronary artery bypass graft (97).

Neonatal testicular infarction is rare. These infarctions can be segmental.

Imaging findings early in the course of an infarction tend to mimic those of a neoplasm. Scintigraphic appearance (using Tc-99m-pertechnetate) of scrotal cellulitis has simulated testicular infarction (98).

Ultrasonography of an infarction reveals a diffuse, inhomogeneous echo pattern. At this stage Doppler US reveals hypoperfusion. Without adequate therapy the testes eventually atrophies and often dystrophic calcifications develop.

Leriche's Syndrome

Contrast-enhanced magnetic resonance angiography (MRA) can detect Leriche's syndrome (occlusion of distal aorta) and, in fact, often provides better femoral artery visualization than does intraarterial digital subtraction angiography (DSA). A 3D MRA classification of Leriche's syndrome is based on the level of aortic occlusion: (1) juxtarenal; (2) infrarenal but cranial to the inferior mesenteric artery origin; and (3) caudal to the inferior mesenteric artery (99).

Acquired Immune Deficiency Syndrome (AIDS) Related

Prostatic tubercular abscesses develop in men with AIDS. Epididymo-orchitis is not uncommon and tends to be more severe than in non-AIDS patients. Unusual opportunistic pathogens are common. At times MRI reveals obliteration of interlobular septa and mimics a cancer. Some of these infections evolve into an epididymocutaneous fistula.

Testicular stromal tumors have developed in HIV-infected men. Fournier's gangrene can also be initial presentation of an HIV patient.

Postoperative Changes

Prostate

A false urethral passage may not fill with contrast after prostatic surgery and thus be missed on a voiding cystourethrogram. At times an introduced catheter elevates an adjacent mucosal flap and identifies the false passage. If needed, US is useful for guidance in inserting a catheter.

Urinary incontinence is a complication after prostatectomy. Evaluation of the bladder outlet sphincter mechanism in these patients is discussed in Chapter 11.

Anecdotal reports describe a gossypiboma (retained surgical sponge) after radical prostatectomy and pelvic lymph node dissection resulting in recurrent bladder neck strictures.

Similar to other surgical procedures, a radical retropubic prostatectomy is associated with thromboembolic complications. Pelvic lymphoceles and hematomas appear to have a role in thrombi formation; postoperative pelvic US detects most lymphoceles and hematomas, although small collections are overlooked.

Postvasectomy

A vasectomy is associated with few complications. Granulomas and cysts develop postvasectomy. Granulomas are probably secondary to spermatozoal extravasation and a resultant inflammatory response. Extravasation presumably is secondary to increased pressure in epididymal tubules. The epididymis enlarges.

A granuloma appears as a hypoechoic tumor within either the epididymis or adjacent structures.

Postbiopsy

Arteriovenous fistulas, detectable with color Doppler US, occur with a minority of endorectal prostate needle biopsies; almost all of these fistulas close spontaneously.

Similar to other sites, US-guided transperineal prostatic biopsy can result in perineal tumor implantation.

Testicular US after testicular biopsy reveals a range of findings, such as focal hypoechoic tumors ranging from well marginated to poorly defined, peritesticular hyperechoic foci or linear striations, and focal contour defects (100); some of these findings even suggest a neoplasm, and thus knowledge of a past biopsy is necessary.

Other Findings

After a pancreas–kidney transplant, with the exocrine pancreatic drainage into the bladder, anecdotal reports describe urethral disruption, presumably secondary to enzymatic digestion.

Vesicourethral dysfunction is a complication of radical rectal surgery. The bladder does not empty normally. Radical transurethral prostate resection appears effective in some.

References

1. Mate A, Bargiela A, Mosteiro S, Diaz A, Bello MJ. Contrast ultrasound of the urethra in children. Eur Radiol 2003;13:1534–1537.

2. Seki N, Senoh K, Kubo S, Tsunoda T. Congenital megalourethra: a case report. Int J Urol 1998;5:191–193.
3. Aggarwal A, Krishnan J, Kwart A, Perry D. Noonan's syndrome and seminoma of undescended testicle. South Med J 2001;94:432–434.
4. Nicolas F, Dubois R, Laboure S, Dodat H, Canterino I, Rouviere O. [Testicular microlithiasis and cryptorchism: ultrasound analysis after orchidopexy.] [French] Prog Urol 2001;11:357–361.
5. Lam WW, Tam PK, Ai VH, Chan KL, Chan FL, Leong L. Using gadolinium-infusion MR venography to show the impalpable testis in pediatric patients. AJR 2001;176:1221–1226.
6. Robert F, Rollet J, Lapray JF, Bey-Omar F, Durieu I, Morel Y. [Agenesis of the vas deferens in male infertility. A tentative classification based on 39 cases.] [French] Presse Med 1999;28:116–121.
7. Stikkelbroeck NM, Suliman HM, Otten BJ, Hermus AR, Blickman JG, Jager GJ. Testicular adrenal rest tumours in postpubertal males with congenital adrenal hyperplasia: sonographic and MR features. Eur Radiol 2003;13:1597–1603.
8. Avila NA, Premkumar A, Merke DP. Testicular adrenal rest tissue in congenital adrenal hyperplasia: comparison of MR imaging and sonographic findings. AJR 1999;172:1003–1006.
9. Goldman SM, Sandler CM, Corriere JN Jr, McGuire EJ. Blunt urethral trauma: a unified, anatomical mechanical classification. [Review] J Urol 1997;157:85–89.
10. Uder M, Gohl D, Takahashi M, et al. MRI of penile fracture: diagnosis and therapeutic follow-up. Eur Radiol 2002;12:113–120.
11. Dee KE, Deck AJ, Waitches GM. Intratesticular pseudoaneurysm after blunt trauma. AJR 2000;174:1136.
12. Frauscher F, Klauser A, Stenzl A, Helweg G, Amort B, zur Nedden D. Ultrasonography findings in the scrotum of extreme mountain bikers. Radiology 2001;219:817–821.
13. Mueller-Lisse UG, Frimberger M, Schneede P, Heuck AF, Muschter R, Reiser MF. Perioperative prediction by MRI of prostate volume six to twelve months after laser-induced thermotherapy of benign prostatic hyperplasia. J Magn Reson Imaging 2001;13:64–68.
14. Shukla-Dave A, Hricak H, Eberhardt SC, et al. Chronic prostatitis: MR imaging and 1H MR spectroscopic imaging findings–initial observations. Radiology 2004;231:717–724.
15. Tisseau L, Zini L, Lemaitre L, Biserte J, Gosselin B, Leroy X. [Prostatic malacoplakia: report of 3 cases.] [French] Prog Urol 2000;10:597–599.
16 Halpern EJ, Hirsch IH. Sonographically guided transurethral laser incision of a Mullerian duct cyst for treatment of ejaculatory duct obstruction. AJR 2000;175:777–778.
17. Francica G, Bellini S, Miragliuolo A. Schwannoma of the prostate: ultrasonographic features. Eur Radiol 2003;13:2046–2048.
18. Stamey TA, Donaldson AN, Yemoto CE, McNeal JE, Sozen S, Gill H. Histological and clinical findings in 896 consecutive prostates treated only with radical retropubic prostatectomy: epidemiologic significance of annual changes. J Urol 1998;160:2412–2417.
19. Villers A, Soulie M, Haillot O, Boccon-Gibod L. [Prostate cancer screening (III): risk factors, natural history, course without treatment. Characteristics of detected cancers.] [Review] [French] Prog Urol 1997;7:655–661.
20. Vantaux P, Schneider P, Le Coz S, Villers A. [Consumption coagulopathy disclosing prostatic cancer.] [French] Prog Urol 2001;11:68–69.
21. Valeri A, Drelon E, Azzouzi R, et al. [Epidemiology of familial prostatic cancer: 4-year assessment of French studies.] [French] Prog Urol 1999;9:672–679.
22. Hoedemaeker RF, van der Kwast TH, Boer R, et al. Pathologic features of prostate cancer found at population-based screening with a four-year interval. J Natl Cancer Inst 2001;93:1153–1158.
23. Hugosson J, Aus G, Becker C, et al. Would prostate cancer detected by screening with prostate-specific antigen develop into clinical cancer if left undiagnosed? A comparison of two population-based studies in Sweden. BJU Int 2000;85:1078–1084.
24. Benchekroun A, Zannoud M, Ghadouane M, Alami M, Belahnech Z, Faik M. [Sarcomatoid carcinoma of the prostate.] [Review] [French] Prog Urol 2001;11:327–330.
25. Lilleby W, Torlakovic G, Torlakovic E, Skovlund E, Fossa SD. Prognostic significance of histologic grading in patients with prostate carcinoma who are assessed by the Gleason and World Health Organization grading systems in needle biopsies obtained prior to radiotherapy. Cancer 2001;92:311–319.
26. Rubin MA, Dunn R, Kambham N, Misick CP, O'Toole KM. Should a Gleason score be assigned to a minute focus of carcinoma on prostate biopsy? Am J Surg Pathol 2000;24:1634–1640.
27 Bocking A. [Cytopathology of the prostate.] [Review] [German] Pathologe 1998;19:53–58.
28. Prando A, Wallace S. Helical CT of prostate cancer: early clinical experience. AJR 2000;175:343–346.
29. Halpern EJ, Strup SE Using gray-scale and color and power Doppler sonography to detect prostatic cancer. AJR 2000;174:623–627.
30. Kuligowska E, Barish MA, Fenlon HM, Blake M. Predictors of prostate carcinoma: accuracy of gray-scale and color Doppler US and serum markers. Radiology 2001;220:757–764.
31. Halpern EJ, Rosenberg M, Gomella LG. Prostate cancer: contrast-enhanced US for detection. Radiology 2001;219:219–225.
32. Lagalla R, Caruso G, Urso R, Bizzini G, Marasa L, Miceli V. [The correlations between color Doppler using a contrast medium and the neoangiogenesis of small prostatic carcinomas.] [Italian] Radiol Med 2000;99:270–275.
33. Ikonen S, Karkkainen P, Kivisaari L, et al. Magnetic resonance imaging of clinically localized prostatic cancer. J Urol 1998;159:915–919.
34. Cruz M, Tsuda K, Narumi Y, et al. Characterization of low-intensity lesions in the peripheral zone of prostate on pre-biopsy endorectal coil MR imaging. Eur Radiol 2002;12:357–365.
35. Scheidler J, Hricak H, Vigneron DB, et al. Prostate cancer: localization with three-dimensional proton

MR spectroscopic imaging—clinicopathologic study. Radiology 1999;213:473–480.
36. Picchio M, Landoni C, Messa C, et al. Positive [11C]choline and negative [18F]FDG with positron emission tomography in recurrence of prostate cancer. AJR 2002;179:482–484.
37. Garcia G, Chevallier D, Amiel J, Toubol J, Michiels JF. [Prospective study comparing ultrasonography guided trans-rectal biopsy and finger guided trans-perineal biopsy in the diagnosis of prostatic cancer.] [French] Prog Urol 2001;11:40–43.
38. Melchior SW, Noteboom J, Gillitzer R, Lange PH, Blumenstein BA, Vessella RL. The percentage of free prostate-specific antigen does not predict extracapsular disease in patients with clinically localized prostate cancer before radical prostatectomy. BJU Int 2001;88: 221–225.
39. Miller JS, Puckett ML, Johnstone PA. Frequency of coexistent disease at CT in patients with prostate carcinoma selected for definitive radiation therapy: is limited treatment-planning CT adequate? Radiology 2000;215:41–44.
40. Kuhn M, Huttmann P, Spielhaupter E, Gross-Fengels W, Schreiter F. [Clinical value of native and contrast enhanced MRI in staging prostatic carcinoma before planned radical prostatectomy.] [German] Rofo Fortschr Geb Rontgenstr Neuen Bildgeb Verfahr 2001; 173:595–600.
41. Wang L, Mullerad M, Chen HN, et al. Prostate cancer: incremental value of endorectal MR imaging findings for prediction of extracapsular extension. Radiology 2004;232:133–139.
42. Qayyum A, Coakley FV, Lu Y, et al. Organ-confined prostate cancer: effect of prior transrectal biopsy on endorectal MRI and MR spectroscopic imaging. AJR 2004;183:1079–1083.
43. Schettino CJ, Kramer EL, Noz ME, Taneja S, Padmanabhan P, Lepor H. Impact of fusion of indium-111 capromab pendetide volume data sets with those from MRI or CT in patients with recurrent prostate cancer. AJR 2004;183:519–524.
44. Dunzinger M, Sega W, Madersbacher S, Schorn A. Predictive value of the anatomical location of ultrasound-guided systematic sextant prostate biopsies for the nodal status of patients with localized prostate cancer. Eur Urol 1997 31:317–322.
45. Amsellem D, Ogiez N, Salomon L, Chopin D, Abbou CC, Colombel M. [Does PSA of less than 20 ng/ml exclude the diagnosis of metastatic prostate cancer?] [French] Prog Urol 1998;8:1018–1021.
46. Epstein JI, Chan DW, Sokoll LJ, et al. Nonpalpable stage T1c prostate cancer: prediction of insignificant disease using free/total prostate specific antigen levels and needle biopsy findings. [Review] J Urol 1998;160: 2407–2411.
47. Soulie M, Grosclaude P, Villers A, et al. [Variations of the practice of radical prostatectomy in France.] [French] Prog Urol 2001;11:49–55.
48. Theodorescu D, Gillenwater JY, Koutrouvelis PG. Prostatourethral-rectal fistula after prostate brachytherapy. Cancer 2000;89:2085–2091.
49. Coakley FV, Hricak H, Wefer AE, Speight JL, Kurhanewicz J, Roach M. Brachytherapy for prostate cancer: endorectal MR imaging of local treatment-related changes. Radiology 2001;219:817–821.
50. Seifert JK, Morris DL. World survey on the complications of hepatic and prostate cryotherapy. World J Surg 1999;23:109–113.
51 Chen JC, Moriarty JA, Derbyshire JA, et al. Prostate cancer: MR imaging and thermometry during microwave thermal ablation-initial experience. Radiology 2000;214:290–297.
52. Gelet A, Chapelon JY, Bouvier R, et al. [Preliminary results of the treatment of 44 patients with localized cancer of the prostate using transrectal focused ultrasound.] [French] Prog Urol 1998;8:68–77.
53. Padhani AR, MacVicar AD, Gapinski CJ, et al. Effects of androgen deprivation on prostatic morphology and vascular permeability evaluated with MR imaging. Radiology 2001;218:365–374.
54. Hugosson J, Aus G. Natural course of localized prostate cancer. A personal view with a review of published papers. [Review] Anticancer Res 1997;17: 1441–1448.
55. Tefilli MV, Gheiler EL, Tiguert R, et al. Role of radical prostatectomy in patients with prostate cancer of high Gleason score. Prostate 1999;39:60–66.
56. Roberts SG, Blute ML, Bergstralh EJ, Slezak JM, Zincke H. PSA doubling time as a predictor of clinical progression after biochemical failure following radical prostatectomy for prostate cancer. Mayo Clin Proc 2001;76:576–581.
57. Gripp S, Haller JC, Metz J, Willers R. Prostate-specific antigen: effect of pelvic irradiation. Radiology 2000; 215:757–760.
58. Leventis AK, Shariat SF, Slawin KM. Local recurrence after radical prostatectomy: correlation of US features with prostatic fossa biopsy findings. Radiology 2001; 219:432–439.
59. Sella T, Schwartz LH, Swindle PW, et al. Suspected local recurrence after radical prostatectomy: endorectal coil MR imaging. Radiology 2004;231:379–385.
60. Beyersdorff D, Taupitz M, Deger S, et al. [MRI of the prostate after combined radiotherapy (afterloading and percutaneous): histopathologic correlation.] [German] Rofo Fortschr Geb Rontgenstr Neuen Bildgeb Verfahr 2000;172:680–685.
61. Passomenos D, Dalamarinis C, Antonopoulos P, Sklavos H. Seminal vesicle hydatid cysts: CT features in two patients. AJR 2004;182:1089–1090.
62. Isotalo T, Tammela TL, Talja M, Valimaa T, Tormala P. A bioabsorbable self-expandable, self-reinforced poly-l-lactic acid urethral stent for recurrent urethral strictures: a preliminary report. J Urol 1998;160:2033–2336.
63. Bertolotto M, de Stefani S, Martinoli C, Quaia E, Buttazzi L. Color Doppler appearance of penile cavernosal-spongiosal communications in patients with severe Peyronie's disease. Eur Radiol 2002;12: 2525–2531.
64. Lebret T, Herve JM, Lugagne PM, et al. [Extra-corporeal lithotripsy in the treatment of Peyronie's disease. Use of a standard lithotriptor (Multiline Siemens) on "young" (less then 6 months old) plaques.] [Review] [French] Prog Urol 2000;10:65–70.

65. Naroda T, Yamanaka M, Matsushita K, et al. [Clinical studies for venogenic impotence with color Doppler ultrasonography—evaluation of resistance index of the cavernous artery.] [Japanese] Nippon Hinyokika Gakkai Zasshi 1996;87:1231–1235.
66. Della Negra E, Martin M, Bernardini S, Bittard H. [Spermatic cord torsion in adults]. [French] Prog Urol 2000;10:265–270.
67. Sanelli PC, Burke BJ, Lee L. Color and spectral Doppler sonography of partial torsion of the spermatic cord. AJR 1999;172:49–51.
68. Baud C, Veyrac C, Couture A, Ferran JL. Spiral twist of the spermatic cord: a reliable sign of testicular torsion. Pediatr Radiol 1998;28:950–954.
69. Paltiel HJ, Connolly LP, Atala A, Paltiel AD, Zurakowski D, Treves ST. Acute scrotal symptoms in boys with an indeterminate clinical presentation: comparison of color Doppler sonography and scintigraphy. Radiology 1998;207:223–231.
70. Sebe P, Haab F, Nouri M, Tligui M, Gattegno B, Thibault P. [Epididymal gaseous abscess after BCG treatment.] [French] Prog Urol 2000;10:99–100.
71. Callejas-Rubio JL, Ortego N, Diez A, Castro M, De La Higuera J. Recurrent epididymo-orchitis secondary to Behcet's disease. J Urol 1998;160:496.
72. Aragona F, Pescatori E, Talenti E, Toma P, Malena S, Glazel GP. Painless scrotal masses in the pediatric population: prevalence and age distribution of different pathological conditions—a 10 year retrospective multicenter study. J Urol 1996;155:1424–1426.
73. Langer JE, Ramchandani P, Siegelman ES, Banner MP. Epidermoid cysts of the testicle: sonographic and MR imaging features. AJR 1999;173:1295–1299.
74. Sirpa A, Martti AO. Results of fibrin glue application therapy in testicular hydrocele. Eur Urol 1998;33:497–499.
75. Mikata N, Imao S, Nakamura K, Tokieda K, Kawahara Y. [The Leydig cell tumor and combined germ cell tumor in the unilateral testis. A case report.] [Japanese] Nippon Hinyokika Gakkai Zasshi 1998;89:507–510.
76. Bussar-Maatz R, Weissbach L. Retroperitoneal lymph node staging of testicular tumours. TNM Study Group. Br J Urol 1993;72:234–240.
77. Renshaw AA. Testicular calcifications: incidence, histology and proposed pathological criteria for testicular microlithiasis. J Urol 1998;160:1625–1628.
78. Kole AC, Hoekstra HJ, Sleijfer DT, Nieweg OE, Schraffordt Koops H, Vaalburg W. L-(1-carbon-11)tyrosine imaging of metastatic testicular non-seminoma germ-cell tumors. J Nucl Med 1998;39:1027–1029.
79. Maszelin P, Lumbroso J, Theodore C, Foehrenbach H, Merlet P, Syrota A. [Fluorodeoxyglucose (FDO) positron emission tomography (PET) in testicular germ cell tumors in adults: preliminary French clinical evaluation, development of the technique and its clinical applications.] [French] Prog Urol 2000;10:1190–1199.
80. Bach AM, Sheinfeld J, Hann LE. Abnormal testis at US in patients after orchiectomy for testicular neoplasm. Radiology 2000;215:432–436.
81. Bachaud JM, Berthier F, Soulie M, et al. [Risk of second non-germ cell cancer after treatment of stage I-II testicular seminoma.] [French] Prog Urol 1999;9:689–695.
82. Hosten N, Stroszczynski C, Rick O, Lemke M, Felix R. [Retroperitoneal recurrence of non-seminomatous testicular tumors: computerized tomography findings before retroperitoneal lymph node excision.] [German] Rofo Fortschr Geb Rontgenstr Neuen Bildgeb Verfahr 1999;170:61–65.
83. Sogani PC, Perrotti M, Herr HW, Fair WR, Thaler HT, Bosl G. Clinical stage I testis cancer: long-term outcome of patients on surveillance. J Urol 1998;159:855–858.
84. Ito K, Iigaya T, Umezawa A. [Case of testicular cancer with malignant transformation in the residual retroperitoneal mature teratoma 8 years after the initial chemotherapy.] [Japanese] Nippon Hinyokika Gakkai Zasshi 1998;89:622–666.
85. Steyerberg EW, Keizer HJ, Sleijfer DT, et al. Retroperitoneal metastases in testicular cancer: role of CT measurements of residual masses in decision making for resection after chemotherapy. Radiology 2000;215:437–444.
86. Ricci Z, Koenigsberg M, Whitney K. Sonography of an arteriovenous-type hemangioma of the testis. AJR 2000;174:1581–1582.
87. Delahunt B, Eble JN, King D, Bethwaite PB, Nacey JN, Thornton A. Immunohistochemical evidence for mesothelial origin of paratesticular adenomatoid tumour. Histopathology 2000;36:109–115.
88. Lachkar A, Sibert L, Gobet F, Thoumas D, Bugel H, Grise P. [Unusual tumor: liposarcoma of the spermatic cord.] [Review] [French] Prog Urol 2000;10:1228–1231.
89. Cast JE, Nelson WM, Early AS, et al. Testicular microlithiasis: prevalence and tumor risk in a population referred for scrotal sonography. AJR 2000;175:1703–1706.
90. Pieri S, Minucci S, Morucci M, Giuliani MS, De'Medici L. [Percutaneous treatment of varicocele. 13-year experience with the transbrachial approach.] [Italian] Radiol Med 2001;101:165–171.
91. Salerno S, Cannizzaro F, Lo Casto A, Romano P, Bentivegna E, Lagalla R. [Anastomosis between the left internal spermatic and splanchnic veins. Retrospective analysis of 305 patients.] [Italian] Radiol Med 2000;99:347–351.
92. Kleinclauss F, Della Negra E, Martin M, Bernardini S, Bittard H. [Spontaneous thrombosis of left varicocele.] [French] Prog Urol 2001;11:95–96.
93. Morvay Z, Nagy E. The diagnosis and treatment of intratesticular varicocele. [Review] Cardiovasc Intervent Radiol 1998;21:76–78.
94. Belli L, Arrondello C, Antronaco R, Curzio D, Morosi E, Fugazzola C. [Venography of postoperative recurrence of symptomatic varicocele in males.] [Italian] Radiol Med 1998;95:470–473.
95. Ruibal M, Quintana JL, Fernandez G, Zungri E. Segmental testicular infarction. J Urol 2003;170:187–188.
96. Sentilhes L, Dunet F, Thoumas D, Khalaf A, Grise P, Pfister C. Segmental testicular infarction: diagnosis and strategy. Can J Urol 2002;9:1698–1701.

97. Kibel AS, Steele GS, Santis WF, Yalla SV. Penile necrosis after coronary artery bypass grafting. Br J Urol 1998;81:508–509.
98. Appelbaum A. Scrotal cellulitis simulating testicular infarction by Tc-99m pertechnetate imaging. Clin Nucl Med 1997;22:499–500.
99. Ruehm SG, Weishaupt D, Debatin JF. Contrast-enhanced MR angiography in patients with aortic occlusion (Leriche syndrome). J Magn Reson Imaging 2000;11:401–410.
100. Yagan N. Testicular US findings after biopsy. Radiology 2000;215:768–773.

Part III

Other Structures

14

Peritoneum, Mesentery, and Extraperitoneal Soft Tissues

This chapter discusses the peritoneum, the intra- and extra-peritoneal soft tissues, pelvic structures, diaphragm, and the anterior abdominal wall. The extraperitoneal abdominal structures are in continuity with the diaphragm superiorly, pelvic structures inferiorly, and the abdominal wall along both flanks. Some authors prefer the term *extraperitoneal* rather than *retroperitoneal* because it more accurately reflects the location, especially for pelvic structures, but both terms are in use synonymously.

The intra- and extraperitoneal portions of the gastrointestinal and genitourinary tracts and other major organs are discussed in their respective chapters.

Technique

Computed Tomography

Multislice computed tomography (CT), especially coronal and three-dimensional (3D) reconstructions, are very useful in defining extraperitoneal tumor spread and tissue planes.

Computed tomography fluoroscopy is useful for guiding abdominal interventional procedures which cannot be managed with ultrasonography (US). Intermittent CT fluoroscopy using real-time fluoroscopic reconstruction at six frames per second confirms the needle position. Patient and operator radiation doses can be decreased with CT fluoroscopy compared to conventional CT guidance by limiting CT fluoroscopy to needle tip scanning rather than the entire needle.

Computed tomography peritoneography is occasionally useful in otherwise inapparent hernias or suspected peritoneal leaks in patients on peritoneal dialysis.

Ultrasonography

The primary limitations of abdominal US are the inherent physical limitations of this technique and, less well appreciated among clinicians, its considerable dependence on the operator. Proficiency in US, especially use of newer techniques and contrast agents, requires considerable training. Unskilled use of US is an invitation to disaster.

New US techniques and addition of contrast agents are changing this field. In the abdomen, tissue harmonic US using pulse-inversion techniques improves image quality and organ structure resolution compared to conventional US. A further improvement in overall image quality consists of combining tissue harmonic US with real-time spatial compound US (1). Yet the type of technique used may need to be tailored to study indication; thus what is optimal for detecting stone disease differs from is ideal in tumor detection.

Similar to intraperitoneal structures, US is useful for extraperitoneal lymph node biopsy. It is efficacious for deep nodes as small as 1 cm in diameter.

Endoscopic US detects enlarged lymph node and tumors. Aspiration biopsy can also be performed using endoscopic US as a guide.

Probes for performing laparoscopic US allow the surgeon to increase visualization of surrounding structures. Such laparoscopic US has a high sensitivity in detecting liver and other metastases. Overall, it improves tumor staging, but additional trocar sites are necessary for the US probe and laparoscopy is prolonged. At some sites the insufflated carbon dioxide makes probe contact with an organ in question more difficult; at times instilling saline into the peritoneal cavity is helpful.

Magnetic Resonance Imaging

Echo planar imaging is a fast imaging technique with images obtained in 50 to 150 msec. Breathing and peristaltic artifacts cause little image degradation with such fast scanning and relatively high-resolution images are obtained with a single breath hold.

Magnetic resonance imaging (MRI) is useful in differentiating extraperitoneal from intraperitoneal tumors. The superior magnetic resonance (MR) soft tissue contrast resolution (compared to CT) makes it more suitable for identifying tumor margins and tumor infiltration of adjacent structures. Similar to CT, a fast MRI technique, together with intraperitoneally instilled saline, visualizes the peritoneal surfaces, omentum, and adjacent mesentery; saline also aids intraperitoneal tumor visualization. Various intraperitoneal recesses are identified. In distinction to CT, retained barium in the bowel does not create artifacts on MRI.

Any fibrosis is accentuated against background fat on T1-weighted spoiled gradient echo (SGE) images. Tumors, abscesses, and other inflammation are best evaluated on intravenous (IV) contrast-enhanced images.

No uniform definition of MR lymphography exists. Whether a conventional MR study focusing on lymph nodes should be called MR lymphography is a matter of definition. Often a more appropriate study consists of heavily T2-weighted images processed using maximum intensity projection accentuating stationary or very slowly flowing fluid, similar to magnetic resonance cholangiopancreatography (MRCP); a limitation of such a study of retroperitoneal structures is incomplete suppression of signals from veins.

Ultrasmall superparamagnetic iron oxide (SPIO) particles are of potential use in MR lymphography (these agents are discussed in more detail in Chapter 7). Using SPIO as an endolymphatic contrast agent results in contrast uptake by normal lymph nodes but not by those replaced by tumor. Potentially, nodal uptake occurs even after IV injection if the iron oxide particles are sufficiently small. Magnetic resonance imaging is typically performed 24 to 36 hours after IV infusion of these contrast agents. The use of IV SPIO in patients with suspected lymph node metastases results in additional diseased nodes being detected than with precontrast scans. Normal lymph nodes decrease in signal intensity on enhanced T2-weighted and T2*-weighted gradient-echo images, indicating uptake of this contrast agent, but nodes infiltrated by tumor have no appreciable contrast uptake and thus reveal no signal change on pre- and postcontrast images (2). Also, postcontrast, T1-weighted signal intensity increases in metastatic nodes, probably due to altered node capillary permeability. These findings are not absolute, and nodes involved by benign disease also tend not to take up contrast.

Scintigraphy

Radionuclide agents used to image inflammation and abscesses are gallium 67, indium-111–labeled leukocytes and technetium-99m (Tc-99m)–labeled leukocytes. Imaging with Ga 67 is performed 48 to 72 hours after injecting the radionuclide; because one of its excretion pathways is via the colon, residual colonic activity interferes with abscess detection, although to a large degree single photon emission computed tomography (SPECT) imaging overcomes this limitation. Indium 111 is cyclotron produced and is not as readily available as the other agents. It is distributed primarily in the liver, spleen, and bone marrow, and bowel activity is less of a concern than with the other two agents. Labeled leukocyte scintigraphy requires in vitro labeling of a sample of the patient's blood with either In 111 or Tc-99m–hexamethylpropyleneamine oxime (HMPAO), a somewhat involved procedure. Most of the nucleotide is labeled to neutrophils, and thus this procedure is most useful for neutrophil-involved inflammatory conditions.

Indium-111–satumomab pendetide (OncoScint) is the first murine origin monoclonal

antibody approved by the Food and Drug Administration for tumor imaging, a technique termed immunoscintigraphy. This specific antibody attaches to a colorectal or ovarian cancer–associated antigen and the attached radionuclide allows cancer detection. Either a diagnostic or therapeutic procedure is possible depending on the radionuclide selected. Its primary use is with suspected intraabdominal metastases, including carcinomatosis. False-positive tests do occur with satumomab pendetide. In an occasional patient increased upper abdominal uptake persists for days in regions of chronic inflammation. Isotope uptake in a nonfunctional adrenal adenoma has resulted in false-positive results.

Lymphoscintigraphy assesses the lymphatic system and, for the most part, has replaced direct lymphography. It is a useful study to investigate chyluria, chyloperitoneum, and chylothorax. Multiple views are obtained for several hours after intradermal injection of Tc-99m–sulfur colloid. Both lymphatic channels and nodes can be evaluated, and the study is used to detect lymphatic obstruction and fistulas. More lymphatic channels and more lymph nodes are visualized using smaller filtration, thus increasing diagnostic certainty in detecting diseased lymph nodes.

The current primary clinical application of positron emission tomography (PET) is to detect cancer using the positron-emitting compound 2-[18F]-fluoro-deoxy-D-glucose (FDG). Transported across cell membranes of metabolically active tumors, the deoxy component of FDG prevents further metabolization, leading to intracellular accumulation and an increase in tumor-to-background of fluorine 18. The amount of FDG accumulating within a tumor is proportional, within broad limits, to the degree of malignancy. Thus in a setting of a tumor of unknown significance detected by another imaging modality, PET suggests whether the tumor is benign or malignant, depending on its metabolic activity. In the abdomen, PET is most useful for lymphoma, colon cancer, and metastases from melanomas and lung and breast carcinoma. It has a role in tumor staging and appears to be of prognostic significance. In general, increased tumor metabolic activity signifies a worse prognosis. Positron emission tomography is also useful after cancer therapy. Its ability to detect recurrent or residual metabolically active tumor is independent of underlying distortion due to fibrosis, and such tumor detection is superior to what is currently available with CT or MRI. Combining PET and CT images improves tumor localization significantly compared with each modality alone.

Test results are degraded by urinary and colon retention of FDG. These artifacts can be minimized by a colon cleansing regimen, patient hydration after FDG injection, administration of furosemide and bladder drainage and instillation of normal saline into the bladder prior to pelvic scanning. Use of oral Gastrografin to outline the intestines during a combined PET-CT study does not degrade FDG images. A limitation of FDG-PET in detecting small tumors is its minimal spatial resolution of about 5 mm. Also, inflammation does lead to false-positive PET results, influencing detection specificity. Recurrent or residual tumor detection is thus best studied after postoperative inflammation has subsided.

Positron emission tomography using oxygen-15–labeled water provides information on tissue perfusion; it is mostly a research tool with limited current clinical use.

Lymphography

Performed more often prior to the introduction of CT, MR, and lymphoscintigraphy, the current indications for lymphography have decreased considerably. It is a relatively prolonged, detailed procedure liked by few radiologists and even fewer radiology residents.

Although CT will detect an enlarged node, differentiation between most benign and malignant is not possible. Lymphography, on the other hand, can identify internal derangement even in a normal-sized node infiltrated by tumor.

The older literature reported rare but varied complications with lymphography, mostly related to contrast overinjection (3), including embolization to brain; a right-to-left cardiac shunt is responsible for some of these complications.

Peritoneography

Direct peritoneography using either a contrast agent or its scintigraphic counterpart has limited indications and is rarely performed. One

use is in a setting of peritoneal carcinomatosis prior to chemotherapy through a catheter implanted in the abdominal wall to evaluate drug distribution.

Biopsy

Either a conventional large core needle or a fine-needle aspiration technique is used for percutaneous biopsy of suspicious tumors; fine-needle aspiration is often preferred, but especially with benign lesions it achieves a low success rate. On average, core needle biopsies obtain a specific diagnosis in over 90% of biopsies, while fine-needle aspirations average only about 50%; the complication rate, chiefly bleeding, is grossly similar with both techniques.

Either CT or US (and occasionally fluoroscopy) is used for biopsy localization and other percutaneous interventional procedures. In general, in most hospitals US equipment is more readily accessible, the study is quicker, and it results in faster patient throughput.

Special interventional equipment designed to be used with MR guidance is available. Little used at present, MR interventional radiology is undergoing rapid expansion with tissue biopsies, fluid drainages, and guidance of other percutaneous therapeutic procedures. An open magnet provides ready patient access.

Endoscopic US-guided fine-needle aspiration biopsy is useful for diagnosis and staging of malignancies. Diagnostic sensitivities and specificities of about 90% are achieved with both extraluminal tumors and lymph nodes.

Nerve Block

Celiac plexus and splanchnic nerve block provides pain palliation for patients with unresectable upper abdominal malignancies. This technique was initially designed to be performed using fluoroscopic guidance, although CT provides more accurate guidance. An alcohol-contrast agent combination provides localization.

Congenital Abnormalities

Situs

Situs refers to orientation of certain organs to the midline. In general, the bilobed lung, left atrium, descending aorta, spleen, and stomach are all located on one side of the body. When these structures are normally placed on the left side the condition is called *situs solitus*. *Situs inversus* is a mirror image and results when these structures are on the right side and the trilobed lung, right atrium, inferior vena cava, gallbladder, and liver are on the left (Fig. 14.1). The prevalence of situs inversus is about 1 in 10,000. These patients are at an increased risk for nasal polyposis, chronic sinusitis, and bronchiectasis (*Kartagener's syndrome*) and a higher than normal risk for congenital heart disease.

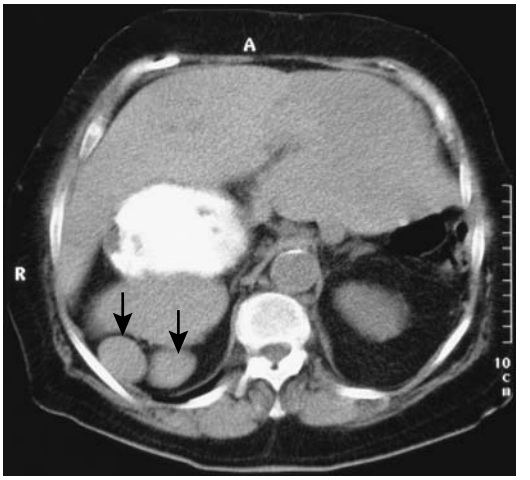

Figure 14.1. Situs inversus in an 85–year-old woman. Polysplenia is present on the right (arrows). The stomach is also on the right.

Situs inversus can be associated with multiple spleens and other defects. Often a conventional radiograph is a good starting point in evaluating these anomalies.

Heterotaxy Syndrome

The term *heterotaxy*, or *situs ambiguous*, describes complex congenital abnormalities differing from situs solitus or situs inversus. Some authors use the terms *asplenia* and *polysplenia* to subdivide heterotaxy into specific categories, but these classifications are incomplete and at times confusing. Others use the terms *left* and *right isomerism*.

Complex familial inheritance patterns exist for heterotaxy. An X-linked recessive inheritance appears to account for a male preponderance.

These patients usually have complex congenital cardiac abnormalities that tend to overshadow abdominal findings. Complex bowel rotation anomalies are encountered with both right and left isomerism. Aortic and gastric positions are variable. Right-sided isomerism results in asplenia. The liver extends across both upper quadrants of the abdomen. Some of these patients have a left-sided inferior vena cava. Gallbladder duplications occur in right-sided isomerism.

Heterotaxy with left abdominal isomerism results in polysplenia. Cardiac anomalies tend to be less severe than in asplenia. Most patients have azygous continuation with interruption of the inferior vena cava. The spleen(s) is (are) on the same side as the stomach. An absent gallbladder is more common in left-sided isomerism. An association exists between polysplenia and biliary atresia. Midgut malrotation is a common associated finding, and midgut volvulus develops in some of these infants.

Traditionally, heterotaxy has been evaluated with angiocardiography. While both CT and pulse and color Doppler US are helpful in outlining some anomalies, MRI is evolving as the preferred modality.

Liver/spleen scintigraphy detects splenic tissue in suspected heterotaxy; in some infants with negative planar imaging, the presence of splenic tissue is shown by SPECT.

Abdominal Wall Defects

Bladder exstrophy is discussed in Chapter 11. Cloacal malformations are discussed in Chapter 12.

Omphalocele

Failure of the abdominal wall to close normally results in several defects. A defect cephalic to the umbilicus results in a supraumbilical ventral hernia, anterior diaphragmatic defects, and related conditions. Additional failure of lateral wall fusion results in an omphalocele. The degree of visceral herniation depends on the size of the defect. Peritoneum covers the viscera, and the defect is obvious. Associated bowel malrotation is common.

Prognosis in these neonates is often limited by other associated abnormalities, at times major. The abdominal organs tend to be malpositioned, leading to unusual imaging findings.

Gastroschisis

Defects in gastroschisis involve the lateral abdominal wall. The gross appearance is similar to that of an omphalocele, but with gastroschisis the umbilicus is in its normal position. Among infants with gastroschisis, about two thirds have a simple defect, and in one third complex defects are identified, ranging from bowel atresia, stenosis, and perforation, to volvulus (4); survival of those with a simple defect was 100%, but those with a complex defect had a mortality rate of 28%.

Neonates with gastroschisis are often premature. Small bowel dysmotility and a prolonged transit time are common. Conventional radiography often reveals bowel wall thickening and lumen dilation. Delayed barium transit suggests obstruction, although actual small bowel obstruction is uncommon. Bowel atresia, if present, does result in a high mortality.

After surgical repair of gastroschisis these infants are at increased risk for necrotizing enterocolitis, although even then overall survival rate is quite high.

Prune Belly Syndrome (Eagle-Barrett Syndrome)

The prune belly syndrome, named after the lax, wrinkled abdominal wall seen in this condition, consists of abdominal wall hypoplasia, genitourinary anomalies—including bilateral cryptorchidism in males—and other, at times major, systemic abnormalities. Occurring mostly in males, the more severely affected neonates die shortly after birth. An incomplete expression of this syndrome exists, and some neonates have only mild manifestations. Unilateral abdominal wall hypoplasia also occurs. An association between congenital cytomegaloviral infection and prune belly syndrome has been raised, but the precise etiology is unknown.

A minority of these neonates have a urethral obstruction such as atresia or valves; most, however, have functional bladder outlet

obstruction. A voiding cystourethrogram reveals a hypertrophied bladder wall. The presence of a urachal remnant is also common. The prostatic urethra is dilated, and a dilated prostatic utricle is often seen. Vesicoureteric reflux is common into dilated, aperistaltic ureters. Renal dysplasia is identified in some patients.

Diaphragmatic Abnormalities

Diaphragmatic development is complex, with the ventral portion evolving from the septum transversum and the dorsal portion originating from the pleuroperitoneal membrane. A Morgagni hernia anteriorly or a Bochdalek hernia posteriorly is a result of incomplete formation of these two diaphragmatic segments. A Bochdalek hernia is more common, usually is on the left, and can be massive to the point that respiratory distress is evident.

Diaphragmatic agenesis is occasionally detected in an asymptomatic adult. Imaging reveals associated herniation of colon, small bowel, and even kidney into the chest, together with a hypoplastic underlying lung.

Inadequate striated muscle development leads to diaphragmatic eventration. Eventration can be complete or partial. When extensive, imaging findings mimic a diaphragmatic hernia. Minor diaphragmatic eventration is of little significance and tends to resolve with age. A partial eventration is difficult to detect in neonates.

Conventional radiography detects most diaphragmatic hernias, although US is useful not only for diagnosis but also for follow-up. A peroral contrast study is generally diagnostic.

Noonan's Syndrome

Noonan's syndrome is a mostly autosomal-dominant condition with facial dysmorphism, a number of congenital cardiac defects, and short stature. It is linked to the cardiofaciocutaneous syndrome, and both probably represent a variable expression of the same genetic defect. An association also exists between neurofibromatosis type 1 and Noonan's syndrome. The reason for including this syndrome in a book on abdominal disorders is that some of these individuals have abdominal lymphangiectasia, at times involving the gastrointestinal tract. About two thirds of children with Noonan's syndrome have poor feeding and gastrointestinal dysfunction—findings suggesting delayed gastrointestinal motor development—and require tube feedings. Also, a number of these patients suffer from various bleeding disorders. In some, lymphangiectasia is associated with pleural effusions, lymphedema, or a protein-losing enteropathy and a resultant hypoproteinemia. Lymphangiectasia can be identified in these individuals by lymphangiography, or, currently more often by lymphoscintigraphy, which reveals dilated and tortuous abdominal and pelvic lymphatic channels and abnormal lymphatic flow.

Computed tomography after bipedal lymphangiography in a 21-year-old man with Noonan's syndrome and protein-losing enteropathy confirmed intestinal lymphangiectasia (5). After cardiac catheterization, a 15-year-old girl with this syndrome developed cutaneous lymphatic fluid oozing from a groin site (6).

Trauma

Unstable Patient

A hemodynamically unstable trauma patient requires immediate resuscitation. Exploration is considered in a patient with clinically evident abdominal trauma who is unresponsive to resuscitation. Imaging simply delays therapy in such a setting. A possible exception is a limited US study for intraperitoneal fluid while the patient is being resuscitated, but keep in mind the limitations of such a study.

Computed tomography of children in shock reveals dilated, fluid-filled bowel; intense enhancement of bowel wall, mesentery, pancreas, kidneys, and adrenal glands; and enhancement of a smaller than normal aorta and inferior vena cava (7). Similar but less pronounced changes are found in adults.

Stable Patient

A pneumoperitoneum in a trauma patient, regardless of whether detected with conven-

tional radiography or CT, generally is an indication for exploration. Other findings, such as organ damage, peritoneal fluid, or a hematoma, in a stable patient are more judgmental. In some, whether to proceed with exploration in an otherwise stable patient with imaging-evident peritoneal fluid or organ damage is not clear, and a policy of observation is adopted; a repeat of appropriate imaging studies is often in order for these patients.

Currently most minor liver and splenic trauma is managed conservatively, although a trend is evident toward nonoperative management of hemodynamically stable patients even with more severe injury. Thus stable patients even with a moderate amount of hemoperitoneum have been managed conservatively, with no differences found between nonoperative and operative groups in resultant abdominal complications and hospital length of stay (8).

Penetrating Injury

The vast majority of gunshot wounds involving the peritoneal cavity require surgical repair. The diagnostic dilemma is determining which of these injuries penetrate the peritoneum. Several diagnostic peritoneal lavage studies in gunshot wound patients achieved a sensitivity of and specificity of over 95% in determining peritoneal penetration. To a large degree CT has supplanted lavage in patients with penetrating trauma, also achieving sensitivities and specificities of over 95% (9).

Most traumatic visceral artery aneurysms (pseudoaneurysm) are due to penetrating injury. A not uncommon scenario is a patient who has surgery shortly after trauma, undergoes arterial ligation, and then presents with a gastrointestinal bleed several weeks later from an aneurysm.

A reasonable approach in stable patients with abdominal stab wounds is to obtain initial CT or US, and in the absence of evidence for immediate surgery to follow them with serial imaging.

Diagnostic Peritoneal Lavage

In the 1980s diagnostic peritoneal lavage was generally considered superior to CT, although its use has decreased markedly over the last decade, having been supplanted by CT and US. Nevertheless, an occasional clinician still recommends that lavage be performed first in a setting of blunt trauma if no contraindications exist.

Diagnostic peritoneal lavage relies on detecting blood in the peritoneal cavity. Generally an arbitrary threshold for a positive test, such as 10,000 red blood cells per cubic millimeter, is assumed. A higher threshold increases the missed injury rate and a lower one increases the false positive rate. The advantages of diagnostic peritoneal lavage include its simplicity and its relatively high sensitivity in detecting intraperitoneal blood. It does not evaluate the severity of injury, and thus is limited in predicting a need for surgery. It is insensitive for retroperitoneal injuries. Even with intraperitoneal injuries, it may miss blood in patients with previous abdominal surgery and extensive adhesions.

A comparison of diagnostic peritoneal lavage and CT in patients with blunt trauma is difficult because each study evaluates different findings.

Peritoneal Fluid

Although a number of investigators believe that US readily detects intraperitoneal fluid, less often discussed is how much fluid is necessary for detection with US. In a blinded prospective study of 100 patients undergoing diagnostic peritoneal lavage, continuous US scanning of Morison's pouch revealed that the mean volume of infused fluid first detected was 619 mL and that detection sensitivity after infusing 1 L was 97% (10). Even keeping in mind that intraperitoneal fluid appears to be twice as common in the pouch of Douglas than in Morison's pouch, statements in the literature about small, moderate, and large amounts of fluid detected with US should be viewed with a jaundiced eye.

Multiple US scans are necessary to detect abnormal fluid; a single view, such as only of Morison's pouch, misses intraperitoneal fluid in a number of patients. In general, in patients with acute trauma evaluated with US, the sensitivity for detecting free fluid is about 65% to 80% and the specificity about 95%, with free fluid in the pelvis being the most common reason for a false-negative finding. Most peritoneal fluid

detected after trauma represents blood; less common is urine, bile, or intestinal content. Pus and chyle develop if presentation is delayed.

The presence of intraperitoneal fluid correlates with injury but does not predict whether surgery will be necessary. Surgical teaching often mandates laparotomy after blunt trauma if isolated intraperitoneal fluid is detected by imaging, yet this is a complex and controversial topic. In general, blunt trauma patients eventually requiring laparotomy have more intraperitoneal fluid than those managed conservatively; an association also exists between the amount of mesenteric fluid and mesenteric laceration.

General Imaging Considerations

Multiorgan damage is common in major trauma; thus a finding of an abnormal collection of intra- or extraperitoneal fluid is not necessarily due to a visible liver or splenic injury, but could also represent a synchronous mesenteric or bowel injury. A US study of over 1000 women of reproductive age with blunt trauma concluded that fluid isolated to the cul-de-sac is likely physiologic, but those with free intraperitoneal fluid usually have clinically important abdominal injuries (11).

If one has the luxury of time, chest and abdominal radiography are reasonable studies, although if CT is available, a strong argument can be made for using it initially. The ready availability of diagnostic CT and its ability to detect other conditions continue to expand the indications for CT in patients with abdominal trauma, and in many centers CT is the first imaging examination performed in a hemodynamically stable patient with a suspected intraabdominal injury. Exceptions include the hemodynamically unstable patient, one with an immediate life-threatening condition, or the patient who is to undergo emergent surgery for nonabdominal trauma.

In spite of an occasional admonition by emergency physicians, radiologists in the United States administer both IV and oral contrast prior to CT to most trauma patients. Very few complications due to contrast are reported. An extensive literature exists on IV contrast reactions, and this topic is beyond the scope of this book. Most radiologists believe that oral contrast aids in study interpretation, and that the advantages of contrast use outweigh any possible disadvantages. Gastroesophageal reflux and aspiration is uncommon even in obtunded or uncooperative patients, and oral contrast is often administered through a nasogastric tube. Lung contrast results if contrast is instilled through a tube placed into a bronchus. The oral iodinated contrast agents used in CT are hypoosmolar and should not be compared to hyperosmolar full-strength contrast agents employed for other examinations.

A pneumoperitoneum can develop after chest trauma. Some of these patients also have an associated pneumothorax, pneumomediastinum, or a retropneumoperitoneum. The pneumoperitoneum can generally be identified with conventional radiography, although occasionally it is detected only with CT.

The vital signs of trauma patients are generally being monitored, and an imaging study should not be relied on to detect hypotension. Nevertheless, on a contrast-CT study the presence of a prolonged nephrogram without excretion into collecting systems should suggest hypotension. A collapsed inferior vena cava should suggest hypovolemia, with or without hypotension. Likewise, the spleen may become smaller than normal. Small bowel ischemia, manifesting as diffuse bowel wall thickening, may develop.

Computed tomography evaluates both the presence of fluid and organ injury. At times a CT study is equivocal. If surgical exploration is not contemplated, repeat CT is often helpful in monitoring the progression of any abnormalities.

In some institutions, especially outside the United States, US rather than CT has replaced diagnostic peritoneal lavage and is often used as a screening modality for suspected abdominal trauma. Use of US in trauma patients has generated strong opinions. Statements such as CT "... is costly, time-consuming, requires sedation, and may be associated with complications in young children ..." while US "... is quick, noninvasive, repeatable, and cost-effective ..." have appeared in the trauma literature (12). Numerous studies extol the virtues of US in trauma patients, yet operator experience is difficult to place in perspective. Pediatric surgeons in particular advocate US as a triage tool in pediatric trauma patients and believe that it alone is sufficient to evaluate children after blunt abdominal trauma. Some believe that only

those with abnormal US should be further studied with CT, a conclusion of dubious validity.

Advocates of US in a setting of trauma rely primarily on detecting intraperitoneal fluid, yet such reliance as a sole indicator of visceral injury does not appear warranted. Although a minority, some patients with later proven visceral injuries develop little or no hemoperitoneum. Nevertheless, screening US studies in patients with blunt abdominal trauma have published sensitivities of 85% to 95% for detecting injuries severe enough to require laparotomy. Abdominal US is considered positive if either intra- or retroperitoneal fluid is detected. False negative studies include retroperitoneal injury, bowel injury and intraperitoneal solid organ injury without presence of a hemoperitoneum. Yet critical analyses of US point to a study of limited value. Major organ damage is missed and active hemorrhage is not identified. The bowel and pancreas are poorly visualized. In a trauma setting, the superiority of CT over US has been established by a number of studies. In one study, CT revealed fluid, organ injury, or both in 33% of consecutive children with blunt abdominal trauma (13); the sensitivity and specificity of US for fluid detection only was 47% to 59% and 79%, respectively (for two observers), and the sensitivity and specificity of US when fluid and organ injury were considered was 65% to 71% and 71% to 79%, respectively; the authors concluded that the low US sensitivity suggests that "a normal screening sonography alone in the setting of blunt abdominal trauma fails to confidently exclude . . . intraabdominal injury" (13). Ultrasonography can probably be justified, however, in those institutions lacking the ready availability of CT.

At times CT is used in patients with minimal trauma to decide whether to discharge a patient or not. Ultrasonography is generally considered not adequate to answer this question and many trauma US studies rely on keeping a patient under observation for some time.

Currently MR is not considered appropriate for screening trauma patients.

Diagnostic/therapeutic laparoscopy has been performed in patients with suspected abdominal trauma, with conversion to open exploration as needed. The role for such laparoscopy is yet to be established.

Bowel Injury/Perforation

In a trauma setting, CT detection of peritoneal fluid, in the absence of any visible solid organ injury, suggests bowel injury. About half of these patients have small bowel or diaphragmatic injury, although isolated intraperitoneal fluid can be associated with unsuspected injury from bowel and mesenteric injuries, to solid organ trauma.

Complicating the issue is that some patients with subsequently detected major bowel injury have no hemoperitoneum on admission CT and US, but bowel and mesenteric injury is detected only hours later; even then, bowel and mesenteric injury can be difficult to diagnose. Currently such injury is probably best studied with CT. Both IV and oral contrast are helpful. A prospective CT study achieved a sensitivity of only 64% but a specificity of 97% in detecting bowel injury in patients with blunt abdominal trauma (14); findings used to detect bowel injury included mesenteric infiltration, bowel wall thickening, extravasation either of vascular or enteric contrast, and the presence of pneumoperitoneum. Bowel wall thickening, in particular, is difficult to put in proper perspective as a finding of major bowel injury. If associated with a mesenteric hematoma, sufficiently severe mesenteric or bowel injury is generally presumed to warrant considering surgery. On the other hand, a focal mesenteric hematoma without adjacent bowel wall thickening occurs both in those patients requiring surgery and those who do not. Computed tomography has a high specificity in detecting a mesenteric hematoma. Nevertheless, the true accuracy of CT in establishing major bowel or mesenteric injury is difficult to judge, and published conclusions vary.

With a perforation, imaging rarely identifies bowel wall discontinuity. Intraperitoneal spill of oral or rectal contrast identified by CT is usually assumed to represent a bowel perforation, but although diagnostic, it is rarely detected. Spill of instilled contrast from a urinary tract perforation is in the differential diagnosis.

In pediatrics the role of CT in detecting bowel perforation appears even more limited than in adults, and CT identifies small bowel injury only in a minority. Clinicians should be aware of this CT limitation and not be lulled into a false sense of security, leading to a delay in surgery.

Mesenteric stranding, often in association with adjacent blood, suggests mesenteric injury, although laceration of an adjacent loop of bowel results in similar findings.

With rare exceptions, the presence of extraluminal gas (either pneumoperitoneum or extraperitoneal gas) is diagnostic of bowel perforation. Extraluminal gas is readily detected with both conventional radiography and CT. The inability to reliably and consistently detect a pneumoperitoneum is a limitation of US.

The small bowel normally contains little gas, and a number of bowel perforations manifest later as an intraabdominal abscess rather than as an immediate pneumoperitoneum. Colonic perforation, on the other hand, commonly results in a pneumoperitoneum, which is readily detected. Other indirect signs for perforation include intraperitoneal fluid, bowel wall thickening, bowel wall contrast enhancement, and bowel lumen dilation. None of the latter signs is specific for a perforation.

Bleeding

Bleeding leads to mesenteric or bowel hematomas, identified by CT as hazy streaking in mesenteric fat, or results in peritoneal or extraperitoneal fluid. Computed tomography scans of direct extravasation of IV contrast is evidence of active bleeding, and such bleeding in a setting of trauma is assumed to represent an injury to the involved viscera. Diffuse extravasation is implied by detecting extravasated contrast material, keeping in mind that extravasated contrast usually has a lower attenuation than the aorta. Not all intra- or extraperitoneal bleeding is due to trauma; a ruptured aneurysm, a vessel weakened by tumor, anticoagulation therapy, or even venous obstruction and superimposed ischemia lead to bleeding and hematoma formation. Other rare causes of hemorrhage include severe pancreatitis or even an intraabdominal pregnancy.

Intraperitoneal blood pools in dependent spaces. Thus with upper abdominal bleeding a common site is Morison's pouch and subphrenic spaces. More inferior locations include paracolic gutters and pouch of Douglas.

Computed tomography attenuation of intraperitoneal blood varies with age; initially it is isodense to intravascular blood. Hemoglobin concentration when blood clots, occurring within several hours, raises the attenuation to over 50 Hounsfield units (HU). Subsequent clot lysis, in a matter of days, gradually leads to an attenuation decrease, and in several weeks may approach the attenuation of water. Lower CT attenuation values are found in patients with preexisting anemia or if blood mixes with ascites or other fluid; thus fluid having a low attenuation does not exclude acute bleeding.

A hematoma often is not homogeneous in appearance. The rate of clot lysis in a hematoma varies, and a lower attenuation may be present at the periphery. Likewise, intermittent bleeding leads to simultaneous clotting and lysis and results in regions containing different attenuation values. If contrast-enhanced CT is performed during active arterial bleeding, the extravasating blood is isodense to adjacent arterial blood. Invariably an associated hematoma is present. A recent bleed can be denser than the rest of a hematoma, and such a sentinel clot tends to be located close to the site of bleeding.

At times nonhemorrhagic ascites also enhances with CT IV contrast.

The MR appearance of a hematoma (and intraperitoneal blood) also varies depending on clot age. Within a day or so of bleeding a hematoma is hypointense on both T1- and T2-weighted images. Then within several days it gradually becomes isointense to hyperintense on T1- but remains hypointense on T2-weighted images. This prominent hypointensity on T2-weighted images allows differentiation of blood from ascites, which is very hyperintense on T2-weighted images. A pneumoperitoneum is also hypointense on T2-weighted images, but other MR sequences and the relative location of gas versus fluid in the peritoneal cavity allow differentiation. Within a week or so a hematoma becomes hyperintense on both T1- and T2-weighted images, but while evolving to this stage some hematomas reveal a hyperintense rim surrounding a hypointense central portion on T1-weighted images. Eventually, if fibrosis develops around a prior hematoma, a hypointense rim on both T1- and T2-weighted images encloses this region.

Diaphragmatic Injury

Diaphragmatic injury is one cause of visceral herniation into the chest. A majority of hemidiaphragmatic ruptures occur on the left side.

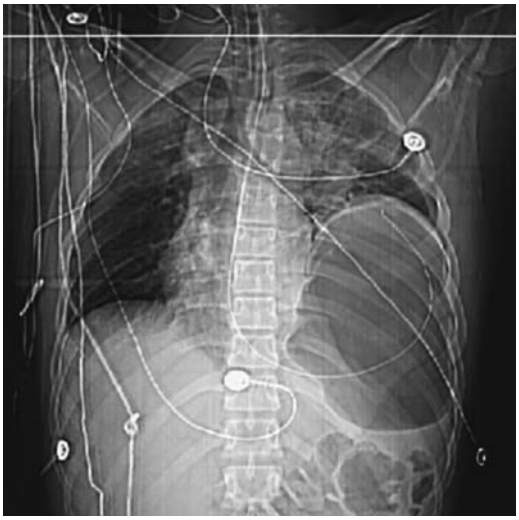

Figure 14.2. Traumatic rupture of left hemidiaphragm. A scout view localizer prior to computed tomography (CT) reveals mediastinal shift to the right, partial left lung atelectasis and an elevated stomach. (Courtesy of Patrick Fultz, M.D., University of Rochester.)

The most common site for rupture is at the diaphragmatic dome, and the least common is at the rib muscular insertions (15). A number of these posttraumatic diaphragmatic ruptures are not initially apparent; herniation increases in size with time, and thus delayed imaging is necessary. Some of these hernias are detected only months later. Intubation appears to hinder the detection of diaphragmatic rupture. Thus an initial chest radiograph or CT detects only about half of diaphragmatic ruptures (Fig. 14.2). These hernias became clinically symptomatic from days to years after trauma, and either conventional chest radiographs or upper gastrointestinal studies are diagnostic (Fig. 14.3). Strangulation of intestinal content has developed, including delayed gastric perforation into the pleural cavity.

A rare cause of diaphragmatic rupture is cardiopulmonary resuscitation.

Computed tomography detection sensitivities for diaphragmatic rupture are disappointing, especially for right hemidiaphragmatic rupture, and are of limited use; keep in mind that detection rates vary with time after trauma. Diaphragmatic crura are not thickened in patients with an injured diaphragm (16); coronal and sagittal reconstructions are also of limited value in detecting subtle diaphragmatic injury. Computed tomography usually does not reveal diaphragmatic discontinuity even with thin sectioning (except in the rare diaphragmatic avulsion); rather, intestinal content not confined by the diaphragm but spilling into the thorax is diagnostic of a hernia, and in the appropriate clinical setting provides indirect

A B

Figure 14.3. Traumatic left hemidiaphragm rupture. A: Chest radiograph reveals gas and fluid at the left lung base. B: A barium study performed through a nasogastric tube identifies part of the stomach in the chest. This study was performed several hours after that in part A, and now considerably more abdominal content has herniated into the chest.

evidence for diaphragmatic rupture. A waist-like intestinal constriction at the site of herniation is occasionally detected if rupture is limited in scope. These traumatic hernias need to be distinguished from congenital diaphragmatic hernias and from hernias through the esophageal hiatus.

Ultrasonography findings in patients with diaphragmatic rupture due to blunt trauma range from diaphragmatic disruption to a non-visualized diaphragm. Occasionally detected is a diaphragm surrounded by fluid or abdominal content herniating through a diaphragmatic defect.

Preliminary reports suggest that MRI is reliable in detecting diaphragmatic injury; coronal and sagittal MRI reveal the site of a diaphragmatic tear and detect abdominal visceral herniating into the thorax, but keep in mind the limitation on early detection, as discussed previously.

Scintigraphy using intraperitoneally instilled Tc-99m–macroaggregated albumin (MAA) detects a diaphragmatic rupture but is rarely necessary.

Arecdotal reports describe spontaneous diaphragmatic rupture.

Barotrauma

A pneumoperitoneum is a rare complication of mechanical ventilation. Detection of free gas in these generally rather sick patients leads to a diagnostic dilemma—Is the pneumoperitoneum secondary to an unsuspected bowel perforation? A number of these patients undergo surgical exploration.

Acute Abdomen

The causes of an acute abdomen are legion, including infection, bowel perforation, inflammation, obstruction, ischemia, volvulus of various structures, gynecologic abnormalities, and tumor infiltration; these conditions are discussed in their respective chapters. At times the first evidence of a serious underlying disease is an acute abdomen, such as Crohn's disease manifesting as bowel perforation. Colonic epiploic appendagitis, a condition diagnosable by imaging, is an example of an acute abdomen not requiring surgical intervention. Less common etiologies for an acute abdomen include lymphoma infiltrating the bowel and resulting in perforation, a perforating primary small bowel neoplasm, and a perforated bowel duplication cyst with spill of the contents into the peritoneal cavity.

In pediatrics, perforation is more common in neonates than in older children. Among neonates with gastrointestinal perforation, most common etiologies are necrotizing enterocolitis, isolated ileal perforations, a combination and sequella of malrotation/volvulus. Etiologic factors in children are trauma, Meckel's diverticula complications, intussusception, pseudomembranous colitis, and post-operative complications.

In children, screening US detects an abdominal abnormality in about half of those with acute or subacute abdominal pain.

Past teaching has been to study an acute abdomen with conventional radiographs, an approach supplanted by CT, generally without IV contrast. At times images with and without IV contrast are useful (Fig. 14.4). Computed tomography has had a major impact in the diag-

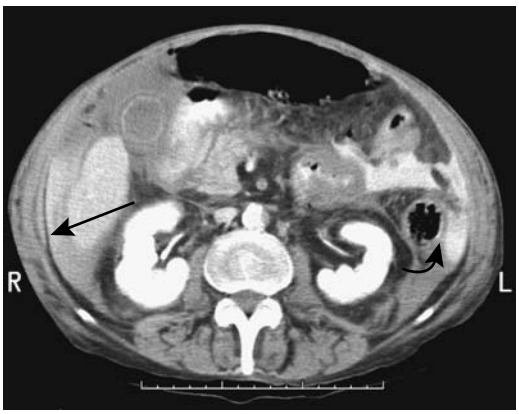

Figure 14.4. Acute abdomen secondary to jejunal perforation. Oral and intravenous (IV) contrast-enhanced CT reveals ascites and pneumoperitoneum. Higher density material is present within this fluid adjacent the liver (arrow) and also in the left upper quadroon (curved arrow). Although angiography revealed patent vessels, surgery suggested emboli and ischemia for the patient's perforation. (Courtesy of Patrick Fultz, M.D., University of Rochester.)

nosis and subsequent management of patients presenting with an acute abdomen. Some studies suggest that CT is superior to clinical evaluation in diagnosing a cause for an acute abdomen. Such an approach appears to hold up regardless of the duration of signs and symptoms and in patients with no prior disease. Nevertheless, rather than use CT in a shotgun approach for all patients presenting with an acute abdomen, a more selective choice of imaging studies often establishes a diagnosis more quickly. For instance, with suspected cholecystitis, US should be the initial imaging modality; suspected acute uncomplicated pancreatitis generally requires little or no imaging, except possibly endoscopic retrograde cholangiopancreatography (ERCP), while pancreatic necrosis calls for contrast-enhanced CT or MR. Ultrasonography is more commonly employed in pediatric patients. CT is especially useful in obese patients, nondiagnostic US, or with suspected bowel obstruction.

In some centers US is used liberally for the initial study of patients with an acute abdomen. It is readily performed and detects a number of acute conditions. One limitation is the presence of dilated bowel. Also, while in experienced hands such diagnoses as appendicitis are readily made, a normal US examination does not exclude appendicitis, pyelonephritis, and other disorders. Likewise, early pancreatitis and bowel ischemia do not have specific US findings.

Laparoscopy is still preferred by some as a diagnostic and therapeutic modality in patients presenting with an acute abdomen. Even if conversion to an open laparotomy is necessary, laparoscopic findings are useful as a guide for the subsequent incision.

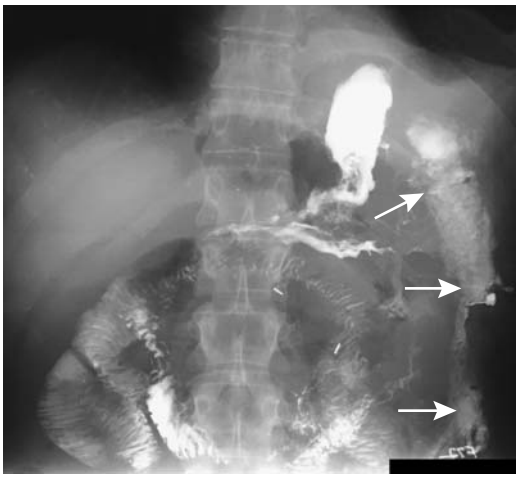

Figure 14.5. Postoperative abscess extending from the left hemidiaphragm inferiorly into left lower quadrant (arrows), communicating with the stomach. Barium sulfate was the contrast material used; it does not affect abscess healing.

Infection/Inflammation

Abscess

Intraperitoneal

Clinical

Some abscesses develop spontaneously, although most are secondary to postoperative complications or spread from a source in an adjacent structure, such as diverticular disease, appendicitis, cholecystitis, and so on. Fluid collections communicating with bowel can become huge, and patients have few symptoms due to the internal drainage (Fig. 14.5). At times an abscess and peritonitis coexist, and the initial inciting event is difficult to identify.

A gallstone falling into the peritoneal cavity during laparoscopic cholecystectomy may not be readily retrievable. Although many of these intraperitoneal gallstones are innocuous, they do serve as a potential nidus for abscess formation, with some of these abscesses manifesting years later. An occasional dropped appendicolith, occurring mostly during laparoscopic appendectomy, results in a similar finding. At times the specific etiology for such an abscess is suggested by CT or US.

Imaging

Computed tomography, US, MRI, or scintigraphy should detect and localize most intraabdominal abscesses, and most can then be drained percutaneously, generally under US guidance. Numerous comparison studies have shown CT and US accuracies of over 90% in detecting intraabdominal abscesses. Whether the greater resolution of CT or the greater portability of US determine the modality used, clinically the availability is the deciding factor.

A note about subphrenic abscesses. It is almost unheard of to have a subphrenic abscess without an associated pleural effusion. Even a chest radiograph should detect such an effusion, and the absence of effusion essentially excludes a subphrenic abscess. If imaging identifies a suspicious abscess beneath the right hemidiaphragm but no pleural effusion is detected, an intrahepatic rather than a subphrenic abscess is more likely.

Gas in a fluid collection generally implies an abscess, but gas bubbles are also seen in retained surgical sponges even without an abscess. Large amounts of gas suggest bowel communication, a finding seen with other benign and malignant conditions (Fig. 14.6).

Computed tomography of a typical abscess shows a fluid-filled structure surrounded by a contrast-enhancing rim. Such a finding is not limited to abscesses and is also seen with some necrotic tumors and other benign conditions such as a hematoma and various cystic structures. Also, not all abscesses have this appearance. Differentiation of an abscess and a benign fluid collection is difficult, especially if the wall is thick. Loculated fluid after abdominal surgery tends to develop primarily in the abdomen and after pelvic surgery loculated fluid is mostly in the pelvis, but this is of limited use in differentiating benign fluid from an abscess.

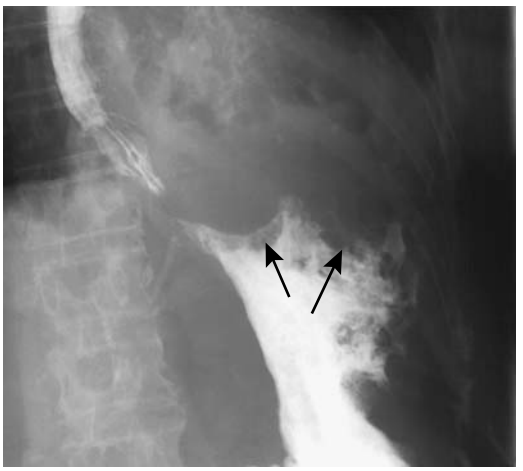

Figure 14.6. Left subphrenic abscess secondary to a perforated gastric fundal adenocarcinoma. The entire fundus is amputated by tumor and abscess (arrows). The study was performed primarily for unexplained weight loss.

Abscesses are hypointense on T1- and hyperintense on T2-weighted MR images; about half are homogeneous in appearance. Gadolinium-enhanced T1-weighted fat-suppressed images identify abscesses as fluid collections surrounded by a contrast-enhancing rim. Gas within an abscess appears as a signal void on both T1- and T2-weighted images. Coronal and sagittal reconstruction aids in differentiating an abscess from bowel. Fluid layering occurs in some abscesses, with hypointense material, presumably representing protein, being dependent on T2-weighted images, and such a finding in the peritoneal cavity is strong presumptive evidence of an abscess. Overall, MR sensitivity in detecting abscesses is close to 100%.

Scintigraphy detects most abdominal abscesses. Useful radiopharmaceuticals include gallium-67 citrate, indium-111 leukocytes, and Tc-99m leukocytes. A major limitation of Ga-67 citrate scintigraphy is the prolonged time required to perform the study.

Therapy

Percutaneous abdominal abscess drainage is an established technique, and almost all well-defined unilocular abscesses can be successfully drained. A majority of abscesses are cured with initial drainage. Recurrent abscesses can be drained percutaneously in most patients and surgery avoided in about half (17). Complex abscesses consisting of loculated, poorly confined, or multiple abscesses or those associated with a fistula have a lower success rate and often require several drains. A single abscess is often drained using US guidance, but multiple abscesses are easier to drain with CT guidance. Distinguishing an abscess from necrotic tissue can be difficult. At times aspirate cytology is helpful. Similar to surgical drainage, attempts to drain infected necrotic tumors percutaneously are rarely successful. Conversion to surgical drainage (and often associated resection) is required with the presence of unhealing abscesses or fistulas and bowel or pancreatic necrosis. Catheter-induced bleeding is an occasional complication requiring surgical correction.

Crohn's disease abscesses can be drained percutaneously using image guidance, and the patient is thus stabilized. These abscesses tend not to resolve completely, especially if they involve an enteric fistula.

Some left subphrenic abscesses cannot be readily drained using a transabdominal approach, and a transpleural approach is necessary. At times a drainage catheter is inserted through the pleura. Regardless of catheter position, most abscesses are successfully drained, although a transpleural approach risks a pneumothorax, requiring its own therapy.

Abscess drainage using a transrectal or transvaginal approach with a combination of endoluminal US and fluoroscopy for needle advancement, tract dilation, and catheter insertion, combined with appropriate antibiotics, is effective therapy for most pelvic abscesses. Patients undergoing transrectal aspiration or drainage have less procedure-related pain and catheter pain than those with a transvaginal approach (18). A viable option for some pelvic abscesses is US-guided transperineal catheter drainage.

Pelvic abscesses are readily drained in children and adolescents. The average hospital stay for children after image-guided transrectal drainage of pelvic abscesses tends to be shorter than after open surgical drainage. Surgical drainage is associated with more complications than percutaneous drainage, but comparison studies often have a built-in bias against surgery—patients undergoing surgical drainage tend to be sicker.

Computed tomography–guided transgluteal percutaneous drainage of deep pelvic abscesses through the greater sciatic foramen is an option in both adults and children (19).

A majority of vancomycin-resistant enterococcal abscesses can be drained percutaneously, although the rate of successful therapy is lower than with more conventional abscesses (20); at times drainage provides a first clue to the presence of vancomycin-resistant enterococci.

Abdominal Wall Abscess

Occasionally diverticulitis or cholecystitis evolves into an abdominal wall abscess. Likewise, an occasional biliary or other neoplasm leads to an abdominal wall abscess. Imaging readily differentiates those abscesses involving the rectus abdominis muscle from intraabdominal conditions.

Psoas Muscle Abscess

An abnormal fluid collection in the psoas muscle region most often is an abscess, and less often a hematoma. In a setting of pancreatitis, a pseudocyst is also in the differential. A primary iliopsoas abscess is not common; a number of these occur in IV drug users and those positive for human immunodeficiency virus. More often these abscesses develop from a gastrointestinal, genitourinary, or spinal source. Some retroperitoneal abscesses involve not only the psoas muscles but also spread along soft tissue planes into adjacent compartments. Psoas abscesses develop in Crohn's patients with disease.

Gram stain and a culture of the abscess contents should establish the responsible organism. Blood cultures are less often helpful. Both gram-positive and gram-negative organisms are involved. In some parts of the world a tuberculous psoas abscess is more common than a pyogenic abscess; a tuberculous abscess tends to involve the adjacent vertebrae. Tuberculous psoas abscesses can be successfully drained percutaneously, although abscess recurrence often requires repeat drainage.

The clinical triad of fever, flank or thigh pain, and limitation of hip movement is found only in about half or fewer patients with a psoas abscess. Sepsis is common.

Computed tomography readily detects psoas abscesses; however, differentiation from a tumor purely on CT criteria is problematic (Fig. 14.7). A hematoma is also often in the differential. Image-guided needle aspiration should be diagnostic and percutaneous catheter drainage therapeutic.

Magnetic resonance imaging is very useful in evaluating psoas muscles. Normal psoas muscle is hypointense on T2-weighted images, while abscesses and the occasional psoas muscle tumor are hyperintense. Contrast-enhanced MR of a psoas abscess reveals a signal void surrounded by intense enhancement.

Conventional therapy of these abscesses is surgical drainage, although percutaneous drainage using CT or US guidance is becoming

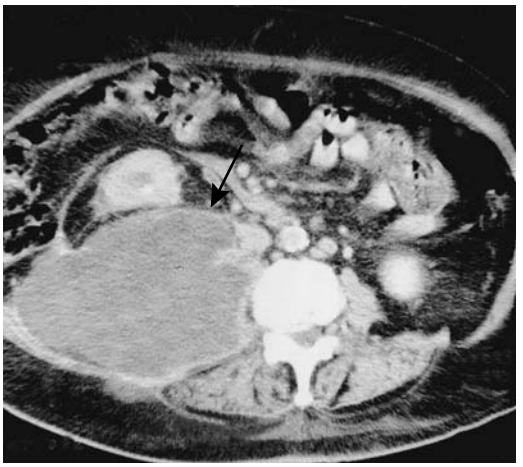

Figure 14.7. Psoas abscess. Transverse CT image reveals an enlarged, mostly hypodense right psoas muscle (arrow) displacing kidney anterior. (*Source:* Paley M, Sidhu PS, Evans RA, Karani JB. Retroperitoneal collections—aetiology and radiological implications. Clin Radiol 1997;52:290–294, with permission from the Royal Collage of Radiologists.)

more common. In distinction to intraabdominal abscesses, surgical psoas abscess drainage appears to result in a shorter patient hospitalization than with percutaneous drainage. On the other hand, serious complications are more common after surgical drainage than after percutaneous drainage (21). Imaging confirms abscess resolution.

Peritonitis

Peritonitis either is primary or develops secondary to an infected adjacent structure. It ranges from localized to diffuse. In the elderly, peritonitis tends to manifest initially in a more advanced or severe form than in a younger patient. At times both peritonitis and ascites coexist. Conditions presenting primarily with ascites are discussed in a later section.

Gastrointestinal perforation is a common cause of acute peritonitis and occurs both in the very young and very old. Peritonitis can develop after inadvertent gallbladder puncture during a liver biopsy or percutaneous nephrostomy. Occasionally encountered is aseptic peritonitis, usually in association with a peritoneal malignancy.

Primary peritonitis is rare in children, but more common in girls. Some of these children are clinically suspected to have appendicitis, and the diagnosis is made only during surgery.

Imaging has a limited role in detecting acute peritonitis. Some degree of ascites is common. Contrast-enhanced CT and MR reveal increased peritoneal enhancement.

Infectious Peritonitis

Discussed here are only some of the more unusual organisms associated with infectious peritonitis.

Patients undergoing peritoneal dialysis are at increased risk of cryptococcal peritonitis. Cryptococcal peritonitis also occurs in patients with cirrhosis and end-stage renal disease.

Listeria is a rare cause of spontaneous bacterial peritonitis. About two thirds of reported patients have chronic liver disease or an underlying malignancy, or the patient was undergoing peritoneal dialysis.

Actinomycosis is a chronic infection by an anaerobic gram-positive commensal bacterium present in body orifices. Typically involved are the genitourinary tract and occasionally bowel. Rarely, it involves the peritoneum or greater omentum. Needle biopsies do not always provide a diagnosis; at times only inflammatory tissue is obtained and only an open biopsy provides the organisms.

Fitz-Hugh–Curtis syndrome, or venereal perihepatitis, is a complication of genital gonococcal or chlamydial infection. In Europe and the United States infection by *Chlamydia trachomatis* is more frequent. A majority of patients are women. Clinically, acute right upper quadrant symptoms mimic those of biliary disease, but liver function tests are normal. Likewise, US of the gallbladder and bile ducts is normal yet gallbladder wall thickening develops in some and multislice CT can detect transient liver attenuation abnormalities (22). Pathologically, perihepatitis consists of adhesions and peritoneal inflammation. Perihepatic fluid is often present. A biopsy should be diagnostic. The diagnosis is confirmed by finding *Neisseria gonorrhoeae* or *C. trachomatis* organisms in perihepatic tissues. Some of these patients have undergone laparoscopy before the true diagnosis is suspected.

A rare cause of peritonitis is acute ascaris peritonitis due to bowel perforation. This con-

dition, more common in children and occurring mostly in China, has a high mortality; on a more chronic basis, ascaris peritonitis leads to peritoneal granuloma formation.

Vernix Caseosa–Induced Peritonitis

An occasional woman develops unexplained abdominal pain after a cesarean section. An exploratory laparotomy reveals an organizing peritonitis, which includes a foreign-body granulomatous reaction. It is believed that this peritonitis most likely is induced by spillage of keratinous material (*vernix caseosa*) derived from amniotic fluid during the cesarean section.

In Cirrhosis

Most spontaneous bacterial peritonitis is encountered in patients with cirrhosis and ascites. Antecedent gastrointestinal bleeding is common in these patients. The clinical presentation is often subtle, and thus evaluation of ascitic fluid should be performed promptly, realizing that ascitic fluid culture is positive only in about half. Most common organisms involved are *Enterobacteriaceae* species and Gram positive cocci. Detection of these and other, less common infectious agents should lead to a search for either underlying cirrhosis or AIDS. Rarely, *Streptococcus pneumoniae* results in primary peritonitis without underlying disease.

Lupus

Acute lupus peritonitis is a rare manifestation of systemic lupus erythematosus. Imaging detects marked bowel wall thickening, intraluminal fluid, and ascites.

Meconium

Meconium peritonitis is a result of intra-utero bowel perforation, spill of meconium, and a resultant sterile chemical peritonitis. These perforations are often associated with congenital bowel obstruction such as small bowel atresia, volvulus, or meconium ileus. At times peritonitis-induced adhesions result in further obstruction. Although usually considered a benign condition, meconium peritonitis can be associated with infarcts secondary to intravascular dissemination of meconium emboli. Meconium in the peritoneal cavity induces an exuberant fibrosis, leading to a multiseptate ascites appearance, which eventually calcifies. In some infants these calcifications are detected as an incidental finding, with the intra-utero bowel perforation having healed.

Imaging shows characteristic calcifications in the peritoneal cavity. These calcifications can extend into the scrotum through an intact processus vaginalis. Ultrasonography identifies these calcifications as hyperechoic linear or irregular abdominal foci, suggesting a cystic appearance.

Sclerosing Peritonitis/Mesenteritis

Clinical

Some authors treat mesenteritis and sclerosing peritonitis as separate entities, although recent thought suggests that these represent different manifestations of the same condition—an acute form (generally a mesenteritis or panniculitis) and a chronic form (often called sclerosing peritonitis). Diffuse mesenteric infiltration consists of inflammation (mesenteritis and panniculitis), fatty dystrophy, fluid, neoplasms, fibrosis, or even amyloid. Some patients develop a combination of inflammation, fatty dystrophy, and fibrosis, although usually one of these predominates. The terminology for this condition(s) is inconsistent and includes *mesenteric panniculitis*, *mesenteric fibromatosis*, *retractile mesenteritis*, *sclerosing mesenteritis*, *mesenteric lipodystrophy*, *mesenteric Weber-Christian disease,* and *inflammatory pseudotumor*. The terms *mesenteritis* and *sclerosing peritonitis* are used here only for description of the primary sites involved. In some patients a sclerosing peritonitis appearance develops during peritoneal dialysis or use of certain drugs, such as practolol and beta-blocking agents. Occasionally mesenteritis is associated with estrogen use. Interestingly, retractile mesenteritis has resolved with progesterone therapy. Intraperitoneal hemorrhage is suggested as a possible link in forming sclerosing peritonitis. The older literature ascribed this condition in some patients to chronic repetitive abdominal trauma caused by vibrations of a pneumatic jackhammer. Mesenteritis has developed in a setting of Crohn's disease, realizing that the clinical and radiologic features of both

are similar. A role for ischemia is occasionally postulated. Its relationship to extraperitoneal fibrosis (discussed below) is uncertain. Retractile mesenteric is associated with a number of neoplasms and immunosuppression therapy. Numerous reports describe sclerosing peritonitis developing in association with a luteinizing thecoma. A rare association exists between retractile mesenteritis and a mesothelioma.

Excessive fatty infiltration of the mesentery, or lipomatosis, may be idiopathic, part of generalized obesity, or associated with steroid therapy. Most lipomatosis is diffuse and tends to infiltrate rather than displace adjacent structures. It is the occasional focal collections of fat that suggest a fat-containing neoplasm in the differential diagnosis.

Mesenteritis presents either as an acute abdomen or, more often, evolves as a chronic condition of diffuse abdominal pain, at times intermittent. Large fibrofatty tumors develop in the abdomen. Histology reveals a fibrofatty infiltrate containing inflammation, fat necrosis, and fibrosis. Multiple mesenteric lymphatic cysts develop in this entity. Mesenteric fat necrosis, or lipodystrophy, also occurs with pancreatitis and some infections. Mesenteric infiltration has led to a protein-losing enteropathy; in fact, enteropathy can be the first manifestation of this condition.

Exuberant small bowel mesenteric fibrosis predominates in some individuals. This variant, often called retractile mesenteritis, also leads to some degree of inflammation, but the primary finding is mesenteric foreshortening and resultant mesenteric and small bowel distortion. Less often the mesocolon or sigmoid mesentery are affected. Normally little omental involvement is found. Rarely, a similar inflammatory process involves primarily the omentum rather than mesentery.

The differential diagnosis of retractile mesenteritis includes mesenteric and other peritoneal neoplasms. In some patients an open biopsy is necessary for diagnosis and to exclude a malignancy.

Imaging

Usually the small bowel mesentery is involved and ranges from a diffuse infiltrate, a focal soft tissue tumor, to discrete inflammatory nodules. The infiltrate typically also involves adjacent small bowel and results in a spiculated, irregular outline to contrast-filled bowel. Valvulae conniventes are thickened and distorted but not destroyed, thus differentiating this condition from most malignant infiltrations. At times the appearance mimics Crohn's disease, which also results in mesenteric inflammation and fibrosis. Occasionally mesenteric calcifications develop, probably within necrotic tissue.

Primarily retractile mesenteritis and panniculitis have separate and distinct CT appearances (23): patients with retractile mesenteritis show a mostly homogeneous soft tissue infiltrate denser than fat that distorts bowel loops. Those with panniculitis have a heterogeneous fat-density infiltrate typically involving the mesenteric root but with preserved fat around the greater vessels (*fat ring sign*), and a loss of the usual sharp outline of enclosed arteries; at times soft-tissue nodules are evident.

Ultrasonography identifies hypoechoic mesenteric tumors, occasionally containing a cystic component.

Magnetic resonance of lipomatosis reveals a fat signal intensity with all imaging parameters. T1-weighted fat-suppressed SGE images are useful to confirm that a focal collection is indeed fat. T1-weighted images of panniculitis (inflammation) reveal hypointense stranding traversing the hyperintense fat.

Sclerosing peritonitis manifests by thickening of the peritoneal lining, diffuse or loculated fluid collections, peritonitis and resultant small bowel obstruction, or simply disordered small bowel motility. Dense adhesions develop. Extensive fibrosis can involve the liver capsule. Peritoneal calcifications develop eventually. Imaging of patients on chronic ambulatory peritoneal dialysis and sclerosing peritonitis detects peritoneal thickening and calcifications; most also have loculated fluid collections and small bowel tethering or dilation.

Aside from calcifications, the imaging appearance of sclerosing peritonitis is similar to that of ovarian carcinoma with carcinomatosis. Both tend to develop adnexal tumors. In carcinomatosis, however, only the peritoneal surface is involved and it has an irregular outline due to malignant nodules; in sclerosing peritonitis not only does the peritoneal thickening have a smooth outline, but also the small bowel and colon walls are thickened. The differential for sclerosing peritonitis also includes diffuse mesothelioma, some chronic infections, and primary and secondary amyloidosis.

Abdominal Cocoon

An abdominal cocoon, also called *sclerosing encapsulating peritonitis*, is a descriptive term for a variant of sclerosing peritonitis consisting of the small bowel being encased by a membrane and displaced centrally. It is a rare condition. Associated soft tissue tumors are evident in some patients. It is not uncommon to see small bowel obstruction.

The etiology of this condition is unknown. Most reported patients have been from the tropics or subtropical zones, with only an occasional report from temperate zones. One group of patients consists of young adolescent girls. Another group includes cirrhotic patients treated with a peritoneovenous shunt for ascites; autopsy in some of these patients simply identifies generalized peritoneal fibrosis. It has developed in a liver transplant recipient (24). A diagnosis of an abdominal cocoon as a separate entity probably is not appropriate if an infectious organism is recognized; peritoneal tuberculosis has resulted in a similar appearance, and this diagnosis should be excluded if an idiopathic abdominal cocoon is encountered.

Once established, a barium small bowel study is diagnostic. Occasionally, a barium study shows the small bowel to have a *cauliflower-like* configuration. Computed tomography reveals most or all of the small bowel encased by a thick membrane. Obstruction tends to develop at the site where the proximal small bowel enters its cocoon. Superficially, the condition mimics a large paraduodenal hernia.

Tuberculosis

Clinical

An increasing prevalence is evident not only for pulmonary tuberculosis but also for its extrapulmonary manifestation. Isolated abdominal involvement is not uncommon in endemic regions. Fatigue, prolonged fever, weight loss, nonspecific bowel symptoms, and a chronic wasting illness are common clinical findings. An erroneous initial diagnosis is common in parts of the world with a low prevalence of abdominal tuberculosis.

Hypercalcemia developed in patients with tuberculous peritonitis without pulmonary involvement. Elevated serum CA 125 tumor marker levels are found in some of these patients; levels decrease after antituberculous therapy.

Tuberculosis ranges from disseminated disease to abdominal involvement only. Abdominal tuberculosis varies in organ involvement considerably, with ulcerative ileocecal involvement not uncommon. Peritonitis, mesenteric and extraperitoneal lymphadenopathy, and genitourinary involvement can occur as separate findings or together; multiorgan involvement, including ulcerative ileocecal involvement is not uncommon. Bowel perforation and obstruction lead to an acute abdomen. Presence vascular and perivascular granulomas, intraluminal thrombi and subintimal fibrosis suggest that bowel ischemia is a common pathway.

A diagnosis of peritoneal tuberculosis is difficult; in spite of clinical, endoscopic, and radiologic evaluation, peritoneal tuberculosis, especially if it involves the ileocecal region, is readily misdiagnosed as Crohn's disease. Differentiating peritoneal tuberculosis from advanced ovarian cancer is difficult. Malignant lymphoma is also often in the differential diagnosis.

Tuberculous ascitic fluid acid-fast stains tend to be negative and not all *Mycobacterium tuberculosis* cultures are positive. Biopsy in some patients reveals epithelioid giant-cell granulomas containing caseous necrosis. At times diagnostic laparotomy and culture of tissue biopsy specimens are necessary for diagnosis.

Imaging

Imaging identifies intra- and extraperitoneal lymphadenopathy. At times these enlarged nodes are focal in location and mimic a malignancy. Nevertheless, CT lymph node location and specific node appearance provide clues aiding the differentiation of these two entities.

Tuberculosis tends to involve more superior para-aortic lymph nodes, while lymphoma more often involves the inferior para-aortic lymph nodes (25). An exception is with disseminated tuberculosis, which affects nodes diffusely and involves the hepatoduodenal and hepatogastric ligaments and mesenteric and extraperitoneal lymph nodes; nondisseminated tuberculosis can involve similar node chains, except the inferior extraperitoneal lymph nodes are mostly spared. The large, confluent lymph nodes found in lym-

phoma are unusual with tuberculosis. An enlarged isolated lymph node chain is nonspecific; for instance, periportal adenopathy, detected by CT, can be an isolated manifestation of tuberculous adenitis, but the differential diagnosis also includes not only malignancies but also such benign diseases as sarcoidosis. Enlarged tuberculous lymph nodes tend toward a lower CT density than lymphomatous nodes. In tuberculous peritonitis a low-density center was seen in some enlarged nodes, and calcification eventually develop in a minority; the low-density portion probably represents caseation necrosis. Even more striking is peripheral rim contrast-enhancement with tuberculosis; lymphomatous nodes are more homogeneous in their enhancement (25).

Fine peritoneal septations are common in tuberculosis, and ascites is often enclosed in a lattice-like mesh. Tuberculous ascites tends to have a higher density than most ascitic fluid. Diffuse peritoneal thickening and infiltration of the greater omentum is common.

In general, CT and US reveal similar findings, although bowel wall thickening is probably better appreciated with CT. At times CT and US complement each other in patients with suspected tuberculous peritonitis. With pelvic involvement the CT appearance often mimics a malignancy. An abdominal cocoon-like appearance can be associated with tuberculous pelvic involvement (26) (Fig. 14.8). Ultrasonography reveals a hyperechoic, thickened mesentery, mesenteric adenopathy, and less often dilated

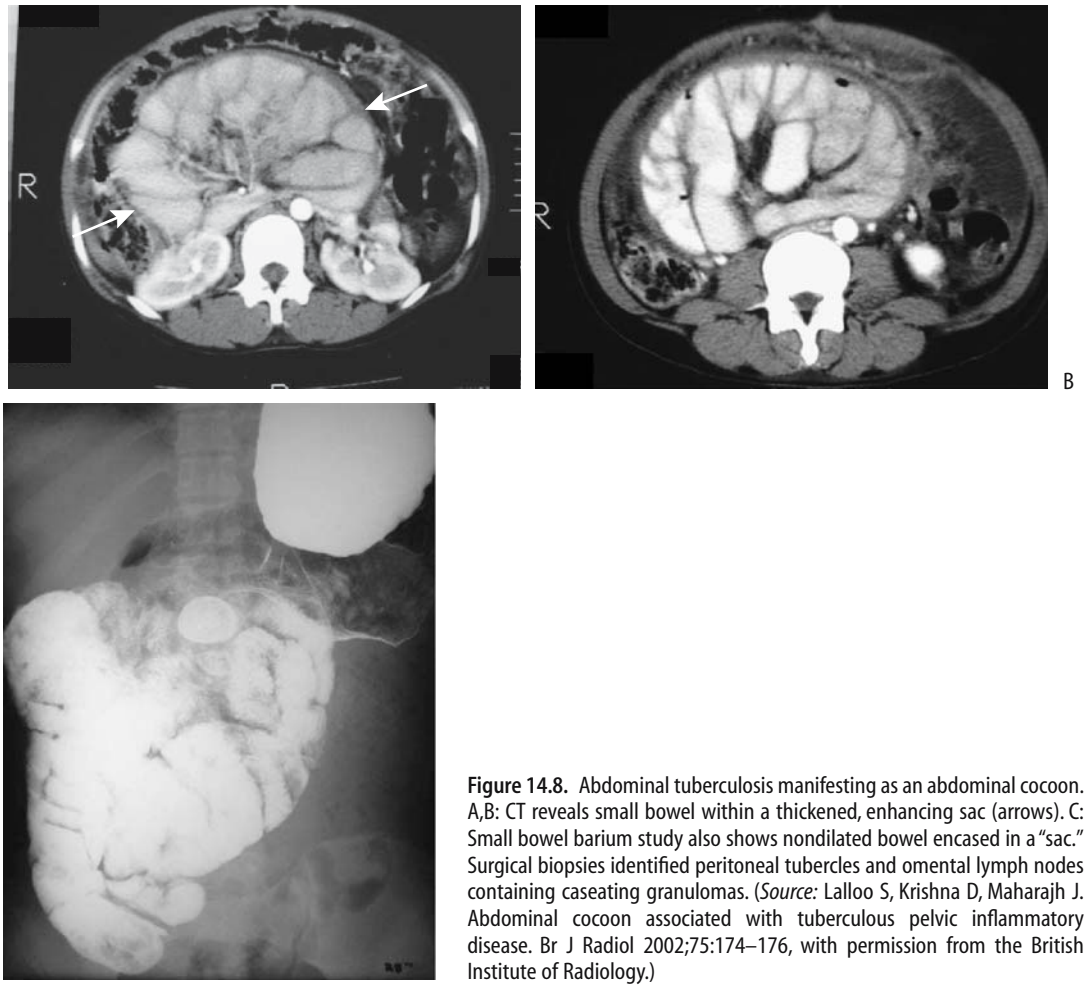

Figure 14.8. Abdominal tuberculosis manifesting as an abdominal cocoon. A,B: CT reveals small bowel within a thickened, enhancing sac (arrows). C: Small bowel barium study also shows nondilated bowel encased in a "sac." Surgical biopsies identified peritoneal tubercles and omental lymph nodes containing caseating granulomas. (*Source:* Lalloo S, Krishna D, Maharajh J. Abdominal cocoon associated with tuberculous pelvic inflammatory disease. Br J Radiol 2002;75:174–176, with permission from the British Institute of Radiology.)

small bowel loops, minor ascites, and occasional omental thickening.

A cone-shaped, contracted cecum and a dilated, edematous terminal ileum are diagnostic findings in the dry type of ileocecal tuberculosis.

Filariasis

Infection with *Wuchereria bancrofti*, *Brugia malayi*, *B. timori,* and *Loa loa* affects not only the lymphatics but also such structures as the kidneys; renal damage can occur even in asymptomatic carriers.

Ultrasonography detects live adult filarial worms by identifying twirling motions in dilated lymph channels; successful chemotherapy ends the worm activity.

Lymphoscintigraphy is of value in assessing lymphatic damage. Extensive lymphoscintigraphic abnormalities are found in *W. bancrofti*-endemic regions even in clinically asymptomatic persons. Chyluria is common. Among patients with filarial chyluria undergoing unilateral pedal lymphography, lymphatic crossover was identified in all and lymphaticorenal fistulas were detected in 98% (27); the authors advocate unilateral lymphography over a bilateral study because lymphatic crossover identifies lymphaticorenal fistulas regardless of the side of involvement.

Echinococcosis

A primary echinococcal cyst in the peritoneum is rare. A study from Tunis found that retrovesical and extraperitoneal sites represent about 10% of their operated hydatid cysts (28); a retrovesical site presumably represents secondary implantation in the pouch of Douglas by intraperitoneal rupture of a more conventionally located cyst (Fig. 14.9).

Parasitic Infestation

Parasitic infestations involve myriad end organs, with the peritoneal cavity often serving as an intermediary pathway. Peripheral eosinophilia often suggests underlying parasitic infestation, although it is present only in about half of infected patients, and generally during the acute phase. Acute or vague abdominal pain is common. Serologic tests (enzyme-linked immunoabsorbent assay) are available for some infestations.

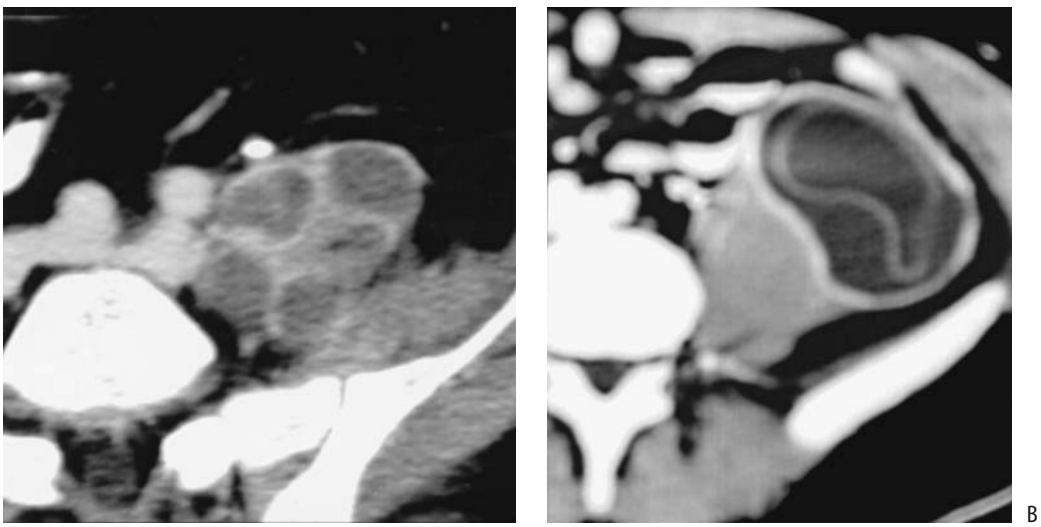

Figure 14.9. Pelvic hydatid disease. A,B: Two contrast-enhanced CT images through the pelvis shows daughter cysts within a denser structure adjacent to the left iliac muscle. Detached membranes are evident in the cyst shown in part B. (*Source:* Polat P, Kantarci M, Alper F, Suma S Koruyucu MB, Okur A. Hydatid disease from head to toe. RadioGraphics 2003;23:475–494, with permission from the Radiological Society of North America.)

Computed tomography detects focal omental, peritoneal, mesenteric, or bowel wall infiltration, often heterogeneous and partly cystic in nature. The imaging differential diagnosis often includes other inflammatory conditions and neoplasms.

Diffuse Infiltration

Fibrosis/Desmoid

Diffuse extraperitoneal fibrosis, also known as *retroperitoneal fibromatosis*, *desmoid tumor*, and *Ormond's disease*, is a locally invasive but benign chronic condition. Extraperitoneal fibrosis is idiopathic in about two thirds of patients. Some evidence suggests an underlying autoimmune response manifesting as a vasculitis and fibrosis. Both mesenteric and extraperitoneal fibromatosis (fibrosis) present most often as a discrete desmoid tumor; a diffuse infiltrate is less common. Fibrous tissue is noncapsulated, poorly marginated, and infiltrates surrounding structures. Its relationship to sclerosing peritonitis and mesenteritis is conjecture. Indeed, some of the patients discussed previously (see Sclerosing Peritonitis/Mesenteritis) probably should be included here (and vice versa).

Etiology

Secondary forms of fibromatosis/desmoid are associated with both malignant and benign disorders. It develops in response to some infiltrating malignancies, and at times the term *malignant retroperitoneal fibrosis* is used to describe a reactive fibrosis secondary to such neoplastic infiltration; malignant cells tend to be scattered throughout the fibrosis. A distinction between malignant and nonmalignant retroperitoneal fibrosis is of obvious clinical importance and thus an extensive biopsy is often indicated.

An association with methysergide and ergotamine use appears to be greater than by chance. Extraperitoneal fibrosis has been reported following treatment of Parkinson's disease with L-dopa analogues; a number of these patients have underlying atherosclerosis and it is difficult to put the relationship among atherosclerosis, drug therapy, and the subsequent development of fibrosis into proper perspective.

An inflammatory abdominal aortic aneurysm is commonly associated with extraperitoneal fibrosis (discussed in Chapter 17). Pathogenesis of fibrosis in this clinical setting is unclear, although severe atherosclerosis appears to induce an immune response in some individuals.

A rare patient develops extraperitoneal fibrosis secondary to actinomycosis and other chronic infection. Extensive extraperitoneal fibrosis develops as a reaction to some foreign bodies. Thus fibrosis is induced by extravasated barium during bowel perforation (29); similar to some of the other reactive fibroses mentioned above, such fibrosis is a local reaction surrounding the barium crystals and is not associated with fibrosis at other sites.

Desmoid tumors are common in familial adenomatous polyposis. In fact, this polyposis syndrome should be suspected in a patient with a newly discovered rectus abdominis muscle desmoid tumor (Fig. 14.10).

Prior abdominal surgery increases the risk for desmoids; in an occasional patient desmoids begin to develop in trocar sites within months after laparoscopy. Less often a desmoid develops in a patient without familial polyposis and at a site unrelated to prior surgery. These sporadic desmoids are less likely to recur after resection than familial ones.

A mesenteric desmoid tumor can develop after radiation therapy. These patients often also develop leg edema and protein-losing enteropathy due to intestinal lymphangiectasia.

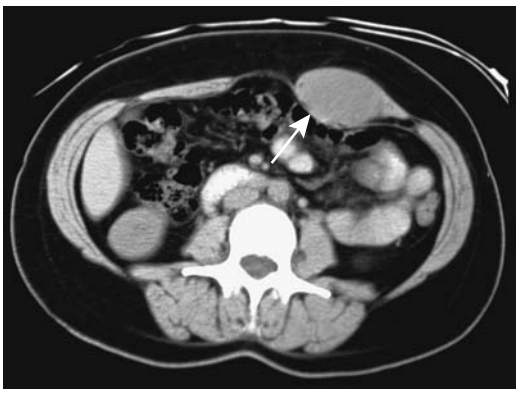

Figure 14.10. Rectus sheath desmoid tumor (arrow). (Courtesy of Patrick Fultz, M.D., University of Rochester.)

Classification of desmoplastic fibroblastomas (*collagenous fibroma*) is not clear. One slowly growing heterogeneous tumor was hypointense on T1-weighted images, mixed hypo- and hyperintense on T2-weighted images and showed heterogeneous contrast enhancement (30); the hypointense regions consisted mostly of collagen.

Clinical

Extraperitoneal fibrosis usually involves structures from the renal hila inferiorly. A somewhat atypical variant is to find fibrosis limited to the pelvis. Although benign, desmoids invade locally and have a high potential for recurrence. Complications of desmoid tumors account for part of the mortality associated with familial adenomatous polyposis.

Symptoms result from the gradual compression of adjacent structures, including ureters, retroperitoneal vessels and nerves, and portions of the gastrointestinal tract. Extraperitoneal fibrosis encasing the ureters results in hydronephrosis, at times unilateral. The ureters are displaced medially. Once a diagnosis of extraperitoneal fibrosis is established, in a setting of hydronephrosis, ureteral decompression is necessary to save the kidney. Laparoscopic ureterolysis is feasible, although often in vain. Placement of double-J ureteric stents is helpful on a temporary basis. With time, soft polyurethane stents tend to become obstructed due to continued extrinsic ureteral compression, and they need to be replaced with more rigid ones.

Occasionally extraperitoneal fibrosis involves the bile ducts and leads to obstructive jaundice; imaging findings can suggest extrahepatic sclerosing cholangitis or a pancreatic malignancy. At times fibrosis leads to both hydronephrosis and biliary obstruction.

Abscesses can develop within a desmoid tumor, at times communicating to the bowel. Some of these abscesses can be managed initially with percutaneous abscess drainage.

Extraperitoneal fibrosis tends to respond to steroid therapy. Immunosuppressive therapy has also achieved some success. Surgical therapy is difficult due to the often-diffuse infiltration. Also, surgery often tends to exasperate recurrence. Once the diagnosis is established, follow-up is by CT or US. Some unresectable desmoid tumors regress after being treated with radiation therapy. The role of hyperthermia is not clear. Spontaneous regression of extraperitoneal fibrosis has also been reported, albeit rarely.

Both growth and response to therapy of a desmoid are readily evaluated with imaging.

Iliac vein and inferior vena caval stenosis secondary to extraperitoneal fibrosis is often approached surgically but can be treated by venous thrombectomy and bilateral iliac stenting, but keep in mind the often temporary nature of such therapy.

Imaging

Most desmoids develop in the mesentery and abdominal wall, with only an occasional one being extraperitoneal in location. A rare one involves both extra- and intraperitoneal structures. In some patients a specific site of origin cannot be determined.

Although at times imaging suggests the diagnosis, no specific finding is pathognomonic. Imaging identifies a desmoid either as a discrete tumor or a poorly marginated infiltration. With diffuse extraperitoneal infiltration, the first task is to establish that the diagnosis is indeed fibrosis rather than an underlying malignancy. Rather than being displaced, adjacent vessels and bowel become encased. Imaging cannot differentiate primary benign fibromatosis from a secondary one due to malignant infiltration, although malignancies increase in size faster than a benign infiltration. Extraperitoneal fibrosis is usually diffuse, but occasionally is well marginated or even nodular. Contour irregularities are not a reliable differential. Either extensive percutaneous biopsies or surgical exploration is often necessary. Negative percutaneous biopsies should be interpreted with caution.

Precontrast CT of most extraperitoneal fibrosis shows a density similar to that of adjacent muscle or is even slightly hyperdense. The tissue tends to enhance postcontrast and may appear somewhat hyperdense. At times the appearance mimics that of a diffuse tumor.

Magnetic resonance imaging of diffuse fibrosis and desmoids usually reveals hypointense signals on both T1- and T2-weighted images. An occasional complex infiltrating tumor exhibits iso- or even hyperintense signal

intensities on T2-weighted images. Postcontrast enhancement is variable.

Desmoids and retroperitoneal fibrosis show Ga-67-citrate uptake. Some correlation exists among clinical symptoms, disease activity, and Ga 67 scintigraphic activity.

Amyloidosis

Amyloid lymphadenopathy is common in uremic patients, in one study being identified in 22% of hemodialysis patients' lymph nodes (31).

Occasionally a patient with amyloidosis develops extensive calcified extraperitoneal amyloid deposits which are visible with conventional radiography and CT.

Sarcoidosis

The CT appearance of abdominal sarcoidosis varies considerably. Often systemic sarcoidosis manifests with hepatosplenomegaly and extraperitoneal adenopathy, at times massive and mimicking lymphoma. Magnetic resonance imaging also readily detects the adenopathy.

Sarcoid-involved lymph nodes show FDG-PET uptake.

Xanthogranulomatosis/Erdheim-Chester Disease

Xanthogranulomatosis is more common in the kidneys than in other extraperitoneal soft tissues. Systemic involvement is called Erdheim-Chester disease, which is a nongenetic systemic condition most often presenting with characteristic and almost pathognomonic bilateral symmetric foci of sclerosis in the long bones, at times containing focal osteolysis within these regions of sclerosis. Bone involvement, however, is only an early manifestation of this systemic condition affecting multiple organs. The etiology of Erdheim-Chester disease is unknown, and its specific histologic classification is unclear. Many pathologists characterize it as a non–Langerhans cell histiocytosis, with histology typically revealing a xanthogranulomatous infiltrate by foamy histiocytes in a bed of fibrosis. Macrophages and giant cells are evident in some biopsies. It is distinct from histiocytosis X. Although it shares similar clinical and radiologic findings with Langerhans cell histiocytosis, most authors believe these are separate entities. Considerable evidence suggests that it is neither a lipid storage disorder nor a primary macrophage cell disorder. It occurs most often in the middle aged and elderly and tends to progress slowly. For instance, in one patient it developed over a 20-year period and led to renal artery stenoses, bilateral ureteric stenosis, and adhesive renal capsule involvement (32). At times it evolves into upper urinary tract obstruction. A diffuse periaortic infiltrate is evident in some, with the CT appearance termed the *coated aorta* (33).

Although case reports mention the rarity of this condition, it is probably not uncommon, and it is underdiagnosed and underreported. In an extensive review of Erdheim-Chester disease, bone pain was the most frequent clinical finding (47%), followed by exophthalmos (27%) and diabetes insipidus (29%) (34); long bone diaphysial osteosclerosis was detected in 76% of patients and extraperitoneal involvement in 39%.

Imaging findings of retroperitoneal Erdheim-Chester disease (and xanthogranulomatosis in general) are those of a diffuse infiltrating solid tumor. Technetium-99m accumulates in regions of bone involvement and presumably also at other sites of involvement. The differential diagnosis includes retroperitoneal fibrosis, diffuse lymphoma, inflammatory fibrosarcoma, malignant fibrous histiocytoma, and other solid tumors, conditions distinguishable only pathologically.

Extramedullary Hematopoiesis

Extramedullary hematopoiesis implies deposits of erythroid precursors outside of bone marrow. The rare patient with retroperitoneal extramedullary hematopoiesis presents with an extensive soft tissue infiltrate.

Systemic Mast Cell Disease (Mastocytosis)

Systemic mast cell disease typically involves the skin, and imaging plays no role in diagnosis, although many patients with systemic mastocytosis have ascites, hepatosplenomegaly, thick-

ened omentum and mesentery and abdominal adenopathy. Some patients develop gastrointestinal lymphonodular hyperplasia. Ascites developed in a patient with systemic mastocytosis and hypertension (35). The usual skin findings point to this condition, but an occasional patient presents with hepatomegaly and lymphadenopathy, and the diagnosis is established from lymph node biopsies.

Fluid Collections

Ascites

Clinical

Ascites means fluid in the peritoneal cavity. Classic ascites is either a transudate or exudate based on total protein concentration, but blood, pus, various organ secretions, or a mixture of fluids can be found in the peritoneal cavity.

The most common cause of ascites in North America and Europe is portal hypertension due to liver disease. Peritoneal carcinomatosis leads to an exudate, often with an obstruction of draining lymphatics. Tumor infiltration of the porta hepatis or liver parenchyma also results in portal hypertension and ascites. Other, less common causes include some infections and conditions leading to hypoalbuminemia.

Congestive heart failure results in increased right heart pressure with concomitant hepatic congestion. Leakage from bile ducts results in bile ascites; often the bile is also infected. Chylous ascites forms from lymphatic obstruction, usually due to a neoplasm such as a lymphoma, or lymphatic transection, usually secondary to surgery.

Ultrasonography in children with mild dengue hemorrhagic fever revealed ascites in 34% (36); in those with severe disease US detected ascites in 95% and pararenal and perirenal fluid in 77%. Ultrasonography thus appears useful for predicting the severity of this condition in children.

Peritonitis, regardless of etiology, is usually associated with varying amounts of peritoneal fluid. Some infections result in blood-tinged ascites. Severe salmonella enteritis or massive *Fasciola hepatica* infection are uncommon causes of moderate ascites.

Common causes of ascites in neonates include urinary tract obstruction with subsequent rupture, and chylous ascites due to birth trauma. Ascites in the young is easier to detect with CT or US than with conventional radiographs.

Ascitic fluid white blood cell count should be routinely obtained on all fluid samples. An elevated count is present with both an inflammation and malignancies. Polymorphocytes predominate in acute bacterial peritonitis, while in more chronic conditions such as peritoneal tuberculosis or carcinomatosis a preponderance of lymphocytes is usually found.

Imaging

As discussed above (see Trauma), the volume of peritoneal fluid first detected by US is about 600 mL. Detection limits for CT and MR are unknown. Larger amounts of fluid are visible even with conventional radiography. Uncomplicated ascites generally has an attenuation of 0 to 40 HU, but in clinical practice the attenuation values alone are not a reliable indicator for differentiating among a transudate, malignant ascites, or a hemorrhage. Most ascites is readily differentiated from other intraabdominal fluid, but care is necessary in the pelvis. An adnexal cyst, such as a fallopian tube cyst, may mimic pelvic ascites.

Although both ascites and intrathoracic fluid abut the diaphragm, CT can nearly always distinguish between them. Fluid in the subphrenic space tends to extend to the paracolic gutters and the posteriorly located Morison's pouch, and forms a sharp outline with abdominal viscera, but there is sparing of the bare area of the liver. With massive ascites CT detects the medial umbilical folds, representing peritoneal reflections, in about two thirds of patients. With the patient supine, intrathoracic fluid extends more medially than ascitic fluid and collects in the posterior sulci.

Occasionally ascitic fluid enhances on delayed contrast-enhanced CT. In most patients this phenomenon is of little significance and is even a potential pitfall suggesting perforation.

Especially in a setting of adhesions or tumor, US is useful in guiding both fluid aspiration and a biopsy or cytology needle.

Lesser sac fluid is readily identified with imaging. Some peripancreatic fluid that appears to be in the lesser sac on CT, however, may actually be located within adjacent tissue planes.

A transudate is hypointense on T1- and hyperintense on T2-weighted images. An exudate has a higher signal intensity on T1-weighted images than a transudate. Although the MR signal intensity varies with fluid protein concentration, considerable overlap in the appearance of various ascitic fluids makes this finding of limited significance.

The gallbladder wall is considerably thicker in patients with ascites due to liver cirrhosis than in patients with noncirrhotic ascites. Most malignant ascites is associated with a normal gallbladder wall thickness.

Portal Hypertension–Induced Ascites

Ascites is common in sinusoidal and postsinusoidal portal hypertension. Pathogenesis is multifactorial, consisting of factors favoring efflux of fluid into the peritoneal space, retention of fluid there, and continued replenishment of the intravascular volume. Peripheral vasodilation is common in patients with cirrhosis and ascites and, to a large extent, appears to be secondary to increased vascular production of nitric oxide, which is a potent vasodilator. In these patients ascites is related to a decrease in portal blood flow. Refractory ascites in cirrhosis often leads to accelerated liver decompensation.

Therapy is tailored for those with nonmalignant versus malignant ascites. In patients with nonmalignant ascites, prior enthusiasm for peritoneovenous shunting using Denver or LeVeen shunts has been tempered by shunt occlusions and other complications such as peritoneal fibrosis, and they are little used today.

Transjugular intrahepatic portosystemic shunt (TIPS) was not initially developed to treat ascites, but in a number of patients with portal hypertension and ascites a successful TIPS improved or even resolved their underlying ascites. Some patients with previously refractory ascites respond to medical management following TIPS insertion. Transjugular intrahepatic portosystemic shunt can control ascites in most patients with refractory ascites, with results influenced by the stage of cirrhosis. Ascites tends to improve in stage B cirrhotics but not those with stage C. In some centers TIPS is performed only in those ascitic patients refractory to conventional therapy; major complications in these patients include intraperitoneal hemorrhage, refractory encephalopathy, and progressive liver and renal failure. Some have new onset or worsening of hepatic encephalopathy. In fact, TIPS in patients with advanced liver and renal failure may hasten death.

Malignant Ascites

One aid in distinguishing benign from malignant ascites is gallbladder US; most malignant ascites is associated with a normal gallbladder wall thickness, while the wall is thickened with most benign causes. Also, benign ascites tends to be mostly in the main peritoneal cavity (greater sac) with relative sparing of the lesser sac, while malignant ascites normally involves both.

Therapy for recurrent, symptomatic malignant ascites consists of therapeutic paracenteses to relieve symptoms in these patients with a limited life span. Alternate therapy consists of insertion of a percutaneous tunneled peritoneal catheter to relieve the symptoms.

Pancreatic Ascites

In pancreatitis, ruptured pancreatic ducts usually lead to pseudocyst formation, but occasionally leakage from a pseudocyst or pancreatic duct into the peritoneal cavity incites an exudate secondary to irritation (pancreatic ascites). If pancreatic ascites persists, endoscopic retrograde pancreatography (ERP) is worthwhile to define the pancreatic duct anatomy and identify a possible site of leakage.

Nephrogenic Ascites

The cause of ascites in a setting of nephrotic syndrome is poorly understood. Refractory ascites in patients with end-stage renal disease, called nephrogenic ascites, appears to be either altered peritoneal membrane permeability or impaired resorption due to peritoneal lymphatic obstruction; the ascitic fluid is rich in protein and contains few leukocytes, and the serum-ascites albumin gradient is decreased. In pediatric patients with nephrotic syndrome, ascites is probably due to general fluid retention, while in adults hypoalbuminemia, superimposed liver disease, and congestive heart failure appear to be factors.

Definitive therapy for nephrogenic ascites is renal transplantation.

In Neonates

An unusual cause of ascites in neonates has been termed *total parenteral nutrition ascites,* developing after infusion through an umbilical vein catheter. These neonates present with ascites, the umbilical vein catheter overlies the liver, and contrast studies through the catheter confirm intraperitoneal extravasation. This complication of total parenteral nutrition is due to liver erosion by the umbilical vein catheter.

Ascitic Hydrothorax

Some patients with ascites develop a hydrothorax, probably due to congenital diaphragmatic defects. At times the hydrothorax predominates, with little evidence of ascites. Most often the peritoneopleural communication is on the right side, although it can be bilateral. Peritoneal communication is confirmed by injecting a Tc-99m–labeled radioisotope (sulfur colloid or macroaggregated albumin) into the peritoneal cavity and scanning over the chest. A similar approach can be used with CT and MRI after intraperitoneal injection of contrast. Even intraperitoneal air injection and appropriate conventional films are diagnostic if the communication is sufficiently large.

Ascitic hydrothorax can be life threatening. Therapy is difficult; chest tube drainage leads to loss of fluids and electrolytes, creates a fistula, and generally is unsatisfactory in these sick patients. Therapy of the underlying cause of ascites should be considered, including TIPS or even liver transplantation, if appropriate.

Biliary Ascites/Biloma

Although bile may leak into the peritoneal cavity and result in bile ascites and bile peritonitis, more often an induced inflammatory response to the intraperitoneal bile results in bile being walled-off, forming a biloma. Most bilomas have a CT attenuation close to water, unless bleeding or infection supervenes.

Magnetic resonance bile signal should be similar to that obtained from gallbladder bile. Bile ranges from hypo- to hyperintense on T1- and hyperintense on T2-weighted images.

Most bilomas are amenable to successful percutaneous catheter drainage.

Chylous Ascites/Lymphocele

Chylous ascites, or chyloperitoneum, is the presence of chyle in the peritoneal cavity, while a lymphocele is a localized collection. Aside from trauma, including injury to the cisterna chyli, chylous ascites develops secondary to major occlusion of intraabdominal lymphatics. Thus thoracic duct ligation during esophagectomy or surgery on the pancreas, aorta, or other major structures leads to postoperative chylous ascites. Some cirrhotic patients develop chylous ascites. Even occlusion of a portosystemic shunt on rare occasion results in chylous ascites. It is a rare complication of severe pancreatic necrosis. Massive chylous ascites can develop secondary to pancreatic transection. In children chylous ascites is found in a setting of small bowel obstruction or a lymphangioma.

Chylous ascites is a rare initial presentation of an abdominal malignancy, presumably secondary to lymphatic obstruction. Chylous ascites is associated with lymphoma and Kaposi's sarcoma in patients with AIDS; it has also developed with *Mycobacterium* infection.

Imaging studies of most patients with chylous ascites are nonspecific. Lymph contains fat and occasionally CT reveals chylous ascites to have a density of negative Hounsfield units—a highly suggestive finding. Likewise, a fluid–fluid level within the peritoneal cavity with the patient recumbent should suggest chylous ascites or a lymphocele.

One of the few indications for lymphangiography or lymphoscintigraphy is suspected chylous ascites. The study identifies a site of leakage or obstruction of extraperitoneal lymphatics. It does not define mesenteric or hepatic lymphatic leakage.

Incidentally, MRCP can define some cisterna chyli, especially if they are dilated.

Most lymphoceles develop after lymphatic disruption due to surgery or other type of trauma. They are relatively common after lymphadenectomy. Most are extraperitoneal in location; intraperitoneal lymph leakage usually results in chylous ascites rather than a lymphocele. They range from a unilocular collection mimicking a simple cyst to a multiseptated, irregular cystic structure containing necrotic

material. Hemorrhage or infection modifies their CT and US appearance. At times imaging differentiation from a urinoma or hematoma is not possible. Some lymphoceles mimic an abscess; also, a lymphocele may become infected. In general, aspiration is required to confirm the underlying condition.

Small lymphoceles tend to resolve spontaneously while larger ones generally require drainage. Simple percutaneous catheter drainage appears to be effective in treating postoperative lymphoceles. Thus percutaneous catheter drainage of symptomatic lymphoceles after radical pelvic lymphadenectomy led to resolution of most lymphoceles (37). If necessary, drainage catheters are inserted using imaging guidance, and lymphocele sclerosis is performed with such sclerotic agents as absolute alcohol. although doxycycline, povidone iodine and bleomycin have been used. Presence of a catheter allows repeat lymphocele ablation as needed. Few complications are associated with this procedure.

At times lymphangiectasia, regardless of cause, results in leakage of chyle percutaneously or into a hollow viscus. Computed tomographic lymphography and MRI are worthwhile in an attempt to define chylous enteric or other drainage. After initial lymphographic opacification for guidance, several patients with uncontrolled postoperative chyle fistulas underwent percutaneous transabdominal puncture and catheterization of the cisterna chyli or lymphatic ducts (38); the thoracic duct could be catheterized in some patients, the fistulas identified with aqueous contrast, and a thoracic duct fistula embolized with coils, leading to resolution of the patient's chylothorax. No morbidity was encountered.

An interesting percutaneous translymphatic thoracic duct embolization in a patient with postoperative chylothorax was started by first performing unilateral lymphangiography, then an abdominal lymph vessel was punctured with a fine needle using fluoroscopic guidance and a 4-French catheter introduced to establish lymph system access (39); the thoracic duct was then embolized with coils and tissue adhesive.

Urinoma

Most localized collections of urine, or urinomas, are extraperitoneal in location. Less often leakage from the urinary tract results in the accumulation of urine in the peritoneal cavity either as single or multiple urinomas or as urinary ascites. The most common cause of urine spill is trauma to the urinary tract, especially bladder dome injury. A cystogram should be diagnostic of a bladder perforation, but may miss the occasional more proximal perforation. Contrast-enhanced CT should detect these. Some urinomas eventually lose their communication with the urinary tract. An occasional urinoma extends through the aortic hiatus into the mediastinum.

Unless complicated by bleeding or infection, most urinomas have a CT attenuation close to that of water.

Technetium-99m–mercaptoacetylglycilglycilglycine (MAG3) renal scintigraphy appears useful to detect urinary leakage into the peritoneal cavity or a more localized collection.

Hemoperitoneum

Bleeding due to trauma has already been discussed in an earlier section (see Trauma).

Common causes of a spontaneous hemoperitoneum are gynecologic diseases and spontaneous rupture of a liver hemangioma or hepatocellular carcinoma. Other reported tumoral causes of hemoperitoneum include bleeding from an enteric sarcoma or even a carcinoid.

At times portal hypertension evolves into unusual variceal formations, rupture of a varix, and intraabdominal hemorrhage. Most esophageal varices bleed intraluminally, but rarely they bleed intraperitoneally. Thus large-volume paracentesis in a setting of portal hypertension can lead to rupture of esophageal or mesenteric varices and an acute hemoperitoneum, a condition having a high mortality rate.

Anticoagulant therapy can lead to a spontaneous intraabdominal hemorrhage and an acute abdomen. Bleeding can occur into the peritoneal cavity, extraperitoneally, into the anterior abdominal wall, or even into bowel wall or lumen.

The most common spontaneous ruptured visceral aneurysm involves the splenic artery. Computed tomography should detect most of these aneurysms.

Spontaneous hemoperitoneum in the pediatric age group is rare. An occasional vascular malformation or ovarian cyst ruptures and bleeds. Hemoperitoneum in a newborn is generally secondary to antenatal hemorrhage.

Loculated blood can mimic a complex cyst or neoplasm, with loculations ranging from single to multiple. Depending on location, some appearances suggest a bowel origin. Computed tomography attenuation of blood in the peritoneal cavity or a hematoma varies with time. An immediate bleed has an attenuation similar to that of intravascular blood, unless it is mixed with other fluid. The hematoma attenuation increases up to 90 HU due to clot formation and red blood cell concentration, and then gradually begins to decrease with clot lysis, reaching water density or slightly higher within several weeks. Bleeding may be intermittent and clot formation and lysis extend for some time, resulting in a heterogeneous CT appearance. Eventual resorption may lead to a normal appearance or evolve into residual fibrosis. A similar change with hematoma age is found with MRI. An acute hematoma is isointense on T1- and hyperintense on T2-weighted images. Within several days the signal gradually becomes hyperintense on T1-weighted images and a hematoma then is hyperintense on both T1- and T2-weighted images.

Presence of hyperechoic pelvic fluid detected with transvaginal US, usually performed for suspected gynecological disease, suggests a hemoperitoneum.

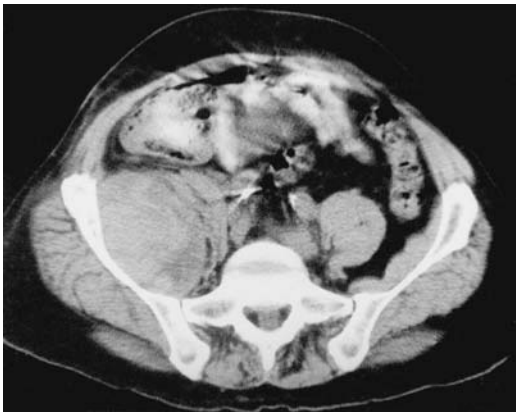

Figure 14.11. Psoas hematoma. Transverse CT image reveals an enlarged, hyperdense psoas muscle. (*Source:* Paley M, Sidhu PS, Evans RA, Karani JB. Retroperitoneal collections—aetiology and radiological implications. Clin Radiol 1997;52:290–294, with permission from the Royal Collage of Radiologists.)

Hematoma

Extraperitoneal Hematoma

Hematomas range from discrete collections to a diffuse infiltrate throughout the involved tissues. The most common site is in the rectus abdominis muscle, with other muscles, such as the internal oblique and gluteus muscles, less often involved.

Conventional radiography cannot identify even an extensive extraperitoneal hematoma, although an abnormality is suggested if the usual fatty tissue planes are obliterated. Computed tomography is generally preferred over US in evaluating suspected extraperitoneal hemorrhage.

As already discussed, CT findings depend on hematoma age, and they range from hyperdense fresh blood, typically >50 HU, to a fluid–fluid level (Fig. 14.11). Ultrasonography findings vary: an inhomogeneous cystic and hyperechoic appearance is common. With some hematomas a hemorrhagic neoplasm is in the differential diagnosis, although rapid onset should suggest the correct diagnosis.

A resolving hematoma has a hyperintense rim on precontrast T1-weighted images.

Spontaneous muscle hematomas are often associated with anticoagulation therapy; if necessary, they are amenable to being percutaneously decompressed.

Abdominal Wall Hematoma

The most common rectus abdominis muscle and sheath tumors consist of desmoids and hematomas. Rectus sheath hematomas occur spontaneously or are traumatic in origin (Table 14.1). Clinically, these hematomas are difficult to detect. A typical hematoma develops in the lower third of the abdominal wall. In the upper abdomen the rectus sheath limits spread, while inferiorly this sheath is incomplete and a hematoma spreads medially and laterally. Also, inferiorly the rectus muscle is separated from the peritoneum and properitoneal fat only by

Table 14.1. Etiology of rectus sheath hematomas

Spontaneous
Anticoagulant therapy
Steroid therapy
Thrombocytopenia
Hemodialysis
Collagen disease
Idiopathic (especially in elderly patients)
Traumatic
Direct trauma, including surgical
Vigorous muscle exertion
Physical exertion
Coughing
Seizures
Pregnancy and labor
Tetanus

transversalis fascia, and rupture of the inferior epigastric artery branches in the preperitoneal fat results in a hematoma throughout this region.

A typical clinical presentation is a rapidly growing painful abdominal wall swelling. Some patients develop anemia. Therapy in most patients is conservative once imaging confirms the diagnosis.

Computed tomography reveals an acute hematoma to be hyperdense compared to adjacent muscles, primarily because of its hemoglobin content. Most so-called rectus sheath hematomas are located posterior to the rectus abdominis muscle but do involve the muscle and result in muscle enlargement. Some hematomas also contain a fluid–fluid level due to a hematocrit effect. In time, a hematoma loses protein and becomes isodense or hypodense relative to adjacent muscle. Some eventually become surrounded by a capsule.

Ultrasonography results vary depending on hematoma age. An inhomogeneous appearance due to blood and blood clots is found in some. Similar to CT, a fluid–fluid level is evident in others, especially larger ones. Ultrasonography, however, can confuse a hematoma with an abdominal wall neoplasm.

Magnetic resonance imaging reveals a heterogeneous hyperintense signals both on T1- and T2-weighted images. Fluid–fluid levels are also detected on MR images.

Cysts

Lymphangiomas, lymphoceles, urinomas, and cystic mesotheliomas are discussed separately in this chapter. Cystic tumors also include rare primary cysts, cystic neoplasms, hematomas, aneurysms, and related entities. Anecdotal reports also describe extraperitoneal bronchogenic cysts (40). Pancreatic pseudocysts (which are not necessarily in the pancreas) and enteric duplications are also in the differential diagnosis if a cyst origin cannot be precisely identified. Incidentally, not all pseudocysts are pancreatic in origin; a pseudocyst developing around the tip of a ventriculoperitoneal shunt contains cerebrospinal fluid (41).

Mesenteric Cysts

The term *mesenteric cyst* is a descriptive one for cystic structures located in the mesentery. Most occur close to the mesenteric root. They have several etiologies, although some cysts are difficult to classify even after histopathologic study. Cyst content varies considerably. Some cysts lack a mucosal lining, thus distinguishing them from a bowel duplication, while others are lined by ciliated, cuboidal or columnar cells. The cyst wall and any septa can contain smooth muscle, fat or lymphovascular tissue. In adults, many are inclusion cysts (discussed later), while in children lymphangiomas are high in the differential.

A number of these cysts are discovered incidentally. Some patients have chronic pain. Cyst rupture or torsion may result in an acute abdomen. A mesenteric cyst tends to change its position as the mesenteric structures shift.

These cysts vary in size. The cyst wall is thin to the point of being barely perceptible, thus differentiating it from an enteric duplication, which has a thick wall. Most of these cysts contain clear fluid, although more proximal jejunal cysts tend to contain chyle. Some of these chylous cysts have a characteristic appearance; they tend to be unilocular and contain a fluid–fluid level visible by imaging. The two fluids are of fat and water densities, with the uppermost containing fat. The two fluids mix with a change in patient position.

Their MR appearance varies depending on cyst content. The cyst wall enhances postcontrast.

Mesenteric cysts should probably be completely excised whenever possible; incompletely excised cysts tend to recur and an occasional one even undergoes malignant transformation.

Omental Cysts

In general, the types of cyst found in the mesentery also develop in the omentum. The most common omental cyst is a lymphangioma.

Inclusion (Mesothelial) Cysts

Peritoneal inclusion cysts, also known as *mesothelial cysts* and *benign cystic mesotheliomas*, are found in premenopausal women and typically are located adjacent to an ovary or surround the ovary. Histologically, the cyst wall is of mesothelial origin, although occasionally it undergoes squamous metaplasia. Their relationship to benign mesotheliomas (discussed in a later section) is unclear. They are not neoplastic or premalignant.

Some peritoneal fluid originates as an exudate from ovaries. This fluid is normally absorbed by the peritoneum, except in a setting of an injured peritoneum and resultant fibrosis when fluid tends to accumulate in discrete cavities surrounded by mesothelial proliferation.

These women present with pelvic pain. Most have had previous surgery, pelvic inflammatory disease, or endometriosis.

Imaging shows a single cyst, at times containing septations, or a multilocular structure. Computed tomography and US identify multiseptated, thin- or thick-walled cysts. In some women a *spider-in-a-web* appearance is found, with the *spider* representing an entrapped ovary (42). In general, in premenopausal women with prior pelvic surgery, an US finding of an ovary inside a complex cyst is typical for a peritoneal inclusion cyst. At times the appearance mimics a hydrosalpinx or an ovarian malignant cystic neoplasm if a separate ovary cannot be identified. A paraovarian cyst is also in the differential diagnosis, although in this entity a distinct and separate ovary is identified.

Endovaginal Doppler US reveals low resistive flow within the septations.

Some of these cysts are adequately treated by simple drainage, while others recur. Recurrent cysts can be treated by transvaginal US-guided drainage and ethanol instillation into the cavity; any subsequent recurrence is also similarly treated.

Presacral Cysts

A list of presacral cystic tumors is rather extensive (Table 14.2). Discussed here are developmental cysts, which include epidermoid cysts, dermoid cysts, enteric cysts, and neurenteric cysts. A rare mesenteric cyst is presacral in location.

As the name implies, these cysts are located anterior to the sacrum and posterior to the rectum, are lined by epithelium, and are believed to originate from residual embryonic tissue. Some manifest in children; in adults these cysts are more common in women. The rare Currarino syndrome consists of an anorectal malformation, a sacral bone defect, and a presacral tumor such as a teratoma, meningocele, or a developmental cyst.

Epidermoid cysts are lined with squamous epithelium and contain a clear fluid. Dermoid cysts are also lined with squamous epithelium but contain additional dermoid components—hair follicles, teeth structures, and so on. They also contain lipid material. Rarely, multiple dermoid cysts develop. The enteric origin tailgut cysts are lined by a variety of epithelium, at times containing columnar, squamous, and transitional epithelium. To be considered a rectal duplication cyst it should be part of the

Table 14.2. Cystic presacral tumors

Development cysts
Epidermoid cysts
Dermoid cysts
Neurenteric cysts
Cystic hamartomas
Rectal duplications
Neoplasms
Sacral origin neoplasms
Chordoma
Teratoma
Cystic meningocele
Necrotic presacral neoplasms
Necrotic rectal neoplasms
Other
Cystic lymphangioma
Abscess
Hemangioma

Figure 14.12. Remnants of a presacral cyst (arrow) after partial resection. The rectum is displaced to the left. (Courtesy of Algidas Basevicius, M.D., Kaunas Medical University, Kaunas, Lithuania.)

rectal wall, contain rectal mucosa, and be surrounded by smooth muscle. The contained fluid has a mucous consistency.

Many presacral cysts are discovered incidentally. Some are detected on rectal examination as a posterior rectal tumor or a chronic fistula posterior to the anus. If sufficiently large, bowel obstructive symptoms or dysuria develop.

Imaging reveals a thin-walled, unilocular cyst, thus distinguishing these cysts from necrotic neoplasms and abscesses. A barium enema shows a soft tissue tumor posterior to the rectum; occasionally contrast outlines a fistulous tract. Calcifications are rare. A typical MR appearance is that of a hypointense lesion on T1- and hyperintense on T2-weighted images. Hyperintense regions on T1-weighted images should suggest fat in a dermoid cyst; occasionally old blood or mucus will have a similar appearance.

Complications include infection, fistula, and malignant degeneration (Fig. 14.12). Especially if infected, a cyst will appear thick-walled. Associated soft tissue nodules or thick septa, especially if irregular in appearance, are seen with a malignancy.

Hemangioma

Hemangiomas represent a developmental anomaly rather than a neoplasm and consist of endothelial-lined blood-filled channels. Most common are cavernous hemangiomas, then capillary ones, and least common and most difficult to diagnose and resect are extraperitoneal venous hemangiomas, which when large are called *monstrous hemangiomas*. Histology of the latter reveals blood vessel walls. A transition from hemangioma to angiomyoma exists with these tumors. At times their large size and slow blood flow preclude even an angiographic diagnosis (43).

In distinction to the liver, most mesenteric hemangiomas occur in the pediatric population; only an occasional one is detected in an adult.

Lymphangioma

Cystic lymphangiomas are either congenital or acquired, with many found in children. Often located at the root of the mesentery, these chyle-containing fluid collections represent lymphatic structures analogous to hemangiomas. They are lined by normal endothelial cells. Lymphoid tissue is often found at the periphery. An occasional one is extraperitoneal in location. They range from unilocular to multilocular, and from single to diffuse lymphangiomatosis.

Some lymphangiomas are detected incidentally. An occasional one results in intractable chyluria, bowel obstruction or an acute abdomen. It is mostly the mesenteric lymphangiomas which result in an acute abdomen due to bowel obstruction and related complications. Some lymphangiomas are associated with recurrent gastric or small bowel volvulus. An occasional one enlarges rapidly secondary to intracystic hemorrhage. Some of these lymphangioma are associated with recurrent gastric or small bowel volvulus.

Some lymphangiomas can be suspected with imaging, with the diagnosis confirmed by aspiration cytology. Especially in children, conventional radiography detects a large, noncalcified tumor. Ultrasonography reveals a cystic tumor containing thin septations. Some cystic lymphangiomas in adults contain calcifications. The solid tumor portion and capsule enhance post-contrast. The cyst content is either of fluid attenuation or higher, presumably because of bleeding or infection. A lipid-containing lymphangioma suggests a lipomatous tumor.

Ultrasonography shows cystic lymphangiomas as cystic tumors containing septations

and occasionally nodules. These lesions are predominantly anechoic. Any hyperechoic debris is presumably secondary to either hemorrhage or infection. Cyst septations are better identified with US than with CT. Magnetic resonance findings vary depending on the amount of protein and blood present. The multilocular appearance and enhancing stroma and capsule as shown by CT should suggest the diagnosis.

An occasional multicystic mesothelioma or cystadenocarcinoma has a similar imaging appearance, and tissue and fluid are necessary to confirm the diagnosis. Aspiration cytology reveals macrophages and abundant lymphocytes.

Percutaneous lymphangioma sclerotherapy with an alcoholic solution results in inconsistent results.

Pseudomyxoma Peritonei

Clinical

Pseudomyxoma peritonei is a poorly understood condition and its definition is controversial. It is characterized by mucinous ascites and peritoneal tumor implants. Rarely, it is associated with a paraneoplastic syndrome. Some authors use the term *pseudomyxoma peritonei* only for a malignancy, while others also include benign tumors. The most common primary site is the ovary; less common is an appendiceal origin, and perhaps least common is an urachal origin. A rare intraductal papillary mucinous neoplasm of the pancreas is associated with pseudomyxoma peritonei (44). At times synchronous mucinous tumors are detected both in the appendix and ovary, or colon and ovary, together with pseudomyxoma peritonei; the former tumors probably are not independent, but originate one from the other and rupture of one of these tumors probably results in pseudomyxoma peritonei, produced by well-differentiated columnar epithelium.

Only rarely does pseudomyxoma involve extraperitoneal tissues, appropriately called *pseudomyxoma retroperitonei*. Most of these are focal rather than diffuse. Thus an occasional mucinous tumor in a retrocecal appendix bursts and results in a retroperitoneal cystic tumor, detectable by imaging.

Some authors subdivide this condition into two distinct categories (45): a disseminated peritoneal adenomucinosis and a peritoneal mucinous carcinomatosis. The former is composed of extracellular mucin and a mucinous epithelium with little cytologic atypia or mitotic activity, at times with an associated appendiceal mucinous adenoma. The latter is composed of a more abundant mucinous epithelium having features of a carcinoma, at times with an associated mucinous adenocarcinoma. In some patients this condition is intermediate between the adenomucinosis and carcinomatosis varieties. The primary reason in subdividing this entity is a difference in prognosis; the 5-year survival rates for patients with adenomucinosis are 84%, with the intermediate form 38%, and 7% for patients with the carcinomatosis variety (45).

Only rarely can the entire tumor be resected, with debulking being the most common operation performed. Because of extensive peritoneal involvement, these patients tend to develop recurrent bowel obstructions. The results of chemotherapy vary.

Imaging

With the peritoneal cavity filled with sebaceous material, abdominal radiography reveals a wide fat stripe between the parietal peritoneum and lateral wall of the ascending colon, mimicking increased intraperitoneal fat. Occasionally curvilinear calcifications develop here. Right lower quadrant calcifications can also be seen in myxoglobulosis.

Computed tomography reveals pseudomyxoma peritonei as numerous, septated, heterogeneous intraabdominal cysts, with cyst content having a density higher than water. The liver and spleen outlines are often scalloped due to adjacent implants. Ultrasonography shows that the viscous fluid is not mobile, with numerous echoes corresponding to the gelatinous masses. Occasionally the viscous fluid and cyst walls have a highly hyperechoic appearance. Ultrasonography is useful in identifying less viscid material for biopsy.

Pseudomyxoma nodules are hypointense on T1-weighted MR images (Fig. 14.13). Any adenocarcinoma component enhances after iv gadolinium.

At times differentiation of pseudomyxoma peritonei from ascites can be difficult. With ascites, small bowel loops tend to float on top;

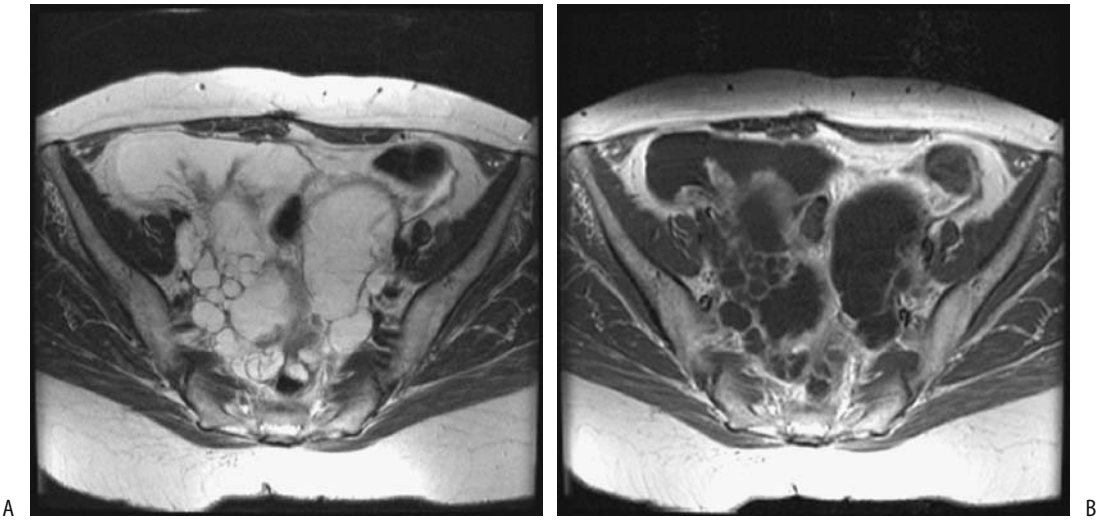

Figure 14.13. Pseudomyxoma peritonei. A: Transverse fast spin echo (FSE) T2-weighted magnetic resonance (MR) image identifies a hyperintense tumor. B: Enhancement of solid component is evident on postcontrast fat-saturated T1-weighted image. (*Source:* Szklaruk J, Tamm EP, Choi H, Varavithya V. Magnetic resonance imaging of common and uncommon large pelvic masses. RadioGraphics 2003;23:403–424, with permission from the Radiological Society of North America.)

with pseudomyxoma peritonei bowel loops are more centrally displaced and compressed.

Solid Tumors

Discussed here are intraperitoneal and primary extraperitoneal tumors originating outside discrete organs. They are not common. A majority are malignant. Clinical presentation with these tumors varies depending on the structure affected. An example of an unusual presentation is a primitive extraperitoneal tumor manifesting as a varicocele (46).

Imaging

Intra- and extraperitoneal tumors show considerable variability in their imaging findings, and the individual tumor types are thus discussed separately. Nevertheless, some general conclusions are apparent. For solid tumor detection MRI appears superior to CT. In patients with known or suspected extrahepatic malignancies, abdominal contrast-enhanced CT detected 70% of proven tumor sites compared with 91% for MRI (47); MRI detected significantly more tumors involving peritoneum, bowel, vascular structures, and bones. For benign disease, on the other hand, no significant differences were evident between the two imaging modalities.

In general, CT criteria do not distinguish between benign and malignant tumors, although a malignancy is suggested if the patient is symptomatic and imaging detects a large tumor with irregular margins. Calcifications suggest a benign tumor, but exceptions do occur. Invasion of surrounding structures is an obvious feature of malignancy tumors. Contrast enhancement of a solid component is common with a malignancy but is also seen with benign tumors.

Adenopathy

Benign lymph node hyperplasia occurs in a number of chronic disorders, with Laënnec's cirrhosis and Crohn's disease being common examples. The prevalence of node hyperplasia increases with the severity of disease, being especially common in end-stage cirrhosis.

Tumor-Associated Adenopathy

Heavily calcified lymph nodes generally imply prior infection, but calcifications, often visible by CT, do occur with malignant infiltration.

Para-aortic adenopathy is more common with non-Hodgkin's lymphoma than with Hodgkin's lymphoma. Imaging shows either discretely enlarged nodes or confluent tumors. These nodes are hypoechoic or even anechoic with US. Nonlymphomatous tumor involvement generally results in a more hyperechoic and heterogeneous lymph node appearance.

With most tumors, including lymphoma, CT and MR simply detect whether lymph nodes are enlarged or not. Most authors simply assume that nodes above a certain size are malignant, with 10 mm often being a cutoff size used; this limit achieves a low sensitivity but specificity is >90% in detecting lymph node metastasis. CT and MRI appear comparable in detecting most lymph node enlargement. Also, one should keep in mind that asymmetry of small pelvic nodes is not uncommon, even with normal nodes. Magnetic resonance readily differentiates lymph nodes from vascular structures, a task occasionally difficult with CT. At times even contrast-enhanced CT does not differentiate between some pelvic lymph nodes and venous structures because some nodes also enhance.

Based on tissue characterization, neither CT nor unenhanced MR differentiates between neoplastic nodal infiltration and inflammatory conditions. T1 and T2 relaxation times of normal, inflammatory, and neoplastic nodes overlap and are not reliable in differentiating these conditions. Even gadolinium-enhanced MRI does not differentiate between normal nodes and metastasis-containing nodes. Exceptions to the above are nodes with central necrosis—regardless of size, these generally represent metastases, although exceptions also occur here because similar changes are found with neurofibromatosis, abdominal tuberculosis, and Whipple's disease.

Potentially, color Doppler US can differentiate between reactive and malignant adenopathy by detecting intranodal focal perfusion defects, aberrant central vessels, displacement of intranodal vessels, and the presence of subcapsular vessels, findings pointing toward a malignancy. One color Doppler US study of superficial lymph nodes achieved a 96% sensitivity and 77% specificity in differentiating reactive and malignant nodes (48).

Laparoscopic US shows most benign lymph nodes to have a hyperechoic center and an oval shape, while neoplastic nodes tend to be more round and inhomogeneous. There is, however, considerable overlap in the appearance of benign and malignant nodes. Also, fatty infiltration makes some nodes blend into the surrounding soft tissues.

Ultrasmall superparamagnetic iron oxide particles (ferumoxtran), however, are taken up by normal lymph tissue but not metastatic foci, and the use of this contrast agent thus selectively decreases T2-weighted signal intensity of even normal-sized nodes but not those containing metastases. Ferumoxtran-enhanced MRI is unique among present-day imaging modalities in being able to detect metastases even in normal-sized lymph nodes. Potentially, FDG-PET has similar capabilities in visualizing lymph node metastases, although it accumulates in the bladder and obscures visualization of pelvic nodes.

Once enlarged lymph nodes are detected, fine-needle aspiration using appropriate image guidance is accurate in differentiating between neoplastic and inflammatory nodes. Some lymph nodes are accessible for endoscopic US-guided aspiration.

Mesenteric Adenitis

Mesenteric adenitis is a description of pathologic findings rather than a specific disease. Clinically, it often mimics appendicitis. A not uncommon presentation is a patient with an acute onset of right lower quadrant pain, imaging reveals enlarged mesenteric lymph nodes, and a normal appendix is found at surgery. Associated ileal or ileocecal wall thickening is identified in some patients. *Yersinia enterocolitica* infection is a common cause, although in only about half of these patients is an eventual etiology identified.

Castleman's Disease

Angiofollicular lymph node hyperplasia, or Castleman's disease, is not common. Enlarged nodes range from unicentric (focal) to multicentric (generalized). An isolated extraperitoneal conglomerate tumor is one form of presentation. Less common is extranodal involvement, including intrahepatic disease. Two histologic types of this disease exist—a more

frequent hyalin vascular type and a plasma cell type—although occasionally found is a mixture of both types. Histologic features consist of lymph node hyperplasia and capillary proliferation.

In a rare patient both multicentric Castleman's disease and primary effusion lymphoma coexist, and presumably lymphoid cells have undergone malignant transformation. Rarely, a high-grade lymphoma develops even in the localized form of Castleman's disease (49). An association with Kaposi's sarcoma has been described.

Castleman's disease occurs in both children and adults. Clinically, it overlaps with some immunologic conditions. Although Castleman's disease is often considered to be benign, the multicentric type has a poor prognosis. Anemia and hypergammaglobulinemia develop, especially with the plasma cell variety. In many of these patients a malignancy is the major differential consideration. One should keep in mind that a pathologist may not be able to differentiate Castleman's disease from Hodgkin's lymphoma on fine-needle aspiration cytology (50), and although imaging defines these tumors, diagnosis is made from biopsy or surgical tissue.

The most common imaging appearance of Castleman's disease is of a well-defined tumor, enhancing homogeneously when small but becoming heterogeneous with growth due to central necrosis (51). Computed tomography and US of extraperitoneal Castleman's disease identify a well-defined, highly vascular tumor mimicking a malignancy (52). Some of these tumors develop vascular encasement. An occasional one develops calcifications. Magnetic resonance imaging also readily detects adenopathy.

Whole-body PET imaging in a patient with Castleman's disease localized FDG to a pelvic tumor identified previously by CT (53); uptake was less than expected for a low- to intermediate-grade lymphoma.

Surgical resection of unicentric Castleman's disease tends to be curative. Clinical and biochemical abnormalities clear after tumor resection.

An example: Computed tomography and MRI identified hydronephrosis and a tumor adjacent to the right ureter in a 45-year-old woman; a right nephrectomy was performed for a presumed primary ureteral tumor, but histology revealed plasma cell type of Castleman's disease (54). A year later CT revealed left hydronephrosis and a tumor adjacent to the ureter; steroid therapy was instituted for presumed Castleman's disease and the tumor resolved.

Necrotizing Lymphadenitis (Kikuchi-Fujimoto Disease)

Necrotizing lymphadenitis, also called *histiocytic necrotizing lymphadenitis*, *apoptotic lymphadenitis,* and *Kikuchi-Fujimoto disease*, develops mostly in young women and usually resolves spontaneously. Fever and lymphadenopathy are the usual clinical findings. Head and neck adenopathy is most common, but some develop retroperitoneal involvement or splenomegaly. Lymph node infiltration by histiocytes and plasma cells in a setting of lymph node necrosis is a common feature, albeit necrosis is not always found. It is a disease of unknown etiology; a hyperimmune reaction to a possible viral infection has been both suggested and denied. Two women developed necrotizing lymphadenitis during remission of diffuse large B-cell lymphoma (55). Necrotizing lymphadenitis and systemic lupus erythematosus have developed in the same patient. In fact, a type of necrotizing lymphadenitis does exist in lupus, and some type of relationship between the two entities would not be surprising.

Imaging identifies adenopathy, either focal or diffuse. Computed tomography and MR in three patients showed uniformly enhancing small lymph nodes in the submandibular, axillary, gastrohepatic, celiac, periportal, paraaortic, retrocrural, mesenteric, and inguinal regions (56); the lymph nodes were <18 mm in diameter.

The differential diagnosis includes infections such as toxoplasmosis and tuberculosis, Castleman's disease, and malignant lymphoma.

Lymphoma

Clinical

The World Health Organization in 1997 classified lymphomas based on clinical, morphologic, immunologic, and genetic grounds. Lymphomas are subdivided into B-cell neoplasms, T-cell neoplasms, and Hodgkin's disease. Both B-cell and T-cell neoplasms are further subdivided into precursor neoplasms

and peripheral neoplasms. Peripheral T-cell neoplasms can be further subdivided into disseminated, primary extranodal, and predominantly nodal. Location and clinical syndrome aid in further defining T-cell lymphoma.

The human herpesvirus type 8 (HHV-8 or Kaposi's sarcoma–associated herpesvirus) is associated with primary effusion lymphoma (or body cavity lymphoma) and multicentric Castleman's disease. This virus may also have a role in other lymphomas, including multiple myeloma and some atypical lymphoproliferations, and in sarcoidosis, although the evidence is not firm.

Primarily splenic and extraperitoneal involvement is a hallmark of Hodgkin's lymphoma. The vast majority of primary extranodal lymphomas are non-Hodgkin's; they involve the extraperitoneum, bowel, mesentery, and other adjacent structures. Lymphomatous omental infiltration is uncommon, with most omental involvement being with non-Hodgkin's lymphoma. Malignant nodal lymphoma prognosis and therapy differ from bowel lymphoma. With the exception of mucosa-associated lymphoid tissue (MALT) lymphomas, most non-Hodgkin's lymphomas are highly malignant.

Abdominal pain is a common presentation. Diffuse infiltration evolving into bowel obstruction and perforation can lead to an initial presentation of an acute abdomen.

The principal therapeutic options with diffuse lymphoma are chemotherapy and radiotherapy. Chemotherapy combined with autologous hematopoietic stem cell infusion improves patient survival in those with relapsing high-grade non-Hodgkin's lymphoma. Considerable current research involves the use of antibodies against lymphoma cells.

Imaging

With clinically suspected lymphoma, lymphangiography has been replaced by CT. Numerous studies show that the ability to detect abnormal extraperitoneal lymph nodes is roughly comparable between lymphangiography and CT, but CT has the advantage of also imaging intraperitoneal and other lymph nodes not normally opacified during lymphangiography. Especially with non-Hodgkin's lymphoma and its high propensity for mesenteric nodal involvement, CT has obvious advantages. Although in the United States CT has also evolved as the dominant imaging modality with Hodgkin's lymphoma, the advantages of CT over lymphangiography in this setting are not as clear-cut, and lymphangiography continues to be performed for Hodgkin's lymphoma more often in parts of Europe. Because lymphangiography can suggest tumor infiltration even in normal-sized nodes, the presence of supradiaphragmatic Hodgkin's lymphoma and a normal abdominal CT is considered in some European centers to be an indication for staging lymphangiography. For an adequate nodal evaluation, however, a technically excellent lymphangiogram is necessary, and appropriate skill in performing these studies is not available in all centers. Also, mild adenopathy and node foaminess do not imply lymphomatous involvement and are seen in a number of nonneoplastic conditions. In any case, staging laparotomy has made a discussion of the relative merits of CT and lymphangiography a moot point in most patients. Although more invasive than lymphangiography, laparotomy staging is considered to be more accurate.

The role of lymphoscintigraphy is still debated. Such scintigraphic agents as Tc-99m–diethylenetriamine pentaacetic acid (DTPA)–human serum albumin show promise in lymphoma staging.

Abdominal lymphomas range from nodular to bulky confluent tumors. Mesenteric nodal involvement is considerably more common with non-Hodgkin's lymphoma than with Hodgkin's lymphoma. Nodal involvement is seen as numerous smooth soft tissue tumors within the mesentery. Extensive nodal involvement results in confluent mesenteric masses surrounding major vessels (Figs. 14.14 and 14.15). Lymphomas tend to have a homogeneous CT density. With the exception of melanoma, carcinomatosis more often leads to a diffuse mesenteric infiltrate. A rare lymphoma involves the peritoneal surfaces diffusely; it is indistinguishable from carcinomatosis.

Most calcifications in a setting of lymphoma develop after therapy, although a rare untreated Burkitt's lymphoma contains calcifications.

Ultrasonography has a limited role in lymphoma detection. Tumor involvement ranges from diffuse and nodular to large confluent masses. Involved nodes are homogeneous and mostly hypoechoic in appearance.

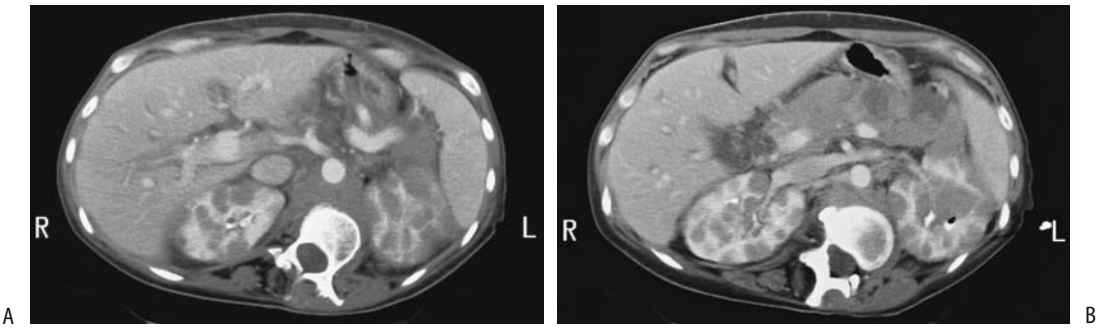

A B

Figure 14.14. Abdominal lymphoma. A,B: Two contrast-enhanced CT images reveal an enlarged pancreas, encased great vessels and numerous renal tumors. (Courtesy of Patrick Fultz, M.D., University of Rochester.)

Computed tomography is often used to follow a patient with prior lymphoma, with MR being a viable alternative. Yet among 78 patients with stages I to III of follicular lymphoma who relapsed, only 14% of recurrences were detected primarily with abdominal or pelvic CT, with clinical, hematologic, and other imaging detecting the rest (57).

Magnetic resonance imaging in initial tumor detection and staging is still evolving. It has established its usefulness during the first 6 months after therapy in following the tumor size, but the signal intensity patterns during this time are not specific for identifying recurrence. However, MRI does differentiate late posttherapy fibrosis (hypointense on T2-weighted images) from viable lymph nodes (hyperintense or heterogeneous on T2-weighted images). Also, fibrotic tissue shows minimal MR enhancement postcontrast, while recurrence generally enhances markedly. Such lymph node enhancement is not limited to lymphoma; many benign conditions and nodal metastases also enhance.

An exception to the use of CT or MR is in patients who have undergone a prior lymphangiogram, where conventional radiography is often sufficient to visualize any change in opacified nodes.

Biopsy, regardless of how it is obtained, is generally diagnostic. Fine-needle aspiration cytology, although usually diagnostic, occasionally cannot distinguish reactive lymphoid hyperplasia from malignant lymphoma.

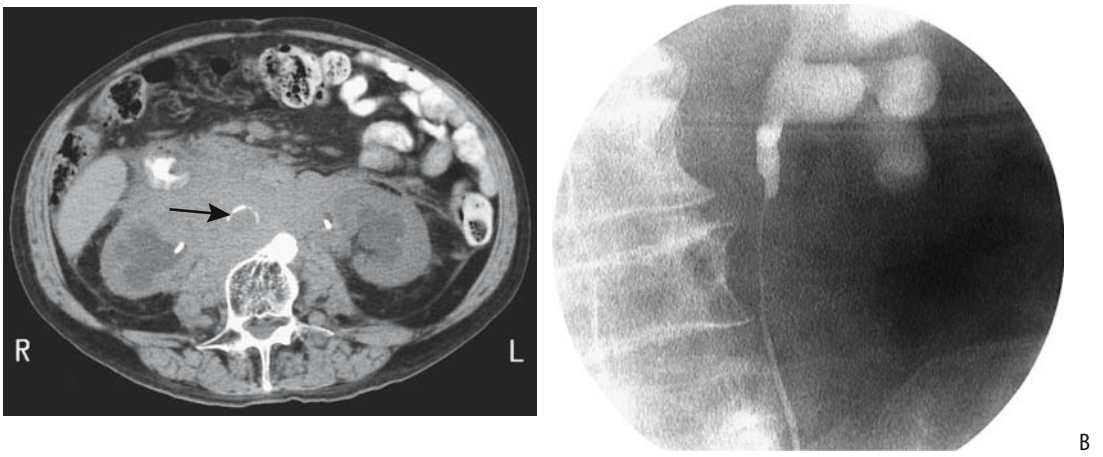

A B

Figure 14.15. Lymphoma obstructing ureters. A: CT identifies a bulky retroperitoneal infiltration encasing a calcified aorta (arrow). Bilateral ureteral catheters are in place. B: Retrograde urethrogram reveals a long extrinsic left ureteral obstruction. (Courtesy of Patrick Fultz, M.D., University of Rochester.)

Some involved lymph nodes do not revert to normal size after successful therapy. In addition, considerable distortion is produced by fibrosis. Magnetic resonance is helpful in this setting; fibrosis is hypointense on both T1- and T2-weighted images. This issue is not always clear-cut, because not only neoplasms but also inflammation and necrosis have an increased signal intensity on T2-weighted images.

Gallium-67 scintigraphy is useful in staging and evaluating lymphoma therapy for both Hodgkin's disease and non-Hodgkin's lymphoma. Viable lymphoma tissue takes up Ga 67, a finding not seen with residual fibrosis or necrotic tissue, and an abnormal uptake of Ga-67 citrate after chemotherapy generally implies residual tumor. Nevertheless, Ga 67 has a relatively low sensitivity with low-grade lymphoma.

2-[18F]-fluoro-deoxy-D-glucose PET is highly sensitive in detecting viable tumor and is superior to both CT and Ga-67 scintigraphy. Computer tomography, however, provides additional information, including localization, and thus the current interest in combined PET-CT units. Of note is that PET-FDG detects both Hodgkin's and non-Hodgkin's lymphomas but does not differentiate between them. It has a low sensitivity in detecting MALT lymphomas. In general, tumor-to-background activity is greatest with high-grade lymphomas. It detects even normal-sized involved lymph nodes, and PET detects both nodal and extranodal involvement, although the sensitivity appears to be lower for bone marrow involvement than for other sites. False-positive findings occur with some nodes affected by inflammatory disease. The reverse is also true—inflammation may obscure tumor involvement because of increased uptake. The current primary role of FDG-PET is in evaluating residual deformity after therapy by accumulating FDG in viable tumors but not in fibrosis, a task not suitable for CT.

Plasmacytoma

An extramedullary plasmacytoma can occur as an isolated manifestation; it can be a metastasis from another site, or evolve into generalized disease (i.e., multiple myeloma). Most extramedullary plasmacytomas occur in lymph nodes. The diagnosis is often unsuspected prior to cytology.

The most common CT finding is that of a hypodense tumor with little contrast enhancement. Pre- and postcontrast T1-weighted MR combined with fast spin echo (FSE) short-time inversion recovery (STIR) sequences should detect both focal bone marrow plasmocytomas and diffuse infiltration.

Lymphangioleiomyomatosis

Lymphangioleiomyomatosis is a rare condition difficult to classify, but probably of hamartomatous origin. It consists of smooth muscle proliferation within lymphatics. A single lymphangioleiomyoma is less common than lymphangioleiomyomatosis. The mediastinum, lungs (pulmonary cysts), and retroperitoneum are most often involved, less often the kidneys and other structures. It is related to tuberous sclerosis; in fact, one of the gene mutations found in tuberous sclerosis is also common in lymphangioleiomyomatosis. Pulmonary lymphangioleiomyomatosis tends to be associated with renal angiomyolipomas and, less often, with abdominal lymphangioleiomyomatosis. Some endothelium-lined lymphangiomas (discussed in a previous section) and lymphangioleiomyomas have a similar imaging appearance, with the difference being that the former contains no smooth muscle cells—a finding established by histology. Their etiologies also appear to differ. Abdominal lymphangioleiomyomatosis is due to proliferation of lymphatic smooth muscle cells and the resultant lymphatic obstruction. Most occur in women of childbearing age, with only an occasional lymphangioleiomyoma described in a young child.

In patients with thoracic lymphangioleiomyomatosis, renal angiomyolipomas were found in 54%, abdominal lymphadenopathy in 39%, lymphangiomyomas in 16%, ascites in 10%, a dilated thoracic duct in 9%, and hepatic angiomyolipomas in 4% (58); a direct correlation existed between abdominal lymphadenopathy and the severity of lung disease.

Imaging detects solid or cystic tumors, mostly in the retroperitoneum. Associated lymph node enlargement is common. Of interest is that some of these lymph nodes are hypodense and contain lymph, while others enhance postcontrast, presumably secondary to their mostly smooth muscle content.

Inflammatory Pseudotumor (Fibrosarcoma)

An unusual entity is the so-called inflammatory pseudotumor or fibrosarcoma, a condition believed to be nonneoplastic by some. A number of terms are used in the literature to describe this condition (Table 14.3) and they reflect divergent views held among pathologists about its pathogenesis. Whether the tumors described represent one entity or are a collection of several conditions, are histogenetically related or not, inflammatory or neoplastic, benign or malignant, is conjecture. These tumors were first described in the lungs but they occur throughout the body, including bowel, mesentery, liver, and extraperitoneum. Histologically they consist of fibroblasts, myofibroblasts, variable amounts of fibrosis, and occasional calcifications, and include an inflammatory infiltrate consisting of lymphocytes, plasma cells, and eosinophils. Myofibroblasts appear to play a central role, hence the inclusion of this term in some of the nomenclature. These tumors differ from granular cell myoblastomas, which are considered to be of neural origin. They also differ from xanthogranulomatosis (discussed earlier; see Diffuse Infiltration).

Pathologically, these tumors exhibit considerable heterogeneity, and a diagnosis from a needle biopsy specimen is difficult; immunohistologic studies are often not helpful. They tend to have benign-appearing cytology and often have relative hypocellularity. Clonal chromosomal aberrations have been detected in some, suggesting a malignant tendency. Polymerase chain reaction studies for Epstein-Barr virus and cytomegalovirus suggest that these viruses do not play a role in this entity.

Table 14.3. Alternate terms used for inflammatory pseudotumor (these do not necessarily represent a single pathologic entity)

Fibrosarcoma
Plasma cell granuloma
Inflammatory myofibroblastic tumor
Inflammatory myofibrohistiocytic proliferation
Xanthoma
Fibroxanthoma
Histiocytoma
Plasmacytoma
Solitary mast cell tumor

Most of these tumors occur in children, but they range from neonates to elderly. Clinically, patients present with pain, anemia, a palpable tumor, or bowel obstruction. Many initially manifest an indolent clinical course and an aberrant response to tissue injury is postulated as a likely pathogenesis. Others, however, act in a malignant fashion. Recurrence is common unless widely excised. Metastases have been reported.

Primary Carcinoma

An unusual entity called *normal-sized ovary carcinoma syndrome*, *primary papillary serous peritoneal carcinoma* and other similar names, consists of diffuse malignant abdominal cavity involvement, normal size ovaries, and no obvious source for a primary malignancy found by either preoperative or operative evaluation. In general, distinguishing primary peritoneal tumors such as malignant mesotheliomas and serous surface papillary adenocarcinomas from metastatic peritoneal tumors is a challenge and involves the use of a hyaluronidase digestion test, electron microscopy, and immunohistochemical antibody studies. Comparing women with primary peritoneal carcinoma with those with primary epithelial ovarian cancer reveals very similar findings.

Ascites is common. Peritoneal involvement is either nodular or diffuse (omental cake). The omentum is affected in most, but adenopathy develops only in a minority. An occasional peritoneal primary papillary serous carcinoma contains calcifications.

These rare primary peritoneal adenocarcinomas are a diagnosis of exclusion. In most patients an adenocarcinoma of unknown primary poses a diagnostic and therapeutic dilemma. In general, the yield from multiple diagnostic procedures aimed at detecting the primary site is low and, even if detected, the therapeutic options are limited. One exception to such a nihilistic approach is in those women presenting with malignant ascites and no pelvic tumor, but who are found to have a peritoneal serous papillary adenocarcinoma. Some of these tumors consist of numerous small nodules throughout the peritoneal cavity, at times beyond the resolution of imaging. A number of these tumors respond to chemotherapy and

have a good prognosis, thus the importance of differentiating this entity from metastatic ovarian carcinoma.

A primary mucinous cystadenocarcinoma, in a setting of normal ovaries, can develop in the extraperitoneum. A number of these tumors originate from ovarian tissue, although some are associated with normal ovaries. A possible origin is in heterotopic ovarian tissue, a teratoma, urogenital rest, intestinal duplication, or even some other metaplasia. One mucinous cystadenoma was in contact with the isthmus of a horseshoe kidney (59); the patient also had congenital absence of the left ovary.

Metastases/Carcinomatosis

Clinical

The most common primary site of peritoneal carcinomatosis is gynecologic; less often seen are gastric and colonic primaries, and rarely breast carcinoma. On rare occasions pancreatic papillary cystic neoplasms (discussed in Chapter 9) lead to peritoneal carcinomatosis, at times after abdominal trauma. Most frustrating, in some patients a primary site simply cannot be found (Fig. 14.16).

Figure 14.16. Primary peritoneal carcinomatosis in a man results in multiple sites of bowel obstruction.

Wilms' tumors spread to the peritoneal cavity; they develop mesenteric, greater omental, and pelvic metastases. Ascites is an inconsistent finding. These tumors range from broad infiltration to focal masses, findings detected by imaging.

Testicular cancers initially metastasize to the extraperitoneum. After successful chemotherapy residual enlarged nodes pose a dilemma: Do these represent necrotic, nonviable tumor or do they contain cancer? Complicating this issue is the rare metastatic testicular germ cell tumor evolving into a mature teratoma after being treated with chemotherapy and resection.

Metastasis to the umbilicus, in the United States often called *Sister Mary Joseph nodes*, is more common than a primary malignancy at this location. Most of these tumors have a gynecologic origin, with an occasional one being a renal cell carcinoma or some other sites. These metastases appear before, during, or after the primary tumor is detected. Associated peritoneal implants are common.

Tissue is generally needed for specific diagnosis, although even this may provide limited information. Image-guided 18-gauge needle biopsies of "omental cake" (which refers to extensive omental infiltration), peritoneal, or adnexal tumors in women with undiagnosed peritoneal carcinomatosis suggested a primary tumor site in only 77% (60); a poorly differentiated adenocarcinoma with an immunohistochemical profile suggesting ovarian cancer was found in another 20%. A peritoneal core biopsy, together with immunohistochemical analysis, establishes a site-specific diagnosis in most of these women.

Cytologic material is obtained from peritoneal washings as a follow-up in some women with ovarian cancer. A peritoneal reservoir can be implanted after tumor debulking and peritoneal washing cytology obtained at several-week intervals; a recurrence is detected in some women by peritoneal cytology prior to other positive findings.

Imaging

Imaging identifies peritoneal tumors, detects any cystic component, and at times suggests the site of origin. Imaging usually does not differentiate between benign and malignant, nor does it differentiate between primary and secondary

neoplasms. Also, the rare diffuse peritoneal leiomyomatosis is in the differential diagnosis. Although most imaging modalities detect widespread peritoneal carcinomatosis, early or small tumors are difficult to identify. Both CT and MR detect enlarged nodes.

Currently CT is the most often used imaging modality to study peritoneal carcinomatosis, although fat-saturated, spin echo contrast-enhanced MR sequences appear superior, being aided by peritoneal contrast enhancement (61). Computed tomography findings in patients with peritoneal carcinomatosis most often consist of peritoneal implants followed by ascites, mesenteric implants, and omental implants (Fig. 14.17). Tumor appearance varies with the site of involvement and the imaging technique used. Peritoneal implants range from small nodules, diffuse infiltration, to an irregular, thickened "cake." Ascites aids CT identification of small nodules. Mesenteric and omental implants likewise have a broad imaging spectrum, including omental cake. Contrast-enhanced CT of carcinomatosis and some infections often shows enhancement of a thickened peritoneum and does not differentiate between these entities. Visible peritoneal calcifications suggest metastatic ovarian carcinoma; most other metastases do not calcify heavily. Prior peritonitis can, of course, result in calcifications and extensive sheet-like deposits generally are due to benign disease rather than a malignancy.

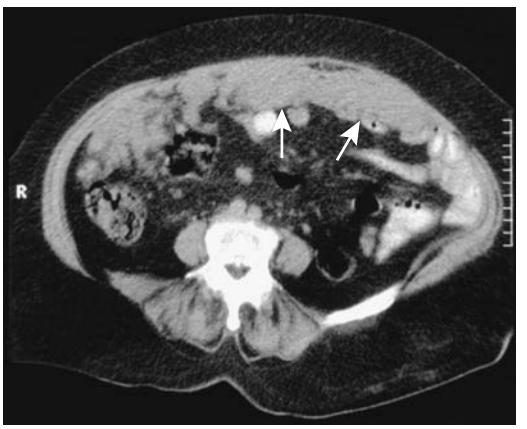

Figure 14.17. Peritoneal metastases from ovarian carcinoma. Computed tomography outlines an irregular cake-like tumor (arrows). (Courtesy of Algidas Basevicius, M.D., Kaunas Medical University, Kaunas, Lithuania.)

Ascites provides an acoustic window for US. In a setting of carcinomatosis US evaluates the extent of ascites, tumor nodules, and adenopathy, and can also image omental and mesenteric involvement.

A fat-suppression MR technique aids visualizing subtle carcinomatosis. Postcontrast MRI identifies an enhancing, thickened peritoneum, achieving sensitivities and specificities of about 90% in detecting peritoneal tumor spread. Peritoneal implants become hyperintense on postcontrast delayed MR images. An MRI finding of enhancing ascites 15 to 20 minutes after IV contrast is not uncommon in peritoneal carcinomatosis. Magnetic resonance lymphography using ultrasmall SPIO particles is a potential aid in detecting nodal disease, but these studies are currently more research than clinical.

An induced pneumoperitoneum during CT visualizes most tumor implants in the peritoneum, with the exception of the pelvis and some peritoneal recesses. A pneumoperitoneum allowed detection of intraabdominal adhesions.

Computed tomography does not detect subtle peritoneal metastases; for some of these, gallium-67 scintigraphy or FDG-PET appear to be superior, but keep in mind that occasionally even disseminated peritoneal carcinomatosis is not detected by PET; only limited data are available on this point. Indium-111–satumomab pendetide planar and SPECT imaging are useful in detecting some carcinomatosis.

In some parts of the world both tuberculous peritonitis and peritoneal carcinomatosis are encountered. The CT findings in both overlap (Table 14.4). Computed tomography, endoscopy, and even biopsy can suggest Crohn's disease, when in reality the patient has peritoneal carcinomatosis. Perforation of an ovarian cystic teratoma with intraperitoneal spill of cyst content also mimics carcinomatosis.

Although not common, hepatocellular carcinoma can result in intraperitoneal metastases, including omental seeding. Imaging reveals discrete single or multiple hypervascular nodules, with larger ones containing necrosis; adjacent vessel engorgement, including prominent draining veins, is identified in some.

Mesenchymal Tumors

A full range of mesenchymal neoplasms are encountered in the peritoneum and extraperi-

Table 14.4. Computed tomography differentiation of tuberculous peritonitis and peritoneal carcinomatosis

	Tuberculous peritonitis		Peritoneal carcinomatosis	
Reference	(62)	(63)	(62)	(63)
Number of patients	42	19	93	19
Peritoneal thickening				
Slight, smooth		79%		26%
Irregular		0%		47%
Peritoneal nodules		0%		37%
Mesenteric nodules		26%		16%
<5 mm in diameter	52%		52%	
≥5 mm	52%		12%	
Omental cakes	8%	21%	20%	37%
Splenomegaly	93%		50%	
Ascites	64%	100%	84%	100%

toneum. In general, a malignant mesenchymal neoplasm is more common than its benign counterpart. Some poorly differentiated sarcomas are difficult to classify (Fig. 14.18). The rare peritoneal adenosarcoma probably originates from regions of endometriosis.

Both malignant and benign fibrous tumors develop in the retroperitoneum and peritoneal cavity. Diffuse fibrosis/desmoid tumors have been discussed earlier.

Mesothelioma

A number of authors list mesothelioma as a separate type of neoplasm, although it is of mesenchymal origin, and the most common form is a sarcoma. Two types of mesothelioma exist: the more common malignant variety and a less common relatively benign form. Whether these represent a variation of the same entity or are different conditions is conjecture. One hypothesis is that the benign variety simply represents a proliferation of mesothelioma cells due to a reaction to an insult. In either case, even the benign mesotheliomas tend to recur unless completely resected.

Both the benign and malignant forms have similar imaging findings, although some benign peritoneal mesotheliomas have a multicystic imaging appearance and thus mimic other cystic tumors. These tumors range from small peritoneal nodules, large tumors, to diffuse peri-

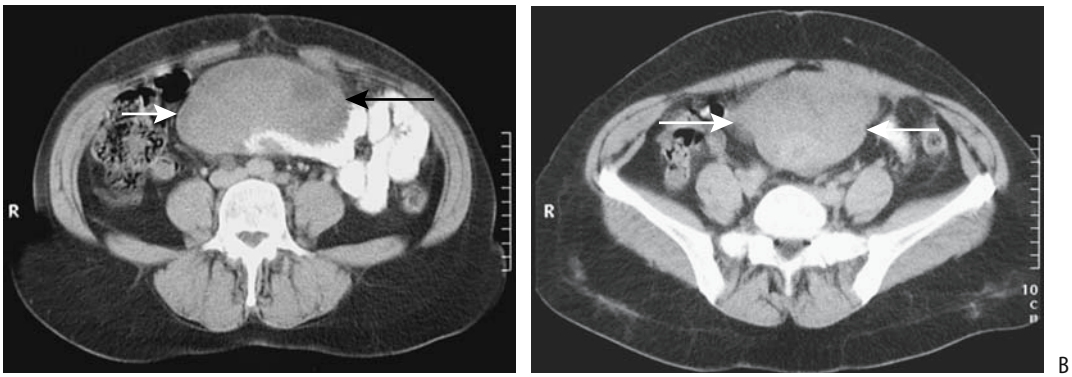

A B

Figure 14.18. Poorly differentiated mesenteric sarcoma. A,B: Two CT images show a homogeneous midabdominal tumor (arrows) displacing contrast-filled small bowel loops. (Courtesy of Algidas Basevicius, M.D., Kaunas Medical University, Kaunas, Lithuania.)

toneal thickening. A thickened mesentery and ascites are evident in some. Pleural plaques and nodules are uncommon.

Malignant

A peritoneal mesothelioma is a rare tumor, being considerably less common than its pleural counterpart. Most patients have had previous asbestos exposure, generally decades earlier, but those with peritoneal mesothelioma tend to be a decade younger than those with a pleural tumor. Nevertheless, pleural thickening and even a concomitant pleural mesothelioma are not uncommon associated findings. At times these tumors grow gradually for several years. The prognosis is grim.

Asbestos comes in two major forms, chrysotile and amphiboles, with most of the asbestos used commercially consisting mainly of chrysotile. The relative carcinogenesis varies between the various types, but why a particular type is more carcinogenic is not known. Asbestos is not directly mutagenic. Asbestos fiber size and other physical and chemical properties appear to be relevant factors in carcinogenesis, but contaminants such as tremolite (a form of amphibole) may also play a role. Chrysotile fibers appear to be cleared from human lungs rapidly, while amphibole clearance half-life is measured in years or decades. A lag period of several decades is necessary after asbestos exposure before a mesothelioma becomes evident. Heavy asbestos exposure increases the risk for abdominal mesothelioma, although considerable individual variability exists. The presumed pathway for abdominal involvement is expectoration of inhaled asbestos fibers, which are swallowed and some then penetrate the bowel wall into lymphatic and splanchnic circulations. Why mesothelial cells are primarily affected after asbestos exposure is speculation. Numerous but inconstant gene changes have been reported. An occasional tumor contains a sarcomatous component.

Not all patients with malignant mesothelioma have a history of asbestos exposure. Prior radiation therapy has been occasionally implicated. A remote history of Thorotrast exposure is found in some. The relationship of a rare peritoneal mesothelioma developing in a setting of recurrent bouts of peritonitis is conjecture.

Spread tends to be intraabdominal and to the pleural cavity, probably by direct extension. Distal metastases are rare. A not uncommon end stage is extensive bowel involvement and small bowel obstructions.

Extraperitoneal malignant mesotheliomas are rare. They readily invade adjacent structures.

Chest radiographs and CT identify pleural plaques in about half the patients with malignant abdominal mesothelioma. A barium study typically shows extensive mesenteric and bowel wall infiltration, thickening and distortion of the valvulae conniventes, bowel wall thickening, sharp angulation of bowel loops, and a narrowed lumen. Some of these tumors have an almost pathognomonic radiographic appearance. Computed tomography findings range from a hypodense tumor with peripheral contrast enhancement to diffuse omental thickening, described as an omental cake; in many patients no discrete tumor masses are identified (Fig. 14.19). Thickening of the parietal peritoneum is more common than visceral peritoneal involvement. Extensive mesenteric thickening is found in some patients. Calcifications are rare. Ascites is common with asbestos-associated mesotheliomas, but it tends to be more limited than that seen with carcinomatosis. It tends to be rather viscous and difficult to remove. Fluid cytology appears worthwhile but tends to be nondiagnostic. Laparoscopic biopsy is useful to establish the diagnosis, although tract seeding by tumor is a potential complication.

The differential includes carcinomatosis and occasionally an infection such as tuberculosis. Even laparotomy has misdiagnosed a mesothelioma as carcinomatosis.

Postoperative chemotherapy is largely ineffective, although anecdotal reports suggest a response to arterial infusion chemotherapy.

Benign

A type of abdominal mesothelioma-like tumor occurs in a younger age group, has no known association with asbestos exposure, women predominate 2:1, and some of these tumors contain a cystic component. The term *solitary benign fibrous tumor* is used by some authors to differentiate this tumor from its malignant counterpart. Pathogenesis is unknown; some authors

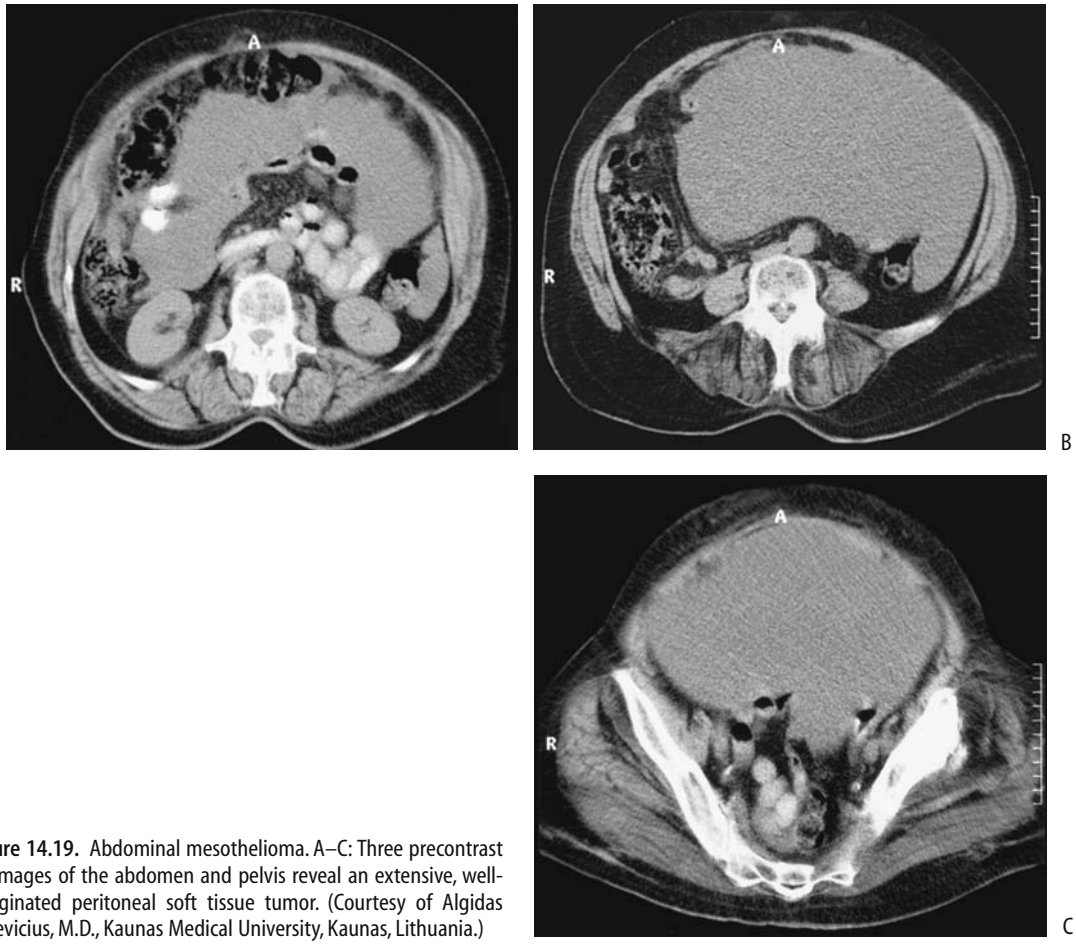

Figure 14.19. Abdominal mesothelioma. A–C: Three precontrast CT images of the abdomen and pelvis reveal an extensive, well-marginated peritoneal soft tissue tumor. (Courtesy of Algidas Basevicius, M.D., Kaunas Medical University, Kaunas, Lithuania.)

regard them as borderline or low-grade malignancies; a response to infection may play a role. Pathologically, these cystic tumors are lined by mesothelium-appearing epithelium, although some evidence suggests that these cells are of fibroblast origin. In either case, a pathologic diagnosis of these benign-appearing tumors is difficult because some contain elements of a low-grade malignant cystic mesothelioma. Immunohistochemical findings can to be helpful.

Diffuse pain is common. A rare patient with a benign cystic mesothelioma is asymptomatic and has the tumor discovered because imaging is performed for unrelated reasons.

Some benign mesotheliomas are focal rather than diffuse (Fig. 14.20). Infiltration results in fixed, spiculated, and narrowed loops of small bowel. The cystic portions are hypointense on T1- and hyperintense on T2-weighted images, while solid components range from slightly hypo- to isointense on T1- and hypointense on T2-weighted images. The appearance can mimic a benign cyst, such as a hemangioma.

Epithelioid Hemangioendothelioma (Epithelioid Angiosarcoma)

These rare malignant endothelial neoplasms involve peritoneal serous membranes, pleura, and pericardium. They have a diffuse sheet-like appearance, and histologically exhibit a tubulopapillary growth pattern and other features often identified with mesotheliomas. Some authors include this endothelial neoplasm in the differential diagnosis of a neoplasm with histologic and clinical features of a malignant mesothelioma.

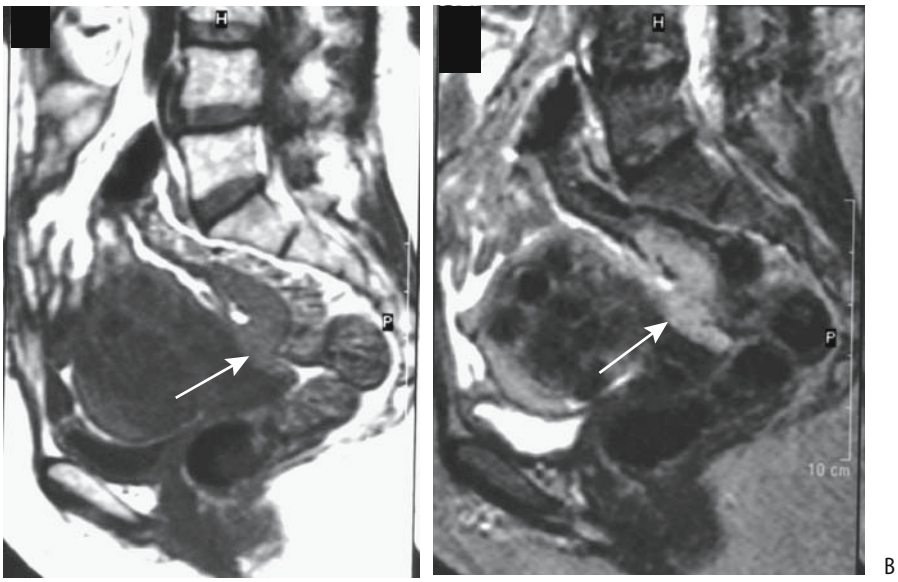

A B

Figure 14.20. Recurrent peritoneal mesothelioma. A: A T1-weighted image identifies numerous uterine myomas. A tumor isointense to muscle is present along the anterior wall in the pouch of Douglas (arrow). B: This tumor is slightly hyperintense on a T2-weighted image (arrow). (Courtesy of Egle Jonaitiene, M.D., Kaunas Medical University, Kaunas, Lithuania.)

These are aggressive tumors with a poor prognosis.

Fat-Containing Tumors

Some lipomas are discovered incidentally. An occasional mesenteric lipoma acted as a nidus for small bowel volvulus. These lipomas are readily detected with CT and MRI; they are well defined and of fat density, are hyperintense on T1- and hypointense on T2-weighted images, and show little contrast enhancement. Color Doppler US and angiography confirms their avascular nature. Central necrosis is not seen. The rare tumor lipomatosis is readily differentiated from obesity (Fig. 14.21).

Most liposarcomas present either as a palpable tumor or as sequelae of compression and impingement on an adjacent structure. An occasional one bleeds. Some of these large, bulky tumors are associated with fever, presumably due to central tumor necrosis. Imaging shows most liposarcomas as large, heterogeneous, poorly marginated and invasive tumors. A cystic component is common. The amount of fat within a liposarcoma varies; more undifferentiated ones tend to contain little fat and consist mostly of soft-tissue–density material, while well-differentiated ones mimic a lipoma. Their CT and MR findings are reflected accordingly. Poorly differentiated liposarcomas are mostly heterogeneous, and are mostly hypointense on T1- and tend toward a hyperintense appear-

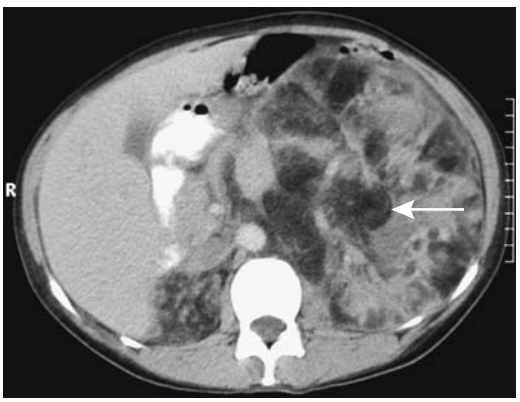

Figure 14.21. Lipomatosis in a woman with tuberous sclerosis. Computed tomography reveals numerous fat-density tumors and small bowel intussusception (arrow). (Courtesy of Algidas Basevicius, M.D., Kaunas Medical University, Kaunas, Lithuania.)

ance on T2-weighted images. The amount of necrosis increases inversely with the degree of differentiation.

Teratomas often contain fat, but other tissue components are also present, including calcifications. Some teratomas exhibit a fluid–fluid level within their cystic component.

The most common site for extraperitoneal angiomyolipomas is in the kidneys (discussed in Chapter 10). Computed tomography and MRI of a rare extraperitoneal extrarenal angiomyolipoma reveal a fatty tumor. Renal involvement is often present, and differentiation of a renal primary with extrarenal extension is often in the differential diagnosis. These tumors tend to be multiple in patients with tuberous sclerosis and involve numerous organs. Some contain sufficient cell atypia to suggest a slow growing low grade malignancy.

An occasional angiomyolipoma contains fat necrosis and mimics a liposarcoma both with imaging and histology.

Most extraadrenal myelolipomas occur in the extraperitoneum. Their imaging findings are similar to those of adrenal myelolipomas.

Hemangiopericytoma

A group of presumed mesenchymal tumors shows a perivascular myoid differentiation and has a varying histologic appearance and classification. These tumors range from myofibromatosis, to spindle cell, to hemangiopericytoma, with some of the latter also showing glomus tumor-like features. Whether these tumors are related neoplasms that simply manifest a spectrum of histologic and clinical findings or whether they are different entities is conjecture. Of these tumors, the hemangiopericytoma type is the most common. It occurs throughout the soft tissues, including the mesentery and omentum. These solid hemangiopericytomas are composed mostly of pericytes and capillaries and range from benign to malignant with gradations in between.

Some patients are relatively asymptomatic in spite of a large tumor, while others develop hypertension, hypoglycemia, or both. One patient with a metastatic hemangiopericytoma developed hypoglycemic coma (64); she had an abnormal insulin-like growth factor and low blood insulin and growth hormone levels that reverted to normal after resection.

Imaging reveals a solid, contrast-enhancing soft tissue tumor.

Recurrence is common after resection.

Leiomyomatous Tumors

Both leiomyomas and leiomyosarcomas occur in the peritoneal cavity and adjacent structures. Detection of a peritoneal leiomyosarcoma raises an obvious question: Did it originate in the peritoneum or is it a metastasis? A rare leiomyoblastoma develops in the omentum (65) or adjacent structures (Fig. 14.22).

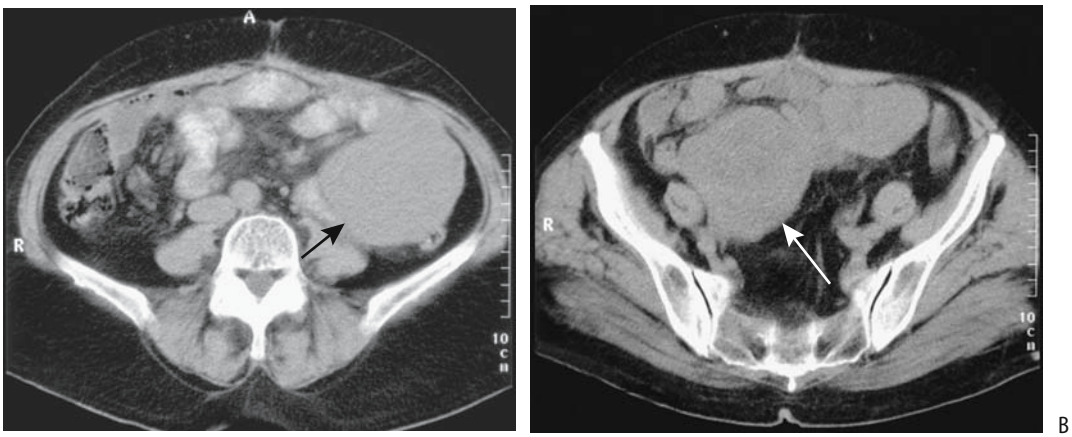

A B

Figure 14.22. Mesenteric leiomyoblastoma. A,B: Noncontrast CT shows this soft tissue tumor extending from the left abdomen into the right lower quadrant (arrows). (Courtesy of Algidas Basevicius, M.D., Kaunas Medical University, Kaunas, Lithuania.)

One variant is disseminated leiomyomatosis, also called *leiomyomatosis peritonealis disseminata*. It is a rare, often benign condition consisting of smooth muscle tumors growing along the peritoneal surface, but an occasional one undergoes malignant degeneration. Whether these tumors originate from metaplasia of submesothelial mesenchymal cells is conjecture. The condition occurs mostly in premenopausal women and is associated with the use of birth control medications or pregnancy. Some of these tumors may regress spontaneously or after oophorectomy. Endometriosis is an associated finding in some these patients. The findings can be quite complex; thus one woman had disseminated leiomyomatosis, endometriosis, and a multicystic mesothelioma (66); preoperatively she was believed to have stage III ovarian cancer.

Computed tomography shows leiomyomatosis as multiple peritoneal nodules mimicking carcinomatosis, except that some of these patients have no ascites. The differential includes ovarian carcinomatosis, leiomyosarcomatosis, mesothelioma, multiple dermoids, lymphoma, and some infections such as peritoneal tuberculosis.

Leiomyosarcomas at other gastrointestinal sites do metastasize to the peritoneum and differentiation from disseminated leiomyomatosis is often not possible. Primary mesenteric or omental leiomyosarcomas have a slow growth rate and are generally quite large at presentation (Fig. 14.23). Occasionally an abscess develops in these leiomyomatous tumors.

A rhabdomyosarcoma is probably the most common sarcoma in the extraperitoneum. Its smooth muscle counterpart, a primary extraperitoneal leiomyosarcoma, is quite rare. A heterogeneous imaging appearance is common, with the larger malignant tumors due to necrosis. Adjacent vessels are often either encased or displaced.

Histiocytic Tumors

Histiocytic tumors range from benign (fibrous histiocytoma) to malignant. A malignant fibrous histiocytoma is not rare. These tumors readily invade adjacent structures; rectal bleeding develops with bowel involvement.

These tumors range from solid to mostly cystic and tend to be large on initial presentation. The site of origin is difficult to establish once extensive invasion of adjacent structures develops. Pelvic ones in women mimic an ovarian neoplasm, a differential diagnosis that can be excluded if a normal ovary is identified.

Imaging reveals malignant fibrous histiocytomas as complex heterogeneous tumors due to their cystic component and necrosis and hemorrhage. They tend to be hypoechoic. Doppler US identifies prominent feeding and draining

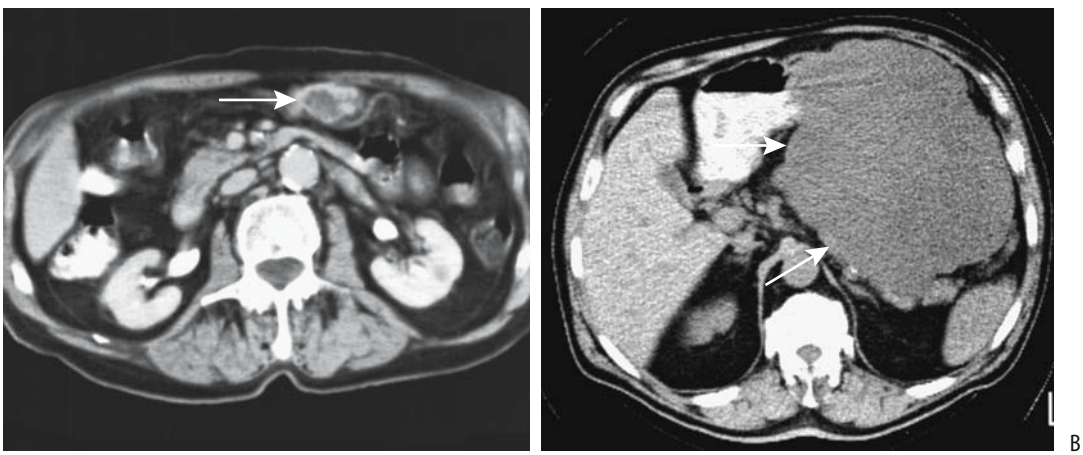

A B

Figure 14.23. A: Omental leiomyoblastoma (arrow). It invades the stomach. B: A poorly vascular retroperitoneal leiomyosarcoma (arrows) in another patient.

vessels. More cystic ones contain thick septa. In an occasional one extensive hemorrhage even suggests a hematoma.

Not uncommonly, a diagnosis is confirmed only after resection. Recurrence is common with malignant ones.

Osteogenic Tumors

An extraskeletal (soft tissue) osteosarcoma is rare. Most occur in adults in the extraperitoneum or in extremities. Some are associated with prior trauma or radiation therapy. Calcifications or even ossification are common in these otherwise homogeneous tumors. Imaging can suggest the tumor extent, but a biopsy is needed for diagnosis.

Malignant Melanoma

Malignant melanoma metastasizes widely throughout abdominal tissues rather than exhibiting a peritoneal carcinomatosis pattern, and for this reason tumor detection strategies differ from those for most other metastases. Computed tomography and MR are often employed, with special attention paid to soft tissues, including abdominal fat. Abdominal wall metastases are seen as soft tissue nodules, often surrounded by cutaneous or properitoneal fat. A FDG-PET scan detects metastases if they are larger than about 1.5 to 2 mm in size; overall, FDG-PET achieves greater sensitivities and specificities than CT in detecting these metastases. Likewise, it is superior to CT in detecting recurrence during follow-up.

Germ Cell Tumors

A primary extraperitoneal germ cell tumor is rare. Most represent metastases from a testicular primary; extensive spread is common on initial presentation (Fig. 14.24). An occasional patient develops peritoneal metastasis after resection; carcinomatosis tends to be rather subtle and is difficult to detect with CT—either Ga-67 scintigraphy or FDG-PET appears more sensitive.

An extraperitoneal choriocarcinoma is associated with elevated β-human chorionic gonadotropin (β-hCG) levels but normal α-fetoprotein levels; CT and MR postchemotherapy may reveal residual tumor, but cannot differentiate between viable tumor and necrotic tissue. Some of this tissue eventually calcifies.

Small Cell Carcinoma

Most peritoneal small cell carcinomas (at times simply called *small cell tumors* to reflect their unknown origin) occur in infants and young males. Imaging in the few reported patients reveals large, lobulated, solid-appearing tumors; some induce a surrounding desmoplastic reaction. Ascites is an inconstant finding.

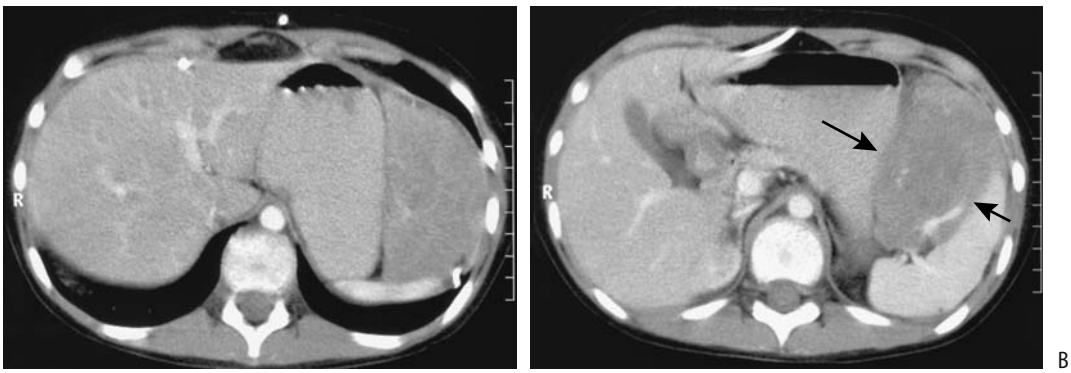

Figure 14.24. Metastatic germ cell tumor in a 12-year-old girl. A,B: Contrast-enhanced CT images reveal a large soft tissue tumor between the stomach and spleen (arrows). Patchy tumoral calcifications are present. (Courtesy of Algidas Basevicius, M.D., Kaunas Medical University, Kaunas, Lithuania.)

A CT finding of large, solid peritoneal tumors without an evident primary site in a pediatric patient or a young adult should suggest a small cell tumor.

Neuroendocrine Tumors

One classification of neuroectodermal origin tumors is based on their origin (Table 14.5). Although these tumors can be differentiated pathologically, from an imaging perspective they often have a similar appearance, and many publications lump them together (Fig. 14.25). They are differentiated in this work as an aid to clinical management rather than to imply that each type has a specific imaging appearance, although quite often a specific diagnosis can be suggested from clinical data and tumor location.

Neuroendocrine tumors originate in the extraperitoneum, mesentery, and bowel wall. Except for neuroblastomas and ganglioneuroblastomas these tumors are found mostly in adults. Tumors adjacent to bowel wall are discussed in Chapters 4 and 5.

Ganglioneuroma

Ganglioneuromas are rare neuroendocrine tumors originating from sympathetic ganglia and are found along the paravertebral sympathetic plexus. Most are extraperitoneal in location. These occur mostly in children and young adults. A rare one is hormonally active. Imaging reveals solid tumors that are nonspecific in appearance. Some contain punctate calcifications. They vary in contrast enhancement. They are hypointense on T1- but of varying intensity on T2-weighted MR images. Hypointense curvilinear bands have been described within these tumors on T2-weighted MR images. Some of these tumors encase blood vessels without narrowing the lumen.

Table 14.5. Classification of neuroectodermal tumors

Nerve sheath (Schwann cell) origin
Neurilemoma
Neurofibroma
Amputation neuroma
Neurosarcoma
Granular cell tumor
Ganglion cell origin
Ganglioneuroma
Neuroblastoma
Paraganglioma tumors*
Pheochromocytoma
Paraganglioma

*The following are similar tumors. The term *pheochromocytoma* is used for paraganglioma tumors located in the adrenal medulla.

Figure 14.25. Extensive retroperitoneal poorly differentiated neuroendocrine tumor. A spine metastasis is present (arrow). Primary site of tumor origin could not be determined; both adrenal glands were involved by tumor. (Courtesy of Algidas Basevicius, M.D., Kaunas Medical University, Kaunas, Lithuania.)

Ganglioneuroblastomas contain both ganglioneuroma and primitive neuroblastoma elements and are considered to be intermediate between benign ganglioneuromas and malignant neuroblastomas. A majority occur in young children. Their imaging appearance varies from a mostly solid to a mostly cystic tumor depending on the degree of cell differentiation.

Neuroblastomas are discussed in Chapter 16.

Paraganglioma (Pheochromocytoma)

Extraadrenal paragangliomas account for about 15% of these tumors. Presumably they arise from embryonic chromaffin cells in parasympathetic tissue and in accessory adrenal glands. A minority are multicentric in origin. Most are detected during the second and third decades of life. An occasional one manifests during pregnancy.

Carney's syndrome (or triad) consists of a gastrointestinal stromal tumor (often a gastric leiomyosarcoma), an extraadrenal paraganglioma, and a pulmonary chondroma. Whether

Carney's syndrome is an autonomic nervous system abnormality or a multiple endocrine neoplasia syndrome or even a multiple hamartoma syndrome makes for an interesting discussion.

Some paragangliomas are nonfunctional. A paraganglioma can compress and displace an adjacent kidney and induce hypertension (Page kidney). As an example, CT of a 25-year-old woman with suspected appendicitis detected a broad ligament tumor, shown to be a nonfunctioning paraganglioma (67).

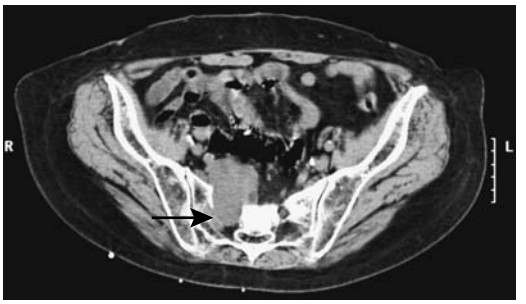

Figure 14.26. Schwannoma exiting sacral foramen. Noncontrast CT identifies a soft tissue tumor widening a sacral foramen on the right (arrow). (Courtesy of Patrick Fultz, M.D., University of Rochester.)

Schwannoma (Neurilemoma)

Schwannomas originate from Schwann sheath cells and are most common in the peripheral neural system. Schwann cells are the peripheral neural system's glial cells. Found mostly in young adults, more often in women, extraperitoneal schwannomas tend to be solid tumors, and their imaging findings are nonspecific. The ones involving the sacral nerves tend to widen the sacral foramina (Fig. 14.26). Preoperative biopsy is often not helpful. A pelvic schwannoma tends to mimic an ovarian neoplasm.

Both MRI and CT are useful in characterizing these tumors (Fig. 14.27). Computed tomography of extraperitoneal schwannomas reveals well-marginated, encapsulated, round or oval tumors. An occasional one undergoes central necrosis, hemorrhage, and central or peripheric calcifications. They show heterogeneous contrast enhancement, with lack of enhancement in cystic regions. Overall, they tend to be somewhat hypovascular. Computed tomography of one pelvic schwannoma revealed only the cyst wall enhancing postcontrast; in some others focal central enhancement is evident.

Neurofibromatous Tumors

Neurofibromatosis type 1 (NF1, *von Recklinghausen's disease*) is a relatively common autosomal-dominant hereditary neurocutaneous syndrome consisting of neurofibromas, café-au-lait spots, and other abnormalities involving various body organs. A mutation in the *NF1* gene occurs roughly in one of 3500 births; *NF1* encodes a tumor suppressor, loss of which leads to neurofibroma formation. Most affected individuals are detected in childhood, but a minority contain a *forme fruste* type first manifesting in adulthood. Although a single neurofibroma most often is an isolated event, the presence of multiple neurofibromas or a single plexiform neurofibroma is strong presumptive evidence for von Recklinghausen's disease. About 50% of affected individuals have spontaneous mutations.

Neurofibromas are complex, noncapsulated tumors originating from Schwann cell lineage in peripheral nerves. Histologically, they differ from neurilemomas. Mast cells appear to play a role in their growth (68). Both somatic and autonomic neural tissue is involved. Because these nerves are ubiquitous and neurofibroma formation sporadic, a wide manifestation of this entity is encountered. Tumors are more common in extraperitoneal tissues, including paraspinal regions, than within the bowel wall. Focal involvement of one organ is unusual but has been reported. Some tumors in the mesentery compress adjacent blood vessels and result in focal ischemia. Extensive extraperitoneal neurofibromas mimic adenopathy.

Neurofibromas tend to be focal, solid, homogeneous, and somewhat hypodense with CT, presumably due to their rich lipid content (Fig. 14.28). Often their appearance mimics that of adenopathy. Cystic degeneration is more common in neurilemomas, but does occur in a minority of neurofibromas. Many are symmetrical bilaterally, with a presacral location also being common. Asymmetry should suggest malignant degeneration. Postcontrast CT reveals a hypovascular soft tissue tumor. Occasional tumors with either peripheral or central contrast-enhancement are described, with the

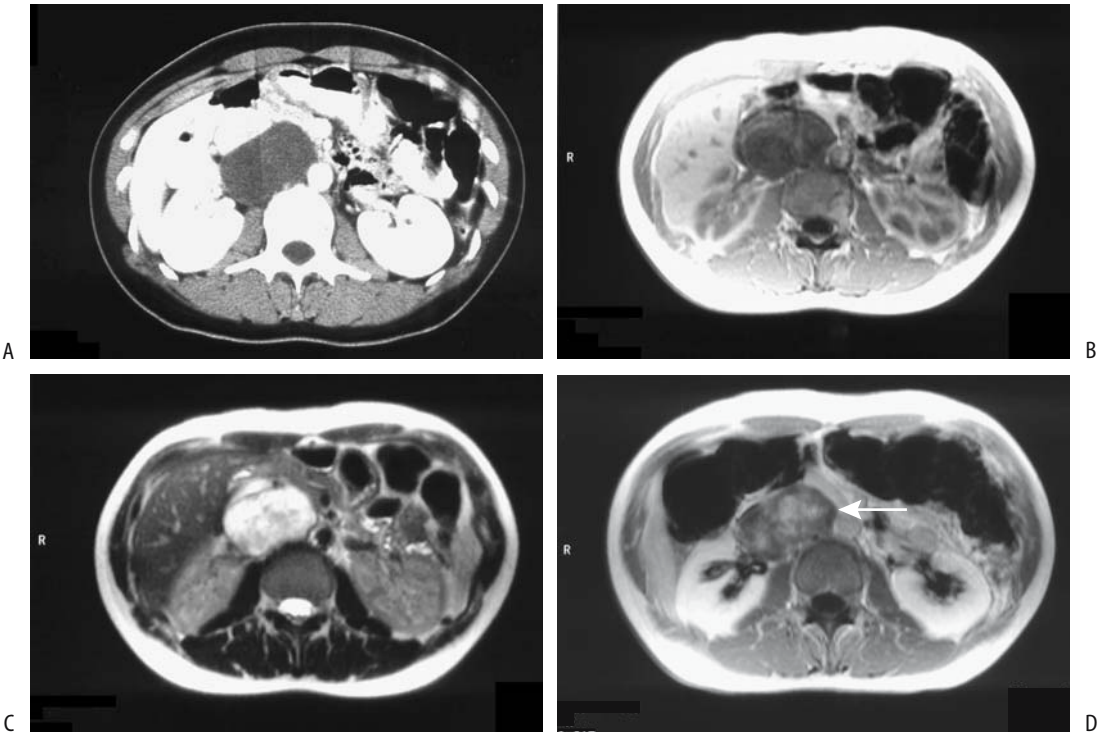

Figure 14.27. Neurilemoma. A: Contrast-enhanced CT identifies a hypodense tumor in right adrenal region, suggestive of a cyst. B: T1-weighted MR image reveals a homogeneous hypointense tumor. C: Turbo spin echo T2-weighted image the hyperintense tumor is located posterior to the inferior vena cava. D: Contrast-enhanced T1-weighted image shows inhomogeneous contrast enhancement (arrow). (*Source:* Rha SE, Byun JY, Jung SE, Chun HJ, Lee HG, Lee JM. Neurogenic tumors in the abdomen: tumor types and imaging characteristics. Radiographics 2003;23:29–43, with permission from the Radiological Society of North America.)

less vascular portion representing lipid-rich Schwann cells and cystic degeneration, while denser segments tend to be more vascular.

Plexiform neurofibromas infiltrate and are poorly marginated. In fact, soft tissue involvement tends to mimic a diffuse infection. Magnetic resonance imaging of some mesenteric plexiform neurofibromas reveals ring-like structures within the tumor on T2-weighted and contrast-enhanced images.

One should keep in mind, however, that mesenteric involvement in von Recklinghausen's disease needs to be distinguished from hereditary intestinal neurofibromatosis, which is a separate genetic disease.

Figure 14.28. Neurofibroma. Contrast-enhanced CT outlines a tumor with target-like enhancement (arrow). The hyperdense center represents nerve tissue, surrounded by more peripheral myxoid degeneration. (*Source:* Rha SE, Byun JY, Jung SE, Chun HJ, Lee HG, Lee JM. Neurogenic tumors in the abdomen: tumor types and imaging characteristics. Radiographics 2003;23:29–43, with permission from the Radiological Society of North America.)

Carcinoid

A mesenteric origin for a carcinoid is not uncommon. In fact, a distinction between bowel

and mesenteric origin is often not possible and some of these tumors are simply identified adjacent to a loop of bowel. Because of the often-associated dense desmoplastic reaction, even CT often cannot identify the exact site of origin for these tumors.

A typical CT appearance is that of a mesenteric tumor surrounded by radiating stellate folds, and such a finding is presumptive evidence for a carcinoid. Adjacent bowel loops are either infiltrated or simply displaced. Atypical appearances, however, are common. A rare carcinoid presents as a large necrotic mesenteric tumor mimicking a necrotic stromal tumor. Associated enlarged lymph nodes are an inconsistent finding.

A percutaneous biopsy is often nondiagnostic; tumor cells are difficult to obtain because of the exuberant fibrosis.

Other Neuroendocrine Tumors

An extrapancreatic gastrinoma is occasionally located in a lymph node. Primary gastrinomas are rare at this location and a small primary pancreatic tumor should be excluded.

Presacral Tumors

Certain tumors are more common in the presacral soft tissues than in other locations and these are discussed here. Overall, however, presacral tumors are uncommon. They originate from any of the soft tissue elements located in this space and range from solid to cystic. Primary presacral neoplasms can invade the sacrum or rectum. Larger presacral tumors tend to displace the rectum laterally. These tumors tend to be insidious, often are quite large when first detected, and thus are diagnosed late.

A triad of anorectal, sacral, and presacral anomalies was described by Currarino et al. (69) in 1981 and is known as Currarino's triad. Both a complete triad and an incomplete form exist. A deformed sacrum is common; anorectal anomalies range from stenosis to an imperforate anus and presacral tumors consist of teratomas, meningoceles and various cysts or cystic neoplasms. Conventional radiographs identify an abnormal sacrum, called a *scimitar sacrum*, but the full extent of abnormalities is better detected with MRI.

Teratoma

The most common presacral tumor in neonates is a teratoma. Most teratomas are benign, although the risk of malignancy increases considerably in older children. Most are large at first presentation. Their imaging appearance is similar to teratomas at other locations and consists of a heterogenous, well-marginated tumor containing both cystic and solid components. The presence of varying amounts of fluid, fat, and calcifications, including teeth, is diagnostic. Malignant ones tend to contain more soft tissue and less of a cystic component than benign ones.

Meningocele

A presacral meningocele is a rare congenital abnormality consisting of herniated meninges and other spinal canal content. An occasional one is familial. Associated abnormalities include sacral abnormalities, spina bifida, and genitourinary defects. Imaging reveals a presacral cystic mass filled with cerebrospinal fluid and containing varying amounts of soft tissue. An associated sacral defect, at times detected even with conventional radiography, should suggest the diagnosis.

Other Presacral Tumors

A chordoma is a low-grade malignant neoplasm resulting in sacral destruction. Extension into the presacral soft tissues is common. A complication after resection of a sacral chordoma is posterior rectal herniation, presumably due to weakness of the posterior pelvic floor.

Widening of a sacral neural foramina should suggest neurofibromatosis.

The rare presacral neuroblastoma has an imaging appearance similar to its counterpart in the adrenal glands.

Ectopic Pregnancy

In general, 1% of all pregnancies are ectopic, and almost all occur in the fallopian tubes; among ectopic pregnancies, about 1% or fewer are intraabdominal. They are thus rare, but their importance lies with the associated high maternal death rate, if undetected. They are believed

to represent the sequelae of a missed ruptured ectopic tubal pregnancy.

Some women with an abdominal pregnancy present with an acute abdomen and undergo emergent surgery; others are managed conservatively, at least initially. Placental attachment to the mesentery is incompatible with fetal life, but some fetuses survive if the placenta is attached to the uterus.

If an abdominal pregnancy is clinically suspected, MRI is the imaging modality of choice; US does not detect all abdominal pregnancies. Imaging findings of an abdominal pregnancy include detection of an extrauterine fetus and placenta; fetal body parts are seen outside the uterus, assuming the uterus can be identified. Also, the placenta is located close to maternal bowel and no uterine wall identified between fetus and maternal abdominal wall. The fetus tends to have an unusual position. Peritoneal fluid is not common in a normal pregnancy but is often identified in an abdominal pregnancy.

A rare cesarean scar pregnancy was confirmed by US, MRI, and cystoscopy (70); her pregnancy was terminated by hysterotomy with uterine preservation, followed by methotrexate therapy.

A rare cause of an intraabdominal calcification is a lithopedion (calcified fetus). Most imaging modalities should suggest the diagnosis.

Hernias

Patients with ascites have increased intraperitoneal pressure, and a number of hernias develop in this setting.

A Richter hernia signifies that only a portion of the bowel wall circumference is incarcerated. Strangulation of the involved bowel segment can occur without anatomic lumen obstruction.

Laparoscopic hernia repair has been extensively adopted, although the prevalence of recurrence and complications have raised questions about such an approach.

Diaphragmatic Hernia

Morgagni Hernia

A hernia through the anteromedially located foramen of Morgagni is not common. These defects are lateral to the midline. Occasionally these congenital hernias (called *Morgagni-Larrey's hernia* in some countries) occur bilaterally. Hernia content ranges from omentum, stomach, and other adjacent structures, and it is surrounded by peritoneum. Some of the smaller ones simply contain fat, at times detectable on chest radiographs and other imaging modalities.

Many of these hernias are discovered incidentally in an otherwise asymptomatic infant or even adult. Symptomatic infants have respiratory distress, recurrent pulmonary infections, or simply failure to thrive. Especially in neonates and infants, other associated anomalies are common. Bowel obstructions in a Morgagni hernia are uncommon.

With gastric herniation, a contrast study with the patient in the lateral position should be diagnostic; a Morgagni hernia is far anterior to the usual esophageal hiatus. Without an associated air–fluid level, conventional chest radiography of a foramen of Morgagni hernia mimics a pericardial cyst or other soft tissue tumor in this location. At times CT is helpful by identifying intestinal content in the chest. Partial diaphragmatic eventration is in the differential diagnosis.

A laparoscopic approach can be used to repair these hernias.

Bochdalek Hernia

A congenital posterolateral diaphragmatic defect, or Bochdalek hernia, is more often detected in neonates on the left side. It varies in size from a barely discernible defect to hemidiaphragmatic agenesis. Almost any intraabdominal organ with sufficient laxity can herniate. Most Bochdalek hernias do not have a hernial sac. If a hernia is large enough, associated pulmonary hypoplasia develops, and it is this hypoplasia that determines the prognosis. Also, these neonates have an increased prevalence of cardiovascular and other anomalies. Pulmonary artery hypertension in this condition is associated with a patent ductus arteriosus.

In neonates a large Bochdalek hernia manifests as respiratory distress. An initial chest radiograph suggests the diagnosis; within several hours air can be identified in the intrathoracic bowel. To prevent further respiratory distress due to bowel distention, once this condition is suspected the stomach should be decompressed with a nasogastric tube. A diag-

nosis is not always obvious and a number of developmental lung conditions, such as lobar emphysema and adenomatoid malformation, have a similar appearance. A barium study confirms the intrathoracic location of portions of the intestine.

At times a Bochdalek hernia manifests later in life. Most of these adult hernias are on the right side. Whether they represent a delayed manifestation of a congenital condition or are an acquired focal diaphragmatic defect is a moot point. A chest radiograph reveals a posterior soft tissue tumor adjacent to the diaphragm, a nonspecific finding also seen with lung neoplasms and other lesions. Computed tomography defines the underlying anatomy and also often outlines a diaphragmatic defect. Hernia content ranges from fat, omentum, or a solid organ such as spleen, to bowel.

Other Diaphragmatic Hernias

Hiatal hernia is discussed in Chapter 2. Diaphragmatic trauma and resultant hernias were discussed earlier in this chapter (see Trauma).

A paraesophageal hernia can contain omentum or other adjacent structure. Chest radiography simply detects an abnormal tumor in the posterior mediastinum; CT or MRI confirms the herniation.

An intrapericardial hernia can be congenital or traumatic in origin. Some of these hernias are asymptomatic. With conventional contrast studies they may mimic a hiatal hernia.

Ventral Hernia

Ventral hernias include umbilical hernias, hypogastric hernias (below the umbilicus) and epigastric hernias. The latter are uncommon, found mostly in obese individuals, often contain properitoneal fat and are detected with CT.

An umbilical hernia is common in the pediatric age group where it is usually considered to be congenital. It develops in adults with increased intraabdominal pressure, such as in a setting of ascites or pregnancy. Especially with ascites, the overlying skin can necrose and rupture, a condition associated with a high mortality. An umbilical hernia can also result in bowel incarceration.

Prior to surgical repair of an acquired umbilical hernia, it appears worthwhile to establish its vascularity with Doppler US. An occasional one contains a herniated paraumbilical collateral vein (71), resulting in major bleeding during repair.

Femoral Hernia

Groin hernias are common in the pediatric age group, but detection of a femoral hernia can be difficult and misdiagnoses are common. Even an incarcerated femoral hernia may be missed clinically.

Computed tomography shows a soft tissue tumor medial to the femoral vein. Problems arise in differentiating a hernia from adenopathy, hematoma, or other tumor.

At times US, including Doppler, aids in differentiating a femoral hernia from other groin masses. Bowel can be identified within a hernia by showing valvulae conniventes, haustrations, or peristalsis.

Inguinal Hernia

Most direct inguinal hernias are acquired, broad-based, and rarely incarcerate. Congenital indirect hernias are due to failure of closure of the processes vaginalis. In adults, an indirect inguinal hernia is acquired and is caused by dilation of the deep inguinal ring. Indirect hernias allow abdominal content to herniate inferiorly. Both direct and indirect hernias can protrude into the scrotum and contain small bowel, large bowel, bladder, omentum, or other contents, including a rare fallopian tube and ovary (72). In general, small bowel is more common in right-sided hernias and colon in left-sided ones, but almost any abdominal organ, including stomach, can herniate (Fig. 14.29). Bowel infarction in a strangulated inguinal hernia is not uncommon; bladder infarction can also develop. Even an acute gangrenous appendicitis has developed in an inguinal hernia. These hernias are accentuated during pregnancy.

Inguinal herniation of the bladder, or inguinal cystocele, can result in urinary obstruction and renal insufficiency. It can result in clinical prostatism without bladder outlet obstruction. Although occasionally identified with CT (Fig. 14.30) the condition is best studied during the filling phase of urodynamic studies with the patient standing.

Figure 14.29. Right inguinal hernia containing sigmoid colon, an uncommon finding. Partial colonic obstruction was present at the hernial ring.

Herniography involves contrast injection into the peritoneal cavity and was performed to detect hernias in infants; it is rarely done today. Peritoneal scintigraphy also detects inguinal hernias. More often either CT or US is performed and should be diagnostic. A bowel-containing hernia is identified if bowel is present distal to the inguinal ring. Fluid adjacent to bowel or bowel wall thickening suggests ischemia, but keep in mind that occasionally a septated hydrocele or hematocele has a similar appearance within a hernia.

Figure 14.30. Bilateral inguinal hernia. Computed tomography identifies contrast-containing small bowel in the right one (arrow) and a portion of bladder in the left one (arrowhead). (Courtesy of Patrick Fultz, M.D., University of Rochester.)

Multidetector CT should readily detect these hernias. Indirect hernias occur lateral to the inferior epigastric vessels, in distinction to direct hernias which are located medial to these vessels.

Ultrasonography using a 7.0-MHz transducer should detect whether an inguinal hernia in present in most children; the US criteria used to define these hernias are a widened internal inguinal ring or inguinal canal fluid or organs either at rest or during straining. Ultrasonography cannot readily differentiate between a direct and an indirect hernia.

Magnetic resonance using T1- and T2-weighted sequences and dynamic sequences readily identifies inguinal rings, including the inferior epigastric vessels.

Most of these hernias are corrected surgically without preprocedure imaging. If the diagnosis is in doubt, US is useful in excluding a hernia containing bladder or other inguinal or testicular tumors. Childhood inguinal herniorrhaphy is one of the causes of seminal tract obstruction; microsurgical vasovasostomy and epididymovasostomy are procedures in adult men to correct such obstruction.

Doppler US is useful in patients with persistent scrotal pain or swelling after inguinal hernia repair. Ischemia, testicular infarction, and fluid collections are readily detected.

Obturator Hernia

An obturator ring hernia is more common in elderly women. It is difficult to diagnose, and small bowel obstruction with strangulation is not uncommon, with its associated relatively high mortality rate. Occasionally a ureter becomes obstructed in an obturator hernia.

These hernias should be visible on CT images. A small bowel barium study should also diagnose these hernias if they contain small bowel, but keep in mind that on a frontal view such a hernia mimics an inguinal or femoral hernia; oblique or lateral views readily differentiate between them.

Spigelian Hernia

A defect in the transversus abdominis muscle aponeurosis lateral to the rectus abdominis

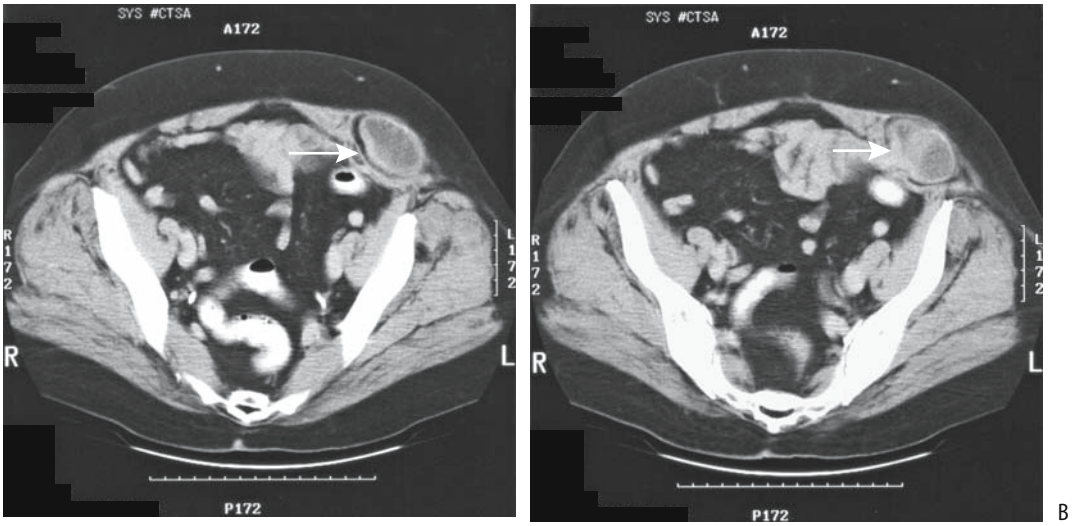

A B

Figure 14.31. A,B: Two CT images of a spigelian hernia (arrows).

muscles and close to the linea semilunaris is the site of a potential hernia. It is a type of ventral hernia but most authors discuss it as a separate entity. Investigators consider a spigelian hernia a fascinating topic for publication. The ratio of articles published to the limited number of patients who have this hernia is probably greater than for any other type of hernia.

The spigelian hernia sac can contain omentum, small bowel, or other adjacent structures. An occasional patient presents with small bowel obstruction, at times with an acute strangulation. Most patients are adults, although an occasional spigelian hernia develops in an infant. A clinically palpable bulge at the hernia site is uncommon because of the overlying external oblique muscle. Most symptomatic hernias, however, are tender to direct palpation.

The hernia should be readily diagnosed with CT (Fig. 14.31). A small bowel barium study is diagnostic if the hernia contains small bowel. Ultrasonography can also identify the abdominal wall defect, hernial sac and contents, and its relationship to the adjacent fascia and muscles; at times a Valsalva maneuver detects intermittent hernia reduction.

Lumbar Hernia

Two potential defects in the posterolateral abdominal wall allow lumbar hernias to develop: a superior (Grynfeltt's triangle) and an inferior (Petit's triangle). Although the literature suggests that most of these hernias are confined to one of these triangles, in reality many consist of a rather extensive abdominal wall defect and do not correspond to a specific superior or inferior site. This is especially true with congenital and postoperative lumbar hernias. Either retroperitoneal fat or bowel herniates through the defect.

Congenital lumbar hernias present during the first year of life with an abnormal protrusion in the lumbar region. They are associated with a meningomyelocele and the lumbocostovertebral syndrome, a syndrome that includes other major malformations.

Acquired lumbar hernias may be spontaneous or traumatic, including postsurgical. A seatbelt injury is associated with some of these hernias; they form mainly in Grynfeltt's triangle. Lumbar hernias have developed in nephrectomy incisions and after iliac crest bone harvesting.

A typical presentation in adults consists of a soft, nontender, smooth flank tumor. It tends to be accentuated with increased abdominal pressure. Bowel within the hernia can incarcerate.

These hernias are readily diagnosed with CT. Recent traumatic ones are associated with an adjacent hematoma. They tend to have a

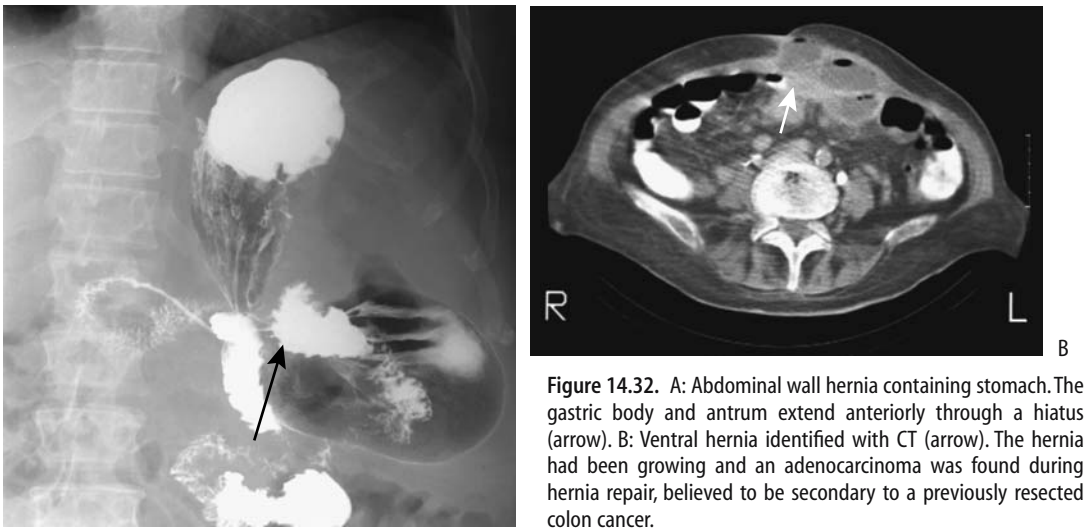

A B

Figure 14.32. A: Abdominal wall hernia containing stomach. The gastric body and antrum extend anteriorly through a hiatus (arrow). B: Ventral hernia identified with CT (arrow). The hernia had been growing and an adenocarcinoma was found during hernia repair, believed to be secondary to a previously resected colon cancer.

wide hiatus. A barium study detects bowel herniation.

These hernias are somewhat difficult to repair because of their wide hiatus and because the surrounding structures tend to be weak. At times extraperitoneal fixation of a prosthetic mesh to the 12th rib superiorly and iliac crest inferiorly is necessary.

Sciatic Foramen Hernia

In a sciatic foramen hernia a loop of bowel or adjacent tissue herniates through one of the sciatic foramina posteriorly. Bowel obstruction and strangulation ensue. These hernias are rare.

Sciatic hernias are a cause of chronic pelvic pain in women; most are left sided, and a rare one can even contain an ovary and fallopian tube. Computed tomography or MRI should identify the hernial content.

Incisional Hernia

Either omentum or part of the stomach or bowel can be part of an incisional hernia (Fig. 14.32). CT should detect these hernias, except that some hernias reduce with the patient supine. A barium study detects herniation if it includes stomach or bowel.

A parastomal hernia is a type of incisional hernia occurring alongside an intestinal stoma on the abdominal wall. Some of these hernias are evident on physical examination while others are detected with a small bowel barium study. A retrograde barium study through the stoma is often helpful in outlining these hernias.

Internal Hernia

Patients with an internal hernia range from those who are asymptomatic, to those who have intermittent nonspecific symptoms, to those who have small bowel obstruction. Especially when intermittent, these hernias are difficult to diagnose with either barium studies or CT. At times only a vague point of obstruction, either partial or complete, is identified with imaging, but the etiology of obstruction is not evident.

Computed tomography findings of symptomatic internal hernias consist of small bowel obstruction, a focal collection of dilated bowel displacing adjacent bowel, and stretched and displaced mesenteric vessels.

Peritoneoceles and enteroceles are discussed in Chapter 5. Cystoceles are discussed in Chapter 11.

Transmesenteric Hernia

A transmesenteric hernia is the most common internal hernia. Although its appearance varies considerably, the presence of dilated small bowel loops close to the abdominal wall without overlying omental fat should suggest this diagnosis (73). Associated small bowel volvulus and

ischemia are common complications, and thus surgical correction without undue delay is imperative with these hernias.

Bowel obstruction due to internal hernia is a complication after orthotopic liver transplantation (74); these obstructions are transmesenteric or retroanastomotic in location and are related to the choledochoenteric anastomosis. Similar to other transmesenteric hernias, some of these patients develop a volvulus and bowel ischemia. Computed tomography findings consist of abnormal mesenteric vessels and focal dilated small bowel loops displacing colon from the abdominal wall, yet a prospective diagnosis of internal hernia is rarely made (74).

Foramen of Winslow Hernia

A small bowel herniation into the lesser sac through the foramen of Winslow can lead to both small bowel obstruction and ischemia. A barium study reveals loops of small bowel posterior to the stomach and displacing the stomach anteriorly and inferiorly. A lesser sac hernia can also develop through a defect in the gastrocolic ligament; CT identifies herniated bowel surrounded by the liver, stomach, and pancreas.

Omentum or colon can also occasionally herniate. Ascending colon herniation through the foramen of Winslow was identified with oral and IV contrast-enhanced CT (75); conventional radiographs revealed this herniated large bowel indenting and displacing the stomach to the left.

Paraduodenal Hernia

A paraduodenal hernia is associated with incomplete midgut rotation. These are also called *mesocolic hernias* and consist of small bowel, usually jejunum, herniating into a right or left paraduodenal fossa. Clinically, these patients range from asymptomatic to those with a small bowel obstruction.

In a left paraduodenal hernia the distal duodenum and proximal jejunum herniate through a peritoneal defect into a left fossa, posterior to the transverse and descending mesocolon.

Imaging of a typical left paraduodenal hernias reveals a discrete focal collection of jejunal loops posterior to the stomach and close to the pancreatic tail, although findings can be confusing. Noncontrast imaging initially suggests a pancreatic tail tumor, but oral contrast should identify this tumor to consist of jejunal loops located between the stomach and pancreas (Figs. 14.33 and 14.34). Bowel obstruction is inconsistent and often intermittent. The inferior mesenteric vein, which is mesocolic in location, outlines the anterior hernial margin and

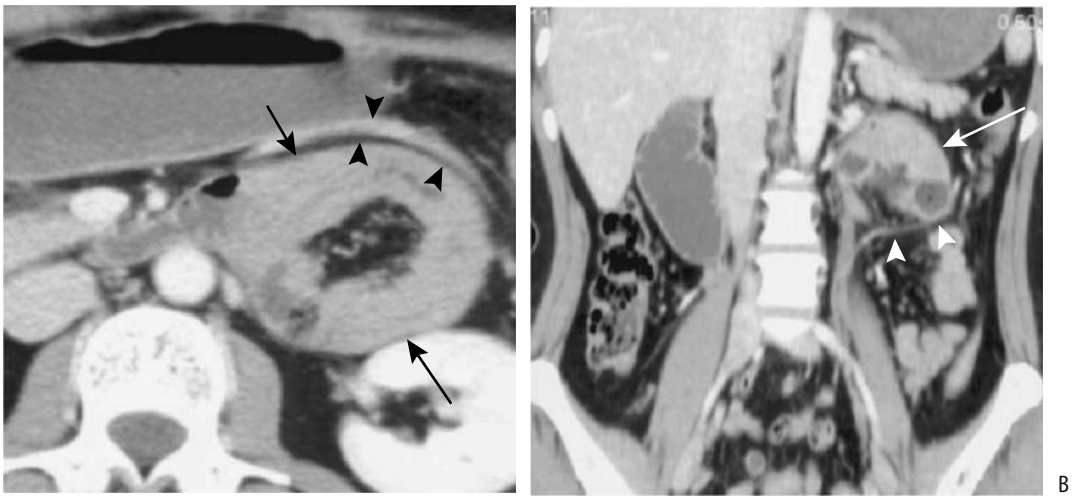

A B

Figure 14.33. Left paraduodenal hernia. Transverse (A) and coronal (B) postcontrast CT show a small bowel loop within the left paraduodenal region (arrows). The inferior mesenteric vein (arrowheads) is displaced anteriorly and laterally. The central hypodense region in part A represents mesenteric fat. (*Source:* Okino Y, Kiyosue H, Mori H, et al. Root of the small bowel mesentery: correlative anatomy and CT features of pathologic conditions. Radiographics 2001;21:1475–1490, with permission from the Radiological Society of North America.)

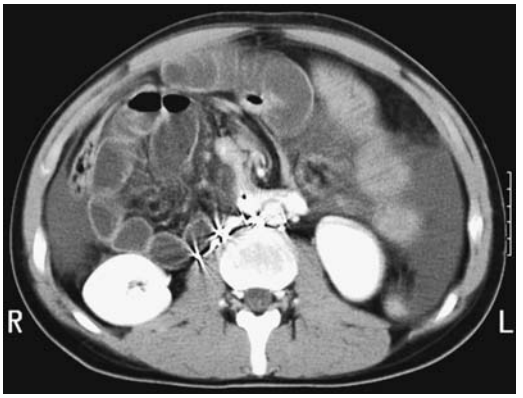

Figure 14.34. Small bowel obstruction in a paraduodenal hernia in a man who had previous testicular carcinoma resection and retroperitoneal lymph node dissection. Contrast-enhanced CT reveals dilated small bowel loops posterior to the duodenum. Involved bowel wall is thickened and enhances considerably. Surgery found a strangulated paraduodenal hernia. (Courtesy of Patrick Fultz, M.D., University of Rochester.)

serves as an anatomic landmark for CT. Occasionally small bowel loops are even located posterior to the pancreas.

A barium upper gastrointestinal study identifies a left paraduodenal hernia as loops of bowel located posterior to the stomach and left of the duodenum. A foramen of Winslow hernia and herniation through a mesenteric defect have a similar gross appearance but can generally be excluded by different bowel position.

A right paraduodenal hernia extends into the mesentericoparietal fossa of Waldeyer, posterior to the small bowel mesentery (Fig. 14.35). Computed tomography reveals the superior mesenteric artery and vein anterior to the hernia. These hernias develop in a setting of midgut malrotation.

Other Internal Hernias

Rare causes of small bowel obstruction and strangulation include herniation through a defect in the falciform ligament (76) and transmesosigmoid herniation; CT should define these. Most retropsoas small bowel herniations are incidental findings.

An uncommon hernia is through a defect in the levator ani muscles. These hernias contain bowel, fat, or simply ascitic fluid in communication with the peritoneal cavity. T2-weighted MR images are useful in detecting these hernias.

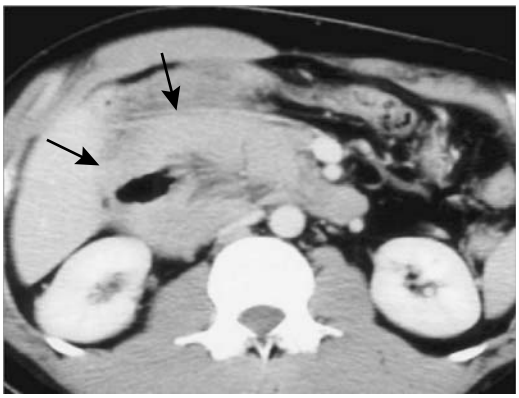

A

B

Figure 14.35. Right paraduodenal hernia. A: Postcontrast CT reveals focal small bowel loops in the right paraduodenal region (arrows) (Waldeyer fossa). (*Source:* Okino Y, Kiyosue H, Mori H, et al. Root of the small bowel mesentery: correlative anatomy and CT features of pathologic conditions. Radiographics 2001;21:1475–1490, with permission from the Radiological Society of North America.) B: Right paraduodenal hernia and midgut malrotation in another patient.

Coronal images allow comparison of one side with the other.

Paracecal hernias are rare. In children, Treves' field hernias predominate. An occasional paracecal hernia in adults results in intermittent small bowel obstruction. A barium study should be diagnostic.

Fibrosis/Adhesions

In spite of an extensive surgical literature on the etiology and pathogenesis of intraperitoneal adhesions, why some patients develop adhesions while others are relatively adhesion-free is not clear. Undoubtedly surgically introduced foreign bodies play a role in postoperative intraperitoneal adhesion development.

Insertion of laparoscopic trocars in patients with previous abdominal surgery and scars can result in bowel injury due to adhesions. In these patients preoperative US of the anterior abdominal wall appears useful to establish regions free of adhesion because many of these patients have adhesions under their scar. Overall, however, US has a low sensitivity in detecting adhesions.

Mesenteric and extraperitoneal fibrosis was discussed earlier (see Diffuse Infiltration).

Fistula

Fistulas and sinus tracts extending to the skin are best studied by direct fistulography. Internal ones are evaluated mostly indirectly. Some fistulas are adequately studied by outlining an adjacent gastrointestinal or genitourinary tract structure with contrast and obtaining conventional radiographs, usually under fluoroscopic guidance. In some patients CT is superior because it not only identifies the full extent of a fistula but also reveals any associated complications such as a tumor, abscess, or even osteomyelitis. Contrast injected into a percutaneous fistula prior to CT often aids in defining internal communications.

Computed tomographic peritoneography can detect a transvaginal leak of peritoneal dialysate.

Magnetic resonance imaging is well suited to evaluate fistulas. Bladder fistulas are best evaluated with gadolinium-enhanced T1-weighted images, while nonbladder fistulas are shown equally well both by nonenhanced and gadolinium-enhanced scans. Perianal fistulas are best studied by MR.

Pneumoperitoneum

A spontaneous pneumoperitoneum without associated peritonitis is not common. Rarely, intrathoracic trauma or an intrathoracic tumor results in a pneumoperitoneum. An uncommon cause of a spontaneous pneumoperitoneum is rupture of an intraabdominal abscess. In patients on mechanically assisted ventilation, air in the anterior mediastinum, or endothoracic fascia, dissects inferiorly through the diaphragm into the extraperitoneal anterior abdominal wall; on a CT study such anterior abdominal wall air can mimic an intraperitoneal location. Complicating the issue, at times this air extends into the peritoneal cavity; such dissection should not be confused with bowel perforation and thus lead to an unnecessary laparotomy.

A postoperative pneumoperitoneum disappears within several days. Generally of importance is not the amount of free air but rather whether it is decreasing from one day to the next; an increase in size should suggest bowel communication.

Over the years the upright posteroanterior chest radiograph was believed to be the most sensitive study to detect a subtle pneumoperitoneum. A lateral radiograph tends to detect a smaller pneumoperitoneum than a frontal radiograph. A major limitation of both of these radiographs is that many of these patients are old, debilitated, in pain, or obtunded, and cannot be upright. Still, as little as 1 cc of intraperitoneal gas can be detected whenever this approach is feasible. Often a radiograph with a horizontal x-ray beam and the patient supine will reveal a pneumoperitoneum adjacent to the liver, in Morison's pouch, or similar locations. Diaphragmatic muscle slips identified on supine abdominal or recumbent frontal chest radiographs or visualization of the ligamentum teres or even gallbladder on conventional radiographs is evidence of a pneumoperitoneum.

Computed tomography is accurate in detecting small amounts of intraperitoneal gas. Some authors have found that CT detects smaller

amounts of gas than conventional radiographs. Computed tomography reveals a pneumoperitoneum as gas between the liver and anterior abdominal wall, subhepatically, in the periumbilical region, in the pelvis, or even trapped between mesenteric folds. With small amounts of gas in unusual locations, differentiation from a small abscess is difficult.

Renal excretion of an oral water-soluble contrast agent should suggest bowel perforation. It should be kept in mind, however, that occasionally orally ingested contrast is absorbed from bowel even in the absence of disease, but these are exceptions.

Ultrasonography can also detect a pneumoperitoneum.

Pneumoretroperitoneum

Focal pneumoretroperitoneum is a hallmark of an abscess. Less often pneumoretroperitoneum alone or in association with pneumoperitoneum is a late sign of bowel ischemia.

Extraperitoneal gas and abdominal wall emphysema have developed after transanal excision of a rectal carcinoma.

Soft tissue gas within the back muscles can mimic a pneumoretroperitoneum on conventional radiographs.

Diaphragm

Diaphragmatic abnormalities include hemidiaphragmatic paralysis, inversion, and eventration.

The classic fluoroscopic "sniff test" detects hemidiaphragmatic paralysis, normally a simple procedure except in the presence of pleural effusion when additional maneuvers are necessary. Bedside US is an alternate technique to detect diaphragmatic paralysis. In some pediatric patients a barium study is useful to define the underlying anatomy and exclude bowel herniation.

Instead of a normal diaphragmatic concavity toward the abdomen, in diaphragmatic inversion the concavity is toward the chest. Inversion is most often secondary to a pleural effusion or neoplasm. The hemidiaphragm is either paralyzed or moves paradoxically.

Abnormal elevation of a hemidiaphragm is defined as eventration. It can be complete or partial, congenital or acquired. Congenital eventration is associated with a muscular defect. A rare congenital eventration is bilateral. Most acquired eventrations are secondary to an innervation defect; with time, muscle atrophy develops. Most partial eventrations are asymptomatic. Complete eventration leads to respiratory distress.

Diaphragmatic neoplasms, although quite rare, tend to manifest late. These tumors include rhabdomyosarcomas, malignant fibrous histiocytomas and others. They grow either superiorly and manifest as an intrathoracic tumor or grow inferiorly and often their imaging appearance mimics a liver, splenic or other upper abdomen organ tumor (77).

Omentum

Omental torsion can be primary or secondary if adhesions involve the free omental edge. Primary omental torsion occurs in both children and adults; the condition mimics acute appendicitis, with acute onset of right lower quadrant pain. A rare omental cystic teratoma results in torsion around its pedicle. Uncorrected omental torsion leads to ischemia and infarction. Omental ischemia also develops in the absence of torsion. Edema, fat necrosis, and eventual fibrosis ensue.

Computed tomography and MRI of omental torsion reveal a characteristic whirling or twisted fatty tumor in the middle and lower abdomen anteriorly (78); MRI also identifies a heterogeneous omentum, suggesting edema.

Ultrasonography of omental torsion reveals a homogeneous noncompressible hyperechoic tumor that can be separated from a normal-appearing gallbladder. Simple torsion is not associated with bowel wall thickening, and, in fact, bowel wall thickening should suggest another diagnosis, such as inflammation of an epiploic appendage. Exception occur, however, and the adjacent bowel wall is thickened if inflammation spreads via the omental tenia.

Ultrasonography and CT reveal omental infarction as hyperechoic, hyperdense regions, often adherent to peritoneum. These findings then evolve and change rapidly. Adjacent organ inflammation is in the differential diagnosis.

Endometriosis

Endometriosis can develop anywhere in the abdomen, including the abdominal wall, inguinal canal, umbilicus, or surgical scar. Endometriosis of the mesentery, omentum, or bowel wall is less common than peritoneal involvement. Endometriosis is associated with a cystic mesothelioma and disseminated leiomyomatosis. It is one of the causes of bloody ascites; in an occasional patient it results in peritonitis and eventually evolves into scarring. A rare endometrioid carcinoma develops at a scar endometriosis site.

Adnexal endometriosis is discussed in Chapter 12.

Most often intraperitoneal endometriosis consists of solid or partly cystic tumors, at times mimicking metastasis. Smaller peritoneal implants are not detected by US. The solid component in larger tumors often appears nodular, and Doppler US reveals blood flow within the tumor.

Magnetic resonance findings vary considerably. Larger endometriomas are readily detected with MRI; fat suppression aids in visualizing smaller foci. With a mostly solid, fibrotic endometrioma, T1-weighted images are iso- to hyperintense and T2-weighted images hypointense. Endometrioma fluid, similar to a hematoma, is hyperintense on both T1- and T2-weighted images. Solid endometrioma nodules enhance postgadolinium.

Diffuse peritoneal endometriosis has an imaging appearance similar to that of carcinomatosis or a chronic infection. Imaging is useful in guiding a diagnostic biopsy.

Peritoneal Foreign Bodies

One of the complications of laparoscopic cholecystectomy is intraperitoneal spill of gallstones and clips. Stones tend to settle in the pelvis and right iliac fossa. Abdominal pain in such a patient often suggests a ureteric calculus or appendicitis and imaging findings of a right lower quadrant calcification may concur with this diagnosis. Surgery in these patients reveals calcifications surrounded by granulomas. Gallstones "lost" in the peritoneal cavity during laparoscopic cholecystectomy are discussed in Chapter 8.

One sequela of colonic epiploic appendiceal inflammation is loose foreign bodies in the peritoneal cavity; some of these are quite large—they measured 6 cm in diameter in one patient (79). Few other conditions lead to loose calcified peritoneal structures. The task of imaging is to prove that such a calcification is indeed loose. Some of these foreign bodies become encased by fibrosis, and then a calcified leiomyoma or similar tumor is in the differential.

Intrauterine contraceptive devices do migrate into the peritoneal cavity. Imaging aids in their localization for laparoscopic removal, although some become encased by adhesions.

Peritoneal spill of ovarian dermoid content or similar structure during resection results in a postoperative granulomatous peritonitis.

Retained barium in the peritoneal cavity or extraperitoneal tissues is discussed in chapter 5. Retained surgical sponges are discussed later (see Examination and Surgical Complications).

Immunosuppression

Most immunosuppression is encountered in HIV-positive patients and in those after organ transplantation. Also, occasionally detected is a primary immunodeficiency state, found mostly in children.

Acquired Immune Deficiency Syndrome (AIDS)

Infection

An immunocompromised 15-year-old boy developed necrotizing myofasciitis of the anterior abdominal wall and clinically presented with an acute abdomen (80).

A common cause of death in African AIDS patients is pulmonary tuberculosis; a majority of these patients also had abdominal tuberculosis, with abdominal lymph nodes, liver, spleen and kidneys involved. These patients tend not to form tuberculous granulomas but do develop tuberculous ascites. Tuberculous HIV patients tend to have larger extraperitoneal and mesenteric adenopathy than nontuberculous HIV patients. Also, adenopathy with a hypodense appearance to lymph nodes suggests *Mycobacterium tuberculosis* source.

Extraperitoneal tuberculous abscesses in AIDS patients are amenable to percutaneous drainage under US guidance (81).

Salmonella bacteremia and septicemia are not uncommon in African seropositive AIDS patients.

Acquired immune deficiency syndrome patients are especially prone to develop systemic *Trypanosoma cruzi* infection, and an extensive literature exists on this topic.

Intestinal perforation secondary to cytomegalovirus (CMV) enteritis is the most common cause of peritonitis in AIDS patients; CMV peritonitis can also occur without a perforation.

Acquired immune deficiency syndrome patients develop bacillary angiomatosis and vascular lesions mimicking Kaposi's sarcoma that are secondary to infection with *Bartonella henselae*. These lesions occur throughout the body, including the abdominal lymph nodes, liver, and spleen. Ascites develops with peritoneal involvement. These lesions contain numerous capillaries, and postcontrast CT reveals marked contrast enhancement.

Tumors

Kaposi's sarcomas develop in AIDS patients not only in the skin but also in the intestinal wall, omentum, mesentery, and other sites. Chylous ascites is not common, except if Kaposi's sarcoma involves the cisterna chyli.

A propensity for AIDS patients to develop lymphoma is well documented.

Posttransplantation

Chronic immunosuppression in patients after transplantation results in a lymphoproliferative condition ranging from lymphoid hyperplasia to lymphoma. Manifestations vary depending on organ involvement. The primary role of imaging is to detect any initial abnormality and in follow-up, with biopsies used to establish a specific diagnosis.

Examination and Surgical Complications

Dialysis

In peritoneal dialysis patients, MR peritoneography is performed by adding an MR contrast agent (about 20 mL) to a 2000 mL dialysate solution instilled into the peritoneal cavity. Images obtained with the peritoneal cavity filled and after drainage are evaluated for leaks, hernias, adhesions, and for any loculated fluid (82). A transvaginal leak of peritoneal dialysate can also be confirmed by CT peritoneography.

The most common causes of peritoneal dialysis catheter occlusion are infection and adjacent soft tissue abutting the end of the catheter. Guide wire-assisted catheter manipulation is often helpful with a suspected catheter occlusion; long-term catheter patency can often be reestablished.

Peritonitis in patients undergoing peritoneal dialysis is often caused by an unusual organism. These include both bacteria and fungi.

Patients undergoing hemodialysis are at risk for mesenteric ischemia involving either the large or small bowel. These ischemias are typically nonocclusive in nature. A mesenteric infarct is a not uncommon cause for an acute abdomen in this patient population.

Ventriculoperitoneal Shunts

Complications of ventriculoperitoneal shunts include shunt migration, shunt fracture, and superimposed infection; an occasional one results in loculated cyst formation.

Laparoscopy

A previous laparotomy is a relative contraindication to laparoscopy because the presence of abdominal wall adhesions increases the risk of bowel injury during pneumoperitoneum induction and trocar insertion.

Laparoscopy in both adults and children has a steep learning curve, but once established it is associated with few complications. Complications encountered include abscesses, hematomas (in the abdominal wall, intraperitoneal, and retroperitoneal), bowel perforation and obstruction, pancreatitis, and splenic infarction. Complications discovered intraoperatively generally result in open surgical intervention.

Hernia Repair

Repair of an inguinal hernia using an extraperitoneal approach should not be associated

with peritoneal complications, although such complication as small bowel obstruction do occur. Other complications encountered include hematoma, seroma, protrusion of the prosthetic mesh, infection, and hernia recurrence. Generally, however, no imaging study is necessary in most patients after laparoscopic hernia repair.

Laparoscopic ventral hernia repair using a mesh does not obliterate completely a preoperative hernial sac, and thus postoperative fluid collections here are common (83); CT differentiation of such fluid from an abscess or recurrent hernia is difficult and, in the absence of symptoms, serial follow-up appears reasonable.

Other Laparoscopic Complications

Incisional hernias through laparoscopic trocar sites are uncommon and develop mostly through trocar sites >10 mm in diameter. Even acute appendiceal strangulation has developed within a laparoscopic port hernia (84).

One complication of laparoscopy is injury to extraperitoneal vessels, often due to blind insertion of needles and trocars. These patients manifest with acute hypotension intraoperatively and require conversion to an open laparotomy.

Small bowel necrosis or mesenteric infarction is rare.

Retained Sponges

A gossypiboma, or textiloma, is a tumor within the body composed of a cotton matrix, such as a laparotomy sponge. Conventional radiography identifies most retained sponges by their radiopaque markers. For a number of reasons CT does not identify radiopaque markers in all patients with retained sponges. Gas bubbles can develop within a gossypiboma without an abscess being present. In time, a sponge becomes encased in fibrosis, a phlegmon, or occasionally an abscess. A rare one migrates into the bowel lumen through a fistula and obstructs (85).

Colonoscopy identified the thread of a surgical sponge at the tip of a granuloma in the sigmoid colon of a patient with a prior hysterectomy (86); conventional radiography identified a radiopaque thread, and CT revealed a gossypiboma. Later study showed that the thread was no longer present and the sponge was presumably spontaneously expelled.

Biopsy

A pneumothorax is relatively common after a lung biopsy. Occasionally not only a pneumothorax but also a pneumoperitoneum develops after a lung biopsy.

Abdominal biopsies and fluid aspirations are performed under sterile conditions, yet the introduction of bacteria and the resultant peritonitis is a recognized complication of these procedures.

An endoscopic suction biopsy can result in small bowel perforation.

Tumor Seeding

Tumor seeding is associated with laparoscopic, biopsy, and catheter drainage procedures and is discussed in the appropriate organ-related chapters. Subcutaneous tumor seeding has even developed along a needle track used for alcohol sclerotherapy of a hepatocellular carcinoma. The type of tumor and probably its pathologic grade are relevant factors in tumor spread. These implants tend to be homogeneous on precontrast CT and heterogeneous and enhancing on postcontrast CT.

The risk of abdominal wall tumor seeding during needle biopsies is probably underestimated in the literature. An unfortunate consequence of tumor seeding after a fine-needle biopsy is that it renders any subsequent attempted curative resection into a palliative one.

Numerous reports describe metastases at laparoscopic trocar sites. These have occurred with both extraperitoneal and intraperitoneal laparoscopy. The relative prevalence of these metastases compared to incisional recurrence after a laparotomy is difficult to place in perspective.

Although rare, tumor seeding also occurs along percutaneous drainage tracts in patients undergoing abscess drainage in a setting of an underlying cancer.

Heterotopic Calcifications

Heterotopic calcification in abdominal incisions is a known sequela of abdominal surgery. These

calcifications often are palpable, and some are painful. They are often visible with not only CT but also conventional radiography. Why they form is not known. Some patients appear to be predisposed to heterotopic bone formation because calcifications recur after the primary one is excised.

References

1. Oktar SO, Yucel C, Ozdemir H, Uluturk A, Isik S. Comparison of conventional sonography, real-time compound sonography, tissue harmonic sonography, and tissue harmonic compound sonography of abdominal and pelvic lesions. AJR 2003;181:1341–1347.
2. Harisinghani MG, Saini S, Weissleder R, et al. Magnetic resonance lymphangiography using ultrasmall superparamagnetic iron oxide in patients with primary abdominal and pelvic malignancies: radiographic-pathologic correlation. AJR 1999;172:1347–1351.
3. Fisher HW. Lymphography. In: Skucas J, ed. Radiographic Contrast Agents. Rockville, MD: Aspen Publishers, 1977:423–436.
4. Molik KA, Gingalewski CA, West KW, et al. Gastroschisis: a plea for risk categorization. J Pediatr Surg 2001;36:51–55.
5. Keberle M, Mork H, Jenett M, Hahn D, Scheurlen M. Computed tomography after lymphangiography in the diagnosis of intestinal lymphangiectasia with protein-losing enteropathy in Noonan's syndrome. Eur Radiol 2000;10:1591–1593.
6. Tsang HY, Cheung YF, Leung MP, Chau KT. Cutaneous oozing of lymphatic fluid after interventional cardiac catheterization in a patient with Noonan syndrome. Cathet Cardiovasc Intervent 2000;51:441–443.
7. O'Hara SM, Donnelly LF. Intense contrast enhancement of the adrenal glands: another abdominal CT finding associated with hypoperfusion complex in children. AJR 1999;173:995–997.
8. Goan YG, Huang MS, Lin JM. Nonoperative management for extensive hepatic and splenic injuries with significant hemoperitoneum in adults. J Trauma 1998; 45:360–364.
9. Shanmuganathan K, Mirvis SE, Chiu WC, Killeen KL, Hogan GJ, Scalea TM. Penetrating torso trauma: triple-contrast helical CT in peritoneal violation and organ injury—a prospective study in 200 patients. Radiology 2004;231:775–784.
10. Branney SW, Wolfe RE, Moore EE, et al. Quantitative sensitivity of ultrasound in detecting free intraperitoneal fluid. J Trauma 1995;39:375–380.
11. Sirlin CB, Casola G, Brown MA, et al. Ultrasonography of blunt abdominal trauma: importance of free pelvic fluid in women of reproductive age. Radiology 2001; 219:229–235.
12. Partrick DA, Bensard DD, Moore EE, Terry SJ, Karrer FM. Ultrasound is an effective triage tool to evaluate blunt abdominal trauma in the pediatric population. J Trauma 1998;45:57–63.
13. Benya EC, Lim-Dunham JE, Landrum O, Statter M. Abdominal sonography in examination of children with blunt abdominal trauma. AJR 2000;174:1613–1616.
14. Butela ST, Federle MP, Chang PJ, et al. Performance of CT in detection of bowel injury. AJR 2001;176:129–135.
15. Scaglione M, Pinto F, Grassi R, et al. [Diagnostic sensitivity of computerized tomography in closed trauma of the diaphragm. Retrospective study of 35 consecutive cases.] [Italian] Radiol Med 2000;99:46–50.
16. Larici AR, Gotway MB, Litt HI, et al. Helical CT with sagittal and coronal reconstructions: accuracy for detection of diaphragmatic injury. AJR 2002;179:451–457.
17. Gervais DA, Ho CH, O'Neill MJ, Arellano RS, Hahn PF, Mueller PR. Recurrent abdominal and pelvic abscesses: incidence, results of repeated percutaneous drainage, and underlying causes in 956 drainages. AJR 2004; 182:463–466.
18. Hovsepian DM, Steele JR, Skinner CS, Malden ES. Transrectal versus transvaginal abscess drainage: survey of patient tolerance and effect on activities of daily living. Radiology 1999;212:159–163.
19. Gervais DA, Hahn PF, O'Neill MJ, Mueller PR. CT-guided transgluteal drainage of deep pelvic abscesses in children: selective use as an alternative to transrectal drainage. AJR 2000;175:1393–1396.
20. Catalano OA, Hahn PF, Hooper DC, Mueller PR. Efficacy of percutaneous abscess drainage in patients with vancomycin-resistant enterococci. AJR 2000;175:533–536.
21. Conde Redondo C, Estebanez Zarranz J, Rodrigues Toves A, Amon Sesmero J, Simal F, Martinez Sagarra JM. [Treatment of psoas abscess: percutaneous drainage or open surgery.] [Review] [French] Prog Urol 2000; 10:418–423.
22. Pickhardt PJ, Fleishman MJ, Fisher AJ. Fitz-Hugh-Curtis syndrome: multidetector CT findings of transient hepatic attenuation difference and gallbladder wall thickening. AJR 2003;180:1605–1606.
23. Sabaté JM, Torrubia S, Maideu J, Franquet T, Monill JM, Pérez C. Sclerosing mesenteritis: imaging findings in 17 patients. AJR 1999;172:625–629.
24. Abul S, Al-Oazweni H, Zalat S, Al-Sumait B, Asfar S. Cocoon abdomen in a liver transplant patient. J R Coll Surg Edinb 2002;47:579–581.
25. Yang ZG, Min PQ, Sone S, et al. Tuberculosis versus lymphomas in the abdominal lymph nodes: evaluation with contrast-enhanced CT. AJR 1999;172:619–623.
26. Lalloo S, Krishna D, Maharajh J. Case report: abdominal cocoon associated with tuberculous pelvic inflammatory disease. Br J Radiol 2002;75:174–176.
27. Koga S, Nagata Y, Arakaki Y, Matsuoka M, Ohyama C. Unilateral pedal lymphography in patients with filarial chyluria. BJU Int 2000;85:222–223.
28. Ben Adballah R, Hajri M, Aoun K, Ayed M. [Retrovesical and retroperitoneal extrarenal hydatid cyst: descriptive study of 9 cases.] [French] Prog Urol 2000;10:424–431.
29. Rollandi GA, Biscaldi E, De Cian F, Derchi LE. [Retroperitoneal fibrosis caused by barium: complication of rectal perforation during double contrast enema of the colon. Report of a case.] [Italian] Radiol Med 1999;97:539–542.
30. Shuto R, Kiyosue H, Hori Y, Miyake H, Kawano K, Mori H. CT and MR imaging of desmoplastic fibroblastoma. Eur Radiol 2002;12:2474–2476.

31. Guz G, Ozdemir BH, Sezer S, et al. High frequency of amyloid lymphadenopathy in uremic patients. Ren Fail 2000;22:613–621.
32. Leluc O, Andre M, Marciano S, Lafforgue P, Rossi D, Bartoli J. [Retroperitoneal complications of Erdheim-Chester disease.] [French] J Radiol 2001;82: 580–582.
33. Serratrice J, Granel B, De Roux C, et al. "Coated aorta": a new sign of Erdheim-Chester disease. J Rheumatol 2000;27:1550–1553.
34. Veyssier-Belot C, Cacoub P, Caparros-Lefebvre D, et al. Erdheim-Chester disease. Clinical and radiologic characteristics of 59 cases. [Review] Medicine 1996;75: 157–169.
35. Gimenez Bascunana A, Torrella Cortes E, Alberca De Las Parras F. [Systemic mastocytosis, portal hypertension and ascites.] [Spanish] Rev Esp Enferm Dig 1999; 91:795–796.
36. Setiawan MW, Samsi TK, Wulur H, Sugianto D, Pool TN. Dengue haemorrhagic fever: ultrasound as an aid to predict the severity of the disease. Pediatr Radiol 1998;28:1–4.
37. Kim JK, Jeong YY, Kim YH, Kim YC, Kang HK, Choi HS. Postoperative pelvic lymphocele: treatment with simple percutaneous catheter drainage. Radiology 1999;212:390–394.
38. Cope C. Diagnosis and treatment of postoperative chyle leakage via percutaneous transabdominal catheterization of the cisterna chyli: a preliminary study. J Vasc Interv Radiol 1998;9:727–734.
39. Schild H, Hirner A. Percutaneous translymphatic thoracic duct embolization for treatment of chylothorax. Rofo Fortschr Geb Rontgenstr Neuen Bildgeb Verfahr 2001;173:580–582.
40. Martin R, Sanz E, de Vicente E, et al. Differential diagnosis of asymptomatic retroperitoneal cystic lesion: a new case of retroperitoneal bronchogenic cyst. [Review] Eur Radiol 2002;12:949–950.
41. Pernas JC, Catala J. Pseudocyst around ventriculoperitoneal shunt. Radiology 2004;232:239–243.
42. Jain KA. Imaging of peritoneal inclusion cysts. AJR 2000;174:1559–1563.
43. Leinung S, Lotz I, Wurl P, Frey A, Lochhaas L, Schonfelder M. [Monstrous venous hemangioma of the retroperitoneum: problems of diagnosis.] [German] Rontgenpraxis 2000;52:302–308.
44. Zanelli M, Casadei R, Santini D, et al. Pseudomyxoma peritonei associated with intraductal papillary-mucinous neoplasm of the pancreas. Pancreas 1998;17: 100–102.
45. Ronnett BM, Zahn CM, Kurman RJ, Kass ME, Sugarbaker PH, Shmookler BM. Disseminated peritoneal adenomucinosis and peritoneal mucinous carcinomatosis. A clinicopathologic analysis of 109 cases with emphasis on distinguishing pathologic features, site of origin, prognosis, and relationship to "pseudomyxoma peritonei." Am J Surg Pathol 1995;19:1390–1408.
46. Signori GB, Martino F, Monticelli L, Mangiarini MG, Chioda C. [Secondary varicocele as a clinical manifestation of primitive retroperitoneal tumor.] [Italian] Minerva Urol Nefrol 1998;50:267–269.
47. Low RN, Semelka RC, Worawattanakul S, Alzate GD. Extrahepatic abdominal imaging in patients with malignancy: comparison of MR imaging and helical CT in 164 patients. J Magn Reson Imaging 2000;12:269–277.
48. Tschammler A, Ott G, Schang T, Seelbach-Goebel B, Schwager K, Hahn D. Lymphadenopathy: differentiation of benign from malignant disease—color Doppler US assessment of intranodal angioarchitecture. Radiology 1998;208:117–123.
49. Sanz Garcia RM, Guerra Vales JM, de Prada I, Martinez MA, Guillen Camargo V. [Localized Castleman's disease associated with high-grade lymphoma.] [Spanish] An Med Interna 1999;16:305–307.
50. Meyer L, Gibbons D, Ashfaq R, Vuitch F, Saboorian MH. Fine-needle aspiration findings in Castleman's disease. Diagn Cytopathol 1999;21:57–60.
51. Meador TL, McLarney JK. Computed tomography features of Castleman disease of the abdomen and pelvis. AJR 2000;175:115–118.
52. Gonzalez Sanchez FJ, Landeras Alvaro RM, Encinas Gaspar MB, Napal Lecumberri S. [Castleman's disease: isolated retroperitoneal mass. Report of a case.] [Spanish] Arch Esp Urol 1999;52:282–285.
53. Murphy SP, Nathan MA, Karwal MW. FDG-PET appearance of pelvic Castleman's disease. J Nucl Med 1997;38:1211–1212.
54. Iwamoto Y, Ueda H, Yamamoto K, et al. [Retroperitoneal Castleman's disease occurred around the bilateral upper ureters. A case report.] [Japanese] Nippon Hinyokika Gakkai Zasshi 1998;89:618–621.
55. Yoshino T, Mannami T, Ichimura K, et al. Two cases of histiocytic necrotizing lymphadenitis (Kikuchi-Fujimoto's disease) following diffuse large B-cell lymphoma. Hum Pathol 2000;31:1328–1331.
56. Miller WT Jr, Perez-Jaffe LA. Cross-sectional imaging of Kikuchi disease. J Comput Assist Tomogr 1999;23: 548–551.
57. Oh YK, Ha CS, Samuels BI, Cabanillas F, Hess MA, Cox JD. Stages I–III follicular lymphoma: role of CT of the abdomen and pelvis in follow-up studies. Radiology 1999;210:483–486.
58. Avila NA, Kelly JA, Chu SC, Dwyer AJ, Moss J. Lymphangioleiomyomatosis: abdominopelvic CT and US findings. Radiology 2000;216:147–153.
59. Azam P, Lang H, Lindner V, Roy C, Saussine C, Jacqmin D. [Retroperitoneal mucinous cystadenoma.] [French] Prog Urol 1999;9:319–321.
60. Spencer JA, Swift SE, Wilkinson N, Boon AP, Lane G, Perren TJ. Peritoneal carcinomatosis: image-guided peritoneal core biopsy for tumor type and patient care. Radiology 2001;221:173–177.
61. Ricke J, Sehouli J, Hosten N, et al. [Fat-saturated, contrast-enhanced spin-echo sequences in the magnetic resonance tomographic diagnosis of peritoneal carcinosis.] [German] Rofo Fortschr Geb Rontgenstr Neuen Bildgeb Verfahr 1999;171:461–467.
62. Ha HK, Jung JI, Lee MS, et al. Computed tomography differentiation of tuberculous peritonitis and peritoneal carcinomatosis. AJR 1996;167:743–748.
63. Rodriguez E, Pombo F. Peritoneal tuberculosis versus peritoneal carcinomatosis: distinction based on CT findings. J Comput Assist Tomogr 1996;20:269–272.
64. Grunenberger F, Bachellier P, Chenard MP, et al. Hepatic and pulmonary metastases from a meningeal heman-

giopericytoma and severe hypoglycemia due to abnormal secretion of insulin-like growth factor: a case report. Cancer 1999;85:2245–2248.
65. Centonze M, Dvornik G, Alberti Di Catenaja A, Cemin S, Della Sala SW. [Epithelioid leiomyoblastoma of the greater omentum: a case report.] [Italian] Radiol Med 2001;101:510–512.
66. Zotalis G, Nayar R, Hicks DG. Leiomyomatosis peritonealis disseminata, endometriosis, and multicystic mesothelioma: an unusual association. Int J Gynecol Pathol 1998;17:178–182.
67. Alamowitch B, Mausset V, Ruiz A, et al. [Non-secreting pheochromocytoma of the broad ligament revealed by appendicular peritonitis.] [French] Presse Med 1999;28:225–228.
68. Zhu Y, Ghosh P, Charnay P, Burns DK, Parada LF. Neurofibromas in NF1: Schwann cell origin and role of tumor environment. Science 2002;296:920–922.
69. Currarino G, Coln D, Votteler T. Triad of anorectal, sacral, and presacral anomalies. AJR 1981;137:395–398.
70. Valley MT, Pierce JG, Daniel TB, Kaunitz AM. Cesarean scar pregnancy: imaging and treatment with conservative surgery. Obstet Gynecol 1998;91:838–840.
71. Killi RM, Ozutemiz O, Elmas N. Color Doppler sonography of herniated paraumbilical collateral vein masquerading as an acquired umbilical hernia. AJR 2000;174:1465–1466.
72. Roth CG, Varma JD, Tello R. Gastrointestinal/genitourinary case of the day. Incarcerated inguinal hernia of the left fallopian tube and ovary. AJR 1999;173:787,791–792.
73. Blachar A, Federle MP, Dodson SF. Internal hernia: clinical and imaging findings in 17 patients with emphasis on CT criteria. Radiology 2001;218:68–74.
74. Blachar A, Federle MP. Bowel obstruction following liver transplantation: clinical and CT findings in 48 cases with emphasis on internal hernia. Radiology 2001;218: 384–388.
75. Pear BL, Plunkett LA. Case 32: Herniation of the ascending colon into the lesser sac. Radiology 2001;218:773–775.
76. Sourtzis S, Canizares C, Thibeau JF, Philippart P, Damry N. An unusual case of herniation of small bowel through an iatrogenic defect of the falciform ligament. Eur Radiol 2002;12:531–533.
77. Puls R, Kreissig R, Hosten N, Gaffke G, Stroszczynski C, Felix R. Tumour of the diaphragm mimicking liver lesion. Eur J Radiol 2002;41:168–169.
78. Grattan-Smith JD, Blews DE, Brand T. Omental infarction in pediatric patients: sonographic and CT findings. AJR 2002;178:1537–1539.
79. Takada A, Moriya Y, Muramatsu Y, Sagae T. A case of giant peritoneal loose bodies mimicking calcified leiomyoma originating from the rectum. Jpn J Clin Oncol 1998;28:441–442.
80. Donnelly LF, Frush DP, O'Hara SM, Bisset GS 3rd. Necrotizing myofasciitis: an atypical cause of "acute abdomen" in an immunocompromised child. Pediatr Radiol 1998;28:109–111.
81. Rendon Unceta P, Amaya Vidal A, Porcel Martin A, Macias Rodriguez MA, Soria de la Cruz MJ, Martin Herrera L. Abdominal tuberculous abscesses in AIDS patients: percutaneous treatment. Rev Esp Enferm Dig 1999;91:439–446.
82. Prokesch RW, Schima W, Schober E, Vychytil A, Fabrizii V, Bader TR. Complications of continuous ambulatory peritoneal dialysis: findings on MR peritoneography. AJR 2000;174:987–991.
83. Lin BH, Vargish T, Dachman AH. Computed tomography findings after laparoscopic repair of ventral hernia. AJR 1999;172:389–392.
84. Goodwin AT, Ghilchik M. Acute strangulation of the appendix within a laparoscopic port-site hernia. Eur J Surg 1998;164:151–152.
85. Dux M, Ganten M, Lubienski A, Grenacher L. Retained surgical sponge with migration into the duodenum and persistent duodenal fistula. Eur Radiol 2002;12 Suppl 3:S74–77.
86. Manabe T, Goto H, Mizuno S, Kanematsu M, Hoshi H. [A case of retained surgical sponge penetrated into the sigmoid colon.] [Japanese] Nippon Igaku Hoshasen Gakkai Zasshi 1997;57:279–280.

15

Spleen

Technique

Magnetic Resonance

Magnetic resonance (MR) relaxation characteristics of focal tumors tend to be similar to normal splenic tissue and thus difficult to detect. With the spleen located in the left upper abdomen close to the left hemidiaphragm, magnetic resonance imaging (MRI) of the spleen requires control of motion artifacts. A number of breath-hold techniques have been developed that allow dynamic contrast-enhanced images. Faster MRI techniques allow postcontrast images to be obtained during perfusion, equilibrium, and more delayed phases. Some focal lesions equilibrate with normal splenic parenchyma within several minutes after contrast injection and thus early postcontrast images accentuate tumors compared to normal tissue.

Superparamagnetic iron oxide contrast agents are taken up by the reticuloendothelial cells and shorten T2, making high signal intensity tumors more conspicuous. While these agents are theoretically advantageous in the spleen, research activity in this field peaked about a decade ago, and little current clinical application exists in the spleen.

Scintigraphy

Some of the more common radiopharmaceuticals useful in splenic imaging are technetium-99m (Tc-99m)–sulfur colloid, indium-111–white blood cells, and Tc-99m–red blood cells.

Biopsy/Drainage

Splenic biopsies are performed in both adults and children with few complications. A variety of needles are used, with 20- and 22-gauge needles being the most common (1). Biopsies establish a specific diagnosis in most patients with a focal splenic abnormality.

Congenital Anomalies

Malposition

The spleen is normally located in the left upper quadrant of the abdomen. Malposition is due to either a congenital maldevelopment or an acquired condition, such as a prior surgical procedure. Excessive mobility to the spleen is secondary to laxity of the splenic suspensory ligaments, including the lienorenal ligament. At times the splenic hilum is located along the superior aspect of the spleen, a condition that is probably a normal variant. The spleen can herniate into a prior lumbar incision.

Many patients with a hypermobile spleen are asymptomatic, and these "wandering spleens" are discovered incidentally when an imaging study is performed for other purposes. An asymptomatic wandering spleen can even be located in the right side of the pelvis, mimick-

ing a pelvic tumor. CT and MR reveal an absent spleen in its usual location and a splenic-sized tumor inferiorly. Contrast enhancement detects a vascular pedicle. A wandering spleen can be diagnosed with sequential liver-spleen scintigraphy and with In-111-leukocyte scintigraphy. An occasional such wandering spleen is associated with dilated feeding vessels within lax ligaments. Lax suspensory ligaments predispose a wandering spleen to splenic torsion and has even caused splenic flexure volvulus. Splenic torsion is a rare cause of an acute abdomen; at times contrast enhanced imaging reveals a partly nonenhancing spleen due to ischemia (2).

Accessory Spleen

The term *accessory spleen* is used to designate additional separate splenic tissue believed to be congenital in origin. It is a common condition, with most accessory spleens located near the splenic hilum, some even being intrapancreatic in location where they can mimic a pancreatic tumor. Although most are relatively fixed in position, an occasional one fits the criteria of a wandering spleen, such as an intrascrotal paratesticular accessory spleen. Similar to a main spleen, cysts can also develop in an accessory spleen. In a setting of splenomegaly an accessory spleen will also enlarge. Thus an accessory spleen enlarges secondary to portal hypertension. Torsion of an accessory spleen vascular pedicle can result in vascular compromise and progress to ischemia and infarction.

An accessory spleen is detected by computed tomography (CT), ultrasonography (US), MRI, and scintigraphy. On noncontrast CT it mimics enlarged lymph nodes, but after contrast it enhances similar to the spleen. Color Doppler US also suggests the diagnosis. Accessory spleens have the same MR signal intensity as normal spleen parenchyma on all sequences.

A Tc-99m–sulfur colloid scan shows uptake similar to the spleen. Occasionally such uptake results in confusion. Thus after a splenectomy somatostatin receptor scintigraphy reveals uptake in an accessory spleen.

Asplenia and Polysplenia

The terms *asplenia* and *polysplenia* are descriptive only, and associated abnormalities are common. These conditions are part of the heterotaxy syndrome (discussed in Chapter 14).

Splenogonadal Fusion

Splenogonadal fusion in males is discussed in Chapter 13. This rare congenital anomaly is associated with orofacial and extremity abnormalities. Imaging detects a tumor in the lower abdomen, with radiocolloid spleen scintigraphy and single photon emission computed tomography (SPECT) showing uptake similar to splenic tissue.

Gaucher's Disease

Gaucher's disease is an autosomal-recessive storage disorder caused by a defect in the lysosomal enzyme β-glucosidase, an enzyme needed to degrade sphingolipids. About 40 mutations of the β-glucosidase gene have been identified, with clinical disease variability depending on the specific type of gene mutation involved. Its hallmark is pathologic storage of glycolipid in mononuclear phagocytes, with a tissue reaction to these lipid-engorged macrophages, or Gaucher cells, probably leading to further organ damage. The diagnosis is made by showing decreased acid β-glucosidase activity in peripheral blood leukocytes. A histologic diagnosis is not necessary in most patients. Genotyping is available and does detect most carriers, but the variable phenotypic expressivity limits the use of genotyping as a practical tool.

Gaucher's disease is subdivided into three types based on the presence or absence of neurologic involvement: type 1, nonneuronopathic; type 2, severe neuronopathic; and type 3, a chronic, less severe neuronopathic form similar to type 1, but with more severe, systemic manifestations. A rare neonatal form leads to hydrops fetalis.

The disease involves multiple organs but varies considerably in its clinical expressivity and severity. Typically, splenomegaly, bone lesions, and eventually central neurologic involvement become evident. These patients are at increased risk of developing lymphoproliferative disorders, including non-Hodgkin's lymphoma.

Moderate-to-severe splenomegaly due to reticuloendothelial hypertrophy and hyperplasia is a common and often the only imaging finding. Hepatomegaly generally is not a prominent feature. A number of CT and US techniques have been developed to measure splenic volume. These are useful in patients with Gaucher's disease who often undergo serial follow-up studies. Follow-up of splenic volume changes are best obtained using the same imaging modality.

A minority of patients have well-defined homogeneous hypodense nodules scattered throughout the spleen. Ultrasonography shows variable echogenicity in these nodules. An irregular, inhomogeneous appearance is seen if these nodules become confluent. Of interest is that splenectomized patients tend to develop retroperitoneal or periportal lymphadenopathy. Magnetic resonance imaging also identifies splenic nodules in some of these patients, with these nodules being isointense on T1- and hypointense on T2-weighted images. Also, MR detects splenic infarcts in these patients.

These patients have decreased plasma levels of low-density lipoproteins. Technetium-99m–low-density lipoprotein scintigraphy shows that these proteins are taken up by the spleen, bone marrow, and liver reticuloendothelial system (3). Such serial studies appear of value in follow-up after therapy.

Splenectomy and heterotopic splenic autotransplantation have been used to treat hypersplenism. Partial splenectomy often leads to enlargement of the splenic remnant. It is not clear if such enlargement is due to splenic tissue regeneration or continued glycolipid deposition or both.

An occasional patient with massive splenomegaly develops a splenic abscess.

Thalassemia

Hypersplenism can be corrected in children with thalassemia by partial or total surgical splenectomy. An alternative is partial splenic embolization. After embolization the spleen decreases in size and fewer transfusions are necessary.

Hereditary Spherocytosis

Patients with hereditary spherocytosis have hemolysis, either compensated or leading to anemia, and are at increased risk for bilirubinate gallstones, erythroid aplasia, and hemolytic crises.

Therapy consists of splenectomy, although partial splenic embolization is an option (4).

Niemann-Pick Disease

Niemann-Pick type C disease is an autosomal-recessive lipid storage disorder, leading to an accumulation of syringomyelin and cholesterol in the brain, liver, and spleen. Most affected patients develop neurologic symptoms. Isolated nodular splenomegaly develops in this condition.

Sickle Cell Disease

Patients with sickle cell disease are at risk for splenic infection, abscess, acute splenic sequestration crisis, hypersplenism, and splenic infarction. Most acute infarctions involve only a portion of the spleen, although total splenic infarction does develop. During an acute sequestration crisis the hematocrit drops and spleen enlarges, at times massively. Computed tomography identifies multiple hypodense foci in the spleen. Multiple episodes of focal splenic infarction eventually result in a small spleen, at times containing calcifications.

In patients homozygous for this condition MRI reveals a signal void on T2-weighted sequences due to a combination of iron deposition and superimposed calcifications (iron overload is discussed in Chapter 7). These patients have impairment of splenic reticuloendothelial function; scintigraphy with Tc-99m–sulfur colloid reveals nonvisualization of the spleen.

Patients with sickle cell disease develop round intrasplenic nodules, shown to represent functioning splenic tissue; this tissue is hypodense on CT, hypoechoic on US, appears as normal spleen on MRI, and manifests uptake of Tc-99m–sulfur colloid. Imaging thus allows distinguishing these nodules from abscesses and infarcts.

Trauma

In the United States, the initial triage of trauma patients classifies them into those who are unstable and require immediate surgery or stable; the latter patients generally undergo contrast-enhanced CT, with a decision for surgery, angiographic therapy, or conservative management based on CT findings. Quite often splenic trauma is only one element of multisystem trauma, and the decision for a specific therapy is modified accordingly. Intravenous contrast is necessary for adequate CT evaluation. Using splenic arteriography as a gold standard, in 78 hemodynamically stable patients CT achieved an 81% sensitivity and 84% specificity in predicting the need for splenic therapy (5). In general, US is believed to be not as sensitive in detecting the extent of injury.

A number of injury severity schemes based on contrast-enhanced CT have been developed. Some use the degree of splenic laceration and devascularization as a classification guide. Both in adults and children these schemes have had limited success in guiding therapy. A splenic injury classification scale, devised by the American Association for the Surgery of Trauma, is outlined in Table 15.1. In general, the injury severity score best correlates with outcome.

Some patients managed conservatively develop delayed complications, including splenic or subphrenic abscess, bleeding from a (pseudo)aneurysm, or splenic rupture. Whether routine follow-up CT is warranted in these patients is controversial. Follow-up CT in otherwise asymptomatic patients does not appear to be routinely warranted. Whether US follow-up, including color Doppler, is warranted is not clear.

Blunt abdominal trauma can result in pseudoaneurysms and a splenic arteriovenous fistula; some of these fistulas resolve spontaneously.

Hematoma

A hematoma can be subcapsular or intraparenchymal in location or, with rupture of the capsule, even perisplenic.

With noncontrast CT, intrasplenic hematomas range from hypodense to hyperdense (density-time variations are discussed in Chapter 14). Contrast-enhanced CT reveals a hematoma as a nonperfused region surrounded by contrast-enhancing normal parenchyma. A subcapsular hematoma tends to have a crescent shape, while perisplenic ones are more irregular. Multiple episodes of spontaneous splenic bleeding can eventually result in a CT "onion skin" appearance.

A recent hematoma has a complex US appearance, and clotted blood in a hematoma can be

Table 15.1. Surgical splenic injury scale

Grade*	Type of injury	
I	Hematoma	Subcapsular, <10% of surface
	Laceration	Capsular, <1 cm in parenchymal depth
II	Hematoma	Subcapsular, 10–50% of surface Parenchymal, <5 cm in diameter
	Laceration	Parenchymal, 1–3 cm in depth, trabecular vessels not involved
III	Hematoma	Subcapsular, >50% of surface or expanding Ruptured Parenchymal, >5 cm in diameter or expanding
	Laceration	Parenchymal, >3 cm in depth or involving trabecular vessels
IV	Laceration	Segmental or hilar vessels involved in devascularization (>25% of spleen)
V	Laceration	Shattered spleen
	Vascular	Hilar injury with devascularized spleen

* Advanced one grade for multiple injuries, up to grade III.
Source: Modified from Moore et al. (6).

isoechoic to splenic tissue. Thus a perisplenic hematoma may simply blend into the spleen until it liquifies later on. In time, a hematoma gradually becomes anechoic.

Most hematomas eventually resolve; an occasional one becomes infected and requires drainage. Some evolve into nonepithelial cysts. Splenic hematomas can be drained percutaneously, although some recur. Gallium-67 subtraction scintigraphy is useful if an infected splenic hematoma is suspected.

Laceration/Rupture

Splenic laceration is usually associated with intraperitoneal hemorrhage; occasionally splenic injury also leads to extraperitoneal hemorrhage into the anterior pararenal space (7).

Although uncommon, delayed splenic rupture does occur after trauma. Occasionally even a minor splenic laceration leads to hemorrhage days later, at times massively. This topic is difficult to place in proper perspective because splenic rupture has been reported even years after prior injury.

Splenic rupture after minor trauma should lead to a search for underlying disease. In Western countries the leading cause of spontaneous splenic rupture is infectious mononucleosis. Rupture is a recognized complication in patients with malaria. Rarely, spontaneous splenic rupture occurs in patients with HIV/AIDS, acute leukemia, sickle cell disease, amyloidosis, hepatitis virus infection, and even *Salmonella enteritidis* infection (8). Splenomegaly due to such entities as Wilson's disease predisposes to rupture. Rupture of a splenic cyst after minor trauma can result in an acute abdomen. Splenic rupture is a complication of various interventional procedures, such as colonoscopy, extracorporeal shock-wave lithotripsy, and even after insertion of an implantable defibrillator using a left subcostal approach.

Precontrast CT of a laceration is seen as an irregular, hypodense defect (Fig. 15.1). Post–intravenous contrast, a laceration is better defined by surrounding contrast-enhancing normal splenic parenchyma; an adjacent subcapsular or extrasplenic hematoma is often present. With active arterial bleeding at the time of study, contrast CT can identify extravasation.

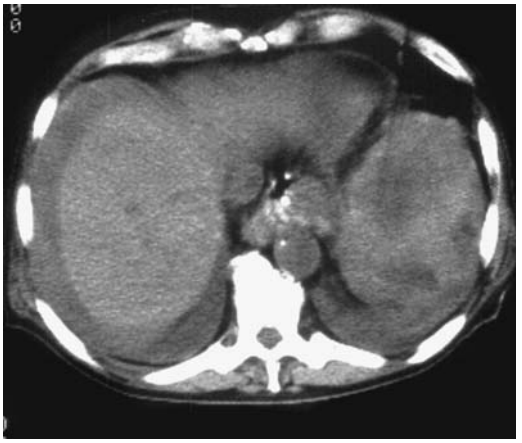

Figure 15.1. Splenic laceration. Ascites is also present.

Avulsion

Most splenic avulsions are secondary to major trauma. Avulsion has occurred, however, secondary to colonoscopy and even in a patient with hyperemesis.

Therapy

The overall trend is to manage conservatively hemodynamically stable patients with splenic injury, generally detected by CT, and with no other indication for laparotomy. Conservative management tends to be unsuccessful if a traumatic pseudoaneurysm or frank extravasation is detected on an initial CT examination; these patients should be treated with early surgical or endovascular therapy. Some of these patients undergo splenic arteriography and, if contrast extravasation is detected, splenic artery embolization is performed. Transcatheter arterial embolization therapy performed in trauma patients with angiographically evident contrast extravasation, arterial disruption, or major arteriovenous fistula is successful in over 90% of these patients.

Computed tomography identifies a splenic artery pseudoaneurysms as contrast blush; arteriography confirms this finding, and a majority of these aneurysms can be successfully embolized.

A subtotal splenectomy, with preservation of the upper splenic pole supplied by splenogastric

vessels, was performed in patients with severe splenic injuries (9). Partial laparoscopic splenectomy following splenic trauma is also feasible.

A preexisting diseased (enlarged) spleen is more prone to laceration/rupture than a normal spleen and patients with such a spleen probably undergo a higher rate of splenectomy than those with a normal-size spleen. Conservative management, however, can be successful in stable patients with trauma to a diseased spleen.

At times heterotopic splenic autotransplantation is performed after abdominal trauma requiring total splenectomy. Whether the autotransplanted splenic tissue is functioning can be evaluated with red blood cell scintigraphy.

Follow-up US in children with blunt splenic trauma found that the time to healing is related to injury severity (10); sequelae include an occasional splenic cyst.

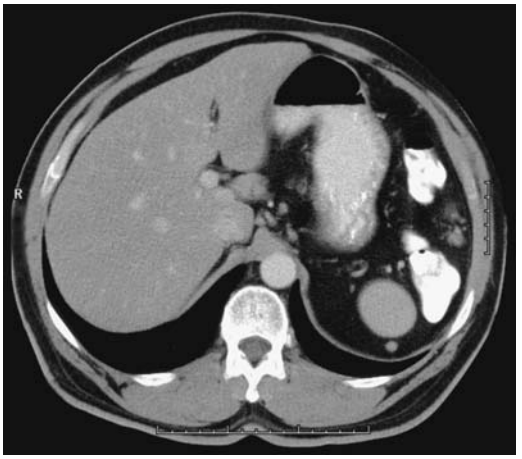

Figure 15.2. Splenosis. The patient had a splenectomy as a child due to trauma. Computed tomography (CT) reveals left upper quadrant soft tissue nodules. Serial studies showed no change. (Courtesy of Patrick Fultz, M.D., University of Rochester.)

Torsion/Volvulus

Occasionally a wandering spleen twists on its axis on either an acute or chronic basis, a condition occurring in both children and adults. Torsion can be suggested in the appropriate clinical setting if the spleen is not in its usual right upper quadrant location (the condition is really a *volvulus*, although the term *torsion* is often used interchangeably in the literature).

When acute, the sudden onset of abdominal pain suggests an acute abdomen. On a more chronic basis, few symptoms are elicited and the condition is often detected incidentally when an abnormal lower abdominal or even pelvic tumor is detected and the splenic fossa empty.

Imaging suggests the diagnosis. Computed tomography reveals a hypodense spleen, at times still showing postcontrast peripheral enhancement. Ultrasonography detects a hypoechoic solid spleen, and Doppler US reveals absent blood flow, confirming the diagnosis.

Torsion and infarction also develop in an accessory spleen, especially if it has a long vascular pedicle. A number of these rare events occur in children.

Laparoscopic splenopexy of a mobile spleen has been performed (11).

Splenosis

Acquired splenic tissue outside the spleen, such as ectopic implantation from prior trauma, is termed splenosis, thus distinguishing it from an accessory spleen, which is a congenital condition. Splenosis tends to present with multiple nodules; accessory spleens, on the other hand, are few in number. Splenosis involves the peritoneum, retroperitoneal tissues, thoracic cavity, and even subcutaneous abdominal wall tissues (Fig. 15.2). It can develop years after splenectomy. Even intrahepatic splenosis has been reported (12). One patient developed cerebral splenosis 15 years after splenectomy (13).

Splenosis can become quite large, even mimicking an adjacent neoplasm. Most of these splenic nodules have a smooth outline. If sufficiently large, splenosis is imaged by CT, US, MRI, and scintigraphy. Ultrasonography reveals homogeneous echogenicity.

Splenosis should be differentiated from polysplenia.

Splenomegaly

The definition of an abnormally enlarged spleen (splenomegaly) is arbitrary. One definition used by ultrasonographers is a spleen that deviates by

Figure 15.3. Massive splenomegaly secondary to myelofibrosis.

either one or two standard deviations from a group of "normal" spleens using the US splenic volume index.

Etiologies of splenomegaly are legion. Some radiologists subdivide splenomegaly into moderate versus massive, with the correspondingly most likely associated etiologies (Fig. 15.3). The most common causes of massive splenomegaly are myelofibrosis, lymphoma, and late-stage leukemia, although these entities are also encountered with lesser splenic enlargement. Splenomegaly is common in patients with portal hypertension. A rare cause of hepatosplenomegaly is systemic mastocytosis.

Infection/Inflammation

Most splenic infections are hematogenous in origin, although in some patients no primary focus of infection can be determined.

Small, focal, hypodense nodules scattered in the spleen on arterial phase CT images suggest an infection. A finding of such a "spotted spleen," however, is also seen with some neoplasms, especially lymphoma, and noninfectious inflammatory conditions such as sarcoid (14).

Abscess

Splenic abscesses are not common. Most develop in a setting of systemic infection, trauma, diabetes, malignancy, or some hematologic disorder. Splenic flexure fistulas in colonic Crohn's disease can involve the spleen and result in abscesses. Some left renal abscesses also involve the spleen. Likewise, a splenic abscess is a complication of a nephrectomy, especially if a nephrectomy is performed for xanthogranulomatous pyelonephritis. Common pathogens encountered are *Staphylococcus* and *Streptococcus* species and *Escherichia coli*. An occasional abscess contains *Clostridium perfringens* or other clostridial species.

Clinical signs and symptoms are nonspecific and include fever, pain, and left upper quadrant tenderness. Splenomegaly is usually present. Undiagnosed, splenic abscesses result in a high mortality rate.

Imaging should suggest the diagnosis (Fig. 15.4). In some patients a chest radiograph reveals a left pleural effusion. Most splenic abscesses are solitary. Computed tomography shows a hypodense region surrounded by

Figure 15.4. Splenic abscess detected by CT. It was of unknown etiology.

a contrast-enhancing rim. Gas within an abscess implies gas-forming bacteria; gas is only rarely secondary to an enteric fistula. A ruptured splenic abscess, however, has led to a pneumoperitoneum.

Most splenic abscesses have a slight heterogeneous MR appearance on precontrast images. Peripheral ring enhancement is common on postcontrast images.

Once imaging suggests a splenic abscess, culture of aspirated material should identify the infectious agent. Traditionally splenic abscesses have been treated by splenectomy, although they are amenable to percutaneous drainage, generally under US guidance, and percutaneous drainage has replaced splenectomy in a number of institutions.

Hydatid Disease

Hydatid disease is discussed in more detail in Chapter 7. Although most echinococcal cysts are located in either the liver or the lungs, an occasional cyst develops in the spleen, kidneys, bones, heart, or peritoneum. Usually splenic involvement is also associated with other disease, at times being recurrent. Rupture of a splenic echinococcal cyst results in peritoneal dissemination of cyst content.

Cyst wall calcifications develop in about half of splenic echinococcal cysts. Most have a well-demarcated outline; some are multiloculated (Fig. 15.5). Postcontrast CT reveals little contrast enhancement in the cyst wall.

Other splenic cysts, including the rare lymphangioma, are in the differential diagnosis.

Tuberculosis

Splenic tuberculosis is rare. Silent splenic involvement is found in some patients with disseminated tuberculosis. Typically multiple small, hypodense lesions are scattered throughout the spleen. No calcification is evident during an acute infection but develop with healing. The imaging appearance is nonspecific and is similar to that seen with a number of other infections and some lymphomas. Computed tomography revealed multiple, round or oval, hypodense tumors (Fig. 15.6). Ultrasonography of diffuse involvement reveals numerous hyperechoic foci. They are hypointense on T1-weighted images and often heterogeneous on T2-weighted images. They do not enhance with contrast but tend to have a slight rim enhancement postcontrast. Splenic tuberculosis is often associated with extraperitoneal adenopathy, with the nodes having peripheral contrast enhancement.

The less common isolated tuberculoma mimics a splenic abscess.

Tuberculous splenic abscesses are photopenic with Tc-99m-sulfur colloid scintigraphy; these abscesses, however, have increased uptake during gallium-67 scintigraphy.

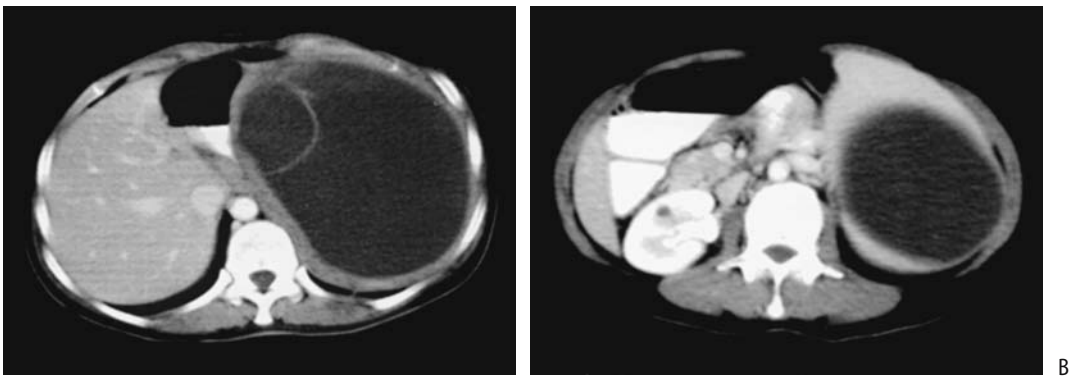

A B

Figure 15.5. Isolated splenic hydatid disease. Contrast-enhanced CT through upper (A) and lower (B) poles reveals a large cystic nonenhancing structure. A daughter cyst is evident in A. (*Source:* Polat P, Kantarci M, Alper F, Suma S, Koruyucu MB, Okur A. Hydatid disease from head to toe. RadioGraphics 2003;23:475–494, with permission from the Radiological Society of North America.)

Figure 15.6. Splenic tuberculosis in an HIV-positive man. Contrast-enhanced CT shows marked splenomegaly and numerous poorly enhancing nodules throughout the spleen. Enlarged retroperitoneal nodes were also identified. (Courtesy of Patrick Fultz, M.D., University of Rochester.)

Candidiasis

A *Candida* sp. splenic abscess in the absence of immunocompromise is rare. Both pre- and postcontrast CT aid in detecting these multiple, often small abscesses. They tend to be hypodense. A typical US appearance is that of a bull's-eye, a finding that is neither specific nor always seen. These abscesses appear hypointense on T1- and hyperintense on T2-weighted images. They do not enhance postcontrast.

If large enough, these abscesses are amenable to percutaneous drainage.

Histoplasmosis

Multiple small, punctate intrasplenic calcifications develop in patients with past histoplasmosis infection. Tuberculosis shows similar findings. In both entities calcifications are indicative of inactive disease.

Imaging readily detects these granulomas.

Brucellosis

Human brucellosis is caused by *Brucella abortus*, *B. suis*, *B. canis,* and *B. melitensis*. The latter is considered to be the most virulent.

Among patients with brucellosis from Beirut, Lebanon, the main presenting symptoms were fever, sweating, fatigue, and joint pain, with osteoarthritic involvement being the most prevalent complication (15). Abdominal complaints were not common.

Calcifications in splenic brucellosis have an irregular and mottled appearance. Of interest is that with most infections calcifications imply disease inactivity within that nidus; brucellosis is unique in that active infection can be present even in a calcified nidus.

Cat-Scratch Disease (Bartonella Infection)

Bartonella henselae infection is related to contact with cats and is the presumed cause of cat-scratch disease. If disseminated, this infection leads to focal multinodular liver and splenic granulomas.

The splenic granulomas eventually calcify, often having a coarse appearance.

Infectious Mononucleosis (Epstein-Barr Virus Infection)

While splenomegaly is common in patients with infectious mononucleosis, in the occasional patient with disproportionate splenomegaly an underlying hematologic malignancy or a storage disorder such as Gaucher's disease should be considered.

Some physicians believe that early splenectomy is indicated in a setting of splenic rupture complicating infectious mononucleosis, and most patients with spontaneous splenic rupture undergo splenectomy, although a nonoperative approach is feasible in selected patients. Even with initial nonoperative management, some eventually require a splenectomy.

Metabolic and Related Disorders

Hypersplenism

Hypersplenism, or increased splenic hemolysis, is a manifestation of several disorders, such as thrombocytopenic purpura and Gaucher's disease. Transcatheter splenic artery embolization is effective therapy for hypersplenism.

Platelets, white blood count, and liver function tests improve significantly after such embolization. Fever, abdominal pain, pleural effusion, and ascites are transient phenomena after splenic embolization.

Partial splenic embolization can be therapeutic in cirrhotic patients with hypersplenism. Residual spleen volumes remain stable in those with infarction rates >80%; on the other hand, in patients with lower infarction rates spleen volume tends to increase. The ideal splenic volume to be embolized is not clear and probably varies depending on disease and age. For instance, children with hypersplenism undergoing 30% to 40% splenic volume embolization have lower morbidity compared with those undergoing more extensive splenic embolization (16); all maintained a platelet count above baseline.

Hyposplenism

The classic example of decreased splenic function is in sickle cell disease. For unknown reasons patients with celiac disease also develop hyposplenism. Decreased splenic function is detected by the presence of abnormal red blood cells and by finding decreased splenic uptake on a Tc-99m–sulfur colloid scan.

Hyposplenism increases the risk of infection and predisposes to spontaneous splenic rupture.

Extramedullary Hematopoiesis

Extramedullary hematopoiesis is most common in patients with congenital hemolytic anemias. Most foci occur in the liver and spleen but are too small to identify with imaging. If large enough, CT reveals a homogeneous hypodense tumor, suggesting an infection or neoplasm.

Iron Overload

Similar to the liver, MRI of the spleen detects relatively low levels of splenic iron overload, but for meaningful results stringent equipment calibration is necessary. Iron overload is difficult to quantify but is occasionally useful in adults with suspected posttransfusion iron overload. In children after autologous bone marrow transplantation, MRI detects earlier iron overload in the liver than in the spleen.

Amyloidosis

Splenic involvement occurs in both primary and secondary amyloidosis. Diffuse rather than focal splenic involvement is more common. Abnormal regions tend to be hypodense on CT. Some foci calcify. Arterial phase CT in a patient with primary liver and spleen amyloidosis revealed lack of contrast enhancement (17); the spleen was hypointense on T2-weighted MR images.

Systemic amyloidosis is associated with hyposplenism. Among patients with suspected liver amyloidosis, a liver-spleen scan is quite sensitive in detecting decreased splenic activity and can suggest disease even before abnormal red blood cells are detected in a peripheral smear.

An amyloid spleen predisposes to a spontaneous splenic rupture.

Sarcoidosis

Splenic abnormalities are present in roughly half of patients with sarcoidosis, with splenic involvement usually being asymptomatic and overshadowed by other organ involvement. The most common abdominal manifestation of sarcoidosis is hepatosplenomegaly, although marked splenic enlargement is rare. Less often seen are splenic nodules (18), an appearance called *spotted spleen*. Usually these splenic nodules are larger than their counterparts in the liver. They are not specific to sarcoidosis and are also found with some malignancies and infections. Punctate calcifications develop in some sarcoid spleens; these calcifications are readily identified by imaging and are similar to those seen with histoplasmosis and tuberculosis. Chest radiography is normal in some patients with splenic sarcoidosis.

Computed tomography reveals sarcoid nodules to be hypodense to splenic parenchyma and hypointense on MRI; they are best identified on T2-weighted fat-suppressed images and on immediate contrast-enhanced images. Ultrasonography reveals solid, hypoechoic foci.

Extraperitoneal adenopathy is common. Computed tomography also often detects an increased number of normal-sized lymph nodes.

Virus-Associated Hemophagocytic Syndrome

Virus-associated hemophagocytic syndrome consists of erythrocyte and other blood element phagocytosis in multiple organs, including the spleen. Magnetic resonance imaging in a patient with acute lymphocytic leukemia and virus-associated hemophagocytic syndrome revealed multiple, round splenic signal voids believed to represent hemosiderin deposits (19).

Tumors

Nonneoplastic

Inflammatory Tumor

The term *inflammatory tumor,* also called *inflammatory pseudotumor* and *inflammatory myofibroblastic tumor*, describes a focal inflammatory and reactive response in the spleen. The etiology of these rare tumors is unknown. They consist of a discrete encapsulated tumor containing a mixture of spindle cells suggesting myofibroblasts, inflammation, fibrosis, and necrosis.

They vary considerably in size and number. Some are quite large. They contain a mix of solid and cystic components. Computed tomography reveals a heterogeneous tumor. A central scar is suggested in some. They enhance less than normal spleen on early phase CT, but delayed enhancement is evident on later phases. They are heterogeneous and hypo- to isointense to splenic parenchyma on T1- and hypo- to hyperintense on T2-weighted MR images. Similar to CT, delayed enhancement is evident postgadolinium. Their overall appearance is nonspecific and a preoperative diagnosis is difficult; the differential includes a malignancy.

A number of patients with an eventually diagnosed splenic inflammatory tumor have undergone a splenectomy.

Hemangioma

Some authors classify splenic hemangiomas under neoplasms, together with angiomas and angiosarcomas. Although imaging findings overlap somewhat for these entities, pathogenetically hemangiomas are generally considered to be development anomalies and probably should be classified under hamartomas, but they have a sufficiently unique imaging appearance that they are discussed separately; keep in mind that an occasional splenic hemangioma exhibits sarcomatoid changes.

Splenic hemangiomas range from single to multiple. Multiple hemangiomas occur in the Klippel-Trénaunay-Weber syndrome. Hemangioma complications include hemorrhage and rupture. One infant with splenic hemangiomatosis had life-threatening thrombocytopenia, anemia and intravascular coagulopathy (Kasabach-Merritt syndrome) (20); whether these tumors indeed represented hemangiomatosis or a hemangioendothelioma is not clear.

Similar to liver hemangiomas, CT shows a low-density tumor with a peripheral hypervascular contrast-enhancing rim. Unlike in the liver, however, splenic hemangiomas less often show progressive central enhancement (Fig. 15.7).

Gray-scale US reveals hemangiomas as well-marginated, homogeneous and hyperechoic tumors (Fig. 15.8).

Figure 15.7. Presumed splenic hemangioma. Early contrast-enhanced CT image reveals a hypodense tumor. Delayed views showed that this tumor fills in from the periphery and becomes nearly isodense with the spleen. A similar tumor was present on CT images 19 months previously. (Courtesy of Patrick Fultz, M.D., University of Rochester.)

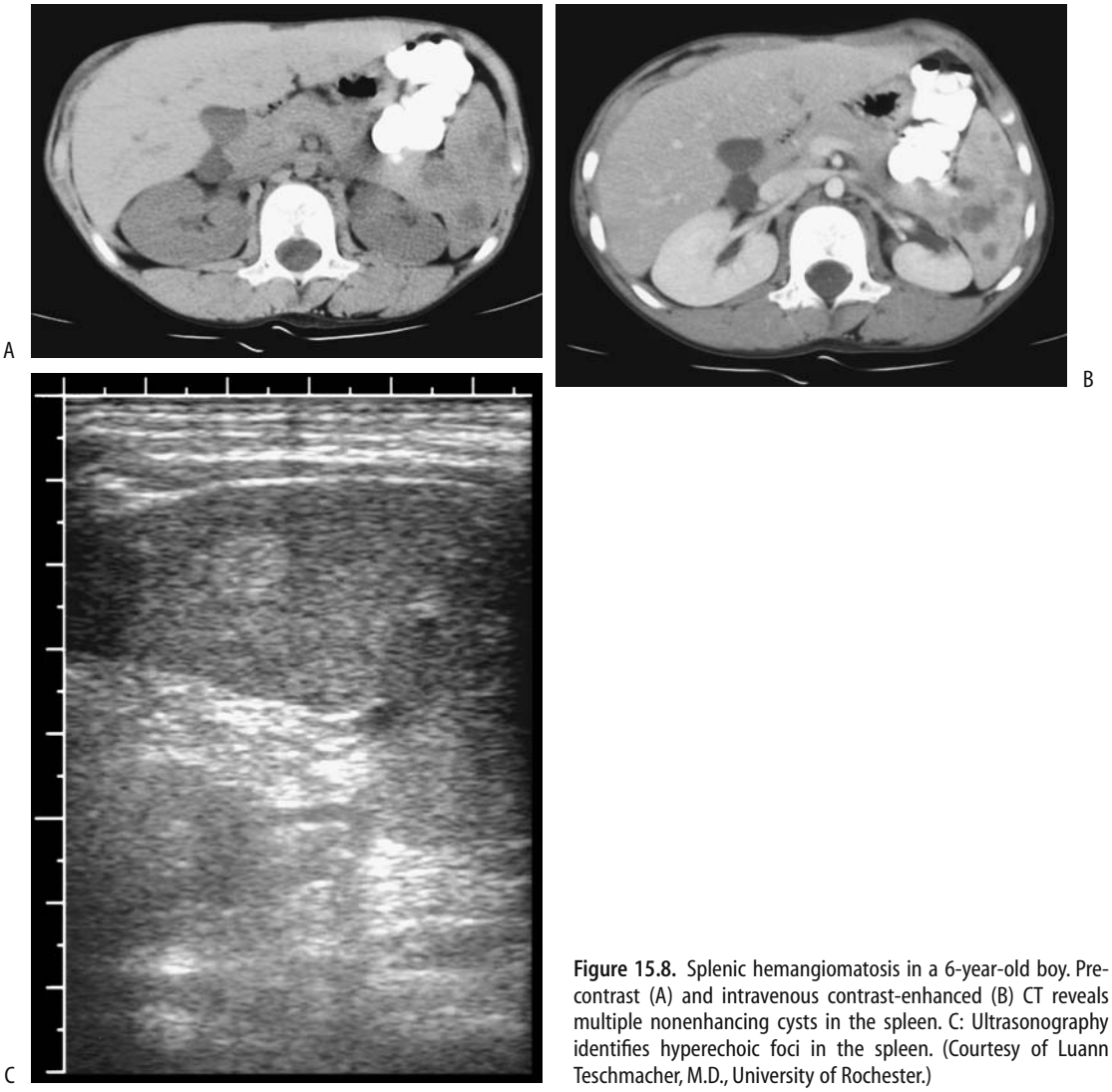

Figure 15.8. Splenic hemangiomatosis in a 6-year-old boy. Precontrast (A) and intravenous contrast-enhanced (B) CT reveals multiple nonenhancing cysts in the spleen. C: Ultrasonography identifies hyperechoic foci in the spleen. (Courtesy of Luann Teschmacher, M.D., University of Rochester.)

A majority of splenic hemangiomas are hyperintense on T2-weighted MRI relative to the spleen; similar to liver hemangiomas, dynamic MRA reveals progressive centripetal enhancement in most, with eventual uniform enhancement. They differ from liver hemangiomas in achieving earlier homogeneous contrast enhancement rather than exhibiting gradual enhancement from the periphery inward.

A Tc-99m–red blood cell scan shows a typical hemangioma as a photopenic lesion during perfusion and on early blood pool images, with subsequent filling-in on delayed images. Technetium-99m–human serum albumin (HSA) reveals radiotracer accumulation within a hemangioma.

With a suspected hemangioma in an asymptomatic patient serial US is useful to evaluate any change.

Peliosis

Splenic peliosis is considerably less common than peliosis hepatis. Peliosis has developed in

splenic hamartomas and in splenic parenchyma (21). Splenic peliosis can result in spontaneous splenic rupture, probably due to minor trauma.

The imaging appearance of splenic peliosis is similar to that seen in the liver. Computed tomography reveals hypodense tumors.

Hamartoma

The rare splenic hamartoma, or splenoma, is believed to be congenital in origin. Two types occur: white pulp, composed of aberrant lymphoid tissue, and red pulp, composed mostly of sinuses. Often a mix of both is found. A histopathologic differentiation from lymphoma is possible with most of these tumors. Most are detected incidentally. An occasional one is associated with thrombocytopenia or pancytopenia.

The CT appearance is similar to that seen with hamartomas in other locations. They range from homogeneous to heterogeneous. Most do not contain calcifications. Some have a cystic component. They tend to be isodense to splenic tissue. Some exhibit prolonged contrast enhancement. US reveals a well-marginated and somewhat hypoechoic tumor, at times containing multiple punctate foci, probably representing necrosis.

Most hamartomas are isointense on T1- and hyperintense on T2-weighted images. They have heterogeneous early postcontrast enhancement, often enhancing more uniformly on delayed images. Some hamartomas, however, have an enhancement pattern similar to hemangiomas. Prolonged enhancement on postcontrast CT and MR images differentiates these lesions from most malignancies. Aside from necrotic regions, angiography reveals them to be hypervascular.

Most hamartoma have similar uptake of Tc-99m-HSA to hemangiomas. Radiocolloid uptake is less within the tumor than in a normal spleen.

Cysts

Pathologically, most splenic cysts can be divided into epithelial-lined cysts, which are developmental in origin, and nonepithelial cysts, which are mostly sequelae of a prior hematoma. Radiologists often refer to both types as *simple cysts*, which is a descriptive term. Except for echinococcal cysts, infections rarely result in a splenic cyst.

A simple cyst, either developmental or posttraumatic, has a well-defined wall, consists of fluid density, and does not enhance postcontrast. Some cysts contain septa. Hemorrhage into a simple cyst or the presence of cholesterol crystals result in hyperechoic fluid. Calcifications eventually develop in some cyst walls.

A large splenic cyst is one of the causes of splenomegaly.

Simple cysts have been treated by laparoscopic spleen-preserving surgery.

Epithelial Cysts

Most developmental cysts, also called *epidermoid cysts*, *mesothelial cysts*, *primary cysts,* and *true cysts*, probably represent sequelae of mesothelial cell remnants trapped in splenic tissue. Several familial splenic cysts are reported. Some authors classify hemangiomas and cystic lymphangiomas as true cysts.

These cysts tend to be asymptomatic until trauma, at times minor, leads to hemorrhage and an increase in cyst size and then rupture. At times infection or compression of adjacent structures reveals its presence. Most are unilocular.

Prenatal US identified a splenic cyst at 31 weeks' gestation (22); the cyst had spontaneously regressed when the infant was 7 months of age.

Nonepithelial Cysts

The majority of cysts encountered in the West are posttraumatic; these do not have an epithelial lining and are also called *pseudocysts*, *hemorrhagic cysts*, and *serosal cysts*. At times prior hematoma-inducing trauma was relatively minor and is not remembered. Eventually a hematoma evolves into a nonepithelial cyst containing serous fluid.

Pancreatic Pseudocyst

Some cysts originating in an adjacent structure involve the spleen to the extent that imaging will suggest a splenic origin. For example, a pancreatic pseudocyst (also called a *false cyst*) arising from the tail of the pancreas can extend into the spleen and appear intrasplenic. Also in the dif-

ferential is an abscess and a cystic or necrotic neoplasm.

These cysts can be drained percutaneously.

Lymphangioma

Splenic lymphangiomatosis consists of multiple endothelial-lined cysts; it is a rare tumor. Some are associated with splenomegaly or hypersplenism. Most are discovered incidentally. Not uncommonly, liver and other site lymphangiomas are also identified.

Imaging typically shows a multilocular cyst or multiple thin-walled cysts, most often subcapsular in location. An occasional one contains curvilinear calcifications. They are hypodense and do not enhance with postcontrast CT. Occasionally diffuse lymphangiomatosis appears on postcontrast CT as a mottled spleen. They are hyperintense on T2-weighted images, except that cyst septa, consisting of fibrous connective tissue, appear hypointense.

Hydatid disease is in the differential diagnosis of a cystic lymphangioma.

Whether these patients should be treated (resection or embolization) or whether observation is appropriate depends on symptomatology.

Neoplasms

Angioma/Angiosarcoma

An angioma is an unusual splenic tumor that is difficult to classify. This rare, benign vascular tumor is composed of anastomosing vascular channels containing papillary projections. Littoral cell angiomas are rare neoplasms originating from cell lining sinuses (littoral cells) rather than larger vessels and have characteristic immunohistochemical properties. For unknown reason, anemia or thrombocytopenia develops in some patients. These tumors range from a focal tumor, to a miliary pattern, to ones replacing most of the spleen. Most are benign, although a littoral cell angiosarcoma also occurs. Littoral cell angiomas are hypodense relative to normal spleen tissue (23); dynamic CT reveals progressive and homogeneous contrast enhancement to the point that they resemble normal splenic parenchyma.

A primary angiosarcoma is a rare but highly malignant splenic neoplasm. It can involve accessory spleens. Splenomegaly is not uncommon and spontaneous splenic rupture does occur with angiosarcomas. Imaging of some of these tumors suggests abscesses.

Only a few MR findings of primary splenic angiosarcomas are reported. One was hypointense both on T1- and T2-weighted images, which differentiates it from most hemangiomas (24); intratumoral hemorrhage and necrosis were evident. Postgadolinium imaging revealed heterogeneous enhancement.

Lymphoma

The most common focal splenic tumor is malignant lymphoma. Most primary splenic lymphomas appear as a large, solitary tumor; multifocal tumors are less common. These tumors tend to enhance less than splenic parenchyma on postcontrast CT. Only an occasional one shows rim enhancement (Fig. 15.9). The majority of primary lymphomas are hypoechoic on US.

Splenomegaly is common but not universal with splenic involvement by lymphoma. Conversely, splenomegaly may be due to some other underlying disorder. Calcifications are unusual, but have developed in both untreated and, more often, treated lymphoma. Large necrotic nodules mimic an abscess (Fig. 15.10).

Aside from splenomegaly, splenic involvement by systemic lymphoma tends to be missed by imaging. In particular, diffuse lymphomatous infiltration is difficult to detect. To put splenic involvement by systemic lymphoma in perspective, among 680 patients with malignant lymphoma, US revealed abnormal splenic texture in only 15% (25); among these, about one third each were Hodgkin's disease, low-grade non-Hodgkin's lymphoma, and high-grade non-Hodgkin's lymphoma.

The US appearance of lymphoma involving the spleen varies considerably (25): diffuse involvement in 37%, small nodular in 39%, large nodular in 23%, and bulky in 2%. High-grade non-Hodgkin's lymphomas were either large nodular or small nodular, while low-grade non-Hodgkin's lymphomas and Hodgkin's disease were either diffuse or had a small nodular pattern.

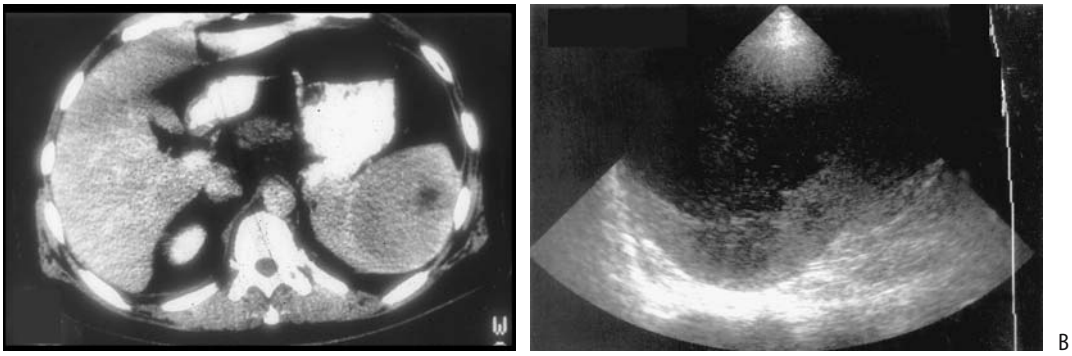

Figure 15.9. Solitary lymphoma. A: Transverse contrast-enhanced CT identifies a hypodense tumor with rim enhancement (arrow). B: The tumor is hypoechoic on longitudinal US (arrows). (*Source:* Dachman AH, Buck JL, Krishnan J, Aguilera NS, Buetow PC. Primary non-Hodgkin's splenic lymphoma. Clin Radiol 1998;53:137–142, with permission from the Royal College of Radiologists.)

Contrast-enhanced MR reveals diffuse splenic infiltration to have immediate heterogeneous enhancement, becoming isointense on delayed views. Focal lymphoma is hypointense on immediate postcontrast images.

Leukemia

Diffuse leukemic infiltration of the spleen results in a homogeneously enhancing enlarged spleen. Associated lymphadenopathy is common.

Laparoscopic splenectomy is feasible in patients with leukemia and Hodgkin's lymphoma.

Plasmacytoma/Multiple Myeloma

The rare primary splenic plasmacytoma most often presents with splenomegaly. Some of these patients develop disease progression after splenectomy but in an atypical fashion for multiple myelomas.

Metastases

An isolated metastasis to the spleen is not common. Presumably most abnormal cells are destroyed in the spleen. Colon, lung, ovarian, and other cancers result in multiple metastases, generally late in the course and most metastases

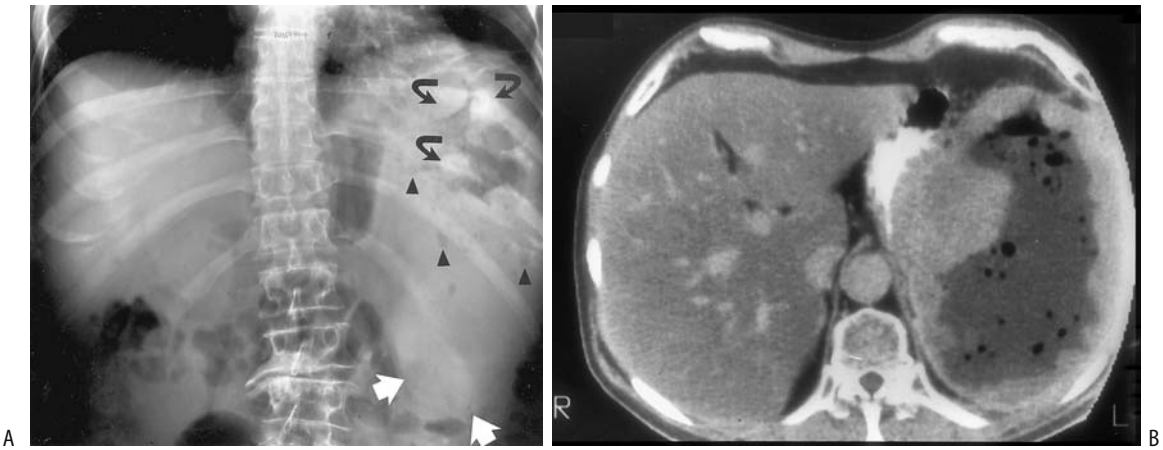

Figure 15.10. Splenic lymphoma. A: Splenomegaly is present (white arrows). Mottled gas (arrowheads) outlines nodules (curved arrows) in a necrotic cavity. B: The necrotic cavity is better identified on contrast-enhanced CT. A gas-fluid level is present in an irregular, nodular cavity. (*Source:* Dachman AH, Buck JL, Krishnan J, Aguilera NS, Buetow PC. Primary non-Hodgkin's splenic lymphoma. Clin Radiol 1998;53:137–142, with permission from the Royal College of Radiologists.)

are small. At times a necrotic metastasis mimics a cyst. Only an occasional melanoma is encountered.

Calcifications develop in an occasional slow-growing tumor. Most metastases are hypodense on CT and are isointense on precontrast MR images; the exception is a melanoma, which often has a heterogeneous appearance. Metastases appear hypointense on immediate postcontrast MR images, becoming isointense on delayed images.

Diffuse splenic metastases can be missed by CT. Thus a diffuse metastatic seminoma was not detected by CT but was evident on FDG-PET (26).

Other Neoplasms

The rare cystadenocarcinoma probably arises from embryonic rests or mesothelium.

Splenic leiomyosarcomas are very rare.

Calcifications

Some of the conditions associated with splenic calcifications (Fig. 15.11) are listed in Table 15.2.

Hepatosplenic silicosis leads to calcifications in both the liver and spleen, and occasionally even eggshell-like calcified lymph nodes. Conventional radiographs reveal numerous calcified nodules, which are better identified by CT. Biopsy reveals birefringent particles within the nodules.

Table 15.2. Conditions associated with splenic calcifications

Posttraumatic cyst
Infection/inflammation
Tuberculosis
Histoplasmosis
Brucellosis
Hydatid cyst
Healed abscess
Atherosclerosis
Hemangioma
Neoplasm
Infarcts
Sickle cell disease
Silicosis
Thorotrast

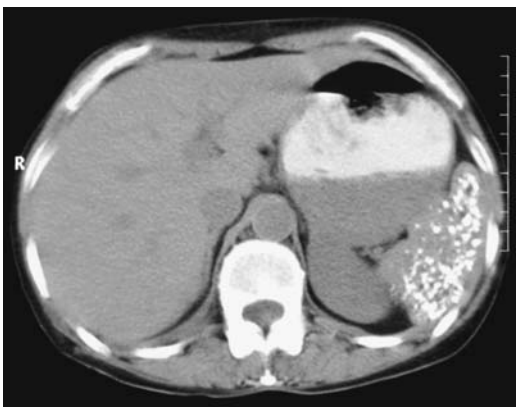

Figure 15.11. Extensive splenic calcifications detected by CT (arrow). Either tuberculosis or histoplasmosis can produce these changes. (Courtesy of Algidas Basevicius, M.D., Kaunas Medical University, Kaunas, Lithuania.)

Vascular Disorders

Portal Hypertension

Idiopathic portal hypertension, or Banti's disease, consists of anemia, splenomegaly, and portal hypertension. It is a distinct entity differing from liver cirrhosis-associated portal hypertension in both its histopathology and portal hemodynamics.

Splenomegaly is common in portal hypertension. Regardless of etiology, the interrelationship between portal hemodynamics and splenomegaly is complex and poorly understood. A rare cause of portal hypertension but entailing a normal-size spleen is a splenic arteriovenous fistula; contrast-enhanced imaging or Doppler US should be diagnostic of a fistula.

Duplex Doppler US appears useful in differentiating between congestive splenomegaly as seen in patients with liver cirrhosis and splenomegaly due to various myelo- and lym-

phoproliferative disorders; the maximum portal flow velocity in patients with proliferative disordersis normal, but is reduced in those with congestive splenomegaly.

Leukopenia and thrombocytopenia develop in patients with cirrhosis, portal hypertension, and hypersplenism. In this clinical setting, patients with a superimposed hepatocellular carcinoma undergoing transcatheter hepatic arterial embolization also underwent partial splenic embolization and infarction (27); the leukopenia and thrombocytopenia were corrected in a majority of patients if more than 50% of their spleens were infarcted.

Infarction

Vascular emboli result in focal splenic infarction, at times multiple. Splenic artery thrombosis is associated with total splenic infarction. Rarely, a splenic infarct occurs in a setting of congestive splenomegaly or pancreatitis, at times together with splenic vein thrombosis and possibly other infarctions. The risk of infarction is increased in a setting of portal hypertension. Rarer causes of splenic infarction include systemic mast cell disease (28) and celiac disease (29); the latter is also associated with splenic venous thrombosis.

Occasionally intrasplenic gas bubbles are detected after a major infarct; they develop even without an infection.

An infarct is a common cause of a focal splenic tumor. A typical infarct is wedge-shaped and located adjacent to the splenic capsule. Less often an infarct has a round or nodular outline. Computed tomography reveals lack of contrast enhancement. Occasionally a neoplasm has a similar appearance. The rare total splenic infarction shows only peripheral contrast enhancement, presumably secondary to a capsular artery supply. Nevertheless, the lack of splenic contrast enhancement is not pathognomonic of a total infarction; a more common cause is severe hypotension.

Initially after an infarct, US reveals a hypoechoic tumor. Later, scarring results in a gradual hyperechoic appearance. Similar to CT, infarcts are identified on delayed postcontrast MRI as hypointense wedge-shaped regions adjacent to the capsule.

Immunosuppression

Abnormal CT scans in HIV patients should not be routinely ascribed to AIDS; a second disease, consisting of either superimposed infection or a neoplasm is most often responsible for abnormal findings.

Hepatosplenic abscesses are not uncommon in AIDS patients, often being secondary to unusual organisms. Most are small and multiple. An US "snowstorm" appearance is found with some opportunistic liver and spleen infections, reflecting fibrosis or a fibrinous exudate. Abdominal US with a 3.5-MHz transducer will miss small abscesses in these patients; a 5-MHz transducer should identify more abscesses.

Similar to other patients, splenic tuberculous abscesses in immunocompetent patients are hypodense on CT and hypoechoic on US.

Examination and Surgical Complications

Splenectomy

Compared to an open splenectomy, in both adults and children a laparoscopic splenectomy requires a longer operative time but the patient's overall hospital stay is shorter. Most laparoscopic splenectomies are performed for a normal-sized or moderately enlarged spleen, although a laparoscopic approach is feasible in a patient with marked splenomegaly. Some surgeons believe that if the spleen is enlarged, preoperative splenic artery embolization makes laparoscopic splenectomy easier (30).

Following splenectomy, residual splenic tissue can be identified with In-111–labeled autologous platelet SPECT.

An increased risk for postsplenectomy infection is well known. Splenectomy results in depressed phagocytosis and a decrease in serum levels of immunoglobulin M (IgM). The consequences of splenectomy are not trivial, especially in children and in those undergoing splenectomy as part of lymphoma therapy. This risk tends to lessen after several years.

A subphrenic abscess is a recognized complication after splenectomy, developing either shortly after surgery or, less commonly, on a

delayed basis. Computed tomography should detect a subphrenic abscess, but keep in mind that an occasional abscess mimics an intact spleen. Image-guided drainage is generally the treatment of choice, with surgery reserved for multiseptated abscesses or if percutaneous drainage fails.

Thorotrast

Thorotrast deposits can be visualized in the spleen with conventional radiography and CT. The spleen tends to be atrophic.

A Thorotrast-induced angiosarcoma is rare in the spleen, with most occurring in the liver. The effect of prior Thorotrast use is discussed further in Chapter 7.

References

1. Lieberman S, Libson E, Maly B, Lebensart P, Ben-Yehuda D, Bloom AI. Imaging-guided percutaneous splenic biopsy using a 20- or 22-gauge cutting-edge core biopsy needle for the diagnosis of malignant lymphoma. AJR 2003;181:1025–1027.
2. Deux JF, Salomon L, Barrier A, Callard P, Bazot M. Acute torsion of wandering spleen: MRI findings. AJR 2004;182:1607–1608.
3. Lorberboym M, Vallabhajosula S, Lipszyc H, Pastores G. Scintigraphic evaluation of Tc-99m-low-density lipoprotein (LDL) distribution in patients with Gaucher disease. Clin Genet 1997;52:7–11.
4. Kimura F, Ito H, Shimizu H, et al. Partial splenic embolization for the treatment of hereditary spherocytosis. AJR 2003;181:1021–1024.
5. Shanmuganathan K, Mirvis SE, Boyd-Kranis R, Takada T, Scalea TM. Nonsurgical management of blunt splenic injury: use of CT criteria to select patients for splenic arteriography and potential endovascular therapy. Radiology 2000;217:75–82.
6. Moore EE, Cogbill TH, Jurkovich GJ, Shackford SR, Malangoni MA, Champion HR. Organ injury scaling: spleen and liver (1994 revision). J Trauma 1995;38:323–324.
7. Sivit CJ, Frazier AA, Eichelberger MR. Prevalence and distribution of extraperitoneal hemorrhage associated with splenic injury in infants and children. AJR 1999;172:1015–1017.
8. Kimpel M, Zander T, Dux M. [Spontaneous occult splenic rupture after Salmonella enteritidis infection.] [German] Rofo Fortschr Geb Rontgenstr Neuen Bildgeb Verfahr 2001;173:380–381.
9. Resende V, Petroianu A. Subtotal splenectomy for treatment of severe splenic injuries. J Trauma 1998;44:933–935.
10. Emery KH, Babcock DS, Borgman AS, Garcia VF. Splenic injury diagnosed with CT: US follow-up and healing rate in children and adolescents. Radiology 1999;212:515–518.
11. Bittar I, Cohen Solal JL, Cabanis P. [Volvulus of the mobile spleen. Conservative laparoscopic treatment.] [French] Presse Med 2001;30:1005–1006.
12. Hierholzer J, Fuchs H, Menzel B. [Intrahepatic splenosis.] [German] Rofo Fortschr Geb Rontgenstr Neuen Bildgeb Verfahr 2001;173:769–771.
13. Rickert CH, Maasjosthusmann U, Probst-Cousin S, August C, Gullotta F. A unique case of cerebral spleen. Am J Surg Pathol 1998;22:894–896.
14. Warshauer DM, Molina PL, Worawattanakul S. The spotted spleen: CT and clinical correlation in a tertiary care center. J Comput Assist Tomogr 1998;22:694–702.
15. Tohme A, Hammoud A, el Rassi B, Germanos-Haddad M, Ghayad E. [Human brucellosis. Retrospective studies of 63 cases in Lebanon.] [French] Presse Med 2001;30:1339–1343.
16. Harned RK 2nd, Thompson HR, Kumpe DA, Narkewicz MR, Sokol RJ. Partial splenic embolization in five children with hypersplenism: effects of reduced-volume embolization on efficacy and morbidity. Radiology 1998;209:803–806.
17. Monzawa S, Tsukamoto T, Omata K, Hosoda K, Araki T, Sugimura K. A case with primary amyloidosis of the liver and spleen: radiologic findings. Eur J Radiol 2002;41:237–241.
18. Thanos L, Zormpala A, Brountzos E, Nikita A, Kelekis D. Nodular hepatic and splenic sarcoidosis in a patient with normal chest radiograph. Eur J Radiol 2002;41:10–11.
19. Zilkha A, Madan V, Leonidas JC, Valderrama E. Liver and spleen MRI findings in virus-associated hemophagocytic syndrome in a patient with acute lymphocytic leukemia. Pediatr Radiol 1998;28:920–922.
20. Schulz AS, Urban J, Gessler P, Behnisch W, Kohne E, Heymer B. Anaemia, thrombocytopenia and coagulopathy due to occult diffuse infantile haemangiomatosis of spleen and pancreas. Eur J Pediatr 1999;158:379–383.
21. Lam KY, Yip KH, Peh WC. Splenic vascular lesions: unusual features and a review of the literature. [Review] Aust N Z J Surg 1999;69:422–425.
22. Yilmazer YC, Erden A. Complete regression of a congenital splenic cyst. J Clin Ultrasound 1998;26:223–224.
23. Levy AD, Abbott RM, Abbondanzo SL. Littoral cell angioma of the spleen: CT features with clinicopathologic comparison. Radiology 2004;230:485–490.
24. Imaoka I, Sugimura K, Furukawa M, Kuroda S, Yasui K. Computed tomography and MR findings of splenic angiosarcoma. Radiat Med 1999;17:67–70.
25. Gorg C, Weide R, Schwerk WB. Malignant splenic lymphoma: sonographic patterns, diagnosis and follow-up. Clin Radiol 1997;52:535–540.
26. Lenzo NP, Moschilla G, Patrikeos A. Diffuse splenic metastases from seminoma visualized on FDG PET. AJR 2004;183:525–527.
27. Han MJ, Zhao HG, Ren K, Zhao DC, Xu K, Zhang XT. Partial splenic embolization for hypersplenism

concomitant with or after arterial embolization of hepatocellular carcinoma in 30 patients. Cardiovasc Intervent Radiol 1997;20:125–127.
28. Maruyama H, Sugihara S, Ishihara K, et al. Systemic mast cell disease with splenic infarction: a case report. Pathol Int 1998;48:403–411.
29. Andres E, Pflumio F, Knab MC, et al. [Splenic thrombosis and celiac disease: a fortuitous association?] [French] Presse Med 2000;29:1933–1934.
30. Poulin EC, Mamazza J. Laparoscopic splenectomy: lessons from the learning curve. Can J Surg 1998;41: 28–36.

16

Adrenals

Technique

Computed Tomography

The current imaging modality of choice to evaluate the adrenal glands is computed tomography (CT), although magnetic resonance (MR) is making strong inroads. Both enlargement and a focal tumor can be detected, assuming it is large enough. Some adrenal abnormalities have a nonspecific CT appearance, although different enhancement patterns and fat content allow differentiation between some benign and malignant lesions.

It is not uncommon to detect adrenal enlargement as an incidental finding when CT is performed for other indications. Once an abnormality is detected, the following specialized techniques are useful for further evaluation: 6β-iodomethyl-19-norcholesterol (NP-59) scintigraphy, unenhanced CT densitometry, opposed phase chemical shift magnetic resonance imaging (MRI), and percutaneous biopsy.

Ultrasonography

Transabdominal US can almost always visualize a normal right adrenal gland, but the left gland is seen in only about two thirds of examinations; endoscopic US, on the other hand, almost always detects the left adrenal gland but identifies the right gland in only a minority of patients.

Magnetic Resonance

Compared to CT and US, MRI has better soft tissue contrast depiction. A disadvantage is its relative insensitivity for visualizing adrenal calcifications. Normal adrenal glands have an intensity similar to that of liver parenchyma on T1-weighted images. They are not as well seen on T2-weighted images, although fat suppression accentuates their signal intensity compared to the adjacent fat, and this technique is commonly used.

Scintigraphy

Scintigraphy has a distinct role in evaluating functional adrenal tissue. The radiopharmaceutical iodine-131–NP-59 is taken up by normally functioning adrenal cells and evaluates cortical function. Increased adrenal uptake of NP-59 occurs in Cushing's syndrome, aldosteronism, and some adrenal tumors. This is a complex procedure; uptake lasts several days and imaging is thus delayed. The delay also decreases background activity. Planar scintigraphy and single photon emission computed tomography (SPECT) can be combined in an attempt to increase study sensitivity. NP-59

appears to be cost-effective for evaluating adrenal incidentalomas.

Selenium-75–methylnorcholesterol scintigraphy is similar to NP-59. Cortical adenomas have either normal or increased uptake, while malignancies show decreased activity. Uptake of this radiopharmaceutical shows a direct relationship with the functional state of hyperfunctioning adenomas.

Iodine-131–metaiodobenzylguanidine (MIBG) is a norepinephrine analogue, and a normal adrenal does not accumulate large amounts of this tracer. It shares some of the norepinephrine pathways and is of use in detecting pheochromocytomas, neuroblastomas, and carcinoids. In some hyperfunctioning endocrine conditions both anatomic and functional information are obtained. Thyroid uptake of iodine 131 is blocked with potassium iodide prior to and after the use of this agent.

Indium-111-octreotide binds to somatostatin receptors throughout the body. These receptors are found in neuroendocrine and other structures, including tumors originating from these structures. Increased somatostatin receptors and thus increased octreotide concentrations occur in carcinoids, pheochromocytomas, and neuroblastomas.

Biopsy

Imaging provides guidance for needle biopsy of adrenal tumors. Most biopsies utilize a posterior approach, although anterior, transhepatic, transpancreatic, and transsplenic approaches have been used. A wider artificial window can be obtained by injecting saline into the adjacent paravertebral space and thus displacing the pleura laterally (1); this allows a wider path and potentially safer adrenal access by avoiding puncture of pleura and diaphragm. A CT-guided approach is often used, although an open MR scanner and MR fluoroscopy using steady-state free precession sequences, if available, provide considerable advantages (2); MR fluoroscopy permits an oblique paravertebral approach without pleural transgression. A sensitivity of >90% can be obtained in detecting a malignancy. Although most biopsies provide a specific diagnosis, a malignancy obviously can be missed; a biopsy of a benign lesion, such as an adenoma, does not exclude the concomitant presence of a carcinoma.

Complications encountered include pneumothorax, perinephric hemorrhage, hepatic hematoma, and needle-track metastases. Adrenal hematomas can also be induced.

Congenital

Bilateral adrenal agenesis is incompatible with life. In unilateral agenesis the contralateral gland hypertrophies. The rare infant with congenital adrenal hypoplasia requires replacement therapy for survival.

Accessory adrenal rests are usually of little significance. An intratesticular location is not uncommon. Most accessory glands contain only cortical tissue, while a heterotopic gland contains both cortex and medulla.

A horseshoe-shaped adrenal gland was reported in an infant with asplenia (3).

Congenital Adrenal Hyperplasia

Congenital adrenal hyperplasia is an autosomal-recessive condition leading to impaired hormone synthesis. A number of such adrenogenital syndromes have been described; they are based on specific hormone synthesis impairment, with 21-hydroxylase deficiency being the most common. Some infants with congenital adrenal hyperplasia also do not synthesize aldosterone and have salt wasting, a potentially fatal condition.

Clinically, girls and women develop virilization and boys have precocious puberty, but keep in mind that similar findings also occur with virilizing tumors.

Imaging of congenital adrenal hyperplasia reveals large adrenals that are cerebriform in outline. Adrenal rest tissue in other locations also enlarges. This condition should be suspected in an infant with enlarged adrenal glands, although not all infants with congenital adrenal hyperplasia have gland enlargement.

Acquired adrenogenital syndrome is most often due to an adenoma, and less often to an adrenocortical carcinoma.

Wolman's Disease

Wolman's disease is an autosomal-recessive condition caused by a deficiency of lysosomal

acid lipase. It is characterized by abnormal storage of cholesteryl esters and triglycerides. Onset is after the first month of life and manifests as hepatosplenomegaly, abdominal distention, and failure to thrive. It is usually fatal in infancy.

Computed tomography in these infants shows hepatosplenomegaly, with the liver being hypodense, and bilateral adrenal calcifications. These imaging findings, in the appropriate clinical setting, should suggest the diagnosis.

Beckwith-Wiedemann Syndrome

Beckwith-Wiedemann syndrome is a congenital overgrowth syndrome having a sporadic occurrence and variable expressivity. These children develop cysts and various childhood solid tumors, including adrenocortical carcinomas. The kidneys are more often affected than the adrenals. Bilateral multilocular cystic adrenal tumors developed in a neonate with Beckwith-Wiedemann syndrome (4); resection revealed benign hemorrhagic macrocysts. Unilateral cysts are more common.

Trauma

Trauma to the adrenal and surrounding structures most often leads to hemorrhage and a hematoma. The right side is more often involved, and trauma to the overlying ribs and liver is common. Associated bleeding often is not confined to the adrenal gland but also involves adjacent extraperitoneal tissues. In some patients a hematoma is asymptomatic and is discovered only later, when trauma is already forgotten.

An adrenal injury classification scale, devised by the American Association for the Surgery of Trauma, is outlined in Table 16.1. Adrenal hemorrhage/hematoma is discussed later in this chapter.

Table 16.1. Surgical adrenal injury scale

Grade*	Type of injury
I	Contusion
II	Laceration involving cortex (<2 cm)
III	Laceration extending into medulla (≥2 cm)
IV	Parenchymal destruction >50%
V	Total parenchymal destruction
	Vascular avulsion

* Advanced one grade for multiple injuries, up to grade V.
Modified from Moore et al (5).

Enlargement

Visualization of normal-appearing adrenal glands essentially excludes a neoplasm. An abnormal gland is identified as a focal bulge, diffuse gland enlargement, or both. A focal tumor can be either neoplastic or hyperplastic. In general, a functioning primary tumor is associated with either an atrophic or normal-size contralateral gland. Most small hyperplastic and neoplastic nodules are isodense on CT and isointense on MR to normal adrenal parenchyma on precontrast images and are identified by their contour abnormalities.

Determining whether a tumor is in the adrenal or is extraadrenal in location is usually straightforward with imaging. The presence of a normal adrenal gland adjacent to a tumor establishes their relationship. Especially when large, however, some extraadrenal tumors invade and obliterate the adrenal gland; the reverse is also true—an adrenal tumor can involve adjacent tissues. With both scenarios it may not be possible to establish the site of tumor origin.

Hyperplasia

A distinction between a normal-sized gland and an enlarged one is a borderline of gradation. With diffuse enlargement the usual adrenal shape is preserved, although on occasion some degree of nodularity to the gland outline is observed. Bilaterally enlargement signifies hyperplasia. It should be kept in mind, however, that some patients with clinical evidence of adrenal hyperfunction have normal-sized glands.

Hyperplasia of the medulla is less common; such hyperplasia appears to be a precursor to a pheochromocytoma.

Hyperplastic adrenal gland MR signal intensity is identical to a normal adrenal with all imaging sequences.

Infection

Adrenal abscesses are uncommon in adults. Some represent the sequelae of an infected

hematoma. These abscesses can be diagnosed by needle aspiration. At times an infected tumor is in the differential diagnosis.

Adrenal hydatidosis is rare (6). Imaging reveals a similar appearance to that seen in other organs.

Involvement by histoplasmosis or tuberculosis is usually bilateral but also asymmetrical. The imaging findings vary depending on the extent of involvement and the degree of necrosis. Initially, histoplasmosis results in bilateral adrenal enlargement, but eventually the glands become atrophic and develop punctate calcifications. Tuberculosis, a cause of adrenal insufficiency, has a similar adrenal enlargement followed by atrophy and calcification appearance.

Other infections are rare. Anecdotal reports describe adrenal coccidioidomycosis or North American blastomycosis involving the adrenal glands even in an immunocompetent patient; the latter infection can also cause adrenal insufficiency. Computed tomography in a patient with adrenal paragonimiasis detected an enhancing right adrenal tumor, with US revealing a dumbbell-like hyperechoic tumor (7); a multicystic structure filled with creamy material was found at surgery.

Initially with gland enlargement a neoplasm is in the differential diagnosis. With an atrophic, calcified gland, however, a neoplasm is less likely.

Cysts

Aside from cystic neoplasms, adrenal cysts are uncommon. Cystic neoplasms include a rare carcinoma, pheochromocytoma, or a postinjection therapy adenoma. Nonneoplastic cysts can be classified as parasitic, epithelial retention cysts, endothelial cysts, and pseudocysts due to prior hemorrhage, with a majority of cysts representing the latter two entities. Imaging cannot differentiate between these various nonneoplastic cysts, with a few exceptions. Endothelium-lined cysts consist of lymphatic and vascular degenerative cysts. They tend to be multilocular and are filled with clear or milky fluid.

Some adrenal hemorrhages evolve into a *pseudocyst*, a poor term because there is nothing "pseudo" about these cysts. They are not related to pancreatic pseudocysts, which have a different etiology. An adrenal pseudocyst is a cortical cyst without a cellular wall, but it has a fibrous capsule. Wall thickness tends to be several millimeters; a thicker or irregular wall should raise suspicion for a neoplasm. These cysts tend to be unilocular and vary in size considerably. Ultrasonography reveals a cyst with internal echoes. Magnetic resonance imaging shows a thick-rimmed cyst. Similar to their US appearance, these cysts' signal intensity varies depending on cyst content. Curvilinear wall or septal calcifications develop in some; an occasional one contains central calcifications.

The CT density of adrenal cysts varies from water to old blood. Some exhibit rim contrast enhancement, but the cystic component should not enhance. Fluid-fluid layering is occasionally found. The relationship of polycystic renal disease and adrenal cysts is not clear.

The differential diagnosis of a cystic adrenal tumor is between one of the above-listed cysts and a cystic or necrotic neoplasm. The presence of soft tissue density nodules suggests a neoplasm. Contrast enhancement of any solid component most often signifies a neoplasm (8). If needed, an aspiration biopsy is obtained, but keep in mind that cysts containing old blood are difficult to drain. If a lesion appears indeed to be a cyst, it can be observed.

One must ensure that a cystic structure is indeed of adrenal origin. For instance, CT or MRI of a gastric cardia diverticulum can minic a left adrenal cyst.

Incidental Tumors

In some patients diffusely enlarged adrenal glands are discovered incidentally; most often this finding is of little significance. An incidentally detected focal adrenal tumor (incidentaloma), on the other hand, probably warrants further study. About 10% to 15% of patients with a focal tumor have autonomous cortisol hypersecretion without obvious stigmata of Cushing's syndrome. Among newly detected single adrenal tumors about half are adenomas, yet even an incidental tumor has about a one-third chance of being a metastasis, even with no known primary.

What is the eventual outcome of incidentally discovered adrenal tumors (incidentalomas)? In patients with a unilateral incidental tumor, 17% had biochemical evidence of adrenal

hyperfunction, consisting of hypercortisolism, hyperaldosteronism, and medullary hyperfunction (9); in patients with bilateral incidental tumors, abnormal adrenal function was detected in 29%, consisting of hypercortisolism, hyperaldosteronism, adrenal insufficiency, and congenital adrenal hyperplasia. A not uncommon incidental functioning adrenal tumor is a pheochromocytoma. Some of these tumors function subclinically and appropriate endocrine testing is useful. Most initially discovered metastases are unilateral and do not produce adrenal insufficiency; bilateral involvement suggests adrenal hemorrhage, especially in a setting of a coagulopathy, and possible lymphoma.

An incidental adrenal tumor discovered in a workup for another condition, without a known primary cancer, has only about a 1% rate of being malignant; most of these malignancies will be larger tumors. As a result, some investigators suggest that smaller tumors, for instance those <3 cm or so in diameter, can be followed with imaging; an exception is with those exhibiting subtle hormone production or in a patient with hypertension or diabetes, and these should be resected. On the other hand, risk of malignancy is increased in a setting of a known primary cancer in another organ, but here also the prevalence of malignancy varies with tumor size.

Both CT and MRI are helpful in defining adrenal tumors (differentiation of benign and malignant tumors is discussed in more detail in the next section). A biopsy is helpful, especially for larger tumors. Similar to other sites, a positive biopsy is diagnostic but a negative one needs to be placed in the proper perspective. One biopsy caution: a pheochromocytoma should be excluded before a biopsy is performed. Also, biopsy rather than cytology is necessary; cytology often cannot differentiate a benign from a malignant tumor.

2-[18F]-fluoro-deoxy-D-glucose positron emission tomography (FDG-PET) appears to have a role in distinguishing benign from malignant adrenal tumors. Benign tumors show no FDG uptake; on the other hand, malignant adrenal tumors have increased FDG uptake, indicative of high glucose metabolism. Whole-body PET also identifies primary extraadrenal tumor sites, thus providing staging.

Occasionally prenatal US identifies a suprarenal tumor, at times even containing small cysts; eventually these tumors tend to disappear and thus a conservative approach with US follow-up appears reasonable in otherwise healthy neonates. Presumably some of these findings represent congenital adrenal hyperplasia.

Adenoma Versus Nonadenoma

A major problem in clinical practice is to differentiate an adrenal adenoma from other tumors, usually a metastasis. Although most adenomas are small, smooth in outline, and homogeneous, while metastases are larger, have an irregular outline, and are heterogeneous, sufficient overlap exists in these characteristics that they are of limited use in any one patient. With a nonfunctioning adenoma or carcinoma the contralateral gland is not atrophic.

Two specific imaging characteristics are useful in differentiating adrenal adenomas from nonadenomas. Initially, emphasis was placed on detecting an adenoma's increased lipid content. While still a useful concept, some overlap exists, and this technique has been supplanted by another almost unique adenoma property—a more rapid contrast washout compared to nonadenomas. Computed tomography and MR differentiation of adenomas from nonadenomas rely primarily on these findings.

Using a variety of techniques, including chemical shift imaging and dynamic contrast enhancement, MRI could differentiate between benign and malignant adrenal tumors with a 89% sensitivity and 99% specificity (10). Sensitivity and specificity can be increased by combining results from several MR sequences, such as dynamic contrast enhanced sequences and chemical shift imaging.

Lipid Content

Most adrenocortical adenomas contain considerable lipid (lipid rich), but the amount of fat is still considerably less than in a myelolipoma. An inverse linear relationship exists between the percentage of lipid-rich cortical cells in adrenal adenomas and their unenhanced CT attenuation; a similar inverse linear relationship exists with MR chemical shift changes. It should be kept in mind, however, that about 20% of adenomas contain little or no lipid (lipid poor).

The reverse is also true—an occasional adrenal cortical carcinoma and metastasis contains sufficient fat to be detectable by CT and MRI, but these tend to be large and irregular in outline at initial presentation.

In general, unenhanced CT attenuation values of a nonfunctioning adrenal tumor are more useful in differentiating between an adenoma and a nonadenoma than size or CT homogeneity. Due to their fat content, most adenomas have lower attenuation values than malignant tumors, with the published sensitivities in making this differential varying depending on the assumed threshold HU; thus in 60 patients with single adrenal nodules, a CT threshold of 19 HU on unenhanced and 41 HU on late postcontrast scans achieved a sensitivity of 93% and specificity of 100% in differentiating benign from malignant tumors (11). As a rough guide, adrenal tumors having a CT density of 0 Houndsfield units (HU) or less can be assumed to be benign and those having a density >20 HU can be assumed to be malignant. It is those with intermediate densities that present a diagnostic dilemma.

Magnetic resonance signal intensities of both benign and malignant tumors vary, presumably due to their inhomogeneous histologic appearance. Nonfunctioning adenomas range from hypo- to mostly isointense to liver parenchyma on both T1- and T2-weighted sequences and show mild-to-moderate postcontrast enhancement. Most adenomas contain insufficient fat to produce a major change on fat-suppressed MR images, and a major decrease in intensity should suggest a myelolipoma. Nevertheless, chemical shift MRI is useful in differentiating lipid-rich adenomas from nonadenomas, achieving sensitivities and specificities similar to those of CT enhancement washout techniques (see next section). This technique is insensitive in characterizing lipid-poor adenomas.

An internal standard is needed to meaningfully evaluate adrenal MR signal intensity. Although liver signal intensity is readily measured, it varies considerably depending on liver fat content. The adrenal-to-spleen ratio appears more useful. Metastases have an adrenal-to-spleen ratio >0.8, while most adenomas have a lower ratio. An overlap exists, however, and the ratio is of limited value in establishing the benign or malignant nature of an adrenal lesion. Some investigators prefer muscle as their standard.

Most adenomas are isointense to muscle or spleen on in-phase spoiled gradient echo (SGE) images and appear hypointense on opposed-phase images. With a chemical shift technique, most adenomas have a loss of signal intensity on opposed-phase images while most benign nonadenomas, pheochromocytomas, and metastases do not. Loss in signal intensity in bone marrow in an adjacent vertebral body is useful confirmation of this technique. With a tendency of adrenal adenomas to contain fat and the high sensitivity of opposed-phase imaging for detecting fat, in a setting of a known malignancy and an adrenal tumor, MRI can be sufficient to differentiate these entities and save these patients a biopsy.

Another option is to use a signal intensity (SI) index, defined as:

(SI in-phase − SI opposed-phase)/SI in-phase

This index differentiates adenomas, metastases and pheochromocytomas (12). One study achieved 100% accuracy in distinguishing adenomas from metastases if the SI index cutoff value was 11.2–16.5% (13); this index was more reliable in differentiating adenomas from metastases than an adrenal-to-liver, spleen, or muscle ratio for signal change on opposed-phase MR imaging..

Which modality is more accurate in differentiating benign from malignant tumors—unenhanced CT attenuation or chemical shift MRI? For most tumors both yield similar results; most adenomas measuring >10 H on unenhanced CT can be characterized with chemical shift MRI (14). Nevertheless, diagnostic uncertainty still exists with a minority of these tumors.

Contrast Washout

Very useful in differentiating adrenal adenomas from nonadenomas is washout of contrast enhancement. Enhancement washout is equal to initial enhanced attenuation minus delayed enhanced attenuation. More rapid washout is a characteristic finding in a majority of adenomas (compared to nonadenomas). Mean CT attenuation measured at specific time delays postcontrast (10 to 30 minutes), is lower for adenomas than for nonadenomas. In one study, the per-

centage loss of enhancement at 10 and 30 minutes was significantly greater for adenomas than for nonadenomas; a 92% sensitivity and 95% specificity were achieved at 10 minutes and a 97% sensitivity and 100% specificity at 30 minutes for differentiating adenomas and nonadenomas (15); washout was more accurate for such differentiation than unenhanced CT densities. A typical assumption is that more than a 40% or 50% washout on a 10-minute postcontrast image implies an adenoma. The time delay is not crucial; thus even with a postenhancement delay of 60 minutes, considerable attenuation differences exist between adenomas and metastases. Various refinements, including percentage enhancement washout and relative enhancement washout, reach sensitivities and specificities approaching 100% in differentiating adenomas from nonadenomas (16). This is a highly specific test for adrenal tumor characterization.

Lipid-poor adenomas warrant special mention. They cannot be differentiated from nonadenomas by their precontrast attenuation values; however, lipid-poor adenomas have enhancement and washout characteristics similar to those of more typical lipid-rich adenomas (17).

Contrast-enhanced MRI of adrenal adenomas revealed a homogeneous capillary blush on immediate images in 71%, rapid washout on 45-second images in 94%, and diminished signal intensity on out-of-phase images in 86% (18); in distinction, on immediate images no malignant adrenal tumors had a homogeneous capillary blush, 50% showed negligible enhancement, 33% revealed a patchy enhancement, 17% had peripheral enhancement, and an irregular enhancement pattern was found in 92% on 45-second images. Thus a majority of adrenal adenomas can be distinguished from malignancies by their characteristic initial homogeneous capillary blush followed by a rapid washout.

Postcontrast MRI reveals peak enhancement of most adrenal adenomas during the early phase, followed by a relatively rapid washout; most metastases exhibit a slower washout. Exceptions include pheochromocytomas, which show little washout and granulomas which reveal minimal enhancement. Especially when small, adenomas tend to have a homogeneous capillary blush, while malignancies are heterogeneous. Overlap in enhancement patterns, however, occurs with benign and malignant lesions.

Primary Cortical Adenoma-Carcinoma

Clinical

About half of adrenal cortical neoplasms are hyperfunctioning, and the other half are nonhyperfunctioning. The hyperfunctioning, or hormone-producing tumors, are discussed later in this chapter. Many nonfunctioning tumors are discovered incidentally. Although nonfunctioning adenomas occur at all ages, the prevalence increases with age. A relationship appears to exist between an adenoma's lipid content and its functional status. Adenomas are more common in diabetic and hypertensive patients. Both adenomas and carcinomas are more common in women and are detected at a younger age in women.

Both adrenal adenomas and carcinomas are more prevalent than usual in patients with Gardner's syndrome. Patients with Li-Fraumeni syndrome have a predisposition to adrenocortical carcinomas; in this autosomal-dominant syndrome adrenal tumors tend to develop in children and young adults.

Cortical carcinomas are rare aggressive tumors. Most have a poor prognosis even if resected. Adrenal cortical carcinomas in children tend to be very malignant and most are functional.

An interesting phenomenon consists of adrenal collision tumors. Thus a contiguous adrenal adenoma and metastasis results in the adenoma component displaying a signal loss on opposed-phase MR images and the metastatic component increasing in signal intensity.

At times neither a biopsy nor a resected specimen allows adequate evaluation of an adrenocortical tumor if only histologic criteria are employed; immunohistologic staining is often helpful. Nevertheless, even then the true nature of a tumor may not be apparent. For example, CT and US discovered an incidental homogeneous adrenal tumor in a 43-year-old woman; endocrine tests revealed preclinical Cushing's syndrome. An adrenalectomy was performed, and histology revealed an adrenocortical

tumor of undetermined nature (19); 4 months later the patient presented with a metastatic cortisol and androgen-producing adrenocortical carcinoma.

Pain is more common with carcinomas. Precocious puberty develops in an occasional patient. About half of these tumors have some type of endocrine abnormality, but in general, endocrine testing per se does not differentiate between benign and malignant tumors.

The role of percutaneous ablation for adrenal tumors is mostly anecdotal.

Imaging

Regions of hemorrhage and necrosis are common in carcinomas and result in a heterogeneous appearance. Necrosis is not specific for a carcinoma and is also seen in adrenal hemangiomas and other larger tumors. Some adenomas and carcinomas develop calcification. Calcifications are more common in larger, heterogeneous-appearing tumors containing central necrosis or hemorrhage; the imaging appearance of these larger tumors does not permit ready differentiation between adenomas and carcinomas.

Especially with the larger adrenal carcinomas, the vena cava should be studied for possible invasion. A right adrenal gland adrenocortical carcinoma can grow as an intracaval tumor thrombus, at times even extending into the atrium. Or, a neoplasm invading the inferior vena cava results in an acute Budd-Chiari syndrome. Imaging, including magnetic resonance angiography (MRA), is useful in evaluating malignant tumor extension into the adrenal veins and inferior vena cava.

A carcinoma tends to have patchy CT contrast enhancement, a somewhat nonspecific finding.

Nonfunctioning adenomas are hypointense to liver on T1- and vary in intensity on T2-weighted MR images (Fig. 16.1). Magnetic resonance is useful in distinguishing a cyst from an adenoma; on T2-weighted images fluid in a cyst is hyperintense.

Metastases

An adrenal metastasis without a known primary tumor is sufficiently rare that it is generally not considered in the differential diagnosis of an incidental adrenal tumor. On the other hand, adrenal gland metastases are common in a setting of a known cancer in another organ. Given the known prevalence of adrenal adenomas, in a setting of a known primary malignancy the chance that an enlarged adrenal gland represents an incidental adenoma is roughly 50%.

Lung and breast carcinoma and melanoma are common metastases. Less common metastases to the adrenal glands include thyroid carcinoma and hepatocellular carcinoma.

Patients with a renal cell carcinoma are at approximately a 2% to 3% risk of ipsilateral

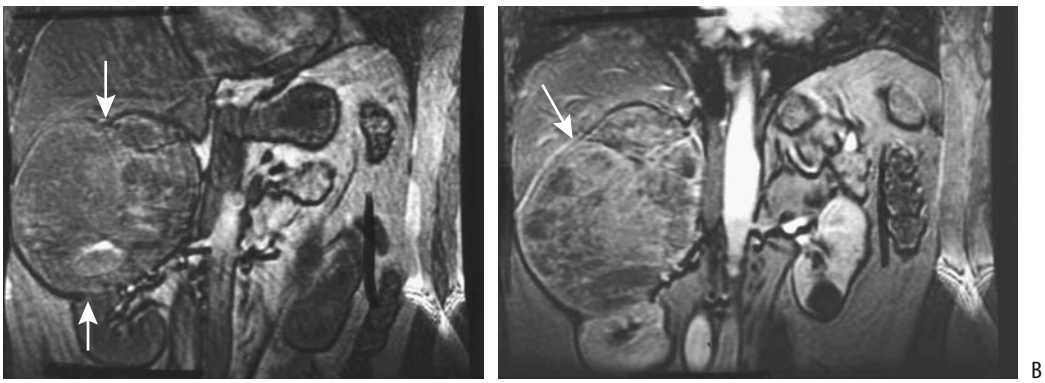

Figure 16.1. Adrenal carcinoma. Precontrast (A) and contrast-enhanced (B) magnetic resonance (MR) images reveal a large, heterogeneous right adrenal tumor (arrows). (*Source:* Burgener FA, Meyers SP, Tan RK, Zaunbauer W. Differential Diagnosis in Magnetic Resonance Imaging. Stuttgart: Thieme, 2002, with permission.)

adrenal metastasis or direct invasion, although these risks increase with larger tumors. Occasionally renal cell carcinoma metastases develop to the contralateral or even both adrenals. After a right radical nephrectomy in a 74-year-old patient CT identified a hypervascular tumor on the left, initially believed to be a splenic artery aneurysm, but arteriography suggested a hypervascular adrenal tumor and adrenalectomy confirmed a metastasis (20).

Small metastases blend into a normal-appearing adrenal gland; with growth, a slight bulge in gland outline may be the only finding. The larger metastases are readily visualized by CT and MRI. Some eventually invade surrounding structures. Small metastases tend to be homogeneous; central necrosis develops with growth, and the imaging findings vary accordingly. Necrosis, however, is seen in both metastases and some primary adrenal neoplasms. Calcifications in a metastasis are rare.

Magnetic resonance signal intensity of metastases varies considerably and is, per se, not a useful guide. Most metastases exhibit heterogeneous contrast enhancement, and the homogeneous capillary blush seen with adenomas is uncommon. Their lack of lipid results in no appreciable signal loss on opposed phase MR images, thus distinguishing most metastases from adenomas. A possible exception is with some renal clear cell carcinomas, which contain intracytoplasmic lipid, and such an adrenal metastasis can potentially be confused with an adenoma.

Iodine-131–NP-59 scintigraphy reveals lack of tracer accumulation in most metastases. A word of caution is also necessary here: some adrenal metastases from renal cell carcinomas accumulate NP-59 (21). Some thyroid carcinoma metastases to the adrenal gland show I 131 uptake.

If needed, a percutaneous biopsy provides confirmation. As in other sites, a negative biopsy is less significant than a positive biopsy.

Whether an adrenal-sparing nephrectomy is a viable option in a setting of a renal cell carcinoma and a normal-appearing adrenal gland by imaging is controversial; preoperative CT does not detect adrenal invasion in some of these patients, because of metastases below the resolution of CT or other reasons.

Percutaneous ethanol injection has been performed on adrenal metastases from hepatocellular carcinoma (22); preliminary results are encouraging. CT-guided radiofrequency ablation appears to be effective local control of adrenal metastases (23).

Cortical Hormone-Producing Tumors

Hyperfunctional cortical adrenal conditions include Cushing's syndrome and aldosteronism. A single predominant hormone activity is evident in the majority of patients with hormone-producing gland hyperplasia or neoplasm. Occasionally encountered are unusual combinations, such as coexisting pheochromocytoma and primary adrenal Cushing's syndrome.

Imaging is not a substitute for an appropriate clinical endocrinological investigation in a patient suspected of having a hyperfunctional adrenal condition.

Cushing's Syndrome

Cushing's syndrome, or hypercortisolism, results from excessive cortisol secretion by the adrenal cortex. Affected individuals have increased urinary free cortisol excretion and an elevated serum cortisol level, with loss of a circadian rhythm. Screening includes an overnight dexamethasone suppression test. It should be emphasized that not all patients appear clinically cushingoid.

Secondary Hyperplasia

Most often Cushing's syndrome is due to adrenal hyperplasia secondary to excessive adrenocorticotropic hormone (ACTH) secretion. The most common cause of excessive ACTH secretion is a pituitary tumor (Cushing's disease), although an occasional pancreatic neuroendocrine tumor, pheochromocytoma, bronchial carcinoid, gastrinoma, functioning ovarian tumor, or a tumor at some other site is responsible for ectopic ACTH production. A pituitary adenoma and an adrenocortical adenoma can coexist, resulting in a complex clinical presentation.

Computed tomography shows that only about 70% of patients with ACTH-dependent Cushing's syndrome have enlarged adrenal glands (24); the adrenals are larger in patients with ectopic ACTH syndrome than in those with

Cushing's disease. These glands are most often smooth in outline, with only a minority containing nodules. The less common nodular appearance mimics an adrenal adenoma, especially if hyperplasia is unilateral.

Primary Adrenal Causes

Primary adrenal causes of Cushing's syndrome, or ACTH-independent causes, are less common and include adenoma, carcinoma, and primary adrenal hyperplasia. A rare variant encountered in pediatrics and young adults is primary pigmented nodular adrenocortical disease, which is due to hypersecretion of cortisol by multiple intraadrenal pigmented or "black" cortical adenomas.

About two-thirds of patients with primary Cushing's syndrome have adenomas and one-third carcinomas. Rarely, adenomas develop bilaterally. Even an adrenocortical carcinoma in one gland and a contralateral adenoma have been described (25); CT simply showed bilateral adrenal tumors.

Primary adrenal hyperplasia is uncommon. It tends to be bilateral, with the adrenal glands having a somewhat nodular appearance. One patient developed unilateral nodular hyperplasia and an atrophic contralateral gland (26).

The 5-year survival rate for those with these carcinomas is about 30%.

Imaging

In a patient with hypercortisolism, a CT or MR finding of an enlarged unilateral adrenal gland is suggestive of an adenoma. A symptomatic adenoma generally is round or oval and several centimeters in diameter. Calcifications are uncommon. An adenoma is homogeneous and of soft-tissue–to-water density. Some of the less dense adenomas mimic a cyst, but their functioning status cannot be predicted from their attenuation values. The contralateral gland tends to be atrophic secondary to ACTH suppression by the hyperfunctioning adenoma. They exhibit little contrast enhancement.

Functioning adenomas have a similar MR appearance to that of nonfunctioning adenomas (discussed previously), although some functioning adenomas contain little lipid and thus do not lose signal intensity on opposed-phase chemical shift images (an exception is with aldosterone-producing tissue, discussed below; see Aldosteronism).

Computed tomography in 11 patients with primary adrenal Cushing's syndrome and later proven primary adrenal hyperplasia revealed massively enlarged, multinodular adrenal glands (27); these glands were hypointense to liver on T1- and hyperintense on T2-weighted MR images.

Magnetic resonance imaging is at least equal to CT and superior to US in detecting hyperfunctioning adrenocortical tumors in patients with Cushing's syndrome; these tumors are hyperintense relative to liver on T2-weighted sequences, thus differing from most nonfunctioning adrenal adenomas, which tend to be hypo- to isointense.

Selenium-75-methylnorcholesterol and I-131–NP-59 scintigraphy detect endocrine functioning adrenal tumors. A rough relationship exists between radiotracer uptake and the degree of functional autonomy and I-131–NP-59 scintigraphy is both a functional and a localization test in Cushing's syndrome. It is an adjunct to CT and MRI. This test has almost 100% specificity and sensitivity in detecting these tumors. Cortical adenomas have increased-to-normal uptake and malignant tumors a decreased-to-absent radiotracer uptake. Symmetric visualization or mild asymmetry of the adrenals in a setting of hypercortisolism almost always represents adrenal hyperplasia. More marked asymmetry suggests an adenoma. Unilateral adrenal gland visualization is typical for an adenoma; the adenoma-produced cortisol decreases pituitary ACTH production, which in turn shuts off function in a normally functioning contralateral adrenal gland. Cysts likewise have no uptake. Prior surgery also results in asymmetric uptake. Scintigraphy allows the localization of any residual postoperative adrenal tissue.

Aldosteronism

Clinical

Primary aldosteronism (*Conn's syndrome*) is secondary to either an aldosterone-secreting neoplasm or adrenal hyperplasia. Over half of

primary aldosteronism is due to a functioning adrenocorticoid adenoma (*aldosteronoma*). Hyperplasia, usually bilateral, accounts for most of the rest, with a carcinoma being rare. Bilateral adenomas have been reported. Some patients with Conn's syndrome have grossly normal-appearing glands. A pheochromocytoma and primary hyperaldosteronism have occurred simultaneously; whether this is a coincidence or an unknown interreaction is conjecture.

The mineralocorticoid aldosterone is involved in blood volume and serum potassium homeostasis, which in turn regulate aldosterone secretion by the zona glomerulosa in the adrenal cortex. Excessive secretion leads to hypertension, hypokalemia, and suppression of plasma renin activity, a condition also known as mineralocorticoid hypertension (28). This is not a simple condition; although in most patients the two stimuli for aldosterone production (potassium and angiotensin II) tend to be low, some patients have normal serum potassium levels. Familial hyperaldosteronism is described. A curious sideshow is pseudohypermineralocorticism, caused by an excess of mineralotropics other than aldosterone.

Although mineralocorticoid hypertension is not common, its significance lies in its being a potentially correctable cause of high blood pressure. One should keep in mind that aldosteronism also develops in primary renovascular hypertension but the latter entity is associated with high serum renin levels while in primary aldosteronism the renin levels are low.

Hypoaldosteronism is rare. It appears to be due to inadequate stimulation of aldosterone secretion or a defect in the adrenal synthesis of aldosterone. An unusual cause of secondary hypoaldosteronism (called pseudohypoaldosteronism by some) is seen in some infants with urinary tract infection, with or without urinary tract obstruction. Clinically, hypoaldosteronism results in hypotension and hyperkalemia. Imaging has no role in its diagnosis.

Imaging

A distinction between unilateral aldosteronomas, which are treated surgically, and bilateral hyperplasia, treated medically, is of obvious importance. The adrenal glands are significantly larger in patients with bilateral adrenal hyperplasia than in those with an aldosteronoma. One study achieved 100% sensitivity when a CT mean limb width of >3 mm was used to diagnose bilateral adrenal hyperplasia, and 100% specificity when limb width was 5 mm or greater (29). Unless imaging identifies a tumor, such differentiation is generally sought by bilateral adrenal venous sampling.

Aldosteronomas tend to be small; discrete nodules are difficult to visualize. Thus among 18 aldosterone-producing adrenal adenomas, 89% were detected with CT but only 28% with US (30). Adrenal hyperplasia in Conn's syndrome ranges from diffuse and bilateral to nodular (Fig. 16.2). Thus one or more nodule may represent either an adenoma or nodular hyperplasia. Complicating this picture is the presence of the occasional unrelated incidental adrenal tumor.

Similar to Cushing adenomas, aldosteronomas contain varying amounts of lipid. As a result, some have CT attenuation values close to that of water and their CT appearance can mimic a cyst.

Calcifications develop only in an occasional benign aldosteronoma.

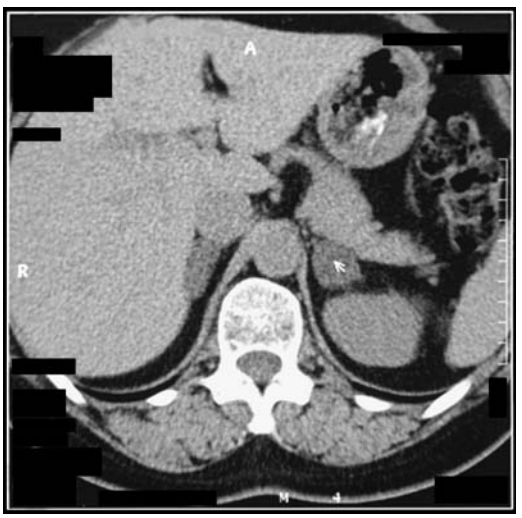

Figure 16.2. Conn's syndrome. Computed tomography (CT) reveals bilateral adrenal hyperplasia. (Courtesy of Algidas Basevicius, M.D., Kaunas Medical University, Kaunas, Lithuania.)

In 20 patients with primary hyperaldosteronism, 50% had aldosterone-producing adenomas and 50% bilateral adrenal hyperplasia (31); MRI detected adenomas with a sensitivity of 70% and specificity of 100%, with adenomas being iso- to hypointense relative to liver on T1- and slightly hyperintense on T2-weighted images. Of interest is that signal intensity decreased on out-of-phase chemical shift images in 86% of adenomas and 89% of adrenal hyperplasia, indicating the presence of lipid.

Iodine-131–NP-59 scintigraphy appears to be complementary to CT and MR in differentiating between adenomas and adrenal hyperplasia, being especially useful with a unilateral hyperplastic nodule. Scintigraphy visualizes these tumors as hot nodules, with an occasional warm nodule.

Bilateral adrenal venous sampling distinguishes most but not all adenomas from hyperplasia. Blood samples are obtained after stimulation with ACTH. With bilateral hyperplasia, after stimulation aldosterone levels increase in blood samples from both adrenals; on the other hand, a more marked unilateral increase is detected with an aldosteronoma.

Therapy

Patients with bilateral glomerulosa hyperplasia and those amenable to glucocorticoid therapy are treated medically. Adenomas are resected, but keep in mind that hypertension persists in 30% to 50% of patients after resection even if they are biochemically cured. Such persistent postoperative hypertension suggests coexisting essential hypertension.

Several patients with Conn syndrome and Cushing's syndrome have been treated by CT-guided acetic acid injected into their adrenal nodules (32); follow-up revealed cystic degeneration. A few aldosteronomas have also been treated by transcatheter arterial embolization with absolute ethanol.

Medullary Tumors

With some adrenal medullary tumors even a combination of histology, immunochemistry, and cytophotometric techniques achieves only a differentiation between benign and malignant states, and even then at times with difficulty.

Pheochromocytoma (Paraganglioma)

Clinical

A pheochromocytoma is a paraganglioma located in the adrenal medulla. An inconsistent terminology is in use when describing corresponding extraadrenal neoplasms; some authors refer to them as *extraadrenal pheochromocytomas* if they are functioning and *paragangliomas* if nonfunctioning, while others call all extraadrenal tumors *paragangliomas* and simply specify the site and functioning status.

A paraganglioma originates from chromaffin neural crest tissue that has migrated to form the paraganglionic system. Most are located between the diaphragm and the inferior renal pole, with the most common extraadrenal site being in the organ of Zuckerkandl near the inferior mesenteric artery origin. An occasional one involves the inferior vena cava, urinary bladder, or even the broad ligament. About 10% occur in children, where a familial prevalence is evident and is more likely to be extraadrenal and multicentric. A number of pheochromocytomas have been detected during pregnancy and postpartum.

A pheochromocytoma produces an excess of catecholamines, and most of these patients have elevated catecholamine levels. An occasional one is part of a complex tumor; thus it can contain mesenchymal elements. Or, a cortical carcinoma or adenoma exhibits neuroendocrine differentiation. About 10% of pheochromocytomas are malignant. In general, extraadrenal paragangliomas are more malignant and metastasize more readily than their adrenal counterparts. The malignant potential of some is difficult to establish even by histology, the one definite finding of malignancy being the presence of metastases at sites normally devoid of chromaffin cells.

Although many patients with a pheochromocytoma are hypertensive, overall this condition is a rare cause of hypertension. Pheochromocytoma-induced hypertension tends to be paroxysmal, but differentiation from other causes of hypertension is difficult. A rare paraganglioma (pheochromocytoma) undergoes spontaneous rupture and extraperitoneal hemorrhage, at times resulting in an acute abdomen (Fig. 16.3).

The prevalence of pheochromocytomas is increased in several disorders—neurofibromatosis, von Hippel-Lindau disease, Sturge-

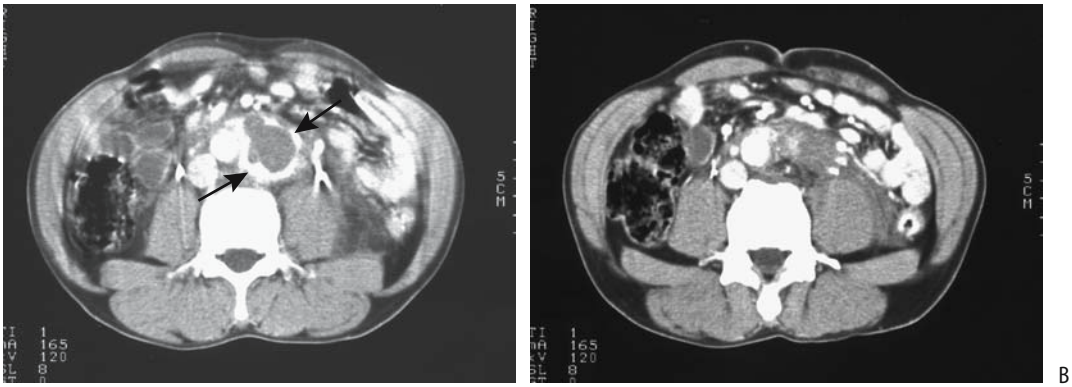

Figure 16.3. Spontaneous rupture of paraganglioma. A: Contrast-enhanced CT shows a retroperitoneal tumor with peripheral enhancement (arrows). B: A more caudad scan identifies left para-aortic fluid and infiltrate, mimicking a ruptured aortic aneurysm. (*Source:* Rha SE, Byun JY, Jung SE, Chun HJ, Lee HG, Lee JM. Neurogenic tumors in the abdomen: tumor types and imaging characteristics. Radiographics 2003;23:29–43, with permission from the Radiological Society of North America.)

Weber syndrome, tuberous sclerosis, and multiple endocrine neoplasia (MEN) syndrome. Anatomically, some pheochromocytoma-containing glands are normal in size. Bilateral tumors are more prevalent in both MEN II patients and those with von Hippel-Lindau disease; some of these patients also develop extraadrenal pheochromocytomas. Thus detection of bilateral or familial pheochromocytomas warrants a search for other unsuspected tumors. Of note is that a large minority of these patients with a pheochromocytoma are asymptomatic and have normal blood pressure and normal catecholamine testing. Nevertheless, in patients with von Hippel-Lindau disease and MEN II syndrome, the measurement of plasma normetanephrine and metanephrine achieves a sensitivity and specificity of over 95% in detecting pheochromocytomas (33).

Intravenous ionic contrast may precipitate a hypertensive crisis in a patient with a pheochromocytoma. Premedication with an α-adrenergic blocking agent appears prudent prior to intravenous (IV) contrast agent administration to prevent an adrenergic crisis, although the need for such blockage is not well established for nonionic contrast agents.

Imaging

A review of 282 patients who underwent pheochromocytoma resection in France between 1980 and 1991, found unilateral tumors in 67%, bilateral ones in 19%, and extraadrenal in 14% (34); the sensitivities of imaging in detecting these tumors were 89% for CT, 98% for MRI, and 81% for I-131-MIBG scintigraphy.

If imaging reveals no adrenal tumor in a patient suspected of a pheochromocytoma, imaging of other extraadrenal sites, including bladder, is necessary. Scintigraphy with I-131-MIBG is useful to detect extraadrenal and bilateral tumors.

Most pheochromocytomas are readily imaged by CT, US, and MRI (Fig. 16.4), yet the clinical and imaging findings are not always straightforward, even in a setting of elevated catecholamines. Intrinsically solid tumors, necrosis, and hemorrhage result in a cystic appearance and, as a result, they have a variable imaging appearances. It is with cystic tumors that the differential diagnosis between cystic pheochromocytomas, necrotic carcinomas, and metastases becomes problematic. An aid to diagnosis is that aside from necrotic regions, these are very hypervascular tumors and postcontrast CT shows marked contrast enhancement.

Another source for confusion is that a minority of adrenal pheochromocytomas contain sufficient microscopic fat to result in a CT attenuation of <10 HU and thus mimic an adenoma (35); after contrast enhancement some of these hypodense tumors also reveal >60% contrast washout on 10-min images, similar to adenomas.

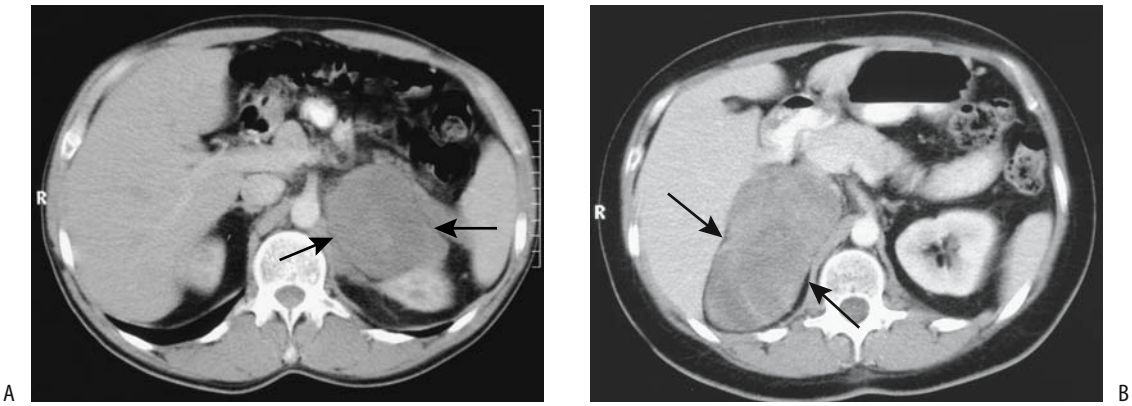

Figure 16.4. A: Left adrenal pheochromocytoma. Computed tomography reveals a large, homogeneous, poorly enhancing tumor (arrows) displacing the left kidney. B: Right adrenal pheochromocytoma. Computed tomography identifies a large, homogeneous, poorly enhancing tumor (arrows). (Courtesy of Algidas Basevicius, M.D., Kaunas Medical University, Kaunas, Lithuania.)

Some contain linear or laminated calcifications (Fig. 16.5). Aside from several anecdotal reports, pheochromocytomas do not contain sufficient lipid to influence their imaging appearance.

Nonnecrotic pheochromocytomas tend to be hypointense-to-isointense to liver on T1- and hyperintense on T2-weighted images. Their lack of fat reflects their hyperintense T2-weighted fat-suppressed appearance. They tend to exhibit progressive enhancement postcontrast MR. Nevertheless, a sufficient number of pheochromocytomas have an atypical low signal intensity on T2-weighted images and not all hyperintense adrenal tumors represent pheochromocytomas, so that reliance on a hyperintense T2-weighted appearance results in a low sensitivity in diagnosing a pheochromocytoma (Fig. 16.6).

Scintigraphy with I-123-MIBG achieves an 80% to 90% detection rate for these tumors; MIBG SPECT sensitivity approaches 100%. This tracer accumulates in adrenergic tissue throughout the body, including metastases. Optimal scan timing is variable, with scans often obtained 24 to 48 hours postinjection. An occasional metastasis is detected only on earlier scans. Indium-111 pentetreotide scintigraphy appears to have similar detection ability as I-123-MIBG, but it has not been studied as extensively.

2-[18F]-fluoro-deoxy-D-glucose PET detected tumors in 76% of patients with pheochromocytomas, with most benign, malignant, and metastatic foci avidly concentrating FDG (36); in fact, several pheochromocytomas not accumulating MIBG showed intense FDG uptake, although MIBG images tended to be as good or better for tumors concentrating both agents. A majority of pheochromocytomas also reveal uptake during (11C)-hydroxyephedrine-PET scanning (37).

Therapy

The treatment of choice for most pheochromocytomas is surgical resection, although an occasional one is treated by catecholamine pharmacotherapy. Resection consists of either adrenalectomy or adrenal-sparing surgery, with a laparoscopic approach commonly employed. A pheochromocytoma has been treated with percutaneous radiofrequency ablation (23).

Neuroblastoma/Ganglioneuroma

Clinical

The most common abdominal neoplasm of early childhood, a neuroblastoma originates from neuroblasts in sympathetic ganglia. The adrenal glands are the most common site, with

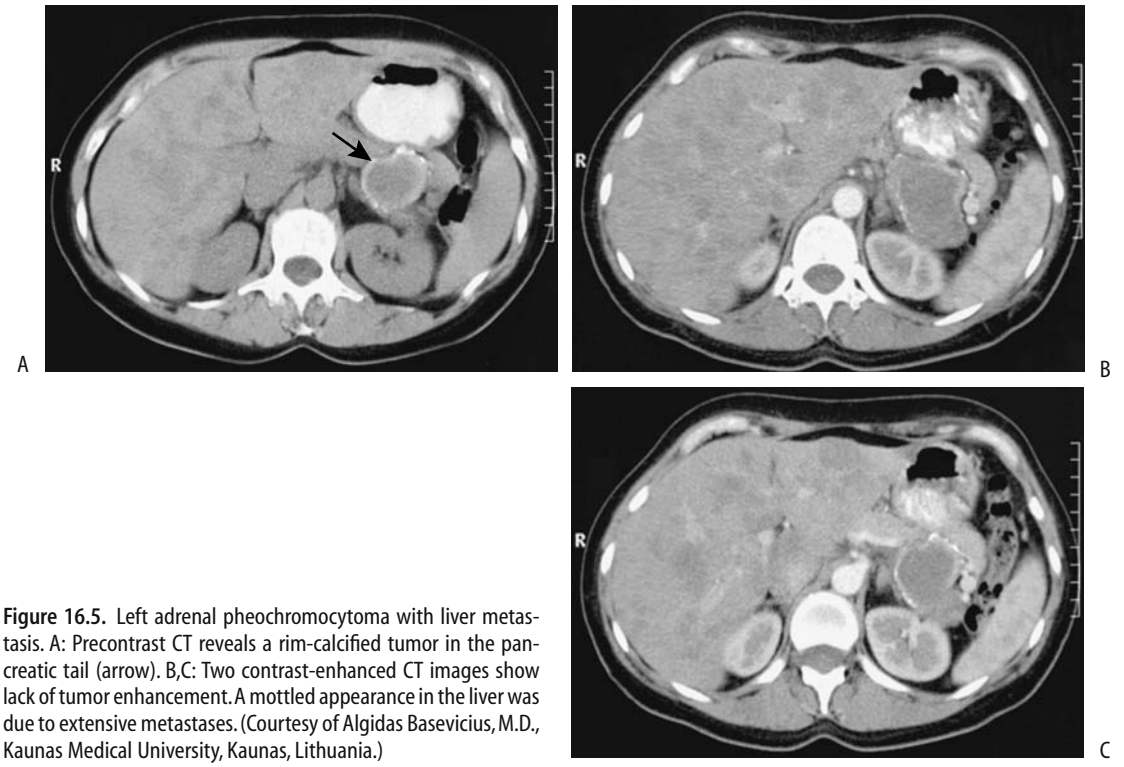

Figure 16.5. Left adrenal pheochromocytoma with liver metastasis. A: Precontrast CT reveals a rim-calcified tumor in the pancreatic tail (arrow). B,C: Two contrast-enhanced CT images show lack of tumor enhancement. A mottled appearance in the liver was due to extensive metastases. (Courtesy of Algidas Basevicius, M.D., Kaunas Medical University, Kaunas, Lithuania.)

other neuroblastomas originating anywhere along the sympathetic chain, with a paraaortic location being the next most common site. The prevalence of extraadrenal origin increases with age at onset. These tumors are prone to metastasize, and metastasis at initial presentation is not uncommon. Bilateral adrenal involvement, from either a synchronous origin or metastasis, is found occasionally. Spread is both hematogenous and lymphatic.

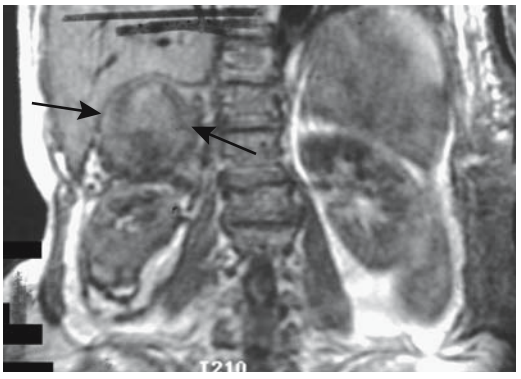

Figure 16.6. Bleeding pheochromocytoma (arrows) identified on T1-weighted coronal image. Hypointensity surrounding the right kidney represents a perinephric and paranephric hematoma. (*Source:* Burgener FA, Meyers SP, Tan RK, Zaunbauer W. Differential Diagnosis in Magnetic Resonance Imaging. Stuttgart: Thieme, 2002, with permission.)

A neuroblastoma, ganglioneuroblastoma, and well-differentiated ganglioneuroma differ from each other in degree of differentiation. In fact, in any one tumor histology often reveals a mixture of tumor cells. Some neuroblastomas undergo spontaneous transformation into a ganglioneuroma, with a benign neoplasm having a solid, homogeneous appearance.

The most common presentation is a palpable hard, fixed abdominal tumor, although a number of these tumors are detected incidentally. Some of these children develop periorbital ecchymoses.

The patient survival rate decreases with age, with the highest survival being in infants less than 1 year of age. Survival also appears to depend on tumor DNA ploidy status. Thus children with diploid tumors do poorly, while

those with aneuploid tumors have a much better survival.

Percutaneous biopsy using 15- or 16-gauge core biopsy needles provides an alternate approach to open biopsy in children with advanced neuroblastoma. Percutaneous biopsy provides both a histologic diagnosis and enough sample for prognosis.

Imaging

Depending on the site of origin, imaging reveals a suprarenal or paraspinal tumor. Neuroblastomas are poorly encapsulated and compress or invade adjacent structures; aortic or inferior vena caval encasement is often found with larger tumors. In adults, ganglioneuromas tend to surround major blood vessels but do not narrow the lumen. Tumor hemorrhage and necrosis result in a heterogeneous imaging appearance. An occasional neuroblastoma contains a cystic component. Coarse, mottled calcifications are common. They have less CT contrast enhancement than muscle and, similar to neuroblastomas, a heterogeneous, predominantly hyperintense signal is evident on T2-weighted MR images. Computed tomography and MRI are preferred over US because of their ability to better image metastases. Bone scans and chest radiographs are obtained preoperatively to detect metastases and establish a baseline.

Gray-scale 2D and 3D US using tissue harmonic imaging identified an adrenal ganglioneuroblastoma in a pregnant woman as an inhomogeneous, encapsulated, solid tumor (38); color and power Doppler showed extensive neovascularity.

Iodine-123-MIBG scintigraphy detects most neuroblastomas but some bone metastases show little or no MIBG uptake (39). SPECT imaging detects more tumors and better defines their location. Both 24-hour and delayed 48-hour scanning appear useful; washout can result in some lesions being missed on delayed scans. Occasionally technetium-99m (Tc-99m)–hydroxymethylene diphosphonate (HMDP) bone scintigraphy is positive in an adrenal neuroblastoma.

Although MIBG scintigraphy appears superior to FDG-PET, the latter does detect most primary neuroblastoma foci and metastases. Also, occasionally FDG-PET is positive when a neuroblastoma fails to accumulate MIBG. PET scanning using carbon-11-hydroxyephedrine (HED) will also locate neuroblastomas.

Combined MIBG scintigraphy and MR imaging achieves a better diagnosis of neuroblastoma foci in children than either study individually. A retrospective study found MIBG scintigraphy, MRI and combined MIBG-MRI sensitivities of 69%, 86% and 99% and specificities of 85%, 77% and 95%, respectively (39).

In a newly discovered tumor the differential often includes a Wilms' tumor. Imaging shows most neuroblastomas to be more inhomogeneous than a Wilms' tumor. the latter is intrarenal in location, while an adrenal neuroblastoma displaces the kidney inferolaterally. Some paraspinal neuroblastomas extend into the spinal canal, a finding not seen with Wilms' tumors. At times an adrenal hemorrhage (hematoma) mimics a neuroblastoma. After the initial presentation, US should distinguish an anechoic and avascular hemorrhage from the hyperechoic and vascular neuroblastoma.

Lymphoma

Primary adrenal lymphoma is rare (40). More common is lymphomatous adrenal involvement from adjacent extraperitoneal lymph nodes, either unilateral or bilateral. Clinically silent adrenal involvement is relatively common with the latter, but adrenocortical insufficiency is a late finding with bilateral adrenal involvement.

Imaging findings range from solid nodules to diffuse homogeneous tumors. Adjacent lymphadenopathy is common. Often the adrenal glands are simply replaced by lymphomatous tissue and appear enlarged while maintaining their usual shape. With growth, lymphomas tend to become heterogeneous in appearance. They are hypoechoic with US. Magnetic resonance imaging reveals a signal intensity similar to that of metastases. Increasing enhancement on delayed postcontrast images is typical.

Necrosis and calcifications develop after therapy.

Less Common Tumors

Rarer adrenal tumors include a bronchogenic cyst, pure lipoma, teratoma, vascular leiomyomas, schwannoma, and even a sarcoma. Occasionally a patient with von Recklinghausen's disease develops bilateral adrenal neurofibromas, although in this disease adrenal pheochromocytomas are more common. Ectopic tissue is occasionally detected in the adrenal glands (i.e., a choristoma), the most common one being ectopic thyroid tissue (41). Except for the latter, no imaging findings suggest a specific diagnosis.

Hemangioma

Adrenal hemangiomas are rare. Some contain calcifications and often are large. The more typical ones have imaging characteristics similar to those of liver hemangiomas. An occasional adrenal hemangioma contains a central stellate hypointense region on MRI. Hemorrhage and necrosis are relatively common, and these influence their imaging appearance. The gradual tumor enhancement from the periphery inward is not seen as often as with liver hemangiomas. An occasional one presents with extraperitoneal hemorrhage.

An adrenal hemangioma-like appearance in an infant should suggest a hemangioendothelioma. Their imaging appearance is similar to those in the liver.

Myelolipoma

Adrenal cortical myelolipomas are rare, benign, nonfunctioning tumors composed of fat and bone marrow tissue. They occur bilaterally. Most myelolipomas are small and are discovered incidentally in asymptomatic patients. Anecdotal reports describe extraadrenal perirenal myelolipomas (42). An occasional patient presents with acute pain secondary to intratumoral or extraperitoneal bleeding.

In a minority of patients a myelolipoma is associated with some type of endocrine abnormality, such as Cushing's syndrome, a pheochromocytoma or hyperthyroidism. Adrenal myelolipomatous tissue reported from the Armed Forces Institute of Pathology consisted either of an isolated adrenal myelolipoma (identified by fat evident at CT) or myelolipomatous tissue within other adrenal tumors (consisting of smaller foci containing less fat but more calcifications) (43); larger myelolipomas contained hemorrhage and necrosis. About 20% of these tumors contain small foci of calcifications.

Unenhanced CT should detect most of these tumors. The amount of fat present varies considerably, but a myelolipoma should not contain only fat; a mixture of fat and nonfatty tissue often results in a heterogeneous appearance (Fig. 16.7). Bleeding can obliterate surrounding fat planes (Fig. 16.8). Contrast-enhanced CT can obscure the fat component and miss a tumor.

Ultrasonography shows a highly echogenic tumor.

Magnetic resonance imaging reveals a variable signal with both T1- and T2-weighted sequences (Fig. 16.9). The signal decreases with fat suppression. These tumors enhance postcontrast. Their MR characteristics are modified by any hemorrhage and necrosis.

As already mentioned, other adrenal tumors, including a rare adenocarcinoma, contain fat. Differential diagnosis for a fat-containing adrenal lesion also includes a teratoma and liposarcoma. Some cysts contain a fatty component.

A biopsy should be diagnostic. Unless symptoms ensue, most of these tumors can be followed conservatively. With time, they can increase, decrease, or remain unchanged.

Hemorrhage/Hematoma

Some of the more common conditions associated with adrenal hemorrhage are listed in Table 16.2. Usually a hematoma is limited to the adrenal glands, without involving adjacent extraperitoneal tissues.

Adrenal hematomas have an imaging appearance similar to that of hematomas at other locations; their appearance changes and evolves with time.

Neonates

Most adrenal hemorrhage in neonates is idiopathic, although birth stress and related factors

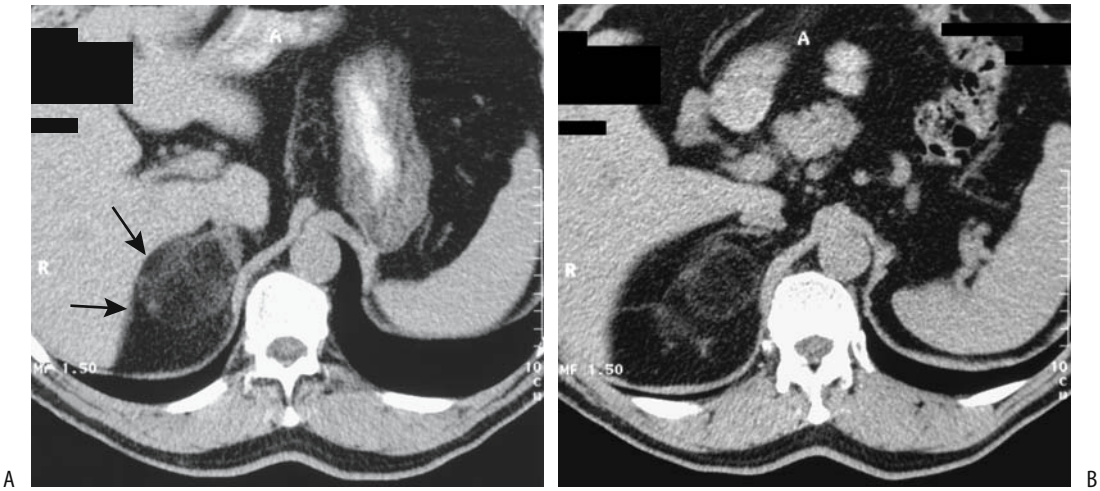

A B

Figure 16.7. Adrenal myelolipoma. A,B: Computed tomography shows a fat-containing structure (arrows) that has replaced the right adrenal gland. It is surrounded by extensive perirenal fat. (Courtesy of Algidas Basevicius, M.D., Kaunas Medical University, Kaunas, Lithuania.)

are implicated. Jaundice may be present. Hemorrhage is more common on the right side, except if associated with renal vein thrombosis when it occurs much more often on the left. With an inferior vena cava thrombus hemorrhage tends to be bilateral.

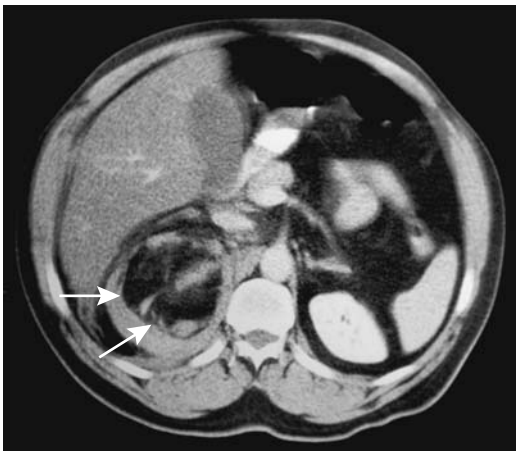

Figure 16.8. Bleeding adrenal myelolipoma. Contrast-enhanced CT reveals a fat-containing tumor superior to the right kidney (arrows). Angiography performed shortly after this study identified a hypovascular tumor. (Courtesy of Patrick Fultz, M.D., University of Rochester.)

Typically, these neonates do not develop adrenal insufficiency. A scrotal hematoma is occasionally the initial presentation of adrenal hemorrhage in neonates.

The primary differential diagnosis in a neonate is a neuroblastoma, although MRI will differentiate these, with the exception of a hemorrhagic, cystic-appearing neuroblastoma (see also the description in Neuroblastoma/Ganglioneuroma, above). Also, hemorrhage should change its appearance over time, become anechoic, and decrease in size. Neonatal adrenal hemorrhage should also be differentiated from adrenal congestion, which develops in perinatal asphyxia and other perinatal stress conditions. Ultrasonography in the latter identifies diffuse adrenal enlargement, a smooth surface, and loss of the central hyperechoic stripe (44); histology in five neonates who died revealed diffuse sinusoidal congestion.

Adults

In adults, spontaneous adrenal hemorrhage ranges from unilateral to bilateral. Aside from trauma, most are associated with stress or a severe illness and are more often unilateral. In a setting of anticoagulant therapy a hematoma usually develops early in the course. If associated with a neoplasm, imaging

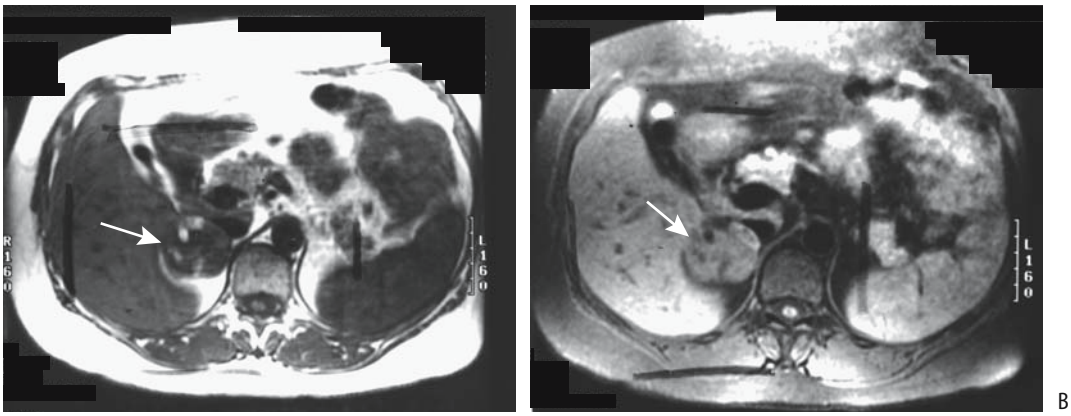

Figure 16.9. Adrenal myelolipoma. A right adrenal tumor (arrows) contains foci which are hyperintense on T1- (A) and hypointense on T2-weighted images (B). (*Source:* Burgener FA, Meyers SP, Tan RK, Zaunbauer W. Differential Diagnosis in Magnetic Resonance Imaging. Stuttgart: Thieme, 2002, with permission.)

should detect tumor enhancement. Adrenal hemorrhage is relatively common in patients with meningococcal sepsis (Waterhouse-Friderichsen syndrome); some hemorrhages extend into adjacent extraperitoneal tissues. In some patients with primary antiphospholipid syndrome hemorrhage is probably due to adrenal vein thrombosis. A right adrenal hemorrhage is a complication of liver transplantation, a not surprising finding because these patients undergo inferior vena caval division and ligation of right adrenal veins.

Table 16.2. Conditions associated with adrenal hemorrhage

Neonates
Idiopathic
Stress
Renal vein thrombosis
Inferior vena cava thrombosis
Adults
Idiopathic
Stress
Surgery
Hypotension
Sepsis
Trauma
Anticoagulant therapy
Underlying neoplasm
Postpartum period
Meningococcal sepsis (Waterhouse-Friderichsen syndrome)
Primary antiphospholipid syndrome
Adrenal vein thrombosis
Inferior vena cava thrombosis
Vasculitis leading to hypercoagulable state and venous thrombosis
Associated with liver transplantation
Adrenomyeloneuropathy

Imaging findings of adrenal hemorrhage are varied and consist of either unilateral or bilateral gland enlargement, at times asymmetrical, or a focal tumor. A typical CT appearance is a heterogeneous tumor having a density of 50 to 90 HU. Some hemorrhages are associated with periadrenal fat infiltration or even involve adjacent diaphragmatic crus. They are hyperintense on both T1- and T2-weighted MR images. A hematoma shows no contrast enhancement with either CT or MRI. Angiography, although rarely performed, identifies a hypovascular tumor. With time, the involved gland shrinks and the hematoma decreases in density.

While unilateral hemorrhage generally has few sequelae, bilateral involvement can result in adrenal insufficiency. In either case, an adrenal hemorrhage should be followed until resolution to exclude an underlying neoplasm. With time, some involved glands atrophy and calcify. Presumably in some adults adrenal calcifications represent sequelae of neonatal hemorrhage. The

hallmark of a remote hemorrhage is an extensively calcified gland with no significant soft tissue component. Prior granulomatous disease usually results in more patchy calcifications.

Insufficiency

Most of the adrenal cortex must be destroyed before adrenal insufficiency (Addison's disease) manifests clinically. Most often insufficiency is idiopathic, although an autoimmune disorder is often suspected. Other less common etiologies include adrenal hemorrhage, tuberculosis, histoplasmosis, rare adrenal involvement by North American blastomycosis, and sarcoidosis. Infiltration by lymphoma or metastatic carcinoma, when extensive, can also lead to adrenal insufficiency.

In an acute setting of shock, adrenal insufficiency should be considered if CT reveals bilateral, enlarged, hematoma-density adrenal glands. In a setting of septicemia, however, shock may be induced by septicemia rather than adrenal insufficiency. Also, at times adrenal gland enlargement in the face of adrenal insufficiency is due to tumors such as lymphoma or metastases.

Imaging in patients with more chronic adrenal insufficiency shows that about half have bilateral adrenal enlargement, at times containing regions of necrosis and calcification. Enlarged glands tend to decrease in size after appropriate therapy. Some patients have calcified, atrophic glands. Noncalcified atrophic glands are difficult to visualize with imaging.

Iron deposition in the adrenal glands in patients with hemochromatosis eventually results in mild adrenal insufficiency. Computed tomography reveals small glands having increased attenuation.

Vascular Lesions

An aneurysm of an adrenal artery is rare; rupture leads to a periadrenal hematoma. Imaging reveals a cystic tumor, hematoma, and possible thrombus in the artery. These aneurysms can be diagnosed by angiography and are amenable to embolization.

Adrenal vein thrombosis can develop in a setting of heparin-induced thrombocytopenia (45).

Immunosuppression

Both fungal and viral adrenal infections are more common in AIDS patients than in the general population. Sufficient gland destruction results in adrenal insufficiency.

Lymphoma predominates among adrenal tumors in AIDS patients. Kaposi's sarcoma is less common. Several adrenal adenocarcinomas have been reported, although the association may be fortuitous.

Postoperative Changes

An adrenalectomy is performed using either an open or laparoscopic approach and either an anterior, posterior, or a thoracoabdominal incision. A transthoracic approach is preferred by some. Using anterior transabdominal approach the left adrenal gland is reached by either mobilizing the spleen and pancreatic tail, or using the lesser sac as a pathway and displacing the pancreas away from the adrenal gland. An open adrenalectomy is generally performed in patients with a suspected malignancy and for tumors larger than about 6 cm. A laparoscopic adrenalectomy is considered for others; it requires minimal access, is least painful to the patient, and results in a shorter hospitalization than an anterior approach.

References

1. Karampekios S, Hatjidakis AA, Drositis J, Gourtsoyiannis N. Artificial paravertebral widening for percutaneous CT-guided adrenal biopsy. [Review] J Comput Assist Tomogr 1998;22:308–310.
2. Konig CW, Pereira PL, Trubenbach J, et al. MR imaging-guided adrenal biopsy using an open low-field-strength scanner and MR fluoroscopy. AJR 2003;180:1567–1570.
3. Shafaie FF, Katz ME, Hannaway CD. A horseshoe adrenal gland in an infant with asplenia. Pediatr Radiol 1997;27:591–593.
4. Akata D, Haliloglu M, Ozmen MN, Akhan O. Bilateral cystic adrenal masses in the neonate associated with the incomplete form of Beckwith-Wiedemann syndrome. Pediatr Radiol 1997;27:184–185.
5. Moore EE, Malangoni MA, Cogbill TH, et al. Organ injury scaling VII: cervical vascular, peripheral vascular,

adrenal, penis, testis, and scrotum. J Trauma 1996;41: 523–524.
6. Ferrozzi F, Cademartiri F, Tognini G. [Adrenal hydatidosis. The computed tomographic picture in a case.] [Review] [Italian] Radiol Med 1999;98:430–431.
7. Hahn ST, Park SH, Kim CY, Shinn KS. Adrenal paragonimiasis simulating adrenal tumor—a case report. J Korean Med Sci 1996;11:275–277.
8. Wang LJ, Wong YC, Chen CJ, Chu SH. Imaging spectrum of adrenal pseudocysts on CT. Eur Radiol 2003;13:531–535.
9. Barzon L, Scaroni C, Sonino N, et al. Incidentally discovered adrenal tumors: endocrine and scintigraphic correlates. J Clin Endocrinol Metab 1998;83:55–62.
10. Honigschnabl S, Gallo S, Niederle B, et al. How accurate is MR imaging in characterisation of adrenal masses: update of a long-term study. Eur J Radiol 2002; 41:113–122.
11. Cataldi A, Cortese G, Corradino R, Porpiglia F, Ali A, Fava C. [Characterization of non-secreting adrenal nodules (incidentalomas): role of multiphasic spiral computerized tomography.] [Italian] Radiol Med 2000;100:257–261.
12. Namimoto T, Yamashita Y, Mitsuzaki K, et al. Adrenal masses: quantification of fat content with double-echo chemical shift in-phase and opposed-phase FLASH MR images for differentiation of adrenal adenomas. Radiology 2001;218:642–646.
13. Fujiyoshi F, Nakajo M, Fukukura Y, Tsuchimochi S. Characterization of adrenal tumors by chemical shift fast low-angle shot MR imaging: comparison of four methods of quantitative evaluation. AJR 2003;180: 1649–1657.
14. Israel GM, Korobkin M, Wang C, Hecht EN, Krinsky GA. Comparison of unenhanced CT and chemical shift MRI in evaluating lipid-rich adrenal adenomas. AJR 2004;183:215–219.
15. Szolar DH, Kammerhuber FH. Adrenal adenomas and nonadenomas: assessment of washout at delayed contrast-enhanced CT. Radiology 1998;207:369–375.
16. Peña CS, Boland GW, Hahn PF, Lee MJ, Mueller PR. Characterization of indeterminate (lipid-poor) adrenal masses: use of washout characteristics at contrast-enhanced CT. Radiology 2000;217:798–802.
17. Caoili EM, Korobkin M, Francis IR, Cohan RH, Dunnick NR. Delayed enhanced CT of lipid-poor adrenal adenomas. AJR 2000;175:1411–1415.
18. Chung JJ, Semelka RC, Martin DR. Adrenal adenomas: characteristic postgadolinium capillary blush on dynamic MR imaging. J Magn Reson Imaging 2001;13: 242–248.
19. Hofle G, Gasser RW, Lhotta K, Janetschek G, Kreczy A, Finkenstedt G. Adrenocortical carcinoma evolving after diagnosis of preclinical Cushing's syndrome in an adrenal incidentaloma. A case report. Horm Res 1998;50:237–242.
20. Joual A, Patard JJ, Chopin D, Abbou CC. [Contralateral aneurysm-like adrenal gland metastasis of a renal adenocarcinoma.] [French] Prog Urol 1998;8:89–91.
21. Tsukamoto E, Itoh K, Kanegae K, Kobayashi S, Koyanagi T, Tamaki N. Accumulation of iodine-131–iodocholesterol in renal cell carcinoma adrenal metastases. J Nucl Med 1998;39:656–658.
22. Shibata T, Maetani Y, Ametani F, Itoh K, Konishi J. Percutaneous ethanol injection for treatment of adrenal metastasis from hepatocellular carcinoma. AJR 2000; 174:333–335.
23. Mayo-Smith WW, Dupuy DE. Adrenal neoplasms: CT-guided radiofrequency ablation–preliminary results. Radiology 2004;231:225–230.
24 Sohaib SA, Hanson JA, Newell-Price JD, et al. CT appearance of the adrenal glands in adrenocorticotrophic hormone-dependent Cushing's syndrome. AJR 1999; 172:997–1002.
25. Midorikawa S, Hashimoto S, Kuriki M, et al. A patient with preclinical Cushing's syndrome and excessive DHEA-S secretion having unilateral adrenal carcinoma and contralateral adenoma. Endocr J 1999;46: 59–66.
26. Otsuka F, Ogura T, Nakao K, et al. Cushing's syndrome due to unilateral adrenocortical hyperplasia. Intern Med 1998;37:385–390.
27. Doppman JL, Chrousos GP, Papanicolaou DA, Stratakis CA, Alexander HR, Nieman LK. Adrenocorticotropin-independent macronodular adrenal hyperplasia: an uncommon cause of primary adrenal hypercortisolism. Radiology 2000;216:797–802.
28. Stewart PM. Mineralocorticoid hypertension. [Review] Lancet 1999;353:1341–1347.
29. Lingam RK, Sohaib SA, Vlahos I, et al. CT of primary hyperaldosteronism (Conn's syndrome): the value of measuring the adrenal gland. AJR 2003;181:843–849.
30. Lorenzo Romero JG, Salinas Sanchez AS, Segura Martin M, et al. [The Conn syndrome. The clinical and surgical aspects of 18 cases of adrenal adenoma.] [Spanish] Actas Urol Esp 1999;23:14–21.
31. Sohaib SA, Peppercorn PD, Allan C, et al. Primary hyperaldosteronism (Conn syndrome): MR imaging findings. Radiology 2000;214:527–531.
32. Liang HL, Pan HB, Lee YH, et al. Small functional adrenal cortical adenoma: treatment with CT-guided percutaneous acetic acid injection–report of three cases. Radiology 1999;213:612–615.
33. Eisenhofer G, Lenders JW, Linehan WM, Walther MM, Goldstein DS, Keiser HR. Plasma normetanephrine and metanephrine for detecting pheochromocytoma in von Hippel-Lindau disease and multiple endocrine neoplasia type 2. N Engl J Med 1999;340:1872–1879.
34. Jalil ND, Pattou FN, Combemale F, et al. Effectiveness and limits of preoperative imaging studies for the localisation of pheochromocytomas and paragangliomas: a review of 282 cases. French Association of Surgery (AFC), and The French Association of Endocrine Surgeons (AFCE). Eur J Surg 1998;164:23–28.
35. Blake MA, Krishnamoorthy SK, Boland GW, et al. Low-density pheochromocytoma on CT: a mimicker of adrenal adenoma. AJR 2003;181:1663–1668.
36. Shulkin BL, Thompson NW, Shapiro B, Francis IR, Sisson JC. Pheochromocytomas: imaging with 2–[fluorine-18]fluoro-2-deoxy-D-glucose PET Radiology 1999;212:35–41.
37. Trampal C, Engler H, Juhlin C, Bergstrom M, Langstrom B. Pheochromocytomas: detection with 11C hydroxyephedrine PET. Radiology 2004;230:423–428.
38. Slapa RZ, Jakubowski W, Kasperlik-Zaluska AA, et al. Adrenal ganglioneuroblastoma in pregnant woman: diagnosis with three-dimensional ultrasound. Eur Radiol 2002;12 Suppl 3:S121–126.

39. Pfluger T, Schmied C, Porn U, et al. Integrated imaging using MRI and 123I metaiodobenzylguanidine scintigraphy to improve sensitivity and specificity in the diagnosis of pediatric neuroblastoma. AJR 2003;181:1115–1124.
40. Tazi K, Achour A, Koutani A, Ibn Attya A, Hachimi M, Lakrissa A. [Primary non-Hodgkin's malignant lymphoma of the adrenal gland. Case report and review of the literature.] [Review] [French] Prog Urol 1999;9: 1102–1105.
41. Shiraishi T, Imai H, Fukutome K, Watanabe M, Yatani R. Ectopic thyroid in the adrenal gland. Hum Pathol 1999;30:105–108.
42. Kumar M, Duerinckx AJ. Bilateral extraadrenal perirenal myelolipomas: an imaging challenge. AJR 2004;183:833–836.
43. Kenney PJ, Wagner BJ, Rao P, Heffess CS. Myelolipoma: CT and pathologic features. Radiology 1998;208:87–95.
44. Koplewitz BZ, Daneman A, Cutz E, Hellmann J. Neonatal adrenal congestion: a sonographic-pathologic correlation. Pediatr Radiol 1998;28:958–962.
45. Bolter S, Meier M, Roeren T. [Adrenal vein thrombosis in heparin-induced thrombocytopenia.] [German] Rofo Fortschr Geb Rontgenstr Neuen Bildgeb Verfahr 2000;172:100–101.

17

Abdominal Vasculature

Technique

Computed Tomography

Contrast-enhanced computed tomography (CT) can visualize the major aortic branches on early-phase and venous branches on late-phase images. Late images also evaluate the portal phase. Most radiologists use a nonionic contrast agent, with a typical intravenous (IV) injection consisting of 150 mL at a rate of about 4 to 5 mL/sec. A faster injection rate produces earlier and greater vascular enhancement than a slower rate. A test bolus injection or automatic bolus triggering optimizes contrast enhancement (more details on CT angiography are in Chapter 7).

Three-dimensional (3D) image reconstruction is helpful in evaluating overlapping arteries and veins; the aorta, main arterial branches, as well as vena cava and portal vein branches are usually identified. Preoperative reconstructed 3D CT angiography is useful to surgeons in planning complex intraabdominal procedures, especially if unusual vascular paths are present. Reconstruction techniques include surface rendering, maximum intensity projection (MIP) and volume rendering; the latter utilizes more of the available data and generally is more accurate. A multiple threshold display technique decreases artifacts and allows better small vessel depiction than a shaded surface display technique. Each technique has its advantages and disadvantages (Fig. 17.1).

Similar to virtual colonoscopy, virtual CT arterial endoscopy is also feasible. In theory, a stenosis, aneurysm, or stent could be evaluated from its endoluminal surface. In practice, such applications are still being developed.

Computed tomography arterial portography and CT hepatic arteriography are discussed in Chapter 7. These techniques are of value primarily in the study of the liver blood supply. Evaluation of CT arterial portography images is not always straightforward, most often due to flow artifacts caused by nonopacified blood.

Ultrasonography

Doppler ultrasonography (US) measures blood flow velocity in larger vessels. Superior mesenteric artery and renal artery blood flow velocities can be measured even in neonates.

The use of intravascular contrast agents enhances portal vein and collateral blood flow during Doppler US studies. One IV US contrast agent is Perflenapent emulsion (EchoGen, Sonus Pharmaceuticals, Bothell, WA), providing enhancement lasting 5 to 15 minutes. Continuous infusion, rather than bolus injection, prolongs enhancement and decreases saturation artifacts.

Transesophageal echocardiography has evolved into a valuable thoracic aortic study, especially in a setting of suspected aortic dissection, postoperative repair, and follow-up. Echocardiography also evaluates the extent

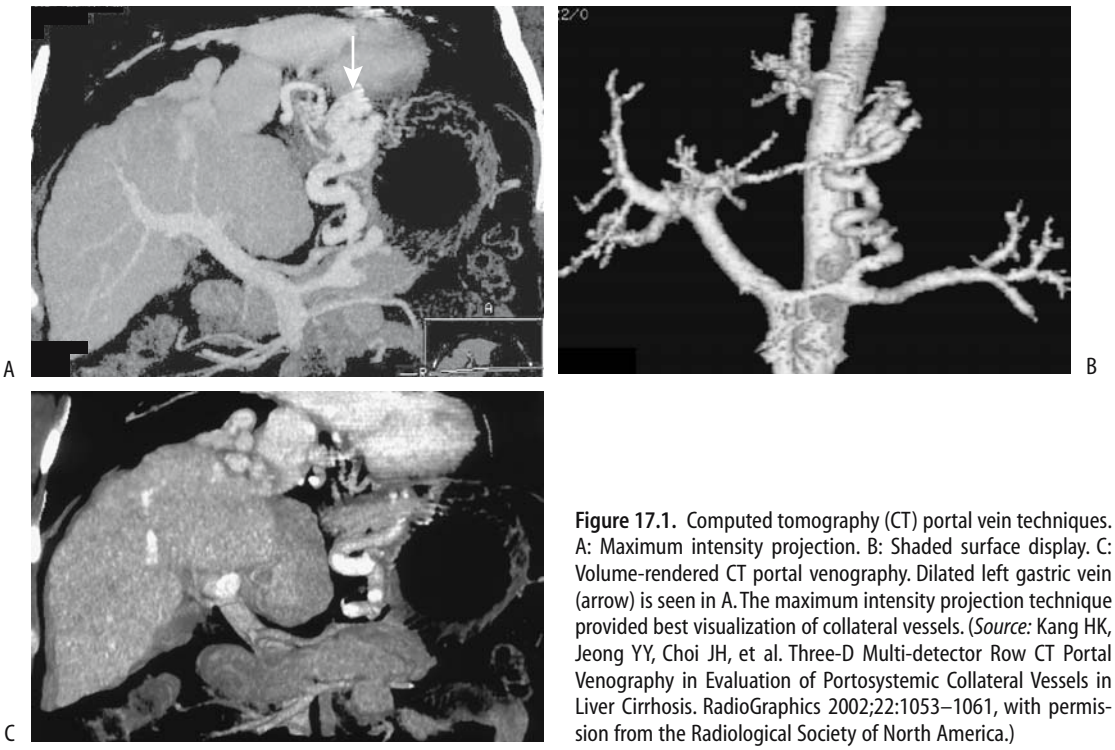

Figure 17.1. Computed tomography (CT) portal vein techniques. A: Maximum intensity projection. B: Shaded surface display. C: Volume-rendered CT portal venography. Dilated left gastric vein (arrow) is seen in A. The maximum intensity projection technique provided best visualization of collateral vessels. (*Source:* Kang HK, Jeong YY, Choi JH, et al. Three-D Multi-detector Row CT Portal Venography in Evaluation of Portosystemic Collateral Vessels in Liver Cirrhosis. RadioGraphics 2002;22:1053–1061, with permission from the Radiological Society of North America.)

of atherosclerosis, aortic ulcers, intramural hematomas, and blood flow.

Intravascular US holds promise in evaluating vessel wall morphology. It has been called a technology in search of an application and is gradually finding a role in endovascular intervention procedures.

Magnetic Resonance

Currently magnetic resonance angiography (MRA) is an alternate vascular imaging modality in patients with a contraindication to iodinated contrast agents. Its future indications will undoubtedly increase considerably, mostly at the expense of invasive angiography.

Intraluminal blood has a varied MR appearance depending on the technique used; it ranges from a signal void on spin echo (SE) sequences to being hyperintense on gradient-recalled echo (GRE) sequences. Conventional T1- and T2-weighted SE techniques result in flowing blood appearing dark. An exception is with slow-flowing blood, which tends to mimic a thrombus and appears bright. Due to the T1-shortening effect of IV contrast, contrast-enhanced MRA sequences result in flowing blood being bright while stationary objects are saturated and appear "dark." A further refinement of this technique is subtraction of precontrast images from postcontrast ones, improving vessel contrast resolution.

Compared to digital subtraction angiography (DSA), the sensitivity and specificity percents of MRA in detecting major vessel stenoses or occlusions are in the high 90% range. Currently, the major constraints of abdominal vessel MRA include the pulsatile nature of blood flow, respiratory motion, and peristalsis. The use of heavily T2-weighted fast turbo spin echo sequences instead of conventional T2-weighted SE sequences improves image quality. Fast GRE sequences allow dynamic contrast-enhanced vascular studies using single breath-hold image acquisition and result in few motion artifacts. Useful techniques include *time of flight* and *phase contrast*. The former consists of a variation in signal intensity with time due to proton motion within a magnetic field, while the latter monitors phase variations; each has certain

advantages and limitations. A 2D time-of-flight technique permits 3D reconstruction images. The phase-contrast technique is useful in evaluating portal vein blood; it measures flow direction and velocity.

The relative merits of MRA versus computed tomography angiography (CTA) are still evolving. Mention of angiography in CT implies the use of an intravascular contrast agent. This is not necessarily true with MRA, because MRA without contrast enhancement is feasible. Flowing fluid can be made to produce a signal void and thus appear black (black blood technique) or appear bright. Limitations of MRA without contrast include the presence of slow flow and spin-dephasing signal voids induced by turbulence. In general, contrast-enhanced MRA of abdominal vessels is superior to noncontrast time-of-flight or phase-contrast MRA.

A T1-weighted 3D MRA technique using gradient-echo [fast imaging with steady-state precision (FISP)] with ultrashort echo and repetition times obtained during the arterial phase after IV contrast overcomes a number of limitations of no-contrast techniques; images are obtained within 20 to 40 seconds during a breath-hold. At times a subtraction technique using precontrast images is helpful. Contrast-enhanced MRA of the portal vein is hampered by slow flow, and in this situation a time-of-flight technique is more appropriate.

Both 2D and 3D gadolinium-enhanced MRA evaluate major vessels. Thus MRA performed with four 3D acquisitions (at 0, 30, 60, and 90 seconds after IV gadolinium) provides an arteriogram (without veins) in most patients during the second or third acquisitions and a venogram by subtracting the arterial phase from an arteriovenous phase (third or fourth acquisition) (1); all major vessels, including portal vein and superior mesenteric vein, can be visualized, but secondary branches are better shown by conventional angiography. Veins <5 mm in diameter are often not well seen with MRA.

Using gadolinium-enhanced MRA, MIP post-processing provides vascular phase images that can then be reformatted into 3D images viewed along a 360-degree axis. The use of gadolinium results in arterial phase images without the need for subtraction, but a subtraction technique is necessary for venous-phase imaging. The entire intraabdominal aorta can be visualized with 3D gadolinium-enhanced MRA, and this technique appears useful in studying aortic aneurysms and dissections. Virtual MR intraarterial endoscopy is feasible using gadolinium-enhanced gradient echo MRI and a postprocessing algorithm to obtain aortic and renal artery images; the clinical usefulness of such a technique remains to be established. Combining gadolinium-enhanced MRA with 3D phase contrast MRA provides additional information than is possible with each technique separately. Both the aorta and renal arteries can be evaluated; the former results in images similar to a contrast arteriogram, while the latter is based on flow characteristics and is useful to identify vascular stenoses.

Similar to CT, either a test dose or an assumed time interval establish a delay between the start of contrast injection and initial image acquisition for optimal arterial enhancement. Another approach is to monitor a single voxel within the aorta and use an increase in signal within this voxel (corresponding to the arrival of injected gadolinium) to trigger MR angiography. Such automatic triggering improves arterial enhancement compared to manual triggering; venous enhancement is also less than with manual triggering. The advantages of such automatic triggering can be used two ways—either to obtain increased arterial enhancement or a similar enhancement to manual triggering but using a reduced contrast dose.

Magnetic resonance contrast agents are discussed in more detail in Chapter 7. Ultrasmall superparamagnetic iron oxide (SPIO) particles shorten both T1 and T2 relaxation times, have a blood half-life measured in hours, and thus are known as blood-pool MR contrast agents. Equilibrium-phase 3D MRA using SPIO readily evaluates abdominal and pelvic arteries, but venous overlap limits their use. They also depict the portal vein and its major branches. These small iron oxide particles pass through capillaries and are eventually cleared by lymph nodes.

Contrast enhanced 3D MR portography identifies the main portal vein and right and left intrahepatic portal veins with their main branches (2); MR portography also detects varices and portosystemic shunts. In a setting of liver tumors it can confuse vein occlusion with narrowing.

Magnetic resonance venography is also feasible. An electrocardiogram (ECG)-triggered

black-blood half-Fourier acquisition single-shot turbo spin echo (HASTE) sequence assesses the vena cava and major veins. Good quality pelvic and abdominal vein images are obtained by using a 2D fast low-angle shot (FLASH) time-of-flight technique without breath-hold but with arterial presaturation (3). Major venous obstructions, thrombi, and intravascular tumors can be detected. Contrast-enhanced 3D MRA is necessary for more detailed study.

Contrast enhanced MR lymphography, performed after interstitial or iv injection is theoretically feasible and undoubtedly will be performed in the future once appropriate contrast agents are available.

Scintigraphy

An estimate of portal blood shunting can be obtained with perrectal portal scintigraphy. A solution of technetium–99m (Tc-99m) pertechnetate is instilled into the rectum, and serial liver and heart scintigrams are obtained and a portal shunt index calculated. In a longitudinal study of patients with liver disease ranging from chronic hepatitis to cirrhosis and varices, the shunt index initially increased gradually as the patient's disease progressed to cirrhosis and then increased rapidly as varices developed (4). The clinical role of this test is not clear.

Angiography

Systemic Circulation

Catheter-based DSA is an often-used gold standard when evaluating other imaging modalities. Although DSA is often supplanted in this role by CTA and MRA, conventional angiography continues to serve as a framework for angioplasty, stent placement, and various embolization techniques.

Compared to conventional DSA, 3D images obtained with subtraction angiography performed by rotating the x-ray tube during contrast injection (*digital rotational subtraction angiography*) tend to be superior in most patients (5).

Percutaneous arterial puncture and catheter manipulation should be performed with caution in patients with Behçet's disease. These patients have a higher than normal prevalence of aneurysms and are at increased risk of (pseudo)aneurysm formation and thrombophlebitis at a puncture site. If feasible, either CTA or MRA is a viable alternate study.

Diagnostic renal angiography and percutaneous renal intervention procedures using carbon dioxide are options in patients with renal insufficiency.

Although gadolinium contrast has been occasionally used for angiographic studies and CT imaging in patients with renal insufficiency or prior severe reaction to an iodinated agent (6), one should keep in mind that the pharmacokinetic properties of Gd-DTPA, with only one gadolinium ion, are similar to iodinated agents containing 3 to 6 iodine atoms. Toxicity of gadolinium agents, at doses achieving equivalent x-ray stopping power, is greater than with nonionic iodinated agents (7). This is in distinction to the use of approved lower gadolinium MR doses, which are insufficient for useful x-ray contrast, but which have negligible nephrotoxicity (8). The European Society of Urogenital Radiology position is that gadolinium-based contrast agents are more nephrotoxic than iodinated contrast agents in equivalent x-ray attenuation doses (9) and their use for angiography and CT is not recommended.

Gelatin sponge is often used as an embolic material. Being inherently radiolucent, contrast agents are often mixed with it if visualization is desired. Some investigators find Lipiodol more useful than a water-soluble contrast material.

Portal System

Direct portography is performed either by injecting an intrahepatic portal vein branch or via splenic pulp injection (splenoportography). A transjugular approach through an intrahepatic portosystem shunt is an option in select patients. Indirect portography is an arteriographic procedure consisting of contrast injection into either the superior mesenteric or splenic arteries.

Direct transhepatic portography is useful to evaluate and treat some portosystemic collateral pathways in patients with portal hypertension; although this technique has been supplanted by newer procedures, in selected patients it pro-

vides excellent opacification of the portal vein and its branches. Selective superior mesenteric vein catheterization permits dynamic portal venous blood flow studies. Direct splenoportography enjoyed its golden age in the early 1970s, being supplanted initially by other angiographic procedures and then by CT arterial portography. It is currently little used, although an occasional investigator rediscovers it as a "new procedure." Computed tomographic portography performed by direct intrasplenic contrast injection using a needle-catheter assembly is a simple procedure having a role in an occasional patient when other access to the portal vein is impractical. Direct splenoportography using carbon dioxide through a small needle fills a useful but rather select niche (10).

Hepatic venography is performed by selective hepatic vein catheterization. If needed, a balloon occludes hepatic vein outflow, thus permitting contrast opacification of hepatic parenchyma, an aid in detecting intrahepatic venous collaterals.

Wedge hepatic venography using carbon dioxide is little used but at times is an adjunct to study the portal venous system. Carbon dioxide hepatic venography can visualize the portal vein in most patients and splenic and superior mesenteric veins in over half of patients.

Congenital Abnormalities

Aorta

Isolated congenital abdominal aortic abnormalities are uncommon; most are associated with other anomalies and are discussed in Chapter 14 under the heading Heterotaxy Syndrome.

Congenital abdominal aortic coarctation is uncommon. Symptoms in these patients range from hypertension, to intermittent claudication, and abdominal pain. A patient with Alagille's syndrome and abdominal aortic coarctation also had an aberrant splanchnic blood supply (11).

Vena Cava

Most inferior vena caval abnormalities occur inferior to the renal veins. The absence of the infrarenal portion is rare; more often, mention of an absent vena cava describes azygous continuation of a patent infrarenal segment, with hepatic veins draining directly into the right atrium. Such azygos inferior vena cava continuation is associated with cardiac and situs anomalies. In these patients the renal artery is located ventral to the azygos vein, a finding detectable by abdominal US. Azygous continuation of the vena cava is common in patients with polysplenia. Occasionally, indirect azygous continuation is associated with an inferior vena caval aneurysm. Hemiazygous continuation is rare.

Agenesis of other inferior vena cava segments is rare. One patient with agenesis of the hepatic segment had the infrahepatic vena cava draining into the portal vein and hepatic veins draining into a suprahepatic inferior vena cava (12). Hypoplasia of the inferior vena cava is also rare; these patients tend to have an extensive collateral circulation.

In inferior vena caval transposition a single vein ascends on the left, crosses the midline at the renal vein level, and continues its ascent to the right atrium. A duplicated left vena cava is rare; when present, the two vena cavae join at the renal vein level. A left vena cava can be differentiated from a dilated gonadal vein by tracing its cranial and caudal extensions. As expected, thrombophlebitis of a left vena cava is difficult to detect; CT and MR tend to suggest adenopathy, and aspiration biopsy or surgical exploration are often performed.

Arteries

An independent hepatic and splenic artery origin from the abdominal aorta occurs in approximately 1% of the population, an anomaly detected with contrast-enhanced CT and angiography. A common origin of the celiac, superior mesenteric, and inferior mesenteric arteries is very rare (13). A middle mesenteric artery, originating from the aorta, also a rare anomaly, usually supplies the right and transverse portions of the colon.

A hepatic artery identified by US in the portacaval space is often believed to have a superior mesenteric artery origin, yet one originating from the celiac artery can also be detected in this space.

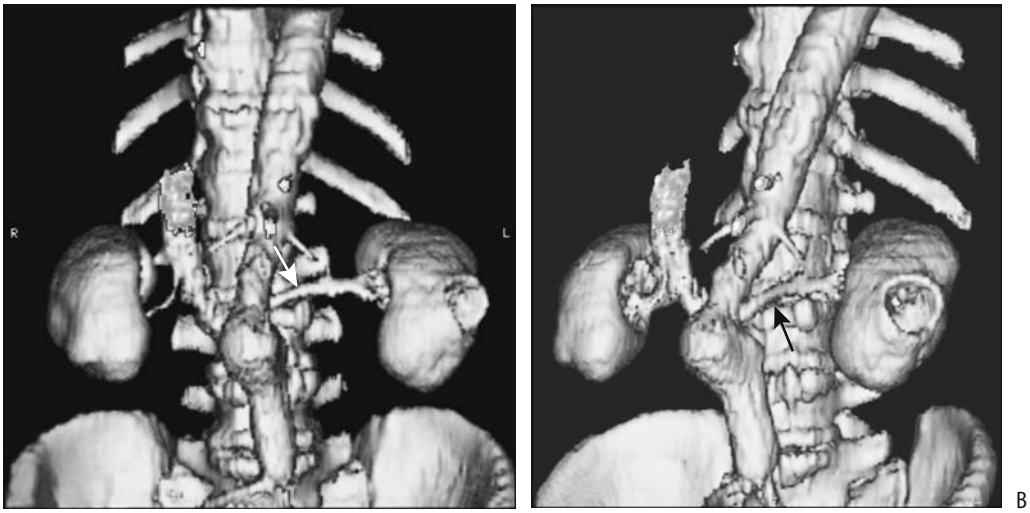

Figure 17.2. Retroaortic left renal vein. Frontal (A) and oblique (B) 3D CT reconstructions reveal the left renal vein (arrows) posterior to a tortuous aorta. (Courtesy of Patrick Fultz, M.D., University of Rochester.)

Veins

Systemic Veins

A retroaortic left renal vein, located either at the same level as a normal renal vein or more caudally, occurs in about 5% of the population (Fig. 17.2). Circumaortic left renal veins consist of a true vascular ring and also occur roughly in about 5%, findings detected with contrast enhanced CT. Gadolinium enhanced 3D MRA detects a retroaortic and circumaortic left renal veins with roughly the same frequency.

An abdominal aortic aneurysm can compress a retroaortic left renal vein and result in renal vascular congestion and induce hematuria (14). Although at times called a *nutcracker* phenomenon, this term is best avoided to prevent confusion with other similarly named conditions.

Portal Venous System

Congenital portal venous absence is rare; most occur in females and tend to be associated with liver tumors and other congenital abnormalities (Fig. 17.3). With an absent portal vein, intestinal

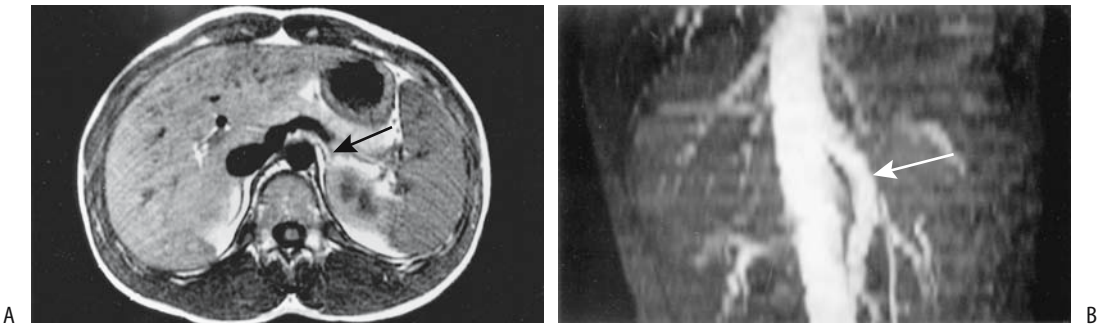

Figure 17.3. Congenital absence of portal vein in an 11-year-old boy. A: Transverse magnetic resonance (MR) imaging shows the splenic vein (arrows) joining the superior mesenteric vein and emptying into the inferior vena cava. B: An MR angiogram identifies the superior mesenteric vein (arrow) draining into inferior vena cava. (*Source:* Kohda E, Saeki M, Nakano M, et al. Congenital absence of the portal vein in a boy. Pediatric Radiology 1999;29:235–237, with permission from Springer-Verlag.)

and splenic venous blood bypasses the liver and drains directly into systemic veins. Some of these patients develop hepatofugal drainage of a large inferior mesenteric vein into systemic veins.

Congenital portal vein duplication or an accessory portal vein is also rare. Some of these mimic a liver hilar tumor. At times direct portography shows an accessory smaller vein located parallel to the main portal vein and draining into the right liver lobe; some of these accessory portal veins drain the coronary veins, thus modifying results obtained after a transjugular intrahepatic portosystemic shunt (TIPS) and preventing coronary vein embolization.

A portal vein located cranial to the gallbladder bed and feeding the right anterior segment is associated with rightward deviation of the ligamentum teres. A portal vein located anterior to the duodenum (and thus prepancreatic in location) is associated with malrotation and polysplenia. Computed tomography and magnetic resonance imaging (MRI) reveal a vascular structure anterior to the head of the pancreas.

Aberrant gastric venous drainage is common and accounts for some of the unusual liver enhancement patterns detected. Veins of Retzius are intestinal veins draining directly into vena cava or its branches—usually the gonadal or renal veins—rather than into portal vein branches. Whether they represent a normal variant or should be considered congenital anomalies is conjecture. These veins can be identified if searched for, including with CT arterial portography.

Ultrasonography can detect portocaval anastomoses in infants; these vessels probably represent continued ductus venosus patency.

Normally the superior mesenteric vein lies to the right and anterior to the superior mesenteric artery. A reversed position of these two vessels suggests but is not pathognomonic of midgut malrotation.

An aberrant right gastric vein supplies segment 4 of the liver and is a cause of a pseudolesion during contrast-enhanced CT or CT portography. An aberrant left gastric vein is less common and is identified on postcontrast CT along the hepatogastric ligament. These veins provide a partial collateral pathway for the portal system.

Trauma

Abdominal aortic injury is considerably less common than to the thoracic aorta. Nevertheless, abdominal aortic and inferior vena caval injuries are associated with a high morbidity and mortality. Unchecked bleeding, shock, and injury superior to the renal vessels all play a role in increased mortality.

On rare occasions intravascular gas is detected after trauma; portal venous gas, hepatic venous gas, and inferior vena cava gas in five patients cleared on follow-up studies and no cause was determined (15).

Aortic Injury

Thoracic aortic injuries are not discussed in this book, but mention should be made of delayed aortoesophageal fistulas developing after swallowing sharp objects or after gunshot wounds.

Abdominal aortic injury should be suspected with lumbar spine transverse process fractures. Handlebar injuries to the duodenum are well known to trauma physicians. Less well known is aortic injury due to a similar mechanism. Fatal delayed abdominal aortic ruptures have occurred after handlebar injury.

In the United States, contrast-enhanced CT is the current imaging modality used to evaluate suspected aortic trauma. A periaortic hematoma detected near the diaphragm level is an insensitive but specific sign of aortic injury (16).

Blunt abdominal aortic injury carries a high morbidity and mortality. Some traumatic inframesenteric abdominal aortic dissections can be successfully treated with implanted stents. In general, surgical repair is preferred for an unstable patient or those with threatened extremities, but angiographic endovascular stent placement appears to be an option in a stable patient with viable limbs.

Arterial Trauma

An arterial (pseudo)aneurysm is a known complication of trauma in both children and adults. The hepatic artery is a common location for these aneurysms, although any artery, even the inferior epigastric artery, can be involved. These aneurysms tend to remain silent until manifest-

ing by bleeding, often weeks or, rarely, even years later. Most such delayed bleeding is into the gastrointestinal tract, with an occasional one to respiratory or urinary tracts. At times bleeding is massive, stops spontaneously, but invariably recurs later.

Less common are posttraumatic arteriovenous fistulas; most are due to penetrating injury. Although CT is often useful in suggesting the diagnosis, arteriography is generally necessary to define the location and extent of these fistulas.

Many detected aneurysms are treated successfully by transcatheter embolization. An unresolved question is whether such embolization is indeed advantageous to the patient or whether conservative management achieves a similar end, especially with smaller, uncomplicated aneurysms. In patients with arterial injuries managed nonoperatively, follow-up arteriography reveals that some injuries heal spontaneously, some improve with residual deformity and others worsen; the dilemma is that pretherapy imaging is not accurate enough in selecting those who are expected to improve and those who progress.

Venous Trauma

Trauma to the inferior vena cava consists of contusion, laceration, transection, and, rarely, dissection. In particular, injury to the retrohepatic portion of the vena cava is associated with a poor prognosis.

Peritoneal lavage readily misses inferior vena cava injuries. Typically CT shows a hematoma surrounding the vena cava. Some hematomas are associated with an intraluminal thrombus. At times CT in patients with traumatic inferior vena cava rupture identifies contrast extravasation. Computed tomography detection of a collapsed inferior vena cava during a trauma study suggests hypovolemia.

Trauma is a rare cause of Budd-Chiari syndrome. Presumably bleeding and extrinsic compression of the intrahepatic inferior vena cava by a hematoma obstruct the hepatic veins or intrahepatic portion of the inferior vena cava, findings detectable by CT. Ascites is common and should be differentiated from intraperitoneal bile or blood, which suggest other etiologies for intraperitoneal fluid. An occasional patient develops traumatic Budd-Chiari syndrome secondary to inferior vena cava thrombosis. On the other hand, with hepatic vein rupture generally not enough time elapses for Budd-Chiari syndrome to develop.

Bleeding

Active hemorrhage in a trauma setting is recognized as contrast extravasation during contrast-enhanced CT. Rapid infusion of a relatively large contrast bolus aids in detecting a site of arterial extravasation, less so with venous bleeding. Multislice CT appears to be superior to more conventional CT in detecting more subtle bleeds. Even if active extravasation is not detected, a high-density region, having a Hounsfield density close to that of adjacent arteries and surrounded by lower density clot, should suggest recent extravasation. These are often subtle findings requiring expertise in interpretation.

Occasionally Tc-99m–red blood cell scintigraphy locates a bleeding site; the radiotracer accumulates in one particular region, with no change in location during the study.

The appearance of a pseudoaneurysm is similar to that of arterial bleeding (Fig. 17.4). Some authors consider bleeding to represent a

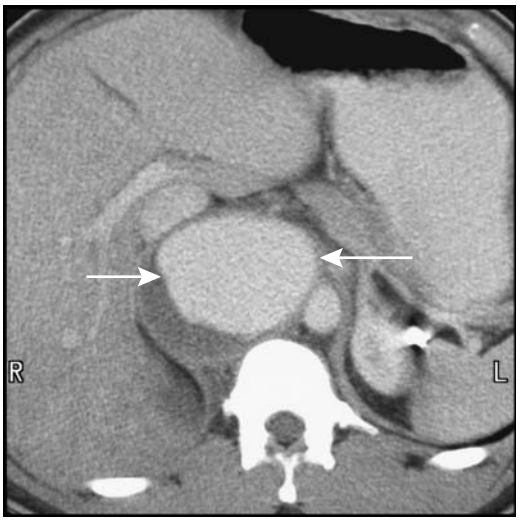

Figure 17.4. Traumatic pseudoaneurysm secondary to gunshot wound. Computed tomography identifies the aneurysm (arrows) between the aorta and inferior vena cava. (Courtesy of Patrick Fultz, M.D., University of Rochester.)

pseudoaneurysm if it is contained, but this distinction is rather subtle. In either case, a pseudoaneurysm should be isodense to its connecting vessel and, being contained, should be sharply marginated.

Aorta

Atherosclerosis/Stenosis

For unknown reasons, smokers and patients with chronic pancreatitis have a higher prevalence of aortic calcifications than controls. Alagille syndrome includes arteriohepatic dysplasia; occasionally aortic calcifications develop even in teenagers with this syndrome.

High-resolution T2-weighted MRI aids in detecting and classifying atherosclerotic plaques (17).

Abdominal aortic stenosis is occasionally discovered in children. A majority of these consist of congenital malformations and a minority of inflammatory aortitis; associated renal and visceral artery involvement is common, together with arterial hypertension. Some stenoses in young adults are isolated, with the aortic bifurcation being a common site; some of these stenoses calcify, even in young patients. Atherosclerotic aortic stenoses are quite common in the elderly, although clinically they are often overshadowed by stenoses at the origin of great vessels.

MRA is useful in detecting and evaluating aortic stenoses.

Isolated stenoses are amenable to surgical correction. More common is diffuse involvement of the aorta, iliac arteries and distal vessels. Percutaneous transluminal balloon angioplasty and, if needed, intraluminal stent placement are the interventional modalities used to treat aortic stenosis. Although generally performed under angiographic guidance, intravascular US guidance is also feasible. Angiography alone probably underestimates vessel diameter in almost two-thirds of patients; incomplete stent deployment is also more readily identified by intravascular US than by angiography.

Aortic stent placement is feasible in patients with failure of percutaneous transluminal angioplasty or presence of ulcers, which increases risk of embolization with angioplasty. In general, similar long-term restenosis rates are found for transluminal angioplasty and stent placement (18); a small aortic diameter is a predictive factor for restenosis.

Follow-up after percutaneous transluminal angioplasty of patients with infrarenal atherosclerotic aortic stenosis shows a clinical patency rate similar to open surgery.

Aneurysm

Atherosclerotic Aneurysm

Most abdominal aortic aneurysms are atherosclerotic in origin. An occasional mycotic one is encountered.

Screening for an abdominal aortic aneurysm is not widely practiced even in hypertensive patients. An abdominal aortic aneurysm in these patients is associated with claudication, and these patients appear to benefit from screening US. An occasional aortic aneurysm is associated with a coagulopathy, which often clears after aneurysm repair.

From a potential therapeutic perspective, an abdominal aortic aneurysm's size and location are of obvious importance. One classification is into infrarenal, juxtarenal, and pararenal aneurysms. Most common are infrarenal ones, fusiform in shape. Pararenal aneurysms extend distal to the superior mesenteric artery and involve the renal arteries.

The role of imaging is to establish that an aortic aneurysm is indeed present, provide information about its size and shape, detect complications, and outline the preoperative anatomy.

Aneurysms vary in size considerably. Measurement of aneurysm dimensions before endovascular therapy is of obvious importance, yet DSA measurements of an aneurysm's diameter and length are inaccurate by up to 15% (19); an indwelling catheter is the only available reference standard. Computed tomography, US, or MRA provides more reliable aneurysm dimensions.

Calcifications develop in long-standing aneurysms, but aortic calcifications do not imply that an aneurysm is present. An occasional aneurysm is suggested from a conventional abdominal radiograph, but this study is rarely employed when suspecting an aneurysm. In particular, measurement of a suspected

aneurysm's diameter is notoriously inaccurate on conventional radiographs, but if such a measurement is necessary, a lateral projection rather than a frontal one should be chosen.

Computed tomography angiography is the current preoperative imaging study of choice. Numerous studies confirm accuracy of CT in measuring an aneurysm's diameter. Multidetector CT in patients evaluated for aortoiliac aneurysms, performed with a 25-second delay after the start of IV contrast injection resulted in aortic enhancement of >200 Hounsfield units (HU) and no superimposed venous filling (20). A 3D shaded surface display is helpful in viewing aneurysms, with image rotation providing multidirectional images. In differentiating among suprarenal, juxtarenal, and infrarenal aneurysms, the use of narrrow collimation and overlapping axial reconstructions aids in correctly classifying most aneurysms and identifies main and accessory renal arteries.

Ultrasonography should identify an aortic aneurysm, outline its shape, and measure its width and rough length in most patients and is often the first screening examination obtained in a patient with a pulsatile abdominal mass. Involvement of other vessels is difficult to evaluate. Obesity and bowel gas limit the information obtained. Doppler US does provide additional information but is generally superfluous if subsequent angiography (CT or other) is obtained.

Magnetic resonance imaging and MRA are evolving into primary imaging modalities for preoperative aneurysm study, at times providing information superior to CT. Potentially 3D MRA can provide definitive pretherapy studies and replace both CT and DSA. Some studies achieve almost perfect agreement between conventional angiography and MRA interpretations of aortic disease. Conventional angiography is often considered the gold standard in aneurysm evaluation primarily because many surgeons are comfortable with its results and rely on its information. Nevertheless, the use of angiography is declining for this indication and is gradually being relegated to those situations where CT and MR are inconclusive.

Magnetic resonance imaging can identify an aneurysm's size and shape. Transverse images tend to provide more information about the distal aorta and iliac vessels compared to coronal images, but sagittal images are helpful in identifying major vessel origins. Gadolinium-enhanced MRA achieves high sensitivity and specificity in determining whether the renal arteries and iliac arteries are involved by an aneurysm; also, gadolinium aids in differentiating between slow blood flow and a mural thrombus. A 3D gadolinium-enhanced MRA technique identifies an aneurysm and aids in establishing its relationship to renal and other major arteries. Stenosis of major vessels is also detected and atherosclerotic plaques and thrombi are evaluated.

One inherent limitation of MRI is its inability to visualize calcifications. Also, multiple sequences are generally necessary. Thus although arterial-phase MRA visualizes a patent aortic lumen, it does not outline the aortic wall or identify thrombi; for the latter axial imaging is necessary.

Inflammatory Aneurysm

An inflammatory abdominal aortic aneurysm is characterized by marked thickening and inflammation in the aneurysm wall. The etiology is unknown, although an immune response appears to be involved in some patients.

Many inflammatory aneurysms are associated with extensive surrounding extraperitoneal fibrosis. At times the ureters become encased and obstruct. The duodenum or inferior vena cava can also be entrapped. The inflammation often subsides after aneurysm repair and ureteric obstruction is relieved. Computed tomography performed several years after inflammatory aortic aneurysm repair reveals no or little persisting inflammatory tissue in most patients.

A MR study of an inflammatory aortic aneurysm reveals a complex, concentric, layered outline; homogeneous enhancement postcontrast distinguishes this condition from the more common atheromatous intima.

Dissecting Aneurysm

Most dissecting aortic aneurysms are thoracic in origin and dissect into the abdomen. These aneurysms are generally subdivided into those involving the ascending aorta and those originating distal to the great vessels. A dissection is diagnosed by detecting both true and false lumens and identifying an intimal flap. Most

false aneurysms are saccular in outline and communicate with the aortic lumen. Some false lumens spiral around the aortic circumference; in these, dissection the inner lumen is invariably the true lumen (21).

Aortography was the traditional gold standard in detecting a dissection, identifying an intimal flap, and establishing an entry site and possible exit site. Postcontrast CT and lately MRI are evolving as noninvasive alternatives to aortography in suggesting the extent and length of a dissection (Fig. 17.5). A helical CT study evaluating various protocols concluded that an optimal CT study consists of two separate but adjacent scans—3-mm collimation for the aortic arch and 5-mm collimation for remaining aorta (22); such a study achieved almost a 100% sensitivity and specificity for detecting a dissection and identifying entry and exit sites.

Some acute dissecting aneurysms have an eccentric hyperdense aortic wall on precontrast CT. A hyperdense wall is also found in some intramural hematomas and nondissecting

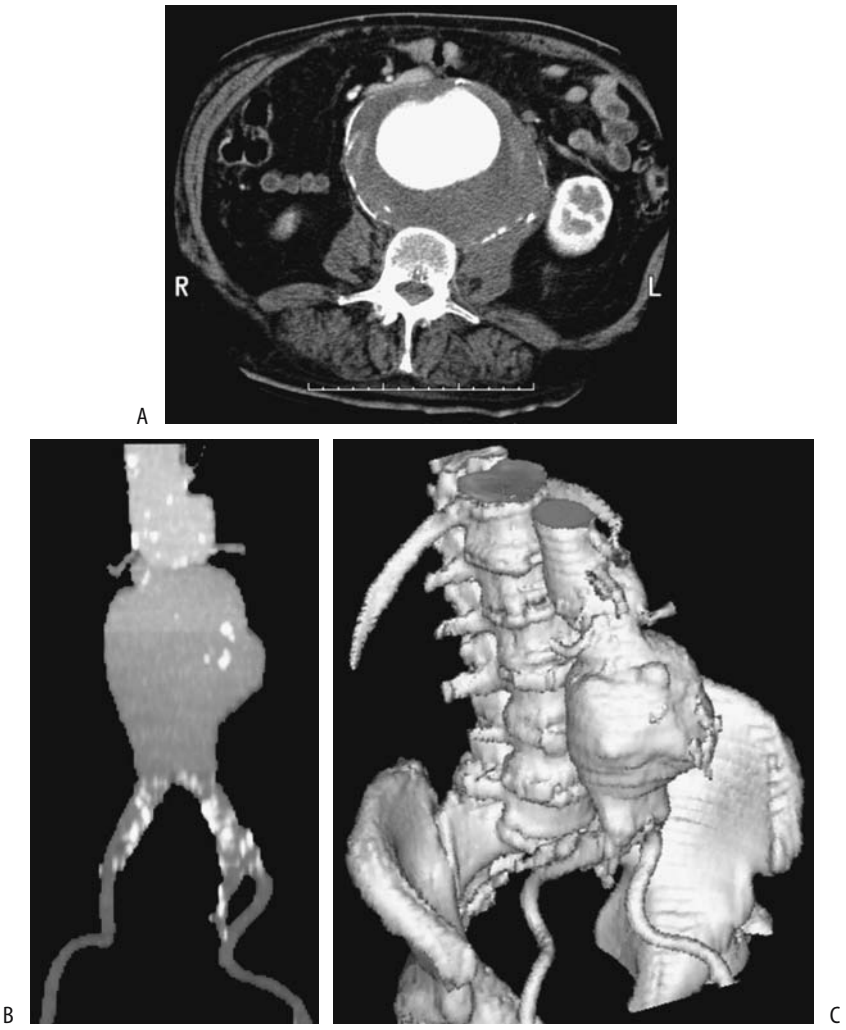

Figure 17.5. Dissecting abdominal aortic aneurysm. Transverse (A), coronal (B), and 3D (C) CT reconstructions each provide slightly different information about the shape and scope of this aneurysm. (Courtesy of Patrick Fultz, M.D., University of Rochester.)

aneurysms, but with the latter the hyperdensity is circumferential rather than eccentric.

Contrast-enhanced CT in a minority of patients with a dissecting aneurysm reveals linear hypodense structures in the false lumen; these fibroelastic bands, described as aortic *cobwebs*, extend from the intimal flap and represent portions of aortic wall incompletely sheared during dissection. These *cobwebs* identify the false lumen and distinguish it from the true lumen.

Ultrasonography identifies most true and false lumens, separated by an intimal flap. Some false-positive Doppler imaging results are probably due to a heavily calcified aorta acting as a strong acoustic reflector, resulting in mirror image artifacts. At times a crescent-shaped hypoechoic zone between a thrombus and aortic wall suggests dissection, but Doppler US does not detect any flow in this region, a condition called *pseudodissection*.

Intravascular US also differentiates the true from the false lumen. It identifies an acute angle between the dissecting flap and false lumen outer wall, and differentiates the three-layered true lumen wall from single-layered false lumen wall. Intravascular US is also useful to differentiate causes of branch vessel compromise—whether a dissection intersects a branch vessel origin or whether a vessel origin was spared but a dissection flap simply compresses the true lumen and covers its origin.

Magnetic resonance detects an intimal flap and identifies both true and false lumens. Flowing blood results in a signal void in both lumens with a SE technique, a finding modified by slow flow or a thrombus. As an aneurysm diameter increases, the false-to-true lumen cross-sectional area ratio also increases, but peak average velocity in the true lumen decreases, findings obtained from MR phase-contrast images. T1-weighted SGE images reveal slow flow in either a true or false lumen as high signal intensity, although, in general, postcontrast 2D or 3D techniques better identify both lumens and an intimal flap, and differentiate slow flow from a thrombus. Contrast-enhanced MR establishes flow patterns in a dissection, including flow in major vessels, and is useful if iodine-based contrast agents are contraindicated. Yet exceptions do occur; in an occasional patient aortic wall thickening is the only sign of dissection on T1-weighted MRI.

The diagnosis is difficult with a thrombosed false lumen; the appearance is similar to that of an eccentric mural thrombus. An intimal flap is not detected with a thrombosed false lumen. Inward displacement of intimal calcifications suggests dissection, but this appearance is mimicked by calcifications within a thrombus and an intramural hematoma. A thrombosed false lumen does not enhance with contrast during an early phase; for reasons unknown, occasionally a false lumen enhances on late-phase images.

Intramural Ulcer/Hematoma

A penetrating atherosclerotic ulcer-like defect is detected in some patients with extensive atherosclerosis, an entity probably distinct from a dissecting aneurysm. The spectrum of findings ranges from an asymptomatic ulcer penetrating through lamina elastica and forming an intramural hematoma, to intramural dissection, aneurysm formation, and even aortic rupture. The evidence suggests that a hematoma, caused by bleeding from vasa vasorum, is the inciting event in this condition, weakening the aortic wall sufficiently to lead to a dissection.

Follow-up CT of some of these ulcer-intramural hematomas reveals the hematoma regressing in size with time (23); some of these patients, however, have ulcer-like cavities that tend to evolve into saccular aneurysms. In others, an intramural hematoma without a patent false lumen is associated with intramural dissection; nonenhanced CT of these focal hematomas often shows a hyperdense rim. A typical appearance is a focal outpouching in a region involved by atherosclerosis and surrounded by a thickened, hyperdense aortic wall that does not enhance with contrast. Aortic intramural hematomas probably need to be followed with imaging.

Transesophageal US identifies an intramural hematoma as a homogeneous aortic wall thickening with intraluminal displacement of intimal calcification.

Hematomas appear hyperintense on T1- and T2-weighted MR images.

Mycotic Aneurysm

An abdominal aneurysm in a patient with fever, abdominal or back pain, and leukocytosis sug-

gests a mycotic etiology, a life-threatening condition. Aneurysm wall tissue and blood often yield positive blood cultures for the involved organism. Complicating matters in the elderly, some atherosclerotic aneurysms become infected. These aneurysms tend to change size faster than atherosclerotic aneurysms.

Less common organisms encountered include *Salmonella enteritides* and other *Salmonella* species, *Yersinia enterocolitica*, and even a hydatid origin. Syphilitic aneurysms are mostly of historical interest. Rare reports describe *Mycobacterium bovis* infected aortic aneurysms after intravesical bacillus Calmette-Guérin therapy for bladder cancer, even to the point of aneurysm rupture. Some aneurysms develop from an adjacent spinal abscess.

Most of these aneurysms are saccular. Early-stage CT findings consist of a hazy aortic wall outline, evolving into a periaortic infiltrate and paraaortic fluid. The false lumen is often thrombosed. An increase in surrounding fat density can suggest the diagnosis, although similar findings are seen with other causes of extraperitoneal fibrosis or hemorrhage. Aortic wall gas is only an occasional finding.

Complications

Rupture

The sudden onset of severe pain is the hallmark of a ruptured abdominal aortic aneurysm. The risk of rupture is directly related to aneurysm size. Rupture continues to be associated with high morbidity and mortality. It is fatal without surgical repair and is considered a surgical emergency. Rupture is unpredictable and can occur during a radiologic examination. Patients with a leaking aneurysm are often hypotensive and hemodynamically unstable. A ruptured aortic aneurysm occasionally occludes the inferior vena cava. A chronic ruptured but contained abdominal aortic aneurysm can result in extensive anterior lumbar spine erosions, findings readily detected with imaging.

A hemodynamically stable patient suspected of harboring a ruptured abdominal aortic aneurysm usually undergoes a CT study. The aneurysm is recognized and the extraperitoneal hemorrhage identified as isodense or hyperdense regions. Less often detected is an actual aortic wall defect. Extravasation of contrast signifies active bleeding.

The CT *crescent sign*, consisting of a hyperdense curvilinear structure within a mural thrombus or aneurysm wall, is found in larger aortic aneurysms and often signifies an aneurysm at risk of rupture or one already ruptured. This sign appears to be caused by hemorrhage within a thrombus or in the aneurysmal wall. It is more common in ruptured aneurysms, and if detected in an unruptured aneurysm, suggests impending rupture. A periluminal halo, on the other hand, consisting of a hypodense internal structure within a thrombus around the lumen, is found in roughly 10% of both nonruptured and ruptured aneurysms and does not have a connotation similar to that of the crescent sign.

In a Dutch study of consecutive patients admitted with a ruptured abdominal aortic aneurysm, an US diagnosis was consistent with rupture in only 51% (24).

A Tc-99m–red blood cell study will occasionally suggest rupture of an aortic aneurysm.

Fistula

Vascular fistulas in general are discussed later (see Vascular Fistulas).

A rare ruptured atherosclerotic aortic aneurysm results in an aortocaval fistula. Surprisingly, some of these patients are relatively asymptomatic. These fistulas can be detected by CT. Early caval contrast enhancement is diagnostic. Multislice CT with overlapping slices improves anatomic depiction of these fistulas.

An aortoduodenal fistula and resultant massive gastrointestinal hemorrhage is a recognized complication after aortic aneurysm repair but is quite rare in the absence of prior surgery. An occasional small aneurysm communicates with a cavity and adjacent duodenum (25); the diagnosis can be suggested by CT.

Mural Thrombus

Mural thrombi are common in an aortic aneurysm. These thrombi tend to be soft and loosely attached to the aortic wall; as a result, they are a source of distal emboli. These thrombi do not strengthen the wall of an aneurysm. In time, calcifications develop within a thrombus.

Mural thrombi can be evaluated and characterized by MRI. Thrombi range from hyperintense signal on T1- and T2-weighted images for an unorganized thrombus, an inhomogeneous signal intensity for a partially organized thrombus, and hypointense signal on both T1- and T2-weighted images for an organized thrombus.

A mural thrombus can be suspected with radionuclide aortic angiography. A photon-deficient region along the aneurysm wall corresponds to a mural thrombus.

Therapy

Surgical

Indications for surgical repair of an abdominal aortic aneurysm vary somewhat among surgeons. Because of the risk of rupture in aneurysms >5 cm in diameter, one recommendation is to consider elective surgery in fit patients with an aneurysm >4.5 cm in diameter. Other indications include significant occlusive disease requiring repair, pain, or a suspected mycotic etiology.

An open, elective aortic abdominal aneurysm repair carries a mortality of about 2% to 4%, which is in contrasts to a mortality of about 80% for emergent repair of a ruptured aneurysm.

Endovascular

The introduction of endoprostheses has markedly changed aortic aneurysm surgery. Instead of an abdominal incision, vessel clamping, and associated major blood loss, the procedure is performed via a femoral artery approach. Instead of direct aneurysm inspection, oversawing of feeding vessels and surgical repair, both initial planning and repair are performed under imaging control. Preoperative CT, often with 3D reconstruction, is used for aneurysm evaluation and to select an appropriate prosthesis, although 3D MRA is assuming an increasing role in preoperative management of these patients. At times arteriography is helpful. C-arm fluoroscopic guidance is used for prosthesis insertion to bridge the aneurysm. If needed, a bifurcation graft or an aorto-uni-iliac graft is inserted. Such percutaneously inserted and deployed grafts have had a variable success rate. Long-term success rates are not available and the borderline between surgical correction and percutaneous stent therapy is poorly defined. Patients with a long life expectancy and low surgical risk continue to undergo surgical repair. Also, infected aneurysms remain in the surgeon's domain.

Endovascular aneurysm repair performed using stent-grafts in patients considered too high risk for conventional repair resulted in complete aneurysm exclusion (based on CT criteria) in 88% (26). Deployment and complete aneurysm exclusion with covered stents is more successful with tube grafts than with bifurcation grafts. Surgical correction is necessary for migrating grafts. Nevertheless, a number of authors have commented that their morbidity rates compare favorably with those of open surgery in these high-risk patients.

A limitation of a transfemoral approach is that the iliac arteries must be accessible and relatively free of major atheromatous disease. A major reason for failure of stent-graft insertion is excessive iliac artery tortuosity or arteriosclerosis, with rates of failure dependent on patient selection factors and operator experience.

Covered stent-grafts have been successfully inserted in patients with aortic aneurysms close to renal artery orifices, with the proximal uncovered stent portion placed across one or both renal artery orifices. Stent-grafts have been deployed across saccular aneurysms.

Complications after initial stent-graft insertion are common, and secondary intervention is often necessary. The significance of leakage outside the graft is not clear.

Postoperative Findings

Postoperative imaging appearances differ after various surgical repairs and after percutaneous endoprosthesis insertion. Some of the complications encountered also differ. Knowledge of specific therapeutic technique used is necessary for postoperative imaging evaluation.

Delayed aneurysm rupture after endovascular repair is rare.

Normal Imaging

Serial postoperative contrast-enhanced CT or MR identifies most major complications after surgical repair, including bleeding, false aneurysm formation, vessel occlusion, and most

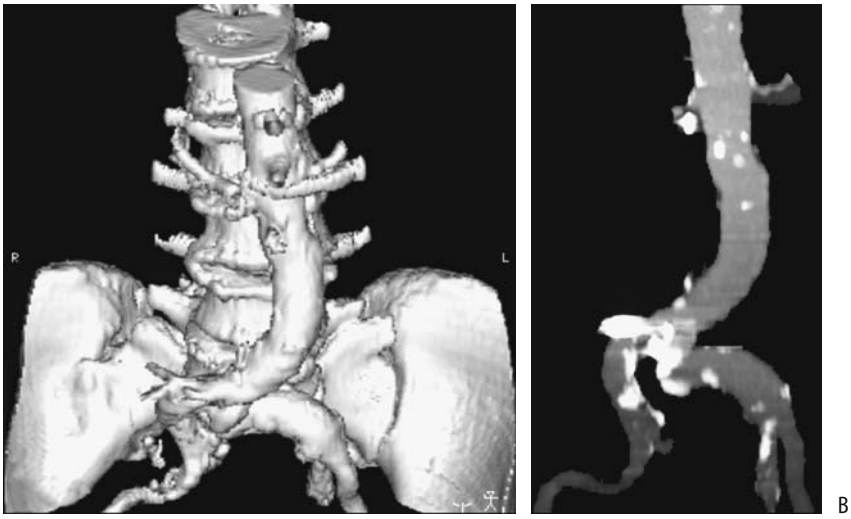

Figure 17.6. Abdominal aortic aneurysm repair. A 3D reconstruction (A) and maximum intensity projection (MIP) reconstruction (B) identify relationship of aorta to adjacent structures. (Courtesy of David Waldman, M.D., University of Rochester.)

fistulas (Fig. 17.6). With an end-to-end anastomosis, the native aneurysm wall is wrapped around a graft. Postoperative fluid is common between a graft and native aorta and is detected with CT or MR. Perigraft fluid in some patients persists for several months. This fluid is gradually reabsorbed; increasing amounts of fluid with time suggest infection.

Postoperative surveillance includes measurement of residual aneurysm size. A measure of maximum residual aneurysm diameter using CT angiography is common, although aneurysm volume is probably more accurate. Magnetic resonance imaging is limited in the immediate postoperative period if metal components are present. Covered nickel titanium stent-grafts used for abdominal aortic aneurysm repair have been safely imaged by 1.5-T MRI, with no ferromagnetism or heating detected (27). In an *in vitro* contrast-MR study of nitinol, tantalum, stainless steel, and cobalt alloy stents, only the latter stent resulted in a signal void inside the lumen (28); MR of some of the stents produces an artificial diameter narrowing.

A CT scan 24 to 48 hours after graft placement should reveal any partial or complete thrombosis of the aneurysmal sac; initially patent channels tend to close subsequently, but can recur. A mottled appearance within the aneurysmal sac is not uncommon. Maximum intensity projections rendered from helical CT a week or so after aortic stent graft placement is useful to evaluate stent deformity or stent angulation; MIP also aids in detecting renal artery occlusion, leaks and thrombi. Computed tomography criteria of successful endovascular repair consist of a decrease or unchanged size aneurysmal sac without the presence of perigraft channels; the latter are often associated with subsequent aneurysm enlargement.

Eventual fibrosis surrounding the surgical site appears hypointense with both T1- and T2-weighted images.

Some evidence suggests that MRA is as sensitive as CTA in detecting endoleaks (29); it also avoids iodinated contrast agents Eventual fibrosis surrounding the surgical site appears hypointense both with T1- and T2-weighted images.

No firm guidelines are established for long-term follow-up of asymptomatic patients after endovascular repair. Pre- and postcontrast CT scans annually appear reasonable. Any symptoms or known complication require more frequent follow-up.

Bleeding/Leak

Precontrast CT is useful in detecting an acute postoperative hematoma; a recent bleed is slightly hyperdense to the surrounding struc-

tures. Postcontrast CT readily detects graft occlusion. A new false aneurysm enhances postcontrast, unless it is thrombosed.

Leakage adjacent to a prosthesis is considered a perigraft leak, while leakage along an aneurysm border is a retrograde leak. Leaks are uncommon in the thrombosed portion of an aneurysm; rather, continued patency of feeding vessels, such as the lumbar and inferior mesenteric arteries, the median sacral artery, and occasionally even the urethral and testicular arteries plays a role in the pathogenesis of leaks after stent-graft repair (30). Inferior mesenteric artery leaks are ventral to the prosthesis and lumbar or median sacral artery leaks are dorsolateral in location. For most leaks CT can thus establish its origin. Perigraft leak rates vary considerably and depend, in part, on the extent of the initial aneurysm. As the number of patent feeding vessels increases, the leak rate also increases, reaching 60% when more than six lumbar arteries are patent (31). A rare contained leak developing after aneurysectomy is sufficiently extensive to result in inferior vena cava compression.

Computed tomography angiography appears reliable in detecting perigraft leakage. The sensitivities and specificities for detecting leakage were 63% and 77% for conventional angiography and 92% and 90% for CTA, respectively (32). An occasional side-branch endoleak is not detected by CT but is identified by duplex US. Preliminary evidence suggests that contrast enhanced US also detects endoleaks after endovascular aneurysm repair, even detecting some missed by CTA (33).

Most leaks can be treated successfully with additional stent-grafts. Some leaks are amenable to coil embolization; embolization results in aneurysmal sac thrombosis. Others can be sealed off with balloon dilation at the end of stent insertion. Still others disappear spontaneously. At times rather creative embolization is helpful. Thus endoleaks due to retrograde flow in the inferior mesenteric artery have been treated by selective superior mesenteric artery catheterization and embolization through the middle colic artery (34).

Infection/Fistula

Fever, leukocytosis, and anemia suggest graft infection as a complication of an aortic aneurysm or aortic bypass surgery. While graft infection is not common, it is associated with a high morbidity and mortality. An extraperitoneal lymphocele can develop after aortic reconstruction. It can become infected.

Some of the initial work with CT detection of graft infection suggested a sensitivity and specificity approaching 100%, but later studies tempered such enthusiasm, and the current belief is that CT detects mostly advanced infections.

Gas adjacent to a graft is identified by CT shortly after surgery in many patients even without infection. Gas developing several weeks or longer after surgery, on the other hand, implies infection or an aortoenteric fistula. Thus in a patient with anemia or gastrointestinal bleeding of unknown cause (sentinel bleed) and a remote history of aortic aneurysm repair, the presence of soft tissue gas, no matter how little, is presumptive evidence of graft infection and often serves as a harbinger for a future major bleed. A CT finding of periprosthetic wrap thickening, an inhomogeneous appearance and thickening of adjacent bowel wall and valvulae conniventes are common with an infection but are nonspecific findings. Perigraft fluid can persist for several months after surgery, although fluid collections for longer periods of time suggest an infection. If necessary, image-guided fluid can be obtained for culture. Some infectious organisms are notoriously difficult to culture, and prolonged incubation is necessary.

Some infections progress to an aortoenteric fistula, with the third and fourth parts of the duodenum most often involved. Direct signs of an aortoenteric fistula are not common; these include either IV contrast extravasating into bowel lumen or orally administered contrast leaking into soft tissues surrounding a graft.

One of the limitations of MR is an inability to detect small amounts of gas in soft tissues. However, MR differentiates persistent inflammation and fluid in an abscess from a hematoma. Fluid appears hypo- to isointense on T1- and hyperintense on T2-weighted images, while a persistent hematoma is hyperintense with both sequences, although these findings vary, depending on age.

Indium-111–white blood cell (WBC) scintigraphy is useful as a primary test for suspected infections or as an adjunct to ambiguous CT

results. Gallium scanning, or more recently, Tc-99m–hexamethylpropyleneamine oxime (HMPAO)–labeled leukocytes appear to have a role in suggesting an infection but have had limited application. An occasional test is false positive; thus an occasional patient with a non-infected pseudoaneurysm will have uptake of Tc-99m-HMPAO–labeled leukocytes.

Primary percutaneous drainage appears reasonable in patients with aortic graft infection and a fluid collection, although some of these patients later require removal of their infected prosthetic grafts.

Other Findings

Postoperative pseudoaneurysms develop both with and without an underlying infection. Iliac artery tortuosity predisposes to iliac artery injury during percutaneous endoprosthesis insertion. An extreme complication of a pseudoaneurysm is blowout of an aortic stump.

In a setting of a pseudoaneurysm, aortography provides a roadmap for future repair, while CT is superior in evaluating surrounding infection.

Ureteric stenosis, periureteritis, and ureteric compression by a false aneurysm are some of the complications of aortic surgery (35); some of these complications manifest only years later. Endovascular repair can also result in a periaortitis and ureteral obstruction (36). At times a portion of a self-expanding stent covers a renal artery; evidence of renovascular compromise, however, is not common.

In a patient with postoperative hematuria the surgical graft coursed through the bladder (37); presumably an intravesical tunnel was created during the original graft insertion.

Aortitis

Nonspecific aortoarteritis, or Takayasu's arteritis, is a panarteritis of unknown etiology. Patient age at onset ranges from pediatrics to old age. In a collection of 31 patients with Takayasu's arteritis, 45% had aortic aneurysms (38); of note is that aortic wall thickening was detected on CT in several of these aneurysms, aneurysms increased rapidly in size, and ruptured during follow-up.

Patients with Takayasu's arteritis develop visceral artery stenoses. Although angioplasty and stent insertion usually have an immediate benefit, these patients suffer from a high rate of restenosis.

Thrombosis Leriche's Syndrome

Acute abdominal aortic thrombosis is not common. Rather than being acute, some of these thrombotic occlusions present with renal failure or congestive heart failure, and the diagnosis is suspected from renal scintigraphy.

A rare cause of aortic occlusion was intra-aortic growth of hydatid cysts (39); recurrent hydatid cysts developed after previous surgery for a paraspinal hydatid cyst.

Leriche originally described obstruction at the aortic bifurcation, but his name is now associated with symptoms due to infrarenal aortic obstruction. Varying degrees of claudication and impotence develop depending on the extent of atherosclerosis and collateral flow. Diminished femoral artery pulses are common.

Three-dimensional contrast-enhanced MRA using MIP and a rotated display in patients with Leriche's syndrome located the level of aortic occlusion as juxtarenal, infrarenal but cranial to inferior mesenteric artery, or caudal to the inferior mesenteric artery (40). Collateral pathways and concomitant renal artery stenoses can often be detected. Although in theory IV DSA provides similar information, increased contrast conspicuity and a 3D rotational display make MRA superior, visualizing even small collaterals. Whether MRA image quality is superior to that of intraarterial DSA is debatable, but the lack of catheter manipulation and arterial injection makes MRA a simpler study.

Inferior Vena Cava

Obstruction

Thrombosis

Most inferior vena caval thrombi originate in an adjacent vein and spread centrally. Thus a lower extremity venous thrombus can extend superiorly, or a renal malignancy, especially originating in the right kidney, not uncommonly invades and obstructs the inferior vena cava. Caval thrombosis is a complication of Crohn's disease, systemic lupus erythematosus, and

Behçet's syndrome. In these settings caval obstruction should be suspected if hepatosplenomegaly, ascites, and lower extremity dependent edema develop.

Imaging detects a thrombus as an intraluminal filling defect or simply as lack of caval filling with contrast (Fig. 17.7). A primary thrombus and a neoplastic thrombus have a similar imaging appearance and can be differentiated only if thrombus neovascularity or other evidence of a neoplasm is detected. Noncontrast CT reveals an acute thrombus to be isodense or slightly hyperdense to blood. With age, a thrombus gradually becomes hypodense. The involved vessel diameter tends to be expanded focally, regardless of etiology. Gas within a thrombus is rare and suggests infection. Calcifications develop in some chronic thrombi.

With incomplete obstruction, postcontrast CT identifies most thrombi as a hypodense tumor surrounded by contrast-opacified blood. A bland thrombus does not enhance postcontrast, while a tumor thrombus does. Complicating the issue is the occasional bland thrombus attached to a tumor thrombus. Still, caution is needed to differentiate a thrombus from incomplete mixing of opacified and nonopacified blood and a resultant transient artifact.

Collateral vessels are common with obstruction of the inferior vena cava. Lower extremity radionuclide venography reveals collateral flow; an occasional patient has diffuse hepatic uptake of the radionuclide. With superior vena caval obstruction, the azygos vein, hemiazygos vein, internal mammary veins, vertebral venous plexus, and lateral thoracic and some superficial thoracoabdominal veins enlarge and become collateral vessels. Because of these collaterals, after contrast injection into an upper extremity CT can reveal enhancement of a liver segment or the inferior vena cava. Early and dense contrast enhancement of liver segment IV occurs due to segmental liver perfusion from epigastric and paraumbilical veins; such a pseudolesion in segment IV is a potential pitfall seen occasionally during both arterial portography and helical CT.

Magnetic resonance readily detects a caval thrombus. With SE sequences the vena cava contains a tumor rather than a signal void as seen with flowing blood. Slow-flowing blood, however, also results in loss of the caval signal void. With GRE sequences flowing blood appears hyperintense, and this technique appears more reliable in detecting a thrombus than a SE technique. In some patients incom-

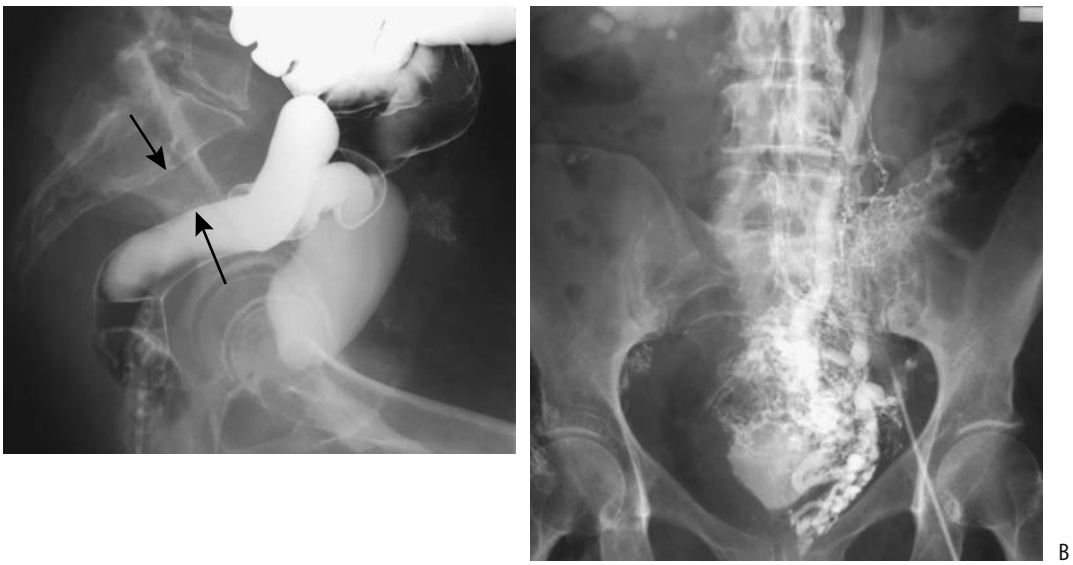

A B

Figure 17.7. Idiopathic inferior vena caval obstruction. A: A lateral view from a barium enema and cystogram reveals widening of the presacral soft tissues (arrows), a common finding with caval obstruction. B: Venogram identifies extensive collaterals veins and confirms lack of vena cava filling.

plete obstruction simply results in hepatosplenomegaly and follows a relatively benign course, while others develop chronic liver disease and esophageal varices. Caudate lobe and left lobe hypertrophy, right lobe atrophy, and a nodular liver outline develop with intrahepatic inferior vena caval obstruction; peripheral linear or wedge-shaped hypodense defects are detected in some patients. Some chronic thrombi are associated with caval wall thickening; MR contrast enhancement extends from the vena cava into surrounding soft tissues, probably reflecting thrombophlebitis.

Occasionally a caval thrombus regresses spontaneously.

Membranous Obstruction

One of the causes of Budd-Chiari syndrome is inferior vena cava obstruction by a membrane (web). This condition is more common in East Asia than in the West and predominates in young adult males. Some of these patients also have hepatic vein membranes.

A congenital inferior vena cava web is rare. After therapy some of these webs restenose and require several dilations. Why an acquired web forms in some patients is not clear. A number of affected patients have suffered prior abdominal trauma. An underlying hypercoagulable state has been suggested; in fact, some patients with membranous obstruction have both an underlying hypercoagulable condition and also had recent trauma.

A membranous obstruction can be detected by either US or cavography but not by CT. Doppler US is useful in evaluating membranous obstruction of both the inferior vena cava and main hepatic veins.

With some membranous obstructions the hepatic veins act as an alternate pathway for blood flow. Thus intrahepatic collaterals can develop between inframembranous and supramembranous hepatic veins; because of these pathways, a Budd-Chiari syndrome does not develop.

Other Obstructions

A rare inferior vena caval obstruction is associated with a diaphragmatic hernia; liver herniation results in torsion and narrowing of the inferior vena cava.

Therapy

Most membranous obstructions are amenable to transfemoral balloon dilatation with excellent results. An occasional membrane, however, is relatively thick and resists balloon dilatation. Endoluminal recanalization and stent insertion are viable options in patients with chronic inferior vena caval obstruction

Unique percutaneous thrombectomy of floating iliocaval thrombi has been performed with an occluding balloon sheath. Using a transjugular access route, the sheath was positioned in the inferior vena cava, a balloon inflated to prevent central thrombi embolization, mechanical fragmentation performed through a working channel using a rotating basket, and residual thrombus fragments then aspirated (41).

Tumor

Primary

Primary inferior vena caval malignancies are rare; they are readily confused with adjacent extraperitoneal tumors. Primary leiomyomas and sarcomas should be distinguished from secondary ones, the latter often representing intravenous leiomyomatosis from a uterine leiomyoma. Some of these women have had a previous hysterectomy for uterine leiomyomas. For example, cavocardiac leiomyomatosis was discovered in a woman who had a hysterectomy 16 years previously for a hemorrhagic fibroma (42); her present tumors were believed to be uterine in origin.

Leiomyosarcoma

The most common primary vena caval malignancy is a leiomyosarcoma. For some reason authors have an urge to publish their experience with vena cava leiomyosarcomas, but these extensive case reports belie the rarity of this condition. A number of these patients have been enrolled in the International Registry of Inferior Vena Cava (IVC) Leiomyosarcomas. Out of 218 patients in this study, over half developed tumor recurrence after radical resection (43). Recurrence consisted of local spread, distant metastases, or both.

Leiomyosarcomas range from an intraluminal tumor obstructing the inferior vena cava, to

a tumor extending primarily outside the caval wall, to a complex tumor having features of both; CT shows a lobulated well-defined heterogeneous tumor, while MRI reveals a tumor having an isointense signal on T1- and an iso- to hyperintense signal on T2-weighted images. Regions of hemorrhage result in a hyperintense T1-weighted signal. These tumors usually enhance markedly with contrast. With a complex appearance, both CT and MRI are useful in differentiating between a neoplasm and a simple thrombus. At times a tumor is so extensive that identification of the site of origin is not possible radiologically, surgically, or even pathologically.

Histiocytoma

Only a few inferior vena caval malignant fibrous histiocytomas have been reported. Contrast-enhanced CT of one revealed a minimally enhancing intraluminal tumor expanding the lumen considerably, findings not seen with a simple thrombus (44); hyper- and hypointense regions were identified on T1- and T2-weighted sequences. Small serpiginous enhancing tubular structures on immediate postgadolinium SGE images were believed to represent feeding vessels.

Secondary

Extraperitoneal tumors readily compress the inferior vena cava or invade and progress to an intraluminal tumor thrombus. Invasion by renal cell carcinoma is familiar to most radiologists. Some of the more unusual invasive tumors include a liposarcoma and adrenal carcinoma. Intracaval extension of these tumors can be determined by transesophageal US.

Magnetic resonance imaging and MRA identify both intraluminal tumors and extrinsic caval compression by a tumor. Collateral vessels are also detected. Magnetic resonance imaging generally provides more information than CT.

Caval Fat

True intracaval fat-density tumors range from a lipoma to renal angiomyolipoma extending through a renal vein.

A fat-density intraluminal caval tumor is rare; a more common reason for such a CT appearance is juxtacaval fat, located medially at the hepatic vein level or slightly superior, artificially projecting into the caval lumen. This fat is contiguous to fat surrounding the subdiaphragmatic esophagus. Either coronal reconstruction images or contrast-enhanced images should suggest a correct diagnosis. Such fat is generally considered to be a normal variant, although it appears to be more common in patients with chronic liver disease (45).

Filters

Clinical

From initial open surgical placement, insertion of inferior vena cava filters has evolved into a percutaneous technique using an introducer sheath. Indications for inserting inferior vena cava filters have expanded from patients who had a pulmonary embolus and could not be anticoagulated to those at risk for emboli. Ease of filter insertion and reduced associated morbidity have expanded the indications further, although in a setting of a pulmonary embolus anticoagulation is generally the first step. Recurrent emboli in the face of adequate anticoagulation or a complication of anticoagulation, such as bleeding, indicates the need for filter insertion. Contraindications to anticoagulation include a recent hemorrhage, with other contraindications often relative and at times subjective.

A number of vena cava filters are available. They differ in their appearance, such as cone, basket, or net; in their construction material and thus radiodensity; and in whether they are readily removable. In broad terms, all filters trap most clots, but some pulmonary emboli are unavoidable. At times vena caval filters are inserted temporarily, such as in the presence of iliac vein or caval thrombi and or in the risk of embolization during thrombolysis.

Carbon dioxide is an alternate contrast agent for vena cavography during filter insertion when iodinated contrast agents are contraindicated or in those patients with renal insufficiency (46).

Complications

Complication rates for radiologic and surgical placement of inferior vena cava filters appear comparable although in one institution radiologists achieved a higher success rate and fewer

complications (47); part of the reason may be that radiologists tended to perform cavography prior to filter placement and surgeons did not. A review of over 1700 implanted filters at one institution (up to 1998) found a 6% prevalence of observed postfilter pulmonary emboli, fatal in 4% of patients, with most fatal pulmonary emboli occurring a median of 4 days after filter insertion (48); the prevalence of observed postfilter caval thrombosis was 3%. Intrafilter clots are not uncommon. Benefit must be balanced against risk.

Other filter complications include malposition, filter tilting, and insufficient opening. Ideally, a filter is positioned between the ileal vein confluence and renal veins. A filter cephalad to the renal veins risks renal vein thrombosis. Mild filter tilting is common, but the ability to trap clots is reduced with excessive tilting. Likewise, insufficient filter opening reduces a filter's clot trapping ability. A filter is designed to prevent pulmonary emboli, and the evidence of such an embolus after filter placement represents filter failure. In such a situation the filter should be investigated for migration, strut failure, or inferior vena cava thrombosis. Filter migration occurs either caudal or cranial. Vena caval thrombosis is a recognized filter complication, regardless of filter design. Some caval thrombi are asymptomatic. Even without a thrombus, extremity venous stasis tends to accentuate after filter placement. Rare complications include myocardial infarction due to filter migration and pericardial tamponade.

Filter perforation is rare. Anecdotal reports describe caval penetration resulting in pancreatitis and even biliary obstructive. Filter struts can fracture and migrate, including to the kidneys. Rare reports describe penetration of a vertebral body and caval perforation leading to small bowel volvulus.

Caval filters are recognized on contrast-enhanced SGE MRI because of their symmetry and magnetic artifacts.

Incidentally, J-tipped guidewires should be used with care around filters; these guidewires are at risk for entrapment.

Aneurysms

Inferior vena cava aneurysms are very rare. Most are believed to be congenital. Acquired ones are secondary to trauma or an arteriovenous fistula. Some are asymptomatic and are incidentally discovered when CT or MR are performed for other reasons. Sagittal reconstruction is helpful in their visualization.

Visceral Vessels

Vasculitides

Systemic vasculitis often involves small visceral vessels, with resultant ischemia leading to ulcerations, perforation, or evolving into a stricture. Vasculitis can involve any part of the gut, even the duodenum, which has a rich blood supply. It often affects multiple bowel segments, in distinction to thromboemboli, which tend to affect continuous segments. De novo duodenal ischemia is almost always secondary to a vasculitis. Concomitant splenic and renal involvement also suggest a vasculitis.

Behçet's Syndrome

A chronic multisystemic disorder, Behçet's syndrome is of unknown etiology. Whether Behçet's syndrome has a primary ischemic basis is debatable; some authors classify it not under ischemia but in a separate category. Also, some authors separate Behçet's syndrome into two forms: complete and incomplete. In Japan, Behçet's colitis patients typically have no eye involvement, and these patients are classified under the incomplete form of Behçet's syndrome.

Resected bowel in these patients reveals multiple punched-out inflammatory ulcers, mostly in the ileocecal region; most ulcers are on the antimesenteric border. Histopathology reveals a nonspecific vasculitis. Granulomas are not identified. Clinically, many patients develop erythema nodosum, arthralgias, oral and genital ulcers, and a relapsing iritis. Gastrointestinal symptoms are common, with abdominal pain and recurrent aphtha mimicking Crohn's disease, ulcerative colitis, or another vasculitis. An acute presentation with bowel perforation and peritonitis is not uncommon. An occasional patient presents with prolonged fever. The diagnosis can be difficult; in 1990 the International Study Group for Behçet's Disease proposed specific diagnostic criteria consisting of oral ulcers and at least two of the following: genital ulcers, specific eye lesions, skin lesions, and a

skin pustule test. A diagnosis of Behçet's syndrome is established mostly on clinical grounds rather than on histopathologic findings.

The most common site of gastrointestinal involvement is the ileocecal region, followed by the colon, small bowel, and, least often, esophagus. Gastric disease is rare. Imaging in affected individuals reveals inflammatory polyps and either aphtha or deep ulcers. In general, deep or punched-out ulcers in either the distal ileum or right colon should suggest Behçet's syndrome. A perforation is not an uncommon acute event. A retrospective CT study of patients with intestinal Behçet's syndrome found intestinal polyps in 36% and thickened bowel wall in 32% (49); enhancement ranged from mild to marked. Both polyps and a thickened bowel wall were more common in patients with complications. Also, severe perienteric infiltration was seen only in patients with complications. Adjacent lymph nodes can be deformed by chronic ileocecal ulcerations.

Most therapy is unsatisfactory in patients with Behçet's syndrome. Some patients' clinical symptoms improve and imaging abnormalities clear after the start of a low residue diet. Even thalidomide treatment has been helpful.

Patients with Behçet's syndrome are prone to develop aortic and arterial aneurysms (50). Stent-grafts are helpful, although artery occlusion is a complication. Thromboses of inferior vena cava, portal vein, and smaller veins also develop.

Postoperative recurrence after bowel resection is common and generally is close to an anastomosis.

Periarteritis Nodosa

Periarteritis nodosa (polyarteritis nodosa), a necrotizing inflammation (arteritis) of small and medium-sized artery walls, eventually results in organ ischemia, with renal arteries more often involved than liver vessels. Hypertension is common. These patients develop arterial aneurysms and stenoses, generally at sites of arterial bifurcation—characteristic but not pathognomonic findings; these findings also occur in other arteritides. Aneurysms tend to be small, saccular, at times having an irregular outline.

Contrast CT shows patchy renal uptake bilaterally due to scarring; wedge-shaped defects develop secondary to focal ischemia. The imaging appearance is nonspecific.

Henoch-Schönlein Purpura

Henoch-Schönlein purpura (nonthrombocytopenic purpura) is a vasculitis of unknown etiology affecting mostly children. Usually a characteristic lower extremity purple rash precedes abdominal symptomatology, with some exceptions. Abdominal pain and bleeding in these patients presumably is secondary to intramural bleeding or a serohemorrhagic effusion.

Imaging reveals a predilection for proximal small bowel involvement. With extensive involvement, a small bowel study reveals intramural fluid as fold thickening and thumbprinting (Fig. 17.8). An intramural hematoma occasionally acts as a lead point for an intussusception. Computed tomography identifies segmental small bowel mural thickening, a nonspecific finding.

In children with Henoch-Schönlein purpura, US detects dilated small bowel segments, decreased motility, and eccentric bowel wall thickening.

Figure 17.8. Henoch-Schönlein purpura resulting in bowel wall edema (arrows) and fold infiltration.

Allergic Granulomatous Vasculitis (Churg-Strauss Syndrome)

Allergic granulomatous angitis (Churg-Strauss syndrome) is a necrotizing vasculitis leading to ischemia due to arterial occlusion. Some patients develop ulcerative colitis–like findings. Symptoms tend to improve with steroid therapy, but disease recurs when steroids are discontinued.

Degos' Disease

Degos' disease (malignant atrophic papulosis) is a rare, progressive disease leading to occlusion of small and medium-size arteries. Bowel involvement results in perforations, peritonitis, and fistulas.

Degos' disease is in the differential diagnosis of small bowel ulcerations.

Systemic Lupus Erythematosus

Some patients with systemic lupus erythematosus develop a gastrointestinal vasculitis with resultant symptoms of diarrhea and pain. The final end point is ischemic bowel disease. In affected patients with acute abdominal pain, CT reveals bowel wall thickening, a target-like appearance and mesenteric vascular engorgement and haziness, findings suggesting ischemic bowel disease (51). In distinction from more common bowel ischemia, bowel wall thickening tends to be multifocal, varies in length, and is not confined to a single vascular field. Unless irreparable damage ensues, the changes should revert to normal after therapy (Fig. 17.9).

A three-phase Tc-99m–pyrophosphate scintigram appears useful in these patients; a positive scan suggests a vasculitis.

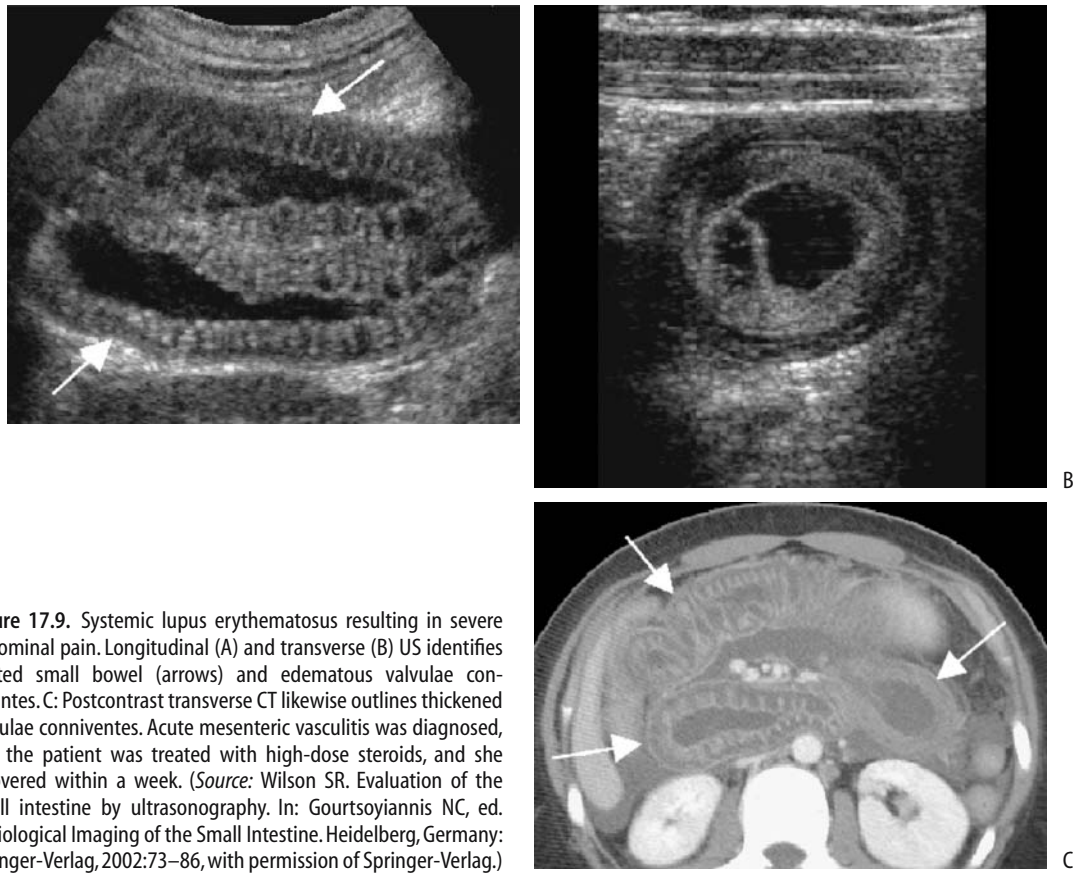

Figure 17.9. Systemic lupus erythematosus resulting in severe abdominal pain. Longitudinal (A) and transverse (B) US identifies dilated small bowel (arrows) and edematous valvulae conniventes. C: Postcontrast transverse CT likewise outlines thickened valvulae conniventes. Acute mesenteric vasculitis was diagnosed, and the patient was treated with high-dose steroids, and she recovered within a week. (*Source:* Wilson SR. Evaluation of the small intestine by ultrasonography. In: Gourtsoyiannis NC, ed. Radiological Imaging of the Small Intestine. Heidelberg, Germany: Springer-Verlag, 2002:73–86, with permission of Springer-Verlag.)

Antiphospholipid Antibody Syndrome

Study of antiphospholipid antibody syndrome belongs mostly in the hematologist's domain. Abdominal imaging enters the picture when venous and arterial thromboses develop in patients with serum antiphospholipid antibodies and thrombocytopenia. Abdominal pain and abdominal distention are the most common clinical presentations. Spontaneous abortions also occur.

Both antiphospholipid antibodies and lupus anticoagulant alter hemostasis and induce a hypercoagulable state. This syndrome exists as a primary form and also in association with systemic lupus erythematosus. Both forms manifest similar clinical findings, although lupus usually leads to venous thrombosis only.

Patients with antiphospholipid syndrome develop major vascular thromboses, including the aorta, inferior vena cava, portal vein, superior mesenteric vein, and splenic vein (52). Resultant ischemia is either localized or diffuse and can progress to infarction and necrosis and involve kidneys, liver, spleen, stomach, and bowel. Adrenal infarction can develop without evident hemorrhage (53). Pancreatitis and hepatic dysfunction associated with portal hypertension develop in some. Inferior vena cava or hepatic vein thrombosis can lead to Budd-Chiari syndrome. In some patients thromboemboli recur at the same site; in others they tend to be limited to either the arterial or venous side. Imaging detection of unusual or recurrent thrombi, especially in a younger patient, should suggest this entity. Histology simply reveals extensive small artery, arteriolar, and venous occlusive disease.

Other Vasculitides

Pseudoxanthoma elasticum is a connective tissue disorder consisting of characteristic skin lesions, angioid streaks in the eyes, and occlusive vascular disease. Presumably the latter findings are responsible for the occasional gastric hemorrhage developing in this condition. Some patients develop ischemic bowel perforations before manifesting peripheral findings.

Dermatomyositis is a vasculitis also affecting the gastrointestinal tract. Underlying ischemia leads to edema, ulcers, gangrene, and, if severe enough, eventual bowel perforation.

A distinct form of vasculitis consisting of a giant cell phlebitis in a 16-year-old girl led to an ischemic colonic stricture (54); arterioles and arteries were not involved.

Ischemia

Clinical

Adults

Acute intestinal ischemia is a result of arterial thrombosis, arterial embolism, venous thrombosis, a vasculitis, or a nonocclusive low blood flow state. (Ischemic enterocolitis is discussed in Chapters 4 and 5, and gastrointestinal tract bleeding is discussed Chapter 4). From a clinical viewpoint, intestinal ischemia is best subdivided into acute and chronic types; some authors also include a subacute category.

Acute intestinal ischemia often presents as an abdominal catastrophe, evolving rather swiftly into a major infarction. Mortality remains high even with rapid diagnosis and ready availability of surgical consultation.

Nonocclusive mesenteric ischemia is difficult to detect and is probably underdiagnosed. Presenting symptoms tend to be vague and wide-ranging. The jejunum is involved in most patients. At its extreme, nonocclusive ischemia leads to necrosis, gangrene, and perforation. Computed tomography, US, and MRI are not reliable in the early detection of this condition, and mesenteric angiography should be considered in a clinical setting of suspected acute mesenteric ischemia.

Mesenteric ischemia can ensue with an aortic dissection involving the origin of the superior mesenteric artery or even compressing it; at times stenting relieves the ischemia.

Cholesterol embolization is associated with atheromatous plaques, angiography, vascular surgery, and even thrombolytic therapy. Such embolization can lead to mesenteric ischemia, gastrointestinal hemorrhage and bowel infarction and perforation (55). Clinically, these patients often also develop extremity ischemia and renal insufficiency. Eosinophilia is detected in some.

Although fibromuscular dysplasia is common in the renal arteries, it is unusual in visceral

arteries; it is an occasional cause of ischemia, especially in a younger patient. Angiography reveals a characteristic "string of beads" appearance seen with fibromuscular dysplasia.

Mesenteric ischemia is more common in patients undergoing chronic hemodialysis than in the general population, probably due to atherosclerosis.

Heroin-related mesenteric ischemia is well known. Ischemia also develops after intranasal cocaine use.

Most chronic ischemia, especially in the elderly, is caused by either arterial stenosis due to atherosclerosis or a vasculitis. It is more common in women. Patients with chronic ischemia present with intestinal angina, weight loss, anemia, and diarrhea. Stenoses and occlusions range from a single visceral artery being involved to a combination of vessels. Collateral flow from the internal iliac or other arteries is not unusual. On a chronic basis, at times the arc of Buehler enlarges to the point that it provides most of the arterial blood supply to the liver and spleen.

Infants and Children

Gastric ischemia in a neonate is usually a complication of acute anoxia or shock. Intestinal ischemia in children is often superimposed on underlying congenital vascular or metabolic abnormalities. Thus vascular thromboemboli are a known complication in a setting of homocystinuria, a rare inborn error of amino acid metabolism manifesting as a multisystemic disease associated with mental retardation and vascular disease, consisting of premature arteriosclerosis and thrombosis.

Does the use of umbilical artery catheters in newborns impair mesenteric blood flow? Doppler US performed before and after removal of umbilical artery catheters found that after catheter removal mean peak celiac artery systolic blood flow velocity increased from 50 cm/sec to 62 cm/sec and superior mesenteric artery flow from 52 cm/sec to 72 cm/sec (56); end diastolic blood flow velocity and vessel diameters did not change significantly.

Umbilical arteriovenous fistulas are uncommon. They can be either congenital or acquired. Even in a neonate an arteriovenous fistula between the umbilical artery and umbilical vein can result in bowel ischemia. Bowel perfusion improves in some after umbilical vein ligation.

Imaging

Angiography is the historic gold standard in suspected acute mesenteric ischemia. It is more time-consuming and often less available than CT, which is the current examination of choice in many centers. Mesenteric CTA detects superior mesenteric artery embolism or thrombosis and superior mesenteric vein thrombosis with a sensitivity approaching that of angiography. In addition to acute ischemia, CT also evaluates other causes of an acute abdomen.

Conventional radiography findings in patients with intestinal ischemia reflect the underlying spectrum of pathologic changes. They are normal initially or reveal variable degrees of gaseous bowel distention and fluid levels. Dynamic CT findings range from early ischemic ileus, bowel wall edema, and hematoma manifesting as bowel wall thickening, major vessel stenosis, or occlusion (either arterial or venous) to eventual bowel wall necrosis identified as intramural gas and lack of bowel wall contrast enhancement. In patients requiring surgery for acute mesenteric ischemia, detection of at least one of these CT findings achieves a specificity of over 90% but a considerably lower sensitivity. At times a contrast-enhanced CT *target sign* is evident during the arterial phase, especially if ischemia is due primarily to venous obstruction.

Gas–fluid levels and dilated bowel loops, both nonspecific signs of acute mesenteric ischemia, are seen equally well with conventional radiography and CT. Major ischemia leads to gas within the bowel wall (pneumatosis intestinalis) and mesenteric and portal vein gas. With few exceptions, in adults detection of mesenteric and portal venous gas implies mesenteric infarction. Such gas occasionally migrates to the internal spinal venous plexus, presumably from the pelvic veins. Pneumoperitoneum and even pneumoretroperitoneum are uncommon manifestations of bowel ischemia and presumably reflect a perforation. Some authors preach the superiority of CT in detecting portal venous gas and probably rightly so, although a formal comparison with conventional radiography is lacking. Nevertheless,

quite often conventional radiographs suffice to suggest the diagnosis.

Computed tomography in patients with acute superior mesenteric artery occlusion identifies intravascular blood clots as high-density regions on precontrast images and as filling defects after contrast enhancement. A sometimes useful finding in acute superior mesenteric artery occlusion is a CT ratio of the external diameter of the superior mesenteric vein divided by the external diameter of the superior mesenteric artery; this ratio becomes <1 in patients with acute occlusion.

Sonographic findings range from normal to nonspecific distended loops of bowel.

Doppler US is useful for detecting high-grade celiac artery and superior mesenteric artery stenoses and occlusion. When successful in evaluating mesenteric vessel patency, however, Doppler US findings need to be placed in a proper clinical perspective because not all stenoses are symptomatic.

Celiac artery narrowing is found in some patients if the study is performed at expiration (median arcuate ligament syndrome), a finding minimized at inspiration (Fig. 17.10). These patients have chronic abdominal pain, at times mimicking gastric outlet obstruction. Doppler US measurement of mesenteric vascular flow is difficult in a setting of suspected acute ischemia, being successful only in a minority of patients.

Various MR techniques such as MRA, cine phase contrast MRA, and flow-independent T2-weighted imaging not only identify anatomic stenoses but also provide physiologic data about blood flow. Currently the use of MRI in bowel ischemia is still in its infancy.

Vessel obstruction is best identified with MRI on early contrast-enhanced images. Thus major arterial or venous thrombosis is seen on postcontrast images as a signal void, often surrounded by increased enhancement in a thickened vessel wall. A similar wall thickening is found with bowel wall edema, such as in hypoproteinemia, but no increased postcontrast wall enhancement is evident. Systolic gating is helpful when using a 3D phase contrast MRA technique to evaluate celiac and superior mesenteric artery stenoses. Gadolinium-enhanced 3D spoiled gradient-refocused acqui-

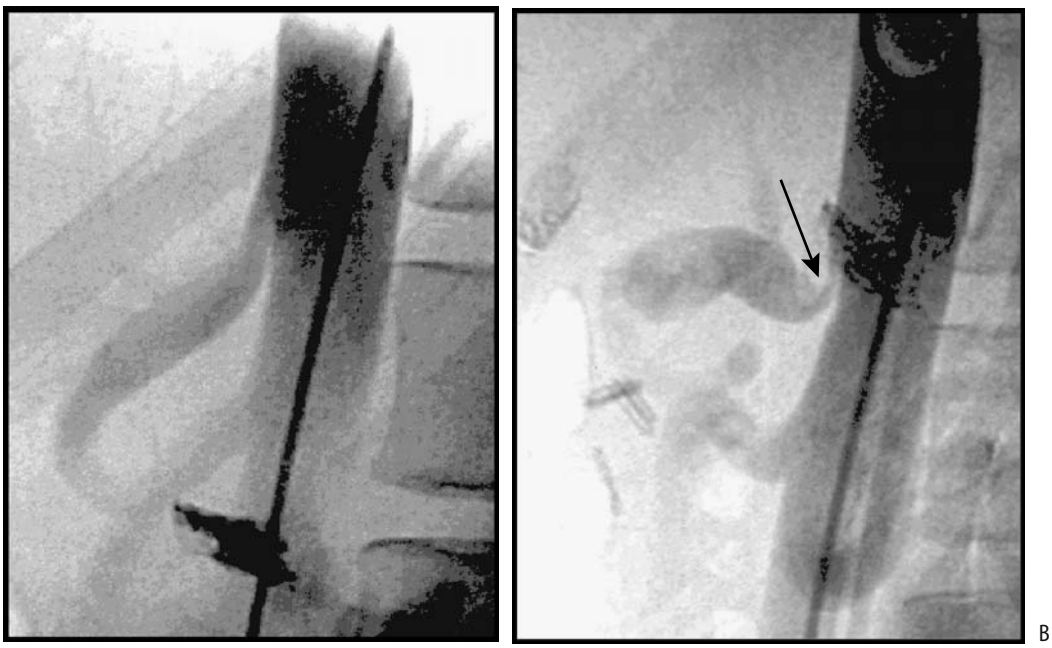

A B

Figure 17.10. Celiac trunk compression by median arcuate ligament. Inspiration (A) and expiration (B) lateral digital subtraction angiography (DSA) views show a transient compression (arrow). (*Source:* Funaki B. Compression of the celiac trunk by the median arcuate ligament. Radiology 2000;214:604–605, with permission from the Radiological Society of North America.)

sition in the steady state (GRASS) MRA identifies any stenosis in celiac and superior mesenteric arteries.

Deoxyhemoglobin in blood cells is paramagnetic, but oxyhemoglobin is not. This difference can be used to measure superior mesenteric vein blood oxygen saturation in hemoglobin, obtained using flow-independent MR T2 data; it appears useful in confirming suspected chronic mesenteric ischemia. In patients without ischemia, superior mesenteric vein blood oxygen saturation increases after a meal, but in symptomatic patients with chronic mesenteric ischemia blood saturation tends to decrease. In spite of research on this topic for over a decade, the clinical relevance of such measurements is yet to be established.

In an occasional patient positive uptake of Tc-99m–HMPAO–labeled leukocytes appears to reflect underlying chronic ischemia rather than primary inflammation.

Therapy

Acute Ischemia

Different therapy is employed for acute and chronic ischemia. Without therapy, acute nonocclusive ischemia often progresses to infarction. The treatment of choice in some patients with nonocclusive ischemia is papaverine infusion via a vascular catheter. Resection and anticoagulation are therapies for infarcted bowel. Recurrent bowel ischemia is a complication of surgical bypass grafting for acute ischemia. Fibrinolytic therapy using urokinase, rather than surgical embolectomy, appears effective in a majority of patients with a mesenteric embolus and without evidence of intestinal infarction; others require laparotomy. The best sign of successful therapy is pain abatement; persistent pain suggested intestinal infarction.

Rather than surgical embolectomy, in selected individuals mechanical thrombolysis of mesenteric and portal vein thrombosis, using a jugular vein approach, is an alternate approach.

Chronic Ischemia

Either percutaneous transluminal angioplasty or a surgical bypass graft is employed in a setting of chronic mesenteric ischemia. At times transaortic endarterectomy is performed. All of these techniques have their associated complications. The published success rates of percutaneous transluminal angioplasty are difficult to put in perspective because different criteria are used (e.g., size of postprocedure luminal diameter, restenosis rate, improved clinical status) and are operator dependent.

Similar to surgical mesenteric vascular graft placement, percutaneous transluminal angioplasty has a technical procedure success rate of about 90% and short-term clinical success of about 80%. Procedure-related mortality and the major complication rate appear similar for operative bypass grafting and percutaneous transluminal angioplasty; long-term pain relief is similar or better with grafting.

Splanchnic Aneurysms

Many splanchnic aneurysms contain only a portion of the vessel wall; therefore, strictly speaking these outpouchings should be called pseudoaneurysms, yet the term *aneurysm* has been adopted in most of the medical literature and is used here.

The most common site for abdominal aneurysms is in the splenic artery, although they occur widely. Detection of a splanchnic aneurysm in a young patient should suggest Ehlers-Danlos syndrome (57). Some patients with multiple visceral artery aneurysms have connective tissue fragility suggesting cystic medial necrosis, even without clinical features of Marfan syndrome; they are prone to excessive hemorrhage during angiography and appear to be at increased risk for developing complications during vascular catheterization procedures.

Pancreatitis and resultant pseudocysts lead to aneurysms in adjacent vessel. Other causes include trauma, such as biopsy, and infection resulting in mycotic aneurysms. Intestinal tuberculosis is an occasional cause of a mesenteric artery aneurysm, generally manifesting as massive gastrointestinal hemorrhage.

Many aneurysms calcify and are identified with conventional radiography. In general, the presence of rim calcifications suggests an atheromatous origin rather than mycotic or traumatic. Some of these aneurysms become quite large. Noncontrast imaging reveals a fluid-filled cavity similar to a cyst or abscess. Thus prior to attempted drainage of a suspected cyst

or abscess, at times it is worthwhile obtaining Doppler US to exclude an aneurysm from the differential diagnosis. Some aneurysms contain a thrombus, making their identification even more difficult.

Currently DSA is considered the gold standard in evaluating splanchnic aneurysms. Evidence is accumulating that CTA is nearly as accurate, but MRA is still in the background although potentially it will evolve into a viable alternative.

In general, once a visceral aneurysm is detected, repair should be considered. Some smaller aneurysms are followed with serial US. These aneurysms tend to increase in size with time and are at increased risk of rupture. Many of these aneurysms undergo primary surgical repair. Angiographic embolization is a viable option but some surgeons still consider this therapy only in the presence of a surgical contraindication.

Temporarily occlusion of a splanchnic feeding vessel during transcatheter embolization appears to decrease the risk of rupture and bleeding during the procedure.

Celiac Artery

Aneurysms of the celiac artery are uncommon. Most are associated with medial degeneration and tend to be silent. These aneurysms can be treated by embolization. Celiac artery occlusion may be tolerated with such a technique as long as patent collateral vessels are present.

Splenic Artery

Underlying atherosclerosis is common in patients with splenic artery aneurysms. A mycotic cause is rare. Prevalence of these aneurysms is higher in women, and pregnancy and multiparity appear to predispose to their formation. Splenic artery aneurysms are uncommon in the pediatric age group, with most aneurysms in this age group being traumatic in origin. Portal hypertension in association with splenomegaly appears to predispose to splenic artery aneurysm formation. They also occur after liver transplantation.

Ultrasonography, MRI, and arteriography in a man with Ehlers-Danlos syndrome, type IV, identified kidney and liver cysts and splenic artery and hypogastric artery aneurysms (58), suggesting a common connective tissue defect for these conditions.

Most splenic artery aneurysms are asymptomatic until they rupture into the peritoneal cavity or an adjacent structure, including the bowel. They are prone to rupture during pregnancy, with rupture being most common during the third trimester, leading to high maternal and fetal mortality. Spontaneous rupture of splenic artery aneurysms occurs after liver transplantation. A rare splenic artery aneurysm erodes into the splenic vein and leads to portal hypertension. An occasional such patient develops a mesenteric steal syndrome.

Splenic artery aneurysms can present as a cystic tumor in the pancreatic tail; Doppler US identifies arterial blood. Rupture into the pancreatic duct results in succus pancreaticus.

Most of these aneurysms are saccular in outline. They are either intra- or extrasplenic in location and occur most often in the distal portion of the splenic artery (close to the spleen). Their size varies considerably, with larger ones being more prone to rupture.

Splenic artery aneurysms can be diagnosed by Doppler US, CT, MRI, or angiography. Gray-scale US does not detect them readily; calcifications tend to produce artifacts. One limitation of Doppler US is that a completely thrombosed aneurysm is missed.

Hepatic Artery

Hepatic artery aneurysms occur in the common hepatic, right and left hepatic, or any branch artery. Most are secondary to atherosclerosis; less common etiologies include trauma, abscess, or inflammation, such as pancreatitis. Rarer causes are related to Marfan's syndrome, Ehlers-Danlos syndrome, lupus erythematosus, and even von Willebrand's disease (59). Some traumatic aneurysms are secondary to instrumentation, such as liver biopsy, or various attempts at drainage procedures.

The major complication of hepatic artery aneurysms is rupture, an event associated with a high morbidity and mortality. Most bleeding is intraperitoneal, or, with erosion into the duodenum, an upper gastrointestinal hemorrhage ensues. Occasionally an aneurysm evolves into an arteriobiliary fistula and results in hemobilia.

Three-dimensional CTA is useful in detecting and defining these aneurysms.

Although color Doppler US provides aneurysm flow characteristics, angiography not only defines its relationship with the hepatic artery but also provides access for therapy. These aneurysms are treated with Gianturco coils, gelatin sponge, polyvinyl alcohol fragments, occlusion with Ivalon particles, or other particles. Embolization controls bleeding in most patients. Percutaneous transluminal angioplasty is emerging as the preferred treatment modality for both intrahepatic and extrahepatic saccular aneurysms, and such an angioplastic technique has a high success rate. Biliary sepsis, liver insufficiency, and gangrenous cholecystitis are some of the complications. An occasional patient with an intrahepatic aneurysm, however, requires a partial hepatectomy.

Superior Mesenteric Artery

Aneurysms of the superior mesenteric artery and its branches are not common. These are often detected only after rupture. Some are infected or are associated with intramural dissection. An aneurysm close to the origin of the superior mesenteric artery was associated with a tight stenosis of the celiac artery (60). These aneurysms develop in patients with systemic lupus erythematosus (Fig. 17.11).

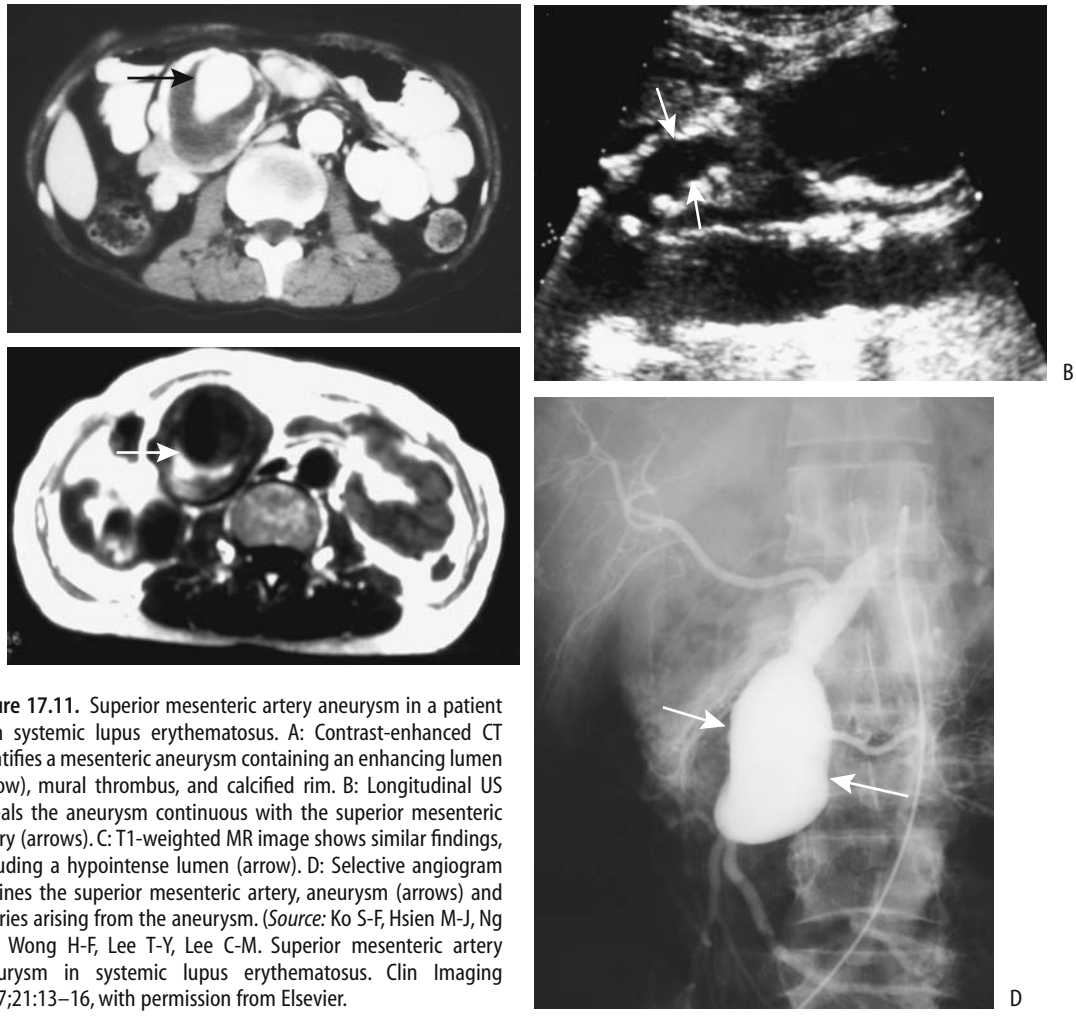

Figure 17.11. Superior mesenteric artery aneurysm in a patient with systemic lupus erythematosus. A: Contrast-enhanced CT identifies a mesenteric aneurysm containing an enhancing lumen (arrow), mural thrombus, and calcified rim. B: Longitudinal US reveals the aneurysm continuous with the superior mesenteric artery (arrows). C: T1-weighted MR image shows similar findings, including a hypointense lumen (arrow). D: Selective angiogram outlines the superior mesenteric artery, aneurysm (arrows) and arteries arising from the aneurysm. (*Source:* Ko S-F, Hsien M-J, Ng S-H, Wong H-F, Lee T-Y, Lee C-M. Superior mesenteric artery aneurysm in systemic lupus erythematosus. Clin Imaging 1997;21:13–16, with permission from Elsevier.

Superior mesenteric artery branch aneurysm embolization using small coils is occasionally performed.

Pancreaticoduodenal Arteries

The pancreaticoduodenal arteries have a greater predilection for aneurysms than expected. For unclear reasons a number of these aneurysms are associated with stenosis or occlusion of the celiac artery.

Some of these aneurysms are secondary to pancreatitis, with a septic etiology or prior trauma being postulated. Not all aneurysms progress if left untreated. Still, these aneurysms tend to rupture even when still small, bleed—extraperitoneally or even into the duodenum—and carry a high mortality rate.

These aneurysms are treated both by transcatheter embolization and surgically, and some are left untreated. Nevertheless, for those aneurysms associated with celiac axis stenosis, correction of the latter condition should also be considered. Surgical options include aneurysm resection or even arterial ligation, although with rupture a partial pancreatectomy may be required to control bleeding.

Other Aneurysms

Aneurysms are rare in the inferior mesenteric artery. An occasional one is associated with obstruction of the superior mesenteric or celiac artery.

Less common sites for an aneurysm include the gastroepiploic artery; rupture of these aneurysms carries a high mortality rate. A gastroduodenal artery aneurysm developed a few months after an episode of acute biliary pancreatitis (60). An occasional middle colic artery aneurysm is reported. These aneurysms are also embolized.

Small vessel aneurysms are rare, but a mycotic source or periarteritis nodosa should be suspected with some of them.

Dissection

A complication of transcatheter arterial embolization is dissection of the feeding trunk. With attempted transcatheter arterial embolization of hepatocellular carcinomas, the two most common sites of dissection are celiac artery and proper hepatic artery; long-term follow-up of these dissections reveals recanalization in approximately one third, a residual narrowed lumen in another third, and complete obstruction in the rest.

A hepatic artery dissection is rare. Superior mesenteric artery dissection is also rare. Three-dimensional CT can identify the false lumen, intimal flap, and both entry and exit points.

Portal Vein

Portal Hypertension

It should be kept in mind that some authors use the term *portal hypertension* rather broadly and include under this topic splenic vein obstruction and resultant gastric varices, a condition without portal vein hypertension. Others use *left-sided portal hypertension* and *localized portal hypertension* to describe splenic vein obstruction. Isolated splenic vein obstruction is discussed in a later section. Some conditions, such as splenic vein thrombosis extending into the portal vein, involve both veins and are covered in this section.

Pressure and Blood Flow Measurements

Normal portal venous pressure ranges from 5 to 10 mm Hg, which is 4 to 6 mm Hg higher than inferior vena cava pressure. Portal hypertension is said to be present if portal venous pressure exceeds 10 mm Hg, is more than 5 mm Hg above inferior vena caval pressure, or if splenic vein pressure is more than 15 mm Hg. Clinically, a useful assumption is that portal hypertension is present if portal pressure is more than twice the normal range, but keep in mind that the portal vein–inferior vena cava pressure gradient is more significant in evaluating portal hypertension than an actual pressure.

Mean normal portal vein blood velocity is about 15 to 30 cm/sec and varies both with respiration and cardiac phase but is hepatopetal. With portal hypertension venous blood flow exhibits a complex pattern. For instance, in some patients hepatopetal flow in the fasting state changes to a to-and-fro flow after a meal and then to hepatofugal flow.

Intraoperative flow measurements show that hepatic artery blood flow is approximately two

thirds that of the portal vein; hepatic artery flow increases significantly with temporary occlusion of the portal vein. Theoretically, percutaneous Doppler US should be able to measure liver and portal venous blood flow; in practice, blood flow measurements vary considerably.

Hepatic venous pressure gradients are obtained by hepatic vein catheterization and portal blood flow velocity and portal vein congestion index measured by duplex Doppler US. No significant correlation exists between venous pressure gradients and Doppler measurements in patients with cirrhosis and portal hypertension, but a significant linear correlation is evident if patients with patent paraumbilical veins are excluded (61).

Duplex portal vein US in patients before TIPS diagnosed portal hypertension with a sensitivity and specificity of 80% if a portal vein diameter >1.25 cm or portal vein velocity <21 cm/sec were detected, but US could not grade hypertension (62). On the other hand, in cirrhotic patients portal blood velocity does not differentiate between those with or without endoscopic evidence of esophageal varices or congestive gastropathy and, in general. Doppler US cannot identify those cirrhotic patients at risk for upper gastrointestinal bleeding.

Phase-contrast MRA has been used to measure portal blood flow. In general, MRA results correlate with data obtained by Doppler US. Phase contrast MRA also provides azygos vein flow changes during the cardiac cycle; flow rates are considerably greater in patients with chronic liver disease and portal hypertension than in healthy individuals. Potentially, such information aids in evaluating progression of diffuse liver disease.

An endoscopic balloon technique measures esophageal variceal pressure. This pressure correlates only partly with portal venous pressure, probably due to the presence of other collateral channels.

Etiology and Pathogenesis

Occasionally portal hypertension is associated primarily with increased portal blood flow, such as an arterioportal fistula, but most often it develops due to increased resistance to portal venous blood flow. A rare malignant vascular intrahepatic tumor leads to portal hypertension; these tumors result in increased portal blood flow due to shunting, intrahepatic portal obstruction caused by massive tumor growth, or both. Occasionally portal hypertension is idiopathic (Banti's syndrome).

Increased Flow

Portal hypertension due to increased blood flow is most often a result of a systemic artery-to-portal vein shunt, either intra- or extrahepatic in location. These shunts, or fistulas, extend to the splenic vein, superior mesenteric vein, or portal vein, including its intrahepatic branches. They can be congenital or acquired. A congenital artery-to-portal vein fistula should be suspected with infantile portal hypertension. At times portal hypertension manifests clinically only years after a fistula is established.

Increased Resistance

Table 17.1 lists some of the causes of portal hypertension due primarily to increased resistance to portal blood flow. Of interest is that portal venous pressure tends to be slightly elevated in some disorders not usually associated with portal hypertension. Thus portal pressure is increased in patients with biliary obstruction, decreasing after biliary decompression. Rarer causes of prehepatic portal venous obstruction include adenopathy at the liver hilum. A number of patients with abdominal tuberculosis and periportal adenopathy have portal hypertension (63). Similarly, periportal lymphoid infiltration in lymphoma or leukemia can result in portal hypertension.

With presinusoidal intrahepatic obstruction the hepatic vein wedged pressure is normal. Thus patients with hepatic schistosomiasis have hyperkinetic systemic and splanchnic circulations but a normal hepatic venous pressure gradient and hepatic blood flow; in those with esophageal varices a normal hepatic venous pressure gradient is indicative of presinusoidal portal hypertension. Of note is that portal hypertension in schistosomiasis patients is not due to fibrosis only but is multifactorial; hemodynamic values are not significantly different between patients with and without liver fibrosis. A rare cause of portal hypertension is portal vein invasion by an intrahepatic peripheral cholangiocarcinoma.

Table 17.1. Causes of portal hypertension (due to increased vascular resistance)

Prehepatic
Portal venous system thrombosis
Extrinsic portal compression or tumor invasion
Congenital atresia or thrombosis
Intrahepatic
Presinusoidal
Conditions leading to diffuse hepatic fibrosis
Gaucher's disease type 1
Polycystic kidney disease and hepatic fibrosis
Mixed connective tissue (collagen vascular) disease
Primary biliary cirrhosis
Schistosomiasis
Postsinusoidal
Laënnec's cirrhosis
Tumor infiltration, such as by a hepatocellular carcinoma
Amyloidosis
Systemic lupus erythematosus
Hepatitis and hepatic failure
Diffuse intrahepatic portal venous system thrombosis
Distal biliary obstruction
Biliary atresia patients post-portoenterostomy (Kasai operation)
After renal transplantation
Systemic mastocytosis
Idiopathic
Posthepatic
Budd-Chiari syndrome
Congestive (right) heart failure
Inferior vena caval obstruction

Blood flow velocity decreases in a number of liver diseases, and duplex Doppler US measurements of blood flow are useful in evaluating disease progression. Increased intrahepatic resistance to flow in patients with chronic liver disease is due not only to intrahepatic morphologic changes but also to a dynamic constriction of the intrahepatic portal drainage bed, believed to be due to decreased synthesis of nitrous oxide in the intrahepatic circulation. Complicating this issue, patients with portal hypertension have increased portal blood flow due to splanchnic arteriolar vasodilation. Endothelins and poorly understood neural and humoral regulation, in part mediated by vasodilators, appear to play a role in increasing intrahepatic vascular resistance. Plasma endothelins, potent systemic and portal vasoconstrictors, are elevated in patients with bilharzial and postviral chronic liver diseases with portal hypertension; a positive correlation exists between plasma endothelin levels and portal vein diameter. On a systemic basis, peripheral arterial vasodilation and an increase in cardiac output ensue in patients with chronic liver disease.

Patients with mixed connective tissue disease (collagen vascular disease) can develop sufficient periportal fibrosis to cause portal hypertension and esophageal varices. Patients with advanced Gaucher's disease type I and a noncirrhotic liver develop portal hypertension. These patients have extensive confluent central hepatic fibrosis, which presumably is responsible for their portal hypertension (64), although Gaucher's cells compressing liver sinusoids and thus increasing resistance to flow is probably also a factor. Extensive perisinusoidal amyloid infiltration will also lead to portal hypertension.

Liver involvement in cystic fibrosis increases with age. With increasing survival, some of these individuals develop biliary cirrhosis and eventual portal hypertension. A liver transplantation is a viable option provided that adequate pulmonary function has been maintained.

A rare patient with sclerosing peritonitis and extensive liver capsule fibrosis develops portal hypertension even with a patent portal vein; the capsule fibrosis presumably prevents hepatomegaly and any liver disease leads to a sufficient increase in intrahepatic pressure to compress intrahepatic portal vein and hepatic vein branches and results in portal hypertension. Some patients with autosomal dominant polycystic kidney disease and extensive hepatic fibrosis also develop portal hypertension; in some, distortion of intrahepatic portal vein branches by extensive hepatic cysts is sufficient to produce portal hypertension.

An association of portal hypertension and pulmonary hypertension exists in patients with underlying liver cirrhosis and those with mixed connective tissue disease. The pulmonary findings are similar to those found in primary pulmonary hypertension.

In long-term surviving neonates with biliary atresia who undergo hepatic portoenterostomy (Kasai operation), about half develop portal hypertension (65); the incidence of subsequent portal hypertension is significantly lower in those with a serum bilirubin <2 mg/dL at 3 months postsurgery than in those with a biliru-

bin level >2 mg/dL. Among those developing portal hypertension, esophageal varices were discovered between 11 months and 5 years of age in more than 70% of children, while thrombocytopenia tended to develop at a slightly older age.

The etiology of Banti's disease, consisting of anemia, splenomegaly, and portal hypertension, is unclear. Portal hypertension is considered to be idiopathic. A rare patient develops portal hypertension several years after renal transplantation; their portal venous pressure decreases and esophageal varices clear after splenectomy.

In some studies of noncirrhotic portal hypertension an idiopathic etiology continues to be a prominent feature.

Clinical Aspects

Portal hypertension is assessed by measuring hepatic venous pressure gradient, a technique that is the gold standard in planning subsequent hemodynamic therapy. Nevertheless, portal hypertension is often assumed to be present if portal vein collaterals are detected. Thus the presence of distal esophageal varices is generally taken to be presumptive evidence of portal hypertension. Splenomegaly may or may not be present in adults, although splenomegaly is more common in children.

A typical scenario with Laënnec's cirrhosis is an increase in intrahepatic resistance to portal blood flow, opening of collateral vessels, and a decrease in portal blood flow to the liver. A compensatory increase in hepatic artery blood flow develops, but due to postsinusoidal obstruction some of this arterial blood is diverted to the portal vein and eventually portal vein blood flow reverses direction (hepatofugal flow). Doppler US in patients with cirrhosis reveals a significant decrease in portal flow with a worsening Child's grade of cirrhosis; patients with ascites and encephalopathy also have a significantly lower portal blood flow rate compared to those without these abnormalities.

Some patients with portal hypertension develop large esophageal varices, while others have small varices or none. Likewise, the prevalence of nonesophageal portosystemic collaterals varies. Some develop both large esophageal varices and nonesophageal portosystemic collaterals.

Physical exercise in patients with liver cirrhosis and portal hypertension increases portal pressure and reduces hepatic blood flow and thus appears to increase risk of variceal bleeding.

Splenic artery occlusion will mask underlying portal hypertension.

A portosystemic shunt reverses gastropathy in most patients with noncirrhotic portal hypertension; in these patients it is presumably venous congestion that causes gastropathy, realizing that gastric mucosal capillary dilation does not signify portal hypertension.

Imaging

The thoracic duct caliber increases in cirrhosis. No direct relationship is apparent between the degree of portal hypertension and the caliber of this duct. The distal end of this duct in the left supraclavicular region can be visualized with US in most patients.

CT is insensitive in detecting hepatofugal flow in the main portal vein in patients with cirrhosis. On the other hand, a main portal vein diameter of <1 cm is highly specific for hepatofugal flow (66).

Doppler US provides a measure of hepatic artery and portal vein pulsatility. Normally the hepatic artery has pulsatile flow, but portal venous blood is nonpulsatile with only minor cardiac and respiratory effects. A significant increase in hepatic artery pulsatility occurs in patients with end-stage liver disease. The hepatic veins, on the other hand, are dampened in cirrhosis and their appearance approaches that of the portal vein.

Detection of portosystemic collateral vessels is often used as proof for portal hypertension (Fig. 17.12). A collateral vein within the ligamentum teres is relatively common and is detectable with Doppler US. One should keep in mind, however, that in a minority of normal individuals Doppler US detects blood flow in a paraumbilical vein; velocity increases in portal hypertension and flow extends anterior to the liver surface, a finding not seen normally. Inferior vena cava dilation is also often found in patients with cirrhosis and portal hypertension.

In a setting of portal hypertension, contrast-enhanced 3D MRA is currently the imaging modality of choice in evaluating portal blood flow and portal vein anatomy. Subtracting the

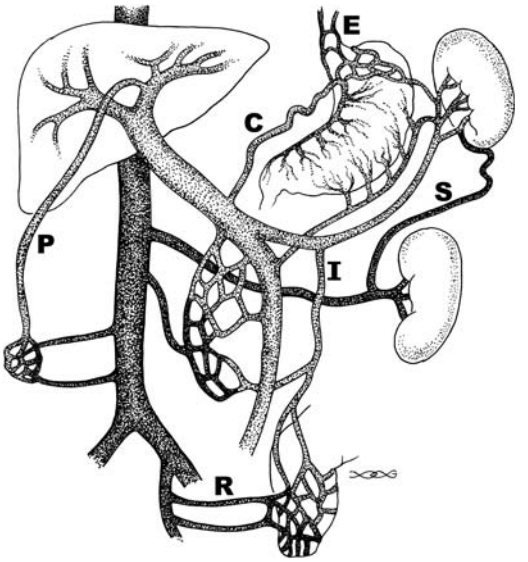

Figure 17.12. Major pathways of portosystemic venous shunting in portal hypertension. E, esophageal varices; P, paraumbilical veins; R, rectal veins; S, splenorenal veins. Reversal of flow occurs in the coronary vein (C) and inferior mesenteric vein (I).

arterial phase from venous phase data aids in visualizing blood flow patterns and shunts using several viewing projections.

Discrepancies exist between Doppler US and contrast-enhanced MRA in assessing portal vein anatomy. Detection of portal vein patency, especially of intrahepatic portal vein branches, is more accurate with MRA. Splenorenal shunts and varices are better detected with MRA.

Portal Vein Obstruction/Thrombosis

A rare cause of portal hypertension is partial obstruction by a portal vein web or membrane. The etiology of these webs is not clear.

Clinical Aspects

Infection, neoplasm, and a hypercoagulable state are associated with portal vein thrombosis. Blood stasis due to decreased flow presumably plays a role in thrombosis developing in a setting of portal hypertension. The reverse is also true, namely, portal vein thrombosis leads to portal hypertension. At times splenic vein thrombosis extends into the portal vein.

The most common cause of massive gastrointestinal bleeding in children is from portal hypertension–induced varices secondary to portal vein thrombosis. Splenomegaly is common in children with portal vein thrombosis. Their liver is normal. In most children thrombosis is considered to be idiopathic, although prior umbilical vein catheterization or omphalitis play a role. Prior umbilical sepsis, even at birth, should be suspected in the child or young adult who develops portal hypertension with no obvious underlying cause. In an interesting US study of 100 neonates with umbilical vein catheterization, clinically silent portal venous thrombosis was detected in 43% (67); follow-up US revealed complete or partial resolution in only about half, with a correlation found between initial thrombus size and subsequent clot resolution. Significant risk factors for thrombosis were catheterization for >6 days and blood transfusion.

Some of the conditions associated with portal vein thrombosis are listed in Table 17.2. Patients

Table 17.2. Conditions associated with portal vein thrombosis

Children
Idiopathic
Prior umbilical vein catheterization
Prior omphalitis
Homocystinuria
Adults
Idiopathic
Inflammation
Pancreatitis
Ascending cholangitis
Ulcerative colitis
Crohn's disease
Adjacent abscess
Tuberculosis involving porta hepatis lymph nodes
Primary hepatic actinomycosis
Penetrating peptic ulcer
Neoplasm
Pancreatic and liver carcinomas
Gastric carcinoma
Bladder carcinoma
Posttherapy
After hepatocellular carcinoma therapy
After splenectomy
Gastric variceal therapy
Other
Hypercoagulation state
Behçet's disease
Postpartum
Myeloproliferative syndromes

with a hepatocellular carcinoma are prone to developing portal vein thrombosis, with the thrombus often consisting of tumor encroaching into portal vein branches rather than being nonneoplastic. Thrombi develop after hepatocellular carcinoma therapy with percutaneous ethanol injection. Fine-needle biopsy of a portal vein thrombus is useful in some patients with hepatocellular carcinoma to identify a neoplastic thrombus if results will influence patient management.

Portal, splenic, and superior mesenteric vein thrombosis is an occasional complication after splenectomy. Most of these patients are symptomatic and an occasional one even develops an acute abdomen. Some authors suspect that endoscopic variceal sclerotherapy predisposes to portal vein thrombosis, although controlled evidence is lacking.

Portal vein thrombosis should be suspected if a patient with Behçet's disease develops splenomegaly. These patients often have cavernous transformation of the surrounding vessels. Patients with homocystinuria, a rare, inherited metabolic disease, are at risk for arterial and venous thromboemboli, including portal vein thrombosis.

In a setting of portal vein thrombosis, an anomalous insertion of the right gastric vein maintains hepatopedal blood flow if the insertion is at the portal vein bifurcation or intrahepatically (distal to the thrombus). Such an anomalous right gastric vein insertion is a pathway for TIPS placement.

Ultrasonography mass screenings can detect extrahepatic portal venous obstruction in asymptomatic patients.

Imaging

Portal vein thrombosis can be assessed with contrast-enhanced CT, gray-scale and Doppler US, contrast-enhanced MRI, and angiography (Fig. 17.13). Most benign thrombi do not widen the portal vein caliber, while a malignant thrombus often does. Also, blood flow (neovascularity) is present in about half of malignant thrombi but not in benign ones.

Contrast-enhanced CT detection of portal vein thrombosis approaches 100% by visualizing an intraluminal thrombus. These thrombi often extend into the splenic and superior mesenteric veins. Coronal or sagittal 3D reconstruction often provides an overall view of these thrombi.

Established portal vein thrombosis often results in a hypodense liver on precontrast CT scans, presumably secondary to fat accumulation. Segmental atrophy develops in an involved segment. The proportion of blood supplied by the hepatic artery increases and as a result postcontrast liver CT shows increased enhancement during the late arterial phase and decreased enhancement during the venous phase. Segmental intrahepatic portal vein thrombi result in transient wedge-shaped parenchymal defects showing increased enhancement during the arterial phase.

Postcontrast CT reveals a benign thrombus as a tubular low-density intraluminal tumor. At times enhancing collateral vessels are evident (cavernous transformation). A thrombus in a nonoccluded portal vein is seen as a nonenhancing tumor surrounded by contrast enhanced venous blood. Mesenteric edema and mesenteric varices are evident in some patients even without a thrombus extending into the superior mesenteric vein. On a chronic basis, CT identifies a cord-like sclerotic portal vein or portal vein calcifications.

Some of these patients develop arterioportal shunts, seen as segmental intrahepatic portal vein enhancement during arterial CT phase.

Controversy surrounds the role of US. Gray-scale US reveals a portal vein thrombus as an intraluminal tumor or abnormal intraluminal echoes. A thrombus ranges from focal to diffuse. Gray-scale US does not detect an anechoic clot, and Doppler US is necessary for these. With complete extrahepatic portal thrombosis, Doppler US reveals an absent portal vein lumen except for a hyperechoic band from which no flow is detected. Usually the site of obstruction can be established. Doppler US evaluates residual blood flow in patients with partial obstruction. Ultrasonography is more problematic in differentiating a benign from a malignant portal vein thrombus in a setting of cirrhosis. Doppler US detection of pulsatile flow in the thrombus is rather specific in diagnosing a malignant thrombus but at the expense of a lower sensitivity, although published results vary considerably. In general, the presence of pulsatile arterial flow, detected by Doppler US, is assumed by some to obviate a need for percutaneous biopsy of the thrombus to estab-

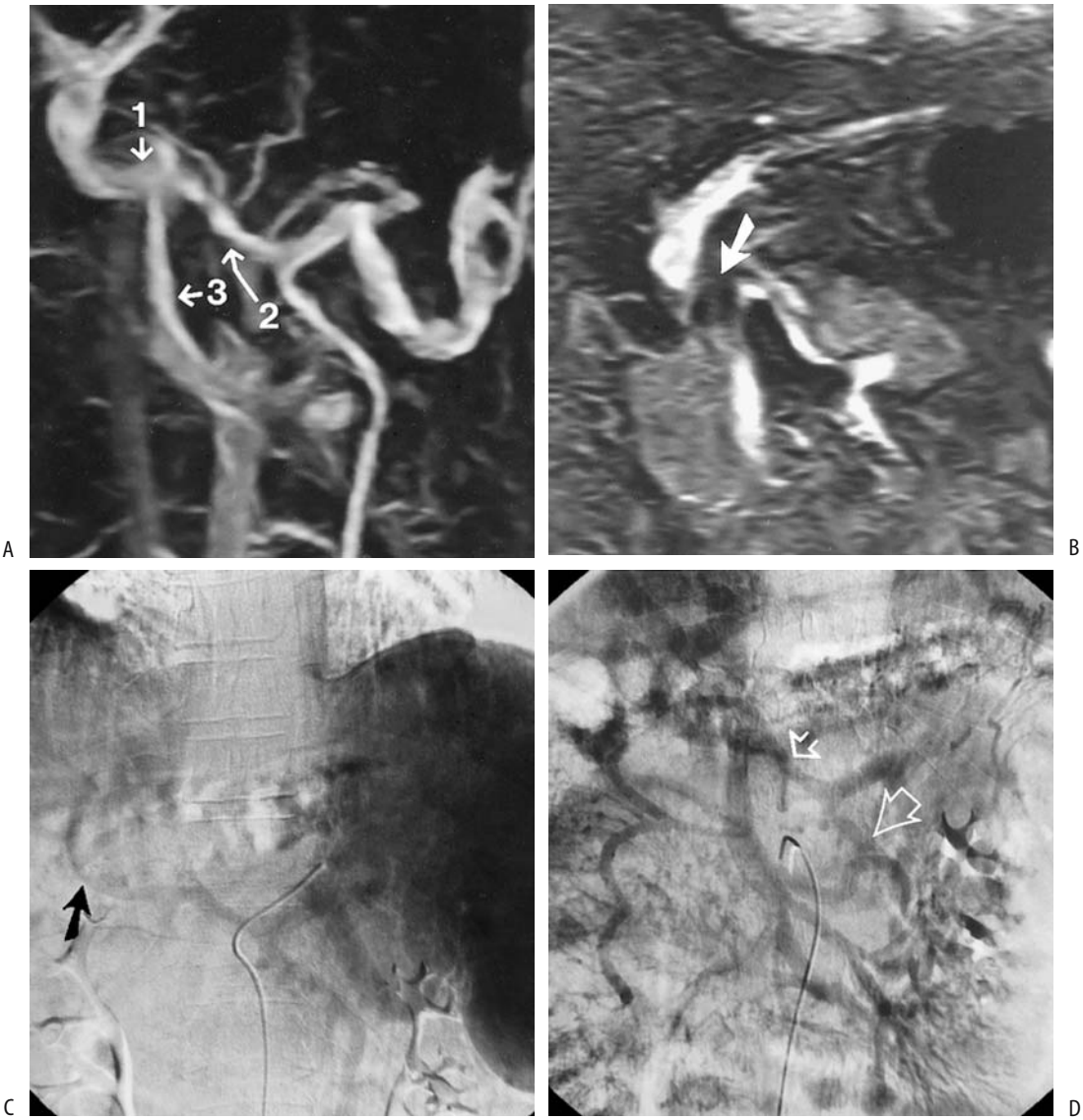

Figure 17.13. Portal vein thrombosis in a man with cirrhosis. A 3D magnetic resonance angiography (MRA) coronal maximum intensity projection (A) and coronal portal venous phase image (B) identify partial portal (1), splenic (2) and superior mesenteric (3) vein thromboses. C: DSA intraarterial splenoportography shows a collateral portal vessel (arrow). D: Mesenteric portography show portal vein thrombosis (small arrow), and retrograde flow is identified in the inferior mesenteric vein (large arrow). For full evaluation both MRA and DSA were necessary in this patient. (*Source:* Kreft B, Strunk H, Flacke S, et al. Detection of thrombosis in the portal venous system: comparison of contrast-enhanced MR angiography with intraarterial digital subtraction angiography. Radiology 2000;216:86–92, with permission from the Radiological Society of North America.)

lish a definitive diagnosis. Continuous flow, on the other hand, is seen with both benign and malignant thrombi. With slow portal vein blood flow Doppler US reveals no flow, but no thrombus is detected by gray-scale US. In patients with portal vein thrombosis Doppler US reveals a significantly lower mean hepatic artery resistive index than controls; such a lower resistive index is a secondary sign of portal vein thrombosis.

Published studies favor MR over US. MRI detects more occlusion or encasement of smaller portal vein branches than US, although occasionally the reverse is true. In general, MRI provides additional information over US in preoperative assessment of the portal venous system and MRA achieves a sensitivity and specificity similar to intraarterial DSA in assessing portal venous system patency or thrombosis in patients with portal hypertension (68). In fact, contrast enhanced 3-D MRA is emerging as the method of choice for studying the portal venous system in patients with portal hypertension, and thus potentially could replace DSA for this application.

Flowing blood within the portal vein appears as a void on both T1- and T2-weighted MR images. A thrombus appears similar to intraluminal soft tissue, although slow flow has a similar appearance (Fig. 17.14). On contrast-enhanced MR the normally hyperintense intraluminal blood is replaced by a hypointense thrombus. At times enhanced collateral circulation is identified. Any enhancing vessels within the thrombus suggest malignant infiltration.

Occlusion of an intrahepatic portal vein branch results in a peripheral wedge-shaped hyperintense segment on immediate contrast-enhanced MR due to a compensatory increased arterial blood supply. This segment gradually becomes isointense. One should keep in mind, however, that contrast-enhanced MRI reveals a signal-intensity decrease in some right (8%) and left (9%) portal vein branches and portal vein (6%) during the equilibrium phase (69); these flow artifacts tend to mimic a portal venous thrombosis.

Portal Vein Cavernous Transformation

Cavernous transformation represents formation of venous channels either within a thrombosed portal vein or in surrounding extraperitoneal tissues. Some fresh portal vein thrombi recanalize within days, but cavernous transformation of surrounding vessels, consist-

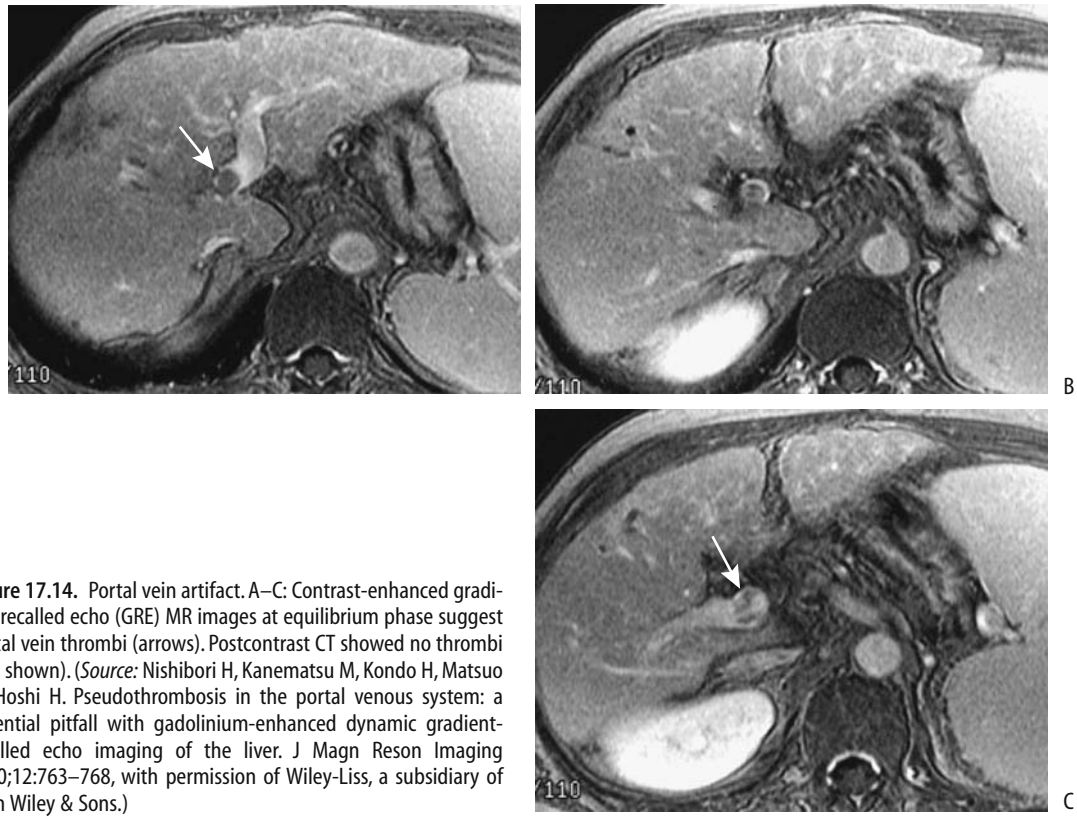

Figure 17.14. Portal vein artifact. A–C: Contrast-enhanced gradient-recalled echo (GRE) MR images at equilibrium phase suggest portal vein thrombi (arrows). Postcontrast CT showed no thrombi (not shown). (*Source:* Nishibori H, Kanematsu M, Kondo H, Matsuo M, Hoshi H. Pseudothrombosis in the portal venous system: a potential pitfall with gadolinium-enhanced dynamic gradient-recalled echo imaging of the liver. J Magn Reson Imaging 2000;12:763–768, with permission of Wiley-Liss, a subsidiary of John Wiley & Sons.)

ing of a sponge-like mass of collateral vessels around the main portal vein, takes several weeks. Collateral circulation develops via two pathways: First, portosystemic shunting such as through a left gastric vein and these portosystemic collaterals usually imply that portal hypertension is present. Second, portoportal channels develop and extend into intrahepatic portal venous branches. Cavernous transformation is associated with such conditions as chronic pancreatitis, tumor infiltration, and intraabdominal sepsis.

In a Spanish study of patients with cavernous transformation, predisposing factors were omphalitis, echinococcal cyst, major abdominal surgery, cirrhosis, Sjögren's syndrome, and idiopathic (70). A hydatid cyst in the porta hepatis can lead to cavernous transformation. The extent of collateralization varies considerably but tends to be more prominent with more chronic portal vein thrombi. Thus patients with portal vein thrombosis during childhood can eventually develop an extensive cavernous transformation involving adjacent structures. Many patients with congenital hepatic fibrosis have cavernous transformation of the portal vein.

Biliary veins (cystic and paracholedochal) represent an alternate blood flow pathway in cavernous portal vein transformation, and thus it is not uncommon to see numerous serpiginous extrinsic bile duct indentations. These bile duct varices can compress the extrahepatic bile ducts to the point of inducing biliary obstruction.

Of interest is that in most patients with cavernous transformation of the portal vein the pancreatic duct is smaller than normal, presumably due to pancreatic venous congestion.

In patients with cavernous transformation of the portal vein confirmed by angiography, color Doppler US detected the transformation in 93%, B-mode US in 64%, and contrast-enhanced CT in 50% of patients (71); color Doppler US was superior to B-mode US in identifying collateral channels.

Therapy

Treatment with heparin alone can result in recanalization of acute portal venous thrombosis. A number of case reports suggest that either intraportal plasminogen infusion or such therapy as plasminogen activator and urokinase through a transjugular intrahepatic catheter approach to the portal vein have dissolved thrombi.

Transjugular intrahepatic portosystemic shunting and thrombolysis appear to be viable therapy in patients with noncavernomatous portal vein thrombosis in order to increase portal output and restore portal blood flow; patent shunts can be achieved, although those with an initial complete thrombosis require more frequent shunt revisions than those with incomplete obstruction. Some of these patients continue to be symptomatic despite a functioning TIPS.

Few surgical options exist for chronic portal vein thrombosis. Lysis and thrombus aspiration, portal vein stenting, and TIPS are potential options.

Collateral Veins

Portosystemic Shunts

Extrahepatic portosystemic shunts are rare in absence of portal hypertension and in such a setting a congenital shunt origin is likely. An extrahepatic shunt, together with intrahepatic portal venous hypoplasia, generally implies a congenital basis. Some of these shunts in patients without portal hypertension can be rather large. Some are associated with hepatic encephalopathy and after successful shunt embolization encephalopathy clears.

In portal hypertension, for significant collaterals to open, the portocaval pressure gradient needs to be >12 mm Hg. Initially, as develops, the portal vein caliber increases, but the caliber tends to decrease once shunts start to form.

Traditionally conventional angiographic portography was used to evaluate portosystemic shunts, but 3D helical CT portography appears to be equal to and at times even superior to angiography (72). Results of CT portography can be used to plan therapy.

Esophagogastric Shunts: Esophageal and gastric fundal varices represent the most common spontaneous portosystemic shunts. A common pathway is from the portal vein, through the left gastric vein (also called the coronary vein) and into the gastroesophageal veins (varices). A common drainage path for these paraesophageal varices is via veins around the aorta into the hemiazygous vein. An alternate path is via a vein located anterior to the

inferior vena cava (precaval vein) and into the inferior vena cava.

Doppler US in the presence of these shunts reveals reversal of flow in the left gastric vein. A parallel pathway is from the splenic vein via the short gastric veins, which tend to dilate. Imaging detection of a dilated coronary vein implies either portal hypertension or splenic vein obstruction. The latter condition, of course, does not result in esophageal varices.

Splenomegaly is common in portal hypertension and the presence of esophageal varices, but little or no correlation exists between splenic size and size of esophageal varices.

Therapy and the resultant imaging of esophagogastric shunts are discussed in Chapters 1 and 2.

Intrahepatic Shunts: Spontaneous intrahepatic portal vein-to-systemic vein shunts are rare in a nondiseased liver. If present, aside from paraumbilical veins, they do not necessarily imply that portal hypertension is present; these shunts develop in either the right or left lobe and consist of either a single dilated vessel or multiple small veins. In the liver the left portal vein forms anastomoses with veins in the ligamentum terres and ligamentum venosum.

Gray-scale US reveals shunts as typical anechoic structures. Color Doppler US establishes flow patterns, such as bidirectional flow. Some shunts have a continuous flat portal vein flow pattern in both the shunt and the related hepatic vein. Computed tomography and MRI simply show abnormal vascular channels.

Patients with large intrahepatic portosystemic venous shunts develop hepatic encephalopathy. In symptomatic patients these shunts can be embolized using various coils and detachable balloons (73); retrograde transcaval obliteration is least invasive in treating simple portosystemic venous shunts.

Paraumbilical Collaterals: Paraumbilical veins are relatively common collaterals (Fig. 17.15). Rather than a single vein, it is usually a collection of veins close to the original obliterated paraumbilical vein. Located in the ligamentum teres, it connects the left portal vein and systemic abdominal wall collaterals and, when present, it is detected by US and the flow is established with Doppler US. Spontaneous formation of dilated umbilical veins should suggest portal hypertension (Cruveilhier-Baumgarten syndrome). Some patients develop a venous hum and a caput medusae. Occasionally esophageal variceal sclerotherapy in a patient with idiopathic portal hypertension leads to portal vein thrombosis at the origin of the umbilical vein and the disappearance of the venous hum and dilated abdominal wall veins characteristic of Cruveilhier-Baumgarten syndrome.

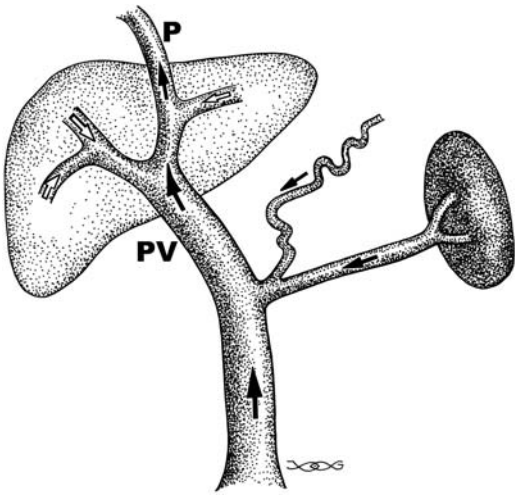

Figure 17.15. Effect of shunting via the paraumbilical vein (P). Hepatopetal portal vein (PV) flow is still maintained, but flow is reversed in the intrahepatic portal vein branches.

Why some patients develop markedly dilated paraumbilical veins rather than other collaterals is not known. In general, those having hepatofugal paraumbilical flow greater than hepatopetal portal vein flow tend not to develop esophageal varices. Turbulent flow is identified in some patients.

A dilated paraumbilical vein most often drains via the inferior epigastric vein into the external iliac vein. Less common is drainage via the superficial epigastric vein into either the internal thoracic vein or saphenous vein, pathways identifiable with color Doppler US.

Other Collaterals: The azygos vein, which drains esophageal varices, dilates in a setting of portal hypertension and esophagogastric varices. Endoscopic US visualizes this vein; its caliber is increased and maximal azygous vein blood velocity is greater in patients with varices compared to controls. An occasional large splenic vein-to-azygos vein shunt is detected in a noncirrhotic patient, presumably on a congenital basis. Similarly, spontaneous left gastric vein to left renal vein shunts can occur, often in a portal hypertension setting.

Less often encountered are gastroepiploic and splenorenal collaterals and shunting from the inferior mesenteric vein to the inferior hemorrhoidal veins (Fig. 17.16). A spontaneous shunt involving the right renal vein is rare. Likewise, portosystemic collaterals through duodenal and other extraperitoneal structures are uncommon.

Colonic variceal bleeding is rare, but at times is massive. Several studies suggest that colonic varices tend to become more prominent after successful sclerotherapy of esophageal varices and the resultant obliteration of coronary-azygous venous anastomoses.

The prevalence of mesenteric varices in portal hypertension is not known. Rupture of a mesenteric varix is a rare cause of hemoperitoneum. In patients with ascites and mesenteric varices, bleeding into the peritoneal cavity can follow large-volume paracentesis, possibly induced by the sudden decrease in intraperitoneal pressure due to fluid withdrawal.

In general, MRI detects more varices in more patients than does US.

In addition to endoscopic obliteration of esophagogastric varices (by sclerotherapy and other procedures), portosystemic shunts can be embolized. Such embolization generally helps control hepatic encephalopathy after the failure of medical management. In a setting of a large portosystemic shunt with considerable superior mesenteric venous blood flowing through the shunt, shunt obliteration tends to improve liver function.

Therapy of Portal Hypertension

Medical Therapy

In a patient with cirrhosis who bled, what are the relative roles of propranolol and sclerotherapy in preventing rebleeding and on survival? A meta-analysis of nine randomized trials concluded that the mean percentage of patients free of variceal rebleeding was 39% in the propranolol group and 55% in the sclerotherapy group, but that adverse events were higher in the sclerotherapy group (74); the mean survival rate, however, did not differ significantly. In this subgroup of patients, although sclerotherapy is more effective than propranolol in preventing variceal rebleeding, the authors suggest that propranolol is the preferred therapy for preventing rebleeding.

Beta-blocking agents reduce portal venous pressure in cirrhotic patients, although the results are somewhat idiosyncratic. The goal is to reduce the portal pressure gradient below 12 mm Hg. Beta-blockers do not achieve such pressure reductions in some patients, and their use is thus limited as prophylactic agents. A reduction in portal pressure appears to be potentiated by combining beta-blockers and isosorbide-5-mononitrate.

Both flow velocity and pulsatility index are obtained with Doppler US, although US is of limited value in discriminating good from poor responders to medical therapy (61).

Rectal Tc-99m–pertechnetate scintigraphy of collateral blood flow from the inferior mesen-

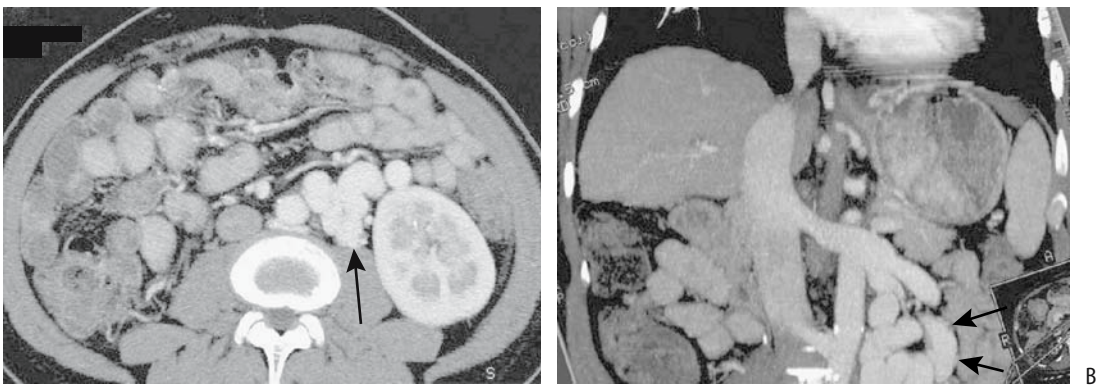

A B

Figure 17.16. Retroperitoneal shunt. A: Postcontrast CT shows tortuous, dilated vessels adjacent to left kidney (arrows). B: Coronal maximum intensity projection CT portal venography detects a tortuous shunt (arrows) communicating with left renal vein. (*Source:* Kang HK, Jeong YY, Choi JH, et al. Three-D multi-detector row ct portal venography in evaluation of portosystemic collateral vessels in liver cirrhosis. RadioGraphics 2002;22:1053–1061, with permission from the Radiological Society of North America.)

teric vein shows that propranolol in cirrhotics does reduce shunting; this response to propranolol appears to depend on the severity of liver disease.

Esophageal and gastric variceal sclerotherapy or variceal ligation helps control variceal bleeding but, theoretically at least, should not reduce portal hypertension. Nevertheless, portal venograms performed before and after variceal ligation reveal that although in a majority of patients portal pressure does increase, in a minority the pressure decreases, presumably due to the opening of other major collaterals.

Surgical Therapy

The ideal therapy of portal hypertension due to cirrhosis is liver transplantation, a procedure both complex and controversial.

Any abdominal surgery in a patient with varices is fraught with bleeding complications. Preoperative CTA, including 3D reconstruction, is very useful in outlining collateral vascular channels, especially in unusual locations, prior to shunting.

A portocaval shunt is performed either end-to-side or side-to-side. The former diverts all portal blood away from the liver. Some surgeons prefer a mesocaval interposition shunt using a graft between the superior mesenteric vein and vena cava, but a distal splenorenal shunt (Warren shunt) is performed more often (Fig. 17.17). The number of these procedures has decreased considerably since the advent of TIPS.

Shunt stenosis or occlusion should be suspected if recurrent variceal bleeding occurs after a surgically constructed shunt. Doppler US evaluates the patency of these shunts in most patients by detecting flow in both limbs and through the anastomosis. Percutaneous transcatheter angioplasty, and if necessary stent insertion, is worthwhile if shunt stenosis or occlusion is detected, but keep in mind that angioplasty of stenotic surgical shunts carries a risk of encephalopathy.

The Sugiura procedure consists of esophageal transection and esophagogastric devascularization, with a splenectomy also included by some surgeons. Hepatic function tends to worsen immediately postoperatively after a modified Sugiura operation but then improves. In patients with previous variceal bleeding, a modified Sugiura procedure results in somewhat greater survival rate than a portosystemic shunt. Esophageal transection does not cure esophageal varices, and in most patients they recur in time. New collaterals are also common at other sites.

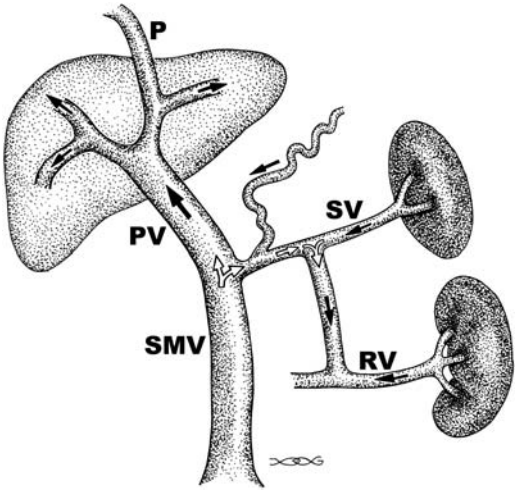

Figure 17.17. Effect of splenorenal shunt. Splenic vein (SV) and part of superior mesenteric vein (SMV) blood are shunted into the left renal vein (RV). Hepatopetal flow is still maintained in the portal vein (PV) and intrahepatic branches, in spite of a patent paraumbilical vein (P). With further increase in intrahepatic resistance portal vein flow will eventually reverse.

Transjugular Intrahepatic Portosystemic Shunting (TIPS)

Clinical Aspects: One reason why surgical portosystemic shunting is not performed more often is difficulty in predicting which patients will progress with their hepatic failure or develop significant encephalopathy. An orthotopic liver transplantation, on the other hand, although having its own morbidity and mortality, is not associated with subsequent hepatic failure or encephalopathy. In a setting of an acute variceal bleed, however, liver transplantation is often impractical and it is in this setting that TIPS evolved as a viable alternative to surgical portosystemic shunting. From a practical point of view, TIPS is less invasive than a surgical portosystemic shunt.

A relatively high prevalence of portal vein thrombosis is found in patients with portal

hypertension. It thus seems prudent to search for portal vein thrombosis, such as with contrast-enhanced CT, prior to TIPS. A finding of an extensive portal vein, splenic vein, and superior mesenteric vein thrombus renders TIPS meaningless.

Currently, TIPS is the therapy of choice for portal hypertension–associated complications in most patients. It decompresses the portal system by creating a side-to-side portosystemic anastomosis. It decreases portal hypertension without the associated mortality and morbidity of a laparotomy, but at the same time introduces its own complications. The current primary indications for TIPS consist of acute variceal hemorrhage not amenable to medical management, prevention of recurrent variceal bleeding, and refractory ascites due to portal hypertension. Less common indications include Budd-Chiari syndrome and cirrhotic hydrothorax. In patients with end-stage cirrhosis, TIPS gains time, and once the patient is stable an elective liver transplantation can be performed. In patients with portal hypertension-associated colopathy, TIPS controls bleeding from angiodysplasia-like colonic lesions. It is effective in high-risk patients with continued bleeding from esophagogastric varices despite sclerotherapy or failure of surgical shunting. Massive bleeding from peristomal ileal conduit varices has been successfully treated with TIPS (75). In a number of patients with varices and a malignancy, TIPS aids subsequent surgery. Thus control of esophagogastric varices allows transcatheter hepatic segmental artery chemoembolization of a hepatocellular carcinoma. Similarly, TIPS in a patient with esophageal varices and an esophageal carcinoma decreases portal venous pressure and lessens the risk of hemorrhage during subsequent carcinoma therapy.

One subgroup of patients consists of those in whom endoscopic sclerotherapy for acute variceal bleeding fails and TIPS is requested on an emergency basis. These are high-risk patients. One study reported a 30-day mortality of 50% in emergency TIPS patients compared to 7% for elective TIPS (76). TIPS may not be justified in patients with uncontrolled acute variceal bleeding and advanced liver disease, sepsis and multiorgan failure.

Current evidence suggests that preoperative TIPS does not directly affect subsequent liver transplantation; TIPS neither hinders nor facilitates surgery, nor influences postoperative survival. Subsequent transplantation operative time and transfusion requirements do not differ from those without TIPS. Malpositioned shunts, on the other hand, do interfere with subsequent orthotopic liver transplantation. They interfere with cross-clamping at the usual vascular sites during liver transplantation and prolong surgery and in such a situation the transplant team should be made aware of a shunt malposition.

Although the experience with TIPS has been limited, it is feasible and appears as safe in children as in adults, although it is technically more difficult in children and takes longer. Only limited experience is available in infants and younger children.

Secondary hypersplenism is commonly associated with portal hypertension and these patients often have leukopenia and thrombocytopenia; TIPS tends to improve secondary hypersplenism.

Technique: Prior to performing TIPS, interventional radiologists prefer to outline the hepatic vascular anatomy, determine the portal venous blood flow direction, and detect any underlying collateral shunts. These factors can be evaluated by several imaging techniques. Overall, MRI appears to provide more useful information than CT or US.

In experienced hands a TIPS shunt is installed in approximately 2 hours. It is performed using conventional angiographic techniques of angioplasty and a transjugular venous approach, the hepatic veins are catheterized and used to create an intrahepatic shunt between a portal vein branch and a systemic hepatic vein. It is a side-to-side portocaval shunt (Fig. 17.18). Color Doppler US during the procedure aids in selecting the most appropriate veins for puncture. If necessary, transjugular cholangiography defines underlying biliary anatomy. Postprocedure Doppler US evaluates shunt patency.

During TIPS, the catheter and guidewire pass through the right atrium, and thus cardiac arrhythmias are to be expected. Even in patients with no known underlying heart or electrolyte abnormality, nonsustained ventricular tachycardias are common.

An ideal shunt diameter is one that maintains the patient's liver function, preprocedure varices or ascites resolves, and no hepatic

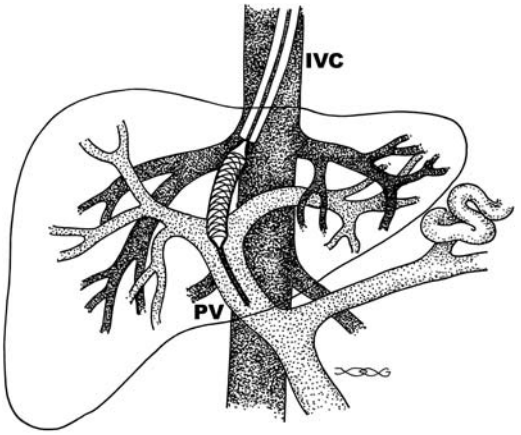

Figure 17.18. Creation of an intrahepatic portosystemic shunt. A mesh stent is shown being inserted through a catheter and over a guidewire. IVC, inferior vena cava; PV, portal vein.

encephalopathy develops. A too-small shunt does not reduce the portosystemic pressure gradient enough to correct an underlying abnormality (Fig. 17.19). An overgenerous shunt, on the other hand, risks hepatic encephalopathy. Also, larger-caliber Wallstents have decreased radial strength and yield poorer results. The optimal shunt diameter is estimated before the procedure from the patient's hepatic reserve, presence of encephalopathy, and potential for bleeding.

Results: A transjugular intrahepatic portosystemic shunt is one of the most difficult intervention procedures performed, and thus the success rates and complications depend considerably on operator skill and experience. In most studies the success rate in achieving a patent portosystemic shunt with TIPS ranges over 90%. Numerous studies point to TIPS as being effective therapy for portal hypertension and a successful technique in managing variceal bleeding or (less often) intractable ascites. Several randomized studies suggest that in a setting of variceal bleeding patient survival is similar in those undergoing TIPS and those undergoing endoscopic variceal therapy. On a short-term basis TIPS appears to be equally effective in controlling both gastric fundal and esophageal variceal bleeding. Reintervention is eventually required in a majority of patients, with most reinterventions occurring during the first year after TIPS.

A meta-analysis of 11 randomized clinical trials containing 750 patients comparing TIPS with endoscopic therapy found that TIPS markedly reduces the risk of rebleeding but at

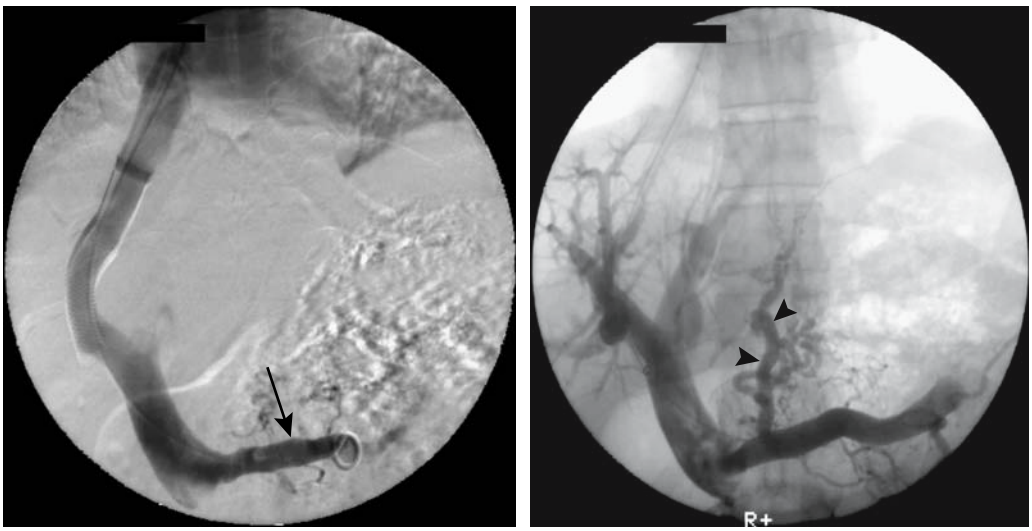

Figure 17.19. A: Transjugular intrahepatic portosystemic shunt (TIPS) insertion in a patient with portal hypertension. B: Angiogram after shunting reveals back-flow into the splenic vein (arrow) and coronary vein (arrowheads). (Courtesy of David Waldman, M.D., University of Rochester.)

an increased risk of encephalopathy and without affecting survival (77); TIPS dysfunction developed in 55% of these patients. Survival, however, appears similar in both groups.

Published TIPS mortality rates depend on patient status pre-TIPS. The most frequent cause of death beyond the acute period is progression of liver failure. Mortality rates correlate with a higher Child's classification.

Long-term follow-up reveals a decrease in blood urea nitrogen, an increase in albumin, and a return of bilirubin to initial levels or lower; surviving patients have an improved quality of life. The progression of acute liver failure is not common after successful TIPS, although in some patients the effects of TIPS on liver function are unpredictable. One measure of liver metabolic function is the arterial ketone body ratio, defined as arterial acetoacetate level divided by β-hydroxybutyrate level. This arterial ketone body ratio appears to have prognostic implications; among patients the 30-day post-TIPS mortality in those with a pre-TIPS ratio ≤0.5 was 75%, a rate higher than the 14% rate in patients with a pre-TIPS ratio >0.5 (76).

The results of TIPS performed primarily for ascites are discussed in Chapter 14; TIPS appears effective in reducing ascites and improving renal function in patients with functional or organic renal disease (78).

One unrelated outcome is that esophageal motor function tends to improve after TIPS without inducing any gastroesophageal reflux. An occasional protein-losing enteropathy associated with portal hypertension also resolves after TIPS.

Transjugular intrahepatic portosystemic shunting has a limited effect if a large spontaneous portosystemic shunt already exists. If necessary, embolization is an option when such a portosystemic shunt is discovered. Also, occasionally complications dictate TIPS shunt obliteration, which can be performed.

Transjugular portosystemic shunting results in systemic hemodynamic changes, with the major long-term hemodynamic alteration being an increase in pulmonary vascular resistance. Right atrial and pulmonary artery pressures increase, cardiac output increases, and peripheral resistance decreases. In patients with an elevated systemic venous pressure, reduction of the portosystemic pressure gradient after TIPS increases right atrial pressure further and accentuates any underlying congestive failure.

As expected, TIPS induces an immediate decrease in portal pressure and an increase in portal blood flow. A typical pre-TIPS portocaval pressure gradient of about 20 to 22 mm Hg decreases to <10 mm Hg. Compensatory hepatic artery flow increases, but no overall splanchnic and liver perfusion changes occur. Although the portocaval pressure gradient decreases after TIPS, eventually the pressure again increases. Patients developing ascites usually have a portocaval pressure gradient >12 mm Hg.

One alternative to Doppler US follow-up is Tc-99m–diethylenetriamine pentaacetic acid (DTPA) liver perfusion scintigraphy. Relative arterial and portal liver inflow can be calculated from a biphasic time-activity curve. Technetium-99m–macroaggregated albumin (MAA) injected into the portal veins evaluates portosystemic shunting by comparing counts in the lungs and liver; the amount of shunting correlates inversely with portosystemic pressure gradient. The clinical application of such scintigraphy remains to be established.

Shunt Stenosis/Occlusion: The most common TIPS complication is shunt stenosis, often requiring revision. Why do shunt stenoses develop? Autopsy study of three livers containing four TIPS tracts revealed short- and midterm TIPS occlusions to be caused by thrombi associated with hepatocyte necrosis and bile leakage, while long-term stenoses consisted of a combination of pseudointimal hyperplasia and hepatocyte ingrowth (79). Biopsies in patients with a shunt stenosis tend to reveal bile within an organising thrombus; the degree of stenosis appears related to amount of bile leakage. A rare shunt thrombosis extends proximally to involve the portal, splenic, and mesenteric veins.

Shunt stenosis or occlusion is suspected either with routine radiologic screening or when the patient develops recurrent symptoms; it is this complication that limits TIPS as an optimal long-term solution for portal hypertension. The prevalence of shunt stenosis or occlusion appears independent of a patient's Child-Pugh class.

Anticoagulation appears to aid early shunt patency but probably does not affect patency on a long-term basis.

Recurrent portal hypertension due to stent thrombosis, stenosis, or stent retraction develops during the first year in over half of patients. Portography and portal manometry serve as gold standards in detecting and characterizing shunt stenoses, but, being invasive, are used only when other imaging is noncontributory. Endoscopic detection of varices is a less sensitive method, but appears superior to Doppler US. Although hepatic vein stenosis appears to be relatively common after TIPS, it is rarely symptomatic.

Ultrasonography is often used in evaluating TIPS shunt patency, although CTA shows considerable promise in detecting most shunt dysfunctions; CTA achieved a 92% sensitivity and 77% specificity in detecting hemodynamically significant TIPS abnormalities (80). Although these values are similar to the results obtained with US, CTA eliminates a subjective bias inherent in performing US through an often narrow acoustic window; 3D multiplanar reconstruction CTA is very helpful.

The degree of stenosis beyond which revision is necessary is not clear. At times lumen reduction of even 10% requires intervention due to a high portosystemic gradient; these mild stenoses are generally due to intimal hyperplasia.

Doppler US of portal venous flow reveals considerable variability in repeat measurements, and published studies are not always comparable. In spite of publications such as "The Inaccuracy of Duplex Ultrasonography in Predicting Patency of Transjugular Intrahepatic Portosystemic Shunts" (81) in the gastroenterology literature, most investigators believe that duplex US identifies flow within a shunt. Typical blood velocities within patent, well-functioning shunts are within the 120 to 200 cm/sec range, often associated with a reversal of intrahepatic portal vein flow. Portal vein velocity increases from about 20 cm/sec to 40 cm/sec. In a thrombosed shunt Doppler US does not detect flow. In the practical sense, the issue is more complex because a shunt Doppler signal is not detected even from some patent shunts.

Either a Doppler US measurement of maximum peak velocity of 50 cm/sec or less within the shunt or a change from hepatofugal to hepatopetal portal venous flow indicates shunt stenosis. Using these criteria, Doppler US identifies TIPS occlusion and confirmed patency in over 95% patients. A choice of 50 cm/sec shunt peak velocity is, of course, not absolute. An assumption of a greater Doppler US shunt peak velocity threshold improves the specificity of detecting normal shunt function. One further refinement is the use of either an increase or decrease in shunt peak velocity of more than 40 or 50 cm/sec from the initial post-TIPS baseline value as a cutoff criterion; such a change in shunt peak velocity appears to be a more sensitive sign of shunt stenosis than simply a low flow state. Also, blood flow in the right anterior portal vein becoming hepatopetal after TIPS is indirect evidence of shunt stenosis or occlusion.

Doppler US shunt velocity varies between the portal vein end and hepatic vein end. Thus in patients with functioning TIPS, median shunt velocity was 60 cm/sec at the portal vein end and increased to 82 cm/sec at the hepatic vein end (82); velocity is reduced in patients with compromised shunts. The use of the IV US signal enhancer Levovist improves color and flow signals (compared to pre-Levovist) at the portal vein shunt end in only 24% of studies but improved hepatic vein shunt end (83); more stenoses are identified with Levovist, with most stenoses being located at the hepatic vein shunt end evaluation of both shunt ends. Evaluation should be performed by Doppler US.

In a number of institutions Doppler US has replaced angiography as the post-TIPS screening modality. Yet published sensitivities and specificities of Doppler US in detecting TIPS stenosis or occlusion are difficult to place in proper perspective. Some of the studies conflict. Several more optimistic studies report almost 100% sensitivity and specificity in detecting stenosis or occlusion. Some authors ascribe Doppler US false-positive or false-negative diagnoses to technical factors, including the type of stent used. Thus, in one study a shunt velocity of <60 cm/sec achieved a sensitivity of only 25% and specificity of 93% in detecting shunt stenosis (84); a high sensitivity (90%) could only be achieved at the expense of poor specificity (<33%). Some studies suggest that shunt or portal vein Doppler US velocities correlate poorly with portal pressure.

In summary, most patent shunts have a velocity >70 cm/sec and hepatofugal flow in the liver portal vein branches; in general, midshunt

velocities of <60 cm/sec should suggest shunt dysfunction. It should be kept in mind, however, that Doppler US rarely identifies the cause of shunt stenosis.

Once a stenosis is suspected and is confirmed by venography, percutaneous transluminal angioplasty is the primary therapy to reestablish shunt patency, with multiple interventions necessary in some patients (Fig. 17.20). Patients treated by dilation tend to develop a restenosis, but those managed by insertion of new shunts tend to remain patent.

A rheolytic thrombectomy catheter is designed to remove thrombi by fragmentation and suction. It uses multiple retrograde high-speed fluid jets to create a recirculating vortex that fragments the adjacent thrombi, and the thrombi are then evacuated through an aspiration lumen. It can recanalize an acutely occluded TIPS stent.

Other Complications: Other complications include intraperitoneal hemorrhage, hematoma, hemobilia, accelerated liver failure, hepatic vein stenosis, and infection. Less commonly encountered are perforation through the liver capsule, stent migration with portal vein perforation and portal vein dissection, thrombosis, and laceration. Occasionally a stent migrates; some of these stents have been successfully retrieved. Inadvertent hepatic artery puncture has resulted in fatal hemorrhage. Likewise, right atrial and aortic perforation during stent placement can lead to hemopericardium and cardiac tamponade.

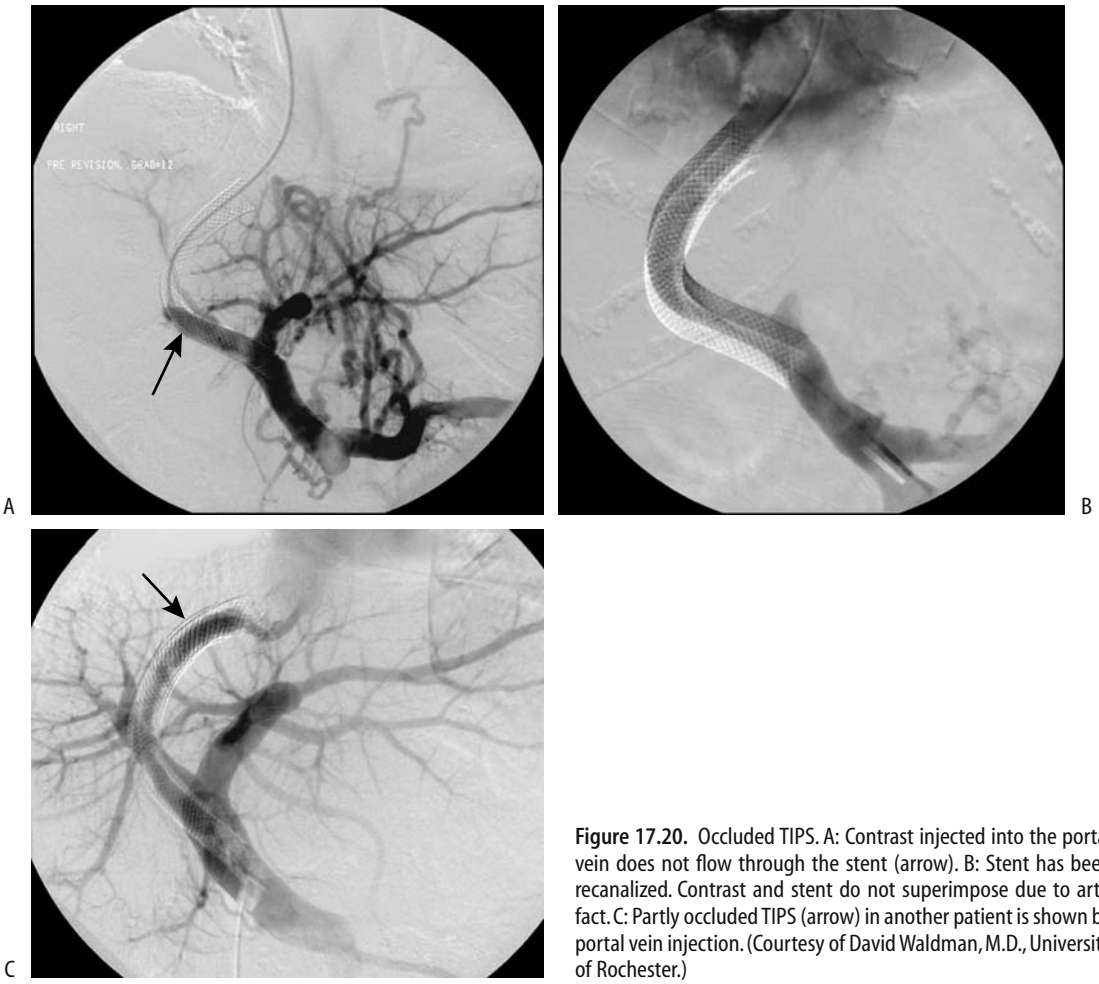

Figure 17.20. Occluded TIPS. A: Contrast injected into the portal vein does not flow through the stent (arrow). B: Stent has been recanalized. Contrast and stent do not superimpose due to artifact. C: Partly occluded TIPS (arrow) in another patient is shown by portal vein injection. (Courtesy of David Waldman, M.D., University of Rochester.)

Sepsis following TIPS is not common, and the significance of TIPS infections is poorly understood. Reported findings in patients believed to have a primary shunt infection include tender hepatomegaly, hypoxemia, septic pulmonary emboli, septic shock, and necrotizing fasciitis; blood cultures tend to be positive.

Hepatic encephalopathy develops in 15% to 30% of patients after TIPS, presumably due to their increased portosystemic shunting. It is more frequent during the first 3 months after TIPS, and a majority of these patients have a portocaval pressure gradient of <12 mm Hg. The prevalence of encephalopathy appears increased in patients undergoing TIPS for refractory ascites. Doppler US appears useful in predicting the risk of encephalopathy; encephalopathy developed in 83% of patients with Doppler US evidence of hepatofugal blood flow in both right and left portal vein branches, but encephalopathy occurred in only 12% of patients with hepatopetal blood flow (85). In most patients encephalopathy can be controlled medically. Symptomatic encephalopathy is a consideration for subsequent liver transplantation.

^{1}H-MR-spectroscopy of brain metabolites is useful in liver transplantation to evaluate hepatic encephalopathy (86); whether such spectroscopy has a role after TIPS-associated hepatic encephalopathy is unclear.

A rare TIPS complication is liver infarction.

Portal Vein Stenting

Portal vein stenting is an option in patients with an unresectable pancreatic or biliary tumor invading the portal vein and leading to portal hypertension. These stents are inserted after percutaneous transhepatic portography evaluates the underlying anatomy. In 13 such patients, the mean portal venous pressure decreased significantly immediately after stent placement, but follow-up revealed increased risk of stent occlusion in those with initial splanchnic vein tumor involvement (87).

Portal Vein Aneurysm

Portal and splenic vein aneurysms, especially those extrahepatic in location, are rare. Most are associated with portal hypertension or an arterioportal fistula. Some are congenital in origin; others are related to previous trauma.

Most portal vein aneurysms are asymptomatic. They occur at any age. A number of these aneurysms gradually increase in size with time, often with progression of portal hypertension.

Some patients have both an arterioportal fistula and a portal vein aneurysm, an association that appears to be more than fortuitous. In some of these patients the aneurysm thromboses after percutaneous arterial embolization closes the fistula.

Portal vein aneurysms tend to be fusiform, while intrahepatic ones are mostly cystic. Unless thrombosed, US reveals these aneurysms to be anechoic. Contrast-enhanced CT or 3D power Doppler US should detect an aneurysm and identify any portosystemic fistulas. Doppler US shows turbulent flow in most. Portal venography is rarely necessary for diagnosis.

Portal Vein Gas

The most common etiology for portal venous gas is bowel ischemia; some of the other reported associations presumably have ischemia as a common pathway (Table 17.3). Some of the listed conditions, especially in pediatric patients, have a benign course. Some cystic fibrosis patients have both portal and systemic venous gas, and presumably gas is shunted from the portal circulation via the inferior mesenteric vein and hemorrhoidal veins into the inferior vena cava.

Table 17.3. Etiologies of portal venous gas (listed from more common to less common)

Bowel ischemia
Necrotizing enterocolitis in babies
After colonoscopy
Trauma
With increased bowel intraluminal pressure due to lumen obstruction
After double-contrast barium enema in pediatric patients
Colonic diverticulitis
Endoscopic retrograde cholangiopancreatography and sphincterotomy
Associated with pneumatosis intestinalis in the pediatric age group
Intraabdominal infection with a gas-forming organism
In a setting of hypertrophy pyloric stenosis
Perforated duodenal ulcer complicated by an abscess
After a seizure
In a patient with cystic fibrosis with bowel obstruction

Traditionally, conventional radiographs have identified portal gas. It appears as multiple, branching, linear lucencies in the liver and is familiar to radiologists. Conventional US, color Doppler flow imaging, and CT have a high sensitivity in detecting portal gas; of these modalities, CT appears most useful in suggesting an etiology. Doppler US reveals venous gas as turbulent flow with fleeting echoes. Gas bubbles result in a highly echogenic appearance, often transient in nature.

Portal Vein Tumors

Primary portal vein neoplasms are rare. An adjacent extrinsic carcinoma often invades the portal vein, encases it, and eventually obstructs. The most common is pancreatic carcinoma, with those originating in the body and tail of the pancreas invading the splenic vein, and pancreatic head cancers invading the portal vein. Similarly, metastases to the porta hepatis invade not only the portal vein but also adjacent bile ducts.

The role of CT and MR in preoperative staging of portal vein invasion is still evolving. Whether Doppler US is comparable to angiography or CT arterial portography in detecting portal vein encasement or occlusion is debatable.

Calcifications

Portal vein calcifications are rare, with the pertinent literature consisting mostly of case reports. One CT study, however, found an 11% prevalence of portal and mesenteric venous calcification in patients with advanced cirrhosis (88). Most patients are adults with long-standing portal hypertension.

Some portal vein thrombi calcify. These calcifications appear as linear or mottled densities corresponding to the portal vein path.

Portal vein calcifications are better identified with CT than with conventional radiography. They should not be confused with intrapancreatic calcifications, atherosclerosis, or aneurysmal calcifications.

Other Findings

Not uncommonly segments of portal vein branches are opacified during CT hepatic arteriography. These arterioportal shunts can be divided into intrahepatic and extrahepatic. Causes for intrahepatic shunting include tumors—mostly hepatocellular carcinomas, previous liver biopsy, and portal vein thrombosis, regardless of cause (89); extrahepatic causes include inflow through adjacent organ portal collateral circulations.

Portal and mesenteric vein septic thrombophlebitis is usually secondary to other foci of infection. Sigmoid diverticulitis, appendicitis, infected pancreatitis, and similar entities are generally responsible; they are discussed in their respective chapters. Computed tomography readily detects such thrombophlebitis.

A portal vein graft was inserted during a pancreatic resection and Whipple procedure (90); rectal evacuation of the portal vein graft occurred as a late complication, presumably induced by graft infection.

Splenic Vein

Splenic vein obstruction is often clinically silent, although in a minority of patients it results in splenic infarction or leads to gastrointestinal bleeding. The most common etiologies of splenic vein thrombosis are pancreatitis and pancreatic carcinoma. An occasional adjacent tumor, such as a pancreatic cystadenoma, compresses the splenic vein. Perihilar splenic varices secondary to a splenic hilar hydatid cyst compressed adjacent hilar vessels (91). An association of celiac disease and splenic venous thrombosis has been raised (92).

Without underlying liver disease, these patients tend to develop gastric varices without esophageal varices, although splenic vein thrombosis tends to extend and involve the portal vein. Occasionally gastric fundal varices are associated with colonic varices. In some patients the spleen becomes enlarged; in fact, splenic vein obstruction should be considered in the differential diagnosis in a patient with gastrointestinal bleeding occurring in a setting of unexplained splenomegaly.

Splenic vein occlusion is diagnosed by CT, conventional and endoscopic US, MRI, or angiography. Computed tomography reveals no splenic vein visualization but perigastric collateral veins are present; these are indirect signs, and an occasional obstruction detected

by angiography is not identified by CT. At times splenic vein thrombosis reveals a hypodense splenic vein, collateral vessels, and a patent portal vein. Ultrasonography shows an echogenic thrombus in the splenic vein lumen.

Splenic vein aneurysms are rare. An occasional aneurysm regresses after resolution of splenomegaly.

Pancreatic pseudocysts occur in the general location of the splenic and portal veins. An occasional one erodes into the splenic vein.

Superior Mesenteric Vein

Superior mesenteric vein thrombosis is idiopathic, associated with an underlying malignancy, develops in hypercoagulable states, and occurs in a setting of pancreatitis, sigmoid diverticulitis, or appendicitis, and as a sequela after abdominal surgery such as a Whipple procedure or even a complicated appendectomy (Fig. 17.21). It occurs in young patients. Acute thrombosis, in the absence of collaterals, often progresses to intestinal infarction. A more chronic course leads to pain, diarrhea, and malabsorption.

The major issue with superior mesenteric vein thrombosis is that the clinical presentation is usually sufficiently vague and the diagnosis is initially overlooked. The mortality from this condition has not changed significantly over the years. Complicating the picture is the frequent presence of other intraabdominal disease.

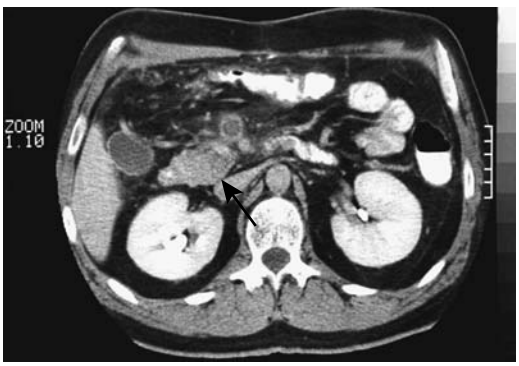

Figure 17.21. Superior mesenteric vein thrombosis after appendectomy. Contrast-enhanced CT reveals an enlarged vein, an intraluminal clot and an enhancing vein wall (arrow). (*Source:* Schmutz GR, Benko A, Billiard JS, Fournier L, Péron JM, Fisch-Ponsot C. Computed tomography of superior mesenteric vein thrombosis following appendectomy. Abdom Imaging 1998;23: 563–567, with permission from Springer-Verlag.)

Figure 17.22. Superior mesenteric vein thrombosis. Contrast-enhanced CT shows an enlarged, enhancing superior mesenteric vein and an intraluminal clot (arrow). (Courtesy of Gérard Schmutz, M.D., Centre Hospitalier Universitaire, Caen, France.)

Occasionally an acute thrombus resolves spontaneously. In most patients, however, prompt diagnosis and therapy with thrombolytic, anticoagulant, antiplatelet, or antispasmodic agents is warranted to prevent complications and reduce mortality. At times selective superior mesenteric artery infusion of urokinase is helpful.

Computed tomography shortly after clot formation reveals a thrombus to have a higher density than does soft tissues. The superior mesenteric vein is often enlarged. Later, a characteristic CT appearance consists of a hypodense central thrombus surrounded by a higher density wall (Fig. 17.22). At times a thrombus extends into the portal vein. With incomplete lumen obstruction, contrast-enhanced blood surrounds a lower density thrombus. The vein wall enhances after contrast. Surrounding mesenteric edema is not uncommon.

Inferior Mesenteric and Pelvic Veins

Septic thrombophlebitis of the inferior mesenteric vein is most often secondary to sigmoid diverticulitis. It is readily detected with CT.

Contrast-enhanced MR venography using a blood-pool contrast agent outlines major pelvic veins and evaluates for pelvic vein thrombosis. Superimposed arterial structures can be minimized by a subtraction technique.

Budd-Chiari Syndrome

Clinical

Budd-Chiari syndrome consists of obstruction to the venous outflow from the liver. The reported prevalence of Budd-Chiari syndrome varies throughout the world, in part due to different reporting criteria. The older literature considered only acute obstruction under Budd-Chiari syndrome, although currently the definition has been expanded to also include a more common chronic form. It is caused by hepatic vein obstruction or, less often, obstruction in the adjacent inferior vena cava (Table 17.4). In Japan, most patients with Budd-Chiari syndrome have a chronic form; the etiology is idiopathic in the majority, and over 90% have obstruction in the intrahepatic portion of the inferior vena cava. The most common direct underlying cause of Budd-Chiari syndrome in Western countries is either hepatic vein or inferior vena caval thrombosis. Patients developing a Budd-Chiari syndrome believed to be idiopathic in origin should be investigated for an undetected latent coagulation disorder. Other causes include a web-like membranous obstruction of the inferior vena cava, a condition more common in the Orient. Trauma is a rare cause of Budd-Chiari syndrome. Major hepatic surgery with compromise of the hepatic veins or intrahepatic portion of the inferior vena cava is an occasional predisposing factor. A renal cell carcinoma, a rare adrenal neoplasm with inferior vena cava invasion, retroperitoneal sarcoma, and malignancies involving the inferior vena cava also result in Budd-Chiari syndrome. Hepatic vein thrombosis is a complication of Behçet's disease, and Budd-Chiari syndrome should be suspected if hepatomegaly and ascites are detected in this disease. A rare cause of acute Budd-Chiari syndrome is percutaneous insertion of a transhepatic inferior vena cava catheter.

Regenerative liver nodules are more prevalent in chronic Budd-Chiari syndrome than expected. The question of whether this syndrome is linked to an increased risk for hepatocellular carcinoma has been raised. Complicating this question, some of these patients have underlying cirrhosis.

The onset of symptoms in Budd-Chiari syndrome ranges from acute to insidious. Initially liver dysfunction is mild, but gradually hepatomegaly, ascites, and complications of portal hypertension ensue. The presentation is complicated by associated portal vein, splenic vein, or superior mesenteric vein thrombosis, which also develop in some patients. A majority of these patients have limited therapeutic options and a poor prognosis.

From a clinical viewpoint it is useful to subdivide Budd-Chiari syndrome into acute and chronic presentations. From an anatomic viewpoint, a subdivision into a partial obstruction limited to thrombosis of one hepatic vein and a more complete obstruction involving more of the liver drainage is more informative. Complete obstruction of the hepatic veins is rare; drainage of the caudate lobe tends to be preserved unless the adjacent inferior vena cava is obstructed. Especially in chronic obstruction, accessory hepatic veins enlarge and become evident. At times the obstruction involves mostly smaller veins, with the main hepatic veins being patent.

Table 17.4. Conditions associated with Budd-Chiari syndrome

Idiopathic
Vascular conditions
Veno-occlusive disease
Inferior vena cava web or membrane
Inferior vena caval narrowing induced by right hemidiaphragm elevation
Behçet's disease
Polycythemia vera
Thrombotic thrombocytopenic purpura in a pregnant patient
Drug induced
Oral contraceptives
Neoplasms
Hepatocellular carcinoma
Inferior vena cava or hepatic vein sarcoma
Adjacent neoplasm invading inferior vena cava
Pregnancy
Infection
Trauma
Other
Hypereosinophilic syndrome
Systemic lupus erythematosus

Imaging

Imaging findings differ between acute and chronic liver outflow obstruction. Hepatomegaly, especially with caudate lobe enlargement and central liver contrast enhancement are common with acute obstruction. Left lobe, and especially caudate lobe hypertrophy and an irregular liver surface develop on a more chronic basis. Liver enhancement varies in chronic obstruction depending on degree of subcapsular collaterals and portal blood stasis. Homogeneous enhancement is found with less severe chronic obstruction, probably due to extensive collateral drainage.

The gold standard in diagnosing Budd-Chiari syndrome is inferior cavography and selective hepatic venography, yet the diagnosis can often be suspected with CT, US, MRI, or scintigraphy. Occasionally the condition is misdiagnosed as an infiltrating tumor. In particular, portal vein blood flow abnormalities are common in Budd-Chiari syndrome, and a misdiagnosis of primary portal hypertension should be avoided.

Computed tomography in patients with acute Budd-Chiari syndrome reveals hepatomegaly, a heterogeneous hypodense liver showing decreased central postcontrast enhancement, and marked ascites. Caudate lobe enlargement is common even with an acute onset, at times compressing the adjacent inferior vena cava. Veins draining the caudate lobe dilate. An irregular liver outline develops, but the liver is not nodular as found in cirrhosis.

Ultrasonography suggests Budd-Chiari syndrome if gray-scale US identifies hepatic veins and Doppler US detects either no blood flow or a reversal of flow. Likewise, the syndrome should be suspected if both gray-scale and Doppler US fail to identify hepatic veins. Normal flow in the inferior vena cava varies with respirations and cardiac cycle, but in some patients with Budd-Chiari syndrome and partial vena caval obstruction either reversed or continuous caval flow is detected by Doppler US. Still, the specificity with US is low.

Not only does the caudal lobe enlarge in Budd-Chiari syndrome, but the caudate vein also becomes prominent. In fact, US detection of a caudate vein equal to or >3 mm in diameter, in the appropriate clinical setting, should suggest Budd-Chiari syndrome (93).

Both morphological and perfusion abnormalities are defined with MR angiography. The MR postcontrast appearance varies depending on chronicity. Acute Budd-Chiari syndrome results in early homogeneous enhancement of an enlarged caudate lobe and heterogeneously decreased enhancement of the rest of the liver; central liver portions enhance considerably more than the periphery. Magnetic resonance imaging identifies ascites, major hepatic vein thrombi, and alternate venous pathways; it detects either hepatic vein thrombosis or simply the absence of hepatic venous flow (94).

During the subacute obstruction phase, postcontrast CT enhancement differences between the central and peripheral liver become less pronounced than during the acute phase. Computed tomography of chronic Budd-Chiari syndrome results in caudate lobe and usually left lobe hypertrophy and varying degrees of right lobe atrophy, with the hypertrophic regions having heterogeneous postcontrast enhancement. Ascites is not as prominent as with an acute syndrome. Computed tomography arterial portography reveals similar heterogeneous liver contrast enhancement in a setting of vascular congestion.

Fibrosis ensues during the chronic phase, identified by its hypointense signal on both T1- and T2-weighted images. Major venous thrombosis is not a prominent feature of chronic Budd-Chiari syndrome; instead, detected are extensive collaterals, caudate lobe enlargement, and regenerative nodules in less affected portions of the liver. These nodules are hyperintense on T1- and iso- to hypointense on T2-weighted images and enhance during the arterial phase. Collateral vessels are best identified during the portal vein phase.

Inferior vena caval involvement ranges from obstruction by a thrombus, to a web resulting in partial obstruction, to the vena cava being compressed by an enlarged caudate lobe. Occasionally vena cavography and hepatic venography fail to identify the full extent of venous outflow obstruction; in such a setting percutaneous transhepatic venography appears useful to define the proximal and distal ends of an occlusion.

With a simple obstruction the portal venous system is not affected, but an extensive obstruction results in flow reversal. Alternate venous

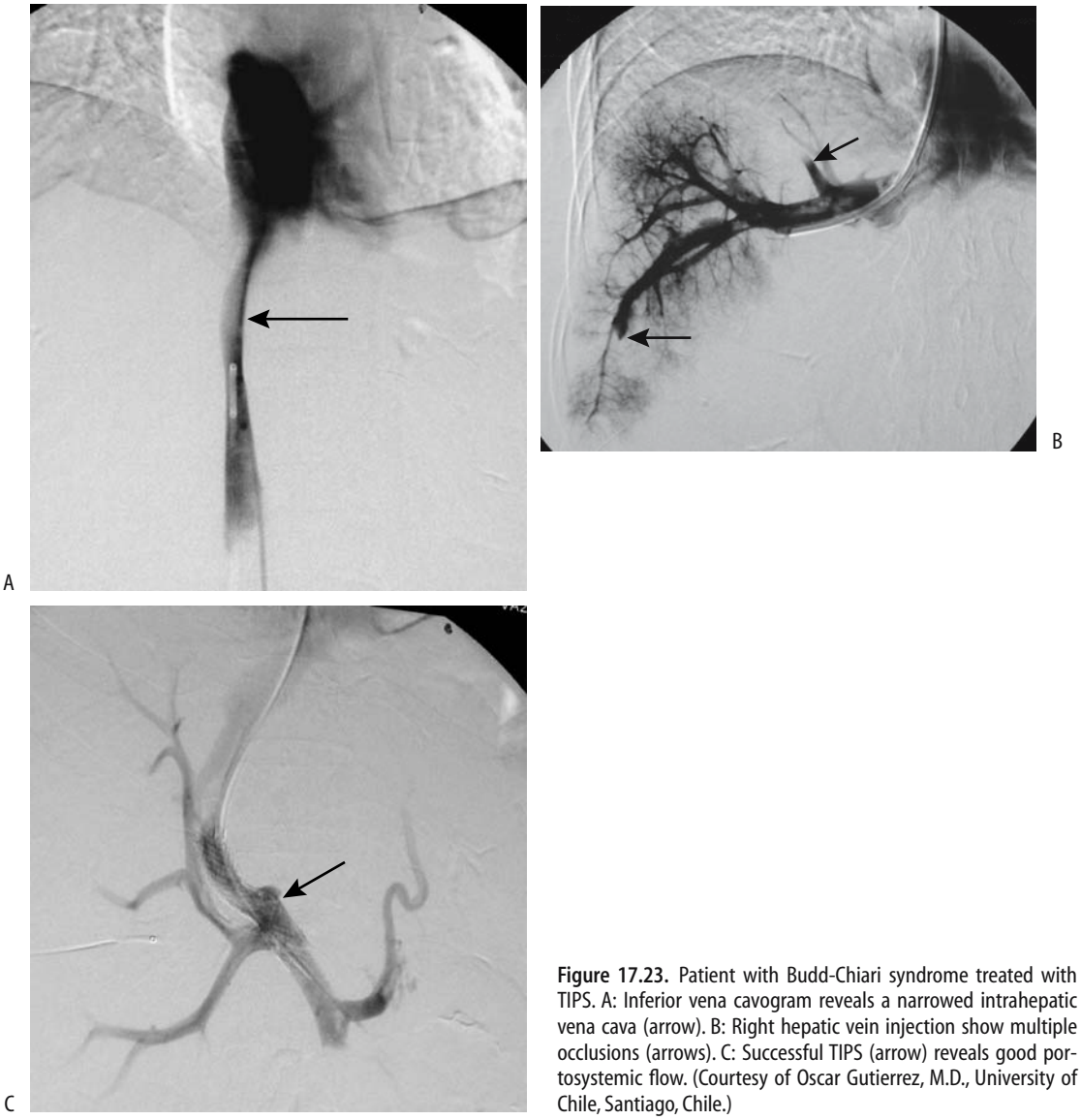

Figure 17.23. Patient with Budd-Chiari syndrome treated with TIPS. A: Inferior vena cavogram reveals a narrowed intrahepatic vena cava (arrow). B: Right hepatic vein injection show multiple occlusions (arrows). C: Successful TIPS (arrow) reveals good portosystemic flow. (Courtesy of Oscar Gutierrez, M.D., University of Chile, Santiago, Chile.)

pathways are common in chronic Budd-Chiari syndrome, although clinically apparent varices are not. Collateral vessels or partial recanalizations often have a spider web–like drainage pattern. Especially capsule-based collaterals become more evident with subacute obstruction. Budd-Chiari syndrome in children is associated with multiple intrahepatic venovenous shunts; the presence of these shunts, detected with Doppler US, should suggest the diagnosis.

Incomplete hepatic vein obstruction results in a partial Budd-Chiari syndrome. In a patient with obstructed middle or left hepatic veins, the affected liver segments appear hypodense on precontrast CT, but vary in appearance on postcontrast images. The margins of involved segments correspond to intersegmental planes, and

such a finding should suggest a partial Budd-Chiari syndrome.

Therapy

Short stenotic segments are dilated with balloon angioplasty; shunt placement, TIPS, or thrombolytic therapy are employed with thrombosed segments. Therapy in some patients is surgical.

Hepatic Vein Thrombosis

The primary problem in patients with hepatic vein thrombosis is to control the underlying hematologic abnormalities; otherwise recurrent thrombosis is common. The type of therapy varies with the underlying lesion. Thus an intraluminal thrombus in an isolated hepatic vein is amenable to fibrinolytic infusion or balloon thrombectomy, more extensive obstruction is treated with venoplasty or stenting, and TIPS should be considered for diffuse intrahepatic venous obstruction.

Although angioplasty is safe and usually successful, recurrent stenosis is common. Therapy often involves several sessions. A stent placed across a stenotic hepatic vein segment reduces the pressure gradient. These stents should be monitored every 6 months or so because intimal fibrosis leads to lumen obliteration.

Transjugular intrahepatic portosystemic shunt placement is effective therapy for some patients with acute and even chronic Budd-Chiari syndrome (Fig. 17.23). Using a transjugular access, puncture from a hepatic vein stump is performed into an engorged intrahepatic vein. At times, puncture is feasible even in the absence of any patent residual hepatic vein, with a stylet perforating from the inferior vena cava through the liver into a portal vein; dilatation and stent placement then establish a venous communication. For unknown reasons stent occlusion is a common complication after TIPS placement for Budd-Chiari syndrome.

A percutaneous transhepatic approach is feasible to recanalize the hepatic veins but is not often employed.

Inferior Vena Cava Obstruction

Percutaneous transluminal angioplasty and stent placement is an option in patients with Budd-Chiari syndrome caused by intrahepatic inferior vena caval obstruction. Percutaneous transluminal angioplasty alone results in about a 50% patency rate; stenting after primary percutaneous transluminal angioplasty decreases the restenosis rate considerably. A residual narrowing is often evident after stent insertion, but a stent keeps the vena cava patent and decreases the risk of Budd-Chiari syndrome recurrence.

Renal Vessels

Hypertension

Nonrenal Causes

Most hypertension is idiopathic. Identified causes can be subdivided into nonrenal, nonvascular renal, and renovascular. Nonrenal causes of hypertension include primary aldosteronism and the presence of a pheochromocytoma, Cushing's syndrome, vasculitis, and other disorders. An unusual cause of nonrenal malignant hypertension was gallbladder hemobilia (95). A rare patient has several conditions responsible for hypertension.

Nonvascular Renal Causes

The final pathway for nonvascular renal causes of hypertension is increased renin production.

Nephroptosis is a rare cause of renal hypertension. Technetium-99m-renography identifies diminished perfusion and excretion on the affected side.

In general, renal cysts are not associated with hypertension. Patients with cysts, however, tend to have systolic and diastolic blood pressures significantly higher than those without cysts, either due to underlying renal disease that is responsible for both or due to renal artery compression caused by an expanding cyst, thus leading to increased renin release. Compression by an adjacent extrarenal tumor, typically an adrenal one, is occasionally implicated in unilateral renal ischemia and the resultant hypertension.

A thrombus or an atheromatous plaque embolizing distally can result in renal hypoperfusion and hypertension, or the involved renal parenchyma infarcts.

A number of glomerular and interstitial renal diseases result in hypertension. Occasionally ureteric obstruction, generally on an acute

basis, leads to increased renin secretion and hypertension. Chronic pyelonephritis is an uncommon cause of hypertension.

Both renal cell carcinomas and Wilms' tumors result in hypertension, either by vascular compression or by intrinsic renin production. Juxtaglomerular tumors also produce renin.

Hypertension after renal trauma is not common even with a renal artery thrombosis. Nevertheless, hypertension has developed after traumatic renal artery narrowing, extrinsic renal artery compression, an arteriovenous fistula, and a traumatic aneurysm. At times a segmental artery is involved. Occasionally a subcapsular hematoma or urinoma compresses the adjacent renal tissue, leads to ischemia, increases the renin production, and manifests by hypertension (Page kidney).

Renal Doppler US in women with pregnancy-associated hypertension reveals markedly prolonged interlobar artery acceleration times (96), suggesting that renal artery or segmental artery stenosis or vasospasm plays a role in this condition.

Hypertension after a renal transplant is not always due to renal artery stenosis. In some, it appears to be associated with rejection. In others, renin production by a native kidney plays a role.

Renal Artery Stenosis

The most common cause of renovascular hypertension is renal artery stenosis, with an occasional renal artery aneurysm or dissection being responsible. The true prevalence of renovascular hypertension is not known because not all patients with hypertension undergo a full diagnostic workup. Many patients with renal artery stenosis are asymptomatic and do not seek medical attention, thus introducing a bias in any statistical analysis. As a rough estimate, among all causes of hypertension, a renovascular etiology accounts for approximately 3% to 5%, with the prevalence of secondary causes being greater in children. Considerable emphasis is placed on renovascular causes because in many patients these are correctable.

Etiology

Among patients with renal artery stenoses, fibromuscular dysplasia is the underlying etiology in about 20% of patients and arteriosclerotic vascular disease in the rest. The primary lesion associated with renal artery narrowing in the elderly is atherosclerosis, while in a younger population fibromuscular hyperplasia predominates.

Fibromuscular Dysplasia

Fibromuscular dysplasia occurs most often in the renal arteries, followed by the carotid and iliac arteries. It is the second most common cause of renal artery stenosis involving the middle to distal portions of the renal artery. The etiology is not known. Fibromuscular dysplasia is often subdivided into medial, intimal, and adventitial (perimedial) dysplasia, with medial fibromuscular dysplasia being the most common. Typically, imaging detects multiple stenotic segments (Fig. 17.24). Rarely, medial dysplasia results in spontaneous arterial rupture and an extraperitoneal hematoma.

Medial dysplasia typically affects middle-aged women and tends to be bilateral, consisting of single or multiple constrictions in the distal two thirds of the renal artery. Segmental renal branches are occasionally involved. A "string of beads" appearance is characteristic.

Intimal fibroplasia manifests as a smooth stenosis of varying length involving distal renal artery segments. Occasionally it has a web-like appearance. The proximal end of the renal artery is often diseased if the aorta is also involved.

Perimedial dysplasia also affects middle-aged women, tends to be unilateral, and involves the distal renal artery segments. Whether perimedial dysplasia and medial fibroplasia are different manifestations of the same process is conjecture.

Complete renal artery occlusion is rare with these dysplasias. Intimal and perimedial dysplasias are associated with vessel dissection and thrombosis—complications uncommon with medial dysplasia.

In distinction to atherosclerotic disease, fibromuscular dysplasia tends not to recur after therapy.

Atherosclerosis

Most renovascular hypertension is due to atherosclerosis, a progressive disease. The proximal one third of the renal artery and its ostium are

Figure 17.24. Fibromuscular dysplasia. A: Right renal arteriography reveals a slightly irregular main renal artery stricture and several mild strictures in the intrarenal arteries. (Courtesy of David Waldman, M.D., University of Rochester.) B: Fibromuscular dysplasia of right renal artery in another patient. (Courtesy of Oscar Gutierrez, M.D., University of Chile, Santiago, Chile.)

most often affected, and usually the adjacent aorta is also involved by atherosclerosis. Some patients also have segmental and diffuse intrarenal atherosclerosis. Bilateral renal artery involvement is common. An older patient population is affected than with fibromuscular dysplasia. This is a progressive and recurrent condition.

Typical presentations include hypertension, renal ischemia, parenchymal loss, and eventual renal failure. As a rough estimate, approximately a 60% stenosis of a main renal artery is necessary to detect renal atrophy with imaging.

Other Etiologies

Renal artery hypoplasia is a developmental anomaly most often found in children and young adults with renovascular hypertension. Renal artery origins are involved.

Takayasu's arteritis, a rare cause of renal artery stenosis and hypertension, results in arterial wall thickening.

A rare patient with neurofibromatosis develops renal artery stenosis and hypertension.

Also rare is acute renal artery occlusion due to necrotizing vasculitis.

Renal artery stenosis is not uncommon after renal transplantation. This topic is discussed in Chapter 10.

Clinical

Sufficient renal artery stenosis leads to decreased renal perfusion, activation and release of renin and angiotensin II, and increased renal prostaglandin, and via a multifactorial feedback mechanism results in hypertension. Especially in long-established hypertension, plasma renin values and related clinical tests serve little purpose in differentiating renovascular from essential hypertension. Clinically, renovascular hypertension manifests similar to essential hypertension.

Progression of severity of renal artery stenosis is common, yet in patients with fibromuscular dysplasia renal perfusion correlates inversely with the degree of stenosis, a finding not seen in patients with atherosclerosis. Rare exceptions to stenosis progression do occur, and renal artery stenosis regresses.

Occasionally seen is the patient with a renal cell carcinoma with an incidentally discovered contralateral renal artery stenosis. Although a simple nephrectomy can be performed, in such a setting the stenosis can be expected to progress, even to occlusion. In this specific setting of renal cell carcinoma and contralateral renal artery stenosis, prophylactic percutaneous transluminal angioplasty of the stenosis appears to be of benefit.

A not uncommon finding is both renal artery disease and infrarenal aortic disease; although simultaneous aortic and renal revascularization can be performed, at times percutaneous transluminal renal angioplasty is preferred prior to surgical revascularization, especially in high-risk patients.

Detection

The first problem encountered is defining the degree of renal artery stenosis. Using angiograms performed with a DSA technique in consecutive hypertensive patients, three experienced radiologists could not distinguish between 50% and 60% stenosis or between 60% and 70% stenosis (97); the authors concluded that statements about degree of renal artery stenosis are not realistic or clinically significant when using DSA. Nevertheless, many authors do use DSA results as their gold standard.

The imaging definition of renal artery stenosis is obviously arbitrary. Most investigators use a lumen narrowing of >50% as a cutoff point, with a minority adopting 60% narrowing as their limit. A pressure gradient across a stenotic segment >10 mm Hg is generally also considered significant. The use of a miniaturized pressure guidewire revealed that a 50% stenosis results in a mean pressure gradient of 22 mm Hg (98).

The definition of an ostial stenosis is also arbitrary; some investigators define an ostial stenosis as any stenosis within 5 mm of the renal artery origin, while others use a 10-mm length adjacent to an atherosclerotic aorta. Regardless of definition, detecting an ostial stenosis is not always clear-cut; most renal arteries originate either anterolateral or posterolateral from the aorta; a completely lateral origin is found only in a minority. In some patients CT angiography identifies an ostial lesion, but DSA shows it to be truncal in location.

In patients with chronic hypertension due to renal artery stenosis, the end-stage finding detected with most imaging modalities is a small, smooth kidney without urinary obstruction. These changes, however, are not always present; also, stenosis of an accessory renal artery rarely leads to a small kidney. A more basic question is whether accessory artery stenosis results in hypertension—some indirect findings suggest that accessory renal arteries are not a direct cause of hypertension (99).

Comparison Studies

Urography is not sensitive in detecting corrective renal artery stenosis as a cause of renovascular hypertension and is not used for this purpose. Aside from an end-stage small, smooth kidney, main renal artery stenosis results in a delayed nephrogram. Likewise, US and scintigraphy, although used at times for screening, are inferior to CTA and MRA in detecting renal artery stenosis in patients with suspected renovascular hypertension (100).

In general, CTA renal artery image quality is worse than intraarterial DSA but is better than intravenous DSA. Also, MRA sensitivity in detecting at least 50% stenoses was higher for MRA (100%) than US (79%), but specificities were similar (101). Although some studies suggest that MRA and DSA are equally effective in detecting significant main renal artery stenoses, MRA and conventional angiography can diverge both by overestimating and underestimating the degree of stenosis by more than 10% (relative to angiography).

Some imaging studies include detection of accessory renal arteries while others do not, thus introducing another variable in study comparisons.

Accessory Renal Artery Detection

Accessory renal arteries are found in about 40% of patients. Renal arteries are end arteries, and the acute occlusion of an accessory renal artery leads to segmental renal infarction. Thus knowledge of renal volume perfused by an accessory artery is of some importance prior to surgical procedures such as an aortic stent or graft implantation over this segment. The perfused vascular bed of an accessory renal artery can be obtained from CT performed with selective accessory renal artery angiography.

A limitation of noninvasive techniques is that some accessory renal arteries are not detected. Several studies have concluded that CTA does not visualize about 20% to 25% of accessory renal arteries, although other studies indicate that CTA does not detect <10%.

Only a minority of accessory renal artery stenoses are detected by US. A not untypical conclusion is that duplex Doppler US detects only about 5% of accessory renal arteries seen at catheter angiography (102).

In general, more accessory renal arteries are detected with MRA than with color Doppler US (101). Comparison of CTA and MRA yields conflicting results, with some studies suggesting that MRA is inferior both in detecting accessory renal arteries and in grading renal artery stenoses. One should keep in mind, however, that MR results are very technique dependent, and results vary accordingly. A realistic estimate is that MRA identifies 75% to 90% of accessory renal arteries.

Computed Tomography

Traditionally, conventional angiography has been the gold standard in evaluating renal artery stenosis. In a number of institutions arterial-phase helical CT has replaced renal angiography. Arterial phase 3D reconstruction images outline a stenosis in most patients. A number of studies have concluded that CTA has essentially the same accuracy for detecting renal artery stenosis ≥50% as DSA, although under- and overestimation of stenosis grade are encountered. The sensitivities and specificities in detecting clinically significant stenoses of the main renal arteries are over 90%, but keep in mind that the accuracy of detecting a proximal renal artery stenosis is greater than in distal segments. As a further refinement, CTA with real-time interactive volume rendering appears faster and is more accurate in detecting renal artery stenoses than the use of other current techniques (103). Nevertheless, clinically significant renal artery stenosis, including stenosis of an accessory artery, can be missed by CTA.

Electron beam CT can determine renal volume, measure perfusion, and identify progressive changes in unilateral renal artery stenosis (104); initially symmetric time-attenuation curves are present, then asymmetric time-attenuation curves but with similar perfusion, and eventually asymmetric curves with impaired perfusion.

Evaluation of renal artery fibromuscular dysplasia presents its own unique problems. Computed tomography angiography in most hypertensive patients with renal artery fibromuscular dysplasia identifies most but not all lesions; arteriography remains the imaging modality of choice in the study of fibromuscular dysplasia.

Ultrasonography

Investigators are deeply divided on the use of Doppler US for evaluating possible renal artery stenosis. The accuracy of Doppler US is reasonable in patients with a tight stenosis, but this test appears to be of doubtful value in screening hypertensive patients where detection of a 50% to 70% stenosis is relevant.

Initial Doppler US studies of renal artery stenosis were directed primarily toward the renal artery and relied on detecting an increased velocity in the stenotic segment, with mixed results. Emphasis then shifted to poststenotic changes in smaller intrarenal branches. Normal intrarenal arteries have a rapid systolic upstroke, while in a setting of renal artery stenosis the upstroke is dampened and time to peak systole is also dampened. Still, even this approach has led to mixed results. Although several studies show that intrarenal Doppler US will detect more severe stenoses (greater than about 70%), US misses less severe stenoses. The sensitivity and specificity for duplex US in detecting a ≥60% diameter main renal artery stenosis were 91% and 97%, respectively (102). In another prospective study, intra- and extrarenal Doppler US achieved a sensitivity and specificity of 79% and 93%, respectively, in detecting at least a 50% renal artery narrowing (101), results similar to a number of other studies. Some investigators assumed a renal artery peak systolic velocity >100 cm/sec or even >180 cm/sec to represent significant renal artery stenosis; although the early work was promising, later studies achieved substantially worse results. Also, duplication of such parameters as acceleration time is inconsistent.

The sensitivity and specificity for detecting significant stenosis in a given vessel (including accessory arteries) in consecutive patients were 97% and 98%, respectively (105); these impressive results were reached by twofold use of Doppler US: a stenosis of >50% was presumed if the main renal artery maximal systolic velocity was >180 cm/sec and velocity in the more distal segment was less than one quarter of the maximum velocity, or, in the absence of

these criteria, stenosis was presumed if the intrarenal segmental artery acceleration time was >70 msec. Arteriography was the gold standard.

The Renal Artery Stenosis Study Group from 14 European centers using the echo-enhancing agent Levovist for renal artery Doppler US found more diagnostic studies with enhanced Doppler US (84%) compared with nonenhanced Doppler US (64%) (106).

Magnetic Resonance

Magnetic resonance angiography is a promising noninvasive screening test in patients suspected of renal artery stenosis, and the indications for its use continue to expand. The results with MRA approach those of conventional angiography in detecting renal artery stenosis. In general, a normal MRA is highly predictive of normal arteries, although some stenoses are under- and overestimated by MRA. Several consecutive data sets with imaging times of 7 seconds or so can be acquired during a single breath-hold; postgadolinium and 3D views are then evaluated. Introduction of MR phase-contrast flow measurements adds functional information. These studies are technically demanding, however, and require optimal contrast bolus timing. Also, most studies have addressed the detection of stenosis only in proximal renal artery segments.

Magnetic resonance angiography is considered especially valuable in patients with chronic renal failure; IV gadolinium in the doses used in MR is less nephrotoxic than iodinated contrast agents. Captopril renography is of limited value in these patients. Thus in an elderly hypertensive patient with suspected proximal renal artery stenosis, MRA can be the primary screening test and, if positive, the patient is referred directly for DSA and possible angioplasty. If necessary, even DSA and angioplasty are performed with gadolinium or carbon dioxide as contrast agents.

Can MRA visualize all renal artery ostial and truncal stenoses? Magnetic resonance angiography tends to overestimate stenosis grade. One constraint of 3D MRA is that a false ostial stenosis can be suggested due to loss of signal intensity at a renal artery origin. Nevertheless, 3D gradient-echo contrast enhanced MRA achieves a >90% sensitivity and specificity for correctly identifying a clinically relevant stenosis. A stenosis is identified as signal extinction, a finding based not only on flow turbulence but also on the MR parameters used. Image subtraction in 3D contrast enhanced reual artery MRA does improve study quality and aids in visualizing distal renal arteries. Gadolinium enhancement increases the apparent precontrast renal artery diameter, probably due to improved visualization of slow-flowing blood along the periphery.

One approach in providing both detailed renal artery evaluation and also abdominal aortic coverage is to first obtain high-resolution, small field-of-view 3D contrast-enhanced renal artery MRA, followed by large field-of-view 3D MRA of the aorta (107); such high-resolution MRA yielded a sensitivity of 97% and specificity of 92% in detecting renal arterial stenosis.

The reliability of phase-contrast MR flow measurements to differentiate between hemodynamically significant renal artery stenosis and nonstenosed vessels is not clear; some have achieved high sensitivity and specificity, but others have found velocity waveforms from phase-contrast data to be inaccurate in predicting renal artery stenosis (108).

The role of MR angiography in fibromuscular hyperplasia is not well established.

Scintigraphy

The glomerular filtration rate is maintained at normal levels through arteriolar vasoconstriction induced by angiotensin II even in renal artery stenosis. Conversion of the inactive angiotensin I to angiotensin II is inhibited by captopril (angiotensin-converting enzyme inhibitor) administration. In a setting of renal artery stenosis, captopril administration results in a decreased glomerular filtration rate as measured with Tc-99m-DTPA or Tc-99m-mercaptoacetylglycilglycilglycine (MAG3). Captopril renography thus potentially detects underlying renal artery stenosis, although the reported sensitivities and specificities of captopril renography in detecting renal artery stenosis vary considerably. Earlier literature suggested that a distinct advantage of captopril renography was that it identified those patients who will most benefit from correction of renal artery stenosis, yet a more recent analysis

concluded that "renal scintigraphy had no significant predictive value" after renal angioplasty (109).

Why some patients have false-negative captopril renography is puzzling, but the response to captopril decreases with poor renal function. Test accuracy tends to be compromised in a setting of renal failure and it is not applicable to a poorly functioning kidney. Because MAG3 is filtered by glomeruli and secreted by tubules, while DTPA is filtered by glomeruli, the former is preferred in those with renal failure. In one study captopril Tc-99m-MAG3 renography achieved a sensitivity and specificity of 85% and 71%, respectively, in detecting a stenosis >50% (110). Occasionally captopril scintigraphy findings of a mobile kidney mimic those seen with renal artery stenosis.

Scintigraphy provides little anatomic detail, but in a setting of a normal serum creatinine level a scintigraphic finding of impaired fractional flow to one kidney is an indication for further investigation. Iodine-131-hippuran renography can detect arterial luminal narrowing in a setting of unilateral renal artery stenosis where the nonstenotic kidney served as a "normal" landmark. In general, studies using Tc-99m are technically superior to I 131, and most institutions prefer the former.

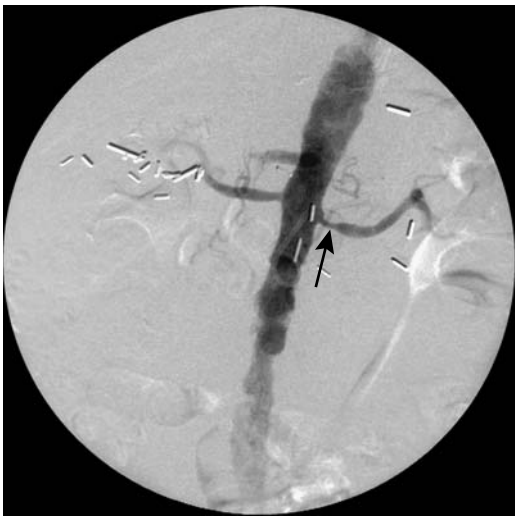

Figure 17.25. Left renal artery stenosis (arrow) in a hypertensive patient. A stent was later inserted. (Courtesy of David Waldman, M.D., University of Rochester.)

Figure 17.26. Renal arteriogram in a woman with renal failure, malignant hypertension and scleroderma reveals marked vasospasm and tortuosity of major and smaller intrarenal vessels. The distal intrarenal arteries are tapered. Vasospasm resulted in slow intrarenal flow and persistence of arterial filling. Similar changes are found both in renovascular hypertension and in scleroderma. (Courtesy of Oscar Gutierrez, M.D., University of Chile, Santiago, Chile.)

Angiography

Digital subtraction angiography using IV contrast injection enjoyed brief popularity as a screening test for renal artery stenosis, but most centers have abandoned this technique for more modern imaging.

Direct injection angiography is the gold standard used in evaluating the main and accessory renal arteries (Fig. 17.25). Angiography is often preferred in patients with fibromuscular dysplasia. One should keep in mind that hypertension, in general, is associated with arterial vasospasm and tortuosity of intrarenal arteries (Fig. 17.26).

Carbon dioxide can be used in place of iodinated contrast to evaluate renal arteries during digital subtraction arteriography. In patients at risk for contrast-related nephrotoxicity or who are allergic to iodinated contrast, carbon dioxide arteriography appears to be a viable alternative.

Venous Renin Assay

Selective renal vein assay for renin is not used either as a screening test or for detecting renovascular causes of hypertension. It is useful, however, to evaluate whether a detected renal artery stenosis is indeed a cause of a patient's hypertension.

Therapy

Although renovascular hypertension often is controlled medically, in a setting of atherosclerotic renal artery stenosis medical therapy often does not prevent renal ischemia and resultant renal insufficiency and, in fact, accelerates parenchyma damage. Therapeutic modalities for renal artery stenosis include percutaneous transluminal angioplasty (balloon dilation), stenting, surgical correction and occasionally some other type of therapy. The primary indications for therapy of renal artery stenosis are hypertension refractory to medical therapy and renal ischemia manifesting by a decrease in renal function; one should keep in mind, however, that because renal artery stenosis exists does not mean that it is responsible for a patient's hypertension or renal failure. Hypertension persisting after successful angioplasty or other therapy is often ascribed to underlying essential hypertension.

Overall therapeutic success is measured by two outcomes: Is hypertension cured and is renal function deterioration arrested? Different results are obtained in patients with fibromuscular dysplasia and atherosclerotic stenosis, and in an analysis of success rates these two patient populations should be separated. Some investigators distinguish ostial stenoses from other stenoses because success rates for ostial stenoses are better with stenting than with simple transluminal angioplasty. One should also keep in mind that hypertension can be caused by stenosis of an isolated accessory renal artery, but for renal function to be impaired generally both main renal arteries need to be involved.

An exception to direct interventional therapy is trauma-induced hypertension; once the underlying defect is identified and appears stable, a number of these patients are initially followed medically because the hypertension resolves spontaneously in some.

When to suggest therapeutic intervention is controversial. Classic dogma is that medical therapy should be exhausted first, yet numerous studies have confirmed that outcomes of angiographic and surgical therapeutic are better if initial renal function is close to normal.

The cure rates for hypertension after reconstructive surgery, angioplasty, and stenting are low and are similar. The current trend in revascularization therapy is away from emphasis on cure of renovascular hypertension and a shift toward control of renal failure progression due to ischemia. One sign of successful revascularization is that serum creatinine levels do not worsen significantly in those with impaired renal function.

Preliminary evidence suggests that intrarenal resistance index identifies patients whose blood pressure or renal function improves after correction of renal artery stenosis. Among patients with a preprocedure resistance index (RI) of <80, mean arterial pressure decreased by at least 10% in 94% of patients, while in patients with a preprocedure RI of >80, pressure did not decrease in 97% (111); a preprocedure RI of >80 thus selects those patients with renal artery stenosis in whom therapy will not improve their hypertension. Captopril assisted Doppler US also appears useful in predicting outcome; multivariate analysis suggests that the best predictors of a favorable therapeutic outcome are a unilateral RI of <0.65 after captopril and a kidney longer than 93 mm (112).

Therapy Comparisons

A French review of published therapies for renal artery stenosis found that most studies were retrospective and uncontrolled, and their success rates overestimated (113); hypertension cure rates after percutaneous angioplasty were 50% in patients with fibromuscular dysplasia but only 19% in those with an atherosclerotic stenosis, while in patients with progressive renal failure due to atherosclerotic disease, surgical revascularization improved renal function in 55% and angioplasty improved function in 41%. Some more pessimistic studies have reported that hypertension was cured only in about 5%, worsened also in about 5%, and renal insufficiency improved in about a third and continued to worsen in slightly fewer patients.

A retrospective study of renovascular hypertension patients who underwent percutaneous transluminal renal angioplasty, percutaneous transluminal renal artery stent placement, or renal arterial bypass grafting found similar procedure success rates (91% to 98%), but complication rates were 13% for angioplasty, 16% for stent placement, and 38% for bypass grafting (114); of interest is that the number of antihypertensive medications returned to baseline in all patients by 12 months. In the Dutch Renal Artery Stenosis Intervention Cooperative Study Group, patients with hypertension and atherosclerotic renal artery stenosis were randomly assigned to either undergo percutaneous transluminal renal angioplasty or receive drug therapy (115); 3 months later no significant differences were evident in either systolic or diastolic blood pressures in the two groups.

Surgical Bypass

The initial therapy for renal artery stenosis consisted of aortorenal bypass surgery, which then was replaced by hepatorenal, splenorenal and other bypass, patch angioplasty, and renal artery endarterectomy. Retrospective surgical studies from the late 1980s and 1990s established standards for postoperative 5-year survival of 52% to 65% or higher and improvements in hypertension and renal insufficiency, and most current authors compare their angioplasty and stenting results against these standards. These comparisons are difficult to place in proper perspective because surgical studies tended to contain "sicker" patients with their correspondingly greater morbidity and mortality. Currently surgical therapy in many institutions is limited to a few specific indications, including failed angioplasty and stenting.

Angioplasty

Percutaneous transluminal revascularization consists of balloon angioplasty, at times supplemented by stenting. If necessary in high-risk patients, carbon dioxide is used as a primary intravascular contrast agent during angioplasty, supplemental when necessary by iodinated contrast.

Angiography is generally used initially to evaluate the success of angioplasty; Doppler US is used by some investigators to assess patency during subsequent follow-up. Roughly half of patients with underlying fibromuscular dysplasia who undergo successful angioplasty are cured and most of the rest are improved, results far superior to those achieved in patients with atherosclerotic disease (Fig. 17.27).

Percutaneous angioplasty appears less appropriate for the relatively uncommon ostial stenosis. A randomized, prospective study compared transluminal angioplasty alone and angioplasty

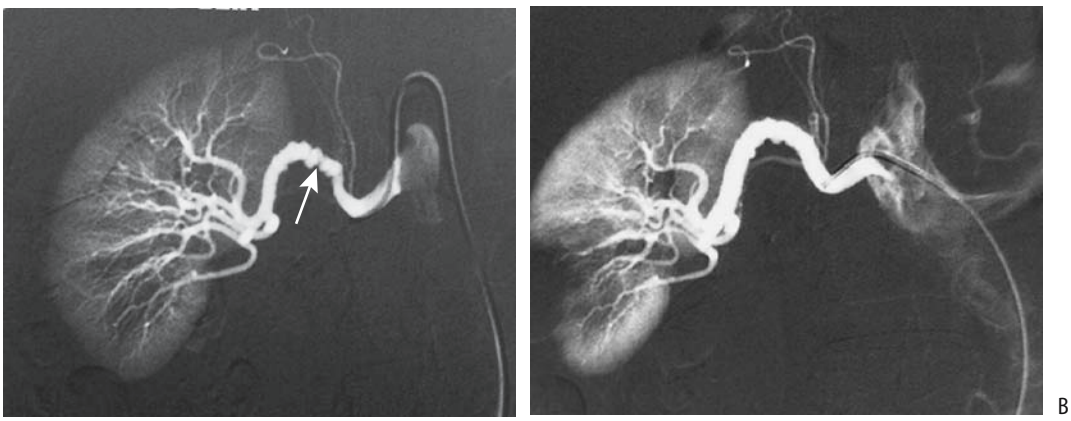

Figure 17.27. Fibromuscular dysplasia in a young woman with severe hypertension. A: Renal arteriogram reveals an irregular, segmented right renal artery stenosis (arrow). B: Arteriogram after angioplasty shows an essentially normal renal artery. (Courtesy of Oscar Gutierrez, M.D., University of Chile, Santiago, Chile.)

with stent placement in patients with ostial atherosclerotic renal artery stenosis (116); the primary success rate, defined as a <50% residual stenosis, of angioplasty alone was 57% compared with 88% for stenting. The 6-month postprocedure primary patency rate was 29% for angioplasty alone, and 71% for stenting. Among patients undergoing angioplasty alone, 29% required secondary stenting for angioplasty failure, with these patients then having a success rate similar to those with primary stenting. The authors concluded that primary stenting is a superior procedure for patients with ostial stenosis.

Stenoses can be dilated in patients with renovascular hypertension due to nonspecific aortoarteritis (Takayasu's disease); the restenosis rate, evident by recurrence of hypertension and restenosis, found at angiography, was 16% at 22 months (117).

Complete renal artery occlusions have been successfully revascularized. Sufficient data are not available to draw firm conclusions about angioplasty for this indication.

Angioplasty complications include renal artery dissection and rupture, embolization of atheromatous fragments, and artery thrombosis. Even including complications due to femoral angiography, angioplasty is associated with fewer complications than surgical correction.

Doppler US detection of residual renal artery stenosis one day after percutaneous revascularization of atherosclerotic renal arteries appears to be a predictor for future restenosis (118).

Stenting

Currently, percutaneously implanted renal artery stents have a role in stenoses that are not amenable to angioplasty, those due to failed therapy, and in a setting of ostial stenosis. Percutaneous renal artery stent insertion has been performed for renal artery involvement in aortic dissection (119). Problems with dissection and residual stenosis are largely overcome with stenting. A review of published studies of stent placement up to 1998, comparing results of renal arterial stent placement and renal percutaneous transluminal angioplasty, concluded that stenting is technically superior and clinically comparable to angioplasty (120); stenting achieves a lower restenosis rate (17%) than angioplasty (26%). The complication rates are similar, but stenting results in fewer patients with a postprocedure residual stenosis. The importance of a postprocedure residual stenosis is its association with a significantly higher rate of eventual restenosis.

In a follow-up study of consecutive patients, renal arterial stent placement did not significantly improve primary patency of proximal and truncal renal arterial stenoses over that achieved by balloon percutaneous transluminal angioplasty (121); stents did, however, improve patency of ostial stenoses.

In general, stenting for angioplasty failure does relieve stenosis, but hypertension is cured only in half or fewer patients; likewise, arrest of clinical renal failure occurs only in about half or so of patients after stenting.

Renal artery stent obstruction can be evaluated with contrast enhanced MRI.

Acute complications of renal artery stent placement include renal artery thrombosis, renal artery emboli, cholesterol embolization to lower limbs, and femoral hematoma.

Renal Ablation/Embolization

Occasionally percutaneous transcatheter renal ablation is considered in patients with uncontrolled hypertension or nephrotic syndrome. A long-term improvement in hypertension and nephrotic syndrome can be achieved with this procedure, often with a lower morbidity and mortality than for comparable surgical nephrectomy.

Transcatheter embolization should be considered in the hypertensive patient with an accessory renal artery or a branch artery stenosis not amenable to usual therapy and if the involved artery supplies only a small renal segment. Eventual scarring and some loss of renal function will occur.

Renal Artery Aneurysm

Renal artery aneurysms can be subdivided into true aneurysms, dissecting aneurysms, arteritis-related aneurysms, and simply aneurysmal dilatation. True aneurysms are saccular, extraparenchymal, and located at bifurcations.

Several etiologies account for these aneurysms: elastic tissue degeneration, possibly on a congenital basis, and atherosclerosis predominate, with an occasional one being secondary to trauma. The prevalence of renal artery aneurysms increases with age, with only a rare one found in children. They are a rare cause of hypertension; in some patients an aneurysm manifests with pain or hematuria, although most patients are asymptomatic.

Small intrarenal aneurysms develop in patients with polyarteritis nodosa, Wegener's granulomatosis, and lupus erythematosus. Dilated renal arteries and aneurysms occur in Behçet's disease.

An occasional true aneurysm ruptures, at times resulting in a loss of that kidney. Similar to rupture of a splenic artery aneurysm, rupture of a renal artery aneurysm during pregnancy carries a high maternal and fetal mortality. Repair of a known aneurysm should be considered prior to conception. Rupture is not necessarily related to hypertension. Calcifications in an aneurysm do not protect against rupture. Some ruptures evolve into an arteriovenous fistula.

Ring-like calcifications are detected with conventional radiography in less than a third of renal artery aneurysms.

Renal artery aneurysms are readily detected with arteriography. Most are also identified during arterial phase helical CT; precontrast and delayed postcontrast CT images show an isodense mass similar to a neoplasm. A majority are saccular in shape, with a minority fusiform or dissecting. Imaging also detects an occasional thrombosed aneurysm.

Some renal artery aneurysms dissect spontaneously or dissect secondary to trauma, including catheter manipulation. A minority of dissections occur bilaterally. Patients with a dissecting aneurysm can develop hypertension.

Arteriography should be diagnostic of a dissecting aneurysm. At times urography reveals delayed contrast excretion, although often this study is normal.

Renal artery aneurysms have been treated with an ex vivo surgical technique and autotransplantation. Of note is that follow-up of aneurysmectomy reveals a better cure rate of hypertension than in patients with renal artery stenosis. Before ascribing hypertension to an aneurysm, however, a stenosis in another artery should be excluded.

Renal Vein Occlusion

Adults

Renal vein thrombosis is often associated with an underlying renal cell carcinoma or inferior vena caval thrombosis. Less common factors are dehydration, coagulopathy, nephrotic syndrome, pancreatitis and other retroperitoneal inflammation, systemic lupus erythematosus, intrinsic renal disorders such as glomerulonephritis, and as an occasional complication of acute pyelonephritis. The prevalence of thrombosis is sufficiently high in nephrotic syndrome to warrant screening these patients for renal vein thrombosis.

Few symptoms are evident in adults if thrombosis develops gradually. On a chronic basis collaterals (sometimes called renal varices) develop, the kidney is no longer enlarged, and venous flow returns to the renal hilum. A complication of renal vein thrombosis is pulmonary emboli.

Renal vein thrombosis with the thrombus extending into the inferior vena cava can be misdiagnosed as a renal cell carcinoma. Precontrast CT of a renal vein thrombus revealed a hyperdense tumor.

With acute thrombosis, contrast-enhanced CT detects renal enlargement and a thrombus-containing enlarged renal vein. The venous wall tends to enhance with contrast. Corticomedullary differentiation is prolonged and a nephrogram delayed. Extraperitoneal hemorrhage is not an uncommon association.

Ultrasonography detects an enlarged, hypoechoic kidney. Initially a thrombus is anechoic. A thrombus is better detected in the shorter right renal vein than in the left. Doppler US findings have been disappointing. With some thrombi, Doppler US does not detect renal vein flow, although often the obstruction is incomplete and flow is present, albeit slow. Normal arterial Doppler US does not exclude venous thrombosis.

Scant literature exists on the use of MRI for renal vein thrombosis, although based on results from other vascular sites MR should be well suited in this setting.

Neonates

Predisposing factors for renal vein thrombosis in the neonate are dehydration, sepsis, maternal diabetes, polycythemia, and umbilical vein catheter manipulation and the rare hereditary thrombophilia. Thrombosis can be limited to small renal veins or extend into the main renal vein or even inferior vena cava. Clinically, these neonates develop hematuria or hypertension.

Gray-scale US is usually the first imaging modality employed. A transient early finding of an intrarenal vein thrombus is a linear echogenic structure. With sufficiently extensive involvement the affected kidney enlarges and assumes a heterogenous appearance. Ultrasonography should also detect any associated vena caval thrombus. Some neonates also have adrenal hemorrhage. Color Doppler US suggests a lack of flow in the intrarenal veins and reversal of arterial diastolic flow. Contrast enhanced MRI reveals persistent cortical enhancement and a lack of medullary enhancement.

Sequelae of renal vein thrombosis in a neonate range from an atrophic kidney, to focal scarring, to the kidney reverting to an essentially normal appearance.

Renal and Ureteric Varices

Not all venous engorgement is due to renal vein obstruction. Portal hypertension has led to intrarenal segmental venous engorgement (renal varices). Rarely, intrarenal varices are idiopathic. Renal varices can lead to recurrent hematuria.

Computed tomography detects tubular contrast-enhancing perineal structures. Color Doppler US should detect these varices. Selective renal phlebography is diagnostic. Of note is that renal arteriography can miss these venous structures.

Ureteric varices are uncommon. Occasionally engorged gonadal veins lead to extrinsic compression and result in a characteristic serpiginous appearance. Somewhat similar findings are seen with dilation of a ureteral artery, generally in association with renal artery stenosis where the ureteral artery provides a collateral blood supply to the kidney.

Vascular Fistulas

A fistula involving the aorta can be either aortovascular or aortoenteric. Fistulas associated with aortic aneurysms were discussed earlier (see Aorta), as were portosystemic shunts and fistulas (see Collateral Veins).

Aortocaval Fistula

Most aortocaval fistulas are related to aortic aneurysms and resultant surgical correction. These patients tend to be elderly and in poor health. A rare malignant fibrous histiocytoma at the aortic bifurcation led to a pseudoaneurysm which evolved into an iliocaval fistula (122).

In a patient with oliguric renal failure and a suspected aortocaval fistula, angiography using carbon dioxide is an alternate diagnostic test. Aortocaval fistulas have been embolized with coils, cyanoacrylate, and other materials.

Aortoenteric Fistulas

The most common cause of an aortoesophageal fistula is a thoracic aortic aneurysm. Esophageal perforation by an ingested foreign body is less common.

Most aortoduodenal fistulas develop in a setting of prior aortic aneurysm repair. Some are related to prior radiotherapy to this region. Rarely, duodenal tuberculosis or even a brucellar aortic aneurysm evolves into an aortoduodenal fistula.

A fistulous tract between an aortic graft and duodenum can be detected by CTA. If performed while the patient is bleeding, a temporal increase occurs in duodenal contrast agent accumulation (123).

Cavoenteric Fistulas

Most cavoenteric fistulas are secondary to trauma, tumor invasion, or prior radiotherapy. Thus a cavo-duodenal fistula developed after a right nephrectomy and radiotherapy for a urothelial tumor 20 months earlier (124). Anecdotal reports describe migrating caval filters resulting in duodenal perforation and a caroduodenal fistula (124).

Arterioportal Fistula

Clinically, arterioportal fistulas manifest through gastrointestinal bleeding, ascites, heart failure, or even diarrhea, findings induced by resultant portal hypertension, ischemia, or vascular erosions.

Dynamic MRA reveals arterioportal shunts as early focal regions of contrast enhancement (Fig. 17.28). Splenic arteriography is diagnostic.

Treatment of these fistulas is not clear. Some believe that embolization is the therapy of choice for acquired intrahepatic arterioportal fistulas but that extrahepatic ones should be corrected surgically. Successful transarterial embolization using coils and detachable balloons has been performed for these often high-flow fistulas (Fig. 17.29).

Arteriovenous Fistula

An arteriovenous fistula is an abnormal communication that bypasses the usual capillary circulation. A congenital fistula usually has multiple connections between an artery and vein. Most acquired fistulas are traumatic in origin. Tumors eroding into vessels also result in fistulas. The most common acquired origin is from the hepatic artery.

Splenic arteriovenous fistulas are either congenital or acquired. The less common congenital ones tend to be intrasplenic in location and their imaging appearance mimics a hemangioma. Acquired fistulas are often associated with atherosclerosis and trauma; an occasional one is related to pregnancy. They are identified by duplex Doppler US and arteriography.

Renal arteriovenous fistulas range from congenital to acquired. Some of these congenital fistulas do not manifest until adulthood. Among acquired ones are those secondary to prior vascular instrumentation or surgical manipulation, although many are idiopathic. Gross hematuria is the usual presentation with a renal fistula. Hypertension develops in some patients. Larger fistulas are associated with an enlarged feeding artery and draining vein. Loss of adjacent renal parenchyma and a resultant scar are evident with some fistulas. Similar to other sites, renal arteriovenous fistulas are detected by Doppler US. Renal arteriography defines the extent of a fistula and allows selective embolization.

At times scintigraphy of a vascular fistula suggests a hypervascular neoplasm.

Many congenital arteriovenous fistulas are difficult to treat with surgery, and recurrence is common.

Arterioureteral fistula

Arterioureteric fistulas are rare. Most are complications of vascular surgery, with atherosclerotic disease, chronic ureteral stenting or prior pelvic radiotherapy occasionally having a role. Clinical presentation consists of hematuria, often intermittent, ranging from mild to massive bleeding. Most aortoureteric fistulas are related to aortic prosthetic graft infections.

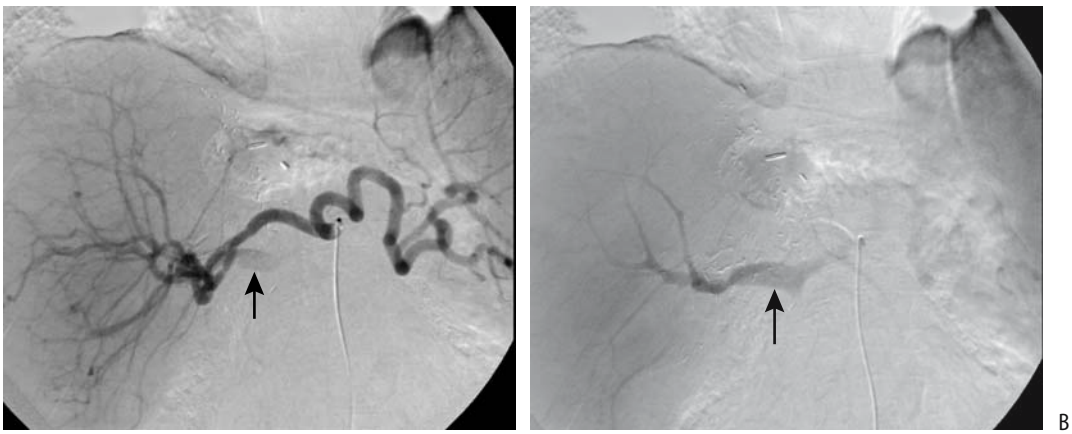

A B

Figure 17.28. Hepatic artery to portal vein fistula. Early (A) and later (B) phase hepatic arteriograms reveal early filling of the portal vein (arrows). (Courtesy of David Lee, M.D., University of Rochester.)

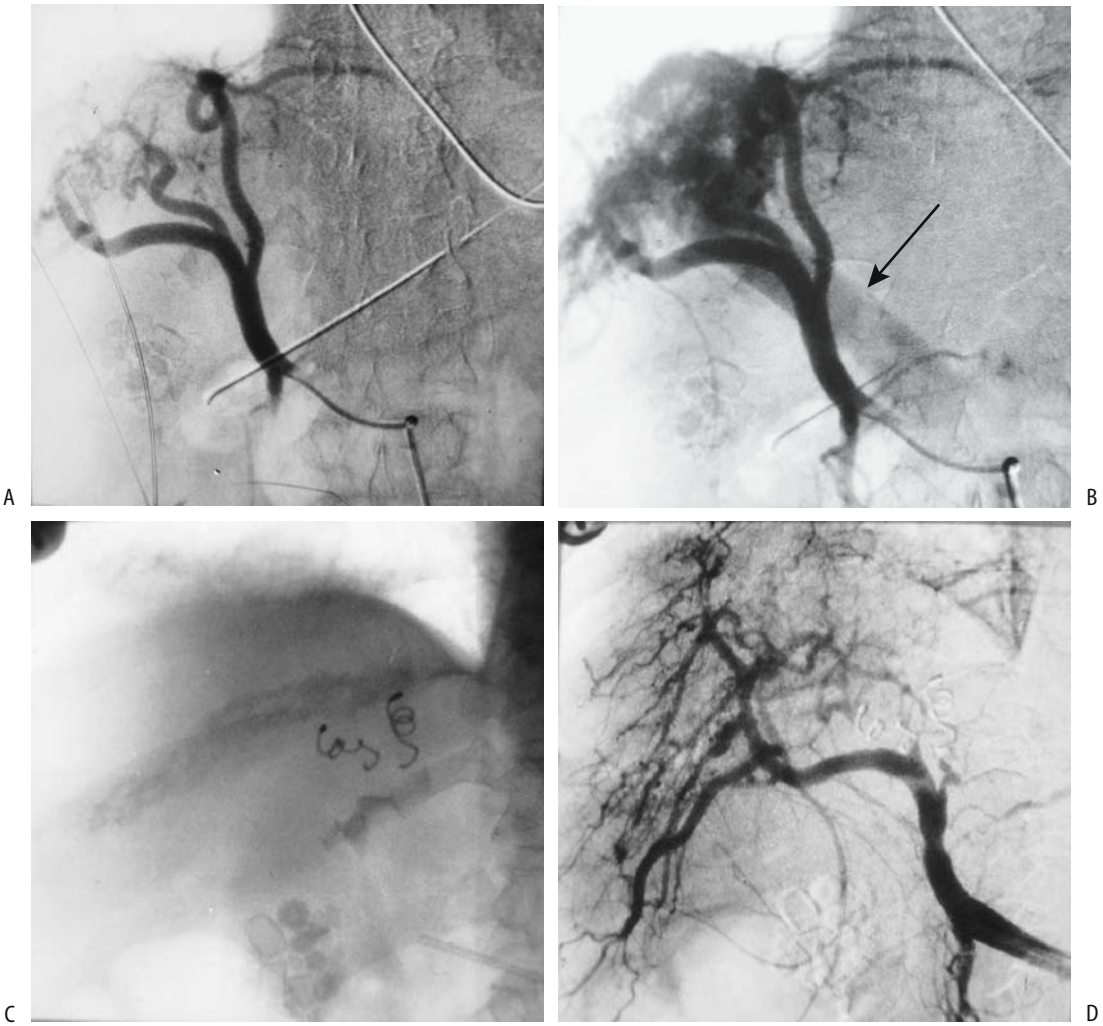

Figure 17.29. Congenital intrahepatic arterioportal fistula in a patient with hypertension. A,B: Hepatic arteriogram reveals portal vein filling (arrow) during arterial phase. C: Left and midright hepatic branches supplying the shunt are embolized with coil. D: Postembolization arteriogram reveals blocked arterial branches and no portal vein filling. (Courtesy of Oscar Gutierrez, M.D., University of Chile, Santiago, Chile.)

In the appropriate clinical setting, arteriography will define these fistulas, but some are initially not detected due to their intermittent bleeding. Some are associated with a pseudoaneurysm. Excretory urography and retrograde ureterography may simply show blood clots. Surgery is difficult in these patients. An empiric nephrectomy is considered in some patients with life-threatening bleeding, but it will miss a more distal site of bleeding. Arterial embolization and endovascular stenting are immediate therapeutic options.

Arteriovenous Malformations

Most mesenteric arteriovenous malformations are a variant of an arterioportal fistula.

Angiography detects the larger arteriovenous malformations. Many are in the pelvis and present difficult management problems. Surgi-

cal excision often is not feasible, while percutaneous embolization tends to be incomplete. Even if embolization is initially successful, invariably new channels develop and the malformation recurs. Ischemia of underlying vital structures is a complication.

Examination and Surgical Complications

One of the complications of transcatheter arterial embolization is iatrogenic dissection of the involved artery and its branches. For example, using the celiac artery to embolize hepatocellular carcinomas, the two most common sites of dissection are the celiac artery and proper hepatic artery. Sequelae of these dissections range from complete vessel recanalization, to stenosis, to complete obstruction.

Inferior vena caval laceration and dissection occur secondary to passage of various catheters and wires.

Temporary bacteremia occurs during angiographic procedures; prevalence is greater during angioplasties than during diagnostic arteriographies.

References

1. Ernst O, Asnar V, Sergent G, et al. Comparing contrast-enhanced breath-hold MR angiography and conventional angiography in the evaluation of mesenteric circulation. AJR 2000;174:433–439.
2. Lin J, Zhou KR, Chen ZW, Wang JH, Yan ZP, Wang YX. 3D contrast-enhanced MR portography and direct X-ray portography: a correlation study. Eur Radiol 2003;13:1277–1285.
3. Alfke H, Ishaque N, Froelich JJ, Klose KJ. [Magnetic resonance phlebography (MRP) of the abdomen and pelvis.] [German] Radiologe 1998;38:591–596.
4. Shiomi S, Sasaki N, Habu D, et al. Natural course of portal hemodynamics in patients with chronic liver diseases, evaluated by per-rectal portal scintigraphy with Tc-99m pertechnetate. J Gastroenterol 1998;3: 517–522.
5. Gattoni F, Dova S, Tonolini M, Uslenghi CM. [Study of the liver and the portal venous system with digital rotational angiography.] [Italian] Radiol Med 2001; 101:118–124.
6. Spinosa DJ, Matsumoto AH, Angle JF, et al. Safety of CO(2)- and gadodiamide-enhanced angiography for the evaluation and percutaneous treatment of renal artery stenosis in patients with chronic renal insufficiency. AJR 2001;176:1305–1311.
7. Nyman U, Elmståhl B, Leander P, Nilsson M, Golman K, Almén T. Gadolinium contrast media for DSA in Azotemia. Acta Radiol 2002;9(suppl. 2):S528–S530.
8. American College of Radiology: Manual on Contrast Media, 4th ed., Reston, Virginia, 1998.
9. European Society of Urogenital Radiology: Guidelines on Contrast Media, Version 4.0, available at www.esur.org, 2004.
10. Caridi JG, Hawkins IF Jr, Cho K, et al. CO2 splenoportography: preliminary results. AJR 2003;180:1375–1378.
11. Quek SC, Tan L, Quek ST, Yip W, Aw M, Quak SH. Abdominal coarctation and Alagille syndrome. Pediatrics 2000;106:E9.
12. Schmid MR, Pfammatter T. Agenesis of the hepatic segment of the inferior vena cava with portal continuation. AJR 2001;177:120–122.
13. Nonent M, Larroche P, Forlodou P, Senecail B. Celiac-bimesenteric trunk: anatomic and radiologic description—case report. Radiology 2001;220:489–491.
14. Puig S, Stuhlinger HG, Domanovits H, et al. Posterior "Nutcracker" phenomenon in a patient with abdominal aortic aneurysm. Eur Radiol 2002;12 Suppl 3:S133–S135.
15. Brown MA, Hauschildt JP, Casola G, Gosink BB, Hoyt DB. Intravascular gas as an incidental finding at US after blunt abdominal trauma. Radiology 1999;210: 405–408.
16. Wong H, Gotway MB, Sasson AD, Jeffrey RB. Periaortic hematoma at diaphragmatic crura at helical CT: sign of blunt aortic injury in patients with mediastinal hematoma. Radiology 2004;231:185–189.
17. Serfaty JM, Chaabane L, Tabib A, Chevallier JM, Briguet A, Douek PC. Atherosclerotic plaques: classification and characterization with T2–weighted high-spatial-resolution MR imaging—an in vitro study. Radiology 2001;219:403–410.
18. Therasse E, Cote G, Oliva VL, et al. Infrarenal aortic stenosis: value of stent placement after percutaneous transluminal angioplasty failure. Radiology 2001;219: 655–662.
19. Biederer J, Link J, Steffens JC, Fronius M, Heller M. [Contrast media-enhanced 3D MR angiography before endovascular treatment of aneurysm in the abdominal aorta, iliac artery and peripheral vessels.] [German] Rofo Fortschr Geb Rontgenstr Neuen Bildgeb Verfahr 2000;172:985–991.
20. Macari M, Israel GM, Berman P, et al. Infrarenal abdominal aortic aneurysms at multi-detector row CT angiography: intravascular enhancement without a timing acquisition. Radiology 2001;220:519–523.
21. LePage MA, Quint LE, Sonnad SS, Deeb GM, Williams DM. Aortic dissection: CT features that distinguish true lumen from false lumen. AJR 2001;177:207–211.
22 Hansmann HJ, Dobert N, Kucherer H, Richter GM. [Various spiral CT protocols and their significance in the diagnosis of aortic dissections: results of a prospective study.] [German] Rofo Fortschr Geb Rontgenstr Neuen Bildgeb Verfahr 2000;172:879–887.
23. Quint LE, Williams DM, Francis IR, et al. Ulcerlike lesions of the aorta: imaging features and natural history. Radiology 2001;218:719–723.

24. Akkersdijk GJ, van Bockel JH. Ruptured abdominal aortic aneurysm: initial misdiagnosis and the effect on treatment. Eur J Surg 1998;164:29–34.
25. Kapadia BJ, Agarwal M, de Silva RD. Primary aorto-duodenal fistulas in minimally aneurysmal aortas: imaging diagnosis. Abdom Imaging 2000;25:51–54.
26. Chuter TA, Gordon RL, Reilly LM, et al. Abdominal aortic aneurysm in high-risk patients: short- to intermediate-term results of endovascular repair. Radiology 1999;210:361–365.
27. Engellau L, Olsrud J, Brockstedt S, et al. MR evaluation ex vivo and in vivo of a covered stent-graft for abdominal aortic aneurysms: ferromagnetism, heating, artifacts, and velocity mapping. J Magn Reson Imaging 2000;12:112–121.
28. Lenhart M, Volk M, Manke C, et al. Stent appearance at contrast-enhanced MR angiography: in vitro examination with 14 stents. Radiology 2000;217:173–178.
29. Cejna M, Loewe C, Schoder M, et al. MR angiography vs CT angiography in the follow-up of nitinol stent grafts in endoluminally treated aortic aneurysms. Eur Radiol 2002;12:2443–2450.
30. Gorich J, Rilinger N, Sokiranski R, et al. Endoleaks after endovascular repair of aortic aneurysm: are they predictable? Initial results. Radiology 2001;218:477–480.
31. Fan CM, Rafferty EA, Geller SC, et al. Endovascular stent-graft in abdominal aortic aneurysms: the relationship between patent vessels that arise from the aneurysmal sac and early endoleak. Radiology 2001; 218:176–182.
32. Armerding MD, Rubin GD, Beaulieu CF, et al. Aortic aneurysmal disease: assessment of stent-graft treatment-CT versus conventional angiography. Radiology 2000;215:138–146.
33. Napoli V, Bargellini I, Sardella SG, et al. Abdominal aortic aneurysm: contrast-enhanced US for missed endoleaks after endoluminal repair. Radiology 2004;233:217–225.
34. Baum RA, Carpenter JP, Tuite CM, et al. Diagnosis and treatment of inferior mesenteric arterial endoleaks after endovascular repair of abdominal aortic aneurysms. Radiology 2000;215:409–413.
35. Clemens L, Bernardini S, Chabannes E, Debiere F, Bittard H. [Ureteral lesions after surgery of the aortic bifurcation. Report of 6 cases.] [French] Prog Urol 2000;10:1156–1160.
36. Simons PC, van Overhagen H, Bruijninckx CM, Kropman RF, Kuijpers KC. Periaortitis with ureteral obstruction after endovascular repair of an abdominal aortic aneurysm. AJR 2002;179:118–120.
37. Kluge A, Bachmann G,Weimar B, Rau WS. Inconspicuous path of an aortic bypass straight through the urinary bladder. AJR 1999;173:246.
38. Sueyoshi E, Sakamoto I, Hayashi K. Aortic aneurysms in patients with Takayasu's arteritis: CT evaluation. AJR 2000;175:1727–1733.
39. Men S, Yucesoy C, Edguer TR, Hekimoglu B. Intraaortic growth of hydatid cysts causing occlusion of the aorta and of both iliac arteries: case report. Radiology 1999;213:192–1944.
40. Ruehm SG, Weishaupt D, Debatin JF. Contrast-enhanced MR angiography in patients with aortic occlusion (Leriche syndrome). J Magn Reson Imaging 2000;11:401–410.
41. Wildberger JE, Schmitz-Rode T, Reffelmann T, Siewert E, Hubner D, Gunther RW. [Percutaneous transjugular thrombectomy in iliocaval thrombosis—initial experience with a newly developed 12F balloon sheath.] [German] Rofo Fortschr Geb Rontgenstr Neuen Bildgeb Verfahr 2000;172:651–655.
42. Le Bouedec G, Bailly C, Penault-Llorca F, Fonck Y, Dauplat J. [Intravascular leiomyomatosis of uterine origin. A case of pseudo-metastatic cavo-cardial thrombus.] [Review] [French] Presse Med 1999;28: 1463–1465.
43. Mingoli A, Sapienza P, Cavallaro A, et al. The effect of extent of caval resection in the treatment of inferior vena cava leiomyosarcoma. Anticancer Res 1997;17: 3877–3881.
44. Kelekis NL, Semelka RC, Hill ML, Meyers DC, Molina PL. Malignant fibrous histiocytoma of the inferior vena cava: appearances on contrast-enhanced spiral CT and MRI. Abdom Imaging 1996;21:461–463.
45. Gibo M, Murata S, Kuroki S. Pericaval fat collection mimicking an intracaval lesion on CT in patients with chronic liver disease. Abdom Imaging 2001;26:492–495.
46. Dewald CL, Jensen CC, Park YH, et al. Vena cavography with CO(2) versus with iodinated contrast material for inferior vena cava filter placement: a prospective evaluation. Radiology 2000;216:752–757.
47. Savin MA, Panicker HK, Sadiq S, Albeer YA, Olson RE. Placement of vena cava filters: factors affecting technical success and immediate complications. AJR 2002;179:597–602.
48. Athanasoulis CA, Kaufman JA, Halpern EF, Waltman AC, Geller SC, Fan CM. Inferior vena caval filters: review of a 26–year single-center clinical experience. Radiology 2000;216:54–66.
49. Ha HK, Lee HJ, Yang SK, et al. Intestinal Behçet syndrome: CT features of patients with and patients without complications. Radiology 1998;209:449–454.
50. Park JH, Chung JW, Joh JH, et al. Aortic and arterial aneurysms in Behçet disease: management with stent-grafts—initial experience. Radiology 2001;220:745–750.
51. Byun JY, Ha HK, Yu SY, et al. Computed tomography features of systemic lupus erythematosus in patients with acute abdominal pain: emphasis on ischemic bowel disease. Radiology 1999;211:203–209.
52. Kaushik S, Federle MP, Schur PH, Krishnan M, Silverman SG, Ros PR. Abdominal thrombotic and ischemic manifestations of the antiphospholipid antibody syndrome: CT findings in 42 patients. Radiology 2001;218:768–771.
53. Riddell AM, Khalili K. Sequential adrenal infarction without MRI-detectable hemorrhage in primary antiphospholipid-antibody syndrome. AJR 2004;183: 220–222.
54. Sharma MC, Deshpande V, Sharma R, Pal S, Sahni P. Giant cell phlebitis as a cause of large intestinal stricture. J Clin Gastroenterol 1998;27:79–81.
55. Lancrenon C, Delacour JL, Floriot C, et al. [Intestinal perforation due to cholesterol crystal embolism.] [French] Presse Med 2000;29:1982–1983.
56. Rand T, Weninger M, Kohlhauser C, et al. Effects of umbilical arterial catheterization on mesenteric hemodynamics. Pediatr Radiol 1996;26:435–438.

57. Heiss U, Helms A, Tietje H, Mundinger A. [Aneurysm rupture of the ileocolic artery, multiple aneurysms, renal arteriovenous fistula and fatal aortic rupture in Ehlers-Danlos syndrome, subtype IV.] [German] Rofo Fortschr Geb Rontgenstr Neuen Bildgeb Verfahr 1999;170:608–610.
58. De Toma G, Plocco M, Nicolanti V, Cavallaro G, Amato D, Letizia C. [Arterial aneurysms associated with cystic hepato-renal disease.] [French] Presse Med 2000;29: 1559–1561.
59. Garaci FG, Gandini R, Romagnoli A, Fasoli F, Varrucciu V, Simonetti G. Hepatic artery pseudoaneurysm in von Willebrand's disease. Eur Radiol 2003;13:1913–1915.
60. Scesa JL, Garcier JM, Privat C, et al. [Aneurysm of the duodeno-pancreatic arcades. Diagnostic imagery and therapeutic indications] [French] Presse Med 2000;29: 1115–1117.
61. Merkel C, Sacerdoti D, Bolognesi M, Bombonato G, Gatta A. Doppler sonography and hepatic vein catheterization in portal hypertension: assessment of agreement in evaluating severity and response to treatment. J Hepatol 1998;28:622–630.
62. Haag K, Rossle M, Ochs A, et al. Correlation of duplex sonography findings and portal pressure in 375 patients with portal hypertension. AJR 1999;172: 631–635.
63. Dutta U, Bhutani V, Nagi B, Singh K. Reversible portal hypertension due to tuberculosis. Indian J Gastroenterol 2000;19:136–137.
64. Lachmann RH, Wight DG, Lomas DJ, et al. Massive hepatic fibrosis in Gaucher's disease: clinicopathological and radiological features. QJM 2000;93: 237–244.
65. Saeki M, Honna T, Nakano M, Kuroda T. [Portal hypertension after successful hepatic portoenterostomy in biliary atresia.] [Japanese] Nippon Geka Gakkai Zasshi 1996;97:648–652.
66. Bryce TJ, Yeh BM, Qayyum A, et al. CT signs of hepatofugal portal venous flow in patients with cirrhosis. AJR 2003;181:1629–1633.
67. Kim JH, Lee YS, Kim SH, Lee SK, Lim MK, Kim HS. Does umbilical vein catheterization lead to portal venous thrombosis? Prospective US evaluation in 100 neonates. Radiology 2001;219:645–650.
68. Kreft B, Strunk H, Flacke S, et al. Detection of thrombosis in the portal venous system: comparison of contrast-enhanced MR angiography with intraarterial digital subtraction angiography. Radiology 2000;216: 86–92.
69. Nishibori H, Kanematsu M, Kondo H, Matsuo M, Hoshi H. Pseudothrombosis in the portal venous system: a potential pitfall with gadolinium-enhanced dynamic gradient-recalled echo imaging of the liver. J Magn Reson Imaging 2000;12:763–768.
70. Cosme Jimenez A, Barrio Andres J, Bujanda Fernandez de Pierola L, et al. Clinical characteristics of non-neoplastic cavernomatous transformation of the portal vein at a Gastroenterology Service in Spain. Rev Esp Enferm Dig 2000;92:448–457.
71. Ueno N, Sasaki A, Tomiyama T, Tano S, Kimura K. Color Doppler ultrasonography in the diagnosis of cavernous transformation of the portal vein. J Clin Ultrasound 1997;25:227–233.
72. Matsumoto A, Kitamoto M, Imamura M, et al. Three-dimensional portography using multislice helical CT is clinically useful for management of gastric fundic varices. AJR 2001;176:899–905.
73. Tanoue S, Kiyosue H, Komatsu E, Hori Y, Maeda T, Mori H. Symptomatic intrahepatic portosystemic venous shunt: embolization with an alternative approach. AJR 2003;181:71–78.
74. Bernard B, Lebrec D, Mathurin P, Opolon P, Poynard T. Propranolol and sclerotherapy in the prevention of gastrointestinal rebleeding in patients with cirrhosis: a meta-analysis. J Hepatol 1997;26:312–324.
75. Medina CA, Caridi JG, Wajsman Z. Massive bleeding from ileal conduit peristomal varices: successful treatment with the transjugular intrahepatic portosystemic shunt. J Urol 1998;159:200–201.
76. Terasaki M, Patel NH, Helton WS, et al. Effects of transjugular intrahepatic portosystemic shunts on hepatic metabolic function determined with serial monitoring of arterial ketone bodies. J Vasc Interv Radiol 1998;9: 129–135.
77. Luca A, D'Amico G, La Galla R, Midiri M, Morabito A, Pagliaro L. TIPS for prevention of recurrent bleeding in patients with cirrhosis: meta-analysis of randomized clinical trials. Radiology 1999;212:411–421.
78. Waggershauser T, Muller-Schunk S, Holl J, Reiser M. [TIPS in patients with therapy refractory ascites and kidney dysfunction.] [German] Radiologe 2001;41: 891–894.
79. Terayama N, Matsui O, Kadoya M, et al. Transjugular intrahepatic portosystemic shunt: histologic and immunohistochemical study of autopsy cases. Cardiovasc Intervent Radiol 1997;20:457–461.
80. Chopra S, Dodd GD 3rd, Chintapalli KN, et al. Transjugular intrahepatic portosystemic shunt: accuracy of helical CT angiography in the detection of shunt abnormalities. Radiology 2000;215:115–122.
81. Owens CA, Bartolone C, Warner DL, et al. The inaccuracy of duplex ultrasonography in predicting patency of transjugular intrahepatic portosystemic shunts. Gastroenterology 1998;114:975–980.
82. Libicher M, Radeleff B, Madler U, et al. [After-care of TIPSS patients. Comparison between color Doppler ultrasound and portography.] [German] Radiologe 1998;38:370–377.
83. Leutloff UC, Richter GM, Libicher M, et al. [Follow-up of TIPSS by color-coded duplex sonography using an ultrasonic signal enhancer. First results.] [German] Radiologe 1999;39:1072–1077.
84. Murphy TP, Beecham RP, Kim HM, Webb MS, Scola F. Long-term follow-up after TIPS: use of Doppler velocity criteria for detecting elevation of the portosystemic gradient. J Vasc Interv Radiol 1998;9:275–281.
85. Kimura M, Sato M, Kawai N, et al. [Evaluation of hepatic encephalopathy and portal hemodynamics by Doppler ultrasonography after a transjugular intrahepatic portosystemic shunt.] [Japanese] Nippon Igaku Hoshasen Gakkai Zasshi 1997;57:233–237.
86. Naegele T, Grodd W, Viebahn R, et al. MR imaging and (1)H spectroscopy of brain metabolites in hepatic encephalopathy: time-course of renormalization after liver transplantation. Radiology 2000;216:683–691.
87. Yamakado K, Nakatsuka A, Tanaka N, et al. Portal venous stent placement in patients with pancreatic and

biliary neoplasms invading portal veins and causing portal hypertension: initial experience. Radiology 2001;220:150–156.
88. Verma V, Cronin DC 2nd, Dachman AH Portal and mesenteric venous calcification in patients with advanced cirrhosis. AJR 2001;176:489–492.
89. Choi D, Choo SW, Lim JH, Lee SJ, Do YS, Choo IW. Opacification of the intrahepatic portal veins during CT hepatic arteriography. J Comput Assist Tomogr 2001;25:218–224.
90. Aldrighetti L, Ferla G. Portal vein graft rectal evacuation after Whipple procedure. The Fabrizio's disease. Hepatogastroenterology 1996;43:1638–1639.
91. El Fortia M, Bendaoud M, Taema S, et al. Segmental portal hypertension due to a splenic Echinococcus cyst. Eur J Ultrasound 2000;11:21–23.
92. Andres E, Pflumio F, Knab MC, et al. [Splenic thrombosis and celiac disease: a fortuitous association?] [French] Presse Med 2000;29:1933–1934.
93. Bargallo X, Gilabert R, Nicolau C, Garcia-Pagan JC, Bosch J, Bru C. Sonography of the caudate vein: value in diagnosing Budd-Chiari syndrome. AJR 2003;181: 1641–1645.
94. Noone TC, Semelka RC, Siegelman ES, et al. Budd-Chiari syndrome: spectrum of appearances of acute, subacute, and chronic disease with magnetic resonance imaging. J Magn Reson Imaging 2000;11:44–50.
95. Seguin P, Le Bouquin V, Campion JP, Malledant Y. [Hemobilia of gallbladder origin manifesting as malignant hypertension.] [French] Presse Med 1998;27:913.
96. Nakai A, Asakura H, Oya A, Yokota A, Koshino T, Araki T. Pulsed Doppler US findings of renal interlobar arteries in pregnancy-induced hypertension. Radiology 1999;213:423–428.
97. van Jaarsveld BC, Pieterman H, van Dijk LC, et al. Interobserver variability in the angiographic assessment of renal artery stenosis. DRASTIC study group. Dutch Renal Artery Stenosis Intervention Cooperative. J Hypertens 1999;17:1731–1736.
98. Gross CM, Kramer J, Weingartner O, et al. Determination of renal arterial stenosis severity: comparison of pressure gradient and vessel diameter. Radiology 2001;220:751–756.
99. Gupta A, Tello R. Accessory renal arteries are not related to hypertension risk: a review of MR angiography data. AJR 2004;182:1521–1524.
100. Boudewijn G, Vasbinder C, Nelemans PJ, et al. Diagnostic tests for renal artery stenosis in patients suspected of having renovascular hypertension: a meta-analysis. Ann Intern Med 2001;135:401–411.
101. De Cobelli F, Venturini M, Vanzulli A, et al. Renal arterial stenosis: prospective comparison of color Doppler US and breath-hold, three-dimensional, dynamic, gadolinium-enhanced MR angiography. Radiology 2000;214:373–380.
102. Nchimi A, Biquet JF, Brisbois D, et al. Duplex ultrasound as first-line screening test for patients suspected of renal artery stenosis: prospective evaluation in high-risk group. Eur Radiol 2003;13:1413–1419.
103. Johnson PT, Halpern EJ, Kuszyk BS, et al. Renal artery stenosis: CT angiography-comparison of real-time volume-rendering and maximum intensity projection algorithms. Radiology 1999;211:337–343.
104. Paul JF, Ugolini P, Sapoval M, Mousseaux E, Gaux JC. Unilateral renal artery stenosis: perfusion patterns with electron-beam dynamic CT—preliminary experience. Radiology 2001;221:261–265.
105. Radermacher J, Chavan A, Schaffer J, et al. Detection of significant renal artery stenosis with color Doppler sonography: combining extrarenal and intrarenal approaches to minimize technical failure. Clin Nephrol 2000;53:333–343.
106. Claudon M, Plouin PF, Baxter GM, Rohban T, Devos DM. Renal arteries in patients at risk of renal arterial stenosis: multicenter evaluation of the echo-enhancer SH U 508A at color and spectral Doppler US. Levovist Renal Artery Stenosis Study Group. Radiology 2000; 214:739–746.
107. Fain SB, King BF, Breen JF, Kruger DG, Riederer SJ. High-spatial-resolution contrast-enhanced MR angiography of the renal arteries: a prospective comparison with digital subtraction angiography. Radiology 2001;218:481–490.
108. Lee VS, Rofsky NM, Ton AT, Johnson G, Krinsky GA, Weinreb JC. Angiotensin-converting enzyme inhibitor-enhanced phase-contrast MR imaging to measure renal artery velocity waveforms in patients with suspected renovascular hypertension. AJR 2000;174:499–508.
109. Soulez G, Therasse E, Qanadli SD, et al. Prediction of clinical response after renal angioplasty: respective value of renal Doppler sonography and scintigraphy. AJR 2003;181:1029–1035.
110. Bongers V, Bakker J, Beutler JJ, Beek FJ, De Klerk JM. Assessment of renal artery stenosis: comparison of captopril renography and gadolinium-enhanced breath-hold MR angiography. Clin Radiol 2000;55: 346–353.
111. Radermacher J, Chavan A, Bleck J, et al. Use of Doppler ultrasonography to predict the outcome of therapy for renal-artery stenosis. N Engl J Med 2001;344:410–417.
112. Soulez G, Therasse E, Qanadli SD, et al. Prediction of clinical response after renal angioplasty: respective value of renal Doppler sonography and scintigraphy. AJR 2003;181:1029–1035.
113. Plouin PF, Raynaud A, Elkohen M, Pannier-Moreau I, Battaglia C. [Non-surgical treatments of renal artery stenoses.] [Review] [French] Presse Med 1996;25: 725–730.
114. Xue F, Bettmann MA, Langdon DR, Wivell WA. Outcome and cost comparison of percutaneous transluminal renal angioplasty, renal arterial stent placement, and renal arterial bypass grafting. Radiology 1999;212:378–384.
115. van Jaarsveld BC, Krijnen P, Pieterman H, et al. The effect of balloon angioplasty on hypertension in atherosclerotic renal-artery stenosis. N Engl J Med 2000;342:1007–1014.
116. van de Ven PJ, Kaatee R, Beutler JJ, et al. Arterial stenting and balloon angioplasty in ostial atherosclerotic renovascular disease: a randomised trial. Lancet 1999;353:282–286.
117. Sharma S, Gupta H, Saxena A, et al. Results of renal angioplasty in nonspecific aortoarteritis (Takayasu disease). J Vasc Interv Radiol 1998;9:429–435.

118. Akan H, Arik N, Saglam S, Danaci M, Incesu L. Selcuk MB. Evaluation of the patients with renovascular hypertension after percutaneous revascularization by Doppler ultrasonography. Eur J Radiol 2003;46:124–129
119. Behrendt P, Do D, Baumgartner I, Triller J, Kniemeyer H, Mahler F. Renal artery stenting following acute aortic dissection: implantation and follow-up. Vasa 2000;29:138–140.
120. Leertouwer TC, Gussenhoven EJ, Bosch JL, et al. Stent placement for renal arterial stenosis: where do we stand? A meta-analysis. Radiology 2000;216:78–85.
121. Baumgartner I, von Aesch K, Do DD, Triller J, Birrer M, Mahler F. Stent placement in ostial and nonostial atherosclerotic renal arterial stenoses: a prospective follow-up study. Radiology 2000;216:498–505.
122. Szucs-Farkas Z, Toth J, Szollosi Z, Peter M, Bartha I. Pseudoaneurysm and ilio-caval fistula caused by malignant fibrous histiocytoma of the aorta–CT diagnosis and angiographic confirmation. Eur Radiol 2002;12:450–453.
123. Roos JE, Willmann JK, Hilfiker PR. Secondary aortoenteric fistula: active bleeding detected with multi-detector-row CT. Eur Radiol 2002;12 Suppl 3:S196–200.
124. Guillem PG, Binot D, Dupuy-Cuny J, et al. Duodenocaval fistula: a life-threatening condition of various origins. J Vasc Surg 2001;33:643–645.

Index

B

C

R

T